Copyrighted Materials
Copyright © 1996 NACE International Retrieved from www.knovel.com

Corrosion-Resistant Alloys in Oil and Gas Production

Volume I and Volume II

Juri Kolts and Stephen W. Ciaraldi, editors

NACE International • Houston • 1996

NACE International

© 1996 by NACE International
All rights reserved.
Printed in the United States of America

Library of Congress Catalog Card Number: 96-069736
ISBN: 1-877914-92-4

Reproduction of contents in whole or part or transfer into electronic or photographic storage without permission of copyright owner is expressly forbidden.

Neither NACE International, its officers, directors, nor members thereof accept any responsibility for the use of the methods and materials discussed herein. No authorization is implied concerning the use of patented or copyrighted material. The information is advisory only, and the use of the materials and methods is solely at the risk of the user.

NACE International, 1440 South Creek Dr., Houston, TX 77084
(713) 492-0535

Copyrighted Materials
Copyright © 1996 NACE International Retrieved from www.knovel.com

Preface

Following decades of low product margins, the "oil crisis" of the 1970s resulted in substantial increases in energy prices. This economic trend produced a surge in oil and gas exploration, development, and production, including the pursuit of deep, highly pressured, and environmentally hostile hydrocarbon reserves. The associated technical hurdles spawned a significant increase in research and other technology activities aimed at addressing the challenges. These technology activities continued through the 1980s and are still ongoing today. Despite lower product prices, technology is now recognized as a critical enabling element for economic feasibility of many oil and gas developments and a substantial contributor to minimizing exploration and production costs.

Materials technology was among those advanced by the recent petroleum industry events just described. Advancements were particularly evident in the use and further development of corrosion-resistant alloys for oil and gas production. Historically, corrosion-resistant alloys had been used in instruments, valve components, and downhole equipment. In the 1980s, use of corrosion-resistant alloys was extended to tubing and liners. This increasingly common application was fueled by the recognition that alloy use could provide considerable cost savings through a project's life cycle, despite higher initial capital expense. More recently, process facilities in offshore production, especially in the North Sea, have utilized increased volumes of corrosion-resistant alloys. This usage also has been driven by life cycle cost savings.

Corrosion-resistant alloys offer technical advantages by virtue of their high corrosion resistance and often higher strength. These properties improve safety and reliability by reducing the need for corrosion-induced workovers and the maintenance of downhole inhibition programs. The higher strengths permit extension to deeper and higher pressure wells. Although each project has its own particular attributes, cost savings associated with corrosion resistant-alloys often are related to:

- the high cost of offshore personnel;
- increased cost of deferred production in high productivity fields;
- increased emphasis on non-staffed or minimally staffed facilities;
- increased cost of remedial work in subsea, deep water, or deep well production;
- cost savings associated with improved safety and reliability.

Selections of specific alloys from among the large number available are made on the basis of mechanical properties, corrosion resistance, and resistance to environmental cracking. Because of the large range of environmental conditions encountered in oil and gas production, the materials options available to resist these environments also is quite broad. This range of materials includes the martensitic stainless steels to the highly alloyed nickel- and cobalt-base alloys. The economic impact of utilizing the "proper" alloy is significant.

Despite the increased use of corrosion-resistant alloys for oil and gas production, the experience base is quite limited. This compilation of selected papers was thus prepared to provide a ready one-source overview. The compilation emphasizes not only the interactions between corrosion-resistant alloys and environments observed in laboratory tests, but also pertinent field experience. It includes contributions of alloy suppliers, component manufacturers, and end users, providing multiple perspectives on the subject.

NOTE: As in all compilations, many excellent publications are left out because of space, scope, or because the editors have missed these in the literature search. We apologize to those authors whose papers have been overlooked. To the authors contributing to this compilation, we extend our compliments because they have provided an excellent data base for the introduction, and continued use, of a new technology in the petroleum industry. Their efforts and dedication have resulted in safe and cost-effective improvements to industry practice.

Juri Kolts Stephen W. Ciaraldi

Copyrighted Materials
Copyright © 1996 NACE International Retrieved from www.knovel.com

Contents

Preface ..... *xi*

VOLUME I

Section 1 Martensitic Stainless Steels

"Failures of Martensitic Stainless Steels in Sweet and Sour Gas Service"
J.D. Alkire, S.W. Ciaraldi **3**
"Development of Sour Resistant Modified 13CR OCTG"
H. Asahi, T. Hara, A. Kawakami, A. Takahashi **12**
"Experiences with 13CR for Mitigating CO_2 Corrosion in the Oilfield, Case Histories: The Gulf of Mexico and Inland Gas Wells"
D.A. Baudoin, D.K. Barbin, J. Skogsberg **26**
"Experience of 13% Cr Tubing II: 10 years and 1 million feet later"
M. Bonis, J.L. Crolet **39**
"Corrosion Behavior of 1 to 22 Percent Chromium Steels and Monel K-500 in CO_2/Brine Environments"
J.R. Bryant, G.B. Chitwood **49**
"Laboratory Test for Evaluating Alloys for H_2S Service"
D.S. Burns **65**
"Corrosion Performance of 13 Cr Stainless Tubulars in Sour Environments"
W.C. Chen **73**
"Some Limitations on the Use of 13Cr Alloys for Corrosive Gas and Oil Production"
S.W. Ciaraldi **82**
"13Cr Tubulars Solve Corrosion Problems in the Tuscaloosa Trend"
J.D. Combes, J.G. Kerr, L.J. Klein **91**
"Effect of Stress and Environment on Failures of 17-4 pH Stainless Steel Valve Stems"
F.S. Gareau, N.A. Chambers, A.M. Martinson **99**
"Corrosion Assisted Cracking of CA-6NM"
D.A. Hansen, T. Doody **110**
"Corrosion Behavior of 9 to 25% Cr Steels in Wet CO_2 Environments"
A. Ikeda, S. Mukai, M. Ueda **112**

"Effect of Microstructure on the Sulfide Stress Corrosion Cracking Resistance of AISI 410 and 420 Steels"
Y. Ishizawa, T. Shimada, M. Tanimura 120
"Operational Experience of Using 13%Cr Tubular Steels"
M.B. Kermani, G. Weighill, T. Pendlington, G. Elliot 138
"Influence of Cathodic Protection on Stress Corrosion Cracking of Martensitic Stainless Steels in Sea Water"
H. Kiesheyer, G. Lennartz 151
"H_2S Cracking Resistance of 420 Stainless Steel Tubulars"
L.J. Klein 153
"9Cr-1Mo and 13Cr Tubulars for Sour Service"
L.J. Klein, R.M. Thompson, D.E. Moore 159
"Stress Corrosion Behavior of 13 Cr Martensitic Stainless Steels in CO_2-H_2S-Cl^- Environment"
H. Kurahashi, T. Kurisu, Y. Sone, K. Wada, Y. Nakai 171
"Stress Cracking of 13 Cr Steels in CO_2-H_2S-Cl^- Environments"
H. Kurahashi, T. Kurisu, Y. Sone, K. Wada, Y. Nakai 179
"Polarization Behavior of High-Alloy OCTG in CO_2 Environment as Affected by Chlorides and Sulfides"
K. Masamura, S. Hashizume, J. Sakai, I. Matsushima 188
" McElmo Dome CO_2 Source Facilities Corrosion Control"
M.H. Nguyen 195
"Behavior of Different Martensitic Stainless Steels Under Oil and Gas Corrosive Environments"
B.J. Orlans-Joliet, F. Blanchard, G.C. Guntz, J.-J. Servier 202
"Effect of Environmental Factors and Yield Strength on SCC Property of AISI 420 Stainless Steel"
S. Sakamoto, A. Kawakami, H. Asahi, A. Nakamura 207
"Development of Resistant OCTG and Its Application to Corrosive Wells"
M. Tanimura 226
"Sulfide Stress Cracking Failures of 12Cr and 17-4PH Stainless Steel Wellhead Equipment"
R.M. Thompson, G.B. Kohut, D.R. Canfield, W.R. Bass 237
"Evaluation of SSC Resistance on Super 13CR Stainless Steel in Sour Applications"
M. Ueda, T. Kushida, T. Mori 245
"Austenitizing Temperature Effect on SCC Resistance of 410 Stainless Steel"
D.D. Vitale, H.E. Ebert 262
"Sulfide Stress Cracking Resistance of Weld Repairs in Wellhead Alloys"
M. Watkins, E.L. Von Rosenberg 274
"Pitting and Stress Cracking of 12 CR-NI-MO Martensitic Stainless Steels in Chloride and Sulfide Environments"
Y. Yoshino, A. Ikegaya 279
"The Application & Field Experience of High Strength 12% Cr Centrifugally Cast Pipe for Gas Gatherystem"
A. Yoshitake, M. Teraoka, T. Torigoe, S. Amako 288

Section 2 Austenitic Stainless Steels

"Sulfide Stress Cracking of AISI 304 Stainless Steel Springs in Sour Water"
B. Craig, B. Hodgson 297
"Sulfide Stress Cracking Resistance of Nitrogen Strengthened Stainless Steels"
R.R. Gaugh 299
"Effects of Residual Stress on Stress Corrosion Cracking
of Non-Magnetic Drill Dollars"
D.S. Kopecki 308
"A Criterion for Evaluating and Predicting the Sour Resistance of High Alloys"
T. Murata, R. Matsuhashi, M. Sakakibara, M. Onayama 318
"The Stress Resistance of Non-Magnetic Stainless Steels
Used in Oil Exploration"
P. G. Smith, J.E. Truman, H.T. Gisborne, G. Oakes 328

Section 3 Duplex Stainless Steels

"Materials Failures in Sour Gas Service"
S.W. Ciaraldi 343
"Evaluation and Application of Highly Alloyed Materials
for Corrosive Oil Production"
B.D. Craig 351
"Evaluation of the Resistance of Some Highly Alloyed Stainless Steels
to Stress Corrosion Cracking in Hot Chloride Solutions
under High Pressures of CO_2 and H_2S"
J.L. Crolet, M.R. Bonis 363
"Special Stainless Steels for Application of Natural Gas Exploitation Systems;
Resistance to Stress Corrosion in Environments Containing
Chlorides and H_2S of Austenitic and Austeno-Ferritic Grades"
A. Desestret, E. Mirabal, D. Catelin, P. Soulignac 375
"Properties of and Experience with Welded Joints in Stainless Alloys"
H. Eriksson, P. Norberg, S. Bernhardsson 397
"Corrosion and Age Hardening Studies of Some Cast Stainless Alloys
Containing Ferrite"
J.W. Flowers, F.H. Beck, M.G. Fontana 407
"The Effect of Cathodic Protection on Duplex Stainless Steels in Sea Water"
R. Francis, G. Byrne, G.R. Warburton 420
"The Corrosion of Duplex Stainless Steels in Sour Service"
R. Francis, G. Byrne 434
"Corrosion Behaviors of Duplex Stainless Steel for Wet CO_2 Environment"
A. Ikeda, M. Miura, S. Mukai, M. Ueda, K. Koso 447
"Effect of Alloying Element and Ferrite-Austenite Ratio on SCC Resistance
of Duplex Stainless Steels in Sour Gas Environment"
Y. Ishizawa, T. Inazumi 464

"Production Technology and Corrosion Properties of Duplex Stainless Steel Line Pipe by HF-ERW Process"
H. Kashimura, M. Onoyama, Y. Watanabe, T. Fujikawa 474
"Full Scale Testing of Duplex Stainless Steel Pipes in Simulated Sour Environments"
Y. Kobayashi, Y. Ishizawa, J. Sakai, M. Itoh, T. Taira, H. Arup 483
"Duplex Stainless Steel Pipelines and Piping on the North Slope"
A.C. Madsen, F.O. Mueller, R. Geisert., J.B. Lee, H.J. Choi 494
Corrosion Behavior of 25 Pct Cr Duplex Stainless Steel in CO_2-H_2S-Cl^- Environments"
S. Mukai, H. Okamoto, T. Kudo, A. Ikeda 501
"Stress Corrosion Cracking Susceptibility of Duplex Stainless Steels in Sour Gas Environments"
P.R. Rhodes, G.A. Welch, L. Abrego 518
"Investigation of the Stress Corrosion Cracking of Duplex Stainless Steel Weldments in Sour Conditions"
M.J. Schofield, R. Bradshaw, R.A. Cottis 557
"Optimizing Welding Condition for Excellent Resistance in Duplex Stainless Steel Linepipe"
K. Tamaki, K. Yasuda, M. Kimura, H. Kawasaki, T. Uegaki 567
"Corrosion Resistance of Duplex Stainless Steel Weldments"
H. Tsuge, Y. Tarutani, T. Kudo 574
"Performance of High Resistant Duplex Stainless Steel in Chloride and Sour Environments"
M. Ueda, H. Okamoto, T. Kobayashi, K. Kondo, K. Ogawa, T. Kudo 588
"Influence of Thermal History on Corrosion Resistance of Duplex Stainless Steel Linepipe"
K. Ume, N. Seki, Y. Naganawa, T. Hyodo, K. Satoh, Y. Kuriki 609
"Effect of Heat Treatment and Microstructure on the Corrosion and SCC of Duplex Stainless Steels in H_2S/Cl^- Environments"
S. Mark Wilhelm, R.D. Kane 621
"Performance of Duplex Stainless Steel Pipes in Sour Gas Wells"
G. Wilken 630

VOLUME II

Section 4 Precipitation-Hardened Nickel Alloys

"Cast Nickel Alloys for Sour Service"
R. Badrak 641
"Effect of Sulfur on Cracking Behavior of CRA's in Simulated Downhole Environments"
W. Coyle 653

"Evaluation and Qualification of a Precipitation-Hardened Material for Deep, Hot, Sour Environments"
T.A. DeBold, N.B. Schmidt, M.F. Bluem, S.R. Herman 666
"Failure of Monel Ni-Cu-Al Alloy K-500 Bolts in Seawater"
K.D. Efird 676
"Stress Corrosion Cracking and Hydrogen Embrittlement of High-Strength Nonmagnetic Alloys in Brines"
J.G. Erlings, H.W. deGroot, J.F.M. van Roy 680
"Development of Large Nickel-Base Alloy 925 Composite Block Trees for Extreme Corrosion, Fire-Resistant Applications on Offshore Platforms"
T. Haeberle, P.J. Kovach 687
"Hydrogen Embrittlement of INCOLOY Alloy 925, MONEL Alloy K-500, and INCONEL Alloy 625 by Slow Strain Method"
J.A. Harris, E.F. Clatworthy 695
"Behavior of Age-Hardenable Alloy UNS NO7725 for Oil Field Applications"
E.L. Hibner 701
"Precipitation-Hardened, Nickel-Base Alloys for Sour Gas Environments"
M. Igarashi, S. Mukai, T. Kudo, Y. Okada, A. Ikeda 709
"Failures of Nickel Copper Bolts in Subsea Applications"
M.W. Joosten, L.H. Wolfe 716
"Heat Treatment and Environmental Embrittlement of High-Performance Alloys"
J. Kolts 722
"Alloy 718 for the Oil and Gas Industry, Superalloy 718 Metallurgy and Applications
J. Kolts 733
"Alloy 718-Alloy Optimization for Applications in Oil and Gas Production"
O.A. Onyewuenyi 749

Section 5 Solid Solution Nickel/Cobalt-Base Alloys

"Corrosion-Resistant Alloys for Hot, Deep Sour Wells: Properties, Experience, and Future Trends"
A.I. Asphahani, J.C. Prouheze, G.J. Petersen 769
"Stress-Cracking Resistance of Stainless Alloys in Sour Environments"
H.E. Chaung, M. Watkins, G.A. Vaughn 779
"Laboratory Testing of Nickel Alloys for H_2S Service"
J.A. Harris, T.F. Lemke 786
"Environmental Cracking Evaluation of Resistant Alloys in H_2S-CO_2-CL^- Environment by Slow Strain Rate Tensile Test"
A. Ikeda, M. Ueda, H. Tsuge 791
"Laboratory Evaluation of Corrosion Resistant Alloys for the Oil and Gas Industry"
J. Kolts 810
"Temperature and Texture Effects on Properties of CRA's"
S.E. Mahmoud, C.W. Petersen 828

"The Use of Strain Rate Testing to Determine the Effect of Elemental Sulfur on Stress Corrosion Cracking of Nickel-Base Alloys"
C.J. Martin, H.S. Ahluwa, F. Blanchard, J. Skogsberg 841
"Development of High-Alloy Tubular Goods for Sour Wells"
H. Ogawa, K. Denpo, K. Ina, K. Shitani, A. Miyasaka, H. Asahi, S. Sakamoto, M. Onoyama 855
"Critical Contents of Nickel and Chromium Required for SCC Resistance of High Alloy OCTG"
J.I. Sakai, M. Honda, K. Masamura, I. Matsushima, Y. Ishizawa 861
"Laboratory and Field Evaluations of Clad Christmas Tree Equipment"
W.J. Sisak, J.R. Gordon 871
"The Effect of Elemental Sulfur on Stress Cracking of Nickel Base Alloys"
N. Sridhar, S.M. Corey 877
"Influence of Elemental S on Corrosion Behavior of CRA in H_2S-CO_2-Cl^- Environment"
M. Ueda, T. Kudo 888
"Wireline Materials for Sour Service"
G.A. Vaughn, H.E. Chaung 905

Section 6 Other Alloys

"Corrosion and Stress Corrosion Cracking of Aluminum Alloy Drillpipe in a Water-Based, Low-Solids, Nondispersed Drilling Mud"
S.W. Ciaraldi, D.R. Grimes, H.F. Nichols, S.O. Moore 915
"Yellow Metal (UNS C69100) for Sour Service"
T. Clark, W. Inglis, C.M. Fowler 923
"Performance of a Beryllium Copper Nonmagnetic Drill Collar Alloy"
F. Dunlevey 936
"Corrosion and Hydrogen Embrittlement Behavior of Titanium in Aqueous Sulfidic Solutions"
Z.A. Foroulis 943
"Engineering Incentives for Utilizing Ti-3Al-8V-6Cr-4Zr-4Mo Alloy Tubulars in Highly Aggressive Deep Sour Gas Wells"
D.R. Klink, R.W. Schutz 952
"Stress Corrosion Behavior of Ti-3Al-8V-6Cr-4Zr-4Mo Alloy Under Deep Sour Gas Well Conditions"
R.W. Schutz, M. Xiao, T.A. Bednarowicz 964
"Stress Cracking Behavior of Ti-38-6-44 In Sour Gas Environments"
D.E. Thomas, S.R. Seagle 982
"The Chloride Stress Corrosion Cracking Behavior of Beryllium Copper and Other Nonmagnetic Drill Collar Alloys"
J.C. Turn Jr. 989

"The Effect of Oxygen and Temperature on Chloride Stress Corrosion Cracking of Beryllium Copper and Other Nonmagnetic Alloys in a Simulated Chloride Drilling Environment"
J.C. Turn Jr. **998**
"The Performance of Zirconium Alloys in Sulfide Solutions"
T. Yau **1,009**

Section 7 Acidizing Corrosion-Resistant Alloys

"Duplex Stainless Steel Behavior During Acidification: Laboratory Versus Field Test Results"
T. Cheldi, I. Obracaj, A. Cagada, M. Cabrini, B. Vicentini, G. Rondelli **1,017**
"Hydrogen-Assisted Cracking and Inhibition of Spring Alloys in Acidizing Solutions"
W.R. Coyle, G.B. Chitwood, P.W. Rice, M.L. Walker **1,026**
"How High Alloy Tubulars React in Acidizing Environments"
J.D. Garber, M. Kantour **1,038**
"Compatibility of Stainless and Nickel Base Alloys in Acidizing Environments"
R.D. Kane, S.M. Wilhelm **1,043**
"Corrosion and Stress Corrosion Cracking of High-Performance Alloys in Simulated Acidizing Environments to 175°C (350°F)"
J. Kolts, S.M. Corey **1,054**
"Corrosion Inhibition of 13Cr, Super 13Cr, and 15Cr Stainless Steels in HCl-HF Acidizing Fluids"
R.D. Mack **1,058**
"Effect of Acidizing Solutions on K_{IEAC} of 13 Cr and 22 Cr Stainless Steels"
T.H. McCoy, S.T. Mackey, M.L. Walker **1,067**
"Corrosion Behaviors of Corrosion-Resistant Alloys in Acid Stimulation Environments"
A. Miyasaka, H. Ogawa **1,088**
"A Field Experience of Corrosion Inhibition During the Acid Fracturing of a Deep Oil Well Completed with 22% Cr Duplex Steel"
A. Valdes, A. Viloria, S. Marcano **1,096**
"Acid Inhibition of CRA's: A Review"
M.L. Walker, J. M. Cassidy, K.R. Lancaster, T.H. McCoy **1,104**

Bibliography **1,127**

Copyrighted Materials
Copyright © 1996 NACE International Retrieved from www.knovel.com

Section 1

MARTENSITIC STAINLESS STEELS

Paper No. 210—CORROSION/88

FAILURES OF MARTENSITIC STAINLESS STEELS IN SWEET AND SOUR GAS SERVICE

J.D. Alkire and S.W. Ciaraldi
Amoco Corporation
Amoco Research Center
P.O. Box 400
Naperville, IL 60566

ABSTRACT

Several failures of Type 410 stainless steel (SS) and CA6NM components in sweet and sour gas well service are reviewed. The sweet corrosion resistance of Type 410 SS wellhead components was exceeded due to high flow velocities and turbulence, resulting in rapid attack. This equipment also simultaneously suffered crevice corrosion in service. A high hardness Type 410 SS subsurface safety valve experienced hydrogen stress-cracking in the absence of H_2S when exposed to a brine completion fluid. Finally, sulfide stress-cracking failure of a CA6NM wellhead valve was contributed to a weld repair made prior to final heat treatment. In this case, weld metal chemistry variation resulted in insufficient temper softening, despite the fact that low hardness was obtained in the valve base metal. The failures discussed further define the limitations of martensitic stainless steels used for corrosive gas production and indicate that additional precautions are necessary to assure failure-free performance.

INTRODUCTION

Corrosion mitigation has become a major concern in the production of many deep, high-pressure gas reserves. CO_2 and H_2S gases often present in deep reservoirs can be extremely corrosive to traditionally used steel tubulars and wellheads. Conditions can be made worse by high formation temperatures and by the presence of aqueous brines containing organic acids. However, such reserves can be successfully produced through use of corrosion inhibition and/or application of corrosion-resistant alloy (CRA) equipment.

Martensitic stainless steels having 12-13% chromium base metal compositions represent economical CRA material selections compared to higher nickel stainless steels and nickel-base alloys. Unfortunately, martensitic stainless steels have limitations, with respect to both corrosion resistance and susceptibility to sulfide stress-cracking (SSC) in sour wells. These limits have been at least qualitatively defined by numerous laboratory investigations. However, the complexities of corrosion and environmentally-induced cracking phenomena can sometimes lead to unanticipated field failures. Several such failures, described below, illustrate the importance of field experience as a supplement to laboratory testing in defining the application limits of martensitic stainless steels for sweet and sour gas production.

SWEET CORROSION OF WELLHEAD COMPONENTS

Types 410 and 420 stainless steels (SS) contain 11.5-14% chromium. These steels have demonstrated excellent sweet (CO_2) corrosion resistance in laboratory tests, within limits of temperature, aqueous chloride content, and CO_2 partial pressure.[1,2] Successful performance as production tubulars, even at somewhat higher temperatures, has been reported.[3] Amoco Production Company has successfully utilized Type 420 stainless steel tubulars for numerous sweet gas wells, with no known corrosion problems. However, corrosion detected in Type 410 SS wellhead components used in a sweet gas field in the Gulf of Mexico necessitated early replacement with equipment having greater corrosion resistance.

Wells in this field typically produced 20-50 MMSCFD of gas containing about 2% CO_2, but no detectable H_2S. Condensate yield was 200-600 BBLS/D with extremely low water cut. Sand production was minimal.

Flowing wellhead pressures and temperatures were about 7,500-9,000 psig (52-62 MPa) and 110°C (230°F), respectively. Separated produced water had low total dissolved solids content of 1,300 ppm. Chloride content was only about 800 ppm. Although carbonate/bicarbonate ions were not detected, organic acids anions, primarily as acetates, were present to about 230 ppm. Measured pH of fluids exposed to air but still CO_2 saturated was typically 4.6.

Wellheads consisted of forged, Type 410 SS (F6a) gate valves and chokes, pressure rated to 15,000 psig (103 MPa). Internal diameter of the valves was 3-1/16 in. (77.8 mm), which have linear flow velocities of 12-31 ft/s (3.7-9.4 m/s). This corresponds approximately to about 0.3-1.1 times the API limiting velocity as defined in RP 14E.[4]

Pressure reduction to the 1,250 psig (8.6 MPa) flow line conditions was accomplished in two stages, using a fixed and an adjustable choke. Although velocities approaching sonic were obtained at choke points and choke outlets, these regions were sleeved with silicon carbide inserts. The choke bodies themselves were exposed to velocities comparable to or only slightly higher than those in the gate valves.

Overall internal appearance of the bottom half of a gate valve after longitudinal sectioning is shown in Figure 1. Pitting corrosion was observed near the inlet flange and from the valve gate to the outlet flange. Corrosion appeared flow/turbulence related just past the gate, Figure 2. Similar, but less severe attack, was observed on the upper half of the valve.

Internal, wetted valve surfaces were covered with a thin green film. This film did not extend into corrosion pits. Scrapings of the film were obtained and analyzed by x-ray diffraction (XRD), Energy Dispersive Spectroscopy (EDS), infrared (IR) analysis, and by reagent chemical tests. In summary, the film was found to be primarily zinc sulfide with small amounts of iron carbonate. Because zinc bromide-containing completion/packer fluids had been used, the zinc sulfide film probably formed by downhole reaction of such fluids with trace amounts of H_2S.

Figure 3 shows overall internal appearance of an adjustable choke body after longitudinal sectioning. Internal surfaces were relatively deposit-free, but showed deterioration in several locations. Within the choke bore, severe metal loss was observed 90° and 270° to the flow inlet, Figure 4. These locations corresponded to flow contact regions, since flow was split by a nickel-base alloy stem, which was reportedly not attacked. Corrosion metal loss was also observed in the threaded region at which the choke insert had been located. An eroded appearance was evident in only part of this threaded region. Within the gas inlet and outlet bores, scattered pitting corrosion had occurred. Note that the outlet bore was shielded from flowing conditions by the silicon-carbide insert. However, because this insert had no downstream seal, stagnant fluids could accumulate between the insert and mating choke outlet base metal, which also thereby exposed insert threads to fluids. Significant crevice corrosion was observed on outlet flange seal ring faces. Type 410 SS components of choke inserts exhibited similar forms of attack, as shown in Figure 5.

Numerous metallographic mounts were prepared from the corroded valve and choke. Typical of CO_2 corrosion, pits were sharp-walled and deep, Figure 6. Pit deposits were determined to be iron and chromium rich using an EDS equipped electron microprobe. All corroded components were confirmed by EDS to be Type 410 SS. Metallurgical structure consisted of the expected quenched and tempered martensite. Hardnesses by Rockwell C-scale (HRC) tests were 17-19 HRC.

Deterioration of the Type 410 SS wellhead components was evidently due to CO_2 corrosion. Because of low TDS of produced fluids, indicating a high proportion of condensed water compared to formation water, pH values of fluids under operating conditions may have been below 4.[5] However, locations of corrosion and lack of apparent attack in Type 420 SS production tubing, which experienced similar linear flow rates, suggests factors other than general corrosivity were prerequisites for corrosion of the wellhead equipment.

Corrosion of stainless steels requires that passive films be locally disrupted.[5] Location of severe attack near inlet ports and just beyond valve gates suggests turbulence was sufficient to destabilize passive films. This conclusion is consistent with reports that Type 420 stainless steel is resistant to CO_2 corrosion under non-turbulent flow conditions at rates up to at least 85 ft/s (26 m/s).[1] Unfortunately, virtually no laboratory corrosion data considering flow turbulence effects are available. Therefore, it is currently unknown if the reported improved CO_2 corrosion resistance of nickel and molybdenum-containing martensitic stainless steels and/or duplex stainless steels is sufficient to resist corrosion in such turbulent applications.[1,6] These alloys could be cost-effective alternatives to use of nickel-base CRA clad equipment.

Although probably not a prerequisite for corrosion, the zinc-sulfide film present on wetted valve surfaces may have contributed to attack. Corrosion performance of Type 410 SS is adversely affected by the presence of

aqueous sulfides.[7] Also, once pitting had initiated, the zinc-sulfide film may have served as a large, active cathodic reaction surface, increasing pit propagation rates.

Corrosion of the Type 410 SS chokes was also observed under crevice conditions, e.g., in insert threads, on areas mated to silicon-carbide sleeves, and in flange seal ring faces. Although laboratory crevice corrosion of Type 410 SS in acidic brines has been reported, additional work of this type is needed, particularly with regard to higher alloy stainless steels.[8,9] Equipment designs which minimize crevices appear desirable for critical wellhead equipment. The importance of crevice corrosion resistance cannot be overstated. Expensive and otherwise serviceable high pressure well control equipment can be easily ruined by crevice corrosion of ring joint seal faces.

SUBSURFACE SAFETY VALVE (SSSV) FAILURE

The susceptibility of Type 410 SS to environmental cracking in H_2S-containing brines has been clearly demonstrated by numerous laboratory investigations.[7,10-12] Similar cracking has been reported in H_2S-free brines, but resistance is generally higher, except when very low pH environments are involved or large cathodic potentials are applied.[13-16] For this reason, less attention is often given to maximum hardness restrictions for equipment intended for sweet service. Unfortunately, as will be described below, brine completion fluids can be quite conducive to hydrogen stress-cracking in unrestricted hardness downhole components.

A tubing retrievable, surface controlled SSSV was installed at a depth of 450 ft (131 m) in a sweet well in the Gulf of Mexico. The valve was tested several times before and after installation, including hydrotesting by the manufacturer. The valve was then closed and the well shut-in for approximately two years.

During the shut-in period, the packer fluid consisted of inhibited calcium bromide brine. Fluid in the valve and the tubing above the valve was a similar, but slightly heavier brine. Well production during completion tests consisted primarily of gas containing 1.9% CO_2. No H_2S was known to be present. Shut-in tubing pressure was approximately 9,600 psig (66 MPa).

SSSV failure occurred while the control line and production tubing were being pressured in an attempt to open the valve. As a result of the failure, 24 days and a considerable amount of expense were necessary to kill the well and retrieve the bottom half of the valve and the rest of the tubing. Upon retrieval, the SSSV was found to have parted due to a fracture near the top of the spring housing

The power spring housing is basically a stepped tube with male threads on the upper end (as installed in the well) and female on the other. It is the primary pressure containing and load carrying member for the valve assembly. Fracture had occurred in the upper pin end section of the housing at the base of the threads. The failure consisted of a fairly flat circumferential of fracture. Visual examination indicated the fracture path was primarily radial from the tube ID to OD. A dark band was observed along the ID over about 270° of the fracture surface. The maximum depth of this dark band was 0.087 in. (2.2 mm). Figure 7 shows a close-up of a typical area.

Metallographic sections through the fracture showed numerous secondary cracks. Orientation of the cracks further confirmed ID to OD radial propagation. The microstructure was quenched and tempered martensitic. EDS analysis indicated the metal composition was typical of Type 410 SS. Hardness values were 41-42 HRC.

The dark band shown in Figure 7 was microscopically observed to be a deposit. EDS analyses of the deposit revealed a chemistry similar to the base metal, with slightly enriched Si, Cr, and Mo. Absence of Na, Ca, Br, and Cl indicated the deposit did not form in the presence of the kill fluid. The deposit was determined to be rich in oxygen with relatively low carbon using Wavelength Dispersive Spectroscopy (WDS). This suggests the deposit was primarily a mixture of oxides rather than a carbonate corrosion product.

The reported tempering temperature used for the housing was 524-551°C (975-1,024°F). A section cut from the failed housing was laboratory tempered at a slightly lower temperature, 499°C (930°F), in attempt to duplicate the dark deposit. An analysis of the oxide formed in the laboratory revealed a composition essentially the same as that found on the fracture surface

EDS analysis was also conducted on deposits found on an uncleaned area of the fracture surface away from the dark band. Major elements identified were Fe, Ba, Cr, Na, Zn, Si, S, and Cl. Most of these would have been corrosion products (Fe, Cr, Cl) or were precipitated by the kill fluid (Zn, Na). The remainder were contaminants, i.e., sand and barium sulfate. All sulfur found was associated with barium, rather than as a sulfide corrosion product.

Sections of the fracture surface were electrolytically cleaned and examined with a Scanning Electron Microscope (SEM). Three main areas of interest were noted and roughly correspond to locations A, B, and C in Figure

7. Figure 8 shows the fracture surface along the ID where the oxide layer was removed by cleaning, area A. The fracture surface was primarily intergranular. Note the absence of corrosion pits as indicated by relatively clean grain facets. Figure 9 shows area B in Figure 7 and was from near mid-wall on the fracture.

The surface was a combination of intergranular and cleavage fractures. The surface had been heavily corroded as shown by the numerous etch pits and lack of grain definition. Area C in Figure 7 is shown in Figure 10. The surface is characteristic of cleavage fracture. Note the total lack of etch pits as was seen in Figure 9. A thin area of dimpled rupture was found at the extreme OD of the housing, and again lacked evidence of corrosion damage (etch pits).

EDS and WDS analyses of the dark band present on the housing ID and the oxide formed by laboratory heat treatment, suggest the fracture surface beneath the dark band was a pre-existing quench crack. Lack of corrosion beneath the band also suggests the crack and deposit did not form in service in the brine kill fluid. An oxide usually forms on quench crack faces during the subsequent tempering operation. Quench cracks are also typically intergranular and can be branched. Both of these characteristics were observed on the failed sample. The orientation of the crack was somewhat unusual for a quench crack, i.e., circumferential at the tube ID. Normally, such cracks form longitudinally on the OD of a quenched tube. However, the manufacturer in this case quenched the material by standing it on end in a furnace basket and lowering it into a water/polymer quench bath. This procedure could produce ID cracks since the inside of the cube can be quenched by percolating fluid before the outside is lowered into the tank. The ID quench would also be more severe, approaching that of water alone, due to depletion of the polymer onto steel surfaces from the percolating fluid as it rises in the cube.

Given the possibility of pre-existing quench crack, calculations were made to determine the flaw depth that could be present and propagate by brittle failure. Based on the manufacturers reported plane strain fracture toughness (KIC) value of 40 ksi • $in.^{½}$ (44 MPa • $m^{½}$) and the maximum load, which occurred during hydrotest, it was estimated that a maximum flaw depth of 0.221 in. (5.61 mm) could be tolerated. This value is considerably greater than the depth of the dark band believed to represent the quench crack. Thus the housing could have been cracked by this amount and still have passed hydrotest.

Based on the initial completion tensile load on the housing and the presumed pre-existing quench crack depth, an in-service applied stress intensity (K) of 23 ksi • $in.^{½}$ (27 MPa • $m^{½}$) was calculated. Thomas, et al., have determined the SCC threshold stress-intensity (K_{ISCC}) for a 44 HRC, Type 420 stainless steel to be 11 ksi • $in.^{½}$ (12 MPa • $m^{½}$) in ambient temperature, acidified 3.5% aqueous NaCl.[17] These workers also found that the K_{ISCC} value in distilled water was only 18 ksi • $in.^{½}$ (20 MPa • $m^{½}$). Therefore, a crack the size of the dark band would be able to grow by SCC under the load on the valve as installed.

A pre-existing quench crack in a brine fluid would be expected to act as a crevice. The resulting low pH and hydrogen generation by corrosion could cause the crack to grow by hydrogen stress-cracking, the mechanism believed responsible for SCC.[18] Corrosion near the center of the fracture surface suggests that the crack grew slowly over a considerable time period. The lack of corrosion on the initial quench crack face can be attributed to the tight oxide layer, which would be protective. No such oxide would be present on cracks formed in service. The lack of corrosion on the rapid failure fracture near the OD caused by final overload dates the corrosion near the center of the fracture. That is, had the corrosion seen near the middle taken place after the valve failed, the final fracture surfaces would have been similarly corroded. Since they were not, sub-critical crack growth and corrosion must have taken place prior to final failure.

The SSSV failure demonstrates the importance of hardness restrictions for Type 410 SS components to be used in sweet service. Lacking more quantitative information, the sour service hardness restriction of 22 HRC max. appears appropriate, albeit possibly conservative. Also, corrosion resistance may be maximized by maintaining such a hardness restriction.[5] The failure also suggests improvements are needed in non-destructive inspection techniques for critical gas well components.

SSC OF CA6NM WELLHEAD VALVE

CA6NM (cast) and F6NM (forged) alloys containing 12Cr-4Ni-0.75Mo offer significant advantages over Type 410 SS in terms of fabricability, corrosion resistance, toughness, and SSC resistance.[6,12,19-21] Improved SSC resistance, in particular, allows more confident application to highly sour wellhead service. Although nickel-containing martensitic stainless steels can be susceptible to chloride-induced SCC at elevated temperatures, recent in-house research yet to be published indicates this possibility is unlikely in realistic, deaerated test solutions, particular at hardnesses below 23 HRC.[22,23]

The failed 10,000 psig (69 MPa), CA6NM gate valve was manufactured and hardness tested to 23 HRC maximum. Gas leakage from the valve body occurred after four years service as an outside wing valve on a sour gas well Christmas tree. Production during this period of time consisted of 48-60 MMSCFD gas, 1,500-2,000 BBLS/D condensate and 1-14 BBLS/D low-salinity water. Gases contained about 14% H_2S and 5% CO_2. Flowing wellhead conditions were approximately 1,160 psig (8 MPa) at 31°C (88°F).

Figure 11 shows overall appearance of the failed CA6NM valve body. Two logitudinal cracks were observed on the internal surface in the same general vicinity. These cracks are shown at higher magnification in Figure 12. Metallographic mounts were prepared through cracked regions and examined. Jagged, branched cracking indicative of SSC was observed, Figure 13. Microstructure of the valve body consisted of quenched and tempered martensite. Although no microstructural difference was discernable, there was a visual difference in response to the chemical etchant used on metallographic mounts at the site of crack initiation compared to the bulk of the valve body.

Because of the different etching characteristics, EDS analyses were performed on metal at the sites of crack initiation and bulk metal using an electron microprobe. Approximate chemical analyses obtained are listed below:

Weight %	Crack Initiation Site	Base Metal
Cr	13.4	13.6
Ni	4.2	3.4
Mo	0.3	0.6
Mn	1.9	1.5
Si	0 5	0.4

With the exception of Mn, which tends to run high by EDS, the analyses were within CA6NM requirements. Note, however, the higher Ni and slightly lower Cr content at the crack initiation site. This difference can only be explained by the metal at the crack initiation site originating from defect repair by welding. Microstructural similarity indicates this repair was made prior to final valve body heat treatment.

Numerous hardness tests were obtained on the flange of the failed valve. Hardness was 18-23 HRC and 248-251 Brinell (HB) in these tests. Additional HRC tests were performed on metallographic mounts, in base metal and suspected weld repair regions. Base metal hardness was again confirmed to be 19-23 HRC. However, hardness at the suspected weld repair where cracking had originated was 26-27 HRC.

Failure of the CA6NM wing valve body was due to SSC. Susceptibility to SSC was a result of high hardness of an apparent weld repair located at the valve body ID. In general, heat treatment of CA6NM to low hardness can be difficult for manufacturers. In this case, the higher Ni content and slightly lower Cr content of the repair weld did not allow satisfactory softening during temper heat treatment. Recent laboratory studies confirm this observation and have shown that high Ni to Cr ratios in welds, as well as high C contents, can lead to insufficient softening during tempering.[19] Interestingly, as has been observed previously, once initiated in the hard repair weld, SSC continued to propagate through the softer valve body bulk metal.[24,25]

Because repair welding of castings is an economic necessity, it seems that additional requirements are needed to assure proper heat treatment response to low hardness. Restricting weld metal chemistry to compositions closer to that of the base alloy is desirable. Also, manufacturer qualification of weld repair techniques and materials could be considered, and accomplished by requiring a valve manufacturer to weld, heat treat, and hardness evaluate test samples using weld metals and procedures intended for actual repair welds.

CONCLUSIONS

1. Sweet corrosion of Type 410 SS wellhead components occurred due to both turbulent and stagnant (crevice) flow conditions. Laboratory studies of flow turbulent effects on CRA materials are needed.
2. Hydrogen stress-cracking failure of a high hardness, Type 419 SS SSSV occurred in an H_2S-free, brine completion fluid. The failure suggests hardness restrictions similar to those used for sour service should be applied to critical Type 410 SS components intended for sweet service.
3. High Ni to Cr content of a CA6NM valve repair weld resulted in insufficient temper heat treatment softening and susceptibility to SSC failure. Better repair weld metal composition match to CA6NM base metal is desirable for proper tempering response to low hardness.

ACKNOWLEDGMENT

Thanks are owed to G.P. Coker, M. Horvat, P. LaCroix, S.M. Polomchak, D. Quellhorst, C.R. Schimpf, C.Q. Sharp, K.A. Sutter, W.R. Warke, and G.A. Zagorce for the valuable assistance with these investigations.

REFERENCES

1. A. Ikeda, S. Mudai, M. Veda, *Corrosion* 41, 4(1985), p. 185.
2. K. Masamura, S. Hashizume, K. Nunomura, J. Sakai, I. Matsushima, "Corrosion of Carbon and Alloy Steels in Aqueous CO_2 Environment," CORROSION/83, paper no. 55 (Houston, TX: NACE, 1983).
3. L.J. Klein, "H_2S Cracking Resistance of Type 420 Stainless Steel Tubulars," CORROSION/84, paper no. 211 (Houston, TX: NACE, 1984).
4. American Petroleum Institute, "Recommended Practice for Design and Installation of Offshore Production Platform Piping System," 3rd ed., RP14E (Dallas, TX: API, 1981).
5. J.L. Crolet, M.R. Bonis, *SPE Production Engineering* 1, 5(1986), p. 344.
6. H. Kurahasi, T. Kurisu, Y. Sone, K. Wade, Y. Nakai, *Corrosion* 41, 4(1985).
7. Y. Ishizawa, T. Shimada, M. Tanimura, "Effect of Microstructure on the Sulfide Stress Corrosion Cracking Resistance of AISI 410 and 420 Steels," CORROSION/82, paper no. 124 (Houston, TX: NACE, 1982).
8. M. Watkins, J.B. Greer, *Journal of Petroleum Technology* 6(1976), p. 698.
9. B.D. Craig, "Evaluation and Application of Highly Alloyed Materials for Corrosive Oil Production," 1982 ASM Metals Congress, paper no. 8201-015 (Metals Park, OH: ASM, 1982).
10. R.S. Treseder, T.M. Swanson, *Corrosion* 33, 7(1977), p. 108.
11. R.N. Tuttle, *Materials Protection* 9, 4(1970), p. 11.
12. R.D. Kane, M. Watkins, J.B. Greer, "The Improvement of Sulfide Stress Cracking Resistance of 12% Chromium Stainless Steels Through Heat Treatment," CORROSION/76, paper no. 137 (Houston, TX: NACE, 1976).
13. H.H. Uhlig, *Metal Progress* 57 (1950), p. 486.
14. H.J. Bhatt, E.H. Phelps, "The Effect of Electrochemical Polarization on the Stress Corrosion Behavior of Steels With High Yield Strength," paper presented at the Third International Conference on Metallic Corrosion in Moscow, USSR, held May 16-26, 1966.
15. H.J. Bhatt, E.H. Phelps, *Corrosion* 17 (1961), p. 420.
16. J.E. Truman, R. Perry, G.N. Chapman, *Journal of the Iron and Steel Institute*, p. 745 (1964).
17. C.J. Thomas, R.G.J. Edyvean, R. Brook, *Materials Science and Engineering* 78 (1986), p. 55.
18. M.F. McGuire, R.F. Hehemann, A.R. Troiano, International Congress on Hydrogen in Materials, Paris, France, 1972, p. 325.
19. E.G. Sherman, C.S. Nalbone, W.D. Scott, "Processing of Low Carbon CA6NM to Meet Hardness Requirements," *Steel Foundry Facts* 353, 1(1983), p. 12.
20. *Metals Handbook*, 9th ed., vol. 3 (Metals Park, OH: ASM, 1980), p. 104.
21. D.S. Burns, *Materials Performance* 15, 1(1976), p. 21.
22. A.P. Bond, H.J. Dundas, *Stress-Corrosion Cracking and Hydrogen Embrittlement of Iron Base Alloys*, NACE-5 (Houston, TX: NACE, 1977), p. 1136.
23. Y. Yoshino, *Corrosion* 42, 10(1986), p. 592.
24. S.W. Ciaraldi, *Materials Performance* 25, 1(1986), p. 9.
25. S.W. Ciaraldi, *SPE Drilling Engineering* 1, 3(1986), p. 233.

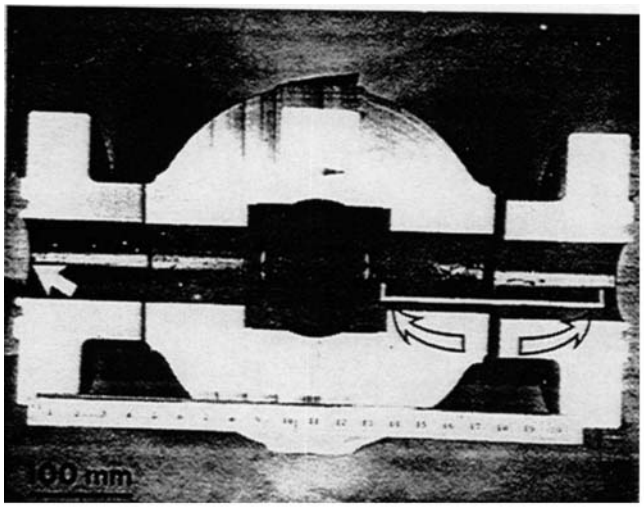


FIGURE 1
Overall internal appearance of lower half of Type 410 SS wing valve. Arrows indicate regions of pitting attack.

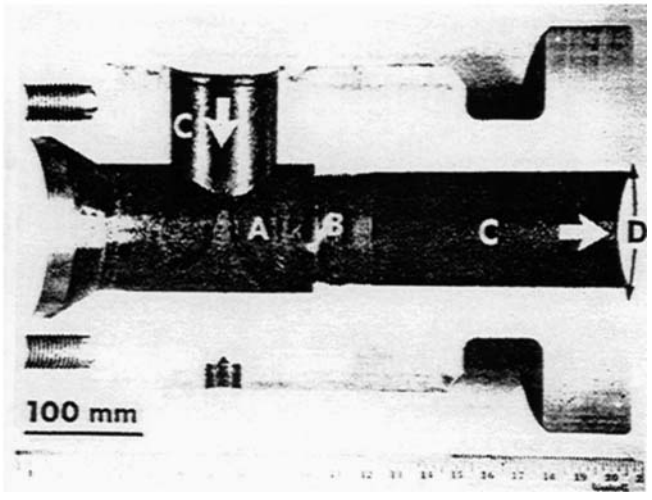


FIGURE 3
Overall internal appearance of Type 410 SS choke body. Gas flow indicated by arrows. Erosion/corrosion (A), crevice corrosion of insert threads (B), pitting corrosion (C), and crevice corrosion of outlet flange seal face (D) indicated.

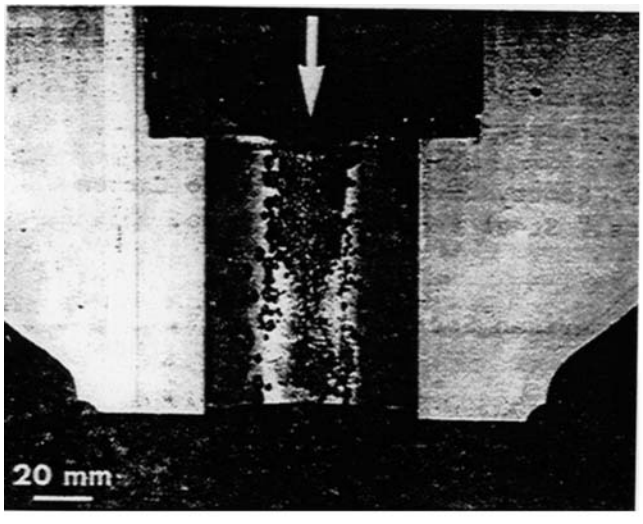


FIGURE 2
Pitting attack, thought to be turbulence related, on outlet port of wing valve. Arrow indicates flow direction.

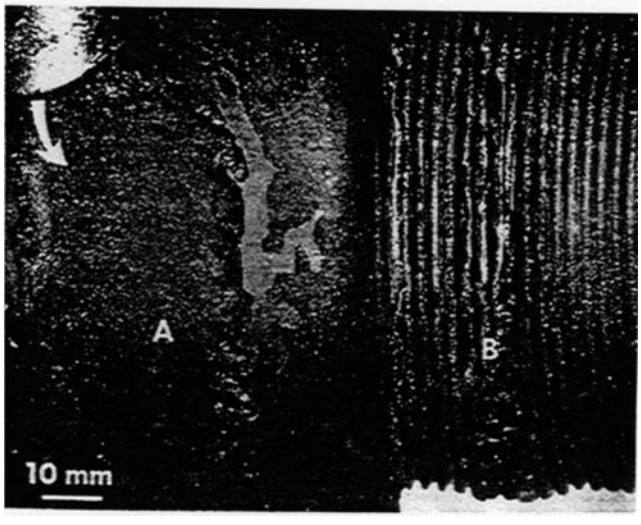


FIGURE 4
Erosion/corrosion (A) and thread insert crevice corrosion (B) of choke body. Arrow indicates flow direction.

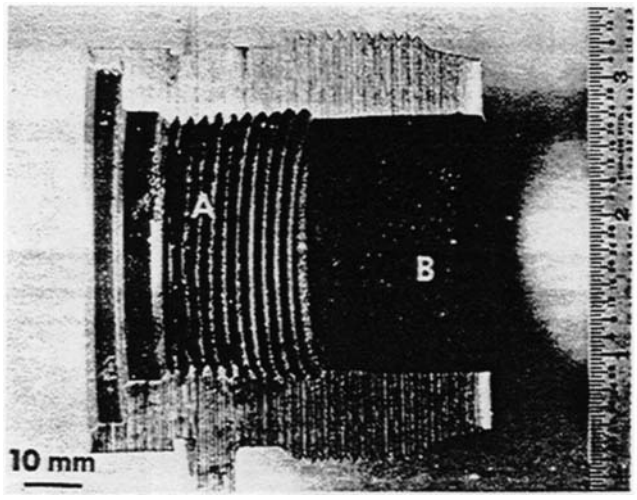


FIGURE 5
Crevice corrosion (A) and pitting attack (B) of Type 410 SS choke insert.

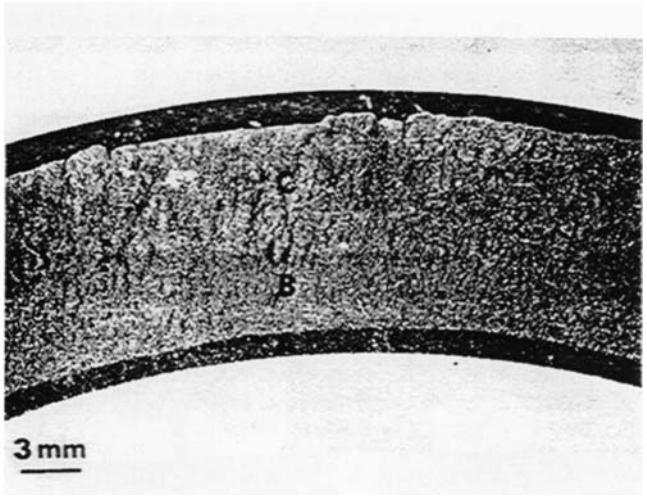


FIGURE 7
Fracture surface of Type 410 SS SSSV housing showing dark oxide on ID (A), possible sub-critical crack growth area (B), and final fast fracture (C). Dark band on OD is a thread flank and not part of fracture surface.

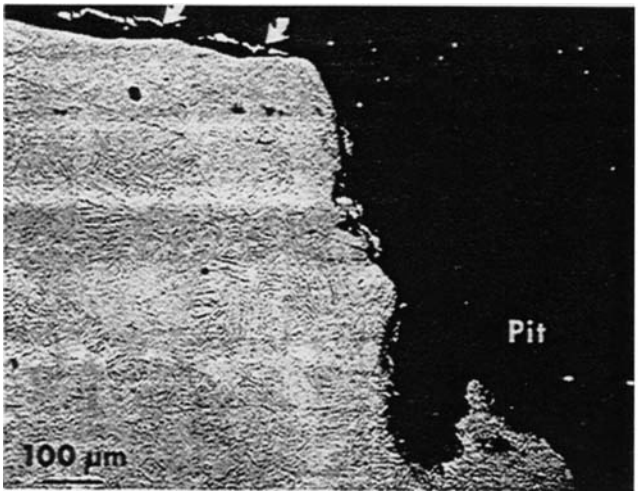


FIGURE 6
Sharp-walled, deep pit in Type 410 SS wing valve body, typical of CO_2 corrosion. Arrows indicate zinc-sulfide film present on wetted surfaces.

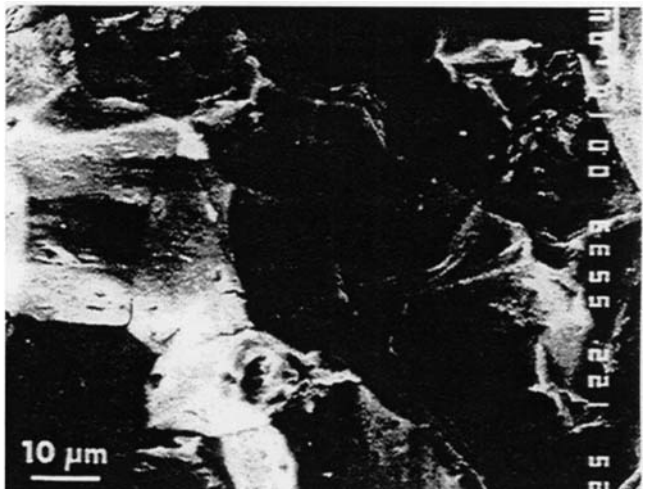


FIGURE 8
Appearance of SSSV fracture surface in dark band near ID, region A, Figure 7.

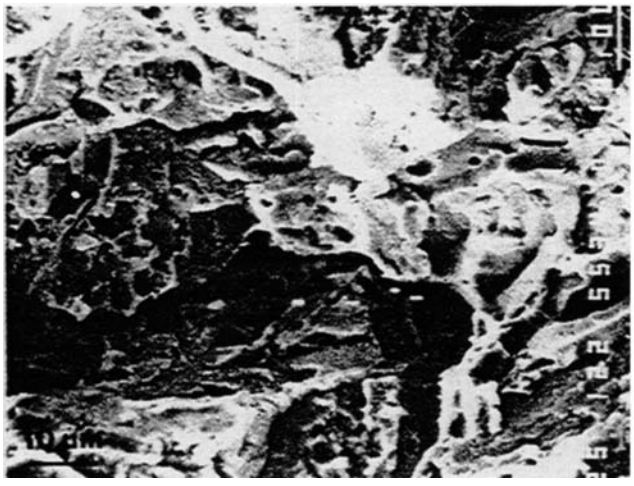


FIGURE 9
Appearance of SSSV fracture surface near mid-wall, region B, Figure 7.

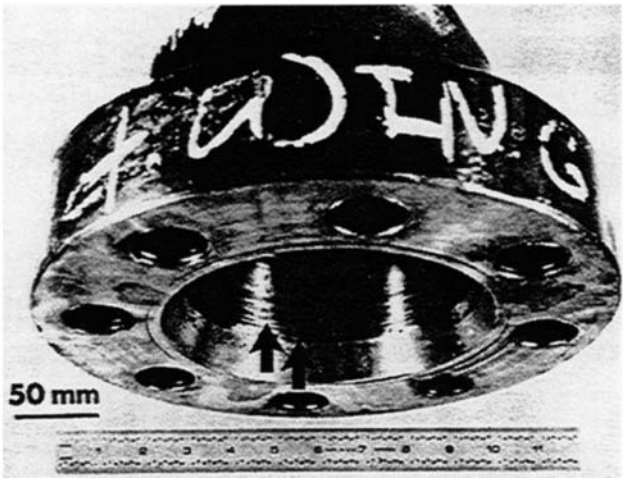


FIGURE 11
Overall appearance of failed CA6NM valve body. Arrows indicate locations of the two longitudinal cracks observed.

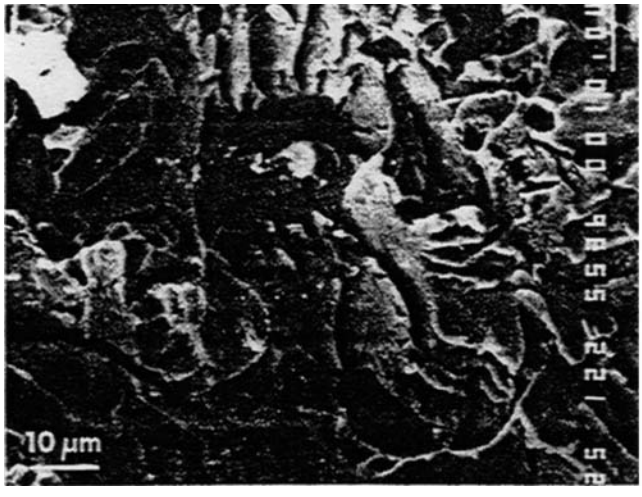


FIGURE 10
SSSV fracture surface near OD of housing in fast fracture area, region C, Figure 7.

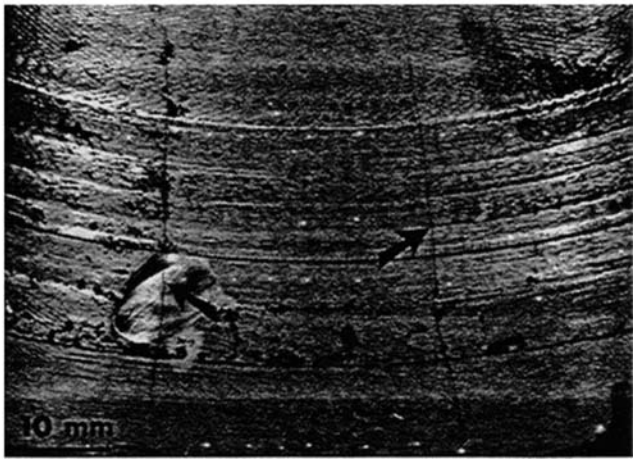


FIGURE 12
Longitudinal cracks (arrows) in CA6NM valve body.

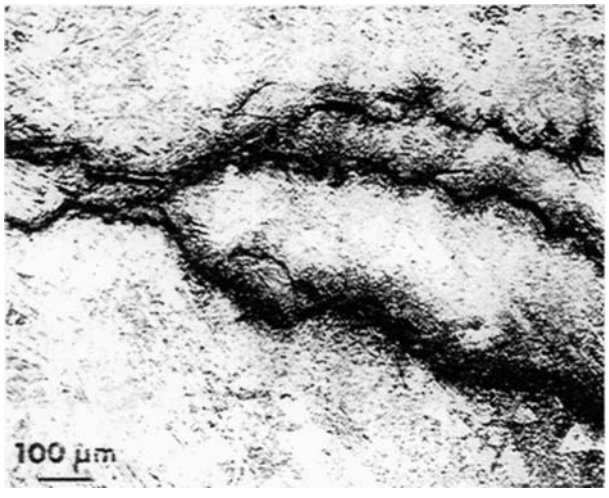


FIGURE 13
Micrograph of crack in CA6NM valve body. Jagged, branched appearance is characteristic of sulfide stress cracking (SSC), Vilella's etch.

Copyrighted Materials
Copyright © 1996 NACE International Retrieved from www.knovel.com

Paper No.
79

CORROSION 95
The NACE International Annual Conference and Corrosion Show

DEVELOPMENT OF SOUR RESISTANT MODIFIED 13CR OCTG

H.Asahi and T.Hara
Nippon Steel Corp., Steel Research Lab.
20-1, Shintomi, Futtsu,
Chiba-ken 299-12, Japan

A.Kawakami and A.Takahashi
Nippon Steel Corp., Yawata R&D Lab.
1-1, Tobihata, Tobata,
Kitakyushu 804, Japan

ABSTRACT

Sour resistant 13% Cr martensitic OCTG (Oil Country Tubular Goods) with so far unexpected high CO_2 corrosion resistance was developed. CO_2 corrosion resistance was remarkably increased by complex additions of Cu and Ni, of which contribution to CO_2 corrosion resistance corresponds to that by a further addition of 6% Cr at 180℃. SSC resistance was improved by an addition of Mo. Based on such knowledge of roles of chemical elements on corrosion properties and phase stability, 0.02%C-12.5%Cr-4.5%Ni-1.5%Mo-1.5%Cu steel was developed. This steel has good hot-workability and was produced into seamless OCTG. Corrosion rates in a high pressure CO_2 environment were less than 0.1 mm/y at temperatures up to 200℃ (392 F) compared with 100℃ of conventional API L80-13CR. No SSC occurred in sour environments with partial pressure of 0.001MPa or less even at low pH of 3.5. At elevated temperatures no cracking and no pitting was observed in H_2S containing CO_2-brine environments. The properties of the developed steel are much better in CO_2 corrosion and SSC resistance compared with those of conventional 13Cr steel and are close to those of duplex stainless steel.

Key words: 13% Cr Stainless Steel, Corrosion Resistant Alloys, Corrosion, CO_2 Gas, Sour Gas, Sulfide Stress Cracking, Molybdenum, Copper,

INTRODUCTION

Field application of 13% Cr stainless OCTG has been increasing[1)] because of its good corrosion resistance in CO_2 containing environments and its low price. Furthermore, high strength is easy to be got for cases of martensitic steels

like 13% Cr stainless steel. However, it is less resistant to CO_2 corrosion at higher temperatures[2] and especially is susceptible to SSC even if a partial pressure of H_2S is very low. In order to expand application limits of 13% Cr stainless OCTG to higher temperature and higher partial pressure of H_2S region, a new type of 13% Cr stainless steel has been attempted to develop.

So far, several types of modified 13% Cr stainless OCTG were proposed[3, 4, 5, 6]. Mostly they are featured by a reduced C content and additions of Ni, Mo or Cu and are reported to show better corrosion resistance. But further study may make it possible to improve corrosion resistance, especially combined properties for both CO_2 corrosion and SSC.

In the present paper, a new alloy design concept for improving CO_2 corrosion resistance will be shown. A new type of SSC resistant 13% Cr martensitic stainless steel developed based on this alloy design concept will be evaluated comparing with API L80-13CR (AISI420 type steel).

EXPERIMENTAL

Materials

In order to clarify effects of alloying elements, laboratory melt steels were used. Ranges of chemical compositions of materials used are listed in Table 1. Steels melted in a vacuum induction furnace and cast were re-heated at 1250 ℃ and then conventionally hot rolled to plates of 12 mm in thickness. All the steels were then heat-treated, typically quenched and tempered. Tests specimens were machined after heat-treatment.

Test Procedures

Measurement of Corrosion Rate. A corrosion rate was determined from the weight loss after descaling, the immersion time and the surface area. A specimen of which dimensions are 3 mm thick, 15 mm wide and 20 mm long were mechanically polished with 320 grid emery paper followed by degreasing in acetone. Descaling was performed by immersing specimens in a boiling 18% NaOH + 3% $KMnO_4$ solution for 5 minutes and subsequently in a boiling 10% $(NH_4)_2HC_6H_5O_7$ (ammonium citrate) solution for 5 minutes. Immersion tests were performed in high pressure autoclaves. A partial pressure of a test gas is indicated as the value at the test temperature. A test solution was deaerated with pure nitrogen gas before introducing a test gas. The solution volume to the specimen surface was 20 ml/cm^2 and the test duration was 96 hours if not mentioned otherwise.

Four-point bent beam test. Four-point bent beam test with or without a notch was used to assess SSC resistance. The dimensions of a notched specimen is illustrated in Fig. 1. Those of a smooth specimen is the same as Fig. 1 except the notch. After stressing specimens based on the formula indicated in Fig. 1, they were immersed in a test solution.

Tensile type SSC test. The tests were performed using dead weight type constant load testers, basically based on the NACE standard TM0177-90 method A. The dimensions of a specimen is shown in Fig. 2. The solution was 5% NaCl acetic acid buffer solution, pH of which was changed by changing a mixture ratio of 1N CH_3COOH and 1mol/l CH_3COONa. The gas was a mixture of H_2S and N_2 or of H_2S and CO_2.

Electrochemical measurement. Polarization curves were measured in a potentiodynamic method. After mechanical polishing, a specimen was coated with silicon resin, leaving an area of 1 cm^2 for measurement. Just before mounting on

the measuring apparatus, the specimens was pickled in 50% sulfuric acid to remove the air-formed film. A sweep rate of 10 mV/min was employed.

Critical pitting potential (V'_c) was determined as the potential corresponding to the current density of 100 $\mu A/cm^2$.

Depassivation pH (pH_D) measurement. Specimens were prepared with the same procedure as that for electrochemical measurement. Specimens activated by pickling were immersed in test solutions with various pH values. After 24 hours, an immersion potential was measured. The value of pH_D was decided as a pH where a corrosion potential suddenly rises on the potential-pH diagram.

ALLOY DESIGN CONCEPT

Effects of Alloy Elements on CO_2 Corrosion Rate

Corrosion test results at elevated temperatures in substitute ocean water (SOW, according to ASTM D 1141) saturated with 4 MPa CO_2 are shown in Fig.3, 4 and 5. Chemical compositions indicated in Fig.5 are base compositions where effect of each element was examined. A reduction of C content decreased the corrosion rate as shown in Fig.3, probably because Cr content in solid solution increases due to a decrease in Cr as chromium carbides. Nitrogen, which also could reduce Cr content in solution as a result of chromium nitride formation, had smaller effect compared with C as shown in Fig.4. Corrosion rates decreased with increases in Cu, Cr and Mo, while Ni had no pronounced effect on corrosion rate as shown in Fig.5. A contribution of Mo to a decrease in corrosion rate was about 1.6 times as great as that of Cr. Copper reduced a corrosion rate remarkably. By an addition of 1% Cu or greater, a corrosion rate fell to below 0.1 mm/y at 180℃.

In order to clarify the Cu effect, the data of Fig.5 and other additional data were replotted in Fig.6 in the relation between Cr+1.6Mo and corrosion rate. In Fig.6, any steels containing Cu also contain Ni. It is very clear from Fig.7 that the remarkable Cu effect on corrosion rate appears under co-existence of Ni. Fig.6 indicates that the contribution of complex additions of Cu and Ni to a reduction of corrosion rate corresponds to an addition of Cr+1.6Mo of 6%.

A type of corrosion of these steels in these environments was general corrosion and no pitting appeared. The corrosion products of Cu free steel was black and thin film. For Cu added steel, the corrosion product was also thin but looked like a color containing yellow or amber.

Role of Mo Addition on H_2S Corrosion

Smooth four-point bent beam (without notch) tests were performed in 3.5% NaCl solution with various pH and H_2S partial pressure for 14 days. The applied stress was 1.0 of the yield strength. As shown in Fig.8, in environments with lower pH and higher H_2S partial pressure, the specimens suffered cracks, fissures or pittings. The critical line for being immune from such degradations moved toward lower pH side by an addition of 1% Mo.

Results of pH_D measurement in 5% NaCl solutions saturated with H_2S partial pressure of 0.001 and 0.01 MPa are illustrated in Fig.9. Values of pH_D in sour environments decreased with increase in Mo and became almost constant at 1.5% Mo or higher.

Phase Stability

Steels which are aimed to develop are required to be fully martensitic,

that is, they must consist of only austenite at elevated temperatures. There would be three reasons for it. First, high strength cannot be obtained if much ferrite exists. Second, low temperature toughness deteriorates if ferrite appears in martensitic structure. Third, small amount of δ-ferrite remarkably deteriorates hot-workability. Good hot-workability is necessary especially for seamless process which is widely applied to high grade OCTG production. Figure 10 illustrates influence of δ-ferrite amount at a heating temperature on reduction of area of smooth tensile test at 900 ℃. A reduction of area of 75% or greater is considered to be necessary for obtaining good surface quality pipes. Therefore, the figure reveals that one necessary condition to keep good hot-workability is that the structure at the heating temperature before rolling was fully austenite, that is, was free from ferrite. Figure 11 shows the relationship between Ips (Index of Phase Stability; Ni + 40C + 34N + 0.3Cu - 1.1Cr -1.8Mo) obtained in the present research and δ-ferrite fraction. Values of Ips should be -9.42 or larger in order to maintain the phase fully austenite.

Alloy Design

In this paragraph, the alloy design concept for sour resistant 13% Cr steel is explained. Aiming properties are that a corrosion rate should be less than 0.1 mm/y at the temperature of 180 ℃ and should be immune from SSC under H_2S partial pressure of 0.005 MPa or smaller. Main points which were considered for the alloy design are the following.

(1)Carbon content must be 0.03% or less.
(2)An amount of Cr + 1.6Mo must exceed 20% for Cu free alloys and 14% for Cu-Ni alloys.
(3)Mo of more than 1.5% must be added.
(4)A value of Ips must be -9.42 or greater.

When Cr + 1.6Mo is equal to 20%, Ips cannot be -9.42 or greater, that is, such a steel cannot be fully martensitic. Therefore, there is no possibility to satisfy above conditions without complex additions of Cu and Ni.

The main chemical compositions finally decided are shown in Table 2. The features are low content in carbon, complex additions of Cu and Ni and an addition of Mo (referred to as 13Cr-Ni-Cu-Mo steel or CRS).

This type of steel cannot transform into any other than martensite at any cooling rate. The steel would be basically normalized and tempered or often tempered at dual phase temperature region followed by final tempering.

PROPERTIES OF DEVELOPED STEEL

Pipes were produced using commercial seamless process in Yawata works, Nippon Steel. The pipes were subjected to heat treatment. The chemical compositions and the mechanical properties of steels evaluated here including the pipes are listed in Table 3 and 4, respectively. As a reference, conventional API L80-13CR from AISI type420 steel was used.

Microstructure and Mechanical Properties

The microstructure of the developed steel was well tempered martensite as shown in Fig.12. The etchant was 5% HCl added saturated picricacid ethanol solution. Low-temperature toughness examined by V-notch Charpy test is indicated in Fig.13. A transition temperature for 50% shear fracture (vTrs) was lower than -100 ℃(-148 F), being excellent level.

CO_2 Corrosion Properties

Temperature dependence. In substitute ocean water saturated with 4 MPa of CO_2, immersion tests for 96 hr were conducted. The results are illustrated in Fig.14. The corrosion rate of 13Cr-Ni-Cu-Mo steel remained less than 0.1 mm/y even at a high temperature of 180℃(356 F), while it slightly increased with increase in temperature. Type 420 steel, however, showed far higher corrosion rate, more than ten times as great. The specimen surfaces of the developed steel after immersion test looked like temper colour (blueing), which indicates the corrosion product was very thin. On the other hand, the corrosion product of type 420 was thick and black. No pitting appeared in both steels.

Effect of chloride ion concentration. Effects of chloride ion concentration were examined in solutions with NaCl up to 20% in concentration under 4 MPa CO_2 at 180℃. Results are shown in Fig.15. Corrosion rate gradually increased with increase in NaCl concentration.

Effect of H_2S on corrosion rate. Effect of H_2S on corrosion rate was examined in SOW solution under 4 MPa CO_2 at 200 ℃. As shown in Fig.16, the corrosion rate increased a bit with the presence of little amount of H_2S but the change was not so pronounced.

Sulfide Stress Cracking Properties

Four-point bent beam test. SSC tests in simulated high pressure environments were conducted in an autoclave using notched four-point bent beam test specimens. The surface stresses were applied to 100% of the actual yield strength, which results in heavy plastic deformation at the notch bottom. The test duration was 336 hours (14 days).

The results are shown in Fig.17. Typical cross sections of notch portion are shown in Fig.18. In SOW at 25 ℃, no crack occurs at H_2S partial pressure of 0.005 MPa or lower for CRS, while cracks occurred even at H_2S partial pressure of 0.001 MPa for AISI 420. In 5% NaCl solution, both steels failed at H_2S partial pressures down to 0.001 MPa at 25℃ while CRA was more resistant to SSC than AISI 420 at 100 ℃. The difference of results between SOW and 5%NaCl is supposed to result from difference in pH value of the solution. Calculated pH values are 3.27 for SOW and 2.87 for 5% NaCl. [7]

Tensile type SSC test. Tensile type SSC test were performed in environments with various H_2S partial pressures and various pH values. The applied stress was 556 MPa (85% of 95 ksi) or 644 MPa (85% of 110 ksi). Results are illustrated in Fig.19 on the pH - H_2S partial pressure diagram. As it is clear from the graph, H_2S partial pressure of 0.01 MPa seems to be a boundary condition at pH of 3.5. Whenever no failure occurred in this condition, the specimen kept its metallic brightness until the end of the test duration. On the other hand, a failed specimen became black. Furthermore, no pronounced effect of an increase in NaCl concentration up to 20% was observed as shown in Fig.19.

DISCUSSION

Mechanism of Improvement in CO_2 Corrosion Resistance

CO_2 corrosion resistance was increased by an addition of Cu and was more remarkably increased by complex addition of Ni and Cu as shown in Fig.7. Although the mechanism of increase in corrosion resistance has not yet been

understood, the probable explanation at present is as follows: Corrosion product of Cr-Ni-(Mo) alloys looked black while that of Cu containing alloys is a color containing yellow or amber. This phenomena may suggest that metallic Cu formed in the layer of corrosion products. This assumption was examined by X-ray analysis. Because X-ray diffractometry requires a thicker layer of corrosion product, specimens corroded at 250 ℃ were used. Copper steel presented weak diffraction peaks determined as Cu. Copper-Ni steel presented stronger diffraction peaks determined as $Cu_{3.8}Ni$ which has the same crystal system and almost the same lattice constant as Cu. These result could indicate that metallic Cu exists in the corrosion product and Ni promotes metallic Cu formation. These layers of Cu metal or Cu-Ni alloy can be expected to work as barrier against corrosion.

Environmental Factors Affecting SSC Occurrence

In the environments where 13% Cr stainless steel tubing are expected to be applied, a cathod reaction of corrosion is basically hydrogen reduction. Therefore, hydrogen embrittlement is probably a mechanism of SSC. If so, no cracking might occur at elevated temperatures. Actually, cracks occurred only at temperatures close to room temperature as shown in Fig.17. Hydrogen embrittlement cracking does not occur when hydrogen entry is none or little, that is, when the steel is passive or an environment has high pH and low partial pressure of H_2S in case of active state. If pitting occurred, pH value in the pit would decrease.[8] Hydrogen entry would increase with decrease in pH, leading to hydrogen embrittlement cracking. Therefore, once a pitting was formed, SSC could finally occur. Pitting could occur when oxidation/reduction potential of S ($S_{OX/RED}$) would be greater than the critical pitting potential (V'_c).[9]

When $S_{OX/RED}$ was smaller than V'_c, no pitting would occur. In this case, if pH of the environment was larger than pH_D, SSC would not occur because hydrogen entry is negligibly small. If pH was lower than pH_D, SSC could occur at lower pH or higher partial pressure of H_2S, that is, at high rate of hydrogen entry.[10]

SSC test results is in accordance with this criteria as shown in Fig.20. It should be noted that 13% Cr steel can be applicable at relatively high pH values which is not far lower than pH_D and at lower partial pressures of H_2S. Modified 13% Cr developed here, however, expands applicable environmental conditions toward lower pH and higher partial pressure of H_2S, compared with API L80-13CR (AISI 420).

CONCLUSIONS

Modified 13% Cr martensitic stainless steel with good SSC resistance and excellent CO_2 corrosion resistance was developed. Obtained results are as follows:

1)Complex addition of Cu and Ni remarkably increases CO_2 corrosion resistance, which is almost equivalent to an addition of Cr + 1.6Mo of 5% at 180℃.

2)An addition of Mo suppresses pittings, fissures and cracks at low pH region and decreases pH_D in environments containing small amount of H_2S.

3)As far as Ips (= Ni + 0.3Cu + 40C + 34N - 1.1Cr - 1.8Mo) is -9.42 or greater, the alloy is fully martensitic and presents excellent hot-workability.

4)Based on the above results, 0.01/0.03%C-13%Cr-4/6%Ni-1/2%Cu-1.5/2%Mo steel was developed.

5)In substitute ocean water saturated with CO_2 of 4MPa, corrosion rate of the developed steel is 0.1 mm/yr or less at 180 ℃, compared with more than 1 mm/yr of AISI 420 steel.

6)The maximum H_2S partial pressure immune from SSC of the developed steel is about 0.005 MPa at pH of 3.5, compared with less than 0.001 MPa of AISI 420.

ACKNOWLEDGEMENTS

The authors wish to thank Nippon Steel Corporation for allowing the publication of this material and also acknowledge many members of Nippon Steel for assistance and corporation.

REFERENCES

1)NACE Technical Committee Report, "Survey of CRA Usage", (Houston, TX: NACE, 1993).
2)A.Ikeda, M.Ueda and S.Mukai, "CO_2 Corrosion Behavior and Mechanism of Carbon Steel and Alloy Steel," CORROSION/83, paper no. 45(Houston, TX:NACE, 1983).
3)A.Miyasaka and H.Ogawa, "Influence of Metallurgical Factors on Corrosion Behaviors of Modified 13% Cr Martensitic Stainless Steels," CORROSION90, paper no. 67(Houston, TX:NACE, 1990).
4)M.Ueda, T.Kushida, K.Kondo and T.Kudo, "Corrosion Resistance of 13Cr-5Ni-2Mo Martensitic Stainless Steel," CORROSION/92, paper no. 55(Houston, TX:NACE, 1992).
5)S.Hashizume, T.Takaoka, Y.Minami and Y.Ishizawa, "Corrosion Resistance of 15% Cr Stainless Steel for OCTG," CORROSION/92, paper no. 54, (Houston, TX:NACE, 1992)
6)A.Tamaki, "A new 13Cr OCTG for High Temperature and High Chloride CO_2 Environments," CORROSION/89, paper no.469(Houston, TX:NACE, 1989)
7)A.Miyasaka, "Thermodynamic Estimation of pH of Sour and Sweet Environments as Influenced by the Effects of Anions and Cations," CORROSION/92, paper no. 5(Houston, TX:NACE, 1992).
8)K.Denpo and H.Ogawa, Corrosion 47, 8(1991): p592.
9)K.Denpo, A.Miyasaka and H.Ogawa, "A Selection Method for High strength Alloy Materials for sour Service," The Second NACE International Symposium, (Houston, TX:NACE, 1989).
10)H.Asahi, M.Ueno and T.Yonezawa, Corrosion 50, 7(1994): p537.

Table 1 Chemical composition ranges of material. (mass%)

C	Cr	Mo	Ni	Cu	N
0.01/0.20	12/20	0/2.5	0/6.0	0/3.0	0.03/0.12

Table 2 Chemical compositions of the developed steel.(mass%)

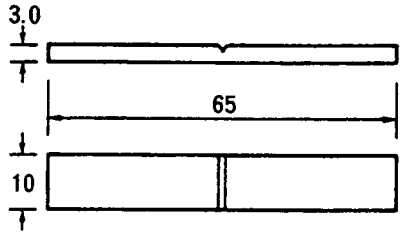
C	Cr	Mo	Ni	Cu	N
0.01/0.03	12/13	1.5/2.0	4.0/6.0	1.0/2.0	0.01/0.08

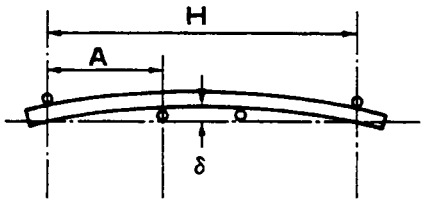
Table 3 Chemical compositions of evaluated materials (mass%).

		C	Si	Mn	P	S	Cr	Mo	Ni	Cu	N
13Cr-Ni-Cu-Mo (CRS)	ST	.028	0.26	0.47	.015	.001	12.6	1.40	4.46	1.55	.041
	MH2	.020	0.09	0.51	.007	.001	12.5	1.54	4.00	1.52	.058
	MO4	.019	0.09	0.47	.011	.001	12.8	1.47	4.00	1.44	.058
AISI420	420	0.20	0.25	0.57	.016	.004	12.7	—	0.13	—	.030

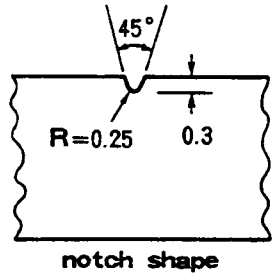
Table 4 Mechanical properties of evaluated material. MPa (ksi)

		YS	TS	Remarks
13Cr-Ni-Cu-Mo (CRS)	ST1	809(117)	904(131)	tubing
	ST2	680(98)	854(124)	tubing
	MH2	748(109)	875(127)	lab. melt
	MO4	743(108)	932(135)	lab. melt
AISI420	420	590(86)	774(112)	tubing
	420H	728(106)	885(128)	tubing





$$\sigma = 12Et\delta/(3H^2 - 4A^2)$$



where:

E : Young's modulus (205800MPa)

σ : surface tensile stress

δ : deflection

t : specimen thickness

H : distance between outer supports

A : distance between inner and outer supports

Fig.1 Dimensions of four-point bent beam test specimen.

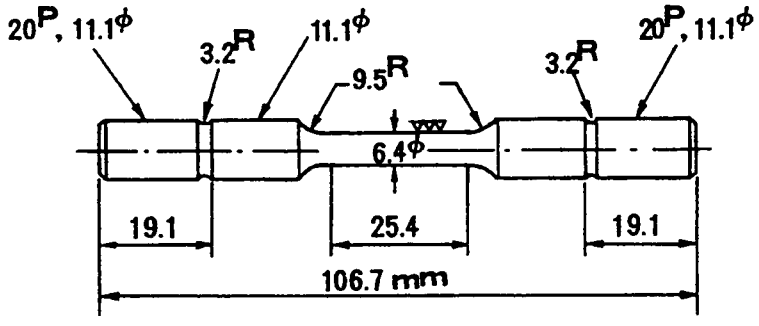


Fig.2 Dimensions of tensile type SSC test.

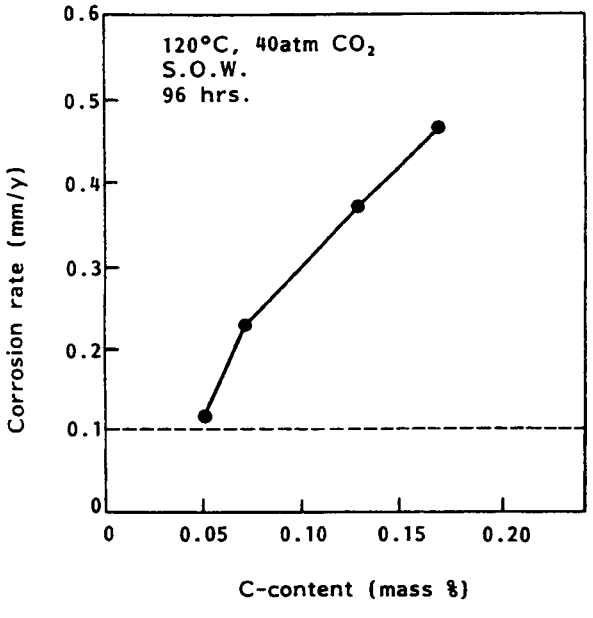


Fig.3 Effect of C content on corrosion rate. (120 ℃, 4MPa CO_2, SOW, 96hr, 13%Cr-0.12%N steel)

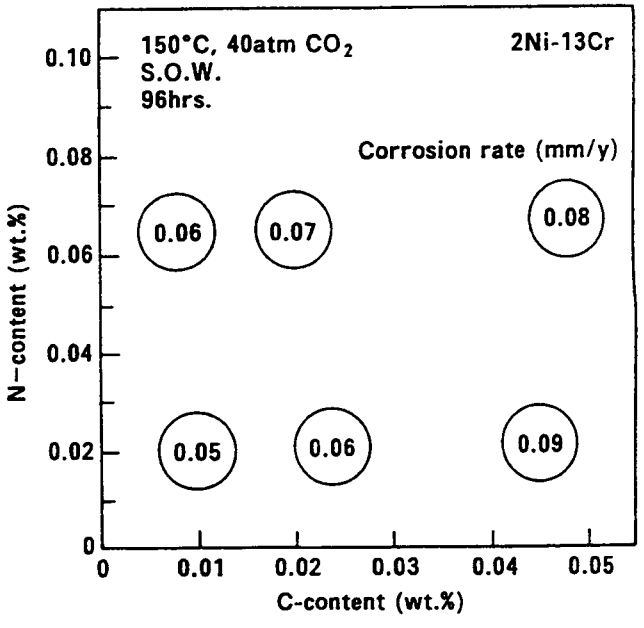


Fig.4 Effects of C and N contents on corrosion rate. (150 ℃, 4MPa CO_2, SOW, 96Hr, 0.02%C-13%Cr-2%Ni steel)

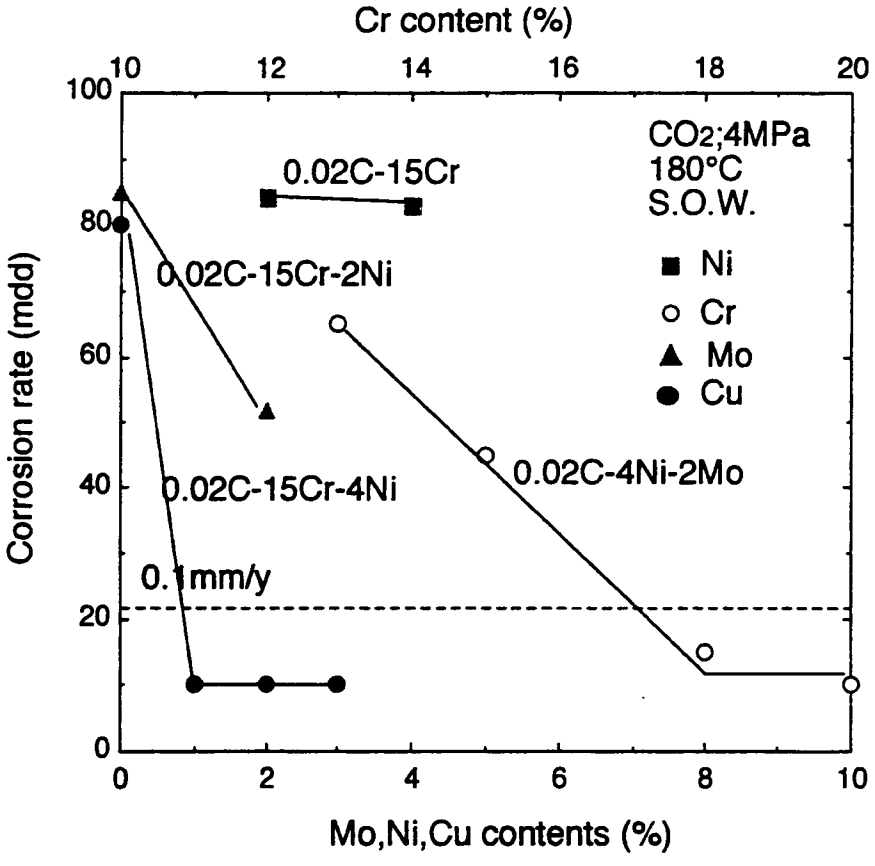


Fig.5 Effects of Ni, Cr, Mo and Cu contents on corrosion rate. (180 ℃, 4MPa CO_2, SOW, 96hr)

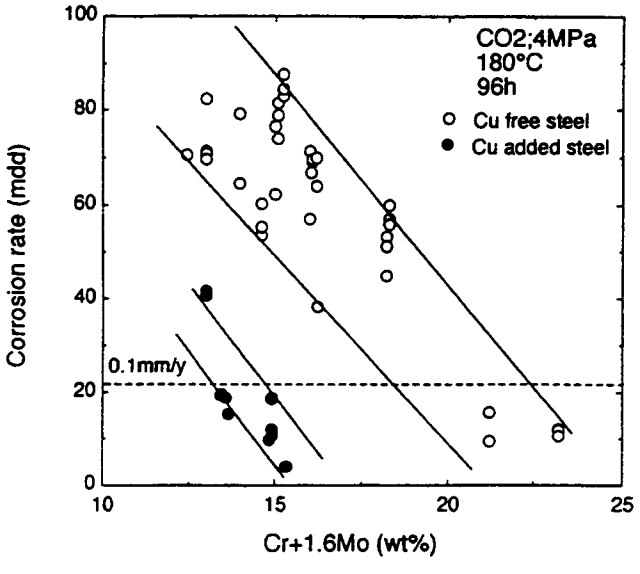


Fig.6 Effect of complex addition of Cu and Ni on corrosion rate. (180℃, 4MPa CO_2, SOW, 96hr)

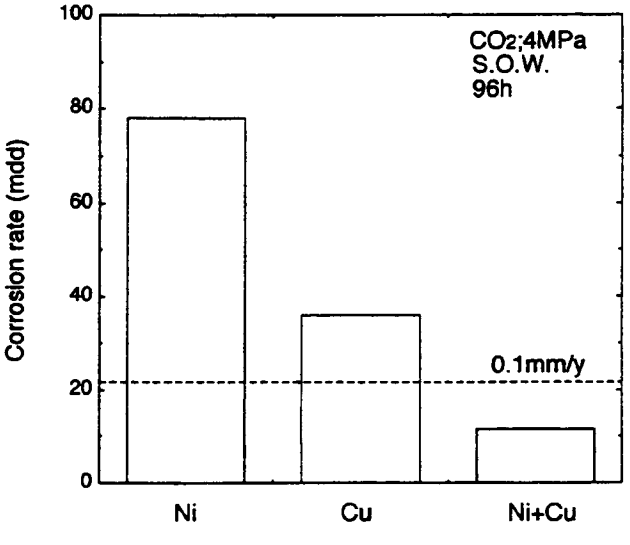


Fig.7 Effect of Ni addition on corrosion rate of Cu added steels. (185℃, 4MPa CO_2, SOW, 96hr, 0.02%C-15%Cr)

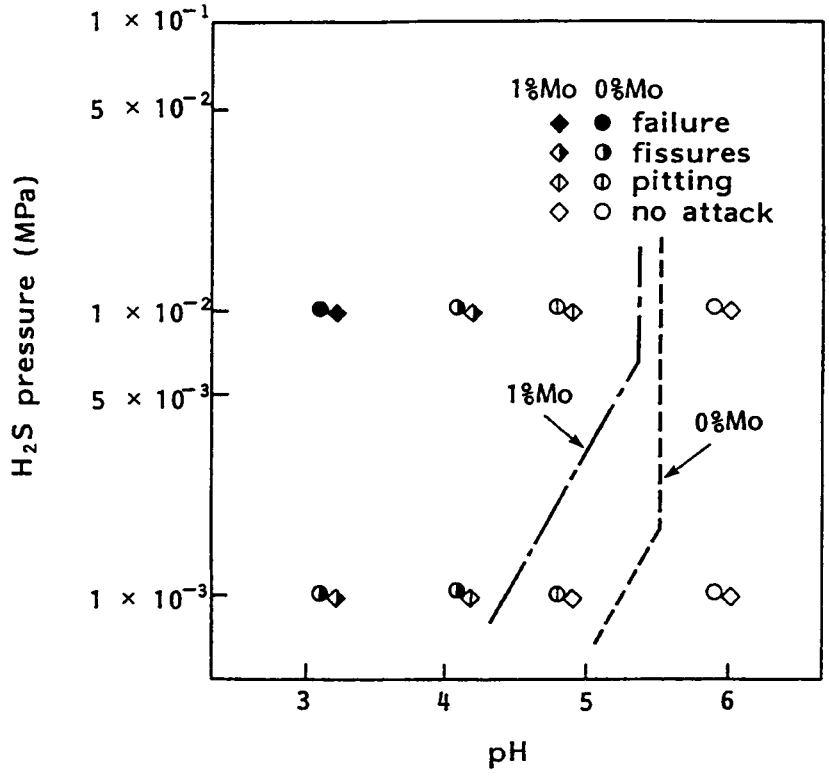


Fig.8 Effect of Mo addition on degradation morphology due to corrosion. (3.5%NaCl acetic buffer solution, 25 ℃, 336Hr, 0.02%C-13%Cr-2/4%Ni steels)

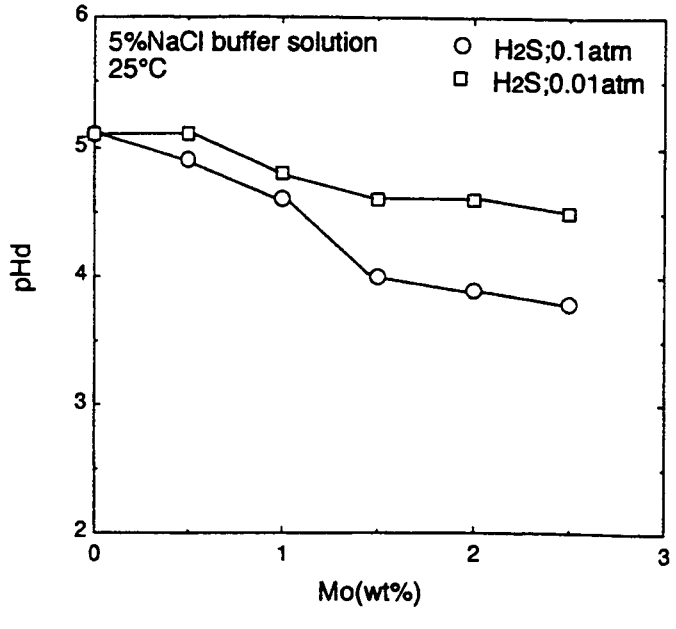


Fig.9 Effect of Mo content on pH_D. (5%NaCl acetic buffer solution, 25℃, 0.02%C-13%Cr-4%Ni-1.5%Cu steels)

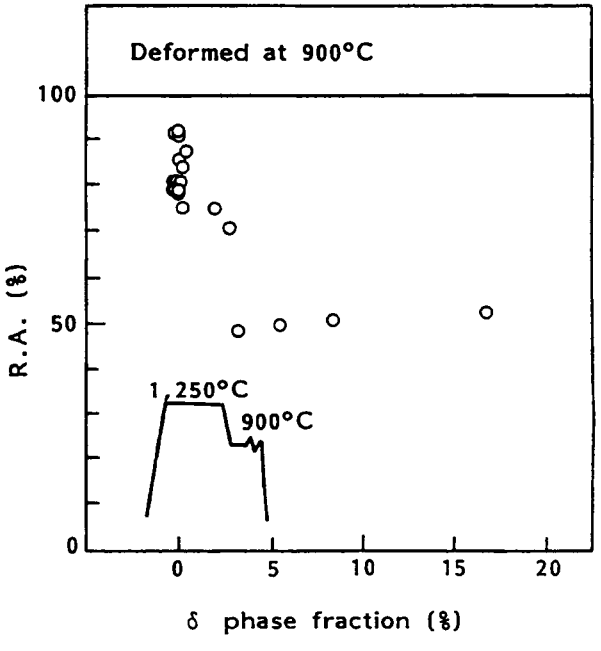


Fig.10 Effect of δ-ferrite amount on hot-workability. (Reduction of area at 900 ℃, smooth tensile test specimen, 13%Cr-Cu free steel)

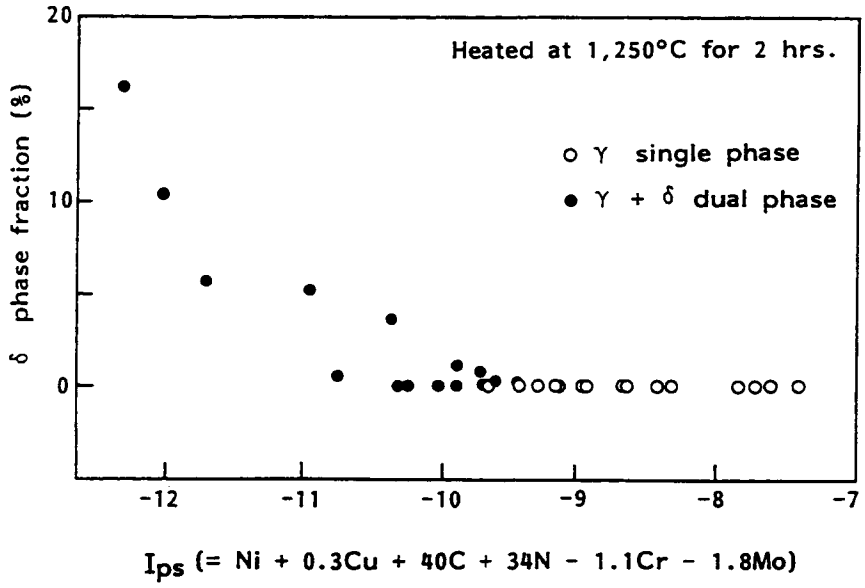


Fig. 11 Relationship between δ-ferrite fraction and chemical composition.

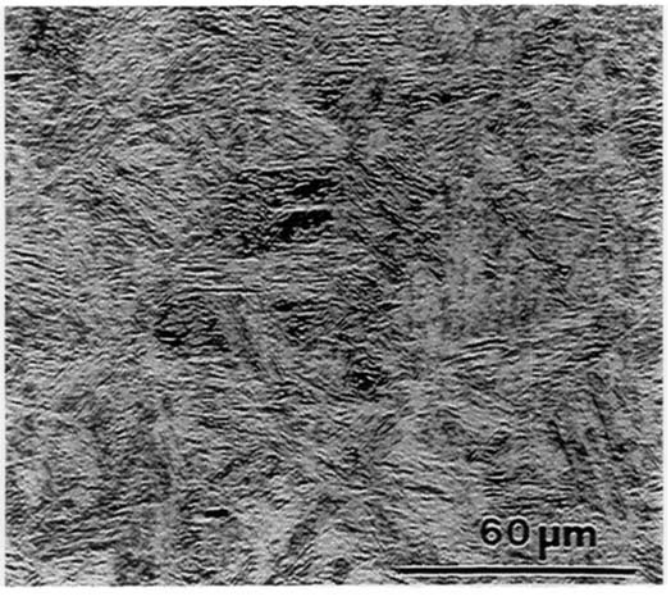


Fig. 12 Microstructure of the developed steel (ST1).

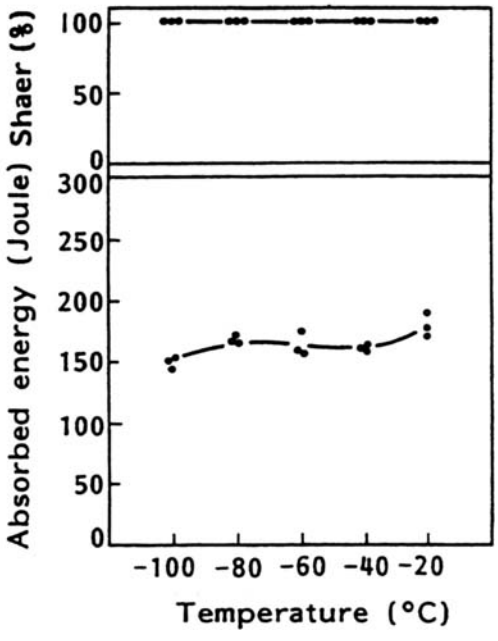


Fig. 13 Result of v-notch Charpy test. (7.5 mm sub-size, ST1)

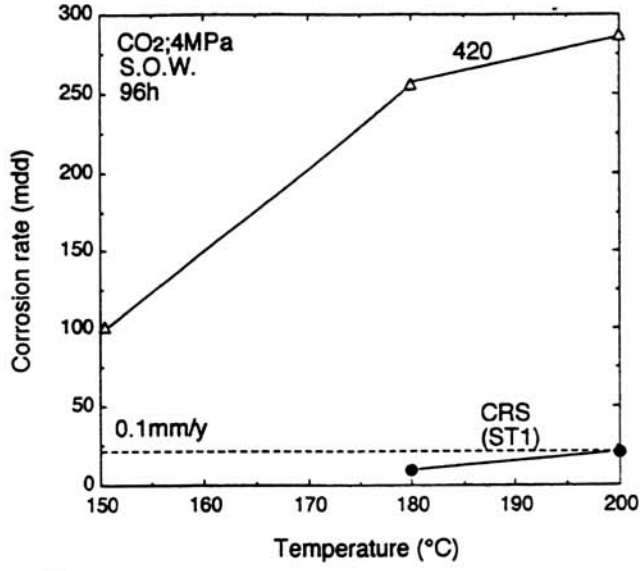


Fig.14 Temperature dependence of corrosion rate. (4MPa CO_2, SOW, 96hr, ST1 and 420)

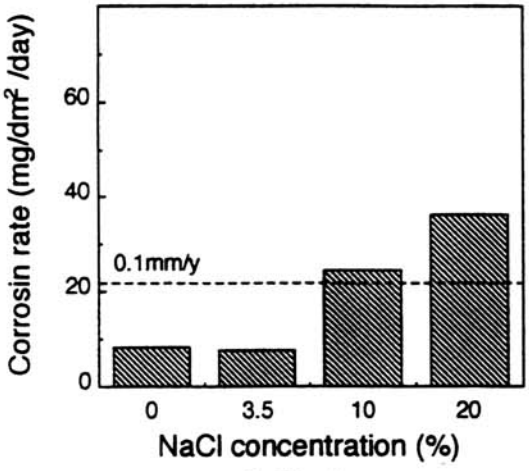


Fig.15 Effect of Cl-ion on corrosion rate. (40MPa CO_2, 180℃, 96hr)

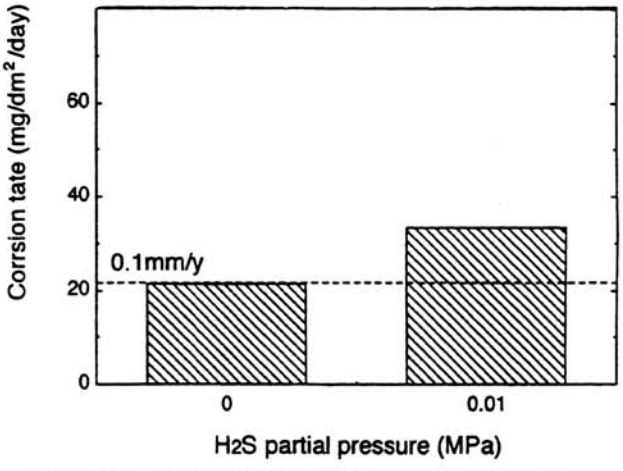


Fig.16 Effect of H_2S on corrosion rate. (4MPa CO_2, 200 ℃, 96hr)

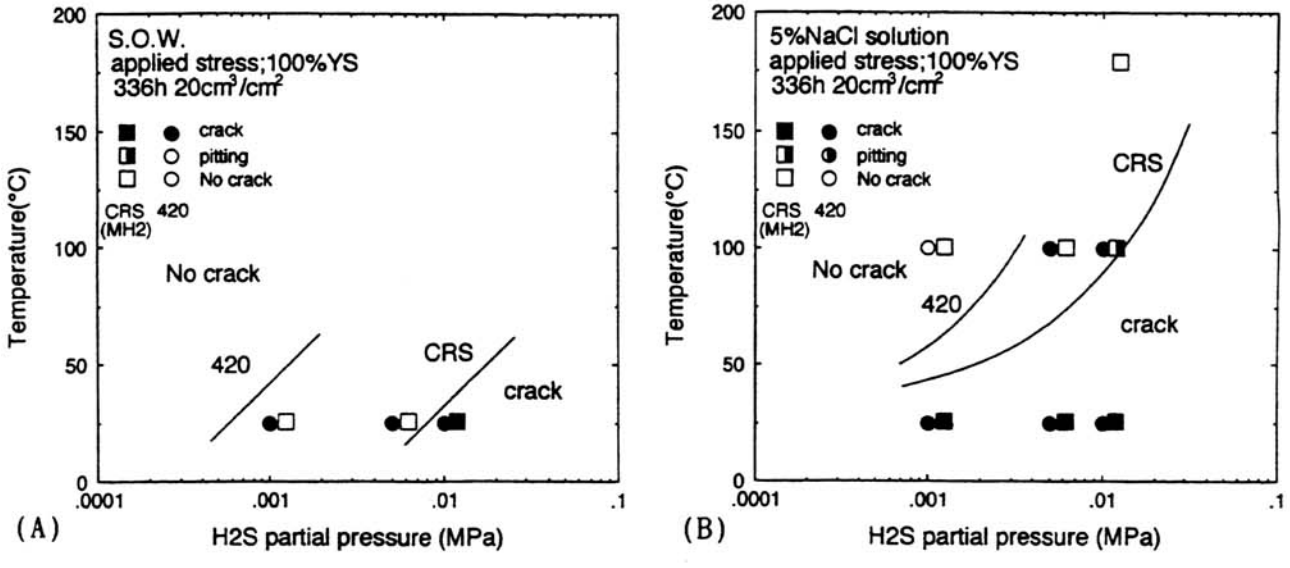


Fig.17 Results of four-point bent beam SSC test. (A) SOW, (B) 5%NaCl solution (4MPa CO_2, Notched specimen, 336hr, 100% of YS)

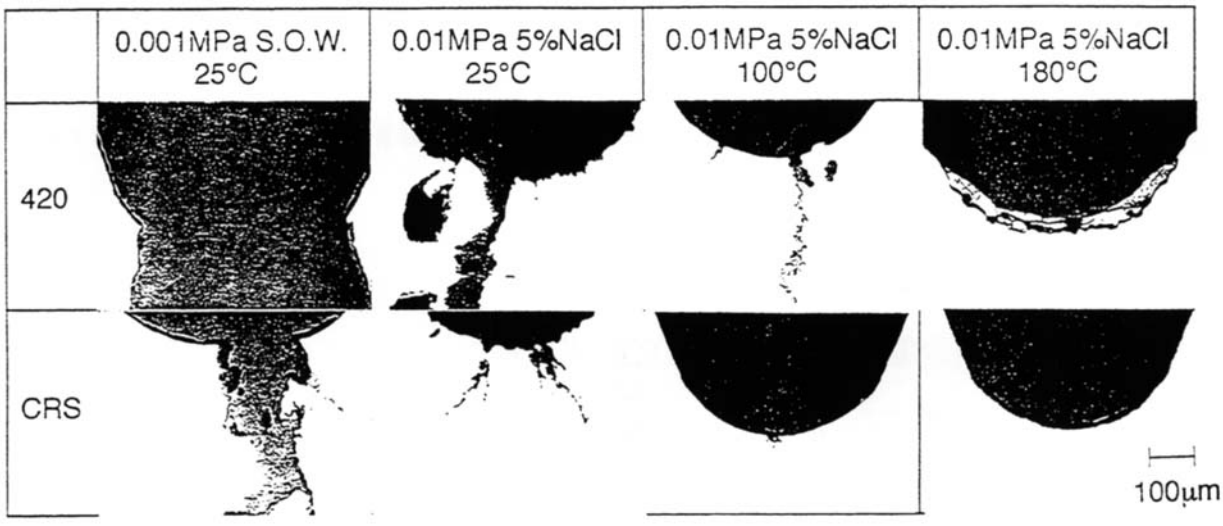


Fig. 18 Cross section photographs of notch portion after four-point bent beam tests.

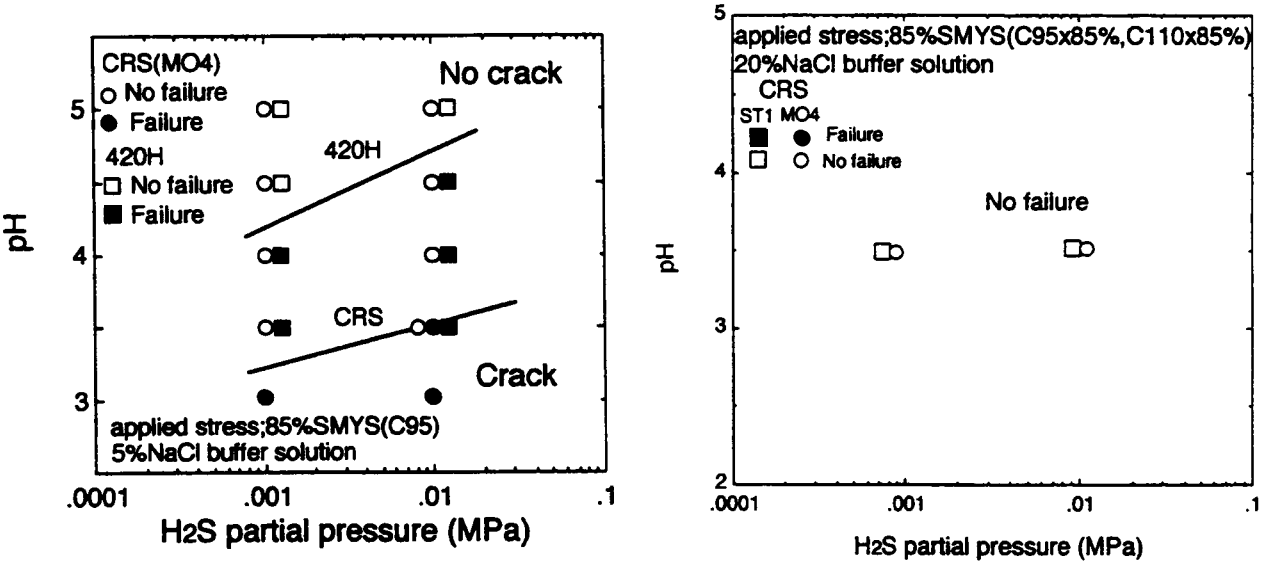


Fig. 19 Results of tensile type SSC test.

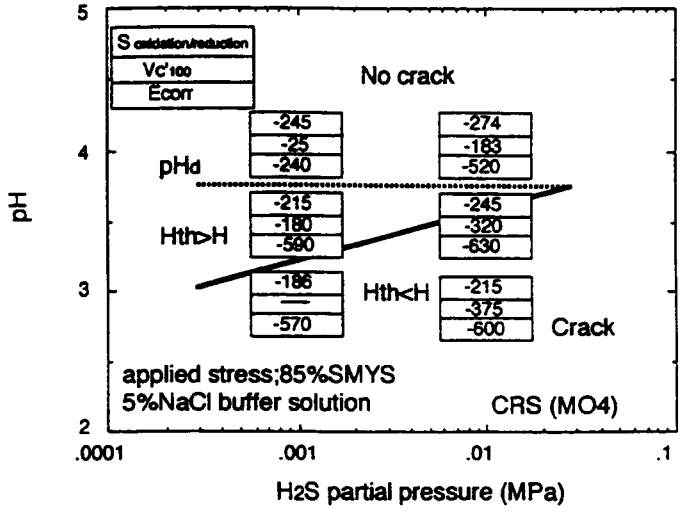


Fig. 20 Electrochemical states of tensile type SSC tests.

Copyrighted Materials
Copyright © 1996 NACE International Retrieved from www.knovel.com

Paper No.
639

CORROSION 95
The NACE International Annual Conference and Corrosion Show

EXPERIENCES WITH 13CR FOR MITIGATING CO_2 CORROSION IN THE OILFIELD CASE HISTORIES: THE GULF OF MEXICO AND INLAND GAS WELLS

Debbie A. Baudoin
Chevron U.S.A. Production Co.
5750 Johnston St.
Lafayette, LA 70503

David K. Barbin
Texaco E & P Inc.
400 Poydras St.
New Orleans, LA 70052

Jim Skogsberg
Chevron Petroleum Technology Co.
2202 Oil Center Court
Houston, TX 77073

ABSTRACT

Material selection for downhole completions in the oilfield is one that is critical to the economic success of a project on a long-term basis. In the past, the selection of downhole tubulars has been routine and basic, with most operators selecting carbon steel as standard procedure. Today, a paradigm shift from the use of traditional carbon steel to 13 percent chrome (13Cr) is taking place as we utilize tools of economics, corrosion engineering, and field data. We also place special emphasis on case-by-case histories of material performance for each well.

Factors to be considered in the decision making process in selecting materials for sweet corrosive environments include:

Field Data (Current and Historical)
Corrosion Engineering
Economics

This paper takes an objective look at the field experiences, conditions, and economics involved in making a materials selection. Of all elements considered, economics is the main driving force. This paper will focus on four case histories from the Gulf of Mexico and inland Louisiana with various temperatures, pressures, chloride content, CO_2 content, and production rates. These case histories, along with proven long term experience will help set the stage for further usage of 13Cr.

Key Words: CO_2 corrosion, decision making process, economics, field experience, flowchart, gas wells, 13Cr

INTRODUCTION

The use of 13Cr in the oilfield has increased over the last several years. The price and lead time for delivery of 13Cr has decreased significantly over the last decade. Some companies have instituted stocking programs as their usage has accelerated. Today many companies are reviewing their methods for tubular selection. Decisions are being made on a case-by-case basis utilizing the tools of economics, corrosion engineering and historical field data.

Studies have demonstrated 13Cr is a viable option to traditional carbon steels that have failed before all intended reserves were produced. It has been further determined 13Cr is an economical replacement for carbon steel when corrosion inhibition, coatings, linings or downhole injection systems are necessary.

The intent of this paper is to present case histories from the Gulf of Mexico and inland waters of Louisiana, and to present the framework of previous experience which provides a basis for the guidelines used in evaluating them. The cases include wells with high chlorides, high bottom hole temperature, wells that failed with carbon steel and wells that are costly to inhibit with chemicals.

Gulf Of Mexico

The Gulf of Mexico is replete with production platforms from virtually all major and independent oil companies. Several hundred platforms are strategically located throughout the Gulf of Mexico, in an effort to capitalize on the oil and gas rich reservoirs. Approximately 1300 producing platforms are located in waters from 10 feet to 1000 feet. At present, majors and independents are producing some 11 billion cubic feet of natural gas per day and over 700,000 barrels of oil per day.[1] Additional reserves are being realized with the advent of three dimensional seismic technology and in the future, production will occur in greater water depths.

Inland Louisiana

The inland waters of Louisiana have produced oil and gas since the 1930's, and for some companies have served as the foundation for their development and future growth in the Gulf of Mexico. Several hundred oil and gas producing fields exist in Louisiana inland waters and land locations. At present, many companies are exploring these areas for new oil and gas reserves.

FIELD DATA

Current

Many production related parameters and corrosion related data should be considered when performing the materials evaluation. Typical data used for the evaluation is as follows:

Reservoir Life	Wellhead Pressure
Gas Rate	Separator Temperature
Condensate Rate	Tubing Size
Water Rate	Tubing Length
Bottom Hole Temperature	CO_2 Content
Bottom Hole Pressure	H_2S Content
Wellhead Temperature	Chloride Content

In addition to the above parameters, the wellbore schematic and details are necessary for modeling the well for corrosivity.

Historical

Upon evaluation for a workover, available corrosion monitoring tools should be considered. These may include tubing caliper surveys, gas analyses, corrosion coupons, and water analyses. In addition to monitoring tools, well and reservoir history should be considered. For example, corrosion related workovers and/or corrosion control programs implemented for wells in the subject producing field should be considered when performing the evaluation.

Production parameters and corrosion related variables may not be available for analysis of a development well. Therefore, data should be gathered from an existing well produced from the same or a similar reservoir. This information should help determine the potential corrosivity of the fluids flowing in the wellbore.

CORROSION ENGINEERING

Essential elements of modeling a well to predict CO_2 corrosion in gas wells include:

Phase Behavior. - Different phases exist at various depths in the production tubing . It is critical to determine if the production tubing will be water wet or oil wet. The presence of liquid water as a free and separate phase is necessary for corrosion to occur, and therefore it is important to determine the depth of water wetting. If the tubular is oil wet, corrosion should not significantly reduce tubing life, unless the flow dynamics of the well disturb the oil film.

Water pH. - The pH of the water at the tubing surface must be calculated taking into account water chemistry, CO_2, H_2S (if any), and temperature. Water pH with temperature relate to the solubility (stability) of iron carbonate (ferrous carbonate) scale, which when formed on the tubing surface may reduce corrosion rates.[2]

Type Flow. - The flow dynamics of the well must be established to determine if the flow pattern is annular or annular mist. The worst case is one in which there is annular mist flow for the entire tubing string. Under this condition, a portion of the fluid actually leaves the wall of the tubing and flows at the velocity of the gas phase. These droplets entrained in the gas can damage the oil or water films on the tubing surface. Protective iron carbonate scales may also be removed or damaged.[3] The best case is fluid flowing in an annular pattern. This will occur at lower velocities and will result in much less disturbance of any film on the tubing, including protective iron carbonate scales.

Flow Velocity. - Velocity is a key parameter in the corrosiveness of the fluid. At higher velocities, it is difficult to maintain the protective iron carbonate scale. As a first look, tubing velocities should be compared to the critical velocity calculated according to API RP-14E, using a constant (C) of 100 for continuous service.[4]

Erosion. - Erosion from sand must be considered as a separate process from corrosion and erosion corrosion.

Predicted Corrosion Rates. - From the above, water wet tubing with annular mist flow and high velocities approaching the API critical velocity will need corrosion control measures. Predicting the approximate life of the tubing will require estimating corrosion rates. One method for doing this is using a PC-based model developed by a joint-industry-program at the University of Southwestern Louisiana.[5] This model calculates all of the above and predicts a corrosion rate and a tubing service life. This computer model has been used for some of the case histories presented in this paper.

ECONOMICS

Materials selection for corrosive wells should be evaluated on a case-by-case basis of economics. Factors such as the initial cost of the tubular must be considered. However, other cost elements such as workover dollars, (both tangible and intangible), lost opportunity, chemical costs, and deferred production due to downtime must also be considered. Economics of some commonly used corrosion mitigation methods are explored as follows:

13Cr Tubing. - This method incurs a higher initial cost, but its life is expected to exceed the reservoir life. The tubing should be reusable if production related workovers are required, whereas internally plastic coated tubing is not considered as reliable for reuse. In addition to corrosion resistance, 13Cr can be a more attractive alternative to carbon steel for high gas rate wells. The erosional constant in the API RP-14E guidelines can be a larger value. This fact results in accelerated production in some cases. Other advantages in using 13Cr include less corrosion monitoring, increased chance of depleting the reservoir, no deferred production or cash flow due to corrosion, reduced maintenance/manpower, no corrosion inhibitor treatments and improved overboard water quality. For the Gulf of Mexico, Chevron purchases 13Cr tubing to API Specification 5CT to the appropriate N-80 or L-80 (sour service) grade. Minimal supplementary requirements include descaling of ID surfaces and disallowance of cold straightening. Complimentary 12Cr surface wellheads and trees are purchased to API Specification 6A with quality assurance set at PSL levels of 2 or 3. For sour service, the appropriate API materials class is specified in order to meet NACE MR-0175. Manufacturer's materials specifications are approved in

advance and therefore no supplementary requirements are used. The company does not specify notch toughness requirements beyond those required by API and does not use CA6NM nor F6NM in the Gulf of Mexico.

Chemical Inhibition via Batch Treating. - This method incurs a lower initial cost than the other alternatives. However, lost cash flow from shutting in the well for treatment is extremely high. Other disadvantages of batch treating are the possibility of formation damage during treatment, anticipated tubing life less than reservoir life, and the inability to treat the well due to decreased reservoir pressure. The predicted life of the reservoir is a key factor when evaluating various corrosion control options. For instance, chemical inhibition may be appropriate for a well expected to produce for only a few years.

Continuous Treating System (CTS). - This method incurs a higher initial cost than batch treatment. The advantage of CTS systems is no lost cash flow due to shutting in the well, and a significantly more effective chemical inhibition treatment. However, the chemical and maintenance costs are quite high. Also, the mechanical risk for this type of completion is much higher than for conventional completions.

Other economic elements which are difficult to assess a dollar figure must also be considered. A cost sometimes overlooked is that associated with insignificant reserves to justify a workover. In some instances, it is uneconomical to workover a well that has failed due to corrosion, leaving behind unrecovered reserves. Another factor that must be considered is that associated with the environmental and safety risks of a corrosion related tubular failure.

FLOW CHARTS

It is sometimes easy to determine the type of material to be run in a well, but there are occasions when the decision is not as evident. Based on concrete data and past experiences, two flowcharts were developed to aid in this decision making process; one for new drills (both exploratory and developmental), and one for workovers. Please refer to Figures 1 and 2.

Based on past field experience, environmental limits have been established for 13Cr production tubing. These limits should be used as rules-of-thumb, because documented field experience usually involves only a few of the parameters which influence corrosion and seldom documents the interrelationship between these parameters. Our defined rule-of-thumb limits include a maximum bottom hole temperature of 300°F; 100,000 ppm to 150,000 ppm chloride in the produced water; 10 ppm H_2S concentration to partial pressures of 1/2 psi to 1 1/2 psi, depending on water pH. These H_2S limits are for grade L-80 tubing.

CASE HISTORIES

Case 1

The cost of corrosion for a downhole failure can translate into millions of dollars. Table 1 illustrates this point for Case Study #1. This well was completed with 13Cr based on the results of the modeling and the economic evaluation. This well produced 12 million cubic feet of gas per day (MMCFD), 700 barrels of condensate per day (BCPD) and 60 barrels of water per day (BWPD). As noted in Table 5, the anticipated production life of the well is 14 years.

Modeling for Case 1 indicates a very corrosive environment. The results show the entire tubing to be water wet. Predictions indicate serious corrosion rates in the entire tubing string and a corrosion failure in 8 months to 1 year. Under downhole conditions, two phase flow (vapor and water) is present throughout the tubing string with 60 barrels of water. Hydrocarbons condensing in the tubing prior to water (at a ratio high enough to keep the tubing oil wet) helps mitigate corrosion. This phenomenon is not occurring in this well. The condensate will be in the vapor phase throughout the entire tubing string, resulting in a mist type flow pattern. Water in the liquid phase will coexist with hydrocarbons in the vapor phase, leaving the tubing water wet. If the tubing is water wet and subject to such high velocities, serious corrosion is likely to occur.

Based on the computer modeling and economic evaluation, 13Cr was selected for corrosion mitigation. A caliper has been run since the well was completed, showing no penetrations in the tubular. As noted in Table 1, a payout period between 1 and 2 years was realized.

Case 2

This case history demonstrates tremendous economic losses when using carbon steel rather than 13Cr. The well was completed with carbon steel and failed due to CO_2 corrosion. This well produced at rates of 36 MMCF, 18 BCPD and 20 BWPD. It failed after being on production for 26 months. The workover costs were $1.2 MM and the deferred revenue costs were $3.5 MM. 13Cr was subsequently run in the well and has been calipered three times over two years. Caliper survey results indicate no pitting in the tubing. Refer to Tables 2 and 5 for economics and production vitals.

Case 3

This exploratory well was completed with L-80 carbon steel. It required downhole corrosion mitigation measures on a three week frequency, in which downtime was approximately 7 hours per treatment. The well produced at rates of 4 MMCF, 400 BCPD and 1500 BWPD. For production vitals refer to Table 5. There were also difficulties when bringing this well back on production after corrosion inhibition treatments.

The economic comparison is based on the subsequently drilled well in which 13Cr was run. As the economics point out, (refer to Table 3) a one year payout was realized when 13Cr was used.

Case 4

This well was completed with 4 1/2 in. internally plastic coated tubing. Production parameters and corrosion related variables can be found in Table 5. Production for the well is 30 MMCFD, 1000 BCPD and 20 BWPD. At the conditions referred to in table 5 and the above production rates, 4 1/2 in. tubing was modeled for this case. Condensate is present in the tubing from 9000 feet to the surface. Therefore, the upper portion of the tubing string is oil wet. The flow regime is in annular flow, and low velocities are present in the lower portion of the tubing. The tubing is water wet in this portion of the string.

The liquid film is not turbulent, rather slow moving with a film velocity of 1.3 feet per second. The predicted life is 28 years for a well with 4 1/2 in. tubing. It is also important to note that an iron carbonate film can be maintained at this low velocity, providing corrosion protection. The worst case prediction is 9 years for this well. Considering that the life of the reservoir is only 3 to 4 years, low carbon steel is sufficient for this application. Also note corrosion inhibition for this well will have a longer film life due to the lower velocities and the iron carbonate formation.

An aggressive monitoring program has been implemented for this well. A caliper was run 6 months after the well began producing. The survey indicated no penetrations in the 4 1/2 in. tubing. The survey included 417 joints of pipe totaling 13,350 feet of tubing with the packer at 13,346 feet. Coupons were pulled on a monthly basis for three months with corrosion rates of 0.19, 0.29, 0.19 MPY respectively. The well has produced at accelerated rates between 38 - 41 MMCFPD. It should be noted that this accelerated rate would not have been possible if 3 1/2 in. tubing was used.

The well was also modeled with 3 1/2 in. tubing. Results indicate very severe corrosion, and velocities that exceed the erosional velocity. The flow regime indicates mist flow. The above information along with the monitoring data from the program implemented for this well will verify the accuracy of the decision making process.

ADDITIONAL EXPERIENCE: LONG-TERM PERSPECTIVE

The company completed their first 13Cr well for the False River field of the Tuscaloosa Trend in the summer of 1975. Other gas fields in Louisiana that were eventually completed include Judge Digby, Moore-Sams, Profit Island, and Elba. Wells in the Tuscaloosa Trend are generally 18,000 to 21,000 feet deep. The conditions were:

- Bottom hole temperature: 375°F maximum
- Bottom hole pressure: 14-16,000 psi
- CO_2 partial pressure: 8%
- H_2S partial pressure: 20-30 ppm = 1/2 psi maximum
- Chlorides up to 100,000 to 150,000 ppm
- Up to 200°F surface wellhead temperatures

The surface equipment included 12Cr/13Cr trees with tubing hangers. The dual 13Cr tubing strings (420 Stainless steel) were a proprietary grade of C-85 with hardness controlled to HRC 23. The liners were low alloy steel of grade P-110.

These wells were originally completed with low alloy steel production tubing that corroded out in one to two years because of CO_2 corrosion from water condensation in the upper third of the tubing strings. The 13Cr was installed to extend tubing life and avoid expensive workovers. Some of these wells have been acidized with mud acid (HCL/HF) and some have been completed with clear brines, including Zinc Bromide.

Not a single one of these gas wells, that has stayed on production, has ever been lost due to corrosion leaks or sulfide stress cracking. One well that had been repeatedly shut in and acidized was lost due to internal pitting corrosion. Tubing strings have shown internal pitting, some of which have exceeded API wall tolerances. Some strings were replaced after 5 years to avoid the high cost of reinspecting used tubing. These tubing strings have never been coated or protected from corrosion by using chemical inhibition.[6]

Other important aspects of this experience were:

- There has been some gas cutting of gates and seats, even those hardfaced with cobalt-based alloys.
- Wireline work has not caused any tubing failures. This is consistent with industry experience. Wireline tools can scratch tubing and remove protective corrosion films on both 13Cr and low alloy steel. This will accelerate corrosion, but rarely leads to failure.
- There has been no observed pitting of 13Cr tubing exposed to clear brines.
- Copper coating the box of the connection and also applying molycoate to both the pin and box have prevented galling during make up of 13Cr tubing.
- Tubing stored in the open air has pitted because of salt water deposits from the humid Gulf Coast atmosphere.
- There have been no brittle fractures of wellhead equipment or production tubing. This equipment was purchased without supplementary notch toughness requirements. Wellheads and trees were generally 12Cr (410 SS) and were not F6NM or CA6NM, which have higher notch toughness.
- There has been no significant corrosion of low alloy steel grade P-110 liners.
- Used tubing must be 100% full-body inspected by EMI for internal pitting. Pitting first appears at the connections.
- This tubing was purchased through a cooperative effort with Mannesmann, NKK, and Sumitomo. Joint specifications were written for each mill. All tubing was purchased with the ID and OD surfaces descaled by pickling and bead blasting.

CONCLUSIONS

These cases cover various spectrums of temperatures, pressures, chlorides, CO_2 content, and production rates. While the current cases cover only CO_2 applications, it must be noted that 13Cr has over time been successful in production applications where 20-30 ppm H_2S has been produced. A paradigm shift from traditional carbon steel to 13Cr use is occurring more rapidly than ever before due to economics, deliverability, proven historical performance, drilling deeper, hotter, more corrosive wells and information sharing of successes using 13Cr .

This paper takes an objective look at the economics and conditions involved in making a materials selection. While the main focus of this paper has been the use of 13Cr, there certainly is and always will be applications for traditional carbon steel tubulars. As this paper demonstrates, economics is the main driving force, however field data and historical performance must be considered in this decision making process.

ACKNOWLEDGMENTS

The authors would like to thank C.D. Adams for his work with the USL Corrosion Modeling Program, R. Braun and J.B. Bates for their contributions.

REFERENCES

1. Offshore Magazine, June 1994

2. R. H. Hausler & D. W. Stegmann, CO_2 Corrosion and Its Prevention by Chemical Inhibition in Oil and Gas Production, Corrosion 88, paper no. 363

3. J. S. Smart, A review of Erosion Corrosion in Oil and Gas Production, Corrosion 90, paper no. 10

4. API Recommended Practice for Design and Installation of Offshore Production Platform Piping Systems, APIRP14E, API Dallas, TX

5. Adams, C. D., J. D. Garber, and A. G. Hill, "Expert System for Predicting Tubing Life in Gas Condensate Wells", Corrosion 92, paper no. 273

6. J.D. Combes, 13Cr Tubulars Solve Corrosion Problems in the Tuscaloosa Trend, Petroleum Engineer International, March 1993

Table 1: Case 1 Economics

BATCH	YR1	YR2	YR3
Tubing Cost	$90,000		
Workover Cost			$1,200,000
Replacement Tubing Cost			$90,000
Mcfd	36,000	36,000	36,000
bcpd	18	18	18
Deferred Prod. Due to Downtime	$0	$0	$3,500,000
Corrosion Inhibition Expenses	$0	$0	$0
YEAR TOTAL	$90,000	$0	$4,790,000
CUMULATIVE COST	$90,000	$90,000	$4,880,000

13 CHROME	YR1	YR2	YR3
Tubing Cost	$216,000		
Workover Cost			
Replacement Tubing Cost			
Deferred Prod. Due to Downtime	0	0	0
Corrosion Inhibition Expenses	0	0	0
YEAR TOTAL	$216,000	$0	$0
CUMULATIVE COST	$216,000	$216,000	$216,000

Table 2: Case 2 Economics

BATCH	YR1	YR2	YR3
Tubing Cost	$137,000		
Workover Cost			
Replacement Tubing Cost			
Mcfd	4,000	4,000	4,000
bcpd	400	400	400
Deferred Prod. Due to Downtime	$48,000	$48,000	$48,000
Corrosion Inhibition Expenses	$75,000	$75,000	$75,000
YEAR TOTAL	$260,000	$123,000	$123,000
CUMULATIVE COST	$260,000	$383,000	$506,000

13 CHROME	YR1	YR2	YR3
Tubing Cost	$213,000		
Workover Cost			
Replacement Tubing Cost			
Deferred Prod. Due to Downtime	$0	$0	$0
Corrosion Inhibition Expenses	$0	$0	$0
YEAR TOTAL	$213,000	$0	$0
CUMULATIVE COST	$213,000	$213,000	$213,000

Table 3: Case 3 Economics

BATCH	YR1	YR2	YR3	YR4
4-1/2" Tubing				
Tubing Cost	$227,000			
Workover Cost				
Replacement Tubing Cost				
Mcfd	30,000	30,000	30,000	30,000
bcpd	1,000	1,000	1,000	1,000
Deferred Prod. due to Downtime	$294,000	$294,000	$294,000	$294,000
Corrosion Inhibition Expense	$7,600	$7,600	$7,600	$7,600
Mcfd	10,000	10,000	10,000	10,000
bcpd	300	300	300	300
Accelerated Prod. Due to > Tubing ID (-#)	$10,001,000	$10,001,000	$10,001,000	$10,001,000
YEAR TOTAL	($9,472,400)	($9,699,400)	($9,699,400)	($9,699,400)
CUMULATIVE COST	($9,472,400)	($19,171,800)	($28,871,200)	($38,570,600)

13 CHROME	YR1	YR2	YR3	YR4
3-1/2 " Tubing				
Tubing Cost	$223,000			
Workover Cost				
Replacement Tubing Cost				
Deferred Prod. due to Downtime				
Corrosion Inhibition Expense				
YEAR TOTAL	$223,000	$0	$0	$0
CUMULATIVE COST	$223,000	$223,000	$223,000	$223,000

Table 4: Case 4 Economics

	Case 1	Case 2	Case 3	Case 4
Reservoir Life	14 Years	7 Years	5 Years	3-4 Years
Gas Rate	12 MMCFD	36 MMCFD	4 MMCFD	30 MMCFD
Condensate Rate	700 BCPD	18 BCPD	400 BCPD	1000 BCPD
Water Rate	60 BWPD	20 BWPD	1500 BWPD	20 BWPD
BHT	259°F	240°F	300°F	210°F
BHP	11,000 psi	6400 psi	10,000 psi	4000 psi
Wellhead Temp	120°F	180°F	170°F	110°F
Wellhead Pressure	8000 psi	6100 psi	7000 psi	3000 psi
Separator Temp	100°F	180°F	160°F	85°F
Tubing Size	2.875 inch	2.875 inch	2.875 inch	3.958 inch
Tubing Length	17,000 feet	15,400 feet	14,000 feet	12,600 feet
CO_2 Content	1.26 mol %	0.84 mol %	1.1 mol %	0.40 mol %
H_2S Content	nil	nil	nil	nil
Chloride Content	127,000 mg/l	40,000 mg/l	20,000 mg/l	11,000 mg/l

Table 5: Summary of Production and Corrosion Related Variables

	Case 1	Case 2	Case 3	Case 4
Economics (Cost) - Carbon Steel	$9,200 M	$4880 M	$ 510 M	-$38,600 M
Economics (Cost) - 13Cr	$289M	$ 216 M	$ 213 M	$ 223 M

Table 6: Summary of Economics

Figure 1: Flowchart of Decision Making Process for Materials Selection New Drills

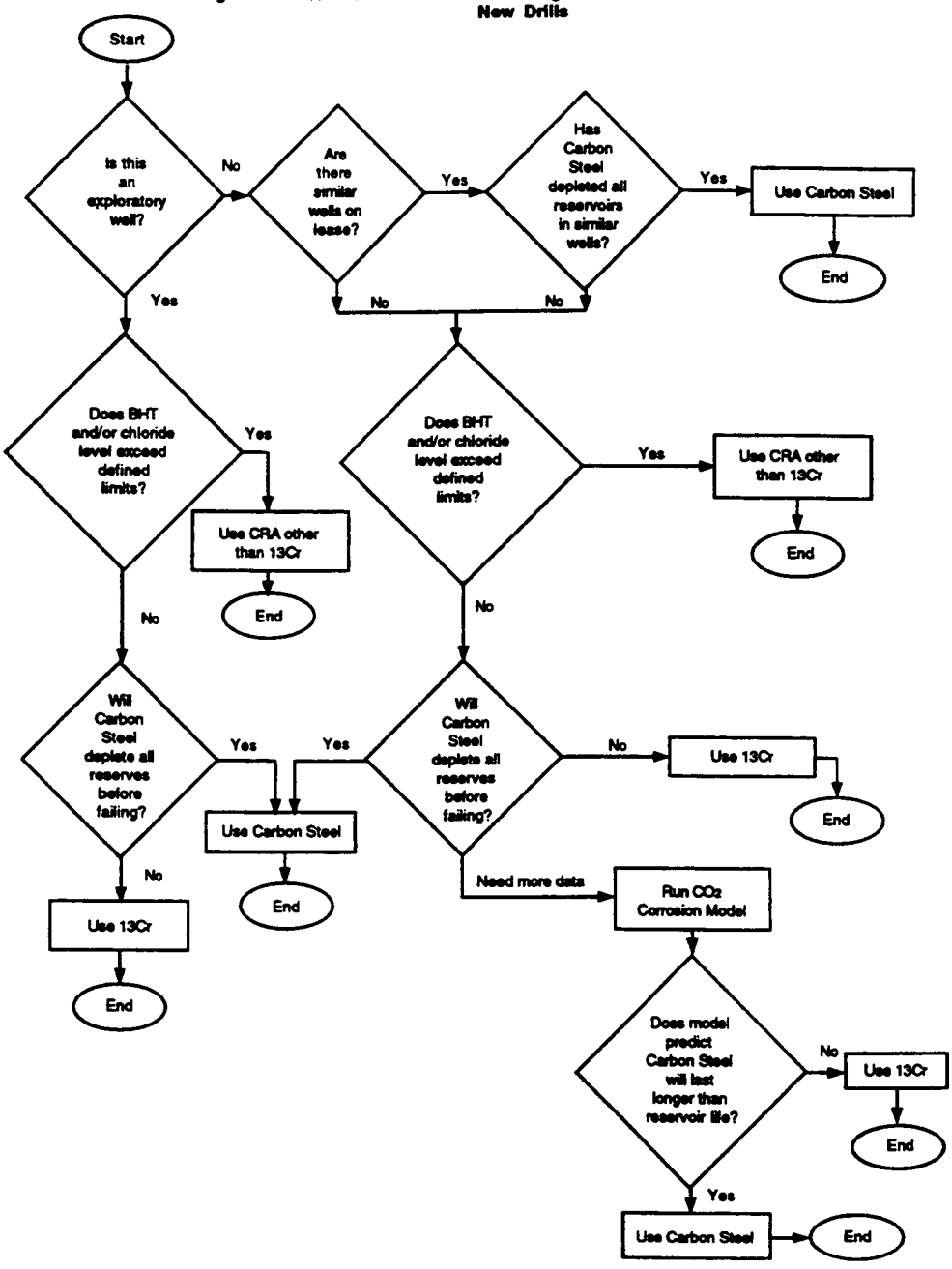
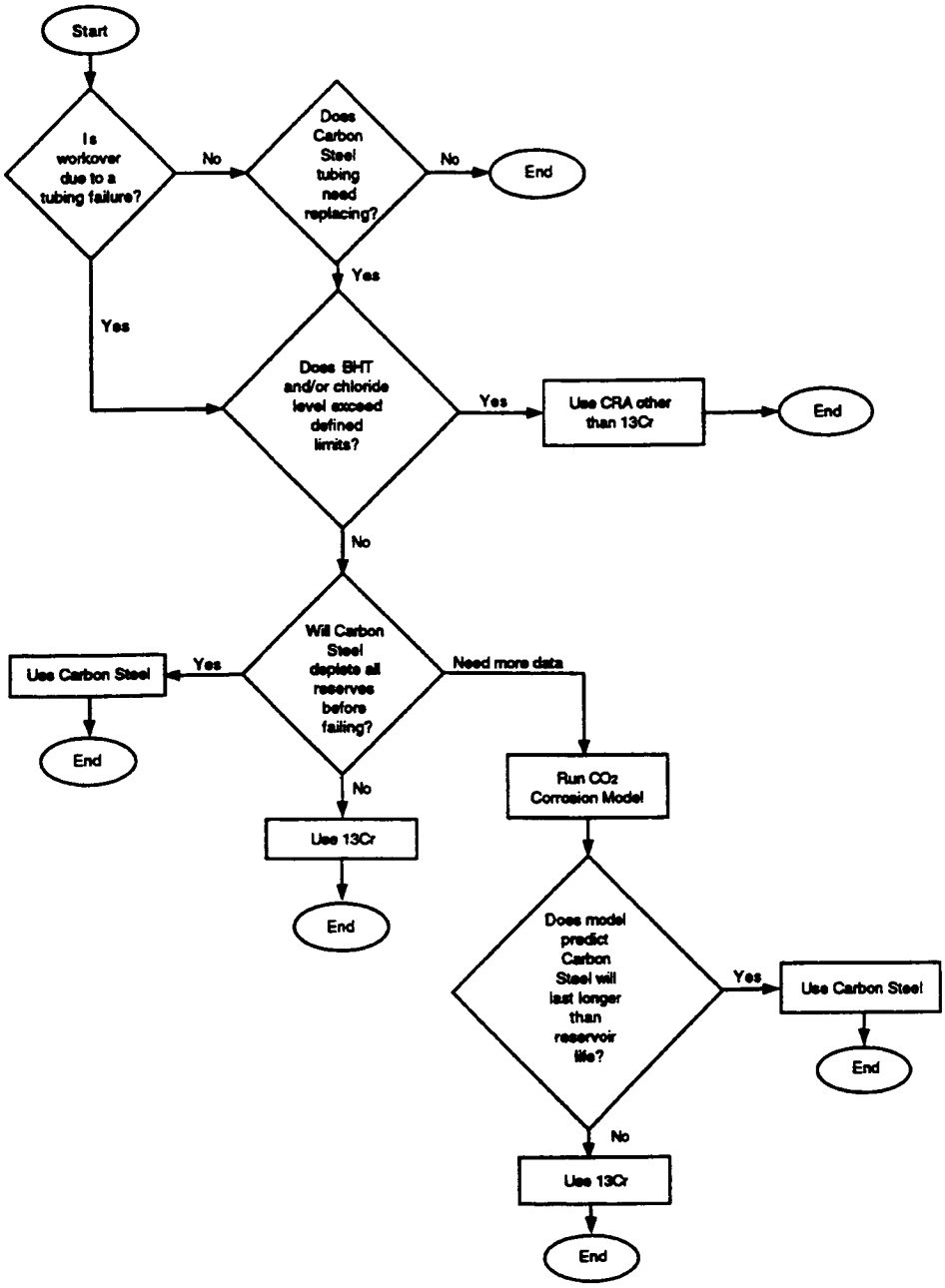


Figure 2: Flowchart of Decision Making Process for Materials Selection Workovers



Copyrighted Materials
Copyright © 1996 NACE International Retrieved from www.knovel.com

Paper No.
7

CORROSION 94
The Annual Conference and Corrosion Show
Sponsored by NACE International

Experience of 13 % Cr Tubing

II : 10 years and 1 million feet later

Michel BONIS and Jean-Louis CROLET
Elf Aquitaine

64018 PAU (France)

Abstract

The Elf Group today has 707 km (2,4 x 10^6 ft) of 13 % Cr steel tubing in service in 279 wells, including 235 oil wells and 44 gas wells. The operating conditions for these tubes have remained practically unchanged for 10 years, and the overall performance is completely satisfactory. The corrosion limits are even much higher than was believed. Altogether, the use of 13 % Cr steel tubing has led to savings of more than 500 milliion $, half of which is due to the use of 13 % Cr steel right from the initial well completion.

Introduction

The beginnings

Our Company installed its first 13 % Cr stainless steel production tubing in 1978, almost simultaneously in Holland and in Gabon. Both cases involved the replacement of standard carbon steel tubing in extremely corrosive CO_2 wells, where perforation had unfortunately occurred too rapidly. Indeed, the life between well workovers had fallen to between 18 and 6 months, and the initial objective was "to try to attain at least 3 years".

At this time, stainless steel was practically unknown in the oil and gas industry, whereas it had already been a standard material for 20 to 30 years in the chemical industry. Applying the principle of cross-fertilization which is a permanent policy between our hydrocarbon and chemical divisions, the experience and methods of the chemicals and special steels industry were therefore adopted. A few polarization curves and laboratory autoclave tests soon showed that, in a strictly deaerated solution, with indeed moderate acidity, even the baseline 13 % Cr alloy presented no risk of either uniform or pitting corrosion. Moreover, cracking was theoretically not a problem, due to the martensitic structure (SCC) and the absence of H_2S (SSC). The use of 13 % Cr steel tubing was thus rapidly introduced in about a hundred wells, corresponding to a total length of about 200 km (0.7 million ft).

In spite of the information available, all the errors usually made when changing from plain carbon to stainless steel were repeated on this occasion. However, an early and systematic examination of all incidents which arose fortunately prevented them from becoming permanent counter references. The code of practice for the use of stainless steel tubing, which has been described in several publications[1-4], was defined at this time.

With hindsight, it is absolutely clear that none of this know-how could have been established by preliminary pilot tests, or by experimental applications. In this field, it must be humbly acknowledged that everything cannot be quantified in advance. From time to time, without taking undue risks, the right policy can thus be to go ahead and take the plunge. In corrosion as elsewhere, the pioneering spirit must not bow down to bureaucracy.

Maturity

After the inspection of several tubing strings withdrawn for verification, 13 % Cr steel was rapidly confirmed to be virtually "indestructible" in CO_2- containing oil or gas wells. Apart from a few mechanical or chemical accidents not particularly related to the nature of the metal, this stainless steel tubing could even be re-used indefinitely, with losses limited to 1 - 2 % per operation.

The costs concerned have been determined, based on the real operational values, and it has been found that :

- Apart from production losses, which are not always easy to assess, the cost of CO_2 corrosion in a well is essentially the cost of the workover operation itself, at least when the latter was not already programmed for production reasons other than corrosion.
- In the Gulf of Guinea, for 2 000 - 2 500 m (7 000 - 8 000 ft) deep wells in calm seas, the extra cost due to the use of 13 % Cr steel was in fact only the tenth of that of a corrosion-imposed workover.
- The supply of new plain carbon steel tubing represented only 3 % of the workover cost (all these ratios were re-confirmed in 1992). Replacement of tubing when a workover was programmed for other reasons was therefore not considered by the operators as an unacceptable corrosion problem, but simply as a normal consumption, without consequence, and therefore not questioned[5-8].
- The costs of down-hole inhibition on the rig, and particularly those associated with the logistics, are always underestimated. In Gabon, it was found that the extra cost of 13 % Cr tubing did not exceed the real operating expenditure for 2 to 3 years of well inhibition[3-4], either by squeeze or continuous downhole injection.

Analysis of these four cost factors reveals that, while the immediate technical purpose of 13 % Cr steel tubing is obviously to resist corrosion, its real economic function is in fact to reduce the offshore personnel requirements associated with corrosion prevention. The overall consideration of these different economic aspects clearly revealed the advantage of equipping corrosive CO_2 wells with 13 % Cr steel from the outset. This led to the apparent need to predict the corrosivity of newly discovered and as yet unexploited wells[5-6].

In fact, since our production fields are essentially offshore in nature, it also became apparent that, even in the case of uncertainty, the financial risks were minimized by equipping the wells with stainless steel. This approach was adopted for two platforms in the Cameroon, for which it was not known at the time whether they would resemble the neighboring corrosive Gabon field or the distant and uncorrosive Frigg field (Norway). It was therefore realized that the essential requirement was to reliably predict, not so much the corrosivity of a well, but rather the absence of corrosivity, in order to be able to maintain standard carbon steel tubing without risk[7-8]. The model used for this prediction has been described in detail elsewhere[7]. Simply an automatic calculation software was developped for making it easily accessible to technicians of Engineering Departments. To date, no exceptions have been encountered to the predictions of this model.

10 years later

The first two stages were very rapid (1978 - 1984), with an intense activity and a strong involvment of the research and central departments Subsequently, the use of 13 % Cr steel tubing has become the standard routine, directly managed by the operating subsidiaries. The recent survey by the NACE Technical Committee T-1F-21 thus took us completely by surprise. Due to a lack of centralized information, we were unable to reply in time, whereas we represent probably a quarter of all 13 % Cr well tubing used in the world, i.e. a fifth of all equipment in corrosion-resistant alloys.

The aim of this paper is to correct this omission, by indicating the state of our knowledge in 1994, the utilization statistics, the present operating procedure and the resistance limits discernible today.

Knowledge update

Utilization statistics

Table 1 summarizes the information communicated to the T-1F-21 Committee concerning the wells presently in production, together with those planned (firm decision). It can be seen that there are 707 km (2.4×10^6 ft) of 13 Cr tubing installed today in 279 wells, compared to 120 wells in 1984[3] and 140 in 1986[4].

The apparent slowdown in the last few years has no technical significance, and this applies also to the ratio between oil and gas wells (235/44). The difference stems simply from the fact that we have more oil fields than gas fields, and that an oil-producing platform generally comprises a greater number of wells than a gas rig. The rapid initial growth simply reflects the retrofitting of the Gabon rigs.

Today's growth is determined only by new discoveries. In this case, the policy remains to install 13 % Cr tubing from the outset. Unfortunately, this is still sometimes due to uncertainty, but this time for silly reasons, related to missing or incomplete water analyses. For example, the absence of 4 samples of reservoir water led to a capital investment penalty of 10 million $. However, this is no longer a technical problem of corrosion, but simply a question exploration organization.

The absence of H_2S in Table 1 is not a deliberate purpose, resulting from a specific selection. It simply reflects the hazards of geology. Although slight souring encountered in the Cameroons did engender traces of H_2S, the partial pressure was always less than 10 mbar (0.15 psi).

In conclusion, by 1996, there will be 815 km (2.7 million ft) of 13 % Cr stainless steel tubing in service.

Operating procedures

Practically nothing has changed compared to 10 years ago. However, the rare modifications are as follows :

Make up torque : The torque levels of VAM couplings were increased shortly after our first publications. In effect, in the high pressure gas fields in Holland, the tensile forces during cooling slightly reduced the tightness of the metal/metal junctions. In any case, the geometries of the connections are now no longer the same as ten years ago. The suppliers (and Computer Assisted Design) have made considerable progress, and the problem has ceased to exist.

Anti-galling coatings on threads : The oxalate coating initially used proved insufficient at the higher torque levels. In agreement with the suppliers, this was therefore replaced by copper plating. This also enabled standardization with the other grades of stainless steel. Copper plating is now limited to the coupling.

Temporary protection during storage : Oily coatings are not necessary[3-4] : rinsing due to rainwater, combined with a suitable drainage slope are sufficient to keep the tubes clean and in a passive condition. Nevertheless, protection is sometimes still used from force of habit.

API grade and heat treatment : Until recently, our purchases were always limited to API L80 grade. This had nothing to do with H_2S, but was a simple metallurgical coincidence, related to the risk of local chromium depletion around chromium carbide precipitates during the more limited tempering treatment required for grade C95.

It is now known that certain suppliers propose a C95 grade which is not sensitive to intergranular corrosion. However, this cannot be guaranteed to be the general case.

Acidification : Responsibility for verifying the suitability of acid inhibitors for 13 % Cr steel is today left to the acid suppliers (except in the case of doubt or extreme temperature conditions).

Loss and regeneration of know-how : Due to the direct effect of size and time on statistics, this aspect is particularly important in Gabon, because of the large number and age of the wells equipped with 13 % Cr steel. As everywhere else, human nature, routine and trouble-free operation gradually induce forgetfulness, then laxity. Changes in personnel, at all levels, periodically bring home the fact

that anything which goes without saying will some day have to be said again, and preferably specified in writing.

In this respect, it is not sure that the operating procedures for 13 % Cr tubing are different from any other type of oil industry know-how.

Limits of use

We still have no idea of the real corrosion resistance of the 13 % Cr steel. However, the limits are obviously well beyond the pessimistic predictions of the literature, based on oversimplified laboratory tests.

Corrosion by CO_2 : For example, for a 10 g/l NaCl solution (0.2 M/l) at 150° C and 48 bars (700 psi) CO_2, the laboratory corrosion rates reported in the literature[9] are 0.8 mm/year. In a Congo project, with much more chlorides, 3.3 M NaCl and 0.5 M $CaCl_2$, at 150° C and 4 bars (60 psi) of CO_2, but with 4.3 mM/l of HCO_3^-, the corrosion rate falls to less than 0.1 mm/yr. The difference is due to the real pH, which is about 4.2, compared to the value of approximately 3.3 for the pure NaCl solution. The depassivation pH was probably somewhere in between.

Similarly, in a high pressure high temperature ("HPHT") project in the North Sea, the C95 grade would have been satisfactory with respect to dissolution in the 1.2 M NaCl + 0.1 M $CaCl_2$ medium with 40 bars of CO_2 and 0.1 bar of H_2S at 190° C, corresponding to a pH of 4, but the mechanical properties of this material were insufficient for the intended application. A super austenitic grade work-hardened to 140 ksi was therefore chosen.

Seawater : The only case of internal corrosion observed in the last 10 years occurred in Gabon, which is statistically not surprising. It was not a breakthrough, but simply a routine inspection after a normal well workover. The appearance of the tubes (non-perforating pits) and the history of the well showed the corrosion to date back to an early injection test carried out without particular precautions concerning the deaeration of the seawater.

Subsequently, it has been shown that production wells equipped with 13 % Cr steel can be directly converted to injection wells at the end of their lives, without having to replace the tubing. It is sufficient simply to ensure that the oxygen content of the injection water is less than 30 ppb during operation, and strictly zero during shutdown periods (addition of excess oxygen scavenger in the latter case).

In any case, there is no risk involved, either physical or financial. Indeed, in the event of breakthrough in a 13 % Cr tubing, the resulting workover would be simply equivalent to the one which would have been required to replace the stainless steel by standard tubing.

Sulfide stress cracking : Figure 1 summarizes the results of sulfide stress cracking (SSC) tests on L80 grade 13 % Cr steel, obtained with smooth tensile specimens under quasi-constant stress (TM 01 77-A), at different pH levels and H_2S partial pressures. It should be noted that the failure observed at 1 mbar and a pH of 3 was not included in the original publication[10].

This figure also indicates the zone authorized in the recommendation MR 0175-93 ; together with the conventional limits for "H_2S service" being prepared by the European Federation of Corrosion. It can be

seen that the 13 % Cr L80 grades resists at least up to these limits, and even significantly further. Where necessary, the ultimate limits must be determined by specific tests.

Thus, while these new limits for the SSC resistance are beyond certain exaggeratedly pessimistic predictions in the literature[11], they also fall significantly short of the excessively optimistic older versions of the MR 01-75. Finally, it must be born in mind that the presence of H_2S can also affect uniform or pitting corrosion. The SSC limit is thus not necessarily the overall service limit for the 13 % Cr steel.

In situ pH, real bicarbonate concentration and water analyses : In CO_2 corrosion, as SSC, it has been seen that the in situ pH is a determining factor for the resistance of 13 % Cr steel. In order to evaluate it either by calculation[12] or by simulation in an autoclave, it is therefore necessary to have a relatively accurate value for the bicarbonate concentration. This implies two absolutely essential conditions :

a) Water sampling together with transport and storage of the specimens, must be performed under anaerobic conditions

By definition, testing prior to the choice of 13 % Cr steel is carried out in carbon steel equipment, so that the corresponding water samples contain significant amounts of $Fe(HCO_3)_2$ corrosion product. In condensed waters (e.g. $Cl^- < 1\,000$ ppm), it must be remembered to eliminate the corresponding alkalinity and to correct the analysis results accordingly.

Conversely, in formation waters accidentally aerated before analysis, the oxidation of Fe^{++} to Fe^{+++}, followed by hydrolysis, can physically eliminate as many meq/l of HCO_3^- as there are meq/l of Fe^{++} in the composition. Here again, it may prove necessary to correct the measured HCO_3^- content, increasing it by the observed amount of Fe^{++} (in meq/l).

Thus, because of the presence of corrosion products, it can be necessary to correct the measured bicarbonate values, either upwards or downwards.

b) Measurement of acetate concentrations

In the presence of acetates or other inorganic anions, as is frequently the case in the corrosive CO_2 fields[7,8,13,14], the standard method for measuring bicarbonate concentrations incorporates part of the organic alkalinity, whereas the latter does not buffer the CO_2 directly[15]. Here again, the total organic alkalinity must be measured independently (by liquid chromatography), followed by correction of the measured bicarbonate value[12].

As for the CO_2 corrosion of carbon steels, the accurate prediction of corrosion behaviour in 13 % Cr grades can require an equally detailed analysis of the water chemistry.

Overall evaluation

The economic justification of the use of 13 % Cr steel tubes is no longer necessary. The installation of 707 km of tubing, representing a considerable tonnage of stainless steel ($\approx$ 12 000 t) has not been undertaken without reason.

The technical balance is also extremely satisfactory : two perforations in 16 years for 279 wells, due in both cases to accidents of acidification following an unfortunate chain of circumstances[3,4]. For the first accident, in 1979, the sequence of events was as follows : a double packer, one of which was not leaktight ; acid not at all consumed, since injected in an unforseen non-limestone formation ; temperature 120° C ; discharge after 36 hours, and total loss of inhibition. The second case also involved a double packer, and a slight leak of acid in the packer fluid (KCl brine), leading to perforating external pits.

Four tubing failures have also been observed during programmed workovers. All were due to rolling cracks which had not been detected by nondestructive inspection during manufacture.

Finally, there have also been several epidemics of rejections, due to mechanical damage of the sealing surfaces during workover operations. It was therefore necessary to cut and re-thread the ends, which although it represented an unexpected expenditure, was not fundamentally serious. For this reason, the instructions for unscrewing the joints must also be repeated regularly[3,4].

While the overall economic balance of 16 years use of 13 % Cr stainless steel tubing is difficult to evaluate with precision, it clearly represents savings of several hundred millions of dollars (about 500 million $ if the cost of an offshore workover is taken to be 2 million $). Half of this amount is due to savings on replacements in wells retrofitted before 1984, and the remainder for wells equipped in this way from the start.

Conclusions

In 1994, the Elf Group has 707 km (2.4 million ft) of 13 % Cr stainless steel tubing in service in 279 wells, 235 producing oil and 44 gas. By the end of 1996, there will be at least 815 km (2.7 million ft).

The operating procedure has remained practically unchanged since our previous publications. Very few incidents have occurred in 16 years, only two of which led to a workover. Moreover, the perceptible limits of corrosion resistance are higher than is often assumed (0.1 bar H_2S or 1.5 psi ; > 200° C, at least in certain cases).

The overall economy resulting from the use of 13 % Cr steel tubing probably amounts to about 500 million $, approximately half of which is due to the equipment of wells with stainless from the outset.

References

1) J.L. CROLET "La corrosion acide dans les puits (CO_2, H_2S) : aspects métallurgiques" Bull. Centres Rech. Explor. - Prod. Elf Aquitaine 6, 1 (1982) ; p. 265

2) J.L. CROLET J. Pet. Techn. 35, 8 (1983) ; p. 1553

3) J.L. CROLET "L'expérience Elf Aquitaine de l'utilisation des tubings à 13 % Cr" Bull. Centres Rech. Explor. - Prod. Elf Aquitaine 8, 1 (1984); p. 15

4) J.L. CROLET and M.R. BONIS, SPE Prod. Eng. 1, 9 (1986) ; p. 344

5) J.L. CROLET and M.R. BONIS, Oil and Gas European Mag. 10, 2 (1984) ; p. 68

6) J.L. CROLET and M.R. BONIS, Materials Performance 25, 3 (1986) ; p. 41

7) M.R. BONIS and J.L. CROLET, "Basics of the prediction of the risks of CO_2 corrosion in oil and gas wells", CORROSION 89, paper 466 (Houston, Tx : NACE, 1989)

8) J.L. CROLET "Which CO_2 corrosion ? Hence which prediction" 10th European Corrosion Congress, Barcelona, 5 - 8 July (London UK : European Fed. of Corrosion,1993)

9) M. NEWSKI, A. DAVILA "Laboratory simulation of some Venezuelan CO_2 corrosive oil wells and their relationship with field experience". CORROSION 87, paper 439 (Houston, Tx : NACE, 1987)

10) M.B. KERMANI, D. HARROP, M.L.R. TRUCHON, J.L. CROLET "Experimental limits of sour service for tubular steels". CORROSION 91, paper 21 (Houston, Tx : NACE, 1991)

11) A. IKEDA, S.MUKAI, M.UEDA, Corrosion 41,4 (1985) ; p185

12) J.L. CROLET and M.R. BONIS "Materials Performance". 46, 7 (1990) ; p. 81

13) "Corrosion in oil and gas - well equipment" (Dallas, Tx ; API, 1958)

14) "Condensate well corrosion" (Tulsa Ok ; NGAA, 1953)

15) J.L. CROLET and M.R. BONIS "The role of acetate ions in CO_2 corrosion". CORROSION 83, paper 160 (Houston, Tx : NACE, 1983)

Table 1 - Wells equipped with grade L80 13 % Cr steel

Country	Wells		Length		% CO_2	NaCl equivalent	BHP		BHT	Installation
	Type	Number	km	(k ft)		g/l	bar	(ksi)	°C	date
Producing wells										
Holland	gas	39	124.8	(416)	0.85 to 4.2	< 1 to 135 *	150 to 345	(2.2) (5.0)	85 to 125	78 to 93
Gabon	oil	170	308.4	(1 028)	0.8 to 3.9	80 to 250	100 to 250	(1.5) (3.6)	65 to 125	78 to 93
The Cameroons	oil gas	16 2	80.5 10.5	(268) (35)	3 2	15 < 1	100 100	(1.5) (1.5)	70 60	83 - 87 83 & 91
Oman	oil	2	6.8	(23)	1	180	200	(2.9)	120	88 - 99
Nigeria	oil	42	83.6	(279)	4	20	143 to 206	(2.1) (3.0)	66 to 80	93 to 94
Norway **	oil gas	5 3	19.3 11.3	(64) (38)	3.1 2.4	40 < 1	322 615	(4.7) (8.9)	115 125	94 94
Planned wells										
The Congo ***	oil	24	88.8	(296)	1	260	410	(5.9)	145	96
Holland	gas	6	19.2	(64)	1.5 to 3.5	< 1	300 to 400	(4.506)	125	96

* 1 well at 135 g/l, 2 at 100 g/l, the rest at < 1 g/l

** subsea wells

*** grade API C95

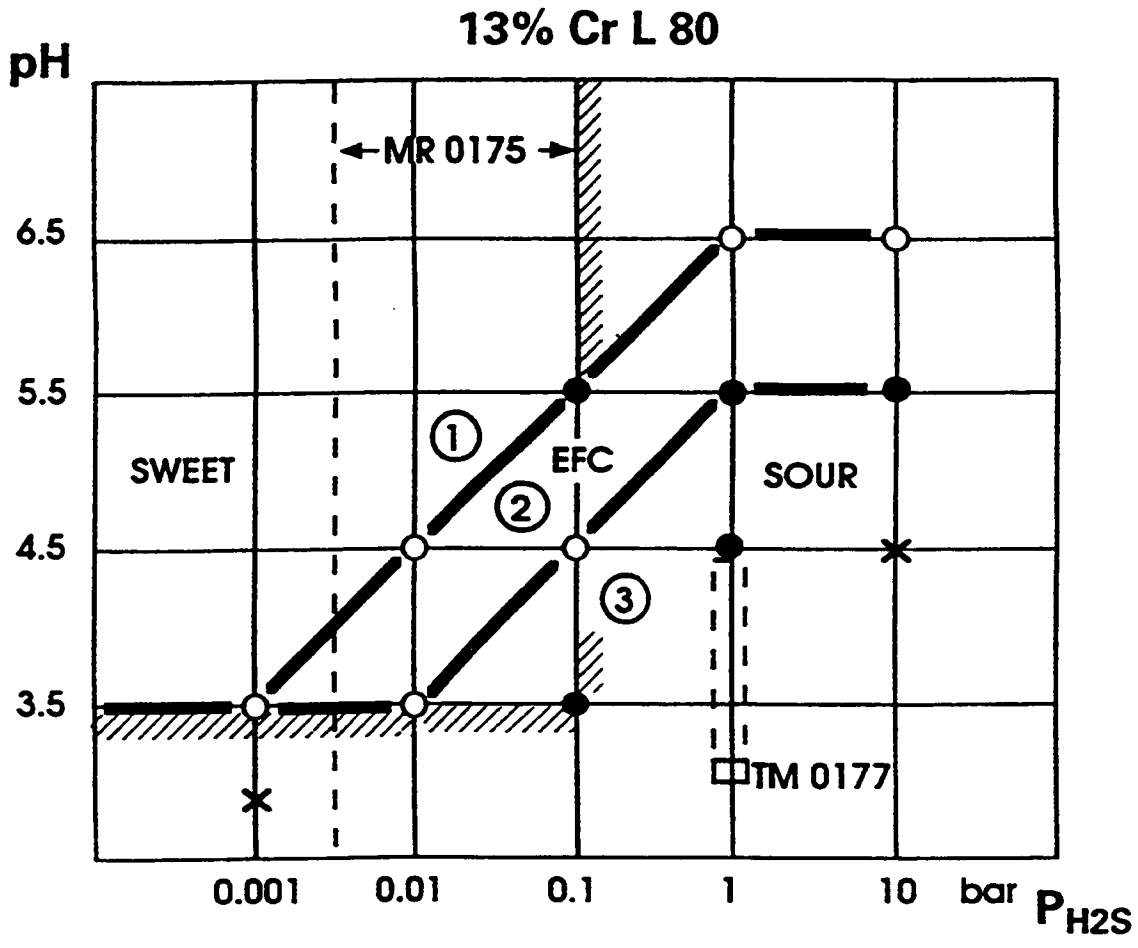


Figure 1 : Resistance of L80 grade 13 % Cr steel tubing to sulfide stress cracking, determined by modified TM 0177 tests : x failure, • experimentally observed non failure, o deduced non failure ; limiting conditions for H_2S service according to NACE MR 0175-93 (—), or prepared by the European Federation of Corrosion (____) ; ACE recommendation for 13 % Cr steel.

Copyrighted Materials
Copyright © 1996 NACE International Retrieved from www.knovel.com

Paper No. 58 - CORROSION/83

CORROSION BEHAVIOR OF 1 TO 22 PERCENT CHROMIUM STEELS AND MONEL K-500 IN CO_2/BRINE ENVIRONMENTS

Jon R. Bryant and Greg B. Chitwood
Otis Engineering Corp.
P.O. Box 34380, Dallas, TX 75234

ABSTRACT

Seven ferrous alloys containing from 1 to 22 percent chromium were evaluated to determine the effect of chromium content in reducing corrosion rate in CO_2 - brine solutions. Additionally, one nickel base alloy was evaluated which contained no chromium. Coupons of each alloy were tested for 72 hours in a matrix of static and turbulent solutions containing 7, 40, or 100 psig CO_2 and zero, 1.93, or 15.17 weight percent chloride. Two solution temperatures -- 65°C (150°F) and 175°C (350°F) -- were used. Corrosion rate was found to decrease steadily and to be strongly dependent on increasing chromium content. The deleterious effects of chloride and CO_2 content on corrosion rate were most prominent at 175°C, where the corrosion rate was typically highest. Corrosion resistance was highest in the 22 chrome and nickel base alloys; their corrosion rate was generally below 1 mpy.

INTRODUCTION

With the increasing demand for energy and the gradual depletion of easily obtainable hydrocarbons, oil and gas are being recovered by new methods and from new sources, most of which impose more strenuous operating conditions on equipment. These newer formations are deeper, hotter and contain higher pressure than ever seen before. In addition, new enhanced recovery methods, e.g. CO_2 injection, steam and fire flooding are being utilized to more efficiently and

completely extract gas and oil from existing formations. It is no longer uncommon to produce reservoirs which have higher partial pressure of CO_2, saline waters, and temperatures as high as 175°C (350°F). This has resulted in some very corrosive conditions[1].

There have been numerous studies on the corrosion behavior of steels in aqueous environments containing CO_2. Many of these date back to the early 1950's and deal with problems of weight-loss corrosion in gas condensate wells. These wells had low to intermediate temperatures (121°C; 250°F) and CO_2 partial pressures from 0 - 40 psig[2]. Previous studies have discussed the severity of corrosion in these environments and the beneficial effects of alloying elements such as nickel and chromium in reducing the extent of corrosive attack in steels. Much of this work is the basis for the use of materials containing high levels of nickel and chromium in aqueous CO_2 environments in the oilpatch.

However, many of these studies have not taken into account some of the variables which could affect the corrosion behavior of materials in aqueous CO_2 environments. This study was undertaken to specifically examine the effects of environmental variables and chromium content on the corrosion of chromium containing steels in CO_2-brine environments. The parameters investigated include: temperature, CO_2 partial pressure, chloride content, solution velocity and chromium content. The materials studied were selected from engineering alloys commonly used in the oilpatch and some proposed for application in particularly severe, corrosive environments.

EXPERIMENTAL PROCEDURE

The corrosion tests were performed with seven ferrous alloys ranging in chromium content from 1 to 22 percent, the compositions of which appear in Table 1. One nickel base alloy, Monel K-500, was also tested and contains no chromium. Two 1/8" thick coupons of each alloy were cut; their shape was dictated by their available product form. Each coupon, however, had a similar surface area to volume ratio.

Specimen Preparation. Both coupons of each alloy were subjected to each of the corrosion tests such that the occurrence of inaccurate results due to chemical fluctuations would be eliminated. Before initiating each test, the coupons were ground to a uniform surface finish, washed, dried with acetone, and weighed to the nearest 0.1 mg. Teflon washers were placed on each side of the coupons to isolate them from the 316 stainless steel specimen holder.

When an exposure experiment was terminated, the coupons were removed from the autoclave, taken off the holder, and washed in tap water. An inhibited, 15 volume percent hydrochloric acid solution was used to remove any adhering corrosion products and surface tarnish.

This cleaning solution would loosen and dissolve the surface corrosion product without attacking the underlying metal. The coupons were immersed in the cleaning solution for approximately 15 minutes. If corrosion products could still be removed from the coupon by rubbing, the coupon was again immersed in fresh cleaning solution for another 15 minutes. The coupons were then rinsed several times in tap water after removal from the cleaning solution and then dried with acetone. Each coupon was re-weighed and the weight loss (or gain) was recorded. Finally, the coupons were visually examined for the nature of corrosion and each coupon was photographed.

Environments. The experiment investigated the corrosion characteristics of each alloy in several CO_2/brine environments, as specified in Table 2. Both static and turbulent flow tests were performed to study the effects of flow on the corrosion behavior of the alloys. Table 3 outlines the turbulent flow tests. A final test contained H_2S to help determine its effect on the corrosion of each alloy.

Solution Preparation. All solutions were prepared with deaerated, deionized water having negligible chloride content. The synthetic seawater solution was prepared volumetrically using a standard sea salt mixture (ASTM D-1141-52, Formula A), such that the chloride contribution from all compounds totaled 1.93 percent. Reagent grade NaCl was added to the sea water solution to achieve the fortified, 15.17 percent chloride solution.

Each solution was deaerated with high purity nitrogen before saturating with CO_2. The pH of the CO_2 saturated solutions ranged from 4.5 to 6.0, depending on the chloride content.

During an experiment, the solution pH was determined by withdrawing a liquid sample from the autoclave and measuring the solution pH by a combination-pH electrode at ambient conditions. When the test solution contained chloride ion (1.93 percent or 15.17 percent), the solution pH was about 5.0 - 6.0. When no chloride ion was present, the solution pH was about 5.0.

The pH measurements should be interpreted carefully because the true solution pH is probably different from the values noted at ambient conditions. Dexter and Culberson[3] report that the dissociation constant for carbonic acid (H_2CO_3) is increased by the presence of soluble salts (such as NaCl and Na_2SO_4). Shannon[4] reports that the dissociation constant for H_2CO_3 in water decreases with increasing solution temperature. Consequently, it is difficult to totally characterize the CO_2-aqueous brines used in this study on the basis of solution pH and CO_2 partial pressure alone.

Corrosion Test Procedure. The corrosion tests were performed by using the following procedure for loading and sealing the autoclaves. The autoclave cavity and lid was thoroughly cleaned with

ethanol and water before each experiment. The test procedure for conducting the autoclave experiments is summarized in steps (1) through (11).

(1) The coupon holder was placed in the autoclave cavity. When the effects of a turbulent solution on the alloys were studied, the rotating coupon holder assembly was attached to the free end of the stirring shaft. Consequently, as the autoclave lid was being lowered onto the seal ring, the rotating holder assembly was simultaneously lowered into the autoclave well.

(2) High purity nitrogen gas (99.999 percent N_2) was flowed through the autoclave for approximately 20 minutes in order to displace air.

(3) The deaerated test solution was transferred to the autoclave.

(4) High purity nitrogen gas was again flowed for 15 minutes to purge the autoclave.

(5) The nitrogen gas in the autoclave was increased to 1000 psig to pressure test.

(6) After the autoclave was properly sealed, the nitrogen was released.

(7) The autoclave was heated to the test temperature.

(8) High purity CO_2 gas was bubbled through the solution for approximately 20 minutes.

(9) The CO_2 partial pressure required for the test was added to the autoclave. At least one-half hour was required to develop a constant CO_2 pressure above the solution because the CO_2-H_2O equilibrium had to be established for the given termperature and pressure.

(10) After the CO_2 pressure above the solution became constant, the autoclave pressure was increased to 1000 psig by the addition of nitrogen gas.

(11) Both the static and turbulent solution exposure tests were conducted for approximately 72 hours.

CO_2/H_2S Corrosion Experiment. The experiment which utilized the H_2S/CO_2 gas mixture was performed in a one liter autoclave. The surface of the autoclave cavity had a Hastelloy C-276 alloy lining (trademark of Cabot Corp., Stellite Division) in order to minimize corrosion of the autoclave during the experiment. Only five corrosion coupons could be placed in the autoclave cavity (samples A, B, D, F, and G).

The test was run for three days at a temperature of 175°C (350°F). The high purity carbon dioxide was added to the autoclave (100 psig CO_2) and then the total pressure was increased to 1000 psig by addition of the H_2S-CO_2-N_2 gas mixture (0.1 percent H_2S, 1.0 percent CO_2, and balance N_2).

RESULTS AND DISCUSSION

Since the primary intent of this study was not to determine specific corrosion rates for the alloys tested, extreme caution must be exercised when applying the actual rates to similar well conditions. The goal was to identify significant trends which might develop as a result of varying the environmental factors of interest. A considerable quantity of data was generated, but only that data which either supported a major premise, denoted observable trends or exhibited interesting anomalies has been included.

Corrosion Rate Studies. Results of the project are presented in three sections and are categorized as (1) static solution tests, (2) turbulent solution tests, and (3) the CO_2/H_2S test. In all cases, the corrosion rate data were calculated by using the standard weight loss equation [5] as

$$\text{corrosion rate (mpy)} = \frac{534W}{DAT}$$

where:

W = measured weight loss of the specimen, mg.

D = specimen density, g/cm^3

A = total surface area of the specimen excluding any coverage by the teflon washer, in^2

T = total time of corrosion test, hours

mpy = mils per year

Each corrosion rate presented for the static tests is an average calculated from duplicate specimens. The corrosion rates reported for the turbulent environments were based on weight loss measurements from only one coupon for each alloy per test. This was done to minimize the mass of the rotating assembly.

Static Solution Experiments. There are several ways of presenting the data graphically, each a slight variation of the other. Semi-logarithmic plots of corrosion rate versus the three major environmental factors of interest (chromium content, partial pressure of CO_2 and percent salt) were chosen and are presented in Figures 1 - 11. Hopefully the data can provide some insight into how a particular alloy chemistry might be expected to behave in well conditions similar to the experimental conditions tested.

Effect of Chromium. The results of this study indicate that a significant improvement in corrosion resistance occurs with increasing chromium content in the ferrous alloys. For most CO_2/brine environments examined, a sharp decrease in corrosion rate occurred between the 5Cr-1/2Mo and the 9Cr-1Mo steels at the 65°C (150°F) temperature level. Figure 1 is indicative of that trend. The remaining two levels of CO_2 exhibited virtually identical results. Note that at this temperature there is very little difference in corrosion rate regardless of the level of chlorides. Only the Monel K-500 and 22 chromium stainless steel (SAF 2205) had corrosion rates of less than 1 mpy in the most severe environments (i.e., high chloride brines at high temperatures).

At 175°C (350°F) the results are a bit more erratic as demonstrated in Figures 2 and 3; however, several significant points should be noted. There is now a much greater difference in the corrosion rates with varying chloride content. The same general trend that was noted at the lower temperature (corrosion rate decreases as chromium content increases) is again seen for the 1.93% and 15.2% chloride levels. At the 0% chloride level, an interesting anomaly occurs. The same trend as seen before is followed up to about 11-12% chromium. At this point, the corrosion rate increases and peaks at about 13% chromium before again decreasing. This was true regardless of CO_2 partial pressure. This may be partially explained by looking at Table 5 which provides a relative analysis of surface corrosion layers. For 9Cr-1Mo material the corrosion film is composed largely of chromium oxides which tend to be quite stable and moderately adherent. The 12 to 13% chromium materials (represented by 410 in the table), exhibit a corrosion film which is mostly carbonaceous (C plus O_2) with very little chromium oxide. This type film tends to spall more readily and is quite friable.

Effect of Chlorides. Figures 4 - 7 are plots of corrosion rate as a function of chloride content for each alloy at both low and high levels of CO_2 and temperature.

Figure 4 represents 7 psig CO_2 and 65°C (150°F) for the various alloys tested. At these conditions there appears to be a significant change in corrosion rate between 0% and 1.93% chlorides, but after that, there is very little change up to 15.2% chloride. Figure 5, 100 psig CO_2 and 65°C (150°F), exhibits the same trend for all the materials except 8Cr-1 1/2Mo and 9Cr-1Mo which seem to be virtually unaffected by the chloride content.

At 175°C (350°F) and 7 psig CO_2, much the same trend as noted at 65°C (150°F) was noted. There was a significant change in corrosion rate between 0% and 1.93% chloride but then there was little change up to 15.2% chloride except for the 4130 material. As the level of CO_2 was increased to 100 psig all the materials exhibited an increasing corrosion rate across the entire range of chloride levels. It is interesting to note that now the 4130 materials corrosion rate begins to flatten out and has corrosion rates similar to the other materials tested at the 15.2% chloride level.

Another important aspect about the static solution experiments concerns the corrosion behavior in 15.2% chloride solutions at 65°C (150°F) and 175°C (350°F). The corrosion rates of 4130 and 5CR-1/2Mo for the 175°C (350° F) environments never exceed the corrosion rates of the respective alloys at 65°C (150°F); however, the higher chromium containing (greater than 8% Cr) alloys exhibited corrosion rates at 175°C (350°F) which were significantly higher than the rates of the respective alloys at 65°C (150°F). This corrosion behavior indicates that these higher chromium containing alloys are sensitive to high chloride brines at high temperatures. The surface analysis data suggest that the 4130 and 5Cr-1/2Mo alloys may possess a surface film which limits the corrosion at 175° C (350° F). The nature of this film is not clear and more studies are necessary to establish its makeup.

Effect of CO_2 Partial Pressure. The last four plots, Figures 8 - 11, represent all the alloys tested as a function of CO_2 partial pressure at 0% and 15.2% chlorides at each temperature. The 1.93% chloride data was omitted because there were no trends noted which are not demonstrated in the plots included.

Figure 8, 0% chloride and 65°C (150°F), shows little effect of CO_2 partial pressure on any of the alloys tested. The corrosion rates for the low (less than 9%) chromium materials show a very gradual increase in corrosion as the partial pressure of CO_2 increases, whereas 9Cr-1Mo and above materials exhibit a gradual decrease. Monel K-500 shows a marked change, but it is insignificant since the highest corrosion rate is less than 1 mpy.

Figure 9 represents 15.2% chlorides at 65°C (150°F). For all the alloys there was a definite inflection point at 40 psig of CO_2. Again for the 8Cr and lower materials the trend was identical to the 0% chlorides. The higher (greater than 12%) chromium steels and Monel K-500 exhibited a sharp decline in corrosion rate up to 40 psig CO_2 and then a sharp increase. The sharp increase for these materials is again not significant since the corrosion rates were less than 1 mpy. More studies at higher partial pressures of CO_2 are needed to determine if this trend above 40 psig CO_2 continues.

The last two plots represent 0% and 15.2% chloride at 175°C (350°F) respectively. At 0% chlorides, there is very little effect of CO_2 partial pressure on corrosion rate for any of the materials tested. The effect on Monel K-500 is again highly exaggerated since the highest corrosion rate is less than 1 mpy.

Figure 11, 15.2% chloride and 175°C (350°F) demonstrates a very pronounced effect of CO_2 partial pressure again up to 40 psig and then there is virtually no effect. The 4130 was the only alloy that showed a general decrease across the entire range of CO_2, but the corrosion rates were quite high. This may again be a function of the corrosion film found for these low chromium materials. Overall, the corrosion rates for all the materials were much higher except for the Monel K-500 and SAF 2205.

Turbulent Solution Experiment. This series of experiments was arranged such that the predominant effects observed in the static tests could be examined in greater detail for turbulent conditions. At 65°C (150°F), for example, the variable of CO_2 was selected for the turbulent exposure test because the corrosion rates for the alloys in static CO_2-brines at 65°C (150°F) seemed to be more dependent on CO_2 partial pressure than upon chloride concentration. Similarly, a variation of chloride concentration for the 175°C (350°F) tests was selected because the corrosion rates for most alloys in static CO_2 brines at this temperature seemed to be more dependent on chloride concentration rather than CO_2 partial pressure.

1. Turbulent Experiment at 65°C (150°F).

In the turbulent tests, the corrosion rates of the chromium containing alloys were found to decrease with higher percent chromium regardless of coupon velocity. At 65°C (150°F), the corrosion rates for all the alloys except the 4130 and 5Cr-1/2Mo have a rather narrow range of corrosion rate values for both the static and turbulent flow conditions. The 4130 and 5Cr-1/2Mo steels in the 1.97% chloride, 100 psi CO_2 solutions exhibits large corrosion rate increases as the coupon velocity increased. All other alloys in this environment did not exhibit a direct correlation between corrosion rate and increasing coupon velocity. The same trend was noted as the CO_2 content was raised in the turbulent tests: 4130 and 5Cr-1/2Mo showed a strong, increasing corrosion dependence with increasing CO_2, whereas the other alloys exhibited very minimal corrosion rate changes.

2. Turbulent Experiment at 175°C (350°F).

At 175°C (350°F), the corrosion rates of 5Cr-1/2Mo, 8Cr-1-1/2Mo, 9Cr-1Mo, AISI 410, and 13Cr were found to pass through a minimum at a coupon velocity of 5.2 ft/sec. The 4130 showed just the opposite effect; that is, the corrosion rate was highest at the 5.2 ft/sec condition. Monel K-500 exhibited more than 8 mpy corrosion in the 11.5 ft/sec environment, which was the highest corrosion rate it experienced of any environment. Corrosion rates of less than 1 mpy were observed with the SAF 2205 in all environments tested.

The effect of chloride content on corrosion rate in the 175°C (350°F) turbulent tests became more prominent as the alloy content decreased. In the turbulent solutions, an increase in corrosion rate was generally seen with increases in chloride content; although the 410, 13Cr, SAF 2205, and Monel K-500 showed only minor changes. The alloys 4130 and 5Cr-1/2Mo exhibited tenfold changes in corrosion rate. Upon comparing the corrosion results between turbulent and static solution tests, it was observed that corrosion rate increased for the 1.93% chloride level when the solution became turbulent. At the 15.2% chloride level; however, the trend was reversed for those alloys containing 8 percent chromium or greater. Corrosion rates of the alloys were found to be higher at this temperature than at 65°C (150°F).

Effect of H_2S. The results for the CO_2-H_2S-brine experiment at 175°C (350° F) are given in Table 4. The data indicate that Monel K-500 and the low chromium-containing alloys (5% Cr and less) have an increased susceptibility to corrosion in H_2S-CO_2 brines over that observed in the equivalent H_2S-free solution. The high chromium materials (12% Cr and greater) exhibited very low corrosion rates in both environments. A great deal more testing along with surface analysis work would be needed in order to better understand the behavior of these materials in these type environments. Little was done in this area since the focus of the study was CO_2 containing environments.

Surface Analysis. The results of the surface analysis experiments were obtained using AES and ESCA techniques. The results obtained by ESCA are given in Table 5. The alloy with the lowest chromium content (excluding Monel K-500) possessed the thickest corrosion layer (4000-5000 angstroms) versus 200 - 650 angstroms for 9Cr-1Mo.

The data indicates important information about the relative concentrations (in atomic percent) of carbon, iron, chromium and oxygen on the surfaces of the eight specimens. The 4130 (Sample A) surface had a carbon-to-oxygen concentration ratio that clearly suggests the presence of a metallic carbonate after exposure in the 65°C (150°F) environments. The carbon-to-oxygen ratio for 4130 exposed in the 175°C (350°F) environments indicates a preponderance of oxygen. Consequently a metal oxide is believed to be present on the 4130 for the 175°C (350°F) environments. Similarly, the 9Cr-1Mo possessed tarnishes which contain much oxygen and a relatively small concentration of carbon for both the 65°C (150°F) and 175°C (350°F) environments. The formation of this tightly adherent metal oxide, at the higher temperature, may provide a clue as to why the 4130 material behaves similar to the higher alloyed stainless materials. The surface layers of the AISI 410 contained very high levels of both carbon and oxygen. By comparison, the tarnish or the Monel K-500 was different than that found on the ferrous alloys. It had relatively high levels of carbon and oxygen as well as the principle alloying elements (nickel and copper).

It is also interesting to note that the AISI 4130 surface contained about 19 atomic percent sodium, whereas, no sodium was detected on any of the other samples examined. The absence of sodium on the surface of the AISI 410 would suggest that this alloy possessed a surface layer significantly different from that on the AISI 4130 alloy exposed to the same brine conditions at 175°C (350°F).

SUMMARY AND CONCLUSIONS

Seven ferrous alloys containing nominally from 1 to 22 percent chromium and one nickel-based alloy (Monel K-500) were evaluated for corrosion performance in brines containing carbon dioxide. Weight loss corrosion measurements were used to evaluate these eight alloys.

The corrosion rate data indicate that the lowest percentage chromium-containing steel which performed well in all of the static and turbulent solutions was the AISI 410 stainless steel (12 Cr). In addition, the 9CR-1Mo steel had good corrosion behavior in a majority of the environments investigated.

The weight loss corrosion test results can be summarized as follows:

The low alloy steel (AISI 4130, 5Cr-1/2Mo) and (to a lesser extent) 8Cr-1 1/2Mo steel exhibit increasing corrosion rates with increasing CO_2 partial pressure at 65°C (150°F). The higher alloy materials (9Cr-1Mo, AISI 410, 13 Cr, SAF 2205 and Monel K-500) showed little or no corrosion rate dependence on CO_2 partial pressure at 65°C (150°F) and 175°C (350°F).

The AISI 4130 and 5Cr-1/2Mo alloys exhibited lower corrosion rates at 175°C (350°F) than in the respective environments at 65°C (150°F).

The other higher alloy materials (excluding Monel K-500) have an increase in corrosion rate with increasing chloride solutions at 175°C (350°F). Consequently, it appears that the higher chromium-containing alloys exhibit sensitivity to high chloride solutions at 175°C (350°F).

The AISI 4130 and 5Cr-1/2Mo alloys have increasing corrosion rates with increasing coupon velocity. However, solution temperature is also an important factor because these two alloys showed lower turbulent flow corrosion rates at 175°C (350°F) than at 65°C (150°F).

The higher chromium-containing alloys (8Cr, 9Cr, 12Cr, and 13Cr) and the Monel K-500 possessed an interesting sensitivity to coupon velocity at 175°C (350°F). The corrosion rates were lower at 5.2 ft/sec than for the respective static solution or at 11.5 ft/sec.

Addition of H_2S to a CO_2-brine at 175°C (350°F) caused a large increase in corrosion rate for the low chromium containing steels tested and the Monel K-500. The AISI 410 and 13Cr alloys exhibited similar corrosion rates (less than 1 mpy) in both environments.

For all environmental conditions, corrosion rates of the steels generally decreased with increasing chromium content.

On the basis of the findings from this work, it seems that two general classes of alloys exist in CO_2-brine service. In one class would be the low chromium-containing steels (AISI 4130 and 5Cr-1/2Mo) while the other class would contain the remaining six alloys (8Cr-1-1/2Mo, 9Cr-1Mo, 12Cr, 13Cr, SAF-2205 and Monel K-500).

REFERENCES

1. Bryant, JR, Materials to Supply the Energy Demand, Metals Park, American Society of Metals, 1981.

2. National Association of Corrosion Engineers. "The Fluid Testing of 32 Alloys in the Flow Stream Condensate Wells." Publication No. 50-3, page 103, July 1950.

3. Dexter, Stephen C. and Culberson, Charles. "Global Variability of Natural Sea Water." Materials Performance, 19 (September, 1980). 16-28.

4. Shannon, D.W. "The Role of Chemical Components in Geothermal Brines on Corrosion". Paper Number 57, Corrosion 1978. Pages 57-1 - 57-19.

5. Fontana, M.G. and Greene, N.D. Corrosion Engineering. New York: McGraw-Hill Book Company, 1967.

TABLE 1. CHEMICAL COMPOSITIONS OF THE ALLOYS EVALUATED IN THE TEST PROGRAM

Alloy	Coupon Designation	Cr	C	Mn	P	S	Si	Ni	Mo	Fe	Cu	Ti	Al
AISI 4130	A	.94	.29	.49	.013	.025	.27	-	.16	bal	-	-	-
5Cr-1/2Mo	B	5.23	.12	.43	.016	.017	.37	.12	.47	bal	-	-	-
8Cr-1-1/2Mo	C	8.65	.10	.42	.010	.010	.37	-	1.64	bal	-	-	-
9Cr-1Mo	D	9.44	.12	.52	.010	.003	.45	.25	.99	bal	.16	-	-
AISI 410	E	11.7	.10	.58	.012	.002	.32	-	-	bal	-	-	-
13Cr	F	13.3	.20	.50	.015	.005	.32	-	-	bal	-	-	-
SAF 2205*	G	22.0	.03	2.0	.03	-	.80	5.5	3.0	bal	-	-	-
Monel** K-500	H	-	.15	.73	-	.001	.07	63.2	-	.89	31.6	.51	2.86

* Registered Trademark of Sanvik, Inc.
** Registered Trademark of Huntington Alloys, Inc.

TABLE 2. SUMMARY OF THE EXPERIMENTS PERFORMED UNDER STATIC SOLUTION CONDITIONS AT 65°C (150°F) AND 175°C (350°F)

CO_2 partial pressure	7 psig CO_2		40 psig CO_2		100 psig CO_2	
Temperature	150°F (65°C)	350°F (175°C)	150°F (65°C)	350F (175°C)	150°F (65°C)	350°F (175°C)
0.00 weight percent chloride	x	x	x	x	x	x
1.93 weight percent chloride	x	x	x	x	x	x
15.17 weight percent chloride	x	x	x	x	x	x

TABLE 3. SUMMARY OF THE EXPERIMENTS PERFORMED UNDER TURBULENT SOLUTION CONDITIONS AT 65°C (150°F) AND 175°C (350°F)

CO_2 partial pressure	7 psig CO_2				40 psig CO_2				100 psig CO_2			
Temperature	150°F (65°C)		350°F (175°C)		150°F (65°C)		350°F (175°C)		150°F (65°C)		350°F (175°C)	
Velocity * (ft/sec)	5.2	11.5	5.2	11.5	5.2	11.5	5.2	11.5	5.2	11.5	5.2	11.5
0.00 weight percent chloride								x				
1.93 weight percent chloride		x				x		x	x		x	
15.17 weight percent chloride							x	x				

* Coupon velocities are stated for the geometric center of a coupon.

TABLE 4

CORROSION RATE DATA FOR ALLOYS EXPOSED TO SEAWATER SOLUTIONS AT 175°C (350°F) WITH AND WITHOUT H_2S

Material Designation	Corrosion Rates (mpy)	
	1.93 percent Chloride 100 psig CO_2 No H_2S	1.92 percent Chloride 100 psig CO_2 0.1 percent H_2S
AISI 4130	35	101
5Cr-1-1/2Mo	13	40
AISI 410	1.4	1.2
13 Cr	---	1.0
Monel K-500	0.12	2.7

TABLE 5

ESCA ANALYSIS OF SURFACE CORROSION LAYERS*

	Relative Concentration Expressesd as Atomic Percent							
	AISI 4130		Monel K-500		9Cr-1Mo		AISI 410	
Element	A	A-1	B	B-1	C	C-1	D	D-1
Calcium	-	2.0	-	---	---	---	--	---
Carbon	21.2	8.1	15.7	16.2	5.0	9.2	47.0	46.6
Chlorine	---	6.1	---	---	---	---	---	1.8
Chromium	7.1	---	---	---	28.9	16.8	5.3	3.1
Copper	---	---	17.8	13.5	---	---	---	---
Iron	3.8	6.1	---	---	2.5	8.7	---	---
Magnesium	---	11.8	---	---	---	---	---	---
Molybdenum	.8	---	---	---	0.6	0.6	---	---
Nickel	1.4	6.1	48.7	51.8	---	6.9	---	2.2
Nitrogen	---	---	---	---	---	---	3.5	---
Oxygen	61.8	40.7	17.8	18.5	63.0	57.8	44.2	42.8
Phosphorus	3.9	---	---	---	---	---	---	---
Silicon	---	---	---	---	---	---	---	1.8
Sodium	---	19.1	---	---	---	---	---	---
Sulfur	---	---	---	---	---	---	---	0.9

* Samples A, B, C and D were subjected to 0.00 percent chloride solution, 100 psig CO_2, and 65°C. Samples A-1, B-1, C-1 and D-1 were subjected to 15.17 percent chloride solution, 100 psig CO_2 and 175°C.

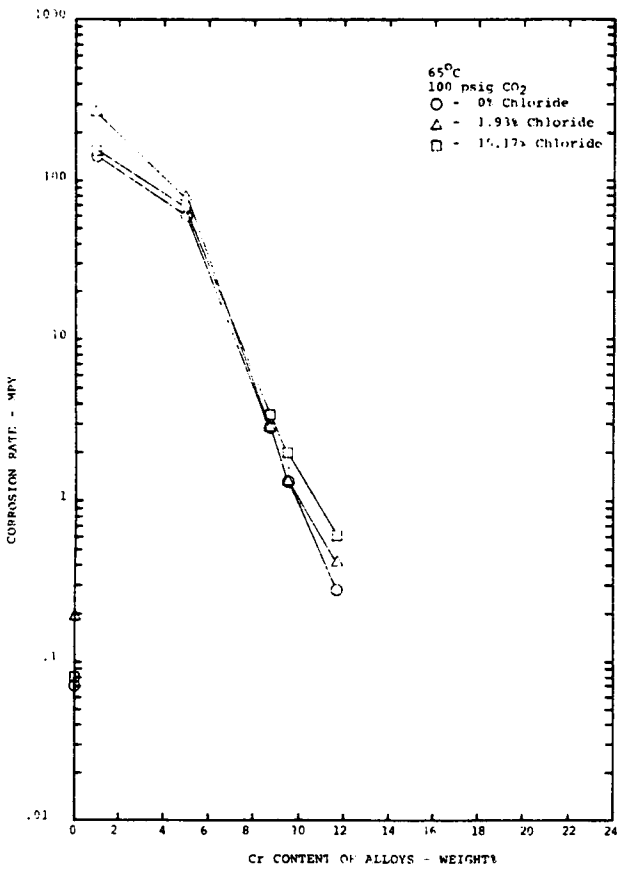


Figure 1 Effect of chromium on corrosion rate for 100 psig partial pressure CO2 at 65°C and variable chloride content.

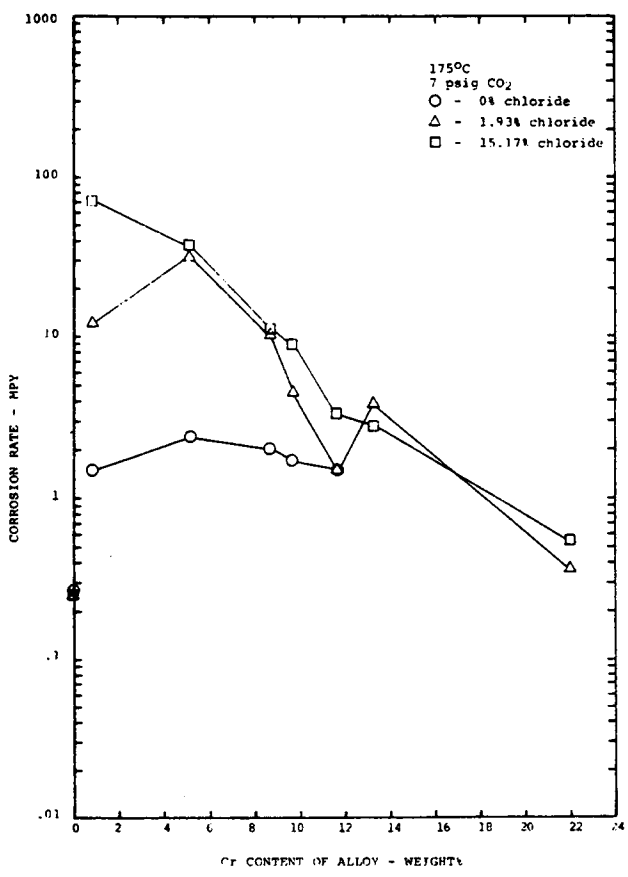


Figure 2 Effect of chromium on corrosion rate for 7 psig partial pressure CO2 at 175°C and variable chloride content.

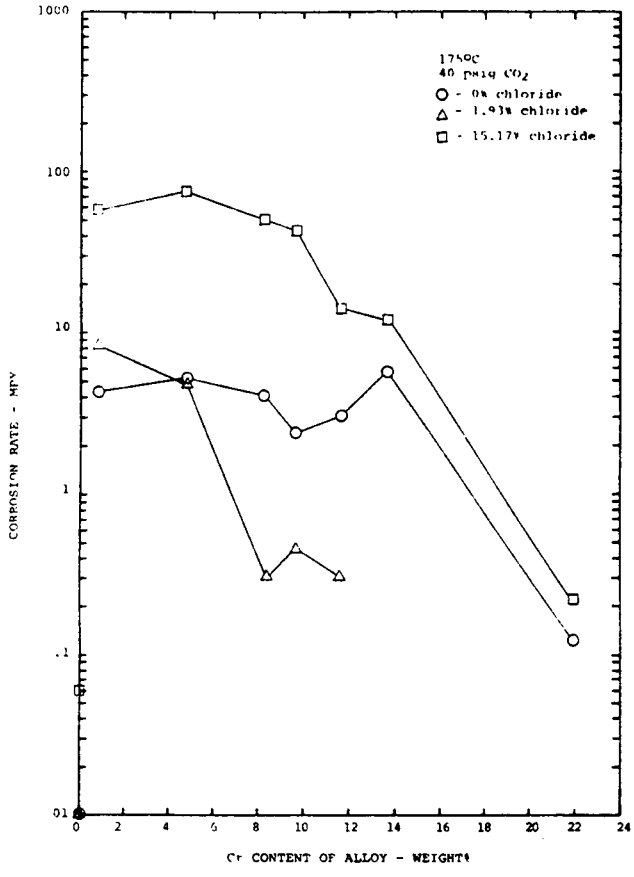


Figure 3 Effect of chromium on corrosion rate for 40 psig partial pressure CO2 at 175°C and variable chloride content.

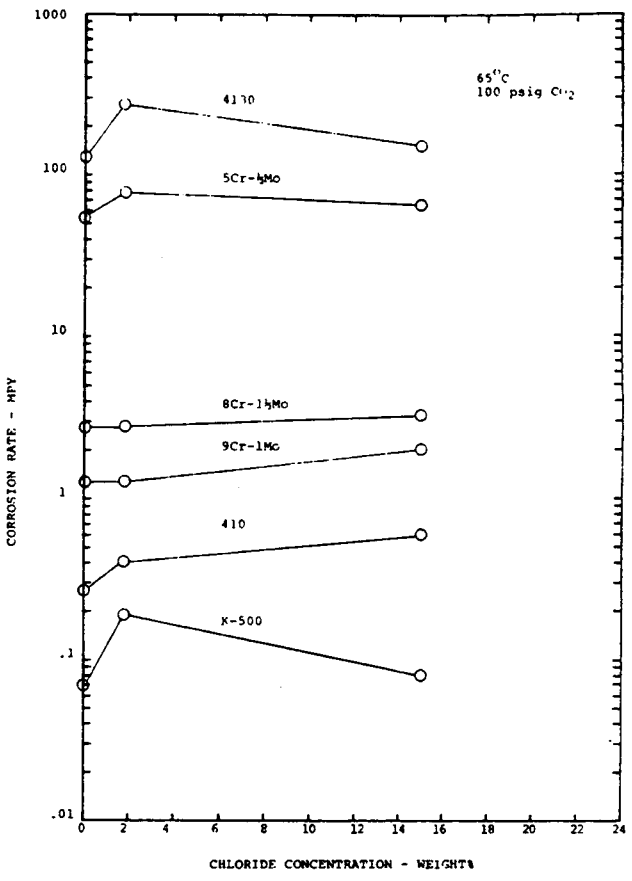


Figure 5 Effect of chlorides on corrosion rate at 100 psig partial pressure CO2 at 65°C for the alloys tested.

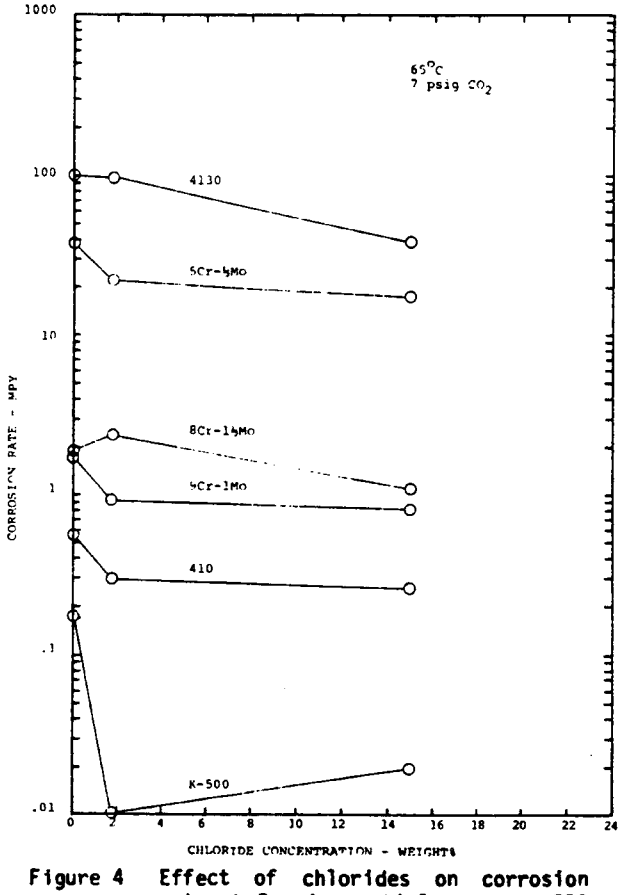


Figure 4 Effect of chlorides on corrosion rate at 7 psig partial pressure CO2 at 65°C for the alloys tested.

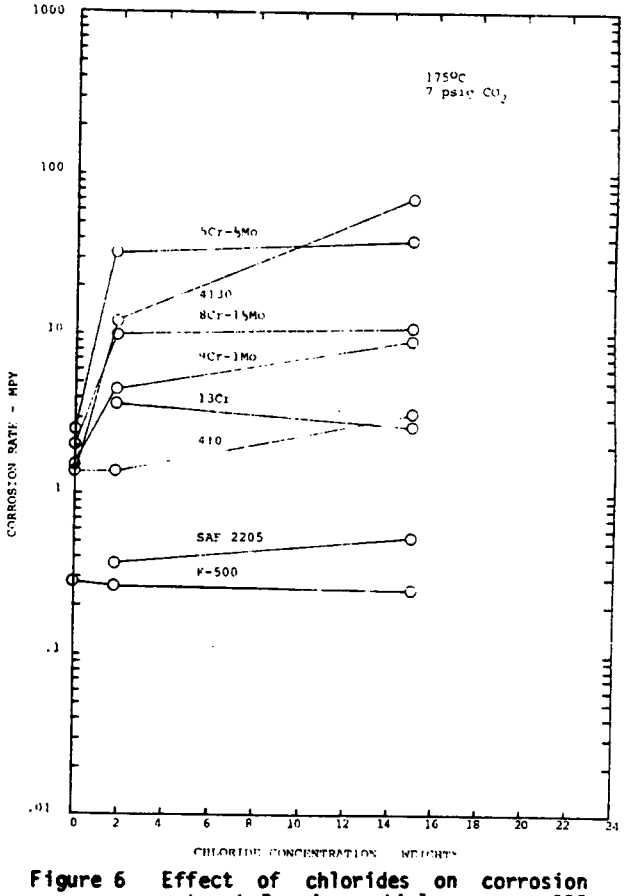


Figure 6 Effect of chlorides on corrosion rate at 7 psig partial pressure CO2 at 175°C for the alloys tested.

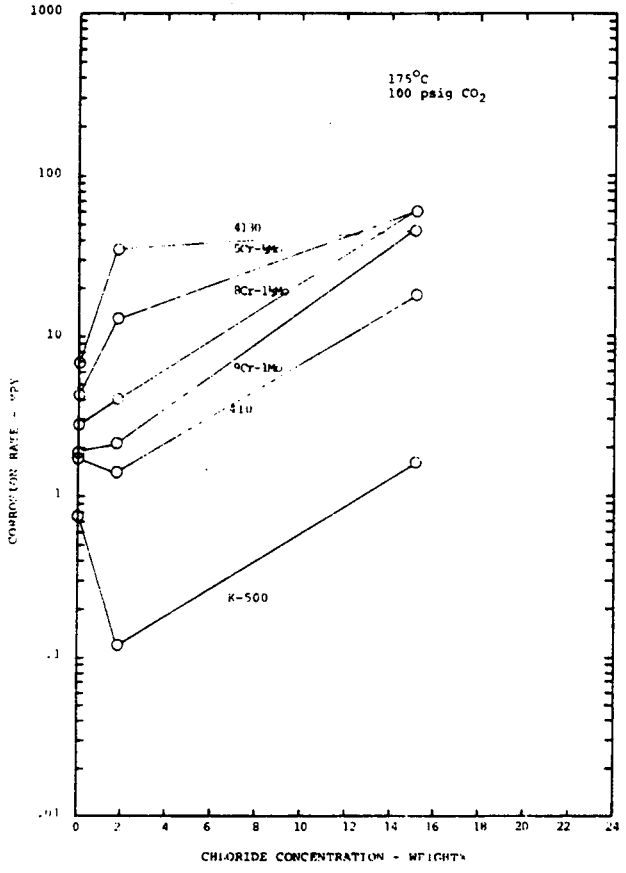


Figure 7 Effect of chlorides on corrosion rate at 100 psig partial pressure CO2 at 175°C for the alloys tested.

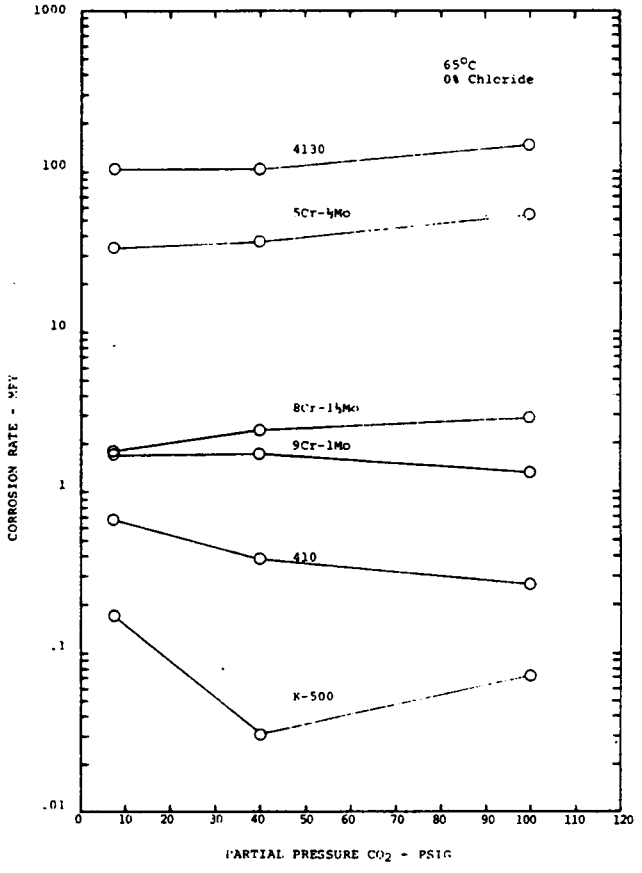


Figure 8 Effect of partial pressure of CO2 on corrosion rate at 0% chlorides and 65°C.

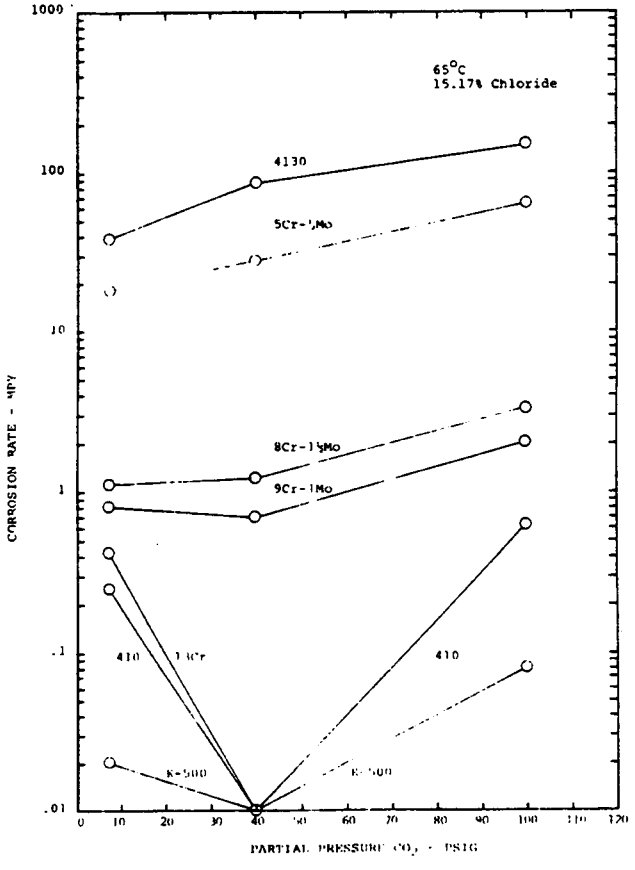


Figure 9 Effect of partial pressure of CO2 on corrosion rate at 15.2% chlorides and 65°C.

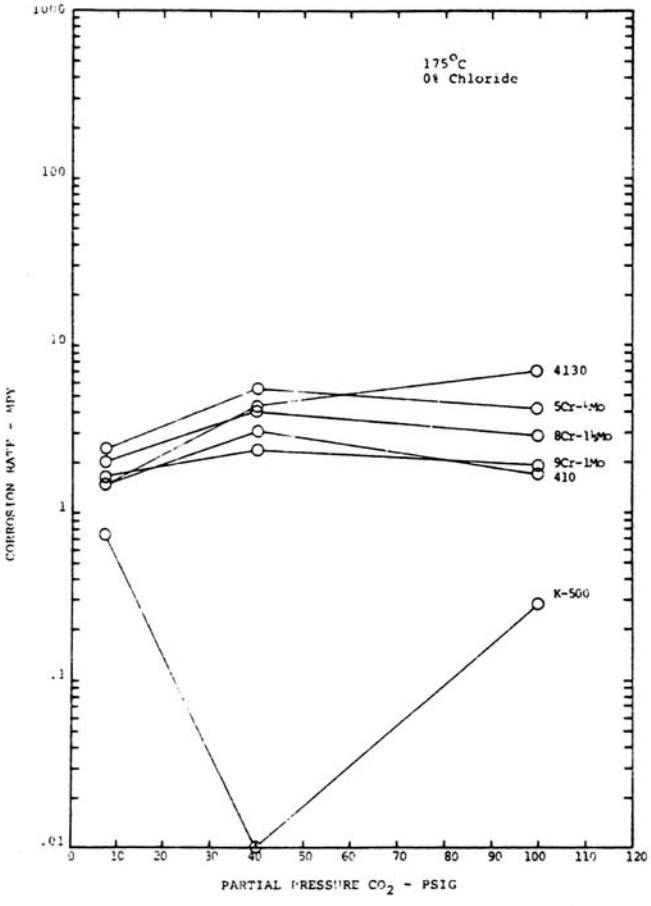


Figure 10 Effect of partial pressure of CO2 on corrosion rate at 0% chlorides and 175°C.

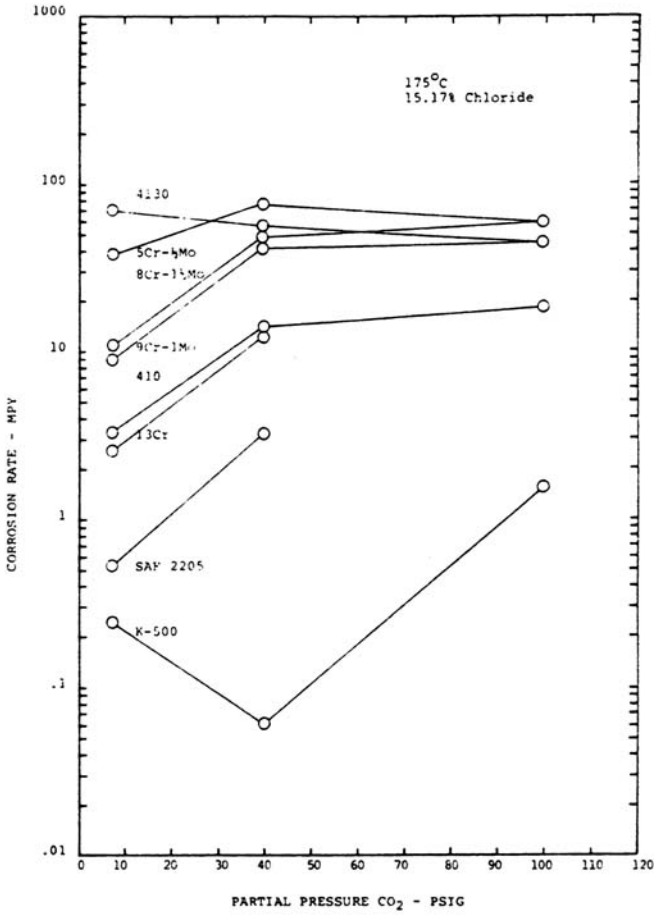


Figure 11 Effect of partial pressure of CO2 on corrosion rate at 15.2% chlorides and 175°C.

Copyrighted Materials
Copyright © 1996 NACE International Retrieved from www.knovel.com

Laboratory Test for Evaluating Alloys for H_2S Service*

DONALD S. BURNS, *Cameron Iron Works, Inc., Houston, Texas*

Accelerated tensile stress tests of materials suitable for petroleum production under hydrogen sulfide conditions approximating a procedure under development by NACE Unit Committee T-1F-9 are described. Welded carbon steel coupons in the range 137 to 200 HBN blistered and failed at less than 43% of designated yield strength, mainly in nonwelded zones, by blistering. Tubular specimens used to approximate hydrogen absorption under field conditions failed with respect to interrelations of wall thickness, stress, time, and method of hydrogen charging. Low alloy steels (AISI 4130 and others; N-80 tubing; low alloy NiCrMo) were tested at 228 to 269 HBN at 95% YS. AISI 410, Carpenter 450, and ASTM A-351 Grade CA6-NM stress cracked at 24 to 67% YS. However, in service AISI 410 at less than HRC 22 performs well. Alloy steels with less than 1% Ni indicated limits of 85% YS. Inconel X-750, Uranus 50, MP 35N, Nimonic 105 did not fail at 100% YS.

MANY ARTICLES have been written on hydrogen sulfide corrosion of engineering materials used in oil field environments. In general, these have been concerned with a state-of-the-art survey,[1,2] theoretical mechanisms,[3,4] laboratory testing,[5-8] or field reports.[9-14] It is clearly evident that although much has been accomplished, more remains to be done.

Sulfide stress cracking or hydrogen blistering of steels has been a serious problem because of the lack of economical alternative alloys. In addition, the problem is quite complex, involving the variables pH, applied potential, applied stress, temperature, inhibition, metallurgical factors, manufacturing factors, and the H_2S concentration. Three of the basic difficulties in corrosion prevention are:

1. Accelerated laboratory tests do not always agree with field data.
2. Accelerated lab test data on conventional acceptable oil field materials are not readily available.
3. There is no universally acceptable way of qualifying new materials or processes for direct substitution of existing acceptable materials with proven field experience.

The purpose of this paper is to present data on known acceptable oil field materials obtained with an accelerated test method. Carbon, low alloy, stainless, and specialty alloy materials were tested. Although the test method does not offer data in complete agreement with field experience, it does provide data from which management decisions can be made more effectively. The purpose of this work was to establish experience with a new test method for development of basic corrosion data on familiar oil field materials. In so doing, confidence levels were developed for progression to an accelerated evaluation of new materials and processes.

Experimental Procedure

Figure 1 offers a composite view of the corrosion testing apparatus. A series of creep machines for dead weight load testing were modified to perform H_2S evaluations in tension according to a proposed test procedure written by NACE Unit Committee T-1F-9. Figure 2 offers an additional view of the appliance accessories for valving, metering, and timing. This laboratory is a remote test facility where safety was a prime concern—the dangers of H_2S as cited by Atherton[15] have been properly considered.

Table 1 gives the composition of the H_2S solution. All tests were accomplished using this test solution at an average pH of 4.0 after an initial deaeration purge with nitrogen gas. A continuous flow of gaseous H_2S was maintained throughout the test at a flow rate of a few bubbles per minute. A positive pressure was maintained on the vessel to ensure exclusion of air.

The experimental plan involved uniaxial tensile tests on materials that are commonly used in oil tool products and other potential materials. Table 2 lists the materials evaluated. The selection included carbon steel, alloy steels, stainless steel, and specialty alloys. The test plan required that the application of different tensile stresses (less than the yield stress) were to be monitored versus time to failure so that the stress corrosion test limit stress (S_{TL}) or test limit time factors might be better understood. Figure 3 shows the manner in which the data were evaluated. It also serves to graphically define certain terms used in the investigation.

Results

General

Figure 4 shows the two mechanisms of failure associated with this sulfide corrosion investigation—blistering and cracking. There was good general agreement that all observed failures of carbon steel were of a blistering nature, whereas the higher strength materials failed due to cracking.

Table 3 lists the test limit stress for each alloy tested. This particular test limit stress is defined as the maximum level of stress (or % of yield strength) to which an oil tool component can be loaded without cracking for at least 30 days immersion. The designer is cautioned that these stress levels are *not intended* for use as design stress levels. These data reflect accelerated testing conditions and should only be used for comparative purposes when comparing similar or substitute materials against a known acceptable material.

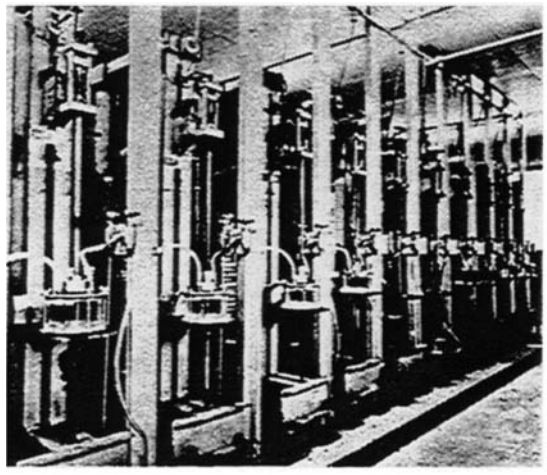
Carbon Steels

Properly processed carbon steels typically in the hardness range of 137 to 200 HBN have been used successfully in H_2S service and have been completely acceptable in this service with no known failures.

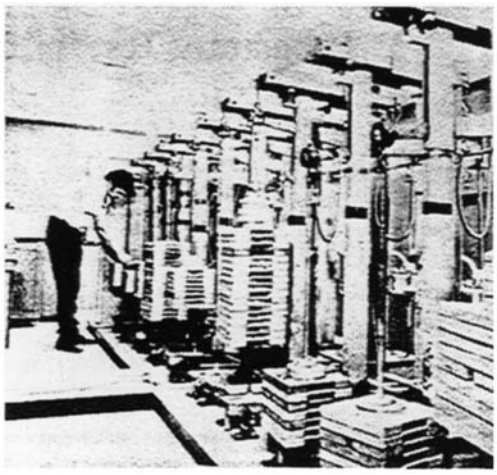
The investigation of carbon steels was prompted by an interest in low carbon steel weldments using CMS 1138 and CMS 1120 (modified AISI 1022 containing 0.22 C max and 1.0% Mn) (Cameron Material Specification). The intent of the investigation was to test weldments of controlled hardness in the as-welded condition to determine the actual necessity of stress relieving when weldments and materials are properly controlled.

Early in the testing program, it became obvious that the weld and heat affected zone (HAZ) was not as susceptible to the test environment as the base metal. All failures were associated with the base metal, as shown in Figure 5.

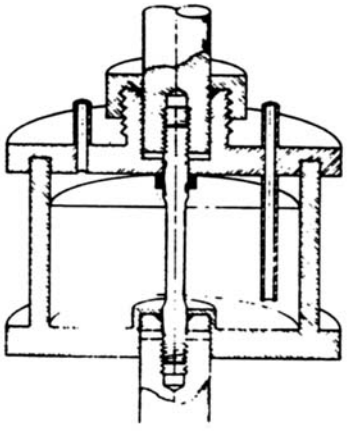
*Presented during Corrosion/75, April 14-18, 1975, Toronto, Ontario, Canada.



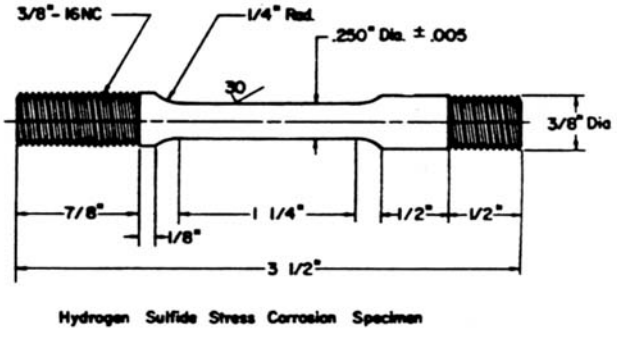
Front View



Rear View



Detail View



Hydrogen Sulfide Stress Corrosion Specimen

NACE Specimen

FIGURE 1 — A composite view of the sulfide corrosion testing equipment.

Several carbon steels were included: (1) CMS 1138 (0.22 C max.); (2) AISI 1029); and (3) ASTM A216, Grade WCB.

Figure 6 shows the relation between time to failure and applied stress. It can be seen from this graph that in this test, carbon steels have a test limit stress (S_{TL}) of approximately 24,000 psi or about 43% of yield. Further metallographic evaluations of the failures indicated that all failures were of a blistering nature.

Tubular Samples

One shortcoming of laboratory stress corrosion testing of solid test samples is that the solid sample does not represent the actual service conditions which the part might experience. Figure 7 shows some basic differences which are involved. Here it is shown that a solid sample can become supersaturated with hydrogen when totally immersed in the H_2S test solution. Tubular samples, on the other hand, can be evaluated for a fixed concentration gradient within a given time if vented appropriately. Herein lies the basis for argumentation between laboratory tests and field data—one prime difference involves the mechanism of hydrogen absorption and removal. In an effort to simulate field situations, this investigation also examined tubular specimens made from low carbon steel and tested in the NACE-H_2S test solution.

Figure 8 gives typical results for hollow specimens. It is seen that hollow and solid samples reacted differently in deaerated H_2S. This difference in behavior is associated with the difference of hydrogen concentration profiles existing in a solid, unvented sample or a hollow, vented sample. Schenk[16] reported that almost any carbon steel will eventually fail in a selected H_2S environment; however, this investigation revealed that such failure is primarily controlled by stress, time, specimen shape, and the method of hydrogen charging.

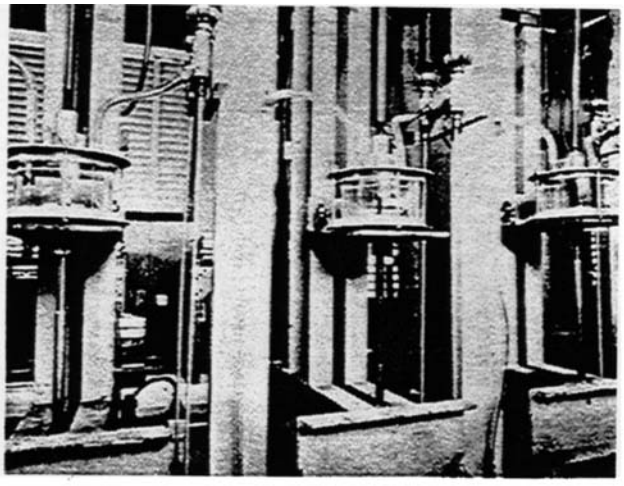
Hollow or tubular type specimens may warrant further evaluation to better explain the failure times of solid specimens as reported by Schenk and confirmed by this paper, versus completely acceptable field use of carbon steels in H_2S environments.

Weld Samples

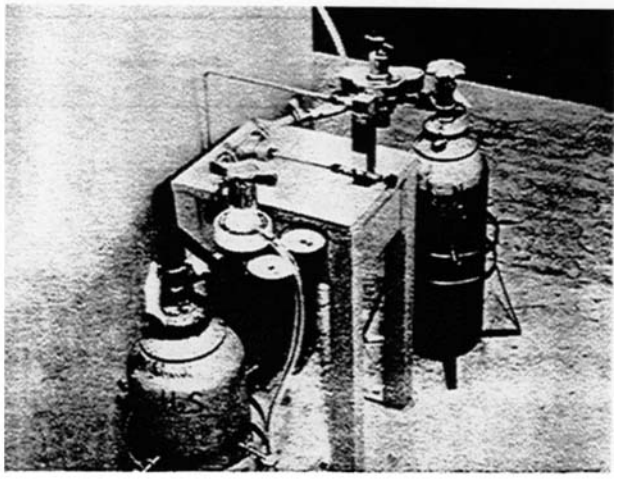
Because welded joints are always present, the effect of hydrogen sulfide on selected examples of either cross-weld or full-weld specimens was investigated.

Figure 5 shows typical results for observations on cross-weld samples. In every case, all failures were in the parent material, and never in the weld bead or heat affected zones. Corrosion tests on full-weld specimens indicate that excellent service life is possible through proper control of the weld process. Tests currently in process reveal that full-weld samples of low carbon steel can endure the NACE test solution for extended periods. This suggests that low carbon steel weldments are considerably more resistant to H_2S service than the parent material. In this sense, good agreement exists between the observations for both cross-weld and full-weld samples. Figure 9 reflects the typical results of the tests on weld samples.

Field data is in complete agreement with these findings. Welds properly made using controlled hardness welding procedures are used in the as-welded condition with complete success throughout the industry. Pipelines and flowlines transmitting sour crude and gas have used as-welded construction with success. Pressure vessels are



Valving



Metering



Timing

FIGURE 2 – Additional experimental details.

manufactured to API RP-942 and used in the as-welded condition.

Recently as-welded construction ball valves have been used in sour (40% H_2S) environments and have performed completely satisfactorily for over 2 years. Examination of one valve after 13 months service revealed no effects on the weldment by the H_2S environment.

Low Alloy Steels

These were of the most interest to the writer because of their common usage by most manufacturers associated with the oil and gas industry. The following alloys were examined using solid tensile samples: (1) AISI 4130; (2) AISI 4135; (3) AISI 4135 (modified); (4) N80 tubing; (5) S00-90 tubing (controlled heat treatment AISI 4130 tubing); (6) AISI 4340; and (7) ZCMS 66 (low Ni-Cr-Mo material, a modified grade of AISI 8620, meets physical requirements of API Type 2).

Also included was one heat of modified AISI 4135, and one heat of AISI 4340. Each grade of steel was tested at varying stress levels starting at 95% of yield and continuing at lower stress levels until a test limit stress (S_{TL}) was reached.

Figures 10 and 11 graphically illustrate the effect of the test solution on each of these steel samples. It is interesting to note that the low alloy steels performed better than other grades of steel, except for the specialty alloys.

Three different hardness levels of 4340 were tested to explore the effects of a material with a Ni content in excess of 1%. The 4340 grade of steel reflects a much lower test limit stress at hardnesses lower than HRC 22 than other low alloy grades of steel. Figure 12 illustrates these data.

Investigation of the modified 4135 was prompted due to interest in higher strength tubular grades. Initial evaluation does not reveal any significant improvement at the higher hardness value of HRC 27. Examination at lower hardness levels may show a favorable

TABLE 1 – Composition of NACE T-1F-9 Test Solution

Constituent	Amount Added
Sodium Chloride	50 g
Glacial Acetic Acid	5 g (4.8 ml)
Deionized Water	945 g
Initial pH = 3.0	Maximum pH = 5.0
System was deaerated by an initial N_2 purge and then saturated with H_2S. H_2S gas was continually metered throughout the test to maintain saturation.	

Material Designation & Type	Heat Number	Metallurgical Condition	Brinell Hardness Number	0.2% Offset Yield Strength (psi)	Ultimate Tensile Strength (psi)	Percent Elongation	Percent Reduction in Area
Carbon Steels							
CMS 1138[1]	D1	Annealed	–	53,100	72,600	35.5	63.0
CMS 1138[1]	D1	Normalized	–	62,200	81,000	29.2	51.1
CMS 1138[1]	D1	Quenched & Tempered	150	55,900	77,600	34.2	74.4
AISI C-1029	P6033	Normalized	200	64,900	96,000	25.5	52.8
ASTM A216-WCB	CIW 1	Normalized	–	55,550	89,550	18.7	24.1
Alloy Steels							
S00-90	B2935	Quenched & Tempered	205	98,500	113,300	23.7	72.6
AISI C-4130	CIW 5	Quenched & Tempered	228	92,500	109,700	26.6	74.0
AISI C-4135	5364	Quenched & Tempered	270	120,200	134,900	21.0	65.5
AISI C-4135 (Mod.)	5388	Quenched & Tempered	270	117,500	130,200	24.0	64.0
N80	CIW 7	Normalized	187	70,100	104,000	27.4	68.1
N80	CIW 6	Normalized	262	94,100	133,500	16.8	46.1
AISI C-4340	06922-1	Quenched & Tempered	321	98,900	185,600	14.7	29.5
AISI C-4340	06922-2	Quenched & Double Tempered	241	104,100	117,600	27.0	64.8
AISI C-4340	06922-3	Quenched & Double Tempered	228	99,300	112,500	27.0	70.3
ZCMS 66	CIW 3	Quenched & Tempered	221	75,000	100,000	18.0	35.0
Stainless Steels							
AISI 410	820651	Austenitized & Double Tempered	237	96,800	114,600	22.8	68.0
Carpenter 450	53204	Overaged	265	82,000	132,000	23.2	70.0
CA6-NM	C790	Austenitized & Double Tempered	243	92,300	119,700	22.4	60.6
CA6-NM	ML93AA	Austenitized & Double Tempered	228	89,100	115,500	22.7	66.3
CA6-NM	ML93AB	Austenitized & Double Tempered	248	112,000	127,100	22.0	67.0
Specialty Alloys							
Inconel X-750	30 F1X	Solutionized & Aged	321	127,000	179,900	26.0	40.0
Uranus 50	83351	Solutionized & Aged	192	60,400	100,800	36.4	70.0
MP35-N	C51804	Cold Worked	437	198,500	250,600	14.3	59.7
MP35-N	C51804	Cold Worked & Aged	495	280,700	300,800	10.0	47.8
Nimonic 105	–	Solutionized & Aged	300	118,000	171,200	21.0	22.0

		Chemical Compositions, Weight %														
		C	Mn	P	S	Si	Cr	Ni	Mo	V	Cu	Al	Fe	Ti	Cb+Ta	Co
CMS 1138[1]	D1	.20	1.02	.015	.029	.26	–	–	–	–	–	–	–	–	–	–
CMS 1138[1]	D1	.20	1.02	.015	.029	.26	–	–	–	–	–	–	–	–	–	–
CMS 1138[1]	D1	.20	1.02	.015	.029	.26	–	–	–	–	–	–	–	–	–	–
AISI C-1029	P6033	.27	.77	.015	.024	–	–	–	–	–	–	–	–	–	–	–
ASTM A216-WCB	CIW 1	.30	1.00	.040	.045	.60	.40	.50	.25	.03	.50	–	–	–	–	–
S00-90	B2935	.30	.47	.010	.028	.24	.97	–	.19	–	–	–	–	–	–	–
AISI C-4130	CIW 5	.29	.58	.007	.023	.26	.82	.06	.14	.01	.02	–	–	–	–	–
AISI C-4135	5364	.34	.69	.018	.022	.28	1.06	–	.19	–	–	–	–	–	–	–
AISI C-4135 (Mod.)	5388	.35	.69	.016	.017	.32	1.01	–	.82	–	–	–	–	–	–	–
N80	CIW 7	.35	1.58	.007	.024	.07	.17	.03	.03	.01	.02	–	–	–	–	–
N80	CIW 6	.41	1.50	.017	.023	.21	.06	.06	.14	.01	.03	–	–	–	–	–
AISI C-4340	06922-1	.39	.72	.011	.016	.27	.79	1.88	.27	.01	.14	–	–	–	–	–
AISI C-4340	06922-2	.39	.72	.011	.016	.27	.79	1.88	.27	.01	.14	–	–	–	–	–
AISI C-4340	06922-3	.39	.72	.011	.016	.27	.79	1.88	.27	.01	.14	–	–	–	–	–
ZCMS 66	CIW 3	.24	1.05	.04	.03	.27	.30	.25	.21	.09	–	–	–	–	–	–
AISI 410	820651	.11	53	.019	.015	.40	12.2	.27	.04	–	.07	.006	–	–	–	–
Carpenter 450	53204	.03	.36	.012	.003	.25	14.9	6.4	.73	–	1.5	–	–	–	–	–
CA6-NM	C790	.05	.41	.009	.024	.52	12.0	4.5	.76	–	–	–	–	–	–	–
CA6-NM	ML93AA	.04	.32	.029	.018	.62	12.4	3.8	.60	.04	.07	.01	–	–	–	–
CA6-NM	ML93AB	.04	.32	.029	.018	.62	12.4	3.8	.60	.04	.07	.01	–	–	–	–
Inconel X-750	30 F1X	.06	.14	.005	.003	.20	15.5	72.9	.04	–	.04	.71	6.6	2.6	.91	–
Uranus 50	83351	.03	.80	.024	.018	.60	21.2	8.07	2.76	–	1.8	–	Bal	–	–	–
MP35-N	C51804	.02	.04	.004	.005	.05	19.4	35.3	9.91	–	–	–	.55	–	–	Bal
MP35-N	C51804	.02	.04	.004	.005	.05	19.4	35.3	9.91	–	–	–	.55	–	–	Bal
Nimonic 105	–	.13	.08	.003	.008	.33	15.6	Bal	5.08	–	–	4.6	.77	1.14	–	21.5

[1]CMS – Cameron Material Specification.

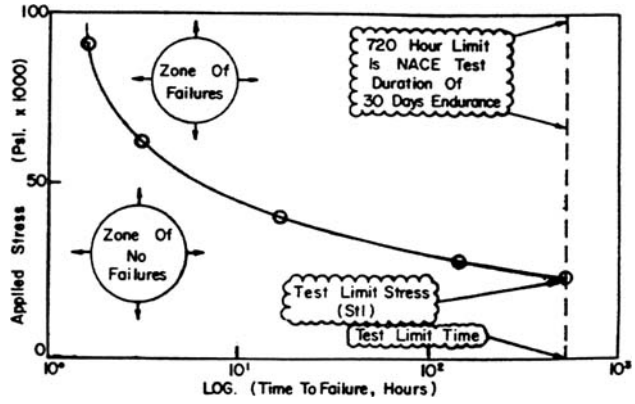


FIGURE 3 — Method of graphical analysis used in this investigation.

trend.

Stainless Steels

The inadequacy of low alloy steels to resist weight loss corrosion in H_2S-CO_2 environments has prompted most designers to utilize components made of martensitic stainless steels. This investigation also examined the sulfide stress cracking resistance of one popular stainless steel composition and two relatively new compositions. (1) AISI 410; (2) Carpenter 450 (a wrought stainless steel similar to ASTM A351 Grade CA6-NM); and (3) ASTM A351, Grade CA6-NM.

These three materials were evaluated in the overaged, austenitized, and single tempered or austenitized and double tempered conditions. Figure 13 shows the relation between test limit stress and time.

The AISI 410 class stainless steels in the quenched and double tempered condition and single tempered CA6-NM offered test limit stress of only 24% of the yield strength. Double tempering of the CA6-NM stainless offered much higher test limit stresses, approximately 67% of their yield strength. The Carpenter 450 alloy performed as well as or better than the double tempered CA6-NM. All failures were caused by stress corrosion cracking.

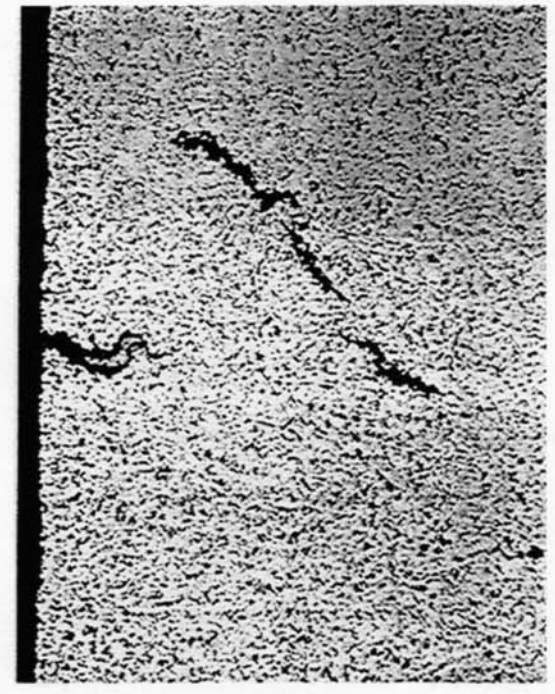
These tests indicate that the martensitic grades of stainless steel, AISI 410, are very susceptible to SCCC and would soon fail in service. To the contrary, the martensitic grades used on valve bodies in the production industry, when weight loss corrosion must be contended with, have stood up well. No known failures of valve bodies made from 410 stainless have been reported when used at hardnesses of less than HRC 22.

These data can be looked upon as an examination of different alloys for comparison when direct substitution is considered.

Specialty Alloys

Under certain conditions where high strength and associated high hardnesses are required, specialty or high alloy steels have been used successfully at hardnesses up to HRC 35 and, in some cases, up to HRC 50. This investigation was sufficient to show that certain alloys are quite acceptable for use under extremely adverse conditions up to and exceeding their yield strength. The alloys examined were: (1) Inconel X-750; (2) Uranus 50 (French designation); (3) MP 35N; and (4) Nimonic 105 (British designation).

Each was tested at 100% of the yield strength, and no failures were noted. This was the only class of steel tested which resisted failures at 100% of the yield strength. Microexamination of these specimens revealed no structural damage.



100X
CMS 1138 Norm 172 BHN
59.1 ksi 95% 6.9 Hours



100X
410 SS QTT 21-22 HRC
96.8 ksi 95% 2.0 Hours

FIGURE 4 — Typical types of failure observed in SSCC evaluations.

Summary

The findings are cited briefly as follows:

1. For carbon steels, the S_{TL} in the NACE-H_2S solution is about 43% of the designated yield strength.

2. For applications involving stainless steel, metallurgical structure can exert a strong influence in H_2S service. Single tempering of CA6-NM and the 400 class stainless samples offered a low S_{TL} of just 24% of the yield strength. Double tempering of CA6-NM

TABLE 3 – Results of Sulfide Stress Corrosion Tests

Material Designation & Type	Heat Number	As Tested Condition	Brinell Hardness Number	0.2% Offset Yield Strength (psi)	Test Limit Stress (psi)
Carbon Steels					
CMS 1138[1]	D1	Annealed	–	53,100	16,992
CMS 1138[1]	D1	Normalized	–	62,200	18,660
CMS 1138[1]	D1	Quenched & Tempered	150	55,900	22,360
AISI C-1029	P6033	Normalized	200	64,900	41,212
ASTM A216-WCB	CIW 1	Normalized	–	55,550	21,665
Alloy Steels					
S00-90	B2935	Quenched & Tempered	205	98,500	78,800
AISI C-4130	CIW 5	Quenched & Tempered	228	92,500	80,013
AISI C-4135	5364	Quenched & Tempered	270	120,200	76,928
AISI C-4135 (Mod.)	5388	Quenched Tempered	270	117,500	75,200
N80	CIW 7	Normalized	187	70,100	49,070
N80	CIW 6	Noramlized	262	94,100	62,341
ZCMS 66[1]	CIW 3	Quenched & Tempered	221	75,000	67,500
Stainless Steels					
AISI 410	820651	Austenitized & Double Tempered	237	96,800	10,648
Carpenter 450	53204	Overaged	265	82,000	42,640
CA6-NM	C790	Austenitized & Double Tempered	243	92,300	62,303
CA6-NM	ML93AA	Austenitized & Double Tempered	228	89,100	58,806
CA6-NM	ML93AB	Austenitized & Single Tempered	248	112,000	30,240
Specialty Alloys					
Inconel X-750	30 F1X	Solutionized & Aged	321	127,000	127,000
Uranus 50	83351	Solutionized & Aged	–	60,400	60,400
MP35N	C51804	Cold Worked	–	198,000	198,000
MP35N	C51804	Cold Worked & Aged	–	280,000	280,000
Nimonic 105	-	Solutionized & Aged	300	118,000	118,000

[1]CMS – Cameron Material Specification.

yielded values as high as 67% of the attendant yield strength.

3. For alloy steels containing less than 1% Ni, the S_{TL} was approximately 85% of the yield strength.

4. For the alloy steel containing more than 1% Ni (AISI 4340) there is a definite indication of susceptibility at hardnesses of HRC 22 and lower.

5. For specialty alloys, S_{TL} values were found to be in excess of the yield strengths.

6. For carbon steel tubular samples, the S_{TL} increases as a function of decreasing wall thickness for the samples examined. It is concluded that SSCC failures are controlled by stress, time, specimen shape, and the method of hydrogen charging.

7. For cross-weld samples of special low carbon steel, all failures occurred in the parent metal.

8. For full-weld metal samples, using controlled welding procedures and processes, the S_{TL} is approximately 90% of the yield strength.

9. As a comparative tool, when known acceptable material curves have been developed, relatively fast comparison of new materials or heat treat processes can be evaluated against a known acceptable standard.

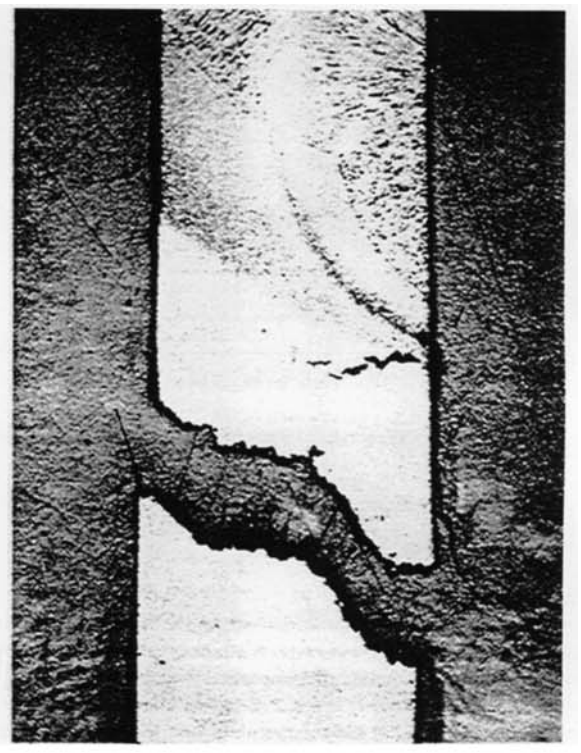
Acknowledgments

The author wishes to acknowledge the willing assistance obtained from Prof. Charles Hays, Texas A&M University, and Mr. John S. Johnston, Metallurgist, Cameron Iron Works, Inc.

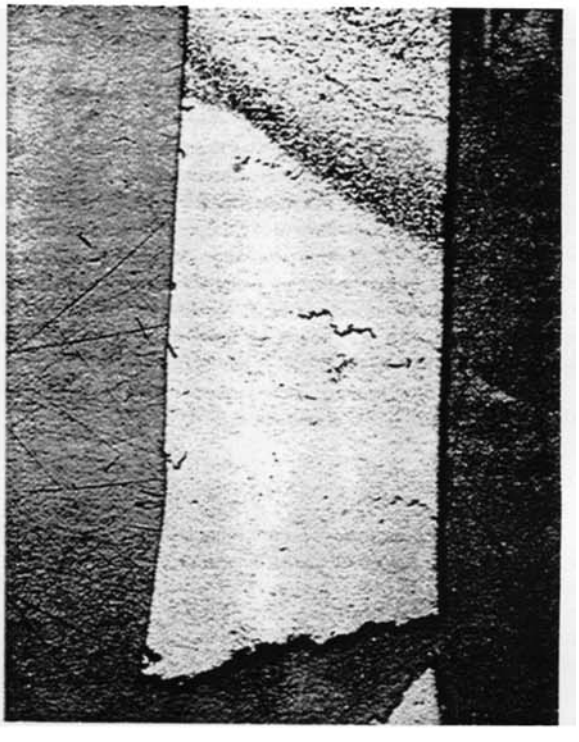
Conclusions drawn and opinions expressed are those of the author and not necessarily concurred in by Cameron Iron Works, Inc. or NACE.

References

1. Zapffe, C. A., Sims, C. E. Trans. AIME, Vol. 145, p. 225 (1941).
2. Schuetz, A. E., Robertson, W. D. Corrosion, Vol. 13, p. 437t (1957).
3. Barth, C. E., Steigerwald, E. A. Met. Trans., Vol. 1, p. 3451



8X
CMS 1138/w A/W 150 BHN
44.1 ksi 100% 45.6 Hours



8X
CMS 1138/w A/W 137 BHN
44.1 ksi 100% 43.4 Hours

FIGURE 5 – Fractures of low carbon steel cross-weld samples. Note that the failures are restricted to the parent material, not the weld or heat affected zones. These failures were each observed to be caused by blistering.

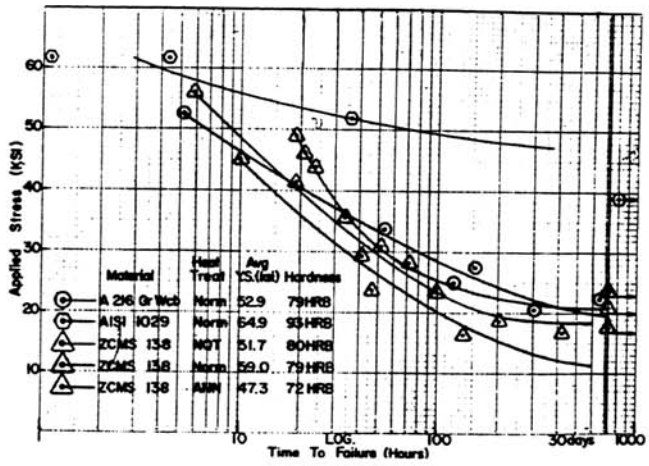


FIGURE 6 — Carbon steels. Correlation of stress vs time to failure.

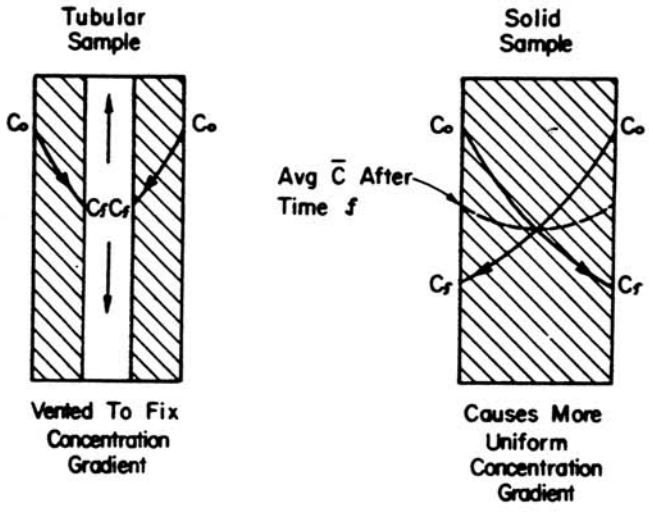


FIGURE 7 — Variations in hydrogen concentrations caused by differences in charging.

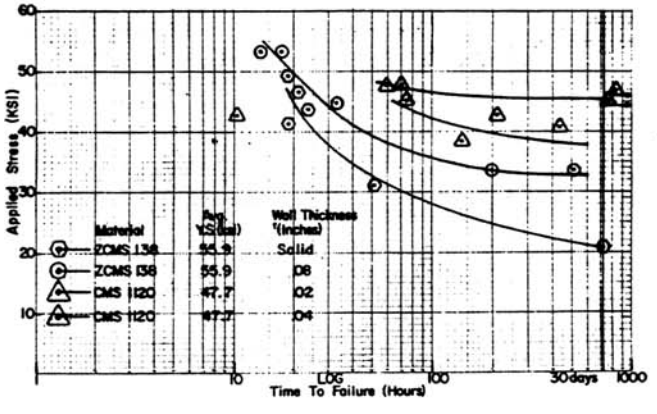


FIGURE 8 — Relationship solid vs hollow specimens. Correlation of stress vs time to failure.

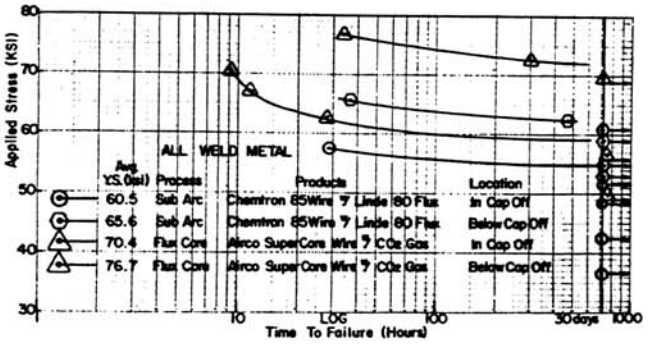


FIGURE 9 — All-weld metal data as welded. Correlation of stress vs time to failure.

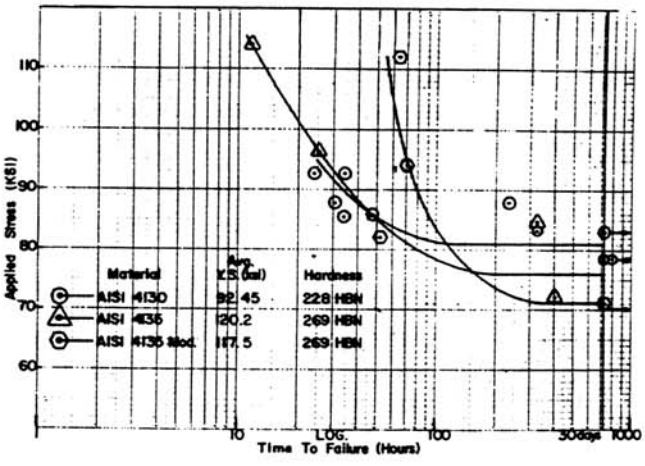


FIGURE 10 — Low alloy steel. Correlation of stress vs time to failure.

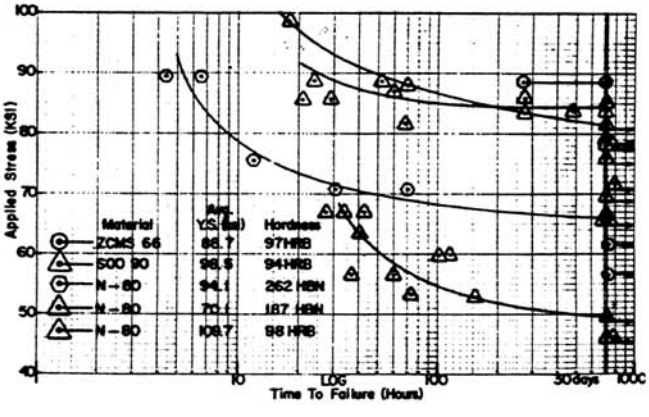


FIGURE 11 — Low alloy steel. Correlation of stress vs time to failure.

(1970).
4. Beachem, C. D. Met. Trans., Vol. 3, p. 437 (1972).
5. Vollmer, L. W. Corrosion, Vol. 14, p. 324t (1958).
6. Baldy, M. F. Corrosion, Vol. 17, p. 509t (1961).
7. Hudgins, C. M., McGlasson, R. L., Mehdizadeh, P., Rosborough, W. M. Corrosion, Vol. 22, p. 238 (1966).
8. Treseder, R. S., Swanson, T. M. Corrosion, Vol. 24, p. 31 (1968).
9. A Report of Technical Practices Committee 1G. Field Experience with Cracking of High Strength Steels in Sour Gas and Oil Wells. Corrosion, Vol. 8, p. 351 (1952).
10. Prange, F. A. Corrosion, Vol. 15, p. 49t (1959).
11. Sewell, E. D. Hydrogen Embrittlement Challenges Tubular Goods Performance. ASEM No. 65-Pet-13, Petroleum Mechanical Engineering Conference, Houston, Texas, September 19-22, 1965.
12. Liebchen, K. H. Materials Protection, Vol. 10, No. 9, p. 50

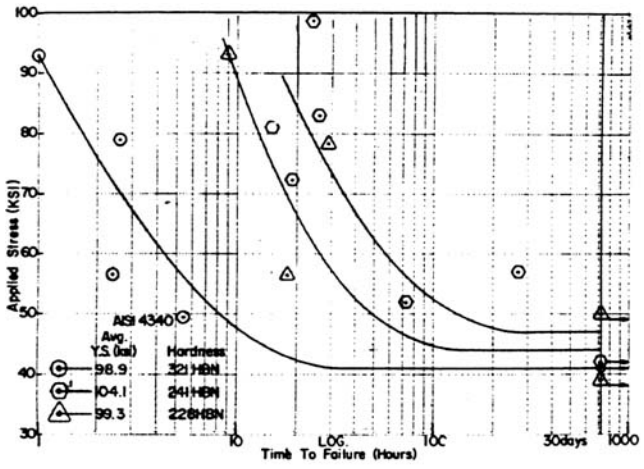


FIGURE 12 – Effects of hardness on AISI 4340. Correlation of stress vs time to failure.

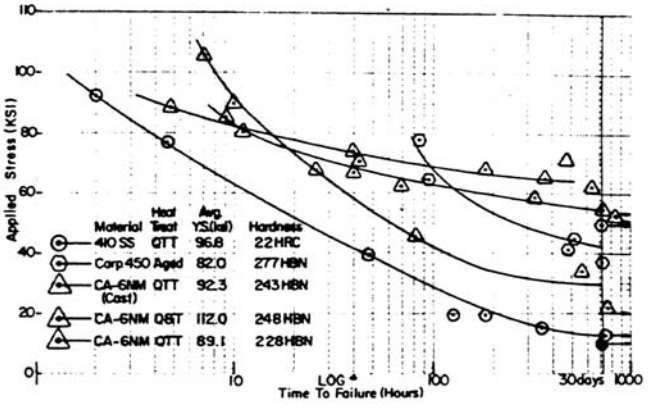


FIGURE 13 – Stainless steel data. Correlation of stress vs time to failure.

(1965).

13. Kohut, G. B., McGuire, W. J. Materials Protection, Vol. 7, No. 6, p. 17 (1968).
14. Garwood, G. L. The Drilling Contractor, p. 39, 50 (1974) March-April.
15. Atherton, S. D. H_2S–A Toxic Gas That Can Kill. AIME (Petroleum Division), Paper No. SPE 3202, Regional Meeting of the Society of Petroleum Engineers of AIME, Lafayette, Louisiana, November 9-10, 1970.
16. Schenck, H. Schmidtmann, E., Klarner, H. F. Stahl und Eisen, Vol. 87, p. 136 (1967).

Copyrighted Materials
Copyright © 1996 NACE International Retrieved from www.knovel.com

Paper No. 61—CORROSION/90

CORROSION PERFORMANCE OF 13 CR STAINLESS TUBULARS IN SOUR ENVIRONMENTS

W.C. Chen
Exxon Production Research Company
P.O. Box 2189
Houston, TX 77252-2189

ABSTRACT

This paper presents results of corrosion and environmental cracking testing of 13 Cr stainless steels in slightly sour environments and provides guidelines for justifying 13 Cr for sour services. The purpose of this paper was to confirm/refute the service limits suggested by manufacturers. The new test results indicate that many of the existing 13 Cr service limits can be relaxed for Grade L-80 by engineering justification on a case-by-case basis.

Keywords: 13 Cr, sour environments, service limits, sulfide-stress cracking, stress-corrosion cracking, weight-loss corrosion, erosion-corrosion, pitting corrosion, engineering justification.

INTRODUCTION

It is well known that 13 Cr stainless steels have good corrosion resistance to CO_2 environments and cost much less than duplex stainless steels and high-nickel corrosion-resistant alloys (CRAs). However, 13 Cr is susceptible to corrosion at high temperatures and is susceptible to sulfide-stress cracking (SSC) in H_2S environments.[1]

Many 13 Cr OCTG manufacturers have suggested service limits of temperature and H_2S/CO_2 partial pressures for using 13 Cr in sour, CO_2 environments.[2-4] However, there is no common agreement on these limits. The limits of H_2S partial pressure and temperature range from 0.15 to 10 psi (1.0 to 69 kPa) and from 93° to 204°C (200° to 400°F), respectively. These limits were derived from the results of different test techniques (e.g., C-ring/bent-beam tests vs. NACE tensile tests; or, unnotched specimens vs. notched specimens; or, a threshold stress of 80 percent vs. 100 percent). Those tests had various degrees of conservatism compared to service conditions. Moreover, there are several successful field experiences in environments that are more severe than those defined by some of these service limits.[5,6]

To determine the usability of 13 Cr for slightly sour, CO_2 environments, it is necessary to explore the resistance of 13 Cr to stress-corrosion cracking (SCC), SSC, erosion-corrosion, pitting, and weight-loss corrosion. The objectives of this work were to confirm/refute the 13 Cr service limits suggested by manufacturers and to establish engineering guidelines for selecting 13 Cr for slightly sour services.

EXPERIMENTS

Because a large number of test techniques are utilized, this paper will not go into the details of each experimental procedure. Much of this information is contained in tables. This section will discuss only the test technique and results for each experiment.

Klein pointed out that 13 Cr appears to be more resistant to H_2S cracking than indicated by NACE tensile tests in slightly sour environments.[7] Whitehead et al. also concluded that the standard NACE tensile test solution is inappropriate for testing the SSC resistance of 13 Cr because the passivity on which the 13 Cr depends to resist SSC cannot be achieved.[8] Therefore, C-rings were chosen as the specimen type for SCC and SSC tests, and NaCl solution without acetic acid was chosen as the basic test solution. Acetic acid was added to some test solutions to evaluate the effect of pH on SCC and SSC resistance of 13 Cr.

Test Materials

Grade L-80 13 Cr stainless steel tubulars were received from various manufacturers and two samples were heat-treated to Grade C-95 in our laboratory. Table 1 lists the chemical compositions and mechanical properties of these test materials.

SCC Test

Eight autoclave tests were conducted to evaluate the SCC resistance of 13 Cr. The autoclaves were replenished with a continuous flow of H_2S/CO_2 gas mixture to maintain the low constant partial pressure of H_2S. Each autoclave was also equipped with a condenser at the gas outlet to prevent water loss due to water vaporization The condenser consists of a water-cooled C-276 pipe attached to the top of the autoclave. The apparatus, as shown in Figure 1, causes the water vapor to liquefy and to return to the autoclave so that a constant NaCl concentration can be maintained.

C-rings stressed to 90 percent of yield were exposed to environments containing about 300 psi (2,068 kPa) CO_2, H_2S levels ranging from 1.5 to 15 psi (10 to 103 kPa), pH ranging from 3.6 to 5.2, and temperature ranging from 93° to 177°C (200° to 350°F). The results and test conditions of these tests are presented in Table 2. The L-80 samples experienced no failures during the 30-day exposure to the test environments. The H_2S partial pressure, NaCl concentration, and addition of acetic acid (pH variation) have no significant effects on the SCC resistance of 13 Cr within the test conditions. Only one C-95 13 Cr sample cracked in a 5-percent NaCl solution saturated with 15 psi (103 kPa) H_2S and 290 psi (2,000 kPa) CO_2 at 200°F (93°C), where the pH is 3.8.

SSC Test

Ten ambient-pressure C-ring tests were conducted at temperatures ranging from 24° to 93°C (75° to 200°F) to evaluate the resistance of 13 Cr material to SSC. The test vessels were replenished with an H_2S/CO_2 gas mixture or with a 100-percent H_2S gas to maintain the low constant partial pressure of H_2S. All C-rings were stressed to 90 percent of yield. Most of the tests had 30-day exposures, except two were extended to 90 days and one to 60 days to evaluate the effect of exposure time to test results. All of the failed samples cracked within the first two weeks of testing. In the 90-day tests, a C-95 sample cracked within the first two weeks and was replaced by a new one of the same material after 30 days of exposure. Again, the new one cracked after it had been exposed to H_2S for two weeks.

The H_2S partial pressures and chloride compositions of the SSC tests match very closely with the compositions utilized to evaluate SCC resistance. Test results and conditions are listed in Table 3. The NaCl concentration ranges from zero to 25 percent; the H_2S partial pressure, from 0.15 to 15 psi (1.03 to 103 kPa); and pH, from 3.5 to 5.1. As in the SCC tests, none of the L-80 samples failed. Only C-95 samples failed in test solutions saturated with 15 psi H_2S.

NaCl concentration, H_2S partial pressure, and the addition of acetic acid (pH variation) have no significant effect on the SSC resistance of L-80 13 Cr within the test conditions. However, increasing the NaCl concentration from 5 to 25 percent made C-95 13 Cr susceptible to SSC when the H_2S partial pressure is 15 psi (103 kPa). Adding acetic acid to the 5-percent NaCl solution also made C-95 13 Cr susceptible to SSC.

These test results compare favorably with the C-ring test data of Tanimura et al.[9] Their critical partial pressure of H_2S derived from data of unnotched C-rings stressed to 90 percent yield and exposed to 5 percent NaCl, 0.5 percent acetic acid, and an H_2S/N_2 gas mixture at room temperature is about 7.5 psi (52 kPa) for L-80 13 Cr and about 3 psi (21 kPa) for C-95 13 Cr.

Weight-Loss Corrosion

Weight-loss corrosion tests to measure the corrosion rate of 13 Cr stainless steels were conducted on AISI 410 and CA-15 stainless steels 5- to 25-percent NaCl brines with zero to 3,000 psi (zero to 20,684 kPa) H_2S and 15 to 3,400 psi (10 to 23,442 kPa) CO_2 at temperatures ranging from 66° to 232°C (150° to 450°F). The results, plotted in Figure 2, show a significant increase in corrosion rate above 200°F (93°C). The solid curve indicates the corrosion rates of 13 Cr in 25-percent NaCl brine saturated with 700 psi (4,826 kPa) CO_2. The dashed curve indicates the corrosion rates of 13 Cr in 25-percent brine with 50 psi (345 kPa) H_2S and 700 psi (4,826 kPa) CO_2. The H_2S in the H_2S/CO_2 environments tends to increase the corrosion rate of 13 Cr above 93°C (200°F).

Erosion-Corrosion

The resistance of 13 Cr to corrosion is dependent upon a protective film developed on the surface. If damage or breakdown of this film occurs, increased corrosion will result. A series of erosion-corrosion tests was conducted on an AISI 420 stainless steel to determine the effect of flow velocity on the surface film and on the corrosion resistance of 13 Cr. The test results are plotted in Figure 3. At a temperature of 65°-107°C (150°-225°F), a CO_2 partial pressure of 15-50 psi (103-345 kPa), and chloride contents ranging from 0.2 to 2 percent, the AISI 420 stainless steel has good corrosion resistance, less than 1.5 mils per year, mpy (0.04 mm per year, mmpy). The flow velocity of 5-65 feet per second, ft/s (1.5-20 meters per second, m/s), has no significant effect on the corrosion resistance of 13 Cr.

Pitting Corrosion

A very localized rupture of the protective film can result in pitting, an aggressive penetration of the metal. No pitting was observed on the test coupons below 121°C (250°F) in the erosion-corrosion tests, and no significant pitting was observed on the L-80 13 Cr C-rings in the SCC and SSC tests.

Pitting corrosion tests of 13 Cr were performed at 24°C (75°F) and 52°C (125°F) using the ASTM G-48 total immersion ferric chloride test method.[10] The test results are summarized in Table 4. Pits were observed only on C-95 13 Cr coupons tested at 52°C (125°F). No pitting was observed on the planar surfaces of L-80 13 Cr coupons. Although the ASTM G-48 test is used for screening purposes, the fact that no pitting was observed after testing is an indication of good pitting resistance of L-80 13 Cr.

Although the above laboratory data reveal that L-80 13 Cr has a good pitting resistance, pits were observed on 13 Cr tubulars that were exposed to temperatures above 125°C (260°F) in a CO_2 producing well. The acidizing as well as producing environment were the contributing factors. Therefore, the pitting problem that may be caused by acidizing needs to be resolved. More discussions on acidizing will be given in the discussion section.

Discussion

The service limits of 13 Cr suggested by manufacturers do not distinguish the effect of strength of 13 Cr corrosion performance. The results of SCC, SSC, and pitting tests reveal that the cracking and pitting resistances of L-80 13Cr is much better than that of C-95 13 Cr. This indicates that the service limits of L-80 13 Cr should be less restrictive than those of C-95 13 Cr.

The C-95 13 Cr susceptible to SCC (Table 2), SSC (Table 3) and pitting (Table 4) under some test conditions. More tests are required in order to establish the range of environments in which C-95 can be used. Therefore, the following discussions on 13 Cr usability will be limited to Grade L-80.

SCC and SSC tests do not reveal a strong cracking or pitting propensity for L-80 13 Cr in test environments containing up to 25 percent brine and up to 15 psi (103 kPa) H_2S at temperatures up to 177°C (350°F); see Tables 2 and 3. The results of this investigation indicate that the susceptibility of 13 Cr to SSC could be detected in a laboratory test within 30 days of exposure to H_2S, and longer exposure times have an insignificant effect on the test results.

The weight-loss corrosion tests reveal a good corrosion resistance of 13 Cr in sour, CO_2 environments up to 93°C (200°F); see Figure 2. The erosion-corrosion tests show that the good corrosion resistance of 13 Cr will not be adversely affected by a flow velocity under 65 ft/s (20 m/s); see Figure 3. Results of the pitting tests do not reveal a pitting propensity for L-80 13 Cr under a severe ferric chloride test solution (Table 4).

Summarizing the above test results, we found that 13 Cr L-80 has appropriate corrosion and cracking resistances in CO_2 environments containing 25 percent brine and 15 psi (103 kPa) H_2S at temperatures up to 93°C (200°F). This implies that many existing 13 Cr service limits can be relaxed for Grade L-80. However, these numbers do not necessarily refer to the service limits because there is no satisfactory correlation between laboratory and field data. Moreover, the desired lifetime and the required design conservatism of 13 Cr string varies from well to well. It would be wise to evaluate 13 Cr service limits with available laboratory and field data on a case-by-case basis.

Although use of L-80 13 Cr stainless steel for slightly sour environments is promising, there are other factors that may affect the performance of 13 Cr in field services. Those factors need to be resolved through proper design and control of operations to ensure the integrity of 13 Cr string, downhole equipment, and wellhead. The following discussion covers the concerns and provides some possible resolutions.

Oxygen Contamination

The lack of oxygen in the downhole environment is believed to minimize pitting. Therefore, the introduction of oxygen during workover operations, etc., should be minimized, and, if the wells are to be exposed to oxygenated solutions for extended periods, an oxygen scavenger is suggested.

Acidizing

Exposure of 13 Cr to acids during routine well stimulation is a primary concern. Hydrochloric and hydrofluoric acids used in the acidizing stimulation are very corrosive. If there is no appropriate acid-inhibitor treatment during acidizing, they will dissolve or will pit the 13 Cr stainless steel. Many investigators have conducted testing on 13 Cr to determine whether the stimulation acids can be effectively inhibited.[11,12] It appears that acid inhibition can successfully control the corrosion of 13 Cr up to 121°C (250°F).

Galvanic Corrosion

Galvanic corrosion caused by contact between 13 Cr (passive) and carbon steel is a possibility.[13] Unless the 13 Cr-carbon steel connections can be completely insulated and carbon steel parts can be properly protected, the full string, the downhole equipment, and the wellhead should be made of 13 Cr. A full string made of 13 Cr is further recommended because the acid inhibitor may not be effective for both 13 Cr and carbon steel.

Crevice Corrosion

The 13 Cr stainless steel is susceptible to crevice corrosion; thus, threaded connections need special design to avoid local crevices. The internally flush design and the metal-to-metal interference seals or back-up seals (such as Teflon seal rings) are required.

Lifetime Prediction

The desired lifetime of 13 Cr strings usually varies significantly, depending on whether they are replacements of failed carbon steel strings or whether they are set up for new wells. Unfortunately, there is insufficient field experience to confirm that the 13 Cr will have the desired lifetime, nor do we have a satisfactory correlation between laboratory and field data that would enable us to make predictions. Based on simple weight-loss data, life prediction appears to be possible, but there does not appear to be a similar technique for predicting crack initiation and growth. In general, the conditions chosen for testing are severe compared to service in order to accelerate cracking. However, there is always an argument regarding how much conservatism is needed. To resolve this problem, engineering judgment is warranted when using test results to design field systems.

Engineering Justification of 13 Cr Serviceability

The engineering justification of L-80 13 Cr for slightly sour service should satisfy the following three requirements: (1) 13 Cr should be free from cracking and pitting propensities under service conditions; (2) tubulars should be designed to tolerate weight-loss corrosion for the desired lifetime; and (3) concerns about damage by oxygen, acidizing, galvanic, and crevice corrosion need to be resolved. The laboratory test results presented in this paper are believed to be adequate for the evaluation of L-80 13 Cr serviceability for slightly sour, CO_2 environments. If necessary, a safety factor on test results, such as chloride concentration, H_2S partial pressure, and corrosion rate, can be incorporated into the evaluation and justification, depending on the required design conservatism.

CONCLUSIONS

1. SCC and SSC tests reveal no cracking nor pitting propensity for L-80 13 Cr in test environments containing up to 25 percent brine and up to 15 psi (103 kPa) H_2S at temperatures up to 177°C (350°F).
2. The weight-loss corrosion tests reveal a good corrosion resistance of 13 Cr in sour, CO_2 environments up to 93°C (200°F). The erosion-corrosion tests show that the good corrosion resistance of 13 Cr is not adversely affected by a flow velocity under 65 ft/s (20 m/s).
3. Results of pitting tests also reveal no pitting propensity for L-80 13 Cr.
4. The test results indicate that many existing 13 Cr service limits can be relaxed for Grade L-80.

5. It is recommended that the 13 Cr serviceability for slightly sour, CO_2 environments be evaluated and justified on a case-by-case basis.
6. Three requirements must be satisfied to justify using 13 Cr tubulars in slightly sour, CO_2 environments: (1) 13 Cr must be free of cracking and pitting propensities under service conditions, (2) tubulars should be designed to tolerate weight-loss corrosion for the desired lifetime, and (3) the concerns about damage by oxygen, acidizing, galvanic and crevice corrosion should be resolved.

ACKNOWLEDGMENT

The author wishes to thank the management at Exxon Production Research Company for supporting this investigation and for permitting publication of this paper. The author also wishes to thank the Corrosion Control Group of the Materials Section, Exxon Production Research Company, for providing the weight-loss corrosion and erosion-corrosion data.

REFERENCES

1. S. Mukai, M. Ueda, T. Tsumura, A. Ikeda, "Corrosion Behavior of 13 Cr Stainless Oil Country Tubular Goods in Wet CO_2-H_2S-Cl^- Environments," Proceeding of the 4th Asian Pacific Corrosion Conference at Tokyo, May 1985, p. 664.
2. "High Alloy OCTG — New SM-Series," Sumitomo Metal Industries, Ltd., 1986.
3. "Corrosion Engineering Map of Martensitic 13 Cr and Duplex 22 Cr Stainless Steels for OCTG," Kawasaki Steel Corporation, March 1984.
4. "Corrosion Resistance of NK Cr 13 in CO_2 Environments," Technical Bulletin, Nippon Kokan K.K., December 1986.
5. J.D. Combes, J.G. Kerr, L.J. Klein, "13 Cr Tubulars Solve Corrosion Problems in the Tuscaloosca Trend," Petroleum Engineer International, March 1983, pp. 50-70.
6. J. Murali, G.L. Boswell, R.R. Schulz, "Selection and Application of Stainless Steel Tubulars for a Deep, Hot Gas Well," Proceeding of the Eighth Annual Energy-Sources Technology Conference and Exhibition in Dallas, Texas, February 17-21, 1985, pp. 117-125.
7. L.J. Klein, "H_2S Cracking Resistance of 420 Stainless Steel Tubulars," *Materials Performance*, 23 10(1984), pp. 29-34.
8. T.D. Whitehead, C.H. Baloun, "Evaluating the Suitability of NACE Standard Test, TM-01-77, for Testing 13% Chromium Martensitic Stainless Steels for Sulfide-Stress Cracking Resistance," ASTM STP 866 (Philadelphia, PA: ASTM, 1985), pp.400-414.
9. M. Tanimuna, Y. Ishizawa, T. Shimada, "The Sulfide Stress Corrosion Cracking Resistance of 13% Cr Steels for OCTG," Nippon Kokan Technical Report (Overseas), Vol. 39, December 1983, pp. 62-67.
10. ASTM Standard G 48-76: "Standard Test Methods for Pitting and Crevice Corrosion Resistance of Stainless Steels and Related Alloys by the Use of Ferric Chloride Solution," *1989 Annual Book of ASTM Standards*, Vol.03.02 (Philadelphia, PA: ASTM, 1989).
11. M.L. Walker, "Tubulars in Harsh Environments Need Special Protection" *Drilling*, 7/8 (1988), pp. 30-33.
12. R.D. Kane, S.M. Wilhem, "The Compatibility of Stainless and Nickel-Base Alloys in Acidizing Environments," CORROSION/89, paper no. 481 (Houston, TX: NACE, 1989).
13. M.G. Fontana, *Corrosion Engineering*, 3rd ed. (New York, NY: McGraw-Hill, 1986), p. 43.

TABLE 1
Chemistry and Mechanical Properties of 13 Cr Stainless Steels

Manufacturer	A		B		C
C	0.20		0.20		0.19
Si	0.52		0.20		0.42
Mn	0.62		0.42		0.69
P	0.013		0.023		0.015
S	0.001		0.007		0.002
Cr	13.12		13.76		13.02
Mo	--		0.10		–
Ni	–		0.24		0.08
Cu	–		0.05		–
Grade	L-80	C-95	L-80	C-95	L-80
Yield Strength, ksi (MPa)	83.9 (578.5)	107.2 (739.1)	83.3 (574.3)	107.7 (742.6)	84.0 (579.2)
Tensile Strength, ksi (MPa)	110.0 (758.4)	134.5 (927.3)	110.8 (763.9)	132.5 (913.6)	110.0 (758.4)
Elongation, %	24.5	20.5	28.0	19.4	30.0
% Reduction of Area	62.6	64	67.6	60.1	68.3
HRC Hardness	21	26	16	26	20

TABLE 2
Results of 30-Day Hot, Sour Autoclave SCC Tests on 13 Cr C-rings

		5% NaCl, w/o Acetic Acid					5% NaCl 0.5% Acetic Acid	10% NaCl w/o Acetic	25% NaCl w/o Acetic
		1.5 psi H_2S, 300 psi CO_2		15 psi H_2S, 290 psi CO_2			15 psi H_2S 290 psi CO_2	15 psi H_2S 290 psi CO_2	15 psi H_2S 290 psi CO_2
Manufactuer	Grade	-- 250°F	-- 350°F	pH 3.8 200°F	-- 250°F	-- 350°F	pH 3.6 250°F	pH 5.0 350°F	pH 5.2 350°
A	L-80	NF	NF	NF	NF	NF	NF	NF	NF
	C-95	NF	NF	NF	NF	NF	NF	NF	NF
B	L-80	NF	NF	NF	NF	NF	NF	NF	NF
	C-95	NF	NF	F	NF	NF	NF	NF	NF
C	L-80	NF	NF	NF	NF	NF	NF	NF	NF

Note: pH of brine was measured after nitrogen-purging at the end of test.
All C-rings were stressed to 90 percent yield.

NF = No Failure. F = Failure.

TABLE 3
Results of 30-Day Ambient-Pressure SSC Tests on 13 Cr C-rings

		No acetic acid added into test solutions					
		0.15 psi H_2S, pH ~ 5.1, 75°F			15 psi H_2S, pH ~ 4.6, 75°F		
Manufactuer	Grade	0% NaCl	5% NaCl	25% NaCl	0% NaCl	5% NaCl[1]	25% NaCl[1]
A	L-80	NF	NF	NF	NF	NF	NF
	C-95	NF	NF	NF	NF	NF	NF
B	L-80	NF	NF	NF	NF	NF	NF
	C-95	NF	NF	NF	NF	NF	F
C	L-80	NF	NF	NF	NF	NF	NF

		Test solutions containing 0.5% acetic acid			
		15 psi H_2S, pH ~ 3.5, 75°F		15 psi H_2S, 5% NaCl, pH ~ 3.5	
Manufacturer	Grade	5% NaCl[2]	25% NaCl	140°F	200°F
A	L-80	NF	NF	NF	NF
	C-95	F	F	F	NF
B	L-80	NF	NF	NF	NF
	C-95	F	NF	NF	NF
C	L-80	NF	NF	NF	NF

Note: [1] Test was continued additional 60 days.
[2] Test was continued additional 30 days.

* All C-rings were stressed to 90 percent yield. NF = No Failure. F = Failure.
pH of brine was measured after nitrogen-purging at the end of test.

TABLE 4
Results of ASTM G-48 Pitting Corrosion Tests on 13 Cr Coupons

		Test Temperature	
Manufacturer	Grade	75°F (24°C)	125°F (52°C)
A	L-80	NP	NP
	L-95	NP	P
B	L-80	NP	NP
	L-95	NP	P
C	L 80	NP	NP

Note: NP = None Pitted. P = Pitted.

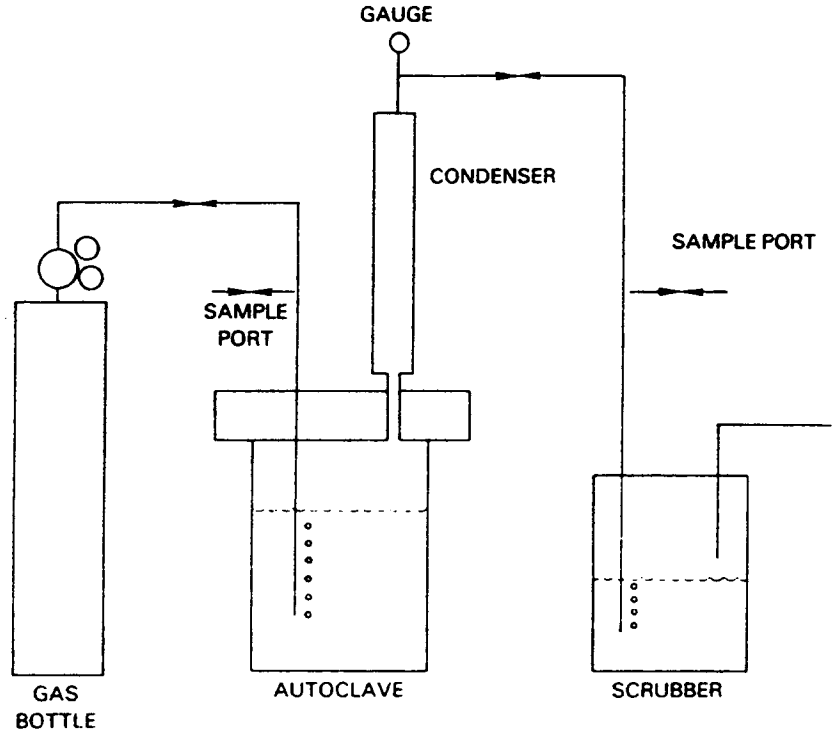


Figure 1. Schematic of SCC test apparatus.

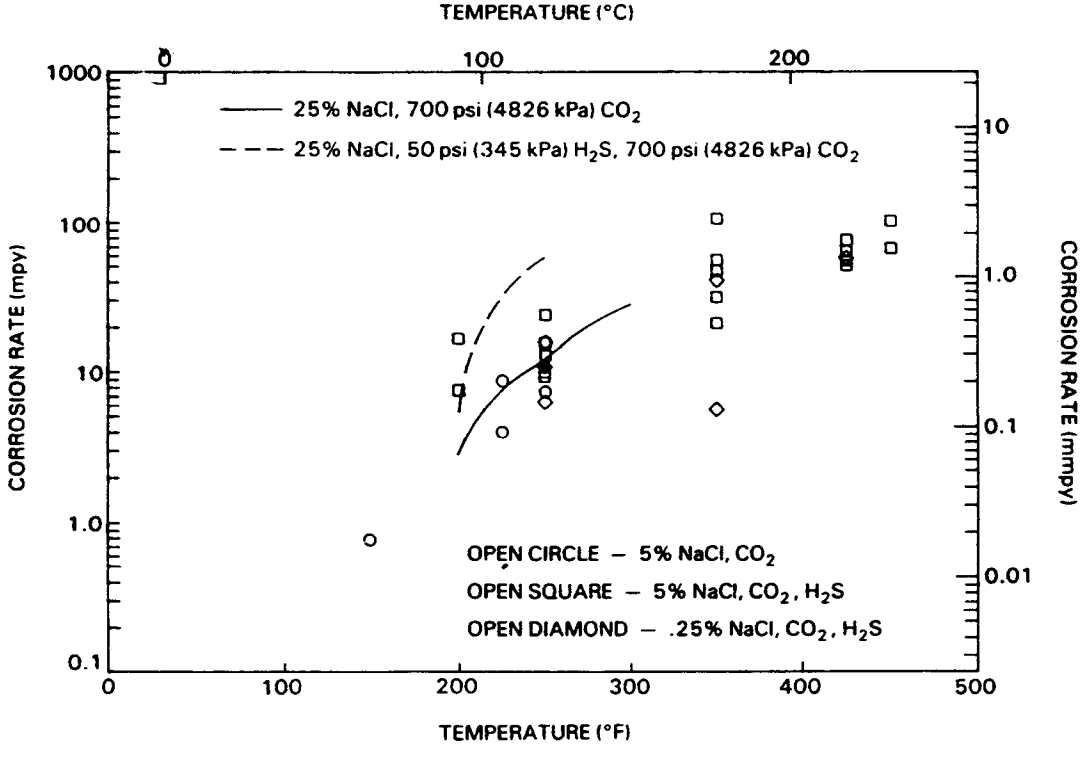


Figure 2. Weight-loss corrosion rate of AISI 410 and CA-15 stainless steels.

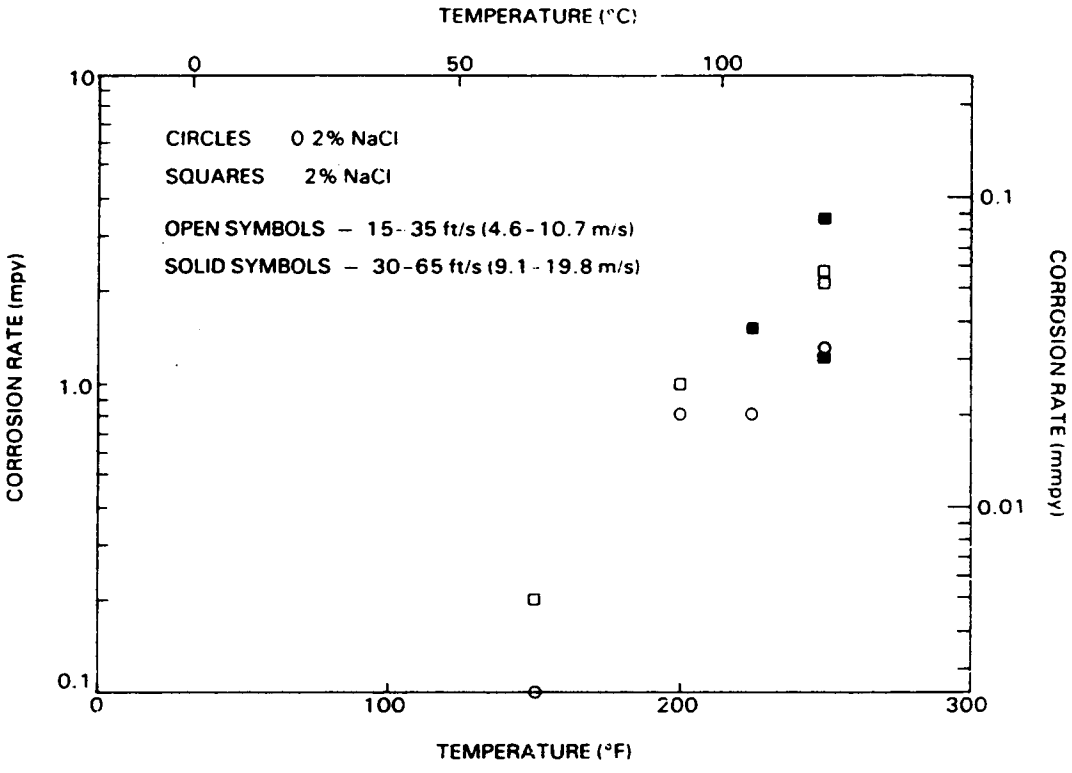


Figure 3. Erosion-corrosion rate of AISI 420 stainless steels.

Copyrighted Materials
Copyright © 1996 NACE International Retrieved from www.knovel.com

Paper No. 71—CORROSION/90

SOME LIMITATIONS ON THE USE OF 13Cr ALLOYS FOR CORROSIVE GAS AND OIL PRODUCTION

S.W. Ciaraldi
Amoco Corporation
c/o Amoco Norway Oil Company
P.O. Box 388
4001 Stavanger
Norway

ABSTRACT

Laboratory investigations and field experience continue to define the application limits of 13Cr alloys. Recent stress corrosion cracking tests have developed a direct relationship between tolerable H_2S levels and acetate anion contents of test brines. Strength level was found to be an important variable in the chloride-induced cracking of nickel containing alloys. Corrosion related service failures have been attributed to organic acid levels of produced fluids and flow related effects. Laboratory tests have demonstrated acetate anions to significantly influence corrosion behavior. A field test unit was developed to study flow related corrosion of stainless alloys and has successfully defined a few acceptable velocity limits in offshore tests.

INTRODUCTION

Use of 13Cr stainless steel (SS) tubulars and wellheads for corrosive gas and oil production has become increasingly common in recent years. Economics of stainless usage are often favorable as an alternative to continuous downhole corrosion inhibition. Further, stainless steel completions are generally regarded as more reliable and hence require less maintenance than conventional wells.

13Cr alloys have several partially defined limitations for successful field performance. Poor resistance to sulfide stress cracking (SSC) in H_2S containing environments is probably the most well known of these.[1] For this reason, usage is often restricted to sweet service as defined by NACE Standard MR-01-75, i.e., H_2S partial pressure below 0.34 kPa (0.05 psia).[2] However, SSC failure free performance has been reported at significantly higher H_2S levels.[3] Further, although demonstrated to be susceptible to chloride-induced stress-corrosion cracking (SCC) in aggressive elevated temperature laboratory tests, SCC service failures of nickel containing 13Cr base alloys CA6NM and F6NM are not known to have been reported in petroleum production operations.[5,6]

Recent field experience has demonstrated additional limitations of 13Cr alloys. Organic acids are inherent to the produced fluids of most gas-condensate wells and are believed to have contributed to the service occurrences of corrosion discussed below.[4] Also, additional flow related sweet corrosion failures of 13Cr alloys have occurred since those reported previously.[7] These field experiences are described below in addition to results of recent laboratory and field corrosion tests performed to better define the limits of 13Cr alloys for corrosive gas and oil production.

STRESS CORROSION CRACKING

Sulfide Stress Cracking of 13Cr Alloys

Numerous laboratory studies have attempted to define the maximum tolerable H_2S level for which SSC of 13Cr alloys does not occur.[3,8-11] Unfortunately, reported values vary appreciably, ranging from about 0.7 to 28 kPa (0.1 to 4 psia). Such critical H_2S values for SSC depend on specific test environment and specimen geometry, but can be difficult to relate to measurable production well parameters.

The results of recent SSC tests on 13Cr alloys are described in detail in a previous publication.[12] However,

an important finding from this work is briefly described here. Specifically, the synergistic effect of organic acid anions and H_2S on SSC.

Table I lists maximum "No SSC" partial pressures obtained for 13Cr alloys in five different ambient temperature test environments. These values were obtained by two week exposures of fatigue precracked double cantilever beam (DCB) specimens to the test environments. Full details of the test procedures can be found in the referenced publication.[12] Also listed in Table I are values of computer calculated acetate anion contents of the test environments.

Figure 1 illustrates that No SSC H_2S partial pressures decreased with increased acetate anion levels of the test environments. The results are consistent with a hydrogen induced cracking mechanism and results of previous research which have demonstrated that at constant pH levels, acetates dramatically increased the diffusion limited current of the reduction of H+ ions.[13] These results may help rationalize successful field performance of 13Cr alloys under nominally sour [i.e., H_2S partial pressure greater than 0.34 kPa (0.05 psia)] conditions, as most wells typically contain less than 0.05 percent (500 ppm) organic acid anions.[3,4]

Stress Corrosion Cracking of Nickel Containing Alloys

In order to assess the likelihood of chloride-induced SCC of nickel containing 13Cr base alloys in simulated production environments, modified NACE TM-01-77 tests were performed at 93°C (200°F).[14] These tests were conducted using an F6NM alloy quenched and double tempered to average hardnesses of 24.2 and 26.8 Rockwell C (HRC). Aqueous test solutions contained 5 percent NaCl and 0.5 percent acetic acid (HAc), but rather than with H_2S, solutions were continuously purged with N_2, CO_2, or air. Again, full details of the testing can be found in the previously referenced paper.[12]

Results of the chloride-induced SCC tests are shown in Table II. The 24.2 HRC F6NM sample resisted SCC at 100 percent of yield strength (YS) under air purge. By contrast, the 26.8 HRC sample resisted SCC at 100 percent YS under N_2 and CO_2 purges, but was quite susceptible to SCC under O_2 purge, even at applied stresses as low as 50 percent YS. Fractographic studies of failed specimens confirmed an SCC mechanism.

In general, produced gases should be free of air. However, the possibility of air contamination can often not be completely precluded over the service life of a well. As lower hardness F6NM did not exhibit the same susceptibility to SCC that the higher hardness sample did, it appears desirable that sour service hardness restrictions also be applied to sweet service equipment to minimize likelihood of chloride induced SCC in nickel containing martensitic stainless steels.

CORROSION

Effects of Organic Acids

In addition to SSC behavior, corrosion rates of 13Cr DCB specimens were determined in the five ambient temperature environments listed in Table I.[12] Again, a significant effect of computer calculated acetate anion concentration was found. These results are shown in Figure 2, along with results obtained for 9Cr-1Mo and F6NM (13Cr-4Ni-0.5Mo) specimens.

Corrosion rates for 9Cr-1Mo specimens were higher than 13Cr rates at low acetate anion levels and showed a gradual increase with increased solution acetates. The 13Cr corrosion rates were low at low acetate contents, but shifted abruptly higher at acetate anion levels between 0.17 and 0.19 percent (1,700-1,900 ppm). Corrosion of 13Cr specimens was in the form of broad pits, approaching a fairly uniform attack mode. F6NM samples exhibited low corrosion rates under all five test conditions.

Although decreased pH levels have been demonstrated to be conducive to corrosion of SS alloys, computer calculated pH values of Table I tests environments did not directly correlate to corrosion rates.[15] However, acetates are known to strongly promote the sweet corrosion of carbon steels and perhaps similarly may contribute to 13Cr corrosion.[13]

Several strings of 13Cr production tubing were recently observed to have experienced corrosion within 2-3 years in sweet gas/condensate service. Relatively high organic acid levels of produced fluids are thought to have contributed to attack. Wells at this offshore field produced 40-60 MMSCFD of gas having typical CO_2 partial pressures of 69-138 kPa (10-20 psia). Flowing bottomhole temperatures were about 81°C (177°F) to 101°C (213°F). Produced waters had high total dissolved solids (TDS) and contained 13,000 to 36,000 ppm chlorides. Total organic acid anion content was about 350 to 470 ppm. Measured pH of ambient pressure fluids after exposure to air but while still CO_2 saturated was about 3.6 to 4.7.

Only certain joints within the tubing strings had experienced corrosion. Location was somewhat random with respect to well depth, but corroded joints were most often in the vicinity of deviated well doglegs. In general, attack was in the form of broad pits which approached uniform corrosion, similar to that observed in the laboratory tests described above. Figure 3 shows an example of this corrosion. Although corrosion had occurred, maximum penetration rate observed was only about 0.13 mm/y (5 MPY).

Computer calculations were made to estimate the pH of fluids under production conditions. Values of these estimates were 3.4 to 4.2. As significant corrosion of 13Cr alloys would not normally be anticipated at this combination of pH, temperature, and CO_2 partial pressure, it seems reasonable to assume that relatively high organic acid anion levels had contributed to corrosion, especially considering attack appearance.[4] Note that although actual anion levels were below those at which high corrosion rates were observed in the above described laboratory tests, these tests had been conducted only at room temperature. It is quite possible that the critical acetate level for inducing corrosion could be lower at elevated temperatures.

Effects of Flow Rate

Flow enhanced sweet corrosion of Type 410 SS wellhead components in sweet gas/condensate service was previously reported.[7] Since that time, two strings of 13Cr production tubing from the same offshore field have experienced attack within one year of service. Wells at this location produced 20-50 MMSCFD of gas with a CO_2 partial pressure of 1.0-1.4 MPa (150-200 psia). Bottomhole and flowing tubing temperatures were about 127°C (260°F) and 110°C (230°F), respectively. The wells produced fluids with extremely low water cut. This water had low TDS and low chloride content of 800 ppm. Organic acid anion contents of up to 230 ppm were present. Measured pH of fluids exposed to air but still CO_2 saturated was about 4.6.

Corrosion of the 13Cr tubing was in the form of attack on the pin end of upper string joints. An example of this attack is shown in Figure 4. The small gap in the internal diameter of the proprietary connection used allowed produced fluids and gases to impinge directly on tubing pin ends. Maximum through-wall pitting rate was about 1.7 mm/y (66 MPY). The more severely attacked tubing string had produced at velocities of 10.7-21.3 m/s (35-70 ft/s). This corresponds to 80-240 percent of the "Limiting Velocity" as defined by API RP 14E.[16] Flow velocity in the less severely attacked string were more constant at about 100 percent of the Limiting Velocity or 12.2 m/s (40 ft/s).

Although acetates may have again contributed, locations and appearances of the 410 SS and 13Cr failures described clearly indicate a predominant influence of flow velocity and related effects. Unfortunately, except for 13Cr tubing connection change to a more flush design, no operational guidelines with respect to flow velocity could be given to field personnel to minimize corrosion failures. This situation prompted the implementation of the flow effects field test program described below.

Studies of Flow Related Corrosion Using a Field Test Unit

A fundamental design concept of the flow effects field test unit was the desire to produce various flow velocities at constant well production rates. This was accomplished by designing a unit in which internal diameter could be changed. Further, direct 90 degree flow impingement onto test coupons was selected as a worst case scenario for flow/turbulence enhanced corrosion.

Figure 5 shows overall design of the flow effects field test unit in its assembled state, with important components and features identified. The unit was designed to be placed into the flowline of a high production rate well. Note that the upstream coupon will be impinged upon at a velocity (V1) characteristic of the normal flowline diameter (Dl). The downstream coupon was designed to protrude 6.35 mm (0.25 in.) into the flow stream and is impinged upon at a velocity (V2) characteristic of the flow tube ID (D2). Four flow tubes having various IDs were fabricated. Length of the flow tubes was chosen to be 10 times the maximum flow tube ID so that steady flow would be re-established prior to impingement onto the downstream coupon. Note in Figure 5 that test coupons were electrically isolated from the flow tubes using TFE spacers, sleeves, and washers.

Table III lists chemical compositions and hardnesses of the 410 SS and F6NM alloys used in the initial flow related effects test program. All ring coupons were ground to a final thickness of 9.5 mm (0.375 in.) from 12.7 mm (0.5 in.) stock subsequent to quench and temper (double temper for F6NM) heat treatments.

The flow effects unit was assembled using flanged connections into the flowline of a producing well at the field at which the 410 SS and 13Cr flow related failures had been observed. Location of the unit was about 3 m (10 ft) downstream of a 90 degree bend which was immediately adjacent to the wellhead chokes. Flowline

pressure and temperature were about 8. 3 MPa (1,200 psig) and 71°C (160°F), respectively. Nominal production rate of the well was 40 MMSCFD of gas, 300 bbl/d condensate and 50 bbl/d water.

Coupons were degreased and weighed before and after exposure in the flow effects test unit. The coupons were visually examined and any weight loss measured and converted into corrosion rate based on the specimen area exposed to the impinging flow stream and well production duration. Additionally, calculations were made to determine flow velocity and and APR RP 14E Limiting Velocity based on actual production data gathered during coupon exposures. Fortunately, few production spikes occurred so that averaging gave a good representation of conditions under which coupons had been exposed.

Results of the initial flow effects field tests are shown in Table IV. Note that test durations varied from 38-69 days. Type 410 SS was exposed to flow at two different velocities. At 58 percent of the Limiting Velocity, no visual change in coupon appearance was observed. However, at 95 percent of the Limiting Velocity, an isolated corrosion pit had initiated on the impinged surface of the coupon. Overall appearance of this coupon is shown in Figure 6, with a close-up view of the corrosion pit shown in Figure 7. By contrast, alloy F6NM coupons resisted attack in the flow effects field test unit at three velocities, the highest of which was 120 percent of the Limiting Velocity.

The limited number of flow effects tests performed to date have demonstrated the feasibility of the technique, which caused minimal disruption to normal production activities. The critical velocity for flow induced attack on 410 SS was bracketed to be between about 60 to 95 percent of the API Limiting Velocity or between 8.5 m/s (28 ft/s) and 14 m/s (46 ft/s). Note that these velocities correspond well to those at which field service failures were observed.[7] Test results for alloy F6NM suggest this alloy would be a suitable replacement for 410 SS, at least at velocities up to 17.9 m/s (58.6 ft/s) or 120 percent of the Limiting Velocity. Additional tests to further define the limits of these and other stainless steel and higher alloys are in progress.

CONCLUSIONS

1. Maximum partial pressures for which sulfide stress cracking (SSC) of 13Cr alloys was not observed were found to decrease with increased acetate anions in laboratory test environments.
2. Strength level of a nickel containing 13Cr base alloy was found to influence the occurrence of chloride-induced SCC in elevated temperature aerated brines. These results suggest hardness restrictions should be applied to sweet service equipment for this alloy type.
3. Acetate anions were found to promote corrosion of 13Cr alloys in laboratory tests and are believed to have contributed to corrosion of 13Cr production tubing in sweet gas/condensate field service.
4. Flow related pin end corrosion of 13Cr production tubing was observed at velocities as low as about 100 percent of the API RP 14E Limiting Velocity in sweet gas/condensate field service.
5. A flow effects field test program was initiated and tests performed with minimal disruption to normal producing operations. Alloy F6NM was found to be superior to 410 SS in resisting attack at flow rates near or above the Limiting Velocity.

ACKNOWLEDGMENTS

Thanks are owed to D.V. Beggs, G.P. Coker, J.A. Franz, M. Horvat, D.R. Larson, R.L. Lee, H.F. Nichols, D.W. North, M.R. Pelligrini, S.M. Polomchak, and C.S. Sistrunk for their valuable contributions to these investigations.

REFERENCES

1. E.H. Phelps, *Metals Engineering Quarterly* 5(1973), p. 44.
2. NACE Standard MR-01-75, "Sulfide Stress Cracking Resistant Metallic Materials for Oil Field Equipment" (Houston, TX: NACE, 1981).
3. L.J. Klein, "H_2S Cracking Resistance of Type 420 Stainless Steel Tubulars" CORROSION/84, paper no. 211 (Houston, TX: NACE, 1984).
4. J.B. Fisher, *Acta Geochemica* 51, 9(1987).
5. A.P. Bond, H.J. Dundas, Stress-Corrosion Cracking and Hydrogen Embrittlement of Iron Base Alloys, NACE-5 (Houston, TX: NACE, 1977), p. 1136.
6. Y. Yoshino, *Corrosion* 42, 10(1986), p. 592.

7. J.D. Alkire, S.W. Ciaraldi, "Failures of Martensitic Stainless Steels in Sweet and Sour Gas Service, CORROSION/88, paper no. 210 (Houston, TX: NACE, 1988).
8. Nippon Kokan K.K., "Test Results of NK CR13, Resistance to Sulfide Stress Corrosion Cracking in Low H_2S Environments," Internal Report, Oct. 1981.
9. R.D. Kane, J.B. Greer, *J. of Petr. Techn.* 29, 11(1977), p. 1483.
10. Y.T. Ishizawa, T. Shimada, N. Tanimura, "The Sulfide Corrosion Cracking of 13% Cr Steels for OCTG," 1983 3rd Asian-Pacific Corrosion Control Conference in Taipei, Taiwan, R.O.C.
11. Nippon Kokan K.K., "Corrosion Resistance of NKK's High-Alloy OCTG," Internal Report, Mar. 1984.
12. S.W. Ciaraldi, "On the Sour Service Limitations of Martensitic Stainless Steels," UK Corrosion 89, Inst. of Corrosion Science and Techn., Beds, UK.
13. J.L. Crolet, M.R. Bonis, "The Role of Acetate Ions in CO_2 Corrosion" CORROSION/83, paper no. 160 (Houston, TX: NACE, 1983).
14. NACE Standard TM-01-77, "Testing of Metals for Resistance to Sulfide Stress Cracking at Ambient Temperature" (Houston, TX: NACE, 1977).
15. M.G. Fontana, N.D. Greene, *Corrosion Engineering*, 2nd ed. (New York, NY: McGraw-Hill Co., 1978), p. 163.
16. American Petr. Inst., "Recommended Practice for Design and Installation of Offshore Production Platform Piping Systems," 3rd ed., RP 14E (Dallas, TX: API, 1981).

TABLE I - EFFECT OF ACETATE ANION ON THE AMBIENT TEMPERATURE SSC OF 13Cr DCB SPECIMENS

Test Environment	No SSC H2S Partial Pressure (kPa)	(psia)	Acetate Anion Content (wt %)
1. 20 % NaCl, 0.5 % HAc	0.34	0.05	0.190
2. 20 % NaCl, 0.1 % HAc	1.38	0.20	0.085
3. 20 % NaCl, 0.5 % HAc, 5.5 MPa (800 psig) CO2	0.69	0.10	0.172
4. 20 % NaCl, 0.1 % HAc, 5.5 MPa (800 psig) CO2	$\geq$ 3.45	$\geq$ 0.50	0.050
5. Synthetic sea water, 0.5 % HAc	$\leq$ 0.34	$\leq$ 0.05	0.345

TABLE II - RESULTS OF MODIFIED NACE TM-01-77 SCC TESTS ON F6NM ALLOYS AT 93 C (200 F)

Hardness (HRC)	Purge Gas	Applied Stress (% yield strength)	Result
24.2	air	100	No failure
26.8	N2	100	No failure
26.8	CO2	100	No Failure
26.8	O2	100	Failure
26.8	O2	80	Failure
26.8	O2	50	Failure
26.8	O2	20	No Failure

TABLE III - CHEMICAL COMPOSITION AND HARDNESS OF ALLOYS TESTED IN FIELD FLOW EFFECTS UNIT

Wt %	Type 410 SS	F6NM
C	0.13	0.15
Mn	0.52	0.66
P	0.016	0.016
S	0.012	0.007
Si	0.45	0.31
Ni	0.17	3.40
Cr	12.04	12.61
Mo	0.04	0.50
Cu	0.03	0.05
Fe	bal.	bal.
Hardness (HRC)	22	23

TABLE IV - RESULTS OF FIELD FLOW EFFECTS TESTING

Alloy	Position	Duration (days)	Velocity (m/s)	Velocity (ft/s)	% Limiting Velocity	Results
410 SS	US (1)	38	8.5	28.0	58	CR(2)<0.025 mm/y (1 MPY) no visible change
410 SS	DS (3)	38	14.0	45.8	95	(4) Isolated corrosion pit
F6NM	US	69	6.6	21.6	44	CR<0.025 mm/y (1 MPY), no visible change
F6NM	DS	39	13.6	44.7	92	CR<0.025 mm/y (1 MPY), no visable change
F6NM	DS	69	17.9	58.6	120	CR<0.025 mm/y (1 MPY), no visable change

(1) - Upstream
(2) - Corrosion rate
(3) - Downstream
(4) - Coupon damaged during removal from test unit, weight loss indeterminate.

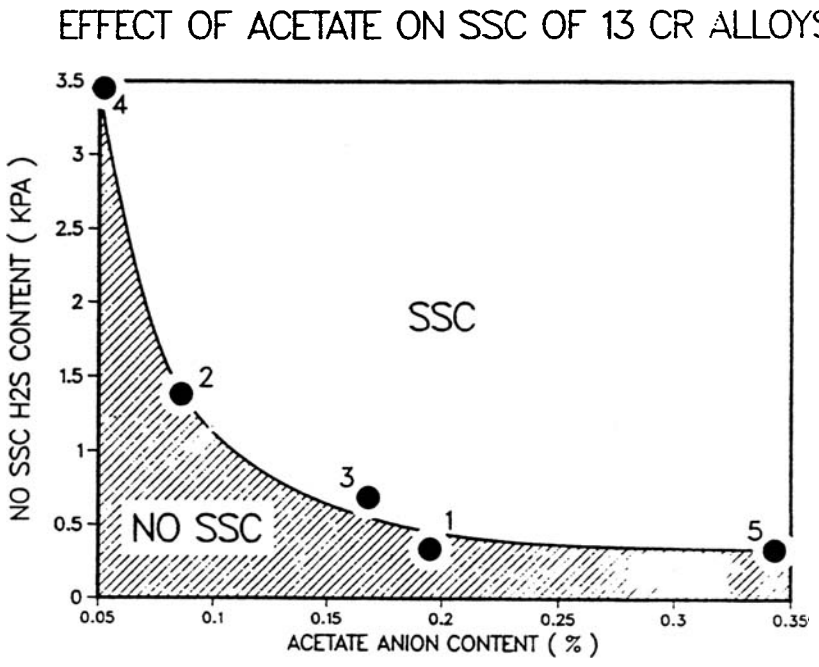


Figure 1 - Effect of H2S partial pressure and acetate anion content on SSC of 13Cr DCB specimens. Numbers near data points correspond to the environments listed in Table I.

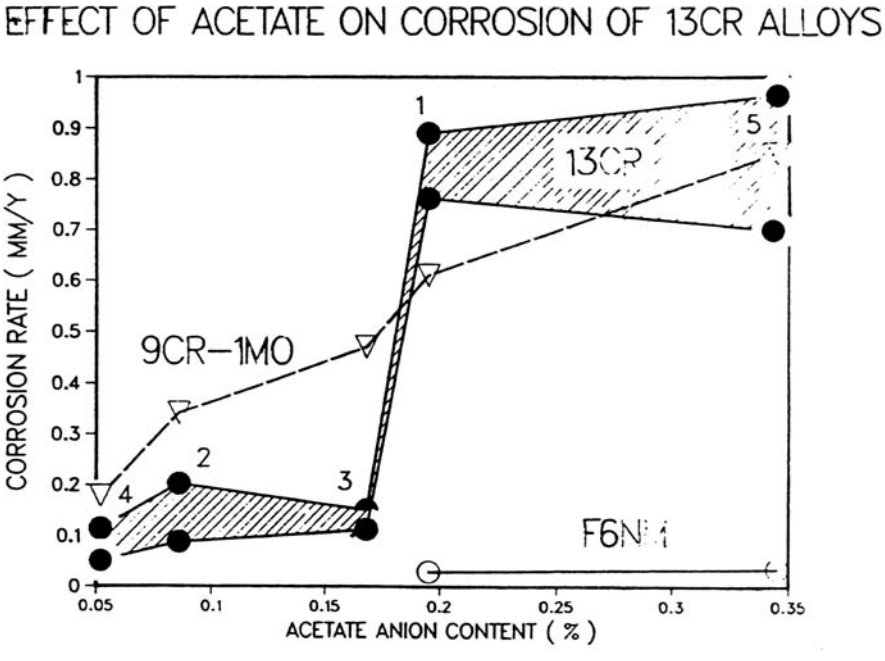


Figure 2 - Effect of acetate anion content on corrosion of martensitic SS alloys. Numbers near data points correspond to the environments listed in Table I.

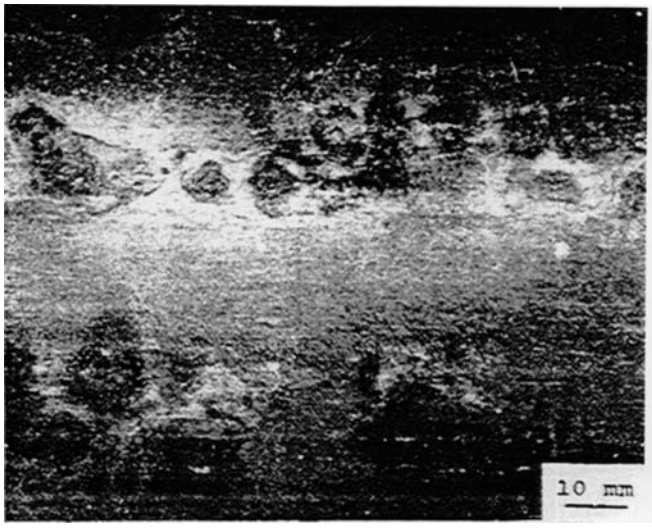


Figure 3 - Sweet service induced corrosion of 13Cr production tubing thought due in part to acetate anion effects.

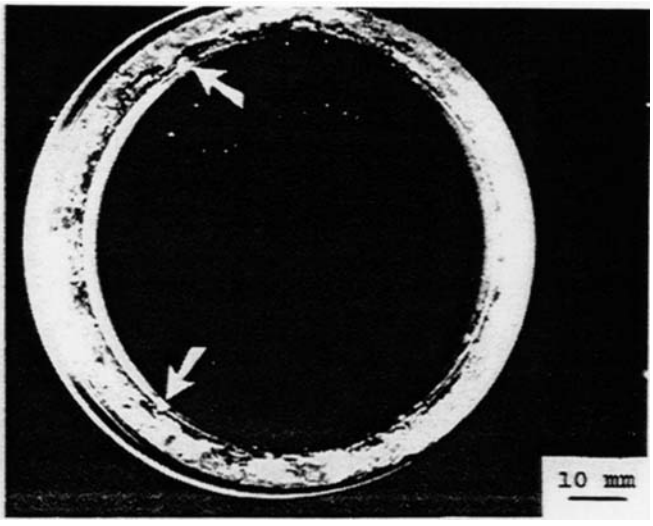


Figure 4 - Pin end attack of 13Cr production tubing due to high flow rate sweet service.

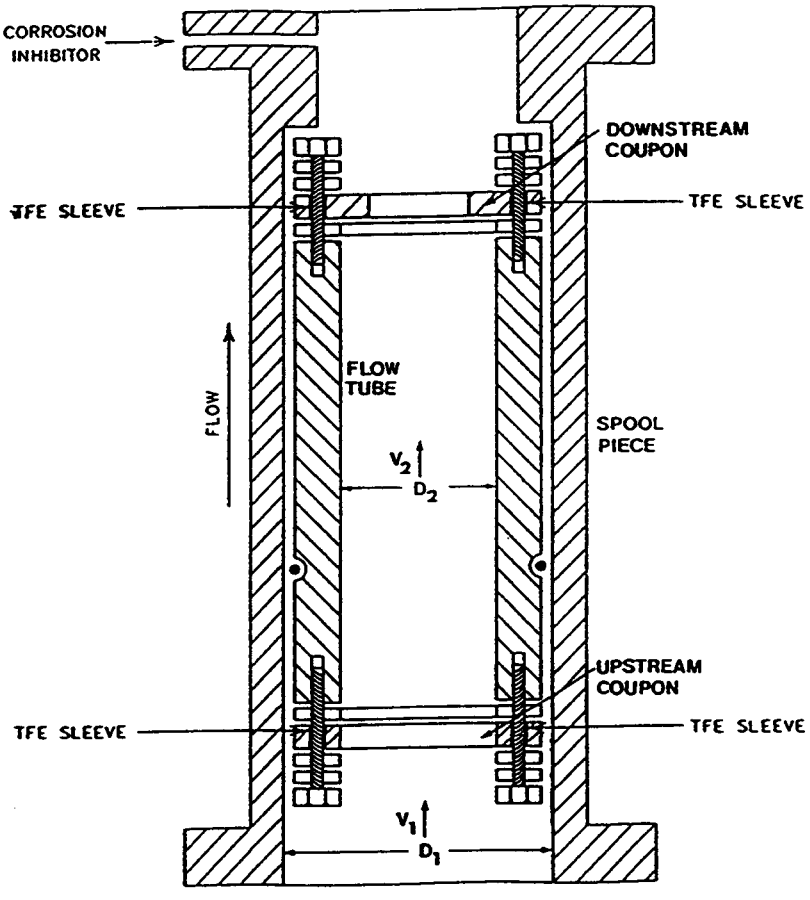


Figure 5 - Field test unit used in offshore well flowline to study velocity effects on sweet corrosion of SS alloys.

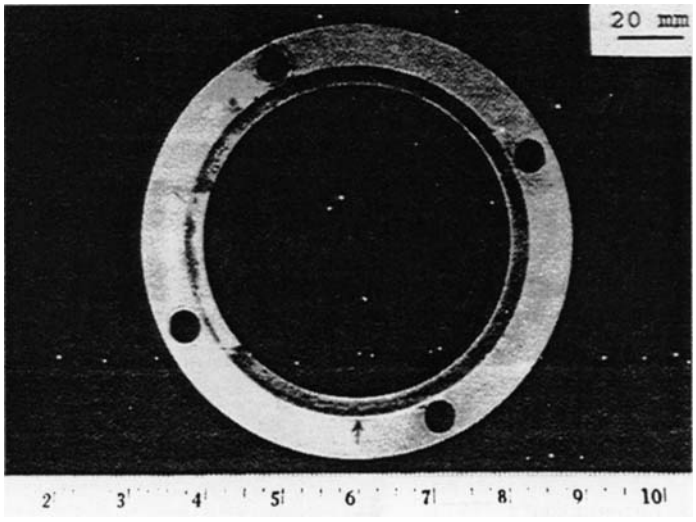


Figure 6 - Overall appearance of 410 SS coupon exposed in the field test unit to flow at 95 percent of the API 14 E Limiting Velocity or 14 m/s (46 ft/s).

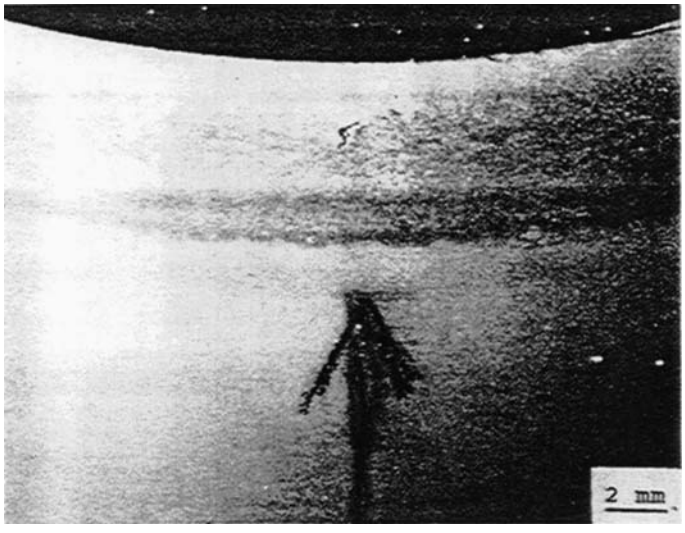


Figure 7 - Closer view of impinged surface of 410 SS coupon shown in Figure 6. Note isolated corrosion pit.

Copyrighted Materials
Copyright © 1996 NACE International Retrieved from www.knovel.com

13Cr Tubulars Solve Corrosion Problems In The Tuscaloosa Trend

by J. D. Combes, J. G. Kerr, and L. J. Klein,
Chevron U.S.A. Inc.

Downhole corrosion problems in the Tuscaloosa Trend can complicate completion and production practices for the operator. Obviously, the inability to control these corrosion problems can cost the producer considerable time and money. Since becoming one of the first operators in the Tuscaloosa, Chevron has made substantial progress in fighting this tough, corrosive environment, and now, with the help of 13Cr tubulars, appears to be winning the battle.

In August 1974, Chevron spudded the Alma 1 well, which turned out to be the discovery well for the False River field in the Tuscaloosa Trend which runs across southern Louisiana (Fig. 1). The well was completed in the summer of 1975. In addition to False River, Chevron also has producing wells in the Judge Digby, Moore-Sams, Profit Island, and Elba fields.

Well Conditions

Wells in the Tuscaloosa Trend are generally 18,000 to 21,000 ft deep. The conditions Chevron encountered at False River and other nearby fields were as follows:

Bottomhole temperature: 375 F
Bottomhole pressure: 14-16,000 psi
CO_2: 8%
H_2S: 20-30 ppm
Chlorides: up to 35,000 ppm
Water production: up to 1,300 b/d
Flowing wellhead temperature: 100-120 F at low rates; over 200 F at 20 MMcfd

Production was essentially dry gas with rates up to 16 MMscfd. Condensate production ranged from 0 to 400 b/d.

Despite the relatively low H_2S content, the wells were still sour by the NACE MR-01-75 definition,[1] because of the high total bottomhole pressure. Partial pressure of H_2S was about 0.3 to 0.5 psia, or 10 times the H_2S partial pressure (0.05 psia) defined by MR-01-75 as the minimum H_2S level necessary for an environment to be considered sour.

Later, another operator reported H_2S cracking of P-110 tubing at a nearby well having similar sour conditions. It was clear that Chevron's Tuscaloosa wells fell into the category of deep, hot, high-pressure sour gas wells.

Completion Design

Chevron's Tuscaloosa Trend well completion design is shown in Fig. 2. A parallel string completion was employed for maximum safety with the kill string available if required. The annulus was packed off and filled with weighted mud above 20,000 ft so that the casing was not exposed to the reservoir fluids, except below the packer. The production tubing strings were 2⅜-in. OD, 5.95 lb/ft (0.254-in. wall) Babcock & Wilcox restricted yield strength, sour-service low-alloy steel, RY-85 grade, with upset ends and Hydril PH-6 premium threaded connections. The RY-85 grade had an 85-ksi minimum yield strength, a maximum hardness of Rc 22, and was internally coated. Wellheads and tubing hangers were made of Type 410 stainless steel.

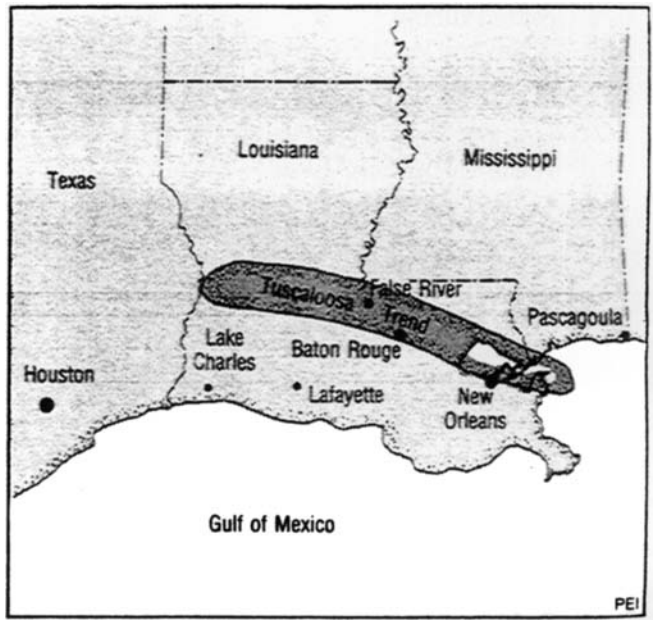


Fig. 1. Location of the False River field, Tuscaloosa Trend.

Corrosion Problems

Commercial gas production began in late 1977 and early 1978. Because corrosion of the tubing strings was expected, a water-soluble inhibitor program was instituted. Inhibitor was pumped continuously down the kill string and up the production string.

This inhibitor program proved to be ineffective, and CO_2 corrosion failures began occurring in the tubing strings after 4 to 11 months. No patterns were noted. Corrosion was randomly distributed in both the production and kill strings. Through-wall corrosion after less than a year's service indicated corrosion was occur-

Courtesy Hart Publications, Inc.

TABLE 1. Comparison of Type 410 stainless steel and low-alloy steels in the NACE tensile test

Material	Condition	Hardness	Yield strength	Threshold stress, % yield strength
Type 410	QTT*	237 BHN	96.8 ksi	11
Type 410	QTT	18 Rc	84.9 ksi	60
Type 410	QTT	22 Rc	90.0 ksi	33
AISI 4130	QT**	228 BHN	92.5 ksi	86
AISI 4135	QT	270 BHN	120.0 ksi	64
AISI 4135 (Mod.)	QT	270 BHN	118.0 ksi	64

*Quenched and double tempered
**Quenched and tempered
Complied from data in References 7 and 11

ring at rates of 250 to 300 mpy, even with inhibitors and coated tubing.

Several wells required workovers between 1978 and 1979 due to tubing corrosion failures. Safety risks occur when the tubing string becomes perforated by corrosion and the reservoir fluids and full reservoir pressure reach the casing. Besides these risks, workovers to replace the tubing cost between $1 million and $2 million in 1979 and took up to 60 days to complete, with consequent lost production.

In addition, a drilling rig was needed to pull the tubing, and with the high level of drilling activity in the Tuscaloosa in 1979, there were only a limited number of drilling rigs available; rigs tied up doing workovers were not available for exploratory drilling elsewhere.

Clearly something had to be done to mitigate CO_2 corrosion. Chevron decided to approach the problem from two different directions. One approach was to find or develop, in conjunction with chemical companies, improved inhibitors which would work in the hot, high-pressure Tuscaloosa well environments. Both water-base and oil-base inhibitors would be evaluated.

The second approach was to use a corrosion resistant, high-alloy tubular material which would resist corrosion without the use of inhibitors. It was not necessary to find a material that would be totally inert in the field environment, but one that would resist H_2S cracking and chloride stress-corrosion cracking and have sufficient general corrosion and pitting resistance to last about 3 to 5 years.

Choosing 13Cr

Chevron did not have laboratory data to aid in determining the best tubing material. Therefore, it was necessary to rely on published literature, field experience, and the opinions of experts most familiar with oil field metallurgy and corrosion. Several alloys were considered, including 9Cr-1Mo, 13Cr, and duplex stainless steels. Both 9Cr-1Mo and 13Cr had the advantage over duplex of being strengthened by heat treatment and therefore were capable of being upset; upset ends with premium threaded connections were desirable. Also, 13Cr and 9 Cr-1Mo have better chloride stress-corrosion cracking resistance than duplex stainless steel, 9Cr-1Mo and 13Cr being essentially immune if properly heat treated.

Chevron expected 13Cr to have better CO_2 and chloride corrosion resistance than 9Cr-1Mo. And, although 9Cr-1Mo has slightly better H_2S cracking

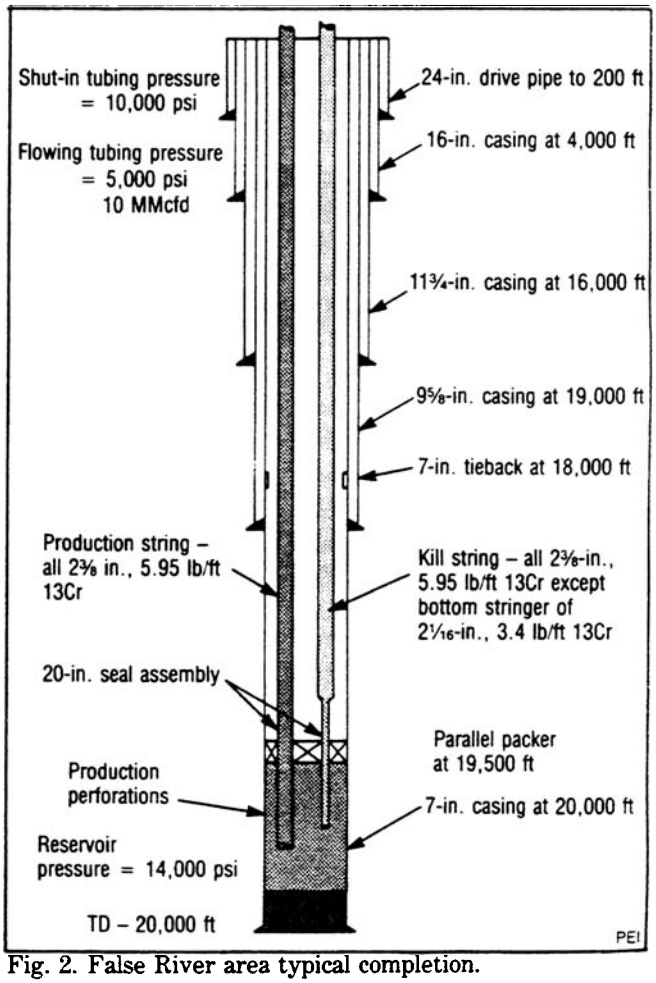


Fig. 2. False River area typical completion.

resistance than 13Cr,[2] it was felt that 13Cr, with 85-ksi minimum yield strength and Rc 23 to 24 maximum hardness, would have sufficient resistance to withstand the Tuscaloosa environment. In 1979, 13Cr (Type 420) was chosen as the tubing material.

H_2S Cracking of 13Cr

Alloys with 12% to 13% Cr had the reputation of performing poorly in laboratory H_2S cracking tests, but performing satisfactorily in the field. Almost all of the laboratory tests which led to these findings were performed on Type 410 stainless steel rather than Type 420. Several reports in the literature demonstrated that Type 410 is significantly more susceptible to H_2S cracking in laboratory tests than low-alloy steels at the same strength level.[4-9]

For example, Table 1 compares results for Type 410 and low-alloy steel tested by the NACE TM-01-77 tensile test.[10] The low-alloy steel, even at slightly higher strength levels than the Type 410, had higher threshold stress values than Type 410. Additional lab tests suggested that Type 410 could be quite susceptible to H_2S cracking in service even below Rc 22,[5,6] especially under severe hydrogen charging conditions.[2]

Limiting the steel hardness to Rc 22 maximum is a widely used guideline for preventing H_2S cracking in sour service environments.

Conversely, other tests showed Type 410 to be resistant to H_2S cracking up to about Rc 25[12] in a solution

similar to the NACE tensile test solution, but without NaCl, as shown in Fig. 3. Cracking occurred only at hardness greater than Rc 25. It was later demonstrated that the presence of NaCl increased Type 410's cracking susceptibility.[5]

There had never been any reported failures of Type 410 at a hardness of Rc 22 or less.[4,7] The only reported failures of Type 410 were at a hardness greater than Rc 25, in environments with high H_2S concentrations.[13,14]

Several attempts to resolve the discrepancy in cracking results between laboratory tests and field experience were reported in the literature. Experimental setups were constructed at well sites to perform laboratory type stressed-specimen tests in actual, produced fluids.

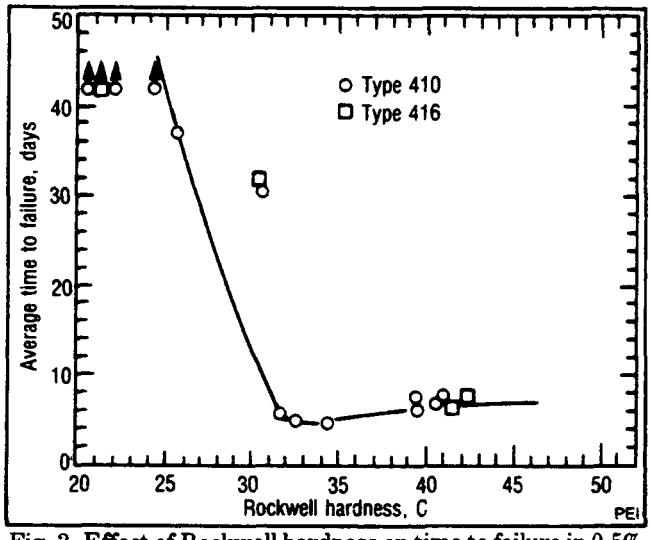


Fig. 3. Effect of Rockwell hardness on time to failure in 0.5% acetic acid solution saturated with H_2S.[12]

At the Lacq sour gas field in France,[16] produced fluids having a gas composition of 74% methane, 15% H_2S, and 9% CO_2 were passed through a test loop at 5,000 psi and 85 to 140 F. Stressed samples were mounted inside the test loop. Several samples of 12% Cr steels (Type 410) in the 80- to 90-ksi yield strength range were tested. Results showed no cracking of any sample which had not been plastically deformed.

Similar tests were conducted in sour gas fields in the U.S., Canada, and Venezuela, with H_2S contents ranging from 0.003% to 11% and CO_2 ranging from 1.0% to 40%.[9] Since laboratory tests were found to provide a lower limit for H_2S cracking threshold stresses in actual oil field H_2S environments, lab test results were used to demonstrate that at least 1% H_2S was needed for Type 410 at 86-ksi yield strength to crack at stresses below its yield strength (Fig. 4). At higher H_2S concentrations the cracking resistance of Type 410 was still inferior to carbon and low-alloy steels at the same or slightly higher strength level.

Although all the published data on H_2S cracking of 13Cr pertained to Type 410, one manufacturer provided laboratory test data on its Type 420 tubular material which showed Type 420 to have H_2S cracking resistance equivalent to AISI Type 4130 low-alloy steel tubular material at the same strength level.[17] The manufacturer believed its H_2S cracking test was more severe than the NACE tensile test and offered this as an explanation of why 13Cr performed the same as 4130 in its laboratory tests.

More recently, additional laboratory tests have been performed on Type 420 stainless steel which report that it has better resistance to H_2S cracking than Type 410.[18] Both the NACE TM-01-77 tensile test and the Shell bent beam test[19] were used to establish the superior performance of Type 420 over Type 410 in the 85- to 95-ksi yield strength range, as shown in Fig. 5. The NACE solution was used for the Shell bent beam tests rather than the original Shell solution, which contained no NaCl, because it was found that the addition of 5% NaCl made the Shell bent beam test more severe, as had been reported earlier.[4]

At the Socal Materials laboratory, NACE tensile tests and Shell bent beam tests also were performed on Type 420 stainless steel. Test samples were taken from the tubing actually being used in Tuscaloosa wells. Material from all three manufacturers supplying 13Cr tubing was tested. The yield strength of the samples tested was between 88 and 90 ksi.

As shown in Fig. 6, a threshold stress in the NACE test of 60% yield strength was estimated for all three manufacturers' materials. Both the tube bodies and heavier wall upset portions were tested. Standard full-size specimens were used for the upsets while subsize specimens were used for the tube bodies, because the 0.254-in. wall was not thick enough to make full-size specimens.

Several subsize tube body samples failed in the shoulder radius due to excessive crevice corrosion against the test chamber, as noted in Fig. 6. This problem was eliminated by shortening the gauge length so the shoulder radius did not contact the test chamber.

These results agree with previously published results shown in Fig. 5 and also with additional unpublished data supplied by one of the tubing manufacturers, which indicated a threshold stress of 65% to 70% yield strength in the NACE tensile test for Type 420 13Cr having yield strength in the 85 to 95 ksi range.[20]

In the Shell bent beam tests, the original Shell solution, without NaCl, was used. The test chamber was purged with H_2S gas twice per day for 20 min, Monday through Friday. The S_c values (critical stress index) obtained ranged from 6.1 to 10.2 for all the samples tested. As expected, these S_c values are higher than those shown in Fig. 5 for Type 420 at a hardness of Rc 21 to 23 because there was no salt in Chevron's test solution. The results do agree with unpublished manufacturer's data which found S_c values between 6.0 and 10.1 for 13Cr in the 85- to 95-ksi yield strength range.

Threshold values in the NACE test of 60% to 70% yield strength compare favorably with results for carbon steels at comparable strength levels which have performed satisfactorily in sour environments. However, the Shell bent beam S_c values of 6.0 to 10.0 are below the values normally obtained for steels which have proven to be resistant to cracking in sour environments. Resistant steels generally have an S_c greater than 10.

Results of the two different tests might lead to con-

tradictory predictions regarding 13Cr performance in a sour environment. The reasons for the apparent discrepancies in test performance are not fully understood; however, results of the NACE tensile tests gave us confidence that the resistance of Type 420 to H_2S cracking was at least better than that of Type 410, which was the alloy that had obtained a reputation for poor performance in laboratory H_2S cracking tests, as discussed previously.

General Corrosion of 13Cr

Another factor to consider in choosing 13Cr tubulars for the Tuscaloosa Trend was the possibility of general corrosion and pitting attack caused primarily by CO_2, H_2S, and chloride ions in the produced brine. As mentioned earlier, Type 410 wellheads, valves, and related equipment had been used extensively to solve aqueous CO_2 corrosion problems.

Furthermore, in tests intended to evaluate corrosion resistance in service environments, and which were performed in onsite field test loops, Type 410 stainless steel generally exhibited corrosion rates of less than 1 mpy[16,21] even when corrosion rates for carbon steel were much higher. In a more severe laboratory test which attempted to simulate a highly corrosive downhole environment, Type 410 still corroded at less than one-third the rate of carbon steel.[22] The tests also demonstrated that 13Cr had better general corrosion resistance than 9Cr-1Mo, as would be expected because of its higher Cr content, and 13Cr was predicted to have adequate resistance to chloride pitting in downhole environments because of the absence of oxygen.[23]

Chevron had used Type 410 tubing hangers in Tuscaloosa wells from the very beginning. Several of the tubing hangers in older wells which used low-alloy steel tubing with continuous inhibitor injection suffered some chloride pitting attack. Pitting rates up to 100 mpy (based on pit depths) were measured.

It is most likely that oxygen was introduced into the well bore along with the injected inhibitor. Because oxygen, or some other highly oxidizing species, must be present for chloride pitting to occur, the oxygen introduced with the inhibitor was probably responsible for the chloride pitting attack.

As long as the wells with 13Cr tubing were not going to be inhibited, there would be no chance for oxygen to enter the well bore and mix with the produced fluids. Because there would be virtually no oxygen in the produced brine, chloride pitting of the 13Cr tubing was expected to be negligible, as predicted by published data.[23,24]

After 13Cr tubing had been purchased for the Tuscaloosa, unpublished laboratory data became available which predicted high corrosion rates for 13Cr above about 300 F, based on autoclave tests intended to simulate a downhole environment. The data showed 13Cr corroding either at about half the rate of carbon steel[25] or at rates greater than that of carbon steel.[26] These data caused some concern that 13Cr might suffer high

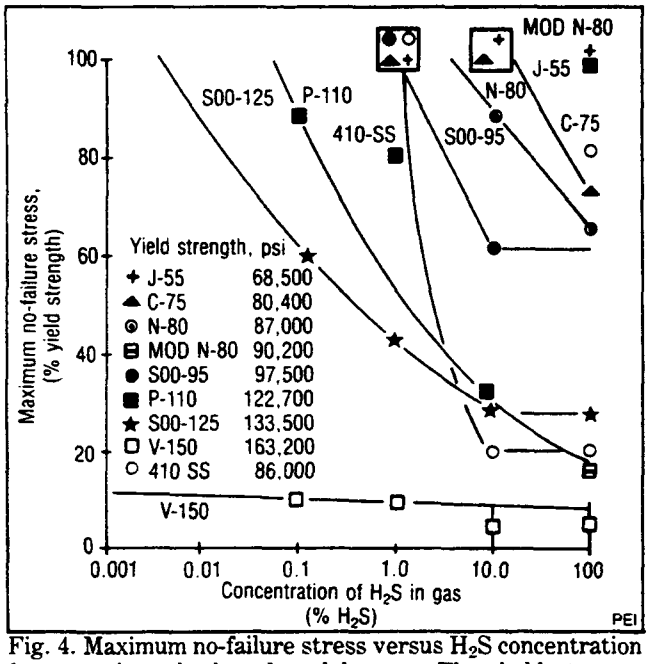


Fig. 4. Maximum no-failure stress versus H_2S concentration for several steels, based on lab tests. Threshold stresses shown give lower limit for threshold stresses in actual field environments.[9]

corrosion rates, particularly in the bottom portion of the well where temperatures are in excess of 300 F.

The explanation for the wide disagreement between these laboratory tests and the field results that became available later is probably related to the oxygen content in the autoclave tests. In general, autoclave tests do not accurately model the flowing downhole multiphase environment, and in these tests the oxygen content was probably not low enough to be representative of the essentially oxygen-free environment found in actual well conditions.

Field Experience

Chevron first became involved with alloy tubulars in corrosive gas wells with the discovery of the Puckett-Ellenberger field, in Texas, in 1952. Wells were 14,000 ft deep with a bottomhole pressure of 6,300 psi and a bottomhole temperature of 235 F. Gas contained 28% CO_2, 15 ppm H_2S, and less than 1 bbl of condensate per MMscf.

Because conditions proved to be corrosive to carbon steel, trials were made with 9Cr-1Mo tubulars in one well. The tubing failed after 1 month due to H_2S cracking. At the time, no hardness controls were employed in tubing manufacture — hardness was about Rc 40. Two additional wells then were completed with 9Cr-1Mo having a maximum hardness of Rc 26. These two wells are still in service more than 25 years later, never needing a corrosion inhibition program.

Several years after the discovery of the Puckett-Ellenberger field, Mobil began producing gas from the Brown-Bassett field, Ellenberger formation.[27] Conditions were similar to Chevron's, except the CO_2 content was 50%. A test program concluded that 9Cr-1Mo

with a maximum hardness of Rc 23 was the most practical tubing material for this field. Today, 9Cr-1Mo is still in service in many of the field's wells.

Although details were sketchy, discussions in 1979 with several people in the oil field tubular business indicated that Type 420 13Cr tubulars had been used in Europe, the North Sea, and other non-U.S. locations to solve CO_2 corrosion problems. However, H_2S content, temperatures, and pressures were generally all lower than those encountered by Chevron in the Tuscaloosa Trend.

It was recently reported [24] that the French company SNEA(P) has 50 wells completed with 13Cr tubing in the Netherlands and Gabon. Since 1979, 13Cr production tubing also was purchased by various oil companies for several U.S. locations, including Texas, Louisiana, and the Gulf of Mexico. Chevron is no longer the only operator in Tuscaloosa Trend using 13Cr tubulars. Furthermore, in 1979, the use of 13Cr tubing was a step beyond the temperature, pressure, and H_2S conditions where 13Cr had been used before. Researchers felt that as long as the strength level was carefully controlled, 13Cr would be sufficiently resistant to avoid H_2S cracking under Tuscaloosa Trend conditions.

Tubing Manufacture

The 13Cr tubing used by Chevron in the Tuscaloosa Trend was supplied by Mannesmann, Sumitomo, and NKK. It had a specified yield strength range of 85 to 100 ksi, a minimum tensile strength of 100 ksi, and an initial hardness limit of Rc 24. The hardness limit was soon reduced to Rc 23 as tubing suppliers refined their manufacturing processes to allow the narrowest possible range of mechanical properties.

Because of the relatively high yield to tensile ratio of Type 420 compared to Type 410 and low-alloy steels, simultaneously meeting the 85-ksi minimum yield strength and Rc 23 maximum hardness limits was a difficult task. The hardness limit effectively restricted the yield strength range to about 85 to 95 ksi.

Heat Treatment

One of 13Cr's advantages over most other stainless steel tubing is that its strength is obtained by quenching and tempering. This allows upset-end tubing to be produced with uniform mechanical properties throughout both the tube body and upset.

The tubes were austenitized at about 1,800 F and air cooled. Early on it was discovered that water quenching would crack Type 420 stainless steel, so either oil quenching or air cooling was necessary. Because of its excellent hardenability, air cooling resulted in a fully martensitic structure throughout the wall of both the tube body and heavier wall upset ends. Tempering was done at about 1,290 F or higher, thus avoiding the critical 750 to 1,100 F range which can cause sensitization problems that, in turn, can result in

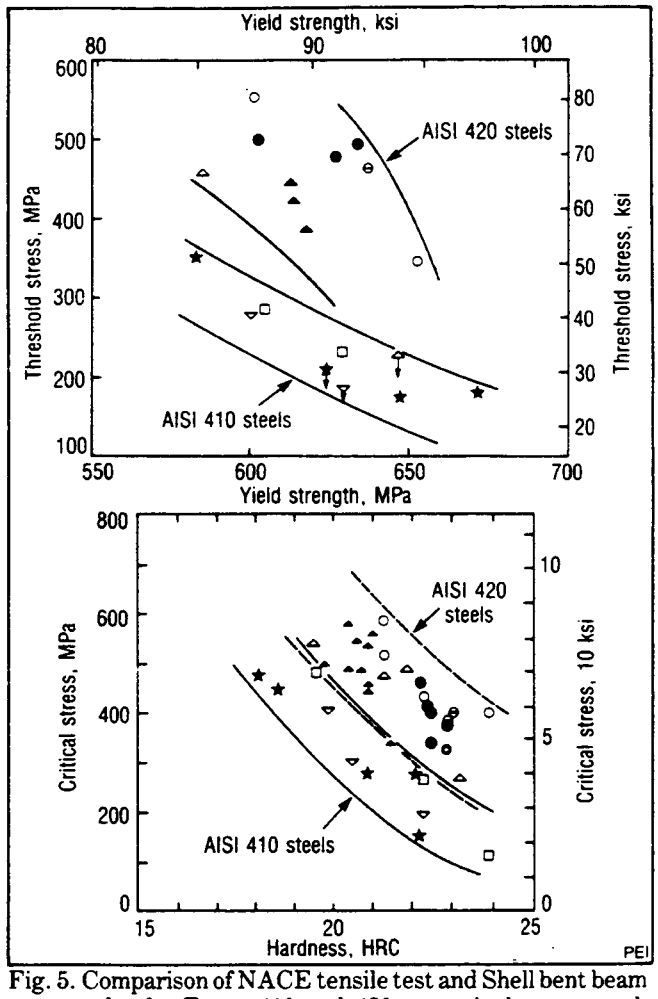


Fig. 5. Comparison of NACE tensile test and Shell bent beam test results for Types 410 and 420 at equivalent strength levels. Shell bent beam solution contained 5% NaCl, that is, the NACE solution.

intergranular chloride stress — corrosion cracking or intergranular corrosion.[2,23,24]

Although NACE standard MR-01-75 requires double tempering for all martensitic stainless steels, tubing used by Chevron was not double tempered. Double tempering improves H_2S cracking resistance of some cast martensitic stainless steels, for example CA6NM,[11] but there is no evidence that double tempering improves the H_2S cracking resistance of either Type 410 or Type 420 stainless steel, as long as they are properly tempered the first time. Unpublished results of tests performed by suppliers verified that double tempering offered no improvement in H_2S cracking resistance.[17]

Quality Control

To ensure strength and hardness uniformity, tensile tests and midwall bench-type hardness tests were required on one out of every 100 tubing joints, which is twice the test frequency required by API 5AC.[28] In addition, tensile and hardness tests of the upset ends were performed on one out of every 200 joints. Because of the upset ends, tensile and bench-type hardness tests required the sacrifice of an entire tube length.

In addition to the destructive mechanical test, surface hardness tests were made at two or three locations

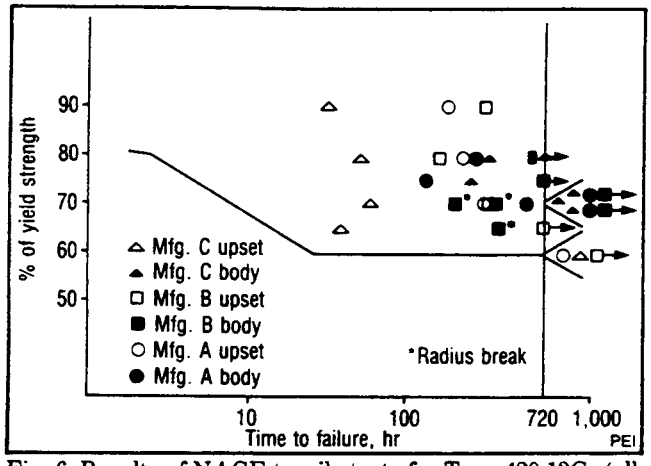


Fig. 6. Results of NACE tensile tests for Type 420 13Cr (all samples 88- to 90-ksi yield strength). Samples which broke in shoulder radius due to crevice corrosion in the test chamber are noted. Specimen was redesigned to shorten gauge length and eliminate shoulder failure problem. Upset samples were full-size; body samples were subsize.

on every tubing length, including the upsets, either using an in-line Brinell tester in the heat treatment mill, or a portable Rockwell-type hardness test after heat treatment was completed. The type of test used depended on the manufacturer's equipment and expertise with a particular type of hardness tester.

To maintain tight control over mechanical properties throughout the entire order, all tensile and hardness data were carefully reviewed and statistically evaluated. Additionally, periodic mill surveillance visits were made to each mill as the tubing was being manufactured. These quality control efforts commonly resulted in finding a hardness variation within a tube of only 1 to 2 Rc points when bench-type hardness tests were performed every foot along the length of sample tubes. An example of this type of test result is shown in Fig. 7. The variation within a heat was generally 3 to 4 Rc points. Heat-to-heat hardness test results were essentially identical.

Current Situation

As of autumn 1982, Chevron has 26 wells completed with parallel strings of 2⅜-in. O.D., 5.95 lb/ft 13Cr tubing, and 21 are currently producing. The parallel string completion design was retained for safety, but no inhibitors have been circulated down the kill string. Production has been alternated between production and kill strings and plans are to eventually produce through both strings.

Several wells have now been producing for about 2 years. There have been a total of nine workovers to date for various mechanical reasons, most of which were performed from 9 months to 2 years after the wells began producing. None of the workovers has been related to any corrosion problems, and there have been no instances of H_2S cracking.

When tubing strings from the nine workover wells were pulled, they were inspected and no significant corrosion of any kind was found. The wells from which the tubing was inspected produced up to 275 bbl/day of water with up to 34,000 ppm chloride.

In the meantime, there are 11 older wells that are still completed with low-alloy steel RY-85 tubing using an improved water-dispersible inhibitor system. Because of field depletion, bottomhole pressures have dropped to 11,000 to 12,000 psi, and flow rates through the production tubing are lower than they were in 1975 to 1979.

The improved inhibitor system and reduced flow rates apparently have solved the low-alloy steel corrosion problem, because in the past 2 years, no workovers were required for any of the older wells completed with RY-85 tubing. Because of the success of both the 13Cr and the improved inhibitor system in fighting downhole corrosion, the choice of which corrosion control method to use becomes primarily an economic one.

Economics

At the time of the most recent purchase, 13Cr tubing had about a $5 to $10/ft cost premium over low-alloy steel tubing, or about $200,000 to $400,000/well for the initial cost of two 20,000-ft strings. Surface facilities for inhibitor injection cost about $250,000/well and the annual cost of chemicals and maintenance is about $125,000. A rigorous economic analysis would require

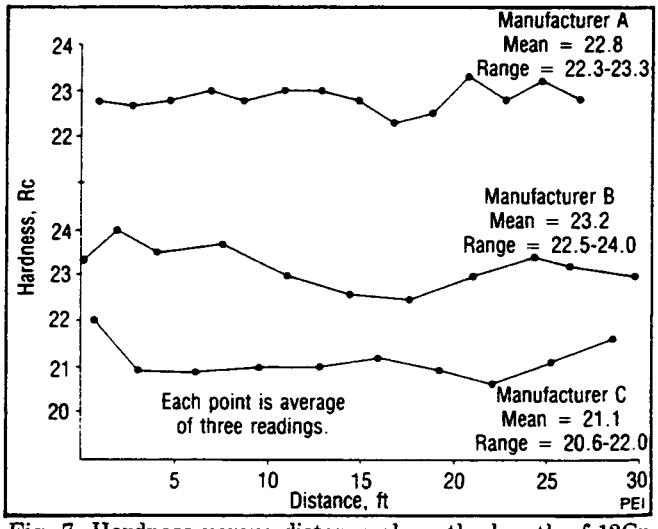


Fig. 7. Hardness versus distance along the length of 13Cr tubulars. One sample from each of the three manufacturers. Tubulars from manufacturers A and B were from early production runs when the specified maximum hardness was Rc 24.

an analysis of tax consequences as well as many assumptions, including the production life of the field, life of the tubing (assuming it would eventually fail), expected inflation rates, workover costs, etc. However, based solely on initial cost of tubing and surface equipment, and on annual cost of inhibitors, 13Cr has an economic advantage over low-alloy steel plus inhibitors, primarily because of the ongoing yearly cost of chemical inhibitors.

Type 420 13Cr tubing was successfully used to solve CO_2 corrosion problems in deep, hot, sour gas wells in the Tuscaloosa Trend. Type 420 has better H_2S cracking resistance than Type 410 at equivalent strength levels, but it still does not perform as well in laboratory

H_2S cracking tests as low-alloy steels of comparable strength. With careful control of mechanical properties and by limiting the hardness to Rc 23 to 24, Type 420 13Cr tubing will resist H_2S cracking in sour gas wells containing low ppm levels of H_2S. 13Cr will also provide excellent corrosion resistance as long as oxygen is not introduced into the well bore by artificial means.

References

1. *Material Requirement, Sulfide Stress Cracking Resistant Metallic Material for Oil Field Equipment*, National Association of Corrosion Engineer's Standard MR-01-75 (1980 revision).
2. Phelps, E. H.: "Stress Corrosion of Ferritic-Martensitic Stainless Steels," *Metals Engineering Quarterly* (May 1973) 44-49.
3. Rice, P. W.: "Evaluating Nickel Base and Stainless Alloys for Subsurface H_2S Service," paper presented at the Energy Technology Conference and Exhibit, Petroleum Division of ASME, Houston, Tex. (Sept. 18-22, 1977).
4. Tuttle, R. N.: "Guidelines Aid in Designing for H_2S Service," *Oil and Gas J.* (Dec. 11, 1978) 108-116.
5. Treseder, R. S. and Swanson, T. M.: "Factors in Sulfide Corrosion Cracking of High Strength Steels," *Corrosion, 24*, No. 2 (1968) 31-37.
6. Tuttle, R. N.: "Selection of Materials Designed for Use in a Sour Gas Environment," *Materials Protection, 9*, No. 4 (1970) 11-14.
7. Burns, D. S.: "Laboratory Test for Evaluating Alloys for H_2S Service," *Materials Performance, 15*, No. 1 (1976) 21-27.
8. Greer, J. B.: "Results of Interlaboratory Sulfide Stress Cracking Using the NACE T-1F-9 Proposed Test Method," *Materials Performance, 16*, No. 9 (1977) 9-15.
9. Kane, R. D. and Greer, J. B.: "Sulfide Stress Cracking of High-Strength Steels in Laboratory and Oilfield Environments," *J. Pet. Tech.* (November 1977) 1483-1488.
10. *Testing of Metals for Resistance to Sulfide Stress Cracking at Ambient Temperatures*, National Association of Corrosion Engineers Standard TM-01-77.
11. Kane, R. D., Watkins, M., and Greer, J. B.: "The Improvement of Sulfide Stress Cracking Resistance of 12% Chromium Stainless Steels Through Heat Treatment," *Corrosion, 33*, No. 7 (1977) 231-235.
12. Bloom, F. K.: "Stress Corrosion Cracking of Hardenable Stainless Steels," *Corrosion, 11*, No. 8 (1955) 351t-361t.
13. Treseder, R. S.: "Oil Industry Experience with Hydrogen Embrittlement and Stress Corrosion Cracking," in *Stress Corrosion Cracking and Hydrogen Embrittlement of Iron Base Alloys*, NACE-5, proceedings of a conference held in Unieux-Firmany, France (June 12-16, 1973); NACE, Houston (1977) 147-161.
14. Tuttle, R. N.: "Deep Drilling – A Materials Engineering Challenge," *Materials Performance, 13*, No. 2 (1974) 42-45.
15. "Corrosion in Hot, Deep, Sour Gas Condensate Wells," transcript of panel discussion at the National Conference of NACE (March 1973); *Materials Performance, 14*, No. 6 (1975).
16. Estavoyer, M.: "Corrosion Problems at Lacq Sour Gas Field," *J. Inst. Pet., 46*, No. 439 (July 1960) 223-233.
17. Popperling, R. K.: Mannesmann Research Institute, private communication.
18. Ishizawa, Y., Shimada, T, and Tanimura, M.: "Effect of Microstructure on the Sulfide Stress Corrosion Cracking Resistance of AISI 410 and 420 Steels," paper No. 124, presented at NACE Corrosion '82 (March 22-26, 1982) Houston, Tex.
19. Fraser, J. P., Eldridge, G. G., and Treseder, R. S.: "Laboratory and Field Methods for Quantitative Study of Sulfide Corrosion Cracking," presented at the Fourteenth Annual NACE Conference (March 17-21) San Francisco, Calif.; reprinted in *H_2S Corrosion in Oil and Gas Production – A Compilation of Classic Papers*, R. N. Tuttle and R. D. Kane, editors, NACE, Houston (1981) 283.
20. "Test Results of NK CR-13; Resistance to Sulfide Stress Corrosion Cracking in Low H_2S Environments," Nippon Kokan K. K. Report (October 1981) unpublished.
21. "Field Test Results of Various Steels in the Flow Lines of Natural Gas Containing CO_2," Sumitomo Metal Industries Report (November 1979) unpublished.
22. Watkins, M. and Greer, J. B.: "Corrosion Testing of Highly Alloyed Materials for Deep, Sour Gas Well Applications," *J. Pet. Tech* (June 1976) 698-704.
23. Brelin, J. L. and Guntz, G.: "Corrosion of Steel by Condensates Containing CO_2," Revue de Metallurgie (December 1979) 799-808.
24. Crolet, J. L.: "Acid Corrosion in Wells (CO_2, H_2S): Metallurgical Aspects," presented at the International Petroleum Exhibition and Technical Symposium of SPE, Bejing, China (March 18-26, 1982).
25. "Resistance of 9 and 13 Chromium Steels Against CO_2 Corrosion," Nippon Kokan K. K. report (October 1980) unpublished.
26. "CO_2 Corrosion Behavior and CO_2 Corrosion Resistant Materials for Oil Country Tubular Goods," Sumitomo Metal Industries Report No. 343, Rev. I (February 1980) unpublished.
27. Blount, F. E., Arnwine, B. C., and Chandler, R. J.: "A Field Study Designed to Select a Tubing Program for Ellenberger Gas – Brown-Bassett Field, Terrell County, Texas," presented at the spring meeting of the Southwestern District of the API Division of Production (March 22-24, 1961) Albuquerque, N.M., condensed version reprinted in *Materials Protection* (December 1962) 24-26.
28. *API Specification for Restricted Yield Strength Casing and Tubing*, API, Washington, D. C., Eleventh Edition (March 1979).

About the Authors



J. D. Combes is principal drilling consultant for Chevron U.S.A. in New Orleans, La. He received a BS in petroleum engineering from the University of Tulsa and immediately went to work in New Orleans for The California Co., predecessor to Chevron U.S.A.'s Eastern Region. Since 1970, Combes has served as consultant to Chevron's Eastern Region production vice president and as advisor to division or overseas managers on special problem wells. He also organized and supervises Socal's Corporate Drilling Training Group.



Leigh J. Klein is a metallurgical engineer with BS and MS degrees from Rensselaer Polytechnic Institute. He has been a materials engineer with Socal's Engineering Department Materials Laboratory in Richmond, Calif., since 1979, working on applications for corrosion-resistant alloys in sour gas production.



James G. Kerr began his career in the oil industry in 1950 and is currently supervisor of Socal's Engineering Department Materials Laboratory in Richmond, Calif. Kerr received a BS in mechanical engineering from the California Institute of Technology and an MS in metallurgy from Lehigh University.

Copyrighted Materials
Copyright © 1996 NACE International Retrieved from www.knovel.com

Paper No.
146

CORROSION 93
The NACE Annual Conference and Corrosion Show

EFFECT OF STRESS AND ENVIRONMENT ON FAILURES OF 17-4 PH STAINLESS STEEL VALVE STEMS

F.S. Gareau
Imperial Oil Resources Limited
237-4 Avenue S.W.
Calgary, Alberta, Canada T2P 0H6

N.A. Chambers
Imperial Oil Resources Limited
3535 Research Road N.W.
Calgary, Alberta, Canada T2L 2K8

A.M. Martinson
Imperial Oil Resources Limited
425 First Street S.W.
Calgary, Alberta, Canada T2P 3L8

ABSTRACT

A case history of sulphide stress cracking of UNS S17400 (17-4 PH) stainless steel valve stems will be presented. Even though the valve stems met the requirements of NACE Standard MR0175-84, failures still occurred. The valves were used in a wet sour gas environment that contained 27% hydrogen sulphide, 7% carbon dioxide and 66% methane. The production environment included elemental sulphur but did not contain liquid hydrocarbons. The range of nominal tensile stem stresses from field experimentation was 74 to 221 MPa--9 to 31 percent of the specified minimum yield strength. Local stresses, near sharply machined corners, were higher. In a NACE TM0177 laboratory test, the threshold stress was less than 20% of the yield strength. Both field and laboratory experience indicated that it is preferable to use alternative materials in sour service. However, one can decrease the probability of sulphide stress cracking failures if purchasing specifications are detailed to include requirements for hardness testing, documentation, manufacturing and pertinent design information.

Keywords: sulphide stress cracking, sulphide stress corrosion cracking, hydrogen embrittlement, precipitation-hardened stainless steels, 17-4 PH, UNS S17400, hydrogen sulphide, sour gas, valve stem

INTRODUCTION

Unified Numbering System (UNS) S17400 stainless steel has been used for many years in oilfield applications. Common applications include chokes, valve internals and tubing hangers. This material has traditionally been used where higher strengths and resistance to corrosion are required.

UNS S17400 is a martensitic stainless steel that is precipitation-hardened or strengthened. The chemical composition of this alloy is shown in Table 1. To obtain resistance to sulphide stress cracking, NACE Standard MR0175, Sulphide Stress Cracking Resistant Metallic Materials for Oilfield Equipment[1], lists two specific heat treatments and a maximum hardness of Rockwell C33 for this material. UNS S17400 supplied in conformance with the double-age heat treatment at 620°C (1150°F) (condition H1150 + H1150) was first accepted in the original MR0175-75 document (for valves) when the entire document was balloted within NACE. On the basis of laboratory and field data, UNS S17400 supplied in conformance with a three step heat treatment process (condition H1150-M) was added to MR0175 in 1978.

In 1977, Gaugh[2] reported on the resistance of UNS S17400 to sulphide stress cracking as a function of heat treatment and the applied stress level. Some of this data is listed in current literature from Armco[3]. In the proposed NACE Standard Tensile Test (which was later approved as NACE Standard TM0177, Laboratory Testing of Metals for Resistance to Sulphide Stress Cracking in H_2S Environments[4]), the time-to-failure was always greater for condition H1150-M compared to condition H1150 + H1150. The threshold stress level, as defined in TM0177, is observed to be lower in this laboratory test compared to high alloy materials[5] and quenched and tempered steels used for tubular components[6]. Thompson[9] reported that the threshold stress for UNS S17400 in the NACE TM0177 test (Method A) was less than 20% of the material yield strength.

Rice[7] presented sulphide stress cracking results from unnotched C-ring tests that used the TM0177 test solution. The C-rings were deflected to a strain corresponding to the yield stress. The specimens with heat treatments that did not comply with MR0175 failed during the first day. Material in condition H1150 + H1150 and condition H1150-M failed within seven and twelve days, respectively. Other materials such as UNS N07718 were intact after 28 days.

From the point of view of cracking in sour environments, the authors are aware of both successful and unsuccessful field experiences. Sulphide stress cracking failures have occurred in the field[8,9, 10,11] when the condition of UNS S17400 did not comply with MR0175. Laboratory results[2,12,13,14] have shown that UNS S17400 is extremely sensitive to sulphide stress cracking in heat treatment and hardness conditions that differ from MR0175. In approximately 1970, Tuttle[15] recommended that precipitation-hardened stainless steels be considered unacceptable for sour service while Hudgins[16] reported that UNS S17400, with hardnesses less than Rockwell C22, had been successfully used for valve trim components. Salter[17] described failures of UNS S17400 and provided engineering guidelines for the use of this material today--the material must be in the H1150 + H1150 condition with a maximum design stress equivalent to forty percent of the specified minimum yield stress, and it should not be used for a critical pressure retaining part.

Thompson et al[9] recently described sulphide stress cracking in a tubing hanger made from UNS S17400 that met the MR0175 hardness limits. This failure occurred in a gas condensate field that contained 14 to 16 percent hydrogen sulphide. Similarly, the case history in this paper involves UNS S17400 material that met the requirements of MR0175 and still failed by sulphide stress cracking. The components that failed were valve stems. UNS S17400 that

conforms to MR0175, is a standard sour service valve stem material used by several valve manufacturers today.

CASE HISTORY

Field Facilities and Environment

These valves were installed as part of a project to produce sour gas from five gas wells. The gas composition was 27% hydrogen sulphide, 7% carbon dioxide and 66% methane, and the total daily raw gas production was 2,400,000 standard cubic meters. Liquid hydrocarbons were not present in the gas. The production rate of elemental sulphur, a waste by-product, varied from 0.2 to 1.4 grams per cubic meter. Formation water was first produced from one well after approximately six months of production, and after ten and fifteen months production from two other wells. These three wells produced approximately 40 to 400 cubic meters of formation water per million standard cubic meters of gas. The formation water included 80,000 mg/l chlorides and 120,000 mg/l total dissolved solids. The other two wells produced condensed water, which contained less than 300 mg/l chlorides, at an approximate rate of 17 cubic meters per cubic meter of gas.

The producing reservoir depth is approximately 4,000 meters. The bottom hole temperature and pressure is 140°C and 38.6 MPa. The gas production rates from the individual wells ranged from 185,000 to 1,000,000 cubic meters per day.

The gas produced from each well passed through two chokes and a line heater at the well site. Gathering lines that transport the wet sour gas to the central battery are 168.3 millimeters in diameter, with lengths that vary from 3600 to 5000 meters. The battery contains a test separator for gas and liquid measurement, an inlet separator to separate the liquids from the comingled gas streams, three silica gel dehydration towers, a salt bath heater for dehydration tower regeneration, flare systems, filters, produced water handling facilities and sulphur solvent handling facilities. The dry gas was then transported through a 323.9-mm diameter 70-km transmission line with twelve remote block valve stations to dedicated sweetening facilities. The sweetening facilities were outside the scope of this project and this case history. Gathering lines were operated at approximately 10 MPa and 45°C. Conditions at the battery outlet were approximately 9 MPa and 40°C. At the sweetening facilities, the pressure and temperature decreased from the battery outlet conditions to 7.6 MPa and 10°C.

The sulphur solvent, diaryl disulphide, was stored centrally at the battery and was distributed to the individual well sites through 60.3-mm pipelines.

Valve Design and Materials

Approximately 185 rising-stem gate valves with UNS S17400 stems were installed throughout the facilities. Table 2 shows the number of valves installed for various pressure classes and sizes. Nominal sizes ranged from two to twelve NPS (nominal pipe size). The valve stems were supplied from eleven separate heats. All valves were purchased with documentation that indicated that the stems met all the requirements of MR0175. One stem was supplied in condition H1150-M and the others were supplied in condition H1150 + H1150. It was not possible to verify the manufacturer's certificate of compliance for seventeen valve stems because the documentation was not complete. One heat treatment certificate indicated that six stems were improperly cooled from the aging temperature (620°C). A water quench was used instead of air cooling. The hardness of each stem, including those improperly heat treated, was individually reported to be less than Rockwell C33. The reported hardnesses (for 177 valves) ranged from

Rockwell C22 to C32. One hardness value was documented for each stem. Some stems received their final heat treatment at the supplier's mill. Others were sold from the mill in a condition which did not meet MR0175 requirements. Independent companies were used to heat treat the latter stems.

All valves were expanding gate valves. The valve bodies and bonnets were ASTM A352-Gr. LCC. For nominal sizes 2 to 4, the gate components and seats were UNS S17400. For nominal sizes 6 to 12, the gate components were ASTM A216-Gr. LCC and the seats were either ASTM A515-Gr. 70 or UNS S31600 with UNS R30006 hardfacing.

Valves were both hand wheel operated and bevel gear operated. Although permanent actuators were not installed on any of the valves, frequently operated valves were opened and closed with a portable hydraulic tool.

The ends of the stems for valves less than or equal to 4 NPS were machined to produce a coarse Acme thread (see Figure 1). The stem screwed into one-half of the two-piece gate. For sizes larger than 4 NPS, symmetrical notches were machined into opposite sides of the stem. The notches fit loosely into one-half of the two-piece gate (see Figure 2). One unique aspect about the design of the 8 NPS valve was the availability of two gear ratios to open and close the gate--a high torque gear and a low torque gear.

Field Failures

Nine stems failed during fifteen months of sour gas production. The first failure occurred in a 4 NPS, Class 1500 valve stem that was located at the battery. The failure occurred approximately forty days after the plant start-up. The second failure occurred eighteen days later in an 8 NPS, Class 2500 valve stem that was located at a gas well site. Both of these failures occurred prior to the production of formation water. Only condensed water with a chloride content less than 300 mg/l was present. Two 6 NPS, Class 900 valve stems failed after seven months of gas production. At this time, one of the five gas production wells was producing formation water. The service temperature of the failed valves did not exceed 45°C.

All stem failures were discovered when the valves did not appear to be functioning properly. In each situation, sour gas did not leak out of the valve because the broken stem was restrained within the packing material.

After seven months of production, eighty-eight of the one hundred eighty-five UNS S17400 valve stems were replaced with UNS NO7718 material. The stems that were replaced were judged to have a high probability of failure or an unacceptable consequence if failure did occur. The risk assessment accounted for the magnitude of the stem stress, the frequency of valve use, safety and the cost of shut-in production if a failure did occur. An additional five more broken stems were discovered when the field was temporarily shut-in, after fifteen months of sour gas production. Table 3 lists all the failures.

Failure Investigation

Analyses of the failed components revealed that the failure mechanism was sulphide stress cracking. The brittle appearance of the failed 4 NPS stem is shown in Figure 3. A cross-section through the stem (Figure 4) shows secondary cracks and the failure location in the root of the last engaged thread. The micrograph in Figure 5 reveals that the failure was primarily transgranular (original magnification = 200X). Measured hardnesses were Rockwell C32 to C33 versus the C33 maximum in MR0175. The hardness (C32 to C33) found for this stem was harder than the hardnesses reported on the manufacturer's material test report which were C22 to C30.

All threads were sharply machined without smooth corner radii. The failure initiated where stresses were concentrated within the thread roots. The 2 NPS stem failures were identical to the failure described above.

The plane of failure for all the other broken stems is shown schematically in Figure 2. All failures initiated at stress concentration points in the reduced cross-section region of the stems. Rough machining left sharp notches that locally concentrated the stress. The location of all failures was predictable; they all occurred where we would expect based on the stem design in these valves. All failures occurred in stems heat treated to condition H1150 + H1150.

Localized corrosion from elemental sulphur was not observed on the failed stems or other valve trim components that were examined in the laboratory. Elemental sulphur was not believed to have played a role in the failure mechanism.

In addition, a 12 NPS stem, that had been in service for one week, was examined in the laboratory. Although it had not failed in service, the hardnesses ranged from Rockwell C34 to C36. These values are higher than the C32 value reported by the manufacturer and the maximum C33 allowed by MR0175.

Field Experiments

Field experiments were conducted to determine the actual valve stem stresses. The torque applied to the handwheel to open and close these valves in service is listed in Table 4. Information from the manufacturer enabled calculation of the stresses in the stem. Tensile stresses and stresses as a percentage of the specified minimum yield stress (SMYS) in the reduced cross-section regions are also listed. On the day that this data was collected, the field operators indicated that none of the tested valves were "locking". Occasionally, the two halves of the two-component gates were reported to have temporarily "locked" when they were being opened or closed. This phenomena is expected to be more of a concern with expanding gate valves compared to slab gate valves. Incidentally, significantly higher torques were measured when the gates were being expanded into the closed position. These values are not reported because the stem was in compression.

Table 5 compares the stem tensile stresses of a number of different sized valves with a constant input torque. On this basis, the highest stem stress was expected in the 8 NPS, Class 2500 valves. One should also be aware of the fact that the valves smaller than 6 NPS are designed with much smaller handwheels and correspondingly lower opening torques would be expected.

LABORATORY TEST RESULTS

Laboratory sulphide stress cracking tests were conducted on specimens cut from a stem that had failed in service and from a new stem. Both stems were UNS S17400 in condition H1150 + H1150. The measured Rockwell C hardnesses of these materials were C33 and C30, respectively. The test was the industry standard NACE tensile test described in TM0177-90, Method A[4].

The threshold stress, which is the highest stress at which failure does not occur in 720 hours, expressed as a percentage of the yield strength, was used to measure the resistance to sulphide stress cracking. The threshold stress for both UNS S17400 materials was less than 20% of the yield stress. The results from all test specimens is shown in Table 6 and Figure 6. The threshold stress values for UNS S17400 which conforms to NACE MR0175 are similar to the results reported by Gaugh[2] and Thompson[9]. The results from Thompson[9] are plotted as circles

in Figure 6. Although there is considerable disagreement over an acceptable threshold stress value from the NACE standard tensile test, the most commonly discussed value is an eighty percent threshold stress.

DISCUSSION

The primary cause of failure was the use of a material relatively susceptible to sulphide stress cracking in the severe environment previously described. The secondary causes of failure were related to design, manufacturing techniques and service fouling from solids such as iron sulphide corrosion-reaction by-products. The experimental stem stresses, reviewed in isolation, did not explain all the failures. With a material sensitive to sulphide stress cracking (as shown by both laboratory and field data) many factors contributed to the failures. The valve and stem design, coupled with service conditions where fouling was expected (which contributed to high opening torques), determined the magnitude of the nominal tensile stresses. Sharp notches increased the nominal stresses. Local material yielding would have occurred for two of the valves listed in Table 5 if we assume that the roughly machined notches had a stress concentration factor of 1.82.

Laboratory data[2,7] indicated that UNS17400 in condition H1150-M was more resistant to sulphide stress cracking than material in condition H1150 + H1150. The single stem (in condition H1150-M) installed in the field conditions described previously did not fail. However, this single data point was not sufficient to conclude that H1150-M was more resistant to sulphide stress cracking in an environment that contained 27% hydrogen sulphide.

The expanding gate valves are designed with a two-piece gate. The friction force, that must be overcome to open and close the valves, varied significantly from day to day, and from one valve to another. This variable was difficult to quantify during the failure investigation.

Although it is preferable to use an alternative material to UNS S17400 in sour service, one can decrease the probability of sulphide stress cracking failures if purchasing specifications are detailed to include requirements for hardness testing (frequency, location and test method), requirements for material documentation (including heat treatment procedures), requirements for manufacturing (including notch radii) and requirements for pertinent design information such as the maximum or design tensile stress. In addition, statistical techniques may be useful to analyze the material processing variables or test data. For example, statistical analysis of hardness data may enhance the purchaser's confidence in the data.

CONCLUSIONS

Our gas production environment, which included 27% hydrogen sulphide, 8% carbon dioxide, 66% methane, condensed water for two failures and formation water for seven failures, was severe enough to result in sulphide stress cracking of UNS S17400 material which was manufactured in compliance with NACE MR0175. Abnormal situations, such as contact with acids, did not occur.

While failures of UNS S17400 have long been known to occur in the laboratory, this case history documents field failures as well. One cannot solely rely on purchasing UNS S17400 to meet the requirements of MR0175, to avoid sulphide stress cracking in the field.

Current usage guidelines in NACE MR0175 do not appear adequate to prevent failures of UNS S17400 under all circumstances. Improved guidelines are necessary. It may be possible to minimize field failures with better design and machining practices, limitations on the maximum design stress and enhanced quality assurance programs. Enhanced quality assurance would

ensure that the proper heat treatments are followed and the required hardnesses are obtained. Statistical techniques may be used to enhance the confidence in hardness data.

For those environments where cracking cannot be tolerated, materials are available with significantly better cracking resistance. For example, UNS NO7718 and other alloys may be a cost effective substitutes where the manufacturer commonly supplies UNS S17400 materials for sour environments.

ACKNOWLEDGEMENTS

The authors would like to acknowledge the contributions of our associates at Imperial Oil Resources over the last several years. In particular, we wish to acknowledge Deryl Neufeld, Alex Watson, Colin Nikiforuk, Jim Bissell, Wayne Williamson and Regan Lazar.

REFERENCES

1. NACE Standard MR0175-90, "Sulphide Stress Cracking Resistant Metallic Materials for Oilfield Equipment", National Association of Corrosion Engineers, Houston, Texas, USA, 1990.

2. R.R. Gaugh, "Sulphide Stress Cracking of Precipitation Hardening Stainless Steels", Materials Performance, p. 24-29, September 1977.

3. Product Data Bulletin No. S-38, "Armco Nitronic 50 Stainless Steel", Baltimore Specialty Steels Corporation, A Subsidiary of Armco Inc., 1990.

4. NACE Standard TM0177-90, "Laboratory Testing of Metals for Resistance to Sulphide Stress Cracking in H_2S Environments", National Association of Corrosion Engineers, Houston, Texas, USA, 1990.

5. R.D. Kane, M. Watkins, D.F. Jacobs, G.L. Hancock, "Factors Influencing the Embrittlement of Cold Worked High Alloy Materials in H_2S Environments", Corrosion, p. 309-320, September 1977.

6. J.A. Straatmann, Y.E. Smith, "Quenched and Tempered Oil Country Tubular Goods Provide Improved Performance Properties for Hostile Oil and Gas Drilling Environments", H_2S Corrosion in Oil and Gas Production--A Compilation of Classic Papers, R.N. Tuttle and R.D. Kane, Eds., NACE, Houston, Texas, USA, 1981, p. 572-578.

7. P.W. Rice, "Evaluating Nickel Base and Stainless Alloys for Subsurface H_2S Service", Materials Performance, p. 16-25, September 1978.

8. R.N. Tuttle, "Deep Drilling--A Materials Engineering Challenge", Materials Performance, p. 42-46, February 1974.

9. R.M. Thompson, G.B. Kohut, D.R. Canfield, W.R. Bass, "Sulphide Stress Cracking Failures of 12Cr and 17-4PH Stainless Steel Wellhead Equipment", Corrosion, p. 216-220, March 1991.

10. W.J. Sisak, G.A. Vaughn, J.L. Harper, "Bleeder Valve Failure", Exxon Production Research Company, December 11, 1986.

11. W.J. Sisak, "17-4 PH Choke Failure at Flomation", Exxon Production Research Company, March 20, 1990.

12. J.P. Fraser, R.S. Treseder, "Cracking of High Strength Steels in Hydrogen Sulphide Solutions", Corrosion, p. 342-350, October 1952.

13. F.K. Bloom, "Stress Corrosion Cracking of Hardenable Stainless Steels", Corrosion, p. 351t-361t, August 1955.

14. G.B. Kohut, W.J.McGuire, "Sulphide Stress Cracking Causes Failure of Compressor Components in Refinery Service", Materials Protection, p. 17-22, June 1968.

15. R.N. Tuttle, "Selection of Materials Designed for use in a Sour Gas Environment", H_2S Corrosion in Oil and Gas Production--A Compilation of Classic Papers, R.N. Tuttle and R.D. Kane, Eds., NACE, Houston, Texas, USA, 1981, p. 159-161.

16. C.M. Hudgins, Jr., "Practical Aspects of Hydrogen Damage at Atmospheric Temperature", H_2S Corrosion in Oil and Gas Production--A Compilation of Classic Papers, R.N. Tuttle and R.D. Kane, Eds., NACE, Houston, Texas, USA, 1981, p. 152-158.

17. N.Y. Salter, M.F. Hallihan, "Valves for Sour Service: Types, Specifications and Metallurgies", NACE Canadian Region Western Conference, Edmonton, Alberta, Canada, February 24-27, 1992.

TABLE 1
CHEMICAL COMPOSITION OF UNS S17400

Element	Weight Percent
carbon	0.07 max
chromium	15 to 17.5
columbium	0.15 to 0.45
copper	3.0 to 3.5
manganese	1.00 max
nickel	3.0 to 5.0
phosphorus	0.040 max
silicon	1.00 max
sulphur	0.030 max

TABLE 2
SIZES OF VALVES INSTALLED

NPS	ANSI Pressure Class	Number of Valves
12	900	14
10	900	5
8	2500	10
6	2500	15
6	900	19
4	2500	5
4	1500	10
4	900	12
3	2500	10
3	900	3
2	2500	20
2	1500	62

TABLE 3
UNS S17400 STEM FAILURES

NPS	ANSI Class	Number of Failures
2	1500	3
4	1500	1
6	900	4
8	2500	1

TABLE 4
VALVE OPENING TORQUES AND STEM STRESSES

Valve Size (NPS)	ANSI Class (Joules)	Measured Opening Torque (MPa)	Nominal Stem Stress (MPa)	Reduced Cross-section Stress* (MPa)	Reduced Cross-section %SMYS
4	2500	47	110	142	20
6	900	47	54	74	10
6	2500	176	200	221	31
8	2500 (high torque gear)	61	165	202	28
8	2500 (high speed gear)	285	-	-	-
10	900	75	63	67	9

* without consideration of stress concentrations

TABLE 5
STEM STRESSES WITH 176 JOULES OPENING TORQUE

NPS	ANSI Class	Reduced Cross-section Region Tensile Stress(MPa)**	Reduced Cross-section Region %SMYS
2*	1500	155	21
4*	1500	395	55
6	900	274	38
6	2500	221	31
8	2500	584	81
10	900	158	22
12	900	169	23

* highest opening torque measured = 47 joules
** without consideration of stress concentration

TABLE 6
LABORATORY NACE TM0177 TEST RESULTS

Stress Level (% of actual yield strength)	Failed Valve Stem time to failure(hr.)	New Valve Stem time to failure(hr.)
20	248	350
30	107	163
50	33	45
70	7.8	14.2

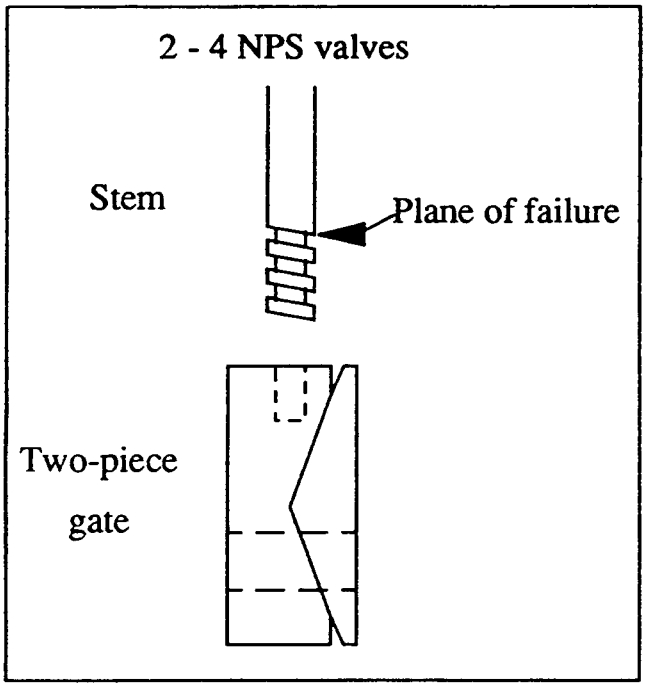


FIGURE 1 - Valve gate/stem schematic

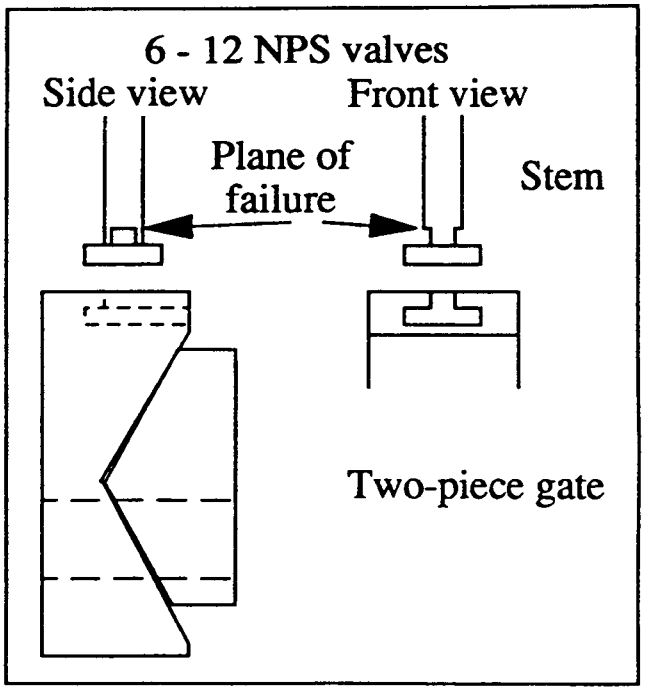


FIGURE 2 - Valve gate/stem schematic

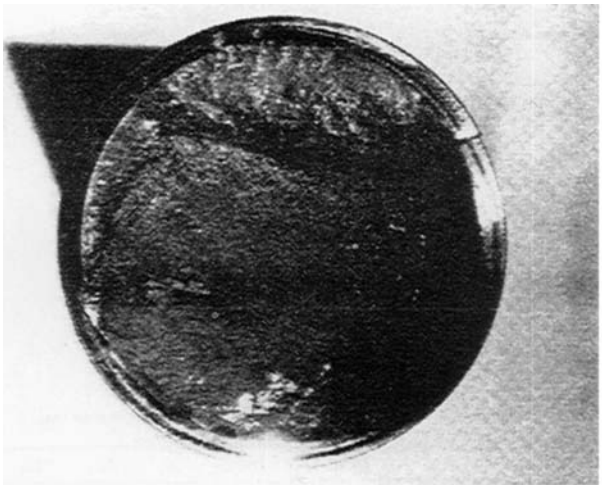


FIGURE 3 - Fracture surface for 4 NPS stem

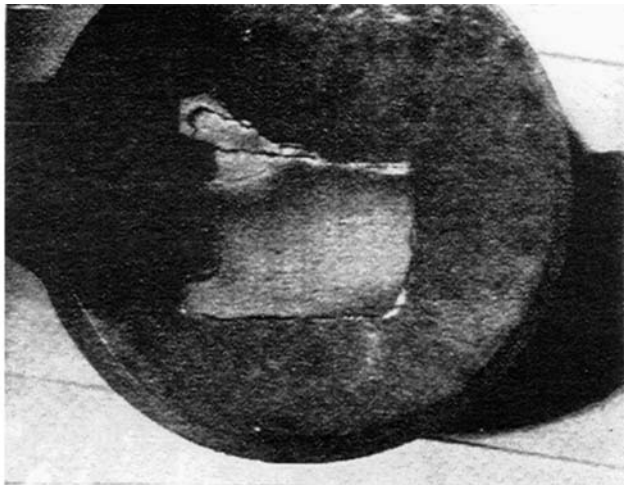


FIGURE 4 - Cross-sectional view

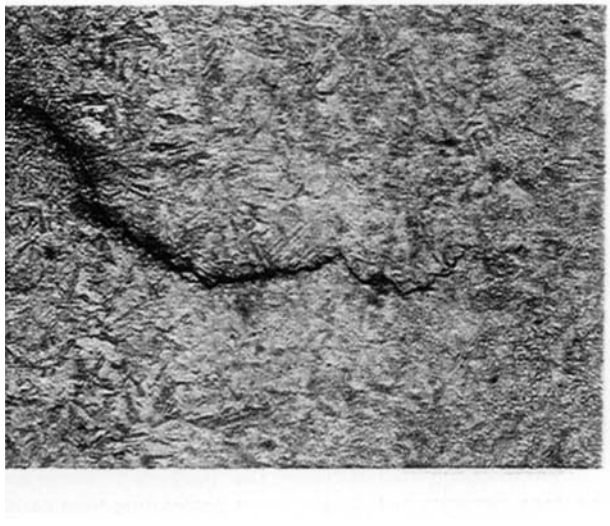


FIGURE 5 - Transgranular cracking

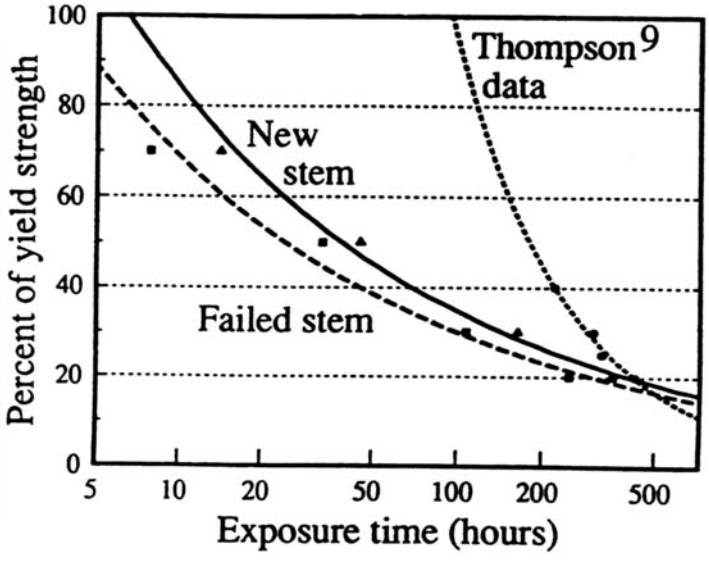


FIGURE 6 - NACE TM0177 test results

Copyrighted Materials
Copyright © 1996 NACE International Retrieved from www.knovel.com

Corrosion Assisted Cracking of CA-6NM*

DAVID A. HANSEN and THOMAS DOODY,
Arabian American Oil Company, Dhahran, Saudi Arabia

Chromium-nickel steel pump impellers (CA-6NM, ASTM A-296, approximately 18-21 Cr, 9-12 Ni + Mo and/or Cu) operating at 180 to 230 psia, 4400 to 4900 rps in 60 C, 6.8 pH oilfield injection water containing Na, Cl, carbon dioxide, and less than 1 mg/l hydrogen sulfide suffered erosion-corrosion of leading edges of impeller vanes, cavitation damage on the suction side, and circumferential cracks in 2300 ± 500 hours. This life is half as long as that obtained with impellers fabricated of CF-8M, an austenitic alloy. Because service life of low C martensitic CF-8M should be longer, it was concluded that damage was chloride assisted.

ASTM A-296 Gr. CA-6NM has been used for impellers in some Saudi Arabian oil field water injection shipping pumps during the past year. These pumps operate at 4400 to 4900 rpm, with suction pressures of 1.2 to 1.6 MPa (180 to 230 psia) and discharge pressures of 4.1 to 4.8 MPa (600 to 690 psia). These are bi-rotor pumps and they are rated at 17.2 MW (23,000 hp), maximum. The pumps normally ship water at 1.9 to 3.2 m^3/s (30,000 to 50,000 GPM).

Normal operating problems include vibration episodes with vibration velocities up to 0.02 m/s (0.8 inch/s), and transient pressure variations are usually less than ± 0.14 MPa (± 20 psi).

The composition of the injection water is given in Table 1. Normal water service temperature at the pumps is 82 to 88 C (180 to 190 F). The compositions of the impellers examined are given in Table 2.

TABLE 1 – Average Composition of Injection Water (mg/l)

Na	Ca	Mg	SO_4	Cl	HCO_3	N_2	CO_2	CH_4	H_2S
1323	393	83	808	2270	191	293	218	34	<1

Note: Average specific gravity is 1.0039 at 16 C (60 F), and average pH is 6.8.

TABLE 2 – Composition of Alloys Examined

Element	CA-6NM (%)	CF-8M [semi quantitative composition check (%)]
C	0.03	
S	0.013	
P	0.010	
Si	0.93	
Mn	0.44	
Ni	4.3	10-14
Cr	12.9	16-18
Mo	0.60	1.75-2.75

Field Experience

Two types of impeller failures have been encountered: (1) Gradually increasing pump vibration due to the shedding of the leading edges of impeller vanes (Type 1 failure), and (2) seizure of pump due to circumferentially cracked impeller capturing the casing wear ring (Type 2 failure).

In all failures to date, moderate to severe cavitation damage has been observed on the suction side, behind the eyes of vanes. Service lives usually are about 2300 ± 500 hours.

Metallography has established that the Type 1 failures are due to stress corrosion and fatigue cracks propagating from cavitation

*Voluntary manuscript submitted for publication November, 1976.



FIGURE 1 — Stress corrosion (intergranular, branched) and fatigue cracks (transgranular, linear) in a CA-6NM impeller vane. Fatigue cracks are thought to be due to corrosion fatigue. Etchant: Kalling's No. 2. 160X

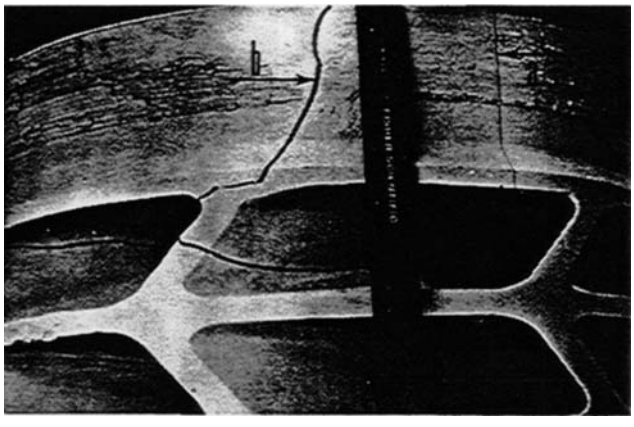


FIGURE 2 — Circumferential fatigue cracks in a CA-6NM impeller. These cracks are thought to be from corrosion fatigue. Arrow A indicates where impeller was cut for a view of the fracture surface indicated by arrow B.



FIGURE 3 — View of the fatigue crack surface indicated by arrow B in Figure 2. Note the striations (beach marks), which are typical of most fatigue cracks.

pits. A typical microstructural view of a Type 1 (vane) crack is shown in Figure 1. A macroscopic view of a Type 2 failure is shown in Figure 2. The large circumferential cracks seen in Figure 2 are thought to be due to corrosion fatigue. The impeller shown in Figure 2 was cut along the line indicated by arrow A, and Figure 3 shows the crack surface indicated by arrow B in Figure 2.

ASTM A-296 Cr. CF-8M impellers have been used in the same pumps for the same water service for up to twice as long as the CA-6NM impellers. In CF-8M impellers, the longest circumferential crack found was about 6 mm (0.25 inch) long. Further, microstructural examinations show no stress corrosion cracks in failed vanes (Type 1 failures) of CF-8M. Since the fatigue life of low-carbon martensitic CA-6NM should be much longer than that of austenitic CF-8M, it was concluded that the fatigue cracking observed in CA-6NM must be accelerated by the water service. Further, since the H_2S levels of the water are low, it was tentatively concluded that the stress corrosion and accelerated fatigue are due to chloride assistance.

Conclusions

Recent field experience indicated that CA-6NM is susceptible to chloride stress corrosion cracking (SCC) and chloride corrosion fatigue in hot saline waters. In view of the lack of detailed knowledge of the susceptibility envelop, due care should be taken when considering CA-6NM for saline water service.

Copyrighted Materials
Copyright © 1996 NACE International Retrieved from www.knovel.com

Corrosion Behavior of 9 to 25% Cr Steels in Wet CO_2 Environments*

*A. IKEDA, S. MUKAI, and M. UEDA**

Abstract

This paper reports the results of an investigation into the effects of various environmental factors on CO_2 corrosion of 9 to 25% Cr steel, with emphasis on the finding that each alloy has application criteria based on critical temperatures and CO_2 partial pressures in a CO_2-Cl^- environment. It is also shown that each alloy would be resistant even in two phase flow at flow rates of up to 26 m/s (in the respective critical conditions). The potential corrosion behaviors of 9Cr-1Mo, AISI 420 (13Cr), and 22 to 25% Cr duplex phase stainless steels in severely corrosive wells was investigated using a CO_2-Cl^- solution with a slight H_2S contamination. In particular, the effects of H_2S partial pressure and temperature on SCC and localized corrosion of these alloys are discussed.

Introduction

Recently, CO_2 corrosion resistant material has become important because of the application of CO_2 injection for enhanced oil recovery and the active exploitation of deep natural gas reservoirs containing CO_2. There are several inconsistencies among various ingestigators' results, e.g., the effect of chloride ion (Cl^-) on CO_2 corrosion, the occurrence of mesa-corrosion, etc.[1-5] In order to mitigate CO_2 corrosion, 9Cr-1Mo and AISI Type 420 (13Cr) martensitic steels and 22 to 25% Cr duplex α-γ phase stainless steels have been widely used; however, application criteria have still not been clearly defined.

In this paper, the corrosion behavior of 9 to 25% Cr steel in a wet CO_2 environment is investigated in detail, and the influence of H_2S contamination on applicability of alloys resistant to CO_2 corrosion is discussed.

Experimental

Materials Tested

Chemical compositions and mechanical properties of the materials tested are shown in Table 1. Materials melted in the laboratory and in the mill were used. The pure iron and chromium steels were melted, hot rolled, and heat treated in the laboratory. These materials were used to study the environmental factors involved in CO_2 corrosion. To identify the materials used in each experiment, the figure numbers corresponding to the experimental results are indicated in the right hand column of Table 1.

Experimental Apparatus

Schematic illustrations of the experimental apparatus are shown in Figure 1. For this work, the autoclave with stirrer was used most of the time. As for the liner of the autoclave, titanium or a Ni base alloy (25Cr-50Ni-6Mo) was used for experiments in a CO_2 or CO_2-H_2S environment, respectively. The material for specimen holders matched that of the liner. To ascertain the corrosion resistance of the alloy in high velocity flow, the gas loop was used. The standard experimental conditions of the corrosion tests in each system are shown in Table 2. Experiments were conducted in closed systems to prevent contamination by air. Test specimens used in each apparatus are shown in Figure 2. In the autoclave, the coupon specimens are mounted parallel to the inner wall using specimen holders. Stress corrosion cracking (SCC) tests are conducted using notched four point bent beam specimens (shown in Figure 2), which are stressed to 100% of 0.2% proof strength (yield strength).

The gas loop was used for the experimental work in gas-liquid two phase flow with relatively low CO_2 pressure (0.15 MPa at 25 C). Temperature is determined by the autoclave temperature and the water cooling system of the specimen, where pressure is determined by the temperature of the flow system, in which a blower is used. Solution is injected through the valve at the bottom portion of the autoclave as shown in Figure 1. The volume is adjusted by a valve and a flow meter. The specimen holder and the specimen dimensions are shown in Figure 2. Both the specimen holder and the specimens were horizontally installed at the testing section. The small specimens mounted at the top and the bottom of the specimen holder pipe are cooled by the circulating cooling water in accordance with the design of the experiment. On the set condition, the center of the specimen is parallel to the inner surface of the specimen holder. In this paper, gas flow velocity was 26 m/s and the ratio of solution to gas was 1:1000. The direct observation of the flow condition via the observation pipe, which is made of a quartz glass installed in the system, shows that annular flow was achieved in the experimental condition. It is consistent with the flow diagram given by Mandhane, et al.[6] Surface temperatures of specimens were measured beforehand with a sheathed thermocouple welded onto the specimen surface. Temperatures measured during the experiment are shown in Figure 3. These will be characteristic factors for the testing apparatus. It is understood from Figure 3 that water could condense on the surface of specimens cooled with water. It should be noted that in the vicinity of 100 C, temperature at the flow pipe is higher than that at autoclave because flow resistance creates friction in the system, thus elevating the temperature.

*Presented during CORROSION/84 (Paper No. 289), April 1984, New Orleans, Louisiana; revised July 1984.

*Central Research Laboratories, Sumitomo Metal Industries Ltd., 1-3, Nishinagasu-hondori, Amagasaki, Japan.

TABLE 1 — Chemical Composition and Mechanical Properties of Materials

Material	Chemical Composition (wt%) C	Si	Mn	P	S	Ni	Cr	Mo	Other	Mechanical Properties Y.S. (MPa)	T.S. (MPa)	Elong. (%)	HRC	Method[1]	History[2]	Materials Tested (Figure No.)
Pure iron	0.003	0.01	0.05	0.003	0.002	0.01	0.01	0.02		127	247	59.0	—	L	N	7
2Cr	0.001	0.004	0.03	0.002	0.004	0.01	2.15	0.02		117	255	52.6	—	L		7
5Cr	0.001	0.005	0.04	0.004	0.004	0.01	4.89	0.03		202	332	43.0	—	L		7
9Cr	0.001	0.007	0.08	0.002	0.004	0.07	9.08	0.01		191	347	43.1	—	L		4, 7
13Cr	0.005	0.012	0.08	0.002	0.007	0.05	13.50	0.01		185	312	34.4	—	L		4, 7
25Cr	0.005	0.020	0.02	0.003	0.006	0.04	24.53	0.01		278	371	21.0	—	L		4, 7
9Cr-1Mo	0.12	0.49	0.41	0.022	0.002	0.11	8.50	0.95		584	718	23.2	18.6	M	QT	8, 9
										651	792	20.0	23.5	M		
	0.12	0.51	0.42	0.024	0.008	0.11	8.27	0.94		520	686	31.9	15.5	M		
										595	750	29.6	20.2	M		
										624	768	29.1	21.5	M	9	
										655	798	28.1	23.1	M		
										710	849	25.2	26.2	M		
										879	1055	25.9	33.9	M		
13Cr(AISI 420)	0.21	0.61	0.64	0.017	0.006	0.15	13.48	0.02		602	785	22.9	20.8	M	8, 9	
										768	926	16.8	29.0	M		
	0.20	0.57	0.63	0.016	0.001	0.06	12.66	0.01		502	691	35.3	15.9	M		
										576	737	33.0	19.7	M		
										656	772	30.3	22.3	M	9	
										675	814	29.0	23.7	M		
										742	874	26.7	27.1	M		
										826	985	25.1	31.2	M		
	0.02	0.53	0.89	0.012	0.005	6.84	25.78	3.03	0.44Cu	553	804	37.8	21.5	M	ST	8, 11
									0.46W	822	938	21.8	29.2	M	ST + CW	
									0.15N							
Duplex stainless steel 25Cr-7Ni-3Mo	0.02	0.27	0.97	0.020	0.001	7.09	25.70	3.20	0.50Cu	568	782	32.4	—	M	ST	
									0.35W	669	814	27.7	—	M	ST + CW	
									0.15N							
										727	850	26.7	—	M		
										760	874	23.3	—	M		11
										747	904	23.0	—	M		
										816	917	20.7	—	M		
										840	940	20.4	—	M		

[1]Method: L = laboratory melting, M = mill melting.
[2]History: N = normalized, QT = quenched and tempered, ST = solution treatment, and CW = cold worked.

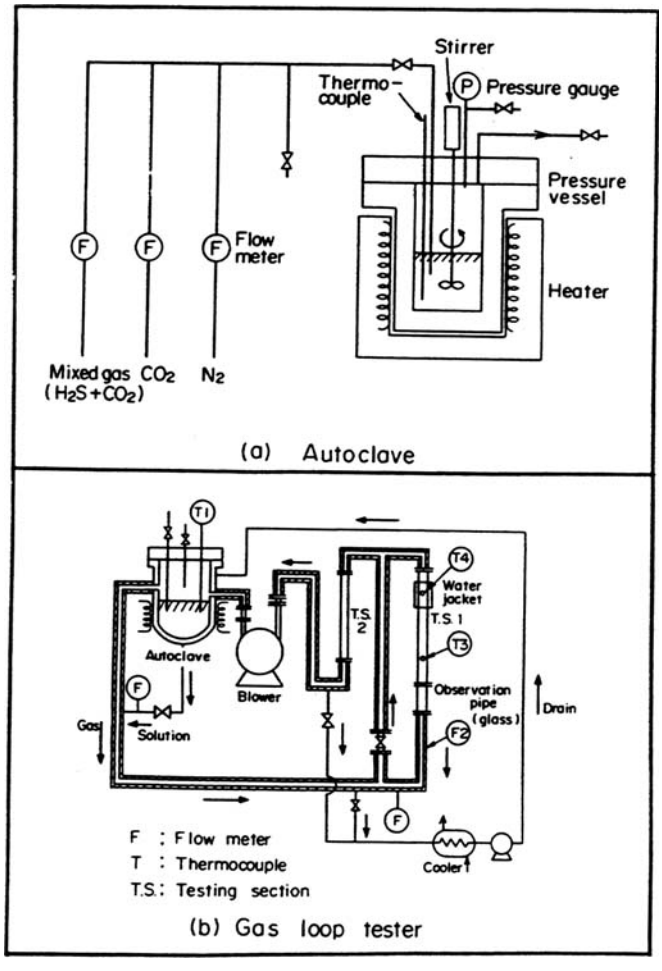


FIGURE 1 — Schematic illustration of test apparatus. Arrows indicate direction of fluid flow. (a) Autoclave, (b) gas loop.

TABLE 2 — Standard Experimental Conditions

	Autoclave	Gas Loop	SCC
Solution	5% NaCl	5% NaCl	5% NaCl
CO_2 pressure (MPa)	0.1, 3.0	0.15	3.0 (with H_2S)
Temperature °C (°F)	30 ~ 250 (86 ~ 482)	100 ~ 150 (212 ~ 302)	30 ~ 250 (86 ~ 482)
Test duration (h)	96	200	336
Flow velocity (m/s)	2.5	26	2.5
Specific volume (mL/cm^2)	25	1000	12

Test Method

The specimens are polished with emery paper (320 mesh) and degreased in acetone and ethanol. After mounting coupons in the specimen holders or fully stressing the four point beam specimens to 100% of their yield strength, the apparatus is closed. Both the evacuation and the nitrogen purging operations are repeated. After that, the deaerated test solution is poured into the autoclave, and nitrogen is bubbled for more than 2 h. After the evacuation, CO_2 gas or CO_2/H_2S mixed gas is charged, and the pressure is raised to the experimental condition. The test solution is stirred during the test in the autoclave. After the corrosion test, visual observation is made and weight loss is measured after cathodic descaling of the test samples. Occasionally, specimens are mounted in epoxy resin and further examined at higher magnification to detect SCC.

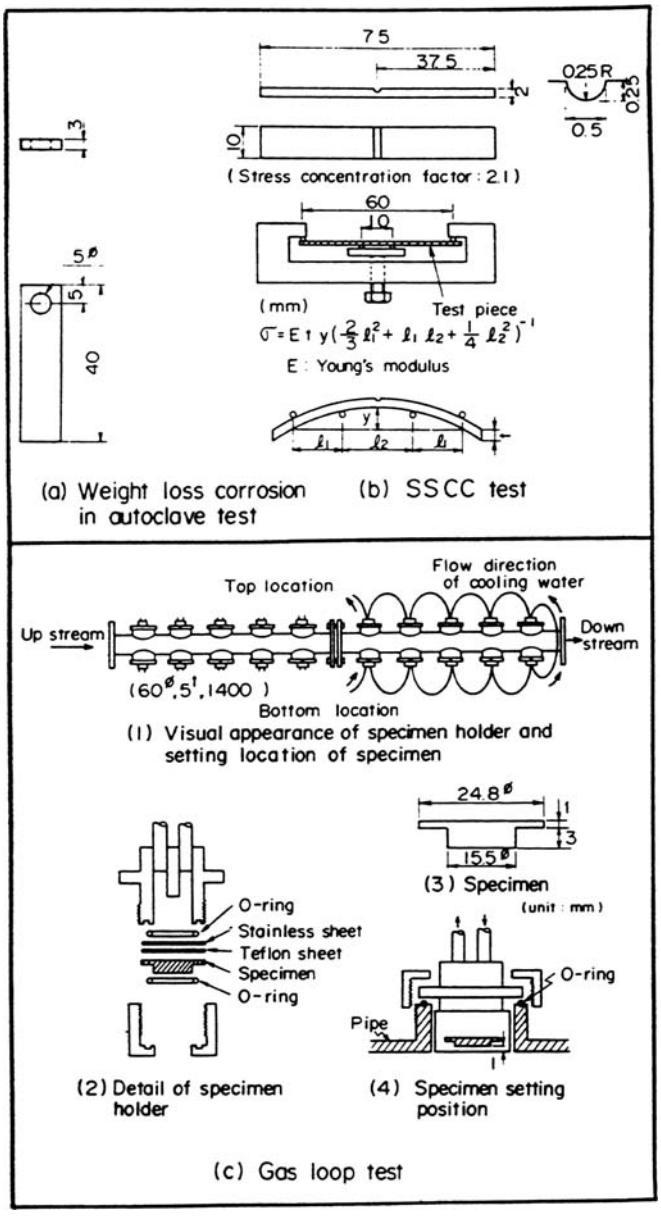


FIGURE 2 — Appearance of test specimens; Young's modulus (E): 2.0 × 10^5 MPa for duplex stainless steel and 2.1 × 10^5 MPa for 9Cr-1Mo and 13Cr steels.

Test Results

Effect of Environmental Factors on CO_2 Corrosion of Cr Steel

Effect of CO_2 Partial Pressure. The influence of CO_2 partial pressure (P_{CO_2}) on corrosion rates of 9, 13, and 25% Cr steels is shown in Figure 4. The corrosion rates of 9 and 13% Cr steels increase dramatically with increasing P_{CO_2} at relatively high temperatures. The critical temperature at which corrosion resistance is achieved via a protective film is 150 and 200 C for 9% Cr and 13% Cr steels at 0.1 MPa, respectively. At 3.0 MPa CO_2, each maximum temperature for CO_2 corrosion resistance decreases to 100 C for 9% Cr steel and 150 C for 13% Cr steel. The 25% Cr steel is very resistant up to 250 C and 3.0 MPa CO_2. In 3.0 MPa CO_2, the temperature indicating maximum corrosion rate is correlated with Cr content in the alloy. Although the analysis of this phenomenon was not a part of this work, it may be surmised that a relationship exists between the formation condition of $FeCO_3$ and the iron dissolution rate.

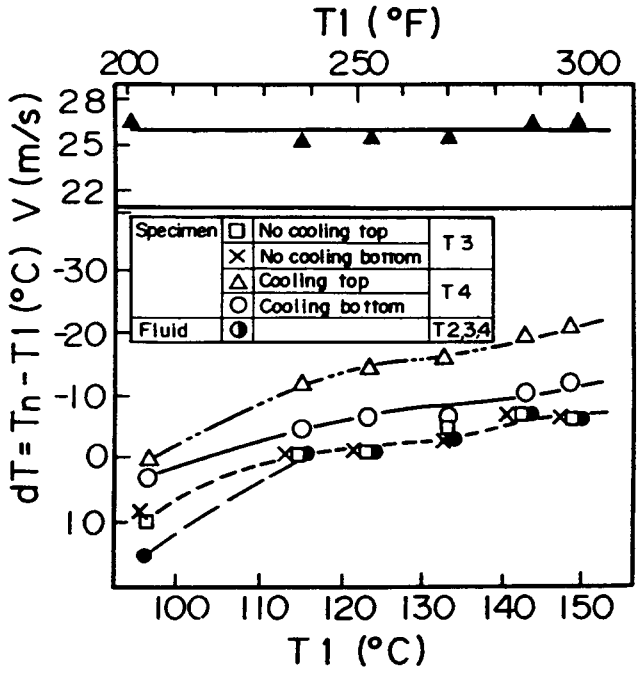


FIGURE 3 — Characteristics of gas loop for temperature and flow velocity; 1:1000 (solution:gas) injection.

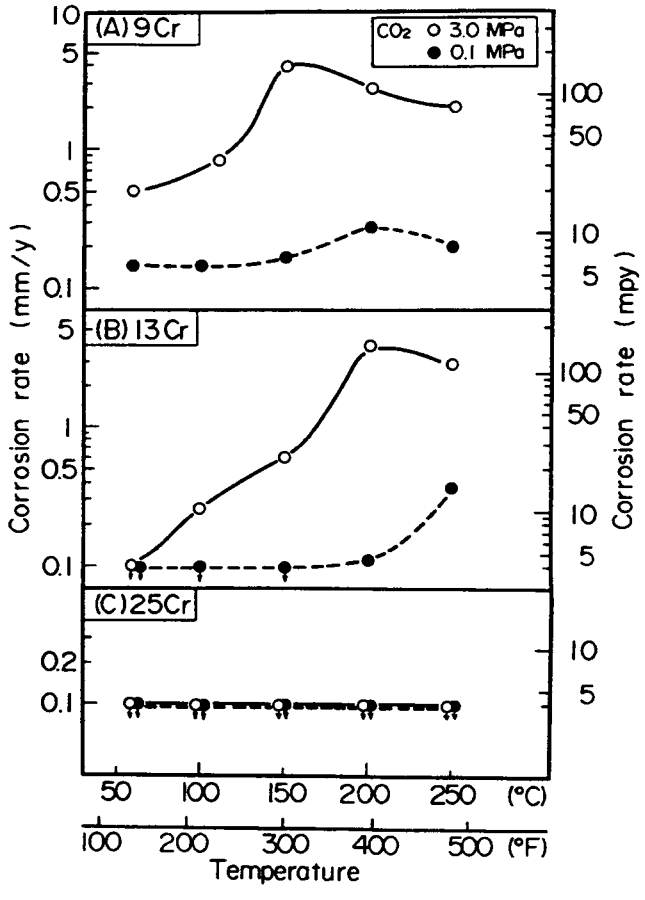


FIGURE 4 — Effect of CO_2 partial pressure and temperature on corrosion rate of Cr steel in the autoclave. (5% NaCl; 3.0 and 0.1 MPa CO_2 at 25 C; test duration, 96 h; flow velocity, 2.5 m/s.)

TABLE 3 — X-Ray Analysis of Corrosion Product in the Autoclave

Temp. (°C)	150				200				250			
P_{CO_2} (MPa)	0.1		0.3		0.1		0.3		0.1		0.3	
Corrosion product	$FeCO_3$	Fe_3O_4	$FeCO_3$	Fe_3O_4	$FeCO_3$	Fe_3O_4	$FeCO_3$	Fe_3O_4	$FeCO_3$	Fe_3O_4	$FeCO_3$	Fe_3O_4
Pure iron	ss[1]	—	ss	—	mw	ww	s	—	mw	mw	s	—
9Cr[2]	w	—	w	—	w w	w ww	s m	— —	— —	w w	ms ms	— —
13Cr[2]	w	—	m	—	—	—	—	—	—	—	—	—
25Cr	—	—	—									

[1]Intensity of x-ray diffraction pattern: ss > s > ms > m > mw > w > ww
Strong — —Weak

[2]Cr steel: Cr compound is not detected, although Cr_2O_3 is detected if baked at 800 C.

The analysis of the corrosion product is shown in Table 3. The tendency for Fe_3O_4 to form in high temperature/low CO_2 conditions and for $FeCO_3$ to form in low temperature/high CO_2 is, appropriately, the same as in the case of a pure iron-CO_2 system. Fe_3O_4 may form more readily on Cr steel than on pure iron.

Effect of Cl^- Ion. The influence of Cl^- ion concentration on the corrosion rate of Cr steel has not been sufficiently clarified. Bryant reported that Cl^- concentration up to 16 wt% has a slight effect on the corrosion rate of 9Cr and 12Cr steels in 175 C, 7 atm CO_2.[4] There is less influence at low temperature (65 C) than at high temperature (175 C). Masamura, et al., reported that the increase of NaCl content from 10 to 20% increases the corrosion rate of 13Cr in high temperature, high pressure CO_2 (55 to 65 atm, 150 to 200 C) while the effect of Cl^- concentration on corrosion rate was not significant in 22% Cr α-γ duplex phase stainless steel.[2]

In this work, the autoclave test results at 150 C, 3.0 MPa CO_2 are shown in Figure 5. The corrosion rates of both 9% Cr and 13% Cr steels slightly increase with increasing Cl^- concentration, a pattern similar to the results of Bryant.[4] The corrosion rate of 25% Cr steel is not affected by the Cl^- ion concentration up to 20% NaCl.

Effect of Test Duration. In the autoclave test, the time dependence of corrosion rate and the initiation of localized corrosion are investigated for Cr steels, as shown in Figure 6.

The 25% Cr steel showed a corrosion rate of less than 0.01 mm/y and did not show any evidence of localized corrosion up to 336 h. In the case of 9Cr and 13Cr steels, there was no evidence of the formation of a protective corrosion product, although their corrosion rates slightly decreased over the duration of the test.

With respect to the effect of time on the corrosion behavior of Cr alloy in a CO_2-Cl^- environment, it is presumed that corrosion resistance can be maintained indefinitely if the application criteria are strictly adhered to; if conditions are outside the limitations of the application criteria, numerous corrosion rates can be observed after long-term exposure to the CO_2-Cl^- environment.

Effect of Flow Velocity. A couple of test results at two phase flow of 26 m/s involving CO_2 gas, water vapor, and hot water of solution:gas ratio 1:1000 are shown in Figure 7. As mentioned above, this flow condition corresponds to the annular flow. In general, corrosion behavior of Cr steel in this two phase flow is similar to that in the flowing solution in the autoclave. It means that the corrosion rate tends to decrease with increasing Cr content in steel. It can also be noted that the corrosion rate is higher at 150 C than at 100 C, and the condition with water cooling may be more severe than without water cooling in two phase flow conditions. It could be related to the condensation of water on the specimen surface. As for the corrosion behavior of pure iron and 2 to 5% steels, it should be mentioned that two phase flow might be a more

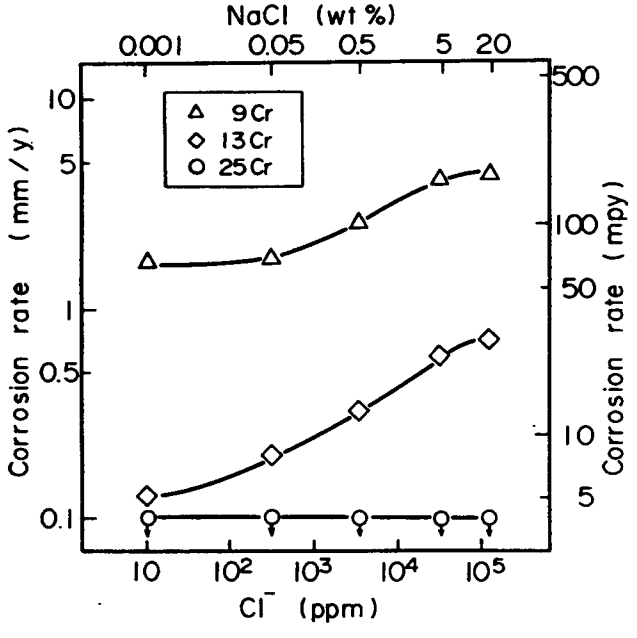


FIGURE 5 — Effect of Cl^- ion concentration on the corrosion rate of Cr steels at 150 C in the autoclave. (3.0 MPa CO_2 at 25 C, test duration, 96 h; flow velocity, 2.5 m/s.)

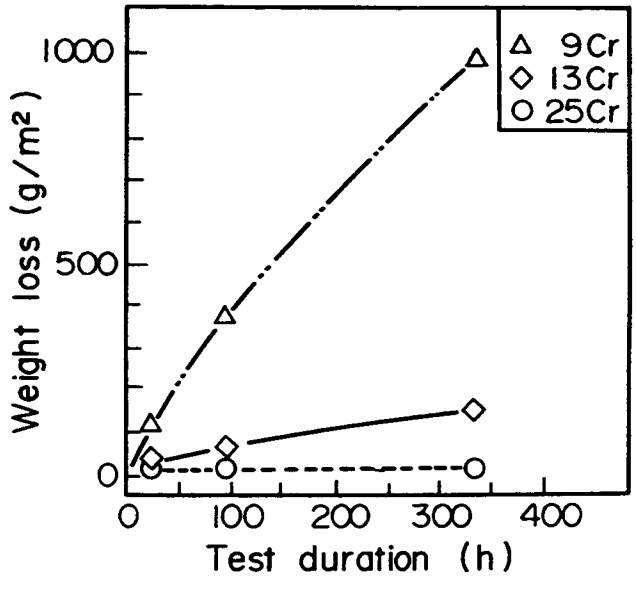


FIGURE 6 — Effect of test duration on weight loss of Cr steels at 150 C in the autoclave.

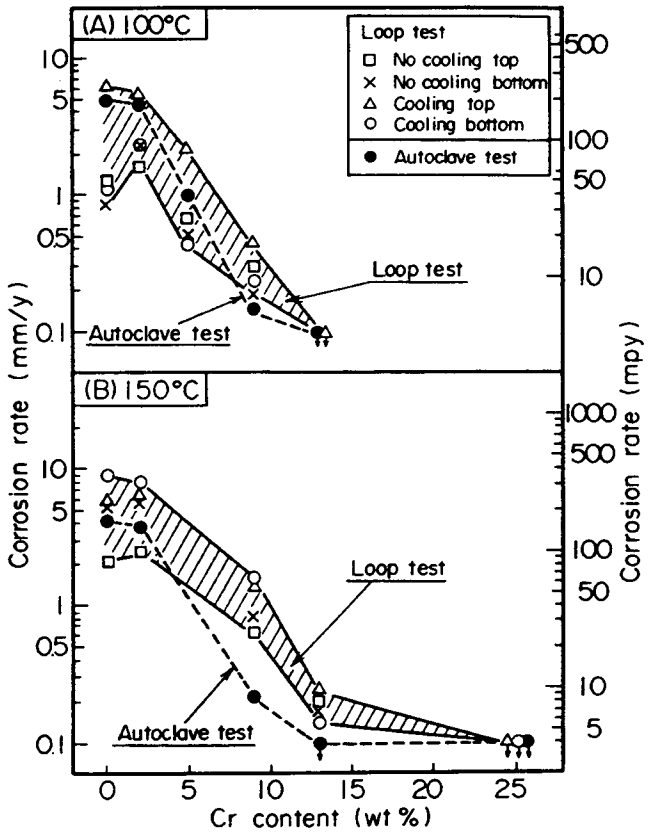


FIGURE 7 — Effect of flow condition and Cr content on corrosion rate at 150 C by gas loop tester. (5% NaCl; 0.15 MPa CO_2 at 25 C; test duration, 200 h; flow velocity, 26 m/s; injected solution gas ratio (solution:gas), 1:1000.)

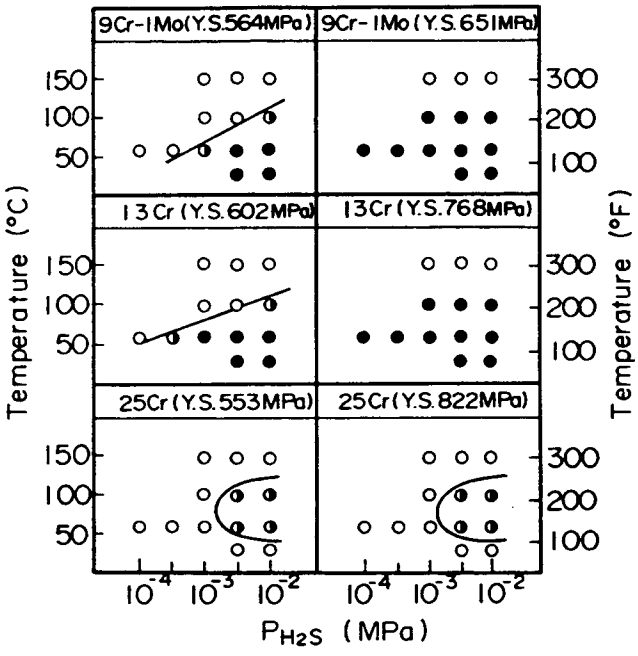


FIGURE 8 — Effect of H_2S partial pressure and temperature on susceptibility to SSCC. [5% NaCl; 3.0 MPa CO_2 + H_2S at 25 C, test duration, 336 h; flow velocity, 2.5 m/s; stress, $1\sigma_y$ with notch; (○) No defect, (◐) localized corrison, (●) SCC.]

severe environment compared with the flowing solution, even with other conditions being the same.

At 100 C, the corrosion rate of 9% Cr steel is higher in the two phase flow than in the autoclave tests, although its extent might be assessed as corrosion resistance. Both 13 and 25% Cr steels are very resistant to corrosion at this temperature. At 150 C, the corrosion behavior of 13% Cr steel is likely to be similar to that of 9% Cr steel, although the corrosion rate in the former is lower than in the latter. The 25% Cr steel is very resistant even in high gas flow rates up to 26 m/s, even in the presence of condensed water. In this experiment, no evidence of localized corrosion such as pitting and crevice corrosion was observed in 9 to 25% Cr steel after testing.

Effect of H_2S Partial Pressure and Temperature on Corrosion and SCC of 9Cr-1Mo, 13Cr, and Duplex α-γ Phase Stainless Steels

The SCC or pitting susceptibility of Cr stainless steels and α-γ duplex stainless steel in an H_2S environment has been discussed for a long time.[7-9] In this section, the influence of H_2S contamination in a CO_2-Cl^- environment on the corrosion behavior of steels mentioned above was investigated. Ikeda, et al., reported that 9Cr-1Mo and 13Cr steels with martensitic microstructure are essentially CO_2 corrosion resistant alloys.[5] The former could be applied up to 100 C, and the latter could be applied up to 150 C. Mukai, et al., reported that the application criteria of α-γ duplex stainless steel depended on environmental and metallurgical conditions such as H_2S partial pressure, Cl^- ion concentration, temperature, and cold work.[10] The criteria for partial pressure of H_2S is one of the most important problems under investigation. Rhodes, et al., reported P_{H_2S} to be around 0.02 atm H_2S.[8] In this work, the autoclave test was conducted in 5% NaCl, 3.0 MPa CO_2/H_2S mixed gas (at 25 C).

Effect of Temperature and H_2S Partial Pressure on SCC. In Figure 8, the effects of temperature and P_{H_2S} are shown. The 9Cr-1Mo steel of C-95 grade is very susceptible to sulfide stress corrosion cracking (SSCC). Even at 1×10^{-4} MPa P_{H_2S}, SSCC occurs. The critical P_{H_2S} for L-80 grade 9Cr-1Mo steel is about 3×10^{-4} MPa. The 13Cr steel is also classified as susceptible to SSCC. In the CO_2-Cl^- environment contaminated with a small amount of H_2S, the dependence of SSCC susceptibility of these materials on the strength level is clearly shown in Figure 9. The critical line for complete SSCC resistance is determined by P_{H_2S} and strength. When the results after 336 h are compared with those after 96 h, the critical line moves to the lower hardness side and/or lower P_{H_2S} side.

The 25Cr duplex stainless steel suffers selective corrosion of the α-phase in the temperature region of 60 to 100 C, as shown in Figure 10. It is presumed that the critical P_{H_2S} for absence of environmental degradation is, in this work, in the region between 1×10^{-3} and 3×10^{-3} MPa. Even though this value should be confirmed in the longer test, it is close to the value determined by slow strain rate tests (SSRT) at the high temperature (177 C) used by Rhodes, et al.[8] In this test result, the different susceptibility between cold worked and solution annealed specimens is not observed; nevertheless, it was detected in the short-term test results (96 h) of Mukai, et al.[10] A detrimental effect of cold work on SSCC or localized corrosion resistance of duplex stainless steel is shown in the next section.

Effect of Cold Work on SCC Susceptibility of 25Cr Duplex Stainless Steel. The effect of temperature and cold work on the SCC susceptibility of duplex stainless steel in a CO_2-Cl^- environment contaminated with a small amount of H_2S is shown in Figure 11. Because 25Cr duplex stainless steel has a good work hardenability, the yield strength of the material linearly increases in accordance with the cold work ratio. Even though the applied stress increases with the cold work ratio, it is clearly seen from Figure 11, as also shown in a previous paper,[10] that (1) cold work increases susceptibility to SCC or

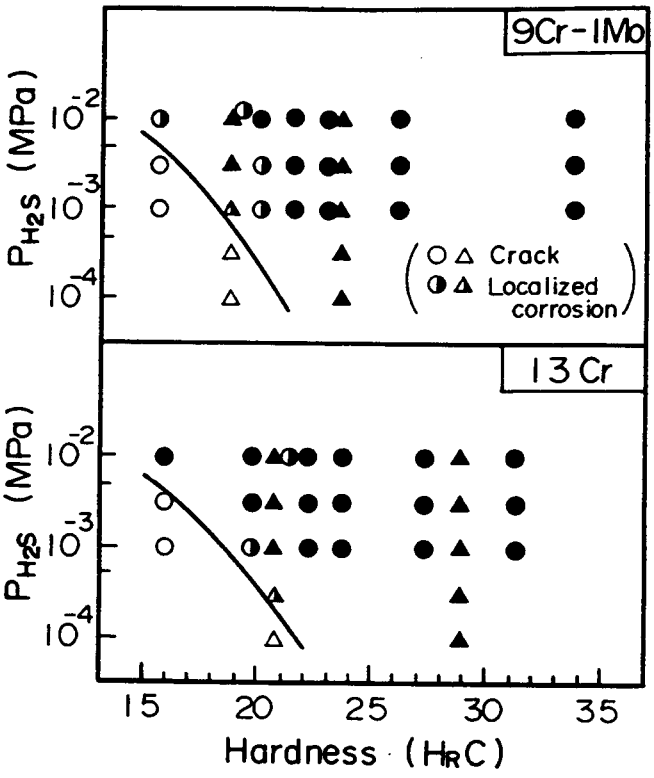


FIGURE 9 — Effect of H_2S partial pressure and strength of 9Cr-1Mo and 13Cr steels on susceptibility to SSCC. [5% NaCl; 3.0 MPa CO_2 + H_2S at 25 C; test temperature, 60 C; flow velocity, 2.5 m/s; stress, 1σ_y with notch; test duration, (○) 96 h, (△) 336 h.]

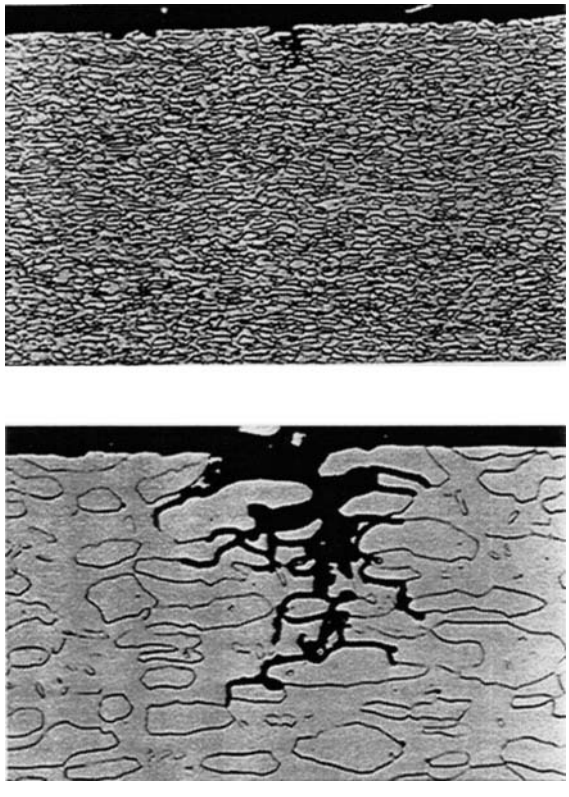


FIGURE 10 — Optical micrograph of selective corrosion of 25Cr α-γ duplex stainless steel. (5% NaCl; 3.0 MPa CO_2 + 0.01 MPa at 25 C, test duration, 336 h; flow velocity, 2.5 m/s; stress, 1σ_y with notch; temperature, 60 C.)

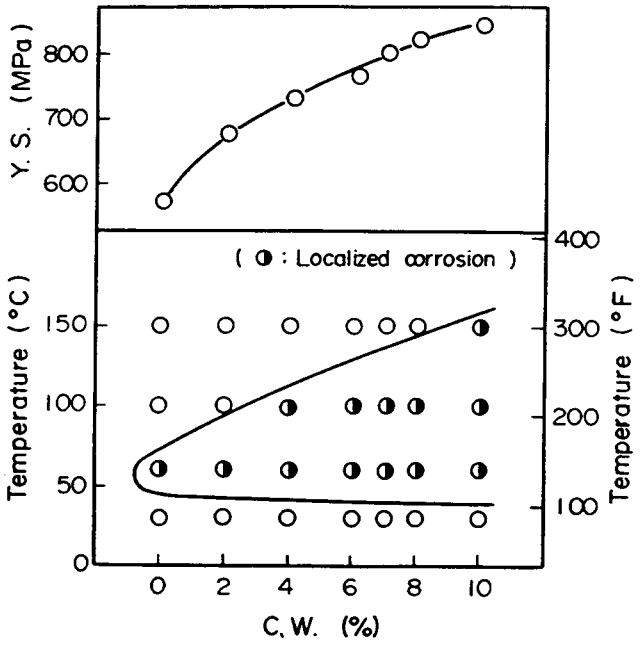


FIGURE 11 — Effect of temperature and strength of duplex stainless steel on susceptibility to SSCC. (5% NaCl; 3.0 MPa CO_2 + 0.01 MPa H_2S at 25 C; test duration, 96 h; flow velocity, 2.5 m/s; stress, 1σ_y with notch.)

selective corrosion of duplex stainless steel, and (2) at approximately 60 C, this material is the most susceptible to SCC or localized corrosion.

Discussion

Utilization of martensitic 9Cr-1Mo and 13Cr steels and 22 to 25% Cr α-γ duplex steel in wells suffused with CO_2 is increasing.[11,12] As discussed in previous papers,[5] the application criteria in a pure CO_2 environment could be given with respect to temperature. Other investigators have also presented essentially the same results.[2,3,13] However, in the CO_2-Cl^- environment contaminated with H_2S, definite criteria for usage have not been presented; nevertheless, these materials, especially 13Cr steel and 22 to 25% Cr duplex stainless steels, were required to produce the critical wells. As a result, a couple of challenging applications have been made.[11,12]

In this paper, the effect of extreme environmental conditions on CO_2 corrosion behavior of these alloys is discussed, and the corrosion resistance of 13% Cr steel and 22 to 25% Cr duplex stainless steels in a CO_2-Cl^- environment will also be discussed in detail. Because the corrosion behavior of 9Cr-1Mo steel is very similar to that of 13%Cr steel, disregarding that the former is less applicable at high temperatures, discussion for 9Cr-1Mo is omitted.

Effect of Environmental Factors on CO_2 Corrosion of 9 to 25% Cr Steels

In this work, it was confirmed that one of the most important factors in CO_2 corrosion of Cr steel was temperature (see the discussion of the stability of protective film primarily composed of Cr-Fe-O-H in a previous publication[5]). However, the corrosion behavior of 9Cr-1Mo and 13Cr steels at relatively high temperature, above 100 and 150 C, respectively, as shown in Figure 4, suggests that the partial pressure (P_{CO_2}) is another important factor. P_{CO_2} could affect both the cathodic and the anodic reactions. For the former, an increase in diffusion limiting current density is accompanied by increasing P_{CO_2}.[5] On the other hand, the anodic reaction is enforced through increasing instability of the Cr-Fe-O-H passivation film because an increase of P_{CO_2} lowers the pH value of the solution.[14] A calculated result for the H_2O-CO_2 system based

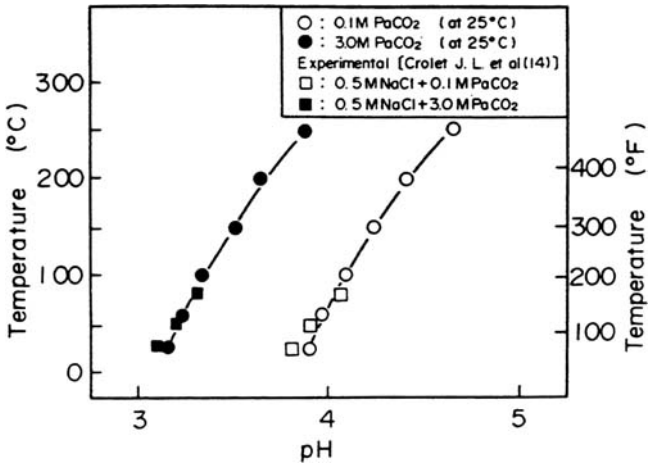


FIGURE 12 — Relationship among CO_2 partial pressure (P_{CO_2}), temperature, and pH value in pressurized CO_2-H_2O system. (Calculation for H_2O-CO_2 system in this work and experimental data for H_2O-CO_2-Cl^- system after Crolet, et al.[14])

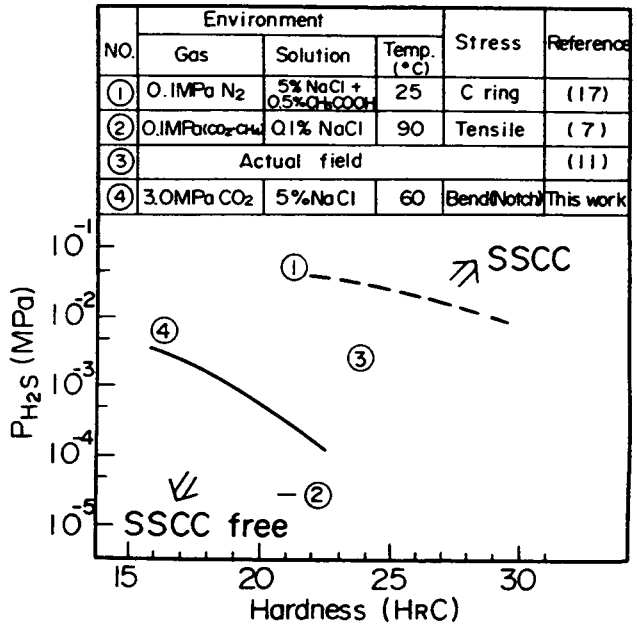


FIGURE 13 — Effect of P_{H_2S} and yield strength on susceptibility to SSCC.

on the thermodynamic equilibrium is shown in Figure 12. Judging from the absolute value of the corrosion rate, it is presumed that the rate determination of corrosion in high Cr steel is an anodic reaction, and therefore, P_{CO_2} contributes to the increase in corrosion rate. As described in the previous section, it is believed that both Cl^- concentration and flow velocity complement CO_2 corrosion behavior in conditions outside the limitations of the application criteria defined by primary factors such as temperature, P_{CO_2}, etc.

13% Cr Martensitic Stainless Steel

The 13% Cr steel is corrosion resistant in a CO_2-Cl^- solution below 150 C; in such conditions, corrosion resistance does not depend heavily on Cl^- concentration (if less than 20% NaCl) or on P_{CO_2}, if less than 3.0 MPa at ambient temperature. Corrosion does, however, increase with increasing CO_2 and Cl^- levels. The corrosion resistance in two phase flow up to 26 m/s is essentially the same as in the solution phase shown in Figure 7. It means, in general, that the flow conditions and two phase flow, including condensed water, would not affect the corrosion resistance of the alloy in the temperature range below a critical temperature. However, it should be noted that it could make the corrosion environment aggressive at the critical or higher temperature, for example, at temperatures higher than 150 C for 13% Cr steel.

Ikeda, et al., presented the corrosion behavior of 420 type 13Cr steel in CO_2-Cl^- contaminated with H_2S, where 13Cr steel would suffer primarily weight loss corrosion at temperatures over 150 C, severe pitting corrosion at intermediate temperatures between 60 and 120 C, and SSCC near ambient temperature.[15]

In addition to general corrosion at high temperatures, the deep pitting at intermediate temperatures and SSCC at low temperatures would limit application of 13% Cr steel. Resistance to deep pitting could be improved with the alloying design of 420 steel.[15] On the other hand, SSCC behavior of 13% Cr steel in high CO_2-Cl^- slightly contaminated with H_2S has not been discussed up to now, although results in NACE Standard TM-01-77 solution and the Shell solution (0.5% CH_3COOH aqueous solution saturated with 1 atm H_2S) were presented. For example, 420 steel with HRC 22, shown in Figure 9, has Sc = 8 on the Shell bent beam test and $\sigma_{th} = 0.3\sigma_y$ on the NACE TM-01-77 test, which are values similar to those presented by other investigators.[9,16] Because the stress concentration factor of the Shell bent beam specimen is equal to 2, Sc = 8 means that σ_{th} in the Shell solution is over σ_y. Thus, care should be taken that characteristics of the testing solution could significantly affect SSCC susceptibility of 13% Cr steel. In Figure 13, the effects of hardness, P_{H_2S}, and SSCC on the stress condition of $1\sigma_y$ are shown. Compared with data of Ishizawa, et al.,[17] based on 0.5% CH_3COOH - 5% NaCl solution bubbled with N_2-H_2S gases (total pressure = 1 atm), the author's data are more extreme, as are the data of Oredssen, et al., although both temperatures in the latter are slightly higher than those in the former.

For example, an actual application of 420 type 13Cr steel with C-85 grade in CO_2-Cl^- with a small amount of H_2S has been in successful operation in the Tuscaloosa field for about two years, as reported by Combs, et al.[11] The environmental conditions are P_{CO_2}, 70 to 100 bar (1 to 1.5 ksi); $Cl^- \leqq 3000$ ppm; P_{H_2S}, 0.02 to 0.03 bar (0.4 psi); and 180 C at well bottom. It is possible that corrosion severity in the actual wells is less than in the laboratory simulation test, although future observation is needed.

22 to 25% Cr Duplex Stainless Steel

The 25% Cr ferritic stainless steel is resistant to corrosion (below 250 C) in the high temperature H_2O-CO_2-Cl^- system. The 22 to 25% Cr duplex stainless shows the same corrosion resistance as 25% Cr ferritic stainless steel because the formation of a stable Cr(III)-O or Cr(III)-OH passivation film.[5] Co-existence of H_2S with CO_2 is significantly detrimental to the corrosion resistance of 22 to 25% Cr duplex stainless steel depending on temperature and P_{H_2S}, as shown in Figure 14.

Through their systematic investigation using a relatively short-term, notched four point bent beam test, Mukai, et al.,[10] showed that the selective corrosion of α phase occurred in the temperature range of 60 to 100 C in a CO_2-Cl^--H_2O system slightly contaminated with H_2S (P_{H_2S} = 0.01 MPa). Their results also suggest that cold work is detrimental. Sakai, et al., using the slow strain rate test (SSRT), also showed that SCC susceptibility of 22% Cr duplex stainless steel was high in the same temperature region.[18] In this work, the investigation by Mukai, et al., was extended to the low P_{H_2S} region using a longer test duration, as shown in Figures 8 and 9. It was clarified that a criterion for the existence of selective corrosion, which could be considered an initiation of SCC, was set at a P_{H_2S} between 0.001 and 0.003 MPa in the temperature range of 60 to 100 C. Craig found a P_{H_2S} limit of 0.05 MPa for establishing an SCC-MPa and at 116 C.[12] The effect of the P_{H_2S}:P_{CO_2} ratio on SCC criteria is an important factor.

NO.	Environment		Stress	Material	Reference
	Gas (P_{CO_2})	Solution (NaCl)			
①	7 MPa	5-15%	Tensile	22 Cr	(7)
②	2.5	20	SSRT	22 Cr	(18)
③	5.0	10	U bend	22 Cr	(19)
④	1.0	20	Bend (Notch)	25 Cr	(10)
⑤	2.0	25	SSRT	22 Cr	(8)
⑥	1.0	20	Bend	25 Cr	(20)
⑦	12.2	11	U bend	22 Cr	(12)
⑧	3.0	5	Bend (Notch)	25 Cr	This work

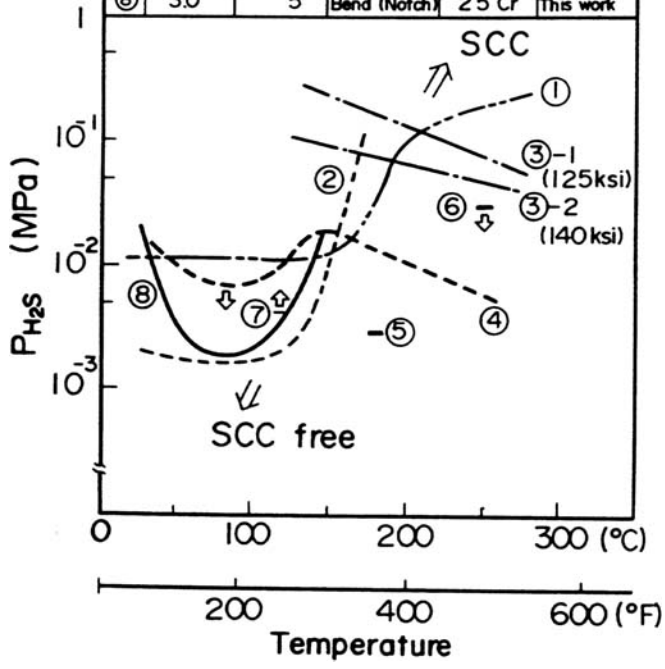


FIGURE 14 — Effect of P_{H_2S} and temperature on susceptibility to SCC.

because P_{H_2S}:P_{CO_2} may be one of the indicators for the transition from H_2S corrosion to CO_2 corrosion.

As clearly shown in Figure 14, there is an inconsistency among the published autoclave data, i.e., the criteria for SCC in the high temperature region over 150 C. Oredsson, et al.,[7] showed that the lower limitation of P_{H_2S} had a tendency to increase with temperature increases, while Mukai, et al.,[10] and Prouheze, et al.,[19] showed that it decreased with temperature increases. In order to understand the reason for this difference, the experimental technique should be discussed in more detail. In this work, the results shown in Figure 11 suggest that the increased cold work and the increased temperature are detrimental to SCC resistance.

Conclusion

1. Reliable corrosion protection in an H_2O-CO_2-Cl^- system is accomplished with high Cr steel such as martensitic 9Cr-1Mo and 13% Cr steels and 22 to 25% Cr duplex phase stainless in both the solution phase and the two phase flow with high flow rate (up to 26 m/s). Temperature and P_{CO_2} are the main environmental factors to be considered in establishing application criteria. The Cl^- concentration and the flow rate of up to 26 m/s could increase corrosion severity in environmental conditions more extreme than those conforming to the application criteria.

2. The application criteria for martensitic stainless steel in a CO_2-Cl^--H_2S environment is limited by P_{H_2S}, temperature, and the strength of the materials. Below 120 C, susceptibility to SSC and localized corrosion is very high. The effect of H_2S on the corrosion behavior of martensitic stainless steel with HRC $\leqq$ 24 is critical in 0.0003 MPa, which is similar to the description in NACE Standard MR-01-75.

3. Generally speaking, SCC susceptibility of 25% Cr duplex stainless steel increases with increasing temperature and P_{H_2S}. However, in the low P_{H_2S} condition, it should be noted that there was a temperature region of maximum susceptibility to selective corrosion, i.e., 60 to 100 C, where P_{H_2S} of 0.003 MPa is a critical condition for SCC or selective corrosion.

Acknowledgment

The authors thank K. Nishioka, Managing Director of the Board and General Manager of Central Research Laboratories, Sumitomo Metal Industries Ltd.; T. Yukitoshi and F. Terasaki, Assistant General Managers; and T. Moroishi, Deputy Manager of Central Research Laboratories, for their helpful advice and support. Thanks are also due Messrs. I. Sakoda, H. Kusagi, T. Hoshino for their assistance with the experimental work.

References

1. A. K. Dunlop, H. L. Hassell, P. R. Rhodes, "Fundamental Considerations in Sweet Gas Well Corrosion," CORROSION/83, Paper No. 46, National Association of Corrosion Engineers, Houston, Texas, 1983.
2. K. Masamura, S. Hashizume, K. Nunomura, J. Sakai, I. Matsushima, "Corrosion of Carbon and Alloy Steels in Aqueous CO_2 Environment," CORROSION/83, Paper No. 55, National Association of Corrosion Engineers, Houston, Texas, 1983.
3. K. Satoh, K. Yamamato, N. Kagawa, "Prevention of CO_2 Corrosion in Gas Gathering Systems," CORROSION/83, Paper No. 56, National Association of Corrosion Engineers, Houston, Texas, 1983.
4. J. R. Bryant, G. B. Chitwood, "Corrosion Behavior of 1 to 22 Percent Chromium Steels and Monel K-500 in CO_2/Brine Environments," CORROSION/83, Paper No. 58, National Association of Corrosion Engineers, Houston, Texas, 1983.
5. A. Ikeda, M. Ueda, S. Mukai, "CO_2 Corrosion Behavior and Mechanism of Carbon Steel and Alloy Steel," CORROSION/83, Paper No. 45, National Association of Corrosion Engineers, Houston, Texas, 1983.
6. J. M. Mandhane, G. A. Gregory, K. Aziz, Int. J. Multiphase Flow, Vol. 1-4, p. 537 (1974).
7. J. Oredsson, S. Bernhardsson, "The Performance of High Alloyed Austenitic and Duplex Stainless Steels in Sour Gas and Oil Environments," CORROSION/82, Paper No. 126, National Association of Corrosion Engineers, Houston, Texas, 1982.
8. P. R. Rhodes, G. A. Welch, L. Abrego, J. Materials Energy Systems, Vol. 5, p. 3 (1983).
9. R. S. Treseder, T. M. Swanson, Corrosion, Vol. 24, No. 1, p. 3 (1968).
10. S. Mukai, H. Okamoto, T. Kudo, A. Ikeda, J. Materials Energy Systems, Vol. 5, p. 59 (1983).
11. J. D. Combes, J. G. Kerr, L. J. Klein, Petrol. Engr. Int., p. 50, March 1983.
12. B. D. Craig, 1982 ASM Metals Cong., 8201-015.
13. M. Matsui, A. Kuhara, A. Yoshitake, T. Ishii, "The Development of High Strength 12% Cr Centrifugally Cast Pipe for Sour Gas Gathering Piping System," CORROSION/83, Paper No. 54, National Association of Corrosion Engineers, Houston, Texas, 1983.
14. I. L. Crolet, M. R. Bonis, Corrosion, Vol. 39, No. 1, p. 39 (1983).
15. A. Ikeda, S. Mukai, Tetsu-to-Hagané, S4186, 1982.
16. R. D. Kane, M. Watkins, J. B. Greer, Corrosion, Vol. 33, No. 7, p. 231 (1977).
17. Y. Ishizawa, T. Shimada, M. Tanimura, Proc. South Asian Pacific Corrosion Control Conf., p. 381, 1983.
18. J. Sakai, I. Matsushima, Y. Kanemura, M. Tanimura, T. Osuka, 1982 ASM Metals Cong., 8201-010.
19. J. C. Prouheze, J. C. Vaillant, G. Guntz, B. Lefebvre, 1982 ASM Metals Cong., 8201-012.
20. T. Kudo, H. Miyuki, H. Okamoto, J. Murayama, T. Moroishi, "Corrosion Behavior of Highly Alloyed Materials in H_2S-CO_2-Cl^- Environments," CORROSION/82, Paper No. 127, National Association of Corrosion Engineers, Houston, Texas, 1982.

Copyrighted Materials
Copyright © 1996 NACE International Retrieved from www.knovel.com

Paper No. 124—CORROSION/82

EFFECT OF MICROSTRUCTURE ON THE SULFIDE STRESS CORROSION CRACKING RESISTANCE OF AISI 410 AND 420 STEELS

Y. Ishizawa, T. Shimada, M. Tanimura
Technical Research Center
Nippon Kokan K.K.
1-1 Minamiwataridacho, Kawasakiku, Kawasaki, 210 Japan

ABSTRACT

The SSCC resistance of AISI 410 and 420 type 13% Cr steels were studied in relation to their microstructures. Two types of the SSCC tests and the optical and electron microscopic observation were conducted on eight laboratory heats and a few mill products. The SSCC tests revealed the higher SSCC resistance of 420 steels over 410 steels. From the results of microscopic observation, the superiority of 420 steels was attributed mainly to the improvement of substructures introduced by the higher carbon content.

INTRODUCTION

The production of oil and gas form the reservoirs that contain significant amounts of hydrogen sulfide and carbon dioxide has been promoted as the demand for energy increases. AISI 410 and 420, 13% Cr martensitic stainless steels have attracted attention for application in these areas, particularly where the oil and gas contain high levels of carbon dioxide along with low levels of hydrogen sulfide, because they offer improved corrosion resistance in comparison with low alloy steels. However, sulfide stress corrosion cracking (SSCC) is a serious problem for high strength 13% Cr steels.

It has been recognized that 13% Cr steels are sensitive to SSCC more than quenched and tempered type low alloy steels, but there are few works on this matter.[1,2] A characteristic feature of 13% Cr steel is that the mircrostructure is significantly affected by the chemical compositions. And the SSCC resistance of these steels is expected to be affected by the change in microstructure. From this viewpoint, the effect of microstructure on the SSCC resistance of AISI 410 and 420 steels was investigated.

MATERIALS AND EXPERIMENTAL PROCEDURES

Materials

Four heats of AISI 410 steels with carbon levels in the range of 0.11% to 0.15%, and four heats of AISI 420 steels with carbon levels of 0.8% to 0.21% were prepared. The chemical compositions of these steels are listed in Table 1. Small amounts of nickel was added to eliminate delta-ferrite in three heats of 410 steels, No. 2, No, 3, and No. 4. One of the 420 steels, No. 8, was alloyed with 0.7% of molybdenum to study the effect of this element on the SSCC resistance. All steels were melted in air as 50 to 150 kg laboratory heats. Ingots were rolled to 13 mm thick plates after reheating to 1523°K. These plates were air cooled from 1223°K and tempered at several temperatures between 893° and 1013°K. Additionally, the steels from mill products with carbon levels of 0.18% and 0.20% were tested. Their chemical compositions were similar to those of steel No. 5 and No. 7, respectively. Mill products were also air cooled and tempered to the strength level of L-80 grade.

Mechanical Properties

Tensile tests were conducted in duplicate on the round bar specimens machined longitudinally after tempering. Rockwell C scale hardness measurements were also conducted.

Microstructures

Microstructures of the tested materials was studied by optical and electron microscopy. Prior austenite grain size was measured by the linear intercept method.

Corrosion Tests

Weight loss corrosion tests were performed on the coupon specimens with the size of 20 x 40 x 5 mm. Specimens were immersed in NACE solution (0.5% acetic acid and 5% sodium chloride solution saturated with hydrogen sulfide) kept at 298°K during the test period of 5 days. Prior to the measurement of the weight loss, the amount of diffusible hydrogen was measured by the extraction method in glycerine at 318°K.

SSCC Tests

The SSCC resistance of the materials was evaluated by two methods. Shell type bent beam test and NACE constant load tension test.[3] Shell type bent beam tests were carried out to obtain the critical stresses (Sc) for failure. The specimen was 4.8 x 1.6 x 76 mm with two drill holes at the center to introduce the stress concentration. Since the preliminary test showed that the presence of chlorine ion accelerates SSCC of 13% Cr steels, NACE solution was adopted instead of the original solution of this test which contains no sodium chloride. The test temperature was 294°K and the duration was 14 days.

The threshold stresses for SSCC were determined by the NACE constant load tension tests on the round bar specimens with a diameter of 2.6 mm in accordance with NACE Standard TM-01-77. Tests were conducted in NACE solution at 298°K and the maximum duration was 30 days. In some cases, SEM fractography was used to investigate the fracture surface of NACE tension test specimens.

RESULTS

Microstructures

Since the martensitic transformation can take place at even a low cooling rate in 13% Cr steels, the microstructure of the tested materials after air cooling from 1,223°K consists of martensite and secondary phases which can exist during austenitizing. According to the equilibrium diagrams of Fe-Cr-C system, the secondary phases of 13% Cr steels are delta-ferrite and/or carbides.[4] The microstructure after air cooling reflects the structural composition at the austenitizing temperature which varies with the contents of carbon of martensite and carbides, and the steels of the lower carbon levels consist of martensite and small amount of delta-ferrite. Optical micrographs of the tested steels after tempering are shown in Figure 1. Delta-ferrite exists in No. 1 (0.12% C), No. 2 (0.11% C-0.5% Ni) and No. 8 (0.20% C-0.7% Mo) steels. Addition of 0.5% Ni to 0.11% C steel (No. 2) reduced delta-ferrite but did not lead to full martensite structure. A small amount of delta-ferrite in No. 8 steel is due to the addition of molybdenum, which is the strong ferrite forming element. The results of grain size measurement is shown in Figure 2. It is evident that carbon content over 0.2% leads to finer grain size. It is attributable to the retarding effect of undissolved carbides on grain growth during austenitizing.

Mechanical Properties

Figure 3 and Figure 4 show the tensile properties and the hardness of No. 1, 3, 4, 5, and 7 steels at each tempering temperature. The strength and the hardness level is in the reasonable order of their carbon content except that 0.15% C steel (No. 4) and 0.18% C steel (No. 5) are almost at the same strength level. The tempering temperature to obtain the same strength level changes with carbon content and it can be seen that the lower carbon content leads to lower tempering temperature. The tensile properties and the hardness of No. 2, 6, and 8 steels are shown in Figure 5 and Figure 6. The strength level of low nickel 0.2% C steel (No. 6) is lower than that of 0.2% C-0.2% Ni steel (No. 7) at each temperature. The strength level of No. 2 steel, in which the amount of delta-ferrite was reduced by nickel addition, is higher than that of No. 1 steel, showing that the presence of delta-ferrite leads to the tempering at the lower temperature to obtain the same strength level. Number 8 steel which contains 0.7% of molybdenum shows high tempering resistance.

It was expected that such effects of chemical composition and structural change on tempering temperature should affect the detailed microstructure of tested steels. So the microstructural aspects such as the morphology of lath or subgrain, the shape and distribution of carbide particles and the arrangement of dislocations were observed with electron microscopy. The examples of thin foil electron micrographs of the tested steels are shown in Figure 7. As mentioned, AISI 420 steels can be tempered at higher temperature in comparison with 410 steels to obtain the same strength level. These micrographs show that 420 steels have more recovered

substructure and large amount of coarser carbides than 410 steels. Thus the degree of recovery and coarsening of carbides depend on carbon content if the strength is at the same level. When 420 steels are tempered to the yield strength of about 600 MPa, recrystallization proceeds and coarse, globular carbides exist at the subgrain boundary. Oppositely, in 410 steels tempered to the same strength level, the lath structure still remains and relatively small, rod-like carbides can be seen at the lath boundary. Such rod-like carbides were also observed in 420 steels when the tempering temperature is low as shown in Figure 7(f) and 7(e). In addition, in 0.18% C 420 steel, the retardation of recovery along with rod-like carbides were often observed even when tempered at higher temperature as is shown in Figure 7(h).

The two-stage replica electron micrographs are shown in Figure 8. The strength level is almost the same for these steels. General tendency is similar to that of the thin foil electron micrographs that carbides become coarser and more spheroidal with the increase of carbon content. Rod-like carbides can be seen in both 410 steels, Figure 8(a) and 8(b). The difference in the carbides configuration between 0.18% C and 0.20% C steels is clear in the SEM micrographs shown in Figure 9. Carbides in 0.18% C steel are relatively small and the number of rod-like carbides is larger than in 0.20% C steel.

Corrosion Test Results

The results of the corrosion tests are shown in Table 2. The data of AISI 4130 type steels with chromium content of 1.0% and 2.0% obtained in the same test condition are listed together for comparison. These data indicate that the corrosion rate becomes higher with the increase of chromium content. The reason for this effect of chromium is not clear, but it can be said that the corrosion resistance of 13% Cr steel is not so high in such a corrosive environment as NACE solution. The measurement of diffusible hydrogen showed no influence of chromium content as is shown in Table 2.

Shell Type Bent Beam Test Results

The results of Shell type bent beam tests are shown in Figure 10. It is clear that 420 steels have higher critical stress than 410 steels at the same hardness level. In both cases of 410 and 420 steels, it seems that high side in the narrow range of carbon content leads to slightly higher critical stresses. The data of mill products, both 0.18% C and 0.20% C steels, are also plotted in Figure 10 and lie in the same range of the steels produced in the laboratory. From these results, it can be said that the SSCC resistance of 420 steels is higher than that of 410 steels.

NACE Constant Load Tension Test Results

The results of NACE constant load tension tests are shown in Figure 11. General tendency is almost the same as that of Shell type tests. AISI 420 steels showed higher threshold stresses than 410 steels at the same strength level. This test method clarify the superiority of 0.20% and 0.21% C steels over 0.18% C steel. Three 410 steels which contain nickel over 0.5% seem to show rather low threshold stresses than that of No. 1 steel which was not alloyed with nickel. The same rating as Shell type tests can be drawn from these results that 420 steels are more resistant to SSCC than 410 steels. In addition, it can be said that higher carbon level leads to higher SSCC resistance in 420 steels.

Fractography

The SEM fractographs of the fracture surface of the constant load tension specimens are shown in Figure 12. It is clear that fracture modes are affected by carbon content and the strength level. In case of 420 steels, dimple-like transgranular fracture is predominant at the yield strength level from 600 to 700 MPa. As a very rare case, quasi-cleavage mode was observed. On the other hand, 0.11% and 0.12% C 410 steels (No. 1 and No. 2 steels) showed the strong tendency of intergranular fracture. At the yield strength of about 600 MPa, 0.11% and 0.12% C steels show three types of fracture modes, dimple-like, intergranular and the intermediate of the two modes as shown in Figures 12(a) to 12(f). But intergranular fracture becomes very predominant with the increase of the strength level. Higher carbon 410 steels, 0.13% and 0.15% C steels, also show intergranular fracture at higher strength level but the damage of the grain boundary is not so severe in comparison with 0.11% and 0.12% C steels as is shown in Figure 12(g). Dimple-like fracture is predominant at the lower strength level in these steels.

DISCUSSION

Microstructure and the SSCC Resistance

Fractography revealed two types of SSCC fracture modes; transgranular and intergranular fractures. Transgranular fractures can be classified into dimple-like and quasi-cleavage fractures. These fracture modes have been known as typical for hydrogen embrittlement and several studies were reported from the viewpoint of the stress state or the stress intensity factor.[5,6] In 13% Cr steels, as was shown in the previous paragraph, dimple-like transgranular fracture and intergranular fracture were predominant and quasi-cleavage type fracture was very few. In most cases the fracture mode of 420 steels is dimple-like irrespective of the degree of the applied stress. This fracture mode is referred as the presence of high stress state and it seems applicable to 13% Cr steels.[6] Observation of the tested specimens and the measurement of the reduction in its diameter revealed that the stress of constant load specimen should increase with the exposure time because of the reduction in cross-sectional area of the specimen by the general corrosion and the stress concentration effect caused by the grooves which generate at the specimen surface through the localized corrosion as is shown in Figure 13. The crack started at the root of the surface groove can be seen in Figure 13(b). Thus 420 steels cause failure after the increase of the actual stress even when the applied stress is low, resulting in dimple-like fracture mode.

Dimple-like fracture surface consists of the fracture units, the region encircled by tear ridge shown in Figure 14. The crack initiation site is relatively brittle part surrounded by tear ridge. The cooperation of high stress and hydrogen cause the void or crack at first. In high stress region, such cracks occur continuously and grow repeating coalescence each other. Coalescence occurs by the mechanical deformation and fracture and tear ridge is formed at this time. The resistance of 13% Cr steels to dimple-like SSCC seems to depend on the conditions of the defective part which becomes the crack initiation site. Possible defective parts concern with inclusions, carbides, lath, or subgrain boundaries. It was shown that in 420 steels, when compared at the same strength level, the substructures are well recovered and carbides are coarser and more globular in comparison with 410 steels. Such substructures seem to relate with higher resistance to dimple-like SSCC. On the other hand in 410 steels, lath structure remains and rod-like carbides were observed at lathe boundary, resulting in poor resistance to dimple-like SSCC. Between 0.18% C and 0.20% C 420 steels, such difference in their substructures was also observed as previously mentioned. Though it is not so distinct difference as that of between 410 and 420 steels, it seems to be one factor that explains the fact that higher SSCC resistance relates with higher carbon content in 420 steels.

One of the microstructural factors which would influence the SSCC resistance is grain size. It is said that finer grains restrict the environmental fracture at grain boundary and the qualitative explanation has been presented in terms of the segregation of impurities at the prior austenite grain boundary.[7,8] As mentioned, intergranular fracture is predominant in 0.11% and 0.12% C steels. It was also observed when the strength level is high in 0.13% and 0.15% C steels. Intergranular fracture seems to be attributable to the cooperation of the mechanisms of temper embrittlement and hydrogen embrittlement. In case of 410 steels, coarse grain size is disadvantageous in terms of impurity segregation and moreover, tempering temperature should be taken low to obtain the specified strength level. It is possible that these factors accelerate intergranular fracture of 410 steels, especially in 0.11% and 0.12% C steels. The influence of grain size seems to relate mainly with intergranular fracture as mentioned here. But, it is possible that finer grains leads to the improvement of substructures, resulting in higher resistance to transgranular SSCC. It may be another explanation of the superiority of the steels with higher side of carbon level in 420 steels.

As has been mentioned, the SSCC resistance of 410 steels are poor in comparison with that of 420 steels. It is not because intergranular fracture occurs in 410 steels. It only means that the susceptibility of grain boundary becomes higher than that of transgranular parts by other factors such as impurity segregation at certain strength level. If the factors which cause intergranular fracture in 410 steels are eliminated, the fracture mode will become intergranular . But, as shown in case of dimple-like fracture in 0.13% and 0.15% C steels, the SSCC resistance is still poor in comparison with 420 steels. Schematic drawing about this matter is shown in Figure 15.

It must be noticed that the effect of substructure on the SSCC resistance mentioned in this report concerns with the comparison of 410 and 420 steels. It cannot be applied directly to other type of steels, though it seems possible partly. For example, it is known that AISI 4130 steels have higher SSCC resistance than 420 steels. But the substructural observation does not offer any explanation for this matter. Further studies about the basic toughness, corrosion properties, hydrogen absorption, and other factors seem necessary. In this study, the corrosion tests were conducted but satisfactory results to clarify this matter was not obtained.

Another microstructural factor of importance with respect to the SSCC resistance of 13% Cr steels is delta-ferrite which exists in 0.11% and 0.12% C steels. The SSCC test results showed that the reduction in the volume fraction of delta-ferrite by adding nickel to 0.11% C steel does not lead to any improvement of the SSCC resistance. The SSCC resistance of 410 steels is poor irrespective of the presence of delta-ferrite. The longitudinal cross section of the NACE tension test specimen of 0.12% C steel is shown in Figure 16. Delta-ferrite does not seem to serve as the crack initiation site. It rather seems to be the obstacle to the crack growth. In Figure 17, optical microstructure and SEM fractograph of the SSCC fracture surface of 0.05% C-13% Cr steel which contains 50 to 60% of delta-ferrite are shown. For the materials of this study, it was difficult to distinguish the difference of the fracture mode between martensite and delta-ferrite because the volume fraction of delta-ferrite is small. It can be seen in Figure 17 that SSCC occurs in martensitic parts (dark area in the figure) and delta-ferrite shows ductile fracture without any damage by hydrogen. These photographs show that delta-ferrite does not act as the crack initiation site probably because the hardness is low enough.

Nevertheless, it maybe said that the presence of delta-ferrite is unfavorable in terms of SSCC because it makes the strength of the steels lower, resulting in the lowering of the tempering temperature to obtain the specified strength level, and it makes the substructure unfavorable to the SSCC resistance.

The next subject is on the effect of alloying elements, nickel and molybdenum, on the SSCC resistance. In 0.11% C steel (No. 2), 0.5% of nickel was added to obtain the simple martensitic structure as previously mentioned. As a result, the tempering temperature for this steel can be taken higher than for 0.12% C-Ni free steel (No. 1 steel). But the SSCC resistance of No. 2 steel is the same or slightly lower than that of No. 1 steel. It suggests the detrimental effect of nickel addition over 0.5%. Though some studies were reported about this matter, further study seems necessary to clarify the role of nickel on the SSCC resistance.[9]

The contribution of molybdenum to improve the SSCC resistance of the low alloy steels has been reported.[10] In 420 steels, however, the addition of 0.7% of molybdenum did not lead to any improvement. This steel contains small amounts of delta-ferrite but because of the high tempering resistance shown in Figure 5 and Figure 6, the secondary detrimental effect of delta-ferrite mentioned can not operate. The study over wide range of molybdenum content should be conducted.

Indicative Parameter of the SSCC Resistance

The last subject concerns with the other indication of the SSCC resistance of 410 and 420 steels. Figure 18 and Figure 19 show the results of Shell type tests and NACE tension tests respectively as a function of the yield to tensile strength ratio (yield ratio) of tested steels. Originally, such plots should be classified according to the strength level. But in the present case, in the yield strength range of 580 to 680 MPa, the SSCC resistance can be arranged by the yield ratio irrespective of carbon content and the strength level. The different lines are drawn for 410 and 420 steels in Figure 18, but it can be said that all data lie in the same band. This result is not contradictory to the fact that the SSCC resistance of 420 steels is higher than that of 410 steels. It seems rather consistent with the effect of microstructure on the SSCC resistance. The yield ratio is the parameter that concerns with the ductility or the capacity of the work hardening of the materials. The SSCC resistance is not independent of these factors. To tell the detailed, the factors which affect the SSCC resistance such as the number and the shape of carbides, grain size, the state of grain and subgrain (lath) boundary and dislocation density would also affect the yield and the tensile strength. The balance of such factors decides the yield ratio and also the SSCC resistance. It seems believed that materials with higher yield ratio is favorable to the SSCC resistance because the hardness can be restricted lower at the same yield strength level. But it is not correct as is shown in Figure 18 and Figure 19.

CONCLUSIONS

The SSCC resistance of AISI 410 and 420 steels were studied in relation to their microstructures and resulted in the following conclusions:

1. The SSCC resistance of 420 steels are higher than that of 410 steels at the same strength level. It is mainly due to the higher carbon content of 420 steels.
2. Higher carbon content steels can be tempered at higher temperature to obtain the specified strength level. It is advantageous to make the microstructure favorable to the SSCC resistance, that is well recovered substructure with coarse and globular carbides.
3. In 420 steels, the higher SSCC resistance relates with higher carbon level. It is attributable partly to finer grain size introduced by higher carbon content.

4. In 0.11% and 0.12% C steels with coarser grain size, intergranular SSCC mode other than dimple-like transgranular one is predominant. But it is not the key factor to explain the poor SSCC resistance of 410 steels. The SSCC resistance of 410 steels is essentially poor, irrespective of the fracture mode.
5. The presence of delta-ferrite is not detrimental directly but it is favorable to eliminate delta-ferrite in terms of SSCC because of its secondary detrimental effect of making the substructures disadvantageous to the SSCC resistance by lowering the tempering temperature.
6. The yield to tensile strength ratio is available to estimate the SSCC resistance of AISI 410 and 420 steels.

REFERENCES

1. R.D. Kane, M. Watkins, J.B. Greer, *Corrosion* 33, 7(1977), p. 231.
2. D.S. Burns, *Materials Performance* 15, 1(1976), p. 21.
3. J.P. Fraser, G.G. Eldredge, R.S. Treseder, *Corrosion* 14, 11(1958), p. 37.
4. *Metals Handbook*, Vol. 8 (ASM, 1973).
5. M. Watkins, M.F. Bluem, J.B. Greer, *Corroison* 32, 3(1976), p. 102.
6. C.D. Beachem, *Metalurgical Transactions* 3,2(1972),p. 437.
7. R.P.M. Proctor, H.W. Paxton, *Transactions of ASM*, Vol. 62 (1969), p. 989.
8. I.M. Bernstein, *Metallurgical Transacitons* 1, 11(1970), p. 3,143.
9. E. Snape, F.W. Schaller, R.M. Forbesjones, *Corrosion* 25, 9(1969), p. 380.
10. P.J. Grobner, D.L. Sponseller, D.E. Diesburg, *Transactions of the ASME*, 29, 2(1976), p. 708.

Table 1. Chemical Compositions of Tested Steels.

	Steel No.	C	Si	Mn	P	S	Cr	Ni	Mo
	1	0.12	0.37	0.56	0.013	0.008	12.55	0.03	-
AISI	2	0.11	0.30	0.49	0.009	0.008	12,90	0.59	-
410 Steels	3	0.13	0.29	0.52	0.010	0.008	13.10	0.69	-
	4	0.15	0.33	0.55	0.009	0.010	12.99	0.69	-
	5	0.18	0.31	0.67	0.006	0.010	12.73	0.22	-
AISI	6	0.21	0.29	0.55	0.008	0.009	13.05	0.09	-
420 Steels	7	0.20	0.27	0.51	0.007	0.008	12.84	0.25	-
	8	0.20	0.25	0.47	0.017	0.009	13.06	0.40	0.73

(wt %)

Table 2. Results of Corrosion Tests and Diffusible Hydrogen Measurements.

Steels		Corrosion Rate mm/year	Diffusible Hydrogen cc/100g·Fe
AISI 410,420 Steels		1.9-4.2	2.2-6.7
Low Alloy Steels	1%Cr	1.4-2.1	2.2-5.5
	2%Cr	1.8-2.4	5.8-9.3



No.1 (0.12%C)



No.3 (0.13%C-0.5%Ni)



No.2 (0.11%C-0.5%Ni)



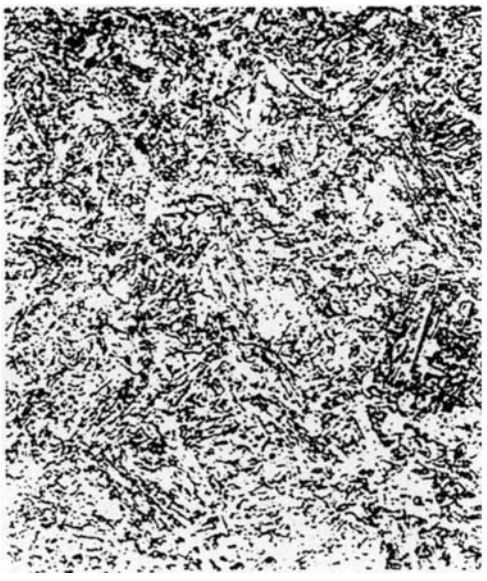
No.4 (0.15%C-0.5%Ni)

50 μm

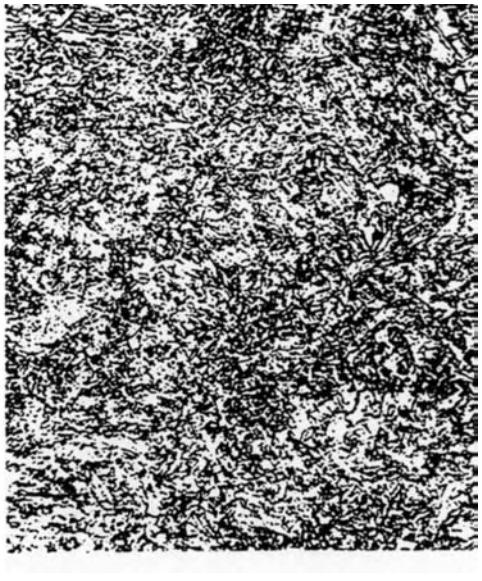
Figure 1 -- Optical microstructures of tested steels.

(Figure 1 continued next page)

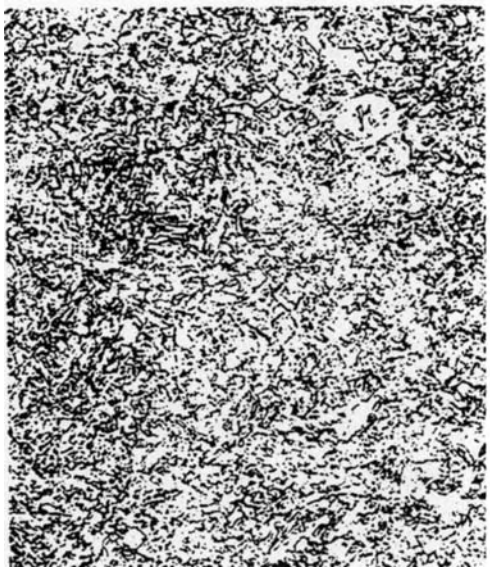
Figure 1 (continued)



No.5 (0.18%C-0.2%Ni)



No.7 (0.20%C-0.2%Ni)



No.6 (0.21%C)



No.8 (0.20%C-0.7%Mo)

50 μm

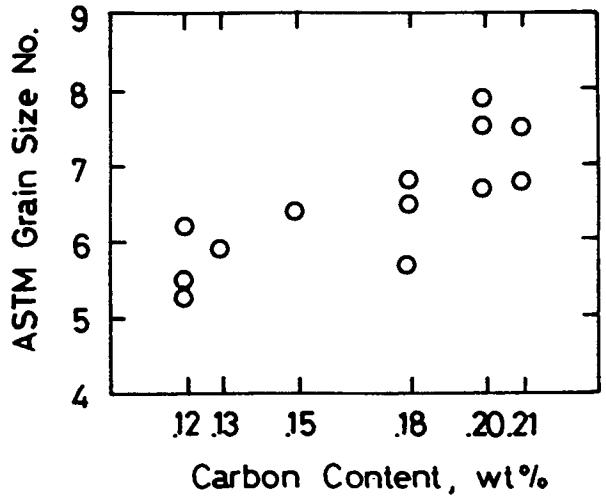


Fig.2 Grain size of tested steels.

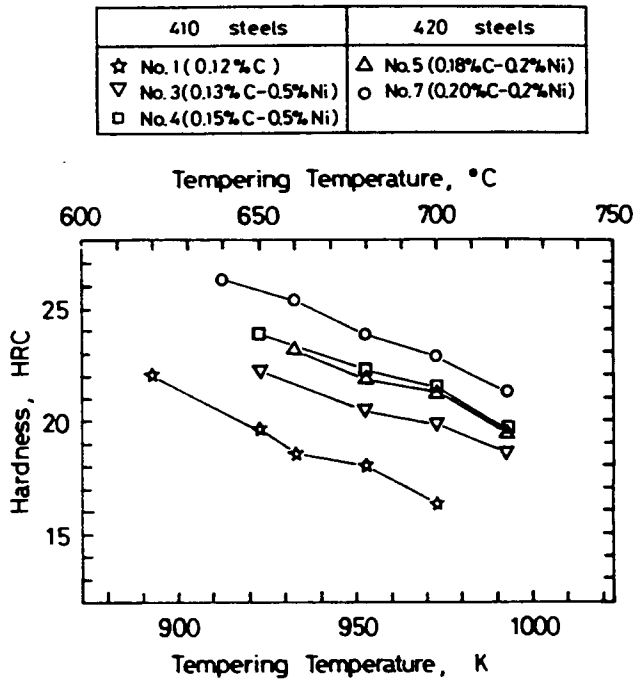


Fig.4 Hardness of No.1,3,4,5, and 7 steels at each tempering temperature.

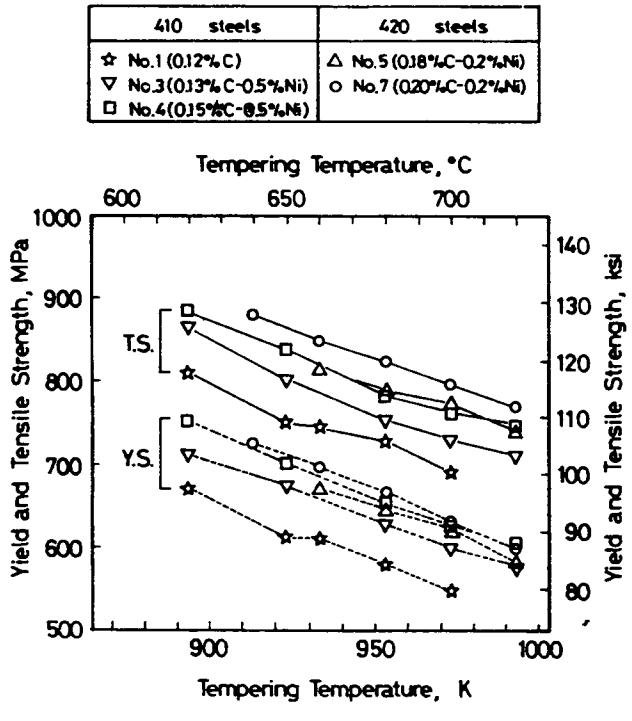


Fig.3 Tensile properties of No.1,3,4,5, and 7 steels at each tempering temperature.

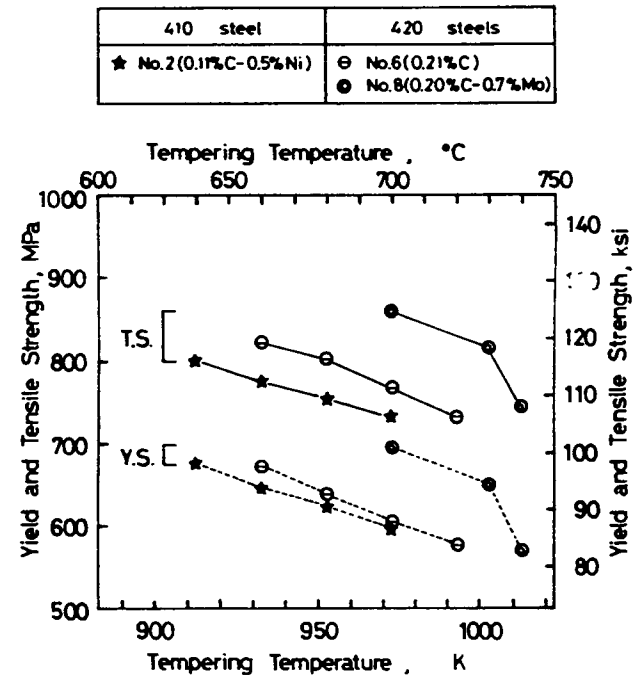


Fig.5 Tensile properties of No.2,6,and 8 steels at each tempering temperature.

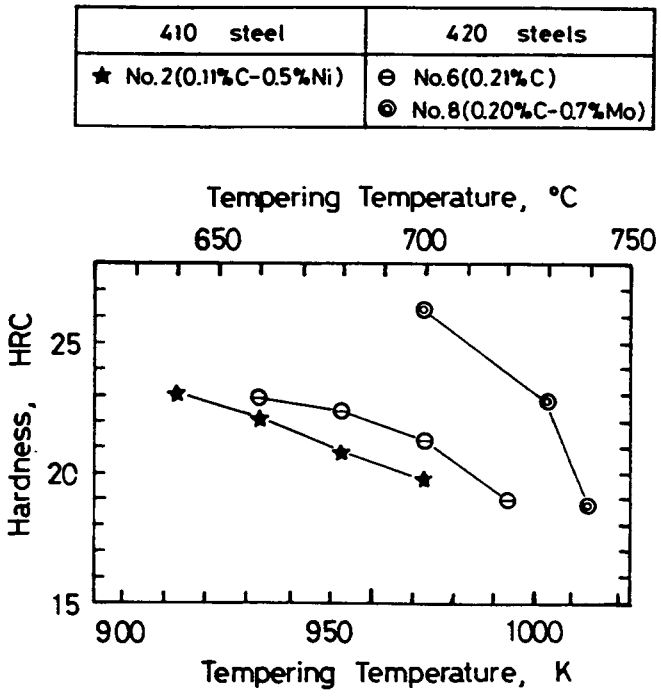
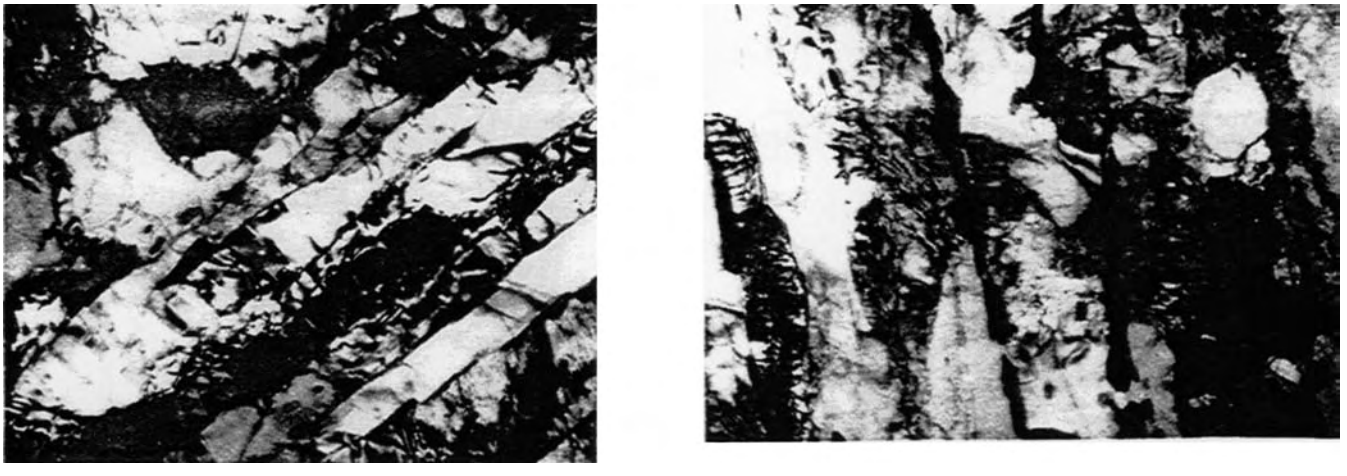


Fig.6 Hardness of No.2,6,and 8 steels at each tempering temperature.



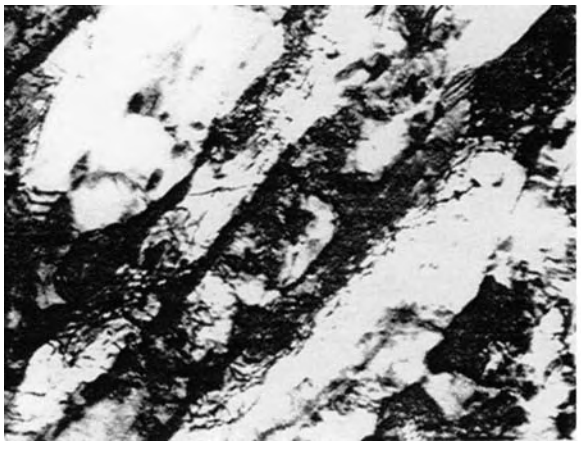
No.2(0.11%C-0.5%Ni)
(a) tempered at 953 K
Y.S.=625 MPa

No.3(0.13%C-0.5%Ni)
(b) tempered at 973 K
Y.S.=610 MPa

Figure 7 -- Thin foil transmission electron micrographs.

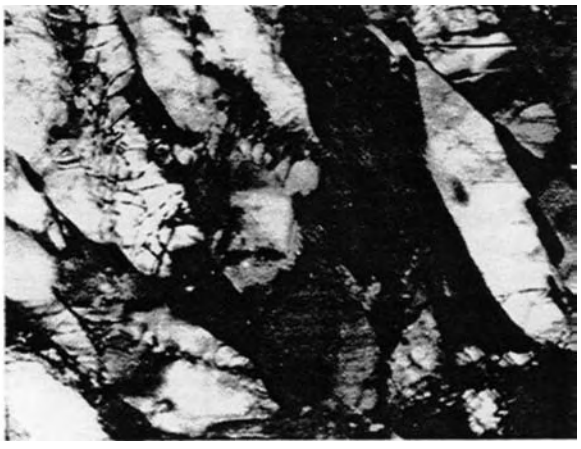
(Figure 7 continued next page)

Figure 7 (continued)



0.5 μm

No.4(0.15%C-0.5%Ni)
(c) tempered at 973 K
Y.S.=630 MPa



0.5 μm

No.5(0.18%C-0.2%Ni)
(f) tempered at 953 K
Y.S.=645 MPa



0.2 μm

No.5(0.18%C-0.2%Ni)
(d) tempered at 993 K
Y.S.=585 MPa



0.5 μm

No.7(0.20%C-0.2%Ni)
(g) tempered at 953 K
Y.S.=665 MPa



0.2 μm

No.7(0.20%C-0.2%Ni)
(e) tempered at 993 K
Y.S.=605 MPa



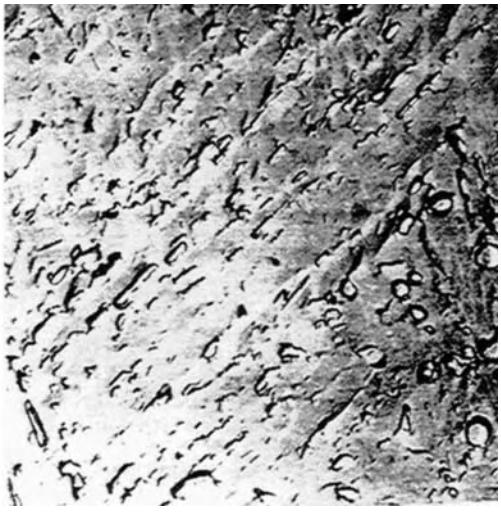
0.2 μm

No.5(0.18%C-0.2%Ni)
(h) tempered at 993 K
Y.S.=585 MPa



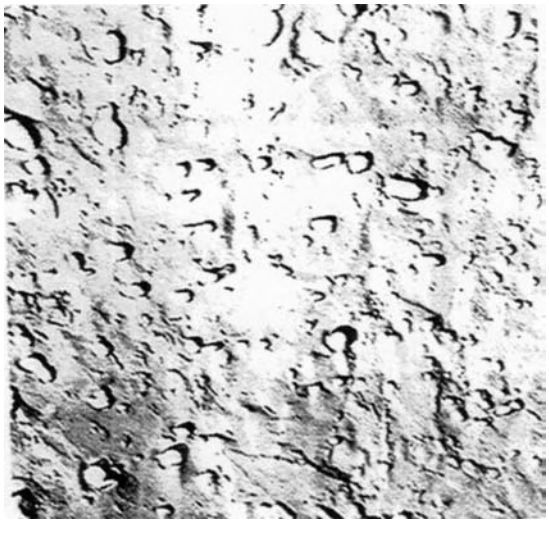
No.1 (0.12%C) 1μm

(a) tempered at 923 K
Y.S.=610 MPa



No.4 (0.15%C-0.5%Ni) 1μm

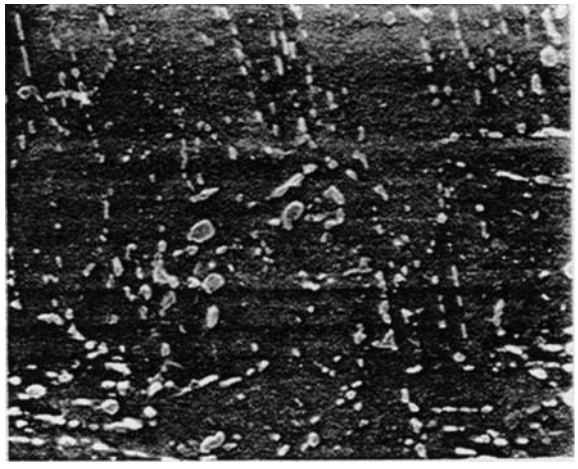
(b) tempered at 953 K
Y.S.=655 MPa



No.7 (0.20%C-0.2%Ni) 1μm

(c) tempered at 973 K
Y.S.=635 MPa

Fig.8 Two-stage replica electron micrographs of No.1,4,and 7 steels.



(a) No.5 (0.18%C-0.2%Ni) tempered at 993 K Y.S.=585 MPa



(b) No.7 (0.20%C-0.2%Ni) tempered at 993 K Y.S.=605 MPa

Fig.9 SEM micrographs of No.5 and 7 steels.

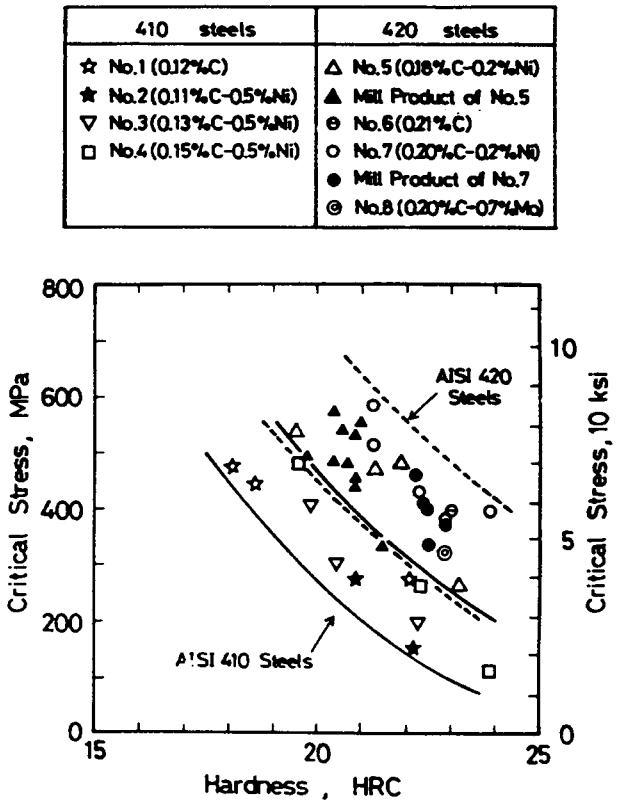


Fig.10 Results of Shell type bent beam tests.

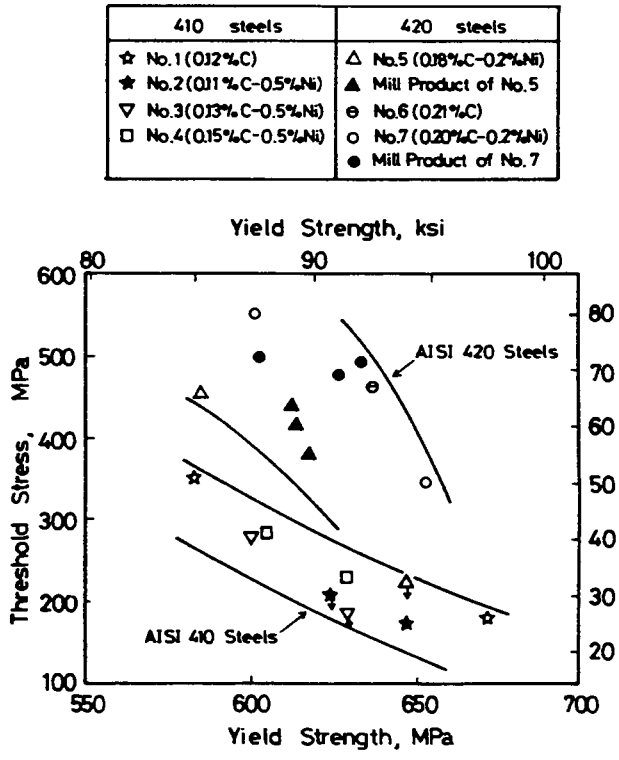
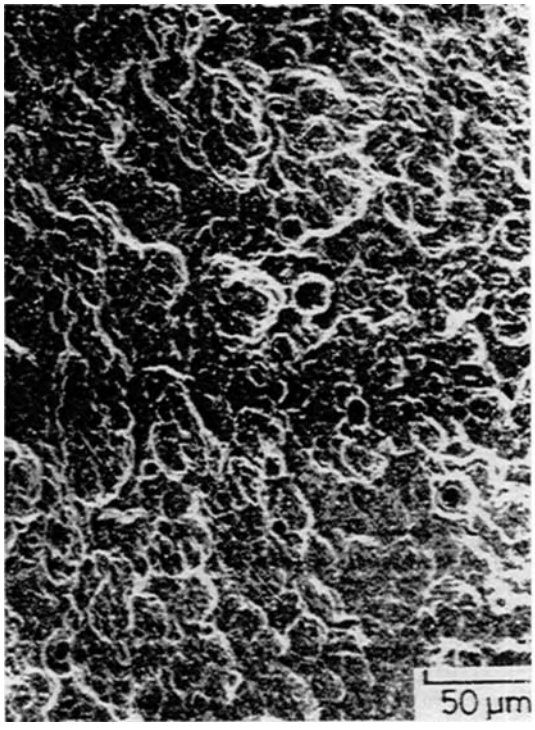
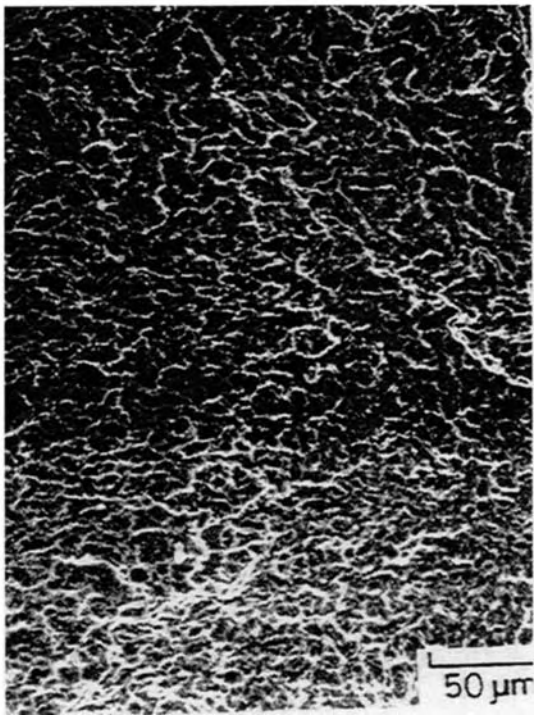


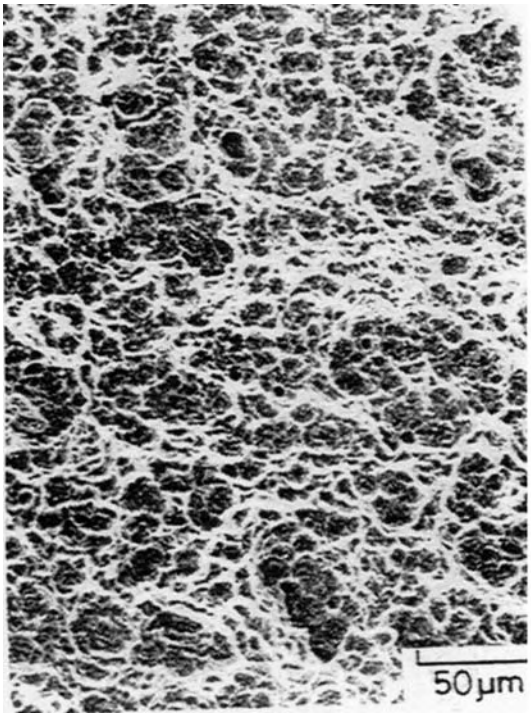
Fig.11 Results of NACE constant load tension tests.



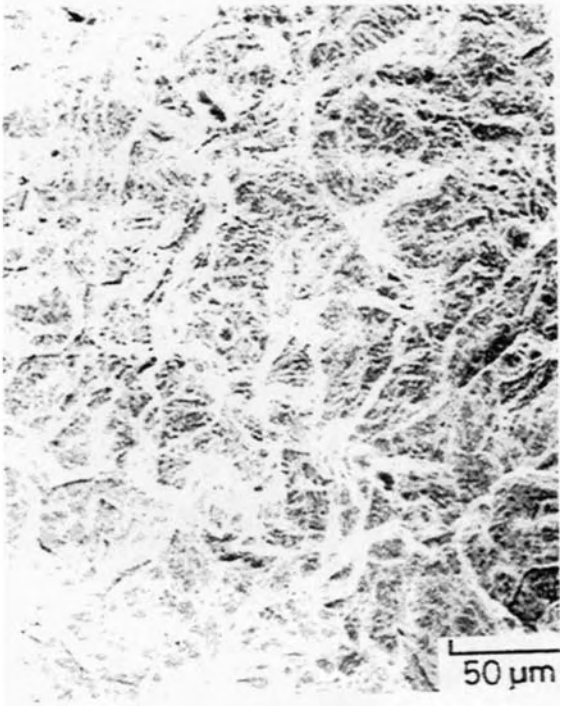
(a)
No.7 (0.20%C-0.2%Ni)
Y.S.=605 MPa



(c)
No.7 (0.20%C-0.2%Ni)
Y.S.=700 MPa



(b)
No.6 (0.21%C)
Y.S.=645 MPa

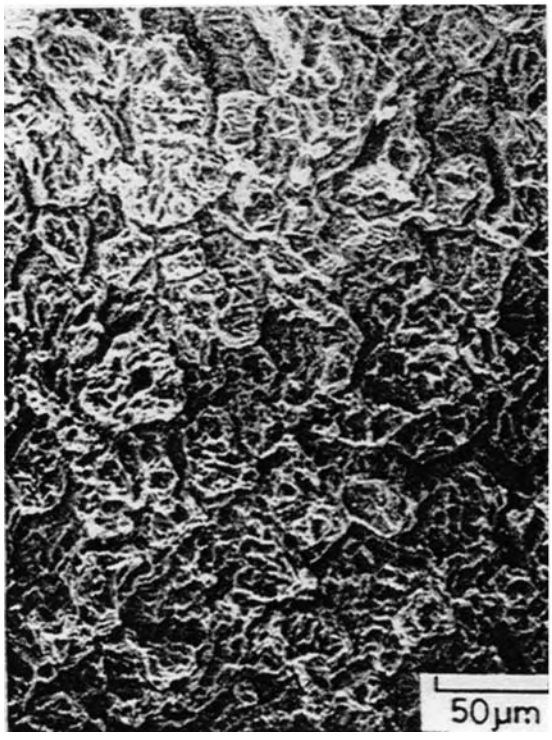


(d)
No.2 (0.11%C-0.5%Ni)
Y.S.=625 MPa

Figure 12 -- SEM fractographs of NACE constant load tension test specimens.

(Figure 12 continued on next page)

Figure 12 (continued)



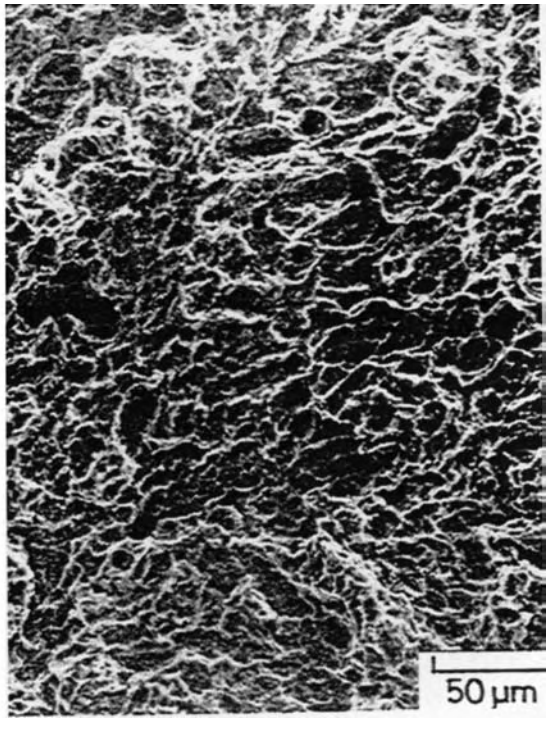
(e)
No.2 (0.11%C-0.5%Ni)
Y.S.=625 MPa



(g) No.1 (0.12%C)
Y.S.=670 MPa

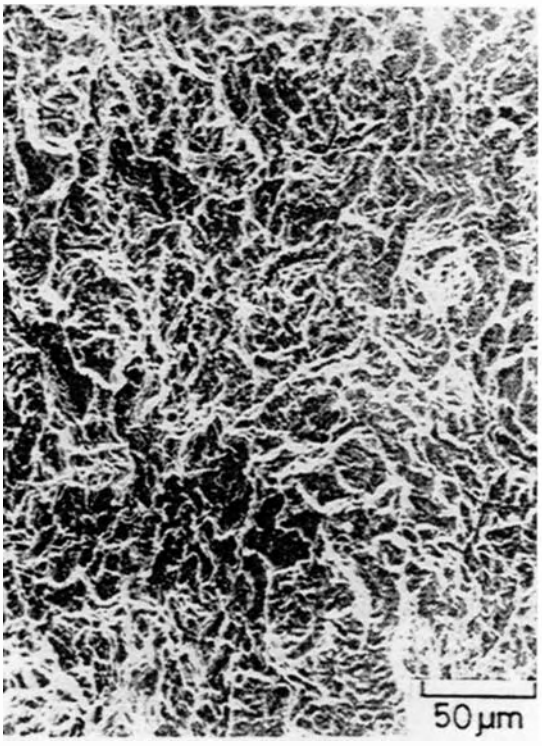


(f)
No.1 (0.12%C)
Y.S.=585 MPa

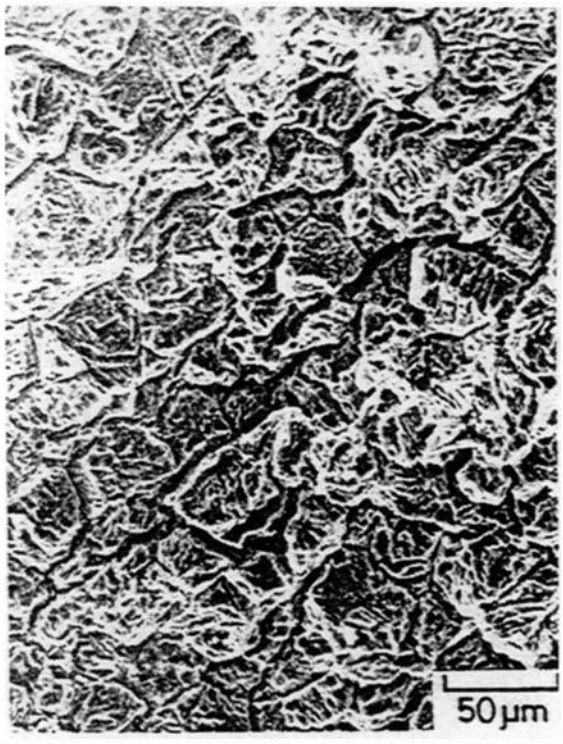


(h)
No.5 (0.18%C-0.2%Ni)
Y.S,=585 MPa

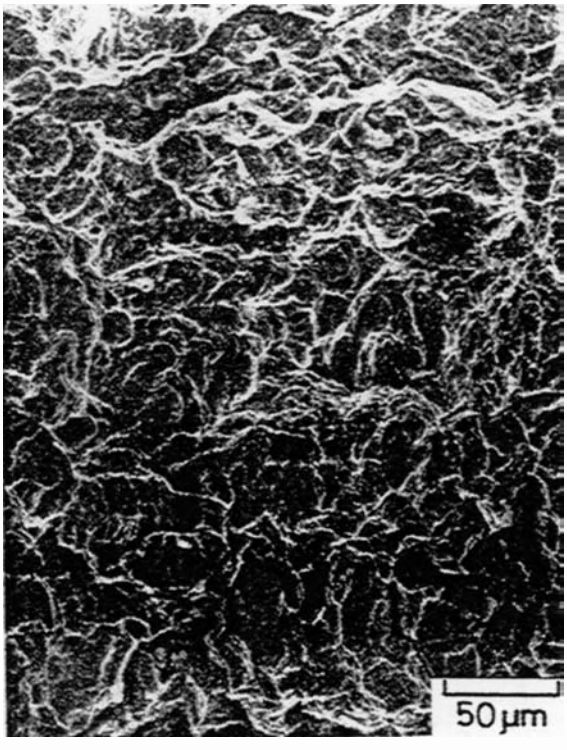
Figure 12 (continued)



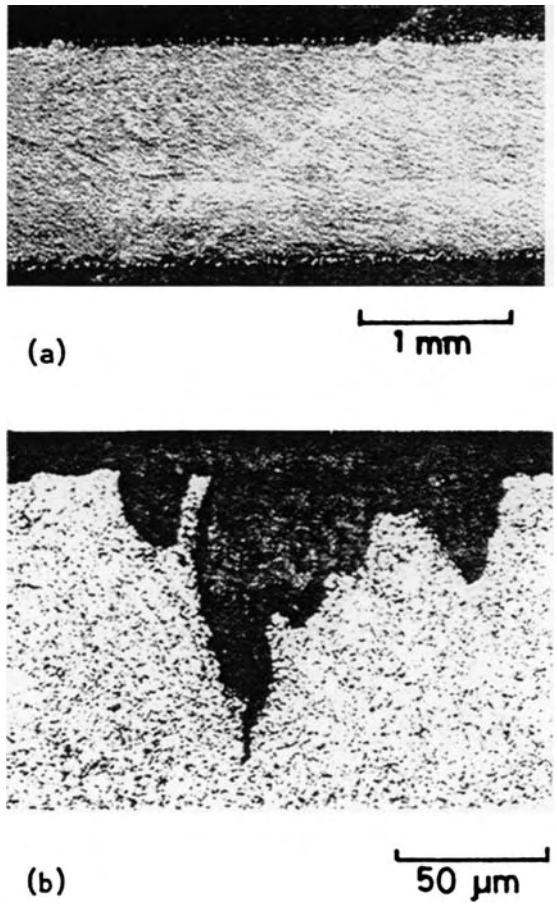
(i) No.5 (0.18%C-0.2%Ni)
Y.S.=645 MPa



(j) No.3 (0.13%C-0.5%Ni)
Y.S.=630 MPa

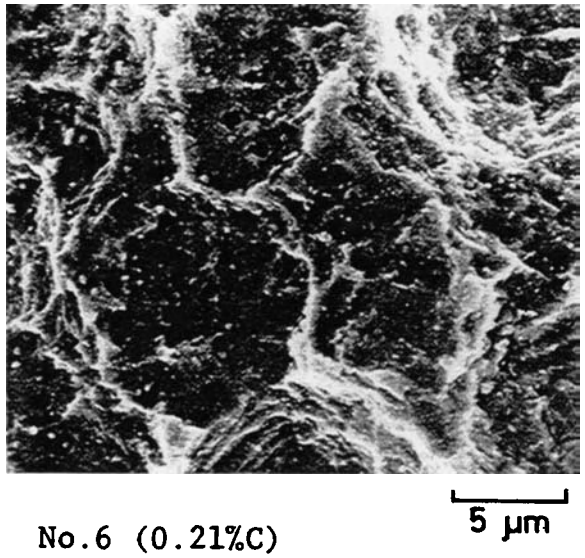


(k) No.4 (0.15%C-0.5%Ni)
Y.S.=600 MPa



No.7 (0.20%C-0.2%Ni)
Y.S.=650 MPa
Applied Stress=360 MPa

Fig.13 Longitudinal cross section of NACE constant load tension test specimen of AISI 420 steel.



No.6 (0.21%C)
Y.S.=645 MPa

Fig.14 Fracture units of dimple-like transgranular fracture (SEM fractograph).

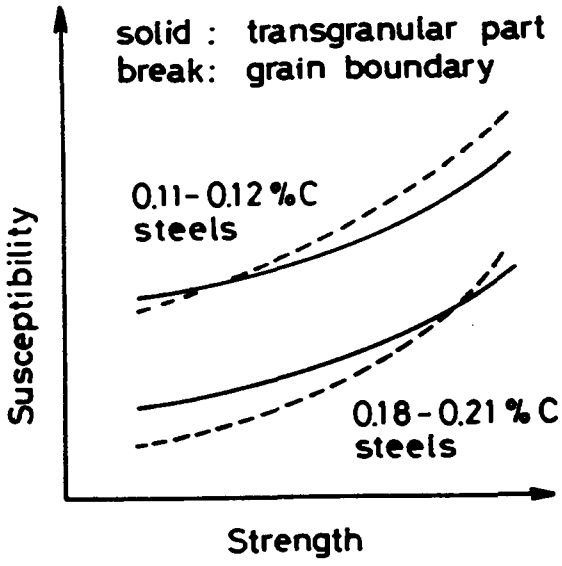
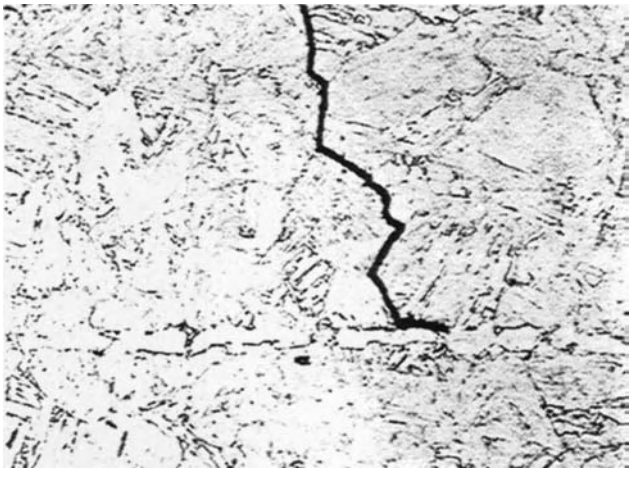


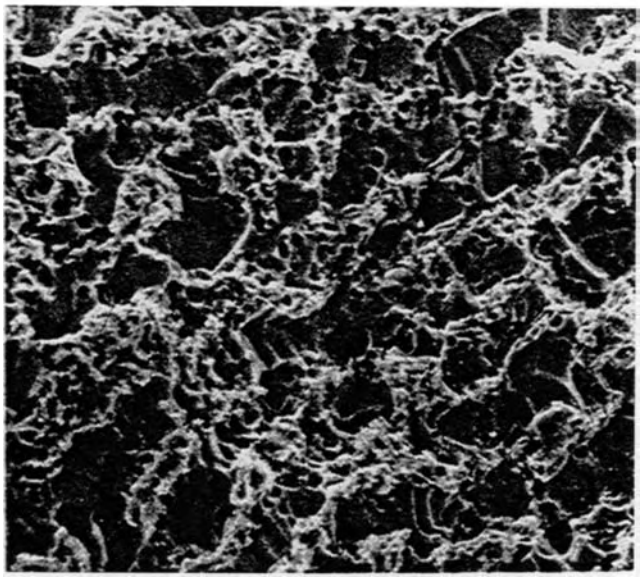
Fig.15 Schematic drawing of the susceptibility to intergranular and transgranular SSCC in 410 and 420 steels.



No.1 (0.12%C)

Fig.16 Obstacle effect of delta-ferrite on crack growth.





0.05%C-13%Cr Steel

Y.S.= 355 MPa

Fig.17 Microstructure and SEM fractograph of 0.05%C-13%Cr steel.

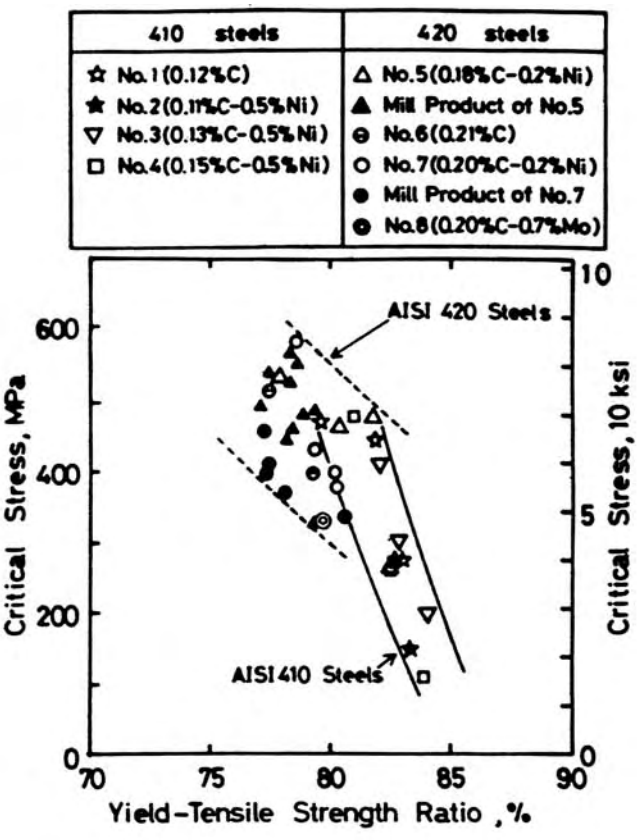


Fig.18 Results of Shell type bent beam tests as a function of the yield to tensile strength ratio.

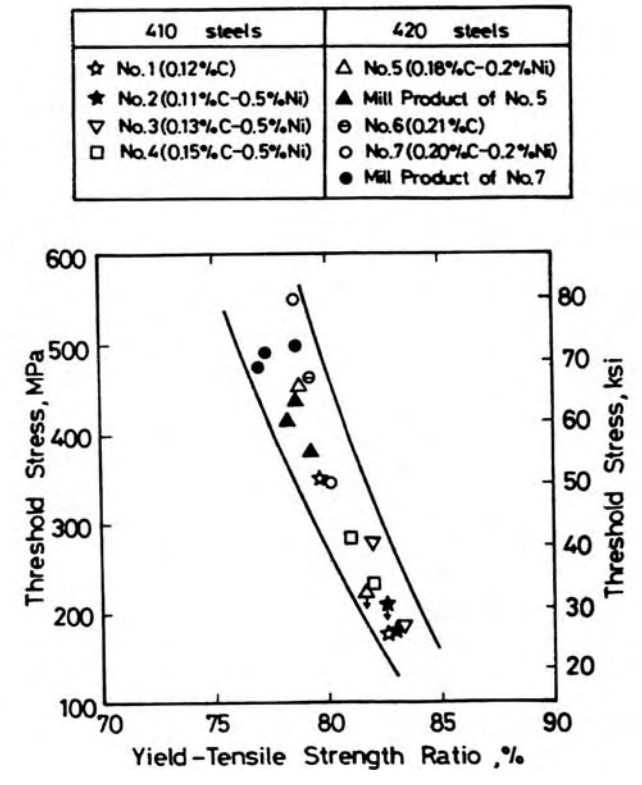


Fig.19 Results of NACE constant load tension tests as a function of the yield to tensile strength ratio.

Copyrighted Materials
Copyright © 1996 NACE International Retrieved from www.knovel.com

Paper No.
96

CORROSION 95
The NACE International Annual Conference and Corrosion Show

OPERATIONAL EXPERIENCE OF USING 13% Cr TUBULAR STEELS

M B Kermani
BP International
Chertsey Road, Sunbury on Thames, UK

G Weighill
BP Exploration
Forusbeen 35, 4033 Forus, Norway

T Pendlington and G Elliot
BP Exploration
Farburn Industrial Estate, Aberdeen, UK

ABSTRACT

Operational experience of using 13% Cr tubing are presented in this article with notable examples of its use as production tubing. The philosophy in deciding to move towards the use of 13% Cr steel tubulars is described based on either laboratory studies indicative of the need for a corrosion resistant alloy or high corrosivity of producing wells on carbon steel tubing. The experience is wide ranging from gas and oil production to sweet and sour conditions. The choice has proved extremely successful in controlling high corrosion in both gas and oil producing fields and in artificial lift oil wells.

INTRODUCTION

In the current climate of squeezed margin, the appropriate and cost effective materials choice in petroleum industry is becoming increasingly vital in sustaining a healthy economy. The choice is governed by mechanical properties, resistance to both corrosion damage and sulphide stress cracking (SSC), availability and cost. Resistance to CO_2 corrosion and SSC are often the principal factors affecting the choice of materials. CO_2 corrosion of carbon and low alloys steels is a major cause of corrosion damage. The resistance to SSC is essential in H_2S-containing environments, since the occurrence of SSC can result in a

catastrophic and potentially hazardous failure (1). These factors often necessitate the selection of highly alloyed, highly priced materials.

The first economical material choice for completion technology continues to be carbon steel which provide sufficient strength backed by economy. The economical advantage of completing a well by carbon or low alloy steel on the initial capital expenditure and its comparison with other options are approximated in Fig. 1. This illustrates the initial capital cost implication of using corrosion resistant tubing. However, in the absence of a true understanding of the long term corrosion behaviour of carbon and low alloy steels and lack of a realistic corrosion predictive tool, alternative choice of materials would need to be considered.

In this paper corrosion experience of three producing fields are described. These cover gas and oil producing fields. Whilst in one example the initial choice was a 13% Cr tubing, others had been initially completed by carbon steel which consequently underwent severe corrosion by CO_2 and necessitated a work-over and replacement of tubing by 13% steel. The experience is wide ranging and reference has been made to the current knowledge of CO_2 corrosion prediction. Prior to describing corrosion experience, an overview of each field is presented.

THE WEST SOLE GAS FIELD

The West Sole Gas Field, discovered in September 1965, was the first commercial gas find in the North Sea and the first to start feeding natural gas into the UK national grid. Following the initial gas developments in the Southern North Sea in the late 1960's the main exploration and production interest moved to the Central and Northern North Sea where oil was the main objective. The discovery of West Sole began a period of gas field discovery and development in the Southern North Sea, which within a decade was supplying almost all of Britain's gas. West Sole gas field is located in the Southern North Sea, some 40 miles east of Spurn Head as shown in Fig. 2. Three offshore platforms and 19 wells are currently available to maintain production rates of up to 280 MMSCF/D to the onshore terminal at Easington, via two submarine pipelines (Fig. 2). Any water produced with the gas is removed by dehydration units located on the platforms. At the terminal the gas is treated to remove condensate prior to delivery into the British Gas transmission system.

Well Conditions and Completion Design

West Sole Field is a sweet gas producing field containing 0.75 mol% CO_2. Well conditions are summarised in Table 1 and an overview of the completion design in shown in Fig. 3. Based on a recent release of the de Waard and Milliams (dWM) algorithm (2), corrosion rate for this field is ca. 9 mm/y hence indicating high corrosivity of the well. Corrosivity assessment using Crolet and Bonis "CORMED" (3) criterion leads to a MEDIUM corrosion risk indicating potential requirement for a premature workover. The corrosivity calculations are included in Table 2.

Completion Tubing

The original material selected for West Sole gas field was grades K55 and N80 carbon steel tubing with a mixture of 13% Cr, 9Cr-1Mo and carbon steel downhole jewellery. The first indication that severe corrosion of carbon steel tubing was occurring came as early as July 1968, when leaking surface valves were inspected. This proved to be indicative of future downhole corrosion problems which was subsequently confirmed by caliper survey and cast considerable doubt on the integrity of tubing strings throughout the field (3).

Early in 1971, it was suspected that the internal upset tubing close to a coupling in one well had parted (4). The well was worked over confirming the initial suspicion - the tubing had parted just below the tubing hanger. A detailed injection revealed the extent of corrosion - this is summarised in Table 3 (4) . In general, corrosion was in the form localised mesa type attack and ring corrosion mostly adjacent to couplings. A widespread shallow pitting corrosion was also evident along the wireline tracks some spreading out from the track.

Detailed studies concluded that the cause of corrosion in West Sole tubular was attributed to a CO_2 corrosion mechanism by the interaction of CO_2 and condensing water in the produced gas forming carbonic acid. As the gas flow proceeds up the tubing, and prevailing conditions exceed dew point, water condensation occurs. This results in the formation of a hanging film of water (water wetting of the surface) leading to corrosion. The factors determining the extent of the film include tubing size, well conditions, gas flow rate and water content. The implication of "hanging film theory" (5) is that the corrosivity of the environment is inversely proportional to depth. Turbulence effect arising from various causes such as changes of section or non-flush couplings may be superimposed on the aforementioned parameters.

As a result of severe corrosion particularly in the top third, some of the wells were worked over after 2-4 years, replacing the corroded carbon steel with 13% Cr grade N80 tuning in the wetted areas (top 3,000 to 4,000 ft).

The first study of the performance of the 13% Cr tubing was made in 1976. It was at this stage that the "hanging film" theory was developed (5). The study revealed satisfactory performance of 13% Cr tubing to the extent that the same tubing was re-run after 5 years service. At that time the aim was to extend the completion life of the wells to 8-10 years minimum. As production continued, the extent of water condensation within the completion increased - finally in early 80s, the full extent of well completions was replaced by 13% Cr due to appearance of corrosion in the lower two third of the wells.

In late 80's, a comprehensive study was carried out on tubings removed from West Sole gas wells. Selected lengths of the N80 tubing and assorted nipples and couplings were examined visually. The conditions of both the low alloy steel and 13% Cr tubings assessed against the known results of previous caliper surveys reiterated earlier findings. In all wells, 13% Cr tubing showed superior performance in comparison to carbon steel tubing, although some superficial pitting corrosion and wireline tracks was identified on some joints. However, these were not considered influential in promoting severe corrosion which led to the conclusion that a useful life significantly well in excess of the required 8-10 years minimum would have been obtained. By contrast, carbon steel tubing suffered severe localised corrosion, mostly associated with wireline tracks, but also spreading out into larger

patches in some cases. The overall corrosion rate approached 0.05" (1.27 mm) per year, although varying from well to well. The corrosion rate of carbon steel in the upper part of the wells reached some 0.16" (4.1 mm) per year. These values are below those determined using dWM algorithm as indicated in Table 2. Damage close to wireline tracks on the tubing surface, appeared to be of fundamental concern, since it appeared to initiate the onset of corrosion. Again, a second form of corrosion was a ring type corrosion on the internal surfaces adjacent to the couplings. The presence of this could not totally be associated with local turbulence effect arising from non-flush transitions across joints. However, this was considered as a likely factor to accelerate metal wastage. Another possible factor was the minor galvanic action arising from a slight difference in the metallurgy of coupling and tubulars. A reasonable correlation between caliper survey results and the subsequent visual examination of corrosion damage experienced on carbon steel tubing was confirmed. On this basis caliper data were considered a determinate technique for assessing the condition of downhole tubulars in the West Sole gas field. However, although results can be misinterpreted if due care is not taken in, for instance, comparing them with previous survey data.

Non-tubular components (downhole jewellery) made from 9Cr-1Mo performed well - some corrosion was present, but this was shallow and restricted in coverage. The adjacent carbon steel tubing manifested only general corrosion which had resulted in greater penetration than any of pits observed on 9Cr-1Mo components with little or no evidence of galvanic attack. The principal corrosion mechanism differed between the wells, but general extent and depth of the damage compared reasonably well with the caliper survey results.

As a result of the experience gained from the West Sole fields all subsequent BP gas field developments in the Southern North Sea basin included the use of 13% Cr completions from initial design. The useful life and cost of replacing carbon steel tubulars on West Sole confirmed that the increased capital cost of 13% Cr completions could be easily justified on a life of field cost analysis.

FORTIES FIELD

BP Forties field, discovered in October 1970, was the first major oil find in the British sector of the North Sea. The field covers an area of 91 hn^2 and is named after the sea area in which it lies, about 177 km north-east of Aberdeen. The position of the field is shown in Fig. 2. Oil production from the field began in 1975, peaked at about half a million barrels per day between 1978 and 1980. By mid-1985, cumulative production had reached one and a half billion barrels, which was over a quarter of all oil produced from the UK Continental Shelf up to that time.

Well Conditions and Completion Design

Forties Field is a sweet oil producing field containing 2.85 mol% CO_2. Well conditions are summarised in Table 1 and an overview of the completion design in shown in Fig. 3. Based on a recent release of the de Waard and Milliams algorithm (2), calculated corrosion rate is ca. 8.7 mm/y hence indicating high corrosivity of the well for a carbon steel tubing. Corrosivity assessment using Crolet and Bonis "CORMED" (3) criterion leads to a HIGH corrosion risk indicating the requirement for a premature workover. The corrosivity calculations are included in Table 2.

Completion Tubing

The original tubing material for all Forties producing wells was carbon steel - a schematic illustration of Forties completion design is shown in Fig. 3. In the mid to late 80's increased corrosion rates were experienced in some wells. While it was recognised the corrosion mechanism was related directly to the formation of carbonic acid, there were several mitigating circumstances that were thought to have influenced the onset and extent of damage amongst which two parameters were considered as having the most influence. These were (i) an increase in concentrations of CO_2 in separator gasses and (ii) the advent of artificial gas lift and the use of submersible pumps both altering corrosion characteristics. The increase in CO_2 concentration in the separator gas with subsequent effect on CO_2 partial pressure was associated with an increase in water cut above a certain limit. In the early 80's the produced water levels in all wells was such that oil rather water wetting of the tubulars occurred and corrosion was not an issue. Under these circumstances the need for tubular replacement was driven by production requirements and not corrosion damage. Lives of up to 10 years for 7" completions were obtained. As the reservoir aged, the water cut increased and the well pressures reduced. Water wetting, and hence, corrosion became apparent and, the use of smaller diameter completions to sustain production increased turbulence in the tubulars. By the late 80's significant corrosion was being experienced on some of the natural lift wells. About the same time artificial lift using gas re-injection or electric submersible pumps (ESP) into the tubulars were installed. Severe corrosion was seen in the very early gas lift completions using carbons steel. In the artificial lift wells using ESP, the increased turbulence and drop in pressure at the suction section of the pump allows gas breakout to occur within the pump which increases the CO_2 concentration in the brine phase above the equilibrium value. This was considered a contributory factor in promoting high rates of corrosion to be observed in ESP lifted wells. Another minor contributory factor was the local turbulence at joints protruding into the flow and increasing the local flow and its subsequent effect on corrosion rate.

A comparison between the corrosion rates determined by caliper survey and those illustrated in Table 2, indicated that, although in the majority of cases, corrosion prediction using available models lead to an overestimation of corrosivity, in some instances, localised corrosion comparable to the extent predicted by the models were experienced.

As a result of severe corrosion experienced in artificial lift wells, a number of producers in Forties field were re-completed with 13% Cr tubing. One string of 13% Cr tubing has been recovered showing little or no corrosion proving the experience of other fields in sustain corrosion by the use of high alloy materials.

Sea water injection is not carried out though 13% Cr tubing.

GYDA FIELD

BP's involvement in the search for oil and gas on the Norwegian Continental Shelf dates back to 1975, when the company farmed in as operator of North Sea Block 7/12. This proved to be the beginning of a long and rewarding engagement for BP in the harsh waters off the coast of Norway. A successful exploration drilling programme on Block 7/12 revealed the Ula field in 1976. Five years later BP discovered the Gyda field in Block 2/1, only 28 kilometres south east of Ula. On these two concessions there now stand offshore drilling and production facilities, designed to safely and efficiently retrieve oil and gas from as much as four kilometres beneath the sea floor.

Location of the Gyda oilfield situated in the Norwegian sector of the North Sea is shown in Fig. 2. First oil from Gyda was produced in 1990 using the natural energy from the reservoir to lift the fluids to surface. The gas is sent to Ekofisk which is either used as a fuel gas at Ekofisk or subsequently transported to a terminal at Emden in Germany. The oil is joined the pipeline from Ula via a Y piece and sent to Ekofisk. From Ekofisk the oil is transported in the existing system to a terminal at Teesside, England.

Well Conditions and Completion Design

Gyda Field is a sour oil producing field containing 2 mol% CO_2 and 22 ppm H_2S. Well conditions are summarised in Table 1 and an overview of the completion design in shown in Fig. 3. Based on a recent release of the de Waard and Milliams (dWM) algorithm (2), corrosion rate is ca. 5.7 mm/y hence indicating high corrosivity of the well for carbon steel tubing. Corrosivity assessment using Crolet and Bonis "CORMED" (3) criterion leads to a MEDIUM corrosion risk indicating potential requirement for a premature workover. The corrosivity calculations are included in Table 2.

Completion Tubing

The original development study identified a high potential for $C0_2$ corrosion from formation water and 13% Cr tubulars were recommended for controlling corrosion in production wells.

Referring to the summary of fluid and reservoir conditions in Table 1, the partial pressure of CO_2 is 51 psia at 3000 psia bubble point pressure and the bottom hole temperature (BHT) is 310 ^oF at 13630 ft total vertical depth (TVD) subsea datum, indicating a high potential for corrosion. A review was carried out to identify the most cost effective method of controlling corrosion when water occurs in producing wells and 13% Cr tubulars were proposed. However, doubts existed over the suitability of 13% Cr at the high bottom hole temperatures. An experimental study was set up in 1987 to determine corrosion rates of 13% Cr under simulated Gyda conditions in a high temperature and pressure autoclave facility.

Laboratory Tests

The tests were carried out under 'worst case' downhole conditions using test solutions of simulated Gyda formation water and sea water and determined corrosion rates of 21 - 43 and 6 - 64 mpy, respectively - latter values refer to the extent of localised corrosion. Seawater tests were included to simulate conditions when injected seawater for reservoir pressure maintenance dominates the produced fluid. Pitting corrosion was seen and the higher rate for each fluid type represented effects of localised corrosion with the removal of the protective film, e.g.: with turbulence due to gas breakout. However, these results were considered pessimistic as reflecting worst case scenario and oil wetting of the surface was omitted from the tests - this could tend to lower the corrosion rates and, at least for the first few years of production, water production was not expected. Other similar experience has shown that subsequent water production may not be detrimental to a tubing which has been producing a dry oil at low production rates (6). Sulphide stress cracking (SSC) was not considered a risk, as the calculated in-situ pH and H_2S partial pressures were within the safe domains for the use of 13% Cr tubing steel (7).

The study considered three options for controlling downhole corrosion - these are shown in Table 4. Also, included is the overall cost (initial capital expenditures plus the operating expenditures) are the operational implications of the 3 options reviewed for the life of the field - the costs are based on 1987 figures.

The decision was taken to install 13% Cr downhole tubulars on Gyda rather than duplex stainless steel because some 70% of the £M 17.3 was for working over the wells and some of these costs may be offset during the field life if wells were worked over for reasons other than corrosion. In addition to this, 13% Cr was considered satisfactory to last for the life of some wells and the up-front capital cost of duplex stainless steel was considered too high. The decision was supported by a review by the suppliers, although Gyda bottom hole temperature was at the limit for the recommended use of 13% Cr and no data were available for corrosion trends at higher temperatures.

Oil Producer Wells

Gyda oil producer completion were specified with 13% Cr stainless steel for all downhole tubulars exposed to producing fluids and typically comprise 5" tubing from surface, crossed over to 4.5" tubing above a seal assembly stabbed directly into a 4.5" liner. A tubing retrievable downhole safety valve is installed in the 5" tubing, typically at 1900 ft. The outer casings are specified in carbon steel and the Xmas tree and flowlines in duplex stainless steel. An overview of completion schematic is shown in Fig. 3.

On Gyda, there are currently 15 natural lift oil production wells completed with 13% Cr tubulars. The completions were installed between 1990 - 94 and the majority of the wells still produce dry oil. However, seawater breakthrough has occurred in 4 wells and they produce predominantly seawater. In addition to these, 1 well produces ca. 5% formation water and seawater breakthrough is expected soon and a further well has cut formation water but is closed in.

To date, there has been no evidence of corrosion in any of the 13% Cr producer completions, either from caliper surveys or flowline corrosion coupon monitoring. Although caliper surveys have been proposed for downhole corrosion monitoring, in practice very few have been run on Gyda for operational reasons. The experience of Gyda in the use of 13% Cr tubing in condition in excess of the temperature and H_2S concentration industry limits for the recommended use of 13% Cr has proven its superior performance.

Water Injection Wells

Gyda standard water injection completions are specified with carbon steel tubulars and are therefore beyond the scope of this paper. However, there are some 4 oil producer wells completed with 13% Cr tubulars which have been turned around to water injection due to changes in reservoir management strategy. There is some potential for oxygen pitting corrosion at couplings, although oxygen residuals in the Gyda injection water are generally ca. 10 ppb and corrosion risk is considered low. To date, no significant corrosion has been observed although recent evidence indicates the potential for chloride pitting.

Laboratory studies have shown that, in general, 13% Cr steel shows good corrosion resistance when exposed to sea water injection under base line conditions, i.e. oxygen

level: 20 ppb, sea water temperature: 14 ^{o}C max., flow velocity 2 m/s max. Increasing any of these parameters could cause severe corrosion attack. They reported that re-injection of chlorine to the injected water should be avoided.

To date, the performance of 13% Cr tubulars on the Gyda oilfield has been good and adds support to the findings of the original laboratory studies. The downhole tubulars will continue to be monitored carefully as more wells cut water and the potential for corrosion increases.

SUMMARY

Well corrosivity identified by initial studies and predictive modelling have reiterated the severity of CO_2 corrosion for carbon steel. The predictive models, although proving essential as an estimate of potential corrosivity, are inadequate in addressing all parameters affecting the long term performance of carbon steel. The high corrosion rates experienced in CO_2 containing produced fluids were successfully contained by the use of 13% Cr steel tubing. The North Sea experience of using well completion by the use of 13% Cr has been satisfactory in the combat against corrosion. This has been further maintained by the regular use of corrosion monitoring to ensure that tubing design is successfully preventing corrosion. On the basis of tubing inspection, caliper data were considered a determinate technique for assessing the condition of downhole tubulars, although results can be misinterpreted if due care is not taken in, for instance, comparing them with previous survey data.

Tubing inspection and running practices have had to be rigorously defined and followed (4). In particular, the importance of: (i) flush couplings; (ii) use of the optimum tubing make-up torque, and (iii) detailed pre-running inspection to eliminate manufacturing defects have been highlighted over the years. Failure in any of these areas can lead to rapid tubing deterioration downhole.

One final point of note is the potential problem of thread galling with the 13% Cr which has to be properly addressed by suitable anti-galling thread coatings. The original 13% Cr tubulars in the West Sole field had the threaded surfaces protected by an oxalation treatment, similar to phosphating treatment (parkerising) for low alloy steel tubulars. Threads in the current generation of 13% Cr tubing are treated by a copper plating for the coupling only. This may be a source of concern when used for the purpose of water injection and industry experience of this is not totally favourable.

ACKNOWLEDGEMENT

The authors wish to thank BP Exploration for permission to publish this paper. Special thanks are due to Miss Tracy Smith, Messrs Don Harrop and Paul Badelek for their valuable comments and contributions to this work.

NOMENCLATURE

BHP	Bottom Hole Temperature	BHP	Bottom Hole Pressure
D	Day	dWM	de Waard & Milliams
ESP	Electric Submersible Pump	GOR	Gas Oil Ratio
MM	Million	mpy	mils per year
SCF	Standard Cubic feet	STB	Standard Barrel
TVD	Total Vertical Depth		

REFERENCES

1. M B Kermani, in the Proceeding of the Conference on Hydrogen Transport and Cracking in Metals, Institute of Materials, in publication, 1994.

2. C de Waard and U Lotz, NACE Annual Conference, CORROSION '93, Paper No 69, 1993.

3. J L Crolet and M R Bonis, NACE Annual Conference, CORROSION '85, Paper No 232, 1985.

4. D J Gair and T P Moulds, Tubular Corrosion in the West Sole Gasfield, Corrosion Prevention & Control, pp 50-57, June 1985.

5. G B Wallis and S Makkenchery, The hanging film phenomenon in vertical annular two phase flow, J Fluids Eng., Sept. 1978.

6. N Blackburn, Society of Petroleum Engineers, SPE 27604, January 1993.

7. M B Kermani, D Harrop, M L R Truchon and J L Crolet, NACE Annual Conference, CORROSION '91, Paper No 21, 1991.

Table 1

Well Conditions

Field	Field Type	GOR (SCF/STB)	CO_2 (mol%)	H_2S (ppm)	BHP (Bubble Point) (psi)	BHT (^oC)
West Sole	Gas	-	0.78	0	1850	85
Forties	Oil - artificial lift	420	2.85	0	2000	110
Gyda	Oil	956	2.0	22	8600 (3,000)	154

Table 2

Calculated Corrosivity of Produced Water for Carbon and Low Alloy Steel Tubing

Field	In-situ pH*	dWM Corrosion Rate (mm/y)	CORMED Corrosion Risk	Tubing
West Sole	4.07	9.00	Medium	13% Cr replacing original CS
Forties	4.69	8.7	High	13% Cr replacing original CS
Gyda	4.3	5.7	Medium	13% Cr

*: Calculated in-situ pH without the effect of gas partitioning
CS: carbon steel

Table 3

Corrosion Damage of Carbon Steel Tubing in West Sole Gas Field

Depth (ft) (below tubing hanger)	Completion Equipment	Description of Corrosion
0 - 30	Wellhead and 1st Joint Tubing	Tubing parted below tubing hanger - severe metal wastage with instances of holes
30 - 600	Tubing	Seep, scattered pits, occasional instances of holes
600 - 1800	Tubing	Isolated areas of light pitting, some grooving at joints
1800 - 1825	Downhole safety valves & 10 ft tubing above and below	Severe metal wastage with small isolated holes
1825 - 9000	Tubing	Light , shallow, scattered pits
9000 - 9100	Packer & tailpipe	No corrosion

Table 4

Gyda Materials Choice

Choice No.	Materials Choice	Tubing Cost (£M)	Implications
1.	Low alloy steel with downhole corrosion inhibition	112.0	Many workovers and no guarantee of success
2.	13% Cr stainless steel production strings	17.3 - 32.2	Assuming 1 workover per well due to corrosion in field life
3.	Duplex stainless steel production strings	9.9	Assuming 1 string per well lasting for field life and not considering workovers for non corrosion related issues

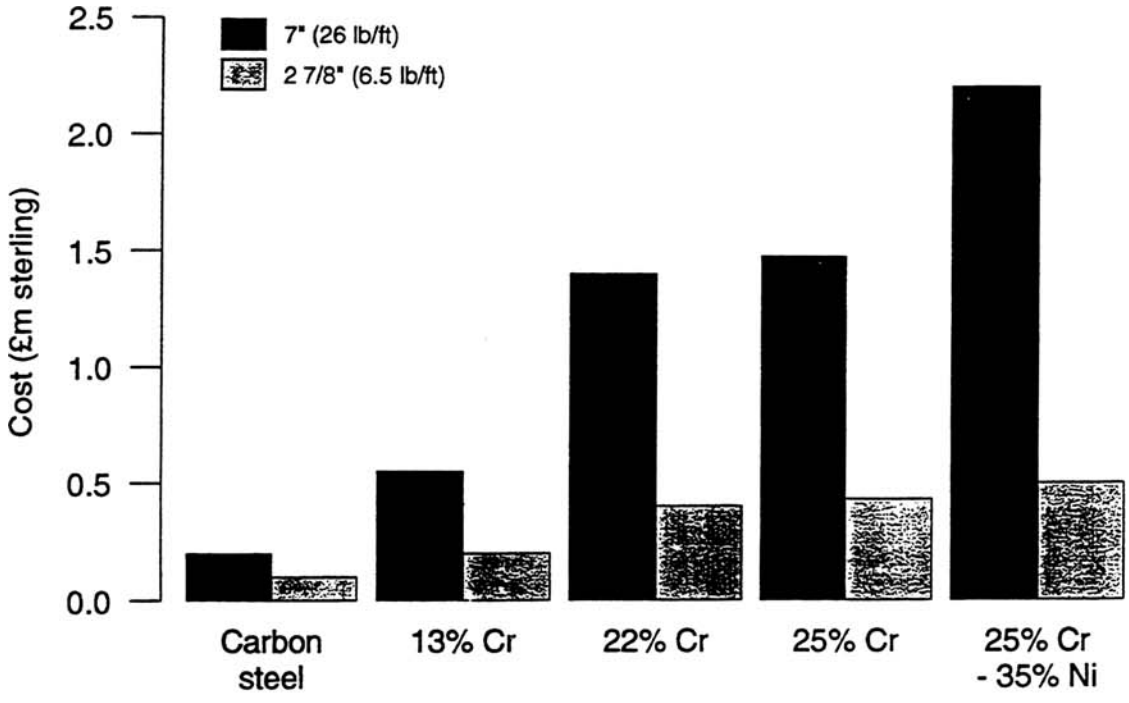


Fig.1 Comparative cost of well completions (5000m with premium threads)



Fig 2. Fields locations

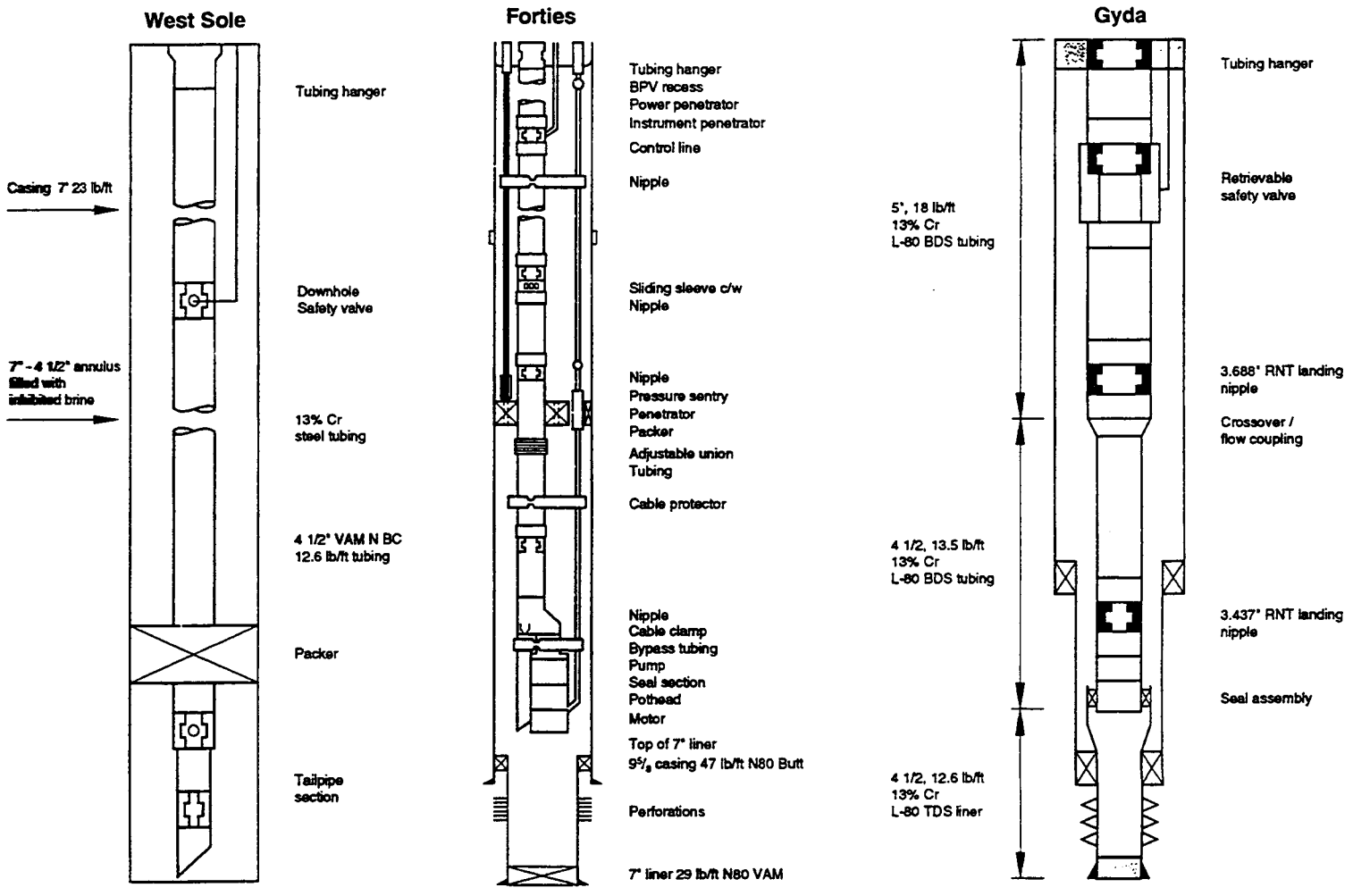


Fig 3. Schematic of typical completion strings

Copyrighted Materials
Copyright © 1996 NACE International Retrieved from www.knovel.com

INFLUENCE OF CATHODIC PROTECTION ON STRESS CORROSION CRACKING OF MARTENSITIC STAINLESS STEELS IN SEA WATER*

H. KIESHEYER and G. LENNARTZ
Thyssen Edelstahlwerke AG, Krefeld, West Germany

Generally martensitic stainless steels exhibit poor resistance against stress corrosion cracking (SCC) in chloride containing media. If the free corrosion potential of the material is more noble than it's pitting potential occuring pits act as initiators of chloride induced SCC, or if the material's potential is so unnoble that hydrogen evolution takes place hydrogen induced embrittlement and SCC is possible. This work's intention is the investigation of SCC immune potential gaps between the pitting and the hydrogen evolution potentials, in which a cathodic protection of these steels is feasible.

Experimental procedure

Three commercial martensitic steels with two strength conditions each were selected for this investigations (Fig. 1):

- the heat treatable steel x 22 CrNi 1 7 (DIN-Mat. Nr. 1.4057 containing 0.22% C, 17% Cr and 1% Ni (- AISI 431),
- the low carbon martensitic type x 4 CrNiMo 16 5 containing 0.04% C, 16% Cr, 5% Ni and 1.2% Mo (DIN-Mat. Nr.1.4418)
- the precipitation hardening steel x 5 CrNiCuNb 17 4 (DIN-Mat. Nr. 1.4512), a 17-4 PH type containing 0.05% C, 16% Cr, 4% Ni, 3% Cu and 0.3% Cb.

In all laboratory tests artificial sea water (DIN 50 907) has been used. They were accomplished with notched tensile test specimens under constant load as well as under slowly alternating stress.

In the range from –1000 up to +300 mVH test potentials of the specimens were set potentiostatically.

At the pilot plant of the ferrous metallurgy engineer association of Germany (VDEh) at Heligoland ground flat specimens were exposed for one year in the three areas of spray water, of tidal and of permanent immersion. Furthermore test pieces with cathodic protection by iron were exposed in the zones of tidal and permanent immersion.

Since May '81 unprotected and iron- or zinc-protected double cantilever beam (DCB) specimens were placed in all three areas. These experiments are just going on.

Test Results

Experiments with constant load

Fig. 2 shows the results for steel x 22 CrNi 1 7 with its two states of strength constantly loaded with 85% of the actual notch tensile strength.

At more noble potentials than the pitting potential of about +100 mVH the times to failure drop down drastically. Even some 50mV below the pitting potential single cracks can appear initiated by crevice corrosion under covers.

In the cathodic area exists a threshold potential under which the times to failure also decrease considerably i.e. under these conditions the steel becomes susceptible to hydrogen induced SCC. This threshold potential is about –800 mVH for the lower and –600 mVH for the higher strength condition, which accordingly is more susceptible to this corrosion type. The low-carbon martensitic steel x 4 CrNiMo 16 5 shows a better corrosion behaviour. At the anodic side the pitting potential is about 100mV more noble that of steel x 22 CrNi 1 7. In the cathodic area only some specimens with the higher strength state failed at very low potentials. This steel shows the most extensive potential gap, in which no corrosion occurs. The most susceptible material is the precipitation hardening steel x5 CrNiCuNb 17 4 especially in the state of higher strength. Its threshold potential of hydrogen induced SCC is about –400mVH.

Without external polarisation the open circuit potentials of all specimens are near the corresponding pitting potentials, but up to 2000 h exposure time neither cracks no any visible pits were observed.

In galvanic contact with the higher chloride corrosion resistant steel x 5 CrNiMo 18 10 (DIN-Mat. No. 1.4401) specimens of the materials x 22 CrNi 1 7 and x 5 CrNiCuNb 17 5 failed by cracking after 100-350 H exposure time.

Experiments with alternating stress

At free corrosion potentials under alternating stress with about two cycles per minute, a minimum stress of 0.2 x R_mK_z and maximum stresses of 0.4 - 0.7 x R_mK_z specimens of all three steels show failure times of about 80% compared with those tested in air (Fig. 3).

Potentiostatic tests have demonstrated, that there also exist distinct threshold potentials depending on the material conditions and the maximum stress. Below these potentials the failure times decrease remarkably, above these potentials the times of exposure get up to those of air tested specimen. Again the order of increasing susceptibility is x 4 CrNiMo 16 5, x 22 CrNi 17 and x5 CrNiCuNb 17 5.

Field tests at Heligoland

In the spraywater zone the steel x 22 CrNi 1 7 shows the most severe corrosion. Caused by severe pitting rust was built up on the surface and under PVC washers crevice corrosion had taken place, whereas the both other steel types exhibit only unimportant discolouring by single small pits.

In the tidal and the permanent immersion zones the unprotected specimens of all three steels show pitting and

**This investigation was sponsored by the Ministry of Research and Technology of West Germany.*

furthermore crevice attack under PVC washers and barnacles.

Cathodically protected by iron all specimens of the permanent immersion zone are free of any kind of corrosion. In the tidal immersion zone only test pieces of steel x 22 CrNi 1 7 show some crevice corrosion under barnacles and washers.

Thus by means of a well tuned cathodic protection it is possible to make use of these high strength martensitic steels for marine applications e.g. for off-shore techniques.

MATERIAL	R_m N/mm²	A_5 %	Z %	NOTCH TENSILE STRENGTH IN N/mm² NOTCH FACTOR $\alpha_K \sim 3{,}5$ d = 5 mm	d = 3 mm
4057	938	16,4	60	1430	1585
4057	1182	13,2	58	1839	2061
4418	893	20,8	72	1412	1573
4418	1032	16,2	65	1723	1809
4542	1121	15,6	60	1765	1972
4542	1401	12,0	55	2244	2430

Fig 1.

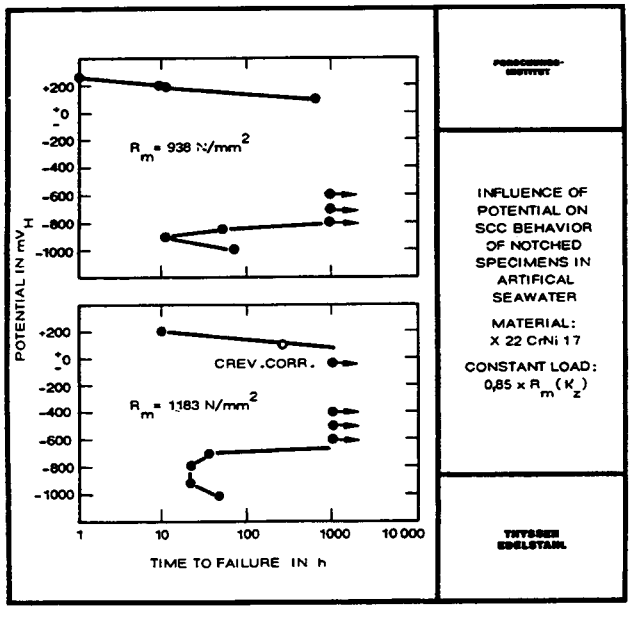


Fig 2.

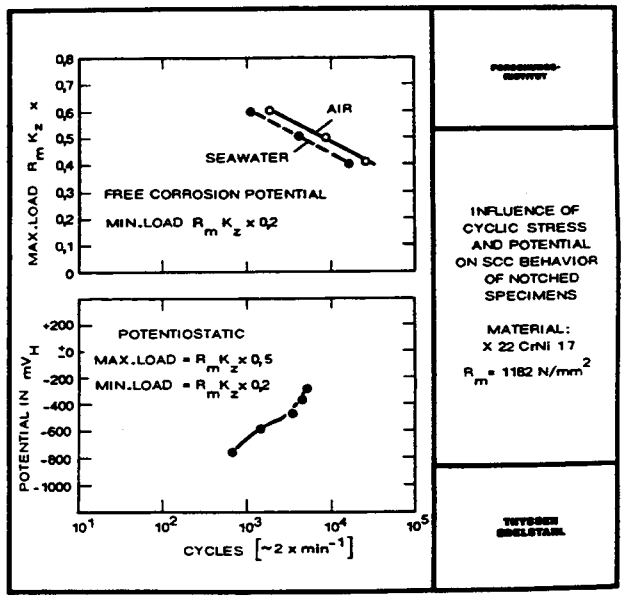


Fig 3.

Copyrighted Materials
Copyright © 1996 NACE International Retrieved from www.knovel.com

H_2S cracking resistance of 420 stainless steel tubulars*

*Leigh J. Klein**

AISI 420 stainless steel (13 Cr) production tubing is being used successfully in deep sour gas wells in the Tuscaloosa Trend Despite their reputation for poor H_2S cracking resistance in laboratory tests, 12-13% Cr steels continue to perform well in sour environments. NACE tensile test and Shell bent beam test results indicate that 420 is more resistant to H_2S cracking than 410, but it is not as resistant as carbon steel at the 586 to 690 MPa (85 to 100 ksi) yield strength level. In addition to evaluating 420 stainless steel in the standard NACE tensile and Shell bent beam tests, the effects of chloride concentration, pH, and H_2S gas concentration on cracking tendency in the NACE test solution were also examined. The cracking tendency of 420 increases as the NaCl concentration in the NACE tensile test is increased from 0 to 5%. Above 5% NaCl, cracking susceptibility remains constant. Cracking susceptibility is reduced when the initial pH of the NACE solution is adjusted to 4.0. Cracking tendency is also reduced when the H_2S concentration in the gas used for the NACE test is reduced below the standard 100%. AISI 420 appears to be more resistant to H_2S cracking than is indicated by standard laboratory tests, at least in low H_2S level sour environments.

Introduction

THE SEARCH FOR OIL AND GAS IN DEEP, hot, sour environments has prompted an increase over the last five years in the study and use of high alloy production tubulars as an alternative to carbon and low alloy steel tubulars protected by corrosion inhibitors. Chevron USA began using high alloy corrosion resistant tubulars in 1980 when AISI 420 stainless steel (13 Cr) was chosen for 60.3 mm (2 3/8 in.) OD 6.45 mm (0.254 in.) wall thickness production tubulars for deep sour gas wells in the Tuscaloosa Trend.[1] Until that time, restricted yield strength [586 to 690 MPa (85 to 100 ksi)], plastic coated, sour service, low alloy steel tubing had been suffering from severe CO_2 pitting corrosion at rates up to 7.6 mm/y (300 mpy). The wells typically contained 8% CO_2 and up to 34,000 ppm chloride ion, but only 20 to 30 ppm H_2S. Bottom hole temperatures were about 190 C (375 F) and bottom hole pressures were about 100 MPa (15,000 psi). At that high pressure, the wells were sour by the NACE MR-01-75 definition. The H_2S partial pressures were about 0.003 MPa (0.4 psi).

To meet the mechanical strength requirements of the well design, a 586 MPa (85 ksi) minimum yield strength for the tubing was needed. Because it was unreasonable to simultaneously require 586 MPa (85 ksi) minimum yield strength and MR-01-75's Rockwell C22 maximum hardness for martensitic stainless steel, the hardness limit for the tubing was initially set at Rockwell C24. As manufacturers obtained experience in heat treating 13 Cr tubing, they were able to maintain tight control over mechanical properties, and so the hardness limit was later reduced to Rockwell C23.

There are two other points on which the 13 Cr tubing does not meet MR-01-75. First, 420 stainless steel is not listed as an acceptable martensitic stainless steel by MR-01-75. Second, MR-01-75 requires double tempering of all martensitic stainless steels, both cast and wrought. The tubing used in the Tuscaloosa Trend gas wells was austenitized, fully hardened by air cooling, and then single tempered only. The tubes could not be water quenched because water quenching causes quench cracks. Test results indicate double tempering does not improve the H_2S cracking resistance of wrought 420 stainless steel as long as it is tempered properly the first time.[2] In contrast, it has been shown that double tempering does improve the H_2S cracking resistance of certain cast 13 Cr alloys, in particular CA-6NM.[3]

In laboratory H_2S cracking tests, 13% Cr alloys generally perform poorly. Most of the laboratory tests have been performed on 410 stainless steel rather than on 420. Reports in the literature indicate 410 performs worse in laboratory H_2S cracking tests than low alloy steels at the same strength level.[4-9] Table 1 compares results from the literature for low alloy steel and 410 tested in the NACE TM-01-77 tensile test for

TABLE 1 — Comparison of 410 stainless steel and low alloy steels in the NACE tensile test[3,7]

Material	Condition	Hardness	Yield strength (ksi)	Threshold stress (%YS)
410	QTT[(1)]	237 BHN	96.8	11
410	QTT	18 Rc	84.9	60
410	QTT	22 Rc	90.0	33
AISI 4130	QT[(2)]	228 BHN	92.5	86
AISI 4135	QT	270 BHN	120.0	64
AISI 4135 (Mod.)	QT	270 BHN	118.0	64

[(1)]QTT = Quenched and double tempered.
[(2)]Quenched and tempered.

*Presented during CORROSION/84 (Paper 211) April 1984, New Orleans, Louisiana.

*Standard Oil Company of California, Materials Laboratory, P.O. Box 4012, Richmond, California.

evaluating resistance of metals to sulfide stress cracking at ambient temperature. As shown in the table, low alloy steel, even at slightly higher strength levels than 410, has higher threshold stress values.

Other laboratory tests suggest that 410 can be quite susceptible to cracking in service, even with hardness below the MR-01-75 approved limit of Rockwell C22,[5,6] especially under severe hydrogen charging conditions.[10]

On the other hand, there have never been any reported H_2S cracking failures of 410 at a hardness of Rockwell C22 or less.[4,7] The only reported cracking failures of 410 were at a hardness greater than Rockwell C25, in environments with high H_2S concentrations.[11,12] The 410 wellheads, valves, and related equipment have been used for years to resist aqueous CO_2 corrosion in both sweet and sour environments.[4,5,7,13] The 410 wellheads were, in fact, being used on the Tuscaloosa Trend gas wells before the switch to 13 Cr tubing. One explanation often given for the successful use of 410 wellhead equipment in sour service is that, besides being manufactured with controlled hardness, the wellhead equipment generally is not subject to high stress.

Attempts to resolve the discrepancy in cracking results between laboratory tests and field experience have been made using equipment constructed at well sites to perform laboratory type stressed specimen tests in actual, produced fluids.[9,14] At the Lacq sour gas field in France produced fluids having a gas composition of 74% methane, 15% H_2S, and 9% CO_2 were passed through a test loop at 34 MPa (5000 psi) and 30 to 60 C (85 to 140 F).[14] Stressed samples were mounted inside the test loop. Several samples of 12% Cr steels (410) in the 552 to 621 MPa (80 to 90 ksi) yield strength range were tested, and there was no cracking of any sample which had not been plastically deformed. Similar tests were conducted in sour gas fields in the US, Canada, and Venezuela, with H_2S contents ranging from 0.003 to 11% and CO_2 ranging from 1.0 to 40%.[9] Laboratory test results provided a lower bound for H_2S cracking threshold stresses in these actual oilfield H_2S environments. The laboratory test results were then used to demonstrate that at least 1% H_2S was needed for 410 at 593 MPa (86 ksi) yield strength to crack at stresses below its yield strength. These results are shown in Figure 1. At higher H_2S concentrations, the cracking resistance of 410 was still inferior to carbon and low alloy steels at the same or slightly higher strength level.

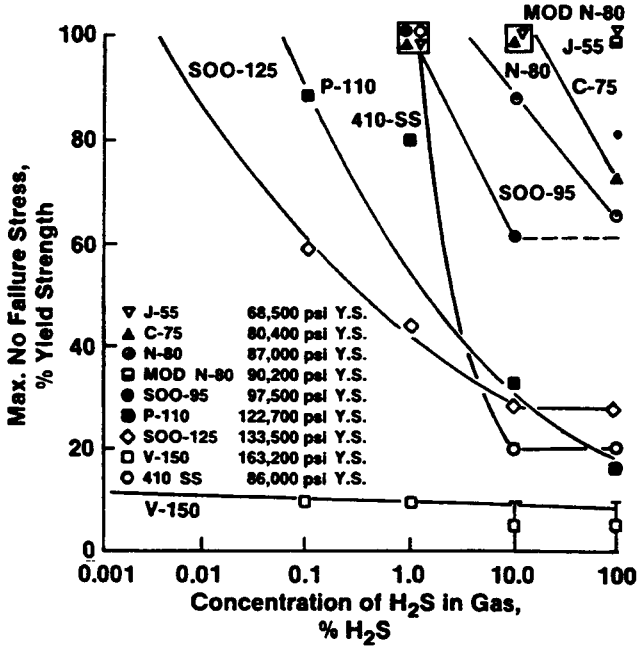


FIGURE 1 — Maximum failure stress vs H_2S concentration for several steels, based on laboratory tests. Threshold stresses shown give lower bound for threshold stresses in actual field environments (Reference 9).

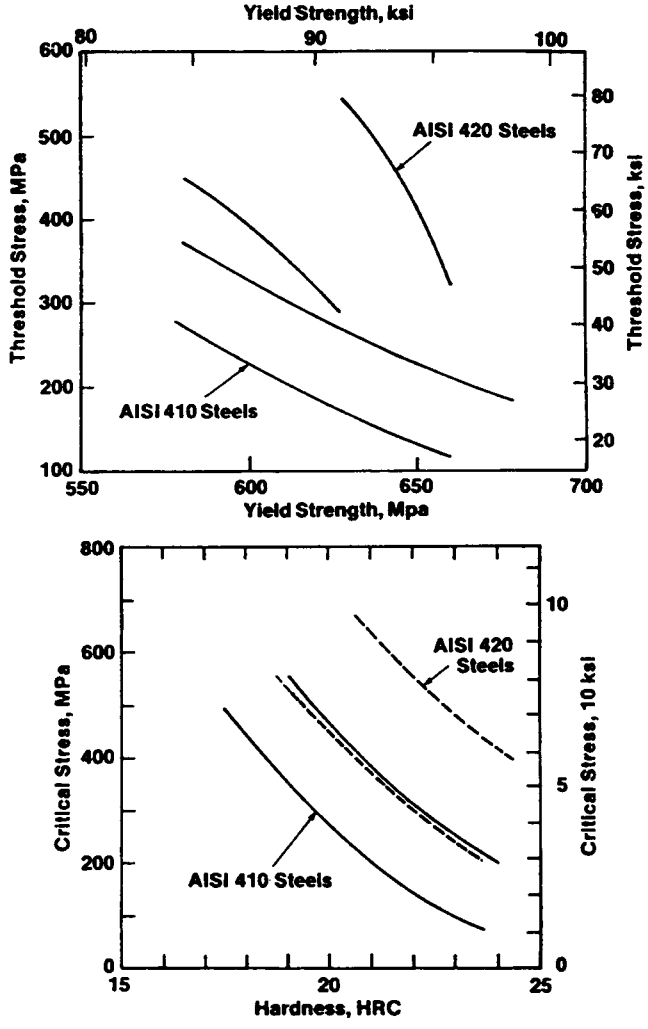


FIGURE 2 — Comparison of NACE tensile test and Shell bent beam test results for 410 and 420 stainless steel showing superior performance of 420 at equivalent strength levels. Shell bent beam solution contained 5% NaCl; i.e., the NACE solution (Reference 15).

Recent laboratory tests have been performed on 420 stainless steel, and it has been shown that 420 has better resistance to H_2S cracking than 410.[15-19] Both the NACE TM-01-77 tensile test and the Shell bent beam test were used to establish the superior performance of 420 over 410 in the 586 to 655 MPa (85 to 95 ksi) yield strength range, as shown in Figure 2.[16] The NACE solution was used for the Shell bent beam tests rather than the original Shell solution,[16] which contained no NaCl. The addition of 5% NaCl makes the Shell bent beam test more severe.

H_2S cracking susceptibility of steel generally diminishes with increasing pH.[5] It has been claimed that the pH of the standard NACE solution is unreasonably low, and therefore the test is too severe, particularly penalizing the most H_2S cracking susceptible materials, including 420 stainless steel.[17] It was further claimed that modifying the standard NACE solution by adding just enough acetic acid to bring the initial pH to 4.0, rather than simply adding a fixed amount (0.5%) of acetic acid, gave results that were more representative of actual service conditions. If 13 Cr performs well in a pH 4.0 NACE solution, and if the pH 4.0 solution is more representative of field conditions, this could help explain why 13 Cr has performed successfully in sour environments when most laboratory tests predict it will fail.

The purpose of this test work was to evaluate the H_2S cracking resistance of 420 (13 Cr) tubing material supplied by

three manufacturers and already performing successfully in Tuscaloosa Trend sour gas wells, in both the standard NACE test and the Shell bent beam test. Next, the effect of chloride ion concentration would be evaluated. It was already known that Cl^- had a detrimental effect on the H_2S cracking resistance of 410 stainless steel.[5] Finally, the effects of raising the pH of the NACE solution and reducing the concentration of H_2S in the gas would be studied separately to see the changes they would make in the cracking results and to see if a better correlation with actual field performance could be obtained.

Experimental procedure

AISI 420 stainless steel (hereafter referred to as 13 Cr) from actual production runs of upset end 60.3 mm OD × 6.45 mm wall (2 3/8 × 1/4 in. wall) tubing was supplied by 3 different manufacturers. Specified mechanical properties for the tubing were 586 to 690 MPa (85 to 100 ksi) yield strength, 690 MPa (100 ksi) minimum tensile strength, and Rockwell C23 maximum hardness. The tubes were austenitized, air cooled, and tempered to obtain a fully martensitic microstructure. Chemical compositions are shown in Table 2.

Tensile properties and hardness were measured along the entire length, including the upsets of all three sample tubes used for testing. No significant differences in mechanical properties were found between the upsets and bodies of the tubes. The average and range of mechanical properties along the tube lengths are shown in Table 3.

The NACE TM-01-77 tensile test was used as the basis for most of the H_2S cracking tests. Standard, full-size specimens were used for testing the heavier wall upset ends of the tubes, while subsize specimens [3.81 mm (0.150 in.) gage diameter] were required when testing the 6.45 mm (1/4 in.) wall tube bodies. The smooth gage section tensile specimens were loaded in uniaxial tension by sustained load, constant deflection proof rings and surrounded by a chamber filled with the test liquid. Initially, samples of three manufacturers' materials for both the bodies and upsets were tested in the standard NACE solution (5% NaCl + 0.5% acetic acid + 945 g deionized water + continuous H_2S bubbling, initial pH 2.7 to 3.0) to compare different manufacturers' materials and upsets with bodies, and to establish baseline results for comparision with later test results. Tests were run for 720 hours at 70 ± 10 F (21 ± 5 C). Failure in less than 720 hours was automatically indicated by shut-off of a digital timer.

In addition, Shell bent beam tests were also conducted to compare bodies and upsets of the three manufacturers' 13 Cr. About 16 individual test specimens were used to obtain each

TABLE 2 — Composition of 13 Cr tubing used for H_2S cracking tests (%)

Material	C	Mn	Si	P	S	Cr	Ni	Mo	Cu	Fe
Manufacturer A	0.17	0.44	0.27	0.032	0.010	13.6	0.23	0.02	0.03	Bal
Manufacturer B	0.21	0.72	0.45	0.024	0.010	13.3	0.24	0.02	0.006	Bal
Manufacturer C	0.18	0.63	0.18	0.001[1]	0.001	12.1	0.10	0.01	0.04	Bal

[1]Less than.

TABLE 3 — Mechanical properties of 13 Cr tubing used for H_2S cracking tests[1]

Material	Yield strength[2] Range (ksi)	Yield strength[2] Avg. (ksi)	Tensile strength Range (ksi)	Tensile strength Avg. (ksi)	Hardness Range (Rc)	Hardness Avg. (Rc)
Manufacturer A	87.3-92.3	88.8	114-119	117	22.3-23.3	22.8
Manufacturer B	89.2-91.7	90.4	116-118	117	21.3-22.5	21.9
Manufacturer C	85.4-89.8	87.5	108-114	111	20.6-22.0	21.1

[1]Values reported are mean values for measurements made along the length of each tube.
[2]0.2% offset, cylindrical shaped specimens.

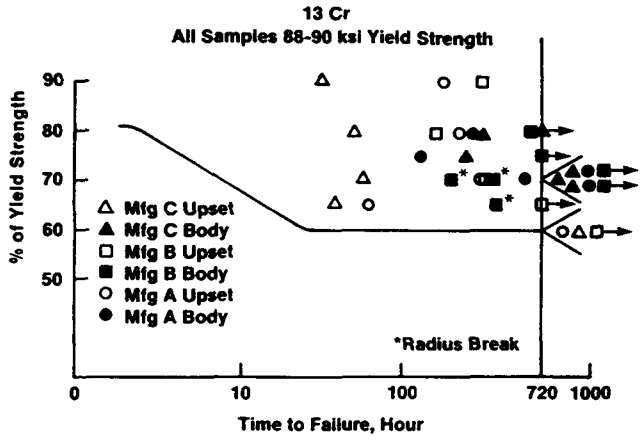


FIGURE 3 — Results of NACE tensile tests for 420 (13 Cr). Samples which broke in shoulder radius because of crevice corrosion in the test chamber are noted. Specimen was redesigned to shorten gage length and eliminate shoulder failure problem. Upset samples were full-size; body samples were subsize.

Sc value. The test solution was a 0.5% acetic acid solution in deionized water (no NaCl) with H_2S bubbled twice per day for 30 minutes, 5 days a week.

To evaluate the effect of chloride ion concentration on the H_2S cracking susceptibility of 13 Cr, the NaCl content of the standard NACE solution was varied. Tests were run identically to the NACE tensile tests described above, except the NaCl concentrations were changed to 0, 1, 2, and 20%. Results for 5% NaCl were already available from the standard NACE test. Subsize tube body specimens were used for these tests.

The effect of pH was evaluated using the NACE solution modified by adding just enough acetic acid to bring the initial pH to 4.0. All other parameters, including the NaCl content, were according to NACE TM-01-77. Again, subsize tube body specimens were used.

The effect of H_2S concentration in the gas was evaluated by bubbling a mixture of H_2S and N_2 through the NACE solution. A single bottle containing the mixed gases was used. Concentrations of H_2S were 0.5, 1, 5, and 20%, with the balance N_2. All other parameters were per TM-01-77. Subsize tube body specimens were used.

Results

NACE tensile test

Results for the NACE tensile test are shown graphically in Figure 3. In Figure 3, all test results have been combined, including samples from all three manufacturers and both upset and tube body samples. The threshold stress below which failure does not occur in 720 hours has been estimated at 60% of yield strength.

The possibility of premature failure exists when subsize specimens are used in the NACE tensile test because of the greater proportion of the cross section that can be lost by corrosion and the higher surface area to volume ratio for absorption of hydrogen at the gage surface. In this series of tests, however, subsize specimens did not suffer premature failure as compared to the full-size specimens. In fact, a careful scrutiny of the data indicates a slightly higher threshold value for the tube bodies compared to the upsets, which was not expected because the upsets and tube bodies all had the same strength and microstructure. Slight differences in test results can be attributed to the experimental scatter that is typically encountered in this test, rather than real differences between the materials. There were no significant differences between any of the materials tested.

TABLE 4 — Shell bent beam test results for 13 Cr

Material	Sc	
	Upset ends	Tube bodies
Manufacturer A	6.1	6.8
Manufacturer B	7.6	7.6
Manufacturer C	—	10.2

In a few instances, subsize specimens broke in the shoulder radius, probably because of stress concentration at the shoulder and excessive corrosion at the solution surface. These are noted in Figure 3. The problem was eliminated by shortening the gage length so that the shoulder radius was well below the liquid surface.

Shell bent beam test

The results of the Shell bent beam tests are shown in Table 4. Sc values ranged from 6.1 to 10.2. This variation may indicate the typical data scatter to be expected for 13 Cr in this test because unpublished results of tests performed by two of the manufacturers also had a range of Sc values from 6 to 10 for 420 13 Cr in the 607 to 634 MPa (88 to 92 ksi) yield strength range. These results are higher than those shown in Figure 2 because the results in Figure 2 were obtained using NaCl in the test solution.

Effect of chloride ion content and pH

Figure 4 shows the effect of NaCl concentration on time-to-failure and threshold stress in the NACE test. Like that which has been reported previously for 410,[5] it was found that the addition of salt also increases the H_2S cracking susceptibility of 420 13 Cr.

From the results shown in Figure 4, it appears that cracking resistance falls off above 1% NaCl (6000 ppm Cl^-) and reaches a minimum between 2 and 5% NaCl (12,000 to 30,000 ppm Cl^-). There appears to be no further decrease in resistance as the NaCl concentration is increased to 20% (120,000 ppm Cl^-).

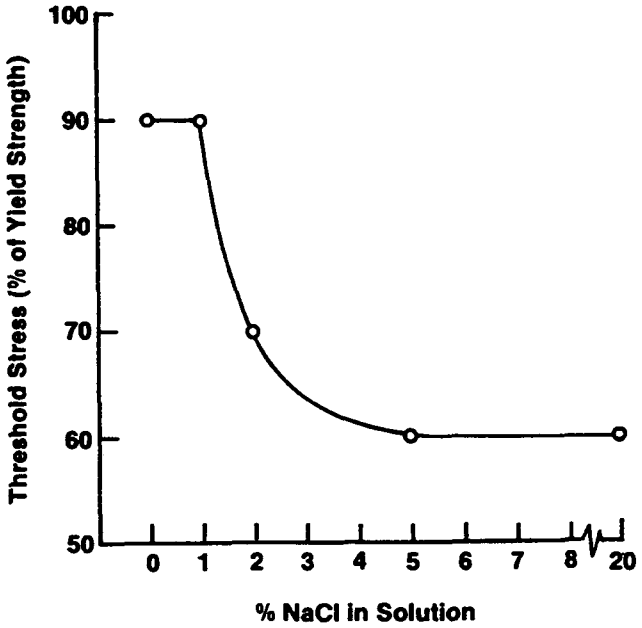


FIGURE 4 — Effect of NaCl concentration in the NACE solution on the threshold stress for 90 ksi yield strength 13 Cr (420 stainless steel).

A secondary effect of changing the NaCl concentration in the NACE test was its effect on the initial pH of the solution. The following pH values were typically measured at the beginning of the test (% NaCl), initial pH: (0), 2.9 to 3.2; (1), 2.9; (2), 2.8; (5), 2.7 to 3.0; and (20), 2.3 to 2.4. The reduced pH for the 20% NaCl solution may have been caused by impurities in the reagent grade NaCl.

This shows that reducing the pH from about 3.0 to about 2.3 has no significant effect on the cracking results since the threshold stress was 60% of yield strength for both the 5 and 20% NaCl solutions. There was little, if any, difference in pH between the 0, 1, 2, and 5% NaCl solutions, with the 2.7 to 3.0 pH range for the 5% solution overlapping the values measured for the other three solutions. Therefore, the higher threshold stresses obtained in the 0, 1, and 2% solutions, compared to the 5% solution, must have been due only to the chloride concentration, and not to changes in pH.

The results of cracking tests in the NACE solution adjusted to pH 4.0 are shown in Table 5. The threshold stress is at least 80% of yield strength. The sample at 90% yield strength failed in 305 hours, but the sample at 100% did not fail in 720 hours. Clearly, raising the pH to 4.0 reduces the tendency for 13 Cr to crack in the otherwise standard NACE environment.

Effect of H_2S concentration

The effect of reducing the concentration of H_2S in the gas bubbled through the NACE solution in the NACE tensile test is shown in Table 6. The threshold stress is 100% of yield strength or greater for concentrations up to and including 5% H_2S. Somewhere above 5% H_2S, the threshold stress begins to fall below 100% of yield strength, and at 20% H_2S, it has decreased to 70% of yield strength. These results are similar to those shown in Figure 1 for 410 stainless steel. As with 410, it appears that a minimum level of H_2S is required to crack 420 stainless at a hardness level of Rockwell C23 maximum. Below this minimum H_2S level, high strength steels, such as API P-110, will still crack.

TABLE 5 — Results of NACE tensile test with the pH adjusted to 4.0

Material	Stress as % of yield strength				
	60	70	80	90	100
Manufacturer A		NF[1]	NF	305	NF

[1]Time to failure in hours, NF = no failure in 720 hours.

TABLE 6 — Results of NACE tensile test with reduced H_2S concentration[1,2]

% H_2S	Threshold stress (% yield strength)[3]
0.5	110
1	110
5	100
20	70
100	60

[1]Balance of gas was N_2.
[2]Threshold stress is highest measured no failure stress.
[3]All tests performed on subsize 13 Cr tube body specimens from tube with 88.8 ksi (612 MPa) yield strength.

Discussion

Each of the three manufacturers' 13 Cr tubes that were tested had yield strengths in the 607 to 621 MPa (88 to 90 ksi) range, and considering the scatter typically encountered with tensile testing, it can be assumed they were equivalent in strength. From the results shown in Figure 3, it can be concluded there is no significant difference between the H_2S cracking susceptibility of the different manufacturers' commercially supplied materials. This applies to both upset ends and tube bodies.

The 60% of yield strength threshold value obtained in the NACE test is similar to previously reported results for 420 (13 Cr) at the same strength level.[15,18] In these other reported results, threshold values of 65 to 70% of yield strength were obtained in the NACE solution for 13 Cr in the 586 to 655 MPa (85 to 95 ksi) yield strength range.

As concluded by other studies,[15,19] it does appear that 420 stainless steel has better H_2S cracking resistance than 410 stainless steel. However, 420 is not nearly as resistant as the sour service AISI 4130 type low alloy steels at the same or somewhat higher strength level. Some grades of sour service, low alloy steel tubing and casing have threshold values in the NACE tensile test of 100% of yield strength or greater.[20] A 60% of yield strength threshold in the NACE test is similar to what has been obtained by others for ordinary carbon steel in a comparable yield strength range, including carbon steel with hardness below Rockwell C22.[7,8] In tests conducted in our laboratory, however, with the same equipment and procedures used to test the 13 Cr, we have obtained threshold values of 75 to 100% of yield strength for quenched and tempered plain carbon steel tubulars in the 586 to 676 MPa (85 to 98 ksi) yield strength range (Rockwell B98 to Rockwell C24).[20]

The Sc values obtained in the bent beam test were generally below 10. Materials with Sc values less than 10 are normally not considered resistant to cracking in a sour environment. For example, API N-80 tubulars, with published Sc values in the 5 to 14 range,[5] are not permitted by MR-01-75 for use in sour service at temperatures below 150 F (66 C). Although the designation "N-80" covers a much wider range of composition, strength, microstructure, and resulting performance than the 13 Cr tested in this program, the bent beam results would indicate 13 Cr with yield strength of about 620 MPa (90 ksi) has H_2S cracking resistance similar to what can be generally expected of N-80.

Results of tests in which the NaCl concentration was varied indicate H_2S cracking resistance of 13 Cr increases as the chloride concentration is decreased below the 5% NaCl level of the standard NACE test. Improved H_2S cracking resistance of 410 stainless in a solution similar to the NACE solution but without NaCl has been reported before,[21] and it was found that cracking occurred only at hardness greater than Rockwell C25. These results at low chloride concentrations may not have practical significance because most oil and gas wells will, at least sometime during their life, produce water containing substantial amounts of chloride.

The test results at the high chloride levels might have some practical significance, however. The fact that cracking susceptibility remained constant above 5% NaCl indicates the actual chloride content of a high chloride well will not affect H_2S cracking susceptibility; e.g., cracking susceptibility of 13 Cr in a 100,000 ppm Cl^- well will be no greater than in a 30,000 ppm Cl^- well.

The H_2S cracking tendency of 13 Cr was reduced significantly in the NACE solution when the pH was adjusted to 4.0, as had been reported previously.[17] One explanation offered for the difference in performance between the NACE solution at pH 3.0 and the same solution at pH 4.0 is that at pH 3.0, 13 Cr is in the active electrochemical state, while at pH 4.0 it is passive.[17] Being in the active state at pH 3.0, the free corrosion potential is more cathodic than at pH 4.0, and more hydrogen is liberated to cause cracking because 13 Cr corrodes faster. The alloy is passive at pH 4.0, the corrosion rate is much lower, and the amount of liberated hydrogen is much less.

The current test results did not verify this theory. At pH 3.0, the corrosion potential for 13 Cr in the NACE solution must be right at the active-passive transition point because in some cases the samples were corroded (active) while in others they were either shiny or only slightly discolored (passive) when removed from the test. There was no correlation between whether the sample corroded or not and whether or not it cracked. Of the 44 samples that corroded, 27 cracked and 17 did not. Of the 11 samples that were shiny or only slightly discolored, five cracked and six did not. At pH 4.0, all four samples were either shiny or slightly discolored when removed from the test, as would be predicted by the theory, including the one that failed in 305 hours. The effect of pH, therefore, appears to be something more than simply the resulting effect on the electrochemical corrosion potential.

The NACE tensile and Shell bent beam test results indicate that 420 (13 Cr), although having better H_2S cracking resistance than 410, is slightly less resistant to cracking than plain carbon steel at the same strength level, especially if the carbon steel is quenched and tempered. Raising the pH to 4 in the NACE test improved the 13 Cr performance, but carbon steel and low alloy steel also demonstrate improved resistance to cracking in the NACE solution when the initial pH is adjusted to 4.0.[17] The standard NACE and Shell bent beam tests may be too severe to accurately predict performance of 13 Cr in low H_2S sour environments like the Tuscaloosa Trend. The NACE test at pH 4 may, in some cases, be more representative of actual field performance, but carbon steel will outperform 13 Cr at the same strength level in the pH 4 NACE test, and carbon steel at Rockwell C23-24 would not be acceptable in the sour Tuscaloosa Trend environment per MR-01-75.

The key factor in explaining the successful use of 13 Cr tubing in a sour environment appears to be H_2S content. In Tuscaloosa Trend gas wells, 13 Cr tubing may be performing well because, despite being classified "sour" by the MR-01-75 definition, there are only 20 to 30 ppm H_2S in the gas. It is quite possible that 586 MPa (85 ksi) minimum yield strength 13 Cr has adequate cracking resistance in low H_2S sour environments, but that higher concentrations of H_2S in field environments could cause it to crack. At 100% of yield strength, 13 Cr resisted cracking when the H_2S concentration in the NACE test was reduced to 5%. A 5% H_2S concentration in the gas used for the NACE test corresponds to a partial pressure of about 0.005 MPa (0.75 psia) for this ambient pressure test. This is the same order of magnitude, but slightly higher than, the 0.003 MPa (0.4 psia) H_2S partial pressure in Tuscaloosa Trend gas wells. If there is a threshold H_2S level needed to crack 13 Cr, corresponding roughly to 0.005 MPa (0.75 psia), this would explain the success of 13 Cr tubing in Tuscaloosa gas wells operating below this threshold. More work is needed to better substantiate and define this threshold.

There are still many unresolved questions concerning the use of 13 Cr in deep sour gas wells, which can probably only be answered by carefully monitored trial usage in actual service environments. For the present, 13 Cr with 586 MPa (85 ksi) minimum yield strength and Rockwell C23 maximum hardness should probably not be used in deep sour gas wells containing more than about 50 ppm H_2S.

Conclusions

1. At 621 MPa (90 ksi) yield strength, 420 stainless steel has better H_2S cracking resistance than 410 stainless steel at the same strength level, but it is slightly less resistant than plain carbon steel at the same strength level. It is significantly less resistant than AISI 4130 type low alloy steels at the same or somewhat higher strength levels.

2. H_2S cracking susceptibility of 420 (13 Cr) decreases when there is less than 2% NaCl in solution (12,000 ppm Cl^-) and remains constant above 5% NaCl (30,000 ppm Cl^-) in the NACE TM-01-77 tensile test modified by adjusting the NaCl concentration.

3. In the NACE tensile test, 420 stainless steel is more resistant to cracking when the initial pH is adjusted to 4.0 than in the standard solution which had an initial pH of 2.7 to 3.0.

4. Reducing the H_2S content of the gas in the NACE tensile test to low concentrations increases the threshold stress of 13 Cr. The threshold stress did not fall below 100% of yield strength until the H_2S concentration exceeded 5%.

5. Production tubing made of 420 has performed successfully in deep sour wells containing 20 to 30 ppm H_2S; however, laboratory tests still indicate it is slightly less resistant to H_2S cracking than plain carbon steel at the same strength level. For now, 13 Cr at 586 MPa (85 ksi) minimum yield strength and Rockwell C23 maximum hardness should probably not be used in deep sour gas wells containing more than 50 ppm H_2S.

Acknowledgment

The author thanks Standard Oil Company of California, Chevron USA, and Chevron Oil Field Research Company for permission to publish this paper. Thanks are also extended to J. G. Kerr, J. W. Coombs, and W. E. Erwin for helpful comments and discussion, and to D. L. Cocke for completing the low H_2S tests in time.

References

1. J. D. Combes, J. G. Kerr, and L. J. Klein, Petroleum Engineer International, Vol. 55, No. 3, p. 50 (1983).
2. R. K. Popperling, Mannesmann Research Institute, unpublished test results.
3. R. D. Kane, M. Watkins, and J. B. Greer, Corrosion, Vol. 33, No. 7, p. 231 (1977).
4. R. N. Tuttle, Oil and Gas Journal, Vol. 76, No. 50, p. 108 (1978).
5. R. S. Treseder and T. M. Swanson, Corrosion, Vol. 24, No. 2, p. 31 (1968).
6. R. N. Tuttle. Materials Protection, Vol. 9, No. 4, p. 11 (1970).
7. D. S. Burns, Materials Performance, Vol. 15, No. 1, p. 21 (1976).
8. J. B. Greer, Materials Performance, Vol. 16, No. 9, p. 9 (1977).
9. R. D. Kane and J. B. Greer, Journal of Petroleum Technology, Vol. 29, No. 11, p. 1483 (1977).
10. E. H. Phelps, H_2S Corrosion in Oil and Gas Production—A Compilation of Classic Papers, R. N. Tuttle and R. D. Kane, Eds., NACE, Houston, Texas, 1981, p. 352.
11. R. S. Treseder, Stress Corrosion Cracking and Hydrogen Embrittlement of Iron Base Alloys, NACE-5, NACE, Houston, Texas, 1977, p. 147.
12. R. N. Tuttle, Materials Performance, Vol. 13, No. 2, p. 42 (1974).
13. Panel Discussion at the NACE Annual Conference, March 1973, Materials Performance, Vol. 14, No. 6, p. 43 (1975).
14. M. Estavoyer, Journal of the Institute of Petroleum, Vol. 46, No. 439, p. 223 (1960).
15. Y. Ishizawa, T. Shimada, and M. Tanimura, CORROSION/82, Preprint No. 124, National Association of Corrosion Engineers, Houston, Texas, 1982.
16. J. P. Fraser, G. G. Eldridge, and R. S. Treseder, H_2S Corrosion in Oil and Gas Production—A Compilation of Classic Papers, R. N. Tuttle and R. D. Kane, Eds., NACE, Houston, Texas, 1981, p. 283.
17. J. L. Crolet and D. P. Perrollet, CORROSION/82, Preprint No. 135, National Association Corrosion Engineers, Houston, Texas, 1982.
18. "Test Results of NK Cr-13; Resistance to Sulfide Stress Corrosion Cracking in Low H_2S Environments," Nippon Kokan K.K. report (October 1981).
19. Y. Ishizawa, T. Shimada, and M. Tanimura, Paper presented at the 3rd Asian-Pacific Corrosion Control Conference, Taipei, Taiwan (June 1983).
20. L. J. Klein and D. L. Cocke, Standard Oil Company of California Materials Laboratory, unpublished test results.
21. F. K. Bloom, Corrosion, Vol. 11, No. 8, p. 351t (1955).

Copyrighted Materials
Copyright © 1996 NACE International Retrieved from www.knovel.com

Paper No. 52—CORROSION/90

9CR-1MO AND 13CR TUBULARS FOR SOUR SERVICE

L.J. Klein, R.M. Thompson, and D.E. Moore
Chevron Corporation
P.O. Box 4012
Richmond, California 94804

ABSTRACT

The effects of strength level, quench medium, and H_2S level on the sulfide stress cracking (SSC) resistance of 9Cr-1Mo and 13Cr alloys were evaluated using the NACE TM-01-77 Tensile Test Method. Reducing the strength level below that of API L-80 and C-75 grades increased SSC resistance. The effect was more pronounced in 9Cr-1Mo than in 13Cr. Quench medium was found to have no significant effect on SSC resistance. Reduced H_2S levels in an otherwise standard TM-0177 test resulted in higher threshold stress values for both alloys. A limiting H_2S partial pressure of 1.5 psia (10 kPa), based on test results and supported by field experience, is suggested for both alloys at the L-80 strength level. Suggestions are offered on areas for future research to develop 9Cr-1Mo and 13Cr alloys with improved SSC resistance.

Keywords: hydrogen sulfide, chrome steel, oil wells, gas wells, petroleum production, laboratory tests, heat treatment

INTRODUCTION

CO_2 corrosion is the most pervasive form of corrosion in the oil field. The traditional, most widely used method of fighting downhole CO_2 corrosion is to use chemical corrosion inhibitors to protect carbon steel or low alloy steel equipment. Nonmetallic coatings are also often used, either alone or in conjunction with corrosion inhibitors.

An alternative approach is to use corrosion-resistant alloy (CRA) tubulars which can withstand the environment without inhibitors. Over the past 10 years, 9Cr-1Mo and 13Cr (Type 420) tubulars have been used increasingly for this purpose.[1-5] In a number of situations 9Cr-1Mo or 13Cr downhole tubulars have been economically competitive with carbon or low alloy steel plus corrosion inhibitors.

In many oil field environments, H_2S is also present. This presents concern for sulfide stress cracking (SSC) of 9Cr-1Mo and 13Cr alloys, because it has been well established that these alloys, as well as other similar martensitic stainless steels (e.g., Type 410, CA6NM, 17-4PH) perform poorly in laboratory SSC tests.[6-15] Despite their poor performance in laboratory SSC tests, there have been relatively few field SSC failures of these alloys, especially when hardness is controlled, considering their widespread use in sour service throughout the world.[2, 9, 16, 17]

Hardness-controlled (HRC 22 maximum) 9Cr-1Mo and 12Cr (Type 410) downhole and wellhead equipment, including packers, mandrels, tubing hangers, and valves, have been used for many years in sour service without restrictions placed on allowable H_2S content of the well. This is largely because their use arose before widespread laboratory testing. On the other hand, use of 9Cr-1Mo and 13Cr for downhole tubulars has mainly been limited to either sweet or mildly sour environments, primarily because their use evolved when laboratory SSC results were known.[1-3]

Because of their significantly lower cost relative to duplex and austenitic CRAs, there is a strong economic incentive to extend the range of application of 9Cr-1Mo and 13Cr tubulars to higher H_2S limits. This can occur in two ways. The first is by demonstrating through a combination of laboratory testing and field experience that current commercial alloys can tolerate higher H_2S levels than is now commonly believed. The second way is by modifying the existing alloys or developing new ones similar in cost to 9Cr-1Mo and 13Cr but with improved SSC resistance.

The purpose of this paper is twofold. First, it presents the results of laboratory tests on a range of manufac-

turers' products. The tests were aimed at quantifying the effects of reduced strength levels, the quench medium, and H_2S partial pressure on SSC resistance of 9Cr-1Mo and 13Cr. The intent of the strength level and quench method studies was to determine if these easily specified parameters could help assure optimum SSC resistance of currently available alloys. The intent of the H_2S partial pressure study was to determine the limiting H_2S partial pressure for L-80 grade 9Cr-1Mo and 13Cr tubulars.

The second purpose of this paper is an attempt to stimulate others, particularly alloy suppliers, to develop 9Cr/13Cr-type alloys with improved SSC resistance. Perhaps some of the results presented here will point to areas for further study.

MATERIALS TESTED

Eight samples of 9Cr-1Mo from five different suppliers were included in the test program. Five were tubing samples and three were forgings. Eight samples of 13Cr from five different suppliers were also included. One was a forging and the rest were tubing samples.

The mechanical properties of the samples in the as-received condition are shown in Table 1, and their chemical compositions are shown in Table 2. Yield strengths for the 9Cr-1Mo ranged from 85 to 94 ksi (586 to 648 MPa), and essentially characterized the L-80 strength range. For 13Cr, the yield strength range was 88 to 102 ksi (607 to 703 MPa), which extends somewhat beyond the L-80 strength range.

EXPERIMENTAL PROCEDURE

SSC testing was done substantially in accordance with NACE Standard TM-01-77 using proof rings for load application. Test duration was 720 hours. Wherever possible, full-size test samples were used. Where the sample size was insufficient, subsize specimens were used.

In order to evaluate the effect of reduced strength level, six samples of 9Cr-1Mo and seven samples of 13Cr were retempered at 760°C (1,400°F) for up to two hours to reduce their strength. The resulting mechanical properties are shown in Table 3. The purpose of this study was to determine whether lower strength grades, e.g., C-75, or perhaps a 65 ksi minimum, restricted yield strength grade (i.e., "C-65"), would provide sufficiently improved SSC resistance to permit the use of 9Cr-1Mo or 13Cr at higher H_2S levels. There may be opportunities in the oil field to economically prevent downhole corrosion by using 9Cr or 13Cr in wells where an API J-SS strength level is all that is needed.

To evaluate the effect of quenching method, six samples of 9Cr-1Mo and six samples of 13Cr were re-austenitized and then either air-cooled (i.e., normalized), oil-quenched, or water-quenched to provide a range of cooling rates. The 9Cr-1Mo was austenitized at 950°C (1,740°F) for 20 minutes, and the 13Cr was austenitized at 920°C (1,690°F) for 20 minutes. The 9Cr-1Mo was then tempered at 700°C (1,290°F) for 30 minutes, and the 13Cr was tempered at 720°C (1,325°F) for 30 minutes. The resulting mechanical properties are shown in Table 4.

The purpose of the quench method study was to determine the effect of quench rate on SSC resistance. It was recognized that 13Cr tubing generally cannot be water-quenched on a commercial scale without suffering quench cracks, and that air cooling is typically used. However, the results of these tests would determine whether more rapid quench rates would be worth pursuing in an attempt to optimize the alloys' SSC resistance.

In order to evaluate the effect of reduced H_2S content, the TM-01-77 test was modified by substituting an H_2S/N_2 gas mixture for the 100% H_2S gas used in the standard test. This same procedure was used previously.[13] Gas mixtures containing 5%, 20%, and 50% H_2S, with the balance N_2, were used, resulting in H_2S partial pressures of 0.74 psia (5.1 kPa), 2.9 psia (20 kPa), and 7.4 psia (51 kPa), respectively. All other test parameters, including test solution, temperature, and duration, were in accordance with the TM-01-77 procedure. The test results were then compared with field experience.

In all cases, the threshold stress (i.e., the maximum no-failure stress) in the NACE Tensile Test was the parameter used to measure SSC resistance. Typically, five to six specimens were used in each case to establish the threshold stress value.

RESULTS

Effect of Strength Level

Figure 1 shows the threshold stress in the NACE Tensile Test (as a percent of actual yield strength) plotted as a function of yield strength for 9Cr-1Mo. A similar plot for 13Cr appears in Figure 2. Similar to other

martensitic steels, the threshold stress for both alloys increases as strength level decreases. The effect is slightly more dramatic for 9Cr-1Mo than for 13Cr.

Although there is far from unanimous agreement within the industry for an acceptance criterion for the NACE Tensile Test, one of the more commonly cited is 80% of specified minimum yield strength (SMYS) as the minimum threshold stress needed to demonstrate adequate SSC resistance. This value is based primarily on the performance of API L-80 steel grades which typically have an 80% SMYS, or higher, threshold stress in the standard NACE test. In addition, API Specification 5CT requires an 80% SMYS minimum threshold stress for API C-90 tubulars.

As Figure 1 shows, decreasing the actual yield strength of 9Cr-1Mo below 80 ksi (552 MPa) results in a threshold stress above 80% of actual yield strength (and by definition, above 80% SMYS). This would indicate that a 65 ksi minimum yield grade of 9Cr-1Mo, with an allowable yield strength range of 65-80 ksi (448-552 MPa), might have SSC resistance similar to API L-80, and thus have adequate SSC resistance in any sour oil field environment without limits placed on H_2S content.

13Cr, on the other hand, does not show quite as good SSC resistance at the lower strength levels, the lower bound of the results only increasing to about 70% of yield strength at strength levels below 80 ksi (552 MPa).

Threshold stress based on % SMYS can best be evaluated by grouping the samples into different grades based on yield strength, i.e.:

C-S (65-80 ksi (448-552 NPa) yield strength)
C-75 (75-90 ksi (517-621 MPa) yield strength)
L-80 (80-95 ksi (552-655 MPa) yield strength)

Threshold stress as % SMYS can then be determined for each grade.

This has been done in Figure 3, where % SMYS has been plotted versus yield strength for C-65, C-75, and L-80 grades. Because of the overlap in strength between grades, many samples appear on more than one graph. Threshold stress as % SMYS will vary for a single test result depending on the SMYS (65, 75, etc.) being considered.

As Figure 3 shows, at the C-65 strength level both 9Cr-1Mo and 13Cr exceed an 80% SMYS criterion. As mentioned earlier, 9Cr-1Mo performed better than 13Cr at this strength level. At the C-75 and L-80 strength levels, both alloys have about equal SSC resistance, but neither satisfies the 80% SMYS criterion.

If a C-65 grade of 9Cr-1Mo or 13Cr could be commercially produced, the test results indicate it would be acceptable in H_2S environments without limits placed on H_2S partial pressure.

Effect of Quench Medium

While all the tubular samples tested in the as-received condition were air-cooled and tempered, the as-received forgings were all liquid-quenched and tempered. Therefore, the SSC performance of the as-received tubulars and forgings were compared to get an initial indication of the effect of quench rate. The comparison is shown in Figure 4 for 9Cr-1Mo. Since the materials had similar yield strengths, it does appear from Figure 4 that the liquid-quenched forgings on average had slightly better SSC resistance than the air-cooled tubulars.

For 13Cr, only one liquid-quenched sample was tested (Sample D3); and as Figure 2 shows, its performance was no different than tubing samples of equal strength.

Figure 5 shows the results of NACE Tensile Tests on samples which were re-austenitized in the laboratory, in order to compare the effects of air cooling, oil quenching, or water quenching before tempering. As Figure 5 shows, there was no consistent difference in threshold stress due to quenching medium for either 9Cr-1Mo or 13Cr. Any differences between results within individual heats in Figure 5 cannot be attributed to differences in strength level or quench rate, but rather are indicative of the range of scatter typically obtained in the NACE Tensile Test.

Thus, it appears that increasing the quench rate alone will not significantly improve the SSC resistance of 9Cr-1Mo and 13Cr. These alloys readily transform to martensite even with air cooling; so cooling rate alone does not appear to be a critical factor. The better performance of the 9Cr-1Mo forgings compared to the tubing in the as-received condition, rather than being due to the quenching medium used by the manufacturer, is likely due to a tempering effect. Tempering times and temperatures can affect microstructure refinement, which has been shown to affect SSC resistance of low alloy and 13Cr steels.[14, 18, 19]

Effect of H_2S Concentration

Figure 6 shows the result of plotting threshold stress of L-80 grade 9Cr-1Mo and 13Cr in the NACE Tensile

Test as a function of % H_2S used in the test. In this figure, % SMYS was used to denote threshold stress. Some of the results for the 13Cr tested at reduced H_2S levels were reported previously.[13]

The results for the two alloys are very similar to each other, and both are shown as falling within a single scatter band. Others have also reported test results showing 9Cr-1Mo and 13Cr having essentially the same SSC resistance at the L-80 strength level.[20, 21] From a user's standpoint, we would consider both alloys to have equivalent SSC resistance in the typical commercial condition.

If one considers a threshold stress of 80% SMYS to indicate a steel is satisfactory for sour service use, then Figure 6 could be used to estimate the maximum recommended H_2S level for 9Cr-1Mo and 13Cr to obtain sour service performance similar to API L-80.

Using the lower bound of the data in Figure 6, it can be seen that 80% SMYS corresponds to an H_2S partial pressure of about 1.5 psia (10 kPa). Thus, one might conclude that the limiting H_2S level for 9Cr-1Mo and 13Cr is 1.5 psia (10 kPa) H_2S. This is higher than the limiting H_2S level for these alloys suggested by some, but similar to that suggested by others.[13, 14, 21]

In order to factor field experience into any limiting H_2S guideline for 9Cr-1Mo and 13Cr tubulars, Chevron field experience with martensitic stainless steels in sour service was reviewed. Figure 7 summarizes this experience, showing the conditions for most of Chevron's sour fields in terms of total pressure and H_2S content. Each field condition plotted represents a separate oil or gas field in which one or more of the following are used: 12Cr (Type 410) Xmas tree valve trim, 12Cr tubing hangers, 12Cr valve bodies, 12Cr or 9Cr-1Mo packers, 9Cr-1Mo subsurface safety valves, 9Cr-1Mo landing nipples and mandrels, 9Cr-1Mo tubing, or 13Cr tubing.

A line has been drawn on Figure 7 at an H_2S partial pressure of 1.5 psia (10 kPa). While martensitic stainless steels (primarily 12Cr wellhead equipment) have been used at higher than 1.5 psia (10 kPa) H_2S, more than half of the experience in terms of both the number of wells and the number of fields is at or below 1.5 psia (10 kPa) H_2S partial pressure. Therefore, a 1.5 psia (10 kPa) limit represents a reasonable guideline for downhole tubulars based on field experience.

DISCUSSION

Improving The SSC Resistance of 9Cr-1Mo and 13Cr

While Figures 1 and 2 showed a wide range of performance among different test samples even at the same strength level, no consistent trends to differentiate the better performers from the poorer ones were identified. There were no consistent differences between manufacturers, nor, as Table 2 shows, were there any major differences in chemical composition among the materials tested. One minor factor in the chemical compositions of the 13Cr may have had some influence on the results. 13Cr samples C2 and C3, which fell near the lower bound of SSC performance (see Figure 2), had 0.32% Ni and 0.40% Ni, respectively. It has been shown that nickel content greater than 0.2% can be detrimental to SSC resistance of Type 420 13Cr.[21]

Clearly, more work is needed to determine whether chemistry modifications can have a significant impact on the alloys' SSC resistance. (Note: Research into steels used for thick-walled refinery pressure vessels has shown that small additions of vanadium can increase the hydrogen embrittlement resistance of 3Cr-1Mo steel.[22] This may provide a direction for further study.)

The quench medium test results indicated that quenching method alone is unlikely to explain differences in performance, nor does it offer much promise for success as a way to improve SSC resistance of 9Cr-1Mo and 13Cr.

The major differences in performance between test samples are most likely due to factors such as thermomechanical processing prior to final heat treatment, tempering time and temperature, variations in chemistry, carbide distribution and size, microstructure uniformity, and/or dislocation density.[14] Investigations into these areas provide the most promise for finding ways to improve the SSC resistance of 9Cr-1Mo and 13Cr. Significant improvements in the alloys' SSC resistance may require alloy development involving more than just minor modifications to existing chemical compositions and manufacturing processes.

Lower Strength Grades of 9Cr-1Mo and 13Cr

It was shown that a C-65 grade of 9Cr-1Mo and 13Cr might be suitable in sour environments without any limit on H_2S content. A C-65 grade of these materials has not been universally available. Therefore, an additional area for study, primarily by manufacturers, is to determine how these alloys can be supplied on a commercial basis at this lower strength level without sacrificing SSC and corrosion resistance. Factors to be considered

include tempering times and temperatures, alterations to chemistry, effect of changes in chemistry and/or manufacturing process on SSC resistance, and economics. An increased cost resulting from increased tempering times or other changes in manufacturing process may be tolerable to end users if the result is an alloy with good corrosion resistance and SSC resistance in a wide range of environments.

H_2S Limit For 9Cr-1Mo and 13Cr

While it can be argued that other laboratory test results would dictate an H_2S limit for 9Cr-1Mo and 13Cr well below 1.5 psia (10 kPa), an argument could also be made that based on the test results reported here, a 1.5 psia (10 kPa) H_2S partial pressure limit is conservative. Even with a reduced H_2S content, the NACE Tensile Test is still severe. Considering that the standard NACE test uses 100% H_2S at ambient pressure, or equivalently a partial pressure of about 15 psia (100 kPa), the same reasoning would lead to a limiting H_2S partial pressure for API L-80 steels of only 15 psia (100 kPa). However, no such limit is imposed; L-80 steel tubulars are used in sour service without limits on H_2S, and have been used successfully in many instances where the H_2S partial pressure is greater than 15 psia (100 kPa). By analogy, it could be argued that 9Cr-lNo and 13Cr should withstand H_2S partial pressures greater than 1.5 psia (10 kPa).

While 9Cr-1Mo and 12Cr have been used with good success for a number of years in downhole and wellhead equipment, 9Cr-1Mo and 13Cr tubulars are untested and unproven in the field at high H_2S levels. It seems a reasonable course of action, therefore, to limit their use to some fixed level of H_2S. When taken together, the test results and field experience reported here seem to indicate that 1.5 psia H_2S partial pressure is a reasonable guideline limit for 9Cr-1Mo and 13Cr tubulars. In the future, additional field experience may justify a change in this guideline.

CONCLUSIONS

1. At the C-75 and L-80 strength levels, 9Cr-1Mo and 13Cr tubulars have about equal SSC resistance as measured by the NACE Tensile Test. Their SSC resistance is inferior to API L-80 steel.
2. Reducing the strength level of 9Cr-1Mo and 13Cr tubulars below the C-75 strength level had a beneficial effect on the SSC resistance of both alloys. The effect was more pronounced in 9Cr-1Mo. At a C-65 strength level, both 9Cr-1Mo and 13Cr exhibited a threshold stress in the NACE Tensile Test of ≥ 80% SMYS.
3. 9Cr-1Mo forgings had better SSC resistance than tubular samples at similar strength levels. The same effect was not evident with 13Cr, however only one 13Cr forging sample was tested.
4. Quench rate from the austenitizing temperature had no significant effect on SSC resistance for either 9Cr-1Mo or 13Cr.
5. Reduced H_2S concentrations in the gas used in an otherwise standard NACE Tensile Test resulted in increased threshold stress values for 9Cr-1Mo and 13Cr at the L-80 strength level. On the basis of these test results and a review of field experience with martensitic stainless steels in sour service, a guideline limit of 1.5 psia (10 kPa) H_2S partial pressure is proposed for 9Cr-1Mo and 13Cr tubulars
6. Future work to improve the SSC resistance of 9Cr-1Mo and 13Cr, and thereby expand their useful range in sour service, may prove most beneficial in the following areas:
   a. Determine why 9Cr-1Mo forgings have better SSC resistance than tubular products, and apply the knowledge to improve the performance of tubulars.
   b. Determine which factors, including thermomechanical treatment, tempering time and temperature, chemistry, carbide distribution and size, and microstructure, will help explain why some samples of 9Cr-1Mo and 13Cr have significantly better SSC resistance than others at the same strength level. Explore ways to improve the alloys' SSC resistance through chemistry or other modifications
   c. Determine whether a restricted yield strength, 65 ksi minimum yield grade of 9Cr-1Mo and 13Cr (i.e. C-65) can be supplied on a commercial basis.

ACKNOWLEDGMENTS

The authors wish to express their thanks to the management of Chevron Corporation for granting permission to publish this paper. Thanks go also to Paul W. Hunter for conducting the laboratory tests, and to G.B. Kohut, J.W. Skogsberg, and W.E. Erwin for reviewing the manuscript and offering helpful suggestions.

REFERENCES

1. J.D. Combes, J.G. Kerr, and L.J. Klein, *Petroleum Engineer International*, 55, 3(1983), p. 50.
2. J.D. Alkire, S.W. Ciaraldi, "Failures of Martensitic Stainless Steels in Sweet and Sour Gas Service," CORROSION/88, paper no. 210 (Houston, TX: NACE, 1988).
3. J. Nurali, *Oil and Gas Journal*, 7(1984), p. 98; 7(1984), p. 66; 8(1984), p. 56.
4. J.L. Crolet, *Journal of Petroleum Technology*, 35, 9(1983), p. 1553.
5. J.L. Crolet, M.R. Bonis, "Experience in the Use of 13% Cr Tubing in Corrosive CO_2 Fields," SPE Paper No. 13552, presented at the International Symposium on Oilfield and Geothermal Chemistry in Phoenix, Arizona, April 9-11, 1985.
6. P.W. Rice, "Evaluating Nickel Base and Stainless Alloys for Subsurface H_2S Service," presented at the Energy Technology Conference and Exhibit (Houston, TX: ASME, September 18-22, 1977).
7. R.S. Treseder, T.M. Swanson, *Corrosion*, 24, 2(1968), p. 31.
8. R.N. Tuttle, *Materials Protection*, 9, 4(1970), p. 11.
9. D.S. Burns, *Materials Performance*, 15, 1(1976), p. 21.
10. J.B. Greer, *Materials Performance*, 16, 9(1977), p. 9.
11. R.D. Kane, J.B. Greer, *Journal of Petroleum Technology*, 29, 11(1977), p. 1483.
12. R.D. Kane, M. Watkins, J.B. Greer, *Corrosion*, 33, 7(1977), p. 231.
13. L.J. Klein, *Materials Performance*, 23, 10(1984), p. 29.
14. M. Tanimura, Y. Ishizawa, T. Shimada, "The Sulfide Stress Corrosion Cracking Resistance of 13% Cr Steels for OCTG," Nippon Kokan Technical Report, Overseas No. 39, 1983.
15. H. Xurahashi, T. Xurisu, Y. Sone, X. Wada, Y. Nakai, "Stress Corrosion Cracking of 13 Cr Steels in CO_2-H_2S-Cl Environments," CORROSION/84, paper no. 212 (Houston, TX: NACE, 1984).
16. R.N. Tuttle, *Materials Performance*, 13, 2(1974), p. 42.
17. R.N. Tuttle, *Oil and Gas Journal*, 12 (1978), p. 108.
18. T. Xaneko, Y. Okada, A. Ikeda, "Influence of Microstructure on SSC Susceptibility of Low Alloy High Strength Oil Country Tubular Goods," CORROSION/87, paper no. 291 (Houston, TX: NACE, 1987).
19. E. Snape, *Corrosion*, 24, 9(1968), p. 261.
20. Y. Ishizawa, T. Shimada, M. Tanimura, "Effect of Microstructure on the Sulfide Stress Corrosion Cracking Resistance of AISI 410 and 420 Steels," CORROSION/82, paper no. 124 (Houston, TX: NACE, 1982).
21. S. Nukai, N. Ueda, T. Tumura, A. Ikeda, "Corrosion Behavior of 13Cr Stainless Oil Country Tubular Goods in Wet CO_2-H_2S-Cl Environments," presented at the 4th Asian-Pacific Corrosion Control Conference, October, 1986.
22. T. Ishiguro, Y. Tanaka, T. Iwadate, K. Ohnishi, "A Study on Hydrogen Embrittlement Susceptibility of Advanced Hydrogenation Pressure Vessel Steels", presented at the International Conference on Interaction of Steels with Hydrogen in Petroleum Industry Pressure Vessel Service in Paris, France, March 28-30, 1989.

TABLE 1

MECHANICAL PROPERTIES OF MATERIALS TESTED - AS-RECEIVED CONDITION

Supplier Code	Product Form	Heat Treatment	Yield Strength (ksi)	Tensile Strength (ksi)	Hardness (HRB)
9Cr-1Mo					
A1	Tubing	N & T	94.0	117	99
A2	Tubing	N & T	93.7	116	100
A3*	Tubing	N & T	--	--	--
B1	Tubing	N & T	89.0	110	97
C1	Tubing	N & T	86.1	111	98
D1	Forging	Q & T	87.8	109	97
D2	Forging	Q & T	85.2	107	98
E1	Forging	Q & T	91.0	114	99
13Cr					
A4	Tubing	N & T	88.0	112	94
B2	Tubing	N & T	95.9	113	97
B3	Tubing	N & T	92.4	111	90
B4	Tubing	N & T	101.9	118	98
C2	Tubing	N & T	91.2	116	96
C3	Tubing	N & T	89.3	116	96
D3	Forging	Q & T	90.4	116	98
F1	Tubing	N & T	88.8	117	100

* Not tested in the as-received condition.

Note that the letter in the Supplier Code refers to a single manufacturer, i.e., A1, A2, A3, (9Cr-1Mo) and A4 (13Cr) were all from the same manufacturer. The different numbers refer to different heats of material.

1 ksi = 6.895 MPa

TABLE 2

CHEMICAL COMPOSITION OF MATERIALS TESTED
(Wt %)

Supplier Code	C	Mn	Si	P	S	Cr	Mo	Ni
9Cr-1Mo								
A1	0.11	0.53	0.51	0.025	0.003	9.0	0.96	0.12
A2	0.11	0.48	0.50	0.027	0.002	8.8	0.93	0.08
A3	0.13	0.47	0.47	0.020	0.005	9.0	1.00	0.07
B1	0.13	0.46	0.35	0.009	0.002	8.9	0.93	0.12
C1	0.12	0.45	0.27	0.013	0.013	8.8	1.06	0.13
D1	0.15	0.44	0.45	0.012	0.006	9.1	0.90	0.19
D2	0.14	0.43	0.44	0.011	0.004	8.4	0.92	0.21
E1	0.13	0.44	0.35	0.010	0.012	8.8	1.00	0.17
13Cr								
A4	0.19	0.72	0.37	0.019	0.001	13.0	0.01	0.07
B2	0.19	0.46	0.25	0.017	0.005	12.4	0.02	0.11
B3	0.20	0.49	0.28	0.014	0.006	13.0	0.03	0.17
B4	0.20	0.47	0.29	0.018	0.007	13.0	0.03	0.11
C2	0.19	0.70	0.32	0.017	0.002	13.4	0.01	0.32
C3	0.20	0.80	0.28	0.016	0.002	12.9	0.01	0.40
D3	0.21	0.58	0.54	0.015	0.003	12.9	0.02	0.15
F1	0.17	0.44	0.27	0.032	0.010	13.6	0.02	0.23

TABLE 3

MECHANICAL PROPERTIES OF MATERIALS RETEMPERED TO REDUCE STRENGTH

Supplier Code	Yield Strength (ksi)	Tensile Strength (ksi)	Hardness (HRB)
9Cr-1Mo			
Tempered 2 Hours at 1400°F (760°C):			
A1	77.0	98.2	92
A2	76.1	99.1	91
A3	76.4	99.4	90
B1	73.0	94.5	92
C1	77.8	96.6	92
D1	74.0	97.2	95
13Cr			
Tempered 2 Hours at 1400°F (760°C):			
A4	80.0	104.2	91
B2	66.6	90.8	89
B3	80.6	100.0	87
B4	81.4	95.8	90
C2	70.0	96.4	96
C3	79.6	105.0	90
Tempered 0.5 Hours at 1400°F (760°C):			
A4	84.4	108	97

1 ksi = 6.895 MPa

TABLE 4

MECHANICAL PROPERTIES OF MATERIALS REHEAT TREATED TO EVALUATE EFFECT OF QUENCHANT

Supplier Code	Quenchant	Yield Strength (ksi)	Tensile Strength (ksi)	Hardness (HRB)
9Cr-1Mo				
A1	Air	102.3	119	99
A1	Oil	103.9	120	98
A1	Water	99.5	115	99
B1	Air	93.4	111	98
B1	Oil	94.5	111	97
B1	Water	91.2	109	94
13Cr				
B2	Air	91.0	106	96
B2	Oil	89.6	108	95
B2	Water	89.4	107	95
C2	Air	95.6	113	98
C2	Oil	92.6	111	96
C2	Water	94.2	111	96

1 ksi = 6.895 MPa

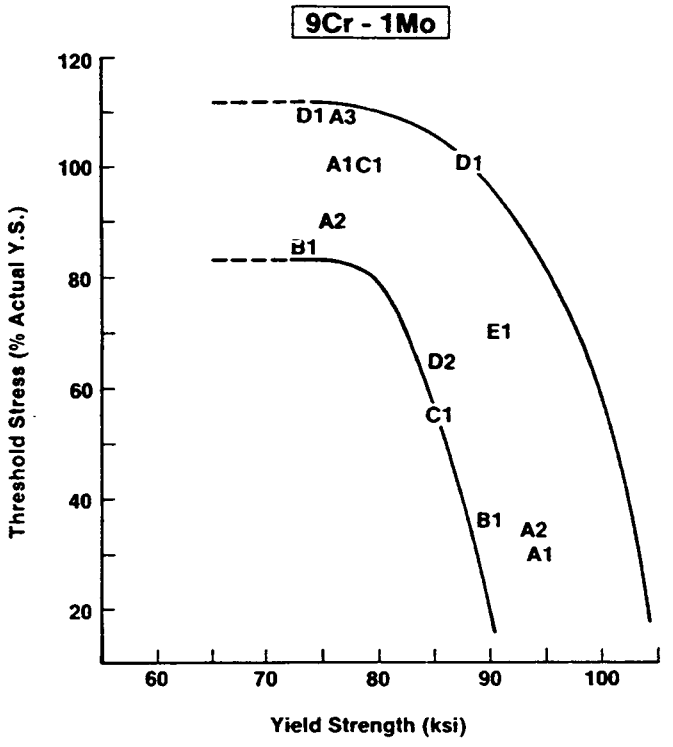


Figure 1 - Effect of yield strength on the threshold stress of 9Cr - 1 Mo. Threshold stress (as % of actual Y.S.) determined using the NACE Tensile Test. (A1, A2, B2, etc. refer to supplier codes. See Tables 1 - 4)

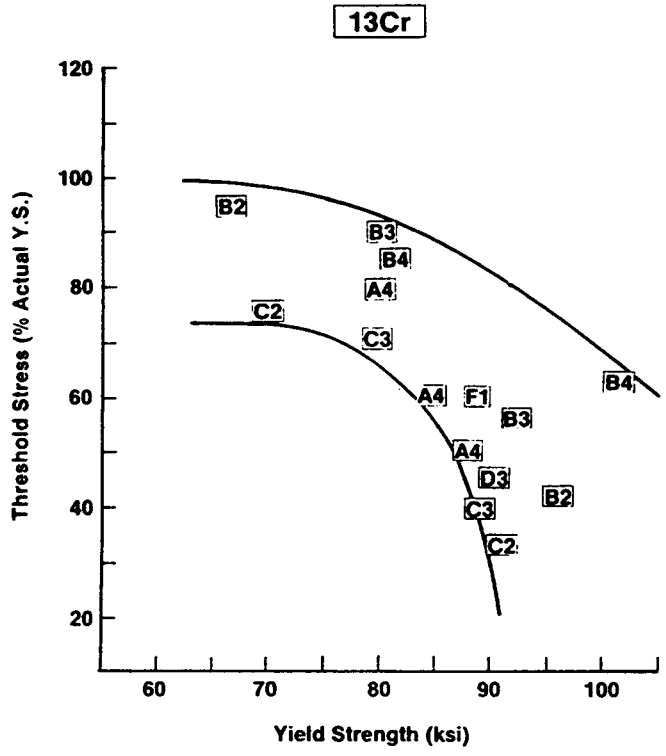


Figure 2 - Effect of yield strength on the threshold stress of 13Cr. Threshold stress (as % of actual Y.S.) determined using the NACE Tensile Test. (A4, B2, B3, etc. refer to supplier codes. See Tables 1 - 4)

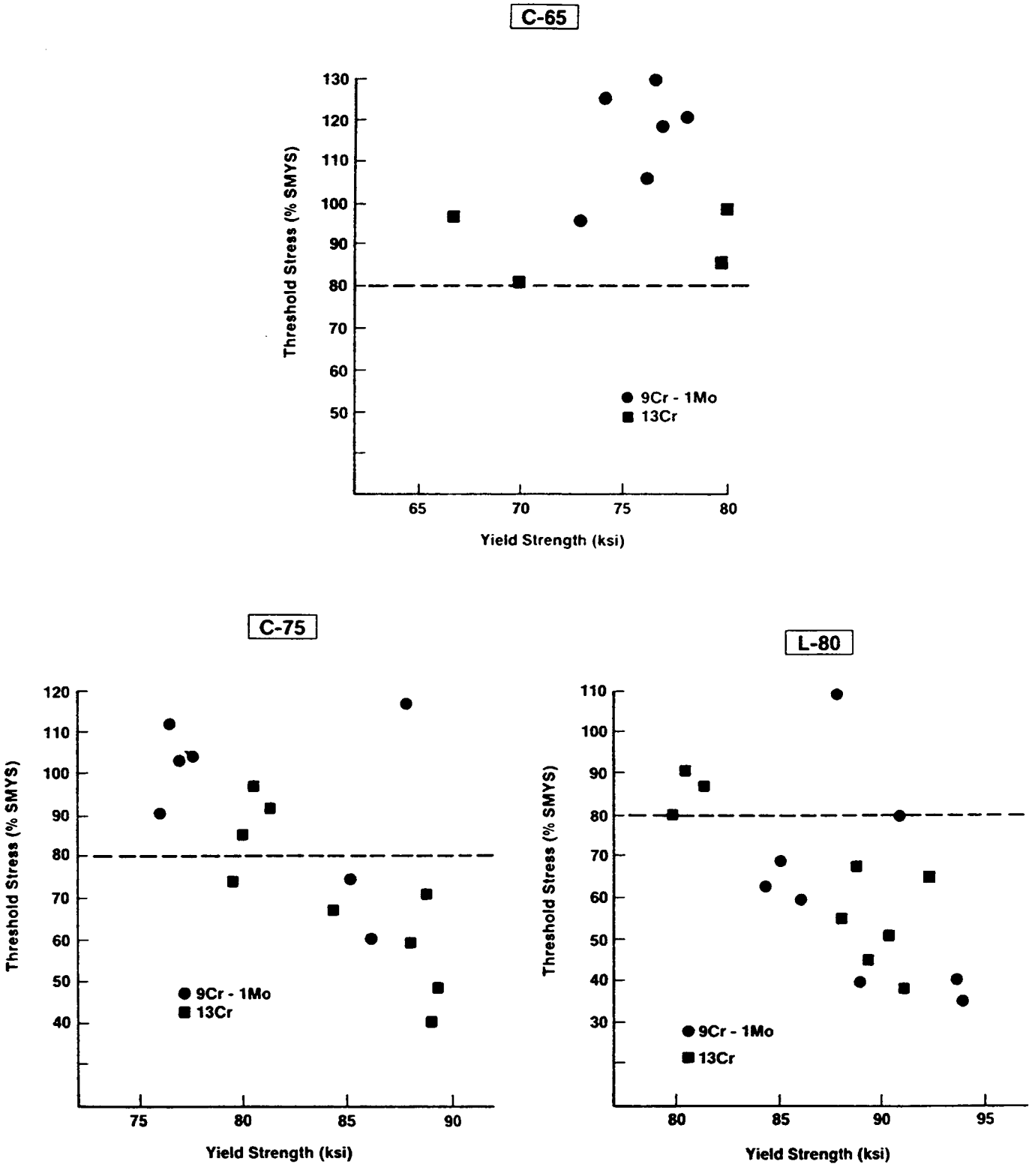


Figure 3 -Threshold stress in the NACE Tensile Test (as %SMYS) for three different strength grades of 9Cr-1Mo and 13Cr. The lowest strength grade, C-65, can satisfy an 80% SMYS minimum threshold stress, while the higher strength grades, C-75 and L-80, clearly do not.

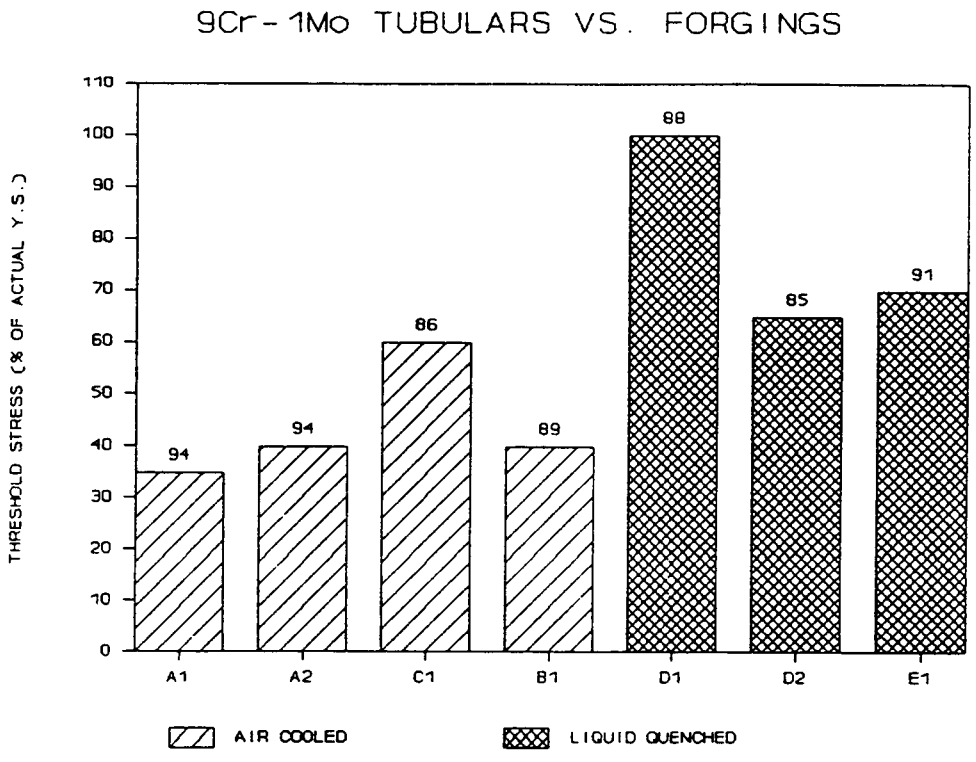


Figure 4 -Comparison of SSC resistance of 9Cr-1Mo tubulars (air-cooled and tempered) versus forgings (liquid quenched and tempered) in the as-received condition. Numbers above the bars are the respective yield strenghts in ksi.

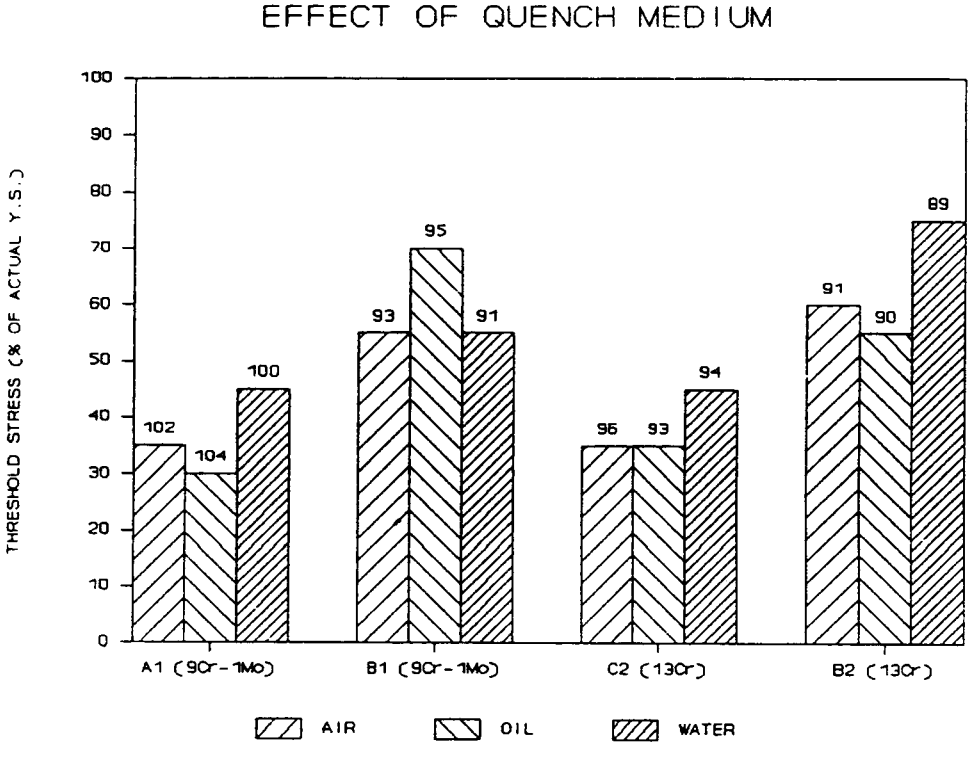


Figure 5 -Effect of quench medium on laboratory heat treated material. Numbers above the bars are the respective yield strengths in ksi.

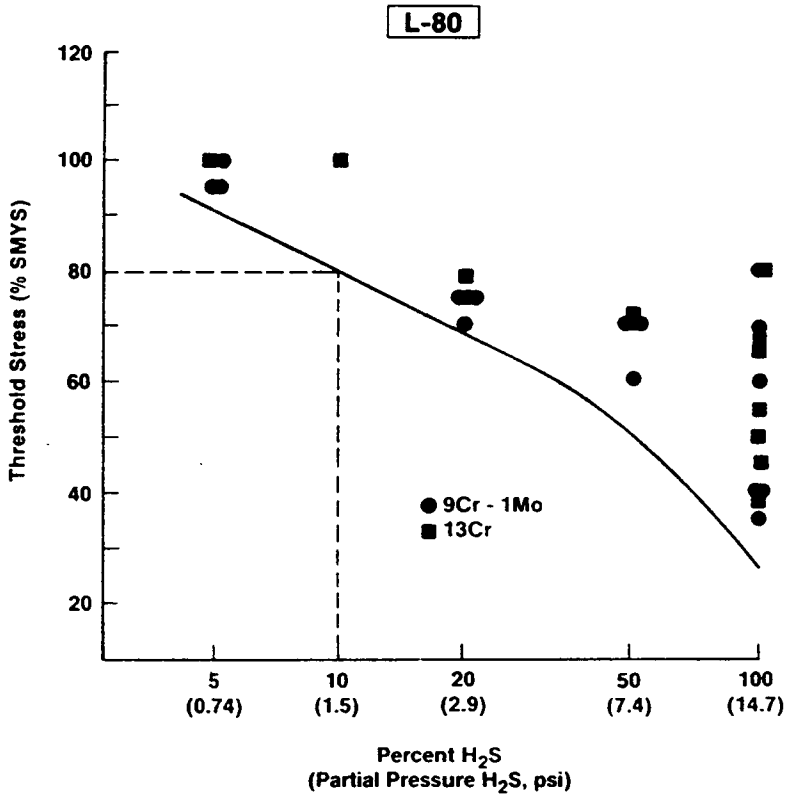


Figure 6 - Effect of H_2S concentration and partial pressure on the NACE Tensile Test results for L-80 grade 9Cr - 1Mo and 13Cr.

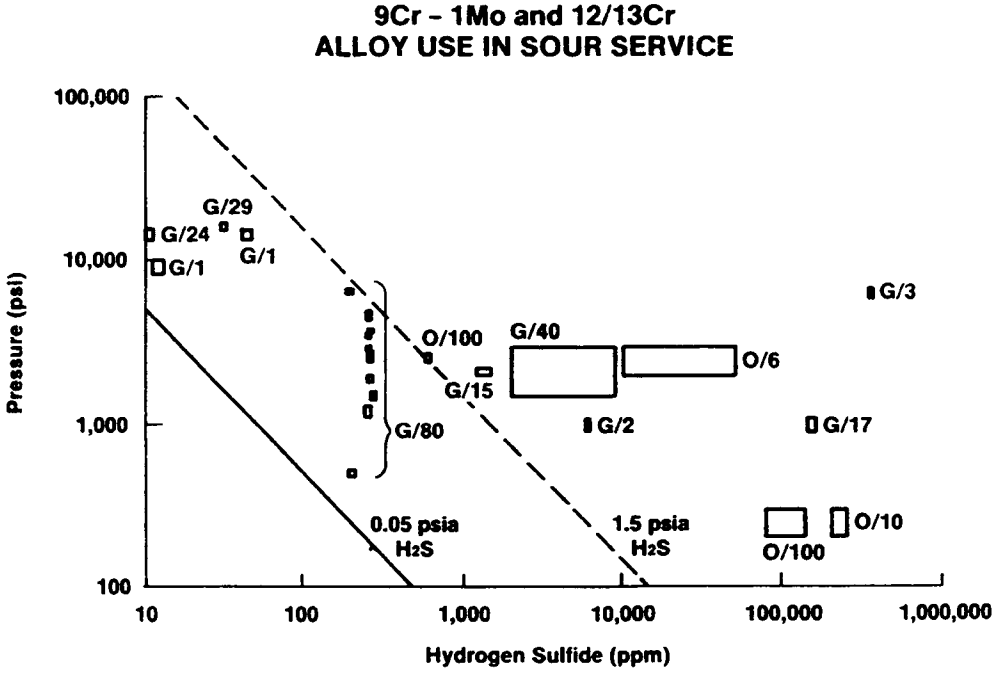


Figure 7 - Chevron field experience with 9Cr - 1Mo and 12/13Cr alloys in sour service. Each plotted rectangle represents the range of H_2S and total pressure encountered in a specific field. The letter next to the field condition indicates either a gas field (G) or an oil field (O). The number represents the number of wells in the field.

Copyrighted Materials
Copyright © 1996 NACE International Retrieved from www.knovel.com

KAWASAKI STEEL TECHNICAL REPORT No. 14 March 1986

Corrosion and Stress Corrosion Behavior of 13 Cr Martensitic Stainless Steels in CO_2-H_2S-Cl^- Environment*



Hayao Kuranashi
Staff Manager,
Electrical Steels & Stainless Steels Dept., Steel Technology Div.



Yuji Sone
Dr. Sci., Senior Researcher, Stainless Steel Lab., I & S Research Labs.



Kayoko Wada
Stainless Steel Lab., I & S Research Labs.



Yoichi Nakai
Staff Manager, Planning & Development Dept. I & S Research Labs.

Synopsis:

Corrosion and stress corrosion behaviors of two types of 13 Cr martensitic stainless steels, C-Cr type (0.2%-13% Cr) and Cr-Ni type (0.02% C-13% Cr-3% Ni), were investigated in CO_2 and CO_2 + H_2S environments. The 13 Cr steels were resistant to CO_2 corrosion at low partial pressure of CO_2. High partial pressure of CO_2 (30 atm), however, increases the corrosion rate of 13 Cr steels at above 150°C. When a small amount of H_2S is mixed into CO_2 environment, crevice corrosion resistance is greatly decreased. Susceptibility to cracking was measured by the slow strain rate technique in CO_2 + H_2S environment and changes in the corrosion potential were measured during the test. The C-Cr type steel reveals an active state in all these environments and its resistance to cracking is inferior to the low alloy steel used. The Cr-Ni type steel reveals a passive state, but is translated into an active state by straining and resistant to cracking.

1 Introduction

The uniform corrosion rates of low alloy steels are significantly increased in sweet environments where solution pH is lowered by CO_2 and non-protective corrosion product films form[1]. On the other hand, sulfide stress cracking (SSC) is a more serious problem than uniform corrosion in sour environments because low alloy steels absorb a large amount of hydrogen due to the action of H_2S and become brittle[2]. The most effective countermeasure against SSC has been considered to be the lowering of the hardness of steels. NACE recommends that the hardness of tubular goods for use in sour environments is lower than a Rockwell C hardness of 22[3].

A number of new developed gas and oil wells contain CO_2 and/or H_2S[4]. Therefore, 13 Cr martensitic stainless steels and duplex stainless steels are often used for tubular goods instead of the low alloy steels used until recently[4]. In recent years, even the use of Ni-based alloys has been considered. Of all such corrosion resistant alloys, 13 Cr steels have been used most widely because they are the least expensive and their strength can be modified easily by adjusting the carbon content and/or tempering temperature.

A minimum level of 13% chromium is required if steel is to exhibit passivity in a wide range of corrosive environments. The corrosion and SSC behavior of 13 Cr steel are more significantly affected by the content of CO_2 and H_2S in environments than those of other stainless steels containing more than 13% Cr and those of Ni-based alloys. The authors previously reported the

* Originally published in *Kawasaki Steel Giho*, 17(1985)3, pp. 299-305

Reprinted with permission of Kawasaki Steel

following experimental results on the stress corrosion cracking of 13 Cr steels in environments containing CO_2 and/or H_2S[5].

(1) 13 Cr steels tempered at above 600°C are immune to stress corrosion cracking in CO_2 environments.
(2) In CO_2 environments containing various amounts of H_2S, the SSC susceptibility of 13 Cr steels increases with partial pressure of H_2S (P_{H_2S}). Some 13 Cr steels are subject to SSC even at 0.07 atm P_{H_2S}.
(3) When the yield strength of 13 Cr steels exceeds 60 kgf/mm^2, failure quickly occurs in the NACE condition. This critical strength (60 kgf/mm^2) is lower than that of low alloy steels by 10 kgf/mm^2.
(4) The higher susceptibility of 13 Cr steels is caused by the fact that such steels absorb hydrogen more easily than do low alloy steels.

In the present work, the effect of temperature and P_{H_2S} on the corrosion rate of 13 Cr steels was investigated in CO_2 and/or H_2S environments. SSC susceptibility was also examined from the view point of corrosion.

2 Experiments

2.1 Materials

Chemical compositions of the materials tested are shown in **Table 1**. There are many kinds of 13 Cr martensitic stainless steels, which can be divided into two main types:

(1) High carbon 13 Cr type (C-Cr type), which does not contain alloy elements other than Cr (such as SUS 420 J1 and J2).
(2) Low C-Ni-13 Cr type (Cr-Ni type), which is strengthen by Ni addition (such as CA6NM).

Steel A is SUS 420 J1 (C-Cr type), while steel B belongs to the Cr-Ni type. Steel C is a low alloy steel KO90SS produced by Kawasaki Steel for oil tubular goods. Steel C was used for comparison with the 13 Cr steels. The specimens of steel A and C were cut from mill-finished seamless pipes produced by the prag mill.

Steel B was a laboratory heat. It was melted in a vacuum induction furnace and hot rolled into 13-mm thick sheet. Tempering temperature and mechanical properties are shown in **Table 2**. Specimens of steel A and B were tempered at both 600 and 710°C. The corrosion tests, however, were performed with specimens tempered at 710°C.

Table 1 Chemical composition of steels used (wt%)

	C	Si	Mn	P	S	Cr	Ni	Mo	Nb
A	0.20	0.75	0.76	0.010	0.004	13.2	—	—	—
B	0.02	0.47	0.50	0.020	0.005	12.8	2.95	—	—
C	0.23	0.29	0.51	0.012	0.004	1.06	—	0.60	0.034

Table 2 Tempering temperature and mechanical properties of steels used

Steel	Heat No.	Tempering temp. (°C)	Yield strength (kgf/mm^2)	Tensile strength (kgf/mm^2)	Elongation (%)
A	A1	710	63.6	78.4	24.1
	A2	600	77.1	96.2	18.8
B	B1	710	81.1	94.2	17.9
	B2	600	76.4	84.7	21.7
C		650	70.4	76.4	25.0

2.2 Corrosion Test

Corrosion tests in a CO_2 environment without H_2S were conducted in a 5-*l* Hastelloy-Alloy-C-lined autoclave in order to examine the effects of CO_2 pressure (P_{CO_2}) and temperature (25-250°C in these tests). Specimens ($3t \times 25W \times 50L$ mm) were polished with 360# wet silicon carbide paper and degreased with acetone. The autoclave was purged, pressurized to 1 or 30 atm with CO_2 gas as required, and heated to a predetermined temperature. 3.5% NaCl solution was used as the corrosive agent. Under some of the conditions, crevice corrosion tests were conducted with the type of specimen shown in **Fig. 1**. The test duration was 100 h for corrosion tests and 72 h for the crevice corrosion tests.

Corrosion and crevice corrosion tests in CO_2 and/or H_2S environments were performed in NaCl solutions saturated with gases containing various amount of CO_2 and H_2S at a pressure of 1 atm balanced with N_2 gas for 30 days. The gas was bubbled in the test cell for the duration of the test period. The gas composition, NaCl concentration, testing temperature, calculated solubility of CO_2 and H_2S, and pH value are tabulated in **Table 3**. The condition I test was conducted in an aerated NaCl solution without CO_2 or H_2S at 80°C in order to examine the effect of oxygen on corrosion. Condition VII is the NACE condition which is widely used to observe the

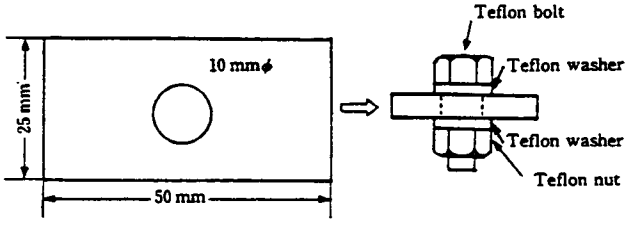


Fig. 1 Specimen for crevice corrosion test

Table 3 Test conditions for immersion test in $CO_2 + H_2S$ environment

	Temp. (°C)	NaCl (wt%)	Gas composition (atm)			Solubility of gas (calculated)		pH*3)	Testing Period
			P_{CO_2}	P_{H_2S}	P_{N_2}	CO_2 (ppm)	H_2S (ppm)		
I	80	3.5	0	0	1.0 air	0.4	0	6.0	720 h (30 day)
II	25	3.5	1.0	0	0	550	0	5.0	
III	25	3.5	0.7	0.007	Bal.	880	21	5.2	
IV	25	3.5	0.7	0.07	Bal.	880	210	4.9	
V	25	3.5	0.7	0.3	0	880	904	4.7	
VI	25	3.5	0	1.0	0	0	3 000*2)	5.0	
VII*1)	25	5.0	0	1.0	0	0	3 000*2)	3.9	

*1) NACE condition (0.5% Acetic acid addition, initial pH 3.0)
*2) Measured value at the end of test was about 2 900 ppm
*3) pH was measured at the end of test

SSC susceptibility of steels and the HIC (hydrogen-induced cracking) susceptibility of line pipe steels. Condition VI was used only for the SSC test mentioned below. The specimen is the same as for the autoclave test mentioned above.

2.3 SSC Test in Environments Containing CO_2 and/or H_2S

SSC behavior of 13 Cr steels was examined with SSRT (slow strain rate technique) in environments containing CO_2 and/or H_2S. While a specimen as illustrated in **Fig. 2** was being strained, the change in corrosion potential (E_{corr}) was measured with a saturated calomel electrode (SCE). After a specimen and a capillary were set in a test cell, a solution saturated with a given gas was circulated through the cell for 24 h prior to the SSRT test. SSRT tests were conducted at a strain rate of 8.3×10^{-5}/s under conditions IV, V, VI and VII as shown in Table 3.

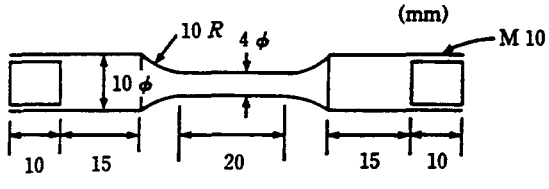


Fig. 2 Specimen for SSRT test

3 Results

3.1 Corrosion Behavior in CO_2 Environments

Figures 3 and 4 show the effect of temperature on corrosion rate at P_{CO_2} of 1 and 30 atm, respectively. At 1 atm P_{CO_2}, the corrosion rate of steel C (low alloy steel) was

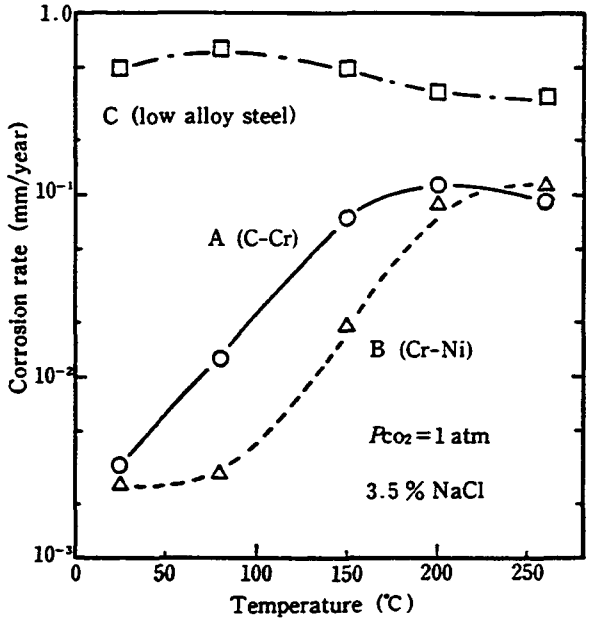


Fig. 3 Effect of temperature on corrosion rate for low alloy steel and 13 Cr steels in sweet environment (P_{CO_2} = 1 atm)

0.6 mm/year at 80°C and 0.4 mm/year at 250°C. On the other hand, the corrosion rate of C-Cr type 13 Cr steel (steel A) increased with temperature and reached a maximum (0.1 mm/year) at 200°C. The corrosion rate of Cr-Ni type 13 Cr steel (steel B) also increased with temperature up to 250°C, but was only 0.1 mm/year even at 250°C. These results show that both types of 13 Cr steels can be used at temperatures of up to 250°C at P_{CO_2} of 1 atm.

At 30 atm P_{CO_2}, steel A was extremely resistant to corrosion up to 80°C but revealed a maximum corrosion rate of 1.4 mm/year at 150°C and corroded at a rate of

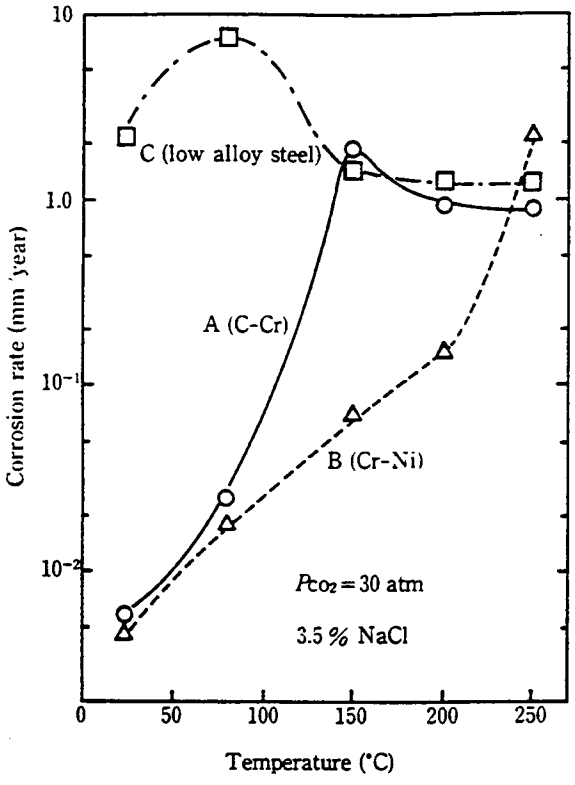


Fig. 4 Effect of temperature on corrosion rate for low alloy steel and 13 Cr steels in sweet environment (P_{CO_2} = 30 atm)

1.0 mm/year at temperatures from 200 to 250°C. Steel C corroded rapidly at a rate of 7.5 mm/year at 80°C. Its corrosion rate, however, decreased drastically at above 150°C, where it became the same as that of steel A. On the other hand, steel B was free from corrosion up to 200°C, but corroded more rapidly than either steel A or C at 250°C. These results show that in higher P_{CO_2} environments, the advantage of high corrosion resistance in 13 Cr steels disappears at above a critical temperature correlated with chemical composition. At P_{CO_2} of 30 atm, this critical temperature is 150°C for C-Cr steel and 250°C for Cr-Ni steel.

Under these conditions, although steel A, B and C all exhibited general corrosion, pitting corrosion was not detected in spite of the use of a 3.5% NaCl solution.

The results of crevice corrosion tests at 150°C and 30 atm P_{CO_2} are shown in **Table 4**. Neither steel A nor B suffered from crevice corrosion.

Table 4 Effect of crevice on corrosion rate for 13 Cr steels in a immersion test under a pressure of 30 atm CO_2 gas at 150°C for 72 h

(mm/year)

A (C—Cr)		B (Cr—Ni)	
Creviced	Crevice free	Creviced	Crevice free
1.36	1.47	0.04	0.05

Consequently, when 13 Cr steels are used in CO_2 environments not containing H_2S, only general corrosion needs to be taken into account at high temperatures and high P_{CO_2}.

3.2 Corrosion Behavior in CO_2 + H_2S Environments

Figure 5 shows the effect of P_{H_2S} on corrosion rate in CO_2 + H_2S environments at 25°C. This figure also contains data obtained in an environment free of CO_2 or H_2S (open air conditions) at 80°C. Both C-Cr and Cr-Ni 13 Cr steels exhibited similar changes in corrosion rate with P_{H_2S}. When the CO_2 environment was contaminated with 0.007 to 0.3 atm P_{H_2S}, their corrosion rates increased slightly, but were only 0.02 mm/year even at 0.3 atm P_{H_2S}. This figure was about one tenth of that of low alloy steel (steel C). The corrosion morphologies of 13 Cr steels are shown in **Photo 1**. Many small pits were detected in C-Cr steel even at 0.07 atm P_{H_2S}, and similar pits were found for Cr-Ni steel at 0.3 atm P_{H_2S}.

The corrosion resistance of 13 Cr steels was drastically reduced under the NACE condition. C-Cr steel had a corrosion rate of 1.3 mm/year . This value was larger than that of steel C (0.9 mm/year). Neither type of 13 Cr steel exhibited pitting corrosion, but both showed

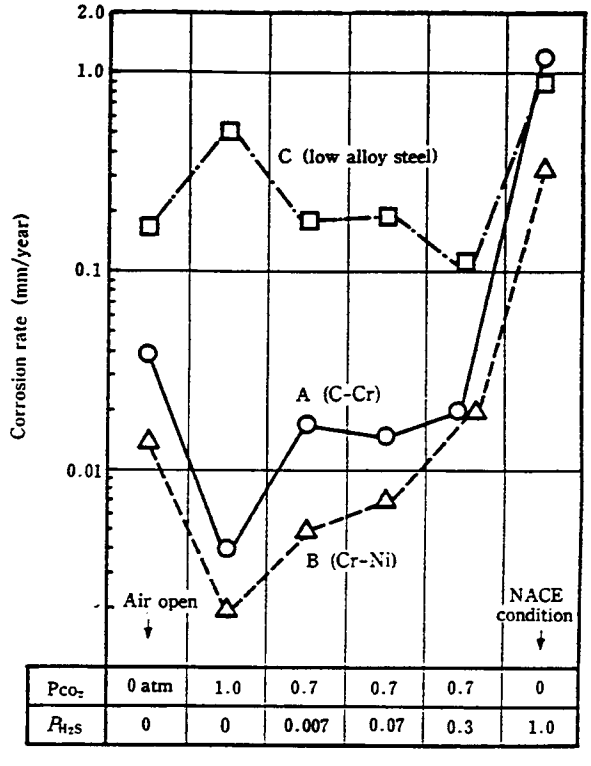


Fig. 5 Effect of H_2S partial pressure on corrosion rate of low alloy steel and 13 Cr steels in CO_2 + H_2S environment at 25°C except air open condition (80°C)

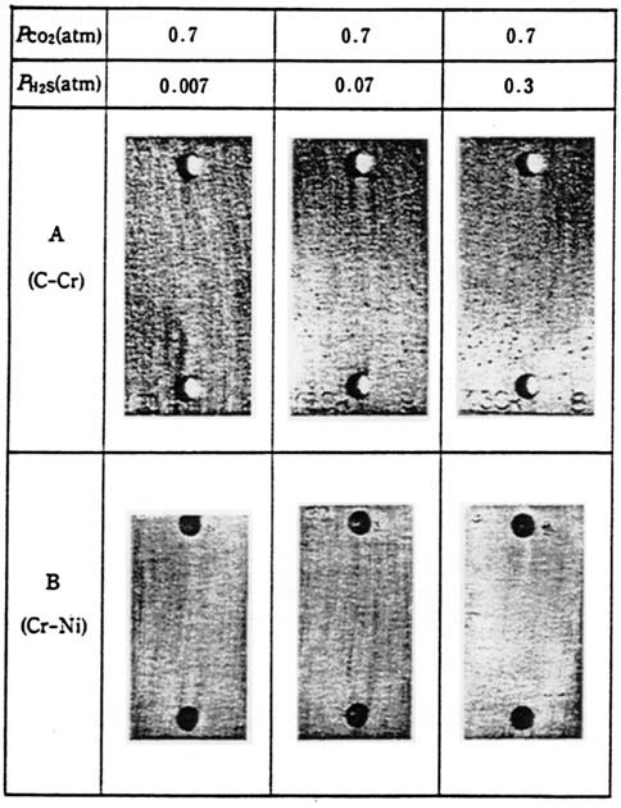


Photo 1 Overall appearance of flat specimens after 720 h exposure in CO_2-H_2S-Cl^- environments at 25°C

general corrosion.

In open air conditions without CO_2 or H_2S, both types of 13 Cr steel suffered from pitting corrosion, with corrosion rates higher than those in all CO_2 + H_2S environments except the NACE condition. This indicates that the corrosion resistance of 13 Cr steels is strongly affected by the presence of oxygen.

On the other hand, the corrosion resistance of low alloy steel (steel C) was significantly inferior in the CO_2 environment without H_2S, with a corrosion rate of 0.5 mm/year . However, when a small amount of H_2S was added to the CO_2 environment, the corrosion resistance of low alloy steel increased with P_{H_2S}. The corrosion rate was 0.18 mm/year at 0.007 atm P_{H_2S} and 0.11 mm/year at 0.3 atm P_{H_2S}. Apparently, sulfide film formed, preventing further attack, as shown by H. Thomason.[6] However, the corrosion resistance of the low alloy steel in the NACE condition was inferior to that in the CO_2 environment without H_2S.

The results of crevice corrosion tests of 13 Cr steels are shown in **Table 5**. The overall appearance of steel A specimens after the immersion test is shown in **Photo 2**. Steel A suffered from crevice corrosion even at 0.07 atm P_{H_2S}. This shows that H_2S is a significant factor in crevice corrosion. Steel B exhibited slight crevice corrosion

Table 5 Test results of crevice corrosion

Environmental test condition					Test result	
Temperature (°C)	NaCl (%)	Gas composition (atm)				
		P_{CO_2}	P_{H_2S}	P_{N_2}	C—Cr	Cr—Ni
80	3.5	0	0	1.0 air	× ×	△ △
80	3.5	1.0	0	0	○ ○	○ ○
25	3.5	0.7	0.007	Bal.	○ ○	○ ○
25	3.5	0.7	0.07	Bal.	× ×	○ ○
25	3.5	0.7	0.3	0	× ×	△ △
25	5.0	0	1.0	0	— —	— —

○: no crevice corrosion
△: slight crevice corrosion
×: heavy crevice corrosion
—: general corrosion

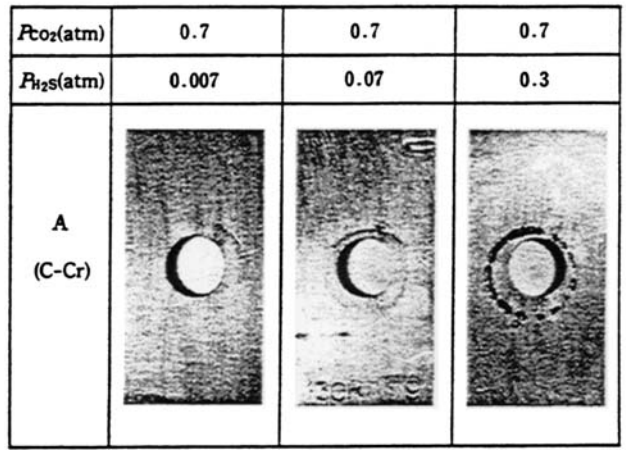


Photo 2 Overall appearance of creviced specimens after 720 h exposure in CO_2-H_2S-Cl^- environments at 25°C

at 0.3 atm P_{H_2S}. Under the NACE condition, 13 Cr steels suffered no crevice corrosion, but showed general corrosion.

These results shows that in a CO_2 environment containing a small amount of H_2S, crevice corrosion is the most serious problem for 13 Cr steels.

3.3 SSC Behavior in CO_2 + H_2S Environments

SSRT tests were conducted under condition IV, V, VI and VII as shown Table 3. The pH values of all conditions except VII were about 4.8, and were not affected by P_{H_2S}. Typical curves of change in E_{corr} during the SSRT test and stress-strain curves are shown in **Figs. 6** and 7. E_{corr} did not change during the tests in Fig. 6, but on the other hand, E_{corr} began to drop in Fig. 7 immediately after the specimen was strained, and fell continuously

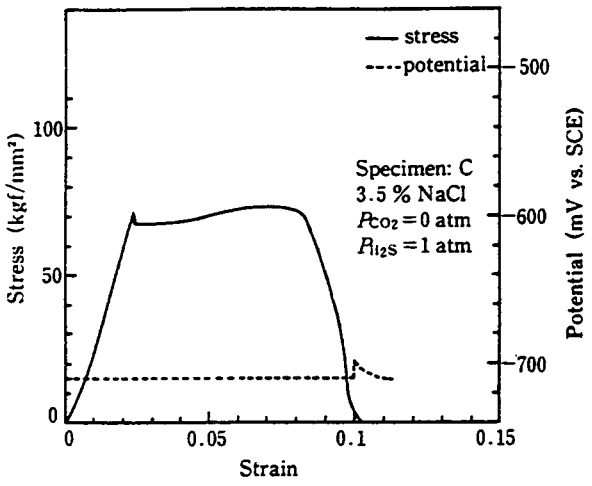


Fig. 6 Stress-strain curve and change of corrosion potential during SSRT test for low alloy steel in 3.5% NaCl solution saturated with 100% H_2S gas

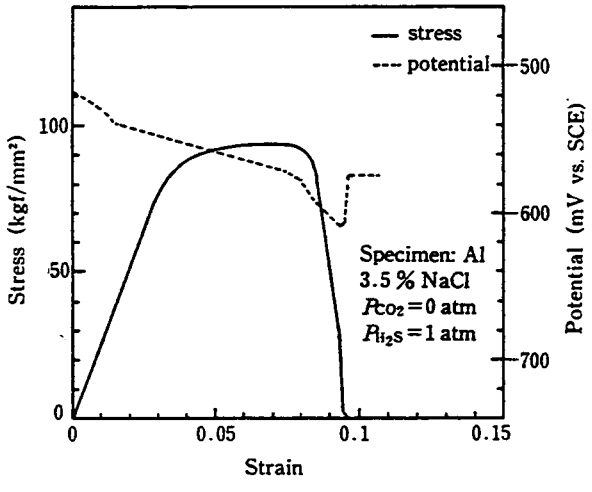


Fig. 7 Stress-strain curve and change of corrosion potential during SSRT test for Cr-Ni steel in 3.5% NaCl saturated with 100% H_2S gas

until the specimen failed. The patterns of change in E_{corr} were divided into the two types illustrated by Figs. 6 and 7. C-Cr 13 Cr steel and low alloy steel showed the former pattern under all conditions used in this work, with an E_{corr} of $-670 \sim -710$ mV (vs. SCE). Cr-Ni 13 Cr steel also exhibited the former pattern under the NACE condition ($E_{corr} \approx -630$ mV), but showed the latter under all other conditions tested. In those cases except NACE condition, E_{corr} dropped from $-470 \sim -590$ mV to -650 mV. E_{corr} before straining was $-470 \sim 500$ mV for Cr-Ni 13 Cr steel tempered at 710°C (B1) and $-550 \sim -590$ mV for that tempered at 600°C (B2).

The effect of H_2S solubility on the degree of embrittlement is shown in **Fig. 8**. The degree of embrittlement was evaluated in terms of the ratio of elongation under each test condition (El_{H_2S}) to elongation in air (El_{air}), and a low ratio indicates a relatively greater degree of embrittlement. Although H_2S solubility under condition VI is the same as that under condition VII (NACE condition), 13 Cr steels were significantly brittle under the NACE condition, with degrees of embrittlement larger than those of the low alloy steel (steel C). Under all conditions, steel A2 exhibited the same degree of embrittlement as that obtained under the NACE condition. Steel A1, B1, and B2 retained their ductilities when H_2S solubility was small. However, steel A1 was more susceptible to SSC than low alloy steel under all conditions used. On the other hand, although the degree of embrittlement of Cr-Ni steel tempered at 600°C was the same as that of the low alloy steel (steel C), that of Cr-Ni steel tempered at 710°C (B1) was smaller than that of steel C. Steel B1 did not show any embrittlement at 0.07 atm P_{H_2S}. Calculated solubility is 160 ppm under this condition.

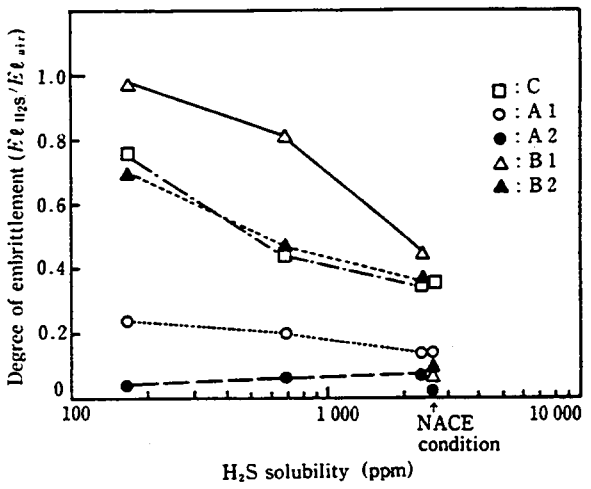


Fig. 8 Effect of H_2S solubility on the degree of embrittlement measured by SSRT test in $CO_2 + H_2S$ environment

From the results of SSRT tests in $CO_2 + H_2S$ environments except the NACE condition, the SSC susceptibility of steels used in this work was ranked as follows.

$$A2 \ll A1 < C \approx B2 < B1$$

In these conditions, steel C, B2, and B1 failed under local elongation, while steel A1 and A2 failed in the brittle mode without local elongation.

4 Discussion

Corrosion of low alloy steels caused by water with a high CO_2 content poses a serious problem and has frequently been studied. D.W. Shannon[1] reported that

corrosion becomes smaller as temperature increases. On the other hand, K. Masamura, *et al.*[7] showed that the corrosion rate reaches its maximum at a temperature lower than 100°C and decreases with temperature at higher temperatures. The results obtained in this work are similar to the latter. The maximum corrosion rate occurred at 80°C. As P_{CO_2} increases, the maximum rate also rises. D.W. Shannon[1] reported that while an unprotective $FeCO_3$ film formed at lower temperatures, Fe_3O_4 film formed at higher temperatures. This Fe_3O_4 film protects carbon steel from corrosion.

The temperature dependence of corrosion behavior of C-Cr 13 Cr steel shows a similar tendency to that of low alloys steel. The critical temperature at which the corrosion rate reaches its maximum is 200°C at 1 atm P_{CO_2} and 150°C at 30 atm P_{CO_2}. C-Cr steel, however, has considerable resistance to CO_2 corrosion at temperatures below 100°C. This shows that the passive film of C-Cr steel is stable in this temperature range. However, the passive film becomes unstable at above the critical temperature, and C-Cr steel does not show the special quality of a stainless steel. That is, C-Cr steel suffers from CO_2 corrosion in the same manner as low alloy steel in this temperature range. Cr-Ni steel also exhibits similar corrosion behavior at 250°C and 30 atm P_{CO_2}, but under all of other conditions it is resistant to CO_2 corrosion. 13 Cr steels suffer little of the crevice or pitting corrosion which are serious problems in stainless steels. Furthermore, as the authors[5] showed in early work, 13 Cr steels tempered at above 600°C were immune to stress corrosion cracking (SCC) in CO_2 environments. From these results, it may be said that when 13 Cr steels are used at below a critical temperature correlated with P_{CO_2} and their chemical composition, they will be immune to pitting corrosion, crevice corrosion, and SCC, and their general corrosion resistances will be superior to that of low alloy steels.

In a CO_2 environment contaminated with a small amount of H_2S, general corrosion of 13 Cr steels increases slightly. On the other hand, crevice corrosion accelerates drastically. S. Tsujikawa, *et al.*[8] have studied the effect of P_{H_2S} on crevice corrosion of SUS 444 ferritic stainless steel in a 3.5% NaCl solution at 80°C. Crevice corrosion resistance is evaluated as the potential denoted E_R at which the growth of crevice corrosion stops. E_R is measured by active to noble polarization of a specimen with crevicing. A higher E_R indicates that crevice corrosion resistance is higher. These researchers reported that the effect of H_2S was not found at P_{H_2S} below 0.003 atm but was found at 0.01 atm P_{H_2S} and saturated at P_{H_2S} above 0.03 atm. The E_R of SUS 444 is $-200 \sim -300$ mV (vs. SCE) in an H_2S-free environment and drops to -530 mV in an environment containing 0.03 atm P_{H_2S}. Since the corrosion resistance of 13 Cr steels is inferior to that of SUS 444, it is reasonable to expect that the crevice corrosion of 13 Cr steels will be strongly accelerated by small amounts of H_2S. Although the present investigation was conducted at a lower temperature (25°C) than that used in S. Tsujikawa's work[8] and crevice corrosion is more difficult to occure, C-Cr 13 Cr steel was found to suffer from crevice corrosion at 0.07 atm P_{H_2S}.

Therefore, when 13 Cr steels are used in CO_2 environments with a small amount of H_2S, care must be given to crevice corrosion as well as to SSC. Special attention should be given to sites where crevice corrosion is thought to occur, that is, at coupling portions and beneath sludge deposits in oil tubular goods.

Generally, the passive film of stainless steel does not exist at below a critical pH. This critical pH is denoted as pH_d. The accelerating effect of H_2S on crevice corrosion indicates that H_2S raises the pH_d of stainless steel. M. Miyuki, *et al.*[9] reported that the pH_d of a duplex stainless steel was under 2.0 in a 5% NaCl + 0.5% acetic acid solution at 200°C, but that the pH_d rose to 2.8 after gas containing 0.1 atm P_{H_2S} was bubbled into the solution. The mechanism of crevice corrosion is considered to be as follows[10]. In a crevice, first the dissolution of a small amount of iron occurs, and the pH is then lowered by hydrosis of iron. When the pH in the crevice reaches the pH_d, active dissolution of stainless steel in the crevice begins immediately. If the environment contains a small amount of H_2S, the pH in the crevice may rapidly reach pH_d and crevice corrosion is thus accelerated. It has not to date been made clear, however, why the pH_d of stainless steel is increased by H_2S.

The SSC susceptibilities of 13 Cr steels in $CO_2 + H_2S$ environments were evaluated by SSRT tests. In an environment where E_{corr} of 13 Cr steels remains unchanged during the SSRT test, both C-Cr and Cr-Ni steels are more susceptible to SSC than is low alloy steel. E_{corr} of C-Cr steels does not change during SSRT test under the conditions used in this work. E_{corr} of low alloy steel also does not change under these conditions. On the other hand, E_{corr} of Cr-Ni steel decreases with strain under all conditions except the NACE condition, and when E_{corr} reaches the value obtained under the NACE condition, specimens ruptured. The degree of embrittlement of Cr-Ni steel under such conditions is the same as or smaller than low alloy steel. Consequently, in environments where 13 Cr steels become active, the degrees of embrittlement are larger than that of low alloy steel in the same manner as under hydrogen charging. On the other hand, in environments where 13 Cr steels do not become active, they reach the rupture point following the destruction of their passive film. In such cases, susceptibility to SSC is suppressed.

It has been made clear that oxygen accelerates pitting and crevice corrosion in 13 Cr steels. D. Combes, *et al.*[11] report that 13 Cr oil tubular goods have been used

without problems in actual well environments, in spite of the presence of CO_2 and small quantities of H_2S. They state that this is attributable to the absence of oxygen in typical drilling conditions. Their findings thus support the view that oxygen is a major cause of corrosion in 13 Cr steels.

5 Conclusions

The following conclusions have been drawn from this study of the corrosion and SSC behavior of 13 Cr steels in $CO_2 + H_2S$ environments.

(1) Both C-Cr and Cr-Ni 13 Cr steel exhibit good corrosion resistance at 1 atm P_{CO_2} without H_2S at temperatures below 250°C and suffer little pitting or crevice corrosion. They cannot, however, be used practically at 30 atm P_{CO_2} or above a critical temperature which is 150°C for C-Cr steel and 250°C for Cr-Ni.

(2) 13 Cr steels exhibit only slight general corrosion but suffer significantly from crevice corrosion in CO_2 environments which contain a small amount of H_2S.

(3) The SSC susceptibility of 13 Cr steels is related to the stability of their passive films in CO_2 environments contaminated with small amounts of H_2S. When the passive film is not stable, SSC susceptibility is higher than that of low alloy steel. On the other hand, when it is stable, the SSC resistance is the same as or superior to that of low alloy steel.

References

1) D. W. Shannon: "Corrosion of Iron-base Alloy versus Alternate Materials in Geothermal Brines" (BATTELE, Pacific Northwest Laboratories), November (1977)
2) R. N. Tuttle and J. W. Kochera: "Control of Hydrogen Embrittlement in Deep Gas Wells", *International Conference on the Effect of Hydrogen on Behavior Materials*, AIME, (1975)
3) NACE standard, MR-01-75 (1984 Editorial Revision), Item No. 5304
4) R. N. Tuttle and T. W. Hamby: *Materials Performance*, 17(1977)9, 9
5) H. Kurahashi, T. Kurisu, Y. Sone, K. Wada, and Y. Nakai: "Stress Corrosion Cracking of 13 Cr Steels in CO_2-H_2S-Cl^- Environments", CORROSION/84, New Orleans, No. 212 (1984)
6) W. H. Thomason: "Formation Rates of Protective Iron Sulfide Films on Mild Steel in H_2S-Saturated Brine as a Function of Temperature", CORROSION/78, New Orleans, No. 41, (1978)
7) K. Masamura and I. Matsushima: Preprint of the 47th Corrosion and Protection Symposium, Japan Society of Corrosion Engineering, (1983), 31
8) S. Tsujikawa and K. Uesugi: Preprint of '84 Spring Meeting of Japan Society of Corrosion Engineering, (1984), 324
9) H. Miyuki, J. Murayama, T. Kudo, and T. Moroishi: "Localized Corrosion of Duplex Stainless Steels in CO_2-H_2S-Cl^- Environment at Elevated Temperature", CORROSION/84, New Orleans, No. 293, (1984)
10) Y. Hisamatsu: *Tetsu-to-Haganė*, **63**(1977)5, 14
11) J. D. Combes, J. G. Kerr, and L. J. Klein: *Petroleum Engineer International*, March (1983), 50

Copyrighted Materials
Copyright © 1996 NACE International Retrieved from www.knovel.com

Stress Corrosion Cracking of 13Cr Steels in CO_2-H_2S-Cl^- Environments*

*H. KURAHASHI, T. KURISU, Y. SONE, K. WADA, and Y. NAKAI**

Abstract

Stress corrosion cracking (SCC) behavior of two 13Cr steels was investigated in aqueous CO_2-H_2S environments. U-bend tests, constant load tensile tests, and corrosion tests were performed in CO_2 environments containing different amounts of H_2S. In addition, the slow strain rate tensile (SSRT) tests and hydrogen absorption measurements were done under cathodic hydrogen charging conditions to determine why 13Cr steels are more susceptible to SCC in H_2S environments than low alloy steels are.

The 13Cr steels were less resistant to SCC in the CO_2-H_2S environments than low alloy steels were, but some 13Cr steels were not subject to SCC even at a hydrogen sulfide partial pressure of 0.3 atm. Furthermore, it was found that SCC in a CO_2-H_2S environment was caused by hydrogen embrittlement and that the SCC susceptibility of 13Cr steels was affected by their intergranular cracking behavior. Thus, their microstructures and carbide dispersions are important factors in defining SCC susceptibility of 13Cr steels.

Introduction

Until recently, low alloy steel tubulars have been used in combination with corrosion inhibitors in gas or oil wells containing hydrogen sulfide (H_2S), carbon dioxide (CO_2), and salt water.[1] This practice is very expensive, however. Moreover, the efficiency of inhibitors is reduced in high temperature wells.[1,2] Under these conditions, the alternative of using special corrosion resistant alloy tubulars has been considered. Of all the corrosion resistant alloys, 13Cr martensitic steel is the least expensive. Its strength can be changed easily by adjusting the carbon content and/or tempering temperature. But a minimum level of 13% chromium is required for steel to exhibit passivity in a wide range of corrosive environments. Therefore, the corrosion and stress corrosion cracking (SCC) behaviors of 13Cr steel are more significantly affected by environmental factors than those of other stainless steels containing more than 13% Cr and those of Ni base alloys. It has been known that 13Cr steels are highly resistant to CO_2 corrosion. But they are more susceptible to SCC in environments containing H_2S than the low alloy steels are.[3-5] Therefore, they should be used in gas and oil fields with higher CO_2 concentrations and lower H_2S concentrations. It is necessary to clarify the critical H_2S concentration at which 13Cr steels undergo SCC. This critical H_2S concentration is affected by the chemical composition, strength, and microstructure of the steel.[3,6]

The primary purpose of this paper is to present the SCC characteristics of two types of 13Cr steels: low carbon Ni-Cr type and high carbon Cr type, in CO_2-Cl^- environments with various H_2S concentrations. In addition, the slow strain rate tensile (SSRT) tests were conducted under cathodic hydrogen charging conditions to determine why 13% Cr steels are more susceptible to SCC in environments containing H_2S than are low alloy steels.

* Presented during CORROSION/84 (Paper No. 212), April 1984, New Orleans, Louisiana.

* Kawasaki Steel Corp. Research Laboratories, 1-Kawasaki-cho, Chiba 260, Japan.

Experimental

Materials

Twenty kinds of 13Cr steel were used in this investigation. They included two types: (1) a high carbon 13Cr type (C type) and (2) a low carbon Ni-13Cr type (Ni type). In addition, three low alloy steels of different strengths were used to compare them with the 13Cr steels. The chemical compositions of the above are listed in Table 1. Various alloying elements such as carbon, nitrogen, niobium, vanadium, nickel, and molybdenum were investigated to determine their influence on SCC for each type of 13Cr steel. The specimens of Heat Nos. 2 and 3 were cut from mill-finished seamless pipes produced by the Kawasaki prag mill and heat treated to their respective strengths. The austenitizing temperature was 950 C. All of the other 13Cr steels were laboratory heats. They were melted in a vacuum induction furnace and hot rolled into 5 mm thick plates. They were heated at 1000 C for 1 h and air cooled or water quenched, and then they were tempered at varying temperatures from 450 to 780 C. The specimens of low alloy steels were cut from mill-finished seamless pipes having strengths of API L80, C90, and C95.

Procedure

The U-bend tests, constant load tensile tests, and corrosion tests were performed in CO_2 environments containing various amounts of H_2S at a pressure of 1 atm. The gas compositions, NaCl concentrations, testing temperatures, and testing periods are shown in Table 2. The Condition I test was conducted in an aerated NaCl solution without CO_2 or H_2S. Condition VII is the "NACE condition," which is used to observe the SCC susceptibility of steels in H_2S environments.

In the U-bend test, 2 mm^t × 20 mm^w 14 mm^H specimens were immersed in a 0.1 m^3 vessel. The gas was continuously bubbled through the vessel after deaerating with nitrogen gas.

In the constant load SCC test, the solution saturated with a given gas was circulated through the cell shown in Figure 1. The specimen was the NACE subsize (2.5 mm^Φ × 25.4 mm^ℓ).

TABLE 1 — Chemical Composition of Steels Used (wt%)

	Steel No.	C	Si	Mn	P	S	Cr	Ni	Mo	Nb	V	N
C-type	1	0.30	0.42	0.51	0.027	0.013	12.2	—	—	—	—	<0.01
	2	0.20	0.75	0.76	0.010	0.004	13.2	—	—	—	—	0.020
	3	0.18	0.49	0.49	0.020	0.005	13.05	—	—	—	—	0.020
	4	0.19	0.49	0.53	0.002	0.004	13.1	—	—	—	—	0.013
	5	0.15	0.50	0.52	0.002	0.003	13.2	—	—	—	—	0.0098
	6	0.15	0.53	0.53	0.002	0.004	13.2	—	—	—	—	0.063
	7	0.14	0.50	0.50	0.003	0.003	13.0	—	—	—	0.10	<0.01
	8	0.14	0.51	0.53	0.002	0.003	13.1	—	—	0.052	0.12	<0.01
	9	0.14	0.50	0.51	0.002	0.003	12.9	—	—	—	0.22	<0.01
	10	0.10	0.49	0.52	0.003	0.003	13.0	—	—	—	—	<0.01
	11	0.10	0.49	0.52	0.003	0.003	13.6	—	—	—	—	0.057
	12	0.10	0.50	0.52	0.003	0.002	11.7	—	—	—	0.11	<0.01
	13	0.10	0.51	0.53	0.003	0.002	11.7	—	—	0.048	0.10	<0.01
	14	0.11	0.49	0.51	0.003	0.002	11.7	—	—	—	0.23	<0.01
Ni-type	15	0.006	0.15	0.52	0.003	0.002	12.8	2.46	—	—	—	0.063
	16	0.019	0.47	0.50	0.020	0.005	12.8	2.95	—	—	—	0.058
	17	0.054	0.49	0.52	0.003	0.004	13.2	3.87	1.0	—	—	0.019
	18	0.003	0.19	0.52	0.002	0.003	12.2	4.66	—	—	—	0.019
	19	0.004	0.28	1.50	0.002	0.004	13.0	5.54	—	—	—	0.018
	20	0.004	0.19	0.53	0.002	0.003	13.3	6.10	—	—	—	0.019
	21	0.003	0.20	1.52	0.003	0.004	12.2	6.11	1.01	—	—	0.019
Low alloy steel	KS80	0.25	0.25	1.40	0.019	0.004	—	—	—	—	—	<0.01
	K090 SS	0.23	0.29	0.51	0.012	0.004	1.06	—	0.60	0.034	—	<0.01
	KS95	0.25	0.24	1.35	0.020	0.007	—	—	—	—	—	<0.01

TABLE 2 — Test Conditions

	Temperature (C)	NaCl (wt%)	Gas Composition (atm) P_{CO_2}	P_{H_2S}	P_{N_2}	Solubility of Gas (calculated) CO_2 (ppm)	H_2S (ppm)	pH[3]	Testing Period
I	80	3.5	0	0	1.0 air	0.4	0	6.0	
II	80	3.5	1.0	0	0	550	0	5.0	
III	25	3.5	0.7	0.007	Bal.	880	21	5.2	720 h
IV	25	3.5	0.7	0.07	Bal.	880	210	4.9	(30 days)
V	25	3.5	0.7	0.3	0	880	904	4.7	
VI	25	3.5	0	1.0	0	0	3000[2]	5.0	
VII[1]	25	5.0	0	1.0	0	0	3000[2]	3.9	

[1]NACE condition (0.5% acetic acid addition, initial pH: 3.0).
[2]Measured value at the end of test was about 2900 ppm.
[3]pH was measured at the end of the test.

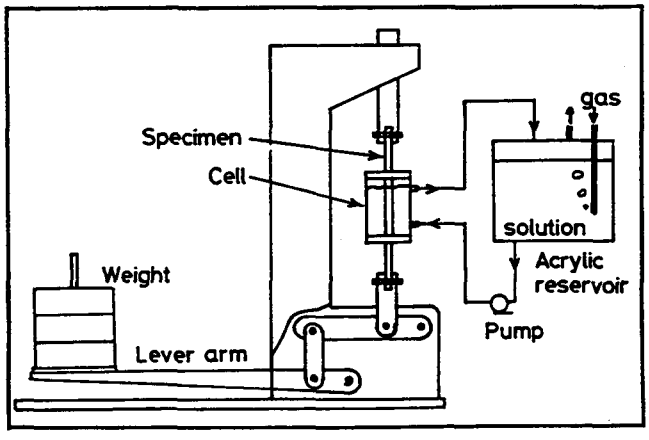


FIGURE 1 — Apparatus for constant load test.

Corrosion rates in each test solution were measured by using 2 mm^t × 40 mm^w × 50 mm^l specimens.

The U-bend SCC tests and corrosion tests in a high temperature, high pressure CO_2 environment were conducted in a 5 L Hastelloy Alloy C lined autoclave. The autoclave was purged with nitrogen gas, pressurized to 30 atm with CO_2, and heated to predetermined temperatures.

The SSRT tests and the hydrogen absorption measurements for 13Cr steel and a low alloy steel (K090SS) were made under cathodic hydrogen charging conditions to investigate their hydrogen embrittlement (HE) susceptibility. The specimens used are illustrated in Figure 2. The hydrogen was charged in a 0.1N NaOH + 0.1N NaCN solution for 24 h prior to the SSRT test. The SSRT test was conducted at a strain rate of 8.3×10^{-5}/s with a constant hydrogen charge. The amount of hydrogen absorption was measured by the vacuum heat extraction method (450 C × 1 h) after a charging time of 24 h.

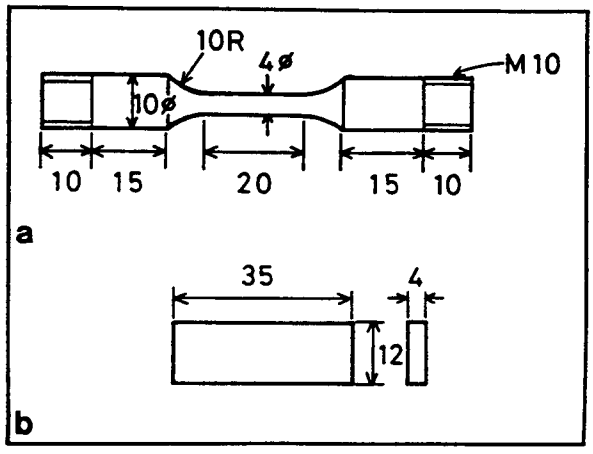


FIGURE 2 — Specimens for SSRT and hydrogen absorption measurement under cathodic hydrogen charging condition: (a) SSRT specimen and (b) specimen for hydrogen absorption.

All of the specimens were polished with #600 wet silicon carbide paper and degreased with acetone. The U-bend specimens were stressed with AISI 316 stainless steel screws and electrically insulated with Teflon washers.

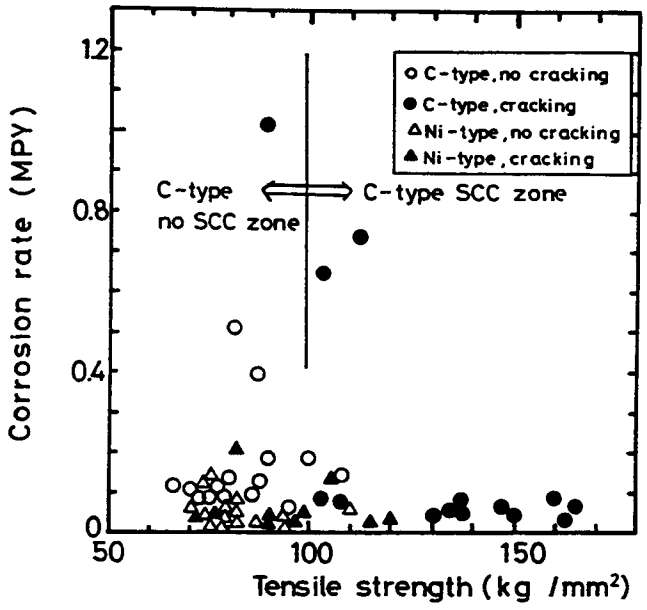


FIGURE 3 — SCC behavior of 13Cr steels tempered at various temperatures (test condition: CO_2 1 atm, 80 C).

Results and Discussion

SCC in CO_2 Environment

The effect of tempering temperature on SCC in a CO_2 environment without H_2S (Condition II) and aerated solution without CO_2 or H_2S (Condition I) is listed in Table 3. These results are plotted in strength-corrosion rate maps shown in Figures 3 and 4. The strength of the C-type decreased with increasing tempering temperature. The strength of the Ni-type fell to a minimum at around 650 C and grew with increasing temperature above 600 C.

The SCC susceptibility of 13Cr steels in these environments was strongly affected by tempering temperature. When each steel was tempered above each specific temperature, it was completely immune from SCC. This specific tempering temperature was designated a critical tempering temperature (CTT). With the exception of 0.30% C steel, CTT of the C-type was 600 C in both conditions. The strengths of the C-types tempered above CTT were 66 to 100 kg/mm^2. On the other hand, when they were tempered below CTT, their strengths were above 100 kg/mm^2 and they suffered from SCC. Therefore, the SCC susceptibility of C-type steels under these conditions is considered to be dependent on their microstructure and strength. The mode of cracking was typically intergranular, as shown in Figure 5. Figure 6 shows transmission electron micrographs of a 0.20C-13Cr steel tempered at 550 and 600 C. At 550 C, small needle-like precipitates were observed within the grains, and at 600 C, spherical particles precipitated along the grain boundaries. The effect of C and N on the SCC of C-type steels was not observed in the CO_2 environment. In the aerated environment, however, even 0.3% C steel tempered at 700 C suffered SCC. This indicates that high carbon contents diminish SCC resistance of C-type steel and that oxygen dissolved in the environment further accelerates SCC. Ni-type steels were divided into two groups according to CTT. One CTT was 550 C. The other's was 600 C, as was that of the C-type steels. A Ni addition above 5.5% or a 1% Mo addition decreased CTT to 550 C. The strengths of Ni-type steels varied in strength from 70 to 120 kg/cm^2, depending on tempering temperature. They suffered SCC when strengths ranged from 70 to 120 kg/mm^2. These results indicate that the Ni-type SCC susceptibility is independent of strength and depends on their tempering temperature. When a 0.003C-13Cr-5Ni specimen was tempered at 600 C, fine needle-like carbides were observed within its grains, as shown in Figure 6. When the material was tempered at 550 C, no precipitates could be observed. This steel's CTT was 600 C. These results indicate that Ni-type SCC susceptibility is significantly affected by changes in microstructure and carbide dispersion.

Both the C-type and Ni-type were highly resistant to CO_2 corrosion (Condition II). Their corrosion rates were below 1 mpy regardless of their tempering temperature, and no pitting

TABLE 3 — Results of SCC Test for 13 Steels Tempered at Various Temperatures

	Nominal Composition (wt%)	3.5% NaCl + 1 atm CO_2, 80 C						3.5% NaCl, aerated, 80 C					
		450 C	500 C	550 C	600 C	650 C	700 C	450 C	500 C	550 C	600 C	650 C	700 C
C-type	0.3C-13Cr	X	—	X	O	O	O	X	X	X	X	X	X
	0.2C-13Cr	X	X	X	O	O	O	X	X	X	O	O	O
	0.15C-13Cr	X	X	X	O	O	O	X	X	X	O	O	O
	0.15C-13Cr-0.06N	X	X	X	O	O	O	X	X	X	O	O	O
	0.10C-13Cr	X	X	X	O	O	O	X	X	X	O	O	O
	0.10C-13Cr-0.06N	X	X	X	O	O	O	X	X	X	O	O	O
								X	X	X	O	O	—
Ni-type	0.006C-13Cr-2.5Ni-0.06N	X	X	X	O	O	—	X	X	O	O	O	O
	0.05C-13Cr-4Ni-1Mo	X	X	O	O	O	O	X	X	X	O	O	O
	0.003C-12Cr-5Ni	X	X	X	O	O	O	X	X	O	O	O	O
	0.04C-13Cr-5.5Ni	X	X	O	O	O	O	X	X	O	O	O	O
	0.004C-13Cr-6Ni	X	X	O	O	O	O	X	O	O	O	O	O
	0.003C-12Cr-6Ni-1Mo	X	X	O	O	O	O						

Note: O = crack-free.
X = cracked.

could be observed on the specimen surfaces. In the aerated condition, however, C-type steels suffered pitting. The degree of pitting corrosion was more severe with specimens subjected to higher tempering temperatures. Based on these results, the presence of oxygen in the environment should be taken into account when using C-type 13Cr steels in CO_2 environments. Conversely, Ni-type corrosion rates were less than 1 mpy under this condition, and there was little pitting. The Ni-type steels were highly resistant to corrosion.

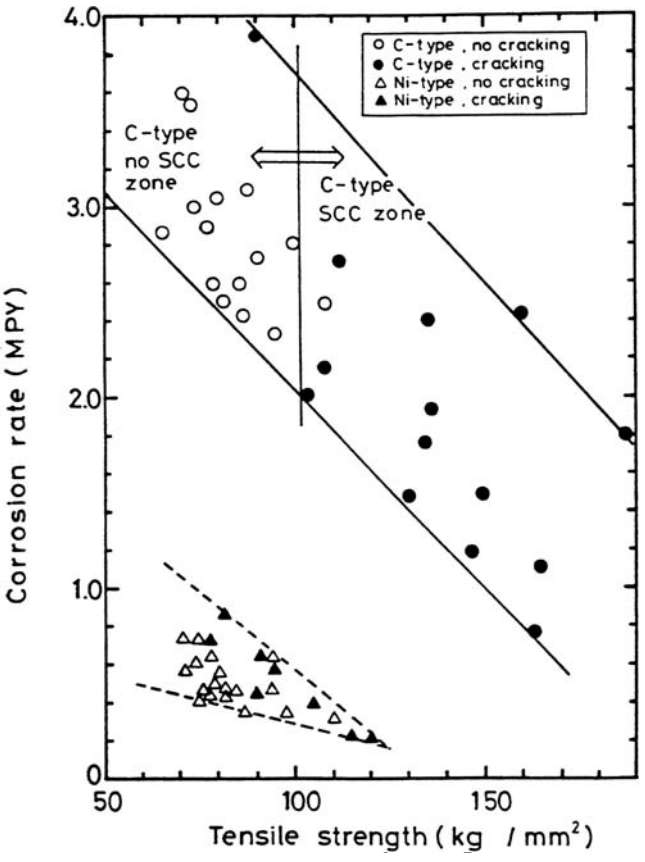


FIGURE 4 — SCC behavior of 13Cr steels tempered at various temperatures (test condition: aerated 3.5% NaCl, 80 C).

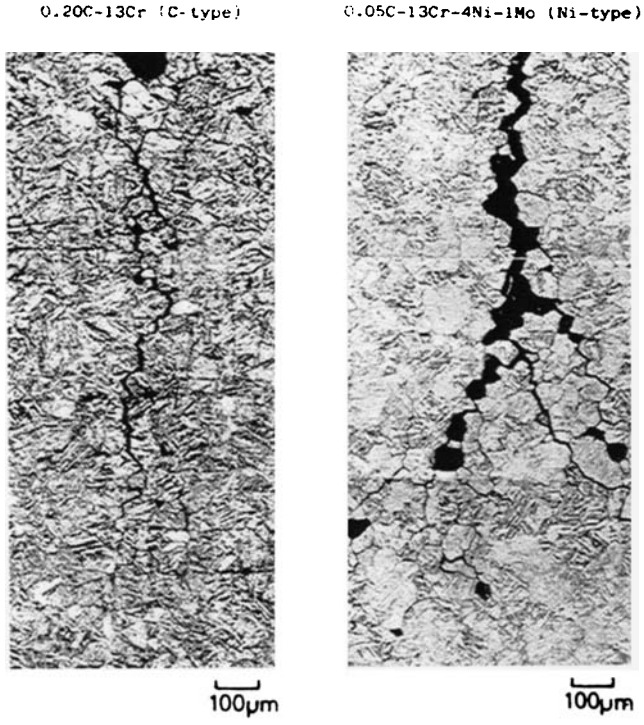


FIGURE 5 — SCC of 13Cr steels tempered at 450 C (test conditions: CO_2 1 atm, 80 C).

SCC in High Temperature, High Pressure CO_2 Environments

The SCC test results in high pressure CO_2 environments at 150 and 200 C are shown in Table 4. Specimen strengths were adjusted to the levels of API L80 and C90. All of them were tempered at temperatures above 600 C. In these environments, no SCC occurred. But these data show that C-type steels should not be applied to these environments because their corrosion resistance was very poor. On the other hand, Ni-type steels revealed a high level of corrosion resistance. Thus, they can be applied to high pressure, high temperature CO_2 environments.

SCC in CO_2 Environments Containing H_2S

U-bend SCC tests of 13Cr steel laboratory heats in CO_2 environments containing H_2S have been made in Conditions III, IV, and V (Table 2). The specimen strengths were adjusted to API L80 and C90. The results are tabulated in Table 5, which also shows tensile properties and corrosion rates. All corrosion rates were under 5 mpy (127 μm/y). The 13Cr steels are highly corrosion resistant in these environments. None of the low alloy steels had ever cracked, regardless of H_2S concentration in CO_2 environments, but the SCC resistance of the 13Cr steels was significantly affected by alloy composition and H_2S concentration. The 13Cr steel test results have been summarized as follows:

1. Carbon was detrimental to C-type 13Cr steel's SCC resistance. The SCC of 0.19C-13Cr steel of both L80 and C90 levels occurred at P_{H_2S} above 0.07 atm.
2. 0.10 to 0.15C-13Cr-0.06N steels were not subject to SCC even at a P_{H_2S} of 0.3 atm. This shows that N addition to C-type steels improves SCC resistance.
3. The SCC for a Ni-type steel containing 0.05% C was observed even at P_{H_2S} of 0.007 atm. This shows that carbon is very detrimental to Ni-type SCC resistance as well as that of the C-type material.
4. The higher the Ni addition for Ni-type, the more SCC resistance improved. But the addition of less than 2.5% Ni had no effect on SCC resistance.
5. The addition of 1% Mo improved Ni-type SCC resistance. For 4 to 6% Ni and 1% Mo bearing steel, SCC did not occur even in P_{H_2S} of 0.3 atm.

The effect of alloying elements on the Ni-type SCC resistance showed the same inclination as the results of SCC tests

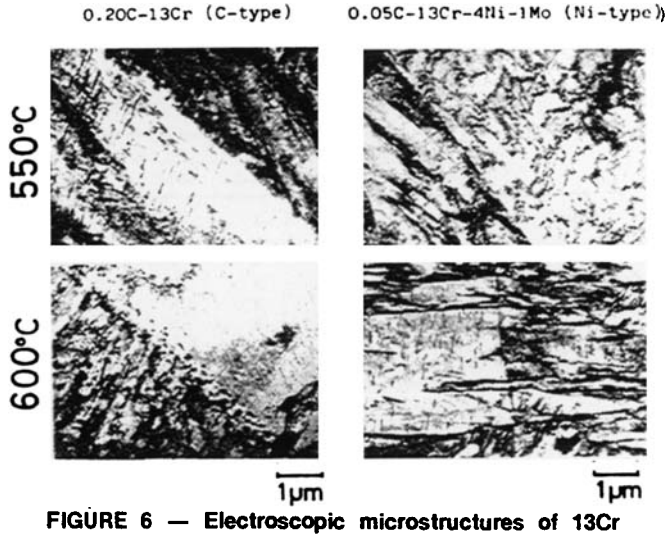


FIGURE 6 — Electroscopic microstructures of 13Cr steels tempered at 550 and 600 C.

TABLE 4 — Results of SCC and Corrosion Tests in High Temperature, High Pressure CO_2 Environments

Strength	Type	Composition	150 C, 3.5% NaCl P_{CO_2} = 30 atm, 72 h	200 C, 3.5% NaCl P_{CO_2} = 20 atm, 100 h
L80 level	C-type	0.20C-13Cr	O (39.4)	O (15.7)
		0.15C-13Cr-0.06N	O	O
		0.10C-13Cr-0.009N	O	O
	Ni-type	0.05C-13Cr-4Ni-1Mo	O	(not tested)
		0.003C-13Cr-4Ni-1Mo	O (3.1)	O (7.1)
	Low alloy steel	K080S	O (39.0)	O (16.0)
C95 level	C-type	0.20C-13Cr	O	O
		0.15C-13Cr-0.06N	O	O
		0.10C-13Cr-0.009N	O	O
	Ni-type	0.05C-13Cr-4Ni-1Mo	O	(not tested)
		0.003C-13Cr-4Ni-1Mo	O	O
	Low alloy steel	K095	O	O

Note: ( ) = corrosion rate (mpy).
O = crack-free.

(Table 3) in the pure CO_2 environment. This indicates that both the SCC in the pure CO_2 environment and the SCC in the CO_2 + H_2S environments involve the same phenomena and that H_2S accelerates SCC.

Figure 7 shows the applied stress-failure time curves measured by the constant load tensile tests under Conditions IV, V, VI, and VII (Table 2). The applied stress is described by the ratio of applied stress (σ) to yield strength (σy). The 0.20C-13Cr steel was used in this test. The specimens were cut from a mill-finished seamless pipe. The failure time in the NACE solution (pH = 3.5) was considerably shorter than that of the other conditions (pH ≥ 4.7), and the threshold stress was much smaller (approximately 0.6σy). If the acetic acid is removed from the solution, the threshold stress was 0.9σy even in the solution containing 3000 ppm H_2S (Condition VI) and 1.0σy in the solution containing less than 900 ppm H_2S (Condition IV and V). This suggests that the decrease in pH considerably accelerates the SCC of 13Cr steels and that the NACE condition is too severe to evaluate their SCC susceptibility.

The depassivation pH of the 0.20C-13Cr steel was measured in NaCl solution containing CO_2. The solution pH was changed by adding hydrochloric acid. Depassivation pH is defined as a critical pH below which a steel cannot passivate. The depassivation pH of the 0.20C-13Cr steel was about 3.5. This fact may be the cause of the significant decrease in the SCC resistance of 13Cr steel in NACE solution.

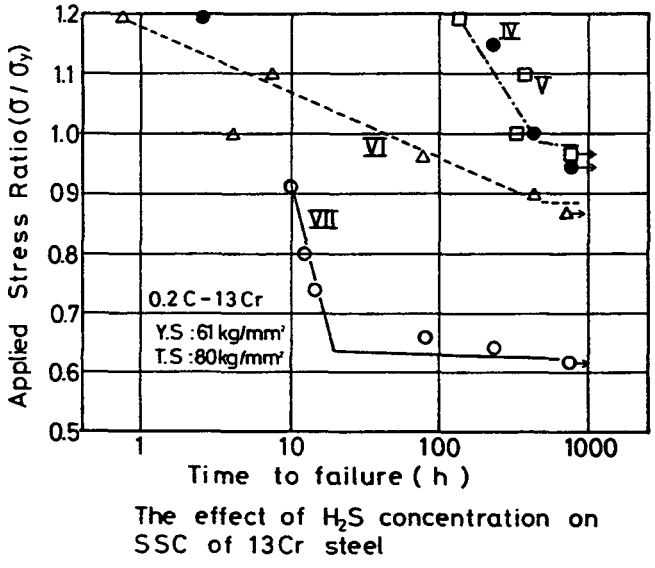


FIGURE 7 — Stress-time to failure curves of a 0.2C-13Cr steel under Conditions IV, V, VI, and VII shown in Table 2.

SCC in NACE Solution

The average corrosion rate of the C-type material was about 63 mpy (1.6 mm/y) in the NACE solution. That of the Ni-type was about 13 mpy (0.3 mm/y). Low alloy steels corroded at rates of 30 to 40 mpy (0.8 to 1.0 mm/y). Therefore, 13Cr steels should not be applied to environments like the NACE solution. However, because this solution has been widely used to study SCC in H_2S environments, constant load tensile tests were conducted in the NACE solution. The result agreed with the often proved fact that the susceptibility of 13Cr steels to SCC in H_2S environments is inferior to that of low alloy steels having the same strength. The effects of strength (σy) on the failure time measured under an applied stress of 0.6σy are shown in Figure 8. When the yield strength of 13Cr steels exceeded 58 kg/mm^2, the failure time decreased rapidly. The critical strength of low alloy steels was about 68 kg/mm^2. This is in agreement with the well-documented fact that the critical hardness for sulfide stress corrosion cracking is approximately HRC 25. Therefore, 13Cr steels have about 10 kgf/mm^2 lower critical strength than low alloy steels. The fracture mode of 13Cr steels was intergranular, as shown in Figure 9, but that of low alloy steels was transgranular.

The data for steel A deviated from the scatter band of the yield strength-failure time curve, taking considerably longer to fail. SCC specimens of steel A were cut from mill-finished seamless pipe. The applied stress-failure time curve of steel A and a laboratory heat are shown in Figure 10. Both 13Cr steels have the same chemical composition and strength. Steel A was more resistant to SCC in the NACE solution than the laboratory heat was. The fracture mode of steel A was trans-

TABLE 5 — The Results of SCC Test in CO_2 + H_2S Environment

	Composition (wt%)	Tempering Temperature (C)	Tensile Strength YS (kg/mm²)	Tensile Strength TS (kg/mm²)	SCC Test Results Condition III P_{CO_2}: 0.7 atm P_{H_2S}: 0.007 atm	SCC Test Results Condition IV 0.7 atm 0.07 atm	SCC Test Results Condition V 0.7 atm 0.3 atm
C-type	0.19C-13Cr	640	73	90	O (0.8)	X (0.6)	X (2.1)
		730	60	78	O (1.3)	X (1.4)	X (2.3)
	0.15C-13Cr	630	70	88	O (0.8)	X (1.0)	X (5.3)
		720	60	75	O (2.6)	O (1.6)	X (2.6)
	0.15C-13Cr-0.06N	630	75	93	O (1.1)	X (1.7)	X (2.0)
		720	60	78	O (1.5)	O (1.6)	O (2.6)
	0.10C-13Cr-0.06N	600	70	90	O (3.4)	O (2.4)	X (2.6)
		680	58	76	O (1.6)	O (1.7)	O (2.4)
Ni-type	0.006C-13Cr-2.5Ni	580	70	78	X (0.5)	X (0.6)	X (0.9)
		650	60	70	O (0.3)	O (0.4)	X (1.0)
	0.05C-13Cr-4Ni-1Mo	600	68	82	X (0.2)	X (0.4)	X (0.7)
		650	62	84	X (0.2)	X (0.3)	X (0.8)
	0.003C-13Cr-4Ni-1Mo	600	72	78	O (0.2)	O (0.3)	O (0.9)
		630	65	78	O (0.2)	O (0.2)	O (0.8)
	0.003C-12Cr-5Ni	580	69	73	O (0.4)	O (2.7)	X (0.9)
		630	62	74	O (0.3)	O (0.6)	X (0.7)
	0.004C-13Cr-6Ni	580	72	78	O (0.4)	O (0.4)	X (0.8)
	0.003C-12Cr-6Ni-1Mo	580	72	79	O (0.3)	O (0.4)	O (0.8)
Low alloy steel	KS80	640	67	79	O (12)	O (15)	O (7.4)
	K090SS	670	63	72	O (6.0)	O (6.5)	O (4.5)
	KS95	600	73	85	O (17)	O (16)	O (7.2)

Note: ( ) = Corrosion rate in mpy.

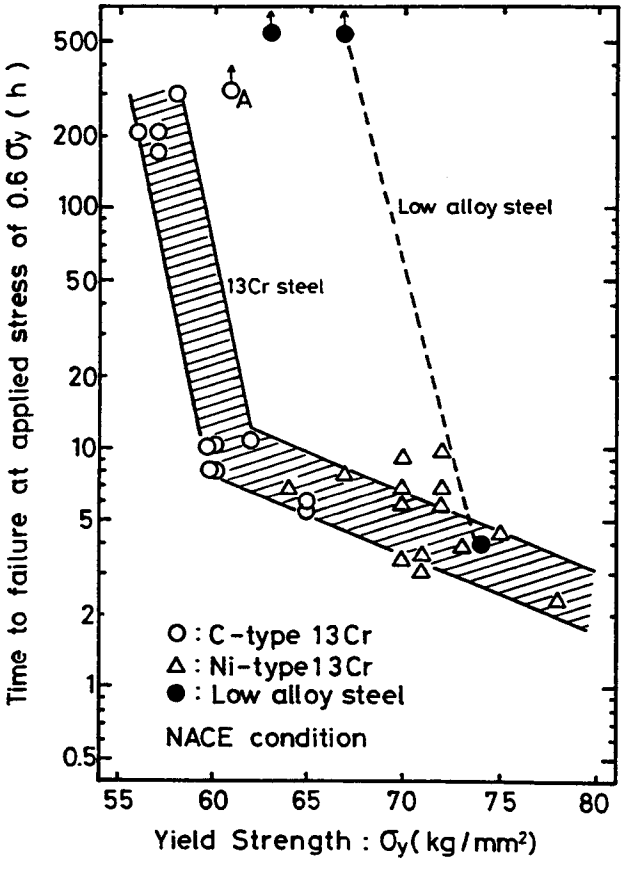


FIGURE 8 — Effect of yield strength on SCC susceptibility of 13Cr steels.

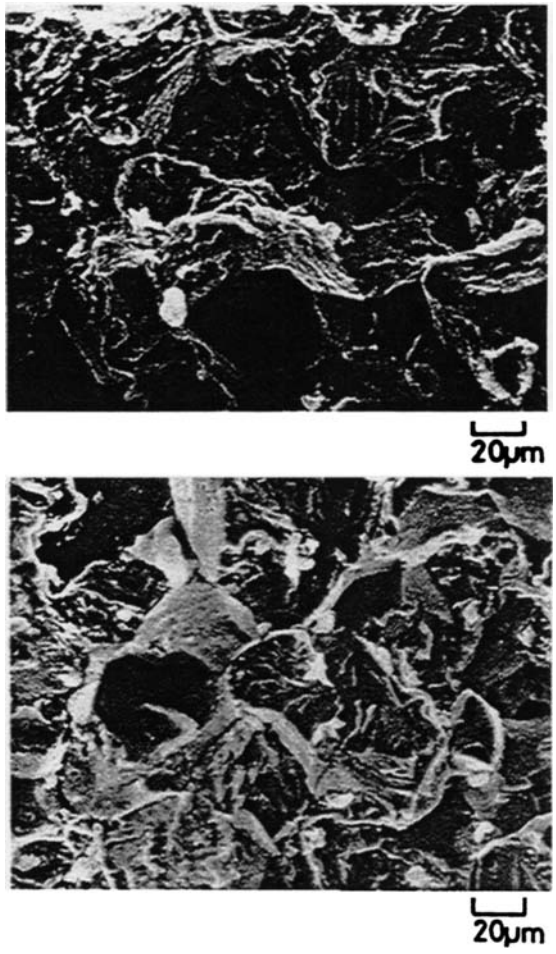


FIGURE 9 — SEM fractographs of constant load tensile test specimens in NACE solution.

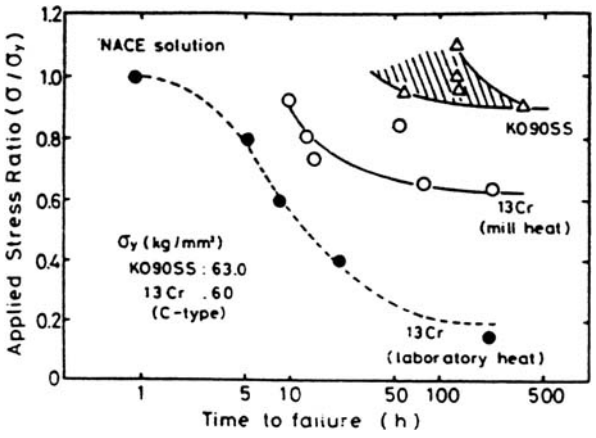


FIGURE 10 — Stress-time to failure curves of 0.20-13Cr steels (mill and laboratory heats) and a low alloy steel in NACE solution.

granular, and laboratory heat specimens had intergranular fractures. The photomicrographs and transmission electron micrographs are shown in Figures 11 and 12, respectively. The microstructure of steel A was very fine. The dislocation density was high, and almost no carbide was detected. Conversely, the laboratory heat recrystallized to some degree, and many carbides precipitated within the grains and along grain boundaries. This grain boundary precipitation is believed to accelerate intergranular SCC in the NACE solution. The C-type steels that contained niobium and/or vanadium had a small amount of delta ferrite, and their strengths were lower than those of other 13Cr steels. Their yield strengths were below 58 kg/mm^2, and SCC susceptibility was lower than that of other 13Cr steels. This is caused not by the addition of Nb and/or V but by the lower strength or delta ferrite. The C-type steels having less than 0.15% C had also some delta ferrite and had higher threshold stresses than C-type steels having above 0.15% C but their threshold stresses were below 0.6σy, with the exception of a 0.10 C steel of which threshold stress was 0.6σy. The effect of other alloying elements such as nitrogen, nickel, and molybdenum on SCC in NACE solution were not observed. This shows that the NACE condition is too severe to evaluate the SCC susceptibility of 13Cr steels.

Hydrogen Embrittlement

It is generally agreed that SCC of low alloy steels in H_2S environments is caused by HE. In comparison with low alloy steels of equal strength, 13Cr steels are inferior in SCC resistance in environments containing H_2S. It has not been determined whether SCC of 13Cr steels is caused by HE or anodic dissolution assisted cracking. Therefore, HE susceptibility has been investigated by SSRT testing under corrosion-free conditions, namely, hydrogen charging. A 0.20C-13Cr steel, a 0.02C-3Ni-13Cr steel, and a K090SS (L80 level) steel were used in this experiment. Both 13Cr steels were tempered at 600 and 710 C.

The degree of HE at each current density is shown in Figure 13. The degree of HE was evaluated in terms of the ratio of elongation under hydrogen charging (El_H) to elongation in air (El_{air}). The small ratio indicates that HE is enhanced. Low alloy steel was not significantly subject to embrittlement, but the embrittlement of 13Cr steels was significant. As mentioned above, the SCC resistance of low alloy steels in CO_2-H_2S environments was higher than that of 13Cr steels. Thus, it is reasonable to speculate that the SCC is caused by HE. The 13Cr steels were divided into two groups based on HE susceptibility. One was less susceptible; those specimens were tempered at 710 C. The other group was highly susceptible; those specimens were tempered at 600 C. It was rather unexpected that although the strength of Ni-type steel tempered at

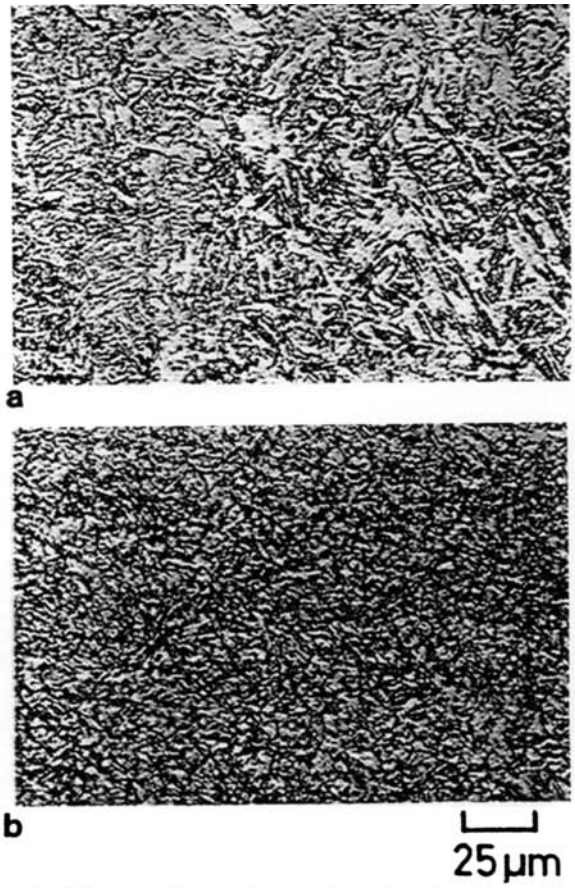


FIGURE 11 — Photomicroscopic microstructures of C-type 13 Cr steels. (a) 0.19C-13Cr, laboratory heat, and (b) 0.20-13Cr, mill heat.

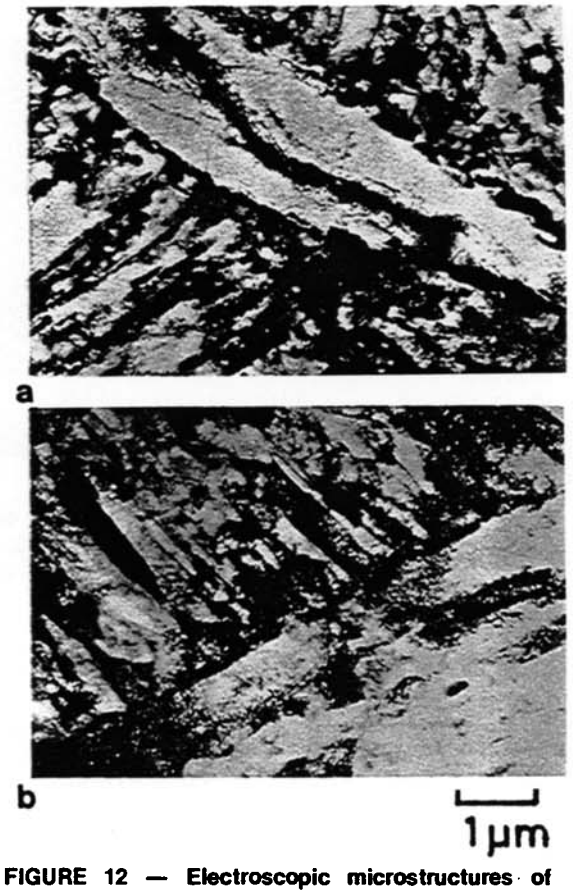


FIGURE 12 — Electroscopic microstructures of C-type 13Cr steels. (a) 0.19C-13Cr, laboratory heat, and (b) 0.20-13Cr, mill heat.

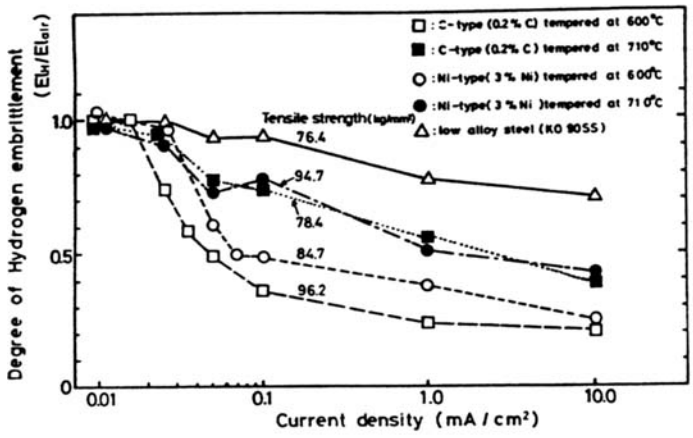
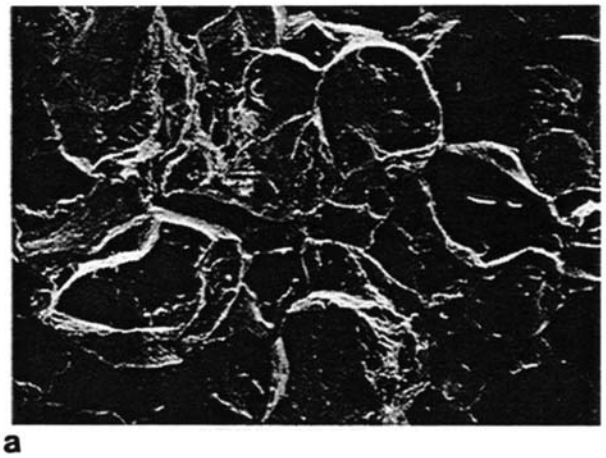
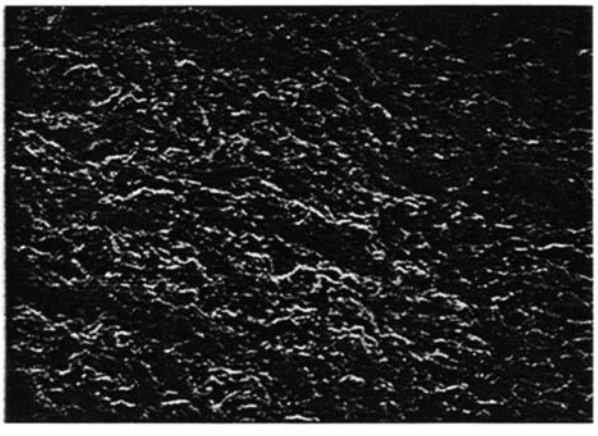


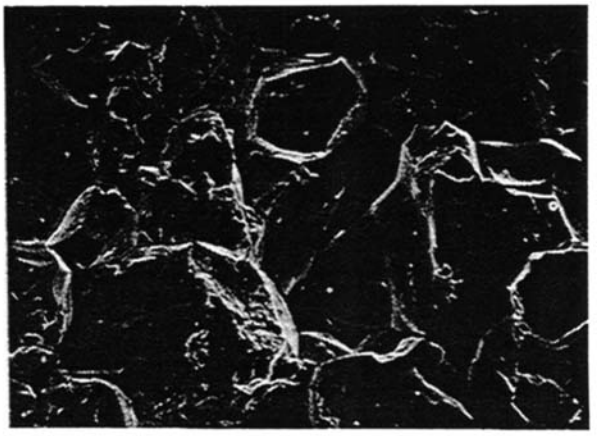
FIGURE 13 — Effect of current density for hydrogen charging on degree of hydrogen embrittlement measured by SSRT testing.



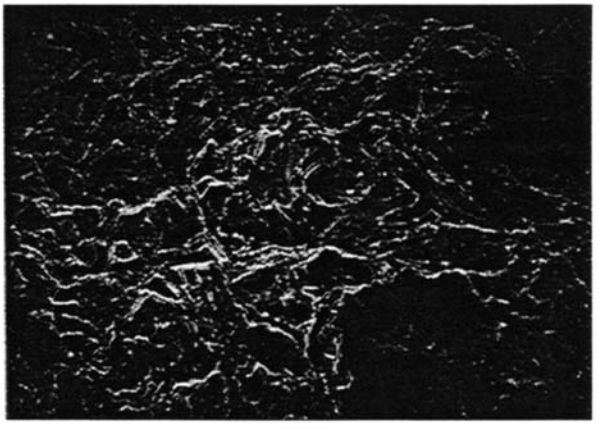
a



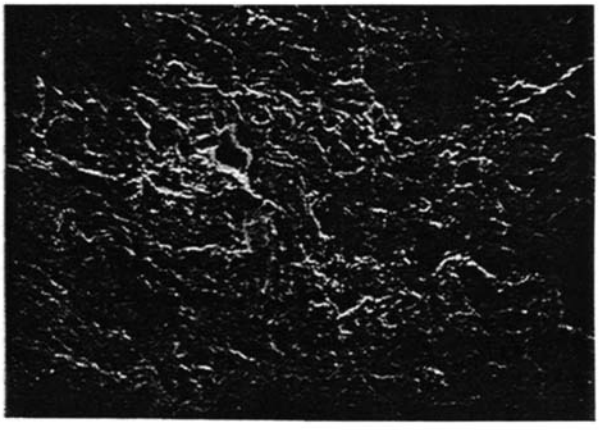
b



c



d



e

FIGURE 14 — SEM fractographs of SSRT specimens under hydrogen charging: (a) and (b): C-type (0.20C-13Cr), 600 and 710 C, respectively; (c) and (d): Ni-type (0.2C-13Cr), 600 and 710 C, respectively; and (e) low alloy steel.

710 C was higher than that of that tempered at 600 C, the former's HE susceptibility was smaller than the latter's. As shown in Figure 14, the characteristic difference between these two groups was that intergranular cracking (IGC) occurred for the more highly susceptible group, but no IGC could be observed for the lower one. The cracking appearance of the low alloy steel was also transgranular. The higher the current density became, the more the area ratio of IGC on the fracture surface increased for the more highly susceptible group. The fracture surfaces of the C-type 13Cr steel tempered at 600 C exhibited IGC entirely under a current density of 10 mA/cm^2.

Figure 15 shows how charge current density is related to the amount of hydrogen absorption. The low alloy steel absorbed less hydrogen at each current density than the 13Cr steels did. The low alloy steel was less susceptible to HE. The C-type and Ni-type steels tempered at 710 C absorbed as much hydrogen as the Ni-type steel tempered at 600 C. But the former were more resistant to HE than the latter. This indicates that HE susceptibility depends on more than the amount of hydrogen absorption. The C-type steel tempered at 600 C absorbed the most hydrogen, and it was most susceptible to HE. Consequently, the reason for the lower HE suscep-

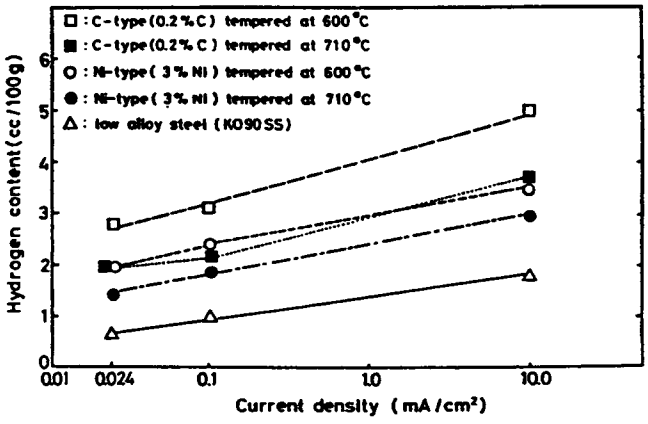


FIGURE 15 — Amount of hydrogen absorption under cathodic hydrogen charging in a 0.1N NaOH + 0.1N NaCN solution.

tibility of the low alloy steel can be explained by its smaller degree of hydrogen absorption. But it is impossible to explain the HE susceptibility difference for the two groups of 13Cr steels only in terms of their different hydrogen absorption levels and their strength. One can conclude that HE susceptibility of 13Cr steels depends heavily on IGC, which is affected by microstructure and carbide dispersion.

Conclusions

The following conclusions have been drawn from this study of SCC behavior of 13Cr steels in CO_2-H_2S environments.

1. When 13Cr steels, with the exception of 0.3% C, are tempered at above 600 C, they are immune from SCC in CO_2 environments without H_2S. But C-type steels suffer pitting in the aerated condition. Their corrosion resistance is worse in higher temperature (above 150 C) and higher pressure CO_2 environments. On the other hand, Ni-type steels are highly corrosion resistant in these environments.

2. In CO_2 environments containing various concentrations of H_2S, SCC susceptibility is affected by alloying elements. The 0.10 to 0.15C-13Cr-0.06N steels are not subject to SCC even at P_{H_2S} of 0.3 atm. The 4 to 6% Ni and/or 1% Mo-bearing 13Cr steels are free from SCC even at P_{H_2S} of 0.3 atm.

3. The SCC behavior is heavily influenced by the material's strength level in the NACE condition. The effect of alloying elements on SCC behavior cannot be determined. When the yield strength of 13Cr steels exceeds 58 kg/mm^2, failure quickly occurs. This critical strength (58 kg/mm^2) is lower than that of low alloy steels by 10 kg/mm^2.

4. The SCC of 13Cr steels in CO_2-H_2S environments is caused by HE rather than anodic dissolution assisted cracking. SCC is affected by IGC, which depends on microstructure and carbide dispersion.

References

1. T. W. Hamby, R. N. Tuttle, Oil Gas J., Vol. 12, p. 114 (1975).
2. J. D. Combers, J. G. Kerr, L. J. Klein, Petro. Engr. Int., p. 50, March 1983.
3. Y. Ishizawa, T. Shimada, M. Tanimura, "Effect of Microstructure on the Sulfide Stress Corrosion Cracking Resistance of AISI 410 and 420 Steels," CORROSION/82. Paper No. 124, National Association of Corrosion Engineers, Houston, Texas, 1982.
4. D. S. Burns, Materials Performance, Vol. 15, No. 1, p. 21 (1976).
5. R. S. Treseder, T. M. Swanson, Corrosion, Vol. 24, No. 2, p. 31 (1968).
6. P. Lillys, A. E. Nehrenberg, Trans. ASM, Vol. 48, p. 327 (1956).

Copyrighted Materials
Copyright © 1996 NACE International Retrieved from www.knovel.com

Polarization Behavior of High-Alloy OCTG in CO_2 Environment as Affected by Chlorides and Sulfides*

K. MASAMURA, S. HASHIZUME, J. SAKAI, and I. MATSUSHIMA*

Abstract

Pitting corrosion resistance of 13% Cr steel, duplex stainless steel, and high Ni austenitic stainless alloys for Oil Country Tubular Goods (OCTG) has been examined by electrochemical measurements in a high temperature, high pressure autoclave, simulating well conditions. Each steel shows the pitting potential in the CO_2-NaCl-H_2O system, the value of which becomes less noble with increased Cl^- concentration and temperature. The presence of H_2S is detrimental. High alloying additions of Cr and Mo enhance pitting resistance whether H_2S is present or not. The corrosion potentials of these alloys in the simulated well conditions, in which oxygen is absent, do not exceed the pitting potential. Therefore, pitting corrosion can not occur by the passivity breakthrough mechanism, and may occur only when some other factor causes breakdown.

Introduction

High alloys with Cr, Ni, and Mo are used in high temperature and high pressure oil and well environments which contain H_2S and CO_2 of high partial pressures and high chloride concentrations.

Resistance of these materials to stress corrosion cracking (SCC) is important because the environments in deep sour wells contain H_2S and chlorides, which in combination constitute very aggressive media, causing SCC in passive alloys. Resistance to pitting corrosion, however, is also a very important characteristic required for Oil Country Tubular Goods (OCTG). Pitting corrosion is not only detrimental in itself, but also provides initiation sites for SCC.

To evaluate resistance to pitting corrosion of alloys, immersion tests in autoclaves are often used,[1,2] but reproducing pits in a resistant alloy requires much time. Electrochemical behavior of steels is an important characteristic that provides basic information for the evaluation of corrosion resistance. Measurements of the pitting potential in autoclaves have been made to evaluate the pitting corrosion resistance of OCTG in deep sour well environments. The recent development of reliable inner reference electrodes has made it relatively easy to measure the electrochemical behavior of metals in autoclaves replicating down hole conditions.

The present study is concerned particularly with the localized corrosion mechanism, which can be postulated by measuring the electrochemical behavior of high alloys in high temperature and high pressure environments containing NaCl, CO_2, and H_2S.

Experimental Technique

Material

Four types of OCTG, i.e., 13% Cr steel (CR13[1]), ferritic-

*Submitted for publication March 1984; revised August 1986.

*Corrosion Laboratory, Technical Research Center, Nippon Kokan K.K., 1-1 Minami-Watarida, Kawasaki-ku Kawasaki, 210, Japan.

[1]Registered trade name, Nippon Kokan K.K., Kawasaki, Japan.

TABLE 1 — Chemical Compositions of Materials Tested (%)

	C	Si	Mn	P	S	Ni	Cr	Mo	Cu	Ti	N
CR13	0.20	0.48	0.46	0.013	0.001	0.24	13.0	0.02	—	—	—
CR22[1]	0.016	0.46	1.44	0.020	0.004	6.02	21.65	3.01	—	—	0.15
NIC42[1]	0.016	0.37	0.47	0.012	0.0006	41.2	21.6	2.83	1.68	0.70	0.01
NIC52[1]	0.012	0.27	0.69	0.005	0.0002	51.3	24.6	7.08	0.91	1.11	—
AISI 304	0.066	0.58	0.82	0.029	0.020	8.75	18.29	0.14	—	—	—

[1]CR22 is a ferritic-austenitic duplex SS; NIC42 and NIC52 are high Ni austenitic stainless alloys.

austenitic duplex stainless steel (SS) (CR22[2]), high Ni austenitic stainless alloys (NIC42[3] and NIC52[4]), and AISI 304 SS were used. Specimens were taken from commercial tubular products. Table 1 lists the chemical compositions. Electrodes measuring 15 × 10 × 2 mm and coupons measuring 50 × 30 × 3 mm were used with a 400-grit finish.

Electrochemical Measurement

Electrochemical measurements were conducted in a 5-L, Ti-lined autoclave equipped with attachments to accommodate three electrodes (working, counter, and reference). An Ag/AgCl electrode[5] that had been developed for use under high temperature and high pressure conditions was applied as the reference electrode. The electrode potential of the Ag/AgCl electrode was checked before and after each test with a reference SCE at ambient temperature.

Experiments were conducted in aqueous solutions containing either chloride ions (0 to 3% NaCl), H_2S [0 to 1 atm at room temperature (RT)], CO_2 (up to 20 atm at RT), or combinations thereof. After holding the specimens for 1 h at a testing temperature (100 to 200 C), polarization curves were obtained using the potentiodynamic method from −1000 mV vs Ag/AgCl in the noble direction. The sweep rate was 20 mV/min. The instantaneous corrosion rate was measured in the autoclave using an AC-impedance monitoring system. This system was originally developed by S. Haruyama using the double frequency method.[3]

Immersion Test

The corrosion rate of the alloys was determined from weight (wt) loss of coupon specimens that had been exposed to H_2S-CO_2-NaCl corrosion media simulating deep sour well environments in an autoclave. The immersion tests were conducted in a Ti-lined autoclave. The test solution occupying 3/4 of the total volume of 4 L was equilibrated with CO_2, H_2S, and N_2 gases of a given pressure for 24 h and heated to a test temperature.

Results

Effects of Temperature and Chlorides on Electrochemical Behavior of 13% Cr Steel

Polarization curves for 13% Cr steel in 0.05M Na_2SO_4 solution at 100, 125, and 150 C (CO_2 = 20 atm at RT) are shown in Figure 1. Passivity is observed and the passive current density (CD) increases with temperature. The anodic dissolution rate in the polarization curves for CR13 also increases with temperature. The corrosion potential (E_{corr}) and the active-passive transition potential (E_c) are ~ −620 and −600 mV vs Ag/AgCl, respectively, regardless of the temperature. At 150 C,

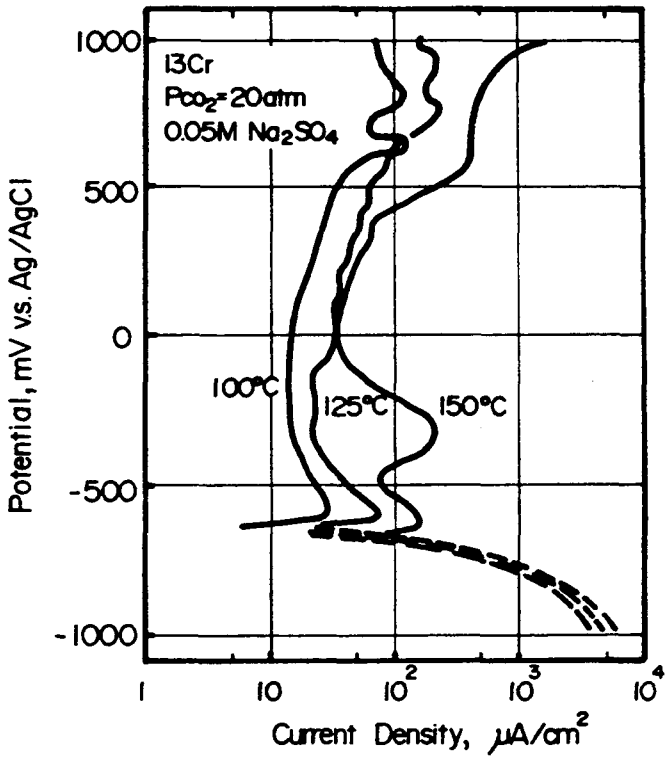


FIGURE 1 — Polarization curves for 13% Cr steel in 0.05M Na_2SO_4 solution at 100, 125, and 150 C (CO_2 = 20 atm at RT).

two current peaks are observed at ~ −600 and −400 mV vs Ag/AgCl. Rapid transpassive dissolution occurs at and above +500 mV vs Ag/AgCl. Although chloride ions are not present in the solution, the passive film on 13% Cr steel becomes unstable at 150 C. These tendencies suggest that the corrosion rate of CR13 increases with temperature in CO_2 environment without chlorides.

Figure 2 illustrates the effects of the NaCl concentration on the polarization curves at 125 C. When NaCl is present in the solution, the pitting potential appears in the polarization curve, the value of which becomes less noble as the Cl^- concentration increases. The peak CD at ~ −600 mV vs Ag/AgCl increases with the NaCl concentration. Figure 3 shows a potential-NaCl concentration diagram that defines the active, passive, and pitting potential regions at 125 C. The critical pitting potential in this study was taken as a potential that gave a CD of 500 μA/cm². When NaCl concentration is low, the passive area is wide, becoming narrower with an increase of the NaCl concentration. This behavior indicates that the passive film on 13% Cr steel becomes less stable with an increase of NaCl concentration.

[2]-[4]Registered trade names, Nippon Kokan K.K., Kawasaki, Japan.

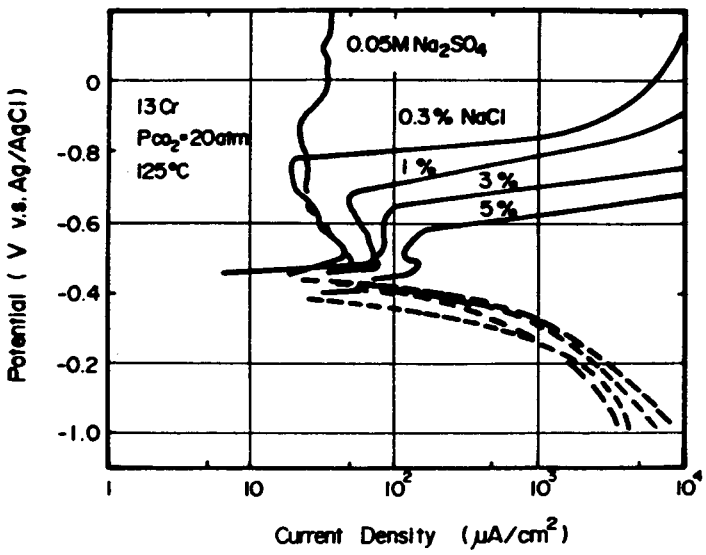


FIGURE 2 — Effects of NaCl concentration on the polarization curves for 13% Cr steel at 150 C (CO_2 = 20 atm at RT).

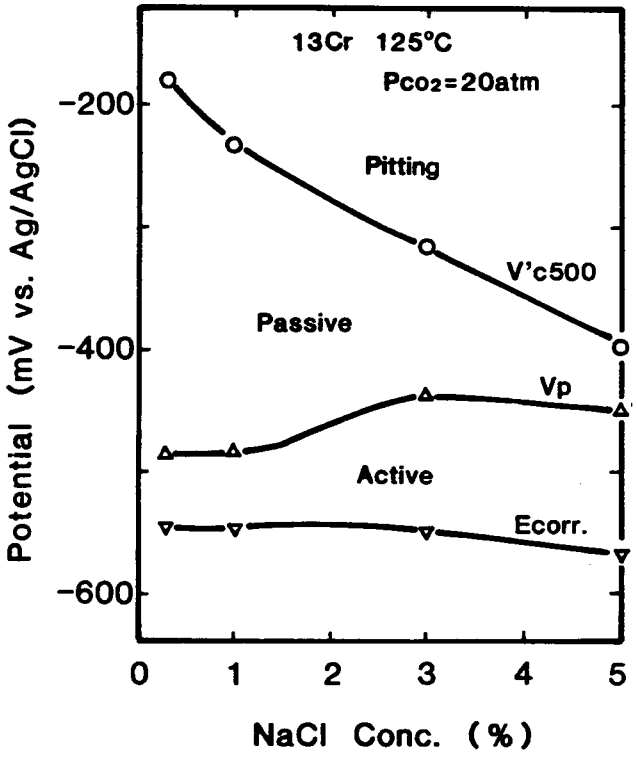


FIGURE 3 — Effects of NaCl concentration on characteristic potentials of 13% Cr steel obtained from polarization curves at 150 C (CO_2 = 20 atm at RT).

The effects of temperature on the characteristic potentials of 13% Cr steel in 3% NaCl solution are shown in Figure 4. The characteristic potentials, i.e., pitting potential, passivation potential, and corrosion potential, shift in the less noble direction with temperature. The solid marks in the figure show the potential at which the anodic CD equals 100 $\mu A/cm^2$ on the polarization curves. At 150 C, the corrosion potential is close to the potential at which the anodic CD equals 100 $\mu A/cm^2$. This fact suggests that the corrosion rate of 13% Cr steel in 3% NaCl solution at 150 C is high. This result is substantiated by an observed corrosion rate greater than 0.5 mm/y in the immersion test at 150 C for 96 h.[4] This diagram shows that temperature and chloride ions act adversely on the stability of the passive film on 13% Cr steel.

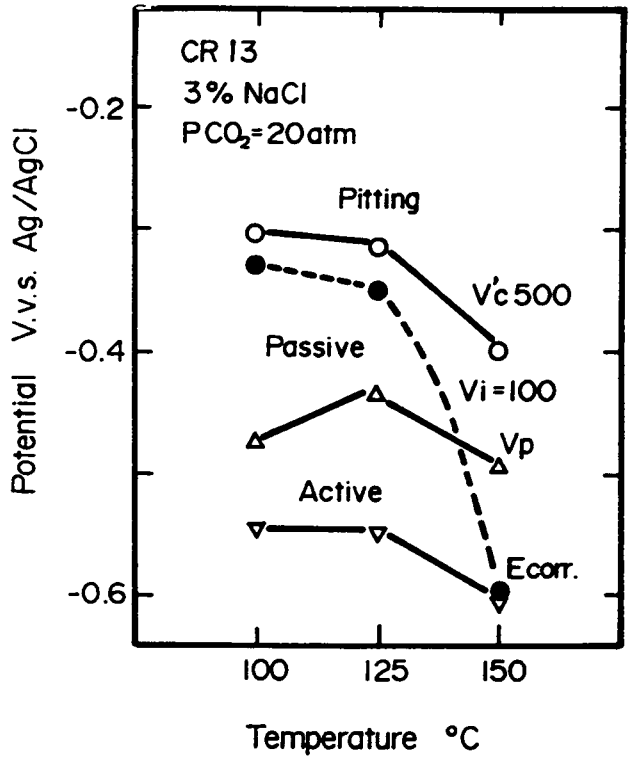


FIGURE 4 — Effect of temperature on the characteristic potentials of 13% Cr steel obtained from polarization curves in 3% NaCl solution (CO_2 = 20 atm at RT).

Corrosion Potential and Corrosion Rate of 13% Cr Steel

The variation of the corrosion potential and the corrosion rate of 13% Cr steel with time in 3% NaCl solution at 150 C (saturated with 20 atm CO_2 at RT) is illustrated in Figure 5. The effect of O_2 is also shown. The instantaneous corrosion rate was measured using an AC-monitoring system. The corrosion rate is shown in mho. A corrosion rate of 10^{-3} mho corresponds to ~0.1 mm/y.

When oxygen is present, the corrosion potential immediately after immersion of 13% Cr steel is much more noble than when oxygen is absent; then the potential shifts in the less noble direction in a short time and levels off at around −520 mV vs Ag/AgCl, which is close to the active state. The corrosion rate is smaller than that obtained in absence of O_2 in the first 100 h, after which, it increases rapidly. This corresponds to the initiation and growth of pitting corrosion by the passivity breakthrough mechanism. The average corrosion rate determined by wt loss method is 0.23 mm/y in the same environment.

When O_2 is absent, the corrosion potential is located at ~ −500 mV vs Ag/AgCl immediately after immersion and then shifts in the less noble direction, levelling off at ~ −550 mV vs Ag/AgCl. This potential corresponds to the active state as shown in Figure 2. The low corrosion rates at the initial stage can be attributed to the presence of the passive film on 13% Cr steel formed in the air before testing. The passive film breaks down in a short time, and then 13% Cr steel corrodes in the active region. The corrosion rate increases with time for at least 500 h, according to present test results. The average corrosion rate determined from wt loss during the measurement was 0.6 mm/y. The corrosion rate estimated by the AC monitoring system is comparable with the results determined by the wt loss method.

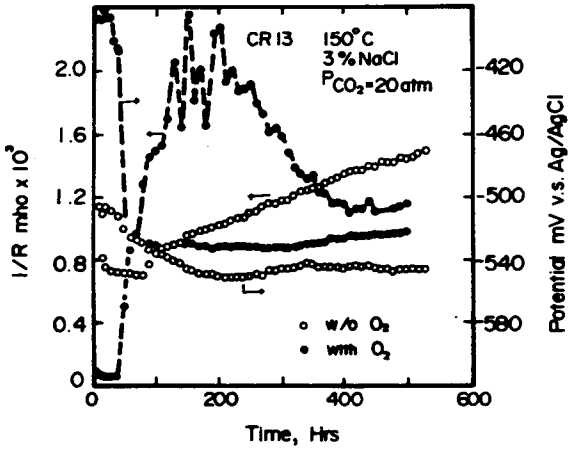


FIGURE 5 — Change of corrosion potential and corrosion rate of 13% Cr steel in 3% NaCl solution at 150 C (CO_2 = 20 atm at RT).

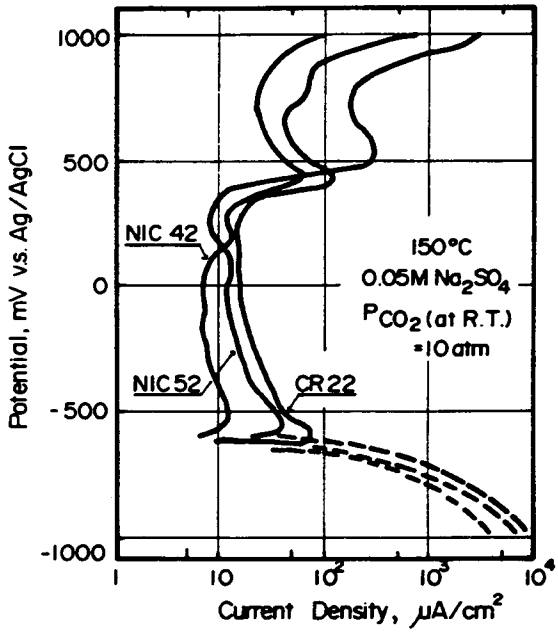


FIGURE 6 — Polarization curves for duplex SS (CR22) and high Ni austenitic stainless alloys (NIC42, NIC52) in 0.05M Na_2SO_4 solution in equilibrium with CO_2 at 150 C (CO_2 = 20 atm at RT).

In view of the observed active corrosion potential of 13% Cr steel in the CO_2-NaCl-H_2O system at high temperatures without O_2, it can be concluded that the corrosion potential does not exceed the pitting potential, thus the breakthrough of the passive film hardly occurs.

Table 2 lists the corrosion rates of 13% Cr steel determined by the wt loss method in 1 and 3% NaCl solutions (CO_2 = 20 atm at RT) at 100 and 150 C for more than 500 h. Pitting corrosion is not observed when O_2 is absent. The highest corrosion rate is observed at 150 C in 3% NaCl solution without O_2. In 1% NaCl solution, the corrosion rate is below that obtained in 3% NaCl solution. The lowest corrosion rate is observed in 3% NaCl solution at 100 C. Only when O_2 is present, even in small amounts, does pitting corrosion occur. This behavior is not surprising considering the tendency to pit in aerated chloride media at ambient temperature. However, the corrosion rate is lower than in the absence of O_2.

Effects of H_2S on Polarization Curves for High Alloys in Absence of Chlorides

Polarization curves for CR22, NIC42, and NIC52 in 0.05M Na_2SO_4 at 150 C (CO_2 = 10 atm at RT) are shown in Figure 6. Passivity is observed at temperatures between 100 to 200 C in solution with or without CO_2. No wt loss was detected for these steels in 96 h of immersion tests in 3% NaCl solution without H_2S up to 200 C, as previously reported.[4]

Figure 7 shows the effects of CO_2 and H_2S on the polarization curves for CR22 in 0.05M Na_2SO_4 solution at 150 C. In the presence of H_2S, the CDs are high in the potential region corresponding to passivity, which is caused by H_2S oxidation in the high temperature solution, as identified by examining polarization behavior of a Pt electrode under the same condition.[6] Thus, the combination of H_2S and CO_2 in absence of Cl^- does not affect the corrosion characteristics of high alloys such as CR22, NIC42, and NIC52.

Effects of H_2S on the Pitting Potential of High Alloys in the Presence of Chlorides

Figure 8 shows polarization curves for CR13, CR22, NIC42, NIC52, and AISI 304 SS in 3% NaCl (CO_2 = 10 atm at RT) at 150 C. When NaCl is present in the solution, all the high alloys examined show a pitting potential, with the more highly alloyed materials having a more noble pitting potential.

Figure 9 shows the effect CO_2 and H_2S in the 3% NaCl solution on the polarization curves for CR22. Pitting potentials are observed. The presence of CO_2 has a little affect on the value of pitting potential. On the other hand, presence of H_2S gives a pitting potential of less noble value. Under this condition, the current increase resulting from H_2S oxidation does not disturb the observed pitting potential of CR22, and it is obvious that H_2S has a detrimental effect on pitting resistance of

TABLE 2 — Test Results of Immersion Test of 13% Cr Steel in NaCl Solution at High Temperatures

Run No.	Temp. (C)	NaCl (%)	CO_2 (atm)	Test Duration (h)	Corrosion Rate (mm/y)	Presence of O_2	Form
1	150	3	20	526	0.60	no	U
2	150	3	20	504	0.23	yes	P
3	150	1	20	672	0.23	no	U
4	100	3	20	672	0.02	no	U

U—Uniform corrosion
P—Pitting corrosion

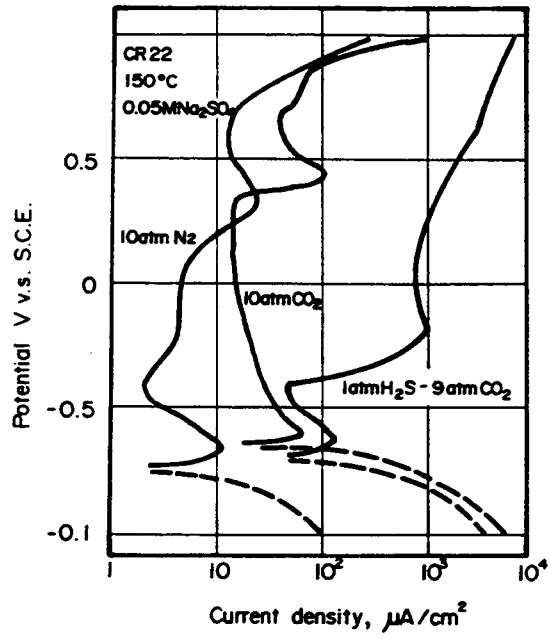


FIGURE 7 — Effect of CO_2 and H_2S gas on the polarization behavior of CR22 in 0.05M Na_2SO_4 solution at 150 C.

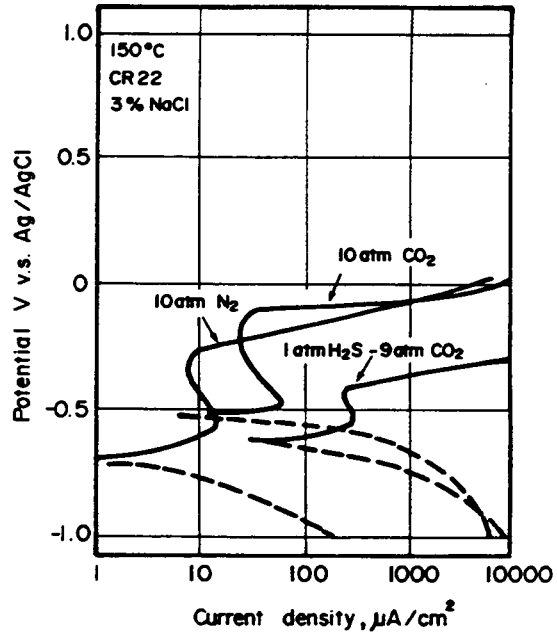


FIGURE 9 — Effect of CO_2 and H_2S on the polarization behavior of CR22 in 3% NaCl solution at 150 C.

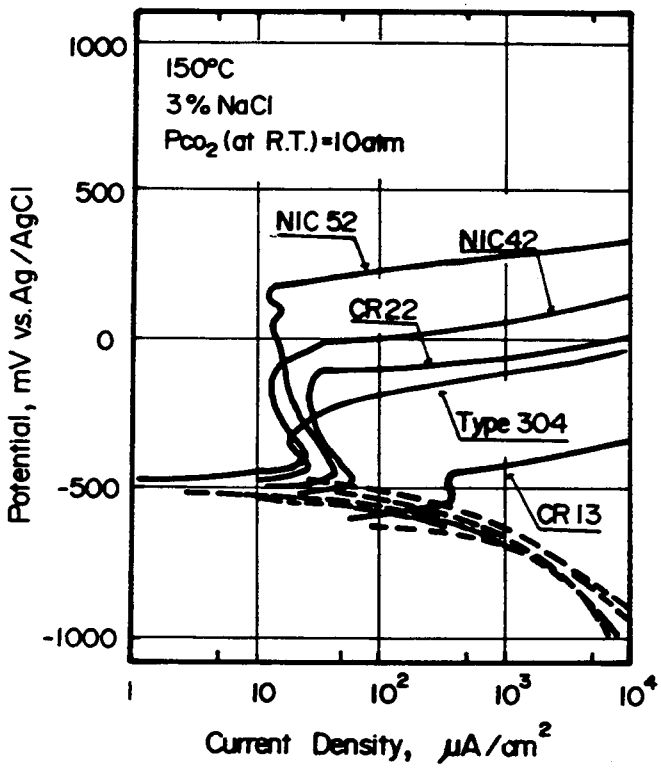


FIGURE 8 — Polarization curves for CR13, CR22, NIC42, NIC52, and AISI 304 SS in 3% NaCl solution in equilibrium with CO_2 at 150 C (CO_2 = 10 atm at RT).

CR22. The same principle applies to NIC42 and NIC52. Cathodic CD on CR22 increases when CO_2 and/or H_2S are present. The anodic dissolution rate of CR22 also increases.

Polarization curves for CR13, CR22, NIC42, NIC52, and type AISI 304 SS in the presence of Cl^- and H_2S are shown in Figure 10. The pitting potential for all the alloys becomes less noble when H_2S is introduced into the chloride-bearing environment. Apparently, H_2S, together with Cl^-, has a detrimental effect on the stability of the passive film.

Figure 11 shows the effect of alloyed Cr and Mo on the pitting potential in the high temperature environments containing H_2S, CO_2, and NaCl. A parameter [Cr(%) + 3Mo(%)], which showed a good correlation with the pitting potential of similar alloys in 20% NaCl (pH 3) at 25 C, was used.[2,6] The plots for austenitic stainless alloys fall on a straight line, although the line is different depending on the presence or absence of H_2S. Two types of duplex SSs, 22%Cr-6%Ni-3%Mo-0.14%N and 25%Cr-7%Ni-3%Mo-0.10%N, were tested. Duplex SSs show less noble values than austenitic stainless alloys regardless of the pressure of H_2S. This is possibly caused by the heterogeneous nature of duplex SSs. Cr and Mo additions are effective in providing high pitting potentials for stainless alloys in environments containing H_2S, CO_2, and NaCl.

Corrosion Rate and Corrosion Potential of Duplex SS

Figure 12 illustrates the change of the corrosion potential and the corrosion rate with time of the duplex SS (CR22) measured in an autoclave at 150 C in 3% NaCl solution saturated with 20 atm CO_2 (at RT). The corrosion potential is located at ~ −360 mV vs Ag/AgCl immediately after immersion and then shifts in the less noble direction for 50 h. The latter potentials correspond to the active state of duplex SS at 150 C. These results indicate that the corrosion potential hardly exceeds the pitting potential in this environment. Similar behavior is expected for NIC42 and NIC52, considering the absence of oxidizing agents that have a noble redox potential.

The corrosion rate illustrated in Figure 12 increases with time during the immersion period from 50 to 600 h. The time when the corrosion rate begins to increase corresponds to the time when the corrosion potential starts to shift in the less noble direction. This fact shows that the passive film, which formed in air before the specimens were introduced in the corrosion environment, protects the substrate while it is intact. Active corrosion starts after the passive film breaks down. The corrosion rate indicated by the AC monitoring system was less than 0.05 mm/y, and the average corrosion rate of the duplex SS during the corrosion rate measurement was found to be 0.005 mm/y by the wt loss measurement. Thus, the duplex SS

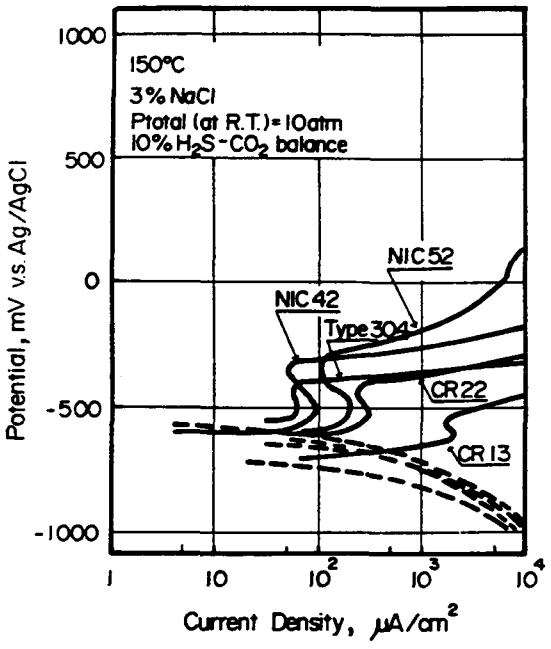


FIGURE 10 — Polarization curves for CR13, CR22, NIC42, NIC52, and AISI 304 SS in 3% NaCl solution in equilibrium with 10% H_2S-CO_2 gas (10 atm at RT).

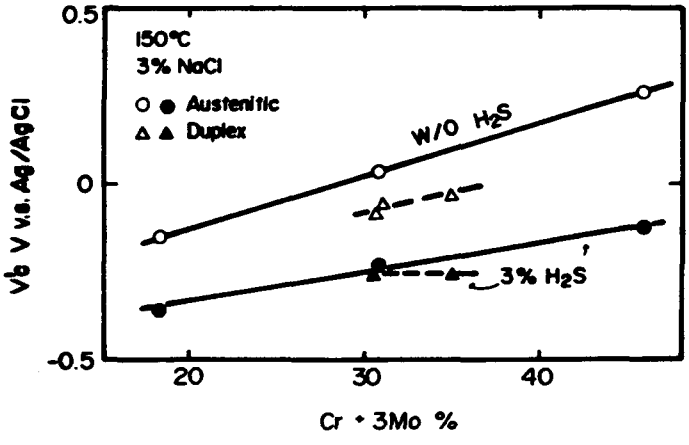


FIGURE 11 — Effect of Cr and Mo additions on the pitting potential of stainless alloys in 3% NaCl solution at 150 C.

shows good corrosion resistance in the simulated well environments. Pitting corrosion is unlikely in the well environment of equivalent temperature that contains chlorides without oxygen or hydrogen sulfide, since the corrosion potential does not exceed the pitting potential.

Discussion

Corrosion Resistance of 13% Cr Steel

Presence of CO_2 in high temperature solution accelerates cathodic reaction on 13% Cr steel. Similar behavior was observed on carbon steel in a solution containing CO_2 at ambient temperature.[7] The corrosion rate of 13% Cr steel in CO_2 environment is lower than that of carbon steel because the anodic dissolution rate of 13% Cr steel is much lower than that of carbon steel in CO_2 environments. The anodic dissolution rate increases with temperature, suggesting that 13% Cr steel corrodes appreciably in a CO_2 environment at high temperatures.

The stability of the passive film on 13% Cr steel becomes

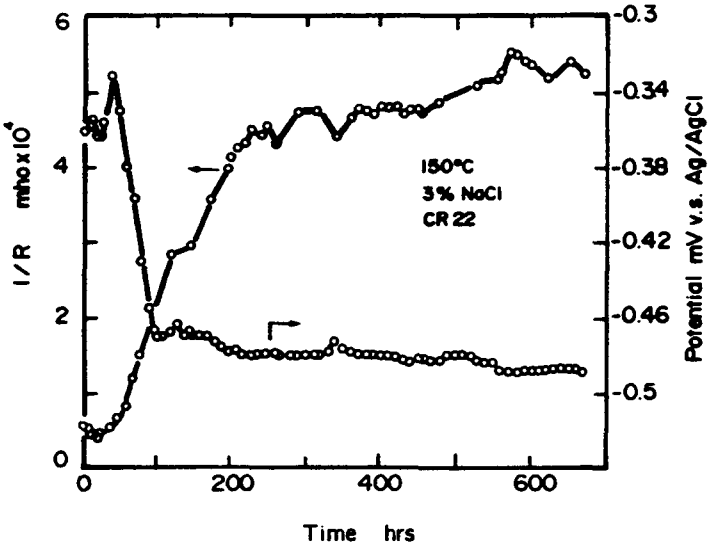


FIGURE 12 — Change of the corrosion potential and corrosion rate with time of CR22 in 3% NaCl solution at 150 C (CO_2 = 20 atm at RT).

lower at high temperatures, particularly when chlorides are present in the environment. Rapid corrosion was observed on 13% Cr steel in immersion tests when the temperature was above 150 C and the NaCl concentration was greater than several percent.[4] The presence of NaCl and CO_2 accelerates the anodic dissolution rate of 13% Cr steel at high temperatures, as indicated by the results of polarization measurements. To ensure the effect of residual O_2 in the autoclave on pitting corrosion in 13% Cr steel, immersion tests were conducted for 600 h in the same environment with and without deaeration. Pitting corrosion was not observed in 13% Cr steel, when deaeration was conducted carefully. Pitting corrosion is observed only with an obvious presence of O_2.

When O_2 is absent, the corrosion potential of 13% Cr steel is rather active in high temperature and high pressure environments, as seen in the results of electrochemical measurements. According to the corrosion theory, pitting corrosion does not occur unless the corrosion potential exceeds the pitting potential. Because oxygen is not present in the sour wells, the corrosion potential of the alloy can never be so noble; thus, there is little probability to pit according to this mechanism.

Role of H_2S for Corrosion of High Alloys

Presence of H_2S in chloride-bearing environments makes the passive film less stable at high temperatures. The pitting potential for high alloys in 3% NaCl solution at high temperature becomes less noble when H_2S is present. Anodic dissolution was also accelerated with H_2S. The presence of H_2S with chlorides creates a potential danger for corrosion to occur, e.g., pitting corrosion, SCC, and general corrosion. However, pitting corrosion does not occur unless the corrosion potential exceeds the pitting potential, similar to the case of 13% Cr steel. As the observed corrosion potential and the corrosion rate of CR22 show (Figure 12), the corrosion potential tends to stay in the active region. In the case of high alloys, pitting corrosion does not initiate through the breakthrough mechanism of the passive film in the well environment because oxidizing agents are absent.

Generally, corrosion rates of high alloys are very low in NaCl solution with CO_2 and H_2S up to 200 C, although corrosion potential stays in the active region. This means that these materials are essentially immune to corrosion in the well environment, unless other factors are introduced into the environment.

Effect of Alloying Elements

Cr and Mo additions are beneficial in improving corrosion resistance of FeCrNiMo alloys. Higher Cr and Mo concentrations give a higher pitting potential and a lower dissolution rate in H_2S environments. These alloying elements are important in improving the corrosion resistance of OCTG.

Summary

1. The lower corrosion rate of 13% Cr steel in CO_2 environment without chlorides or H_2S, as compared to carbon steel, is not caused by the establishment of passive films on 13% Cr steel, but results from the lower anodic dissolution rate of 13% Cr steel in the active state.

2. The passive film on 13% Cr steel is relatively weak in the high temperature environments containing CO_2 and NaCl, and the pitting potential is very low (−490 mV vs Ag/AgCl in 3% NaCl solution at 150 C).

3. The corrosion potential of 13% Cr steel is located in the active region and does not exceed the pitting potential in NaCl solutions containing CO_2 at 150 C; therefore, passivity breakthrough hardly occurs in the environments.

4. When chlorides are absent, H_2S does not affect corrosion properties of duplex and high Ni austenitic stainless alloys in high temperature environments containing CO_2. The presence of CO_2 and/or H_2S accelerates anodic dissolution of high alloys in the active region on polarization curves and also accelerates cathodic reaction on these alloys.

5. Pitting potentials for duplex and high Ni austenitic SSs are affected by H_2S when chlorides coexist in the environments and shift in the less noble direction, with an increase of the H_2S concentration. The corrosion potential, however, does not exceed the pitting potential in the environment containing H_2S, CO_2, and NaCl. Passivity breakthrough hardly occurs in the environments.

6. Cr and Mo have beneficial effects on the pitting potential in environments containing H_2S, CO_2, and NaCl at high temperatures.

References

1. Z. Szklarska-Smialowska, Corrosion, Vol. 27, No. 6, p. 23, 1971.
2. G. Herbsleb, K. Poepperling, Corrosion, Vol. 36, No. 11, p. 611, 1981.
3. S. Haruyama, T. Tsuru, "Electrochemical Corrosion Testing," ASTM STP 727, F. Mansfeld, U. Bertocci, Eds., ASTM p. 167, Philadelphia, Pennsylvania, 1981.
4. K. Masamura, J. Sakai, K. Nunomura, M. Honda, S. Hashizume, I. Matsushima, CORROSION/83, Paper No. 55, National Association of Corrosion Engineers, Houston, Texas, 1983.
5. Katsumi Masamura, Shuji Hashizume, Iwao Matsushima, Boshoku Gijutsu, Vol. 34, p. 107, 1985.
6. I. Matsushima, M. Tanimura, Y. Ishizawa, T. Shimada, K. Masamura, J. Sakai, CORROSION/85, Paper No. 233, National Association of Corrosion Engineers, Houston, Texas, 1985.
7. K. Masamura, I. Matsushima, Transactions of the Iron and Steel Institute of Japan, Vol. 23, p. 676, 1983.

Copyrighted Materials
Copyright © 1996 NACE International Retrieved from www.knovel.com

Paper No. 442—CORROSION/87

MC ELMO DOME CO_2 SOURCE FACILITIES CORROSION CONTROL

M.H. Nguyen
Shell Western E & P Inc.
P.O. Box 576
Houston, Texas 77001

ABSTRACT

The corrosion surveillance program for McElmo Dome CO_2 source facilities incorporates a variety of corrosion monitoring techniques in order to locate areas where corrosion may be occurring and to permit remedial measures to be taken as early as possible. This paper reviews the materials used in various equipment and discusses the locations to be monitored, the monitoring techniques, and the results obtained up to date.

INTRODUCTION

The McElmo Dome CO_2 source field in southwestern Colorado has been on production since spring of 1984. The current rate is approximately 600 MMSCFD. In an effort to minimize corrosion related problems associated with operation of the facilities, corrosion resistant alloys were used at critical locations and low alloy steels were used where corrosion is expected to be minimal. To monitor the condition of the equipment and locate corrosion problem areas, a corrosion monitoring program was set up and implemented in early 1985. This paper reviews materials selection and presents information about the corrosion monitoring program for the Yellow Jacket and Hovenweep CO_2 source facilities.

CO_2 SOURCE FACILITIES AND MATERIALS SELECTION

Wellhead and Bottom Hole Assemblies

Wet CO_2 gas and liquid are produced from 22 flowing wells. The wellheads were made of 410 SS and the bottom hole assemblies were 9Cr 1Mo or 13Cr (420 S.S). Initially, the 4½ in. (11.43 cm) OD tubings were API J-55, internally plastic coated. But due to corrosion failures, they were replaced by 13Cr tubing which, from information gathered to date, appears to be adequately corrosion resistant in the McElmo Dome CO_2 field.

Gathering Lines

From the wellheads, the CO_2/water mixture is transported to the 12 cluster facilities where the free water is separated from the 2-phase CO_2. The wellhead cluster gathering lines are 6 in. (15.24 cm), 316L SS, externally coated with polyethylene. 316L SS was chosen over duplex SS due to the return of HCl used for downhole stimulation through these lines.

Clusters

Each cluster is equipped with 3-phase test and production separators, a hydrate inhibitor tank, and a produced water tank. The separators are low alloy steel (A516 Grade 70) and internally weld clad with 316L SS with the exception of one cluster; at cluster YA, carbon steel without cladding was used for those separators to provide a long-term corrosion test. Valves, piping, and auxiliary components are 316L SS at all clusters. Water tanks and hydrate inhibitor tanks are internally protected with polyester glassflake or high build epoxy coating. Free water separated from the wet CO_2 is transported to two salt water disposal wells via 3 in. carbon steel, externally coated and cathodically protected flowlines. A hydrate inhibitor (DEG/A20 mixture) is added to the 2-phase CO_2 stream at the well cluster facility and the mixture is transported to the central facility via duplex SS

(22 Cr, 5 Ni, 3.5 Mo) lines. The duplex SS lines externally coated with polyethylene, cathodically protected, and share the same trench as the carbon steel water disposal lines.

Central Facilities

At the two central facilities, Yellow Jacket and Hovenweep, the water-DEG mixture is separated out, the liquid CO_2 is vaporized, recombined with the gaseous CO_2, dehydrated and compressed to 2,100+ psig (14.5 MPa) before shipment to the Cortez Pipeline. Equipment and piping handling wet CO_2 are 316L SS and those handling dehydrated CO_2 are bare low alloy steel. The DEG dehydration systems (glycol contactor, reboiler, rich glycol flash tanks, heat exchangers, coolers, piping) are carbon steel. Figure 1 summarizes the dehydration process of CO_2 from wellhead to the CO_2 pipeline. Operating conditions as well as materials used are included.

CORROSION MONITORING PROGRAM

The corrosion surveillance program incorporates a variety of corrosion monitoring techniques in order to best evaluate the condition of the equipment. These techniques include borescope examination, ultrasonic measurement, pair probe readings, corrosion coupons, IRIS (Internal Rotary Inspection System) inspection, visual inspection, and chemical analyses. A brief description of these techniques, the monitoring program details and results are presented in this section.

Corrosion Monitoring Techniques

Borescope examination. Borescope examination is performed mainly at the wellhead. The cross horizontal bore, the first wing valve bore and the second wing valve inlet are examined. The examination allows the detection of localized or pitting attack. The length and depth of the pits are determined by taking measurements in the bore and by replicating the pits with a molding compound. The well is shut in and depressured during examination.

Ultrasonic measurement of wall thickness. Ultrasonic measurement is a rapid and inexpensive method to determine metal loss due to general corrosion or erosion. This technique is used throughout the facilities (wellheads, piping, vessels).

The instantaneous corrosion rate instruments. Pair probes are used mainly in the water disposal lines. Pair probes are installed downstream of the corrosion inhibitor pump and at the water disposal wellsites to monitor corrosion rates. The pair probe electrodes are also used as weight loss coupons.

Corrosion coupons. Corrosion coupons are installed downstream of the wellhead and can be removed under pressure for evaluation. Currently, 420 SS corrosion coupons are installed at the wellhead to monitor the performance of 13 Cr tubing.

IRIS inspection. The ultrasonic internal calipering of small diameter heat exchanger and cooler tubes or IRIS inspection are used to determine the extent of corrosion. The IRIS device allows the detection of general or localized ID wall loss of tubes 2 in. (5.08 cm) or less in diameter. This technique requires the shutdown of the facilities and the tubes need to be clean for good results.

Visual inspection. Visual inspection of the interior surfaces of vessels and piping is the most effective way to detect pitting or localized attack. Past experience with corrosive CO_2 streams indicate that the localized pitting attack is more likely to occur and this is the most difficult to detect by other means. Visual inspection requires the shutdown and draining of the equipment prior to inspection.

The chemical analyses. Produced water and glycol analyses allow the detection of any changes in the process conditions.

Corrosion Monitoring Program

The method, location, and frequency of monitoring are listed in Tables 1, 2, and 3. The program has been updated several times and the changes were based on initial results. Borescope examination has been extended to every wellhead at different frequencies according to the observed pitting severity. Based on favorable visual inspection results and initial readings, ultrasonic measurement has been extended from monthly to quarterly for carbon steel items. Glycol and water analyses are taken quarterly unless drastic changes in any of the ion concentrations arise.

Results

Borescope examination of twenty-one wellheads showed pitting and/or erosion on 62% of the wells. Pits ranged from 0.51 mm to 4.06 mm wide and less than 0.76 mm deep. No corrosion was detectable on the 420 SS wellhead corrosion coupons. The monthly chromium count stayed low (< 1 ppm).

At the clusters, coating failure have been reported in the produced water and glycol/produced water tanks. Failures were primarily attributed to poor surface preparation and application. Inspection of these tanks showed isolated pitting. Consequently, coatings were replaced and magnesium anodes were added to provide additional corrosion protection to the tanks. Corrosion protection of the salt water disposal lines is accomplished with corrosion inhibitor. The recommended dosage is 200-240 ppm of a water soluble inhibitor. The corrosion rate recorded at the salt disposal well site remains consistently low (<.025 mm/y).

Visual inspection of the production separators and test separators at YA and YB clusters (the "corrosion test" cluster and a standard cluster) in January 1986 showed slight pitting on the carbon steel production separator at YA, slight discoloration on the carbon steel test separator at YA, and no corrosion on the 316L lined vessels at YB.

At the central facilities, the corrosion monitoring program is based on ultrasonic measurements, visual inspection, IRIS inspection and glycol analyses. No corrosion has been detected by ultrasonic measurements. Visual inspection and IRIS inspection done in January 1986 showed no corrosion in the stainless steel vessels and carbon steel heat exchanger tubes. Multiple pittings of 0.38 mm - 0.51 mm deep were identified in the carbon steel high and low pressure flash tanks. The pH and chloride concentration in glycol have been monitored closely to avoid corrosive conditions. Glycol pH is kept at 7-8 using DEA and chloride concentration is kept below 1,000 ppm.

CONCLUSION

The purpose of the McElmo Dome corrosion monitoring program is to locate areas where corrosion may occur and allow remedial measures to be taken as early as possible. As a side benefit, it provides valuable corrosion information for future facility designs. Results of the monitoring program to date indicate minimal corrosion problems at Yellow Jacket or Hovenweep source facilities.

ACKNOWLEDGMENT

Acknowledgments are expressed to L. Abrego, A.F. Breckwoldt, C.M. Bulovas, R.C. Hulsey, R.H. Klug, and J.P. Tralmer of SWEPI and SDC for information obtained from internal company reports authored by them which provided information helpful to the preparation of this paper.

TABLE 1

McELMO DOME PRODUCTION UNIT
PRODUCING WELLS CORROSION MONITORING PROGRAM

MONITORING METHOD	LOCATION FOR MONITORING	FREQUENCY
1. Visual Inspection	All downhole equipment	As possible
2. Water Analyses (Fe, Cr, pH, Cl, HCO_3)	All wells	Monthly
3. Weight-loss Coupons (25% of wells)	At wellheads(1)	Quarterly
4. Casing Pressure	Annulus	Monthly
5. Analyze Debris	All equipment	As necessary
6. Ultrasonics (Westhollow) (25% of wells)	Wellheads(1)	Semi-annually
7. Borescope (Westhollow)	Wellheads(2)	

(1) Change in initial frequency:

- For weight loss coupons: Change from "monthly" to "quarterly"
- For wellhead ultrasonic: Change from "quarterly" to "semi-annyually"

2) Borescope Inspection Frequency:

- YA-1, YB-1, YB-3, YC-2, HB-1, HC-2, HD-2, HF-1: 12 months
- YA-2, YF-1, HB-2, HC-3, HE-2: 18 months
- YB-2, YD-1, YD-2, YE-1, HA-1, HC-1, HD-1, HE-1: as necessary
- YC-1: based readings ASAP

TABLE 2

McELMO DOME PRODUCTION UNIT
WELL CLUSTER FACILITIES AND GATHERING SYSTEM
CORROSION MONITORING PROGRAM

	LOCATION	MONITORING METHOD	FREQUENCY
1.	3" C.S. Water Line at HA, HB, HC, HD, HE, HF, YA, YB, YC, YD, YE, YF Clusters	Weight-loss Coupons Pair Probes(1)	Monthly Monthly
2.	3" C.S. Water Line at Injection Well	Weight-loss Coupons Pair Probes(1) Water Analysis(2)	Monthly Monthly Monthly
3.	Duplex Stainless Steel Pipe at three Bellhole Locations (Hovenweep)	Ultrasonics	Every 6 Months
4.	Production Separators at Clusters (316L Overlaid & C.S.) a) Upper & Lower Parts of Shell and at Drain Section	Ultrasonics	Every 6 Months (316L) Every 3 Months (C.S.)
	b) Interior Portions	Visual Inspection	During Shutdown
5.	Test Separators at Clusters (316L Overlaid & carbon steel) a) Upper & Lower Parts of Shell and at Drain Section	Ultrasonics	Every 6 Months (316L) Every 3 Months (C.S.)
	b) Interior Portions	Visual Inspection	During Shutdown
6.	Produced Water Storage Tanks (Epoxy-lined C.S.)	Visual Inspection O_2 Analysis	During Shutdown Every 2 Months
7.	Hydrate Inhibitor Storage Tanks (Plastic Coated)	Visual Inspection	During Shutdown
8.	Produced Water (C.S.) Cathodic Protection System	Potential Measurements (Shell Pipeline)	Yearly
9.	Gas Gathering (Duplex) Cathodic Protection System	Potential Measurements (Shell Pipeline)	Yearly

(1) Change in initial frequency from twice monthly to monthly

2) Items added to the program

TABLE 3

McELMO DOME PRODUCTION UNIT
CENTRAL FACILITIES CORROSION MONITORING PROGRAM

	LOCATION	MONITORING METHOD	FREQUENCY
1.	Inlet Separator (V-101) (316L Overlaid)	Visual I.D. Inspection Ultrasonics	During Shutdown Every 6 Months(1)
2.	Glycol Contactor (V-103) (316 S.S. Trays, C.S. Vessel)	Visual I.D. Inspection Ultrasonics Glycol Analysis (Rich Glycol and Lean Glycol)(2)	During Shutdown Every 3 Months(1) Quarterly
3.	Second Stage Compressor Suction Scrubber (V-104) (C.S. Vessel, 316 S.S. Demister)	Visual I.D. Inspection Ultrasonics	During Shutdown Every 3 Months
4.	H.P. Rich Glycol Flash Tank (V-105) (C.S. Vessel)	Visual I.D. Inspection Ultrasonics	During Shutdown(1) Every 3 Months
5.	Glycol Still (V-118) (316L Clad, 316 S.S. Trays)	Visual I.D. Inspection Ultrasonics(2)	During Shutdown Every 6 Months
6.	Second Stage Discharge Bottle (V-121) (C.S.)	Ultrasonics(2) Visual Inspection	Every 3 Months During Shutdown
7.	Water Pump Discharge Bottle (V-127) (304 S.S.)	Ultrasonics	Every 6 Months
8.	Water Surge Tank (V-129) (Coated C.S.)	Water Analysis	Monthly
9.	Inlet Vapor Separator (V-201) (316L Overlaid)	Visual I.D. Inspection Ultrasonics	During Shutdown Every 6 Months
10.	First Stage Compression Suction Scrubber (V-202) (316L Overlaid)	Visual I.D. Inspection Ultrasonics Water Sample Off Bottom	During Shutdown Every 6 Months Every 2 Months
11.	First STage Discharge Bottle (V-204) (C.S.)	Ultrasonics Visual Inspection	Every 3 Months During Shutdown
12.	V-150 (E-101 Knockout pot) (C.S.)	Ultrasonics(2) Visual I.D. Inspection(2)	Every 3 Months During Shutdown
Tanks			
13.	Glycol Storage Tank T-108 (C.S.)	Visual I.D. Inspection	During Shutdown
14.	Produced Water Storage Tank (T-110) (Epoxy-lined C.S.)	Visual I.D. Inspection Water Analysis O_2 Analysis	During Shutdown Monthly 2 Months
15.	Fuel Oil Storage Tank (T-113) (C.S.)	Visual I.D. Inspection	During Shutdown
16.	Utility Water Storage Tank (T-114) (C.S.)	Visual I.D. Inspection	During Shutdown
17.	Slop Oil/Water Tank (T-115) (C.S.)	Visual I.D. Inspection	During Shutdown

(1) Change in initial frequency: Change from "every 2 months" to "quarterly" for carbon steel and "semi-annually" for stainless steel

(2) Items added to the program

(3) Change in initial frequency: from "yearly" to "during shutdown"

TABLE 3 (CONTINUED)

McELMO DOME PRODUCTION UNIT
CENTRAL FACILITIES CORROSION MONITORING PROGRAM

	LOCATION	MONITORING METHOD	FREQUENCY
	Heat Exchangers and Heaters		
18.	Glycol Contactor Residue Gas Cooler (E-102) (C.S. Tubes)	Internal Tube Caliper (Contract Firm)	During Shutdown(3)
19.	Compressor Discharge Cooler (E-103) (C.S. Tubes)	Internal Tube Caliper (Contract Firm)	During Shutdown(3)
20.	Hot Lean-Rich Glycol Heat Exchanger (E-105) (C.S. Tubes and Shell)	Internal Tube Caliper (Contract Firm) Ultrasonics (shell)(2) (Contract Firm)	During Shutdown(3) Every 3 Months
21.	Jacket Water Cooler (E-116) (C.S. Tubes)	Internal Tube Caliper (Contract Firm)	During Shutdown(3)
22.	First Stage Compressor Discharge Heat Exchanger (E-201) (316L Tubes/C.S. Shell)	Internal Tube Caliper (Contract Firm) Ultrasonics (shell)(2) (Contract Firm)	During Shutdown(3) Every 3 Months
23.	Glycol Reboiler (H-102) (C.S.)	Visual O.D. & I.D. Inspec. Ultrasonics (shell)(2)	During Shutdown(3) Every 3 Months
24.	Start-up Heater (H-101) (C.S.)	Visual I.D. Inspection(2)	During Shutdown
	Compressors		
25.	Compressor (K-101) (C.S.)	Visual Inspection	During Shutdown
	Valves		
26.	Control Valve (LV-331) on Line from Vessel V-201	Visual Inspection	During Shutdown
27.	Control Valve (PV-350) on Line into Vessel V-201	Visual Inspection	During Shutdown
28.	Control Valve (LV-303) on Line from from Vessel V-202-A)	Visual Inspection	During Shutdown
	Piping		
29.	Piping (24"-W-147-DS) Downstream of Control Valve (LV-331)	Ultrasonics	Every 6 Months(1)
30.	Piping (24"-W-140-ES) Downstream of Control Valve (PV-350)	Ultrasonics	Every 6 Months(1)
31.	Piping (2"-A-118-DS) Downstream of Control Valve (LV-303)	Ultrasonics	Every 6 Months(1)
32.	On Carbon Steel Flange/Piping on Couple Between 4"-R-100-ES (Drain Line from V-103) and 4"-R-101-BC (Going to E-106A) for Possible Galvanic Effects	Ultrasonics	Every 6 Months(1)
33.	Piping (18"-D-103-FC) from E-101 to E-103	Ultrasonics	Every 3 Months(1)
34.	Piping (4"-R-108-BC) from E-106A to E-104A	Ultrasonics	Every 3 Months(1)
35.	Piping (2"-J-113-ACS) from V-129	Ultrasonics	Every 3 Months(1)

(1) Change in initial frequency: Change from "every 2 months" to "quarterly" for carbon steel and "semi-annually" for stainless steel

(2) Items added to the program

(3) Change in initial frequency: from "yearly" to "during shutdown"

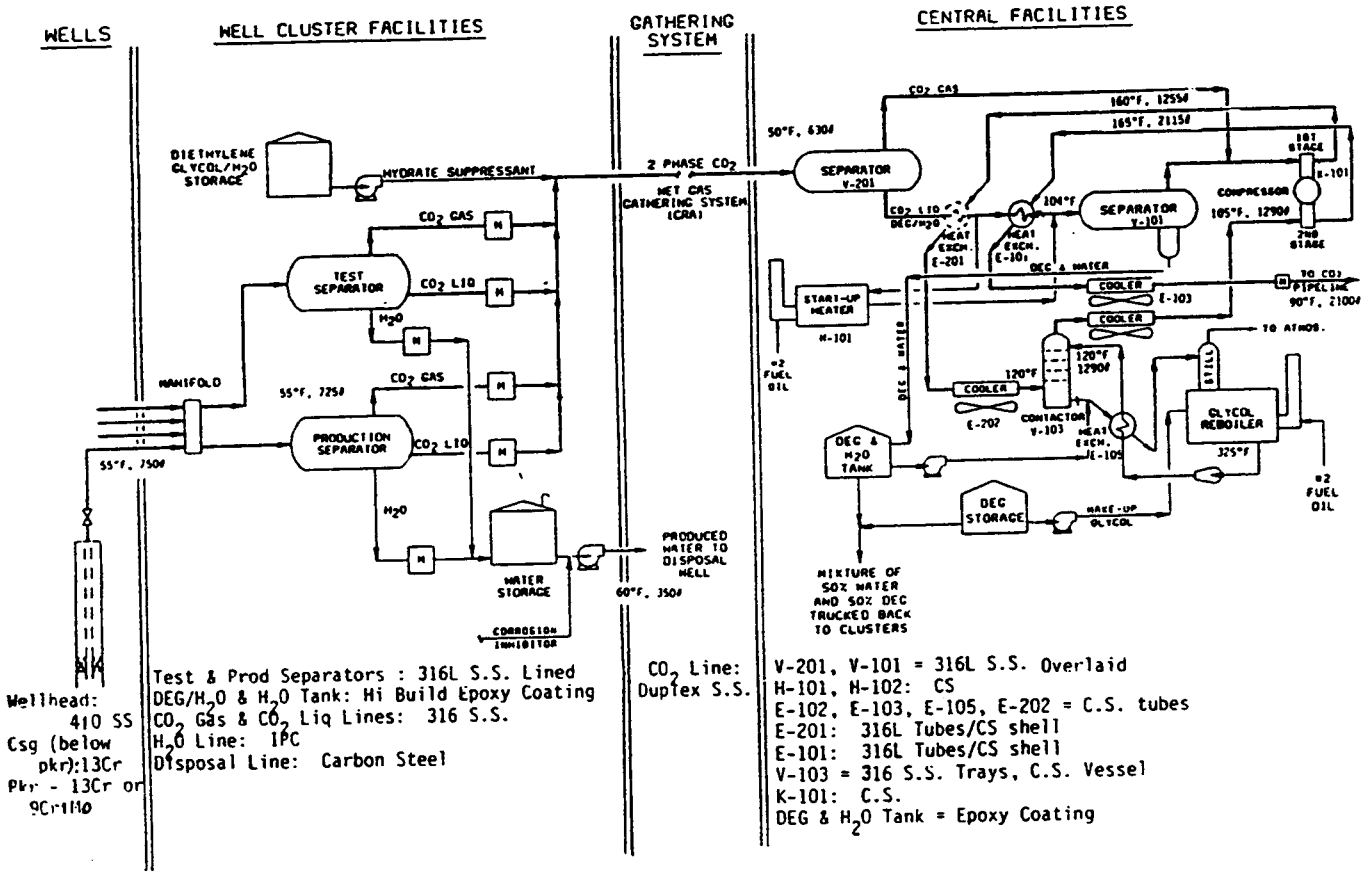


FIGURE 1 - Yellow Jacket and Hovenweep
CO_2 Source Facilities

Copyrighted Materials
Copyright © 1996 NACE International Retrieved from www.knovel.com

Paper No.
85

CORROSION 95
The NACE International Annual Conference and Corrosion Show

BEHAVIOR OF DIFFERENT MARTENSITIC STAINLESS STEELS UNDER OIL AND GAS CORROSIVE ENVIRONMENTS

B.J. ORLANS-JOLIET, F. BLANCHARD and G.C. GUNTZ
Vallourec Research Center
P. O. Box 17
59620 Aulnoye Aymeries, France

J-J. SERVIER
Vallourec Oil & Gas
P. O. Box 1
59620 Aulnoye Aymeries, France

ABSTRACT

The tests described in this paper are aimed at evaluating the performances of different martensitic stainless steels regarding on the one hand general and crevice corrosion in sweet environments at elevated temperatures, and on the other hand regarding sulfide stress cracking.

Keywords : 13Cr stainless steels, corrosion, carbon dioxide, sulfide stress cracking, hydrogen sulfide.

INTRODUCTION

API 5CT L80 type 13Cr grade is widely used in oil and gas fields with a high CO_2 content. NACE MR0175-94 Standard [1] states that casings and tubings in this grade are acceptable up to a maximum H_2S partial pressure of 0.1 bar (1.5 psia, 10 kPa) in production environments with a produced water pH $\geq$ 3.5. The addition of these materials in MR0175-94 Standard has been based on an experience representing over 100 wells with 13Cr being used in fields for times ranging from 1 to 12 years.

Laboratory results as published for the NACE MR0175 ballot in 1992 show that the API 5CT L80 type 13Cr grade is acceptable up to a threshold stress of 80% Specified Minimum Yield Strength (SMYS), with 0.1 bar H_2S [2,5]. The statistical exploitation of these published

data gives an estimated minimum value close to 70% SMYS with ± 2 times the standard deviation.

In severe well conditions, increased performances can be necessary for yield strength, impact properties and localized corrosion with an improved SSC resistance. In this study, we present the behavior obtained for these different aspects on 13Cr with Ni and Mo added respectively up to 5% and 2% in comparison with a standard 13Cr.

EXPERIMENTAL PROCEDURE

Materials

The different 13Cr martensitic stainless steels tested were a standard 13Cr and two 13CrNiMo : 13-4-1 and 13-5-2.

Element analysis of steels was determined using the glow discharge spectrometer technique. The actual composition of these three 13Cr martensitic steels is given in Table 1.

Testing methods

Mechanical tests. The actual yield strength values (0.2% offset) were measured by tensile tests on round specimens taken longitudinally at mid-wall thickness. For impact tests, Charpy V-notched specimens taken in the longitudinal and transverse direction were tested at 0°C. Considering the wall thickness, energy values were normalized per unit of area.

Corrosion tests. The test conditions were :

- for general corrosion : PCO_2 = 10 bars or 50 bars
  NaCl = 100 g/l or 300 g/l
  Temperature = 150°C or 180°C
  Deaeration with nitrogen
  Stirring = 200 rpm
  Test duration = 7 days.

The 34,5 x 15 x 5 mm specimens degreased with aceton were weighed before and after the test.

- for crevice corrosion : PCO_2 = 50 bars
  NaCl = 100 g/l
  Temperature = 80°C
  Deaeration with nitrogen
  Test duration = 7 days.

The 30 x 30 x 5 mm specimens were polished with 120 grit paper, pickled in 50% HCl solution at 50°C for 15 minutes, passivated in 30% HNO_3 solution for 10 minutes, rinced and dried. The device used was a PTFE multicrevice assembly.

SSC tests. Tests according to the method A of NACE TM0177-90 [6] were carried out to assess the resistance of these products to SSC with a gas mixture of 10% H_2S in CO_2. These tests were performed with proof ring devices in the following test solution :

- NaCl = 50 g/l
- Sodium acetate = 10,464 g/l

The pH = 3.5 was adjusted by HCl addition at the beginning of the test. Double walled glass vessels were used to control and record the temperature of the solution continuously throughout the test.

After machining, the specimens were polished with 600 grit paper and electrolytically. The applied stress level was 80% SMYS of the grade (L80 or C95).

RESULTS

Mechanical properties

The results show that mechanical characteristics are mainly influenced by chemical analysis. The improved martensitic 13-5-2 can easily meet the tensile properties of the C95 grade; the C110 grade can also be reached without impairing elongation and toughness. On the other hand in the case of 13-4-1, the level of C95 can only be met with low tempering temperature; this difference of behavior is mainly due to Ti content which has a significant hardening effect in the former alloy.

The longitudinal ductility, evaluated by impact tests at 0°C is rather high with no cristallinity in any case, especially for the two improved martensitic alloys, in spite of the higher grade. The transverse impact tests are sensitively lower in the case of standard 13Cr and 13-4-1, but still without any cristallinity.

Corrosion resistance

Uniform corrosion is also drastically influenced by the type of alloy. At 150°C or 180°C in NaCl solutions under high pressure of CO_2, the corrosion rates are roughly tenfold lower in the case of 13-5-2 or 13-4-1 alloy in comparison with standard 13Cr : the two improved martensitic steels being hardly distinguishable in that case. This behavior can be ascribed to the higher free Cr content in the case of low Carbon alloys (heats A and B); Ni could also have a complementary beneficial influence. The effect of Mo which is more doubtful in that case, is obvious on the other hand, in the crevice corrosion tests at 80°C where 13-5-2 is the only alloy to be free of attack.

SSC results

The standard 13Cr L80 grade show no failure at 80% SMYS for NACE TM0177-90 standard tensile tests in the conditions suggested by NACE MR0175-94 for tubing and casing (§10.2.1). The improved martensitic 13-5-2 also behaves without any cracks, but for higher yield strengths : C95 grade. These good results were obtained after an optimization of Ni and Mo contents regarding appropriate heat treatment and structure. The higher sensitivity of 13-4-1 is due to the lower tempering temperature necessary to meet the C95 grade.

CONCLUSIONS

The improved 13Cr alloyed with additions of Nickel (5%) and Molydbdenium (2%) is intended to be used in sweet environments where

the use of a standard 13Cr is prohibited by elevated temperatures and in sour environments due to presence of H_2S.

With 13-5-2 steel, the corrosion rates in sweet environments are far lower than with API 5CT 13Cr and the crevice corrosion resistance is increased too in comparison with 13-4-1.

High toughness values and no failures during NACE TM0177-90 tests show the superiority of 13-5-2 steel against standard 13Cr for L80 and 13-4-1 for C95.

REFERENCES

1. NACE MR0175-94 Standard (1994)

2. M.B. Kermani, D. Harrup, M.L.R. Truchon and J-L. Crolet, Corrosion 91, Cincinnati, paper 21 (1991)

3. L.J. Klein, R.M. Thompson and D.E. Moore, Corrosion 90, Las Vegas, paper 52 (1990)

4. W.C. Chen, Corrosion 90, Las Vegas, paper 61 (1990)

5. S.W. Ciaraldi, Corrosion 90, Las Vegas, paper 71 (1990)

6. NACE TM0177-90 Standard (1990)

ACKNOWLEDGEMENTS

Thanks to TISL, BSST for their participation at this research program.

TABLE 1 : CHEMICAL COMPOSITION OF THE DIFFERENT HEATS (wt%)

Type	Heat	C	Mn	Si	P	S	Cr	Mo	Ni	Ti
13 Cr	A	0.21	0.46	0.25	0.01	0.004	13.09	0.02	0.14	-
13-4-1	B	0.01	0.58	0.41	0.01	0.006	13.40	0.37	3.78	-
13-5-2	C	0.01	0.50	0.14	0.02	0.006	12.68	1.85	5.82	0.21

TABLE 2 : MECHANICAL PROPERTIES

Type	Heat	Dimensions OD x WT (mm)	Grade	YS (ksi)	UTS (ksi)	E (%)	CVN - Cristallinity at 0°C (J/cm²) Long.	Trans.
13 Cr	A	160 x 20	L80	84	109	22.7	174 (0%)	123 (0%)
13-4-1	B	139.7 x 7.72	C95	104	114	21.3	212 (0%)	106 (0%)
13-5-2	C	177.8 x 10.36	C95	102	117	22.6	243 (0%)	194 (0%)
"	"		C110	118	122	22	242 (0%)	182 (0%)

TABLE 3 : GENERALIZED CORROSION RESULTS

Type	Heat	Grade	NaCl : 100 g/l P CO_2 : 10 b Temperature :150°C	Corrosion rate (mm/year) 100 g/l 50 b 150°C	 100 g/l 50 b 180°C	 300 g/l 50 b 180°C
13 Cr	A	L80	0.46 0.47	1.28 1.43	3.08 3.19	3.24 3.02
13-4-1	B	C95	- -	0.06 0.03	0.35 0.34	- -
13-5-2	C	C95	0 0	0.03 0.02	0.32 0.34	0.33 0.34

TABLE 4 : CREVICE CORROSION RESULTS

Type	Heat	Grade	Corroded sites NaCl :100 g/l P CO_2 :50 b Temperature :80°C
13 Cr	A	L80	9/40 14/40
13-4-1	B	C95	6/40 7/40
13-5-2	C	C95	0/40 0/40

TABLE 5 : NACE TENSILE TEST RESULTS

Type	Heat	Dimensions OD x WT (mm)	Grade	YS (ksi)	UTS (ksi)	Failure time at 80% SMYS 10% H_2S in CO_2 pH = 3.5
13 Cr	A	160 x 20	L80	84	109	> 720 h > 720 h
13-4-1	B	139.7 x 7.72	C95	104	114	**160 h** **178 h**
13-5-2	C	177.8 x 10.36	C95	102	117	> 720 h > 720 h
"	"	"	C110	118	122	**166 h** > 720 h

Copyrighted Materials
Copyright © 1996 NACE International Retrieved from www.knovel.com

Paper No.
82

CORROSION 95
The NACE International Annual Conference and Corrosion Show

EFFECT OF ENVIRONMENTAL FACTORS AND YIELD STRENGTH ON SSC PROPERTY OF AISI 420 STAINLESS STEEL

S.Sakamoto and A.Kawakami
Nippon Steel Corp.,Yawata R & D Lab.
1-1,Tobihatacho,Tobata-ku,Kitakyushu 804,Japan

H.Asahi
Nippon Steel Corp.,Steel Research Labs.
20-1,Shintomi,Futtsu,Chiba 299-12,Japan

A.Nakamura
Japan National Oil Corp.,Technology Research Center
2-2,Hamada 1-chome,Mihama-ku,Chiba 261,Japan

A B S T R A C T

Study on service limit of AISI 420 stainless steel for sour environment is conducted. Since SSC is a phenomenon of hydrogen embrittlement,the measurement of hydrogen content in steel is a key factor to the predict SSC occurrence. SSC occurs if hydrogen content entering into steel exceeds a critical hydrogen content for the steel. Comparison of both values of hydrogen contents enables to estimate critical environmental conditions and yield strength. Estimation results by this method coincides well with data in several literatures. Through this appraisal,specially heat-treated low yield strength 13Cr steel was found to be a good candidate for sour service.

Keywords : hydrogen sulfide, sulfide stress cracking, hydrogen embrittlement, hydrogen content, 13Cr steel, yield strength, heat treatment

INTRODUCTION

AISI 420 stainless steel(13Cr steel) has been generally recognized as being susceptible to sulfide stress cracking(SSC),although it has good CO_2 corrosion resistance.

An extensive research work has been carried out to clarify the application limit of 13Cr steel in terms of SSC resistance. So far,it has been reported that SSC property of 13Cr steel depends on both environmental conditions as pH and H_2S partial pressure and material characteristics of yield strength,microstructure and chemical compositions[1-7]. However,the safety use limit of H_2S partial pressure has not been determined consistently. The critical H_2S partial pressure ranges from 0.003MPa to 0.1MPa in literature[2-6],which may be due to inconsistency of tests:difference in material strength,experimental techniques and evaluation criteria. Therefore,a new concept is needed for systematically estimating SSC occurrence.

For low alloy steel,H.Asahi et al. proposed a method of predicting SSC occurrence by considering that SSC is a phenomenon of hydrogen embrittlement,where hydrogen content is a principal parameter determing the SSC susceptibility of a material[8]. A similar concept can be applied for 13Cr steel,because the SSC of 13Cr steel is also closely related to hydrogen embrittlement[9]. This paper has focussed primarily on establishing a prediction method of SSC property of 13Cr steel using the criterion of hydrogen content in steel,so that critical conditions for SSC occurrence in 13Cr steel could be systematically understood.

Furthermore,SSC resistant 13Cr steel with low yield strength(e.g.65-ksi grade) has potential needs[4]. This paper also discusses the performance of low strength 13Cr steel.

EXPERIMENTAL

Materials

Commercial seamless pipe of 13Cr steel of chemical compositions listed in

Table 1 was used in this study. Two kinds of additional heat treatment were applied to this pipe in order to prepare test samples with different yield strength: a normalizing and tempering process(N-T) and three steps of normalizing,dual phase treatment and tempering process(N-L-T),as shown in Figure 1. Heat treatment conditions and the corresponding mechanical properties are listed in Table 2.

Electrochemical hydrogen permeation test

Electrochemical hydrogen permeation method was used for determing the hydrogen uptake in steel exposed to a corrosive environment. The test device is illustrated in Figure 2. During test,hydrogen entered steel from the cathode-side surface where the specimen was corroded,and diffuses toward the anode-side surface hydrogen was oxidized to hydrogen ion. The potential of anode-side surface Ni-plated beforehand was maintained at +0.1V vs S.C.E. during the test. Specimens were 1mm thick and 3.14 cm^2 in tested area. Hydrogen uptake into steel was obtained by Eq.(1).

$$[H] = 0.42 \times I/D \quad \cdots\cdots (1)$$

Where, [H] : hydrogen uptake just beneath the cathode-side surface (ppm),

J : hydrogen permeation current ($\mu A/cm^2$),

D : apparent diffusion coefficient ($\times 10^{-7} cm^2/sec$) .

Apparent diffusion coefficients of tested materials were determined by electrolytic hydrogen charging method as shown in Figure 3. The charging current was changed in two or three steps to obtain the build-up and decay curves of hydrogen permeation current. The apparent diffusion coefficient was obtained by the build-up and decay curves utilizing diffusion theory.

SSC test

SSC susceptibility was mainly evaluated by V-notched four point bent beam test. The dimensions of the specimens and stress calculation formula are shown in Figure 4. Specimens were loaded to 100% of yield strength neglecting the stress concentration caused by the notch. The loaded specimen were immersed in test solution for 72 hours to allow hydrogen saturation in a specimen. The short time can minimize the raise of pH of test solution.

The NACE tensile test was also carried out in accordance with NACE TM-0177 method-A in order to compare the results with those by V-notched four point

bent beam test.

Test environments

The test solution used for both hydrogen permeation measurement and V-notched four point bent beam test was 1 mol/ℓ acetate buffer solution containing 3%NaCl saturated with test gases of 0.1%,1%,10% H_2S balanced with N_2 or 100% H_2S at ambient pressure. The partial pressure of H_2S was 1×10^{-4} to 1×10^{-1} MPa(1.5×10^{-4} to 1.5×10^{-1}psi). The pH value of the solution was adjusted in the range of 2 to 6. Testing temperature was maintained at 25 ℃.

For the NACE tensile test,the standard NACE solution(0.5% acetic acid + 5%NaCl, 0.1MPa H_2S) and modified solution(0.5% acetic acid + 5%NaCl, 0.01MPa H_2S) were used.

RESULTS AND DISCUSSION

Hydrogen uptake

Experiments to investigate the influence of environmental factors on hydrogen uptake into steel were carried out for steel 13L under various environmental conditions. The apparent diffusion coefficient of steel 13L was determined to be 1.92×10^{-7}㎠/sec by hydrogen charging method. Figure 5 shows the hydrogen uptake in relation to pH of test solution. In pH region below 5.0,the logarithm of hydrogen uptake decreases proportionally with the increase in pH. In pH region over 5.0,hydrogen uptake could not be detected since 13Cr steel presented a passive state. Figure 6 shows the hydrogen uptake plotted as a function of partial pressure of H_2S. The logarithm of hydrogen uptake increases proportionally with the increase in H_2S partial pressure.

Experiments to investigate the influence of strength level on hydrogen uptake were also carried out. The apparent diffusion coefficients of test samples were determined as shown in Figure 7. Hydrogen uptake is plotted in Figures 8 and 9 as a function of yield strength. It is apparent that the logarithm of hydrogen uptake increases proportionally with the increase in yield strength.

By regression analysis,the following empirical equation was obtained.

$$\log[H] = 0.86 \times 10^{-3} \times YS - 0.041 \times pH + 0.28 \times \log P(H_2S) + 1.21 \quad \cdots\cdots (2)$$

Where, [H] : hydrogen uptake into steel in ppm,

YS : yield strength in MPa,

P(H_2S) : partial pressure of H_2S in MPa.

It is noted here that Eq.(2) is applicable in the condition of pH below 5.0. Figure 10 shows the relation between the measured hydrogen uptake and calculated one by Eq.(2). The correlation factor,"r" of 0.949 is considered to be sufficient for precisely estimating the hydrogen uptake in 13Cr steel.

SSC susceptibility by notched bent beam test

Table 3 lists the SSC test results by V-notched four point bent beam method. It also lists hydrogen uptake calculated by Eq.(2). It seems that SSC susceptibility increases with increase in acidity, H_2S partial pressure and yield strength. These data are rearranged to the relation between hydrogen uptake and SSC susceptibility in Figure 11. The critical hydrogen uptake in terms of SSC occurrence decreases with the increase in yield strength. The relation between critical hydrogen content and yield strength is written as Eq.(3).

$$\log[H]_{CRIT} = -2.69 \times 10^{-3} \times YS + 2.46 \quad \cdots\cdots (3)$$

Here, $[H]_{CRIT}$: critical hydrogen content in ppm,

YS : yield strength in MPa.

Critical conditions for SSC occurrence by notched bent beam test

Since the SSC mechanism of 13Cr steel is considered to be hydrogen embrittlement,SSC occurrence of 13Cr steel can be predicted by comparing the hydrogen uptake into steel exposed in a sour environment([H]) and critical hydrogen uptake for SSC of a material($[H]_{CRIT}$). If [H] exceeds $[H]_{CRIT}$,SSC will occur. In the opposite case,SSC will not occur. The critical conditions for SSC occurrence,therefore,can be written as Eq.(4).

$$[H] = [H]_{CRIT} \quad \cdots\cdots (4)$$

Hereby,both [H] and $[H]_{CRIT}$ are already determined as Eqs.(2) and (3). Equations.(2) through (4) are reduced to the following equation.

$$3.45 \times 10^{-3} \times YS - 0.041 \times pH + 0.28 \times \log P(H_2S) = 1.20 \quad \cdots\cdots (5)$$

Using this equation,the critical yield strength free from SSC can be estimated when environmental conditions(pH and H_2S partial pressure) are known.

Otherwise,critical environmental conditions can be estimated when yield strength is specified. The value of pH can be estimated from CO_2 and H_2S partial pressures,concentration of chloride and bicarbonate and so on,for example,by the method established by A.Miyasaka et al[10,11].

Comparison with the results by NACE tensile test

Figure 12 shows the NACE tensile test results. In this figure,the points of A_1 and A_2 mean the critical yield strength up to which R_s (σ_{th}/YS) value is estimated at 1.0. Yield strength at the point A_1(0.1MPa H_2S pressure) is ca.450MPa,and at A_2(0.01MPa H_2S pressure) is ca.520MPa. By using the proposed appraisal mentioned above,as shown in Figure 13,the estimated critical yield strengths corresponding to A_1 and A_2 are presented at the points of B_1 and B_2,respectively. Yield strength at the point B_1(0.1MPa H_2S pressure) is ca.460MPa,and B_2(0.01MPa H_2S pressure) is ca.540MPa. In comparing two results, the estimated critical yield strengths at B_1 and B_2 coincide well with ones at A_1 and A_2 by the NACE tensile test. This fact means that no SSC susceptibility by V-notched four point bent beam test at stress application of 100% yield strength is equivalent to the immunity against SSC in NACE tensile test under the applied stress of 100% yield strength(R_s = 1.0). This may also suggest that the proposed criterion is too conservative,if threshold stress of 80% yield strength or higher by NACE tensile test is considered to indicate a steel satisfactorily resistant for sour service.

If a criterion is based on the threshold stress of 80% yield strength(R_s =0.8) by NACE tensile test,the above mentioned Eq.(3) should be modified. In figure 12,the points of a_1 and a_2 mean the critical yield strengths at which threshold stress σ_{th} is 80% yield strength. Yield strength at the point a_1(0.1MPa H_2S pressure) is ca.570MPa,and at a_2(0.01MPa H_2S pressure) is ca.620MPa. Since the solution pH after 720 hours of testing is 3.5,hydrogen uptake corresponding to the points a_1 and a_2 can be calculated by Eq.(2) resulting in 18.9ppm and 10.9ppm,respectively. These hydrogen amounts mean the critical hydrogen content based on the criterion of the threshold stress of 80% yield strength by NACE tensile test. These critical hydrogen contents are plotted in Figure 13. it is found from this figure that yield strength dependence of critical hydrogen content by the above mentioned NACE criterion is equivalent to Eq.(3) which is based on the criterion by V-notched bent beam test at stress application of 100% yield strength,and only the constant term is

different from Eq.(3). Thus,the Eq.(3) is modified as the following equation,

$$\log[H]_{CRIT} = -2.69\times 10^{-3}\times YS + 2.76 \quad \cdots\cdots(6)$$

which also changes Eq.(5) to the following.

$$3.45\times 10^{-3}\times YS - 0.041\times pH + 0.28 \times \log P(H_2S) = 1.50 \quad \cdots\cdots(7)$$

Estimation of critical use limit of 13Cr steel in terms of SSC property

Using Eq.(5) or Eq.(7),critical conditions for avoiding SSC problem can be estimated. For example,Figure 14 shows the estimation results of critical H_2S partial pressure as influenced by yield strength under the pH condition of 3.5. For immunity against SSC,H_2S partial pressure is calculated by Eq.(5) to be 0.0005MPa for the API L-80 grade(max.Y.S.:95 ksi). If one considers the SSc resistance of R_s value of 0.8 or higher to be enough for practical use,allowable H_2S pressure for the L-80 grade is estimated to be 0.006MPa in accordance with Eq.(7). Furthermore,a 65-ksi grade(max.Y.S.:80ksi) is expected to be SSC resistant up to 0.1MPa of H_2S partial pressure on the criterion of R_s value of 0.8 by NACE tensile test. The low strength 13Cr steel is worthwhile in a well where API J-55 can be applied and the SSC problem is a serious concern.

Comparison with some published data

Some published data[2,3,4,5,12] are given in Table 4 together with the critical partial pressure of H_2S calculated by Eq.(5) or Eq.(7). The relation of critical partial pressure of H_2S between published data and calculation results are shown in Figure 15. The calculation results appear to coincide well with experimental results in the literature[2,3,4,5,12],irrespective of test methods. Therefore,the proposed method is recognized to be useful for predicting whether SSC problem may occur for 13Cr steel with a specific yield strength exposed in a specific environment.

CONCLUSIONS

(1) Hydrogen content into steel can be predicted by the following equation:

$$\log[H] = 0.86\times 10^{-3}\times YS - 0.041\times pH + 0.28 \times \log P(H_2S) + 1.21 ,$$

[H] : ppm, YS : MPa, $P(H_2S)$: MPa.

(2) Critical hydrogen content based on the criterion of no SSC by v-notched four point bent beam test at stress application of 100% yield strength can be expressed as following:

$\log[H]_{CRIT} = -2.69 \times 10^{-3} \times YS + 2.46$, $[H]_{CRIT}$: ppm, YS : MPa.

Based on the criterion of R_s (σ_{th}/YS) value of 0.8 by NACE tensile test,critical hydrogen content can be written as following:

$\log[H]_{CRIT} = -2.69 \times 10^{-3} \times YS + 2.76$, $[H]_{CRIT}$: ppm, YS : MPa.

(3) By solving the above equations,critical conditions of pH,$P(H_2S)$ and yield strength can be estimated to avoid SSC problem.

(4) Critical H_2S partial pressure for the L-80 grade to get R_s value of 0.8 or higher is predicted to be 0.006MPa under the pH condition of 3.5.

(5) Lowering the strength level of 13Cr steel considerably improves its SSC resistance. For example,low strength grade with maximum yield strength of 80ksi or lower presents excellent SSC resistance ($R_s \geqq 0.8$) even under the standard NACE condition($P(H_2S)$=0.1MPa).

ACKNOWLEDGEMENT

The authors wish to thank Japan National oil Corporation and Nippon Steel Corporation for permission to publish this paper. The assistance of and discussion with co-workers at Nippon Steel's research laboratories is also gratefully acknowledged.

REFERENCES

1. Y.Ishizawa, T.Shimada,and M.Tanimura, "Effect of Microstructure on the Sulfide Stress Corrosion Cracking Resistance of AISI 410 and 420 Steels" ,CORROSION/82,Paper No.124,National Association Corrosion Engineers,Houston,Texas,1982

2. L.J.Klein, Material Performance,Vol.23,No.10,p.29,1984

3. A.Ikeda, S.Mukai,and M.Ueda, Corrosion,Vol.41,No.4,p.185,1985

4. L.J.Klein, R.M.Thompson,and D.E.Moore, "9CR-1MO and 13CR Tubulars for Sour Service", CORROSION/90,Paper No.52,National Association of Corrosion Engineers,Houston,Texas,1990

5. M.B.Kermani, D.Harrop, M.L.R.Truchon,and J.L.Crolet, "Experimental Limits of Sour Service for Tubular Steels",CORROSION/91,Paper No.21,National Association of Corrosion Engineers,Houston,Texas,1991

6. W.C.Chen, "Corrosion Performance of 13Cr Stainless Tubulars in Sour Environments",CORROSION/90,Paper No.61,National Association of Corrosion Engineers,Houston,Texas,1990

7. S.Mukai, M.Ueda, T.Murata,and A.Ikeda,"Corrosion Behavior of 13Cr Stainless Oil Country Tubular Goods in Wet CO_2-H_2S-Cl^- Environments",presented at the 4th Asian-Pacific Corrosion Control Conference,October,1986

8. H.Asahi, M.Ueno,and T.Yonezawa,Corrosion,Vol.50,No.7,p.537,1994

9. T.Kushida, M.Ueda, T.Kudo, T.Kobayashi,and A.Nakayama,"SSC Susceptibility and Its Evaluation Method of 13Cr Martensitic Steel",CORROSION/93,Paper No.124,National Association of Corrosion Engineers,Houston,Texas,1993

10. A.Miyasaka, K.Denpo,and H.Ogawa, ISIJ International,Vol.29,p.85,1989

11. A.Miyasaka, "Thermodynamic Estimation of pH of Sour and Sweet Environments as Influenced by the Effect of Anions and Cations",CORROSION/92,Paper No.5,National Association of Corrosion Engineers,Houston,Texas,1993

12. M.Ueda, T.Kushida, T.Mori,and T.Okazawa,"Corrosion Resistance of 13Cr Martensitic Stainless Steel in H_2S Containing CO_2 Environment",presented at the Asian Symposium on Corrosion and Protection in Oil and Gas Operation,Oil Refineries,and Petrochemical Industries,Osaka,June,1994

Table 1

Chemical composition of tested steel (wt.%)

C	Si	Mn	P	S	Ni	Cr	Al	N
0.198	0.37	0.41	0.0094	0.0027	0.149	12.91	0.0065	0.025

Table 2

Additional heat treatment conditions and mechanical properties of test materials

Category	Steel code No.	Temperature(℃)			0.2 P.S.		T.S.	
		Norma.	L	Temper.	(MPa)	(ksi)	(MPa)	(ksi)
Mill-produced	13L	———	———	———	577.2	83.8	748.7	108.7
N-T processed	LA	990	———	650	711.5	103.3	885.9	128.6
	LL	990	———	710	644.9	93.6	815.3	118.3
	LS	990	———	750	568.5	82.5	753.5	109.4
N-L-T processed	LP	990	800	600	477.8	69.4	680.1	98.8
	LN	990	800	650	473.6	68.7	678.4	98.5
	LE	990	800	700	461.2	66.9	668.9	97.1
	LQ	990	820	600	455.7	66.1	679.1	99.0
	LM	990	820	650	460.6	67.1	678.2	98.9
	LF	990	820	700	449.8	65.6	671.3	97.9
	LJ	990	840	600	424.0	61.5	681.5	98.9
	LH	990	840	650	397.4	57.7	657.2	95.4
	LC	990	840	710	375.6	54.5	636.4	92.4
	LB	990	840	750	339.1	49.3	623.3	90.5
	LY	990	860	600	507.7	73.9	748.2	109.1
	LW	990	860	650	463.5	67.5	710.5	103.6
	LV	990	860	700	433.2	63.1	680.1	99.1
	LZ	990	880	650	580.4	82.8	755.9	109.7
	LX	990	880	700	492.1	71.4	697.4	101.2
	LU	990	880	750	423.2	61.4	653.7	94.9

Table 3

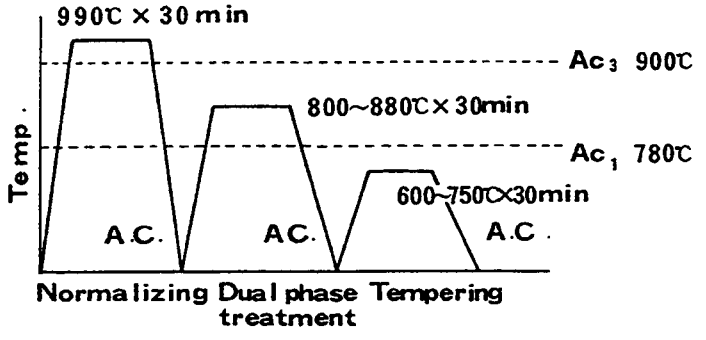
Results of V-notched four point bent beam test at stress application of 1.0 Y.S.

Steel code	Y.S. [MPa]	$P(H_2S)$ [MPa]	pH Initial	pH Final	Result Fail or Not	$[H]_{CALC.}$ [ppm]
LB	339.1	0.1	2.12	2.75	NF	12.8
LC	375.6	0.1	2.12	2.75	NF	13.8
		0.1	4.01	4.08	NF	12.2
LH	397.4	0.1	2.12	2.75	NF	14.4
		0.1	4.01	4.08	NF	12.7
		0.1	4.58	4.53	NF	12.2
LJ	424.0	0.1	2.12	2.75	NF	15.2
		0.1	4.01	4.08	NF	13.4
		0.1	4.58	4.53	NF	12.8
LE	461.2	0.1	3.06	3.04	NF	15.9
		0.01	2.08	2.68	NF	8.6
		0.01	4.06	4.00	NF	7.6
LN	473.6	0.1	3.06	3.04	NF	16.3
		0.01	2.08	2.68	NF	8.8
		0.01	4.06	4.00	NF	7.8
LX	492.1	0.1	3.06	3.04	F	16.9
		0.01	2.08	2.68	NF	9.1
		0.01	4.06	4.00	NF	8.1
13L	577.2	0.1	3.95	4.02	F	18.2
		0.1	4.49	4.56	NF	17.3
		0.01	3.99	4.05	F	9.5
		0.01	4.93	5.09	NF	8.6
		0.001	2.49	2.70	NF	5.7
		0.001	3.48	3.57	NF	5.2
		0.001	4.52	4.62	NF	4.7
		0.0001	2.50	3.06	NF	2.9
		0.0001	4.50	4.41	NF	2.5
LS	568.5	0.01	5.03	5.05	NF	8.5
		0.001	3.06	3.15	NF	5.4
		0.001	4.06	4.03	NF	4.9
LL	644.9	0.01	5.03	5.05	F	9.9
		0.001	3.06	3.15	F	6.2
		0.001	4.06	4.03	NF	5.7
		0.0001	2.93	3.09	NF	3.3
LA	711.5	0.1	5.00	5.02	F	21.6
		0.0001	2.50	3.06	NF	3.7
		0.0001	4.50	4.41	NF	3.3

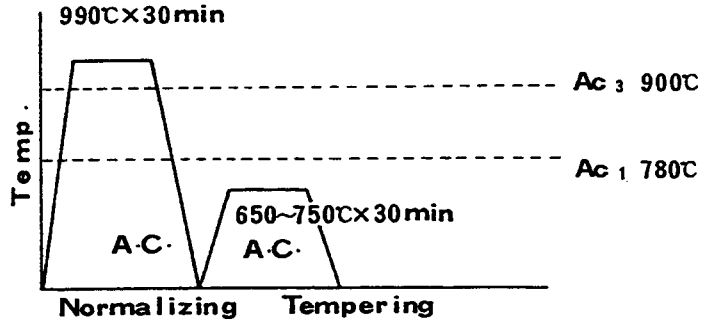
Table 4
Published data and estimation results of critical H_2S partial pressure for L-80-13CR

No.	Y.S. (MPa)	Test method	Applied stress	Base environment	P(H_2S) [MPa]		Estimation		Ref.
					Failure	No failure	Criterion*	Crit. P(H_2S) [MPa]	
①	602	Notched bent beam	1.0× Y.S.	5%NaCl, 3 MPa CO_2 (pH* =3.0)	1×10^{-3}	3×10^{-4}	A	2×10^{-3}	[3]
②	620	Notched bent beam	1.0× Y.S.	5%NaCl, 3 MPa CO_2 (pH* =3.0)	3×10^{-3}	1×10^{-3}	A	1×10^{-3}	[12]
③	L-80 grade	NACE tensile	0.8× SMYS	Pre-NACE soln.	——	1×10^{-2}	B	6×10^{-3}	[4]
④	612	NACE tensile	0.8× Y.S.	Pre-NACE soln.	2×10^{-2}	5×10^{-3}	B	2×10^{-2}	[2]
⑤	595	NACE tensile	0.9× Y.S.	5%NaCl, Acetate buffer, pH=3.5	——	1×10^{-2}	B ~ A	3×10^{-2} ~ 3×10^{-3}	[5]
⑥	594	Notched bent beam	1.0 × Y.S.	S.S.W., 3 MPa CO_2 (pH* =3.7)	1×10^{-2}	——	A	3×10^{-3}	[13]
⑦	577	Notched bent beam	1.0× Y.S.	0%NaCl, Acetate buffer , pH=4.0	——	1×10^{-1}	B ~A	5×10^{-2} ~ 5×10^{-3}	[6]

pH * : estimated pH by the method established by A. Miyasaka [10,11].
Criterion A : the critical conditions, the Eq. (5), obtained by notched bent beam rest(σ_{AP}=1.0YS).
Criterion B : the critical conditions, the Eq. (7), obtained by NACE tensile test (σ_{AP} = 0.8YS).



(a) Three steps(N-L-T) process



(b) Conventional N-T process

Figure 1 Heat treatment process

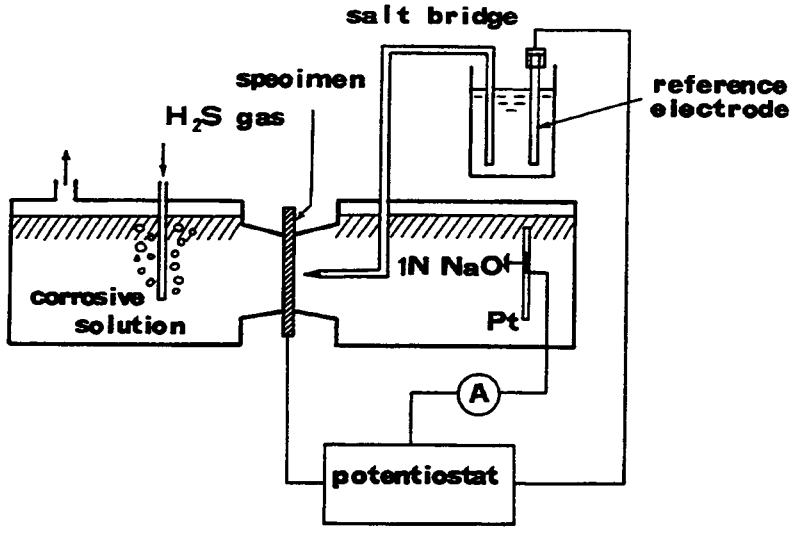


Figure 2 Hydrogen permeation test apparatus

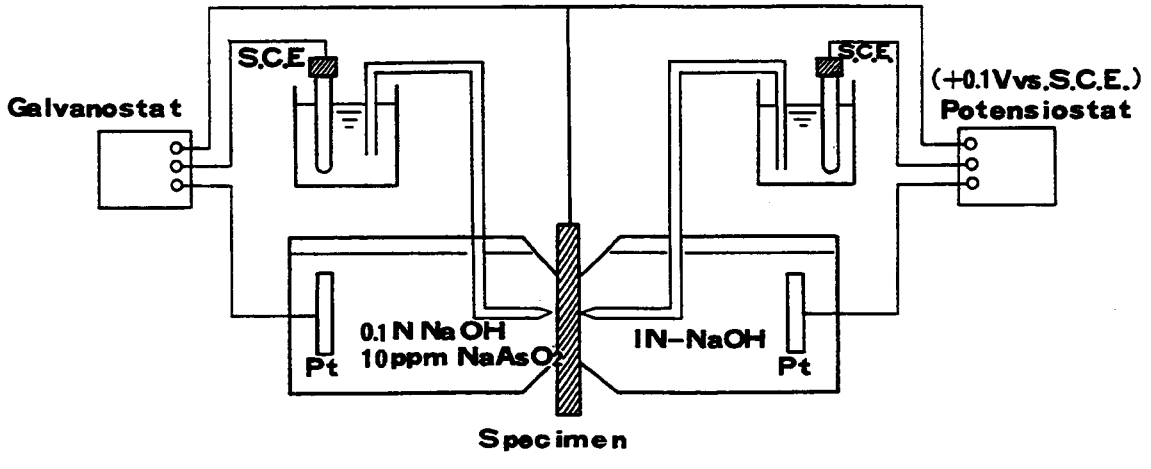


Figure 3 Hydrogen permeation test apparatus using electrolytic hydrogen charging method

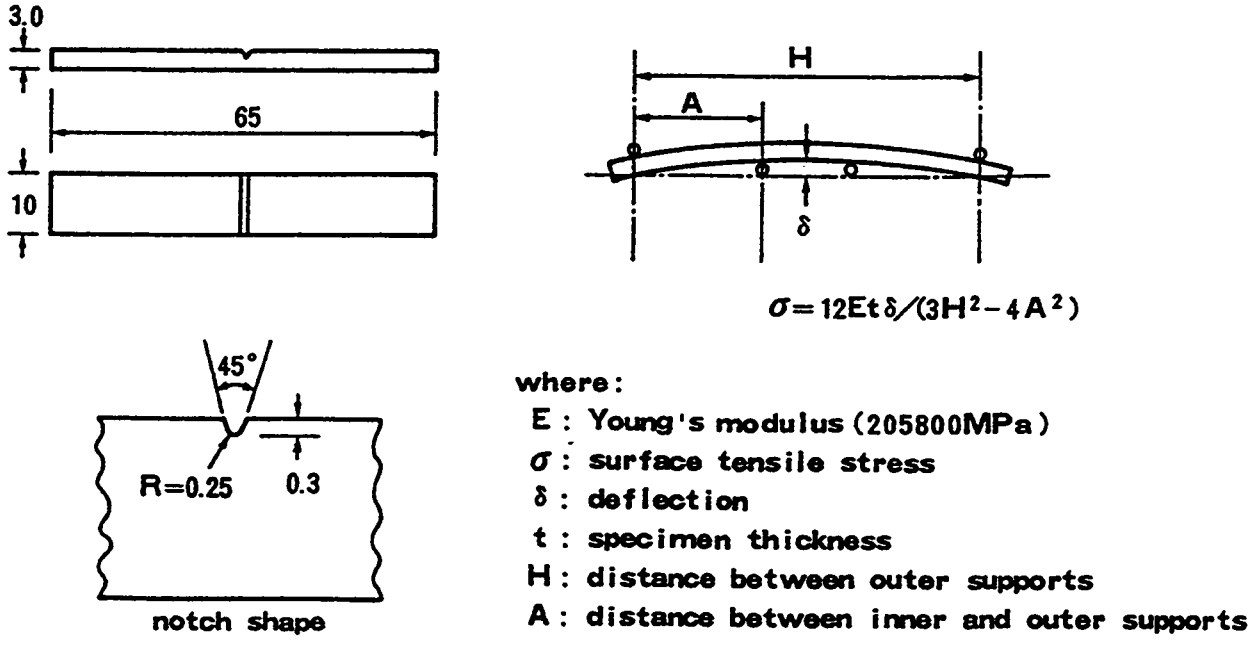


Figure 4 Dimensions of V-notched four point bent beam test specimen and stress calculation formula

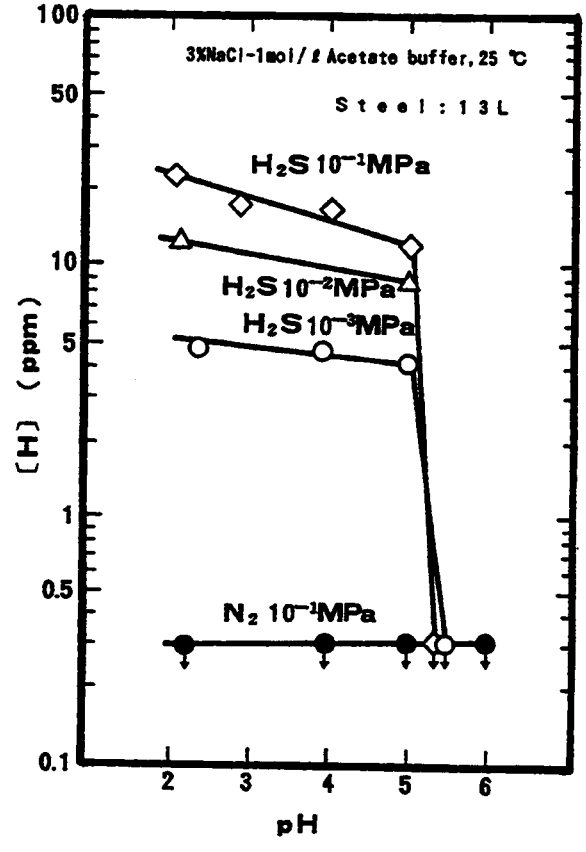


Figure 5 Effect of pH on hydrogen uptake

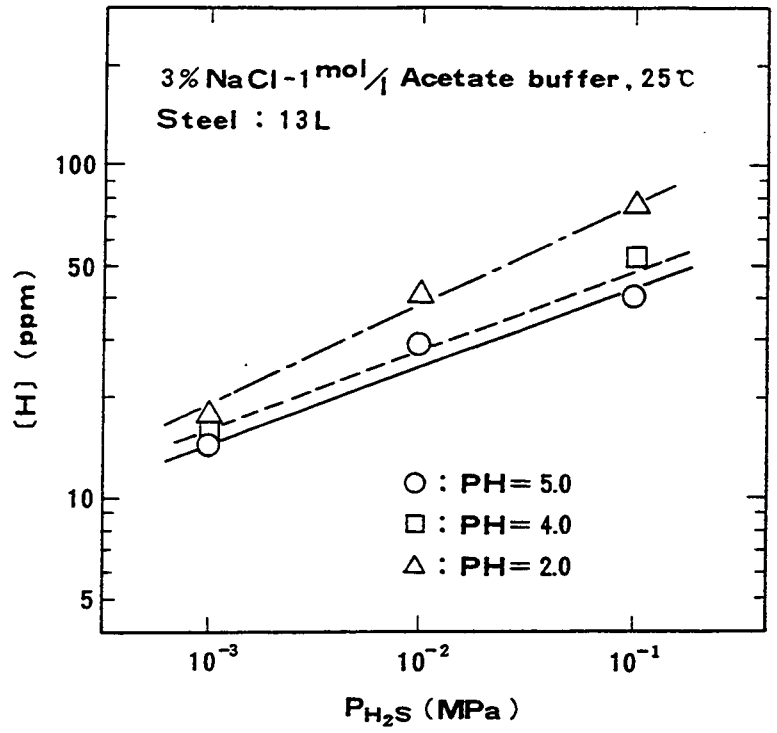


Figure 6 Effect of H_2S partial pressure on hydrogen uptake

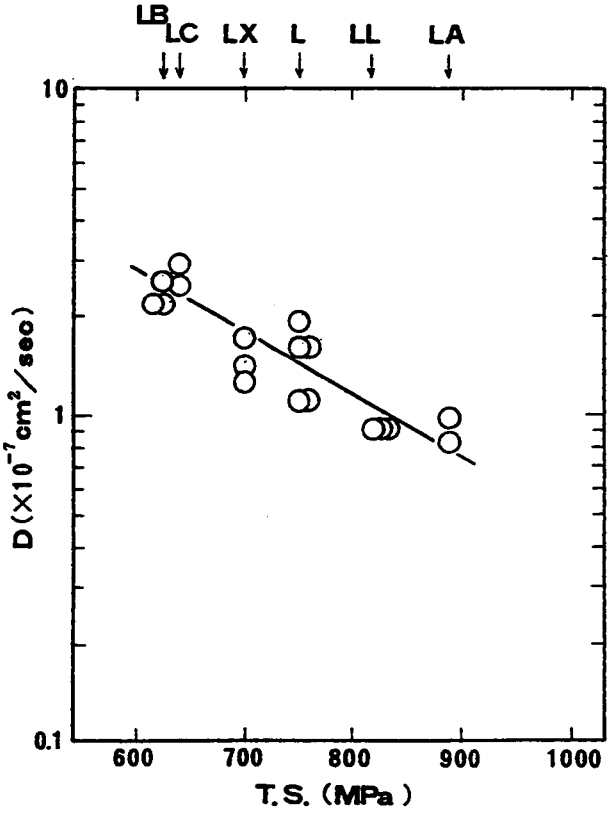


Figure 7 Apparent diffusion coefficient in relation to tensile strength

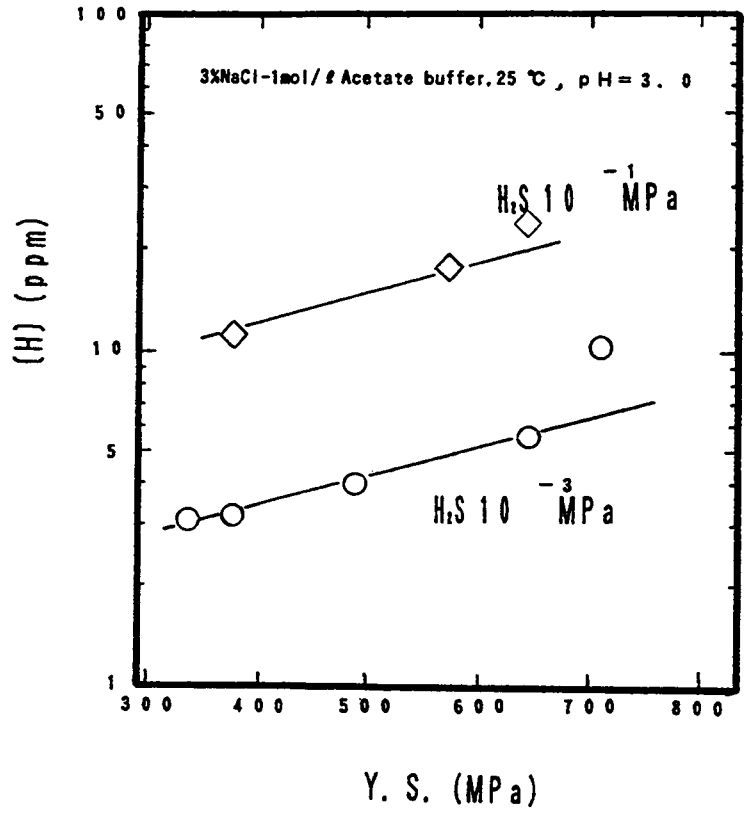


Figure 8 Effect of yield strength and H_2S partial pressure on hydrogen uptake

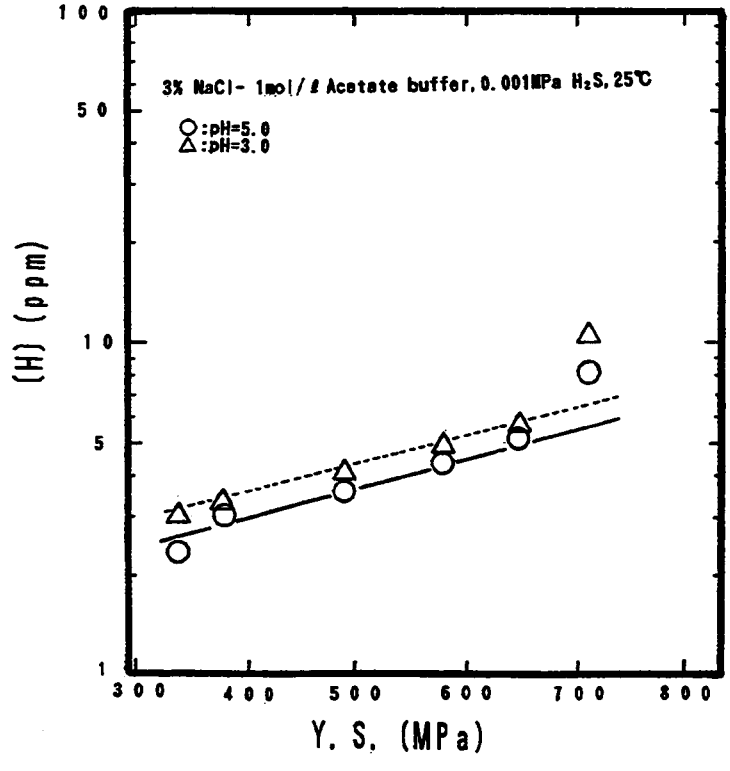


Figure 9 Effect of yield strength and pH on hydrogen uptake

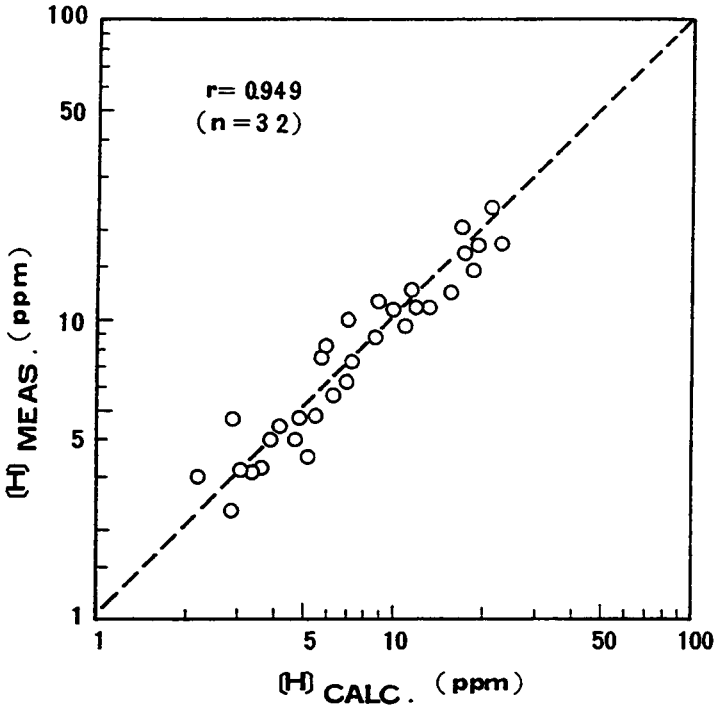


Figure 10 Relation between calculated hydrogen uptake and measured one

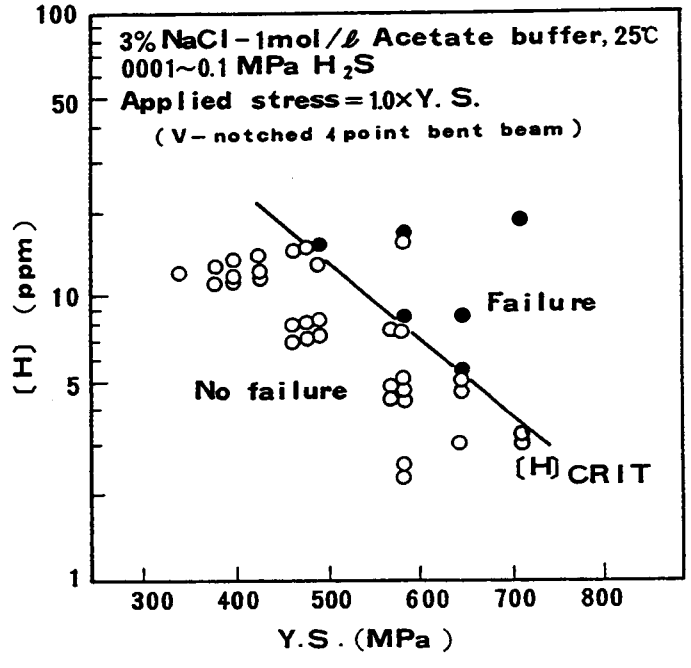


Figure 11 Plots of SSC susceptibility as a function of yield strength and hydrogen uptake

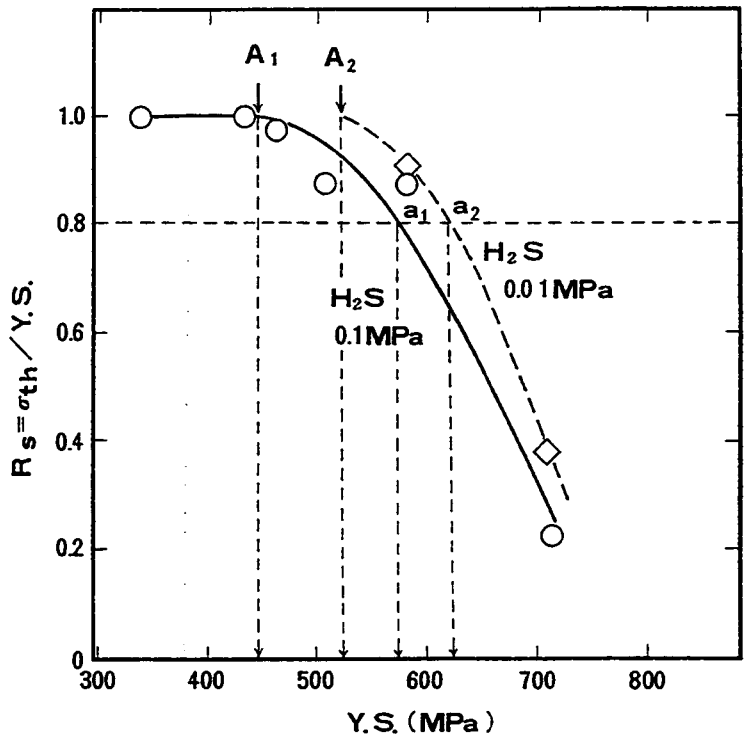


Figure 12 NACE tensile test results

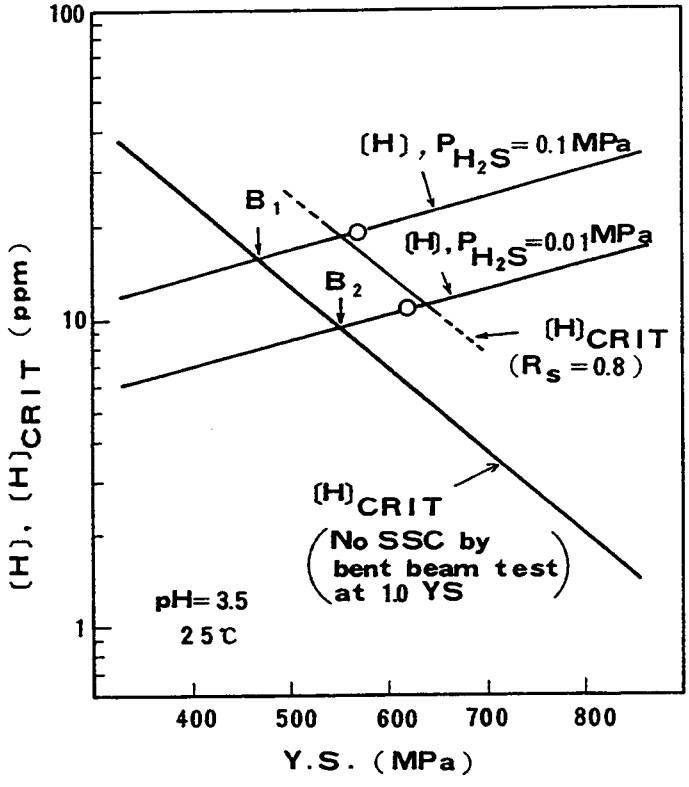


Figure 13 Effect of yield strength on hydrogen uptake and critical hydrogen content based on the criterion of no SSC by V-notched bent beam test at stress application of 100% yield strength or R_s value of 0.8 by NACE tensile test

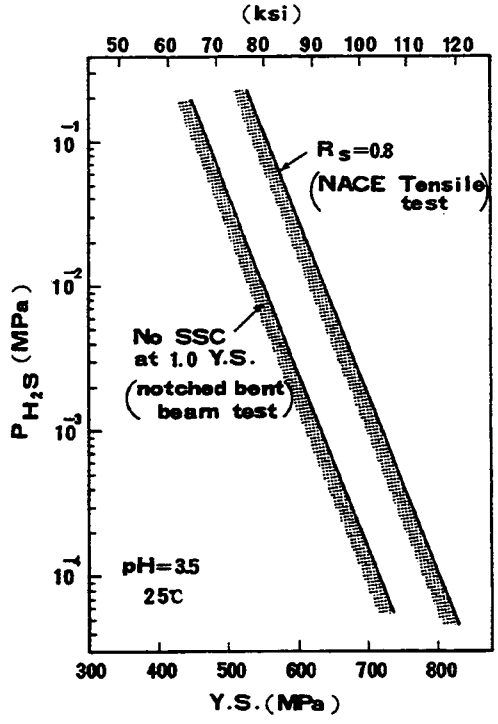


Figure 14 Estimation results of allowable partial pressure of H_2S as a function of yield strength

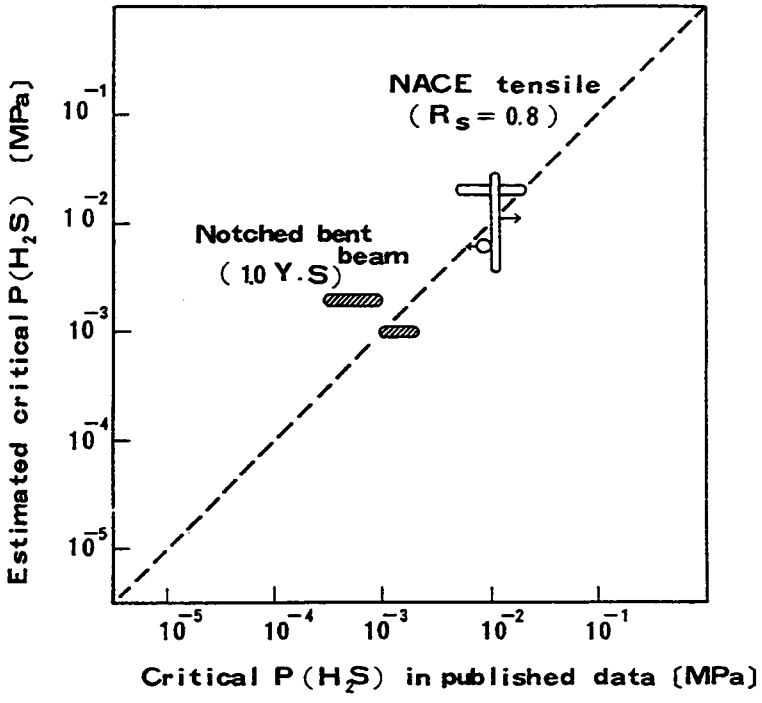


Figure 15 Comparison of estimated critical H_2S partial pressure with published data

Copyrighted Materials
Copyright © 1996 NACE International Retrieved from www.knovel.com

NIPPON KOKAN TECHNICAL REPORT
Overseas No. 46 (1986)

Development of Corrosion Resistant OCTG and its Application to Corrosive Wells

Masayuki Tanimura*

Drilling activity of deep sour oil and gas well has increased sharply in resent years, and use of corrosion resistant OCTG is increasing.

We have classified oil and gas wells according to corrosion environments, and studied on the effects of metallurgical factors on corrosion resistance.

Based on the experimental results, we have developed NK AC series for H_2S corrosion, NK CR series for CO_2 corrosion and NK NIC series for H_2S-CO_2 corrosion.

This report presents an outline of corrosion properties and applied conditions of these OCTG.

1. Introduction

With the oil shock as its opportunity, the development of oil and natural gas fields severe in natural environment and corrosive environment as well as the secondary and tertiary oil recovery have been executed actively to cope up with the escalation in oil and natural gas pricings and to secure the energy resources. In the meanwhile, there appeared some examples where corrosion resistant alloys of high cost are employed in the OCTGs (oil country tubular goods) in the development of oil and gas fields severe in corrosion or the secondary and tertiary recoveries.

In general, the economy in the development of oil and natural gas fields depends extensively on the selection of adequate materials and countermoves to prevent corrosion. For the development of oil and natural gas fields severe in corrosion, the method of using corrosion inhibitors or surface treated pipes is also being studied without having a recourse on the corrosion resistant materials that are high in cost, but in many cases, they are not always considered appropriate from the limit of their effectiveness or the economical problems.

The corrosion problems in oil and natural gas wells attribute to the chlorides (to be abbreviated as "Cl" hereinafter), H_2S and CO_2 that are contained within the oil and natural gas, and can roughly be classified into the H_2S corrosion, the CO_2 corrosion and the mixture corrosion of H_2S and CO_2. Especially, the need for deeper drilling wells leads to the rise in temperature, which makes the corrosion severer. NKK has emphatically executed the development and research of OCTGs resistant to these corrosion problems. In this report, the corrosive environments of oil and natural gas fields are orderly arranged, and based on it, NKK's corrosion resistant OCTGs and the range of their application to wells are being described herein.

2. The environmental conditions of wells and the evaluation of corrosion resistance

Some important factors out of the environmental conditions of wells influencing the corrosion of OCTGs are as cited under[1].

(a) Ratio between oil and water.
(b) Corrosive substances such as H_2S, CO_2, O_2, Cl plus organic acids within water.
(c) Temperature
(d) Bacteria
(e) Stress

The natural gas well causes a severer corrosion than oil well because the preventive effect to corrosion due to oil film can not be expected. Generally such factors as H_2S, CO_2 and Cl that are corrosive substances, plus temperature and stress are used for selecting the adequate materials for OCTGs. According to the NACE standard MR-01-75, the gas well whose H_2S partial pressure exceeds the level of 0.0035 atm has danger of causing a stress corrosion cracking due to H_2S, and hence is defined as a sour well, thus being discriminated from the sweet well with a low H_2S partial pressure. The CO_2 corrosion is caused to appear even with the sweet well if there exists the CO_2. From the aspect of materials for OCTGs, the corrosive property of well can be sub-

Reprinted with permission of Nippon Kokan

*Manager (Dr.), Alloy Development Lab., No. 2 Materials Research Dept., Technical Research Center

divided into the following three kinds by environment.

(1) A well mainly containing H_2S with temperature level lower than 100°C... A well of H_2S corrosion (212°F)

Due to the formation of FeS film by H_2S, the general corrosion is rather of small scale, so a carbon steel or a low alloy steel can be used. However, the H_2S is problematic since there may appear the stress corrosion cracking if the H_2S coexists with the stress. For the appearance of stress corrosion cracking, the strength and stress of OCTG are important factors in addition to the H_2S partial pressure and temperature conditions of well.

(2) A well mainly containing CO_2 with temperature level higher than 60°C... A well of CO_2 corrosion (140°F)

The accident examples where a local corrosion was caused to appear on OCTG because of CO_2 have been reported since about 40 years ago[2]. The principal factors influencing on the CO_2 corrosion are CO_2 partial pressure, Cl concentration and temperature. Since Cr is the alloying element which enhances the resistance against CO_2 corrosion, the high Cr steels such as martensitic stainless steels and duplex stainless steels are economically applicable steel grades. The 18% Cr-8% Ni, austenitic stainless steel has a fear of causing the stress corrosion cracking to appear due to Cl.

(3) A well where H_2S coexists with CO_2 with temperature level higher than 60°C... A well of H_2S-CO_2 corrosion

The natural gas field discovered in the Southern area in USA covers the extremely deep wells containing a plenty of H_2S and CO_2. The H_2S functions not only to promote the local corrosion due to CO_2 but also to cause the stress corrosion cracking due to H_2S and Cl. The corrosive property of a well may vary with the H_2S partial pressure and the temperature condition, but the high Ni austenitic materials are considered economical OCTGs from the view point of stress corrosion cracking.

Beside these environmental conditions of well, the influence of material conditions should be taken into account to understand the corrosion properties of OCTGs. In other words, the mechanical properties such as strength, ductility and toughness required for OCTGs as fundamental chracteristics must be satisfied. The OCTGs of high strength are required from the need for deeper wells and reduction in material cost. Generally, the OCTG made of carbon steel or low alloy steel can be strengthened by heat treatment, but in case of the OCTG made of duplex stainless steel or high Ni austenitic steel, it is necessary to take into consideration the influence of cold working or the influence of aging when exposed to a well temperature because the said material is strengthened by cold working after the step of heat treatment.

The evaluation items for the corrosive property of OCTG are as cited under: In addition to the stress corrosion cracking due to H_2S and Cl general corrosion, pitting corrosion, crevice corrosion, intergranular corrosion, along with the hydrogen embrittlement cracking due to galvanic corrosion, it is necessary to consider also the characteristics against heavy brine and acidizing.

While tracing up the historical process of the development of corrosion resistant OCTGs, Paragraph 3 introduces the concept of alloy design as to the corrosion resistant OCTGs of NKK and also the scope of application of these products to wells.

3. Corrosive environment of wells and corrosion resistant OCTGs

3.1 The H_2S corrosive wells

The failure accidents of OCTGs that happened mainly with the sour gas wells in USA, Canada and France in the beginning of 1950s gave a considerable shock to the development of sour oil and natural gas fields, but it was made clear that the cause for the failure was the stress corrosion cracking due to H_2S and that strength and hardness of OCTG greatly influenced the sensitivity to cracking. For this reason, the OCTG for sour wells was selected in view of the hardness of OCTG. Upon the basis of these usage actual showings, the C75 grade and the L80 grade were established in the API specification in the years of 1965 and 1975 respectively. NKK not only carried out the production study of these OCTGs meeting the API specification but also produced and delivered the 2% Cr-Mo-V-Al steel, EL tubings in 1967 that have the actual usage record in the Lacq gas field well known for its sour gas in France.

The study of stress corrosion cracking due to H_2S can roughly be classified into the study for evaluating the sensitivity of OCTG to stress corrosion cracking and the development of OCTG resistant to stress corrosion cracking. As to the former study, NKK also took a part in the joint study with NACE T-1F-13 Task Group on the stress corrosion cracking test method that was started from the year of 1972 and contributed to the establishment of NACE standard TM-01-77 that is the testing method using a round bar tensile specimen[3]. Because some oil companies adopt the test method using the Shell Bent Beam specimen or the DCB specimen apart from this testing method, NKK carried out the test of confirming the reproducibility of testing method jointly with the associated companies and thus set up the testing method and the evaluation standard for stress corrosion cracking. The latter research led to the study on the influence of strength, chemical composition, microstructure and non-metalic inclusions of OCTG against the stress corrosion cracking, which was put into practical application in development of the OCTGs resistant to stress corrosion cracking. The characteristic research results are shown in *Fig. 1* and *Fig. 2*. *Fig. 1* shows the relation between the hardness after tempering the AISI 4130 steel when changing the microstructure under varied quenching conditions and the threshold stress value of stress corrosion

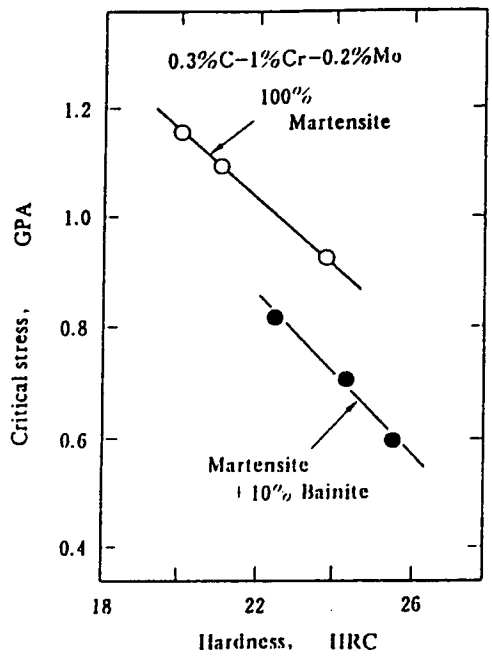


Fig. 1 Effect of microstructure on stress corrosion cracking due to H_2S.

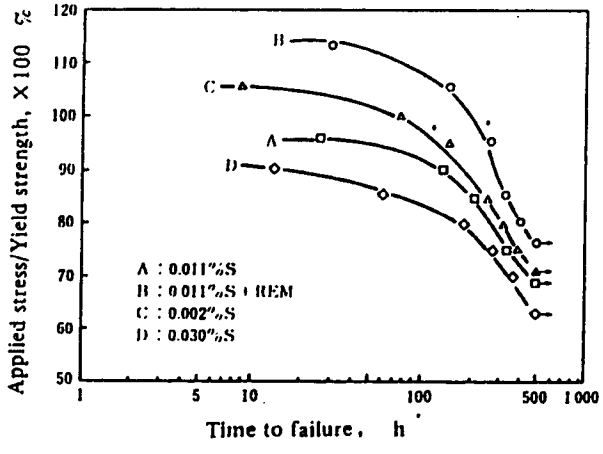


Fig. 2 Effect of S content on stress corrosion cracking due to H_2S.

cracking by means of the Shell Bend Beam method. The tempered martensite structure that has been tempered after perfectly hardened proves to provide a considerable resistance against the stress corrosion cracking[4]. In order to obtain a favorable microstructure, NKK's quenching equipment adopts the method of quenching both the inner and outer surfaces of steel pipes simultaneously. *Fig. 2* shows the test result where the sulfide inclusion was noticed as the initiation site of stress corrosion cracking, indicating the influence of S content and inclusion shape control of 0.3%C-1.3%Mn steel on the stress corrosion cracking[5]. The extremely low S content and the shape control of inclusion prove to be the method effective for improving the resistance against stress corrosion cracking. NKK applied this research result to the production of OCTGs resistant to stress corrosion cracking and played a pioneering role in the alloy design of OCTGs.

In the development of deeper sour natural gas fields discovered in the latter half of 1960s, there appeared the need for C90 grade OCTG having higher strength and higher stress corrosion cracking resistance than C75 and L80 grades in API specification. By revising the chemical composition from C-Mn type to Cr-Mo type and further adopting the said result, NKK succeeded in developing the AC90 and AC95 for the high strength OCTGs. With the advent of 1980s, there has appeared the need for higher stress corrosion cracking resistance than AC90 and AC95. For this reason, the study of reviewing in wider scope the influence of chemical compositions and nonmetalic inclusions on stress corrosion cracking was carried out. The typical results are given in *Fig. 3* and *Photo 1*. *Fig. 3* shows the result of having investigated the influence of Mo in the 0.25% C-1% Cr steel and the 0.3% C-1% Cr steel adopting the Shell Bent Beam testing method, from which it can be known that the increase of Mo serves to improve the resistance to stress corrosion cracking[4]. *Photo 1*, on the other hand, shows the fact that the presence of TiN inclusion, if any, causes to appear the stress corrosion cracking from TiN itself or its interface and proves hazardous. Based on these results, NKK developed the AC90M and AC95M OCTGs that have more favorable resistance to stress corrosion cracking than

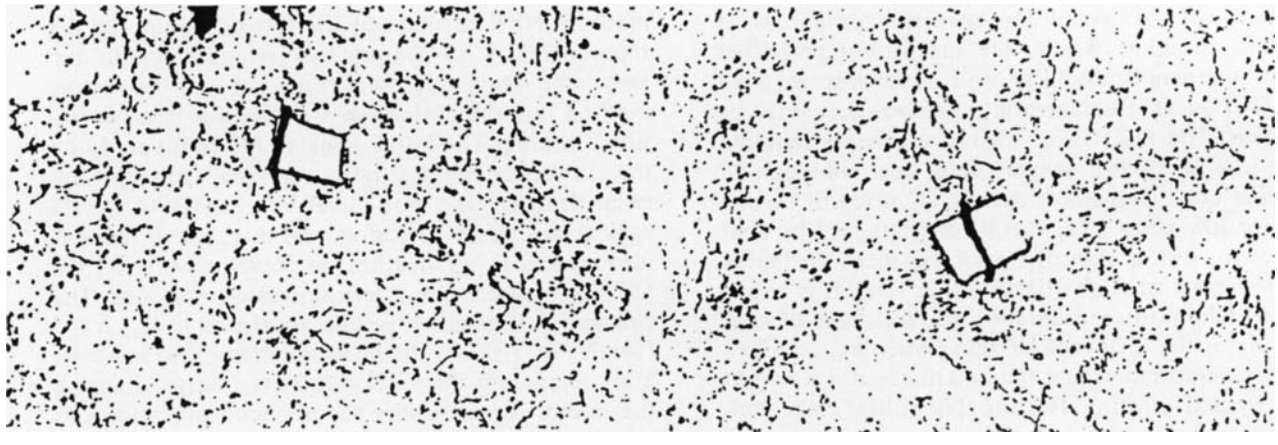


Photo 1 Formation of crack at TiN inclusion.

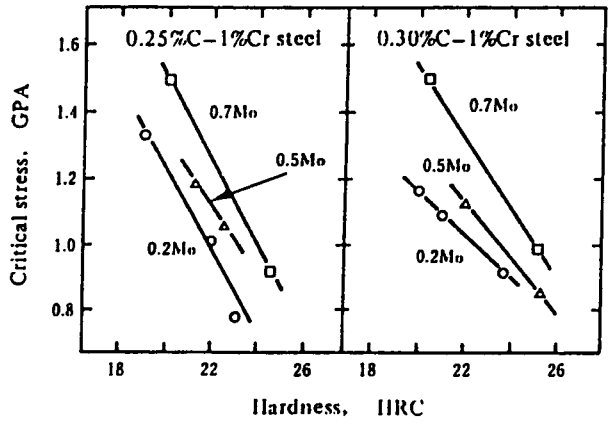


Fig. 3 Effect of Mo content on stress corrosion cracking due to H_2S.

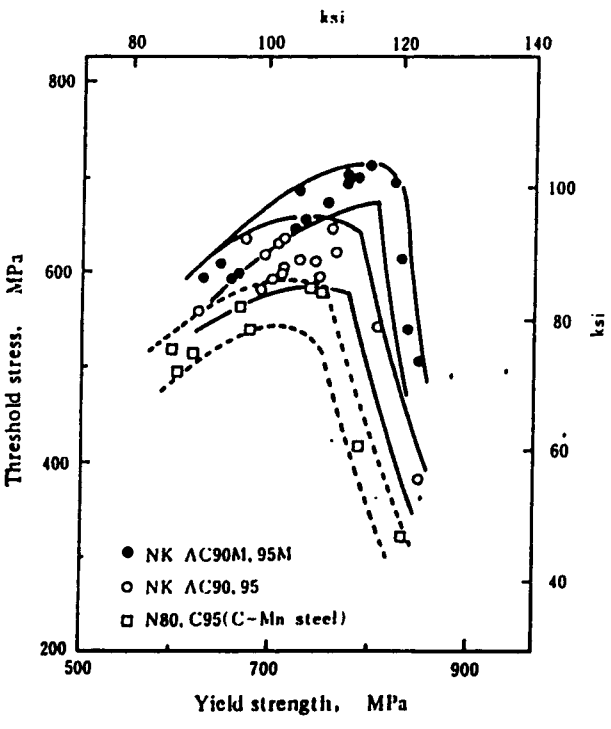


Fig. 4 Threshold stress for the NACE TM-01-77 test method conducted on NK AC, NK ACM and C-Mn steel.

the AC90 and AC95. *Fig. 4* shows the result of comparing the stress corrosion cracking characteristics measured by NACE TM-01-77 on conventional C-Mn steel, AC90 and 95 steel, and AC90M and 95M steel[4]. The AC90 and 95 steels have a higher threshold stress of stress corrosion cracking on the higher strength side as compared with the C-Mn steel. What's more, that for AC90M and 95M systems have a still higher stress. Though the C90 grade was established in the API specification of 1984 version and the provision was given to the threshold stress of NACE TM-01-77 test, even the AC90 and 95 steels prove to be the OCTGs that can well satisfy the requirements in the specification. These OCTGs passed the quality guarantee tests at majour petroleum companies in USA, and their excellent properties are recognized among them, and have a great deal of production actual showings to data.

On the other hand, the need for the OCTGs high in collapse strength and still more excellent in stress corrosion cracking resistance is increasing. Higher the strength, higher becomes the collapse strength, but a higher strength increases the sensitivity to the stress corrosion cracking, so the steel pipe of low strength is desirous. For this reason, the development of the OCTG enhanced both in characteristics of collapse strength and stress corrosion cracking resistance has been considered difficult. For upgrading the collapse strength of steel pipes, NKK adopted the hot straightening technique of post heat treatment, and has produced the OCTGs higher in collapse strength than the worldwide standards. Consequently, the AC80T OCTG featuring the high collapse strength and stress corrosion cracking resistance by putting this technique in practical application has been developed, which attracts attention from leading petroleum companies.

The principal codes of NKK for the low alloy steel OCTGs durable to the H_2S corrosion are summarized in *Table 1*.

3.2 CO_2 corrosive wells

The accident examples of local corrosion of OCTGs due to CO_2 have been reported since many years ago[2], and the API subdivided the degree of

Table 1 Chemical composition and mechanical properties of NK AC series for H_2S corrosion.

	Chemical composition %							Mechanical property		
	C	Si	Mn	P	S	Cr	Mo	Y.S MPa	T.S MPa	Hardness HRC
NK AC 85	≤0.30	≤0.35	≤0.75	≤0.030	≤0.005	0.85	≤0.30	586/689	≥689	≤23
NK AC 90	≤0.35	≤0.35	≤0.75	≤0.030	≤0.005	1.00	≤0.40	620/724	≥710	≤24
NK AC 90 M	≤0.35	≤0.35	≤0.75	≤0.030	≤0.005	1.00	≤0.80			
NK AC 95	≤0.35	≤0.35	≤0.75	≤0.030	≤0.005	1.00	≤0.40	655/758	≥724	≤25
NK AC 95 M	≤0.35	≤0.35	≤0.75	≤0.030	≤0.005	1.00	≤0.80			
NK AC 80 T	≤0.30	≤0.35	≤1.60	≤0.030	≤0.015	–	–	551/655	≥689	≤22

El : In accordance with API Spec.

Table 2 Chemical composition of NK CR series for CO_2 corrosion, %.

	C	Si	Mn	P	S	Cr	Mo	Ni	N
NK CR 9	≤0.22	≤1.0	≤1.0	≤0.025	≤0.005	9	1	–	–
NK CR 13	≤0.22	≤1.0	≤1.0	≤0.025	≤0.005	13	–	–	–
NK CR 22	≤0.03	≤1.0	≤2.0	≤0.030	≤0.005	22	3	5.5	0.15
NK CR 25	≤0.03	≤1.0	≤2.0	≤0.030	≤0.005	25	3	7	0.15

corrosion by CO_2 partial pressure based on experiences into three kinds and has been urging the attention against the CO_2 corrosion of OCTGs.

(1) The corrosive property appears when the CO_2 partial pressure exceeds the level of 2.1 atm.

(2) The corrosive property does not appear when the CO_2 partial pressure is lower than 0.5 atm.

(3) There is a probability for corrosion when the CO_2 partial pressure is at the middle.

This similar conception is adopted by a number of petroleum companies though a more or less difference is recognized in the numerical values of CO_2 partial pressure. Where the environments of a well involves a danger of causing the CO_2 corrosion, the prevention of corrosion is made generally using the corrosion inhibitors. When viewing the CO_2 corrosion from the aspect of materials on the other hand, it is widely known that Cr stands for the alloy element to enhance the corrosion resistance. As a matter of fact, in developing the Ellenburger natural gas field containing some 50% CO_2 in 1957 the on-site test was carried out for selecting the adequate materials, and it was clarified that the steel containing Cr at 9% or above was necessary from the viewpoint of corrosion resistance[6]. Consequently, the 9 to 13% Cr steels have been used for the components where the effect of corrosion inhibitor can not be expected conventionally.

In the European natural gas fields since 1970; the OCTGs made of 9% or 13% Cr martensitic stainless steel or of 22% Cr, duplex stainless steel have been used for prevention of CO_2 corrosion. The duplex stainless steel was adopted because, due to the rise in well temperature, the 9% and 13% Cr steels have insufficient corrosion resistance and because the 18% Cr-8% Ni, austenitic steel has a danger for stress corrosion cracking due to Cl. With the reference being made to the actual usage showings in Europe, this grade of steel pipes has been used widely to the CO_2 corrosive wells in USA as well. What needs to be cared about in the CO_2 corrosive wells is the need for considering the corrosion due to H_2S,especially the stress corrosion cracking since almost all the wells contain a small amount of H_2S.

With special attention paid to the OCTG made of high Cr stainless steel being used for the CO_2 corrosive wells, NKK has started the research and development for this kind of OCTG since 1979. *Table 2* and *Table 3* shows the principal codes of NKK's high Cr OCTGs. The CR9 and CR13 as well as the CR22-65 grade plus CR25 are the steels that are just heat treated, whereas the high grade of CR22 is given the cold work after heat treatment. *Photo 2* illustrates

Table 3 Grade and mechanical properties of NK CR series.

	Grade	Y.S MPa	T.S MPa	El %	Hardness HRC
CR 9	80	551/655	≥689		≤23
CR 13	85	586/689	≥724		≤24
	95	655/758	≥758		–
CR 22	65	448/586	≥655	API formula	18/23
	110	758/896	≥862		26/32
	125	862/1 000	≥931		28/36
	140	965/1 103	≥1 000		29/37
CR 25	80	551/689	≥689		20/26

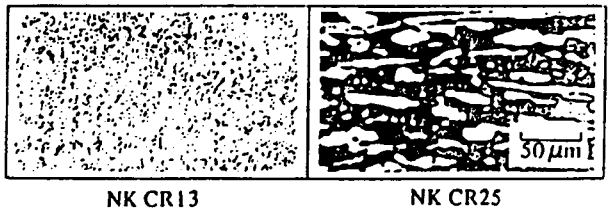


Photo 2 Microstructure of CR13 and CR22.

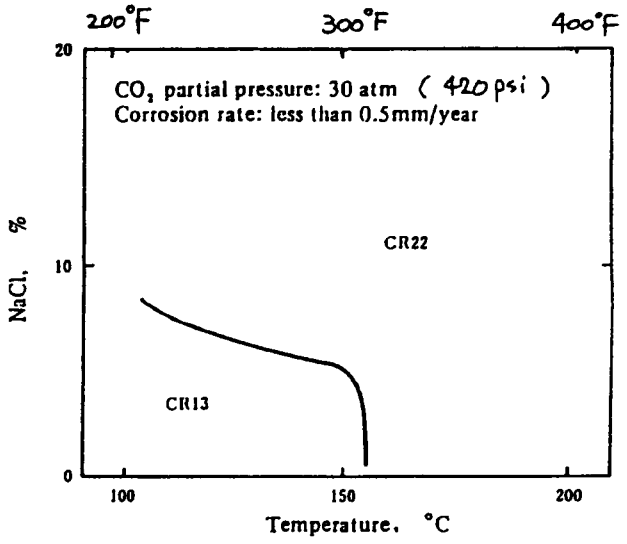


Fig. 5 Material selection under condition of CO_2 corrosion.

the microstructure of typical CR13 and CR22. The CR13 is the fine tempered martensite structure while the CR22 is the duplex structure consisting of some 50% austenite and some 50% ferrite. As the Cr content increases, higher becomes the corrosion resist-

ance against the CO_2 corrosion, and the examples of applicable well conditions from the viewpoint of the CO_2 corrosion are shown in *Fig. 5*[7]. This *Fig. 5* is the example that has been prepared on the basis of test result conducted in the laboratory. The CR13 is suitable in case of the well temperature lower than 150°C while the CR22 is suited to the temperature higher than that. The CR9 does not differ so much from the CR13 pricewisely, but its working temperature will be around 100°C or lower, so it is difficult to consider it as a characteristic OCTG. However, some petroleum companies prefer the adoption of CR9 to the other kinds.

The keypoints of the contents of study that has been carried out in commercializing the high Cr OCTGs in *Table 2* are being described in terms of the martensitic steels and the duplex stainless steels respectively.

3.2.1 Martensitic stainless steels

Conventionally, the steels belonging to this category covers the 9% Cr-1% Mo steel and the AISI 410, 13% Cr steel, and are used also for the parts of well. In the comparison of these two steels, it has been said that the 13% Cr steel is more excellent in the CO_2 corrosion resistance while the 9% Cr-1% Mo steel has a higher resistance against the stress corrosion cracking due to H_2S. Noticing the 13% Cr steels excellent in the resistance to CO_2 corrosion, NKK decided to improve the resistance against stress corrosion cracking of this steel. As a result of studying the influence of metallurgical factors being given on the stress corrosion cracking of 13% Cr steel, it was made clear that the effect of microstructure is considerable and that the alloy composition has its influence through the microstructure[8]. The result where the threshold stress of stress corrosion cracking obtained through the testing method of NACE TM-01-77 has been arranged orderly by the C-content of test material is shown in *Fig. 6*. Like the case of a low alloy steel described in 3.1, its threshold stress decreases more as the strength increases. When the comparison is made with the level of yield strength being around 600 MPa, higher becomes the threshold stress as the C content among AISI 420 steels becomes higher in addition to the fact that the AISI 420 steel has a higher threshold stress than the AISI 410 steel. Studying this result from the microstructure of test material, it can be known that the AISI 410 steel presents the tempered martensite structure containing a bit of δ ferrite and must adopt a lower tempering temperature for obtaining the same level of strength, and thus the recovery of hardened structure is insufficient. On the other hand, the AISI 420 steel presents a tempered martensite simplex structure, but the low C steel presents coarser crystal grains than the high C steel does. Because, in general, the stress corrosion cracking resistance depends on the crystal grain size, it can be imagined that the high C steel of finer grains showed a higher threshold stress. From the result of this study, it can be hinted that the adoption of finer tempered martensite structure is able to enhance the stress corrosion cracking resistance for the 13% Cr steel. The chemical composition and the heat treatment for NK CR 13 have been set up from the point of view as mentioned above.

The 9% Cr-1% Mo steel or the 13% Cr steel has a greater sensitivity to stress corrosion cracking as compared with the low alloy steel for use in H_2S corrosive wells, so its application to sour wells is restricted. For this reason in order to clarify the applicable range of NK CR13 to the sour wells, NKK pursued the relation between the H_2S partial pressure and the stress required for stress corrosion cracking due to H_2S. *Fig. 7* shows the test result of stress

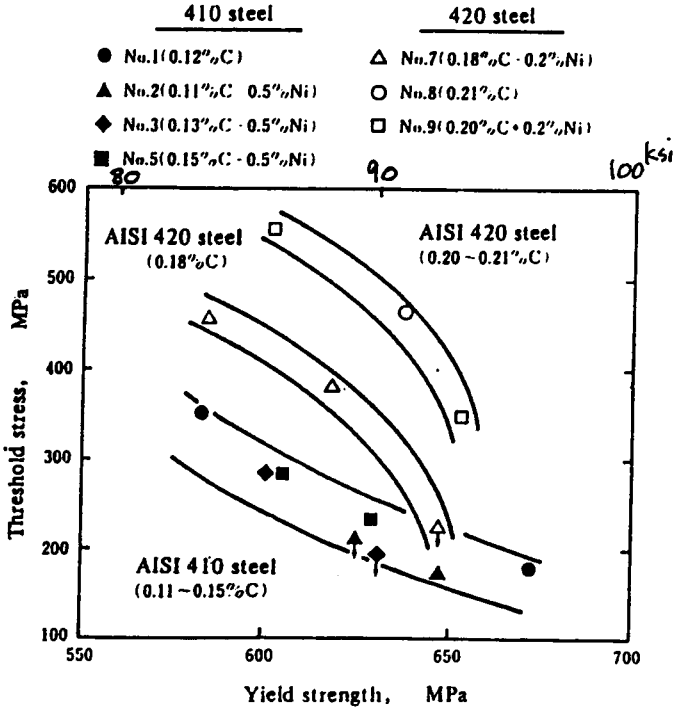


Fig. 6 Threshold stresses of various 13% Cr steels by NACE TM-01-77 test method.

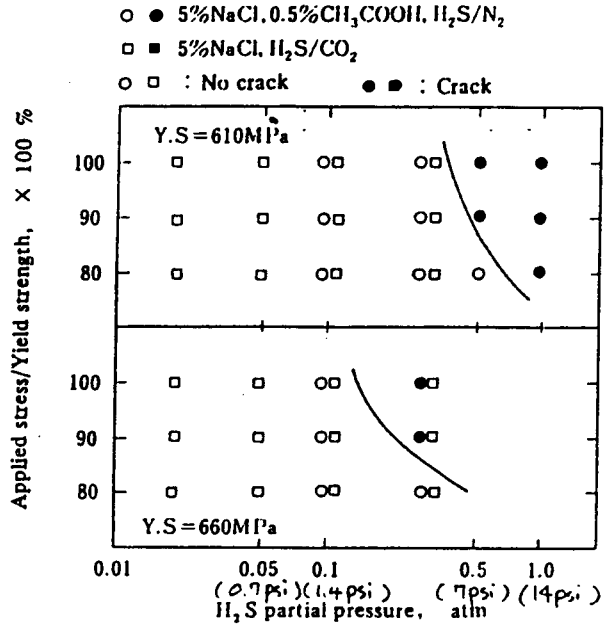


Fig. 7 Effect of H_2S partial pressure on stress corrosion cracking of CR 13.

corrosion cracking under a low H_2S partial pressure using C ring specimens[9]. Because of the tempered martensite structure, the cracking is likely to appear with a lower pH value of test solution, namely in the 5% NaCl + 0.5% acetic acid solution system. So, when the judgement is made under this condition, there is a less danger for causing the stress corrosion cracking in case of the H_2S partial pressure lower than 0.1 atm.

The NK CR13 is being produced and delivered to various foreign countries including the domestic market, but there is Chevron's natural gas field at Tuscaloosa Trend as the well that is noticed for the use of 13% Cr steel OCTG[10]. This well has the environment conditions of 8% CO_2, 20 to 30 ppm H_2S, 3.8% Cl, bottom hole pressure of 1 000 atm and bottom hole temperature of 190°C and stands for a sour gas well. The H_2S partial pressure is at around 0.03 atm and within the safety region against the stress corrosion cracking as known from *Fig. 7*. The bottom hole temperature, on the other hand, exceeds a bit the line of applicable range that is shown in *Fig. 5*, but even today when more than 2 years has passed since its installation no abnormality has been reported thus far. NKK delivered to this well about 320 tons of NK CR13 85 grade. The mechanical test result at Chevron showed that the mechanical properties had been controlled narrow range as given below and was highly reputed.

- Yield point: 589 to 615 MPa. Mean value at 603 MPa.
- Tensile strength: 745 to 786 MPa. Mean value at 765 MPa.
- Hardness: HRC 20.6. to 22.0 Mean value at HRC 21.1.

3.2.2 Duplex stainless steels

As the temperature of CO_2 corrosive well becomes higher, the martensitic stainless steel fails to satisfy the required corrosion resistance which needs the use of the steel of higher Cr content. Since the austenitic stainless steel of 18% Cr-8% Ni has a danger of causing the stress corrosion cracking due to Cl, the stainless steel having the duplex structures of austenite and ferrite which is favorable in the corrosion resistance and the stress corrosion cracking due to Cl is attracting the attention. This steel has a problematic aspect in strength as use for OCTGs in the state as it is heat treated, so its strength is intensified usually by cold working.

NKK also took up the duplex stainless steel as the OCTG having the corrosion resistance in excess of that offered by the 13% Cr steel, and conducted a variety of studies necessary for the alloy design. *Fig. 8* presents the result where various corrosion test results are shown in the relation between the main components, Cr and Ni contents[11]. The influence of metallurgical factors on general corrosion, pitting corrosion and intergranular corrosion has been summarized to one trend since these corrosions are likely to show almost the same inclination. In other words, the corrosion resistance varies with the ratio between austenite phase and ferrite phase, and the range of 40 to 70% ferrite phase indicates the favorable corrosion resistance. In addition, suppose the

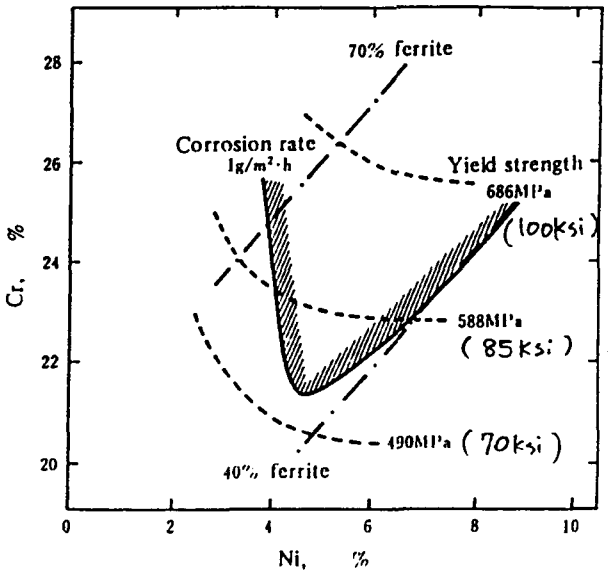


Fig. 8 Effect of Cr and Ni content on corrosion properties, yield strength and ferrite content of duplex stainless steels.

(1.1 mm/y = 43.5 mil/y)

corrosion rate at lower than 1 $g/m^2 \cdot h$, then it proves the upper side than the curve shown by the solid line. For this reason, the hatched region in the figure proves to be the adequate Cr and Ni contents. The alloy elements such as Mo, N, etc. other than Cr and Ni function to enhance the corrosion resistance[11]. Generally, the pitting corrosion resistance is expressed by the pitting index PI = Cr + 3Mo + 16N, and NKK's test results can also be put in order by this formula, requiring to make the PI more than some 30%. Since the resistance against the stress corrosion cracking due to Cl is proportioned approximately to the yield strength of steel, the resistance can be estimated with use of the yield strength[11].

Based on the aforementioned test result, the chemical composition in *Table 2* has been set up, but the stress corrosion cracking tends to be caused when there exists H_2S. As to the mechanism of stress corrosion cracking, the hydrogen being caused to appear due to the H_2S corrosion is estimated to be the cause for cracking since the cracking is likely to happen at the temperature level lower than 100°C, and as a result of observing the fracture surfaces, the characteristics of hydrogen embrittlement cracking are recognized on the ferrite phase, and since the sensitivity to cracking is enlarged by the cathodic polarization[12]. From the practical viewpoint, the H_2S partial pressure for causing the stress corrosion cracking has been looked after by the C-ring specimen. The test result is given in *Fig. 9*. Using the materials of three kinds of strength as to both the steels of CR22 and CR25 respectively, the test was conducted in the 5% NaCl water saturated with the mixed gas of H_2S and CO_2. The stress corrosion cracking is caused to appear at the H_2S partial pressure of 0.1 atm or above in case of a low strength material, and at the pressure of 0.05 atm or above in case of a high strength material, so tends to appear more easily than the case of CR13, and the threshold H_2S partial pressure needs to be set at a lower level.

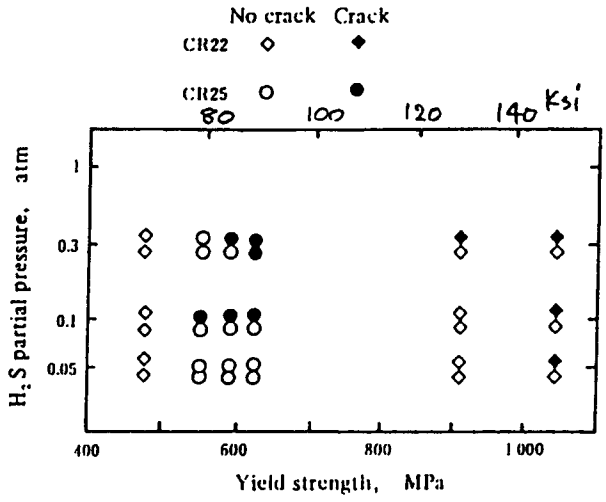


Fig. 9 Effects of H_2S partial pressure and yield strength on stress corrosion cracking of CR 22 and CR 25.

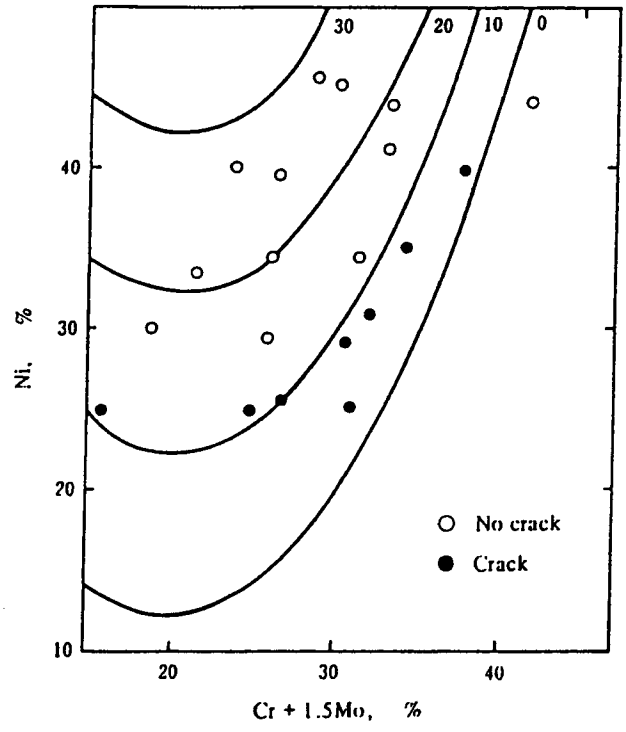


Fig. 10 Effects of Cr, Mo and Ni contents on stress corrosion cracking of Ni alloys due to $MgCl_2$.

3.3 H_2S-CO_2 corrosive wells

It is necessary to develop the OCTGs resistant to the H_2S-CO_2 corrosion because many oil and natural gas fields contain H_2S. In the development of deeper natural gas fields with H_2S of some 45%, CO_2 of some 10% and bottom hole temperature of around 200°C from the end of 1960 upto the first half of 1970s, the study was carried out for selecting the adequate OCTGs, and it is reported that the Ni, Co and Ti alloys are the most competent candidates[13]. NKK is of the view that this natural gas well is an example of extremely severe corrpsive well and estimates that most of wells have lower H_2S and temperature levels. This is the region difficult to apply the martensitic and duplex stainless steels even if the H_2S and temperature of well are rather low, and NKK understands that the OCTG needs to be developed in consideration of the corrosion conditions and economy of well. Thus, noticing Ni alloys, NKK examined the influence of metallurgical factors on the corrosion resistance and the stress corrosion cracking resistance. It was confirmed that the pitting index PI quoted in Paragraph 3.2.2 is applicable to the pitting corrosion resistance which is better as this value is higher[14], and further that intergranular corrosion depends on C-content and heat treatment conditions and carbides should not be allowed to be precipitated in order to increase the resistivity. The test result of stress corrosion cracking due to $MgCl_2$ is shown in *Fig. 10*[15]. The result is illustrated in the relation between the principal alloy elements such as Cr, Mo and Ni and the sensitivity to stress corrosion cracking. It was reported conventionally that the material containing Ni at more than 45% would not allow the stress corrosion cracking to appear[16], but the stress corrosion cracking will not be caused to appear even under the value lower than that so long as Cr and Mo are at adequate contents, and there is also the range where it is difficult to judge the sensitivity to cracking simply with the Ni content. Respective curves in the figure indicate the contour lines of stability "Δ" of austenite structures according to the following formula[17]:

$$\Delta = \mathrm{Ni} - \left[\frac{(\mathrm{Cr} + 1.5\mathrm{Mo} - 20)^2}{12} - 0.5\mathrm{Mn} - 35\mathrm{C} - \mathrm{Cu} - 27\mathrm{N} + 15 \right]$$

It has been clarified that the sensitivity to stress corrosion cracking due to $MgCl_2$ has something to do with the stability of austenite structure and that the alloy composition with the Δ higher than 10 does not have the sensitivity to cracking.

Fig. 11 shows the exmaple of test result of stress corrosion cracking when there exists H_2S[18]. This is the result when the H_2S has been changed to two levels of 1 atm and 10 atm where the test environment is at high Cl and high CO_2 partial pressures at temperature level of 250°C. The sensitivity to stress corrosion cracking at low H_2S partial pressure corresponds to the curve of "Δ" = 10 in *Fig. 10*, and shows approximately the same trend as the sensitivity to stress corrosion cracking due to $MgCl_2$. In case of high H_2S partial pressure, the stress corrosion cracking is likely to appear, requiring a further high structure stability. For this reason, as regards the stress corrosion cracking, its sensitivity to cracking can be estimated with the stability of austenite structure.

The Ni alloy OCTGs is reported to cause the hydrogen embrittlement cracking due to the galvanic corrosion when getting in touch with a low alloy steel[19]. NKK's research result can be summarized as given in *Fig. 12*, and it was made clear that the hydrogen embrittlement is caused to appear when the Ni content is more than 40% and its yield strength is higher than 1 000 MPa.

With the reference being made to the aforesaid

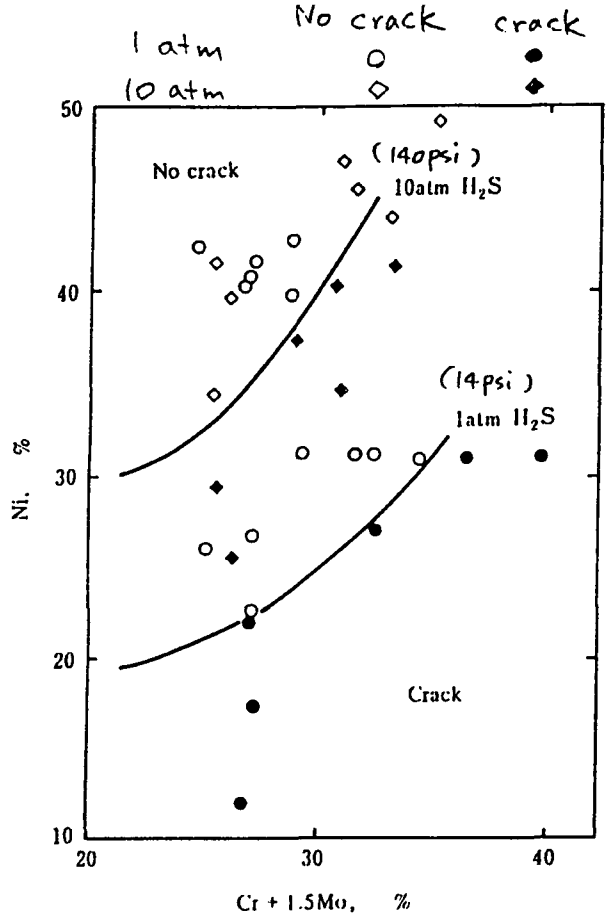


Fig. 11 Effect of Cr, Mo and Ni contents on stress corrosion cracking of Ni alloys due to H_2S-CO_2-Cl.

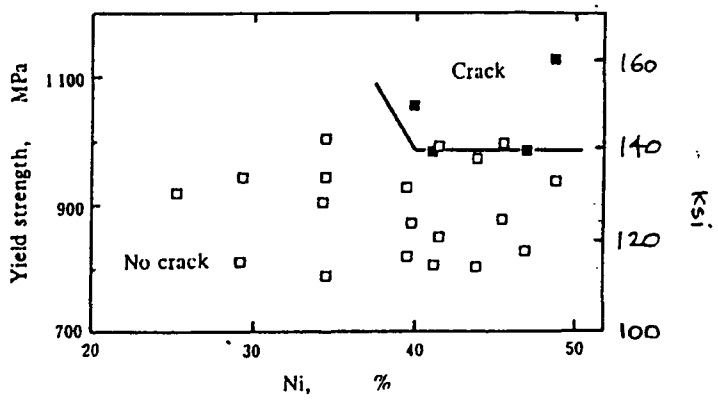


Fig. 12 Effect of Ni content and yield strength on hydrogen embrittlement cracking of Ni alloys.

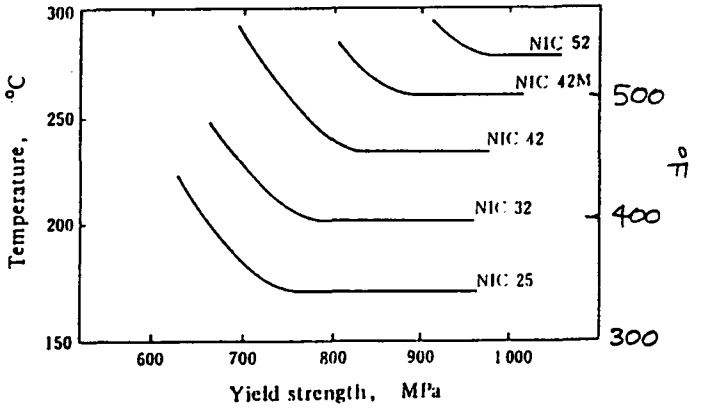


Fig. 13 Summary of resistance to stress corrosion cracking of NIC series OCTG.

Table 5 Grade and mechanical properties of NK NIC series.

	Grade	Y.S MPa	T.S MPa	El %	Hardness HRC
NK NIC 25	80	551/758	≥689	≥18	18/26
	110	758/931	≥793	≥15	24/32
	125	862/1 000	≥896	≥12	26/34
NK NIC 32	80	551/724	≥689	≥18	17/25
	110	758/896	≥793	≥16	22/30
	125	862/1 000	≥896	≥12	26/34
NK NIC 42	110	758/896	≥793	≥15	22/30
	125	862/1 000	≥896	≥12	26/34
NK NIC 42M	125	862/1 000	≥896	≥12	27/35
	135	931/1 069	≥965	≥10	28/36
NK NIC 52	125	862/1 000	≥931	≥12	27/35
	140	965/1 103	≥1000	≥10	29/37

research result, the Ni alloy OCTGs given in *Table 4* are being produced. *Table 5* shows the mechanical properties of these pipes, but are strengthened through application of cold working because these alloys are low in strength at as-heat treated conditions.

Since the cold worked pipes have a high sensitivity to stress corrosion cracking, the test of stress corrosion cracking was carried out under the environment of H_2S-CO_2-Cl from practical application viewpoint. *Fig. 13* indicates the relation between the yield strength of OCTGs and the critical temperature for the occurrence of stress corrosion cracking[18]. Each curve indicates the upper limit temperature where the

Table 4 Chemical composition of NK NIC series for H_2S-CO_2 corrosion, %.

	C	Si	Mn	P	S	Cr	Mo	Ni	Cu	Ti
NK NIC 25	≤0.03	≤0.5	≤1.0	≤0.030	≤0.005	22	3	25	–	–
NK NIC 32	≤0.03	≤0.5	≤1.0	≤0.030	≤0.005	22	4.5	32	–	–
NK NIC 42	≤0.03	≤0.5	≤1.0	≤0.030	≤0.005	22	3	42	1.8	0.9
NK NIC 42M	≤0.03	≤0.5	≤1.0	≤0.030	≤0.005	22	6	42	1.8	0.9
NK NIC 52	≤0.03	≤1.0	≤1.0	≤0.030	≤0.005	25	7	52	1.0	1.0

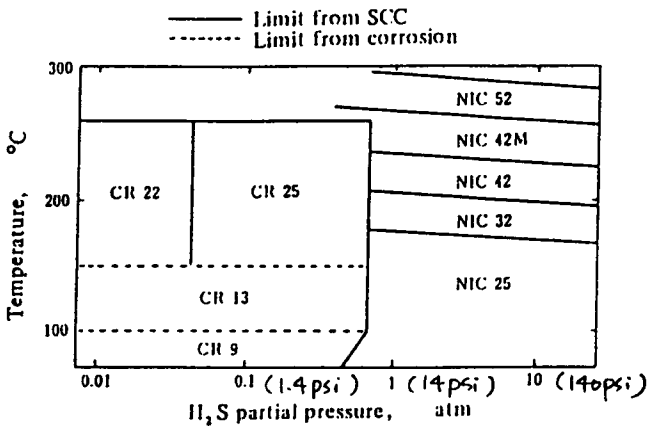


Fig. 14 Relationship between CR series and NIC series OCTG, and service condition.

stress corrosion cracking will not appear, and there is the need for using the OCTGs of higher Ni alloys as the well temperature is getting higher.

3.4 How to select the corrosion resistant OCTGs in view of the corrosive environment of well

The characteristics of low alloy steel system AC series, high Cr stainless steel system CR series and Ni alloy system NIC series have been discussed by classifying the corrosive environment conditions of well into the H_2S corrosion, the CO_2 corrosion and the H_2S-CO_2 corrosion, but practically, how to select the adequate OCTGs concretely in view of well conditions is important. Especially in case of CR series and NIC series, its selection is complicated. For this reason, NKK has prepared such a chart as shown in *Fig. 14* so as to select the corrosion resistant OCTGs in consideration of corrosive conditions of well[18]. This is the figure where the relation of H_2S partial pressure with temperature has been arranged in order upon the presumption that the CO_2 and Cl contents inside a well are sufficiently high, and is popularly utilized as the guide line for selecting the corrosion resistant OCTGs currently by many majour petroleum companies.

4. Summary

It is expected that the development of oil and natural gas fields severe in corrosive property is becoming increasingly popular, and that, following such a trend the need for corrosion resistant OCTGs will be increasing. NKK has produced the product of more than 10 000 tons even if they are restricted to the high Cr stainless steel, CR series and Ni alloy, NIC series. The study of counterplan other than material itself to prevent corrosion is also being carried out because the enhancement of corrosion resistance of OCTGs leads to the rise in pricing. Since the development of oil and natural gas fields needs to have the cost minimum concept as its premises even if any of these methods is to be adopted, it is necessary to execute the study for producing the corrosion resistant OCTGs at lowest possible attractive pricing level in addition to the study for enhancing the performance of OCTGs along the users' desire.

On the other hand, since the sealing performance of coupled sections becomes important in case of the oil and natural gas wells high in pressure and severe in corrosive property, the special threads need to be developed in parallel with the study of materials on corrosion resistant OCTGs. NKK has already succeeded in developing and producing NKEL, NK2SC and NK3SB. The details on special threads are to be reported at another opportunity.

What's more, there are many aspects whose explanation has not been made because the entirety of corrosion resistant OCTGs has been treated here in this report, but you are kindly asked to refer to the reference literatures listed at the end of this paper.

References

1) *Foroulis, Z. A.* "Corrosion and corrosion inhibition in the petroleum industry". Werkstoffe und Korrosion. Vol. 33, No. 3, p. 121-131 (1982).
2) *Crolet, J. L.* "Acid corrosion in wells: Metallurgical aspects". J. of Petroleum Technology. Vol. 35, No. 8, p. 1553-1558 (1983).
3) *Greer, J. B.* "Results of interlaboratory sulfide stress cracking using the NACE T-1F-9 proposed test method". Materials Performance. Vol. 16, No. 9, p.9-15 (1977).
4) *Tanimura, M; Ishizawa, Y; Shimada, T.* "SSCC-resistant oil country tubular goods for sour oil and gas services". Corrosion Prevention & Control. Vol. 31, No. 1, p. 5-13 (1984).
5) *Ohki, T; Tanimura, M; Kinoshita, K; Tenmyo, G.* "Stress Corrosion-New approaches". ASTM STP 610. American Society for Testing and Materials. 1976. p. 399-419.
6) *Blount, F. E; Arnwin, B.C; Chandler, R.J.* "Results of a field study to select a tubing program for Ellenberger gas". Materials Protection. Vol. 1, No. 12, p. 24-26 (1962).
7) *Masamura, K; Hashizume, S; Nunomura, K; Sakai, J; Matsushima, I.* "Corrosion of carbon and alloy steels in aqueous CO_2 environment". CORROSION/83. Paper No. 55, Anaheim (1983).
8) *Ishizawa, Y; Shimada, T; Tanimura, M.* "Effect of microstructure on the sulfide stress corrosion cracking resistance of AISI 410 and 420 steels". CORROSION/82. Paper No. 124, Houston (1982).
9) *Ishizawa, Y; Shimada, T; Tanimura, M.* "The sulfide stress corrosion cracking resistance of 13% Cr steels for OCTG". Proc. of 3rd APMACA. Taipei. 1983. p. 381-389.
10) *Combes, J. D; Kerr, J. G; Klein, L. J.* "13 Cr tubulars solve corrosion problems in the Tusca-

loosa trend". Petroleum Engineer Inter. Mar. p. 50-70 (1983).
11) *Sakai, J; Matsushima, I; Kamemura, Y; Tanimura, M; Osuka, T.* "Effects of metallurgical factors an service performance of duplex stainless steel for deep sour gas wells". J. of Materials for Energy Systems. Vol. 5, Sept., p. 105-111 (1983).
12) *Ishizawa, Y; Shimada, T; Tanimura, M.* "SCC behavior of a duplex stainless steel in sour gas environments". CORROSION/83. Paper No. 167, Anaheim (1983).
13) *Watkins, M; Greer, J.B.* "Corrosion testing of highly alloyed materials for deep sour gas well environments". CORROSION/76. Paper No. 139, Houston (1976).
14) *Masamura, K; Hashizume, S; Sakai, J; Ono, T; Matsushima, I.* "Pitting corrosion resistance of high-alloy OCTG in CO_2 environment as affected by chlorides and sulfides". CORROSION/84. Paper No. 292, New Orleans (1984).
15) *Sakai, J; Honda, M; Masamura, K; Matsushima, I.* "Critical contents of nickel and chromium required for SCC resistance of high alloy OCTG". Corrosion. Vol. 41, No. 2, p. 80-84 (1985).
16) *Rhodin, T.N.* "Physical metallurgy of stress corrosion fracture". New York, Interscience Publishers, 1959. p. 247-272.
17) *Peckner, D; Bernstein, I.M.* "Handbook of Stainless Steels". New York, McGraw-Hill, 1977. p. 4-27.
18) *Matsushima, I; Shimada, T; Ishizawa, Y; Masamura, K; Sakai, J; Tanimura, M.* "Effects of alloy composition on corrosion and SCC resistance of high alloy OCTG in sour well environments". CORROSION/85. Paper No. 233, Boston (1985).
19) *Kane, R.D; Watkins, M; Jacobs, D.F; Hancock, G.L.* "Factors influencing the embrittlement of cold worked high alloy materials in H_2S environments". Corrosion. Vol. 33, No. 9, p. 309-320 (1977).

Copyrighted Materials
Copyright © 1996 NACE International Retrieved from www.knovel.com

Paper No. 53—CORROSION/90

SULFIDE STRESS CRACKING FAILURES OF 12CR AND 17-4PH STAINLESS STEEL WELLHEAD EQUIPMENT

R.M. Thompson and G.B. Kohut
Chevron Corporation
Materials Division
P.O. Box 4012
Richmond, California 94804

D.R. Canfield and W.R. Bass
Chevron U.S.A. Inc.
6400 South Fiddler's Green Circle
Englewood, Colorado 80111

ABSTRACT

Sulfide stress cracking case histories of 12Cr and 17-4PH stainless steel tubing hangers are presented along with the results of NACE TM-01-77 laboratory tests performed on the failed material. Even though the hangers both met NACE MR0175-88 hardness requirements, failure still occurred. These failures demonstrate the limitations of these alloys in high H_2S service even when MR0175 requirements are met. The need for better usage guidelines is discussed.

INTRODUCTION

The 12% chromium (Type 410, CA-15) and 17-4PH (Type 630) stainless steels have been used for many years in oil field applications where CO_2 corrosion resistance is required. Common wellhead applications include chokes, valve bodies, valve internals, and tubing hangers. These materials have traditionally been chosen over more costly, higher-alloy alternatives such as Type 660 stainless steel, Alloy 718, Alloy 625, and others. The high level of chromium in 12Cr and 17-4PH is responsible for their good corrosion resistance in CO_2 service. The chemical composition of the two alloys is shown in Table I. Because of higher chromium and the addition of nickel, 17-4PH generally shows better corrosion resistance than 12Cr.

Although they have excellent corrosion resistance, the 12Cr and 17-4PH materials are not without shortcomings. The most serious is susceptibility to sulfide stress cracking (SSC). Laboratory test results show that these materials are sensitive to cracking in sour service, and yet use of 12Cr and 17-4PH continues within the industry because of generally good field experience.[1-4] While the corrosion resistance of 17-4PH is better than 12Cr, the sulfide cracking resistance of these two alloys in laboratory tests is equally poor.

The industry has long known that an important variable affecting sulfide stress cracking susceptibility is the strength level of the material.[5,6] Because hardness is directly related to strength level and is easily measured, maximum hardness limits for both of these alloys in sour service have been established for manufacturing and quality assurance purposes. As defined in NACE MR0175-88, the maximum allowable hardness for 12Cr is HRC 22 and for 1/-4PH; HRC 33.

Field sulfide stress cracking failures of 12Cr and 17-4PH have been known to occur, however those which have been reported have generally been in material which exceeds NACE MR0175-88 hardness requirements.[7-9] Chevron has recently experienced several SSC failures of these alloys in high H_2S (≈15%) gas condensate wells. Two of these were in excessively hard material and were attributed to quality control problems. However, two tubing hanger failures have occurred in material which met the NACE hardness limits. These tubing hanger failures demonstrate that the SSC resistance of 12Cr and 17-4PH is questionable in high H_2S service.

FIELD ENVIRONMENT RESPONSIBLE FOR FAILURES

The failures described in this paper both occurred in the same gas condensate field. H_2S levels in this field range from 14 to 16%. Flowing tubing pressure and temperature are about 1000 psi (6.9 MPa) and 38°C (100°F), respectively. CO_2 levels are 5 to 6% and water production typically ranges from 50-300 BPD. Gas production is typically 10 to 30 MMCFD.

12CR STAINLESS STEEL MANDREL TUBING HANGER

The purpose of a tubing hanger is to support the weight of the tubing string and seal the annular space between the production casing string and the tubing. The hanger seats in the tubing head and can be of several different designs. For the commonly used mandrel hanger design, the uppermost tubing joint is threaded into the base of the hanger. Stresses are induced in the hanger by well pressure, tubing string weight, and metal-to-metal annular seals between the hanger and the tubing head.

The first tubing hanger incident occurred in a 410 SS hanger which had been in service for six years. The well had been shut-in for three years due to high water production. The tubing and the annulus contained an inhibited 2% KCl brine fluid during the shut-in with plugs set at 2,500 and 2,600 feet (760 and 790 m). A leak around the downhole plugs likely permitted gas (containing H_2S and CO_2) to enter the upper section of tubing and come into contact with the hanger during the shut-in.

Pressure had been detected in the annulus for approximately one year prior to failure. The pressure was periodically bled-off and, at one time, a sample of the gas revealed 600 ppm H_2S.

After the three year shut-in, a workover was instituted in an effort to return the well to production. During this workover, the hanger parted while lifting the tubing string under a load of about 60,000 lbs (267,000 N). The air weight of the string was 182,000 lbs (82,500 kg).

Initial observation by field personnel supported the theory that the hanger was cracked for some time prior to failure. A black corrosion deposit was reportedly present over 80-90% of the fracture surface while the remaining 10-20% was clean.

The 7" x 3-1/2" (17.8 cm x 8.9 cm) hanger is shown as-received in Figure 1. The fracture surface (Figure 2) appeared brittle and a small shear lip was present at the outside diameter. Small, secondary cracks found during the metallographic investigation established that cracking propagated from the hanger ID to the OD. The hanger cross-section is shown in detail in Figure 3. Cracking initiated at the plug socket on the ID (shown in Figure 3) and followed the prior austenite grain boundaries. The secondary cracks contained iron sulfide corrosion deposits as determined by microprobe analysis. The existence and morphology of these cracks, which are shown in Figure 4, and the presence of sulfide deposits identified the failure mechanism as sulfide stress cracking.

The results of mechanical testing are shown in Table II. Hardness of the hanger ranged from HRC 18-21 with an average hardness of HRC 19; meeting the hardness requirements listed in NACE MR0175-88. Hardness near the crack initiation site was also measured and was found to be no different than the bulk hardness. The microstructure shown in Figure 3 appeared normal for 410 SS.

The specific shut-in conditions in this well caused by gas leakage around the downhole plugs are believed to have been a significant factor in this failure. Although the hanger material was within specification, its inherent susceptibility to sulfide cracking coupled with the shut-in environment caused the failure.

17-4PH STAINLESS STEEL MANDREL TUBING HANGER

A second tubing hanger failure was discovered in the same field approximately one year after the first. This second failure occurred in a 17-4PH hanger which was in service for 10 months. The failure was found during a workover to up-size the tubing, but it was evident that the hanger had parted prior to the workover.

A large acid stimulation job was performed on this well about 7 months prior to the discovery of the failure. A total of 160,000 gallons (606 m^3 of inhibited 28% HCl was pumped at 8,500 psig (59 MPa) at a rate of about 60-70 BPM. Following stimulation, the well was shut-in for three days prior to flow back.

The 7-1/2" x 4-1/2" (19.1 cm x 11.4 cm) mandrel hanger was manufactured in accordance with the H1150M heat treatment in NACE MR0175-88. The resulting mechanical properties are listed in Table II. Hardness ranged from HRC 25-30 with an average of HRC 27, well below the NACE maximum of HRC 33.

The hanger is shown as it was received in Figure 5. The hanger parted at the plug socket on the ID, which was the same location as the previous 12Cr failure. The fracture surface, which is shown in Figure 6, appeared brittle with radial markings emanating from the ID.

Secondary cracking just under the fracture surface was found by metallographic analysis. These cracks, which are shown in Figure 7, were primarily transgranular, and their orientation established that the primary crack propagated from ID to OD. The microstructure (Figure 7) appeared normal for 17-4PH.

Stress analysis work performed by the manufacturer of the hangers has shown that stresses in the failed hanger range from 60-75% of the actual yield strength. As expected, the location of highest stress (the plug socket at the ID) corresponded to the fracture location. Although stress analysis was not performed on the 12Cr hanger, results would be expected to be similar.

Corrosion product (scale) was present in the secondary cracks, on the fracture surface, and on the ID of the hanger. This scale was analyzed and found to contain primarily iron, chromium, and sulfur.

Based on the scale analysis and the crack morphology, the 17-4PH tubing hanger failure was due to sulfide stress cracking (SSC). The acidizing treatment is believed to have played a significant role in this failure, although no conclusive evidence was found to support this theory. If the failure did occur during or immediately following acidizing, the hanger seals must have remained intact because annular pressure was not detected.

LABORATORY TEST RESULTS

Laboratory SSC tests were conducted on both hangers and the results showed clearly the high susceptibility of 410 SS and 17-4PH to sulfide cracking. The test method used was the industry standard NACE TM-01-77, "Testing of Metals for Resistance to Sulfide Cracking at Ambient Temperatures."

The threshold stress, i.e., the highest stress at or below which no failure occurs in 720 hours, expressed as a percentage of the yield strength was used to measure SSC resistance. While there is considerable disagreement over an acceptance criteria for the NACE test, the most commonly discussed value is 80% threshold stress. For example, API C-90 grade tubulars are considered suitable for sour service if a threshold stress of 80% of specified minimum yield strength (SNYS) or higher is obtained in this test. A threshold stress of 10% of actual yield strength was obtained in the laboratory test on the 410 SS hanger material and 15% of actual yield for the 17-4PH hanger. These test results are presented in Table III.

IMPLICATIONS OF FAILURES

The 12Cr and 17-4PH materials have historically been used in sour service because of their good corrosion resistance. As long as the material has met NACE hardness requirements, selection and use has been made without regard to H_2S level. However, these tubing hanger SSC failures show that a more careful look at the widespread use of these materials in sour service is warranted.

The 12Cr and 17-4PH alloys have performed generally well in the field as opposed to poor performance in the laboratory. The reason for this is believed to be that field environments do not often approach the severity of the laboratory NACE environment. Field environments can increase in severity, however, especially when there is a deviation from normal field production conditions. When this occurs, the likelihood of cracking is increased and field failures of these marginal materials can occur. For example, the acid stimulation performed prior to the discovery of the 17-4PH failure and the intrusion of sour gas into the completion brine in the tubing string in the case of the 410 SS hanger probably played a significant role in promoting these failures.

The case histories presented in this paper demonstrate clearly that properly heat treated material which meets the requirements of NACE MR0175-88 can fail in field environments. This has long been known to occur in the laboratory, but now has been documented in the field as well. This implies that the NACE hardness requirements cannot be solely relied upon to prevent field SSC failures.

Better criteria are needed for the cost effective use of 12Cr and 17-4PH alloys. Substantial favorable field experience is believed to exist for these alloys as they have been used extensively above the NACE sour service definition. The authors have been surveying some of these satisfactory applications with the objective of developing a better usage guideline than presently exists. While there are some who will argue that these alloys should not be used in any H_2S service, this approach is overly conservative based on the long history of satisfactory field experience. With appropriate guidelines, users can continue to take advantage of the cost effectiveness of these materials while limiting the risk of costly failures.

CONCLUSIONS

1. Examples of field SSC failures of 12Cr and 17-4PH tubing hangers have been presented and discussed. The most important aspect of these failures was that the material in both cases met NACE MR0175-88 hardness requirements and yet still failed.

2. These alloys are most vulnerable to SSC during conditions which deviate from normal production environments. The failures presented in this paper are believed to have occurred under such conditions.
3. Current usage guidelines in NACE MR0175-88 do not appear to be adequate to prevent failures of 12Cr and 17-4PH under all circumstances. Improved guidelines are needed, and the authors encourage users to place a priority on this issue.
4. To avoid failures in environments which are too severe for 12Cr and 17-4PH, materials with higher cracking resistance, such as Alloy 718 or higher alloys, are necessary.

ACKNOWLEDGMENT

Special thanks to L.J. Klein, J.W. Skogsberg, P.W. Hunter, S.L. Hardy, and L.F. Rivas for assistance in the investigations described in this paper.

REFERENCES

1. R.D. Kane, M. Watkins, J.B. Greer, *Corrosion* 33, 7(1977), p. 231.
2. R.R. Gaugh, *Materials Performance* 16, 9(1977), p. 24.
3. P.W. Rice, *Materials Performance* 17, 9(1978), p. 16.
4. Y. Ishizawa, T. Shimada, M. Tanimura, "Effect of Microstructure on the Sulfide Stress Corrosion Cracking Resistance of AISI 410 and 420 Steels," CORROSION/82, paper no. 124 (Houston, TX: NACE, 1982).
5. J.P. Fraser, R.S. Treseder, *Corrosion* 8, 10(1955), p. 342.
6. F.K. Bloom, *Corrosion* 11, 7(1955), p. 351.
7. R.N. Tuttle, *Materials Performance* 13, 2(1974), p. 42.
8. J.D. Alkire, S.W. Ciaraldi, "Failures of Martensitic Stainless Steels in Sweet and Sour Gas Service," CORROSION/88, paper no. 210 (Houston, TX: NACE, 1988).
9. J.A. King, P.S.C. Badelek, "Performance of Valve Materials in Wet H_2S and CO_2 Contaminated Hydrocarbons," CORROSION/82, paper no. 134 (Houston, TX: NACE, 1982).

TABLE I

Chemical Composition of Hanger Materials

Element	12Cr (UNS S41000)	17-4PH (UNS S17400)
Carbon	0.15 max wt %	0.07 wt % max
Chromium	11.5 - 13.5	15 - 17.5
Columbium	--	0.15 - 0.45
Copper	--	3.0 - 3.5
Manganese	1.00 max	1.00 max
Nickel	0.75 max	3.0 - 5.0
Phosphorous	0.040 max	0.040 max
Silicon	1.00 max	1.00 max
Sulfur	0.030 max	0.030 max

TABLE II

Mechanical Properties of Hanger Materials

Property	12Cr Hanger	17-4PH Hanger
Yield Strength	97.1 KSI (669 MPa)	118.3 KSI (816 MPa)
Tensile Strength	115.0 KSI (793 MPa)	132.4 KSI (913 MPa)
% Elongation	21.0 %	23.4 %
% Reduction of Area	63.5 %	64.5 %
Hardness	19 HRC	27 HRC

TABLE III

Laboratory NACE TM-01-77 SSC Test Results

Specimen	% Actual YS	Time to Failure (Hrs)	Hardness
12Cr	10	No Failure	13.5 HRC
12Cr	20	156	15.2 HRC
12Cr	20	148	15.5 HRC
12Cr	30	115	17.3 HRC
12Cr	40	133	16.2 HRC
12Cr	50	67	16.0 HRC
17-4PH	10	No Failure	25.1 HRC
17-4PH	15	No Failure	24.2 HRC
17-4PH	20	424	24.8 HRC
17-4PH	25	324	25.2 HRC
17-4PH	30	303	25.4 HRC
17-4PH	40	220	25.2 HRC

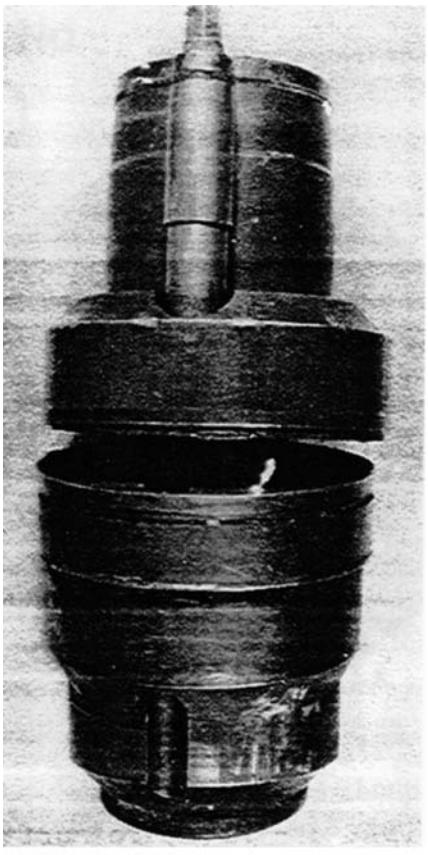


FIGURE 1 - Type 410 SS tubing hanger in the as-received condition.



FIGURE 3 - Cross-section of 410 SS hanger showing location of fracture.

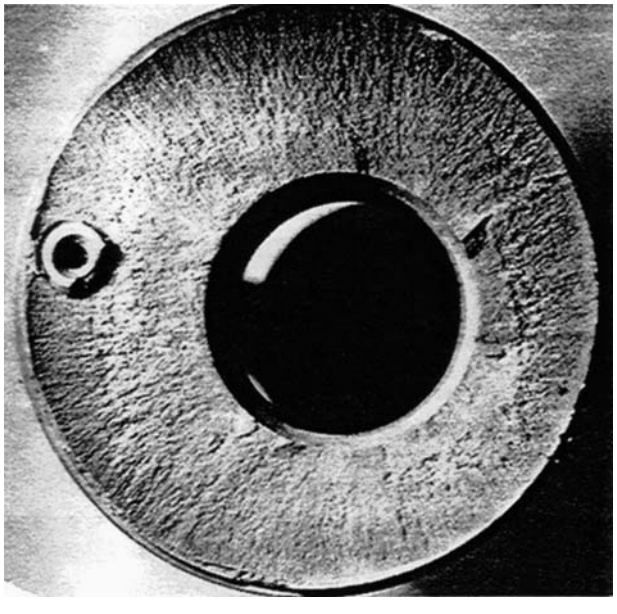


FIGURE 2 - Fracture surface of 410 SS hanger. Note small shear lip at the OD.

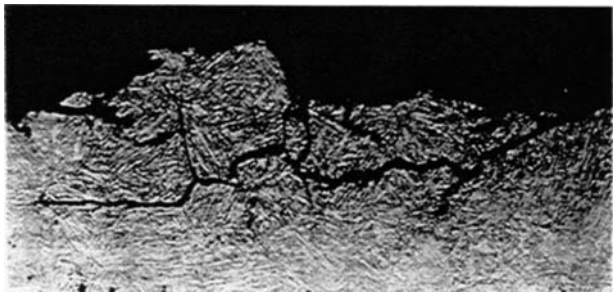
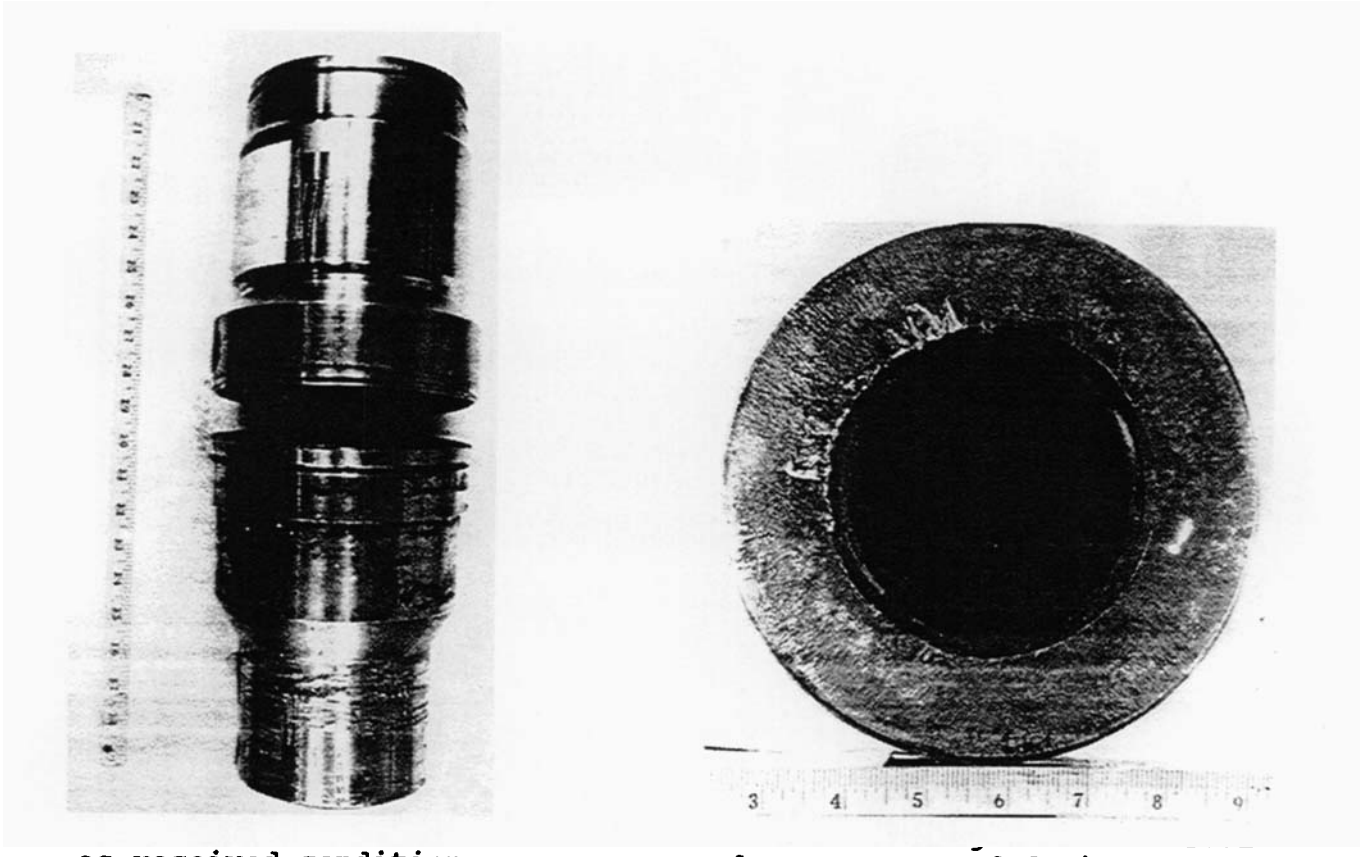


FIGURE 4 - Secondary cracking in 410 SS hanger found just below the fracture surface.
200x Villella's Etch



as-received condition.

damage occurred during the workover when the failure was discovered.

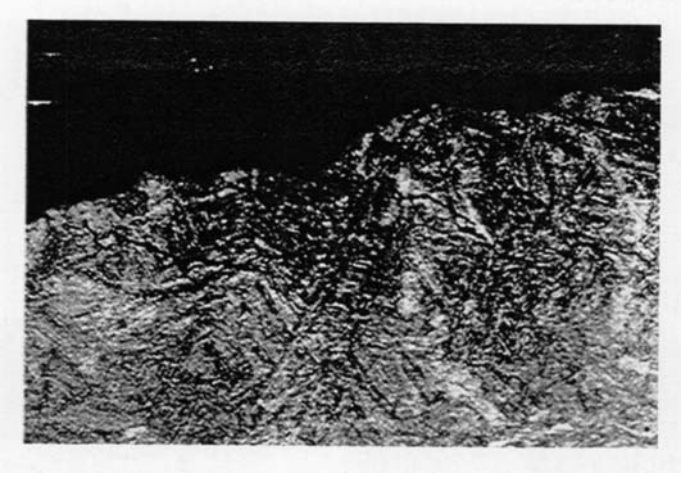


FIGURE 7 - Example of secondary cracks found along the fracture surface of the 17-4PH hanger. 200x Fry's Reagent

Copyrighted Materials
Copyright © 1996 NACE International Retrieved from www.knovel.com

Paper No.
80

CORROSION 95
The NACE International Annual Conference and Corrosion Show

EVALUATION OF SSC RESISTANCE ON SUPER 13CR STAINLESS STEEL IN SOUR APPLICATIONS

Masakatsu Ueda and Takahiro Kushida
Sumitomo Metal Industries, Ltd.
Iron & Steel Research Labs.
1-8, Fuso-cho, Amagasaki, Japan

Tomoki Mori
Sumitomo Metal Industries, Ltd.
Wakayama Steel Works
1850 Minato, Wakayama, Japan

ABSTRACT

The super 13Cr martensitic stainless steel consists of low C content below 0.03mass%, 13mass% Cr 5.5mass% Ni and 2mass% Mo and has good resistance of both sulfide stress cracking(SSC) at room temperature and localized corrosion at elevated temperatures compared with conventional 13Cr steel(AISI 420). The buffer solution containing CH_3COONa-CH_3COOH with high buffer power has been developed in order to carry out a more exact experiment under a constant pH between 3.0 and 5.5 The effect of H_2S partial pressure and pH on SSC resistance of the super 13Cr stainless steel was evaluated in the newly developed buffer solution by constant strain method, slow strain rate technique(SSRT) and the cyclic SSRT in which the tensile and compression tests were repeated 15 times at the strain rate of 4×10^{-6} s^{-1} between 0.95 and 0.60 x yield strength. The SSC resistance was characterized and quantified by means of correlating H_2S partial pressure and solution pH. SSRT gave the most severe evaluation for the SSC resistance of all the methods tested because SCC susceptibility in SSRT was evaluated under the plastic deformation condition up to failure. The constant strain tests which are 4 point bent beam test with notch and NACE tensile test according to NACE TM0177-90, and the cyclic SSRT showed almost the same evaluation result. Therefore, the cyclic SSRT was recommended as a very effective quick evaluation method for the SSC resistance of the super 13Cr stainless steel.

Key words: Martensitic stainless steel, Sulfide stress cracking(SSC), Carbon dioxide(CO_2), Hydrogen sulfide((H_2S), Oil country tubular goods(OCTG), Slow strain rate technique(SSRT), Cyclic SSRT

INTRODUCTION

The field application of conventional 13Cr martensitic stainless steel(AISI 420, hereafter referred to as 13Cr steel) has been increasing due to the good corrosion resistance in CO_2 environments[1]. However, it is well known that 13Cr steel is susceptible to sulfide stress cracking(SSC) in the CO_2 environment with a H_2S partial pressure of more than 0.0003MPa in laboratory tests and less resistant to general and localized corrosions at elevated temperatures[2]. The SSC susceptibility of 13Cr steel depends on environmental factors such as H_2S partial pressure, pH and Cl^- ion concentration. Klein et. al. indicated that the SSC susceptibility was reduced when the initial pH of NACE solution was adjusted to 4.0 or there was less than 2% NaCl in solution[3]. Kermai et. al. presented the effect of pH and H_2S partial pressure on the SSC susceptibility[4]. Based on these test results and field experiences, it was described in NACE MR0175-94 that API 5CT grade L-80 type 13Cr tubing and casing are acceptable up to a maximum H_2S partial pressure of 0.01MPa(1.5psi) in production environments with a produced water pH greater than or equal to 3.5[5].

Recently, a number of new 13Cr steels with the improved-corrosion resistance at ambient and elevated temperatures have been proposed by some researchers[6-8]. In the super 13Cr stainless steel which has been developed by Sumitomo Metal Industries Ltd., the carbon content is reduced to below 0.03mass% in order to suppress the reduction of Cr concentration in the matrix in the form of the Cr carbide precipitation; 5mass% Ni content is added to obtain the martensitic single phase, and 2mass% Mo content is added to improve SSC and localized corrosion resistance[9]. Further, in previous work, it was shown that the super 13Cr stainless steel had a passive film in environments containing a small amount of H_2S, but 13Cr steel did not. The H_2S limit of the former was 0.001 to 0.003MPa[9]. Because of these superior properties, the super 13Cr stainless steel has been used in the North Sea[10] and will be widely applied for OCTG. In field application, the effect of pH and H_2S partial pressure on the SSC resistance is very important information. In general, the NACE tensile test, Method A, according to NACE TM0177-90, is used as a conventional evaluation method for SSC resistance[11]. However, this test method under a constant pH has had the following problems:

1. Though the experiment is carried out by using a buffer solution, keeping the pH constant during 720h is difficult because the pH increased by the cathodic reaction of corrosion, $2H^+ + 2e^- \rightarrow H_2$.
2. The test period is very long, namely 720h.

Therefore, a buffer solution with a high buffer power and a quick test method were needed to carry out an exact and rapid SSC evaluation. SSRT(Slow strain rate technique) and ESSRT(Elastic SSRT) are known as rapid SSC evaluation methods. In the ESSRT proposed by Gelder et. al.[12], a specimen is pre-stressed to UTS(Ultimate tensile stress) in air, unloaded and strained at a constant strain in hostile environments. However, the material tested suffers a plastic deformation from the pre-stress, and the mechanical properties of the material change from their original condition.

In this paper, a new buffer solution for keeping the pH constant in test solutions over a long duration is first investigated. Then, the SCC resistance of the super 13Cr stainless steel is evaluated by constant strain, SSRT, cyclic SSRT methods using the buffer solution developed. The cyclic SSRT shown in this paper is the method in which the tensile and compression tests are repeated at a constant strain under a plastic deformation. Finally, the SSC resistance of the super 13Cr stainless steel and the possibility of the cyclic SSRT as a quick test are discussed based on the SSC evaluation results obtained.

EXPERIMENTAL

Materials

Materials with the chemical composition and the tensile properties given in Table 1 were used in this study. These materials were manufactured by the mannesmann-mandrel mill process, quenched in water from 900C in mill and tempered in the laboratory to get the 0.2 % yield strengths of 550MPa(80ksi) 654MPa(95ksi) and 757MPa(110ksi) grades. The figures which show the experimental results for each of the materials tested are indicated in the right hand column of Table 1.

Corrosion test

Buffer solutions with pH 3, 3.5, 4.5 and 5.5 were first investigated by using the dissolution constants of CH_3COOH, H_2CO_3 and H_2S, and by measuring the buffer power with titration tests using 0.01N NaOH and 0.01N HCl solutions.

The SSC resistance on super 13 Cr stainless steel was evaluated by using constant strain, SSRT and cyclic SSRT methods with a buffer solution of H_2S and CO_2. Test specimens shown in Figure 1 were stressed longitudinally in the rolling direction. They were polished with silicon carbide No.600 paper rinsed with distilled water and then degreased in ethanol and acetone. Deaeration was carried out by the application of a vacuum and/or the bubbling of N_2 gas. H_2S and CO_2 gases were charged to test pressure at 25C.

In the constant strain test, 4 point bent beam and NACE tensile specimens were used as shown in Figure 1. The 4 point bent beam specimen had a notch with the stress concentration factor of 2.1 and was stressed to 100% of yield strength. The standard test period was 336h, but a 720h test was also carried out to investigate the effect of the notch on SSC susceptibility. The NACE tensile test in the buffer solution , which was bubbling 0.1MPa CO_2 gas with various H_2S gas partial pressures, was carried out according to method A in NACE TM0177-90 by using the proof ring type test apparatus.

In the SSRT test, the tensile test was carried out at the strain rate of 4×10^{-6} s^{-1} in the buffer solution containing H_2S and CO_2 gases, and the following indices were used to evaluate the cracking susceptibility:

1. L_T^e/L_T^o: a ratio of plastic strain between hostile(L_T^e) and inert(L_T^o) environments.
   (The plastic strain means the strain in plastic region between 0.2% yield strength and failure)
2. R_T^e/R_T^o: a ratio of reduction in area between hostile(R_T^e) and inert(R_T^o) environments
3. Whether a secondary crack is observed or not using an optical microscope at 30X.

In the cyclic SSRT test, the tensile and compression tests, as shown in Figure 2, were repeated 15 times between 0.95 and 0.60 x yield strength at the strain rate of 4×10^{-6} s^{-1} in hostile environments Namely, both load and strain are controlled in this test. The cracking susceptibility was evaluated by using the following indices:

1. Cycle number to failure
2. Whether a crack is observed or not on the gauge section of the specimen after tested.

The cyclic SSRT has the following advantages:

1. The test can be carried out within the elastic strain region of materials, the same condition that is used in actual fields
2. The provability of SCC occurrence becomes high by repeating the tensile and compression tests at a constant strain.

The disadvantage might be that the cyclic SSRT can only evaluate materials with a passive film.

RESULT AND DISCUSSION

Buffer Solution

The buffer solution using CH_3COONa and CH_3COOH was investigated in this study. This solution had been used by Kermani et al[4] and can be prepared by the following two methods.

1)Addition of HCl to CH_3COONa solution; Dissolution reaction of CH_3COOH and its dissolution constant in the equilibrium state at 25C are given as follows:

$$CH_3COOH \rightarrow CH_3COO^- + H^+ \qquad (1)$$

(Initial)		A	B
(Final)	C	A-C	B-C

$$(A-C)(B-C)/C = 10^{-4.87} \qquad (2)$$

where A is the concentration, M, of CH_3COONa and was 0.05M in the solution of Kermani et al[4], and B-C corresponds to the controlled pH value. Therefore, the added-quantity of HCl, B, can be calculated from equation (2).

2)Addition of CH_3COOH to CH_3COONa solution; The dissolution equation in this case is given as follows:

$$CH_3COOH \rightarrow CH_3COO^- + H^+$$

(Initial)	D	A	
(Final)	D-E	A+E	E

$$(A+E)E/(D-E) = 10^{-4.87} \qquad (3)$$

where D is the added-quantity of CH_3COOH and can be calculated from equation (3).

The calculation result of HCl or CH_3COOH quantities, which is added to each of the buffer solutions, is shown in Table 2. In general, it is known that buffer power is stronger when the ratio of CH_3COOH/CH_3COO^- is equal to 1 and both of their concentrations are large. So, considering the buffer power and the small added-quantity, in order to minimize the influence of CH_3COO^- ion on corrosion, the preparation methods of buffer solutions with a pH of 3.0, 3.5, 4.5 and 5.5 were

determined as follows:

pH 3.0 and 3.5: prepared by the addition of CH_3COOH to the 0.005M CH_3COONa solution
pH 4.5 and 5.5: prepared by the addition of CH_3COOH to the 0.01M CH_3COONa solution

The buffer power of the developed buffer solutions was investigated by titrating each of the solutions with 0.01N NaOH and HCl solutions. The result in buffer power for alkali and acid solutions is given in Figure 3 and 4, respectively. The pH change in testing solutions is estimated by assuming the following corrosion reaction:

$$Fe \rightarrow Fe^{2+} + 2e^-, \qquad 2H^+ + 2e^- \rightarrow H_2 \qquad (4)$$

The corrosion rate of 0.01mm/y corresponds to 7.5ml addition of 0.01N NaOH to 100ml of the buffer solution in the condition where the specific volume is $20ml/cm^2$, test duration is 720h and specific gravity is $7.8g/cm^3$. Furthermore, the buffer solutions proposed have excellent buffer power at pH 3.0 3.5 and 4.5, but the buffer power is poor at pH 5.5. Further, the result in Figure 5 shows that the buffer solution adding CH_3COOH, has better buffer power than that adding HCl.

In the case of pH 4.5 and 5.5 buffer solutions, it is necessary to consider the buffer effect of $H_2CO_3(aq)$ and $H_2S(aq)$ in CO_2 and H_2S environments. Each of added-quantities of $NaHCO_3$ and NaSH was calculated based on the following constants at 25C and the first dissolution reactions of $H_2CO_3(aq)$ and $H_2S(aq)$:

$$[H_2CO_3(aq)] = 6.8 \times P(CO_2), \quad [HCO_3^-][H+]/[H_2CO_3(aq)] = 10^{-6.352} \qquad (5)$$
$$[H_2S(aq)] = 10.06 \times P(H_2S), \quad [HS^-][H^+]/[H_2S(aq)] = 10^{-7.00} \qquad (6)$$

where $P(CO_2)$ and $P(H_2S)$ are partial pressure(MPa) of CO_2 and H_2S. Table 2 also shows the calculation result of $NaHCO_3$ and NaSH quantities added under 0.1MPa CO_2 and H_2S to the buffer solutions at pH 4.5 and 5.5. In experiment, the $NaHCO_3$ and NaSH quantities, which were calculated from the partial pressures of H_2S and CO_2, were added to the buffer solution

Constant Strain Test

4 point bent beam with notch: The experiment using 4 point bent beam specimen with notch was carried out in a 3.0MPa CO_2-H_2S environment and 3.0MPa CO_2-H_2S environment containing the buffer solution. The result is shown in Figure 6. The calculated-pH in a 3.0MPa CO_2 environment is 3.15 and that is equal to the pH estimated from the $P(CO_2)+P(H_2S)$ vs. pH diagram proposed by Bonis et al[13] The H_2S limit of super 13Cr stainless steel(654MPa[95ksi] grade) in a 3.0MPa CO_2-5%NaCl environment is 0.001 to 0.003MPa as previously described by Ueda et al[9]. This H_2S limit is higher than 0.0003MPa in a 3.0MPa CO_2-5%NaCl environment for the 13Cr steel of 550MPa[80ksi] grade by Ikeda et al[2]; therefore, the super 13Cr stainless steel has superior SSC resistance than 13Cr steel. The long term test result in a 0.002MPa H_2S-4.0MPa CO_2-10%NaCl environment, which has the calculated-pH of 3.0, is shown in Figure 6. The 4 point bent beam specimen without notch of super 13Cr stainless steel(654MPa[95ksi] grade) did not suffer SSC in the test. This fact suggests that the notch introducing a stress concentration accelerates SSC susceptibility. When the pH is increased up to 4.0, the super 13Cr stainless steel did not suffer SCC even in the 0.01MPa H_2S environment.

NACE tensile: The effect of applied-stress on SSC resistance of super 13Cr stainless steel is shown in Figures 7 and 8. The super 13Cr stainless steels with the yield strengths of 550MPa(80ksi) 654MPa(95ksi) and 757MPa(110ksi) grades were used in this experiment. The steel of 757MPa (110ksi) grade indicated less SSC resistance than the steels of 550MPa(80ksi) and 654MPa(95ksi) grades. The SSC resistance of 654MPa(95ksi) grade was almost the same as that of 550MPa(80ksi) grade Although it is well known that the SSC resistance in the 13Cr steel of 550MPa(80ksi) grade strongly depends on the yield strength[14], the SSC resistance in the super 13Cr stainless steel decreased from a higher yield strength point compared to the 13Cr steel. In 0.1MPa H_2S environments, SSC did not occur in the steels of 550MPa(80ksi) and 654MPa(95ksi) grades when the pH was increased to 4.5. The pH after the 720h test in pH 3.5 environments rose only about 0.1 and it confirmed that the proposed buffer solution had high buffer power. The effect of H_2S partial pressure and pH on SSC resistance is shown in Figure 9. The super 13Cr stainless steel of 654MPa(95ksi) grade was used in the test and the applied stress was 90%SMYS. The steel did not suffer SSC in a 0.002MPa H_2S, pH 3.0 environment, and this result was in agreement with the long term test result using the 4 point bent beam specimen without notch shown in Figure 6 in spite of the difference in Cl^- ion concentration. In 0.01MPa H_2S environments, the pH limit for the SSC resistance was between 3.0 and 3.5.

SSRT

The evaluation result of both the ratios of plastic strain and reduction in area in SSRT test is shown in Figure 10. SSRT gave a very severe evaluation of SSC resistance. Namely, the super 13Cr stainless steel of 654MPa(95ksi) grade suffered in the 0.001MPa H_2S-pH 3.5 environment. A Secondary crack was observed on the gauge section of the specimen after being tested when both L_T^e/L_T^o and R_T^e/R_T^o was less than 0.8. Because SSRT is a evaluation method to evaluate SSC susceptibility up to the plastic strain region, it is thought that SSRT gave a high SSC susceptibility.

Cyclic SSRT

In H_2S environment, the super 13Cr stainless steel has passive film as shown in a previous paper[9] but 13Cr steel does not have passive film. The cyclic SSRT test, which is able to evaluate SSC susceptibility of materials with passive film, was applied to the steel of 654MPa(95ksi) grade. The effect of strain rate on SSC resistance is shown in Figure 11. SSC was observed on both strain rates of 4×10^{-6} and 4×10^{-7} s^{-1}, but was not on that of 4×10^{-5} s^{-1}. Therefore, the cyclic SSRT under 4×10^{-6} s^{-1} was carried out in this study because test period was about 1 day. Figure 12 gives the effect of H_2S and pH on the SSC resistance. The result was similar to that of the NACE tensile test shown in Figure 9 SSC in the 0.001MPa H_2S-pH 3.5 environment was not observed even after 150 cycles. Further, the effect of Cl^- ion concentration on the SSC resistance is shown in Figure 13. The SCC on the super 13Cr stainless steel did not occur even in the 0.01MPa H_2S-pH 3.0 environment when Cl^- ion concentration was 100ppm. The result was also same as that obtained by 4 point bent beam test with notch as described in a previous paper[9]. Accordingly, it is thought that the cyclic SSRT gives almost the same evaluation result as the 4 point bent beam test with notch and the NACE tensile test.

Comparison of Evaluation Results on SSC Resistance

Comparison of evaluation results on SSC resistance among constant strain, SSRT and cyclic SSRT tests is shown in Figure 14. SSRT gave a high SSC susceptibility, and the pH limit for SSC occurrence

using SSRT was about 1.0 higher than that in the same H_2S partial pressure environments compared with the evaluation results by other methods. The 4 point bent beam with notch, NACE tensile, and cyclic SSRT tests had almost the same evaluation results. However, the decreasing of SSC resistance by the notch must be considered. The SSRT result suggests that the plastic deformation up to failure in SSRT which does not exist in actual usage, greatly increases the SSC susceptibility.

From these results, it is clear that the cyclic SSRT is a very effective quick test method instead of NACE tensile test for the super 13Cr stainless steel. Further, the cyclic SSRT could be applied to corrosion resistant materials with a passive film in sour environments. Namely, that would be effective for austenitic and duplex stainless steels, because those steels had the cracking susceptibility under elastic strain region in sour environments by SSRT as described by Tsuge et al[15]. However, the cyclic SSRT might not be suitable for Ni base alloy because Ueda et al presented that Alloy 825 suffered SCC(Stress corrosion cracking) under plastic strain region in sour environments by SSRT[16].

CONCLUSION

Buffer solutions with high buffer power were investigated and the SSC evaluation of the super 13Cr stainless steel were carried out using these buffer solutions by various test methods including the cyclic SSRT as a quick test method. The results obtained are summarized as follows.

1.The following buffer solution has been developed:

pH 3.0 and 3.5: prepared by the addition of CH_3COOH to the 0.005M CH_3COONa solution
pH 4.5 and 5.5: prepared by the addition of CH_3COOH to the 0.01M CH_3COONa solution

At pH 4.5 and 5.5, $NaHCO_3$ and NaSH must be added to the buffer solution corresponding to the partial pressures of CO_2 and H_2S.

2.The SSC resistance of the super 13Cr stainless steel by constant strain, SSRT and cyclic SSRT was characterized and quantified by means of correlating H_2S partial pressure and solution pH.

3.SSRT gave the most severe evaluation for SSC resistance of all the methods tested. 4 point bent beam test with notch, NACE tensile test and cyclic SSRT showed almost the same evaluation result although the decreasing of SSC resistance by the notch must be considered. The plastic deformation up to failure in SSRT, which does not exist in actual usage, is thought to greatly decrease the SCC resistance.

4.The cyclic SSRT from the above results was recommended as a very effective quick evaluation method for the SSC resistance of the super 13Cr stainless steel.

ACKNOWLEDGMENTS

The authors wish to thank Sumitomo Metal Industries Ltd. for allowing publication of this research The assistance and discussion of co-workers in laboratories are gratefully acknowledged.

REFERENCES

1.J.D.Combes, J.G.Kerr and L.J.Klein, "13Cr Tubulars Solve Corrosion Problems in Tuscaloosa Trend" Petroleum Engineer International, March, (1983)

2.A.Ikeda, S.Mukai and M.Ueda, Corrosion, 45, 4(1985): p.185.

3.L.J.Klein, Material Performance, October(1984): p.29.

4.M.B.Kermani, D.Harrop, M.L.R Truchon and J.L.Crolet, "Experimental Limits of Sour Service for Tubular Steels", Corrosion/91, paper no.77, (Houston, TX:NACE, 1991).

5.NACE Standard MR0175-94, NACE International(1994).

6.A.Tamaki, "A New 13Cr OCTG for High Temperature and High Chloride Environment" Corrosion/89, paper no.469, (Houston, TXNACE, 1989).

7.S Hashizume, T.Takaoka, Y.Minami, Y.Ishizawa and T.Yamada, "A New 15 Percent Steel Developed for OCTG", Corrosion/91, paper no.28, (Houston, TX:NACE, 1991).

8.A.Miyasaka and H.Ogawa, "Influence of Metallurgical Factors on Corrosion behaviors of Modified 13Cr Martensitic Stainless Steels", Corrosion/90, paper no.67, (Houston, TX:NACE, 1990).

9.M.Ueda, T.kushida, K.Kondo and T.Kudo, "Corrosion resistance of 13Cr-5Ni-2Mo martensitic stainless Steel in CO_2 Environment Containing a Small Amount of H_2S", Corrosion/92, paper no.55 (Houston, TX:NACE, 1992).

10.M.Barteri, A.Cigada, D.Condanni and M.Marangon, "Corrosion resistant Alloy Tubing for T-Block Conditions", European federation of corrosion(1993): p.551.

11.NACE Standard TM0177-90, NACE(1990).

12.K.Van Gelder, J.G.Erlings, J.W.M. Damen and M.M.Festen, "Limiting Conditions for the Application of Duplex Stainless Steel and Corrosion-resistant Clad Materials in Sour Service", Pipe Technology International conference at Rome, Italy on November 17 to 19(1987): p.I-2.

13.M.Bonis and J.L.Crolet, Corrosion science, 27, 10/11(1987): p.1059.

14.L.J.Klein, R.M.Thompson and D.E.Moore, "9Cr-1Mo and 13Cr Tubulars for Sour Service" Corrosion/90, paper no.52, (Houston, TX:NACE, 1990).

15.H.Tsuge, Y.Tarutani, T.Kudo, K.Fujikawa and T.Moroishi, "Corrosion Resistance of 22%Cr Duplex Stainless Steel in Cl^--H_2S environment", International Conference on Duplex Stainless Steel, The Hague, 26-28 October(1986): p.33B.

16.M.Ueda and T.Kudo, "Evaluation of SCC Resistance of CRAs in Sour Service", Corrosion/91, paper no.2, (Houston, TX:NACE, 1991).

TABLE 1
CHEMICAL COMPOSITION AND TENSILE PROPERTIES OF MATERIALS USED IN THIS STUDY

No.	C	Si	Mn	P	S	Cr	Ni	Mo	Y. S. MPa	Y. S. ksi	T. S. MPa	T. S. ksi	HRC	Figure No.
1	0. 016	0. 18	0. 45	0. 018	0. 001	12. 0	5. 36	1. 93	682	99	896	130	26	6, 10
2	0. 02	0. 18	0. 45	0. 019	0. 001	11. 95	5. 50	2. 06	703	102	861	125	26	6*
3	0. 013	0. 25	0. 46	0. 013	0. 001	11. 90	5. 39	1. 92	585	85	791	115	22	7, 8
4	↓	↓	↓	↓	↓	↓	↓	↓	715	104	839	122	25	7, 8, 9 11, 12 13
5	↓	↓	↓	↓	↓	↓	↓	↓	839	122	949	138	30	7, 8

*:used for 720h test

TABLE 2
NEW BUFFER SOLUTION FOR THE EXPERIMENT UNDER PH CONTROLLED

1)Buffer solution

	CH_3COONa	Additive		pH3	pH3. 5	pH4. 5	pH5. 5
1	0. 05M	Initial	HCl(M)	0. 05	0. 0483	0. 0351	0. 0095
		Final	CH_3COOH(M)	0. 0493	0. 0480	0. 0350	0. 0095
			CH_3COO^-(M)	0. 0007	0. 002	0. 0150	0. 0405
2	0. 01M	Initial	CH_3COOH(M)	0. 815	0. 241	0. 0235	0. 0023
		Final	CH_3COOH(M)	0. 814	0. 242	0. 0235	0. 0023
			CH_3COO^-(M)	0. 011	0. 010	0. 01	0. 010
3	0. 005M	Initial	CH_3COOH(M)	0. 445	0. 125	0. 0118	0. 0012
		Final	CH_3COOH(M)	0. 444	0. 125	0. 012	0. 0012
			CH_3COO^-(M)	0. 006	0. 005	0. 005	0. 005

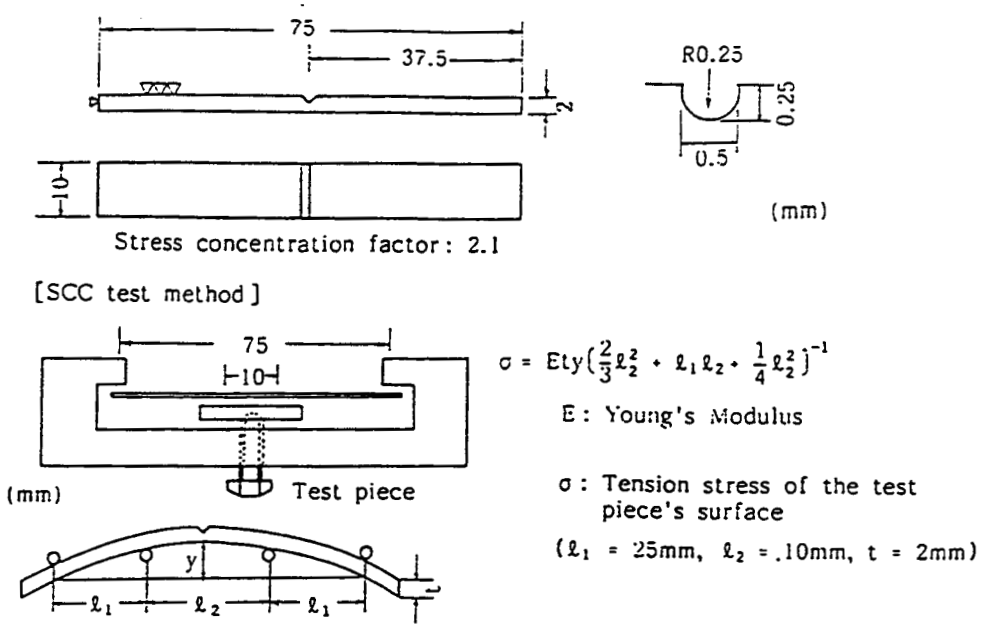
: new method

2)In H_2CO_3(aq) solution under 0. 1MPa CO_2

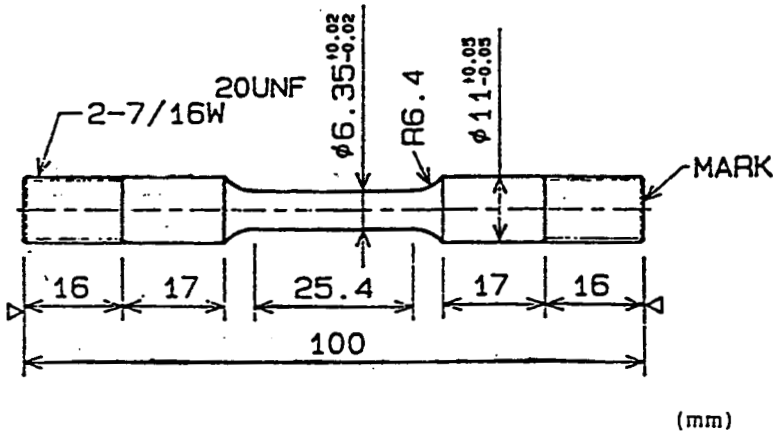
	Additive		pH 4. 5	pH 5. 5
4	Initial	$NaHCO_3$(M)	0. 0095	0. 0318
	Final	H_2CO_3(M)	0. 68	0. 68
		HCO_3^-(M)	0. 0095	0. 0956

3)In H_2S(aq) solution under 0. 1MPa H_2S

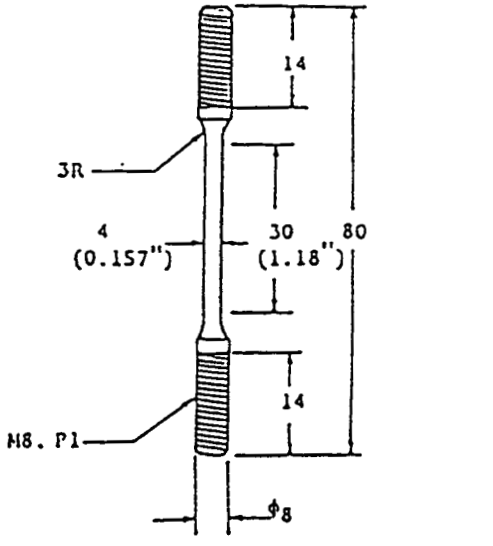
	Additive		pH 4. 5	pH 5. 5
5	Initial	NaSH(M)	0. 00315	0. 0318
	Final	H_2S(M)	1. 006	1. 006
		HS^-(M)	0. 00312	0. 0318



(a) 4 point bent beam specimen with notch



(b) Tensile specimen used in proof ring test



(c) Tensile specimen used in SSRT and cyclic SSRT

FIGURE 1 - Schematic illustration of test specimens

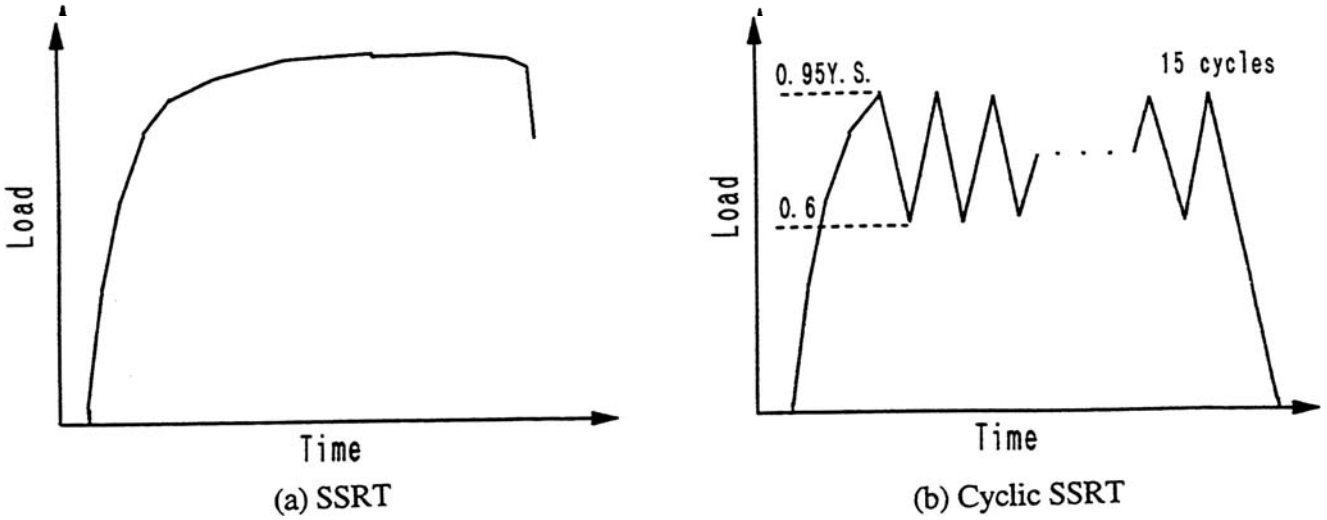


FIGURE 2 - Schematic illustration of load vs. time curves in SSRT and cyclic SSRT

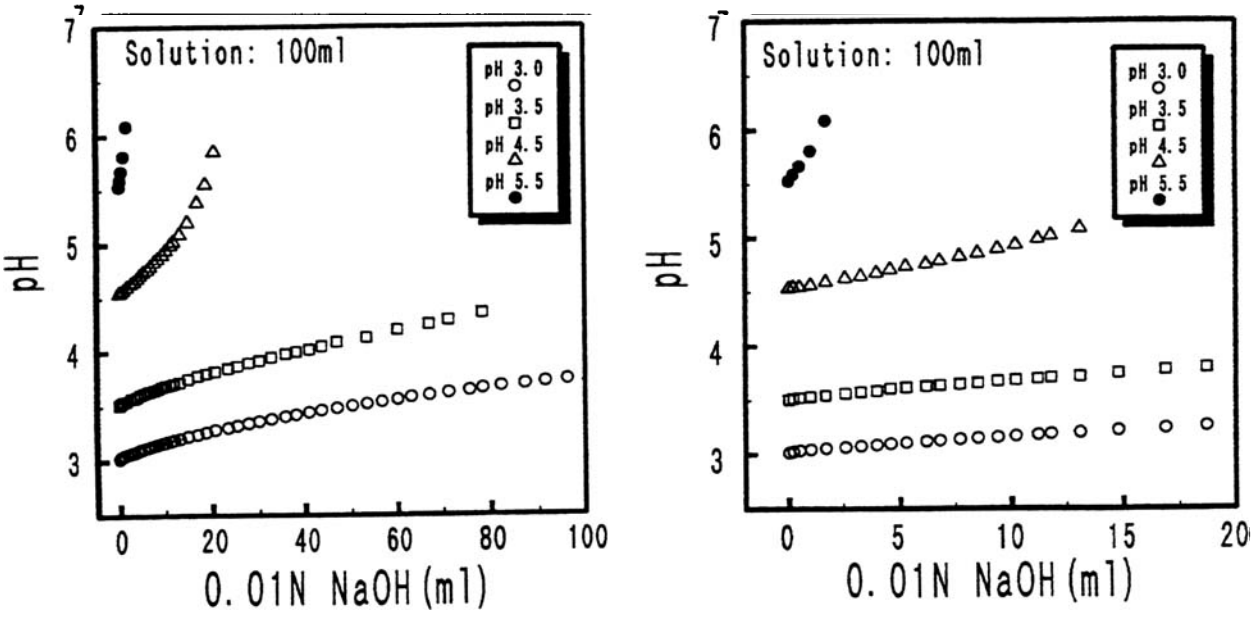


FIGURE 3 - Buffer power of new buffer solution for the addition of 0.01N NaOH solution
(5%NaCl-new buffer solution: 100ml, Titration solution: 5%NaCl-0.01N NaOH)

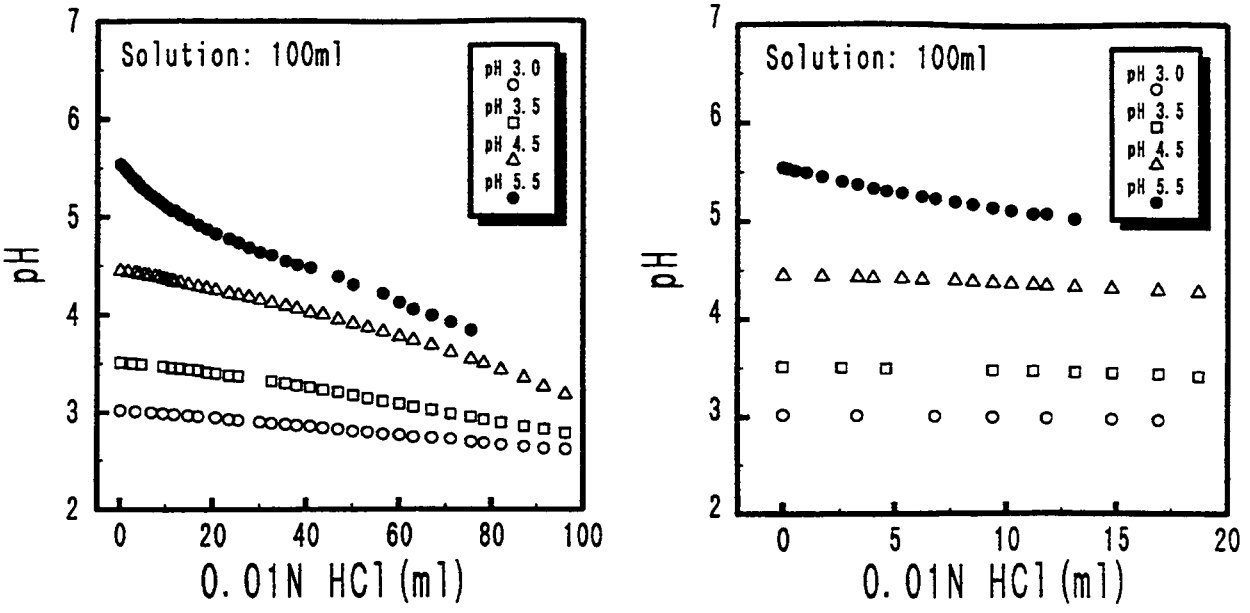
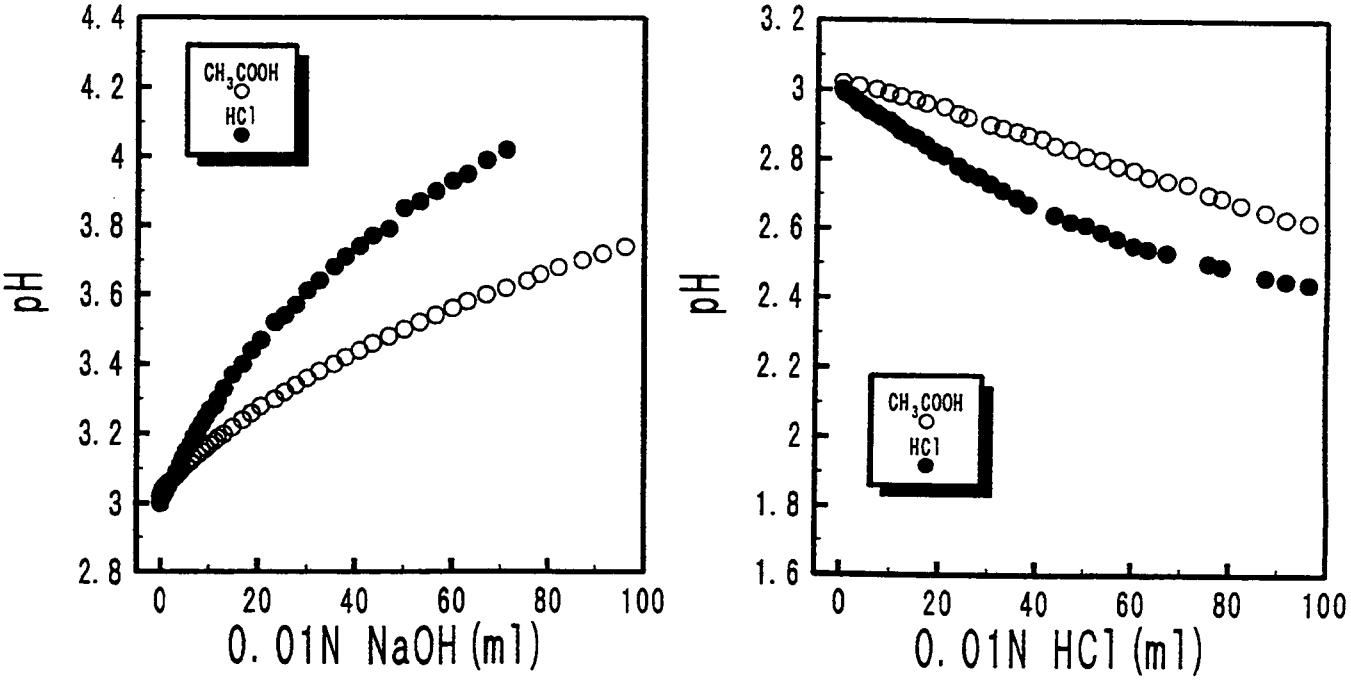


FIGURE 4 - Buffer power of new buffer solution for the addition of 0.01N HCl solution
(5%NaCl-new buffer solution: 100ml, Titration solution: 5%NaCl-0.01N HCl)



(a) For Alkaline solution

(b) For acid solution

FIGURE 5 - Comparison of the buffer effect between pH 3 solutions adjusted by CH_3COOH and HCl additions
(CH_3COOH: 0.005M CH_3COONa-CH_3COOH, HCl: 0.05M CH_3COONa-HCl)

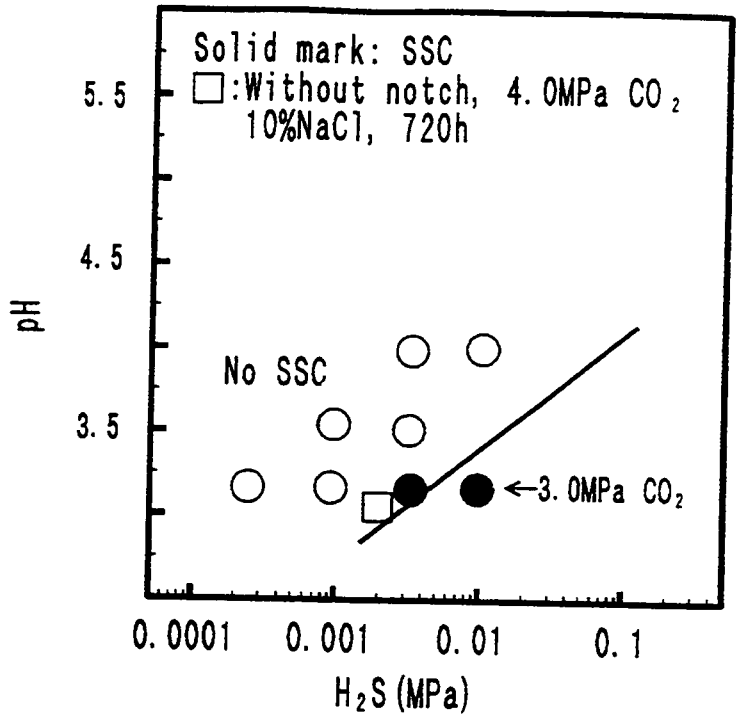


FIGURE 6 - Effect of H_2S partial pressure and pH on SSC resistance by 4 point bent beam test with notch
(5%NaCl-the buffer solution in Table 2, 3.0MPa CO_2-H_2S, 336h, 1.0σ_y)

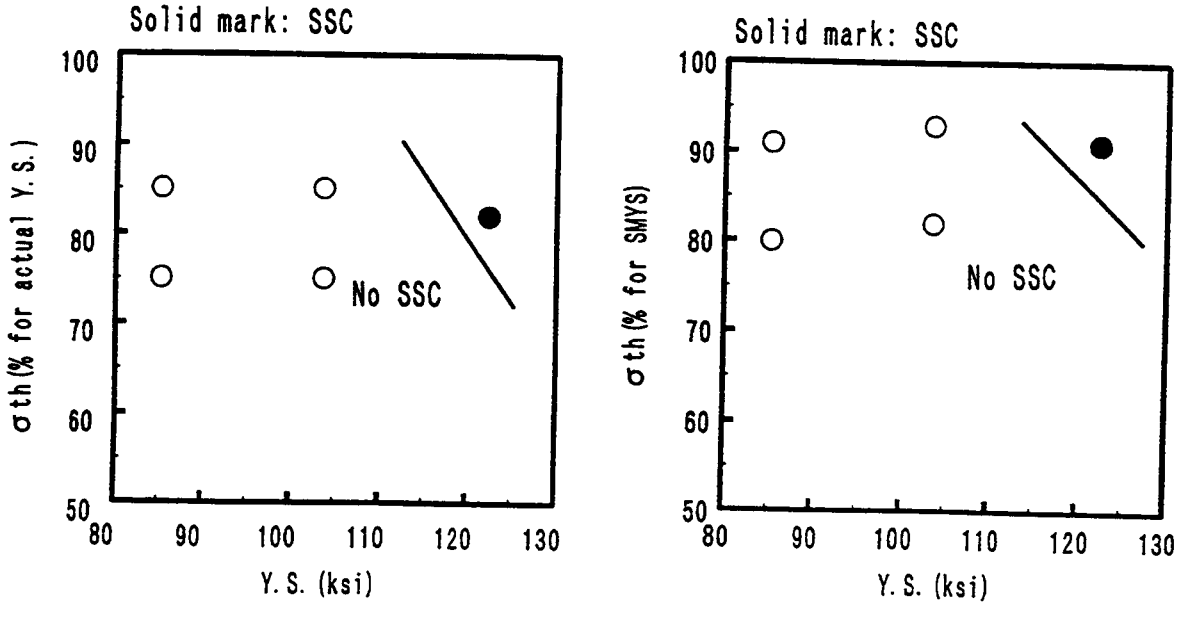


FIGURE 7 - Effect of applied-stress on SSC resistance by NACE tensile test
(pH 3.5: 5%NaCl-the buffer solution in Table 2, 0.002MPa H_2S(CO_2 balance) bubbling)

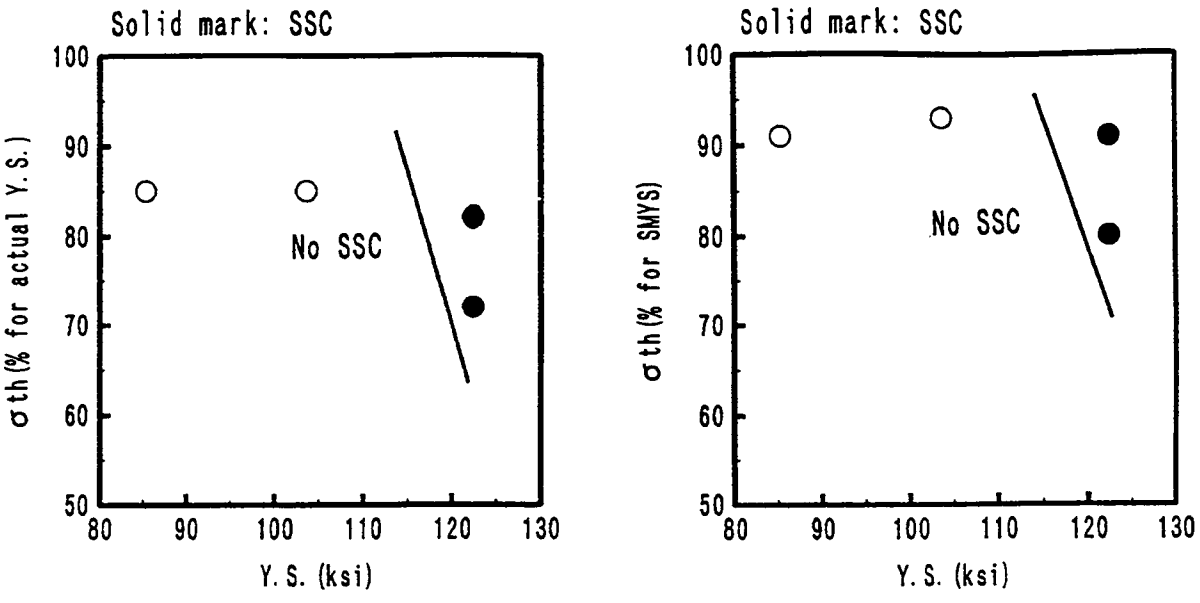


FIGURE 8 - Effect of applied-stress on SSC resistance by NACE tensile test
(pH 4.5: 5%NaCl-the buffer solution in Table 2, 0.01MPa H_2S(CO_2 balance) bubbling)

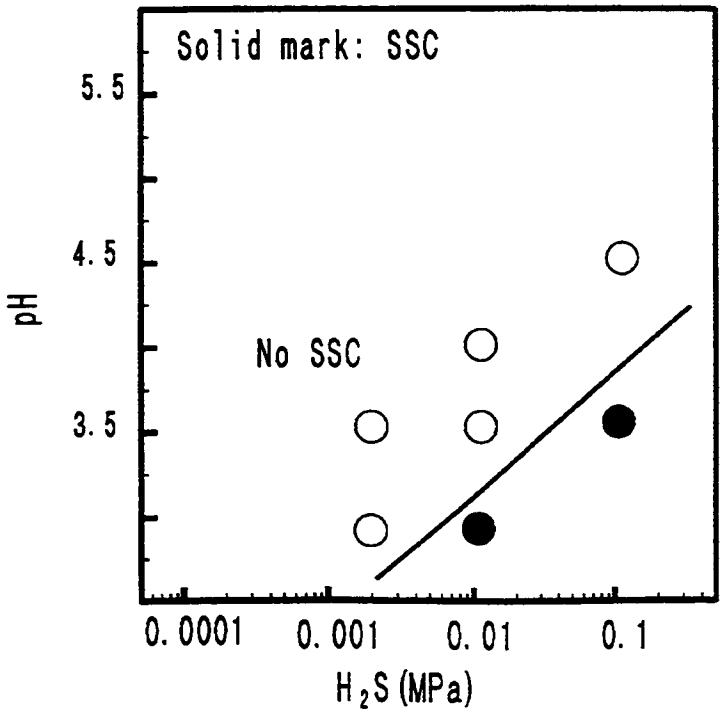


FIGURE 9 - Effect of H_2S partial pressure and pH on SSC resistance by NACE tensile test
(Material: 654MPa(95ksi) grade, 5%NaCl-the buffer solution in Table 2
H_2S-CO_2 gas bubbling under 0.1MPa, Applied stress: 0.9SMYS)

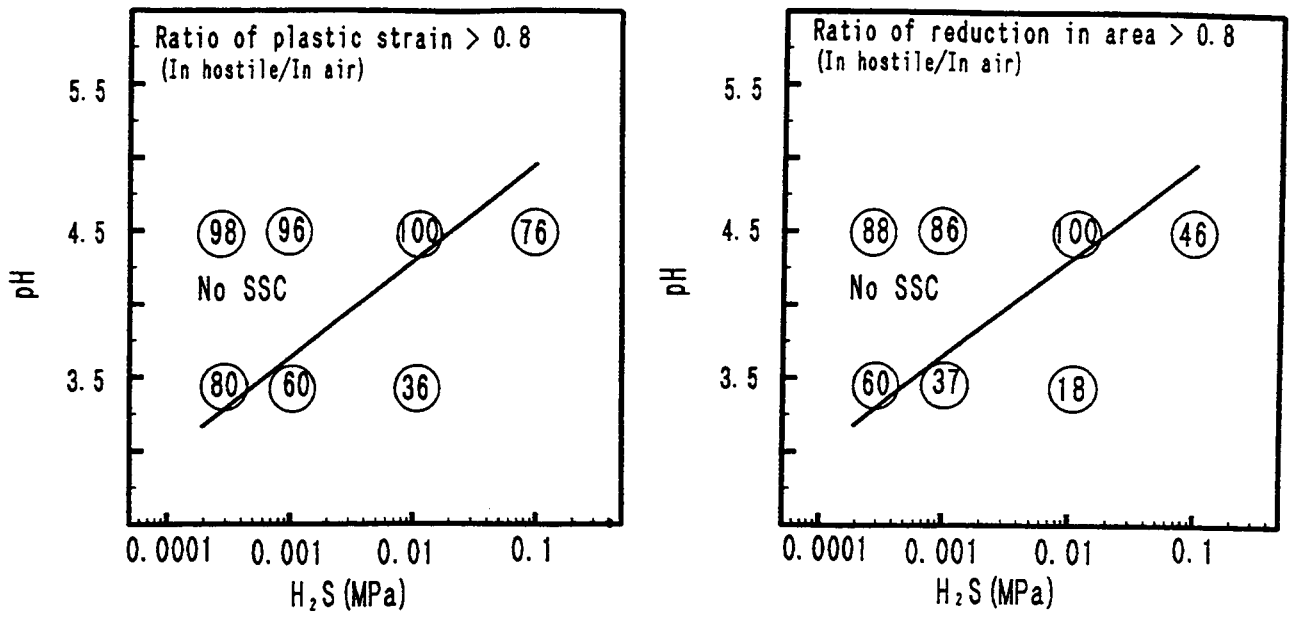


FIGURE 10 - Effect of H_2S partial pressure and pH on SSC resistance by SSRT test
(Material: 654MPa(95ksi) grade, 5%NaCl-the buffer solution in Table 2
H_2S-CO_2 gas(Total pressure: 0.1MPa))

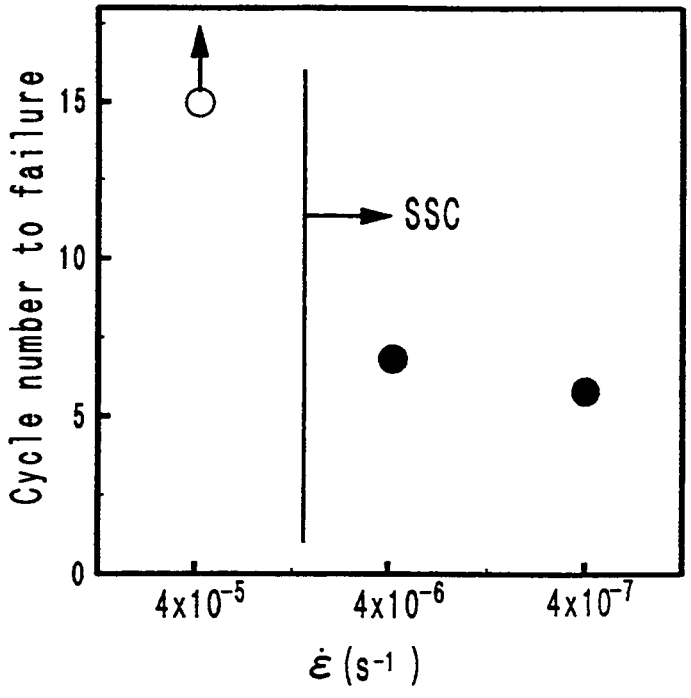


FIGURE 11 - Effect of strain rate on SSC resistance by cyclic SSRT test
(Material: 654MPa(95ksi) grade, pH 3.0: 5%NaCl-the buffer solution in Table 2
0.01MPa H_2S(CO_2 balance))

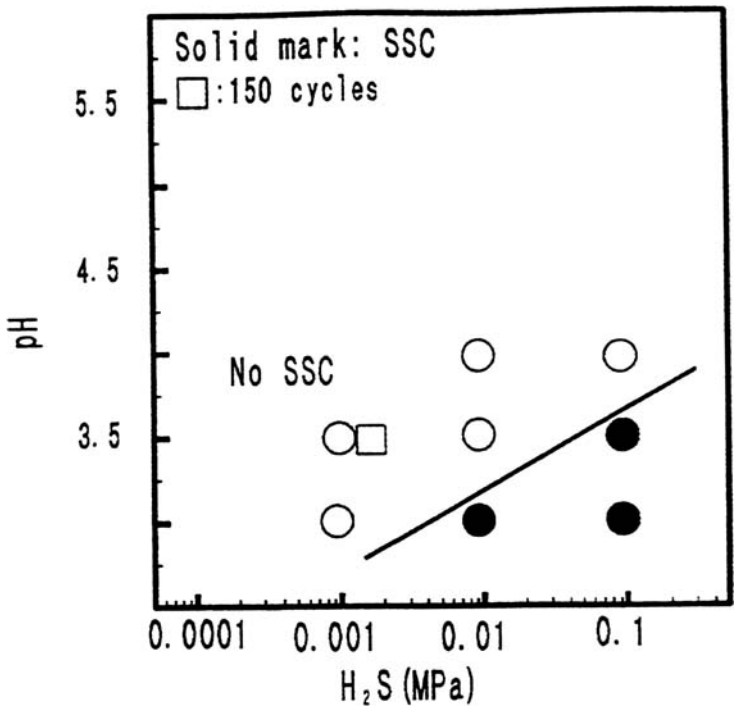


FIGURE 12 - Effect of H_2S partial pressure and pH on SSC susceptibility by cyclic SSRT test
(Material: 654MPa(95ksi) grade, 5%NaCl-the buffer solution in Table 2
H_2S-CO_2 gas(Total pressure: 0.1MPa))

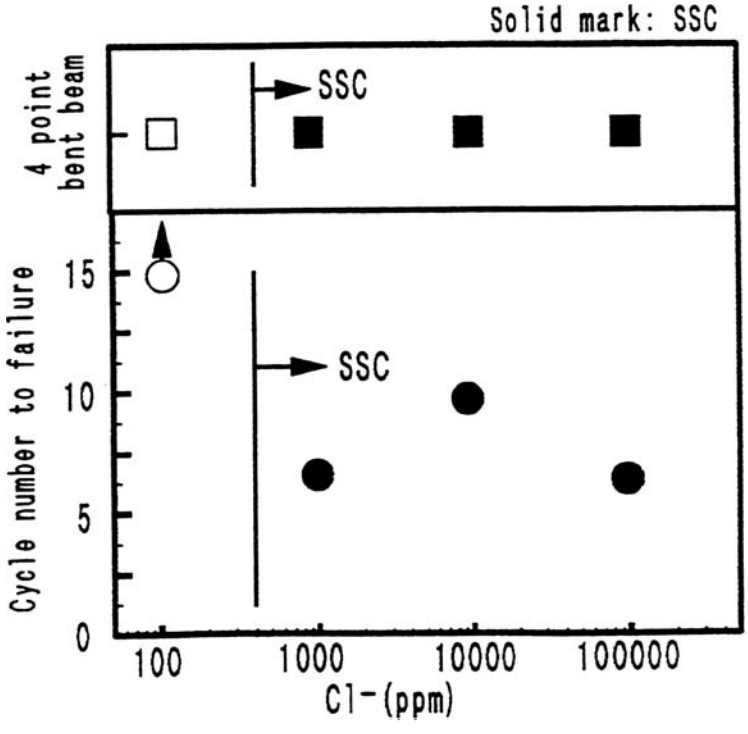


FIGURE 13 - Effect of Cl^- ion concentration on SSC resistance by cyclic SSRT
(Material: 654MPa(95ksi) grade, pH 3.0: 5%NaCl-the buffer solution in Table 2
0.01MPa H_2S(CO_2 balance), 4 point bent beam test result: after Ueda[9])

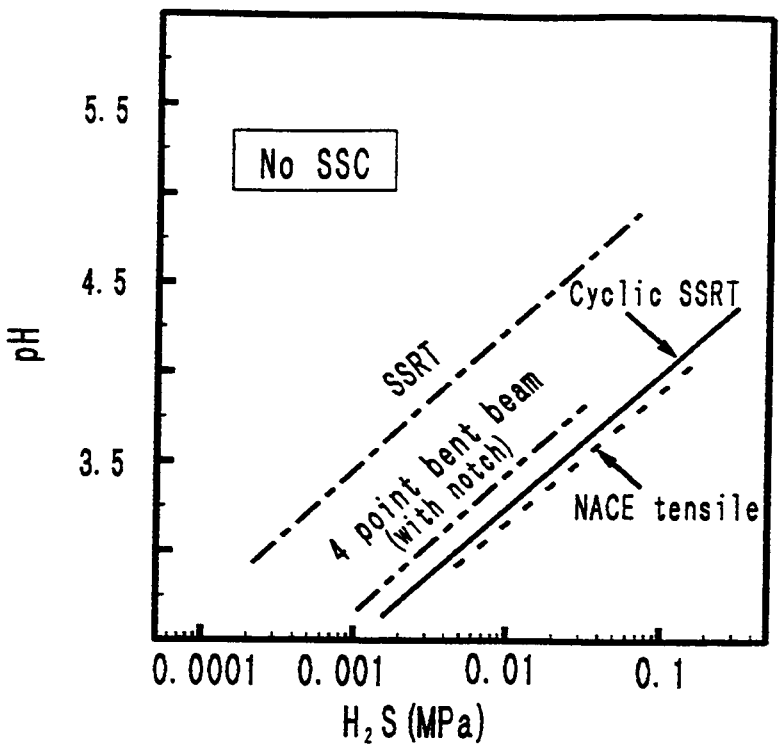


FIGURE 14 - Comparison between evaluation results in 4 point bent beam with notch, NACE tensile, SSRT and cyclic SSRT tests

Copyrighted Materials
Copyright © 1996 NACE International Retrieved from www.knovel.com

Paper No.
139

CORROSION 93
The NACE Annual Conference and Corrosion Show

AUSTENITIZING TEMPERATURE EFFECT ON SSC RESISTANCE OF 410 STAINLESS STEEL

D. D. Vitale and H. E. Ebert
Dresser-Rand Company
P. O. Box 560
Olean, New York 14760

ABSTRACT

This paper describes a program to determine the effect of austenitizing temperature on the impact strength and sulfide stress cracking (SSC) resistance of 410 stainless steel. Impact tests and sulfide stress cracking tests were performed on material austenitized at 1650°F(900°C) and 1800°F(982°C).

Austenitizing at 1650°F(900°C) versus 1800°F(982°C) has a significant effect on increasing the impact strength and increasing the SSC threshold stresses.

Keywords: sulfide stress cracking, SSC, 410 stainless steel, austenitizing temperature, impact strength

INTRODUCTION

There are many reports in the literature indicating the effect of austenitizing temperature on impact toughness. The widely accepted austenitizing temperature for some 400 series martensitic stainless steels is 1800°F(982°C). One reason for the selection of this temperature, rather than some lower temperature, is that this type of material is known to be rather "sluggish" during transformation and that existing carbides go into solution rather slowly. Another reason for the higher temperature is improved creep rupture properties, which is not a concern in compressor applications.

The purpose of the project was to determine the effects of austenitizing 410 stainless steel (SS) at 1650°F(900°C). Properties to be measured included grain size, impact strength, tensile properties, and SSC resistance. A secondary purpose was to compare the properties of oil quenched versus atmosphere quenched material. Because of its high hardenability, this material is atmosphere cooled as a normal procedure. Austenitizing at 1650°F(900°C) with an atmosphere quench would have less distortion and cracking than austenitizing at 1800°F(982°C) with an oil quench.

TEST PROCEDURE

One heat of 1-3/4 inch(44.5mm) diameter bar stock was used for all testing. The chemical analysis is listed in Table 1. The material was cut into appropriate test bar length and quartered lengthwise prior to heat treating.

All heat treating was done in accordance with the requirements of NACE Standard MR0175 for sour gas service. Samples were austenitized at 1650°F(900°C) or 1800°F(982°C), quenched, and double tempered. Heat treating cycles are shown in Table 2. All samples were heat treated in a laboratory furnace certified by survey to be less than ±10°F(±5.5°C) from setpoint.

RESULTS

Tensile Tests

The results of the room temperature tensile tests are listed in Table 3. Comparing heat treatments A to C and heat treatments B to D, it appears that the 1800°F(982°C) heat treatment yields slightly higher tensile and yield strengths and lower percentage elongation and percentage reduction of area than a 1650°F heat treatment when tempered at the same temperature.

Air Quenching resulted in slightly higher tensile and yield strengths than oil quenching from the same temperature.

Impact Tests

The Charpy V notch impact test results are listed in Table 4. Two specimens were tested at each of the following temperatures: +50°F(10°C), 0°F(-18°C), -25°F (-31.5°C), -50°F(-45.5°C), and -75°F(-59.5°C). One test each was performed at +70°F(21°C) and -100°F(-73.3°C).

Figure 1 shows that the 1650°F(900°C) heat treatment gives higher impact values at all test temperatures. With the 1800°F(982°C) heat treatment, oil quenched impact values are greater than those obtained with air quenching. This confirmed earlier work done in our laboratory. Air quenched and oil quenched impact test results are very similar with the 1650°F(900°C) heat treatment.

SSC Tests

Three specimens of each heat treatment were stressed according to the test matrix shown in Table 5. The testing was done at Cortest Laboratories and the samples were exposed to NACE TM0177 solution (5.0 weight percent sodium chloride, 0.5 weight percent glacial acetic acid in distilled water) saturated with hydrogen sulfide at ambient temperature and pressure.

Test results are shown in Table 6 and Figures 2 and 3. Threshold stress is defined as the strength at which a specimen completes a 720 hour exposure without rupture. Although only a limited number of samples were tested it is evident that the 1650°F(900°C) heat treatment gives significantly greater resistance to SSC under standard test conditions.

The threshold stress of the standard 1800°F(982°C) heat treatment is approximately 22 ksi(152 MPa) or 30% of the actual yield strength, 73 ksi(496 MPa). The threshold stress for the 1650°F(900°C) heat treatment is between 51 and 65 ksi (351 and 448 MPa) or 70-90 % of actual yield strength.

Further testing would be needed to confirm that an air quench gives superior threshold stresses and to establish the actual threshold stresses. However, the data for all samples tested is consistent and indicates the threshold stress for a 1650°F(900°C) austenitizing temperature is approximately twice that of the standard heat treatment.

Metallographic Study

Samples were taken from each of the four heat treatments and prepared in a plane parallel to the longitudinal axis. The samples were all similarly etched to examine grain size, microstructure and carbides. Figures 4 through 11 show the microstructure at 100X and 1000X of each austenitizing temperature and quench.

Note the much finer grain size of the 1650°F(900°C) austenitizing temperature (size 8 and finer) compared to the 1800°F(982°C) austenitizing temperature (size 3-4).

Lath martensite prevails in the microstructures of all 1800°F(982°C) austenitizing cycles. It is not as obvious in any of the 1650°F(900°C) cycles.

Scanning Electron Microscope (SEM) Study

The shear and cleavage topographies of the room temperature impact specimens were studied using the SEM. The shear zone of all samples had ductile microvoid coalescence. The cleavage zone of the 1650°F(900°C) austenitizing cycles was nearly all transgranular cleavage while the corresponding 1800°F(982°C) austenitizing cycles produced varying degrees of intergranular cleavage (Figures 12-15).

Polished and etched photos of these samples are shown in Figures 16-19. The higher austenitizing temperature appears to have resulted in more migration of carbides to grain and martensite boundaries.

CONCLUSIONS

1. The 1650°F(900°C) austenitizing temperature results in a much finer grain size than the 1800°F(982°C) austenitizing temperature.

2. The lower austenitizing temperature gives considerably higher impact values at all temperatures tested.

3. The 1650°F(900°C) austenitizing temperature results in SSC threshold stresses approximately two times greater than those obtained with 1800°F(982°C) heat treatment cycles.

4. Air quenching from the 1650°F(900°C) austenitizing temperature is equal to oil quenching from this temperature and has better impact toughness and SSC resistance than oil or air quenching from 1800°F(982°C).

5. A 1650°F(900°C) austenitizing temperature should be considered when greater impact toughness or resistance to SSC is required than can be obtained with the standard 1800°F(982°C) heat treatment.

6. The microstructure observations are consistent with the test results in that the fine grained microstructure and finer martensite are responsible for the superior toughness, the SSC threshold cracking stress and the increased percentages of transgranular fracture.

TABLE 1

CHEMICAL ANALYSIS

ELEMENT	WT.%
Carbon	0.136
Silicon	0.34
Manganese	0.41
Sulfur	0.019
Phosphorus	0.02
Copper	0.09
Nickel	0.16
Chromium	12.90
Cobalt	0.009
Titanium	0.021

TABLE 2

HEAT TREAT CYCLES

IDENTIFICATION	AUSTENITIZE TEMP.	1ST TEMPER	2ND TEMPER
Set A	1800°F(982°C), 5Hr. Oil Quench	1300°F(705°C), 5Hr. Air Cool	1200°F(649°C), 3Hr. Air Cool
Set B	1800°F(982°C), 5Hr. Air Cool	1300°F(705°C), 5Hr. Air Cool	1200°F(649°C), 3Hr. Air Cool
Set C	1650°F(900°C), 5Hr. Oil Quench	1300°F(705°C), 5Hr. Air Cool	1200°F(649°C), 3Hr. Air Cool
Set D	1650°F(900°C), 5Hr. Air Cool	1300°F(705°C), 5Hr. Air Cool	1200°F(649°C), 3Hr. Air Cool

TABLE 3

MECHANICAL PROPERTY RESULTS

IDENTIFICATION	T.S.,Ult., psi (MPa)	Y.S., psi (MPa)	%, El.	%, R.A.	HARDNESS (HB)
Set A	99,403 (685)	73,558 (507)	28.0	67.1	207
Set B	101,703 (701)	76,152 (525)	32.0	68.4	207
Set C	94,433 (651)	70,079 (483)	36.0	71.6	196
Set D	96,918 (668)	72,067 (497)	33.0	71.6	207

TABLE 4

CVN Ft * lb (Joules) AT TEMPERATURES INDICATED

TEMPERATURE, °F (°C)	SET A	SET B	SET C	SET D
+70 (21)	99.0 (134)	82.0 (111)	95.0 (129)	103.0 (140)
+50 (10)	89.0 (121) 63.0 (85)	66.5 (90) 76.0 (103)	102.0(138) 95.0 (129)	93.0 (126) 96.0 (130)
0 (-18)	47.5 (64) 42.0 (60)	34.0 (46) 26.5 (36)	84.0 (114) 78.0 (106)	78.5 (106) 75.0 (102)
-25 (-31.5)	31.0 (42) 19.0 (26)	25.0 (34) 24.0 (33)	67.0 (91) 62.0 (84)	54.5 (74) 70.0 (95)
-50 (-45.5)	25.0 (34) 21.0 (28)	19.0 (26) 16.0 (22)	37.0 (50) 37.5 (51)	32.5 (44) 39.0 (53)
-75 (-59.5)	15.0 (20) 18.5 (25)	21.0 (28) 18.5 (25)	29.0 (39) 34.0 (46)	35.0 (47) 34.5 (47)
-100 (-73.3)	15.5 (21)	15.5 (21)	23.5 (32)	22.0 (30)

TABLE 5

SSC SPECIMEN TEST MATRIX

IDENTIFICATION NO.	YIELD STRENGTH ksi (MPa)	STRESS APPLIED ksi (MPa)	PERCENT OF Y.S.
A1	73.0 (503)	43.8 (302)	60
A2	73.0 (503)	36.5 (251)	50
A3	73.0 (503)	21.9 (151)	30
B1	73.0 (503)	43.8 (302)	60
B2	73.0 (503)	36.5 (251)	50
B3	73.0 (503)	21.9 (151)	30
C1	73.0 (503)	43.8 (302)	60
C2	73.0 (503)	51.1 (352)	70
C3	73.0 (503)	65.7 (453)	90
D1	73.0 (503)	43.8 (302)	60
D2	73.0 (503)	51.1 (352)	70
D3	73.0 (503)	65.7 (453)	90

TABLE 6

SSC TEST RESULTS

IDENTIFICATION NO.	STRESS APPLIED ksi (MPa)	INITIAL pH	FINAL pH	FAILURE TIME (HRS)	CONDITION OF GAGE SURFACE
A1	43.8 (302)	2.80	3.80	244.1	N/A
A2	36.5 (251)	2.80	3.60	213.6	N/A
A3	21.9 (151)	2.80	3.70	NO FAIL	PITTED
B1	43.8 (302)	2.80	3.80	243.3	N/A
B2	36.5 (251)	2.80	3.80	133.1	N/A
B3	21.9 (151)	2.80	3.70	NO FAIL	PITTED
C1	43.8 (302)	2.80	3.80	NO FAIL	NO CRACKS
C2	51.1 (352)	2.80	3.70	NO FAIL	NO CRACKS
C3	65.7 (453)	2.70	3.60	227.4	N/A
D1	43.8 (302)	2.80	3.80	NO FAIL	NO CRACKS
D2	51.1 (352)	2.80	3.65	NO FAIL	NO CRACKS
D3	65.7 (453)	2.70	3.65	NO FAIL	NO CRACKS

N/A = No Attack

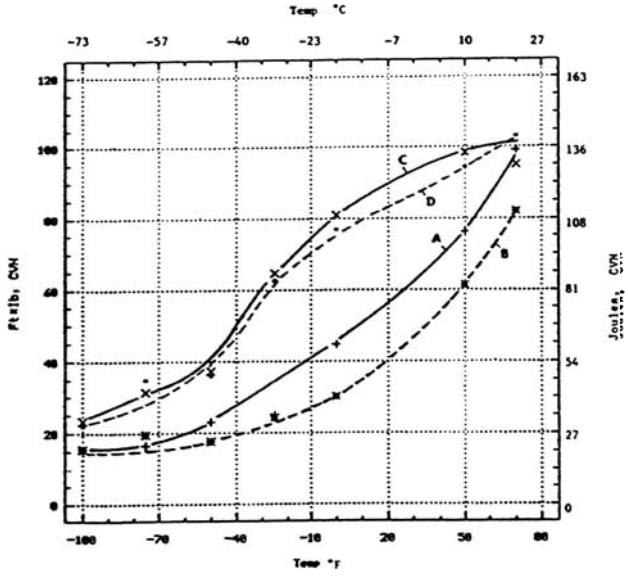


Figure 1

+: Set A - 1800°F(982°C),OQ, 1300°F(705°C) + 1200°F(650°C) Double Temper.

*: Set B - 1800°F(982°C),AC, 1300°F(705°C) + 1200°F(650°C) Double Temper.

×: Set C - 1650°F(900°C),OQ, 1300°F(705°C) + 1200°F(650°C) Double Temper.

•: Set D - 1650°F(900°C),AC, 1300°F(705°C) + 1200°F(650°C) Double Temper.

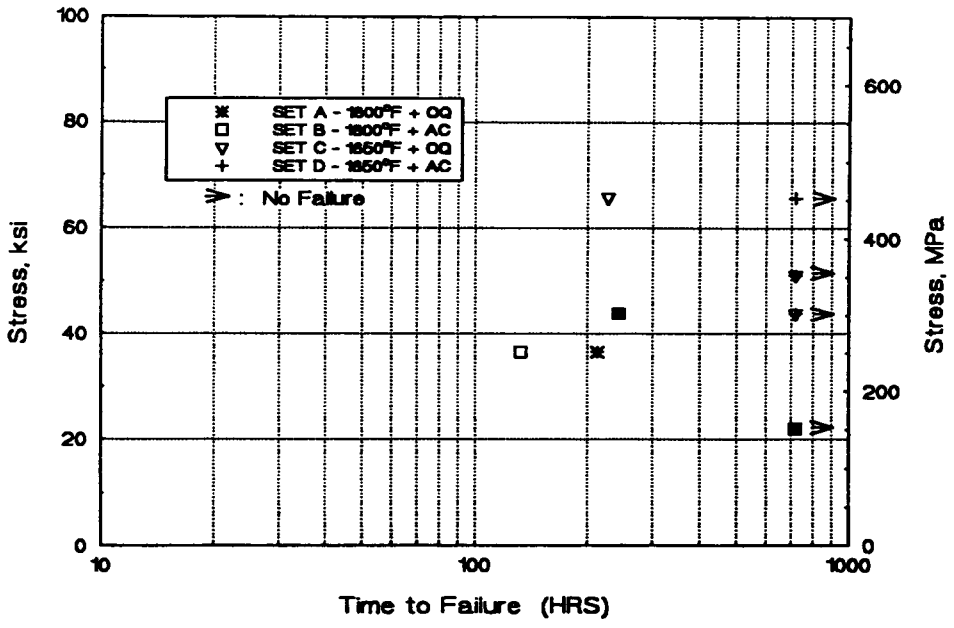


Figure 2 - SSC resistance of 410SS with different heat treatments. Stress vs. Time to Failure.

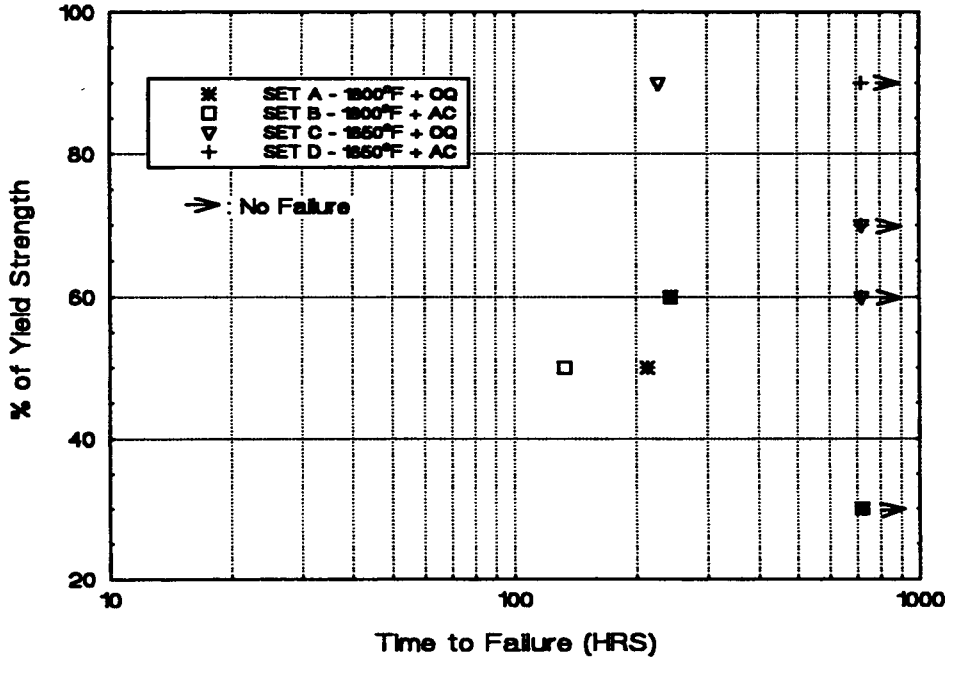
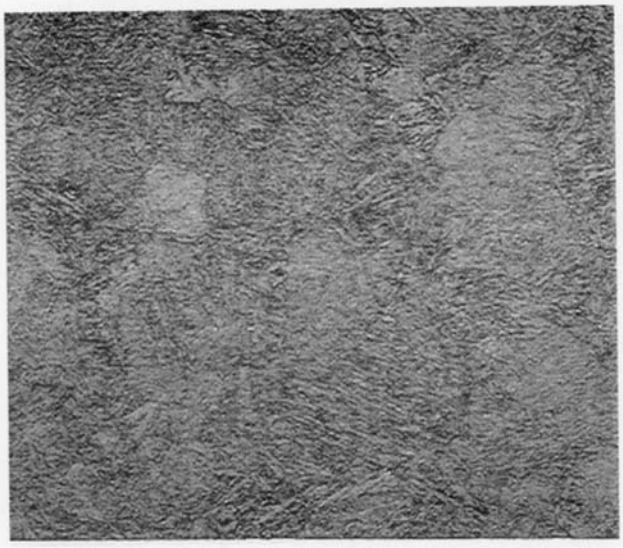


Figure 3 - SSC resistance of 410SS with different heat treatments. Percent of Y.S. vs. Time to Failure.



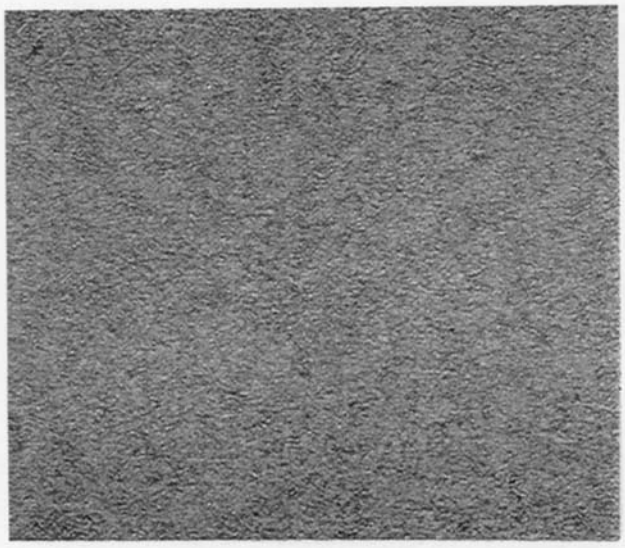
Vilella's Etch 100X

Fig. No. 4 - Set A (1800°F + OQ) microstructure.



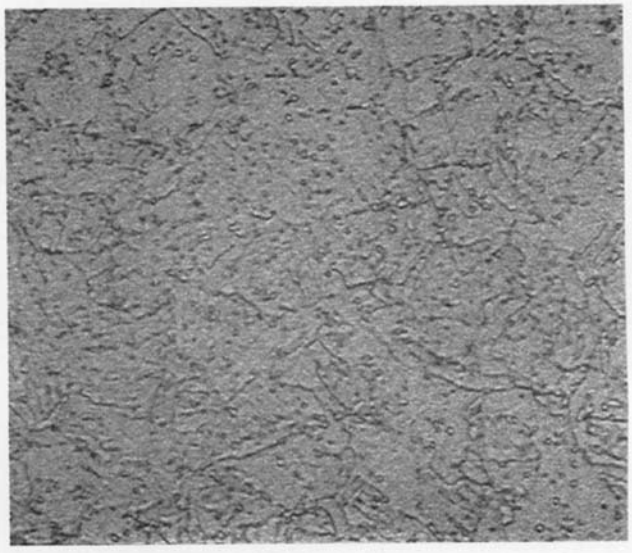
Vilella's Etch 1000X

Fig. No. 5 - Set A microstructure.



Vilella's Etch 100X

Fig. No. 6 - Set C (1650°F + OQ) microstructure.



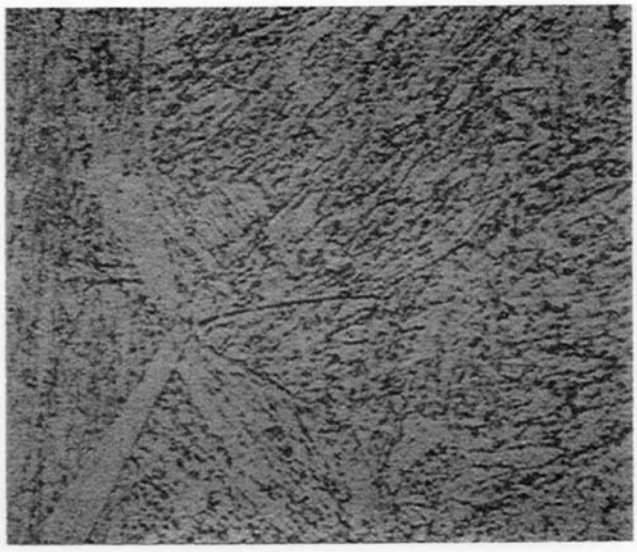
Vilella's Etch 1000X

Fig. No. 7 - Set C microstructure.



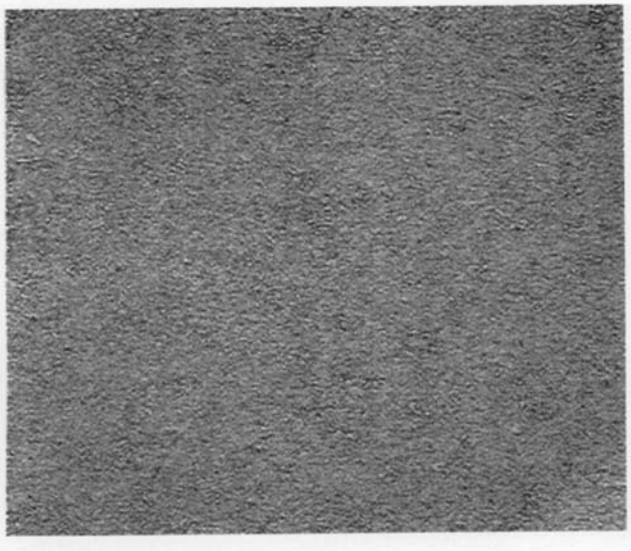
Vilella's Etch 100X

Fig. No. 8 - Set B (1800°F + AC) microstructure.



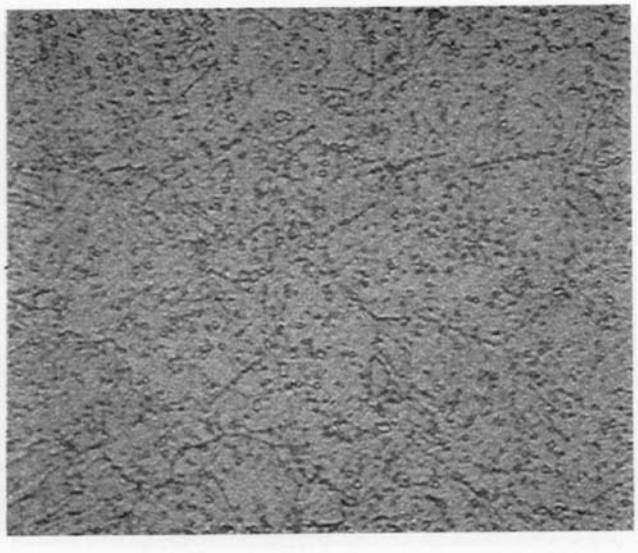
Vilella's Etch 1000X

Fig. No. 9 - Set B microstructure.



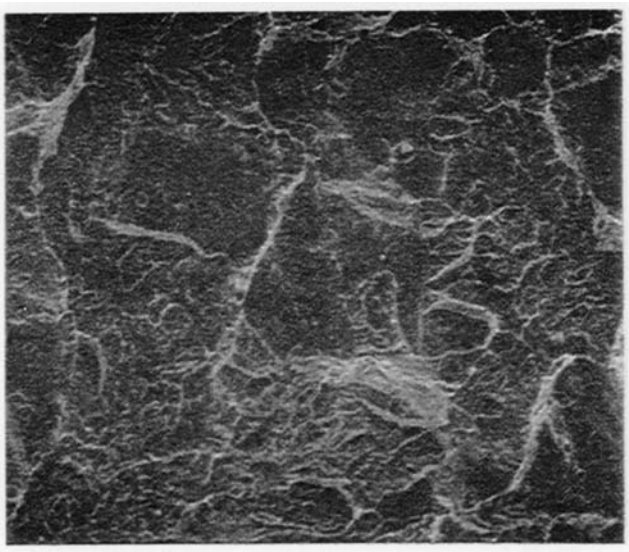
Vilella's Etch 100X

Fig. No. 10 - Set D (1650°F + AC) microstructure.



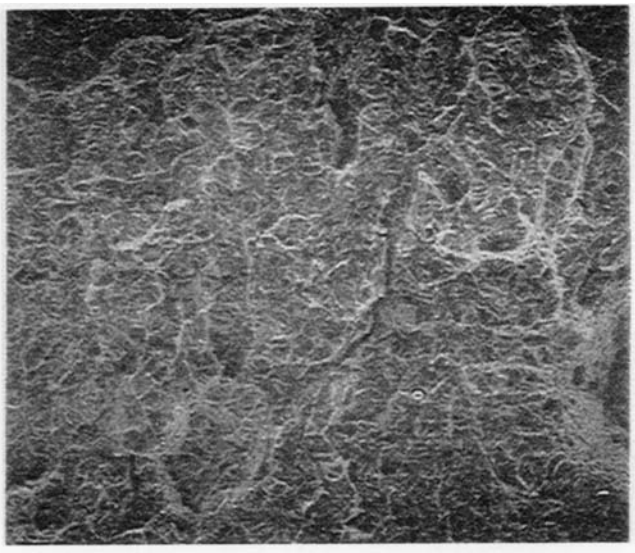
Vilella's Etch 1000X

Fig. No. 11 - Set D microstructure.



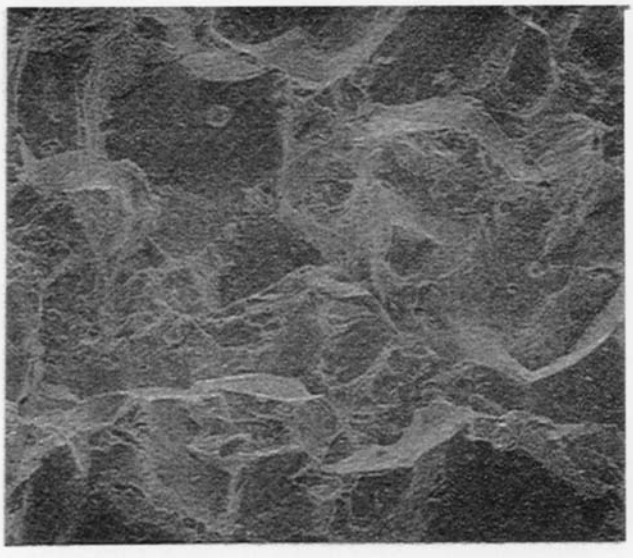
Vilella's Etch 250X

Fig. No. 12 - Set A (1800°F + OQ) impact fracture in cleavage zone, 75-90% transgranular.



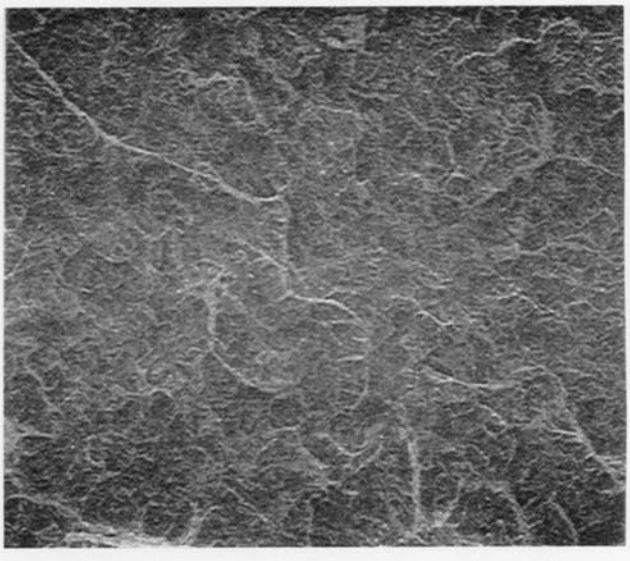
Vilella's Etch 250X

Fig. No. 13 - Set C (1650°F + OQ) impact fracture in cleavage zone, nearly all transgranular.



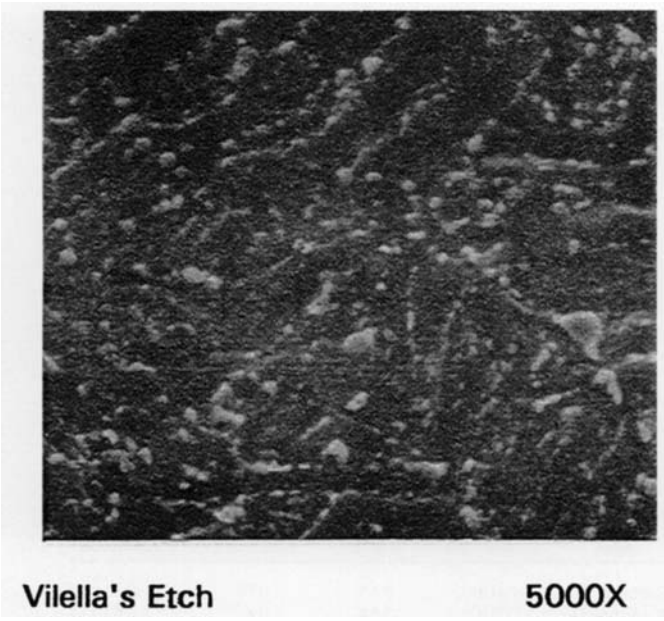
Vilella's Etch 250X

Fig. No. 14 - Set B (1800°F + AC) impact fracture in cleavage zone, transgranular.



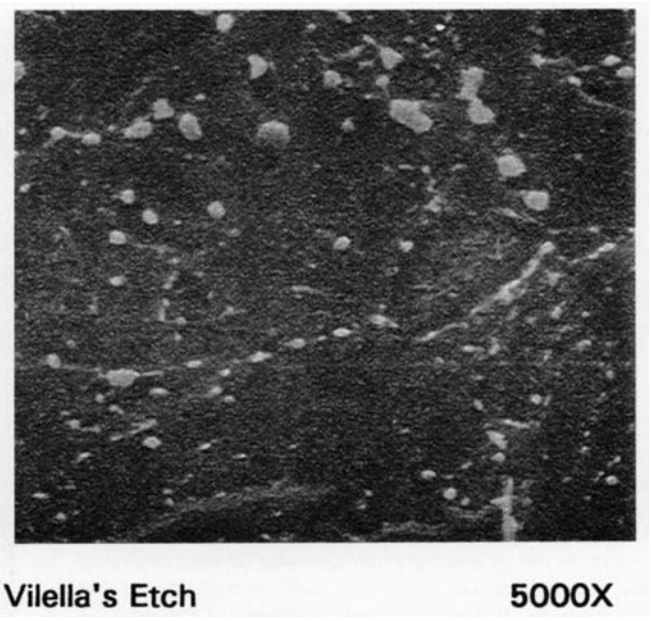
Vilella's Etch 250X

Fig. No. 15 - Set D (1650°F + AC) impact fracture in cleavage zone, transgranular.



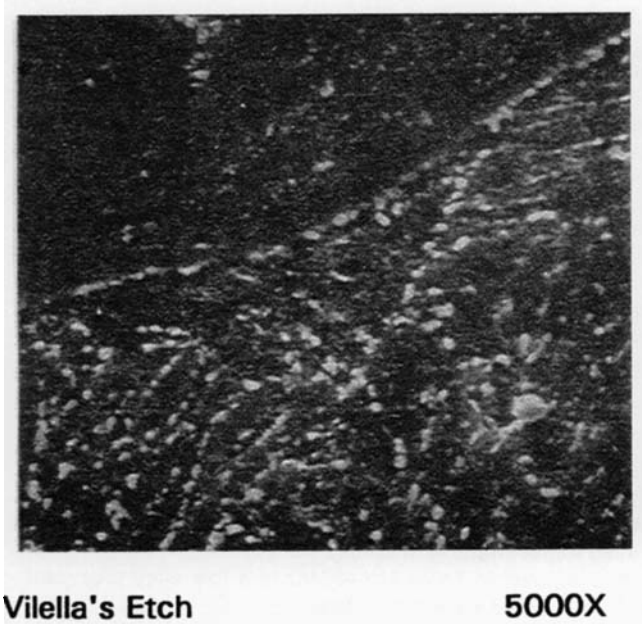
Vilella's Etch 5000X

Fig. No. 16 - Set A (1800°F + OQ) etched microstructure, carbides follow lath martensite and grain boundaries.



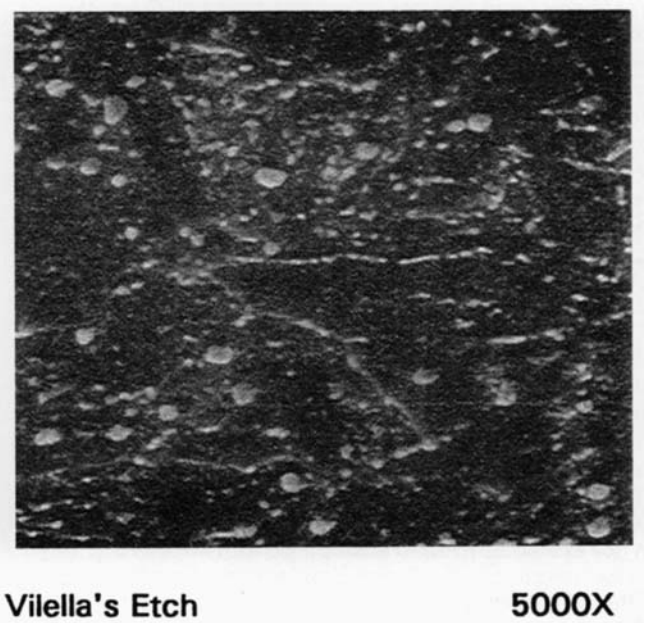
Vilella's Etch 5000X

Fig. No. 17 - Set C (1650°F + OQ) etched microstructure, carbides generally dispersed throughout matrix.



Vilella's Etch 5000X

Fig. No. 18 - Set B (1800°F + AC) etched microstructure, carbides follow lath martensite and grain boundaries.



Vilella's Etch 5000X

Fig. No. 19 - Set D (1650°F + AC) etched microstructure, carbides generally dispersed throughout matrix.

Copyrighted Materials
Copyright © 1996 NACE International Retrieved from www.knovel.com

Sulfide Stress Cracking Resistance of Weld Repairs in Wellhead Alloys*

*M. WATKINS and E. L. VON ROSENBERG**

The sulfide stress cracking (SSC) resistance of weld repairs in A487-9Q and CA-15, two commonly used wellhead casting alloys, was evaluated in NACE TM-01-77 sour acid-chloride solution. The SSC resistance of weld repairs in the as-welded condition was inferior to that of the unrepaired casting. Poor SSC resistance of the repairs was attributed to high hardness in the heat affected zone. Stress relieving at 593 C (1100 F) reduced hardness and improved SSC resistance marginally. Stress relieving at 649 C (1200 F) and 704 C (1300 F) produced significant reductions in hardness and improvements in SSC resistance. In these stress relieved conditions, the SSC resistance of the A487-9Q weldments exceeded that of the unrepaired base metal. However, the SSC resistance of weld repairs in the CA-15 alloy, although improved after postweld stress relief heat treatments, was still not equivalent to the SSC resistance of the unrepaired base metal. The only postweld heat treatment that produced the same level of SSC resistance in the weld repair of CA-15 alloy as in the unrepaired base metal used austenitization at 982 C (1800 F) and tempering at 704 C (1300 F). The heat affected zone of the weld repair, even when stress relieved, was more susceptible to SSC than the base metal in an unrepaired component.

Introduction

A STUDY WAS INITIATED to determine if the sulfide stress cracking (SSC) resistance of weld repairs to wellhead equipment is equivalent to that of unrepaired components. Defective areas in the cast valves are routinely repaired by burning or grinding out the suspect cast metal, then replacing it with weld metal. If the valve is intended for sour service, it should be stress relieved at 621 C (1150 F) to produce a hardness that does not exceed 22 HRC, in accordance with MR-01-75.[1]

One literature survey[2] cites several references that question the effectiveness of postweld heat treatments to restore the SSC resistance of weldments to levels inherent in the base metal. Considering the wide variation in composition and hardenability of low alloy steel and stainless steel alloys that are used to manufacture valves, it is unlikely that a stress relieving temperature of 621 C (1150 F) would be adequate to modify the hardness of local hard spots in the associated heat affected zones (HAZ). Moreover, since many valves were originally given a quenched-and-tempered heat treatment prior to welding, there is a good possibility that the microstructure of the weld repair will be different from, and probably inferior to, the microstructure of the base metal. Several studies have shown that the SSC resistance of a low alloy steel similar to alloys used in the manufacture of valves for wellhead equipment was greatly dependent on microstructure.[3-7] A martensitic structure resulting from a quenched-and-tempered heat treatment was superior to other microstructures. Consequently, the SSC resistance of the weld repair, even if given a stress relieving heat treatment, may be significantly different from that of the base metal.

The primary objective of this study, therefore, is to characterize the SSC resistance of weld repairs in typical wellhead cast alloys and to determine if it is equivalent to the SSC resistance of unrepaired components.

TABLE 1 — Chemical Compositions of Alloys Tested (Wt%)

Alloy	A487-9Q	CA-15	AWS E10018 Electrode	E410-16 Electrode
Carbon	0.31	0.15	0.08	0.11
Manganese	0.97	0.54	0.42	0.53
Phosphorus	0.021	0.047	0.009	0.019
Sulfur	0.025	0.017	0.016	0.011
Silicon	0.91	0.51	<0.02	0.48
Nickel	0.08	0.38	<0.02	0.03
Chromium	1.15	12.53	0.03	12.94
Molybdenum	0.22	0.37	<0.02	0.08

Experimental Methods

Materials

ASTM A487-9Q and Cast Alloy Institute CA-15 were the two alloys studied. Both are representative of alloys commonly used to manufacture wellhead components. Their compositions are given in Table 1. A487-9Q is a low alloy steel and CA-15 is a 12% Cr stainless steel.

Both alloys were in the form of rectangular keel blocks 100 × 100 × 200 mm (4 × 4 × 8 in.) from a commercial foundry that supplies major valve manufacturers. Keel blocks are poured along with the castings and are used to determine mechanical properties of the castings. The keel blocks were heat treated by a commercial heat treater to 187-225 HBN, which is consistent with the practices of valve manufacturers. MR-01-75 specifies a maximum hardness of 22 HRC, which is approximately equivalent to 235 BHN. Alloy A487-9Q was austenitized at 890 C (1650 F), air cooled, re-austenitized at 871 C (1600 F), water quenched, then tempered at 649 C (1200 F).

• Presented during CORROSION/83 (Paper 159), April, 1983, Anaheim, California.

*Exxon Production Research Company, Houston, Texas.

some accelerated attack followed by a long period of denting inhibition.[1]

Summary

The results are consistent with the conclusion reached earlier that denting is caused by an acid chloride attack of carbon steel in the tube-plate crevice. The dent aggravating role of Cu^{++} ion is also confirmed. A neutral chloride + CuO test produced active denting similar to that obtained in 1% seawater + CuO. The tests in which either Fe_3O_4 or SiO_2 were added to 1% seawater produced denting which stopped after several weeks. Denting in these two tests was reinitiated following a subsequent CuO addition. The freshwater + CuO environment did not produce denting, probably because of the alkaline forming tendency of the lake water when heated.

Acknowledgment

This work was sponsored by the Steam Generator Owners Group for the Electric Power Research Institute and the Westinghouse Electric Corp.

[1]*Editor's Note:* Post test photomicrographs are available in the original preprint which can be obtained from NACE in Houston.

References

1. E. P. Morgan, F. W. Pement, N. J. Esposito, R. G. Aspden, "Examination of Denting and Characterization of Associated Materials in the Plate Tube Intersections of Westinghouse Nuclear Steam Generators," presented at NACE Research in Progress, San Francisco, CA, March, 1977.
2. G. Economy, M. J. Wootten, A. R. Pebler, W. T. Lindsay, Jr., "Laboratory Studies of the Denting Phenomena," presented at NACE Research in Progress, San Francisco, March, 1977.
3. M. J. Wootten, G. Economy, A. R. Pebler, W. T. Lindsay, Jr., Materials Performance, Vol. 17, No. 12, p. 30 (1978).
4. W. M. Connor, G. Economy, A. R. Vaia, G. E. Von Nieda, M. J. Wootten, Proceedings of Water Chemistry II, BNES, Bournemouth, U.K., Paper No. 11, 1980.
5. G. E. Von Nieda, G. Economy, M. J. Wootten, Materials Performance, Vol. 20, No. 6, p. 38 (1981).
6. PWR Steam Side Chemistry Follow Program, Palo Alto, CA: Electric Power Research Institute, August 1982, NP 2541.
7. Proceedings: Support Structure Corrosion in Steam Generators, Palo Alto, CA: Electric Power Research Institute, January 1983, NP 2791.

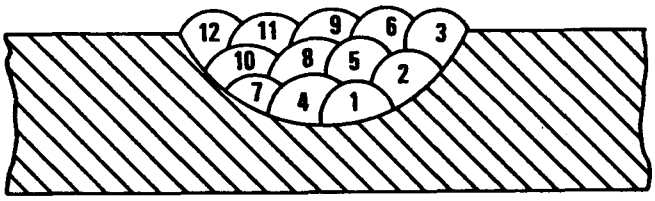


FIGURE 1 — Weld bead geometry used to fill the machine groove.

TABLE 2 — Welding Parameters

	A487-9Q	CA-15
Electrode	E10018-D2	E410-16
Preheat (F)	300 min.	400 min.
Interpass (F)	250 min.	400 min.
Wire diameter (mm)	30	30

TABLE 3 — Postweld Heat Treatments[1]

Code	Alloy	Condition
A1	A487-9Q	As received[2]
A2	A487-9Q	As welded
A3	A487-9Q	Welded + 593 C (1100 F)
A4	A487-9Q	Welded + 649 C (1200 F)
A5	A487-9Q	Welded + 704 C (1300 F)
B1	CA-15	As received[2]
B2	CA-15	As welded
B3	CA-15	Welded + 593 C (1100 F)
B4	CA-15	Welded + 649 C (1200 F)
B5	CA-15	Welded + 704 C (1300 F)
B6	CA-15	Welded + 982 C (1800 F), 593 C (1100 F)
B7	CA-15	Welded + 982 C (1800 F), 649 C (1200 F)
B8	CA-15	Welded + 982 C (1800 F), 704 C (1300 F)
B9	CA-15	Welded + 1038 C (1900 F), 982 C (1800 F), 593 C (1100 F), 593 C (1100 F)
B10	CA-15	Welded + 1038 C (1900 F), 982 C (1800 F), 649 C (1200 F), 621 C (1150 F)
B11	CA-15	Welded + 1038 C (1900 F), 982 C (1800 F), 704 C (1300 F), 677 C (1250 F)

[1]Air cooled after each heat treatment step.
[2]Condition prior to weld repairs.

The CA-15 alloy was austenitized at 1038 C (1900 F), air cooled, re-austenitized at 982 C (1800 F), air cooled, tempered at 704 C (1300 F), air cooled, then retempered at 677 C (1250 F). These heat treated conditions are designated "as-received" in this study.

Weld Repairs

Elliptical grooves approximately 19 mm (3/4 in.) wide and 12 mm (1/2 in.) deep were machined across the width of the keel blocks. The number of grooves per block was limited so that excessive heating during welding would not occur. The grooves were filled with weld metal, simulating weld repairs in a casting. Figure 1 shows the pattern of filling the groove with weld metal.

The weld repair procedures used in this study were representative of procedures used by valve manufacturers. These procedures were reviewed and discussed with three valve manufacturers. The specific welding parameters are given in Table 2. Adhering slag and scale were completely removed prior to the deposition of the next weld bead. All starts and stops were subjected to grinding. The welds were radiographed to locate defects.

Three types of postweld heat treatments were used: (1) stress relief; (2) normalize and temper; and (3) double normalize and double temper. Heat treatment temperatures are given in Table 3. Heat treatment time at temperature was 1 h/in. of thickness. All blocks were air cooled after each heat treatment step. Some keel blocks were kept in the as-welded condition.

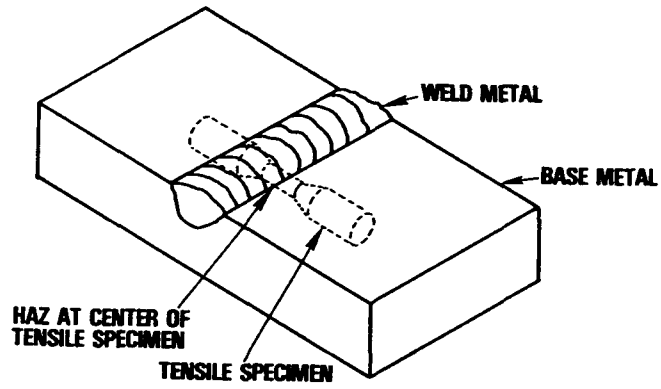


FIGURE 2 — Orientation of the tensile specimen with respect to the weld.

TABLE 4 — Tensile Properties

Code	Yield Strength (MPa)	Yield Strength (ksi)	Tensile Strength (MPa)	Tensile Strength (ksi)	Elongation (%)	Reduction of Area (%)
A1	597	86.7	766	111.2	22	49
A2	60	87.8	78	113.3	18	53
A3	54	79.2	74	108.3	14	44
A4	57	83.2	76	110.7	22	68
A5	56	82.1	76	110.7	20	57
B1	59	86.2	75	109.7	18	55
B2	58	84.4	75	109.4	16	54
B3	56	81.8	73	106.2	15	54
B4	58	84.7	76	110.7	18	55
B5	555	80.6	74	108.7	20	61
B6	777	112.8	92	134.2	17	51
B7	682	99.0	83	121.0	20	58
B8	615	89.3	78	113.3	19	57
B9	777	112.8	940	136.5	15	49
B10	703	102.0	854	124.0	17	57
B11	632	91.8	808	117.3	19	59

Specimen Preparation

Standard 6.25 mm (0.250 in.) diameter specimens were used to determine representative tensile properties of the weld repairs and for NACE specimens. Tensile specimens were machined such that the HAZ of the weld repair was at the midpoint of the gage length (Figure 2). Tensile properties are given in Table 4. The yield strengths of the base metal for A487-9Q and CA-15, respectively, were 597 and 593.9 MPa (86.7 and 86.2 ksi).

Sulfide Stress Cracking Tests

SSC resistance was measured in terms of threshold stress in accordance with NACE procedure TM-01-77.[8] A tensile sample, stressed in uniaxial tension, was immersed in NACE solution, an aqueous solution containing 5% sodium chloride, 0.5% acetic acid, and saturated with hydrogen sulfide gas. The threshold stress was determined for each condition by finding the highest stress the specimen sustained for 30 days without failure.

Results

SSC Resistance

Threshold stresses for the A487-9Q alloy are given in Table 5. Three observations are readily apparent. First, welding caused significant degradation of the SSC resistance of the alloy. The threshold stress of the base metal prior to welding was 45% YS. In the as-welded condition, the threshold stress of the weld repair was less than 10% YS. Second, stress

TABLE 5 — SSC Data for A487-9Q Alloy

Code	Yield Strength (MPa)	Yield Strength (ksi)	Threshold Stress (MPa)	Threshold Stress (ksi)	Threshold % YS
A1	597	86.7	269	39.0	45
A2	605	87.8	61	8.8	10
A3	546	79.2	109	15.8	20
A4	573	83.2	316	45.8	55
A5	566	82.1	311	45.2	55

TABLE 6 — SSC Data for CA-15 Alloy

Code	Yield Strength (MPa)	Yield Strength (ksi)	Threshold Stress (MPa)	Threshold Stress (ksi)	Threshold % YS
B1	594	86.2	238	34.5	40
B2	582	84.4	115	16.7	20
B3	564	81.8	115	16.2	20
B4	584	84.7	175	25.4	30
B5	555	80.6	167	24.2	30
B6	777	112.8	78	11.3	10
B7	682	99.0	136	19.8	20
B8	615	89.3	246	35.7	40
B9	777	112.8	116	16.9	15
B10	703	102.0	176	25.5	25
B11	632	91.8	221	32.1	35

relieving at 593 C (1100 F) produced only marginal improvement in SSC resistance compared to the as-welded condition. The SSC resistance of the weld repair in the 593 C (1100 F) stress relieved condition, however, was not equivalent to that of the unrepaired component. The threshold stress of the 593 C (1100 F) stress relieved condition was 20% YS. Third, the 649 and 704 C (1200 and 1300 F) stress relieved conditions possessed threshold stresses of 55% YS, which were higher than the threshold stress of the unrepaired base metal. Therefore, the SSC resistance of the weld repair was not only restored, but improved by means of high stress relieving temperatures.

Similar results were obtained for the CA-15 alloy and are given in Table 6. The threshold stress of the unrepaired base metal was 40% YS. In both the as-welded and the 593 C (1100 F) stress relieved condition, the threshold stress was less than 20% YS. Unlike the A487-9Q alloy, stress relieving at higher temperatures did not by itself improve the SSC resistance of the weld repair over that of the unrepaired base metal. The threshold stress in both the 649 and 704 C (1200 and 1300 F) stress relieved condition was 30% YS.

Postweld heat treatments B8 (austenitized at 982 and tempered at 704 C) and B11 (double-austenitized at 1038 and 982 C, double-tempered at 704 and 677 C) produced the highest SSC resistance in weld repairs for the CA-15 alloy. The threshold stresses were 40 and 35% YS for postweld heat treatments B8 and B11, respectively. Only heat treatment B8 restored the SSC resistance of the weld repair to that of the unrepaired base metal.

Metallographic Examination

Representative NACE tensile specimens were selected for metallographic examination. All except one of the A487-9Q specimens failed in the HAZ (Figure 3). The one exception was the 1300 F stress relieved specimen that was stressed at 90% YS; it failed in the weld metal. Most of the CA-15 specimens also failed in the HAZ; however, each specimen that was stressed at 90% YS, representing the as-welded and the three

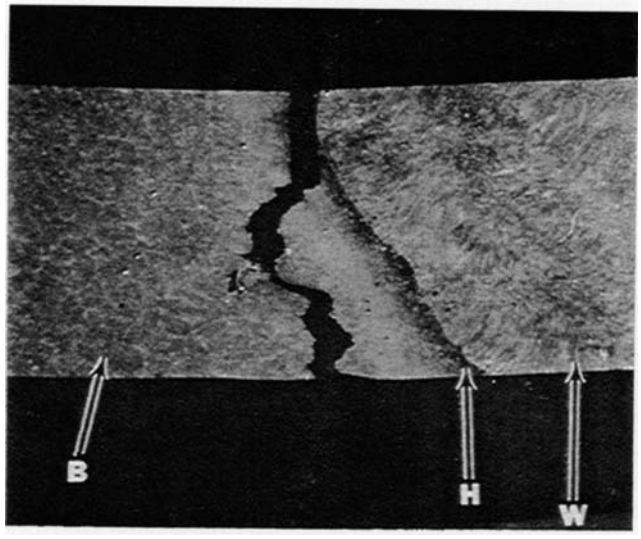


FIGURE 3 — Metallographic specimen showing that fracture initiated in the HAZ of the tensile specimen. Arrow H points to the HAZ, arrow B points to the base metal, and arrow W points to weld. Nital etch.

TABLE 7 — Maximum Hardness in HAZ

Code	Hardness (HV)	HRC Equivalent
A2	339	34
A3	321	32
A4	257	24
A5	257	24
B2	339	34
B3	321	32
B4	297	40
B5	283	27
B6	299	30
B7	283	27
B8	268	25
B9	290	28
B10	287	28
B11	280	27

stress relieved conditions, failed in the base metal. Even in these cases, though, the HAZ contained multiple cracks.

The microhardness of the base metal of A487-9Q was approximately 230 HV. The hardnesses in a given HAZ were quite variable. The hardest areas were always observed adjacent to the fracture surface for those samples that failed in the HAZ. The maximum hardnesses measured in the HAZ of the various samples are listed in Table 7. The maximum hardness measured in the as-welded specimen was 339 HV, which is approximately 34 HRC. In the 593 C (1100 F) stress relieved condition, the maximum hardness was still high at 321 HV (HRC 33). Thus, the poor SSC resistance of both the as-welded condition and the 593 C (1100 F) stress relieved condition was consistent with high hardness in the HAZ. Likewise, improvements in the SSC resistance of the 649 and 704 C (1200 and 1300 F) stress relieved conditions were consistent with significant reductions in hardness to 257 HV (23 HRC).

Similar trends were observed for the CA-15 alloy. The same high hardness levels were characteristic of the as-welded condition and the 593 C (1100 F) stress relieved condition. Moreover, the hardnesses remained at fairly high levels, 297 and 283 HV (29 and 28 HRC), respectively, for the 649 and 704 C (1200 and 1300 F) stress relieved conditions. Lower hard-

nesses were obtained for heat treatments using austenitizing. Since the hardness of the base metal was 247 HV, which is significantly lower than the hardness of any of the stress relieved conditions, the SSC resistance would be expected to be higher in the base metal than in any of the stress relieved conditions.

Microstructural differences in the HAZ were consistent with the hardnesses reported in Table 7. The HAZ in the as-welded condition in the A487-9Q alloy was primarily martensite that had been tempered lightly during welding. However, the characteristic acicular structure was prominent and showed no evidence of decomposition. The HAZ in the 593 C (1100 F) stress relieved condition consisted of tempered martensite, but remnants of the acicular martensitic structure remained. The HAZ in the 649 and 704 C (1200 and 1300 F) stress relieved condition were characterized by completely recrystallized martensite, which is significantly softer than the acicular structure.

Similar findings were observed for the CA-15 alloy. The HAZ contained martensite. The HAZ of specimens that were stress relieved at progressively higher temperatures contained progressively lesser amounts of the remnant acicular structure.

Fractographic Examination[1]

The fracture surfaces of NACE tensile specimens were examined with a scanning electron microscope (SEM). The fracture initiation areas were easy to identify because of the flat, 90° orientation to the tensile axis. All specimens exhibited multiple-origin fractures. Two types of fracture surfaces were observed for the A487-9Q alloy. Specimens tested at loads that were large percentages of yield stress were characterized by initiation areas that were usually confined to the outer rim of the cross section with a rough, fibrous zone at the core. The fracture mode in the initiation areas was mixed, consisting of both intergranular fracture and quasi-cleavage fracture. The initiation areas of specimens tested at lower applied loads were fewer in number and extended greater distances into the cross section, sometimes across the entire fracture surface. At higher magnifications, these fracture surfaces exhibited extensive grain boundary cracking.

The fracture surface of a typical CA-15 specimen was relatively flat, exhibiting little evidence of a shear lip or fibrous fracture. The fracture mode was primarily intergranular.

Discussion

Sulfide Stress Cracking Resistance

The results of this study show that the SSC resistance of cast wellhead alloys was severely degraded by welding. As expected, in the as-welded condition in both the A487-9Q and CA-15 alloys, weld repairs were characterized by hard HAZ and poor SSC resistance. The purpose of the stress relieving heat treatment is to reduce hardness. It is implicitly assumed that the 621 C (1150 F) stress relieving temperature is adequate to reduce hardness of the weld repair sufficiently to restore SSC resistance. Our results show that this assumption is not always correct. A stress relieving temperature of 704 C (1300 F) did not restore the SSC resistance of the weld repair in the CA-15 alloy to a level equivalent to that of the unrepaired base metal. Postweld heat treatment B8, which used austenizing, was the only heat treatment that produced an equivalent level of SSC in CA-15 weld repairs.

The 593 C (1100 F) stress relief temperature was unsatisfactory for both the A487-9Q and CA-15 alloys. The SSC resistance of both alloys stress relieved at 593 C (1100 F) was not significantly improved over that of the as-welded condition. High hardness (321 HV) in the HAZ is one explanation for the poor SSC resistance for the 593 C (1100 F) stress relieved condition. Tempering data for the A487-9Q alloy, the basis for the 621 C (1150 F) temperature in MR-01-75, does not predict this high hardness level. During welding, the microstructure in the HAZ transforms to austenite. Since the temperature in the weld changes rapidly because of high cooling rates, however, homogenization by diffusion of carbon and the other alloying elements cannot take place. Thus, there are areas of alloy segregation that these areas will remain at higher hardness levels. Thus, higher stress relieving temperatures are needed to achieve the desired lower hardnesses.

The detrimental effects of weld repairs were also indicated by the predominant occurrence of failures in the HAZ associated with the repairs. This phenomenon occurred in the stress relieved specimens that had threshold stresses higher than those of the base metal. The few samples that did not fail in the HAZ contained extensive multiple cracks in the HAZ. If stress relieving heat treatments could have truly restored the SSC resistance of the weld repair to that of the nonwelded component, the locations of the failures would have been more evenly distributed between the weld and the base metal. Thus, the microstructure of the HAZ, even after stress relieving, was more susceptible to SSC than the base metal.

[1] *Editor's Note:* SEM micrographs are presented in the preprint, available from NACE Headquarters.

Summary

1. The SSC resistance of weld repairs in the as-welded condition was inferior to that of the base metal for both A487-9Q and CA-15 alloy. Poor SSC resistance of the weld repairs was attributed to high hardness (339 HV) in the HAZ.

2. The SSC resistance of the 593 C (1100 F) stress relieved condition was only marginally better than that of the as-welded condition in both alloys. Areas of high hardness (321 HV) were still present in the HAZ.

3. Stress relieving at 649 and 704 C (1200 and 1300 F) produced significant reductions in the HAZ hardness and, consequently, significant improvements in SSC resistance. In these stress relieved conditions, the SSC resistance of the A487-9Q alloy exceeded that of the base metal. The SSC resistance of the weld repairs in the CA-15 alloy, however, although improved, was still not equivalent to the SSC resistance of the unrepaired component.

4. Austenitization at 982 C (1800 F) followed by a 704 C (1300 F) temper was the only postweld heat treatment that restored the SSC resistance of welds in the CA-15 alloy to the same level as in the unrepaired base metal.

5. Most failures occurred in the HAZ of the weld repair, indicating that the microstructure, even when stress relieved, was more susceptible to SSC than was the base metal.

References

1. NACE Standard MR-01-75, 1980 Revision.
2. A. A. Omar, R. D. Kane, W. K. Boyd, CORROSION/81, Preprint No. 186, National Association of Corrosion Engineers, Houston, TX (1981).
3. J. B. Greer, Materials Performance, Vol. 14, No. 3, p. 11 (1975).
4. R. D. Kane, M. Watkins, J. B. Greer, Corrosion, Vol. 33, No. 7, p. 231 (1977).
5. E. Snape, Corrosion, Vol. 24, No. 9, p. 261 (1968).
6. P. J. Grobner, D. L. Sponseller, D. E. Diesburg, Corrosion, Vol. 35, No. 6, p. 240 (1979).
7. M. Hill, E. P. Kawasaki, G. E. Kronbach, CORROSION/71, Preprint No. 10, National Association of Corrosion Engineers, Houston, TX (1971).
8. NACE Standard TM-01-77, 1977.

Copyrighted Materials
Copyright © 1996 NACE International Retrieved from www.knovel.com

Pitting and Stress Cracking of 12Cr-Ni-Mo Martensitic Stainless Steels in Chloride and Sulfide Environments*

YUICHI YOSHINO and AKIHIKO IKEGAYA***

Abstract

Laboratory melted 12Cr-Ni-Mo steels were tested in chloride/sulfide solutions at 60 C and at room temperature to evaluate their resistance to pitting and stress cracking in connection with environmental and metallurgical factors. H_2S had significant adverse effects on the pitting resistance of the martensitic stainless steels tested. Stress cracking at 60 C was associated in many cases with the formation of pits in chloride/sulfide solutions. Potentiostatic stress cracking tests revealed that in a sulfide solution at room temperature, cracking occurs by hydrogen embrittlement and in chloride/sulfide solutions, by active path corrosion. These steels were tempered at 600 C for the single temper treatment and 700 C followed by 600 C for double tempering. The double temper treatment intensified pitting and stress cracking at 60 C while improving stress cracking resistance at room temperature, as reported elsewhere. Fracture was mixed mode in the single temper condition and transgranular quasi-cleavage with double tempering regardless of solution temperature. The metallurgical changes associated with the temper treatments were studied and discussed.

Introduction

Straight 12Cr martensitic steels, AISI 410 and 420, have been widely used by industry for many CO_2 applications. However, the use of 12Cr stainless steels has been limited to environments of a very low H_2S concentration because their resistance to sulfide stress cracking (SSC) is significantly inferior to that of low alloy quenched and tempered steels.[1,2] In addition, low impact toughness of these steels is a serious concern, especially for wellheads of a high pressure rating.

The petroleum industry has increasingly given considerable attention to low carbon ASTM A-182, class F6NM, as a potential wellhead and valve material for corrosive production fluids containing both CO_2 and H_2S. By comparison, F6NM steel has an excellent low temperature impact property and adequate SSC resistance. Its SSC resistance can be improved by double tempering with the first temper being well into the intercritical temperature range.[3,4] NACE Standard MR-01-75 (1980 Revision[1]) requires that F6NM and other martensitic stainless steels be double tempered for H_2S applications.

The steel must be resistant not only to SSC, but also to pitting and chloride stress corrosion cracking (SCC) because a certain concentration of chloride ions is always expected to occur with H_2S. H_2S is known to promote pitting and SCC of stainless steels,[5,6] e.g., critical pitting temperature is significantly decreased by H_2S. Because F6NM steel contains approximately 4% Ni, it is so sensitive to chloride SCC that it cracks readily in 42% $MgCl_2$ solution. Therefore, evaluating the SCC resistance of the Ni-containing martensitic stainless steel in the sour environment has significant practical importance. However, to the authors' knowledge, only a few works have considered pitting and SCC resistance of this steel while a relatively large volume of work has been conducted with regard to SSC.[7,8]

The purpose of this paper is to elucidate the effects of some environmental and metallurgical factors on the performance of low carbon 12Cr-Ni-Mo martensitic stainless steels in chloride/sulfide environments. The effects of double tempering are highlighted.

Experimental

Material

Chemical compositions of all the steels tested in this study are listed in Table 1. The concentrations of Si, Mn, P, and S are 0.4 to 0.6%, 0.5 to 0.55%, 0.015 to 0.020%, and 0.010 to 0.015%, respectively. They are all vacuum melted laboratory heats except for two that are air melted. Most of the steels are slightly modified from ASTM A-182 class F6NM composition. After hot rolling to 8 mm thick plates, they were normalized at 1020 C and quenched from 980 C. The tempering temperature was 600 C for the single temper condition and 700 C followed by 600 C for the double temper condition, and the holding time was 6 h. Although NACE MR-01-75 calls for a slightly different temper treatment, for simplicity, the steels for this study were tempered at 700 C to produce approximately 50% austenite.

Electrochemical Test

Potentiodynamic anodic polarization experiments were performed at a scan rate of 20 mV/min in several deaerated solutions containing NaCl and/or H_2S at 60 C. The specimen mounted in a holder as described in ASTM G 61 was immersed in the solution for 30 min prior to the experiment, and the polarization was terminated at a current density of 1 mA/cm^2.

In the tests using deaerated 3.5% NaCl at 25 C, the specimen was passivated at −300 mV vs Ag/AgCl for 10 min and anodically polarized at 50 mV/min until the current density reached 100 μA/cm^2; then the potential scan was reversed to

*Submitted for publication March 1984; revised June 1984.

*Materials Research Laboratory, The Japan Steel Works Ltd., Chatsumachi 4, Muroran, Hokkaido 051 Japan.
**Formerly with The Japan Steel Works Ltd.

[1]NACE Standard MR-01-75 (1980 Revision): "Sulfide Stress Cracking Resistant Metallic Material for Oil Field Equipment," National Association of Corrosion Engineers, Houston, Texas 1975.

TABLE 1 — Chemical Composition and Hardness of 12Cr-Ni-Mo Steels Tested

Heat	Chemical Composition (wt%) C	Cr	Ni	Mo	Cu	Ti	Zr	Al	HRC Hardness Single[2]	Double[2]
B1	0.027	12.70	5.08	—	—	—	—	—	20.7	18.3
C0	0.009	12.68	3.75	0.59	1.01	0.06	0.04	0.055	22.9	20.7
C4	0.004	12.57	3.84	0.60	—	—	—	—	17.1	ND
F1	0.021	12.79	3.79	0.57	0.10	0.06	0.08	—	22.1	ND
H0	0.021	12.81	3.76	0.58	0.54	0.07	0.06	0.059	21.8	18.3
N	0.021	12.96	5.09	0.60	0.53	0.11	0.10	—	22.8	ND
X1	0.019	12.97	3.87	0.58	—	0.10	—	—	21.7	15.3
X2	0.024	13.14	3.91	0.60	—	0.16	—	—	24.2	ND
0[1]	0.020	12.33	3.74	0.48	—	—	—	—	17.0	17.2
9[1]	0.020	12.44	3.71	0.48	—	0.24	—	—	20.0	16.5

ND denotes no determination of hardness.
[1]Denotes air melted steel.
[2]Denotes temper treatment.

measure the repassivation potential. The specimen was sealed with Teflon tape after the passivation treatment in 65% nitric acid, and the test surface was polished with No. 320 SiC paper just before the experiment to avoid preferential pitting at the edge of the tape.

Pitting Test

In addition to the electrochemical tests described above, an immersion test was conducted in dilute (0.6% and 1%) $FeCl_3$ solutions at room temperature for 24 h. Weight measurements were taken before and after the test.

Stress Corrosion Cracking Test

U-bend specimens, 2.5 mm thick and 10 mm wide, were used for the evaluation of SCC resistance. The specimen was bent and bolted until straight ends of the specimen were parallel, thus avoiding metal contact between the specimen and Inconel 625 bolt. The calculated strain at the bend surface was approximately 13.5%. Boiling 30% $MgCl_2$ and boiling 25% NaCl (pH 1.5) solutions were used for H_2S-free chloride SCC, as well as 0.5% acetic acid, 0.5% acetic acid-5% NaCl (NACE), 5% NaCl, and synthetic seawater solutions all saturated with 0.5 atm H_2S-0.5 atm CO_2 at 60 C for chloride/sulfide SCC. After a predetermined test duration (two to four weeks depending on the test solution), the specimen was descaled with steel wool and cleanser to allow observation of cracks.

Sulfide stress cracking sensitivity was determined by the four-point bend test at room temperature. The four-point bend test utilized the Shell test specimen described by Fraser[9] and three different H_2S-saturated solutions, namely 0.5% acetic acid, 5% NaCl, and NACE. The test duration was two weeks.

Potentiostatic SCC tests were conducted to elucidate the cracking mechanism in several H_2S-saturated solutions using four-point bend and U-bend specimens. The specimen was examined at 24 h intervals to determine the time to failure.

In all of the tests with H_2S solution, the solution was deaerated by purging with argon gas at 500 mL/min for 1 h prior to the introduction of H_2S. After the saturation, H_2S gas was continuously supplied at a rate of a few bubbles per second. The same procedure was repeated when the test was interrupted and resumed.

Metallurgical Study

Transmission electron microscopy (TEM) was conducted together with electron diffraction and optical and scanning electron microscopy (SEM) to characterize microstructure. The transmission electron microscope was 200KV JEM-200CX. Samples for optical and scanning electron microscopy were polished and etched with 10% HCl-1% picral-methanol.

Some of the SCC test specimens were subjected to SEM fractography and cross section microscopy after observation under low power magnification. The volume of retained austenite was determined by a magnetic flux saturation technique and x-ray diffraction method described by Miller.[10] X-ray diffraction was also conducted to analyze the residue of electrolytic extraction conducted at 18 mA/cm^2 in 10% acetylacetone-1% tetramethylammonium chloride-methanol cooled to 15 C. The weight loss caused by dissolution was 2.2 to 2.3 g. Heights of three diffraction peaks were averaged for Fe_3C [(210),(211),(122)], Fe_7C_3 [d = 2.27, 1.82, 1.79], and $Cr_{23}C_6$ [(422), (511),(531)] and normalized by the peak height of Fe_3C to find the relative volume of these carbides.

X-ray microanalysis was performed using a line scanning technique to determine redistribution of Ni and Cr caused by the partition at the tempering temperature. The acceleration voltage was 30 kV, and the sample current was 100 μA with a beam diameter of 3 μm.

Results and Discussion

Environmental Effects

Pitting Resistance. The anodic polarization curves of Heat F1 in chloride/sulfide solutions were measured as a function of H_2S partial pressure at 60 C. As a parameter for pitting resistance, the overpotential from the corrosion potential to the potential at 100 μA/cm^2, defined here as the pitting overpotential, was plotted against H_2S partial pressure, as shown in Figure 1. The pitting overpotential decreased sharply from 610 to 275 mV upon the introduction of only 0.005 atm H_2S. It further decreased linearly with logarithmic H_2S partial pressure in the range of 0.005 to 0.5 atm. Thus, H_2S has a

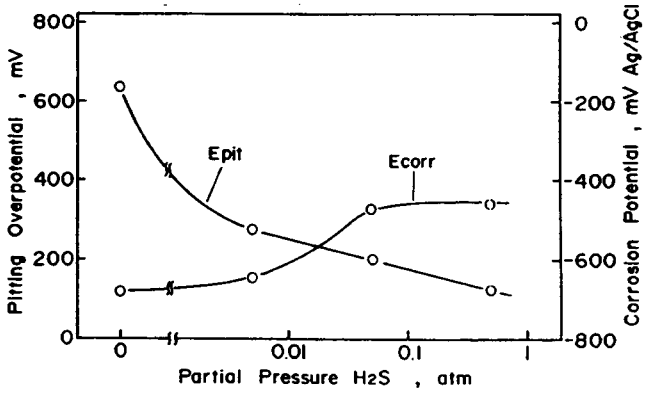


FIGURE 1 — Variations in the pitting overpotential and corrosion potential of Heat F1 with H_2S partial pressure in 1% NaCl solution at 60 C.

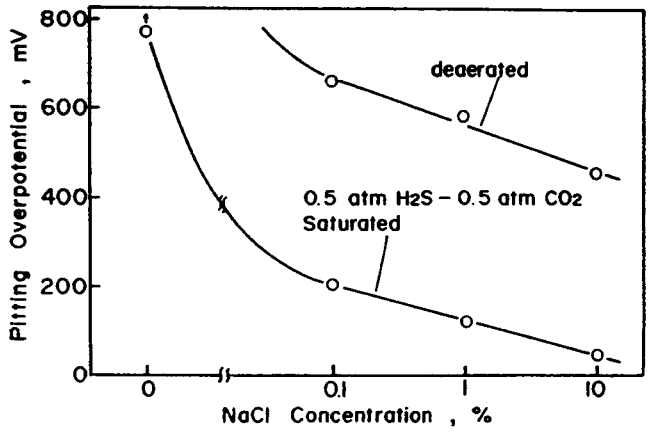


FIGURE 2 — Effect of NaCl concentration on the pitting overpotential of Heat F1 in H_2S-free and H_2S-containing solutions at 60 C.

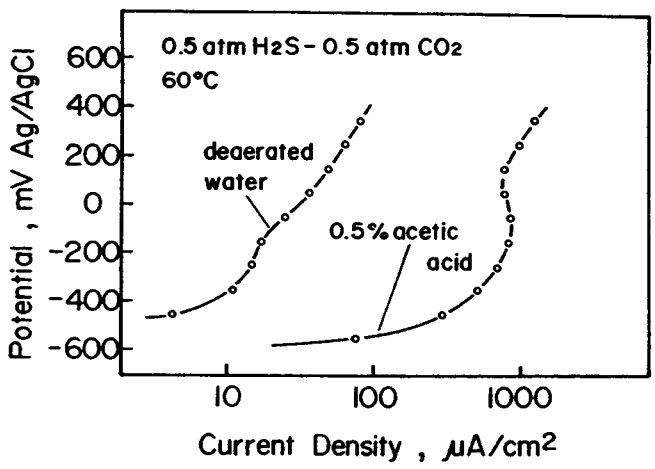


FIGURE 3 — Anodic polarization curves of Heat F1 in chloride-free, 0.5 atm H_2S-0.5 atm CO_2-saturated solutions at 60 C.

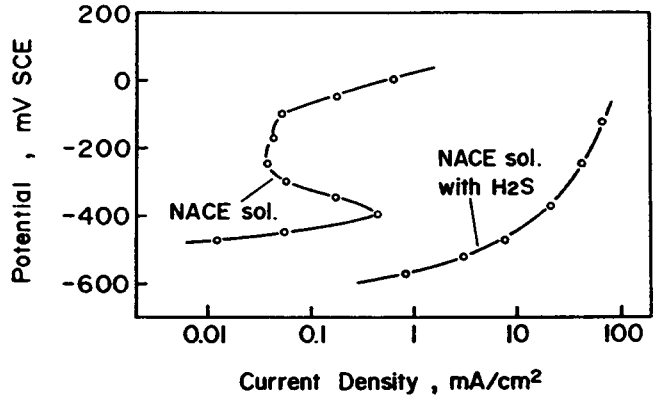


FIGURE 4 — Effect of H_2S on anodic polarization curve of Heat 9 (double tempered) in NACE solution at 20 C.

strong adverse effect on the stability of passive film, thereby promoting pitting corrosion. The corrosion potential increased with H_2S because of the enhancement of the cathodic reaction. This partially accounts for the reduction of the pitting overpotential.

The pitting overpotential was measured as a function of NaCl concentration at the same temperature in solutions saturated with 0.5 atm H_2S-0.5 atm CO_2 mixed gas and some that were not. As shown in Figure 2, the pitting overpotential decreased with NaCl concentration and with H_2S partial pressure, regardless of atmosphere, as would be expected from the work by Johnson.[11] It decreased significantly with the H_2S/CO_2 mixed gas, a shift of about 450 mV in the less noble direction. A careful comparison of the data in Figures 1 and 2 revealed that the effect of 0.5 atm CO_2 is not appreciable, being masked by the predominant effect of H_2S. When the solution contained no NaCl, however, pitting did not take place in either neutral or acidic solution saturated with the mixed gas (Figure 3). Consequently, there seems to be a synergism between H_2S and NaCl, i.e., H_2S promotes pitting only, or at least much more effectively, when NaCl is present.

Figure 4 demonstrates the effect of H_2S in NACE solution at room temperature on the anodic polarization curve. The saturation of 1 atm H_2S resulted in active metal dissolution with no passivation, as took place in the H_2S-free solution. Unlike in the 1% NaCl solution at 60 C (Figure 1), the corrosion potential decreased with H_2S at room temperature, as a result of the promotion of the anodic reaction. The anodic reaction is considered the oxidation of chromium in the H_2S-free solution and the sulfidation of iron in the H_2S-saturated solution.

Stress Corrosion Cracking. Two heats of 12Cr-Ni-Mo steels were used in the U-bend SCC tests using chloride and chloride/sulfide solutions at 60 C. Table 2 summarizes the results. These steels were intact after two weeks' immersion in 0.5% acetic acid solution saturated with the H_2S/CO_2 mixed gas, whereas they cracked or pitted in the 5% NaCl and synthetic seawater solutions. As typically shown in Figure 5(a), there was a tendency in the synthetic seawater for pits to form perpendicular to the direction of applied stress, successively nucleating a new pit in the vicinity of the existing ones. Thus, they looked like a crack. In the 5% NaCl solution, cracks were much sharper, having initiated at the side corner of the specimen, as shown in Figure 5(b). Nevertheless, they were often associated with or initiated from pits. The NACE solution is so aggressive at this temperature that the steels were severely attacked, but no cracking took place.

Both steels cracked in 30% $MgCl_2$ solution with no apparent indications of pitting as is usually the case for austenitic stainless steels in a high concentration of $MgCl_2$. Heat B1 cracked in 25% NaCl (pH 1.5) solution, probably because of a high Ni content, i.e., 5%.

TABLE 2 — Results of U-Bend Tests in Chloride and Chloride/Sulfide Solutions for Heats B1 and X2

	0.5 atm H_2S-0.5 atm CO_2 Saturated, 60 C				H_2S-free, Boiled	
Heat	0.5% HAC	NACE	5% NaCl	Syn. Seawater	25% NaCl	30% $MgCl_2$
B1	intact	attack	crack	pit	crack	crack
X2	intact	attack	crack	pit	pit	crack

Intergranular cracking was predominant in 5% NaCl solution saturated with the H_2S/CO_2 mixed gas (Figure 6). Cracking was also intergranular in 30% $MgCl_2$ solution. The cracking mode in relation to temper treatment will be discussed in more detail later in this paper.

Table 3 shows the effects of temperatures on SCC in synthetic seawater saturated with the mixed gas. The specimen cracked at low temperatures while only fine shallow cracks were observed at and above 60 C. However, as was observed in the previous test, the specimen was pitted at all temperatures and to a greater degree at higher temperatures.

The resistance to SSC was evaluated on two steels of similar composition in three different H_2S-saturated solutions at room temperature using four-point bend specimens. The results are summarized in Table 4, where it is obvious that the aggressiveness of the solutions could be ranked: NACE, 5% NaCl, and 0.5% acetic acid solutions. As pointed out by Phelps,[12] a few percent NaCl promoted SSC to a considerable degree. As is widely recognized, SSC of low alloy steels is due to hydrogen embrittlement. The 0.5% acetic acid solution is more aggressive to these steels than 5% NaCl in terms of pH and less aggressive in terms of NaCl concentration. The net ef-

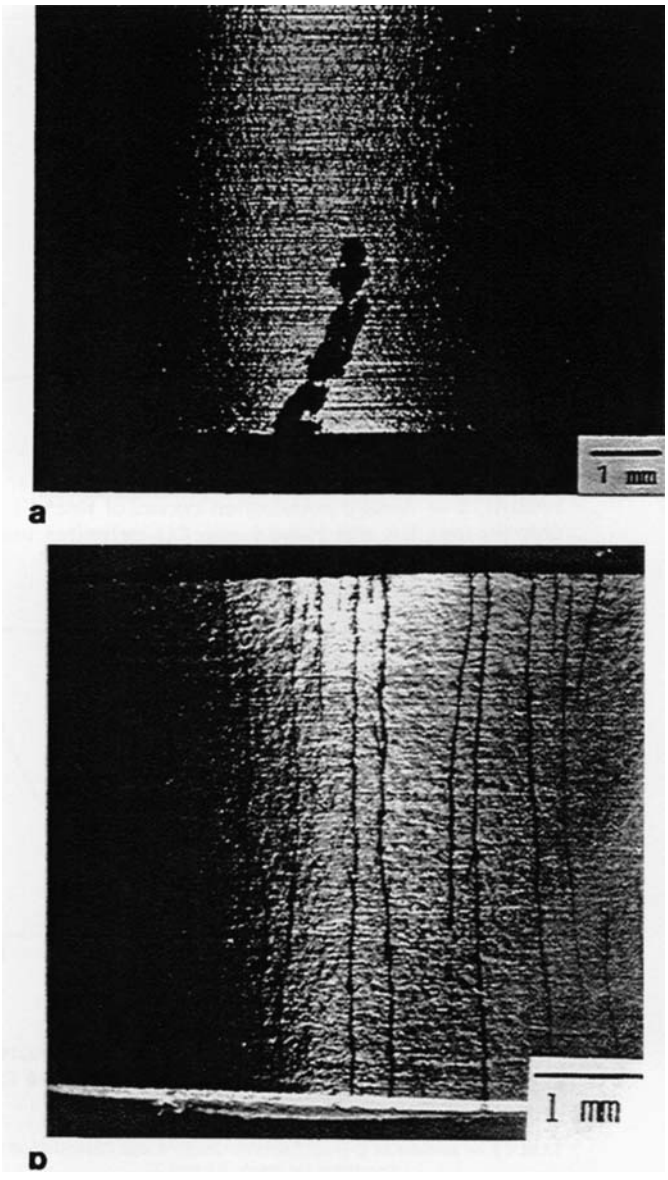


FIGURE 5 — Appearance of U-bend specimen after immersion in H_2S/CO_2-containing solutions at 60 C. (a) Successive formation of pits in synthetic seawater and (b) stress corrosion cracks in 5% NaCl solution.

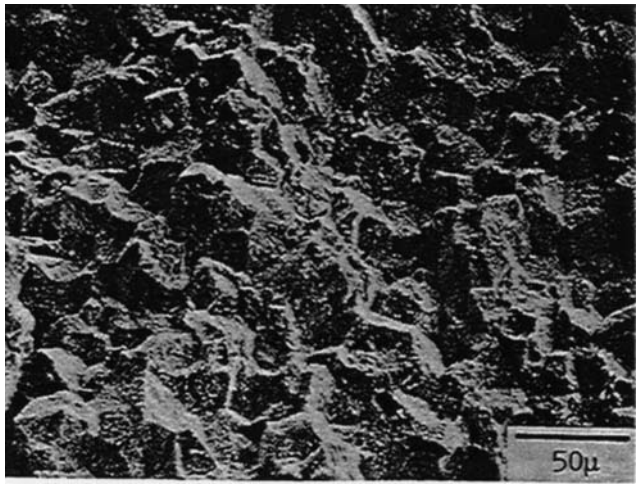


FIGURE 6 — SEM fractograph of U-bend specimen immersed in H_2S/CO_2-saturated 5% NaCl solution at 60 C (Heat X2).

TABLE 3 — Effect of Temperature on U-Bend SCC of Heat C4 in Synthetic Seawater with 0.5 atm H_2S-0.5 atm CO_2

Temperature (°C)			
20	40	60	80
crack	crack	fissure	fissure

TABLE 4 — Results of Four-Point Bend Tests in H_2S-saturated Solutions at Room Temperature

		Applied Stress (ksi)			
Heat	Solution	110	100	90	80
N	0.5% HAC	NF,NF	NF,NF	NF,NF	NF,NF
N	5% NaCl	F,F	F,F	F,F	NF,NF
N	NACE	F,F	F,F	F,F	F,F
X1	0.5% HAC	NF,NF	NF,NF	NF,NF	NF,NF
X1	5% NaCl	F,F	F,NF	NF,NF	NF,NF
X1	NACE	F,F	F,F	F,F	,F,F

NOTE: NF and F denote no failure and failure within two weeks, respectively.

fect is that SSC sensitivity is virtually the same.[13] In this experiment, however, the considerable difference observed between these solutions seems to suggest an involvement of an active path corrosion mechanism.

Potentiostatic stress cracking tests at room temperature showed a promotion of cracking in anodic polarization and retardation in cathodic polarization for both 1% NaCl and NACE solutions, and vice versa in 0.5% acetic acid solution (Table 5 and Figure 7). Thus, active path corrosion is the mechanism of the stress cracking in chloride-containing solutions while hydrogen embrittlement takes place in the chloride-free solution. The fact that all of the failed samples were pitted except the one that failed in 0.5% acetic acid solution indicates a critical role of pitting in stress cracking, i.e., pits trigger stress cracking.

Single Temper vs Double Temper

Pitting Resistance. Figure 8 demonstrates the influence of temper treatment on anodic polarization behavior in H_2S-free 3.5% NaCl solution. The double tempered steel exhibited an appreciably less noble breakdown potential than did the single tempered steel. The same effect was observed to a lesser extent in H_2S-free NACE solution. The reduction of breakdown potential was on the average about 60 mV in the NACE solution. As can be seen in Table 6, single tempering benefits the resistance to pitting in dilute $FeCl_3$ solutions. At 1% $FeCl_3$, all of the specimens pitted, but the single tempered steels showed approximately 25% smaller weight losses.

In the double temper treatment, the first temper was 700 C, or 100 C higher than the single temper. The volume of austenite was dilatometrically about 50% at 700 C in most of steels tested. The partition of carbon as well as alloying

TABLE 5 — Effect of Applied Potential on Failure Time (hours) in U-Bend Test at Room Temperature for Heat C4

	Potential Relative to Corrosion Potential (mV)							
Solution	−400	−300	−200	−100	0	200	300	400
0.5% HAC	120	NF	NF	NF	NF	NF	NF	NF
NACE	NF	NF	24	—	24	—	24	24

NOTE: Corrosion potential was −450 mV vs Ag/AgCl in 0.5% HAC and −680 mV in NACE solution. NF denotes no failure within seven days (168 h).

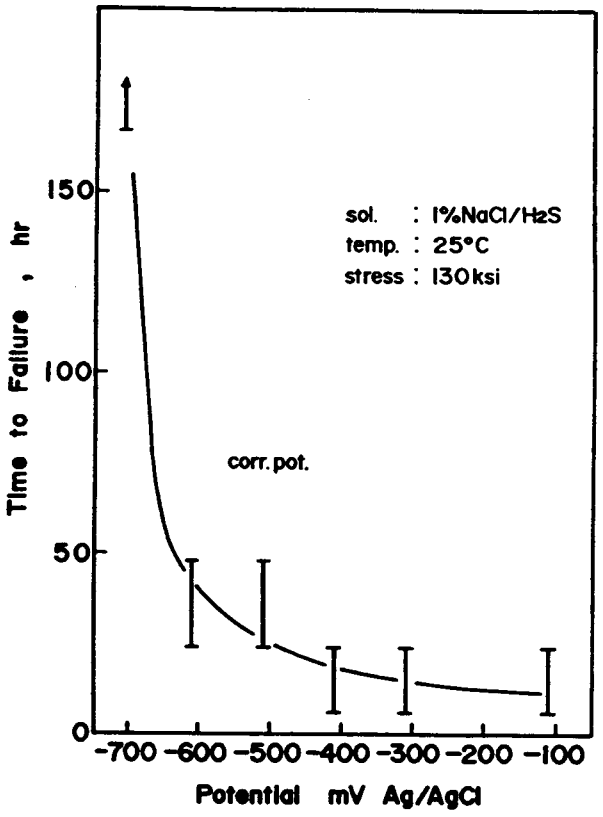


FIGURE 7 — Variation of failure time with applied potential in four-point bend test in H_2S-saturated 1% NaCl solution at 25 C (Heat C4 stressed at 130 ksi).

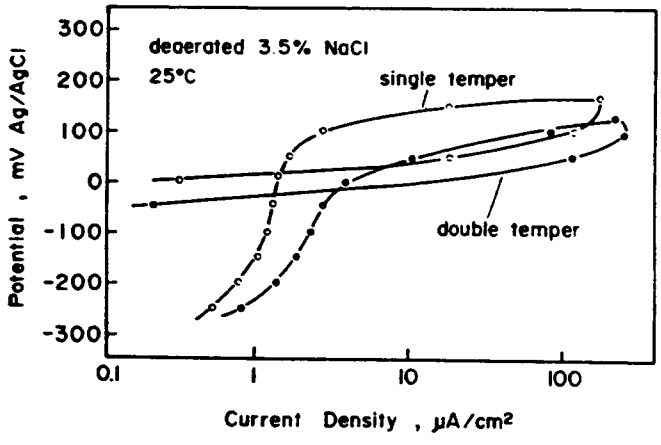


FIGURE 8 — Effect of tempering on anodic polarization curve of Heat C0 in deaerated 3.5% NaCl solution at 25 C.

elements such as Cr and Ni occurs at this temperature. In fact, x-ray microanalysis revealed that the concentration of Ni in the double tempered steel varies with a greater amplitude and interval than in the single tempered steel, as shown in Figure 9. However, no appreciable difference was observed with the distribution of Cr, nor with carbon.

In addition to the alloy partition, double tempering affects the precipitation of carbide. Results of x-ray analysis of extracted residue are summarized in Table 7 to show relative volume of Fe_3C, Cr_7C_3, and $Cr_{23}C_6$. The volume of $Cr_{23}C_6$ was significantly greater in the double temper condition than in the single temper condition. This indicates that double tempering enhances successive transformation of Fe_3C to Cr_7C_3 and $Cr_{23}C$.[14,15] The precipitation of these Cr carbides results in the depletion of Cr in the surrounding matrix and provides a site for pitting.[16]

Stress Corrosion Cracking. Table 8 summarizes the results of a U-bend test in 5% NaCl solution saturated with the H_2S/CO_2 mixed gas at 60 C. In the single temper condition, only one specimen out of six tested failed within two weeks. Microfissures were barely visible only on the side of the specimen. On the other hand, all but one specimen failed in the double temper condition. Many sharp cracks extended from the side corner across the whole width of the specimen, as shown in Figure 5(b). Thus, the double temper has an adverse effect on SCC resistance. In the single tempered steel, intergranular microcracks were observed together with pits formed at the grain boundary [Figure 10(a)]. Cracks undoubtedly started from the bottom of pits in the double temper condition, but grew transgranularly in this case [Figure 10(b)]. This observation is partly supported by the SEM fractograph

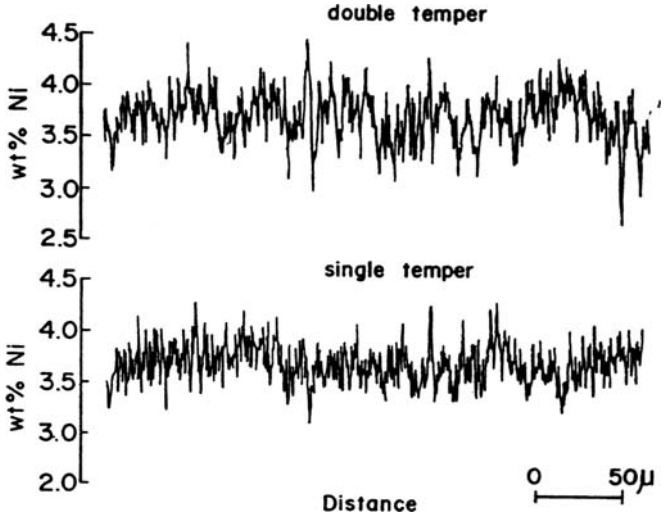


FIGURE 9 — Effect of tempering on distribution of nickel in Heat 9.

TABLE 6 — Influence of Tempering Treatment on Pitting Resistance of Heats C0, H0, and X1 in Dilute $FeCl_3$ Solutions

Heat	Temper	0.6% $FeCl_3$	1% $FeCl_3$
C0	single	intact	pit
	double	pit	pit
H0	single	intact	pit
	double	pit	pit
X1	single	intact	pit
	double	pit	pit

TABLE 7 — Variation of Relative Volume of Carbides with Tempering Treatment for Heat X2

Temper	Fe_3C	Cr_7C_3	$Cr_{23}C_6$
single	1	2	1.8
double	1	2	2.8

NOTE: The volume of Cr carbides is relative to that of cementite.

(Figure 6) where intergranular failure of single tempered Heat X2 is apparent.

Table 9 summarizes the results of four-point bend SSC tests in two solutions at room temperature. The double tempered steels had greater resistance to stress cracking in both solutions. As described earlier, the solutions used in this test

TABLE 8 — Effect of Tempering Treatment on SCC Resistance of Heats C0, H0, and X1 in H_2S/CO_2-Containing 5% NaCl Solution at 60 C

Heat	Tempering Treatment	
	Single (600 C)	Double (700/600 C)
C0	NF,NF	crack,crack
H0	NF,crack	crack,crack
X1	NF,NF	NF,crack

NOTE: NF denotes no failure within two weeks, but microfissures did form on the lateral face of specimen.



a



b

FIGURE 10 — Microscopic nature of stress corrosion cracks in U-bend test in H_2S/CO_2-saturated 5% NaCl solution at 60 C (Heat C0). (a) Microintergranular cracks in single tempered Heat C0 (top view of lateral face) and (b) pit-initiated transgranular crack in double tempered Heat C0 (longitudinal cross section).

both cause stress cracking, but by different mechanisms, i.e., hydrogen embrittlement in 0.5% acetic acid solution and active path corrosion in 5% NaCl solution. SEM fractography of failed specimens revealed the involvement of intergranular failure in the single temper condition and solely transgranular failure in the double temper condition regardless of the solution (see Figure 11). The intergranular cracking was predominant in 5% NaCl solution while it was about 50% of the total fracture surface and appeared to be accompanied by a significant deformation in 0.5% acetic acid solution. This may be because of a difference in applied stress, i.e., 100 vs 130 ksi. The change of fracture path observed here is in good agreement with the results of SCC tests at 60 C shown in Figure 10. Thus, the grain boundary of single tempered steels seems to be inherently weak. The beneficial effect of double tempering was attributed to the reduction of hardness and increase of retained austenite resulting from this treatment.[3,4] However, the change of fracture mode should also be taken into account because transgranular quasi-cleavage fracture generally requires more energy for crack extension than does intergranular fracture.

Figures 12 and 13 show SEM and TEM micrographs for both temper treatments. Using SEM for the single temper condition, the grain boundary appeared as a sharp edge of grain interior. Transmission electron microscopy combined with selected area diffraction technique revealed $Cr_{23}C_6$ carbide and retained austenite at the prior austenite grain boundary. The retained austenite was present chiefly inside the grain, i.e., at the lath boundary. On the other hand, grain boundary in the double temper condition was not as sharp as in the single temper condition. A fine lamellar structure was observed inside the grain by SEM. It is thought to be the result of etching topography, which in turn reflects the partition of Ni. The laths protruded into neighboring grains; thus, the grain boundary was not clearly distinguishable [Figure 13(b)]. The grain boundary carbide was barely discernible.

The degree of interlath carbide precipitation was not appreciably different under TEM between the temper treatments despite the fact that x-ray analysis of the extracted residue demonstrated a more pronounced precipitation of $Cr_{23}C_6$ in the double temper condition.

The double temper treatment generally reduces hardness and increases the volume of retained austenite in Ni-containing martensitic stainless steels.[3,4] In the present study, hardness was reduced by 2 to 7 HRC with the exception of Heat 0. This can account for the greater resistance of the double tempered steels in 0.5% acetic acid solution. However, because hardness is not as critical in active path corrosion SCC as in hydrogen embrittlement, the hardness reduction cannot fully explain the effects of double tempering. Furthermore, in view of the fractographic change associated with the tempering treatments, it is likely that the microscopic nature of the grain boundary plays a more important role in stress cracking than hardness per se.

The volume of retained austenite was measured, and the results were summarized in Table 10 for five steels. Because the x-ray method generally gives a lower volume than the magnetic method, the results for Heats C0 and X2 should only

TABLE 9 — Results of Four-Point Bend Tests in H_2S-Saturated Solutions at Room Temperature in Relation to Tempering Treatment

Solution	Heat	Temper	Applied Stress (ksi)					
			130	120	110	100	90	80
0.5% HAC	0	single	F,F	F,NF	NF,NF	NF,NF		
		double	F,NF	NF,NF	NF,NF	NF,NF		
	9	single	F,F,	F,F	F,NF	NF,NF		
		double	F,F	NF,NF	NF,NF	NF,NF		
0.5% NaCl	B1	single			F,F	F,F	F,F	F,NF
		double			F,F	F,F	NF,NF	NF,NF
	C0	single			F,F	F,F	F,F	F,NF
		double			F,F	F,F	F,NF	NF,NF
	F1	single			F,F	F,F	F,F	F,NF
		double			F,F	F,F	NF,NF	NF,NF

NOTE: F and NF denote failure and no failure within two weeks, respectively.

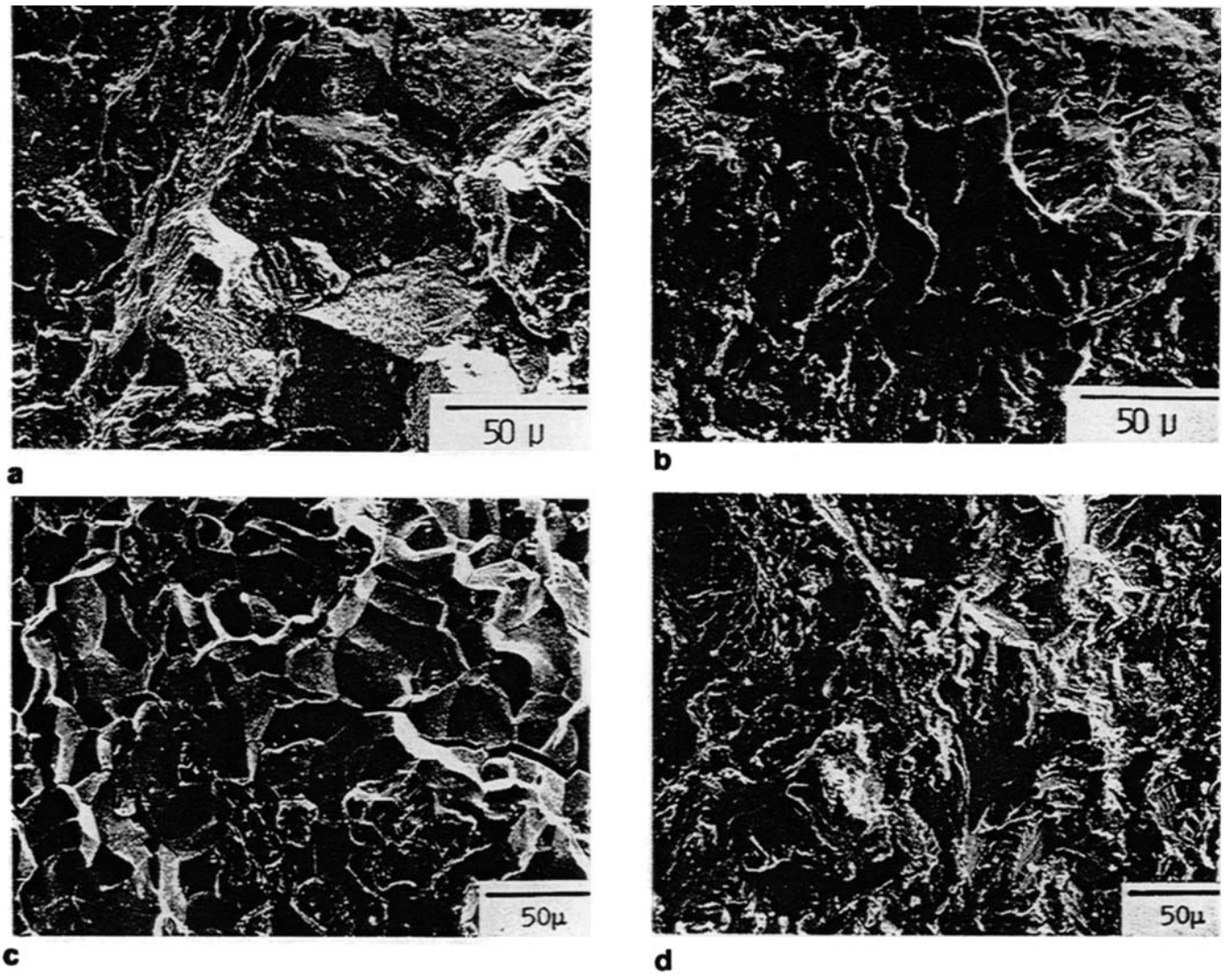


FIGURE 11 — SEM fractographs of four-point bend specimens failed in H_2S-saturated 0.5% acetic acid and 5% NaCl solutions at room temperature. (a) Single tempered Heat 0 in H_2S-saturated 0.5% acetic acid solution, (b) double tempered Heat 0 in H_2S-saturated 0.5% acetic acid solution, (c) single tempered Heat C0 in H_2S-saturated 5% NaCl solution, and (d) double tempered Heat C0 in H_2-saturated 5% NaCl solution.

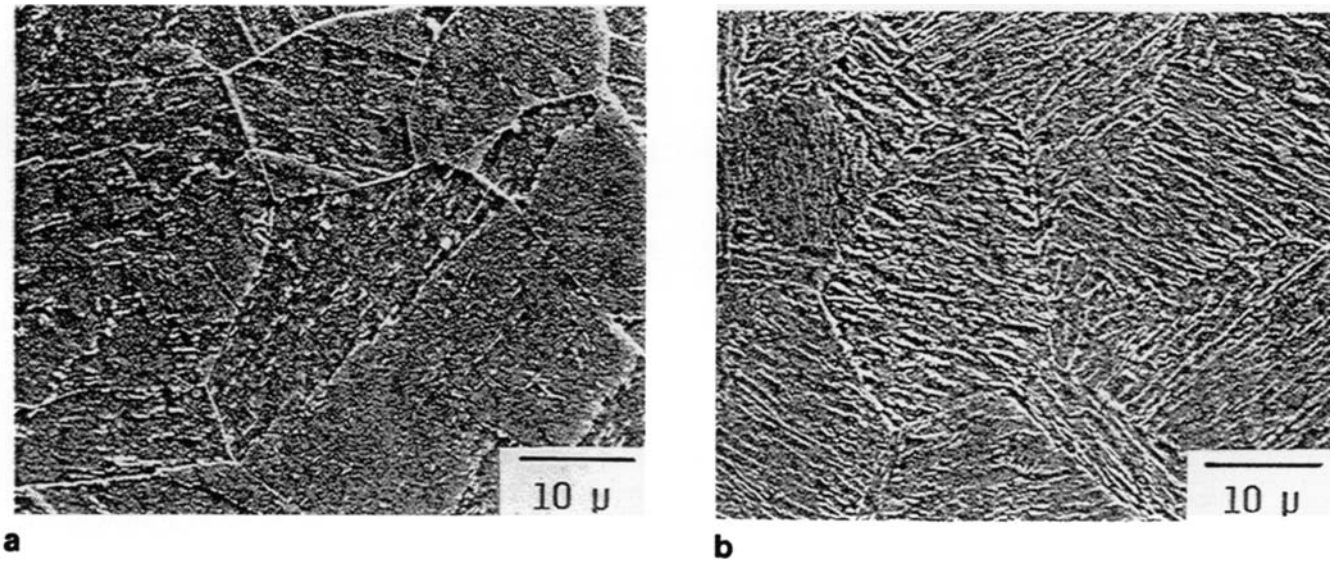


FIGURE 12 — SEM micrographs of Heat C0: (a) single tempered at 600 C and (b) double tempered at 700 C/600 C.

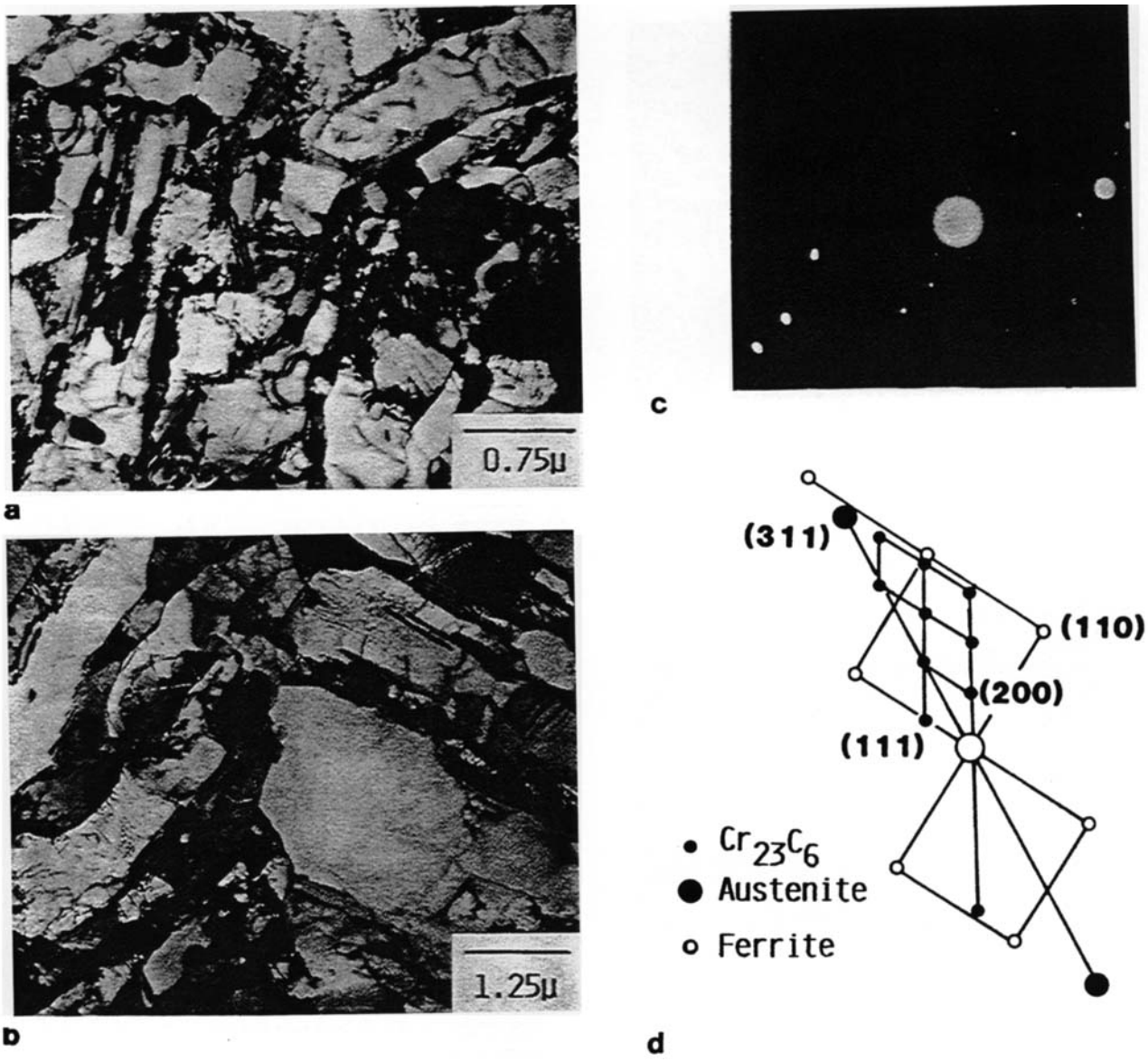


FIGURE 13 — TEM micrographs and electron diffraction pattern of Heat C0. (a) Bright field image of single tempered Heat C0, (b) bright field image of double tempered Heat C0, (c) selected area diffraction pattern for Figure 13(a), and (d) schematic key diagram of Figure 13(c).

TABLE 10 — Variation in Volume of Retained Austenite with Tempering Treatment

Heat	Temper	Volume Retained Austenite (%)	Technique
C0	single	0.4	x-ray
	double	12.6	x-ray
X2	single	2.0	x-ray
	double	10.9	x-ray
0	single	21.0	magnetic
	double	14.5	magnetic
9	single	15.5	magnetic
	double	16.5	magnetic
X1	single	18.0	magnetic
	double	19.5	magnetic

be regarded as a reference.[16] The volume of retained austenite was practically the same for Heats 9 and X1, regardless of the temper treatment, and even reduced in Heat 0 by the double temper. On the other hand, Heats C0 and X2 appeared to show a significant increase. The retained austenite serves as a microcathode, anodically polarizing the neighboring area.[17] It absorbs hydrogen to a much greater extent than the surrounding matrix. It also causes incompatible deformation at the interface. Furthermore, it may be transformed into martensite under stress[18] and/or by hydrogen.[19] All of these can happen in combination in a stressed specimen exposed to the corrosive environment. Whichever mechanism is operative, the total volume of retained austenite cannot explain the change of fracture mode because the retained austenite is predominantly at the lath boundary inside the grain.

Consequently, $Cr_{23}C_6$ carbide and retained austenite observed at the grain boundary of single tempered steels in TEM [Figure 10(a)] seem to be playing a critical role in the initiation and propagation of stress cracking. $Cr_{23}C_6$ carbide particles at the grain boundary promote intergranular SCC in chloride environments, as is well recognized.[20,21] The presence of retained austenite at the grain boundary probably enhances this process, anodically polarizing the adjacent area. The grain

boundary carbide also enhances intergranular hydrogen induced cracking.[22] The retained austenite attracts hydrogen atoms because of its greater solubility. The hydrogen atoms interact with dislocations generated by incompatible deformation of the two phases, thereby eventually resulting in the formation of cracks. If it is transformed into martensite, it provides a preferential path for crack extension. These mechanisms become relatively insignificant at 60 C because the solution is so aggressive at this temperature that no preferential pitting takes place at the grain boundary. Thus, pitting resistance of the bulk structure dominates SCC resistance. As the x-ray diffraction of extracted residue demonstrated, the double tempered steels contain a much greater volume of $Cr_{23}C_6$ and are therefore more sensitive to pitting and SCC.

NACE MR-01-75 (1980 Revision) calls for double tempering of martensitic stainless steels to be used in sour environments. The results of this study indicate that the double tempering impairs pitting and SCC resistance of these steels at intermediate temperatures. The NACE standard requires F6NM steel to be tempered at 675 C and then at 600 C. The first temper is 25 C lower than the tempering temperature used in the present work, but still lies deep in the intercritical temperature range; hence, the same effect will be observed to a greater or lesser extent with the NACE heat treatment. H_2S is often accompanied by a fair amount of salt, usually a few hundred ppm to a few percent, in oil production fluids. When dealing with such an environment, one must face a delicate problem of whether to use a double tempered steel to gain a greater margin for SSC resistance at the expense of pitting and SCC resistance or vice versa. The decision must be based on careful evaluation of major environmental factors such as temperature and concentrations of H_2S and chloride, and the consequences of possible failure.

Conclusion

The following conclusions can be drawn from the results of the present work with regard to the performance of 12Cr-Ni-Mo steels, chiefly F6NM steel, in the wellhead environment containing chloride and sulfide. Pitting resistance deteriorates considerably in the presence of a small volume of H_2S and NaCl in the production fluid. However, F6NM steel is very resistant in the environment containing no chloride ions. In NaCl-containing solutions, stress cracking is triggered by pits. As for sulfide stress cracking at room temperature, cracking sensitivity is enhanced by NaCl much more significantly than in low alloy steels. The promotion of stress cracking is associated with the change in fracture mechanism from hydrogen embrittlement to active path corrosion. Double tempering undoubtedly improves the resistance to sulfide stress cracking at room temperature, which supports the NACE requirement of double tempering for martensitic stainless steels. The improvement is often, but not always, accompanied by the reduction of hardness, as well as dissipation of intergranular failure. However, it impairs pitting and SCC resistance at intermediate temperatures. This is an important finding in view of actual wellhead temperature. The effects of double tempering are considered to be related to carbide and retained austenite at the prior austenite grain boundary.

References

1. R. S. Treseder, T. J. Swanson, Corrosion, Vol. 24, No. 2, p. 31 (1968).
2. P. J. Grobner, R. Garber, Climax Molybdenum Company Report RP-33-80-17, March 10, 1982.
3. D. L. Sponseller, Climax Molybdenum Company Report J-4573, January 1981.
4. R. D. Kane, M. Watkins, J. B. Greer, Corrosion, Vol. 33, No. 7, p. 231 (1977).
5. G. Herbsleb, R. F. Poepperling, Corrosion, Vol. 36, No. 11, p. 611 (1980).
6. Y. Yoshino, unpublished work.
7. H. J. Dundas, "Variations of Microstructure in Seamless Pipe and Their Effect on Resistance to Sulfide Stress Cracking," CORROSION/79, Preprint No. 173, National Association of Corrosion Engineers, Houston, Texas, 1979.
8. H. J. Dundas, Climax Molybdenum Company Report J-4642, December 31, 1980.
9. J. P. Fraser, G. G. Eldredge, R. S. Treseder, Corrosion, Vol. 14, No. 11, p. 517t (1958).
10. R. L. Miller, Trans. ASM, Vol. 57, p. 892 (1964).
11. M. J. Johnson, "Relative Critical Potentials for Pitting Corrosion of Some Stainless Steels," Localized Corrosion—Cause of Metal Failure, ASTM STP 516, ASTM, Philadelphia, Pennsylvania, p. 262, 1972.
12. E. H. Phelps, Metals Engineering Quarterly, No. 5, p. 44 (1973).
13. Y. Yoshino, unpublished work.
14. A. Inoue, T. Masumoto, Met. Trans., Vol. 11A, No. 5, p. 739 (1980).
15. R. G. Baker, J. Nutting, J. Iron Steel Inst., Vol. 187, No. 7, p. 257 (1959).
16. N. D. Tomashov, G. P. Chernova, O. N. Marcova, Corrosion, Vol. 20, No. 5, p. 166t (1964).
17. S. Shimodaira, M. Takano, Y. Takizawa, H. Kamide, "Mechanisms of Transgranular Stress Corrosion Cracking of Duplex and Ferritic Stainless Steels," Stress Corrosion Cracking and Hydrogen Embrittlement of Iron Base Alloys, NACE-5, R. Staehle. J. Hochmann, R. McCright, J. Slater, Eds., National Association of Corrosion Engineers, Houston, Texas, p. 1003, 1977.
18. G. M. Gordon, "Physical Metallurgy of Fe-Cr-Ni Alloys," Stress Corrosion Cracking and Hydrogen Embrittlement of Iron Base Alloys, NACE-5, R. Staehle, J. Hochmann, R. McCright, J. Slater, Eds., National Association of Corrosion Engineers, Houston, Texas, p. 893, 1977.
19. R. J. Asaro, A. J. West, W. A. Tiller, "Hydrogen Induced Phase Transformation of Austenite to Martensite," Stress Corrosion Cracking and Hydrogen Embrittlement of Iron Base Alloys, NACE-5, R. Staehle, J. Hochmann, R. McCright, J. Slater, Eds., National Association of Corrosion Engineers, Houston, Texas, p. 1115, 1977.
20. H. Tomari, et al., "Influence of Chemical Composition on the Intergranular Stress Corrosion Cracking Susceptibilities of Ferritic Stainless Steels in High Temperature Aqueous Environments," CORROSION/81, Preprint No. 121, National Association of Corrosion Engineers, Houston, Texas, 1981.
21. WRC Bulletin 138, February, 1969.
22. C. L. Briant, Met. Trans., Vol. 9A, No. 5, p. 731 (1978).

Copyrighted Materials
Copyright © 1996 NACE International Retrieved from www.knovel.com

Paper No.
86

CORROSION 95
The NACE International Annual Conference and Corrosion Show

THE APPLICATION & FIELD EXPERIENCE OF HIGH STRENGTH 12% Cr CENTRIFUGALLY CAST PIPE FOR GAS GATHERING SYSTEM

A. Yoshitake, M. Teraoka, T. Torigoe
Hirakata Plant, Kubota Corporation
1-1 Nakamiya Ohike 1-Chome, Hirakata-shi
Osaka 573 , Japan

S. Amako
Kubota America Corporation
World Houston Plaza
15710 JFK Blvd Ste 288
Houston , TX77032

ABSTRACT

Centrifugal cast method is one of the processes to provide high quality seamless pipe. The advantages of the process are

① heavy wall pipe can be manufactured.

② relatively flexible in material selection for manufacturing pipe.

For sweet corrosion environment caused by CO_2 [1][2] where carbon steels can not be used, centrifugally cast 12% Cr martensitic stainless steel pipes and fittings have been developed. One of the key factors of this material applied to pipeline is the weldability, especially high hardness of the welds or its heat affected zone which causes for brittle rupture as well as stress corrosion cracking of the pipeline. Cast 12%Cr pipe which has high strength with low hardness even at the weld joint has been developed. Besides of the development of straight pipe, several types of fittings have been developed. These pipes and fittings have been used for natural gas gathering lines and booster compression lines in sweet corrosion service.

Keywords: centrifugal casting, 12%Cr steel, martensitic stainless, sweet corrosion, welding, fittings,

INTRODUCTION

In the oil and gas production services, there are a number of corrosive wells where corrosion resistant materials for their piping systems are required. It is noted that the internal corrosion of the pipeline may take place when the fluid contains CO_2, H_2S, O_2, and/or brine[2].

In the natural gas wells contains 13 to 15% CO_2, 50 to 100ppm H_2S, and water, with the gas pressure of 4500psi [8] and the gas temperature at 350F(177°C) [9] 、 carbon steel gathering lines were suffered from corrosion problems, although it had been anticipated that the interaction of CO_2 and H_2S would react with carbon steel to form a protective film[3][7]. Generally this type of environment, however, was classified into sour corrosion[1][2], it was rather considered as sweet corrosion because the corrosion was mainly caused by CO_2 dissolved in water.

Martensitic stainless steel pipe has been considered to be adopted as the replacement of the carbon steel pipeline, since valve bodies of 12%Cr alloys (Type 410) had been used without any corrosion problems[3]. Furthermore it is well known that martensitic stainless steel such as AISI 410 or CA15 was the best choice[1][5] for the material of this type of corrosion pipeline to handle high pressure corrosive oil and gas from the wellhead to some central processing facility where either the corrosive product or water is removed.

This type of material normally has high strength as well as corrosion resistance, but has high hardness especially at the weld joint. It is pointed out that toughness reduction and degradation in stress corrosion cracking resistance may be occured with increasing the hardness of the material. NACE standard, MR-0175 [6] stated that the hardness of this type of grade should be less than HRc 22 (Hv 248) including at weld joint.

Centrifugal cast 12%Cr pipe (KCR-13A)Note 1 which has high strength with low hardness even at the weld joint has been developed [4].

Furthermore, in order to make fittings from the centrifugal cast pipe, high temperature properties of the material were investigated. It was found that the material had enough ductility at temperature of 700 to 800°C. From these studies, several fittings such as elbows, tees, and reducers of 8 to 26 inches nominal diameter was produced.

Thus, centricast 12%Cr pipe has been used not only for natural gas gathering lines, but also booster compression piping systems in sweet corrosion service.

MATERIAL

Centrifugal casting

The outline of the centrifugal casting process is as follows. First, well refined molten metal is poured into a rotating metallic mould. Then, the molten metal is subjected to the centrifugal force (around 100 to 200G) to form a cylindrical shape. Solidification will take place from outside in. During the solidification, the centrifugal force is applied to the molten metal which result in the greater compactness of the metal and high quality casting. By controlling the weight of the molten metal poured, the required wall thickness of the pipe can be adjusted.

Material requirement

Centrifugal cast 12%Cr pipe which has high strength with low hardness even at the weld joint has been developed. Required mechanical properties of the base metal are as follows. The hardness requirement of Hv 238 max. is somewhat lower than that of NACE requirement.

0.2% Proof Strength	:	415MPa min.
Yield Ratio	:	0.80 max.
$vE_{10°C}$	:	20J (34J Average) min.
Hardness	:	Hv 238 max. (including the highest hardness point at HAZ)

From the corrosion resistance view point, the chemical composition range of cast 12%Cr has been specified as shown in Table 1 [4]. In order to achieve the specified mechanical properties which are conflicting each other, the effect of each element on the mechanical properties was investigated . With increasing C and Ni content, the hardness was increased. As shown in Figure 1, C and Si affects the toughness. On the other hand, the microstructure of 12%Cr cast material consists of tempered martensite and delta ferrite. The delta ferrite also affects mechanical properties.

Note 1. KCR-13A is the trade name of Kubota Corporation.

For the purpose of finding suitable chemical balance, each mechanical property was arranged by the ratio of Cr equivalent to Ni equivalent (Cr_e/Ni_e). Figure 2 shows an example of the effect of Cre/Nie on the yield strength and hardness. Through these invesigations, it was found that the ratio of Cr equivalent to Ni equivalent (Cr_e/Ni_e) should be within 5 to 6.5, and Si content should be less than 0.5%. Thus , the target value of each element of cast 12%Cr material was determined within the specified chemical range shown in Table 1

Heat treatment

From thermal analysis of the material, it was found that the cast 12%Cr had AC_1 transforming point at around 800°C and AC_3 at 860°C. Besides of these investigations, the isothermal transformation of the material was also investigated. As the results, the following heat treatment was applied to the cast 12%Cr pipe.

920/950°C → air cool
730/760°C → air cool

The mechanical properties of each size of production pipes are shown in Table 2.

Corrosion resistance [4]

The corroison tests were performed on various Cr content materials in a CO_2 saturated aqueous solution, with and without NaCl at a temperature of 350F (177°C). The test specimens were put in a autoclave in which CO_2 gas was pressurized to 210 psig in the solution and heated. The duration time was 120 hours, and corrosion weight losses were measured after tests. As shown in Figure 3, the corrosion rate decreased markedly as Cr content is increased. 12% Cr material shows enough corrosion resistance compared with carbon steel. In order to verify the corrosion resistance of this material, anodic polarization measurements were performed potentiodynamically at scanning rate of 20mV/min. [9]. In comparison between cast and wrought 12%Cr materials, the corrosion potential (Ecorr) of both materials are similar, but the passive current density (ip) of cast 12%Cr material is lower which means more stable than that of type 410 material in CO_2 saturated 0.05M Na_2SO_4 solution where carbon steel has no passive range.

Stress corrosion cracking (SCC) properties were studied with the slow strain rate technique. Susceptibility to SCC was evaluated by the rate of elongation to failure in solution to that of in air (Ef in sol. : Ef in air)、in a word, the larger the ratio, the less susceptible the alloy. Table 3 summarizes the test data, and it is clear that cast 12%Cr is less susceptible to SCC than type 410 and carbon steel.

FITTINGS

Availability of fittings is one of the interesting points for the materials applied to pipeline systems. For the purpose of making fittings from a centrifugal cast pipe, high temperature properties of the material were investigated. Figure 5 shows elevated temperature tensile test data of cast 12%Cr materials which indicate that the material has peculiarity in ductile at the temperature between 700 to 800°C. By using these characteristics, hot forming fittings can be produced. By high frequency induction bending process, stick type bends with a radius of more than 1.5 times of the outside diameter can be produced. Short radius and long radius elbows can be produced by hot-die bending or hot-mandrel bending processes(Figure 6). Tees can be produced by hot-extruding forming (Figure 7). Needless to say, heat treatment after hot forming is required as the same as straight pipe.

WELDING

Welding is one of the key technologies for the 12%Cr pipe to be adopted in oil and gas pipelines. The important points of quality in the weld joints with this materials are the hardness and the toughness. As described before, by controlling the chemical compositions, high strength with low

hardness 12%Cr martensitic stainless steel casting has been developed. It was found that the hardness even at heat affected zone where the highest hardness can be expected satisfied the specification.

Several types of welding processes were tested such as GTAW, GTAW+GMAW, GTAW+SMAW. One example of welding and it's properties are summarized in Table 4 to 6, and Figure 8. Furthermore, fracture toughness at the weld joint was investigated by COD method at -20°C in accordance with BS 5762. Even at the heat affected zone where the highest hardness distributed, COD value of δc was 0.32mm which satisfied the pipeline quality.

Prior to welding, preheating at 200°C was applied. After welding, all welds received a minimum 2 hours PWHT at around 730°C. A local annealing devices in the form of a coil was used. Skin temperature was measured and recorded with at least two thermocouples.

CONCLUSIONS

By controlling chemical compositions, centrifugal cast 12%Cr pipes which have high strength with low hardness even at the weld joints have been developed. Several types of fittings such as elbows, tees, and reducers can be produced from centrifugal cast pipes.

When considering the development of a new oil and gas field or providing new equipment for an existing facility, there are many factors to consider. Costs are obiously significant but other matters must be considered such as continuous and safe operation : avoidance of unscheduled failure which may cause leakage and hence pollution. Due to the ability to provide a full range of high quality pipe, fittings and bends, there are many attractive applications.

Primarily, the material has been developed for natural gas gathering line in sweet corrosion service where 8 inch O.D. and Sch120 straight pipes were required [4]. These pipes have been supplied for more than 10 years and total length more than 24km. Periodical check by ultrasonic inspection detected no decrease in wall thickness of the pipes. By a pipe through visual inspection performed for the cast gathering lines, no localized corrosion such as pitting or erosion was detected.

Based on these field experience, and by the development of fittings, centrifugal cast 12%Cr pipes have been adopted to another application such as booster compression piping systems where 13 to 15% CO_2, 80 ppm H_2S, and water were contained with the gas pressure of 600 to 960 psig and maximum temperature of around 290F (143°C). Nominal diameter of 8 to 26 inch centrifugal cast pipes and fittings have been supplied.

REFERENCES

1. S. Karlsson : " Technical and economic Aspects of Stainless Steels in Corrosive Downhole Environments" Stainl Steels ('84) P438-445
2. R.D. Kane, "Corrosion of Stainless Alloys in Oilfield Production Environments" Stainless 84 (GBR), (1985), P429-437.
3. J.R. Seipel : "Arun Field Development Phase", Offshore South-east Asia 82 Conference, 1982
4. M. Matsui et al : "The Development of High Strength 12%Cr Centri Cast Pipe for Sour Gas Piping System", Corrosion '83, P No. 54
5. R.S. Treseder and T.M.Swanson, Corrosion, Vol. 24, No. 2, P31 (1968)
6. NACE Standard MR0175.
7. A. Ikeda et al : "Influence of Environmental Factors on Corrosion in CO_2 Source Well", Corrosion '85, P No. 29
8. L.H. Bolt, M. Soeparidi, and D. Suherman : "Drilling of Arun Gas Field", Offshore Southeast Asia '82 Conference, 1982
9. J. Soeryanto : "Transmission, Storage,and Export of Products from the Arun Field", Offshore Southeast Asia '82 Conference, 1982

TABLE 1
Chemical composition of cast 12%Cr material (wt%)

C	Si	Mn	P	S	Ni	Cr	Mo	Fe
0.08 max.	0.80 max.	1.00 max.	0.04 max.	0.03 max.	1.00 max.	11.0 13.5	0.6 max.	Bal.

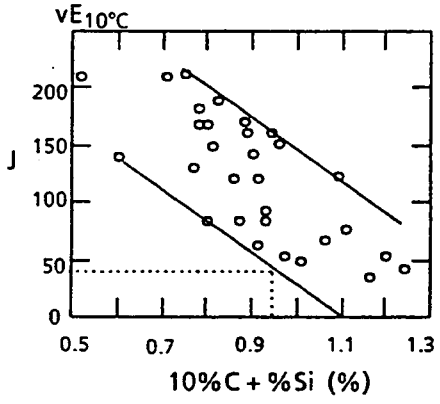


FIGURE 1—Relation between C content and charpy absorbed energy of cast 12%Cr

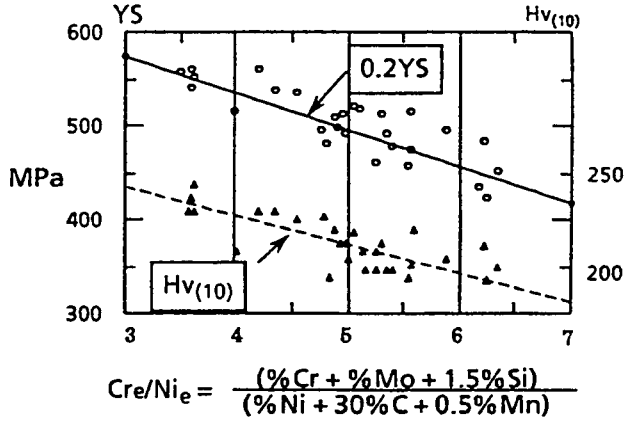


FIGURE 2—Relation between mechanical properties and Cr_e / Ni_e

TABLE 2
Mechanical properties of centricast 12%Cr pipes

Pipe size	Tensile test					$vE_{10°C}$ J	Hv(10)
	YS MPa	TS MPa	YR	EL %	RA %		
8inch	460	587	0.78	30.4	71.4	237	192
18inch	447	594	0.75	30.6	75.5	190	190
26inch	441	587	0.75	31.6	73.1	147	188

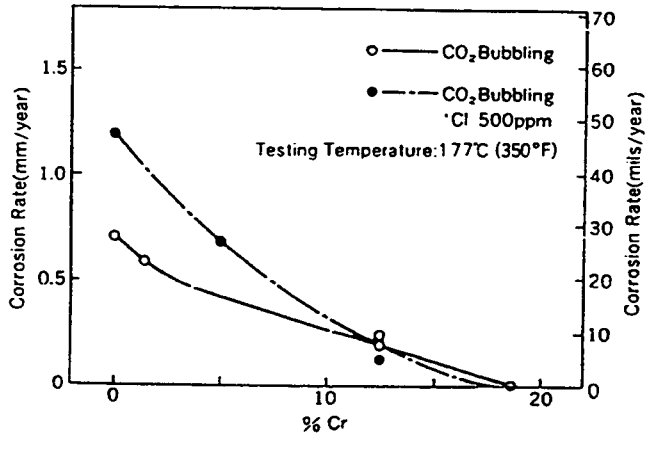


FIGURE 3—Influence of Cr content on CO_2 corrosion in various materials

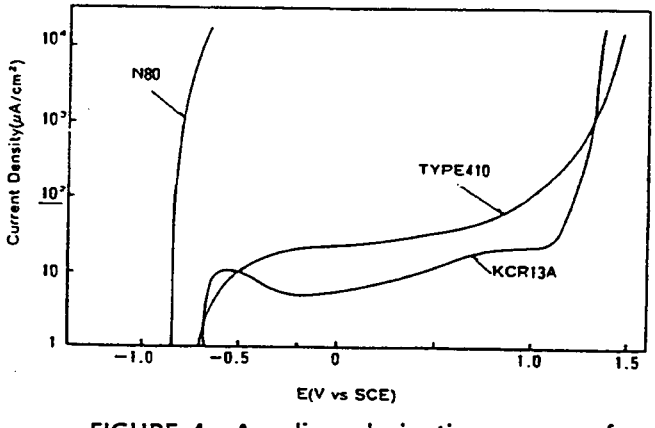


FIGURE 4—Anodic polarization curves of N-80 (carbon steel), and 12%Cr stainlesss steels (0.05M Na_2SO_4 saturating CO_2 gas at 25°C. Sweep rate 20mV/min.)

TABLE 3
Ratio of elongation to failure in the environment employed to that in air for the materials

	CO_2 (22atm) Efs/Efa	0.5Mol NaCl +	
		CO_2 (22atm) Efs/Efa	CO_2 (44atm) Efs/Efa
N-80	0.79	0.49	0.55
$2_{1/4}$%Cr	0.37	0.34	0.40
5%Cr	0.52	0.48	0.65
Type410	0.61	0.52	0.50
Cast 12%Cr	0.80	0.69	0.70
Type304	—	0.32	—

strain rate : 4.2×10^{-6}/S

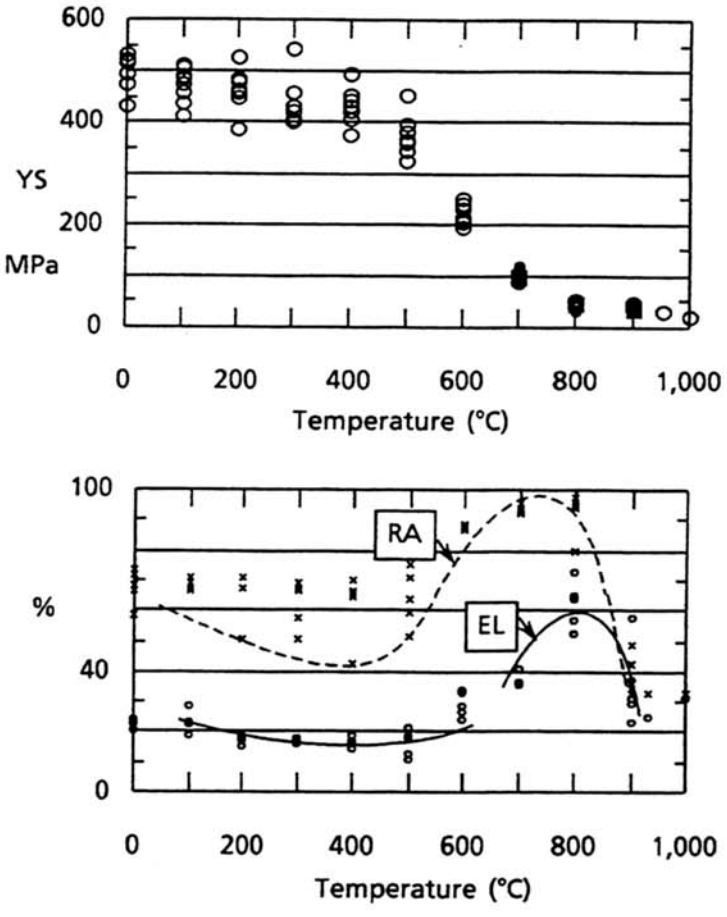


FIGURE 5—Elongation and reduction of area at elevated temperature of cast 12%Cr



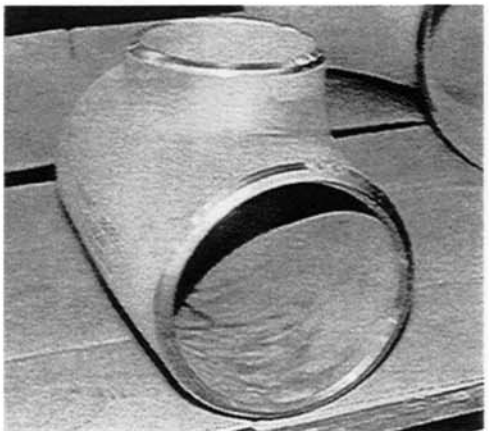


TABLE 4
Welding condition

Pass No.	Welding process	Dia. Wire	Shield Gas (Ar) ℓ/min.		Amp.	Volt
			Trail	Back		
1	GTAW	2.4	15	30	110	15
2	GTAW	2.4	15	30	110	15
3	SMAW	3.2	—	—	100	25
4	SMAW	3.2	—	—	120	30
5	SMAW	4.0	—	—	120	30
6	SMAW	4.0	—	—	120	30

Position 5G
Preheat 200°C
PWHT 730°Cx2H

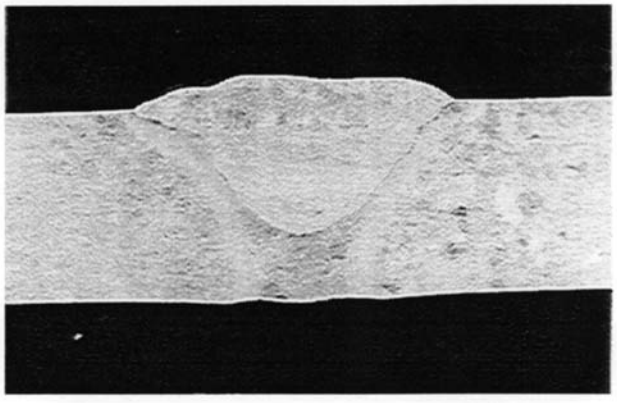


FIGURE 8—Macrostructure of weld joint (26" Sch40 12%Cr centricast pipe)

TABLE 5
Tensile properties

	YS MPa	TS MPa	EL %	YR %	Break
Base metal	479	603	30	79	—
Weld joint	—	609	—	—	B.M.

TABLE 6
Toughness & hardness

	$vE_{10°C}$ J	$Hv_{(10)}$
Base metal	198	190
Depo.	109	190
Bond	140	190
HAZ	236	210max.

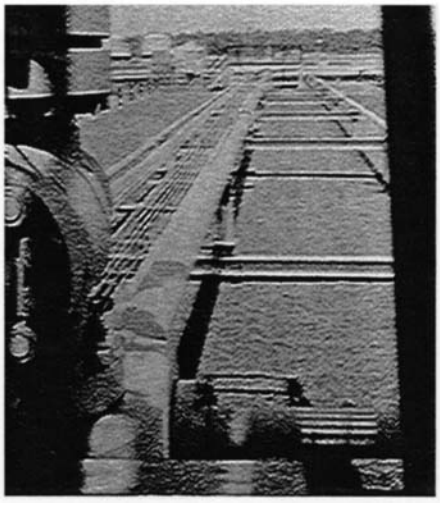


FIGURE 9—The centrifugal cast 12%Cr pipe installed in gas gathering line

Copyrighted Materials
Copyright © 1996 NACE International Retrieved from www.knovel.com

Section 2

AUSTENITIC STAINLESS STEELS

Technical Note

Sulfide Stress Cracking of AISI 304 Stainless Steel Springs in Sour Water*

BRUCE CRAIG and BRIAN HODGSON***

Background

A NEW FILTER HOUSING was installed recently in a water injection system to improve water quality and, hence, injectivity. The housing contained 80 triple length filter cartridges. Each cartridge was sealed at one end by spring loaded seal plates. Both the springs and the seal plates, shown in Figure 1, were made of AISI 304 SS. The composition of the springs is given in Table 1. One week after startup, the unit was shut down because the expected differential pressure increase normally seen across property functioning filters was not observed. The housing was opened and many of the springs were found to be cracked, allowing some of the water to bypass the filter elements.

The composition of the water being filtered, and to which the springs were exposed, is given in Table 2. The temperature of the water was 114 F (45 C) and the operating pressure was 225 psi. The pH of the water was 6.3.

Failure Analysis and Remedial Action

The fracture surface from one of the springs was examined using a JEOL JSM 35C scanning electron microscope (SEM). A black deposit on the fracture surface was left intact and analyzed by energy dispersive spectroscopy. The results showed that the principle aggressive species was sulfur. It is assumed the sulfur is present as some form of iron sulfide. A similar analysis of the spring material adjacent to the fracture showed no indication of sulfur or other corrodent.

After removing the deposit, the fracture surface was examined on the SEM. The fracture mode was predominantly transgranular with some secondary intergranular cracking present. The exact point of crack initiation could not be determined.

Since stainless steel springs are typically highly cold worked, a metallographic mount was made of the spring material and examined by optical microscopy to evaluate the extent of cold work. The austenite grains were found to be elongated in the axial direction of the wire, and subsequent microhardness testing confirmed the high degree of cold work. The hardness was measured to be Knoop Hardness 477 which is approximately equivalent to a tensile strength of 218 kpsi.

It was concluded from the accumulated data that failure most probably occurred by sulfide stress cracking. This is consistent with the work of Vaughn and Chaung[1] who found that high strength (212 ksi) 316 wire used for wirelines failed in less

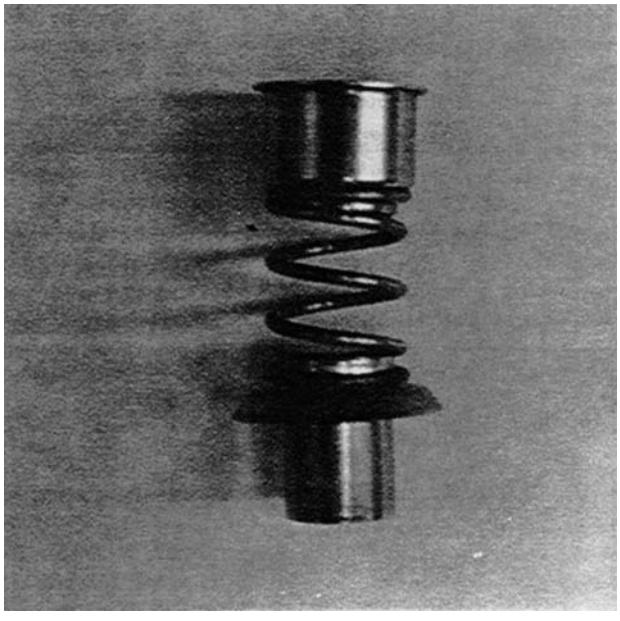


FIGURE 1 — Spring and seal plate assembly shown at approximately one-half original size.

TABLE 1 — Chemical Composition of Filter Springs (Wt%)

C	Mn	Si	Cr	Ni	Mo	P	S
0.06	1.33	0.38	19.02	8.20	0.15	0.023	0.005

TABLE 2 — Injection Water Analysis (ppm)

Total Dissolved Solids	3636
H_2S	318
Cl	173
CO_2	150
Dissolved Oxygen	50-100 ppb

*Technical note submitted for publication June, 1983.
*Metallurgical Consultants, Inc. of Denver, Denver, Colorado.
*Marathon Oil Company, Littleton, Colorado.

than seven days under laboratory conditions in a sodium chloride solution in contact with 100% H_2S at 93 C. The fracture mode was predominantly transgranular. These investigators also observed rapid failure of 316 SS wire after 30 days field exposure to an environment of mixed chlorides 11% H_2S and 40% CO_2. It should be noted, however, that both their laboratory and field tests were much more severe than the actual field conditions described in this paper. Thus, it becomes apparent that milder environments can still promote sulfide stress cracking, and that marginally resistant alloys such as 304 and 316 SS should not be used when high strength is required.

Contacting the manufacturer of the filter system proved discouraging, as their only other alloy for springs was AISI 316 which they considered superior to 304 SS in resistance to sulfide stress cracking. The only difference between these two alloys is the greater Mo content of the 316 SS which provides enhanced pitting resistance but little, if any, increase in sulfide stress cracking resistance.

Most sulfide stress cracking resistant alloys described in the literature are not readily available as spring wire material, especially in the small quantity needed for this application. In addition, there was a time constraint since the filters were shut down awaiting new springs. In light of these considerations, the alloy most easily obtainable at the lowest cost and with the greatest resistance to sulfide stress cracking was Hastelloy C-276. The hardness of these springs was Rockwell C 41 which corresponds to an approximate tensile strength of 190 kpsi. These springs have been in service ten months without incident and are expected to operate successfully for many years.

Acknowledgment

The authors thank Marathon Oil Company for permission to publish this paper.

Reference

1. G. A. Vaughn, H. Chaung, Materials Performance, Vol. 21, No. 1, p. 44 (1982).

Copyrighted Materials
Copyright © 1996 NACE International Retrieved from www.knovel.com

OTC 4150

SULFIDE STRESS CRACKING RESISTANCE OF NITROGEN-STRENGTHENED STAINLESS STEELS

by Robert R. Gaugh, ARMCO, Inc.

©Copyright 1981 Offshore Technology Conference
This paper was presented at the 13th Annual OTC in Houston, TX, May 4-7, 1981. The material is subject to correction by the author. Permission to copy is restricted to an abstract of not more than 300 words.

ABSTRACT

Although the bulk of the materials used in oil field operations are carbon steel or alloy steel, stainless alloys are employed in critical areas where salt water, CO_2, and H_2S may be present. Relatively recently, a number of nitrogen-strengthened austenitic stainless steels have become commercially available. They have substantially higher strength than the 300 series of stainless steels, plus other attractive features.

This report describes sulfide stress cracking tests performed on a number of these alloys. Most were found to be somewhat susceptible to cracking, depending on the stress level. It was determined that this was due to their high manganese content. The mechanism responsible for cracking was not firmly established. One commercial nitrogen-strengthened stainless steel, XM19, was highly resistant to sulfide stress cracking despite a manganese content of 5%. This difference is attributed to the superior corrosion resistance of the alloy.

INTRODUCTION

Although the bulk of the materials used in oil field operations are carbon steel or alloy steel, stainless alloys are employed in critical areas such as pumps, valves, and down-hole instrumentation housings. In many such operations, significant amounts of salt water, CO_2, and H_2S are present, creating severe problems of general corrosion, pitting, and sulfide stress cracking. Corrosion-resistant materials also are required in other supporting areas, such as work and supply boats for off-shore platforms.

Among the alloys that have been used in this area are Type 410 and S17400 stainless steels, and nickel alloys N05500, and N07750. While all of these alloys have adequate strength, each has certain deficiencies. Both Type 410 and S17400 stainless steels are subject to sulfide stress cracking, pitting, and crevice corrosion. The nickel alloys, although highly resistant to the environment, are considerably more expensive than the stainless steels and less readily available.

Most austenitic stainless steels have adequate corrosion resistance for oil field operations, and are immune to sulfide stress cracking as long as they are free from α'martensite resulting from cold work. However, they do have rather low strength, with only 30 to 35 ksi 0.2% yield strength in the annealed condition.

Relatively recently, a number of nitrogen-strengthened austenitic stainless steels have become commercially available. These alloys have nearly twice the 0.2% yield strength of the 300 series of stainless steels, giving them a definite design advantage over the older alloys. Several also have other attractive features, such as excellent resistance to brine, seawater, and other corrosive environments, and one alloy (S21800) is much less subject to galling and seizing than other corrosion-resistant alloys. All are completely non-magnetic, even when severely cold worked. This is important for certain instrument applications, where magnetism can seriously affect their operation.

This report describes the propensity of a number of nitrogen-strengthened stainless steel alloys to stress crack in H_2S environments.

The investigation was performed in two parts. The first was to determine the resistance of various commercial nitrogen-strengthened stainless steels to sulfide stress cracking as a function of applied stress. When most of these were found to be somewhat susceptible to cracking, additional work was performed on experimental alloys to determine the cause.

EXPERIMENTAL WORK

The test specimens used for the first phase of this work were made from commercially produced bar stock of the following stainless steels: XM11, XM17, XM19, XM28, XM29, S21800, and Type 304N. Specimens of Type 304 and Type 316 were included for controls. All were tested in the annealed condition except for the Type 304N, which was cold drawn. XM19 and XM28 bars also

References and illustrations at end of paper.

© OTC Reprinted with the permission of the Offshore Technology Conference

were tested in the high-strength (hot rolled) condition, since these are commercially available, and have minimum yield strengths of 90 and 105 ksi respectively in small bar sizes, as compared with 55 ksi for annealed material. The chemical analyses of these materials are listed in Table 1.

All testing was carried out using either sub-size or standard tensile test specimens as described in NACE Standard TM-01-77. [1] After machining, the annealed specimens were re-annealed at 1900 or 1950F for 10 to 15 minutes to remove the residual stresses. Those samples that were in the hot rolled or cold drawn condition were left as-machined. The annealed specimens were mechanically polished with emery cloth or, in a few cases, bead blasted to remove all scale. They were subsequently electropolished as a final operation to remove the cold worked layer that was produced by the previous polishing or blasting operations. For surface uniformity, the samples that were not re-heat treated also were electropolished.

All specimens were stressed in direct tension, using units similar to creep frames. The test cells were simply constructed from 165mm lengths of 64mm O.D. glass tubing, which were closed at both ends with #12 rubber stoppers. Figure 1 shows a close-up view of a test cell and specimen.

The tests were performed by submerging the gage length sections of the specimens in a 5% NaCl-0.5% acetic acid solution (standard NACE solution), purging with argon for 1/2 hour to remove oxygen, saturating with H_2S, and then loading to various stress levels. Oxygen was excluded from the cells during the tests by means of traps containing small amounts of water which were attached to the vents.

Most of the requirements of NACE TM 01-77 were met for this work. One exception is that the H_2S was bubbled through the test cells for one 10-minute period three times weekly, instead of continuously. This was simple to do and thought to be sufficient to keep a high concentration of H_2S in the test solution, which reacts with stainless alloys much less than carbon and alloy steels. The test solution was kept within the prescribed pH limits of 3 to 4.5 by means of weekly additions of acetic acid. It was not possible to control the temperature any closer than 27 + 8.4C (80 + 15 F), which was the ambient temperature range in the laboratory.

The times to failure for the various commercial materials tested are shown graphically in Figure 2 as a function of applied stress. Their susceptibility to cracking was unexpected, since the mechanism of sulfide stress cracking generally is believed to be hydrogen embrittlement, [2] and these alloys, like the other austenitic stainless steels, are highly resistant to this type of failure.

Figure 3 shows the mode of cracking of annealed XM29. These cracks, which looked very much like chloride stress-corrosion cracks, were typical of all of the failed nitrogen-strengthened stainless steels. This resemblance was puzzling, since these alloys, like other austenitic stainless steels, are not normally subject to chloride stress corrosion cracking at temperatures below about 140-150F.

There did not appear to be any great difference in sulfide stress cracking resistance among the various nitrogen-strengthened alloys that were tested in the annealed condition, except for XM19. This material did not crack even when tested at 100 ksi applied stress, which is well above its 0.2% yield strength of about 60 ksi. When in the high-strength (hot rolled) condition, the alloy did become slightly susceptible to cracking, but only when stressed to very high levels approaching the ultimate tensile strength of the material.

The superior resistance of XM19 to sulfide stress cracking, compared to the other nitrogen-strengthened stainless steels, is ascribed to the very high corrosion resistance of the alloy. Of all of the alloys tested, only XM19 and Type 316 remained completely free of corrosion after exposure to the NACE solution for 1000 hours. It is believed that without attack of the surface, there is no atomic hydrogen liberated to diffuse into the metal and cause cracking.

Control samples of annealed Type 304 and Type 316 did not crack when tested at 60 ksi applied stress (well above their 0.2% yield strengths of 30-35 ksi) However, when stressed to 75 ksi, Type 304 failed from sulfide stress cracking in 131 hours. This susceptibility was attributed to the formation of α'martensi in the specimen due to cold work produced by loading (This was determined by a hand magnet, since α'martensite is magnetic.)

The data from Figure 2 have been replotted in Figure 4, with the results obtained from the annealed nitrogen-strengthened stainless steels (excluding XM19) grouped together. Included for comparison are test data from a previous study [3] of S17400 stainless in the two heat treated conditions considered acceptable by NACE [4] for sulfide service (Conditions H1150 + 1150 and H1150M). Note that although the nitrogen-strengthened stainless steels are subject to sulfide stress cracking in laboratory tests, they are at least as resistant as S17400 stainless (a widely used alloy) in the NACE-approved heat treated conditions.

The discovery that all of these nitrogen-strengthened stainless steels (except XM19) were to some extent susceptible to sulfide stress cracking was surprising because all austenitic stainless alloys heretofore have been virtually immune to this mode of failure as long as they remained free of α'martensite produced by cold working. This was puzzling, because the nitrogen strengthened alloys all are very stable, and never transform to α'martensite (as determined by magnetic measurements) despite any amount of cold working. Because of this, additional work was done in an attempt to determine the reason for this behavior.

The major differences in composition between the AISI 300 series of stainless steels and the nitrogen-strengthened alloys are higher levels of manganese and the addition of nitrogen to the latter materials.

For this phase of the study, two series of 30-lb. induction-melted laboratory heats were prepared. Additions of manganese up to 12%, both singly and in combination with .20-.26% nitrogen were made to a base alloy of 18% Cr-10%Ni-Balance Fe composition. Their chemical analyses are listed in Table 2.

These heats were hot forged to 1/2" sq. bars, which were then machined into standard NACE sulfide test specimens. After machining, all specimens were annealed at 1950F for 15 minutes and water quenched. The specimen preparation and test procedure were as described previously in this paper.

The test results are shown graphically in Figures 5 and 6, plotted as times to failure vs. applied stress for each alloy. For both series of heats there was a strong correlation between susceptibility to sulfide stress cracking and increasing manganese content. The alloys containing both manganese and nitrogen appeared to be somewhat more resistant to cracking than the materials containing manganese alone. However, if the applied stresses were plotted as percent of yield strength rather than absolute values, this difference probably would be minimal, due to the strengthening effect of the nitrogen.

The sample containing only 0.5% Mn and no nitrogen transformed to α'martensite on loading to 75 ksi stress, thus explaining its increased susceptibility to cracking at that stress level.

Although this work indicated that high manganese contents in austenitic stainless steels increase their propensity toward sulfide stress cracking, the reason for this behavior was not obvious.

One possible explanation was that even though these alloys remain completely non-magnetic after exposure to sub-zero temperatures or when heavily cold worked (do not transform to α'martensite), they might contain another transformation product such as ε-martensite. This hexagonal crystal structure has been found to occur reversibly with applied stress in some stainless steels. [5] It was postulated that if small amounts of ε-martensite were present in the austenitic matrix, the material might then become subject to sulfide stress cracking.

To check this out, X-ray diffraction studies were performed on several samples of annealed and cold worked commercial nitrogen-strengthened stainless steels, and also on annealed XM29 sheet that was stressed to approximately 50 ksi. Nothing other than austenite was found in any of these samples. This work was considered inconclusive, since the detection of ε phase reportedly is quite difficult. [5]

Some effort also was directed toward determining whether the mechanism of cracking of these alloys was hydrogen embrittlement or chloride stress-corrosion cracking. Although neither would be expected to occur in an austenitic stainless steel at room temperature, there has been at least one example of hydrogen embrittlement of an austenitic nickel-base material (NO5500) reported in the literature. [6]

To help resolve this question, XM19, XM28, Type 304, Type 316, and two of the experimental Cr-Ni-Mn-Fe alloys were tested in the NACE solution as before, except iron anodes (1 to 1 surface area ratio) were attached to the specimens just below the gage lengths. This was expected to greatly reduce or eliminate the cracking altogether if chloride stress-corrosion cracking were the mechanism. On the other hand, if hydrogen embrittlement were the cause of failure, then cathodic protection was expected to increase the tendency for cracking. The results obtained appeared to be contradictory. See Table 3.

Coupling with iron greatly prolonged the time to failure of XM28 and the experimental Cr-Ni-Mn-Fe alloys, although metallographic examination revealed small radial cracks in the gage length sections of each test specimen. This behavior indicated that the mechanism of cracking of the uncoupled specimens of these alloys was chloride stress-corrosion cracking.

On the other hand, coupling with iron produced microcracks in the gage length sections of specimens of XM19, Type 304, and Type 316. This was unexpected, since uncoupled specimens of these alloys showed no cracking whatsoever after 1000 hours in test. The results indicated that perhaps these formerly resistant alloys now were being hydrogen embrittled.

An additional experiment was performed, where several specimens of XM19 and XM28 were tested in the NACE solution as before, except at boiling (104C-220F) instead of at room temperature. It was thought that if hydrogen embrittlement were the cause of the cracking at room temperature, it should not occur at the boiling point, and conversely, if chloride stress-corrosion cracking were the cause, it would become more severe at higher temperatures.

In the case of XM28, the time to failure was extended from an average of about 30 hours to over 1000 hours by the increased temperature. For XM19, no cracking occurred either at room temperature or at boiling. This indicated that the mechanism of failure in the standard NACE test was hydrogen embrittlement, in agreement with the results of the galvanic coupling experiment on XM19, but in opposition with the work on XM28.

Further work presently is in progress to help clarify the mechanism of sulfide stress cracking of these alloys. At present it appears that perhaps both hydrogen embrittlement and chloride stress-corrosion cracking may be operating together in a manner not yet understood.

CONCLUSIONS

1) Most of the nitrogen-strengthened austenitic stainless steels were found to be somewhat susceptible to sulfide stress cracking, as measured by NACE Test Method TM 01-77, even though all were in the annealed condition and were fully austenitic.

2) The degree of susceptibility of these materials to cracking varied with the composition of the alloy, but in general was at least as good as that of S17400 alloy in the NACE-approved H1150 + 1150 and H1150M conditions.

3) The propensity of the nitrogen-strengthened stainless steels toward sulfide stress cracking was found to be directly related to increasing manganese content of the alloy. The addition of nitrogen to high-manganese stainless steels did not appear to increase their susceptibility to sulfide stress cracking.

4) One commercial nitrogen-strengthened stainless steel, XM19, was virtually immune to sulfide stress cracking, despite a manganese content of 5%. This difference is attributed to the superior corrosion resistance of the alloy, which prevented attack of the surface and hence precluded the liberation of atomic hydrogen from the test solution. This alloy is included in NACE Standard MR-01-75, which lists metallic materials that can be used in sulfide environments. [4]

5) The mechanism by which high manganese content causes austenitic stainless steels to become susceptible to sulfide stress cracking is as yet unknown.

NOMENCLATURE

1) SXXXXX and NXXXXX refer to Unified Numbering System for Metals and Alloys (UNS) - SAE HS 1086a and ASTM DS-56A.

2) "XM" grades are ASTM designations.

REFERENCES

1. NACE Standard TM-01-77; "Testing of Metals for Resistance to Sulfide Stress Cracking at Ambient Temperatures", National Association of Corrosion Engineers, Houston, Texas, July 1977.
2. Chu et al; "Mechanism of Stress Corrosion Cracking of Steels in H_2S", Corrosion, September 1980, p. 475-481.
3. Gaugh, R. R.; "Sulfide Stress Cracking of Precipitation Hardening Stainless Steels", Materials Performance, September 1977, p. 24-29.
4. NACE Standard MR-01-75, 1980 Revision; "Sulfide Stress Cracking Resistant Metallic Material for Oil Field Equipment", National Association of Corrosion Engineers, Houston, Texas, Revised August 1979.
5. Lepistö, T., and Ketunnen, P.; "Embrittlement Caused by ε-Martensite in Stainless Steels", Scandinavian Journal of Metallurgy, Vol. 71 (1978), p. 71-76.
6. Harris, J. A., Scarberry, R. C., and Stephens, C. D., "Effects of Hydrogen on the Engineering Properties of Monel Nickel-Copper Alloy K-500", Corrosion, February 1972, p. 57-62.

TABLE 1

Chemical Analyses of Commercial Alloys Studied

Alloy	Y.S.,KSI*	C	Mn	P	S	Si	Cr	Ni	N	Other
XM11	60	.03	9.29	.024	.008	.72	20.45	6.81	.28	
XM17	60	.06	7.80	.023	.022	.71	19.44	5.85	.31	2.22 Mo
XM19	60	.05	5.04	.021	.009	.47	21.29	12.50	.28	2.21 Mo,.17Cb,.18V
XM28	60	.11	12.38	.021	.006	.54	17.88	1.63	.33	
XM29	60	.05	12.83	.025	.004	.67	17.52	3.63	.28	
S21800	60	.08	7.98	.028	.008	4.02	16.87	8.13	.16	
Type 304N	60	.05	1.74	.048	.026	.62	19.33	8.03	.27	
Type 304	35	.06	.83	.022	.018	.65	18.00	8.39	--	
Type 316	35	.03	1.65	.027	.024	.69	17.70	12.78	--	2.81 Mo

*Typical 0.2% yield strengths of annealed material. XM19, XM28, and Type 304N also are available as high-strength bars, with mechanical properties dependent on the size.

TABLE 2

CHEMICAL ANALYSES OF EXPERIMENTAL ALLOYS STUDIED

Alloy Type	Y.S.,KSI*	C	Mn	P	S	Si	Cr	Ni	N
18Cr-10Ni-0.5Mn	35	.036	.65	.010	.020	.44	17.83	9.88	--
18Cr-10Ni-2.5Mn	35	.036	2.42	.008	.024	.45	17.52	9.67	--
18Cr-10Ni-5Mn	35	.034	5.27	.001	.023	.42	17.79	9.70	--
18Cr-10Ni-8Mn	35	.043	7.90	.004	.016	.51	18.56	10.04	--
18Cr-10Ni-12Mn	35	.039	12.13	.007	.018	.31	18.36	9.83	--
18Cr-10Ni-2Mn-N	50	.045	2.12	.007	.018	.33	18.54	10.14	.20
18Cr-10Ni-5Mn-N	50	.042	5.07	.004	.014	.47	18.55	10.14	.22
18Cr-10Ni-8Mn-N	50	.035	8.03	.004	.014	.51	18.67	10.03	.22
18Cr-10Ni-12Mn-N	50	.040	12.20	.007	.015	.41	18.42	9.84	.26

*Estimated 0.2% yield strengths of annealed material.

TABLE 3

SULFIDE STRESS-CRACKING OF COUPLED VS. UNCOUPLED SPECIMENS

Alloy	Condition	Stress, Ksi	Coupled to Iron	Uncoupled
XM28	Annealed	75	Microcracks @ 1000 Hr.	Fractured @ 30 Hr.
XM28	High Strength	100	Fractured @ 730 Hr.	Fractured @ 166 Hr.
18Cr-10Ni-2.5Mn	Annealed	75	Microcracks @ 1000 Hr.	Fractured @ 67 Hr.
18Cr-10Ni-8Mn	Annealed	50	OK @ 1000 Hr.	Fractured @ 20 Hr.
XM19	Annealed	100	Microcracks @ 1000 Hr.	OK @ 1000 Hr.
XM19	High Strength	100	Microcracks @ 1000 Hr.	OK @ 1000 Hr.
Type 304	Annealed	60	Fractured @ 867 Hr.	OK @ 1000 Hr.
Type 316	Annealed	75	Microcracks @ 1000 Hr.	OK @ 1000 Hr.

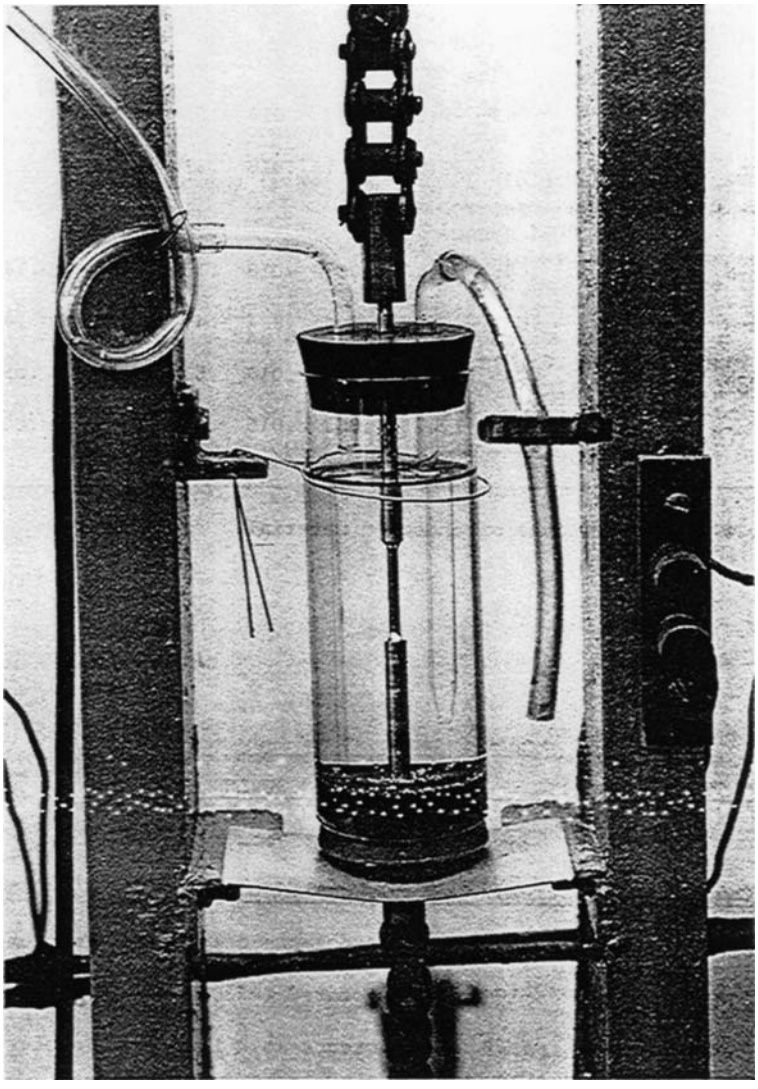


Fig. 1 - Close-up view of test cell and specimen.



Fig. 3 - Mode of cracking of annealed XM 29.

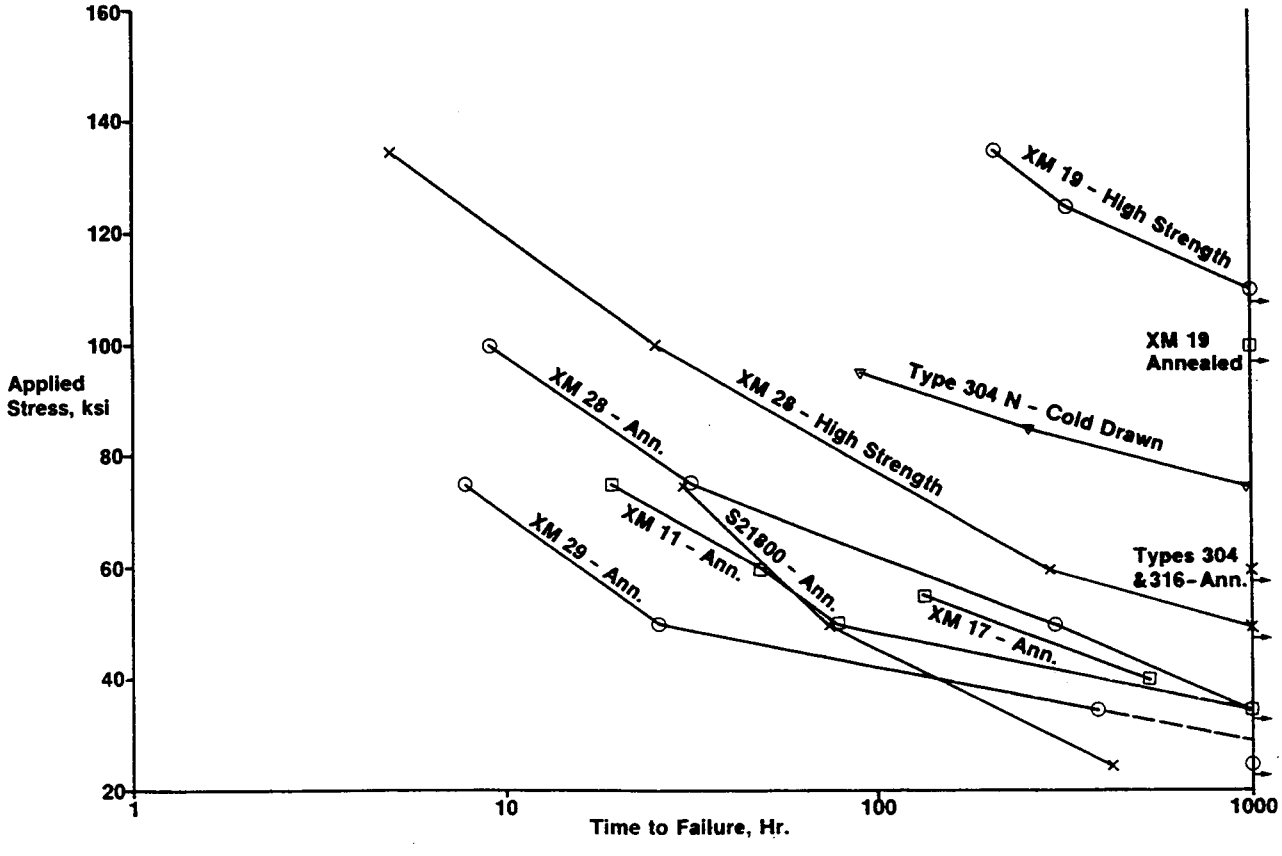


Fig. 2 - Sulfide Stress Cracking of Nitrogen-Strengthened Stainless Steels.

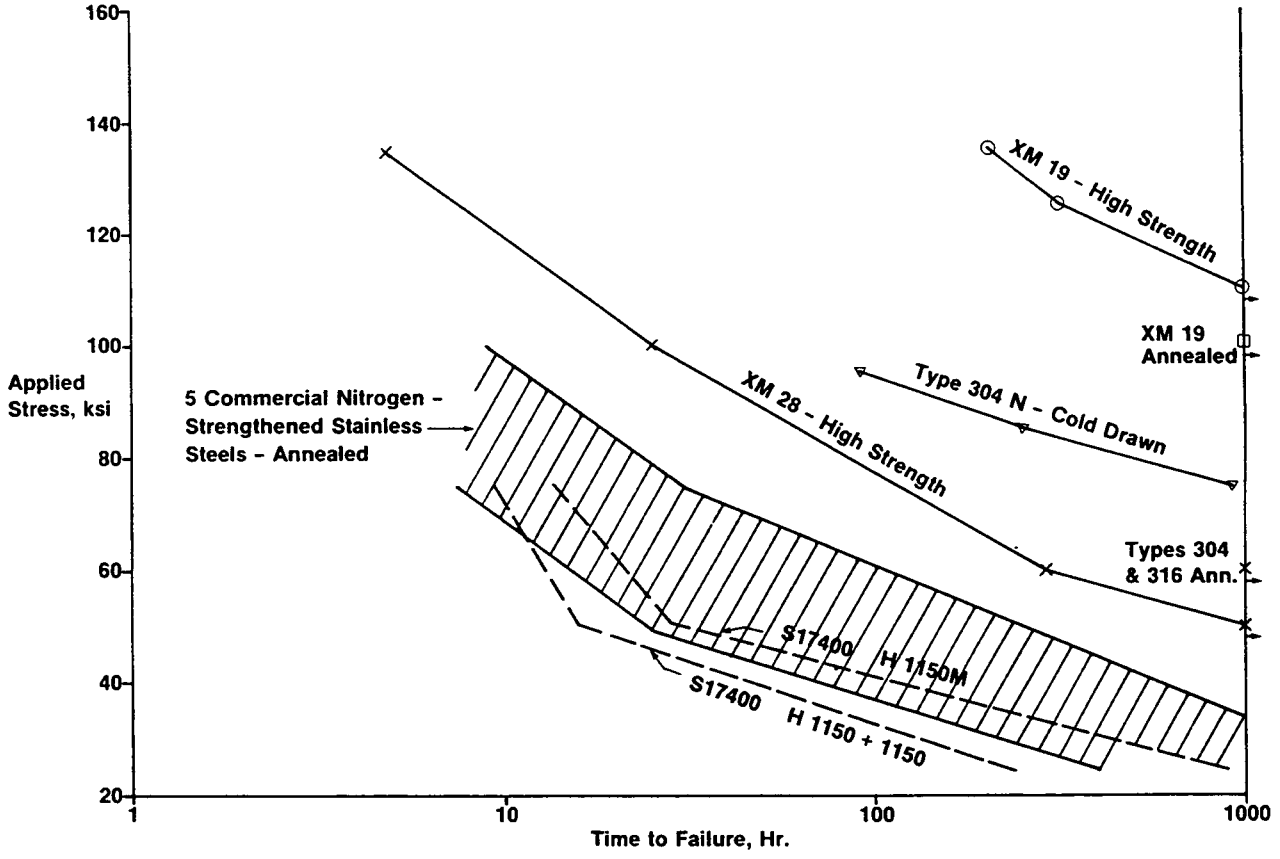


Fig. 4 - Sulfide stress cracking of nitrogen-strengthened stainless steels vs. S17400.

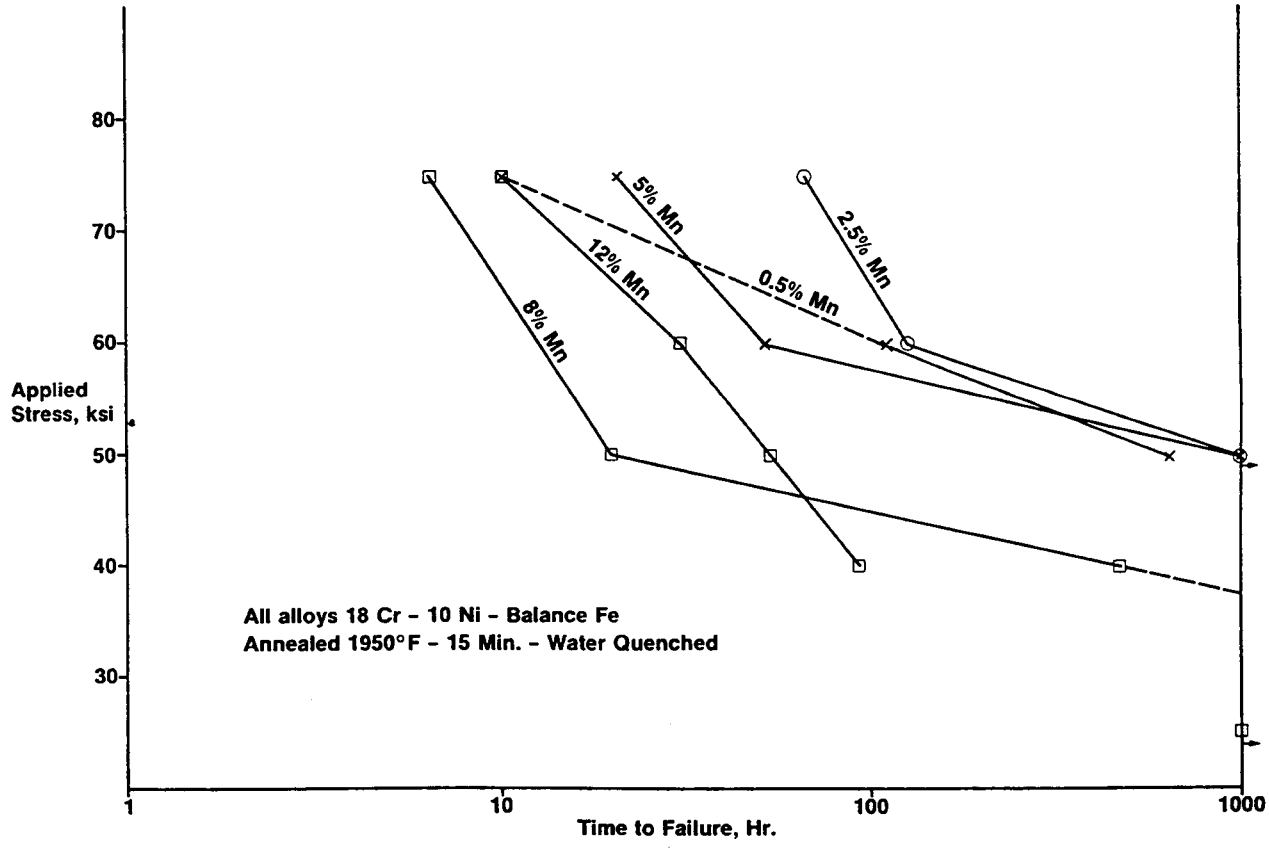


Fig. 5 - Sulfide Stress cracking of experimental Cr-Ni-Mn steels.

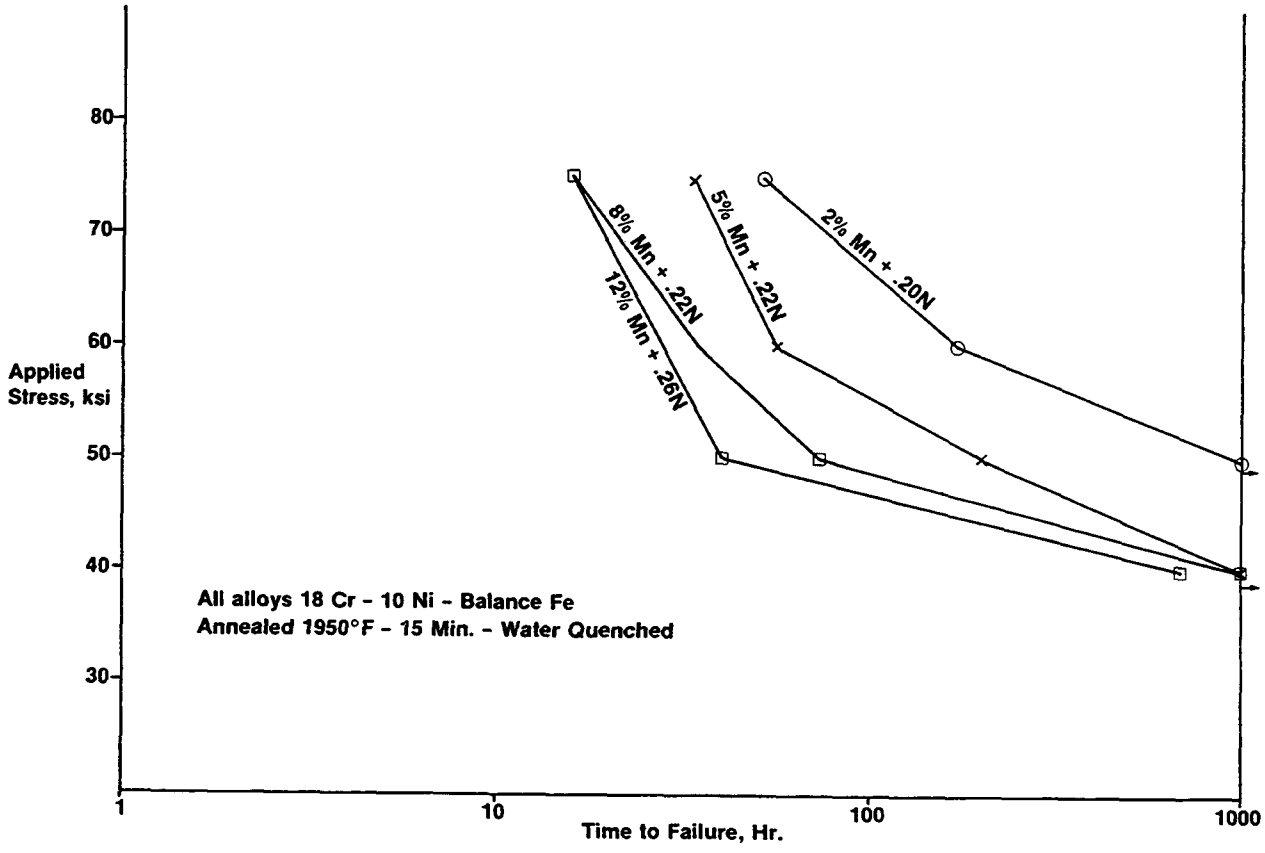


Fig. 6 - Sulfide stress cracking of experimental Cr-Ni-Mn-N steels.

Copyrighted Materials
Copyright © 1996 NACE International Retrieved from www.knovel.com

Paper No. 161—CORROSION/86

EFFECTS OF RESIDUAL STRESS ON STRESS-CORROSION CRACKING OF NON-MAGNETIC DRILL COLLARS

D.S. Kopecki
Eastman Whipstock
2525 Holly Hall
Houston, TX 77054

ABSTRACT

Non-magnetic drill collars (NMDCs) are known to crack, especially when used in drilling fluids with a high concentration of chlorides. The cause is stress corrosion cracking driven by residual tensile stresses on the collar I.D. Residual stress measurements and subsequent stress corrosion tests show that generally chrome-manganese (Cr-Mn) austenitic stainless steel NMDCs have greater residual hoop tensile stress on the I.D. than the material can tolerate in chloride bearing drilling fluids. These data are presented. A realistic solution is to specify controlled residual stresses for Cr-Mn collars, since Cr-Mn austenitic stainless steel is the most economical material for NMDCs. A number of such NMDCs are in service and their performance is briefly presented and discussed .

INTRODUCTION

Non-magnetic drill collars (NMDCs) are used in drill strings when magnetic instruments will be used to survey a well bore. An NMDC permits magnetic compasses and magnetometers placed in the bore of the NMDC to react accurately. Steel components in the vicinity of survey instruments would distort the earth's magnetic field and lead to false measurements.

For background, NMDCs are usually 30 feet (9.1 m) long with threaded ends and range in sizes beginning at 4-1/8 inch O.D. x 2 inch I.D., up to 10 inch O.D. x 3 inch I.D. (105 mm O.D., x 51 mm I.D. up to 254 mm O.D. x 76 mm I.D.). Very few NMDCs have O.D. and I.D. outside of this range.

The most common material is essentially Cr-Mn stainless steel, and a typical composition (in weight %) is below.

C 0.08-0.20	Mo 0.16-0.27
Cr 15.0-19.0	Cu 0.50-1.0
Mn 9.5-14.0	N 0.20-0.50
Ni 1.00-3.00	P & S are controlled

Other austenitics in which Ni replaces Mn are also in use. NMDCs are usually produced by warm forging in order to affect workhardening. A minimum yield strength of 110 ksi (758 MPa) for small collars and 100 ksi (690 MPa) for large collars is often specified. The final operations are often turning the O.D. and boring the I.D.

Over the past ten years and perhaps longer, the users of austenitic NMDCs have experienced stress corrosion cracking (SCC). The environmental agent which leads to SCC in austenitic NMDCs is the chloride ion in drilling fluid or, as it is commonly called, drilling mud. This fluid contacts both the I.D. and O.D. of a collar. It can have a range of salt concentration from very low (where actually none is added) to "salt saturated." Sometimes the source of chloride is sea water or brine used to make the drilling fluid. Some constituents in the fluid originate from the formations being drilled. In general, drilling fluid exists in a great variety of salt concentration and concentration of other constituents. The chlorides sometimes present in drilling fluid are NaCl, KCl, $CaCl_2$, and $MgCl_2$. $MgCl_2$ seems to be the most aggressive .

Temperature and pressure play a significant role in the cracking of NMDCs, generally, geologic temperature increases with the depth of a well. Normal petroleum drilling temperatures range from 100° to 400°F (38° to 204°C), and geothermal drilling reaches higher temperatures. Pressure does not have a direct effect, but its

indirect effect is to suppress boiling and allow temperatures above the atmospheric boiling point. Hydrostatic pressure effecting an NMDC increases as the depth of a well increases. (Generally, it has not been possible to test NMDC materials in laboratories at service temperatures due to lack of pressure test vessels.)

In response to the cracking problem, producers have directed efforts to reduce failures toward both metallurgical improvements and control of residual stress. However, most manufacturers have concentrated on metallurgical improvements which, in almost all cases, have not resulted in a practical solution to completely eliminate SCC, although SCC resistance has been generally improved. Higher cost materials with low or no susceptibility to SCC can be used to eliminate cracking, but it is more economical to control residual stresses on Cr-Mn even though it is susceptible. In fact, NMDCs made of Cr-Mn with properly controlled residual stress do perform with immunity to longitudinal stress corrosion cracking.

The residual stresses in austenitic NMDCs are likely to be larger than ordinary tubes because of the very thick wall and because austenitic stainless requires temperatures for stress relief that are usually absent from the last part of the forging cycle. Unfortunately, residual stress has not been a significant part of nearly all investigations of cracked NMDCs due mainly to lack of knowledge in this matter. The general result has been neglect of this aspect which is paramount to any other. Better results would have been achieved if the residual stress had been quantified before making any metallurgical changes or running any corrosion studies.

Nevertheless, based on an energy analysis of a fracture process such as Griffith's approach to brittle fracture, it is necessary to have a tensile stress to cause stress corrosion cracking. Theoretically, a threshold stress is required for susceptible materials in each particular environment. In collars, this threshold can be translated to a maximum allowable residual tensile stress. Users could select collars that are below the maximum allowable or, instead, have collars produced to their specification for maximum residual stress. However, without good knowledge of the entire variety of drilling fluids and drilling conditions, a much safer approach is to seek compressive residual stresses on the exposed surfaces. This can be expected to prevent SCC under virtually all conditions.

DESCRIPTION OF FAILURES

Crack patterns in failed collars have some variety. One type has two deep, wide cracks 180° apart, Figure 1. Some shorter cracks are usually present with deep, wide cracks. At the other extreme is a large number of shallow cracks that radiate from the I.D. surface, Figure 2. In all cases, cracks begin on the I.D. and they tend to have great length in the axial direction of the collar.

Inspection of just a few cracked collars can lead to a realization that cracks such as shown in Figure 1 have opened to dimensions up to approximately 0.020 inches (0.5 mm) which indicates tensile hoop residual stress on the order of 50 ksi (345 MPa) on the I.D. However, due to the total absence of crack initiation on the O.D. and the estimated high tensile residual stress on the I.D., it seems likely that a significant hoop compressive stress exists on the O.D. In contrast, service stresses, which can reach at most 10 ksi (70 MPa) under severe conditions, are insignificant compared to such high residual stress.

Stress corrosion cracks in NMDCs have been discovered over a wide range of exposure times. The shortest instance of failure on EW records is about 100 hours. For a fleet of collars made with susceptible materials, failures are continuous for the life of the fleet. Even though there is attrition from wear and tear on any such fleet, some collars remain in service over ten years. So it is likely that some collars over ten years old will eventually crack.

The accumulated failure percentage is somewhat difficult to ascertain with reasonable accuracy for a number of reasons. However, to give a general indication, it is possible to state the failure rate is in the range of 10 to 40% depending on what particular alloy and manufacturing sequence has been employed.

Finally, the few thorough investigations of SCC failures that have occurred after a few months in service indicate that these failures are related to high chloride concentrations between 150,000 ppm chloride and saturation with a chloride salt. Such chloride levels are now common. So there is considerable risk with the use of Cr-Mn NMDCs, especially in the as-bored condition .

MEASUREMENTS AND RESULTS

The introduction covered the basic concept that a threshold tensile residual stress exists for SCC of each particular austenitic stainless. Based on this concept, the most fundamental path on which to proceed is to first measure the residual stress present in NMDC products from different manufacturers, and then to perform stress

corrosion tests at stress levels corresponding to the measured residual stress. To be rigorous, each size collar from each manufacturer under consideration would require testing. Such data can reveal which collars are acceptable for service (i.e., those materials that do not crack at a stress equal to the actual residual stress of the collar should not crack in service). If tests predict cracking on a particular collar, then it is possible to correct this by specifying a maximum tensile residual stress to the manufacturer.

Tests have been made by EW on products from different manufacturers. Table I shows the I.D. residual stress on various products. The samples in the upper part of the table are placed in order of increasing hoop tensile stress and show a range of 28 to 75 ksi (193 to 520 MPa). The lower part of the table deals with samples that have been treated after boring to induce compressive I.D. stress. Compressive I.D. layers will be discussed later.

In general, residual stress testing on collars without an I.D. treatment indicates a residual stress profile as shown in Figure 3. Roughly half the wall nearest the I.D. is in tension. The other part of the wall nearest the O.D. is in compression, due to a requirement for force equilibrium.

Following these residual stress tests, some stress corrosion tests were run to discover whether or not it is possible to use particular collars with the residual stresses in the as-bored condition. The results are in Table II. The data in this table shows that all Cr-Mn collars with tensile residual stress can be expected to crack at stress levels roughly equivalent to their respective residual stress.[1] It was also decided that tests at 30 ksi (207 MPa) would be of benefit. This is a rough guess at the minimum residual stress that could be achieved by good control of present processing methods without instituting additional processing steps. These lower stress tests indicate that practical reductions in the present levels of hoop tensile stress are not a general solution for Cr-Mn because cracking still occurs.

Besides these purely lab tests, there is correlation between measured residual stress and the field performance of collars from the same source. Table III shows these results. This table shows that doubling the residual stress from 30 to 60 ksi (207 to 414 MPa) leads to accumulation of nearly equal failure percentage in one fourth the time. On the other hand, compressive stress has prevented failures for nine months of service.

One final result is that the residual stress tests show compressive hoop residual stress on the O.D., even on the samples that were treated on the I.D. Consequently, in the field no cracks have been initiated on the O.D. of collars due to this compression. Therefore, in reality, the absence of O.D. cracks in service constitutes the strongest possible proof that compressive residual stress is perfectly effective against stress corrosion cracking. The two stress corrosion tests run with compressive stress, are certainly consistent with this conclusion.

SOLUTION

The most practical solution to eliminate stress corrosion cracking on Cr-Mn NMDCs seems to be introducing compressive hoop residual stress on the I.D. after boring. Substitution of another alloy type that is not susceptible is a second possibility but, at this time, that particular solution is not cost competitive against Cr-Mn stainless steel with controlled residual stress.

An acceptable residual stress profile for Cr-Mn NMDCs is represented in Figure 4. In this case, compressive hoop stress must be present on both the I.D. and the O.D. of the collar. For the O.D., this entails altering the I.D. stress considerably while maintaining the O.D. compression that exists after boring. One way of expressing the requirements for magnitude and depth of compression is by the two cross hatched rectangles in Figure 4. The curve for hoop residual stress must pass below both rectangles .

DISCUSSION

The use of grain boundary corrosion or grain boundary sensitization tests, such as ASTM A262 practices A and E, can be of use in two ways. First, these tests allow a user to choose a material that is preferable. Second, such tests are an important means that producers can use to control quality. However, such tests are well known and understood; they need not be discussed in detail here.

One shortcoming of such tests is that stress is not a variable. NMDC materials that pass such tests can crack when stresses are sufficiently high. On the other hand, NMDC materials that fail these tests can be used successfully, in some cases, when compressive stress is introduced on all exposed surfaces. To correct this shortcoming, grain boundary tests on Cr-Mn NMDCs need to be complemented by residual stress controls.

In this particular study, however, there is little need to apply grain boundary tests because the C-ring stress-corrosion tests in conjunction with residual stress tests provide better information on each NMDCs corrosion or stress corrosion behavior .

[1] For cases where tensile residual stress was measured, stress corrosion tests were run at stresses slightly higher than the measured hoop tensile residual stress to account for the influence of axial residual stress in the collar, superimposed service stresses, a safety factor, and the likely possibility that a manufacturer would produce some colllars with a higher residual stress than the sample that was measured.

Based on the behavior of most of the C-rings, the test solution used for these tests is very severe for chloride SCC, general corrosion and pitting. It has an extreme pH relative to normal drilling fluids. Therefore, this test solution is appropriate for accelerated tests as is desired in this case. However, the solution does not closely resemble any actual drilling fluid except that it has a high chloride concentration and has an oxygen scavenger. Details of the solution and the test procedure are in Appendix 1.

Relative to a requirement for a compressive layer on the I.D. of a Cr-Mn NMDC, it is possible in principle that a very thin compressive layer with no imperfections or windows would be adequate to prevent SCC. However, there are a number of reasons for desiring much greater depth as allows:

1. Insure an area without imperfections or windows so that no cracks can initiate and propagate.
2. Durable against abrasive wear for many years of service.
3. Thicker than the deepest scratches and corrosion pits.

Relative to a compressive stress to prevent SCC, this need not be more than sightly compressive. However, there are small tensile stresses applied during service which must be overshadowed by the compressive residual stresses. Internal pressure can superimpose a maximum of 5,000 psi x 1.58 = 7,500 psi hoop tension at the I.D. (34 MPa x 1.58 = 52 MPa hoop tension at the I.D.).[2] The second possibility for superimposed stress is due to thermal transients which, for example, might occur after a drill string has been tripped in a well bore and the first flow of drilling fluid through the collar is colder than the collar. This may contribute a few thousand psi hoop tension at the I.D. Altogether, the minimum level of compression induced by treating the I.D. must be some moderate value to maintain net compression during service.

The last point for discussion is the reasons why the application of compressive residual stress layers to Cr-Mn NMDCs is particularly ideal. First, there is ample wall on NMDCs to permit thick compressive layers without detrimentally affecting the required strength of a collar. Second, employing NMDCs with compressive layers has the advantage that good knowledge of the environment is not required since this technique is almost universally effective, independent of the environment.

SUMMARY AND CONCLUSIONS

1. Residual stress plays a role equal to any other parameter in causing stress corrosion cracking in Cr-Mn NMDCs. Applied stresses are not significantly involved in the failures that have been experienced.
2. The results of field failures indicate that Cr-Mn NMDCs with the very best metallurgical processing to improve chloride SCC do not achieve flawless performance. These NMDCs crack on their I.D. due to high hoop tensile residual stresses. Furthermore, field results indicate that compressive residual stress on the O.D. is 100% effective in preventing crack initiation on the O.D.'s of Cr-Mn NMDCs. Tension and compression C-ring tests in conjunction with residual stress tests have been used to verify the mechanism for I.D. cracking and the mechanism for the absence of cracking on the O.D.
3. Rather than approaching the SCC problem with a specification for maximum tensile residual stress based on a measured threshold stress, it is more practical to specify compressive layers on exposed surfaces of Cr-Mn NMDCs. This is compatible with the abilities of present manufacturing technologies and is more cost effective than a change to more expensive materials.
4. Cr-Mn NMDCs with properly controlled residual stress on both I. D. and O.D. will not undergo SCC. Proper control includes allowances for manufacturing tolerances on residual stress parameters, abrasive wear and other service conditions, and allowances for minor service stresses.

ACKNOWLEDGMENTS

Eastman Whipstock has supported the development work described in this paper and has encouraged publication of this paper. The author wishes to acknowledge Cary Touchton of EW for the residual stress measurements and Dale McIntyre of Cortest Laboratories for coordinating the C-ring stress corrosion tests. The test solution used for C-ring tests originated in the corrosion laboratories at Carpenter Technology Corporation.

REFERENCES

1. W.H. Friske, "Shot Peening to Prevent the Corrosion of Austenitic Stainless Steels," Rockwell International, A1-75-52 (Sept., 1975).
2. D.R. McIntyre, *Chemical Engineering*, Part I, II, 4(1980), p. 107; 5(1980), p. 131.
3. R.N. Parkins, *Materials Performance* 24, 8(1985), p. 9.

[2] Calculated from 5,000 psi (34 MPa) pressure differential between I.D. to O.D. and a Lame' formula applied to a 4-3/4 inch O.D. x 2-1/4 inch I.D. (121 mm O.D. x 57 mm I.D.) collar.

4. M. Mesnager, *Comp. rend.*, 169 (1919), pp. 1391-1393.
5. G. Sachs, *Zeitschrift fur Metallkunde*, 19 (1927), pp. 352-357.
6. V. Weiss, Proceedings of SESA, held 1957 (Vol. XV, No. 2), p. 53.

APPENDIX I

C-Ring Test

NaCl with Oxygen Scavenger

A. Apply stress to ring. If the stress is compressive, then the sides and the tensile surface (either I.D. or O.D.) of the ring must be coated.

B. Test Solution and Practices: Dissolve reagent grade NaCl in distilled water at room temperature [22-23°C (72-73°F)] until the solution is saturated (about 26 w/o NaCl). Place 570ml of the saturated solution in a 1-liter wide-mouth Erlenmeyer flask or any similar vessel. Add 30ml of ammonium bisulfite solution (reagent grade between 45 and 50% ammonium bisulfite).

Add 30ml of the ammonium bisulfite solution to the test vessel after 7, 14, 21...days during the test. Do not remove test solution from the vessel.

Use a cold-finger condenser that conforms to ASTM A262, Practice C. Use other glassware that conforms to ASTM A262, Practice C when possible.

The test vessel should be at the boiling point during the test. The test period is 28 days.

APPENDIX II

Residual Stress Measurement

1. This procedure is for testing 6-7 inches (152-178 mm) O.D. NMDCs.

   Sample length will be 110% of sample O.D. Obtain a smooth and circular I.D. that is constant and concentric to the O.D.

2. Face the ends parallel to each other and perpendicular to the bore.

3. Measure several I.D.'s and O.D.'s. Measure length several times next to the I.D. Record these measurements.

4. Turn material from the O.D.

5. Repeat Steps 3 and 4 until the wall is about .080 inch (2.0mm) thick.

6. Calculate hoop strain and axial strain relative to the initial I.D. and length for each value of the machined O.D.

7. Plot hoop strain vs. machined O.D., see Figure 5. Plot axial strain vs. machined O.D. On each plot, extrapolate to the point where the wall has zero thickness. Net hoop strain and axial strain are the results of the extrapolations, respectively.

8. Finally, calculate stresses using the formulae:
   — $\sigma_{hoop} = E (\upsilon \varepsilon_a + \varepsilon_h) / (1 - \upsilon^2)$ (1)
   — $\sigma_{axial} = E (\upsilon \varepsilon_h + \varepsilon_a) / (1 - \upsilon^2)$ (2)

   where σ = stress
   E = elastic modulus
   υ = Poisson ratio
   ε = strain

Discussion of Residual Stress Measurement Technique. Certain steps in the procedure lead to approximate but useful results rather than rigorously correct quantitative values. Some of the reasons for this are mentioned briefly below.

A length of 1.10 x O.D. does not ensure that axial stress is constant along the length. Obviously, the axial stress is zero on the ends and there is probably neither a uniform length in the middle nor is the axial stress in the middle the same as that in a long bar from which the sample has been cut. Another way to express this is that the axial stress in the entire sample has relaxed as a result of cutting such a short length. This relaxation of the axial stress affects the hoop stress everywhere in the sample through a cross strain which is often calculated using the Poisson ratio. Therefore, the general conclusion is that both axial and hoop residual stresses are relaxed to some extent by cutting a short sample.

The length of the sample has been justified on the basis of the weight that a technician or machinist can easily handle without lifting equipment. For an O.D. of 6 to 7 inches (152-178 mm), the weight becomes excessive beyond a length of 1.10 x O.D. Keeping the length always 1.10 x O.D. allows comparison of the results on different sizes on a somewhat relative basis. However, it has been necessary to test some 8 inch O.D. (203 mm O.D.) samples since these were the only samples available. These were shortened to 6 inches length (152 mm length) to limit their initial weight. Due to the different ratio of length to O.D., comparison with the main body of data is less than ideal.

There has been no determination of the errors in using such short samples or the relative errors in comparisons between samples with different ratios of length to O.D. Nevertheless, there is a high level of confidence that the large tensile hoop stresses which lead to failure would be well enough measured by this technique to permit correct discrimination against particular products that have unsafe levels of residual stress. The technique is also very likely to indicate compressive stress and the depth of compression when there is adequate compressive stress and adequate depth of compression.

The technique cannot be used proficiently to investigate residual stress within approximately 0.060 inches (1.5 mm) of the I.D. or where there are large stress gradients. When the wall of the sample is machined below 0.125 inch (3.2 mm), there are numerous problems with lathe turning. Other techniques such as light grinding or electrochemical machining exist, but these are not applicable to the rapid metal removal desired for the major portion of this test .

It is quite evident, from a plot of the data for the I.D. (see Figure 5) or for a plot of the length, that both measurements for this test must generally be precise to the limit of mechanical measuring instruments. In fact, the initial test made by EW was preceded by an investigation which, first, determined that instruments had adequate precision; second, determined detailed steps necessary to relocate instruments exactly on the same contact points; and third, determined the minimum number of measurements which yielded repeatable averages.

To avoid all the critical steps necessary for good mechanical measurements, strain gauges could be mounted on the I.D. This has not been attempted by EW because there were initially neither strain gauge recording equipment nor personnel trained for this work. Furthermore, a major problem with the use of strain gauges is either that the O.D. must be machined while the sample is stationary or that resistance errors are introduced by disconnecting and later reconnecting gauge wires in order to turn the sample.

There are more complete techniques which could be used instead of the method described above. These lead to an end result that is a plot of the hoop residual stress versus radius. The earlier technique is a method of boring the I.D. progressively larger and is known as the Sachs boring technique.[4,5] An alternative, developed later, is a method of metal removal from the O.D. similar to that done here which results in a plot of hoop residual stress versus radius.[6] Although the data collected for this study could be transformed to hoop stress versus radius, the results in their present form have been adequate to solve the problem at hand.

TABLE I

Residual Stress in Cr-Mn, Cr-Mn-Ni, and Cr-Ni NMDC's

Sample	I.D. Hoop Residual Stress ksi (MPa)	O.D. X I.D. inches (mm)
A	28.0 ± 1.5 (193 ± 10)	6-3/4 X 2-13/16 (171 X 71)
B	33.5 (230)	6 X 2-13/16 (152 X 71)
C	42.5 (290)	6-1/4 X 2-13/16 (159 X 71)
D	50.4 (348)	6 X 2-13/16 (152 X 71)
E	51 (350)	6-1/2 X 2-13/16 (165 X 71)
F	57 (390)	7 X 2-13/16 (178 X 71)
G	60 (410)	6-3/4 X 2-13/16 (171 X 71)
H	62 (430)	6-1/4 X 2-13/16 (159 X 71)
I	73.5 (510)	8 X 2-13/16 (203 X 71)
J	75 (520)	8 X 2-13/16 (203 X 71)

Sample	I.D. Hoop Residual Stress ksi (MPa)	Estimated Depth of Compression inches (mm)	O.D. X I.D. inches (mm)
K	-104 (comp.) (-720)	0.11 (2.8)	6-1/4 X 2-13/16 (159 X 71)
L	-120 (comp.) (-830)	0.11 (2.8)	6-1/2 X 2-13/16 (165 X 71)

TABLE II

C-ring Stress-Corrosion Tests on Austenitic NMDC Materials

Sample	Grade	Stress, ksi (MPa)	Result
R	Cr-Mn	-100 (-690)	No visible cracks in 28 day test.
		-100 (-690)	No visible cracks in 28 day test.
S	Cr-Mn	30 (210)	Crack observed visually in 4 days.
		0 (0)	No visible cracks in 21 day test.
		-20 (-140)	No visible cracks in 28 day test.
T	Cr-Mn	78 (540)	Crack observed visually in 21 days.
		78 (540)	Crack observed visually in 24 days.
U	Cr-Mn	65 (450)	Crack observed visually in 20 days.
		65 (450)	Crack observed at end of 28 day test.
V	Cr-Mn	62 (430)	Crack observed visually in 4 days.
		62 (430)	Crack observed visually in 8 days.
		30 (210)	No crack observed visually at 10 days, corrosion product obscured view until end of 28 day test when a crack was observed.
W	Cr-Mn	33 (230)	Crack observed visually in 6 days.
		33 (230)	Crack observed visually in 12 days.
		20 (140)	Crack observed microscopically at end of 28 day test.
		15 (100)	Crack observed microscopically at end of 28 day test.
X	Cr-Mn-Ni	56 (390)	Crack observed visually in 1 day.
		56 (390)	Crack observed visually in 12 days.
		30 (210)	Crack observed visually in 8 days.
Y	Cr-Ni	80 (550)	No visible cracks in 28 day test.
		80 (550)	No visible cracks in 28 day test.

See Appendix I for details of the test.

TABLE III

Measured Residual Stress and Field Failures

Measured I.D. Hoop Residual Stress	Fraction of Collars Cracked In Average Months of Service
30 ksi (210 MPa) tension	8% in 30 months
60 ksi (410 MPa) tension	7% in 7.5 months
Compression due to I.D. treatment	0% in 9 months

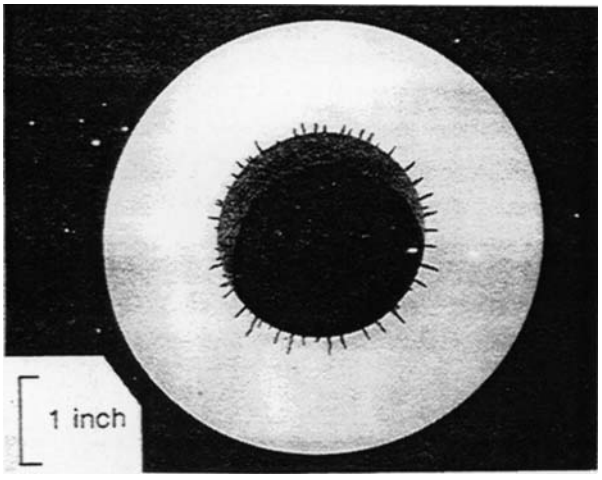


Figure 1. Stress corrosion cracking pattern in an NMDC. Two deep, wide cracks at 180° are present.

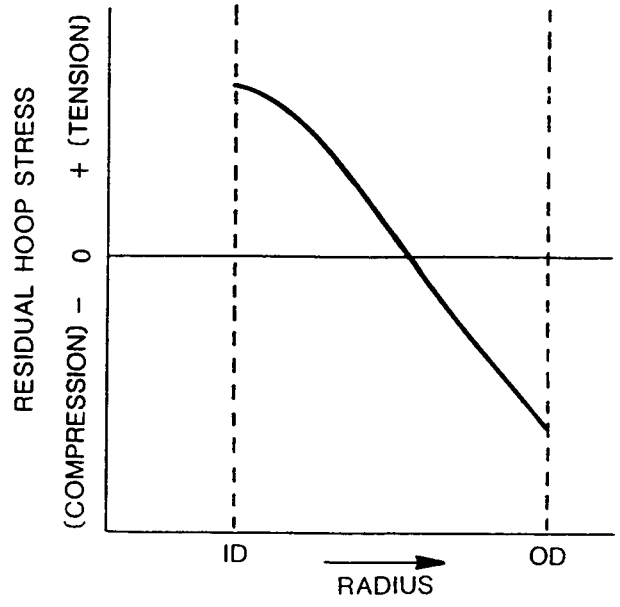


Figure 3. Schematic showing the residual hoop stress in an NMDC in the as-bored condition. Note that the material on the O.D. is in compression.

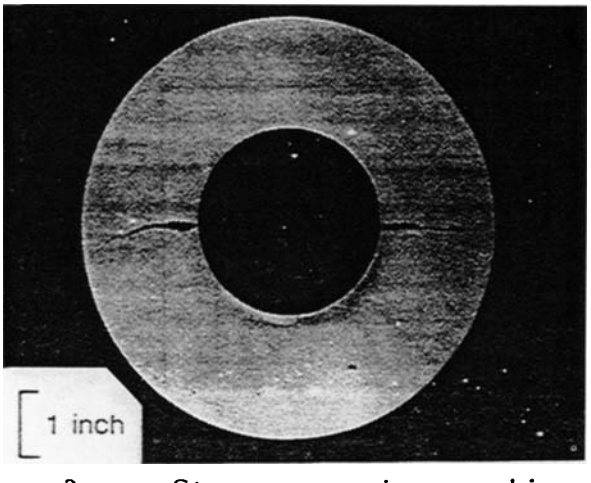


Figure 2. Stress corrosion cracking pattern in an NMDC. Multiple shallow cracks are shown.

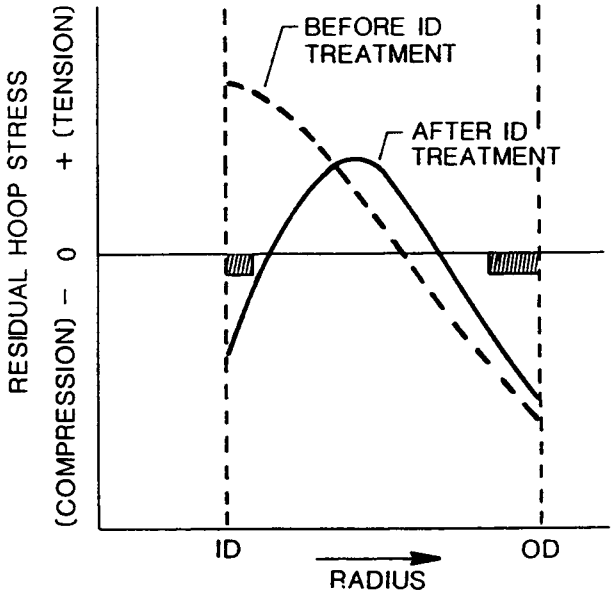


Figure 4. Schematic showing the residual hoop stress in a collar after treating the I.D. to control residual stress.

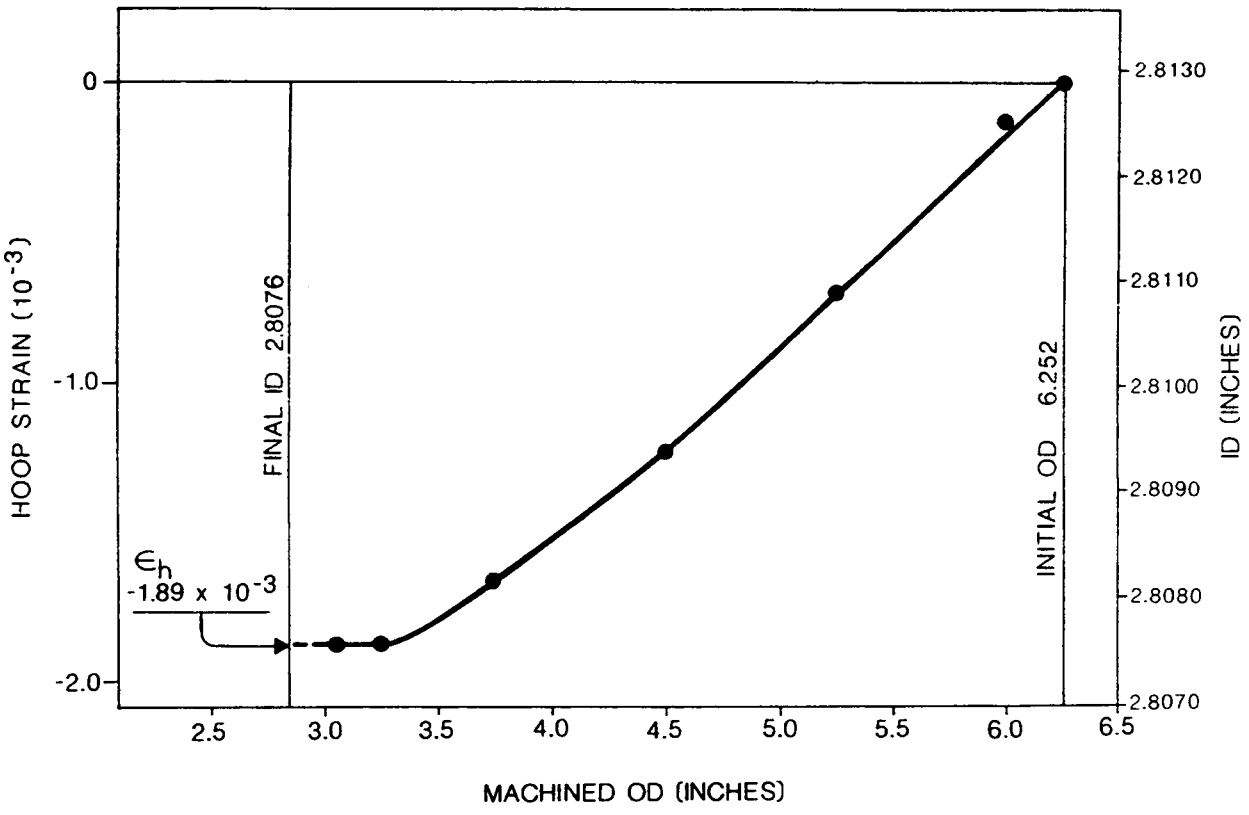


Figure 5. Relaxation data from a residual stress test on a 6-1/4 inch O.D. X 2-13/16 inch I.D. sample (159 mm O.D. X 71 mm I.D. sample).

Copyrighted Materials
Copyright © 1996 NACE International Retrieved from www.knovel.com

Paper No. 208—CORROSION/84

A CRITERION FOR EVALUATING AND PREDICTING THE SOUR RESISTANCE OF HIGH ALLOYS

Tomomi Murata, Ryo Matsuhashi,
Mizuo Sakakibara, Masao Onoyama
R & D Laboratories-I, Nippon Steel Corporation
1618 Ida, Nakahara-ku, Kawasaki 211 JAPAN

ABSTRACT

A criterion for evaluating and predicting the sour resistance of high alloy is presented through multiple regression analysis of laboratory data with the aid of a computer. *Sour Resistance* is defined as a polarization resistance in anodic dissolution of metals which do not form passive films in sour environments. *Sour Resistance* value defined in this study, SR, consists of major alloy components and their coefficients which are the function of given environmental parameters.

SR value showed useful relationships with corrosion behaviors of high alloys tested in NACE solution and brine solution under high partial pressure of H_2S and CO_2 at temperature up through 250°C (482°F).

INTRODUCTION

In deep oil/gas wells, engineering materials frequently encounter aggressive high temperature environments containing high levels of H_2S, CO_2, sulfur and concentrated brine solutions together with hydrocarbons where corrosion of materials is a main concern to attain the designed life performance. Tuttle and Kane's dialogue appeared in the special issue of *Materials Performance* clearly states that material selection process becomes critical in the deep wells because of the cost and environments.[1] The aim of this study is to assess the selection guideline of high alloys for sour application through multiple regression analysis of laboratory obtained corrosion data. A part of this approach was presented at CORROSION/83.[2]

EXPERIMENTAL

Materials: Fifteen commercially available high alloys were employed for this study. Main alloy compositions are listed in Table 1. Each alloy was machined to dimensions of test specimens shown in Fig. 2 and 3 as received materials conditions. Specimens were mechanically polished with Emery paper of # 320 followed by decrease in aceton for five minutes using ultrasonic vibration before testing.

Corrosion Tests: Immersion tests for weight loss measurements repassivation potential measurement with crevice and SSRT for evaluating the susceptibility to SCC were conducted. Employed test apparatus are schematically illustrated in Fig. 1-3.

After each corrosion test, specimen was visually examined for localized corrosion, and surface film analysis was carried out with the specimens of interest by IMA and ESCA for in-depth profile of alloy elements and their bond states. As test solutions, NACE solution and CO_2 and H_2S saturated synthetic sea water were employed. Corrosion rate is expressed in mdd unit throughout this study.

Multiple Regression Analysis: In order to obtain a useful tool in material selection, multiple regression analysis which is well established in statistical analysis was conducted with the obtained corrosion data and SR which consists of alloy components such as Cr, Mo, and Ni in this particular study and their coefficients. These coefficients are functions of environmental parameters.

The essential idea of this approach is based on the following observations:

1. Passive films formed prior to tests in sour environments tend to be destroyed or reduced depending on the severeness of the given environments, and stability of the passive films,
2. Instead of passive films, which are amorphous, crystalline sulfides or sulfides and oxides (sometimes hydro-oxides) mixtures tend to be dominant,
3. In accelerating tests, corrosion behaviors of alloys could be treated as anodic dissolution in active or semi-active state, e.g., polarization resistance could be a suitable measure of corrosion resistance in accelerating sour environments in most cases.

RESULTS AND DISCUSSION

Immersion Tests: Immersion test were conducted in both NACE solution and CO_2 and H_2S saturated synthetic seawater systems. Multiple regression analysis of the corrosion rates, CR, was made so that linear relationship is found between log (CR) and SR values. In this study, Cr, Mo, and Ni were chosen as important components. In case of Co-base alloys Co could be treated as equivalent to Ni.[3] In this analysis, the coefficient of Cr was set as unity for convenience sake, and weight percent was used for alloy compositions. The obtained results are shown in Table 2 and 3 for CO_2 and H_2S brine solutions and NACE solution respectively. The corrosion rates of some alloys were negligible and their data were not included in multiple regression analysis, but shown in each figure as CR = O. The multiple correlation coefficient is not high enough for CO_2: 79 atm and H_2S: 8.77 atm at 250°C (482°F) where SR has to be reconsidered. Except for the above case, good correlations were found between log (CR) and SR values as indicated in Fig. 4 through 11. It is to be noted that there exists three distinct zones:

1. severe weight loss corrosion;
2. pitting corrosion; and
3. immune zone, as pointed for each figure.

Surface film analysis made with stainless steels for 24 hr exposure tests are shown in Fig. 12 where in-depth profile of alloy elements and bond states suggest that the outer layer consists of mainly NiS and the inner layer consists of Cr and Mo oxides and Cr hydro-oxide.[4] This analysis was made with 316 and alloy A before breakdown occurred in contrast to 430 and 304 which underwent breakdown of pre-formed passive films within 24 hr exposure in NACE solution. These data are typical examples of the change of the pre-formed passive films during immersion tests. In case pre-formed passive films persist, then the alloy behaves immune to the environment: 316 showed immune to NACE solution at 25°C (77°F) for five days but showed severe corrosion at 90°C (194°F) where only sulfides were observed. In order to examine the stability of the films in a given corrosion system, repassivation potential, E_r, was determined in the presence of a crevice by way of potential sweep method usually employed in the crevice corrosion study. The obtained E_r values plotted against SR values for 80°C (176°F) in NACE solution is shown in Fig. 13 which suggests again the usefulness of SR value as a measure of the film stability.

Stress Corrosion Cracking Tests: Stress corrosion cracking tests were conducted using slow strain rate test method in NACE solution at 25°C (77°F). The obtained results were plotted against SR values as shown in Fig. 14 which indicates that above 35 of SR value alloys become immune to SCC. The same tendency is being found for the other corrosion systems. It is very interesting to notice that immunity zone without external stress will be shifted to higher SR values when stress is applied in corrosive environments. Since stress corrosion cracking is closely related to film stability and reformation rate upon breakdown under stress, it is reasonable to observe the SR value dependence of the susceptibility to SCC expressed as the inverse of $\varepsilon_{NACE}/\varepsilon_{air}$ where ε is a fracture strain.

Electrochemical Meaning of SR Value: The data shown so far indicate that alloys exposed to aggressive sour environments may: 1) keep the pre-formed passive films; 2) form new films which are usually non protective crystalline nature; 3) become film free or; 4) show the intermediate state as schematically summarized in Fig. 15. The approximately linear relationship between log (CR) and SR values except for those in immunity may suggest that activation process of electrochemical anodic dissolution is rate controlling rather than diffusion of reacting species through films on alloys.

Present understanding of SR value is the followings:

To the first order approximation, alloys are considered as solid solutions so that they are different pure metals each of which has a unique free energy for anodic dissolution, ΔG, at corrosion potential in a given corrosive environment. The general expression for the corrosion rate, CR is:

$$CR = i_o/nF \exp(nF\eta/RT)$$
$$= A \exp(-\Delta G/RT) \exp(nF\eta/RT).$$

Therefore,

$$\log (CR) = B - \Delta G + nF\eta$$
$$= B' - C(SR)$$

where A, B, B' and C: constants

i_o: exchange current density of a given solid solution in a given environment
η: overpotential for anodic dissolution of a given corrosion system.

At constant pressure and temperature, Gibbs free energy for anodic dissolution of solid solution can be expressed as a summation of mole fraction of each component times chemical potentials of its dissolved state. SR values, therefore, are directly related to ΔG. The overpotential term, on the other hand, is difficult to assess because of the presence of complicated cathodic reactions such as reduction of H_2S. The contribution of this term to SR value may cause the deviation of the data from the linearity with log (CR).

The cathodic polarization measurements suggest that cathodic reactions at high alloys are little influenced by alloy compositions in contrast to anodic reactions. Therefore η term in equation (2) can be treated as a constant in a given environment. Both kinetic and thermodynamic viewpoints on this matter are described in an appendix.

CONCLUSIONS

The following concluding remarks could be drawn from this study:

1. SR value presented in this study may provide a useful mean in evaluating and predicting corrosion behaviors of engineering alloys for sour environments.
2. SR values consist of major alloy components and their coefficients which are the functions of environmental parameters.
3. For a given environment, low SR alloys show severe weight loss corrosion whereas high SR alloys show immunity or localized corrosion if the value is not high enough.
4. Apparently SR value is directly related to free energy for anodic dissolution. General expression for SR value is the following:

$$\log (CR) = B' - C (SR)$$

5. This concept is useful from engineering viewpoint, but more work should be done for clear meaning in corrosion kinetics.

ACKNOWLEDGMENT

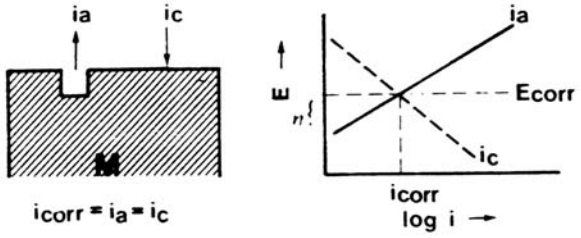
The present authors would like to acknowledge the useful discussion and stimulation by Dr. S. Itoh and Mr. H. Kihira.

REFERENCES

1. Tuttle, R.N., Kane, R.D., *Materials Performance* 22, 1(1983), p. 9.
2. Murata, T., Sato, E., Matsuhashi, R., CORROSION/83, paper no. 53.
3. Vaughn, G.H., Ghaung, H., *Materials Performance* 21, 1(1982), p. 44.
4. Hashimoto, M., Murata, T., to be published.

Appendix 1 - Theoretical background for SR values.

a. Discussion From Kinetics Viewpoint



$i_{corr} = i_a = i_c$

Anodic Reaction (Oxidation)

$M \longrightarrow M^{n+} + ne^-$

$$\log i_{corr} = \log i_a = A + B \cdot \eta_{corr} - C \cdot \Delta G_a \quad \cdots\cdots(1)$$

Cathodic Reaction (Reduction) ---- const.

for example,

$2H^+ + 2e^- \longrightarrow H_2$

$$\log i_{corr} = \log i_c = A' - B' \cdot \eta_{corr} - C' \cdot \Delta G_c$$

$$= \alpha - B' \cdot \eta_{corr} \quad \cdots\cdots(2)$$

$$\therefore E_{corr} = [(\alpha - A)/(B + B')] + [C/(B + B')] \cdot \Delta G_a \quad \cdots(3)$$

$$\therefore \log i_{corr} = \left[A + \frac{B(\alpha - A)}{(B + B')}\right] - \left[C - \frac{B \cdot C}{(B + B')}\right] \cdot \Delta G_a$$

$$= a - b \cdot \Delta G_a \quad \cdots\cdots(4)$$

b. Discussion From Thermodynamical Viewpoint

if T, P : const.,

$$d\Delta G_a = \sum (\partial \Delta G_a / \partial n_i)_{T,P,n_j \cdots} dn_i$$

$$= \sum \mu_i \, dn_i \quad \cdots\cdots(5)$$

$$\therefore \Delta G_a = \sum \mu_i \cdot n_i = \sum \mu_i \cdot z_i \cdot [M_i] \quad \cdots\cdots(6)$$

$$\log i_{corr} = a - b \cdot \sum \mu_i \cdot z_i \cdot [M_i]$$

$$= a - b_1 [Cr] - b_2 [Ni] - b_3 [Mo] \cdots\cdots(7)$$

$$[SR] = [Cr] + (b_2/b_1) \cdot [Ni] + (b_3/b_1) \cdot [Mo]$$

$$= [Cr] + X[Ni] + Y[Mo] \quad \cdots\cdots(8)$$

$$\therefore \log i_{corr} = a - b_1 [SR] \quad \cdots\cdots(9)$$

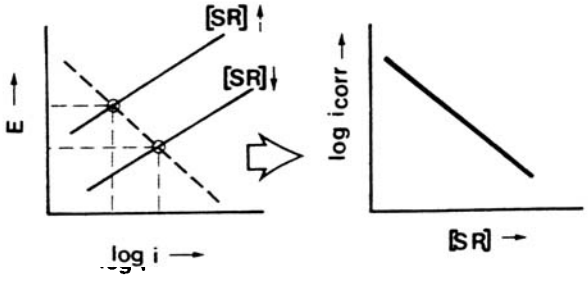


TABLE 1
Major chemical composition of tested alloys

Chemical Composition of Tested High-alloy Steels

Alloy \ Comp.	C	Mn	Cr	Ni	Mo	others
410W	0.02	0.51	11.98	0.05	—	—
430	0.059	0.37	16.35	0.09	—	—
A	0.004	0.07	18.84	—	1.90	—
B	0.001	0.19	26.03	0.14	1.08	—
C	0.024	0.48	25.17	5.83	3.05	Nb ; 0.61
304	0.049	0.94	18.36	9.25	0.08	—
316	0.055	1.02	18.34	8.54	2.97	—
316C	0.06	1.11	17.45	7.15	0.93	Cu ; 1.94
D	0.052	0.67	17.14	13.2	—	Si ; 3.95 Cu ; 0.81
E	0.049	1.48	24.18	12.7	0.8	N ; 0.315
310S	0.05	1.02	24.9	19.95	—	—
F	0.042	1.01	24.85	15.93	3.02	Cu ; 2.09
329J$_1$	0.038	0.53	24.59	5.35	2.15	Cu ; 1.15
G	0.043	0.84	22.5	35.86	—	Ti ; 0.58 Al ; 0.66
H	0.06	0.03	17.9	66.03	0.5	W ; 14.96 Y ; 0.017

TABLE 2
List of SR equations for various environmental conditions
R: multiple correlation coefficient

① CO_2-H_2S-Brine

No.	ENVIROMENT	ELEMENT	COEFFICIENT	T-VALUE	CORROSION RATE EQUATION / SR EQUIVALENT EQUATION	R
①	CO_2 : 81atm H_2S : 0.03atm T : 130°C	Cr Ni Mo	-0.107 -0.103 -0.125	-3.48 -1.64 -0.45	log C.R. = 2.40 - 0.107·[SR] [SR] = [Cr] + 0.96[Ni] + 1.17[Mo]	0.87391
②	CO_2 : 67atm H_2S : 1.22atm T : 60°C	Cr Ni Mo	-0.104 -0.023 -0.428	-6.58 -0.88 -2.73	log C.R. = 2.32 - 0.104·[SR] [SR] = [Cr] + 0.22[Ni] + 4.12[Mo]	0.95472
③	CO_2 : 79atm H_2S : 8.77atm T : 250°C	Cr Ni Mo	-0.060 -0.014 -0.049	-4.96 -2.33 -1.64	log C.R. = 2.84 - 0.060·[SR] [SR] = [Cr] + 0.23[Ni] + 0.82[Mo]	0.84094
④	CO_2 : 1atm H_2S : 0.04atm T : 90°C	Cr Ni Mo	-0.111 -0.024 -0.116	-7.04 -1.15 -2.02	log C.R. = 2.22 - 0.111·[SR] [SR] = [Cr] + 0.22[Ni] + 1.05[Mo]	0.90212

TABLE 3
List of SR equations for NACE solution at various temperatures

⑪ NACE

t/°C	Elem.	Coeff.	T-value	Corrosion Rate Eq. / [SR] Equivalent Eq.	R
25	Cr Ni Mo	-0.082 -0.037 -0.262	-3.341 -6.586 -2.949	log C.R. = 3.57 - 0.082[SR] [SR] = [Cr] + 0.45[Ni] + 3.20[Mo]	0.9323
60	Cr Ni Mo	-0.091 -0.038 -0.374	-2.918 -5.275 -3.297	log C.R. = 4.45 - 0.091[SR] [SR] = [Cr] + 0.41[Ni] + 4.10[Mo]	0.9152
80	Cr Ni Mo	-0.082 -0.046 -0.564	-3.037 -7.396 -5.718	log C.R. = 4.47 - 0.082[SR] [SR] = [Cr] + 0.56[Ni] + 6.83[Mo]	0.9536
90	Cr Ni Mo	-0.122 -0.037 -0.248	-3.292 -4.305 -1.840	log C.R. = 4.88 - 0.122[SR] [SR] = [Cr] + 0.30[Ni] + 2.03[Mo]	0.8881

$n_{Cr} = 15$ $t_{Cr} = 2.16$
$n_{Ni} = 14$ $t_{Ni} = 2.18$
$n_{Mo} = 10$ $t_{Mo} = 2.31$
(95%)

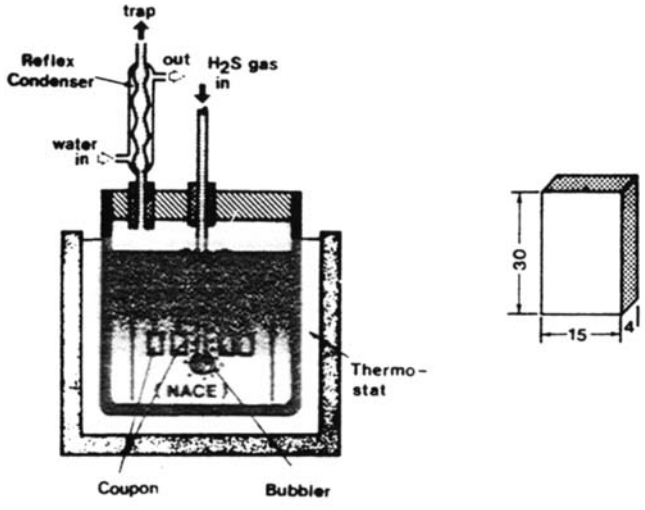


Fig. 1 - Schematic illustration of a high pressure and high temperature corrosion test apparatus.

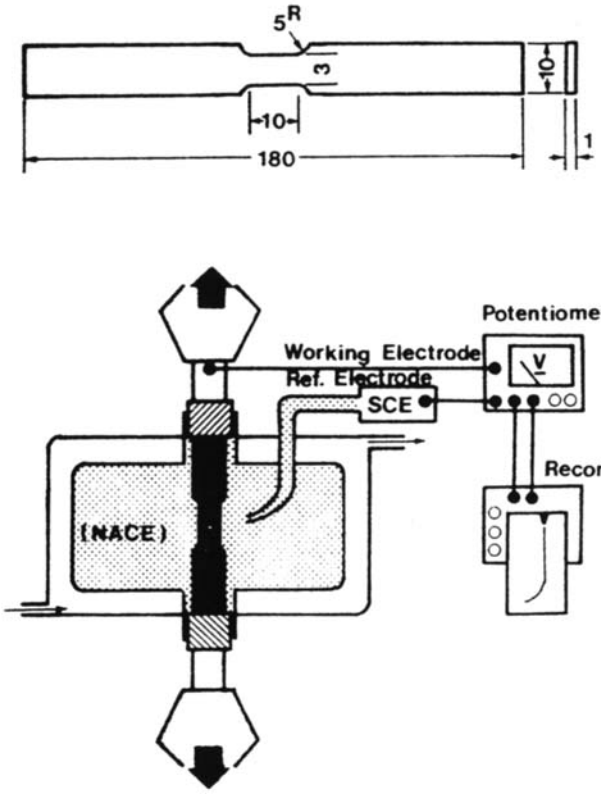


Fig. 3 - Schematic illustration of SSRT test apparatus and dimension of cylindrical specimen.

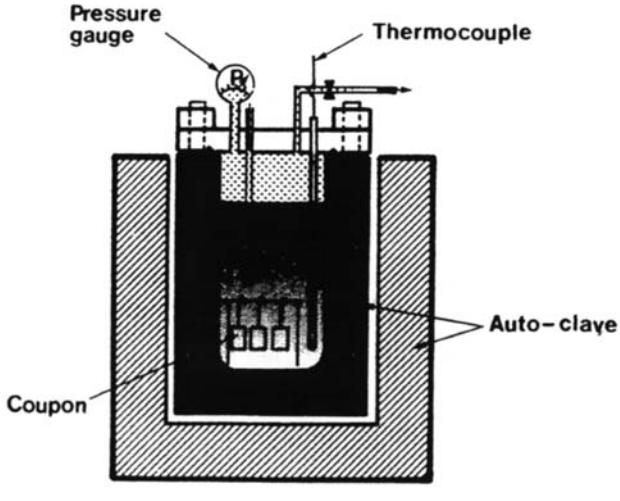


Fig. 2 - Schematic illustration of an ambient temperature corrosion test apparatus and test coupon dimension.

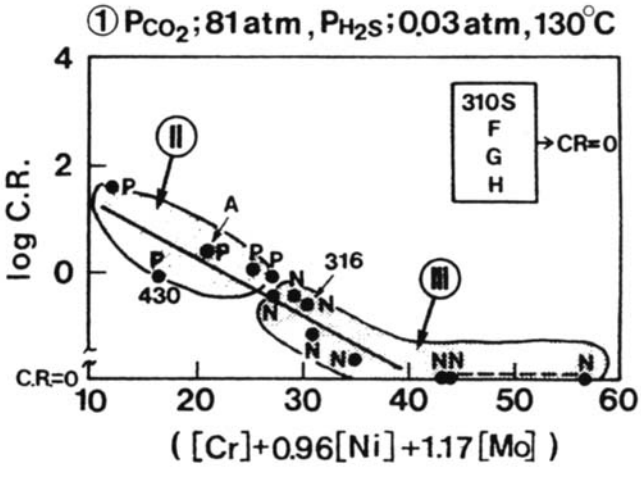


Fig. 4 - Relationship between SR and corrosion rates in solution saturated with CO_2: 81 atm. and H_2S: 0.03 atm. at 130 C.

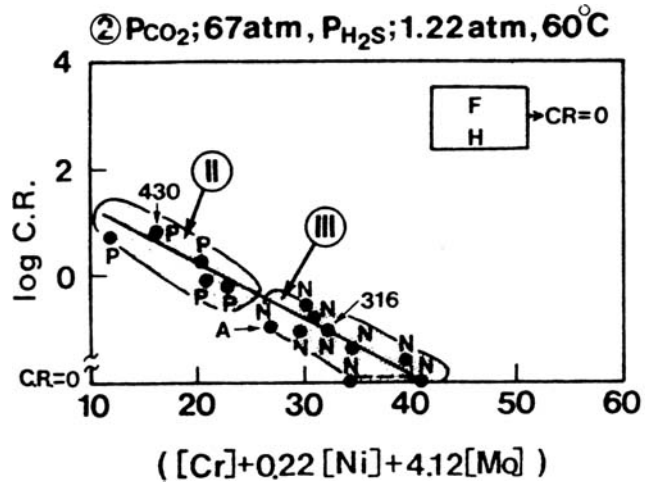


Fig. 5 - Relationship between SR and corrosion rates in solution saturated with CO_2: 67 atm. and H_2S: 1.22 atm. at 60 C.

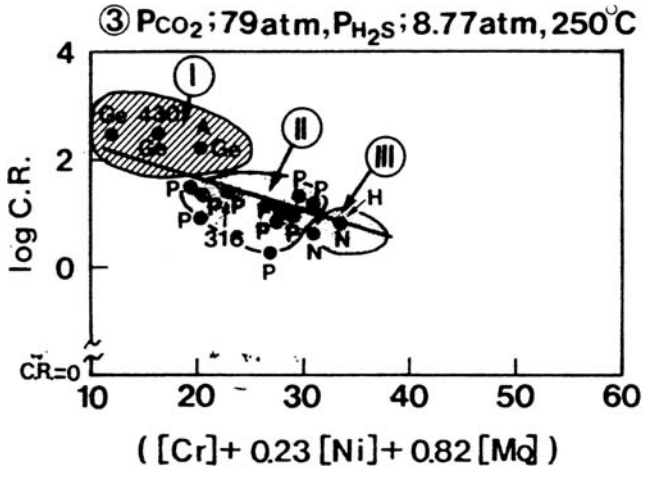


Fig. 6 - Relationship between SR and corrosion rates in solution saturated with CO_2: 79 atm. and H_2S: 8.77 atm. at 250 C.

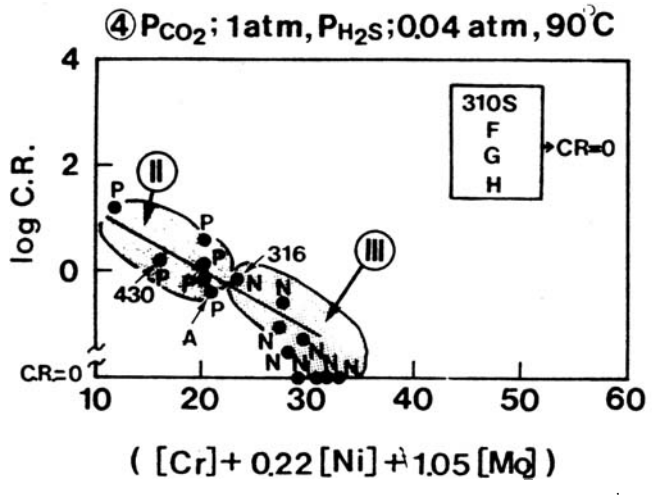


Fig. 7 - Relationship between SR and corrosion rates in solution saturated with CO_2: 1 atm. and H_2S: 0.04 atm. at 90 C.

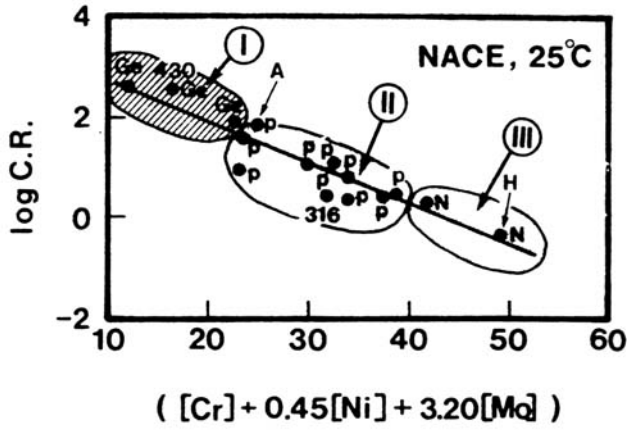


Fig. 8 - Relationship between SR and corrosion rates in NACE solution at 25 C.

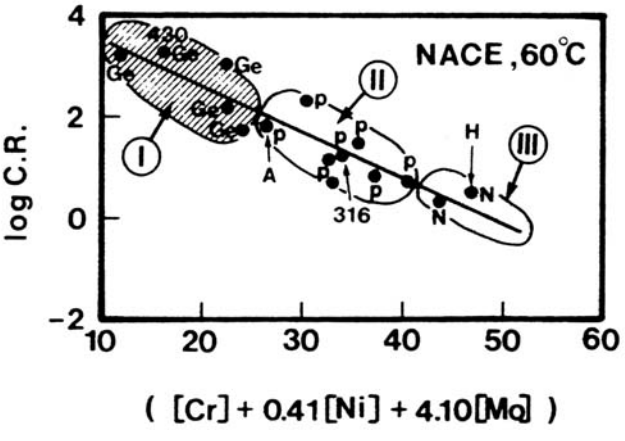


Fig. 9 - Relationship between SR and corrosion rates in NACE solution at 60 C.

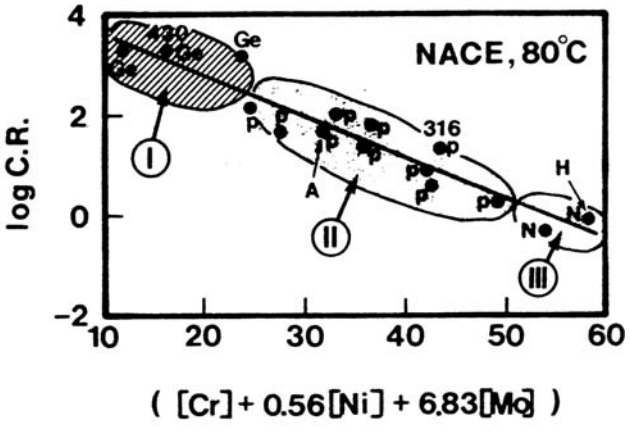


Fig. 10 - Relatioship between SR and corrosion rates in NACE solution at 80 C.

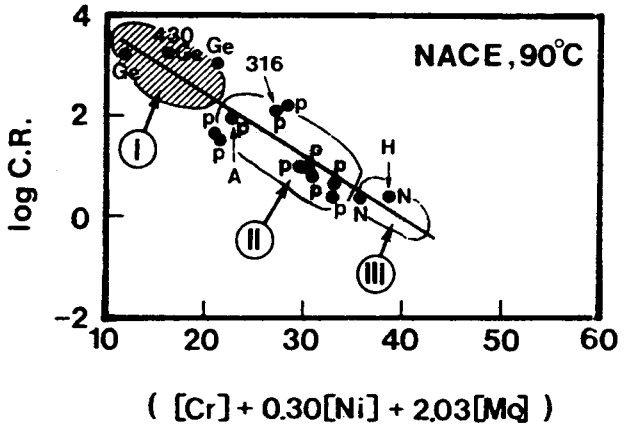


Fig. 11 - Relationship between SR and corrosion rates in NACE solution at 90 C.

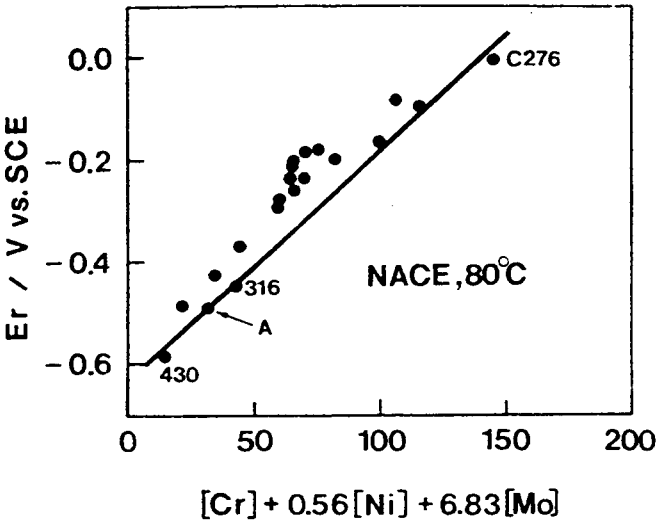
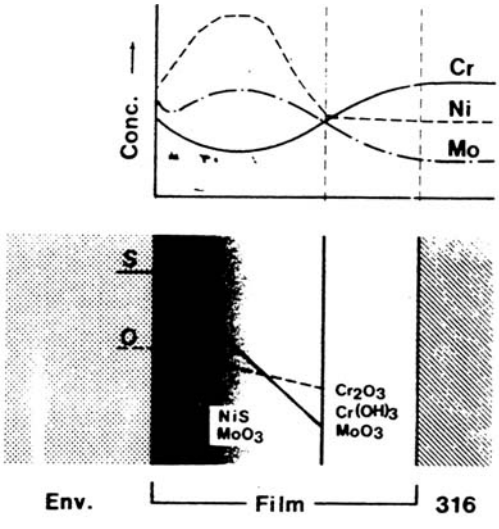


Fig. 13 - Repassivation potential measurements of alloys in NACE solution at 80 C.



NACE, 25°C, ESCA

Alloy	Comp.	Cr	Ni	Mo	O	S
430	17Cr	Cr_2O_3 . CrO_3	—	—	-OH	M-S
A	19Cr -2Mo	Cr_2O_3 . $Cr(OH)_3$	—	MoO_3	-OH	M-S
304	18Cr-9Ni	Cr_2O_3 . $Cr(OH)_3$	NiS	—	-OH	M-S
316	17Cr-11Ni-2Mo	Cr_2O_3 . $Cr(OH)_3$	NiS	MoO_3	-OH	M-S

Fig. 12 - Example of surface film analysis after exposure to H_2S bearing environments for a day.

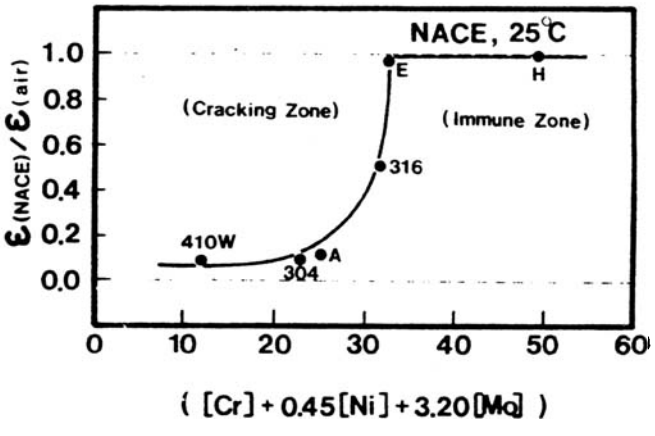


Fig. 14 - SSRT results against SR values.

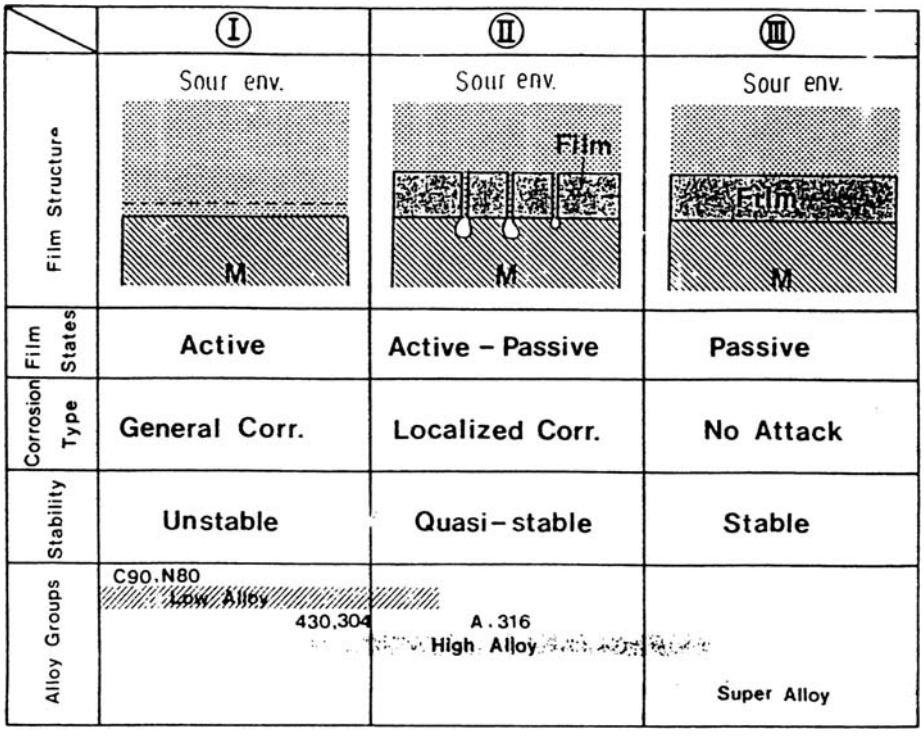


Fig. 15 - Summary of this study.

Copyrighted Materials
Copyright © 1996 NACE International Retrieved from www.knovel.com

The Stress Corrosion Resistance of non Magnetic Stainless Steels Used in Oil Exploration

P. G. SMITH, J. E. TRUMAN, H. T. GISBORNE, and G. OAKES

Austenitic Steels of the Cr-Mn-(Ni)-N2 type are being used in the work hardened condition in substantial section size for some applications, notably as drill collars and stabilizers in the directional drilling of oil wells.

Service can involve contact with chloride bearing fluids and as drilling to greater depths can involve high temperature some instances of stress corrosion cracking have been reported. Resistance to stress corrosion cracking of several compositions has been assessed in solutions of several chlorides with variation of a number of factors. An important feature in determining resistance to cracking has proved to be carbon content and degree of sensitization. Effect of carbon content, strain and thermal treatment on behavior and mode of cracking are discussed.

INTRODUCTION

The technical requirements for materials for the manufacture of drill collars and stabilizers used in oil exploration are given in Table I, these being based on engineering needs. In addition to this moderate strength and good toughness, items used for directional drilling must also have a very low magnetic permeability due to the use of magnetic field measuring instruments. It is this latter need which restricts the choice of ferrous alloys to those with a face-centered cubic structure (austenitic steels) and then care must be taken to ensure that the austenite is sufficiently stable and is free from traces of magnetic phases. The strength of annealed alloys such as the '300' series stainless steels is inadequate but can be improved by the following applied separately or in combination:

(1) Solution hardening using interstitial and/or substitutional elements.

(2) Cold working.

(3) Warm working at a temperature below that of recrystallization (approximately 850 °C).

(4) Suitable additions of alloying elements to allow strengthening by precipitation hardening.

Of these various options, (1) is not really practicable alone to give A.P.I.7. properties but can contribute. Option (2), while being a very convenient method of strengthening steel in small section form, is less attractive with the larger sections (drill collars are commonly 4 to 11 in. diameter) involved here. Precipitation hardening of austenitic steels is feasible and alloys do exist but are not widely used and invariably have low impact strength. In the main, option (3) is utilized. While strengthening of the standard austenitic steels is possible by this means, modified alloys are most often used so that less strain is required to achieve the desired strength. Increased contents of nitrogen and manganese and reduced nickel are common. A range of types is shown in Table II and to these may be added types 304 and 316.

Service Conditions

In service the equipment is in an environment which can be corrosive. A drilling mud is pumped down the bore of the drill string towards the bottom of which the non-magnetic components are positioned and this flows back to the surface

P. G. SMITH, Commerical Manager, J. E. TRUMAN, Product Metallurgist, H. T. GISBORNE, Product Development Manager, and G. OAKS, Research Manager, are all with Sheffield Forgemasters, Sheffield, England. This paper was originally presented at the ASM International Conference on New Developments in Stainless Steel Technology, September 17–21, 1984, Detroit, MI.

 ©1985 AMERICAN SOCIETY FOR METALS
Courtesy ASM International (formerly American Society for Metals)

Table I. Mechanical Property Requirements for Drill Collars, A.P.I.7

	Outside Diameter	
	3–6 in.	7–10 in.
Minimum yield strength N/mm^2 (ksi)	759 (110)	690 (100)
Minimum tensile strength N/mm^2 (ksi)	966 (149)	931.5 (135)
Minimum elongation pct	13	13

outside the string serving a variety of purposes including lubrication, removal of the drilling debris and preventing hole cave-in by exerting a high hydrostatic pressure. Depending on local conditions, the solid, inert component of the mud may be suspended in an oil or water based medium. The water used may be saline or may have soluble salts added, these latter usually being chlorides to prevent the solution of strata through which the drillings may pass or to inhibit the swelling of clay layers. The water based muds are often made alkaline (pH 10–12) and can have additions of bisulphite to reduce the corrosion of carbon and low alloy steel components. The temperature down-hole can be substantially above normal and temperatures above 100 °C have been reported. Contact time is limited, however, service being intermittent and down-hole time being only a proportion of service life.

Stresses on a collar are complex and not well documented. They would appear from service conditions, however, to consist of torsional, hoop and bending stresses; the magnitudes of which are not known.

SERVICE FAILURES

Life of drill collars is limited as there is considerable wear and tear of the threaded ends leading to the necessity of cutting back and rethreading which can only be done a limited number of times before length is inadequate. Lately there have been reports of cracking before discard of collars for the above reason and this has been identified as stress corrosion cracking. While the total incidence of failure appears to be low, the view has been expressed that it is increasing. It may well be that some collars are now meeting more arduous environmental conditions, notably higher temperatures resulting from an increasing number of deeper wells, temperature having a marked relevance to incidence of stress corrosion cracking (S.C.C.).

A number of lengths cut from the ends of collars showing cracks became available for examination. On analysis it became obvious that these were in a variety of materials. In all cases the major cracking was radial with branching of some cracks; these occasionally propagated parallel to the bore surface. Cracking was much deeper from the bore than from the outer surfaces and indeed, was never more than superficial from the latter even when cracks from the bore had fully penetrated the wall. Initiation had been from numerous points with propagation both radially and axially so that there could be parallel, overlapping cracks; only a limited number of cracks progated to a marked extent however. Both intergranular and transgranular cracks were noted but only in one case were both types found in one collar, the intergranular mode predominating in this instance. The pattern of intergranular cracking in an 8.5-in. diameter collar is shown in Figure 1; the outer surface cracks are not visible

Table II. Details of Materials Tested

Identification	C	Si	Mn	Cr	Ni	Mo	N	Tensile Strength N/mm^2 (ksi)		A262 Tests	
								Rp.2	Rm	A	E
Staballoy A*	0.040	0.32	10.13	17.70	6.43	0.14	0.325	644 (93.4)	820(121.8)	Step	Pass
Staballoy B*	0.059	0.31	10.39	17.39	6.31	0.32	0.31	707(102.5)	882(127.8)	Dual	Pass
Staballoy C*	0.075	0.42	10.65	17.98	6.27	0.21	0.34	669 (97.0)	877(126.1)	Mainly Ditch	Fail
Staballoy D*	0.16	0.15	10.52	17.38	6.51	0.27	0.25	634 (91.9)	845(122.5)	Ditch	Fail
E*	0.073	0.55	19.23	13.40	2.06	0.48	0.26	758(109.8)	870(126.1)	Dual	Pass
F*	0.030	0.71	18.35	12.82	2.66	1.23	0.25	527 (76.4)	758(109.9)	Step	Pass
G*	0.163	0.40	9.21	14.94	11.98	0.23	0.27	662 (95.9)	857(124.2)	Ditch	Fail
H*[2]	0.125	0.29	17.46	17.79	0.46	0.97	0.46	854(123.8)	1030(149.3)	Ditch	Fail
304[1] W.W.	0.050	0.58	1.14	18.74	10.06	0.40	0.03	460 (66.7)	676 (97.9)	Step	Pass
304 Soft	0.050	0.58	1.14	18.74	10.06	0.40	0.03	553 (80.2)	553 (80.2)	Step	Pass
304[1] W.W.	0.030	0.39	2.85	18.90	10.50	0.06	0.192	689.3(99.)	861(124.8)	Step	Pass
304N[1] Soft	0.030	0.39	2.85	18.90	10.50	0.06	0.192	328 (47.5)	683 (99.0)	Step	Pass

*Materials extracted from full scale drill collars.
[1]Materials extracted from rolled plate.
[2]Also contains 0.94 pct Cu.

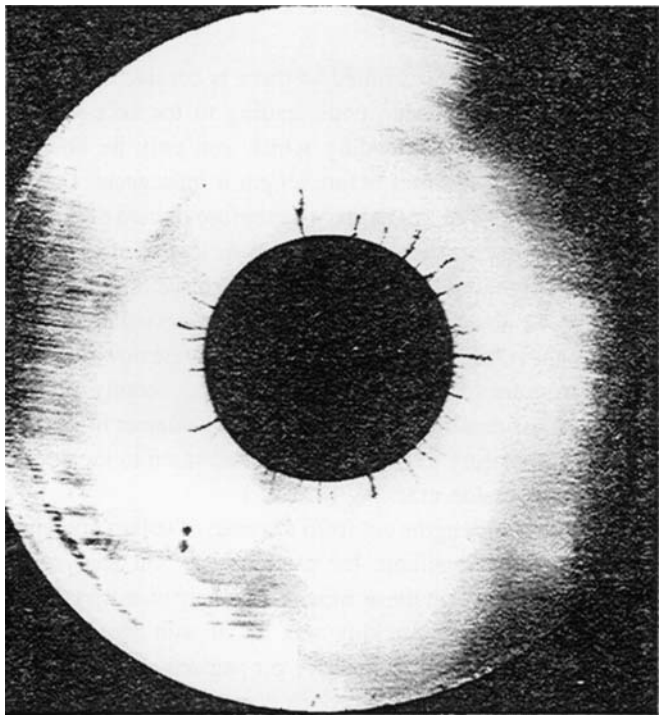


Fig. 1—Cracks in a drill collar section (material H) shown by dye penetrant. (Magnification ⅓ size.)

but penetrated at most to only 0.015 in. A detail of a bore crack is in Figure 2. The features of the transgranular cracks so far observed were generally similar except that no example of really deep cracking has yet been seen, the deepest being 0.15 in. even from the bore surface: an example is in Figure 3.

The observations made on failures demonstrate the need to study the cracking mechanism of these materials in hot chloride media.

MATERIALS USED FOR TESTING

The majority of the materials under test were taken from full scale drill collars. A to D in Table II were produced at Sheffield Forgemasters, as per Appendix I and consisted of two standard STABALLOY® collars and two experimental high C collars. For completeness and comparison purposes material from life expired collars of different composition to STABALLOY was evaluated. All results obtained were compared with data obtained from earlier investigations on 304 and 304N hot-rolled plate, the finishing temperature for which was low enough to give warm work. Tests were as rolled and after annealing.

®Owned by Sheffield Forgemasters.

All the materials were assessed for susceptibility to intercrystalline corrosion by ASTM A 262 practices A and E. Test material was taken from the same position as that for stress corrosion cracking testing as described below. Results are in Table II.



Fig. 2—Detail of a crack in collar in Fig. 3. Magnified 85 times.

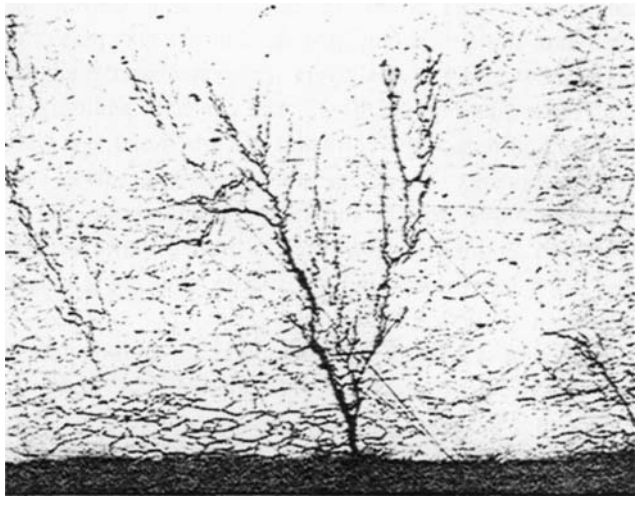


Fig. 3—Transgranular cracking in the bore of a 316 type collar. Magnified 150 times.

STRESS CORROSION CRACKING STUDIES

Test Procedures

Two modes of stressing were used for stress corrosion cracking testing. A bend test involved samples 4 in. × 0.5 in. × 0.125 in. Details of pre-forming and stressing are given in Appendix II. This represents a severe procedure as not only is stress at near yield but the latter is also increased by the pre-forming operation. Use of uniaxial stressing in tension allows more realistic loading although less conveniently. This procedure also is detailed in Appendix II. With both types of stressing, the test pieces were machined tangentially so that the mid-points came from points near to the bore surface or from an equivalent position in the case of the solid forgings.

Table III. Tests on Material From Several Drill Collars: Bend Tests in Biling NaCl Solutions: Times to Crack Initiation (Hours)

Temperature	Concentration	G	H	A	E	F
Boiling	Sat.	<24	<24	<24	<24	24–48
	10 pct	<24	<24	48–72	<24	
	10 pct, pH12	<24	<24	72–96	24–96	72–96
	3 pct	<24	<24	1176–1248	24–96	
	3 pct, pH12	<24	<24	>1032		720–816
80 °C	10 pct	<24		48–72	48–96	
	10 pct, pH12		<24	48–96	48–96	120–168
	3 pct			72–168		>1000
	3 pct, pH12		<24	>1032	864–1032	>1000
60 °C	Sat.	<24	<24	144–168	528–600	
40 °C	Sat.	72–144	<24	>2132	>1036	
20 °C	Sat.	240–288	96–120	>2452	>1032	

Sat = Saturated @ 20 °C.

Comparison of Some Materials

The bend test method was used to give comparisons of several drill collar compositions, sodium chloride solutions being utilized at various concentrations and temperatures. The samples were examined at low magnifications at intervals for signs of cracking, being removed from the solution for this purpose but not washed. Time out of the solution was as short as possible. Inspection was initially at 24-hour intervals but was less frequent as total time extended. The time ranges within which crack initiation was noted are shown in Table III. Subsequent crack growth rates varied but in the main the materials giving rapid initiation also suffered the most rapid crack extension. Sections prepared through a number of cracked specimens in each material showed the cracking to be branched in all cases but to be intergranular in the case of G and H and transgranular with A, E, and F. The cracks closely resembled those found in collars in service.

Tests were also carried out in boiling 42 pct magnesium chloride solution with entirely transgranular cracking being produced in all materials very quickly.

Effect of Anion Species

The effect of the chlorides of sodium, potassium, calcium, and magnesium were investigated using the bend test and one material, STABALLOY. Saturated solutions were made at room temperature to simulate practice and so actual concentrations varied. To give comparison without such variation tests were also carried out in solutions whose chloride contents were similar to that of 10 pct sodium chloride. In some cases testing was at normal pH, in others the pH was adjusted to 12 with sodium hydroxide. The higher temperatures were not covered on the whole because of the rapid cracking in sodium chloride solutions. Results are in Table IV.

Effect of Bisulfite Addition

To demonstrate any bisulfite effect, a saturated (at ambient temperature) sodium chloride solution was used. The effect of a 2 pct sodium metabisulfite addition was investigated at pH 6 and pH 12, the material being STABALLOY from collar A and collar C as warm worked or after treatment of 2 hours @ 650 °C. Times to crack initiation are in Table V. It should be noted that while access of air to the solutions was restricted it was not excluded. Analyses immediately after test termination showed that all the bisulphite had been oxidized in the solution.

Effect of Test Interruptions

Bend test samples from collar A were used to observe the effect of test interruption, the corrodent being boiling 10 pct sodium chloride solution. Without interruption, cracks started between 72 and 96 hours, the cracks then growing rapidly and penetrating the sample after 216 hours. Three other samples were tested similarly but were interrupted after 72 hours, and not returned to the test solution until a further 96 hours had elapsed, this pattern of 72 hours "in" and 96 hours "out" being continued. Samples which were merely allowed to dry or were washed briefly after the "in" cycle both developed cracks in the next "in" cycle and these cracks grew just as quickly as those of the "continuous" sample. A sample which was washed thoroughly (five minutes in swiftly flowing water) each time it was removed from the test solution, however, still had no cracks after a total of 1000 hours in the test solution. When the periodic

Table IV. Relative Effects of Chlorides of Na, Ca, K and Mg Steel A, Bend Tests, Times to Crack Initiation (Hours)

Temperature	Solution	NaCl	$CaCl_2$	KCl	$MgCl_2$
Boiling	Sat.	<24			
	Sat. pH12	<24			
	10 pct	48–72			120–192
	10 pct, pH12	72–96			48–120
	3 pct	1176–1284			
	3 pct, pH12	>1032			
80 °C	10 pct	48–72			
	10 pct, pH12	48–96			
	3 pct	72–168			
	3 pct, pH12	>1032			
60 °C	Sat.	144–168	24–72	120–192	24–72
	Sat. pH12	48–120	24–72	>2136	24–72
	10 pct	144–192	192–240	216–288	1128–1200
	10 pct, pH12	262–336			384–456
55 °C	Sat.	216–288	120–168	1032–1128	456–504
40 °C	Sat.	>2136	312–456	>2136	1850–2132
20 °C	Sat.	>2452	>2452	>2452	>2452

Sat = Saturated @ 20 °C.
"10 pct" solutions all had Cl content equivalent to 10 pct NaCl.

Table V. Effects of Addition of 2 Pct Sodium Metabisulphite

		Boiling Saturated NaCl Time to Crack Initiation	
Steel	pH	No Bisulphite	With Bisulphite
A	6	<24	48–72
A	12	<24	504–528
C + 2 h 650 °C	6	<24	<24
C + 2 h 650 °C	12	<24	<24

washing was discontinued however cracks, were noted within 72 to 96 hours.

Effect of Stress

The tensile stressing technique was used to investigate the effect of stress on cracking tendency. The behavior of the softened standard grade 304 is shown in Figure 4 as a basis of comparison, the two cracking corrodents used being the commonly used, aggressive 42 pct magnesium chloride solution and 30 pct sodium chloride solution. Plotted on the same illustration are data for the same material in the warm worked state. Figure 5 contains similar information for the high nitrogen content 304. Generally similar testing was carried out for two drill collar materials, the 10Mn, 18Cr, 6Ni, Staballoy and the 18Mn, 13Cr, 2Ni, 1Mo material, results being in Figures 6 and 7. The sodium chloride solutions were a little stronger (saturated at room temperature) and the effect of increasing pH level was also covered in this solution. All the failed samples (304 and drill collar materials) from these tests showed only transgranular cracking. Limited testing was also carried out on the very high carbon experimental STABALLOY type F, results are not plotted to avoid confusion but are in Table VI. Micrographs of sections through fractures are in Figures 8 and 9.

Effect of Carbon Content

To investigate the influence of carbon content 4 Staballoy collars of otherwise similar composition were subjected to the bend test in three boiling sodium chloride solutions. Times to crack initiation are shown in Table VII, together with comments on type of cracking determined by metallography.

Effect of Aging at 650 °C

In view of the observed mode of failure in service it was deemed prudent to examine the effect of isothermally aging at 650 °C. This was carried out on collars A, B, and C and the results obtained are given in Table VIII while results of A 262 A and E assessment are in Table IX.

As the above results are for material in a strained condition some comparative tests have been carried out on one collar (collar C) after softening. Bend test blanks were first softened by heating at 1050 °C for 30 minutes and cooling

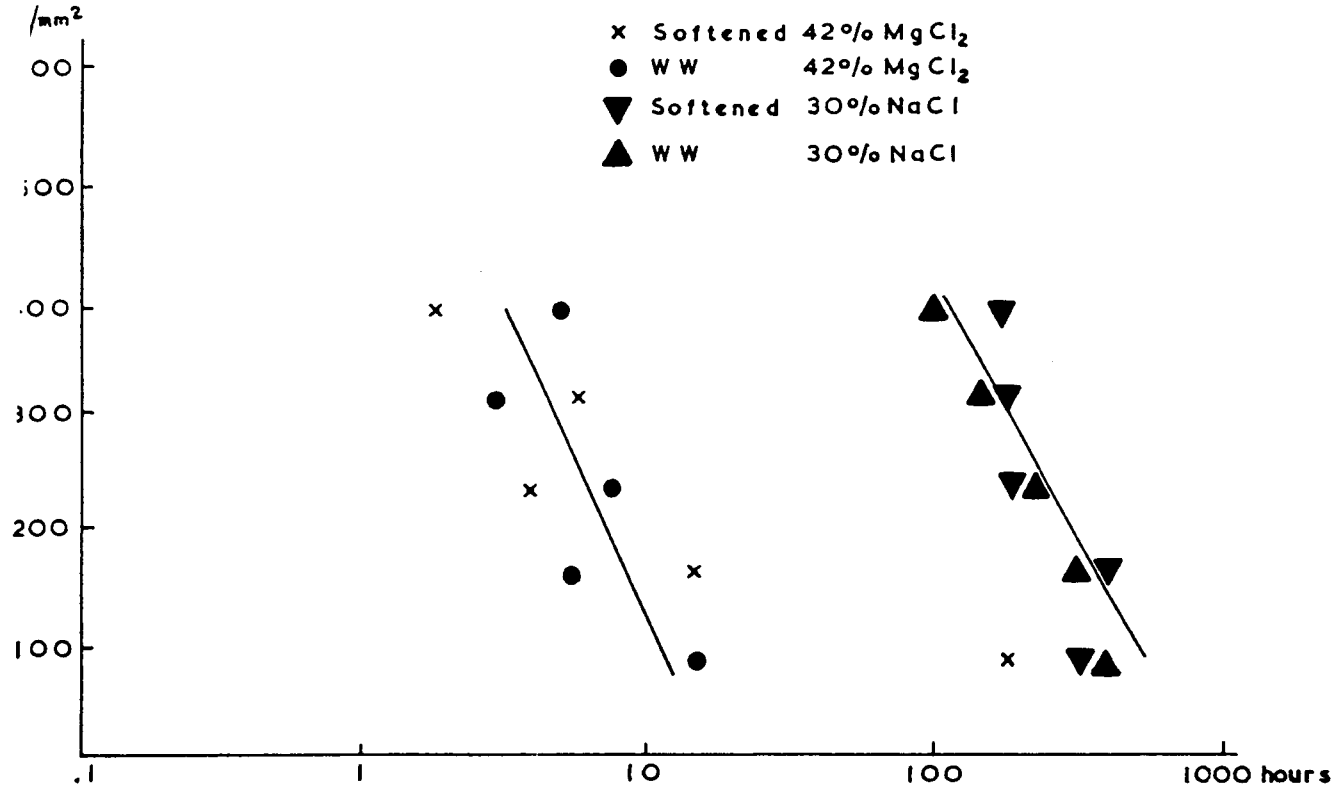


Fig. 4—Times to rupture in boiling solutions: 304 steel.

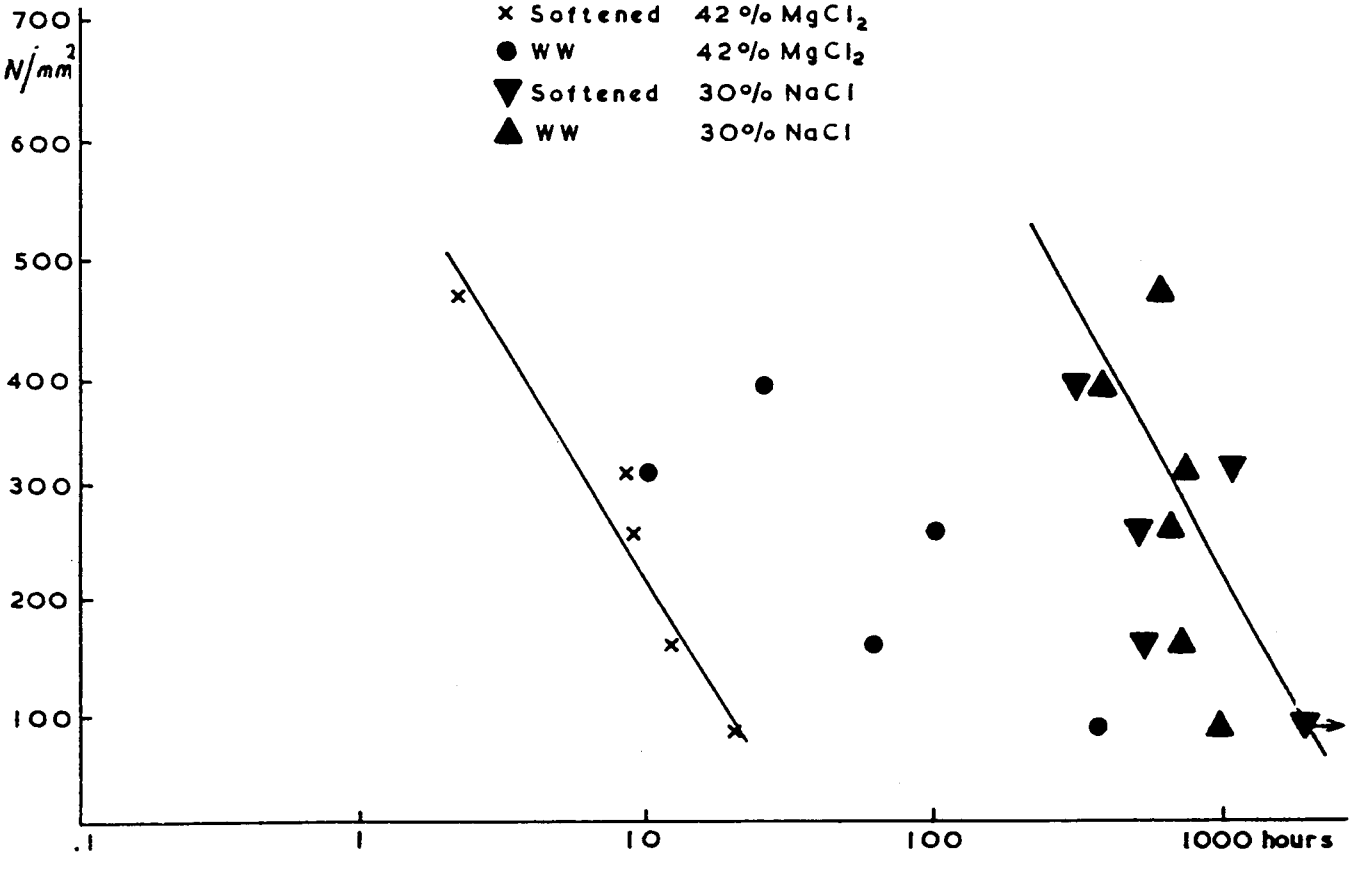


Fig. 5—Times to rupture in boiling solutions; 304 + nitrogen.

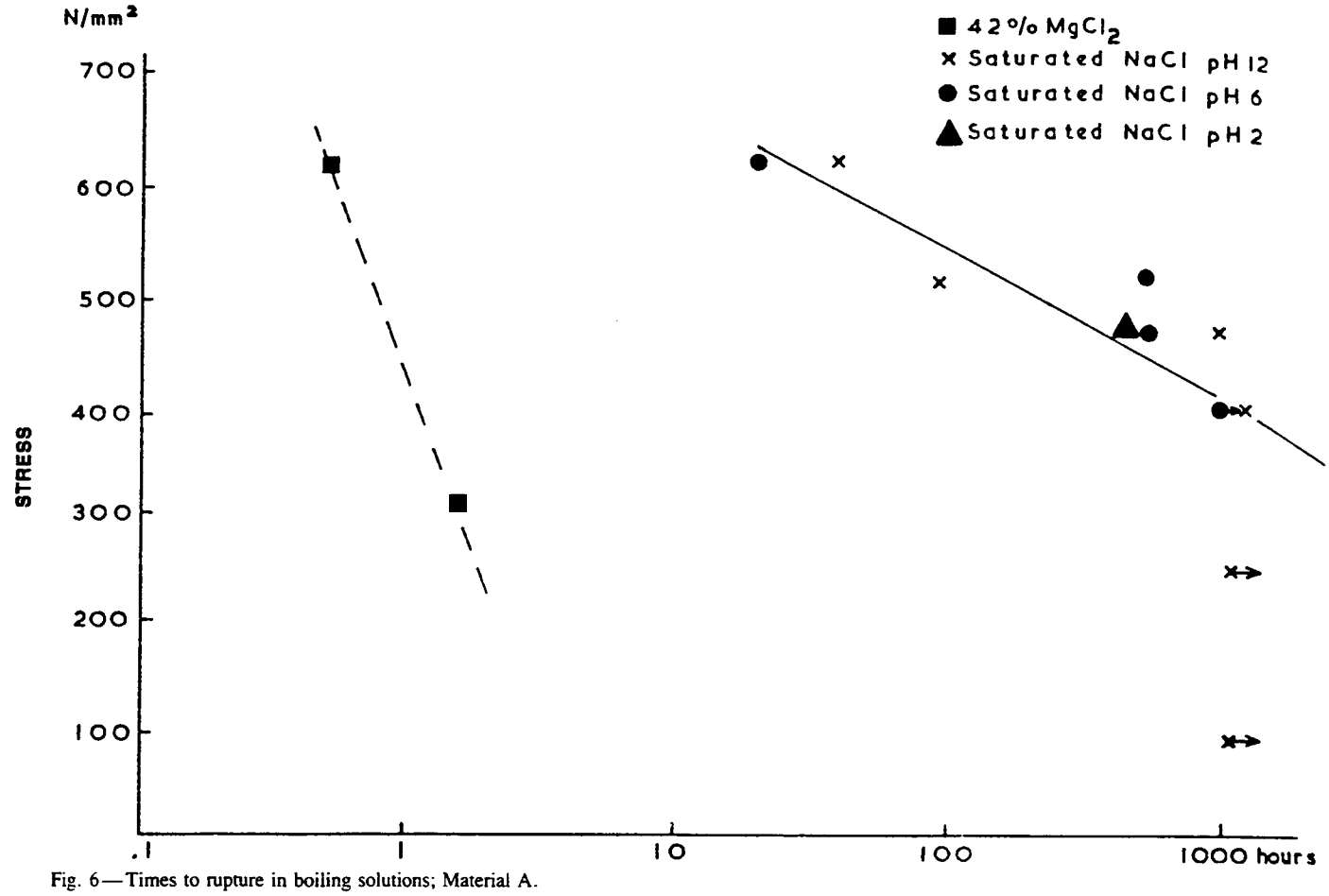


Fig. 6—Times to rupture in boiling solutions; Material A.

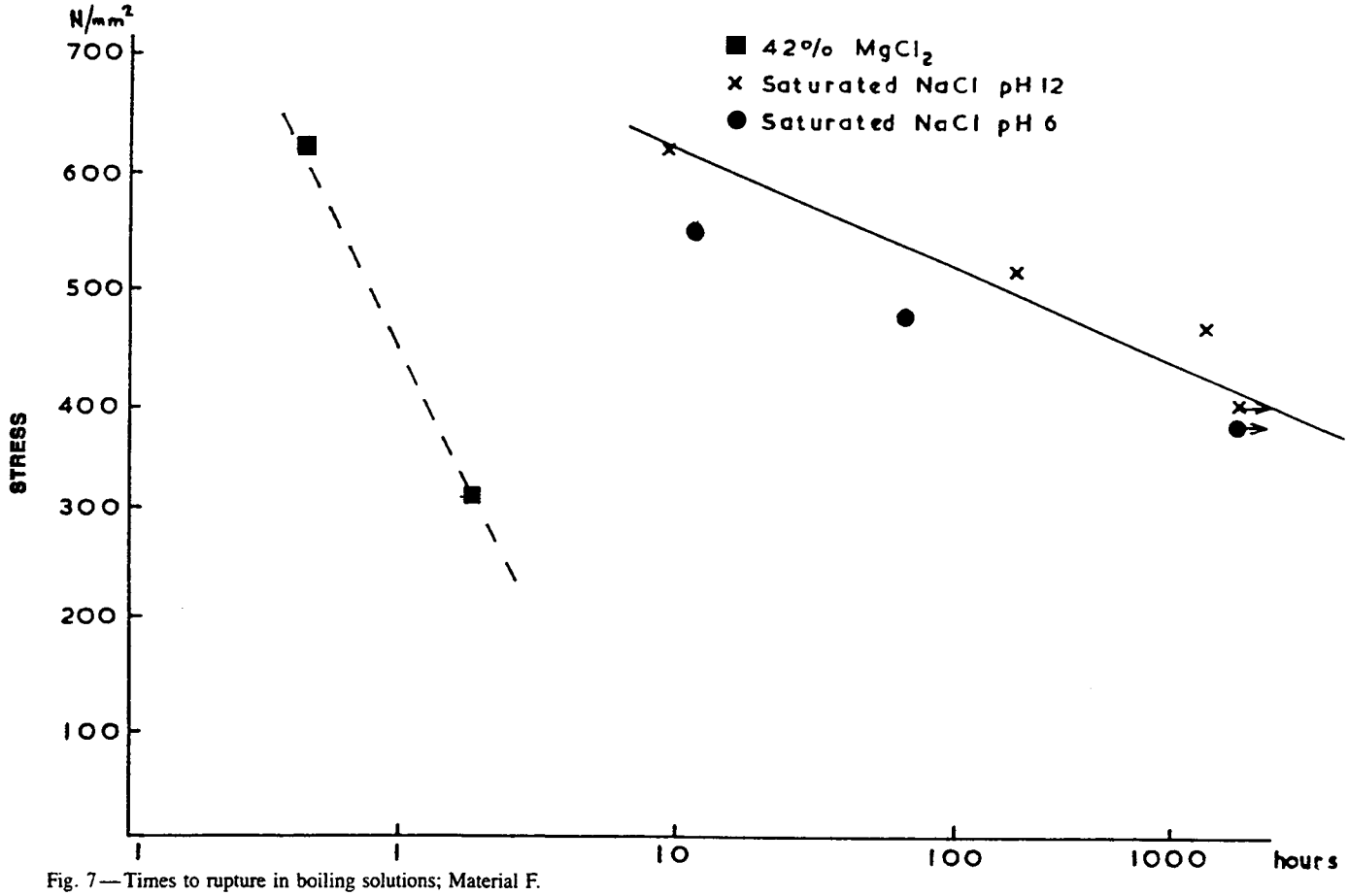


Fig. 7—Times to rupture in boiling solutions; Material F.

Table VI. Tests in Boiling Solution at 309 N/mm², Times to Rupture, Hours

Steel	C Pct	42 Pct $MgCl_2$	Saturated NaCl
A	0.040	1.5 T.C.	1000 h*
D	0.16	0.9 T.C.	2.1 I.C.

I.C. = Intercrystalline cracking.
T.C. = Transcrystalline cracking.
*Tests at high stress gave T.C. cracking.

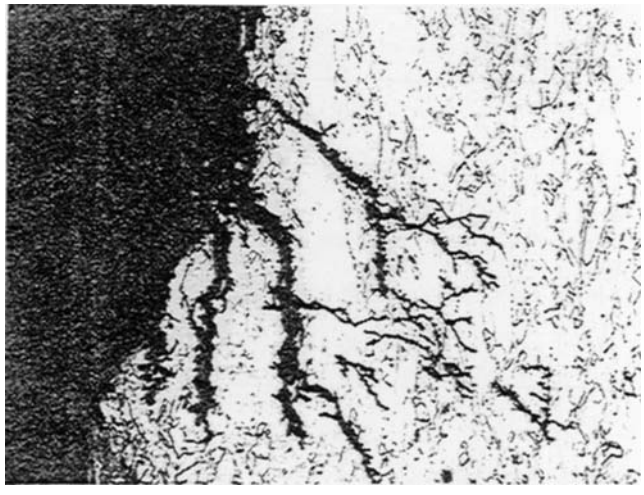


Fig. 8 — Section through fracture of warm-worked STABALLOY material tested at 620N/mm² in boiling saturated sodium chloride solution (pH 12). Magnified 100 times.

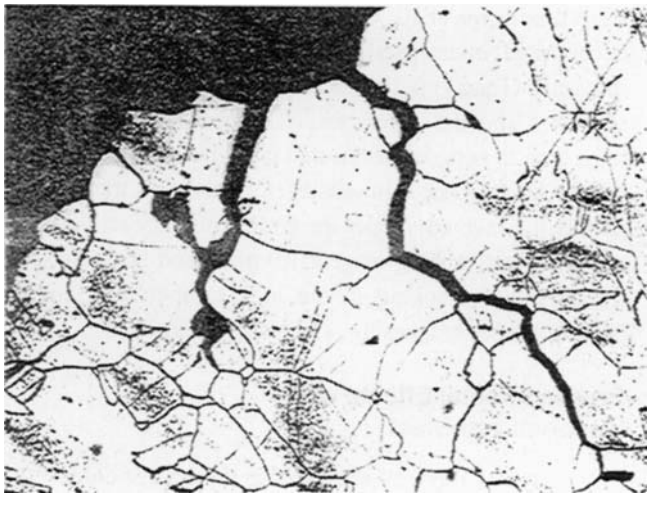


Fig. 9 — Section through fracture of a high carbon (0.16 pct) collar material tested @ 409N/mm² in boiling saturated sodium chloride solution (pH 12). Magnified 100 times.

in air. Some were then treated for various times at 650 °C after which they were ground free from oxide and lightly pickled in hydrochloric acid — nitric acid — water mixture

Table VII. Bend Tests in Boiling NaCl Solutions Times to Crack Initiation, Hours

Steel	C Pct	3 Pct NaCl	10 Pct NaCl	Saturated
D	0.16	∠24 I.C.	∠24 I.C.	∠24 I.C.
C	0.075	936–1032 I.C.	48–72 I.C.	∠24 I.C.
B	0.059	1300	72–96 T.C.	∠24 T.C.
A	0.040	1176–1224 T.C.	48–72 T.C.	∠24 T.C.

I.C. = Crack growth intercrystalline.
T.C. = Crack growth transcrystalline.

Table VIII. Effect of Iso Thermal Treatment @ 650 °C on S.C.C. Behavior; Times to Crack Initiation in Boiling 3 Pct NaCl Solution, Hours

Time @ 650 °C	C (0.075 Pct)	B (0.059 Pct C)	A (0.040 Pct C)
0	936–1032 I.C.	>1300	1176–1224 T.C.
1	∠24 I.C.	96–144 T.C.	408–480 T.C.
4	∠24 I.C.	96–144 I.C.	216–288 T.C. + some I.C.
16	∠24 I.C.	72–96 I.C.	72–96 I.C. + some T.C.

I.C. = Intercrystalline cracking.
T.C. = Transcrystalline cracking.

at 50 °C. Other softened samples were ground and then bent to the bend test pre-form shape before being treated at 650 °C and acid pickled. All were then stressed in the normal way and tested in boiling 3 pct sodium chloride solution. Where there was no cracking after 500 hours tests were duplicated but with boiling 10 pct sodium chloride solution. Test results are in Table X while A 262 assessment results are in Table XI.

DISCUSSION

Comparison of Service and Laboratory Cracking

The tests on the various drill collar materials, highly stressed in sodium chloride solutions gave cracking characteristics very similar to those found after service, that is, intergranular and transgranular failure modes were observed.

Table IX. Testing to A262 Practices A and E of Test Material of Table VIII

Time @ 650 °C(h)	C(0.075 Pct)		B(0.059 Pct C)		A(0.040 Pct C)	
	A	E	A	E	A	E
0	Ditch	Severe I.C.	Dual	Unaffected	Step	Unaffected
1	Ditch	Severe I.C.	Ditch	Very slight I.C.	Step	Unaffected
4	Ditch	Very severe I.C.	Ditch	Very severe I.C.	Dual	Very slight I.C.
16	Ditch	Very severe I.C.	Ditch	Very severe I.C.	Dual	Very severe I.C.

Table X. Collar C Material Treated 1050 °C and Air Cooled, Bend Tests in Boiling NaCl Solutions

Treatment	3 Pct NaCl	10 Pct NaCl
None	>500	528–600 Deep T.C. Cracks 720 h
20 min 650 °C	>500	576–648 T.C. Crack, 0.002 in. deep, 720 h
1 h 650 °C	>500	432–480 T.C. Cracks 0.005 in. deep, 720 h
4 h 650 °C	>500	240–264 I.C. Cracks 0.01 in. deep, 720 h
Bend + 20 min 650 °C	<24 Deep I.C. Cracks 24 h	No test
Bend + 1 h 650 °C	<24 Deep I.C. Cracks 24 h	No test
Bend + 4 h 650 °C	<24 Deep I.C. Cracks 24 h	No test

Table XI. Testing to A262 Practice A and E Test Material of Table X

Condition	Practice A	Practice E
No treatment	Step	Unaffected
20 min 650 °C	Dual	Severe I.C.
1 h 650 °C	Dual	Very severe I.C.
4 h 650 °C	Ditch	Very severe I.C.
Bend + 20 min 650 °C	Ditch	No test
Bend + 1 h 650 °C	Ditch	No test
Bend + 1 h 650 °C	Ditch	No test

The intergranular failures were predominantly restricted to the high carbon material (0.12/0.16 pct) and the transgranular to the low carbon grades (0.03/0.073). In addition there was correlation with the results of the intercrystalline corrosion tests to A 262 A and E, the intergranular mode being apparent with those materials having a "ditch" or "fail" classification respectively.

Relative Resistance of the Grades

All the types tested showed (Table III) rapid failure in the higher concentration, boiling solutions but distinct advantage was obvious for the lower carbon grades at lower temperatures. It has been noted many times[1-6] that chloride induced S.C.C. is only likely in hot solutions except very special environmental conditions not usually encountered and this has been demonstrated for 304 steel by techniques quite similar to those used here,[7] some limited cracking being observed at 60 °C but none at 40 °C or below. The low carbon, warm worked grades in the current work did not show any cracks in the saturated sodium chloride at 40 °C and below despite prolonged exposure but in contrast the high carbon materials suffered intergranular cracking within short times even at 20 °C. There is no doubt that this is stress accelerated intercrystalline corrosion,[5] the two relevant materials G and H failing the A 262 E intercrystalline corrosion test and the others (A, E, F) not doing so. It is of relevance to note, however, that intergranular cracking does not necessarily occur in sensitized material, a transgranular path being favored despite the grain boundary active path in some severe cracking reagents. Both G and H showed only transgranular cracking in the high temperature (140 °C) boiling 42 pct magnesium chloride solutions.

Environmental Effects with Unsensitized Steel

The results of Table IV show that in the case of unsensitized material the tendency for cracking in the chlorides of sodium, calcium, potassium, and magnesium are generally similar especially when the chloride contents are rationalized on a wt pct basis, one possible exception being the rather acid magnesium salt. However, when the pH of this solution was increased, the results obtained were very similar to those of the others.

Temperature thresholds did appear somewhat lower than for 304[7] but it must be remembered that the applied stress was much higher in these drill collar tests; higher than possible in practice. Thus these data serve to illustrate the relative behavior of composition and variability of aggressivness of salt solutions rather than a realistic simulation of service, that is they are very much accelerated tests.

There are a number of features which favor materials in service. One, not covered in the work, is the dynamic nature of the corrodent as it is known that depassivation is favored by static conditions. The increased pH, which it is understood applies to at least some muds, showed only modest advantage in itself but does appear to render the presence of bisulphite much more effective. In these tests with very adverse stress, chloride content and temperature (Table V) failure only occurred in an alkaline (pH 12) solution when the sulphite had been oxidized. The beneficial effect is presumably due to prevention of the cathodic reaction (oxygen and water to the hydroxyl ion), by scavenging of the oxygen and ineffectiveness of sulphite addition at lower pH to the presence of an alternative reaction. The ineffectiveness of bisulphite addition in suppressing cracking of the high carbon material should be noted.

The intermittant nature of down-hole service could be advantageous. These admittedly, idealized laboratory tests indicated that immersion periods less than time for crack initiation are not cumulative if the material is thoroughly washed between periods. Whether this is feasible in practice is questionable but it is in any event good practice to wash stainless steel with fresh water prior to storage.

Effect of Stress

The effect of stress on time to failure in chloride environments has been extensively studied[1-6] for 304 steel. Figure 4 shows that reducing applied stress results in increased time to rupture but does not prevent cracking, at least down to quite low stress levels while the pattern for a less aggressive environment is the same but with the plot moved to longer times. The results for warm worked material, which was substantially stronger though not as strong as drill collars, were similar. The same general patterns are obvious for 304 steel with a nitrogen addition (Figure 5) although here the warm worked material (yield strength quite similar to drill collars) gave, if anything, rather better results. This demonstrates no adverse effect for the nitrogen increase and for warm work *per se*. Two drill collar compositions, both resistant to the intercrystalline corrosion tests, were similarly tested (Figures 6 and 7) and these showed similar patterns for sodium chloride testing, with the plot slopes actually shallower than for 304, and no consistent effect of pH. It thus appears that at temperatures of 100 °C and slightly above, there should be a prolonged life for collars even in the presence of chloride bearing muds unless the stress is excessive. Failures in shorter time, however, could presumably occur if the chloride bearing mud temperature was substantially higher.

Effect of Sensitization

Increasing carbon content in STABALLOY (Alloys A to D) results in an increasing degree of 'sensitization' and a reduced resistance to stress corrosion cracking. This reduction in stress corrosion cracking resistance is attributed to 'sensitization' (Table VII). Examination of other competitive systems illustrate a similar feature as demonstrated by the inferior stress corrosion resistance of G and H relative to A, E, and F (Table III).

It is clear from the data that high carbon levels (0.12/0.16 pct) have only limited resistance to stress corrosion cracking in the environments tested. It is difficult, however, to specify the permissible carbon content required in the products under discussion to meet the service requirements. The effect of intermediate carbon levels (Table VII) indicates no very marked influence over the range 0.040 to 0.075 pct carbon although the latter did show intercrystalline cracking in this maintaining correlation with A 262 assessment (Table II). Differences in stress corrosion cracking behavior were emphasized by additional sensitization by iso-thermal treatment at 650 °C (Tables VIII and IX). An interesting feature of these results is that they confirm that there can be reduction in stress corrosion cracking resistance from sensitization without the actual cracking being intergranular; presumably the effect in such cases is on time to crack initiation, this being at a grain boundary. The effect will vary with the tendency of the corrodent to cause transgranular cracking in unsensitized material; even extremely sensitized material cracks transgranularly in boiling 42 pct magnesium chloride solution but the life is affected.[3]

It is known that cold strain can affect the sensitization behavior of standard austenitic steels[8] and the results in Tables X and XI confirm that this is the case with drill collar steels. Solution treatment removed all precipitated carbides in the 0.075 pct carbon material C, as assessed by optical metallography, and delayed the initiation of cracking in the boiling 10 pct sodium chloride test to a substantial degree. The treatment removed all precipitated carbides but the improvement noted could be at least, in part, due to a reduction in stress. Treatment at 650 °C for various times up to 4 hours introduced and progressively increased sensitization (Table XI) but did not have a correspondingly obvious effect on crack initiation time while crack propagation of the 650 °C treated samples was very slow. Moreover, only the 4 hours 650 °C sample showed intergranular cracking. In contrast, the specimens strained by bending after softening/solution treatment, but before the sensitization treatment, were not stressed any more but suffered rapid deep intergranular cracking. While the above tests involved iso-thermal sensitization, similar effects would be achieved

from warm working. Solomon[9,10] has demonstrated sensitization of 304 steel during slow cooling as a result of prior strain and also from warm strain while cooling through the carbide precipitation temperature range. These results emphasize the importance of carbon content magnified by the effect of strain but also demonstrate that material with suitably controlled carbon content can be strengthened by warm work without detriment to the S.C.C. resistance. Freedom from sensitization does not give immunity to cracking in all chloride bearing environments, nor does sensitization mean that cracking will occur in all environments, but suitable attention to carbon content will ensure that as wide a range of corrodents as possible will be tolerable.

CONCLUSIONS

As would be expected, the austenitic stainless steels commonly used for the manufacture of non-magnetic drill collars and stabilizers can suffer stress corrosion cracking when stressed in hot chloride bearing solutions. There will however be very many environmental conditions where there is no great risk. The potentially dangerous environments will be more numerous if the steel is in a sensitized state and this is especially difficult to avoid with the large sections involved and consequent limited cooling rates unless the carbon content is controlled to suitably low levels. The sensitizing effect is exacerbated by the strain involved in producing the desired strength of the components but even so can be avoided by due care. The ASTM A 262 practice E appears to be a suitably rapid assessment method. There is no evidence that warm working *per se* increases the tendency for transgranular stress corrosion cracking and, indeed, at least two of the warm worked compositions utilized have favorable stress/time to failure relationships in hot sodium chloride solutions relative to 304 steel. This extension of life with reduced stress is obviously of advantage for down-hole service where life is in any event finite for other reasons and there are some other features which may counteract adverse effects of chloride bearing environments.

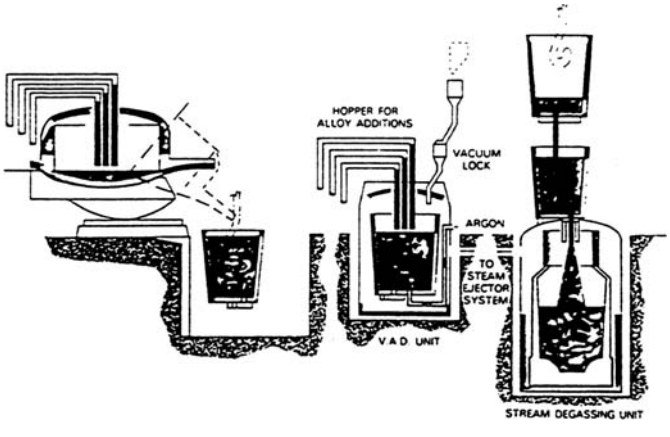


Fig. 10—Primary secondary and degassing steel-making units.

Even with all the available measures to ensure best service there is a practical hazard should the environment conditions become very aggressive (*i.e.*, higher chloric content with high temperature). It is understood that fears c this have led to consideration or use of expensive materials such as the precipitation hardening nickle base, nickle copper and copper-beryllium alloys. Considerable savings could be achieved if a superior stress corrosion resistant steel were available and material development is well advanced.

APPENDIX I

Production at Sheffield Forgemasters. The steelmaking operations at Sheffield Forgemasters are outlined in Figures 10 and 11, the V.O.D. facility allowing the production of very low carbon contents if desired. Ingots may be forged by a variety of conventional forging means and also available is the largest forging machine currently in service, the G.F.M. SXP 65 (Figure 12).

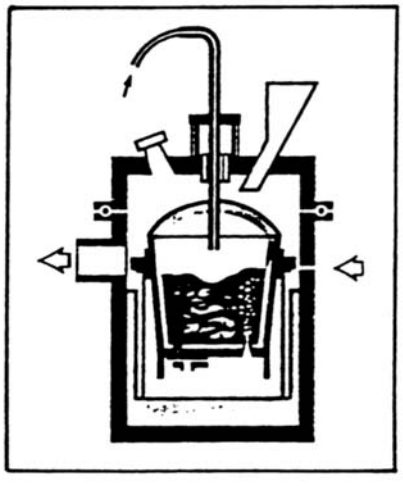


Fig. 11—VOD unit.

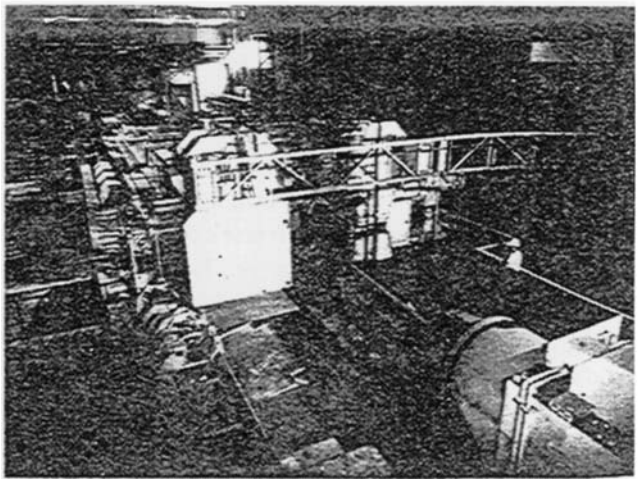


Fig. 12—G.F.M., SXP 65 forging machine.

Table XII. Reproducibility of Mechanical Properties in Staballoy Collars Standard Test Position 1 in. below Machined Outer Surface

Collar Diameter	7.5 in.–8 in.						6.25 in.–7.25 in.						4.5 in.–4.75 in.					
Test Position	Front End			Back End			Front End			Back End			Front End			Back End		
	N	M	SD	N	M	SD	N	M	SD	N	M	SD	N	M	SD	N	M	SD
Rp 0.2 N/mm²	74	802	7	74	808	7	63	818	9	63	854	7	13	886	6	13	958	12
(k.s.i.)		(116)			(117)			(119)			(123)			(128)			(139)	
Rm N/mm²	74	931	6	74	958	6	63	975	7	63	900	6	13	1043	6	13	1102	18
(k.s.i.)		(135)			(139)			(141)			(143)			(151)			(160)	
Elongation pct	74	37	3	74	35	3	63	35	4	63	34	4	13	33	1.5	13	31	4
Charpy J	74	230	24	73	221	20	63	216	17	63	220	17	13	184	28	13	192	2
(ft lbs)		(166)			(160)			(156)			(159)			(133)			(139)	

N = Number of collars, M = Mean of results, S.D. = Standard Deviations.

The composition chosen for drill collar manufacture, designated 'Staballoy' is an 18 pct chromium type with 10 pct manganese, 6 pct nickel, and 0.3 pct nitrogen, these changes from the standard 304 type analysis serving to facilitate the attainment of desired strength by solid solution hardening and/or increasing rate of strain hardening. To obtain the desired strength consistently and reproducibly over the long length involved calls for careful choice of a hot reduction sequence and very precise control of reduction and temperature over the latter, colder stage of forging. The SXP 65 forging machine is ideal for this purpose, the very precise control of reduction and forging rate allowing a balance between kinetic heating and heat loss to be maintained. Test data illustrating uniformity of properties and distribution of strength through the wall thickness are in Table XII and Figure 13.

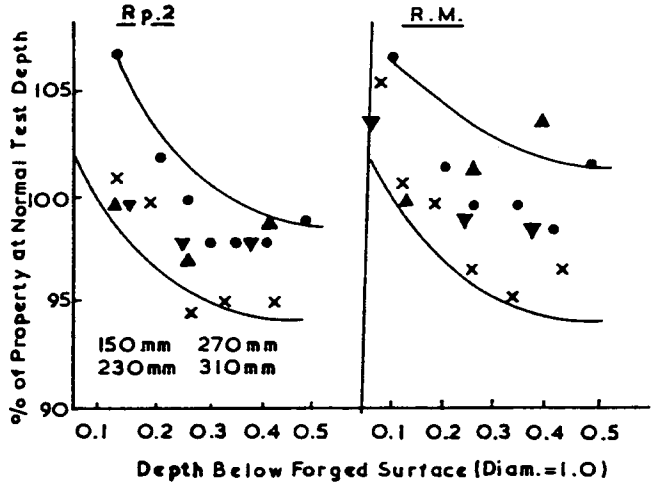


Fig. 13—Distribution of strength through the thickness of warm worked drill collars: normal test position is 1 in. below machined outer surface.

APPENDIX II

Stress Corrosion Cracking Test Procedures. (a) *Bend Test.* The bend test specimen was 4 in. × 0.5 in. × 0.125 in. and was abraded to a 120 grit finish. It was bent to a "pre-form" shape by pushing into a U shaped die by a round tipped wedge (tip radius 0.5 in.) until the angle between the "legs" was 110 deg (after relaxing). Closure was then continued between parallel jaws until the outer ends of the legs were 1.125 in. wide. On relaxation the warm worked drill collar materials opened to 1.75 in. The bend was then again compressed by "knife edge" contacts applied 0.5 in. from the leg ends until a retaining clip with aperture of 1 in. could just be slipped over the ends.

The clips were made of ferritic stainless steel and electrical contact with the test piece was prevented by plastic inserts. There was relaxation of approximately 0.0625 in. on withdrawing the knife edges.

Tests were in liter flasks or in beakers fitted with "cold finger" condensers or cover glasses. The condensers were not air tight and there was ready access of air into beakers. Temperature was maintained either by hot plates or liquid thermostat baths, 400 ml of solution was used; any losses due to evaporation were made up by periodic water additions.

For inspection the samples were removed at intervals, initially of 24 hours but at lower frequency as time proceeded. Time out of solution was the minimum possible and the samples were not washed. Sometimes corrosion product had to be brushed off to allow examination. Examination was by hand lens or low power microscope if necessary. Initiation of cracks was noted after which the test was allowed to continue until cracks had almost penetrated the thickness or for some finite time.

(b) *Tensile Test.* The specimens were of orthodox, round tensile test design with parallel 1 in. long × 0.125 in. diameter. They were stressed uniaxially by weights and levers. The corrodent was in concentric glass containers heated by external windings with concentration changes prevented by reflux condensers through which there was access to the atmosphere. Time to rupture was recorded.

ACKNOWLEDGMENTS

The authors thank the directors of Sheffield Forgemasters P.L.C. for permission to publish this paper.

REFERENCES

1. A. J. Sedriks: *Corrosion of Stainless Steels,* J. Wiley & Sons, p. 139, 1979.
2. R. M. Latanision and R. W. Staehle: *Proceedings of the Conference on Fundamental Aspects of Stress Corrosion Cracking,* N.A.C.E., Houston, TX, 1969, p. 214.
3. J. E. Truman, I.S.I. Publication 117, p. 101, 1969.
4. G. J. Theus and R. W. Staehle: *Proceedings of Conference on Stress Corrosion Cracking and Hydrogen Embrittlement of Iron Base Alloys,* N.A.C.E. Houston, TX, 1977, p. 843.
5. J. E. Truman: *Ibid,* p. 111.
6. H. E. Haninen: *Int. Met. Rev.,* 1979, vol. 24, no. 3, p. 85.
7. J. E. Truman: *Corros. Sci.,* 1977, vol. 17, p. 737.
8. V. Cihal: *Proceedings 4th Bolton Landing Conference,* 1974.
9. H. D. Solomon: *Corrosion,* 1984, vol. 40, no. 2. p. 51.
10. H. D. Solomon: *Corrosion,* 1980, vol. 36, no. 8.

Copyrighted Materials
Copyright © 1996 NACE International Retrieved from www.knovel.com

Section 3

DUPLEX STAINLESS STEELS

Materials failures in sour gas service*

Stephen W. Ciaraldi*

Three analyses of materials failures in sour gas service are reviewed. The failures include stress corrosion cracking (SCC) of a duplex stainless steel (SS) wireline; sulfide stress cracking (SSC) of moderate hardness L-80 casing, and SSC of two forged carbon steel, gathering system fittings. The failures demonstrate the significant effects of stress level, environmental aggressiveness, and localized hard zones in promoting SCC and SSC.

Introduction

DESPITE RECENT ADVANCES IN MATERIALS for sour gas service, failures can still occur. These failures can be unexpected, due to apparent conformance to available sour service guidelines, or because materials selections were based on the current literature. However, factors not considered in either guidelines or the literature can promote failures. In particular, high stress levels, environmental severity and localized regions of high hardness can cause susceptibility to SCC and SSC and will be shown. The occurrences of such failures indicate the limitations of currently accepted sour service guidelines.

Duplex SS wireline failure

The susceptibility of cold worked, duplex SS to SCC in chloride-containing, aqueous, hydrogen sulfide environments has been documented.[2-4] This susceptibility is exhibited in both ambient and elevated temperature environments. Controversy still exists concerning SCC mechanism (hydrogen embrittlement or anodic dissolution) within various temperature regimes; this question will not be addressed here. The laboratory data is convincing enough so that few cold worked duplex SS have been applied to sour service. Indeed, cold worked duplex SS are not recommended for sour service according to the 1980 Revision of NACE Standard MR-01-75.[5]

Few data are available on duplex SS wirelines, particularly in field environments. A recent publication by Vaughn and Chaung addressed these aspects of duplex SS SCC.[6] Using stressed wireline specimens, the workers found duplex SS to resist SCC up to 30 days at 93 C in both a laboratory, aqueous chloride-hydrogen sulfide environment, and a typical sour field environment. Failures occurred in similar tests at 149 C.

Despite the documented SCC susceptibility of duplex SS, such materials are sometimes used in sour wells. Availability of more resistant materials is often poor, particularly without long lead times. In gas well completions, long lead times can cause substantial monetary losses. This was the case with the current wireline (slickline) failure. Because exposure time of the wireline in the well was to be short, failure was not anticipated. However, the failure did occur, and resulted in a time consuming and costly fishing job.

The failed duplex SS wireline had been used to run a bottom hole pressure recorder. Well conditions at the time of failure were reported to be:

H_2S	3.5 to 4.0%
CO_2	12 to 20%
Pressure at failure location	189 bar (2750 psig) maximum
Total Depth	4200 m (13,800 ft)
Liquid Level	3660 to 3960 m (12,000 to 13,000 ft)
Aqueous chlorides	73,000 to 85,000 ppm
pH	7 approximately
Temperature at failure location	90 C approximately

The wireline had a diameter of 2.3 mm (0.092 in.) and was stressed to approximately 360 MPa (52 ksi) by hanging weight. Specified wireline mechanical properties were not known. Parting of the line took place approximately 335 m (1100 ft) above the recorder at a depth of 3810 m (12,500 ft). Note that the line parted in the vicinity of the fluid level. Failure occurred after an exposure period of only 8 h, 45 min.

Overall appearance of failed wireline sections is shown in Figure 1. Cracking occurred both parallel and perpendicular to the wireline axis. Failed sections curled outward from the line, apparently in response to residual stresses imparted in the material by cold working during manufacture. The wireline was covered with a thin black scale, identified by Energy Dispersive Spectroscopy (EDS) as iron sulfide containing small amounts of nickel, chromium, and chlorine.

Several metallographic mounts of failed wireline sections were prepared. These mounts were examined optically and with a scanning electron microscope (SEM). Figure 2 is a low magnification cross section of a wireline piece containing both longitudinal and transverse cracks. Figures 3 and 4 show longitudinal and transverse cracking, respectively, at somewhat higher magnifications. The elongated grain structure of the material indicated the wire had been heavily cold worked during manufacture. Approximately equal percentages of austenite and ferrite were present in the microstructure.

Examination of metallographic mounts showed that

*Presented during CORROSION/85, Paper No. 217, NACE, Houston, TX, 1985.

*Standard Oil Company (Indiana), Amoco Research Center, P.O. Box 400, Naperville, IL 60566.

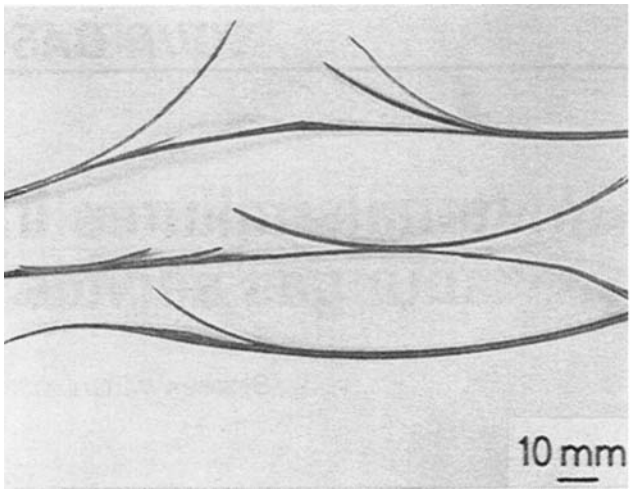


FIGURE 1 — Overall appearance of failed duplex SS wireline.

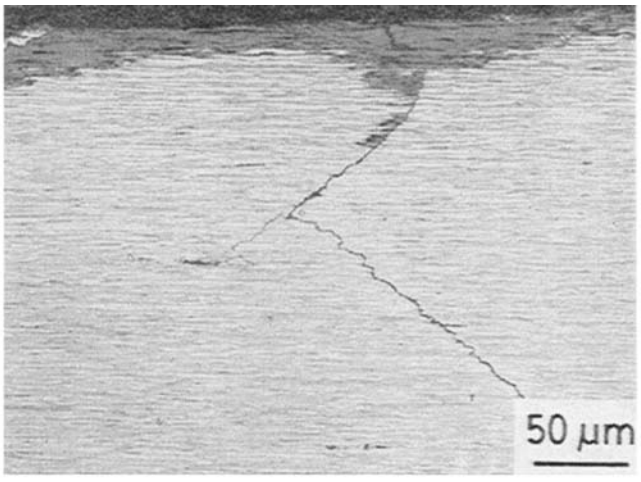


FIGURE 4 — Transverse cracks in duplex SS wireline (glyceregia etch).

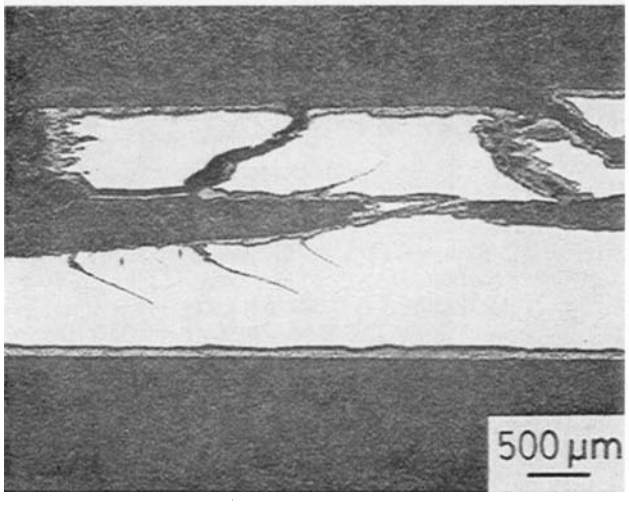


FIGURE 2 — Cross sectional view of wireline showing large longitudinal and smaller transverse cracks (glyceregia etch).

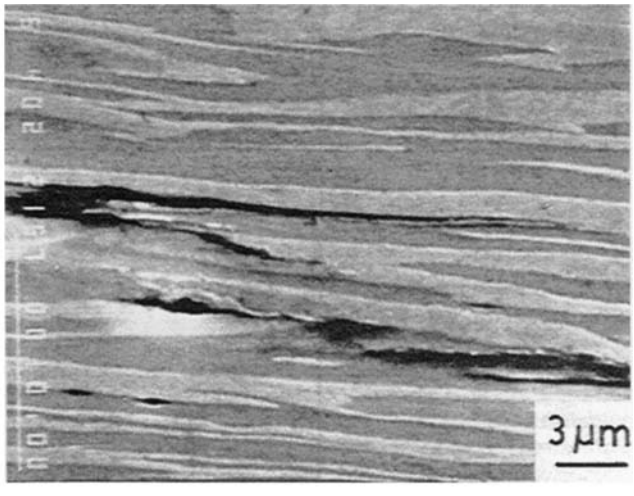


FIGURE 5 — SEM showing intergranular, longitudinal cracks in duplex SS wireline. Light phase is ferrite, dark phase is austenite (glyceregia etch).

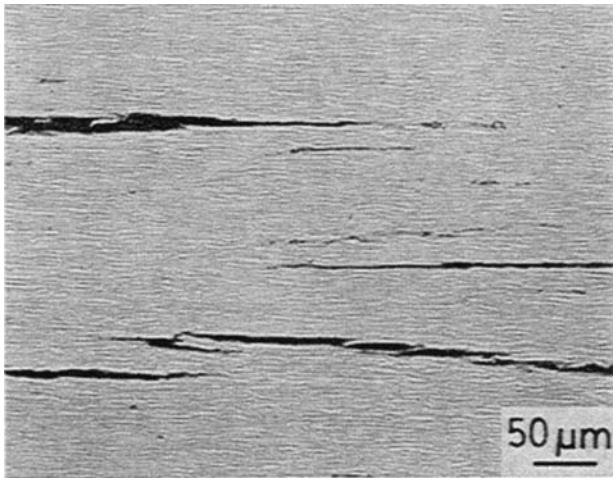


FIGURE 3 — Longitudinal cracks on duplex SS wireline (glyceregia etch).

longitudinal cracking occurred primarily intergranularly (Figure 5). SEM fracture surface examination of longitudinal cracks confirmed them to be intergranular (Figure 6). Transverse cracking (Figure 7) occurred transgranularly through both microstructural phases. Near crack tips, however, preferential cracking was observed in the light-contrast microstructural phase. Standardless EDS chemical analyses of the phases gave the following approximate results:

	wt%		
	Light phase	Dark phase	Overall
Mn	1.7	1.9	1.9
Si	0.5	0.5	0.5
Ni	6.6	8.2	6.9
Cr	23.8	21.5	23.3
Mo	2.4	1.9	2.3
Cu	1.9	1.2	1.9

These results indicate the light phase to be ferrite and the dark phase to be austenite. Overall chemical composition was typical of duplex SS.

A suitable area for SEM fracture surface examination of transverse cracking was not found. Also, due to the deteriorated condition of the wireline, it was not possible to

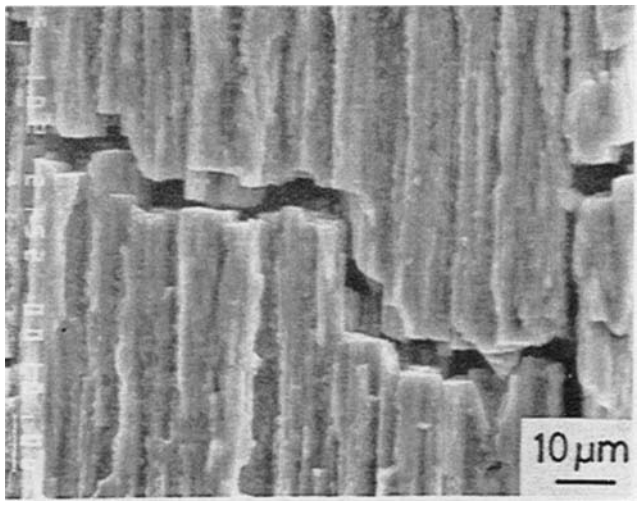


FIGURE 6 — Scanning electron fractograph (SEF) showing intergranular nature of lontigudinal cracking in duplex SS wireline.

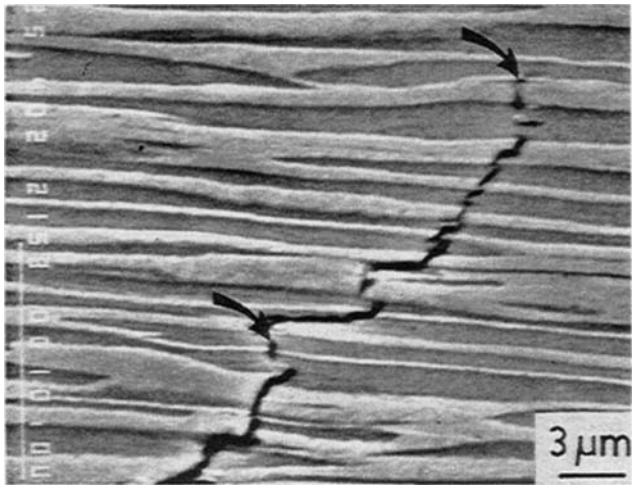


FIGURE 7 — SEM showing transverse cracking of duplex SS wireline. Light phase is ferrite, dark phase is austenite. Arrows denote regions of preferential ferrite cracking (glyceregia etch).

perform satisfactory tensile tests. However, microhardness measurements were performed on the material. Results were 380-480 KHN (38-46 HRC equivalent) indicating the wireline to have a tensile strength of approximately 1380 MPa (200 ksi).

Failure of the wireline resulted from SCC induced by the presence of hydrogen sulfide and aqueous chlorides. Longitudinal cracking of the wireline was more prevalent than transverse cracking. This observation suggests SCC to have initiated and propagated primarily from residual stresses from cold working. The observation also suggests the SCC resistance of the wireline in this orientation was significantly lower than that in the transverse direction.

Longitudinal SCC in the wireline occurred intergranularly. This duplex SS SCC morphology has been reported in laboratory tests only at temperatures equal to or greater than 100 C, which is higher than the actual failure temperature.[7] Transverse cracking of the wireline occurred transgranularly, and apparently somewhat preferentially in the ferrite phase. This SCC fracture mode has been reported in lower temperature regimes.[7,8] The two cracking morphologies observed suggest the possibility that more than one SCC mechanism was involved in the failure.

It is interesting to note that although Vaughn and Chaung did not obtain SCC of duplex SS wirelines in their laboratory and field tests at 93 C, the current field failure occurred quite rapidly near this temperature.[6] This fact illustrates that despite the popular opinion that typical laboratory test environments are more severe than comparable service environments, field conditions can approach and exceed this severity. In the case of the current failure, it is suspected that environmental aggressiveness was influenced by the presence of the liquid-vapor level, through either a meniscus, or wetting and drying effect. The failure illustrates the need for caution in accepting new materials into sour service guidelines and recommended practices.

L-80 Casing failure

NACE Standard MR-01-75 states that quenched and tempered carbon-steels are acceptable for sour service at a maximum hardness of 22 HRC.[5] The document further lists the API 5AC L-80 specification as being applicable to all temperature sour service. However, API 5AC requirements for the L-80 grade allow maximum hardness to 23 HRC.[1] This apparent contradiction in MR-01-75 has been a source of confusion, particularly with field personnel. Current oil industry practice generally applies L-80 grade tubulars to sour service without hardness restrictions or testing beyond the API 5AC specification requirements.

Literature indicates that increased steel hardness generally results in decreased SCC resistance.[9,10] The maximum hardness level at which field failures cannot occur has generally been accepted as being 22 or 23 HRC. Although carbon steels at 23 HRC might be expected to give satisfactory sour service performance, the current casing failure occurred by SSC near this hardness level. The failure shows the importance of factors in addition to hardness in determining SSC susceptibility.

Failure of the L-80 casing was discovered subsequent to flow testing after a second acidizing treatment of the subject well. Packer seal leakage had allowed excessive pressure from the formation to accumulate within the casing tubing annulus during well unloading by nitrogen injection. Together with string weight stresses, it was estimated that axial tension at the casing failure location had approached 100% specified minimum yield strength (SMYS). Conditions in the casing-tubing annulus during completion operations were:

H_2	2.3%
CO_2	3.0%
Pressure	310 bar (4500 psig)
Annular Fluid	Inhibited 2% KCl water

The failed L-80 casing measured 178 mm (7.0 in.) OD by 9.5 mm (0.375 in.) wall thickness. Weight was 38.6 kg/m (26 lb/ft). Failure occurred at a depth of 31.4 (103 ft) in the top joint of this particular size casing. Heavier-wall casing had been set above the failed joint.

Figure 8 shows one half of the parted casing. Overall appearance of the fracture surface is shown in Figure 9. One large and several small seams or blisters were observed near the casing ID in regions of apparent crack initiation. Figure 10 shows a section of the fracture surface after it was cut from the casing and cleaned. Several blisters can be seen, and it appears the cracking initiated at the ID near the blisters and then propagated through the wall thickness.

Metallurgical structure of the seamless casing consisted of quenched and tempered martensite. Nonmetallic inclusion content was moderate. Sulfide inclusions were in the form of stringers, and had a higher density near the ID of the casing. Some moderate banding, attributed to manganese segregation, was observed near the ID of the failed casing.

Figure 11 shows a cross section of the primary fracture in the casing. Cracking exhibited jagged characteristics typical of SSC. In addition to the large blisters described previously, many blister-type micro-cracks were found (Figure

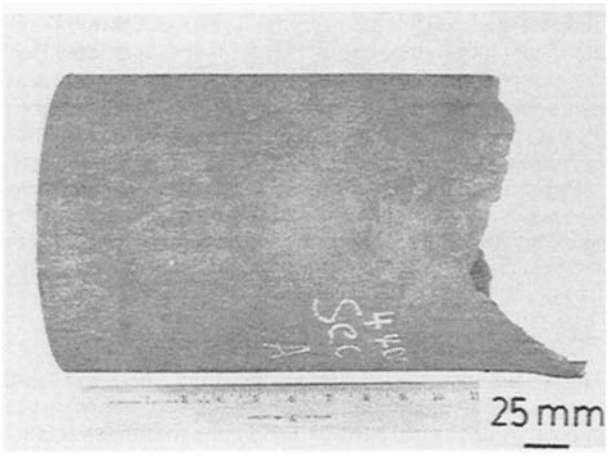


FIGURE 8 — Overall appearance of failed L-80 casing.

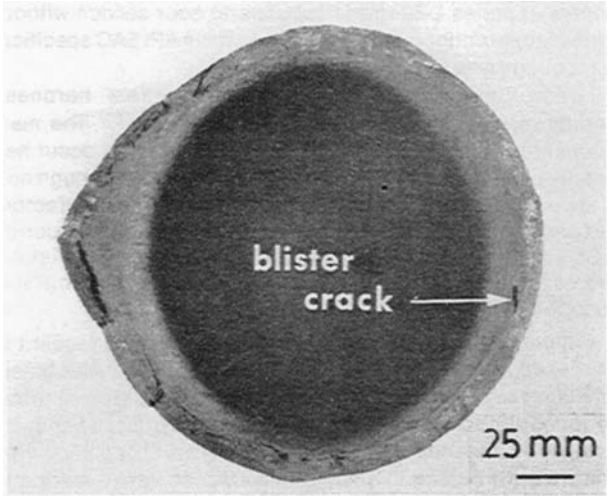


FIGURE 9 — Fracture surface appearance of failed L-80 casing. (Note presence of blister-type crack.)

12). Examination of crack tips showed cracking had propagated in the longitudinal direction and likely had initiated at sulfide stringer inclusions (Figure 13). The cracks were similar in appearance to hydrogen-induced step cracking, which has historically been associated with sour service failures of lower-strength linepipe.[11-13] Dye penetrant tests on a ring cut from the failed casing showed the material to contain many micro-cracks. This cracking was generally located in regions 1.3 to 2.5 mm (0.05 to 0.10 in.) from the ID to mid-wall.

Through-wall hardness tests were performed on a ring cut from the failed casing. Test surfaces were ground under liquid coolant to avoid overheating. It was difficult to obtain valid readings near the ID because of the presence of extensive micro-cracking. It is thought that some of the results obtained near the ID were less than the actual hardness, due to proximity to cracking (Table 1). Nine Rockwell C scale impressions were made in four locations approximately 90° apart. Of the nine per quadrant, three impressions each were made near OD, mid-wall, and ID. Although overall average hardness of the failed casing was 22.2 HRC, ID readings may have been influenced by the micro-cracks. If this were indeed true, actual overall average hardness of the casing may have been closer to 23 HRC. Micro-hardness tests on the casing resulted in values from 256-269 KHN (21-23.5 HRC equivalent). Banded regions had micro-hardnesses as high as 275 KHN (24.5 HRC equivalent).

Tensile properties of the casing were determined using

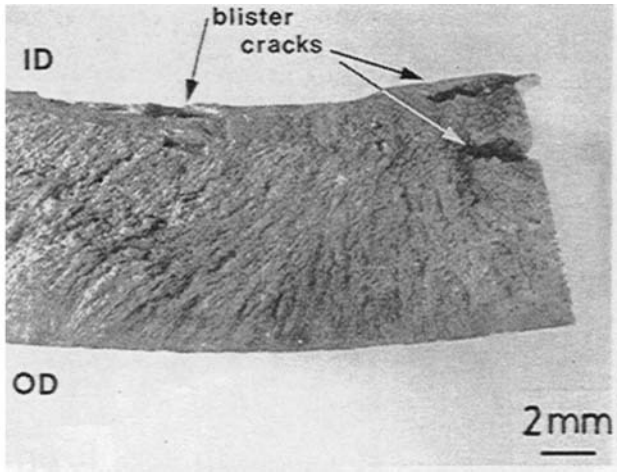


FIGURE 10 — Section of L-80 casing fracture surface. (Note presence of blister-type cracks.)

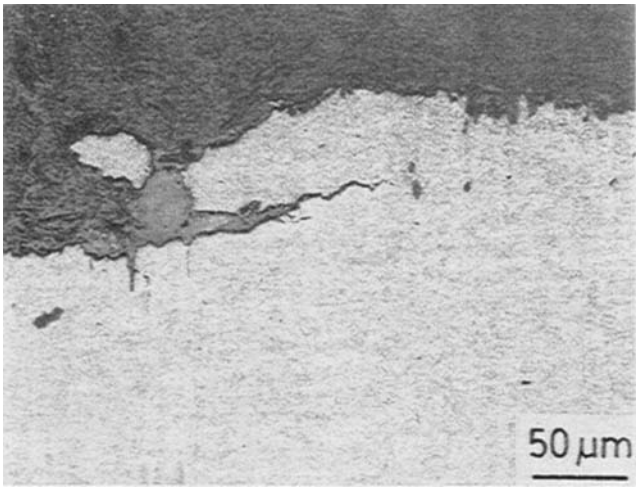


FIGURE 11 — Cross sectional view of primary fracture surface of failed L-80 casing. Cracking exhibits jagged characteristics of SSC (nital etch).

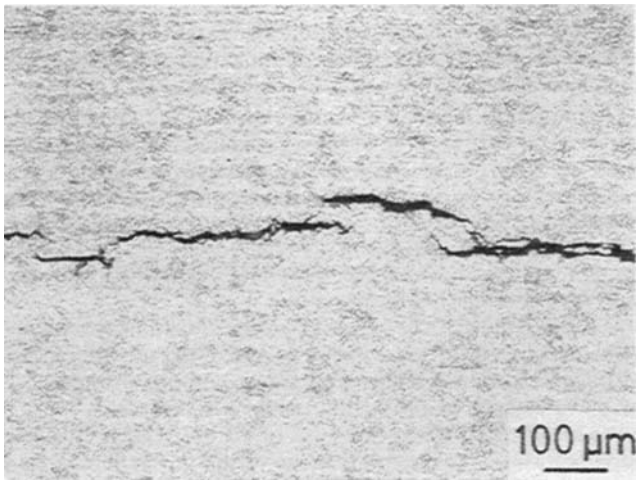


FIGURE 12 — Blister-type micro-cracks in failed L-80 casing, similar in appearance to hydrogen-induced step cracking (nital etch).

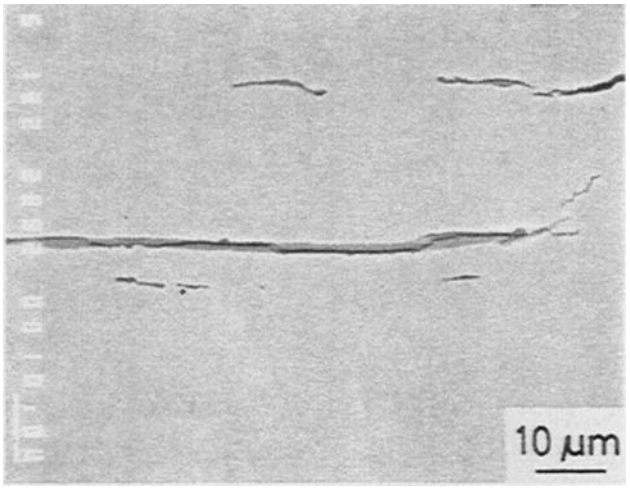


FIGURE 13 — Tip of L-80 casing blister-type micro-crack showing preferential propagation at sites of stringer-type sulfide inclusions (nital etch).

TABLE 1 — Hardness and mechanical properties of failed L-80 casing

		Hardness (HRC)				
		0°	90°	180°	270°	Average
ID	(1)	21.5	21.0	21.0	21.5	21.0
	(2)	19.0	21.5	22.0	21.5	
	(3)	17.5	22.0	20.5	22.5	
Midwall	(1)	21.0	22.0	22.5	22.5	22.7
	(2)	23.0	23.0	23.0	23.0	
	(3)	23.0	23.0	23.0	23.0	
OD	(1)	23.5	23.5	21.0	23.5	23.1
	(2)	23.5	24.0	21.0	23.0	
	(3)	23.0	24.0	22.0	23.5	

Overall average = 22.2 HRC

Yield strength MPa	Yield strength ksi	Tensile strength MPa	Tensile strength ksi	Elongation (%)	Reduction of area (%)
680.5	98.7	795.7	115.4	23.6	66.6

machined bars having 6.35-mm (0.25-in.) diameter gage sections. Full-strip specimens were not used to eliminate effects of surface corrosion. Results of the tensile tests are also listed in Table 1. The values reported are averages from two tests. Note that yield strength apparently exceeds API 5AC L-80 requirements.[1] However, use of machined bars, as well as the possibility of casing strain during running/pulling, may result in somewhat higher values compared to strip tests performed on newly manufactured casing. Approximate tensile-strength hardness conversion predicts a hardness of about 23 HRC.

Chemical composition of the failed casing was determined (Table 2). The composition conforms to API 5AC.[1] Note that the sulfur content of 0.015% is well below the API maximum of 0.060%.

Laboratory SSC tests were performed on the casing material according to NACE Standard TM-01-77.[14] Test loads were applied in increments of 5% SMYS. SSC Threshold Stress, confirmed by tests on duplicate specimens, was determined to be 85% SMYS (68.9% actual yield strength).

Failure of the L-80 casing resulted from SSC. Failure evidently occurred in two stages. Crack initiation resulted from the formation of blister-type, micro-cracks, essentially similar to hydrogen-induced step cracks. Conventional SSC

TABLE 2 — Composition of failed L-80 casing

Element	Wt%
Carbon	0.31
Manganese	1.44
Silicon	0.25
Phosphorus	0.020
Sulfur	0.015
Chromium	0.13
Molybdenum	0.003
Nickel	0.01
Aluminum	0.002

resulted from the presence of the micro-cracks, and eventually led to casing failure. Relatively good SSC resistance was obtained in laboratory tests on the casing steel. However, it is thought that factors other than inherent SSC resistance contributed to the failure. Primary among these is temporary occurrence of an axial stress level close to 100% SMYS. Laboratory SSC test results predict failure at this stress level.

Another possible contributing factor to the failure was the presence of acidizing fluids. The occurrence of hydrogen-induced blister-cracks in a high-strength steel suggests a very large effective hydrogen fugacity. It is possible that corrosion by acidizing fluids contributed to the hydrogen fugacity. Interestingly, hydrogen-induced cracks were not observed in the heavier-wall casing joint set immediately above the failed joint, which was also examined. This joint was stressed to approximately 80% SMYS during completion operations. Average hardness was 18.4 HRC and sulfur content was 0.013%. The fact that cracks were not observed in this joint suggests the lighter-wall casing failure to be caused primarily by the combination of maximum L-80 hardness and high stress levels. Minimizing both applied stresses and maximum hardness should prevent such failures. Based upon these facts, and the MR-01-75 document, it would appear a hardness limitation of 22 HRC for sour service L-80 steels should be considered.[1]

Failed gathering system fittings

NACE Standard MR-01-75 states that carbon steels are acceptable for sour service at hardnesses to 22 HRC in several heat treatment conditions, including hot rolled.[5] Forged components could be interpreted to be in this latter condition. The document also lists steels manufactured according to ASTM A234 (WPA, WPB, and WPC) to be applicable to sour environments. The requirements of ASTM A234 for carbon steel forgings do not mandate heat treatment after forging, provided final forming is completed above 620 C.[15] At this minimum temperature, ferrite recrystallization would not be expected, but significant stress-relief should occur. Carbon-steel hardness specifications by ASTM A234 are 197 BHN max. (92.8 HRB equivalent), but actual testing is not required. The specification requires removal of crack-like defects between 5 and 12½% of wall thickness. Grinding and machining are acceptable.

The two sour gas gathering system failures described below occurred within two weeks of each other. One failed component was a drip system liquid sample pot, basically consisting of a 165 mm (6.5 in.) OD × 102 mm (4 in.) OD tee, the single smaller OD branch being fitted with a cap. Wall thickness was approximately 9.5 mm (0.375 in.). The second failed component was a 203 mm (8 in.) to 152 mm (6 in.) reducer, having a 6.4 mm (0.25 in.) wall. According to stamped identification numbers, both fittings were manufactured to ASTM A234 WPB.

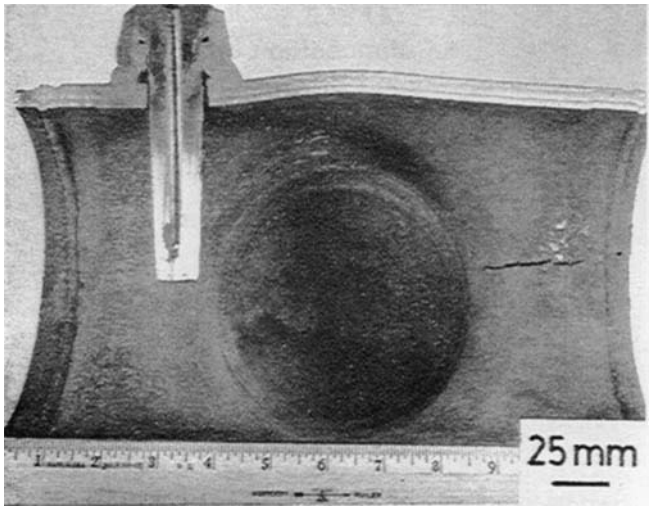


FIGURE 14 — Internal appearance of failed sample pot (tee) from sour gas gathering system.

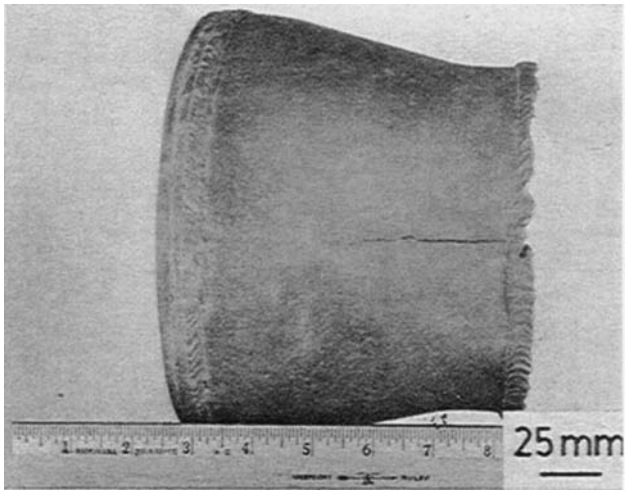


FIGURE 15 — External appearance of failed reducer from sour gas gathering system.

The failed fittings had been exposed to similar internal conditions, summarized below:

H_2S	13.5 to 15.0%
CO_2	4.5 to 5.2%
Pressure	76 bar (1100 psig) maximum
Aqueous chlorides	30,000 ppm approx.
pH	7 approximately
Temperature	43 C maximum

Internal liquids consisted of sour water and hydrocarbon condensate containing corrosion inhibitor from downhole carryover and gathering system injection.

There were suspicions that high stresses had been generated in the failed fittings. In the case of the sample pot, hydrate (hydrocarbon-ice compound) formation had completely fouled the line prior to the failure. It is possible that expansion during hydrate formation had generated significant stresses. For the reducer, which was set at a lateral tie-in below ground, high stresses were evidently the result of ground settling. When this fitting was removed, the vertical leg of the tie-in moved approximately 152 mm (6 in.). The fitting was also found to be slightly distorted into an oval shape.

Internal appearance of the failed tee after sectioning is shown in Figure 14. Cracking occurred longitudinally and was not associated with girth welds. Figure 15 shows overall external appearance of the failed reducer. The longitudinal crack observed was, again, unassociated with girth welds. Fracture surfaces from the failed fittings were visually examined. Although largely obliterated by erosion and corrosion, the reducer fracture surface contained regions exhibiting a brittle appearance. By contrast, the fracture surface of the failed tee showed regions of apparent ductile overload. These failure modes were confirmed by SEM examination. However, these observations indicated only final failure mechanisms, and not the causes of failure initiation.

Metallurgical structure of both fittings was ferritic-pearlitic. Examination of internal and external surfaces of the fittings showed the presence of numerous defects. These defects included tears, seams, and laps (Figures 16 and 17). Note the deformed grains near the seam in Figure 17. Appearance suggests this deformation occurred during forging. Further examination revealed the presence of deformed grains to depths of 0.05 to 0.13 mm (0.002 to 0.005 in.) uniformly distributed over both internal and external surfaces of the fittings. Many of the internal forging defects were found to have

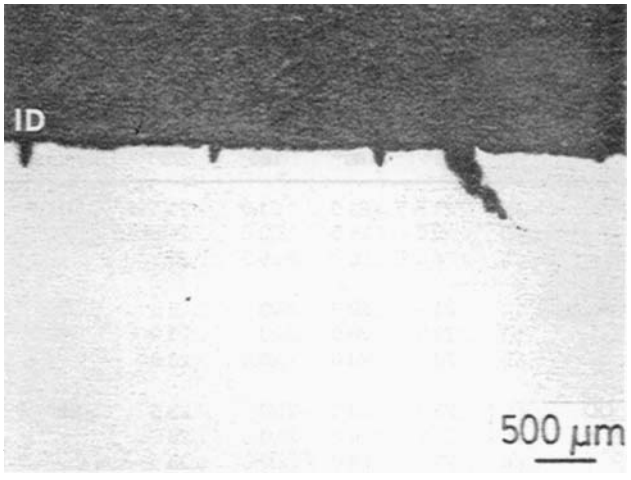


FIGURE 16 — Internal defects, most likely forging tears, in failed sample pot (tee) (nital etch).

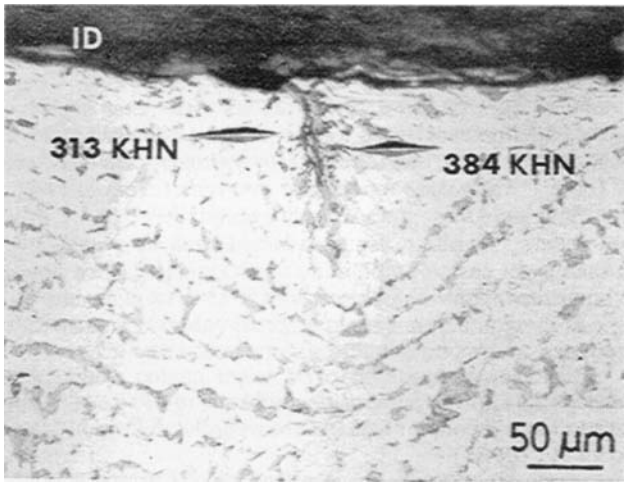


FIGURE 17 — Internal defect, most likely a forging seam, in failed reducer. (Note grain deformation near defect.) Results of microhardness tests (100 g load) noted (nital etch).

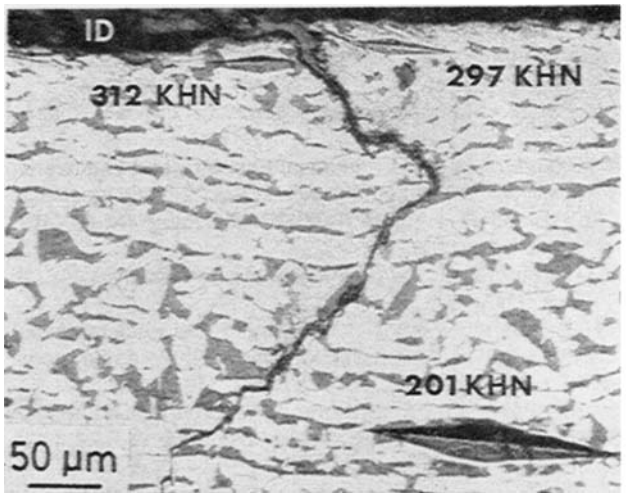


FIGURE 18 — Secondary crack initiated at internal surface of sample pot (tee) in region of elevated skin hardness. Cracking shows jagged characteristics of SSC. Results of microhardness tests (100 g load near surface, 500 g load internally) indicated (nital etch).

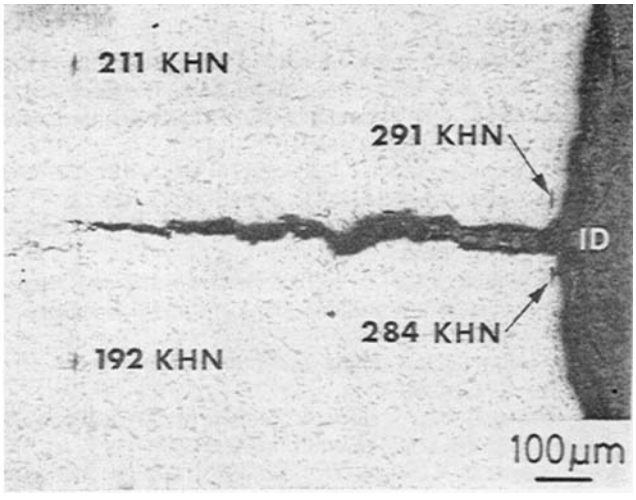


FIGURE 19 — Secondary crack initiated at internal surface of failed reducer in region of elevated skin hardness. Cracking shows jagged characteristics of SSC. Results of microhardness tests (100 g load) indicated.

propagated into jagged cracking, characteristic of SSC (Figures 18 and 19).

As indicated in Figures 17 to 19, microhardness measurements were performed in regions containing deformed grains. Results of 284-318 KHN (26-31 HRC equivalent) were obtained. Similar measurements in undeformed regions, into which cracking propagated, gave results of 192-211 KHN (88-92 HRB equivalent). Direct HRB bulk hardness measurements confirmed these latter microhardness test results. Chemical compositions of the fittings met specifications.

Tensile properties of the fittings were determined, with the following results:

	Tee	Reducer
Yield strength (MPa)	348.9	468.2
Yield strength (ksi)	50.6	67.9
Tensile strength (MPa)	514.4	575.7
Tensile strength (ksi)	74.6	83.5
Elongation (%)	33.0	18.5
Reduction of area (%)	66.8	59.4

Although the yield and tensile strengths were somewhat high, the determined values meet specifications. Because brittle fracture surface regions were observed on the reducer, charpy impact tests were performed on the fittings. Unfortunately, only longitudinal specimens could be obtained. All specimens were notched on ID surfaces. Good impact resistance was obtained for the tee at temperatures down to −40 C. Brittle, low-energy fracture was obtained for the reducer at −17.8 C. Service temperature may have decreased to near this level.

Failure of the gathering system fittings was most likely caused by SSC, followed by ductile overload of the tee, and brittle fracture of the reducer. Because bulk hardness of the fittings was low, SSC susceptibility was not anticipated. This susceptibility apparently resulted from the combination of forging defects, high skin hardness, and large service stresses. It should be noted that none of the forging defects observed were of a rejectable size. It is particularly interesting to note that once initiated, SSC was not arrested by softer base metal.

The cause of elevated skin hardness of the fittings is not conclusively known. Appearance of deformed grains near forging defects suggests the deformation results from forging at too low a temperature. However, the occurrence of elevated hardness in these regions further suggests forming to have been performed below the stress-relief temperature, as well as below the recrystallization temperature. It is difficult to envision forging at such a low temperature without significant evidence of deformation through the wall thickness. If elevated skin hardness was caused by final cold sizing operations, the fittings should have been normalized according to ASTM A234.[15] Because elevated skin hardness was observed uniformly over both internal and external surfaces, skin hardness is not thought to be from handling/installation of the fittings. Uniformity of elevated skin hardness also suggests that grinding was probably not responsible.

If elevated skin hardness was indeed caused by forging at too low a temperature, the problem could be alleviated by normalizing heat treatment subsequent to forging. Earlier versions of ASTM A234 had required heat treatment of all fittings rated for over 20.7 bar (300 psig).[16] Had the current fittings been normalized after forging, SSC failures would not have occurred, suggesting this practice should be required by appropriate sour service standards.

Conclusions

1. SCC failure of the heavily cold-worked duplex SS wireline shows the unsuitability of such materials for elevated temperature sour service in the presence of aqueous chlorides. The failure also illustrates that the aggressiveness of sour service field environments can exceed the severity of comparable laboratory tests.

2. Failure of the L-80 casing by SSC demonstrates the influence of applied stress level and possibly acidizing fluids, in addition to steel hardness, on SSC susceptibility.

3. Forged fitting elevated skin hardness, possibly the result of low temperature forming, can result in SSC susceptibility of moderate hardness carbon steel fittings. Normalizing subsequent to forging should alleviate this problem.

Acknowledgment

Thanks are owed to G. P. Coker, M. Horvat, S. M. Polomchak, T. J. Ryan, C. R. Schimpf, M. Schultz, A. J. Walker, and W. R. Warke for their valuable assistance in these investigations.

References

1. API, "Specification for Restricted Yield Strength Casing and Tubing," API Spec 5AC, 13th Ed., p. 16, March 1982.
2. G. Herbsleb, R. K. Popperling, CORROSION/80, Paper No. 13, NACE, Houston, TX, 1980.
3. S. O. Bernhardsson, J. Oredsson, M. Tynell, CORROSION/80, Paper No. 14, NACE, Houston, TX, 1980.
4. A. I. Asphahani, CORROSION/80, Paper No. 12, NACE, Houston, TX, 1980.
5. NACE Standard MR-01-75 (1980 Revision), "Sulfide Stress Cracking Resistant Metallic Material for Oil Field Equipment," NACE, Houston, TX, 1979.
6. G. A. Vaughn, H. E. Chaung, Materials Performance, Vol. 21, No. 1, p. 44, 1982.
7. Y. Ishizawa, T. Shimada, M. Tanimura, CORROSION/83, Paper No. 167, NACE, Houston, TX, 1983.
8. M. Onayama, N. Hayashi, K. Shitani, T. Suehiro, "Evaluation of Corrosion Resistance of a Duplex Stainless Steel in H_2S-CO_2-Chloride Environments," 1982 Metals Congress International Symposium on Duplex Stainless Steel, ASM, St. Louis, MO, p. 19, October 1982.
9. C. M. Hudgins, R. L. McGlasson, P. Mehdizadeh, W. M. Rosborough, Corrosion, Vol. 22, No. 8, p. 238, 1966.
10. J. B. Greer, Materials Performance, Vol. 14, No. 3, p. 11, 1975.
11. A. Ikeda, M. Kowaka, Chemical Economy and Engineering Review, Vol. 10, No. 5 to 6, No. 117, p. 12, May/June 1978.
12. T. V. Bruno, R. T. Hill, CORROSION/80, Paper No. 6, NACE, Houston, TX, 1980.
13. E. M. Moore, J. J. Warga, Materials Performance, Vol. 15, No. 6, p. 17, 1976.
14. NACE Standard TM-01-77, "Testing of Materials for Resistance to Sulfide Stress Cracking at Ambient Temperature," NACE, Houston, TX, 1977.
15. ASTM, "Piping Fittings of Wrought Carbon Steel and Alloy Steel for Moderate and Elevated Temperatures," A234-82a, Section 1, p. 163, January 1983.
16. ASTM, "Piping Fittings of Wrought Carbon Steel and Alloy Steel for Moderate and Elevated Temperatures," A234-75, Part 1, p. 157, 1976.

Copyrighted Materials
Copyright © 1996 NACE International Retrieved from www.knovel.com

EVALUATION AND APPLICATION OF HIGHLY ALLOYED MATERIALS FOR CORROSIVE OIL PRODUCTION

Bruce D. Craig
Research Engineer
Marathon Oil Company
Denver Research Center
Littleton, Colorado 80160

ABSTRACT

Selection of materials for production of oil from the Brae Field, operated by Marathon Oil Company, in the North Sea required extensive testing of highly alloyed steels and Nickel base alloys. Elevated bottomhole temperatures in combination with a high partial pressure of carbon dioxide and the presence of hydrogen sulfide ruled out the use of carbon or low alloy steels for the production tubing.

Testing of U-bend and crevice specimens in a simulated environment provided the basis for final selection of a duplex stainless steel for the tubing material. Laboratory test methods employed and results are discussed. Testing of tube connections for galling and gas leakage is also reviewed.

INTRODUCTION

The search for new sources of oil and gas by the petroleum industry in recent years has lead to production from more hostile environments. Many of these wells are deep (greater than 15,000 ft) and as a result have high reservoir temperatures and pressures. They may also contain significant concentrations of CO_2, H_2S and chlorides. These corrodents have been effectively dealt with in the past using plastic coatings and chemical inhibitors, however, the high temperatures and pressures being encountered now often reduces the effectiveness of these methods of corrosion control. Furthermore, the high strengths required for

© 1983 *J. Materials for Energy Systems* Courtesy ASM International (formerly American Society for Metals)

tubulars in deep wells renders them susceptible to other modes of failure such as sulfide stress cracking or, in the case of stainless steel tubulars, chloride stress corrosion cracking.

The decision to produce the Brae Field in the United Kingdom sector of the North Sea brought about the need to evaluate materials for tubing and wellhead valves suitable in an aggressive environment. Preliminary data gathered from other operators with similar fields and data from the literature suggested the use of plastic coated carbon steel tubulars and inhibitor injection would probably be uneconomical as well as pose a potential safety problem. Failures of such wells onshore often resulted in serious well control problems which would be even more critical offshore. Therefore, a conservative approach to materials testing and selection was adopted for this field.

EXPERIMENTAL PROCEDURE

In an effort to simulate field conditions, the following data extracted from drill stem tests were used to establish a test environment.

240°F (116°C)	Bottomhole Temperature
7000 psig	Bottomhole Pressure
11% NaCl 80 ppm H_2S 24 mol % CO_2	Reservoir Fluids
35% CO_2	Surface Produced Gas
200°F (93°C)	Surface Producing Temperature

This data was taken and translated into the following procedure for autoclave testing of U-bend specimens. A 2 liter autoclave was filled with distilled water containing 70,000 ppm chloride as NaCl. The autoclave was sealed after the specimens were immersed and the temperature was raised to 240°F (116°C). Then, the autoclave was purged with nitrogen to eliminate any oxygen present and CO_2 was added until a pressure of 260 psig was obtained, representing the partial pressure of 35% CO_2 at 760 psig. This pressure, lower than bottomhole, was the design for the first stage of separation on the platform and was used to include evaluation of alloys for wellhead metallurgy and topside processing as

well as taking into consideration the limits of our test equipment.

After two sets of tests with just CO_2 were completed for wellhead evaluation a third was run using 300 ppm Na_2S to produce H_2S in the test solution. This did in fact occur as the pressure was found to increase to 360 psig after one week of testing. When the cell was vented to return to test pressure, H_2S was evolved and at the end of the test the solution contained 10-12 ppm sulfide. Later on in the testing it was felt more control on the exact content of H_2S was necessary so it was added as a gas at approximately 5 psig or a concentration of 70 ppm.

U-bend specimen used in testing stress corrosion cracking resistance were nominally of the size shown in Figure 1 and run in duplicate.

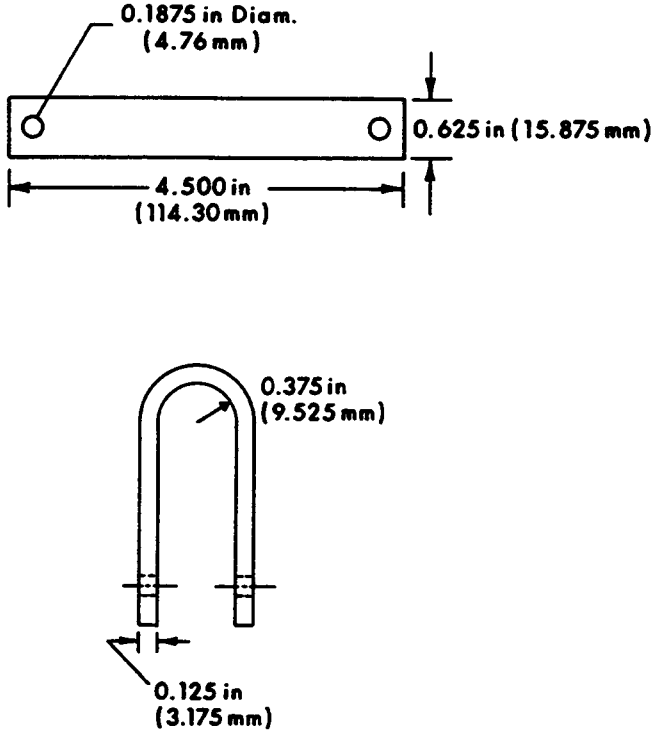


Figure 1. Dimensions of U-bend Specimens Used For Stress Corrosion Cracking Tests. Legs Held By Stainless Steel Bolt.

A stainless steel bolt was used to hold the legs parallel to maintain the stress after the sample was bent around a 3/8 inch mandrel. For all specimens the full thickness of the plate or tube provided for samples was used--most often this was 1/8 inch. These specimen were suspended in the solution from a Teflon tree and electrically isolated from each other and the container walls.

Crevice corrosion tests were also run using coupons 1-1/2" x 1-1/2" with serrated Teflon washers bolted to both sides as shown in Figure 2.

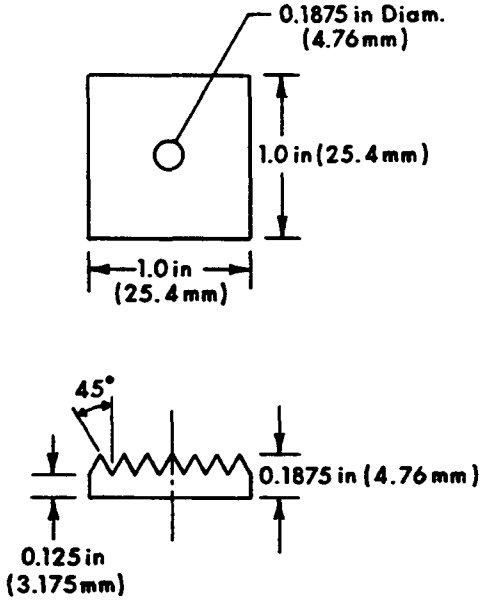


Figure 2. Teflon Washer Used For Crevice Corrosion Testing. Fastened to Both Sides of Test Coupons with Stainless Steel Bolt.

These samples were also suspended from a Teflon tree and isolated from the container walls and each other.

Additionally, corrosion weight loss tests were run using the above-mentioned coupons without Teflon washers to better distinguish general and pitting corrosion behavior. Duplicate samples were run for each alloy.

All testing was performed for 30 days after which specimens were cleaned in water, descaled in inhibited acid when appropriate and rinsed in acetone. Specimens were examined under a 25X binocular microscope for cracks and crevice attack and certain representative samples were prepared for metallographic examination to investigate the possibility of microcrack formation.

Alloys tested in this program are shown along with their composition in Table I. Mechanical properties and processing of the material are presented in Table II as supplied by the manufacturer. No additional evaluation was performed on these alloys except hardness testing.

RESULTS

Table III presents the results of U-bend testing, Table IV of crevice corrosion testing and Table V of weight loss corrosion testing. Test #3 for the U-bend specimen was run with carbon steel bolts to hold the legs rather than stainless steel to evaluate galvanic coupling. This was the only test to use a galvanic couple. Zeron 25 (a duplex stainless steel) failed by intergranular cracking at the top of the U-bend but showed no other corrosion. The 9 Cr-1 Mo failed in a mixed mode manner, predominately by intergranular fracture, Figure 3. A heavy corrosion scale covered the specimen. Several other specimen from each test environment were metallographically prepared and examined but no microcracking was observed. No cracking of the high strength, 862-966MPa, (125-140 ksi) duplex alloys was found.

Crevice corrosion tests showed very little effect except for 410 stainless steel although even 410 was not as seriously attacked as would be expected. The crevice attack on Ferralium 255 was a very light etch, the depth of which was not measurable.

TABLE I

Chemical Composition (wt%)

Alloy	C	Mn	Si	P	S	Al	Cr	Mo	Ni	Fe	Nb	Ti	Co	V	Cu	Other
Carpenter 20 Cb-3 (1)	0.07	2.0	1.0	0.035	0.035	-	20.0	2.5	35.0	Bal	-	-	-	-	3.5	Nb + Ta, 1% max
9Cr-1Mo	0.14	0.52	0.46	0.014	0.013	0.024	9.04	0.96	-	Bal	-	-	-	-	-	
410 Stainless Steel	0.15	1.00	1.00	0.035	0.035	-	12.0	-	-		-	-	-	-	-	
Inconel X 750 (2)	0.08	1.0	0.50	-	0.010	0.8	15.0	-	Bal	7.0	1.0	2.5	1.0	-	0.50	
Inconel 718	0.08	0.35	0.35	0.015	0.015	0.5	19.0	3.1	52.0	Bal	5.0	0.9	1.0	-	0.30	
Nitronic 60 (3)	0.072	8.06	3.99	-	-	-	16.96	0.18	8.45	Bal	0.01	-	-	0.04	-	0.12N
Nitronic 50	0.035	4.78	0.40	-	-	-	20.69	2.14	12.40	Bal	0.13	-	-	0.15	-	0.23N
Zeron 25 (4)	0.059	0.555	0.845	0.014	0.011	0.045	23.62	2.38	6.01	Bal	0.013	0.010	0.024	0.106	.053	0.076N, 0.58W
Monel K500	0.15	0.60	0.15	-	0.005	2.8	-	-	65.0	1.0	-	0.50	-	-	29.5	
Paralloy 208 (5)	0.04	0.69	0.65	0.017	0.018	-	20.9	3.99	26.5	Bal	0.39	-	-	-	1.72	
Paralloy 20A	0.06	1.19	0.92	0.015	0.015	-	20.9	2.50	28.8	Bal	-	-	-	-	3.16	
Uranus 50 (6)	0.03	-	-	-	-	-	20.0	2.5	8.0	Bal	-	-	-	-	1.5	
Firth-Vickers 734 (7)	0.04	3.76	0.40	0.010	0.004	-	21.25	2.75	9.40	Bal	0.31	-	-	-	-	0.003B
Inconel 625	0.10	0.50	0.50	0.015	0.015	0.40	22.0	9.0	Bal	5.0	4.0	0.40	1.0			
Mann AF-22 (8)	0.023	2.94	0.44	0.023	0.003	-	22.41	3.11	5.58	Bal	-	-	-	-	-	
Ferralium 255 (9)	0.02	0.65	0.33	0.022	0.005	-	25.46	3.47	5.54	Bal	-	-	0.20	-	-	0.17N
Hastelloy G (10)	0.023	1.37	0.44	0.014	0.002	-	22.15	6.45	Bal	19.17	-	-	1.85	-	1.60	Nb + Ta-2.17,0.64W
Sanicro 28 (11)	0.018	1.61	0.03	0.02	0.003	-	26.4	3.48	30.9	Bal	-	-	-	-	0.99	
Sandvik SAF 2205	0.027	1.67	0.35	0.026	0.003	-	22.1	3.0	5.7	Bal	-	-	-	-	-	0.15N
Sumitomo DP3 (12)	0.014	0.87	0.45	0.028	0.001	-	24.95	3.18	6.8	Bal	-	-	-	-	0.5	0.14N,0.3W
Vallourec VS22 (13)	0.021	1.68	0.39	0.027	0.013	-	22.08	3.05	5.32	Bal	-	-	-	-	-	0.12N
NKK-Cr22 (14)	0.016	1.44	0.46	0.020	0.004	-	21.85	3.01	6.02	Bal	-	-	-	-	-	0.15N

(1) Carpenter Technology Corporation
(2) International Nickel Company
(3) Armco Steel Corporation
(4) Mather-Platt, Ltd.
(5) APV, Ltd.
(6) Crousot-Loire Steels
(7) Firth-Vickers Special Steels, Ltd.
(8) Mannesmannröhren-Werke AG
(9) Bonar Langley Alloys, Ltd.
(10) Cabot Corporation
(11) Sandvikens Jernverks Aktiebolag
(12) Sumitomo Metal Industries, Ltd.
(13) Vallourec
(14) Nippon Kokan

TABLE II

Thermal/Mechanical Treatment and Mechanical Properties of Alloys

Alloy	Treatment	Y.S., ksi (MPa)	U.T.S., ksi (MPa)	Elong (%)	Rockwell Hardness
Carpenter 20 Cb-3	Solution Annealed	-	-	-	B86
9 Cr-1Mo	Annealed	-	-	-	C22
410 Stainless Steel	Annealed	-	-	-	B80
Inconel X-750	Annealed	-	-	-	B87
Inconel 718	Annealed	-	-	-	B91
Nitronic 60	Solution Annealed	-	-	-	B85
Nitronic 50	Solution Annealed	-	-	-	B95
Zeron 25	Solution Annealed	-	-	-	B97
Monel K500	CD, Ann and Age Hd	-	-	-	C32
Paralloy 208	As Cast	-	-	-	B80
Paralloy 20A	As Cast	-	-	-	B78
Uranus 50	Solution Annealed	-	-	-	B97
FV 734	Solution Annealed	65.3 (450)	127.2 (878)	42	B93
Inconel 625	Annealed	-	-	-	B90
Mann AF22	Solution Annealed	83.5 (567)	1110.6 (763)	24	B87
Ferralium 255	Solution Annealed	-	-	-	C26
Hastelloy G	Solution Annealed	-	-	-	B85
Sanicro 28	Cold Worked	120.0 (830)	133.0 (916)	-	C30
Sandvik 2205	Cold Worked	140.0 (964)	146.0 (1004)	-	C31
Sumitomo DP3-80	Solution Annealed	83.8 (575)	111.7 (771)	33	C21
Sumitomo DP3-110	Cold Worked	122.9 (848)	130.4 (900)	24	C30
Sumitomo DP3-140	Cold Worked	145.7 (1005)	154.7 (1067)	18.5	C33
Vallourec VS22-65	Solution Annealed	78 (540)	110.1 (760)	26	B96
Vallourec VS22-125	Cold Worked	160.9 (1110)	173.9 (1200)	12.5	C31
NKK Cr22-140	Cold Worked	148.0 (1021)	154.0 (1063)	16	C33

TABLE III

Results of Stress Cracking Tests

Alloy	Test #1 (No H_2S)	Test #2 (300 ppm Na_2S Added)	Test #3 (300 ppm Na_2S Added + C-Steel Bolt)	Test #4 (H_2S Added
Carpenter 20 Cb-3	NC (no cracking)	-	-	-
9 Cr-1Mo	One specimen of two cracked	-	One specimen cracked, heavy scale	-
410 S.S.	NC	-	-	NC, light pitting
Inconel X750	NC	-	-	-
Inconel 718	NC	-	-	-
Nitronic 60	NC	-	-	-
Nitronic 50	NC	-	-	-
Zeron 25	NC	IGC both specimens	-	-
Monel K500	NC	NC, heavy pitting, blue scale	-	-
Paralloy 20B	NC	-	-	-
Paralloy 20A	NC	-	-	-
Uranus 50	NC	NC, light pitting	-	-
FV 734	-	NC, pitting, black scale	-	-
Inconel 625	-	NC	NC	-
Mann AF-22	-	NC, severe pitting	NC, excellent condition	-
Sanicro 28	-	-	NC	NC
Sandvik 2205	-	-	NC	NC
Sumitomo DP-3-140	-	-	-	NC
Vallourec VS22-65	-	-	-	NC
-125	-	-	-	NC
NKK-Cr22	-	-	-	NC
Ferralium 255	-	-	-	NC

TABLE IV

Crevice Corrosion Results in Same Environment as U-Bend Test #4

Alloy	Result
Sumitomo DP3-80	No Attack
DP3-110	No Attack
Sandvik 2205	No Attack
Inconel 625	No Attack
Mann AF22	No Attack
Ferralium 255	Light Crevice Attack
410 S.S.	Light Crevice Attack & Some Pitting

TABLE V

Weight Loss and Pitting Corrosion Rates After 39 Day Exposure (Test Environment #4)

Alloy	General Wt. Loss	General Corr. Rate	Max. Pit Depth	Pitting Rate
Sanicro 28	50.4 mg	0.4 mpy	10.1 mils	94.5 mpy
	25.0	0.2	3.4	31.8
Sandvik 2205	69.4	0.7	2.1	19.7
	89.7	0.9	9.7	90.8
AF 22	79.7	0.7	8.4	78.6
	38.9	0.4	6.3	59.0
Inconel 625	4.2	0.0	0	-
	3.1	0.0	0	-
Ferralium 255	2.8	0.0	0	-
	1.5	0.0	0	-
Hastelloy G	3.3	0.0	0	-
	4.3	0.0	0	-

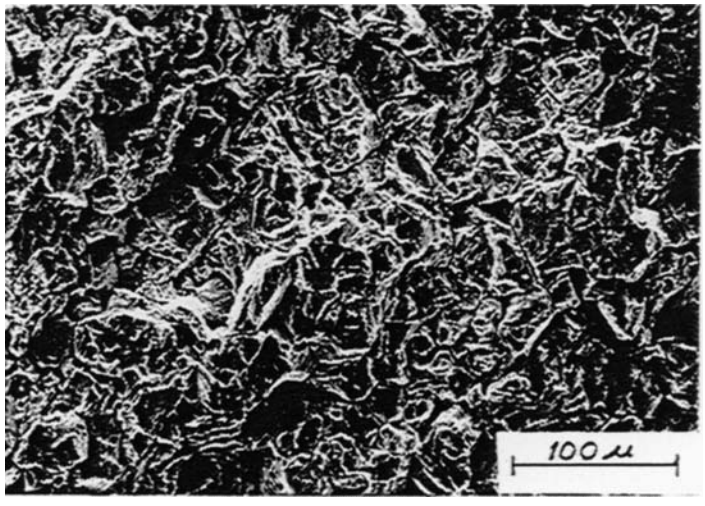


Figure 3. Mixed Mode Fracture of 9 Cr-1 Mo in Test Environment #3.

The general corrosion rates and pitting corrosion were surprising in that all the duplexes were expected to behave in a similar manner, however the Ferralium 255 was not attacked while the other two, AF22 and SAF 2205, were pitted. Furthermore, pitting varied considerably from one specimen to the next for the same alloy. An example of pitting on the Sanicro 28 sample is shown in Figure 4.

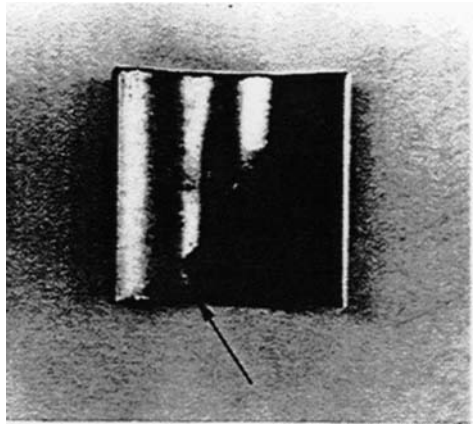


Figure 4. Sanicro 28 Corrosion Coupon Showing Localized Pitting After 39 Days Exposure in Test Environment #4.

This austenitic alloy pitted just as badly as the duplex 2205. Pitting was always quite localized often limited to one region of the coupon.

The high alloy materials listed at the top of Table I with the exception of 9 Cr-1 Mo were tested in the annealed condition since they were being considered for use in wellhead components such as Christmas tree valves. Application of these alloys were anticipated to be as weld overlays on low alloy steel base material and as process piping. Alloys from Mannesmann AF22 through NKK-22 Cr in Table I were considered for downhole tubulars.

Two cracking failure mechanisms were of concern in the service environment both downhole and on the surface. First, the high bottomhole temperatures and high surface temperatures presented a potential for chloride stress corrosion cracking with the high chloride content (70,000 ppm) of the produced water. Additionally, the concentration of H_2S was significant enough to consider hydrogen sulfide cracking to be a potential mechanism for failure, especially with decreasing temperature, although high surface temperature somewhat reduced the effect of this mechanism.

Other corrosion considerations were pitting attack because of the high CO_2 and chloride content and general weight loss corrosion from the high CO_2 content.

Table III shows the effect of adding a small concentration of H_2S to the test environment. The Zeron 25 duplex alloy failed by intergranular cracking whereas in the absence of H_2S it did not. Monel K500, which did not crack, was severely corroded in the presence of H_2S. Both the Firth-Vickers 734, a fully austenitic alloy, and AF22 were pitted. Uranus 50, another duplex stainless steel, also showed light pitting attack. The 9 Cr-1 Mo ferritic steel failed both with and without H_2S present in a predominately intergranular mode.

Coupling of alloys with carbon steel bolts through the legs in Test #3 stopped the pitting attack previously observed on the AF22 alloy probably because the galvanic effect afforded cathodic protection to the duplex stainless steel.

DISCUSSION

Previous work on AF22 by Herbsleb and Popperling[1] in brine solutions with H_2S showed failure did not occur when the H_2S concentration was 0.1g/L or less for specimens loaded to 90% of the yield strength. Further, they found chloride pitting resistance diminished in the presence of H_2S and with increasing temperature. These results agree with data presented in this work even though the stress condition (U-bend) was more severe.

Sandvik SAF 2205 was found to be resistant to chloride stress corrosion cracking in a simulated oil field brine at 100°C at a yield strength of 116 ksi by Bernhardsson et al[2]. Although cracking occurred in the NACE solution, they suggested the threshold for cracking in lower H_2S concentration could be substantially increased. This supposition is supported by the data gathered in this investigation and further agrees with their belief that SAF 2205 would be effective in CO_2 rich low H_2S content environments.

Work of Asphahani[3] on highly alloyed materials in CO_2/H_2S environments showed no cracking for Uranus 50, AF22, Ferralium 255, 20Cb-3, and Hastelloy G when subjected to 5% NaCl + (99% CO_2 and 1% H_2S) at 90°C (195°F) with various degrees of cold work up to 50% for 1000 hour exposure.

Kolts[4] studied the chloride stress cracking of a group of alloys in 25% NaCl at various temperatures and stressed beyond their yield strength. At 250°F (121°C) no cracking was observed for Ferralium 255, Sanicro 28 and Carpenter 20Cb-3 even when these alloys were cold worked as much as 50% .

Results from unpublished studies[5,6] showed that NKK-Cr22 and DP3 cold worked to 140 ksi yield failed by transgranular cracking in the NACE test solution (5% NaCl, 0.5% acetic acid and saturated with H_2S at 25°C) while in environments with less H_2S, but high CO_2 cracking did not occur.

The concensus from all the above referenced work and this investigation is that duplex stainless steels are resistant to environmental cracking at low H_2S concentrations and at temperatures less than 250°F (121°C).

It is difficult to explain whey Ferralium 255 showed indications of crevice attack when the other duplex alloys

did not, especially since the compositions of all the duplex stainless steels were quite similar. Mo, Cu, Ni, N and W have all been demonstrated to be effective in reducing crevice corrosion. Since Mo and W partition to the ferrite and Ni, Cu and N partition to the austenite, the explanation may lie in the relative amounts of ferrite and austenite and their respective resistance to pitting and crevice attack. This may also explain why the reverse behavior was observed for pitting corrosion. No further work was done to elucidate this behavior.

From the data obtained through this testing program and knowledge of different manufacturers' capabilities, it was decided to weld overlay all Christmas tree valves with Inconel 625 and specify a duplex stainless steel for downhole tubing. Since stainless steel is notorious for galling and tubing is coupled by threaded connections, another test program to evaluate coupling performance was undertaken.

Premium threaded pup joints of duplex stainless steel were requested from the manufacturers of DP3, NKK Cr22, SAF 2205 and VS22. These samples were run through a series of laboratory tests which included ten make and break tests to determine galling resistance, three cycles of internal hydrostatic pressure to 5000 psi for 5 minutes, thermal cycling tests from ambient temperature to 250°F (121°C) ten times while the connection was loaded in tension to 400,000 lbs (881 kg) and simultaneously pressure to 5000 psi with nitrogen gas, and an internal pressure test under tension (400,000 lbs) and bending at an equivalent of 6°/100 ft deviation for three cycles. Finally, those alloys that performed satisfactorily under these conditions were used for manufacture of full size joints that were subjected to actual rig floor testing on a drilling rig to evaluate field behavior.

One type of proprietary connection passed all laboratory and rig testing for galling. Another initially failed the full scale rig testing but later passed after changing the method of surface preparation. A third failed and was rejected although further work on surface preparation or design may have corrected the shortcomings.

These results emphasize another area of concern for duplex alloys, that of susceptibility to galling. Furthermore, even when laboratory testing indicated a particular connection was suitable for anti-galling, actual field handling showed otherwise.

CONCLUSIONS

The use of duplex stainless steels can provide superior corrosion resistance for downhole tubing in aggressive environments at yield strengths to 140 ksi (966 MPa). Small quantities of H_2S can increase the corrosion of these alloys, especially by pitting attack.

While these alloys offer good protection against severe corrosion, the joining of pipe by threaded connections can present another area of problems primarily due to galling.

ACKNOWLEDGEMENT

I would like to thank Marathon Oil Company, Marathon Petroleum Company and the participating companies in the Brae project for permission to publish this paper.

REFERENCES

1. G. Herbsleb and R. K. Popperling, NACE Annual Meeting, Corrosion/80, Paper 13, Chicago, Ill. 1980.

2. S. O. Bernhardsson, J. Oredsson and M. Tynell, Ibid, Paper 14.

3. A. I. Asphahani, Ibid, Paper 12.

4. J. Kolts, NACE Annual Meeting, Corrosion/82, Paper 241, Houston, Texas, 1982.

5. Nippon Kokan K. K., unpublished research.

6. Sumitomo Metal Industries, Ltd., unpublished research.

7. H. Nagano, T. Kuda, Y. Inaba and M. Harada, International Colloquium on Stainless Steels, 19th Hournees des Aciers Speciaus, St-Etienne, France, May, 1980.

Copyrighted Materials
Copyright © 1996 NACE International Retrieved from www.knovel.com

Paper No. 232—CORROSION/85

EVALUATION OF THE RESISTANCE OF SOME HIGHLY ALLOYED STAINLESS STEELS TO STRESS CORROSION CRACKING IN HOT CHLORIDE SOLUTIONS UNDER HIGH PRESSURES OF CO_2 AND H_2S

J.L. Crolet, M.R. Bonis
Societe Nationale Elf-Aquitaine (Production)
64018 Pau, France

ABSTRACT

SCC tests under high temperatures and high pressures of acid gas are presented. They try to give the best representation of the actual service conditions of ultra deep petroleum developments, by reproducing in their corrosive media the temperature, the chloride content, the partial pressure of H_2S and the natural acidity of produced waters (through their native alkalinity and the real pressures of the two acid gases, CO_2 and H_2S, and not by any other addition of acids). Results are reported for duplex stainless steels (22%Cr - 5% Ni) and austenitic nickel alloys (VS28, Alloy 825, Hastelloy G3).

The SCC resistance is shown to be influenced by the chloride content, the partial pressure of H_2S and the acidity of the corrosive medium. As expected, the more highly alloyed grades exhibit the better resistance. The SCC resistance of duplex stainless steels is strongly reduced then their level of cold work is increased. As a result, these grades are not good candidates for ultra deep applications under high temperatures and high pressures of H_2S. On the other hand, with just a slight amount of cold work, their behavior remains quite satisfactory for many others applications, even under many bars of H_2S and elevated temperatures.

The intermediate nickel alloys with 30 to 40% Ni perform fairly well up to very high temperatures and acid gas pressures, even with a high level of cold work. This makes them excellent candidates for ultra deep applications. Finally, the interest of adjusting the severity of the test conditions to the addressed application is emphasized.

INTRODUCTION

During the last 2 or 3 years, many studies have been devoted to the stress corrosion cracking (SCC) of stainless and nickel alloys in the presence of H_2S in corrosive media aimed as representing the expected conditions of some ultra deep petroleum developments.[1-6] This means temperatures higher than 150 to 200°C (302 to 392°F), absolute pressures exceeding 1,000 bars, and CO_2 + H_2S content reaching 50% or more. Obviously such conditions are rather unusual. In addition, they have been studied only recently. Therefore, unlike sulfide stress cracking and the recommended TM 01 77 procedure, no standard test medium is still available. Consequently, maybe for fear of underestimating the severity of a rather new type of damage, or for matching the most difficult possibilities, recent studies have been carried out under extreme conditions of temperature (up to 350°C [662°F]) and acidity (down to pH 2 or 0.5). Naturally, very highly alloyed stainless steels are then required for resistance such extraordinary conditions.

Anyway, these studies have already demonstrated the ability of some (expensive) metallic materials to be used in ultra deep wells. They have also indicated the influence of alloying elements, Cr, Ni, Mo, N on the SCC resistance, particularly through the evolution of the passive layer in the presence of H_2S.[2,6] However, efforts are still necessary for properly adjusting the composition and the properties of the materials to the effective severity of the expected corrosive conditions.

For an end user in the oil and gas industry, such an accurate adjustment is indeed mandatory. Obviously, any excessive alloy would burden the already high cost of well equipment in stainless steels. In this respect, many deep or ultra deep wells which are to be developed in the near future do appear to be less severe than most of the

tests. On the other hand, stainless steels may also be interesting in conditions of relatively low severity. For instance, their use may be aimed merely at avoiding the inhibition of carbon steel, in case of hostile natural environments or remote geographic positions.

For all these reasons, we tried first to appreciate how a relevant severity of produced waters under pressures of acid gas could be expressed. Naturally, this started with the knowledge of the in situ pH and the comprehension of the solubility equibria of the corrosion products. Thus it has been shown that the only way for reproducing both the acidity of the water and the solubility of corrosion products is to exactly reproduce the alkalinity of water and the natural partial pressures of CO_2 and H_2S.[7] Similarly, it is felt that temperature has to be limited "realistic" values, that is not exceeding 200°C (392°F).

This study is also focused on the less expensive materials, namely the less alloyed candidates for this type of stainless applications. Therefore the study is primarily aimed at appreciating accurate limits for the possible use of duplex stainless steels or intermedate nickel alloys, in corrosive media being as representative as possible of the incoming ultra deep developments.

In addition, in order to apply uniform and well known stresses through the samples (which is not always the case in the usual bent beam tests), a special technology has been developed for stressing smooth tensile specimens in high pressure autoclaves (possibly up to 2000 bars).

EXPERIMENTAL

Testing Device

The experimental device is defined for matching the three following requirements:

1. Testing under very high pressures of gas (up to 2000 bars), with CO_2 and H_2S in any proportion in the gas.
2. Use of smooth tensile specimens.
3. Istantanteous detection of sample ruptures.

Autoclaves

The standard autoclaves in our laboratory are designed for 500 bars and 200°C (392°F), with an internal diameter of 74 mm (internal volume 1.13 l). This standard type is used for most of the tests.

For this study, additional 1,000 bars/200°C (392°F) and 2000 bars/300°C (572°F) autoclaves have also been built, with the same internal geometry. They are made of a precipitation hardened stainless steel, type ASTM A286 (Ugine Aciers Fluginox 130). In order to prevent any corrosion problem for the autoclaves themselves, the corrosive medium (0.5 l), usually bearing chlorides, is contained in a quartz beaker inside the autoclave.

Due to the intended very high pressures, tensioning the samples from the outside, through gliding seals, was not considered reasonable. Therefore, internal proof rings have been preferred.

Test Specimens

The test specimen is derived from the subsize sample of the TM 01-77 procedure. In autoclave tests, however, the tensile samples are entirely immersed in the corrosive medium. Due to the stress concentration factor in the threads, this resulted in abnormal failures out of the gauged length. These troubles have been solved by reducing the diameter of the gauged length to 2 mm. According to our past experience on SSC, the surface finish of samples is not that of lathe turning, but of smooth grinding for a final surface roughness better than 0.2 µm.[8]

Proof Rings

The rings are designed according to the following requirements:

A. resistance to corrosion in all the media to be tested. Rings were first machined in the high strength titanium alloy TA6V. However, they did corrode in high chloride high H_2S conditions. Then Hastelloy C-276 was chosen and one cold worked bar was especially supplied by the Cabot Corp. All the subsequent rings have been machined from it. They behave quite satisfactorily.

B. mechanical strength, allowing loading samples up to 1,500 MPa without any plastic strain of the ring. This is not an easy task for rings which have to keep small external diameters. The design of the adopted ring is shown in Figure 1a. This design is optimized following Ikeda's analysis.[9] The challenge here is to increase the yield strength of the ring as much as possible, along with keeping its stiffness similar to

that of the samples.

C. good electrical insulation between ring and sample. Because of this, the end nuts (Figure 1b), machined from the same batch of metal as the sample, bear on trued up quartz washers. Unfortunately, these are very brittle. Therefore, they are themselves fretted in a metallic socket, for preventing the cracking of the insulating washer when loading the samples.

D. Perfect knowledge of the applied stress. This is achieved by the loading procedure of the samples.

The ring is first preloaded with the help of a small tension testing machine, 1 ton in capability (Figures 2 and 3). During this step, the strength-strain diagram of the ring is determined; the strength is measured by the tension testing machine, the strain is marked by a strain gauge which is stuck on the side of the ring (Figure 4).

Then the end nuts of the samples are manually screwed. The goal is to just ensure a good mechanical contact between the sample and the ring, but no real torque is applied. Finally the tension testing machine is slowly unloaded. As a result, the sample is progressively loaded by the partial relaxation of the ring (Figure 5).

Initially, the required preload of the ring is calculated from the relative stiffness of ring and sample, and from the expected stress level in the sample. At the end, this level is measured (at room temperature), by comparing the final readings of the strain gauge and the known strength/strain diagram of the ring.

At the temperature of the test, this stress level is of course slightly shifted, due to the differences between the two constitutive metals of the ring and the sample. This shift can be calculated by taking into account their different coefficients of thermal expansion and the different variations of their elastic modulus with temperature (Figure 5). For a ring in Hastelloy C, this leads to a decrease of the effective applied stress of 7 to 21%, depending on the alloy, the stress level and the test temperature. However, the overall error on the applied stress during the test is probably less than 3%.

Instantaneous Detection of Ruptures

Five identical samples are simultaneously tested in the same autoclave. The five corresponding rings are tightly screwed on a holder, which is itself tightly fixed on the head of the autoclave (Figure 6).

On this head, but on the outside, a very sensitive accelerometer is also fixed (Figure 7). It allows each rupture of a sample to be individualy detected.

In fact, contrary to SSC tests, the samples either did not crack or cracked so early that, most often, the detection system was not yet operating.

Test Conditions

Tested Materials

Four grades of duplex stainless steels (22% Cr, 5 % Ni) and three grades of austenitic alloys are studied. Samples are cut from commercial cold worked tubings, kindly supplied by their manufacturers:

Trade name	UNS	API grade	Manufact.
VS 22	S31803	L 80, Q 125	Vallourec
SAF 22-05	S31803	P 110, V 150	Sandvik
VS 28		P 110	Vallourec
Alloy 825	N08825	Q 125	Cabval
Hastelloy G3	N06007	V 150	Cabval

Their chemical compositions and mechanical properties at room temperature are given in Tables 1 and 2.

Corrosive Media

Aqueous solutions are prepared from deionized water and reagent grade salts, NaCl and $NaHCO_3$. Since the influence of methane is known to be neglible, the acid was in equilibium with the solution is a simple 50-50 mixture of CO_2 and H_2S.

This mixture is prepared in advance in a cylinder, from commercially pure gases. Most of the tests are performed under a pressure of 350 bars (5,000 psi). This is thought to represent "reasonable" ultra deep condi-

tions. Some tests are also performed under lower pressures.

The most severe conditions in this study are 100g/l NaCl and 200°C. All materials are first tested in this medium. In case of rupture, the severity is then lowered, by reducing the salinity per decade (10, 1, 0.1 g/l), or the temperature (150°C [302°F]), or the pressure of acid gas.

The influence of various accounts of sodium bicarbonate $NaHCO_3$, representing the natural alkalinity of reservoir waters, is also studied, as well as the effect of a dilution from a given reservoir water (i.e., 100 g/l NaCl + 10 meq/l $NaHCO_3$).

For all these media, the pH values under pressure have been evaluated from our previous studies, and they are reported with the results.[7]

Applied Stress

The tubing strings of deep high pressure wells are usually made of joints and threaded couplings with tight metal to metal seals. In this type of connection, the yield point of the metal is always more or less reached, but never exceeded too much. From the point of view of the corrosion resistance, the relevant stress level is then the yield strength of the metal, whatever the actual working rate of the tubing can be.[8]

For the purpose of safety, the nominal stress level in our tests is chosen as 90% of the yield strength at room temperature. As mentioned before, the absolute applied stress at the temperature of the test is lower. However, the yield strength YS also decreases with temperature. Altogether, the normalized stresses /YS at the temperature of the test finally stand between 80 and 100%. Exact values depend on the alloy. They are given in Table 3.

Testing Procedure

The samples are first loaded on their respective proof rings. Just before being introduced into the autoclaves, they are degreased in a mixture of alcohol-acetone, decontaminated for 15 min. in 15% HNO_3, rinsed in deionized water and dried.

After the autoclaves have been closed, the corrosive medium is deaerated by bubbling nitrogen and saturated in the test was under atmospheric pressure. Then pressure and temperature are raised up to the final test conditions. The saturation in gas is achieved by bubbling the test gas through the solution at the pressure and temperature of the test.

RESULTS

All the results are given in Table 4. Most often, all the five samples of a given test have or have not cracked. The simultaneous presence of failed and unfailed specimens is only found for borderline conditions. In this case, the residual scatter of the stress values or mechanical properties is probably high enough for making the rupture to occur or not.

Nickel Alloys

All the tested nickel alloys resist the most severe conditions of this study. Therefore testing was not developed further.

Duplex Stainless Steels

Influence of Cold Work

As expected, the sensitivity of duplex stainless steels to SCC increases with their degree of cold work. Thus, the very slightly cold worked grade 80 VS 22 resists SCC in the most severe conditions, 100 g/l NaCl and 200°C (392°), when the steel SAF 22-05 -P 110 already cracks for 10 g/l and 150°C (302°F). For the most cold worked grade, even a salinity as low as 0.1 g/l NaCl does not prevent cracking.

It results in only the less cold worked grade 80 VS 22 resisting possible ultra deep environments. Unfortunately, its mechanical properties will often be considered too low.

Influence of Chloride Content

Table 5 gives the limiting content in sodium chloride, below which SCC does not occur under a pressure of 350 bars of the CO_2-H_2S mixture. This illustrates the determining role of chloride ions in the severity of the corrosive medium.

Influence of Temperature

Since only 2 temperatures have been tested, just a rough estimate of the influence of temperature is possible. Nevertheless, from tests ≠ ≠ 11 and 13 on 125 VS 22, a higher temperature appears to represent more severe conditions. In Table 5, the higher temperature then correspond to a lower limiting content in sodium chloride.

Influence of Acidity

In our test conditions, the primary parameters for the acidity of the corrosive medium are the partial pressure of the acid gas and the content of the water in alkaline species HCO_3. Temperature and ionic strength have only secondary effects.

Table 4 clearly shows that a sufficient addition of bicarbonate can be a very effective moderator of SCC, at least when the panel salinity temperature-cold work is not too severe.

Thus, for 125 VS 22 in 10 g/l NaCl at 150°C (302°F), cracking occurs with 1 meq/l HCO_3^- (pH 2.7), but it disappears with 20 meq/l CO_3 HCO_3^- (pH 3.7). On the other hand, between test ≠ ≠ 21 and 22, the addition of 0.1 meg/l HCO_3^- does not change significantly the severity of cracking but pH also is unchanged.

In the case of 125 VS 22 and SAF 22 05-V 150 at 150°C (302°F), we have also tested the influence of the dilution of a water, a reservoir type of water (100 g/l NaCl + 10 meq/l HCO_3^-), by pure water (condensed water). From tests ≠ ≠ 8, 9, 11 and 19, 20, 21, 24, it can be seen that, in this case, only strong dilutions (99 or 99.9%) may suppress SCC. During the first 90%, the effect of the decrease in the chloride content is in fact balanced by the parallel decrease of the alkalinity and then of the pH.

Beyond 90%, that is below 1 meq/l HCO_3^-, pH finally becomes stable. Then, and only then, is dilution really beneficial.

Influence of the Pressure of Acid Gas

The influence of a decrease of the acid gas pressure has been studied for the grade 125 VS 22 in pure NaCl solutions. In these conditions, it results in a decrease of the pH (by 0.5 unit per decade of pressure). As expected, the decrease of the acid gas pressure is proven to be very beneficial (tests ≠ ≠ 7, 14, 15). Even at nearly constant pH values (tests ≠ ≠ 8, 14, 15), a decrease of the acid gas pressure is still beneficial.

Combining the respective beneficial or detrimental effects is also of interest. Thus, from tests ≠ ≠ 9, 10, 11, it can be seen that for a constant partial pressure of acid gas, a tenfold increase of the chloride content is compensated by an increase of the in situ pH by one unit.

DISCUSSION

The results of these SCC tests in the presence of H_2S are in perfect agreement with the usual parameters and mechanisms of this type of corrosion.[10] In particular they emphasize the determining roles of the chloride content and the acidity of the corrosive medium (defined by the acid gas pressure *and* the water alkalinity), and also of the composition and the degree of cold work of the material. The partial pressure of H_2S, as such, seems here to be of less importance.

These results agree fairly well with those of Ikeda et al.[5] For these authors, temperature and are also the primary parameters for the SCC resistance; then come the chloride content and the partial pressure of H_2S. Our results are also consistent with those of Poepperling despite differences in the experimental procedure and test conditions.[11]

However, the multiplicity of additive and competitive influences results in several important consequences.

Evaluation of the Severity of Test Conditions in SCC Studies

From the previous discussion, it follows that the expression of the severity of SCC tests is probably not unique. It will depend both on the particular context of each study, and for each material, on the proximity of its own limit of resistance.

Determination of the Limit of the Use of a Given Material

In the vicinity of a limit of resistance, all the additive or competitive influences are emphasized. Therefore,

when a study is aimed at selecting a material which has to be safe but nevertheless not excessive, the severity of the test can no longer be expressed by only one or even several of the presently studied parameters. All together are mandatory:

- Temperature;
- Chloride content;
- Natural alkalinity of the water;
- Partial pressures of the two acid bases, CO_2 and H_2S; and
- Applied stress.

It results that a precise limit of use for a given material cannot be but a complex function of all these parameters. Then it will be very difficult to determine it systematically in advance for all the candidate materials. On the other hand, for a well defined application, it will be easy to check check the good behavior of such and such anticipated material.

Approximate Guidelines

For the sake of simplicity, it is also possible to consider only approximate guidelines. These are expressed through a limited number of parameters: for example chloride content and temperature, temperature and partial pressure of H_2S or, as often, chloride content and partial pressure of H_2S. These guidelines represent an envelope, which naturally includes a safety margin with respect to the actual limit of resistance.

Such an envelope, however, may also introduce economic penalties; increasing levels of simplification obviously lead to using more and more uselessly sophisticated alloys.

Supposedly approximate guidelines may also prove patently erroneous when one of the parameters which has been considered for their evaluation is overly unrealistic. In our example, this will be the case for all SCC studies which would be carried out in simultaneously very acidic (pH < 2) and very concentrated brines.

As a matter of fact, despite geological exceptions, the reservoir waters always bear some alkalinity. Then their pH cannot be lower than pH 3, even under several hundred bars of acid gas. On the other hand, the most acidic waters are primarily condensed waters, the salinity of which is then very low (< 1 g/l). Nevertheless, it is still worth noting that even for a condensed water, about 1,000 bars of acid gas would be necessary for getting pH values lower than 2.5. It results that a corrosive medium made of a both very acidic and very concentrated brine may yet have an academic interest, but it will represent only exceptionally the actual corrosive media which can be encountered in oil and gas wells.

Furthermore, our tests on dilution show that the most severe conditions for SCC are the reservoir waters themselves. Wherefore, the use of corrosive media at pH < 3 is perhaps useful for ranking materials at the top level, but it will most often be of low interest in the selection of materials for the equipment of ultra deep wells. In addition, several authors have also pointed out how the evolution of the passive layer is the prefence of H_2S is important for SCC, in particular with respect to the possibility of formation of Ni or Cr sulfide layer.[4] This formation itself is also influenced by the acidity of the corrosive medium and not solely by the partial pressure of H_2S.[5,7]

Therefore, tests under high pressure of H_2S at the natural pH of the water are in no way equivalent to tests under lower H_2S pressure, in a solution acidized to the same pH by adding mineral or organic acid.[7]

Interest of Performant Testing Facilities

In all SCC studies, the decisive role of the applied stress is well recognized today, and one can recall all the harmful misconceptions which may have been suggested in the past from U-bend tests.

Unfortunately, tensioning samples at a known stress level and under high pressures of acid gas is not exactly easy. We do believe, however, that it is altogether more economical to invest in sophisticated high pressure test facilities than to pay for miles of tubing in an excessively high alloyed material.

Behavior of Duplex Stainless Steels

The minimally cold worked duplex stainless steels, grade API N 80, have an excellent SCC resistance up to already very severe conditions: 100 % YS, 200°C (392°F), 100 g/l of pure NaCl and 350 bars of the CO_2-H_2S mixture. This makes them excellent candidates for numerous applications, for example in sheet metal work: heat exchangers for heating sour hydrated crude oils (desalting units) or for cooling sour associate gases (enhanced

condensate recovery).

This makes them also excellent candidates for the equipment of corrosive wells, when the use of 13% Cr martensitic stainless steels is prevented by too high a partial pressure of H_2S (risk of sulfide stress cracking during the periods of well shut down and cooling).

This evaluation, indeed, is not in contradiction with some papers of the literature setting the limit of the use of duplex steel near 0.1 to 0.3 bars of H_2S.[3,12,13]

Actually, these figures correspond to highly cold worked steels or to both concentrated and very acidic brines. In such conditions, we have also observed failures. These simply mean that sour ultra deep wells will never be equipped with high strength tubing in duplex stainless steel.

On the other hand, it has also been shown that up to 150°C (302°F), with limited acidities or chloride contents, the cold worked grades are still able to sustain respectable pressures of H_2S. As an example, in Lacq, the ultra deep field of the early fifties (gas composition: 15% H_2S, 9% CO_2; bottom hole conditions: 125 to 140°C, 3500 to 4500 m and 700 bars at the beginning, 63 g/l Cl ions, in situ pH 3.8), all the wire-lines are in Uranus 50, a similar duplex alloy with 21% Cr and 8 % Ni. These have been used for 14 years, with the number of runs before failure averaging 100 per line. The final failures were analyzed, and they were shown to be merely mechanical failures, due to wear (reduceion in section) or to improper operating conditions.

To sum up, it seems that the possibilities of using duplex stainless steels have been basically underestimated. Their corrosion resistance is far from negligible and they remain the less expensive candidate materials after the 13% Cr steels.

Behavior of Austenitic Alloys with Intermediate Nickel Contents

As in Vaughn's results the very promising results on the commercial tubings VS 28 and Alloy 825 show that there are possibilities of solving the corrosion problems, associated with the production of ultra deep sour fields without resorting to extreme alloys with 70% Ni.[14] In particular, the less alloyed composition, VS 28 by Vallourec or Sanicro 28 by Sandvik, will probably cover a great number of applications, provided that their good behavior is verified in each case. The permanent need of having appropriate high pressure testing facilities at one's disposal is again emphasized.

CONCLUSION

This study of the SCC resistance of stainless steels under pressure of H_2S finally leads to three main conclusions. First, for being useful to the end user in the oil and gas industry, the available data on SCC resistance must be issued from tests carried out in conditions not too far from the envisaged service conditions. Due to the multiplicity of the basic parameters of this corrosion, and their mutual imbrication, it does not seem reasonable to compare the severity of too different corrosive media. Therefore, a representative corrosion test has to reproduce simultaneously the temperature, the chloride content and the acidity of the corrosive medium (through the alkalinity of water and the actual partial pressures of the two acid gases, CO_2 and H_2S, and not by any other acid), and also naturally a well defined stress level throughout the samples.

Present results show that duplex stainless steels, type 22% Cr - 5% Ni, are not suitable for the equipment of ultra deep wells under high pressures of H_2S and high temperature. However, with a low level of cold work, they will be successful in a lot of other uses, even under respectable pressures of H_2S. This is an important statement because the cost of these materials still remains acceptable for many applications in petroleum production.

For more severe circumstances the austenitic alloys, type VS 28 (28% Cr - 33% Ni), still offer wide possibilities, before considering alloys with higher nickel contents.

REFERENCES

1. J. Kolts, A. Asphahani, *Corrosion* 37, 6(1981), p. 327.
2. J.A. Harris, T.F. Lemke, "Laboratory Testing of Nickel Alloys for H_2S Service," paper no. 137, NACE Annual Conference (Houston, TX: NACE, 1982).
3. J.C. Prouheze, J.C. Vailland, *J. Mat. Energy Sys.* 5, 1(1983), p. 19.

4. T. Kudo, H. Miyuki, J. Murayama, "Effect of Cr, Ni, and Mo On Corrosion Resistance of Highly Alloyed Materials in Sour Wells Environments," paper no. 209, NACE Annual Conference (Houston, TX: NACE, 1984).
5. A. Ikeda, T. Kudo, Y. Okada, S. Mukai, F. Terasaki, "Corrosion Behavior of High Alloy Oil Country Tubular Goods for Deep Sour Gas Well," paper no. 206, NACE Annual Conference (Houston, TX: NACE, 1984).
6. J. Sakai, M. Honda, K. Masamura, T. Ono, Y. Matsushima, "Critical Contents of Nickel and Chromium Required for SCC Resistance of High Alloy OCTG," paper no. 207, NACE Annual Conference (Houston, TX: NACE, 1984).
7. J.L. Crolet, M.R. Bonis, *Materials Performance* 33, 5(1984), p. 35.
8. J.L. Crolet, C.P. Perrollet, "SCC Tensile Tests: Comparison Between the Regular NACE Test, the SNEA(P) Test and a Modified NACE Test at pH 4," paper no. 135, NACE Annual Conference (Houston, TX: NACE, 1982).
9. A. Ikeda, T. Kaneko, H. Kajimura, "Influence of Various Factors on the Uniaxial Tension Load Test for Sulfide Stress Cracking," paper no. 161, NACE Annual Conference (Houston, TX: NACE, 1983).
10. J.C. Charbonnier, *Memoires et Etudes Scientifiques de la Revue de Metallurgie* 78, 2(1981), p. 65.
11. R.K. Poepperling, Erdoel und Kohle, Erd gas, *Petroch.* 37,3(1984), p. 119.
12. J. Oredsson, S.O. Bernhardsson, "The Performance of High Alloyed Austenitic and Duplex Stainless Steels in Sour Oil and Gas Enviroments," paper no. 126, NACE Annual Conference (Houston, TX: NACE, 1982).
13. G. Herbsleb, R. Poepperling, *Corrosion* 36, 11(1980), p. 611.
14. G.A. Vaughn, H-E. Chaung, "Wire Line Materials for Sour Service," paper no. 182, NACE Annual Conference (Houston, TX: NACE, 1982).

Table 1 : Composition of the tested alloys (w %)

TRADE NAME	API GRADE	C	Si	Mn	Cr	Ni	Mo	Cu	S	P	Co
80 VS 22	N 80	0.02	0.27	1.58	21.5	5.3	2.5	-	0.020	0.028	
SAF 22-05	P 110	0.018	0.34	1.76	20.8	6.3	2.4	-	0.020	0.018	
125 VS 22	Q 125	0.05	0.35	2.29	20.2	5.5	2.5	-	<0.01	<0.01	
SAF 22-05	V 150	0.024	0.33	1.30	21.0	7.5	2.5		0.022	0.016	Al0.13 V 0.14
VS 28	Q 125	0.025	0.20	1.50	26.0	33.0	2.7	0.70	0.019	0.012	
Alloy 825	Q 125	0.005	0.46	0.68	20.0	41.0	3.0	0.87	0.001	0.018	
Hastelloy G3	V 150	0.006	0.40	0.71	22.5	64.2	7.0	1.92	0.002	0.018	Co3.24

Table 2 : Mechanical properties at 20°C

TRADE NAME	API GRADE	Y.S MPa (KSI)	UTS MPa	ELONGATION %
80 VS 22	N 80	744 (107.9)	810	27
SAF 22-05	P 110	843 (122.2)	1 072	22.2
125 VS 22	Q 125	996 (144.4)	1 046	16.1
SAF 22-05	V 150	1 124 (163)	1 187	16
VS 28	Q 125	885 (128.2)	949	13.5
Alloy 825	Q 125	907 (131.5)	933	13.2
Hastelloy G3	V 150	1 048 (151.8)	1 118	12.4

It appears that duplex stainless steels are cold worked for yield strengthes approaching the maxima of their corresponding API grades.

Table 3 : Applied stresses (MPa)

TEMPERATURE		20°C		150°C				200°C			
TRADE NAME	API GRADE	YS	σ = 0.90 YS	YS	σ	$100\frac{\sigma-\sigma_0}{\sigma_0}$	$100\frac{\sigma}{YS}$	YS	σ	$100\frac{\sigma-\sigma_0}{\sigma_0}$	$100\frac{\sigma}{YS}$
80 VS 22	N 80	744	670	631	618	- 7.7	98.0	593	596	- 11.0	100.5
SAF 2205	P 110	843	759	728	703	- 7.3	96.6	691	680	- 10.4	98.4
125 VS 22	Q 125	996	896	895	835	- 6.8	93.3	862	809	- 9.7	93.8
SAF 2205	V 150	1 124	1 012	1 042	946	- 6.5	90.8	1 012	918	- 9.3	90.7
VS 28	P 110	885	796	774	678	- 14.8	87.6	735	630	- 2.1	85.7
ALLOY 825	P 110	907	816	842	716	- 12.2	85.0	826	675	- 17.3	81.7
HASTELLOY G3	V 150	1 048	943	944	877	- 7.0	92.9	905	847	- 10.2	93.6

Table 4 : Results

ALLOY GRADE	PRESSURE OF CO_2-H_2S	TEST NUMBER	TEMPERATURE °C	CORROSIVE MEDIUM			NUMBER OF RUPTURES FOR 5 SAMPLES
				NaCl g/l	HCO_3^- meq/l	in situ pH *	
80 VS 22	350	1	200	100	0	2.65	0
N 80	350	2	150	100	0	2.65	0
SAF 22-05		3	200	10	1	2.7	1
P 110	350	4	150	10	1	2.7	2
		5	200	1	0	2.7	0
		6	200	100	0	2.65	5
		7		100	0	2.65	5
		8		100	10	3.3	5
125 VS 22	350	9	150	10	1	2.7	5
		10		10	20	3.7	0
		11		1	0	2.75	0
Q 125		12		1	0.1	2.75	0
		13	200	1	0	2.75	1
	30	14	150	100	0	3.2	5
	10	15	150	100	0	3.42	0
		16		10	0	3.45	0
		17	200	100	0	2.65	5
		18		100	0	2.65	5
SAF 22-05		19		100	10	3.3	5
	350	20		10	1	2.70	5
V 150		21	150	1	0.1	2.75	2
		22		1	0	2.75	3
		23		1	20	3.7	0
		24		0.1	0	2.80	1
VS 28-P 110		25					0
825-P 110	350	26	200	100	0	2.65	0
G3-V 150		27					0

* calculated at 100°C with the help of our computer program[7] "pH calc".

Table 5 : Limiting content L in sodium chloride (in g/l), below which SCC does not occur under 350 bars of CO_2 + H_2S.

MATERIAL	80 VS 22	SAF 22-05/P 110	125 VS 22	SAF 22-05/Q 150
at 150°C	L > 100	1 < L < 10	1 < L < 10	L < 0.1
at 200°C	L > 100	L < 10	L < 1	L < 0.1

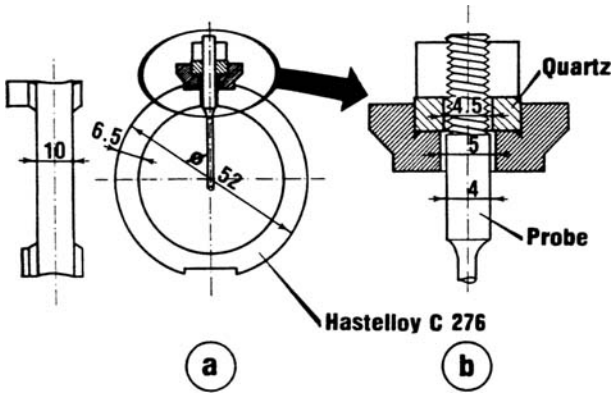


FIGURE 1 : Design of the optimized proof ring

a) ring dimensions (mm)
b) isolating washer

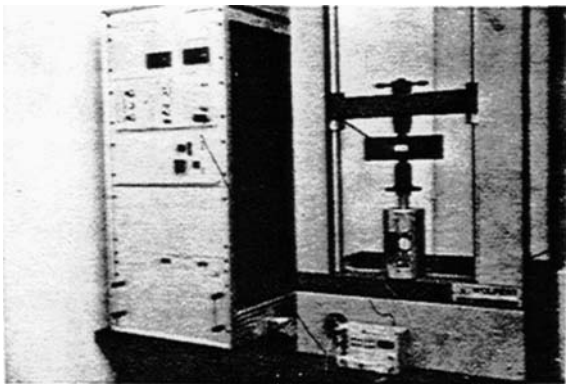


FIGURE 2 : View of the loading machine

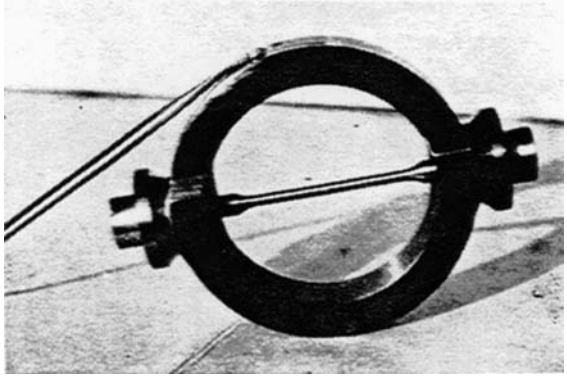


FIGURE 4 : View of the proof ring with the strain gauge used for calibration

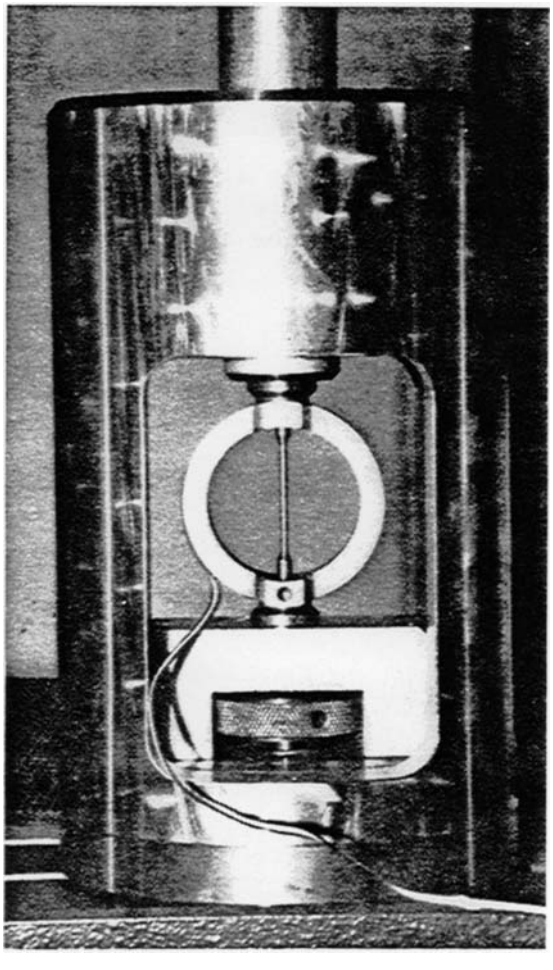


FIGURE 3 : View of the loading device

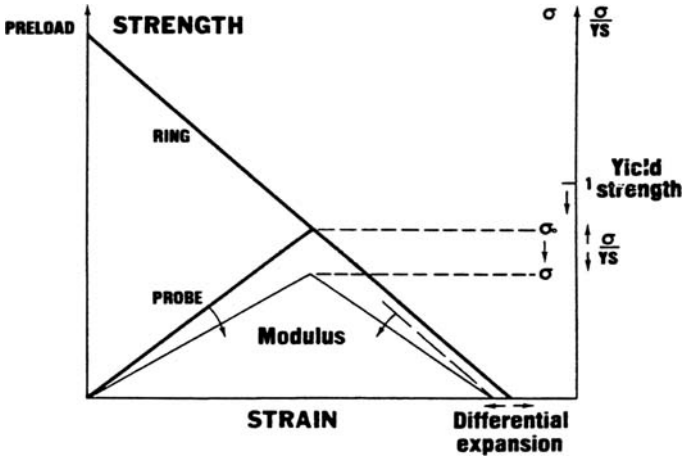


FIGURE 5 : Illustration of the calculation of the final stress in the sample

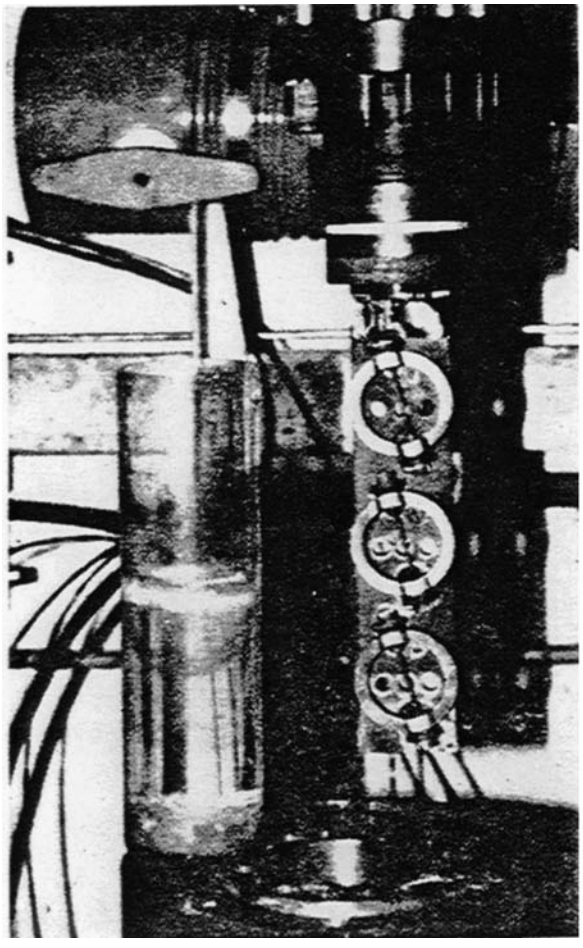


FIGURE 6 : View of the samples before closing the autoclaves

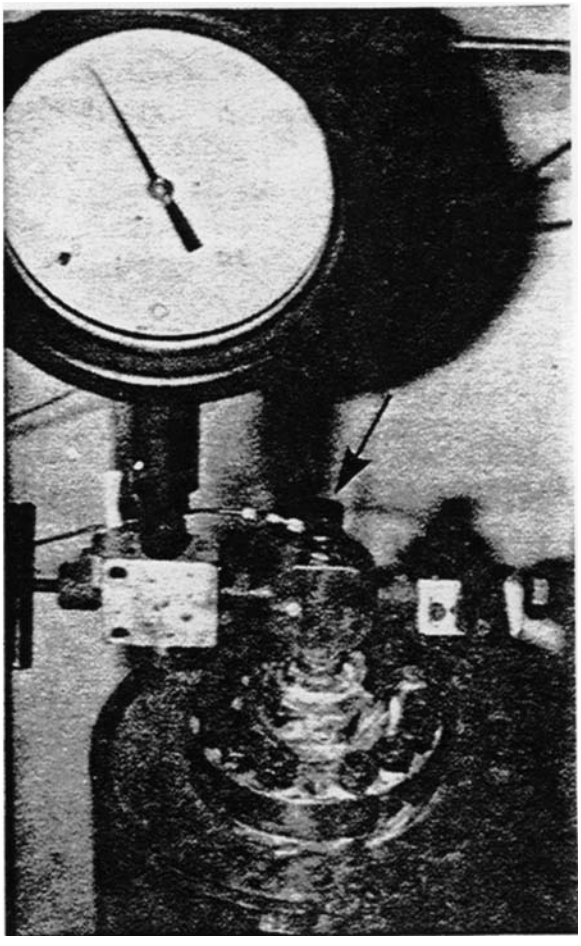


FIGURE 7 : View of the accelerometer for detecting the rupture of samples from the outside of the autoclave

Copyrighted Materials
Copyright © 1996 NACE International Retrieved from www.knovel.com

Paper No. 229–CORROSION/85

SPECIAL STAINLESS STEELS FOR APPLICATION IN NATURAL SOUR GAS EXPLOITATION SYSTEMS

RESISTANCE TO STRESS CRACKING IN ENVIRONMENTS CONTAINING CHLORIDES AND H_2S OF AUSTENITIC AND AUSTENO-FERRITIC GRADES

A. Desestret
Société UNIREC, Groupe USINOR
Centre de Recherches d'Unieux - B.P. 34
42701 FIRMINY (France)

E. Mirabal
Universidad Simon Bolivar
Caracas, Venezuela

D. Catelin, P. Soulignac
Société CREUSOT LOIRE
Division Tôles Fortes Creusot Marrel
B.P. 31 - 71208 LE CREUSOT (France)

ABSTRACT

The resistance to sulfide stress corrosion cracking of special stainless steels, austenitic, and duplex austeno-ferritic, was evaluated in various conditions, at temperatures up to 150°C (302°F) under 1 to 15 bar H_2S in the NACE TM-01-77 solution. The study of mechanical and electrochemical processes was undertaken in the duplex stainless steels: influence of mechanical twinning of the ferrite phase which causes strong local depassivations, and of the electrochemical processes, both anodic and cathodic. The first results seem to show the primary importance of the anodic dissolution process initiated by twinning of the ferrite phase, while cathodic hydrogen seems to exert a lesser influence, at least in most electrochemical situations studied here. Indeed, at this stage of the work, embrittlement by hydrogen cannot be ruled out, but it seems to play only a secondary role, at least at low pressures of H_2S and in the electrochemical situations obtaining in the conditions investigated. Increasing the temperature seems to increase very much the relative influence of the anodic dissolution process, but at high pressures of H_2S the participation of hydrogen can still be significant. In addition, one must take into account the complex influence of temperature increases on the mechanical twinning of the ferrite phase, which first becomes less important up to about 200°C (392°F), to augment again above. This can explain the better resistance of duplex stainless steels at 100°C and 150°C (212°F and 302°F), whereas austenitic steels become very sensitive to cracking. Better knowledge of the several processes involved in the cracking phenomena made thus possible a more precise formulation and design of the duplex stainless steels in such a way that the resistance to cracking is much greater at room temperatures, up to about 80% to 90% of the yield strength. A more precise control of metallurgical factors and of fabrication procedures have been shown to improve very markedly the resistance of industrial products, castings, rolled plates, and forgings. In the last case, the resistance in the transverse direction becomes about the same as in the longitudinal direction whereas in more conventional common hot-worked material, the transverse direction can be very sensitive to cracking.

INTRODUCTION

These last ten years, fields of sour natural gas have been more and more exploited although the gas may contain up to several parts percent of CO_2 and H_2S, with waters very rich in chlorides. This draws the attention back again to corrosion problems which had been much investigated in France in the late fifties and in the sixties when the gas field of Lacq was first put in operation.[1] It should indeed be mentioned that this deposit of sour (15% H_2S) gas was very probably the first to be commercially operated in an everyday manner. The favorable experience of 20 years so gained led us to try and investigate this important application for the material which had proved quite successful in the field of Lacq, namely the duplex austeno-ferritic stainless steel Uranus 50† (UNS 31803 + Cu 1.5%) (Cr 21/23 - Ni 5/8 - Mo 2/3 - Cu 1/2 - N ≤ 0.15-C ≤ 0.03) which was used to fabricate about 100 cast valves and chokes, and numerous wirelines.[1-2] To that aim, reference was made to NACE standards MR-01-75 and TM-01-77 as up to then the tests carried out were those of Société ELF-Aquitaine, in a very similar solution, but at pH 4.[3-5] Thus, experiments were done, mostly on cast materials, in compliance with Standard TM-01-77. Surprisingly, and at apparent variance with what was obtained at pH 4 and with the successful field experience, the first results turned out to be quite scattered and sometimes even poor.[6] We were thus led to undertake further investigations in order to understand the discrepancies between these mediocre test results and the very successful field experience, and also to better adapt and improve the design of the alloys in that respect.

The experiments were done in the solution described in Standard TM-01-77, at temperatures up to 150°C (302°F). At the higher temperatures, the pressure of H_2S was increased to 15 bar in order to maintain a high enough concentration in the solution. In all cases the tensile specimen used was the one specified as "sub-size" in the standard, except when wires were tested .

The influence of all the relevant metallurgical factors was thus reviewed and analyzed: composition, structure, and fabrication procedures. We investigated simultaneously: castings, forgings, rolled plates and bars, as well as highly cold-worked drawn wires. The cast metal exhibited in general a lower resistance than the wrought one. Rolled and forged products are more resistant in the longitudinal direction but can be quite sensitive to cracking in the transverse direction. Beside Uranus 50†, other duplex stainless steels were investigated: Uranus 45† N (UNS 31803) (Cr 21/23 - Ni 5/7 - Mo 2.5/3.5 - Cu 0 - N ≤ 0.15 - C ≤ 0.030), Uranus 52† N (UNS 32550) (Cr 24.5/25.5 - Ni 7/8 - Mo 2.5/3.5 - Cu 1/2 - N ≤ 0.20 - C ≤ 0.03), and Uranus 47† N (UNS 31200 + Mo 3%) (Cr 24.5/25.5 - Ni 7/8 - Mo 2.5/3.5 - Cu = 0 - N ≤ 0.20 - C ≤ 0.03). The latter two steels display an excellent resistance in very varied conditions. The fundamental phenomena were investigated in order to try and understand the observations summed up above: electrochemical processes, both anodic and cathodic. The former were assumed to be related to local depassivation and repassivation, while the latter could be presumed to cause hydrogen embrittlement of the ferrite phase. Special attention was given to local depassivation of this ferrite phase due to mechanical twinning, which had been investigated in previous papers and which had been to exert a very important influence.

In an earlier work it was found that the electrochemical conditions in which cracking can occur correspond in general to low potentials (ca -500 mV vs SCE), while the samples which stay at higher potentials (-100 to -200 mV vs SCE) usually do not crack.[6] At the lower potentials, the influence of cathodic hydrogen could be assumed, while in the higher range of potentials the anodic processes could be thought to be rate determining. It had been also shown that cracking phenomena of duplex stainless steels seem to involve complex mechanical and electrochemical couplings between the two phases, ferrite and austenite. In many cases the former can initiate cracks by twinning up to high temperatures. This tendency of ferrite to mechanical twinning is markedly enhanced by heat treatments which cause various phases to precipitate, with consequent hardening, at temperatures 300°C (572°F) and 900°C (1,652°F).[6,8,10-11]

TESTS ON CAST DUPLEX STAINLESS STEELS

Figure 1 sums up the results of tests carried out according to NACE Standard TM-01-77 on fourteen heats of the cast steel URANUS 50 M† (UNS 31803 + Cu 1.5 %) (Cr 21/23 - Ni 5/8 - Mo 2/3 - Cu 1/2 - C ≤ 0.03 - N 0.1/0.2). The scatter is obviously quite important, as the threshold stress which does not cause cracking in one month can vary between 200 MPa and 300 MPa, or 50% and 70% of the average yield strength, for compositions within the normal composition range of the alloy. Let us remark the poor resistance of heats which contain

† Trademarks registered by Compagnie Français des Forges and Fonderies (UNISOR Group) and Sté CREUSOT LOIRE, Division Creusot-Marrel.

between 40% and 50% of ferrite. This important scatter could perhaps be in relation to the type of specimen: all these data were obtained with the "sub-size" tensile test-piece, as described in NACE standard TM-01-77, whereas a few comparison tests done with the standard specimen seemed to give less scattered and significantly longer times to rupture, in such a manner that the threshold stress could then well correspond to the highest value obtained with "sub-size" test-pieces, i.e. 70% of the yield strength minimum.[4] For instance, for a given heat containing 30% ferrite, a sub-size tensile specimen cracked in 50 hours under a stress of 385 MPa, or about 95% of the yield strength, and at 355 MPa, or 80% of the yield strength, one specimen cracked in 110 hours while others survived for more than 1,000 hours without rupture. Contrary to these results, a standard test-piece machined from the same heat and stressed at 400 MP, that is very near 100% of the yield strength, cracked only after 700 hours. These discrepancies could be related to the coarse micrographic structure of cast duplex stainless steels, with quite often very large grain sizes. The poor resistance of heats containing 50% of ferrite shows high contents of this phase to be detrimental, and this leads to think that such dangerous situations can exist accidentally, locally, on the smaller specimens, due to large grain sizes. This could well explain the important scatter observed in our tests and in the threshold stresses thus inferred. In particular, the four obviously erratic results shown in Figure 1 with a question mark (?), could be accounted for in this manner as they are situated within the scatter band of heats containing about 50% of ferrite, although these latter specimens came from a heat found to contain between 25% and 29% of ferrite by macroscopic magnetic measurements. These arguments are bolstered by previous data which showed cracking of duplex stainless steels to be often initiated by mechanical twinning of the ferrite phase, which can therefore be thought to be sometimes the cause of cracking of the steels.[6-8] Detailed investigations of the cracking processes of austeno-ferritic stainless steels have indeed brought to light complex mechanical and electrochemical coupling phenomena between ferrite and austenite which can be strongly accelerated by the mechanical twinning of stressed ferrite, as already mentioned.[9] Now, on the basis of such know-how, it has then been possible to design "optimized" alloys, within the normal ranges of metallurgical variables for a given type (composition, metallurgical processing, ...) in such a way that resistance to cracking is increased in a very important manner. Figure 1 shows an example of the much improved resistance so obtained, as an "optimized" heat of cast Uranus 50 M has been found not to crack for periods longer than 1,000 hours under stresses as high as 85% or even 90% of the yield strength. Let us remark that this excellent resistance was observed on "sub-size" test-pieces which can be thought to be highly susceptible, much more so than the "standard" specimens, as discussed above. A higher grade duplex stainless steel was also "optimized" in a like manner: Uranus 52 M (Cr 25 - Ni 8 - Mo 3 - Cu 1.5 - C $\leq$ 0.03 - N $\leq$ 0.20). Sub-size specimens of this alloy were stressed at 80% and 100% of the yield strength (400 and 540 MPa): neither sample had cracked when the tests were discontinued after more than 1,000 hours. This last result is all the more remarkable as the ferrite content was about 50%, which shows that in "optimized" duplex stainless steels, ferrite content can be increased to that level without deteriorating significantly the resistance to cracking, as it is the case with "conventional" heats, as described above.

Test Under Cathodic Polarization

As it was mentioned in a previous paper, the electrochemical potential of the samples was continuously monitored during the tests.[6] It was thus found that the samples could exhibit potentials which were situated in two different regions: the first region is above -350 mV vs SCE, usually from -200 to -300 mV vs SCE, in which case cracking does not occur or occurs only after very long periods of time, while samples giving potentials lower than -300 or -350 mV vs SCE, and sometimes as low as -450 or -500 mV vs SCE, are much more sensitive to cracking. It may however happen that the most resistant steels can withstand these latter seemingly aggressive conditions. In view of this, additional tests were carried out on optimized material which consisted in imposing potentiostatically the most severe cathodic potential of -455 mV vs SCE, sometimes after a previous test without any applied polarization, at the freely corroding potential. The samples, stressed at 80% of their yield strength some of which had already lasted about 1,000 hours, were potentiostatically brought down to the cathodic potential of -455 mV vs SCE: cracking occurred then in 105, 179, and 731 hours. Thus, in these very aggressive and severe conditions, the shortest time to rupture is at least equal to and on the hole longer than the longest lifetime of freely corroding non-optimized specimens, as Figure 1 shows. The polarization current was continuously monitored during the tests, and this showed that the shortest time to rupture was related to polarization currents in the anodic direction, with peak bursts as high as 5 milliamperes. On the contrary, very low anodic currents, for instance 10 microamperes, or cathodic currents, which were observed to be as high as 1

milliampere, were measured on specimens that survived the longest times. These observations already suggest that anodic processes are very important in the conditions of the tested solution.

Influence of the test temperatures 90°C/100°C (194°F/212°F)

As it has been previously mentioned, tests were also carried out in the NACE TM-01-77 solution at temperatures up to 90°C or 100°C (194°F or 212°F) under a pressure of H_2S up to 15 bar. The resistance of the austeno-ferritic steel were not found to deteriorate and the threshold stresses observed were very similar to that indicated in Figure 1. This can be explained by the improved resistance of the ferrite phase to twinning when temperature increases as well as by a probable decrease of hydrogen embrittlement effect on that phase.[8,12]

TESTS ON FORGED DUPLEX STAINLESS STEELS

About ten industrial heats of Uranus 50 type (UNS 31803 + 1.5% Cu) (Cr 21/23 - Ni 5/7 - Mo 2.5/3.5 - Cu 1/2 - C ≤ 0.03 - N ≤ 0.15) of austeno-ferritic stainless steel were investigated in the product form of forged billets, the dimensions of which varied approximately between 150 to more than 300 millimeters, about square or rectangular. The forged products contain usually more ferrite than the cast material, i.e., 40% to 50%. In all cases, the longitudinal and transverse directions were very well defined as the forging operations had been done in one direction only, starting from the ingot. Sub-size tensile specimens were cut in both directions, along the length of the billets, and across.

These heats were tested according to the procedure described in NACE Standard TM-01-77: the results are summed up in Figure 2. As these results are much more consistent and very much less scattered than in the case of the cast material, it is quite possible to draw curves showing the variation of the time to rupture with the stress, including the different data from the several heats tested. This figure brings again forward the great importance of designing the several metallurgical factors involved in the processing: in spite of the fact that all the tested heats were comprised within the normal composition range, very marked differences are apparent. When a close metallurgical control of the processing has been exercised, resistance to cracking is nearly as good in both longitudinal and transverse directions, whereas the transverse direction can be very prone to cracking when the metallurgical processing is done more loosely: in this latter case, the threshold stress can be as low as 10% of the yield strength, or about 40 MPa, while a proper control of the processing brings this threshold stress up to 80% or 90% of the yield strength, practically on the level of the threshold stress determined for the longitudinal direction. It must be remarked in addition that the optimized metallurgical processing improves also the resistance in the longitudinal direction, albeit in a lesser degree as the more common material is already quite resistant, with a threshold stress at about 75% of the yield strength.

The following examples give actual values for the threshold stress determined on three typical optimized heats of Uranus 50 (UNS 31803 + 1.5% Cu) and Uranus 45 N (Cu ≤ 0.1) (UNS 31803).

	Direction of Test-Piece	Yield Strength	Threshold Stress No Rupture After More Than 1,000 Hours	
		MPa	MPa	% of Yield Strength
		URANUS 50 (UNS 31 803 + 1.5% Cu)		
1)				
	Longitudinal	485	485	100
	Transverse	436	390	80
2)				
	Transverse	509/539	484	90/95
		URANUS 45 (UNS 31 803)		
1)				
	Longitudinal	477/512	438	90
	Transverse	487/495	429	90

Test Under Cathodic Polarization

The same test as that described in the case of cast steels was done on an optimized transverse sample; the sample had first been stressed at 80% of the yield strength and had not cracked after 1,168 hours in freely corroding conditions. The electrochemical potential stayed around -200 mV vs SCE, always above -300 mV vs SCE. At the end of this preliminary test, the potential was brought down to -455 mV vs SCE potentiostatically. A slight cathodic current was measured, of a few microamperes, with very frequent bursts the cathodic direction, up to 10^{-4} Amperes, and only some rare similar anodic peaks. The test-piece was still standing intact after 744 hours when the experiment was discontinued. This good resistance suggests again that cathodic charging at -455 mV vs SCE is not too harmful for an optimized austeno-ferritic steel.

TESTS ON PLATES DUPLEX STAINLESS STEELS URANUS 45 N AND URANUS 47 N

Tests were carried out on material cut from plates hot rolled to the dimensions 13,000 x 2,800 x 5 to 12 mm, from several heats of duplex stainless steels, types Uranus 45 N and Uranus 47 N.

Uranus 45 N (UNS 31 803)

Cr 21/23 - Ni 5/7 - Mo 2.5/3.5 C ≤ 0.03 - N 0.1/0.2 - Ferrite content: ca - 50% - Y.S.: 540 to 570 MPa (Tables Ia & Ib).

Tests were first done in the NACE TM-01-77 solution at 25°C (77°F) and 1 atmosphere H_2S: the threshold stress which does not cause rupture after durations of 1,000 hours and more, is about the same in the two directions, i.e., 460 MPa which is around 80% of the yield strength. When the tests are done in the NACE TM-01-77 solution at the temperature of 90°C (194°F) under a pressure of 15 bar of H_2S, the threshold stress is a little lower in the transverse direction than in the longitudinal direction: 400 MPa or about 70% of the yield strength in the first case against 450 MPa, or around 80% of the yield strength, in the second. The increase in temperature causes only a very slight decrease in the resistance of the duplex alloy.

Likewise welding does not decrease the resistance, as is shown by the results of Table Ib: the threshold stress remains at about 75% or 80% of the yield strength for the two types of welding processes evaluated, MIG and TIE.

Uranus 47 N (UNS 31 200 + 3 % Mo)

Cr 24.5/25.5 - Ni 7/8.5 - Mo 2.5/3.5 - C≤ 0-03 - N 0.15/0.20 - Ferrite content: ca 50% - Y.S.: 600 to 637 MPa (Tables IIa & IIb).

The results of Table IIa show that at 25°C (77°F) the threshold stress is very probably higher than 480 MPa, or 80% of the yield strength, both in the longitudinal and transverse direction. When the conditions are made more aggressive, at 90°C (194°F) under a pressure of 15 bar H_2S, the resistance is only a little lower as the threshold stress remains at about 75% or 80% of the yield strength, at 480 MPa.

As for Uranus 45 N, welding does not deteriorate the resistance of Uranus 47 N plates. Table IIb shows that welded samples resist at a stress of 460 MPa, that is about 75% of the yield strength.

TESTS ON COLD WORKED MATERIAL (WIRES, BARS)

Tests at 24°C (75°F) and 1 bar H_2S

Seven different heats and lots of cold worked Uranus 50 wires have been tested at room temperature in the NACE TM-01-77 solution (Table III).

Figure 3 shows the heat containing 47% ferrite to be less resistant, with a threshold stress (σ 720 h) at about 45% of the yield strength (ca 550 MPa), whereas the other heats containing about 30% ferrite are more resistant in that respect, as their "minimum" threshold stress is about 60x of yield strength, about 540 MPa. These data allow to compare the resistance of Uranus 50 cold worked wires and that of AISI 316 cold worked wires. At 24°C (75°F), resistance of cold-worked AISI 316 is very similar to that of cold worked Uranus 50. It must be remembered that in the fully annealed condition AISI 316 is resistant up to its yield strength, whereas annealed

Uranus 50 can be more sensitive to cracking when some metallurgical precautions (optimized heats) are not taken as we saw above.

Figure 4 sums up the main results obtained at room temperature on Uranus 50 and AISI 316. This figure shows very clearly that cold worked AISI 316 and Uranus 50 behave in a very similar manner at 24°C (75°F). While austenitic stainless steels such as type AISI 316 (L) are fully resistant at stresses up to yield point when tested by the NACE TM-01-77 standard procedure, when they are solution annealed, the data given above show that cold work can reduce very significantly this resistance.[3]

Duplex stainless steels exhibit resistances which can vary widely when the fundamental metallurgical features of the alloys are changed, as it was mentioned above: composition, structure, etc... i.e., ferrite content and heat treatment. For instance, at 24°C (75°F), duplex stainless steels can be less resistant than AISI 316 (L): wires fabricated from standard Uranus 50 heats can crack at stresses higher than 75% of the yield strength.[6] It should however be remembered that "optimized" compositions within the range of the Uranus 50 offer a resistance at 24°C (75°F) about equal to that of AISI 316. We shall now see that the Uranus 47 composition is likewise very resistant, as the following results show:

Tests on Uranus 47 (UNS 31 200 + 3 % Mo)
Yield Strength: 1,367 MPa or 198 Ksi
Ultimate Tensile Strength: 1,677 MPa or 243 Ksi

(1) First test
Applied stress: 75% of Y.S. = 1,022 MPa or 148 Ksi

(a) at free corrosion potential, i.e., from -175 to -150 mV/SCE
1,085 hours, not failed
The sample was then polarized to cathodic potentials, successively at -455 and -500 mV/SCE.

(b) -455 mV/SCE
Cathodic current varied between 0 and 10 microamperes.
360 hours, not failed

(c) -500 mV/SCE
The cathodic current was in general lower than 10 microamperes with spurts in the anodic direction of about 50 to 100 microamperes.
980 hours, not failed

Total duration of test:
- 1,085 hrs at -175/-150 mV/SCE (free corrosion potential)
- 360 hrs at -455 mV/SCE (cathodic)
- 980 hrs at -500 mV/SCE (cathodic)

2,425 hrs at stress: 75% of Y.S. (20°C [68°F])

(2) Second Test
Applied stress: ca 90% of Y.S. = 1,227 MPa or 178 Ksi

(a) At free corrosion potential, i.e., from -250 to -150 mV/SCE
1,085 hours, not failed
Sample was then polarized to cathodic potentials, successively -455, -500, and -700 mV/SCE.

(b) -455 mV/SCE
Cathodic current was around 10 microamperes with spurts both in the anodic and cathodic directions of about 20 microamperes.
360 hours, not failed

(c) -500 mV/SCE
Cathodic current was about same as above (2b).
650 hours, not failed

(d) -700 mV/SCE
Polarization current was strongly cathodic and varied around 20 milliamperes.
330 hours, not failed

Total duration of test:

— 1,085 hrs at -250/150 mV/SCE (free corrosion potential)
— 360 hrs at -455 mV/SCE (cathodic)
— 650 hrs at -500 mV/SCE (cathodic)
— 330 hrs at -700 mV/SCE (cathodic)

2,425 hrs at stress: 90% of Y.S. (20°C [68°F])

These tests show that Uranus 47, cold worked, resist cracking even under quite strong cathodic polarization, and stressed up to yield strength.

Tests at 50°C (122°F), 75°C (167°F), and 90°C (194°F) under a pressure of 1 at. of H_2S

In spite of the decrease of H_2S concentration in the solution, these conditions turned out to be quite aggressive, particularly for cold worked AISI 316. Figure 4 shows a marked decrease in the resistance of cold worked AISI 316 wires, whereas the Uranus 50 cold worked wires exhibited the same behavior as that observed at 24°C (75°F).

Tests at 50°C (122°F) and 75°C (167°F) under 15 bar (217 psia) H_2S

A wire sample of Uranus 47 N was tested in the following conditions: applied stress: ca 80% of Y.S. (20°C [68°F]) = 1,095 MPa or 159 Ksi.

After 1,610 hours the sample was still standing and the temperature was then increased to 75°C (167°F), at which temperature the wire had not failed after 1,000 hours.

50°C (122°F), 15 bar H_2S : 1,610 hours
75°C (167°F), 15 bar H_2S : 1,000 hours

Total:

(50°C(122°F) + 75°C(167°F), 15 bar H_2S) : 2,610 hours not failed at 80% Y.S. (20°C [68°F])

Comparison tests were done on AISI 316 and Uranus 50 wires

Applied stress ca 80% Y.S. (20°C [68°F])	Duration
AISI 316 848 MPa or 123 Ksi	1,350 hrs NF
UR. 50 925 MPa or 134 Ksi	1,000 hrs NF

The test on Uranus 50 had to be stopped because of a leakage in the cell... At 50°C (122°F) the three steels are quite resistant.

Similar tests carried out at 75°C (167°F) showed wires of AISI 316 to have initiated cracks at a stress as low as 50% of yield strength, whereas wires of Uranus 50, Uranus 47, and Uranus 50 had not failed after more than 1,000 hours.

It would thus seem that between 50°C and 75°C (122°F and 167°F) the sensitivity of cold worked AISI 316 increases markedly, whereas the two duplex stainless steels Ur 50 and Ur 47 maintain their resistance, as does also Uranus B6.

Tests at 90°/100°C (194/212°F) under 15 bar (217 psia) H_2S

Test-pieces from AISI 316 and Uranus 50 cold-worked wires were tested in these conditions at a stress of about 85% of the yield strength determined at 20°C (68°F). The sample of Uranus 50 was not failed after 700

hours when the test was discontinued, whereas four identical samples of AISI 316, similarly stressed, all cracked in less than 20 hours, although the absolute stress was very significantly lower. Table IV sums up these results. It should be remarked that 85 % of the (20°C [68°F]) yield strength corresponds to at least 100 % of the Y.S. at 100°C.

Consequently, it must be concluded that at 90°/100°C (194°/212°F), in sharp contrast to what obtains at 24°C and 50°C (75°F and 122°F), AISI 316 is much less resistant to cracking than the duplex steel Uranus 50. The results of Table IV show in addition that at 100°C (212°F) the resistance of cold worked Uranus B6 is quite good, as good as that of cold worked Uranus 50.

Tests at 150°C (302°F) under 15 bar (217 psia) H_2S

AISI 316, Uranus 86, Uranus 50, and Uranus 47 N were tested in the above conditions, at the stresses indicated in Table V. This Table V shows that AISI 316 can be resistant only when the stress is lowered to 30% of the yield strength at 20°C (68°F), or 50% of yield strength at 150°C (302°F), i.e., 315 MPa or 46 Ksi. On the contrary, the two duplex steels exhibit an excellent resistance: cold worked Uranus 50 did not fail at stresses as high as 75% Y.S. (20°C [68°F]) or 124% to 162% of Y.S. (150°C [302°F]), i.e., 880 or 890 MPa or 130 Ksi.

Likewise cold worked Uranus 47 N did not crack at stresses at least equal to the yield strength at 150°C (302°F), or equal to 75% of the yield strength at 20°C (68°F), i.e., 1,022 MPa or 148 Ksi. Contrary to this, the resistance to cracking of cold worked Uranus B6 is quite markedly decreased, as samples were observed to fail at a stress as low as 26% of the yield strength at 20°C (68°F), or 75% of the yield strength at 150°C (302°F): this behavior is similar to that found for cold worked AISI 316, reported above.

These tests brings to light the much better resistance to cracking of the duplex stainless steels, as compared to austenitic grades, even an highly alloyed austenitic alloy, i.e., Uranus B6 (UNS N 08 904).

The following conclusions can be drawn from the results described above, from tests at low and high temperatures, which are summed up in Table VI.

1. Cold worked AISI 316 (austenitic) is relatively resistant at 24°C (74°F) and 50°C (102°F), but becomes very sensitive to cracking above 50°C, at 75°C (167°F), 100°C (212°F), and 150°C (302°F).
2. Cold worked Uranus B6 (austenitic), is very resistant at temperatures up to 100°C (212°F), but may be sensitive to cracking at higher temperatures for instance 150°C (302°F).
3. Uranus 50 (duplex) cold worked wires are very resistant at temperatures above 24°C (74°F). At 24°C their resistance can be less than that of AISI 316 if the steel composition and metallurgy has not been "optimized". In fact, Uranus 50 wire lines have been in use since 1969 in the sour (15% H_2S, gas field of Lacq in France, where they have shown excellent resistance provided they were free of surface defects, such as micro-cracks due to poor processing during fabrication.[2] The above results are in agreement with this good field experience. Cold worked Uranus 47 N (duplex) exhibits an excellent resistance at all temperatures between 24°C and 150°C (302°F). In addition, at 24°C, the steel is resistant also under cathodic polarization, which means it is fairly resistant to hydrogen.

INVESTIGATIONS ON THE CRACKING PROCESSES

In order to better understand the results reported above and the apparently intricate behavior of the austeno-ferritic stainless steels, investigations have been carried out on these duplex compositions, and on ferritic alloys the composition of which was as similar as possible to that of the ferrite phase. A typical composition for the latter is the following: C = 0. 004, Mn = 0.4, Si = 0.6, S = 0.004, P = 0.009, Ni = 6, Cr = 25, Cu = 0 or 1.5, N = 0.010.

The composition with Cu = 0 corresponds to the ferrite phase of type Uranus 45, and the composition with Cu = 1.5 corresponds to the ferrite phase of Uranus 50. These last alloys were laboratory alloys melted in small ingots of about 10 kilograms, forged and rolled as small bars.

The duplex materials were taken from industrial products: plates 5 to 12 mm thick for Uranus 45N and Uranus 47N, and forged billets for Uranus 50. Tensile specimens were machined both along the rolling direction (longitudinal) and in the perpendicular direction (transverse).

Study of the Duplex Stainless Steels

Constant extension rate tests were done at previous speeds from 10^{-1} s^{-1} down to 10^{-8} s^{-1}: fast elongation rates were used to evaluate the influence of depassivation by straining which ruptures the passive film, while slow rates were employed in order to obtain precise criteria on the kinetics of stress cracking, which could complement the results of the constant load tests described above.

Preliminary slow strain rate tests showed that maximum sensitivity for cracking is observed at very slow strain rate i.e., below 10^{-6} s^{-1}, at about 5.10^{-7} s^{-1} or at 5.10^{-8} s^{-1}. It should indeed be remarked that these very slow strain rates, not very different from creep rates of austenitic stainless steels, can cause the austenitic grade AISI 316 L to crack as it can be seen on Figure 5: when strained at 5.1 x 10^{-7} s^{-1} this steel does not form cracks and the stress-strain curve is practically identical to that determined in non aggressive environments, while straining at 5 x 10^{-8} s^{-1} causes a marked deterioration which is due to the occurrence of cracks. This experimental technique comes out as more aggressive and sensitive than the constant load test. Three duplex steels were then evaluated, Uranus 45N, Uranus 50, and Uranus 47N, some heats having been fabricated following the optimum procedures already mentioned above. Uranus 47N strained at 4.10^{-7} s^{-1} can be observed to withstand cracking as well in the transverse direction as in the longitudinal. Uranus 45 exhibits a greater difference between the two kinds of samples, even if its resistance looks still fair. These results are in good agreement with those of the constant load tests, where Uranus 47N was generally found better than Uranus 45 N. At this straining rate, 4 x 10^{-7} s^{-1}, Uranus 47 and AISI 316 L behave in a like manner, as regards particularly both elongation and reduction of area which are quite important, higher than those observed on Uranus 45 samples, which are however still good. Lowering the straining rate down to 5.10^{-8} s^{-1} damages markedly 316 L which gives then poor elongations and reductions of area even in the longitudinal direction. In the same condition and for the same type of transverse sampling, Uranus 50 comes out better, as its transverse direction resists as well (or as poorly !) as the longitudinal direction of 316 L. However, when Uranus 50 has been produced by the best procedures, the transverse direction so optimized turns out to be quite resistant, giving elongations of 15% to 19%, and reductions of area around 22%, which compares very favorably with the longitudinal direction of the purely austenitic grade 316 L.

Constant extension rates tests were also done at 90°C (194°F) under a 15 bar pressure of H_2S. Because of the higher aggressivity of this environment, the "higher" straining rate of 4.10^{-7} s^{-1} proved to be very sensitive and discriminating, as Figure 6 shows: the test piece of 316 L, cut lengthwise, exhibits a very poor resistance with an elongation of only a few per cent while the reduction in area is practically nil. The comparison with Uranus 45 and Uranus 47 evidences the better resistance of these latter alloys which display a much higher energy of rupture and reductions of area, between 5% and 16%. Contrary to what was observed at 25°C (77°F), the sample taken in the transverse direction of the Uranus 47 plate exhibits a lower resistance than the sample cut along the length. It should be recalled that constant load tests did not cause cracking of any of these two test pieces.

The constant extension rate test proves then to be a very sensitive and severe method for comparing the several alloys studied. It can be thought that in addition to the criteria already mentioned, energy for rupture, reduction of area, elongation, the maximum stress observed on the stress-curve could give an indication of the maximum stress an alloy can withstand without cracking in the corrosive environment. On the basis of such a criterion, it could be anticipated that AISI 316 L is very prone to cracking at 90°C (194°F), under a pressure of 15 bar of H_2S, which could be expected, but also that cracking at 25°C (77°F) under 1 atmosphere of H_2S is possible, as the maximum stress of the stress-strain curve recorded at the slowest rate, 5.10^{-8} s^{-1}, is not far from the yield strength, i.e., 210 MPa. Let us point out again that this extension rate is not too far from the creep rate of usual stainless steels. The maximum stress observed on the duplex steels coupons are on the contrary markedly higher than the yield strength, except in the case of the transverse direction of the non-optimized, more common, Uranus 50 specimen. But, when this alloy has been properly processed, the transverse test-pieces afford maximum stresses which are above 600 MPa, whereas the yield strength is between 450 and 500 MPa. It should be recalled here that a transverse test-piece of this optimized Uranus 50 material withstood a stress of 90/95% of yield strength in a constant load test without cracking for about 1,500 hours (see § III). The curves recorded at 90°C (194°F) (Figure 6) are much more sharply outlined, and it is obvious that the austenitic grade 316 starts cracking at stresses much lower than the yield point, i.e., 141 MPa while the duplex steels test-pieces initiate cracking only when the stress is above 400 MPa.

Study of the Ferrite Phase

The behavior of the ferrite phases has been studied, first by slow strain rate cracking tests, then by fast depassivation straining which does not initiate cracking but general corrosion, because of the mechanical rupture

of the passive film over the whole surface of the specimen.

Figure 7 exhibits stress-strain curves obtained with two synthetic alloys corresponding to the ferrite phase of Uranus 50, at the straining rate of 10^{-6} s^{-1}, in three different solutions:

A: the solution indicated in NACE standard TM-01-77, NaCl 5% + CH_3 COOH 0.5%, pH 3, H_2S : 1 atmosphere at 25°C (77°F)

B: the same solution as in A, but without H_2S, into which nitrogen (or argon) was instead bubbled continuously for deaeration

C: a solution of 5% NaCl, not acidic, at neutral pH (7), under nitrogen bubbling (or argon).

In solution A, the two samples tested cracked very rapidly, as soon as mechanical twinning occurred, which can happen at very low stresses and strains, as shown by the second specimen. The electrochemical potential was quite low in both cases, about -500 Mv vs SCE, which agrees quite well with the potentials observed on samples most likely to crack in the constant load tests.

In solution B, the two samples tested displayed very different spontaneous electrochemical potentials, due to differing random chemical conditions: the first one, at -600 mV vs SCE, cracked as soon as mechanical twinning appeared, in a way very similar to that already observed in solution A, while the second one, situated between 0 and 100 mV vs SCE, was not cracked in spite of the profuse mechanical twinning which took place, as it is evidenced by the numerous small indentations on the stress-strain curve. Obviously, in the latter electrochemical situation, twinning cannot initiate cracks in the ferritic alloy.

In solution C, none of the two test-pieces did crack, although the first one displayed a strong twinning tendency and an electrochemical potential of -650 mV vs SCE. Notwithstanding this very low potential, the strong mechanical twinning was unable to cause cracking, very probably due to the neutral, non acidic, pH of the solution.

Let us remark in tests B2 and C2 the steep fall of the potential when the test-pieces broke. Similarly, in test Cl, a very important and rapid drop of the potential took place when the specimen was first strained. These drops in potential can be interpreted as caused by the activation, or depassivation, of the metal, related to the rupture of the passive film, or to the impossibility for this film to reform or to heal fast enough. These experiments show indeed that the rupture of the passive film is also in the case of solution A the perquisite for cracking to happen. At the slow strain rate used here the passive film breaks in discrete locations situated on twinning lines, as shown in previous papers, from where cracks can propagate when the chemical and electrochemical conditions so allow.[7-8]

In order to evaluate the influence of H_2S on the cracking processes, experiment C was complemented by another experiment which was begun in the same manner as C2, that is straining a sample of the ferritic alloy at the rate of 1.10^{-6} s^{-1} in the pH 3 solution containing 5% NaCl and 0.5% CH_3COOH, with pure argon in place of H_2S (see Figure 8).

After 17.5 hours, when elongation was about 7%, and as numerous jagged indentations caused by mechanical twinning were clearly visible on the stress-strain curve, H_2S was bubbled into the solution, instead of argon. Cracking followed then rapidly, after 1.7 hours, whereas in the absence of H_2S, cracking had not occurred as shown by experiment C2. Exactly coincident with the introduction of H_2S, and before the drop in stress, the electrochemical potential fell from ca -200 mV vs SCE down to -400 or -600 mV vs SCE: we recognize here the two domains of potential observed in the deadload tests. The higher one was found to be related to a very low probability of cracking, while the lower potentials were measured on specimens most likely to break. From the experiment of Figure 8, E2-4, it is obvious that such a situation arises when the passive film has been ruptured in the presence of H_2S, in the chloride solution of pH 3. But experiment Bl shows the presence of H_2S is not absolutely necessary for the onset of cracking provided the electrochemical potential is at very low values, i.e., -450 mV vs SCE, or below, and the pH very low.

From these results, it can be concluded that the rupture of the passive film is the necessary condition for cracking to initiate, but the electrochemical conditions must also be such as to make possible propagation due to the impossibility of repassivation of the regions at which the passive film has been locally damaged by twinning. It must be pointed out that if the environment is so aggressive so as to cause general depassivation all over the metal, general corrosion can set in instead of localized corrosion, i.e., cracking. But this last situation is possible only if hydrogen embrittlement does not come into play as this can also cause cracking of ferritic alloys. Now, in the low potentials situation, hydrogen discharge is quite possible and the combined effects of anodic active dissolution and of hydrogen discharge could account for cracking.

Therefore, we endeavored to check these assumptions by carrying out experiments on the ferritic alloy polarized at -480 mV vs SCE or at -242 mV vs SCE. In the first case, cracking occurs, but not at the second higher potentials, as we saw above. The two tests consisted in depassivating rapidly the potentiostated samples in order to break completely the passive film all over the surface. In these conditions no localized corrosion, or cracking can occur, but only general corrosion, unless the influence of hydrogen is very rapid and important. The fast straining rate, chosen on the basis of earlier experiments, was 10^{-2} s^{-1}. The solution was the standard NACE TM-01-77 solution with H_2S at 25°C (77°F). Figure 9 shows the results of the two tests: in test B, at -242 mV vs SCE, as it could be expected, fast straining causes a marked increase of the polarizing current in the anodic direction: film rupture makes possible a strong acceleration of the anodic dissolution process. But, more surprisingly, an increase of the polarizing current in the anodic direction was also observed when the sample was set at the lower potential, -480 mV vs SCE, at which potential the polarizing current was cathodic before straining. It can consequently be concluded that also at the last tested potential, the main influence is due to the anodic dissolution process: hydrogen very probably discharged at this potential seems to play only a secondary role. But, although secondary, this role may not be minor and negligible as suggested by experiment E2-4 of Figure 8 above. However, the acceleration by straining of the cathodic process of hydrogen discharge is obviously less important than that of the anodic dissolution process.

CONCLUSIONS

The different results reported above can be summarized in the following manner:

1. High ferrite contents can be detrimental as regards the resistance of austeno-ferritic steels to stress corrosion cracking. Previous investigations have indeed shown that the ferrite phase can sometimes initiate cracking due to its tendency to mechanically twin when stressed, or more exactly, strained.
2. It is quite possible to minimize to a large extent this detrimental influence by designing properly the austeno-ferritic alloys and by controlling closely the several processing operations down to the finished products. It is thus possible to tolerate rather high ferrite contents, around 50% which makes possible to design alloys the yield strength of which is high, i.e., higher than 400 MPa (58 Ksi) up to about 600 MPa (87 Ksi), while retaining an excellent resistance to corrosion in general, and particularly to stress corrosion cracking.
3. The test described in NACE Standard TM-01-77 seems to be a very severe and discriminating method to evaluate the resistance of duplex stainless steels and to check their metallurgical conditions, making possible to compare products in a seemingly valid manner.
4. Cold work, at least up to about 20%, does not seem to decrease very much the resistance of duplex stainless steels, contrary to what is observed with the austenitic grades such as AISI 316 (L).
5. Temperature increases up to 150° or 200°C (302° or 392°F) seem to increase the resistance of the duplex stainless steels, even when not optimized, of the usual common types. In sharp contrast to this, austenitic grades are very much deteriorated
6. Welding does not deteriorate much the resistance to stress corrosion cracking provided it is done with a close control of the welding processes and procedures.

These observations can be accounted for on the basis of current knowledge on the several phenomena involved. First of all, it must be kept in mind that duplex austeno-ferritic stainless steels are aggregates of two phases, austenite and ferrite, and that the properties of this aggregate are not necessarily the simple sum of the properties of both phases, due to complex interactions between them. Now, on the basis of the current knowledge, the following interpretations can be offered to try and explain the cracking phenomena of duplex stainless steels in the TM-01-77 solutions:

1. Both phases can initiate cracking depending upon the conditions of temperature, and the chemical or electrochemical conditions
2. Mechanical twinning of ferrite can play an important role because of its important effect of local rupture of the passive films, which makes possible, first, a strong acceleration of the localized anodic dissolu-

tion process, and probably also, but in a lesser degree, the discharge and entry of hydrogen.

3. The good resistance of the duplex stainless steels must be ascribed to complex interactions between the two phases: mechanical interactions, as ferrite mechanically strengthens the aggregate, while austenite bears most of the stress, or more exactly, the strain, and electrochemical interactions due to favorable galvanic couplings between the two phases. In addition, it may be surmised that austenite can act as an hydrogen trap, affording thus protection in that respect to ferrite which is much more sensitive to hydrogen. When only limited amounts of hydrogen are discharged, this protection can probably be quite effective: such a situation seems fortunately to obtain in the chloride solutions containing H_2S we have tested, in the electrochemical conditions we found to exist.
4. It is possible to take advantage of these complex interactions when designing duplex stainless steels in order to set the best resistance to the several types of corrosion, and particularly to stress corrosion cracking.

Duplex stainless steels containing Cr, Ni, Mo, and also Cu, exhibit in a general manner better mechanical properties and a better resistance to corrosion than the conventional austenitic stainless steels of the AISI 300 series, including type 316 or even more alloyed steels. Copper additions are made in steels used in very aggressive environments, such as acidic chloride solutions, particularly with the presence of H_2S, as this increases resistance to general and crevice corrosion. The reasons for these better properties are complex and must be fully understood in such a way that manufacturing procedures can be closely controlled in order to achieve and maintain the best properties and avoid pitfalls which could deteriorate these alloys.[6-13]

The research work thus carried out to investigate the cracking processes led to a better understanding of the respective role of the two phases, ferrite, and austenite, and of the complex mechanical and electrochemical couples which are operative, and which can exert widely varying influences depending upon the different possible mechanical and/or electrochemical situations. Because of variations in these situations, and also in the metallurgical conditions of the duplex steels, resistance to corrosion and particularly to stress corrosion cracking can vary very much. The important influence of the ferrite phase on these variations has been shown, and earlier work brought to light the importance of precipitations which can occur in the ferrite phase during heat treatments.[6,8-11] Further investigations have shown the cracking processes of duplex stainless steels to be determined by both the anodic and cathodic coupled half-reactions of the overall corrosion reaction. Mechanical twinning of ferrite causes strong local depassivation by rupturing the passive film, which depolarizes strongly the anodic dissolution reaction in the twinned regions. The coupled cathodic reaction then causes hydrogen to discharge and this may also influence the cracking process if a sufficient amount of hydrogen is discharged onto the depassivated region, with hydrogen entry and embrittlement.

In order to understand the reasons for the better resistance of the duplex stainless steels at the higher temperatures it is necessary to go back to the rather complex cracking processes operative in these alloys. It has been shown that stress cracking is controlled by the mechanical twinning of the ferrite phase.[7-8] When the influence of mechanical twinning of the ferrite phase is minimized, the resistance to cracking of the duplex steel is very much increased. As twinning is due to the lack of mobility of screw dislocations, an increase of temperature can be thought to improve dislocation mobility, as this process is thermally activated. And actually, experience shows that the ferrite phase is much less prone to mechanical twinning at 100°C (212°F) or 150°C (302°F) than at room temperature. This can explain the better resistance to SCC of the duplex stainless steel at the higher temperatures.

Now, it has proved possible to minimize the detrimental influence of the twinning tendency of the ferrite phase by carefully controlling the metallurgy and the metallurgical processing of the duplex stainless steels.

Depending upon the electrochemical conditions, the temperature, the composition of the aggressive solution (chlorides, sulfides, pH, complexing species, etc ...), the kinetics of the several processes involved in stress corrosion cracking can be influenced in an important, but different manner, which may accelerate or slow down cracking.

Among the several processes involved, one must take into account the effect of discharged hydrogens atoms into the ferrite phase of the duplex steel, as this phase can be prone to hydrogen embrittlement, much more so than the austenitic phase.

A precise knowledge of the different metallurgical and electrochemical features involved allowed to consider more precise formulation for the duplex stainless steels.

INDUSTRIAL APPLICATIONS

This know-how makes possible an accurate control of the manufacturing procedures in order to obtain the best properties and to avoid harmful metallurgical conditions: composition, heat treatments, hot and cold working, welding ... The critical parameters which must be carefully watched are, first, of course, composition and more exactly the balance between alpha-forming and gamma-forming alloying elements. This led to the development of several industrial compositions, in their different product forms: castings, forgings, rolled plates, bars, or wires. Hot working (rolling, forging) is more difficult for duplex stainless steels than for austenitic compositions. Likewise, the wire drawing operations can be tricky if hot working has not been carefully controlled, as this can initiate "hotshortness" cracks and slivers detrimental to the quality of the finished products, i.e., wires, sheets, bars, forged parts. It must be indeed underlined that the resistance of the duplex material can also be impaired very significantly by surface defects as it is the case for any other alloy. These small defects can initiate several types of corrosion in very aggressive environments (crevice corrosion and stress corrosion cracking). But they may also be, more generally, the cause of mechanical failures. However, the most important cause of failures may be an improper heat treatment which brings about embrittlement of the duplex structure.[6,9-11] This can happen if the annealing temperature is too low, below 1,000°C (1,830°F), or if the quenching operation after solution annealing is faulty, which may cause a slow cooling during which the duplex stainless steel can remain for long periods of time, in the dangerous temperature zones, between 400°C (750°F) and 900°C (1,650°F), for instance 30 minutes at 800°C (1,470°F). This has been extensively investigated. All this being said, it must be emphasized that the industrial production of satisfactory duplex stainless steels is quite possible on a large scale, when the very well known metallurgical factors are correctly controlled during processing and fabrication. The current industrial experience gathered in the production of numerous thousand tons, all over the world, of quite satisfactory plates, forgings, castings, tubings, bars, and wires, as well as welded pipings and vessels, over a period of about 50 years, bears witness to this industrial feasibility. Welding processes and procedures have been developed over the years which ensures good fabrication conditions. Duplex stainless steels have been extensively employed for various equipments in fields of sour gas and oil, both on land and offshore because of the excellent combination of properties they offer: good resistance to various types of corrosion (general, pitting, crevice, stress cracking, fatigue) high mechanical properties, good weldability. This gives an overall good cost efficiency. Some typical examples are listed in Table VII: welded pipes, fittings, valves chokes, wire-lines, flow-lines, gathering systems, reinjection pumps, and lines, etc...[13-19]

REFERENCES

1. N. Estavoyer, "Corrosion Problems at Lacq Sour Gas Field," *Journal of the Institute of Petroleum* 46, 439, 7(1960), pp. 223-233.
2. J. Gratcos, M. Garcia, Etude de la corrosion sous tension des lignes de mesures en acier inoxydable 304, 316, Uranus 50. C.R. SNPA, Centre de Recherches de Pau - Etude no. 238 a/69, 12(1969) Patent SNPA 1970.
3. NACE Standard MR-01-75, "Material Requirement. Sulfide Stress Cracking Resistant Material for Oil Field Equipment" (Houston, TX: NACE).
4. NACE Standard TM-01-77, "Test Method. Testing of Metals for Resistance to Sulfide Stress Cracking" (Houston, TX: NACE).
5. C. Perrolet, J.L. Crolet, Evaluation di la susceptibilité à la fragiliation par H_2S à l'aide d'essai de rupture différé sur éprouvettes lisses cylindriques : comparaison entre l'es sai NACE normal, l'essai SNEA (P) et un essai NACE modifié à pH 4. *Mémoires Scientifiques de la Revue de Métallurgie*, p. 5, 1(1982) CORROSION/82, paper no. 135.
6. A. Desestret, "Sulfide Stress Corrosion Cracking Resistance of Several Austenitic and Duplex Stainless Steels in Chloride Solutions Containing H_2S. Influence of Structure, Hardening Head Treatments, Cold-Worked and of Temperature of the Solutions," CORROSION/82, paper no. 165 (Houston, TX: NACE, 1982).
7. A. Desestret, R. Oltra, *Corrosion Science* 20, 6(1980), p. 799.
8. T. Magnin, J. Le Coze, A. Desestret, "Twinning and Stress Corrosion Cracking of Ferrite Phases of Duplex

Stainless Steels," *ASM Conference Proceedings*, ed., R.A. Lula, held October 23-28, 1982 in St. Louis, MO (Metals Park, OH: ASM, 1982).

9. J. Hochman, A. Desestret, P. Jolly. R. Mayoud, "Properties of High Cr Ferritic Stainless Steels and Austeno-ferritic Stainless Steels," International Congress on SCC and HE of Iron Base Alloys, Firminy, Juin 1973, ed., NACE, 1977, pp. 956/1,002. Publié en français dans Métaux, Corrosion, Industrie, 591-592, Nov-Dec 1974 et 593, Dec 1975.
10. P. Combrade, A. Desestret, P. Jolly, R. Mayoud, "Use of Duplex Stainless Steels to Retard Stress Corrosion Cracking in Predictive Methods for Assessing Corrosion Damage to BWR Piping and PWR Steam Generators," *USA-Japan International Conference*, Mt Fuji, May 28-June 2, 1982, ed., NACE, pp. 153/173.
11. H.D. Solomon, T.M. Devine, "Influence of Microstructure on the Mechanical Properties and Localized Corrosion of a Duplex Stainless Steels Mi Cor 78. Optimization of Processing, Properties and Service Performance Through Microstructural Control," ASTM STP No. 672 (Philadelphia, PA: ASTM, 1979), pp. 430/461.
    H.D. Solomon, E.F. Koch, "High Temperature Precipitaiton of ??? in a Multicomponent Duplex Stainless Steel," *Scripta Metallurgica* 13 (1979), pp. 971/974.
    H.D. Solomon, "Age Hardening in a Duplex Stainless Steel," General Electric Company Corporate Research and Development, Report No. 82 CRD 27, October 1982.
    H.D. Solomon, T.M. Devine, Jr., "Duplex Stainless Steels – A Tale of Two Phases," General Electric Company Corporate Research and Development, Report No. 82 CRD 276, November 1982, Duplex Stainless Steels, *ASM Conference Proceedings*, ed., R.A. Lula, 1983.
12. P.R. Rhodes, G.A. Welch, L. Abrego, "Stress Corrosion Cracking Susceptibilty of Duplex Stainless Steels in Sour Gas Environments," R.A. Lula, ed., *ASM Conference Proceedings* (Metals Park, OH: ASM, 1983).
13. R. Mayoud, S. Béchet, "Uranus 50 – Half a Century of Successful Experience," *Molybdenum Mosaic* 7, 1(1984), p. 6.
14. A. Desestret, R. Mayoud, "Les aciers inoxydables austéno-ferritiques. Nouveaux développements fondés sur 50 ans d'expérience," *Revue de Métallurgie*, CIT Avril 1984, p. 321.
15. G. Herbsleb, R.K. Poepperling, "Corrosion Properties of Austeno-ferritic Duplex Steel AF 22 in Chloride and Sulfide Containing Environments," CORROSION/80, paper no. 13 (Houston, TX: NACE, 1980), p. 587.
16. S.O. Bernhardsson, J. Oredson, M. Tynell, "Properties of Duplex Stainless Steels for Use in Corrosive Oil and Gas Wells," CORROSION/80, paper no. 14 (Hoston, TX: NACE, 1980).
17. A.I. Asphahani, "Highly Alloyed Stainless Materials for CO_2/H_2S Environments,"CORROSION/80, paper no. 12 (Houston, TX: NACE, 1980).
18. J.C. Prouheze, J.C. Vaillant, C. Guntz, B. Lefebvre, "Production of Tubng of Duplex Steel US 22. Influence of Cold Working on Mechancal Properties. Behavior in Corrosion Sour Gas and Oil Environments," Duplex S.S., *ASM Conference Proceedings*, R.A. Lula, ed. (Metals Park, OH: ASM, 1983).
19. "Duplex Stainless Steels," R.A. Lula, ed., *Conference Proceedings of the ASM Congress*, held October 25-28, in St. Louis, MO (Metals Park, OH: ASM, 1983).

TABLE I

S.SCC Tests on URANUS 45 N Plates - Thickness 6/7 mm (UNS 31 803)

.023 - Mn 1.74 - Si 0.472 - S 0.006 - P 0.021 - Cr 22.12 - Ni 5.67 - Mo 2.80 - Cu 0.161 - N 0.142 - α % $\simeq$ 45 %

2/607 MPa - UTS 772/818 MPa - Elongation 35-40 % - Reduction of Area = 60 %

Table Ia

Tensile tests after NACE TM-01-77 at 25°C / 1 atm. H_2S

E DIRECTION	Stress MPa	Stress % YS	Duration (hours)	Observations
UDINAL	428	$\simeq$ 70 %	> 1690	No rupture/No cracks
	460	$\simeq$ 80 %	> 985	- ID -
	515	$\simeq$ 90 %	603	Cracks
ERSE	429	$\simeq$ 75 %	> 1470	No rupture/No cracks
	457	$\simeq$ 80 %	> 1450	- ID -
	460	$\simeq$ 80 %	180	Rupture
	470	$\simeq$ 85 %	> 1200	No rupture/No cracks

Tensile tests in the NACE TM-01-77 solution at 90°C / 15 bar H_2S

UDINAL	400	$\simeq$ 70 %	> 1200	No rupture/Small crack initiations
	428	$\simeq$ 75 %	> 960	No rupture/No cracks
	450	$\simeq$ 80 %	> 1178	- ID -
ERSE	400	$\simeq$ 70 %	> 1060	- ID -
	450	$\simeq$ 80	377	Cracks

Table Ib

Welded assemblies URANUS 45 N Plates - 6/7 mm (UNS 31 803)

Specimens transverse to weld seams

Tensile tests after NACE TM-01-77 at 25°C / 1 atm. H_2S

ELDS Filler wire : C 0.017, Mn 1.85, Si 0.44, S 0.007, P 0.019
Cr 22.95, Ni 5.71, Mo 2.85, Cu 0.08, N 0.13

YS 591/607 MPa - UTS 770/783 MPa - Elongation $\simeq$ 19 %

Stress MPa	Stress % YS	Duration (hours)	Observations
480	$\simeq$ 80 %	> 816	No rupture/No cracks
540	$\simeq$ 90 %	385	Cracks

ELDS Filler wire : C 0.015, Mn 1.85, Si 0.44, S 0.007, P 0.021
Cr 22.84, Ni 5.60, Mo 2.85, Cu 0.10, N 0.125

YS 608/618 MPa - UTS 793/796 MPa - Elongation $\simeq$ 28 %

Stress MPa	Stress % YS	Duration (hours)	Observations
427	$\simeq$ 70 %	> 960	No rupture/No cracks
450	$\simeq$ 75 %	> 1180	- ID -
488	$\simeq$ 80 %	205	

TABLE II

S.SCC Tests on URANUS 47 N Plates - Thickness 6/7 mm (UNS 31 200 + 3 % Mo)

025 - Mn 1.20 - Si 0.34 - S 0.002 - P 0.029 - Cr 24.75 - Ni 6.82 - Mo 3.00 - Cu 0.10 - N 0.195 - α % 45 %

00/637 MPa - UTS 792/794 MPa - Elongation 34/42 % - Reduction of aera : 84/76 %

Table IIa

Tensile tests after NACE TM-01-77 at 25°C / 1 atm. H_2S

IRECTION	Stress MPa	Stress % YS	Duration (hours)	Observations
UDINAL	480	$\simeq$ 80 %	950	No rupture/Some small crack initiations
ERSE	480	$\simeq$ 75 %	1010	No rupture/No cracks

Tensile tests in the NACE TM-01-77 solution at 90°C / 15 bar H_2S

IRECTION	Stress MPa	Stress % YS	Duration (hours)	Observations
UDINAL	480	$\simeq$ 80 %	1100	No rupture/No cracks
ERSE	480	$\simeq$ 75 %	740	No rupture/Some small cracks initiations

Table IIb

Welded assemblies - URANUS 47 N Plates - 6/7 mm (UNS 31 200 + 3 % Mo)

Tensile tests after NACE TM-01-77 at 25°C / 1 atm H_2S

RON Beam Weld (no filler wire)

E taken along the weld seam α = 65 % - YS = 690 MPa

S 637 MPa - $\simeq$ 90 % YS - Duration > 840 hours - No rupture/No cracks

D electrode : Boehler Fox CN 26-7N

41 - Mn 4.87 - Si 0.53 - S 0.004 - P 0.013 - Cr 25.0 - Ni 7.13 - Mo 2.21 - Cu 0.104 - N 0.295 - α 35 % - YS = 610 MPa

ES TRANSVERSE TO WELD SEAMS

Stress MPa	Stress % YS	Duration (hours)	Observations
549	$\simeq$ 90 %	39	Rupture
488	$\simeq$ 80 %	610	- id -
460	$\simeq$ 75 %	1450	No rupture/No cracks

TABLE III

COLD WORKED WIRES OR BARS

	Cr	Ni	Mo	Cu	C	N	%	MECHANICAL PROPERTIES AS COLD WORKED TYPICAL & APPROXIMATE VALUES			
								YS		UTS	
								MPa	Ksi	MPa	Ksi
AISI 316 (austenitic)	17	12	2.5	-	0.03	0.1	0	1000 — 1200	145 — 174	1250 — 1350	181 — 195
• URANUS 50 (α / γ)	20/23	5/8	2/3	1/2	0.03	0.15	30/55	1200 — 1400	174 — 203	1800 — 1700	218 — 247
• URANUS 45 UNS 31 803	ID	ID	ID	≤ 0.1	ID	ID	ID	ID	ID	ID	ID
• URANUS 52 (α / γ)	24/26	7/8	2.5/3.5	1/2	0.03	0.10/0.20	40/55	1400	203	1700	247
• URANUS 47 UNS 31 200	ID	ID	ID	0	ID	ID	ID	ID	ID	ID	ID
• URANUS B6 (γ) AISI 904 L UNS N 0 8904	20	25	4.5	1.5	0.02	0.15	0	1100	160	1270	184

URANUS 45. 50. 47. 52. B6 ARE TRADE MARKS REGISTERED BY THE DIVISION CREUSOT MARREL OF THE SOCIÉTÉ CREUSOT LOIRE. AND BY THE COMPAGNIE DES FORGES ET FONDERIE (C3F) OF THE GROUP USINOR

TABLE IV

COLD WORKED MATERIAL (WIRES - BARS) - S.SCC TENSILE TESTS

NACE TM-01-77 SOLUTION 100°C (212°F) - 15 BAR H_2S (15 ATMOSPHERE)

STEELS (COLD WORKED)	MECHANICAL PROPERTIES					S.SCC TESTS	
		YS	UTS	EL %	RA %	APPLIED STRESS	TIME TO RUPTURE (HOURS)
AISI 316 L AUSTENITIC Cr 18/Ni 12/Mo 2.5	20°C	1060 MPa 154 Ksi	1283 MPa 186 Ksi	13	45		6
						897 MPa (130 Ksi)	2
	150°C	630 MPa 92 Ksi	1225 MPa 177 Ksi	5	42		21
						0.85 YS (20°C) 1.42 YS (150°C)	19
DUPLEX S.S. α / γ Cr 21/Ni 6/Mo 2.5/Cu 1.5 (URANUS 50) UNS 31803 + Cu 1.5 %	20°C	1190 MPa 154 Ksi	1520 MPa 221 Ksi	7	40		
						1027 MPa (149 Ksi)	700 NF
	150°C	552 MPa 85 Ksi	1229 MPa 179 Ksi	7	41		
						0.86 YS (20°C) 1.86 YS (150°C)	
AUSTENITIC S.S. γ Cr20/Ni 25/Mo 4.5/Cu 1.5 (URANUS B6) UNS N 08904	20°C	1140 MPa 165 Ksi	1480 MPa 215 Ksi	8	25		
						908 MPa (132 Ksi)	1300 NF
	150°C	400 MPa 58 Ksi	1150 MPa 168 Ksi	8	57		
						0.80 YS (20°C) 2.27 YS (150°C)	

TABLE V

STRESS CORROSION CRACKING TESTS IN THE NACE TM-01-77 SOLUTION AT 1050°C (302°F) UNDER A PRESSURE OF 15 ATMOSPHERE OF H_2S

COLD WORKED MATERIAL (WIRES - BARS)

NF : NO FAILURE

		MECHANICAL PROPERTIES				S.SCC TESTS			
						APPLIED STRESS			TIME TO RUPTURE (HOURS)
		YS	UTS	EL %	RA %	% YS (20°C)	% YS (150°C)		
AISI 316 L F/Ni 12/Mo 2.5 AUSTENITIC γ	20°C	1060 MPa 154 Ksi	1285 MPa 186 Ksi	13	45	50	84	530 MPa 77 Ksi	33-120-80-30
	150°C	630 MPa 92 Ksi	1225 MPa 177 Ksi	5	42	45	75	472 MPa 69 Ksi	51
						30	50	315 MPa 46 Ksi	> 900 NF > 1000 NF
DUPLEX S.S. F/Ni 6/Mo 2.5 Cu 1.5 URANUS 50) NS 31 803 1.5 % Cu) α/γ	20°C	1190 MPa 173 Ksi	1520 MPa 221 Ksi	7	40	75	162	893 MPa 130 Ksi	> 750 NF
	150°C	552 MPa 80 Ksi	1229 MPa 179 Ksi	7	41	35	75	414 MPa 60 Ksi	> 1000 NF
	20°C	1200 MPa 174 Ksi	1500 MPa 218 Ksi	8	53	73	125	877 MPa 127 Ksi	> 1100 NF
	150°C	704 MPa 102 Ksi	1367 MPa 198 Ksi			44	75	528 MPa 76 Ksi	> 1050 NF
DUPLEX S.S. 25/Ni 7/Mo 3 URANUS 47) 1 200 + 3 % Mo) α/γ	20°C	1367 MPa 198 Ksi	1677 MPa 243 Ksi	3		50	80	682 MPa 99 Ksi	> 1750 NF
	150°C	700 MPa 100 Ksi				75	100	1022 MPa 148 Ksi	> 1220 NF
FERRITIC S.S. F/Ni 25/Mo 4.5 Cu 1.5 URANUS B6) NS NO 8904 γ	20°C	1140 MPa 165 Ksi	1480 MPa 215 Ksi	8	35			300 MPa 44 Ksi	547 372
	150°C	400 MPa 58 Ksi	1160 MPa 168 Ksi	8	37				
TRIPHASE ALLOY 20 Mo 7 Co 40 (PHYNOX)	20°C	1125 MPa 163 Ksi	1668 MPa 242 Ksi	11	54	90	100	1013 MPa 147 Ksi	> 1000 NF
	150°C								

TABLE VI

COLD WORKED MATERIAL (BARS - WIRES)

THRESHOLD STRESS FOR RESISTANCE (720 HOURS TO 1000 HOURS) TO SULFIDE STRESS CORROSION CRACKING IN THE NACE TM-01-77 SOLUTION (NaCl 50 G/L), CH_3COO 0.5 G/L, H_2S)

COLD WORKED STEEL	R 0.002 (20°C) MPa (YIELD STRENGTH AT 68°F, Ksi)	TEMPERATURE OF TEST AND PRESSURE OF H_2S				
		1 ATM H_2S	5 TO 15 BAR H_2S			
		25°C (76°F)	50°C (122°F)	75°C (167°F)	90/100°C(212°F	150°C (302°F)
AISI 316 L (δ)	1060 (154)	$\simeq 0.65$ R 0.002/YS (20°C)	$\geqslant 0.8$ R 0.002/YS (20°C)	$\leqslant 0.5$ R 0.002/YS (20°C)	$\ll 0.8$ R 0.002/YS (20°C)	$\leqslant 0.3$ R 0.002/YS (20°C)
* URANUS 50 (UR 45) (α - δ) UNS 31 803	1200 (174)	$\simeq 0.65$ R 0.002/YS (20°C)	$\geqslant 0.8$ R 0.002/YS (20°C)	$\geqslant 0.8$ R 0.002/YS (20°C)	$\geqslant 0.9$ R 0.002/YS (20°C)	$\geqslant 0.8$ 0.002/YS (20°C)
* URANUS 47 (UR 52) (α - δ) UNS 31 200 + 3 % Mo	1400 (203)	$\geqslant 1$ R 0.002/YS (20°C)	$\geqslant 0.8$ R 0.002/YS (20°C)	$\geqslant 0.8$ R 0.002/YS (20°C)		$\geqslant 0.8$ R 0.002/YS (20°C)
* URANUS B6 (δ) UNS NO 8904	1100 (160)	$\geqslant 1$ R 0.002/YS (20°C)	$\geqslant 0.8$ R 0.002/YS (20°C)	$\geqslant 0.8$ R 0.002/YS (20°C)	$\geqslant 0.8$ R 0.002/YS (20°C)	$\leqslant 0.3$ R 0.002/YS (20°C)

TABLE VII

TYPICAL USES OF DUPLEX S.S. IN SOUR GAS & OIL EXPLOITATION SYSTEMS

FACTORS INFLUENCING CORROSION PERFORMANCE OF STEELS							
EXAMPLE OF USE	GAS COMPOSITION			pH CONDENSATE	TEMPERATURE	PRESSURE	CHLORITES
	H_2S	CO_2	OTHERS				
GAS FIELD (LACQ - FRANCE)	15 %	20 %	CH_4...	4	90°C (230°F) NOW INCREASING	MAX 500 BAR (7200 Psi) NOW DECREASING	USUALLY LOW BUT CHLORIDE INJECTIONS 1000-60 000 PPM
NORTH SEA FLOW LINES (HOLLAND, NORWAY, U.K.)	UP TO 25 %	9 %		5	UP TO 150°C (300°F)	MAX 450 BAR (6300 Psi)	ABOUT 1000 PPM
CORTEZ CO GATHERING SYSTEM		WET CO_2			40°C	65 BAR (910 Psi)	USUALLY LOW BUT CHLORIDE

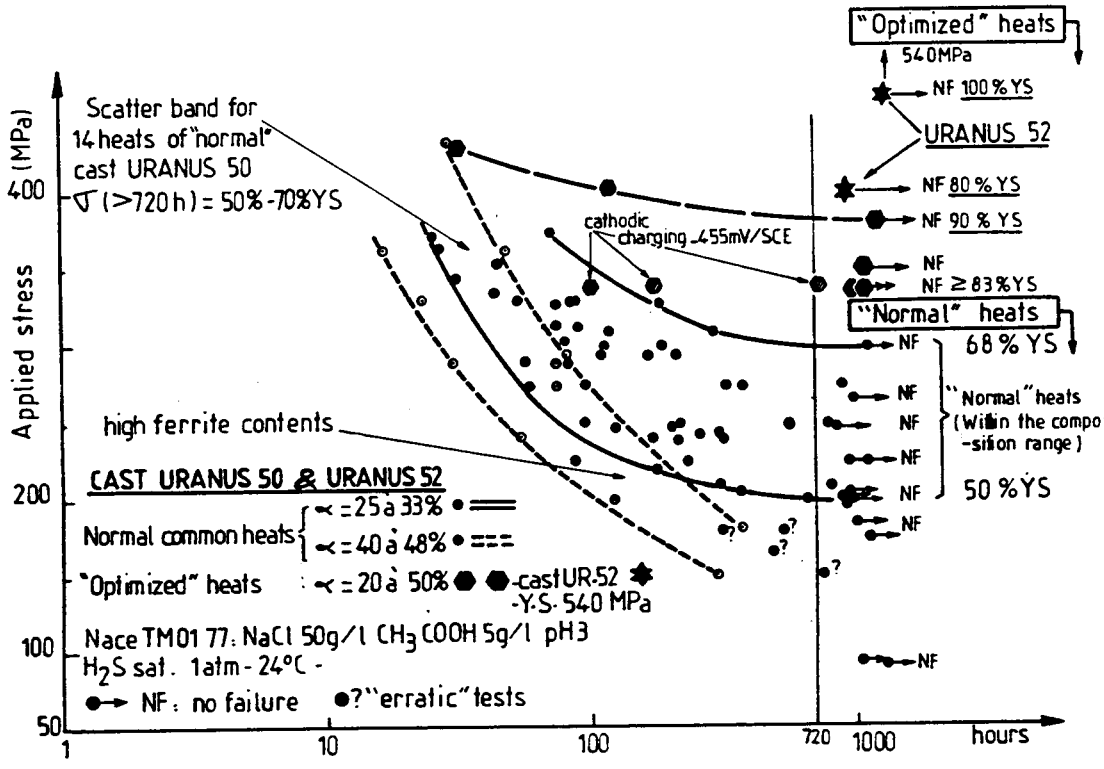


Figure 1

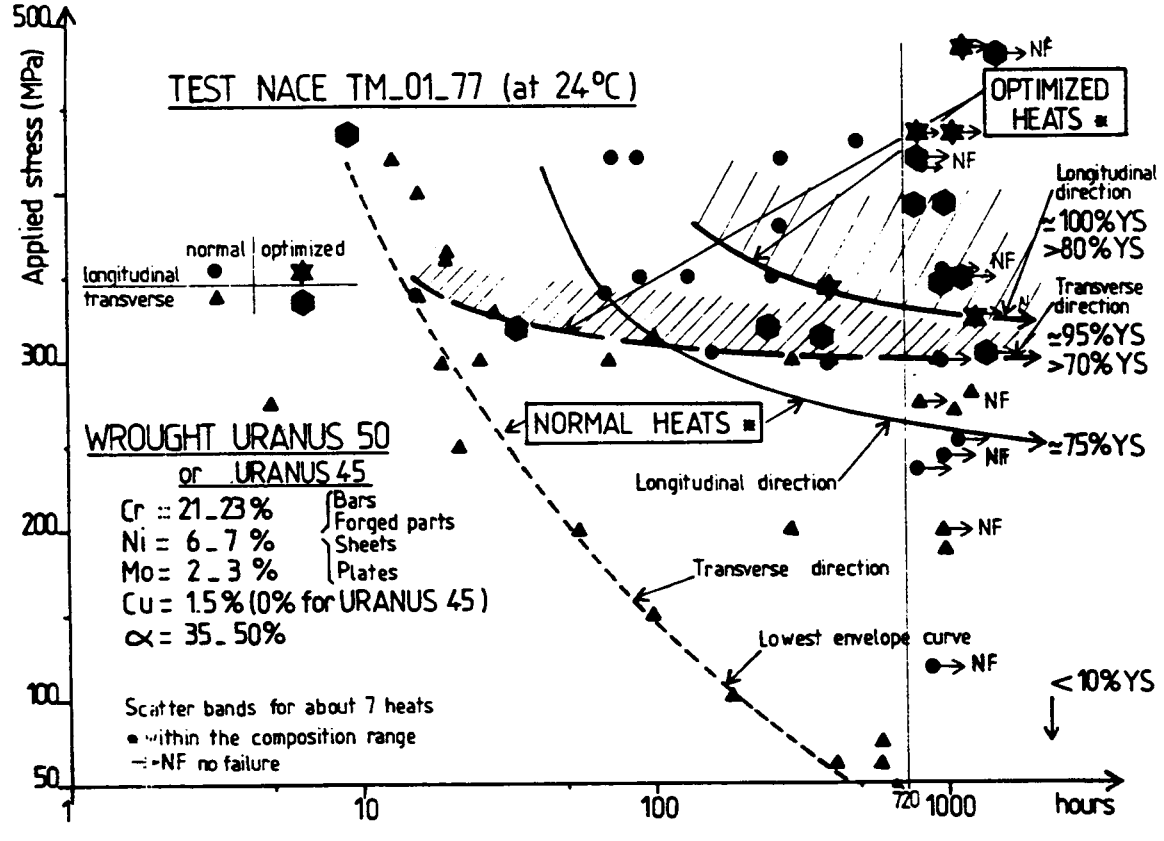
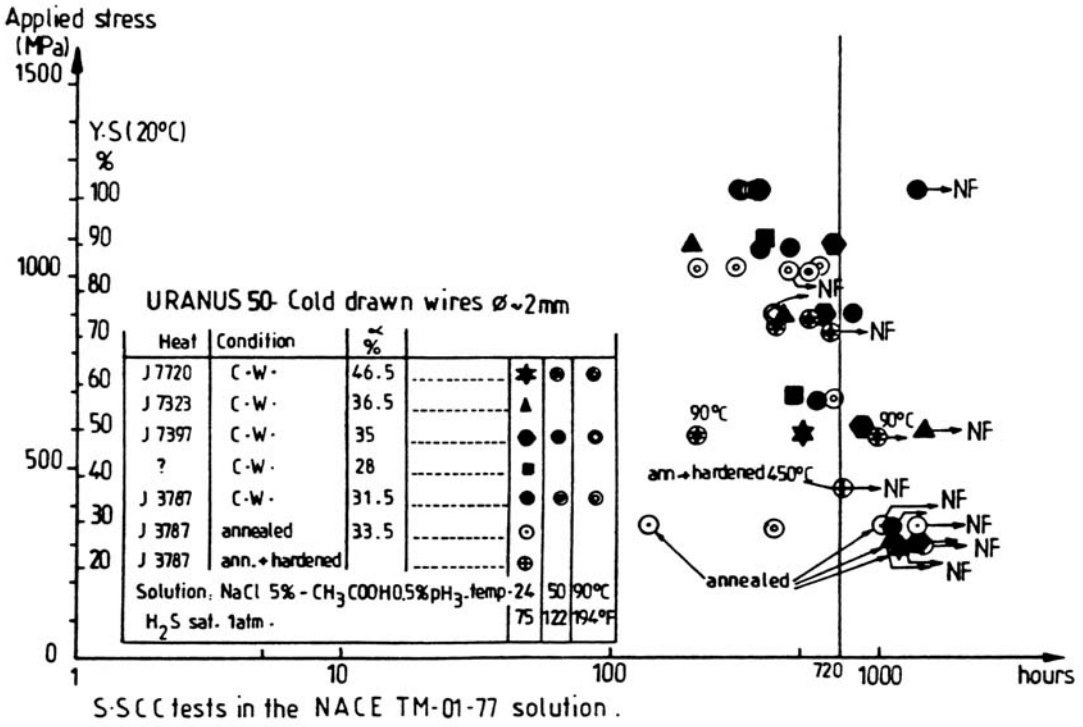
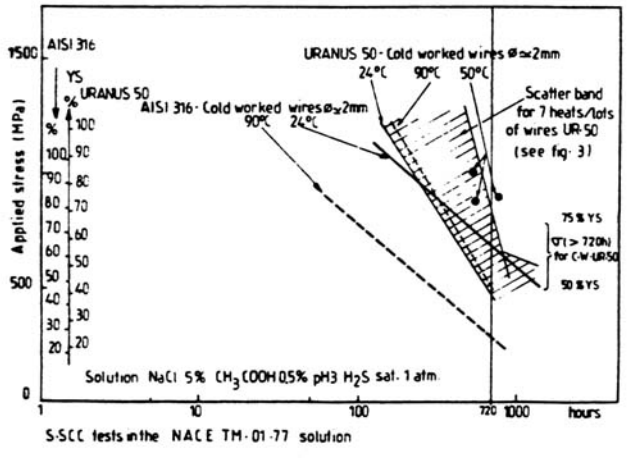


Figure 2



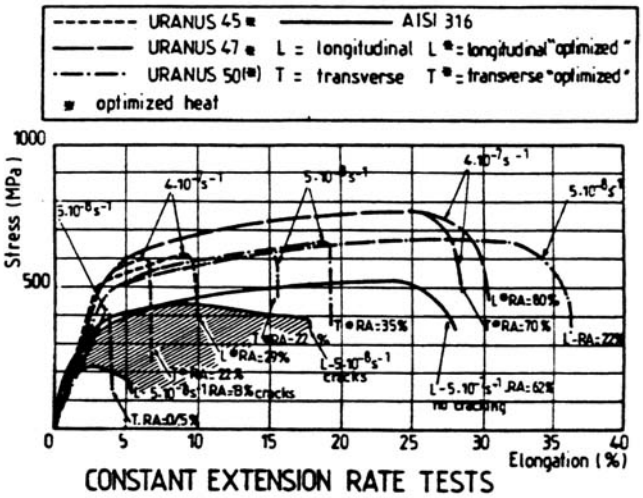
S-SCC tests in the NACE TM-01-77 solution.

Figure 3



S-SCC tests in the NACE TM-01-77 solution

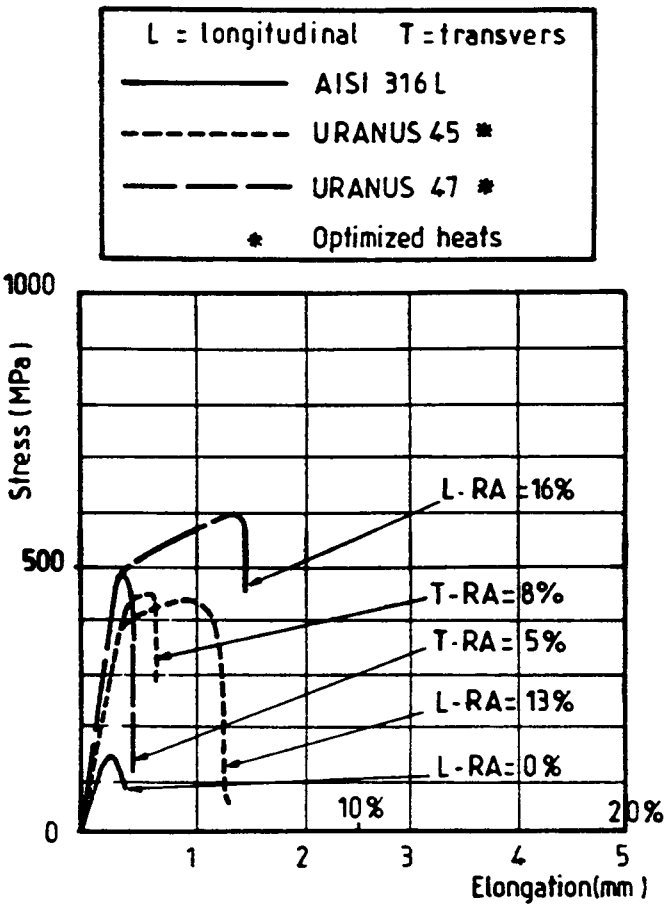
Figure 4



CONSTANT EXTENSION RATE TESTS

Solution: NaCl 5% + CH3COOH 0.5% - H2S 1atm. - 24°C -
Straining rate: $4.10^{-7}\,s^{-1}$ - $5.10^{-8}\,s^{-1}$

Figure 5



CONSTANT EXTENSION RATE TESTS

Solution :

NaCl 5%

CH_3 COOH 0.5%

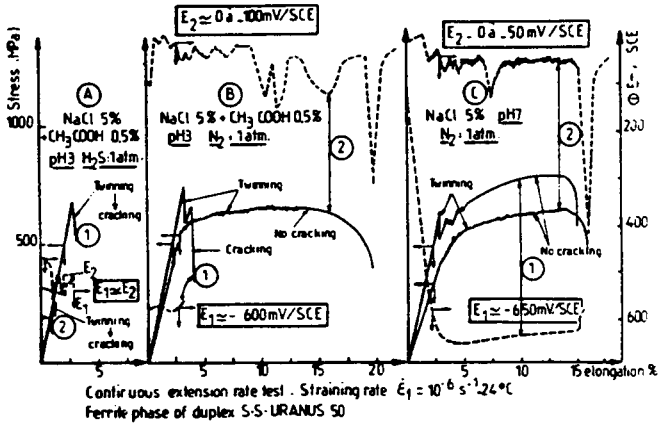
H_2S = 15 bar

90° C

Straining rate :

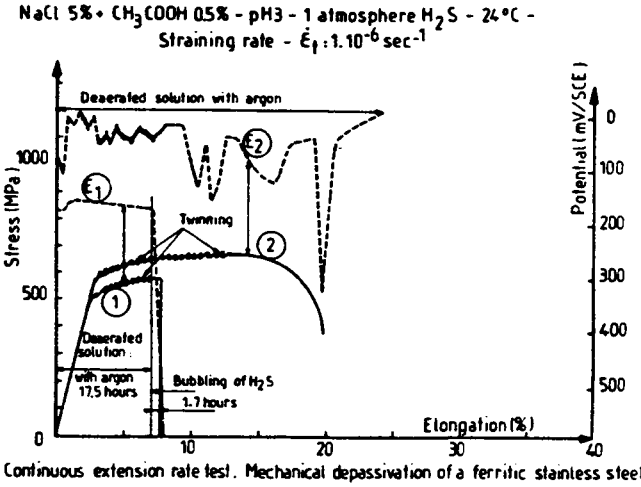
$4.10^{-7} s^{-1}$

Figure 6



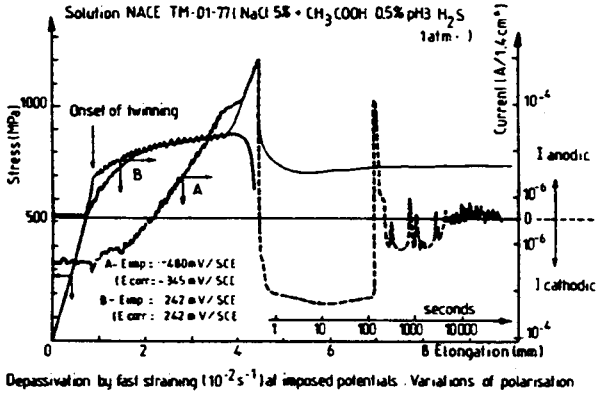
Continuous extension rate test . Straining rate $\dot{\varepsilon}_1 = 10^{-6} s^{-1}$ 24°C
Ferrite phase of duplex S-S- URANUS 50

Figure 7



Continuous extension rate test. Mechanical depassivation of a ferritic stainless steel.
The ferrite phase of duplex S-S. URANUS 50

Figure 8



Depassivation by fast straining ($10^{-2} s^{-1}$) at imposed potentials . Variations of polarisation current during straining . Ferrite phase of duplex S-S-URANUS 50 .

Figure 9

Copyrighted Materials
Copyright © 1996 NACE International Retrieved from www.knovel.com

PAPER NUMBER
308

Corrosion 87
March 9-13, 1987
Moscone Center / San Francisco, California

PROPERTIES OF AND EXPERIENCE WITH WELDED JOINTS IN STAINLESS ALLOYS

Hans Eriksson
Peter Norberg
Sven Bernhardsson

AB Sandvik Steel
S-811 81 Sandviken
Sweden

INTRODUCTION

Stress corrosion cracking (SCC) is a very common problem with stainless steels in numerous industrial applications. Especially susceptible are the standard austenitic stainless steels AISI 304 and 316. These steels have displayed SCC at as low temperatures as 50 or 60°C in chloride containing solutions (1).

In most cases the SCC problems can be solved if the standard austenitics are replaced by duplex stainless steels or by high-nickel austenitic alloys.

However, some doubts has been expressed regarding the weldability of these two groups of material. Especially the corrosion resistance of the weldments has been discussed. The purpose of this paper is to give some aspects of the SCC-resistance of weldments in two duplex stainless steels, SAF 2304 and SAF 2205, and one high-nickel austenitic alloy Sanicro 28 in some relevant environments. Both experimental results and practical experience are considered.

A suitable method for testing and ranking stainless steels with respect to their SCC resistance is the 40% $CaCl_2$ test. The $MgCl_2$ test, on the other hand, may give misleading results (2,3), e.g. by indicating a negative effect of Mo-alloying. Autoclave tests at different temperatures and chloride contents can give valuable information about the applicability or limitations of the tested grade.

Since the mid 70's more and more oil and gas wells have been taken into production although they cannot be regarded as

easily accessible. Of course, this has been costly, partly because they are often extremely corrosive. This is mostly owing to the presence of hydrogen sulphide and chlorides in combination. The conditions are normally oxygen free and often also involve high temperatures. The material must be selected carefully. Especially SCC has to be avoided. More and more corrosion resistant alloys have therefore been put into service.

The resistance to H_2S/Cl^--induced SCC may, for instance, be tested in autoclave equipment at varying H_2S-partial pressure and temperatures. However, the old NACE TM-01-77 is still utilized very frequently, although originally it was developed for carbon steels and does not give exact applicability limits for stainless steels. These limitations of the test are mainly due to the high proportion of H_2S (100%) and unrealistically low pH. However, it is possible to use the test for the ranking of steels and for the evaluation of weld quality.

Materials

Nominal compositions of the duplex stainless steels SAF 2304 and SAF 2205, and the high-nickel austenitic alloy Sanicro 28 are shown in Table 1. The duplex alloys typically contain 45% ferrite and 55% austenite after normal quench-annealing. Owing to the duplex microstructure, these alloys possess a yield strength which is nearly twice that of the standard austenitic grades. The ultimate tensile strength is also high, or some 30% higher than for the austenitics.

The materials involved in this study were mostly tubes in the extruded and quenched condition or quench-annealed after cold pilgering. In one case, 20 mm thick plate in SAF 2205 was used.

The weldability of the three materials is good. Butt-welded joints were produced according to the welding recommendations summarized in Table 2. In addition, however, SAW joints in the SAF 2205 plate were made with arc energies up to 6.0 kJ/mm using Sandvik 22.8.3.L wire.

SCC-resistance in O_2/Cl^- environments

Constant-load tests on tensile specimens were performed in aerated 40% $CaCl_2$, pH=6.5, at 100°C. The specimens were machined from welded joints as well as from parent metals in SAF 2304 and SAF 2205. The applied initial stress was varied so as to enable the determination of the threshold stress relative to the tensile strength at the testing temperature. The threshold stress was defined as the lowest stress below which no SCC failure occurred during the 500 hours of testing.

Figure 1 shows the threshold stress for TIG and MMA welded joints in SAF 2304. The parent metal was a tube in size OD 108 x WT 9.7 mm. The SCC resistance of the welded joints in SAF 2304 was not different from that of the parent metal. All conditions exhibited a threshold stress of $0.8 \times R_m$ at the testing temperature.

Results of similar tests on SAF 2205 in various welded conditions are displayed in Figure 2. Welds produced by TIG, SAW and MMA were included. The SCC resistance of the welded joints was negligibly lower than that shown by the unwelded material. The indicated difference in threshold stress between unwelded material and welded joints is only about 3%. It is doubtful whether this is significant, and

in any case it should not be of importance to practical situations.

In order to copy the conditions encountered in industries utilizing water for process cooling, SCC tests have been performed in dilute chloride solutions at high temperatures. The autoclaves employed worked at a total pressure of 100 bar and with once-through flow of the solution. The chloride content was varied between 30 and 16000 ppm Cl^-, added as NaCl. The oxygen content of the inlet solution was 7 $\pm$ 1 ppm and the pH at room temperature 6 $\pm$ 0.5.

The tests were performed at temperatures between 100 and 250°C on spring-loaded tensile specimens stressed to $R_{p0.2}$ at the testing temperature. The testing time was 1000 h and at least 4 specimens were involved in each combination of chloride content and temperature.

So far, very few tests involving welded joints have been run. Figure 3 shows results for SAF 2205. Unwelded material as well as TIG joints were tested. A tube in size OD 110 x WT 8 mm was used as parent metal. All eight specimens, represented by the unfilled triangle at 150°C, 300 ppm Cl^-, passed the test without any sign of SCC. This indicates that there is very little difference, if any, in SCC resistance between unwelded material and welded joints in SAF 2205 when exposed to this type of environment.

The laboratory results are also supported by service experience from a large variety of applications, see Figure 4. It can be assumed that most points in this diagram involve welds of some kind.

SCC-resistance in $H_2S/CO_2/Cl^-$-environments

Figure 5 shows results from tests with SAF 2205 in NACE-solution (5% NaCl, 0.5% HAc, 100% H_2S, atmospheric pressure). It can be seen that tests of the all weld metal give somewhat higher resistance than the parent metal (OD 168 x WT 12 mm). MMA welded joints seem to have slightly lower resistance than the parent metal. The differences are small, however. They might be due to small variations in yield strength as a result of minor variations in microstructure, for instance ferrite content. Another explanation could be that the welding operation induces stresses which are superimposed on the applied load. Locally this could imply an effective applied load which is greater than the nominal one.

In Figure 6 results from NACE-tests of a TIG welded tube are presented (OD 110 x WT 8 mm). When comparing with MMA welds it is obvious that TIG gives a comparable threshold stress in the NACE-solution. All failures indicated in Figure 6 occurred in the parent metal except the failure at 600 N/mm^2 after around 200 h. This failure occurred in the weld metal.

All this goes to prove that welding does not have negative effects on SCC-resistance in H_2S environment.

In Figure 7 practical experience and laboratory results for SAF 2205 have been compiled. The laboratory tests were performed in NACE-solution at different temperatures and partial pressures of H_2S. The applied stress was equal to the yield stress at the testing temperature. The acceptance criteria was 500 h testing time without failure. The material emanated from a tube in size OD 168 x WT 12 mm. It should be

pointed out that the practical applications are likely to include weldments in varying numbers. Performance in practical service has been successful. This may seem somewhat surprising when comparing with the experimental points at 90°C which indicate failure when the partial pressure of H_2S is greater than 10 kPa. However, the experiments have been performed in NACE-solution which has a very low pH, around 2.5, while the practical applications have a pH-value between 4.5 and 6.

The pH-value has been shown to have a dramatic influence on the SCC susceptibility of SAF 2205 in H_2S-environments (5). Typically, the tolerable partial pressure is increased more than one order of magnitude if the pH is increased from 2.5 to 3.9 in NACE-solution tests between room temperature and 90°C.

A similar comparison for Sanicro 28 between practical experience and laboratory results have been compiled in Figure 8. The laboratory tests (see Table 3) involved a tube in size OD 177.8 x WT 9.19 mm which was TIG butt-welded. Also in the case of Sanicro 28 it is reasonable to expect the presence of weldments in applications of annealed material. As can be seen, the experience in practice is good also in the case of Sanicro 28.

It is of some interest to compare the data with results from tests of cold-worked material. Sanicro 28 in cold-worked condition has proved to withstand far higher hydrogen sulphide pressures and temperatures than indicated by the points in Figure 8 (6). Cold-working of high-nickel stainless steels and nickel-base alloys has turned out to have a slight negative effect on the SCC-resistance in H_2S-environments (7). Thus, it could be anticipated annealed material including weldments that would be possible to use in significantly more severe conditions including higher H_2S-pressures and temperatures.

In some applications containing hydrogen sulphide oxygen can be present. This could be the case in piping systems equipped with pumps with leaking seals or even down-hole if non-deareated injections are made. The effect of oxygen contamination has been investigated (8) in an environment containing 100 ppm H_2S, 2% CO_2 and the rest He at a total pressure of 10 MPa (100 bar).

This gives a partial pressure of H_2S of 1 kPa. The temperature was 100°C and the NaCl-content 5%. The tests were performed both with and without the addition of 40 ppm oxygen. Tested materials were SAF 2205, SAF 2304, AISI 316 and 904L in the form of TIG welded joints. The resistance to SCC and pitting was investigated. The results are summarized in Table 4. As can be seen all materials were resistant in both environments. There was no indication that the presence of oxygen made the conditions more severe.

DISCUSSION

Data in the present study lead to the general conclusion that the presence of weldments in SAF 2304, SAF 2205 and Sanicro 28 does not have any significant influence on the SCC-resistance. A prerequisite for this is, of course, that the welding operation has been performed according to the recommendations provided by the supplier. The recommendations aim at a welding procedure ensuring that the mechanical and corrosion properties are not affected by

any microstructural anomalities in the weld metal or HAZ.

Generally a high arc energy leads to a slow cooling rate. This could, especially in the case of highly alloyed materials, lead to precipitation of unwanted carbides or intermetallics.

A very low arc energy will, on the other hand lead to low productivity. In the case of duplex stainless steels a low arc energy also could give too rapid cooling. This will lead to insufficient austenite reformation in the completely ferritic-ly solidified structure. The austenite content has to be sufficient, otherwise the toughness in HAZ may be reduced.

Also another problem could arise. The austenite dissolves the main part of the nitrogen, an alloying element which is added in all modern duplex stainless steels. The solubility of nitrogen in the ferrite phase is low, and if the austenite content is too low there is a risk of chromium nitride (Cr_2N) formation in the ferrite phase. These nitrides could, for instance, reduce the pitting corrosion resistance (9). It has to be pointed out, however, that nitrogen is an austenite former and contributes to the austenite reformation.

The effect of different welding conditions, among other parameters the arc energy, was recently investigated (9). In many cases a significantly increased arc energy resulted in better productivity and properties because of more extended austenite reformation.

In this context it also has to be stressed that proper austenite reformation is only possible if the filler and parent metal have a carefully balanced chemical composition. The nickel content in the filler metal of duplex stainless steels is normally increased by a few percent in comparison with the parent metal. The parent metal has to contain sufficient amounts of austenite formers, such as nickel and nitrogen. The latter is especially effective in giving quick austenite reformation. This nitrogen addition also has more positive effects. Most important are increased strength and pitting corrosion resistance. Therefore, modern duplex stainless steels typically have a nitrogen content between 0.1 and 0.3 wt.%.

REFERENCES

1. The Society of Chemical Engineers, Japan, Japan Society of Corrosion Engineering, and Japan Stainless Steel Association: Stress Corrosion Cracking in Shell and Tube Exchanger Made of Stainless Steel - Collection of Data on the Results of Use in Practice, Sept, 1979

2. S Bernhardsson. Paper No 266, NACE Corrosion/84, New Orleans, LA, April, 1984

3. H Eriksson and P Norberg. The SCC-resistance of ferritic-austenitic and high-nickel stainless alloys. 10th Scandinavian Corrosion Congress, Stockholm 1986

4. E Sato et. al. Corrosion of Steels in a Wet H_2S and CO_2 environment, 2nd Asian-Pacific Corrosion Control Conference, Kuala Lumpur/Penang, 1981, 28.6-10.7.

5. J Oredsson and S Bernhardsson. Materials Performance , Vol. 22, No. 1, Jan., 1983, p 35.

6. S Bernhardsson et. al. Paper No 225, NACE Corrosion/85. Boston, MA, March, 1985.

7. H E Chaung et. al. Paper No 227, NACE Corrosion/85. Boston, MA, March, 1985.

8. B. Johnsson, Corrosion in production systems, offshore. Final Report, Research Project JK 4310/85, May, 1986, Jernkontoret, Sweden (In Swedish)

9. B. Lundqvist, P. Norberg and K. Olsson. Paper No 10, Duplex Stainless Steels '86, The Hague, The Netherlands, 26-28 Oct, 1986.

Table 1 Chemical composition (wt-%) and microstructure of the stainless steels tested

Grade	UNS	C max	Cr	Ni	Mo	Cu	N	Microstructure
SAF 2304	S32304	0.030	23	4	-	-	0.1	Duplex
SAF 2205	S31803	0.030	22	5.5	3.0	-	0.14	Duplex
Sanicro 28	N08028	0.020	27	31	3.5	1.0	-	Austenitic

Table 2 Recommendations for welding SAF 2304, SAF 2205 and Sanicro 28

Grade	Welding method	Filler metal Sandvik	Arc energy kJ/mm	Remarks
SAF 2304/SAF 2205	TIG/MIG	22.8.3.L	0.5-2.5	Preheating or post-weld heat treatment not necessary
	MMA	22.9.3.LR		
Sanicro 28	TIG/MIG	27.31.4.LCu	max 1.0	Preheating or post-weld heat treatment not necessary
	MMA	27.31.4.LCuR		

Table 3 Summary of corrosion testing of welded joints in Sanicro 28

Test	Testing, time hours	Specimen type	P_{H_2S} kPa (psi)	Temperature °C (°F)	NaCl wt-%	Acidified with HAc	P_{CO_2} kPa (psi)	No. of specimens	Result
A	527	Tensile stressed to yield point	100 (14.5)	20 (68)	5	To pH = 2.5	-	2	NC
B	336	U-bends	100 (14.5)	20 (68)	9	To pH = 3	-	4	NC
C	336	U-bends	38 (5.5)	90 (194)	9	To pH = 3	-	4	NC
D	144	U-bends	500 (72.3)	20 (68)	9	-	1180 (171)	6	NC
E	144	U-bends	500 (72.3)	90 (194)	9	-	1180 (171)	6	NC

NC = No Corrosion

Table 4 Results from tests of TIG welded SAF 2205, SAF 2304, AISI 316 and 904L in 5% NaCl and 1 kPa H_2S at 100°C without (environment 1) and with (environment 2) the presence of 40 ppm oxygen

Material	SCC	Pitting	Comments
Environment 1			
SAF 2205	No	(Yes)	One in HAZ, complete cover of black deposit
SAF 2304	No	Yes	Mainly in welds, complete cover of black deposit
AISI 316	No	Yes	Mainly in welds, complete cover of black deposit
AISI 904L	No	(Yes)	One in HAZ
Environment 2			
SAF 2205	No	No	
SAF 2304	No	Yes	One in HAZ
AISI 316	No	Yes	One in HAZ
AISI 904L	No	No	

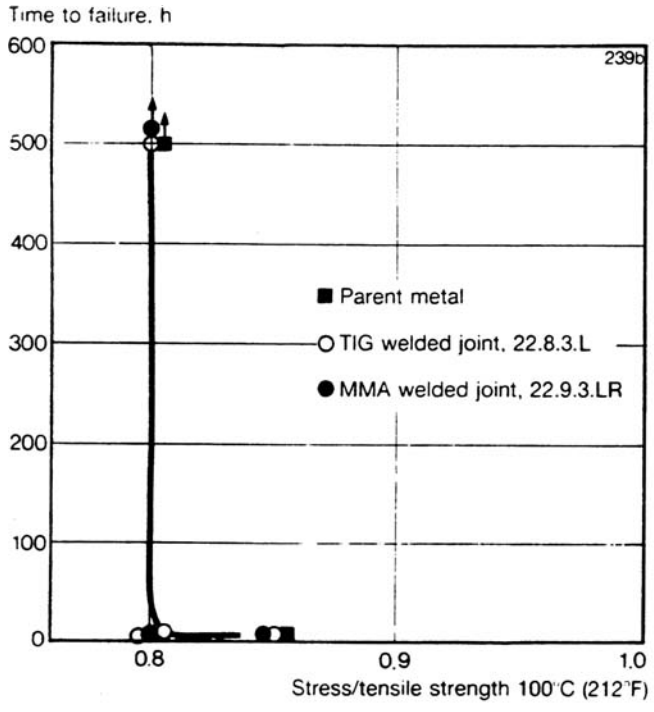


FIGURE 1 - Constant-load SCC tests of welds in SAF 2304. Aerated 40% $CaCl_2$, pH=6.5, at 100°C.

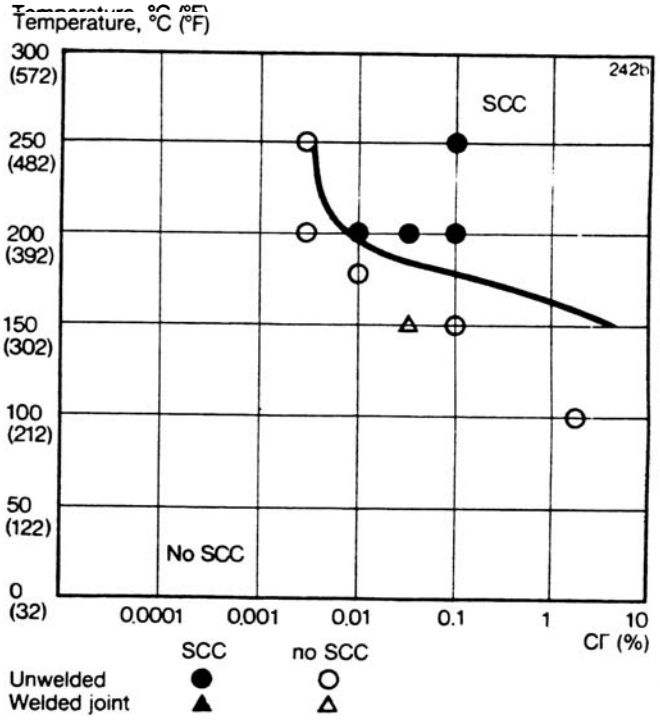


FIGURE 3 - SCC tests of SAF 2205 in undeaerated chloride solutions at 100 bar total pressure. Tensile specimens stressed to $R_{p0.2}$.

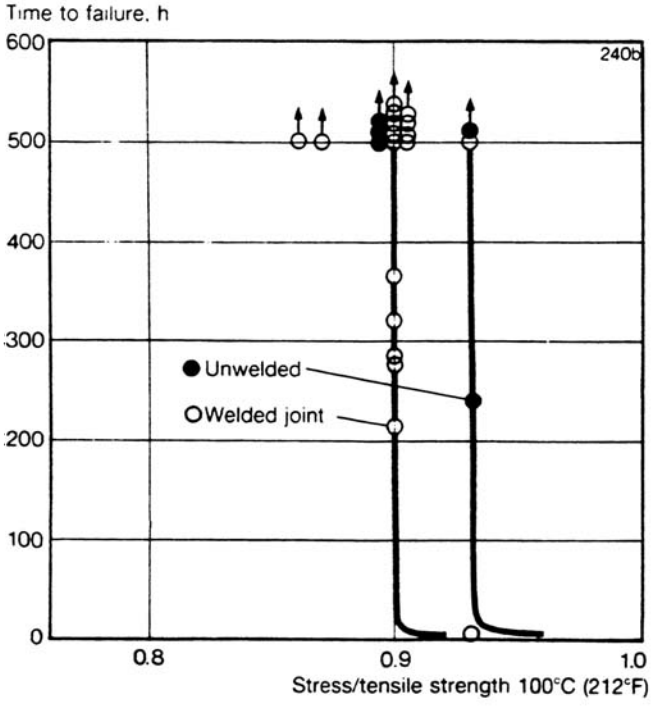


FIGURE 2 - Constant-load SCC tests of TIG, SAW and MMA joints in SAF 2205. Aerated 40% $CaCl_2$, pH=6.5, at 100°C

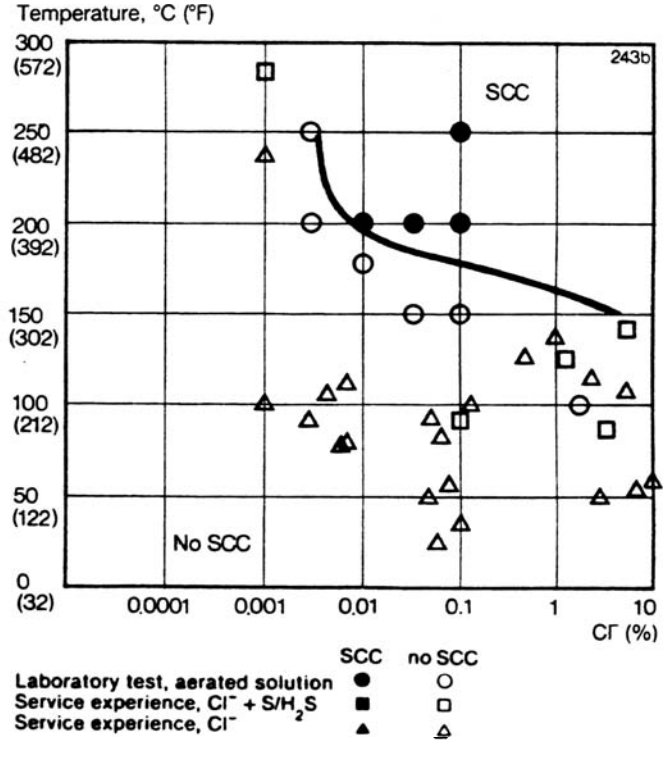


FIGURE 4 - Compilation of practical experience and laboratory test results for SAF 2205.

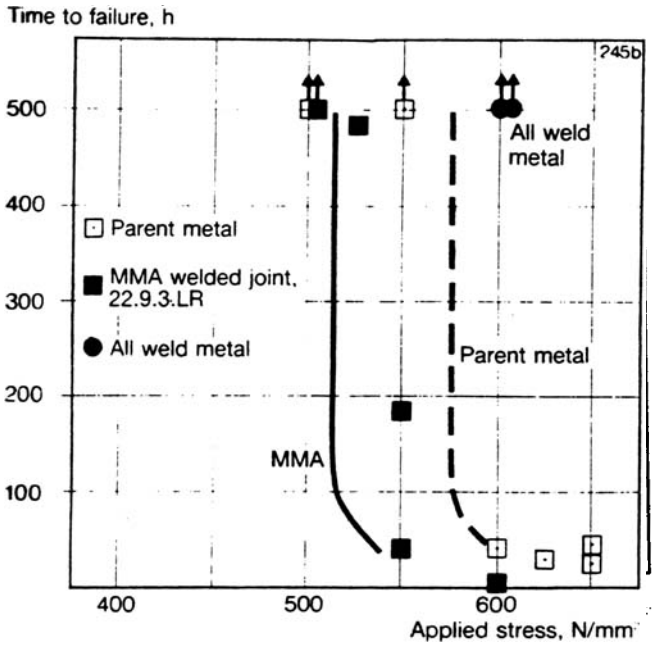


FIGURE 5 - Tests according to NACE TM-01-77 of SAF 2205 in welded and unwelded conditions.

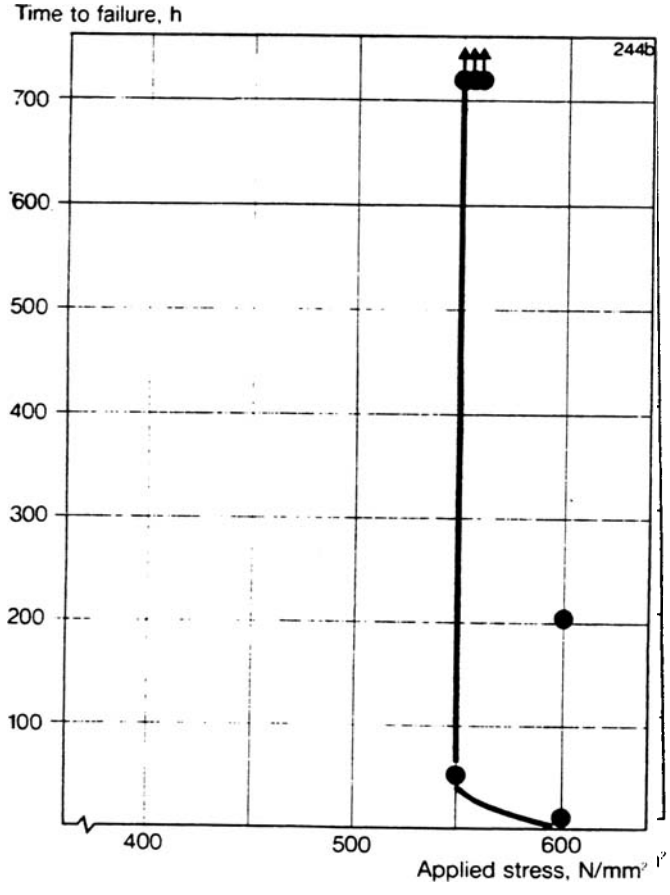


FIGURE 6 - Tests according to NACE TM-01-77 of TIG welded SAF 2205.

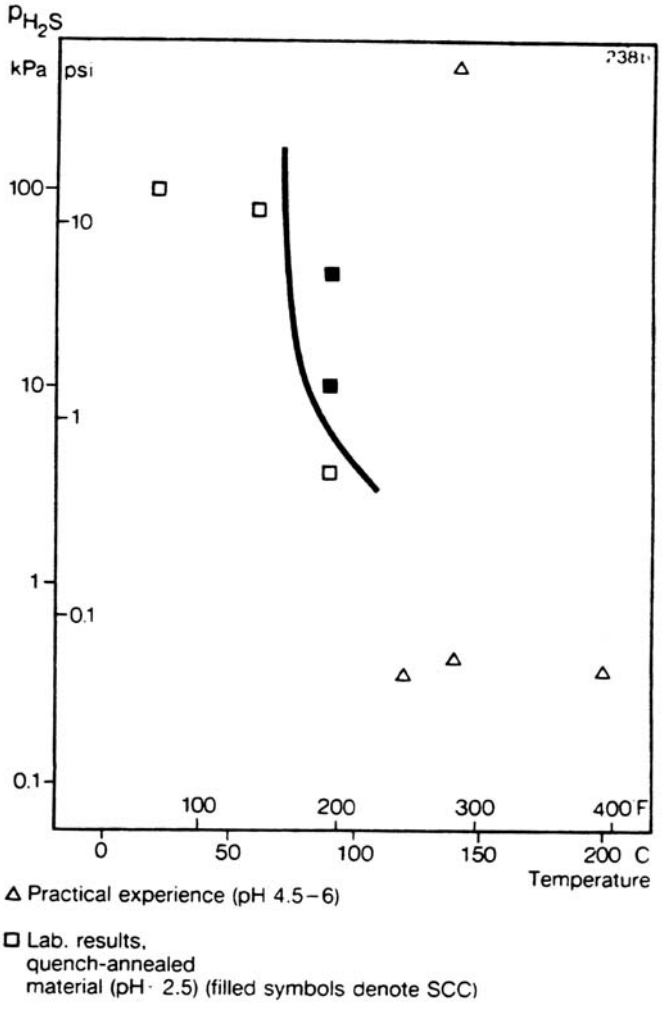


FIGURE 7 - Comparison between practical experience and laboratory test results of SAF 2205 in H_2S-containing environments.

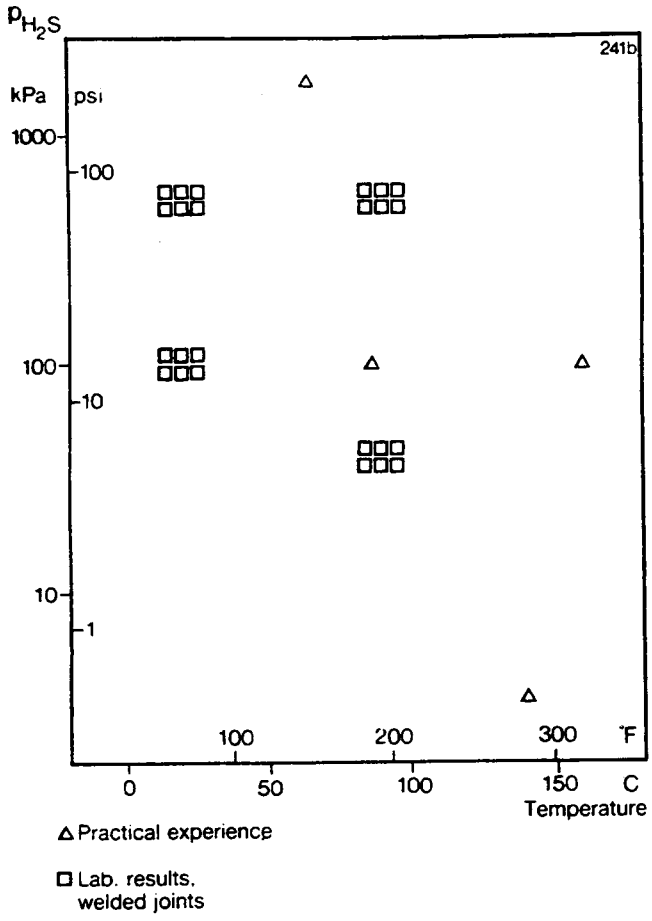


FIGURE 8 - Comparison between practical experience and laboratory test results of Sanicro 28 in H_2S-containing environments.

Copyrighted Materials
Copyright © 1996 NACE International Retrieved from www.knovel.com

Corrosion and Age Hardening Studies Of Some Cast Stainless Alloys Containing Ferrite*

By J. W. FLOWERS,* F. H. BECK** and M. G. FONTANA**

Abstract

A high-strength, corrosion-resistant alloy is described. This alloy, ACI type CD-4MCu, which is predominantly ferrite, possesses corrosion resistance equal to or better than that of austenitic stainless steels. High strength and corrosion resistance are obtained for the alloy in either the solution-annealed or aged condition. High resistance to stress corrosion cracking and pitting by chloride environments is also inherent in this alloy.

ACI cast alloys of the 19 Cr-9 Ni types, CF-3 (low carbon), CF-8 (normal carbon), CF-3M (low carbon, molybdenum bearing), CF-8M (normal carbon, molybdenum bearing) and CF-8C (normal carbon, columbium stabilized) containing from 0 to 44 percent ferrite in the austenite matrix are discussed with respect to corrosion resistance. Laboratory corrosion data from a number of environments are reported. Data are presented illustrating a marked increase in resistance to chloride stress corrosion cracking and improved mechanical properties with increasing amounts of ferrite in the alloys.

Introduction

CORROSION OF CAST STAINLESS ALLOYS with duplex (ferrite-austenite) microstructures has not been extensively explored. One purpose of this article is to present a research effort concerned with the effect of ferrite (0-65 volume percent ferrite in austenite) on the corrosion and stress corrosion of several cast alloy types. Particular emphasis is placed on the 19 Cr-9 Ni (CF-3, CF-8, CF-3M, CF-8M and CF-8C)[1] type alloys and on the CD-4MCu[1] alloy. The latter is of great interest because of its high strength and high corrosion resistance.

During the laboratory development of alloy CD-4MCu it was found that solution annealing by water quenching from approximately 2000 F (treatment normally used for 19 Cr-9 Ni alloys) produced an excellent combination of strength and corrosion resistance provided the carbon content of the alloy was maintained below 0.04 percent. An improvement in mechanical properties with no loss in corrosion resistance was attained upon aging the annealed material at 900 F for 3 hours. Later attempts to produce commercial castings of heavy or variable section thickness were unsuccessful due to quench cracking from the above solution annealing treatment. A modified solution annealing treatment which involves furnace cooling from 2050 F to 1750 F and oil quenching (treatment described in detail in the procedure) was employed to prevent quench cracking, and is the only recommended heat treatment for the alloy. The second objective of this article is to present studies of metallurgical changes in the annealed and aged alloy and the effects of these changes on corrosion resistance.

Experimental Procedure

Material Description

Chemical compositions of 23 of a total of 27 alloy compositions used in this study are reported in Table 1. These include cast alloys of the 19 Cr-9 Ni (CF-3, CF-8, CF-3M, CF-8M and CF-8C)[1] type prepared by induction melting of virgin materials (chemistry of alloys was designed to yield zero-, intermediate- and high-ferrite contents in each group) and one representative commercially produced heat each of cast alloys CD-4MCu,[1] CE-30,[1] CG-8M[1] and columbium-bearing Ni-Cr alloy.[2] The remaining four compositions included cast and wrought commercially produced alloy[2] and commercially produced wrought alloys, AISI Types 304 and 316. These latter materials were used in the stress corrosion program for comparison with the columbium-bearing Ni-Cr alloy[2] and the zero-ferrite CF-8 and CF-8M alloys which are the cast counterparts of the wrought 304 and 316 alloys, respectively.

Hardening Mechanism of CD-4MCu

All work on the hardening mechanism of alloy CD-4MCu was performed on material of the composition given in Table 1. Experimental solution-annealing treatments were made at temperatures within the range 1750-2150 F, followed by air, oil or water quenching. A solution-annealing treatment which prevents quench cracks in castings with heavy or variable sections was also employed. In this treatment, the test specimens were held at 2050 F for 2 hours, furnace-cooled to 1750 F, held at 1750 F for ½ hour and oil quenched. (Heavy sections are held at 2050 F for 2 hours plus 2 to 3 hours per inch of section thickness, furnace cooled to 1750 F and held until a uniform temperature is obtained throughout the section and finally oil quenched). Aging treat-

★ Submitted for publication February 25, 1963. A paper presented at the 19th Annual Conference of the National Association of Corrosion Engineers, March 11-15, 1963, New York, N. Y.
• Army Materials Research Agency, Watertown Arsenal, Watertown, Mass.
** Dept. of Metallurgical Engineering, Ohio State Univ., Columbus, Ohio.
[1] Alloy Casting Institute designation.
[2] Inconel, a product of International Nickel Company.

TABLE 1—Chemical Composition, Ferrite Content and Mechanical Properties of Alloys.

Alloy Designation	ACI Type	Volume % Ferrite	Percent Composition C	Mn	Si	Cr	Ni	Mo	N	Room Temperature Properties T.S. psi	Y.S. psi	% Elongation	% Reduction in Area	Charpy Impact V-Notch ft-lbs	Hardness BHN
A —	CF3 — 0		0.020	0.78	1.20	16.97	13.35	—	0.030	61,200	25,400	63	74	149	116
B —	CF3 — 4		0.020	0.83	1.29	19.28	10.07	—	0.075	71,800	31,800	73	68	122	133
K —	CF3 — 20		0.023	0.84	1.21	20.36	8.25	—	0.013	—	—	—	—	—	—
C —	CF3 — 37		0.020	0.83	1.50	21.81	7.68	—	0.056	89,100	51,000	48	67	102	164
D —	CF8 — 0		0.080	0.74	1.22	18.08	12.20	—	0.050	66,900	29,900	60	65	145	127
E —	CF8 — 5		0.070	0.80	1.25	19.99	9.38	—	0.062	77,600	36,300	60	68	122	158
F —	CF8 — 16		0.080	0.78	1.28	21.37	8.08	—	0.077	86,800	47,100	52	64	100	156
L —	CF3M-0		0.026	1.28	0.90	17.16	13.46	2.48	0.051	67,600	28,600	70	73	155	116
M —	CF3M-20		0.026	0.91	1.43	20.31	10.86	2.59	0.039	89,600	46,200	53	67	128	149
N —	CF3M-39		0.021	0.77	1.14	21.59	9.50	2.78	0.015	92,500	55,000	43	65	78	172
G —	CF8M-0		0.080	0.85	1.12	16.72	15.02	2.51	0.042	67,000	30,000	57	65	140	129
H —	CF8M-2		0.070	0.61	1.30	18.99	11.36	2.60	0.074	80,200	42,000	60	58	88	160
J —	CF8M-15		0.070	0.79	1.39	20.17	9.55	2.40	0.064	87,800	48,400	45	64	96	164
P —	CF8M-16		0.070	0.58	0.95	21.76	8.86	2.35	0.110	91,200	49,800	47	70	119	174
O —	CF8M-38		0.050	0.82	1.27	21.87	9.64	2.65	0.035	93,000	52,700	42	65	100	173
R —	CF8C-0		0.080	1.43	0.79	18.34	11.17	Cb 0.56	0.054	72,000	29,200	52	41	51	128
T —	CF8C-13		0.080	1.29	1.93	20.60	8.53	0.78	0.110	93,200	50,700	38	37	19	164
S —	CF8C-44		0.070	1.04	1.54	22.35	8.34	0.80	0.042	89,400	52,000	38	42	34	168
CD 4MCu(S.A.) - 65			0.025	0.89	0.90	25.03	5.52	Mo 2.08	Cu 3.15	107,500	97,900	17	44	44	228
CD 4MCu(Aged-65)			0.025	0.89	0.90	25.03	5.52	2.08	3.15	138,800	100,700	9	10	10	306
	CE30 — 28		0.250	0.54	1.80	28.16	9.64	—	—	100,200	62,500	11	18	—	190
	CG8M — 17		0.056	1.12	1.06	20.17	10.40	3.52	—	86,800	44,600	42	59	—	156
	CN7M — 0		0.040	0.70	0.88	20.22	29.78	2.75	3.50	65,000	28,300	45	69	—	140
Inconel (Cb) — 0			0.052	0.79	1.28	14.20	73.20	Cb 1.89	—	78,200	28,600	41	39	—	132

Note: Except for alloy CD-4MCu, all specimens were water quenched from 2050°F.
Alloy CD-4MCu given modified solution anneal and modified solution anneal plus age
S.A. - 2050°F, 2 hrs., F.C. to 1750°F 0.5 hr. and oil quench, stress relieve 600°F 2 hrs. and air cool.
S.A. and age - S.A. as above + 3 hrs. at 900°F

ments were performed for time periods up to 24 hours at 800, 900 and 1000 F, 1500 hours at 1000 F and 3500 hours at 900 F in order to study the mechanism of the aging process. The decomposition of the ferrite of the alloy into sigma phase and austenite was studied in the range 1200-1700 F by heating specimens at temperatures within this range for time periods sufficiently long for the reaction to go to completion.

Conventional mechanical polishing was employed on specimens prepared for light microscopy. Vilella's reagent (10 cc HCl, 100 cc methyl alcohol, 1 gm picric acid) served as a general etchant for most of the metallography. The etching procedure developed by Gilman[1] was used to check for the presence of sigma phase.

X-ray diffraction was used to verify the metallographic phase identifications made on specimens heated in the 1200-1700 F range and to provide a preliminary survey of the phases precipitating during age-hardening. For these purposes normal metallographic specimens which had been deeply etched in 20 percent hydrochloric acid in methyl alcohol or Vilella's reagent were mounted in a diffractometer unit in such a manner so that the X-ray beam grazed the etched surface. Filtered chromium radiation was employed.

Surface replicas from many of the specimens, particularly those in the annealed and aged conditions, were prepared for electron microscopy, since the important structural details were not resolvable in the light microscope. A mixture of 45 parts lactic acid, 45 parts methyl alcohol and 10 parts hydrochloric acid by volume was selected for solution-annealed specimens and specimens aged for relatively short time periods; a lower concentration of hydrochloric acid was used for specimens aged for long time periods. This reagent was used electrolytically at a potential difference of 6 volts for 10 seconds or less. A two-stage replica technique was employed.

Transmission electron diffraction through selected areas of extraction replicas was performed in the electron microscope as a means of identifying the structures of fine precipitates. The procedure for indexing electron diffraction patterns is covered in detail by Hall.[2]

Two methods of obtaining extraction replicas were employed. The method originally developed by Fisher[3] was found to be effective in extracting copper precipitate particles. In this technique, the specimen was first lightly etched in 10 to 20 percent hydrochloric acid in methyl alcohol, then covered by a thin film of 1 to 4 percent collodion. The specimens was then etched again with the hydrochloric acid solution through the plastic to free the precipitate particles, washed with methyl alcohol and dried. The film was then stripped as described by Hall.[4]

TABLE 2—Effect of Annealing and Aging Treatments on Microstructure and Hardness of Alloy CD-4MCu.

	Solution-Annealing Temperature, F*				
	2150	2050	1950	1850	1750
Quench	**Brinell Hardness**				
Water	285	278	262	234	230
Oil	252	244	240	241	231
Air	250	244	237	227	235
	Volume Percent Austenite				
Water	12	20	22	29	35
	Brinell Hardness Subsequent to Aging at 900 F for 3 Hours after Solution-Anneal Indicated				
Water	326	325	305	296	296
Oil	297	289	292	300	281
Air	292	292	284	274	287

* For two hours.

A second method of preparing extraction replicas was found effective for extracting small particles of sigma phase and a body-centered cubic transition precipitate. Specimens were electrolytically etched in the lactic-hydrochloric-methyl alcohol baths and after allowing to stand for a few seconds in the bath after etching, a film containing numerous precipitate particles formed on the surface of the specimen. This film was transferred intact to a carbon replica by means of the surface replica technique. All electron diffraction patterns were recorded with the electron microscope operated at 80 KV.

Quantitative metallography was employed to obtain a measure of the volume percent of the major phases present in annealed specimens and specimens heated in the 1200-1700 F range. The method used was point-counting, as described by Howard and Cohen.[5]

Stress Corrosion Studies

Except for alloy CD-4MCu, which was studied in both the solution-annealed and aged conditions, all materials employed in the stress corrosion study were water quenched from 2050 F. Heat treatments are described in the footnote to Table 1.

Stress corrosion specimens measuring approximately 1.3 inches long by 0.4 inch wide by 0.1 inch thick were prepared from each of the materials. After heat treating, the specimens were polished through 500 emery on the side to be placed in tension during the susceptibility test. The specimens were then deflected a predetermined amount by means of a screw acting against a knife edge at the center of the specimen which spans the opening of a C-clamp. Stress was determined from the relationship of stress and deflection for center loaded beams,

$$S = 12\,\frac{Ecy}{l^2}$$

in which S = tensile stress on specimen directly opposite knife edge (stress is maximum at this point), E = Young's modulus of elasticity, c = ½ thickness of specimen, y = specimen deflection in inches, and l = gage length over which deflection is determined.

After the specimen was loaded to produce the desired stress level, the assembly was placed in an autoclave containing 875 ppm sodium chloride in double distilled water. The pH of this solution was in the range of 6.0 to 6.5. Approximately 200 ml was added to the experimental 550-ml autoclave for each test.

Specimens were placed in autoclaves with the stressed surfaces facing up to receive the condensate which fell from the autoclave top. This was essential since the wetting and drying action was necessary for the promotion of stress corrosion cracks. The specimen was centered in the autoclave above the solution level to ensure these conditions. Upon completion of an 8-hour exposure, the specimen was removed, given a very light metallographic polish and examined on the tension side for cracks. More complete details of the apparatus and procedure are described elsewhere.[6]

Corrosion of CF Alloys

Corrosion tests were made on solution-annealed and aged CD-4MCu as described above and on CF type materials which were either solution-annealed (heated to 2050 F for 2 hours followed by a water quench) or sensitized (reheating the solution-annealed specimen to 1300 F, holding at temperature for 1 hour and finally quenching in water).

Except for the stress corrosion work described above, the surfaces of all corrosion specimens were prepared on 120 grit emery cloth. The specimens were then degreased in acetone and subjected to the corrosive environment.

All corrosion tests were performed in solutions prepared from reagent grade chemicals and double distilled water. Percentages are reported on a weight basis except for the chloride solutions used in the stress corrosion work. Approximately 200 ml of solution per square inch of specimen surface was employed, using fresh solution for each test period.

Experimental Results

Metallurgical Structures in Alloy CD-4MCu

Solution-Annealed Structures. Experimental work was undertaken on the solution-annealing of CD-4MCu in an effort to provide a better understanding of the structural changes which occur as a result of variations in thermal treatments. Hardness and microstructural changes were observed for specimens heated to 1750, 1850, 1950, 2050 and 2150 F for 2 hours and cooled in water, oil and air. Brinell hardness data after these treatments are presented in Table 2, along with the results of point counts made on the specimens water-quenched from each temperature and the hardnesses for the complete set of specimens after an aging treatment of 3 hours at 900 F. The hardness values after annealing



Figure 1—Annealed microstructure of alloy CD-4MCu (water quenched after 2 hours at 2050F). Etch, Vilella's Reagent. 225X.



Figure 2—Annealed microstructure of alloy CD-4MCu (heat 2050F 2 hours, furnace cool 1750F, oil quench, reheat 600F 2 hours and air cool). Etch, Vilella's Reagent. 225X.



Figure 3—Electron micrograph of alloy CD-4MCu specimen described in Figure 1. Etch, lactic acid-hydrochloric acid solution. 6500X.

generally increased with annealing temperature and severity of quench. All specimens showed response to the hardening heat treatment. The volume percent austenite decreased to a significant degree with increasing temperature. No sigma phase was detected metallographically in any of the annealed specimens.

A typical photomicrograph of the alloy in the solution-annealed condition is shown in Figure 1. The matrix is ferrite and the pools and plates are austenite, which appears in a dendritic form, also as Widmanstätten structure within the ferrite. The fine structure within the ferrite probably results from copper precipitated during cooling. Another characteristic of the microstructures produced by quenching specimens from 1950 F or higher is the presence of sub-boundaries within the ferrite grains. These are often referred to as "veins" in the literature on ferrous metallurgy. It has been shown that such sub-boundaries can be produced by deformation caused by applied loads at elevated temperatures or by the volume changes accompanying a phase change.[7-9] Guinier[9] has emphasized that the formation of sub-boundaries is a manifestation of polygonization. In this alloy, it appears that the sub-boundary formation is related to the formation of austenite during solution-annealing or during the quench itself. Figure 2 shows the microstructure with an increased amount of austenite and very little evidence of the subgrain structure characteristic of specimens quenched from 1750 F and 1850 F.

The annealed microstructures show some evidence of precipitation within the ferrite; this was investigated employing the electron microscope. Figure 3 is an electron micrograph of a surface replica which was obtained from a specimen which had been water-quenched from 2050 F. The microstructure shows evidence of fine precipitation within the ferrite and at sub-boundaries. Indications of larger precipitate particles and of precipitation at austenite-ferrite interfaces occur upon air cooling from 2050 F.

Electron diffraction patterns taken from extraction replicas permitted identification of the precipitate particles as a face-centered cubic phase with interplanar spacings very close to those of pure copper. The exact composition was not determined, but the precipitate was probably similar to the epsilon phase in the iron-copper system and was perhaps nearly pure copper. The presence of the copper-rich phase at internal boundaries within the specimens, as indicated by the electron micrographs, may have been a contributing factor in the cracking of castings of the CD-4MCu alloy when quenched from the higher annealing temperatures.

Aged Structure. The age-hardening of CD-4MCu was investigated with specimens in two initial conditions. One set of specimens was solution-annealed for 2 hours at 2050 F and water-quenched, and a duplicate set was given the modified solution-annealing treatment described previously. Hardness measurements were made on these specimens prior to and subsequent to aging for periods up to 24 hours at 800 F, 3500 hours at 900 F and 1500 hours at 1000 F.

These hardness data show some evidence of at least a two-stage hardening process. A slight maximum is attained early in the aging periods, followed by a gradual increase in hardness on continued aging at 800 F and 900 F. At 1000 F there is evidence of definite overaging of the alloy followed by a rather sharp rise in hardness

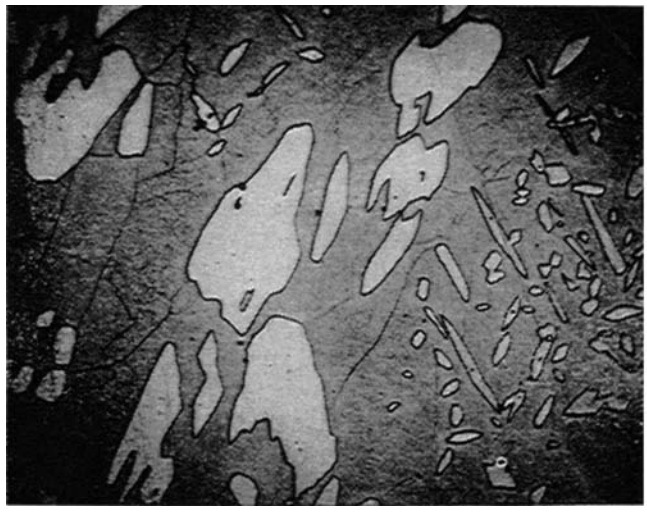


Figure 4—Microstructure of aged alloy CD-4MCu (aged 3 hours at 900 F subsequent to anneal described in Figure 1). Etch, Vilella's Reagent. 380X.

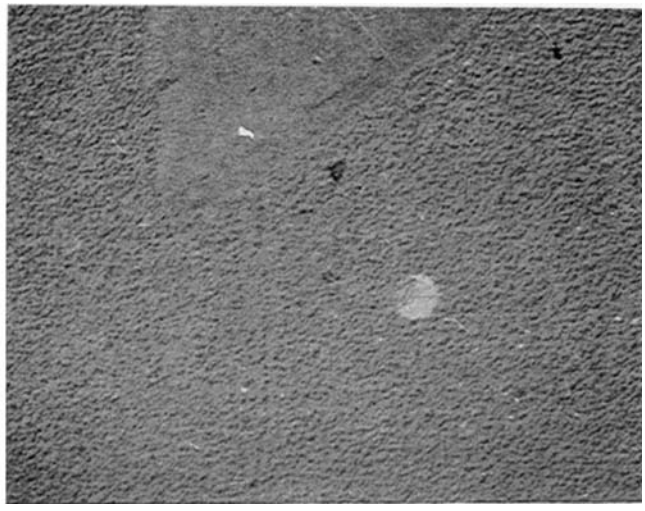


Figure 5—Electron micrograph, microstructure of aged alloy CD-4MCu described in Figure 4. Etch, lactic acid-hydrochloric acid solution. 6500X.

after aging times in the order of 1000 hours. The material initially water-quenched from 2050 F generally maintains a hardness advantage over the material which had received the modified solution-anneal. This may be due in part to the difference in the amount of austenite in the microstructure, because the specimens quenched from 2050 F contain 20 percent austenite, while those given the modified treatment are 36 percent austenite.

Microhardness data on some of the aged specimens showed that the hardness of the austenite remains constant during aging while the hardness of the ferrite increases, thus demonstrating that the processes producing the hardening occur only in the ferrite phase.

Structural Changes at 900 F. Metallographic investigations with the light microscope produced only a limited amount of information about the structural changes occurring at 900 F (Figure 4). The principal changes noted were a general darkening of the matrix with increased aging time and indications of accelerated aging at sub-boundaries within the ferrite. There was definite evidence of precipitation within the ferrite but the finer details of the structural changes were not resolvable. X-ray diffraction patterns from etched surfaces of the specimens showed evidence for the presence of a nearly pure copper precipitate after 500 hours of aging and sigma phase was detected after 2000 hours.

Figure 5 shows an electron micrograph of a surface replica taken from a specimen aged 3 hours at 900 F. A somewhat greater degree of precipitation is evident in comparison with the annealed structure discussed previously. A diffraction pattern otbained from an HCl extraction replica was indexed as face-centered cubic with a lattice parameter of 3.62 ± 0.01 Å. Within the limits of accuracy of electron diffraction, the lattice parameter of this phase remained constant throughout the aging period. X-ray diffraction patterns of the same phase obtained from specimens aged 500 hours or more gave a lattice parameter of 3.620 Å, which is slightly larger than the lattice parameter, 3.6153 Å, of pure copper. These data show that this first precipitate probably was nearly pure copper.

The number of particles apparently increased during the 3-hour aging period and the particles appeared essentially spherical in shape, with an average diameter of 100 to 150 Å. Slow growth of the particles during aging apparently occurs with the spheres attaining an average diameter in the order of 300 Å after 3500 hours of aging.

Electron micrographs of the alloy were made after 24 hours of aging and a diffraction pattern from a lactic acid-HCl extraction replica disclosed the first two lines on the diffraction pattern to be the first experimental evidence of the occurrence of a body-centered cubic, chromium-rich transition precipitate. An extraction replica and diffraction pattern after 250 hours of aging, also obtained with the lactic acid-HCl technique, provided further evidence of this phase. Small, essentially spherical particles visible in the etching film produced an electron diffraction pattern which was indexed as body-centered cubic with a lattice parameter of 2.88 ± 0.01 Å, in comparison with the X-ray lattice parameter of the ferrite (2.872 Å in the annealed condition), and the lattice parameters for pure iron and pure chromium, which are 2.8664 Å and 2.8845 Å, respectively. The apparent average diameter of the sphere-like particles of the body-centered cubic phase increased very slowly from about 100Å or less after 24 hours of aging to about 200Å after 3500 hours.

From the lattice parameter of the body-centered cubic phase, it appears to be related to the chromium-rich body-centered cubic phase found by Fisher, Dulis and Carroll[10] and Williams and Paxton[11] in ferritic stainless steels and very pure iron-chromium alloys; this phase was found to contain about 80 percent Cr.

A lactic acid-HCl extraction replica of the aged structure after 1000 hours is a complex pattern resulting from the superposition of rings from the copper precipitate, the body-centered cubic precipitate, and sigma phase, which was first detected after this aging period. At this point there are at least five phases in the microstructure. Small amounts of carbides and nitrides would also be expected to form, but no evidence of their presence was obtained.

After 2000 hours of aging, particles of sigma phase were readily discernible in electron micrographs as plate-like precipitate within the ferrite. Some sigma particles formed at austenite-ferrite interfaces and grew into the ferrite. Definite evidence was found for the gradual replacement of the ferrite and transition precipitate with sigma phase.

Specimens aged 3500 hours at 900 F illustrate further growth of sigma phase into the aged ferrite. The aging is rather heterogeneous and large areas can be found within the ferrite which apparently contain little or no sigma phase. Even after 3500 hours the aging process is evidently far from completion.

Structural Changes at 1000 F. The first changes in microstructure observed for specimens aged at 1000 F were a general darkening of the ferrite and indications of precipitation at sub-boundaries. Specimens aged 24 hours at 1000 F contained the copper-rich precipitate. The average particle diameter is about 250 Å, showing that growth of this precipitate is much more rapid at 1000 F than at 900 F. Growth of these particles is apparently responsible for the overaging effect noted for the hardness curve at this temperature.

With continued holding at 1000 F the structural changes within the ferrite were very different from those occurring at 900 F. Fine austenite began to form within the ferrite, and could first be resolved with the light microscope after 100 hours. There was also some growth of previously existing austenite into the ferrite. Particles of sigma phase were first seen in electron micrographs after 160 hours of aging. Lactic acid-HCl extraction replicas produced no evidence for the existence of the body-centered cubic transition precipitate at 1000 F.

Laminar aggregates of sigma phase and new austenite formed with prolonged exposure. Austenite-ferrite interfaces were preferred sites, but some aggregates also formed within the ferrite. On further holding, the decomposition of the ferrite continued, with about 50 percent of the original ferrite being replaced by sigma phase and new austenite after 1500 hours at 1000 F.

Decomposition of Ferrite Between 1200 and 1700 F. Specimens in both of the annealed conditions were reheated for varying time periods in the temperature range 1200 to 1700 F for the purpose of studying the decomposition of the ferrite in the initial microstructures. Since the data obtained for both initial conditions were very similar, only those for specimens solution-annealed at 2050 F and water-quenched are presented.

Microstructural investigations showed that the structural changes occurring during the periods of softening were the formation of new austenite and probably the growth and coalescence of the copper-rich precipitate present in the annealed microstructure. The new austenite could be detected almost immediately after the start of reheating and was usually seen in a Widmanstätten form, although some growth of the austenite originally present did occur. The only evidence for agglomeration of the copper-rich precipitate was the change in etching response with time as studied with the light microscope. X-ray diffractometer patterns of specimens lightly etched with 20 percent HCl did verify the presence of the copper-rich precipitate throughout reheating at 1200, 1400 and 1550 F. No X-ray evidence of the precipitate was obtained at 1650 F. The microstructures of the 1650 F specimens showed little if any evidence for the precipitate after several hours of aging.

During the later stages of reheating, formation of large amounts of sigma phase occurred within the ferrite in the form of a lamellar aggregate with new austenite. The transformation often began at the original austenite-ferrite interfaces and occasionally the lamellar product was nucleated at a ferrite-inclusion interface. Growth of the lamellar aggregates then proceeded into the ferrite. After the transformation products filled the ferritic areas, there was a tendency for the new austenite to thicken and for the sigma phase to assume the form or rather irregularly shaped small particles. The amount of sigma phase present and the degree of dispersion of the sigma particles increased with decreasing temperature. Results of point counts showed that the volume percentages of sigma phase present in the final microstructures were 35, 41 and 49 at 1550, 1400 and 1200 F, respectively.

At 1650 F, only 10 volume percent of sigma phase had formed after 150 hours of reheating, and no sigma phase was detected after 150 hours at 1700 F. From the microstructural investigation, the times for the start and finish of sigma phase formation at the temperatures investigated were determined approximately and those data are exhibited in Figure 6, which shows the expected C-shaped curve.

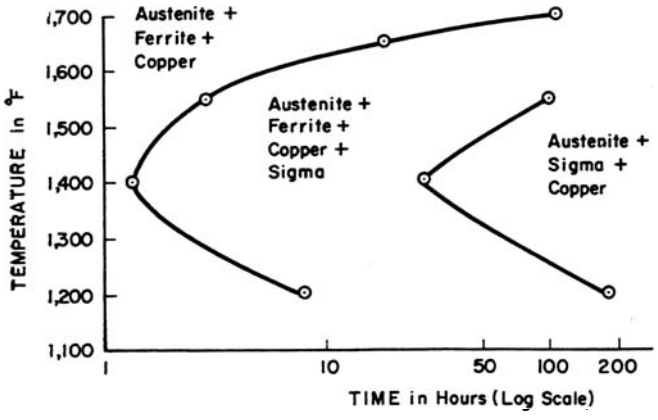


Figure 6—Partial isothermal transformation diagram for alloy CD-4MCu in the temperature range 1200-1700 F.

Discussion

The study of the solution-annealing of CD-4MCu showed that the volume percentage of austenite in the annealed structure increases with decreasing temperature, and that a nearly pure copper precipitate was present in the annealed condition, even when the alloy was water-quenched from 2050 F. There was apparently a quench-hardening effect, because the hardness of the alloy tended to increase with annealing temperature and severity of quench. In addition, there was some microstructural evidence of deformation of the ferrite during quenching which may have been produced by transformation stresses caused by austenite formation.

Recent theoretical and experimental work has emphasized the role of vacancies in quenching phenomena and precipitation. Federighi[12] and DeSorbo, Treaftis and

Turnbull[13] have advanced the belief that the excess vacancies retained for a short time when a metal is rapidly quenched from a high temperature may be responsible for the otherwise anomalously high rates of clustering observed during the early stages of aging aluminum alloys. Hauser, Capenos and Banerjee[14] have recently obtained experimental evidence for the formation of small dislocation loops by the collapse of vacancy disks in the ferrite of a thin foil of Type 410 stainless steel upon quenching the foil from 1500 F. This is apparently the first time that this phenomenon has been observed in a body-centered cubic alloy. Whether either or both of these effects of vacancies are at least partially responsible for the precipitation and hardening observed upon quenching CD-4MCu is open to question. Thin foil studies with the electron-microscope would be required to resolve the issue.

Experimental results from electron microscopy and electron diffraction of specimens aged at 900 F indicate that the hardening observed in CD-4MCu at this temperature is caused by a three-stage precipitation process. In the first few hours of aging the hardening seems to be mainly associated with the precipitation of a fine dispersion of nearly pure copper particles within the ferrite. The second stage appears to be associated with the precipitation of small particles of a body-centered cubic transition precipitate which is probably higher in chromium than the parent ferrite. The third stage involves growth of sigma phase at the expense of the transition precipitate; it was far from complete after 3500 hours at 900 F.

However, it is quite possible that the hardening in the first few hours at 900 F is actually the result of a superposition of the effects of the copper-rich precipitate and small particles of the transition phase which were undetected by the extraction replica techniques. The existence of the copper-rich precipitate in the annealed specimens also interferes with observations. However, the overaging observed at 1000 F where copper alone was detected does serve to illustrate the hardening effect of copper

The question of why particles of copper harden and strengthen the alloy, whereas in bulk form, copper is much softer than stainless steel, is most interesting. Hornbogen and Glenn,[15] in their study of the precipitation of copper from alpha iron, performed an experiment which seems to answer the question, to a degree. These authors deformed an aged specimen by rolling, extracted the copper particles, and examined them in an electron microscope. The particles were thin enough for transmission of electrons and lines were observed which were not present in the particles before deformation; these lines were thought to indicate thin twins or stacking faults in the particles. This was interpreted as showing that the particles were sheared during the deformation and that strengthening was provided by the energy required to shear a particle in its own system of deformation.

Replacement of the body-centered cubic transition phase with sigma phase in this duplex stainless steel occurs much more rapidly than the similar process in ferritic stainless steels. Sigma phase was first detected after 1000 hours at 900 F, whereas several years is sometimes required to form sigma phase in ferritic stainless steels.[16] The main contributing factor may be the composition differences between the ferrite phases involved. Due to the partitioning of the alloying elements between the austenite and ferrite in the duplex alloy, this ferrite contains a considerably higher concentration of sigma phase-promoting elements than the gross composition indicates.

The hardening effect conferred by the transition precipitate may be produced by coherency stresses. Williams and Paxton[11] examined with X-rays single crystals of iron-chromium alloys containing the chromium-rich precipitate which forms in this system. They also examined extracted particles of the precipitate. The single crystal patterns showed no evidence of precipitate spots but the extracted particles had a larger lattice parameter than the ferrite. A possible explanation is that in bulk specimens the chromium-rich precipitate is completely coherent with the ferrite matrix, whereas, in the extracted form it is unconstrained and exhibits the lattice parameter characteristic of its composition. A similar effect may be possible for the alloy studied in the present investigation.

Corrosion Studies

Due to the high resistance displayed by CD-4MCu alloy to both general and stress corrosion in several environments, a program was undertaken to examine the corrosion behavior of a series of ferrite-containing CF type alloys, prepared for studies of mechanical properties. These corrosion studies are discussed below. Mechanical properties, ferrite contents and chemical compositions of these materials are given in Table 1.

Stress Corrosion

Specimens of each alloy were stressed in tension to predetermined values and exposed individually in autoclaves containing 875 ppm sodium chloride in water for a time period of 8 hours. These tests were continued on new specimens at various stress levels until the minimum stress to cause cracking of each during the 8-hour test period was determined. This stress is shown in Figure 7 at the black to grey transition zone in each of the bars, which are identified by alloy type and ferrite content. The lower zone of each bar represents the non-cracking stress range, the upper zone shows the stress range for cracking, and the total height represents the yield of stress for each alloy. It is of interest to note that only three of the alloys, CN-7M, Ni-Cr alloy(2) and CE-30, are free of the transition zone. Of these three alloys CN-7M displays stress corrosion cracks in the above environment when stressed slightly over the yield stress. Cracking has not been observed at any time for alloys CE-30 and Ni-Cr alloy(2) even when stressed far in excess of the yield stress. Columbium-free Ni-Cr alloy(2) (cast and wrought) and columbium-bearing Ni-Cr alloy(2) (cast) were included in these tests. All three of the Ni-Cr materials are represented by a single bar.

With the exception of the high ferrite-containing CF-8M alloy, all CF type materials display an increase in resistance to stress corrosion cracking with increasing ferrite content. This effect is observed in each of the five groups of alloys which are arranged in the orders of increasing ferrite content and increasing alloying elements. Except for the low carbon alloys and alloy CF-8C

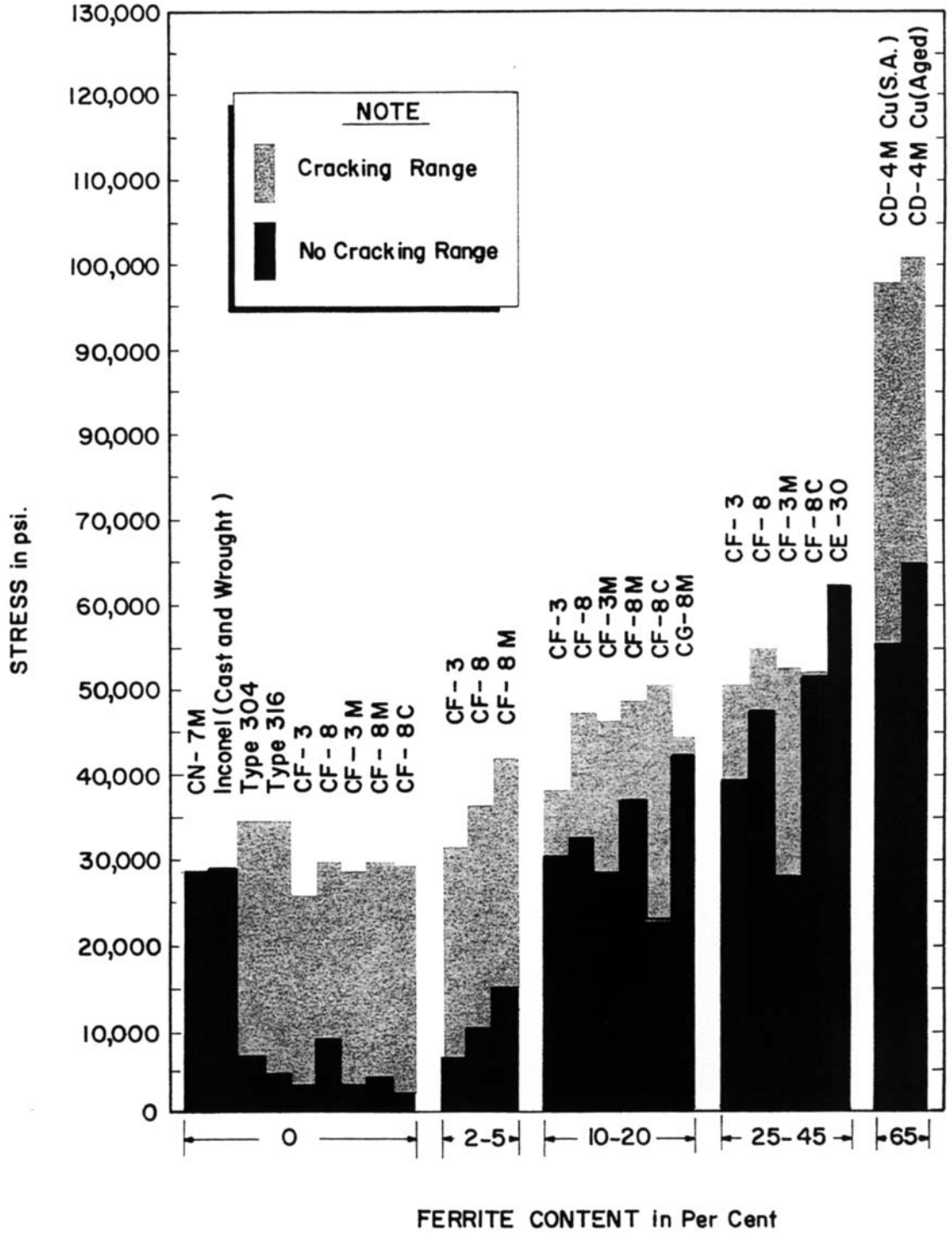


Figure 7—Effect of ferrite on the stress corrosion susceptibility of alloys by condensate from 400F water, containing 875 ppm sodium chloride, 8-hour tests. Total bar length indicates yield strength; black to grey transition indicates stress required to promote cracking.

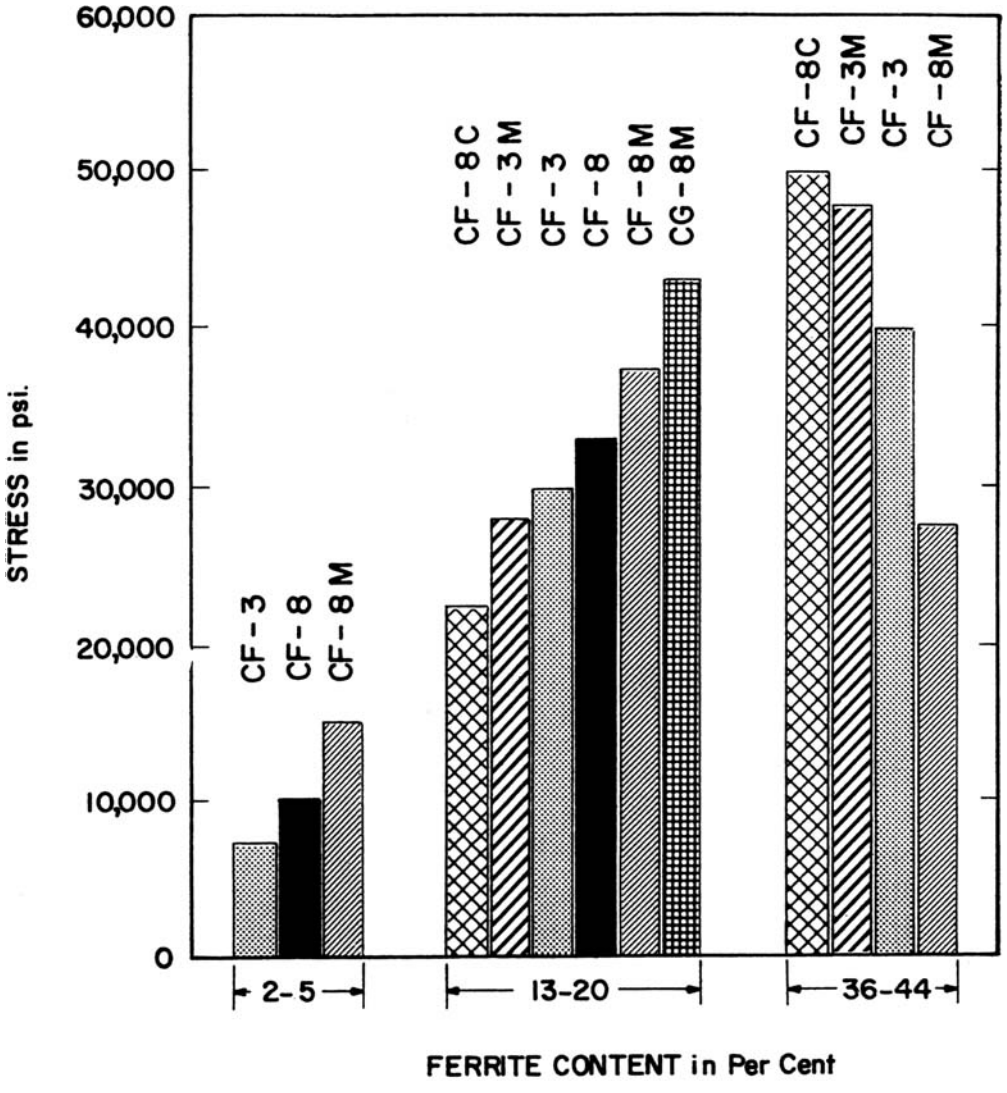


Figure 8—Effect of ferrite, carbon and total alloy content on stress corrosion susceptibility of some CF type alloys. Total bar length indicates stress required to produce cracking under conditions described in Figure 7.

which show marked improvements at the high ferrite level, the most significant increase in resistance to cracking is observed in going from the zero and very low ferrite level to the intermediate ferrite level (10-20 percent ferrite).

Figure 8 lists the order of the alloys in the very low and intermediate ferrite group with respect to carbon content and total alloy content as a function of increasing resistance to cracking. It is immediately evident that high carbon is superior to low carbon alloys. Further improvement is observed with increasing alloy content of the high carbon heats, i.e., CF-8 on the low end and CG-8M on the high end. Alloy CF-8C, which must be considered as having the lowest carbon content of the group (carbon combined as columbium carbide rather than in solid solution) shows the poorest resistance of all alloys in the intermediate ferrite range. Alloy CF-3 displays the best resistance of the low carbon heats. Alloy CF-3M, normal and high nitrogen heats, is represented by a single bar which falls between the CF-3 and CF-8C materials.

This figure also shows the high ferrite-containing alloys arranged in the same order as in the very low and intermediate groups. A complete reversal in corrosion resistance is observed. That is, the CF-8C shows the greatest resistance to cracking, followed by CF-3M, CF3 and finally CF-8M with the lowest resistance to stress corrosion cracking.

These data are interesting from the standpoint of the mechanism of stress corrosion cracking. They suggest possible major variations in the stabilities of the austenites of the different alloys which can occur as a result of partitioning of the elements in the two phases. The importance of alloy composition, for example, the content of carbon and molybdenum, in addition to that of ferrite is realized from the data. An important area for future study is indicated; that is, complete and detailed analyses of the various alloys by microprobe studies, could provide information leading to formulation of a more stress corrosion resistant material.

Figure 9, alloy F-CF8-16, represents a structure containing 16 volume percent ferrite in an austenite matrix. The yield strength of this alloy is 47,100 psi. A stress in the order of 33,000 psi is required to crack this material in the test. Close examination reveals that the increased cracking resistance is derived from the "keying" action of ferrite. The termination point of one end of a crack is illustrated. The crack did not pass through

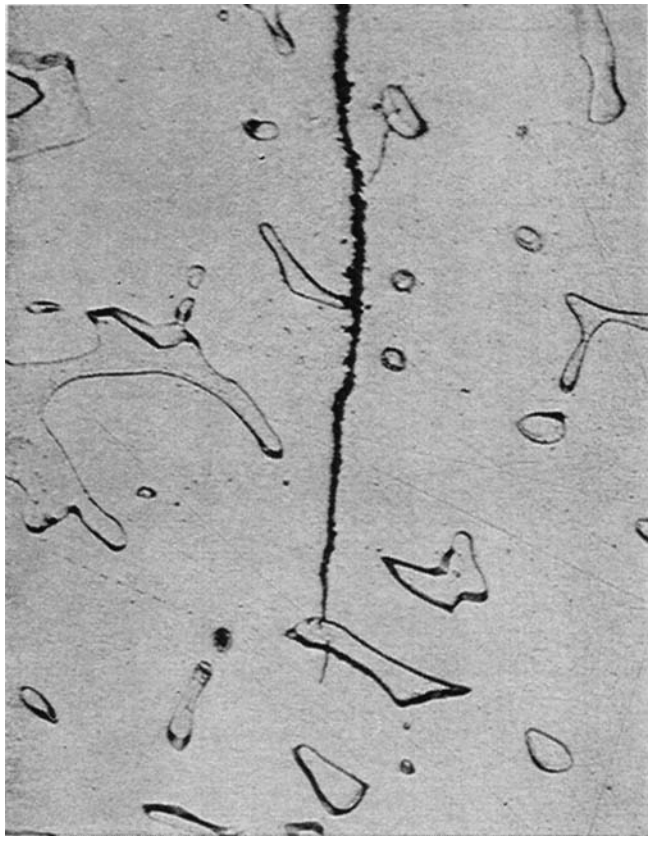


Figure 9—Stress corrosion crack showing "keying effect" of ferrite in alloy F-CF8-16. Specimen stressed at 33,000 psi and tested per description in Figure 7. Oxalic acid etch, electrolytic. 500X.

the ferrite, but propagated through the austenite beneath the ferrite grain and again emerged on the lower side of the ferrite grain. A similar observation was made at the other extremity of the crack.

General Corrosion

Corrosion by Boiling 65 percent Nitric Acid. Specimens from all ferrite levels of the CF-3, CF-8, CF-8M and CF-8C type alloys were solution-annealed at 2050 F and exposed to boiling 65 percent nitric acid. Although this environment is normally used to detect sensitivity to intergranular corrosion associated with chromium depletion during carbide precipitation and/or sigma phase formation, its main purpose here was to detect possible effects of the duplex structure. Results of these tests are presented in Table 3.

An increase in corrosion resistance results when the ferrite content of the CF-3 and CF-8 alloys is increased from 0 to approximately 20 percent. An increase in the ferrite content of alloy CF-3 from 20 to 37 percent results in a slight increase in corrosion rate. Considerable improvement in corrosion resistance is observed for the CF-8M alloy when the ferrite content is increased from 0 and 2 percent to 16 percent (high nitrogen alloy) and to 38 percent (alloy 0). Figure 10 is a cross section of alloy 0 showing a typical high ferrite content structure. The intermediate ferrite containing CF-8C alloy, alloy T, displays a considerable increase in corrosion rate over the 0 and 44 percent ferrite-containing R and S alloys. This effect is related to carbide precipitation at the ferrite-austenite boundaries of the T alloy. The ferrite stringers in this case are thin and quite continuous in comparison to the massive ferrite in alloy S.

TABLE 3—Effect of Ferrite in CF-3, CF-8, CF-8M and CF-8C Type Alloys on Corrosion by Boiling 65 Percent Nitric Acid (48-hour Periods).

Alloy Code-Designation-% Ferrite	Corrosion Rate in Mils Per Year					
	1	2	3	4	5	Average
A-CF3-0	15.5	10.5	9.6	12.0	10.4	11.6
B-CF3-4	11.0	6.0	9.6	10.5	8.6	9.2
K-CF3-20	11.0	6.8	6.2	9.4	7.9	7.9
C-CF3-37	9.5	8.8	7.3	11.0	9.4	9.2
D-CF8-0	16.0	13.5	8.2	13.0	12.5	12.6
E-CF8-5	9.1	15.0	5.7	12.0	11.5	10.7
F-CF8-16	6.3	9.1	8.4	5.7	8.6	7.6
G-CF8M-0	24.0	16.5	19.5	24.0	15.5	19.5
H-CF8M-2	25.0	20.0	24.0	27.0	22.0	23.6
J-CF8M-15	21.0	16.5	13.5	17.5	18.0	17.3
P-CF8M-16	14.5	9.6	8.8	10.5	10.5	10.8
O-CF8M-38	9.7	10.0	12.0	10.5	12.0	10.8
R-CF8C-0	9.5	7.0	9.6	6.9	8.2	8.2
T-CF8C-13	18.5	18.0	21.0	20.0	14.0	18.3
S-CF8C-44	11.0	9.7	11.5	11.5	15.5	11.8

Note: All specimens water quenched from 2-hour solution-anneal at 2050 F.

TABLE 4—Effect of Ferrite in CF-3, CF-3M and CF-8M Type Alloys on Corrosion by Aqueous 10 Percent Nitric Acid-3 Percent Hydrofluoric Acid Solution at 175 F. (Five Half-hour Periods).

Alloy Code-Designation-Percent Ferrite	Average Corrosion Rate in Mils Per Year		
	Solution-Annealed*	Sensitized**	Ratio***
A-CF3-0	13.20×10^3	13.80×10^3	1.0
B-CF3-4	6.20×10^3	3.90×10^3	0.63
K-CF3-20	4.40×10^3	0.98×10^3	0.22
C-CF3-37	2.00×10^3	0.68×10^3	0.34
L-CF3M-0	2.50×10^3	2.10×10^3	0.84
M-CF3M-20	0.61×10^3	0.41×10^3	0.67
N-CF3M-39	0.32×10^3	0.36×10^3	1.1
G-CF8M-0	2.50×10^3	8.10×10^3	3.2
J-CF8M-15	0.62×10^3	1.90×10^3	3.1
P-CF8M-16	0.57×10^3	0.64×10^3	1.1
O-CF8M-38	0.35×10^3	0.42×10^3	1.2

* Solution-anneal; water quench from 2 hours at 2050 F.
** Sensitization; water quench from 1 hour at 1300 F subsequent to solution-anneal.
*** Sensitized/solution annealed.

Corrosion by 10 Percent Nitric Acid-3 Percent Hydrofluoric Acid at 80 C. This environment, designed to reveal carbide precipitation and susceptibility to intergranular corrosion, is used here to determine the effect of ferrite on corrosion by mixed acids. In all cases, a pronounced increase in corrosion resistance was displayed with increasing ferrite content for CF-3, CF-3M and CF-8M alloys.

Table 4 shows the average corrosion rates of five half-hour test periods. Corrosion rates are high as is normally observed in this environment. The test can be used quantitatively with Type 316 L stainless steel in which the ratio of the rates for the sensitized specimens to those of the solution-annealed specimens indicates the degree of sensitization. If the sensitization is marked, the ratio is 2:1 or higher.

The ratios for the sensitized to solution-annealed specimens are 1:1 or less for the low carbon CF-3 and CF-3M materials. Again, the beneficial effect of increasing ferrite content is evident for the above two materials. As might be expected, the normal carbon CF-8M sensitized specimens display higher corrosion rates and ratios for the low ferrite heats. Decreased corrosion rates and low ratios are observed for intermediate and high ferrite contents. The great difference between the J and P alloys, of equivalent ferrite content, is probably related to the difference in nitrogen contents of the alloys. Nitrogen affects the degree of partitioning of the elements in the two phases of the alloy.

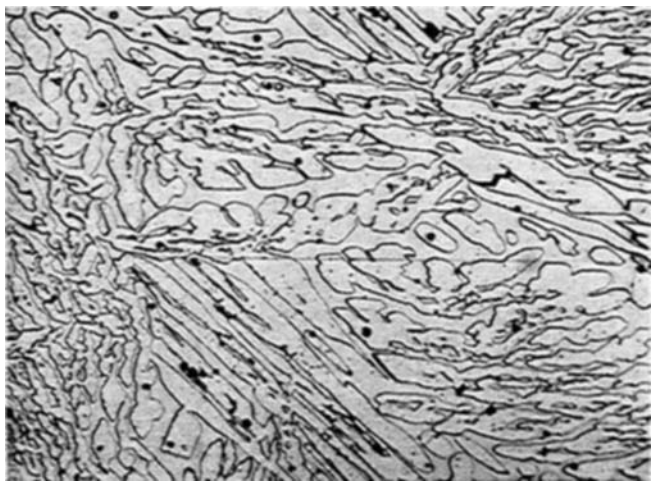


Figure 10—Typical microstructure of high ferrite-containing alloy, O-CF8M-38, illustrating ferrite stringers and pools in austenite matrix. Oxalic acid etch, electrolytic. 200X.

Corrosion by Boiling 75 Percent Acetic Acid. Boiling 75 percent acetic acid represents an environment which produces a relatively mild corrosion attack on Type 316 stainless steel. Thus, its effect on the CF-8M series of ferrite-containing alloys was of primary concern, although the C-F8 series was also tested in order to determine any effect of ferrite in the non-molybdenum bearing material. Although passivity was displayed for all specimens during the second period, the beneficial effect of ferrite was evident for both groups, as indicated in Table 5. The corrosion rate was greatly reduced for the CF-8 alloys and all of the CF-8M specimens containing ferrite were attacked at a rate less than 1 mil per year, while the fully austenitic G-CF8M-0 alloy displayed a rate of 19 mils per year in the first period.

If the assumption is made that passivitity is produced by the polarization currents between the austenite and ferrite, as was reported in earlier work on CF type alloys, these data were as expected. The anodic polarization of ferrite was shown to reduce the corrosion attack of acetic acid on CF-8 and CF-8M alloys.[17]

Corrosion of CF-8M by Glacial Acetic, Phosphoric and Sulfuric Acids. Corrosion by boiling glacial (99.7) percent acetic acid (Table 6) provided data similar to that observed for the boiling 75 percent acid. Although the first period rates in the glacial acetic acid were lower than those observed for the 75 percent acid, the effect of passivity was demonstrated. All corrosion rates of the CF-8M alloys were low, the highest being only 2 mils per year for the first two periods of the G-CF8M-0 alloy. The H-CF8M-2 alloy had a rate of 1 mil per year for each of the first two periods. All alloys containing more than 2 percent ferrite displayed rates of less than 1 mil per year in all test periods.

The CF-8M alloys displayed high resistance to corrosion by boiling 40 percent phosphoric acid. A reduction in corrosion rate was found when the ferrite content of the CF-8M alloy was increased from 0 to 38 percent (Table 6).

TABLE 5—Effect of Ferrite in CF-8 and CF-8M Type Alloys on Corrosion by Boiling 75 Percent Acetic Acid (48-Hour Periods).

Alloy Code-Designation-% Ferrite	Corrosion Rate in Mils Per Year		
	1	2	3
D-CF8-0	160	<1	<1
E-CF8-5	110	<1	<1
F-CF8-16	70	<1	<1
G-CF8M-0	19	<1	<1
H-CF8M-2	<1	<1	<1
J-CF8M-15	<1	<1	<1
P-CF8M-16	<1	<1	<1
O-CF8M-38	<1	<1	<1

Note: All specimens water quenched from 2-hour solution-anneal at 2050 F.

TABLE 6—Effect of Ferrite in CF-8M Type Alloys on Corrosion by Glacial Acetic, Phosphoric and Sulfuric Acids (48-Hour Periods).

Alloy Code-Designation-% Ferrite	Corrosion Rate in Mils Per Year					
	1	2	3	4	5	Average
Boiling Glacial Acetic Acid						
G-CF8M-0	2.2	2.1	<1	<1	<1	
H-CF8M-2	1.1	<1.	<1	<1	<1	
J-CF8M-15	<1.	0	0	<1	<1	
P-CF8M-16	<1.	<1.	0	<1	<1	
O-CF8M-38	<1.	<1.	0	<1	<1	
Boiling 40% Phosphoric Acid						
G-CF8M-0	1.0	1.0	1.5	2.0	2.0	1.6
J-CF8M-15	0.5	0.5	0.9	0.9	0.9	0.74
O-CF8M-38	0	0.3	0.3	0.5	0	0.22
85% Phosphoric Acid, 200 F						
G-CF8M-0	37.0	5.5	40.0	42.0	51.0	35.1
H-CF8M-2	4.2	7.6	6.4	6.6	5.6	6.1
J-CF8M-15	4.0	2.5	4.9	12.0	12.0	5.9
P-CF8M-16	2.9	2.2	9.0	9.0	7.9	5.2
O-CF8M-38	2.7	2.2	3.0	2.8	1.9	2.1
15% Sulfuric Acid, Ambient Temperature						
G-CF8M-0	3.1	0	3.1	0	0	....
J-CF8M-15	3.8	0	0	0	0	
O-CF8M-38	0.9	0	0	0	0	

Note: All specimens water quenched from 2-hour solution-anneal at 2050F.

An excellent demonstration of the effect of ferrite on corrosion resistance is illustrated in Table 6 for the corrosion of CF-8M by 85 percent phosphoric acid at 200 F. Here, even as small an amount of ferrite as 2 percent causes a drop in corrosion rate from 35 mpy for the fully austenitic material to 6 mpy. Further reductions in corrosion rates to 2 mils per year are brought about by increasing the ferrite content to 38 percent. Little difference is indicated when increasing the ferrite content from 2 to 15 percent.

Data for the corrosion of CF-8M in sulfuric acid at ambient temperature are presented in Table 6. All rates are low; the improvement in resistance brought about by ferrite is evident in alloy 0-CF8M-38.

Corrosion of Alloy CD-4MCu by Nitric and Sulfuric Acids. Alloy CD-4MCu, which possesses corrosion resistance equivalent to and frequently far superior to that of the CF alloys, was investigated in several concentrations of nitric and sulfuric acids at temperatures up to the acid boiling points. Complete results of these investigations are provided in Figures 11 and 12 for nitric and sulfuric acid, respectively. These figures are iso-corrosion diagrams which show the relationships of temperature, acid concentration and corrosion rate.

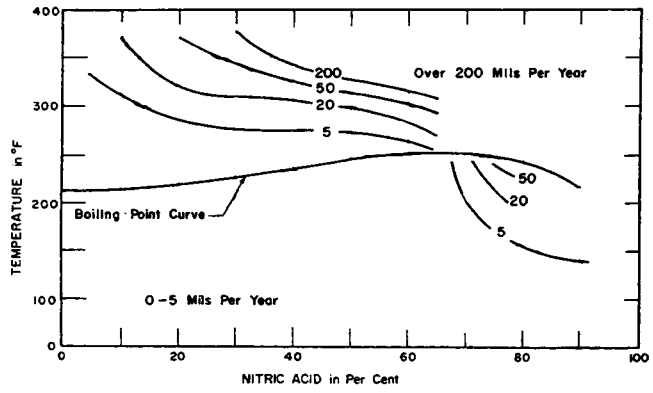


Figure 11—Iso-corrosion diagram for alloy CD-4MCu in nitric acid.

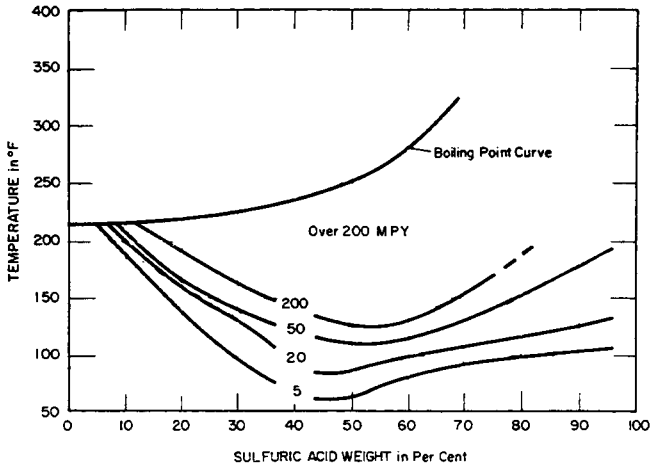


Figure 12—Iso-corrosion diagram for alloy CD-4MCu in sulfuric acid.

Solution-annealed specimens (2050 F and modified treatments) with and without subsequent aging (3 hours at 900 F) were used. In general, there was a tendency for the rates on modified solution-annealed specimens to be slightly higher than those of 2050 F solution-annealed alloys. Aging caused a slight additional loss in corrosion resistance.

Discussion

All of the experiments involving acetic, phosphoric and sulfuric acids displayed increasing corrosion resistance with increasing ferrite content of the alloys. This effect is most pronounced in the first period corrosion rates for alloys CF-8 and CF-8M in 75 percent acetic acid and for alloy CF-8M in 85 percent phosphoric acid.

The passivity effect illustrated in these experiments was investigated earlier for CF-8 type alloys in boiling 75 percent acetic acid and was found to result from anodic polarization of the ferrite.[17] Impressed current studies on fully austenitic and fully ferritic alloys (vacuum melted) revealed anodic polarization of the ferrite. Anodic current densities required to polarize the ferrite and austenite were approximately 0.4 and 0.7 ma/sq in, respectively. Galvanic couples of these two materials, designed to provide different ratios of ferrite to austenite, revealed current flow from ferrite to austenite. Ratios corresponding to approximately 15 volume percent and higher ferrite in a duplex alloy greatly increased the tendency toward passivation. Individual specimens containing 15 percent or more ferrite displayed the same strong tendency to passivate.

This interpretation probably explains the behavior observed in the present investigation which includes observations on environments of phosphoric and sulfuric acids as well as acetic acid. Molybdenum-bearing CF-8M material, which possess greater resistance than CF-8 to the above environments, displays a greater tendency toward passivity at lower ferrite levels than those observed for CF-8. This is verified in the data reported in Tables 5 and 6.

The propagation of stress-corrosion cracks in duplex alloys is through the austenite only. Ferrite interrupts the cracks and finally the ferrite fails mechanically. Other investigators including Copson[18] and Snowden[19] have made reference to the effect of ferrite.

The complicated microstructure of the CD-4MCu and the still incomplete micro-probe studies on this alloy and on the CF type alloys described above prevent further discussion at this time.

Summary and Conclusions

Metallurgical Structures in Alloy CD-4MCu

The amount of austenite present in the annealed microstructure increases with decreasing annealing temperature in the range 1750-2130 F. The hardness after annealing is sensitive to the annealing temperature and the quenching practice. A copper-rich precipitate was identified in annealed specimens water-quenched and air-cooled from 2050 F. In the early stages of aging at 900 F, the copper-rich precipitate contributed a hardening effect. A body-centered cubic precipitate was first identified after 24 hours at 900 F. The composition of the precipitate was not determined, but was believed to be similar to that of the chromium-rich precipitate which forms and has been identified in iron-chromium alloys and ferritic stainless steels. Sigma phase was first identified at 900 F after 1000 hours of aging. Further aging resulted in growth of the sigma phase at the expense of the body-centered cubic precipitate.

Aging at 1000 F resulted in the precipitation of the copper-rich precipitate after short aging periods followed by the formation of sigma phase without any intermediate precipitate.

The ferrite in the annealed microstructure decomposed into sigma phase and new austenite upon reheating in the range of temperature from 1200 to 1650 F.

Stress Corrosion

The threshold stress required to cause stress corrosion cracking in 8 hours was determined for a number of alloys exposed to the vapor condensation phase of a 400 F aqueous solution containing 875 ppm sodium chloride.

Alloy CD-4MCu, which has a yield strength in the order of 100,000 psi, displayed threshold values for stress corrosion of 55,000 and 60,000 psi for the non-aged and aged material, respectively.

A pronounced improvement in stress corrosion cracking resistance was observed for all CF alloys when the ferrite was increased to the intermediate 13-20 percent ferrite range. The higher carbon alloys showed the greatest improvement and the resistance increased with increasing alloy content. The stabilized CF-8C alloy displayed the lowest resistance to stress corrosion.

High ferrite-containing alloys (36 to 44 percent ferrite) show a reverse effect of carbon content as com-

pared to the intermediate group. That is, the low carbon materials are less susceptible to cracking. Except for alloy CF-8M, the alloys of high ferrite content are more resistant to stress corrosion than those of the intermediate group.

CE-30, CN-7M and Ni-Cr alloy[2] were not subject to stress corrosion cracking under the above test conditions when stressed to values of the yield strength and below. Stresses in excess of the yield strength resulted in stress corrosion of alloy CN-7M. CE-30 and Ni-Cr alloy[2] did not stress-corrode at stress levels far in excess of the yield strengths of these materials.

Fully austenitic CF-type alloys and AISI Types 304 and 316 displayed the highest susceptibility to stress corrosion cracking.

General Corrosion

Data for the corrosion of ferrite-containing alloys are presented for several environments. CF alloys show ferrite to have no detrimental effect on corrosion. Those cases in which increased corrosion resistance was observed are believed to result from polarization (passivity) originating from the two-phase structure.

Acknowledgment

The interest and support of the Alloy Casting Institute, which sponsored this research, are greatly appreciated.

References

1. J. J. Gilman. Electrolytic Etching—The Sigma Phase Steels. *Trans. ASM*, 44, 566 (1952).
2. C. E. Hall. Introduction to Electron Microscopy, p 254. McGraw-Hill Book Company, Inc., New York (1953).
3. R. M. Fisher. Electron Microstructure of Steel by Extraction Replica Technique. *Symposium on Techniques for Electron Metallography, ASTM*, p 49 (1953).
4. C. E. Hall. Reference 2, p 339.
5. R. T. Howard and M. Cohen. Quantitative Metallography by Point-Counting and Lineal Analysis. *Trans. AIME*, 172, 413 (1947).
6. R. W. Staehle, F. H. Beck and M. G. Fontana. Mechanism of Stress Corrosion of Austenitic Stainless Steels in Chloride Waters. *Corrosion*, 15, 373t-381t (1959) July.
7. N. P. Goss. Subboundary Structure of Recrystallized Iron. *Trans. AIME*, 145, 272 (1941).
8. Hultgren and B. Herrlander. Hot Deformation Structure, Veining, and Red-Shortness Cracks in Iron and Steel. *Trans. AIME*, p 493 (1947).
9. A Guinier. Structures in Crystals; Imperfections in Nearly Perfect Crystals, p 402, John Wiley and Sons, New York (1952).
10. R. M. Fisher, E. J. Dulis and K. G. Carroll. Identification of the Precipitate Accompanying 885 F Embrittlement in Chromium Steels. *Trans. AIME*, 197, 690 (1953).
11. R. O. Williams and H. W. Paxton. The Nature of Aging Binary Iron-chromium Alloys Around 500 C. *J. Iron and Steel Institute*, 185, p e88 (1957).
12. T. Federighi. Quenched-in Vacancies and Rate of Formation of Zones in Aluminum Alloys. *Acta Metallurgica*, 6, 379 (1958).
13. W. DeSorbo, H. N. Treaftis and D. Turnbull. Rate of Clustering in Al-Cu Alloys at Room Temperature. *Acta Metallurgica*, 6, 401 (1958).
14. J. J. Hauser, J. M. Capenos and B. R. Banerjee. Submicroscopic Structures in Tempering 410 Stainless Steels. *Trans. ASM*, 54, No. 3, p 514 (1961).
15. E. Hornbogen and R. C. Glenn. A Metallographic Study of Precipitation of Copper from Alpha Iron. *Trans. AIME*, 48, 1064 (1960).
16. J. J. Heger. Discussion to Reference 10. *Trans. AIME*, 200, 665 (1954).
17. G. A. Mancini. The Effect of Ferrite on the Corrosion of CF Type Alloys. Master's Thesis, Ohio State University (1958).
18. H. R. Copson. Effect of Composition on Stress Corrosion Cracking of Some Alloys Containing Nickel. Phy. Met. of Stress Corrosion Fracture. N.Y. Interscience Publ. (1959).
19. P. P. Snowden. Comparative Stress Corrosion Behavior of Some High Alloy Steels. *JISI*, 197 (1961).

Copyrighted Materials
Copyright © 1996 NACE International Retrieved from www.knovel.com

Paper No.
290

CORROSION 95
The NACE International Annual Conference and Corrosion Show

THE EFFECT OF CATHODIC PROTECTION ON DUPLEX STAINLESS STEELS IN SEA WATER

R Francis, G Byrne and G R Warburton
Weir Materials Ltd
Park Works
Newton Heath, Manchester, M40 2BA

ABSTRACT

The report reviews the available data on the embrittlement of duplex stainless steels under cathodic protection in sea water. Much of this data has previously been unpublished. The results show that while hydrogen enters duplex alloys at typical protection potentials (-1V SCE) the risk of failure is very low. The austenite phase tends to block cracks in the ferrite, and very high stresses are needed to produce fracture of the austenite or austenite-ferrite phase boundaries to enable crack propagation to occur. The smaller the grain size the more resistant duplex stainless steel is to embrittlement. The report also shows that currently used design stresses for duplex alloys are well below the stresses needed to produce failure. The service experiences with cathodically protected duplex are reviewed and the few failures explained. The report concludes that at normal protection potentials the risk of failure of duplex stainless steel due to hydrogen embrittlement is extremely low.

INTRODUCTION

In the early 1980's a number of oil companies experienced failures of corrosion resistant alloy fasteners on cathodically protected subsea structures. Some of the early failures were on riser clamps although bolts in other areas also failed. The bolts were of alloy K-500 (UNS N05500) and the failures were ascribed to hydrogen embrittlement.

These failures led to a number of research efforts to identify the cause and suggest actions to prevent embrittlement. The only published results are those of Efird (1) who suggested that by controlling the hardness of K-500, embrittlement could be prevented. However, unpublished work by Francis and Campbell (2,3) at BNF Metals Technology Centre, showed that embrittlement could occur on fully solution annealed material with a hardness of 296 HV. They also showed that cracking could occur on unstressed K-500 polarised to -1000mV SCE in sea water.

Alloy K-500 has not generally been used as a corrosion resistant bolting material subsea since that time. A number of alternatives were tried; these included B7 steel, high strength copper alloys, nickel-base alloys and 25Cr duplex stainless steel.

Early laboratory tests (2) suggested that duplex stainless steel could suffer from embrittlement. For this reason there has only been limited use of duplex stainless steel fasteners in the North Sea.

With the increasing use of subsea completions and flowlines with aggressive wells there is a desire to use duplex stainless steels for subsea manifolds, flowlines and bolts. Because of the high temperatures of the process fluids these systems frequently require cathodic protection to prevent localised corrosion on the sea water side and there is a need to determine the risk of cracking of duplex stainless steels under cathodic protection in seawater. The present paper reviews the body of unpublished data on hydrogen embrittlement of duplex stainless steel and also records some service experiences.

LABORATORY TEST RESULTS

Effect of Hydrogen on Mechanical Properties

Francis and Campbell (2) charged specimens of cold worked 25Cr duplex stainless steel (UNS S32550) at -1V SCE for 60 days and then carried out mechanical testing to investigate any change in properties. The results are shown in Table 1. There was no significant change in the yield stress or the UTS. However, there was a substantial reduction in both the elongation and the reduction in area, showing some embrittlement had occurred. Figure 1 shows a typical fracture face with transgranular cleavage at the perimeter and ductile shear in the centre. Similar tests have been carried out at WML on cold worked Zeron 100 (UNS 32760), a super duplex stainless steel which was additionally overstrained by 50% to simulate the severe cold work which can be produced during thread rolling of fasteners. The results are shown in Table 1. As for S32550, there was no significant change in the proof stress or the UTS, but there was a reduction in the elongation and the reduction in area. This reduction was not so great as that seen for S32550. A typical fracture face is shown in Figure 2, and although it is similar to that in Figure 1, the depth of embrittlement is much less.

Critical Potential for Hydrogen Evolution

The severity of embrittlement depends on the amount of hydrogen being evolved and the ability of it to adsorb on the surface and then diffuse inside. Unpublished work of Francis and Campbell (3) showed that significant hydrogen embrittlement of K-500 occurred at potentials of -750 mV SCE and below. Valdez-Vallejo (4) carried out slow strain rate tests on S32760 under cathodic charging over a range of potentials. Figure 3 shows the elongation ratio (ie., elongation/elongation in air) versus potential. Data in the next section suggests that an elongation ratio of 75% does not result in a detrimental loss of properties. This means that the critical potential for the onset of appreciable embrittlement is about -900 mV SCE. A typical potential for aluminium alloy anodes is -1V SCE and thus a potential drop between the anodes and the stainless steel of only 100 mV will significantly reduce the hydrogen charging of duplex stainless steel.

Slow Straining Rate Tests

Valdez-Vallejo (4) conducted slow strain rate tests on both solution annealed S32760 and on cross weld tensiles. The specimens were exposed to synthetic sea water and charged at -1.1 Volt SCE, with a strain rate of 1×10^{-6}/sec. The results in Figures 4 and 5 show that there was no loss in proof strength or UTS and only a small reduction in elongation (~ 75% of elongation in air) for both solution annealed and welded material. Similar results were obtained for material precharged for several weeks prior to testing. More recent work (5) has shown similar results for cold worked S32760 (~900MPa UTS). Microsections of the specimens show that cracks initiate in the ferrite but are blocked by the austenite, which does not embrittle. (See Figure 6). In fact cracks can propagate parallel to the stressing direction because of the blocking action of austenite as shown in Figure 6.

Hutchings (5) also carried out slow strain rate tests on S32760 produced via the powder route. This produces material with a much finer grain size than bar produced by conventional rolling from ingot. The results are shown in Figure 7. The powder route material showed very little loss of elongation (90%) compared with air, even after pre-charging with hydrogen.

Examination of the specimens showed that although very small cracks had originated in the ferrite these had blunted when the cracks met austenite. Hence the finer the grain size the greater the resistance of duplex stainless steels to hydrogen embrittlement.

The conclusion from both these research projects was that cracks will only propagate under very high loads where the austenite can be plastically deformed such that the crack can propagate through the austenite or along the ferrite/austenite phase boundary. Also the finer the grain size the slower the uptake of hydrogen, and the greater the resistance to embrittlement.

Ripple Load Tests

These tests were to see whether the passive film would crack during cyclic loading such as could occur due to process pressure changes or wave action.

Valdez - Vallejo (4) conducted ripple load tests on hydrogen charged S32760 specimens. The ripple parameters are shown in Figure 8, with a slow strain rate curve for comparison. This type of test is thought to be more aggressive than a constant load test, but less aggressive than a slow strain rate test. After 360 hours no failures occurred and no cracks were observed on the sample. A more aggressive test with a $\pm$ 60MPa amplitude ripple was also conducted, but no failures occurred in this test either.

WML have conducted cyclic tests in the elastic region at slow strain rate speeds (3 x 10^{-6}/sec) on heavily cold worked S32760, (yield stress = 900MPa) as shown in Figure 9. Specimens were polarised to -1V SCE in sea water for 60 days and then cycled while still at -1V SCE for a further 60 days. Specimens were then examined for any indications of surface defects or cracks in an SEM. No such defects or cracks were found.

Corrosion Fatigue

Mayaki (6) carried out fatigue tests on S32760 under hydrogen charging conditions. He used 3-point bend tests at 50Hz with a load ratio of 0.1. Hydrogen charging produced a slight reduction in fatigue strength for S32760, but this was negligible compared with the change for high strength steels.

Threshold Stress

Murata et al (7) determined the threshold stress for failure under hydrogen charging conditions for a 25Cr duplex stainless steel. The results in Figure 10 show the threshold stress to be about 650 MPa, well above the yield stress of 550 MPa. This confirms the results of the slow strain rate tests in that gross plastic deformation is required for a crack to propagate.

In addition, Murata et al made experimental alloys with a range of ferrite contents, and determined the threshold stress for each composition under hydrogen charging conditions. Figure 11 shows the threshold stress as a function of the ferrite content. It can be seen that there is a decrease in the threshold stress between 50% and 60% ferrite. Even so the threshold stress at ferrite contents of 60% and above is still 90% of the yield stress. It should be noted that these are experimental alloys with the nickel content varied to control the austenite fraction. In commercial alloys the phase balance is also determined by the temperature at which solution annealing is carried out and such alloys may not necessarily produce the same shape of curve as shown in Figure 11.

SERVICE EXPERIENCES

Marathon

Sentance (8) reports the cracking of 25Cr duplex stainless steel (UNS S32160) downhole tubulars. The tubulars did not fail in service but cracked when they were subjected to excessive impact damage on removal during a routine workover. The cause of failure was identified as hydrogen embrittlement, caused by the galvanic couple between the duplex stainless steel tubulars and the carbon steel casing under the downhole conditions. The tubulars were cold worked in the range 140-160ksi (965 - 1103 MPa).

It was noticed that the failures were in the higher strength tubulars, and replacement tubulars in both S31260 and 22Cr (UNS S31803) with yields nearer the lower limit have performed satisfactorily. ie., hydrogen has entered the tubulars but no cracking has occurred.

It can be concluded that very heavy cold work severely reduces the resistance to cracking under hydrogen charging conditions. It should be noted that manifolds and flowlines would normally use solution annealed material with a yield strength of 550MPa (80ksi) and bolting would be lightly cold worked (max yield 900MPa [130ksi]). Under these conditions cracking would obviously be much less likely.

BP

There have been a few failures of cathodically protected 25Cr duplex bolts (UNS S32550) on one of BP's North Sea platforms. Figure 12 shows a typical bolt and Figure 13 shows the microstructure. It is clear even to the naked eye that the structure is rich in ferrite and well above the normal 50/50 balance. The measured value was 70%. However, the strength of these bolts was not achieved by cold work, but by ageing at about 500°C. This precipitates a fine phase known as alpha prime, which is only visible in the TEM. It has been shown (5) that material which is aged in this manner suffers a dramatic drop in resistance to embrittlement in the slow strain rate test. Figure 14 shows the SSRT curves for aged material saturated with hydrogen at -1.1V at 80°C for 3 weeks and tested at -1.1V SCE in 3.5% NaCl. The dramatic loss of ductility is clearly visible. Hutchings also showed (5) that material heat treated to increase the ferrite content to ~70% also showed a big increase in susceptibility to hydrogen embrittlement. The reduction in elongation was similar to that shown in Figure 14 for aged material. Obviously, the combination of ageing and a high ferrite content together would dramatically increase the susceptibility to embrittlement, and explains the reason for the failure of the BP bolts.

It is for this reason that the high strength of bolting grade S32760 produced by Weir Materials is achieved by cold work and not by ageing.

Weir Pumps

Weir have supplied a large number of submerged sea water pumps to offshore platforms in duplex stainless steel. Many of these are cathodically protected, either by design or because they are in contact with the rest of the platform, which is CP'd. The casings and motors are usually secured with Zeron 100 fasteners and no failures have been reported. The oldest of these pumps has been in use since 1986.

Subsea Developments

A number of projects have utilised 22Cr duplex (S31803) or super duplex (S32760) for subsea applications such as manifolds and flowlines. Many of these have been subject to cathodic protection. In the case of 22Cr duplex this is because of its poor resistance to crevice corrosion in sea water. With the 25Cr super duplex CP has been considered necessary where the process temperature is very high and crevice corrosion of the surface in contact with sea water was considered possible. Table 2 shows some of the projects which have utilised duplex and super duplex with CP. No failures due to hydrogen embrittlement have been reported.

DESIGN STRESSES

Pipework Systems

Pipework systems are usually designed to codes such as ANSI B31.3. For duplex and super duplex alloys this gives design stresses which are typically 45% to 50% of yield stress at temperature. More recently BS8010 Pt 3 has been used, permitting design stresses up to 72% of yield. Hence the gross plastic deformation required to enable embrittlement cracks to propagate is highly unlikely to occur in practice.

Bolting

Fasteners on such items as riser clamps and flanges are usually loaded with bolt extenders to maximum loads of 50% to 60% of yield. Swivel flanges with severe misalignment can give rise to bending moments which can increase the load to yield or even a little over. Even at loads of 110% yield there is insufficient plastic deformation to lead to failure of super duplex stainless steel under normal cathodic protection.

CONCLUSIONS

1) Hydrogen enters duplex stainless steels under cathodic protection in sea water.

2) Hydrogen embrittlement is reduced by a fine grain size and 50% or more austenite.

3) Ageing of duplex stainless steel greatly increases the susceptibility to hydrogen embrittlement.

4) Cold working up to about 35 HRC does not significantly increase the susceptibility to hydrogen embrittlement.

5) Crack propagation is blocked by austenite.

6) High stresses sufficient to plastically deform the austenite are needed to initiate and propagate cracks.

7) There is evidence of up to seven years successful service experience with cathodically protected duplex alloys subsea.

8) The known service failures are due either to excessive cold work or to ageing and a high ferrite content, all of which reduce the resistance to embrittlement.

9) In view of the severe loads necessary to cause cracking and the relatively low design stresses used for duplex stainless steels the risk of cracking under cathodic protection is extremely low.

REFERENCES

1) K D Efird Mater. Perf. 24, 4 (1985) 37.

2) R Francis and H S Campbell Confidential BNF Metals Technology Centre Report R538/1 June 1986.

3) H S Campbell and R Francis "Simulated Service Test for Hydrogen Embrittlement of Cathodically Protected Sub-sea Bolting Materials", UK Corrosion '94, Bournemouth, Uk, November 1994, I.Corr.

4) F R Valdez-Vallejo Ph.D Thesis, University of Manchester, June 1990.

5) D Hutchings, Ph.D Thesis, University of Manchester, March 1994.

6) M.C Mayaki Ph.D Thesis, University of Nottingham 1989.

7) M Murata; Y Mukai and J Wang 5th Int. Symposium of the Japan Welding Society. April 1990 Tokyo.

8) P Sentance Duplex Stainless Steels '91 Beaune, France Oct 1991 p 895.

TABLE 1 Mechanical properties of 25Cr duplex stainless steels charged at -1 volt for 60 days

Alloy	Exposure Conditions	0.2% Proof Stress(MPa)	UTS (MPa)	Elong.n (%)	Red.n in Area(%)
S32550	air	905	947	21	63.2
(cold worked;	air	1079	1092	12	59.5
334 - 404HV)					
	sea water	994	1011	6	N.D.
	sea water	1080	1096	6	18.4
	sea water	970	994	8	27.4
S32760	air	957	995	22	81
(cold worked;	air	965	999	21	81
34 - 36HRC)					
	sea water	939	1045	19	66
	sea water	998	1045	14	68

N.D. = not determined

TABLE 2 Some subsea projects using duplex stainless steels with CP

PROJECT	ALLOY	TEMP (C)*
Lillefrigg	S32760	NK
Draugen	S32760	NK
Statfjord Satellites	S32760	110
Nelson	S32760	104
Tommelieten	S31803	NK
Inde	S31803	NK
Embla	S31803	150
Brae A-C	S31803	102
Scott	S31803	135

* These are manifold temperatures.

NK - Not Known (believed to be around 100 C)

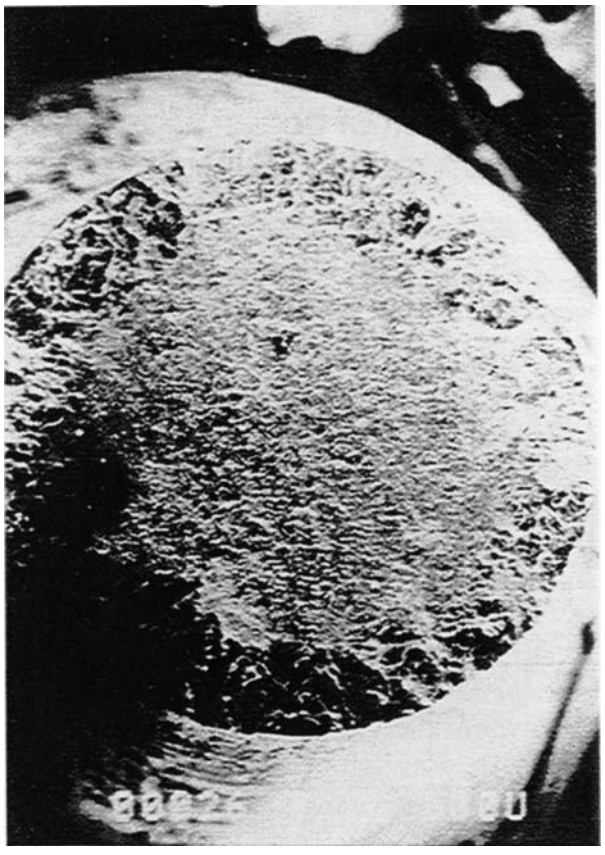


FIGURE 1 - FRACTURE FACE OF UNS S32550 SPECIMEN AFTER 60 DAYS CHARGING AT -1V SCE IN SEA WATER

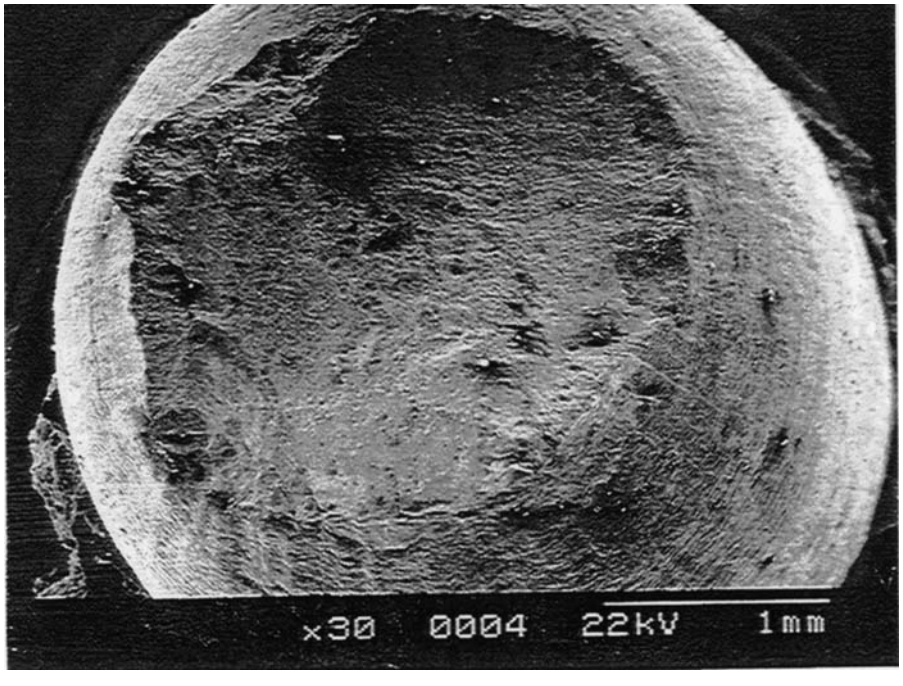


FIGURE 2 - FRACTURE FACE OF UNS S32760 SPECIMEN AFTER 60 DAYS CHARGING AT -1V SCE IN SEA WATER

FIGURE 3 Effect of potential on the elongation ratio in SSRT tests

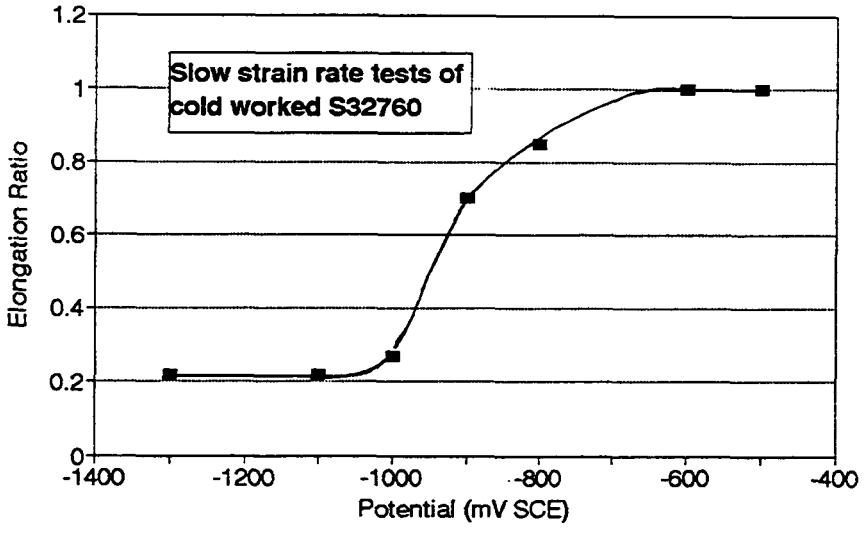


FIGURE 4 Slow strain rate tests on super duplex S32760 charged at -1V SCE

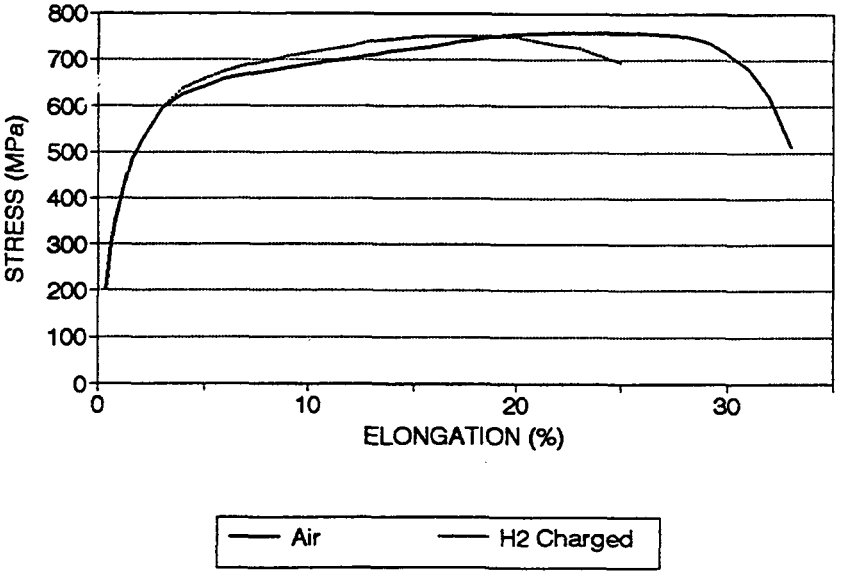
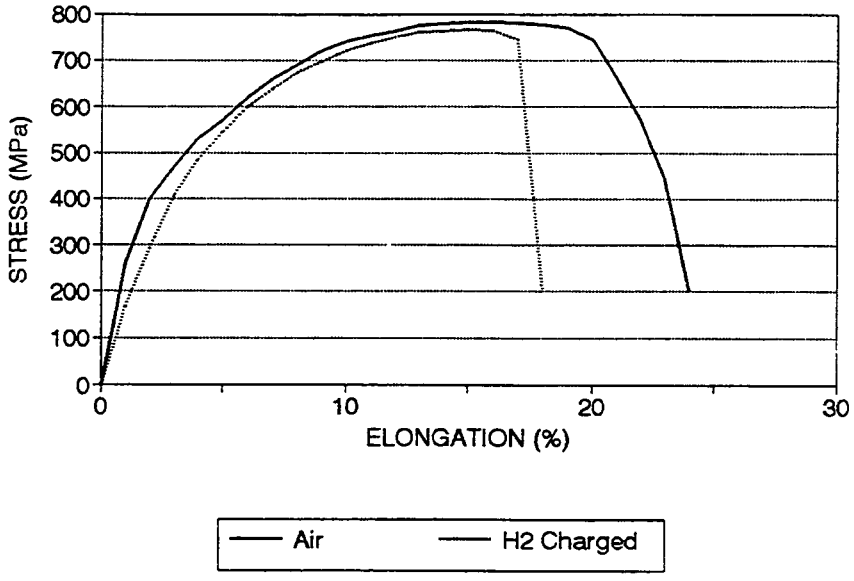


FIGURE 5 Slow strain rate tests on welded super duplex S32760



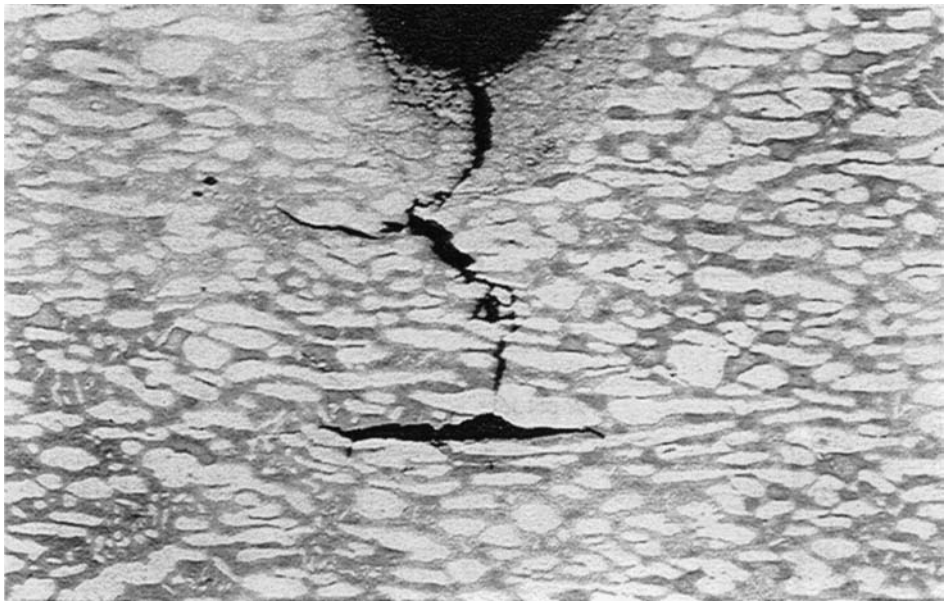


FIGURE 6 - CRACK IN S32760 NOTCHED SPECIMEN AGED FOR 6 HOURS AT 475°C TESTED BY SLOW STRAIN RATE METHOD WITH HYDROGEN CHARGING AFTER PRE-CHARGING FOR 3 WEEKS AT 80°C. (-1V SCE IN 3.5% NaCl)

FIGURE 7 Slow strain rate tests on powder S32760 charged at -1V SCE

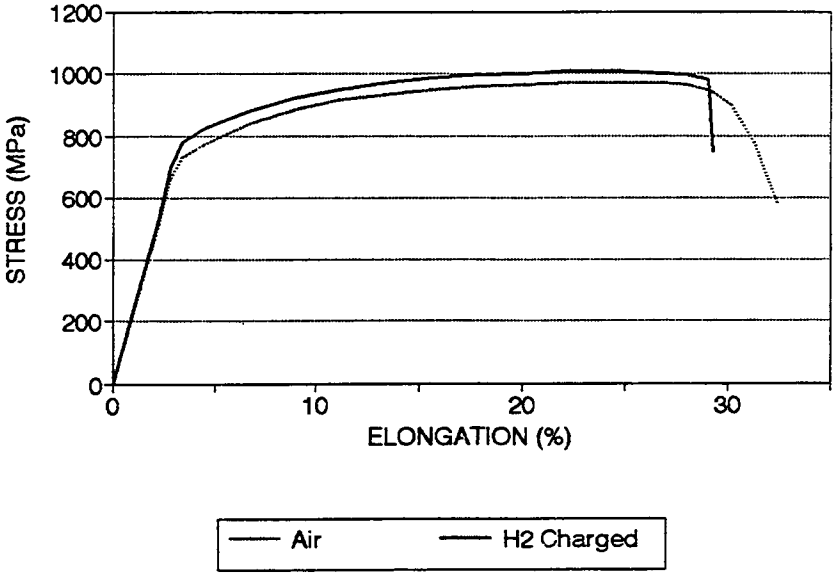


FIGURE 8 Ripple load tests on super duplex S32760 charged at -1100mV SCE

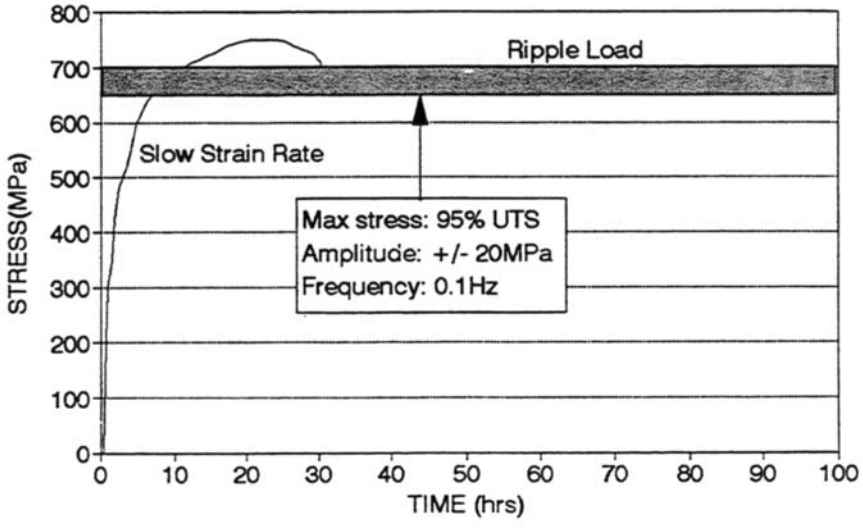


FIGURE 9 Ripple load tests on S32760 (strain rate = 3 E-6/sec: -1000mV SCE)

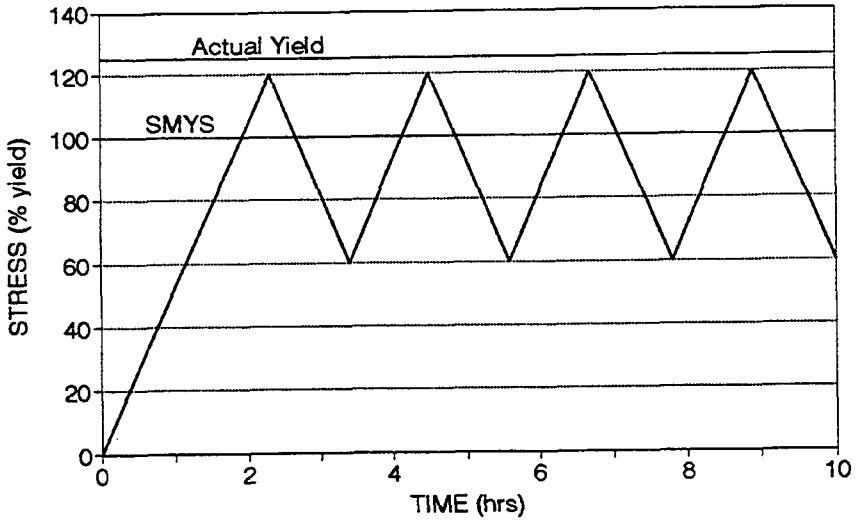


FIGURE 10 Time to failure of hydrogen charged 25Cr duplex stainless steel

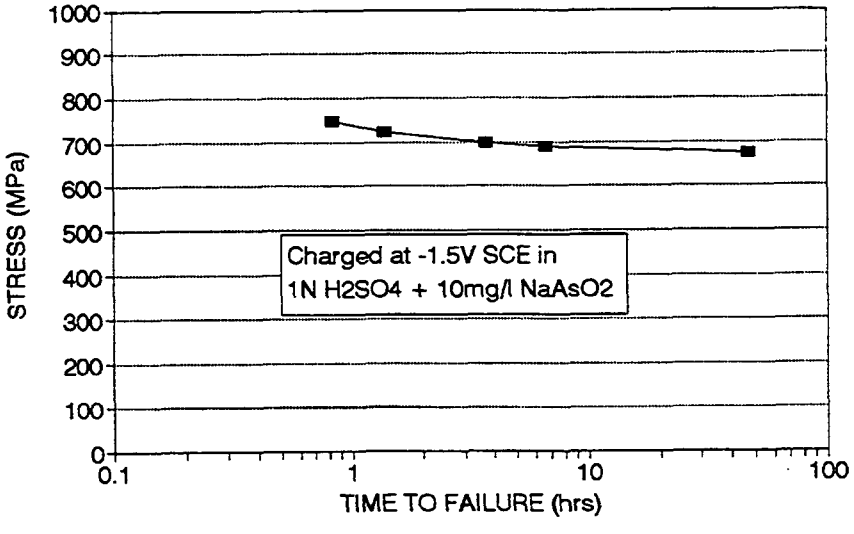
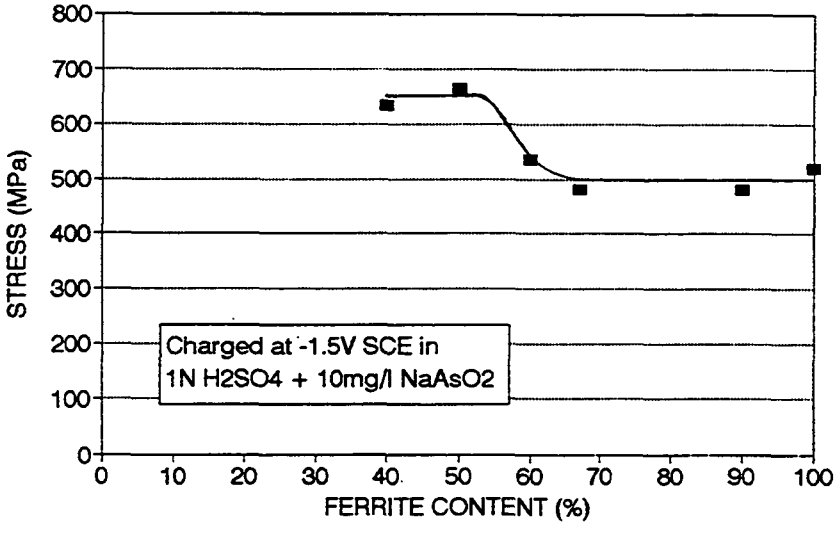


FIGURE 11 Threshold stress versus ferrite content (25Cr duplex)



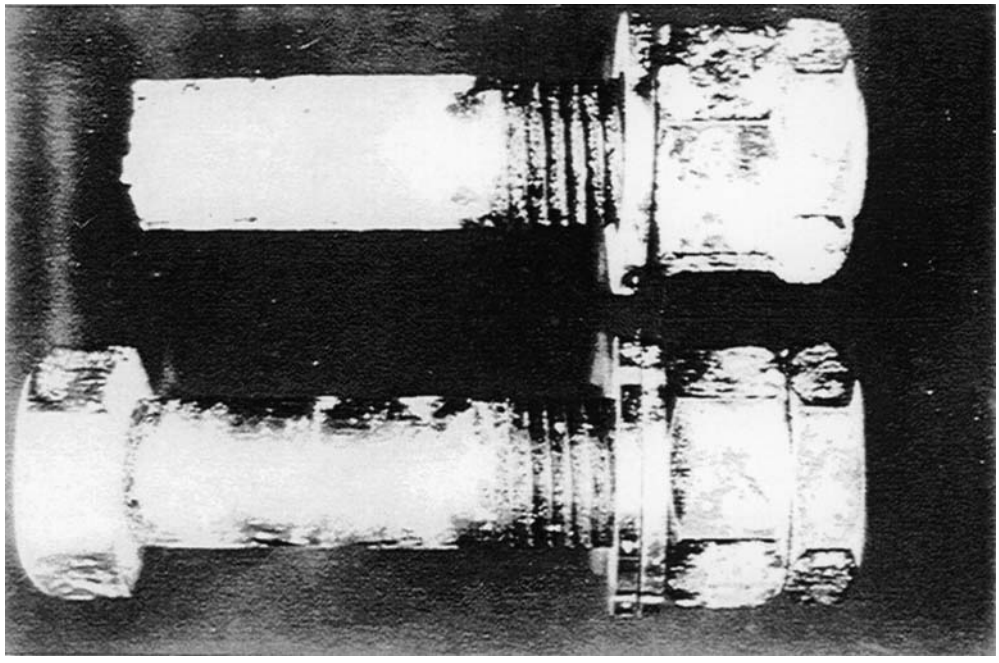


FIGURE 12 - DUPLEX BOLT (UNS S32550) FROM BP NORTH SEA PLATFORM WHICH FAILED DUE TO HYDROGEN EMBRITTLEMENT.

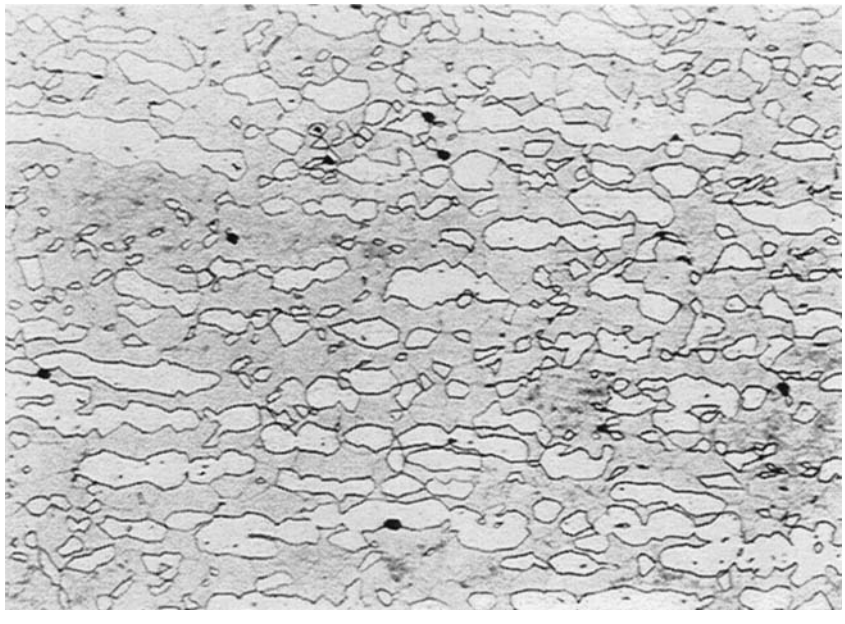
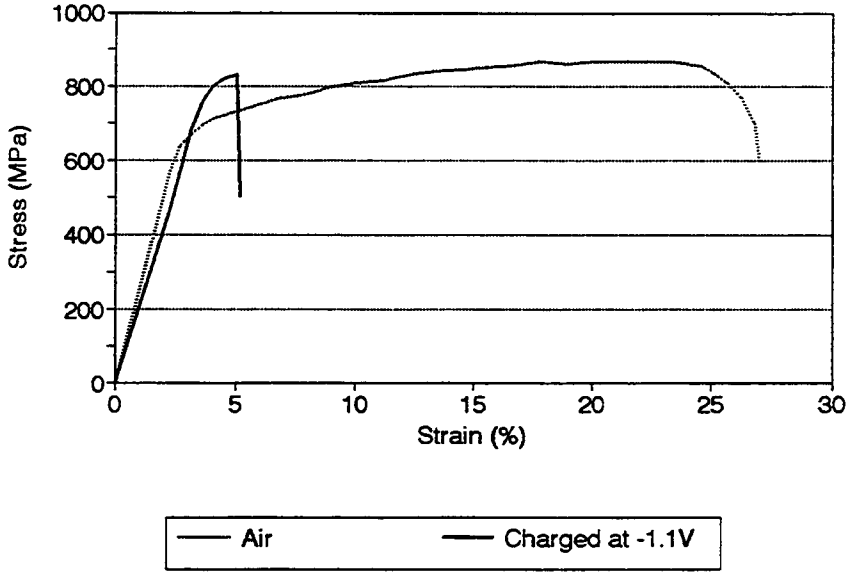


FIGURE 13 - MICROSECTION OF FAILED BOLT (UNS S32550) FROM BP PLATFORM.

FIGURE 14 Slow strain rate tests on S32760 aged at 475°C for 6 hours



Copyrighted Materials
Copyright © 1996 NACE International Retrieved from www.knovel.com

Paper No.
64

CORROSION 94
The Annual Conference and Corrosion Show
Sponsored by NACE International

THE CORROSION OF DUPLEX STAINLESS STEELS IN SOUR SERVICE

R. FRANCIS & G. BYRNE

Weir Materials Limited
Park Works
Newton Heath
Manchester M10 6BA
UK

A B S T R A C T

The high resistance to corrosion of 22 Cr, 25 Cr and super duplex stainless steels in chloride containing environments is well known. In sour service, resistance to stress corrosion cracking, pitting and crevice corrosion in the presence of CO_2 and H_2S is required. This paper presents the results of tests to determine the resistance of three duplex stainless steels to stress corrosion cracking, pitting and crevice corrosion at elevated temperature in a synthetic brine containing different concentrations of H_2S. The three alloys were UNS S31803, UNS S32550 (low Cu) and UNS S32760.

All three materials were tested in the cold worked condition, and loaded to about the 0.2% proof stress. The tests were conducted with 93 bar (9.3 MPa) CO_2 and either 0.125, 0.25 or 0.375 bar (12.5, 25 or 37.5 KPa) H_2S. The results showed that only the super duplex alloy, UNS S32760, was resistant to SCC at 80°C at all of the H_2S concentrations. Pitting and crevice corrosion occurred at 121°C only at the highest H_2S concentration on all the alloys. The depth and severity of attack varied from alloy to alloy and indicated that super duplex UNS S32760 is more resistant than 25Cr, UNS S32550 (low Cu), which is more resistant than 22Cr UNS S31803.

Keywords: Sour brines, Sulphide SCC, pitting corrosion, crevice corrosion, duplex stainless steels.

INTRODUCTION

The resistance to pitting and crevice corrosion of duplex stainless steels in chloride containing environments is well known. Alloys with high chromium, molybdenum and nitrogen contents have the greatest resistance to corrosion, which can be broadly reflected by an empirical relationship known as the PREN number (PREN = %Cr + 3.3 x %Mo + 16 x $\%N_2$). Downhole environments have chloride concentrations which commonly range from the 19,000 mg/l found in seawater to concentrations of 150,000 mg/l. In addition to chloride appreciable quantities of CO_2 and H_2S are usually also present. In this environment not only is resistance to pitting and crevice corrosion important, but also resistance to stress corrosion cracking (SCC). Weir Materials Ltd joined several other companies in a programme to evaluate the suitability of different grades of duplex stainless steel for an offshore project in the North Sea.

EXPERIMENTAL

Tests were conducted to assess the resistance of three duplex stainless steel alloys to stress corrosion cracking, pitting and crevice corrosion in a simulated process brine. The duplex grades were distinguished by their alloy content.

Materials

Three duplex alloys were tested, UNS S31803, UNS S32550, (low Cu) and UNS S32760. S31803 is a 22Cr duplex stainless steel commonly known as 2205. S32550 (low Cu) is a 25Cr duplex alloy without the usual copper addition. Copper was originally added to S32550 to confer improved corrosion resistance in non-oxidising acids, such as sulphuric acid. In sea water and brines copper has not been shown to contribute to pitting/crevice corrosion resistance and many commercial alloys contain little or no copper. Zeron 100, Alloy S32760, is a super duplex alloy containing higher levels of molybdenum and nitrogen[1]. The chemical compositions of the alloys are shown in Table_ 1.

The three alloys were supplied cold-worked to a minimum 0.2% proof stress of 758 MPa (110 ksi). In addition, S32760 was tested in the solution annealed condition (specified minimum yield stress = 550MPa). The measured mechanical properties and hardnesses are shown in Table_ 2.

1. Trade name of Weir Materials Limited.

The pipe sizes were as follows:-

S31803: 88.9mm od x 7.34mm wall
S32550: 108mm od x 7.55mm wall
S32760: 94.8mm od x 4.20mm wall
(CW)
S32760: 88.9mm od x 3.05mm wall
(SA)

Stress Corrosion Cracking

SCC tests were conducted in Alloy C-276 (UNS N10276) autoclaves. It is widely accepted that the resistance of duplex stainless steels to SCC passes through a minimum in the temperature range 80-100°C. Hence the present tests were conducted at 80°C.

Two C-rings and one 3-point bent beam specimen from each alloy were exposed in each autoclave. The C-rings were full wall thickness of the pipe with no machining except for cut ends. The rings were internally stressed using Alloy C-276 fasteners to about 100% of the specified minimum yield stress at room temperature, in accordance with the NACE TM0177 stressing equation for C-rings.

$$\text{Deflection} = \frac{\pi\, d(d-t)(S+0.002E)}{4.tE}$$

Where d = pipe O.D
t = pipe wall thickness
S = 0.2% proof stress
E = Young's Modulus

This was checked by the use of strain gauges. After the 30 day exposure the deflection of the C-rings was measured and no measurable reduction in deflection was observed. This indicated that no stress relief occurred during testing.

The 3-point bent beam specimens were prepared from the longitudinal direction of the pipe, at approximately mid-wall position. This was done to evaluate the stress corrosion resistance of these alloys when stressed in the longitudinal direction as would be the case when 'self weight forces' are experienced in a production string. The specimens measured 74 x 4.5 x 1.2mm and were of machined finish. They were stressed to 100% of the specified minimum yield stress of each material (room temperature properties), in accordance with the ASTM G39 stressing equation, in Alloy C-276 bending jigs.

After stressing, all specimens were placed in the relevant autoclave and the deaerated test solution was introduced. The test solution volume to surface area ratio employed was approximately 9 ml/cm^2. A CO_2/H_2S gas mix was bubbled through each autoclave for approximately 24 hours until measurements on the exit gas indicated that equilibrium conditions had been achieved, i.e. the exit gas composition was equal to the inlet gas composition. The autoclaves were heated to 80°C and the total pressure was adjusted to a nominal 93 bar (9.3MPa).

The yield stress for these duplex stainless steels falls significantly with increasing temperature, resulting in a reduction of at least 10% between 20°C and 100°C. Thus the specimens could be considered to have been overstressed. However, actual yield strengths for the 22 Cr, 25 Cr and super duplex materials were 12.7, 10.3 and 16.8% respectively over the minimum specified. Hence the specimens were stressed to approximately 100% of the yield stress at temperature.

Pitting and Crevice Corrosion Tests

Two pitting corrosion coupons (in the form of stressed, bent beam specimens as described above) and one crevice corrosion coupon (25 x 20 x 1.1mm, drilled and fitted with two castellated glass-filled PTFE crevice formers, with 20 crevice sites per former) of each material were exposed in each of the three autoclaves at 121°C for 30 days. Excepting the test temperature, conditions in the three autoclaves were as described for the SCC tests above.

Test Environment

All tests were conducted in a synthetic brine similar to that which has been observed in some North Sea Fields. The composition is shown in Table 3. All tests were carried out at a total pressure of 93 bar (9.3MPa) which comprised CO_2 containing a small quantity of H_2S. Three H_2S concentrations were evaluated, designated as follows:-

low H_2S 0.125 bar (12.5KPa)
mid H_2S 0.25 bar (25 KPa)
high H_2S 0.375 bar (37.5 KPa)

RESULTS

The test specimens were examined under a low power microscope, and microsections were prepared of interesting features.

The results from the C-ring stress corrosion cracking tests are shown in Table 4, from the pitting tests in Table 5 and from the crevice corrosion tests in Table 6. No cracking occurred on any of the bent beam SCC specimens.

DISCUSSION

Visual Appearance

There was more black corrosion product on the corrosion test specimens than on the SCC samples. This is not surprising in view of the higher test temperature used in the pitting corrosion tests. There was also a difference in the appearance of the corrosion product with H_2S concentration at each temperature. At the low H_2S level, the black corrosion product was loose and poorly adherent. At the mid H_2S level, the scale was more adherent, while at the high H_2S level, the black product was thicker and very adherent.

Stress Corrosion Cracking

No cracking was observed on any of the bent beam specimens, but some of the C-rings in S31803 and S32550 showed cracks. It is possible that the difference in behaviour between the ring specimens and the beams is due to surface condition; it is frequently found that sulphide stress corrosion cracking initiates at sites of imperfections on a surface, e.g. bore-side machining marks, and the pipe material supplied for testing was of variable quality in this respect. A secondary testing factor which may have an influence is the possible difference in mechanical properties in the longitudinal (as tested by the bent beams) and transverse (as tested by the C-rings) directions. All cracks that were found were associated with the edge of the C-rings and they were all in the position of maximum stress on the rings. Stressing was nominally to 100% of the room temperature yield strength. From a consideration of the reduction in yield strength at 80°C and the differing actual yield strength of the test materials, all the materials were stressed to about their actual yield strengths.

The loss of yield strength between 20 and 80°C is approximately 10% for cold worked material and 13% for annealed material and the actual stresses were: 22Cr(98% of actual yield strength); 25Cr, 101%; super duplex (cold worked), (95%); super duplex (annealed) 98%.

The cracks in the C-rings were typically as shown in Figures 1 and 2. The portions near the surface bear some resemblance to corrosion pits, with preferential phase dissolution evident along their entire length. All the cracks were located at the point of maximum stress on the C-rings. The cracks look somewhat of a cross between traditional fine intergranular/transgranular cracks and hemispherical pits. However, the attack on the C-rings was very different to the pitting in the stressed beams, shown in Figures 3 and 4.

The results from the C-rings show that alloy S31803 can suffer cracking at all the H_2S levels in the present tests. The S32550 (low Cu) alloy was more resistant to cracking, but cracking was observed at both the mid and high H_2S concentrations. Alloy S32760 showed no cracking at all three H_2S levels, in both the cold worked and solution annealed conditions.

The appearance of the attack on the SCC specimens indicates that the cracks originated from the base of corrosion pits. It seems likely that the more aggressive conditions found at the base of pits (i.e. low pH and high chloride concentrations) are required to initiate cracking.

This, plus the fact that alloy S32760 showed no signs of pitting or cracking, suggests that the more resistant an alloy is to pitting, the more resistant it will be to sulphide stress cracking.

There is a wealth of data to show that the higher the chromium, molybdenum and nitrogen content of a duplex stainless steel, the higher is its resistance to pitting in aerated, chloride solutions, such as seawater. There is less data for process conditions with high CO_2 and H_2S. However, work by Sandvik (1) has shown the beneficial effects of chromium and molybdenum on pitting resistance, while Tsuge (2) also found that 25 Cr duplex alloys had improved resistance to pitting compared with 22 Cr alloys. Finally Japanese work (3) has shown that high nitrogen containing alloys have superior pitting resistance in a sulphide containing environment. Hence there is evidence to support the conclusions of the present work that higher alloy content improves pitting resistance.

The PREN value ($Cr\% + 3.3 \times \%Mo + 16 \times \%N_2$) is commonly used as an assessment of the resistance of an alloy to pitting in aerated chloride solutions (see Table 1). The present work suggests that it can also be used in process environments, not only as an indicator of pitting resistance, but also as an indicator of resistance to SCC.

Pitting/Crevice Corrosion

No detectable corrosion was observed on either the pitting or crevice corrosion specimens at both the low and mid H_2S concentrations. At the high H_2S level all three alloys suffered pitting and crevice corrosion to some degree. However, the results in both Tables 5 and 6 show that S32760 was more resistant to both pitting and crevice corrosion than S31803 and S32550. This is shown by the lower depth of attack in the pitting tests for S32760 and the fewer number of segments attacked in the crevice tests. The solution annealed S32760 showed no crevice attack, indicating a slightly superior resistance to crevice corrosion compared to cold worked material. Solution annealed material was not exposed in the pitting corrosion tests.

The morphology of the pits in alloys S31803 and S32550 (low Cu) is shown in Figures 3 and 4. They clearly show that preferential dissolution of the ferrite phase was prevalent.

CONCLUSIONS

The present tests indicate that there is a definite ranking order in resistance to SCC, pitting and crevice corrosion for the materials under test. S32760, super duplex, was superior to S32550 (low Cu), 25 Cr duplex, which was superior to UNS S31803, 22 Cr duplex stainless steel in the cold worked condition. This behaviour is consistent with the level of alloy additions in each material, the more highly alloyed being more corrosion resistant.

The results show that cracking originated from the base of the corrosion pits. This supports the view that in sour process environments the relative resistance to cracking can be indicated by the PREN value, previously used as a guide to pitting resistance.

No difference in the resistance to SCC of cold worked and solution annealed S32760 was discernible under the present test conditions as no cracking occurred. The solution annealed material appeared to be slightly more resistant to crevice corrosion than cold worked S32760.

ACKNOWLEDGEMENTS

The author would like to thank Cortest Laboratories Limited who carried out the tests described in this paper, and the participants in the research project for permission to publish some of the results.

REFERENCES

1) P. Gustaffson et al - Paper 9. Duplex Stainless Steels '86, The Hague, Amsterdam, 1986, Published by Nederlands Instituut Voor Lastechniek.

2) H. Tsuge et al - Metaux Corrosion Industrie No 667 1981, p337.

3) M. Onoyama - Duplex Stainless Steels Conference, St. Louis, USA, 1983, published by ASM p191.

TABLE 1: Chemical composition of test alloys.

ALLOY	WT %											PREN
	Cr	Ni	Mo	N	W	Cu	C	Si	Mn	P	S	
UNS S31803	22.7	4.77	2.64	0.17	-	0.18	0.022	0.42	1.31	0.015	0.005	34.1
UNS S32550 (LOW Cu)	24.6	6.52	3.15	0.195	-	0.21	0.03	0.63	0.76	0.020	0.006	38.1
UNS S32760 (COLD WORKED)	25.8	7.02	3.51	0.22	0.51	0.79	0.021	0.46	0.946	0.02	0.007	40.9
UNS S32760 (SOLUTION ANNEAL)	25.1	6.9	3.52	0.21	0.65	0.59	0.021	0.30	0.60	0.023	0.005	40.1

TABLE 2: Mechanical properties of test alloys (room temperature)

ALLOY	0.2% PROOF STRESS (MPa)	UTS (MPa)	ELONGATION (%)	HARDNESS (HRC)
UNS S31803	855	931	25.5	32
UNS S32550 (LOW Cu)	836	985	19.2	31
UNS S32760 (COLD WORKED)	886	1013	14.7	35
UNS S32760 (SOL ANNEALED)	646	889	27	23

TABLE 3: Composition of test brine.

$Ca\ Cl_2\ 6H_2O$	3.3616	g/l
$Mg\ Cl_2\ 6H_2O$	0.9447	g/l
K Cl	3.1079	g/l
$Sr\ Cl_2\ 6H_2O$	0.1978	g/l
$Ba\ Cl_2\ 6H_2O$	1.3969	g/l
Na Cl	70.3995	g/l
$Na\ HCO_3$	2.2785	g/l
TRUE Na	28318.366	mg/l
CHLORIDE	46,000	mg/l

TABLE 4: Results from C-ring SCC tests at 80°C and 100% of the 0.2% proof stress.

ALLOY	H_2S PRESSURE (BAR)		
	0.125	0.25	0.375
UNS S31803	No Crack/ Fine Crack	Crack/Crack	Several Cracks/ Several Cracks
UNS S32550 (Low Cu)	No Crack/ No Crack	Pits and Cracks/ Pits and Cracks	Several Cracks/ Several Cracks
UNS S32760 (Cold Worked)	No Crack/ No Crack	No Cracks/ No Cracks	No Cracks/ No Cracks
UNS S32760 (Sol Annealed)	No Crack/ No Crack	No Cracks/ No Cracks	No Cracks/ No Cracks

TABLE 5: Results of pitting corrosion tests at 121°C

ALLOY	H_2S PRESSURE (BAR)		
	0.125	0.25	0.375
UNS S31803	No Pits	No Pits	Deep Pitting (>0.5mm) Both Samples
UNS S32550 (Low Cu)	No Pits	No Pits	Deep Pitting (>0.5mm)/ 3 Shallow Pits
UNS S32760 (Cold Worked)	No Pits	No Pits	No Pits/3 Shallow Pits

TABLE 6: Results of crevice corrosion test with PTFE multiple crevice washer assembly at 121C.

ALLOY	H_2S PRESSURE (BAR)		
	0.125	0.25	0.375
UNS S31803	No Attack	No Attack	6 Segments Attacked
UNS S32550 (Low Cu)	No Attack	No Attack	4 Segments Attacked
UNS S32760 (Cold Worked)	No Attack	No Attack	2 Segments Attacked
UNS S32760 (Sol Annealed)	No Attack	No Attack	No Attack

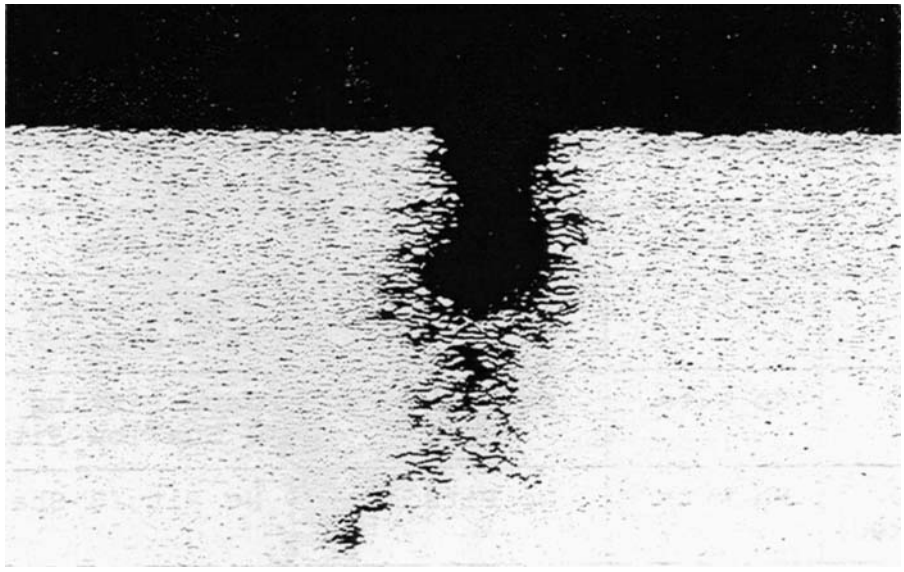


FIGURE 1: Crack in 22Cr C-ring tested with 0.25 bar H_2S (x 200)

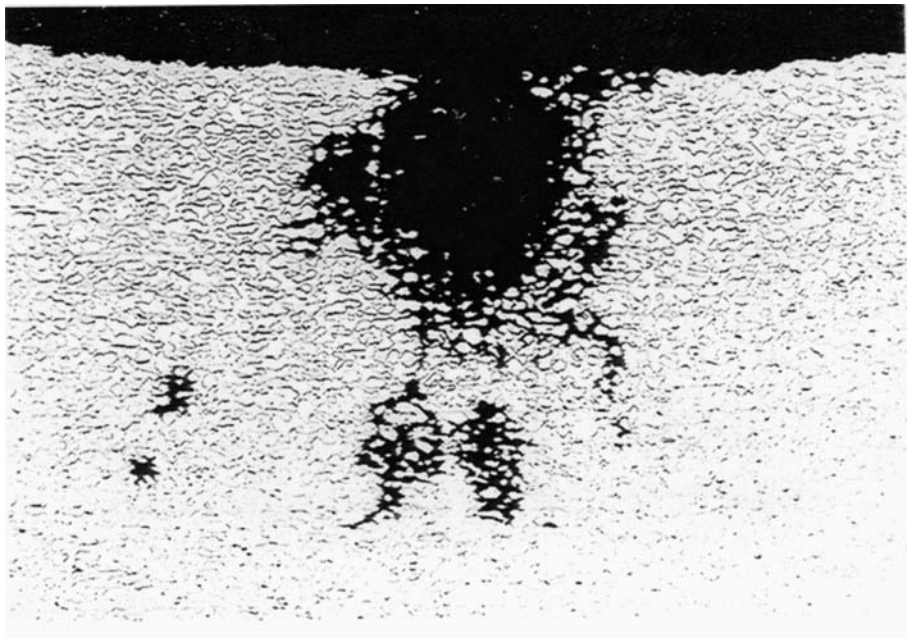


FIGURE 2: Crack in 25Cr C-ring tested with 0.25 bar H_2S (x 200)



FIGURE 3: Pitting corrosion on 22Cr bent beam specimen tested at 121°C, 93 bar CO_2, 0.375 bar H_2S (x 200).

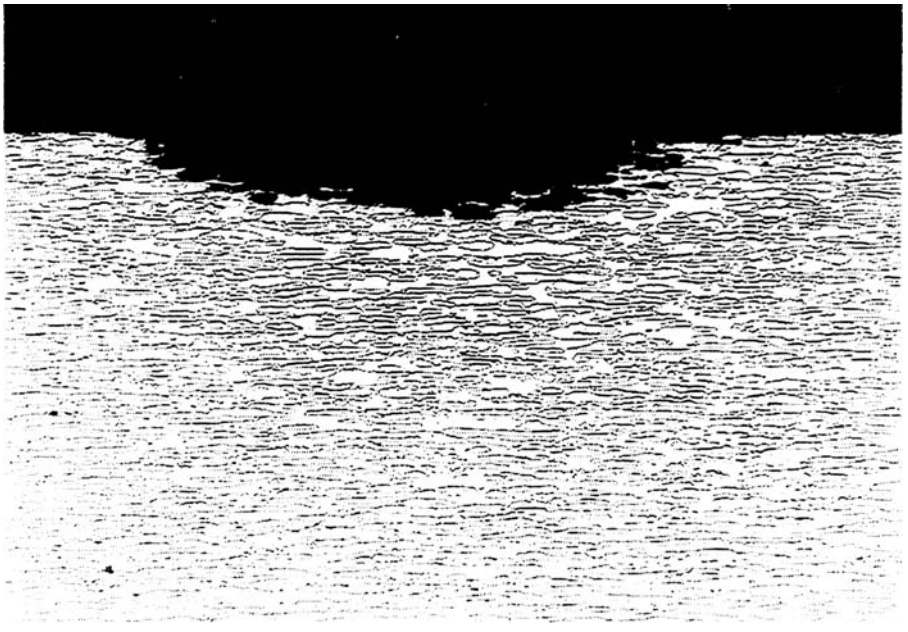


FIGURE 4: Pitting on 25Cr bent beam specimen tested at 121°C, 93 bar CO_2, 0.375 bar H_2S (x 100).

Copyrighted Materials
Copyright © 1996 NACE International Retrieved from www.knovel.com

PAPER NUMBER

333

Corrosion 86

The International Corrosion Forum Devoted Exclusively to The Protection and Performance of Materials

March 17-21, 1986
Albert Thomas Convention Center
Houston, Texas

Corrosion Behaviors of Duplex Stainless Steel for Wet CO_2 Environment

A. Ikeda, M. Miura, S. Mukai, M. Ueda and K. Koso

Central Research Laboratories,
Sumitomo Metal Industries, Ltd.
1-3, Nishinagasu-hondori, Amagasaki 660, Japan

ABSTRACT

22 ∿ 25%Cr α-γ duplex phase stainless steels are suitable for CO_2-brine system. The pitting resistance in the ferric chloride test at 30°C is improved by means of regulating alloying elements both in a pitting index and a fraction of austenite phase. As concerning the duplex stainless steel, it is preferable to include the term of nitrogen content in the expression of pitting index, e.g. P.I. = Cr + 3Mo + 16N.

By the newly developed welding materials, the pitting resistance of welds could be improved.

Influence of H_2S and O_2 contamination on CO_2 corrosion of duplex stainless steels are also discussed.

1. INTRODUCTION

Recently, CO_2 corrosion problems have come out on the exploitation of deep well. A prosperity of enhanced oil recovery (E.O.R) system has also increased an aggressiveness of environment in oil and gas production. These situations have improved a development of economical corrosion resistant alloy tubular products in order to make a performance of well string and pipe line for oil and gas production more reliable. Since a late 1970's, martensitic Cr steels such as 9Cr-1Mo, 13Cr etc. have been successfully applied for a production tubing for gas wells including CO_2(1)-(3). 22 to 25Cr α-γ duplex phase stainless steels are more beneficial than those Cr steels, because a corrosion resistance of the former is more stable than the latter(1)(4)-(6). The epoch making application of α-γ duplex phase stainless steel OCTG was the usage at the Brae field of Marathon Oil in United Kingdom Sector of the North Sea(7). Since 1983, the wells have been operated in no trouble. However, the performance of duplex stainless steel is not always reliable in CO_2-H_2S-Cl^- environment(5)(6). Recently, it was suggested that the regulation of design stress and microstructure would be necessary for the successful application of 22Cr-5Ni-3Mo type duplex

stainless steel tubing on the basis of the field experience(8).

During the post five years, lots of investigations have been done to make a corrosion performance of duplex stainless clear. There is a confliction of corrosion behavior among the publishments, i.e. a temperature and H_2S pressure dependence of corrosion behavior. There is still unsolved the application criteria of it in the CO_2-H_2S-Cl^- environment.

In the past five years, lots of investigations were done to make clear a corrosion performance of duplex stainless steel in the oil and gas production. However, there is still unsolved the application criteria of it in the CO_2-Cl^- system contaminated with any cathodant such as H_2S and O_2. Moreover, there is a confliction among the published data as concerning corrosion behavior, i.e. a temperature and H_2S partial pressure (P_{H_2S}) dependence of SCC susceptibility. In addition of it, there are many unknown subjects in the application of duplex stainless steel for pipe line, because a complexity of microstructure by welding affects significantly corrosion behavior.

In the present paper, the influence of H_2S and O_2 contamination on CO_2 corrosion of duplex stainless steel is investigated. Especially, various factors affecting localized corrosion are discussed in the vicinity of 60°C, in which temperature SCC or selective corrosion of duplex stainless steel was the most sensitive(6). Finally, the improvement of corrosion resistance of duplex stainless steel including both mother metal and weldments are discussed also with the extention of application criteria due to regulation of corrosion environment.

2. EXPERIMENTAL

2.1 Materials tested

Chemical compositions and tensile properties of materials tested are shown in Table 1 and 2. In Table 1, the commercial products of conventional stainless steels and high Ni-Cr steels, which are melted in AOD process are shown. SM22Cr and SM25Cr which are representative α-γ duplex stainless steel prodycts were, especially, used through a course of this work. In Table 2 where Cr, Mo, Ni and N contents were intentionally varied, α-γ duplex stainless steels melted in a vacuum RF furnace of laboratory are shown. These are especially used for investigations of metallurgical factor affecting a pitting corrosion. The numbers of figure and table designated at the most right hand column mean that each materials was used in them.

2.2 Corrosion test

In order to investigate a relative pitting corrosion susceptibility in CO_2-brine systems, a pitting potential (Vc') was evaluated by the potentiodynamic method in accordance with the procedure in JIS G 0577-1981. The potential sweep rate is 20 mV/min. The Vc' is defined as a potential at the polarization current of 100 $\mu A/cm^2$, In this work, 5%NaCl solution saturated with 0.1 MPa CO_2 of which oxygen contamination was below 20 ppm was mainly used. Another pitting test was examined by the ferric chloride test in accordance with ASTM G48. Alternate test temperatures were also used. In order to decide a critical temperature in the ferric chloride test, a temperature increasing method of 2.5°C or 5°C in each step was also carried out. A cycle of test period of this test is usually 24 h.

Weight loss corrosion and SCC behaviors of materials in the high pressure CO_2-brine or CO_2-H_2S-brine environment were investigated with the four point bent beam test with notch in autoclaves cited in elsewhere(5). U bent test was also used. Two different crevice corrosion tests by both metal to metal crevice and teflon crevice with 20 groups(9) as shown in Fig. 1 were applied. As a teflon washer was used for mounting specimens on the holder, the situation of crevice corrosion under the washer was also assessed for the additional information.

Standard test conditions mentioned above are shown in Table 3. In addition to them, various corrosion tests were carried out for conventional α-γ duplex stainless steels i.e. SM22Cr and SM25Cr in Table 1. Those test conditions are tabulated with the

results in Table 4 of section 3.2.

2.3 Welding conditions and mechanical properties

These technical items are described with results at the later section, because the results are closely related with them. The charpy impact test was carried out with the 2 mm V notch specimen.

3. TEST RESULTS

3.1 Corrosion behavior of conventional alloy in brine-corrosive gas system

In order to rank up materials for marine corrosion, a ptting potential in brine and a critical temperature in the ferric chloride test have been conventionally used for the indexes(10). Nurimen at al. developed a relationship between chromium and molybdenum for pitting and crevice corrosion(11). Rockel shows a meanful relationship between a pitting index (P.I.) of Cr + 3Mo and a pitting and crevice resistance of materials in the chloride environment(12). Nowadays, there are a couple of expressions of pitting index for materials including nitrogen, e.g. Cr + 3Mo + 10N, Cr + 3Mo + 16N etc.(13)(14).

Pitting potential values of conevntional stainless steels and alloys cited in Table 1 were studied in 5% NaCl aqueous solution saturated with CO_2 at 0.1 MPa. The result is shown in Fig. 2. As concerns the austenitic stainless steels and alloys, the pitting potential linearly increases with the pitting index of either Cr + 3Mo or Cr + 3Mo + 16N. On the other hand, the pitting potential of duplex stainless steel does not correlate with P.I. = Cr + 3Mo, but with P.I. = Cr + 3Mo + 16N. Because nitrogen content contributes significantly to the pitting resistance of duplex stainless steel, the latter expression i.e. P.I. = Cr + 3Mo + 16N, is possively more preferable, even though a physical meaning of coefficient to nitrogen content is not clear. The ranked pitting resistance in brine including CO_2 is mostly the same as one in no CO_2 brine(13).

A relationship between critical pitting temperature in the ferric chloride test (10%$FeCl_3 \cdot 6H_2O$, 24 h) and the pitting index is shown in Fig. 3. As same as the case of pitting potential, the importance of nitrogen content on the pitting resistance of α-γ duplex stainless steels is also clarified. Therefore, the pitting index for duplex phase stainless steel will be discussed with using P.I. = Cr + 3Mo + 16N, hereafter.

It is one of important phenomena that 10%$FeCl_3 \cdot 6H_2O$ test at 30°C is very critical to the pitting initiation of the conventional 22Cr α-γ duplex stainless steel. A typical average composition of that alloy is constituted from 22Cr-5.5Ni-2.7Mo-0.12N, which corresponds to P.I. = 32.0. This value is slightly less than the critical P.I. at 30°C, i.e. 33. Thus, it is necessary to regulate an alloy composition, if 22Cr type α-γ duplex stainless were required to clear a criterion of no pitting at 30°C. The 25Cr type α-γ duplex stainless steel such as SM25Cr cited in Table 1 has a good reputation as a stainless steel resistant to sea water corrosion. The minimum P.I. of its alloy is about 33.3 corresponding to 24Cr-6.5Ni-2.5Mo-0.11N, which is slightly higher than the critical P.I. at 30°C, i.e. P.I. = 33. Therefore, the ferric chloride test at 30°C in accordance with the procedure of ASTM G48 would be useful for the investigation of either improvement of pitting resistance of 22Cr type alloy or deterioration of pitting resistance due to welding, at least.

The Vc' of the conventional stainless steel in 5% NaCl aqueous solution saturated with 0.001 MPa H_2S is shown in Fig. 4. In this environment, also, nitrogen contents affects significantly the pitting resistance of duplex stainless steel. The P.I. dependence of Vc' in the brine-H_2S system is very resemble to that in the brine-CO_2 system.

3.2 Corrosion behavior of conventional 22Cr and 25Cr α-γ duplex stainless steels

The influence of fundamental three elements, i.e. Ni, Cr and Mo on CO_2 corrosion was investigated with the materials in Table 2. Generally, the

higher the contents of Cr and Ni, the more resistant to SCC the α-γ duplex stainless steel in the brine-CO_2 at high temperature. Both SM22Cr and SM25Cr steels locate the corrosion resistant region in the map as shown in Fig. 5. SM22Cr is more critical than SM25Cr at 200°C, although there is no difference in the susceptibility to SCC of both steels at 150°C. Asphahani show the similar results, although his study was carried in a little different conditions(15).

Corrosion test results in the various conditions are summarized in Table 4. The difference in corrosion resistance between solution annealed SM22Cr and SM25Cr is clearly appeared only in the result of pitting test due to the ferric chloride test.

The effect of Cl^- ion concentration and temperature on both general and crevice corrosion behaviors in the CO_2-brine system is shown in Table 5 and Fig. 6. In these tests, the O_2 contamination in CO_2 gas was 20 ppm in average. Both corrosion behaviors of 9Cr-1Mo and 13Cr steels are mostly consistent with their temperature or Cl^- dependence in the published data(6)(16)(17). The corrosion of 13Cr steel at 150°C in relation to the groove should be essentially categorized to the general corrosion. Both SM22Cr and SM25Cr duplex steels shows an excellent corrosion resistant in all conditions examined. There was no evidence of crevice corrosion even under the fluoride resin washers. The excellent corrosion resistances in brine-CO_2 system is maintained even in the oxygen level up to 700 ppm, as shown in Table 6.

In the brine-CO_2-H_2S system, a localized corrosion resistance of both SM22Cr and SM25Cr was examined. The test results are shown in Table 7 and Fig. 7. Both 9Cr-1Mo and 13Cr steels suffers a general corrosion in every conditions as same as the published data(16). A small amount of H_2S accelerates CO_2 corrosion especially at low temperatures. Both SM22Cr and SM25Cr were immune to crevice corrosion both in the grooved teflon and the metal-metal crevice, although some evidence of crevice corrosion under the fluoride resin washer was observed in SM22Cr at 50°C.

3.3 Influence of environmental and metallurgical on pitting corrosion of duplex stainless steel

Effect of environmental factors on pitting corrosion : Both pitting potential (Vc') and corrosion potential (E_{corr}) are affected by environmental factors. The potential difference, i.e. $\Delta Vc' = Vc' - E_{corr}$, is, in a sense, a probability of pitting initiation.

The influence of environmental fractors on pitting potential (Vc') of SM22Cr cited in Table 1 is shown in Fig. 8. The higher the temperature, the lower the Vc'. The Vc' decrerases significantly with increasing temperature from 30°C to 60°C. Miyuki et al. show that this tendency continued up to 100°C(18). In Fig. 8, the Vc' decreases linearly with log $[Cl^-]$. As for pH value, the contribution is not so large at the range over 4. CO_2 in the environment attributes decreasing pH value of solution. Therefore, pH value over 3.0 should be taken into consideration in the CO_2 environment(6)(19). Miyuki et al. also show that the effect of CO_2 on the Vc' at pH 2.7 was little in the high pressure CO_2 (3.0 MPa P_{CO_2} at 25°C) at 200°C(18). As shown in Fig. 8, $\Delta Vc'$ is almost constant at pH more than 3. This means that P_{CO_2} would hardly affect a pitting initiation, although it might contribute the growth rate of pitting.

E_{corr} is affected by the potential and reaction rate of cathodic reaction. The concentration of cathodant means a probability of cathodic reaction. Therefore, corrosion potential is significantly affected by the concentration of cathodant. For example, effect of $FeCl_3$ concentration on E_{corr} is shown in Fig. 9. The pH value of 10%$FeCl_3 \cdot 6H_2O$ aqueous solution is about 1.5. The corrosion potential of SM22Cr in this solution is about 0.4 V vs S.C.E, which is mostly decided with the redox potential of reaction $Fe^{2+} \rightleftarrows Fe^{3+} + e^-$. In considering a pitting initiation in this system, the meaning of critical temperature of pitting initiation can be clearly explained. When E_{corr} becomes higher than Vc', the pitting corrosion initiate. Because the shift of the redox potential is not so large, the decrease of Vc' with temperature increases come out important,

relatively. For example, the pitting will occur easily in this solution at 60°C, because corrosion potential locates at the much higher potential in comparison with the Vc' as shown in Fig. 8.

Considering CO_2 corrosion problems in the oil and gas production, H^+ and H_2S are usual cathodants. When the water injection and the hydropressure test are applied, the contamination of O_2 and other cathodant would join to the brine-CO_2 corrosion system. The influence of a couple of reactants on CO_2 corrosion is shown in Fig. 10, where 5% NaCl-0.1 MPa CO_2 including 0.1 M of each regend is used. All of them does not affect Vc', but E_{corr}. $NaHSO_3$ reduces slightly E_{corr}. Na_2SO_3 also reduces it in no CO_2 condition. The increase or recovery up to the base level of E_{corr} with injecting CO_2 mean probably a oxidation of Na_2SO_3 or a reduction of CO_2. These reactants are not harmful to the pitting initiation of duplex stainless steel. However, $NaClO_3$ could increase a susceptibility to pitting corrosion of it, because $\Delta Vc'$ could be extremely lowered by the addition of $NaClO_3$. Even though the actual concentration of contamination were significantly lower level than 0.1 M, the corrosivity of brine used for the operation should be taken into consideration.

The effect of metallurgical factors on pitting corrosion ; As discussed at the previopus section, a corrosion behavior of duplex stainless steel attributes nitrogen content in steel. The effect of nitrogen on duplex phase stainless steel is constituted with two factors, i.e. corrosion reaction itself and α-γ phase ratio or γ phase fraction in the equilibrium microstructure. The pitting resistance of α-γ duplex stainless steel could be assessed by the pitting index (P.I.) and the Ni balance, where $Ni_{bal} = Ni + 30(C + N) + 0.5Mn + 8.2 - 1.1(Cr + Mo + 1.5Si)$. Each result as for mother metal and welds metal by GTAW and SMAW are shown in Figs. 11 and 12. The expression due to a γ phase fraction instead of Ni balance was also used in order to make a physical meaning clear.

A pitting resistance of mother metal appears to be dependable only on the pitting index, if the fraction of phase would be over 50%. The critical pitting index is about P.I. = 33. The critical pitting index increases with decreasing γ fraction at the γ fraction below 50%. Although this pnenomenon could not be accurately explained, a distribution of alloying element to α and γ phases and the precipitation such as nitride and carbide might be ralated to the local deterioration of passivation film. The pitting resistance of heat affected zone is mostly the same as mother metal, if the alloying element does not locate at the critical region in Fig. 11.

As concers welds, the pitting behavior is more complicate as shown in Fig. 12. The map for pitting initiation could be divided into four regions. Region 1 is one with fraction over 78%. It is presumed that the change of solidification mode would contribute the increased susceptibility to pitting corrosion in this region. It could drastically happen at the fraction between 73% and 78% as shown in Fig. 13. At the higher fraction, $\alpha + \gamma$ solidification could occur, while solidification occurs at the lower fraction. Because the solubility of alloying element in each α or γ phase depends upon the temperature, the intermetallic compounds precipitate easily at the grain boundaries even during the cooling process after welding. The chemical analysis of extracted residue ascertained this explanation as shown in Fig. 14. The deterioration of corrosion resistance of intercrystalline region could be also clarified by the Huey intergranular corrosion test in Fig. 15.

The region 2 in Fig. 12 is the same region susceptible to pitting as mother metals as shown in Fig. 11. The welds are immune to the pitting corrosion in the region 4.

The welds are only susceptible to pitting in the region 3, nevertheless the mother metals are immune to pitting there. Therefore, it is presumed that any characteristic metallurgical change due to welding is related to the deterioration of passivation film.

Development of girth welding for improv ing pitting resistance ; A welding rod for SMAW and a welding wire for GTAW were developed in order to improve a

pitting resistance at the girth weld. The chemical compositions of deposited metal are shown in Table 8. The welding sequence is shown in Table 9. As for mother metal, the five alloys with different pitting index and fraction cited in Table 1 were used. They are DP8-1 to -5, which correspond to the number illustrated in Fig. 11.

Both corrosion and Charpy impact test results are shown in Table 10. All materials in SMAW is free from pitting. GTAW is more sensitive. In exception of DP8-1, mother metal of which is rather sensitive itself, other materials are almost pitting free. As for ductility of welds, average absorbed energy at -46°C is 114 J in GTAW and 32.6 J in SMAW, respectively.

Thus, if mother metal of α-γ duplex stainless steel is designed with P.I. $\geqq$ 33 and Ni balance of 7.5 to 9.5, it is possible to make both mother metal and SMAW for pipe line application free from pitting in 10%$FeCl_3 \cdot 6H_2O$ at 30°C. If the P.I. of mother metal are increased up to 34, both welds in GTAW and SMAW could be free from pitting.

3.4 Localized corrosion behaviors of duplex stainless steels in CO_2-Cl^- System contaminated with O_2 and O_2-H_2S

Locarized corrosion behaviors of seven duplex stainless steels with the different pitting resistance, i.e. SM22Cr, DP8-1 $\sim$ 5 and SM25Cr were examined by the metal-metal crevice corrosion test shown in Table 1. The metallurgical characteristics relating to pitting corrosion of these materials are cited on Fig. 11. The base environmental condition is 5% NaCl-3.0 MPa CO_2. Both O_2 and H_2S concentrations in CO_2 gas were varied. The effect of elemental sulfur on localized corrosion was also studied, because the reaction $2H_2S + O_2 \rightleftarrows 2S + 2H_2O$ could be assumed in the coexistence of H_2S with O_2. SCC test by the four point bent beam test was partly carried out.

The results are shown in Table 11. In both systems of brine-O_2 and brine-H_2S-O_2, there was no evidence of pitting corrosion. Any crevice corrosion was not observed at the metal-metal crevices settled in the original experimental design. However, some initiation of crevice under teflon washers, which were used for the electric isolation between specimens and holders was observed on some combination among materials and environmental conditions as shown by the asterisk in Table 11. A relationship between the pitting index of materials and the probability of crevice corrosion observed under the teflon washer is shown in Fig. 16. In the relatively low H_2S concentration, the tendency of crevice corrosion decreases with increasing P.I. This means that a resistance of duplex stainless steel to localized corrosion in CO_2-H_2S-(O_2)-brine system could significantly depend upon its pitting index at any critical environmental conditions, although it would be discussed later whether the corrosion behavior underneath teflon washers were important or not. It was clarified that the coexistence of elemental sulfur in brine-CO_2-H_2S system degraded the resistance of duplex stainless steel to localized corrosion. It shall be noted that the pitting corrosion took place at the free surface in no relation with crevices in the environment added with free sulfur. It is also cited that the pitting corrosion occurs mainly at the side surface of specimen with somewaht low pitting indexes. The occurrence of SCC is closely related to P_{H_2S}. That is to say, it occurred at the P_{H_2S} over 0.01 MPa in all materials in no relation with both oxygen contamination and P.I. of materials. This criterion of P_{H_2S} for SCC is consisted with the published data(6).

In order to make clear a relationship between localized corrosion susceptibilities and metallurgical factors in CO_2-O_2-Cl^-, the various duplex stainless steels as solution annealed were examined by the U-bend test in 5% NaCl, 3.0 MPa CO_2 systems contaminated with both O_2 contamination of 5 ppm and 6670 ppm. SCC did not occur in all specimens. In the case of 5 ppm O_2 partially, there was no evidence of localized corrosion at all. In the case of 6670 ppm O_2, the initiation of crevice corrosion underneath teflon washers was observed in relation with both γ-fraction and P.I. as shown in Fig. 17. On the P.I.

over 35, no crevice corrosion occurred. On the other hand, crevice corrosion initiated on the P.I. below 34, excluding the high γ-fraction over 70%.

In order to make clear a relationship between the initiation of SCC and the susceptibility to pitting corrosion, the influence of applied stress on the pitting potential was investigated by the measurement to four point beam specimen. The results are shown in Figs. 18 ∿ 20. In the case of pure CO_2, applying stress hardly affects the pitting potential of SM22Cr, which is classified into, somewhat, the poor pitting resistance. It is noted, however, that the pitting potential is lowered by the applied stress even in the extremely low H_2S concentration, i.e. 0.001 MPa H_2S, nevertheless the initiation of SCC or selective corrosion has not been observed hitherto(6). On the other hand, in the case of DP8-5, which is classified into the relatively high pitting resistance as shown in Fig. 11, the degradation of resistance to pitting does not appear at 0.001 MPa H_2S, but at 0.01 MPa H_2S. As summarized in Fig. 20, it is presumed that the pitting resistance could attribute the SCC resistance in brine CO_2-H_2S system. Materials with high pitting resistance such as DP8-5 and SM25Cr have a more stable performance to SCC than ones with low pitting resistance such as SM22Cr, although their SCC susceptibilities could increase significantly at P_{H_2S} over any critical value.

4. DISCUSSION

4.1 Corrosion in brine-CO_2-O_2

Various corrosion behaviors of duplex stainless steel in brine-CO_2 system contaminated with oxygen from 5 ppm to 6670 ppm in CO_2 gas were presented in Figs. 5 and 17 and Tables 4, 6, 7 and 11. From these results, the contribution of O_2 concentration on the initiation of localized corrosion could be made clearly.

Pitting, metal-metal crevice, and grooved teflone crevice : As concerns 22 ∿ 25Cr duplex stainless steel in 5% NaCl-3.0 MPa CO_2, O_2 contamination up to 6670 ppm, which corresponds to O_2 concentration in 0.1 MPa air, does not affect the initiation of pitting corrosion on free surface and that of crevice corrosion both in the metal-metal crevice and the rigid teflon crevice with groove.

Crevice underneath teflon washer : As concerns 22 ∿ 25Cr duplex stainless steel in 5% NaCl-3.0 MPa CO_2, at least, O_2 contamination upto 700 ppm does not affect the initiation of crevice corrosion even in the crevice underneath teflon washer. O_2 contamination of 6670 ppm could initiate crevice corrosion underneath teflon washer at 60°C and 200°C. In this condition, the susceptibility of crevice corrosion at 60°C does not depend upon the pitting susceptibility of materials. At 200°C, however, it is related to that. As shown in Fig. 17, the initiation of crevice corrosion is not observed at the P.I. over 34.5. It is noted that the initiation site of crevice corrosion locates around the entrance of crevice. As concerning the initiation of crevice corrosion underneath teflon washers, the cause cannot be clearly explained. However, the following is a possible explanation. The teflon washer would make locally a plastic deformation by tightening a bolt. Therefore, an extremely small amount of air could be shut in the surface irregularity. It could not be loosed during the deaeration process, but during the corrosion tests, slowly. So, the superposition of O_2 dissolved in the bulk solution and the confined O_2 underneath washer would contribute to the cathodic reaction and the initiation of crevice via inducing a pitting corrosion around the entrance of teflon washer. Ikeda et al. show that O_2 contamination accelerated CO_2 corrosion by the addition of the following cathodic reaction, i.e. $O_2 + 4H^+ + 4e \rightleftarrows 2H_2O$, which resulted in the increase of corrosion rate of pure iron and the increase of pitting corrosion susceptibility of Cr steel(20). The previous description as for crevice corrosion underneath teflon washer in the present paper does not conflict with it.

SCC : It is concluded from the results shown in Figs. 5 and 17 and Table 6 that the SCC susceptibility of 22 ∿

25Cr duplex stainless steel in brine-CO_2-O_2 system is small, but it could be correlated to its susceptibility to pitting corrosion in the critical conditions, which depend upon O_2 concentration, Cl^- concentration, temperature etc.

4.2. Corrosion in brine-CO_2-H_2S-O_2

Corrosion behaviors of duplex stainless steel in brine-CO_2 system contaminated with both H_2S and O_2 are discussed by the results shown in Tables 7 and 11 and Figs. 16 and 20. The reaction between O_2 and H_2S at the ambient temperature could make a colloidal sulfur in the solution as shown in Formula (1)

$$2H_2S + O_2 \rightleftarrows 2H_2O + 2S \qquad (1)$$

The elemental sulfur could degrade the corrosion resistance of duplex stainless steel through the following cathodic reaction as shown in Formula (2)

$$S + 2H_2O + 2e^- \rightleftarrows H_2S + 2OH^- \qquad (2)$$

The results of corrosion test added with 1 g/ S in Table 11 support the previous presumption. However, it was shown also in Table 11 that the coexistence of H_2S with O_2 upto 6670 ppm could attribute neither initiation of pitting corrosion nor crevice corrosion in the metal-metal crevice. Even though the collidal sulfur were formed in the solution, its concentration might affect the probability for realization of corrosion reaction. On the other hand, the crevice corrosion underneath teflon washers could be observed in the couple of test conditions as same as CO_2-O_2 systems. The same reason as CO_2-O_2 system, i.e. the contribution of O_2 confined under the teflon washer could be rationally presented to the occurrence of crevice corrosion underneath teflon washers in CO_2-H_2S system. A relationship among H_2S, O_2 and pitting index to that corrosion is summarized in Fig. 21. As both representative of low P.I. and high P.I., SM22Cr and SM25Cr are selected, respectively. In Fig. 21, each material with different P.I. has a different immune region to crevice corrosion underneath washers, respectively. The higher the pitting index, the larger the immune region. Both increases of H_2S and O_2 concentration assist mutually the initiation of crevice corrosion underneath teflon washers.

When the applied stress is little, this type of corrosion had better to be ignored, because the situation confining O_2 such as crevice underneath washer could not be always realized. However, in the relatively higher stress application, it is presumed that the effect of colloidal sulfur formation would be detrimental to the initiation of pitting or localized corrosion. It shall be confirmed in tthe future test.

4.3. On the initiation of SCC in brine-CO_2-H_2S

Ikeda et al. show that the critical H_2S concentration for SCC initiation in 5% NaCl-3.0 MPa at σ_{th} = 100% SMYS located at between 0.001 MPa and 0.1 MPa. Present test data is closely consistent with it. It is presumed that SCC initiation is closely related to the pitting initiation, because the pitting potential at 60°C is significantly lowered by the stress application. However, the critical H_2S concentration for SCC in the environment without oxygen contamination will be precisely examined in the future, because it could be possibly higher than 0.01 MPa for material with the relatively higher pitting resistance.

5. SUMMARY

1. The pitting corrosion resistance of duplex phase stainless steel can be effectively evaluated in 10% $FeCl_3 \cdot 6H_2O$ solution at 30°C. In order to overcome that criteria, both P.I. designated with Cr + 3Mo + 16N and γ-fraction in microstructure are useful factors.
2. The pitting resistance of welds is poorer than that of matrix. Both regulation of P.I. and γ-fraction of welds could improve the pitting resistance as same as matrix. The α-γ solidification make significantly detrimental the

pitting resistance of welds. Therefore, that solidification mode should be avoided in the weldments.

3. P_{CO_2} affect hardly the initiation of pitting.
4. Generally speaking, 22 ∿ 25Cr duplex stainless steel is resistant to localized corrosion system contaminated with O_2 or H_2S-O_2. However, a crevice corrosion underneath teflon washers is accelerated by increasing both H_2S and O_2. This type of crevice corrosion initiate in the pitting. Therefore, the material with higher P.I. improve the resistant to this type of crevice corrosion. The confined O_2 in the teflon washers could result in the occurrence of it.
5. Elemental sulfur accelerates both initiation of pitting and crevice corrosion.
6. The cathodant, such as $NaClO_3$ could increase a probability of pitting initiation.

ACKNOWLEDGEMENT

The authors would like to thank Dr. K. Nishioka, General Manager of Central Research Laboratories, for the approvement of this paper submission. They also would like to thank Drs. F. terasaki, T. Matsuoka and T. Moroishi for their encouragement through the course of this work. Thanks owe to Messrs. T. Kobayashi, I. Sakoda and H. Kusagi for their helpful assistant in this work.

References

(1) J. Oredsson, S. Bernhardsson, Intern. Corro. Forum, Corrosion 182, Paper No. 126(1982)
(2) J.D. Combes, J.G. Kerr, L.J. Klein, Petrol. Engr. Int. p.50(Mar., 1983)
(3) Y. Tomoe, M. Nakamura: Proc. 4th APCC at Tokyo, p.997 (1985)
(4) G. Herbsleb, R.K. Pöpperling : Intern. Corro. Forum, Corrosion/80, paper No. 13(1980)
(5) S. Mukai, H. Okamoto, T. Kudo, A. Ikeda, J. Materials Energy Systems vol. 5, p.59(1983)
(6) A. Ikeda, S. Mukai, M. Ueda: Corrosion vol. 41, No. 4, p 185-192(1985)
(7) B.D. Craig 1982 ASM Metals Conmg., 8201-015(1982), J. Materials Energy Systems, vol. 5, p53 (1983)
(8) G. Wilken, Intern. Corro. Forum, Corrosion/85, paper No. 225(Mar., 1985)
(9) ASTM No. STP-576 (1976)
(10) R.J. Brigham: E.W. Loser, Corrosion, 30, (1974), p.161
(11) N. Passal, J.I. Nurimen, Corrosicen, 30, (1974), p.381
(12) M.B. Rockel, ACHEMA Conference at Frankfurt (1979)
(13) M. Miura et al., Sumitomo Metal, vol. 36, No. 4, p.383(1984)
(14) J. Preva, B. Johansson, Intern. Corro. Forum, Corrosion/84, paper No. 218(1984)
(15) A.I. Asphahani, Corrosion 37, p. 327(1981)
(16) S. Mukai, M. Ueda, T. Tsumura and A. Ikeda, Proc. 4th APCC at Tokyo, p.664(1985)
(17) A. Ikeda, M. Ueda, S. Mukai, Intern. Corro. Forum, Corrosion/83 paper No. 45(1983)
(18) H. Miyuki et al., Intern. Corro. Forum, Corrosion/84, paper No. 293, Houston (1984)(NACE)
(19) I.L. Crolet and M.R. Bonis, Corrosion 39, No. 1, p.39 (1983)
(20) A. Ikeda, M. Ueda, S. Mukai, Intern. Corro. Forum, Corrosion/85 paper No. 29(1985)

Table 1. Chemical composition and mechanical peoprerties of materials

Mark	Chemical composition (wt %)												Tensile properties			Designation of Figure No	Designation of Table No
	C	Si	Mn	P	S	Cu	Ni	Cr	Mo	O	N	others	Y.S. (MPa)	T.S. (MPa)	El. (%)		
9Cr-1Mo	0.15	0.42	0.41	0.011	<0.003	0.01	0.09	8.49	0.96	0.002	0.0234		650	801	24.3	6, 7	5, 7
13Cr	0.20	0.48	0.49	0.015	<0.003	0.02	0.14	12.37	0.02	0.002	0.0196		583	793	27.3	6, 7	5, 7
SUS304	0.05	0.57	1.52	0.027	0.004	0.14	9.58	18.59	0.15	0.003	0.0521		294	639	69.7	2, 3, 4	
SUS316	0.06	0.66	1.52	0.026	<0.003	0.26	12.79	16.29	2.05	0.001	0.0079		317	608	65.3	2, 3, 4	
SUS316L	0.02	0.50	1.73	0.025	<0.003	0.26	14.45	17.16	2.17	0.002	0.0355		266	549	65.7	2, 3	
SM22Cr	0.02	0.37	1.62	0.028	0.001	0.09	5.48	22.34	3.00	0.004	0.130		557	761	39.7	2, 3, 4, 6, 7, 9, 11, 16, 18, 20, 21	4, 5, 6, 7, 11
DP8-1	0.008	0.41	1.82	0.025	0.001	0.05	5.95	22.50	3.04	0.003	0.142		592	798	35.0	2, 3, 4, 11, 16	9, 10, 11
DP8-2	0.014	0.38	1.82	0.025	0.001	0.06	6.25	22.40	3.00	0.003	0.150		580	803	36.0	2, 3, 4, 11, 16	9, 10, 11
DP8-3	0.014	0.41	1.76	0.025	0.001	0.50	6.30	22.80	3.05	0.003	0.150		607	815	37.0	2, 3, 4, 11, 16	9, 10, 11
DP8-4	0.014	0.43	1.21	0.024	0.001	0.05	6.35	22.70	3.12	0.003	0.171		630	825	39.0	2, 3, 4, 11, 16	9, 10, 11
DP8-5	0.022	0.43	1.78	0.026	0.001	0.05	6.35	23.65	3.35	0.002	0.181		643	854	34.0	2, 3, 4, 16, 19, 20	9, 10, 11
SM25Cr	0.026	0.41	1.00	0.023	0.001	0.50	6.77	25.16	3.16	0.006	0.129	W : 0.27	616	802	34.0	2, 3, 6, 7, 11, 16, 21	4, 5, 6, 7, 11
SM2025	0.020	0.37	0.59	0.015	0.006	0.04	25.26	22.03	2.77	0.001	0.0185		640	730	25.0	2, 3	
SM2030	0.021	0.31	0.60	0.019	0.001	1.52	31.19	20.90	4.06	0.001	0.0225	Ti : 0.14	797	823	15.3	2, 3	
SM2035	0.012	0.51	0.52	0.014	0.001	0.57	36.97	22.08	4.83	0.001	0.0169	W:0.53, Ti:0.26	897	921	16.7	2, 3	
SM2535	0.017	0.25	0.55	0.017	0.002	0.99	38.07	24.96	3.72	0.001	0.0309		862	902	15.3	3	
825	0.037	0.32	0.83	0.010	0.001	2.05	43.33	21.01	3.07	0.001	0.0084	Ti : 0.84	803	845	17.0	2, 3	
SM2550	0.018	0.35	0.61	0.019	0.001	0.80	48.16	24.04	5.42	0.001	0.0096	Ti : 1.01	837	889	23.3	3	

Table 2. Chemical composition and mechanical properties of materials used for investigation of fundamental effect of alloying element on corrosion behavior

Materials		Chemical composition (wt %)					Tensile properties			Designation of Figure No.
		Mn	Cr	Ni	Mo	others	Y.S. (MPa)	T.S. (MPa)	El (%)	
α-γ duplex phase stainless steel	Mother Metal	0.7/0.9	19/26	4.5/10	0/3	—	902/1068	1047/1164	7/13	5, 11, 17
	Weld Metal	0.8/1.1	22/25	5/15	2.7/3.3	Cu:0.1/0.4 W:0.01/0.3	—	—	—	12, 13, 14 15

(C; ≦0.04, Si; 0.3/0.5, P; ≦0.025, S; ≦0.01)

Table 3. Standard test condition

Autoclave Test		
H_2S	0 - 0.1 MPa	
CO_2	3.0 MPa	
Solution	5% NaCl	
Temperature	60°C	50~150°C
Test duration	96 h	200 h
Specibic volume	37 ml / Cm^2	
Velocity	2.5 m/s	
Electrochmical Test		
H_2S (N_2 balance	0.001 - 0.1 MPa	
Solution	5% NaCl	
Temperture	60°C	
Scan speed	20 mV/min	

Table 4. Corrosion test results of conventional 22Cr and 25Cr duplex stainless steels

Item	Test condition	SM22Cr	SM25Cr
Huey	ASTM A262 Prac C 65%HNO_3, 48h x 5 times, Boiling	0.123 g/m^2/h (Average)	0.099 g/m^2/h (Average)
Pitting	ASTM G48 10%$FeCl_3 \cdot 6H_2O$, 24h, 30°C	Slightly pitting	Pitting free
SCC-1	90g/l NaCl, 0.1MPa CO_2, Boiling 28 days, U-bend	Crack free	Crack free
SCC-2	90g/l NaCl, 0.05MPa CO_2+0.05MPa Air, Boiling, 28 days, U-bend	Crack free	Crack free
Modified NACE-1	20°C, 9%NaCl+CH_3COOH (pH3) 0.1 MPa H_2S, 14 days, U-bend	Crack free	Crack free
Modified NACE-2	90°C, 9%NaCl+CH_3COOH (pH3) 0.1 MPa H_2S, 14 days, U-bend	Crack free	Crack free

Table 5. Corrosion test results on crevice and general corrosion in CO_2-Cl^- environment with various Cl^- ion concentration and temperature

Environment		9 Cr		13 Cr		22 Cr		25 Cr	
Temp.	NaCl concentration	G	C	G	C	G	C	G	C
100 °C	0.05%	GC	GC	NC	NC	NC	NC	NC	NC
	0.5	↓	↓	↓	↓	↓	↓	↓	↓
	5	↓	↓	↓	↓	↓	↓	↓	↓
	20	↓	↓	↓	↓	↓	↓	↓	↓
150 °C	0.05	GC	GC	GC	GC	NC	NC	NC	NC
	0.5	↓	↓	↓	↓	↓	↓	↓	↓
	5	↓	↓	↓	↓	↓	↓	↓	↓
	20	↓	↓	↓	↓	↓	↓	↓	↓

G : 20 Grooves crevice test . C : Crevice test .
NC: No crevice corrosion GC General corrosion
[3.0 MPa CO_2-(20ppm O_2)-200h]

Table 6. Effect of O_2 contamination on corrosion resistance in CO_2-Cl^- environment

Test condition		Corrosion-rate (mm/y)	Remarks
100°C	O_2 200ppm	< 0.01	No SCC and No localized corrosion
	O_2 700ppm	< 0.01	
150°C	O_2 200ppm	< 0.01	
	O_2 700ppm	< 0.01	

(5% NaCl-3.0MPa CO_2)

Table 7. Localized corrosion resistance of various stainless steels in CO_2-H_2S-Cl^- environment

Environment		9 Cr		13 Cr		22 Cr		25 Cr	
P_{H_2S}	Temp. (°C)	G	C	G	C	G	C	G	C
No H_2S	50	NC	NC	NC	NC	NC	NC	NC	NC
	75	↓	↓	↓	↓	↓	↓	↓	↓
	100	↓	↓	↓	↓	↓	↓	↓	↓
	125	GC	GC	↓	↓	↓	↓	↓	↓
	150	↓	↓	GC	GC	↓	↓	↓	↓
0.01MPa H_2S	50	CC	CC	CC	CC	NC*	NC*	NC	NC
	100	↓	↓	↓	↓	↓ *	↓ *	↓	↓
	150	GC	GC	GC*	GC*	↓ *	↓ *	↓	↓

G: 20 Grooves crevice test. C: Crevice test.
NC: No crevice corrosion. CC: Crevice corrosion.
GC: General corrosion *: Slightly crevice corrosion
●: Slightly crevice corrosion underneath teflon washer
[3.0 MPa CO_2 -(20ppm O_2)-5%NaCl, 200h]

Table 8. Chemical composition of deposited metal for duplex stainless steel (wt %)

Welding rod & wire		Chemical composition (wt %)										
Materials	Diameter	C	Si	Mn	P	S	Cu	Ni	Cr	Mo	W	N
GTAW #DP3T	2.0φ	0.007	0.33	1.36	0.009	0.001	0.49	8.96	25.56	3.30	0.30	0.125
SMAW #DP3	3.2φ	0.035	0.42	0.80	0.021	0.005	0.47	8.76	25.37	2.98	0.28	0.150

Table 9. Welding condition of girth weld

Welding process		Welding current (A)	Arc voltage (V)	Welding speed (cm/min)	Heat input (kJ/cm)	Welding material	Welding sequence
GTAW + SMAW	1	120	12	6	14	φDP3T	240φ×11t
	2~9	90	22	6	20	φDP3	
SMAW	1	150	25	16	14	φDP3	240φ×11t
	2~5	100	23	7	20		
GTAW	1	120	12	6	14	φDP3T	240φ×11t
	2~11	90	22	6	20		

Table 10. Pitting corrosion resistance of girth weld

Materials	Pitting Corrosion Test (1) (ASTM G48 10%FeCl3·6H2O 30℃, 24 h)								Charpy Impact (2) Test vE-46 (J) (full size 2mmV)	
	Base metal		SMAW		GTAW + SMAW		GTAW		GTAW + SMAW	GTAW
	Surface	Side	I (3)	E (4)	I	E	I	E		
DP8-1	P.F.	P (Slightly)	P.F.	P.F.	P	P.F.	—	—	41.2	—
DP8-2	P.F.	P.F.	P.F.	P.F.	P.F.	P.F.	—	—	42.2	—
DP8-3	P.F.	P.F.	P.F.	P.F.	P.F.	P.F.	—	—	45.8	—
DP8-4	P.F.	P.F.	P.F.	P.F.	P.F.	P.F.	—	—	42.2	—
DP8-5	P.F.	P.F.	P.F.	P.F.	P.F.	P.F.	P.F.	P.F. (5)	41.8	114

(1) Assessment; P: Pitting, P.F.: Pitting free
(2) Sampling method of Charpy impact test specimen.

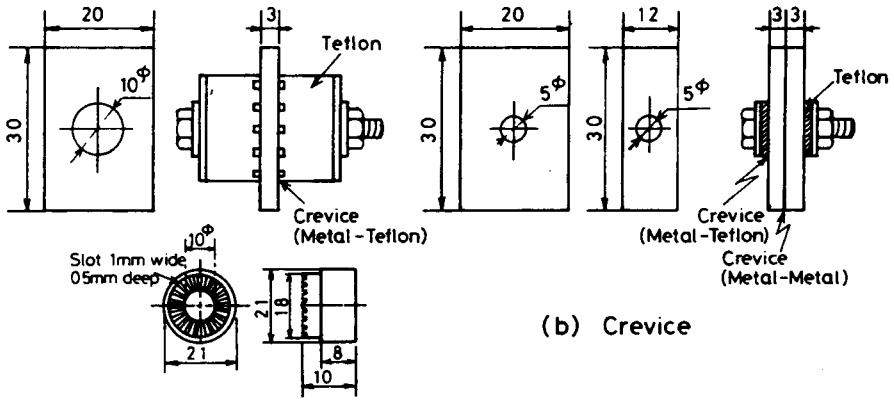


(3) I: Internal bead
(4) E: External bead
(5) Side surface: (Initial bead) No pitting, (Final bead; 5th pass) No pitting
(Internal bead; 2nd 4th pass) Pitting

Table 11. Corrosion behavior in H_2S-CO_2-O_2-Cl^- environment of duplex phase stainless steels

Mark	No.	1		2		3		4		5		6		7	
	O_2(ppm)	200		6670		200		200		200		6670		200	
	H_2S(MPa)	—		—		0.001		0.01		0.1		0.01		0.01	
	S(g/l)	—		—		—		—		—		—		1	
	Evaluation P.I.	C.R. (mm/y)	C.M.	C.R. (mm/y)	C.M.	C.R. (mm/y)	C.M.	C.R. (mm/y)	C.M.	C.R. (mm/y)	C.M.	C.R. (mm/y)	C.M.	C.R. (mm/y)	C.M.
SM22Cr	33.4	<0.01	N.S. / N.C.	0.03	N.S. / N.C.*	<0.01	N.S. / N.C.*	<0.01	S.C.C. / N.C.*	<0.01	S.C.C. / N.C.*	0.02	S.C.C. / N.C.*	0.11	S.C.C. / N.C.P.
DP8-1	33.9	<0.01	N.C.	0.04	N.C.*	<0.01	N.C.*	0.01	S.C.C. / N.C.*	<0.01	N.C.*	0.02	N.C.	0.27	N.C.*, P.
DP8-2	33.8	<0.01	N.C.	0.04	N.C.*	<0.01	N.C.*	0.01	S.C.C. / N.C.*	<0.01	N.C.*	0.03	N.C.*	0.91	N.C.*, P.
DP8-3	34.4	<0.01	N.C.	0.01	N.C.*	<0.01	N.C.*	<0.01	S.C.C. / N.C.*	<0.01	N.C.	0.02	N.C.	0.03	N.C.*
DP8-4	34.8	<0.01	N.C.	0.02	N.C.	<0.01	N.C.*	<0.01	S.C.C. / N.C.*	<0.01	N.C.*	0.02	N.C.	0.07	N.C.*, P.
DP8-5	36.6	<0.01	N.C.	0.05	N.C.*	<0.01	N.C.	<0.01	S.C.C. / N.C.*	<0.01	N.C.*	0.02	N.C.*	0.08	N.C.*
SM25Cr	36.7	<0.01	N.C.	0.01	N.C.*	<0.01	N.C.	<0.01	S.C.C. / N.C.*	<0.01	N.C.	0.02	N.C.*	0.08	N.C.*

Notation
P.I.: Pitting Index (Cr+3Mo+16N wt%), C.R.: Corrosion rate, C.M.; Corrosion mode
N.S.: NoSCC, N.C.; No crevice corrosion, P.; Corrosion under sulfur deposit
*: slightly crevice corrosion underneath teflon washer



(a) Crevice 20grooves

Fig. 1. Appearance of crevice test specimens

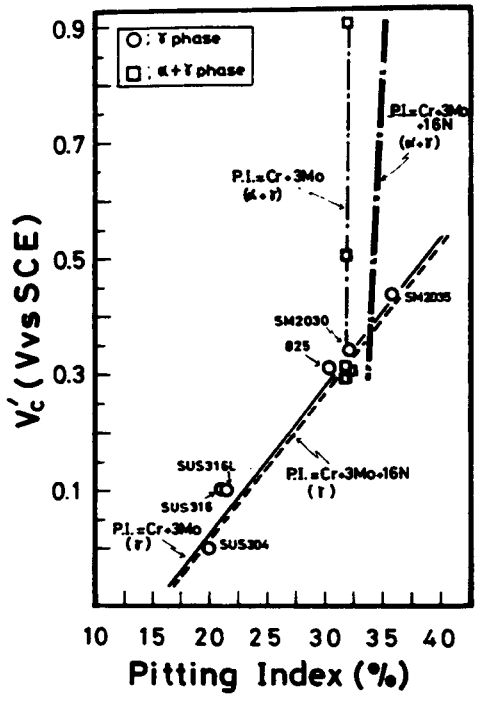


Fig. 2. Pitting potential of various stainless steels (60°C, 0.1 MPa CO_2, 5% NaCl, 20 mV/min)

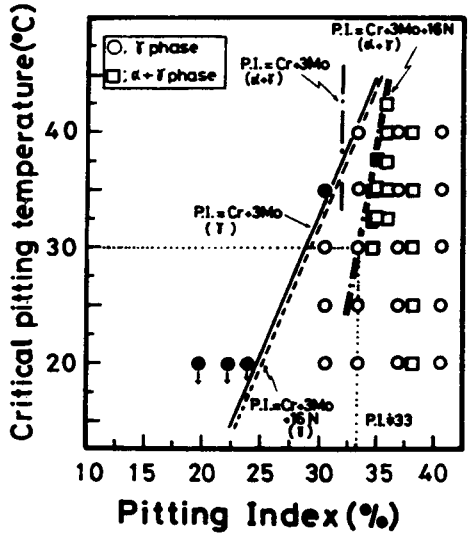


Fig. 3. Relationship between pitting index (P.I.) and critical pitting temperature with various stainless steels (10% $FeCl_3 \cdot 6H_3O$, 24 h)

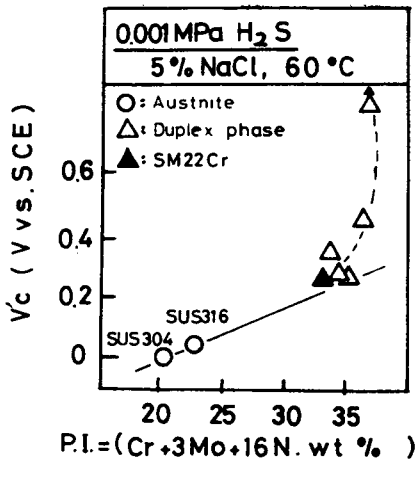


Fig. 4. Pitting potential of various stainless steels in environment including a small amount of H_2S (60°C, 0.001 MPa H_2S(N_2 balance), 5% NaCl, 20 mV/min)

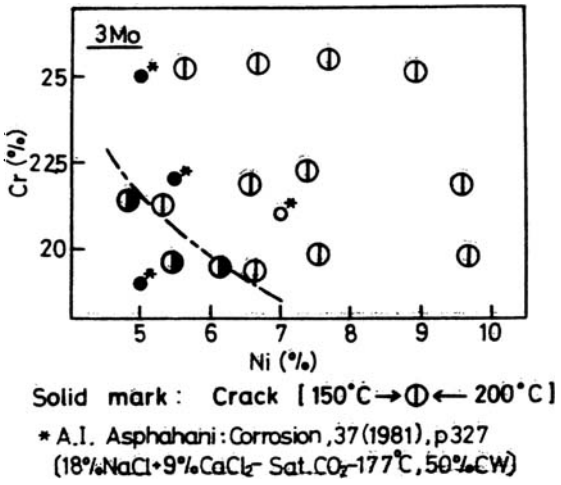


Fig. 5. Effect of Ni and Cr content on SCC susceptibility of α-γ duplex stainless steel in CO_2-Cl^- environment
(25%NaCl, 3.0 MPa CO_2, 30% CW)

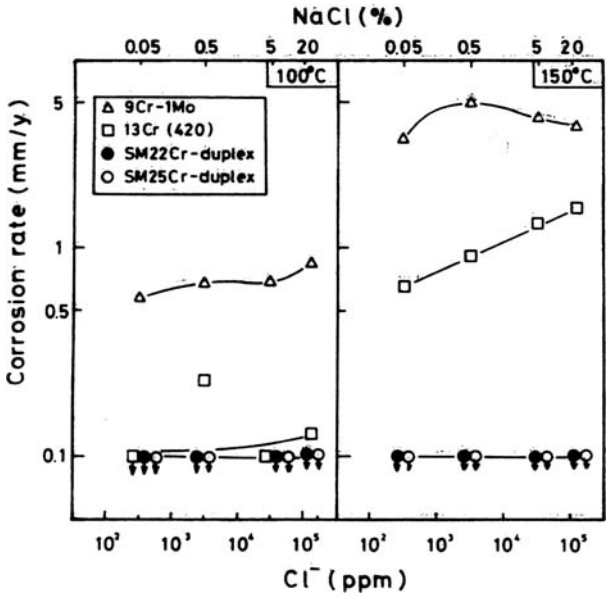


Fig. 6. Effect of Cl^- ion concentration and temperature on corrosion rate in CO_2-Cl^- environment

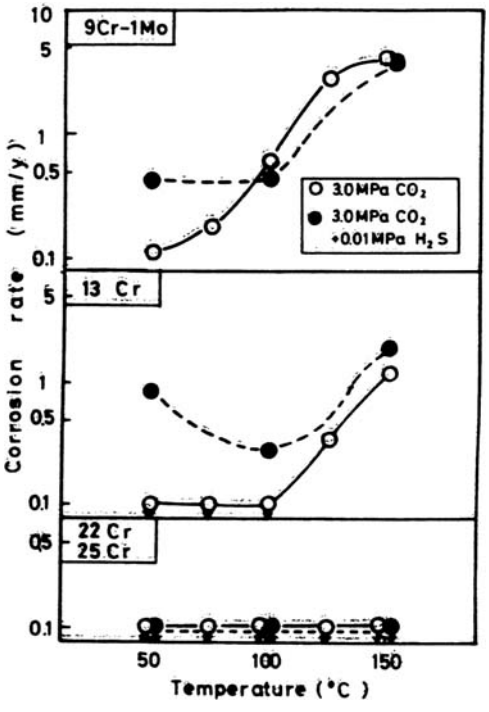


Fig. 7. Effect of H_2S and temperature on corrosion rate in CO_2-H_2S - Cl^- environment
(3.0 MPa CO_2-20 ppm O_2-0/0.01 MPa H_2S-5% NaCl, 200 h)

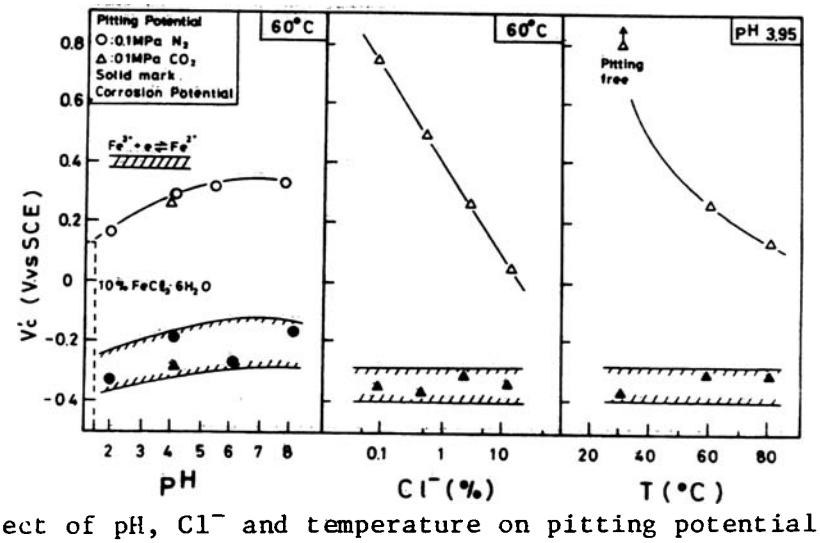


Fig. 8. Effect of pH, Cl^- and temperature on pitting potential and corrosion products.
○ ; 5% NaCl, 0.1 MPa N_2, 20 mV/min
(△ ; 5% NaCl, 0.1 MPa CO_2, 20 mV/min)

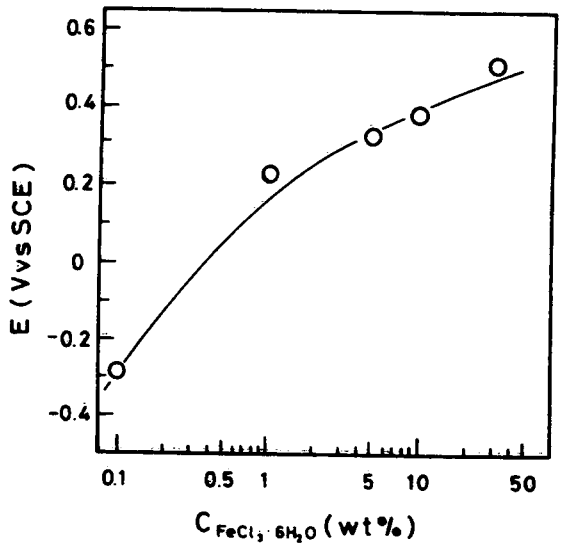


Fig. 9. Effect of $FeCl_3 \cdot 6H_2O$ concentration on corrosion potential of SM22Cr at 20°C

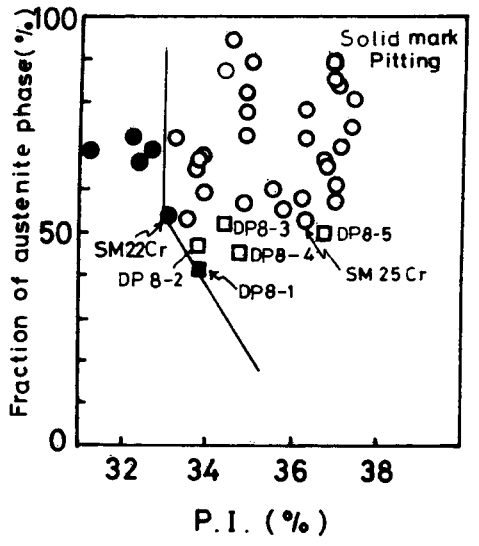


Fig. 11. Effect of pitting index, Ni-balance and fraction of austenite phase on pitting corrosion of mother metal (P.I. = Cr + 3Mo + 16N)

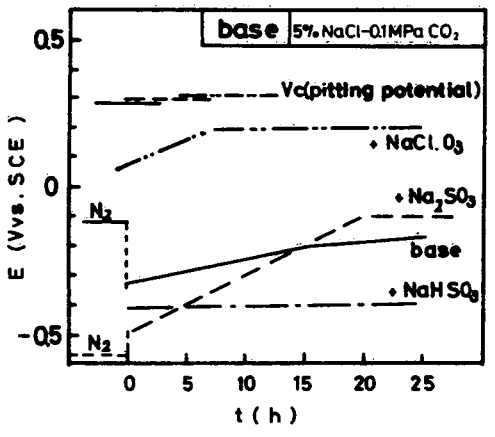


Fig. 10. Effect of cathodant on corrosion potential of SM22Cr in CO_2-Cl^- environment.
(60°C, 5% NaCl, 0.1 MPa CO_2)

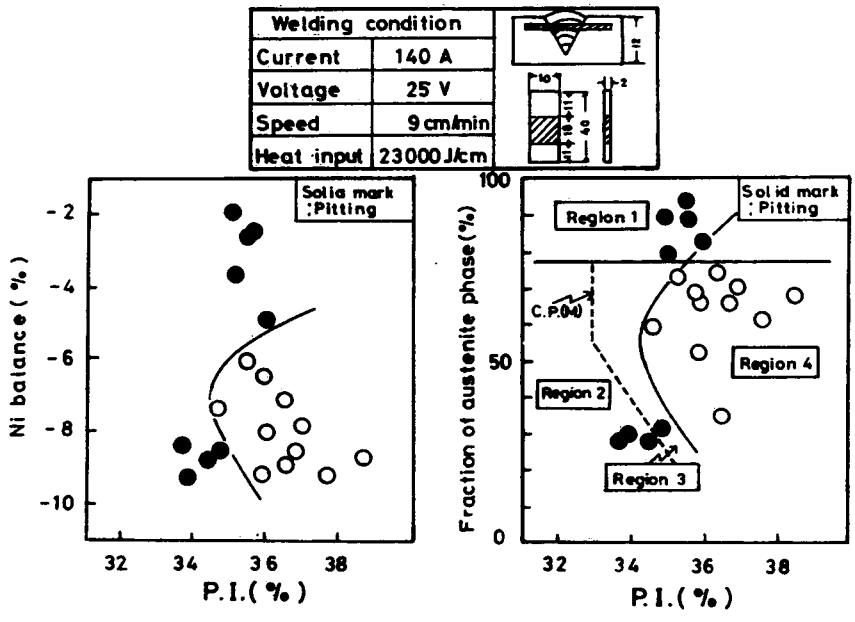


Fig. 12. Effect of pitting index, Ni balance and fraction of austenite phase on pitting corrosion of weldment (SMAW)
(C.P.(M) means critical pitting line for mother metal
P.I. = Cr + 3Mo + 16N
Ni balance = 30(C + N) + 0.5Mn + Ni + 8.2 - 1.1(Cr + Mo + 1.5Si))

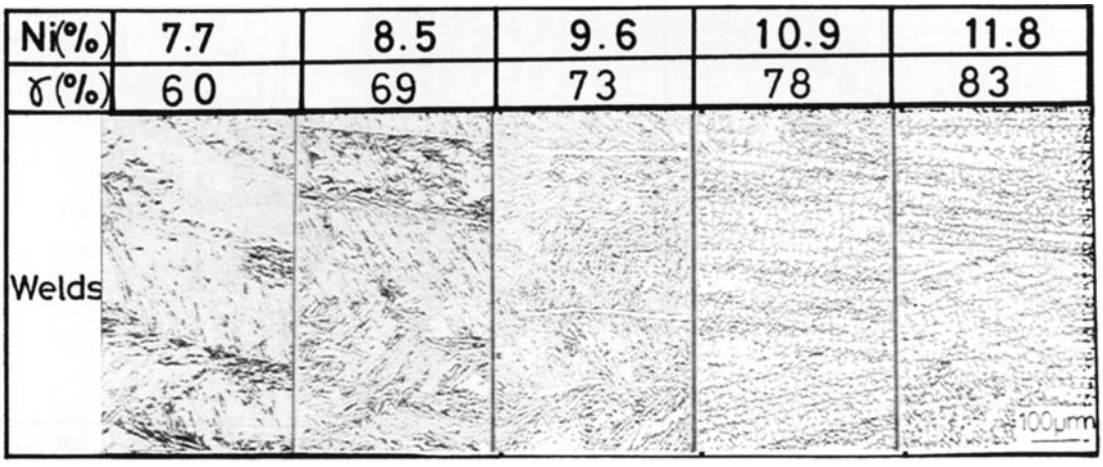


Fig. 13. Effect of Ni content on microstructure of α-γ duplex stainless steels (25Cr-3Mo-0.14N base)

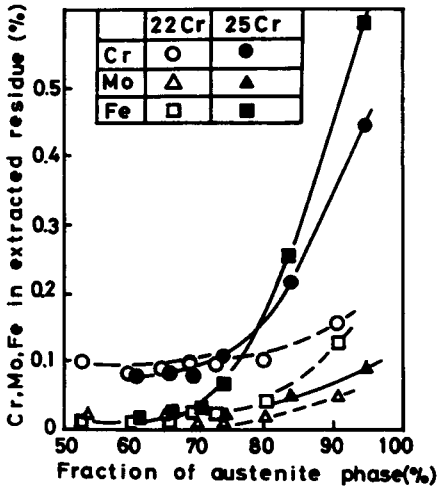


Fig. 14. Content of Cr, Mo and Fe in extracted residue on weldment (SMAW)
(Electrolytic extraction method
Solute ; 10 vol% acetylacetone + 1 wt% TMAC
Solvent; methanol
Current density; 20 mA/cm^2)

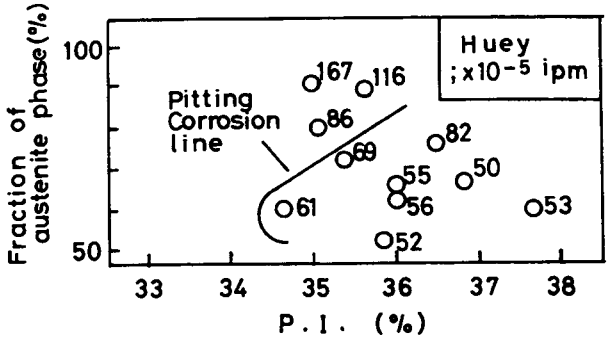


Fig. 15. Effect of pitting index (P.I.) and fraction of austenite phase on intergranular corrosion of weldment (SMAW)

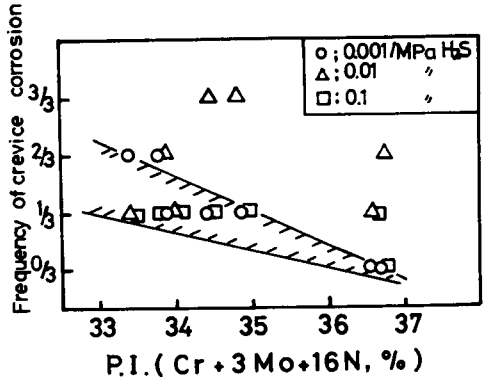


Fig. 16. A relationship between the pitting index of materials and the probability of crevice corrosion

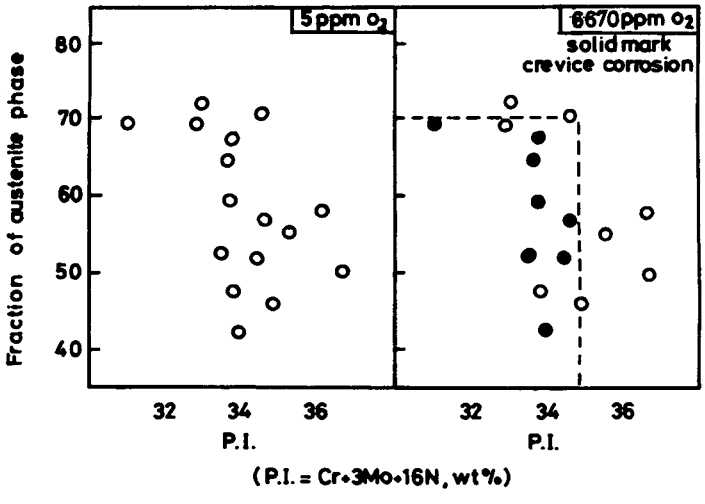


Fig. 17. Effect of O_2 concentration on crevice corrosion in CO_2-O_2-Cl^- environment
(5%NaCl, 3.0 MPa CO_2, 200°C, 96 h)

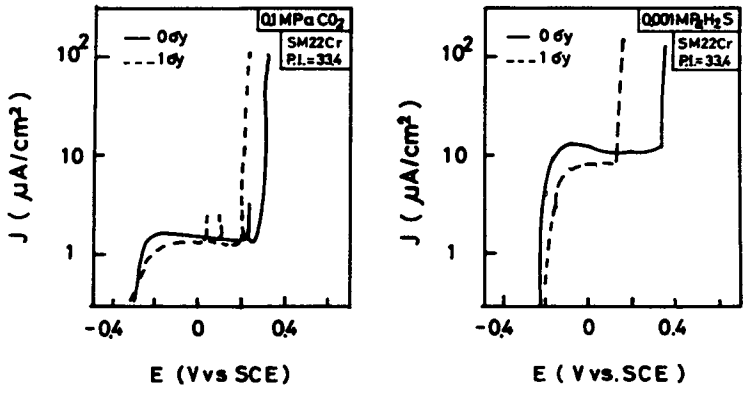


Fig. 18. Effect of applied stress on anodic polarization curves of conventional SM22Cr (5%NaCl, 60°C, 20 mV/min)

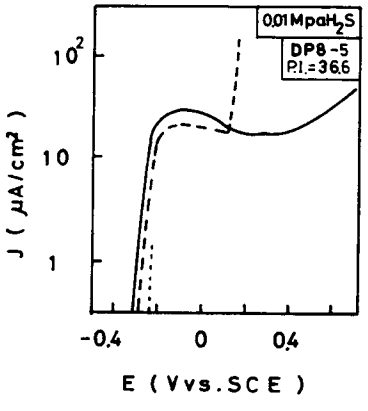


Fig. 19. Effect of applied stress on anodic polarization curves of duplex stainless steel with high pitting index (5%NaCl, 60°C, 20 mV/min)

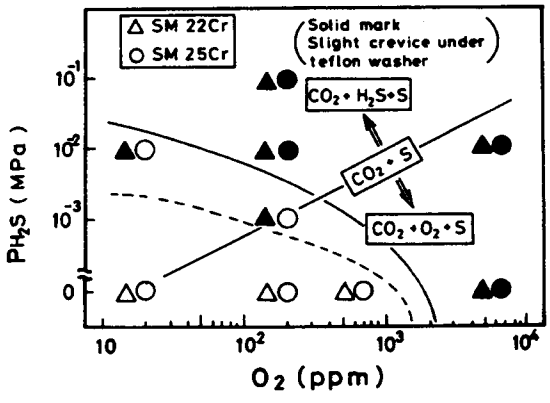


Fig. 21. A relationship among H_2S, O_2 and pitting index on corrosion behavior in H_2S-CO_2- O_2-S environment

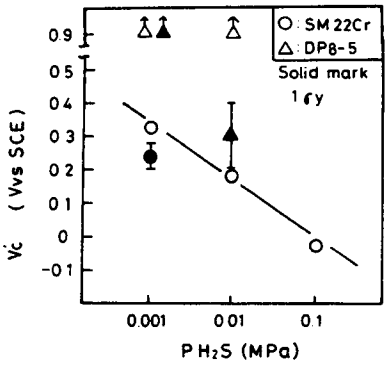


Fig. 20. Effect of applied stress on pitting potential (5%NaCl, 60°C, 20 mV/min)

Copyrighted Materials
Copyright © 1996 NACE International Retrieved from www.knovel.com

PAPER NUMBER

159

Corrosion 86

The International Corrosion Forum Devoted Exclusively to The Protection and Performance of Materials

March 17-21, 1986
Albert Thomas Convention Center
Houston, Texas

EFFECT OF ALLOYING ELEMENT AND FERRITE-AUSTENITE RATIO ON SCC RESISTANCE OF DUPLEX STAINLESS STEELS IN SOUR GAS ENVIRONMENT

Y. Ishizawa
Nippon Kokan K.K., Technical Research Center
1-1, Minamiwatarida-cho
Kawasaki, 210 Japan

T. Inazumi
T. Shimada
M. Tanimura

ABSTRACT

Stress corrosion cracking resistance of duplex stainless steels in the environment containing hydrogen sulfide and chlorides was evaluated for many steels with different chemical compositions and ferrite-austenite ratio. It is indicated that the resistance to cracking is affected by the compositions of ferrite and austenite which constitute the steel structure rather than by the ferrite-austenite ratio. There is an optimum value in Cr content. And alloying with N is beneficial for improving cracking resistance.

INTRODUCTION

Duplex stainless steels are more resistant to stress corrosion cracking (SCC) in high temperature chloride environments, and have better strength than fully austenitic stainless steels. By virtue of these properties, they have been used in various corrosive environments extensively. However, they are known to be susceptible to SCC when the environment contains hydrogen sulfide and chlorides.[1-5] Such a property has frequently prevented the application of duplex stainless steels to sour gas wells.

Many studies have been conducted on the corrosion characteristics of duplex stainless steels and the influence of metallurgical variables such as chemical composition and microstructure on the properties. The structural feature of these steels composed of ferrite and austenite has been taken the major factor that controls the corrosion property. It has been reported that SCC resistance of duplex steels in boiling $MgCl_2$ solutions increases as the volume fraction of ferrite increases to about 40%, and decreases at higher amount of ferrite.[6,7] The SCC behavior in environments containing hydrogen sulfide and chlorides have been also studied with respect to the effect of environmental factors and material conditions.[4,8-10] Studies have revealed that the steels are susceptible to cracking in a wide range of temperature from ambient to about 250°C in the presence of hydrogen sulfide more than a critical concentration. There

have been few studies, however, on the effect of metallurgical variables such as steel composition and phase balance. Although an increase in the amount of ferrite produced by heat treatment is reported to reduce SCC resistance at ambient temperature,[9] it is still obscure if an optimum material condition exists in this phenomenon.

In this study, SCC tests were conducted on steels with various chemical compositions and ferrite-austenite ratio at ambient temperature in order to study the effect of these factors on SCC susceptibility of duplex stainless steels in sour gas environments. As there is an interrelation between chemical composition and ferrite-austenite ratio, the effect of these parameters are difficult to be interpreted discriminately. In the present study, therefore, tests were conducted on many steels which involved duplex steels alloyed with different amounts of Cr, Ni, and N, as well as ferritic and austenitic single phase steels so as to understand the influence of these parameters clearly. The results indicated that the susceptibility of duplex stainless steels to cracking in sour environments was essentially affected by the compositions of ferrite and austenite, and could be improved by controlling the compositions which are resulted from the amount of alloying elements and the phase balance.

EXPERIMENTAL

Material

The present study was conducted on laboratory melted steels with compositions shown in Table 1. Two series of steels were prepared to evaluate the effect of Cr and Ni, and ferrite-austenite ratio (or volume fraction of ferrite).

In series A, the contents of Cr and Ni were varied to change the volume fraction of ferrite, but contents of other elements were not varied intensionally. Series A involves three groups of duplex steels with different (Cr+Ni) levels; (Cr+Ni)% was 29 in the first group, 31 in the second group and 27 in the third group. It also involves a fully austenitic steel and a fully ferritic steel. In the fully ferritic steel nitrogen content was reduced to a low level in order to avoid the loss of ductility due to nitrogen.

In series B, the contents of all elements other than trace elements, C, S, and P, were varied to change the amount of ferrite so that the compositions of ferrite and austenite might be kept constant in this series. Series B involves a fully ferritic steel of low nitrogen as well as series A.

These steels were melted with a vacuum induction furnace and cast as 50 kg ingots. They were hot rolled to 10 mm thick plates, annealed at 1323K (1050C) for 30 min, and quenched in water. All tests were conducted on materials in this solution-annealed state.

Volume fraction of ferrite was measured metallographically by linear intercept method. In order to measure the distribution of alloying elements between ferrite and austenite, the concentration of major elements was analyzed by EPMA for both phases except that nitrogen concentration was measured for only austenitic phase because nitrogen less than 0.1% was difficult to be analyzed by EPMA. Tensile tests were conducted at ambient temperature on round bar specimens of longitudinal and transverse directions to measure the tensile properties of tested materials.

SCC Test

SCC tests were conducted by 4-point bent beam method. Specimens, 76 mm long, 6 mm wide, and 2 mm thick, were cut from the plates perpendicular to the rolling direction. Aqueous solutions of 5% NaCl and 0.5% acetic acid saturated with hydrogen sulfide or gas mixtures of hydrogen sulfide and carbon dioxide at 1 atmosphere were used as the test solution. Thus, SCC susceptibility was evaluated at three different partial pressures of hydrogen sulfide of 1, 0.3, and 0.1 atm. All tests were run at ambient temperature (25°C). Normaly, three specimens for each steel were stressed to 1.0YS (transverse yield strength) and exposed to each test environment for 30 days. In some cases, additional three specimens were tested again to confirm the test results.

RESULTS

Microstructure

The steels investigated are in a great variety of chemical composition and microstructure. Typical microstructures of tested steels are shown in Figure 1. The volume fraction of ferrite is given in Table 1.

Distribution of Alloying Elements

Although the steels were originally characterized by the volume fraction of ferrite and total amounts of each element, the compositions of ferrite and austenite were thought an important factor in the steels of duplex structure. The EPMA analysis of both phases showed clearly that ferrite forming elements, Cr, Mo, and Si, were enriched in ferrite and conversely austenite forming elements, Ni, Mn, and N, were enriched in austenite. The contents of Ni, Cr, and Mo, which showed remarkable enrichment, measured on the steels of series A and B are shown in Figures 2 and 3, respectively.

In series A, the total amounts of Ni and Cr were varied to obtain the duplex structures of different phase balance, but the amounts of other elements were held nearly constant as mentioned before. As a result, the concentrations of alloying elements in ferrite and austenite were varied with varying volume fraction of ferrite as shown in Figure 2. On the other hand, the concentrations of these elements were almost in the same levels in series B as shown in Figure 3.

The results of EPMA analysis for nitrogen in austenite indicated that nitrogen concentration remarkably incresed with increasing amount of ferrite in series A, while it was closely constant in sries B as shown in Figure 4. Consequently, the ferritic and austenitic phase of the steels in series B are almost in the same compositions respectively, independently on the volume fraction of ferrite.

As nitrogen concentration in ferrite must change in proportion to the concentration in austenite, it must increase also as the volume fraction of ferrite increases in the steels of series A. Therefore, precipitation of nitride may occur in the steels of large amount of ferrite. Accordingly in order to check the precipitation, the microstructure of the steels with ferrite more than 50% was examined by thin foil transmission electron microscopy. Chromium nitrides were found to form on dislocations in ferrite, as shown in Figure 5, at volume fraction of ferrite more than 70% in series A (steel No.7, 11, and 15). No precipitates were found at lower amount of ferrite in series A and in the steels of series B. However, the precipitates would not exert a significant effect on the properties of interest because they were very small and formed in a small quantity.

Tensile Properties

Tensile properties of tested steels were varied in a wide range according to volume fraction of ferrite. The longitudinal tensile propertied are illustrated in Figure 6 as a function of the amount of ferrite. The increase in ferrite content generally increased yield strength and reduced elongation and reduction of area. The transverse tensile properties were almost identical with those of longitudinal ones except that yield strength was slightly higher than that of longitudinal direction.

SCC Test Results

Table 2 shows the results of SCC tests. These data indicated that most of the steels were susceptible to cracking in the environment saturated with 1 atm H_2S, the susceptibility reduced as H_2S partial pressure decreased, and several steels resisted cracking in the solution of lower H_2S partial pressures.

The fully austenitic steel and several duplex steels exhibited good resistance to cracking in series A. The resistance to cracking seems to be controlled by factors other than the phase balance, because the duplex steels that showed resistance were in various volume fraction of ferrite and the steels of series B indicated no remarkable difference in cracking susceptibility.

The results at 0.1 atm H_2S

partial pressure for series A were plotted in Figure 7 with total amounts of Ni and Cr. This figure suggests that there is an optimum value in Cr content ranging from 22 to 24%, and there is no significant effect in Ni content.

In series B, however, most steels showed cracking even at the lowest H_2S partial pressure despite Cr contents were within the optimum range observed for series A. It is also noted that the fully ferritic steel of sereis B resisted cracking unlike the ferritic steels of series A.

Crack morphologies are shown in Figure 8. Cracks were propagated transgranularly in ferrite and austenite. Preferential dissolution of austenite was observed occurring within the cracks in the duplex steels containig Cr less than about 24%. In the steels of high Cr which are in high amount of ferrite did not show such tendency as shown in Figure 8 c).

DISCUSSION

Results of the present study indicated clearly that the duplex structure was not always resistant to cracking more than fully austenitic steel in sour gas environments. Such a tendency arising in this system is considered to be related to the cracking mechanism which may differ from that of SCC in boiling $MgCl_2$ solutions. The present authors indicated previously that hydrogen embrittlement mechanism of ferritic phase would be involved in the cracking process at temperatures lower than about 100°C.[8] Wilhelm and Kane reported the acceralation of cracking resulted from cathodic charging, and proposed hydrogen embrittlement mechanism for the cracking at ambient temperature.[9] In this case, the increase in the amount of ferrite is expected to increase cracking susceptibility as indicated in their study. However, it is clear from the results that SCC susceptibility is not governed only by the amount of ferrite. Several steels of large amount of ferrite, in fact, exhibited better resistance to cracking. Therefore, the cracking process should not be considered to be governed by a single mechanism. Probably localized breakdown of passivity is the initial and necessary step of the process and hydrogen embrittlement of ferritic phase assists crack propagation, as indicated by Desestret et al.[11]

An optimum Cr content ranging from 22 to 24% appeared in the results for series A. Such results may be attributed to the improvement of corrosion resistance caused by the increase in Cr content. However, it is not clear why the steels containing Cr above 25% exhibited cracking. On the other hand, the results for series B indicated that the steels were susceptible to cracking despite the Cr contents were within the optimum range.

In order to explain the result of whole steels synthetically, concentration of nitrogen should be taken into account because nitrogen concentration in austenite was changed remarkably in the steels of series A. Thus the SCC data at 0.1 atm H_2S were replotted along with those for the steels of series B in Figure 9 with the contents of Cr and N in austenite. As seen in this figure, good performance against SCC is obtained when N content in austenite is in a high level and Cr content in austenite is about 22%. Such an effect of Cr and N can be explained in terms of corrosion resistance of austenite.

The observation of crack morphology revealed that austenitic phase dissolved preferentially within the cracks of lower Cr steels. This indicates that the austenitic phase tends to be more active than ferrite in the test environments probably because Cr and Mo which are ferrite forming elements distribute lower in austenite than in ferrite. On the other hand, nitrogen, which is known to have a beneficial effect on pitting corrosion, is enriched in austenite, and therefore, can contribute effectively to the corrosion resistance of austenite in duplex steels. Hence, the improved corrosion resistance of austenite resulted from high Cr and N would suppress the breakdown of passivity and prevent the steel from cracking.

Two duplex steels of higher Cr content showed susceptibility to cracking. These results could not be interpreted from the above explanation. As these steels are mainly composed of ferrite, the property of these steels would be decided mostly by nature of the

ferrite. The chromium contents in ferritic phase of these steels were 26-27% and close to that of the fully ferritic steel of series A, as shown in Figure 2. And this ferritic steel (No.16) was more susceptible to cracking than steel No.29 which was also fully ferritic but of lower Cr content. These facts suggest that high Cr is detrimental for the cracking of ferritic steels in sour gas environments. Probably much high Cr enhanced the embrittlement of ferritic phase of these duplex steels.

The properties of duplex stainless steels are decided finally by the nature of ferrite and austenite constituting the steel structure. The optimum range of Cr can be considered to appear from the combination of above mentioned effects of this element for the two phases.

CONCLUSIONS

SCC resistance of duplex stainless steels with various chemical compositions and ferrite-austenite ratio was evaluated in H_2S-chloride containing environments at ambient temperature. From the results the following conclusions can be drawn.

(1) SCC resistance of duplex stainless steels in sour gas environments depends on chemical compositions of ferrite and austenite rather than on ferrite-austenite ratio.
(2) The contents of Cr and N in austenitic phase are the controlling parameters for SCC resistance, because the increased corrosion resistance of austenitic phase due to these elements suppresses the breakdown of passivity at the initial process of cracking.
(3) Much high Cr may exert a detrimental effect on SCC resistance, which probably enhances the embrittlement of ferritic phase.
(4) The optimum Cr content from 22 to 24% provides good performance against SCC in the steels containing 3% Mo and N more than 0.15%. N has a beneficial effect on SCC resistance.

REFERENCES

1. G.Herbsleb, R.K.Poepperling, Corrosion, Vol.36, p.611 (1980).
2. S.O.Bernhardsson, J.Oredsson, CORROSION/80, Paper No.14, National Association of Corrosion Engineers, Houston, Texas, 1980.
3. A.I.Asphahani, Corrosion, Vol.37, p.327 (1981).
4. J.Oredsson, S.O.Bernhardsson, CORROSION/82, Paper No.126, National Association of Corrosion Engineers, Houston, Texas, 1982.
5. P.R.Rhodes, G.A.Welch, L.Abrego, Duplex Stainless Steels, American Society for Metals, Metals Park, Ohio, p.757, 1983.
6. T.Suzuki et al., Nippon Kinzoku Gakkaishi, Vol.32, p.1171 (1968).
7. K.Takizawa et al., Transactions ISIJ, Vol.22, p.325 (1982).
8. Y.Ishizawa, T.Shimada, M.Tanimura, CORROSION/83, Paper No.167, National Association of Corrosion Engineers, Houston, Texas, 1983.
9. S.M.Wilhelm, R.D.Kane, Corrosion, Vol.40, p.431 (1984).
10. A.Ikeda, S.Mukai, M.Ueda, CORROSION/84, Paper No.289, National Association of Corrosion Engineers, Houston, Texas, 1984.
11. A.Desestret et al., CORROSION/85, Paper No.229, national Association of Corrosion Engineers, Houston, Texas, 1985.

Table 1. Chemical compositions (wt.%) and volume fraction of ferrite of tested steels.

Steel No.	Cr	Ni	Mo	Si	Mn	C	N	volume % of ferrite
(Series A)								
1	18.2	11.2	3.0	0.39	1.35	0.013	0.1969	0
2	20.5	9.1	3.1	0.45	1.57	0.012	0.1566	17.4
3	21.1	8.2	3.1	0.52	1.57	0.014	0.1661	23.4
4	22.1	7.2	3.1	0.49	1.57	0.016	0.1778	37.0
5	22.8	6.1	3.1	0.42	1.54	0.011	0.1680	46.4
6	23.6	5.1	3.1	0.40	1.49	0.011	0.1994	55.6
7	25.2	4.0	3.1	0.54	1.60	0.009	0.1785	75.0
8	21.3	6.2	3.0	0.44	1.42	0.012	0.1695	35.6
9	21.9	5.1	3.1	0.47	1.50	0.009	0.1698	50.2
10	22.8	4.0	3.1	0.43	1.45	0.008	0.1578	64.1
11	24.0	3.0	3.1	0.47	1.46	0.009	0.1442	79.5
12	22.8	8.0	3.1	0.46	1.47	0.013	0.1708	35.4
13	23.9	7.0	3.1	0.46	1.48	0.010	0.1687	45.7
14	25.0	6.0	3.1	0.45	1.50	0.010	0.1706	60.5
15	26.0	5.0	3.1	0.49	1.50	0.009	0.1785	70.6
16	26.4	3.1	3.0	0.39	1.50	0.010	0.0040	100
(Series B)								
23	21.4	8.6	2.3	0.37	1.12	0.005	0.2195	12.2
24	22.2	7.9	2.9	0.40	1.05	0.006	0.2299	21.7
25	23.1	7.4	3.2	0.40	0.99	0.006	0.1615	38.7
26	23.4	6.8	3.5	0.41	1.04	0.007	0.1359	51.2
27	23.8	6.3	3.7	0.40	0.95	0.008	0.1106	62.2
28	23.6	5.6	3.6	0.45	0.96	0.010	0.0685	71.9
29	23.9	4.6	4.2	0.43	0.91	0.007	0.0066	100

Table 2. SCC test results.

Steel No.	Volume % of ferrite	Yield[1] Strength MPa	SCC Test Results[2] H_2S Partial Pressure, atm		
			1.0	0.3	0.1
(Series A)					
1	0	355	0/3	2/3	0/6
2	17.4	410	2/3	2/3	2/6
3	23.4	441	3/3	3/3	1/6
4	37.0	484	3/3	0/6	1/6
5	46.4	523	3/3	0/6	0/6
6	55.6	560	3/3	0/6	0/6
7	75.0	645	1/3	1/6	0/6
8	35.6	475	2/3	3/3	1/3
9	50.2	517	2/3	3/3	1/3
10	64.1	565	2/3	1/3	0/3
11	79.5	608	2/3	0/3	0/3
12	35.4	469	0/3	0/3	0/3
13	45.7	519	1/3	0/3	0/3
14	60.5	567	2/3	2/3	1/3
15	70.6	611	1/3	1/3	1/3
16	100	537	2/3	3/3	2/6
(Series B)					
23	12.2	427	4/6	1/3	2/6
24	21.7	464	0/6	1/3	0/6
25	38.7	485	2/6	0/3	2/6
26	51.2	509	2/6	0/3	2/6
27	62.2	548	3/6	1/3	4/6
28	71.9	546	3/6	0/3	2/6
29	100	534	0/6	0/3	0/6

(1) Transverse yield strength.
(2) Number of cracked specimen / number of tested specimen.

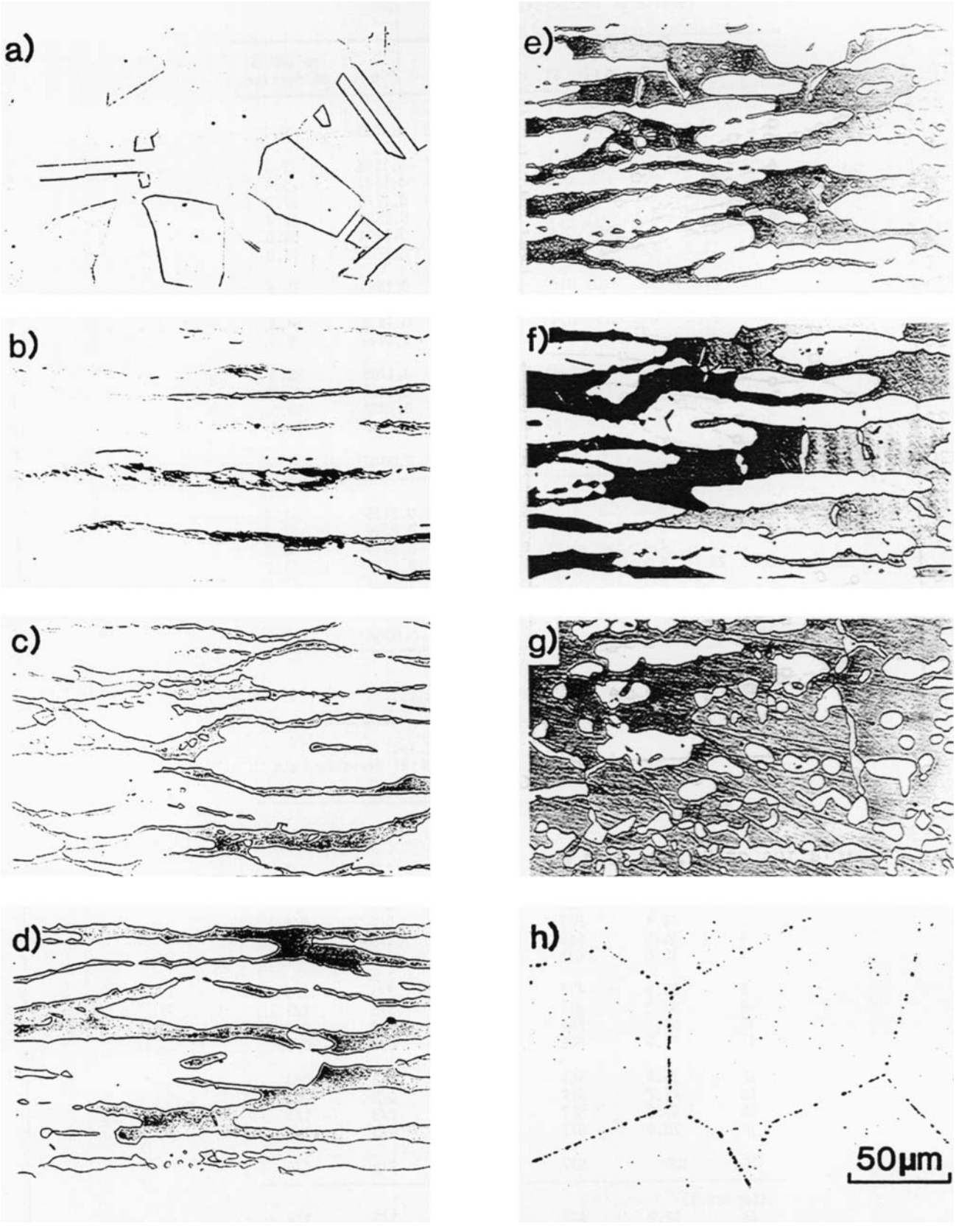


Figure 1—Microstructure of a) fully austenitic steel No.1, duplex steels with volume fraction of ferrite of b) 17.4%, c) 23.4%, d)37.0%, e) 46.4%, f) 55.6%, and g) 75.0%, and h) fully ferritic steel No.16. Dark area is ferrite. Longitudinal cross section.

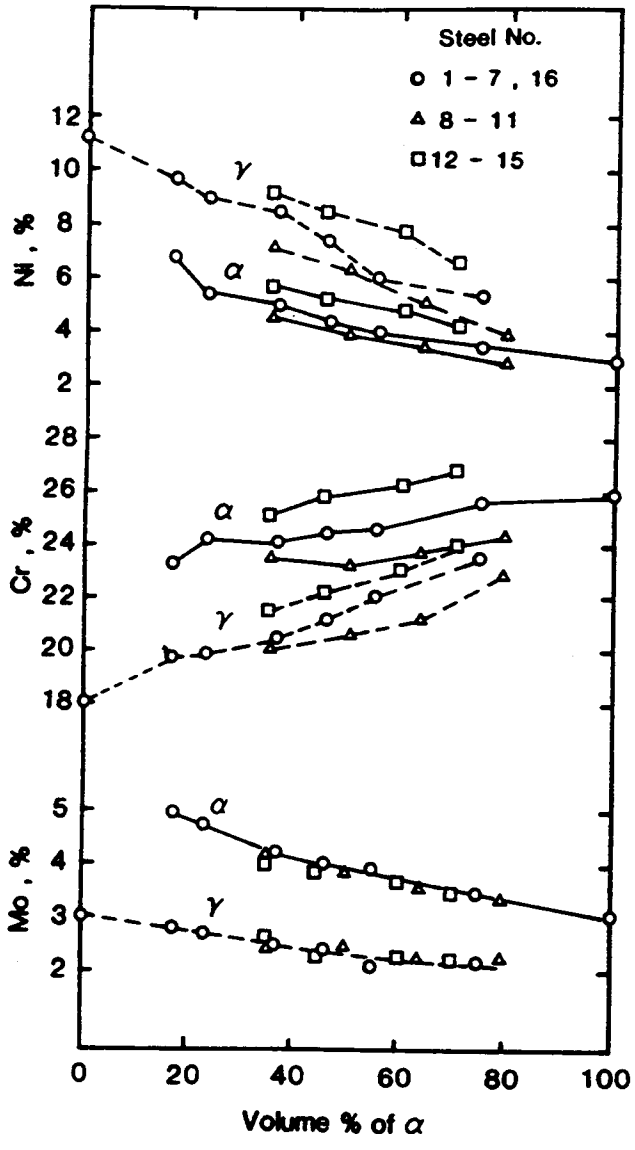


Figure 2—Variation of Ni, Cr, and Mo concentrations in ferrite (α, solid lines) and austenite (γ, broken lines) of series A with volume fraction of ferrite.

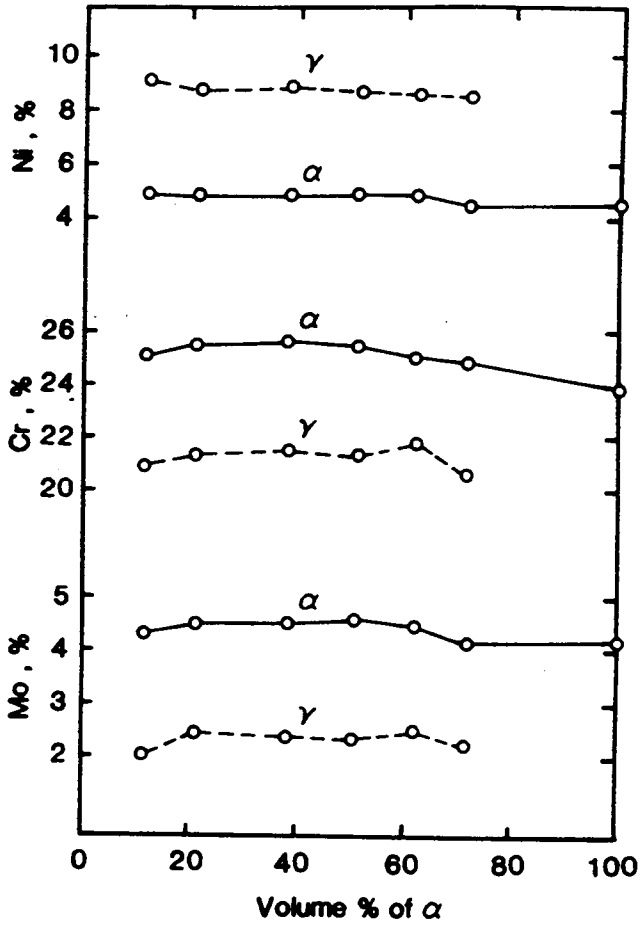


Figure 3—Variation of Ni, Cr, and Mo concentrations in ferrite (α, solid lines) and austenite (γ, broken lines) of series B with volume fraction of ferrite.

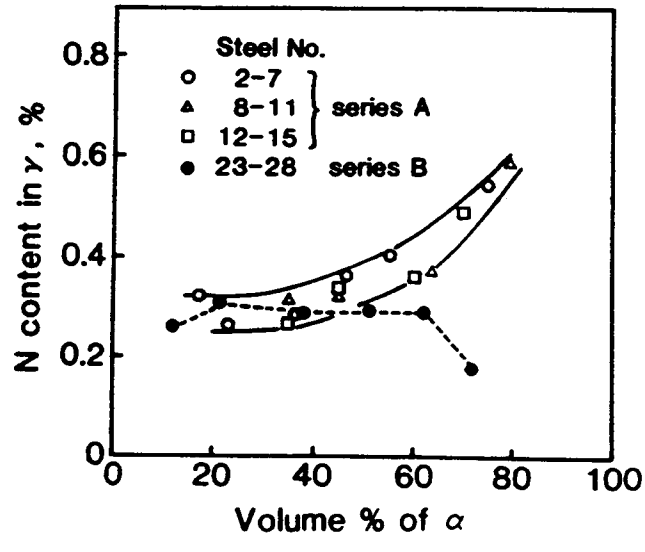


Figure 4—Variation of N concentration in austenite of duplex steels with volume fraction of ferrite.

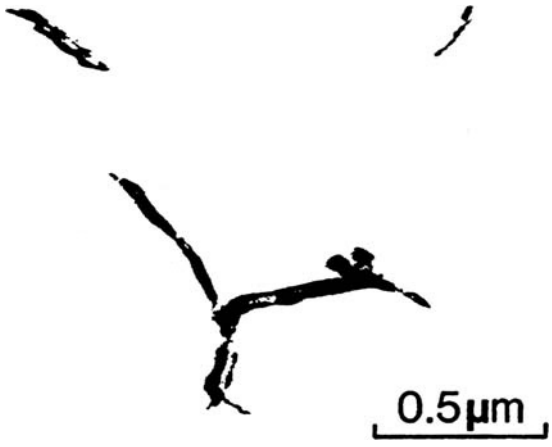


Figure 5—Chromium nitrides (Cr_2N) formed in ferritic phase of steel No.15. TEM.

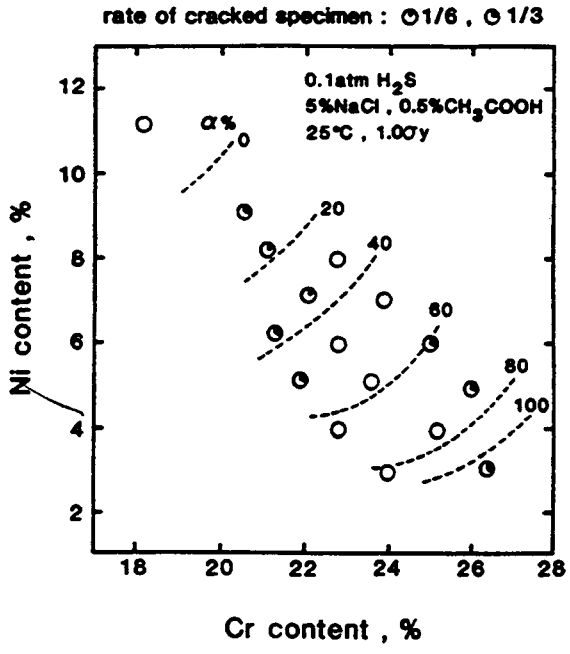


Figure 7—Effect of total amount of Ni and Cr on SCC susceptibility in 0.1 atm H_2S solution. Steels of series A. Open marks denote no cracking and semi-filled marks denote cracking at a rate illustrated.

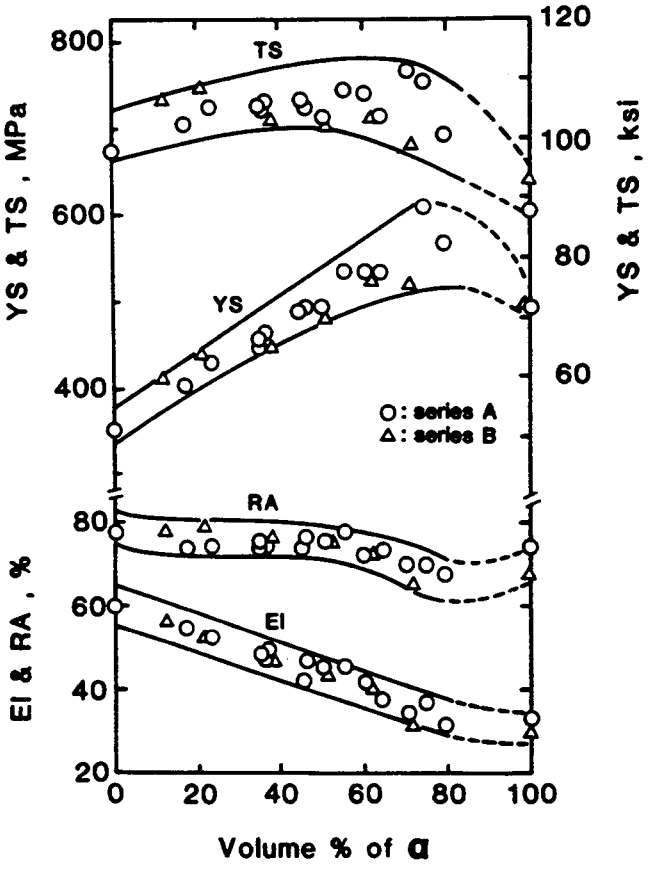
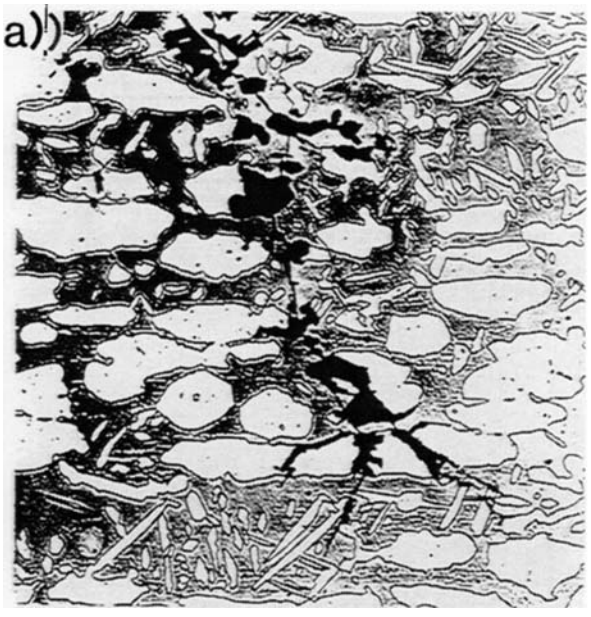
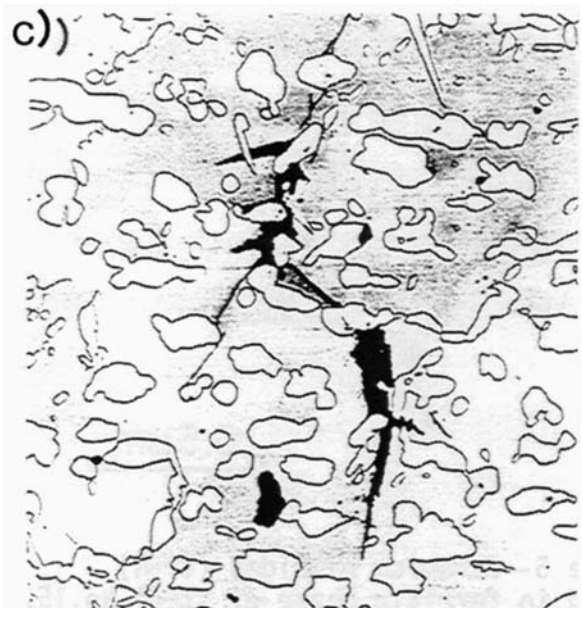


Figure 6—Variation of tensile properties of tested steels with volume fraction of ferrite.





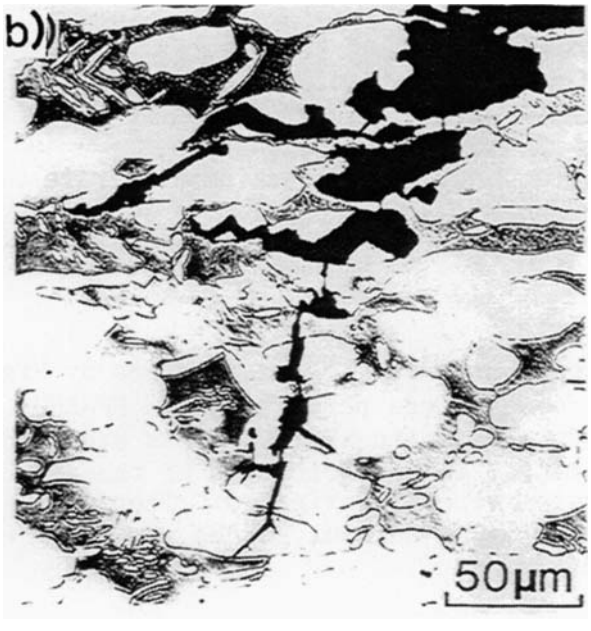


Figure 8—Cracks observed in SCC specimens of steels a) No.9, b) No.25, and c) No.7.

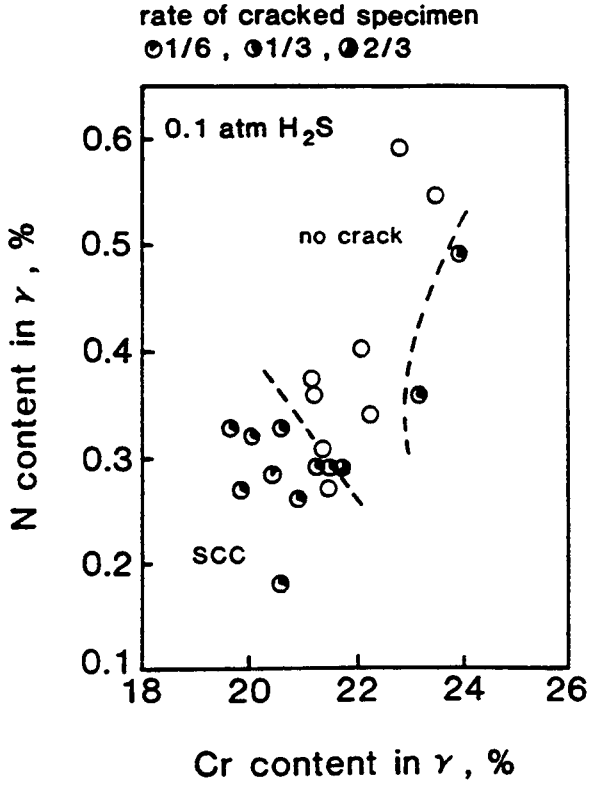


Figure 9—Effect of N and Cr concentration in austenitic phase on SCC susceptibility in 0.1 atm H_2S solution. Whole duplex steels investigated. Open marks denote no cracking and semi-filled marks denote cracking at a rate illustrated.

Copyrighted Materials
Copyright © 1996 NACE International Retrieved from www.knovel.com

PAPER NUMBER
59

Corrosion 88
March 21-25, 1988
Cervantes Convention Center / St. Louis, Missouri

PRODUCTION TECHNOLOGY AND CORROSION PROPERTIES OF DUPLEX STAINLESS STEEL LINE PIPE BY HF-ERW PROCESS

H. Kashimura
Nippon Steel Corporation, Hikari Works
3434 Shimada
Hikari, Yamaguchi, 743 Japan

M. Onoyama
Y. Watanabe
T. Fujikawa

ABSTRACT

The trial production of 10-3/4" O.D. duplex stainless steel line pipes by High Frequency Electric Resistance Welding (HF-ERW) process was performed. In HF-ERW welding, micro oxide inclusions are more likely to occur in the stainless steel than in the carbon steel.(1) First the effect of quantity and distribution of those oxides in the weld seam on the material properties were investigated. Then the optimum welding conditions were established in which no harmful oxides appear in the weld line.

The metallographical examinations showed that the micro structure of weld zone was as uniform and as fine grained as base metal and that the ferrite/austenite ratio in the weld zone was almost same as that of base metal. The weld area was exposed to pitting corrosion resistance tests and stress corrosion cracking tests, and all tests showed acceptable and much the same corrosion resistances as the base material. The mechanical and impact tests also showed no significant differences between weld and base metal. From this study HF-ERW process was recognized as an economical and reliable process for manufacturing duplex stainless steel or even other corrosion resistant alloy line pipes.

INTRODUCTION

As the offshore and onshore exploitations of more aggresive fields increase, the interest in the duplex steel line pipe is growing throughout the world, due to this material's exceptional corrosion resistance with uncompromising mechanical properties. At present the duplex pipes manufactured only by seamless or arc

welding processes are available and almost no research or production result on HF-ERW duplex pipes has been reported.

On the other hand, HF-ERW processes have already been applied to manufacture high grade carbon steel line pipes used in the arctic area at -45°C or severe sour gas service environments. This is due to the fact that remarkable progress in HF-ERW technologies and much improvement in the weld and base metal quality have been achieved, together with the economical merit of this process. Therefore if there is not any weld defect problem nor its detrimental effect on corrosion properties, the application of the HF-ERW process to duplex line pipes would give a couple of advantages. One thing is a economical merit and the other is the preferable characteristics of HF-ERW weldment equal or superior to arc welded pipes,[3] because the weld zone is narrow, no filler material is added, and as a result the micro structures are easily made similar to base material.

The purposes of this study are, (1) to investigate the influence of micro oxides in the HF-ERW weld seam on corrosion and mechanical properties, (2) to find out the optimum welding conditions for defect-free weld especially from the view point of corrosion resistance, and (3) to evaluate the various properties of HF-ERW duplex stainless steel line pipes under the estimated service environment.

EXPERIMENTAL PROCEDURE

Sample preparation

The base materials used were 22Cr and 25Cr duplex stainless steels conforming to ASTM A790 UNS S31803 and S31250 with 6 mm thickness. The both materials were melted by electric furnace, refined in AOD furnace, continuous cast and hot rolled into skelps. The chemical compositions of test materials are shown in Table 1.

The seam welding of the 22Cr steel pipe was performed by the Thermatool type high frequency electric resistance welder in the 24 inch O.D. pipe mill. For the 25Cr steel, the specially designed HF-ERW simulator in the laboratory was used. In order to control micro oxides inclusion, welding test was conducted varying main welding factors such as atmosphere, weld squeez amount, and V-convergency angle. The heat input was kept constant by the automatic welding control system.

The size of welded pipe sample was 273 mm O.D. x 6.35 mm W.T. x 12 m, and the sample made by the weld simulator was 6.0 mm t x 60 mm w x 4 m. All samples were solution annealed at 1040°C-1080°C for 11 seconds by off-line high frequency induction heating followed by water quenching. Surface scales were removed by special salt treatment and subsequent pickling by nitric acid and fluoric acid. For various evaluation tests, specimens were cut out of above samples and wet ground to a 500 grit finish.

Metallographical Examination

Micro structures of HF-ERW weld seam line were compared with that of base metal. The line analysis of the concentration of Cr, Ni, Mo and N across the weld seam was conducted by EPMA. The ferrite/austenite ratio was measured by the microscopic point count method according to ASTM E-562-83. The amount and distibution of micro oxides inclusions were investigated by the observation of fractured surface of Charpy test specimens by point count method.

Mechanical Test

The transverse tensile tests with determination of yeild strength, tensile strength, and elongation were performed for base metal and for seam weld area just tensile strength was determined. The API type flattened rectangular specimens were used. The 5 mm subsize Charpy impact tests according to ASTM E-23 were conducted for two locations, that is the base metal and the weld in which the notch is located in the center of HF-ERW fusion line. The hardness was measured across the weld seam by Vickers method with 1 kg load and converted to Rockwell hardness.

Corrosion Test

The corrosion resistance properties of HF-ERW weld seam were evaluated under the estimated actual service environment. Assuming external surface is exposed to sea water, pitting potential tests in 3.5% NaCl according to JIS G 0577 and pitting corrosion test in 10% $FeCl_3$ $6H_2O$ according to ASTM G48 A were conducted. For critical pitting temperature (CPT) determination, test temperature was varied between 30°C and 65°C with 5°C increments. And assuming severest environment of the internal surface as brine including hydrogen sulfide gas, pitting potential tests and stress corrosion cracking (SCC) tests in 3.5% to 20% NaCl solution with 0.01 atm to 1.0 atm H_2S were performed by 4-point bent beam method. Specimen of 67 mm length, 10 mm width and 2 mm thickness were cut out of the weld perpendicular to longitudinal seam. Besides, resistance to intergranular corrosion was evaluated using Strauss test (ASTM A-262 Practice E) and Huey test (ASTM A-262 Practice C).[3]

RESULTS AND DISCUSSION

Defect-free Welding

In the HF-ERW welding of duplex stainless steel, there apt to appear oxides type inclusions in the weld line under inappropriate welding conditions. Most small oxides have no influence on mechanical properties but those located near the surface may decrease corrosion resistance. Therefore, at first, the type, amount and distribution of oxides in the weld seam under different welding conditions were studied. Then the influence of those oxides on mechanical properties and corrosion resistances was invetigated. And at the last, optimum welding conditions for defect-free welding were found out.

Defect Analysis. Figure 1 shows the typical oxides inclusions inside the weld line found on the factured surface of Charpy test at 100°C. As shown in the EDAX analysis data, those oxides are chromium-, silicate- and manganese-type. The amount of oxides were evaluated in terms of Oxide Area Ratio (OAR) defined as the area % of all oxides observed in the above mentioned Charpy fractured surface. For the reference, the OAR for a penetrator type weld defect is in the level of 5-10% and the OAR for a base metal is about 0.05%. Figure 2 shows the distributions of micro oxides inclusion in the thickness direction for different level of OAR. When the OAR is higher, oxides distribute through the thickness and when the OAR is lower, they are located only in the center zone.

Evaluation. For the case of high OAR in which some oxides are exposed to the surface, the pitting corrosion resistance of the weld was measured in comparison with the low OAR case. As shown in Figure 3, oxides inclusions in the surface could be the cause of pitting corrosion and possible stress corrosion cracking. Figure 4 shows the relationship between the OAR for whole thickness and the OAR for surface zone. It is estimated that if the OAR can be controlled less than 0.1%, no oxide inclusion exists in the surface zone. Although the value is rather empirical, it can be used as an index for determination of various conditions for defect-free welding.

Determination of welding conditions. Table 2 shows the various welding factors tested. The welding speed and power in-put were kept constant to each optimum level by the automatic control system. The most important factor for preventing oxides inclusions is the welding atmosphere. All HF-ERW weldings were conducted under argon gas shielding and dry welding conditions. Oxygen concentration near the weld point was measured. Squeez pressure and V-convergency angle at weld point are also important parameters to minimize the OAR level.[2] By the conbination of each optimum range of these welding parameters, it was made possible to realize the defect free weld with OAR of less than 0.1%. All samples for further evaluation tests have this level of weld quality.

Metallographical Examination

Micro structures of the weld and the base material after solution heat treatment are shown in Figure 5. The dark etched area is ferrite and the light etched area is austenite. Even in the center of HF-ERW fusion line, the phase formation in which island like gamma phase uniformly scatters among alpha phase is quite similar to that of base metal, except that metal flows in the weld area are up-turned toward the surface almost perpendicular to that of base metal. The ferrite/austenite ratio at weld center is 49% and very comparable to 45% of base metal. The result of line analysis of Ni, Cr, Mo and N across the weld EPMA showed no deviation of concentration from base metal and no precipitation in the phase boundaries (Figure 6). This fine-grained, uniform structure of HF-ERW weld line is considered due to a strain caused by weld squeezing and subsequent heat treatment, and also due to no addition of filler material.

Mechanical Properties

Table 3 shows tensile and hardness test results. There is no difference between the weld and the base metal. The weld hardness of duplex steels, contrary to austenitic steels, has a certain importance as it indicates the resistance to H_2S cracking. To ensure sufficient resistance to cracking in hydrogen sulfide, maximum 25 HRc (266 Hv) is sometimes specified for this type of material.[4] The hardness distribution was uniform through the weld. Figure 7 shows the impact toughness properties of 22 Cr duplex steel pipe. Although absorbed energy value of the weld is smaller at lower temperature than base metal, the transition temperature is about -70°C and high enough for arctic services. Besides, flattening tests according to API 5LX were performed and the results were satisfactory.

Corrosion Resistance Properties

Figure 8 shows the result of pitting potential (Vc'100) measurement in 3.5% NaCl solution. There is no difference between the pitting corrosion resistance HF-ERW weld seam and that of base material, so far as the weld is free from detrimental oxides inclusion. In austenitic stainless steels, it is sometimes observed that the edge of rolled sheet has more susceptibility to pitting corrosion than the surface. The surface of HF-ERW weld area which has metal flows similar to rolled edge, however, did not show any decrease of pitting corrosion resistance. This seems again due to the recrystalization caused by strain of weld squeez and subsequent heat treatment. Figure 9 shows the pitting corrosion rate in the $FeCl_3$ solution. The critical pitting temperature (CPT) for 22 Cr steel 25 Cr steel are 30°C and 55°C respectively. The CPT of weld area is comparable to that of base metal. Figure 10 shows the pitting potential test in NaCl + H_2S solution. Here again, weld seam has almost same potential value as base metal though each value is subject to strong influence of H_2S partial pressure. The SCC test result is shown in Figure 11. There is also no significant difference of the critical partial pressure between base metal and HF-ERW weld.

CONCLUSIONS

The production trial of duplex stainless steel line pipe by High Frequency Electric Resistance Welding (HF-ERW) process was carried out. Assuming the estimated pipe line environment as under sea water, the weld area was evaluated by metallographical examinations, corrosion resistance tests and mechanical tests. The influence of welding parameters on weld defects and corrosion properties was investigated. The following conclusions can be drawn.

(1) The HF-ERW weld area of duplex stainless steel showed almost same ferrite/austenite ratio and uniform fine-grained microstructure as base material.

(2) The mechanical and corrosion resistance properties of defect-free HF-ERW weld were in the same level as those of base material.

(3) Micro oxides in the surface area of weld seam caused by inappropriate welding condition may increase the pitting corrosion susceptibility, but by special control of welding parameters including welding atmosphere, weld squeez amount, V-convergency angle, and so forth, the HF-ERW weld without any harmful defect can be achieved.

(4) The HF-ERW process can be a future practical process to manufacture duplex stainless steel or other corrosion resistant alloy pipes as it is more efficient and economical way compared to conventional arc welded pipes while keeping the same quality level.

REFERENCES

1. Y. Watanabe, T. Ikemoto, Tetsu-to-hagane 72, S1142, P.350 (1986)
2. H. Haga, K. Aoki, T. Sato, The Welding Journal, P.208-s, July 1980
3. Y. Watanabe, "Evaluation of welded duplex stainless steel pipes", Interim Report of Nippon Steel Technical laboratory, 1986, unpublished.
4. A certain user's specification for duplex flowlines (seamless and ERW pipes) April, 1983

TABLE 1
CHEMICAL COMPOSITIONS OF TESTED MATERIALS (wt. %)

No.	Material	C	Si	Mn	P	S	Ni	Cr	Mo	N
1	22Cr steel	0.018	0.49	1.77	0.019	0.001	5.85	22.40	3.05	0.143
2	25Cr steel	0.028	0.60	0.61	0.015	0.001	7.09	24.50	2.93	0.160

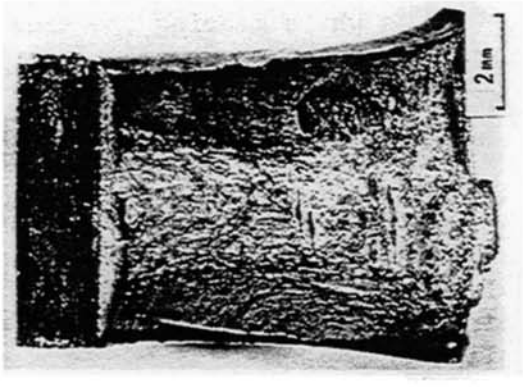
TABLE 2
HF-ERW WELDING CONDITIONS

	Item	Condition
1	Skelp thickness	6.0mm
2	Welding speed	20m/min
3	Heat input	2nd weld phenomena
4	Apex angle	2.5-7.0 degree
5	Upset amount	1.2-4.5mm
6	Shielding gas	Argon gas
7	roll coolant	Nitrogen gas

TABLE 3
TENSILE PROPERTIES (22Cr STEEL)

	Base	Weld
0.2% proof stress (MPa)	560	—
Tensile strength (MPa)	780	781
Elongation (%)	31.8	—
Hardness (HRB)	23	23

(1) Oxide inclusion



(2) EDAX - profile

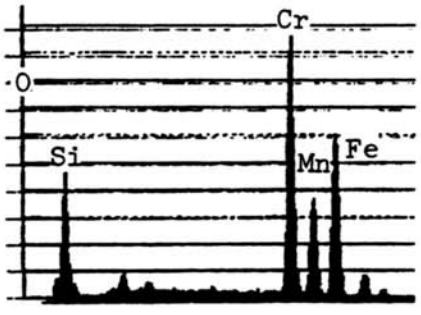


FIGURE 1 - Oxide inclusion in weld

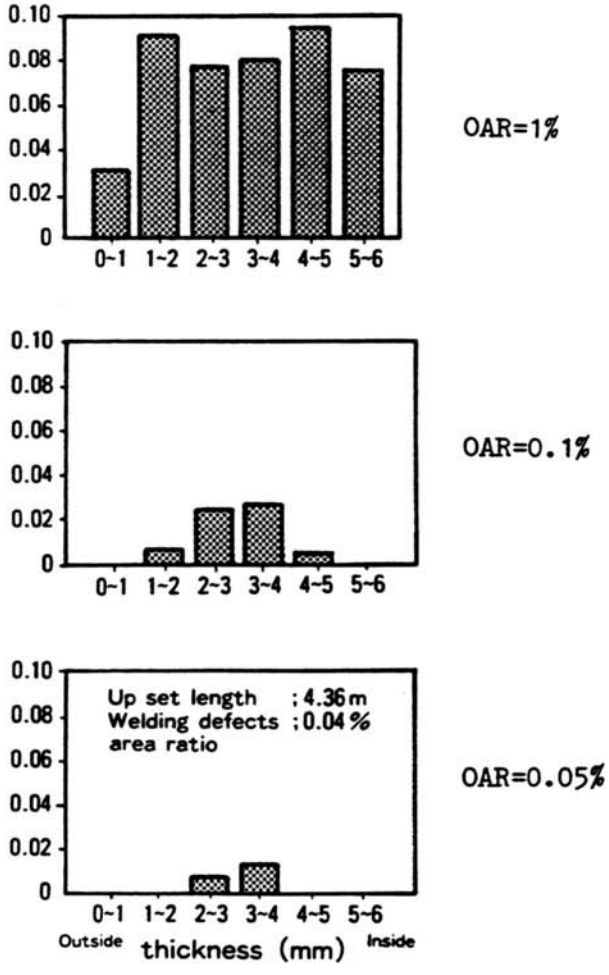


FIGURE 2 - Oxides distribution

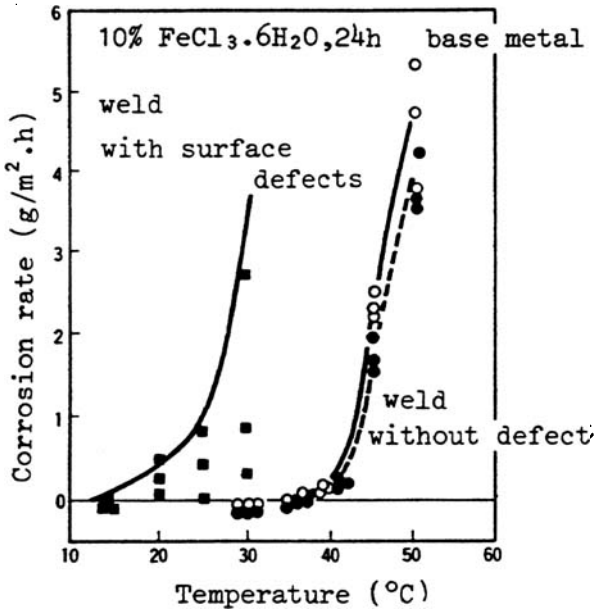


FIGURE 3 - Influence of oxides on CPT

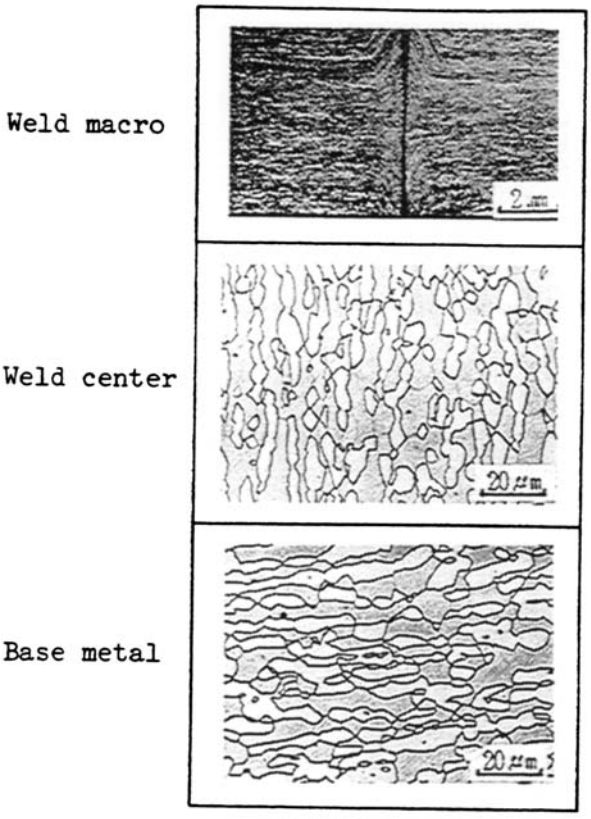


FIGURE 5 - Micro structure (22Cr steel)

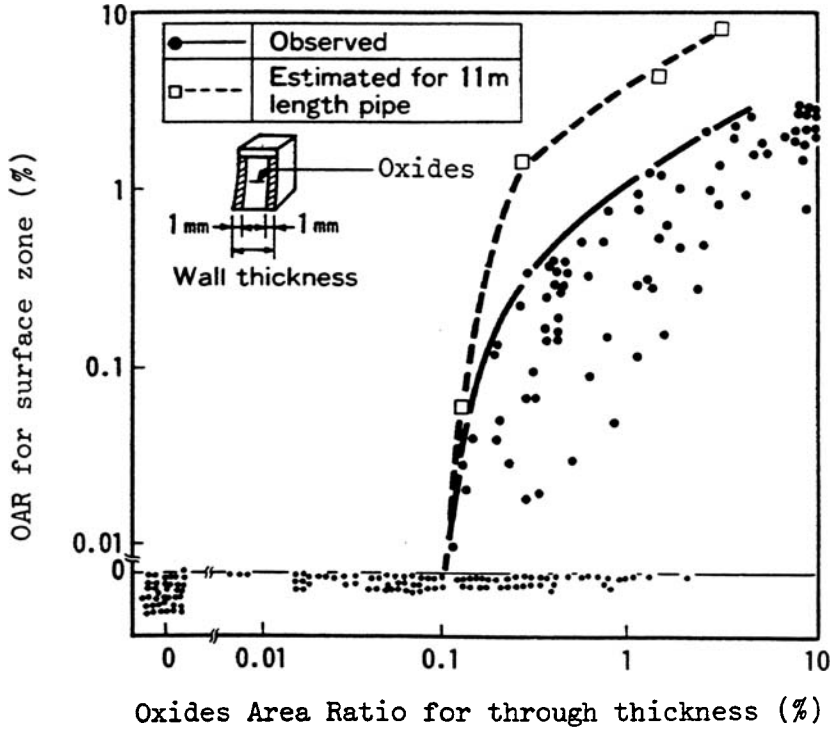


FIGURE 4 - Relationship between OAR for through thickness and OAR for surface zone (22Cr steel)

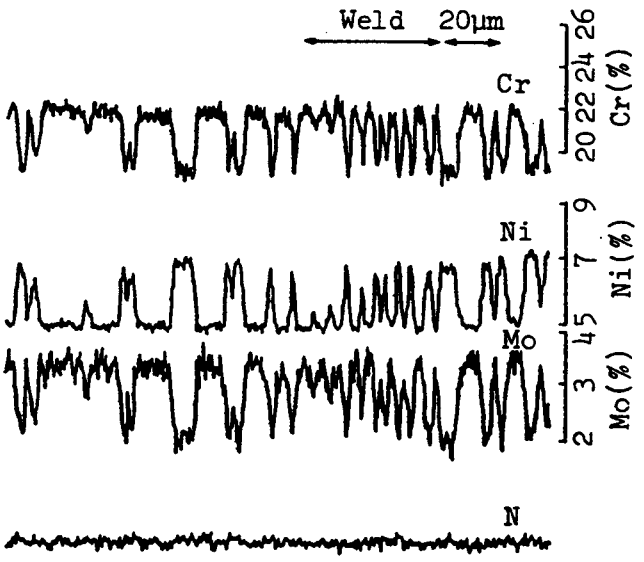


FIGURE 6 - Line analysis (22Cr steel)

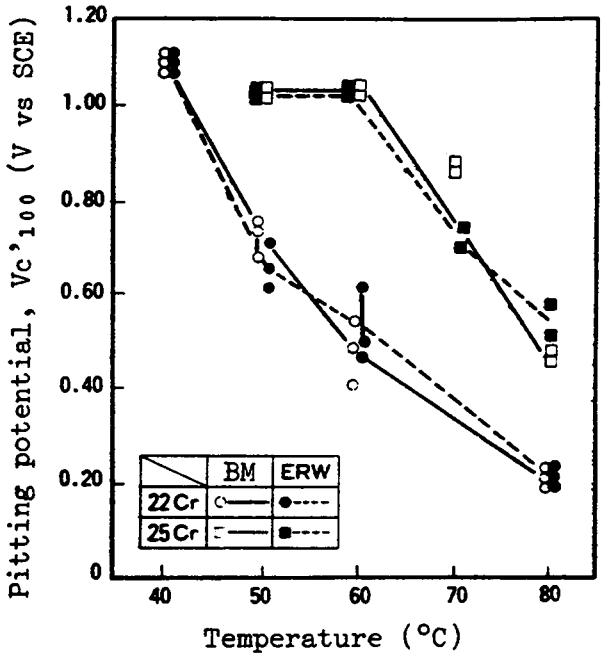


FIGURE 8 - Pitting potential (in 3.5% NaCl)

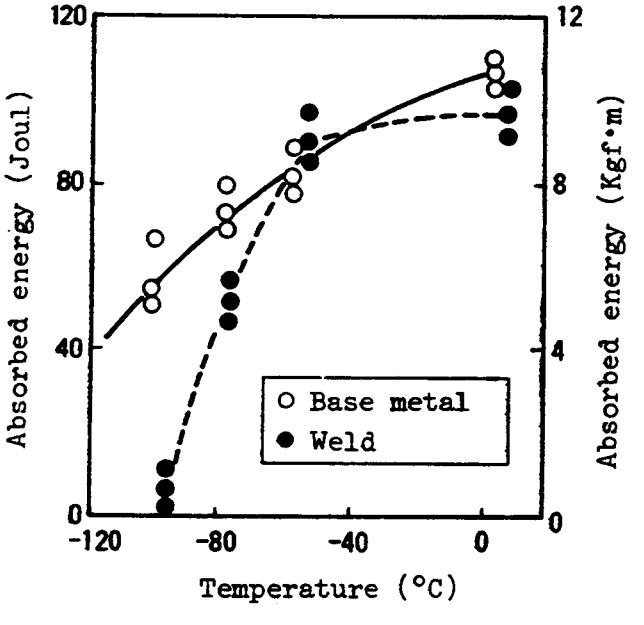


FIGURE 7 - Impact toughness (22Cr steel)

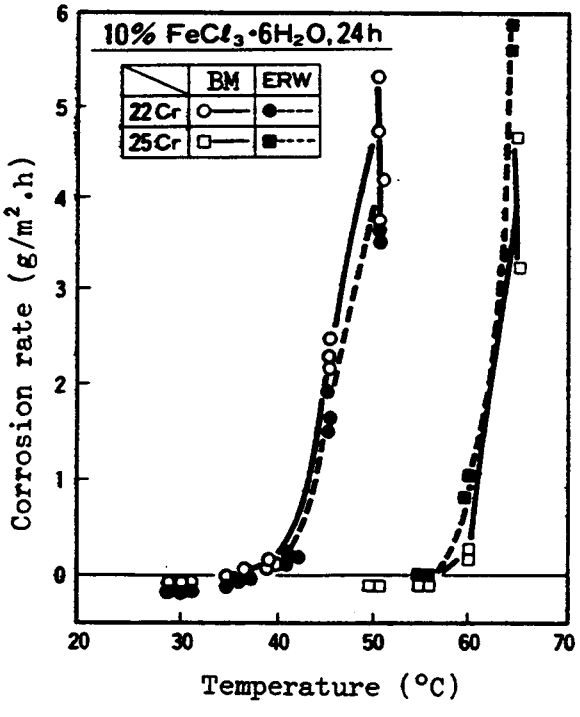


FIGURE 9 - Pitting corrosion (in 10% $FeCl_3$)

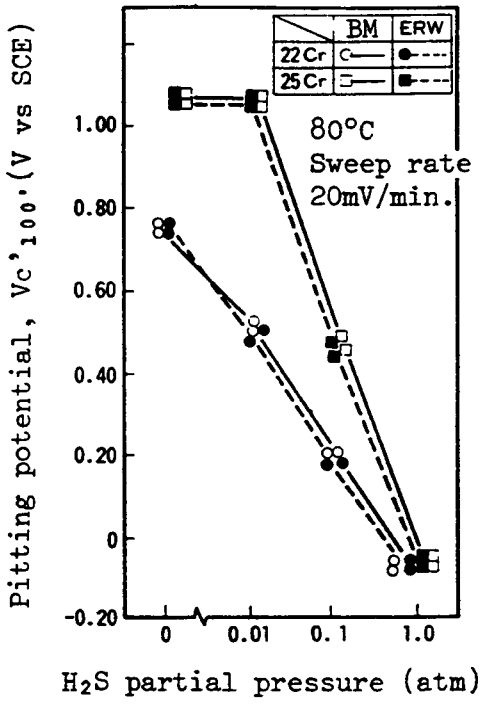


FIGURE 10 - Pitting potential
(in 3.5% NaCl+H_2S)

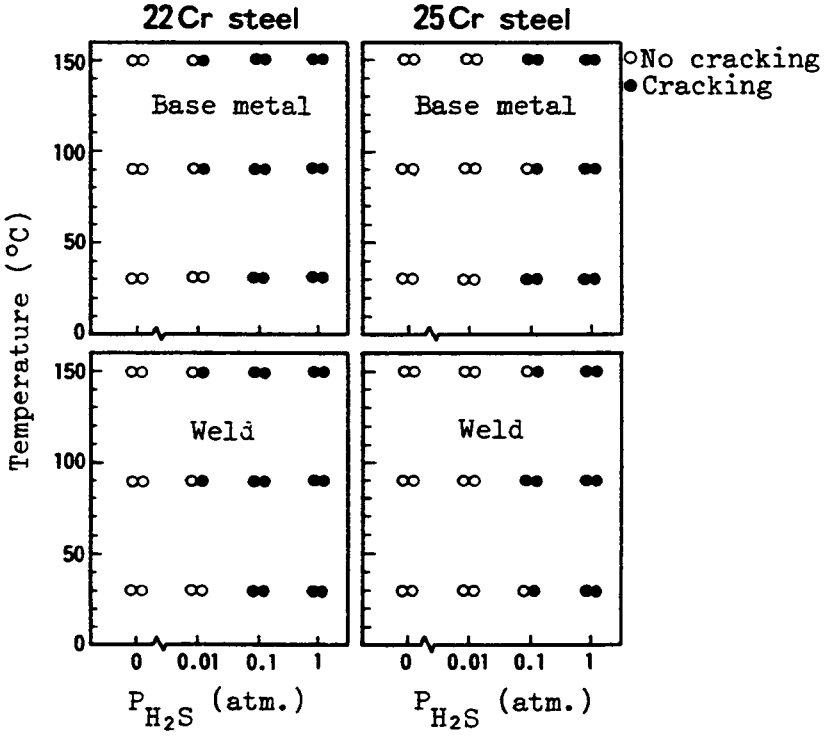


FIGURE 11 - SCC resistance
(20% NaCl+H_2S, σ=617MPa)

Copyrighted Materials
Copyright © 1996 NACE International Retrieved from www.knovel.com

PAPER NUMBER
52

Corrosion 88
March 21-25, 1988
Cervantes Convention Center / St. Louis, Missouri

FULL SCALE TESTING OF DUPLEX STAINLESS STEEL PIPES IN SIMULATED SOUR ENVIRONMENTS

Y. Kobayashi
NKK Steel Research Center, Kokan-cho, Fukuyama 721 JAPAN

Y. Ishizawa and J. Sakai
NKK Steel Research Center, Minamiwatarida, Kawasaki 210 JAPAN

M. Itoh
NKK Pipe and Tube Tech. Dept. Minamiwatarida, Kawasaki 210 JAPAN

T. Taira
Fukuyama Works NKK, Kokan-cho, Fukuyama 721 JAPAN

H. Arup
Danish Corrosion Center, 345 Park Alle DK 2605 Brondby DENMARK

ABSTRACT

Four kinds of duplex stainless steel pipes including girth welds were tested in flows of H_2S-CO_2 containing brines at about 90°C for 4 weeks. Immersion tests with use of test coupons and U-bend specimens were also performed in a variety of the brines differing in H_2S concentrations, temperatures, and acidity. Corrosion behaviors of duplex stainless steels were differentiated by changes of these environmental variables. The heat-tinted areas of girth welds were the most susceptible to occurrence of pitting or surface corrosion attacks in all duplex stainless pipes when exposed to the brines containing H_2S ranging from 100 ppm to 260 ppm in the full scale tests. Increases of Mo contents in duplex stainless steels were found to improve resistance to sour environments, but even duplex stainless steels of 3.4 Mo showed slight corrosion under the presence of 200 ppm H_2S or more. The presence of 11 vol% heavy hydrocarbon mixed with the brine made the pipe surfaces repellent to water and prevented corrosion.

INTRODUCTION

Use of duplex stainless steel linepipes has been recently increasing in corrosive gas/oil transportation because of their high strength, good weldability as well as high corrosion resistance(1-5). Regarding applicability of duplex stainless steels, a number of researches have indicated that they maintain high resistance to localized corrosion in CO_2 containing brines at high temperatures but become

corrosion-prone in the brines containing overcritical amounts of H_2S(6-9). The critical contents of H_2S were mostly in the range from 0.02 bar (2×10^{-3} MPa) of H_2S partial pressure (PH_2S) to 0.1 bar (10^{-2} MPa) when determined by a variety of stress corrosion cracking (SCC) tests(6-8,10,11). As occurrence of SCC is a stress-dependent phenomenon, pitting type corrosion seems more likely to occur than SCC and the critical H_2S contents may vary from the above values(8). In actual gas/oil fields, operation conditions such as acidity of brines, oil or condensate to water ratios and flow conditions vary from one place to another and affect performance of materials to a significant degree(12,13). Effects of these operation conditions as well as H_2S contents should be analized to use duplex stainless steel pipes in H_2S-CO_2-Cl^- environments.

In the present study, full scale corrosion tests were carried out on 22% Cr and 25% Cr type duplex steel pipes in simulated sour environments. Additional corrosion tests were also performed by immersion of test coupons or U-bend specimens in H_2S and CO_2 containing brines to investigate the effects of environmental variables separately. Operation variables investigated in the study were H_2S contents, temperatures, acidity of brines and hydrocarbon mixed with brine. From the standpoint of materials, effects of Cr and Mo contents and surface conditions have been also discussed.

EXPERIMENTAL

Material

Two kinds of 12.75 in. OD x 0.375 in. WT (323.9mm OD x 9.5mm WT) seamless pipes and two kinds of 24 in. OD x 0.688 in. WT (609.6mm OD x 17.5mm WT) UOE welded pipes were used for the present study, investigating the effects of alloy chemistry on resistance to H_2S-CO_2-Cl^- environments. The seamless pipe surfaces were finally finished with grinding and then pickled with acid, and the UOE pipe surfaces with shot blasting and acid pickling. All pipes were commercially produced duplex stainless steel products, involving a 25% Cr duplex stainless steel with a high Mo content (PipeA, CR25M), 22%Cr duplex stainless steels with alloy chemistries of the ordinary S31803 type (Pipes B & D, CR22), and a 22% Cr duplex stainless steel with a high Mo content (PipeC, CR22M). Chemical composition, heat treatment, and mechanical properties of each pipe are given in Tables 1 and 2.

Four pipe sections of 900mm or 500mm in length were welded together by mechanized GTAW to make 3600mm or 2000mm long test sections. Welding consumables and conditions for the girth welds are given in Table 3. Combinations of 7%Ni and 9%Ni type duplex stainless steel filler wires were used to obtain a favorable ferrite/austenite phase ratio in the welds.

Full scale corrosion test

Figure 1 shows schematic drawing of experimental setup used for full scale testing of 12.75in. OD pipes. The setup was specially designed to provide a flow rate of 0.5m/sec. for the liquid in the test pipes while the liquid was kept at a given pressure by an accumulator. The test section was composed of four 900mm long pipes, three or four girth welds and flanges. The whole test section was thermally insulated by wrappings of glass wool, and heated by electric heaters. The pipes were first filled with prescribed amounts of CO_2 and H_2S gases. The test brine was prepared in a separate tank, deaerated below 50 ppb O_2 by vigorous N_2 bubbling, and pumped into the test section. After the filling procedures, the H_2S-CO_2 dissolving brine was circulated through an inner duct pipe by an axial pump. The test solution was sampled at the beginning of the test and periodically once a week at least, and adjusted for acidity, H_2S and CO_2 concentrations. A full scale corrosion test of 24 in. OD pipes was performed with use of other setup, in which the test solution was saturated with a H_2S-CO_2 gas mixture of 8 bars (0.8MPa) in a tank and continuously circulated to the test section at the rate of about 30 L/Hr.

Test materials and test conditions selected for the study are summarized in Table 4. Test pipes were stressed at either 80% of SMYS (368MPa) or 42% of SMYS (189MPa) by internal pressure. Temperatures were about 90°C for all tests. CO_2 concentrations were about 3500ppm, which resulted from saturation with CO_2 gas at 8 bars (0.8 MPa). H_2S concentrations were kept in the range from 220 ppm to 260 ppm in the first test and from 100 ppm to 180 ppm in the second test, which corresponded to H_2S partial pressures from 0.17 bars (0.017 MPa) to 0.20 bars (0.02 MPa) and from 0.08 bars (0.008 MPa) to 0.14 bars (0.014MPa), respectively. For the third test, a hydrocarbon mixture of 11 vol% was added in the brine, to investigate their effects on corrosion behaviors, because fluids in gas pipelines often contain significant amounts of heavy hydrocarbons mixed with brines. Acidity of the brine was also adjusted to pH5 by an addition of 18meq./L $NaHCO_3$ in the third and forth tests.

Immersion test

Corrosion tests were performed by immersion of 50mm x 50mm test coupons and U-bend specimens in brines differing in contents of H_2S and CO_2, temperatures, and acidity of the brines. The specimens were machined from UOE welded pipes and their girth welds and prepared for the tests without disturbing original surfaces. Test conditions are given in Table 5. In Test A and C, H_2S gas or H_2S/CO_2 gas mixtures were periodically injected in the brines at 90°C under atomospheric pressure. In Test B, the test brine in sealed test containers was saturated with the 10%H_2S- 90%CO_2 gas mixture under atmospheric pressure at 25°C and heated to either 60°C or 90°C to maintain similar H_2S concentrations at any temperatures. Test periods were 4 weeks for tests A and B, and 2 weeks for Test C. Measurements of H_2S concentration and pH were carried out at the end of each test.

RESULTS

First full scale corrosion test

CR22 seamless pipes with girth welds were stressed at 80% of SMYS by the internal pressure of 212 bars (21.2 MPa) and tested in a flow of the 0.2 bar H_2S-8bar CO_2-6%NaCl brine at 90°C. The pH value and H_2S concentration of the brine were determined as 4.2 to 4.4 and 220 ppm to 260 ppm, respectively, mostly in the period of the test. After completion of the test, internal surfaces of the tested pipes were visually examined for corrosion attacks. The pipe surfaces were tarnished to greyish brown color, and showed numerous blackish stains in the base metal and small pits along the girth welds, as seen in Fig.2. It is seen in Fig.3-(a) & (b) that the blackish stains in the base metal were corrosion products formed over shallow corrosion attacks. Depth of the corrosion attacks was about 0.1 mm for a maximum. EDAX analysis of the corrosion products indicated that they were rich in Cr, Ni and S but lean in Fe, as compared with chemical compositions of the base metal.

Corrosion pits of 2 to 5 mm in dia. were generated in blue or brown-colored areas near the girth welds, namely heat-tinted areas. A number of faint linear blackish spots of 1 or 2 mm in length were found in the same areas. Surface corrosion attacks were also developing in several areas of the weld metal. Longitudinal cross-sections of these corrosion attacks are shown in Fig.3-(c) & (d). The pits in the heat-tinted areas were open to the surface and about 1mm in depth.

Second full scale test

A CR22 pipe section (PipeB) and a CR25M pipe section (PipeA) were connected to each other by use of flanges and tested in a flow of 0.135 bar H_2S-8 bar CO_2-3%NaCl brine at 93°C. Internal pressure was reduced to 114 bars (11.4MPa): 42% of SMYS as a hoop stress from 212 bars in the first test. The pH value of the brine was from 4.5 to 4.6 which was a little higher than that in the first test. The H_2S concentration was fluctuating mostly in the range from 100 ppm to 180 ppm.

As compared with the first test, these test conditions alleviated corrosion of the CR22 pipes to some extent, but corrosion attacks still appeared in two distinct areas in the base metal of CR22 pipe and in the heat-tinted areas of both pipes, as shown in Fig.4. No signs of corrosion were found in the base metal of CR25M pipe except that minute pitts were found in grinding scars by SEM observations.

Figure 5 shows SEM observation and cross-sections of these surface attacks. Dark indications in the CR22 pipe were revealed as shallow corrosion attacks in the base metal and as small pits with embryonic cracks preferentially propagating in the ferrite phase in the heat-tinted areas. Dark linear spots in the heat-tinted areas of CR25M pipe were very shallow corrosion trenches with no cracks.

No features of corrosion were visible in the flanges of CR22 and CR25M nor in the part of the welded area where the heat tinted colors were removed by grinding prior to the test. These findings indicated surface conditions of materials had significant influences on corrosion resistance and in particular the presence of oxide films on the metal surface was detrimental.

Third full scale corrosion test

The third full scale test was carried out in a flow of 0.135 bar H_2S-8 bar CO_2-3%NaCl brine (89vol%) and hydrocarbon (11vol%) mixture at 93°C. The pH value of the brine was adjusted to 5.2 to 5.4 by an addition of $NaHCO_3$. The other environmental conditions were similar to those in the second test.

Oily sludge was seen inside the test section, and the internal surfaces of the pipes appeared water repellent after cleaned with water, as seen in Fig.6. Qualitative chemical analysis showed the sludge to contain large amounts of sulfur but almost no metallic elements. No signs of corrosion were found anywhere in both CR22 and CR25M pipes. It is evident by comparison with the results from the former two tests that hydrocarbon played a significant role as an corrosion inhibitor.

Fourth full scale corrosion test

CR22 and CR22M UOE welded pipes (Pipes C and D) were tested in 0.135 bar H_2S - 8 bar CO_2-3%NaCl brine at 93°C. The test conditions were similar to those for the second test except that the pH was adjusted to 4.9 to 5.2 by an addition of 18 meq./L $NaHCO_3$ and movement of the brine was slow. The H_2S concentrations were in the range of 150 ppm to 250 ppm.

A number of blackish stains were found scattering in the base metals. Many small stains were seen in non-ground areas of longitudinal welds as well as in the heat-tinted areas and weld metal along girth welds. These features of corrosion attacks were similar in both pipes. Appearances and cross sections of representative stains or small pit indications are shown in Figs.7 and 8, respectively. These were revealed as shallow surface corrosion. A predominant feature of corrosion was preferential dissolution of austenite phase in the base metal and the seam welds of CR22 and CR22M UOE pipes. In contrast, dissolution of ferrite phase occurred in the HAZ and weld metal in the girth welds of both pipes. The latter was also a common feature to corrosion of CR22 and CR25M seamless pipes. Parameters inducing such differences in metallographic features of corrosion are unknown.

Immersion tests

Immersion tests of coupons and U-bend specimens were performed in a variety of test conditions, in order to the effects of H_2S concentrations, temperatures and acidity. Examples of corrosion attacks are shown in Figs 9 and 10, and a summary of the test results in Table 5. Increases of H_2S concentrations led to increasing tendency towards corrosion and caused visible pitting in CR22 at about 180 ppm H_2S and fine surface cracks in the U-bend specimens of CR22 and CR22 weld at 290 ppm H_2S. Further increases of H_2S concentrations caused the surface cracks in all U-bend specimens. When immersed in the brine of about 60 ppm H_2S and 90°C for 2 weeks, in contrast, the base metal showed no visible signs of corrosion and the

heat-tinted area of CR22 weld exhibited only discoloration which seemed an earlier indication of pitting.

Temperatures of the brines also affected occurrence of pitting or cracking to a significant degree. No corrosion occurred in any specimens immersed in the brine of 25°C, while very minute pitts were observed in the base metal of CR22 after the immersion tests at 60°C. In the tests at 90°C, a few of surface cracks were developing in all U-bend specimens and small pits in the base metal of CR22.

Regarding effects of acidity, marked differences of corrosion behaviors were found between the brines of pH4 and pH5. No corroion attacks were visible in any specimens after immersion in the brine of 80 ppm H_2S, pH5 and 90°C. On the other hand, shallow corrosion attacks surrounded by brown-colored areas were generated in the base metals and the heat-tinted areas of weld during immersion in the brine of pH4.

DISCUSSION

Full scale corrosion tests and immersion tests with a variety of H_2S-CO_2 containing brines indicate that duplex stainless steel pipes suffer localized surface attacks under the presence of H_2S. In the following, performance of the pipes in sour environments is discussed from the aspects of environmental conditions and materials.

Effects of environmental parameters

Corrosion attacks were alleviated in the second full scale test. The immersion tests in the 3% NaCl brines at 90°C indicate that changes of H_2S concentrations from 60 to 290 ppm causes marked differences in corrosion behaviors of duplex stainless steels. It is also suggested that the H_2S concentration critical for pitting is close to that for SCC in highly-stressed specimens. The H_2S partial pressure from 2 x 10^{-3} MPa to 10^{-2} MPa, which is known as a critical condition for occurrence of SCC, corresponds to dissolution of about 25 ppm to 130 ppm H_2S in the brine at 90°C. The present experiments show a reasonable agreement with the previous finding and indicate that the critical H_2S concentration for occurrence of pitting and SCC is somewhere around 100 ppm with a little higher values for CR22M and CR25M than for CR22.

Immersion tests in the 3%NaCl brines at three different temperatures have demonstrated that occurrence of corrosion is differentiated by a change of temperature from 90°C to 25°C and duplex stainless steels of these kinds probably resist the presence of 200ppm H_2S or more in the brines at ambient temperatures. The presence of hydrocarbon mixed with brines significantly alleviates corrosiveness of sour environments when uniformly distributed to form films on pipe surfaces. In practical pipelines, however, beneficial effects of heavy hydrocarbon may not be consistent because flow characteristics of two or three phase fluids usually vary depending on operation parameters such as flow velocity and liquid to gas volume ratio, or geographical features. Further studies and relevant experiences are needed to confirm the effects of heavy hydrocarbon on performance of duplex stainless steel pipes.

Effects of pipe materials and surface conditions

It is noted in the second full scale test that CR25M duplex stainless steel has better corrosion resistance in a low H_2S-CO_2-Cl^- environment at high temperatures as compared with an ordinary S31803 type duplex stainless steel : CR22. A beneficial effect of Mo content is also found in the immersion tests A and B. However, the effect of Mo content is limited and high Mo duplex stainless steels are prone to corrode by the presence of about 200 ppm H_2S or more.

Oxide films formed during welding have more influences on corrosion resistance of linepipes than alloy chemistry because pitting or surface corrosion attacks are first generated in the heat-tinted areas of girth welds. The areas in which corroion attacks are frequent are located particularly 4 to 6 mm away from the

fusion line. After removal of the heat-tinted colors, areas of the same location show good corrosion resistance comparable to the base metal. These indicate that corrosion resistance of the alloys is hardly affected by heating. Instead, thin oxide films may form a crevice on the metal surface and promote occurrence of corrosion. In H_2S-containing solutions, deposit of sulfides, which is recognized by dark color, is formed faster on the heat-tinted areas than on oxide-free surfaces, and this seems to facilitate the crevice formation under the oxide films.

SUMMARY

Applicability of duplex stainless steel pipes to sour environments were investigated by full scale corrosion tests and immersion tests. The results are summaried in the followings.

1) Corrosion behaviors of duplex stainless steels were differentiated by changes of H_2S concentrations, temperatures and acidity of the brines. The presence of about 100 ppm H_2S (0.08 bars) in the brines of 3% NaCl at 90°C seems critical for occurrence of small pits or embryonic cracks in the base metal of an ordinary S31803 duplex stainless steel. The critical H_2S concentration was raised by lowering the temperature, and the same material showed no corrosion in the brine of 200 ppm H_2S at ambient temperatures.

2) Beneficial effects of a high Mo content were found in the full scale corrosion test and immersion tets. However, the effects of Mo contents are limited and duplex stainless steels of 3.4 Mo are prone to corrode at the presence of about 200 ppm H_2S or more.

3) Pitting or shallow corrosion attacks with faint linear indications were more likely to occur in the heat-tinted areas of girth welds than in the base metal. In the case of CR22 seamless pipe, the corrosion attacks in the heat-tinted areas were revealed as small pits with embryonic cracks preferentially propagating in the ferrite phase when exposed to the brine at 90°C under the presence of 100 to 180 ppm H_2S. In the case of CR25M seamless pipe, in contrast, they were shallow corrosion trenches with no crack-like appearances. The detrimental effects of oxide films formed in the heat-tinted areas are considered attributable to formation of a crevice on the metal surface.

4) The presence of 11 vol% heavy hydrocarbon mixed with the brine made pipes surfaces repellent to water and prevented corrosion of CR22 and CR25M pipes in the full scale test under the presence of 100 to 160 ppm H_2S in the brine phase at 90°C. Heavy hydrocarbon can play a role as a corrosion inhibitor when unformly distributed over pipe surfaces.

Further studies on duplex stainless steel pipes and high-Ni alloy clad pipes are now in progress with focusses on the effects of heavy hydrocarbon and other environmental parameters, and applicability of these corrosion resistant alloy pipes to sour environments.

REFERENCES

1) T. Taira, O. Hirano, Y. Nishino, T. Kitada, K. Ume, and Y. Naganawa, Nippon Kokan Tech. Report Overseas, No.46, pp25-34(1986).
2) T. Taira and A.K. Singh, "Duplex Stainless Steel Linepipe for Arctic Use," OMAE Sixth Intn'l Symp., Houston, 1987.
3) T. Kitada, T. Ishihara, K. Ume, M. Tsuji, T. Taira, and M. Itoh, "Duplex Stainless Steel Linepipe for Service in CO_2-Cl^- Environments, "TWI Intn'l Conf. Duplex Stainless Steel '86, Hagane The Netherlands, Oct. 1986.
4) A.C. Madsen, F.O. Mueller, R. Geisert, J.B. Lee, and H.J. Choi, Material performance, Feb. 1987, pp49-55.
5) M. Swiss, Welding and Metal Fabrication, Dec. 1979, pp723-724.
6) J. Sakai, I. Matsushima, Y. Kamerura, M. Tanirura, and T. Osuka, J. Materials for Energy Systems, vol.5 No.2, pp105-111 (1983).

7) Y. Ishizawa, T. Shimada, and M. Tanimura, "SCC Behavior of a Duplex Stainless Steel in Sour Gas Environments," NACE CORROSION 83, Anaheim California, April 1983, paper No.167.
8) J. Sakai, S. Hashizume, Y. Kuriki, Y. Naganawa, M. Itoh, and I. Matsushima, "Corrosion Resistance of Duplex Stainless Steel and Its Weldment of Pipeline Service," NACE CORROSION 87, San Francisco, March 1987, Paper No.292.
9) A.I. Asphahani, Corrosion, Vol.37 No.6, pp327-335(1981).
10) K. van Gelder, J.G. Erlings, J.W.M. Damen, and A. Visser, "Stress Corrosion Cracking of Duplex Stainless Steel in $H_2S/CO_2/Cl^-$ Environments," conf. on Hydrogen Sulfide Induced Environment Sensitive Fracture of Steels, Amstermad The Netherland, Sept. 1986.
11) A. Ikeda, H. Mukai, and M. Ueda, Corrosion vol.41 No.4, pp185-192(1985).
12) J. Oredsson and S. Beruhardsson, Material Performance, Jan. 1983, pp35-42.
13) N.L. Crolet and M.R. Bonis, Material Performance, March 1986, pp41-49.

Table 1 Chemical compositions and heat treatments of test pipes

Pipe	Manufacturing	Size OD x WT(mm)	Chemical Compositions wt% C	N	Cr	Mo	Ni	Fe	Heat Treatment*
A	CR25M S'less	323.9 x 9.5	0.012	0.15	24.7	3.4	6.7	Bal.	Sol. Ann. at 1050°C
B	CR22 S'less	ditto	0.012	0.13	23.2	3.0	5.2	Bal.	ditto
C	CR22M UOE	609.6 x 17.5	0.013	0.14	22.3	3.4	5.7	Bal.	ditto
D	CR22 UOE	ditto	0.018	0.14	22.5	3.2	5.8	Bal.	ditto

Note *) UOE welded pipes were solution annealed after longitudinal welding.

Table 2 Mechanical properties of test pipes

Pipe	Mechanical Properties (Trans.) 0.2%PS	TS	Elong.	Hardness
A	586Mpa	776Mpa	31%	HRC21
B	582	747	35	21
C	633	789	38	21
D	638	798	43	21

Table 3 Welding consumables and conditions for girth welding

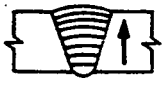
Consumables		Edge Shape and Piling	Welding Conditions		
Filler Wire	Shield Gas	(Outside)	0.375 in. WT. S'less (5 layers)		
			A	V	mm/min.
TGS329(7%Ni) or TGS329M(9%Ni)	100% Ar		170 ∿ 240	9.0 ∿ 10.7	80
			0.688 in. WT. UOE (10 layers)		
			A	V	mm/min.
		(Inside)	120 ∿ 200	8.0 ∿ 10.0	75

Table 4 Test pipes and test conditions of full scale corrosion tests

	1st test	2nd test	3rd test	4th test
Test pipes	A A A A 12.75"ODx0.9Mx4sec. A : CR22 S'less pipe	A A B B 12.75"ODx0.9Mx4sec. A : CR22 S'less pipe B : CR25M S'less pipe	A A B B 12.75"ODx0.9Mx4sec. A : CR22 S'less pipe B : CR25M S'less pipe	C C D D 24"ODx0.5Mx4sec. C. CR22 UOE pipe D. CR22M UOE pipe
Test press.	212bars (80% of SMYS)	114bars (42% of SMYS)	114bars (42% of SMYS)	111bars (42% of SMYS)
Test temp.	90°C	93°C	93°C	93°C
Test sol.	100% brine (6%NaCl)	100% brine (3%NaCl)	89% brine (3%NaCl)* Plus 11% hydrocarbon**	100% brine (3%NaCl)*
Dissolved Gas	PH_2S = 0.20 bars PCO_2 = 8 bars	PH_2S = 0.135 bars PCO_2 = 8 bars	PH_2S = 0.135 bars PCO_2 = 8 bars	PH_2S = 0.135 bars PCO_2 = 8 bars
Flow velocity	0.5 M/sec.	0.5 M/sec.	0.5 M/sec.	Circulation (30L/H)

Note *) 18meq./L of $NaHCO_3$ were added to change pH to 5.

**) $11.9\%C_7+21.6\%C_8+16.8\%C_9+15.5\%C_{10}+34.3\%C_{11}$

Table 5 Summary of immersion tests

TEST CONDITIONS	TEST SOL.	TEST A			TEST B			TEST C		
		3% NaCl			3% NaCl			3%NaCl+CH_3COOH/CH_3COONa		
	DURATION	4 WEEKS			4 WEEKS			2 WEEKS		
	H_2S CONC.	180ppm	290ppm	400ppm	150~200 ppm			60~90 ppm		
	TEST TEMP.	90°C			25°C	60°C	90°C	90°C		
	pH	ABOUT 4.5			ABOUT 4.5			5.1	4.7	3.9
IMMERSION TEST	CR22 BM [1]	Pit	Pit	Pit	No corr.	(Pit)	Pit	No corr.	No corr.	Pit
	CR22M BM [2]	No corr.	Pit	Pit	No corr.	No corr.	No corr.	No corr.	No corr.	Pit
	CR22M WELD [3]	(Pit)	Pit	Pit	No corr.	No corr.	No corr.	No corr.	Discol.	Pit
	CR25M BM [4]	No corr.	Pit	Pit	No corr.	No corr.	(Pit)	No corr.	No corr.	Pit
SCC TEST (U-bend)	CR22 BM	No crack (D)	Crack	Crack	No crack	No crack	Crack	No crack	No crack	Crack
	CR22M BM	No crack	No crack (P)	Crack	No crack	No crack	Crack	No crack	No crack	Crack
	CR22M WELD	No crack (P)	Crack	Crack	No crack	No crack	No crack (P)	No crack	No crack (D)	Crack
	CR25M BM	No crack	No crack (P)	Crack	No crack	No crack	Crack	No crack	No crack	Crack

Note) Test material: 1)UOE pipe of a similar alloy chemistry to pipe B, 2)pipe C, 3)girth weld of pipe C, 4)UOE pipe of a similar alloy chemistry to pipe A.
BM: Base metal, WELD: One side weld by multi-pass GTAW simulating girth welding
No corr.: No corrosion, Discol.: Discoloration, (P): Pit, (D): Discoloration
(Pit) means that pits were very minute and recognized only under a microscope.

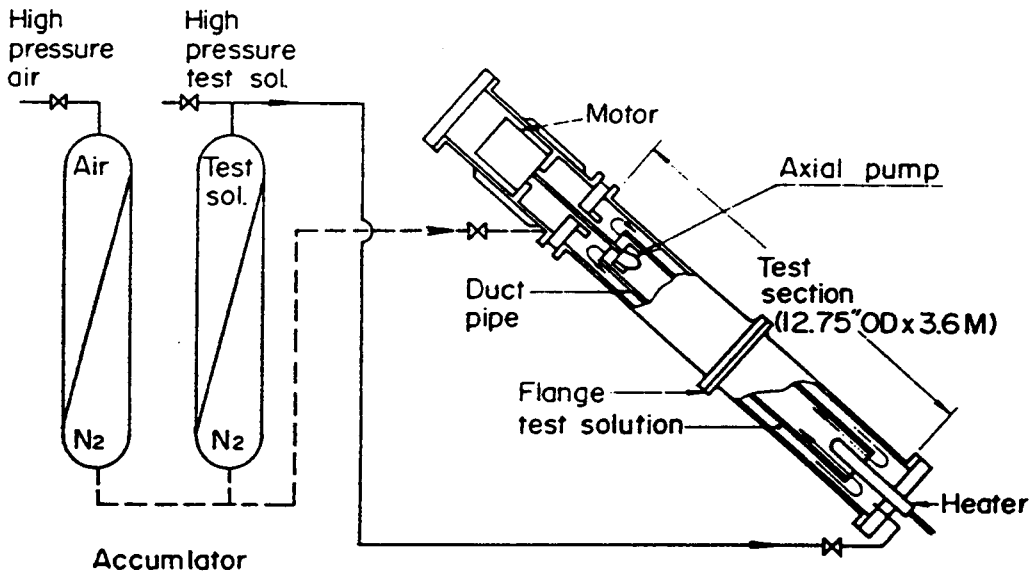


Fig.1 Schematic drawing of setup for full scale corrosion test

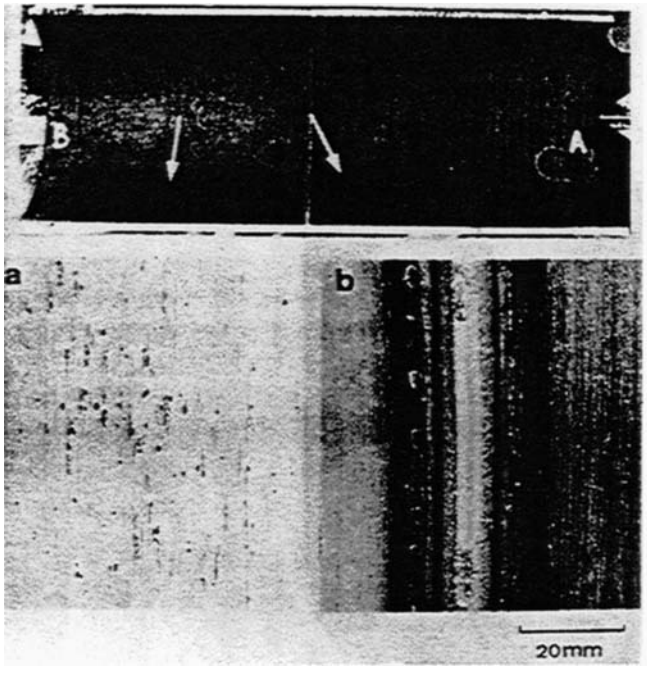


Fig.2 Typical appearances of tested pipes (1st test, CR22 seamless pipe)
a: the base metal, b: the girth weld

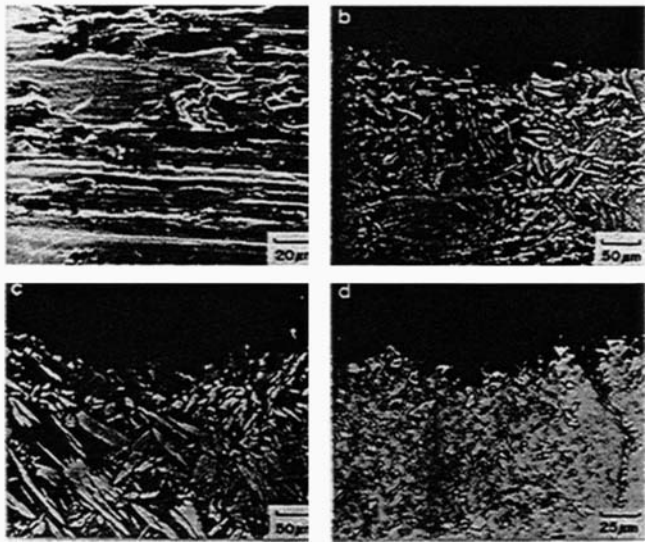


Fig.3 Microscopic features of stains and pitts shown in Fig.2
a: SEM photo of stains in the base metal, b: cross section of a, c: pit in the heat tinted area, d: pit in the weld metal.

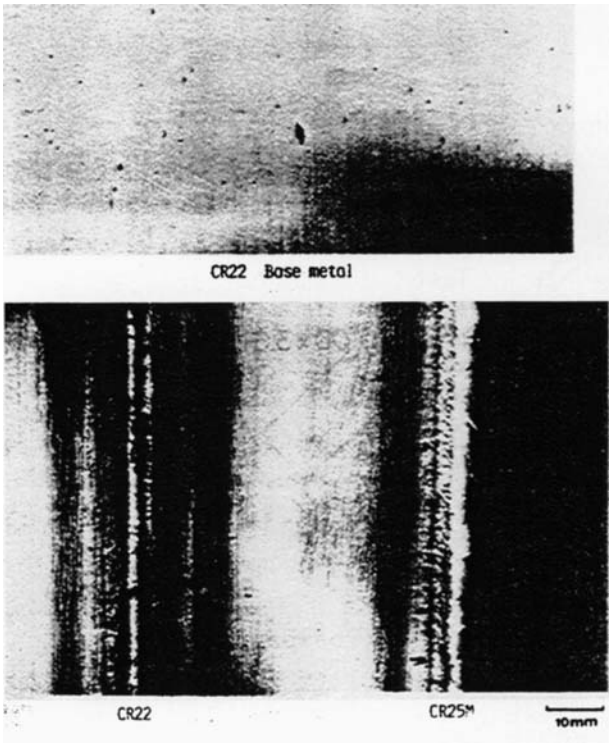


Fig.4 Typical appearances of tested pipes (1st test, CR22 and CR25M seamless pipe)

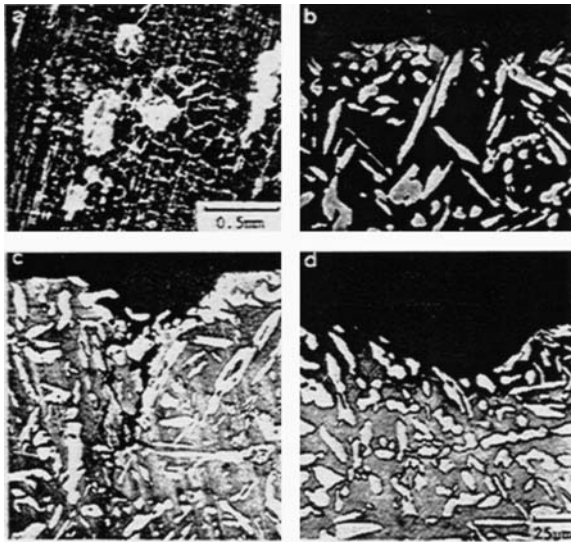


Fig.5 Microscopic features of stains and linear indications shown in Fig.4 a: SEM photo of stains in the base metal of CR22, b: cross section of a, c: small pit in the heat tinted area of CR22, d: small pit in the heat tinted area of CR25M

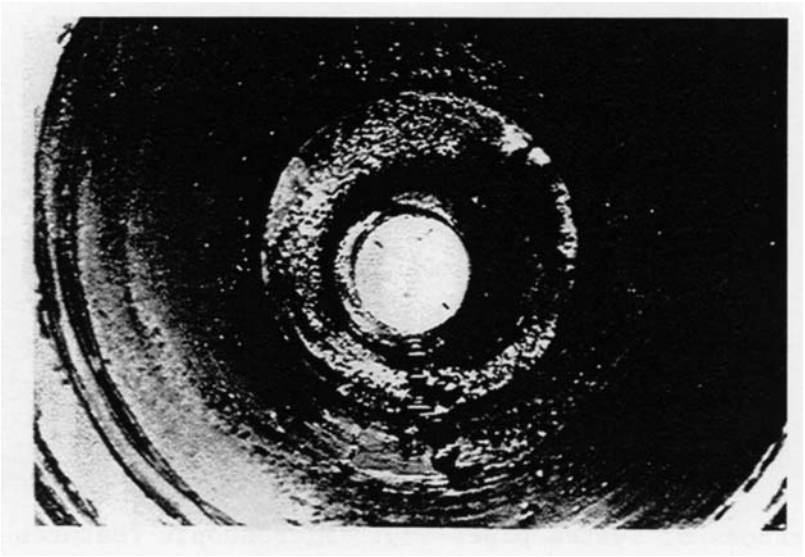


Fig.6 Water repellent appearances of tested pipes (3rd test, CR22 and CR25M seamless pipes)

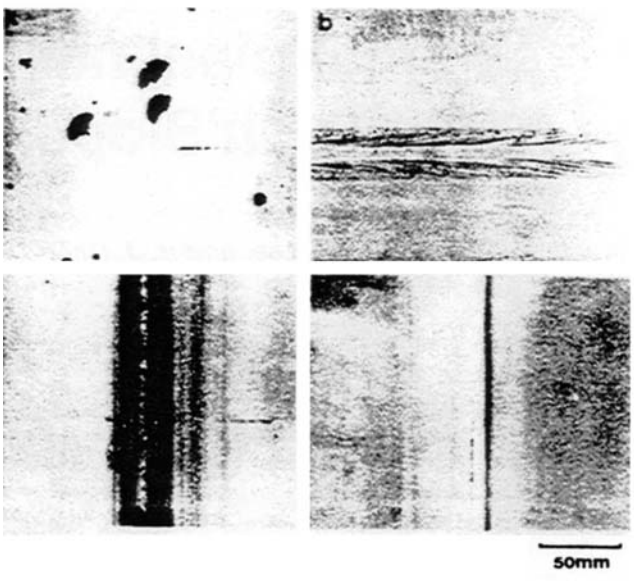


Fig.7 Typical appearances of tested pipes (4th test, CR22 and CR22M UOE pipes) a: the base metal of CR22, b: the seam weld of CR22, c: the girth weld of CR22 (as welded), d: the girth weld of CR22 (polished).

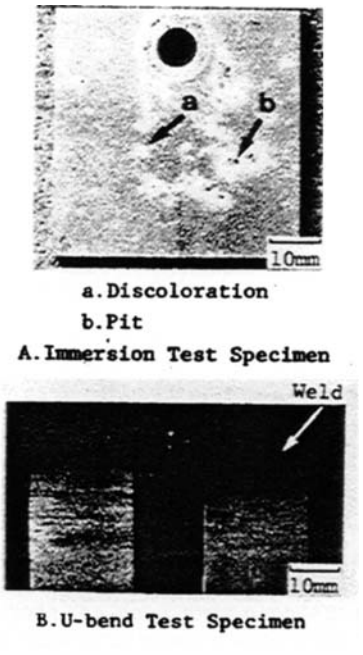


Fig.9 Typical appearances of test coupon and U-bend specimen after immersion test (Immersion test A, 290ppm H_2S, 90°C)

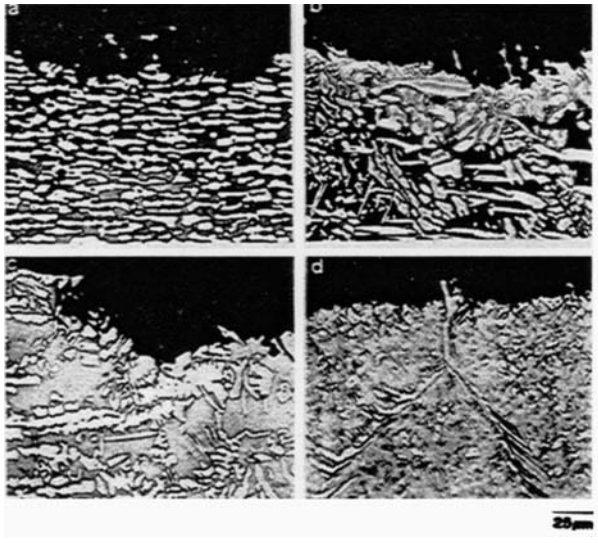


Fig.8 Microscopic features of stains and small pitts shown in Fig.7 a: the base metal, b: the seam weld, c,d: the heat tinted area and weld metal of girth weld.

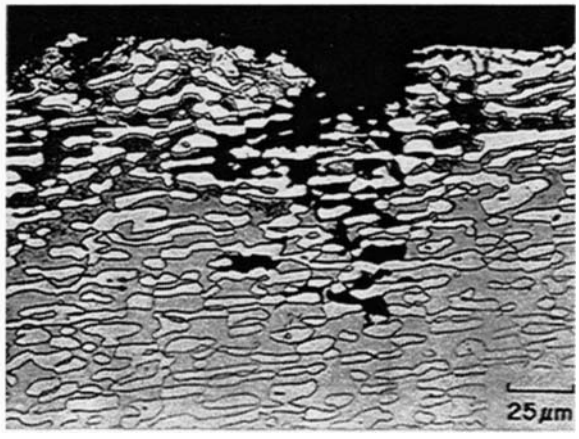


Fig.10 Cross-section of surface crack in U-bend specimen (Immersion test A, 400ppm H_2S)

Copyrighted Materials
Copyright © 1996 NACE International Retrieved from www.knovel.com

Duplex stainless steel pipelines and piping on the North Slope*

A. C. Madsen, F. O. Mueller, R. Geisert, J. B. Lee, and H. J. Choi***

Three duplex stainless steels (SSs) and their welds were tested to determine their acceptability for use on a major Alaskan offshore project. Long- and short-term tests were performed to evaluate resistance to pitting, crevice corrosion, and sulfide stress cracking (SSC) in a simulated crude oil environment containing large amounts of carbon dioxide, produced water, and up to 300 ppm H_2S. Low-temperature (−54 C) toughness and weldability were also evaluated. Duplex SS, conforming to ASTM A790, UNS 31803 modified, had acceptable properties and was selected for a large diameter common line, well lines, and module piping on a major North Slope offshore project.

Introduction

IN 1982, STANDARD OIL began investigating materials of construction suitable for the three-phase pipelines on its offshore project. A highly reliable pipe material was required for this environmentally sensitive area located east of Prudhoe Bay and is the first offshore development on the Alaska North Slope. Duplex stainless steel (SS) appeared to be the most cost effective material offering acceptable mechanical properties and sufficient corrosion resistance to the three phase fluid (Table 1).

The project consists of two gravel islands connected both to each other and to the mainland by gravel causeways. The pipelines will be located on the causeways. Cost studies showed that duplex SS compares favorably to carbon steel systems with inhibitors when the whole life of the field is considered.

Although duplex SS appeared acceptable for the predicted service conditions, Standard Oil seeked assurance that duplex SS pipe: (1) is readily weldable, (2) has sufficient weld metal and heat affected zone (HAZ) toughness (both long seam welds, where applicable, and field girth welds), and (3) is sufficiently resistant to corrosion in the welds as well as in the base metal. At the beginning of the studies, no relevant data existed for weld toughness and corrosion resistance.

*Presented during CORROSION/86, Paper No. 396, NACE, Houston, TX, 1986.

*Standard Alaska Production Company, P.O. Box 196612, Anchorage, AK 99519.
**Standard Oil Production Company, Cleveland, OH 44128.

Experimental procedure

Weldability

Three different duplex SS pipe materials conforming to

TABLE 1 — Pipe materials included in corrosion tests

Material code	Description	Composition—% specified/reported										
		C	Cr	Cu	Mn	Mo	Ni	P	Si	S	N	Other
A	10-3/4 in. OD × 0.690 in. wt	0.04 max	24.0-27.0	1.5-2.5	1.5 max	2.00-4.00	4.50-6.5	0.040 max	0.25-1.0	0.030 max	0.10-0.25	—
		0.03	25.2	1.70	0.90	3.10	5.70	0.020	0.50	0.005	0.15	
B	6 in. OD × 0.750 in. wt	0.03 max	24.0-26.0	0.20-0.80	1.10 max	2.5-3.5	5.5-7.5	0.030 max	0.75 max	0.03 max	Added	0.1-0.5W
		0.017	25.0	0.45	0.89	3.07	7.0	0.026	0.39	0.001	0.138	0.29
C	6 in. OD × 0.432 in. wt	0.030 max	21.0-23.0	—	2.0 max	2.50-3.50	4.50-6.50	0.030 max	1.0 max	0.20 max	0.08-0.20	
		0.02	22.10	—	1.58	2.90	5.31	0.011	0.36	0.011	0.12	

TABLE 2 — Weld filler metals used in test programs

Weld filler type code	Description	Chemical analyses stated on material test reports										
		C	Cr	Cu	Mn	Mo	Ni	P	Si	S	N	Other
A	Bare wire	0.02	25.4	1.9	0.8	3.4	5.3	0.019	0.7	0.003	0.17	
	coated electrode	0.02	25.4	1.9	0.8	3.4	5.3	0.019	0.7	0.003	0.17	
B	Bare wire	0.021	25.25	0.49	0.91	3.18	6.8	0.025	0.48	0.004	0.137	0.32%W
	coated electrode	0.04	27.36	0.46	0.42	3.02	7.58	0.023	0.52	0.008	0.128	0.29%W
C	Bare wire	0.015	22.63	—	1.66	3.01	6.07	0.018	0.45	0.005		
	coated electrode	0.028	22.7	—	0.64	3.1	9.3	0.034	1.0	0.011	0.14	
D	Bare wire	0.015	22.63	—	1.66	3.01	6.07	0.018	0.45	0.005		
E	Bare wire	0.011	22.49	—	1.59	3.00	9.02	0.015	0.17	0.005	0.077	
	coated electrode	0.011	22.49	—	1.59	3.00	9.02	0.015	0.17	0.005	0.077	
F	Bare wire	0.011	22.49	—	1.59	3.00	9.02	0.015	0.17	0.005	0.077	

TABLE 3 — Charpy V-notch test data—girth weld procedures

Pipe material code	Welding procedure	Notch location	FT-LBS (J) @ −29 C[1]				FT-LBS (J) @ −46 C[1]				Notes
			Test data			Average	Test data		Average		
A (Pipe)	- 07/12/83	Weld	8(11)	8(11)	5(7)	7(9)	8(11)	7(9)	3(4)	6(8)	
	(GTAW Root and	HAZ	18(24)	10(14)	23(31)	17(23)	13(18)	12(16)	10(14)	12(16)	
	SMAW Fill)	Base Metal	17(23)	55(75)	101(137)	58(79)	8(11)	12(16)	11(15)	10(14)	
B (Pipe)	800 R&DP #503	Weld	17(23)	12(16)	16(22)	18(24)	8(11)	9(12)	7(9)	8(11)	
	(GTAW Root and	HAZ	150(203)	133(180)	140(190)	141(191)	62(84)	110(149)	106(144)	92(126)	
	SMAW Fill)	Base Metal	248(336)	222(301)	262(355)	244(331)	239(324)	245(332)	261(354)	248(336)	
C (Pipe)	- 6/8/83	Weld	28(38)	31(42)	34	31(42)	31(42)	30(41)	4(46)	32(43)	
	(GTAW Root and	HAZ	78(106)	60(81)	36(49)	56(76)	42(57)	69(94)	91(123)	67(91)	
	SMAW Fill)	Base Metal	148(201)	124(168)	152(206)	141(191)	114(155)	126(171)	144(195)	128(174)	
D (Plate)	BLN-0683-5A	Weld	—				40(54)	49(66)	51(69)	47(64)	63(85)[3,4]
	(GTAW Root and	HAZ	—				60(81)	58(79)	57(77)	59(80)	78(106)
	Fill)	Base Metal	—								
E (Plate)	BLN-0683-5B	Weld	—				38(52)	36(49)	36(49)	37(50)	
	(GTAW Root and	HAZ	—				105(142)	100(136)	102(138)	102(138)	
	SMAW Fill)	Base Metal	—				205(278)	208(282)	226(306)	213(288)	
E (Plate)	BLN-0683-5C	Weld	—				40(54)	39(53)	40(54)	40(54)	
	(GTAW Root and	HAZ	—				97(132)	97(132)	106(144)	100(136)	
	SMAW Fill)	Base Metal	—				205(278)	208(282)	226(306)	213(289)	
F (Pipe)	SCC-IX-2205-001	Weld	—				78(106)	79(107)	61(83)	73(99)	122(165)[2,4]
	(GTAW Root and	HAZ	—				120(163)	120(163)	120(163)	120(163)	199(269)
	Fill)										

[1]10 × 10 mm (full-size specimens) unless otherwise noted.
[2]6 × 10 mm specimens.
[3]7.5 × 10 mm specimens.
[4]Values in parenthesis are adjusted to full size.

the chemical analyses shown in Table 1 were used for testing. The wall thicknesses and diameters of these materials are also shown.

The pipes were cut into sections 7 to 10 in. (18 to 25 cm) in length. The section ends were beveled, and the sections from the same pipe were welded together using weld procedures and filler materials recommended by the supplier. For these pipe materials, the girth welds were made with tungsten inert gas root pass (GTAW) and shielded metal arc (SMAW) filler passes using the filler materials shown in Table 2.

Additionally, several duplex SS plate materials (Material Codes D, E, and F) were welded using the filler materials and procedures shown in Tables 2 and 3, respectively.

Specimens were cut from the aforementioned welds and subjected to Charpy V-Notch and hardness tests. These results are shown in Tables 3 and 4, respectively. Ferrite/austenite ratios were determined for the base metal, HAZ and weld metal (Table 5).

Corrosion tests

The resistance of duplex SS in the as-welded condition to crevice corrosion and stress corrosion cracking (SCC) when exposed to the project fluids was of particular concern. The program included long-term (six-month exposure) SCC and crevice corrosion tests, slow strain rate tests (SSRTs), and scanning electron microscopic (SEM) examination.

TABLE 4 — Hardness test data

Pipe material code	Welding procedure	Hardness location	Hardness HRC[1]		
			Base metal	HAZ	Weld metal
A	Root - GTAW	Top	26.5	28.5	28.5
	Fill - SMAW	Mid wall	26	28.5	28.0
		Root	27	31.0	31.0
B	Root - GTAW	Top	22	25	27
	Fill - SMAW	Mid wall	21	27	28.5
		Root	22	26	27
C	Root - GTAW	Top	22	20.5	17.5
	Fill - SMAW	Mid wall	21	22	21
		Root	22	24	25.5
D	Root - GTAW	Top	20	20	19
	Fill - SMAW	Mid wall	20	20.5	20.5
	Low heat	Root	21	22	20.5
E	Root - GTAW	Top	20	20.5	19.5
	Fill - SMAW	Mid wall	20.5	21	20
	High heat	Root	22	22	19
F	GTAW only	Top	20	20.5	21
		Mid wall	18.5	22	22
		Root	18	23	23

[1]Hardness values are reported as Rockwell C values (HRC).

TABLE 5 — Ferrite content of weld coupons

Pipe material code	% Ferrite/austenite[1]		
	Base metal	HAZ	Weld metal
A	65/35	70/30	60/40
B	50/50	75/25	65/35
C	55/45	65/35	40/60 (SMAW fill) 55/45 (GTAW root)

[1]Ferrite measurements were made using the metallographic point count method. Reported results are an average of three counts.

The tests were performed in one or several of the simulated project environments shown in Table 6. These environments represent the extremes expected in production ranging from sweet to sour corrosion conditions. Oxygen was added to Test Fluids 2 and 4 to simulate possible air intrusions. The 1759 ppm H_2S provides an H_2S partial pressure of 0.175 psi (1.2 KPa) at the test pressure of 100 psi (0.69 MPa). This corresponds to the original design condition of 200 ppm H_2S at 800 psi (5.5 MPa) total pressure [i.e., 0.16 psi (1.1 KPa) H_2S] and to the revised worst-case condition of 300 ppm H_2S at 600 psi (4.4 MPa) total pressure [i.e., 0.15 psi (1.0 KPa) H_2S].

Immersion tanks

Glass-lined reactors were used for the immersion tanks. The tanks were jacketed for steam and hot water heating. Controllers maintained the tank temperatures at 93 C ± 2.8 C. The gases were introduced into the bottom of each tank individually. Tensile and crevice specimens were installed in the immersion tanks as described.

Stress corrosion test (long-term)

Each tensile specimen was machined to the dimensions

TABLE 6 — Test environments

Field number	Environment
1	Synthetic brine/93 C/100 psi (0.69 MPa) CO_2
2	Synthetic brine/93 C/100 psi (0.69 MPa) CO_2 + 2 ppm O_2
3	Synthetic brine/93 C/100 psi (0.69 MPa) CO_2 + 1750 ppm H_2S
4	Synthetic brine/93 C/100 psi (0.69 MPa) CO_2 + 1750 ppm H_2S + 2 ppm O_2

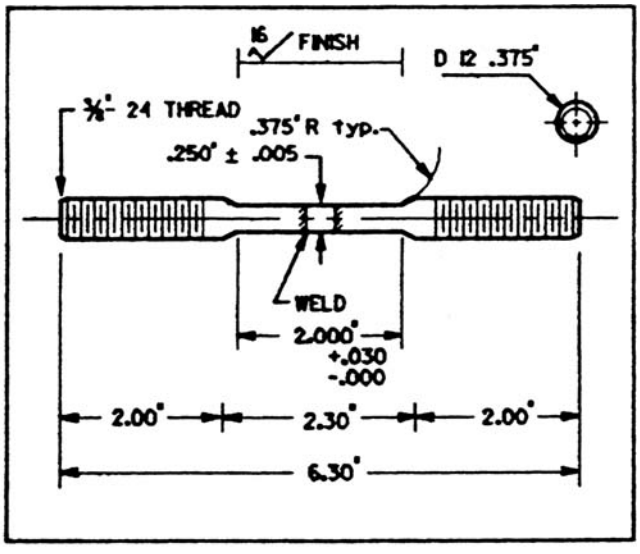


FIGURE 1 — Duplex stainless steel corrosion test specimen.

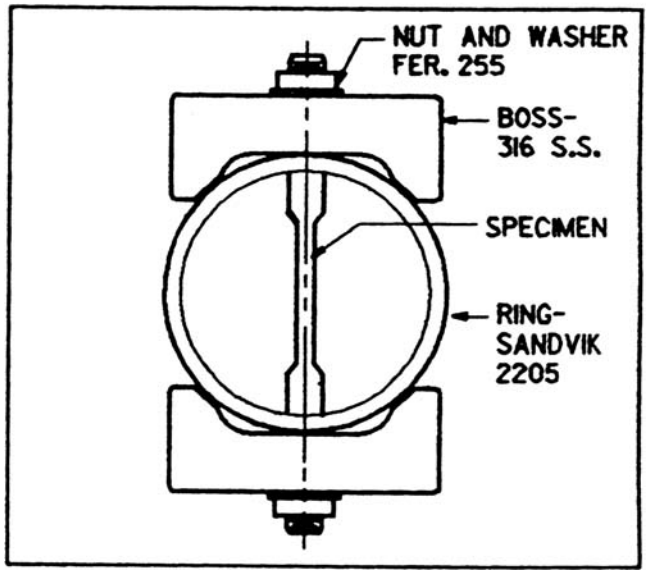


FIGURE 2 — Tensile specimen and loading fixture.

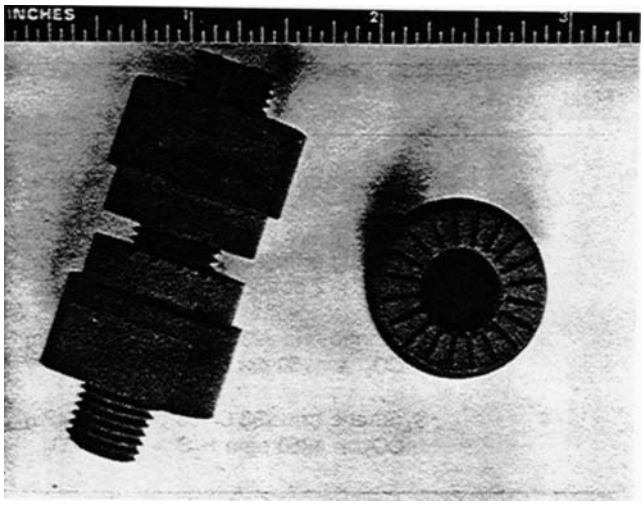


FIGURE 3 — Photograph of the multiple crevice washer test fixture.

shown in Figure 1 and was loaded in a fixture such as that shown in Figure 2.

The stress levels were based on 80 to 100% of the actual yield strength of the alloy. The mechanical properties were determined from the average of three tensile tests using a tensile test machine with an autographic recorder. From the resultant stress-strain curves, the amount of extension for the required load was calculated. Using an extensionometer on the specimen, the nuts were tightened until the required extension was achieved. The test fixtures were then installed on racks and inserted into the autoclaves. One set of fixtures was installed in the vapor zone and another in the liquid zone.

Crevice corrosion tests

The multiple crevice corrosion test technique developed by Anderson was employed to investigate the crevice corrosion properties of the duplex SSs in laboratory simulated oilfield corrosive conditions.[1]

Figure 3 shows the multiple crevice corrosion specimen holder. Two grooved Rulon[1] washers are pressed on each side of a test specimen using a threaded rod. This design offers 40 uniform crevices (20/washer) that can provide statistical data.

These washers were attached to the crevice corrosion test specimens shown in Figure 4 and the assemblies were installed in the autoclaves. One set of assemblies was installed in the vapor zone and another in the liquid zone of each tank.

Autoclave test procedure

After the test specimens were installed, the tanks were closed, heated, and pressurized. The tanks were then leak checked and the lids were retightened. Initially, the various gases were introduced into the tanks for 24 h with the vent valve open slightly. This was to ensure that all entrained gases were purged from the brine and that the brine was completely saturated with the test gas. After the initial purge, the vent valve was closed and the tank pressure was maintained at 100 psi (0.69 MPa). The tanks were then purged weekly to maintain a constant gas composition in the brine. The procedure was to vent the tanks to 90 psi (0.62 MPa) and repressurize to 100 psi (0.69 MPa) in the case of the H_2S/CO_2 mixture and then to 103 psi (0.71 MPa) with O_2. This maintained the oxygen concentration at the 2 to 3 ppm range in solution.

Slow strain rate tests

Specimens for the SSRTs conform to NACE TM0177[2]

[1]Registered trade name.

[2]TM0177, "Testing of Metals for Resistance to Sulfide Stress Cracking at Ambient Temperatures."

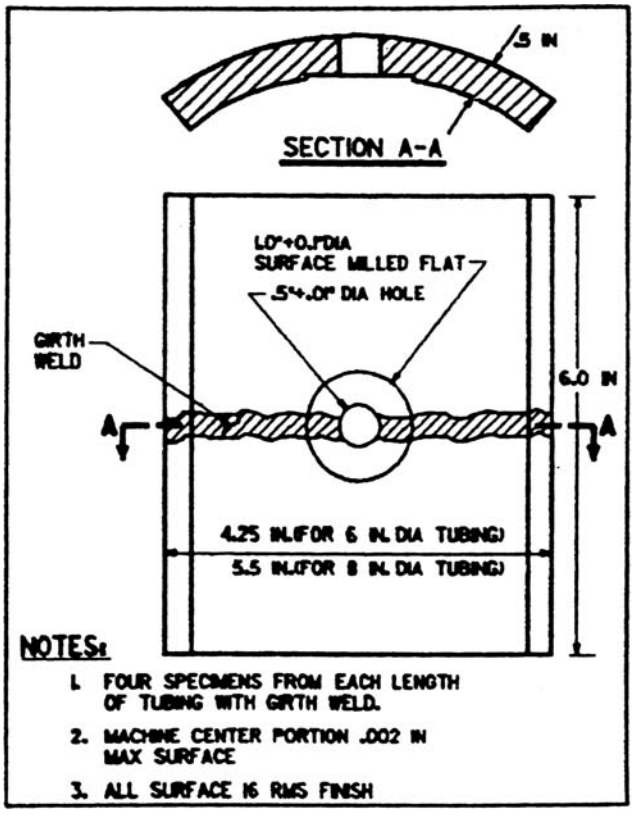


FIGURE 4 — Crevice corrosion test specimen.

subsize specimen dimensions and are shown in Figure 5. Both welded and base metal specimens for each alloy were tested. The same four environments were used for the SSRT as were used for the immersion tests. Prior to testing, each specimen was polished with 600 grit silicon carbide paper to remove machining marks and to ensure a polished surface. Specimens were fitted into a 250 mL Hastelloy C276[3] autoclave. Teflon[4] washers insulated the specimen from the autoclave to prevent galvanic corrosion.

The slow strain apparatus applies a load at a constant strain rate. For this test, the strain rates were 10^{-6} s^{-1} and 5 $\times$ 10^{-7} s^{-1}. The load was measured by a load cell and recorded on a strip chart recorder.

After installing the autoclave and specimen into the slow strain rate tester, the autoclave was filled with synthetic brine and heated to 93 C. While heating, the autoclave was pressurized with the test gases. The strain rate was then initiated and the time-to-failure and ultimate load were recorded on the strip chart recorder.

After failure, the fractured surfaces of the specimens were examined with a SEM to determine SCC or sulfide stress cracking (SSC) susceptibility. SEM examination was then followed by metallographic examination to determine crack morphology. For each alloy, a specimen was tested in air to provide a base of comparison.

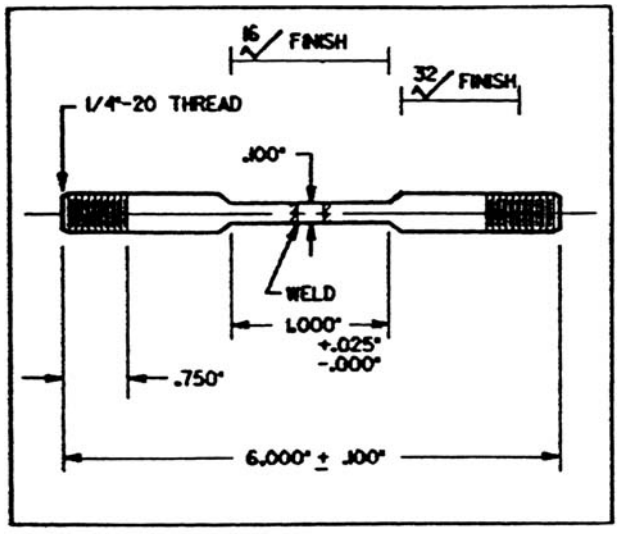
Charpy V-notch tests

Charpy V-Notch tests were performed on Materials A, B, and C at −29 and −46 C. These tests were also performed on Materials D, E, and F at −46 C. The weld, HAZ, and base metal were tested in each case.

Hardness tests

Hardness tests were performed on the base metal, weld metal, and HAZ of each material.

[3],[4]Registered trade names.



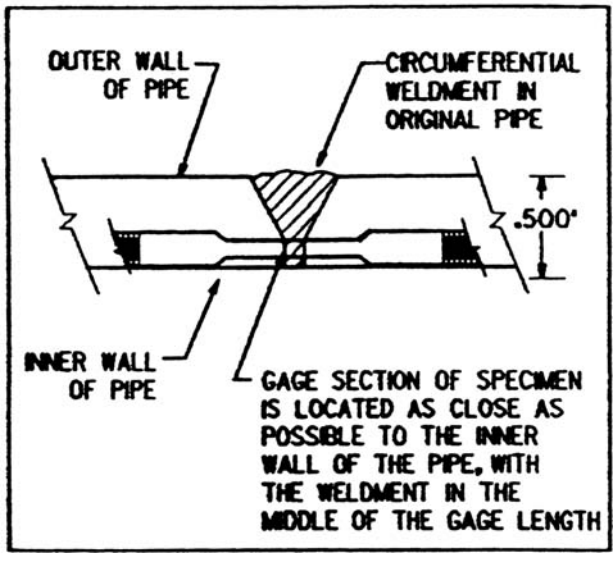


FIGURE 5 — Slow strain rate specimens.

Microstructure

Ferrite content was determined by the point count method in three locations and the results were averaged.

Results and discussion

Immersion tests

Stress corrosion tests. There were no SCC failures of any of the three alloys in the simulated Endicott environments after six months of exposure. These duplex SSs are also resistant to general corrosion, since none of the specimens had corroded. Three specimens showed crevice corrosion under rust deposits: Material C (two specimens) and Material A (one specimen). The rust deposits apparently originated from the specimen racks or from the backing of clad samples that were also being tested. The crevice corrosion attack found on Materials C and A is consistent with the results of the crevice corrosion tests.

Crevice corrosion tests. The results of the crevice corrosion test are shown in Table 7. They show that the environments containing oxygen are the most severe for causing crevice corrosion attack. The three duplex SSs all suffered varying degrees of crevice corrosion in the two oxygen-containing environments. Material C was the most susceptible, followed by Material A. Material B showed attack only in Environment 4 (oxygen containing).

TABLE 7 — Crevice corrosion immersion test results

Test solution	Material phase	Code	No. of crevice attacks out of 40 crevice test sites		Depth and location of the crevice attacks[1,2,3]
1. Brine + CO_2	Solution	A	0		—
		B	0		—
		C	2		OO (HAZ)
	Vapor	A	0		—
		B	0		—
		C	0		—
2. Brine + CO_2 + O_2	Solution	A	1		x (weld)
		B		0	—
		C	4		O (weld) OOO (HAZ)
	Vapor	A	0		—
		B	0		—
		C	0		—
3. Brine + CO_2 + H_2S	Solution	A	0		—
		B		0	—
		C	0		—
	Vapor	A	0		—
		B	0		—
		C	0		—
4. Brine + CO_2 + H_2S + O_2	Solution	A	3		O △△ (weld)
		B	5		O (HAZ) OOO△ (weld)
		C		2	O x[2] (HAZ)
	Vapor	A	0		—
		B	0		—
		C	6		O O△△△△ (HAZ)

[1] O less than 1 mL (25.4 μm), O 1 to 5 mL (25.4 to 127 μm), △ 5 to 10 mL (127 to 254 μm), x 10 to 15 mL (254 to 381 μm).
[2] Under rust deposit away from crevice washer.
[3] Each symbol represents one crevice attack.

Material A also suffered crevice attack when exposed to the CO_2 containing solution (Environment 1). Two areas of attack occurred in the HAZ and both measured less than 0.001 in. (25 μm). In each case, the crevice corrosion attack was either in the HAZ or in the weld metal. There was no corrosion in the base metal portions.

The depth of attack when measured with a pointed micrometer ranged from less than 0.001 in. (25 μm) to between 0.010 and 0.015 in. (250 to 380 μm). The deepest attacks (0.010 to 0.015 in. (250 to 380 μm) occurred on Material A in Environment 2 (CO_2 + O_2) and on Material C in Environment 4 (CO_2 + H_2S + O_2), both oxygen containing environments. With Material C, the attack was under a deposit of rust away from the crevice washer.

Effects of test environments

The environments with oxygen (2 and 4) were the most severe for causing corrosion. The coating on the specimen test racks and on SCC loading fixtures suffered damage in these environments. Test Environment 4 (CO_2 + H_2S + O_2) was the most severe. The test-rack coating failed, exposing portions of the steel racks. The corrosion of the racks resulted in higher iron content in the test solutions. However, the coating was intact in areas where the test specimens were in contact with the racks.

In Test Environment 4, AISI 316 SS bosses suffered pitting and crevice corrosion. Pitting was evident on the flat surface of some bosses. The areas prone to crevice corrosion were the points of contact between bosses and test rings and the holes for the specimens. In Material C, Specimen 1, a rust deposit formed on the specimen from the hole in the fixture. This deposit resulted in crevice corrosion of the specimen. This observation corresponds with the results of the crevice corrosion test where Material C was found susceptible to crevice corrosion.

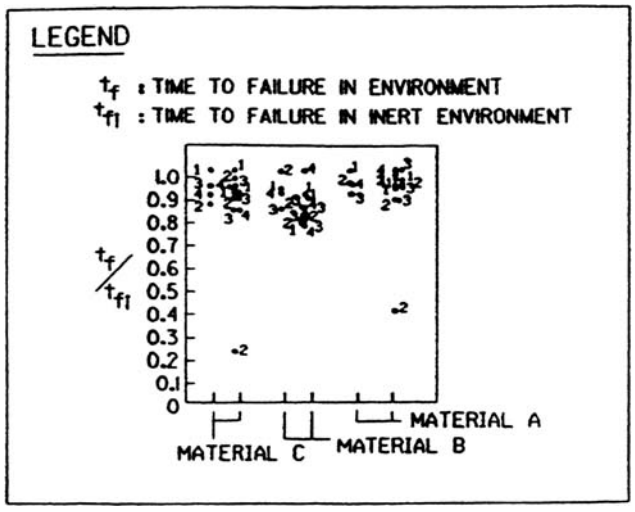


FIGURE 6 — Slow strain rate test results. The numbers indicate the following test environments: (1) synthetic brine/93 C/100 psi (0.69 MPa) CO_2; (2) synthetic brine/93 C/100 psi (0.69 MPa) CO_2 + 2 ppm O_2; (3) synthetic brine/93 C/100 psi (0.69 MPa) CO_2 + 1750 ppm H_2S; and (4) synthetic brine/93 C/100 psi (0.69 MPa) CO_2 + 1750 ppm H_2S + 2 ppm O_2.

Material A, Specimen 2 also had a rust deposit on it. The most probable source for this rust was from the steel backing of the clad crevice specimens that were also being tested.

Slow strain rate tests

Slow strain rate results are reported as a ratio of the time-to-failure in the test environment (T_f) to the time-of-failure in an inert environment (T_{fin}). The test results of the three alloys in four environments are summarized in Figure 6. Each test was run in triplicate at a strain rate of 10^{-6} s^{-1}. The ratio of 0.8 to 1.0 and the reproducibility of results indicate no susceptibility to SCC or SSC. The two low values noted were related to weld defects. At the completion of each test, the specimens were measured to determine elongation, and the fractured surfaces were examined with SEM. Material C was the most ductile and had the greatest elongation. Material A was the least ductile. The strain rate used in this test has been reported as being the most severe for SSC in H_2S saturated NaCl solution (NACE solution).[2] To determine the effect of strain rate, SSRTs were repeated at a slower strain rate of 5×10^{-7} s^{-1}. Again, there was no appreciable difference in T_f and T_{fin}.

SEM examination

Sections of fractured SSRT specimens were examined by SEM to confirm the absence of SCC and SSC.

Figure 7 indicates mechanical fracture occurred in Material C base metal tested in the CO_2 and H_2S environment. The presence of only dimpled structure and substantial necking on the fracture surface shows the absence of SCC and SSC. The Material C welded specimen did not exhibit SCC and SSC but did exhibit welded defects or lack of fusion (Figure 8).

Material B base and weld metals did not show any evidence of SCC or SSC because ductile failure was observed showing substantial necking and mechanical failure.

In contrast, Material A suffered an anomalous fracture. Figure 9 is a SEM fractograph of a welded specimen tested in a CO_2 + H_2S + O_2 environment. It appears that transgranular cracking with tear ridges occurred on the fracture surface, but it was a pure mechanical fracture because the morphology did not shorten T_f. The cracking may have been related to an inhomogeneity in the microstructure because it occurred only at

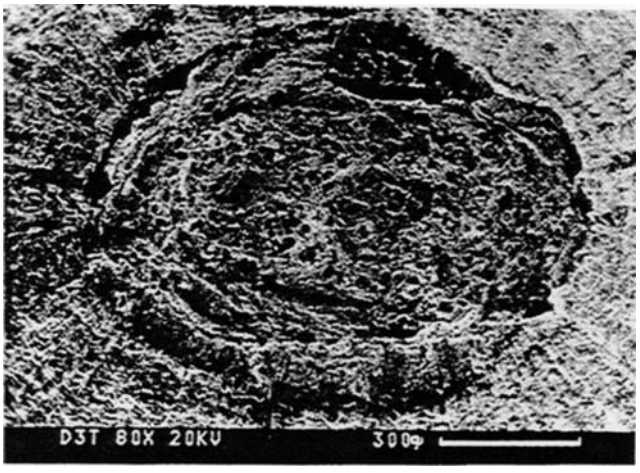


FIGURE 7 — Material C, base metal test environment CO_2 and H_2S SEM fractograph.

H_2S - SEM fractograph.

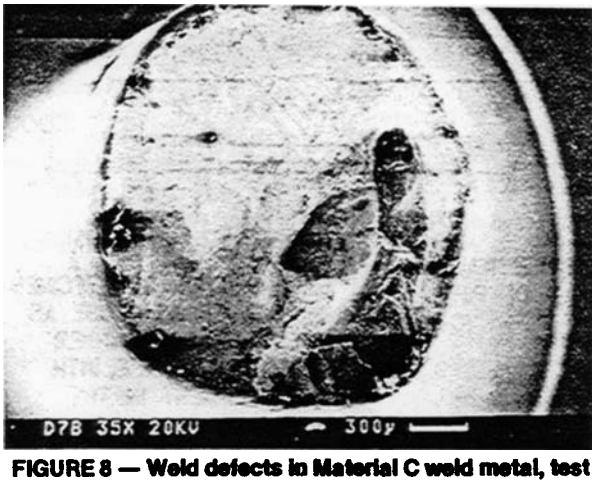


FIGURE 8 — Weld defects in Material C weld metal, test environment CO_2 and O_2 SEM fractograph.

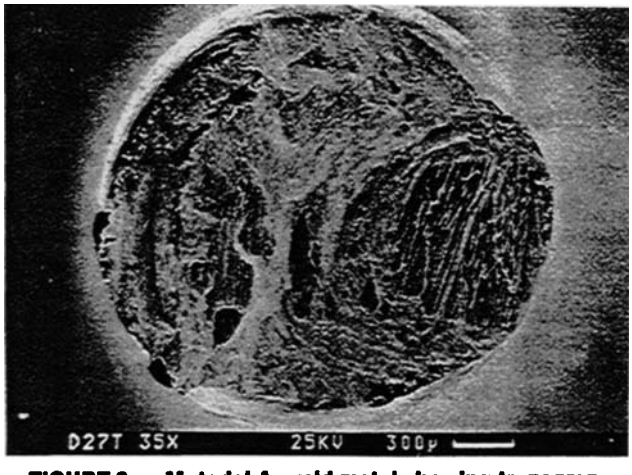


FIGURE 9 — Material A, weld metal showing transgranular cracking, test environment CO_2, H_2S, and O_2, SEM fractograph.

the center of the specimen. Even the pure CO_2 containing solution promoted an anomalous cracking morphology. Therefore, this cracking mode was induced by mechanical fracture. No pitting attack was detected on any of the specimens.

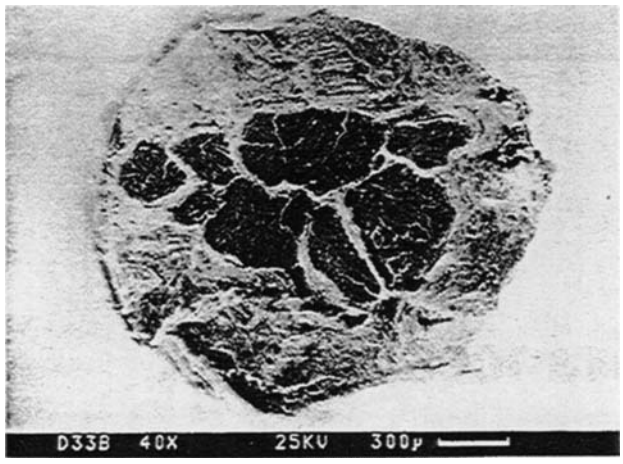


FIGURE 10 — Material A, base metal, showing anomalous fracture mode, test environment CO_2, H_2S and O_2 SEM fractograph.

Charpy V-notch tests (low temperature toughness evaluations)

The results of low temperature toughness tests on as-welded materials are shown in Table 4. These data show that Material C has excellent toughness in the base material, HAZ, and weld when welded with the GTAW process. (Note: Materials C, D, E, and F have the same UNS designation). Weld toughness with the SMAW process is significantly less but may be adequate for most applications.

Furthermore, Material C shows a good tolerance for variations in weld parameters without detriment to the properties.

Material B has excellent base metal toughness. However, the weld has very low toughness. The HAZ showed a sharp drop in toughness that may indicate a sensitivity to heat input.

Material A has very low toughness in the base material, HAZ, and weld.

As-welded hardness evaluation

The hardness test results are shown in Table 5. These tests were performed as part of a standard metallurgical evaluation and to verify compliance with NACE Standard MR0175.[5] This standard limits the hardness of duplex SSs to HRC 28 maximum.

Material C (as-welded) should meet the NACE criterion, but Material B showed marginal hardness and Material A was too hard.

Welding process/filler material evaluation

Evaluation of welding processes and filler materials for duplex SSs was performed by observing the welding operation, recording weld data for each weld, recording welder comments, reactions, and problems, and evaluating the results.

The recommended welding process for duplex stainless is GTAW for the entire weld. This is based on the following:

1. The anticipated maximum wall thickness of the Endicott pipeline was 0.312 in. (0.8 cm).
2. Welders can readily adapt to duplex stainless using the GTAW process.
3. The CVN toughness at −46 C of Material C welds is excellent with the GTAW process (Table 4).

The SMAW process is not recommended at this time for the following reasons:

1. The average welder has difficulty adjusting to the SMAW electrodes currently available. It is estimated that a welder previously qualified for austenitic SS would require two to five days training to become reasonably proficient.
2. The CVN toughness obtained with SMAW is significantly less than with GTAW (Table 4).
3. The additional grinding to remove slag and excess crown between passes would cancel any theoretical advantages in productivity that SMAW offers over GTAW.
4. The reject rate from radiographic inspection is anticipated to exceed acceptable limits based on inclusions occurred in spite of extraordinary grinding and interpass cleaning.

GTAW filler materials showed no significant differences in weldability of the various types, grades, and manufacturers tested.

SMAW electrodes showed significant differences in weldability between manufacturers. These differences are considered to be the result of coating formulations.

Ferrite-austenite contents of the test welds are shown in Table 5. Material A pipe material showed a very nonhomogeneous structure. Some portions showed the expected "wrought" structure. However, other areas exhibited an "as-cast" structure. The ferrite/austenite ratio was generally within the desired range of 40 to 60% ferrite, except for the HAZ which showed 70% ferrite. The ferrite matrix of Material A etched darker than the other types of duplex stainless tested. High magnification examination indicated the possibility of other phases within the ferrite. No further effort was made to identify these phases since this material was essentially eliminated for arctic use because of its inadequate toughness.

Material B showed acceptable ferrite/austenite contents except for the HAZ, which contained approximately 75% ferrite.

The UNS 31803 alloys represented by Materials C, D, E, and F showed satisfactory ferrite/austenite contents in the base material, HAZ, and weld.

Conclusions

1. Material C (which conforms to UNS 31803) has the optimum properties for the Endicott service conditions.
2. The three duplex SS alloys and their welds were not susceptible to SCC or SSC in simulated oilfield environments after six months of immersion of stressed specimens and by SSRTs.
3. The three alloys were susceptible to crevice corrosion in oxygen-containing environments. Material C (UNS 31803) was slightly susceptible to crevice corrosion in the environments containing CO_2 and brine.
4. Material C (UNS 31803) has excellent toughness at 46 C as measured by the CNV test. The weld and HAZ of this material also have excellent toughness when welded with the GTAW process.
5. Material C (UNS 31803) SSs have good tolerance for variations in welding parameters without degradation of weld and HAZ toughness or microstructure.
6. Materials A and B did not have satisfactory CVN toughness in the welds at −46 or −29 C.
7. Duplex SSs are readily welded by the GTAW process, but the SMAW process is difficult for the average welder.
8. Filler materials (GTAW and SMAW) should contain 7 to 9% nickel to achieve welds having optimum toughness and microstructure when in the as-welded condition.
9. The hardness of Material C (UNS 31803) was satisfactory; Material B was marginal; and Material C was too hard.

Acknowledgments

The authors thank the management of Standard Oil Production Company and Standard Alaska Production Company for their permission to publish this paper.

References

1. D. B. Anderson, *Galvanic and Pitting Corrosion—Field and Laboratory Studies, STP 576*, p. 231, ASTM, Philadelphia, PA, 1976.
2. M. Onyama, *Materials for Energy Systems*, Vol. 5, Nov. 2, 1983.

[5]MR0175, "Sulfide Stress Cracking Resistant Metallic Materials for Oilfield Equipment."

Copyrighted Materials
Copyright © 1996 NACE International Retrieved from www.knovel.com

Corrosion Behaviour of 25%Cr Duplex Stainless Steel in CO_2-H_2S-Cl^- Environments

Shiro Mukai, Hiroshi Okamoto, Takeo Kudo and Akio Ikeda

Sumitomo Metal Industries, Ltd., Central Research Laboratories
3, 1-chome, Nishinagasu-Hondori, Amagasaki, Japan

ABSTRACT

Effects of environmental factors and alloying elements on corrosion behaviors of duplex stainless steels were investigated in CO_2-H_2S-Cl^- environments, and also the corrosion resistance of DP3 (Sumitomo duplex stainless steel, 25Cr-7Ni-3Mo) which has been developed for hot sea water heat exchangers was compared with that of other materials.

The corrosion resistance of duplex stainless steels increased with the increase of Cr, Ni and Mo contents in CO_2-H_2S-Cl^- and CO_2-Cl^- environments. SCC occurred on duplex stainless steels with Ni content below 6% even in the H_2S free conditions at high temperature. Low temperature aging treatment increased the susceptibility to SCC of duplex stainless steels with lower Ni content.

DP3 is resistant to SCC at least up to the temperature of 250°C in CO_2-Cl^- environments, though the application of this alloy to H_2S environments is limitted.

I. INTRODUCTION

There is considerable interest in exploiting deep, high-pressure reservoirs. The environments encountered in such wells usually contain substantial amount of hydrogen sulfide (H_2S), carbon dioxide (CO_2) and salt water. It is known that these environments are very severe and iron base low alloys are not acceptable because of high corrosion rate and/or stress corrosion cracking (SCC). Now as an alternative to steels, duplex stainless steels, high nickel stainless steels and nickel base alloys are being evaluated for their corrosion

© 1983 *J. Materials for Energy Systems* Courtesy ASM International (formerly American Society for Metals)

resistance to various sour well conditions [1~6]. In these materials, duplex stainless steels are characterized as more resistant alloys than iron base low steels and cheaper alloys than high nickel ones. Duplex stainless steels, however, have been originally developed for chemical industries. So there is limited information available for the mechanical properties and the corrosion behaviors in sour well environments on duplex stainless steels as tublar goods.

In this work, effects of environmental factors and alloying elements on corrosion behaviors of duplex stainless steels were investigated, and also the corrosion resistance of DP3 which has been developed for hot sea water heat exchangers was compared with that of other materials in CO_2-H_2S-Cl^- environments. The criteria for the application of the alloy to sour wells were discussed.

II. EXPERIMENTAL

1. Materials

The effect of alloying composition of duplex stainless steel on the corrosion behavior was examined with 17 kg vacuum melted materials as shown in Table 1. The billets were forged, hot-rolled to 10 mm in thickness, heat-treated at 1100°C for 30 minutes and then water-quenched. They were cold-worked by 30% in thickness to increase the mechanical strength.

Table 1 Materials tested for the effect of alloying elements on corrosion behavior of α-γ duplex stainless steel (%)

C	Si	Mn	P	S	Ni	Cr	Mo	N
≤0.02	0.4	0.9	≤0.005	≤0.005	4.5 ~10	19 ~26	0 ~3	0.15

Corrosion properties of DP3 were examined on sheets and tubings which was melted commercially. The nominal chemical composition is given in Table 2. Type 317L was also prepared in order to be compared with the corrosion behavior of DP3.

Table 2 Materials tested

	C	Si	Mn	P	S	Ni	Cr	Mo	Cu	W	N
DP3	0.02	0.5	0.8	≤0.02	≤0.02	7.0	25.0	3.0	0.5	0.3	0.15
Type 317L	0.01	0.66	1.56	0.027	0.001	13.0	18.7	2.9	0.09	—	0.03

2. Experimental Method

SCC tests were conducted using notched and smooth 2 x 10 x 75 mm specimens. They were stressed to 100% of their 0.2% proof strength (yield strength) by both three and four point bend beam holders shown in Figs. 1 and 2. The specimens were

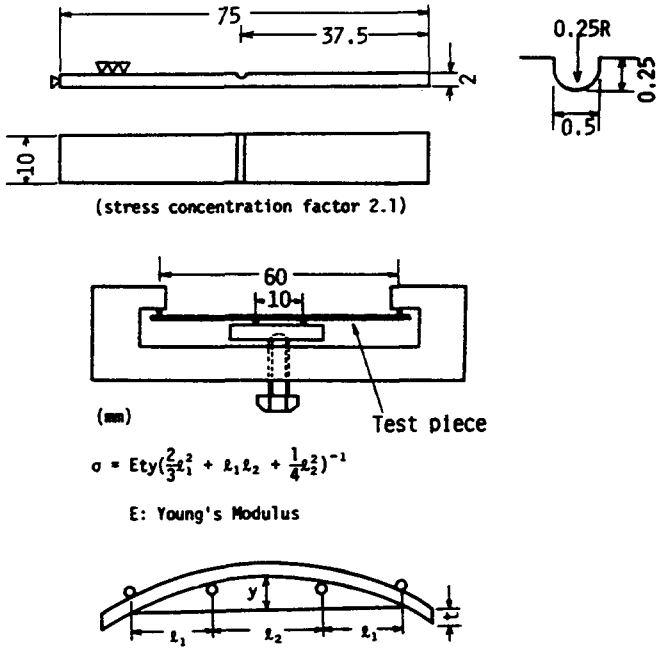


Fig. 1 4 point beam bend test method

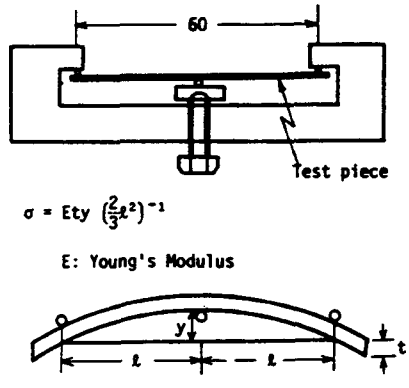


Fig. 2 3 point beam bend test method

stressed transverse to the original rolling direction, except for the investigation of rolling direction. Uniaxial constant load SCC tests were performed on smooth tensile specimen shaped from cold-worked seamless tubings. C ring tests were also performed for the examination of actual tubings.

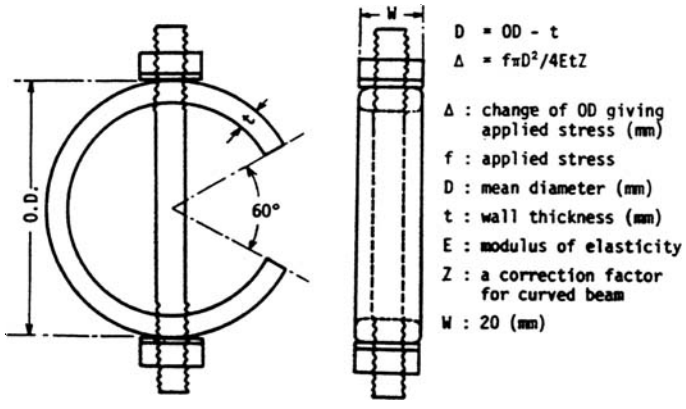


Fig. 3 C-ring test method by ASTM G38-73

Effect of environmental factors on the susceptibility to SCC and the weight loss corrosion was examined in CO_2-H_2S-Cl^- environments. The experiments were conducted in autoclaves of 10 liters in capacity shown in Fig. 4. Test procedures are as follows. The specimens were placed in the autoclave containing test solution. The autoclave was purged with nitrogen to deaerate the solution, and then vacuum was maintained. Finally, the autoclave was purged with H_2S and/or CO_2, and pressurized to the desired partial pressure before heating. The test was conducted mainly for 336 hours (2 weeks). The test solution was stirred all the time during the test duration. After the corrosion test, optical examination at 30X was done to detect SCC. In addition, the weight loss by corrosion was measured after descaling in NaOH + $KMnO_4$ solution. Occasionally, specimens were mounted in epoxy and further examined at higher magnifications. Uniaxial constant load SCC tests were con-

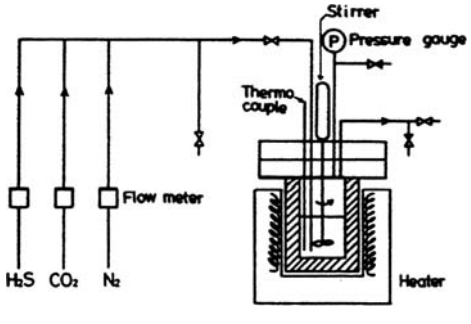


Fig. 4 Corrosion test autoclave apparatus

ducted in 15 liter sized autoclave with lever type loading system shown in Fig. 5. The preparation procedures were same as those described above.

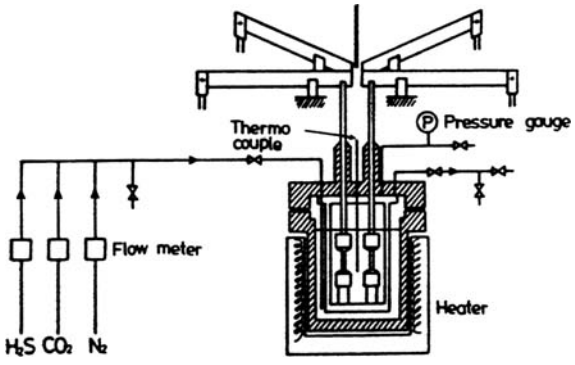


Fig. 5 Constant load type SCC test apparatus

III. MECHANICAL PROPERTIES AND MICROSTRUCTURE OF COLD WORKED DP3

Mechanical properties of DP3 were compared with Type 317L as shown in Fig. 6. The yield strength of annealed DP3 is higher than that of Type 317L. DP3 can easily attain a higher strength level by a relatively slight cold working in comparison with Type 317L.

The microstructure of DP3 consists of two phases, approximately the same amount of ferritic (α) and austenitic (γ) phases. After cold working, the structure becomes more anisotropic with elongated lamellae of ferrite and austenite in rolling direction as shown in Fig. 7.

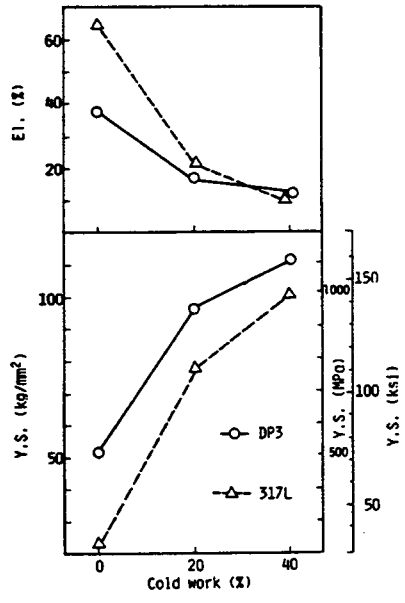


Fig. 6 Effect of cold work on mechanical properties

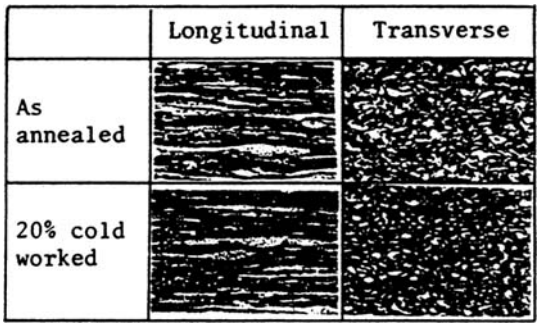


Fig. 7 Microstructure of DP3

IV. CORROSION PROPERTIES IN CO_2-H_2S-Cl^- ENVIRONMENTS

IV-1. Influence of Alloying Elements on Corrosion Behavior of Duplex Stainless Steels

There are few studies on the effect of alloying elements of duplex stainless steels on corrosion behaviors in CO_2-H_2S-Cl^- environments. So, at first, the effect of basic alloying compositions on the corrosion behavior was studied. Fig. 8 shows the effect of Cr, Ni and Mo on the corrosion rate in 25% NaCl - 30 atm CO_2 - 200°C system. Cr and Ni had no significant effect on the corrosion rate. SCC was, however, observed on duplex stainless steels containing relatively lower Cr and Ni as shown in Fig. 9. On the other hand, the

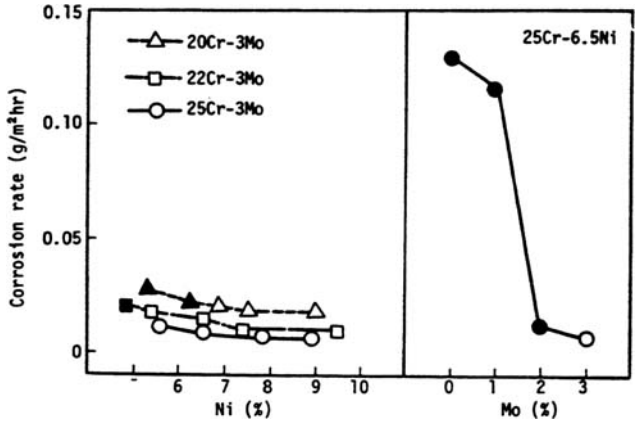


Fig. 8 Effect of Cr, Ni and Mo content on general corrosion and SCC susceptibility (25% NaCl, 30 atm CO_2, 200°C,30% C.W.)

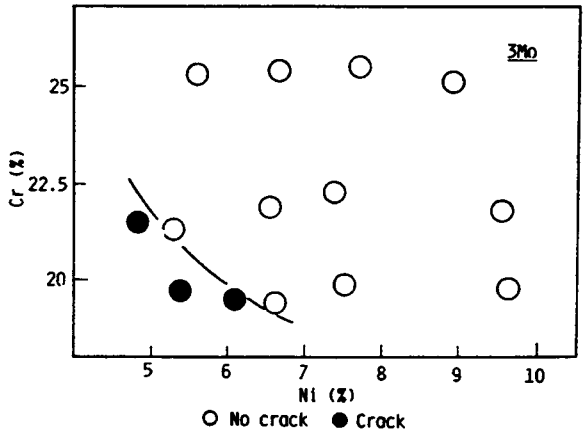


Fig. 9 Effect of Ni and Cr content on SCC susceptibility
(25%NaCl, 30 atm CO_2, 200°C, 30% CW)

increase of Mo content decreased drastically both the corrosion rate and the susceptibility to cracking. It was observed that the alloys below 2% Mo suffered cracking even in the H_2S free condition at high temperature. The result shows that duplex stainless steels containing more than 3% Mo is preferable for the application to high temperature CO_2-Cl^- environments.

It is said that H_2S in CO_2-Cl^- environments remarkably increases the SCC susceptibility of duplex stainless steels [4]. In this work, the presence of 0.5 atm H_2S in 25%NaCl-30 atm CO_2 environment at 200°C caused cracking on all of the alloys shown in Fig. 9. As the concentration of Cl^- decreased, the SCC susceptibility decreased. Fig. 10 shows the test result in the case of 0.1% NaCl solution. It was also shown that Ni content above 6% was necessary to maintain the SCC resistance in this environment.

Next, the effect of low temperature aging treatment at 350°C on the corrosion resistance was investigated in consideration of long term usage of tubings at high temperature. Figs. 11 and 12 show the SCC test results in CO_2-Cl^- and CO_2-H_2S-Cl^- environments respectively. SCC susceptibility was increased by the aging treatment. However, high Ni containing alloys above about 6% Ni maintained the resistance to cracking. It is suggested from these results that DP3, which is composed of 25%Cr, 7%Ni and 3%Mo, has good corrosion

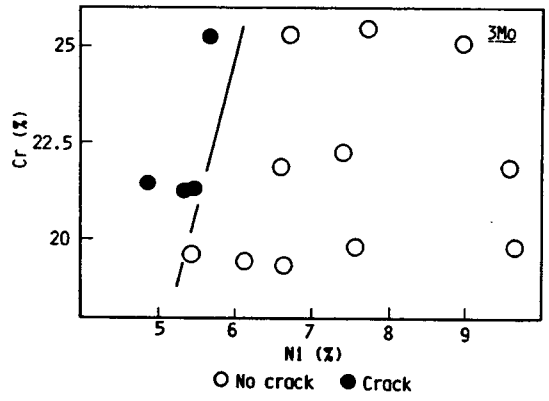


Fig. 10

Effect of Cr and Ni on SCC susceptibility ($0.1\%NaCl, 0.5atm\ H_2S$, $30atm\ CO_2$, 200°C, 30% C.W.)

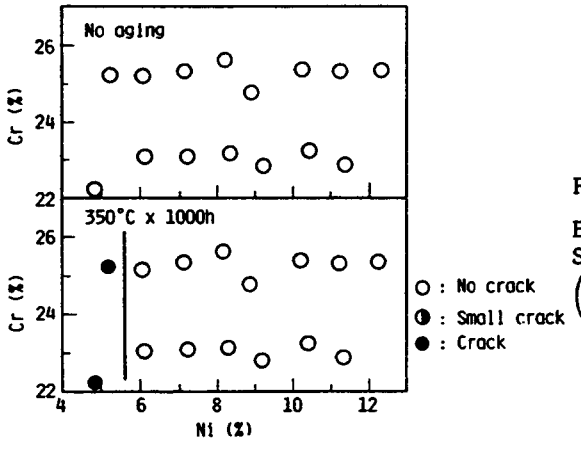


Fig. 11

Effect of aging on SCC susceptibility ($25\%NaCl, 30atm\ CO_2$, 200°C, 30% C.W.)

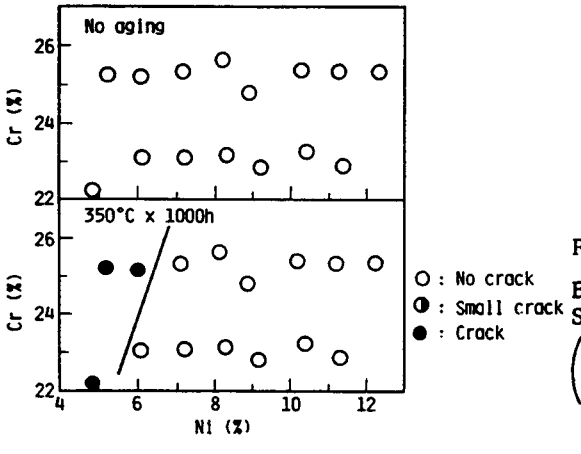


Fig. 12

Effect of aging on SCC susceptibility ($1\%NaCl, 0.1atm\ H_2S$, $30atm\ CO_2$, 200°C, 30% C.W.)

resistance in high temperature CO_2 environments even after low temperature aging.

Ⅳ-2 Corrosion Behavior of 25%Cr Duplex Stainless Steel DP3

1. NACE TM-01-77 test result

The corrosion resistance of DP3 with various strengths ie, as annealed and cold worked materials, was examined by NACE TM-01-77 test method. In the condition without carbon steel coupling, the threshold stress of cracking was higher than the yield strength. The carbon steel coupling decreased the threshold stress to about 70% of the yield strength in the case of cold worked DP3. The results suggest that the cracking of cold worked DP3 in NACE solution at room temperature is due to hydrogen embrittlement.

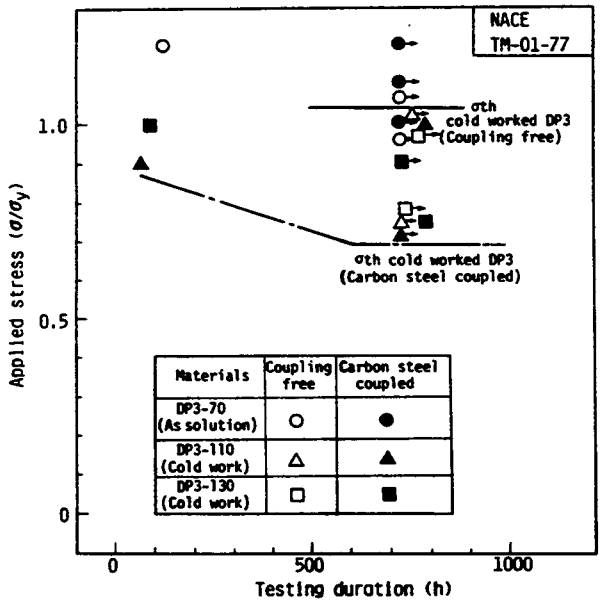


Fig. 13 SCC properties of DP3 by NACE TM-01-77

2. CO_2-H_2S-Cl^- environments at high temperature

(1) Effect of environmental factors

Corrosion resistance of duplex stainless steels is

changeable depending upon the environmental conditions. The effect of partial pressure of H_2S (P_{H_2S}), temperature and Cl^- concentration on corrosion resistance of DP3 was examined in detail. Fig. 14 shows the effect of P_{H_2S} and temperature on SCC of annealed and cold worked DP3 in 5%NaCl-30atmCO_2-H_2S environments. 7% cold worked DP3 has P110 grade strength. The corrosion behavior of Type 317L was also studied in order to be compared with that of DP3. The test results after 96 hour immersion shows the SCC susceptibility of annealed DP3 is lower than that of cold worked DP3, although it is not so clear in the test result by the specimens without notch. SCC resistant region of DP3 on P_{H_2S} and temperature was wider than that of Type 317L, although these alloys have almost the same Mo content. The poor corrosion resistance of Type 317L is considered to be due to the lower Cr content of this alloy. The selective corrosion of α phase was observed on cold worked DP3 between 60°C and 100°C under the condition of 0.1 atm P_{H_2S}. Fig. 15 also shows the test result of DP3 with

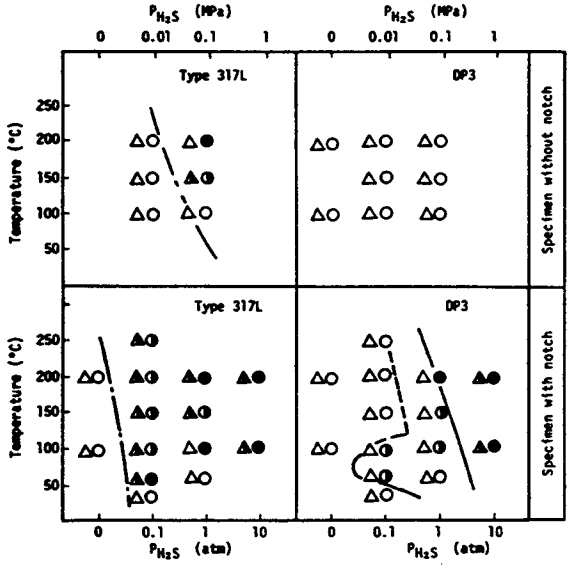


Fig. 14 Effect of temperature and partial pressure of H_2S(P_{H_2S}) on SCC susceptibility of Type 317L and DP3 (5%NaCl-30atm CO_2-96hr)
Δ annealed ○ Cold worked (P110 grade)
Δ○ : Cracking free, ▲◐ ; Small crack or
▲● : Cracking pitting

V140 grade strength in 25%NaCl-30atmCO_2 environments. There exists a critical limit for cracking in terms of P_{H_2S} and temperature. As the temperature was raised from 100°C to 200°C, the critical P_{H_2S} decreased from between 0.1atm and 0.5atm to below 0.1atm. The corrosion rate was below 0.05 mm/y in all the tested environments.

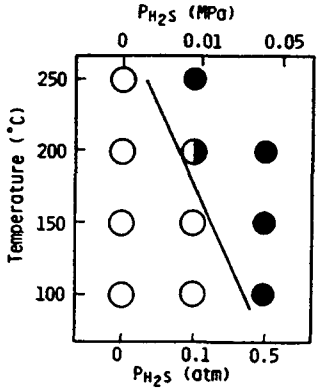


Fig. 15 Effect of partial pressure of H_2S(P_{H_2S}) and temperature on SCC susceptibility of DP3 (30atmCO_2, 25%NaCl)

Fig. 16 shows the effect of P_{H_2S} and Cl^- concentration on corrosion behavior of DP3 with V140 grade strength in 30atmCO_2-200°C system. The SCC susceptibility also depends on the concentration of Cl^-. If the Cl^- concentration was lower than 0.1%NaCl, SCC did not occur even in the presence of 0.5atm P_{H_2S}.

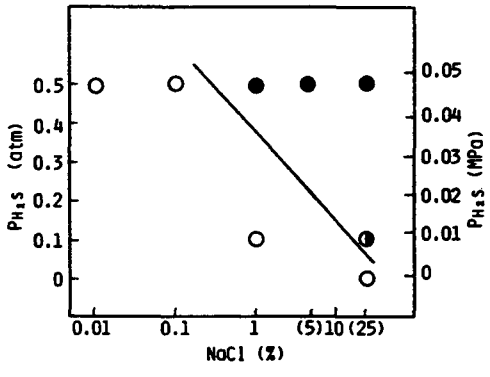


Fig. 16 Effect of partial pressure of H_2S(P_{H_2S}) and Cl^- concentration on SCC susceptibility of DP3 (200°C-30atm CO_2,40% C.W.)

(2) Effect of metallurgical factors

Effect of cold work and rolling direction on SCC susceptibility was investigated in the severe condition of 10atm-H_2S-10atm CO_2-150°C. The test result is given in Fig. 17.

The annealed DP3 did not crack under the applied stress equal to the yield strength. The cold working drastically decreased the threshold stress. The threshold stress of longitudinal direction existed around 80% of the yield strength, while that of transverse direction decreased below 60%. Figs. 18 and 19 show the results on the specimens shaped from the tubings by the uniaxial constant load SCC tests. The similar tendency was also observed. Although the threshold stress in terms of the ratio threshold stress (σth)/yield strength (σ_y) was drastically decreased by cold work, the threshold stress in the representation of applied stress was not so different by cold work as shown in Fig. 18. The cracks of DP3 were observed to propagate mainly through α-phase and to be inhibitted sometimes by γ-phase as shown in Fig. 20. From these observation, it is considered that the lower SCC resistance of transverse direction is caused by the configuration of γ grains which has keying effect [7].

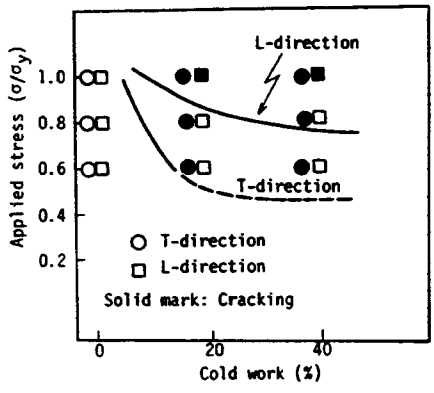


Fig. 17 Effect of cold work and rolling directions on SCC susceptibility of DP3 (10atmH_2S-10atmCO_2-5%NaCl-150°C-96hr, 3 point beam bend test, smooth specimen)

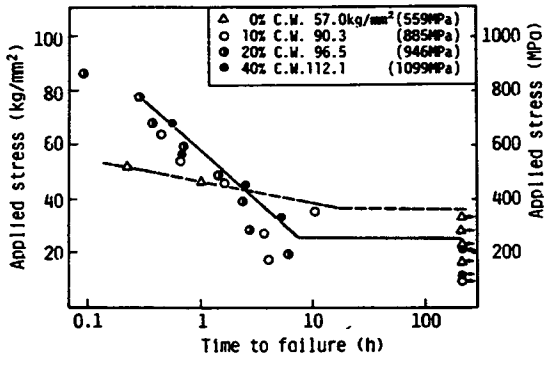


Fig. 18 Effect of cold work on SCC susceptibility of DP3 by uniaxial tensile test (20%NaCl 10atm H_2S 10atm CO_2 150°C)

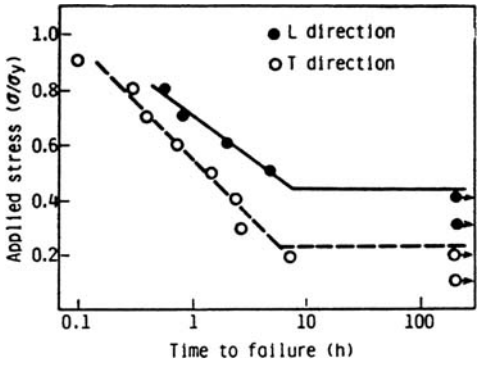


Fig. 19 Effect of rolling direction on SCC susceptibility of DP3 by uniaxial tensile test (20%NaCl, 10atmH_2S-10atmCO_2-150°C, 20% C.W.)

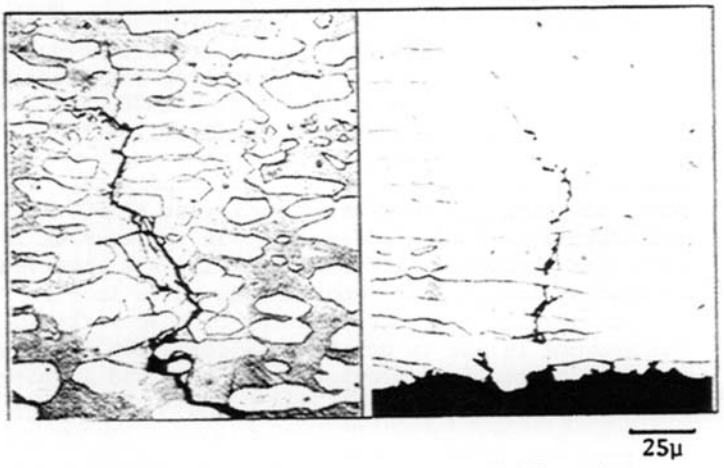


Fig. 20 Observation of cracking of DP3 (20%NaCl, 10atm H_2S, 10atm CO_2, 150°C)

C ring tests were also performed to confirm the effect of the yield strength of DP3 tubings on SCC in the severe condition of 10atm H_2S-10atm CO_2-225°C. Fig. 21 shows that the SCC susceptibility of DP3 had same cold work dependency as that of the test results on sheets shown in Fig. 17. The annealed DP3 did not crack under the applied stress equal to the yield strength even after 30 days. The threshold stress of cold worked DP3 decreased below 40% of the yield strength. There were observed no significant difference between 10% and

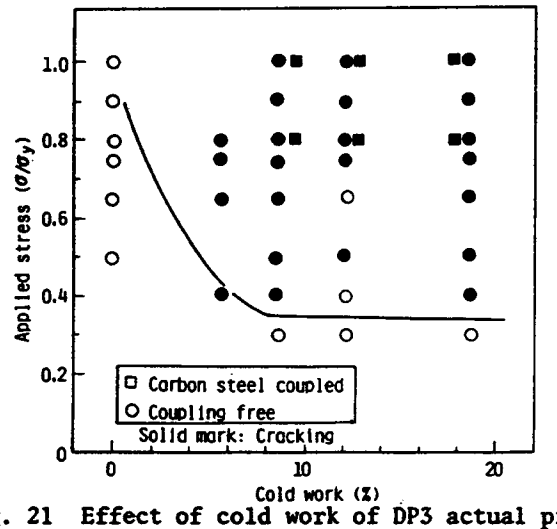


Fig. 21 Effect of cold work of DP3 actual pipes on SCC susceptibility by C ring test method (10atm H_2S, 10atm CO_2, 225°C, 7%NaCl+0.9%$MgSO_4$ +0.4%$CaCl_2$+0.6%$MgCl_2$+0.2%KCl)

20% cold worked materials. In this condition, the carbon steel coupling had no preventing effect of SCC at the high temperature of 225°C in Fig. 21. In the case of 150°C, however, the threshold stress of cracking was observed to be increased by carbon steel coupling as shown in Fig. 22. This result suggests that the cracking of cold worked DP3 at high temperature is due to active pass corrosion, although this cathodic protection effect was not observed in more severe condition as shown in Fig. 21.

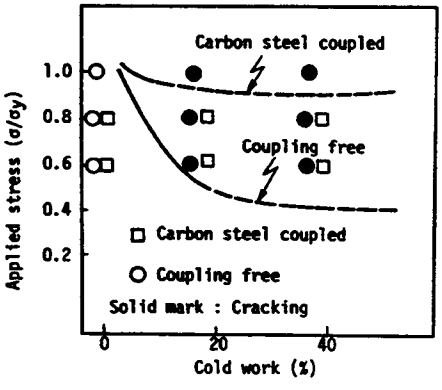


Fig. 22

Effect of iron coupling on SCC susceptibility of DP3 (10atm H_2S-10atm CO_2-5%NaCl-150°C-96hr, 3 point beam bend test, smooth specimen)

V. DISCUSSION

1. Corrosion Resistance of Duplex Stainless Steel DP3 in CO_2-Cl^- Environments

It has been clarified that corrosion resistance in CO_2-Cl^- environments mainly depends on Cr content of steels and 9Cr-1Mo steel is resistant below 100°C and 13Cr steel below 150°C [9]. This work showed that the duplex stainless steel DP3 had high resistance up to 250°C in CO_2-Cl^- environments. It seems that the formation of Cr-oxide film has an important roll to increase the corrosion resistance in CO_2-Cl^- environments [10]. It was proved, on the other hand, from this study that Mo in duplex stainless steels increases notably both the resistances to general corrosion and cracking, and Mo content more than 3% is necessary to sustain the corrosion resistance in high temperature CO_2-Cl^- environments. Duplex stainless steels with 3%Mo which contain Ni less than 6% was also proved to have high susceptibility to cracking, especially when they were aged at 350°C for 1000 hours.

Asphahani [1] showed that 19Cr-5Ni-3Mo, 22Cr-5.5Ni-3Mo and 25Cr-5Ni-3Mo which were cold worked by 50% suffered SCC in 18%NaCl + 9%$CaCl_2$ + CO_2 environment at 177°C, while 21Cr-7Ni-2.5Mo did not. It shows that duplex stainless steels with higher Ni content is desirable for the application to high temperature CO_2-Cl^- conditions.

DP3 which contains 7%Ni has good corrosion resistance at least up to 250°C in CO_2-Cl^- environments in the case of yield strength of 140 ksi grade as shown in Fig. 15.

2. Corrosion Resistance of Duplex Stainless Steel DP3 in CO_2-H_2S-Cl^- Environments

Generally speaking, duplex stainless steels are more susceptible to SCC than nickel base alloys in the presence of H_2S, and the application of duplex stainless steels to sour wells is limited.

In this study, however, annealed DP3 was shown to be more resistant to SCC than the cold worked material, and was estimated to be acceptable below 1 atm P_{H_2S} in 5%NaCl at the temperature below 200°C, even though the confirmation through long term tests are necessary.

Cold worked DP3 has less corrosion resistance than

annealed one in the presence of H_2S, so the application is limitted to the lower P_{H_2S} conditions, for example, below 0.1 to 0.5 atm at 100°C, or below 0.1 atm at 200°C in 25%NaCl solution. As the corrosion resistance also depends on the concentration of Cl^- the critical limits of P_{H_2S} and temperatures are changeable and increase with the decrease of Cl^- concentration. At low temperatures between 60°C and 100°C in 0.1 atm P_{H_2S} environment, preferential attack of α-phase was observed as shown in Fig. 14. The similar phenomena for 22Cr duplex stainless steel was reported by Oredsson et al.[4]. It is not so clear why the selective corrosion occurred, but it is supposed that the stability of passive film on stainless steel is affected by the little variation of solution condition, for example, the change of H_2S concentration in solution by the interaction between temperature and P_{H_2S}.

The effect of alloying elements of duplex stainless steels with 3%Mo on SCC was studied. There were no significant difference of these alloys in severe environments. As the test condition became mild, the effect of alloying elements on SCC was observed. For example, duplex stainless steels with 3%Mo which contain Ni more than 6% was proved to have resistance to cracking in 0.1%NaCl-0.5atm H_2S-30atm CO_2-200°C environment. DP3 which contains 7%Ni has good corrosion resistance in such a mild condition.

VI. CONCLUSION

1. Duplex stainless steel DP3 has an excellent workhardening property compared with austenitic Type 317L stainless steel, and can be applied for the high strength OCTG up to 140 ksi.

2. DP3 is resistant to SCC in CO_2-Cl^- environment at least up to the temperature of 250°C.

3. The presence of H_2S and cold work make DP3 more sensitive to cracking. The application of cold worked DP3 is limited to low P_{H_2S}. The critical P_{H_2S} for cracking increased with the decrease of temperature, ie below 0.1atm at 200°C and between 0.1atm and 0.5atm at 100°C. Its value was, however, adversely decreased below 0.1atm between 60°C and 100°C.

4. Cr, Ni and Mo in duplex stainless steels increase the corrosion resistance both in CO_2-Cl^- and CO_2-H_2S-Cl^- environments. Duplex stainless steels which are composed of

3%Mo and Ni content more than 6% maintained the corrosion resistance in high temperature CO_2-Cl^- conditions even after low temperature aging treatment.

Acknowledgements

The authors would like to thank Dr. K. Nishioka, General Manager of Central Research Laboratories, Dr. F. Terasaki and Dr. T. Moroishi, Deputy General Manager of Central Research Laboratories for their helpful advices and supports. We also acknowledge Y. Nakamura, H. Kusagi and T. Nakagawa for their experimental work.

REFERENCES

1. A.I. Asphahani; Corrosion/80, Paper No. 12

2. Günter Herbsleb, Rolf K Pöpperling; Corrosion/80, Paper No. 13.

3. S.O. Bernhardsson, J. Oredsson, M. Tynell; Corrosion/80 Paper No. 14.

4. Jan Oredsson, Sven Bernhardsson; Corrosion/82, Paper No. 126.

5. B. Lefebvre et al.; Corrosion/82, Paper No. 128.

6. T. Kudo, H. Miyuki, H. Okamoto, J. Murayama and T. Moroishi; Corrosion/82, Paper No. 127

7. H. Nagano, T. Kudo, Y. Inaba and M. Harada; Extrait de Métaux, Corrosion Industrie, mars 1981, No. 667.

8. J.W. Flowers, F.H. Beck and M.G. Fontana; Corrosion 19 (1963), p.186.

9. A. Ikeda and M. Tanaka: Tetsu-to-Hagane 66 (1980), S383.

10. A. Ikeda et al.; to be published.

Copyrighted Materials
Copyright © 1996 NACE International Retrieved from www.knovel.com

STRESS CORROSION CRACKING SUSCEPTIBILITY OF DUPLEX STAINLESS STEELS IN SOUR GAS ENVIRONMENTS

P. R. Rhodes (Shell Development Company)
G. A. Welch (Shell Oil Company)
L. Abrego (Shell Development Company)

ABSTRACT

The stress corrosion cracking (SCC) susceptibility of duplex stainless steel tubulars in oxidant-free NaCl/H_2S solutions simulating downhole sour gas well environments has been evaluated. The alloys tested had compositions of 21-25% Cr, ~ 5% Ni, and ~ 3% Mo and included both annealed and cold reduced products.

The SCC tests were conducted in autoclaves pressured with H_2S/CO_2 and $H_2S/CO_2/CH_4$ gas mixtures. Test specimens included a variety of statically loaded specimens (U-bends, C-rings, notched C-rings, tensiles, and pre-cracked double cantilever beams) as well as dynamically strained specimens. SCC susceptibility increased with yield strength, comparing specimens stressed to their yield point.

In Cl^-/H_2S solutions free of oxidants, SCC initiated under anodic (pitting corrosion) rather than cathodic conditions, similar to a Cl^-/H_2S synergism promoting both pitting and active corrosion. SCC susceptibility was measured over the full range of test temperatures: 23°C to 288°C. The composition-temperature region of SCC immunity has been partially defined and is largely dependent upon minimizing the H_2S partial pressure, NaCl content, and the acidity established by the CO_2 partial pressure. Temperature is shown to be a complex variable and can be rationalized by a number of mechanistic hypotheses.

© 1983 *J. Materials for Energy Systems* Courtesy ASM International (formerly American Society for Metals)

INTRODUCTION

A number of duplex stainless steels having an approximate composition range of 21-25% Cr, 5% Ni, 3% Mo, and 0.15% N are under evaluation for use as a corrosion resistant alloy in high pressure gas wells and surface lines. Typically, corrosive solutions contain NaCl and dissolved H_2S and CO_2 but no oxidant. Such gas is referred to as "sour", due to the presence of H_2S.

One of the attractive features of these duplex alloys is strength. As annealed, yield strengths can range from 450 to 620 MPa (65 to 90 ksi). Cold worked seamless pipes can have yield strengths in excess of 1100 MPa (160 ksi), with several manufacturers marketing downhole tubing at minimum yield strength up to 960 MPa (140 ksi). Cold worked wirelines to 1200 MPa (175 ksi) are also available.

The major limitation to the application of these duplex alloys appears to be their susceptibility to stress corrosion cracking (SCC) which is aggravated by a unique synergism between Cl^- and H_2S. This paper addresses the many experimental variables than can influence SCC susceptibility, including test procedures, in aqueous Cl^-/H_2S solutions.

EXPERIMENTAL PROCEDURES

Alloys

A number of annealed and cold worked seamless tube samples have been tested. Samples were obtained from six manufacturers as representative commercial product. Four commercial compositions were represented; all have the approximate composition: 21 to 25% Cr, ~ 5% Ni, ~ 3% Mo, and 0 or 0.14% Ni. In addition, an experimental duplex alloy having higher alloy content was tested. With one exception (identified as "alternate route"), all tube products were produced by a hot extrusion/cold forming route. Microstructures were typically ~ 50% ferrite, with a highly elongated grain due to hot working procedures. The final cold reduction varied from 0% to 50%, and the corresponding yield strength ranged from 520 MPa (75 ksi) to 1120 MPa (162 ksi). Alloy designation is by mill (designations A through F) and by yield strength (σ_y) and, when appropriate, by tube dimensions. Table 1 lists compositions and mechanical properties of test alloys.

TABLE 1. CHARACTERISTICS OF DUPLEX ALLOY TUBULAR PRODUCTS

NORMAL COMPOSITION[1], %	MILL DESIGNATION	FINAL COLD REDUCTION, % CR	LONGITUDINAL TENSILE PROPERTIES		
			σ_y, MPa	σ_u, MPa	% El
22 Cr-5.5 Ni-3.0 Mo-0.14 N	B	0	520	770	32
		17	~ 840		
		~ 18	850	990	17
		~ 50	1020	1100	14
		50	1120	1230	11
"	C	0	540	720	330
		20	~ 830	950	26
		20	870	1000	20
"	F	?	1030	1070	
25 Cr-5.5 Ni-2.5 Mo-1.7 Cu-0.2 N	A	0	560	800	39
		48[2]	1100		
25 Cr-6.5 Ni-3.3 Mo-0.5 W-0.1 N	D	21	930	1020	11
		?	1050	1100	11
21 Cr-7.0 Ni-2.5 Mo-1.5 Cu	E	30	980	1010	13
Higher Composition: Cr+Ni+Mo = 35%	X	~ 17	910	990	13

(1) All compositions have less than 0.03% C.
(2) Alternate route.

In addition, one mill product was tested as a heavily cold drawn wire for downhole wireline applications.

Loading

Static Tests. Four types of statically stressed specimens were used: round tensile bars, C-rings, U-bends, and double cantilever beam (DCB) fracture mechanics specimens.

Tensile specimens were 10 cm x 1.11 cm rods with a 2.5 cm x 0.65 cm gage. Specimens were enclosed in an environmental chamber and externally loaded via a calibrated proof ring with an attached timer to signal time-to-fracture (Cortest, Inc.).

C-rings were compressed with a Hastelloy C-276 bolt to a calculated stress as shown in Figure 1. In some cases, a Charpy V-notch was added to a depth of 20 percent of the wall thickness. From the diametric deflection (δ), the outer fiber (tensile) strain at the apex was calculated via

$$\varepsilon = \frac{4t}{\pi d(d-t)}\ \delta \qquad (1)$$

where d is the OD and t is the wall thickness. Conversion of ε to σ was made as follows:

(a) Elastic region ($\sigma/\sigma y < 0.75$) $\quad \sigma = E\varepsilon$

(b) Plastic region ($\sigma/\sigma y < 0.75$) via stress-strain curves for longitudinal tensile specimens; i.e., $\varepsilon_y = \sigma_y/E + 0.002$ at the yield point.

Equation (1) derives from a stress analysis of compressed C-rings within the elastic region.[1] It appears to be a reasonable approximation (± 5%) when the C-rings are compressed to the yield point. In most cases, C-rings were tested with the original OD surface intact. Thick tubes had the ID increased to reduce t and therefore to increase δ for more convenient and precise loading. Young's modulus (E) was assumed to be 193 GPa (28 x 10^6 psi). For the C-ring specimens under test, values of δ calculated via Equation (1)

are 1 to 2 percent higher than calculated via ASTM Standard G-38

U-bends were normally 0.64 cm strips 0.16 cm thick bent into a U-shape and held with a Hastelloy C-276 wire fastener. Both longitudinal and transverse U-bends were tested.

Fatigue Pre-cracked DCB Tests. Full wall longitudinal specimens were cut from 2-7/8 inch OD x 0.276 inch wall (73 mm x 7 mm) tubing. Specimens had side grooves, were fatigue pre-cracked, and were wedge loaded, as shown in Figure 2.[2]

Initially, it was thought that the specimen curvature had little effect upon the DCB compliance (load vs. deflection) and that the calculations of K for flat specimens[2] would therefore be approximately applicable to these curved specimens. Subsequent compliance measurements[3] have shown that significant corrections were required for this type of DCB specimen. Values of the stress intensity, K, referred to in this report have included these curvature-induced corrections.

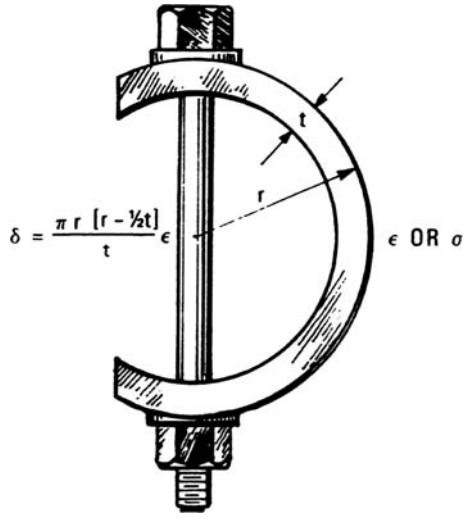
Test specimens were normally wedge loaded to $K > 60$ MN $m^{-3/2}$ (> 55 ksi$\sqrt{\text{inch}}$) . Plane strain conditions were not normally met[2], due to the high fracture toughness of these alloys. After autoclave testing, the wedge lift-off load was measured and the specimens were then cut to measure crack length and surface characteristics of crack growth, if any. The final K value was calculated from the crack length and lift-off load.

Slow Strain Rate Tests. In each autoclave tests, two longitudinal tensile specimens having a 0.25 cm diameter were pulled at a strain rate of 1×10^{-6} sec^{-1} until fracture. Test specimens were sometimes inadvertently coupled to the Hastelloy C-276 autoclave.

This test mode offered two unique features. Crack initiation and possibly crack propagation were enhanced by the application of a continual slow strain, resulting in a continued state of rupture of protective surface films. Secondly, the test procedure was rapid, and therefore well suited to evaluating the deleterious effects of trace levels of H_2S. Very low levels of H_2S were monitored on site.

For comparative purposes to judge SCC susceptibility the most useful test result appears to be the crack depth derived by the test period (16 to 37 hours), though the actual period

C–RING TEST PROCEDURE



ORIGINAL WALL
COMPRESSION (δ) VIA HASTELLOY C-276 BOLT

1% ACCURACY – ELASTIC REGION
GOOD ACCURACY – TO YIELD POINT (ASSUME $\epsilon_y = \sigma_y/E + 0.002$)

σ CALCULATED VIA LONGITUDINAL TENSILE
σ–ϵ CURVES AT RT
($E = 28 \times 10^6$ psi $= 1.9 \times 10^{11}$ Pa)

Figure 1. C-Ring Test Procedure

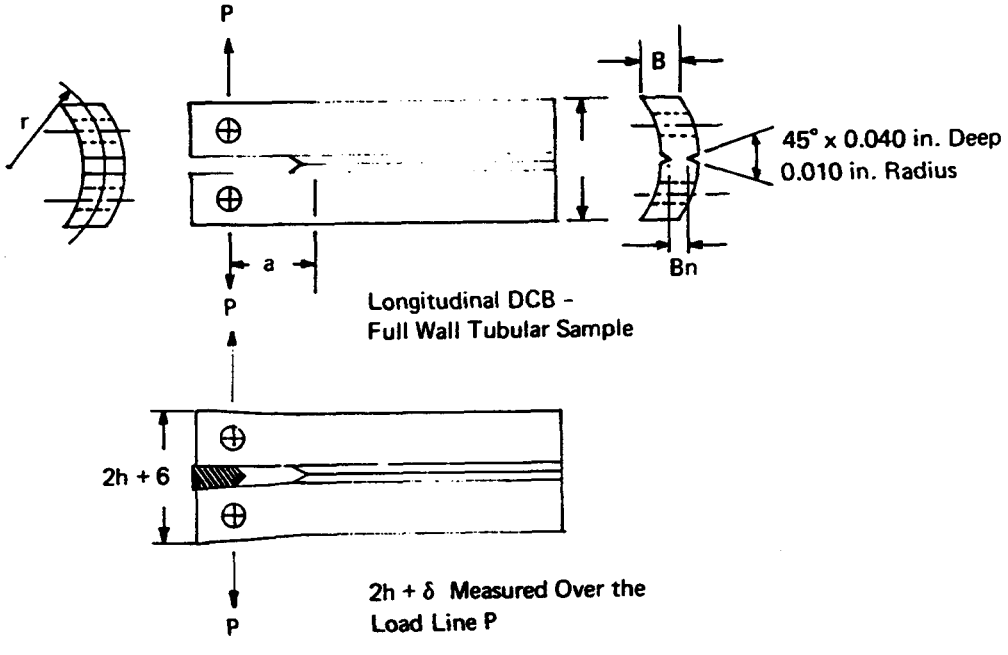


Figure 2. Geometry of Fracture Mechanics DCB Specimens

of crack propagation was probably confined to the final 5 to 10 hours of the test. Crack depths were measured by scanning electron microscopy (SEM) of the fractured surface.

Test Environments

Ambient Pressure Tests. Most tests at ambient temperature (24°C) were conducted in buffered solutions of 1 M NaCl or 5 M NaCl (5.6 and 24.6% NaCl) saturated with 1 bar H_2S. Dilute citric acid (0.02 M) with NaOH was chosen as a buffer. There was no observable interaction of the buffer with the corrosion reactions and buffering over a pH range was possible. Test solutions are identified as 1 M Cl^- (pH = 4.0)/1 bar H_2S and 5 M Cl^- (pH = 3.0)/1 bar H_2S.

Additional tests were made with more acidic solutions to investigate the role of Cl^-: 0.1 M HCl + 1 M NaCl, 0.1 M $HClO_4$ + 1 M $NaClO_4$, and 0.1 M H_2SO_4 + 1 M Na_2SO_4.

Elevated Temperature Tests. To investigate the effect of temperature, tests in 5 M Cl^- (pH = 3)/1 bar H_2S were made at temperatures to 190°C. At 60°C, tests were conducted at ambient pressure, so that the H_2S partial pressure was reduced to 0.85 bar (taking into account the effect of salt in lowering the water vapor pressure). At higher temperatures, autoclaves were used, with 1 bar H_2S added at test temperature, with final test pressure monitored throughout the test.

Autoclave Tests. Initially, tests were conducted with partial pressures of H_2S and CO_2 to be encountered in the field environment. Typically, partial pressures were ~ 0.2 bar H_2S, ~ 50 bar CO_2, and ~ 150 bar CH_4 added to the pressure limit of the autoclave. However, gas analyses established that O_2 contaminants were present in the CO_2 and CH_4 (~ 40 ppm O_2) gas cylinders. Subsequent tests therefore eliminated CH_4 and specified an O_2-free grade (< 5 ppm) of CO_2, and incorporated procedures to insure complete deaeration prior to gas addition.

In autoclave tests with statically loaded samples, gas was charged sequentially from the cylinders at test temperature or at 120°C, if a higher test temperature was used. Normally, the CO_2-H_2S (0.2 to 1.0% H_2S) mixtures and CO_2 were charged directly from the gas cylinder and CH_4 added via an intensifier. The amount of H_2S was calculated from both gas volume and H_2S solubility in the aqueous phase (a function of

temperature and salinity). There was reasonable agreement between calculated and measured values of the H_2S partial pressure. In slow strain rate autoclave tests, comparable charging procedures were used or, alternately, pre-mixed CH_4-CO_2-H_2S gases were added via an intensifier.

In autoclave tests, gas samples were periodically taken and analyzed for H_2S content via gas chromatography. In high temperature tests, it was necessary to reduce the measured H_2S fraction in the analysis due to the contribution of the H_2O partial pressure at the test temperature. Decay of H_2S to below a pre-set partial pressure resulted in H_2S replenishment via a CH_4-H_2S gas mixture added at test temperature via an intensifier. In this way, reasonable control of the H_2S partial pressure during the test was assured. However, in slow strain rate tests, H_2S analyses were performed only in tests at very low H_2S partial pressures. In these cases, multiple gas samples were analyzed, employing Gastec Detector Tubes (Bendix Corp.) having a useful range of 10-120 ppm H_2S.

Electrochemical Tests

All potentials were measured versus a Ag/AgCl, 1 M Cl^-/ cracked glass seal reference electrode. Due to slow H_2S diffusion into the reference electrode tube, which then altered the reference electrode potential, the 1 M Cl^- solutions was replaced daily and frequent checks were made to insure dependability of potential readings.

As long-term potentiostatic tests were therefore risky, galvanostatic tests were chosen to explore the potential dependence of SCC, with constant current supplied by a DC power supply and a large resistor. The Cortest tensile test unit was modified for electrochemical tests by adding a reference electrode and converting the gas inlet tube to double as a counter electrode. In all tests, a corrodable stainless steel counter electrode was used.

Current-potential curves were obtained (except for tensile specimens) on specimens spot welded to 316 SS wire leads, and then exposed to the test solution.

Specimen Evaluation

Stressed specimens were examined carefully for cracks with an optical binocular microscope (X70). At the end of a

test, U-bends not forming visible cracks were then compressed further to open up any fine microcracks. In cases where previously invisible cracks were identified in this way, it was necessary to resolve whether such cracks were stress corrosion cracks or had resulted from cracking of a hydrogen enriched surface layer during compression. Microcracks resulting from stress corrosion were identified by the presence of corrosion products on the crack face near the specimen surface. Specimens showing pitting corrosion but no obvious evidence of cracking were cross-sectioned and examined for cracks at the base of the pits.

In slow strain rate tests, SCC was usually noted by the presence of secondary cracks. Marginal cases were judged by SEM examination of the fractured surface. However, selective corrosive attack of ferritic (or austenitic) phases resulted in some ambiguity, and a clear distinction between SCC and localized corrosion could not always be made (see later section). Supplemental cross sectioning of pitted areas was therefore employed in marginal cases.

Hydrogen Analyses

Hydrogen analyses were performed in a Leco RH-2 unit. Blank corrections were made, i.e., duplicate runs were made but without metal specimens added. Calibration employed National Bureau of Standards' Standard for Hydrogen No. 352 (0.003% H in Ti) with tin powder added to aid fusion.

Artificially higher values of H were measured on specimens that contained adherent corrosion product. Usually a brief electropolish, followed by rinsing and drying, was sufficient to eliminate this surface effect. Test results reported have employed lathe turnings successfully removed from cathodically charged round tensile specimens. Care was taken to eliminate oil and to perform the analysis within ~ 20 min of cutting the turnings. This approach was employed in order to evaluate the hydrogen profile with the specimen, and assumed that the H diffusion coefficient was sufficiently low so as to avoid major egress of H from the lathe turnings.

RESULTS AND DISCUSSIONS

General Features of Cl^-/H_2S SCC

Transgranular SCC of all duplex stainless steels was observed. Anodic rather than cathodic test conditions accelerated SCC, as was first reported by Herbsleb and Poepperling[5]. Cracking is thus promoted by corrosion rather than by external hydrogen charging.

Figures 3 and 4 show typical crack tip morphology. Transgranular cracking of both ferrite and austenite occurred, though some cracking also occurred at the ferrite/austenite grain boundary (Figure 4). In most cases, heavy selective corrosion of the ferrite (dark) phase also occurred.

Anodic Initiation. Figure 5 shows the potential dependence of SCC of "anodically activated" specimens, and clearly demonstrates that SCC develops under anodic rather than cathodic test conditions. Longitudinal tensile specimens of 20% CR "C" were stressed to 870 MPa (0.95 σy) immersed in 1 M NaCl (pH = 4)/1 bar H_2S at room temperature (RT), then anodically activated for 2 hours at + 50 $\mu A/cm^2$, followed by application of cathodic or anodic current for the duration of the test. During anodic activation, the potential initially shifted to - 0.1 V (versus Ag/AgCl, 1 M Cl^-), pit initiation developed and the potential then drifted negatively to a value of about - 0.35 V. Following subsequent adjustment of the applied current, little potential drift was noted, so that constant potential test conditions were approximated, as listed in Table 2. A typical current-potential curve showing the potential range of pit initiation and repassivation is shown in Figure 6.

The electrochemical potential alone, however, is not a sufficient determinant. In the absence of anodic activation, the specimen remained immune to both pitting corrosion and SCC, as noted in Table 2. Specimens maintained at the same potential, but with pitting corrosion previously initiated, failed rapidly by SCC. Conditions that promote localized corrosion such as the presence of a crevice, dynamic straining, or non-metallic inclusions can significantly influence test results. Most tests reported have been selected to favor the initiation of localized corrosion, i.e., a more acidic solution, high NaCl concentration, or higher test temperatures.

TABLE 2. EFFECT OF POTENTIAL ON Cl^-/H_2S SCC IN TENSILE TESTS

Tests in 1 M Cl^- (pH = 4)/1 bar H_2S at 24°C
20% CR "A" ($\sigma = 0.95\ \sigma_y = 870$ MPa)

Anodic activation results from application of + 50 $\mu A/cm^2$ for two hours, which generally resulted in formation of several pits and a final potential of -0.35 V (versus Ag/AgCl, 1 M Cl^-).

Impressed current is then applied for the duration of the test.

ANODIC ACTIVATION	APPLIED CURRENT $\mu A/cm^2$	CORROSION POTENTIAL V(vs. Ag/AgCl, 1 M Cl^-)	COMMENTS	TIME-TO-FAILURE, HOURS
No	None	-0.39 initially drift to -0.29	No pitting developed	> 164
Yes	+ 50	-0.35	Vigorous H_2 liberated from advancing crack	18
Yes	+ 5	-0.48		51
Yes	0	-0.49	Pitting corrosion (and H_2 evolution) continued	115
Yes	- 4	-0.55	Pits repassivated	> 162
Yes	- 85	-0.70		> 188

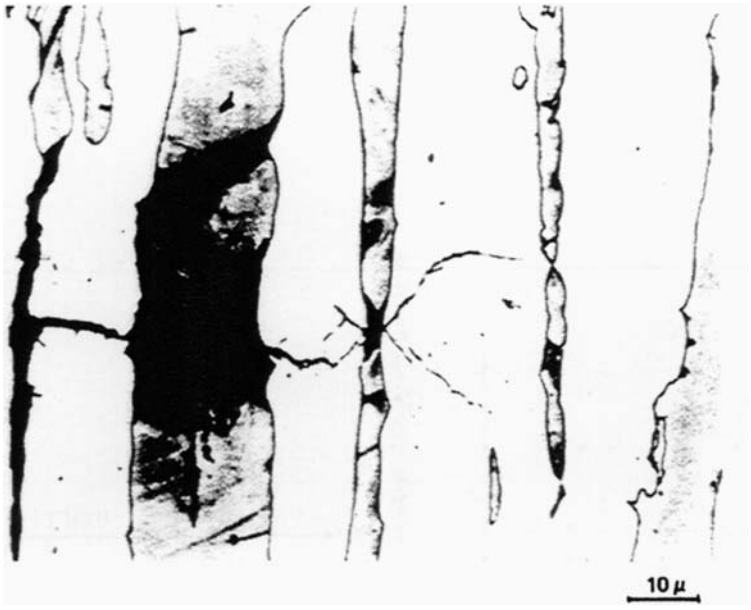


Figure 3. Typical Crack Tip Morphology
Longitudinal tensile specimen of 20% CR "C" in Cl^-/H_2S at 24°C
SCC noted in both phases, with subsequent corrosion of ferrite (dark) phase.
Magnification: 1000X

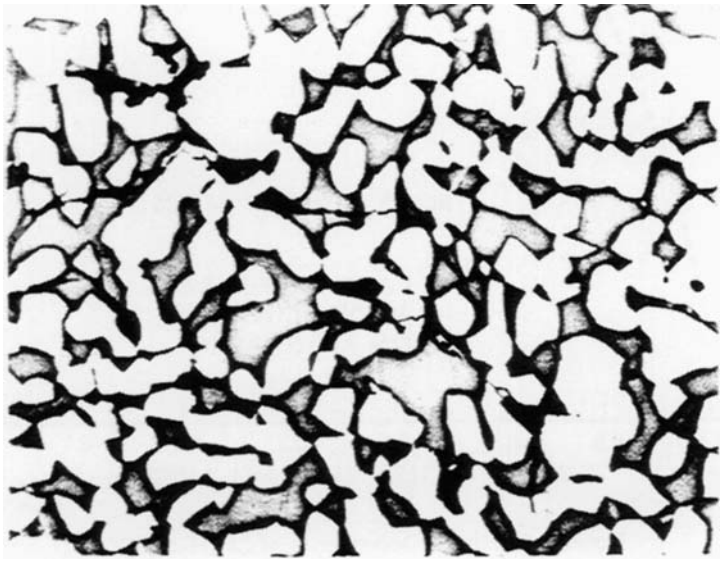


Figure 4. Typical Crack Tip Morphology
Transverse C-ring sample of 30% CR "D" in Cl^-/H_2S at 24°C
SCC along grain boundaries as well as through both phases
Magnification: 1000X

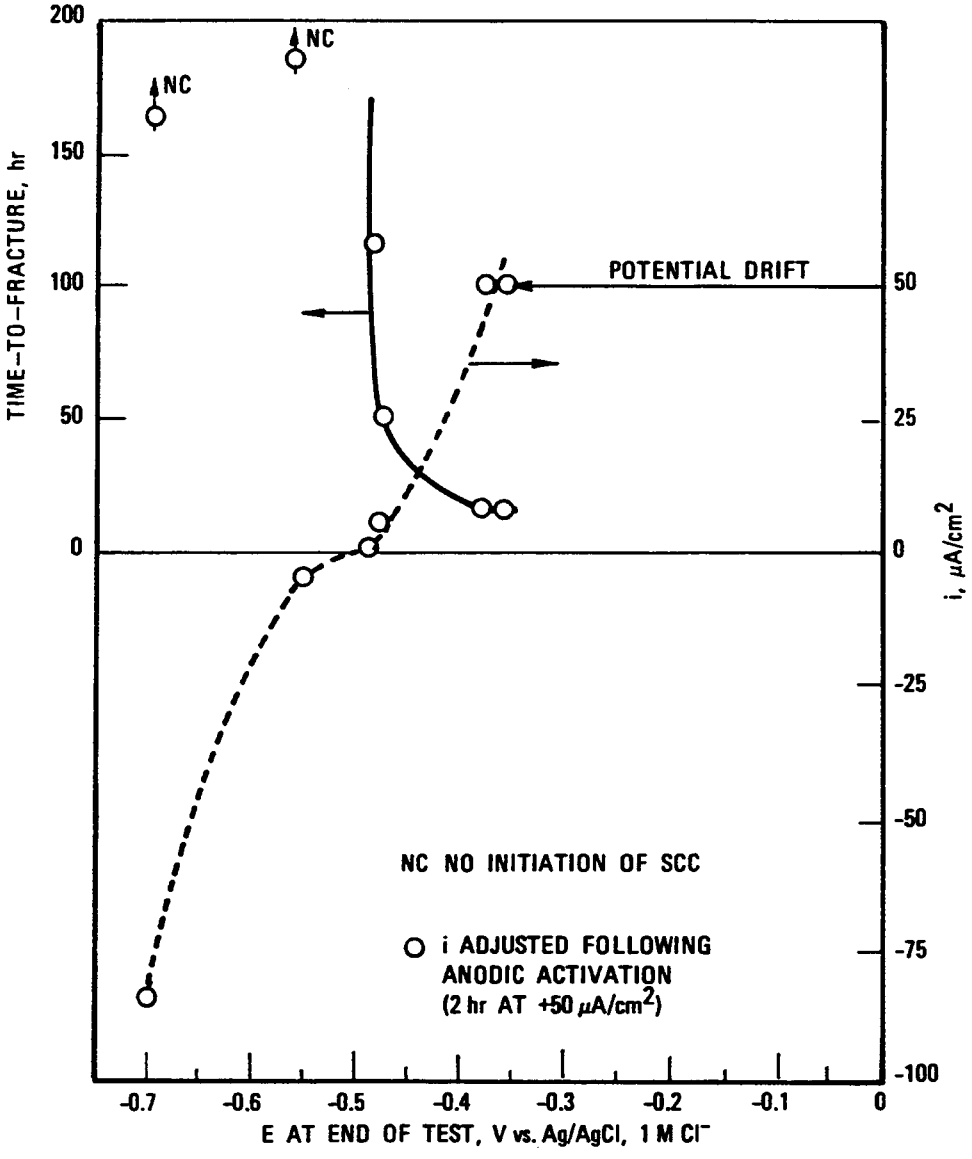


Figure 5. Potential Dependence of Cl^-/H_2S SCC
Tests with 20% CR "C" loaded to 870 MPa (= 0.95 σ_y)
in 1 M NaCl (pH = 4)/1 bar H_2S at 24°C

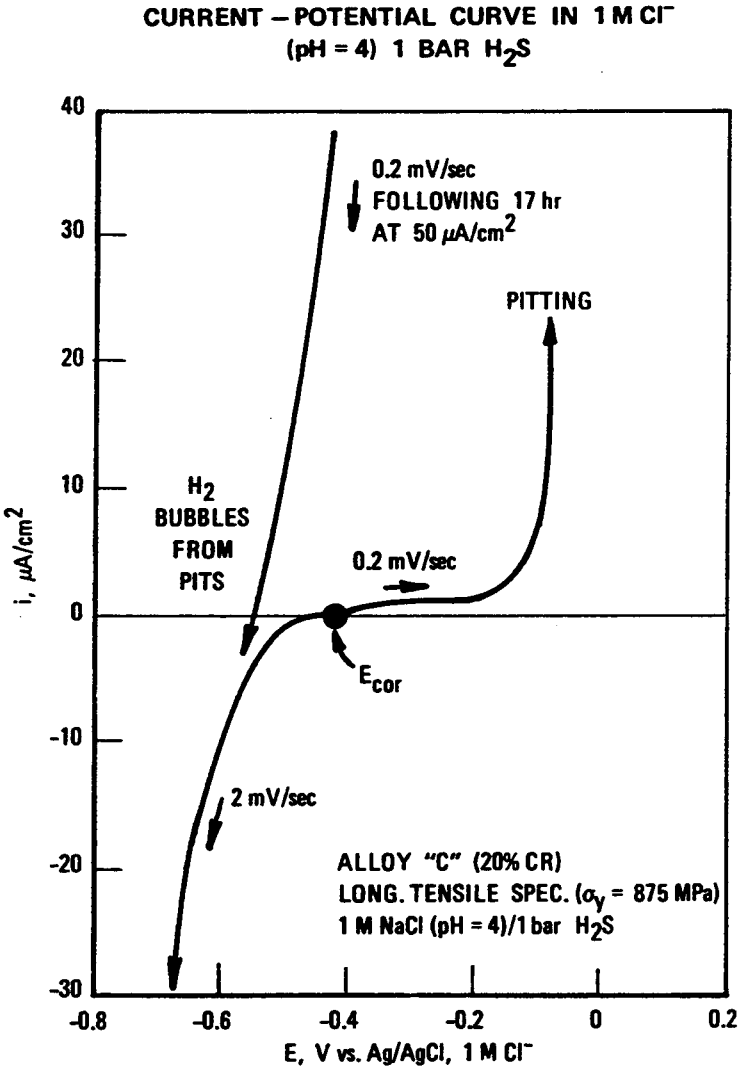


Figure 6. Current - Potential Curve in 1 M Cl⁻ (pH = 4) 1 Bar H_2S

03541

In more acidic solutions, there is a tendency toward general corrosion, as opposed to pitting corrosion, which can also result in SCC.

Cathodic Activation. In sufficiently acidic solutions, SCC appears to occur more readily under cathodic rather than anodic conditions. An example is alloy "D" in NACE solution (5% NaCl + 0.5% acetic acid/1 bar H_2S). Because of the higher Cr and Mo content of this duplex, compared to other compositions evaluated, pitting resistance was greater. Attempts to employ anodic activation in 1 M Cl^-/H_2S solutions were not successful because of this greater pitting resistance. However, SCC did occur readily in the more aggressive 5 M Cl^-/H_2S solution as well as under conditions of cathodic polarization in NACE solution.

Table 3 compares test results on a set of 5 transverse U-bend specimens of alloy D (σ_y = 1050 MPa) exposed for 16 hours in NACE solution at RT. Applied current densities varied from -200 to +260 $\mu A/cm^2$. Only specimens cathodically polarized to -10 and -50 $\mu A/cm^2$ showed SCC initiation, indicated by multiple microcracks. At higher cathodic current densities (-200 $\mu A/cm^2$), the specimen remained free of SCC, as did specimens at open circuit and under anodic polarization (+260 $\mu A/cm^2$). The latter specimens appeared to have remained fully passive in this test.

This detrimental effect of mild cathodic polarization appears to be a result of depassivation and subsequent selective corrosion rather than absorption of cathodically charged hydrogen.

The microcracks, examined by SEM-EDAX, are in fact corrosion grooves of Ni-rich sulfide (see later section). Cross-sectioning confirmed that SCC had actually initiated. This fact, plus the observation of a thin sulfide corrosion product film at -0.59 V (versus Ag/AgCl, 1 M Cl^-), indicates that active corrosion can initiate in the acidic (pH ~ 2.5) H_2S solution under mild cathodic test conditions. The above U-bend test, repeated in the less corrosive 1 M Cl^-/1 bar H_2S solution, did not result in SCC under any test condition.

Role of Absorbed Hydrogen. No evidence of stress cracking under sufficiently cathodic test conditions was noted (see Table 2 and 3). As anticipated from the previous section, some cracking of cold worked alloys cathodically coupled to carbon steel in the NACE solution did occur, however, and examination showed that the resultant cracks were associated with localized corrosion. The SCC

TABLE 3. SCC INITIATION VIA CATHODIC ACTIVATION

Set of five transverse U-bends of alloy "D" (σ_y = 1050 MPa) was exposed 16 hours in NACE solution. Galvanostatic control was via a DC voltage source (32 V) and individual resistors to each of the three cathodic specimens. Specimens and reference electrode were positioned to minimize iR errors in measurement of specimen potentials.

APPLIED CURRENT, $\mu A/cm^2$	MEASURED POTENTIAL START, V vs Ag/AgCl, 1 M Cl	MEASURED POTENTIAL END, V vs Ag/AgCl, 1 M Cl	SCC INITIATION	COMMENTS
-200	-0.745	-0.722	No	No evidence of SCC or corrosion. Rebending caused surface cracks to form as a result of absorbed H.
- 50	-0.638	-0.593	Yes	Tarnished surface. Multiple microcracks noted, and identified as corrosion grooves. Transgranular SCC in austenitic phase.
- 10	-0.558	-0.564	Yes	Multiple microcracks noted.
0	-0.536	-0.520	No	No evidence of SCC or corrosion.
+260	+0.9	+1.6	No	No evidence of SCC or corrosion. Surface coated with anodic deposit (free S?).

susceptibility of alloys in H^+/H_2S solutions referred to below (including tests with Type 304 SS) was also eliminated upon application of sufficient cathodic current density (~ 0.2 mA/cm^2).

The profile of H absorbed under cathodic test conditions is shown in Figure 7. A transverse tensile sample (A, 20% CR) loaded to 875 MPa (127 ksi) was cathodically charged at 50 μA/cm^2 for 12 days in 1 M Cl^- (pH = 4.0)/1 bar H_2S. Analyses of successive lathe turnings, which admittedly will result in some egress of H prior to analyses, indicated that significant concentrations of H exist in the near surface layers. A hydrogen surface concentration of 148 ppm and a diffusion coefficient of 1.4×10^{-10} cm^2/sec was calculated. Values of the surface concentration and diffusion coefficient were calculated by fitting the H profile to the curve for semi-infinitive diffusion with a fixed boundary layer[4]. A second experiment with a tensile specimen having the normal longitudinal orientation yielded a diffusion coefficient of $\sim 0.7 \times 10^{-10}$ cm^2/sec.

Some embrittlement due to cathodic charging at 50 μA/cm^2 was observed, as measured by loss of ductility in tensile and bend tests. Table 3 cites results with U-bend specimens. However, there was no indication of hydrogen induced delayed failure or crack initiation at stresses to $\sim 1.2\sigma_y$ in tests with hydrogen charged cold worked alloys. Table 4 summarizes test results with cold worked tensile specimens following a more moderate hydrogen charge via high temperature charging with hydrogen gas.

Additional tests explored a potential embrittlement effect of hydrogen absorbed in an active crack under anodic test conditions (conditions of Table 2), since a stream of H_2 invariably was seen to be issuing from active cracks. This observation implied very much high rates of H^+ reduction and therefore absorption within the advancing crack compared to the cathodic test conditions cited above. However, no evidence was found that SCC was a direct consequence of hydrogen evolution. Several anodic tests were interrupted at mid point. Upon application of cathodic current, crack growth stopped, and no crack extension occurred upon increasing the load. When subsequently pulled in air to failure, a brittle area ahead of the crack tip was suggestive of hydrogen embrittlement. However, parallel tests with partially cracked specimens that had been out gassed (3 days at 200°C in vacuum) also showed a comparable brittle area when subsequently pulled to failure.

TABLE 4. EFFECT OF HYDROGEN ON MECHANICAL PROPERTIES

21 ppm H absorbed during charging in 120 bar H_2S at 300°C
20% CR alloy "C"; subsize tensile specimen

	LONGITUDINAL				TRANSVERSE			
	STRENGTH		DUCTILITY		STRENGTH		DUCTILITY	
	YS MPa	UTS MPa	% RA	% El	YS MPa	UTS MPa	% RA	% El
As Received	920	940	80	20.0	890	940	40	10.4
Hydrogen Charged		985	40	15.4		1000	21	10.4
		980	55	20.2		970	25	11.1

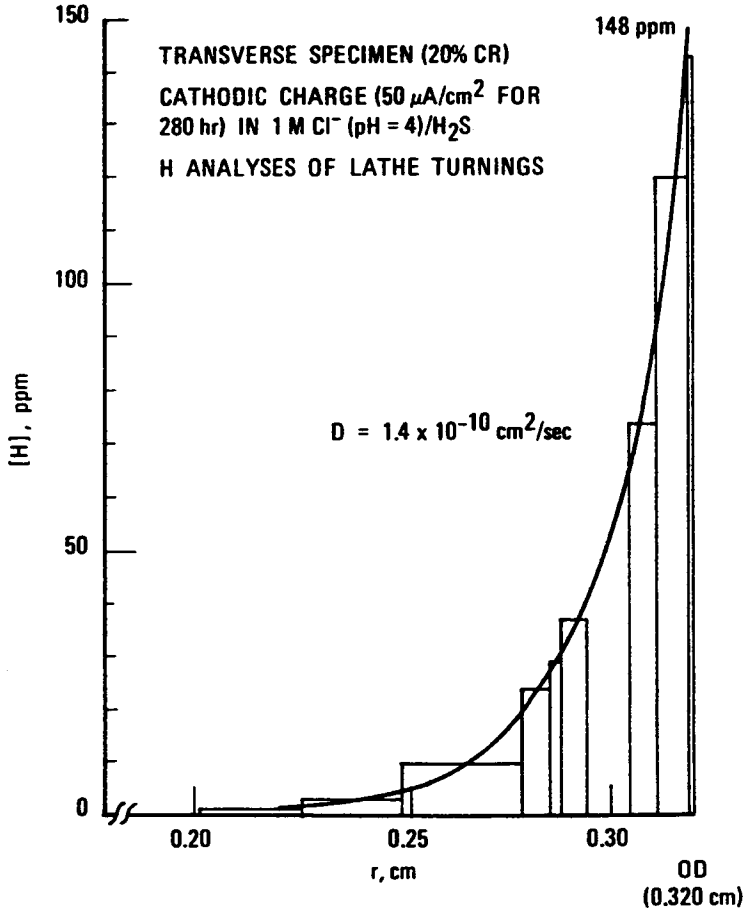


Figure 7. Hydrogen Profile in Cathodically Charged "C" Specimen

Consequently, any contribution of absorbed hydrogen to crack extension would appear to be coupled to sustaining the anodic reaction.

Cl^-/H_2S Synergism. Several reports indicate the detrimental effect of increasing H_2S[6-8] and Cl^-.[8] The presence of H_2S was found to enhance both general corrosion and localized corrosion.[5] Figure 8 shows the effect of trace H_2S on accelerating active corrosion. As little as 1.4×10^{-6} M H_2S, which corresponds to 0.02 ppm soluble H_2S or an equivalent vapor pressure of 1.4×10^{-5} bar, was found to accelerate corrosion in 0.1 M HCl + 1 M NaCl.

The effect of H_2S on pitting corrosion in Cl^- solutions is summarized in Table 5. Pit initiation is shifted toward more active potentials, as is pit repassivation, which suggests a change in electrochemical reactions occurring within the pit. This is illustrated in potentiostatic tests which show pitting rates to cycle in response to the presence or absence of H_2S. Two effects of H_2S can be identified which sustain localized corrosion: (1) accelerated active corrosion, as noted in Figure 8 and (2) formation of more acidic solutions due to precipitation of more stable Ni and Mo sulfide (versus Cr oxides in the absence of H_2S). For all but the very lowest H_2S levels tested, a characteristic black sulfide film was found in regions of SCC and pitting corrosion. EDAX analyses indicate a sulfide corrosion product enriched in Ni but depleted in Fe (Mo could not be determined).

No significant effect of H_2S on the cathodic reaction was noted when tests were compared in solutions of comparable acidity. Under test conditions associated with O_2 contamination, however, a stable soluble oxidant was noted at low but significant levels in hot H_2S solutions. Earlier studies have shown that O_2 reacts rapidly with H_2S to form colloidal sulfur, which is not a corrodent in acidic solutions; however, a soluble by-product is formed which does promote corrosion. This species has been tentatively identified as H_2S_2 or a derivative acidic polysulfide species.[9]

At elevated temperatures, i.e., above 120°C, interpretation of anodic polarization curves has been complicated by parallel oxidation of H_2S to elemental sulfur.

SCC in Absence of H_2S or Cl^-. A number of reports indicate that duplex stainless steels are susceptible to Cl^-

TABLE 5. EFFECT OF H_2S ON PITTING CORROSION

Tests in 1 M NaCl (pH = 4.0) at 40°C.
Purge gas is either N_2, CO_2, or H_2S at ambient pressure.

Pit initiation potential, E_{PIT}, defined during slow anodic scan (1 mV/sec) from corrosion potential, E_{COR} at potential where anodic current exceeds 10 $\mu A/cm^2$.

Following accelerated pitting corrosion to 1 mA/cm^2, scan direction is reversed and the pit repassivation potential, E_{REP}, is defined as the potential where the current approaches zero or becomes negative.

	POTENTIAL (V versus Ag/AgCl, 1 M Cl^-)		
PURGE GAS	E_{COR}	E_{PIT}	E_{REP}
N_2	- .350	+ .270	+ .130
CO_2	- .320	+ .760	+ .105
H_2S	- .400	- .280	- .370

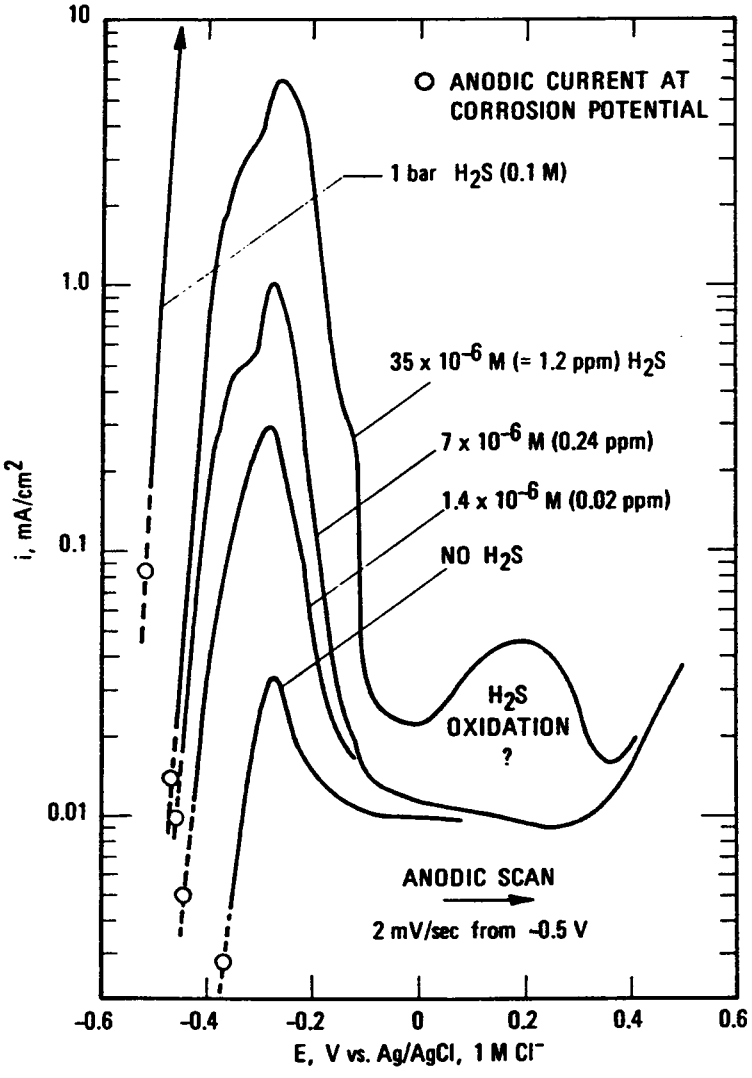


Figure 8. Effect of H_2S Upon Anodic Dissolution of "C" in 0.1 M HCl/1 M NaCl

SCC in sufficiently aggressive solutions, e.g., boiling 45% $MgCl_2$. This study found, in contrast to LeFebvre, et al. [10], that both annealed and cold worked duplex stainless steels are highly susceptible to SCC in boiling 52% LiCl solutions (150°C). To date, duplex alloys have been found consistently resistant to SCC in deaerated 25% NaCl solutions.

Stress corrosion cracking has also been observed in acidified H_2S solutions containing no Cl^-. Tests in 0.1 M H^+/H_2S containing perchlorate (ClO_4^-) and sulfate ($SO_4^=$) showed transgranular SCC of Type 304 and 316 stainless steels as well as the duplex alloys under study. General corrosion rather than localized corrosion resulted, and was confirmed by electrochemical studies showing that H_2S dramatically enhances general corrosion (as in Figure 8) even in the absence of Cl^-. Ni-rich corrosion product films were also present on the surface. As noted above, SCC did not occur in these same tests under conditions of cathodic protection (~ 0.2 mA/cm^2).

Temperature. Literature references disagree as to the effect of test temperature[6-8,11]. Tests were made in 5 M Cl^- (pH = 3)/1 bar H_2S solutions at temperatures from 24°C to 190°C. Tests were made with C-ring specimens cut from alloy "B" at 17% CR and 50% CR and exposed over a range of compressions in order to establish an apparent minimum stress level at each test temperature. Results, plotted in Figure 9, show a clear beneficial effect of testing at temperatures above 80°C.

In part, this temperature effect may also be dependent upon H_2S pressure, and appears to be less evident when testing at H_2S pressures above 10 bar[6] or possibly in solutions acidified by adding acetic acid.[7]

Subsequent data on the temperature effect is presented in the context of autoclave tests in CO_2-H_2S environments.

Crack Initiation Sites. It is probable that a variety of crack initiation sites are operative, which may vary with test temperature, acidity (general versus localized corrosion) and test method. Herbsleb and Poepperling cite pitting corrosion.[5] Our slow strain rate tests invariably show greater susceptibility to localized corrosion in the necked regions, indicating that plastic deformation can significantly promote localized corrosion.

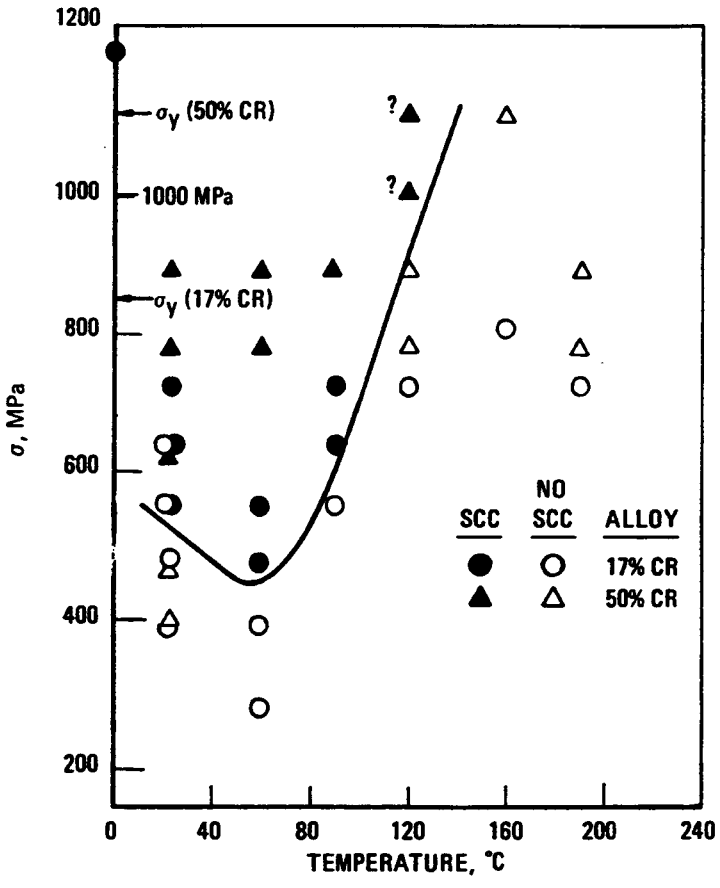


Figure 9. Temperature Dependence of Cl^-/H_2S SCC of "B"
C-ring tests in 5 M NaCl (PH = 3)/1 bar (at T) H_2S
Test periods were 2 weeks at T < 100°C,
1 week at higher temperatures

03541

In a number of tests, particularly at 60°C, multiple ridges of corrosion products were noted, as shown in Figure 10. The dark grooves shown in Figure 10 are the characteristic Ni-rich sulfide product, with cracks in the sulfide running along the middle of the groove. However, cross-sectioning revealed that the cracks did not necessarily extend into the alloy. These grooves were also noted during cathodic polarization at RT (Table 3) under conditions where SCC did follow. Both grooves and pits therefore appear to be effective sites for SCC initiation.

The effect of temperature upon crack initiation sites appears to follow a sequence that is not yet understood, and may bear on resolving the SCC temeprature dependence:

(a) At ambient temperature, cracks tend to form with little or no evidence of pitting corrosion.

(b) At temperatures on the order of 120°C, pitting corrosion becomes increasingly dominant. In some cases, micro-cracks are associated with pitting corrosion indicated (as in Figure 11) but cross-sectioning showed no real evidence of SCC.

(c) At higher temperatures (up to 260°C), susceptibility to pitting corrosion is decreased, but a Ni-rich tarnish film develops on the surface. Kudo, et al. [6] report the tarnish film formed at 200°C to be primarily FeS.

Orientation. A modest effect of transverse versus longitudinal orientations has been reported.[5] A more pronounced effect has been found, as shown in Figure 12, with tensile specimens tested under "anodic activation" conditions. A variety of tests comparing transverse and longitudinal U-bend specimens have also revealed an orientation effect. Specimens oriented so that the crack propagate transverse to the rolling direction therefore represent a more severe test mode.

Conversely, the highly elongated and fine grained wire lines were found to be more resistant to SCC due, presumably due to this same orientation effect.

Cold Working. Studies with cold reduced sheet and tubing indicate that, when tested at the yield point, SCC susceptibility increases with increasing cold reduction. When



50 μ

Figure 10. Corrosion Grooves as Potential Crack Initiation Sites
Annealed "C" C-ring exposed to 5 M Cl^- (pH = 3)/
1 bar H_2S at 60°C for 2 weeks.
Section shown is machined cross-section surface away
from region of maximum stress (see text).
Magnification: 200X

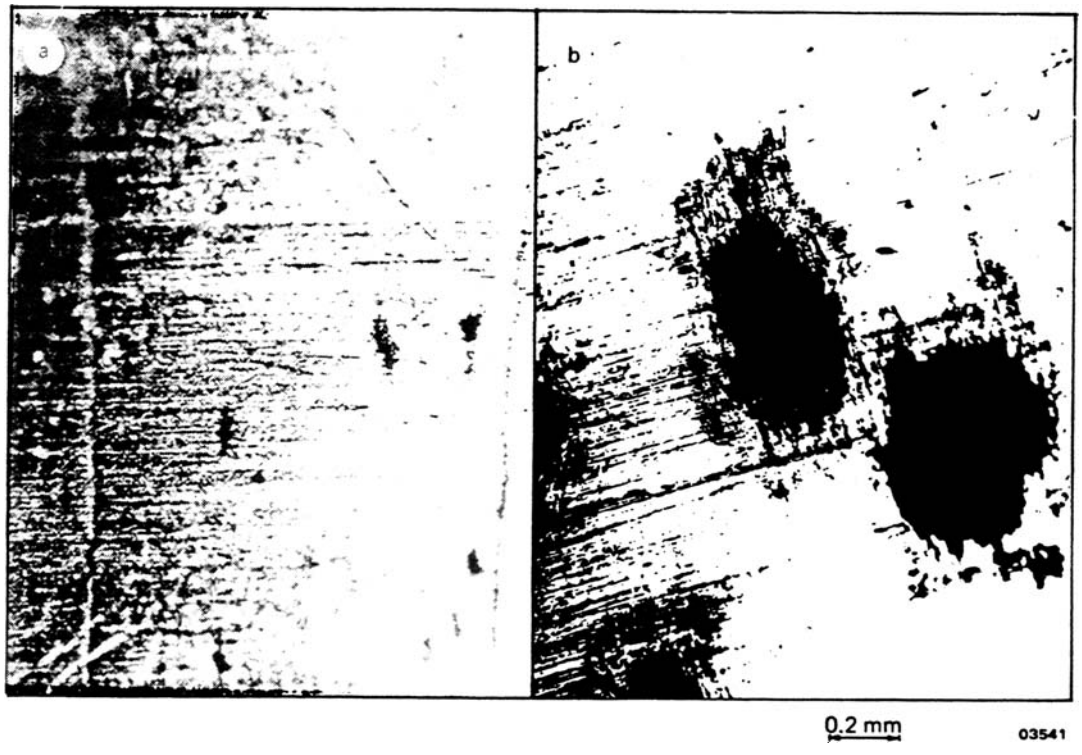


Figure 11. Effect of Temperature Upon Corrosion/SCC Morphology
C-ring tests with 30% CR "D" in 5 M NaCl (pH = 3)/1 atm H_2S
Photos show apex of C-ring at end of test
a) 24°C (σ = 400 MPa) Multiple deep cracks present when cross-sectioned
b) 120°C ($\sigma \sim$ 1000 MPa) Only pits present. Microcracks appear to be at periphery of the pits,
but cross-sectioning revealed no cracking at periphery or base of pits

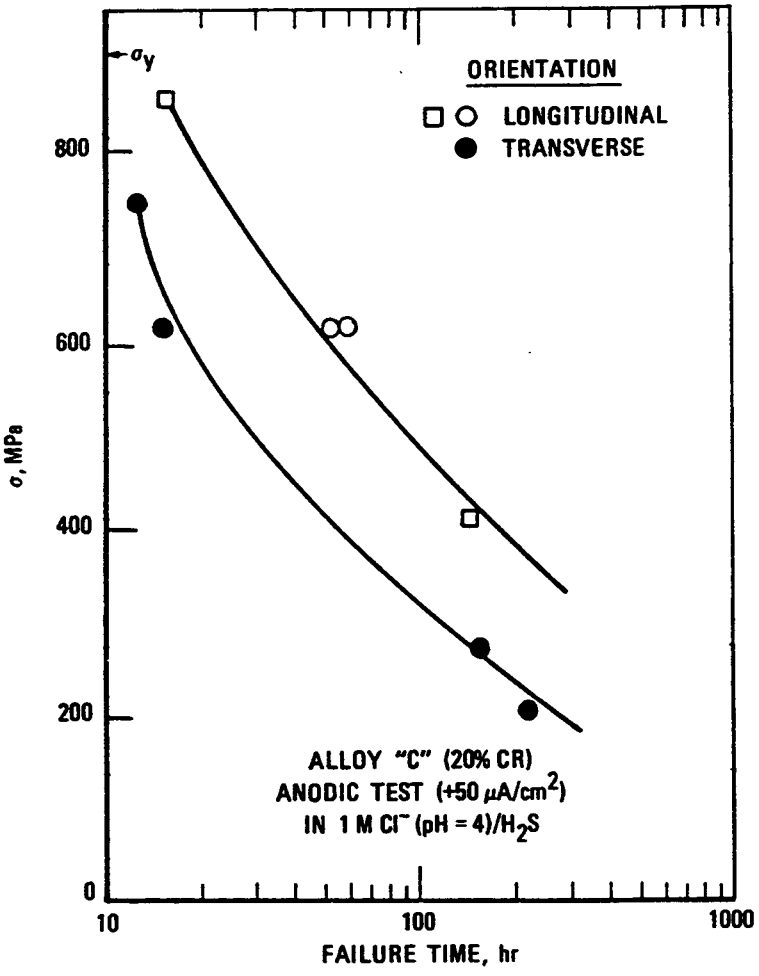


Figure 12. Effect of Load and Orientation on Cl^-/H_2S SCC
Tensile tests with 20% CR "C" under anodic conditions
(+50 $\mu A/cm^2$) in 1 M NaCl (pH = 4)/1 bar H_2S

03541

compared at equivalent stress levels, however, there is some uncertainty as to whether cold work is detrimental.[6,8,12]

Tubing samples of "B" were available having yield strengths varying from 520 MPa (75 ksi) to 1120 MPa (162 ksi) and were tested as C-rings over a wide range of stresses. The results of tests at RT in 5 M Cl^- (pH = 3)/1 bar H_2S are plotted in Figure 13 as applied stress versus crack initiation times, and indicate a threshold stress level of somewhat less than 350 MPa (50 ksi) for cold reduced specimens, based upon tests lasting 2 to 3 months. A higher threshold stress is indicated for the annealed sample, but tests with an equivalent annealed product indicate a threshold stress below 410 MPa (60 ksi).

Similar results were obtained on the other duplex alloys. Estimates of the RT threshold stress for each sample alloy tube have been made. As in the above case, most cold worked alloys showed SCC susceptibility at long exposure times, indicating that the minimum applied stress was still slightly above the threshold stress. This uncertainty is shown in Figure 14 which plots results for each alloy as a function of the degree of cold reduction. A threshold stress value somewhat less than 350 MPa is indicated for all alloys, independent of cold reduction. Additional data obtained in sour gas environments is presented in the following section.

SCC Susceptibility in Sour Gas Environments

The majority of tests have evaluated SCC susceptibility in at H_2S partial pressures of 0.2 bar of less. Salt concentraions were either 1.8 M (10%) or 5.1 M (25%) NaCl, and the CO_2 partial pressure on the order of 50 bar, irrespective of test temperature. Calculated pH values (neglecting salt effects) range from 3.1 (25°C) to 3.7 (200°C).

Applied Stress. A variety of C-ring specimens (as in Figure 13) were exposed in 1.8 M Cl^-/CH_4-CO_2-H_2S at 0.2 bar H_2S and 60°C for two weeks. Test results, plotted as stress vs % CR in Figure 15, indicate a threshold stress on the order of 600 MPa (85 ksi), independent of σ_y and alloy source. In view of the limited number of tests and short test period, however, this result must be considered only as indicative of a trend.

Test Method. A variety of test specimens were exposed to 5.1 M Cl^-/CH_4-CO_2-H_2S at 177°C and ~ 0.2 bar H_2S, employing

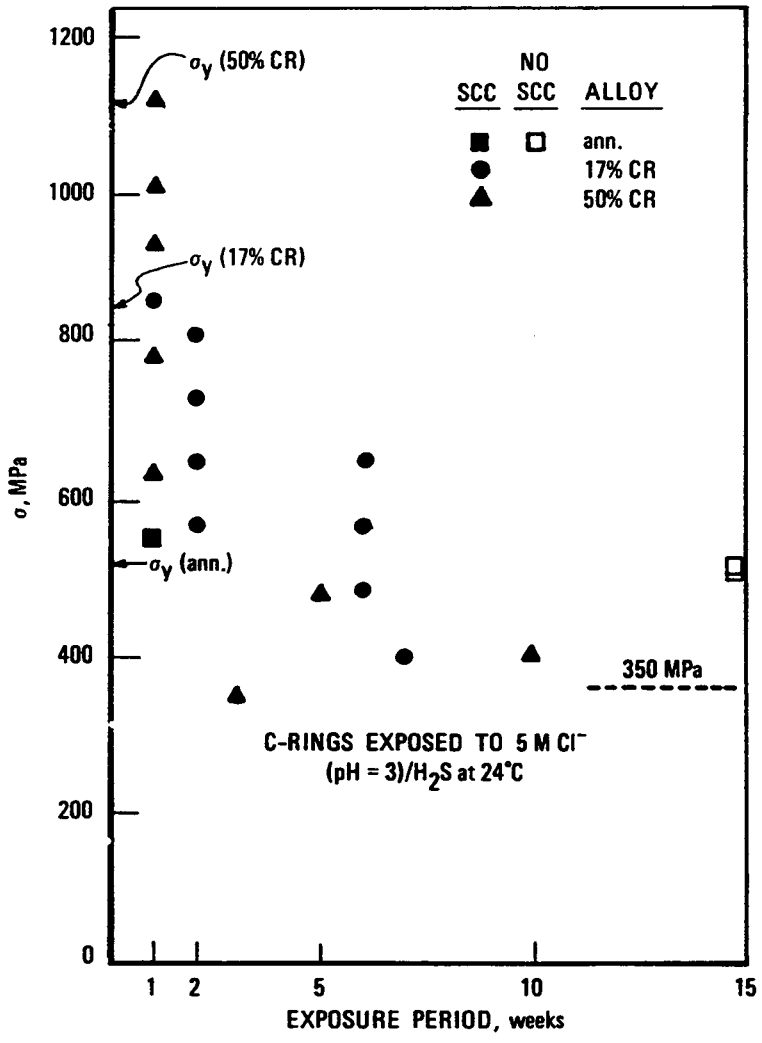


Figure 13. Stress Dependence of Cl^-/H_2S SCC of "B"
C-ring samples cut from annealed and cold reduced tubes and exposed to 5 M NaCl (pH = 3)/1 bar H_2S at 24°C. Filled points indicate time when crack initiation was noted.

03541

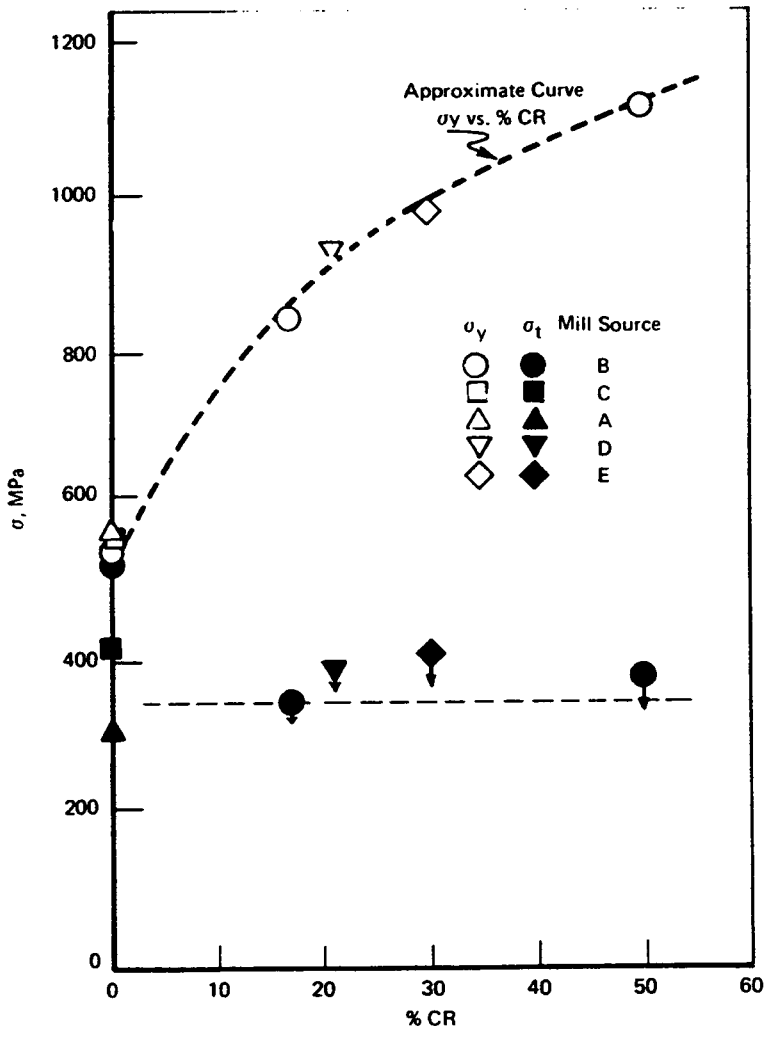


Figure 14. Independence of SCC Threshold Stress on Yield Strength
Values of SCC threshold stress (σ_t) were estimated at RT from Tests in 5M Cl^-/1 Bar H_2S with C-Rings with Test Periods to 15 Weeks
(cf Figure 12)

03541

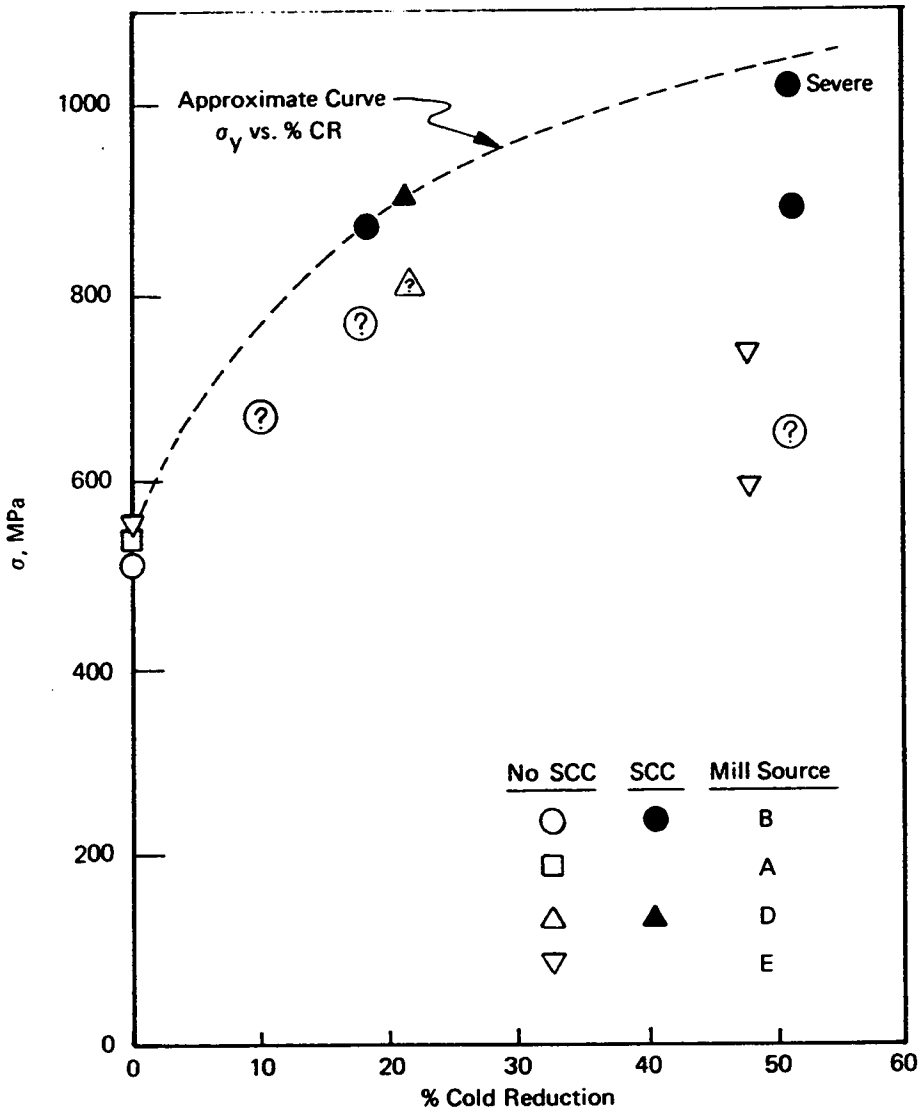


Figure 15. Effect of Cold Reduction on Cl^-/H_2S SCC
Two week tests with C-rings in 1.8 M NaCl/150 bar CH_4 + 50 bar CO_2 + 0.2 bar H_2S at 60°C

several cold worked duplex alloys having yield strength in excess of 1000 MPa (145 ksi). Test results, summarized in Table 6, show that no SCC was noted in a C-ring compressed to the yield point, but that SCC did occur on a notched C-ring, a DCB, and a slow strain rate test specimen.

H_2S Partial Pressure. Table 7 summarizes test results employing the slow strain rate technique. H_2S partial pressure varied from 0.003 bar to 1.8 bar (0.045 to 26 psi) in tests in 5.1 M Cl^-/~ 40 bar CO_2 + ~ 150 bar CH_4 at 177°C. Tests employed specimens from the higher alloyed experimental duplex alloy (with higher Cr+Mo) as well as a high strength version (σ_y = 1100 MPa) formed by an alternate processing route. The detrimental effect of increasing H_2S partial pressure is clear from test results, and indicates that SCC under these test conditions can occur at H_2S partial pressures as low as 0.04 bar (0.6 psi).

Trace H_2S. The effect of as little as 1×10^{-4} bar H_2S was noted in slow strain rate tests in 5.1 M NaCl/55 bar CO_2 at 130°C. Figure 16 compares photographs of the fractured areas in cross-section employing 17% CR "B" (σ_y = 850 MPa). In the absence of H_2S, no environmental effects were noted (Figure 16a). In Figure 16b, with trace H_2S present, localized corrosion was observed, and the ductility was reduced accordingly. However, SCC did not occur in this case. Pitted areas, at higher magnification (Figure 17), show no evidence of crack initiation, though selective phase corrosion was noted. In this case, the austenitic phase was selectively corroded, whereas selective corrosion of the ferrite phase was observed in most tests at lower temperature and higher H_2S pressure.

In the above case, it appears that the H_2S content was sufficient to initiate localized corrosion but not to establish crack initiation conditions. EDAX analysis of residual corrosion product films showed no evidence of sulfide normally observed at higher H_2S levels. The H_2S analysis of gas phase samples ranged from 20 to 30 ppm, both at the start and termination of the test.

A second test showing localized corrosion but not SCC at low H_2S levels is also of interest. Tests with DCB specimens lasting six weeks in 10% NaCl/~ 50 bar CO_2 + 0.011 bar H_2S at 60°C showed no evidence of SCC (Table 6). Both the fatigue pre-cracked surface and at least 95 to 99% of the surface remained fully passive. However, random sections were "stained". Upon examination, these areas were shown to be

TABLE 6. TEST METHOD DEPENDENCE OF Cl^-/H_2S SCC

Tests in 5.1 M Cl^-/CH_4-CO_2-H_2S at 177°C and ~0.2 bar H_2S.

SPECIMEN	LOAD	RESULT
C-ring	to σ_y = 1020 MPa	No SCC in 4-week test
Notched C-ring	to σ_y = 1020 MPa	SCC (4-week test)
DCB (See Table 6)	to K ~ 50 MN $m^{-3/2}$	SCC in 6-week test; 2.5 mm crack growth; final K = 42 MN $m^{-3/2}$
Slow Strain Rate (See Table 5)	to failure	SCC

TABLE 7. EFFECT OF H_2S ON SLOW STRAIN RATE TESTS

Tests in 5.1 M (25%) NaCl at 177°C with CH_4 added to a total test pressure of ~ 200 bar.

TEST CONDITIONS			AVERAGE CRACK GROWTH RATE, mm/day	
P_{H_2S} bar	P_{CO_2} bar	INSULATION	17% CR "X" (σ_y = 910 MPa)	48% CR "A" (σ_y = 1100 MPa)
1.8	40	?	0.84	0.68
0.4	60	Yes	0.18	0.26
0.25	60	?	0.46	0.34
0.09	30	Yes	0.24, 0.14	
0.04	30	?	0.20	
~0.02*	~20	?	0.03**	0.02**
0.003	20	?	< 0.005**	

* Gas leak during test resulted in steady decrease of P_{H_2S} and P_{CO_2}. Estimates are average value for final 1/3 test period.

** Judged to be pitting corrosion, not SCC.

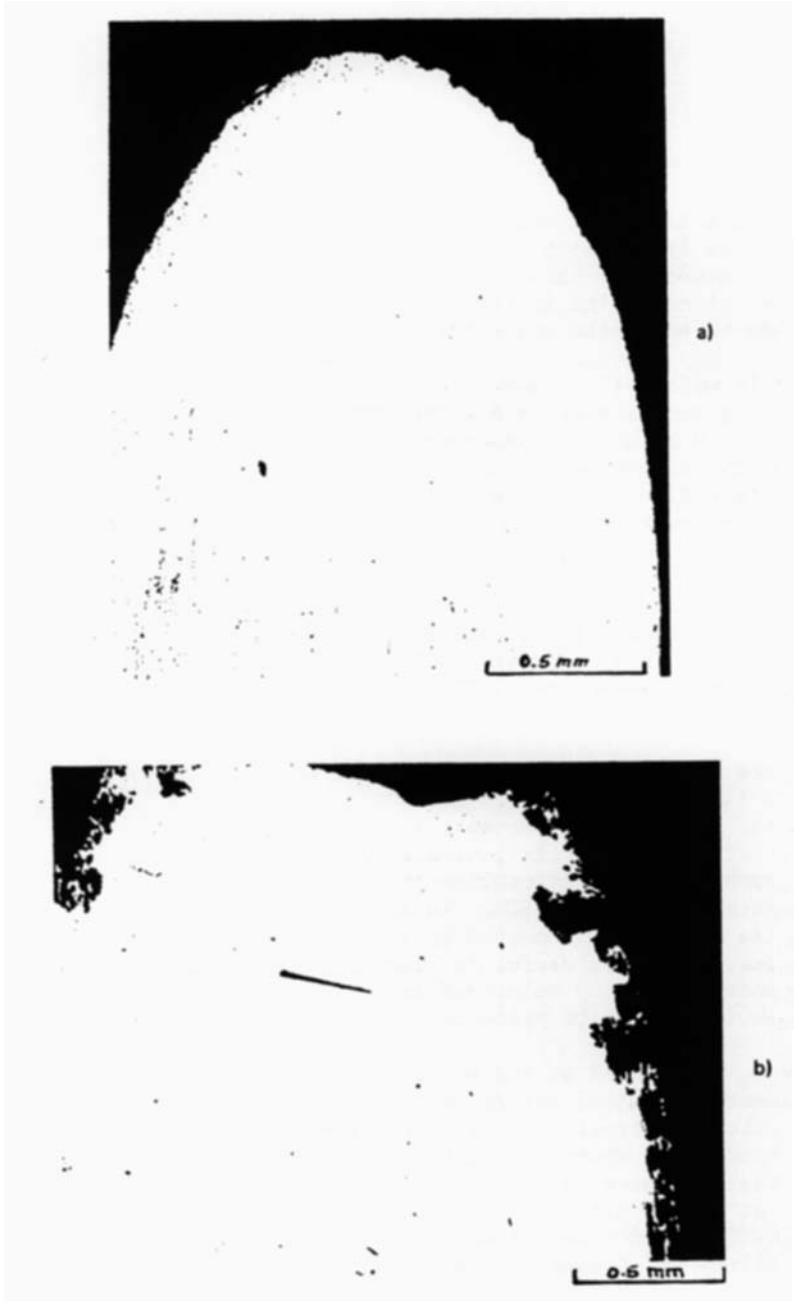


Figure 16. Effect of Trace H_2S on Slow Strain Rate Fracture
17% CR "B" (σ_y = 875 MPa) in 5.1M NaCl/55 Bar CO_2
at 130°C: (a) No H_2S (b) 3×10^{-5} Bar H_2S.
Magnification: 50X.



Figure 17. Enlargement of Localized Corrosion on Figure 15b
Preferential Corrosion of Austenite Phase.
Magnification: 500X.

porous sulfide corrosion product films and were associated with regions of active corrosion (to a depth of 0.2 mm in six weeks). Accordingly,the SCC immunity in this test appears to be conditional on the absence of corrosion in the fatigue pre-crack region, rather than to an innate immunity.

Temperature Effect. Tests with C-rings show a strong beneficial effect of increasing test temperature above 60°C, as is shown in Figure 18. At ~ 0.2 bar H_2S, immunity at 120°C is indicated, even for the alloys having maximum cold reduced strength. For each test temperature, results of several alloys and applied stresses have been included, i.e., results in Figure 18 at 60°C correspond to data displayed in Figure 15.

Tests with DCB specimens also show a beneficial effect of temperature, as is indicated in Table 8. However, SCC persisted (at 0.2 bar H_2S) at temperatures to 177°C, with immunity indicated only at 230°C.

Test with slow strain rate tests also show a beneficial effect of temperature, as is indicated in Table 9 and Figure 19. As with DCB tests, full immunity appears to require temperature of 230°C or higher. It is probable that several factors need to be considered to rationalize this unexpected effect of temperature upon anodic SCC. In addition to classical passive film rupture or absorbed hydrogen (via localized cells) concepts, it may be useful to also examine the temperature dependence of many solutions and surface reactions that can be influenced by presence of H_2S.

O_2 Contaminants. Trace O_2 introduced at the start of the autoclave tests (see experimental section) was found to increase susceptibility to pitting corrosion. This trend was particularly evident under conditions where the test specimens otherwise remained virtually immune to pitting corrosion, such at 10% NaCl at 60°C. Evidence presented in a prior section postulates H_2S_2 (derived from O_2) as responsible for enhanced susceptibility to pitting corrosion.

In all studies to date, this residual effect of trace O_2 has not been found to significantly accelerate SCC susceptibility. A slight detrimental effect may be inferred from data summarized in Table 5, however.

Galvanic Coupling. Coupling to Hastelloy C-276 appears not to be an important variable in the current series of tests. In slow strain rate tests, some accelerated localized

TABLE 8. TEST RESULTS WITH PRE-CRACKED DCB SPECIMENS

Tests at ~ 50 bar CO_2. Crack growth indicated in parenthesis in mm.

Alloys tested:
(1) "B", σ_y = 850 MPa; (2) "B", σ_y = 1020 MPa; (3) As (2), but aged 260°C/1000 hrs; (4) "F", σ_y = 1030 MPa

TEST CONDITIONS[a]				K, MN $m^{-3/2}$					
				CO_2-H_2S			CH_4-CO_2-H_2S[b]		
T, °C	t, WEEKS	P_{H_2S}, bar	NaCl, M	(1)	(2)	(4)	(1)	(2)	(3)
60	6	0.011	1.8	51 (None)	68 (None) 48 (None)	50 (None)			
60	5	0.07	5.1	48 (5)	40 (11)				
60	6[c]	0.20	5.1				47 (None)	23 (12)	22 (13)
130	6	0.11	5.1	58 (1.5)	55 (3)	43 (4)			
177	2	~ 0.1	5.1	47 (None)	46 (None)				
177	6[c]	0.16	5.1				50 (None)	42 (2.5)	44 (7)
230	4	0.11	5.1						52 (None)

(a) Average H_2S analysis was determined by frequent H_2S analysis in the gas phase. Some decay was noted in CH_4-CO_2-H_2S tests, necessitating additional H_2S charging to maintain the desired level. In the CO_2-H_2S tests, the H_2S content showed only a modest decay during the test.

(b) Tests with CH_4 (charged to ~ 200 bar) also contained trace O_2.

(c) Tests were interrupted every two weeks to note crack growth.

TABLE 9. EFFECT OF TEMPERATURE ON SLOW STRAIN RATE TESTS

Tests in 5.1 M (25%) NaCl at ~ 0.15 bar H_2S with CO_2 and CH_4 added (plus H_2O vapor pressure) to a test pressure of ~ 200 bar.

Insulation is uncertain on most specimens.

TEST CONDITIONS			AVERAGE CRACK GROWTH RATE, mm/day	
T, °C	P_{H_2S} bar	P_{CO_2} bar	17% CR "X" (σ_y = 910 MPa)	48% CR "A" (σ_y = 1100 MPa)
74	~ .16	35	0.26	0.16
121	.17	70	0.18, 0.19	
177	.15*	~45	~ 0.26*	
232	~ .15	60	0.15 (? SCC)	0.06 (No SCC)
288	~ .14	8	0.06 (No SCC)	0.11 (?)
288	~ .11	25	0.03 (No SCC)	0.04 (No SCC)

* Results at 177°C at P_{H_2S} = 0.15 bar interpolated from data in Table 7 at higher and lower H_2S partial pressures.

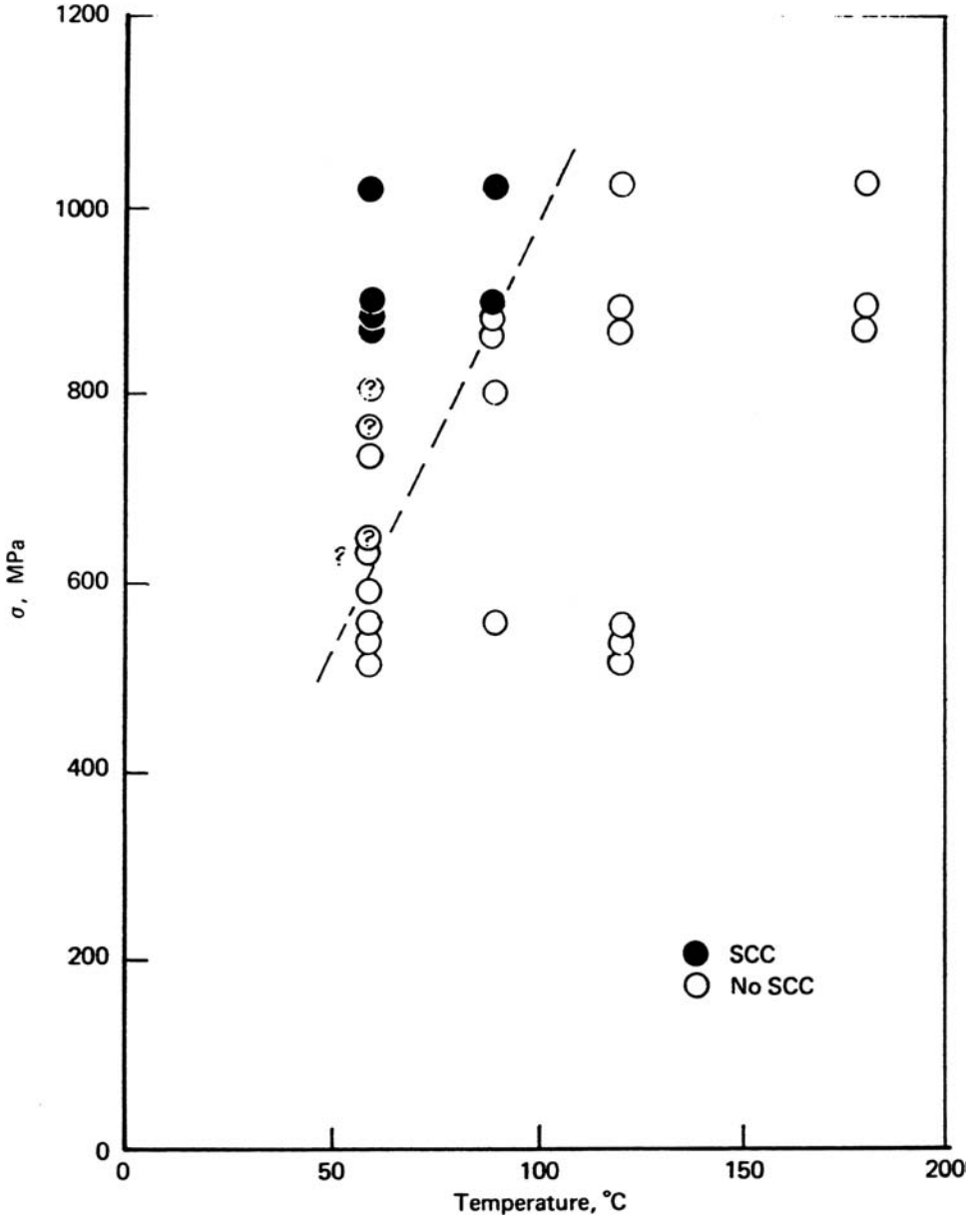


Figure 18. Temperature Effect on Cl^-/H_2S SCC
Two week tests with C-rings in 1.8 M NaCl/150 bar CH_4 + 50 bar CO_2 + 0.2 bar H_2S

03541

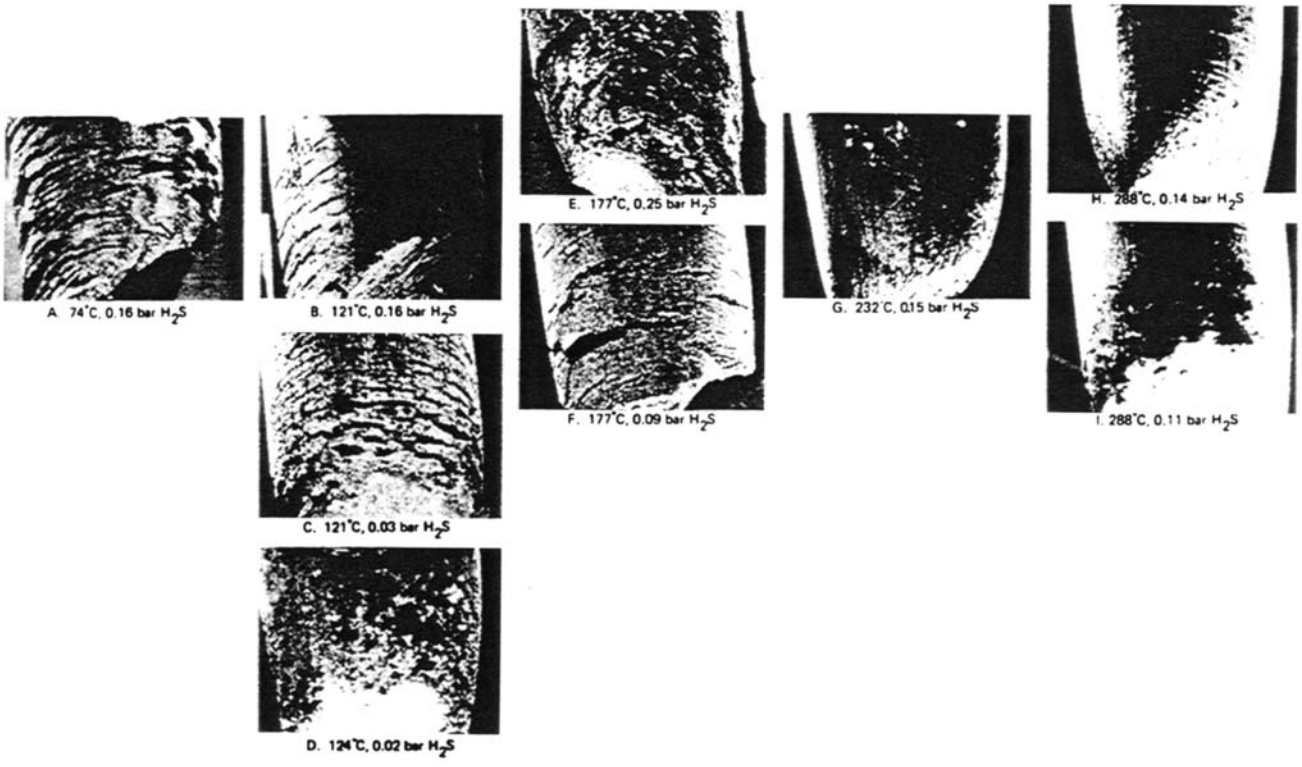


Figure 19. Effect of Temperature on SCC Susceptibility in Slow Strain Rate Tests
(See details in Tables 7 and 9)

corrosion may have occurred, but no strong effect upon SCC susceptibility was noted.

Alloy Content. No significant effect of alloy content was noted. The experimental composition, which had a higher Cr+Mo content, showed no beneficial effect with C-ring or DCB tests at temperatures above 120°C. Some benefit was noted at 60°C, however.

Low Temperature Aging. No detrimental effect was noted upon aging at 260°C for 1000 hours. Comparative DCB tests indicated no effect on SCC susceptibility (Table 8). More extensive tests with C-rings led to the same conclusion.

CONCLUSIONS

There appear to be risks of SCC of duplex stainless steels in saline sour gas environments, as evaluated in autoclave tests at 200 bar, even at H_2S partial pressures of 0.1 bar (= 1.5 psi H_2S) or less. SCC risks are attributed to a Cl^-/H_2S synergism in promoting an anodic mode of initiation and crack propagation, which is operative at ambient temperatures as well as elevated temperatures. However, increasing test temperatures above 150°C results in an improved resistance to SCC. SCC risks increase as the H_2S partial pressure increases. SCC risks also increase with yield strength when comparing specimens stressed to their yield point. No detrimental effect of low temperature aging was noted.

The occurrence of SCC in any particular test medium was found to be sensitive to test techniques. In particular, specimen orientation, notch effects, and dynamic straining appear to be important variables influencing SCC initiation in marginal environments (high temperature or low H_2S).

In order to adequately describe the mechanism of Cl^-/H_2S SCC of duplex stainless steels, it appears that a number of corrosion reactions need to be considered; i.e., the solution chemistry within active pits, the contribution of absorbed hydrogen, the protective properties of sulfide corrosion product films, and the anodic and cathodic reactions of freshly exposed metals.

REFERENCES

1. T. R. Bates, unpublished results, Shell Development Company, 1978.

2. R. B. Heady, Corrosion, 33, 98 (1977).

3. O. A. Onyewuenyi, unpublished results, Shell Development Company, 1982.

4. R. E. Reed-Hill, "Physical Metallurgy Principles", p. 250f, D. Van Nostrand Co., Inc., Princeton (1964).

5. G. Herbsleb and R. K. Poepperling, Corrosion, 36, 611 (1980).

6. T. Kudo, H. Miyuki, H. Okamoto, J. Murayama, and T. Moroishi, Paper No. 127, CORROSION/82, NACE Conference, Houston, March 1982.

7. J. Kolts, and A. I. Asphahani, Paper No. 99, CORROSION/81, NACE Conference, Toronto, April 1981.

8. J. Oredsson and S. Bernhardsson, Paper No. 126, CORROSION/82, NACE Conference, Houston, March 1982.

9. P. R. Rhodes, "H_2S Corrosion in Oil and Gas Production - A Compilation of Classical Papers", R. N. Tuttle and R. D. Kane, eds., p. 843, NACE, Houston, 1981.

10. B. LeFebvre, G. Guntz, J. C. Prouheze, J. C. Vaillant, J. R. Mantelle, P. Bounie, and J. P. Giraud, Paper No. 128, CORROSION/82, NACE Conference, Houston, March 1982.

11. A. I. Asphahani, Paper No. 99, CORROSION/81, NACE Conference, Toronto, April 1981.

12. S. O. Bernhardsson, J. Oredsson, and M. Tynell, Paper No. 14, CORROSION/80, NACE Conference, Chicago, March 1980.

Copyrighted Materials
Copyright © 1996 NACE International Retrieved from www.knovel.com

Paper No.
59

CORROSION 95
The NACE International Annual Conference and Corrosion Show

Investigation of the Stress Corrosion Cracking of Duplex Stainless Steel Weldments in Sour Conditions

Michael J Schofield
Cortest Laboratories Ltd
23 Shepherd Street
Sheffield
S3 7BA, UK

Roy Bradshaw and R A Cottis
Corrosion and Protection Centre
UMIST
Manchester M60 1QD, UK

ABSTRACT

Duplex stainless steels are increasingly widely used in the oil and gas production industry for a variety of applications. The stress corrosion cracking (SCC) behaviour of wrought material is reasonably well understood, and limits of use are placed upon these alloys in NACE MR0175, for sour service. However, the SCC behaviour of weldments is less well understood, and this has limited the use of welded material in H_2S-containing conditions.

The SCC resistance of duplex stainless steels is influenced by their microstructure as well as their chemical composition and the objective of the research reported in this paper is to investigate the SCC behaviour of welded 22%Cr and 25%Cr alloys in a simulated oilfield environment. Mechanised orbital TIG was used to butt weld 168mm outside diameter tubes. The shielding gas contained nitrogen additions of up to 10% (in the case of UNS S32760) and 7% (in the case of UNS S31803). Slow strain rate testing (SSRT) was conducted on cross-weld specimens in sodium chloride solutions overpressured with varying partial pressures of H_2S and CO_2. The SSRT results, in terms of ductility parameters and secondary cracking, are correlated with fractography and metallurgical examination of crack morphology in order to establish the effects of the welding process and the nitrogen content of the shielding gas.

It was found that the nitrogen uptake from the shielding gas has a detrimental effect on SCC resistance of duplex stainless steel weldments. Whilst this effect is only modest, it is in direct contrast to the beneficial effect it has on pitting corrosion resistance.

Keywords: duplex stainless steel, welds, nitrogen, stress corrosion cracking, sour.

INTRODUCTION

The stress corrosion cracking behaviour of duplex stainless steels (DSS) is reasonably well understood in terms of some of the limits of use of these alloys.[1] In this paper cracking is considered only in H_2S-containing environments. Limits of use are nowadays placed on materials in NACE MR0175[2], e.g. UNS S32750 is limited to 1.5 psi H_2S partial pressure. Hardness limitations apply to all materials in MR0175 and temperature, chloride ion levels and pH are applied to some. All such limits must be considered somewhat arbitrary inasmuch as some key details of the mechanism of H_2S SCC of DSS are not yet understood. Almost all published data relate to non-welded material, typically for tubulars and other downhole equipment. No limits of use have been proposed for welded DSS although there is a widespread assumption that in MR0175 welded materials are subject to the same limits of use as non-welded material at the same hardness level. For DSS there is a further complication, that of nitrogen additions made to the shielding, plasma or root (backing) gas in order to improve resistance to localised corrosion.[3,4,5] Pitting corrosion resistance is significantly increased, especially for the lower-alloyed duplex grades. No published data exist on any effect this nitrogen may have on SCC behaviour.

The primary aim of the work reported in this paper is to examine the influence of nitrogen pick-up from shielding gas on the SCC behaviour of 22Cr and 25Cr DSS. This was evaluated by the means of the slow strain rate test technique, with a further objective of assessing the technique for its predictive capability compared with conventional constant load or constant strain test methods. Testing was undertaken in three simulated sour oilfield environments. Some results have been reported previously[6] and the present paper extends that work.

TEST MATERIALS

UNS S31803(1) duplex and UNS S32760(2) superduplex stainless steel were tested in this programme. The compositions of parent metals and consumables are presented in Table 1. The 0.2% proof stresses were 565 and 659 MPa respectively. Schedule 40 (168mm OD X 7.11mm wall thickness) tube was butt welded by mechanised GTAW.

Full details are provided in reference 1. The tubes were machined down to 5.5mm wall thickness and welded in three passes as shown in Ref. 1. Welding was achieved in three passes. All welding parameters were the same for the three welds made in both materials; the shielding gases employed for this investigation were Ar, Ar + 2% N_2, Ar + 5% N_2, Ar + 10% N_2. In addition some tests were conducted on parent metal.

(1) Avesta SAF 2205
(2) Zeron 100

STRESS CORROSION CRACKING TESTING

Full details of the test technique and conditions have been presented[6] and are summarised below:

Smooth tensile (sub-size TM0177 Method A) specimens were subjected to monotonic slow strain rate testing at 4 x 10^{-6} s^{-1} at 90°C in air and three test environments: (1) 20% NaCl solution with 0.2 bar H_2S and 19.8 bar CO_2; (2) 20% NaCl solution with 0.05 bar CO_2 and 20 bar CO_2; (3) 5% NaCl solution with 0.05 bar H_2S and 20 bar CO_2.

TEST RESULTS

Some test results have been presented[6], but further testing has been undertaken to investigate some anomalies. The test results are presented in Figures 1 - 8 and summarised in Tables 2 and 3. Further pertinent details are given below:

- specimens that exhibited ductility on the fracture face generally showed no secondary cracking
- air tests resulted in ductile tearing of the weld metal
- welded SCC test specimens failed at the fusion line
- the extent of nitrogen pick-up into the weld metal is shown in Table 4
- the influence of the nitrogen content of the shielding gas on the phase balance of three regions of the weldment is shown in Table 5.

DISCUSSION

Failure Mode and Location

The main fracture face exhibited transgranular cracking of the austenite phase, with some preferential dissolution of the ferrite phase in all instances except one. Preferential ferrite dissolution is generally observed in relatively reducing (typically acidic, H_2S-containing) environments. Furthermore the ferrite phase has greater ductility than austenite, which is susceptible to cold working. Austenite dissolution with ferrite cracking occurred in the least severe test environment in a UNS S31803 non-welded specimen; in this parent material the austenite content was roughly 50% whereas in all the welded specimens of this material the austenite content at the failure location was significantly lower. Whilst preferential phase dissolution is best attributed to compositional differences between the phases and the redox potential of the test environment, the observed difference in cracking behaviour may be more influenced by simple phase balance.

All welded specimens failed at the fusion line, with cracks initiating in the ferritised area of the high temperature heat affected zone. In this region especially, chromium and molybdenum partition into the ferrite phase, which has the effect of increasing its corrosion resistance. Simultaneously, nitrogen partitions into the austenite which increases its pitting resistance above that of the ferrite. In corroding, the ferrite serves to cathodically protect the austenite, thus conferring some degree of stress corrosion cracking resistance. Careful metallographic examination of these areas has failed to

reveal any detrimental third phase, such as sigma, or precipitates such as chromium nitrides.

Failure Criteria

The presence of secondary cracking on the test specimens correlates well with the appearance of the fracture faces. Where a few shallow cracks are observed on a specimen (usually, one or two were seen at X50 magnification in plan but more were detected by metallurgical cross sectioning) the fracture appeared to be very ductile. In all other cases except one the specimens exhibited no observable ductility and many secondary cracks were seen. These observations correlated completely with the appearance of the load extension curve; ductile specimens exhibited a full curve which is analogous with the material's stress-strain curve whereas cracked specimens exhibited abbreviated curves.

The absolute time to failure gave a general correlation with cracking behaviour but could not be considered to be a good failure criterion. This is largely due to the variation in ductility across the range of materials tested. The incorporation of nitrogen during welding increased the ductility of the weldment but this was not reflected in the load extension curves in the test environments. In the extreme case the time to failure of UNS S31803 parent metal in environment 1 (which cracked) was 70% of the time to failure of Ar welded UNS S32760 tested in air.

The normalised time to failure (given in Tables 2 and 3) varied from 0.27 - 0.59 in environment 1, with a narrower range of 0.35 - 0.48 in the less severe environment 2. By definition, an air test has a value of 1.0 therefore normalised TTF could be a useful parameter for these tests.

The normalised UTS (i.e. ratio of maximum load in test to maximum load for the test material in air) has previously been proposed as a pass/fail criterion. However, in these test values the range 0.76 - 0.96 were obtained in environment 1 and 0.75 - 0.99 in environment 2. To compare this with 1.0 for an air test (i.e. clear pass) would be meaningless.

Influence of Nitrogen

Nitrogen is added to the shielding gas in TIG welding to prevent the loss of nitrogen from the weld, which would cause loss of corrosion resistance and a reduction in austenite content. Additions of 2.5-3% N_2 are recommended[8] and higher levels should be avoided since they destabilize the arc causing spatter and porosity. Chromium nitride precipitation is reported to be reduced in weld metal despite the incorporation of nitrogen from the shielding gas[10]. The procedure developed for the preparation of test material used in this work[7] has been shown to give no such problems even with nitrogen additions as high as 7% for UNS S32760 and 10% for UNS S31803.

The effect of the nitrogen content of the shielding gas on SCC behaviour proved to be slightly detrimental. The level of nitrogen pickup is quantified in Table 4. The welds in all cases cracked sooner (i.e. at lower strains) than parent metal. The effect of nitrogen

was to decrease the SCC performance of the weld; shorter times to failure were observed for welds made with nitrogen in the shielding gas compared with those made with argon only. This is despite the fact that the nitrogen increased the ductility of welds (as shown in the air test of UNS S32760).
Inspection of Figures 7 and 8 indicates the difference between welds and parent metal; the range of elongation at failure values is wider for welds than it is for the parent metals and is similar for all the welds irrespective of nitrogen content.

These results contrast greatly with the beneficial effect that nitrogen has on pitting corrosion resistance.[10] Presumably crack initiation is not in these cases related to pit formation. Examination of the test results show no correlation between time to failure and the austenite content at the cracking location. No correlation is observed between time to failure and the degree of nitrogen pick-up during welding.

Comparison of Test Methods

The SSRT results presented here indicate a much greater degree of SCC susceptibility than has been reported elsewhere for constant deflection tests on these parent materials in the same test conditions. C-ring and 4 point bent beam tests on UNS S32760 stressed to its measured 0.2% proof stress in environment 1 conditions have shown no cracking in 30 days. This may imply that the presence of plastic strain (i.e. plastic deformation or cold work which is caused during the SSRT test) is responsible for the observed cracking.

In order to quantify the degree of cold work that occurred during testing, microhardness testing was undertaken on a number of the test specimens. The results, which are presented in Tables 2 and 3, fail to show any correlation between the increase in hardness and the failure mode or time to failure. All specimens exhibit a high degree of hardening; the UNS S31803 welds were all below 200μH_V prior to testing and after testing had increased to 259-347. A similar extent of hardening was experienced by the UNS S32760, though this was harder initially than the UNS S31803.

The slow strain rate test technique has not been universally accepted for evaluating the stress corrosion cracking behaviour of duplex stainless steels. This work does not increase the confidence in results obtained by this method.

CONCLUSIONS

From the results of this investigation it can be concluded that:

- the stress corrosion cracking resistance in sour conditions of welded duplex stainless steel is inferior to that of parent metal.
- the effect of nitrogen in the shielding gas is detrimental to stress corrosion cracking in our conditions, despite its widespread use as a means of improving resistance to pitting corrosion.
- slow strain rate testing of welded duplex stainless steels is not to be preferred over conventional constant displacement or constant strain techniques.

REFERENCES

1. M.J. Schofield, 'Defining safe use limits for duplex stainless steels', Proc. Duplex Stainless Steel '91. Les éditions de physique, Vol. 1, p. 241-255.

2. Standard Material Requirements - Sulfide Stress Cracking Resistant Metallic Materials for Oilfield Equipment, MR0175, NACE 1994.

3. O. Jonsson et al 'The Role of Nitrogen in Longitudinal Welding of Tubing in Duplex Stainless Steels', Proc. Duplex Stainless Steel '91. Les éditions de physique, Vol. 1, p. 461- 468.

4. B. Josefsson et al 'Phase Transformations in Duplex Stainless Steels and the Relation Between Continuous Cooling and Isothermal Heat Treatment', Proc. Duplex Stainless Steel '91. Les éditions de physique, Vol. 1, p. 67-78.

5. B. Bonnefois et al 'Some Aspects of Nitrogen Introduction in the Duplex Weld Pool', Proc. Duplex Stainless Steel '91. Les éditions de physique, Vol. 1, p. 469 -478.

6. M. J. Schofield et al, 'Investigation of the Stress Corrosion Cracking Susceptibility of Weldments in Duplex Stainless Steels', Paper 29, Duplex Stainless Steels '94, Glasgow, 1994.

7. R. Bradshaw and R.A. Cottis 'The Effect of Nitrogen Additions to Argon Shielding Gases on the Properties of Duplex Stainless Steel GTA Welds', Paper 31, Duplex Stainless Steel '94, Glasgow, 1994.

8. C.A. Pettersson and S.A. Fager, 'Welding Practice for the Sandvik Duplex Stainless Steels', Sandvik R & D S-91-57-ENG, April 1994.

9. R.A. Walker and B.J. Ginn, 'A Magnetic 'Etching' Technique for Phase Identification in Duplex Ferric-Austentitic and other Stainless Steels' Microstructural Science, Volume 15, EMG 909, 1986.

10. O. Jonsson et al, 'The Role of Nitrogen in Longitudinal Welding of Tubing in Duplex Stainless Steels', Avesta Sheffield ACOM 2-1994.

Table 1 Composition of parent material and consumables

	C	Si	Mn	P	S	Cr	Ni	Mo	Cu	Nb	W	N	PRE_N
UNS S31803	.015	.51	0.85	.020	.001	22.0	5.59	3.10	-	-	-	.15	34.7
Avesta 2205	.014	.47	1.58	.017	.001	22.3	8.8	3.10	.09	-	-	.14	34.9
UNS S32760	.027	.53	0.79	.014	.007	25.5	6.90	3.58	.69	-	.72	.29	41.95
Z 100X	.016	.33	0.78	.020	.001	25.2	9.16	3.66	.64	<.02	.58	.23	40.9

Note: PRE_N = Cr + 3.3 Mo + 16 N

Table 2 SSRT results for UNS S31803 - time to failure

Test environment	Test (i) material	Normalised TTF (ii)	Normalised UTS	Material hardness (μHv) before	after test
Air	Ar	29.3 (iii)	736.7 (iv)		
20% NaCl 0.2 bar H_2S 19.8 bar CO_2	PM Ar 2% N_2	0.59 0.28 0.28	0.94 0.84 0.91	177	294
20% NaCl 0.05 bar H_2S 20 bar CO_2	Ar 2% N_2 5% N_2	0.35 0.38 0.47	0.75 0.91 0.92	195 197 188	272 347 259
5% NaCl 0.05 bar H_2S 20 bar CO_2	PM 2% N_2 5% N_2	n/a n/a n/a	n/a n/a n/a	177 197 199	283 286 298

Notes: (i) PM = parent metal, Ar = Argon welded, 2% N_2 = Ar + 2% N_2 in shielding gas , 5% N_2 = Ar + 5% N_2 in shielding gas

(ii) TTF = $\frac{\text{time to failure in test}}{\text{time to failure in air}}$

(time to failure in environment 3 is taken where no air test was performed)

(iii) Absolute values for air tests (hours)

(iv) Absolute values for air tests (MPa)

Table 3 SSRT results for UNS S32760 - time to failure

Test environment	Test (i) material	Normalised TTF (ii)	Normalised UTS	Material hardness (μHv) before	after test
Air	Ar 5% N_2	41.3 (iii) 21.6 (iii)	837.8 (iv) 857.3 (iv)	208	355
20% NaCl 0.2 bar H_2S 19.8 bar CO_2 20 bar CO_2	PM Ar 2% N_2 5% N_2	0.39 0.38 0.32 0.27	0.96 0.90 0.88 0.76	208 208 215 210	358 321 315 355
20% NaCl 0.05 bar H_2S 20 bar CO_2	Ar 2% N_2	0.51 0.48	0.89 0.99	208 225	283 346
5% NaCl 0.05 bar H_2S 20 bar CO_2	PM 2% N_2	n/a n/a	n/a n/a		

Notes: (i) PM = parent metal, Ar = Argon welded, 2% N_2 = Ar + 2% N_2 in shielding gas , 5% N_2 = Ar + 5% N_2 in shielding gas

(ii) TTF = $\frac{\text{time to failure in test}}{\text{time to failure in air}}$

(iii) Absolute values for air tests (hours)

(iv) Absolute values for air tests (MPa)

Table 4 Nitrogen content (wt %) of weld metal

Weld	Uns S31803		UNS S32760	
	Root	Cap	Root	Cap
Ar	0.09	0.11	0.24	0.17
Ar+ 2% N_2	0.16	0.17	0.28	0.28
Ar+ 5% N_2	0.17	0.20	0.29	0.29
Ar+ 7% N_2	0.19	0.22	0.31	0.32
Ar+ 10% N_2	0.21	0.24		

Note: determined by Leco infra red technique

Table 5 Ferrite content (vol %) at fusion line of weld

Weld	UNS S31803	UNS S32760
Ar	73.9	58.0
Ar+ 2% N_2	76.9	57.3
Ar+ 5% N_2	68.6	54.2
Ar+ 7% N_2	76.4	57.6
Ar+ 10% N_2	66.8	

Note: determined on 10 fields at X50 magnification using Magiscan image analysis system after magnetic etching, per reference 9.

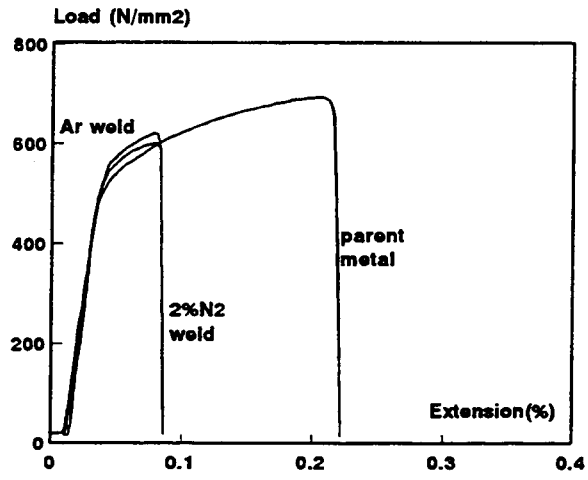


Figure 1. SSRT data for UNS S31803 in environment 1.

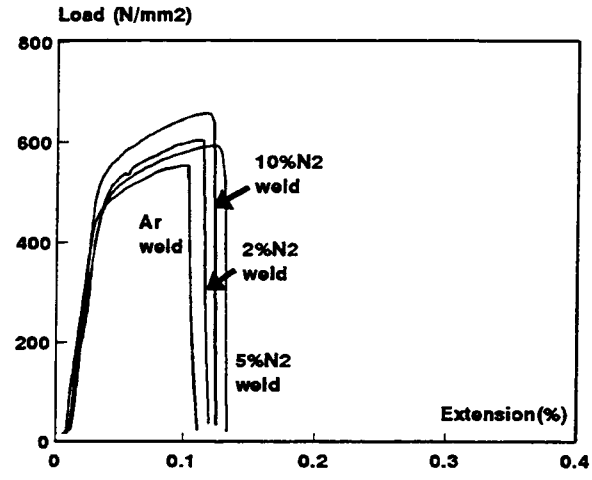


Figure 2. SSRT data for UNS S31803 in environment 2.

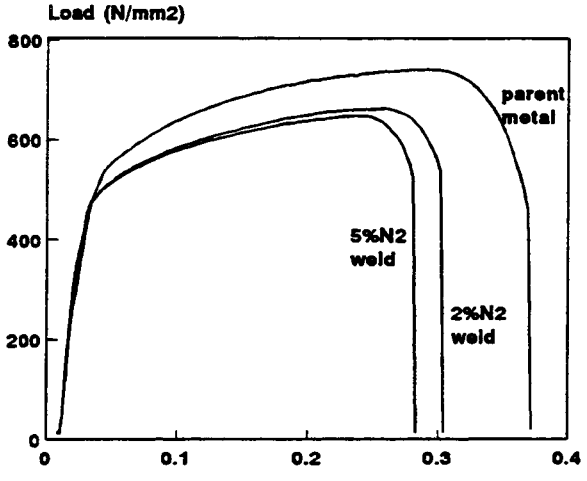


Figure 3. SSRT data for UNS S31803 in environment 3.

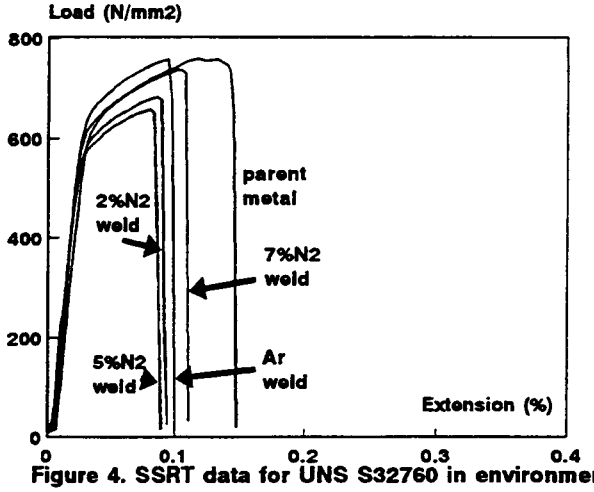


Figure 4. SSRT data for UNS S32760 in environment 1.

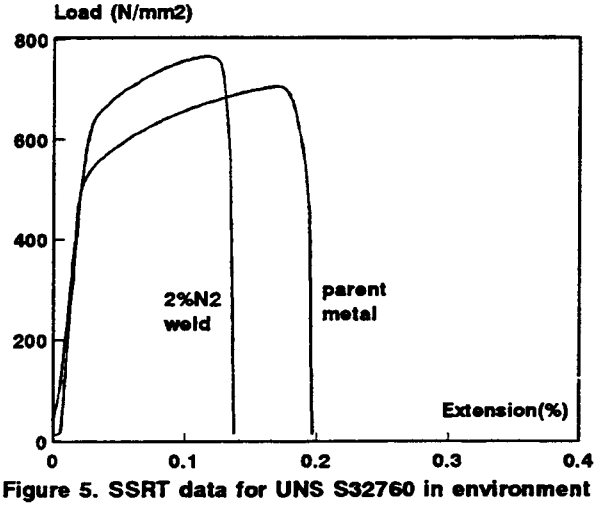


Figure 5. SSRT data for UNS S32760 in environment 2.

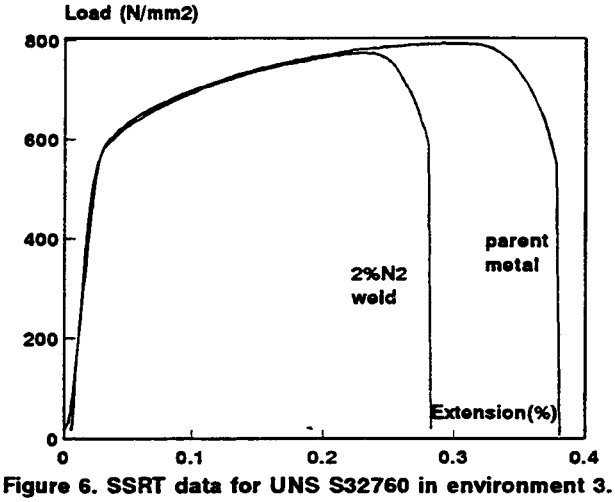


Figure 6. SSRT data for UNS S32760 in environment 3.

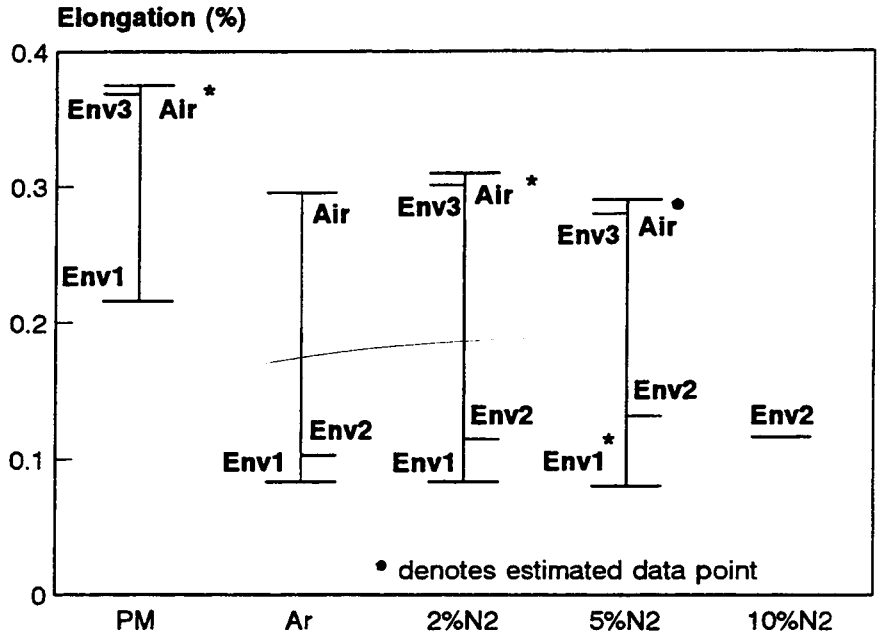


Figure 7. Elongation at failure UNS S31803

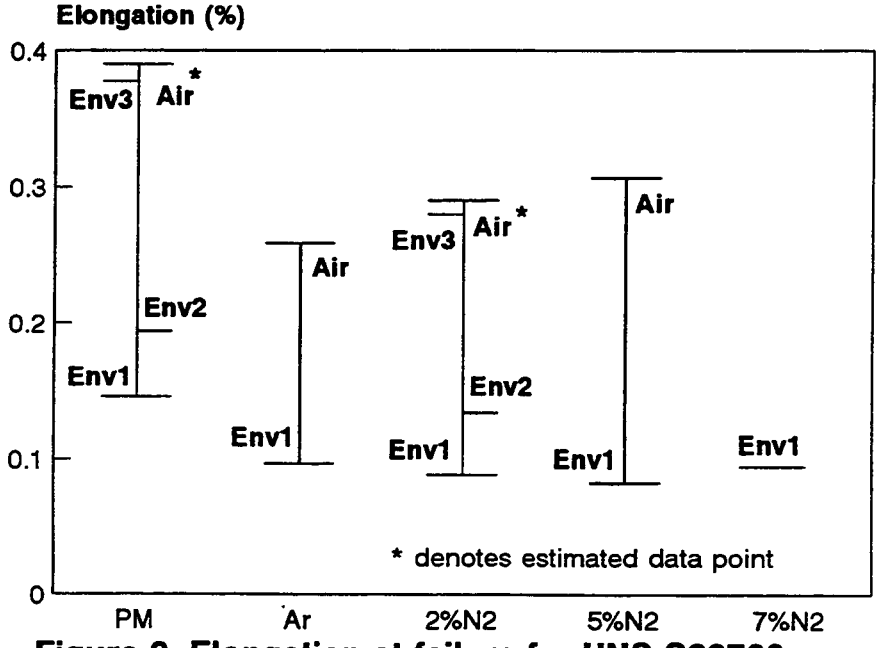


Figure 8. Elongation at failure for UNS S32760.

Copyrighted Materials
Copyright © 1996 NACE International Retrieved from www.knovel.com

KAWASAKI STEEL TECHNICAL REPORT No. 19 November 1988

Optimizing Welding Condition for Excellent Corrosion Resistance in Duplex Stainless Steel Linepipe*



Katsuomi Tamaki
Senior Researcher, Tubular Products Lab., Heavy Steel Products Research Dept., I & S Research Labs.



Koichi Yasuda
Senior Researcher, Joining & Physical Metallurgy Lab., Heavy Steel Products Research Dept., I & S Research Labs.



Mitsuo Kimura
Senior Researcher, Joining & Physical Metallurgy Lab., Heavy Steel Products Research Dept., I & S Research Labs.



Hiroaki Kawasaki
Staff Manager, Technical & Quality Control Sec., Technology & Production Control Dept., Chita Works



Tatsutumi Uegaki
Staff Assistant Manager, Pipe Control Sec., Technical Control Dept., Chiba Works

Synopsis:

The corrosion resistance of the girth weld heat affected zone(HAZ) of duplex stainless steels was discussed in connection with hostile environment linepipe applications.

The girth weld HAZ produced with a slow cooling rate welding procedure using a high pitting index base metal (Cr + 3Mo + 16N = 34.0%) showed the same corrosion resistance as the base metal, even in the as-welded condition. This is considered that the slow cooling rate allows sufficient time for the chromium to heal the chromium depleted area adjacent to chromium nitride precipitates.

1 Introduction

With the development of corrosive oil and gas fields and further the application of the secondary recovery method to such fields, stainless steel, which offers excellent anti-corrosion properties, has been adopted as an essential material. Duplex stainless steel has been attracting attention, in particular, as a linepipe material for natural gas which contains large volumes of CO_2.

Duplex stainless steel consists of ferrite and austenite, with an optimum combination ratio of the phases (generally 40–60% austenite; the rest ferrite)[1]. Duplex stainless steel possesses both the excellent resistance to chloride SCC of ferritic stainless steels and the good notch toughness and the resistance to other types of corrosion of austenitic stainless steels.

However, caution must be paid to the deterioration of the corrosion resistance of the weld metal and HAZ of the girth weld joints which results from an unbalance of the austenite/ferrite fraction in the microstructure.

This paper discusses methods of improving the corrosion resistance of the girth weld joint, which is generally not solution annealed after welding.

2 Experimental Procedure

The materials used for tests were three kinds of API 5L X70 grade pipe, a double submerged arc welding (DSAW) UOE pipe (508 mm OD × 14.3 mm *t*, pitting index (PI)[2] = Cr + 3Mo + 16N = 34.1) and two seamless pipes (219.1 mm OD × 19.05 mm *t*, PI = 32.2 and 34.1), the nominal chemical compositions of which were 22Cr-5.5Ni-3Mo-0.15N (ASTM A790 S31803, DIN 1.4462).

The austenite fraction, toughness, and resistance to pitting corrosion of the HAZ were studied with simulated HAZ specimens (PI = 32.2, N = 0.13%).

The influence of welding heat input on pitting corrosion resistance was tested in a 10% $FeCl_3 \cdot 6H_2O$ solution at 30°C for 24 h. Two kinds of seamless pipes were examined, one with a high pitting index (PI = 34.1) and one with a low pitting index (PI = 32.2). Test specimens were taken from the melt-run gas tungsten arc weld (GTAW) beads. The welding heat input was varied

* Originally published in *Kawasaki Steel Giho*, 20(1988)3, pp. 197–202

Reprinted with permission of Kawasaki Steel

from 3 to 42 kJ/cm by changing the welding speed while maintaining a constant current of 200A and voltage of 12V. Furthermore, welded specimens produced by submerged arc welding (SAW), gas metal arc welding (GMAW), and GTAW, with 9% nickel matching wires were prepared. The specimen sizes were 40 mm$W$ × 50 mm$L$ × 6 mm$t$ (W, transverse to welding direction; L, welding direction; and t, thickness) for the melt run GTAW beads and 40 mm$W$ × 50 mm$L$ × 2 mm$t$ for the others. Each specimen had the weld metal at the center of the specimen. To understand the influence of heat input more precisely, the simulated HAZ specimens were examined.

For girth welding, the shielded metal arc welding (SMAW) method was employed. Test specimens were taken from the location of 1 mm inside the root pass. All specimens were polished with #240 abrasive paper.

3 Results and Discussion

3.1 Metallurgical Characteristics of the Girth Weld HAZ

A weld metal of chemical composition similar to the base metal shows a ferrite-rich microstructure in the as-welded condition and thus requires the addition of austenite formers if an appropriate austenite fraction is to be maintained.

Girth weld joints, which are field fabricated and generally used in the as-welded condition, needs the above-mentioned measure for chemical composition, while seam weld metals of welded pipes do not, because solution annealing after factory welding (short-time solution treatment) is expected to recover the amounts of austenite fraction in the seam weld metals. The design concepts of the chemical composition of the two weld metals differs in two cases accordingly. Basically, however, appropriate austenite fractions can be easily obtained by controlling the chemical composition of the welding materials.

Figure 1 shows that the austenite fraction increase in proportion to increases in nickel content. It appears that the nickel content needed to obtain a weld metal with a 40 to 60% austenite fraction should be controlled in the range of 6.0 to 7.5% for seam welds and in the range of 7.0 to 8.5% for girth welds, with a 0.13 to 0.14% nitrogen content.

Absorbed energy improved with short time solution treatment or weld reheating, contributing to low temperature toughness of the weld metal. The absorbed energy of a seam weld metal was 160 J at −40°C and that of a GTA girth weld metal was 170 J at −40°C in the as-welded condition.

On the other hand, the HAZ in the as-welded condition shows a low austenite fraction as shown in **Photo 1**, because the chemical compoisition of the HAZ is determined by that of the base metal.

In seam welds, the base metal adjacent to the longitudinal weld is subjected to heat cycles in the seam welding process itself as well as in the girth welding, as shown in **Fig. 2**. Furthermore, a short-time solution treatment is usually applied after seam welding. Effects of reheating through multi-pass girth welding or short-time solution treatment were examined with simulated heat cycles. **Figure 3** shows the austenite fraction and toughness of a simulated HAZ (PT = 1350°C, using a cooling time from 800°C to 500°C of 11 sec) in the cross welded area. As shown, both the austenite

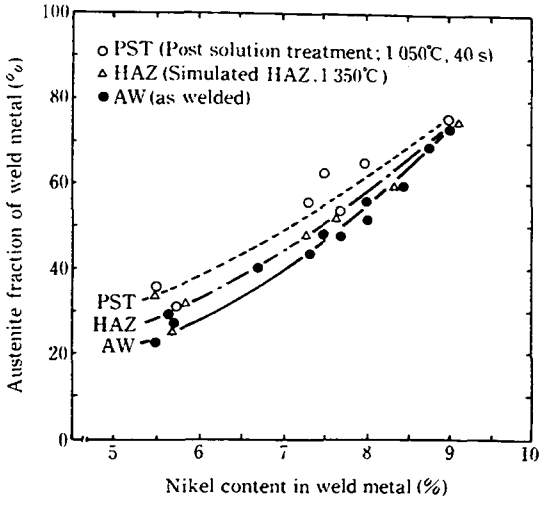


Fig. 1 Relationship between Ni content and changes in austenite fraction of the weld metals due to weld reheat thermal cycle, and short-time solution treatment

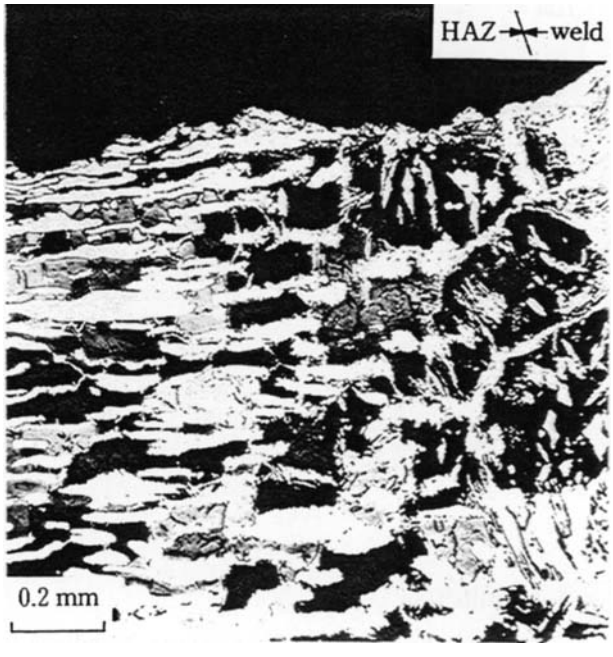


Photo 1 A microstructure of the shielded metal arc girth weld HAZ

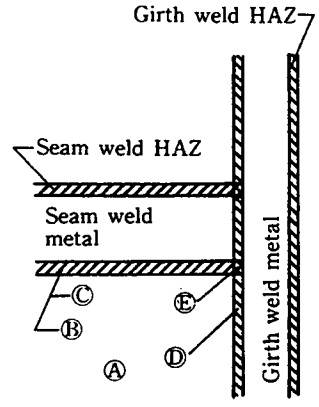


Fig. 2 Schematic showing of the cross welded area in a DSAW-UOE pipe resulting from a seam and a girth weldings

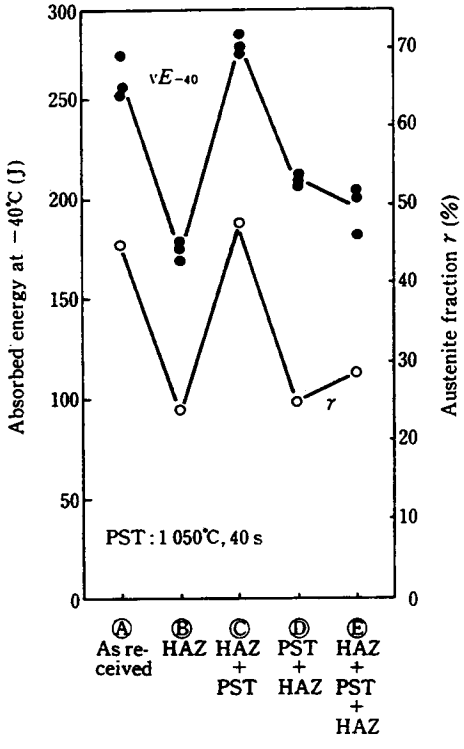


Fig. 3 Absorbed energy and austenite fraction of the simulated HAZ in a cross welded area

fraction and toughness were reduced by the welding thermal cycles (Ⓑ), but were improved by short-time solution treatment following welding (Ⓒ). The seam weld HAZ of a DSAW pipe is consequently expected to have almost the same corrosion resistance as the base metal. **Table 1** is an example of the results of a corrosion test of a DSAW pipe and its seam weld which was short-time solution treated. Both the HAZ and seam weld metal show performance equal to that of the base metal.

However, the austenite fraction and toughness again deteriorated as a result of girth welding thermal cycles after the short-time solution treatment (Ⓓ, Ⓔ), meaning these properties depend on the final thermal cycle.

Toughness should be no problem (absorbed energy at −40°C was about 180 J) even if the thermal history ends with a welding thermal cycle (girth welding HAZ). The austenite fraction, however, falls to the range of 20 to 30% in the as-welded heat affected condition. Although in multi-pass girth welding, the reheating effect of subsequent passes should improve the corrosion resistance of the HAZ, the root pass HAZ, which is in contact with the environment, is not always reheated by subsequent passes.

These results indicate that a decrease in the austenite fraction of the HAZ resulting from field girth welding is generally unavoidable. The girth HAZ is an area where much care should be taken from the standpoint of corrosion damage assessment.

3.2 Corrosion Properties of Girth Weld Joint

Pitting corrosion resistance of the girth weld HAZ was examined from the viewpoints of welding heat input, welding method, and the pitting index of the base metal. This section will describe methods of improving the pitting corrosion resistance of grith weld joints.

3.2.1 Influence of welding heat input on pitting corrosion

The results of pitting corrosion tests in a ferric chloride solution are given in **Fig. 4**. The corrosion rates can be regarded as the result of the corrosion behavior of the weld HAZ, because most pits were located in the HAZ adjacent to the weld fusion line. Pitting corrosion resistance markedly improved with an increase in the welding heat input in both the high and the low pitting index base metals. It also significantly improved with an increase in the pitting index of the base metal. How-

Table 1 Corrosion test results of DSAW pipe

Test	Solution	Condition	Results	
			Base metal	Seam weld
Intergranular corrosion	65% HNO_3	Boiling, 48 h, 5 times	0.175 g/m²·h	0.181 g/m²·h
Chloride SCC	90 g/l NaCl+1 bar CO_2	Boiling, 500 h	No cracking	No cracking
Pitting corrosion	10% $FeCl_3 \cdot 6H_2O$	30°C, 24 h	No pitting	No pitting

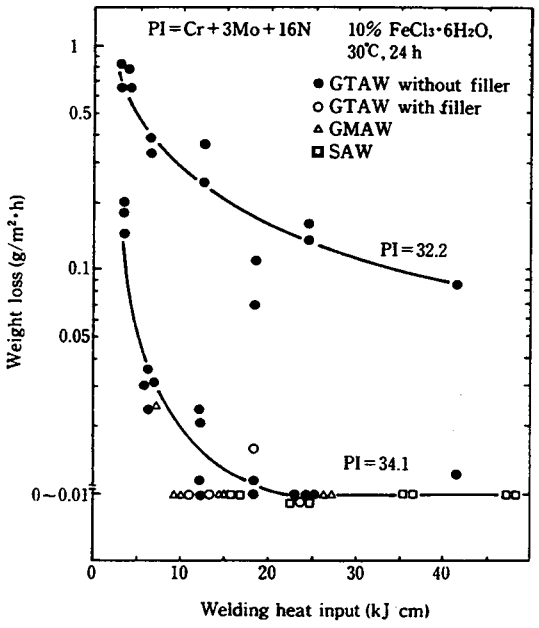


Fig. 4 Influence of welding heat input on the pitting corrosion resistance of the weld HAZ

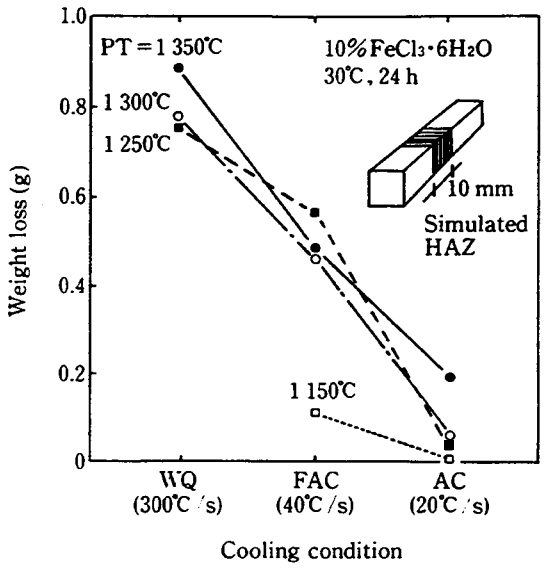


Fig. 5 Influence of cooling rate on the pitting corrosion resistance of the simulated HAZ

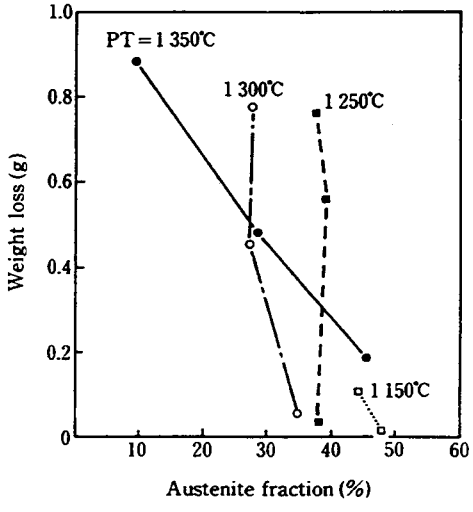


Fig. 6 Relationship between weight loss and the austenite fraction (An rearrangement of Fig. 5 by means of the austenite fraction)

ever, pitting corrosion performance appears to be independent of welding method.

Girth weld joints of high pitting index base metals (PI $\geqq$ 34.0) produced with a welding heat input greater than 10 kJ/cm are almost free of pitting corrosion problems.

Microstructures of the HAZ resulting from low heat input welding do not differ greatly from those with large heat input welding. To understand the influence of cooling rate on pitting corrosion resistance, simulated HAZ specimens were examined. Specimens (11 mm*W* × 100 mm*L* × 11 mm*t*) cut from the low pitting index base metal were heated to elevated temperatures and cooled at three different rates: 300°C/s (water quenching), 40°C/s (forced air cooling), and 20°C/s (air cooling). Holding time at the peak temperature was 3 sec for each specimen.

Results of the pitting corrosion tests in a 10% $FeCl_3 \cdot 6H_2O$ solution at 30°C for 24 h are plotted in **Fig. 5**. Weight loss declined in proportion to reduction of the cooling rate. Slow cooling from an elevated temperature can give a higher austenite fraction than rapid cooling because of the acceleration of austenite precipitation. A rearrangement of Fig. 5 for the austenite fraction is shown in **Fig. 6**, which clearly demonstrates that the same austenite fraction specimen does not necessarily result in the same corrosion weight loss, and further, that the corrosion resistance of the simulated HAZ is greatly influenced by the cooling rate. A distinctively microstructural aspect of the pitted specimens was the preferential attack of the ferrite phase and the ferrite/ferrite boundary when cooled rapidly. The initiation site of the pitting corrosion of the HAZ of an actual GTAW joint was identified as the ferrite/ferrite grain boundary, as shown in **Photo 2**. The reason for the difference in the pitting corrosion resistance of the HAZs with low and high welding heat input will presumably be the difference in the pitting corrosion resistance of their respective ferrite phases.

3.2.2 Mechanism of improvement in pitting corrosion resistance due to slow cooling

The ferrite phase in the simulated HAZ of the low pitting index base metal was examined in detail to elucidate the mechanism of pitting corrosion behavior as influenced by the cooling rate during welding.

Photo 3 shows microstructures etched electrically with

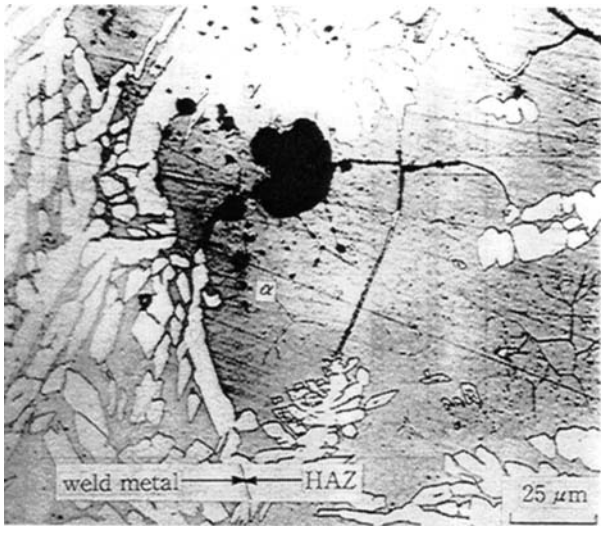


Photo 2 Initiation sites of the pitting corrosion in HAZ (22°C, 10% $FeCl_3 \cdot 6H_2O$)

a 10% oxalic acid solution. Simulated HAZs were heated to 1250°C and cooled (rapid, 300°C/s; slow, 20°C/s). The ferrite/ferrite grain boundaries and ferrite matrix in the rapidly cooled HAZ were attacked severely and deeply. **Photo 4** shows an electron micrograph of precipitates found on the extraction replicas. Precipitates were found in both the rapidly and the slowly cooled HAZs. These precipitates were identified as chromium nitride (Cr_2N, CrN) by electron diffraction analysis, EDX (Energy dispersive X-ray) analysis, and EELS (Electron energy loss spectroscopy) analysis.

These results suggest that the solute nitrogen, formed in the ferrite phase as a result of the decrease in the austenite phase during the weld heating process, is precipitated as chromium nitride regardless of the cooling rate. However, during rapid cooling, chromium near the nitride precipitates is depleted because the time available for diffusion is insufficient for chromium to heal the chromium depletion. During slow cooling, chromium diffusion heals the depleted area.

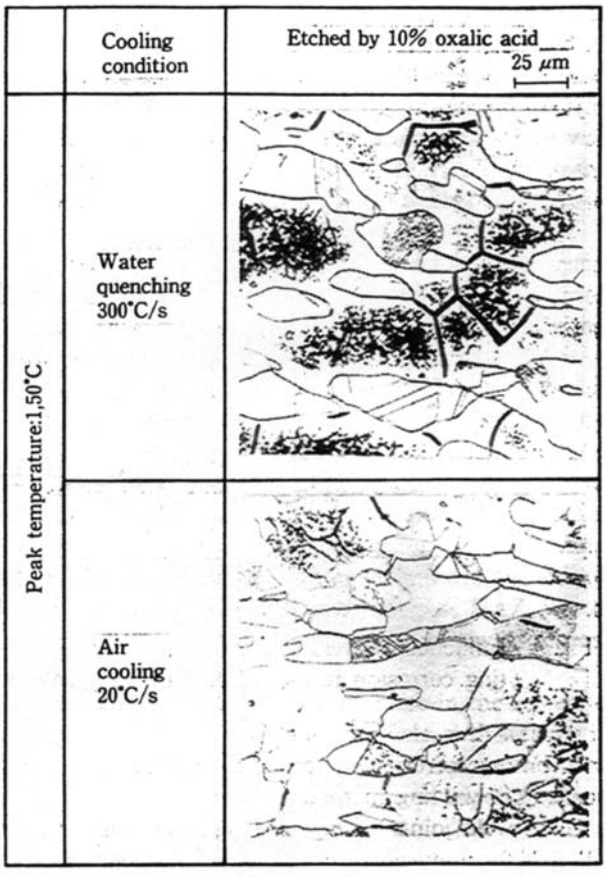


Photo 3 Comparison of sensitization between the simulated HAZs cooled rapidly and slowly

Furthermore, less nitride could be precipitated during slow cooling because more nitrogen could diffuse to the austenite phase. Supporting this conjecture is the result that even in rapid cooling the ferrite phase adjacent to the austenite phase was not sensitized, as shown in **Photo 5**.

The influence of the welding heat input on the corrosion resistance was obtained in 65% nitric acid test (ASTM A262 Practice C) as shown in **Photo 6** as well as

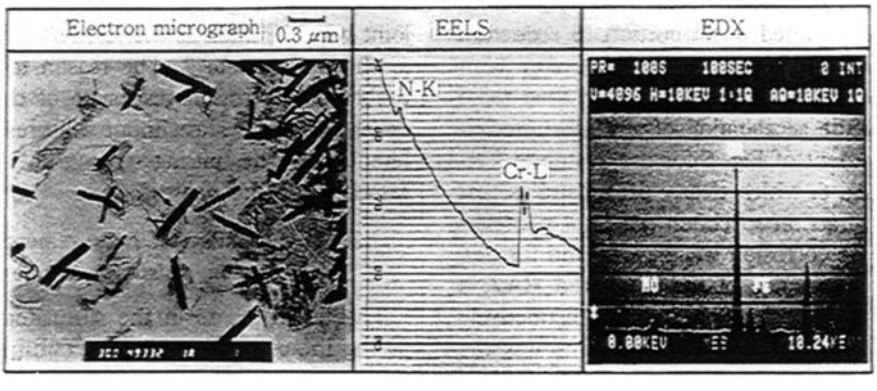


Photo 4 An example of electron micrograph and EELS analyses of precipitates found in the both simulated HAZs cooled rapidly and slowly

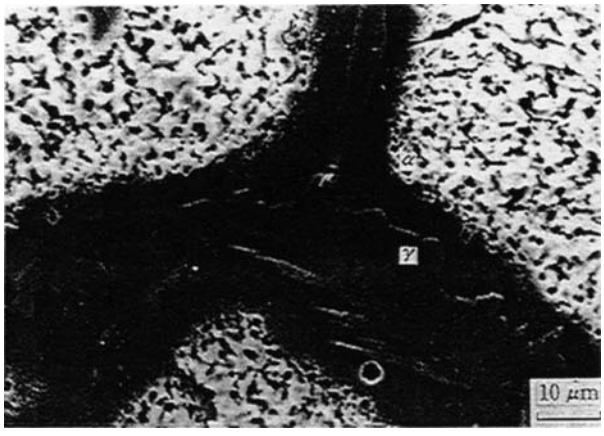


Photo 5 A SEM observation of an oxalic acid etched specimen (PT = 1350°C, water quenched)

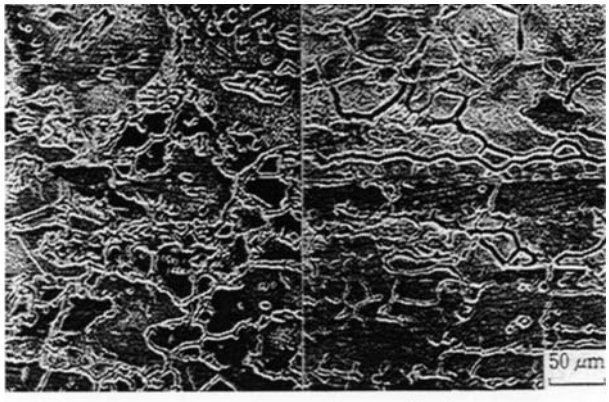


Photo 6 SEM observations of the gas tungsten arc girth weld HAZs after ASTM A262 prac. C test (The rapidly cooled specimen—low heat input specimen—shows ditch structure.)

in the ferric chroride pitting test.

From the above test results, the improvement of the corrosion resistance in girth weld HAZ due to the slow cooling rate is not attributed to the recovery of austenite fraction, but to the disappearance of the chromium depleted area. The girth weld is applied in the as-welded condition and the root pass which is in contact with the environment is not always reheated by subsequent passes. Therefore a welding procedure with slow cooling rate is recommendable from the view point of the pitting corrosion resistance of the HAZ.

3.3 Corrosion Test Results of Two Kinds of Girth Weld Joints

The materials used were an API 5L X 70 grade seamless pipe (PI = 34.1) and a DSAW pipe of the same grade, and their shielded metal arc girth weld joints in the as-welded condition. Root pass welding was carried out with a heat input of 10 to 15 kJ/cm.

The results are summarized in **Table 2**. The corrosion performance of the root pass weld metal and HAZs with a slow cooling rate was found to be identical to that of the base metal.

3.4 H_2S SCC Tests in Autoclave

Although duplex stainless steels have the excellent resistance to SCC in CO_2-Cl^- environments, even a small quantity of H_2S can affect the SCC resistance of duplex stainless steels. A seamless pipe (PI = 34.1) and its shielded metal arc girth weld joint were used for tests. **Figure 7** shows the influence of temperature and partial pressure of H_2S on SCC susceptibility. Duplex stainless steel is very susceptible to crack at around 100°C. All the cracks started at the bottom of pits and passed through the ferrite phase, as shown in **Photo 7**. The H_2S SCC of the weld joint occurred mainly in the HAZ.[3] Increased chloride concentration reduces the critical partial pressure of H_2S. An example is shown in **Fig. 8**. The critical partial pressure of H_2S for SCC is estimated at 10^{-2}MPa in a 5% NaCl solution and at 10^{-3}MPa in a 20%NaCl solution.

4 Conclusions

The metallurgical characteristics and corrosion performance of girth weld joints of the duplex stainless

Table 2 Results of corrosion tests under the atmospheric pressure

		Seamless pipe		UOE pipe girth joint
		Pipe body	Girth joint	
Intergranular corrosion test	ASTM A262 Prac. E ($CuSO_4$-H_2SO_4)	No IGC*	No IGC	No IGC
	ASTM A262 Prac. C (Boiling 65%HNO_3)	No IGC (0.151)**	No IGC (0.171)	No IGC (0.182)
Pitting corrosion test	10%$FeCl_3$·$6H_2O$, 30°C, 24 h	No pitting	No pitting	No pitting
	150 g/l NaCl-0.1 MPa CO_2, 80°C, 28 d	No pitting	No pitting	No pitting
Cl^--SCC U-bend test	$CaCl_2$ (pH=6.5), 100°C, 500 h	No cracking	No cracking	No cracking
CO_2-SCC U-bend test	90 g/l NaCl-0.1 MPa CO_2, Boiling, 28 d	No cracking	No cracking	No cracking

* Intergranular corrosion, ** weight loss (g/m²·h)

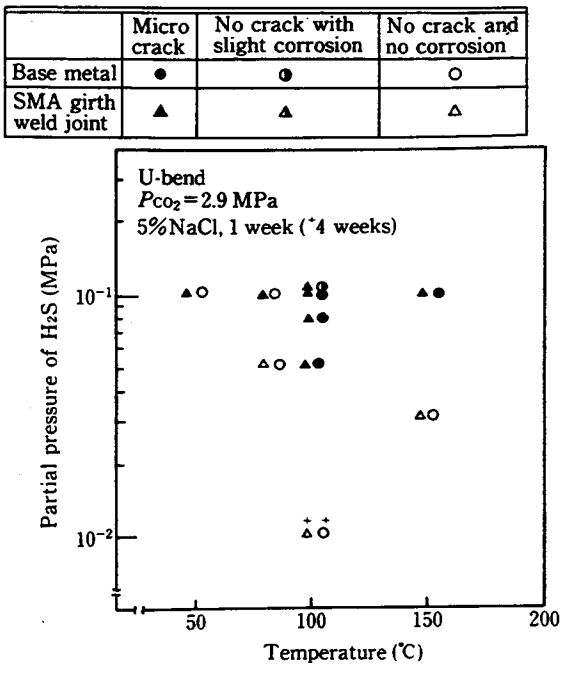


Fig. 7 Influence of temperature and partial pressure of H_2S on the SCC susceptibility

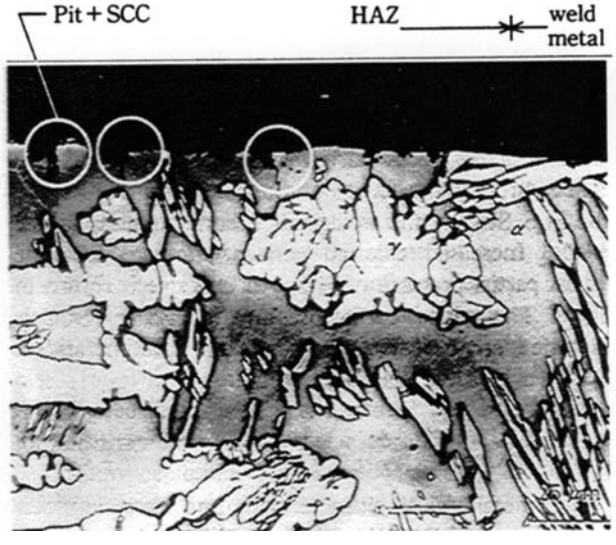


Photo 7 A cross sectional view of a shielded metal arc girth weld joint (White part, austenite; dark part, ferrite. Micro cracks initiated from the related pit bottom were located in the HAZ)

steel specified by ASTM A790 S31803 and DIN 1.4462 were examined in connection with the application of these materials to CO_2-Cl^- environment pipe.

The main results of this study are as follows:

(1) Poor corrosion resistance of HAZ is attributed not to the reduction of the austenite fraction but mainly to the chromium depleted area adjacent to chromium nitrides precipitated during the cooling.

(2) Short time solution annealing after seam welding

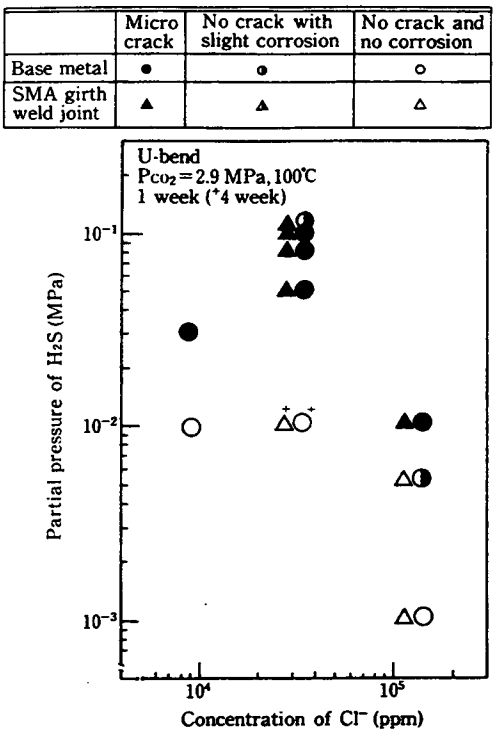


Fig. 8 Influence of chloride concentration on SCC susceptibility

will eliminate the chromium depleted areas and thus restore the corrosion resistance of the seam weld HAZ.

(3) The girth weld HAZ is applied in the as-welded condition and the root pass HAZ which is in contact with the environments is not always reheated by subsequent passes. Therefore the girth weld joint is an area where much care must be taken from the aspect of corrosion damage assessment.

(4) Improvement of the pitting corrosion resistance of the girth weld joints in the as-welded condition required the use of a high pitting index base metal (Cr + 3Mo + 16N = 34.0) and slow cooling rate welding procedures, independently of the welding method.

(5) Duplex stainless steel pipe can be applied with satisfactory results at a H_2S partial pressure up to 10^{-2}MPa in a 5% NaCl solution and 10^{-3}MPa in a 20% NaCl solution.

References

1) M. Kowaka: *Bulletin of the Japan Institute of Metals*, 17(1978)8, 657-665

2) J. Pleva and S. Nordin: "Properties of different MMA welds on modified type 329 ferritic-austenitic stainless steel", Proceedings of Duplex Stainless Steels, Paper No. 8201-30, ASM, St. Louis (USA), September (1982)

3) K. Yasuda, K. Tamaki, S. Nakano, K. Kobayashi, and N. Nishiyama: "Metallurgical characteristics of weld metals and corrosion performance of girth weld joints of duplex stainless steel pipes", Proceedings of Duplex Stainless Steel '86, Paper No. 24, Hague (Netherlands), October (1986)

Copyrighted Materials
Copyright © 1996 NACE International Retrieved from www.knovel.com

PAPER NUMBER

156

Corrosion 86

The International Corrosion Forum Devoted Exclusively to The Protection and Performance of Materials

March 17-21, 1986
Albert Thomas Convention Center
Houston, Texas

CORROSION RESISTANCE OF DUPLEX STAINLESS STEEL WELDMENTS IN WET CO_2 AND H_2S ENVIRONMENT

H. TSUGE, Y. TARUTANI and T. KUDO

Sumitomo Metal Industries, Ltd.,
Central Research Laboratories
3-1 chome, Nishinagasu-Hondori, Amagasaki 660
Japan

ABSTRACT

Effect of nitrogen which is one of the most important elements in duplex stainless steels was investigated on resistances to pitting corrosion and stress corrosion cracking (SCC) in various environments. The increase in nitrogen content increases these resistances in the base metal, which is due to the improvement in the resistance of γ- phase which has lower chromium and molybdenum contents compared to α-phase. Nitrogen is an essential element to sustain the corrosion resistance of the heat affected zone (HAZ) which is heated up to 1350°C or higher, because nitrogen accelerates the formation of γ-phase during the cooling process after welding and avoids the precipitation of chromium carbides or nitrides at grain boundaries. When the nitrogen content is less than 0.08% in 22%Cr, 5.5%Ni and 3%Mo base composition the HAZ has little γ-phase to lead to the high susceptibility to intergranular corrosion and IGSCC occurs even in pure CO_2-Cl^- environment containing no H_2S. Nitrogen has little effect on the precipitation behavior of the base metal by aging heat treatment around 700°C.

INTRODUCTION

The recent search for new sources of hydrocarbons has led to the production from more severe environments. Such wells are deep and often constructed at off-shore. The environments usually contain considerable amounts of carbon dioxide (CO_2), hydrogen sulfide (H_2S) and concentrated brine. Oil and gas production from these wells exposes construction materials such as tubulars and line pipes to very severe corrosion condition.

Iron base alloys are not suitable because of their high corrosion rate and high susceptibility to sulfide stress corrosion cracking. The corrosion resistance of highly alloyed materials, for example, duplex stainless steels, high nickel stainless steels and nickel base alloys have been evaluated for the purpose of selecting proper materials depending on the various well condition(1∿6). Among those high-

ly alloyed materials, 22%Cr duplex stainless steel line pipes have been widely used in the field which contains CO_2 and chloride ions with small amounts of H_2S. Duplex stainless steels usually contain some amount of nitrogen to improve the corrosion and mechanical properties at welded joints. The corrosion behaviors such as pitting, intergranular corrosion and SCC of 22%Cr duplex stainless steel have been investigated by many investigators(7,8). The effect of nitrogen on the corrosion behavior, however,has not been clarified yet.

In this paper, the effect of nitrogen content on the corrosion resistance of 22%Cr duplex stainless steels was investigated with respect to each of base metal, low temperature HAZ and high temperature HAZ which is heated up to 1350°C or higher.

EXPERIMENTAL

Materials Used

The chemical compositions of materials used are shown in Table 1. The materials which are composed of 22%Cr, 5.5%Ni and 3%Mo containing 0.04% to 0.2% nitrogen were melted in laboratory. The ingots were forged, hot rolled to plates of 5 mm in thickness, and then solution heat treated at 1050°C for 30 min, followed by water quenching.

The mechanical properties at room temperature and the ferrite content (α-content) are presented in Fig. 1. The tensile strength increases with nitrogen content, while the 0.2% yield strength is approximately 500 MPa independent of nitrogen content.

In order to investigate the corrosion behavior of the low temperature HAZ of which the microstructure does not change, the specimens were heat-treated at 500°C to 900°C for 0.1 to 30 hours.

The corrosion resistance of the high temperature HAZ which is heated up to 1350°C or higher was studied using the simulated HAZ whose heat pattern is shown in Fig. 2.

Test Method

The pitting potential was measured potentiodynamically in 5% NaCl solution at 60°C at a sweep rate of 20 mV/min with a potentiostat. The saturated calomel reference electrode (SCE) and the platinum counter electrode were used in this study. The test specimen was a disk of 15 mm in diameter and 2 mm in thickness, which was polished with No. 600 emery paper, washed with water and alchol, and then degreased with acetone. The potential at which the anodic current density increases drastically by the occurrence of pitting was adopted as the pitting potential (Vc').

Pitting corrosion test in $FeCl_3$ solution was also conducted by the measurement of the critical pitting temperature (CPT) of the materials using 25 mm x 50 mm x 2 mm specimens polished with No. 600 emery paper. The pitting corrosion resistance was evaluated by the highest temperature below which the material doesn't suffer pitting corrosion attack after 24 hour exposure in 10% $FeCl_3 \cdot 6H_2O$ solution. The solution temperature was increased by 2.5°C until the critical pitting temperature was reached.

Uniaxial constant load SCC tests were conducted in 15 liter sized autoclave with lever type loading system shown in Fig. 3. The constant load SCC test specimen had a nominal gage length of 20 mm and a diameter of 3 mm. The autoclave was purged with nitrogen to deaerate the solution, and then the vacuum was maintained. Finally, the autoclave was purged with H_2S and pressurized to the desired partial pressure before heating. SCC resistance was evaluated by a time to failure in 20% NaCl solution with 1 atm H_2S at 100°C. The U-bend SCC test was also performed in CO_2-H_2S-Cl^- environments.

ASTM A262 Practice C (Huey test) and Practice E (Strauss Test) were selected for the evaluation of intergranular corrosion susceptibility. Huey test was performed in five boiling periods of 48 hours. Strauss test duration was 16 hours. These specimens were 10 mm x 40 mm x 3 mm and polished with No. 320 emery paper.

TEST RESULTS

Duplex stainless steels have a characteristic morphological change in phase structure of welded joint as

shown in Fig. 4. In general, there exist two kind of HAZs at the welded joint, that is, the low temperature HAZ where the microstructure does not change and the high temperature HAZ which is heated up to 1350°C or higher and different phase structure from the base metal. These HAZs are defined as HAZ(A) and HAZ(B) respectively in this paper.

Fig. 5 shows the typical example of microstructure of the base metal and the HAZ(B) with different nitrogen content. In the simulated HAZ(B), the phase structure is strongly affected by the nitrogen content. 0.077% nitrogen alloy has almost single α-phase, while the precipitation of the needle type austenite phase (γ-phase) is observed at grain boundaries of 0.137% nitrogen or higher containing alloy.

Corrosion Resistance of Base Metal

The effect of nitrogen content on the pitting potential of 22%Cr duplex stainless steels in NaCl solution is shown in Fig. 6. The pitting potential of 22%Cr duplex stainless steel increases above 0.12% nitrogen in 5% NaCl solution. The addition of a small amount of H_2S deteriorates the pitting corrosion resistance, though the benefical effect of nitrogen on the pitting resistance is still observed.

Corrosion test results in $FeCl_3$ solution are shown in Fig. 7. The CPT of 22%Cr duplex stainless steels also increases with nitrogen, which is similar to that in NaCl solution. The nitrogen content more than 0.12% is necessary to obtain the CPT value higher than 30°C in $FeCl_3$ solution.

SCC test was conducted under the applied stress of 45 kg/mm^2 (441 MPa) which is almost same as the 0.2% yield strength. Fig. 8 shows the effect of the nitrogen content on the SCC susceptibility in 20% NaCl solution with 1 atm H_2S. The time to failure increases drastically with increasing nitrogen content. The materials above 0.14% nitrogen suffer no failure, although small cracks were observed on the surface of the specimen after 200 hour exposure.

From these results, it is clarified that nitrogen is a benefical element for increasing the resistance to the corrosions such as pitting corrosion and SCC of the base metal.

Corrosion Resistance of Low Temperature HAZ

In order to study the effect of nitrogen content on the corrosion behavior of the low temperature HAZ which is defined as HAZ(A), the specimens were heated at 500 to 900°C for 0.1 to 30 hours. Fig. 9 gives Strauss test results. Intergranular corrosion is not observed in every heating condition examined independent of nitrogen content. Sigma (σ)-embrittlement is, however, found after the high temperature aging around 900°C when the specimens are bent through 180°. The difference in σ-phase precipitation behavior among the materials with 0.07 to 0.16% nitrogen is found to be not so large by the microstructure observation.

Huey test results are shown in Fig. 10. There exists an area of increased corrosion rate in time-temperature diagram, the lower limit of which depends on the heating time. It is clarified that nitrogen has little effect on the intergranular corrosion susceptibility by Huey test. The typical corroded surface which is given in Fig. 11 shows that the intergranular attack occurs not only at α/γ grain boundaries but also at α/α ones. The extraction replicas are shown in Fig. 12. The fine particles which was observed at grain boundaries at 700°C for 1 hour are $Cr_{23}C_6$. However, little Cr_2N is observed in the material which was aged at 700°C for 30 hours. These results indicate that the intergranular corrosion by Huey test is caused mainly by the precipitation of $Cr_{23}C_6$.

The effect of heating on the pitting potential of 22%Cr duplex stainless steel with various nitrogen contents is presented in Fig. 13. There exists an area of decreased pitting corrosion resistance in time-temperature diagram, the lower limit of which depends on the heating time. The results show the small effect of nitrogen content on the pitting potential.

The high corrosion rate in Huey test is found after heat treatment in the range of 600 to 800°C, while the decreased pitting potential in NaCl solution is found above 700°C as shown

in Fig. 14. It is considered that the susceptibility to intergranular corrosion by Huey test is increased mainly by the precipitation of $Cr_{23}C_6$ and the pitting resistance is decreased by the precipitation of σ-phase as well as $Cr_{23}C_6$.

Corrosion Resistance of High Temperature HAZ

In order to investigate the effect of nitrogen content on the corrosion behavior of the high temperature HAZ, that is, HAZ(B) in Fig. 4, the materials were heated with the simulated heat pattern shown in Fig. 2. Fig. 15 shows the effect of peak temperature at heat-cycle on SCC susceptibility of 22%Cr duplex stainless steel containing 0.14% nitrogen. SCC occurs only at the peak temperature of 1375°C, whose microstructure is shown in Fig. 16. The duplex phase transforms to single α-phase when the peak temperature exceeds 1350°C and then needle shaped γ-phase precipitates during the cooling process. So the peak temperature of 1375°C was selected for the investigation of the effect of nitrogen content on the corrosion behavior of HAZ(B)

Fig. 17 gives the effect of nitrogen content on intergranular corrosion of simulated HAZ(B) of 22% Cr duplex stainless steels. The alloys with nitrogen content below 0.077% suffer the intergranular attacks in Strauss and Huey tests. The high sensitivity to intergranular corrosion of 0.077% or lower nitrogen alloys, whose structure is single α-phase after heating, is due to the formation of the chromium depleted zone along α/α grain boundaries by the precipitation of $Cr_{23}C_6$ and/or Cr_2N.

It is indicated in Fig. 18 that nitrogen is benefical in the improvement of the pitting resistance in NaCl solution as well as in $FeCl_3$ solution. If the CPT value in $FeCl_3$ solution is required to be more than 30°C at HAZ(B), 0.14% or higher nitrogen content is necessary for 22% Cr, 5.5% Ni and 3% Mo base composition. The pitting potential and the CPT of the simulated HAZ(B) with high nitrogen of 0.238% are lower than those of the base metal shown in Fig. 6 and Fig. 7.

Fig. 19 shows SCC test results in 20% NaCl solution with 1 atm H_2S at 100°C. The SCC susceptibility of the simulated HAZ(B) is greater than that of the base metal shown in Fig. 8. The materials suffer SCC in a short time under the high applied stress of 45 kg/mm^2 (441 MPa). When the applied stress is decreased to 35 kg/mm^2 (343 MPa), the alloys containing more than 0.123% nitrogen sustain the resistance to cracking. The alloys below the nitrogen content of 0.077%, which have the almost single α-phase, have high sensitivity to SCC even under the low applied stress of 35 kg/mm^2.

SCC Resistance in CO_2-H_2S-Cl^- Environment

Table 2 shows the results of SCC susceptibility of 22% Cr duplex stainless steels in CO_2-H_2S-Cl^- environments using the single U-bend method. SCC occurs on all materials in the condition of 0.1 atm H_2S + 10 atm CO_2. SCC susceptibility becomes lower as the partial pressure of H_2S decreases. The simulated HAZ of the alloy with 0.047% nitrogen content still has SCC susceptibility when H_2S is absent.

Fig. 20 is SCC observation of the simulated HAZ of 22% Cr duplex stainless steels. In the condition of 10 atm CO_2, the cracks of the alloy with 0.047% nitrogen content, which is sensitive to intergranular corrosion mentioned above, are intergranular which is considered to propagate along the chromium depleted zone at α/α grain boundaries.

DISCUSSION

It is clarified that nitrogen is benefical to improve the pitting corrosion resistance of the base metal. The reason why nitrogen increases the resistance is considered as follows; chromium and molybdenum contents in ferrite and austenite phases are almost constant independent of nitrogen content as shown in Fig. 21. The austenite phase has approximately 21% Cr-2.5%Mo, while the ferrite phase has 23% Cr-3.5%Mo. Assuming that the pitting index equation is Cr + 3Mo + 16N(9) and the nitrogen exists only in austenite phase of 60% as shown in Fig. 1, then the nitrogen content required to get the same pitting corrosion resistance

in austenite phase as that in ferrite phase is about 0.18%. So the pitting corrosion is considered to initiate at the austenite phase below the nitrogen content of 0.18% from this rough estimation. Fig. 22 shows the microscopic observation of pitting initiation of 22% Cr duplex stainless steel in NaCl solution. At the alloys with nitrogen content of 0.137%, the pitting corrosion is observed to initiate in austenite phase. When nitrogen content increases to 0.164%, it can be seen that the pitting occurs at random on ferrite and austenite phases. The estimation mentioned above almost agrees with the observation. So the role of nitrogen to the increase in pitting corrosion resistance is attributed to the improvement of the austenite phase of the duplex stainless steel.

It was observed that nitrogen has little effect on intergranular corrosion of the materials aged at the temperature around 700°C in Huey test, which suggests that the determining factor of this corrosion may be mainly the precipitation of $Cr_{23}C_6$. In fact, the precipitation of $Cr_{23}C_6$ was observed at α/γ and α/α grain boundaries.

As mentioned above, the solved nitrogen itself increases the corrosion resistance of the base metal. Moreover nitrogen is an essential element to get the proper microstructure for the corrosion resistances and the mechanical properties at HAZ. Below the nitrogen content of 0.077%, the simulated HAZ(B) has the single ferrite phase, which leads to the sensitization at α/α grain boundaries owing to the formation of chromium carbides and nitrides during the cooling process. So HAZ(B) which has the single ferrite phase is very sensitive to intergranular corrosion and IGSCC can occur in CO_2-Cl^- environments containing no H_2S. To get the dual phase which is desirable for the corrosion resistance in high temperature HAZ, the nitrogen content is required at least to be 0.12% or higher for 22% Cr, 5.5% Ni and 3% Mo base composition.

CONCLUSION

The effect of nitrogen content of 22% Cr duplex stainless steel on the corrosion resistance was investigated. The results obtained are as followed;

1. The increase in nitrogen content increases the resistances to pitting corrosion and SCC of the base metal, which is due to the improvement in the resistance of austenite phase by the solved nitrogen itself.

2. Nitrogen has little effect on the intergranular corrosion at the low temperature HAZ in Huey test.

3. Nitrogen more than 0.12% is required for 22% Cr, 5.5% Ni and 3% Mo base alloy to maintain the corrosion resistance at high temperature HAZ which is heated up to 1350°C or higher.
   When nitrogen content is less than 0.077%, the HAZ which contains little austenite phase has the high susceptibility to intergranular corrosion and IGSCC.

ACKNOWLEDGEMENT

The authors would like to thank Dr. K. Nishioka, General Manager of Central Research Laboratories of Sumitomo Metal Industries, Ltd. and Dr. T. Moroishi, Asistant to General Manager of Central Research Laboratories. We also acknowledge Mr. M. Miura, Mr. S Kiyama and T. Nakagawa for their helpful discussion and their experimental work.

REFERENCES

1. J. Ored, S. Bernhardsson; CORROSION/82, Paper No. 126, National Association of Corrosion Engineers, Houston, 1982.

2. G. Herbsleb, R.F. Poepperling; CORROSION, Vol. 36, No. 11, p. 611 (1980).

3. A. Desestrel; CORROSION/83, Paper No. 165, National Association of Corrosion Engineers, Anaheim, 1983.

4. P.R. Rhodes, G.A. Welch, L.J. Abrego; Materials for Energy System, Vol. 5, No. 1, p. 3 (1983).

5. S.M. Wilhelm, R.D. Kane; CORROSION/83, Paper No. 154, National Association of Corrosion Engineers, Anaheim, 1983.

6. H. Miyuki, J. Murayama, T. Kudo, T. Moroishi; CORROSION/84, Paper No. 293, National Association of Corrosion Engineers, New Orleans, 1984.

7. G. Herbsled, P. Schwaad; Duplex Stainless Steel, American Society for Metals, p. 15, 1983.

8. S. Bernhardsson, J. Ordsson, C. Martension; Duplex Stainless Steel, American Society for Metals, p. 267, 1983.

9. J.E. Truman; Private comunication, 1981.

TABLE 1 - Chemical Composition of 22Cr Duplex Stainless Steels (mass %)

Alloys	C	Si	Mn	P	S	Ni	Cr	Mo	N
A	0.014	0.49	1.72	0.004	0.004	5.57	21.89	3.22	0.047
B	0.012	0.49	1.74	0.004	0.004	5.58	21.72	3.16	0.077
C	0.010	0.51	1.77	0.004	0.004	5.60	21.92	3.22	0.123
D	0.016	0.49	1.83	0.004	0.005	5.56	21.75	3.30	0.137
E	0.008	0.50	1.73	0.004	0.004	5.51	21.70	3.14	0.164
F	0.015	0.50	1.70	0.003	0.004	5.51	21.70	3.16	0.238

TABLE 2 - Results of SCC Susceptibility of 22%Cr Duplex Stainless Steel

Base metal : Single U-bend method ; 100°C, 20% NaCl, 500 h

Test condition / Specimen	10 atm CO_2	0.01 atm H_2S + 10 atm CO_2	0.1 atm H_2S + 10 atm CO_2
N=0.047%	No SCC	No SCC	SCC
N=0.077%	No SCC	No SCC	SCC
N=0.123%	No SCC	No SCC	SCC
N=0.137%	No SCC	No SCC	SCC
N=0.164%	No SCC	No SCC	SCC
N=0.238%	No SCC	No SCC	SCC

Simulated HAZ : Single U-bend method ; 100°C, 20% NaCl, 500 h

Test condition / Specimen	10 atm CO_2	0.01 atm H_2S + 10 atm CO_2	0.1 atm H_2S + 10 atm CO_2
N=0.047%	SCC	SCC	SCC
N=0.077%	No SCC	No SCC	SCC
N=0.123%	No SCC	No SCC	SCC
N=0.137%	No SCC	No SCC	SCC
N=0.164%	No SCC	No SCC	SCC
N=0.238%	No SCC	No SCC	SCC

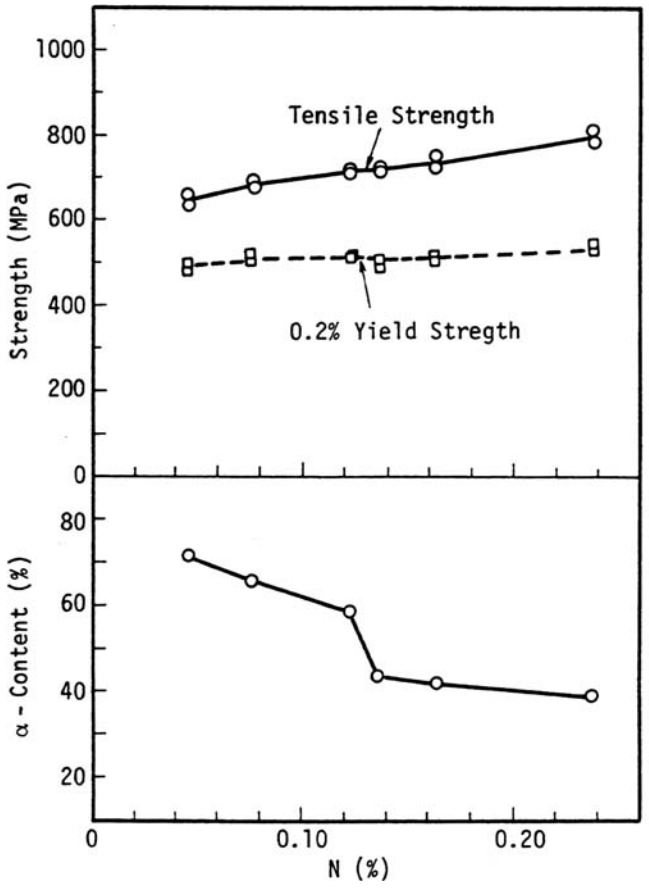


FIGURE 1 - Effect of N Content on Mechanical Properties and Ferrite Content of 22Cr Duplex Stainless Steel

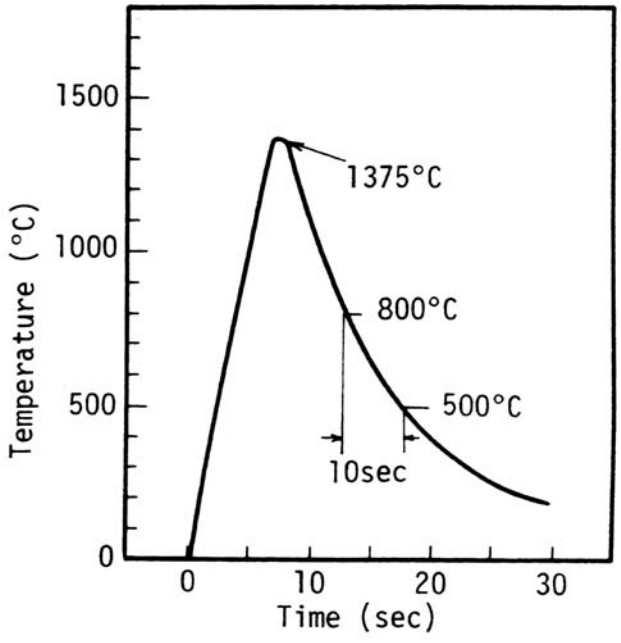


FIGURE 2 - Heat Pattern of Simulated HAZ

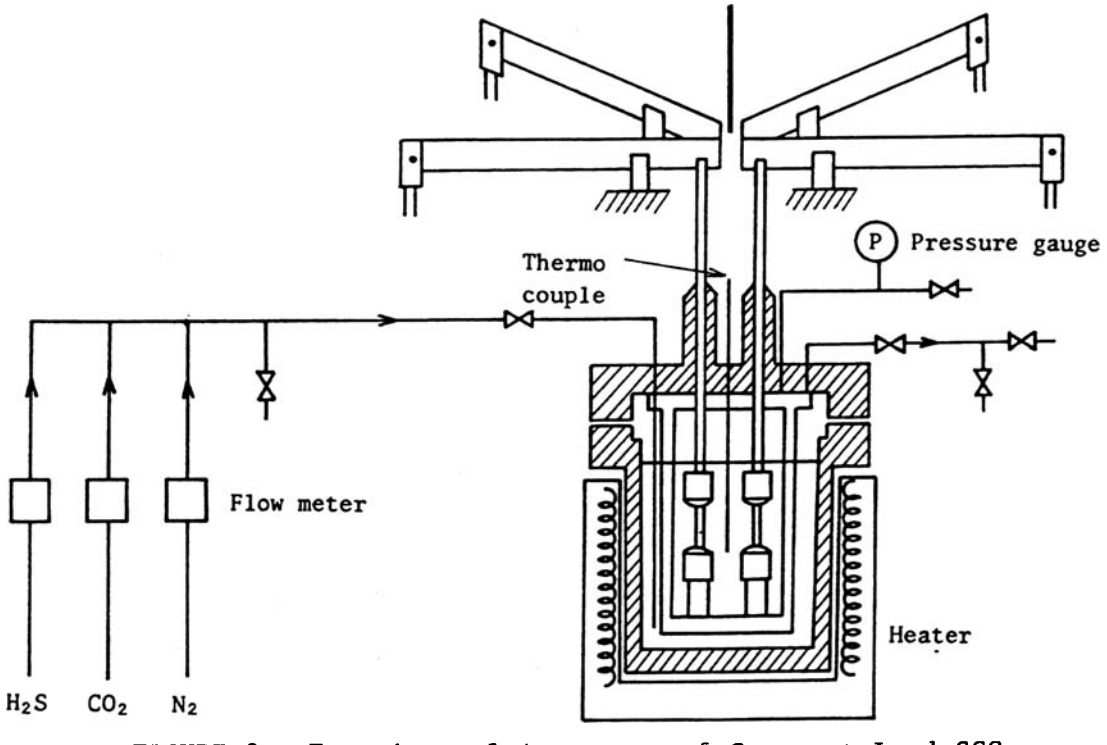


FIGURE 3 - Experimental Apparatus of Constant Load SCC

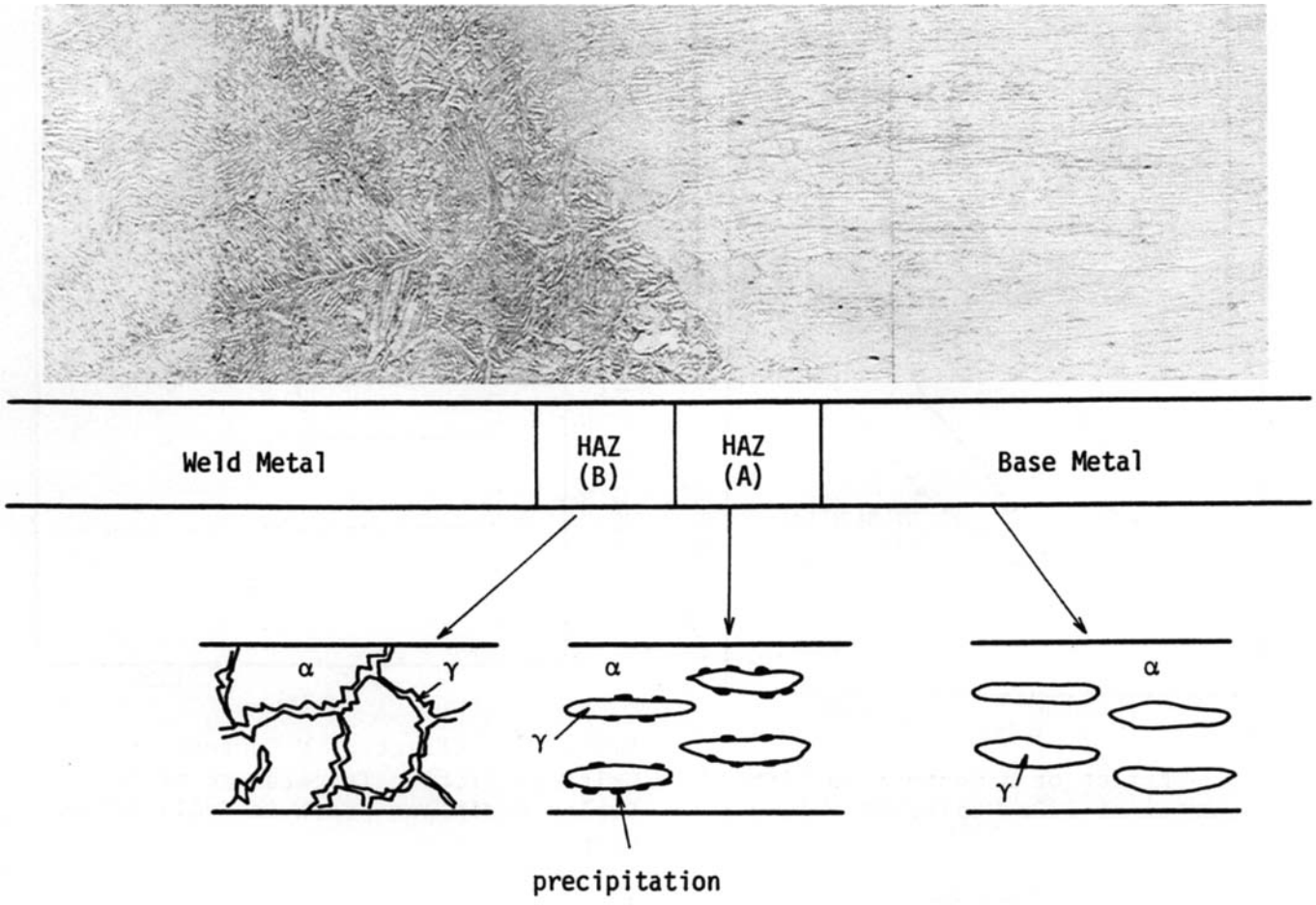


FIGURE 4 - Schematic Diagram of Morphological Phase Change at Welded Joint of Duplex Stainless Steel

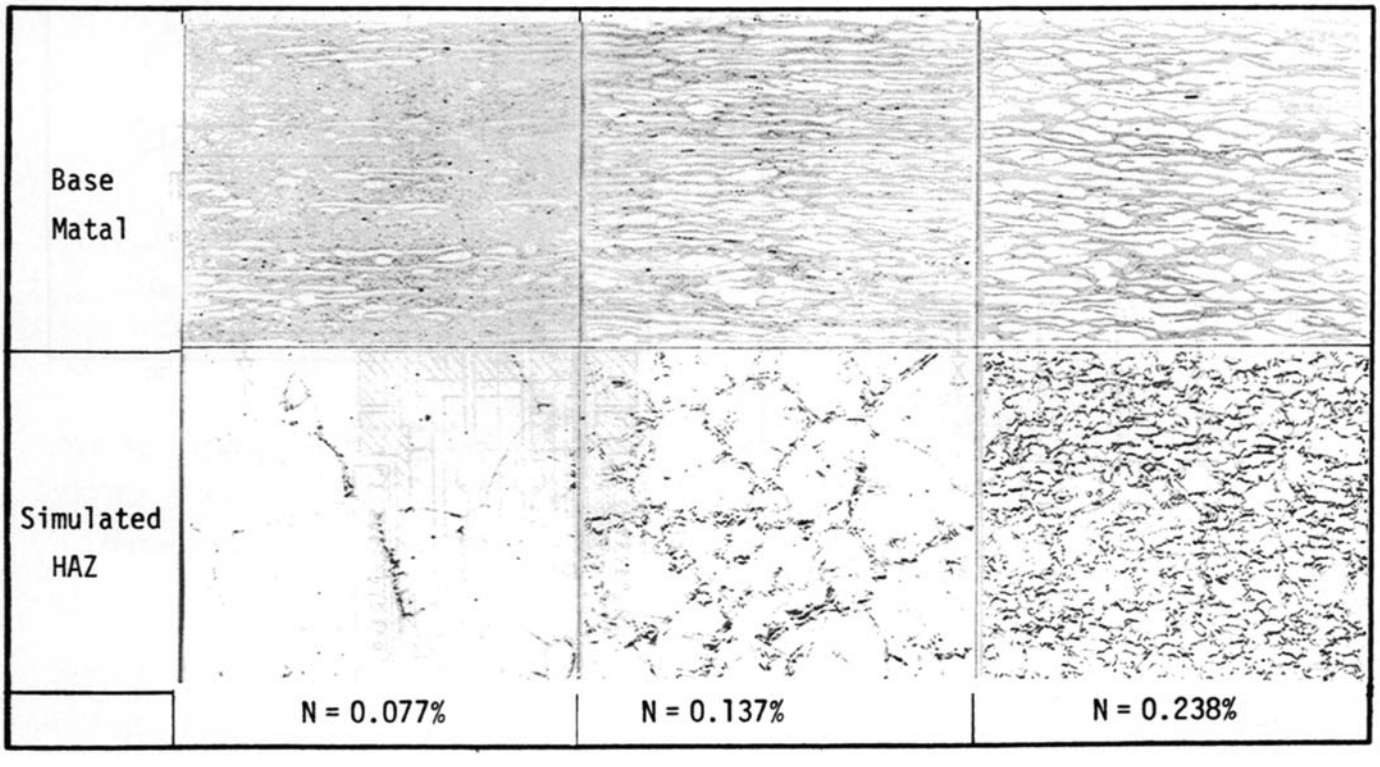


FIGURE 5 - Microstructure Observation of 22Cr Duplex Stainless Steel

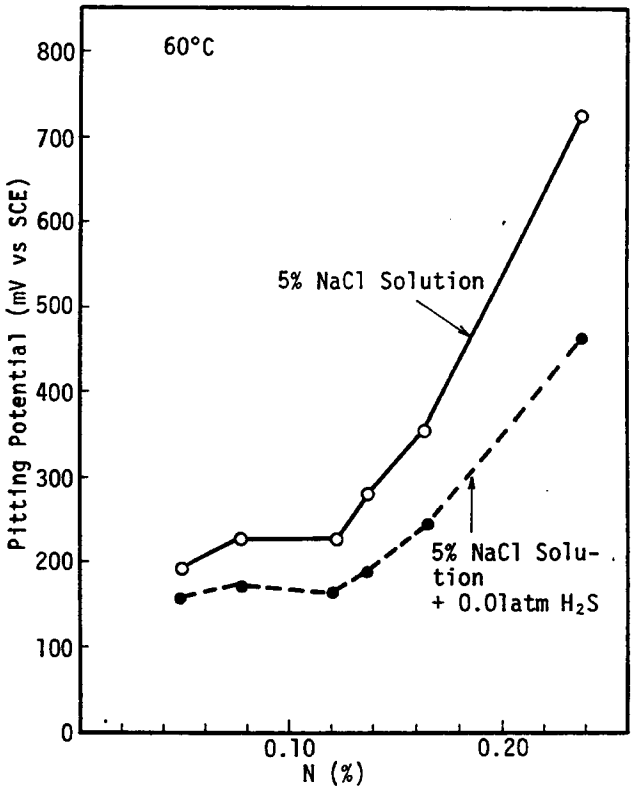


FIGURE 6 - Effect of N Content on Pitting Potential of 22Cr Duplex Stainless Steels

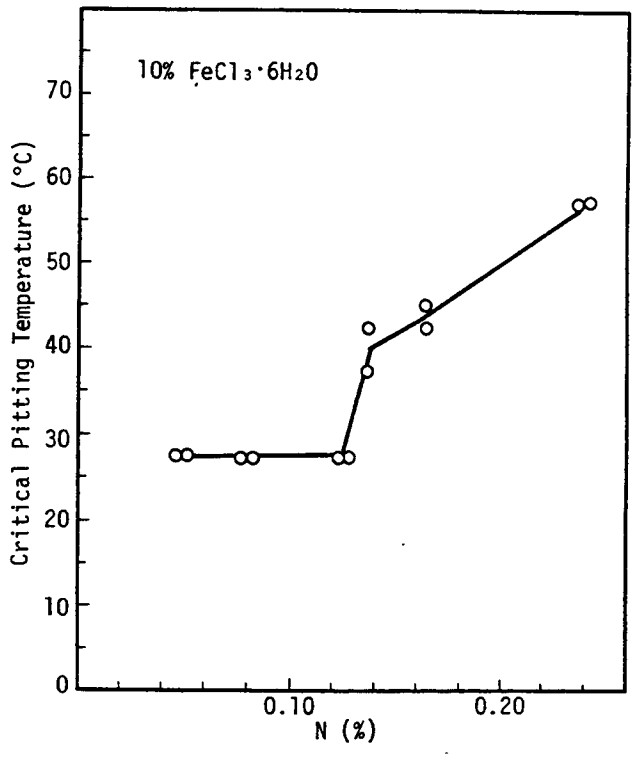


FIGURE 7 - Effect of N Content on Critical Pitting Temperature of 22Cr Duplex Stainless Steel in $FeCl_3$ solution

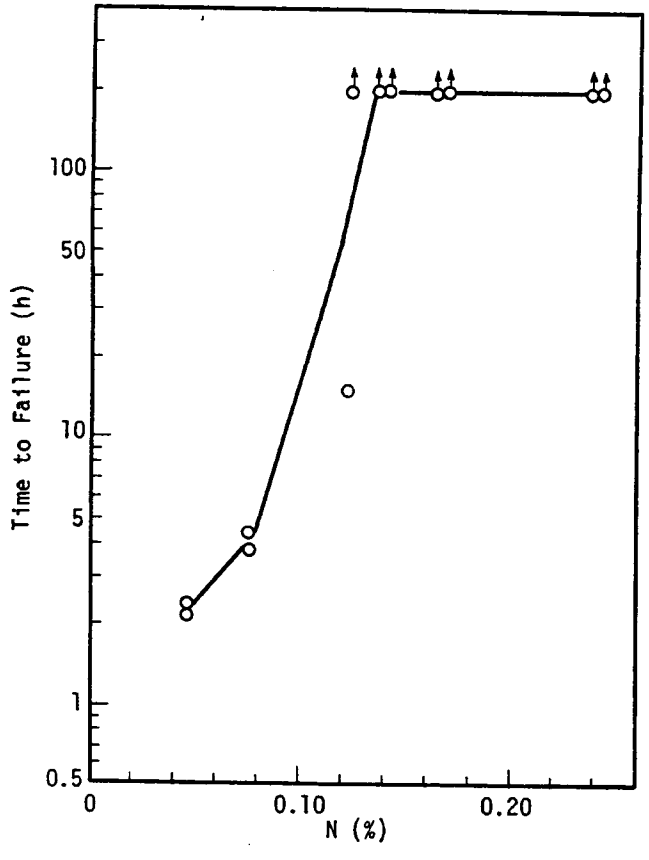


FIGURE 8 - Effect of N Content on SCC Susceptibility of 22Cr Duplex Stainless Steel (100°C, 20% NaCl, 1 atm H_2S, 45 kg/mm^2)

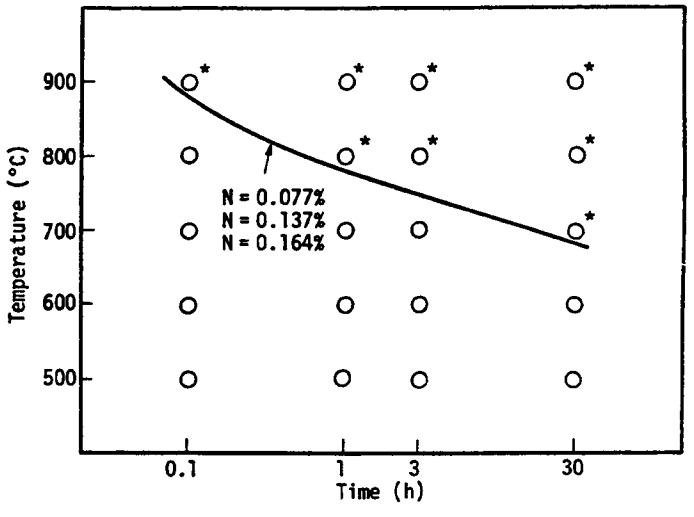


FIGURE 9 - Strauss Test Results of 22Cr Duplex Stainless Steels
(ASTM A262, Practice E)
○ : No crack, * : σ embrittlement

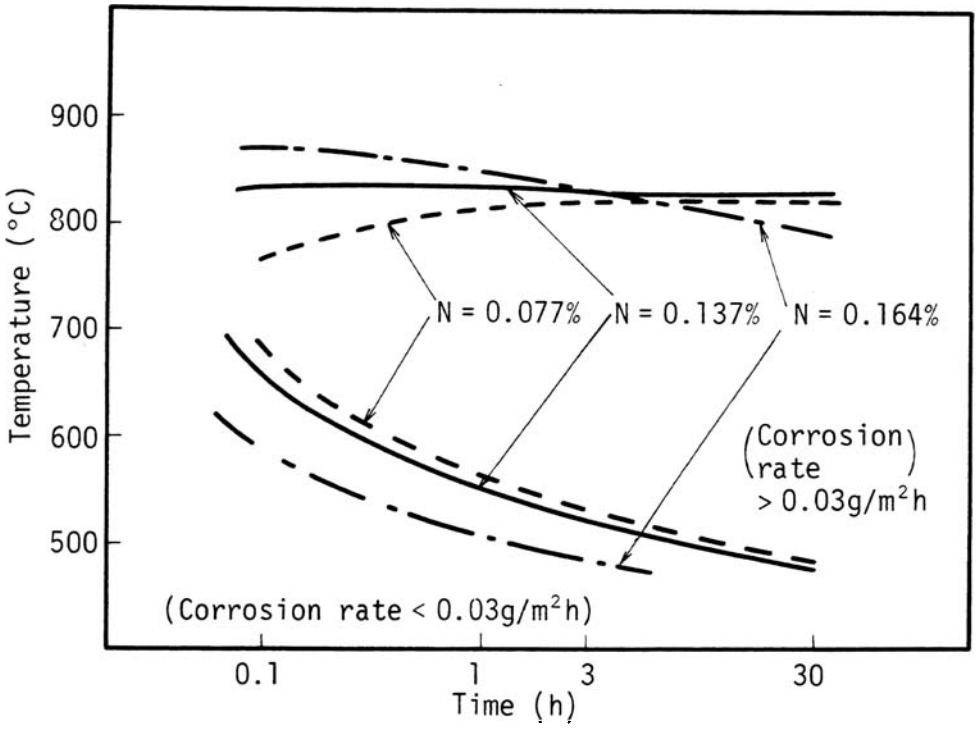


FIGURE 10 - Huey Test Results of 22Cr Duplex Stainless Steels (ASTM A262, Practice C)

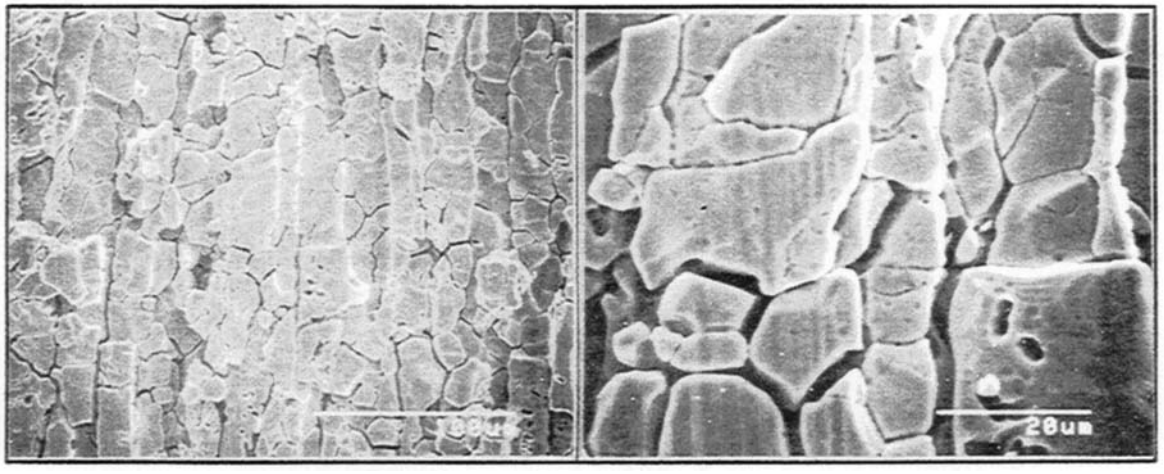


FIGURE 11 - Corroded Surface Observation of 22Cr Duplex Stainless Steel after ASTM A262, Practice E Test (N = 0.137%, Heat Treated for 1 hour at 600°C)

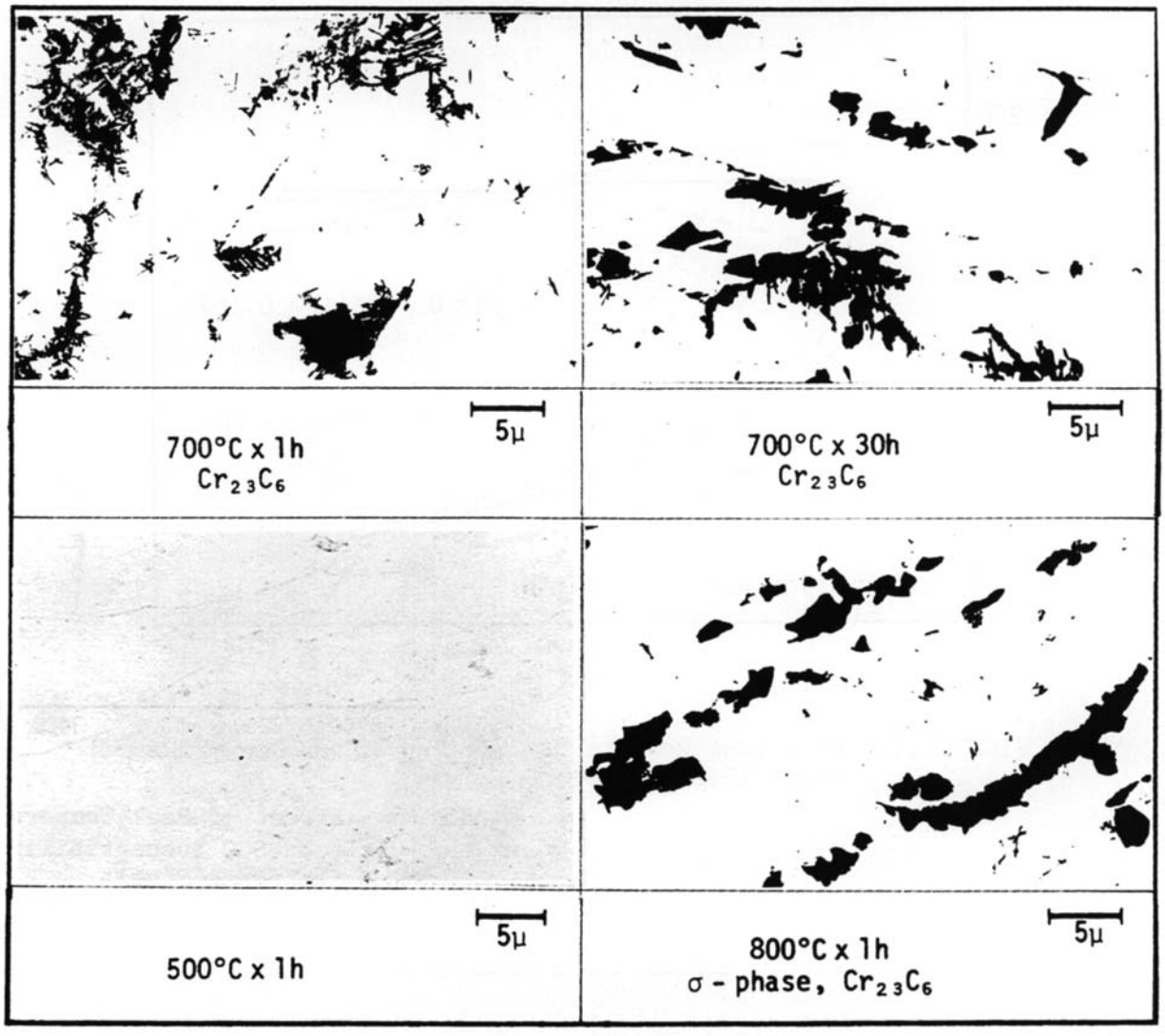


FIGURE 12 - Extraction Replica of Heat Treated 22Cr Duplex Stainless Steel (N = 0.137%)

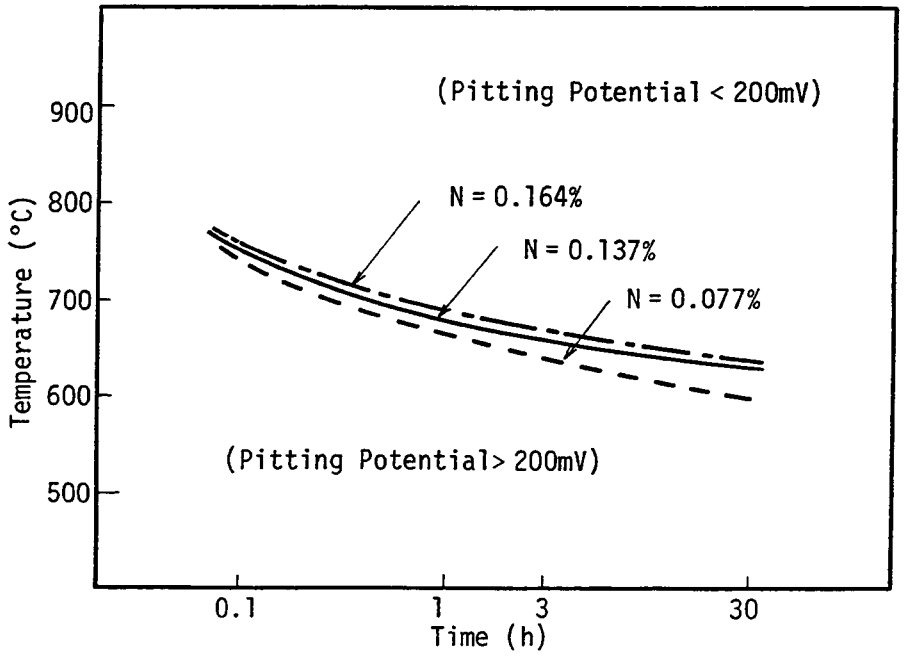


FIGURE 13 - Effect of Heating on Pitting Potential of 22Cr Duplex Stainless Steels (5% NaCl, 60°C)

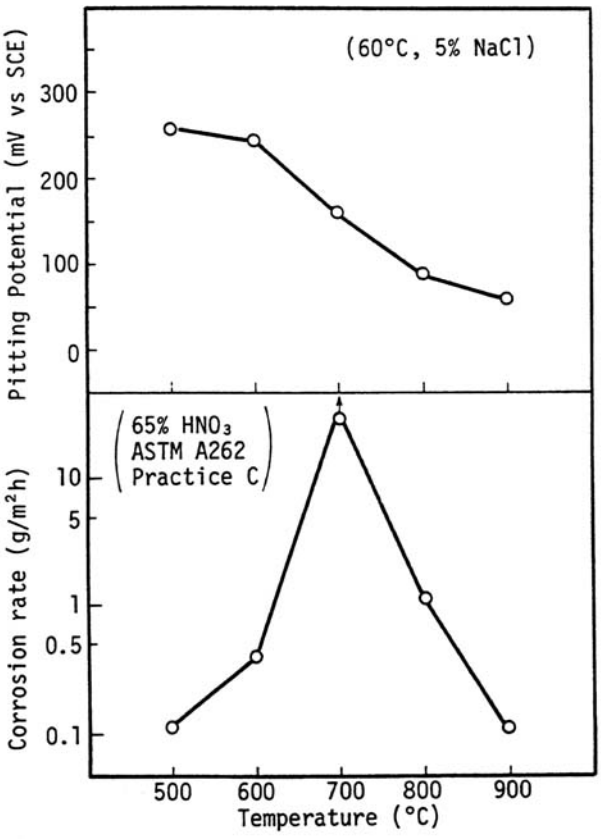


FIGURE 14 - Effect of Heating Temperature on Pitting Potential in NaCl Solution and Corrosion Rate in HNO_3 for 22Cr Duplex Stainless Steel
(N = 0.137%, Heated for 1 hour)

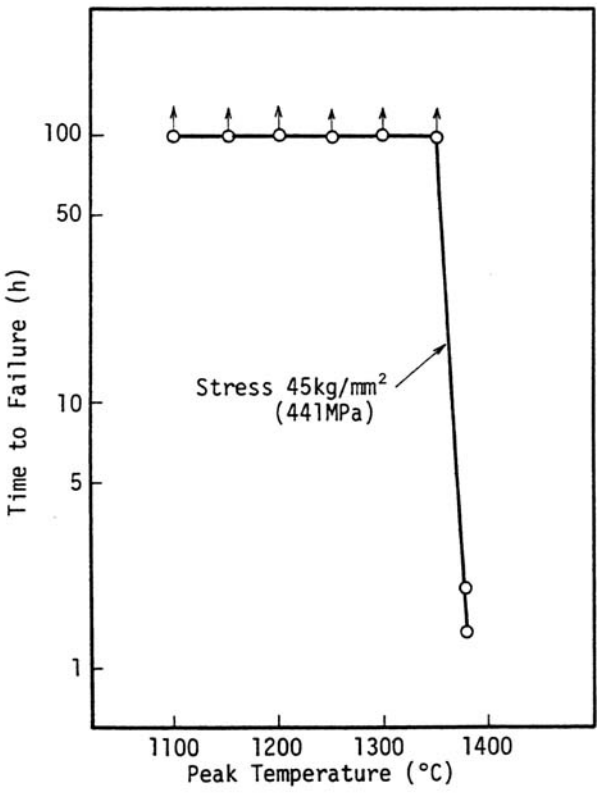


FIGURE 15 - Effect of Peak Temperature at Heat-Cycle on SCC Susceptibility of 22Cr Duplex Stainless Steel
(N = 0.137%, 100°C, 20% NaCl + 1 atm H_2S)

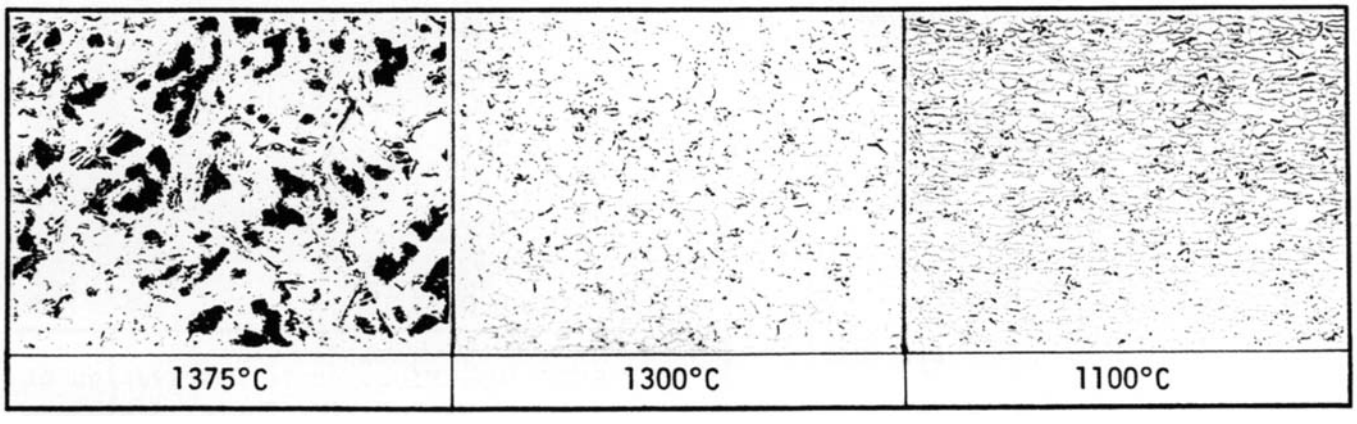


FIGURE 16 - Microstructure of 22Cr Duplex Stainless Steel (N = 0.137%) on Simulated HAZ with Various Peak Temperature

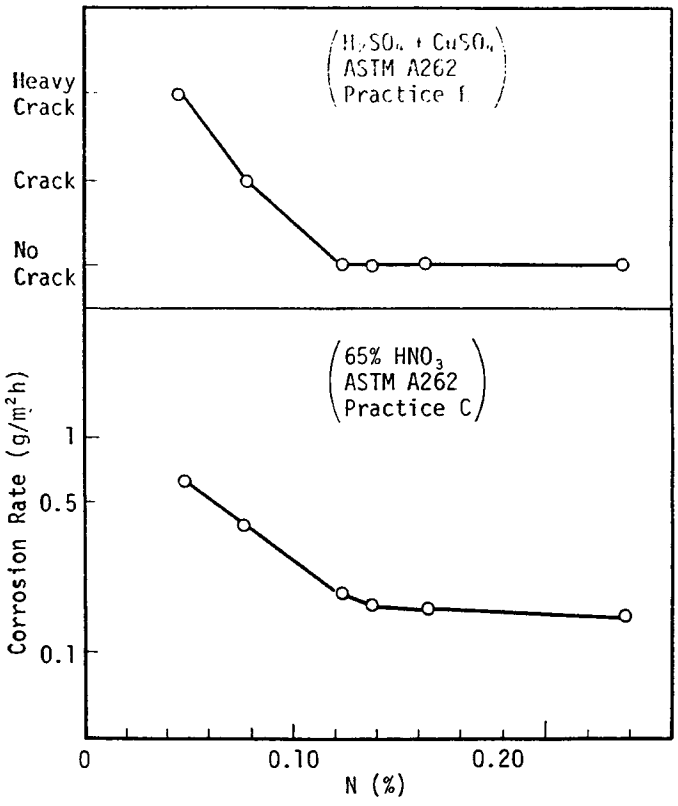


FIGURE 17 - Effect of N Content on Intergranular Corrosion of Simulated HAZ of 22Cr Duplex Stainless Steels

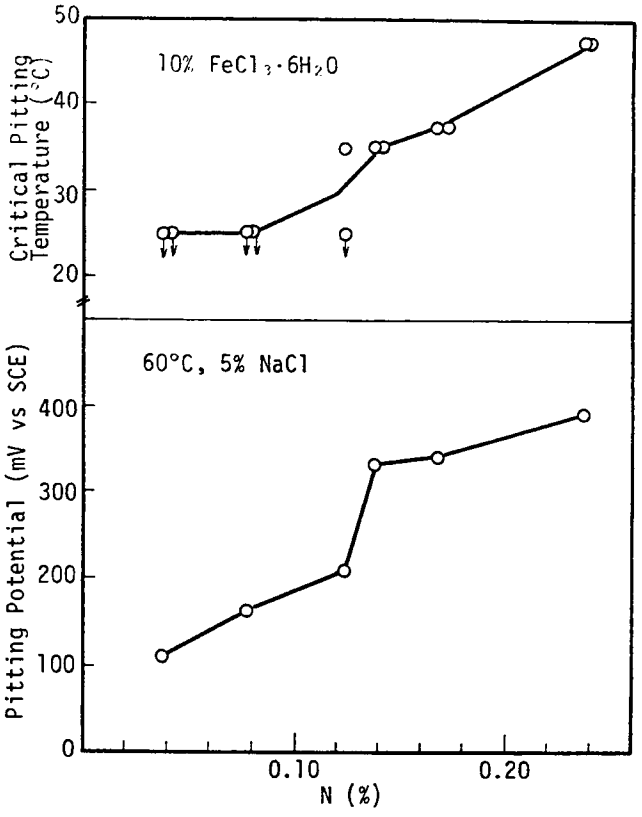


FIGURE 18 - Effect of N Content on Pitting Corrosion Resistance of Simulated HAZ of 22Cr Duplex Stainless Steels

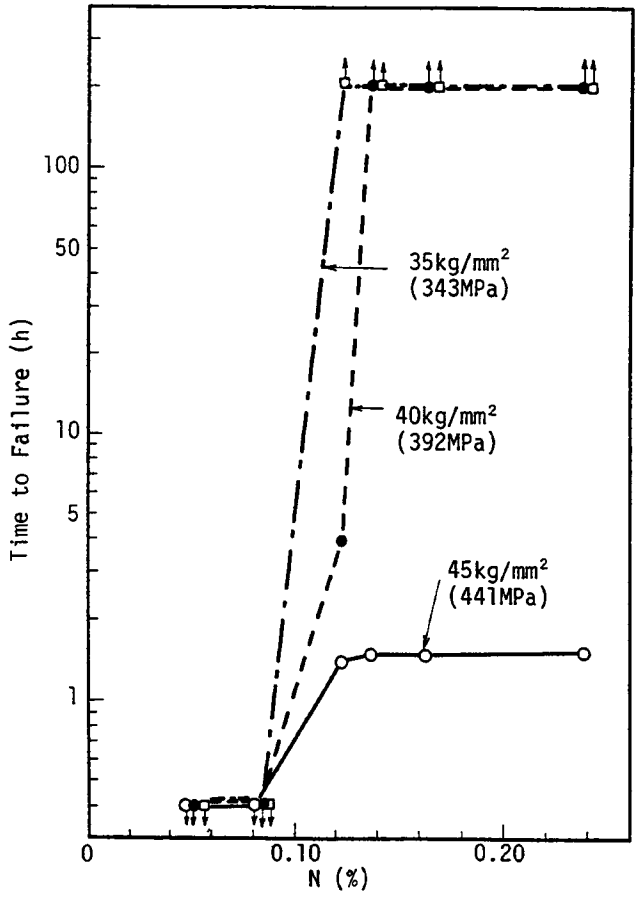


FIGURE 19 - Effect of N Content on SCC Susceptibility of Simulated HAZ of 22Cr Duplex Stainless Steels (100°C, 20% NaCl + 1 atm H_2S)

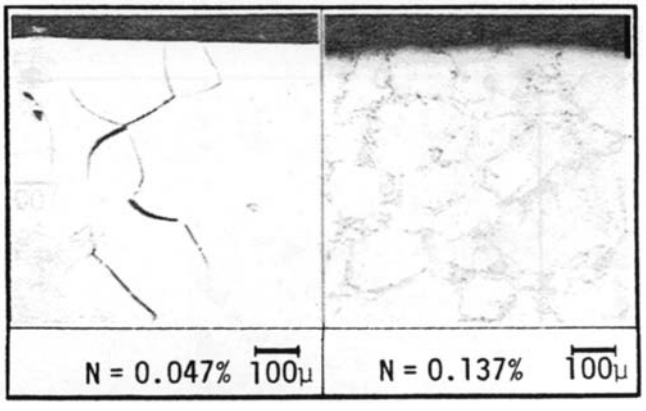


FIGURE 20 - Microscopic Observation of Simulated HAZ of 22Cr Duplex Stainless Steel after Single U-bend SCC Test (100°C, 20% NaCl + 10 atm CO_2, 500 h)

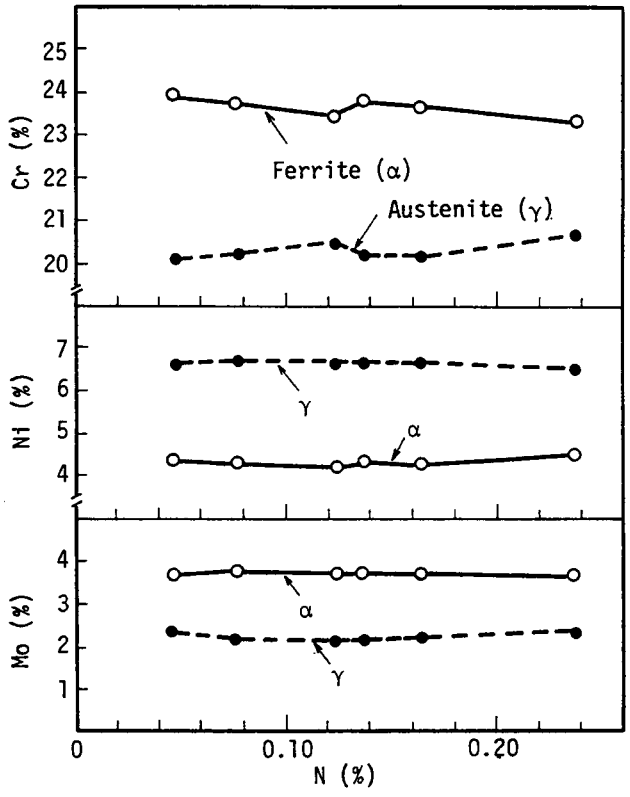


FIGURE 21 - EPMA Analysis of Ferrite and Austenite Phases of 22Cr Duplex Stainless Steels (N : 0.047 ∿ 0.238%)

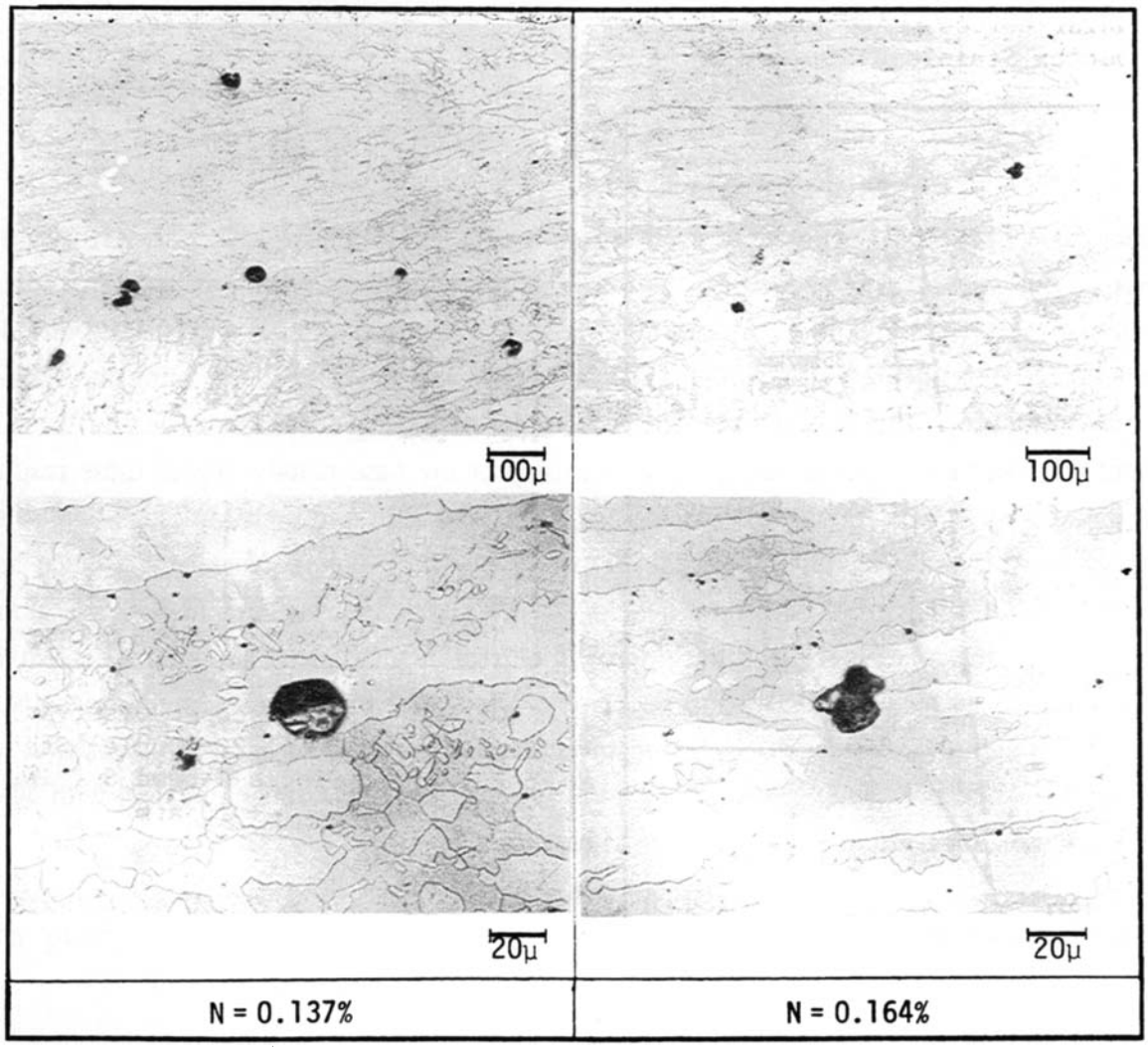


FIGURE 22 - Microscopic Observation of Pitting Initiation of 22Cr Duplex Stainless Steel (60°C, 5% NaCl)

Copyrighted Materials
Copyright © 1996 NACE International Retrieved from www.knovel.com

Paper No.
125

CORROSION 93
The NACE Annual Conference and Corrosion Show

PERFORMANCE OF HIGH CORROSION RESISTANT DUPLEX STAINLESS STEEL IN CHLORIDE AND SOUR ENVIRONMENTS

M.Ueda[1], H.Okamoto[2], T.Kobayashi[3]
K.Kondo[1], K.Ogawa[1] and T.Kudo[1]

Sumitomo Metal Industries, Ltd.
Iron & steel research Labs.[1]
Steel Tube Works[2]
Wakayama Steel Works[3]

ABSTRACT

Effect of W, Mo and N contents on pitting corrosion resistance of 25Cr and 23Cr base duplex stainless steels was investigated using the ferric chloride test according to ASTM G48. The improving effect by W addition for pitting corrosion was found out, and the modified pitting resistance equivalent(PREW) of Cr+3.3(Mo+0.5W)+16N was determined by using the least-squares method. In addition, effect of W, Mo and N contents on pitting corrosion at heat-affected zone in weldment was studied to decide the proper chemistry of the base metal. From these results, 25Cr duplex stainless steel with 2mass% W(25Cr-7Ni-3Mo-2W-0.3N), and high Mo-23Cr duplex stainless steel(23Cr-7Ni-4.5Mo-0.3N) have been developed as high pitting corrosion resistance materials. Further, corrosion behavior of the new developed-steels was investigated in H_2S containing CO_2 environment and these steels showed the improved-corrosion resistance compared with conventional 25Cr duplex stainless steel. Finally, pitting corrosion resistance of the duplex stainless stainless steel with high N content was discussed based on the corrosion test results and the calculation result of PREW in each phase of α and γ, and it was indicated that the duplex stainless steel with 40-45% α content has the most excellent pitting corrosion resistance.

Keywords: duplex stainless steel, sea water, hydrogen sulfide, carbon dioxide, pitting corrosion, stress corrosion cracking(SCC), flow line, oil country tubular goods(OCTG)

INTRODUCTION

Ferric-austenitic stainless steels have been known for more than thirty years and their tubular products have been widely used in annealed and cold worked conditions for line pipe, oil country tubular goods(OCTG) and chemical process services(1). The major reason for the use of duplex stainless steel in oil and gas production is their excellent resistance to marine and CO_2 corrosions, as well as their high mechanical strength and good weldability. The most widely used alloy is 22Cr duplex stainless steel(UNS S31803), which contains 22mass% Cr, 5.5mass% Ni, and 0.12mass% N.

For marine corrosion, the family of duplex stainless steels with 25mass% Cr and superior localized corrosion resistance has been recently developed(2). The 25Cr family, which is a highly alloyed duplex grade, has several variants depending on Mo content, and the presence of Cu and/or W. The latest developments in these grades are the super duplex stainless steels, where chemical compositions such as Mo, N, W and Cu are enriched, with a pitting resistance equivalent(PRE=Cr+3.3Mo+16N) guaranteed over 40(3). However, the 25Cr family has inferior weldability to conventional 22Cr duplex stainless steel. Localized corrosion resistance and microstructure with respect to 25Cr family have been investigated by many researchers(4-9). They have clarified the improving effect of N addition on localized corrosion resistance and the effect of chemical compositions such as Cr, Mo and W on the formation of precipitates such as nitride, and intermetallic phases(σ, χ, R etc).

For CO_2 corrosion, 22Cr(UNS S31803) and 25Cr(UNS S31260) duplex stainless steels have been widely used and have excellent corrosion resistance. The presence of H_2S, however, deteriorates their resistance to corrosions such as stress corrosion cracking(SCC) and localized corrosion. The applicable environmental conditions of duplex stainless steels have been discussed based on both the experimental corrosion test results and the actual application experience(10-12). The effects of alloying elements and the microstructure on the corrosion resistance also have been studied by many researchers to improve the corrosion resistance(13-16).

However, no detailed investigation has been carried out on the localized corrosion resistance of 25Cr duplex stainless steel with W addition more than 1mass%, the effect of Mo and N contents on the localized corrosion of the duplex stainless steel which was expected to improve weldability with Cr content lower than 25mass%, and their corrosion behavior in H_2S containing CO_2 environment.

In this paper, effects of W, Mo and N additions and α content on pitting corrosion resistance of 25Cr and 23Cr base duplex stainless steels were investigated concerning the base metal and the heat-affected zone(HAZ) by welding. Then, the corrosion behavior of the new steels was studied in a CO_2 environment containing a little amount of H_2S.

EXPERIMENTAL

Materials

Materials with chemical composition given in Tables 1 and 2 were used for the investigation of corrosion resistances in the base metal and the heat-affected zone(HAZ). These materials were melted in the laboratory, hot rolled to plates and then solution heat treated at 1100C for 30 minutes, followed by water quenching. SCC resistance in H_2S environment was studied using the new W containing 25Cr and high Mo-23Cr duplex stainless steel pipes which were melted and manufactured in the mill. Chemical composition and mechanical properties of the new steel pipes are shown in Table 3. The new W containing 25Cr duplex stainless steel has a yield strength of more than 550MPa(80ksi).

Experimental Methods

Schematic illustrations of specimens used in this study are shown in Figure 1. The test specimens were polished with a silicon carbide 600 grit paper, washed with water, degreased with ethanol and acetone, and then tested. The pitting corrosion test was carried out in 6% $FeCl_3$ solution according to ASTM G48. The critical pitting temperature(CPT) was determined as the temperature where pitting corrosion was first observed as temperature was increased by 5C in each step. A test period cycle was 24 hours. Anodic polarization measurement in order to evaluate quantitatively pitting corrosion resistance was carried out potentiodynamically at a sweep rate of 20 mV/min with potentiostat, and pitting potential(Vc') was represented as the potential at which the anodic current density exceeded 100 μ A/cm^2. The saturated calomel electrode(SCE) was used as the reference electrode. A weld joining test and simulated HAZ test were conducted to evaluate the effect of weld thermal cycle. The welded joints were produced by TIG welding using the 9mm thick plate and employing the welding condition in Table 4, where the root pass welding was conducted without filler metal. In the ferric chloride test, the specimen from the root side of welded joints was coated just in the weld metal to evaluate the HAZ. The simulated HAZ test was performed using the specimens affected by the simulating weld thermal cycle of type B or C as shown in Figure 2. Precipitates in the HAZ were analyzed by electrolytic extraction method. Then, the precipitate was identified by the electron diffraction pattern using a transmission electron microscope(TEM). Toughness of the HAZ was evaluated by the Charpy impact test with a V notch at 2mm away from fusion line as shown in Figure 1. For SCC resistance in H_2S environment, slow strain rate technique(SSRT) and constant strain tests were conducted using the specimens given in Figure 1. The specimens used in SSRT and constant strain test were taken longitudinally and transversely to the rolling direction, respectively, but all the specimens which were made from pipe were taken longitudinally. In constant strain test, 4 point bent beam specimen with notch was used and stressed to 100% of yield strength. The specimens were settled in autoclave both in SSRT and constant strain test, the autoclave was purged with nitrogen gas to deaerate the test solution, and bubbled with mixed gas of H_2S and N_2 or CO_2 to give the desired partial pressure of H_2S before heating. In the SSRT test, a tensile test was carried out at a strain rate of 4 x 10^{-6} s^{-1} in H_2S and inert environments and the following indices, shown in detail in previous paper, were used to evaluate the cracking susceptibility(17):

1.a ratio of plastic elongation in H_2S environment(L) to that in inert environment(Lo).
2.a ratio of reduction of area in H_2S environment(RA) to that in inert environment(RAo).
3.whether secondary crack is observed or not.

The SCC occurrence in constant strain rate test was evaluated by observing the specimen at high magnification after test.

RESULTS

Pitting Corrosion Resistance of Base Metal

In order to evaluate marine corrosion resistance, a critical pitting temperature(CPT) and a pitting potential have been conventionally used in ferric chloride and brine environments, respectively. In general, increase of Cr, Mo and N contents in steel is said to be effective for the prevention of marine corrosion. Several equations of pitting resistance equivalent(PRE) have been proposed by various researchers, e.g. Cr+3Mo, Cr+3Mo+10N, or Cr+3.3Mo+16N(18-20). In this study, PRE will be discussed using a PRE of Cr+3.3Mo+16N. Further, duplex stainless steel consists of α and γ phases, and the ratio of α to γ is also an important factor for pitting corrosion. It has been shown that the pitting corrosion resistance considering base metal and welding portion was mostly excellent on the material with α content between 40 and 60%(21). For high corrosion resistant duplex stainless steels which have the α content of 40 to 55% and the Mo, W and N contents more than those of conventional duplex stainless steel, the relationship between CPT and PRE is shown in Figure 3. The CPT of the steels with W content more than 0.5mass% has not been classified by the PRE equation. Therefore, the effect of W on pitting corrosion was quantitatively investigated using the electrochemical technique. The pitting potential of duplex stainless steels with high Mo, W and N contents in 20%NaCl solution at 80C was fitted to a linear function of Cr, Mo, W and N contents by applying the least-squares method as shown in Figure 4. Then, the modified PRE equation containing W content(PREW) was determined as follows:

$$PREW = Cr + 3.3(Mo+0.5W) + 16N \quad \text{--- (1)}$$

The improvement of pitting corrosion by W is thought to be similar to that of Mo. Because the coefficient of W in the PREW equation which converted mass% into mole% is the same as that of Mo, and W element belongs to the same group 6A in periodic table as Mo element. The relationship between CPT and PREW is given in Figure 5 rearranging the data in Figure 4. The PREW equation fully represented a tendency of the pitting corrosion. Particularly, 25Cr-3Mo-0.3N base steels with W content more than 2mass%, and 23Cr-0.3N base steels with Mo content more than 4.5mass% indicated excellent corrosion resistance.

Effect of α content on pitting corrosion resistance is shown in Figure 6 to concern duplex stainless steels with high Mo, W and N contents compared with conventional duplex stainless steel. The pitting corrosion resistance deteriorated as α content increased to above approximately 55%. Further, Figure 7 gives the effect of α content on CPT in the ferric chloride test. Maximum CPT was obtained at about 45% α content and high CPT was sustained even in steel with about 35% α content.

Accordingly, the suitable α content for the prevention of pitting corrosion on the duplex stainless steels with high Mo, W and N contents is not 40 to 60% in which conventional duplex stainless steel indicated excellent pitting corrosion resistance, but moves to a slight γ rich region. This behavior could be explained as follows:

The distribution of chemical compositions such as Cr, Mo, W and N in α and γ phases on the duplex stainless steel with high Mo, W and N contents is not equal to that on conventional duplex stainless steel. Therefore, the most suitable α content in the former on which a pitting corrosion resistance becomes equal both in α and γ phases is different from that in the latter.

Pitting Corrosion Resistance of Heat-affected Zone by Welding

The corrosion and mechanical properties of duplex stainless steel deteriorate as a result of precipitates such as Cr nitride and σ phase caused by weld thermal cycle(1). The effects of W, Mo and N contents on pitting corrosion resistance and toughness in the HAZ were investigated using ferric chloride and Charpy impact tests, respectively. The materials used are the 23Cr and 25Cr base duplex stainless steels which had excellent corrosion resistance in the pitting corrosion test of base metals. The following three types of weld thermal cycles, shown in Figure 2 and Table 4, were employed:

A; Heat-affected zone(HAZ) in the actual welded joints by 5 pass GTAW
B; Thermal cycle simulating in the single-pass welding
C; Thermal cycle simulating in the multi-pass welding

Effect of W content on pitting corrosion resistance. 25Cr-3Mo-0.3N base duplex stainless steels with various W contents were used in this investigation. CPT of base metals in the ferric chloride test was 80C in the steels with W content not less than 2mass% as shown in Figure 8. The test result of the materials affected by the thermal cycle A in Figure 8 indicated the highest CPT in the steel with W addition of 1 and 2mass%, although the CPT decreased with increasing W content above 3mass%. Further, CPTs of materials affected by the thermal cycle C having W content above 3mass% also decreased as shown in Figure 9. But the CPT of materials affected by the thermal cycle B which simulated single pass welding did not decrease at W addition up to 4mass%. In order to investigate the cause of decrease of CPT in the high W-added steel, Cr, Mo, Fe, W contents in extracted residue and N content precipitated as nitride were determined by chemical analysis using 25Cr-3.5Mo-0.3N duplex stainless steels with 0 to 3.3mass% W which underwent the thermal cycle A. The W content in extracted residue from 3.3mass% W containing steel increased remarkably as shown in Figure 10. TEM analysis indicated that the precipitate was produced mainly at the interface of α and γ phases, and consisted of Laves phase, $(Fe,Cr)_2(Mo,W)$ as shown in Figure 11. The formation of Laves phase would be the characteristic of excess W in duplex stainless steels though the formation of σ phase arises generally in conventional duplex stainless steel. Furthermore, the formation of Cr_2N slightly occurred as W content increased. This behavior suggests that the decrease of CPT in the steel containing W content above 3mass% in the HAZ is related to the increasing of α phase at high temperature such as 1400C, and the formation of precipitates such as Cr_2N and Laves phase at relatively lower temperature such as 1000C that followed. The decreasing of Mo content from 3.5 to 3.0% led to an extreme drop of Cr content in the extracted residue. Therefore, W addition below about 3mass% to 25Cr-3Mo base duplex stainless steel is very effective from the view point of pitting

corrosion prevention and precipitation such as Cr_2N, σ phase and Laves phase in the HAZ. Thus, a 25Cr-3Mo-2W-0.3N duplex stainless steel has been developed.

Effect of Mo and N contents on pitting corrosion resistance. 23Cr base duplex stainless steels with various Mo and N contents were used in this investigation.

a)Effect of Mo content: CPT of base metals was 80C in the steels with Mo content above 4.5mass% as shown in Figure 12. The CPT of materials affected by the thermal cycle A in Figure 12 decreased at 5.5mass% Mo content and that affected the thermal cycle C in Figure 13 decreased as Mo content increased to not less than 5mass%. The steels affected by the thermal cycle B increased in CPT with increasing Mo content, though the CPT was lower than that of base metals. The Cr, Mo and Fe contents in extracted residue and N content precipitated as nitride are given in Figure 14 with respect to 23Cr-0.3N base duplex stainless steels which were affected by the thermal cycle A. Cr, Mo and Fe contents in extracted residue increased with increasing of Mo content in steel and particularly, their quantities were great in the steel containing 5.5mass% Mo. The precipitate was mainly identified as σ phase by TEM analysis. Nitride was almost not detected in Mo containing 23Cr-0.3N duplex stainless steels.

b)Effect of N content: CPT of base metals and materials affected the thermal cycle A increased with the N content up to 0.3mass% as shown in Figure 15, and was saturated at 0.3 and 0.33mass% N content. The CPT of materials affected by the thermal cycle B, shown in Figure 16, increased as N content increased. Then, the CPT decreased in the steel with 0.33mass% N which underwent the thermal cycle C. This behavior is thought to be related to the nucleation of precipitates by the first thermal cycle with the peak of 1400C and the growth of precipitates by the second cycle at 1000C.

From these results, 23Cr-4.5Mo-0.3N duplex stainless steel has been developed and the new steel showed excellent pitting corrosion resistance as high as W-added 25Cr duplex stainless steel considering heat influence by welding. The Mo addition of 5.5mass% or N addition of 0.33mass% increased in susceptibilities of pitting corrosion and formation of precipitate such as σ phase or nitride.

Effect of Cr, Mo and W contents on toughness. The effect of Cr, Mo and W contents on 4Mo-0.3N, 23Cr-0.3N and25Cr-3.5Mo-0.3N base duplex stainless steels was investigated by Charpy impact test in HAZ at 0C. Test results are shown in Figure 17. The impact value in Cr-varied duplex stainless steels extremely decreased as Cr content increased from 23 to 25mass%. This behavior coincides with the fact that 22Cr conventional duplex stainless steel has very excellent toughness compared with 25Cr conventional duplex stainless steel in HAZ. The effect of Mo content on the impact value was slight in the 23Cr base duplex stainless steel. The addition of W content up to about 2mass% did not affect HAZ toughness, but W addition of 3.3mass% reduced remarkably the impact value. Accordingly, it would clarify that the decrease of Cr content is effective for the improvement of HAZ toughness. From the view point of toughness, high Mo-23Cr duplex stainless steel would be superior than 25Cr duplex stainless steel with W addition.

Stress Corrosion Cracking Resistance in H_2S Environment

SCC resistances of the new W containing 25Cr(new steel A) and high Mo-23Cr(new steel B) duplex stainless steels melted in mill, which have CPT more than 80C, were investigated at 80C which is a temperature with most high susceptibility for the SCC of conventional duplex stainless steel in the environment containing a small amount of H_2S. SCC susceptibility was evaluated by SSRT and constant strain method.

Evaluation by SSRT. Effects of chloride content and partial pressure of H_2S have been obtained by Kudo et al concerning conventional Type 316L, 22Cr(UNS S31803) and 25Cr(UNS S31260) duplex stainless steels using SSRT(23). The test results of new steels A and B in SSRT are shown in Figure 18 to superimpose on the previous result. Type 316L suffered SCC under the condition of partial pressure of 0.001MPa H_2S containing high chloride content of 10^5 ppm. 25Cr duplex stainless steel was more resistance to SCC than 22Cr duplex stainless steel in Cl^--H_2S environments, though the superiority of 25Cr duplex stainless steel diminished with increasing the chloride content and the partial pressure of H_2S. It is thought that the critical partial pressure of H_2S for SCC of duplex stainless steels locates around 0.01MPa, where the chloride content has remarkable effect on the SCC susceptibility. So effect of chloride content on SCC susceptibility of 25Cr duplex stainless steel and the new steels was studied in the environment of 0.01MPa H_2S. Conventional 25Cr duplex stainless steel was susceptible to SCC in the environment containing 2×10^4 ppm Cl^- as shown in Figure 19, but new steels A and B were not susceptible to SCC in that. Therefore, SCC resistance of the new steels is superior to that of conventional 25Cr duplex stainless steel.

Evaluation by constant strain method. Effect of W, Mo and N contents on SCC resistance in 5%NaCl(3×10^4 ppm Cl^-) solution containing 0.003 to 0.01MPa H_2S was investigated by using 4 point bent beam specimen with notch concerning 25Cr and 23Cr base duplex stainless steels. The test results are given in Figure 20. 25Cr-3Mo-W and high Mo-23Cr duplex stainless steels did not suffer SCC in the environment with H_2S partial pressure up to 0.005MPa, but conventional 25Cr and 25Cr-3Mo-0.3N duplex stainless steels did. Then, it is obvious that the steels added W above 1mass% and Mo above 4.5mass% with N content more than 0.25mass% have the same improvement effect for the SCC susceptibility. The SCC of materials tested propagated through α phase and stopped at γ phase by the keying effect(24). Effect of welding on SCC resistance of the new steels in Cl^--H_2S environment was also investigated by using 25Cr-3Mo-2W-0.3N(new steel A) which was welded by TIG welding with filler metal containing 2 and 3mass% W. The critical H_2S partial pressure for SCC of weldment as shown in Table 5 coincided with that of base metal. This fact suggests that the deterioration effect of SCC resistance by welding is small in H_2S containing environment. The crack in welded specimen was observed in α phase at fusion line.

From these results, SCC resistance of the new 25Cr-3Mo-2W-0.3N and 23Cr-4.5Mo-0.3N duplex stainless steels is superior to conventional 25Cr duplex stainless steel. The critical H_2S partial pressure for SCC of the new steels would be around 0.005MPa, although that highly depends on chloride ion concentration in solution.

DISCUSSION

Corrosion resistance of high corrosion resistant duplex stainless steels with high N content and W addition or high Mo content is discussed based on the distribution of chemical compositions such as Cr, Ni, Mo, W and N in α and γ phases. Figure 21 shows the effect of α content on the ratio of Cr, Ni, Mo and W contents in α phase to that in γ phase. The ratios were calculated to use Cr, Ni, Mo and W contents in each α and γ phases which were determined by EPMA analysis. The α content was varied by the following two treatments:

1. Ni content ranged from 4.0 to 8.4mass% for 25Cr-4Mo-0.3N duplex stainless steel. Annealing temperature was 1100C.

2. Annealing temperature ranged from 1050 to 1175C. Materials used was 25Cr-3Mo-2W-0.3N duplex stainless steel. The relationship between annealing temperature and α content is shown Figure 22.

The ratio of Cr, Ni, Mo and W contents was able to represent as a linear function of α content using all the data, though that is theoretically functions of temperature and chemical compositions. Cr, Mo and W elements which promote the formation of ferrite were enriched in the α phase, in the order W > Mo > Cr, and their contents decreased as α content increased. On the other hand, Ni element was enriched in the γ phase and its content increased as α content increased. N content in γ phase can not analyze because the solubility in α phase is very small and nitrogen almost dissolves in γ phase. In general, the equilibrium solubility limit for nitrogen is said to be in the range 0.03-0.05mass% on conventional annealed duplex stainless steel(2). PREW values in each phase of α and γ were estimated using above results and the following calculation methods:

1. Chemical compositions in each phase, $C(\alpha)$ in α phase and $C(\gamma)$ in γ phase, are

$$C(\gamma)=Cx100/(\alpha\%xF(\alpha/\gamma)+100-\alpha\%) \quad \text{---- (2)}$$

$$C(\alpha)=F(\alpha/\gamma)xC(\gamma) \quad \text{---- (3)}$$

where C is chemical composition of base metal, $\alpha\%$ is α content and $F(\alpha/\gamma)$ is the ratio of chemical composition in α phase to that in γ phase and a linear function of α content. Then, the two cases of (a)N content in α phase=0mass% and (b)N content in α phase=0.05mass% were considered with respect to calculation of N content.

2. Substituting $C(\alpha)$ and $C(\gamma)$ of Cr, Mo, W and N in PREW equation (1), PREW values in α and γ phases are obtained, respectively.

The results of PREW calculated for 25Cr-3Mo-2W-0.3N and 23Cr-4.5Mo-0.3N duplex stainless steels are shown in Figure 23. The α content, in which PREW was the same both in α and γ phases, was around 40-45% even if N content in α phase is 0.05mass%. Further, the difference of PREW between α and γ phases becomes 2-4mass% at 55% α content and this difference becomes even bigger as α content increases, while the difference at 35% α content is about 2-3mass% and smaller than that at 55% α content. These calculated results were in agreement with the test results of pitting corrosion resistance in base metal shown in Figures 6 and 7. These facts can be thought relating to N

content in the base metal. N element contributes only to the increasing of PREW in γ phase as N content in α phase is 0mass%. Then, in the case of 50% α content, PREW value in α phase is about 41.5 and the differences between PREW value in α phase and that in γ phase are 2.4mass% in 23Cr-4Mo-0.3N steel and 2.9mass% in 25Cr-3Mo-2W-0.3N steel. From these values, N contents in the base metals in order to obtain the same PREW value both in α and γ phases are estimated to be 0.23mass% in the former and 0.21mass% in the latter, though the performance of pitting corrosion resistance is not satisfied in the steels with the N content. Namely, the 40-45% α content, in which PREW is the same both in α and γ phases, is a characteristic of the high N containing duplex stainless steel.

CONCLUSIONS

Effect of W, Mo and N contents on pitting corrosion resistance of 25Cr and 23Cr base duplex stainless steels was investigated with respect to the base metal and the HAZ in the weldment. Corrosion behavior of the duplex stainless steels which showed excellent pitting corrosion resistance was also studied in H_2S containing environment. Further, the pitting corrosion resistance of duplex stainless steel was discussed based on calculation result of PREW in each phase of α and γ. The results obtained are summarized as follows:

1. The improvement for pitting corrosion due to W addition was found and the modified pitting resistance equivalent(PREW) of Cr+3.3(Mo+0.5W)+16N was determined by using the least-squares method.

2. 25Cr duplex stainless steel adding 2mass% W(25Cr-7Ni-3Mo-2W-0.3N) has been developed as a excellent pitting corrosion resistance material.

3. 23Cr duplex stainless steel with high Mo of 4.5mass%(23Cr-7Ni-4.5Mo-0.3N) which is expected to have superior weldability has also been developed and showed the similar pitting corrosion resistance as the new W-added 25Cr duplex stainless steel.

4. The new W containing 25Cr and high Mo-23Cr duplex stainless steels indicated the improved-corrosion resistance compared with conventional duplex stainless steel in H_2S containing CO_2 environment.

5. From corrosion test results and calculation of PREW in each phase of α and γ in these high corrosion resistant duplex stainless steels with high N content, it was clarified that the most excellent pitting corrosion resistance is obtained at the α content of 40-45% to be slightly γ rich.

ACKNOWLEDGMENTS

The authors wish to thank Sumitomo Metal Industries Ltd. for allowing publication of this research. The assistance and discussion of co-workers in laboratories are gratefully acknowledged.

REFERENCES

1.C.V.Roscoe and K.J.Gradwell, Duplex Stainless Steel'86 Conference,126-132, 1986
2.J.Charles, Duplex Stainless Steel'91 Conference, 3-48, 1991
3.G.Martin and F.Blanchard, Corrosion/92 Paper No. 409, National Association of Corrosion Engineers, Houston, Texas, 1992
4.C.V.Roscoe, K.J.Gradwell, M.R.Watts and W.J.Nisbet, Stainless Steel Conference, York(U.K.), 325, 1987
5.S.Bernhardsson, Corrosion/90 Paper No. 164, National Association of Corrosion Engineers, Houston, Texas, 1990
6.L.Van Nassau, H.Meelker and J.Hilkes, Duplex Stainless Steel'91 conference, 303, 1991
7.W.Nicodemi, R.Roberti and G.M.La Vecchia, Stainless Steel'92 Conference, 270, 1992
8.J.O. Niesson, A.Wilson, B.Josefsson and T.Thorvaldsson, Stainless Steel'92 Conference, 280, 1992
9.H.Okamoto, Stainless Steel'92 Conference, 360, 1992
10.P.R.Rhodes, GA.Wech and L.Abgero, J.Materials for Energy Systems, Vol. 5, No.1, 3, 1983
11.A.Ikeda, S.Mukai and M.Ueda, Corrosion, Vol. 41, 185, 1985
12.T.kudo, H.Miyuki, H.Okamoto, J.Murayama and T.Moroishi, Corrosion/82 paper No.127, National Association of Corrosion Engineers, Houston, Texas, 1982
13.J.Oredsson and S.Bernhardsson, Corrosion/82 Paper No.126, National Association of Corrosion Engineers, Houston, Texas, 1982
14.S.Mukai, H.Okamoto, T.Kudo and A.Ikeda, J Materials for Energy Systems, Vol. 5, No. 1, 59, 1983
15.J.Sakai, I.Matsushima, Y.Kanemura, M.Tanimura and T.Otsuka, ASM Metals Congress, 8201-010, 1982
16.B.D.Craig, ASM Metal Congress, 8201-015, 1982
17.M.Ueda and T.Kudo, Corrosion/91 Paper No.2, National Association of Corrosion Engineers, Houston, Texas, 1991
18.M.B.Rockel, ACHEMA Conference at Frankfurt, 1979
19.M.Miura, Sumitomo Metal, Vol.36, No. 4, 383, 1984
20.J.Preva and B. Johnsson, Corrosion/84 Paper No.218, National Association of Corrosion Engineers, Houston, Texas, 1984
21.A.Ikeda, M.Miura, S.Mukai, M.Ueda and K.Koso, Corrosion/86 Paper No.333, National Association of Corrosion Engineers, Houston, Texas, 1986
22.I.Ikeda, S.Mukai and M.Ueda, Corrosion/84 Paper No.289, National Association of Corrosion Engineers, Houston, Texas, 1984
23.T.Kudo, H.Tsuge and T.Moroishi, Corrosion/88 Paper No.62, National Association of Corrosion Engineers, Houston, Texas, 1988
24.J.W.Flowers, F.H.Beck and M.G.Fontana, Corrosion, Vol. 19, 186, 1963

Table 1. Chemical composition of materials used in pitting corrosion test of base metal

Cr	Ni	Mo	W	N	Others
22/26	4/8.5	3/5.5	0/4.0	0.25/0.35	C:0.02, Cu:0.5

Table 2. Chemical composition of materials used in pitting corrosion test in HAZ and SCC test

	No	C	Si	Mn	P	S	Cu	Cr	Ni	Mo	W	N
W	1	0.022	0.32	0.48	0.022	0.001	0.53	25.2	7.44	2.86	<0.01	0.332
	2	0.022	0.28	0.47	0.022	0.002	0.53	25.6	7.68	2.92	0.98	0.332
	3	0.024	0.28	0.48	0.020	0.002	0.47	25.2	7.55	2.86	2.05	0.335
	4	0.027	0.26	0.45	0.022	0.002	0.45	25.6	7.51	2.93	3.05	0.339
	5	0.027	0.27	0.47	0.021	0.002	0.46	25.5	7.60	3.02	4.26	0.332
Mo	6	0.020	0.28	0.50	0.018	0.001	0.46	22.6	7.03	4.47	0.30	0.301
	7	0.023	0.24	0.51	0.019	0.001	0.54	22.8	6.98	4.94	0.30	0.293
	8	0.019	0.31	0.51	0.017	0.001	0.55	22.5	7.14	5.54	0.30	0.302
N	9	0.028	0.27	0.49	0.016	0.002	0.54	22.7	6.97	4.60	0.59	0.239
	10	0.019	0.26	0.52	0.021	0.002	0.54	22.7	7.02	4.68	0.30	0.328

Table 3. Chemical composition and mechanical properties of the new high corrosion resistant duplex stainless steels manufactured by mill

Material	Chemical composition(mass%)											Y.S.		T.S.		RA
	C	Si	Mn	P	S	Cu	Cr	Ni	Mo	W	N	MPa	ksi	MPa	ksi	%
New steel A	0.015	0.33	0.52	0.015	0.004	0.51	24.6	6.85	3.11	2.10	0.260	594	86.2	848	122.0	46.7
New steel B	0.017	0.39	0.54	0.023	0.001	0.72	22.5	7.05	4.60	0.26	0.310	541	78.7	818	119.0	47.6

Table 4. Welding condition used

(a) in pitting corrosion test

Pass	Voltage (V)	Current (A)	Speed (cm/min)	Heat input (kJ/cm)
1	13	170	10	13.3
2-5	14	200	10	16.8

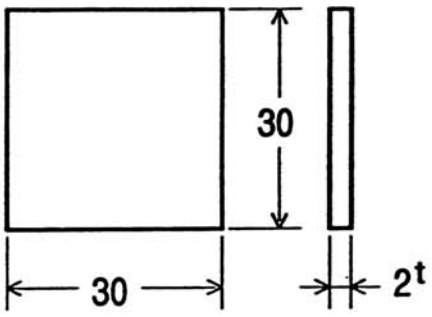
(b) in SCC test

Pass	Voltage (V)	Current (A)	Speed (cm/min)	Heat input (kJ/cm)
1	14	120	10	10.1
2-13	17	150	10	15.3

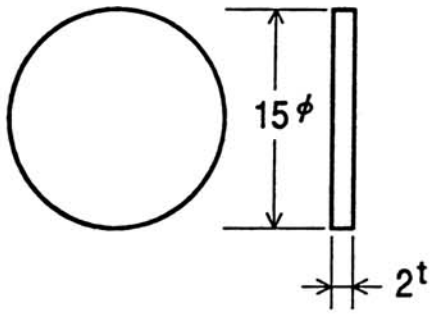
Table 5. Effect of H_2S partial pressure on SCC resistance of 25Cr-3Mo-2W-0.3N duplex stainless steel and its weldment

Type	Filler metal(mass%)					Partial pressure of H_2S		
	Cr	Ni	Mo	W	N	0.003MPa	0.006MPa	0.01MPa
Weldment	25.4	9.5	3.2	2.1	0.26	No SCC	No SCC	SCC
	25.1	9.4	3.1	3.0	0.27	No SCC	No SCC	SCC
Base metal	———					No SCC	No SCC	SCC

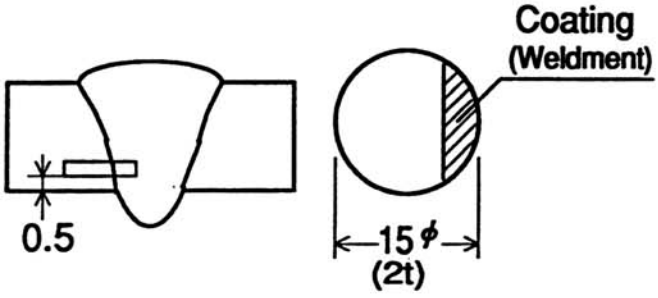
Test condition: 5%NaCl, H_2S+3.0MPa CO_2, 80C, 720h
4 point bent beam, 1σ,



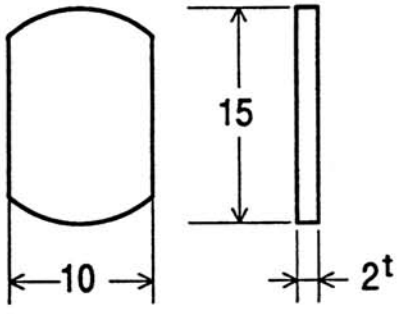
(a) CPT specimen(Base metal)



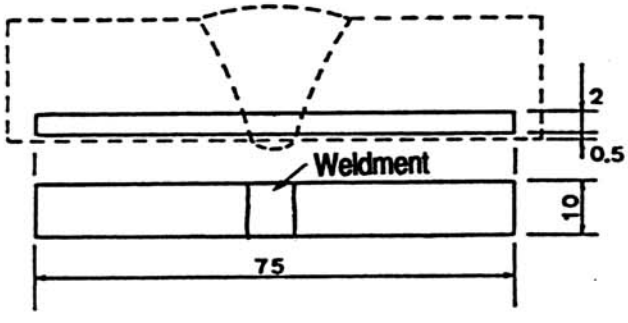
(b) Elcctrochemical specimen



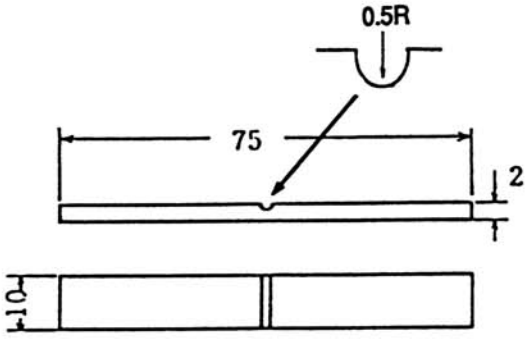
(c) CPT specimen(Welded joints)



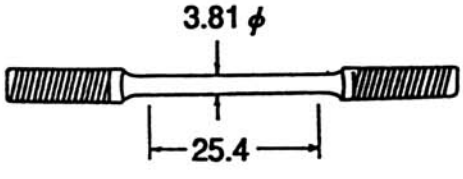
(d) CPT specimen(Simulated HAZ)



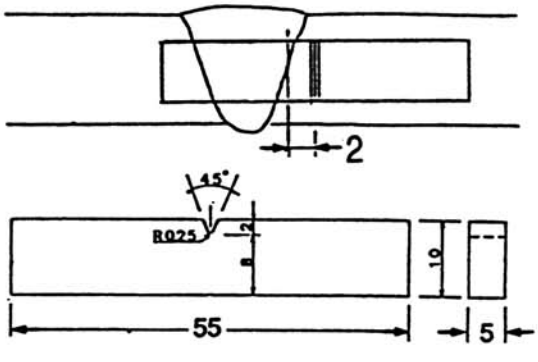
(e) 4 point bent beam specimen (Welding)



(f) 4 point bent beam specimen (Base metal)



(g) SSRT specimen



(h) Charpy impact test specimen

Figure 1. Schematic illustration of test specimens used for this study (Unit: mm)

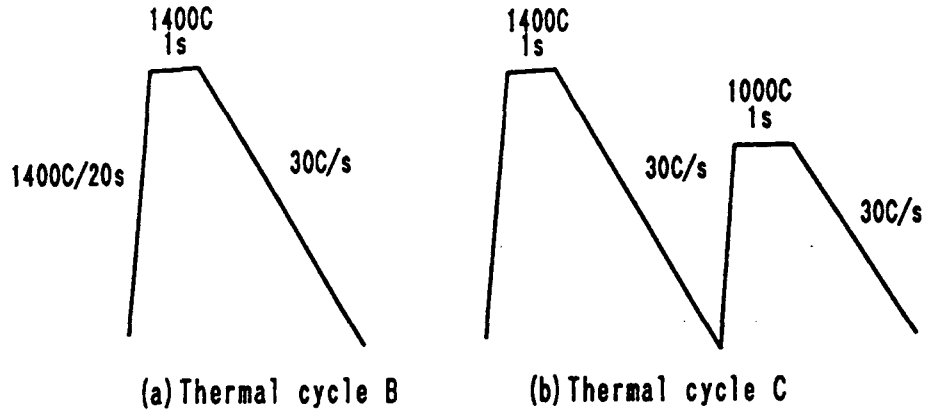


Figure 2. Thermal cycles employed for the simulated HAZ test

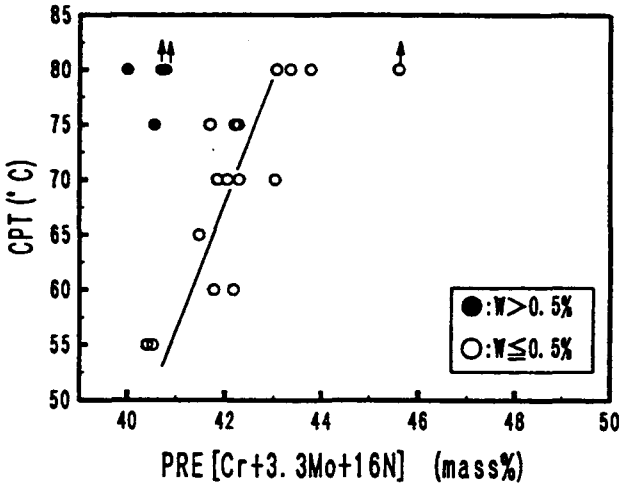


Figure 3. Relationship between critical pitting temperature (CPT) and pitting resistance equivalent(PRE)
(6%$FeCl_3$, a cycle of test period: 24h)

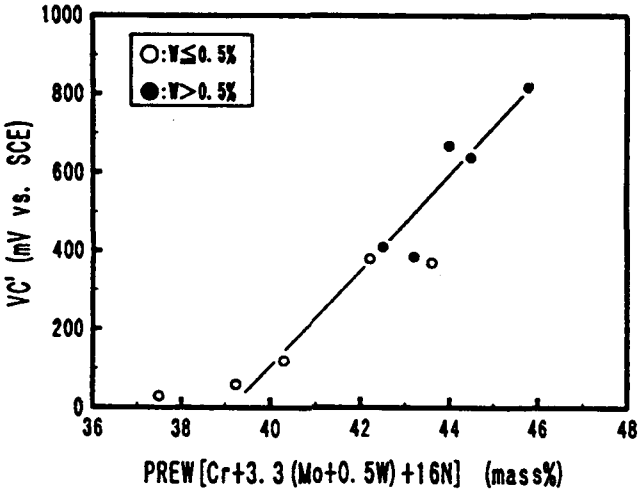


Figure 4. Relationship between pitting potential(Vc') and modified-pitting resistance equivalent(PREW)
(80C, 20%NaCl, Scan rate: 20mV/min)

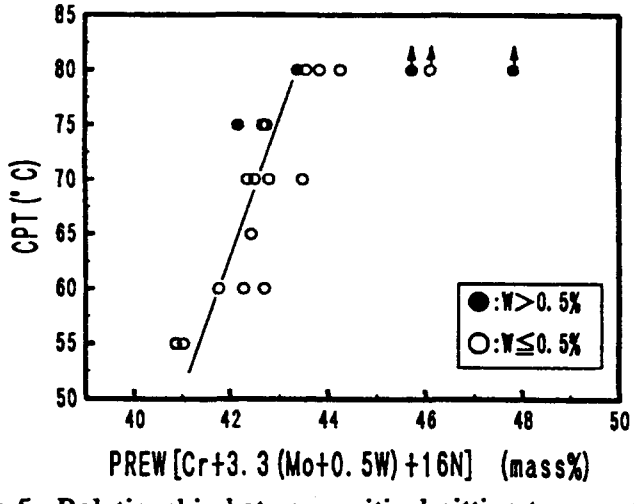


Figure 5. Relationship between critical pitting temperature(CPT) and modified-pitting resistance equivalent(PREW)
(6%$FeCl_3$, a cycle of test period: 24h)

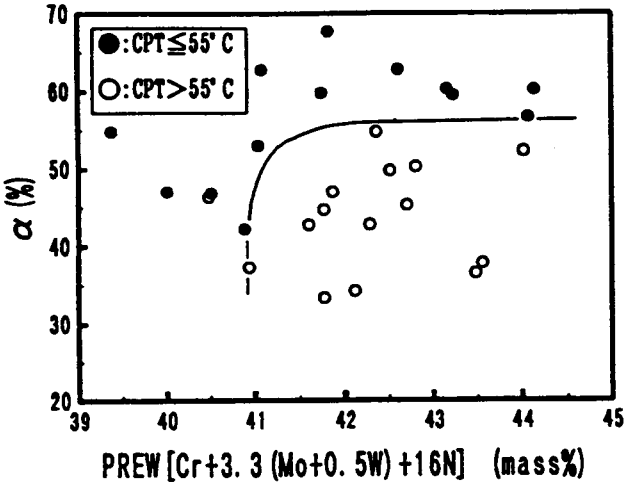


Figure 6. Relationship between α content and modified pitting resistance equivalent(PREW)
(55C, 6%$FeCl_3$, 24h)

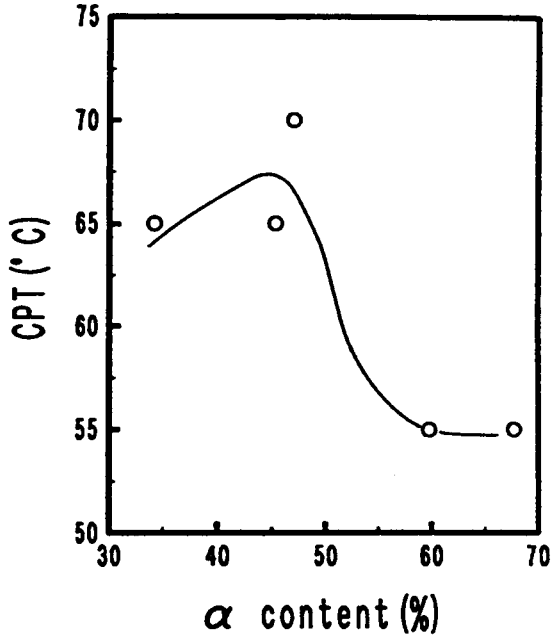


Figure 7. Effect of α content on critical pitting temperature(CPT)
(25Cr-Ni-3.5Mo-0.3N, 6%$FeCl_3$, a cycle of test period: 24h)

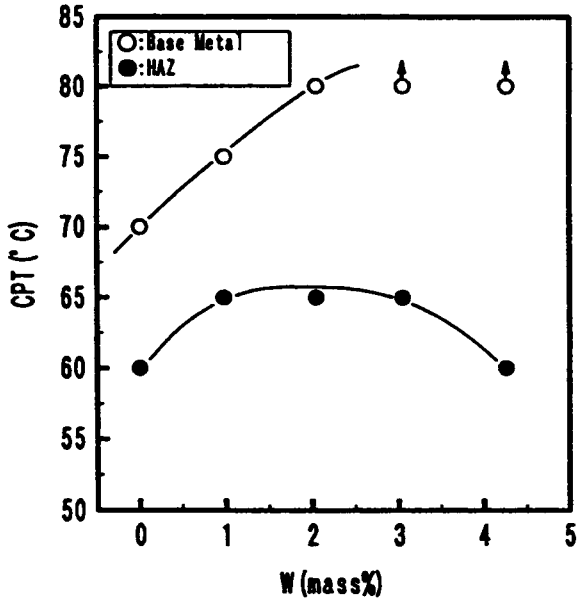


Figure 8. Effect of W content on critical pitting temperature (CPT) of base metal and in HAZ
(25Cr-7Ni-3Mo-W-0.3N, 6%$FeCl_3$, a cycle of test period: 24h)

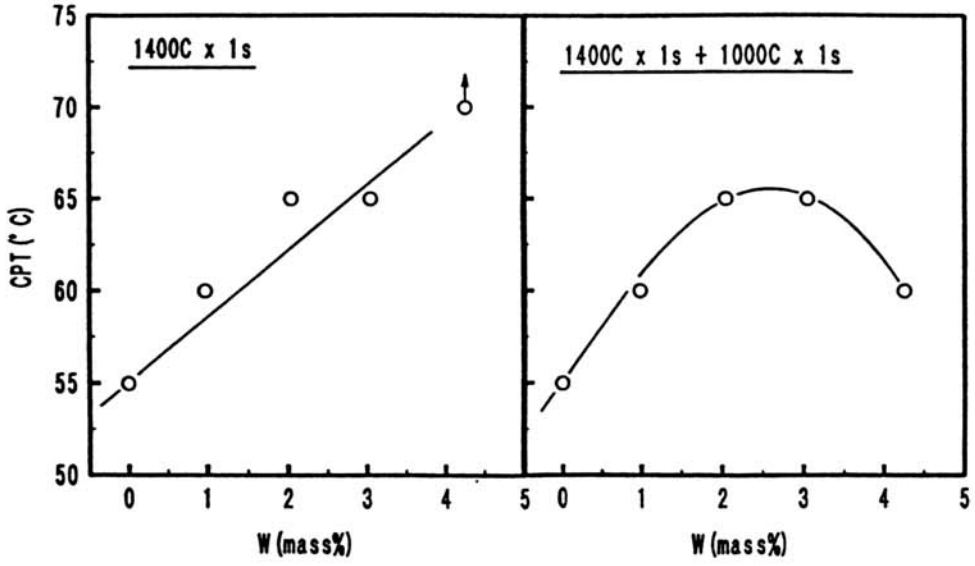


Figure 9. Effect of W content on critical pitting temperature(CPT) in simulated HAZ
(25Cr-7Ni-3Mo-W-0.3N, 6%$FeCl_3$, a cycle of test period: 24h)

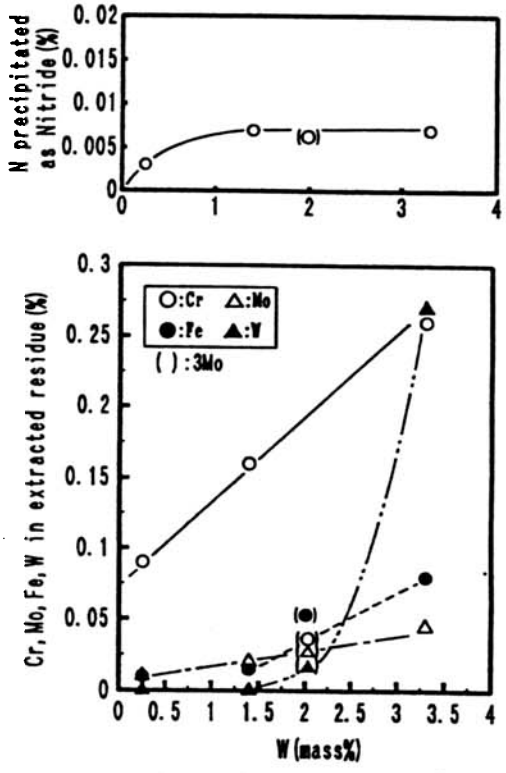


Figure 10. Effect of W content on formation of precipitations in HAZ by analysis of extracted residue
(25Cr-7Ni-3.5Mo-W-0.3N)

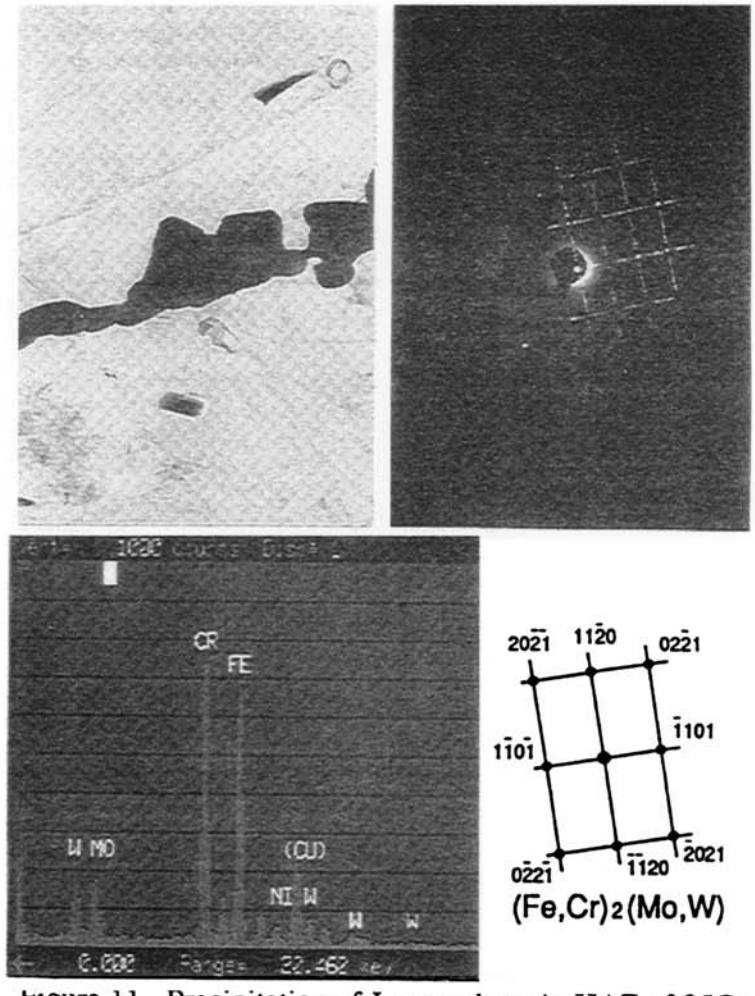


Figure 11. Precipitation of Laves phase in HAZ of 25Cr-7Ni-3.5Mo-3.3W-0.3N steel observed with TEM by extraction replica

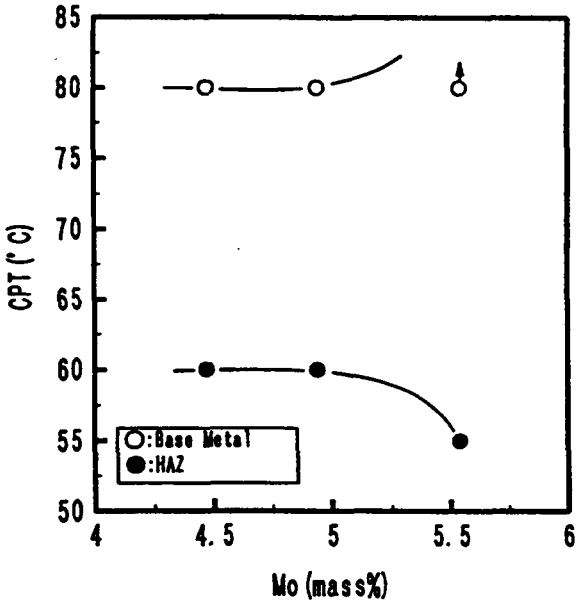


Figure 12. Effect of Mo content on critical pitting temperature (CPT) of base metal and in HAZ
(23Cr-7Ni-Mo-0.3N, 6%$FeCl_3$, a cycle of test period: 24h)

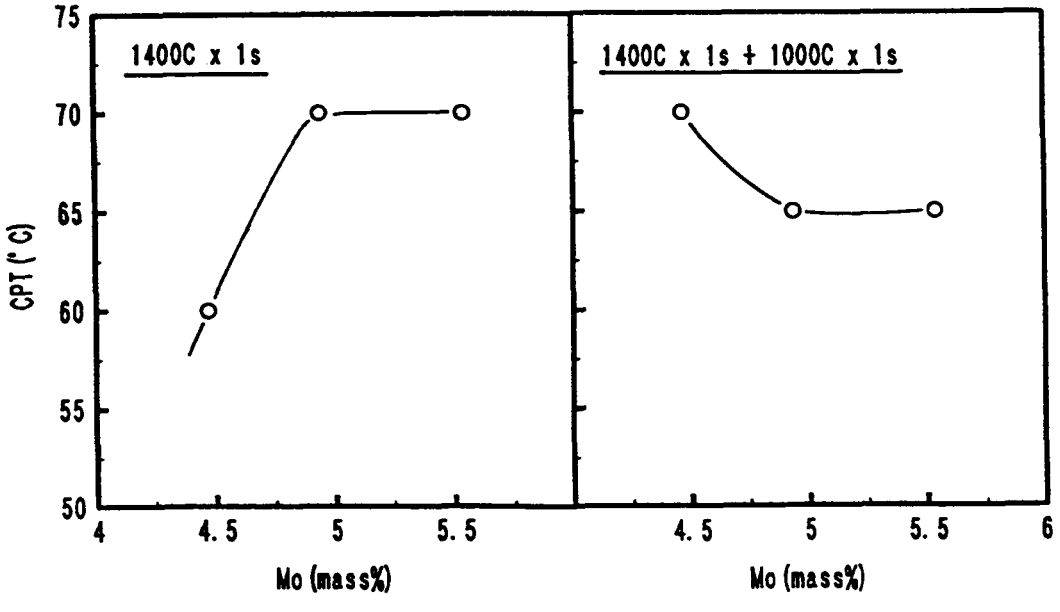


Figure 13. Effect of Mo content on critical pitting temperature(CPT) in simulated HAZ
(23Cr-7Ni-Mo-0.3N, 6%$FeCl_3$, a cycle of test period: 24h)

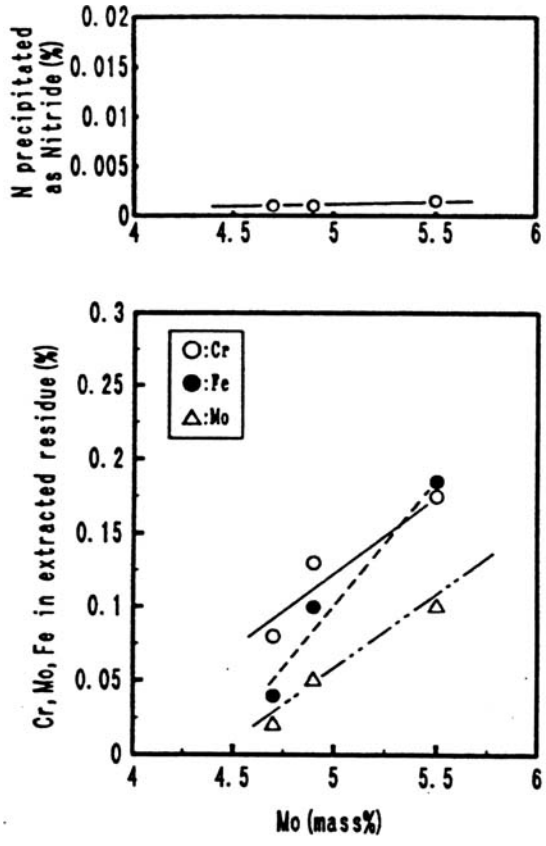


Figure 14. Effect of Mo content on formation of precipitations in HAZ by analysis of extracted residue
(23Cr-7Ni-Mo-0.3N)

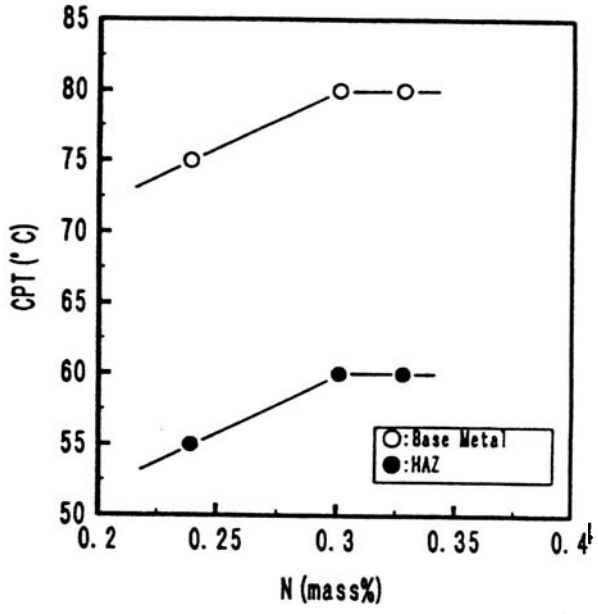


Figure 15. Effect of N content on critical pitting temperature(CPT) of base metal and in HAZ
(23Cr-7Ni-4.5Mo-N, 6%$FeCl_3$, a cycle of test period: 24h)

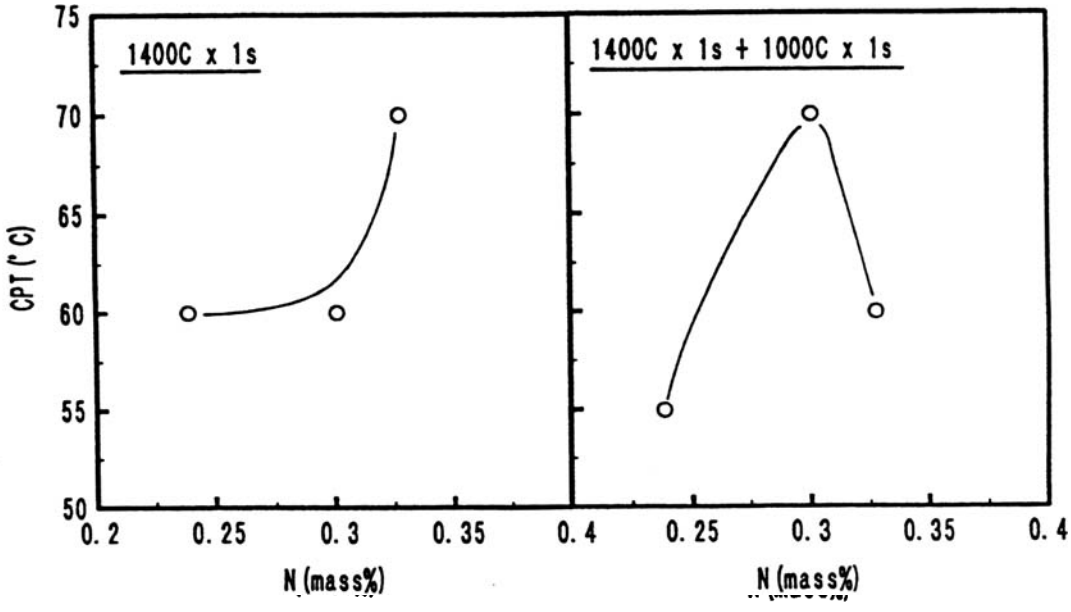


Figure 16. Effect of N content on critical pitting temperature(CPT) in simulated HAZ
(23Cr-7Ni-4.5Mo-N, 6%$FeCl_3$, a cycle of test period: 24h)

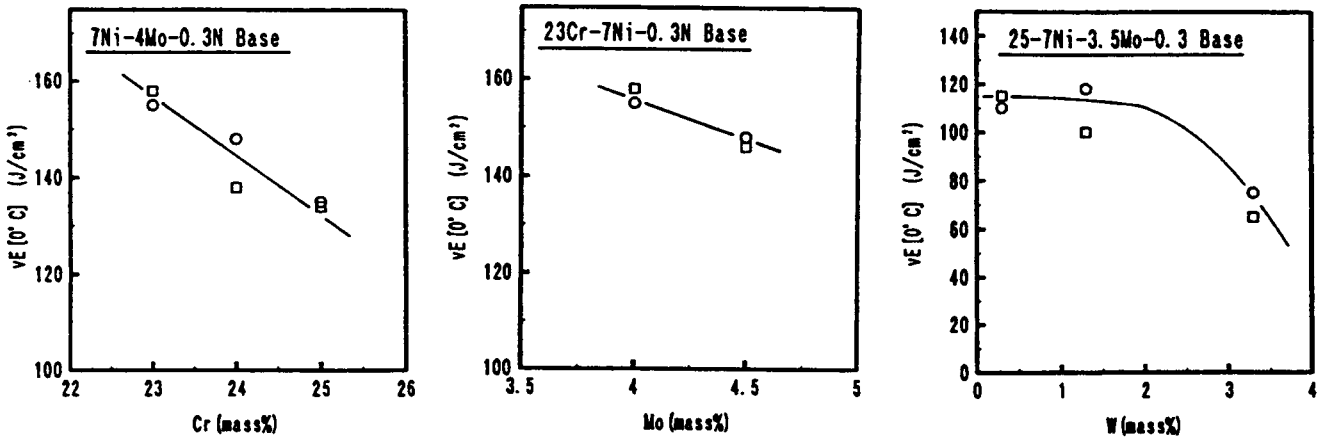


Figure 17. Effect of Cr, Mo and W contents on Charpy impact value at 0C

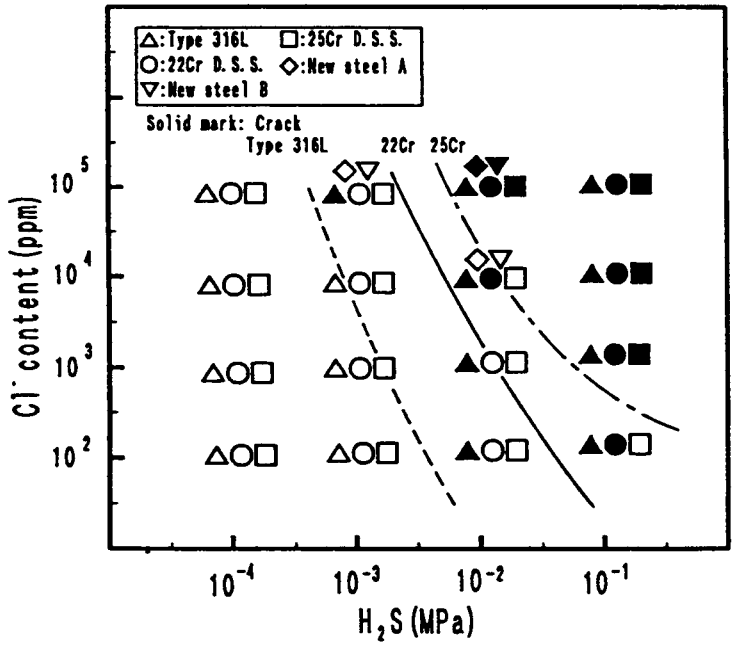


Figure 18. Effect of H_2S partial pressure and Cl^- content on SCC susceptibility of the newly developed duplex stainless steels
(New steel A: 25Cr-7Ni-3Mo-2W-0.3N, New steel B:23Cr-7Ni-4.5Mo-0.3N
SSRT, 80C, Strain rate 4.2 x 10^{-6} s^{-1})

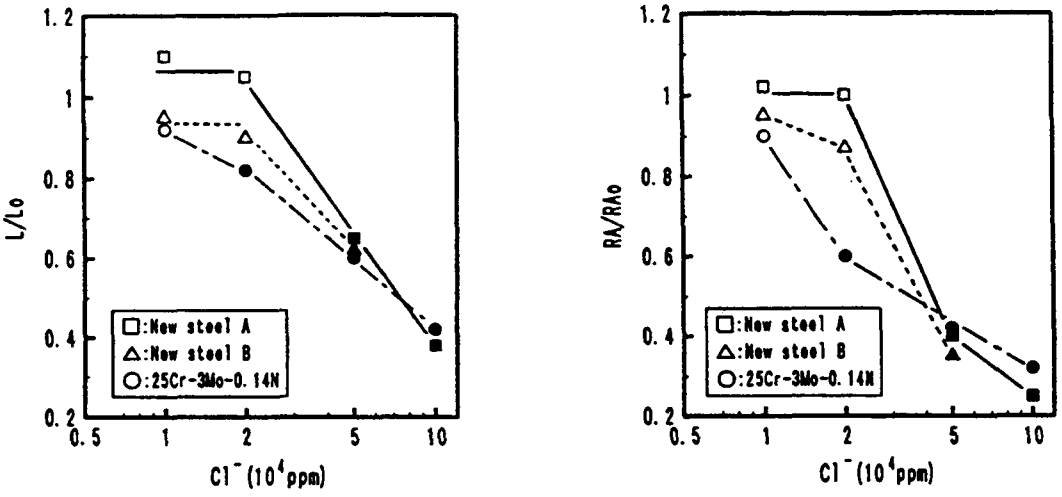


Figure 19. Effect of Cl^- content on SCC susceptibility of the newly developed duplex stainless steels in H_2S containing environment
(New steel A: 25Cr-7Ni-3Mo-2W-0.3N, New steel B:23Cr-7Ni-4.5Mo-0.3N
SSRT, 80C, 0.01MPa H2S, Strain rate 4.2 x 10^{-6} s^{-1})

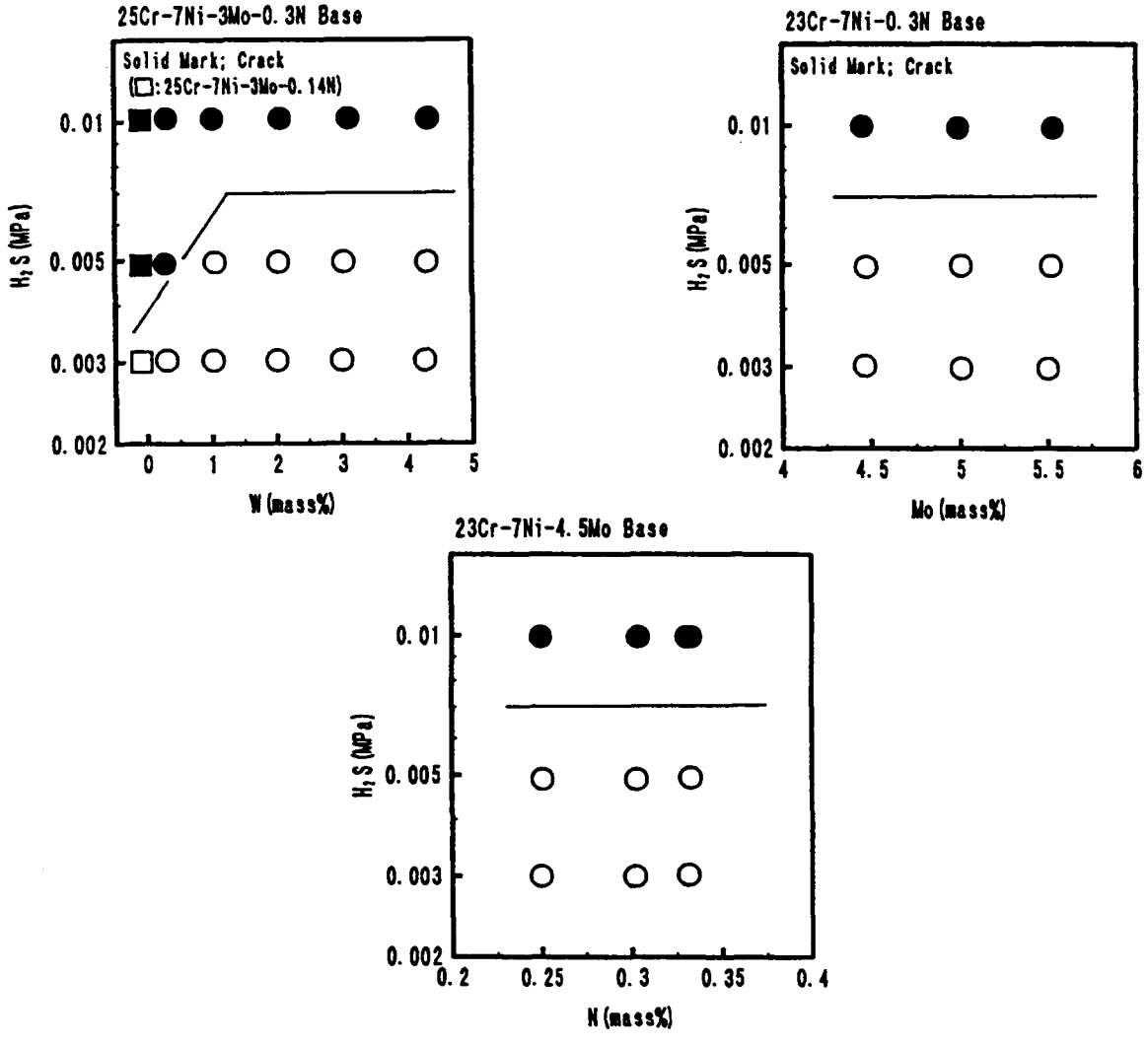


Figure 20. Effect of H_2S partial pressure and alloying elements on SCC susceptibility of duplex stainless steel
(4 point bent beam with notch, applied stress: 1σ_y, H_2S+3.0MPa CO_2, 5%NaCl,336h)

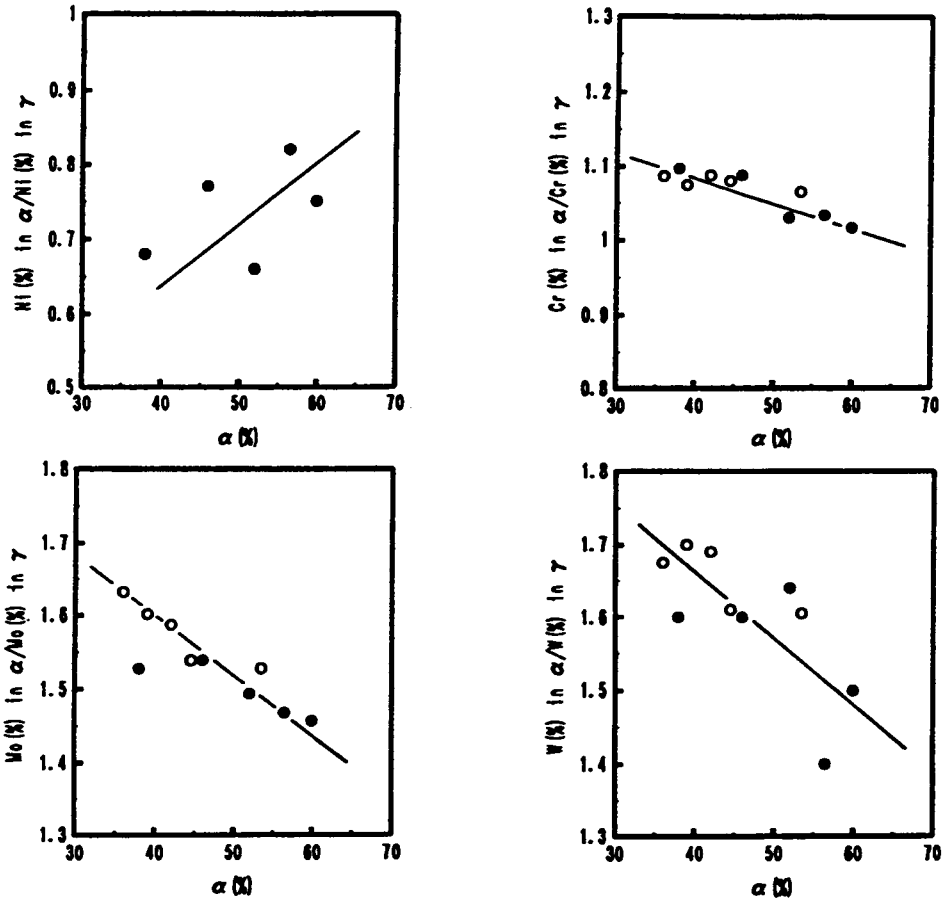


Figure 21. Effect of α content on the distribution ratios of Ni, Cr, Mo and W content in α phase to that in γ phase
(O: varied Ni content[25Cr-Ni-4Mo-0.3N], ●:varied solution treated temperature[25Cr-3Mo-2W-0.3N])

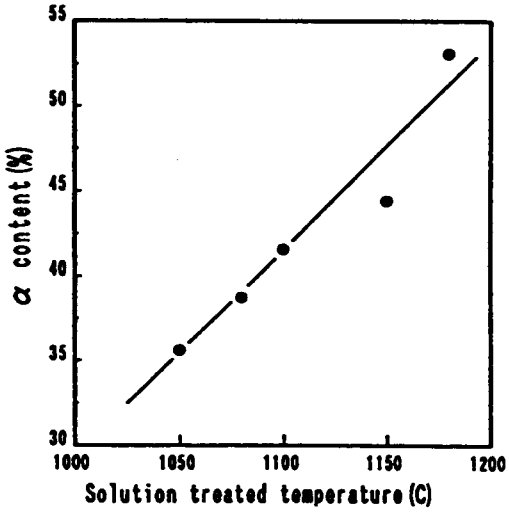


Figure 22. Effect of solution treated temperature on α content of 25Cr-7Ni-3Mo-2W-0.3N steel

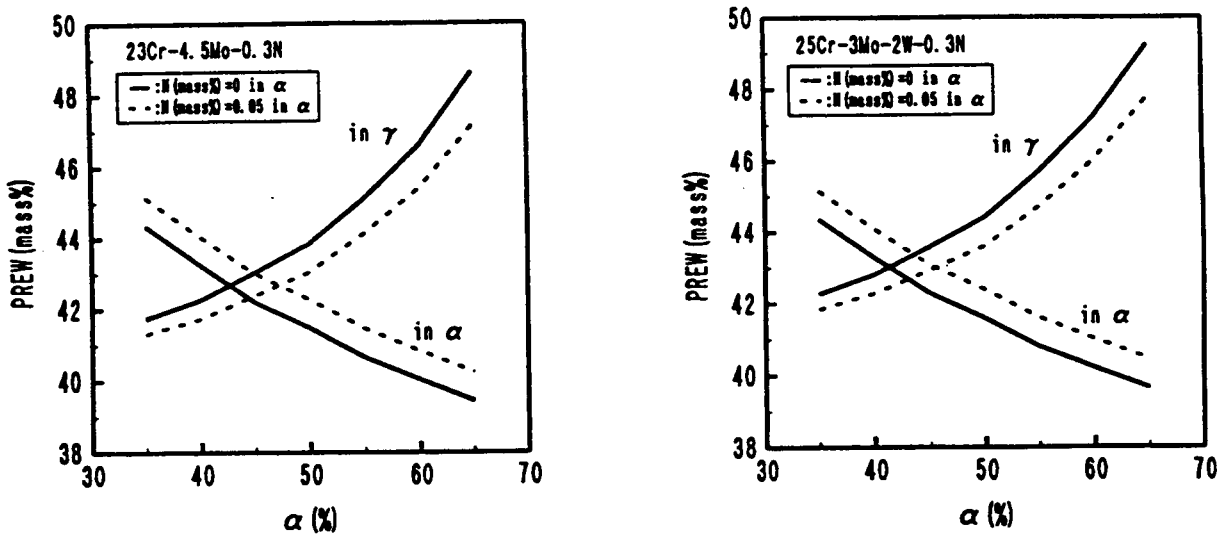


Figure 23. Effect of α content on modified-pitting resistance equivalent(PREW) of the newly developed duplex stainless steels in each phase of α and γ (calculated based on the ratios shown in Fig. 21)

Copyrighted Materials
Copyright © 1996 NACE International Retrieved from www.knovel.com

PAPER NUMBER

155

Corrosion 86

The International Corrosion Forum Devoted Exclusively to The Protection and Performance of Materials

March 17-21, 1986
Albert Thomas Convention Center
Houston, Texas

INFLUENCE OF THERMAL HISTORY ON CORROSION RESISTANCE OF DUPLEX STAINLESS STEEL LINEPIPE

K. Ume*, N. Seki**, Y. Naganawa***, T. Hyodo*, K. Satoh***, Y. Kuriki***

* Fukuyama Res. Labo's, Technical Research Center, Nippon Kokan K.K. Kokan-cho, Fukuyama, 721, Japan
** Fukuyama Works, Nippon Kokan K.K.
*** Material Res. Div., Technical Research Center, Nippon Kokan K.K.

ABSTRACT

Using NK CR22® duplex stainless steel of 22%Cr-5.5%Ni-3%Mo, the extensive research has been carried out to analyze influences of various types of thermal cycles on corrosion resistance. Special attention was paid to the resistance to pitting corrosion in the weld heat affected zone (HAZ) through the complicated metallurgical aspect.

The optimum range of welding heat input exists for the improvement of pitting corrosion resistance in the HAZ. Lower heat input brings about the deterioration of the resistance near the fusion line, higher one on the contrary degrades the HAZ apart from the fusion line. Both these phenomena are closely related to the sensitization of grain boundaries caused by the precipitation of chromium nitrides.

Solution annealing is much effective in giving satisfactory pitting resistance in the HAZ. The annealing at high temperature over 1100°C, however, rather increases the susceptibility to pitting corrosion also by the sensitization of ferrite boundaries. Furthermore, the characteristics of the HAZ in the case of multi-pass welding are also mentioned, reflecting the girth welding of linepipe.

INTRODUCTION

Much attention has recently been paid to the duplex stainless steels as linepipe suited to the service in CO_2-Cl^- environments, since they have high corrosion resistance in such environments and the advantages of high strength levels and good weldability almost comparable to austenitic stainless steels. Duplex stainless steel welded pipes used for flow and gathering line systems are generally manufactured by either the continuous forming or the press bending forming process followed by welding and solution annealing[1]. Individual pipes are jointed by the field girth welding

NK CR22® is a registered trademark of Nippon Kokan K.K.

as pipeline.

Duplex stainless steels, however, are much sensitive to thermal history such as welding and heat treatment, thus showing the complicated metallurgical behavior through the change of microstructure and secondary precipitates[2,3]. This fact requires comprehensive studies on the correlation among thermal cycles, metallurgy and corrosion properties in pipe manufacturing and in girth welding.

The objective of this paper is to study fundamentally the influence of various types of thermal cycles on corrosion properties of duplex stainless steel linepipe. Special attention was paid to the pitting corrosion resistance in the HAZ with respect to the influence of weld heat input, multi-pass welding and solution annealing.

EXPERIMENTAL PROCEDURE

Tested Materials

NK CR22 duplex stainless steels containing approximately 22%Cr, 5.5%Ni, 3%Mo, 0.15%N were used for this study. The aiming and typical chemical compositions of NK CR22 are given in Table 1, which are almost identical with that of ASTM A 790 specification. The steels were hot rolled to 15 mm in thickness, then followed by the solution annealing at 1050°C. The ferrite percentage of steels tested was around 55% after solution annealing.

Thermal Cycles and Preparation of Specimens

Tests are roughly classified to four parts according to the purpose, as summarized in Table 2. Each thermal cycle applied is shown in Figure 1 (A)-(D).

Test A was carried out to investigate fundamentally the influence of weld heat input on microstructures in HAZ and corrosion properties. On the groove of a steel plate, single bead was laid by the tungsten inert gas (TIG) welding, in the range of 6.0-62.2 KJ/cm in heat input with 9% Ni matching duplex stainless filler metal. The sheet specimen was sampled at welded portion including the weld metal. In addition, two-pass welding was also carried out with 30 KJ/cm to examine the influence of interpass temperature on corrosion properties.

Test B was planned to understand the effect of solution annealing. The thermal cycle was applied by using Gleeble tester, being conducted to the solution annealing at 1050°C subsequent to the simulation of welding thermal cycle corresponding to 50 KJ/cm in heat input, which is compared with that of the submerged arc welding of heavy wall thickness duplex stainless steel.

The ranges of temperature in solution annealing is specified to 1020-1100°C in A790. In test C, the effect of annealing conditions on corrosion properties was investigated. The annealing conditions included the ones deviated from A790 specification. The range of 1050-1200°C in temperature, 5 min in holding time and 0.8 (air cooling)-25°C/s in cooling rate were selected in thermal cycles, by using the salt bath. The behavior of microstructure over 1100°C is also related to that of partial transformed HAZ.

Test D was conducted to examine the effect of multi-pass welding, reflecting the girth (circumferential) welding of pipeline. The thermal cycle was applied to the specimen by Gleeble tester. The heat pattern near the fusion line in actual girth welding was simulated, in the selection of heat input of each filler pass to around 15KJ/cm.

Test Method

Each specimen given a thermal cycle was submitted to the corrosion test after abrading to a 220 emery finish. The corrosion resistance was mostly assessed by the pitting corrosion test using 10%$FeCl_3 \cdot 6H_2O$ solution. Preliminary evaluation was based on an exposure time of 24 hours at 30°C. The pitting corrosion test with ferric chloride media does not necessarily reflected actual environments, but is convenient as the ranking test. The Huey tests (ASTM A262 Prac. C) were partially carried out to examine the intergranular

corrosion.

Metallography was examined by using optical and electron microscopy. Furthermore, energy dispersive Xray (EDX) spectrometry and electron energy loss spectrometry (EELS) were also used to identify the precipitates.

RESULTS

General Concept

Figure 2 shows the changes of microstructures in HAZ according to thermal cycles, together with 70%Fe-Cr-Ni phase diagram[4]. The microstructure in HAZ remarkably changes, depending on the peak temperature reached. The HAZ near the fusion line (P) which was heated to the region of ferrite single phase consists of coarse ferrite grains and the austenite precipitated at ferrite grain boundaries on cooling, whereas in the HAZ slightly apart from the fusion line (Q), partial transformation of austenite to ferrite on heating can be observed. Copious precipitation can occur also within ferrite grains. These microstructures are greatly different from that in parent metal. Thus, it is significantly important to make clear the influence of microstructures on the corrosion resistance.

Influence of Heat Input and Interpass Temperature (Test A)

Figure 3 shows the influence of heat input on corrosion rate and the appearance of pittings after FeCl test. Test temperature was selected to 22°C rather than 30°C, so that the pitting might not occur in weld metal. Because the occurrence of pittings in weld metal complicates the analysis of corrosion behavior in HAZ. The resistance to pitting corrosion was improved with the increase of heat input, but rather deteriorated in the excess of heat input. The tendency of improvement of pitting corrosion resistance to around 45KJ/cm is very similar to that in weld metal observed by Sridhar et al.[5]. The pittings occurred along the fusion line in lower heat input, as also shown in Fig.3. On the other hand, in higher heat input, a few pittings were observed in the HAZ about 3 mm apart from the fusion line in addition to the one along the fusion line. It is very interesting phenomenon that the initiation sites of pittings are different, depending on the heat input.

Figure 4 shows the influence of interpass temperature in two-pass welding (30KJ/cm x 2 times). Despite there was no pit in the case of single pass, the pittings occurred in two-pass welding and the corrosion rate increased with interpass temperature. The pittings occurred only in HAZ about 3 mm apart from the fusion line, which was similar to the appearance in high heat input such as 62 KJ/cm.

Typical microstructures around the pittings are compared in Figure 5 in cases of low and high heat input. In low heat input (pits near the fusion line), the pits appear to mainly initiate at the ferrite/ferrite grain boundaries, while at both ferrite-austenite and ferrite-ferrite grain boundaries, in high heat input (pits apart from the fusion line). The observation also indicated that the microstructure of initiation site of pittings in two-pass welding was similar to the latter case. (Fig.5 Right). The pittings near the fusion line in high heat input were microscopically confirmed to be associated with fine austenite precipitated within ferrite grains.

In this connection, the microstructures in HAZ near the fusion line are shown in Figure 6 for each heat input, together with the ferrite percentage along the fusion line. In the case of low heat input, the microstructure near the fusion line consists of ferrite and copious micro-austenite within ferrite grain, and the austenite precipitated at ferrite grain boundary cannot be observed so much. On the other hand, the widmanstatten austenite grows at ferrite boundaries in high heat input.

In general, the sensitization is easy to occur with the increase of ferrite percentage. Thus, such microstructure in low heat input seems to be closely related to the cause of pittings. In Figure 7, the surface appearance after Huey test is shown by focussing the HAZ near the fusion line.

The attack can be observed, mainly at ferrite boundaries. Namely, the sensitization by precipitation at ferrite boundaries seems to be responsible for the cause of pitting occurred near the fusion line in low heat input.

Effect of Solution Annealing (Test B)

In duplex stainless UOE linepipe, it has been already well known that the solution annealing after straight seam welding indicates the beneficial effect on corrosion resistance[1]. Figure 8 shows the effect of solution annealing on pitting corrosion properties and austenite content, in the case of welding with 50KJ/cm. 60 and 180 sec. were selected as annealing time at 1050°C. Corrosion rate was remarkably decreased, and austenite percentage recovered by the solution annealing, even though the holding time was short such as 60 sec.

Figure 9 compares the microstructures of as welded condition and after the solution annealing of 180 sec. It can be seen that the increase of austenite percentage is mainly due to the precipitation and the growth of austenite within ferrite grain. Beneficial effects by solution annealing can be interpreted by the shift of ferrite-austenite ratio to the optimum range[6] and by the extinction of precipitates formed in as welded condition.

Effect of Annealing conditions (Test C)

In test C, the high temperature effect on corrosion properties was investigated. This type of thermal history is also associated with that in the portion of partial transformation in HAZ, such as photo. b in Fig.2. Figure 10 shows the influence of annealing temperatures and cooling rates at the mid-thickness on corrosion rates. Annealing time of each condition is constant, 5 min. It became clear from this figure that the corrosion resistance was decreased with higher temperature and larger cooling rate. In the temperature at 1150°C and over, corrosion rates were dependent on cooling rates, whereas independent on them at 1050°C satisfied A790 specification. The annealing at 1150°C resulted in no pitting in air cooling, in spite of many pittings in higher cooling rate.

A typical microstructure around the pittings is shown in Figure 11, in the case of 1150°C and 25°C/s. The pits appeared to nucleate predominantly at ferrite/ferrite grain boundaries and to develop into ferrite matrix. And this microstructure is also characterized by the appearance of ferrite/ferrite boundaries. Namely, the ferrite/ferrite boundaries are possible to be sensitized by some precipitates.

This can be estimated from Figure 12. The figure compares microstructures of surfaces of specimens after Huey test between 1150°C and 1050°C in annealing temperature. At higher temperature, ferrite/ferrite grain boundaries were more remarkably attacked in comparison with normal annealing temperature (1050°C).

The tendency of sensitization in higher temperature and larger cooling rate were confirmed also in another thermal test. Figure 13 presents the variation of microstructures in each simulated thermal condition. Only in the specimen with 1150°C and 20°C/s, ferrite/ferrite boundaries can be recognized clearly, compared with other two specimens.

Effect of Multi-Pass (Test D)

Finally, the corrosion properties at HAZ in the case of multi-pass welding such as girth welding are tested. Figure 14 shows the effect of number of heat cycles on the corrosion rate and the austenite content. 1st and 2nd cycles corresponds to the root pass and hot pass welding, respectively, and subsequent cycles, to the filler passes. The corrosion resistance was already improved after the third pass. On the other hand, the austenite content increased with number of cycles, approaching to 30%.

Figure 15 presents the change of microstructure by multiple cycles. Similar to that shown in Fig.9, as the number of heat cycles increases, the austenite within ferrite grains precipitates or grows, thus increasing

the austenite content. The improvement of corrosion resistance in HAZ of inner wall in multi-pass welding can be estimated to be the contribution of the beneficial effect of solution annealing through subsequent passes.

DISCUSSION

Summarizing test results described above, main discussions are focussed on the following two items;
(i) metallurgical factors affected on pitting initiation in HAZ,
(ii) beneficial effect of solution annealing
The former is related to Test A and C, while the latter to Test B and D. Further study was carried out by using electron microscope to investigate the factor of pitting initiation.

Metallurgical Factors in As Welded Condition

The initiation sites of pittings in HAZ are roughly classified into three portions.

First is the portion near the fusion line where thermal cycle reached to the region of ferrite single phase by heating. Second is also near the fusion line where the austenite transformed to the ferrite partially. In those portions, the pittings are generated only at the cooling rate over a critical value. The initiation sites are located almost at ferrite/ferrite grain boundaries, as shown in Fig.5 (Left) and 11, even though the pitting rarely occurs at fine austenite within ferrite grains in higher heat input such as 62.2 KJ/cm.

The third is the portion about 3 mm apart from the fusion line, where the pittings occur in case of either higher heat input or double thermal cycles. In this case, the pittings initiate both at ferrite/austenite and ferrite/ferrite grain boundaries, as shown in Fig. 5 (Right).

Figure 16 shows the appearance of precipitates in HAZ near the fusion line. In the specimen with 6.0 KJ/cm, the cluster of granular precipitates like a film can be observed at grain boundaries. Quite similar precipitates were observed also at the portions apart from the fusion lines in the specimens with 62.2KJ/cm and with double thermal cycles. Thus, such precipitates seem to be the most probable to degrade the resistance to pitting corrosion. On the other hand, near the fusion line in the specimen with 62.2 KJ/cm, copious rod-like precipitates can be found in the ferrite matrix. This type of precipitates can be also recognized in HAZ with lower heat input and in weld metal, but most remarkably in the specimen with 62.2 KJ/cm.

Both types of precipitates can be identified as Cr nitride rather than Cr carbide. As an example, the results of identification by using the EDX and EELS are shown in Figure 17, on the granular precipitates like a film. Small amount of Mo and Fe as well as Cr was detected in the precipitates.

On the other hand, Figure 18 indicates a transmission electron micrograph in a specimen rapid-cooled from 1150°C in the range of partial transformation. Granular precipitates of Cr_2N were also observed at the ferrite/ferrite grain boundary. Furthermore, the appearance of the Cr depleted zone can be detected through EDX spectrometry, as shown in Figure 19. Converting the ratio of Xray intensity to the concentration of Cr, Cr percentage at the vicinity extremely close to the precipitates is around 3% lower than that in the ferrite matrix.

The facts mentioned above suggest that the sensitization is raised by the precipitation of film-like or granular Cr nitride at ferrte/ferrite grain boundaries. Similar behavior has been observed by other researchers[7,8], but the extensive interpretation over the whole of HAZ where the microstructure changes continuously to base metal has not attempted yet.

A possible mechanism of the metallurgical behavior in HAZ is shown schematically in Figure 20. This concept is based on the assumption that the time-temperature region of sensitization is different according to the microstructure. In general, the solubility of carbon or nitrogen in ferrite is extremely low in comparison with that in austenite. This fact brings about the difference in the characteristics of the sensitization between ferritic and austenitic

stainless steel. Accrodingly, the assumption can be deduced that the tendency of sensitization is different each other between the microstructure with higher ferrite content and with almost 50% ferrite structure.

In the HAZ near the fusion line with higher ferrite content, the nose of Cr nitride precipitation is presumably projected in extremely shorter time. In rapid cooling (A) such as with lower heat input, the ferrite/ferrite boundaries are sensitized through the precipitation of film-like Cr nitride, thus deteriorating the corrosion resistance due to the occurrence of Cr depleted zone. In moderate cooling (B), the diffusion assisted healing of Cr depleted zone can be presumed to occur, in addition that the sensitization itself is hard to occur, due to the precipitation of austenite at ferrite/ferrite boundaries. This assumption is supposed also by the facts that the solubility of nitrogen to the austenite is much larger than to the ferrite, and that the diffusivilities of Cr and N in the ferrite are much higher than in the austenite. In slow cooling, the susceptibility to corrosion near the fusion line is not strong, even though many Cr nitrides precipitate or grow within ferrite grains. On the contrary, the HAZ apart from the fusion line, which thermal cycle is applied to the temperature at around 700°C, tends to sensitize, thus causing the degradation by slow cooling (C).

Beneficial Effect of Solution Annealing

The changes of appearances of precipitates in HAZ by solution annealing and multi-pass welding are shown in Figure 21. The precipitates can disappear through the solution annealing, while most of precipitates through multi thermal cycles which possess the beneficial effect like solution annealing. Accordingly, the beneficial effect of solution annealing can be interpreted by such disappearance of precipitates. High temperature annealing over A790 specification, however, rather degrades the corrosion resistance of duplex stainless steel as shown in Fig.10. The optimum condition of solution annealing and welding should be selected in pipe manufacturing and in the girth welding.

CONCLUSIONS

Using 22Cr-5.5Ni-3Mo-0.15N duplex stainless steels, the extensive research was carried out to investigate the influence of various types of thermal cycles on pitting corrosion resistance. Four types of thermal cycles simulating the welding and heat treatment were applied to study the influence of heat input, annealing condition and multi-pass welding. Especially, the corrosion resistance in HAZ was focussed through the metallurgical aspects. The results are summarized as follows:

(1) The corrosion resistance in HAZ improves with the increase of welding heat input, whereas the excess heat input rather brings about the degradation of corrosion resistance. In lower heat input, the HAZ near the fusion line was attacked, while higher one deteriorates the HAZ apart from the fusion line.
(2) Both types of degradation are closely related to the sensitization of grain boundaries by the precipitation of film-like Cr nitride.
(3) In the HAZ near the fusion line with higher ferrite content, the occurrence of Cr depleted zone through the sensitization deteriorates the corrosion resistance mainly at ferrite/ferrite grain boundaries in rapid cooling, while the corrosion resistance recovers due to the healing of Cr depleted zone in moderate cooling. On the contrary, the HAZ apart from the fusion line with ferritic austenitic structure becomes easy to sensitize with the decrease of cooling rate.
(4) The solution annealing is much effective to recover from the degradation in HAZ. The multi-pass welding also displays the beneficial effect like as solution annealing through subsequent heat cycles, by optimizing the welding conditions.

ACKNOWLEDGEMENT

The authors would like to thank Mr. M. Itoh, Pipe and Tube Technology Dept., Dr. T. Kitada and Mr. Y. Kobayashi, Fukuyama Res. Labo's, Mr. J. Sakai and Mr. Y. Ishizawa, Material Res. Div., for many helpful advices and useful discussion.

REFERENCES

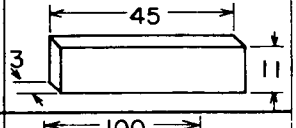
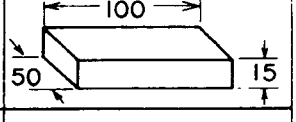
1. K. Uma, T. Kitada, K. Kanero, Y. Naganawa, T. Taira, K. Yano, Int. Conf. OMAE, to be published, Tokyo, 1986
2. T. G. Gooch, Duplex Stainless Steels, Paper No. 8201-029 ASM Publications, P573, 1983
3. H. D. Solomon, T. M. Devine Jr., Duplex Stainless Steels, Paper No. 8201-089, P693, 1983
4. S. J. Acello et al., Corrosion, vol. 18 P286, 1962
5. N. Sridhar, L. H. Flasche, J. Kolts, J. Proc. of ASM Conf. on Advances in Stainless Steel Technology, Detroit Mich. 1984
6. J. Sakai, I. Matsushima, Y. Kamemura, M. Tanimura, T. Osuka, J. Materials for Energy Systems, vol.5, No.2, P105, 1983
7. J. Kolts, L. H. Flasche, D. C. Agarwel, H. M. Tawancy, Corrosion /82 Paper No. 190, Houston, Texas, 1982
8. N. Sridhar, J. Kolts, L. H. Flasche, J. Metals vol.37, P31, 1985

TABLE 1 - Tested steels

	C	Si	Mn	P	S	Cr	Mo	Ni	^{T}N
Aiming	<0.02	0.40/0.60	0.8/1.2	<0.020	<0.003	21/24	2.5/3.5	4.5/6.5	0.08/0.20
Typical	0.013	0.48	0.88	0.017	0.001	23.04	2.91	5.0	0.124

wt%

TABLE 2 - Test conditions

Test	Objective (Parameter)	Thermal Cycle	Specimen Size mm	Test Method
A	Heat Input	TIG Welding Filler: 9Ni Matching Duplex Metal	20^{L} × 75^{C} × 2^{T}	10%FeCl3 6H2O 22°C×72hrs 30°C×24hrs
	Interpass Temperature		20^{L} × 75^{C} × 2^{T}	
B	Effect of Solution Annealing	Gleeble Tester		(65%HNO3 boiling×48hrs 5times)
C	Condition of Solution Annealing	Salt Bath		Metallography
D	Multi-Pass	Gleeble Tester	Same as Test B	

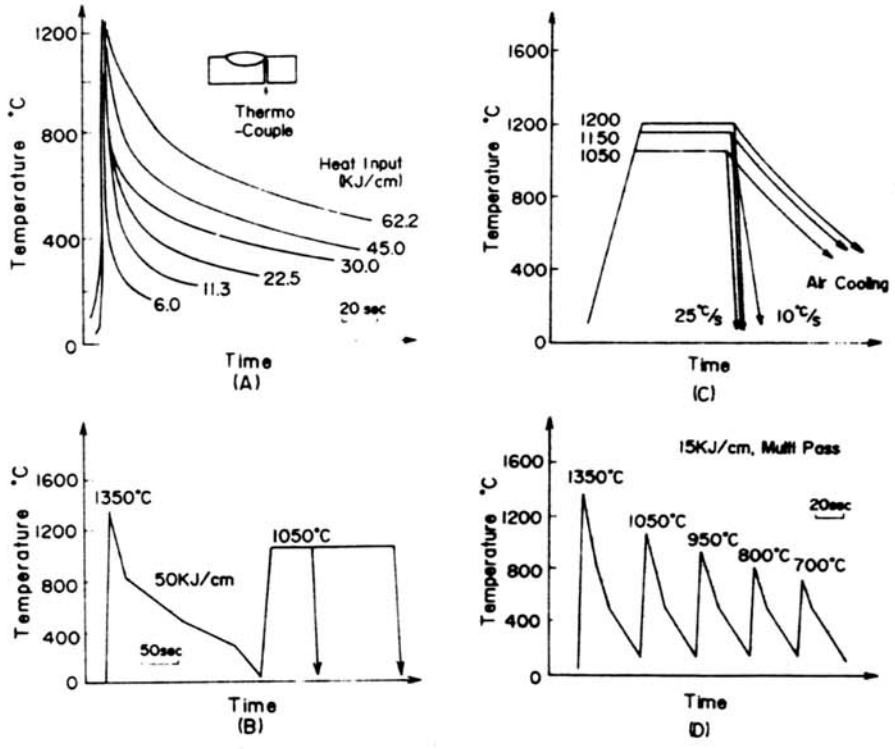


FIGURE 1 - Thermal cycles applied

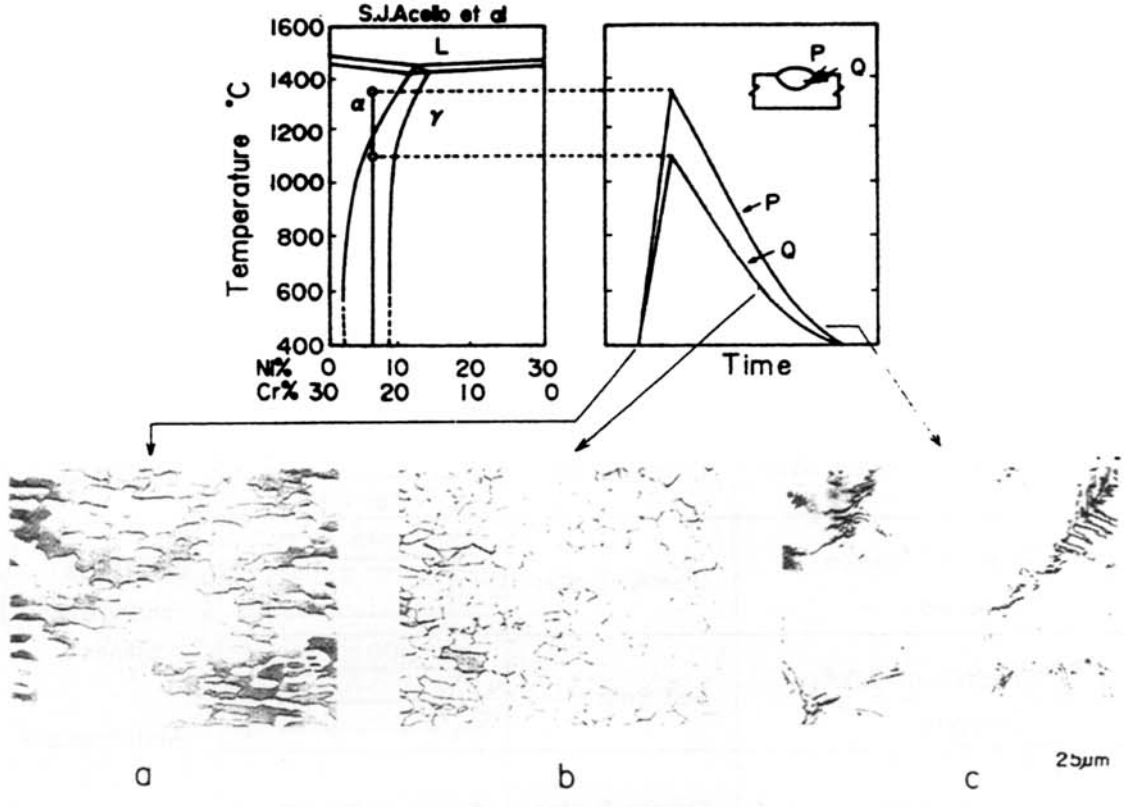


FIGURE 2 - Change of microstructure in HAZ

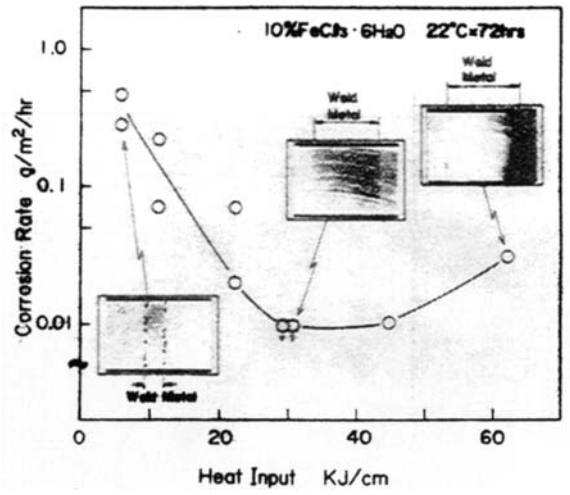


FIGURE 3 - Influence of heat input on corrosion rate ($10\%FeCl_3 \cdot 6H_2O$ 22°C x 72 hrs)

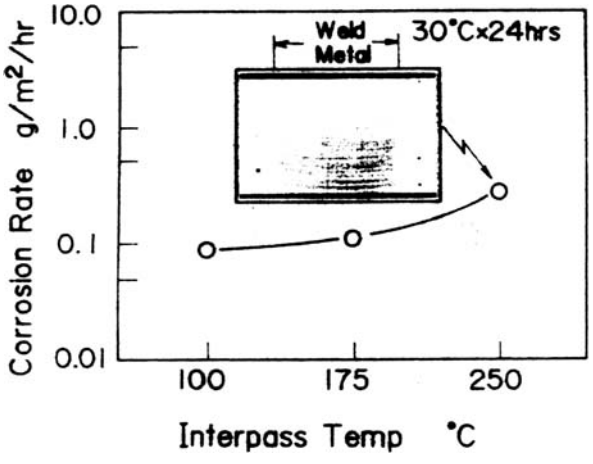


FIGURE 4 - Influence of interpass temperature on corrosion rate in two pass welding ($10\%FeCl_3 \cdot 6H_2O$ 30°C x 24 hrs)

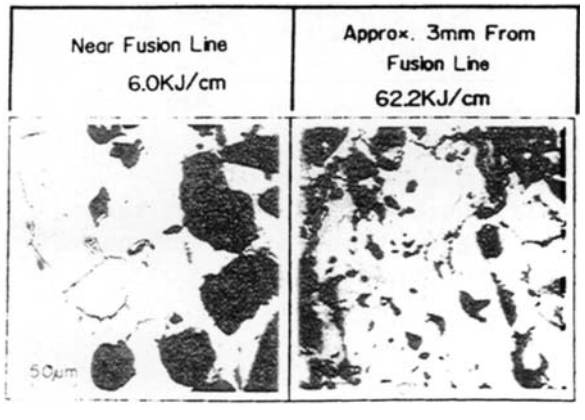


FIGURE 5 - Typical microstructures near pittings

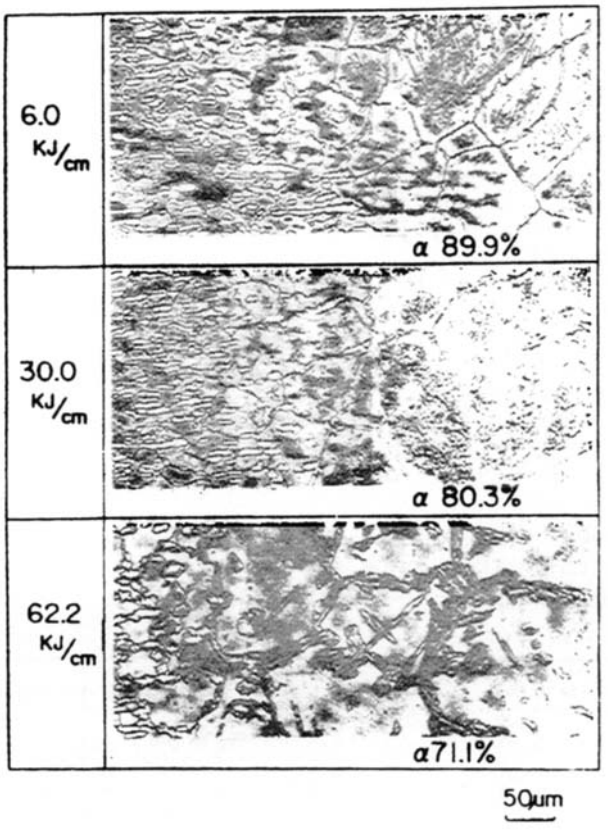


FIGURE 6 - Relation between heat input and microstructure in HAZ

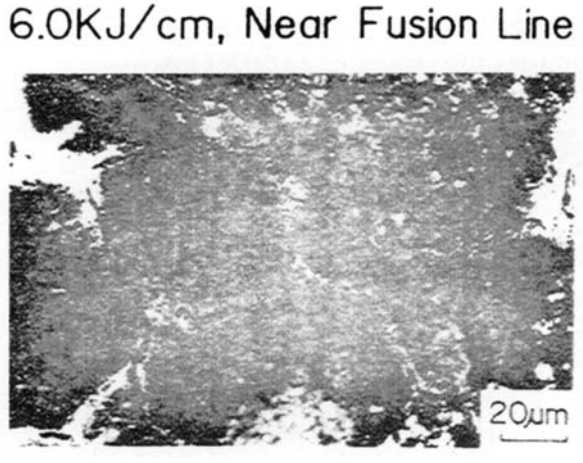


FIGURE 7 - Appearance in HAZ near fusion line after $65\%HNO_3$ test

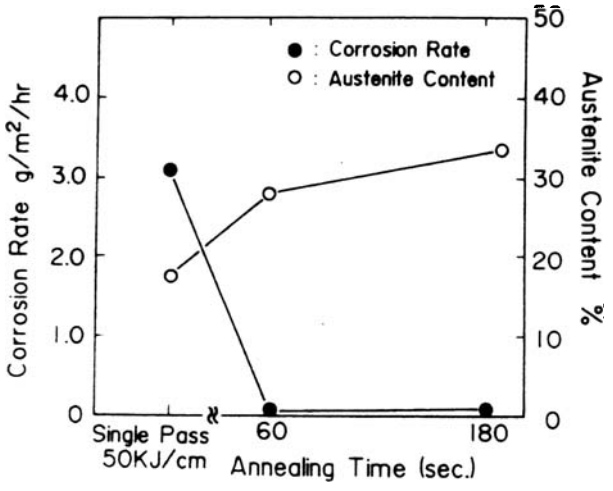


FIGURE 8 - Effect of solution annealing on corrosion rate and austnite content ($10\%FeCl_3 \cdot 6H_2O$ 30°C x 24 hrs)

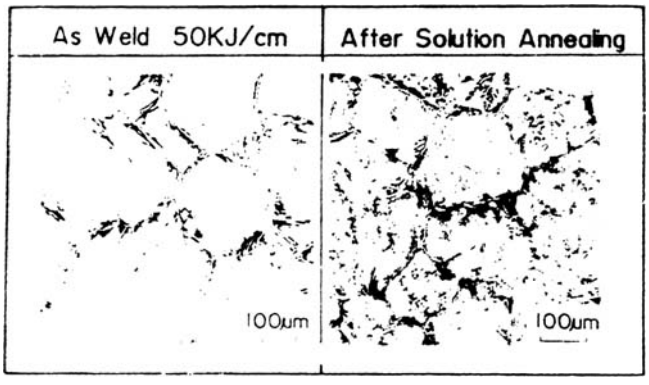


FIGURE 9 - Effect of solutiion annealing on microstructure

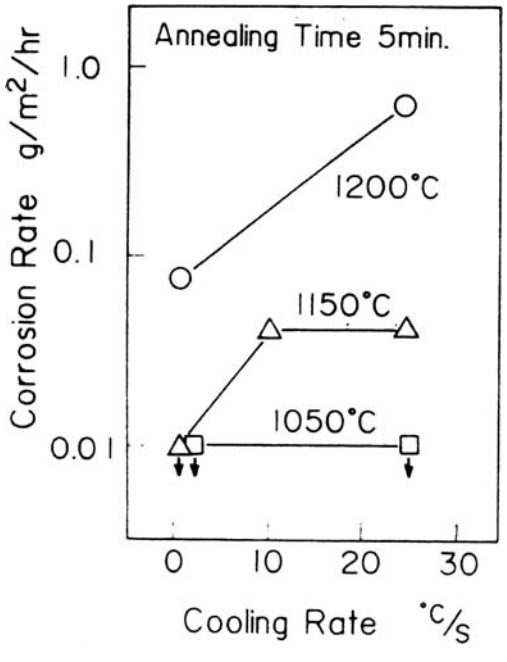


FIGURE 10 - Influence of annealing temperature and cooling rate on corrosion rate ($10\%FeCl_3 \cdot 6H_2O$ 30°C x 24 hrs)

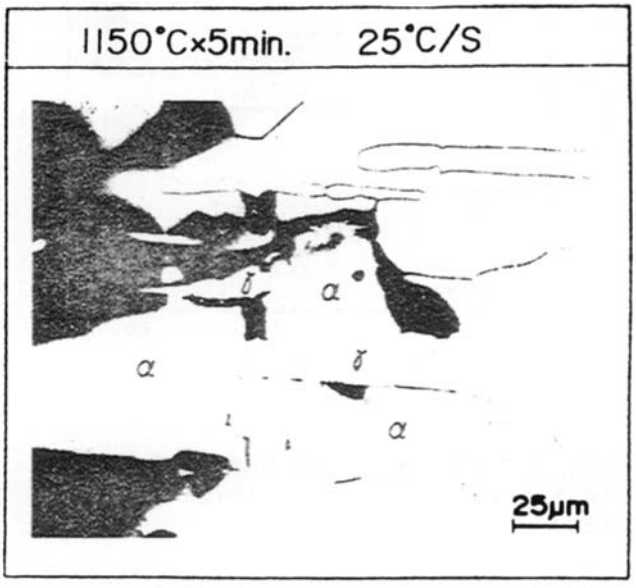


FIGURE 11 - Typical microstructure near pittings after pitting corrosion test

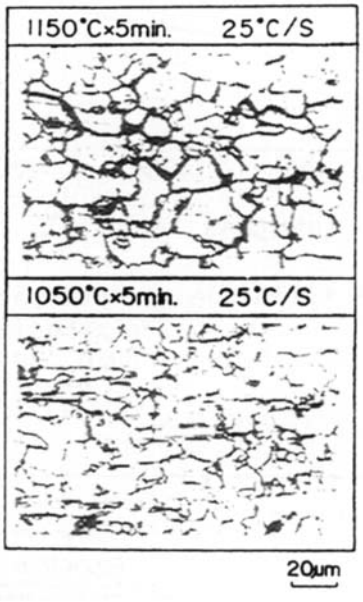


FIGURE 12 - Comparison of microstructures after $65\%HNO_3$ test between higher temperature and normal temperature annealing

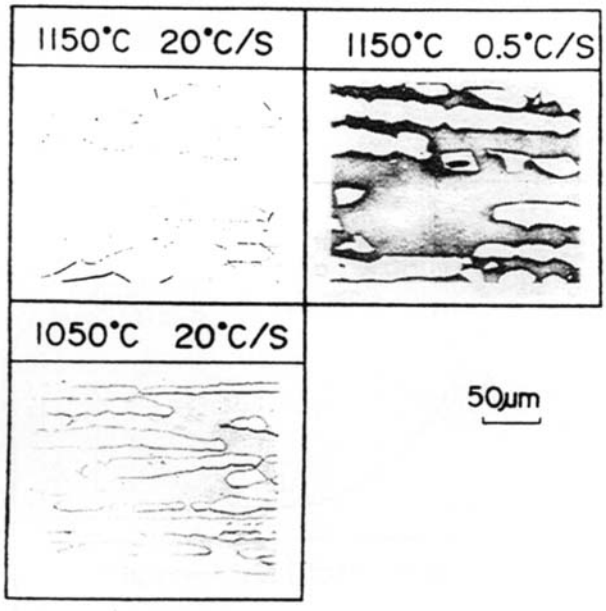


FIGURE 13 - Variation of microstructures according to annealing conditions (10% oxalic acid + 20%NaOH etching)

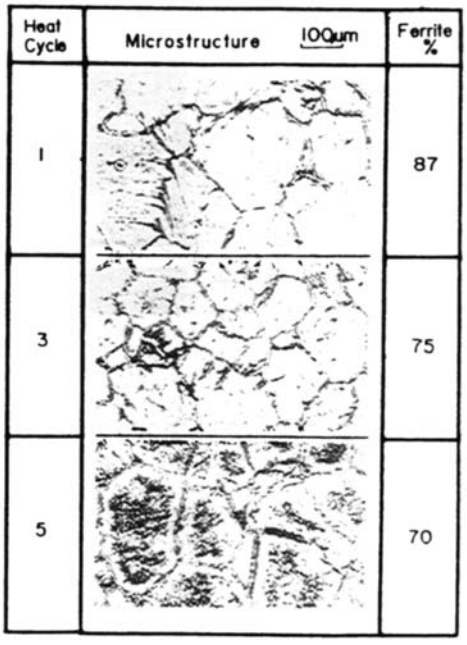


FIGURE 15 - Change of microstructure through multi-pass welding

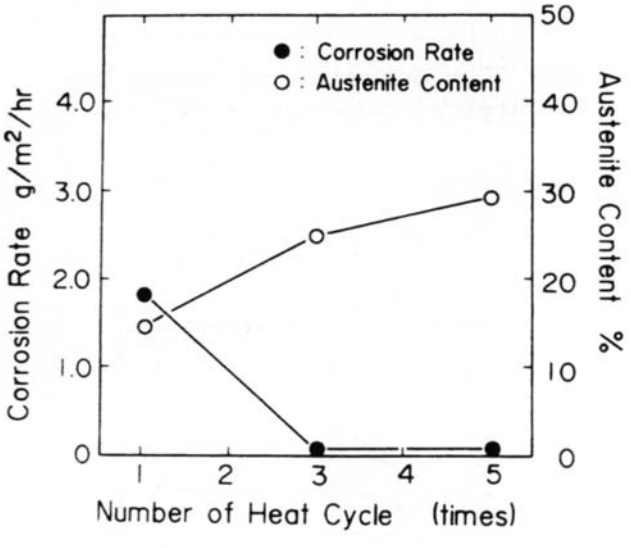


FIGURE 14 - Effect of multi-pass on corrosion rate and austenite content (10%$FeCl_3 \cdot 6H_2O$ 30°C x 24 hrs)

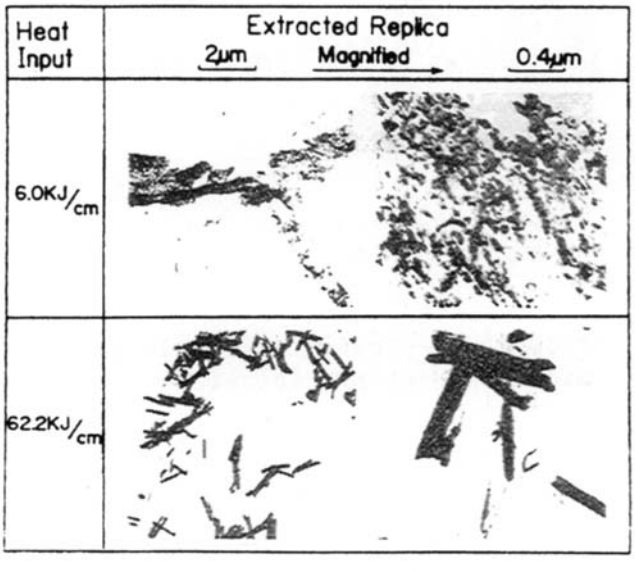


FIGURE 16 - Appearance of precipitates in HAZ near fusion line (Extracted replica)

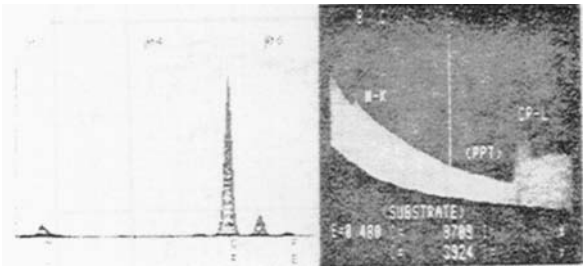


FIGURE 17 - Identification of precipitates

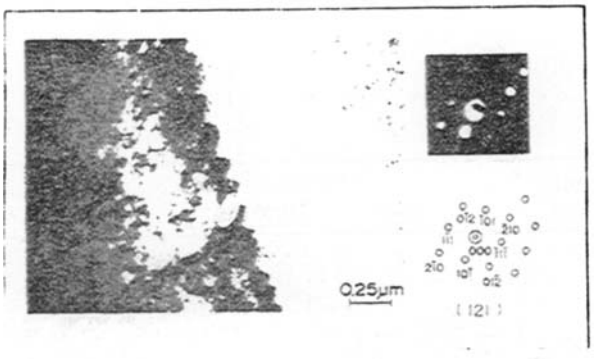


FIGURE 18 - Transmission electron micrograph of precipitates

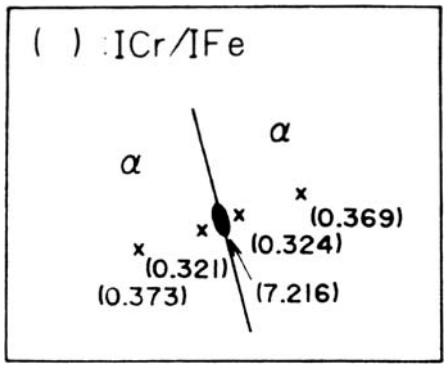


FIGURE 19 - Analysis at vicinity of precipitates through EDX spectrometry

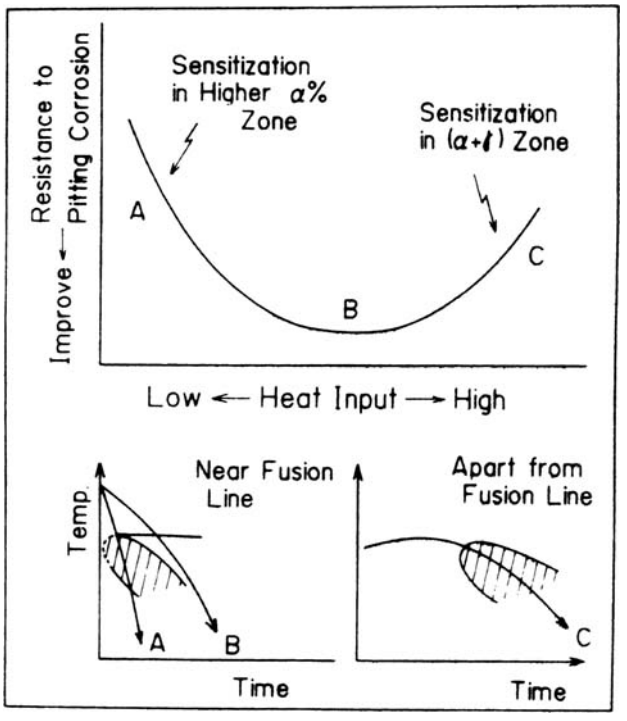


FIGURE 20 - Schematic mechanism for metallurgical behavior in HAZ

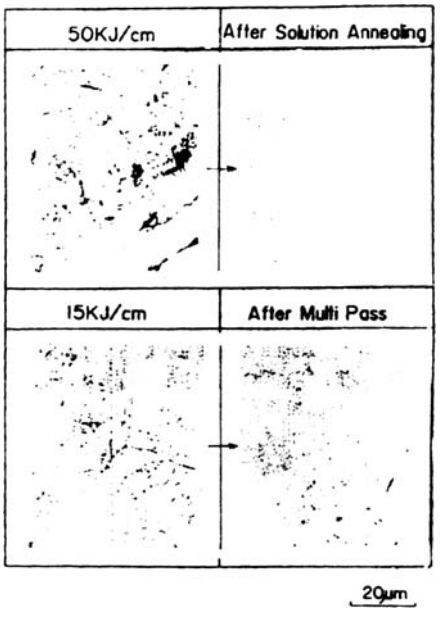


FIGURE 21 - Changes of appearances of precipitates in HAZ by solution annealing or multi-pass welding

Copyrighted Materials
Copyright © 1996 NACE International Retrieved from www.knovel.com

Effect of Heat Treatment and Microstructure on the Corrosion and SCC of Duplex Stainless Steels in H_2S/Cl^- Environments*

S. MARK WILHELM and R. D. KANE***

Abstract

A duplex stainless steel was heat treated at 2200 F (1200 C) (1 hour/water quench) and 2400 F (1315 C) (1 hour/water quench) to change the ferrite:austenite ratio from approximately 50:50 to 77:23 and 94:6, respectively. Slow strain rate (SSR) (4×10^{-6} s^{-1}) experiments in brine solution containing H_2S were conducted to determine the mechanism of environmentally caused cracking and to determine if these heat treatments affect cracking susceptibility. The experiments indicated that hydrogen is the primary cause of embrittlement at ambient temperature. Anodic stress corrosion cracking is the principal form of degradation at 350 F (177 C) in environments that contain H_2S and chloride. Sulfides and chlorides act synergistically to facilitate loss of ductility of SSR tensile specimens at both low [75 F (24 C)] and high [350 F (177 C)] temperature. Heat treatment [600 and 500 F/250 h (316, 260 C)] to simulate downhole service age of cold worked tubes did not produce any deleterious effects with regard to susceptibility to embrittlement.

Introduction

Duplex (austenitic/ferritic) stainless steels are a relatively new class of engineering materials used in oilfield applications. They have been used in wellhead components and, more recently, as high strength tubular goods. They are of interest because they typically have better corrosion resistance than 13% Cr and AISI 410 type steels. However, many aspects of duplex stainless steels in sour gas production environments are still controversial. Important questions center around what the mechanism of cracking is in duplex stainless steels in environments containing H_2S and chlorides, how H_2S affects these materials, and what the limiting concentrations of H_2S are that restrict the use of duplex stainless steels.

This paper examines some of the effects of microstructure and heat treatment on the environmental cracking behavior of a 22Cr-5.5Ni-3Mo duplex stainless steel in H_2S/chloride-containing environments. Particular emphasis has been placed on the interaction between these metallurgical variables and exposure conditions in order to elucidate the cracking mechanism(s) of these materials in oilfield environments. The parameters investigated in this study were: (1) microstructure, (2) low temperature aging, (3) environment temperature, and (4) electrochemical polarization.

Background

Duplex stainless steels were originally developed with the intention that they be stainless steels with corrosion resistance similar to conventional AISI 3XX type stainless steels, but also having better strength and stress corrosion cracking (SCC) resistance in high temperature, chloride-containing environments. Studies have revealed that duplex stainless steels do, in fact, have better SCC resistance than fully austenitic stainless steels in boiling 42% $MgCl_2$ solutions.[1] In addition, the resistance of these materials to SCC increases when ferrite content is between 0 and approximately 40% (Figure 1). However, at greater ferrite content, resistance to SCC decreases. Much of the beneficial effect of ferrite in the 0 to 40% ferrite range has been attributed to the higher resistance of the ferrite phase to SCC crack propagation. This has been supported by observations that duplex stainless steels in high temperature $MgCl_2$ solutions typically exhibit cracking in the austenite phase. In $MgCl_2$, SCC is arrested when the crack intersects a ferrite grain.[2] On the other hand, in high temperature solutions containing NaCl (100 ppm) and O_2 or in solutions containing $FeCl_3$, it has been observed that cracking of the ferrite phase predominates.[3]

The results of controlled potential experiments conducted on 22% Cr duplex stainless steels in high temperature $MgCl_2$ environments indicated that cracking is accelerated by anodic polarization and retarded by cathodic polarization.[4] These results suggest that SCC of these materials in high temperature $MgCl_2$ solutions is governed by anodic cracking processes, and 22% Cr duplex stainless steels show no indication of a hydrogen embrittlement cracking mechanism.

Of interest in this study is the behavior of duplex stainless steels (22 to 25% Cr, approximately 50% austenite/50% ferrite) in H_2S/chloride-containing environments like those in sour gas production. Many studies have been conducted on these materials in a variety of test environments and material conditions. From this work, it appears that the cracking behavior of duplex stainless steels in H_2S/chloride environments is complex, and controversy exists on many aspects of the behavior of these materials. Of particular interest, and at the center of controversy, is the mechanism of embrittlement/cracking of duplex stainless steel in these environments. Two mechanistic points of view are prevalent in this controversy. One is that embrittlement/cracking of these materials in sour brines is caused by hydrogen, i.e., sulfide stress cracking (SSC). The other is that cracking is caused by anodic stress corrosion, i.e., stress corrosion cracking (SCC).

*Submitted for publication May 1983; revised September 1983.
*Battelle Houston Operations, 1100 Rankin Road, Houston, TX 77073.
**CorTest Laboratories, Inc., Cypress, Texas.

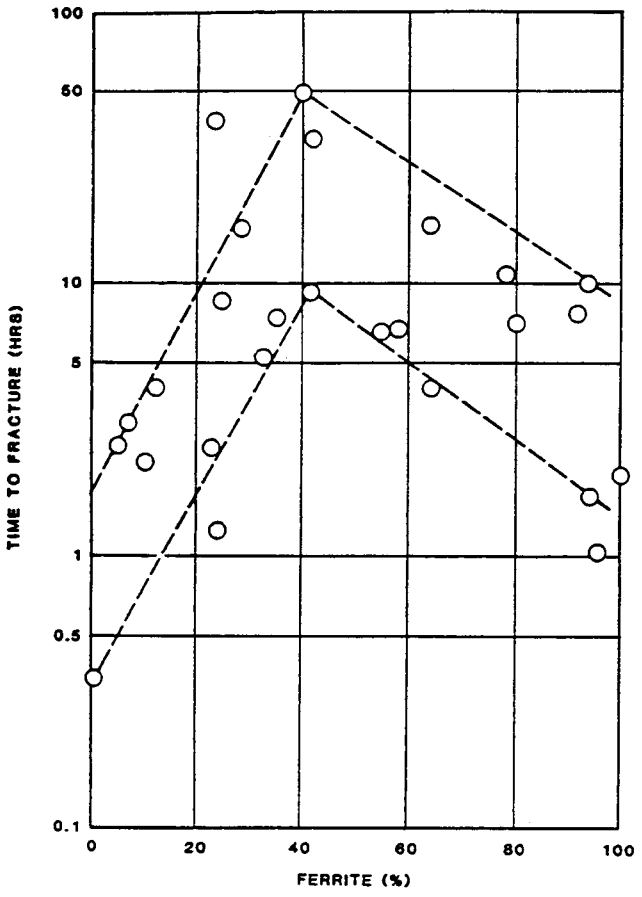


FIGURE 1 — Effect of ferrite content on time to fracture for tensile specimens of various duplex alloys in boiling 42% $MgCl_2$. Applied stress: 25 kg/mm².

To clarify some of the existing data on SCC/SSC of duplex stainless steels in H_2S/chloride environments, the following short discussion is presented.

Effects of Temperature and H_2S Concentration on SCC

Many of the investigations presented in the literature deal with the parametric relationship of temperature and H_2S concentration to the cracking behavior of duplex stainless steels. Two investigations report a maximum susceptibility to embrittlement at higher H_2S concentrations and low testing temperature. Indications are that the limiting H_2S partial pressure for no embrittlement in 22Cr-5.5Ni duplex stainless steels increases with temperature from approximately 0.2 psia (1380 Pa) at 100 to 200 F (38 to 93 C) to over 10 psia (0.07 MPa) at 400 F (204 C). However, other studies have shown susceptibility to SCC/SSC in similar duplex stainless steels at 0.3 psia (2070 Pa) H_2S at approximately 500 F (260 C) in H_2S/CO_2/brine[6] and at 0.75 psia (5170 Pa) H_2S at 350 to 400 F (177 to 204 C) in NACE solution type environments.[7,8] In addition, there are data which indicate that a maximum susceptibility to SCC/SSC may exist around 200 F (93 C).[3] The reason for this complex behavior has not been explained. Likewise, little evidence exists as to what mechanism best explains the cracking behavior of duplex stainless steels.

Effect of Polarization

Some investigators have documented the effects of potential on the cracking susceptibility of duplex stainless steels. As indicated previously, cracking susceptibility of duplex stainless steels in boiling $MgCl_2$ solutions is increased by anodic polarization and decreased by cathodic polarization. By comparison, some investigators who have studied the effect of potential on SCC/SSC of these materials in H_2S/chloride environments have noted beneficial effects of cathodic polarization.[8,9] These studies were conducted at room temperature [~75 F (24 C)] where potential was applied by galvanically coupling the test specimens to steel. In all cases, specimens were statically stressed and loaded to less than the material yield strength. This behavior suggests that anodic SCC processes prevail at low temperatures in H_2S/chloride environments. However, other data suggest that cracking can also be accelerated by cathodic charging.[11,12] Therefore, the cracking mechanism in these materials currently is in doubt.

Observations of Cracking Modes

Observations of cracking mode and crack path are speculative and subject to much interpretation on the part of the investigator. However, results published in the literature indicate that in H_2S/chloride environments, SCC of 22 to 25 duplex stainless steels traverses both the austenite and ferrite phases as well as along the austenite/ferrite boundaries.[6,8] At low temperatures [~75 F (24 C)] these studies have indicated cracking in both the austentic and ferritic phases. At high temperatures [400 to 500 (204 to 260 C)], in H_2S/chloride-containing solutions, SCC has been observed primarily in the ferrite phase or along the interphase boundary. In many cases, preferential dissolution of the austenite phase occurs along the crack path. This behavior is in contrast with that observed in boiling $MgCl_2$ solutions where duplex stainless steels fail by cracking in the austenite phase.

It has also been observed[6] that a fully ferritic stainless steel (30Cr-2Mo) exhibits very good resistance to SCC in high temperature [>300 F (149 C)] H_2S/chloride environments. However, when cold worked to high levels (~40%) this material readily fails by SCC in these environments. For this alloy, SCC occurs by transgranular cracking in the ferrite grains.[6]

Experimental

Material

A section of commercially produced duplex stainless steel tubing (cold reduced 57%) was used as the base material for this investigation. Mechanical properties and chemical composition are given in Tables 1 and 2, respectively. Cylindrical specimens [2.5 × 0.315 in. (6.4 to 0.8 cm)] were machined from the as-received tube and heat treated as described in Table 3. Sub-size NACE tensile specimens with gage section dimensions 1 in. long by 0.1 in. (2.5 × 0.25 cm) diameter were used in all tests.

The effect of heat treatment on microstructure is illustrated in Figures 2 through 4. The as-received material (Figure 2) exhibits a typical duplex microstructure in which the austenitic phase appears as islands in the continuous ferrite phase when viewed perpendicular to the rolling direction of

TABLE 1 — Mechanical Properties of As-Received Duplex Tubing

Yield Strength (ksi)	Ultimate Tensile Strength (ksi)	Percent Elongation	Hardness
128.2	135.8	24.6	31 RC

TABLE 2 — Chemical Composition of As-Received Duplex Tubing (wt%)

Fe	C	Cr	Ni	Mn	Mo	S	P	Si
Bal	0.011	22.50	5.58	1.66	3.25	0.013	0.031	0.44

TABLE 3 — Heat Treatment of Duplex Samples

Sample	Treatment
A (as-received)	Solution anneal: 1922 F/30 min Water quench/cold work
B (sample machined from A)	2200 F/1 hour, water quench
C (sample machined from A)	2400 F/1 hour, water quench
D (sample machined from A)	500 F/250 hours, air cool
E (sample machined from A)	600 F/250 hours, air cool



FIGURE 2 — Microstructure of as-received material, section perpendicular to rolling direction. (500X) (Reduced to 74% for reproduction)



FIGURE 3 — Microstructure of as-received material heat treated at 2200 F for 1 hour. (500X) (Reduced to 74% for reproduction)

the tube. When viewed parallel to the rolling direction, the austenitic phase is elongated in the direction of working (see Figure 14). The austenitic phase constitutes approximately 48% of the matrix. The heat treatment at 2200 F (1204 C) causes a reduction in the volume of the austenitic phase to approximately 23 vol% (Figure 3). Treatment at 2400 F (1315 C) (1 h, water quench) causes a further reduction in austenite content to about 6% (Figure 4). Both heat treatments allow substantial grain growth.

Environmental Cracking Experiments

SSR experiments were conducted at a constant extension rate of 4×10^{-6} in./s using a servo-hydraulic testing machine (MTS). Test environments were contained in either a plexiglass



FIGURE 4 — Microstructure of as-received material heat treated at 2400 F for 1 hour. (125X) (Reduced to 74% for reproduction)

vessel (ambient temperature tests) or in a specially designed Hastelloy C-276 autoclave [350 F (177 C) tests]. The autoclave was designed such that the test specimen was electrically insulated from the vessel. Experiments at constant current were conducted using a regulated power supply. By this method, tensile specimens were tested under open circuit and cathodic and anodic polarization conditions.

Experiments were also conducted at constant stress using the sub-size tensile specimens in a proof ring apparatus such as that described in NACE Standard Test Method TM-01-77. Procedures were followed as set forth in that NACE document.

Environments

Two environmental conditions were examined in the cracking investigations. In tests conducted at ambient temperature, tensile specimens were exposed to a solution that was saturated with H_2S gas (1 atm) and contained 5 wt% NaCl and 0.5% acetic acid. This solution is generically referred to throughout the text as NACE solution. In tests at 350 F (177 C), the solution contained identical concentrations of NaCl and acetic acid but was in equilibrium with 100 psi (0.7 MPa) of H_2S gas at temperature.

Electrochemical Experiments

Electrochemical measurements were conducted in NACE solution at ambient temperature. Open circuit potentials were measured using a high impedance (10^{16} ohm) voltmeter. Galvanic currents were measured using a "zero" (10^{-16} ohm) resistance ammeter. Potentiodynamic experiments were conducted at a scan rate of 0.5 mV/s in the cathodic to anodic direction.

Results

Tests at Ambient Temperature

Stress-strain curves for as-received and heat treated samples are shown in Figures 5 through 7. Curves designated as cathodic or anodic correspond to galvanostatic charging of the tensile specimens at negative or positive 100 $\mu A/cm^2$, respectively. Observations of secondary cracking and area reduction measurements are summarized in Table 4. The effect of environmental parameters on the stress-strain behavior of as-received material at ambient temperature is illustrated in Figure 8 and summarized in Table 5. Two experiments were conducted at constant stress using sub-size NACE tensile specimens. The results of these experiments are summarized in Table 6.

It was generally observed that cathodic charging shortened the time to failure while anodic charging prolonged

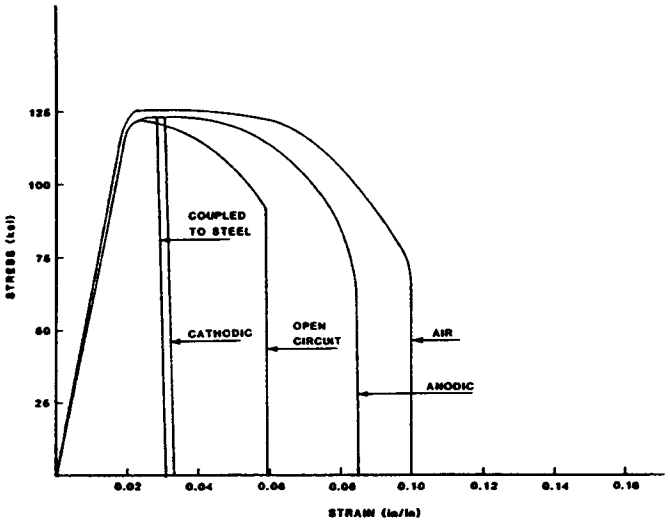


FIGURE 5 — As-received material, 75 F, in NACE solution, saturated H_2S.

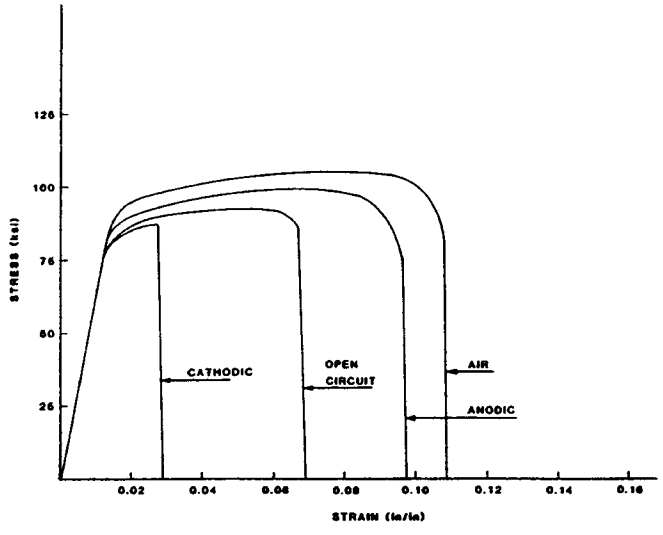


FIGURE 6 — 2200 F, 1 hour, water quench, heat treatment, 75 F, NACE solution.

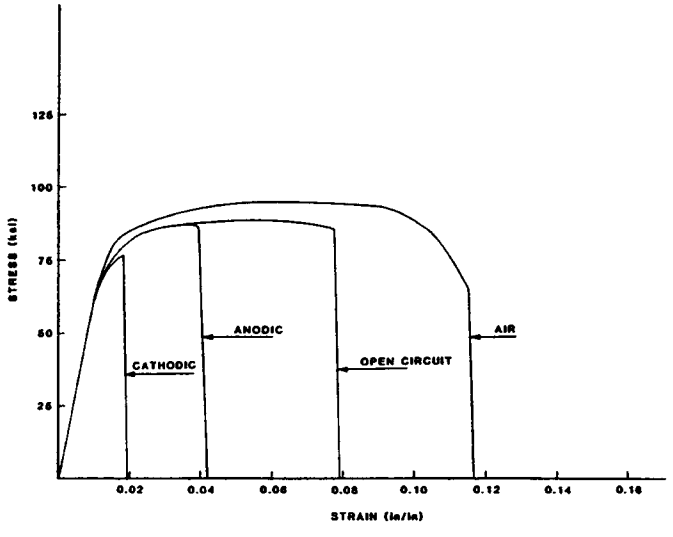


FIGURE 7 — 2400, 1 hour, water quench, heat treatment, 75 F, NACE solution.

TABLE 4 — Slow Strain Rate Data: Ambient Temperature/NACE Solution

Sample Heat Treatment	Charging	Time to Failure (% Air Value)	Secondary Cracks	Reduction in Area (RA) (%)	RA RA^{air}
As-received	Air	100	No	75.5	1
As-received	Open circuit	60	Yes	47.1	0.62
As-received	Anodic*	81	Yes	62.1	0.82
As-received	Cathodic**	34	Yes	13.7	0.18
As-received	Coupled to steel	30	Yes	13.5	0.18
2200	Air	100	No	56.6	1
2200	Open circuit	64	No	20.4	0.36
2200	Anodic*	86	No	8.2	0.14
2200	Cathodic**	27	Yes	3.0	0.05
2400	Air	100	No	88.1	1
2400	Open circuit	68	Yes	17.2	0.20
2400	Anodic*	36	No	24.6	0.28
2400	Cathodic**	16	Yes	8.0	0.09
500	Air	100	No	80.6	1
500	Open circuit	68	Yes	13.7	0.17
600	Air	100	No	86.4	1
600	Open circuit	67	Yes	47.4	0.55
600	Anodic*	93	No	77.4	0.89
600	Cathodic**	33	Yes	5.9	0.07

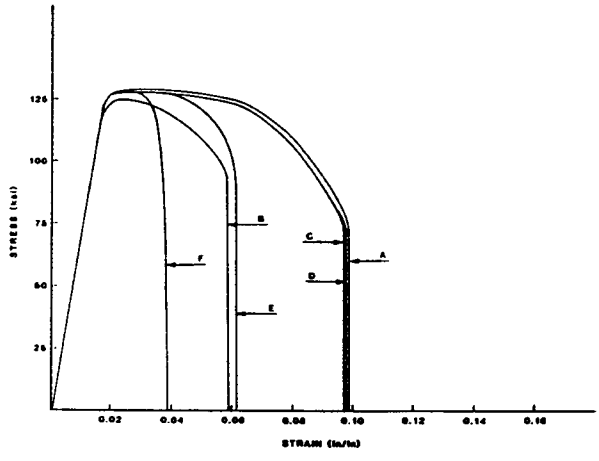


FIGURE 8 — As-received material, 75 F: (A) air; (B) NACE solution, saturated H_2S (1 atm), open circuit; (C) 5% Na_2SO_4, 0.5% acetic acid, saturated H_2S (1 atm), open circuit; (D) 25% NaCl, 0.5% acetic acid, no H_2S, open circuit; (E) 5% NaCl, 0.5% acetic acid, no H_2S, cathodic charge 100 $\mu A/cm^2$; and (F) 5% Na_2SO_4, 0.5% acetic acid, saturated (1 atm) H_2S, cathodic charge 100 $\mu A/cm^2$.

TABLE 5 — Slow Strain Rate Data: Effect of Environmental Variables, As-Received Material

Environment	Time to Failure (% Air Value)	Secondary Cracks	Reduction in Area (RA) (%)	RA RA^{air}
Air	100	No	75.5	1
NACE solution saturated H_2S (1 atm) open circuit	60	Yes	47.1	0.62
1% Na_2SO_4, 0.5% CH_3COOH, saturated H_2S (1 atm) open circuit	98	No	78.8	1.04
25% NaCl 0.5% CH_3COOH, no H_2S, open circuit	98	No	65.2	0.86
5% NaCl, 0.5% CH_3COOH, cathodic charge – 100 $\mu A/cm^2$	64	Yes	45.2	0.60
5% Na_2SO_4, 0.5% CH_3COOH, saturated H_2S cathodic charge – 100 $\mu A/cm^2$	40	Yes	45.6	0.60

TABLE 6 — Constant Stress Experiments: NACE Solution, Saturated H_2S

Sample	Applied Stress (ksi)	Percent of Yield	Time to Failure
As-received	128	100%	>700 hours[2]
As-received Coupled to Steel[1]	128	100%	5 hours

[1]Equal areas (3 cm^2) of tensile specimen and steel couple were exposed.
[2]Specimen did not fail.

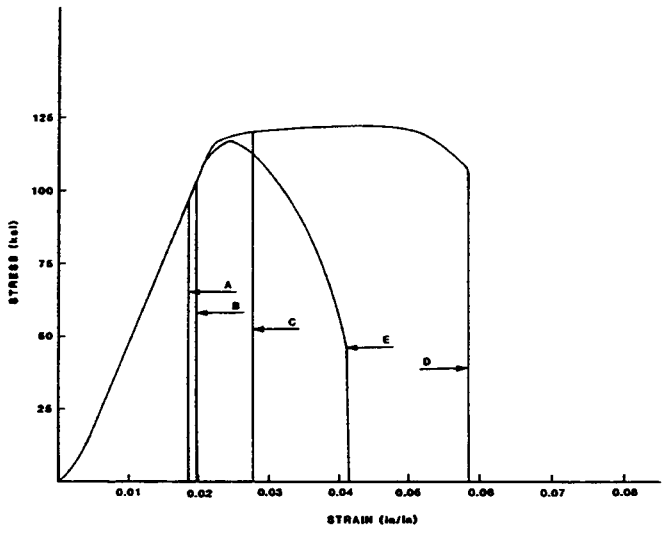


FIGURE 9 — As-received material, 350 F: (A) NACE solution, 100 psi H_2S anodic charge 100 $\mu A/cm^2$; (B) NACE solution, 100 psi H_2S, open circuit; (C) NACE solution, 100 psi H_2S, cathodic charge 100 μ/cm^2; (D) NACE solution, 100 psi H_2S, cathodic charge 1 mA/cm^2; and (E) 25% NaCl, 0.5% acetic acid, no H_2S.

the failure time of all heat treated materials. The absence of either H_2S or chloride at ambient temperature was sufficient to preclude embrittlement under open circuit conditions.

Tests at 350 F (177 C)

Stress-strain curves for as-received material at 350 F (177 C) are shown in Figure 9. Observation of secondary cracking and reduction in area measurements are summarized in Table 7.

It was observed that cathodic charging prolonged the time to failure at 350 F (177 C) and that an environment containing chlorides without any H_2S was sufficient to cause a reduction in ductility.

Electrochemical Data

Open circuit corrosion potentials (Table 8) and galvanic currents (Table 9) for as-received material and samples heat treated at 2200 and 2400 F (1204 and 1315 C) were measured in NACE solution at ambient temperature. Polarization curves were also generated in NACE solution at a scan rate of 0.5 mV/s (cathodic to anodic) for as-received material and samples heat treated at 2200 and 2400 F (1204 and 1315 C). These curves are shown in Figure 10.

TABLE 7 — Slow Strain Rate Data: 350 F

5% NaCl, 0.5% CH_3COOH, 100 psi H_2S

Sample	Charging	Time to Failure (% of Air Values[1])	Secondary Cracks	Reduction in Area (RA) (%)	RA / RA^{air}[1]
As-received	Open circuit	20.0	Yes	17.0	0.22
As-received	Anodic	18.6	Yes	3.9	0.05
As-received	Cathodic 100 A/cm^2	27.3	Yes	7.9	0.10
As-received	Cathodic 1 mA/cm^2	57.9	Yes	19.0	0.25
	25% NaCl, 0.5% CH_3COOH, no H_2S				
As-received	Open circuit	42.1	Yes	37.9	0.50

[1]Air at ambient temperature.

TABLE 8 — Open Circuit Corrosion Potentials[1]

A	B	C	D	E
As-received −302 mV	2200 F −253 mV	2400 F −206 mV	500 F −306 mV	600 F −308 mV

[1]vs saturated calomel electrode, 5% NaCl, 0.5% acetic acid, saturated H_2S.

TABLE 9 — Galvanic Current

	A	B	C
A	—	Cathode[1]	Cathode
B	Anode[2]	—	Cathode
C	Anode	Anode	—

A = As-received material
B = 2200 F heat treatment
C = 2400 F heat treatment
[1]Current flow in the external circuit *away from* electrode in column when coupled to electrode in row.
[2]Current flow *to* electrode in column when coupled to electrode in row.

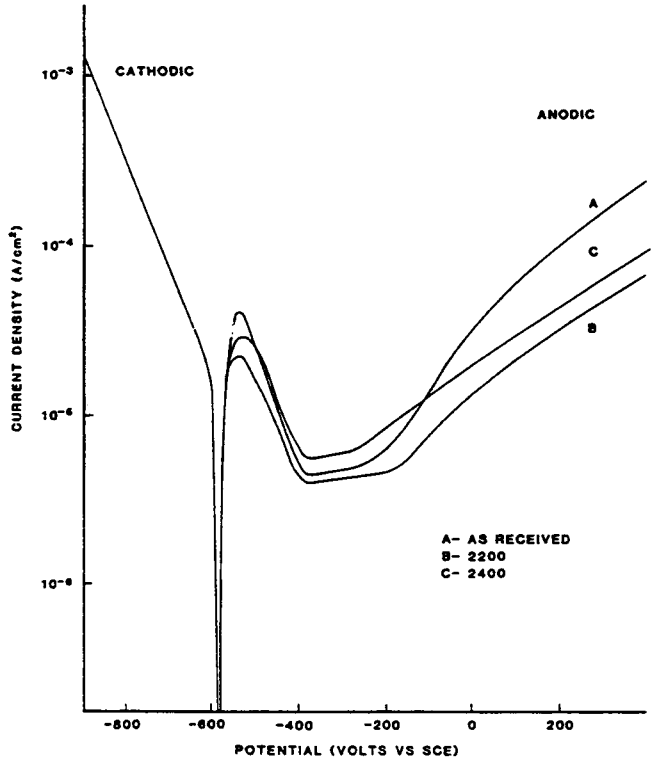


FIGURE 10 — 75 F, NACE solution.

The ordering of open circuit corrosion potentials and the direction of galvanic currents indicates that in ambient temperature NACE solution, the austenite phase is more active than the ferrite phase.

Discussion

Environmental Embrittlement and Corrosion at Ambient Temperature

All experiments conducted suggest that hydrogen embrittlement of the ferrite phase is primarily responsible for the environmentally induced cracking of this particular duplex alloy at ambient temperature under conditions of dynamic tensile strain in NACE solution. The evidence is summarized in the following sections.

SSR Experiments. Cathodic charging (i.e., generation of hydrogen) or coupling to a more active metal (steel) caused a shorter time to fracture than the freely corroding situation (open circuit) for the as-received material and all of the heat treatments. Similarly, anodic charging caused an increase in time to fracture in all experiments with the exception of the 2400 F (1315 C) heat treatment.

The time to failure as well as the percentage reduction in area are reduced for those heat treatments that have higher amounts of ferrite. In other words, a greater ferrite content results in more brittle behavior in environments that contain H_2S/chloride, in spite of the fact that the heat treatments effectively anneal the original cold worked material (20 to 30% reduction in yield strength).

Microstructural Analysis. Microstructural analysis of the gage section of test specimens after removal from the test substantiated the general conclusions drawn from the SSR experiments. Cathodically charged specimens (all heat treatments) always exhibited a significant amount of secondary cracking (transgranular in the ferritic phase) at distances considerably removed from the fracture area.

Anodically charged specimens, on the other hand, exhibited few if any secondary cracks, and when they occurred, they were always located in close proximity to the fracture. Anodically charged specimens exhibited microscopic pitting, but cracks did not initiate from the pits.

In most cases, the austenitic phase corroded preferentially. It is not possible to determine conclusively if cracks propagated through both phases and dissolution occurred subsequent to cracking or if dissolution of the austenite was a requisite step in crack propagation. This type of selective attack is illustrated in Figures 11 and 12. In Figure 11, cracking is clearly indicated in the ferritic phase, while blunt dissolution of the austenite occurs at the crack tip.

Constant Stress Tests. Constant stress experiments (Table 6) also support the contention that hydrogen is the embrittling agent at ambient temperature. The specimen coupled to steel failed in less than 1 day while the uncoupled specimen did not fail during a 1 month exposure. Crack morphology of the failed specimen was identical to cathodically charged SSR specimens.

Effect of Environmental Parameters. The synergistic effect of chlorides and H_2S on cracking susceptibility is illustrated in Figure 8. When neither is present in the environment at ambient temperatures, no cracking is observed.

Either chlorides or sulfides can act to destabilize the chromium oxide films that protect stainless steels. The chromium oxide film also serves as a barrier to the entry of atomic hydrogen. It appears from these data that the combined action of chlorides and sulfides is sufficient to allow the entry of atomic hydrogen, thus permitting embrittlement. Charging experiments (Figure 11, Table 5) indicate that H_2S facilitates the entry of hydrogen and has a stronger influence on embrittlement at ambient temperature than does chloride.



FIGURE 11 — As-received material. Secondary cracking of cathodically charged (−100 μA/cm²) SSR tensile specimen, 75 F NACE solution. (625X) (Reduced to 77% for reproduction)



FIGURE 12 — 2200 F heat treatment. Secondary cracking of cathodically charged (−100 μA/cm²) SSR tensile specimen, 75 F NACE solution. (125X)

Environmental Embrittlement at Elevated Temperature

Experiments conducted at 350 F (177 C) suggest that anodic SCC is the primary cause of embrittlement in aqueous H_2S/chloride environments at elevated temperature. The evidence is summarized below.

SSR Experiments. Cathodic charging of SSR specimens produced greater times to failure than specimens that were tested at open circuit or anodically charged. This fact sug-

gests that inhibition of the oxidative portion of the corrosion reaction retards cracking. It should be noted, however, that the galvanostatic method is not entirely successful, i.e., loss of ductility is still observed at substantial cathodic current densities. This may be attributed to the fact that localized corrosion processes in cracks initiated by dynamic strain may not be readily influenced by externally applied currents. A similar situation was observed at ambient temperature in cathodically charged specimens. At ambient temperature, the austenite phase exposed in the cracks dissolved in spite of the externally applied cathodic current (Figure 12).

Anodic charging produced a slightly shorter time to failure than open circuit conditions. The reduction in failure time by anodic charging could occur by either initiation of cracks (i.e., via pitting) or by increasing the anodic dissolution process inside of cracks. Microstructural analysis of secondary cracks did not indicate that they initiated from pits. The extremely short time to failure under open circuit conditions indicates that crack propagation (anodic dissolution) is rapid, and hence, anodic charging may not produce a significant change in the localized dissolution rate.

Microstructural Analysis. Whereas in boiling $MgCl_2$ cracks appear to prefer the austenite phase,[2] results obtained here suggest that the cracks prefer the ferrite phase. This type of behavior is illustrated in Figures 13 and 14. This is especially graphic in Figure 14 where cracks clearly avoid the austenite phase.

Effect of Environmental Parameters. When H_2S is not present in the environment, a reduction in ductility of the received material at 350 F (177 C) is still observed (Figure 9). Microstructural analysis of specimens tested in 25% NaCl (no H_2S) showed that the ductility loss occurred by preferential dissolution of austenite. No clearly formed cracks in the ferrite phase were observed. These results demonstrate the synergism between H_2S and Cl^- in causing cracking in sour brines at elevated temperature.

Electrochemical Effects on Corrosion and Embrittlement

Polarization curves (Figure 10) for as-received and heat treated samples [2200, 2400 F (1204, 1315 C)] are essentially identical. This is not unexpected in view of the fact that the average chemical compositions of the three specimens are the same. The rise in current density around −200 mV (SCE) is due mostly to localized dissolution (pitting), but a portion may also be caused by oxidation of sulfide:

$$H_2S \rightarrow S^\circ + 2H^+ + 2e^- \quad (1)$$



FIGURE 13 — As-received material. Secondary cracking of anodically charged (+100 $\mu A/cm^2$) SSR tensile specimen, 350 F NACE solution. (250X) (Reduced to 76% for reproduction)

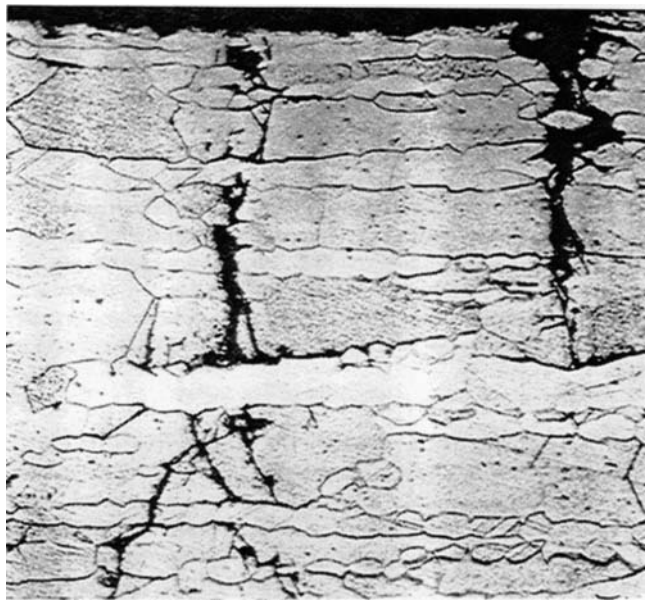


FIGURE 14 — As-received material. Secondary cracking of SSR tensile specimen, open circuit conditions, 350 F NACE solution. (125X)

It is not entirely accurate, therefore, to describe the potential of current increase in sulfide-containing solutions as a pitting potential because of competing reactions.

Cathodic charging at $-100\ \mu A/cm^2$ places the potential in the hydrogen evolution region (Figure 13) around −700 mV. In sulfide/chloride environments, this potential is sufficient to reduce partially the passive film that is normally present at open circuit (−300 mV). Galvanostatic charging, therefore, acts in a dual role to facilitate the entry of hydrogen into the metal. Anodic charging at $+100\ \mu A/cm^2$ places the potential in the pitting region at around +250 mV. At this potential, the hydrogen reaction is essentially zero. It should be pointed out, however, that the externally applied currents (or potentials) are not necessarily distributed to the interior of cracks. Therefore, anodic dissolution inside cracks on specimens being cathodically charged is not precluded, and likewise, hydrogen can be produced inside cracks on specimens being anodically charged.

The chemical compositions of the ferritic and austenitic phases in duplex stainless steels are not equal. Ferrites usually contain more chromium and slightly less nickel.[9] A purely thermodynamic prediction would be that the austenite is the more active phase electrochemically. Among the samples heat treated to change the ferrite:austenite ratio, one could also predict that the higher ferrite material would be slightly more noble.

This trend was verified by measuring galvanic currents and open circuit corrosion potentials at 75 F (24 C) in NACE solution (Tables 8 and 9). It can be concluded, therefore, that under conditions of localized corrosion, a galvanic couple exists between the two phases such that the ferrite would be cathodic to austenite. In all experiments conducted, preferential attack, if it occurred, always involved the austenite (e.g., Figure 12).

It was observed in all cases that localized attack of the austenite only occurred in cracks. Anodic polarization, for instance, did not selectively dissolve austenite on the surface of electrodes. This fact implies that the environment in the occluded cell of a crack is considerably different from the external environment.

Effect of Low Temperature Heat Treatment on Mechanical and Environmental Cracking Properties

To simulate aging that may occur at downhole temperatures, two heat treatments were performed: (1) 500 F (260 C) for 250 hours and (2) 600 F (316 C) for 250 hours. SSR tests were

then conducted on tensile specimens taken from these materials under open circuit and cathodic and anodic polarization conditions. The results of these experiments (Table 4) were similar to those of SSR tests conducted on the as-received duplex stainless steel. This is to say that cracking which was accelerated by cathodic charging and lessened by application of anodic polarization was observed under open circuit conditions. There was no indication of detrimental effects from the formation of second phases or carbides. In fact, the material aged at 600 F (316 C) for 250 hours exhibited considerably greater ductility than the as-received materials at essentially the same yield strength level. This behavior is most likely the result of relaxation of the cold worked structure upon aging.

Effect of High Temperature Heat Treatment on Mechanical and Environmental Cracking Properties

The primary effects of the elevated temperature heat treatments were to (1) eliminate cold work from processing and (2) increase the percentage of ferrite in the microstructures. It is interesting that the as-received material and that heat treated at 2200 F (1204 C) exhibited similar environmental cracking behavior at 75 F (24 C). In both cases, cracking that was accelerated by cathodic charging and reduced by anodic polarization was observed at open circuit conditions. Even though the differences between the as-received material and that heat treated at 2200 F (1204 C) include changes in residual stress caused by cold work and changes in the ferrite content, the response was essentially the same. Metallographic analysis of these materials following SSR testing at 75 F (24 C) indicated that the ferrite phase is more severely affected by the test environment and by application of current.

Comparison of the materials heat treated at 2200 and 2400 F (1204 and 1316 C) indicates that in the SSR tests under open circuit conditions, both exhibit cracking which is accelerated by cathodic charging. Based on strain to failure, however, anodic polarization appears to have beneficial effects on the material heat treated at 2200 F (1204 C) whereas it has a detrimental effect on the material heat treated at 2400 F (1316 C). If reduction in area is used as the criterion for cracking susceptibility, the material heat treated at 2400 F (1316 C) shows the same type of behavior as the as-received material and the material heat treated at 2200 F (1204 C). This is the only discrepancy between strain (time) to failure and reduction in area noted in this study. The discrepancy may be caused by the extremely coarse grain structure of the material heat treated at 2400 F (1316 C). As shown in Figure 15, the cracking is extremely crystallographic in this material. Consequently, the orientation of the few grains going across the gage section may have a large effect on the total strain to failure.

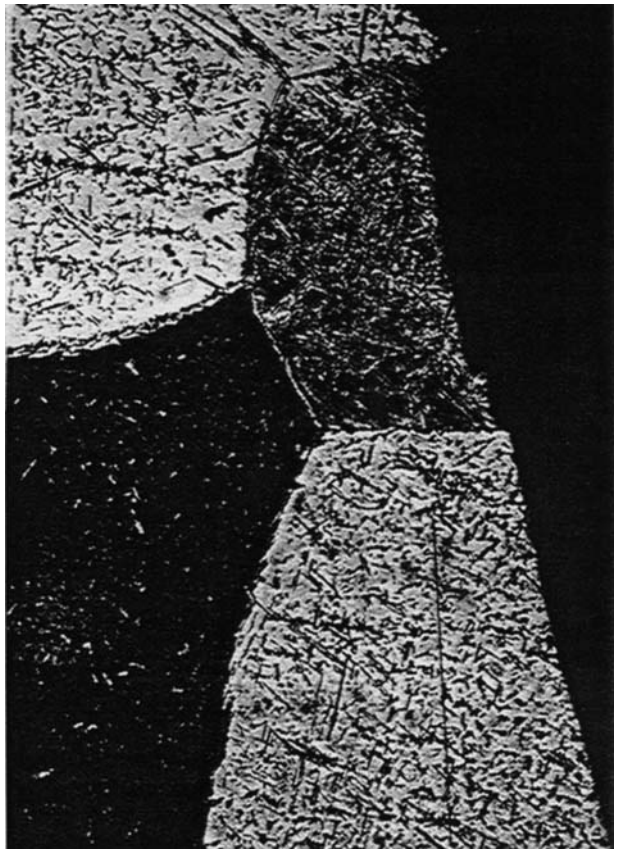


FIGURE 15 — 2400 F heat treatment. Fracture surface of anodically charged (+100 $\mu A/cm^2$) SSR tensile specimen 75 F, NACE solution. (63X)

Summary and Conclusions

It is apparent that hydrogen can act as an embrittling agent when duplex stainless steels are tested at ambient temperature conditions of dynamic strain. Questions arise as to whether hydrogen alone is sufficient to produce embrittlement or if other environmental constituents can also induce cracking. A case can be made that anodic dissolution of the austenitic phase is a necessary condition for cracking because preferential dissolution of austenite is observed even under conditions of cathodic charging (Figure 11). Under conditions where hydrogen is not present in sufficient quantity to cause embrittlement, or if the mechanical properties of the material are such that hydrogen does not induce embrittlement, duplex stainless steels might also fail by an anodic SCC mechanism. If this is the case, it might explain some seemingly anomalous data[8] which suggest that coupling to steel improves cracking susceptibility. It is interesting to note that H_2S and chlorides act synergistically to cause hydrogen embrittlement (SSC) at ambient temperature.

Electrochemical measurements show that a galvanic couple which favors generation of hydrogen on ferrite and anodic dissolution of austenite exists between austenite and ferrite.

At elevated temperature [350 F (177 C)], the mechanism of cracking is probably anodic SCC that is analogous to chloride stress cracking. Here again the pronounced detrimental effect of sour brines is that H_2S and chlorides together are worse than either alone. It is not possible to conclusively determine if hydrogen also plays a role at elevated temperature. The evidence opposed to such participation is that cathodic charging improves performance at 350 F (177 C) while anodic charging has the opposite effect. The supporting evidence comes from the microstructural analysis which shows preferential cracking of the ferrite phase in a manner similar to that observed at ambient temperature.

Heat treatments that increase the amount of ferrite have a generally detrimental effect on cracking susceptibility at ambient temperature, presumably because the ferrite phase is more sensitive to hydrogen. Low temperature heat treatments that simulate service aging of cold worked material have no detrimental effect (and possibly a beneficial effect) on cracking susceptibility.

Acknowledgment

The authors appreciate the assistance of D. A. Vaughan in conducting the SSR experiments and in providing the metallographic analysis.

References

1. Suzucki, et al., Nippon Kinzoku Gakaishi, Vol. 32, p. 1171 (1968).
2. S. Shimodaira, M. Takano, V. Takizawa, H. Kamide, "Mechanisms of Transgranular Stress Corrosion Cracking of Duplex and Ferritic Stainless Steels," Stress Corrosion Cracking and Hydrogen Embrittlement of Iron Base Alloys,

R. Staehle, Ed., National Association of Corrosion Engineers, Houston, Texas, p. 1008, 1977.
3. J. Hochmann, A. Desestret, P. Jolly, R. Mayoud, "Properties of High Chromium Ferritic Stainless Steels and Austeno-Ferritic Stainless Steels," Stress Corrosion Cracking and Hydrogen Embrittlement of Iron Base Alloys, R. Staehle, Ed., National Association of Corrosion Engineers, Houston, Texas, p. 992, 1977.
4. J. Sakai, et al., TMS-AIME Fall Meeting, Paper Preprint No. 8201-010, October, 1982.
5. J. Oredsson, S. Bernhardsson, "The Performance of High Alloyed Austenitic and Duplex Stainless Steels in Sour Gas and Oil Environments, CORROSION/82, Preprint No. 126, National Association of Corrosion Engineers, Houston, Texas, 1982.
6. T. Kudo, et al., "Corrosion Behavior of Highly Alloyed Materials in H_2S-CO_2-Cl^- Environments," CORROSION/82, Preprint No. 127, National Association of Corrosion Engineers, Houston, Texas, 1982.
7. A. I. Asphahani, "Highly Alloyed Stainless Materials for CO_2/H_2S Environments," CORROSION/80, Preprint No. 12, National Association of Corrosion Engineers, Houston, Texas, 1980.
8. J. Kolts, A. I. Asphahani, "Effect of Temperature on the Chloride-Sulfide Stress Cracking of Stainless Tubulars," CORROSION/81, Preprint No. 99, National Association of Corrosion Engineers, Houston, Texas, 1981.
9. G. Herbsleb, R. K. Popperling, "Corrosion Properties of Austenitic-Ferritic Duplex Steel AF 22 in Chloride and Sulfide Containing Environments," CORROSION/80, Preprint No. 13, National Association of Corrosion Engineers, Houston, Texas, 1980.
10. S. Bernhardsson, J. Oredsson, M. Tynell, "Properties of a Duplex Stainless Steel for Use in Corrosive Oil and Gas Wells," CORROSION/80, Preprint No. 14, National Association of Corrosion Engineers, Houston, Texas, 1980.
11. Sumitomo Metal Industries, Ltd., "Properties of DP3 (SM-25Cr) Series for Corrosive Conditions of Oil & Gas Well," No. 801 F No. 518, February 1981.
12. Y. Ishizawa, T. Shimada, M. Tanimura, "SCC Behavior of a Duplex Stainless Steel in Sour Gas Environment," CORROSION/83, Preprint No. 167, National Association of Corrosion Engineers, Houston, Texas, 1983.

Copyrighted Materials
Copyright © 1996 NACE International Retrieved from www.knovel.com

Paper No. 226—CORROSION/85

PERFORMANCE OF DUPLEX STAINLESS STEEL PIPES IN SOUR GAS WELLS

Gerdt Wilken
Mobil Oil AG
P.O. Box 110
D - 3100 Celle, W. Germany

ABSTRACT

Severe weight-loss corrosion affected the lowest part of carbon steel tubing strings in concentric completed sour gas wells in several German sour gas fields. To combat this corrosion problem the carbon steel pipes of the lower sections of the tubing string were replaced by duplex stainless steel pipes. Sour gas corrosion effects on duplex stainless steels can be described as chloride induced stress corrosion cracking or as general corrosion. The analysis of the corrosion effects emphasize the limitations of using duplex stainless steel pipes in sour gas wells.

INTRODUCTION

For over 20 years Zechstein sour gas has been produced in North Germany. The gas contains not only the sour components H_2S and CO_2 up to levels of 25% but also elemental sulfur up to the saturation level under downhole conditions. The gas is completely free of liquid hydrocarbons. To prevent plugging of the tubing by sulfur during production, a packerless concentric completion which allows the circulation of a sulfur solvent was introduced. From the start of the production an aqueous ethylamine solution was circulated as sulfur solvent.[1,2] The lowest part of the carbon steel tubing string was affected by severe weightloss corrosion caused by the reaction of H_2S, CO_2, formation water and elemental sulfur at high temperatures 120°C to 135°C. The trial introduction of pipes made of different high alloy steels to combat this corrosion lead to the result that in this corrosive environment duplex stainless steel pipes show the best corrosion resistance. Since 1977, MOAG has applied as a conventional practice duplex stainless steel pipes for the lowest part of the tubing string (= tailpipe) in sour gas wells. This paper reviews the downhole corrosion behavior of duplex stainless steels in sour gas wells. The observed corrosion phenomena are compared with the numerous data published in the literature.[3-5]

COMPLETION

The completion design must be able to allow the circulation of a sulfur solvent. This is achieved by using a packerless concentric completion as shown in Figure 1. The concentric 5-1/2 x by 5 in. tapered casing with an interior 3-1/2 x 2-7/8 in. tapered tubing string permits the circulation of the solvent through the tubing/casing annulus. Initially the tubing string was made of API grade C 75/2 carbon steel pipes. Since 1977, the lowest part of the tubing string (below the 3-1/2 x 2-7/8 in. cross-over) is made of duplex stainless steels, while the remaining upper part of the tubing is furthermore made of API C 75/2 carbon steels. The pipes are equipped with a premium coupling using a conical thread and a metal-to-metal seal (Mannesmann TDS coupling). For the pipe couplings in the 5 in. casing a reduction of the coupling O.D. was selected to improve the annular clearance around the coupling. This coupling and the tubing design satisfied all factors affecting pipe strength and joint strength (Table 1).

MATERIAL DESCRIPTION

The microstructure of the selected duplex stainless steels contains about 50% austenitic in a ferritic matrix. The material strength is improved by interstitial solid solution hardening due to nitrogen alloying. In the sour gas wells only solution annealed duplex stainless steels without any cold working were used. The physical properties are summarized in Table 2; the chemical analysis of the duplex stainless steels is shown in Table 3. The duplex pipes are equipped with a coupling joint, the nominal wall thickness of the 2-7/8 in. pipes is 5.51 mm, the regular O.D. of the coupling is 88.9 mm while the reduced O.D. is 82 mm. Each pipe is equipped with a coupling which is fitted by the pipe manufacturer at the steel mill. The duplex stainless steel tubing used by MOAG in the Zechstein sour gas production was supplied by Mannesmann with the designation AF 22 - 65.

CORROSION EFFECTS IN SOUR ENVIRONMENTS

The types of corrosion that can occur when using duplex stainless steel pipes in sour gas wells are mainly pitting and stress corrosion cracking, which are induced by the presence of chloride and sulphide ions. General corrosion is less likely to occur. The description of the potential range where the types of corrosion mentioned can occur can be found in the literature.[4-7] An investigation performed on steel specimens taken from pulled or recovered duplex stainless steel pipes elucidated the corrosion behavior under particular sour gas well conditions.

The occurence of corrosion attack in tubing materials is due to the presence of carbon dioxide, hydrogen sulfide, chlorides and elemental sulfur in the sour gas well environment. The main damage to duplex stainless steels is caused by stress corrosion cracking (SCC) and weightloss corrosion (pitting or general corrosion). Duplex stainless steel combines the advantages and particular susceptibilities of austenitic and ferritic stainless steels in view of the corrosion in sour gas environments.[3,4]

From the start of the production of sour gas containing elemental sulfur an aqueous ethylamine solution was circulated to prevent sulfur deposition in the tubing string. This process is based on the chemical reaction between sulfur and the injected solution of aqueous ethylamine to form polysulfide. The initial weight-loss corrosion of the carbon steel pipe could be reduced by preloading the ethylamine with approximately 10 g S/l elemental sulfur.[1,8,9] This measure has no effect on a severe corrosion phenomena affecting the lowest part of the tubing string. This corrosion was aggrevated by the sour gas components, the saline formation water, elemental sulfur as well as by high temperatures and high pressures. The backproduced fluid contains sodium chloride with an average of 0.2 g/l, fluctuations in salt content occur up to levels of 8 g/l. The pH of the solution containing aqueous ethylamine amounts to pH 8.5.

To prevent this so-called tailpipe corrosion, pipes made of different high alloy steels were tested in the wells (Table 4). The required corrosion resistance is related more to pitting and weight-loss corrosion, than to stress corrosion cracking. In comparison with the austenitic, ferritic or martensitic stainless steels, the 23 Cr - duplex stainless steel shows the best corrosion behavior. Nevertheless, mainly the usage of duplex steel pipes is limited to the lowest part of the tubing as shown in the completion configuration of Figure 1. In the course of the production history the length of tubing made of duplex stainless steel pipes was extended up to 1,000 m. The maximum load for the duplex pipes was limited to 50% of the minimum specified yield strength.

STRESS CORROSION CRACKING

The string design and the working load of the tubing string in the sour gas wells described shows no evidence of a particular susceptibility of the duplex stainless steel pipes to stress corrosion cracking in view of the well documented lab data. Failures of duplex stainless steels has not been experienced under normal sour gas production conditions when these pipes are used as tailpipes.

The first failure of duplex stainless steel pipes occurred in 1978. After drilling, the sour gas well was completed in the conventional manner as shown in Figure 1 using a tapered 3-1/2 x 2-7/8 in. production string with a total length of 3,350 m. The well was then shut-in for two weeks. Immediately, an unexpected influx of formation water took place and raised the water level to a depth of 1,240 m. The complete 2-7/8 in. duplex stainless steel string was immersed for this time in the H_2S/CO_2 saturated formation water containing 288.5 g NaCl/l at temperatures in the range of 115 to 130°C. The relevant well data are summarized in Table 5. The string was subsequently pulled and subjected to a visual inspection. This showed that all 27 duplex stainless steel couplings with reduced O.D. had longitudinal cracks as shown in Figure 2. The cracks affected all the couplings, both those made up by the manufacturer as well as those made up at the rig site.

The metallographic analyses of the cracked couplings gave clear indications of chloride induced stress corrosion cracking. The microsections exhibit the prevailing transgranular crack path without branching. This means that the sum of the stresses applied to the pin/coupling combination with reduced O.D. exceeded the threshold stress during make-up and/or loading. An analysis of the joint stresses revealed that for a given make-up torque, the hoop stress of couplings with reduced wall thickness exceeds the threshold stress established in lab tests. The corrosion attack starts at the outer surface of the coupling where the hoop stress is greatest. The crack runs longitudinally to the end of the coupling.

The make-up torque induces a load against the biconical shoulder and against the thread flanks. When the coupling is submitted to a hanging load, a stress maxima is caused at the bevel shoulder and at equal distances on each side of the threaded area. The chloride-induced cracks started in the area of maximum stress and opened one side of the coupling, diverting the stress. A cross section of the coupling with the crack path can be seen in Figure 3. The crack penetrates the inner and outer surface of the coupling radially. In the middle of the coupling wall the crack is aligned at an angle of 60° to the radial axis. The crack shows transcrystalline and intercrystalline fracture modes. The cleavage plane of the crack exhibits numerous pits (Figure 4).

The second SCC-failure of duplex stainless pipes occurred in a sour gas well in 1984 during start-up of production. Using the same completion design as shown in Figure 1, 1.100 m of the API C 75/2 pipes were replaced by 3-1/2 in. duplex stainless pipes below 800 m depth to combat the coupling corrosion.[2,8] At the start-up of the production the string was parted. The failure could be localized at 900 m depth; the string was parted within a pin of a duplex stainless pipe. Both parts of the failed pipe could be recovered during the workover job.

The failure analysis gave indications for SCC, however, no other duplex stainless steel pipe of this string shows cracks on the internal surface of the pin area. The microsection of the material structure at the cracked pin exhibits an unusual austenite/ferrite distribution (> 70 % ferrite), (Figure 6). In addition, the yield strength of the pin material was much higher than of the pipe body material. The impact behavior excludes the presence of the sigma phase (Table 6).

Unpublished investigations carried out by the pipe manufacturer established an increasing susceptibility to SCC with increasing ferrite content in the duplex stainless steel structure.[10] The unusual structure obviously was caused by the solution heat treatment at higher temperatures.

Figure 7 shows the effect of heating temperature on the ferrite content. Up to about 1.150°C the ferrite content increases linearly, but above this temperature exponentially with the temperature increase.[11] The disadvantageous effect of the heat treatment and microstructure on the corrosion and SCC of duplex stainless steels in chloride containing sour gas environments are reported in the literature.[12]

PITTING CORROSION

Because of its unpredictability, pitting corrosion is a major problem affecting the use of stainless steels in chloride environments. The severity of attack is exponentially related to the chloride content and the acidity. High chloride levels locally break down the passive layer of a stainless steel.

In order to predict the possible failures due to pitting corrosion, as well as for corrosion prevention, a knowledge of critical potential ranges for susceptibility to pitting corrosion is of great practical importance.

In environments containing chloride ions, the pitting potential of duplex stainless steels in the passive state is shifted markedly to more negative values by H_2S. This is equivalent to a decreased pitting resistance. This corrosion behavior, combined with the knowledge that chloride-induced pitting is the initial step in stress corrosion cracking, underlines the risk for duplex steel pipes installed in environments containing chloride. In addition, duplex stainless steels in contact with liquid elemental sulfur, assuming the same sour gas environment, can be in the active state. This potential shift causes pitting or weight-loss corrosion and can initiate SCC in the same manner as chloride.

Pitting corrosion to our experience does not occur during conventional sour gas production even in cases where the fluid contains a high amount of formation water. The occurence of local attack on duplex stainless steel pipes is mostly related to environments containing aqueous acid solutions and/or liquid sulfur.

CORROSION BEHAVIOR IN ACID (HCl)

The corrosion behavior of high alloy steels in aqueous acid solutions (pH < 4) is often described by the curves relating corrosion rate to the potential. With increasing potential the materials pass through the active, passive, and transpassive potential ranges. Corrosion is rendered passive at the so-called passivation potential as the potential is shifted from more negative to more positive values.[6] When duplex stainless steel is used in sour gas wells the acid attack is generated by direct contact with acid solutions during acid treatments and/or by the backproduction of low-pH liquids. Especially, the latter production phase leads to circumstances in which the duplex stainless steel could pass through the potential curve from passive to active conditions. For this reason the corrosion behavior of the high alloy steel at acid treatments could not be predicted precisely. Figure 5 shows a general corrosion attack as well as the preferential attack of a single phase of the duplex structure.

This corrosion attack on the duplex stainless steels occurred after a tubing failure at the 3-1/2 x 2-7/8 in. crossover pin. The cross-over was made of a Cr-Mo-steel (type AISI 4130) and failed due to severe weight-loss corrosion.[2] The tubing parted, and the duplex stainless steel pipes are now below the point of reversal of the inhibitor containing sulfur solvent. These pipes are in conditions of free corrosion. The steel surface of the duplex pipes exhibit overall corrosion with a scarred surface structure. The nominal environment in this well, chlorides, sulfur, H_2S and CO_2 at temperatures above 100°C in combination with acid solutions, are responsible for the high corrosion rates, especially in this case where the acid treatment was performed under the assumption that the tubing had not parted. The time of direct contact of the duplex stainless steel pipes with the sour gas and the acid environment could not be estimated. The acid batch was pumped through the tubing into the lowest part of the production casing and/or to some extent into the formation. The separated string of duplex pipes was totally immersed in this corrosive solution. Other than the different types of weightloss corrosion, there is no indication for stress dependent cracks in the duplex stainless material.

The corrosion behavior of duplex stainless steels in environments containing aqueous hydrochloric acid solutions could be improved by using commercial corrosion inhibitors during acidizing treatments. Although the inhibitor formulations are designed for corrosion prevention of carbon steels, good results were also obtained for duplex stainless steels. The limited stability of the corrosion inhibitor as function of temperature lead to the limitation of the interaction of hydrochloric acid and duplex stainless steels. In the case of inhibitor malfunctions the risk of pitting corrosion increases; therefore, the retention time for hydrochloric acid solutions within the tubing was limited to 4 h.[2]

DISCUSSION

Tubing failures in sour gas wells caused by severe weightloss corrosion of API grade C 75/2 steel pipes lead to the introduction of stainless steel pipes. Duplex stainless steel pipes have shown their superior

behavior compared to austenitic or ferritic stainless steels. The sour gas corrosion performance of duplex stainless steels is greatly affected by the operating parameters and environmental factors, especially pH, temperature, chloride, and sulfur levels. In accordance with the laboratory tests, the highest probability of failure occurs when the sour gas environments contain both chlorides and liquid elemental sulfur. Pitting corrosion is normally the first step in the initiation of chloride induced stress cracking. High chloride levels locally break down the passive layer. In the presence of H_2S the pitting potential of duplex stainless steels is shifted markedly to more negative values.

Tensile stresses are necessary for the propagation of the stress cracks. Numerous data in the literature show the threshold stress, as a percentage of the actual yield strength above which the stress corrosion cracking susceptibility increases. Solution annealed duplex stainless steels are supposed to be less susceptible than the cold worked, higher strength duplex stainless steels. However, the danger of SCC occurring in solution annealed duplex stainless steels under the combined effect of chlorides, hydrogen sulfide, and elemental sulfur in aqueous environments can be alleviated by decreasing the stress levels. This synergistic effect must be considered at the time of tubing string design.

Using an uniaxial model for the stress calculation of the tubing pipes, the maximum load of the duplex pipes was calculated to be 50% of the minimum yield strength. In the case of grade 65 ksi, this reduces the length of the duplex pipe string to 2.300 m. As mentioned previously only duplex stainless steels in the solution annealed condition arc used in sour gas wells.

A further important effect is the observation that the carbon steel pipe and the duplex stainless steel pipe do not show any indications for bimetallic corrosion. The coupling joint between duplex and carbon steel is not a region of preferential corrosion. Furthermore, bimetallic corrosion does not occur between duplex pipes of the tubing and the carbon steel pipes of the casing at unavoidable existing contact points. The reason for this observation may be the high pH of the circulating aqueous liquid, e.g. the sulfur solvent ethylamine.

The failures described related to a corrosion attack of the duplex stainless steel pipes are particular instances. If the production system works without any problems with respect to the downhole equipment, the duplex stainless steel reveals no corrosion attack. This is valid also in those cases where the produced fluid contains high concentrations of chlorides, hydrogen sulfide, and liquid elemental sulfur. Stress corrosion cracking can be avoided by limitation of the leading to 50% of the specified minimum yield strength.

CONCLUSION

The corrosion performance of duplex stainless steels in sour gas wells depends on the production parameters in the particular well. At low working loads ($\leq$ 50% YS) the duplex stainless steel satisfies the corrosion prevention requirements even at high H_2S contents in the gas and high chloride concentrations in the produced liquids. Problems may occur if the applied stress exceeds the established threshold stress for the initiation of SCC. A special risk arises during acid treatments with hydrochloric acid through the tubing string. It is recommended that the retention time of the inhibited acid solution within the tubing be limited. Corrosion failures of duplex stainless steels are always related to abnormal production conditions.

ACKNOWLEDGMENT

The author expresses his appreciation to Mobil Oil AG for granting permission to prepare and publish this paper.

REFERENCES

1. F.F. Lyle, et al., *Material Performance* 17/1(1978): pp. 24 - 31.
2. G. Wilken, paper no. 158, CORROSION/83, Anaheim, 1983.
3. S.O. Bernhardsson, J. Oredsson, M. Tynell, *Corrosion* 36 (1980).
4. G. Herbsleb, R.K. Popperling, *Corrosion* 36 (1980): pp. 611-618.
5. A. Desestret, paper no. 165, CORROSION/83, Anaheim, 1983.
6. G. Herbsleb, et al., *Werkstoffe und Korrosion* 30 (1979): pp. 1-8.
7. Herbsleb, G. et al., *Werkstoffe und Korrosion* 30 (1979) 322 - 340.
8. W. Bruckhoff, Erdol - Erdgas Z. 95 (1979): pp. 82-89.
9. G. Schmitt, B. Rothmann, *Werkstoffe und Korrosion* 28 (1977): pp. 59-71.
10. Mannesmann Research Dept., unpublished communication.
11. G. Herbsleb, P. Schwaab, ASM, Int. Symp., St. Louis (October, 1982).
12. S.M. Wilhelm, R.D. Kane, CORROSION/40 (1984), pp. 8,431-8,439.

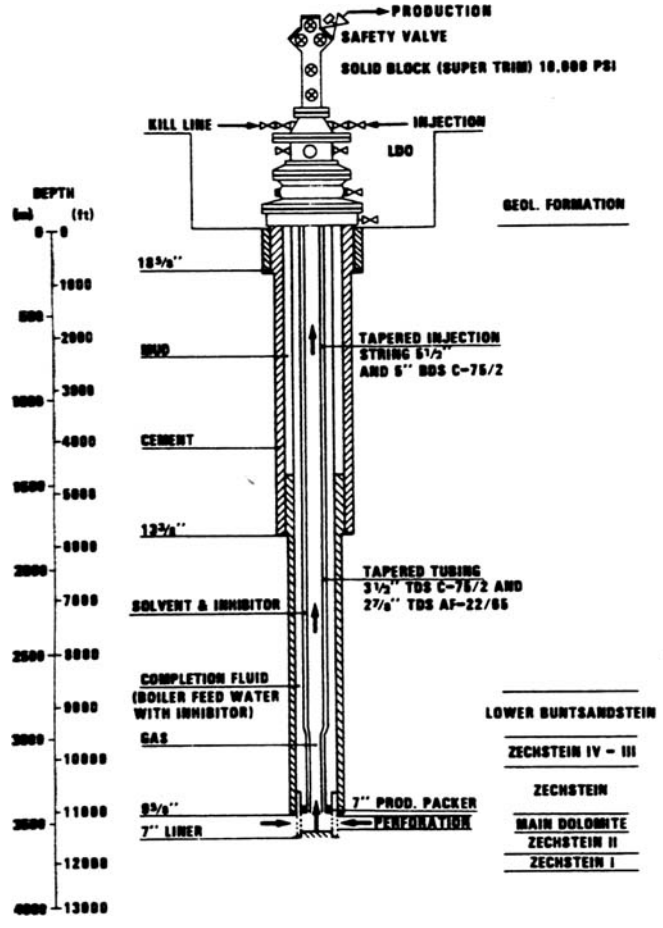


Fig. 1 Completion design of a sour gas well to allow the circulation of a sulfur solvent through the well

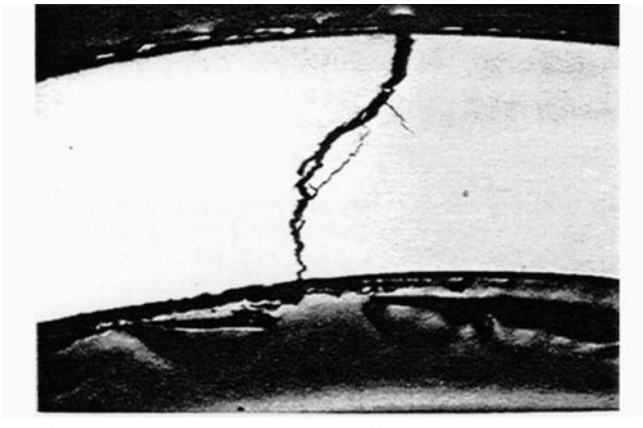


Fig. 3 Cross-sectional through the cracked coupling

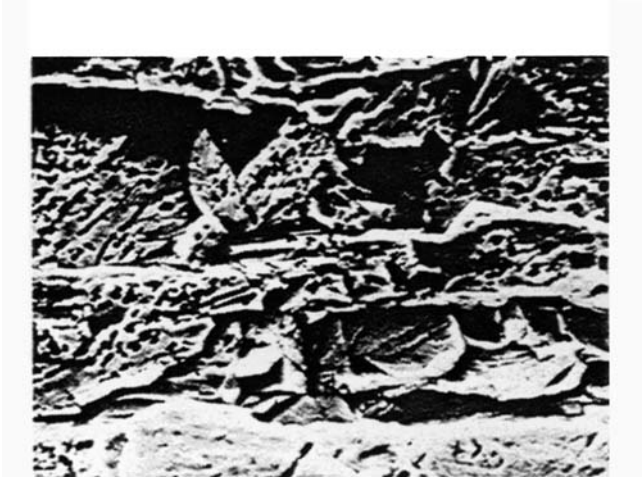


Fig. 4 SEM micrograph of the crack surface

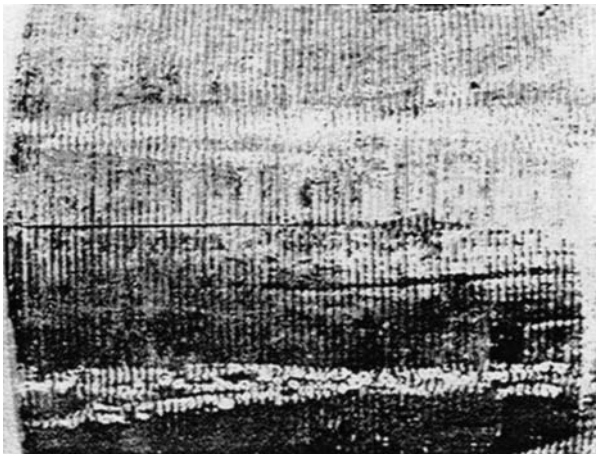


Fig. 2 Longitudinal SCC crack of the duplex coupling

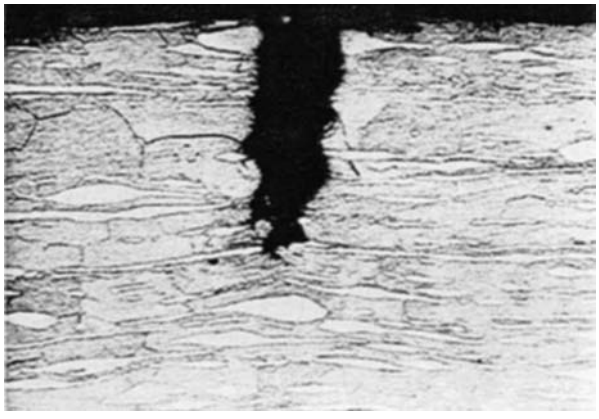


Fig. 5 Preferential dissolution of the ferrite with general corrosion



Fig. 6 Austenite-ferrite distribution of the duplex structure at the crack area

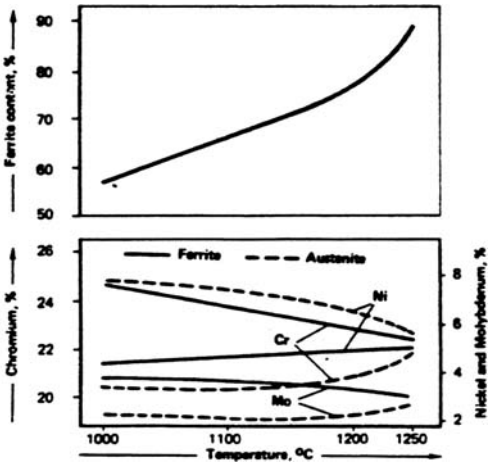


Fig. 7 Effect of annealing temperature on ferrite content of AF 22 and phase composition (10)

TABLE 1

Dimensions and specifications of completion tubulars
(x = with reduced coupling O.D.)

Tubing size	Grade (ksi)	Wall thickness (mm)	Weight (lbs./ft.)	Joint strength (lb.)
Production casing				
5 1/2"	75	9.17	20	497 000
5"	75	9.19	18	452 000
Production tubing				
3 1/2"	75	6.45	9.2	194 260
2 7/8"	AF 22-65	5.51	6.4	135 900 (x)
Crossover				
3 1/2" x 2 7/8"	AF 22-65	6.45	9.2	

TABLE 2

Physical properties of 23 Cr duplex steel
(solution annealed condition)

	Yield strength (N/mm^2)	Tensile strength (N/mm^2)	Elongation (%)
nominal	min. 450	680 - 900	min. 25
checking test coupling	666	807	25.4

TABLE 3

Chemical composition of the duplex steel (wt %)

	C	Si	Mn	Cr	Ni	Mo	N
nominal	0.03	1.0	2.0	21/23	4.5/6.5	2.5/3.5	0.08/0.20
checking test coupling	0.02	0.28	1.82	21.6	5.4	3.2	0.165

TABLE 4

High alloy steels used in sour gas wells

Structure	Elements
Austenitic	18 Cr-10 Ni
Austenitic	17 Cr-13 Ni-5 Mo
Duplex	20 Cr
Duplex	23 Cr
Ferritic	13 Cr
Martensitic	13 Cr

TABLE 5

Gas composition and water analysis in a sour gas well in which an SCC failure of duplex steel couplings was experienced.

Gas analysis	Vol. %
H_2S	10
CO_2	11
CH_4	75
N_2	4

BHSIT = 130 C - 135 C

BHSIP = 340 bar

Water analysis	mg/l
Li	150
Na	69 250
K	2 950
Sr	2 760
Ca	38 500
Mg	1 500
Cl	175 000

TABLE 6

Physical properties of cracked duplex pipe
(SCC caused by high ferrite content in the structure at the pin)

	Yield strength N/mm^2	Tensile strength N/mm^2	Reduction %	Toughness (RT) J
nominal	min 450	680 - 900	min 25	-
pin	645	735	30	-
pipe body	562	752	24	92/90/99

Copyrighted Materials
Copyright © 1996 NACE International Retrieved from www.knovel.com

Section 4

PRECIPITATION-HARDENED NICKEL ALLOYS

Paper No.
62

CORROSION 92
The NACE Annual Conference and Corrosion Show

CAST NICKEL BASE ALLOYS FOR SOUR SERVICE

Robert P. Badrak
Hydril Company
3300 North Sam Houston Parkway East
Houston, Texas 77032-3411

ABSTRACT

Cast nickel base alloys (CRA's) have been viewed by some as not suitable for service in sour environments. Two cast precipitation hardenable nickel base alloys, 718 and 925, were compared with their wrought counterparts. Room temperature SSC tests per method A of NACE TM0177 as well as elevated temperature C Ring tests were conducted. The relative pitting corrosion resistance in chloride environments was examined using accelerated immersion tests.

The SSC resistance of the cast alloys was identical with the wrought counterparts and no SCC was detected in C Ring tests. There was a slight difference in the initiation of pitting. The microstructure and microporosity were found to have an effect upon elevated temperature slow strain rate tests (SSRTs). For the more severe applications, good microstructural and porosity control need to be exercised.

Key Words: Castings, nickel base alloys, pitting, precipitation hardening alloys, sulfide stress cracking, UNS N07718 and UNS N09925.

INTRODUCTION

CRA's have a variety of uses in the production and exploration of oil and gas. Generally, nickel base alloys are used in instances where a combination of high strength and good corrosion resistance are required. Alloys which are required to exhibit resistance to sour (hydrogen sulfide) containing environments must meet the requirements of NACE MR0175[1].

Nickel base alloys can be broadly categorized as those which are precipitation hardening or cold work hardening. The precipitation hardening alloys have gained wide industry acceptance and are used extensively in those instances where the geometry of the component manufactured does not permit strengthening through cold working. Typical applications include downhole accessories (such as packers, side pocket mandrels and safety valves), wellhead equipment (such as valves and hangers) and drilling equipment (such as drill string safety valves).

These precipitation hardening alloys can be produced in either the wrought or cast forms. There has been reluctance to use cast nickel base alloys, demonstrated by the editorial addition of the word "wrought" to all nickel base alloys in MR0175 that did not possess cast data as part of the balloted information (T1F Committee discussion and decision at NACE 90). The cast forms suffer from this lack of industry acceptance and listing in NACE MR0175.

The purpose of this paper was to examine the corrosion resistance of cast and wrought forms of two precipitation hardening alloys, UNS N07718 (718) and UNS N09925 (925). The resistance to stress corrosion cracking (SCC) in sour environments and localized pitting corrosion in chloride containing environments were investigated.

EXPERIMENTAL

Materials and Processing

The vacuum casting procedures[2] involved the following steps: (1) loading mold and crucible with a measured amount of virgin bar stock into the vacuum chamber, (2) induction heating of bar stock until molten, holding melt at temperature for a short period of time to permit vacuum degassing, (3) pouring molten metal into mold and (4) removing from chamber. The 718 heats were cast in a two chambered furnace and the 925 heats were cast in a single chamber furnace.

In centrifugal casting, molten metal is poured into a spinning mold; the centrifugal force drives the metal to the mold wall. This results in the higher density metal being forced to the outer cast surface with the lighter constituents which include the nonmetallics, gas ,sulfides etc migrating to the inner cast surface. The critical variables include the centrifugal force and length of time during solidification. This process has been successfully used to cast high quality 718 using an inert gas blanket instead of the conventional vacuum atmosphere[3]. One of the heats examined herein, number C7D, was made in this manner.

The 925 heats cast were experimental production heats prepared for this investigation. Each heat yielded about 35 lbs (16 kg) and was poured from 2750°F (1510°C) under a partial vacuum of about 25 microns. The melt was allowed to stabilize at the pour temperature for degassing purposes and the time from the start to the end of the pour was about 1 second.

The exact heat treatment cycles used are presented with the corrosion test results; the tested state is always the solution annealed and precipitation hardened condition. With the exception of two batches of test specimens from one heat, all heats of 718 were homogenized after casting and prior to solution annealing.

Pitting Corrosion Tests

The relative resistance of these alloys to pitting corrosion was examined using two different

immersion type environments. The two tests were selected on the basis of wide use and relevance to real world situations.

The first series of pitting tests was performed in accordance with ASTM G48 Method A[4]. This was reputedly the most widely known and utilized immersion test[5]. The environment was a 6% (anhydrous) by weight $FeCl_3$ solution with a standard 24 hour immersion time. The test temperature was varied to determine minimum pitting temperature and relative extent of pitting.

Pitting tests were also performed using $Fe_2(SO_4)_3$ (ferric sulfate) as the oxidizing species with 4% NaCl and 0.01 M HCl. The samples were finished with 120 grit wet, dried with methanol and immersed for 24 hours at a set temperature. This test was selected because of good correlations that had been developed between results and service performance and potentiodynamic polarization scans run in 4% NaCl 0.01 M HCl with a 360 mV/hr scan rate[5,6]. The pH of the test environment was found to be about 1.8.

Stress Corrosion Tests

SSC tests were conducted per NACE TM0177 Method A[7]. The test environment was the standard NACE solution (5% NaCl and 0.5% acetic acid in distilled water). The environment was first purged with nitrogen and then saturated with H_2S, continually bubbling about 10 bubbles/minute after initial saturation. An oxygen trap was utilized. Duplicate samples were run coupled and uncoupled to mild steel. The steel couple was accomplished by wrapping a low carbon steel wire around the tensile shoulder section.

Elevated temperature and pressure autoclave testing was performed using the C-Ring type of specimen. Each test specimen was galvanically isolated from other type materials. The test environment was a deaerated 15% aqueous solution of NaCl with 400 psi (2.76 Mpa) CO_2 and 200 psi (1.38 Mpa) H_2S. ASTM G38[8] was utilized as the method of calculating C-Ring deflections based upon desired outer fiber stresses. Multiple specimens were used and stressed at levels ranging from 70% to 100% of actual YS. The maximum temperature tested (and reported) was 300°F (150°C). The test duration was 30 days and samples were examined afterwards at 30X for evidence of SCC.

Slow strain rate tests of 718 were performed using a strain rate of 4×10^{-6}/sec in inert oil at 300°F (150°C) and a deaerated 5% NaCl environment with 700 psi (4.83 Mpa) CO_2 and 75 psi (0.52 Mpa) H_2S at 300°F (150°C). Each test specimen was connected to a UNS N10276 rod but was galvanically isolated from other materials. The samples were examined at 30X for evidence of SCC and ratios of the elongation and reduction of area between the inert and test environments reported.

RESULTS

Five vacuum induction remelted (VIR) 718 heats, one centrifugally cast 718 heat and four VIR 925 heats were used in this investigation. Two wrought 925 and three wrought 718 heats were used for comparison purposes. The composition of all the heats examined are presented in Table 1.

Two of the 925 heats listed in Table 1, numbers C9B and C9C, were reanalyzed to determine change due to the VIR process. Very little compositional change was observed and the chemistry before and after casting is presented in Table 2. It appeared that minute amounts of carbon, phosphorus and manganese were lost during the melt process.

All of the NACE TM0177 tests passed (No Failure) with no detectable cracking. The actual stress levels, heat treatments etc. are presented in Table 3. A feature noted was the failure in air of one tensile specimen during stressing to 100% of actual YS. An examination of the fracture surfaces and microstructure revealed extensive microporosity and the presence of undesirable phases, primarily Laves. Photomicrographs of the microporosity and Laves phase are presented in Figures 1 and 2 respectively.

None of the C-Ring tests exhibited evidence of SCC. A summary of the C-Ring tests with materials and stress levels is presented in Table 4.

All the 718 SSRT specimens exhibited very low ductility. One cast heat was examined, No. C7C, in two forms: cast rod and a section of a large casting (about 2" (5.1 cm) maximum cross section). The results are presented in Table 5. An examination of the fracture surfaces of the SSRT specimens using a scanning electron microscope (SEM) revealed that the cast rod exhibited large regions of dendritic structure on the fracture surface (see Figures 3 and 4). No metallographic evidence of SCC was detected. The large casting section was found to contain evidence of secondary phase(s) on the fracture surface (see Figure 5). No extensive porosity was found to be evident but evidence of secondary cracking was found at high magnifications.

The results of the pitting tests are presented in Tables 6 and 7 for the ferric chloride and ferric sulfate immersion tests respectively. The comparison of cast and wrought alloys yielded mixed results in the ferric chloride from these tests; the cast alloys appeared to pit first, but pit propagation (extent) indicated no significant difference. The ferric sulfate tests revealed no significant differences between cast and wrought products. In both environments, the 718 materials exhibited superior pitting resistance.

DISCUSSION

Comparison of Stress Corrosion Cracking Resistance

The room temperature tests performed in accordance with NACE TM0177 indicate that neither of the materials tested were susceptible to SSC in cast or wrought conditions. Though not a designed part of this investigation, it was noted that even when processed incorrectly with extensive amounts of embrittling Laves phase and microporosity, the samples did not exhibit susceptibility to environmental cracking at room temperature.

The C-Ring tests indicated that both wrought and cast forms of 718 and 925 were immune to SCC up to 300°F (150°C) in the environment tested. Both of these alloys should have been resistant to SCC at 300°F (150°C), though SCC has been reported in 925 alloy C-Rings at 350°F (177°C) in the standard NACE solution with 90 psi (0.62 Mpa) H_2S when stressed beyond the YS[9].

The SSR tests of 718 were inconclusive in that the material tested possessed unintended microstructural defects. It was noteworthy that the presence of a cast microstructure with extensive microporosity did not exhibit secondary cracking. However, microstructural phases (such as Laves) could have and apparently did adversely affect the resistance to elevated temperature SCC. The SCC resistance of 718 has been related to the presence of Laves phase[10]; the presence of Laves promoted SCC.

In the specimens for some of the NACE TM0177 tensiles and all of the SSRT tensiles from cast

718 heat C7C, the homogenization processing step was omitted in error. In 718, a homogenization treatment was required redissolving the Laves phase prior to further processing. The homogenization process is related to time and temperature. Other researchers have found that 10 hours at 2050°F (1121°C), 4 hours at 2100°F (1150°C) or 1-2 hours at 2150°F (1177°C) are required to effectively remove Laves phase[11]. However, the final product grain size increases with increasing homogenization temperature. For example, the following ASTM grain sizes/homogenization temperatures have been reported: 6 at 2000°F (1093°C), 5 at 2050°F (1121°C), 3 at 2100°F (1150°C) and 1 at 2150°F (1177°C)[3]. A balance between a very small Laves phase content and a reasonable grain size appeared to be the optimum condition.

Pitting Corrosion Resistance

The pitting tests were performed to conduct a rough ranking of the alloys in the cast and wrought forms. The cast alloys exhibited earlier pit initiation in the ferric chloride environments and identical pit initiation in the ferric sulfate containing environment. Corrosion pits on 718 in the solution annealed -precipitation hardened condition are reported in the literature[12] for material tested at 40°C in the ferric sulfate containing environment which is in agreement with the initiation of pits observed in this investigation.

Examination of cast and wrought surfaces just starting to pit indicated that the pits were initiating at surface discontinuities (inclusions, machining marks etc). As indicated by the literature, it was found that minor deviations in chemistry would not be detectable in pitting tests but that inclusions exhibited a greater effect[13]. It was observed here in the ferric chloride tests that the specimen orientation made a difference with respect to pitting resistance, the 925 alloy bar and the centrifugally cast 718 showing direction effects in that one orientation exhibited pitting at least 5°C lower than the other orientation. A direction effect was neither observed in the 718 bar and VIR cast materials nor in the ferric sulfate tests.

Cast 925 Alloy

Heat treatment and microstructural characterizations were conducted on the VIR 925 heats made for this investigation. The time-temperature-transformation (TTT) relationships have been studied for this alloy[14]. The initial heat treatment consisted of solution annealing at 1875°F (1023°C) for 1 hour and precipitation hardening at 1365°F (740°C) for 8 - 12 hours followed by a furnace cool to 1150°F (621°C) and holding an additional 8 - 12 hours. The mechanical properties obtained (88 - 98 ksi (605 - 675 Mpa) did not achieve the desired 100 ksi (690 Mpa) minimum yield strength. The strength was increased to the desired range by increasing the temperature and length of time for the solution annealing cycle to 3 hours at 1925°F (1052°C). This altered solution annealing cycle produced yield strengths up to 107 ksi (738 Mpa).

Optical microscopy and SEM were performed on the heat treated sections to detect the presence of any secondary phases, inclusions or microporosity that may be present. A small amount of microporosity was found and very small islands in the interdendritic area were found to contain secondary phases. The islands were found to contain mostly delta phase with a minute amount of what appeared to be Laves phase. Examples of the microporosity and secondary phases are presented in Figures 6 and 7 respectively. The secondary phase particles were too small for positive identification using energy dispersive spectroscopy.

An as-cast section from heat C9D was examined. Regions of secondary phases, Laves and delta,

were detected in the interdendritic regions. Energy dispersive spectroscopy on the SEM was used to identify the Laves phase; this phase was found to contain about 28% niobium. A SEM photomicrograph of the as-cast structure is presented in Figure 8.

An examination of the microstructure using transmission electron microscopy (TEM) revealed coarse austenite grains with a fine dispersion of spherical γ' precipitates. A photomicrograph using darkfield imaging of the superlattice reflections to reveal the precipitates is presented in Figure 9. The γ' precipitates were found to be in the 8 - 16 nm range. No intermetallic phases were detected in the grain boundaries.

Though no adverse effects of the secondary phases upon SSC were detected here, the presence of these microstructures indicated that additional heat treat/structure work needed to be performed on the cast form of 925 to optimize properties and SSC resistance. It may be that a longer solution annealing cycle is required to dissolve these phases, or that a separate homogenizing cycle is necessary.

Castings

In addition to the well known effects of chemistry and heat treatment on performance of materials in sour environments, the user of castings also needs to be concerned with quality. The defects which can be present in castings such as porosity, inclusions and segregation can act as crack initiation sites and propagation paths. The inclusions and gross segregation can be readily controlled through modern melting and refining practices.

The casting process involves a liquid to solid transformation with an accompanying volume change. This volume change (shrinkage) can be result in porosity. The larger and more intricate the casting configurations the more difficult it is to prevent microshrinkage and compositional segregation. The degree of segregation is controlled by the dendrite spacing which forms during solidification. Control and design of melt practice and part and mold geometry can minimize porosity and segregation. The processes used to produce the castings evaluated herein were produced using both VIR and centrifugal cast methods. Both of these techniques, when carefully controlled, yield very high quality castings with a refined structure and very low inclusion levels.

The casting process needs to be tailored to the application. As the stress levels and the environment become increasingly severe, more attention and limitations on the casting process needs to be imposed. These limitations may increase to the point where castings are excluded when the temperature/environment limitations of the base alloy are reached. A harder characteristic of castings to overcome is their inherent microstructural coarseness. New fine grain casting techniques[15,16] which alleviates this coarseness may be required for very aggressive, high temperature applications.

CONCLUSIONS

The following conclusions have been drawn from this investigation:

1) Both cast and wrought forms of 718 and 925 were immune to room temperature SSC in TM0177 tests.
2) Both cast and wrought forms of 718 and 925 were immune to SCC up to 300°F (150°C) in C-Ring tests with 15% NaCl, 400 psi (2.76 Mpa) CO_2 and 200 psi (1.38 Mpa) H_2S.
3) Microporosity and Laves decreased the ductility in cast 718 as measured by room temperature tensile tests and SSR tests at 300°F (150°C); the Laves phase was found to promote SCC.

4) No difference in pitting resistance was detected between the wrought and cast alloys tested in the ferric sulfate containing environment. Pit initiation was found on the cast alloys about 5°C below the corresponding wrought forms in the ASTM G48 pitting tests.
5) The cast version of 925 required modified heat treat cycle(s) to achieve high strength and good microstructural control.

ACKNOWLEDGEMENTS

The author wishes to convey his appreciation to the following colleagues/companies who have supported this investigation: Mr. Rashmi Bhavsar of Camco, Mr. Greg Chitwood of Otis Engineering, Mr. Ed Hibner of INCO Alloys, Mr. Roy Trent of Howmet, and Mr. Jerry Gapinski of Wisconsin Centrifugal.

REFERENCES

1. NACE Standard MR0175 - Sulfide Stress Cracking Resistant Metallic Materials for Oilfield Equipment.
2. D.A. Ford, Foundry Trade Journal, **Vol. 134**, January, 1973, pp 71-75.
3. G.E. Gapinski and T.J. Devine, *Superalloy 718, Metallurgy and Applications*, ed. E.A. Loria, (TMS, 1989), pp 533-544.
4. ASTM Standard G48 - Test Method for Pitting and Crevice Corrosion Resistance of Stainless Steels and Related Alloys by the use of Ferric Chloride Solution.
5. J.W. Oldfield, International Materials Reviews, **Vol. 32**, No. 3 (1987), pp 153-170.
6. P.E. Manning, Corrosion, **Vol. 39**, No. 3 (March, 1982), pp. 98-102.
7. NACE Standard Test Method TM0177 - Testing of Metals for Resistance to Sulfide Stress Cracking at Ambient Temperatures.
8. ASTM Standard G38 - Practices for Making and Using C-Ring Stress Corrosion Cracking Test Specimens.
9. J. Kolts, CORROSION/86, paper no. 407, (Houston, Texas) 1986
10. I.L.W. Wilson and M.G. Burke, *Superalloys 718, 625 and Various Derivatives*, ed. E.A. Loria, (TMS, 1991), pp 681-704.
11. R.G. Carlson and J.F. Radavich, *Superalloy 718, Metallurgy and Applications*, ed. E.A. Loria, (TMS, 1989), pp 79-95.
12. J. Kolts, *Superalloy 718, Metallurgy and Applications*, ed. E.A. Loria, (TMS, 1989), pp 329-344.
13. J. Degerbeck, J. Electrochemical Society, **Vol. 120**, No. 2 (February, 1973), pp 175-182.
14. P. Ganesan, E.F. Clatworthy, and J.A. Harris, CORROSION/87, paper no. 286, (Houston, Texas).
15. J.K. Tien, J.C. Borofka, and M.E. Casey, J. of Metals, **Vol. 38**, No. 12 (December, 1986), pp 13-17.
16. D.A. Chang, R. Nasser-Rafi and S.L. Robertson, *Superalloys 718, 625 and Various Derivatives*, ed. E.A. Loria, (TMS, 1991), pp 271-286.

TABLE 1: CHEMICAL ANALYSIS OF CRA TEST MATERIALS

Material Code	Alloy Type	Description	WEIGHT, %													
			C	Mn	Si	P	S	Cu	Nb	Ni	Cr	Mo	Ti	Al	Co	Fe
C9A	925	VIR Cast	0.011	0.61	0.14	0.019	0.001	1.72	0.19	42.94	19.95	2.84	2.16	0.22	na	bal.
C9B	925	VIR Cast	0.009	0.61	0.16	0.017	0.001	2.01	0.21	42.51	20.17	2.78	2.07	0.22	na	bal.
C9C	925	VIR Cast	0.014	0.88	0.10	0.016	0.001	1.74	0.08	42.20	20.07	2.71	2.08	0.21	na	bal.
C9D	925	VIR Cast	0.010	0.60	0.15	0.014	0.001	1.66	0.13	44.65	21.22	2.86	2.19	0.24	0.31	bal.
W9A	925	2.5" bar	0.011	0.62	0.17	0.015	0.001	1.72	0.13	43.90	20.58	2.72	1.99	0.21	na	bal.
W9B	925	1.5" bar	0.020	0.64	0.30	na	0.001	1.79	0.36	43.15	21.88	2.79	2.05	0.24	na	bal.
C7A	718	VIR Cast	0.05	0.05	0.06	0.007	0.003	0.03	5.14	51.84	19.08	3.17	1.03	0.54	0.27	bal.
C7B	718	VIR Cast	0.06	0.05	0.05	0.005	0.004	na	4.81	51.54	18.24	3.10	0.93	0.50	0.72	bal.
C7C	718	VIR Cast	0.05	0.04	0.04	0.006	0.003	0.01	5.04	51.54	18.09	3.11	0.88	0.52	0.31	bal.
C7D	718	Centrif. Cast	0.07	0.15	0.07	0.004	0.001	0.017	4.96	52.68	18.99	3.21	0.85	0.47	.003	bal.
C7E	718	VIR Cast	0.06	0.02	0.02	0.010	0.001	0.02	5.33	52.80	18.66	2.95	0.80	0.57	0.02	bal.
C7F	718	VIR Cast	0.035	0.10	0.08	0.007	0.003	0.10	5.30	51.73	18.50	3.20	0.79	0.42	na	bal.
W7A	718	3.0" bar	0.037	0.08	0.05	0.004	0.001	0.03	5.13	52.05	17.45	2.88	1.02	0.49	0.19	bal.
W7B	718	0.5" bar	0.04	0.15	0.09	0.007	0.007	0.10	5.3	52.5	19.0	3.2	0.79	0.45	na	bal.
W7C	718	2.0" bar	0.035	0.73	0.20	0.004	0.001	0.05	4.90	51.73	17.77	2.88	0.88	0.53	0.22	bal.

TABLE 2: COMPARISON OF REMELT CHEMICAL ANALYSIS WITH MELT STOCK CHEMISTRY

Material Code	Source of Analysis (MTR = Material Test Report)	WEIGHT, %													
		C	Mn	Si	P	S	Cu	Nb	Ni	Cr	Mo	Ti	Al	Co	Fe
C9B	melt stock MTR	0.009	0.61	0.16	0.017	0.001	2.01	0.21	42.51	20.17	2.78	2.07	0.22	na	bal.
C9C	melt stock MTR	0.014	0.88	0.10	0.016	0.001	1.74	0.08	42.20	20.07	2.71	2.08	0.21	na	bal.
C9B	VIR casting	0.006	0.53	0.28	0.014	0.001	1.87	0.28	43.36	19.78	2.83	2.03	0.26	na	bal.
C9C	VIR casting	0.006	0.73	0.20	0.011	0.003	1.68	0.10	42.80	20.04	2.78	2.11	0.41	na	bal.

TABLE 3: NACE TENSILE TEST RESULTS PER TM0177

Mat'l Type	Mat'l Code	Heat Treatment	Specimen Properties					Results of Tests under Noted Conditions (NF = no failure at 720 hrs)	Solution pH	
			YS ksi (Mpa)	TS ksi (Mpa)	Elng %	ROA %	HRc		start	finish
925 cast	C9A	1875°F 1 hr WQ, 1365°F 8 hr, FC to 1150°F 8 Hr AC	97.5 (672)	134.9 (930)	20.0	24.2	32.1	NF @ 100% YS NF @ 100% YS steel coupled	2.70 2.70	2.80 3.80
925 cast	C9B	1925°F 1 hr AC, 1365°F 12 hr, FC to 1150°F 12 Hr AC	88.8 (612)	131.6 (907)	31.8	40.0	27.8	NF @ 100% YS NF @ 100% YS steel coupled	2.69 2.69	3.04 3.90
925 cast	C9C	1925°F 3 hr AC, 1365°F 8 hr, FC to 1150°F 8 Hr AC	106.7 (736)	127.5 (879)	23.1	36.4	28.6	NF @ 100% YS NF @ 100% YS steel coupled	2.69 2.69	2.87 3.99
718 bar	W7B	1925°F 1 hr AC, 1400°F 10 hr, FC to 1200°F 20 Hr AC	170.1 (1173)	204.8 (1412)	30.1	20.5	45.0	NF @ 90% YS NF @ 80% YS		
718 cast	C7F	1950°F 1 hr AC, 1400°F 10 hr, FC to 1200°F 20 Hr AC	147.6 (1018)	175.5 (1210)	10.1	14.9	41.5	NF @ 80% YS NF @ 70% YS		
718 cast	C7A	2050°F 3hr AC, 1925°F 1hr WQ, 1325°F 8hr FC to 1150°F 18 Hr AC	146.9 (1013)	168.8 (1164)	18.0	29.8	40.8	NF @ 100% YS NF @ 100% YS steel coupled	2.7 2.7	2.7 3.7
718 cast	C7B	2050°F 3hr AC, 1925°F 1hr WQ, 1325°F 8hr FC to 1150°F 18 Hr AC	146.5 (1010)	167.2 (1153)	17.3	31.1	41.1	NF @ 100% YS NF @ 100% YS steel coupled	2.7 2.7	2.7 3.7
718 cast	C7C	2050°F 3hr AC, 1925°F 1hr WQ, 1325°F 8hr FC to 1150°F 18 Hr AC	121.8 (840)	139.5 (962)	13.0	25.3	39.6	NF @ 100% YS NF @ 100% YS steel coupled	2.7 2.7	2.8 3.8
718 cast	C7C	1925°F 1hr WQ, 1400°F 10hr FC	96.3 (664) 88.3 (609)	103.0 (710) 117.0 (807)	4.0 15.8	4.5 20.3	32.6 30.9	bar: (100% spec broke during stressing) NF @ 95% coupled NF @ 100% YS NF @ 100% YS steel coupled	2.7 2.7 2.7	3.85 3.65 3.85
718 cast	C7D	2100°F 3 hr AC, 1925°F 1 hr AC & 1400°F 5 hrs AC	144.2 (994)	161.6 (1114)	16.0	22.0	41.0	NF @ 100% YS NF @ 100% YS steel coupled	2.69 2.69	

TABLE 4: ELEVATED TEMPERATURE C-RING TEST RESULTS*

Material Code	Material Description	Stress Level (% of Actual YS)	Result
C7C	VIR cast 718	100% 80% 70%	no cracking no cracking no cracking
W7A	3.0" 718 bar	100% 80% 70%	no cracking no cracking no cracking
C9A	VIR cast 925	100% 85% 70%	no cracking no cracking no cracking
C9D	VIR cast 925	100% 85% 70%	no cracking no cracking no cracking
W9B	1.5" 925 bar	100% 85% 70%	no cracking no cracking no cracking

* 30 Days in 15% NaCl, 400 psi (2.76 Mpa) CO_2, 200 psi (1.38 Mpa) H_2S Test Environment at 300°F (150°C)

TABLE 5: SLOW STRAIN RATE TEST RESULTS

Material Description[1]	Test Envirn.	Time to Failure	UTS ksi (Mpa)	Elong %	ROA %	E_1/E_2[2]	R_1/R_2[3]	SCC ?
cast 718 bar	hot oil	1.6 hrs	88.9 (613)	0.1	5.2	-	-	-
cast 718 bar	H_2S test	1.8 hrs	90.2 (622)	0.7	5.2	7.00	1.00	no
cast 718 section	hot oil	3.5 hrs	105.3 (726)	3.2	14.6	-	-	-
cast 718 section	H_2S test	2.2 hrs	99.3 (685)	1.3	8.9	0.41	0.61	yes

note 1) All materials were from Material Code C7C.
note 2) Ratio of Elongations (H_2S test/hot oil)
note 3) Ratio of Reduction of Areas (H_2S test/hot oil)

TABLE 6: Fe_2Cl_3 PITTING TESTS PER ASTM G48

TIME and TEMP	HEAT CODE	SAMPLE	WEIGHT LOSS (mg)	SURFACE AREA (cm^2)	WT LOSS/ UNIT AREA (mg/cm^2)	COMMENTS
1 Hr @ 48°C	W7C	718 Bar	4.5	15.10	0.30	5 small pits
	C7D	718 Cast	6.3	24.32	0.26	several very small pits
	W9A	925 Bar	10.7	14.00	0.76	extensive deep pitting
	C9B	925 Cast	7.7	19.35	0.40	many pits
20 Hrs @ 35°C	W7C	718 Bar	1.60	14.19	0.11	very light pitting
	C7D	718 Cast	168.3	22.97	7.33	extensive deep pitting on all 4 sides
	W9A	925 Bar	185.7	13.61	13.64	extensive deep pitting on 2 sides
	C9B	925 Cast	134.5	15.16	8.87	shallow pitting on all 4 sides
16 Hrs @ 30°C	W7C	718 Bar	0.0	14.19	0.00	no pitting
	C7D	718 Cast	62.4	18.39	3.39	deep pitting on 2 sides
	W9A	925 Bar	65.5	13.61	4.81	deep pitting on 2 sides
	C9B	925 Cast	77.5	15.16	5.11	extensive pitting on all 4 sides
24 Hrs @ 25°C	W7C	718 Bar	0.0	14.19	0.00	no pitting
	C7D	718 Cast	1.0	7.74	0.13	very light pitting
	W9A	925 Bar	3.1	12.84	0.24	very light pitting
	C9B	925 Cast	40.6	20.39	1.99	light pitting

TABLE 7: PITTING TESTS IN CHLORIDE CONTAINING $Fe_2(SO_4)_3$

TIME and TEMP	HEAT CODE	SAMPLE	WEIGHT LOSS (mg)	SURFACE AREA (cm^2)	WT LOSS/ UNIT AREA (mg/cm^2)	COMMENTS
24 Hrs @ 36°C	W7C	718 Bar	0.0	14.19	0.00	no pitting
	C7D	718 Cen Cast	2.0	22.97	0.09	no pitting
	C7E	718 Vac Cast	3.6	25.52	0.14	1 small pit visible
	W9A	925 Bar	4.9	13.74	0.36	2 small pits visible
	C9B	925 Cast	6.8	17.70	0.38	light pitting visible at 10X
24 Hrs @ 33°C	W7C	718 Bar	0.0	14.19	0.00	no pitting
	C7D	718 Cen Cast	2.4	22.97	0.10	no pitting
	C7E	718 Vac Cast	0.5	25.52	0.02	no pitting
	W9A	925 Bar	4.5	13.74	0.33	light pitting on one corner only
	C9B	925 Cast	6.0	15.16	0.40	very light pitting
24 Hrs @ 28°C	W7C	718 Bar	0.0	14.19	0.00	no pitting
	C7D	718 Cen Cast	1.5	22.97	0.07	no pitting
	C7E	718 Vac Cast	0.5	25.52	0.02	no pitting
	W9A	925 Bar	2.2	13.74	0.16	no pitting
	C9B	925 Cast	4.5	17.70	0.25	no pitting

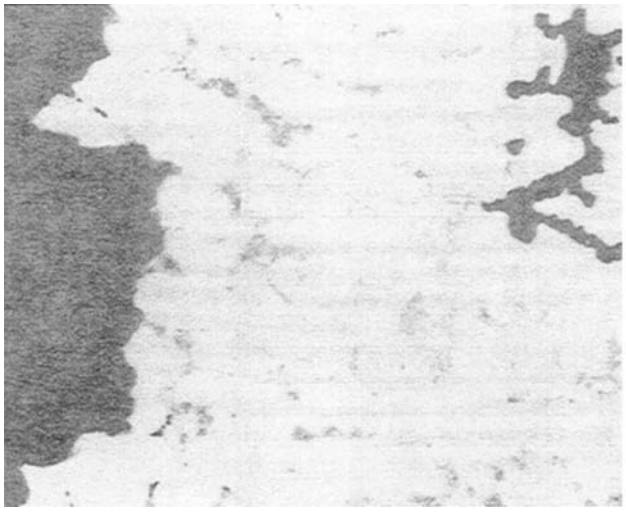


FIGURE 1: Microporosity in Cast 718 (Material Code C7C) Used in TM0177 Test at 100X Etched in Kalling's Reagent

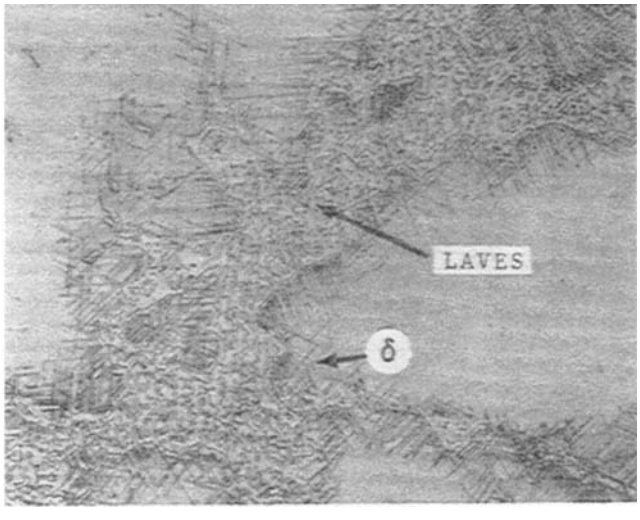


FIGURE 2: Laves and Delta Phase Islands In Figure 1 at 500X Etched in Kalling's Reagent

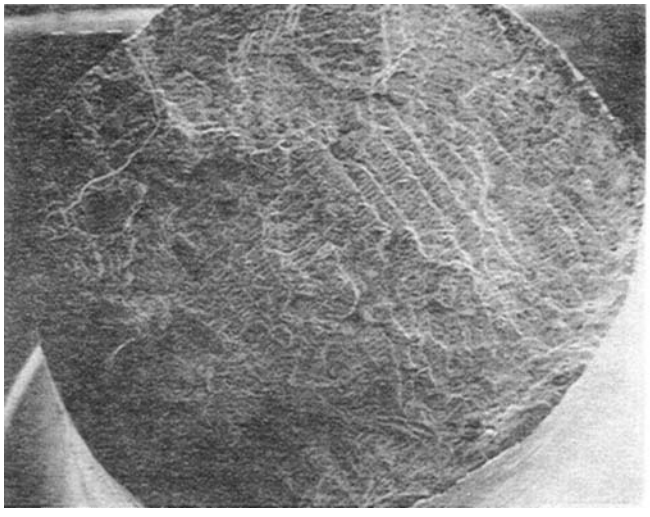


FIGURE 3: SEM photograph of SSR specimen fracture surface tested in H_2S environment at 20X. Fracture surface exhibits cast dendritic features.

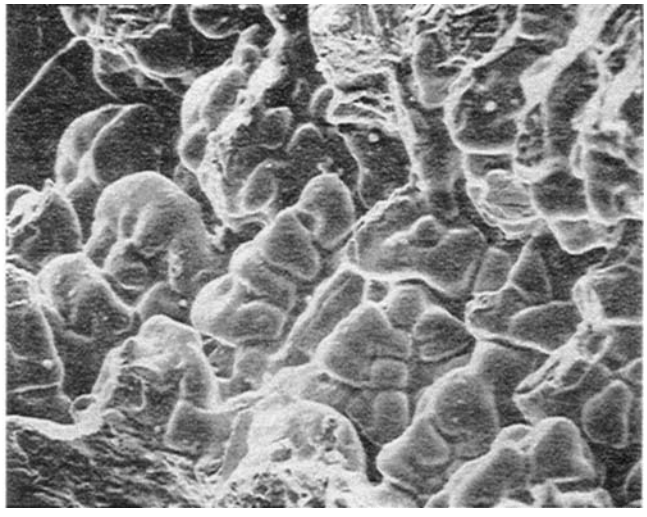


FIGURE 4: SEM photograph of a dendritic region from surface in Figure 3 at 400X. Features are typical of cast surface containing internal porosity.

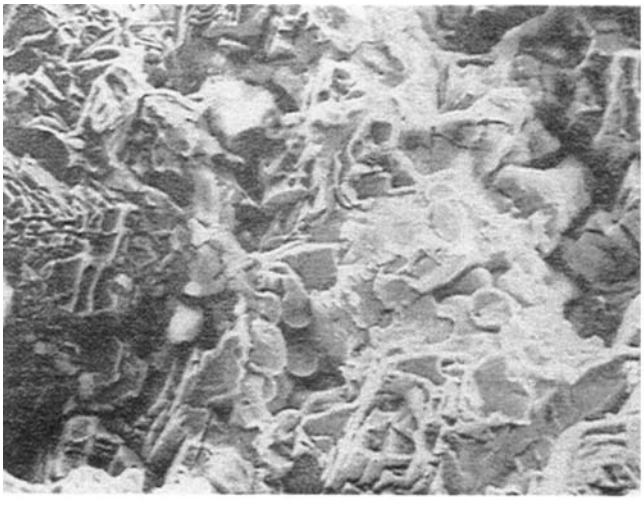


FIGURE 5: SEM photograph of SSR specimen fracture surface tested in H_2S environment at 750X. Fracture surface exhibits features of secondary phase particles; an energy dispersive spectroscopy examination of the secondary particles revealed a high concentration of Nb.

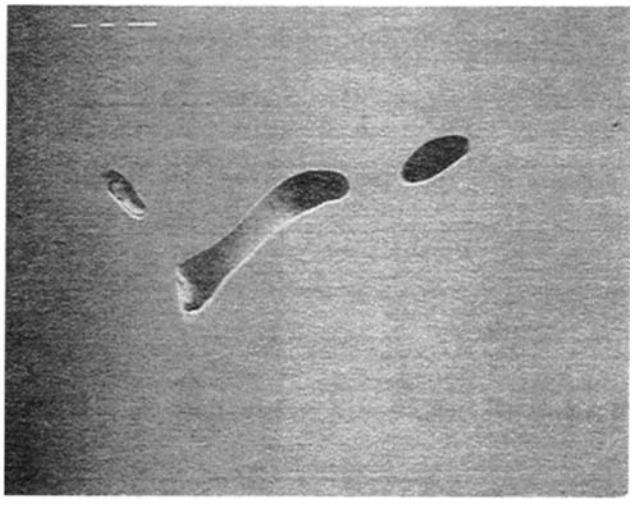


FIGURE 6: Microporosity in cast 925, material code C9B; SEM photomicrograph at 500X.

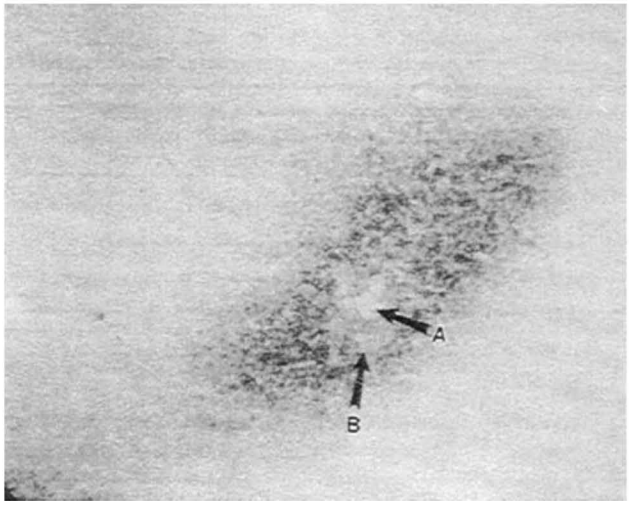


FIGURE 7: Etched microstructure from Figure 6; "A" appears to be Laves phase, "B" is Delta Phase.

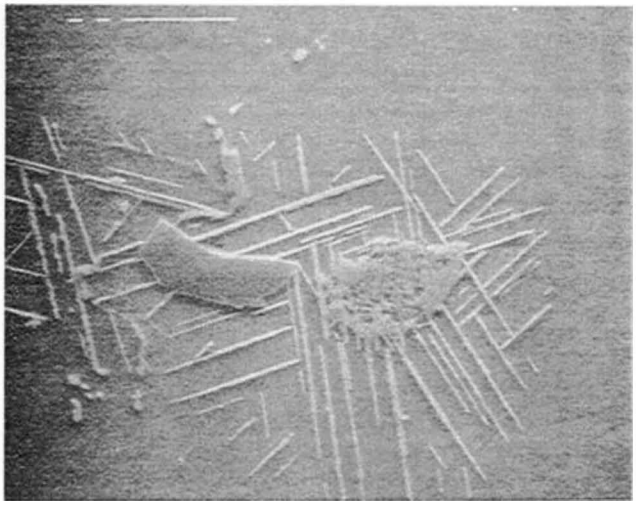


FIGURE 8: SEM photograph of secondary phases in as-cast structure of 925, material code C9D at 2000X. Needle-like phase is delta and large masses are Laves phase.

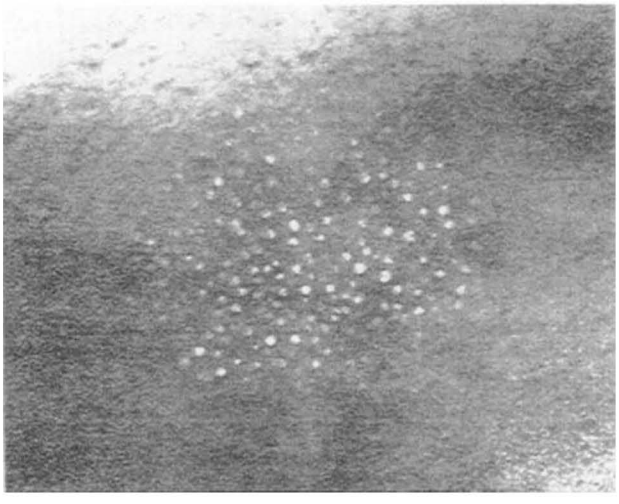


FIGURE 9: TEM photograph using darkfield imaging of the superlattice reflections to reveal the γ' precipitates at 180000X.

Copyrighted Materials
Copyright © 1996 NACE International Retrieved from www.knovel.com

Paper No.
131

CORROSION 93
The NACE Annual Conference and Corrosion Show

EFFECT OF FREE SULFUR ON CRACKING BEHAVIOR OF CRA'S IN SIMULATED DOWNHOLE ENVIRONMENTS

William R. Coyle
Otis Engineering Corporation
2601 Beltline Road
Carrollton, Texas 75006

ABSTRACT

New alloys have been developed that are resistant to the aggressive conditions typically encountered in oil and gas production from deep, hot, sour environments. C-ring and slow strain rate tests (SSRT) were performed to investigate the hydrogen embrittlement resistance and the effect of sulfur on the stress corrosion cracking resistance of several age-hardenable, corrosion-resistant alloys (CRA's). The alloys studied included UNS N07718, N09925, N07048, N07716, N07725, N10276, and R58640. These alloys are often specified for completion equipment for hot, sour wells where highly saline brine and free sulfur are produced along with natural gas containing CO_2 and H_2S. C-rings of each alloy were stressed to 100% of yield and tested in accordance with NACE TM0177.[1] The results of the C-ring tests indicated that all of the CRA's tested were resistant to sulfide stress cracking (SSC). The simulated downhole environment for the SSRT program consisted of 20% NaCl, 75 psi (5.2 bar) hydrogen sulfide (H_2S), 700 psi (48.3 bar) carbon dioxide (CO_2), with and without 1 g/L elemental sulfur. All SSR tests were conducted at 300°F (149°C). Nearly all of the alloys tested showed some susceptibility to stress corrosion cracking (SCC) in the environment containing free sulfur; only UNS N10276 and UNS R58640 were immune to cracking under the laboratory test conditions. The results indicate that the presence of sulfur increases susceptibility to stress corrosion cracking. In the non-sulfur containing environment, UNS R58640 and the nickel-base alloys with at least 48% nickel and 6% molybdenum were resistant to SCC.

Keywords: sulfide stress cracking (SSC), stress corrosion cracking (SCC), elemental sulfur, corrosion-resistant alloys (CRA's), completion equipment, slow strain rate test (SSRT)

INTRODUCTION

Exploration for oil and gas into deep, hot, sour environments has brought about the need for new alloys that are resistant to these aggressive conditions. There are many factors that influence the proper selection of materials for downhole use. These include bottomhole temperature and pressure, concentrations of H_2S and CO_2, and presence of other chemical species such as free sulfur and mercury.[2] All of these factors must be considered when selecting materials. Numerous studies have been conducted to help determine the performance envelope for various CRA's. These studies typically utilize either constant strain or constant load specimens in the environment(s) of interest.

For completion equipment destined for these hostile wellbore environments, there exists a need for materials that are available in large diameter bar with a minimum yield strength of 120 ksi (827 MPa). This product form usually drives the alloy manufacturers to develop alloys that are strengthened by precipitation-hardening heat treatment. This technique uses the precipitation of specific intermetallic constituents by appropriate heat treatment and requires specific alloy composition.[3] Several alloys have been developed which are based on the chemical composition of existing alloys UNS N06625 and UNS N06985 with additions of precipitate forming elements. These alloys, which include UNS N07716, UNS N07725, and UNS N07048, have been introduced to the marketplace recently to address the needs of the energy industry. A test program was initiated in an effort to evaluate these "new" alloys and to compare their performance to that of other commercially-available alloys used in the oil field.

EXPERIMENTAL PROCEDURE

Materials Tested

Several commercially available corrosion-resistant alloys (CRA's) were investigated (UNS N07718, N09925, N07048, N07716, N07725, N10276, R58640). All alloys were supplied in round bar in the size and metallurgical condition listed in Table 1. The mechanical properties and nominal composition of the alloys are presented in Tables 2 and 3, respectively.

C-Ring Experiments

The NACE standard test method TM0177 was followed. Unnotched C-ring specimens were used in the laboratory tests to determine SSC susceptibility. Two C-rings of each of the above materials were tested. The preparation, instrumentation, stressing and fixturing of the C-rings was similar to the technique used by Rice.[4]

The total elastic plus plastic strain at the 0.2% offset yield stress was calculated by dividing the yield strength of the material (as determined from tensile tests performed on the actual bar material) by the modulus of elasticity and adding 0.002 plastic strain. Strain-diametrical decrease data were developed for one C-ring of each material evaluated. A strain gage was bonded on the outer circumference of the C-ring at a position 90 degrees from the load points where the outer fiber stress is at a maximum. The C-ring was placed in a steel test fixture and strained to the predetermined value (see Figure 1). The original and final diameter of the C-ring were noted. The decrease in diameter was calculated for use on the second specimen of the same material. Since the C-rings were identical, this technique ensured that the same amount of plastic strain was induced in both specimens. The actual diametrical decrease value was in close agreement with the values obtained by calculations as described by Hay and Williamson.[5] Carbon steel fixtures allowed for close simulation of field conditions where galvanic corrosion and hydrogen charging can occur. The

test fixture containing the stressed C-rings was placed in the test container and completely immersed in the NACE solution which consists of an acidified, deaerated brine solution saturated with hydrogen sulfide. The test duration was 30 days.

Slow Strain Rate Experiments

The slow strain rate test is one of several used to assess resistance of an alloy to embrittlement in a given environment. The SSRT is of particular utility because it is an accelerated corrosion test, usually taking less than 24 hours to complete. Stainless steels and nickel-base alloys gain their corrosion resistance partially by virtue of a thin oxide film that forms on their surfaces. If this film is disrupted in the presence of an aggressive environment, it may or may not repair itself. In a slow strain rate test, a small-diameter tensile specimen is dynamically strained to failure in the environment of interest. The cracking susceptibility is evaluated by comparing the results in a corrosive environment to those obtained in an inert environment. Kane, et al.[6] should be consulted for a more comprehensive discussion of slow strain rate testing.

Several SSR specimens were machined from each material. The procedure and equipment used for slow strain rate testing was in accordance with current industry practice; NACE T-1F-9 is currently working on a standard test method entitled, "Slow Strain Rate Test Method for Screening Corrosion-Resistant Alloys (CRAs) for Stress Corrosion Cracking in Sour Oilfield Service."

The specific test environment chosen consisted of a 20% brine solution (15.17 wt.% chloride ion), 75 psi (5.2 bar) H_2S (@ Temp.), 700 psi (48.3 bar) CO_2 (@ Temp.), and 300°F (149°C) test temperature, with and without 1 g/L of elemental sulfur. A 20% (by weight) sodium chloride (NaCl) solution was prepared using reagent grade NaCl and distilled water. Deaeration of the brine was initiated by placing an Erlenmeyer flask containing the solution on a hot plate. High purity (certified low-oxygen) CO_2 gas was bubbled through a dip-tube positioned inside the flask. The solution was then brought to a boil while bubbling CO_2 at a rate of 0.1 cubic feet (3 liters) per minute. A reflux condenser was used to prevent evaporation of the solution and to maintain a positive pressure of CO_2. After the solution had been boiled for approximately one hour and before it was transferred to the autoclave, it was allowed to cool to about 95°F (35°C). This procedure consistently achieved a concentration of less than 5 ppb dissolved oxygen as determined by a colorimetric test technique.

In order to ensure that no sulfur contamination could occur, separate annealed N10276 autoclaves (total volume 335 ml) were utilized for the sulfur and non-sulfur tests. For the tests in the sulfur-containing environment, 1 g/L of dry powderized sulfur (0.275 g for 275 ml of solution) was added to the test vessel. The test vessel was then sealed and pressure tested with argon or nitrogen to ensure no leaks. The tubing and the test vessel were evacuated to 20 inches of vacuum and then pressurized with argon to 1000 psi (69 bar). This evacuation and purging procedure was repeated three times to remove any oxygen that may have been present in the lines or test vessel prior to transferring the solution. The last step was evacuation of the test vessel and transfer lines. By manipulating the appropriate valves in the deaerating and transferring apparatus, the brine solution moved from the flask to the test vessel without being exposed to the atmosphere. The vacuum on the test vessel and the transfer lines made this possible. After the transfer had been completed, the remaining solution in the flask was tested for dissolved oxygen to ensure that complete deaeration was achieved.

Utilizing a linear variable differential transformer (LVDT) and a computer-based data acquisition unit, the SSR machine was calibrated prior to each series of tests. For the tests discussed in this paper, the linear displacement rate was calibrated to 0.0144 in/hr. The current industry standard is to express this crosshead separation rate as a test specimen strain rate of $4 \times 10^{-6}\ s^{-1}$. In an effort

to better understand the true meaning of strain rate, a series of experiments was conducted using the LVDT with and without a specimen in the load frame. With a specimen in place, measurements indicated that the linear displacement rate in the elastic range was approximately one-fourth that measured in the plastic range. There was no significant difference between the rates measured when there was no specimen and when the specimen was well into the plastic region. This is an area that would benefit from further study; one might investigate cracking susceptibility while using a feedback controller to maintain a constant strain rate throughout the entire test period and compare the results with those obtained using "standard" techniques.

All slow strain rate specimens were machined on a numerically-controlled (NC) lathe; the specimens nominally measure 0.150 in. (3.8 mm) diameter x 1 in. (25.4 mm) gage length with ¼-20 UNC threaded ends. The surface finish is better than 32 rms in the as-machined condition. After final machining, the gage section of the specimen was lightly polished using 320-grit silicon carbide abrasive cloth. Slow strain rate specimens were degreased and threaded to N10276 pull rods which were electrically isolated from the autoclave. After the 20% brine solution was mixed, deaerated and transferred to the test vessel, H_2S gas was introduced into the assembled test vessel and the pressure maintained for 20 minutes to allow the gas to dissolve in the test solution and come to equilibrium. In the same manner, CO_2 gas was introduced into the test vessel and maintained for 20 minutes. The test vessel was brought up to temperature (300°F or 149°C) and the drive mechanism energized to initiate testing. The partial pressures (at test temperature) for H_2S and CO_2 were 75 psi (5.2 bar) and 700 psi (48.3 bar), respectively.

RESULTS / DISCUSSION

Results of SSC Testing

At the conclusion of the 30-day NACE TM0177 test, all C-rings were intact with no cracking observed. Table 4 summarizes the results of testing. Two steel-coupled C-rings of each alloy were tested at 100% of 0.2% offset yield strength. Based upon these results, the alloys tested were deemed to be resistant to sulfide stress cracking. This class of alloys is generally regarded as resistant to hydrogen embrittlement. The results obtained agree with those of other investigators.[7,8,9]

Results of SCC Testing

The SSRT acceptance criteria used by many researchers to indicate resistance to cracking in any given environment involves calculations of relative ductility. These factors are expressed as ratios of elongation and reduction of area in the test environment to the average elongation and average reduction of area in an inert environment (either air or other suitable inert heat transfer medium). In addition, the presence of secondary cracking in the gage section is determined by examination of samples using low-power optical microscopy. The evaluation of SSR test results is subjective to some extent. However, five (5) classes of behavior ranging from immune to susceptible have been identified by Kane, et al.[6] At least two specimens of each alloy were tested in an inert oil environment at the test temperature of 300°F (149°C). The data are presented in Table 5. The average elongation and reduction of area values in the inert environment were used to calculate the ductility ratios for each alloy. Figure 2 ranks the alloys using the average elongation and reduction-of-area ratios in both simulated downhole environments; however, the data for the sulfur-containing environment varies widely; therefore Figure 2 should not be used without reference to the raw data in Tables 6 and 7.

The strain rate of 4×10^{-6} sec^{-1} was chosen because it is a widely used rate. At a given strain rate, SSRT data from different laboratories can be compared. A round robin SSRT program was organized through NACE subcommittee T-1F-9; the results of this study should provide insight into the compatibility of laboratory results.

Non Sulfur-Containing Environment. The results of slow strain rate testing in the NaCl + H_2S + CO_2 environment is shown in Table 6. Three specimens of each alloy were tested in the environment consisting of 20% NaCl, 75 psi (5.2 bar) H_2S, and 700 psi (48.3 bar) CO_2 at 300°F (149°C). The results were fairly consistent for each alloy tested. Both UNS N09925 and N07718 exhibited mild to moderate susceptibility in this environment; UNS N07048 was practically immune, and the remaining four alloys (UNS N07716, N07725, N10276 and R58640) were immune to SCC.

Sulfur-Containing Environment. The presence of elemental sulfur in the test fluid resulted in more variation in the test results, therefore making it more difficult to predict resistance to SCC. Based upon visual examination of the specimens and interpretation of the ductility ratios (E/E_t and R/R_t), all of the alloys tested, with the exception of UNS N10276 and UNS R58640, showed some susceptibility to stress corrosion cracking in the sulfur-containing environment. These results tend to confirm the findings of other researchers.[3,10,11,12,13,14,15] UNS N07718 was the most susceptible alloy tested in the free-sulfur environment; all specimens contained secondary cracks in the gage section, and ductility ratios were less than 0.5. UNS N09925 was moderately susceptible to SCC; all specimens contained some secondary cracks, and the ductility ratios were between 0.5 and 0.75. The performance of UNS N07048, UNS N07716 and N07725 in the free sulfur environment varied depending on whether or not molten sulfur contacted the gage section of the specimen.

Visual examination of SSR specimens tested in the NaCl + H_2S + CO_2 + elemental sulfur revealed tenacious black sulfide deposits on most of the specimens; when the deposit was in the gage section, the material fractured prematurely. In some cases, the sulfide deposits were located outside the gage length. After removing these deposits, it was noted that the base material under the deposit had suffered severe localized pitting corrosion. In the cases where the deposit was located adjacent to the final fracture, secondary cracks were visible. Ikeda, et al.[15] theorized that the elemental sulfur accelerates the cathodic reaction and creates a crevice at the point of deposition. Adjacent to the sulfur deposit, there is a local enrichment of the H_2S level, which tends to destabilize the protective oxide film(s). This corroded area acts as a stress raiser where cracks can initiate. A longitudinal section of a typical slow strain rate specimen was prepared for metallographic examination. Figure 3 shows the pitting on the diameter underneath the sulfide deposits. Secondary cracks, visible near the fracture surface, are shown in Figure 4. At high magnification, it can be seen that the corrosion pits beneath the deposits act as initiation sites for stress corrosion cracks (Figure 5).

The results obtained in the sulfur-containing environment tend to agree with those cited by G. Schmitt[16] who stated, "It is known that systems containing elemental sulfur may induce SCC at elevated temperatures, especially above 150°C," and "It appeared that even nickel- and cobalt-base alloys are susceptible to SCC at elevated temperatures in H_2S saturated brines, particularly in the presence of elemental sulfur. The risk of SCC increases with the chloride content, presence of elemental sulfur, H_2S partial pressure, acidity, alloy strength, and stress level."

CONCLUSIONS

1. Slow strain rate testing provides a quick method to rank candidate alloys in a simulated downhole environment. However, since a correlation between the SSRT and field performance has not been reliably established, selection of materials for downhole conditions using only SSRT may be too conservative.

2. For all alloys except UNS N10276 and R58640, severe localized corrosion resulted when molten free sulfur in the autoclave contacted the specimen. When the deposits were in the gage section, the specimen failed prematurely with a significant reduction in ductility.

3. UNS N10276 and R58640 were immune to the NaCl + H_2S + CO_2 environment with and without the addition of 1 g/L elemental sulfur.

4. All materials were resistant to hydrogen embrittlement as determined by 30-day TM0177 tests of steel-coupled C-rings stressed to 100% of the 0.2% offset yield strength.

Further Work

Future testing is necessary to better understand stress corrosion cracking in free sulfur environments. There are many interrelated factors which affect cracking susceptibility in a given environment. They include SSR specimen surface finish and method of sulfur addition,[14] as well as strain rate. There are differences in the results obtained using C-rings and slow strain rate tests.[17] This is an important subject which requires more investigation. The ideal goal would be to accurately reproduce field conditions in the laboratory. Obviously the science and art of laboratory corrosion testing has a long way to go in this endeavor.

REFERENCES

1. National Association of Corrosion Engineers, Standard TM0177, "Laboratory Testing of Metals for Resistance to Sulfide Stress Cracking in H_2S Environments."

2. P. W. Rice, W. R. Coyle, G. B. Chitwood, "Select Materials For Downhole Conditions," World Oil, December, 1991, p. 81.

3. R. H. Moeller, H. H. Ruble, R. B. Bhavsar, D. M. Currie, "Large Diameter Cold Worked C-276 For Downhole Equipment," CORROSION/91, paper no. 30, p. 2 (Houston, TX: NACE, 1991)

4. P. W. Rice, "Evaluating Nickel Base and Stainless Alloys for Subsurface H_2S Service," Materials Performance, Vol. 17, No. 9, p. 16-25

5. A. I. Williamson, M. G. Hay, "Selection of CRA Tubing and HCL Corrosion Inhibitors for Burnt Timber/Limestone Wells," CORROSION/91, paper no. 11, p. 4 (Houston, TX: NACE, 1991).

6. D. R. McIntyre, R. D. Kane, S. M. Wilhelm, "Slow Strain Rate Testing for Materials Evaluation in High Pressure H_2S Environments," CORROSION/86, paper no. 149, p. 7-9, (Houston, TX: NACE, 1986).

7. J. R. Bryant, M. Kohler, U. Heubner, P. W. Rice, W. R. Coyle, "Age Hardening Response, Precipitation Phenomena and Corrosion Behavior of a New Ni-Cr-Mo-Fe Alloy for Oil Field Applications," CORROSION/90, paper no. 51, (Houston, TX: NACE, 1990).

8. E. L. Hibner, "A New Age-Hardenable Corrosion Resistant Alloy for Deep Sour Gas Well Service," CORROSION/90, paper no. 50, (Houston, TX: NACE, 1990).

9. R. B. Frank, T. A. DeBold, "Heat Treatment of an Age-Hardenable, Corrosion-Resistant Alloy - UNS N07716," CORROSION/90, paper no. 59, (Houston, TX: NACE, 1990).

10. P. R. Rhodes, "Stress Cracking Risks in Corrosive Oil and Gas Wells," CORROSION/86, paper no. 322, (Houston, TX: NACE, 1986).

11. J. Kolts, "Laboratory Evaluation of Corrosion Resistant Alloys for the Oil and Gas Industry," CORROSION/86, paper no. 323, (Houston, TX: NACE, 1986).

12. S. E. Mahmoud, H. E. Chaung, C. W. Petersen, "Localized Corrosion of Corrosion-Resistant Alloys in Sulfur-Chloride-Containing Environments," CORROSION/90, paper no. 70, (Houston, TX: NACE, 1990).

13. M, Ueda, T. Kudo, S. Kitayama, Y. Shida, "Corrosion Behavior of Titanium Alloys in a Sulfur-Containing H_2S-CO_2-Cl^-, Environment," CORROSION/90, paper no. 271, (Houston, TX: NACE, 1990).

14. H. J. Choi, "The Effect of Elemental Sulfur and Surface Condition on Stress Corrosion Cracking of High Nickel Alloys Under Hot Sour Environments," CORROSION/92, paper no. 59, (Houston, TX: NACE, 1992).

15. M. Ueda, H. Tsuge, A. Ikeda, "Influence of Elemental Sulfur on Corrosion Behaviour of CRA in H_2S-CO_2-Cl^- Environment," CORROSION/89, paper no. 8, (Houston, TX: NACE, (1989).

16. G. Schmitt, "Present Day Knowledge of the Effect of Elemental Sulfur on Corrosion in Sour Gas Systems," CORROSION/90, paper no. 39, (Houston, TX: NACE, 1990).

17. H. E. Chaung, M. Watkins, G. A. Vaughn, "Stress-Corrosion Cracking Resistance of Stainless Alloys in Sour Environments," CORROSION/85, paper no. 227, p. 3-4 (Houston, TX: NACE, 1985).

Table 1. Size and Condition of Alloys Tested

Alloy ID	Product Form	Condition	Heat Treatment Procedure
UNS N07718	4 in. (102 mm) Bar	Solution Annealed + Age Hardened	1875°F (1024°C) - W.Q. 1450°F (788°C) f/6.5 hrs. - A.C.
UNS N09925	5 in. (127 mm) Bar	Solution Annealed + Age Hardened	1850°F (1010°C) - W.Q. 1385°F (752°C) f/4 hrs., F.C to 1200°F (649°C), hold f/ 8 hrs. - A.C.
UNS N07048	6.25 in. (160 mm) Bar	Direct Aged	Hot Finished - W.Q. 1350°F (732°C) f/8 hrs., F.C. 30°F (16.7°C) per hr. to 1075°F (579°C) - A.C.
UNS N07725	7.5 in. (191 mm) Bar	Solution Annealed + Age Hardened	1900°F (1038°C) - W.Q. 1350°F (732°C) f/ 8 hrs., F.C. to 1150°F (621°C), hold for 10 hrs - A.C.
UNS N07716	6 in. (152 mm) Bar	Solution Annealed + Age Hardened	1900°F (1038°C) - A.C. 1350°F (732°C) f/ 8 hrs., F.C. to 1150°F (621°C), hold for 8 hrs - A.C.
UNS N10276	6 in. (152 mm) Bar	Cold Worked	None
UNS R58640	3 in. (76 mm) Bar	Solution Annealed + Age Hardened	1500°F (816°C) - A.C. 1025°F (552°C) f/ 18 hrs., A.C.

Table 2. Mechanical Properties of Alloys Tested

Alloy	Test Direction[1]	0.2% Yield Strength ksi (MPa)	Tensile Strength psi (MPa)	% Elongation	% Reduction in Area	Hardness (Rc)
UNS N07718	L	127.4 (878)	176.5 (1217)	32.3	47	37
UNS N09925	L	119.5 (824)	166.0 (1145)	26.5	32	34
	T	123.0 (848)	166.0 (1145)	19.0	28	
UNS N07048	L	125.6 (866)	169.0 (1165)	27.5	46	40
UNS N07725	T	102.0 (703)	152.0 (1048)	37.0	52	37
UNS N07716	L	132.0 (910)	184.5 (1272)	31.5	53	39
	T	126.0 (869)	175.0 (1207)	32.0	50	
UNS N10276	L	151.0 (1041)	156.0 (1076)	26.0	59	32
	T	123.0 (848)	140.0 (965)	24.0	45	
UNS R58640	L	162.0 (1117)	169.0 (1165)	11.0	26	40

1. Test Direction: L = Longitudinal, T = Transverse

Table 3. Chemical Composition Limits of Alloys Tested

Alloy	C	Mn	Si	P	S	Ni	Cr	Fe	Mo	Ti	Al	Other
N09925	.03	1.0	.5	.03	.03	42.0-46.0	19.5-22.5	22.0 min	2.5-3.5	1.9-2.4	.1-.5	1.5-3.0 Cu .5 Cb
N07718	.08	.35	.35	.015	.015	50.0-55.0	17.0-21.0	Bal	2.8-3.3	.65-1.15	.2-.8	4.75-5.5 Cb
N07048	.015	.50	.20	.015	.010	Bal	21.0-23.5	18.0-21.0	5.0-7.0	1.5-2.0	.4-1.0	1.5-2.2 Cu
N07716	.03	.20	.20	.015	.010	59.0-63.0	19.0-22.0	Bal	7.0-9.5	1.0-1.6	.35	2.75-4.0 Cb
N07725	.03	.35	.20	.015	.010	55.0-59.0	19.0-22.5	Bal	7.0-9.5	1.0-1.7	.35	2.75-4.0 Cb
N10276	.01	1.0	.08	.04	.03	Bal	14.5-16.5	4.0-7.0	15.0-17.0	---	---	3.0-4.5 W 2.5 Co
R58640	.05	---	---	---	---	---	5.5-6.5	.3	3.5-4.5	Bal	3.0-4.0	7.5-8.5 V 3.5-4.5 Zr

Table 4. Results of NACE TM0177 C-Ring Test

Alloy ID	Result After 30 Days
UNS N07718	No Cracking
UNS N09925	No Cracking
UNS N07048	No Cracking
UNS N07716	No Cracking
UNS N07725	No Cracking
UNS N10276	No Cracking
UNS R58640	No Cracking

Table 5. Slow Strain Rate Data - Inert Environment: Ucon Oil, 300°F (149°C)

Alloy ID (UNS No.)	Time to Failure (hrs)	Plastic Elongation (%)	Reduction of Area (%)
UNS N09925	11.3	14.0	27.7
	11.2	13.9	23.1
UNS N07718	12.2	15.1	42.7
	13.0	16.1	45.9
	12.8	16.0	48.3
	12.8	15.8	45.5
UNS N07048	13.6	16.8	42.0
	13.3	17.0	40.0
UNS N07716	15.4	19.7	54.6
	16.6	21.5	57.3
	16.8	21.7	57.0
UNS N07725	16.9	21.5	51.7
	16.0	20.2	55.0
UNS N10276	9.7	11.6	59.2
	9.2	10.7	56.1
	9.3	10.4	56.1
UNS R58640	6.7	6.4	21.7
	6.9	6.5	27.5
	6.8	6.2	16.1

Table 6. Slow Strain Rate Data - Environment:
20% NaCl, 75 psi (5.2 bar) H_2S, 700 psi (48.3 bar) CO_2, 300°F (149°C)

Alloy ID (UNS No.)	Time to Failure (hrs)	Plastic Elongation (%)	Elongation Ratio	Reduction of Area (%)	Reduction of Area Ratio
UNS N09925	7.9	9.0	0.64	17.0	0.67
	7.5	8.8	0.63	17.6	0.69
	7.7	8.8	0.63	16.5	0.65
UNS N07718	10.1	12.2	0.78	24.3	0.53
	11.0	13.8	0.88	26.9	0.59
	10.1	12.2	0.78	27.3	0.60
UNS N07048	12.1	14.9	0.89	34.9	0.83
	12.1	15.0	0.89	22.5	0.54
	13.8	17.3	1.02	21.4	0.53
UNS N07716	16.8	22.0	1.05	53.5	0.95
	16.5	21.6	1.03	52.6	0.93
	15.3	19.9	0.95	55.3	0.98
UNS N07725	16.7	21.7	1.04	55.6	1.04
	16.0	20.7	1.00	53.5	1.00
	16.3	21.0	1.01	54.4	1.02
UNS N10276	8.9	10.4	0.95	56.1	0.98
	9.2	10.7	0.98	56.1	0.98
	8.9	10.2	0.94	55.3	0.97
UNS R58640	6.8	6.6	1.04	26.5	1.22
	6.1	5.5	0.86	26.4	1.21
	7.0	6.8	1.07	19.6	0.90

Table 7. Slow Strain Rate Data - Environment:
20% NaCl, 75 psi (5.2 bar) H_2S, 700 psi (48.3 bar) CO_2, 1 g/ℓ Sulfur, 300°F (149°C)

Alloy ID (UNS No.)	Time to Failure (hrs)	Plastic Elongation (%)	Elongation Ratio	Reduction of Area (%)	Reduction of Area Ratio
UNS N09925	7.4	8.1	0.58	17.9	0.70
	7.8	9.0	0.64	12.9	0.51
	6.8	7.5	0.53	14.3	0.56
UNS N07718	6.3	6.4	0.41	11.7	0.26
	7.5	8.2	0.52	18.3	0.40
	6	6.6	0.42	14.8	0.32
	5.1	4.9	0.31	12.4	0.27
UNS N07048	11.8	13.9	0.82	33.4	0.81
	10.8	13.1	0.78	32.4	0.79
	5.6	5.4	0.32	16.1	0.39
	12.5	15.6	0.92	24.8	0.61
UNS N07716	6.8	7.3	0.35	19.7	0.35
	12.5	15.4	0.74	33.2	0.59
	5.5	5.6	0.27	13.2	0.23
	13.9	17.5	0.83	33.8	0.60
UNS N07725	8.8	10.3	0.49	24.3	0.46
	9.5	11.6	0.56	26.7	0.50
	19.8	26.6	1.28	53.1	1.00
	11.3	14.3	0.69	24.2	0.45
UNS N10276	10.0	11.7	1.08	61.2	1.07
	10.4	12.1	1.12	58.0	1.01
	10.2	11.8	1.08	60.1	1.05
	9.7	11.3	1.04	58.3	1.02
UNS R58640	5.8	5.1	0.81	21.7	1.00
	6.5	6.0	0.95	18.0	0.83
	6.7	6.3	1.00	17.9	0.82
	6.3	5.6	0.88	24.0	1.11

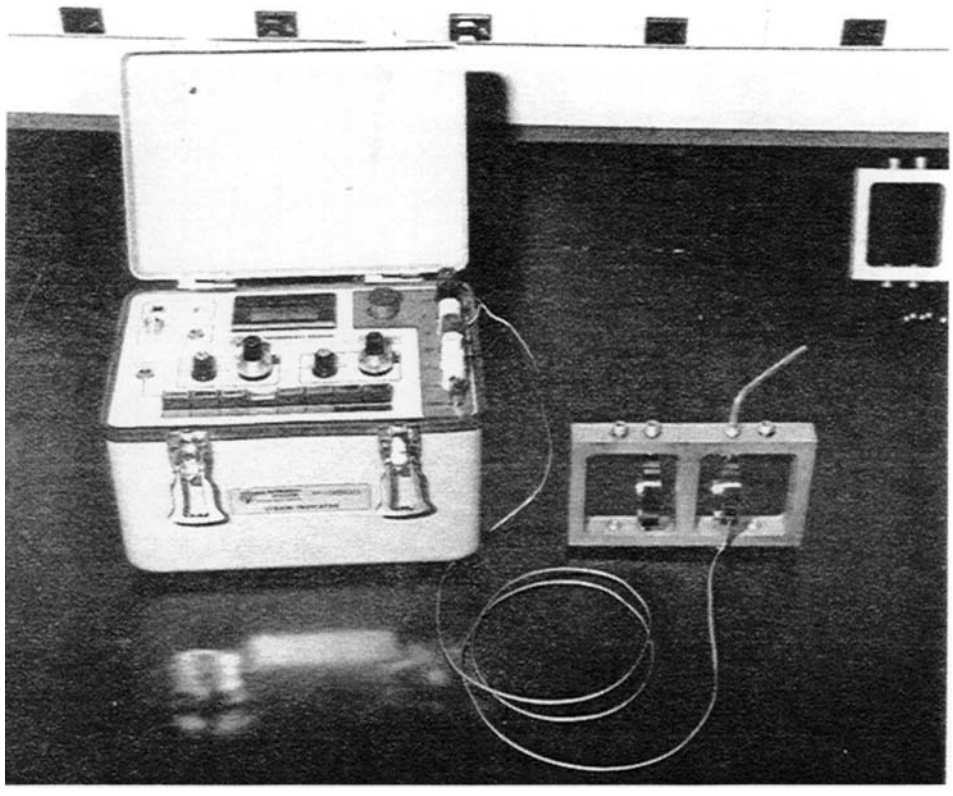


Figure 1. Strain measurement being made on C-ring installed in fixture.

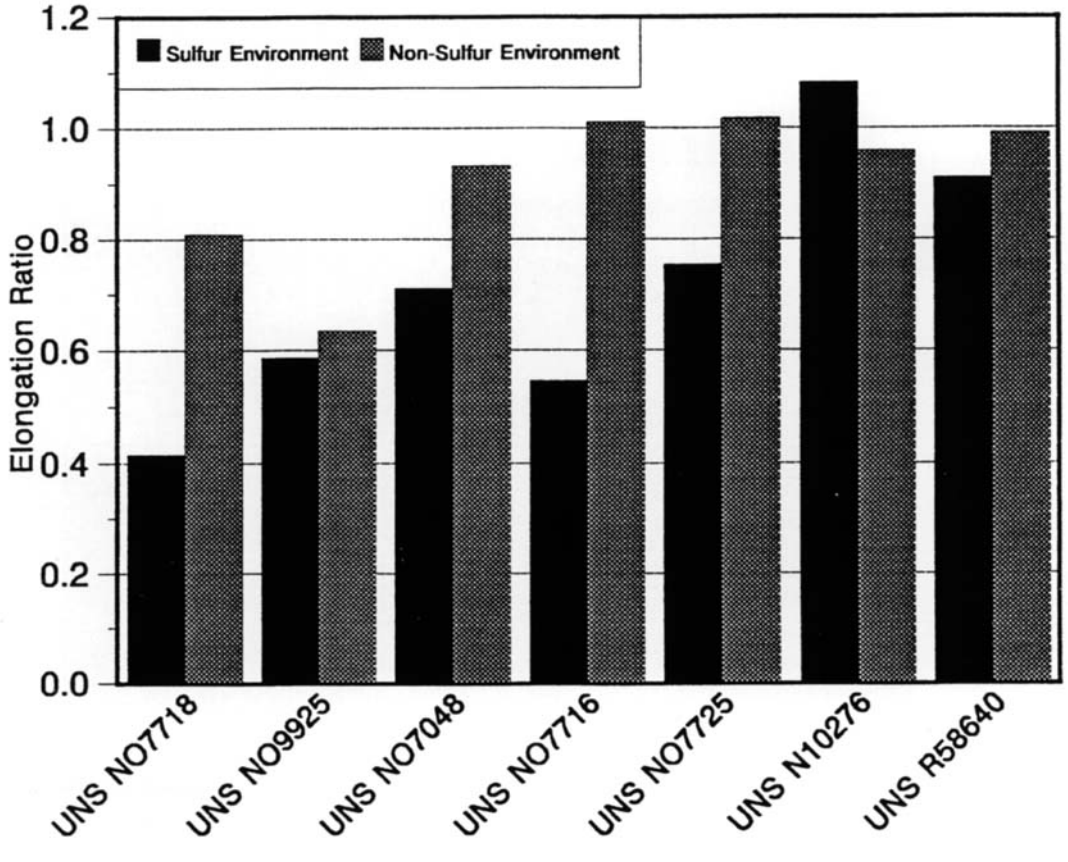


Figure 2. Comparison of average elongation ratio of all alloys tested.

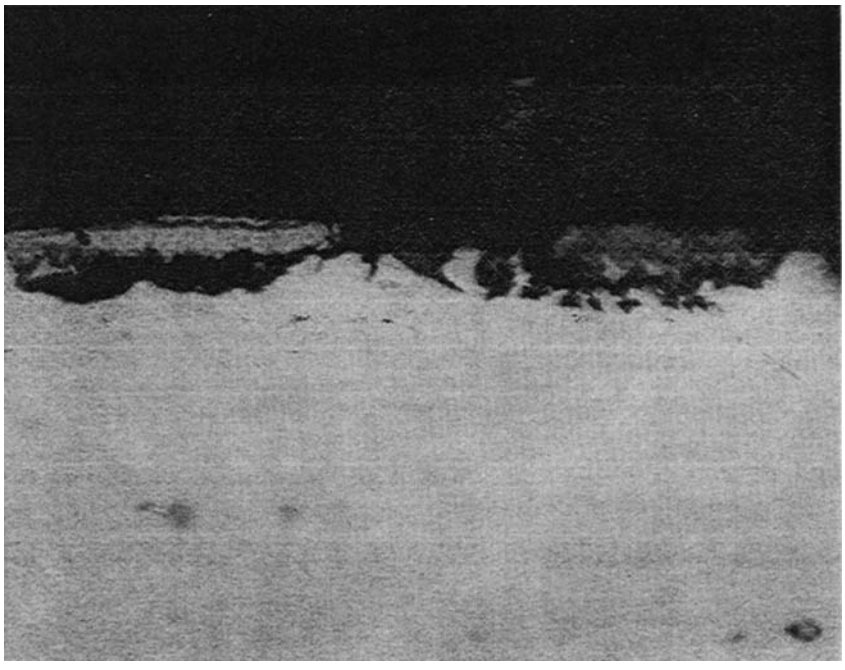


Figure 3. Side wall of typical specimen showing pitting and cracking under sulfide deposit.

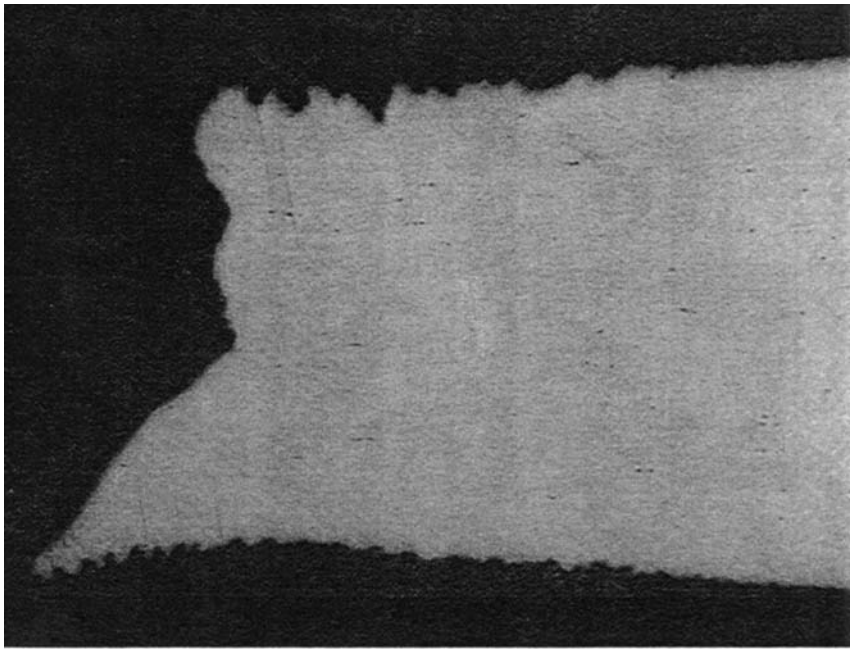


Figure 4. Longitudinal section through the fracture surface showing profile and secondary cracks in necked-down region.

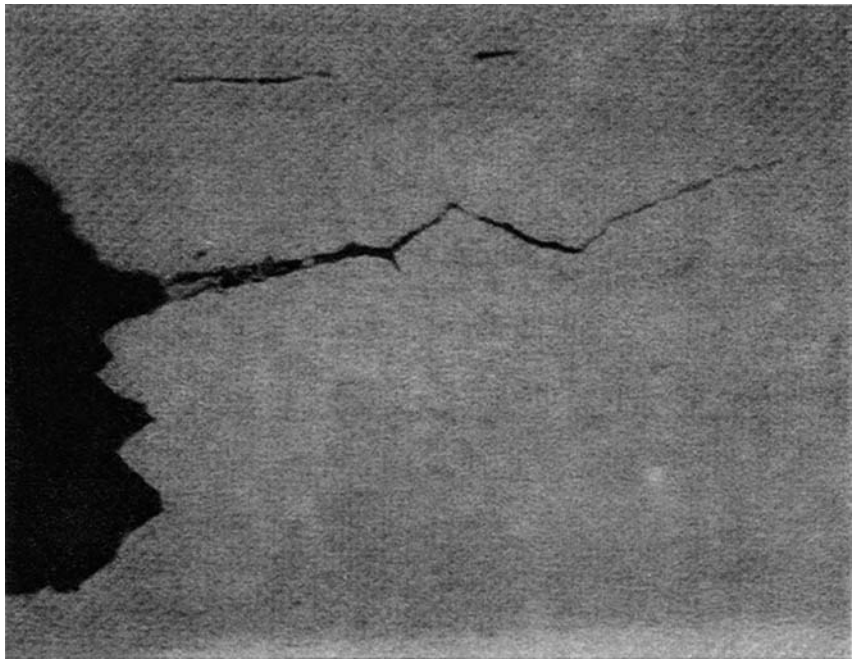


Figure 5. Secondary crack emanating from corrosion pit on surface of specimen.

Copyrighted Materials
Copyright © 1996 NACE International Retrieved from www.knovel.com

Paper No.
49

CORROSION 92
The NACE Annual Conference and Corrosion Show

EVALUATION AND QUALIFICATION OF A PRECIPITATION-HARDENED MATERIAL FOR DEEP, HOT, SOUR ENVIRONMENTS

T. A. DeBold and N. B. Schmidt
Carpenter Technology Corporation
P. O. Box 14662
Reading, PA 19612-4662

M. F. Bluem and S. R. Herman
Exxon Company USA
P. O. Box 61707
New Orleans, LA 70161

ABSTRACT

Exxon identified a need for highly corrosion-resistant precipitation-hardening alloys for use in down hole gas well equipment for severely corrosive environments, such as Mobile Bay. The Exxon fields are expected to contain up to 9.8% hydrogen sulfide with bottom-hole temperatures reaching 420°F (216°C). UNS N07716 was evaluated and specified for use in tubing-retrievable, surface-controlled, subsurface safety valves (TRSV). This paper reviews the service conditions and specific application as well as the processing and testing of UNS N07716 to qualify the material for this application. Slow strain rate test (SSRT) and C-ring data are provided in elevated-temperature sour environments.

Keywords: hydrogen sulfide; Mobile Bay; deep, sour gas wells; subsurface safety valves; UNS N07716; slow strain rate tests; C-ring tests

INTRODUCTION

Exxon holds leases on 62,000 acres located where Mobile Bay meets the Gulf of Mexico, spanning both state and federal waters. Large geologic formations containing natural gas underlie the area, and facilities for the industry's largest offshore sour gas development are under construction. The locations of the leases, wells and onshore treating facility are shown with the surrounding regions in Figure 1. Twelve wells from three different fields will produce through 23 miles of flowline connecting remote wells to the production platforms. At the production platforms the raw produced fluids are separated, metered and dehydrated. A 32-mile gathering system collects the gas from the production platforms and transports it to the onshore treating plant.

The environmental conditions of the initial 22,000' deep wells involve bottom-hole temperatures as high as 420°F (216°C) and hydrogen sulfide up to nearly 10%. These conditions dictated a need for highly corrosion-resistant precipitation-hardening alloys for certain downhole components.

Exxon selected UNS N07716 (Custom Age 625 PLUS®) alloy for its TRSV's because of its resistance to stress-corrosion cracking, sulfide-stress cracking, pitting and crevice corrosion at yield strengths of 120 ksi (827 MPa) and above. This material is aged to produce increased strength and provides corrosion resistance similar to that of cold-worked alloy 625 and superior to that of aged alloy 718 in most or all environments.

Previous papers dealing with UNS N07716 presented effects of alloying elements[1] and heat treatment[2] as well as mechanical properties, corrosion data[3,4] and welding information[5]. This paper reviews Exxon requirements for service in its Mobile Bay wells and the testing necessary to qualify UNS N07716 for this application.

SERVICE CONDITIONS

The H_2S concentration in the fields varies from 0.02-9.8%. The bottom hole temperatures of 420°F (216°C), and the high production rates are predicted to develop wellhead temperatures of 310°F (154°C). Formation water contains total dissolved solids exceeding 300,000 ppm. These conditions have presented a materials selection challenge for Exxon's Mobile Bay TRSV's.

MATERIAL SPECIFICATION

The high pressures at Mobile Bay force the use of high strength materials to avoid undesirable constriction of the flow path and excessive velocity. Many corrosion resistant alloys can be manufactured in a tubular form by extrusion, heat treatment and cold work to a specified strength. Bar is the preferred raw material for TRSV fabrication because of the relatively large wall thickness of the valves. Bar is most readily strengthened by heat treatment rather than cold work. The composition must be optimized to assure that the material provides the desired response to solution annealing and aging. The yield strength range of 120-140 ksi (827 to 965 MPa) was selected as a compromise between the need for high design strength and a concern over increased susceptibility to embrittlement as strength increases.

The need for resistance to embrittlement at high temperatures led to imposition of a slow strain rate tensile (SSRT) test for material to be used in its highest strength condition and continuously stressed at a high percentage of yield strength in service. The test conditions are listed in Table 1. The test conditions were selected to reflect a high level of resistance to stress corrosion cracking rather than to relate to actual service conditions. The test performance requirements reject material for secondary cracking along the uniform gage section at the 300°F (149°C) test temperature. Some evidence of embrittlement on the final fracture surface of the specimen may be accepted, but the time to failure ratio (TFR) should exceed 0.80 times that of a specimen tested in a benign environment. The test is severe because the uniform elongation is relatively extensive and considerable work hardening can occur. A heat is qualified if a minimum of 4 specimens are tested and perform satisfactorily. If one specimen fails, eight more specimens from the piece may be selected for test. If the additional specimens are acceptable, the heat is qualified in spite of the single specimen failure in the first four tested. Test requirements allow a maximum of one failure in 12 specimens tested.

Hydrogen embrittlement at temperatures below 100°F (38°C) is considered a low risk even with the high strength of the materials required. Tests were conducted in accordance with NACE TM0177[6] to assure adequate resistance to the lower temperature failure mechanism, but performance was sufficiently good to avoid a need to include such a test in the procurement specification. This is supported by published results for UNS N07716 in the NACE TM0177 environment.[1-4]

®Registered trademark, Carpenter Technology Corporation.

Resistance to pitting and crevice corrosion is an additional consideration for material selection. Indices which reflect the contribution of elements such as chromium, molybdenum and tungsten on pitting resistance have been used to estimate the performance of corrosion resistant materials. The Pitting Index used by Exxon to rank several alloys used in its well completions is as follows (PI = %Cr + 3%Mo + 1.5%W).

Precipitation hardenable materials
UNS N07716 PI = 45
UNS N09925 PI = 30
UNS N07718 PI = 29

Cold worked materials
UNS N06975 PI = 43
UNS N06985 PI = 43
UNS N10276 PI = 65

A high pitting index decreases the risk of a corrosion related failure in very severe environments. The pitting and crevice corrosion resistance of N07716 was considered to be at least comparable to that of nickel-iron-chromium-molybdenum alloys. Previous work showed that the pitting and crevice corrosion resistance of UNS N07716 is similar to that of UNS N06625 and superior to that of UNS N07718.[1,3,4]

Microstructure is evaluated for each heat and heat treat lot. Corrosion and embrittlement tests are documented with microstructure of the tested material. Adequate information has been accumulated by testing a number of heats to allow use of a microstructural check on each heat treat lot.

Hardness is limited to 40 HRC or 363 HB to assure individual pieces or heat treatment lots are reasonably similar to previously tested material. Also, in ultrasonic evaluation, UNS N07716 has met commercially available inspection test requirements.

MATERIAL EVALUATION

UNS N07716 was evaluated as part of an ongoing program to assure a consistent product and evaluate any effects that variations in heat treatment or processing might have. Slow strain rate tests (SSRT) were conducted according to an Exxon specification, as discussed above. In addition, C-ring specimens were evaluated in elevated-temperature sour environments pertinent to the Exxon fields at Mobile Bay. Results were supported with metallography and fractography. The evaluation of one of the heats tested is described below.

Experimental Procedure

Processing. The SSRT and C-ring specimens were machined from 1.6" (4 cm) round bar of UNS N07716, heat 85002. The heat analysis is found in Table 2.

After hot rolling, the bar was solution annealed in a mill furnace at 1040°C (1904°F) for 2 hours at temperature and air cooled. A workpiece thermocouple showed that the variation in annealing temperature from one end of the 1200 lb (544 kg) load to the other was less than 5°C (9°F). Samples of the mill annealed bar were aged in small laboratory furnaces using double-aging treatments. The primary age consisted of either a 1325°F (718°C), 1350°F (732°C) or 1375°F (746°C) treatment for 8 hours. This was followed by a furnace cool at 100°F/hour (55°C/hour) to the secondary aging temperature, 1150°F (621°C), where the material was held 8 hours and air cooled.

Specimen Preparation and Testing. A location midway between mid-radius and 3/4 radius (5/8 radius) was chosen for testing of mechanical properties and corrosion resistance as well as the metallographic examination.

SSRT specimens were machined and tested according to an Exxon specification. Longitudinal SSRT specimens were machined with the 0.250" diameter x 1" long gage section finished according to the specified 32 RMS or better (actual surface 8 RMS or better).

Slow strain rate tests were performed in an 835 ml (0.22 gallon) autoclave with 75% liquid and 25% gas phase using an extension rate of $4X10^{-6}$ per sec. The autoclave was deaerated with a vacuum and helium purge procedure. Deaerated 25% NaCl + 0.5% acetic acid was added and saturated to 100 psi (690 kPa) of H_2S at 75°F (24°C). The test cell was heated to 300°F (149°C) and allowed to stabilize before beginning the test.

C-ring specimens were produced (from material with primary aging temperatures of 1350°F and 1375°F [732°C and 746°C]) by rough machining annealed bar samples to oversize tubes, aging, finish machining and polishing with 120 grit and 320 grit papers. The 1325°F (718°C) primary age was omitted because this lower temperature typically provides a slightly lower yield strength. Consequently, this material would be expected to resist cracking as well as or better than material aged at higher temperatures. Final dimensions of the C-rings were 1" O. D. X 0.1" wall X 3/4" wide (2.54 cm O. D. X 0.25 cm wall X 1.9 cm wide). This outside diameter placed the test area at 5/8 radius.

All C-rings were stressed to 72 or 90% of the longitudinal 0.2% Y. S. (assumed to be 80 or 100% of the transverse 0.2% Y. S.) as stipulated by NACE TM0177-90. Duplicate specimens from each stress level and primary aging treatments of 1350°F and 1375°F (732°C and 746°C) were exposed to the three environments below. A 1 liter (0.26 gallon) autoclave with 750 ml (0.2 gallon) of solution at room temperature was employed.

(a) 25% NaCl + 200 psi (1379 kPa) H_2S + 750 psi (5171 kPa) CO_2 + 2000 psi (13,790 kPa) N_2 charged at room temperature and tested at 300°F (149°C) for two 3-month periods.

(b) As above, but at 350°F (177°C).

(c) 25% NaCl + 1200 psi H_2S (charged as 43.7 grams of liquid H_2S at room temperature) + 750 psi CO_2 + 2000 psi N_2 charged at room temperature and tested at 350°F for one 3-month period followed by an additional 2-month period.

Results

Mechanical Properties. Results for duplicate room temperature tensile specimens appear in Table 3. The average 0.2% Y.S. varied from 120 to 136.5 ksi (827 to 941 MPa). This covers most of the 120 to 140 ksi (827 to 965 MPa) range generally of interest.

Metallographic Examination. Metallographic results are summarized in Table 3. The material has a recrystallized grain structure with precipitation of fine, discrete Nb-rich carbides in the matrix. Small amounts of Cr and Mo-rich grain boundary carbide can be observed in material with the 1325°F (718°C) and 1350°F (732°C) primary aging treatments. Some increased grain boundary precipitation occurred with the 1375°F (746°C) primary age. Photomicrographs of UNS N07716 with these three primary aging treatments have been published previously [3]

Stress-corrosion cracking tests. Results for SSRT tests exposed at 300°F (149°C) in deaerated 25% sodium chloride with 0.5% acetic acid and 100 psi (690 kPa) hydrogen sulfide (added at 75°F [24°C]) are found in Table 4. Stress-corrosion cracking resistance was evaluated using ratios of time-to-fail and reduction in area in the test environment vs. corresponding values in an inert environment along with evaluation of the gage section and fracture surface. As seen in Table 4, the range of ratios was generally similar for the three conditions evaluated. Time-to-fail ratios varied from 0.81 to 1.07 and reduction of area ratios ranged from 0.72 to 0.97.

Examination of the uniform gage section revealed no secondary cracking and nearly all of each fracture surface exhibited a clean, dimpled fracture. Each fracture surface, however, did contain a small amount of dark surface, indicative of corrosion. A typical example is shown in Figure 2 (corroded area indicated with arrow). The corrosion product was removed ultrasonically in 20% potassium permanganate (200°F, 93°C) followed by 10% ammonium citrate (room temperature) and the underlying surface examined with the scanning electron microscope (SEM). Figure 3 shows the edge of this corroded area in a specimen aged at 1350°F (732°C). The corroded area appears to have fatigue-like striations adjacent to the dimpled fracture of the unaffected surface. Typically, the corroded areas failed in a transgranular path via cleavage and/or quasi-cleavage. Corrosion during the test altered the fracture morphology in these areas making observation of classic fracture morphologies difficult.

Overall, the SSRT tests demonstrated that UNS N07716 was resistant, although not totally immune to the test environment. Variation in the primary aging temperature from 1325°F to 1375°F (718°C to 746°C) did not significantly affect resistance in these tests.

Results for the C-ring tests are shown in Table 5. No failures or localized corrosion occurred for material aged at 1350°F or 1375°F (732°C or 746°C) stressed at 80 or 100% of the transverse 0.2% Y. S.

UNS N07716 (1.6" [4 cm] diameter bar) displayed good resistance in all of the above tests. Larger material (6" [15.2 cm] diameter bar) also produced satisfactory SSRT results in separate studies. In addition, UNS N07716 with primary aging treatments from 1325°F to 1375°F (718 to 746°C) has demonstrated resistance to sulfide stress cracking (NACE TM0177[6]) and intergranular corrosion.[2]

APPLICATION OF MATERIAL

The largest quantity of UNS N07716 bar was manufactured for use in tubing retrievable, surface-controlled subsurface safety valves (TRSV's). The valves will be installed approximately 300 feet below the mudline in the tubing string for shut-in of gas flow in the case of an emergency (Figure 4). The 15,000 psi (103 MPa) working pressure valves have an outside diameter approaching six inches and a length exceeding seven feet. Valve features include metal-to-metal seals in the threaded tubular connections and flapper mechanism. The flapper valve is held open by hydraulic pressure from the surface under normal conditions, and the valve closes when the hydraulic pressure is released.

Limited world-wide industry experience with 15,000 psi (103 MPa) TRSV's prompted the manufacture and testing of prototype valves prior to placing the valve production order. The testing simulated the ability of the valve to function in the environmental conditions of the well. This included repetitive valve cycling at 325°F (163°C) and 15,000 psi (103 MPa) internal pressure with axial loads of 300,000 pounds (136,080 kg). Valve closure tests at 2 to 63 MCFD (0.06 to 1.8 million cubic meters per day) verified the dynamic sealing ability of the valve. Flapper differential pressure opening tests established the ability of the valve to open without damage with pressure below the sealing flapper. Additional, but less stringent testing, was performed to conform with industry quality standards such as API-14A[7]. Table 6 depicts the testing program and the major anomalies found in testing three prototype valves. There were no alloy deficiencies responsible for these anomalies. Post-test disassembly analysis revealed minor mechanical damage to highly stressed contact points but it did not alter the ability of the valve to function. Maximum operating stress levels in the machined components approach 80% of the material specified minimum yield strength.

The primary housing bodies are constructed of UNS N07716. Figure 5 depicts a typical TRSV design. Each valve contains over 60 metallic components machined to close tolerances. Manufacturing times averaged 4 to 6 months. Manufacturing procedures were specially developed for the alloy. Final fluorescent penetrant inspections of the finished components typically did not locate any surface defects.

CONCLUSIONS

Many years of sour production experience, combined with technical resources, have allowed Exxon to qualify well equipment for Mobile Bay service conditions. UNS N07716 has been specified, manufactured, tested and machined into production equipment. Static autoclave and SSRT testing in hot, sour environments supports the use of this material as well as its superior performance in prototype valve testing. Installation of the completed TRSV's is scheduled for Mid-1992 with production operations to start in the second quarter of 1993. Cooperation between the material manufacturer, equipment manufacturers and the operator contributed to the success of the development. The alloy should be considered for use in future applications where its resistance to embrittlement, strength and corrosion resistance are advantageous.

ACKNOWLEDGMENTS

The authors wish to acknowledge W. J. Sisak for his assistance in planning and conducting the static autoclave tests. We also wish to acknowledge R. B. Frank for his role in the development of this alloy along with his review and support in the publishing of this paper.

REFERENCES

1. R. B. Frank, T. A. DeBold, "Custom Age 625 PLUS - A New Age-Hardenable, Corrosion-Resistant Alloy," presented at the ASM Materials Conference, Orlando, FL, October 1986; technical article printed by Carpenter Technology Corporation, Reading, PA.

2. R. B. Frank, T. A. DeBold, "Heat Treatment of an Age-Hardenable, Corrosion-Resistant Alloy - UNS N07716," Corrosion/90, paper no. 59, (Houston, TX: NACE, 1990).

3. R. B. Frank, T. A. DeBold, "Properties of an Age-Hardenable, Corrosion-Resistant, Nickel-Base Alloy," Corrosion/88, paper no. 75, (Houston, TX: NACE, 1988); edited version, Materials Performance, 27, 9(1988): p. 59.

4. R. B. Frank, "Custom Age 625 PLUS® Alloy, - A Higher Strength Alternative to Alloy 625," Superalloys 718, 625 and Various Derivatives, E. A. Loria, Ed., The Minerals and Materials Society, Warrendale, PA, p. 879-893, (1991).

5. M.J. Cieslak, T. J. Headley, R. B. Frank, "The Welding Metallurgy of Custom Age 625 PLUS Alloy," Welding Research supplement, 68, 12(1989): p. 473.

6. NACE Standard TM0177, "Standard Test Method - Laboratory Testing of Metals for Resistance to Sulfide Stress Cracking in H_2S Environments," (Houston, TX: National Association of Corrosion Engineers, 1990).

7. API-14A, "Specification for Subsurface Safety Valve Equipment," 7th Edition, (Washington, DC: American Petroleum Institute, 1988).

TABLE 1 - SLOW STRAIN RATE TEST CONDITIONS OF EXXON SPECIFICATION

1. Environment
   - Deaerated 25% Sodium chloride brine
   - 0.5% acetic acid
   - 100 psi (690 kPa) hydrogen sulfide added at 75°F ± 5°F (24°C ± 2.8°C)
   - Tested at 300°F (149°C)

2. Test Method
   - Slow strain rate at 4 x 10^{-6}/sec.
   - Inert comparison tests in a benign environment at 300°F (149°C).

TABLE 2 - CHEMICAL COMPOSITION OF UNS N07716 HEAT 85002

Element	Weight Percent
Carbon	0.015
Manganese	0.09
Silicon	0.06
Phosphorus	0.006
Sulfur	0.001
Chromium	20.96
Nickel	60.86
Molybdenum	8.00
Aluminum	0.18
Titanium	1.31
Columbium	3.31
Iron	5.09

TABLE 3 - MECHANICAL PROPERTIES AND MICROSTRUCTURE OF 1.6" (4 cm) ROUND BAR OF UNS N07716, HEAT 85002

		Room Temperature Tensile						Microstructure	
Heat Treatment Temperatures °F (°C)	Hardness (HRC)	0.2% Y.S. ksi	(MPa)	U.T.S. ksi	(MPa)	Elong. (%-4D)	R.A. (%)	Grain Size ASTM No.	Grain Boundary Precipitation
1904+1325/1150	34-36	121	(834)	181	(1248)	33	58	5/7	<10%
(1040+718/621)		119	(821)	180	(1241)	36	57		
1904+1350/1150	37-38	129	(889)	185	(1276)	32	56	5/7	<10%
(1040+732/621)		130	(896)	185	(1276)	30	57		
1904+1375/1150	38-38.5	136	(938)	187	(1289)	29	51	5/7	≤25%
(1040+746/621)		137	(945)	187	(1289)	30	52	some 4	

Specimens: 0.252" gage diameter longitudinal tensiles from 5/8 radius location (Hardness and microstructure were also evaluated using longitudinal specimens from the 5/8 radius location).
Heat Treatment: Solution anneal at 1904°F (1040°C) for 2 hours at temperature, AC followed by a primary age for 8 hours, furnace cool at 100°F/hour (55°C/hour) to 1150°F (621°C), 8 hours, AC.

TABLE 4 - SLOW STRAIN RATE TEST RESULTS FOR UNS N07716
Deaerated 25% NaCl with 0.5% acetic acid and
100 psi H_2S (added at 75±5°F, 24±2.8°C), exposed at 300°F (149°C)

Heat Treatment Temperatures °F (°C)	0.2% Y.S. ksi (MPa)	Time To Fail* Tf(env) Hours	Ratio of Tf (env.) to Tf (inert)	R.A. (env) %	Ratio of R.A. (env.) to R.A. (inert)	Secondary Cracking	Attack Found on Frac. Face
1904+1325/1150	120	24.3	0.87	40.3	0.72	No	Yes
(1040+718/621)	(827)	24.5	0.89	43.8	0.78	No	Yes
		25.0	0.91	50.1	0.89	No	Yes
		27.2	0.99	45.6	0.81	No	Yes
1904+1350/1150	129.5	25.3	0.99	46.6	0.82	No	Yes
(1040+732/621)	(893)	24.7	0.97	46.0	0.81	No	Yes
		27.4	1.07	52.6	0.93	No	Yes
		24.3	0.95	43.6	0.77	No	Yes
		25.6	1.0	44.2	0.78	No	Yes
		23.8	0.93	47.7	0.84	No	Yes
		24.5	0.96	47.0	0.83	No	Yes
		24.1	0.95	45.6	0.81	No	Yes
1904+1375/1150	136.5	24.3	0.95	49.8	0.97	No	Yes
(1040+746/621)	(941)	20.6	0.81	37.2	0.72	No	Yes
		24.6	0.96	48.5	0.94	No	Yes
		23.4	0.92	45.6	0.86	No	Yes

- All material from heat 85002, 1.6" (4 cm) round, longitudinal specimens cut from 5/8 radius.
- All tests conducted at 4 x 10^{-6}/sec. including inert tests in 300°F (149°C) helium. (inert data not shown).
- Autoclave capacity 835 ml, with 75% liquid phase and 25% gas phase.
- Specimen gage 0.250" (.635 cm) diameter x 1" (2.54 cm) length.

• Yield (initial deviation from elastic linearity) to failure (hours).

TABLE 5 - RESULTS FOR C-RING SPECIMENS OF UNS N07716 IN 25% NaCl
AUTOCLAVE ENVIRONMENTS
1.6" (4 cm) round from heat 85002

	Test Parameters					Results[c]	
Heat Treatment Temps. °F(°C)	Partial Pressures[a] H_2S psi(kPa)	CO_2 psi(kPa)	N_2 psi(kPa)	Test Temp. °F(°C)	Total Time[b] mo.	For % of Transverse 0.2%Y.S.Below 80%	100%
1904+1350/1150	200	750	2000	300	6	NF,NF	NF,NF
(1040+732/621)	(1379)	(5171)	(13790)	(149)			
"	200	750	2000	350	6	NF,NF	NF,NF
"	1200	750	2000	350	5	NF,NF	NF,NF
	(8274)			(177)			
1904+1375/1150	200	750	2000	300	6	NF,NF	NF,NF
(1040+746/621)							
"	200	750	2000	350	6	NF,NF	NF,NF
"	1200	750	2000	350	5	NF,NF	NF,NF

a. 25% NaCl environment includes the partial pressures of H_2S, CO_2 and N_2 shown, added at room temperature. The 1200 psi H_2S was charged as 43.5 grams of liquid H_2S.

b. Tests were conducted for two 3-month periods or for one 3-month period followed by an additional 2-month period.

c. Specimens stressed according to NACE TM0177 (for 100% 0.2% Y.S., desired outer fiber stress was [0.2% Y.S. + 0.002 X modulus of elasticity]). Transverse 0.2% Y.S. assumed to be 0.9 x longitudinal 0.2% Y.S.

TABLE 6

MOBILE BAY TRSV TESTING

TESTING	PURPOSE	RESULTS
VENDOR API - 14A	CYCLIC WATER & SAND FLOW AND PRESSURE TEST	FLAPPER SAND ACCUMULATION
API - 14A VERIFICATION	CYCLIC WATER & SAND FLOW AND PRESSURE TEST	MINOR FLAPPER PITTING
HOT TEST	CYCLIC TESTING AT WORKING PRESSURE AND TEMPERATURE	MINOR HYDRAULIC PISTON ELASTOMER EXTRUSION
GAS SLAM	FLAPPER CLOSURE AND SEALING AT RATES TO 63 Mcf / D	NO LEAKAGE. MINOR FLAPPER DAMAGE
UNEQUALIZED OPENINGS	FLAPPER OPENING AGAINST DIFFERENTIAL PRESSURE	MINOR FLOW TUBE DEFORMATION (AT INLET TIP)
EXXON RESEARCH TEST	CYCLIC WATER & SAND FLOW AND PRESSURE TEST (PERFORMED AT 325° F AND 300 k # AXIAL)	MINOR HYDRAULIC PISTON PITTING. (MAJOR HYDRAULIC AND BODY LEAKS ON ONE PRODUCT)
MOBILE BAY FUNCTIONAL	QUALITY CHECK OF OPERATING PRESSURE & PRODUCTION TRSV's	NOT YET PERFORMED

207-5918

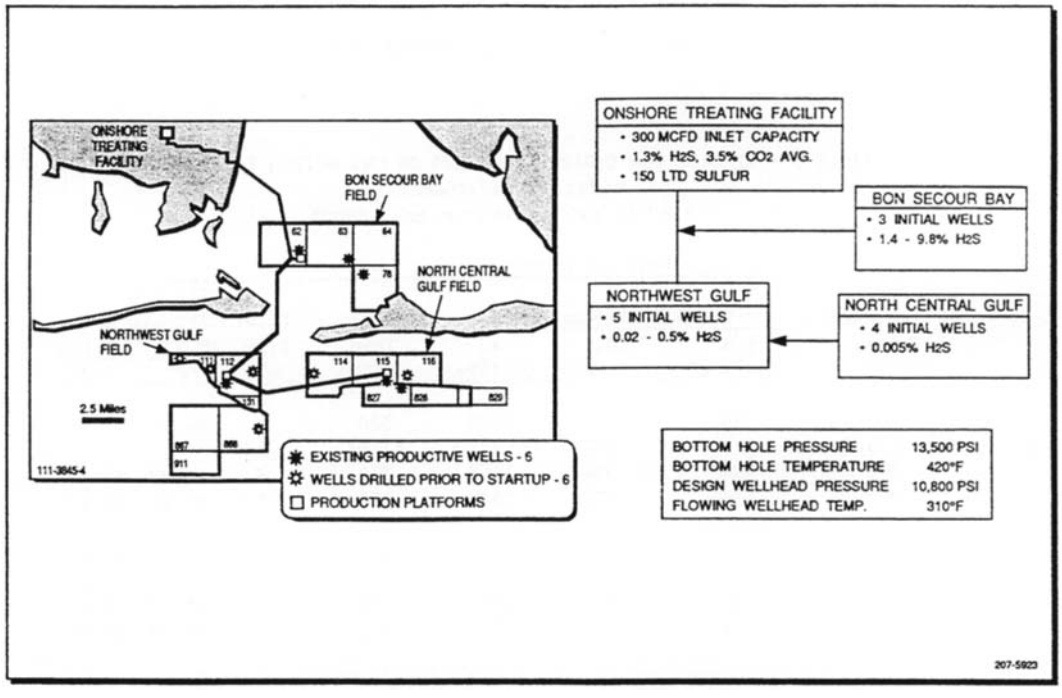


Figure 1 - LOCATION AND BRIEF DESCRIPTION OF WELLS IN EXXON MOBILE BAY PROJECT

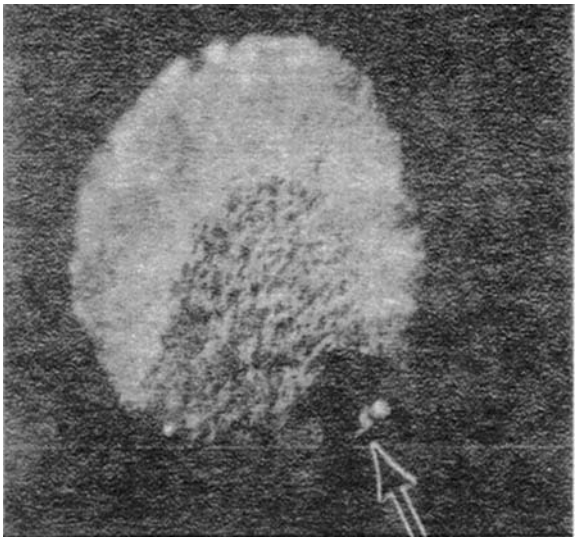


FIGURE 2 - Fracture Surface of UNS N07716 After SSRT in Environment Described in Table 4
- From 5/8 radius of 1.6" (4 cm) round bar from heat 85002, primary age at 1350°F [732°C]
- Original magnification 10X.

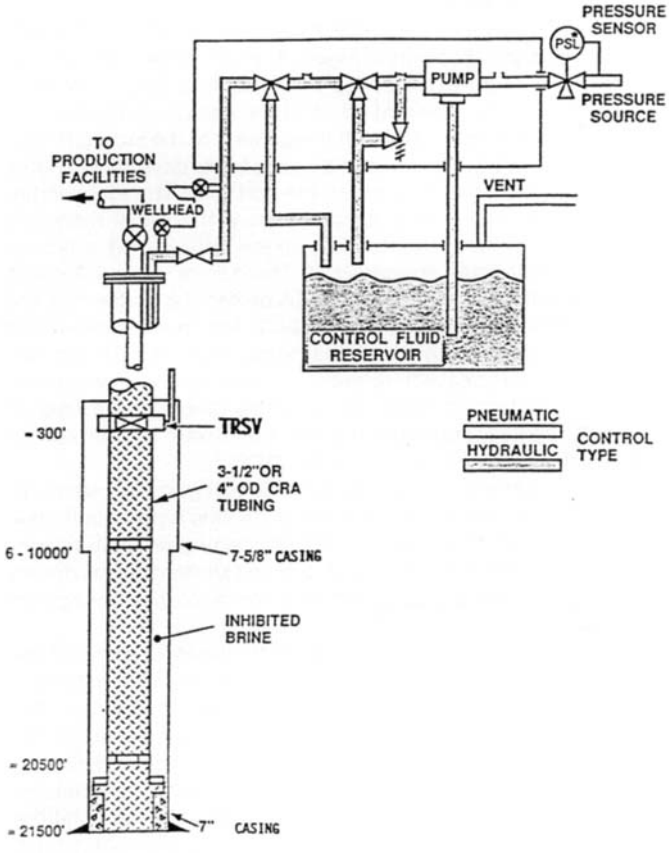


FIGURE 4 - Typical Schematic Showing Application of TSRV
*PSL - Pressure Sensor Low

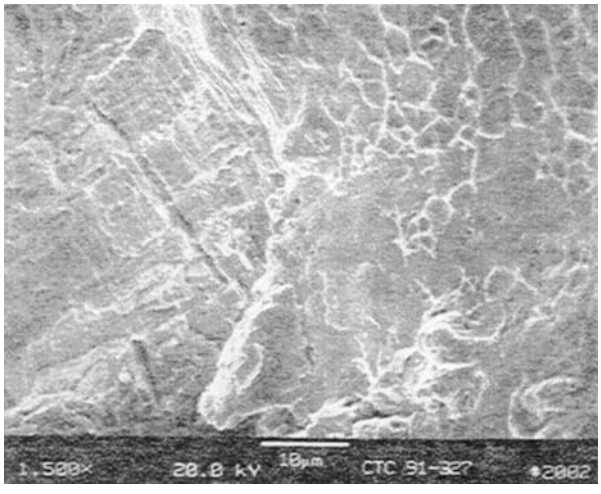


FIGURE 3 - SEM Photograph of Edge of Corroded Area on Fracture Face of SSRT After Testing as in Table 4
- Corroded plus cleaned area to left with fatigue-like striations; clean mechanical fracture to right with dimpled fracture mode.
- From 5/8 radius of 1.6" (4 cm) round bar from heat 85002, primary age at 1350°F [732°C].

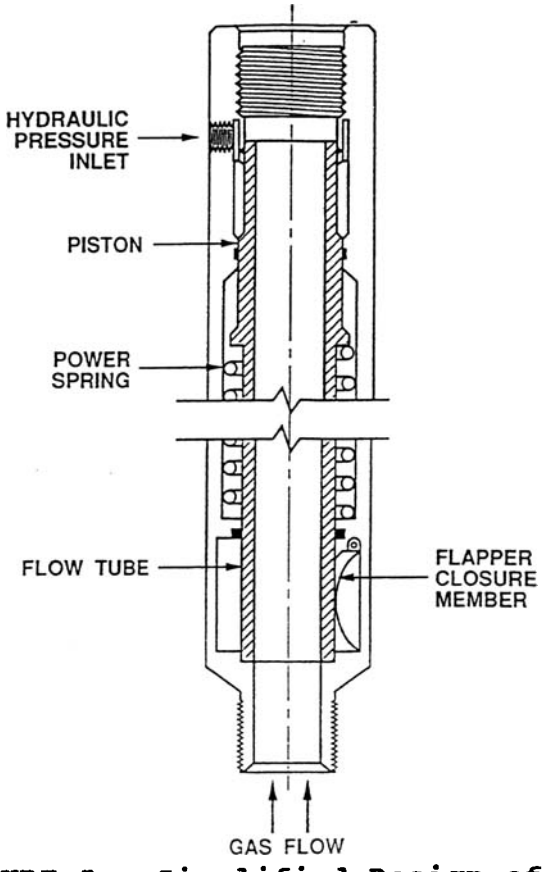


FIGURE 5 - Simplified Design of a Typical TSRV

Copyrighted Materials
Copyright © 1996 NACE International Retrieved from www.knovel.com

Failure of Monel Ni-Cu-Al Alloy K-500 bolts in seawater*

K. D. Efird*

Monel Ni-Cu-Al Alloy K-500 bolts failed by cracking after short periods of service as subsea riser clamp bolts on Occidental Petroleum Caledonia, Ltd.'s Piper Alpha platform in the UK North Sea. All of the bolt failures occurred in the most highly stressed clamps for each riser. The failure mechanism was hydrogen embrittlement caused by a specific set of material and environmental conditions. Severely cold worked material from the thread machining operation, followed by the precipitation hardening heat treatment resulted in localized areas of high hardness (above HRC 35) in the thread root. This, coupled with the high stress level on the bolts in these clamps and cathodic polarization from the platform cathodic protection system, resulted in hydrogen charging of the thread root followed by failure from hydrogen embrittlement. As a result of this experience, a specification for Monel Alloy K-500 bolts has been implemented that has prevented a recurrence of this type of failure.

Introduction

FAILURES OF MONEL ALLOY K-500 riser anchor clamp bolts on the Occidental Petroleum Caledonia, Ltd.'s Piper ALpha platform in the UK North Sea were discovered by divers during a routine yearly inspection. The failures occurred in the main, load-bearing, riser clamps where the bolts were under the highest stress. The portions of the broken bolts remaining in the clamps were recovered for failure analysis. The critical nature of these clamps made a resolution of the problem imperative.

A detailed and comprehensive laboratory investigation was performed on the failed bolts by N. C. Farr of Inco's Henry Wiggin Company, Ltd., Hereford, England. This investigation provides the basis of the data used in this paper. Determination of the failure mechanism was followed by preparation and implementation of a manufacturing specification for Monel Alloy K-500 bolting in order to mitigate this type of failure.

Since the initial riser clamp failures were discovered, a number of additional failures of Monel Alloy K-500 bolts occurred that were not related to riser clamps. These failures all occurred in bolts that were highly stressed in seawater service and under cathodic protection. All of the failures were very similar in their physical characteristics, and the failure mechanism was concluded to be the same as for the riser clamp bolts.

Intergranular cracking of Ni-Cu alloys (Monel Alloy 400 and K-500) has been observed only under very specific conditions.[1-4] These are:

a. Under cathodic protection in HF and in HF vapors (K-500)
b. In high temperature, high pressure steam (Monel Alloy 400)
c. In seawater at 260 C (Monel Alloy 400)
d. In the presence of Hg or Hg salts (Monel Alloy 400 and K-500)
e. In H_2S environments under high stress (K-500)

Reports of intergranular cracking failures of this alloy in ambient seawater are virtually nonexistent in the literature, making correlation of the failure analysis results to the literature difficult.

Failure analysis

A general view of a failed bolt from the Piper Alpha platform riser clamp is given in Figure 1, which shows the appearance of the fracture. A closeup of the fracture face is shown in Figure 2, with the apparent origin of the fracture indicated. The failure occurred in the first full thread next to the shank. Propagation was highly branched and appeared to develop at angles of approximately 45 degrees to the bolt axis. The crack initiation point in Figure 2 is assumed from the radial markings eminating from that point. This general appearance is typical of all of the failures encountered. There were varying degrees of calcareous deposit from cathodic protection on the fracture faces, indicating that some of the bolts had been cracked for a period of time. Analysis of the calcareous deposit did not reveal any information relevant to the failure mechanism. Cathodic protection readings, taken by divers in the area of the bolt failures, indicated that the bolts were at a protected potential of approximately -1.0 V (SCE).

The general microstructure of the bolt material, shown in Figure 3, is a normal microstructure for this type of bolt, having fully recrystallized grains. The hardening precipitate cannot be seen, since the $Ni_3(Ti,Al)$ precipitate that forms during precipitation hardening is too fine for resolution by optical microscopy.

The microstructural analysis of the fracture areas of the bolts revealed that cracking was intergranular with extensive secondary intergranular cracking, as shown in Figure 4. The thread area had a fine-grained microstructure adjacent to the threaded surface, followed by a band of coarser grains just below them, as shown in Figure 5. This indicated an influence of cold work from thread machining on the alloy recrystallization. A shallow layer of internal oxidation was also observed in the threaded surfaces. Microhardness tests in the thread region showed that the threaded surface was significantly harder than other portions of the bolt. Since the entire bolt had undergone the same heat treatment, this supports a direct connection to the machining operation. A plot of microhardness variations with depth below the outer surface for the bolt shank and threaded area is shown in Figure 6.

• Voluntary paper submitted for publication August 1984.
*Occidental Exploration and Production Company, Bakersfield, California 93309.



FIGURE 1 — A general view of a failed Monel Alloy K-500 riser clamp bolt. Note the calcareous deposit on the bolt shank and nut.

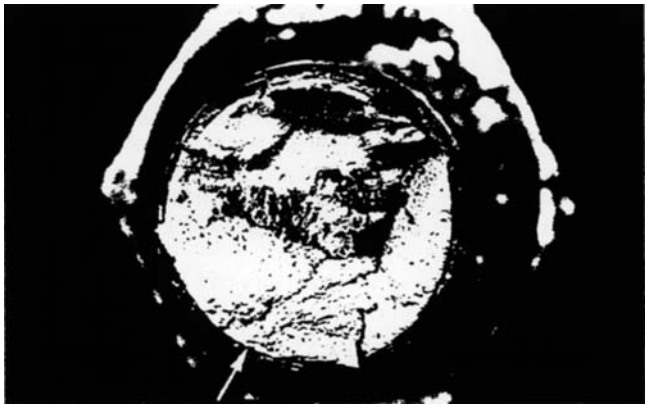


FIGURE 2 — The fracture face of the Monel Alloy K-500 Bolt in Figure 1, showing the apparent fracture origin (arrow) with emanating radial marks and secondary cracking.



FIGURE 3 — The general microstructure of a failed Monel Alloy K-500 riser clamp bolt. Etchant: Carapella's Reagent. (100X)

The mechanical property tests conducted on the bolts were tensile, charpy impact, and hardness. These values were all within the range required for the material in the specified heat treatment and will not be discussed in detail. Important conclusions from these tests were that the material had been heat treated properly; there was no mechanical weakening of the grain boundary area (all the test failures were trans-

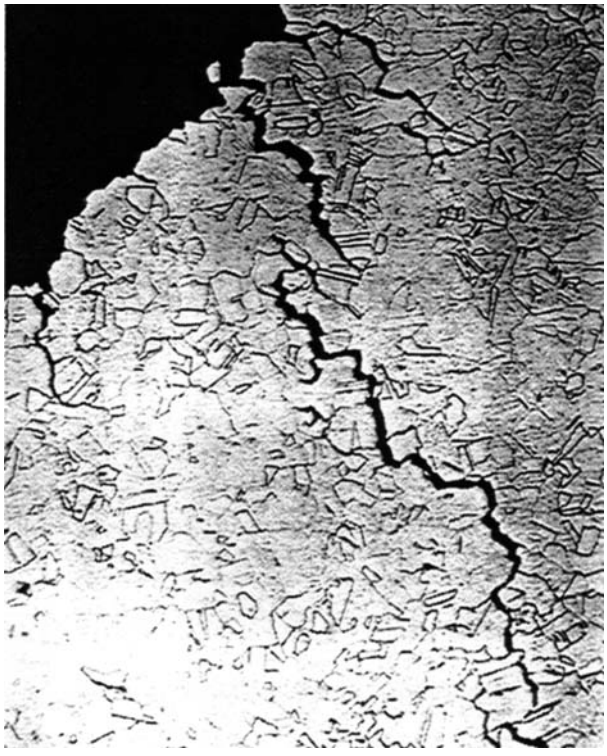


FIGURE 4 — Cross-section of a Monel Alloy K-500 riser clamp bolt failure, showing the secondary intergranular cracking associated with the primary intergranular fracture. Etchant: Carapella's Reagent. (100X)



FIGURE 5 — Cross-section of a Monel Alloy K-500 riser clamp bolt failure at the thread root, crack-initiation area. Note the zone of fine grains adjacent to the threaded surface, followed by a band of course grains. Etchant: Carapella's Reagent. (100X)

granular), and the test failures for both tensile and impact loading were ductile. The service failures encountered were all intergranular and brittle.

The results of detailed compositional analyses of two of the bolts are given in Table 1. These are within the nominal limits specified by ASTM F468. Hydrogen analysis of the bolt shank gave concentrations up to three parts per million (ppm) at the center and only slightly higher values near the outer surface. In the thread root area at the fracture face, however, the hydrogen concentration rose significantly to 18 ppm as indicated in Table 2.

Discussion

The major objective after examining the results of the failure analysis is to determine a failure mechanism that accounts for all of the observed phenomena. The clues to the

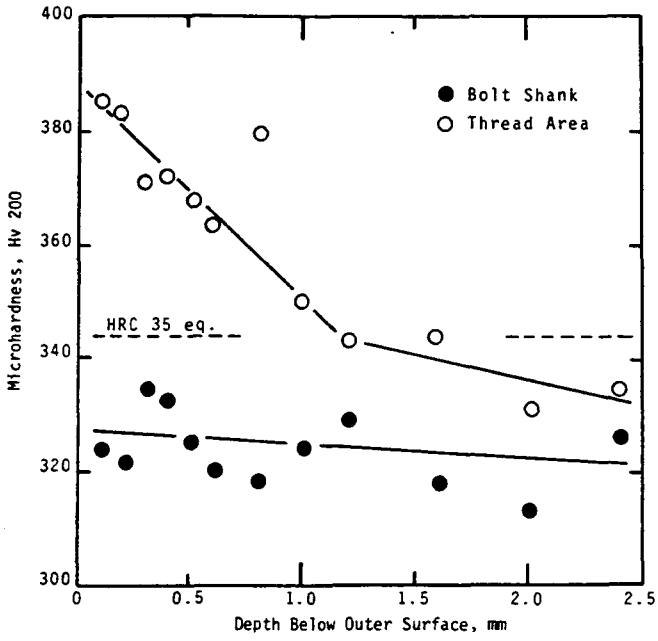


FIGURE 6 — Microhardness profile of the cross-section of a fractured Monel Alloy K-500, riser clamp bolt.

cause of failure considered to be most significant are as follows:

1. The failed bolts are in the most highly stressed clamps on each riser.
2. The failure occurs at the root of the first full thread.
3. Cracking is intergranular and highly branched.
4. There is a high hydrogen concentration at the thread surface.
5. The microhardness at the thread surface is much higher than the body of the bolt.
6. An alteration in grain structure has occurred at the thread surface.

Intergranular cracking of Monel Alloy K-500 is symptomatic of stress corrosion cracking or hydrogen embrittlement.[3] If this assumption is made, there are certain criteria which must be met before Monel Alloy K-500 will crack:

1. The stress level must be above the threshold level for stress corrosion cracking or hydrogen embrittlement.
2. The local hardness at the crack initiation site must be greater than HRC 35.
3. There must be a source of hydrogen for hydrogen embrittlement.

The surface of the thread root area has a hardness greater than HRC 35, as shown in Figure 6. This high local hardness is probably due to severe cold work of the threads during the machining operation, coupled with the precipitation hardening heat treatment. The effect of cold work on the resulting hardness of Monel Alloy K-500 after precipitation hardening is given in Figure 7. This demonstrates that, with severe cold work, the observed local hardness could be achieved on precipitation hardening.

TABLE 2 — Hydrogen analysis of a failed Monel Alloy K-500 riser clamp bolt

Location	H_2 Content, ppm
Shank near outer edge	4.0 - 4.5
Shank at center	2.5 - 3.0
Near fracture	17.0 - 18.5

The stress level on the bolts was very high in this particular case, since the failures occurred in the primary load bearing clamps for the risers. There is no question that the threshold stress for hydrogen embrittlement or stress corrosion cracking could be exceeded under these conditions. In addition, this high stress would serve as an accelerating factor for hydrogen entrance into the metal, as has been documented for sour environments.[3]

The source of hydrogen is the platform cathodic protection system. Aluminum sacrificial anodes in the vicinity of the clamps have shifted the potential to approximately −1.0 V (SCE). This would not normally cause hydrogen to enter the metal; however, the very high stress level could produce this effect.

The two cracking mechanisms can be distinguished by the effects of cathodic protection.[6] Stress corrosion cracking is inhibited or prevented by cathodic protection, while hydrogen embrittlement is accelerated by cathodic protection. At the measured potential of the bolts (−1.0 V, SCE), stress corrosion cracking could not occur, and hydrogen embrittlement would be accelerated.

Although there is no conclusive data from separate corrosion tests that these bolts did fail by hydrogen embrittlement, the evidence pointing to this as the cause of failure is overwhelming. As a result, a specification was written for Monel Alloy K-500 bolts designed to prevent this type of failure. The principle of failure prevention was to eliminate the excessively hard areas at the bolt thread root.

To prevent hardening of these areas, the specification requires that all Monel Alloy K-500 bolts be full annealed after all machining and before age hardening. Annealing eliminates the highly cold worked areas in the bolt threads before the age hardening heat treatment. The detailed specification for Monel Alloy K-500 bolting is given in Table 3.

This specification has been in use for over two years, and there have been no failures of bolts with the new heat treatment. There have, however, been additional failures of the bolts that had not undergone the specified heat treatment. As

TABLE 1 — Chemical composition of failed Monel Alloy K-500 riser clamp bolts and nominal composition limits

	Composition, wt% (Bal Ni)								
	Cu	Fe	Mn	Al	Ti	C	Si	S	P
Bolt A	29.8	0.97	0.72	2.96	0.56	0.19	0.08	0.004	0.0008
Bolt B	29.7	1.04	0.74	2.97	ND	0.15	0.12	0.004	0.011
Nominal limits	27-33	2.0, max	1.50, max	2.3-3.2	0.35-0.85	0.25, max	0.5, max	0.01, max	—

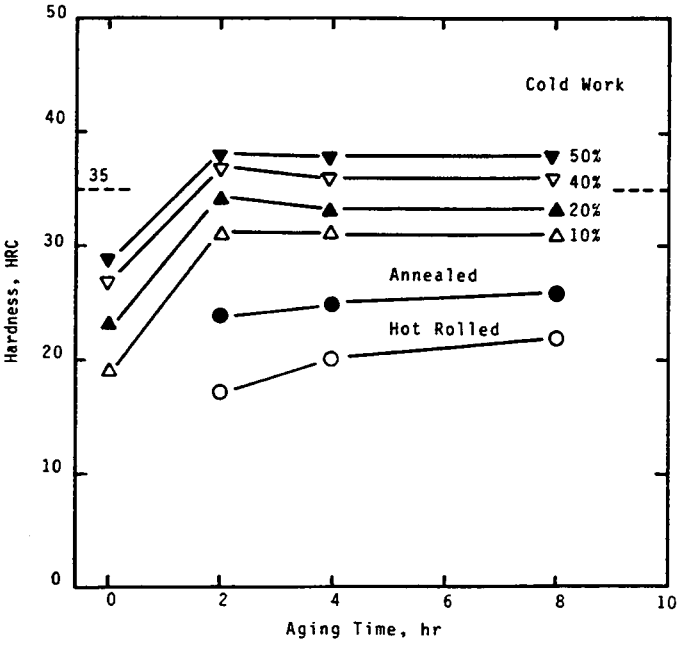


FIGURE 7 — The effect of aging at 595 C (1100 F) on the hardness of cold-worked Monel Alloy K-500.

a result of this experience, all Monel Alloy K-500 bolts for use in seawater are now specified using the requirements given in Table 3.

Conclusions

1. Monel Ni-Cu-Al Alloy K-500 can fail by hydrogen embrittlement in seawater. A very specific set of conditions is required which includes high hardness as a result of extensive cold work preceding precipitation hardening, high stress in service, and cathodic polarization.

2. Full annealing is required after threading and before precipitation hardening to eliminate the cause of high hardness in the thread root and to prevent the hydrogen embrittlement failures of Monel Alloy K-500 in seawater.

References

1. W. K. Boyd and W. E. Berry, Stress Corrosion Cracking of Metals—A State of the Art, STP 518, ASTM, Philadelphia, Pennsylvania, p. 58, 1972.
2. H. R. Copson and C. F. Cheng, Corrosion, Vol. 12, No. 12, p. 647t, 1956.
3. M. R. Chance, H_2S Corrosion in Oil and Gas Production—A Compilation of Classic Papers, National Association of Corrosion Engineers, Houston, Texas, p. 464, 1981.
4. Metals Handbook, 8th ed., Vol. 9, "Fractography and Atlas of Fractographs," American Society for Metals, Metals Park, Ohio, p. 77, 1974.
5. Monel Nickel-Copper Alloys, 4th ed., Huntington Alloys Inc., Huntington, West Virginia, p. 47, 1981.
6. F. L. LaQue, Marine Corrosion, John Wiley & Sons, New York, New York, p. 215, 1975.

TABLE 3 — Specification for Monel Alloy K-500 bolts for seawater applications

1.0. The basic requirement shall be to ASTM specification F 468 (F 468M) "Non Ferrous Bolts, Hex Cap Screws, and Studs for General Use," with the supplementary requirement S5 "Heat Control," and as modified in the following sections.

2.0. Only hot or cold rolled stock material shall be permitted. Extruded material shall not be used. The chemical analysis shall conform strictly to ASTM F 468, with particular emphasis on sulfur. A sulfur level above the 0.01% maximum shall not be used.

3.0. Preheat Treatment Requirements

3.1. All bolt forming and threading operations shall be completed before any heat treatment.

3.2. Sulfurized cutting lubricants shall be removed completely by cleaning in a sodium cyanide or chromic/sulfuric acid bath prior to any heat treatment. Prolonged exposure to the cleaning solution must be avoided.

4.0. Finished machined bolts shall undergo a two-stage heat treatment of a full annealing followed by precipitation hardening.

4.1. The bolt annealing parameters shall be:
Temperature range: 1800-1850 F (980-1010 C)
Time at temperature: 10 minutes
Cooling: Water quench

3.2. The bolt precipitation hardening parameters shall be:
Temperature range: 1100-1125 F (593-616 C)
Time at temperature: 16 hours
Cooling rate: 15-25 F/h (8-14 C/h)
Controlled cooling to: 900 F (480 C)

Copyrighted Materials
Copyright © 1996 NACE International Retrieved from www.knovel.com

Stress corrosion cracking and hydrogen embrittlement of high-strength nonmagnetic alloys in brines*

J. G. Erlings, H. W. deGroot, and J. F. M. van Roy*

Unexpected brittle failures of UNS N05500 drill string parts and nonmagnetic drill collars have recently been observed in cases where the UNS N05500 components were galvanically coupled to carbon steel in concentrated salt solutions at temperatures between ambient and higher than 373 K (100 C). Cracking occurred preferably at locations with a tri-axial stress condition (roots of threads) and has been ascribed to hydrogen embrittlement. Mechanical and slow strain rate tests with UNS N05500, either at the free corrosion potential or galvanically coupled to carbon steel, have been carried out in $MgCl_2$ mud to determine the conditions under which hydrogen embrittlement occurs. A number of alternative high-strength nonmagnetic alloys were included in the tests. It was found that under all test conditions, UNS N05500 was embrittled by hydrogen when galvanically coupled to carbon steel. It was immune to cracking at its free corrosion potential. Under the conditions of our tests, alloys SCF 19, N 10276, and R 30035 were not susceptible to either stress corrosion cracking (SCC) or hydrogen embrittlement.

Introduction

AT A RECENT SEMINAR in Paris on materials for downhole equipment, it was reported that alloy UNS N05500 accessories had cracked extensively under severe conditions at 408 K (135 C). Cracking had been found to be related to hydrogen charging of the parts and had often been initiated at mechanical damage spots. Hydrogen charging (up to concentrations of 100 to 200 ppm) had been caused by cathodic polarization of the alloy owing to its being galvanically coupled to actively corroding carbon steel components.

At a later stage, we measured hydrogen evolution on noncorroding UNS N05500 galvanically coupled to carbon steel in various concentrated chloride-bearing muds at temperatures above 318 K (45 C). In $MgCl_2$ mud, at 408 K (135 C), maximum hydrogen reduction current densities on UNS N05500 were approximately 0.3 A/m^2. Under comparable service conditions, viz. concentrated-chlorides-based on dolomite muds, galvanic coupling to carbon steel and temperatures above 373 K (100 C), we experienced cracking of UNS N05500 drill collars, primarily intergranular but also transgranular. Cracking preferentially started at the roots of threads, where micro-Vickers hardness measurements showed a hardened layer of 0.5 to 1 mm depth of 370 to 400 Vickers hardness. The parent metal hardness was 300 to 330 Vickers.

Other investigators previously reported that hydrogen-charged UNS N05500: (1) exhibits delayed failure when statically stressed at temperatures in the range 443 to 533 K (170 to 260 C) and (2) shows embrittlement during slow straining at lower temperatures.[3,4] Further, UNS N05500 electrolytically charged with hydrogen proved embrittled.[5] Failure of hydrogen-charged UNS N05500 was found to begin with cracking at or near the surface when the material was subjected to strain.[5] Failure of UNS N05500 bolts by hydrogen embrittlement under cathodic protection (CP) in seawater has also been reported.[6] This failure was ascribed to high hardness (HV (200) > 350) as a result of extensive cold work, high service stress and CP. Application of a full annealing treatment after cold work followed by precipitation hardening prevented any further cracking of the bolts. In normal drilling practices, cold work of threads and shoulders of nonmagnetic drill collars (NMDC) is inevitable; hence an increased hardness at these locations cannot be eliminated.

The experience with UNS N05500 has stimulated a further investigation into its cracking behavior under drilling conditions, comparing it with that of other nonmagnetic, high-strength materials. Here we concentrate on hydrogen embrittlement and stress corrosion cracking (SCC) behavior and do not address other important aspects.

Experimental procedures

In uni-axial tensile tests where: 1 = 5 d round bars [gage length (1) = 17.5 mm, diameter (d) = 3.5 mm], the ultimate tensile strength (σ_{UTS}), the strain at fracture (ϵ_f) and the reduction of area (ROA) of UNS N05500 from a failed NMDC were measured. These properties were also measured after the test bar had been electrochemically charged with hydrogen in a solution containing 0.5 g As_2O_3 + 2 mL (96%) H_2SO_4/L at a current density of 10 to 50 A/m^2 at 363 to 368 K (90 to 95 C). Tensile tests were also carried out at room temperature with a number of other nonmagnetic materials both in the as-received condition and after 570 h of exposure in aerated

• Presented during CORROSION/86, Paper No. 162, NACE, Houston, TX, 1986.

*Koninklijke/Shell Laboratorium, Amsterdam (Shell Research B. V.), P.O. Box 1003, Amsterdam, The Netherlands.

$MgCl_2$ mud at 398 K (125 C) under compressed air or 40 to 80 bar CO_2. The alloys tested are listed in Table 1.

Impact testing was carried out with Charpy V-notch specimens (ASTM 1983, E23) both in the as-received condition and after approximately 30 days exposure to a stirred aerated $MgCl_2$ brine at 398 K (125 C). The exposed specimens were galvanically coupled to carbon steel plates with equal surface areas exposed in the same vessel. The galvanic current between the alloy tested and carbon steel was measured as a function of time with a zero resistance ammeter.

Slow strain rate (SSR) tests were used to determine the susceptibility to SCC and hydrogen embrittlement. Tensile bars were pulled to fracture at a slow strain rate (approximately 1.6×10^{-6}/s), while being exposed to the relevant environmental conditions either at their free corrosion potential or galvanically coupled to a piece of carbon steel. The SSR tests carried out are shown in Table 2.

Results and discussion

The fracture strain measured for UNS N05500 taken from a failed NMDC is given in Table 3. The results in this table show that, after 1 y storage at room temperature, the fracture strain has increased significantly. This must be attributed to reduced embrittlement from the absorbed hydrogen diffusing out during the storage period. Fracture strain and also reduction of area are known to decrease by absorption of hydrogen.[7] With a hydrogen diffusion coefficient $D \sim 5 \times 10^{-14}$ m²/s $\sqrt{Dt}$ (t is time) for 1 y is about 1.3 mm, which is nearly half the diameter of our stored tensile bars.[5,8,9] The same effect, but more pronounced, was measured previously with UNS N05500 that had seen severe downhole service. By heating the latter material at 473 K for 5 days, both ϵ_f and ROA increased from 13 to 24%. Charging the same material with hydrogen for 67 h (same conditions as described in Experimental Procedures) reduced ϵ_f and ROA to 7 and 3%, respectively. In the present

TABLE 1 — Chemical composition (in wt%) and heat treatments of the materials tested

	C	S	P	Si	Mn	Ni	Cr	Mo	V	Cu	Nb	Al	Co	Fe	Ti	Be
1. UNS N05500	a. not determined															
	b. 0.16	0.001	—	0.15	0.67	65.23	—	—	—	29.00	—	2.80	—	0.56	0.55	—
	c. 0.14	<0.001	<0.005	0.09	0.89	bal.	0.06	0.01	<0.01	27.4	<0.01	2.93	0.10	0.98	—	—
2. UNS C17200	—	—	—	0.1	0.003	0.03	0.003	—	—	bal.	—	0.04	0.20	0.07	—	1.78
	(0.003 Ca, 0.003 Li, 0.06 Mg, 0.01 Sn)															
3. SCF 19	0.026	<0.001	0.02	0.37	4.87	17.3	19.7	5.12	0.10	0.22	0.02	<0.05	0.18	bal.	—	—
4. Pyromet 31	0.044	<0.001	0.01	0.07	0.10	bal.	22.5	2.01	0.03	0.09	1.00	1.48	0.04	14.8	—	—
5. SC 2205	0.038	0.003	0.02	0.68	18.3	0.28	11.9	1.10	0.02	0.02	0.01	<0.05	<0.01	bal.	—	—
6. XM 19	0.043	0.001	0.03	0.71	18.8	2.01	12.4	1.04	0.03	0.03	0.04	<0.05	0.03	bal.	—	—
7. Incoloy 925	0.02	0.001	—	0.28	0.64	41.81	22.87	2.75	—	1.75	—	0.25	—	27.52	2.11	—
8. UNS N10276	<0.002	0.006	0.006	<0.02	0.42	bal.	15.57	15.52	0.13	—	—	—	2.30	6.15	(W 3.75)	
9. UNS R30035	0.009	0.003	0.005	0.02	0.02	35.60	20.54	9.35	—	—	—	—	bal.	0.45	0.85	—

1. (a) annealed and aged
   (b) annealed
   (c) aged to 900 MPa
2. AT temper
3. hot/cold worked, contains nitrogen
4. solution annealed, aged and c.g.
5. cold deformed to 1000 MPa
6. cold deformed to 1000 MPa, contains nitrogen. Aubert and Duva alloy
7. annealed at 1311 K (1038 C), aged 16 h at 991 K (718 C), air cooled
8. heat treatment unknown
9. heat treatment unknown

TABLE 2 — Summary of slow strain rate tests and results

No.	Material	Medium	Gas cap	T (K)	σ_{UTS} (MPa)	ϵ_f (%)	ROA (%)	Observations on fractured bars and remarks
1	UNS N05500 (a)	air	air	298	1142	22.0	34	strain rate 3.2×10^{-4}/s
2	UNS N05500 (b)	$MgCl_2$-mud	air	348				no cracks, ductile fracture
3	UNS N05500 (b) polarised at the potential of a piece of co-exposed C-steel	$MgCl_2$-mud	air	348				some small cracks, ductile fracture
4	UNS N05500 (a) galv. coupled to C-steel	$MgCl_2$-mud	air	353	1074	16.2	21	some small cracks, ductile fracture
5	UNS N05500 (a)	$MgCl_2$-mud	air	373	1026	15.8	28	no cracks, ductile fracture
6	UNS N05500 (a) galv. coupled to C-steel	$MgCl_2$-mud	air	373	1060	-	24	cracks in bar, brittle areas on fracture face
7	UNS N05500 (a)	$MgCl_2$-mud	air	398	1031	19.4	10-15	no cracks, ductile fracture
8	UNS N05500 (a) galv. coupled to C-steel	(i) $MgCl_2$-mud	air	398	1044	11.7	12	cracks in bar, brittle areas on fracture face
		(ii) $MgCl_2$-mud	air	398	1055	14.9	23	cracks in bar, brittle areas on fracture face
9	UNS N05500 (a) galv. coupled to C-steel	$MgCl_2$-mud	60 bar CO_2	398	1060	13.2	15	cracks in bar, brittle areas on fracture face
10	UNS N05500 (a)	$CaCl_2$-mud	air	423	1040	20	32	only 2 small cracks in necked

Continued on next page

TABLE 2 Continued — Summary of slow strain rate tests and results

								region
11	UNS N05500 (a) 90 hours pre-exposed	$MgCl_2$-mud	65 bar CO_2	433	1008	16.1	24	cracks in bar and pitting
12	UNS N05500 (c)	air	air	298	924	28	40	strain rate $3.2x10^{-4}$/s
13	UNS N05500 (c)	$MgCl_2$-mud	air	373	927	21.5	35	no cracks in bar, ductile fracture
14	UNS N05500 (c)	$MgCl_2$-mud	air	398	815	23	40	no cracks in bar, ductile fracture
15	UNS N05500 (c)	$MgCl_2$-mud	60 bar CO_2	398	826	22	35	no cracks in bar, ductile fracture
16	UNS C17200	air	air	298	964	12.4	24	strain rate $3.2x10^{-4}$/s
17	UNS C17200 galv. coupled to C-steel	(i) $MgCl_2$-mud (ii) $MgCl_2$-mud	air	353 358	1049 948	11.2 10	25 15-19	no cracks in bar, ductile fracture no cracks in bar, ductile fracture
18	UNS C17200	$MgCl_2$-mud	air	373	959	11.2	22	no cracks in bar, ductile fracture
19	UNS C17200 galv. coupled to C-steel	$MgCl_2$-mud	air	373	1019	-	20	no cracks in bar, ductile fracture
20	UNS C17200	$MgCl_2$-mud	air	398	971	10.1	16-20	no cracks in bar, ductile fracture
21	UNS C17200 galv. coupled to C-steel	$MgCl_2$-mud	air	398	1096	8.8	5-7	no cracks in bar, ductile fracture other material with lower ϵ_f and ROA in the as received condition
22	UNS C17200	$MgCl_2$-mud	60 bar CO_2	398	933	9.8	12	no cracks in bar, ductile fracture
23	UNS C17200 112 hours pre-exposed	$MgCl_2$-mud	80 bar CO_2	433	898	4.7	13	cracks in bar and severe corrosion
24	SCF 19	air	air	298	1045	36	52	strain rate $3.2x10^{-4}$/s
25	SCF 19	$MgCl_2$-mud	air	398	895	25	52	no cracks in bar, ductile fracture
26	SCF 19 galv. coupled to C-steel	$MgCl_2$-mud	air	398	953	22	55	no cracks in bar, ductile fracture
27	Pyromet 31	air	air	298	1280	24.6	30	strain rate $3.2x10^{-4}$/s
28	Pyromet 31	$MgCl_2$-mud	air	373	1229	17.8	21	stress corrosion cracking
29	Pyromet 31	$MgCl_2$-mud	air	398	1224	11.8	17	stress corrosion cracking
30	SC 2205	air	air	298	1012	40	56	strain rate $3.2x10^{-4}$/s
31	SC 2205	$MgCl_2$-mud	air	398	830	14.3	21	stress corrosion cracking
32	XM 19	air	air	298	903	44	57	strain rate $3.2x10^{-4}$/s
33	XM 19	$MgCl_2$-mud	air	398	651	8	10-15	stress corrosion cracking
34	Incoloy 925	$MgCl_2$-mud	air	398	1071	18.5	35	no cracks in bar, ductile fracture
35	Incoloy 925 galv. coupled to C-steel	$MgCl_2$-mud	air	398	1034	5.2	8	no cracks in bar, some pits in reduced area, brittle intergranular fracture
36	N10276	air	air	298	1315	14	55	strain rate $3.2x10^{-4}$/s
37	N10276	$MgCl_2$-mud	air	398	1157	13	55	no cracks in bar, ductile fracture
38	N10276 galv. coupled to C-steel	$MgCl_2$-mud	air	398	1244	10	45	no cracks in bar, ductile fracture
39	R30035	air	air	298	1453	15	55	strain rate $3.2x10^{-4}$/s
40	R30035	$MgCl_2$-mud	air	398	1379	13	55	no cracks in bar, ductile fracture
41	R30035 galv. coupled to C-steel	$MgCl_2$-mud	air	398	1376	10	36	no cracks in bar, ductile fracture

1 — °C = °K — 273

investigation, we see a significant reduction in ϵ_f and ROA by hydrogen charging for 136 h (Table 3). The fracture features change correspondingly toward more brittle behavior. These observations indicate that in the UNS N05500 failures embrittlement by hydrogen played a dominant role. As mentioned before, the hydrogen can be generated on the noncorroding NMDC in hot $MgCl_2$ and $CaCl_2$ mud by the galvanic coupling to carbon steel drill string components.[2]

In UNS N05500 bolts, which most likely failed by hydrogen embrittlement, Efird found a higher concentration of hydrogen at the root of threads than at other locations.[6] This suggests that the embrittlement in the severe tri-axial stress situation existing at the roots of the threads of the NMDC, where cracking often started, may be significantly more severe than measured in the tensile tests reported here, although the application of a uni-axial tensile stress also increases the amount of absorbed hydrogen.[10] The higher hardness at the root of the threads is believed not to affect the amount of hydrogen absorbed, although it will enhance embrittlement by a greater notch sensitivity.[5]

The results of Table 4 show that exposure of alternative NMDC materials at their free corrosion potentials to hot $MgCl_2$ mud (S.G. 1.4 KG/L) with and without dissolved CO_2 had no significant effect on their mechanical properties, which were determined at room temperature. In the absence of diffusion barriers on the surface, the exposure time was long enough to establish a constant hydrogen concentration in the tensile bars, if hydrogen should have been absorbed at the surface. Hence, hydrogen embrittlement of the materials tested at their free corrosion potentials was not possible under the applied environmental conditions. For UNS N05500, this agrees with measured free corrosion potentials, which were more positive than the hydrogen equilibrium potential, and the observed passivity of the alloy.[2] None of the materials tested was affected by general and/or localized corrosion.

In the impact tests pre-exposure of the Charpy V-notch im-

TABLE 3 — Mechanical properties of UNS N05500 from a failed NMDC, as received and after various treatments (uni-axial tensile tests)

Material condition	σ_{UTS} (MPa)	ϵ_f (%)	ROA (%)	HV	Type of fracture
As received	—	16.8	—		NMDC failed partly trans- and intercrystalline, brittle
After 1 y storage at room temperature	1139	22.6	30		ductile
As received and charged with hydrogen for 48 h	1100	18.1	37		ductile, some transgranular, brittle
As received and charged with hydrogen for 136 h	1111	13.3	16	325	ductile, transgranular, brittle at the circumference of the fracture plane, several small brittle cracks in the gage

TABLE 4 — Mechanical properties (in air at ambient temperature) of various NMDC candidate materials after 571 h in aerated $MgCl_2$ at 398 K (125 C) in equilibrium with compressed air/40-80 bar CO_2

	σ_{max} (N/mm²)	ϵ_f (%)	ROA (%)
UNS C17200	958/945	12.7/11.9	21/23
UNS C17200, blank	964	12.4	24
UNS N05500	1121/1105	19.2/17.8	26/23
UNS N05500, blank	1142	22.0	34
Pyromet 31	1280/1270	26.6/27.0	30/30
Pyromet 31, blank	1280	24.6	30
XM-19	923/897	41/43	48/58
XM-19, blank	903	44	57
SC 8001	924/907	25/20	37/38
SC 8001, blank	924	28	40
SC 2205	975/982	43/34	59/55
SC 2205, blank	1012	40	56

TABLE 5 — Charpy V-notch impact tests on as received material and material exposed to $MgCl_2$ mud at 498 K (225 C), galvanically coupled to carbon steel. (Values are averages of three measurements)

Material	Impact energy, J	
	As received	After exposure
UNS N05500	36	32
UNS C17200	27	27
UNS N10276	219	228
UNS R30035	68	66

pact specimens had no noticeable effect, although a cathodic current density of approximately 0.05 to 0.4 A/m² was impressed on the surface (Table 5). The observed current densities decreased initially somewhat but were always of the same order of magnitude as those previously found in galvanic cell measurements.[2] When the effect of absorbed hydrogen is caused by diffusion of hydrogen to highly deformed areas, the impact test is too short to reveal any effect. Papp, et al., reported that at strain rates higher than about 1/s (which is slower than the impact strain rate) embrittlement is eliminated at room temperature.[4] It should be noted that some effects have been reported by Milliams and Harris, et al., for materials with higher impact energies.[1,5]

The results of SCC and hydrogen embrittlement (HE) tests are given in Table 2. UNS N05500 was not susceptible to cracking at its free corrosion potential in aerated muds. However, at 433 K (160 C) and 65 bar CO_2, cracking and pitting were found at the free corrosion potential. When UNS N05500 was coupled to carbon steel, intergranular and transgranular brittle cracks were found at all test temperatures. The extent of cracking outside the necked region increased with increasing test temperature (Figure 1). As the surface area ratio of carbon steel to slow strain rate bar was one to one, these results indicate that a UNS N05500 NMDC may suffer from hydrogen embrittlement close to the position where it is coupled to carbon steel components.

In a test at 433 K (160 C) with 80 bar CO_2, cracking and severe corrosion of UNS C17200 were found. Under all other conditions applied in our tests, UNS C17200 was susceptible neither to SCC nor to HE. Alloy SCF 19 was immune to SCC and HE at 398 K in aerated $MgCl_2$ mud. At 373 and 398 K (100 and 125 C, respectively), alloy Pyromet 31 was susceptible to SCC at its free corrosion potential. Extensive transgranular cracking was found (Figure 2). Predominantly transgranular stress corrosion cracking (TGSCC) at the free corrosion potential was also found with alloys SC 2205 and XM 19 at 398 K (125 C) (Figures 3 and 4). As a result of SCC, ϵ_f and ROA were large-

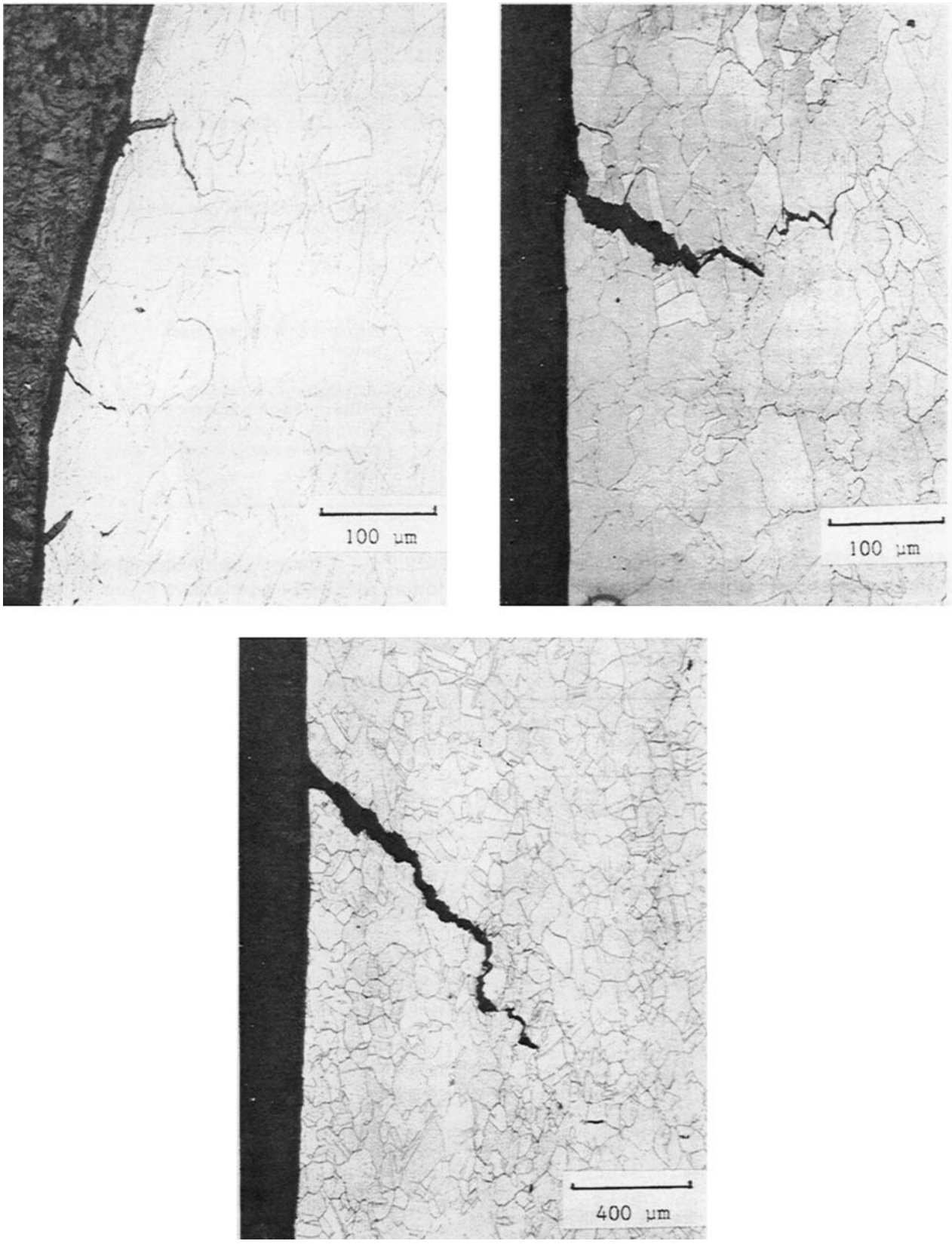


FIGURE 1 — Diametral cross section of UNS N05500 tensile bars after slow strain rate testing in aerated $MgCl_2$ mud. The bars were galvanically coupled to equally large areas of carbon steel: (a) 348 K (75 C), (b) 373 K (100 C), and (c) 398 K (125 C).

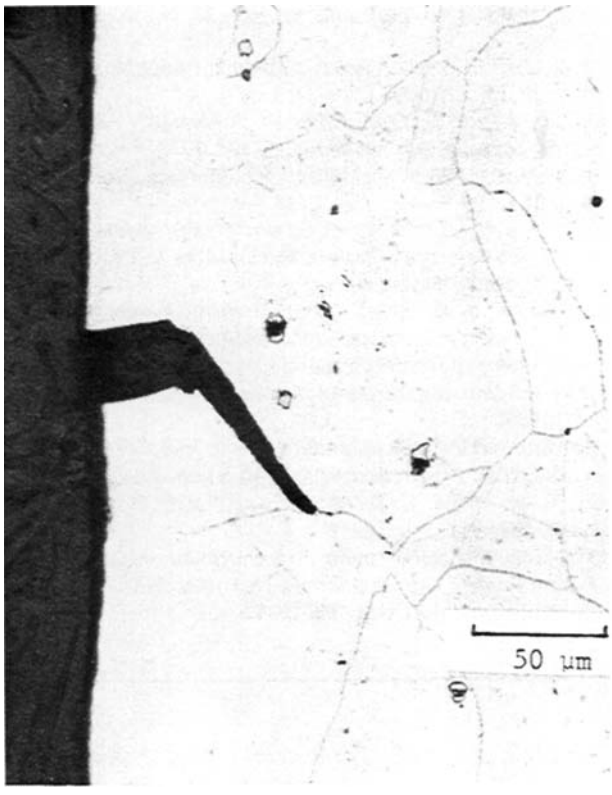


FIGURE 2 — Diametral cross-section of Alloy Pyromet 31 tensile bar after slow strain rate testing in aerated $MgCl_2$ mud at 398 K (125 C).

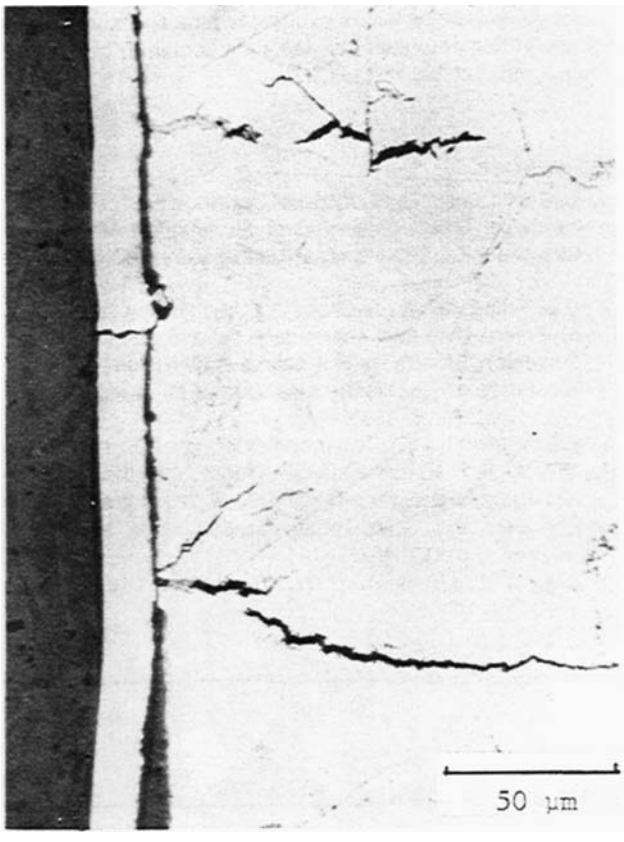


FIGURE 4 — Diametral cross-section of Alloy XM 19 tensile bar after slow strain rate testing in aerated $MgCl_2$ mud at 398 K (125 C).

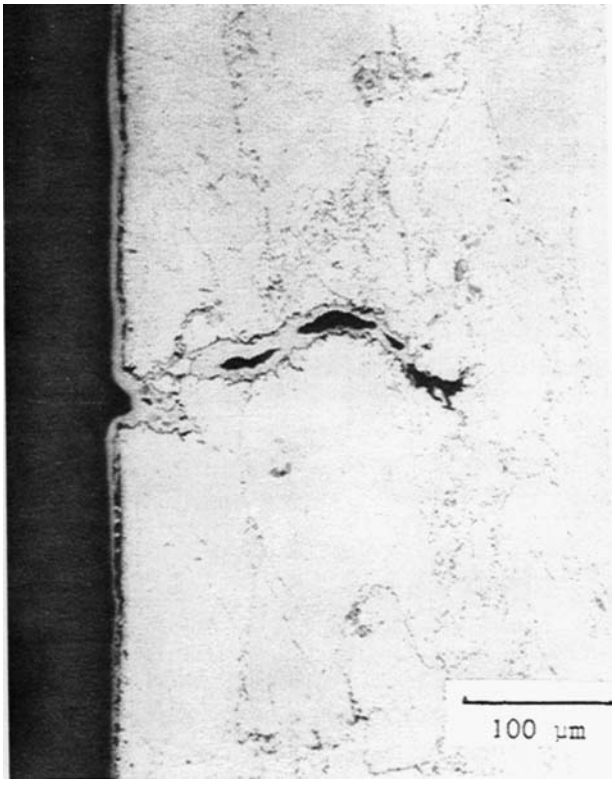


FIGURE 3 — Diametral cross-section of Alloy SC 2205 tensile bar after slow strain rate testing in aerated $MgCl_2$ mud at 398 K (125 C).

ly decreased (Table 2). The behavior of alloy Incoloy 925[1] was extremely brittle in $MgCl_2$ mud when coupled to carbon steel. The embrittlement is also clearly illustrated by a decrease in ROA from 35 to 8%. The same effect was previously found with Incoloy 925 containing sigma phase. The brittle fractures were predominantly intergranular. Alloys N10276 and R30035 were susceptible neither to SCC nor to HE at 398 K (125 C). The resistance to HE was already expected on the basis of results reported by Vaughn and Greer Stroup, et al., and Troiano and Hehemann.[11-13]

Conclusions

1. Alloy UNS N05500 nonmagnetic drill collars failed in service from hydrogen embrittlement. Cracks preferably started at locations with a severe tri-axial stress situation. The hydrogen charging was caused by galvanic coupling to carbon steel.

2. Alloy UNS N05500 is susceptible to hydrogen embrittlement when galvanically coupled to carbon steel in aerated $MgCl_2$ in the temperature range studied, viz. 348 to 398 K (75 to 125 C). At its free corrosion potential alloy UNS N05500 is susceptible neither to SCC nor to HE under these conditions.

3. At their free corrosion potentials and when galvanically coupled to carbon steel, alloys UNS C17200, SCF 19, N10276, and R30035 are susceptible neither to SCC nor to HE at 398 K (125 C) in aerated $MgCl_2$ mud. This was also found for UNS C17200 at 353 K (80 C) and 373 K (100 C).

4. At their free corrosion potentials in $MgCl_2$ mud at 398 K (125 C), alloys Pyromet 31, SC 2205, and XM 19 are susceptible to SCC but not to HE.

---

[1]Registered trade name.

5. Alloy Incoloy 925 is extremely sensitive toward hydrogen embrittlement when galvanically coupled to carbon steel in $MgCl_2$ mud at 398 K (125 C).

References

1. D. E. Milliams, "The Combat of Downhole Corrosion Caused by Sweet Gas," presented at Seminar on Materials for Downhole Equipment, organized by Vallourec, Paris, June 1985.
2. J. G. Erlings, H. W. de Groot, J. F. M. van Roy, "Application of Electrochemical Techniques in a Study of Galvanic Corrosion Effects in Hot Concentrated Salt Solutions," Workshop on Electrochemical Corrosion Testing, Ferrara, Italy, Sept. 11-13, 1985.
3. J. L. Mihelich, A. R. Troiano, *Nature,* Vol. 197, p. 996, 1963.
4. J. Papp, R. F. Hehemann, A. R. Troiano, "Hydrogen Embrittlement of High Strength FCC Alloys," *Hydrogen in Metals,* I. M. Bernstein, A. W. Thompson, Eds., ASM, Metals Park, PA, Vol. 4, p. 657, 1973.
5. J. A. Harris, R. C. Scarberry, C. D. Stephens, *Corrosion,* Vol. 28, p. 57, 1972.
6. K. D. Efird, *Materials Performance,* Vol. 24, No. 4, p. 37, 1985.
7. J. A. Harris, T. F. Lemke, CORROSION/82, Paper No. 137, NACE, Houston, TX, 1982.
8. G. Alefeld, J. Volkl, Eds., Hydrogen in Metals. I. Basic Properties, Springer Verlag, Berlin, p. 327, 1978.
9. K. A. Lee, R. B. McLellan, Scripta Metallurgica, Vol. 18, p. 859, 1984.
10. M. R. Chance, *H_2S Corrosion in Oil and Gas Production—A Compilation of Classic Papers,* R. N. Tuttle, R. D. Kane, Eds., NACE, Houston, TX, 1981.
11. G. A. Vaughn, J. B. Greer, "High-Strength Nickel-Alloy Tubulars for Deep, Sour Gas Well Application," 55th Annual Fall Technical Conference and Exhibition of the Society of Petroleum Engineers of AIME, Dallas, TX, Sept. 21 to 24, 1980.
12. J. P. Stroup, A. H. Bauman, A. Simkovich, *H_2S Corrosion in Oil and Gas Production—A Compilation of Classic Papers,* R. N. Tuttle, R. D. Kane, Eds., NACE, Houston, TX, p. 426, 1981.
13. A. R. Troiano, R. F. Hehemann, *H_2S Corrosion in Oil and Gas Production—A Compilation,* R. N. Tuttle, R. D. Kane, Eds., NACE, Houston, TX, p. 426, 1981.

Copyrighted Materials
Copyright © 1996 NACE International Retrieved from www.knovel.com



OTC 5478

Development of Large Nickel-Base Alloy 925 Composite Block Trees for Extreme Corrosion, Fire-Resistant Applications on Offshore Platforms

by T. Haeberle and P.J. Kovach, Vetco Gray Inc.

Copyright 1987 Offshore Technology Conference

This paper was presented at the 19th Annual OTC in Houston, Texas, April 27-30, 1987. The material is subject to correction by the author. Permission to copy is restricted to an abstract of not more than 300 words.

ABSTRACT

This case study presents the development of the first large components to be manufactured from nickel-base Alloy 925 for oilfield use: nine composite block trees used on an offshore production platform producing gas/condensate containing H_2S, CO_2 and chlorides. Details are provided on the material selection process, as well as the manufacture (forging, heat treating and machining) of the composite blocks and smaller equipment. This report introduces Alloy 925 as a candidate for future oilfield applications, providing performance benefits for special design requirements.

INTRODUCTION

Prior to production of the equipment described in this paper, nickel-base Alloy 925 (UNS-N09925) had not been utilized for commercial oilfield gate valves. This significant application for large composite block trees on an offshore platform was designed to capitalize on the corrosion resistance and high temperature properties of this relatively new material, in order to meet performance requirements often required offshore but usually not specified in combination:

- Space savings through composite block design;
- Resistance to H_2S, CO_2 and chlorides;
- Fire-resistant performance to 2000°F (1093°C) external/1200°F (650°C) internal

Nine of these composite block trees were manufactured during 1986, requiring close cooperation and interaction between the equipment designer/manufacturer (Vetco Gray Inc.); the raw material supplier (Inco Alloys International); and the forging company (C-E Beaumont). Since this material had previously only been used in the oil and gas industry for smaller components (such as tubing hangers and downhole production equipment), new techniques were developed for the forging, heat treating and machining of these massive components. The block forgings each weighed more than 10,000 lbs. (4500 kg) and measured 19 in. x 22 in. x 72 in. tall (48 cm x 56 cm x 183 cm), representing the largest components made to date from this new age hardenable nickel-base alloy.

In terms of commercial alloys, nickel-base Alloy 925 is a relatively new material, having first been offered to the market in 1983. As seen in Table 1, Alloy 925 represents basically a minor modification of Alloy 825 (UNS-N08825), an established corrosion-resistant solid solution nickel-base alloy. The increase in titanium content permits significant strengthening by the formation of gamma prime during an aging cycle. The strengthening effect is not only beneficial at room temperature, but also provides increased strength levels at temperatures up to and above 1200°F (650°C). The resistance of Alloy 925 to hydrogen embrittlement, stress corrosion cracking, and general corrosion has been demonstrated by laboratory testing (1).

EQUIPMENT DESIGN CRITERIA

The composite block trees are destined for use on an offshore platform producing gas/condensate containing CO_2, H_2S and chlorides in significant amounts. The basic design criteria, set forth by the end user (operator), were:

In order to achieve maximum space savings on the offshore platform, the trees were to be of a composite block valve design, incorporating the following:

- 5-1/8 in., 5,000 psi lower master valve, manually operated, fire-resistant
- 5-1/8 in., 5,000 psi upper master valve, with hydraulic actuator, fire-resistant
- 5-1/8 in., 5,000 psi wing valve, manually operated
- 2-1/16 in., 5,000 psi wing valve, manually operated
- 5-1/8 in., 5,000 psi swab valve, manually operated

References and figures at end of paper.

© OTC Reprinted with the permission of the Offshore Technology Conference

Figure 1 shows the finished composite block tree, unpainted, with the tubing head attached during assembly and test. Independent wing valves (flanged, 2-1/16 in. and 5-1/8 in., 5,000 psi, with hydraulic actuators) and a positive choke are also attached. The composite block tree is illustrated in Figure 2a.

Considerable space savings were achieved by use of the composite block design for a multiple valve tree. The composite tree incorporated five valves into a finished package approximately 73 in. high by a maximum width of 36 in. (185 cm x 91 cm). If independent flanged API gate valves were used to construct a tree of equal configuration, it would have a height of approximately 104 in. by a maximum width (across the wing section) of 57 in. (264 cm x 145 cm) (Figure 2b).

This composite block design offered savings of 31 in. (79 cm) in height and 21 in. (53 cm) in overall width. This space savings can translate into structural steel on every deck, and is a critical cost consideration.

Corrosion Resistance:

The composite block trees had to be resistant to an environment containing significant corrosion: greater than 5 psia H_2S (34.47 kPa); 150 psia CO_2 (1034.2 kPa); 12,000 ppm chlorides; all at temperatures to 250°F (120°C).

Fire-Resistant Performance:

To provide a maximum of safety, the end user specified that the manual lower master valve and the actuated upper master valve meet the requirements of API RP 6F, 3rd Edition, Fire Test for Valves (Table 2). Under these guidelines, the valves had to be designed to experience external flame temperatures of 2000°F (1093°C) and internal temperatures up to 1200°F (650°C), and still maintain the seal.

Forged Structure:

The composite block trees were required to be manufactured of forged material, since the operator's specification did not accept casting as a means of fabricating the large composite trees. Additionally, per the operator's requirements, the blocks were to be solid alloy construction.

MATERIAL SELECTION

Initially, the operator specified 22% chromium duplex stainless steel for the composite block trees. After reviewing the basic design criteria, however, nickel-base Alloy 925 was recommended (and approved) as the material of choice for this application.

Use of a duplex stainless steel, as originally requested by the end user, would have compromised other design criteria, particularly the requirement for fire-resistant performance. Duplex stainless steels are subject to formation embrittling phases at elevated temperatures. The formation of both sigma phase and alpha prime in NACE MR-01-75 approved duplex stainless steels (i.e., UNS-S32550 and Z6CNDU20.08M,NF A 320-55 French National Standard) can occur in the temperature ranges to which equipment might be exposed during a fire. The formation of either of these phases can result in Charpy V-Notch impact strengths below 10 ft.-lbs. (13.5 J) at room temperature (2,3). Since the maximum design temperature for fire-resistant equipment is above the temperature range where alpha prime forms, the use of duplex stainless steels is not recommended for this application.

If the fire-resistant requirement were eliminated, duplex stainless steel would still not be recommended for the large forged blocks. It is doubtful that duplex stainless steel blocks of this size could be cooled rapidly enough from the annealing temperature to avoid the formation of sigma phase or alpha prime. While the Charpy V-Notch impact values may not be reduced to the single digit level, the stress corrosion cracking resistance would be reduced by the formation of sigma phase. The negative effect of slow cooling on the general corrosion resistance of duplex stainless steels has also been demonstrated (4).

If both the fire-resistant and forging requirements were eliminated, duplex stainless steel would have been an acceptable material. The use of a casting for the composite tree would have resulted in a much thinner cross section, and this would have allowed an acceptable cooling rate.

Weld-cladding with Alloy 625 is another option which should be considered for this type of application because of its cost-effectiveness. Cladding is a proven technology, which would allow the use of low alloy steel for the body mass, lined on the inner wetted surfaces with Alloy 625 (easily weldable and widely recognized as a better alloy for sour service than Alloy 925). This minimal use of exotic alloy significantly reduces the raw material cost versus the use of solid body Alloy 925. However, cladding was not considered an option in the customer's request for quotation.

Additionally, in the case of the smaller components, there is a point where the additional manufacturing costs associated with weld cladding cannot be offset by the savings realized in raw material costs.

As constructed, the Alloy 925 composite block trees utilize Vetco Gray's proven fire-resistant sealing technology in both the lower and upper master valves. This technology incorporates full metal-to-metal sealing and has demonstrated zero leakage to atmosphere in API RP 6F 'Improved' or SIPM test programs (5). The manually operated lower master valve in the block trees is designed to automatically backseat in the event of a fire, regardless of whether the valve is in the open or closed position. The hydraulically actuated upper master valve is designed to fail-closed and provide a backseat in this position.

By using Alloy 925 for this fire-resistant application, Vetco Gray was able to utilize higher allowable design stress levels than would have been feasible if other materials such as low alloy steel had been used. As illustrated in Table 3, Alloy 925 possesses excellent retention of mechanical properties at high temperatures.

While the high strength of Alloy 925 at elevated temperatures is an advantage from the design standpoint, this high strength must be considered during the various manufacturing steps required to produce the finished tree.

MANUFACTURING PROCESSES

Forging

Forging of the composite block trees represented an advance in current technology, in that they are the largest nickel-base Alloy 925 forgings made to date. The starting stock for the forgings consisted of remelt ingots produced by Inco Alloys International at their Huntington, West Virginia facility. Electric furnace melting followed by argon oxygen decarburization (AOD) was the primary melting method. The remelt method utilized was vacuum arc remelting (VAR). The resultant VAR ingots had nominal dimensions of 30 in. diameter and 90 in. length (76 cm x 229 cm).

With a nominal weight of 19,500 lbs. (8845 kg), the mere size of the VAR ingots drastically limits the number of vendors capable of producing the required forgings. Consideration was given to the capacity of forging presses and also to the equipment used for manipulation of the blocks during forging. Both open and impression die forging techniques were considered, but with only nine composite blocks needed, open die forging offered the most cost-effective method, although it increased rough cutting and machining requirements.

Forging of the composite blocks was performed by C-E Beaumont at its Houston, Texas facility. The ingots were conditioned and heated for a sufficient time to allow complete temperature stabilization prior to forging. The ingot was initially upset and redrawn to impart sufficient thermo-mechanical work to the center of the forging (Figures 3 and 4). After reheating, the material was formed into a rectangular block to make the major dimensions of the finished block (Figure 5). The smaller end was then incrementally drawn to dimension and the final dimension passes produced a finished forging (Figure 6).

The forging sequence included several wash-heat cycles due to the narrow temperature range in which Alloy 925 can be successfully worked. Alloy 925, as with most nickel-base alloys, is much more temperature sensitive than the alloys normally used by the oil and gas industry (low alloy and martensitic stainless steels). If the working temperature is not closely controlled, excessive surface tearing will result (7).

While the sheer size of the composite block forgings makes them noteworthy, the smaller Alloy 925 components produced for this project should also be mentioned. As illustrated in Figure 1, an independent flanged valve is attached to each wing of the composite blocks. Each tree had an independent 2-1/16 in., 5,000 psi Alloy 925 wing valve and an independent 5-1/8 in., 5,000 psi Alloy 925 wing valve. These valve bodies and bonnets, as well as all the bonnets on the composite block tree, were forged by C-E Beaumont.

Forging of the small Alloy 925 valve bodies and bonnets was accomplished in impression (closed) dies. Billet stock was used as the starting raw material for these components. Although the size and configuration of the small valve bodies and bonnets allowed for more normal forging practices, the reduced forgeability and temperature sensitivity of Alloy 925 had to be taken into consideration in the die design and forging practice (7). Figure 7 shows a finished 5-1/8 in., 5,000 psi Alloy 925 gate valve complete with actuator, attached to a 5,000 psi positive choke ready for shipping.

Thermal Processing

Alloy 925 is an age hardenable nickel-base alloy and is therefore thermally processed similarly to Alloy 718 or Alloy X750. To develop the required mechanical properties, the Alloy 925 was solution annealed and age hardened. However, Alloy 925 is susceptible to the formation of sigma phase and special consideration must be given, particularly when working with components the size of the composite block tree.

Data presented in Figure 8 shows the drop in impact strength which occurs in Alloy 925 as a result of sigma phase formation. When this isothermal time-temperature curve is compared to data for duplex stainless UNS-S32550 (2) or duplex stainless Z6CNDU20.-8M,NF A 320-55 French National Standard (9), it is obvious that the rate of sigma phase formation in Alloy 925 is much slower than that for duplex stainless steels.

Nonetheless, care must be taken when thermally processing Alloy 925 to ensure freedom from sigma phase. The aging time and temperature combination selected must avoid the range where sigma phase will form. Additionally, the forgings must be cooled from the solution annealing temperature at a rate sufficiently fast enough to avoid sigma phase formation. The latter consideration is particularly important when processing extremely large forgings such as the composite block trees.

To ensure freedom from sigma phase, the large composite block trees were thermally processed somewhat differently than the smaller components. After forging, the solid blocks were solution annealed and water quenched. Then the forgings were rough machined to within approximately 0.5 in. (1.27 cm) of finished dimensions, including flow bores and valve body cavities. Subsequent to rough machining, the composite block valves were again solution annealed and water quenched, and then age hardened.

Smaller components such as the independent 2-1/16 in. and 5-1/8 in. 5,000 psi valve bodies were produced as closed die forgings and did not require rough machining prior to solution annealing, water quenching, and age hardening. The cross-sectional thickness of these components was small enough to avoid the formation of sigma phase during quenching from the solution annealing temperature.

Machining

Machining of the large Alloy 925 composite block trees, like forging, represented a departure from practices normally used for low alloy steel wellhead components.

As previously discussed, the composite block trees were rough machined prior to heat treating. To achieve this semi-finished state, turning, milling, drilling and boring operations were all performed on the forging. Turning of the bottom Grayloc-style hub was accomplished on a four-axis vertical turret lathe. A large slab mill with a 12-in. face mill and a CNC horizontal boring mill were used to mill the two main faces (front and back) and the nine side faces, respectively. Main flowbore drilling over a length of approximately 73 in. (185 cm) was done on a horizontal ejector drill. Drilling and boring of the cavities was a combination of ejector drilling and trepanning.

Subsequent to the final heat treating operation, the entire composite block tree was finished machined (Figure 9) in three basic operations on CNC horizontal boring mills. Tooling required for these machines ranged from small 1/8-in. high speed steel twist drills to large face mills with multiple indexable carbide inserts. Carbide grades from C-2 to C-5, both coated and uncoated, were used to cut the Alloy 925. Special tooling was also developed, including seat pocket bars and cutters; tooling for contouring heads; roller burnishers for seat pockets; etc. As expected, cutting speeds were much lower than those used for low alloy steel and tool life was poor in all operations.

The surface finish obtained, however, was quite good. Because of the requirements for fire-resistant performance, the sealing surfaces of the bonnets, the valve seat pockets, and Grayloc connection at the tree/tubing head interface required a better surface finish than that required for standard API equipment. Aside from the details already provided, no other special procedures were required to meet these tight surface tolerance requirements.

CONCLUSIONS

1. Technology has been developed to provide complex Alloy 925 wellhead equipment which can meet a unique combination of requirements, including:
   a. Corrosion resistance to H_2S, CO_2, and chlorides
   b. Fire-resistant performance at internal temperatures up to and exceeding 1200°F (650°C)
   c. No embrittlement on large cross-sections or after exposure to extreme design temperatures
2. Alloy 925 is capable of being used for extremely large open die forgings or small complex shaped impression die forgings. However, the unique metallurgy of this material must be understood if it is to be used successfully.
3. Slow cutting speeds and poor tool life are to be expected when machining Alloy 925, but the resulting surface finish is good.
4. It is expected that future applications for Alloy 925 will see more requirements for smaller components, such as the independent flanged valves, than for large composite block trees. Weld cladding is more cost-effective for the large components because of the savings realized in the raw material, but requires additional manufacturing procedures. In the smaller components, the cost of the special alloy raw material may be less than the additional manufacturing required for cladding.

ACKNOWLEDGMENTS

The authors acknowledge the contributions of Mark Elliot, Vetco Gray Inc., and Ben Dickey and Gary Kingry, C-E Beaumont, for their contributions to this program and this presentation.

REFERENCES

1. Lemke, T. F. and J. A. Harris: "High Alloy Materials for Offshore Applications," Proceedings of the 1983 Offshore Technology Conference, Paper No. 4451.
2. Shridar, N., J. Kolts and L. H. Flasche: "A Duplex SS for Chloride Environments," Journal of Metals, Vol. 37, No. 3, March 1985 pages 31-35.
3. Soloman, H.D.: "Age Hardening in a Duplex Stainless Steel," Duplex Stainless Steels, published by American Society for Metals, 1983.
4. Shridar, N., J. Kolts, S. K. Srivastava, and A. J. Asphahani: "Physics, Metallurgy, Properties and Industrial Applications of Ferralium Alloy 255", Duplex Stainless Steels, published by American Society for Metals, 1983.
5. Karr, M. A.: "A New Approach to the Development of Fire-Resistant Wellhead Equipment," presented at the SPE/IADC 1985 Drilling Conference, Paper No. 13447.
6. Kirk, S. D., Inco Alloys International Inc., unpublished correspondence, February 3, 1986.
7. Dickey, B. and G. Kingry, C-E Beaumont, unpublished correspondence, January 28, 1987.
8. Clatworthy, E., Inco Alloys International Inc., unpublished correspondence, March 14, 1986.
9. Jolly, P. and J. Hochmann: Mem. Sci. Rev. Metal, 1973, 70, 117.

TABLE 1

COMPARISON OF THE CHEMICAL COMPOSITION OF ALLOY 825 AND ALLOY 925

ELEMENT	ALLOY 825 (UNS-N08825) %	ALLOY 925 (UNS-N09925) %
NICKEL	38.0 - 46.0	42.0 - 46.0
CHROMIUM	19.5 - 23.5	19.5 - 22.5
IRON*	22.0 minimum	22.0 minimum
MANGANESE	1.0 maximum	1.0 maximum
CARBON	0.05 maximum	0.03 maximum
COPPER	1.5 - 3.0	1.5 - 3.0
SILICON	0.5 maximum	0.5 maximum
SULFUR	0.03 maximum	0.03 maximum
ALUMINUM	0.2 maximum	0.1 - 0.5
TITANIUM	0.6 - 1.2	1.9 - 2.3
MOLYBDENUM	2.5 - 3.5	2.5 - 3.5

*Element determined arithmetically by difference.

TABLE 2

VALVE PRINCIPAL TEST CRITERIA
API RP 6F 'Improved'*

Flame Temperature 1" from Wall	2000°F (1100°C)
Stabilization Temperature of Internal Seal Surface Within 3-1/2 Hours	1200°F (650°C)
Total Duration of Burn	4 to 4-1/2 Hours
Test Pressure (High) Test Pressure (Low) Gas Service Test Pressure (Low) Oil Service	75% WP 500 psi 100 psi
Test Media: During Heat Up & Hold Period During Cooldown	 Water N_2
Hold Period at Stabilization Temperature	One (1) Hour
Allowable Leakage: Through Vessel (Internal) for Burn Period External both during Burn Period and Cooldown Through Valve (Internal) after Cooldown at Low Pressure External after Cooldown at Low Pressure	 Zero Zero Zero Zero
Functional Test after Valve Cooldown: Hold Full Working Pressure with Zero Leakage Open Valve Once Under Full Working Pressure Replace Stem Packing Assembly	 Yes Yes **Optional

*API RP 6F 'Improved' courtesy of Shell Group of Companies
** If necessary to allow opening of the valve.

TABLE 3

TENSILE TEST DATA FOR ALLOY 925[6]

TEST TEMPERATURE °F (°C)	YIELD STRENGTH 0.2% OFFSET KSI (MPa)	TENSILE STRENGTH KSI (MPa)	ELONGATION %	REDUCTION OF AREA %
80 (27)	113.5 (782.6)	169.5 (1168.7)	25.5	43.5
400 (204)	106.3 (732.9)	151.7 (1045.9)	23.0	47.0
1150 (621)	100.2 (690.8)	138.9 (957.7)	26.0	53.5
1200 (649)	100.3 (691.5)	135.8 (936.3)	26.0	55.0
1250 (677)	96.9 (668.1)	126.7 (873.6)	29.0	54.5

Heat No. HH2443XG
Heat Treatment - 1850°F (1010°C) / 1 hr. W.Q.
1350°F (732°C) / 8 hrs. F.C., 100°F (38°C) hr. to 1150°F (621°C) / 8 hrs. A.C.

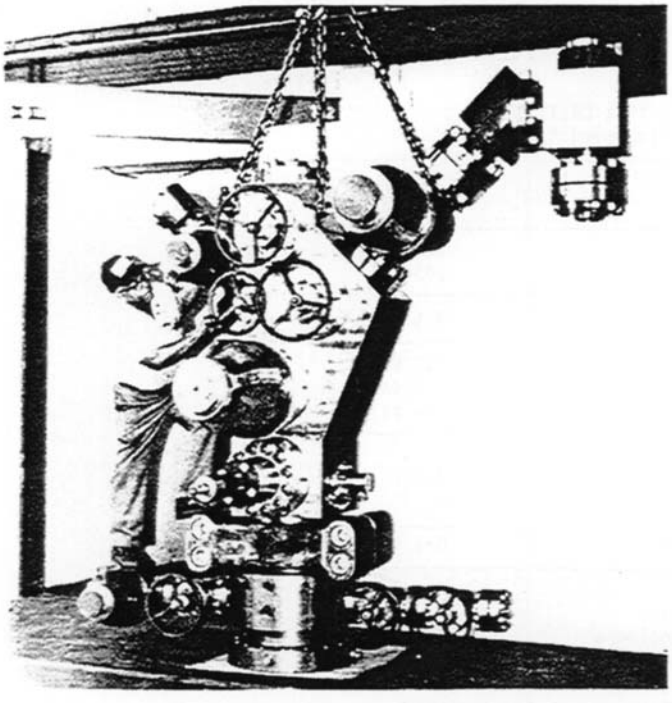


Fig. 1—Composite block tree with tubing head, independent wing valves, and choke attached for testing.

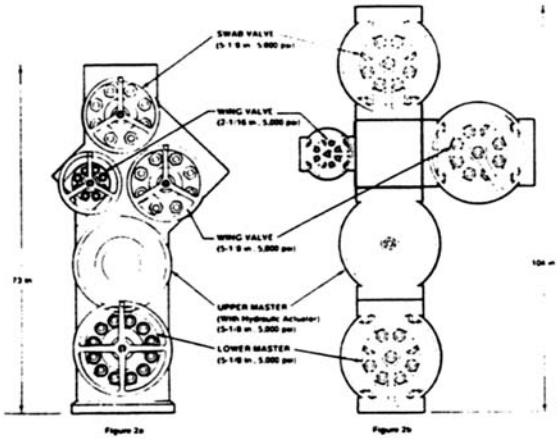


Fig. 2—(a) Composite block tree and (b) independent flanged valves (5⅛ in., 5,000 psi) in comparable tree.



Fig. 3—Alloy 925 VAR ingot in the forging press at the start of the upset operation.



Fig. 4—Alloy 925 ingot during the upset operation.

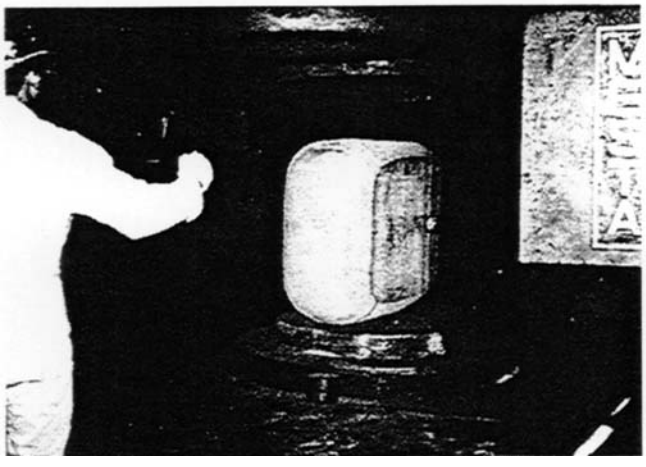


Fig. 5—Forming of a rectangular block from the upset VAR ingot.

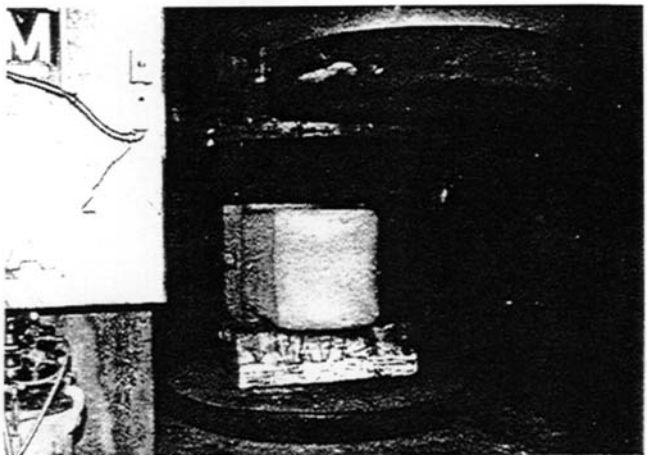


Fig. 6—Forging the small end of the block into shape.

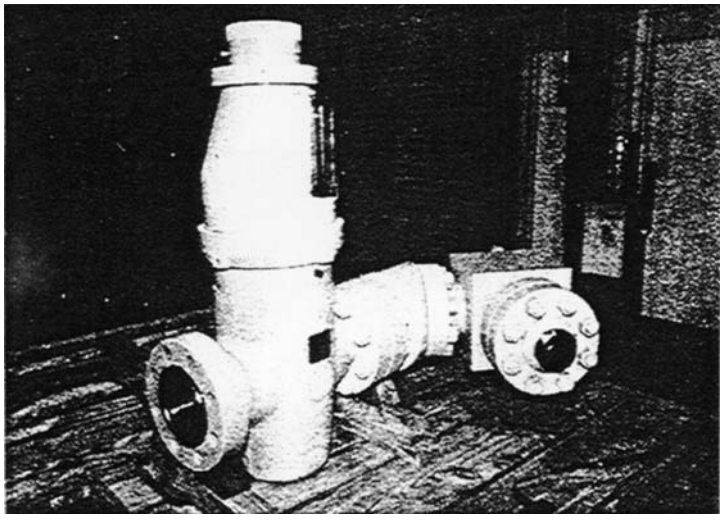


Fig. 7—5⅛-in., 5,000-psi Graygate valve manufactured with Alloy 925 valve body (formed by impression die forging).

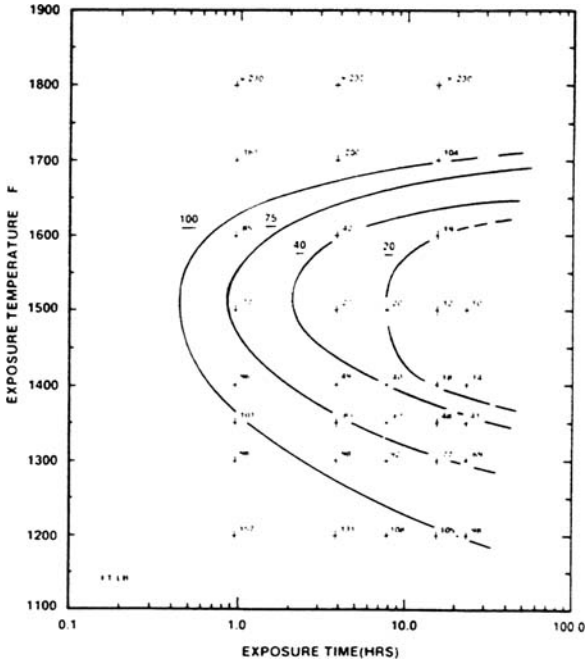


Fig. 8—Isothermal time-temperature-impact strength contours for Alloy 925 solution annealed (1850°F) Base CVN = >236.5 ft-lb.

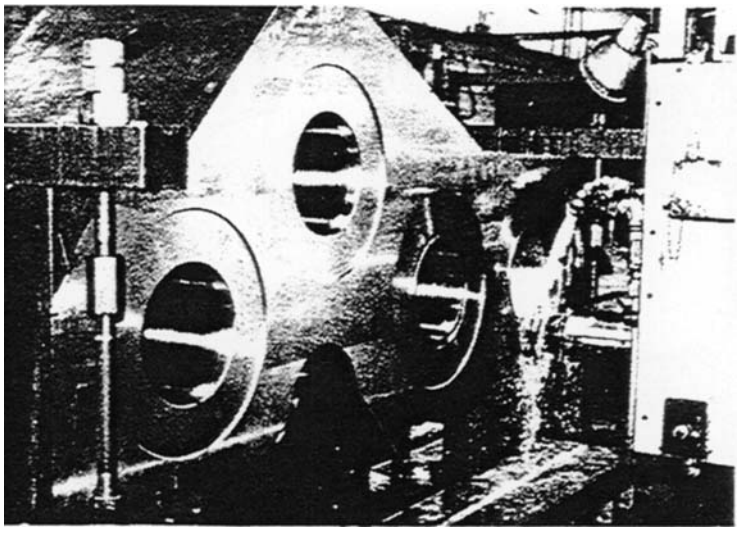


Fig. 9—Finish machining of composite block valve body.

Copyrighted Materials
Copyright © 1996 NACE International Retrieved from www.knovel.com

PAPER NUMBER

150

Corrosion 86

The International Corrosion Forum Devoted Exclusively to The Protection and Performance of Materials

March 17-21, 1986
Albert Thomas Convention Center
Houston, Texas

Hydrogen Embrittlement of INCOLOY alloy 925, MONEL alloy K-500, and INCONEL alloy 625 By Slow Strain Method

J. A. Harris and E. F. Clatworthy
Inco Alloys International, Inc.
Huntington, West Virginia 25720

ABSTRACT

The slow strain rate test technique was used to study several corrosion resistant alloys for susceptibility to hydrogen embrittlement (HE). Cathodic charging of tensile specimens undergoing slow strain rate extension produced hydrogen embrittlement of MONEL* alloy K-500 (UNS No. 5500) and INCOLOY* alloy 925 (UNS No. 9925) but not INCONEL* alloy 625 (UNS NO. 6625). The latter finding contrasts with results obtained by conventional testing of precharged tensile specimens. The effects of material condition on hydrogen embrittlement of INCOLOY alloy 925 could be assessed using the slow strain rate technique.

INTRODUCTION

The conventional method of testing for (HE) is to cathodically charge a tensile specimen for 10-30 days in a cell containing an acid or base and usually a poisoning agent to retard the hydrogen recombination reaction. The NACE steel coupled C-ring test is essentially a hydrogen embrittlement test applied to corrosion resistant alloys (CRAs). The slow strain rate (SSR) test should provide a dynamic HE situation, the only problem being that of finding the proper strain rate--charging current combination necessary to effectively study the problem.

The three alloys selected for this study are INCOLOY alloy 925, MONEL alloy K-500, and INCONEL alloy 625. Evidence of hydrogen embrittlement occurrences of alloy 625 as a C-ring and a cathodically charged tensile specimen was reported by Harris and Lemke (1). The hydrogen embrittlement of alloy K-500 is well documented in the literature (2-5). Alloy 925 was tested for HE resistance as a steel coupled C-ring in the NACE solution (6), where no failures occurred in a yield strength range of 113-185 ksi after 1000 hours.

EXPERIMENTAL

Tensile specimens were machined from the wall of an alloy 925 and alloy 625 cold drawn tube, 2.875" (73 mm) OD x 0.276" (7.0 mm) wall, and from an alloy K-500 hot rolled flat. All specimens were taken with a longitudinal orientation. The specimen had a gage length of 1.00" (25.4 mm) and a gage diameter of 0.140" (3.6 mm). The gage length was dry sanded with 320 and 500 grit papers. The alloys were evaluated in the following conditions:

1. alloy 925:

   as cold drawn (25%)
   as cold drawn + 1250°F (677°C)/1h, AC
   as cold drawn + 1700°F (927°C)/1h, WQ, + 1350°F (732°C)/8h, AC
   as cold drawn + 1850°F (1010°C)/1h, WQ + 1350°F (732°C)/8h, AC

*MONEL, INCOLOY, and INCONEL are registered trademarks of the Inco family

2. alloy K-500 - 1125°F (607°C)/8h FC 25°F (14°C) to 900°F (482°C)/6h, AC

3. alloy 625 - 39% tube reduced.

One specimen was tested in air and a duplicate in 2% NaCl with 200 psi H_2S and 300 psi CO_2 + 500 microamps/sq. cm. current density of hydrogen. Tests were run at room temperature. A constant extension rate of 2 x 10^{-6} (5.08 x 10^{-5} mm/mm/sec) in/in/sec was used in order to allow time for hydrogen diffusion.

Time-to-fracture, % RA and % elongation were determined from the slow strain rate test. The presence or absence of secondary cracks were also recorded. Finally, a longitudinal section through the fracture area was mounted to examine for extent of cracking due to hydrogen embrittlement.

In related studies, hydrogen embrittlement resistance of these alloys was measured by pulling hydrogen charged tensiles. These results were compared to the SSR data.

RESULTS

Chemical analyses of materials tested are listed in Table 1. Slow strain rate results in air and hydrogen charging are given in Table 2. The ratios of SSR parameters obtained during hydrogen charging to those in air [i.e., TTF(H_2)/TTF (air)] are presented in Table 3. Table 4 lists results of hydrogen charged tensile tests showing the effects of cathodic charging on elongation, hydrogen content and depth of hydrogen attack. Slow strain rate curves of alloy 925 obtained in air and hydrogen charging conditions are plotted in Figures 1 and 2. Similar SSR curves for alloy K-500 and alloy 625 are plotted in Figures 3 and 4.

DISCUSSION

Hydrogen embrittlement resistance is an important consideration for potential applications of alloy 925, particularly in oil and gas production and in seawater applications. Alloy K-500, which is used extensively in both these areas, has recently come under increasing criticism for suspected hydrogen embrittlement failures (7). Alloy 925 with its high iron content would seem to be a good replacement for alloy K-500.

Table 2 lists results of SSR testing for the 3 alloys tested. Cold drawn or CD + aged alloy 925 showed time to fracture of about 15 hours in air while annealed + aged reached 30 hours TTF. Hydrogen charging in a sour environment at room temperature results in a decrease in TTF, % RA and % El as well as the area under the curve. The ratios of these parameters in H^2 to air are shown in Table 3 and help to quantify the effects. It can be seen from Table 3 that cold drawn alloy 925 is the least affected condition with all parameter ratios totalling 3.62 out of 4.0 (a total of 4.0 would indicate no effect of hydrogen charging and/or the sour environment). Next best is the cold drawn + aged condition. In the annealed + aged condition, the ductility and total area parameters suffer greater percentage losses than they do in unannealed materials. Retained ductilities are higher for aged material annealed at 1850°F (816°C)1h, WQ compared to that annealed at 1700°F (927°C)/1h, WQ.

The following results compare % loss in elongation obtained by SSR testing with those shown by cathodically charged tensile tests of alloy 925 listed in Table 4.

Alloy Condition	*SSR*	*% Loss in Elong. Cathodic Charging (30 Days)*
As Cold Worked	15.5	26.4
1850°F(1010°C/1h + 1350°F (732°C)/8h,AC	45.0	23.8

Notice that 30 days cathodic charging shows both conditions to be similar in loss in elongation while SSR tests show anneal + aging to be more deleterious. These results seem to leave open the question of whether or not the greater initial ductility of annealed + aged material would offer a better choice than the less ductile but seeming more resistant CD or CD + aged conditions when faced with an obvious hydrogen embrittlement situation.

Tables 2 and 3 clearly show that SSR testing does not cause hydrogen embrittlement of alloy 625 during 13 hours duration of the test. However, as shown below, considerable hydrogen embrittlement of alloy 625 occurs during cathodic charging tests (Table 4):

Alloy Condition - 625	*SSR*	*% Loss of Elongation Cathodic Charge*
As cold worked	0	40% (10 Days) 68% (20 Days) 75% (30 Days)

Cathodic charging of alloy 925 and alloy 625 resulted in almost equal amounts of hydrogen content per time. It would appear that hydrogen did not diffuse into alloy 625 during the slow strain rate test.

Previous studies using cathodic charging had indicated that alloy K-500 was susceptible to hydrogen embrittlement (Table 4). SSR test results also showed susceptibility; however, as shown below, this method was not as aggressive as testing cathodically charged tensiles:

Alloy Condition - K-500	*SSR*	*% Loss in Elongation Cathodic Charge*
CRS + Aged	31	28% (4 Days) 69% (16 Days) 90% (32 Days)

According to the totals column in Table 3, SSR testing rates alloy K-500 about equal in hydrogen embrittlement resistance to INCOLOY alloy 925 in the 1850°F/1h, WQ + aged condition. However, cathodic charging (Table 4) shows alloy 925 to be more resistant than alloy 625.

The intergranular nature of hydrogen embrittlement attack on alloy 925 is shown in Figures 5 and 6.

CONCLUSIONS

1. Tensile tests of cathodically charged specimens showed that alloy 925 absorbs much less hydrogen than alloy K-500. The % loss in elongation in this test is significantly lower in a given charging time for alloy 925 than for either alloy K-500 or alloy 625. The depth of hydrogen diffusion is lower for alloy 625 and alloy 925 than for alloy K-500.

2. Charging with hydrogen during slow strain rate testing produces hydrogen embrittlement in INCOLOY alloy 925 and MONEL alloy K-500.

3. Alloy 625 did not appear to suffer hydrogen embrittlement during the slow strain rate test. In contrast, pulling tensiles of cathodically charged specimens does produce hydrogen embrittlement in alloy 625.

4. SSR testing showed that the degree of hydrogen embrittlement in alloy 925 depends on material condition. The extent of HE damage increases in the order:

   CD
   CD + 1250°F/1h, AC
   CD + 1850°F/1h, WQ + 1350°F/8h, AC
   CD + 1700°F/1h, WQ + 1350°F/8h, AC

   (CD = Cold Drawn)

REFERENCES

1. J. Harris, T. Lemke, Materials Performance, Vol. 23, No. 1, p. 11 (1983).

2. A. Troiano, J. Scholler, ARL 133, Wright Patterson AFB, 1961.

3. A. Troiano, J. Mickelich, Nature, March, 1965, Vol. 197, p. 4811.

4. J. Papp, R. Heckemann, A. Troiana, Hydrogen in Metals, No. 2, ASM Materials/Metalworking Tech. Series, p. 2657.

5. J. Harris, R. Scarberry, C. Stephens, Corrosion, Vol. 28, No. 2 (1972).

6. J. Harris, T. Lemke, D. Smith, R. Moeller, "Development of a Corrosion Resistant Alloy for Sour Gas Service", CORROSION/84, Paper No. 216, National Association of Corrosion Engineers, New Orleans, LA, 1984.

7. K. D. Efrid, Materials Performance, Vol. 25, No. 4, p. 37 (1985).

Table 1

Chemical Analyses

Alloy Heat No.	alloy 925 Y9050G	alloy 625 UNK	alloy K-500 UNK
C	.02	.02	.15
Mn	.44	.19	.58
Fe	27.10	3.03	1.37
S	.001	.006	.002
Si	.15	.46	.17
Cu	1.87	.39	30.25
Ni	42.78	60.59	63.91
Cr	22.38	21.89	.12
Al	.25	.07	2.73
Ti	2.07	.07	2.73
Co	.35	.16	.50
Mo	2.90	8.84	.01
Cb + Ta	.46	3.64	.01
P	.03	.004	.011

Table 2

SSR Test Results
Air and Hydrogen Charging

Alloy	Material Condition	Test Media	Y.S. (Ksi)	TTF % RA	% El	(in^2)	Area
alloy 925	As CD	Air	125.0	16.4	58.4	12.9	206.3
alloy 925	As CD	H_2	116.7	15.1	58.4	10.9	178.4
alloy 925	As CD + 1250°F (677°C/1h, AC	Air	158.7	14.7	47.1	8.9	175.3
alloy 925	As CD	H_2	145.6	13.3	34.3	8.5	152.1
alloy 925	As CD + 1700°F (927°C)/1h, WQ + Age 1	Air	109.5	27.0	37.1	19.6	368.0
alloy 925	As CD	H_2	110.7	14.2	13.0	6.7	149.4
alloy 925	As CD + 1850°F (1010°C)1h, WQ + Age 1	Air	91.9	33.7	48.5	26.0	443.6
alloy 925	As CD	H_2	92.4	21.6	39.1	15.2	233.8
alloy 625	As CD	Air	167.7	13.4	39.5	6.2	165.5
alloy 625	As CD	H_2	152.3	13.2	41.5	6.7	159.8
alloy K-500	CRA + Age 2	Air	115.7	18.2	47.0	12.0	279.5
alloy K-500	CRA	H_2	113.3	14.5	30.1	8.3	183.9

1 - 1350°F (816°C)/8h, AC

2 - 1125°F (607°C)/8h, FC 25°F (13.9°C)/h to 900°F (482°C)/AC

Table 3

SSR Test Results
Ratios

Alloy	Material Condition	Ratio (Soln/Air) TTF	% RA	% EL	Area	Total
alloy 925	**As CD**	**.92**	**1.00**	**.84**	**.86**	**3.62**
alloy 925	**CD + 1250°F (677°C)/1h, AC**	.90	.73	.96	.87	3.46
alloy 925	CD + 1700°F (927°C)/1h, WQ + Age 1	.53	.35	.34	.41	1.63
alloy 925	CD + 1850°F (1010°C)/h, WQ + Age 1	.64	.81	.58	.53	2.63
alloy 625	As CD	.98	1.05	1.08	.96	4.07
Alloy K-500	CRA + Age 2	.80	.64	.69	.66	2.79

1 - 1350°FK (816°C)/1h, AC

2 - 1125°F (607°C)/8h, FC 25°F (13.9°C)/h to 900°FK (482°C)/AC

Table 4

Mechanical Properties vs. Hydrogen Charging

Materials: alloy 925, HH1598XG
alloy 625, NX2378AG

Alloy/Condition	Charge Time (Days)	Hard. (Rc)	0.2% Y.S. (ksi)	UTS (ksi)	% Elong. (1 in.")	H Content (ppm)	Depth of Attack (in." x 10^{-3})
925 CR (20%)	0	29.5	130.3	135.7	10.6	3.4	--
925 CR (20%)	10	29	125.7	132.9	7.7	15.8	3.1
925 CR (20%)	20	28.5	129.2	137.4	6.0	31.9	5.2
925 CR (20%)	30	29	130.2	138.1	7.8	27.2	7.4
925 CR + 1850°F (1010°C)/1h,	0	35	118.5	171.5	21.0	3.1	--
WQ + 1350°F (816°C)/8h	10	34.5	116.6	167.1	20.6	24.4	4.5
FC 100°F (59°C)/h to	20	34.5	115.8	164.5	17.0	27.4	6.1
1150°F (621°C)/8h, AC	30	34.5	117.9	161.7	16.0	26.2	7.4
625 CR (39%)	0	33.5	136.9	152.3	20.1	4.4	--
625 CR (39%)	10	33.5	140.3	146.5	12.0	15.4	3.5
625 CR (39%)	20	33	139.0	142.5	6.5	29.5	5.4
625 CR (39%)	30	34	138.0	148.0	5.0	27.6	6.8
alloy K-500	0	30.31	93.9	147.9	19.5	5.0	--
CRA + 1100°F (593°C)/16h	2	30.31	89.6	124.2	14.0	79.9	4.0
FC 1000°F (538°C)/6h/FC	4	30.31	94.9	130.4	14.0	75.3	6.0
900°F (482°C)/6h, AC	16	30.31	93.7	99.0	6.0	--	14.0
	32	30.31	83.9	85.8	2.0	396.0	--

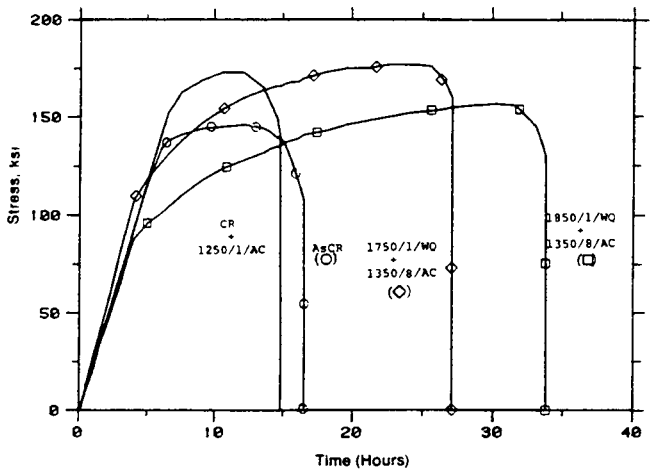


Figure 1 SSR Tests in air at RT-INCOLOY 925.

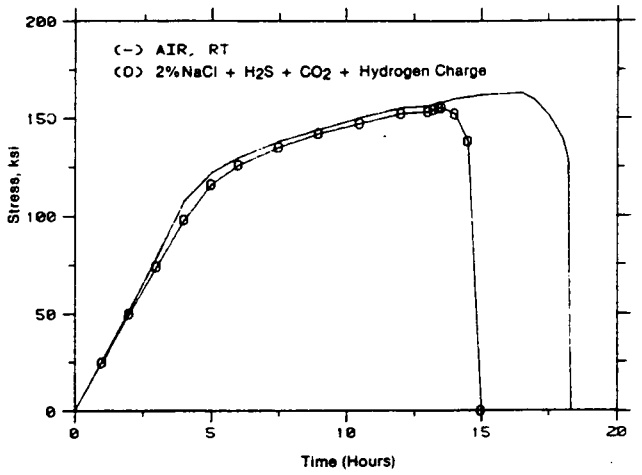


Figure 3 SSR Tests in 2%NaCl with Hydrogen Charging-Monel K500.

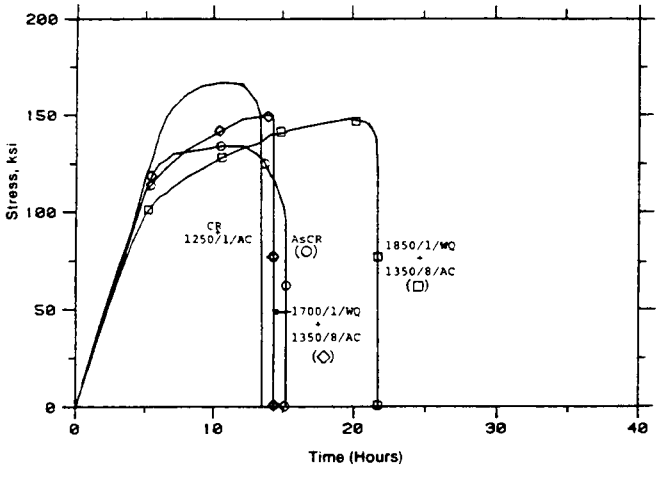


Figure 2 SSR Tests in 2%NaCl with Hydrogen Charging-INCOLOY 925.

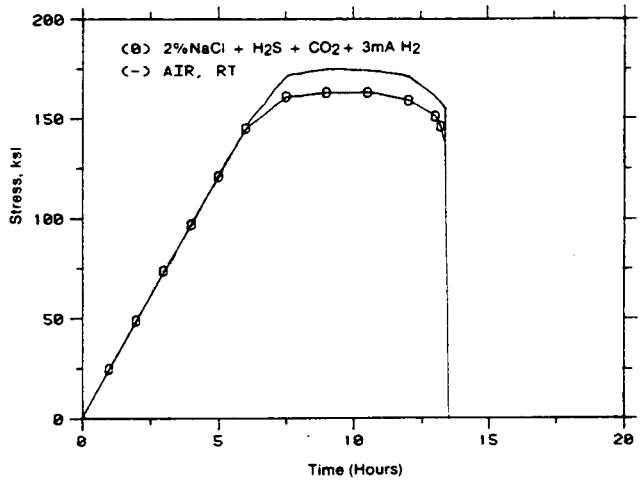


Figure 4 SSR Test in 2%NaCl with Hydrogen Charge-INCONEL 625.

Copyrighted Materials
Copyright © 1996 NACE International Retrieved from www.knovel.com

Paper No. 18—CORROSION/91

CORROSION BEHAVIOR OF AGE-HARDENABLE ALLOY UNS N07725 FOR OIL FIELD APPLICATIONS

Edward L. Hibner
Inco Alloys International, Inc.
Huntington, WV 25720

ABSTRACT

Alloy 725 (UNS N07725) is a highly corrosion resistant alloy capable of being age-hardened to 0.2% yield strengths of 100 to 140 ksi (690 to 965 MPa), while maintaining a high level of ductility and toughness.[1] As alloy 725 is an age-hardenable alloy, large section sizes can achieve uniform hardening throughout the cross section. The alloy is resistant to pitting and stress corrosion cracking (SCC) in environments containing NaCl, H_2S and S at temperatures up to about 232° to 260°C (450° to 500°F), and to sulfide stress cracking (SSC) in the NACE TM-0177 environment. The corrosion resistance of alloy 725 is similar to that of cold-worked alloy 625 (UNS N06625) and is superior to that of age-hardened alloy 718 (UNS N07718).

Keywords: stress corrosion cracking (SCC), hydrogen embrittlement, sulfide stress cracking (SSC), corrosion prevention, INCONEL†, gas wells, sour gas environments, hydrogen sulfide, chloride, sulfur, seawater, mineral acids.

INTRODUCTION

The trend in oil and gas production has been toward deeper wells, enhanced recovery methods and offshore field exploration. Deeper wells and enhanced recovery methods, such as steam injection, in-situ combustion and CO_2 injection, result in hostile environments due to increased temperatures, pressures and environmental H_2S and CO_2 and chloride content. For several decades there has been a need to develop new materials for use in production of oil and gas.[2] Much of the research has centered around the need for high strength Corrosion Resistant Alloys (CRA's) that can withstand the high temperature, high pressure, corrosive oil field production environments INCONEL alloy 625 (UNS N06625) and INCO† alloy C-276 (UNS N10276) have the necessary corrosion resistance, but can only be strengthened through cold work and the desired section sizes are too large to be produced on normal cold working equipment. Age-hardened alloys such as INCONEL alloy 718 (UNS N07718) and INCONEL alloy X-750 (UNS N07750), have been used in these applications but have insufficient corrosion resistance in the most severe environments.[3] INCONEL alloy 725 (UNS N07725) is a highly corrosion resistant alloy which can be age-hardened to yield strength levels of 120 ksi (827 MPa) and above for deep sour gas well applications. As alloy 725 is an austenitic nickel base alloy which is strengthened by precipitation of a gamma double-prime [Ni_3, (Nb, Ti, Al)] during aging, large section sizes can achieve uniform hardening throughout the cross section. Alloy 725 also exhibits excellent corrosion resistance to other commercially significant environments, such as seawater and mineral acids.

PROCEDURE

Materials for testing came from commercially produced tubing, round rod and sheet. The nominal compositions of the alloys are given in Table 1. Materials were tested either as-produced or solution annealed to obtain suitable structures before aging. Yield strengths were in the 117 to 139 ksi (807 to 958 MPa) range obtained by aging alloy 725 and 718 and in the 127 to 168 ksi (876 to 1,158 MPa) range obtained by cold drawing alloys 625

†INCO and INCONEL are registered trademarks of the Inco family of companies.

and C-276. C-rings were prepared from tubing and were stressed to 100% of the 0.2% Yield Strength as per ASTM Standard Practice G38. The specimens were finished to a 120 grit surface finish using aluminum oxide paper.

Sulfide Stress Cracking (SSC) Tests

Tests were conducted on steel coupled C-rings in the NACE TM-01-77 environment for 720 to 1,000 hours of exposure.[4]

Stress Corrosion Cracking (SCC) Tests

C-rings were exposed to 3.2 liters of corrodent contained in a 4 liter autoclave at temperatures from 177° to 260°C (350° to 500°F). The specimens were suspended from a TFE fluorocarbon coated rack in the autoclave so that electrical isolation was maintained. The C-rings were exposed for 14 days at 177°C (350°F). At the end of the 14 day test period, specimens were removed and examined for SCC. If no SCC was observed, the temperature was raised -3.8° or 9.9°C (25° or 50°F) and the C-rings were again exposed to the environment (a fresh solution). The 14-day exposures were continued until SCC was observed or the material was tested at 260°C (500°F).

Crevice Corrosion Tests

Crevice corrosion tests were conducted (1) on sheet and strip in flowing seawater at 30°C (-1.1°F) for 30 days using an acrylic plastic crevice torqued to 25 in.-lbs (2.9 Nm) and (2) on welded and machined tubing with flowing seawater on the I.D. surface at a mean temperature of 14.4° ± 4.4°C (58° ± 40°F) for 180 days using a vinyl sleeve secured by clamps to join sections of tubing. This sleeve-joint acts as a crevice former on the O.D. of the tube.

Mineral Acid Tests

Immersion tests were performed in unsaturated, non-deaerated solutions of reagent grade mineral acids. Sheet specimens were ground to a 120 grit surface finish with aluminum oxide paper and cleaned with l, l, 1-trichloroethane just prior to testing. Mass loss corrosion rates were determined in mpy (1 mpy = 0.025 mm/y).

RESULTS AND DISCUSSION

Mechanical Properties

As mentioned, alloy 725 is an austenitic nickel base alloy which is strengthened by precipitation of a gamma double-prime [Ni_3(Cb, Ti, Al)] during aging. A solution anneal of 1,038° ± 3.89°C (1,900° ± 25°F) air cooled or water quenched, is required to put the material in the proper condition before aging. Tables 2 to 7 display various room temperature tensile (RTT), charpy-v-notch (CVN), hardness (HD) and grain size properties for alloy 725 tubing and rod products. While other age-hardening treatments will strengthen the alloy, a 1,027°C (1,900°F) anneal followed by a dual age of 725°C/8h (1,350°F/8h), Furnace Cool (FC) at 37°C/h to 615°C/8h/ Air Cool (100°F/h to 1,150°F/8h/Air Cool) (AC) was found to provide the best combination of strength and toughness.

The effect of aging treatment on hardness and room temperature tensile properties of 0.217 in. (5.51 mm) x 2.375 in. (60.3 mm) outside diameter (O.D.) tubing is shown in Table 2. Yield strengths of 128 to 133 ksi (883 to 917 MPa) along with high ductility were obtained by dual aging after anneal of the cold drawn tubing.

For 0.562 to 6 in. (14.3 to 152.4 mm) hot finished round rod in the 1,027°C (1,900°F) mill annealed condition, Table 3, yield strengths of 125 to 137 ksi (862 to 945 MPa) along with high ductility were observed. For rod of 3 to 6 in. (76.2 to 152.4 mm) diameter, similar strengths and ductilities were observed for longitudinal and transverse orientations.

After a 1,027°C (1,900°F) anneal and 725°C (1,350°F) dual age, Table 4, round rod which had been cold worked (drawn) 2 and 32% showed no effect of degree of cold work on strength or ductility. For round rod cold worked 12%, Table 5, no effect of annealing temperature (1,850° to 1,900°F) was observed on room temperature tensile properties when tested in the 725°C (1,350°F) dual aged condition. Slightly higher impact properties were obtained for material annealed at 1,014° or 1,027°C (1,875° or 1,900°F) before aging.

Table 6 displays room temperature tensile data for 7.5 inch (190.5 mm) round rod annealed at 1,014° and

1,027°C (1,875° and 1,900°F) before aging at 752°C/6h (1,400°F/6h). No effect of annealing temperature on mechanical properties was discernible. Similar strengths and ductilities were observed for center, mid-radius and edge in both longitudinal and transverse orientations. Yield strengths were in the 117 to 123 ksi (807 to 848 MPa) range with the material showing excellent ductility.

Table 7 shows the grain size for as-forged, annealed, and annealed plus aged 7.5 inch (190.5 mm) round rod. Little difference in grain size is observed between the center, mid-radius and edge of the large diameter rod.

Corrosion Testing

Table 8 contains sulfide stress cracking (hydrogen embrittlement) data for steel coupled nickel alloy C-rings evaluated in various heat treated conditions in the NACE TM-0177 environment. For alloy 725, material representing yield strengths up to 139 ksi (958 MPa) and hardnesses up to 40 HRc did not crack when coupled to carbon steel for 720 to 1,000 hours. Alloy 718 , yield strength 130 ksi (896 MPa) and hardness HRc 34, did not crack in 720 hours of exposure.

Stress corrosion cracking data for C-rings evaluated in a 25% NaCl + 0.5% acetic acid + 120 psig H_2S + 1 g/L sulfur environment is displayed in Table 9. This autoclave environment was designed to simulate conditions in severe deep sour gas wells. Alloy 725 was resistant to SCC up to 232° to 260°C (450° to 500°F). Alloy 718, age-hardened to 130 ksi (896 MPa) yield strength, cracked at 135°C (275°F) in this environment. Cold-drawn alloy 625, yield strength 144 to 160 ksi (993 to 1,103 MPa), cracked at 191°C (375°F). And, cold-drawn alloy C-276, yield strength 127 to 168 ksi (876 to 1,158 MPa, resisted SCC up to about 260°C (500°F). As a result of excellent stress cracking resistance, alloy 725 (N07725) in the solution annealed plus aged condition (HRc 40 maximum) has been included in the NACE MR-0175 document.

Table 10 is a summary of crevice corrosion test data for alloy 625 and alloy 725 sheet specimens, evaluated in flowing seawater at 30°C (86°F) for 30 days using an acrylic plastic crevice torqued to 25 in.-lbs. (2.9 Nm). Alloy 625 suffered significant corrosion, with a large percentage of the crevices attacked up to a maximum depth of 0.66 mm. In the 1,000°C/1h/WQ + 739°C (1,850°F/lh/WQ + 1,375°F) dual aged condition, alloy 725 exhibited excellent crevice corrosion resistance, with no attack observed in the 30 day exposure.

A summary of crevice corrosion test results for alloy 625 and alloy 725 tube sections, evaluated with flowing seawater on the inside surface (I.D.) of tubes is shown in Table 11. Vinyl sleeves which connected the tube specimens provided crevice formers in the seawater environment. The triplicate alloy 625 specimens initiated crevice corrosion in 1 to 30 days, which penetrated to a maximum depth of 0.12 mm in 180 days of exposure. For the duplicate alloy 725 specimens in the 739°C (1,375°F) dual aged condition, only one specimen was attacked, with a maximum penetration of 0.01 mm in 180 days.

Corrosion results for alloy 725 in mineral acids, compared to alloys 625 and C-276 are shown in Table 12. In all of the mineral acid environments of this study, both annealed and annealed plus aged alloy 725 exhibited corrosion resistance comparable to mill annealed alloys 625 and C-276.

CONCLUSIONS

1. Alloy 725 (UNS N07725) is an austenitic nickel based alloy strengthened by precipitation of gamma double-prime during aging. Depending on the mill form, 0.2% Yield strengths from 117 to 137 ksi (807 to 945 MPa) were obtained by dual aging after annealing. Excellent ductility and toughness properties were retained following age-hardening.
2. Stressed C-rings of alloy 725 resisted sulfide stress cracking (hydrogen embrittlement) in the NACE TM-0177 environment, stress corrosion cracking in environments containing NaCl, H_2S and S at high pressures and at temperatures up to 232° to 260°C (450° to 500°F).
3. The corrosion resistance of alloy 725 is similar to that of cold-worked alloy 625 (UNS N06625) and is superior to that of age-hardened alloy 718 (UNS N07718).
4. Alloy 725 is resistant to pitting and crevice corrosion by seawater and to general corrosion in various mineral acid environments.

REFERENCES

1. E.L Hibner, "A New Age-Hardenable Corrosion Resistant Alloy for Deep Sour Gas Well Service," CORROSION/90, paper no. 50 (Houston, TX: NACE, 1990).
2. R.D. Kane, *International Metals Reviews*, 30, 6(1985), p. 291.

3. T.A. DeBold, R. Frank, *Materials Performance*, 27, 9(1988), p. 59.
4. Standard TM-01-77, "Testing of Metals for Resistance to Sulfide Stress Cracking at Ambient Temperatures," (Houston, TX: NACE, 1986 revision).
5. As communicated by the Department of the NAVY, Naval Sea Systems Command, Washington, D.C.

Table 1
Chemical Composition (wt.%)

	Alloy 725 (UNS N07725)	Alloy 625 (UNS N06625)	Alloy 718 (UNS N07718)	Alloy C-276 (UNS N10276)
Ni	57	65*	52.5	59*
Cr	21	21.5	19	15.5
Mo	8	9	3	15.5
Nb	3.5	3.5	5.1	-
Ti	1.5	-	0.9	-
Fe	9*	-	19*	5
W	-	-	-	4

* Balance element, approximate composition.

Table 2
Room Temperature Tensile Properties for Alloy 725 (UNS N07725) Cold-Drawn* 0.217in.(5.51mm) Wall x 2.375in.(60.3mm) O.D. Tubing

Anneal	Age	HD (Rc)	0.2%YS (ksi)	TS (ksi)	El (%)
1850°F	1375°F Dual Age	40	128	184	28
1875°F	1375°F " "	39	132	183	28
1900°F	1375°F " "	39	133	183	27
1900°F	1350°F " "	38	133	185	30

°C = 5/9 (°F - 32); 1 ksi = 6.89 MPa
* Cold-Drawn 17%; Longitudinal Properties Given.
Heat Treatment:
ANNEAL = Temp. °F/1h/Water Quench
DUAL AGE = Temp. °F/8h, Furnace Cool 100°/h to 1150°F/8h/Air Cool

Table 3
Room Temperature Tensile Properties for Alloy 725 (UNS N07725) Hot Finished Round Rod in the 1900°F Mill Annealed + 1350°F/8h, FC at 100°/h to 1150°F/8h/AC

Rod Diameter	Orientation	0.2%YS (ksi)	TS (ksi)	El (%)	RA (%)	HD (Rc)
0.562 inch	longitudinal	126	179	37	45	34/36
1 "	longitudinal	129	188	29	46	36/38
3 "	longitudinal	135	181	30	43	37/38
3 "	transverse	137	187	27	35	
4 "	longitudinal	132	174	33	47	33/36
4 "	transverse	134	178	31	35	
5 "	longitudinal	132	181	31	45	36/39
6 "	longitudinal	130	182	29	44	35/37
6 "	transverse	125	175	31	38	

(1 in. = 25.4 mm; 1 ksi = 6.89 MPa)

Table 4
Room Temperature Tensile Properties for Alloy 725 (UNS N07725)
Cold Drawn Round Rod in the 1900°F/1h/WQ +
1350°F/8h, FC at 100°/h to 1150°F/8h/AC

Diameter	% Cold Work	0.2%YS (ksi)	TS (ksi)	El (%)	RA (%)	HD (Rc)
1.341 in.	12	127	180	31	47	39
1.270 in.	22	127	180	32	48	39
1.187 in.	32	127	179	33	47	37

(1 in. = 25.4mm; 1 ksi = 6.89 MPa)

Table 5
Room Temperature Tensile and Charpy-V-Impact Properties for Alloy 725
(UNS N07725) Cold Drawn* 1.341 Inch Round Rod

Anneal	Condition	0.2%YS (ksi)	TS (ksi)	El (%)	RA (%)	HD (Rc)	Impact** (ft-lbs)
1850°F	1350°F Dual Age	129	183	29	48	38	58;66
1875°F	1350°F Dual Age	129	182	30	47	39	64;70
1900°F	1350°F Dual Age	127	180	31	47	39	66;69

°C = 5/9 (°F - 32); 1 ksi = 6.89 MPa
*Cold Drawn 12%. **Duplicate specimens.
Anneal = Temp.°F/1h/Water Quench.
Dual Age = Temp.°F/8h, FC at 100°/h to 1150°F/8h/Air Cool.

Table 6
Room Temperature Tensile Properties for Alloy 725
(UNS N07725) Forged 7.5 in. (190.5mm) Round Rod

Condition	Orientation	0.2%YS (ksi)	TS (ksi)	El (%)	RA (%)	HD (Rc)
1	Long.(mid.-rad.)	117	169	32	49	38
1	Trans.(edge)	124	173	30	49	34
1	Trans.(mid.-rad.)	120	170	34	47	37
2	Long.(edge)	117	171	32	47	37
2	Long.(mid.-rad.)	121	169	31	45	38
2	Long.(center)	123	172	35	48	37
2	Trans.(edge)	120	170	31	45	35
2	Trans.(mid.-rad.)	121	168	36	49	35
2	Trans.(center)	118	168	33	45	36

Condition:
1. As-Forged + 1875°F/1h/WQ + 1400°F/6h/AC
2. As-Forged + 1900°F/1h/WQ + 1400°F/6h/AC
°C = 5/9 (°F - 32); 1 ksi = 6.89 MPa

Table 7
ASTM Grain Size for Alloy 725 (UNS N07725) Forged 7.5 in. (190.5mm) Round Rod

Condition	ASTM Grain Size No. Center	Mid-Radius	Edge
As-Forged	6	6	7-1/2
As-Forged + 1900°F Anneal	5-1/2	5	6
As-Forged + 1900°F Anneal + 1375°F/8h, FC at 100°/h to 1150°F/8h/AC	5-1/2	4	5-1/2

°C = 5/9 (°F - 32)

Table 8
Sulfide Stress Cracking Data for Steel Coupled Nickel Alloy C-rings, Evaluated in Various Heat Treated Conditions in the NACE Environment*

Alloy	Condition	Mill Product	Properties 0.2% YS (ksi)	HRc	Test Duration (hours)	Cracking Yes(Y) or No(N)
725 (N07725)	1	Tubing	139	35	720	N;N
"	1	"	129	40	720	N;N
"	2	"	138	39	720	N;N
"	2	"	132	36	1000	N;N
"	3	"	134	39	1000	N;N
"	4	"	133	38	720	N;N
718 (N07718)	5	"	130	34	720	N;N

* NACE TM-01-77, 5%NaCl + 0.5% Acetic Acid + H_2S saturated at 75°F.
Condition:
(1) 1850°F/1h/WQ + 1375°F/8h, FC 100°/h to 1150°F/8h/AC
(2) 1875°F/1h/WQ + 1375°F/8h, FC 100°/h to 1150°F/8h/AC
(3) 1900°F/1h/WQ + 1375°F/8h, FC 100°/h to 1150°F/8h/AC
(4) 1900°F/1h/WQ + 1350°F/8h, FC 100°/h to 1150°F/8h/A
(5) 1875°F/1h/WQ + 1425°F/8h/AC
°C = 5/9 (°F - 32); 1 ksi = 6.89 MPa

Table 9

C-ring SCC Test Data For Nickel Alloys*, Evaluated at 100%YS in 25% NaCl + 0.5% Acetic Acid + 120psig H_2S + 1 g/L S

Alloy - UNS# (mill form)	Condition	YS (ksi)	SCC in 14 Days - Yes(Y) or No(N) Temperature(°F) 350	375	400	425	450	475	500
725 - N07725	1	118	N;N	N;N	N;N	N;N	N;N	N;Y	N
"	2	129	N;N	N;N	N;N	N;N	Y;Y		
"	2	139	N;N		N;N		N;N		N;Y
'	3	133	N;N	N;N	N;N	N;N	N;N	N;Y	N
"	4	132	N;N	N;N	N;N	N;N	N;N	N;N	N;N
"	4	138	N;N		N;N		N;N		N;N
"	5	133	N;N		N;N		N;N		N;N
718 - N07718	6	130	Y;Y**						
625 - N06625	7	144	N	Y					
"	7	160	N	Y					
C-276 - N10276	7	127		N	N	N	N	N	N
"	7	155		N	N	N	N	N	Y
"	7	167		N	N	N	N	N	N
"	7	168		N	N	N	N	N	Y

* Multiple specimens as indicated.
** Alloy 718 cracked at 275°F in this environment.
°C = 5/9 (°F - 32)
Condition:
1. 1850°F/1h/WQ + 1400°F/6h/AC
2. 1850°F/1h/WQ + 1375°F/8h, FC 100°/h to 1150°F/8h/AC
3. 1850°F/1h/WQ + 1400°F/8h, FC 100°/h to 1150°F/8h/AC
4. 1875°F/1h/WQ + 1375°F/8h, FC 100°/h to 1150°F/8h/AC
5. 1900°F/1h/WQ + 1350°F/8h, FC 100°/h to 1150°F/8h/AC
6. 1875°F/1h/WQ + 1425°F/8h/AC
7. As-drawn

Table 10

Summary of Crevice Corrosion Test Data for Sheet and Strip Specimens of Alloy 625 (N06625 and Alloy 725 (N07725), Evaluated in Flowing Seawater at 30°C for 30 Days Using an Acrylic Plastic Crevice Torqued to 25 in.-lbs. (2.9 Nm)

Alloy	Observed Initiation (days)	Percent of Sites Attacked	Maximum Depth of Attack (mm)
625 (N06625)*	2 to 5	25 to 75	0.02 to 0.66 (Average 0.26)
725 N07725)**	None at 30 days	0	0.00

* Data for 4 heats of mill annealed commercial sheet.
** Data for 1 heat of hot rolled commercial strip in condition: 1850°F/1h/AC + 1375°F/8h, FC at 100°/h to 1150°F/8h/AC.

Table 11

Summary of Crevice Corrosion Test Data for Specimens of Alloy 625 (N06625) and Alloy 725 (N07725), Evaluated with Flowing Seawater on the I.D. Surface at a Mean Temperature of 14.4°C ± 4.4°C for 180 Days Using Vinyl Sleeves Secured with Clamps as a Crevice Former

Alloy	Observed Initiation (days)	Maximum Depth of Attack (mm)
625 (N06625)*	1 to 48	<0.01 to 0.12
725 (N07725)**	30 (1 specimen only)	0.01 (1 specimen only; second specimen no attack)

* Data for 3 specimens of commercially produced welded tubing.
** Data for 2 machined tube specimens in condition: 1875°F/1h/AC + 1375°F/8h, FC at 100°/h to 1150°F/8h/AC

Table 12

Corrosion Results for Alloy 725 (N07725) in Mineral Acids*, Compared to Literature Data for Alloy 625 (N06625) and Alloy C-276 (N10276)

	Corrosion Rate (mpy)				
Alloy 725 Condition	3%HCl 150°F	10%HCl 150°F	Boiling 10%H_2SO_4	Boiling 10%HNO_3	Boiling 30%H_3PO_4
1	<1;<1	104;105	19;31	<1;<1	3;3
2	<1;<1	262;273	20;29	<1;<1	2;7
3	<1;<1	237;262	20;29	<1;<1	3;3
4	<1;<1	216;219	23;33	<1;<1	<1;3
Literature					
Alloy 625	<1	80-105	18	<1	<10
Alloy C-276	<5	20	20	16	<5

*Duplicate specimens. 1 mpy = 0.0254 mm/y.
Condition:
1. As-mill-annealed
2. As-mill-annealed + 1400°F/6h/AC
3. As-mill-annealed + 1375°F/8h, FC at 100°/h to 1150°F/8h/AC
4. As-mill-annealed + 1350°F/8h, FC at 100°/h to 1150°F/8h/AC

°C = 5/9 (°F - 32)

Copyrighted Materials
Copyright © 1996 NACE International Retrieved from www.knovel.com

Precipitation-Hardened, Nickel-Base Alloys for Sour Gas Environments☆

*M. IGARASHI, S. MUKAI, T. KUDO, Y. OKADA, and A. IKEDA**

Abstract

Stress corrosion cracking (SCC) in sour gas environments of γ′ [gamma prime: Ni_3(Ti and/or Al)] and γ″ (gamma double prime: Ni_3Nb) precipitation-hardened, nickel-base alloys has been studied using the slow strain rate tensile (SSRT) test, anodic polarization measurement, and transmission electron microscopy (TEM). The γ′-type alloy containing Ti was more susceptible to SCC in the SSRT tests up to 350 F (450 K) than the γ″-type alloy containing Nb. The susceptibility to SCC was related to their deformation structures in terms of stress localization and sensitivity to pitting corrosion in H_2S solutions. TEM observation showed that the γ′-type alloy deformed by superlattice dislocation pairs in coplanar structures. This mode of deformation induced stress localization at some boundaries, such as grain boundaries and as a result, the susceptibility to SCC of the γ′-type alloy was increased. On the other hand, the γ″-type alloy deformed by single dislocations, not in coplanar structures, so that it was less susceptible to SCC in terms of stress localization. The anodic polarization measurements suggested that the γ′-type alloy was more susceptible to pitting corrosion compared to the γ″-type alloy.

Introduction

Precipitation-hardened, nickel-base alloys, such as Alloys 718 (UNS N07718) and 925, have been applied for down-hole and well-head equipment in certain sour gas environments.[1-4] They require high strength with toughness and corrosion resistance comparable to tubing even in heavy-wall thickness goods. They are easily strengthened by precipitation of γ′-Ni_3(Ti and/or Al) and/or γ″-Ni_3Nb in adequate aging conditions without cold working.[5] However, these heat-treatable alloys have been considered to be more susceptible to stress corrosion cracking (SCC) in sour gas environments than the conventional cold-worked alloys.[1,3]

Silcock[6] showed that, in the γ′-type FeNi alloys with less than 21% Ni, precipitation of the γ′-Ni_3Ti promoted SCC in boiling $MgCl_2$ solutions. She concluded that it mainly resulted from slip planarity induced by γ′ formation on aging. She also showed that this stress localization would be released by the Orowan looping after prolonged aging. However, our recent transmission electron microscopic (TEM) observation suggested that those were an intrinsic mode of deformation in the γ′-type alloys, but the slip planarity in the alloys with higher than 40% Ni content was not decreased, even in the over-aged conditions. Moreover, the present authors also showed that, in the γ″-type alloys, no planar dislocations were observed in every aging conditions.[7] This suggests that the γ″-type alloys are less susceptible to SCC in hostile environments than the γ′-type alloys in terms of stress localization induced by γ′ and/or γ″ formation.

In this study, SCC in certain sour gas environments of γ′ and γ″ precipitation-hardened, nickel-base alloys was studied using the slow strain rate tensile (SSRT) test, anodic polarization measurement, and transmission electron microscopy (TEM). This article describes the roles of Nb and Ti in SCC of precipitation-hardened, nickel-base alloy from the standpoints of the deformation structures in terms of stress localization and stability of passive films in H_2S solutions. It is also suggested that the γ″-type alloys containing Nb in an aged condition are less susceptible to SCC than in a cold-rolled condition.

Experimental

A survey on SCC and hydrogen embrittlement (HE) using four-point, bent-beam specimens was conducted in the composition range of Ni, 40 to 60%; Cr, 19 to 25%; Mo, 3.0 to 6.0%; and Nb, 2.0 to 5.0% for the γ″-type alloys, or Ti, 1.0 to 3.0% for the γ′-type alloys, respectively, to fix the adequate base compositions for precipitation of the γ′ or γ″ phase, and then to fix the adequate Nb and Ti content for this study. The materials used in this survey were vacuum induction melted and processed by hot-forging and hot-rolling to 7-mm-thick sheets. They were solutionized for 1 h at 2100 F (1423 K), followed by a water quench (WQ), and aged for 20 h in the temperature range between 1200 F (823 K) and 1380 F (1023 K). The four-point, bent-beam-type specimens (0.25-mm R-notched) for SCC and HE were cut from the sheets. The test conditions are described elsewhere.[1]

*Submitted for publication November 1987; revised April 1987.

*Presently at the Laboratory for Research on the Structure of Matter, University of Pennsylvania, 3231 Walnut St., Philadelphia, PA 19104-6272; home institute is at the Technical Research Laboratories, Sumitomo Metal Industries, Ltd., 1-3 Nishinagasu-hondori, Amagasaki, Hyogo 660, Japan.

TABLE 1 — The Chemical Compositions of the Materials Used (in wt%)[1]

	C	Si	Mn	P	S	Ni	Cr	Mo	Ti	Nb	Al
Alloy P(γ'')	0.014	0.01	0.30	0.002	0.002	52.4	22.6	3.49	0.00	4.73	0.09
Alloy A($\gamma' + \gamma''$)	0.005	0.01	0.30	0.003	0.001	51.4	18.8	2.95	0.86	5.14	0.66
Alloy B(γ')	0.005	0.01	0.30	0.001	0.001	42.8	21.8	2.95	2.67	0.10	0.13
Alloy C(γ')	0.014	0.01	0.30	0.001	0.002	51.8	22.3	3.44	2.52	0.11	0.10

[1]Bal Fe.

Subsequently, 52%Ni-22%Cr-3.5%Mo-Fe(bal) system was selected as the base composition, and 4.8% Nb (3.0 at%) was added for the γ''-type alloy (denoted Alloy P) and 2.5%Ti (3.0 at%) was added for the γ'-type alloy (denoted Alloy C), respectively. Two other alloys, Alloys A ($\gamma' + \gamma''$-type) and B (γ'-type), were also studied for comparison. The chemical compositions of the materials are given in Table 1. They were also vacuum induction melted and processed to 9-mm-thick sheets. The sheets were solutionized for 1 h at 1830 to 2100 F (1273 to 1423 K), followed by a water-quench and aged for up to 300 h in the temperature range between 1200 F (923 K) and 1380 F (1023 K). Some sheets were cold rolled 15 to 40% in reduction in thickness after solution treatment. Tensile and SSRT test specimens with 4-mm diameters and gage lengths of 30 mm were obtained from the sheets in the transverse direction, and Charpy impact test specimens, 5 x 10 x 55 − 2 mm V- notched, were also obtained. Specimens for the anodic polarization measurements, 20-mm diameters and 2.0-mm thick, were cut from the sheets.

Specimens for thin foils were cut from the sheets and deformed 5% in tension at room temperature to examine the deformation structures. Thin foils were prepared by an electrolytic jet-polishing technique using a 10% perchloric acid-90% acetic acid bath at 50 F (283 K).[7]

Tensile tests at room temperature and the Charpy impact tests at 32 F (273 K) were performed to study their aging behaviors. High-temperature tensile tests were also performed at 300, 350, and 400 F (422, 450, and 477 K).

The SSRT tests[8,9] were conducted to study the susceptibility to SCC in 25%-NaCl and 0.5%-CH_3COOH solutions saturated with 7 atm H_2S at 300 to 400 F (422 to 477 K) with a strain rate of 4.0 x $10^{-6}s^{-1}$.

The stabilities of passive films were examined by the measurement of pitting potentials of the materials. Anodic polarization curves were obtained potentiodynamically at a sweep rate of 20 mV/min with a potentiostat in H_2S-Cl^- environments at 140 F (333 K).

The deformation structures in the specimens were examined by TEM in the JEM-200CX.

Results

Figure 1 shows the typical corrosion-resistant region of the γ''-type alloys evaluated from the first survey on SCC at 482 F (523 K) and HE at room temperature using the four-point, bent-beam-type specimens. The specimens with less than 40% Ni were very susceptible to SCC even with high-Cr content, while the specimens with more than 45% Ni were less susceptible to SCC, particularly with high-Cr content. On the other hand, the susceptibility to HE increased with Ni content, and the specimens with more than 55% Ni were completely failed, except the 55%Ni-19%Cr specimen. The specimens with around 50%Ni were the least susceptible to SCC and HE, so the base composition was fixed to 52%Ni-22%Cr-3.5%Mo-Fe(bal). This composition is free from the precipitation of topologically close-packed phases, such as sigma or Laves phase.

Second, to fix the adequate Nb and Ti content for this study, various heats with different Nb and Ti content were examined.

Figure 2 shows the effect of Nb and Ti content on the susceptibility to SCC evaluated from the four-point, bent-beam-type tests at 392 F (473 K) using the specimens [52%Ni-22%Cr-3.5%Mo-(Nb or Ti)] aged at 1200 (923), 1290 (973), and 1380 F (1023 K). Their hardening behaviors are described elsewhere.[10] All of the γ''-type alloys containing Nb showed good corrosion resistance to SCC in every aging condition. On the other hand, the susceptibility to SCC of the γ'-type alloys containing Ti was substantially increased with Ti content and with aging temperature. From these results, two

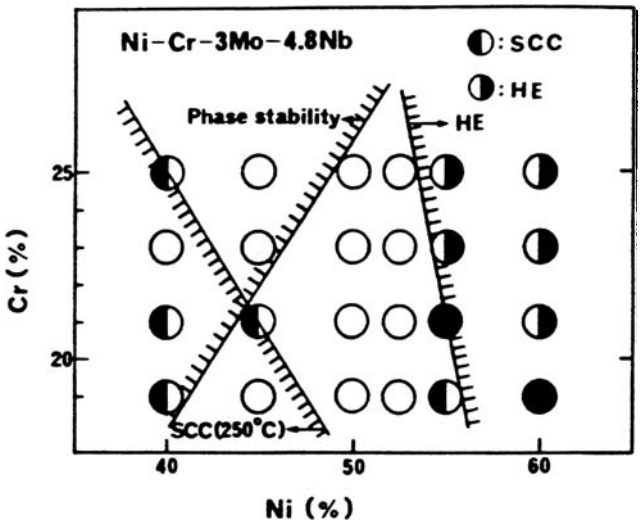


FIGURE 1 — Effect of Ni and Cr on SCC and HE susceptibilities of the specimens with 4.8% Nb. Aging condition: 2100 F x 1 h (WQ) + 1290 F x 20 h (AC). SCC: 20%NaCl-0.5%CH_3COOH, 10 atm H_2S + 10 atm CO_2. HE: 5%NaCl-0.5%CH_3COOH, 1 atm H_2S, 77 F, 1σy, 720 h, with iron coupling. Phase stability: vEo > 3.0 kgf-m/cm².

alloys were finally chosen for this study; i.e., 52%Ni-22%Cr-3.5%Mo-4.7%Nb for the γ''-type alloy and 52%Ni-22%Cr-3.5%Mo-2.5%Ti for the γ'-type alloy. Note that 4.7%Nb is comparable to 2.5%Ti in terms of at% (3.0 at%).

Figure 3 shows isochronal aging behaviors of Alloy P (52%Ni-22%Cr-3.5%Mo-4.7%Nb; γ''-type), and Alloys A ($\gamma' + \gamma''$-type) and B (γ'-type) solutionized at 2100 F (1423 K) and aged for 20 h at 1200 to 1380 F (923 to 1023 K). The highest yield strength (denoted at 0.2% proof stress in this study) was obtained by aging around 1290 F in the specimens from Alloy P, while they were obtained by rather high temperature aging in two other alloys. The elongation and impact values of the specimen from Alloy P decreased with aging temperature. Low-impact values were obtained by aging at higher temperatures than 1290 F (973 K), even with decreasing yield strength. The elongation and impact curves of the specimens from Alloys A and B are similar to those for Alloy P, but the minimum values were lower than for those of Alloy P. Note that the specimens from Alloy P show rather high ductility with higher strength as a result of aging at lower temperatures. This is one of the advantages in the γ''-type alloys compared to the γ'-type alloys.

Figure 4 shows isothermal aging curves of the specimens solutionized at 1965 F (1348 K) and aged at 1290 F (1023 K). The specimens from Alloy P and also Alloy A are strengthened more rapidly than the Alloy B specimens, and then the yield strength is reduced with prolonged aging in Alloy P. However, the yield strengths of Alloys A and B increased after prolonged aging, with markedly reduced toughness.

Figure 5 and Table 2 show the susceptibilities to SCC of Alloy P (γ''-type), and Alloys A ($\gamma' + \gamma''$-type) and B (γ'-type) evaluated from the SSRT tests at 300 to 400 F (422 to 477 K). All specimens were solutionized for 1 h at 2100 F (WQ) and aged for 20 h at 1290 F. In this test, ductility ratio [ratio of time to failure (TTF) in H_2S environment vs TTF in air] corresponds to the susceptibility to SCC of the specimens.[8,9] Alloy P showed an excellent corrosion resistance to SCC up to 350 F (450 K), though it was susceptible to SCC

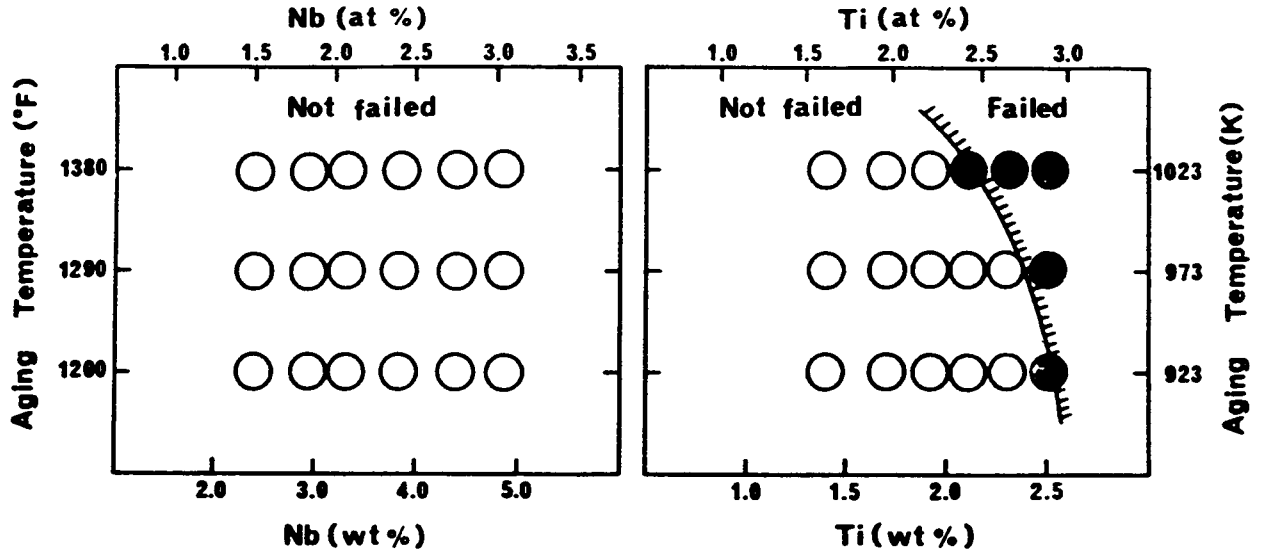


FIGURE 2 — Effect of Nb- and Ti-content on SCC susceptibility of the specimens with 52%Ni-22%Cr-3%Mo solutionized for 1 h at 2100 F (WQ) and aged for 50 h at 1200 to 1380 F. Test condition: 20%NaCl-0.5%CH_3COOH, pH 2, 10 atm H_2S-10 atm CO_2, 392 F, 1σy, 720 h.

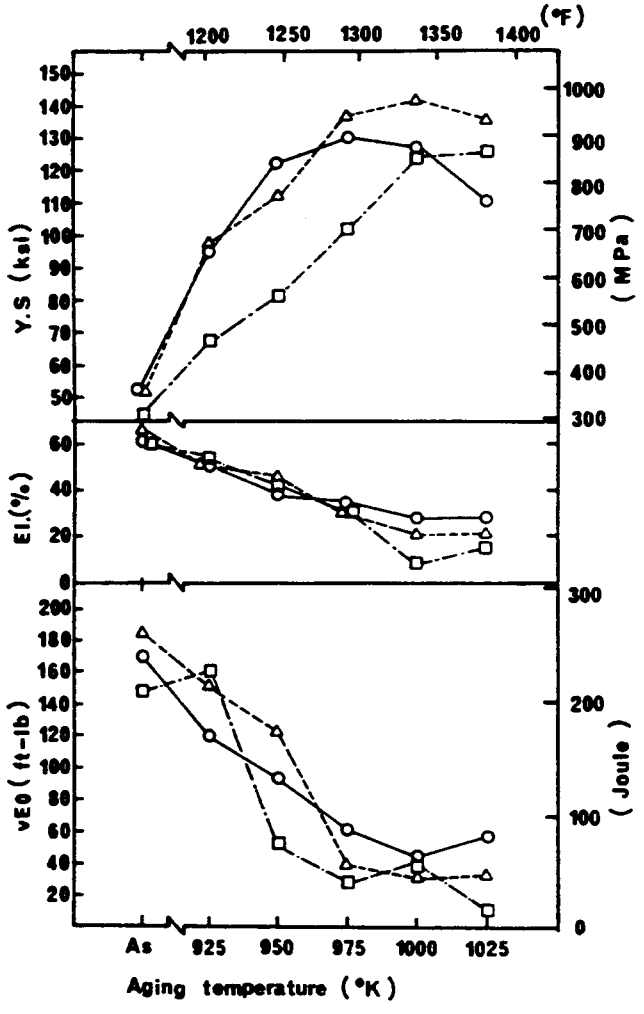


FIGURE 3 — Comparison of aging behaviors of Alloys P, A, and B solutionized for 1 h at 2100 F (WQ) and aged for 20 h at 1200 to 1380 F.

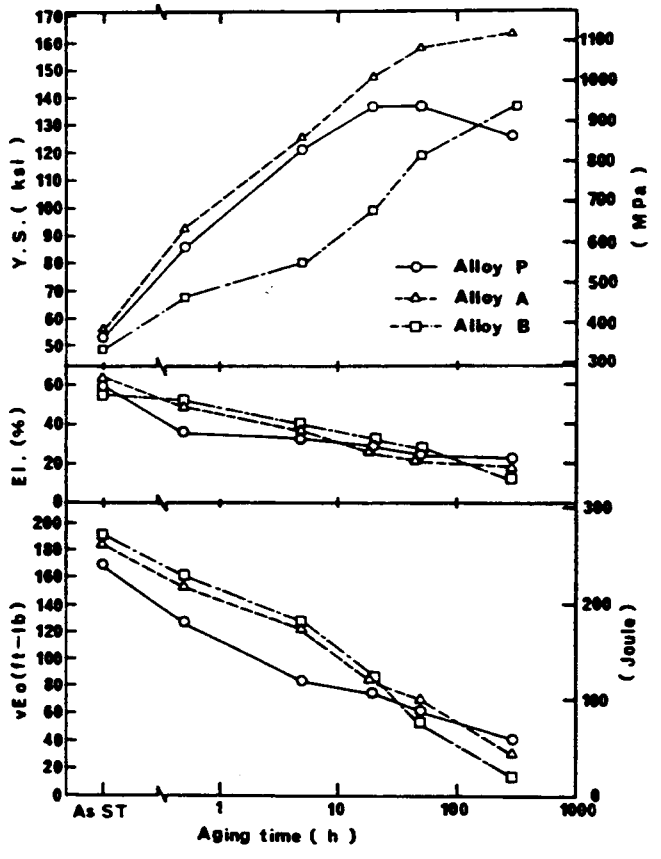


FIGURE 4 — Isothermal aging curves of the specimens solutionized for 1 h at 1965 F (WQ) and aged at 1290 F.

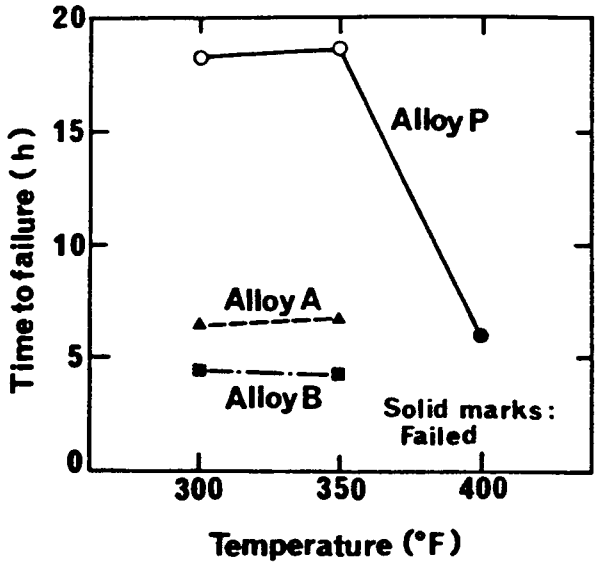


FIGURE 5 — Effect of testing temperature on SCC susceptibility of Alloys P, A, and B solutionized for 1 h at 1965 F (WQ) and aged for 20 h at 1290 F. Test condition: 25%NaCl-0.5%CH_3COOH, 7 atm H_2S, $\epsilon = 4.0 \times 10^{-6} s^{-1}$.

TABLE 2 — The SSRT Test Results of Alloys P, A, and B Aged[1]

Specimens	TTF (h) in H_2S/in Air		
	Testing Temperature (F)		
	300	350	400
Alloy P	16.7/16.8	16.3/16.9	4.0/17.0
Alloy A	6.3/17.7	6.9/17.2	—
Alloy B	4.5/19.6	4.4/18.2	—

[1]Aging condition: 2100 F x 1 h (WQ) + 1290 F x 20 h (AC).

at 400 F (477 K). On the other hand, both Alloys A and B were very susceptible to SCC even at 300 F (422 K).

These differences seemed to come from the alloy chemistry. However, the present authors focused only on the two major elements, Nb and Ti, in this study, which form the different hardening phases, the γ″ and γ′ phases.

To clarify the effect of Nb and Ti on the SSRT behavior, Alloys P and C were studied in detail. Alloy C (52%Ni-22%Cr-3.5%Mo-2.5%Ti) has the same composition as Alloy P except for equivalent substitution of Ti for Nb. Figures 6 and 7 show the elongation and yield strength curves of Alloys P and C in aged and cold-rolled conditions. The cold-rolled specimens from both Alloys P and C were strengthened with increasing reduction in thickness and their elongations were reduced with increasing yield strength. The elongation of the aged specimens was also reduced with increasing yield strength but had higher values than in the cold-rolled condition.

The present authors conducted the SSRT tests using specimens with yield strength ~130 ksi, numbered in the Figures 6 and 7. The summary of the tests are listed in Table 3. No degradation in TTF in the H_2S environment was observed up to 350 F (450 K) in Alloy P in an aged condition compared with that in air. However, in Alloy C in an aged condition, marked degradations in TTF were observed with secondary cracks in the H_2S environment even at 300 F (422 K), as observed in Alloys A and B (Figure 5). On the other hand, in a cold-rolled condition, a slight degradation in TTF without secondary cracks was observed at 350 F (450 K) in Alloy P, though no degradation in TTF was observed at 300 F (422 K). However, in Alloy C in a cold- rolled condition, marked degradations were observed with secondary cracks at both 300 and 350 F (450 K).

The γ″-type alloy containing Nb showed good corrosion resistance to SCC in the SSRT tests compared to the γ′-type alloy containing Ti and also two other alloys. It is also suggested that the

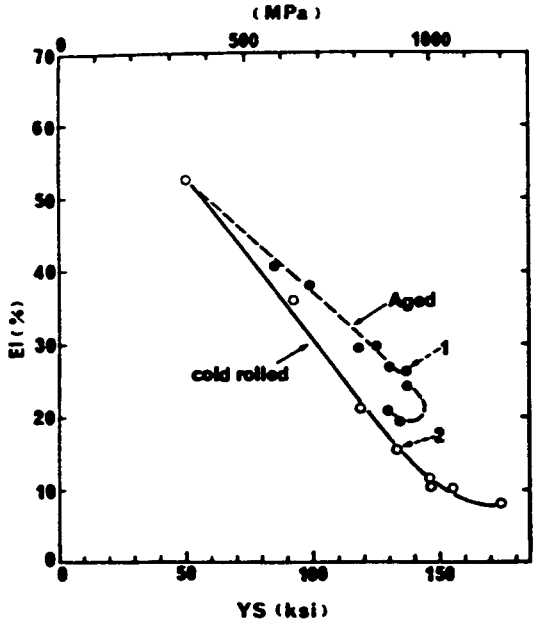


FIGURE 6 — Comparison of El-YS curves of the γ″-type Alloy P between cold rolled and aged at 1290 F. (The specimens with the numbers were examined in the SSRT tests listed in Table 3.)

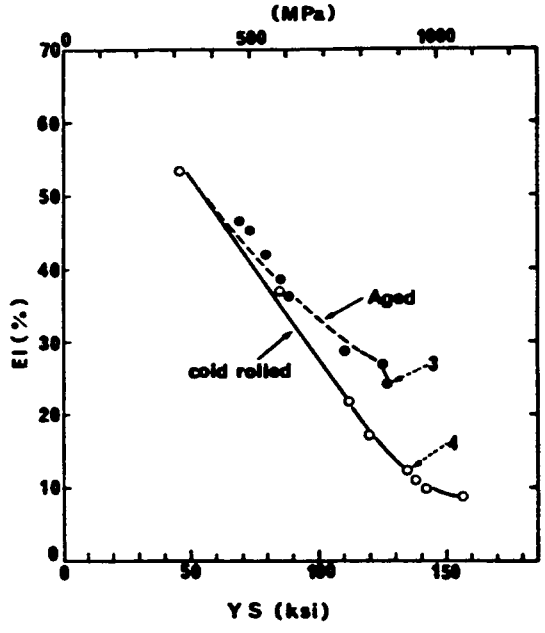


FIGURE 7 — Comparison of El-YS curves of the γ′-type Alloy C between cold rolled and aged at 1290 F. (The specimens with the numbers were examined in the SSRT tests listed in Table 3.)

TABLE 3 — Summary of the SSRT Tests of the γ′- and γ″-type Alloys

Specimens		TTF (h) in H_2S/in Air	
		Testing Temperature (F)	
		300	350
Alloy P (γ″-type)	Aged[1]	18.0/18.2	18.8/18.9
	CW[2]	7.4/8.1	7.1/8.2
Alloy C (γ′-type)	Aged[3]	4.6/17.8	5.9/18.1
	CW[4]	3.7/7.9	5.0/8.3

[1]1965 F x 1 h (WQ) + 1290 F x 20 h (AC).
[2]Cold-rolled 25%.
[3]1965 F x 1 h (WQ) + 1290 F x 300 h (AC).
[4]Cold-rolled 30%.

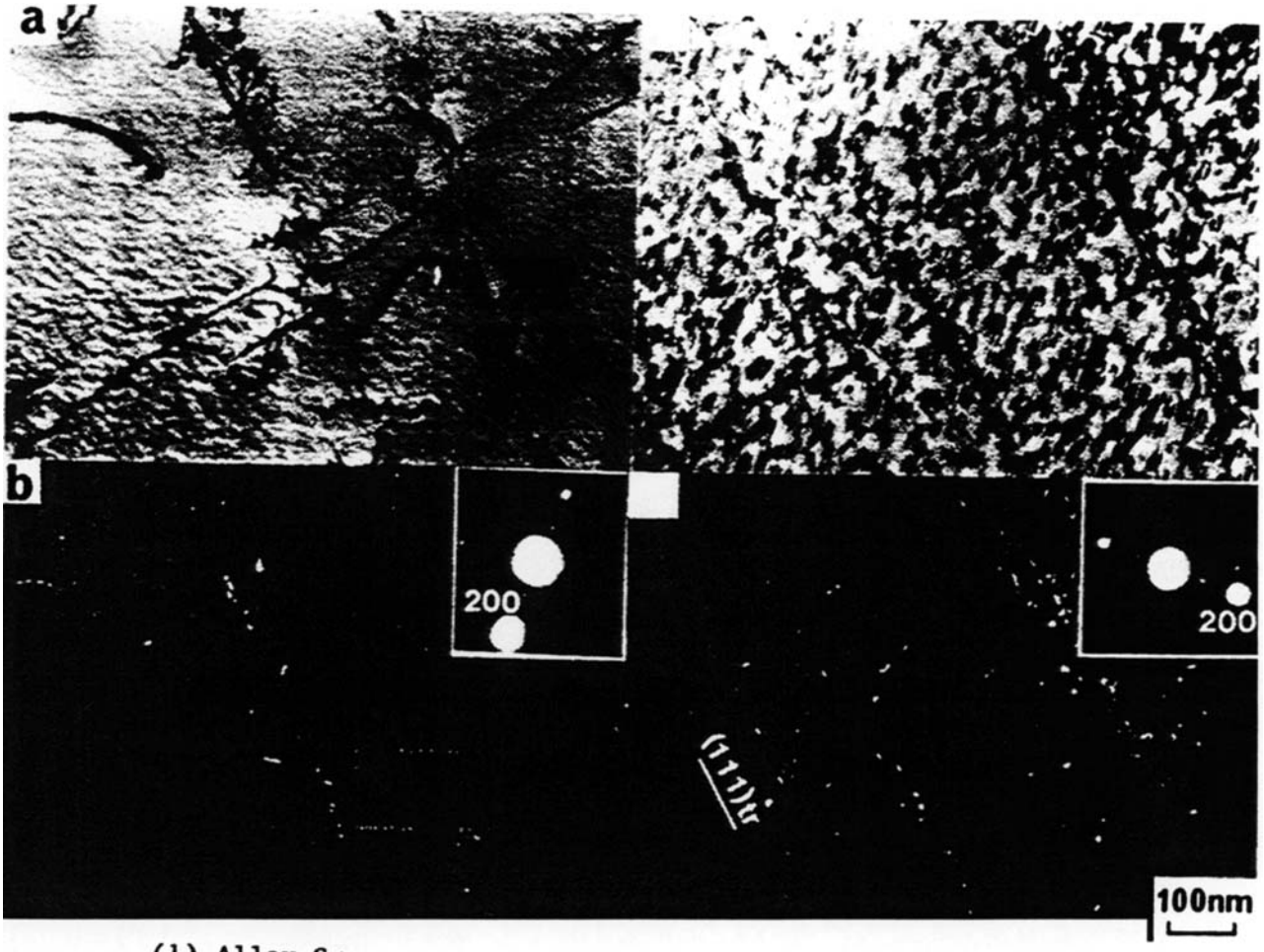


FIGURE 8 — Deformation structures in the specimens aged for 30 min at 1380 F and deformed 5% in tension at room temperature. (a) Bright field, (b) dark field.

γ″-type alloys in aged conditions were less susceptible to SCC than those in cold-rolled conditions. Therefore, the corrosion resistance to SCC of the γ″-type alloy from the standpoints of the deformation structures and anodic polarization in certain H_2S solutions was studied. The deformation structures are related to stress localization, which induces SCC, but the anodic polarization is related to SCC through stability of passive films.

Figure 8 shows deformation structures at room temperature in the specimens from Alloy C containing the γ′ phase and Alloy P containing the γ″ phase aged for 30 min at 1380 F (1023 K). The weak beam technique[11] was used to resolve the dislocation contrasts from the strain contrasts induced by the γ′ and γ″ phases.

Typical superlattice partial dislocation pairs were mainly observed in coplanar structures in Alloy C [Figure 8(1)]. The γ′ particles were sheared by {111}<110> type dislocations in this mode of the deformation.[12] This mode of the deformation occurs preferentially in the same slip plane, and as a result, it induces stress localization at some boundaries, such as grain boundaries. In Alloy P, however, single dislocations not in coplanar structures were observed, with typical {111}<112>-stacking faults in the γ″ particles [Figure 8(2)].[7,13] This mode of the deformation minimizes planar slip so that in this sense, it induces less stress localization at boundaries.[7,14,15] It is concluded that the γ″-type alloys are less susceptible to SCC than the γ′-type alloys because of their differences in stress localization. These stress localization models are schematically illustrated in Figure 9.

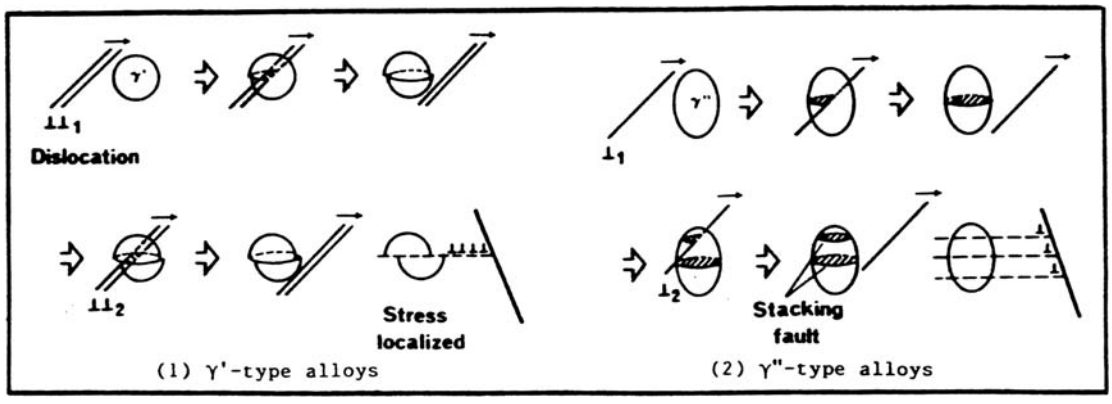


FIGURE 9 — Schematic illustration of the deformation structures related to stress localization at some boundaries.

In the γ'-type alloys, superlattice partial dislocation pairs with the Burger's vectors of 1/2{111} <110> cut through γ' particles, and no faults are left in the γ' particles, except that a step is formed at the particle/matrix interface equal in size to the magnitude of the Burger's vector. Then the second and subsequent dislocation pairs are likely to cut through the γ' particles in the same slip plane because the alloy with Ti is more likely to exhibit coplanar slip because of its low-stacking fault energy, as measured by Beeston, et al.[16] As a result, it induces stress localization at boundaries.

On the other hand, in the γ''-type alloys, a single superlattice dislocation with the Burger's vectors of 1/6{111}<112> and also 2/3{111}<112> in some cases, is likely to cut through the γ'' particles, leaving a stacking fault in the γ'' particles and a smaller step at the particle/matrix interface. Then the subsequent dislocations are more likely to cut through the γ'' particles in the different slip planes because that the coplanar slip could not occur since complex faults would be formed, and the alloy with Nb has rather higher stacking fault energy (SFE) that decreases the ease of the coplanar slip. As a result, it induces less stress localization at boundaries.

The anodic polarization measurements were conducted to evaluate the sensitivities to pitting corrosion of the specimens in certain H_2S environments. The results are listed in Table 4. The specimens from Alloy P showed a good resistance to pitting corrosion up to 0.1 atm H_2S, while the specimens from Alloy C were susceptible to pitting corrosion even in a 0.01 atm H_2S solution. It is concluded that the γ''-type alloy containing Nb is less susceptible to pitting corrosion in certain H_2S environments than the γ'-type alloy containing Ti.

TABLE 4 — Anodic Polarization Behaviors of Alloys P and C Aged

Environment[1]	Specimen	E_{cor} (V vs SCE)	E_{pit} (V vs SCE)
0.01 atm H_2S + N_2	P	−0.23	>+1.0
	C	−0.24	+0.49
0.1 atm H_2S + N_2	P	−0.27	>+1.0
	C	−0.27	+0.35
1.0 atm H_2S + N_2	P	−0.28	+0.05

[1]5% NaCl, N_2 balance, 140 F, scan speed: 20 mV/min.

Discussion

Our study concludes that the γ''-type alloys with Nb are less susceptible to SCC in certain sour gas environments than the γ'-type alloys with Ti in terms of stress localization at boundaries and sensitivity to pitting corrosion.

Silcock[8] showed that the susceptibility to SCC in boiling $MgCl_2$ solutions of the FeNi alloys with less than 21%Ni was reduced by overaging at 1380 F (1023 K). She concluded that it resulted from the reduction in the slip planarity by overaging. However, in our study, the susceptibility of the γ'-type alloys with Ti was increased by overaging at 1380 F (1023 K) (Figure 2). It is considered that this comes from the differences in the base compositions. It is noted that the slip planarity is directly related to the SFE of alloy systems. The SFE of

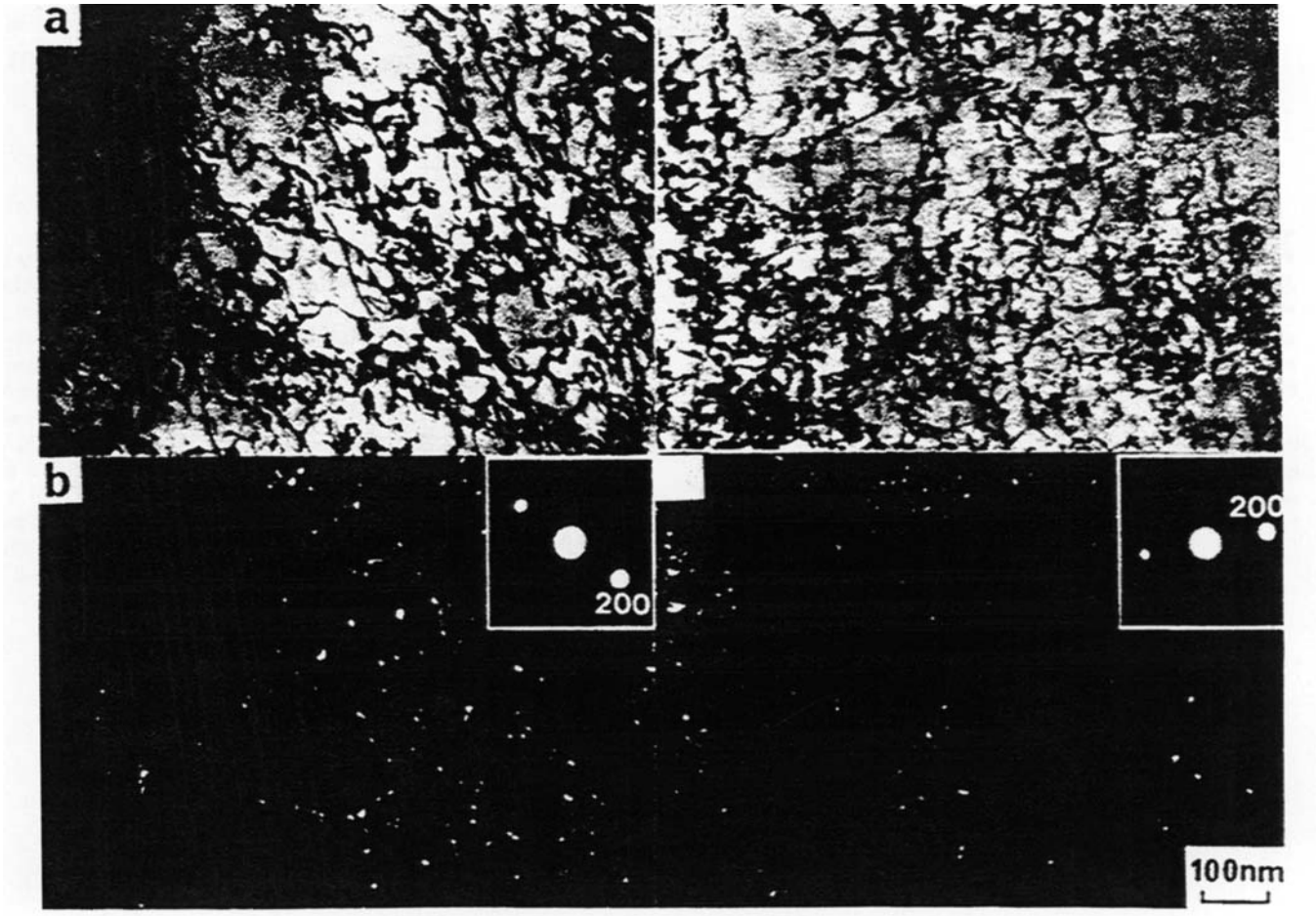


FIGURE 10 — Deformation structures in the specimens cold rolled 25% and deformed 5% in tension at room temperature. (a) Bright field, (b) dark field.

the alloys in this study is decreased by aging, while the SFE of their alloys is increased by aging.[16,17] Consequently, it is suggested that the susceptibility of the γ′-type alloys with Ti in this study was increased by overaging with increasing slip planarity.

It is generally considered that the precipitation hardened alloys are more susceptible to SCC in sour gas environments than the conventional cold-worked alloys.[1,3] However, this study showed that the γ″-type alloys in an aged condition were less susceptible to SCC in the SSRT tests than that in a cold-rolled condition (Table 2). It was suggested that it could be explained from the standpoint of the stress localization. Figure 10 shows the deformation structures of Alloys P and C cold-rolled 25% and deformed 5% in tension at room temperature. Comparing them to those in an aged condition shown in Figure 8, it is suggested that extensive dislocations introduced by cold-working induce stress localization at boundaries in the cold-rolled specimens. It is suggested that this stress localization induces SCC in both Alloys P and C.

Conclusions

1. SCC in sour gas environments of γ′- and γ″-precipitation-hardened, nickel-base alloys were studied using the SSRT test, anodic polarization measurement, and TEM. A first survey on SCC and HE using the constant strain method showed that 52%Ni-22%Cr-3.5%Mo-Fe(bal) was the adequate base composition for precipitation of the γ′ and γ″ phases.

2. The γ″-type alloy containing Nb (52%Ni-22%Cr-3.5%Mo-4.7%Nb) showed a good corrosion resistance to SCC compared to the γ′-type alloy containing Ti (52%Ni-22%Cr-3.5%Mo-2.5%Ti) and also two other alloys (the γ′ + γ″-type and the γ′-type) in the bent-beam and SSRT tests.

3. This γ″-type alloy was easily strengthened up to 130 ksi by aging about 20 h.

4. The susceptibility to SCC was related to their deformation structures and the anodic polarization in certain H_2S solutions.

5. The γ′-type alloy deformed by the superlattice dislocation pairs in coplanar structures. This mode of deformation-induced stress localization at some boundaries, such as grain boundaries and as a result the susceptibility to SCC of this alloy, was increased.

6. The γ″-type alloy deformed by the single dislocations not in coplanar structures so that it was less susceptible to SCC in terms of the stress localization.

7. The anodic polarization measurement showed the γ′-type alloy was more susceptible to pitting corrosion compared to the γ″-type alloy.

8. The γ″-type alloy in aged conditions was less susceptible to SCC than that in cold-rolled conditions. This can be also explained by the slip planarity-induced stress localization.

Acknowledgment

The authors would like to thank Y. Itoh and T. Yukitoshi of Sumitomo Metal Industries, Ltd. for permission to publish this paper. Helpful discussions with F. Terasaki, D. Moroishi, and A. Seki are gratefully acknowledged. The considerable assistance in specimen preparation, testing, and examination of Y. Nishioka, H. Kusagi, S. Asayama, T. Hoshino, M. Fujisawa, and H. Nagai are also acknowledged.

References

1. A. Ikeda, T. Kudo, Y. Okada, S. Mukai, F. Terasaki, CORROSION/84, Paper No. 206, National Asosociation of Corrosion Engineers, Houston, Texas, 1984.
2. T. F. Lemke, J. A. Harris, 15th Annual OTC, Paper No. OTC 4451, National Association of Corrosion Engineers, Houston, Texas, 1983.
3. J. A. Harris, E. F. Clatworthy, CORROSION/86, Paper No. 150, National Association of Corrosion Engineers, Houston, Texas, 1986.
4. J. A. Harris, T. F. Lemke, CORROSION/82, Paper No. 137, National Association of Corrosion Engineers, Houston, Texas, 1982.
5. J. M. Oblak, D. F. Paulonis, D. S. Duvall, Met. Trans., Vol. 5, p. 143, 1974.
6. J. M. Silcock, Brit. Corros. J., Vol. 18, No. 3, p. 132, 1983.
7. M. Igarashi, Y. Nishioka, Y. Okada, to be published in Proc. of Ann. Mtg. of Japan Institute of Metals.
8. H. E. Chaung, M. Watkins, G. A. Vaughn, CORROSION/85, Paper No. 227, National Association of Corrosion Engineers, Houston, Texas, 1985.
9. D. R. McIntyre, R. D. Kane, S. M. Wilhelm, CORROSION/86, Paper No. 149, National Association of Corrosion Engineers, Houston, Texas, 1986.
10. M. Igarashi, Y. Okada, Trans. Iron Steel Inst. Japan, Vol. 25, p. B-29, 1985.
11. C. T. Chou, P. B. Hirsch, M. McLean, E. Hondros, Nature, Vol. 300, p. 621, 1982.
12. B. H. Kear, J. M. Oblak, A. F. Giamei, Met. Trans., Vol. 1, p. 2477, 1970.
13. I. Kirman, D. H. Warrington, Met. Trans., Vol. 1, p. 2667, 1970.
14. M. Yamaguchi, Y. Umakoshi, Intermetallic Compound, Nikkankogyo press, Tokyo, Japan, p. 45, 1985.
15. M. Igarashi, Y. Okada, 4th Japan Institute of Metals Int. Symp., supplement to Trans. JIM, Vol. 27, p. 891, 1986.
16. B. E. P. Beeston, L. A. France, J. Inst. Met., Vol. 96, p. 105, 1968.
17. R. E. Schramm, R. P. Reed, Met. Trans., Vol. 7A, p. 359, 1976.

Copyrighted Materials
Copyright © 1996 NACE International Retrieved from www.knovel.com



OTC 5553

Failures of Nickel-Copper Bolts in Subsea Applications

by M.W. Joosten and L.H. Wolfe, Conoco Inc.

Copyright 1987 Offshore Technology Conference

This paper was presented at the 19th Annual OTC in Houston, Texas, April 27-30, 1987. The material is subject to correction by the author. Permission to copy is restricted to an abstract of not more than 300 words.

ABSTRACT

Slow strain rate tests in ASTM seawater using specimens prepared from a failed nickel-copper alloy bolt have shown that precipitation hardened UNS N05500 (MONEL K-500®) is embrittled by cathodic protection with sacrificial aluminum anodes. Some loss of ductility also occurred when annealed UNS N05500 was coupled to aluminum anodes and when the hardened alloy was coupled to steel. Brittle fractures produced by slow strain rate tests were intergranular and were very similar in appearance to the field fractures. While the slow strain rate tests were conducted on an alloy from only one source, there is no reason to assume that UNS N05500 alloy from other sources would resist hydrogen embrittlement from standard cathodic protection systems.

INTRODUCTION

Bolts of alloy UNS N05500, a precipitation hardening nickel-copper alloy commonly referred to as MONEL K-500® failed in a brittle manner on North Sea platforms sometime prior to August of 1984.[1] The failures, which originated at thread roots where the hardness was about Rockwell C 39, occurred in bolts that had been hardened after threading. The failures were attributed to hydrogen embrittlement that was a result of cathodic protection. It was concluded that hydrogen embrittlement of MONEL K-500 would not occur if the hardness was below HRC 35 which is the acceptable hardness of UNS N05500 in sour systems.[2] To insure proper hardness of the thread roots, it was recommended that annealing and hardening treatments be done after the threading.

Since that time, subsea clamp bolts of UNS N05500 alloy with the recommended heat treatment and hardness have failed in a brittle manner on two North Sea platforms. These failures, occurred while the bolts were coupled to steel and cathodically protected with aluminum anodes or a combination of aluminum anodes and impressed current. The bolts had been roll threaded, annealed at 980 to 1050 C, water quenched, and precipitation hardened at 500 to 600 C for 16 hours. This produced hardnesses of about HRC 25.

The later failures occurred in bolts that were loaded to 344 Mpa (49,890 psi) during installation. This was 59 percent of the specified minimum yield strength of the material. Following the failures, the broken bolts and other cathodically protected alloy N05500 bolts that were in critical subsea applications were replaced with steel bolts.

The remainder of this paper discusses the more recent failures. Results of slow strain rate tests on hydrogen charged samples from one of the failed bolts are presented along with studies of the fracture surfaces.

SUBSEA FAILURES

Since the more recent failures occurred in bolts that had the recommended heat treatment and were below the critical hardness level, the material was traced through the various heat treating and threading steps to the original alloy supplier to see if the failures were restricted to the alloy from a particular vendor or processor. It was found that both sets of failed bolts were heat treated and threaded by the same shops, but the material was supplied by two different companies. A few bolts that were purchased for use on the platforms had been heat treated in an oxidizing atmosphere, but the failures were not limited to these bolts. Thus it is thought that the failures are generic to the alloy and were not caused by improper manufacturing processes.

Alloy compositions of the failed bolts were determined by several independent analyses, and these analyses plus heat analyses of all Alloy N05500 fasteners that were in use on the platforms were studied to see if the failures correlated to composition variables or to tramp elements such as sulfur or selenium. The failures occurred in bolts

References and illustrations at end of paper.

*(MONEL is a trademark of Inco Alloys International Inc.)

© OTC Reprinted with the permission of the Offshore Technology Conference

of the proper alloy composition, and we believe that the failures were not caused by tramp elements or unusual alloy compositions.

Typical microstructure of a failed bolt is shown in Figure 1. All of the failed bolts had grain growth at the thread surfaces, and some had detectable $Ni_3(Ti,Al)$ precipitates, particularly in the larger grains.

Applicable alloy specifications were:

CHEMICAL COMPOSITION

	Ni	Co	Cu	Fe	Al	Si	Mn	Ti	Cr	C	S
Min.	63*	-	27	-	1.3	-	-	0.3	-	-	-
Max.	-	2.0	33	2.0	3.2	0.5	1.5	0.85	-	0.25	0.01

*Ni+Co

MECHANICAL PROPERTIES

Yield Strength	Tensile Strength	Elongation	Hardness
585 MPa Min. (84,850 psi)	900 MPa Min. (130,530 psi)	20% Min.	HRC 35 Max.

The cathodic protection system of the platform on which the most recent bolt failures occurred was designed to produce a current density of 130 mA/m^2 using a combination of impressed current and aluminum anodes.[3] Under normal operating conditions the cathodic protection system delivers a current density of 35 mA/m^2 at a potential of -990 to -1140 mV versus silver/silver chloride.[4]

SLOW STRAIN RATE TESTS

Slow strain rate tests are popular for determining the susceptibility of materials to stress corrosion cracking and hydrogen-induced environmental cracking. Test specimens are subjected to a constant rate of extension until failure occurs. This test method will promote stress corrosion cracking in alloy/environment systems that do not produce cracking in static tests. However, the data produced by the tests must be interpreted cautiously since the absence of stress corrosion cracking in slow strain rate tests is not sufficient evidence to eliminate cracking concerns.

Slow strain rate tests were conducted in air and in circulating ASTM seawater that was exposed to the atmosphere. During the tests, the specimens were contained in plexiglass vessels equipped with two small anodes which were about 1 cm from the gauge sections of the samples.

The slow strain rate tests were conducted in a 20,000-pound capacity load frame specially modified to achieve low strain rates. To calibrate the stiffness of the machine and test fixtures, the specimen strain over a two-inch gauge length was monitored with an extensometer during the first test. For subsequent tests, the crosshead travel was set at the same speed, but an extensometer was not used. Strain rates were in the order of $5x10^{-6}$ per second. For nickel-based alloys, this strain rate reportedly results in the maximum susceptibility to hydrogen embrittlement.[5]

Samples for the slow strain rate tests had 1/4-inch-diameter by 2-inch-long gauge sections. They were machined from the body of a 45-mm-diameter MONEL K-500 bolt that had failed in the threads while in service on one of the North Sea platforms. This bolt, which had been in service about 1 year, had been threaded, annealed, water quenched, and precipitation hardened to Rockwell C 25. Except for two samples that were annealed at 1850 F (1010 C) and one that was baked at 350 F (177 C) for 6 hours after they were machined, the slow strain rate samples had the as-received heat treatment.

Mechanical properties, as determined by the slow strain rate tests, are shown in Table 1. Hardness of the as-received alloy was HRC 25. The annealed hardness was HRB 72.

CHEMICAL COMPOSITION OF SLOW STRAIN RATE SAMPLES

Ni	Cu	Fe	Al	Si	Mn	Ti	Cr	C	S	Se	P
64.6	29.1	1.6	2.8	.07	1.2	.5	.03	.08	.004	<.01	.022

Potentials of the slow strain rate samples versus a silver/silver chloride reference electrode were:

Aluminum anodes	-900 mV
Steel anodes	-620 mV
DC Power supply	-800 mV

Thus the experimental conditions were actually less severe than the field conditions in terms of hydrogen generated on the surface of the specimens.

RESULTS OF SLOW STRAIN RATE TESTS

As is shown in Table 1 and Figure 2, precipitation hardened samples that were tested in air or in ASTM seawater without cathodic protection failed in about 36 hours. These samples elongated at least 19 percent, and the failures were typical ductile fractures (shear or cup and cone, Figure 3). However, when precipitation hardened samples were coupled to small aluminum anodes or to a potentiostat (potentials between -800 to -900mV versus Ag/AgCl), the time to failure was less than 6 hours, and the elongation was less than 5 percent. One sample that was precharged with hydrogen by connecting it to aluminum anodes eight days before a load was applied had only 3.5 percent elongation. The fracture regions of the hydrogen charged specimens were brittle and had numerous secondary cracks (Figure 4).

Two slow strain rate specimens of precipitation hardened MONEL K-500 were coupled to steel anodes which produced a potential of -620mV. One specimen was coupled to the steel for the duration of the test only, and the other was coupled to it for eight days before the load was applied. These specimens failed in about 30 hours, and exhibited good elongation and reduction of area values. The fractures were ductile and did not have secondary cracking. Both specimens had less elongation but more reduction of area than the sample that was tested in seawater without cathodic charging (Table 1 and Figure 2). The duration of the coupling did not affect the failure time or the fracture appearance.

One annealed specimen was strained while coupled to aluminum in artificial seawater. Another was tested in air. The air sample elongated about 30 percent, and the aluminum coupled specimen elongated 21 percent (Table 1). While both had reasonably good elongation, their fracture appearance was much different. The air sample was a typical cup and cone, ductile break that was accompanied by necking, while the aluminum coupled sample displayed many of the brittle fracture characteristics shown by the hardened specimens. It had secondary cracking and only limited necking. This embrittlement suggests that even annealed MONEL K-500 which has insufficient strength for bolting applications is somewhat susceptible to hydrogen embrittlement in cathodically protected systems.

FRACTOGRAPHY

The subsea fractures were intergranular and very brittle (Figure 5). They also had occasional parallel lines that resembled fatigue striations.[6] All of the cathodically protected slow strain rate fractures of the annealed and as-received alloy were intergranular, brittle, and similar to the subsea fractures except that some slow strain rate fractures had ductile dimples on the grain faces (Figures 6 & 7). The fracture of the slow strain rate sample that had been hydrogen charged with aluminum anodes for eight days before testing was intergranular, brittle, and virtually identical to the subsea fracture surfaces, including the parallel lines (Figure 7). It had only a few ductile dimples on the grain surfaces. Slow strain rate fractures that were created in air, or in ASTM seawater without cathodic protection were typical dimpled, ductile fractures (Figure 8).

Fatigue was considered as a possible failure mechanism for the subsea bolts because some features of the fracture resembled fatigue fractures of MONEL 400[6]. Since there were no fractographs of MONEL K-500 fatigue available for comparison, a fatigue test was initiated. A full-sized, hardened UNS N05500 alloy bolt was cycled between 2,800 and 30,000 psi (19.3 and 206.7 N/mm^2) at 0.1 Hertz while the threads were in air and the body was exposed to ASTM seawater and coupled to aluminum anodes. This bolt failed in the threads in 21,613 cycles. This sample failed in air. Therefore, direct correlation of fracture features was not possible. However, the fatigue fracture surface (Figure 9) was dominated by striations and was very different from the subsea and slow strain rate fractures (Figures 5-7). Results of the fatigue and slow strain rate tests and the striking differences between the fatigue and subsea fractures lead to the conclusion that the subsea failures were caused by hydrogen embrittlement, and not fatigue.

CONCLUSIONS

1. Precipitation hardened MONEL K-500 is severely embrittled by cathodic protection.

2. Hardened MONEL K-500 loses some ductility when it is coupled to steel.

3. The alloy in the annealed condition is slightly embrittled by cathodic protection.

4. Based on slow strain rate testing and fractography, the subsea failures were caused by hydrogen induced environmental embrittlement, and not fatigue.

ACKNOWLEDGMENTS

The authors express their gratitude to Conoco Inc. and Conoco (U.K.) Limited for permission to publish this paper. We also appreciate the contributions of Jerry Tyson of Conoco (U.K.) Ltd., and the experimental work of Colin Burnette and Gary Welch.

REFERENCES

1. Efird, K. D.: "Failure of Monel Ni-Cu-Al Alloy K-500 Bolts in Seawater," Materials Performance, Vol. 24, (April 1985) No. 4, 39-40.

2. NACE Standard MR-01-75, "Sulfide Stress Cracking Resistant Metallic Material for Oil Field Equipment," (1984).

3. Vennett, R. M., Seager, R. W., Warne, M. A.: "Design of the Cathodic Protection System for Conoco's North Sea Murchison Platform," Materials Performance, Vol. 22, (Feb.1983) No 2, 22-30.

4. Payne, G. E.: "A History of Corrosion Protection of a North Sea Platform Jacket," Maritime and Offshore Structure Maintenance, Thomas Telford Ltd, London (1986) 19-28.

5. McIntyre, D. R., Kane, R. D., Wilhelm, S. M.: "Slow Strain Rate Testing for Materials Evaluation in High Pressure H_2S Environments", Corrosion 86, Houston, Paper No. 149.

6. ASM Metals Handbook, 8th ed., Vol. 9, "Fractography and Atlas of Fractographs", American Society for Metals, Metals Park, Ohio, (1974) 77.

TABLE 1
RESULTS OF SLOW STRAIN RATE TESTS
(PRECIPITATION HARDENED SPECIMENS)

Environment	Failure Time Hours	Elongation %	0.2 Yield psi	Tensile psi	RA %
Air	36.3	24.6	83,525	140,970	36
Seawater (no anode)	39.8	27.4	87,280	143,750	42
Baked, Seawater (no anode)	37.2	26.2	86,170	140,610	45
Coupled to steel (-620 mV)	28.0	19.0	90,810	141,380	45
Coupled to steel (8 days (-620 mV)	30.0	21.0	83,550	137,250	46
Coupled to Al (-900 mV)	6.1	4.2	85,220	96,310	8
Coupled to Al 8 days (-900 mV)	4.1	3.5	81,480	91,800	7
Potentiostat (-800 mV)	5.8	4.0	85,320	94,170	-
		(ANNEALED SPECIMENS)			
Air	49.1	29.9	29,260	80,210	73
Coupled to Al (-900 mV)	32.3	21.3	28,980	75,520	23



Fig. 1—Photomicrograph of typical microstructure of bolts that failed on the North Sea platforms. The bolts have large grains below the threads, and small grains elsewhere. This bolt had hardening precipitates that were visible at higher magnifications.

70x Carpella's etch

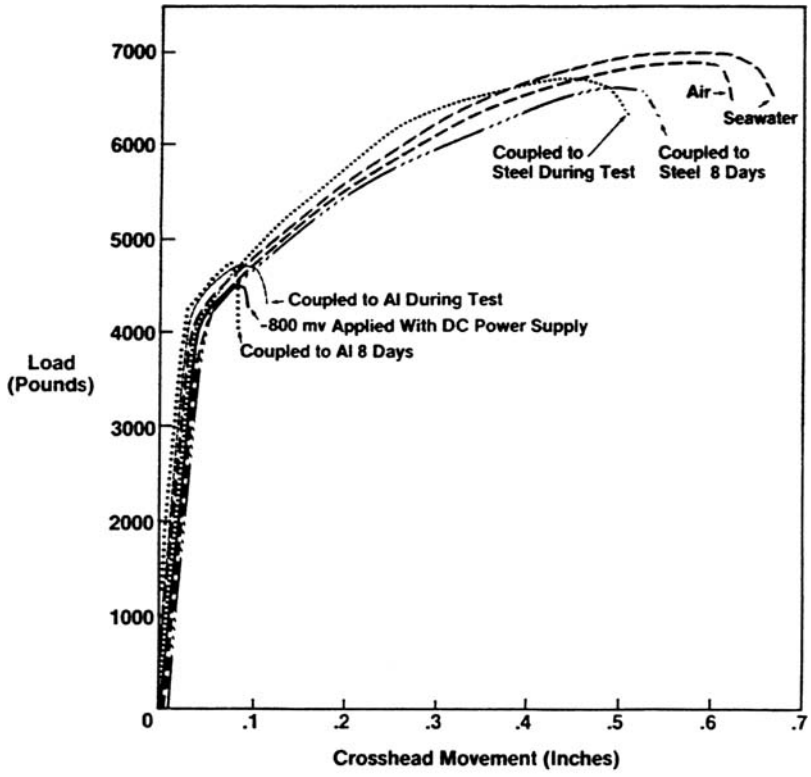


Fig. 2—Slow strain rate graphs of precipitation hardened MONEL K-500.

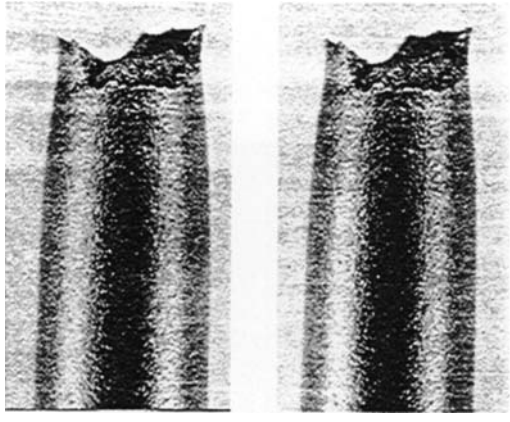


Fig. 3—Ductile fracture of precipitation hardened slow strain rate sample that was tested in seawater without being coupled to a more reactive metal.

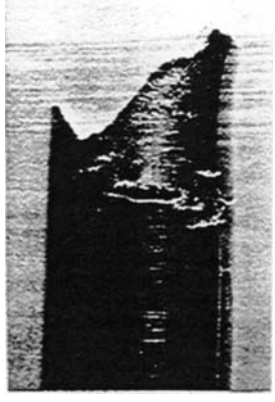


Fig. 4—Brittle fracture of precipitation hardened MONEL K-500 specimen that was coupled to aluminum anodes during slow strain rate tests in ASTM seawater.

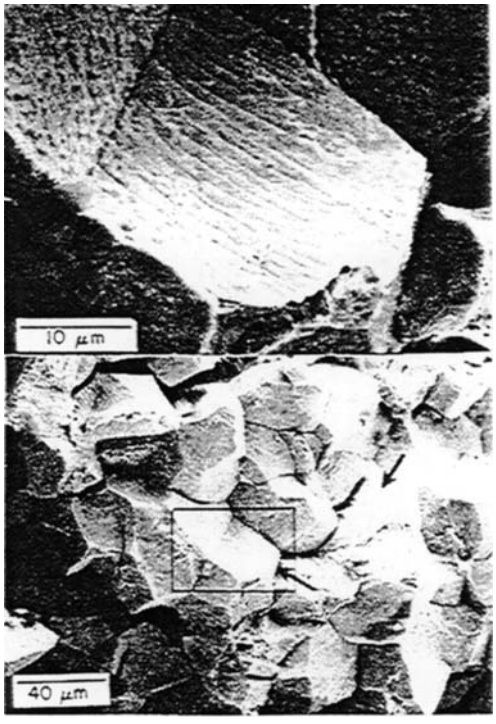


Fig. 5—Fractographs of a subsea failure. The fractures were intergranular and very brittle. The parallel lines (shown by arrows) were also present in the brittle slow strain rate fractures (Fig. 7). They were very similar to lines that have been described as fatigue striations in Model 400, Ref. 6.

500x 2500x

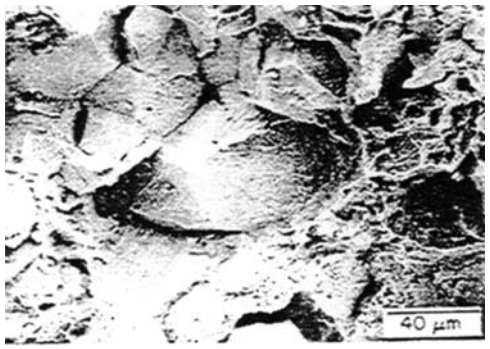


Fig. 6—Fractograph of precipitation hardened MONEL K-500 slow strain rate sample that was coupled to aluminum anodes for the duration of the test only. The fracture is intergranular and brittle, but it has ductile dimples on most of the grain faces.



Fig. 7—Fractograph of precipitation hardened slow strain rate sample that was coupled to aluminum eight days before it was tested. The parallel lines shown by the arrow were also found in subsea failures.

500x

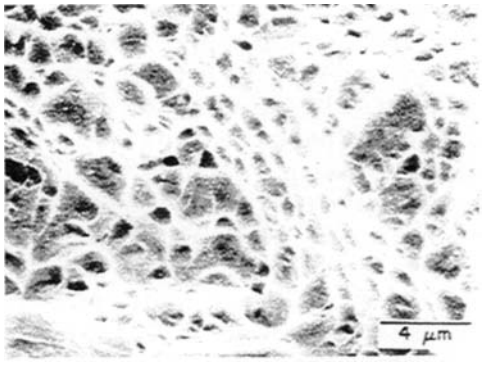
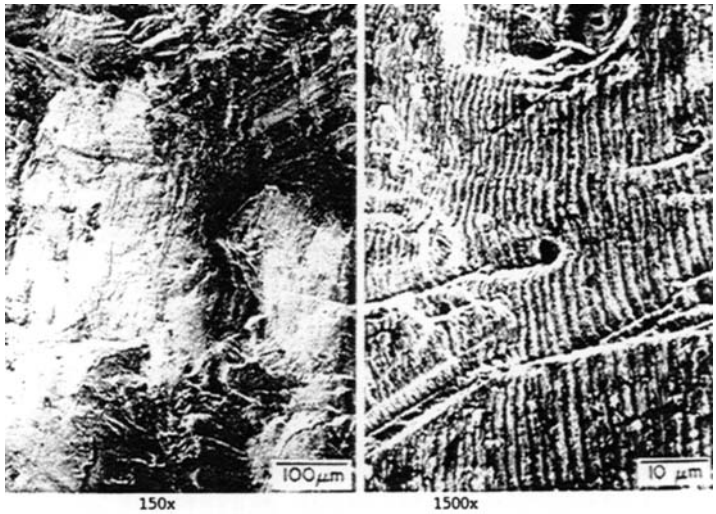


Fig. 8—Fractograph of precipitation hardened slow strain rate sample that was tested in air. The fracture was dimpled.

5000x



150x 1500x

Fig. 9—Fractographs of air fatigue of precipitation hardened MONEL K-500. The fracture has numerous fatigue striations, and it looks significantly different from the slow strain rate and subsea fractures.

Copyrighted Materials
Copyright © 1996 NACE International Retrieved from www.knovel.com

PAPER NUMBER

407

Corrosion 86

The International Corrosion Forum Devoted Exclusively to The Protection and Performance of Materials

March 17-21, 1986
Albert Thomas Convention Center
Houston, Texas

HEAT TREATMENT AND ENVIRONMENTAL EMBRITTLEMENT OF HIGH-PERFORMANCE ALLOYS

Juri Kolts
Cabot Corporation
Technology Department
Kokomo, Indiana 46902-9013

ABSTRACT

The selection of materials for use in specific geothermal environments is often made on the basis of stress corrosion cracking or hydrogen embrittlement resistance. This paper will discuss the effect of various heat treatments of selected alloys on the resulting properties. The heat-treatment parameters include precipitation hardening and annealing prior to cold working.

The data demonstrate that composition plays a major role in establishing environmental embrittlement resistance. Aging above temperatures around 1300° to 1400°F improves hydrogen embrittlement resistance of a number of alloys. The stress corrosion cracking resistance of Alloy 718 and Alloy No. R-41 are reduced by precipitation-hardening heat treatments

INTRODUCTION

Corrosion resistant alloys hold a high potential for use in the very severe geothermal applications. The Salton Sea KGRA poses severe environments indeed. The severity of the environments toward both localized corrosion and toward stress corrosion cracking preclude the use of stainless steels and thus nickel-base, high performance alloys, need to be considered. The selection of corrosion-resistant alloys for geothermal service requires consideration of mechanical properties as well as stress corrosion cracking, hydrogen embrittlement, and corrosion resistance of these alloys. The environments considered should include production fluids and well stimulation (acidizing) fluids if their use is anticipated. No single environment can be used to evaluate the performance of alloys. A few environments have been selected in hopes that the results are representative of relative performance of the alloys in some of the severe geothermal applications.

Resistance to stress corrosion cracking is one of the critical properties in selection of high performance nickel-base alloys for severe geothermal or sour oil and gas applications. The environmental embrittlement resistance of nickel- and cobalt-base alloys is excellent, and a relative prediction of their resistance can often be made on the basis of alloy composition. However, nickel- and cobalt-base corrosion-resistant alloys are often supplied in three conditions: as-cold worked, for example, HASTELLOY® alloy C-276; as-cold worked and aged, for example, HAYNES® alloy No. 188 or MP 35N® alloy; or precipitation- hardened, for example, Alloy 718. The environmental embrittlement resistance of each of these alloy groups can be reduced by improper heat treatment. Alloys which are intended for use in the cold-worked condition are not heat treated after leaving the mill; consequently, the probability of receiving an improper heat treatment is minimal for these alloys. Processing of the other alloys must be carefully controlled to avoid deleterious heat treatments. This paper will discuss some of the heat treatments examined for different nickel- and cobalt-base alloys and the response of the respective alloys to corrosion or embrittlement.

MATERIALS AND PROCEDURE

Commercially available alloys were utilized in this investigation. The compositions are listed in Table 1. These alloys were cold rolled as sheet products or heat treated as specified in the respective tables.

Stress corrosion cracking tests were performed on samples that were 0.040 inch (1 mm) thick. The length of the sample was perpendicular to the rolling direction. The samples were stressed into a C-shape, beyond the flow stress of flat samples as described previously.[1,2] Holders were made of the same alloy as the samples unless otherwise specified.

The specimens were exposed in HASTELLOY alloy C-276 autoclaves in the high-temperature tests. Glass hooks or boats were used to electrically isolate samples. The autoclaves were cooled and opened at specified intervals and filled with new solutions when tests were resumed. Some tests were deaerated by consecutive evacuation with a reciprocating vacuum pump and purging by nitrogen. Other test solutions, as specified in the tables, were not deaerated and air was used to fill the vapor space in the autoclaves.

Cracking was determined by visual inspection at a magnification of 20X. Where uncertainty existed at the end of the final exposure period, samples were metallographically examined for the presence of cracks.

RESULTS AND DISCUSSION

Role of Environmental Parameters in High Temperature Stress Corrosion Cracking

Before the metallurgical parameters which cause stress corrosion cracking in high performance alloys are discussed, it is necessary to appreciate the environmental factors involved in geothermal applications. Only the most severe geothermal environments present high temperature stress corrosion cracking potentials for the alloys discussed. Table 2 presents results of stress corrosion cracking tests in a number of different environments. Some of the environments include HCl at high levels. Levels of concentration at 1 to 2% are usually not anticipated in geothermal environments.

The results in Table 2 show that stress corrosion cracking can occur in the austenitic stainless steels and duplex stainless steels in concentrated brine solutions. Even alloy 825 can show susceptibility to stress corrosion cracking. Alloys G-3, C-276 and C-22 show resistance to stress corrsoion cracking in the described environments as long as high concentrations of acids are not added.

Table 3 shows that the acid concentrations to cause cracking of alloys H, G-3 or C-22 must be quite high since no cracking was observed in NaCl solutions with levels controlled as low as pH = 2.

Additions of Zr, Sr, Fe and Pb salts were made to examine the effects of these salts. The concentrations of the salts were selected to represent the most severe geothermal applications. Type 317L stainless steel cracked in all of the environments at 400°F (204°C), except in the environment at pH=4. Only superficial fissuring was seen (as noted in Figure 3) in FERRALIUM® alloy 255 in the 400°F environments except in the presence of $FeCl_2$. It is anticipated that this environment also contains some $FeCl_3$ which would tend to accelerate cracking. Severe stress corrosion cracking was noted on FERRALIUM alloy 255 in this environment.

Cracking of 317L stainless steel was more severe in the Sr, Fe and Pb containing electrolytes as is evidenced by severe stress corrosion cracking at 300°F. The oxidizing nature of the Fe and Pb containing environments could attribute to increased severity. No explanation is given for the effect of Sr on stress corrosion cracking resistance in 317L stainless steel.

Solid Solution Alloys - Effect of Annealing Prior to Cold Work

It was of interest to determine whether high-temperature heat treatment prior to cold working of solid solution alloy 825 and HASTELLOY alloy G-3 had an effect on high-temperature stress corrosion cracking. The corrosion resistance of alloy 825 is sensitive to heat treatments[3] in the temperature range investigated (1725° to 2200°F, 940 to 1200°C). Samples of alloy 825 manufactured by two producers were evaluated to determine if subtle composition differences were of importance. Two heat treatments were selected for HASTELLOY alloy G-3 to serve as comparisons. The alloys were cold worked by rolling prior to being tested.

The stress corrosion cracking resistances of these alloys were measured in an environment selected for its severity toward these alloy systems. This environment is an accelerated one in comparison to actual geothermal environments and consists of 5% NaCl, 1/2% CH_3COOH deaerated prior to saturating with H_2S at 100 psig (0.69 MPa). The autoclaves are then heated to the respective temperatures. The specimens were examined once a month.

Tables 4 and 5 show that no significant differences in stress corrosion cracking of alloy 825 can be attributed to the heat treatments prior to cold working. Two heat treatments of HASTELLOY alloy G-3 showed the stress cracking performance to be insensitive to these heat treatments. As has been established previously,[4] the performance of alloy G-3 was confirmed to be superior to that of alloy 825, in spite of the higher strength of alloy G-3.

The above results indicate that the annealing temperature prior to cold working does not play an important role in determining the stress corrosion cracking resistance of alloys 825 and G-3. The major alloying elements are of importance in determining stress corrosion cracking performance as can be seen by the consistently better properties of alloy G-3 over alloy 825. However, there is no clear difference between the performance of the alloys 825 showing that the effects of the minor alloying elements are less than that of the major alloying elements.

Effects of Aging on Stress Corrosion Cracking

Because of the use of precipitation hardened alloys in wellheads and other components in thick sections, the role of precipitation hardening on materials performance has commercial significance.

Through the work of Copson, the beneficial role of nickel on the stress corrosion cracking resistance of alloys

has been appreciated for many years. However, the role of other elements (especially molybdenum) and metallurgical structure have received much less publicity. Precipitation hardening heat treatments can alter the environmental embrittlement resistance[5,6] by structural changes due to the presence of the precipitate or by compositional changes due to partitioning[7-11] of elements between the precipitate and matrix. Precipitation of the γ' results in depletion of nickel in the matrix, and this in itself should reduce the stress corrosion cracking resistance in comparison to cold-worked or solution-annealed alloys. The presence of precipitates can alter the mode of slip and thus have an effect on the stress corrosion cracking resistance.

Stress corrosion cracking tests were performed in two aerated environments: 20.4% $MgCl_2$ and 25% NaCl. C-shaped samples similar to those of the previous experiments were employed in autoclave exposures. The autoclaves were opened at intervals of 1, 2, 3, 6, 10, 17, 31, and 42 days. The results of stress corrosion cracking experiments are shown in Tables 6 and 7. In Table 6 the three alloys compared, 718, G-3, and C-276, contain approximately 54%, 45%, and 56% nickel, respectively. From Table 6 there is a large difference in the stress corrosion cracking resistance among alloys 718, G-3, and C-276, with the last alloy showing the highest resistance. This relationship holds even when 718 is compared in the solution-annealed condition. Much of the difference in the stress corrosion cracking performance is thought to be due to the molybdenum and tungsten contents of the alloys. However the presence of precipitates is thought to be important.

Heat treatment of Alloys 718 and No. R-41 is detrimental to transgranular stress corrosion cracking performance as is shown in Tables 6 and 7. Previous testing[12] utilizing these test samples and the results from Table 5 have shown that a strong dependence on strength level is not seen when using the C-shaped samples, thus the increased susceptibility is due to the changes in microstructure. These observations are consistent with those on 25% Ni- containing stainless steels where decreases in stress corrosion cracking resistance are observed as a result of γ' precipitation.[6] A similar response is shown for Incoloy® alloy 925 in Table 8. When the strength is achieved by cold work in the solution annealed alloy, the resulting stress corrosion cracking resistance is higher than when the strength is achieved by precipitation hardening. It is not known whether the increased susceptibility to stress corrosion cracking caused by precipitation hardening is the result of elemental partitioning or whether the mode of slip in precipitation hardened alloys promotes stress corrosion cracking. Both increased planarity of slip and nickel depletion are known to result from precipitation hardening. Possibly a combination of both factors is involved.

Corrosion rates were determined on alloy 718 following the specified heat treatments shown in Table 9. These environments in Table 9 are not applicable to performance in severe geothermal environments but are indicators that chromium depletion may have occurred. In the boiling sulfuric acid, no effect on corrosion rate is found. However, in the ASTM 262 Practice B test (oxidizing sulfuric acid), the heat treatments result in large degradation in corrosion resistance. A corresponding reduction in pitting resistance is noticed. The latter two data imply a chromium depletion as a result of the heat treatment. This may be associated with precipitaion of carbides and may not be necessarily caused by partitioning due to precipitation hardening.

Effects of Aging on Low Temperature Environmental Embrittlement

The mode of cracking reported in this section is different from that reported

in previous sections. Whereas cracking occurs predominantly as transgranular stress corrosion cracking at high temperatures, the cracking reported in this section is mainly intergranular embrittlement near ambient temperatures. The behavior is similar to classical hydrogen embrittlement in high strength steels.

The effects of low-temperature aging on the hydrogen embrittlement of some nickel-base alloys such as alloy 625 and HASTELLOY alloy C-276 are well documented in the literature[13,14] and will not be repeated here. The higher temperature aging limits have been less fully explored and are examined here. In the γ' and γ'' precipitation-hardenable nickel-base alloys such as Pyromet® alloy 31 and Alloy 718,[15] minimum annealing temperatures have been established below which hydrogen embrittlement resistance is no longer adequate. Similarly, a minimum annealing temperature has been shown for MP35N® [15] alloy below which hydrogen embrittlement can be detected. These temperatures are all near 1400°F (760°C).

Data on three additional alloys with very different metallurgical structures are presented. HASTELLOY alloys X and C-276 and HAYNES alloy No. 188 were cold worked 60 percent as sheet samples followed by aging at temperatures between 1200° and 1700°F (650 and 930°C). The first two alloys are not intended for use in the aged condition but were included for the sake of information. The 60-percent cold work represents extremely severe conditions of cold work and was required for these materials to exhibit hydrogen embrittlement. Accelerated hydrogen embrittlement tests were performed on these alloys as C-shaped samples coupled with carbon steel holders. Table 10 presents the data. Notice that all three of these alloys show behavior similar to the precipitation-hardenable alloys where aging temperatures below 1400°F (760°C) represent structures where hydrogen embrittlement becomes detectable. The actual value of the temperature to produce embrittlement-susceptible structures should shift with test technique. If less severe test specimens or environments were employed as has been done in other studies, then the aging temperature for detecting embrittlement would be lowered. Also, longer annealing times tend to reduce the aging temperature at which embrittlement becomes detectable.

It is interesting that alloys with diverse metallurgical structures and aging responses such as Alloys 718, Pyromet alloy 31, MP35N alloy, HASTELLOY alloys X and C-276, and HAYNES alloy No. 188 all exhibit an increase in hydrogen embrittlement susceptibility following aging at 1200°F (650°C), and that each exhibits a minimum temperature near 1350°-1400°F (730-760°C) above which hydrogen embrittlement becomes negligible.

A number of metallurgical events can occur in these alloys at 1200°F (650°C) including precipitation of carbides or other phases, ordering in some alloys as well as partitioning of a number of elements at grain boundaries. No attempts were made to determine which (if any) of the above phenomena were responsible for increasing the susceptibility to embrittlement of the various alloys.

Although hardness is reduced by increasing aging temperatures, hardness or strength alone is not necessarily the governing parameter which determines hydrogen embrittlement resistance in the heat-treatable nickel-base alloys. One example is shown in Table 11 where as-cold worked + aged (400°F 200°C) alloy 718 at a hardness level of HRC 37 may be susceptible to embrittlement, while heat-treated alloy at HRC 44 is not susceptible. Thus the beneficial effects of overaging nickel-base alloys are apparent.

The above information does demonstrate that the hydrogen embrittlement resistance of these alloys is sensitive to heat treatment. Knowledge of those

heat treatments that render the alloys less susceptible to cracking will aid in proper materials selection for geothermal applications. While this paper has addressed some of the aspects of heat treatment and environmental embrittlement, it has not examined the effects of welding or other fabrication techniques where the alloys see only a short time at temperature. This topic is worthy of investigation.

CONCLUSIONS

1. Heat treatment in the temperature range 1725° to 2200°F (940-1200°C) prior to cold working alloy 825 does not greatly influence high temperature stress corrosion cracking behavior in the environment examined.

2. Aging at temperatures above approximately 1300° to 1400°F (700-760°C) improves the ambient temperature hydrogen embrittlement resistance of heavily cold-worked HASTELLOY alloys X, C-276 or HAYNES alloy No. 188 in a manner previously reported for MP35N alloy and Pyromet alloy 31.

3. The high temperature stress corrosion cracking resistance of HASTELLOY alloy C-276 is greater than that of HASTELLOY alloy G-3 which is still greater than that of alloy 718, showing that additional factors other than nickel content determine this property.

4. Aging of alloys 718, No. R-41 and 925 reduces resistance to high temperature stress corrosion cracking.

5. Aging of alloy 718 also reduces resistance to corrosion in oxidizing sulfuric acid.

REFERENCES

1. J. Kolts, JOURNAL OF MATERIALS FOR ENERGY SYSTEMS, Vol. 5, No. 2 (1983), p. 71.

2. A. I. Asphahani, CORROSION, Vol. 37, No. 6 (1981), p. 327.

3. M. H. Brown, CORROSION, Vol. 25, No. 10 (1969), p. 438.

4. J. Kolts, J.B.C. Wu, A. I. Asphahani, METAL PROGRESS, September 1983, p. 25.

5. R. J. Walker, W. T. Chandler, "Influence of Gaseous Hydrogen on Metals," NASA Report, NASA CR 124410, 1973.

6. J. M. Silcock, BRITISH CORROSION JOURNAL, Vol. 18, No. 3 (1983), p. 132.

7. O. H. Driege, ASTM STP 557, 1974, p. 220.

8. R. L. Dreshfield, NBS SP 496, 1977, p. 624.

9. O. H. Driege, C. P. Sullivan, TRANS ASM, Vol. 61 (1968), p. 228.

10. O. H. Kriege, J. M. Varis, TRANS ASM, Vol 62 (1969), p. 195.

11. W. T. Loomis, J. W. Freeman, D. L. Sponseller, MET TRANS, Vol. 3 (1972), p. 989.

12. J. Kolts, Paper No. 241, CORROSION '82, 1982.

13. A. I. Asphahani, Paper No. 42, CORROSION '78, 1978.

14. N. F. Fiore, J. A. Kargol, HYDROGEN EFFECTS IN METALS, Bernstein & Thompson, Eds., AIME, 1981, p. 851.

15. NACE Standard MR-01-75, National Association of Corrosion Engineers, Houston, Texas.

TABLE 1

Composition of Alloys

Alloy	Ni	Cr	Mo	Fe	Mn	Cu	Si	C	Others
HASTELLOY alloy C-22*	58	22	13	3	.5*	-	.08*	0.015*	V=.35* W = 3
HASTELLOY alloy C-276*	56	16	16	5.4	0.50	-	0.03	0.003	V=.35* W = 4
HASTELLOY alloy H*	46	22	9.0	19	.5	-	1.0*	.03*	W = 2
HASTELLOY alloy G-3	45	22	6.8	19	0.73	1.9	0.30	0.006	Cb = 0.39
alloy 825 (Supplier A)	41	21	2.9	30	0.50	1.8	0.30	0.01	Ti = 1.0
alloy 825 (Supplier B)	42	21	2.5	30	0.24	1.9	0.20	0.024	Ti = 0.95
HASTELLOY alloy X*	47	22	9.0	19	1.0**	-	1.0**	0.10	Co = 1.5 W = .5
HAYNES alloy No. 188*	22	22	-	3.0**	1.25**	-	0.35	0.10	Co = 39 W = 14 La = 0.07
CABOT® alloy No. 718	54	18	3.0	18	0.14	0.02	0.16	0.05	Cb = 5.0 Ta = 0.13
CABOT alloy No. R-41	52	19	10	5.0**	0.10*	-	0.5*	0.09	Co = 11 Al = 1.5 Ti = 3.1 B = 0.006

* Nominal Composition

** Maximum

Table 2

Stress Corrosion Cracking
C-Shaped Samples, Like Alloy Holders

ALLOY	ENVIRONMENT				
	1000 Hour Test 54g/l $MgCl_2$ + 170 g/l KCl + 155 g/l NaCl + 320 g/l $CaCl_2$ + 10 mg/l Na Br 240°F (115C) 75 psi (.52 MPa)N_2	168 Hour Test 25% NaCl 1 atmosphere Air 400°F, (200°C)	720 Hour Test 5% $MgCl_2$ + 10% NaCl + 10% $CaCl_2$ + 400°F, (200°C) 90psi(.62 MPa)CO_2	720 Hour Test 5% Mg Cl_2 + 10% Na Cl + 10% Ca Cl_2 + 2% HCl 90 psi (.62 MPa)CO_2 400°F (200°C)	1000 Hour Test 1% HCl 400°F (200°C)
316 Stainless Steel	C*	C	-	-	C
Alloy 255	C	C	C	C	-
Alloy 825	- **	NC	C	D****	C
Alloy G-3	NC ***	NC	NC	C	C
Alloy C-276	NC	NC	NC	C	C
Alloy C-22	NC	NC	NC	C	C

* C Denotes cracking
** Not tested
*** NC denotes no cracking
**** D denotes excessive corrosion

Table 3

Stress Corrosion Cracking
C-Shaped Samples, Like Alloy Holders
Deaerated Solution, 40 psi (0.28 MPa) N_2
1 Week Exposure

ALLOY	25% NaCl pH = 4 300°F (150°C)	400°F (200°C)	25% NaCl pH = 2 300°F (150°C)	400°F (200°C)	25% NaCl pH = 2 2100 ppm $ZnCl_2$ 300°F (150°C,200°C)	400°F	25% NaCl pH = 2 1800 ppm $SrCl_2$ 300°F (150°C,200°C)	400°F	25% NaCl pH = 2 2300 ppm $FeCl_2$ 300°F (150°C,200°C)	400°F	25% NaCl pH = 2 135 ppm $PbCl_2$ 300°F (150°C,200°C)	400°F
316	NC	NC	NC	C	NC	C	C	C	C	C	C	C
255	NC	SC	NC	SC	NC	SC	NC	NC	NC	C	NC	NC
H	NC	NC	NC	NC	NC	NC	NC	NC	NC	NC	NC	NC
G-3	NC	NC	NC	NC	NC	NC	NC	NC	NC	NC	NC	NC
C-22	NC	NC	NC	NC	NC	NC	NC	NC	NC	NC	NC	NC

* C Denotes cracking
** - SC denotes fissuring on surface
*** NC denotes no cracking

TABLE 4

350°F (1776°C) Stress Corrosion Cracking of Cold Worked Alloys
5% NaCl + 0.5% CH_3COOH + 100 psig (.69 MPa) H_2S
0.040-Inch (1mm) Thick Sheet
C-Shaped Samples, Like Alloy Holders, Time to Failure (Months)

Alloy	Cold Reduction (%)	Heat Treatment Prior to Cold Rolling: 5 Min./2200°F/WQ (1200°C)	5 Min./2000°F/WQ (1090°C)	15 Min./1750°F/WQ (955°C)	5 Min./1200°C/WQ + 1 Hr./1725°F/WQ (940°C)	10 Min./2100°F/WQ (1150°C)
825 (Supplier A)	30	11, 11, 11, 11	NC*, NC, NC, NC	11, 11, 11, NC	11, 11, 11, NC	
	50	11, 11, 11, 11	11, 11, 11, 11	11, 11, 11, 11	11, 11, 11, 11	
825 (Supplier B)	30	9, 9, 9, 9	9, 9, 10, 9	9, 10, 10, 10	10, 10, 10, 10	
	50	9, 9, 9, 9	9, 9, 9, 9	9, 9, 10, 9	9, 5, 9, 9	
G-3	30	NC, NC, NC, NC				NC, NC, NC, NC
	50	NC, NC, NC, NC				NC, NC, NC, NC

*NC Denotes No Failure in One Year

TABLE 5

400°F (200°C) Stress Corrosion Cracking of Cold Worked Alloys
5% NaCl + 0.5% CH_3COOH + 100 psig (0.69 MPa) H_2S
0.040-Inch (1 mm) Thick Sheet
C-Shaped Samples, Like Alloy Holders, Time to Failure (Months)

Alloy	Cold Reduction (%)	Heat Treatment Prior to Cold Rolling: 5 Min./2200°F/WQ (1200°C)	5 Min./2000°F/WQ (1090°C)	15 Min./1750°F/WQ (955°C)	5 Min./2200°F/WQ + 1 Hr./1725°F/WQ (940°C)	10 Min./2100°F/WQ (1150°C)
325 (Supplier A)	30	6, 6, 6, 6	6, 6, 6, 6	6, 6, 6, 7	6, 6, 6, 6	
	50	7, 6, 6, 6	6, 6, 6, 6	6, 6, 6, 6	6, 6, 6, 6	
825 (Supplier B)	30	5, 5, 5, 5	5, 5, 5, 5	5, 9, 5, 5	5, 5, 9, 5	
	50	5, 5, 5, 5	5, 5, 5, 5	5, 9, 5, 9	9, 5, 3, 5	
G-3	30	10, 11, 11, 11				10, 11, 11, 11
	50	10, 10, 10, 10				10, 10, 11, 10

TABLE 6

Stress Corrosion Cracking, Aerated Solutions
0.040-Inch (1 mm) Thick Sheet
Triplicate C-Shaped Samples, Like Alloy Holders, Time to Failure (hours)

Alloy	Heat Treatment	Hardness	20.4% $MgCl_2$ 350°F (177°C)	20.4% $MgCl_2$ 450°F (230°C)	25% NaCl 400°F (200°C)
718	Mill Annealed	HRB 80	408/408/408	744/744/1008	48/48/504
718	8 hr/1225°F (663°C)	HRC 26	72/144/240	72/72/72	48/48/48
718	8 hr/1325°F (718°C)	HRC 38	72/144/144	72/72/72	48/48/48
718	8 hr/1450°F (788°C)	HRC 34	72/144/240	72/72/144	48/48/240
718	168 hr/1450°F (788°C)	HRC 29	72/72/240	72/72/144	48/48/48
718	Mill Annealed + 8 hr/1325°F/ 8 hr/1150°F (718°C ;& 620°C)	HRC 42	72/72/144	72/72/72	48/48/48
G-3	50% Cold Rolled	HRC 37	1008/NC/NC*	144/744/NC	NC/NC/NC
C-276	30% Cold Rolled	HRC 33	NC/NC/NC	NC/NC/NC	NC/NC/NC

* NC Denotes No Cracking in 1008 Hours

TABLE 7

Stress Corrosion Cracking, Aerated Solutions
0.040-Inch (1 mm) Thick Sheet
Triplicate C-Shaped Samples, Like Alloy Holders, Time to Failure (hours)
Alloy No. F-41

Heat Treatment	Hardness	Boiling 45% $MgCl_2$ 154°C (309°F)	25% NaCl 400°F (200°C)	25% NaCl 450°F (230°C)
Mill Annealed (1975°F (1080°C), WQ)	HRB 100	NC/NC/NC*	NC/NC/NC	NC/NC/NC
Cold Rolled	HRC 45	NC/NC/NC	NC/NC/NC	NC/NC/NC
1975°F/WQ + 30 min/1950°F/AC + 16 hrs/1400°F (1080°C, 1065°C, 760°C)	HRC 42	72/72/96	48/96/NC	48/48/48
30 min/2050°F/AC + 16 hrs/1650°F (1120°C & 900°C)	HRC 36	312/312/312	48/48/96	48/48/48

* NC Denotes No Cracking in 1008 Hours

TABLE 8: Stress Corrosion Cracking Results
C-Shape (.040" [1 mm] thick) samples, like alloy holders
Time to failure, hrs

Alloy	Condition	Hardness HRC	Boiling 45% $MgCl_2$	Time To Failure NACE Solution at 350°F(177°C) PH_2S ~ 90 psi(.62 MPa)
Alloy 925	Cold Rolled	23	72 96 456	NC NC NC
Alloy 925	Heat Treated	30	24 24 24	744 744 744
Alloy G-3	Cold Rolled	30	NC NC NC*	NC NC NC

* NC Denotes no cracking in 1000 hours

TABLE 9

Corrosion Resistance of Alloy 718

Condition	Boiling 5% H_2SO_4 Four 24-Hour Periods mpy (mm/y)	Boiling 50% H_2SO_4 + 2.5% $Fe_2(SO_4)_3$ 120 Hours mpy (mm/y)
Mill Annealed	81 (2.1)	14 (.36)
8 hr/1250°F (677°C)	77 (1.8)	58 (1.5)
8 hr/1325°F (718°C)	62 (1.6)	200 (5.1)
8 hr/1450°F (788°C)	56 (1.4)	280 (7.1)
168 hr/1450°F (788°C)	77 (2.0)	3600 (9.1)
8 hr/1325°F/18 hr/1150°F (718°C) (620°C)	51 (1.3)	260 (6.6)

TABLE 10

Effect of Aging Temperature on Hydrogen Embrittlement of Alloys
5% NaCl + 0.5% CH_3COOH + H_2S, Room Temperature
0.040-Inch (1 mm) Thick Sheet, Aging Time = 4 Hours
C-Shaped Samples, Carbon Steel Holders, Fraction of Samples Failed in 1000 Hours

Alloy & Treatment	As-Rolled	1200°F (650°C)	1300°F (705°C)	1400°F (760°C)	1500°F (815°C)	1600°F (870°C)
Alloy No. 188 60% Cold Rolled	6/6	4/6	0/6	0/6	0/6	
Alloy X Cold Rolled 60%	0/6	4/4	4/4	0/4	0/4	
Alloy C-276 Cold Rolled 60%	0/6	6/6	3/6	0/6	0/6	

TABLE 11

Hydrogen Embrittlement of Alloy 718
5% NaCl + 0.5% CH_3COOH + H_2S, Room Temperature
0.040-Inch (1 mm) Thick Specimens, C-Shaped Samples, Carbon Steel Holders
Samples Aged 200 Hours at 400°F (200°C) Prior to Testing

Condition	Hardness	Time to Failure (hours)
10% Cold Rolled	HRC 37	106/168/384
20% Cold Rolled	HRC 43	82/276/864
Mill Annealed + 8 hr/1325°F/8 hr/1150°F (718°C) (620°C)	HRC 44	NC/NC/NC*

* NC Denotes No Cracking in 1008 Hours

HASTELLOY is a registered trademark of Cabot Corporation.

HAYNES is a registered trademark of Cabot Corporation.

CABOT is a registered trademark of Cabot Corporation.

MP35N is a registered trademark of SPS Technology Incorporated.

FERRALIUM is a registered trademark of Bonar Langley Alloys Ltd.

INCOLOY is a registered trademark of The Inco Family of Companies.

PYROMET is a registered trademark of Carpenter Technology Corporation.

Copyrighted Materials
Copyright © 1996 NACE International Retrieved from www.knovel.com

ALLOY 718 FOR THE OIL AND GAS INDUSTRY

Juri Kolts

Conoco Inc.
P. O. Box 1267
Ponca City, OK 74603

Abstract

This paper examines some of the properties of Alloy 718 required by the oil and gas industry for the completion of corrosive wells. The properties of interest include strength, toughness, pitting and general corrosion resistance, hydrogen embrittlement resistance, and stress corrosion cracking resistance. The effects of heat treatment on some of these properties are discussed.

Heat treatment temperatures can affect each property differently. Thus high aging temperatures may improve hydrogen embrittlement resistance while low aging temperatures may improve toughness and corrosion resistance. The stress corrosion cracking performance determines the limits for use in the most aggress environments containing elemental sulfur.

Superalloy 718—Metallurgy and Applications
Edited by E.A. Loria
The Minerals, Metals & Materials Society, 1989

Courtesy The Minerals, Metals & Materials Society (TMS)

Introduction

Alloy 718 is used as a corrosion-resistant alloy in the oil and gas industry because of its combination of high-strength, corrosion resistance, and ability to be heat treated to various strength levels. While Alloy 718 was developed for high-temperature use, it's properties have been modified for the oil industry through processing and heat treatment. The properties of most interest to the oil and gas industry are corrosion resistance, strength, toughness, hydrogen embrittlement resistance, and stress corrosion cracking resistance. Since Alloy 718 can be heat treated to the required strength levels, it finds use as thick sections and complicated shapes for downhole and surface components. This paper will discuss some of the oil industry uses of Alloy 718, the corresponding mechanical properties and heat treatments, the corrosion resistance in typical oil field environments.

Applications of Alloy 718 in the Oil and Gas Industry

Alloy 718 is used where high strength and corrosion resistance are required. While a number of alloys can provide high strength and corrosion resistance, many are strengthened only by cold work and, therefore, are not suitable for thick sections or complicated shapes. Other alloys, such as carbon and low-alloy steels, do not have sufficient corrosion resistance, although they may have the desired mechanical properties. Thus, for thick sections or complicated shapes, an alloy must be heat treated rather than cold worked to the desired mechanical properties. An additional advantage of heat-treatable alloys is inventory reduction since one inventory can supply materials for applications requiring different strength levels. In thick sections, heat-treatable alloys such as Alloy 718 provide more uniform mechanical properties through the cross section as compared to cold-worked materials. The cold-worked materials in thick sections often possess high residual stresses, thus increasing difficulty in maintaining tolerances during machining. For these reasons, heat-treatable alloys are often selected for downhole and surface equipment which is machined to final dimensions.

A frequent application of Alloy 718 is in valve stems. These stems are often used in service which is slightly corrosive. Low corrosion rates are needed for low torque to open and close valves, thus, Alloy 718 valve stems are used in combination with noncorrosion resistant alloys. Figure 1 shows a cutout of a valve with parts typically manufactured from Alloy 718. A common use is in gates and seats for corrosion-resistant applications. Alloy 718 valve stems, gates, seats, set screws, and other fasteners requiring high strength have been used for a number of years. Other common applications include springs and components in downhole safety valves which require high tolerances, for example, flappers and seals for downhole safety valves. Alloy 718 components for side-pocket mandrels (chemical injection valves) have been used. These applications constitute the bread-and-butter usage of Alloy 718 in the petroleum industry.

Newer applications of Alloy 718 are found in extremely corrosive wells using only corrosion-resistant alloy equipment. These wells have very high downhole temperatures, high pressures, and high concentrations of both carbon dioxide and hydrogen sulfide. While tubular products in corrosion-resistant alloy completions are cold worked nickel-based alloys, Duplex stainless steels, or 13-chrome stainless steels, these completions require increased use of Alloy 718. Alloy 718 has been used as tubing hangers, bodies for safety valves, downhole polished bore receptacles, chemical injection valves, downhole packers, landing nipples, and extension seals

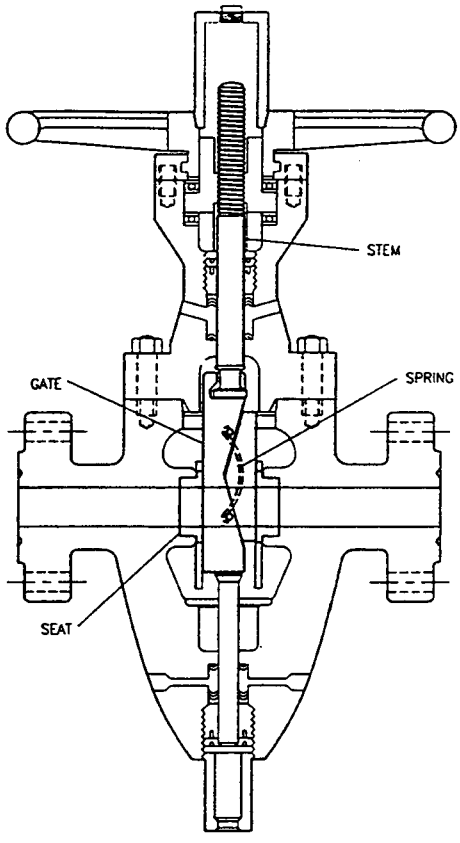


Figure 1. Schematic drawing of a valve showing common Alloy 718 components used in corrosive service.

(1). A large number of these safety valves has been manufactured to date. These constitute the larger equipment constructed from Alloy 718.

Mechanical Properties

The yield strength of precipitation-hardened, corrosion-resistant alloys required for the oil and gas industry ranges from 65,000 to 160,000 psi (450-1100 MPa). The range for Alloy 718 is usually from 110,000 psi (758 MPa) to approximately 150,000 psi (1100 MPa). The NACE specification MR0175 (specification to control hydrogen embrittlement) limits the maximum hardness of Alloy 718 to HRC 40. Thus, the very high-strength levels used in the aviation and aerospace industry are not required nor permitted in oil and gas applications. Therefore, the heat treatments are different from those for high-temperature applications. Consequently, the double-aging treatments used to maximize the strength and creep resistance of Alloy 718 are not used; rather, single-aging treatments are preferred.

In addition to the strength requirement, alloy toughness is extremely important. A Charpy v-notch toughness of 20 to 40 foot-pounds for corrosion-resistant alloys is often specified. This also limits the maximum strength of Alloy 718. Thus, the processing and heat treatment of Alloy 718 should provide the necessary strength and good toughness. In addition, Alloy 718 is heat treated to provide adequate hydrogen embrittle-

ment resistance and stress corrosion cracking resistance. These will be discussed in later sections.

Single-step aging treatments are used to develop the mechanical properties in oil and gas applications. The annealing temperatures are usually in the range 1850 to 1950 F (1210 to 1265 C) followed by a one-step age at 1200 to 1450 F (648 to 988 C). This achieves yield strengths of 130,000 to 140,000 psi (896 to 965 MPa). Figure 2 displays the yield strength and toughness of Alloy 718 and Alloy PH3 after solution annealing and aging between 1200 and 1400 F (648 to 760 C). The strength can be achieved either by underaging near 1275 F (690 C) or overaging near 1400 F (760 C). Depending on the requirements, either of these heat treatments are used for a given yield strength. The toughness (2,3) decreases with increasing aging temperature, although the yield strength reaches a peak between 1200 and 1400 F (648 to 760 C). Thus, for best toughness, underaging may be preferable. There are other considerations for developing toughness in Alloy 718. For example, grain boundary precipitation may affect toughness, as is indicated by either the ductile (4) or intergranular nature of fracture surfaces obtained in toughness tests (5). These factors will not be considered in detail.

The political metallurgical requirement of NACE Specification MR0175 permits the use of Alloy 718 to maximum hardness of HRC 40. It is necessary, for some applications, to obtain the highest yield strength achievable with the imposed maximum HRC 40 hardness. Table 1 shows that under these restrictions, a minimum yield strength of 140,000 psi (965 MPa) can be attained. Alloy 718 as shown in Table 1 has been supplied and installed in oil field applications for corrosive environments. The use at these very high strength levels is contrary to the justification for the recent changes made in NACE Specification MR0175. The increase in the Rockwell hardness to HRC 40 in MR0175 was justified by easier manufacturing of Alloy 718 to the 120,000 minimum yield strength (827 MPa).

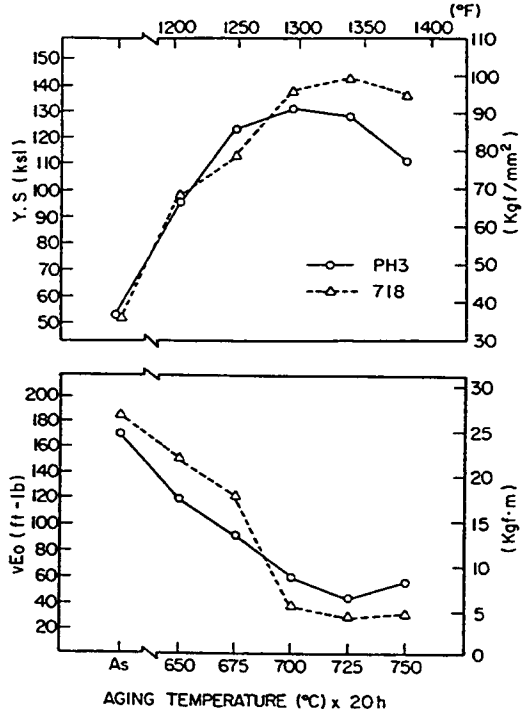


Figure 2. Comparison of aging behavior of PH3, 718,

TABLE 1
ALLOY 718 WITH
SPECIFIED MAXIMUM HARDNESS HRC 40

Yield Strength ksi	MPa	Tensile Strength ksi	MPa	RA %	Charpy V-Notch foot-lbs	Hardness HRC
148	(1020)	183	(1262)	21	79/80/80	39
151	(1041)	183	(1262)	45	69/72/74	40
148	(1020)	188	(1296)	44	68/69/77	39

This paper has not addressed the use of multiple heat treatments which may be detrimental in providing the mechanical properties necessary for the oil field. However, the user should be aware that most of Alloy 718s applied to the market are destined for high-temperature use. These are heat treated to the "standard" two step aging treatments. Reheat treating of these alloys may not provide the required properties for oil and gas applications since the heat treatment history (not only to the last heat treatment) has an effect on the microstructure. For example, grain boundary precipitates or second phases can remain in the grain boundaries to subsequently coarsen in future heat treatments. Therefore, the oil and gas industry should take into consideration heat treatment history. Further study is necessary in this area.

Corrosion Resistance of Alloy 718

Alloy 718 is used for oil and gas applications because of its good corrosion resistance. Since downhole environments are totally deaerated, the likelihood of either general corrosion or pitting corrosion in production environments is low (6). Alloy 718 has been found to be highly resistant to carbon dioxide, hydrogen sulfide, and acetic acid containing environments as shown in Table 2. Corrosion rates of less than 1 mil per year (.025 mm/y) are encountered to high temperatures. Only with acid, oxygen, or elemental sulfur does corrosion of Alloy 718 become significant. Therefore, the pitting corrosion resistance is considered only in the most severe environments encountered in the industry. Figure 3 shows the pitting potentials of alloys used in the industry. These alloys are considered to be corrosion resistant in most production environments. Alloy 718 has pitting corrosion resistance equivalent to duplex stainless steels. Alloys such as 410 stainless steel, nine-chrome one-moly, 304 stainless steel, CA6NM, F6NM, and 17-4 PH stainless steel are limited in use because of their corrosion resistance. Alloy 718 applications are generally not limited by corrosion resistance.

TABLE 2
CORROSION RESISTANCE OF ALLOY 718
IN SIMULATED PRODUCTION ENVIRONMENTS

Environment	Temperature	Gas	Corrosion Rate mpy	(mm/y)
3% NaCl	400 F (204 C)	1% H_2S + 50% CO_2 + 49% CH_4, 1000 psi	0.1	(.0025)
Seawater	240 F (115 C)	CO_2, 250 psi	0.2	(.0050)

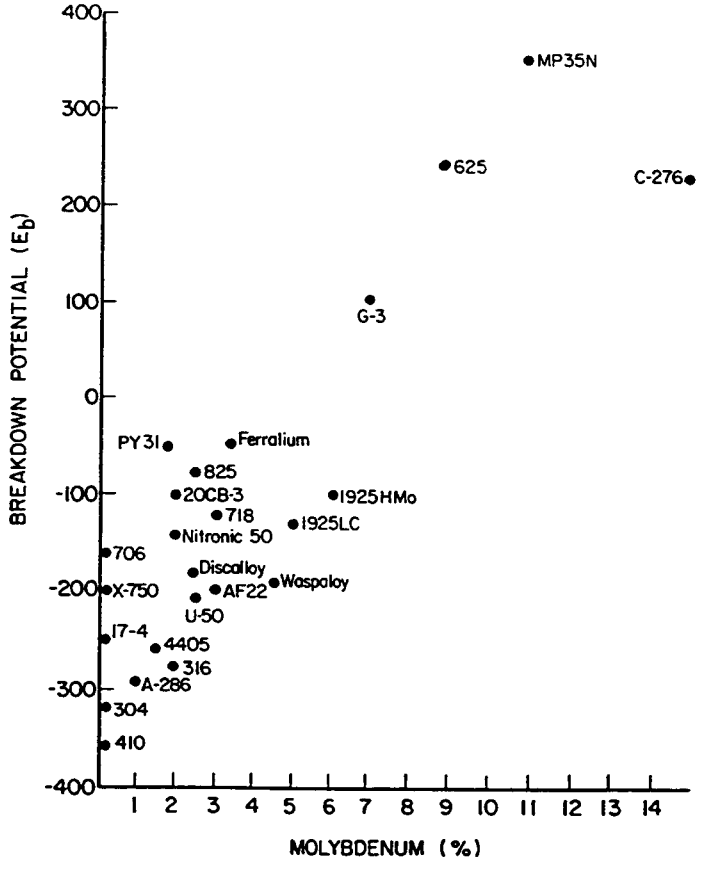


Figure 3. Pitting breakdown potentials of alloys used in the oil and gas industry. Eleven percent NaCl, 250 F, 500 psi CO_2 (after Paul J. Kovach, Vetco Gray).

Both the general corrosion resistance and the pitting corrosion resistance of Alloy 718 are affected by heat treatment. Table 3 shows the influence of aging temperature on the pitting corrosion resistance in the "Yellow Death Solution." In this test, increasing pitting temperatures reflect improved corrosion resistance. The reproducibility of this test is within 5 C. Heat treatments to 1350 F (732 C) do not have a detrimental effect on the pitting temperature in the "Yellow Death Solution." However, heat treatment at 1450 F (788 C) affects the pitting corrosion resistance. The reduction in pitting corrosion resistance can be attributed to both the precipitation of carbides and to the segregation of alloying elements during the precipitation hardening treatments. The trend shows that higher annealing temperatures are detrimental to pitting corrosion resistance of Alloy 718. However, except in the most severe cases, pitting corrosion resistance is not a limiting property, even in the 1450 F heat-treated conditions shown in Table 3. Table 4 shows a corresponding decrease in the general corrosion resistance of Alloy 718 with increasing temperature of heat treatment. This corrosion is associated with the chromium depletion in localized regions due to heat treatment. Thus, both the localized corrosion and generalized corrosion resistance decrease with increasing temperature aging treatments.

TABLE 3
ALLOY 718

Pitting Temperature in "Yellow Death Solution"
4% NaCl + 0.1% $Fe_2(SO_4)_3$ + 0.01M HCl
24-Hour Test

Conditions	Temperature Where Pitting Was Observed C
Mill Annealed	45
8 Hr/1250 F (677 C)	45
8 Hr/1350 F (718 C)	45
8 Hr/1450 F (788 C)	40
168 Hr/1450 F (788 C)	30

TABLE 4
CORROSION RESISTANCE OF ALLOY 718

Conditions	Boiling 5% H_2SO_4 mpy (mm/y)	Boiling 50% H_2SO_4 + 2.5% $Fe_2(SO_4)_3$ mpy (mm/y)
Mill Annealed	81 (2.1)	14 (.36)
8 Hr/1250 F (677 C)	77 (1.8)	58 (1.5)
8 Hr/1325 F (718 C)	62 (1.6)	200 (5.1)
8 Hr/1450 F (788 C)	56 (1.4)	280 (7.1)
168 Hr/1450 F (788 C)	77 (2.0)	3600 (9.1)

Alloy 718 possesses sufficient resistance to corrosion in acidizing environments. Table 5 shows relative corrosion rates of alloys in 10 percent boiling hydrochloric acid. This acid is uninhibited and shows maximum corrosion rates expected for short-term exposures. Alloy 718 corrodes at 4 mils (0.10 mm) per day, even in the uninhibited acid. The corrosion resistance is comparable to Alloys 825, SM2550, or G3, which are a likely combination with Alloy 718 in the most severe completions. From a practical standpoint, the corrosion resistance of Alloy 718 in oil field acidizing environments is adequate, especially since these environments will contain corrosion inhibitors to reduce the corrosion rates even further. The effect of heat treatment on corrosion resistance of Alloy 718 in hydrochloric acid has not been examined. The effects of H_2S on acidizing have also not been examined.

TABLE 5
CORROSION RESISTANCE OF ALLOYS

Uninhibited 10% HCl Acidizing Solution
Boiling Test, 24-Hours

Alloy	Corrosion Rate	
	mpy	(mm/y)
304 Stainless Steel	>20,000	(>500)
Duplex Stainless Steel (2205)	>20,000	(>500)
Alloy 718	1,500	(38)
Alloy SM 2550	1,150	(29)
Alloy G-3	1,050	(27)
Alloy 825	1,000	(25)
Alloy C-276	230	(5.8)

Hydrogen Embrittlement Resistance of Alloy 718

Alloy 718 is susceptible to hydrogen embrittlement (7,8), especially in the high strength heat-treated conditions. However, most of the investigations of hydrogen embrittlement have been performed with high strength (170,000 psi (1172 MPa) yield) materials. Thus, the results from work with these high strength materials for the aerospace industry may not be relevant in predicting the likelihood of failure in oil field applications (9,10). However, the effects of heat treatment or other environmental parameters may still be relevant to oil industry use. High temperature aging treatments (11) near 1400 F (760 C) improve the hydrogen embrittlement resistance of Alloy 718. Table 6 shows the effect of heat treatment on the hydrogen embrittlement resistance in high-pressure hydrogen at room temperature (12). As shown, Heat Treatment No. 1 provides the highest resistance to hydrogen embrittlement. Other work has shown that grain boundary precipitation (13) is detrimental to hydrogen embrittlement

TABLE 6
EFFECT OF HEAT TREATMENT ON
HYDROGEN EMBRITTLEMENT RESISTANCE OF
ALLOY 718, 1,000 PSI PRESSURE OF GAS

Heat Treatment	Strength Ratio H_2/He in Tensile Tests
1900 F/20 min/AC/1400 F/11 hr/1200 F/9 hr	.91
1800 F/1 hr/AC/1325 F/8 hr/1180 F/12 hr	.66
1950 F/1 hr/AC/1350 F/9 hr/1200 F/11 hr	.51

resistance. Fine grained structures are more resistant to embrittlement (14). The hot-worked plus direct-aged condition has better hydrogen embrittlement resistance than hot-rolled + solution-annealed + aged condition. This may be interpreted as an effect of grain boundary precipitation (15) on the hydrogen embrittlement resistance of Alloy 718.

The resistance to sustained crack growth is relatively independent of temperature between ambient and minus 100 F. There is some evidence that the gamma double prime precipitate is more resistant to hydrogen embrittlement than the gamma prime precipitate in nickel-based alloys. Also solution-annealed + cold-worked condition is more susceptible to hydrogen embrittlement (16) than precipitation-hardened Alloy 718. This susceptibility to embrittlement is especially enhanced after well-aging (17) treatments at 400 to 600 F (204 to 315 C).

In spite of the proven susceptibility of Alloy 718 to hydrogen embrittlement at high strength levels, it shows high resistance to cracking at strength levels used in the oil industry (18). Various laboratories have shown that, even at a hardness of HRC 40, Alloy 718 is not susceptible to delayed failure in the NACE TM0177 tests containing hydrogen sulfide and acetic acid, even when coupled to carbon steel and in the well-aged condition (19). Table 8 demonstrates the resistance to delayed failure in the TM0177 tests. These results imply that hydrogen embrittlement of Alloy 718 in properly heat treated conditions does not pose the primary limitation for use in oil field applications. This applies for constant temperature exposures as well as cycling between high and low temperature environments, as is shown in Table 7. Since the strength level is the critical parameter which determines sulfide stress corrosion cracking resistance, controlling the strength level to acceptably low values minimizes the risk for sulfide stress cracking in the oil field. Thus, the HRC 40 maximum hardness appropriately reduces the risk of hydrogen embrittlement in the oil and gas applications to low values.

Stress Corrosion Cracking of Alloy 718

Alloy 718 is susceptible to stress corrosion cracking in high temperature waters (20), in caustic solutions, and in high-temperature chloride solutions (16,21) containing hydrogen sulfide or acids. Most of the stress corrosion cracking investigations performed for the aerospace industries (water or caustic environments) are not relevant to the oil and gas industry applications because of the specificity of environments required for stress corrosion cracking. In deionized water and caustics (22), the

TABLE 7*
RESISTANCE OF ALLOY 718 TO
HYDROGEN EMBRITTLEMENT IN THE NACE
TM-01-77 TEST SOLUTION, ROOM TEMPERATURE,
5 PERCENT NaCl + 1/2 PERCENT ACETIC ACID + 1 ATMOSPHERE H_2S

720 Hours

Alloy Condition	Hardness, HRC	Test Condition	Threshold Stress
1875 F/1 hr/WQ/1425 F/12 hr/AC/1490 F/8 hr AC	38	U-Bend	NF
1875 F/1 hr/WQ/1475 F/12 hr AC	40	U-Bend	NF
1750 F/1hr WQ/1325 F/8 hr FC/1150 F/8 hr AC	41	NACE Tensile	NF
1950 F/1 hr/WQ/1325 F/8 hr FC/1150 F/8 hr AC	41	C-Ring + Steel Couple $\sigma = \sigma_y$	NF
1925 F/1 hr/WQ/1450 F/1 hr/AC	32	C-Ring + Steel Couple $\sigma = \sigma_y$	NF
1750 F/1 hr/WQ/1325 F/8 hr FC/1150 F/8 hr/AC	43	NACE Tensile Steel Couple	NF σ_y
Cold Roll + 1325 F/8 hr/FC/1150 F/8 hr/AC	46	Bent Beam Steel Couple	54 Days
1925 F/1 hr/AC/1400 F/10 hr/FC/1200 F/20 hr AC	45	TM0177	NF

*Data From Reference (19).

TABLE 8
AVERAGE CRACKING TIME FOR COMMERCIAL Fe-Ni-Cr
ALLOYS EXPOSED IN BOILING $MgCl_2$ at 154 C*

Alloy Designation	Nickel Concentration (wt. pct.)	Average Time to Cracking (minutes)++
Type 304	9	590
Type 310	20	600
Alloy 800	32	1,800
Alloy 825	42	6,700
Alloy 718	53	10,000

*Specimens 0.38 mm diameter wires, vacuum annealed and rapidly cooled, stressed at 90% of 0.2% offset yield strength.

++Each value the average of ten specimens.

Reference 31.

stress corrosion cracking resistance improves with increased aging temperature similar to that for hydrogen embrittlement. It is not known whether this is relevant to the stress corrosion cracking in high-temperature chloride solutions typical of oil and gas field environments. The effect of heat treatment on the chloride stress corrosion cracking resistance of Alloy 718 in oil field environments has not been thoroughly examined. This is ironical since the stress corrosion cracking behavior limits the application in the most severe environments. Alloy 718 is susceptible to chloride cracking in boiling magnesium chloride (23) solution at 154 C (309 F) (Table 8) and other high-temperature environments containing chloride, sulfur (24), oxygen, or acids. Although not specific to Alloy 718, the presence of hydrogen sulfide greatly accelerates the high-temperature chloride stress corrosion cracking of nickel-based alloys.

High-temperature chloride stress corrosion cracking limits the maximum environmental temperature for Alloy 718 in the oil industry. While Alloy 718 exhibits good resistance to chloride stress corrosion cracking in many high-temperature chloride containing solutions, it is very susceptible in the presence of elemental sulfur (25) (Table 9). Elemental sulfur is found in environments with high H_2S partial pressures. Therefore, in the presence of elemental sulfur, the maximum temperature limit for Alloy 718 is estimated to be 250 to 300 F (121-149 C). In fact, wellhead temperatures and temperatures of safety valves are controlled below 260 F (127 C) in some applications.

TABLE 9
EFFECT OF ELEMENTAL SULFUR ON STRESS CORROSION CRACKING

C-Shaped Samples, Like Alloy Holders
Deaerated 25% NaCl + 1 g/l Sulfur (No Acid Added)
ANNEALED ALLOYS
Time to Failure, Months, 12-Month Exposure

	350 F 100 psi H_2S pH = 4.5	450 F 100 psi H_2S pH = 4.5
Duplex Stainless Steel	1, 1, 1	1, 1, 1
Alloy 28	1, 2, 2	1, 1, 1
Alloy 925, Aged	1, 1, 1	1, 1, 1
Alloy 718 (Heat Treated HRC 45)	1, 1, 1	1, 1, 1
Alloy 825	2, 2, 2	1, 1, 2
Alloy G-3	7, 8, 8	1, 2, 3
Alloy C-276	NC, NC, NC	NC, NC, NC

NC - No Cracking

Some investigations have shown the gamma double prime alloys to be less susceptible to stress corrosion cracking than gamma prime alloys similar to findings on hydrogen embrittlement. While the data are sparse on Alloy 718, information on other precipitation hardenable alloys similar to 718 suggest that higher-temperature heat treatments and the absence of grain boundary precipitation is beneficial for chloride stress corrosion cracking resistance. Consequently, as a practice, where stress corrosion cracking limitations apply, higher-temperature aging treatments are used to prolong life and improve resistance to chloride stress corrosion cracking.

Selection of Precipitation Hardenable Alloys for the Oil and Gas Industry

Only a few highly corrosion-resistant precipitation hardenable alloys are considered for use in the oil and gas industry. Among these alloys are 17-4 PH stainless steel, Custom 450 stainless steel, A-286, Alloy K500, Alloy 718, Alloy 925, Alloy 625, Alloy Custom-Aged 625+, and a new Alloy PH3. The Alloy X750 has been used historically but is finding less usage because of its susceptibility to hydrogen embrittlement and stress corrosion cracking. The first few alloys are of lower-cost and are used as environmental considerations permit. However, these alloys are more highly susceptible to sulfide stress corrosion cracking and are not considered for the severe applications. In the severe applications, the alloys include 925, 718, PH6, 625, and Custom-Aged 625+. Of these alloys, only Alloy 718 can achieve the very high-yield strengths (140,000 psi minimum yield) for application requiring these strength levels. Table 10 displays the yield

TABLE 10
MECHANICAL PROPERTIES OF HEAT TREATABLE
ALLOYS USED FOR CORROSION RESISTANT
APPLICATIONS IN PETROLEUM PRODUCTION

Alloy	Heat Treatment	Yield Strength Solution Annealed + Aged ksi	(MPa)	Tensile Strength ksi	(MPa)	RA %
625	1700 F/1 hr/WQ/1200 F/16 hr	88	(607)	146	(1007)	36
925	1800 F/1 hr/WQ/1400 F/8 hr FC/ 1150 F/8 hr/AC	114	(786)	170	(1172)	38
Custom Age 625	1800 F/4 hr/WQ/1375 F/8 hr/ FC 1250 F/8 hr/AC	126	(869)	182	(1255)	55
PH6	1960 F/WQ/1275 F/20 hr/AC	133	(917)	160	(1103)	42
718	1875 F/2 hr/WQ/1425 F/8 hr/AC	142	(979)	184	(1269)	36

strengths obtainable and typical values used in the industry. In this respect, Alloy 718 has the advantage over the other alloys. However, for the most severe applications, the Alloy 625, Custom-Aged 625+, and PH6 alloys exhibit higher chloride stress corrosion cracking resistance (26-30) and, therefore, are considered for the highest severity environments.

Subsurface safety valves require alloys with higher strength than those in production tubing because design stress levels are lower. Since the restriction of the I.D. bore should be minimized, the strength requirement for complicated parts is pushed to higher levels. Therefore, one of the most critical components in high-pressure gas wells, a subsurface safety valve, presently imposes the greatest restrictions for material usage in severely corrosive applications. Alloy 718 remains the material of choice for the severe sour applications.

Conclusions

1. The stress corrosion cracking resistance of Alloy 718 determines the limits of application in the most severely corrosive high-pressure sour gas wells.

2. Alloy 718 is susceptible to hydrogen embrittlement in the extremely high-strength levels. However, for oil field applications, the limit of HRC 40 maximum hardness provides good resistance to hydrogen embrittlement.

3. Increasing aging temperatures result in lower toughness in Alloy 718. Toughness is an important material selection criteria for this alloy.

4. Increasing aging temperatures reduce both the general corrosion resistance and the pitting corrosion resistance of Alloy 718.

5. The heat treatment of Alloy 718 is necessarily customized for applications in the oil industry, and heat treatments historically used for high-temperature applications are generally not suitable for general oil field usage. High temperature aging treatments are preferred for improved resistance to environmental embrittlement.

References

1. D. R. Ray, Abu Dhabi; Offshore Khuff Gas Completions Using Exotic Metallurgy, SPE 15755, SPE, 1987.

2. M. Igarashi, S. Mukai, T. Kudo, Y. Okada, A. Ikeda, Precipitation-Hardenable, Nickel-Base Alloys for Sour Gas Environments, Corrosion, Volume 44, No. 3, 1988, p. 169.

3. Oliver Onyewuenyi, Properties of Alloy 718, 1987 ASM Houston Materials Conference, Houston, Texas, April 8, 1987.

4. W. J. Mills, L. D. Blackburn, Fracture Toughness Variations in Alloy 718, Trans. ASME, Vol. 110, July 1988, p. 286.

5. M. Igarashi, Y. Okada; Intergranular Fracture in Precipitation-Hardened, Nickel-Based Superalloys; Symposium in "Grain Boundary Structure and Related Phenomena;" Minakemi Spa, Japan, November 25-29, 1985.

6. T. F. Lemke, J. A. Harris, High-Alloy Materials for Offshore Applications, OTC Paper No. OTC4451, 198?.

7. D. L. Dull, L. Raymond; A Test Procedure to Evaluate the Relative Susceptibility of Materials to Stress Corrosion Cracking; Corrosion, Vol. 29. May 1975, p. 205.

8. D. L. Dull, L. Raymond, Surface Cracking of Inconel 718 During Cathodic Charging, Metallurgical Transactions, Vol. 4, June 1973, p. 1635.

9. J. A. Harris, T. F. Lemke, Laboratory Testing of Nickel Alloys for H_2S Service, Materials Performance, Volume 12, No. 1, 1983.

   Also, Paper No. 137, Corrosion/82, 1982.

10. P. W. Rice, Evaluating Nickel-Base and Stainless Alloys for Subsurface H_2S Service, Materials Performance, Vol. 17, p. 16, 1978.

11. R. J. Walter, W. T. Chandler; Influence of Gaseous Hydrogen on Metals, Final Report Contract NASA-25579, Report for Marshall Space Flight Center, Prepared by Rocketdyne, A Division of Rockwell International; October 1973.

12. R. P. Jewett, R. J. Walter, W. T. Chandler, R. P. Fromberg; Hydrogen-Environment Embrittlement of Metals, A NASA Technology Survey, Contract NASA-19(C) for NASA by Rocketdyne, A Division of North American Rockwell.

13. N. S. Stoloff, L. Klein, J. E. Grossman, H. L. Marcus; Hydrogen Embrittlement of an Aligned Γ/Γ' - Γ Eutectic Alloy, Scripta Met. Vol. 10, p. 889, 1976.

14. R. J. Walter, W. T. Chandler, "Influence of Hydrogen Environments on Crack Growth in Inconel 718," Conference on Environmental Degradation of Engineering Materials, Blacksburg, Virginia, October 11-12, 1977.

15. J. Prybylowski, R. Ballinger, The Influence of Microstructure on Environmentally Assisted Cracking of Alloy 718; Paper No. 244, Corrosion/86, 1986.

16. J. Kolts, Heat Treatment and Environmental Embrittlement of High-Performance Alloys, Paper No. 407, Corrosion/86, NACE 1986.

17. Russell D. Kane, Accelerated Hydrogen Charging of Nickel and Cobalt-Base Alloys, Corrosion, Vol. 34, No. 12, 1978, p. 442.

18. M. Watkins, J. B. Greer, Corrosion Testing of Highly Alloyed Materials for Deep, Sour Gas Well Environments, J. of Petroleum Technology, June 1976, p. 648.

19. Ballot, Item No. 7, Attachment G, MR01-75 Revision, September 1982, NACE, Houston, pp. 48-67.

20. K. Hosoya, R. Ballinger, J. Prybylowski, I. S. Hwang, Microstructural Role in Environmentally Assisted Cracking of Nickel Base Alloys, Corrosion, November 1988, p. 838.

21. Glen A. Vaughn, Hung-Erh Chuang, Wireline Materials for Sour Service, Paper No. 182, Corrosion/81, NACE 1981.

22. H. T. Michels, S. Florren, The Relationship Between Microstructure Deformation Behavior and Stress Corrosion Cracking Resistance at an Age Hardened Ni Base Alloy, Met. Trans. A, Vol. 8A, 1977, p 617.

23. A. J. Sedriks, Stress-Corrosion Cracking of Stainless Steels and Nickel Alloys, J. of the Inst. of Metals, Volume 101, 1973, p. 225.

24. R. D. Kane, J. B. Greer, D. F. Jacobs, H. R. Hanson, B. J. Berkowitz, G. A. Vaughn, Stress Corrosion Cracking of Nickel and Cobalt-Based Alloys in Chloride Containing Environments, Paper No. 174, Corrosion/79, NACE 1979.

25. Juri Kolts, Laboratory Evaluation of Corrosion Resistant Alloys for the Oil and Gas Industry, p. 323, Corrosion/86, NACE, 1986.

26. SSRT Test Results of Precipitation-Hardened, Nickel-Base Alloys for Downhole Equipments, Sumitomo Metal Industries, Ltd., March 1986.

27. R. B. Frank, T. A. DeBold, A New Age-Hardenable Corrosion-Resistant Alloy, ASM Material Conference, Orlando, Florida, October 7, 1986.

28. J. D. Byrd, Properties of Alloy 625, 1987 ASM Houston Materials Conference, Houston, Texas, April 8, 1987.

29. Stress Corrosion Cracking of Precipitation Hardenable Nickel-Based "PH6" Alloy, Sumitomo Metal Industries, Ltd., March 1988.

30. R. B. Frank, T. A. DeBold, Properties of an Age-Hardenable, Corrosion-Resistant, Nickel-Based Alloy, Material Performance, September 1988, p. 59.

31. R. M. Latanision, R. W. Staehle, Stress Corrosion Cracking of Iron-Nickel-Chromium Alloys, Dept. of Metallurgical Eng., The Ohio State University, 1968.

Copyrighted Materials
Copyright © 1996 NACE International Retrieved from www.knovel.com

ALLOY 718 - ALLOY OPTIMIZATION FOR APPLICATIONS IN OIL AND GAS PRODUCTION

O. A. Onyewuenyi

Shell Development Company
P. O. Box 1380
Houston, Texas 77001

Abstract

Alloy 718 is extensively used by the oil and gas industry for Critical Service applications involving both wellhead components and downhole auxiliary equipment for corrosive/sour service. This study addresses the metallurgy and precipitation behavior of this alloy and their effects on fracture resistance. The use of heat treatment and microstructural control to tailor the alloy to the specific needs of oil and gas production applications, in contrast to aerospace applications is highlighted.

Superalloy 718—Metallurgy and Applications
Edited by E.A. Loria
The Minerals, Metals & Materials Society, 1989

Courtesy The Minerals, Metals & Materials Society (TMS)

Introduction

In the last ten years, Alloy 718 has become the preferred material for manufacture of wellhead components, auxiliary and downhole tools for oil and gas wells containing corrosive and crack sensitive species such as CO_2, chlorides and H_2S. For many such applications, the alloy now replaces other corrosion resistant alloys (CRA) candidates such as K-monel, 17-4 pH and Inconel X750. This increased interest stemmed primarily from various factors, namely: (a) reported lab and field failures of production equipment made from the above CRAs[1,2], (b) ability to fabricate heavy wall and/or complex shaped components and still achieve a desired combination of strength, toughness, corrosion and environmental cracking resistance, and (c) discovery that slight modifications in composition and heat treatment can be used to tailor the alloy to the needs of specific environmental applications.

The objectives of this paper are to report typical applications of Alloy 718 in oil and gas production, and the special requirements imposed by its use in deep high pressure sour gas wells. The relative characteristics of underage, peak age, and overage heat treatments of Alloy 718 provides the basis for preferred heat treatments which optimize desired properties. The factors which affect fracture resistance are highlighted and the criteria for toughness requirements of Alloy 718 in critical applications are presented.

Application Requirements

Table I shows the typical components commonly made of Alloy 718. In general, the strength requirements fall into two classes. For wellhead equipments such as valve trims and valve bodies for American Petroleum Institute's Specification 6A PSL4 service, the minimum yield strength is 75 ksi. For fasteners, downhole and auxiliary equipments designed to connect to threaded members such as high strength tubing, and/or to contain high internal pressures, typical minimum strength is 120 ksi. In all cases involving exposure to H_2S, required compliance with National Association of Corrosion Engineer's Standard (NACE) MR-01-75 limits the maximum acceptable hardness to HRC 40.

Table I. Typical Applications of Alloy 718 in Oil and Gas Production

	Typical Minimum Yield Strength, ksi	Maximum Hardness, HRC
Subsurface Safety Valves	120	40
Packers	120	40
Hangers	75-120	40
Valve Gates, Seats, and Stems	75	40
Fire Safe Valves	75	40
Blowout Preventers	75	40
Side Pocket Mandrels	75	40
Fasteners	120	40

010544-2

Auxiliary components such as tubing hangers, packers, and subsurface safety valve body components, are considered particularly critical since they can be highly stressed with tensile loads up to 90,000 psi, and with internal pressures of 15,000 psi, while being exposed to corrosive well fluid containing H_2S, CO_2, and aqueous chlorides. Typical service temperatures can range from ambient during acidizing treatments to 350°F at normal production. Failure of such components can result in substantial monetary risks, and release of deadly toxic gases such as H_2S. Thus such concerns demand special material properties with tight process controls in manufacturing of Alloy 718 components.

For application in deep sour gas wells, the critical requirements therefore are (1) resistance to general and localized corrosion, (2) resistance to environmentally induced cracking for both sulfide stress cracking and anodic stress corrosion cracking, based on a maximum hardness of HRC 40, (3) high strength typically above 120 ksi for both tubing hangers, safety valves and packer components which must be compatible with the strength and thread design of the production tubing, and (4) fracture toughness. The goal of the toughness optimization is to ensure that a leak-before-break type of failure is achieved for pressure containment boundary components, or as a minimum, a catastrophic brittle fracture is precluded. A further consideration is that the metallurgical factors which optimize toughness at a given strength also promote corrosion and cracking resistance. These factors include specific controls on alloy composition, melting and refining practices, degree and uniformity of hot working, and heat treatment.

Metallurgical Considerations

Compositional and Microstructural Effects

The role of the various alloying elements as well as the microstructural phases in Alloy 718 have been extensively studied[3] These microstructural phases include intermetallic compounds such as γ'-body centered tetragonal structure [$Ni_3(TiAlNb)$], γ''-orthorhombic structure (Ni_3Nb), and Laves phase [$Fe_2(Ti, Nb)$]. By controlling the time and temperature at which the alloy is exposed, the amount of each phase or a combination of phases which form can be varied to meet specific requirements. The predominant hardening phase in Alloy 718 is γ'', though some γ' is also present. Carbide phases such as MC, M_6C, Cr_7C_3, and $Cr_{23}C_6$ where M refers to metallic elements like niobium or titanium can also form along with the intermetallic phases, and can affect the attainment of the desired properties. In addition, depending on oxygen and nitrogen levels in the original melt, some dirt in the form of nitride and oxide phases can be present, but to a lesser extent in vacuum processed melts. The mechanical properties as well as the corrosion resistance of Alloy 718 thus depend on the relative amount of these phases as well as their morphology (spherical, angular, film, or needle-like) and location (within grains or at grain boundaries) in the microstructure. The phase volume fractions, morphology and distribution are in turn determined by such factors as alloy composition, melt practice (air melt or vacuum melt), refining practice (vacuum refined or electroslag refined), degree of wrought structure achieved by hot working, and finally, heat treatment. Thus Alloy 718 composition used in the current application is limited to lower carbon grades (0.045% max) and higher minimum levels on Ti, Al and Nb (0.80%, 0.40%, 4.87%, respectively) compared to the aerospace material specifications AMS 5596. Also the maximum levels of the metalloid elements such as P, S, Pb, Se, and Bi were lowered, since these are known to affect toughness and environmental cracking resistance due to their influence on surface activity and grain boundary properties.

Heat Treat Response and Strengthening Behavior

Annealing Behavior. Tensile strength in Alloy 718 in the solution annealed and aged condition is controlled primarily by γ'' and γ' phases, and to a lesser degree by the carbides, nitrides, and the matrix solid solution. An annealing treatment is used prior to aging in order to: (1) dissolve various intermetallic phases in the wrought structure, (2) refine the microstructure by recrystallizing new and uniform grains, and (3) provide homogeneity in the alloy so that properties developed by subsequent aging treatment are less dependent on prior thermomechanical processing history of the alloy. Such annealing effects can be assessed by an annealing response curve which shows the effect of annealing temperature on strength (hardness).

Figure 1 shows typical anneal curves for Alloy 718. They show that as the annealing temperature increased, the hardness decreased. The decrease in hardness also depends on the rate of cooling from the annealing temperature. The hardness of the as-annealed product increases in the slow cooled condition versus water quenched condition. This effect is attributed to the reprecipitation of grain boundary secondary carbides such as $M_{23}C_6$ as the alloy is slow cooled through 1550 to 1650°F. This effect is particularly significant in mill annealed products where variability in properties have been observed. The microstructural changes associated with annealing are shown in Figure 2. It shows the mixed structure associated with low annealing temperature (<1650°F), and the coarse grain structure associated with high annealing temperature (>1950°F). An annealing temperature in the range 1825 to 1925°F provides a more homogeneous structure by eliminating the effects of prior processing history which can influence aging response. Low annealing temperatures close to 1700°F are not sufficient to wipe out the effects of prior processing history such as duplex grain structure, precipitation of deleterious phases, and chemical inhomogeneity. However, the fine grain structure associated with low annealing temperature results in increased strengthening. As a compromise between sufficient chemical and microstructural homogeneity versus strength and toughness, an annealing temperature in the range of 1825°F to 1925°F is often used.

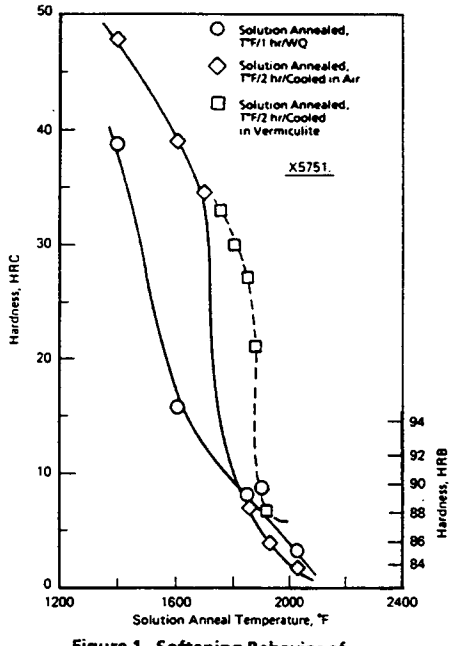


Figure 1. Softening Behavior of Alloy 718 Valve Stem Materials

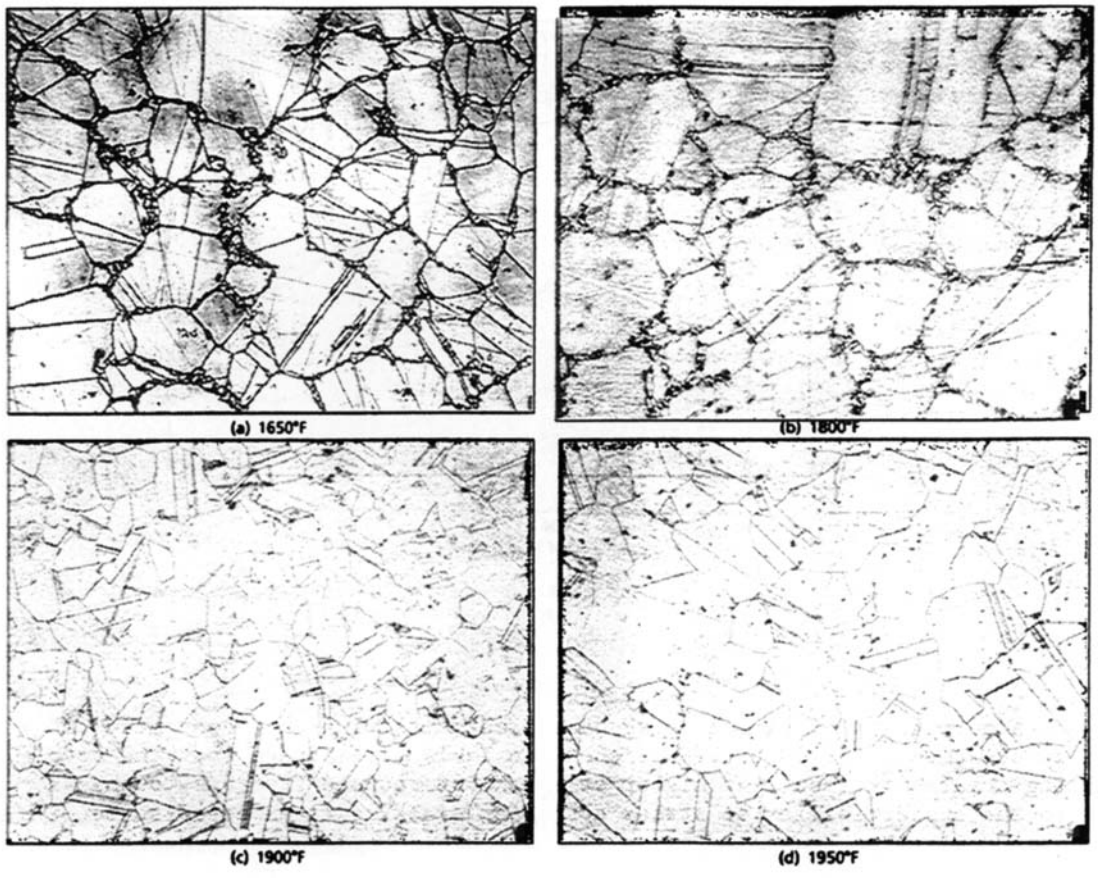


Figure 2. Microstructural Changes Associated with Annealing Treatment in Alloy 718
Annealed: Temperature °F/1hr/Water Quench; ***Magnification:*** 100X

Aging Behavior. For high strength or optimum creep rupture life, the common aerospace heat treatments involve 1950°F or 1725°F anneal treatments, respectively, followed by a double aging cycle. However, such heat treatments were not designed to provide high fracture toughness, and stress corrosion cracking resistance, both of which are major objectives for application to deep sour gas production.

Figure 3 shows the effect of annealing treatment on the age hardening response of Alloy 718. The data shows three conditions representing underaging (1300°F), peak aging (1400°F) and overaging (1500°F). It is evident that for a given prior hot (cold) working history, the age hardening response in the underage or overage conditions is directly affected by the anneal treatment. Increasing the anneal temperature results in softer as-aged material in the underage or overage conditions, whereas, at or near the peak aged condition, the anneal temperature has no significant influence on strength of as-aged material. The dependence on anneal temperature perhaps explains the variabilities in strength observed in underaged annealed bars, where the production furnace temperatures can vary by up to 200°F during annealing. Thus strength uniformity can be better assured by annealing between 1825 to 1925°F, followed by single aging at 1450°F $\pm$ 25°F. The proposed aging temperature range provides the desired strength and hardness requirements, without the need for the second aging cycle.

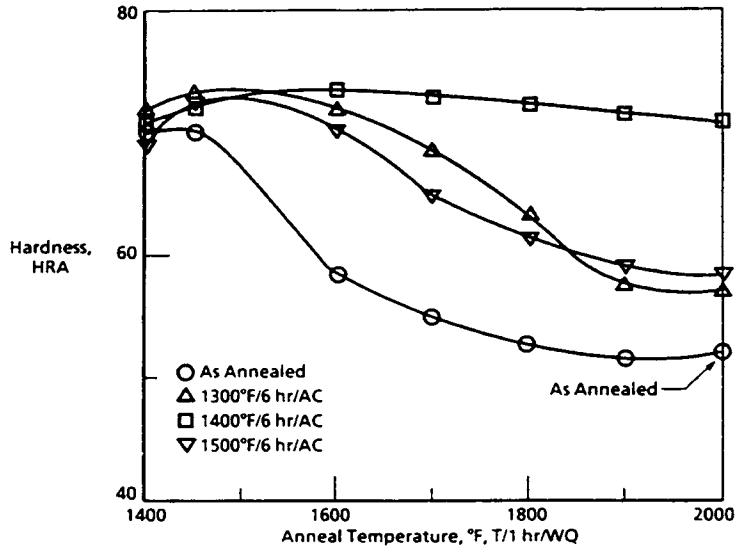


Figure 3. Effect of Anneal Treatment on Age Hardening Response in Alloy 718

013551-2

A comparison of single aging heat treatments with the "conventional" heat treatments for Alloy 718 is shown in Table II. Notice that the double aging treatments result in higher strength but reduced fracture toughness. Also the susceptibility to stress corrosion cracking is expected to be higher due to the increased hardness above HRC 40. The dependence of fracture resistance on heat treatments is evaluated in the next section.

Table II. Effect of Heat Treatment on Typical Room Temperature Properties of Alloy 718

Heat Treatment	Tensile Strength, psi	Yield Strength (0.2% Offset), psi	Elongation	% RA	Hardness, HRC	Fracture Toughness J_{IC}, psi-in.
Solution Anneal: 1875°F/1 hr/WQ Age: 1450°F/6-8 hr/AC	174	124	28	51	35	1908
Solution Anneal: 1925°F/1 hr/WQ Age: 1400°F/6 hr/AC	175	124	27	42	38	1631
Solution Anneal: 1750°F/2 hr/WQ or AC Age: 1325°F/8 hr/Cool 100°F/hr to 1150°F/8 hr/AC	193	164	23	48	42	572
Solution Anneal: 1925°F/1 hr/AC Age: 1400°F/6 hr/FC 100°F/hr to 1200°F/8 hr/AC	205	182	17	41	44	480
Solution Anneal: 1950°F/1 hr/AC Age: 1400°F/10 hr/FC 100°F/hr to 1200°F/8 hr/AC	190	161	19	NR	40	546

010544-5

Effects of Heat Treatment on Fracture Resistance of Alloy 718

To assess the effects of heat treatment on fracture resistance, Charpy impact toughness and fracture toughness based on J-integral and equivalent energy techniques were used. Impact toughness measurements comply with ASTM E23. Elastic plastic fracture toughness tests were based on methods of ASTM E813 for J_{IC} and $K_{IC}(J)$ toughness, and on ASTM E992 for K_{EE} toughness. Single specimen unloading compliance method was used so that both J_{IC} and K_{EE} were obtained from a single specimen test. Figure 4 shows a typical load-displacement record for Alloy 718. Figure 5 shows the associated crack growth J-resistance curve. In most cases fracture initiation occurred near the maximum load, and the K_{EE} toughness was close to the calculated $K_{IC}(J)$ toughness.

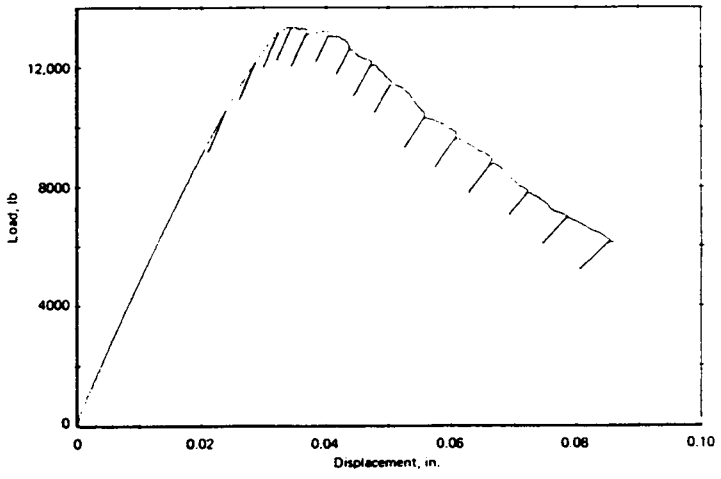


Figure 4. Computerized Load-Displacement Record for K_{EE} and J-Integral Fracture Analysis of Alloy 718 by Unloading Compliance Technique
Note the absence of a linear elastic behavior commonly observed in low toughness (brittle) materials.

07347

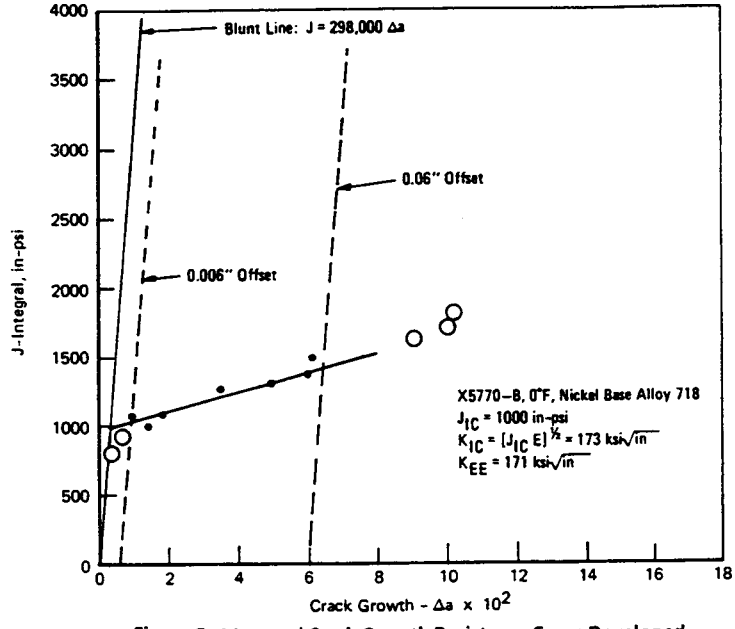


Figure 5. J-Integral Crack Growth Resistance Curve Developed for Nickel Base Alloy 718 by Unloading Compliance Technique

For the heat treat evaluation, sections of Alloy 718 billet or forging stock were heat treated in accordance to a test matrix. Compact tension and/or Charpy specimens were prepared from the samples and tested according to the above techniques. Figure 6 shows the effect of annealing temperature on the equivalent energy toughness. Notice that high anneal temperature $\geq$ 1925°F resulted in lower toughness.

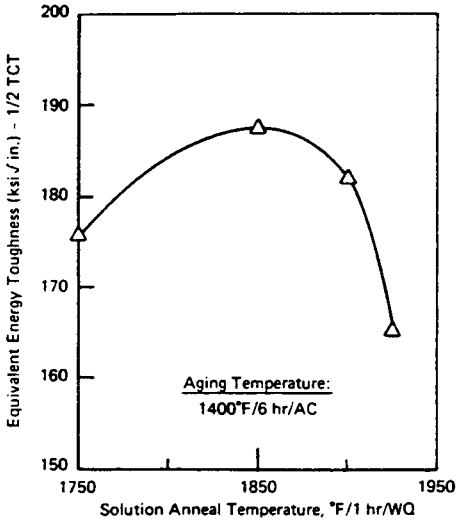


Figure 6. Effect of Annealing Temperature on Toughness of Alloy 718

07847

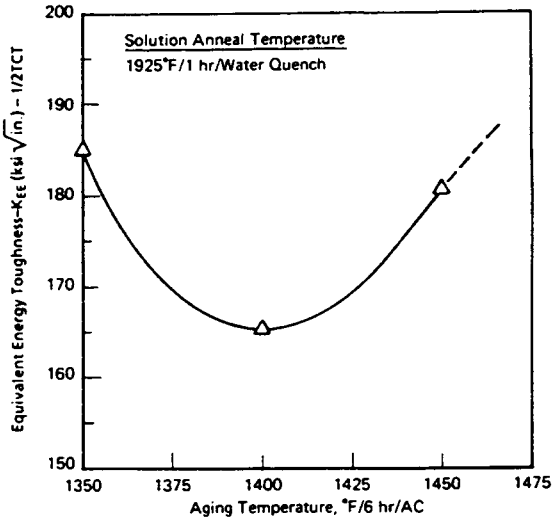


Figure 7. Effect of Aging Treatment on Toughness of Alloy 718

07847

The maximum fracture toughness occurs in the anneal temperature range of 1825 to 1875°F. When a higher anneal temperature such as 1925°F is used, improved toughness can still be achieved by choice of aging treatment. This is shown in Figure 7. Together these results indicate that for a given composition and alloy fabrication, the choice of specific heat treat parameters for anneal and single aging treatments can provide a optimum combination of fracture toughness >200 ksi $\sqrt{in}$, at yield strength $\geq$ 120 ksi, and hardness $\leq$ HRC 40.

Thus, from the foregoing heat treat response studies, the following inferences follow:

1. For the typical annealing temperature range of 1750°F to 1950°F, fracture resistance can vary significantly depending on the annealing cycle and the aging treatment. Improved toughness can be achieved by a relatively intermediate annealing temperature such as 1875°F $\pm$ 25°F, while satisfying the high yield strength requirements of 120 ksi minimum.

2. With a high annealing temperature (1925°F), improved toughness could be achieved with an overaging treatment, but decreased strength can be expected.

3. Single aging treatments rather than conventional double aging treatments can be used to achieve both high tensile strength and high

fracture toughness. An aging treatment of 1450 ± 25°F/6 hours/air cool is capable of meeting such requirements. This saves time, money, and complication of waivers relative to more complicated two step aging treatment.

Toughness Uniformity in Mill Production Samples

To assure that Alloy 718 purchased for Critical Service application has been processed and heat treated for high fracture toughness and environmental cracking resistance, materials heat treated as described above are required to achieve a minimum impact toughness of 40 ft-lb, in order to achieve a fracture toughness greater than 180 ksi √in. Figure 8 demonstrates that for billet sizes up to 5 1/2", this requirement can be readily met. However, for larger billet sizes or large forgings, the fracture resistance becomes significantly inferior.

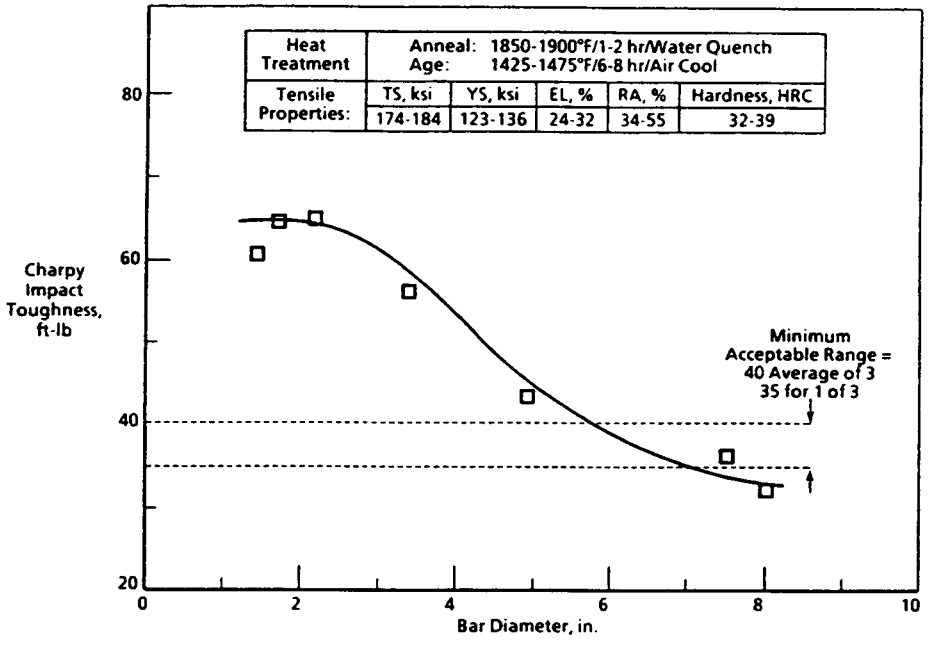


Figure 8. Effect of Heat Treat Section Size on Toughness of Production Samples of Alloy 718

013551-1

The decrease in fracture toughness with increased section size can be caused by factors such as (1) non-uniformity of hot work which affects heat treat response and microstructure and (2) density and distribution of carbide and carbonitride precipitates.

Table III compares the impact and fracture toughness values measured at the center and midwall locations of a heat treated 8" diameter stock used for tubing hanger. Here, the midwall location in the hanger component corresponds to 3/4 radius from center of the bar. Notice the center region shows inferior toughness which is less than the specified 40 ft-lb, or K_{IC} (J) of 180 ksi $\sqrt{in}$ for the component. This difference is attributed to the differences in microstructure between the two regions. Figure 9 shows the thru-wall microstructures in the bar. Compared to the mid-wall and OD regions, the center region shows more coarse grain size, higher density of NbC inclusions, and more grain boundary precipitates. Even though the fracture in the center and midwall region are both ductile, the above characteristics make void initiation and growth more favorable, resulting in low energy ductile tearing. This is supported by the slope of the J-resistance curve as shown in Figure 10. This slope is a measure of the tearing modulus of the alloy. Notice that in addition to the lower fracture toughness, the center region also shows a lower tearing modulus compared to material in the mid-wall region.

Table III. Variability in Impact and Fracture Toughness in 8" Diameter Forging for Alloy 718 Tubing Hanger

Location/ Orientation	Temp., °F	Impact Toughness		Fracture Toughness	
		Cv, ft-lb	Lateral Expansion, mils	J_{IC}, psi-in.	K_{IC}, J ksi$\sqrt{in.}$
Center/CR	0	31	20	975	170
Center/CR		32	19	900	163
Center/CR		31	20	975	170
3/4 Radius/CR	0	41	25	1560	214
3/4 Radius/CR		37	23	1662	221
3/4 Radius/CR		37	24	1885	236

013551-4

As stated earlier, differences in thru wall fracture resistance can also be caused by the density and distribution of carbide precipitates. Figure 11 shows how such precipitates can lower fracture resistance by promoting ductile fracture initiation. As the matrix deforms, local stress concentrations and plastic strain incompatibility between the matrix and the hard precipitates result in early cracking and decohesion of the inclusions. The resulting microcrack nuclei can then propagate into the matrix.

When the inclusions are aligned and occur in high volume fraction, they provide a low energy ductile fracture path. Figure 12 depicts the effect of such precipitate alignment. In this figure, the microstructure normal to the fracture plane in a compact tension specimen is shown. The top is the profile of the crack growth. Notice that when the inclusions

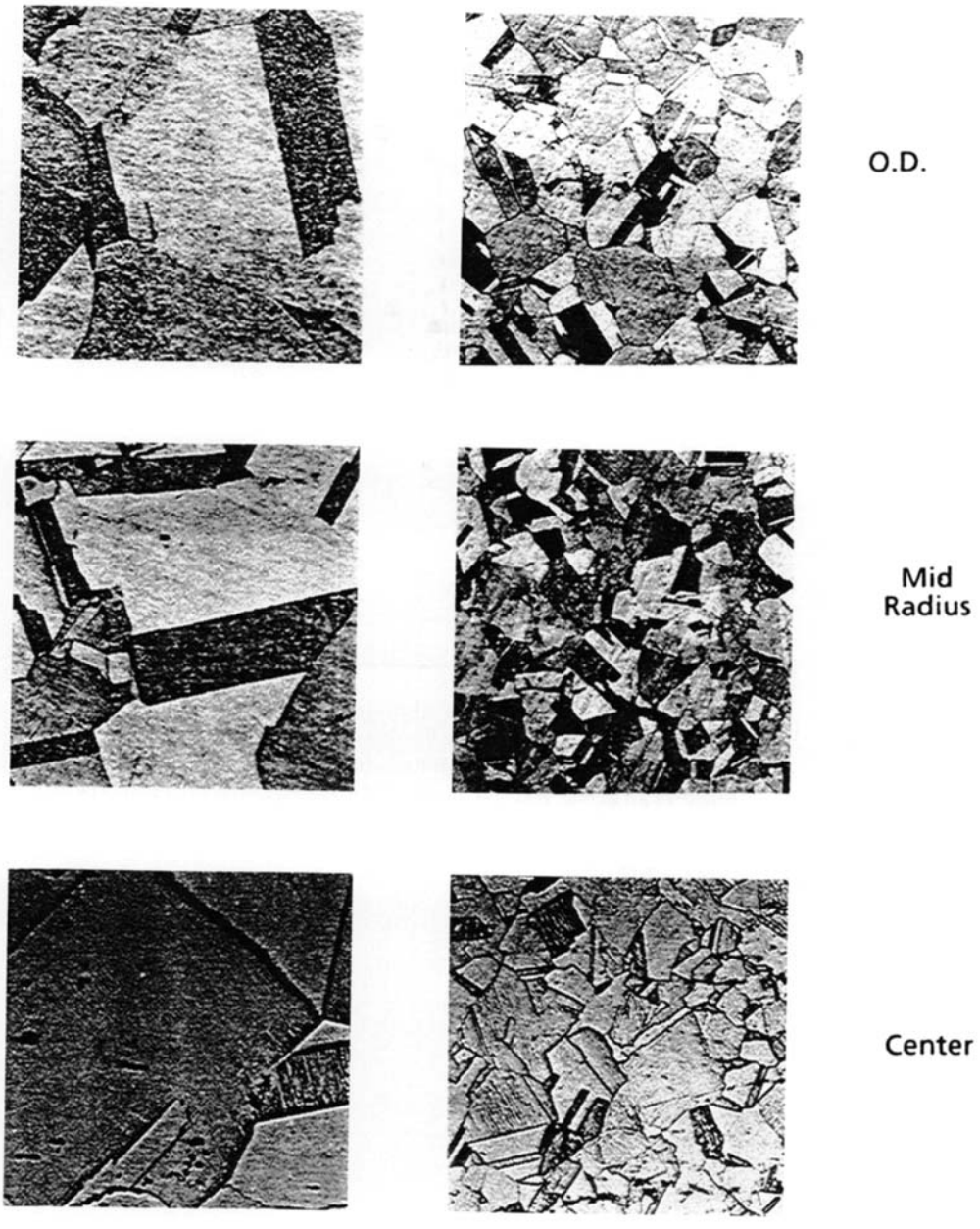


Figure 9. Thru Wall Microstructure in the Longitudinal Orientation of 8" Diameter Forging for Alloy 718 Tubing Hanger

013551

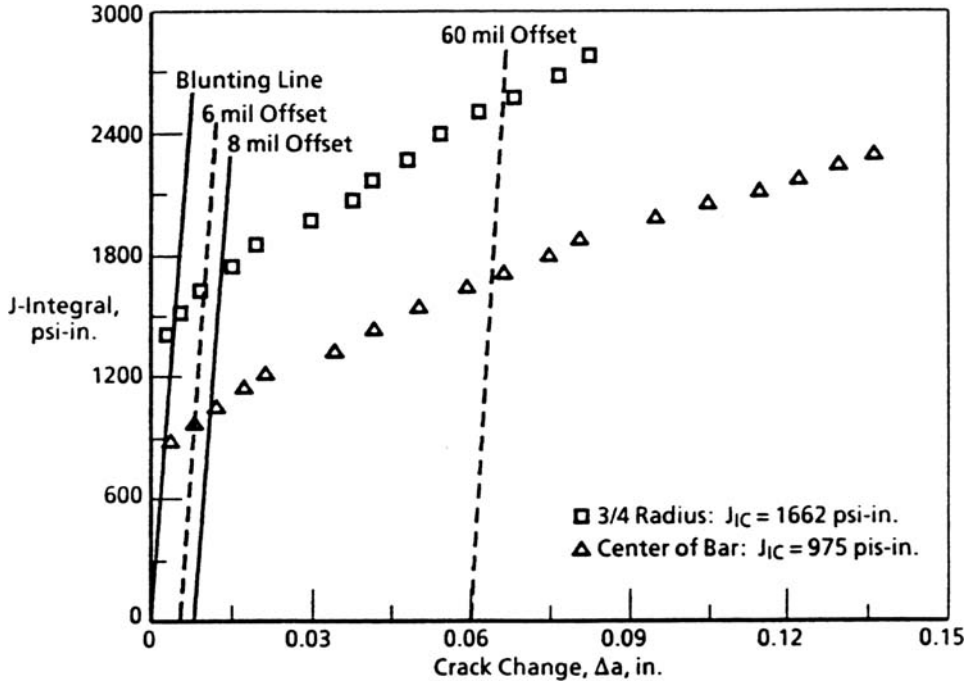
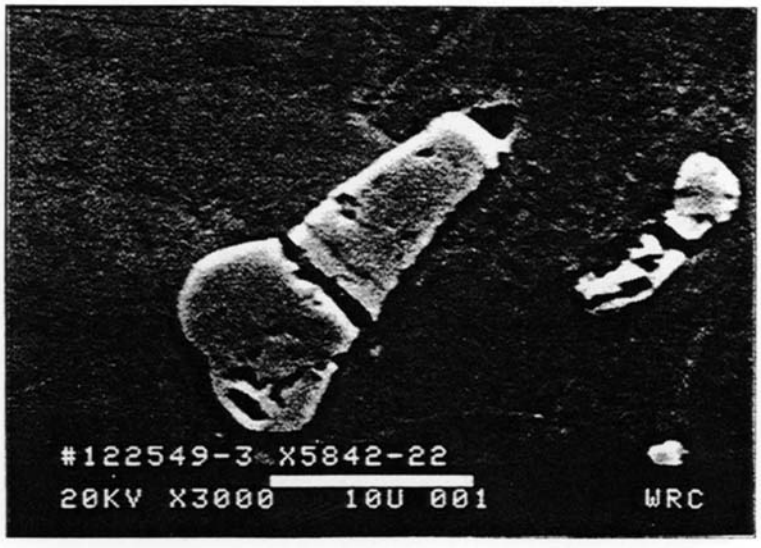
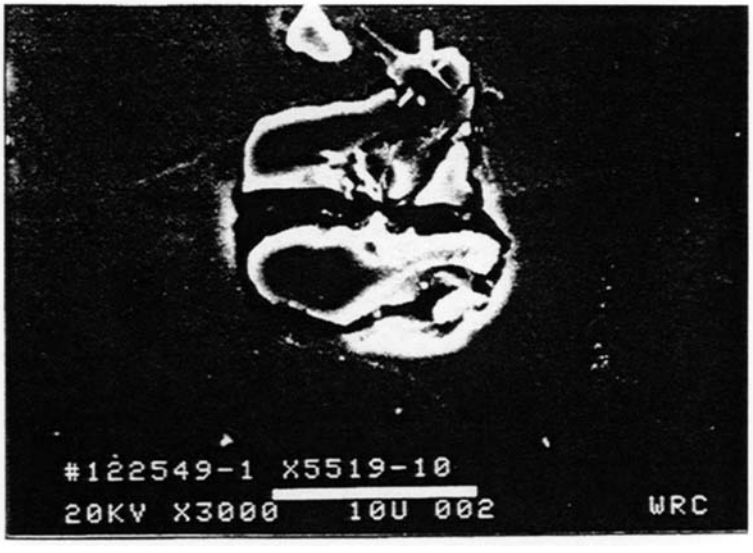


Figure 10: Crack Growth Resistance Curves in 8" Diameter Alloy 718 Tubing Hanger (X-6437) Showing Differences in Fracture Initiation and Ductile Tearing Modulus at Center and 3/4 Radius of Bar

013551-3



(a)

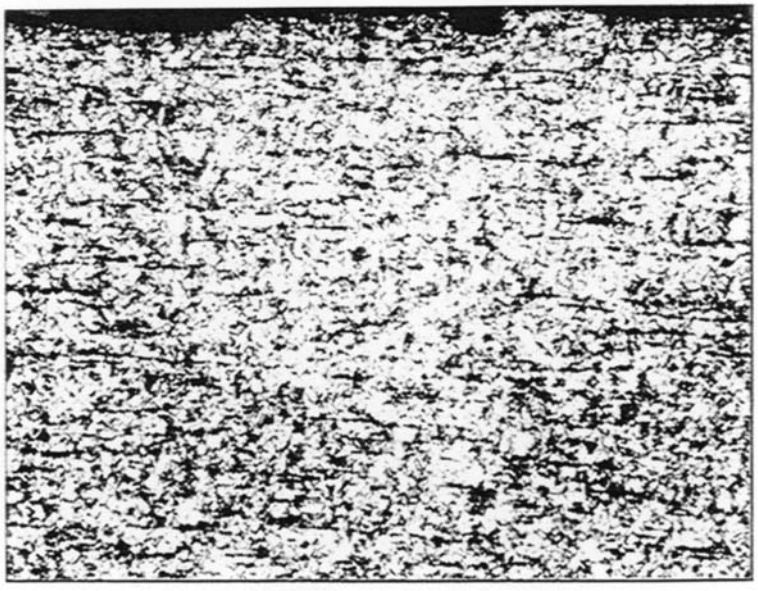


(b)

Figure 11. Micrographs Showing Role of Carbides and Inclusions in Initiating Cracks
As the matrix deforms, local stress concentration and incompatibility result in cracking of the inclusions. The resulting microcrack nuclei can then propagate into the matrix.

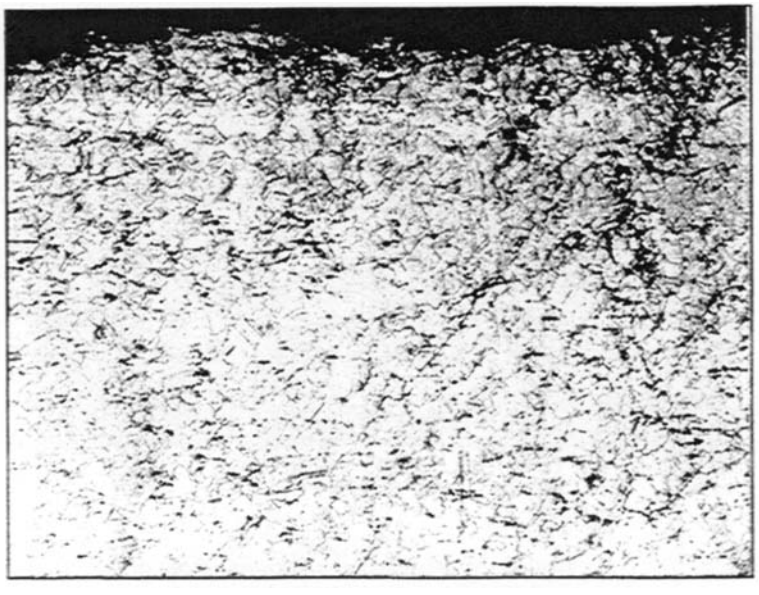
07347

← Crack Propagation



(a) Fracture parallel to inclusion stringers (dark streaks). The alligned NbC precipitates control the fracture and cause low fracture resistance.

← Crack Propagation



(b) Uniform structure and little amount of inclusions. Note jagged texture of the crack profile indicative of high fracture resistance.

Figure 12. Fracture Profile and Microstructure in Alloy 718 Showing Effect of Alligned Precipitates
Magnification: 16X; *Etchant:* Mixed Acid
Magnification: 16X; *Etchant:* Mixed Acid

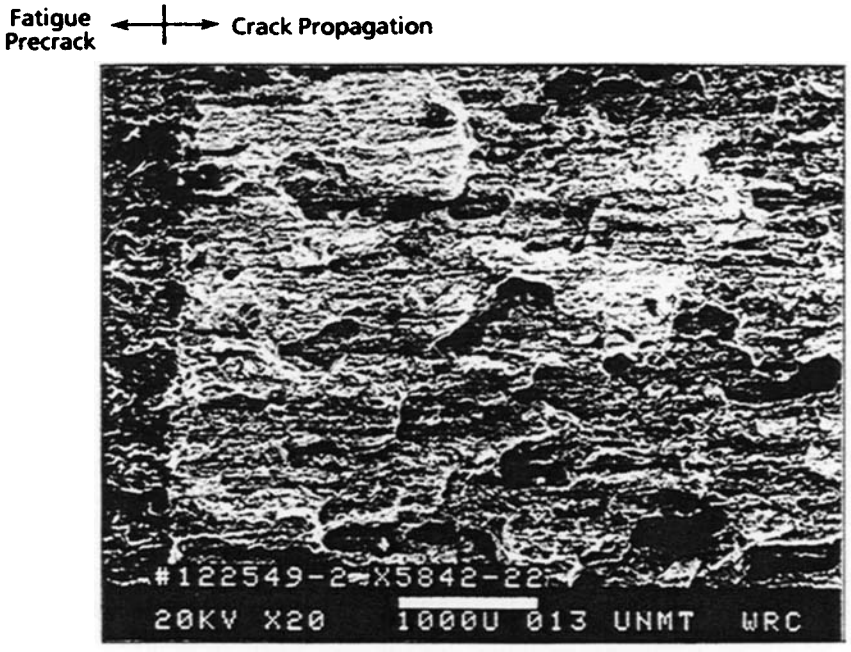
are aligned, the crack profile is more stepped and planar. In contrast, when the inclusions are dispersed and nonaligned, the crack profile is more jagged as shown in Figure 12b. The differences in crack profile associated with precipitate alignment also shows up as differences in the fractography of ductile fracture. As shown in Figure 13 precipitate alignment results in "woody" texture and faceted ductile fracture compared to the randomly dispersed case. Thus, even though in both cases, the fracture is ductile, the differences in the micromechanics explain the difference in measured fracture toughness.

Evaluation of Environmental Cracking Resistance

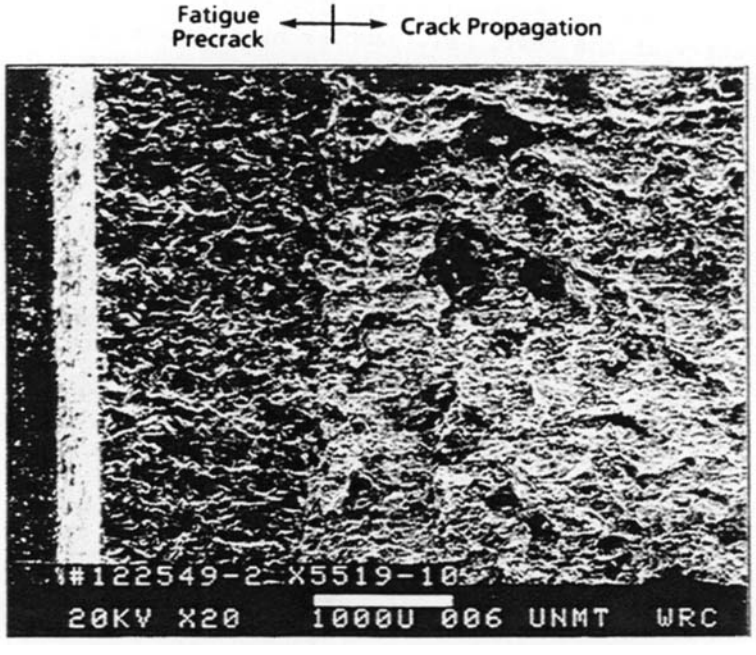
Environmentally assisted cracking in production environments containing $H_2S_{(aq)}$, CO_2, and chlorides can occur by cathodic or anodic mechanisms. Though the conditions at which both mechanisms synergistically interact are unknown, it is clear that anodic cracking predominates at high temperature, and cathodic cracking occurs at lower temperature where hydrogen embrittlement predominates. Table IV shows the conditions and results of cathodic cracking experiments. Precracked double cantilever specimens (DCB) were used to measure the threshold stress intensity factor for unset of crack growth. C-rings prestressed to yield loads assess crack initiation resistance, and the slow strain rate (SSR) test evaluates the dynamic effects of plastic straining during hydrogen absorption.

In general, Alloy 718 shows good resistance to H_2S induced cracking under cathodic conditions. As shown in Table IV, even the heat treatment conditions which show low fracture toughness did not show cracking. The intergranular cracking observed in the SSR test has been attributed to the higher severity of the test. All samples heat treated in accordance to the conditions proposed in the previous sections of this paper did not show cracking.

Table V shows the conditions and results of anodic cracking experiments, using U bend specimens of Alloy 718 samples heat treated to standard aerospace specification. Samples heat treated as proposed in this paper did not crack under the test conditions shown in Table V. In addition, the results suggest that for high H_2S levels, anodic cracking susceptibility increased with yield strength. Also at high strength levels the results suggests that cracking susceptibility increases with H_2S concentration.



(a) Note the "woody" and flat texture of the fracture characteristic of low energy ductile tearing. No evidence of embrittlement.



(b) Note more dimpled, ductile fracture, consistent with the higher fracture resistance of this sample of 718.

Figure 13. Fracture Details Just Ahead of Fatigue Precrack in Alloy 718
Sample with (a) high localized coarse precipitates, (b) fine and uniformly dispersed precipitates.
Magnification: 20X

07347

Table IV. Hydrogen Embrittlement Resistance of Alloy 718

Specimen ID/Type	Heat Treat	Hardness, HRC	Test Temp., °F	Condition	Result
X5322-5,2/DCB	*	37-38	RT-250°F	25% NaCl + 200 psi H_2S, C-S Coupled, 4 Weeks	No Cracking
X4140-38,41/C-Rings	*	38-39	RT-250°F	25% NaCl + 200 psi H_2S, 4 Weeks	No Cracking
X5322-1/DCB	*	38	32	NACE Solution + C-S Coupled 4 Weeks	No Cracking
X5058-5,7/C-Ring	**	38-41	RT	NACE Solution + C-S Coupled 2 Months	No Cracking
X5322-4/SSR	**	38	RT	NACE Solution + C-S Coupled 40 Hours	Intergranular Cracking

* *1925°F/1 hr/WQ + 1400°F/8 hr/AC*
** *1950°F/1 hr/AC + 1325°F/8 hr/FC*
1150°F/8 hr/AC

010544-13

Table V. U-Bend Stress Corrosion Cracking Tests Alloy for 718
25% NaCl – 6-Day Tests

	Test #1	Test #4	Test #5
Heat Treatment	1950°F/1 hr/AC 1325°F/8 hr/FC 1200°F/10 hr/AC	1950°F/1 hr/WQ 1325°F/8 hr/FC 1150°F/8 hr/FC	1950°F/1 hr/WQ 1325°F/8 hr/FC 1150°F/8 hr/FC
Yield Strength, psi	~135,000	~156,000	~156,000
Stress	>y.s.	>y.s.	>y.s.
Temperature, °F	400	400	400
Pressure, psi	14,000	14,000	1500
H_2S, %	3.5	3.5	1
CO_2, %	10	10	10
P_{H_2S}, psi	490	490	22.5
SCC Results, # Failed/# Tested	0/2	2/2	0/2

010544-15

Conclusions

1. Alloy 718 subjected to anneal plus single age heat treat cycles provides the required properties for application in deep, corrosive oil and gas wells.

2. For optimum combination of strength, toughness, and environmental cracking resistance an anneal temperature within 1825 to 1925°F followed by water quench and an aging temperature of 1450 $\pm$ 25°F is proposed.

3. Conventional aerospace heat treatments which optimize strength and creep rupture properties are unacceptable due to decrease in fracture toughness, and environmental cracking resistance.

4. Degradation in fracture resistance is related to the amount and distribution of carbide inclusions and grain boundary precipitation, both contributions are higher in large section components.

References

1. J. W. Kochera, A. K. Dunlop, and J. P. Tralmer, Corrosion/76, Paper No. 50.

2. P. W. Rice, Materials Performance, 1978, pp. 16-25.

3. Ya. Fangttan, P. Deb, and M. C. Chaturvedi, Met. Sci., 1982, 16, p. 555.

Copyrighted Materials
Copyright © 1996 NACE International Retrieved from www.knovel.com

Section 5

SOLID SOLUTION, NICKEL/COBALT-BASE ALLOYS



OTC 6067

Corrosion-Resistant Alloys for Hot, Deep Sour Wells: Properties, Experience, and Future Trends

by A.I. Asphahani, Haynes Intl.; J.C. Prouheze, Vallourec; and G.J. Petersen, Cabval

Copyright 1989, Offshore Technology Conference

This paper was presented at the 21st Annual OTC in Houston, Texas, May 1–4, 1989.

This paper was selected for presentation by the OTC Program Committee following review of information contained in an abstract submitted by the author(s). Contents of the paper, as presented, have not been reviewed by the Offshore Technology Conference and are subject to correction by the author(s). The material, as presented, does not necessarily reflect any position of the Offshore Technology Conference or its officers. Permission to copy is restricted to an abstract of not more than 300 words. Illustrations may not be copied. The abstract should contain conspicuous acknowledgment of where and by whom the paper is presented.

ABSTRACT

Nickel-base, corrosion-resistant alloys (CRA) have been subjected to extensive corrosion testing and evaluation for potential use in hot, deep sour wells. Of these CRA, the Ni-Cr-Mo-W system has been used in sour gas wells in South Mississippi, Wyoming and Mobile Bay. Corrosion data, mechanical properties and resistance to environmental stress cracking are described for several Oil Country Tubular Goods (OCTG) products. Better understanding of metallurgical factors and of the role of alloying for enhanced resistance to corrosion, along with advances in materials processing, are reviewed in terms of their impact on OCTG product reliability, improved safety and cost effectiveness.

INTRODUCTION

Decreasing reserves and the energy crisis of the early seventies accelerated ventures in sour gas wells, enhanced recovery, deepwater offshore platforms and arctic explorations. These ventures brought major challenges to materials engineers. In particular, the extremely corrosive and toxic deep sour gas wells highlighted issues related to material reliability and safety of operations.[1] Conventional steel tubing and other components were rapidly deteriorated by general weight loss, localized pitting/crevice corrosion, stress corrosion cracking and hydrogen embrittlement. Extensive testing and evaluation programs were initiated for a large selection of corrosion-resistant materials, as an alternative to limitations on the use of inhibitors.

© OTC Reprinted with the permission of the Offshore Technology Conference

Of these materials, the high performance alloys of Ni-Cr-Mo-W system offered an optimum combination of corrosion resistance, strength and ductility that is required for deep sour well production tubing.

Despite the oil and gas doldrums of the eighties, experimental studies continued and some corrosion-resistant alloys (CRA) were used in sour gas wells both inland and offshore. This paper provides an overview of the corrosion properties of several high-nickel alloys (chemical compositions shown in Table 1), lists the field usage of CRA tubular products, describes further development, covers present issues and illustrates future trends where high performance alloys might be required to enhance reliability and safety in offshore service.

PROPERTIES OF CRA PRODUCTS

The inability to inhibit corrosion of conventional steel tubing effectively in deep sour gas production led to the testing of CRA products.[2] In addition to the presence of the highly corrosive H_2S/brines and to bottom-hole temperatures approaching 500°F (260°C), the CRA tubulars must possess strength levels capable of handling bottom-hole pressures up to 23,000 psi at depths in excess of 15,000 feet.[3] To meet these severe stress levels, higher yield strength of CRA tubular products can be achieved by cold working (110 to 180 ksi), by precipitation strengthening (140 to 200 ksi) and by cold working plus aging heat treatments (180 to 280 ksi). Even at strength levels exceeding 140 ksi, the CRA tubulars retain their resistance to various forms of corrosive attack , including hydrogen sulfide stress cracking[2]. The corresponding threshold stresses for CRA were much higher than those for stainless steels. (Table 2)

While initially the CRA were identified as "inert" in various laboratory tests, further evaluation uncovered a susceptibility of high strength CRA tubulars to hydrogen embrittlement. This susceptibility was specifically observed for highly cold worked materials that were heat treated for a few hundred hours at temperatures as low at 400°F (simulating the aging of tubulars at bottom-hole well temperatures). Cathodic hydrogen, produced by direct charging or via galvanic coupling to carbon steel, [4] induced stress cracking of the best corrosion resistant alloys that were cold worked and aged (Table 3). The least corrosion resistant of the nickel-base alloys (containing low to moderate amounts of molybdenum and more iron; e.g. alloys G and 718) did not fail in this hydrogen stress cracking test at room temperature. However, when tested at bottom- hole conditions (brine plus H_2S at 400°F), alloys G and 718 failed while alloy C-276 did not stress corrosion crack (Table 4). The high-iron containing alloys were extremely susceptible to stress corrosion cracking. [4,5] Furthermore, when evaluating the CRA for resistance to localized attack in chloride environments,[2,4,5] alloys G, and 718 suffered pitting corrosion. Of the tested CRA, alloy C-276 offered the best resistance of all to localized corrosion in acidizing, chloride- containing environments (Figure 1).

In view of the need for the Ni-Cr-Mo-W system's resistance to localized corrosion and to stress corrosion cracking at bottom-hole conditions (H_2S, Cl^-, $T \geq 400°F$), along with the requirement to resist hydrogen stress cracking at ambient temperatures led to further evaluations of lower strength CRA. Alloy C-276, cold worked to moderate strength levels of 110 to 150 ksi,[5] was identified as the optimum choice for deep sour gas wells liners and production tubulars. Typical tubular sizes and tensile properties are presented in Table 5. Also, representative microstructure is illustrated in Figure 2, for 23 percent cold worked HASTELLOY alloy C-276 tubing.

FIELD USAGE OF CRA TUBULARS

The selection process of appropriate material for liners and production tubulars is usually dependent on the well environment. Representative field environments are listed in Table 6. Well depth and bottom-hole temperature and the presence of hydrogen sulfide/free sulfur (along with other corrosive species: brine, completion fluids, acidizing agents) greatly complicate the material selection process.

Over the last decade, production tubulars from different alloys have been used. Table 7 lists a group of CRA tubulars that have been placed in deep, sour well applications.[6] The logic behind the selection of a specific CRA over another is based on the corrosion characteristics of the well and the laboratory and field data available. In general, duplex stainless steels (alloys AF22 and VS25) and highly alloyed austenitic stainless (alloys 28 and 825) along with some moderate corrosion-resistant nickel alloys (alloys 2550 and G-3), are used in sour wells containing low H_2S at medium bottom-hole temperatures (less than 350°F).

Under aggressive conditions of hydrogen sulfide (1 percent and higher plus free sulfur) at elevated bottom-hole temperatures (350°F and higher), the Ni-Cr-Mo-W system (alloy C-276) is most often specified. Table 8 lists some examples of field usage of HASTELLOY® alloy C-276 tubular products in deep, sour gas wells. Several thousand feet of liners have been used in Thomasville wells (Mississippi). Also, liners have been installed in Big Horn wells (Wyoming). In addition, production tubing and casings of HASTELLOY alloy C-276 are being used in production of sour gas from offshore wells, specifically in the Mary Ann gas field [7,8] Mobile Bay (Alabama).

FURTHER DEVELOPMENTS IN Ni-Cr-Mo-W SYSTEM

Research on the subject of H_2S corrosion is an ongoing activity.[9] Following the original CRA work of the seventies, a good level of materials evaluation and research activities has continued to keep pace. A multitude of innovative approaches to CRA products have occurred in the early eighties. These approaches were prompted by the need for better performance and the requirement for lower cost.

On the alloy design side, the better understanding of the specific roles of chromium, molybdenum and tungsten in imparting corrosion resistance to the Ni-Cr-Mo-W system, has led to a new generation of the C-type alloys: HASTELLOY alloy C-22 (Ni- 22Cr- 13Mo- 3W- 3Fe).[10] C-22™ alloy is an improvement over the old alloy C-276 in terms of its resistance to hydrogen stress cracking. This is demonstrated when both alloys are specifically tested as cold worked and aged at temperatures simulating well bottom-hole conditions. The data presented in Table 9 show the high strength (40% cold worked and aged) C-22 alloy specimens to resist cathodic stress cracking in the NACE/TM-01-77 test solution (coupled to carbon steel). In this same test, alloy C-276 specimens failed within two weeks. In addition, C-22 alloy offers better resistance to anodic stress corrosion cracking than alloy C-276 in various sulfur/chloride/bromide environments (Table 10). Further testing in simulated deep sour gas environments is underway on C-22 alloy tubular products at strength levels of 120 to 150 ksi yield. Preliminary data from such tests show a comparable performance between alloy C-276 and the C-22 alloy tubulars (Table 11). Nevertheless, when testing for resistance to localized corrosion attack in acidizing chloride environments,[11] C-22 alloy tubular products outperformed those made of alloy C-276 (Figure 3). Also, C-22 alloy offers better fatigue properties for bellows/flexural hosing than alloy 625; and a single layer of the C-22 alloy

weld overlay resists crevice corrosion better than two layers of alloy 625 (Figure 4).[12,13]

On the processing side, great efforts were devoted by process metallurgists to enhance materials properties, improve quality and reduce cost. Among most promising processes, the VALLOUREC Powder Metallurgy (P/M) billet manufacturing and tubular production (ANVAL P/M process) has been proven successful on a large commercial scale. Hundreds of thousands of feet of tubing have been produced of CRA grades (stainless steels and nickel alloys). When combined with an optimum chemistry of alloying elements for corrosion resistance, the ANVAL P/M process is capable of yielding product with performance close to that of alloy 625, yet at the moderate cost of a G-type alloy. Such a product: HASTELLOY® alloy G-50 (Ni- 15Fe- 20Cr- 9Mo) has been successfully made in different OCTG sizes. An example of G-50™ alloy seamless product is illustrated in Figure 5. Full density and good mechanical properties can be achieved at very competitive production costs. Preliminary results from stress corrosion cracking tests show the G-50 alloy to offer better resistance than most nickel alloys (825, 718, 2550 and G-3).

PRESENT ISSUES AND TRENDS FOR OFFSHORE

In addition to further evaluation of existing and new CRA products, materials engineers involved in deep sour well projects are very interested in detailed compilation of service performance. A task group within NACE (T-1F-21d: information on the field use of CRA) is attempting to provide such compilation, with limited success.

Another issue for project engineers is related to quality control of CRA tubular products. Several extensive programs are proposed on the subject of standardization of testing for resistance to stress corrosion cracking. The slow strain rate test is being scrutinized for its adaptability as a quality control measure. The main quality issue is that applicable specifications do not guarantee optimum resistance to the aggressive deep sour well environments. Several grades of CRA tubulars are available from various suppliers and, due to differences in melting technique and thermo-mechanical processing, the end users may be receiving the same alloy tubular form but at different metallurgical quality levels. An example is illustrated in Figure 6 for alloy C-276 (UNS N10276).

As experience continues to be gained from involvement in deep sour wells, the knowledge base on performance of CRA products is being adapted to offshore applications. (HASTELLOY alloy C-276 control lines, production tubulars and liners are already in use in offshore wells). In addition to concerns about safety and reliability, the Ni-Cr-Mo-W system has been proven cost effective answer to heat exchangers corrosion on platforms. Figure 7 shows an inefficient, troublesome "double cooling" heat exchanger that was replaced with a spacesaving "single coolant" exchanger. The combination of traces of H_2S and of seawater proved to be aggressive to most stainless steels. Even alloys 825 and 625 lasted only a few months. Data on the Ni-Cr-Mo-W system from deep sour gas testing were considered and applied. At present, several heat exchangers made of HASTELLOY alloy C-276 have been installed at offshore platforms and continue to perform without a reported failure, for more than six years. In addition, the improved HASTELLOY alloy C-22 is being used on offshore platforms to handle combustor-scrubber effluents. Also, C-22 alloy is being designed into subsea connectors and evaluated as weld overlay to solve corrosion-erosion of elbows in pipelines. This alloy is presently being tested for wire line services and as weld filler metal for flow line applications.

CLOSURE

- Deep sour wells represent great challenges to materials engineers. A host of CRA are providing answers to these challenges.
- The Ni-Cr-Mo-W system emerges as the premier CRA product to handle the most aggressive deep sour gas well environments.
- Liners and production tubulars of HASTELLOY alloy C-276 have been used over the last ten years, without reported failures.
- Further developments continue to identify new, improved CRA products and cost effective tubular processing (powder metallurgy).
- Product quality is presently a major issue for materials and project engineers involved in deep sour gas wells.
- The deep sour gas wells knowledge base on CRA is being adapted for safe, reliable and cost effective applications offshore.

REFERENCES

1. Hamby, T.W., Broussard, L.P., and Taylor, D.B.: "Producing Mississippi's Deep, High-Pressure Sour Gas", JPT (June 1976) 629-638.

2. Watkins, M. and Greer, J.B.: "Corrosion Testing of Highly Alloyed Materials for Deep, Sour Gas Well Environments", JPT (June 1976) 698-704.

3. Tuttle, R.N.: "Corrosion in Oil and Gas Production", JPT (July 1987) 756-762.

4. Asphahani, A.I. and Hodge, F.G.: "H_2S Interaction with Corrosion Resistant Austenitic Alloys", NACE-CORROSION/77, T-1F Symposium/Panel Discussion, San Francisco, 1977.

5. Asphahani, A.I.: "High Performance Alloys for Deep Sour Gas Wells", Proceedings of the 7th Int. Congress on Metallic Corrosion (Rio de Janeiro 1978) 976-990.

6. Schillmoller, C.M.: "Deep Sour Gas Production", Ni DI Technical Series, No. 10013, Section 1, January, 1987.

7. "Mobil's Mary Ann: Alabama's First Offshore Production", Ocean Industry (August 1988) 31.

8. "Mobil Salvages Mary Ann Wells with Casing Replacements", Ocean Industry (November 1988) 34-37.

9. "H_2S Corrosion in Oil & Gas Production: A Compilation of Classic Papers", Tuttle, R.N., and Kane, R.D., Co-Editors, NACE publication, 1981.

10. Asphahani, A.I., Manning, P.E., and Straatmann, J.A.: "New Advances in Molybdenum Containing Corrosion Resistant Alloys", Molybdenum Mosaic (Vol. 10, No. 1, 1987) 1-5.

11. Asphahani, A.I., Matthews, S.J. and Silence, W.L.: "Alloy Selection for Reheater Tubes", Tube International (January 1989) 44-49.

12. Nickerson, J.L. and Asphahani, A.I.: "Corrosion Evaluation of Alloys for Flexural Hosing in the Space Shuttle Launch Environment", Conference on Aerospace Corrosion control, Perthshire, Scottland (February 1989)

13. "Corfacing Weld Overlays with HASTELLOY alloy C-22", Haynes International, Inc., Technical Information No. H-2054, 1988.

MP35N is a registered trademark of SPS Technologies, Inc.

17-4PH is a registered trademark of ARMCO Steel Corp.

HASTELLOY, C-22 and G-50 are trademarks of Haynes International, Inc.

TABLE 1: Nominal Chemical Composition (Weight %)

Alloy	Ni	Fe	Co	Cr	Mo	W	Other
718	Bal	19	--	18	3	-	Cb+Ta=5
G/G-3	Bal	19	--	22	6	-	Cu=2
625	Bal	3	--	22	9	-	Cb+Ta=3
C-276	Bal	3	--	16	16	4	V=.35
MP35N	35	--	35	20	10	-	--

TABLE 2: Hydrogen Sulfide Stress Cracking

5% NaCl + .5% Acetic Acid, Saturated H_2S, R.T.

Resistant Alloys	Yield (ksi)	Threshold (ksi)
718	143	139
G/G-3	217	213
625	193	189
C-276	218	214
MP25N	291	285
Susceptible Alloys	**Yield (ksi)**	**Threshold (ksi)**
17-4-PH	125	13
410	90	30

TABLE 3: Hydrogen stress cracking

5% NaCl + .5% Acetic Acid, Saturated H_2S, R.T.
C-shape specimens, coupled to carbon steel

Alloys	Cold Work (10 to 60%)	60% Cold Work + 200 Hrs at 400°F
718	No Cracking	No Cracking
G/G-3	No Cracking	No Cracking
625	No Cracking	Failure
C-276	No Cracking	Failure
MP35N	No Cracking	Failure

TABLE 4: Stress Corrosion Cracking

5% NaCl + .5% Acetic Acid, Saturated H_2S, 400°F
C-Shape and C-Ring Specimens (Autoclave)

Alloys	Cold Work (10 to 60%)	60% Cold Work + 200 Hrs at 400°F
718	Failure	Failure
G/G-3	Failure	Failure
625	Failure	Failure
C-276	No Cracking	No Cracking
MP35N	Failure	Failure

TABLE 5: Typical alloy C-276 Tubular Products (Hardness range of RC = 27 to 36)

Type	OD X Wall (inch)	Y.S. (ksi)	Min UTS (ksi)	Min $\Delta l/l$ (%)
Tubing	2.875 x .276	125-140	140	25
Tubing	3.500 x .254	125-140	140	25
Tubing	4.000 x .226	110-140	140	25
Tubing	4.000 x .380	110-140	140	25
Casing	5.000 x .422	110-140	140	25
Casing	5.000 x .478	125-140	140	25
Coupling	3.475 x .673	125-140	140	25
Coupling	4.053 x .636	125-140	140	25
Coupling	5.000 x 1.074	110-140	140	25
Coupling	6.000 x 1.000	110-140	140	25
Coupling	6.000 x 1.100	125-140	140	25
Accessory	3.500 x .750	120-140	140	25
Accessory	4.500 x 1.250	120-140	140	25
Accessory	5.500 x .750	120-140	140	25

TABLE 6: Representative Field Environments

Location	Downhole Pressure (ksi)	Downhole Temp. (°F)	Depth (Kft)	H_2S (%)
Thomasville (Mississippi)	17-23	275-410	20-24	28-46
LaBarge (Wyoming)	6.5	280	14	4.5
Jackson Dome (Smackover, MS)	11	300-350	16	1
Miocene (Gulf of Mexico)	12	300-350	14-20	.01
Deep Wilcox (So. Texas)	13-20	285-500	13-20	.01
Leadville (Tuscaloosa)	14-16	375	18-21	.002

Ref. 3: R.N. Tuttle, JPT (1987)

TABLE 7: Deep Well Applications (1978-1985)

Alloy	User	Location	Product
2205	Tenneco	Gulf of Mexico	Tubing
2205	Tenneco	Gulf of Mexico	Liner
2205	Shell	Gulf of Mexico	Tubing
2205	ARCO	Gulf of Mexico	Liner
2205	Chevron	Tuscaloosa	Tubing
DP-3	ARCO	Gulf of Mexico	Liner
S-28	Shell	Southwest Texas	Tubing
S-28	ARCO	Gulf of Mexico	Tubing
S-28	Exxon	Big Escamble, AL	Tubing
825	O.I.L.	Arbuckle, OK	Liner
825	Shell	Miocene, TX	Tubing
825	Mesa	Gulf of Mexico	Tubing
825	Gulf	Gulf of Mexico	Tubing
2550	Hunt	Smackover, MS	Liner
2550	Exxon	LaBarge, WY	Tubing
G-3	Shell	Southwest Texas	Tubing
G-3	Shell	Miocene, TX	Tubing
C-276	Shell	Southwest Texas	Casing
C-276	Exxon	Smackover, MS	Casing
C-276	Mobil	Mobile Bay, AL	Liner

2205 : Fe - 5.5 Ni - 22 Cr - 3 Mo - .14 N
DP 3 : Fe - 6 Ni - 25 Cr - 1.5 Mo - .1 N
S-28 : Fe - 31 Ni - 27 Cr - 3.5 Mo - 1 Cu
825 : Fe - 42 Ni - 22 Cr - 3 Mo - 2.25 Cu
2550 : Fe - 50 Ni - 25 Cr - 6 Mo

Ref. 6: C.M. Schillmoller, NiDI (1987)

TABLE 8: Examples of HASTELLOY alloy C-276 usage

Year	Field	OD x Wall(in)	Conditions
1977,78 81,82	Smackover (Mississippi)	Tubing 2 3/8 x .190 Liner: 4 1/2 x .250 Liner: 5 x .478	22,000 ft. depth 350-400°F BH Temp 20,000 psi BH Press. 28-46% H_2S (Cl,CO_2)
1984	Mobile Bay (Alabama)	Liner: 5 x .422	21,000 ft. depth 400°F BH Temp. 15,000 psi BH Press. 9% H_2S (S,CO_2)
1985,87	Mobile Bay (Alabama)	Tubing: 2 7/8 x .276 Tubing: 3 1/2 x .254 Liner: 5 x .422	21,700 ft. depth 400°F BH Temp 11,000 psi BH Press. 3-5% H_2 (Cl,S,CO_2)
1987	Big Horn (Wyoming)	Liner: 5 x .478	22,000 ft. depth 425°F BH Temp. 10,350 psi BH Press. 11.5% H_2S (Cl, CO_2)

TABLE 9: Hydrogen Stress Cracking

5% NaCl + .5% Acetic Acid, Saturated H_2S, R.T.
C-shape specimens coupled to carbon steel

	Hours to Failure	
	Alloy C-276	C-22 Alloy
40% Cold Work	NC/NC/NC*	NC/NC/NC
40% C.W. + 200 hrs at 400°F	312/312/816	NC/NC/NC

*: No cracking, 869 hours

TABLE 10: Stress Corrosion Cracking; C-shape specimens (Mill Annealed Material)

	Alloy C-276	C-22 Alloy
25% NaCl + H_2S + 1 g/l S (450°F)	Failure	No Cracking
20% $MgCl_2$ (450°F)	Failure	No Cracking
4.7% $ZnBr_2$ (400°F)	Failure	No Cracking
1% HCl (350°F)	Failure	No Cracking

TABLE 11: Stress Corrosion Cracking

C-ring specimens; applied stress = 100% yield
2 7/8" OD x .276" wall; yield = 132 ksi

25% NaCl + .5% Acetic Acid + 1 g/l S + H_2S

	Hours to Failure	
	400°F	450°F
Alloy C-276	336,336,336	96,336,336
C-22 alloy	336,336,336	96,336,336

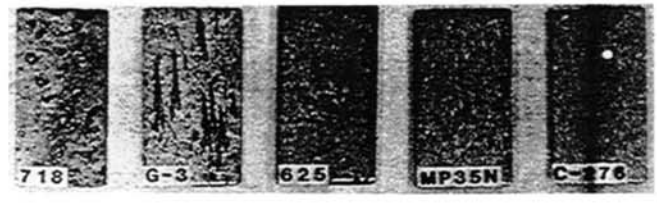


Figure 1: Resistance to Localized Corrosion; 24-Hour Exposure; 1/2 X. 11.5% H_2SO_4 + 1.2% HCl + 1% $FeCl_3$ + 1% $CuCl_2$ at 102°C (216°F).

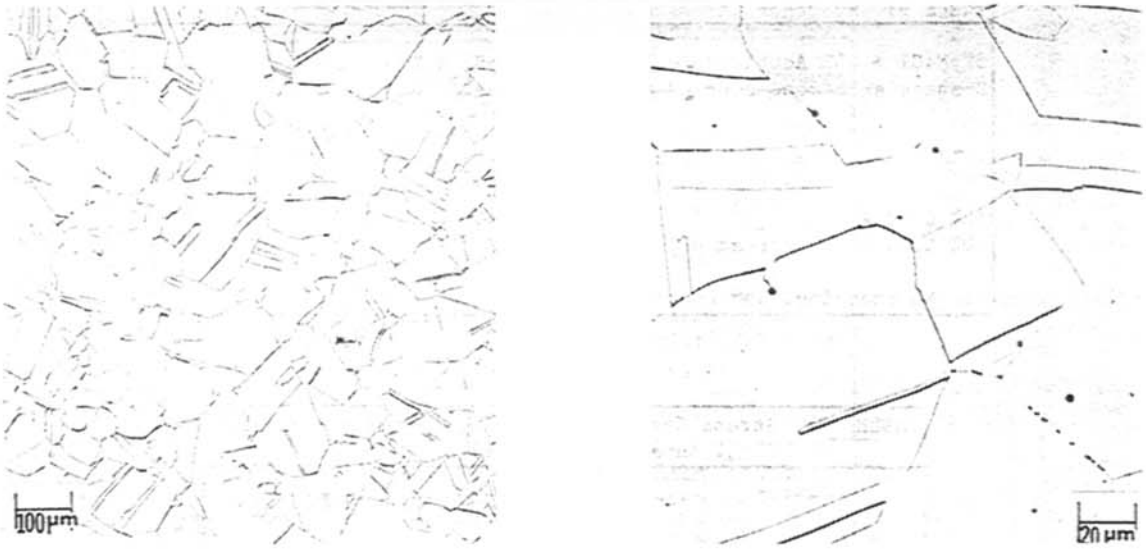


Figure 2: Transverse Cross-Section of HASTELLOY alloy C-276 Tubing.
(4.053" OD x .636" Wall; Y = 125 ksi, UTS = 140 ksi, Δ l/l = 31%)
No apparent primary precipitates; minor/intermittant G.B secondary precipitates

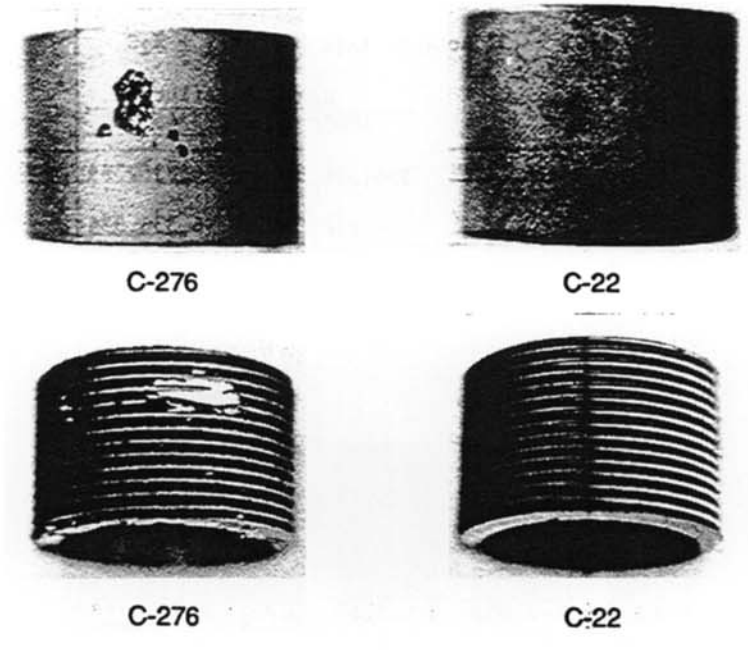


Figure 3: Localized Corrosion of Tubular Products; 24-Hour Exposure.
11.5% H_2SO_4 + 1.2% HCl + 1% $FeCl_3$ + 1% $CuCl_2$ at 125°C (257°F).

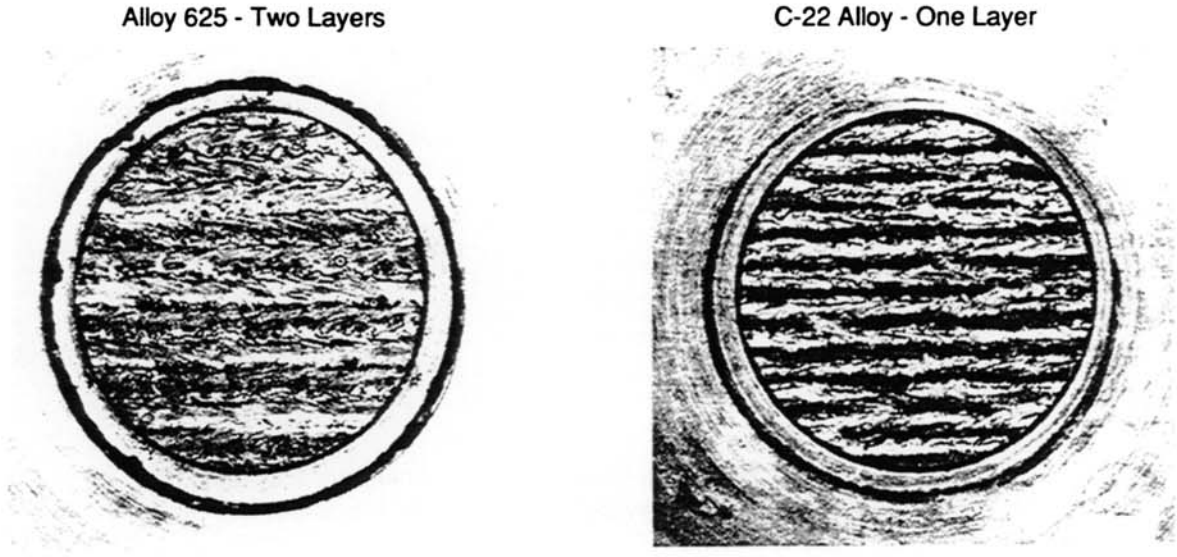


Figure 4: Resistance to Crevice Corrosion; 120-Hour Exposure.
Weld Overlays Tested in 10% $FeCl_3$ at 40°C (140°F).

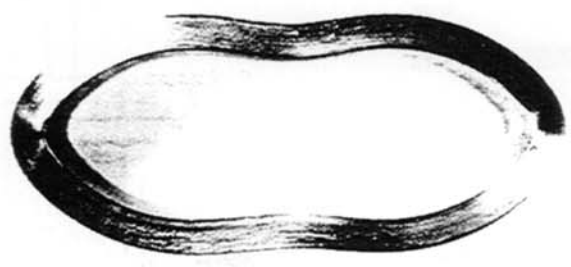


Figure 5: HASTELLOY alloy G-50 Tubular; ANVAL P/M Process.
5" OD x .422" wall; Y = 141 ksi, UTS = 149 ksi, $\Delta l/l$ = 22%.

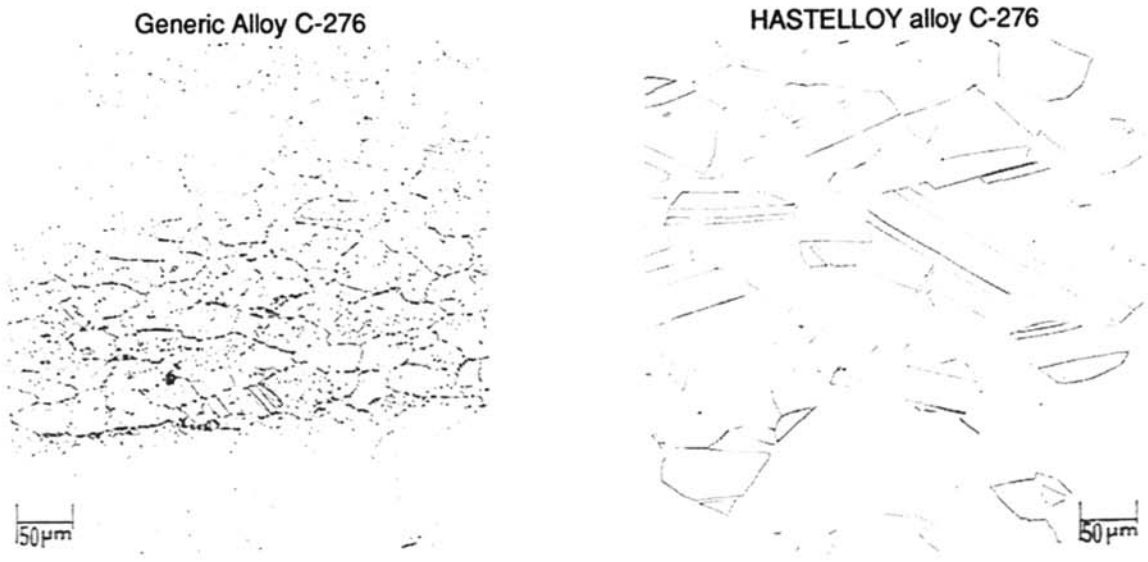


Figure 6: Tubular Products Within Alloy C-276 Chemistry Specifications.
Left: Generic Alloy C-276; Heavy G.B. Precipates and Stringers.
Right: HASTELLOY alloy C-276 Clean Microstructure

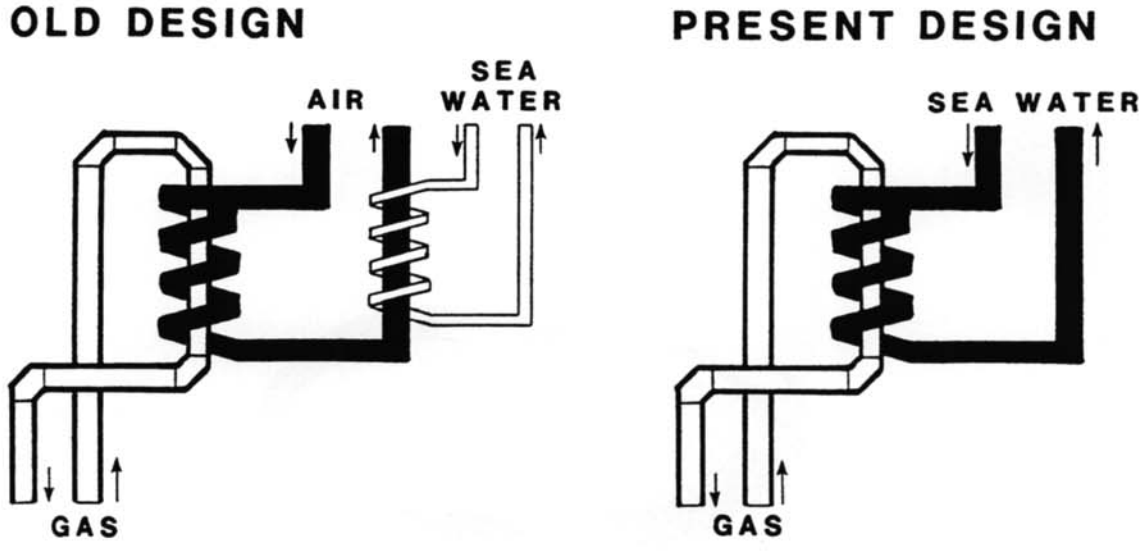


Figure 7: Offshore Platform Heat Exchangers - Gas Coolers
Left: Original Design, Cumbersome and Inefficient
Right: Improved Design; Ni-Cr-Mo-W HASTELLOY alloys

Copyrighted Materials
Copyright © 1996 NACE International Retrieved from www.knovel.com

PAPER NUMBER
227

CORROSION 85
The International Corrosion Forum Devoted Exclusively to The Protection and Performance of Materials
March 25-29, 1985 / Sheraton Hotel
Hynes Auditorium / Boston, Massachusetts

STRESS-CORROSION CRACKING RESISTANCE OF STAINLESS ALLOYS IN SOUR ENVIRONMENTS

H. E. Chaung, M. Watkins, G. A. Vaughn
Exxon Production Research Company
P. O. Box 2189
Houston, Texas 77001

ABSTRACT

The stress-corrosion cracking (SCC) behavior of several stainless alloy samples in sour environments was evaluated using the constant-strain C-ring test method and slow-strain-rate tensile test method. SCC resistance was a function of nickel content, temperature, and processing. SCC resistance increases with increasing nickel content in the alloy. For a specific alloy, SCC was more severe at higher temperatures, higher stress levels, and higher yield-strength levels.

INTRODUCTION

In recent years, there has been very high interest in using tubulars manufactured from iron- and nickel-based stainless alloys in gas wells that contain carbon dioxide, hydrogen sulfide, and salt water at high temperatures and pressures. These conditions are very corrosive to conventional tubulars manufactured from carbon and low-alloy steels. Studies have shown that various types of stainless alloys are capable of resisting the corrosive attack of gas-well environments; however, stainless alloys may be susceptible to hydrogen embrittlement and SCC.[1-4]

Considerable effort(1-8) has been devoted to solving hydrogen embrittlement and SCC problems of stainless alloys for oil-field tubulars. Several of these studies have indicated that stainless alloys can be processed to very high strength levels by cold work and yet be relatively immune to SCC in simulated gas-well environments. One significant limitation to much of these data is that they represent relatively short exposure times, mostly one to two months, while the anticipated life of a well is approximately 20 years. The data presented in this study were obtained using significantly longer exposure times. Therefore, these data should prove useful in studying the SCC behavior of stainless alloys in gas-well environments.

EXPERIMENTAL PROCEDURE

Materials

The chemical compositions of the alloys evaluated are given in Table 1. Samples 1 and 2 are duplex stainless steels;

their microstructures contain approximately equal amounts of ferrite and austenite. The other samples are austenitic stainless alloys containing varying amounts of nickel in the range of 25-50 percent. The austenitic alloys will be referred to by their nominal nickel content.

All samples were furnished as tubular products. The outer diameters were 2-3/8 to 3-1/2 inches (60-90 mm). All samples were strengthened by cold work; tensile properties are given in Table 2.

Constant-Strain Tests

C-ring specimens (Figure 1) were stressed at various percentages of transverse yield strength. Most specimens were stressed to 90 percent of transverse yield, although a few were stressed to 50 and 70 percent. The transverse yield strength was estimated to be 90 percent of the longitudinal yield strength for these cold-worked tubulars. The nuts and bolts used to stress each C-ring were manufactured from the same alloy as the C-ring.

The C-rings were tested in autoclaves at temperatures of 300°F (149°C), 350°F (177°C), and 400°F (204°C). Each specimen was electrically isolated from the autoclave and from other specimens. The test environment was an aqueous solution containing 25 percent sodium chloride, 0.5 percent acetic acid, one gram/liter sulfur, and saturated with hydrogen sulfide gas to a pressure of 100 psi (0.7 MPa).

Specimens were exposed to the test environment for intervals of approximately one month. After each test period, specimens were examined for cracks at 100X magnification. A specimen was designated as "failed" at the first evidence of cracking and was removed from test. The specimens that did not contain cracks were put back into the autoclave for another one-month period. Fresh solution was charged into the autoclave at the beginning of each cycle.

Slow-Strain-Rate Tensile Tests

Tensile specimens, machined along the longitudinal direction of tubulars, were nominally 3.5 inches (8.9 cm) long with a one-inch (2.54-cm) gauge section, as shown in Figure 1. The width and thickness of the gauge section were 0.15 inch (0.38 cm) and 0.125 inch (0.32 cm), respectively. The specimens were pulled to failure in unaxial tension at a strain rate of 4×10^{-6} sec^{-1}. Specimens were tested at temperatures between 75°F (24°C) and 400°F (204°C) both in air and in an aqueous solution containing 25 percent sodium chloride and 0.5 percent acetic acid saturated with hydrogen sulfide gas to a pressure of 100 psi (0.7 MPa) at ambient temperature. Tests in solution were performed in an autoclave that was mounted on the tensile tester. The specimens were electrically isolated from the autoclave and from the specimen holder.

RESULTS

Constant-Strain Tests

Data from constant-strain tests are given in Table 3. Several trends were observed in the data. Very good resistance is exhibited by samples that survived more than six months without failure. Thus, good resistance was exhibited by samples 4 and 5 (Alloy 31), samples 8 and 10 (Alloy 42), and samples 11 and 12 (Alloy 50). Significantly poor resistance was exhibited by samples 1 and 2 (duplex), sample 3 (Alloy 25), sample 6 (Alloy 31), sample 7 (Alloy 35), and sample 9 (Alloy 42). In general, cracking resistance increases with increasing nickel content. Alloy 50 has the highest nickel level of the alloys tested, and none of the specimens of Alloy 50 have failed after more than two years. Samples of the duplex alloy and Alloy 25 have the lowest nickel content, 7 and 25 percent, respectively, and have the shortest failure times. Failure times as well as nickel contents for samples of Alloy 31, Alloy 35, and Alloy 42 are between those for Alloy 25 and Alloy 50.

The poorer performance of sample 6 compared to the other Alloy 31 samples, and sample 9 compared to the other Alloy 42 samples indicates that factors other than chemical composition and yield strength affect SCC behavior. Since samples were furnished by different manufacturers, processing variables may have a prominent effect on SCC behavior. The effects of processing variables on the SSC behavior of cold-worked tubulars are being studied.

Other factors that affect SCC are temperature and applied stress. Cracking resistance decreases with increasing temperature and stress. For example, data for sample 8 show that failure occurred after nine months at 350°F (177°C) and 400°F (204°C), and after 21 months at 300°F (149°C). Similarly, data at 350°F (177°C) for sample 2 show that failure occurred in less than one month at 90 percent of yield stress, but that the sample survived for more than 11 months without failing at 50 and 70 percent of yield stress.

Slow-Strain-Rate Tensile Test

Tensile properties were measured both in air and in the aqueous solution. However, yield and tensile strengths were not reported because they were essentially the same for tests performed in air and in solution. SCC was manifested by decreases in time to failure (t_f) and reduction of area (RA). Ratios of both properties in air and in solution are reported in Table 4. Ratios less than 0.90 were indicative of SCC, and specimens usually exhibited secondary cracks along the gauge section. Ratios greater than 0.90 corresponded to specimens that exhibited good SCC resistance and usually no secondary cracks. Although some of the specimens with ratios between 0.90 and 0.95 did not exhibit secondary cracks, evidence of SCC was present in the primary fracture surface. SSC was confirmed with a scanning electron microscope and was manifested by brittle, transgranular fracture features.

Results show that the duplex alloy exhibited SCC at 75°F (24°C), and only the duplex alloy and Alloy 25 exhibited SCC at 250°F (121°C). At higher test temperatures, more samples exhibit SCC. For example, at 350°F (177°C), all samples except sample 8 (Alloy 42) contained secondary cracks. Although the ratios were only 0.89, fractographic examination with a scanning electron microscope did not reveal any evidence of SCC on the primary fracture surface. Other samples, such as samples 9 and 10, contained evidence of SCC in the primary fracture surface, although secondary cracks were not present.

Nickel content of the alloy had a very pronounced effect on SCC. It can be seen from the data that the higher the nickel content of the alloy, the higher the temperature at which the alloy resisted SCC. Results also showed that temperature has a pronounced effect on all the alloys evaluated; the t_f and RA ratios decrease with increasing temperature, and SCC susceptibility increases with increasing temperature.

Metallographic Examination

Figures 2 and 3 show representative stress-corrosion cracks in C-ring specimens and in tensile specimens. In duplex alloys, cracks propagated through the ferrite matrix and along the austenite grain boundaries. Transgranular cracking, which is characteristic of chloride-induced SCC in stainless alloys, was observed in all other alloys.

DISCUSSION

SCC Test Methods

The constant-strain test and the slow-strain-rate tensile test were used to assess the resistance of stainless alloys to SCC. The guidelines for each test were derived from these and other unpublished laboratory data. The six-month no-failure criterion for the constant-strain tests was set arbitrarily. Data show that a one-month test period was too short, since failures occurred in most samples after longer times. Although six-month tests are time-consuming and expensive to run, the data clearly indicate that samples with the same chemical composition can have significantly different failure times and, consequently, different SCC resistance. Therefore, it seems reasonable to conclude that samples 4 and 5 (Alloy 31) had significantly different SCC resistance, since their failure times were 10 and two months.

The results of the slow-strain-rate tensile tests were somewhat surprising, particularly the data for the Alloy 50 samples. Although these samples exhibited the best SCC resistance of all specimens in the constant-strain test, several lesser-alloyed samples exhibited better SCC resistance in the slow-strain-rate tensile test than Alloy 50. Additional unpublished data obtained from samples of alloys with similar chemical compositions show similar trends. Currently, there is no completely satisfactory explanation for the differences obtained by the two test methods. Until

these differences can be resolved, the continued use of both long-term constant-strain tests and slow-strain-rate tensile tests appears justified to evaluate the SCC resistance of cold-worked stainless alloys.

Effect of Alloy Composition

Nickel had the most pronounced effect on SCC. Alloys with the higher nickel contents possessed the higher resistance to SCC. The classical study by Copson[10] suggests that an alloy should contain approximately 40 percent nickel to obtain immunity to chloride stress-corrosion cracking. Alloys containing less than 40 percent nickel were shown to be susceptible to chloride stress-corrosion cracking in environments containing hydrogen sulfide. Nickel appeared to have a more pronounced effect on SCC resistance in the constant-strain test and less effect in the slow-strain-rate tensile test. Since the slow-strain-rate tensile test measures the ability of an alloy to re-passivate under dynamic straining conditions, data for Alloy 50 samples indicate that elements in addition to nickel affect the ability of an alloy to re-acquire SCC resistance in hydrogen sulfide environments. Additional study is required to define these relationships.

Effect of Temperature

In general, temperature has a pronounced effect on all the alloys evaluated; susceptibility increases with increasing temperature. Therefore, as expected, data support the belief that SCC is a thermally activated process. In almost every case, the t_F and RA ratios in the slow-strain-rate tensile test decreased with increasing temperature. In the constant-strain test, C-ring specimens usually survived longer without failing at lower temperatures.

Effect of Microstructure

The microstructures of alloy tubulars evaluated in SCC studies are currently being characterized using ordinary light microscopy, scanning electron microscopy (SEM), and transmission electron microscopy (TEM). Preliminary data indicate that specimens of Alloy 42 with the poorest SCC resistance also had chromium carbides in the prior austenitic grain boundaries, whereas specimens with higher SCC resistance did not have any significant amount of chromium carbides present in the microstructure. It should be noted that cracks in the failed specimens were transgranular and were not usually associated with grain boundaries associated with chromium carbides. Although the precise role played by carbides in SCC resistance of stainless alloys is not clearly defined at this time, these results indicate that metallurgical and processing variables affect SCC resistance.

CONCLUSIONS

1. Nickel had a very pronounced effect on resistance to SCC; cracking resistance increases with increasing nickel content in the alloy.

2. For a specific alloy, SCC was more severe at higher temperatures, higher stress levels, and higher yield-strength levels.

3. For a given alloy type, processing and manufacturing variables have a significant effect on SCC resistance.

4. Good SCC resistance is represented by alloys surviving six months in constant-strain tests and by time-to-failure and reduction-of-area ratios of 0.9, no secondary cracking, and no evidence of SCC on primary fracture surface in the slow-strain-rate tensile test.

REFERENCES

1. H_2S Corrosion in Oil and Gas Production - A Compilation of Classic Papers, edited by R. N. Tuttle and R. D. Kane, NACE Publication, 1981.

2. M. Watkins and J. B. Greer, Journal of Petroleum Technology, Vol. 28, p. 698 (1976).

3. P. W. Rice, Material Performance, Vol. 17, No. 1, p. 16 (1978).

4. A. I. Asphahani, Corrosion, Vol. 37, p. 327 (1981).

5. J. Kolts and S. M. Corey, Corrosion/84, Paper 217, New Orleans, Louisiana (1984).

6. J. Oredsson and S. Bernhardson, Corrosion/82, Paper 126, Houston, Texas (1982).

7. T. Kudo, H. Miynki, H. Okamoto, J. Murayama, and T. Moroishi, Corrosion/82, Paper 127, Houston, Texas (1982).

8. B. Lefebvre, G. Guntz, J. C. Prouheze, J. C. Vaillant, J. R. Mantelle, P. Bounite, and J. P. Giraud, Corrosion/82, Paper 128, Houston, Texas (1982).

9. Stress Corrosion Cracking - The Slow Strain-Rate Technique, edited by G. M. Ugiansky and J. H. Payer, ASTM STP 666, 1979.

10. H. R. Copson, Physical Metallurgy of Stress Corrosion Fracture, edited by T. N. Rhodin, Interscience, New York, 1959.

TABLE 1 - Chemical Compositions (in Weight Percent)

Alloy	Sample	Ni	Cr	Fe	Mo	Mn	C	Si	Cu	Ti	Co	W	Cb & Ta
Duplex	1	6.8	24.2	64.0	3.4	1.0	0.037	-	0.49	-	-	-	-
Duplex	2	6.8	24.8	64.0	3.4	1.0	0.026	-	0.48	-	-	-	-
25	3	25.9	21.8	44.6	4.9	1.6	0.040	0.60	0.10	0.47	-	-	-
31	4	30.1	26.3	37.4	3.2	1.7	0.019	0.01	0.78	0.07	-	-	-
31	5	31.0	27.0	34.0	3.5	2.0	0.020	0.01	1.00	-	-	-	-
31	6	31.9	26.9	34.9	3.4	1.8	0.020	0.04	1.02	-	0.05	-	-
35	7	35.8	20.9	35.6	5.3	0.5	0.010	0.44	0.53	0.30	-	0.46	-
42	8	44.1	22.1	27.5	3.0	0.4	0.020	0.30	1.70	0.97	-	-	-
42	9	44.0	21.7	27.8	3.4	0.4	0.019	0.07	1.77	0.84	-	-	-
42	10	44.5	22.3	19.7	6.9	0.7	0.007	0.14	1.75	-	2.8	0.79	0.27
50	11	50.1	25.5	15.4	5.8	0.6	0.020	0.49	1.00	1.12	-	-	-
50	12	50.1	25.5	15.4	5.8	0.6	0.020	0.49	1.00	1.12	-	-	-

TABLE 2 - Tensile Properties

Alloy	Sample	Outside Diameter (in.)	Outside Diameter (cm)	Wall Thickness (in.)	Wall Thickness (cm)	Yield Strength (ksi)	Yield Strength (MPa)	Tensile Strength (ksi)	Tensile Strength (MPa)	Elongation (%)
Duplex	1	2-3/8	6.03	0.190	0.48	96	662	112	772	-
Duplex	2	2-3/8	6.03	0.190	0.48	119	821	144	993	-
25	3	2-7/8	7.30	0.200	0.51	142	979	149	1027	13
31	4	2-7/8	7.30	0.276	0.70	122	841	-	-	-
31	5	2-7/8	7.30	0.309	0.78	101	696	110	758	37
31	6	2-7/8	7.30	0.250	0.64	124	855	132	910	20
35	7	2-7/8	7.30	0.200	0.51	138	952	148	1020	12
42	8	2-5/8	6.67	0.310	0.79	132	910	139	958	20
42	9	2-7/8	7.30	0.250	0.64	147	1013	157	1083	16
42	10	2-7/8	7.30	0.276	0.70	116	800	131	903	25
50	11	2-7/8	7.30	0.210	0.53	130	896	142	979	20
50	12	3-1/2	8.89	0.289	0.73	152	1048	157	1082	-

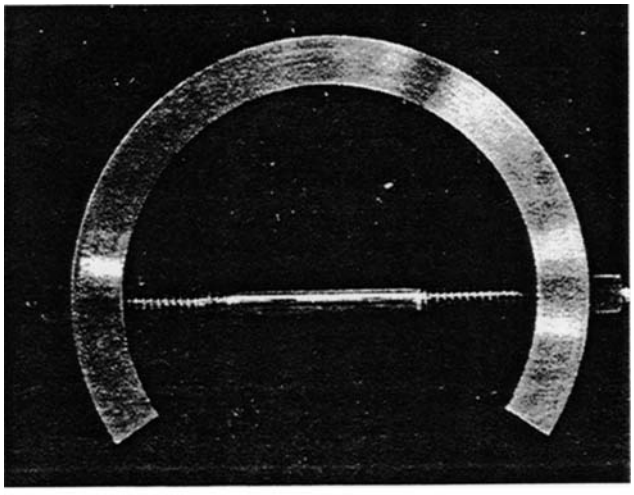
TABLE 3 - Constant-Strain Test Results

Alloy	Sample	Transverse Yield Strength (ksi)	(MPa)	Applied Stress (% TYS)	Test Temperature (°F)	(°C)	Exposure Time (months)
Duplex	1	96	662	90	350	177	(1)
				70	350	177	11
				50	350	177	11
				90	300	149	(6)
Duplex	2	107	738	90	350	177	(1)
				70	350	177	(3)
				50	350	177	11
25	3	128	882	90	350	177	(1)
31	4	110	758	90	400	204	(10)
				90	350	177	(10)
31	5	91	627	90	400	204	(12)
				90	350	177	(13)
31	6	111	765	90	350	177	(2)
35	7	124	855	90	350	177	(3)
				90	300	149	(9)
42	8	119	821	90	400	204	(9)
				90	350	177	(9)
				90	300	149	(21)
42	9	132	910	90	350	177	(2)
42	10	101	696	90	350	177	(15)
50	11	117	807	90	350	177	24
50	12	137	943	90	350	177	18

( ) - Failed in time indicated.

TABLE 4 - Slow-Strain-Rate Tensile Results

Alloy	Sample	Temperature (°F)	(°C)	Time to Failure (hr) Solution	Air	t_f Solution / t_f air	Reduction of Area (%) Solution	Air	RA Solution / RA Air	Secondary Cracking	SCC
Duplex	2	75	24	4.6	8.8	0.52	29	74	0.39	Yes	Yes
		250	121	2.8	9.3	0.30	8	36	0.22	Yes	Yes
		350	177	3.4	7.9	0.43	3	23	0.13	Yes	Yes
25	3	75	24	8.2	6.7	1.22	39	35	1.12	No	No
		250	121	3.6	6.3	0.57	4	24	0.17	Yes	Yes
		350	177	3.4	5.9	0.58	1	11	0.09	Yes	Yes
31	5	75	24	12.2	13.6	0.90	54	55	0.98	No	No
		250	121	10.1	10.2	1.00	52	52	1.00	No	No
		300	149	9.2	9.4	0.98	50	50	1.00	No	No
		350	177	6.8	9.1	0.75	30	50	0.60	Yes	Yes
31	6	75	24	10.4	10.4	1.00	50	51	0.99	No	No
		250	121	7.1	7.4	0.96	47	53	0.88	No	No
		300	149	6.3	7.8	0.81	22	32	0.68	No	Yes
		350	177	4.2	8.2	0.51	13	33	0.39	Yes	Yes
35	7	75	24	8.4	8.4	1.00	42	42	1.00	No	No
		250	121	6.5	6.4	1.02	39	40	0.98	No	No
		300	149	6.0	6.7	0.90	23	62	0.37	Yes	Yes
		350	177	5.3	6.6	0.80	17	61	0.28	Yes	Yes
42	8	75	24	9.5	9.4	1.01	53	52	1.02	No	No
		250	121	6.9	7.9	0.87	45	47	0.95	No	No
		350	177	7.2	8.1	0.89	39	44	0.89	No	No
42	9	75	24	11.6	10.8	1.07	41	40	1.03	No	No
		250	121	7.7	8.1	0.95	35	40	0.88	No	No
		300	149	7.2	8.5	0.85	30	37	0.82	No	Yes
		350	177	6.4	8.8	0.73	21	31	0.68	Yes	Yes
42	10	75	24	18.9	19.5	0.97	53	58	0.91	No	No
		250	121	16.0	18.0	0.89	52	50	1.03	No	No
		300	149	14.1	17.2	0.82	38	50	0.76	No	Yes
		350	177	10.8	16.1	0.67	21	53	0.4	Yes	Yes
50	11	75	24	13.6	14.5	0.94	51	54	0.94	No	No
		250	121	11.3	10.8	1.05	38	39	0.98	No	No
		350	177	6.5	7.9	0.82	18	40	0.45	Yes	Yes
50	12	75	24	8.7	8.4	1.04	37	36	1.02	No	No
		250	121	7.1	7.8	0.91	35	35	1.00	No	No
		300	149	6.3	7.7	0.82	29	35	0.82	No	Yes
		350	177	5.2	7.6	0.68	13	33	0.40	Yes	Yes



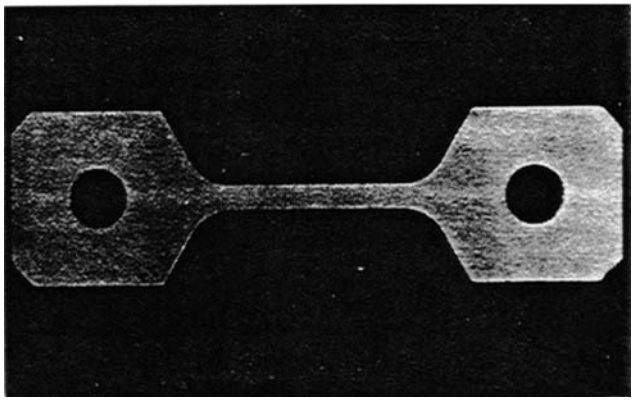


FIGURE 1 - (a) Constant-strain C-ring specimen; (b) slow-strain-rate tensile specimen.

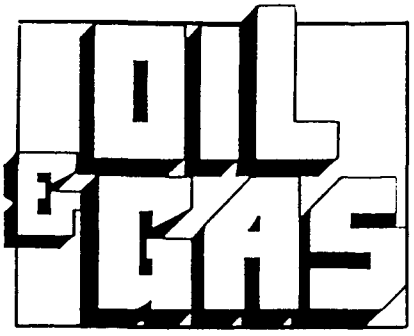


FIGURE 2 - Representative photomicrograph showing SCC in duplex stainless steel. Etch; 200X.



FIGURE 3 - Representative photomicrograph showing SCC in austenitic stainless alloy. Etch; 200X.

Copyrighted Materials
Copyright © 1996 NACE International Retrieved from www.knovel.com



Laboratory Testing of Nickel Alloys for H_2S Service*

J. A. HARRIS and T. F. LEMKE*

The corrosion behavior of several Ni alloys are examined in laboratory tests designed to evaluate materials for H_2S service. Resistance to hydrogen embrittlement, sulfide SCC, and chloride SCC is evaluated. Cathodically charged tensile specimens and steel coupled C-rings are used to characterize hydrogen embrittlement in a 5% NaCl/0.5% acetic acid solution saturated with H_2S. C-rings in 15 to 25% sodium chloride solutions containing H_2S and CO_2 are used to study SCC at elevated temperatures. The results indicate that hydrogen embrittlement is best resisted by cold worked or age hardened alloys having yield strengths under 1103 MPa (160 ksi). For resistance to chloride SCC, alloys with more than 40% Ni should be used.

Introduction

OIL PRODUCERS ARE more interested recently in high strength Ni alloys which are corrosion resistant in increasingly severe well environments.

Practically every commercially available Ni alloy has been tested in a variety of simulated and actual well environments. This flurry of testing has yielded these facts:[1-5]

1. Hydrogen embrittlement must be considered. This is especially important in areas where Ni alloys are cathodically protected by contact with less noble materials or in situations where, even though there is no galvanic corrosion, the Ni alloy is corroding in the presence of H_2S.

2. At elevated temperatures downhole, with sodium chloride brines, CO_2, and H_2S present, SCC replaces hydrogen embrittlement as the primary corrosion problem.

3. High strength requirements amplify the problems of both hydrogen embrittlement and chloride SCC.

This study rates the performances of several Ni alloys in environments that incorporate the above factors. Table 1 lists the compositions of the alloys tested.

Experimental Procedure

Hydrogen Embrittlement

Studies on hydrogen embrittlement of Ni alloys have been ongoing in our company laboratory since early 1969. The most important test procedure involves determination of ductility losses resulting from cathodic hydrogen charging. The method is attractive as it offers simplicity in equipment, design, testing, and interpretation.

Testing was done on smooth, round tensile specimens, 102 mm (4.0 in.) long with a 6.35 mm (0.250 in.) reduced gage area. The specimens were cathodically charged in a 4% sulfuric acid solution saturated with carbon disulfide, a hydrogen recombination poison. The charging cells were connected in series with a DC power supply, a 1-25 mA meter and a variable resistor to maintain a 10 mA total series current. Charging current density was approximately 2 mA/cm^2. When hydrogen analyses were required, 230 mm (0.250 in.) square tabs could be snapped off after hydrogen charging. The tabs were analyzed in a Leco vacuum fusion hydrogen analyzer. The hydrogen charged tensile specimens were pulled to failure at an extension rate of 0.38 mm/mm/minute (0.015 in./in./minute) until fracture.

Low Temperature Stress Corrosion Cracking

NACE steel coupled C-ring tests were conducted at 24 and 75 C (75 and 167 F) in a solution containing 5% NaCl and 0.5% CH_3COOH and saturated with H_2S. H_2S was continuously bubbled through the solution during testing. C-ring specimens were stressed to 100% of the longitudinal yield strength (0.2% offset) with steel bolts and nuts. The steel bolt passed through an additional strip of mild steel which was bent to conform to the C-ring. This ensured adequate galvanic contact and consequent hydrogen evolution on the stressed C-ring surface. Tests were conducted to failure or a minimum of 1000 hours. The formula for stressing the C-rings was obtained from Exxon Production Research, and was applied by assuming transverse yield strength to be identical to longitudinal yield strength.

High Temperature Stress Corrosion Cracking

High temperature testing was done in autoclaves using C-ring specimens. A 25 mm (1 in.) square Teflon bar was machined with slots to hold the C-rings and keep them electrically isolated. Specimens were stressed to 100 and 90% of yield strength and bolted with alloy materials (INCONEL alloy 718, INCOLOY alloy 825, and Hastelloy alloy C-276).

Two high chloride test solutions, both saturated with H_2S, were used. One solution consisted of 25% NaCl, 0.5% CH_3COOH, and 1 g/L of sulfur. That solution was used in conjunction with an overpressure of 1.0 MPa (150 psi) of H_2S at 177 C (350 F). The other solution was 15% NaCl at an overpressure of 6.9 MPa (1000 psi) of 1% H_2S, 20% CO_2, 79% N_2 at 204 C (400 F). Solutions were made with reagent grade chemicals and distilled water. Nitrogen (low oxygen) was passed through the solutions for 3 hours followed by H_2S for 2 hours. The solutions were then transferred to the evacuated autoclave by suction. Final gas pressurization was done after the autoclave reached test temperature.

*Presented during Corrosion/82 (Paper 137), March, 1982, Houston, Texas.

*Huntington Alloys, Inc., Huntington, West Virginia and Houston, Texas.

TABLE 1 — Compositions (%), (Major Elements) of Alloys Tested

Alloy	Ni	Cr	Fe	Mo	Al	Ti	Other
INCONEL 600	76.0	15.5	8.0	—	—	—	—
601	60.5	23.0	14.1	—	1.4	—	—
617	52.0	22.0	1.5	9.0	1.2	—	12.5 Co
625	61.0	21.5	2.5	9.0	—	—	3.6 Cb
690	61.0	29.0	9.0	—	—	—	—
706	41.5	16.0	40.0	—	0.2	1.8	2.9 Cb
718	52.5	19.0	18.5	3.0	0.5	0.9	5.1 Cb
X-750	73.0	15.5	7.0	—	0.7	2.5	1.0 Cb
INCOLOY 800	32.5	21.0	46.0	—	—	—	—
801	32.0	20.5	44.5	—	—	1.1	—
802	32.5	21.0	46.0	—	—	—	0.4 C
825	42.0	21.5	30.0	3.0	—	0.9	2.2 Cu
NI-SPAN-C 902	42.2	5.3	48.5	—	0.6	2.6	—
INCOLOY 903	38.0	—	42.0	—	0.7	1.4	15.0 Co, 3.0 Cb
NIMONIC 86	65.0	25.0	—	10.0	—	—	—
IN-103	66.0	19.0	—	14.0	0.2	0.2	0.5 Cb

Results

Hydrogen Embrittlement

Hydrogen charging lowered the ductility, as measured by reduction of area (RA) in tensile tests, of all alloys tested. In general, there was also a decrease in elongation at failure and in tensile strength, while yield strength was relatively unaffected.

INCOLOY Alloys. The simple Fe-Ni-Cr ternary, alloys 800, 801, and 802 proved highly resistant to hydrogen embrittlement. As Table 2 indicates, 50 days of hydrogen charging were required before any meaningful loss in %RA occurred. Alloy 801 was also tested in the cold drawn condition at approximately 4 times higher yield strength than when annealed, and suffered only a 20% loss in %RA with no measurable loss in elongation. The resistance of these alloys to hydrogen embrittlement compares favorably with that of the austenitic stainless steels. Alloy 825 is more highly alloyed than the simple ternary alloys, but nevertheless showed comparable resistance. Alloys 902 and 903 are age hardenable materials used commercially for their low uniform coefficients of expansion. These alloys contain 5.75 and 0.1% Cr, respectively, and are not as corrosion resistant as other INCOLOY alloys, but alloy 903 has been evaluated for possible high pressure hydrogen containment.[6] Alloy 902 was tested over a range of yield strengths, 230 MPa (34,000 psi) to 1240 MPa (180,000 psi), and as expected, the stronger material showed lower resistance to hydrogen embrittlement. Noteworthy was the relatively good resistance of cold drawn alloy 902 having a yield strength of 1034 MPa (150,000 psi). The bar graphs in Figure 1 summarize the effects of 50 days of hydrogen charging for this class of alloys.

INCONEL Alloys. Mechanical properties of these alloys charged 0, 10, 20 and 30 days are given in Table 3. The percent losses in reduction of area for 30 days of hydrogen charging are plotted in Figure 2. The results show that annealed materials with yield strengths in the 210 to 410 MPa (30,000 to 60,000 psi) range are the most resistant to hydrogen embrittlement, and that the age hardenable alloys are the least resistant when in the aged condition. Alloys 600, 625, and 718 are the least resistant of the annealed materials. Alloys 706 and X-750 were tested in two aged conditions: (1) direct aged; and (2) stabilized plus aged. In both cases, the stabilized plus aged material was less resistant (Figure 2) than direct aged material. The difference was significant in the case of alloy 706.

Some consideration has been given to using alloys, 617, 625, and 718 with higher yield strengths produced by cold working. Yield strengths at the 1030 MPa (150,000 psi) level can be reached by cold reductions of approximately 25%. Above 25% reduction, the ductility falls off rapidly, rendering the alloys undesirable for most commercial applications. Tensile tests on those cold worked alloys indicate that hydrogen embrittlement would still be a problem, occurring to about the same extent as with age hardenable alloys.

TABLE 2 — Mechanical Properties of Hydrogen Charged INCOLOY Alloys

Alloy	Material Condition	Charging Time (days)	YS[1] (ksi)	UTS[1] (ksi)	%El	%RA	Hardness
800	Cold Rolled,	0	50.6	95.5	42	66.2	Rb 83-84
	Annealed	25	51.6	94.1	42	69.8	77
		50	50.6	94.6	40	59.2	78
801	Cold Drawn plus	0	30.9	77.3	56	78.8	Rb 71
	1093 C/1 h, AC	25	31.7	79.5	58	79.2	65
801	Cold Drawn	0	120.0	122.1	16	76.4	Rc 23
		25	118.9	119.5	18	75.0	27
		50	119.7	120.4	20	62.2	24
802	Hot Rolled,	0	40.2	97.4	48	58.9	Rb 79
	Annealed	25	52.1	95.7	50	54.5	71
		50	40.2	94.3	47	47.3	74
825	Cold Rolled,	0	43.6	101.7	47	69.7	Rb 94
	Annealed	25	45.0	100.7	46	53.83	91
		50	44.1	99.4	44	55.5	91
902	Cold Drawn plus	0	34.1	88.4	47	67.1	Rb 71
	1093 C/1 h, AC	25	34.4	89.3	46	61.4	69
		50	32.4	86.3	44	46.8	69
902	Cold Drawn	0	148.2	152.4	11	50.0	Rc 26-27
		25	151.4	152.2	11	44.5	32
		50	150.6	151.4	12	33.3	27
902	Cold Drawn plus	0	188.2	205.1	12	41.2	Rc 38
	649 C/5 h, AC	25	187.0	205.1	8.5	24.6	38
		50	185.7	202.3	8.0	12.3	41
903	Cold Drawn,	0	99.9	169.1	20	47.0	Rc 36
	Solution Annealed	25	115.4	164.7	20	27.3	31
		50	130.0	166.8	18	28.0	31
903	CD Sol Ann + 843 C/	0	176.8	202.2	16	42.0	Rc 43
	3 h, AC + 718 C/8 h	25	176.5	203.5	12	22.5	40
	FC 60/h to 621 C/8 h,	50	180.9	201.7	8	11.6	41
	AC						

[1]Multiply by 6.895 to obtain MPa. Yield strength is stress for 0.2% offset.

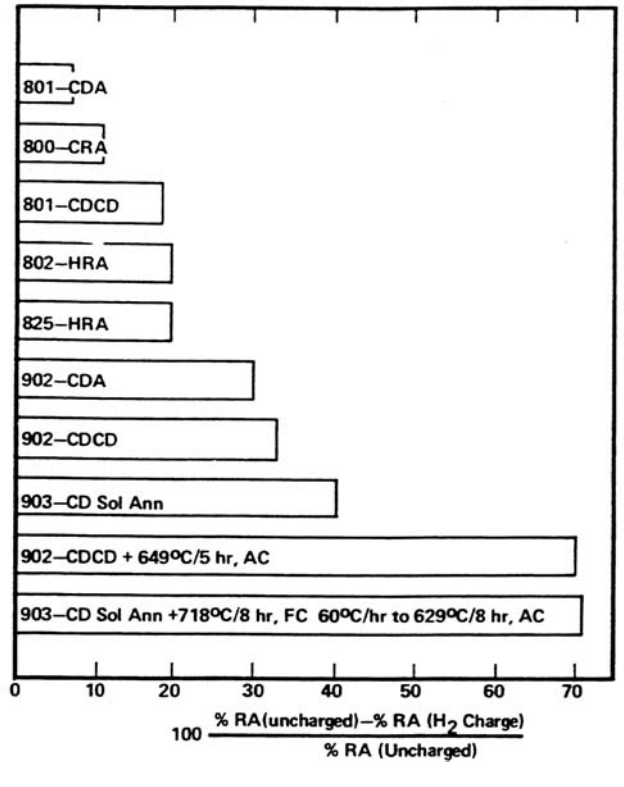


FIGURE 1 — Ductility losses, % change in reduction of area for INCOLOY alloys after 50 days of hydrogen charging.

Low Temperature Stress Corrosion Cracking

The most extensive testing in this environment (NACE steel coupled C-ring test) was conducted on INCONEL alloy 718 tubing. Table 4 lists the results for that alloy at three levels of cold work. An extensive heat treating study was done on the 24% cold drawn tube. Normal aging and overaging, with and without a "well age" (a heat treatment that simulates long

TABLE 3 — Mechanical Properties of Hydrogen Charged INCONEL Alloys

Alloy	Material Condition	Charging Time (days)	YS[1] (ksi)	UTS[1] (ksi)	%RA	%El	Brittle Layer Depth in.[2]
600	Cold Rolled, Annealed	0	53.4	111.8	59.3	44	—
		10	53.1	108.3	40.1	38	—
		20	55.2	105.9	34.5	42	—
		30	55.2	106.9	41.3	39	0.0008
601	Cold Rolled, Annealed	0	32.0	90.4	55.0	66	—
		10	33.1	87.6	47.8	63	—
		20	34.1	85.7	47.8	60	—
		30	31.0	84.8	46.7	60	0.0052
617	Cold Rolled, Annealed	0	46.3	117.6	55.0	64	—
		10	48.2	112.0	44.9	62	—
		20	49.1	110.4	43.8	65	—
		30	46.8	110.9	48.2	60	0.0055
625	Cold Rolled, Annealed	0	84.7	144.0	42.0	37	—
		10	89.9	137.2	30.5	36	—
		20	Lost	133.7	37.5	33	—
		30	88.6	135.5	26.7	36	0.008
690	Cold Rolled, Annealed	0	40.6	106.0	64.1	49	—
		10	48.3	101.2	55.2	46	—
		20	42.9	99.1	50.9	46	—
		30	40.4	99.7	52.1	44	0.0075
706	Cold Rolled, Annealed	0	69.2	132.4	57.6	48	—
		10	67.5	127.5	41.5	46	—
		20	66.4	126.1	48.1	46	—
		30	62.8	122.3	45.2	49	0.006
706	CDA + 883 C/3 h, AC + 718 C/8 h, FC 60 C/h to 621 C/8 h, AC	0	158.1	188.1	27.1	18	—
		10	159.6	181.7	10.7	10	—
		30	157.9	177.5	10.9	9	0.0054
706	CRA + 718 C/8 h FC 60 C/h to 621 C/8 h, AC	0	153.0	186.3	47.9	28	—
		10	156.5	183.6	37.4	25	—
		20	155.7	181.5	30.3	22	—
		30	151.6	179.2	32.0	23	0.0055
718	Cold Rolled, Annealed	0	64.6	126.9	54.5	50	—
		10	62.0	120.9	39.5	50	—
		20	65.0	122.6	33.7	42	—
		30	60.5	115.8	32.8	45	0.009
718	CRA + 718 C/8 h FC 60 C/h to 621 C/8 h, AC	0	163.0	193.0	37.8	24	—
		10	167.2	189.0	24.2	18	—
		20	167.0	182.4	18.1	18	—
		30	166.2	184.8	17.7	14	0.0066
X-750	Hot Rolled	0	110.4	171.4	49.0	30	—
		10	114.7	170.0	30.7	29	—
		20	110.0	162.1	23.2	27	—
		30	110.1	160.9	23.9	25	0.007
X-750	HRA + 704 C/20 h, AC	0	133.5	188.0	45.5	29	—
		10	136.7	187.0	31.8	24	—
		20	134.3	181.0	26.4	24	—
		30	134.0	181.6	25.8	24	0.0053
X-750	HRA + 885 C/3 h, AC + 704 C/20 h, AC	0	126.9	188.3	37.9	24	—
		10	125.8	183.7	13.3	15	—
		20	123.0	173.1	14.4	11	—
		30	125.1	174.4	16.6	15	0.0061

[1]Multiply by 6.895 to obtain MPa. Yield strength is stress for 0.2% offset.
[2]Multiply by 25.4 to obtain mm.

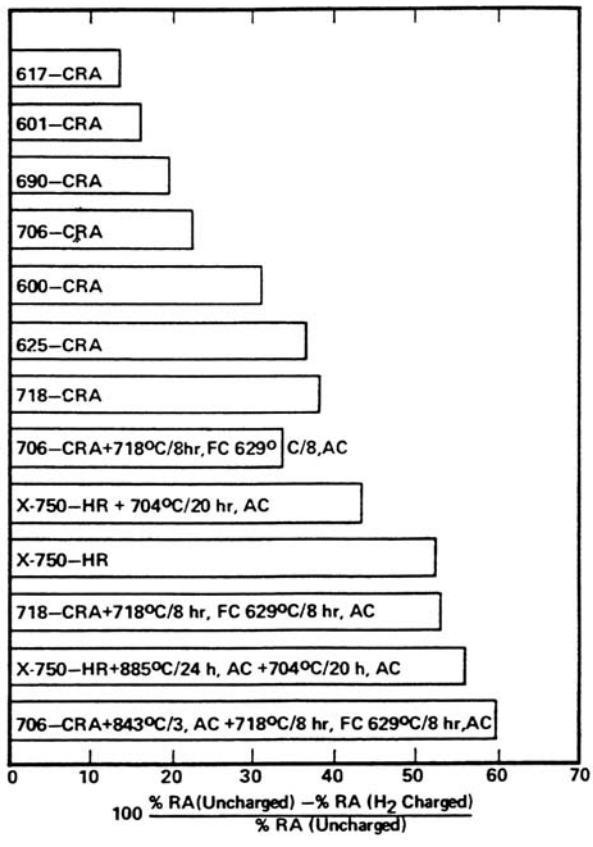


FIGURE 2 — Ductility losses, % change in reduction of area for INCONEL alloys after 30 days of hydrogen charging.

time downhole exposure), were performed on test samples. In general, overaging was effective in increasing resistance. However, if either heat treatment raised the yield strength to 1170 MPa (170,000 psi), cracking would occur. Well aging to accelerate effects of downhole conditions had no deleterious effects on time to cracking. The combination of a high temperature anneal at 1093 C (2000 F) and aging produced materials with yield strengths below 1172 MPa (170,000 psi) which did not fail. The tube with 36% cold work was tube reduced instead of cold drawn and had a yield strength of 1360 MPa (197,000 psi). The tube cracked even when stressed to a strength level below 1170 MPa (170,000 psi). As-tube reduced material is susceptible to cracking and requires an anneal to change this highly stressed condition.

Results for other alloys tested are given in Table 5. INCONEL alloy 625 was tested in the 70% tube reduced condition and failed in 5 days. The two heat treatments shown in Table 4 increased the yield strength of the alloy and decreased failure time to one day. Results for INCONEL alloy 706 indicate that this tube was not attacked by the NACE solution at yield strengths as high as 1290 MPa (187,000 psi).

INCOLOY alloy 825 possessed good resistance to hydrogen embrittlement in the previous tests, and this was reflected in complete resistance of cold worked, steel coupled C-rings to the NACE solution. Heat treating at 316 C for 1000 hours (a simulated well age) had no effect on the alloy's resistance to this environment.

TABLE 4 — Results of NACE C-Ring on INCONEL Alloy 718

Tube Size (OD and Wall) (in.)[1]	Cold Work (%)	Heat Treatment[2]	Test Temp. (C)	Test Strength (ksi)[3]	Time to Failure (days)
3.25 x 0.229	24 (Drawn)	None	75	129.5	>75
		WA (Well Age)	24	129.5	>75
		1065 C/1 h + 843 C/3 h + Over Age	24	140.8	>75
		1065 C/1 h + Age	24	154.6	>75
		1065 C/1 h + Age + WA	24	154.6	>75
		1065 C/1 h + Over Age	75	163.5	>75
		954 C/1 h + Over Age	75	165.0	>75
		954 C/1 h + Over Age + WA	24	165.0	>75
		954 C/1 h + Age	75	170.0	7-8
		954 C/1 h + Age + WA	24	170.0	63
		Over Age	75	186.5	5
		Over Age + WA	24	186.5	56
		696 C/18 h	75	195.5	9
		696 C/18 h + WA	24	195.5	9
3.50 x 0.280	70 (Tube Reduced)	None	75	186.0	9
		954 C/1 h + Over Age	75	157.5	>51
		1065 C/1 h + Over Age	75	165.0	31
		954 C/1 h + Age	75	176.0	4
		843 C/3 h	24	190.8	1
		500 C/24 h	75	198.0	6
		Over Age	75	211.0	6
2.75 x 0.305	36 (Tube Reduced)	None	24	197.0	2
		None	24	180.0	3-5
		None	24	175.0	5-7
		None	24	165.0	25-30
		1038 C/1 h + Age	24	143.0	>42
		593 C/1 h	24	216.0	1
		649 C/1 h	24	230.0	2
		704 C/1 h	24	227.0	1
		760 C/1 h	24	213.0	1

[1]Multiply by 25.4 to obtain mm.
[2]Well age (simulated): 260 C/250 h, AC Over age: 788 C/8 h, FC 60 C/h to 649 C/8 h, AC Age: 718 C/8 h, FC 60 C/h to 625 C/8 h, AC. Tubes given multiple treatments were air cooled between each.
[3]Multiply by 6.895 to obtain MPa.

TABLE 5 — Results of NACE C-Ring Tests

Alloy	Tube Size (OD and Wall) (in.)[1]	Cold Work (%)	Heat Treatment	Test Strength (ksi)[2]	Time to Failure (days)
INCONEL 625	3.5 x 0.281	70 (Tube Reduced)	None	173.5	5
			500 C/9 h, AC	214.5	1
			621 C/9 h, AC	215.0	1
INCONEL 706	3.25 x 0.240	24 (Drawn)	843 C/3 h, AC + 732 C/8 h, FC 60 C/h to 621 C/8 h, AC	128.9	>75
			Above + 260 C/250 h, AC	128.9	>75
			982 C/1 h, AC + 732 C/8 h, FC 60 C/h to 621 C/8 h, AC	157.3	>75
			Above + 260 C/8 h, AC	157.3	>75
			732 C/8 h, FC 60 C/h to 621 C/8 h, AC	187.1	>75
			Above + 260 C/250 h, AC	187.1	>75
NIMONIC 86	2.65 x 0.300	36 (Drawn)	None	168.0	>1
			None	179.3	>1
			None	158.3	>1
IN 103	2.65 x 0.300	36 (Drawn)	None	166.5	2
			None	151.2	>1
INCOLOY 825	2.875 x 0.310	27 (Drawn)	None	105.0	>48
			316 C/1000 h, AC	111.9	>48
	2.650 x 0.330	49 (Drawn)	None	114.2	>48
			316 C/1000 h, AC	127.4	>48
	1.900 x 0.190	63 (Drawn)	None	133.4	>48
			316 C/1000 h, AC	133.5	>48
	2.875 x 0.276	51 (Drawn)	None	147.1	>50

[1] Multiply by 25.4 to obtain millimeters.
[2] Multiply by 6.895 to obtain MPa.

TABLE 6 — Results of High Temperature Autoclave Tests

25% Sodium Chloride + 0.5% Acetic Acid + 1 g/L sulfur, saturated with H_2S, 150 psi H_2S overpressure at 177 C (350 F)

Alloy	Material Condition	YS (ksi)[1]	Test Strength (ksi)[1]	Time to Failure[2] (days)
INCONEL 718	36% TR (Tube Reduced)	197.0	177.3	45-57
	36.7% TR + 1038 C/1 h, AC + 718 C/8 h FC 60 C/h to 621 C/8 h, AC[2]	143.0	143.0	<22
INCOLOY 825	27% TR + 316 C/1000 h, AC	111.9	101.0	>43
	49% TR	114.2	103.0	>43
NIMONIC 86	11% TR	166.9	166.9	>66

15% Sodium Chloride, saturated with H_2S and 1000 psi overpressure of gas mixture of 1% H_2S + 20% CO_2 – Bal N_2 at 204 C (400 F).

Alloy	Material Condition	YS (ksi)[1]	Test Strength (ksi)[1]	Time to Failure[2] (days)
INCOLOY 825	27% TR	105.0	94.5	>47
	49% TR	111.1	100.0	>47
	51% TR	147.1	132.4	>47
NIMONIC 86	11% TR	158.3	158.3	>22

[1] Multiply by 6.895 to obtain MPa. Longitudinal tests. Yield strength is stress for 0.2% offset.
[2] Tested at 204 C (400 F).

High Temperature Stress Corrosion Cracking

Table 6 lists results for the two environments used for high temperature autoclave testing. In the more severe environment (25% NaCl, 0.5% CH_3COOH, 1 g/L S, H_2S saturated), INCONEL alloy 718 failed in both the tube-reduced condition and the tube-reduced plus annealed and aged condition. The failure mode in both cases was transgranular branching cracks typical of chloride SCC. In that environment, INCOLOY alloy 825 did not fail in the 32 day test period. In the other environment, alloy 825 did not fail in 40 days of exposure.

Discussion

All of the alloys tested were rendered less ductile by hydrogen charging. In general, the INCOLOY alloys were more resistant than the INCONEL alloys. It was apparent while performing tensile tests on hydrogen charged material that the INCONEL alloys would develop numerous circumferential cracks normal to the direction of tensile stress, whereas the more resistant INCOLOY alloy specimens did not develop such cracks. Metallographic examinations revealed uniform, intergranular cracking on the INCONEL alloy specimens, ranging from 0.13 to 0.20 mm (0.005 to 0.008 in.) in depth. The age hardened specimens showed a shallower embrittled depth than annealed specimens. This layer obviously was related to the diffusion rate of hydrogen, with crack depth corresponding to depth of hydrogen diffusion. Figure 3 shows that hydrogen diffuses more slowly in alloy 800 than in alloy 706, which exhibited behavior typical of INCONEL alloys. Hydrogen analyses in Figure 4 show that two materials had about the same hydrogen contents, indicating that diffusion in the alloy and not a hydrogen absorption step is rate controlling. Of the

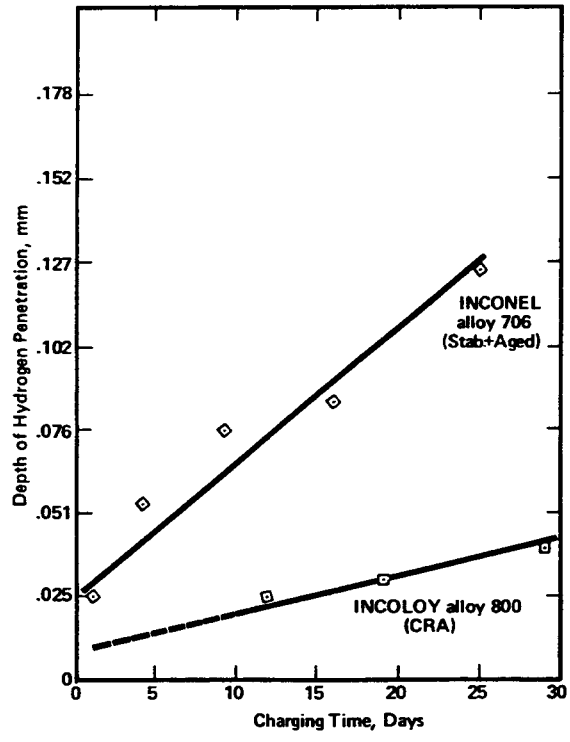


FIGURE 3 — Hydrogen penetration as a function of charging time for INCOLOY alloy 800 and INCONEL alloy 706.

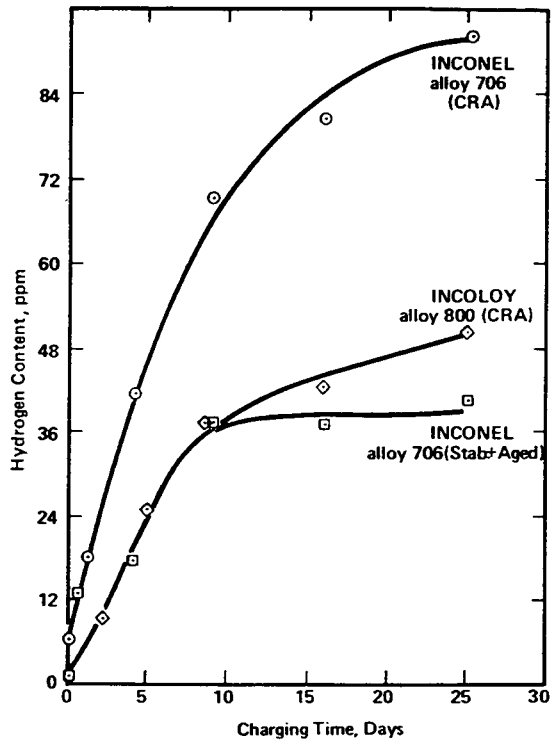


FIGURE 4 — Hydrogen pickup as a function of charging time in 4% H_2SO_4 saturated with CS_2. Current density, 1 mA/cm².

annealed materials, alloys 600, 625, 718, and X-750 had greater embrittled layer depths, and this possibly accounts for their relatively lower resistance. As expected, high strength, age hardened materials exhibited the least resistance to hydrogen embrittlement. Alloy 706 in the annealed and aged condition was the most resistant of these alloys.

Heat treatment plays an important role in an age hardenable alloy's ability to resist hydrogen embrittlement. Consider the alloy 706 data in Table 3 for direct aged vs stabilized and aged material. The 843 C (1550 F)/3 h stabilizing treatment did not appear to affect yield and tensile strengths, but did result in lower ductility, as shown by comparing the %RA and %El (elongation) values with those of direct aged material. As Figure 2 shows, the direct aged alloy 706 was considerably more resistant to hydrogen embrittlement than the stabilized and aged alloy. An identical effect is seen with alloy X-750, *i.e.*, the 885 C (1625 F)/24 h anneal prior to aging also resulted in lower ductility and increased susceptibility to hydrogen embrittlement.

Results of the steel coupled, NACE solution test paralleled those of cathodic charging. Alloy 718 in the direct aged condition possesses low hydrogen embrittlement resistance and low cracking resistance in the NACE test. This alloy resists cracking when given a high temperature anneal of 1065 C (1950 F) and aged to yield strengths under 1100 MPa (160,000 psi). Alloy 706 exhibited good hydrogen embrittlement resistance in the annealed and aged condition and did not fail in the NACE solution at yield strengths as high as 1290 MPa (187,000 psi). The stabilized and aged alloy 706, which exhibited poor resistance to hydrogen embrittlement, did not fail in the NACE solution, probably because of the low yield strength of 890 MPa (129,000 psi). Alloy 625 does not possess good resistance to hydrogen embrittlement and fails in the NACE solution. Alloy 825 cold worked as much as 50% does not fail in the NACE solution at yield strengths as high as 1014 MPa (147,000 psi).

Alloy 718, as-tube reduced, failed after approximately 50 days in the 25% sodium chloride, high temperature autoclave test at a stress level of 1220 MPa (177,000 psi). In contrast, a NIMONIC alloy 86 tube (64 Ni, 25 Cr, 10 Mo) that failed the steel coupled NACE test in 1 day did not fail the autoclave test. The reason for the behavior of this tube lies in the corrosion mechanisms operating in the two tests. The NACE solution causes hydrogen embrittlement, while the autoclave test promotes chloride SCC with the H_2S possibly having no effect. The high Ni content of NIMONIC alloy 86 renders it susceptible to hydrogen embrittlement but resistant to chloride SCC. The Ni content of INCONEL alloy 718 is about 51%, and the alloy's resistance in the two tests depends more on material condition than Ni content. Annealed and aged material will pass either test while heavily cold worked or direct aged material will fail both tests. INCOLOY alloy 825 possesses a favorable Fe:Ni ratio for immunity to hydrogen embrittlement while having enough Ni to resist chloride SCC in all but very aggressive environments.

Summary

The results obtained indicate that the following points should be considered when selecting an alloy for H_2S service: (1) If the environment offers a potential for hydrogen embrittlement (low temperature, H_2S, low pH, galvanic contact), cold worked alloys, or age hardenable alloys in the annealed and aged condition, with yield strengths below 1100 MPa (160,000 psi) will be good choices; and (2) chloride SCC environments (high temperature, high chlorides, with CO_2 and H_2S present) are best handled with alloys of greater than 40% Ni content.

References

1. Kochera, J. W., Dunlop, A. K., Tralmer, J. P. T-1F Paper No. 50, NACE Corrosion/76, Houston, March, 1976.
2. Tuttle, R. N. Materials Performance, Vol. 13, No. 2, p. 42 (1974).
3. Kane, R. D., Watkins, M., Jacobs, D. F., Hancock, G. L. Corrosion, Vol. 33, No. 9, p. 309 (1977).
4. Asphahani, A. I. Proceedings of the 7th International Congress on Metallic Corrosion, Rio de Janeiro, October, 1978.
5. Kane, R. D., Greer, J. B., Jacobs, D. F., Hanson, H. R., Berkowitz, B. J., Vaughn, G. A. Stress-Corrosion Cracking of Nickel and Cobalt-Base Alloys in Chloride-Containing Environments, Paper No. 174, Corrosion/79, March, 1979.
6. Rhodes, C. G., Thompson, A. Met. Trans. A, Vol. 8A (1977).

Copyrighted Materials
Copyright © 1996 NACE International Retrieved from www.knovel.com

PAPER NUMBER

7

CORROSION 89

April 17-21, 1989
New Orleans Convention Center, New Orleans, Louisiana

ENVIRONMENTAL CRACKING EVALUATION OF CORROSION RESISTANT ALLOYS IN H_2S-CO_2-CL^- ENVIRONMENT BY SLOW STRAIN RATE TENSILE TEST

A. Ikeda, M. Ueda and H. Tsuge
Sumitomo Metal Industries, Ltd.
Tubular Products Technology Department
15 Kitahama 5-chome, Higashi-ku, Osaka, Japan 541

ABSTRACT

A slow strain rate test (SSRT) is effective to survey materials selection for a hostile well such as deep sour gas. In order to use effectively data from different sources, it is necessary to make causes of error or variance clear and minimize data variance.

In this paper, various factors affecting SSRT evaluation of corrosion resistant alloys (CRA) in H_2S-CO_2-Cl^- environment are investigated. Those are evaluation index, specimen dimensions, alloys and environmental factors. Through the course of this investigation, a guide line in SSRT evaluation is proposed in relation to stress corrosion cracking mechanism.

INTRODUCTION

Recently, corrosion resistant alloys(CRA) tubing and casing have been conventionally used on the exploration of deep sour gas wells. These materials are not only resistant to general corrosion, but also localized corrosion and stress corrosion cracking(SCC). [1]~[7] Particularly, CRA tend to be a favourable choice for offshore critical well, because they are suitable for a maintenance free well and a well design possible to high production rate in small bore. It will result in saving a well cost.

CRA are, however, not always immune, but corrosion resistant to SCC.[2] SCC could be realized in combination of both alloy and environmental conditions. Because a history of usage of CRA for hostile wells is not so long, a performance of CRA in the actual well has not been clarified, so far. Therefore, usage of CRA has been, hitherto, not critical, but conservative. CRA which were immune to SCC in the acceleration test in severer environmental condition than one presumed in the actual well have been

only applied to the actual field. It will be, however, required in the near future to select any economical CRA suitable to environmental condition. Thus, performance of CRA and any reasonable evaluation criteria will have to be discussed more rigidly.

A slow strain test(SSRT) has been used to assess whether materials were susceptible to environmental cracking in some environment or not, i.e. SCC "go" or "not go". [3][8]~[12] As concerning hydrogen embrittlement(HE) of carbon steel or low alloy steel, Ikeda et al. show that its evaluation was not enough and any quantitative expression was necessary in order to use SSRT effectively. [10][11] They proposed on the basis of their field experience of sulfide stress cracking(SSC) resistant tubulars that when a ratio of plastic elongation in environment to in air is less than 10%, that material is not recommendable for sour application [10]. As a cracking mechanism between HE and active pass SCC(APSCC) is different, that criteria for HE could not be applied to APSCC, which would usually be observed in CRA - H_2S-CO_2-Cl^- system. SSRT is effective to shorten evaluation time, even though a meaning of data were not completely clear. Accordingly, it is favorite for surveying materials and quality assurance of materials under any reasonable conditions and criteria.

In this article, various factor affecting SSRT in CRA - H_2S-CO_2-Cl^- system are studied. Particularly, how to minimize errors or variance of data, compare data from different sources, evaluate quantitatively degradation of materials and extend an application of SSRT are subjects. Accordingly, evaluation index, specimen dimension, alloys and environmental factors are examined and discussed in relation to SCC mechanism.

EXPERIMENTAL

Materials

Materials used are shown in Tables 1 and 2. Materials in Table 1 are melted, forged, hot-rolled to thickness 15mm, solution treated and cold-rolled at reduction ratio of 30% in laboratories. Materials in Table 2 are tubular products. In order to investigate a variance of mechanical properties, commercial products of both SM C276[1] and SM2550[2] are also used.

Apparatus

A schematic illustration of used SSRT apparatus is shown in the previous report [13]. A test specimen is installed in autoclave. Maximum loads of the SSRT testers are both 1 tonnage and 3 tonnages.

The SSRT is carried out at a strain rate from 1×10^{-5} to 1×10^{-7} s^{-1} in air and in hostile environment. Specifically, 4×10^{-6} s^{-1} is conventionally used. As a tensile property of material varies with test temperature, each tensile property measured both in air and in environment at the same temperature shall be compared in order to get an index of environmental degradation. The inner wall of autoclave is lined with SM2550. A pull rod is made of the same material as the autoclave linings. In the present article, an electrical insulation between specimen and pull rod is not designed.

Test Specimen

A standard test specimen in this article is a round tensile specimen as shown in Fig. 1. For purpose to investigate an effect of specimen dimensions on SSRT evaluation, gauge length (G.L.) and specimen diameter are changed from 25.4 to 30mm and from 3.8 to 4.2mm, respectively.

---

[1] SM C276 : UNS No. N10276, 16Cr-60Ni-16Mo Alloy
[2] SM2550 : UNS No. N06975, 25Cr-50Ni-6Mo Alloy

Environmental Condition

The following seven media are used at the various temperatures from 80°C to 232°C ;

Condition (1) : 25%NaCl-0.5%CH_3COOH, 7 bar H_2S

Condition (2) : 25%NaCl, 10 bar H_2S-10 bar CO_2

Condition (3) : NaCl-0.5%CH_3COOH, 10 bar H_2S-10 bar CO_2
(NaCl concentration : 0, 1, 3, 5, 10, 20, 25%)

Condition (4) : 25%NaCl-0.5%CH_3COOH 1 bar H_2S-10 bar CO_2

Condition (5) : 25%NaCl-0.5%CH_3COOH, 10 bar CO_2

Condition (6) : 5%NaCl, 1 bar H_2S-20 bar CO_2

Condition (7) : 5%NaCl-0.5%CH_3COOH 1 bar H_2S

, where gas pressure is one at room temperature, i.e. about 25°C.

Experimental Procedure

In air, a tensile test is carried out at any constant strain rate, after a temperature of test specimen attained to test one. In environment, a test specimen is amounted on the test apparatus. A autoclave is closed and evacuated. Test brine deaerated by pure nitrogen is filled into the autoclave. The pure nitrogen is blowed for about 15 min into the autoclave. After it has been evacuated for about 10 min again, H_2S and/or CO_2 gases are filled up to a test condition. Then, a tensile test is carried out on any constant strain rate, after a temperature of test specimen attained to the test one. After the test specimen has been fractured, the autoclave is cooled down, depressurized and toxic gas is degased from it. During SSRT, a stress - strain curve (S-S curve) is recorded. Whether secondary cracks occurred on the fractured test specimen or not is visually observed. When a degradation is critical, examination of fracture surface is also carried out by a scanning electron microscope (SEM).

SSRT Evaluation

Various evaluation methods have been worldwidely used as shown in Fig. 2. In the present article, a ratio of plastic elongation in environment (L) versus one in air (Lo), i.e. L/Lo, is mainly used for in index of environmental degradation except a preliminary examination. In each SSRT, an average value of two data for both L and Lo values are usually used.

RESULT

Specimen Dimension and Evaluation Index

Precision of Dimension. Most important things taken into account in tensile test is that fracture occurs at gauge section. Specifically, in SSRT test in hostile well condition, it is experienced that any notched effect at the narrow off gauge section shifting from parallel section to tapered one could affect significantly a loss of homogeneous plastic elongation. In spite of no secondary crack and showing a good reduction of area, a poor elongation is frequently experienced. In order to avoid such situation, it is recommended that a specimen diameter at the gauge section is machined smaller in the range of precision than that at the off gauge section.

Inhomogeneity of Material. Every material has some variance on the tensile properties itself. Accordingly, duplicated numbers of test are necessary to decide a mechanical property even in a conventional tensile test. In addition to it, both test specimens tested in air and in environment shall be sampled at the same portion as much as possible. CRA tubulars for oil and gas well are usually produced by cold working to get its high strength. Along both directions of through wall thickness and axis, mechanical properties depend on the sampling location, possibly. Particularly, a heavy wall tends to have a major variance depending upon the cold working method. In conducting SSRT, a sampling location itself shall be considered one of factors affecting test results.

Effect of Specimen Dimension and Evaluation Indices. The material used is SM2242-125, i.e. alloy 825 type[3] with specified minimum yield strength (SMYS) of 125 ksi. A test environment is the Condition (1), i.e. 25%NaCl-0.5%CH_3COOH, 7 bar H_2S. SSRT was carried out at 150°C and on 4 x 10^{-6} s^{-1}. For evaluation indices, Time to Failure (TTF), i.e. elongation, Reduction of area (Ra), Plastic elongation (L or Lo) and (L/Lo) were used. As D.R. McIntyre et al show that a stiffness of frame of tensile equipment could affect the SSRT evaluation[12], all tests in this section were carried out with the same equipment.

Results are shown in Figs. 3 to 6. An absolute value of TTF, i.e. elongation, increases with increasing the specimen diameter and decreases with increasing the gauge section. An absolute value of Ra, reversely, decreases with increasing the specimen diameter and increases with increasing the gauge section. It is natural as shown in Fig. 5 that a tendency of evaluation due to an absolute value of plastic elongation (L) should be the same as the case of TTF. The index of L/Lo is effective to normalize the effect of specimen dimension on SSRT. Besides it, it is noted that the errors due to the difference of frame stiffness of tensile equipment could be minimized by the evaluation due to plastic elongation. If an evaluation index in SSRT were dependent on the test method itself, the data would lose a generalized physical meaning and also lose a comparability among different data sources. Therefore, L/Lo as well as existence of secondary crack is mainly used, hereinafter, in this article as the index of degradation in SSRT.

It is suggested, specifically, that such specimen preparation could become a major source of variance more in hostile environment than in air and it should be taken into account on the analysis.

Environmental Factors

Alloy and Temperature. Ikeda et al show in the systematical study by means of four point bent beam SCC test that corrosion resistance of CRA in the remarkably hostile environment such as brine-H_2S-CO_2-free S depended upon Mo content and temperature.[7] The same alloys used in the previous work[7] and the various CRA tubular products as shown in Tables 1 and 2 were investigated by SSRT. A test environment is the Condition (1), i.e. 25%NaCl-0.5%CH_3COOH, 7 bar H_2S. The SSRT was carried out at the temperature 121 (250), 149 (300), 177 (350), 204 (400) and 232 (450) °C (°F) and on 4 x 10^{-6} s^{-1}. The strength of materials is yield strength of 120 to 140 ksi.

Results are shown in Fig. 7. In this figure, the evaluation of SSRT was done with either SCC or no SCC. It is noted that SCC was not observed, when L/Lo is more than 0.8 and either SCC or no SCC was observed, when L/Lo is less than 0.8. In this environment, temperature and molybdenum content are critical to a SCC susceptibility of CRA in SSRT method. This result is similar to the corrosion and SCC behavior due to other SCC test method of CRA both in brine-H_2S-CO_2-free S and brine-H_2S-CO_2 acidized to low pH.[2][7] It is noted, specifically, that remarkably higher Mo content is required to prevent SCC in the SSRT than in the four point bent beam test.

(3) SM2242 / Alloy 825 : UNS No. N088825, 22Cr-42Ni-3Mo

Alloy and Strength level. On the critical temperature of each alloy which is presumed in Fig. 7, an effect of strength of CRA on SCC behavior by SSRT is investigated. Materials are tubular products of SM2550, SM2060Mo and SM-C276. Each test temperature is 149 (300) °C (°F) for SM2550 or 232 (450) °C (°F) for SM2060Mo and SM-C276, respectively. A test environment is the Condition (1) i.e. 25%NaCl-0.5%CH_3COOH, 7 bar H_2S. The SSRT was carried out on 4 x 10^{-6} s^{-1}. The strength of SM2550 is SMYS 110 grade. The one of SM2060Mo is SMYS 110 and 155 ksi grades. The one of SM-C276 is SMYS 110, 130, 150 and 170 ksi grades.

Results of SSRT are shown in Figs. 8 and 9. All specimens have no evidence of SCC in this examination. This shows that each presumed critical temperature is stable in the safety side and does not depend on the strength level. An absolute value of TTF, that is to say, total elongation in SSRT, decreases with increasing the yield strength of materials both in air and in hostile environment. This phenomenon is commonly observed in the usual tensile properties of CRA. It is noted that any elongation itself does not represent an extent of environmental degradation. As shown in Fig. 9, the environmental degradation could be normalized by the index of L/Lo, in no relation to not only alloy, but also strength of materials. The L/Lo values vary from 0.89 to 1.12 in these SSRT data, in spite of the materials with a conventional homogeneity and without SCC. As this variance in L/Lo values corresponds to 5% variance in elongation, these data are not abnormal in comparison with the conventional tensile test.

Addition of Acetic Acid in Brine. Materials used are SM2242-125, which yield strength (YS.) is in a range of 125 to 145 ksi. In this case, two materials with YS. 138 and 142 ksi were tested. The environments in SSRT are the Condition (2): 25%NaCl, 10 bar H_2S-10 bar CO_2 and the Condition (3): 25%NaCl-0.5%CH_3COOH, 10 bar H_2S-10 bar CO_2. The strain rate is 4 x 10^{-6} s^{-1}. The SSRT is carried out at 100, 125, 175 and 200 °C.

The SSRT result is shown in Fig. 10. As shown in Fig. 7, a type of alloy 825 is critical at 150 °C in the Condition (1). The Condition (3) is different on the gas condition from the Condition (1). In the brine without acetic acid, a critical temperature of this alloy could be raised the higher temperature more than 200 °C as shown in Fig. 10. It is presumed, on the other hand, that the critical temperature in the condition added with acetic acid might still locate in the vicinity of 150 °C as shown in the Condition (3) in Fig. 10. At 150 °C, a L/Lo value of one of SM2242 alloys decreases up to 0.8, although no secondary crack was observed. Thus, it is noted that an addition of acetic acid in brine makes corrosion condition severe in the SSRT and SCC is free on the higher L/Lo value more than 0.8.

Partial pressure of H_2S. Materials used are SM2030-110, which yield strength (YS.) is in a range of 110 to 130 ksi. In this case, material with YS. 126 ksi was tested. The environments in SSRT are the Condition (3): 25%NaCl-0.5%CH_3COOH, 10 bar H_2S-10 bar CO_2, the Condition (4): 25%NaCl-0.5%CH_3COOH, 1 bar H_2S-10 bar CO_2 and Condition (5): 25%NaCl-0.5%CH_3COOH, 10 bar CO_2. The strain rate is 4 x 10^{-6} s^{-1}. The SSRT is carried out at 150°C.

The result of SSRT is shown in Fig. 11. The L/Lo values of SM2030 alloy decrease linearly with increasing H_2S pressure. In 1 bar H_2S, the value of L/Lo is 0.77, although there is no evidence of SCC. In 10 bar H_2S, the value of L/Lo is 0.62 and many secondary cracks are observed at the gauge section.

Chloride Ion Concentration. Materials used are SM2030-110, which yield strength (YS.) is in a range of 110 to 130 ksi. In this case, material with YS. 126 ksi was tested. The environments in SSRT are the Condition (3): NaCl-0.5%CH_3COOH, 10 bar H_2S-10 bar CO_2. The concentration of NaCl changed in the range from 0 to 25%. The strain rate is 4 x 10^{-6} s^{-1}. The SSRT is carried out at 150 °C.

Results of SSRT are shown in Fig. 12. In this hostile conditions, a Cl^- dependence of this material is not so remarkable in the concentration up to 10% NaCl, but in one

of more than 20%. In 20% NaCl, the value of L/Lo is 0.85, although there is no evidence of SCC. In 25% NaCl, the value of L/Lo is 0.62 and many secondary cracks are observed at the gauge section.

Alloy - Environment. Materials used are SM2030, SM2535 and SM2242. The yield strength of materials is almost SMYS 110 ksi grade. As concerns SM2030, partly, SMYS 125 ksi grade are also tested. The environments in SSRT are the Condition (2): 25%NaCl, 10 bar H_2S-10 bar CO_2, the Condition (3): 25%NaCl-0.5%CH_3COOH, 10 bar H_2S-10 bar CO_2, the Condition (6): 5%NaCl, 1 bar H_2S-20 bar CO_2 and the Condition (7): 5%NaCl-0.5%CH_3COOH, 1 bar H_2S. The strain rate is 4×10^{-6} s^{-1}. The SSRT is carried out in the range from 80 to 200 °C. The variance of L/Lo values is also studied.

Results of the SSRT are shown in Figs. 13 to 16. In Fig. 13, effects of temperature on the SSRT results in the Condition (3) are presented. SM2030 is critical in the vicinity of 125 °C, as a tendency of degradation in the L/Lo value is observed and SCC does not occur at 125 °C, but at 150 °C. SM2535 with higher Cr and Ni contents than SM2030 is critical in the vicinity of 150 °C as same as SM2242. In comparison of Fig. 13 with Fig. 10, a strength level of SM2242 does not affect notably for the critical temperature in SSRT.

In Fig. 14, a temperature dependence of SSC susceptibility in the Condition (2) is shown. SM2030 is also critical in the vicinity of 125 °C. On the other hand, no evidence of environmental degradation on both alloys of SM2535 and SM2242 is observed even at 200 °C. In comparison with Fig. 13, it is noted that an addition of acetic acid in brine does not affect the SCC susceptibility of the former alloy, but the susceptibilities of the latter alloy. In comparison with Fig. 10, it is also shown that a strength level of SM2242 is not notable for the critical temperature in SSRT. It is noted that secondary cracks are observed on the gauge sections of specimens with the L/Lo value lower than 0.8.

In Fig. 15, a temperature dependence of SCC susceptibility in the Condition (6) is shown. All alloys are free of SCC in this relatively low Cl^- and low H S condition. In comparison with Fig. 14, it is clarified that these two environmental factors could affect remarkablly a SCC susceptibility of SM2030.

In Fig. 16, variances of L/Lo values of both SM2030 and SM2535 alloys in the SCC free condition are shown. In these cases, the data show 0.91 to 1.04. These are normal variances, because less than 5% variance of each elongation could result in those variances in L/Lo. It is noted that both SM2030 and SM2535 are enough resistant to SCC in the Condition (7), as recognized easily from Fig. 13.

Strain Rate

An effect of strain rate on the critical temperature to environmental cracking of CRA is studied. Both SM2550 and SM2535 alloys with SMYS 110 ksi are examined. A test condition is the Condition (1): 25%NaCl-0.5%CH_3COOH, 7 bar H_2S. The SSRT is carried out on the strain rates of 4×10^{-5} s^{-1}, 4×10^{-6} s^{-1} and 4×10^{-7} s^{-1}. As shown in Fig. 8, each critical temperature of alloys is 150 °C for SM2550 and 125 °C for SM2535 on the strain rates of 4×10^{-6} s^{-1}, respectively.

A result is shown in Fig. 17. There is neither evidence of SCC nor degradation of L/Lo in any conditions. Although strain rate dependence of SCC susceptibility of CRA shall be essentially studied in relation to a mechanism of SCC, it is concluded that a strain rate 4×10^{-6} s^{-1}, which is mainly used in this article, should be acceptable for a standard one in a surveying test.

DISCUSSION

Evaluation Method

A ratio of plastic elongation in environment to one in air at the same temperature

(L/Lo value) is a useful index for evaluation of environmental degradation by SSRT, because an error originated from either specimen dimension or frame stiffness of SSRT machine could be minimized and the data from different sources could be compared with each others in normalizing.

From the results clarified in this article, environmental degradation of CRA by SSRT could be schematically described in Fig. 18. When corrosion resistance of material is sufficient to environmental condition, there is no evidence of degradation in the L/Lo value. It corresponds to the situation "A" in Fig. 18. The more is the severity of corrosion environment, the more apparently becomes the evidence of degradation in the L/Lo value. It is divided to two situations. i.e. "B" and "C" in Fig. 18. In the situation "B", there is no evidence of SCC or secondary crack on the gauge section. On the other hand, SCC and secondary cracks are observed in the situation "C". It is presumed that a boundary between "B" and "C" locates in the vicinity of L/Lo value of 0.7 in the present article. At least, it is clarified that there is no evidence of environmental cracking on the L/Lo value more than 0.8. Because a passivation film on the surface of CRA is continuously destroyed during SSRT, some degradation in the L/Lo value might be, more or less, observed in the critical condition. However, as long as SCC does not occur, it should be recognized that the combination of material and environmental conditions located on the safety side against SCC.

As for variance of the L/Lo value, 5% variance of elongation in tensile test corresponds to L/Lo value of about 0.9 for minimum value. Accordingly, it shall be recognized that the L/Lo value more than 0.9 means no evidence of environmental degradation for materials with conventional homogeneity. If an inhomogeneity of material were more as any CRA with heavy wall thickness, it is noted that the minimum L/Lo value could decrease lower than 0.9 even in no evidence of environmental degradation.

Effect of Environmental Factors and Alloying Element on SCC Behavior of CRA

In one of the severest corrosion environments such as 25%NaCl-0.5%CH_3COOH, 7 to 10 bar H_2S-CO_2, a tendency of SCC behavior of CRA in SSRT depends upon remarkably temperature and Mo content as shown in Fig. 7. This is similar to corrosion behavior by four point bent beam tests in the lower pH and higher temperature[2] and in the higher temperature including free sulfur[7]. This similarity might result from a balance of both abilities for amending and destroying passivation film. In SSRT, the destruction is mainly enforced with the mechanical deformation continuously introduced in materials, while it is mainly done by the chemical or electrochemical reaction in bent beam test. In a critical condition at relatively low temperature, Cr and Ni contents also affect corrosion behavior. As Alloy 825 shown in Figs. 10 and 13, other metallurgical factors might also affect it.

In brine without acetic acid, both Cr and Ni contents contribute corrosion behavior. The effect of environmental factors on corrosion behavior, i.e. temperature, partial pressure of H_2S, Cl^-, appears predominantly in the combination of critical environmental conditions and rather lower grade material such as SM2030.

It is a fact that the evaluation of CRA by SSRT is always more conservative than that due to other SCC tests such as constant load, bent beam, C-ring and DCB tests. However, a tendency of contribution of alloying element and environmental factor obtained by the SSRT in this investigation is consistent with one obtained by the other measures. This means that SSRT could be a beneficial measure for surveying test and quality assurance of material under any reasonable conditions and criteria.

An environmental cracking model of CRA in the hostile well conditions is presented in Fig. 19. In relation to performance of material in the actual well, presently, there is nothing to say. At least, it could be only pointed out that SSRT could give the most conservative assessment, except the following phenomenon; pH value could be changable and go down in pit or crevice on stainless steel and/or CRA through corrosion process for long periods.[14]-[16]

It is clarified in Figs. 8 and 9 that SCC susceptibility of CRA by SSRT hardly depends upon strength level, but alloying elements. This is a new information for the properties of CRA.

CONCLUSION

1. SSRT is useful for evaluation of environmental cracking of CRA in the hostile well conditions.
2. A value of L/Lo is suitable for an index of environmental degradation. It could minimize error originated from equipment and dimension of specimen.
3. SCC was not observed in this article, when a value of L/Lo was more than 0.8. When an elongation in tensile test has 5% variance, about 0.9 on L/Lo corresponds to a minimum value of L/Lo variance.
4. Effect of alloy and environmental factors on corrosion behavior of CRA by SSRT does not conflict with one clarified by other test method, even though the SSRT evaluation is more conservative than other one.
   In severer condition, temperature and Mo content are predominant. In a critical condition of relatively low temperature, Ni, Cr, H_2S and Cl^- affect corrosion behavior.
5. SCC susceptibility of CRA by SSRT hardly depends upon strength level, but alloying element.
6. A concept of environmental degradation of CRA in the hostile well condition is presented on the basis of observation results due to both SSRT and other test measures.

REFERENCE

[1] R.N. Tuttle, Materials Performance 13 (2) p.42 (1974)
[2] A. Ikeda, T. Kudo, Y. Okada, S. Mukai, F. Terasaki, "Corrosion behaviors of high alloy oil country tubular goods for deep sour gas well", Corrosion/84, No.206 (1984) [NACE]
[3] H.E. Caung, M. Watkins, G.A. Vaughn, "Stress-corrosion cracking resistance of stainless alloys in sour environment", Corrosion/85, No.227 (1985) [NACE]
[4] F. Terasaki, A. Ikeda, J. Japanese Association of Petroleum Technology 50 (2) (Mar., 1985) in Japanese
[5] P.R. Rhodes, "Stress cracking risks in corrosive oil and gas well"
[6] S.W. Ciaraldi, "Application of a double cantilever beam specimen to stress corrosion evaluation of high alloy production tubulars" Corrosion/83, No.162 (1983) [NACE]
[7] A. Ikeda, Y. Morita, T. Moroishi, N. Matsuki, "Up-to-date technology in the field of casing and tubing manufacturing "Proc. 4th. Adriatic Sympos. on Oil Well Technology (1985)
[8] A. Ikeda, M. Igarashi, M. Ueda, Y. Okada, H. Tsuge, "On the evaluation methods of Ni-base corrosion resistant alloy for sour gas exploration and production", Corrosion/88, No.65 (1988) [NACE]
[9] G.M. Ugiansky, J.H. Payer, Stress corrosion cracking - The slow strain rate technique, STP665, (1977) [ASTM]
[10] F.F. Lyle Jr., E.B. Norris, Corrosion 34, (1978) No.6, p.193
[11] A. Ikeda, T. Kaneko, T. Moroishi, Critical issues in reducing the corrosion of steels at Nikko, Japan, (Mar., 1985) p.51 [NACE]
[12] A. Ikeda, T. Kaneko, Y. Ando, Corrosion Science, vol.27, No.10/11 pp.1099-1115 (1987)
[13] D.R. McIntyre, R.D. Kane, S.M. Wilhelm, Corrosion/86, No.149 (1986) [NACE]
[14] T. Kudo, H. Miyuki, H. Okamoto, J. Okamoto, T. Moroishi, Corrosion/82 No.127 (1982) NACE
[15] M.G. Fontana, N. Greene, Corrosion Engineering (1967) McGraw-Hill
[16] A.J. Sedriks, Corrosion of stainless steels (1979) John Wiley & Sons
[17] H. Ogawa, I. Itoh, A. Nakata, Y. Hosoi, H. Okada, Tetsu-to-Hagané 63 (1977) p.605 in Japanese

Table 1 Materials tested [Laboratory melted and worked to plate]

Chemical composition (wt%)								Y.S.
P	Ni	Cr	Mo	Ti	Nb	Cu	W	(kg/mm^2)
0.001 / 0.03	30 / 70	15 / 25	3 / 15	0.002 / 1.0	0.001 / 2.0	0.01 / 1.0	0.01 / 4.0	70 / 140

C : 0.003~ 0.007, Si : 0.01, Mn : 0.3~ 0.6, S : 0.002, Al : 0.1, Mg : 0.01, N : 0.002, O : 0.001

Table 2 Materials tested [Tubular products]

Mark	UNS No.	Chemical composition (wt.%)			
		Ni	Cr	Mo	Others
SM2030		28/32	20/25	3.5/4.5	
SM2535		30/40	24/28	3.0/4.0	
SM2242	N08825	38/46	20/23	3.0/4.0	1Ti, 2Cu
SM2550	N06975	48/53	24/27	5.0/7.0	Cu
SM2060Mo		54/58	20/23	12/14	Nb, W, Cu
Alloy G	N06007	48/53	20/23	6.0/7.5	1W, 1Nb
Alloy 625	N06625	60/67	20/23	8.0/10	3Nb
SM-C276	N10276	58/65	14/17	15/17	3W, 5Fe, 1Co

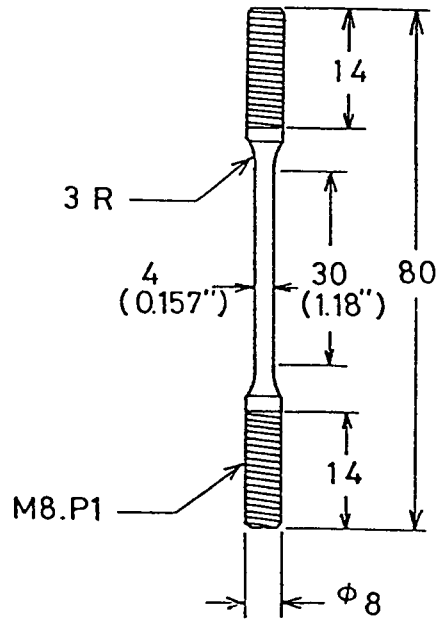
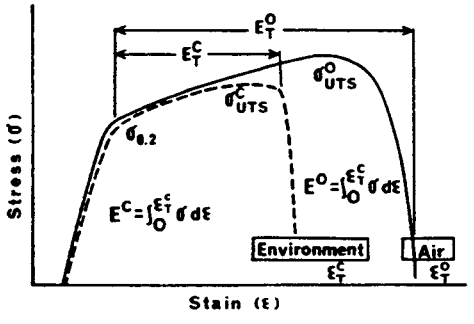


Fig. 1 Dimension of a standard SSRT specimen



Evaluation

(1) $\frac{\sigma^{O}_{UTS}}{\sigma_{UTS}}$

(2) $\frac{\varepsilon^{C}_{T}}{\varepsilon_{T}}$ or $\frac{\varepsilon^{O}_{T} - \varepsilon^{C}_{T}}{\varepsilon_{T}}$

Reduction of area (Ra)

(3) $\frac{E^{C}}{E^{O}}$

(4) $\frac{R^{C}_{a}}{R^{O}_{a}}$

(5) Go, no-go criteria
: with or without secondary crack

(6) Ratio of embrittled fracture surface area

(7) $\frac{E^{C}_{T}}{E^{O}_{T}}$ or $\frac{L}{L0}$ [Ratio of plastic strain (or elongation) in corrosion environment to in air at the same temperature]

Fig. 2 Various SSRT evaluation indices

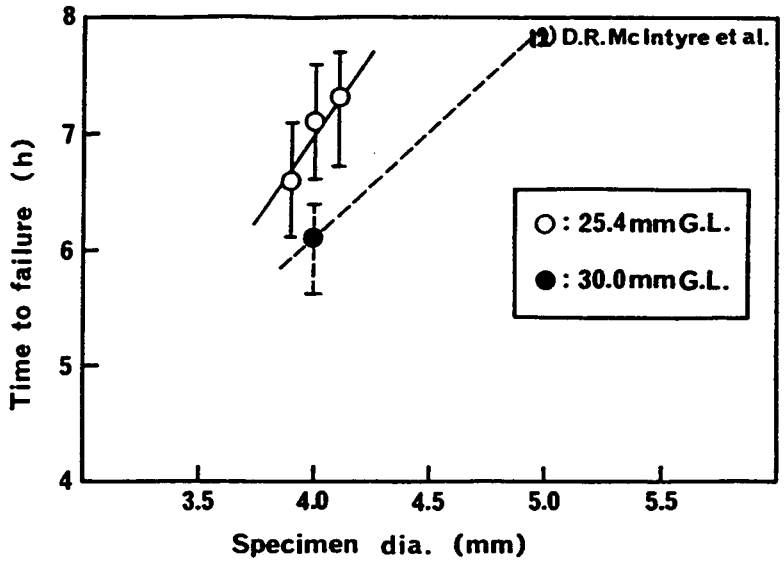


Fig. 3 Effect of specimen dimension on TTF(total elongation) in the SSRT of CRA. [Environment : Condition (1); 25%NaCl-0.5%CH_3COOH, 7 bar H_2S, 150°C, Materials : Alloy 825, Strain rate : 4 x 10^{-6} s^{-1}]

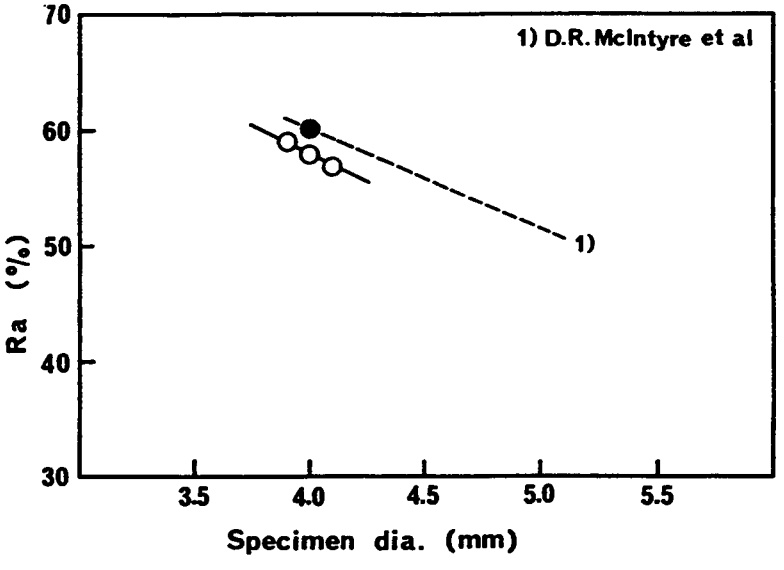


Fig. 4 Effect of specimen dimension on RA in the SSRT of CRA. [Environment : Condition (1); 25%NaCl-0.5%CH_3COOH, 7 bar H_2S, 150°C, Materials : Alloy 825, Strain rate : 4 x 10^{-6} s^{-1}]

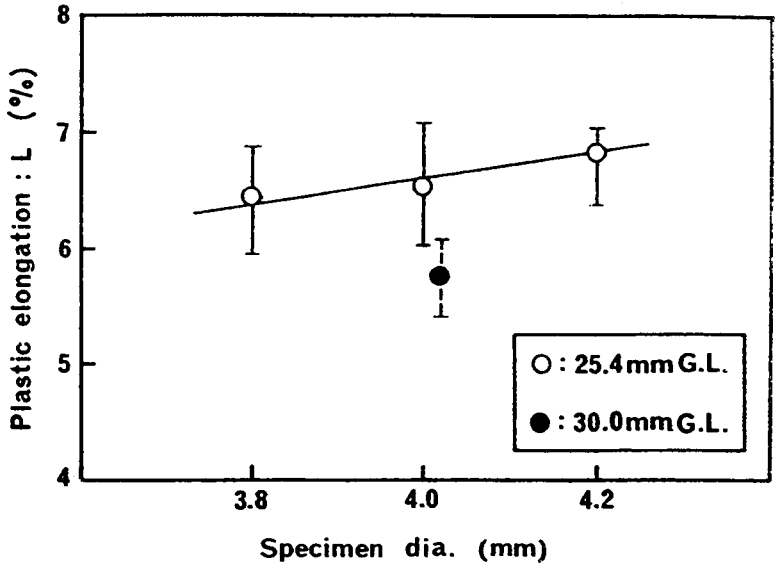


Fig. 5 Effect of specimen dimension on plastic elongation in the SSRT of CRA. [Environment : Condition (1); 25%NaCl-0.5%CH_3COOH, 7 bar H_2S, 150°C, Materials : Alloy 825, Strain rate : 4 x 10^{-6} s^{-1}]

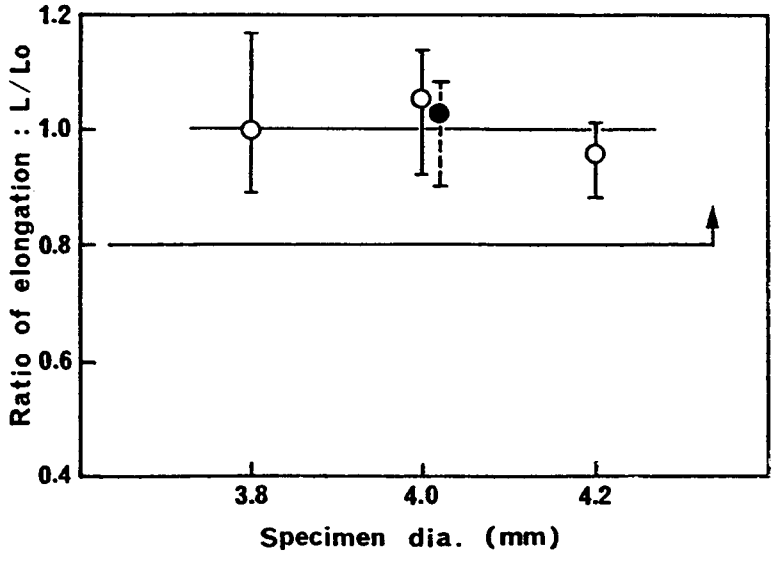


Fig. 6 Effect of specimen dimension on ratio of plastic elongation L/Lo in the SSRT of CRA. [Environment : Condition (1); 25%NaCl-0.5%CH_3COOH, 7 bar H_2S, 150°C, Materials : Alloy 825, Strain rate : 4 x 10^{-6} s^{-1}]

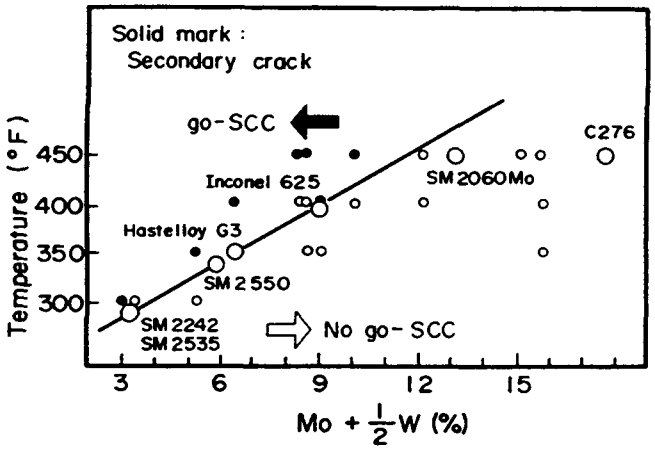


Fig. 7 A relationship between testing temperature and Mo content on SCC occurrence in SSRT of CRA in H_2S-Cl^- environment.
[Environment : Condition (1); 25%NaCl-0.5%CH_3COOH, 7 bar, Strain rate : 4 x $10^{-6}s^{-1}$]

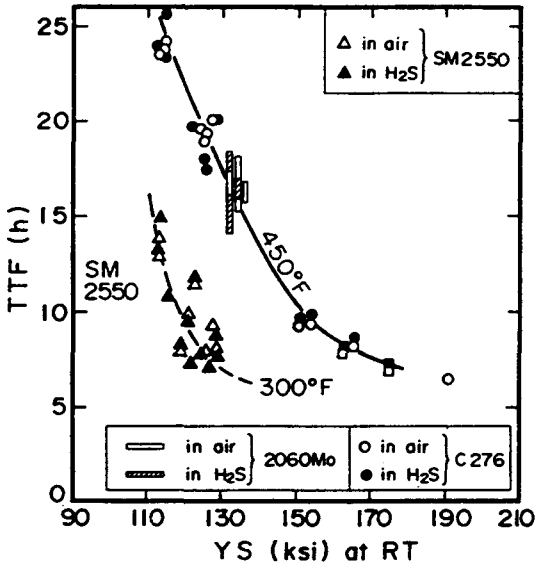


Fig. 8 A relationship between TTF, i.e. elongation, in SSRT and yield strength of alloys SM2550, SM2060Mo and SM-C276
[Environment : (A); Condition (1)/ 25%NaCl-0.5%CH_3COOH, 7 bar, (B); Air, Temperature : 300°F(148.9°C) for SM2550, 450°F (232.2°C) for SM2060Mo and SM-C276, Strain rate : 4 x $10^{-6}s^{-1}$]

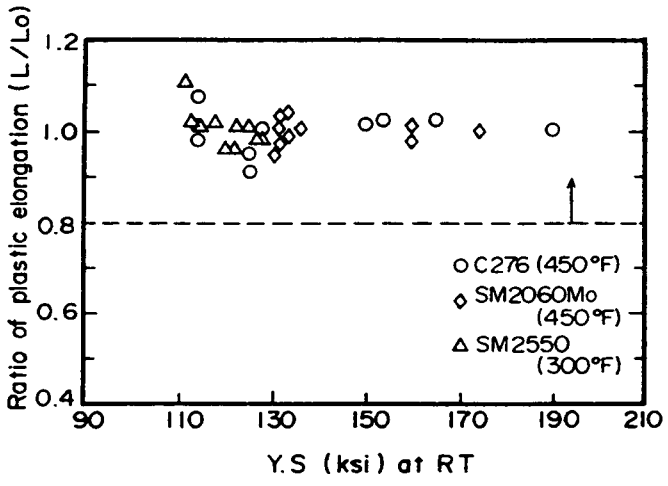


Fig. 9 Effect of strength and alloys on variance of L/Lo value in the SCC free condition on SSRT
[Environment : (A); Condition (1)/ 25%NaCl-0.5%CH_3COOH, 7 bar, (B); Air, Temperature : 300°F(148.9°C) for SM2550, 450°F(232,2°C) for SM2060Mo and SM-C276, Strain rate : 4 x 10^{-6} s^{-1}]

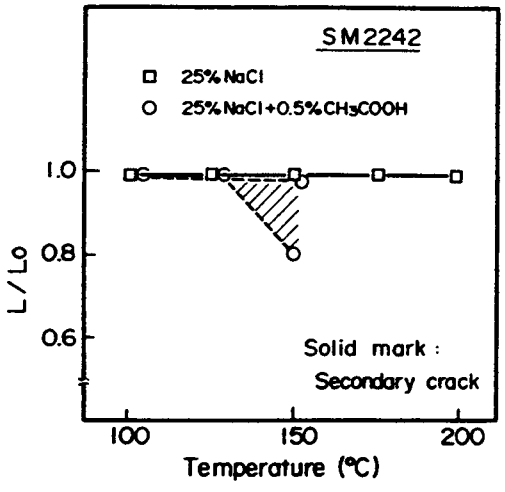


Fig. 10 Effect of acetic acid addition in brine on SCC susceptibility of SM2242-125 alloy
[Environment : (A); Condition (2)/ 25%NaCl, 10 bar H_2S-10 bar CO_2, (B); Condition (3)/ 25%NaCl-0.5%CH_3COOH, 10 bar H_2S-10 bar CO_2. Strain rate : 4 x $10^{-6}s^{-1}$]

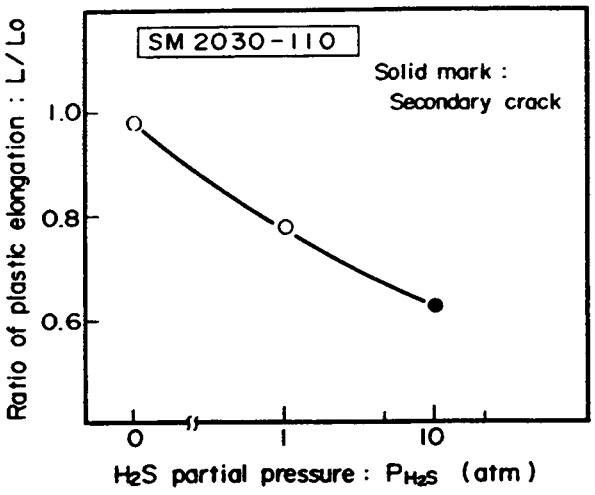


Fig. 11 Effect of partial pressure of H_2S on SCC susceptibility of SM2030-110 alloy
[Environment ; Condition (3), (4) and (5)/ 25%NaCl-0.5%CH_3COOH, H_2S-10 bar CO_2, Temperature : 150°C, Strain rate : 4 x $10^{-6}s^{-1}$]

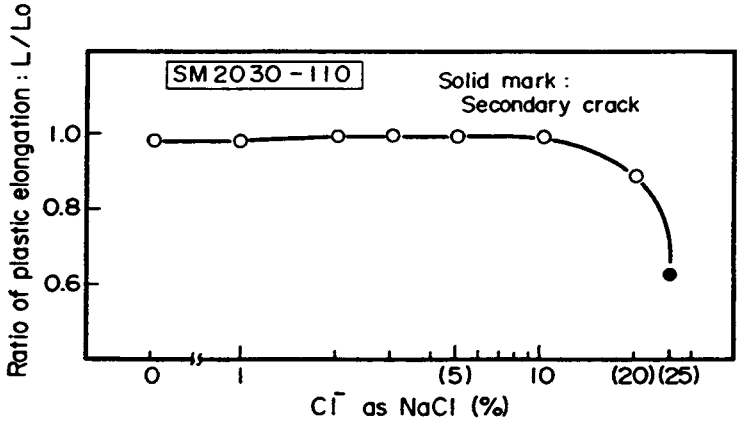


Fig. 12 Effect of chloride ion concentration on SCC susceptibility of SM2030-110 alloy
[Environment : Condition (3)/ NaCl-0.5%CH_3COOH, 10 bar H_2S-10 bar CO_2, Temperature : 150°C, Strain rate : 4 x $10^{-6}s^{-1}$]

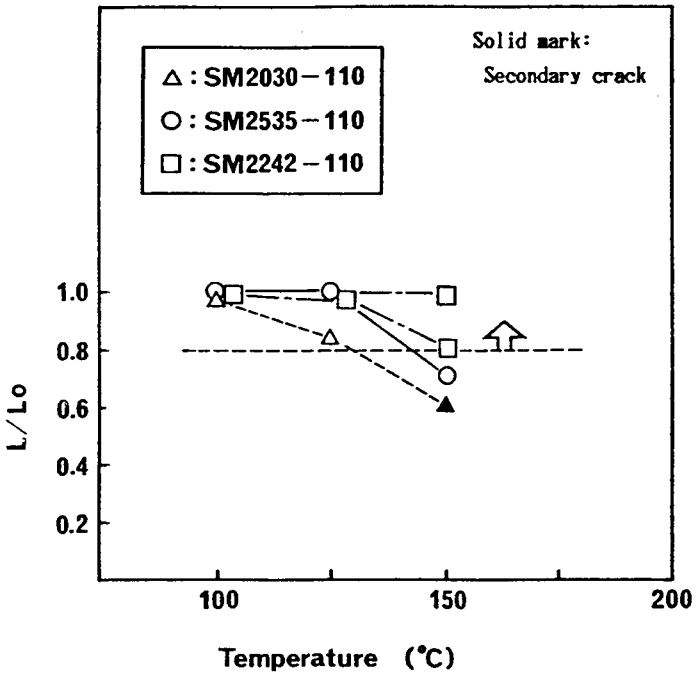


Fig. 13 Effect of alloys and temperature on SCC susceptibility of CRA [Environment : Condition (3)/ 25%NaCl-0.5%CH_3COOH, 10 bar H_2S-10 bar CO_2, Strain rate : 4 x 10^{-6} s^{-1}, Alloys : SM2030-110, SM2535-110 and SM2242-110]

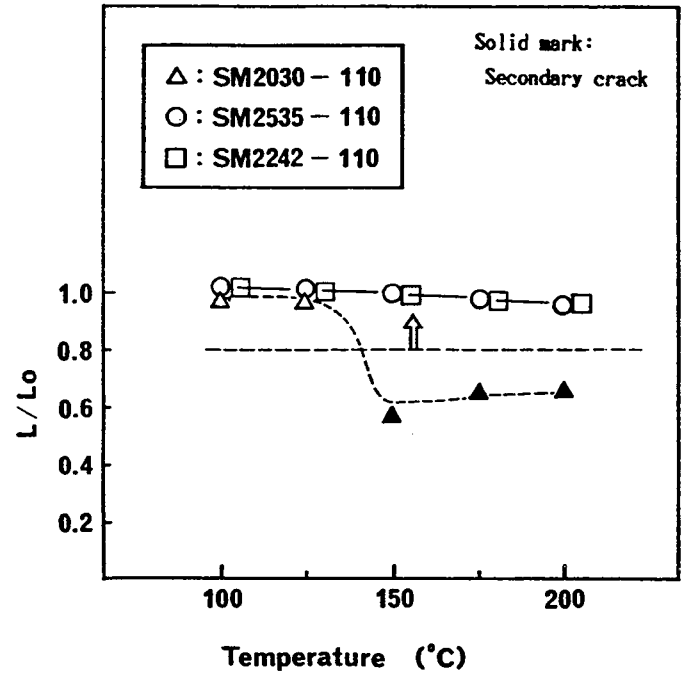


Fig. 14 Effect of alloys and temperature on SCC susceptibility of CRA [Environment : Condition (2)/ 25%NaCl, 10 bar H_2S-10 bar CO_2, Strain rate : 4 x $10^{-6}s^{-1}$, Alloys : SM2030-110, SM2535-110 and SM2242-110]

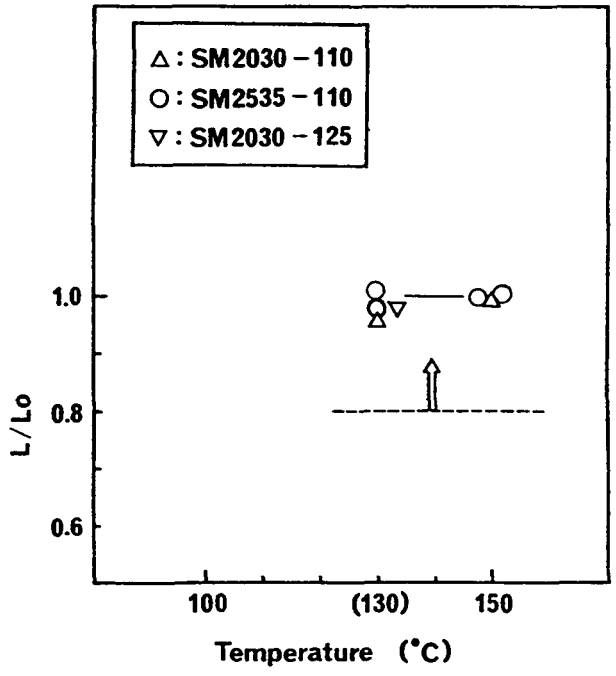


Fig. 15 - Effect of alloys and temperature on SCC susceptibility of CRA [Environment : Condition (6)/ 5%NaCl, 1 bar H_2S-20 bar CO_2, Strain rate : 4 x 10^{-6} s^{-1}, Alloys : SM2030-110, SM2030-125 and SM2535-110]

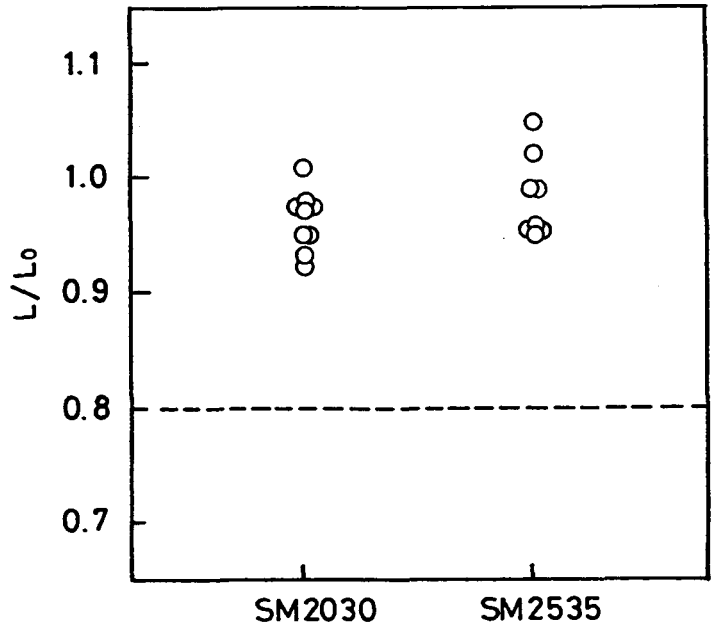


Fig. 16 Variances of L/Lo values of SM2030-110 and SM2535-110 in the SCC free condition
[Environment : Condition (7)/ 5%NaCl-0.5%CH_3COOH, 1 bar H_2S, Temperature : 80°C, Strain rate : 4 x 10^{-6} s^{-1}]

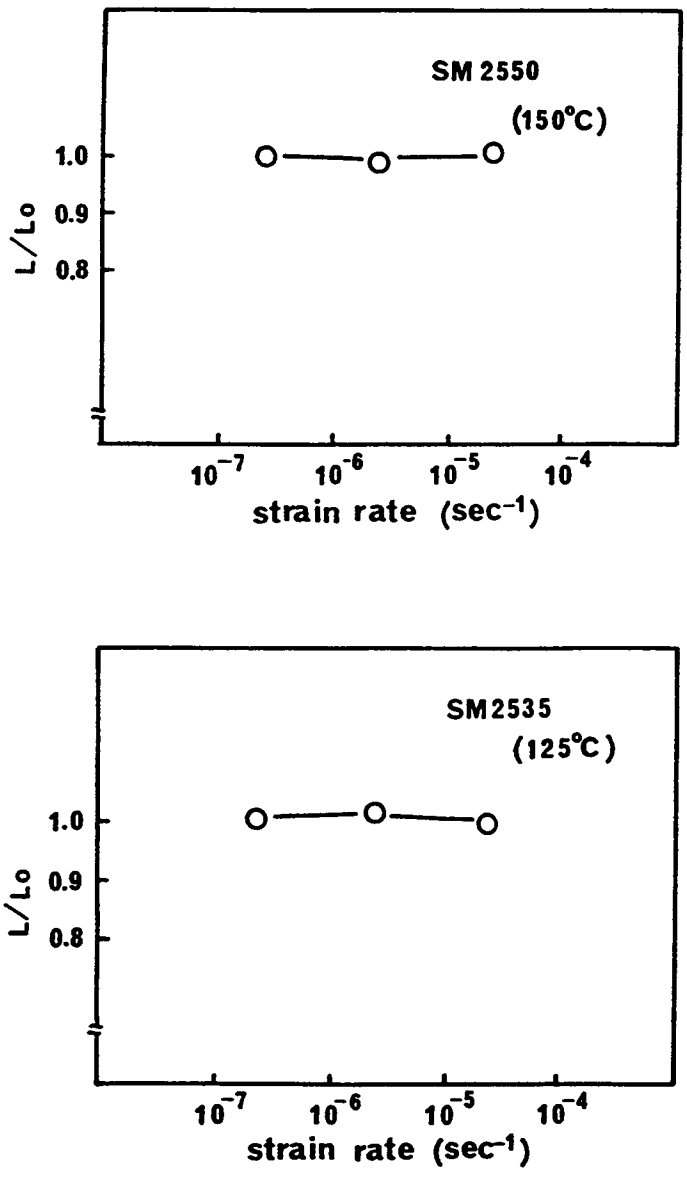


Fig. 17 Effect of strain rate on environmental cracking susceptibility of CRA at the critical temperature
[Environment : Condition (1) ; 25%NaCl-0.5%CH_3COOH, 7 bar, Strain rate : 4 x $10^{-6}s^{-1}$]

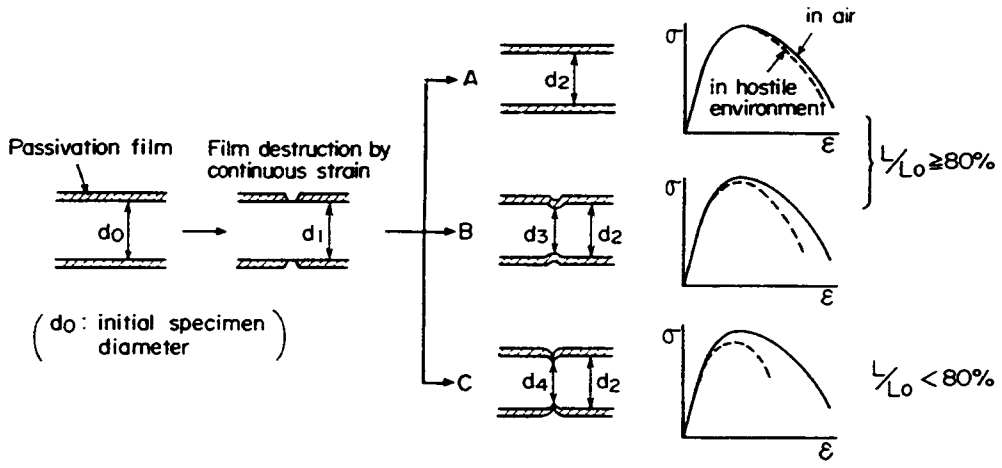


Fig. 18 Schematic illustration of environmental cracking behavior of CRA in hostile well environment by SSRT

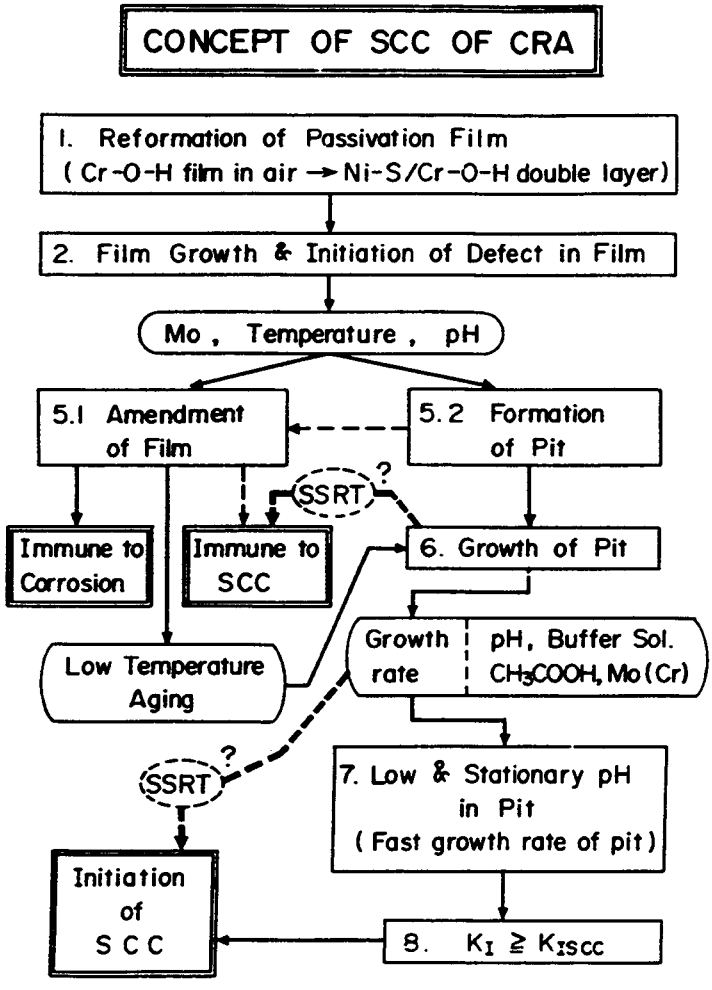


Fig. 19 Concept of SCC initiation of CRA in hostile well environment

Copyrighted Materials
Copyright © 1996 NACE International Retrieved from www.knovel.com

Paper No. 323—CORROSION/86

LABORATORY EVALUATION OF CORROSION RESISTANT ALLOYS FOR THE OIL AND GAS INDUSTRY

Juri Kolts
Cabot Corporation
1020 W. Park Avenue
Kokomo, IN 46902-9013

ABSTRACT

The environmental embrittlement of corrosion-resistant alloys (CRA), determined from laboratory experiments over the last five years, is reviewed in this paper. A number of environments, including ambient temperature production environments, high temperature production environments, high temperature packer fluids and low or high temperature acidizing fluids, cause cracking of some stressed CRA. Data is presented to identify the specific environment — alloy combinations which result in environmental embrittlement.

INTRODUCTION

The corrosion resistant alloys are used in the oil and gas industry because of their excellent corrosion resistance. In many cases the economics of using corrosion-resistant alloys is favorable over that of using corrosion inhibition. However, the basis for selection of corrosion-resistant alloys from among the many that are available, is generally not corrosion resistance but is rather resistance to environmental embrittlement. There are large differences in the environmental cracking resistance of corrosion resistant alloys being used in the oil and gas industry. Detailed knowledge of the cracking phenomena is needed to use the lowest cost materials that will provide acceptable performance. This paper is not an exhaustive literature review of cracking phenomena; rather it highlights the results of laboratory testing conducted at Cabot Corporation over the past five years. Table 1 describes the different alloys that are presently considered for use as corrosion-resistant alloys in oil and gas wells. There are four types of alloy systems, these being the martensitic stainless steels, the duplex (austenitic/ferritic) stainless steels, the fully austenitic stainless steels, and nickel-base alloys. For most applications, such as tubular goods, the duplex stainless steels, the austenitic stainless steels, and nickel-base alloys are utilized in the cold worked condition.

The early application of corrosion-resistant alloys was made on the basis of extensive testing in the laboratory. In these earlier tests, much of the data was obtained by exposure in environments containing 5% sodium chloride with acetic acid and H_2S. Test data in this environment, both at room temperature and elevated temperatures, was partially a basis for establishing a relative ranking in resistance to both hydrogen embrittlement and stress corrosion cracking. Subsequently, much testing has been done utilizing environments which more closely simulate those of actual field conditions. Examples of such environments include 25% NaCl solutions with or without alkalinity in the presence of acid bases, acidizing environments pressurized with acid bases, and various deaerated packer fluids .

Most laboratory results are conservative (where the most severe conditions are taken into consideration). Table 2 describes the factors which are important in determining both stress corrosion cracking and crevice corrosion resistance of alloys. These factors include time, temperature, salinity, pH or acidity, the redox and/or corrosion potential, the crevice geometry (in crevice corrosion) and both stress and the strength level of the alloy (in stress corrosion cracking). Stress corrosion cracking tests in the laboratory are generally conducted at or near the yield strength or even above the yield strength of the alloy in the pretested condition.

The pH of oil/gas production environments is a very important parameter in materials selection. The pH downhole can be directly determined by the partial pressure of CO_2 and H_2S, the presence of oxidants, alkalinity of the water and the temperature. It is often the secondary parameters, such as partial pressure of CO_2 and H_2S,

that are known in oil and gas wells. Often these vary with depth, time, temperature, and operating conditions of the well. Some important conditions of produced fluids, such as alkalinity, are often not even reported for different oil and gas wells. The amount and location of condensed water can change the above parameters within a well. Thus the conditions within a single well may vary considerably and local pH in a producing well may be difficult to determine. Consequently, much laboratory test data is required to simulate all of the conditions even in one well. Nevertheless, laboratory tests have been used to successfully select corrosion-resistant alloys in oil and gas applications.

EXPERIMENTAL PROCEDURE

Throughout the course of this investigation of stress corrosion cracking and crevice corrosion, a number of test techniques have been utilized. In the study of stress corrosion cracking, both C-shaped samples and C-ring samples described previously have been used.[1-3] Commercially available alloys were tested in these investigations. Deaerated analytical grade chemical solutions were used in autoclaves which were pressurized with appropriate gases containing either CO_2, H_2S, or premixed gases of H_2S and CO_2. Some tests are performed with air in the vapor space of the autoclaves. The partial pressures of the gases were controlled at room temperatures, subsequently the autoclaves were heated to the operating temperature. Pressures reported as partial pressure of H_2S or CO_2 are those measured at room temperature and not at the elevated temperatures. The partial pressures reported at ambient temperature are expected to be close to those at operating temperature since most of the pressure increase during heating is generated from steam. The pH of the solutions was controlled by appropriate NaOH additions to the solution prior to purging with gases. The pH measurements were made after equilibrium had been reached with the purge gas at atmospheric pressure. Autoclaves were periodically opened, the samples were inspected for stress corrosion cracking, new solutions added and the same samples were placed back into the autoclaves.

The crevice corrosion tests were run with procedures in autoclave exposures similar to those for stress corrosion cracking. Because of initial difficulties with the erratic results using TEFLON® crevice blocks which tended to creep at the elevated temperatures, ceramic crevice blocks with serrated configuration were employed. Samples were abraded prior to testing.

RESULTS AND DISCUSSION

Crevice Corrosion

At elevated temperatures, the crevice corrosion resistance of alloys can be of importance in selecting corrosion-resistant alloys for oil and gas service. In this investigation a number of alloys were exposed with ceramic blocks to produce crevices at 400°F (200°C) exposed to the environment for 60 days. Six environments listed in Table 3 are evaluated. All environments were deaerated except for the one listed were air was used to fill the vapor space in the autoclave. These tests evaluate the effect of pH at levels of 4.5 and 6, the effect of addition of about 1 psi H_2S to the environment, the effect of elemental sulfur additions, and the effects of aeration .

In the deaerated 25% NaCl solutions containing both carbon dioxide and hydrogen sulfide at pH 4.5 and 6.0, no serious crevice corrosion was found in any of the nickel-base alloys, such as H_2S, G-3, 8700, or C-276. However both 304 and 410 stainless steels are heavily affected at 200°C (400°F), both at pH 4.5 and at pH 6.0. Although few pits and/or slight crevice corrosion was detected on some of the stainless steels as shown in Table 3, no measurable weight loss was recorded. The environments, without air or elemental sulfur, were not particularly aggressive to the alloys other than 410 and 304 stainless steels.

Elemental sulfur was found to greatly accelerate the crevice corrosion attack of the alloys. Severe crevice corrosion occurred on the duplex stainless steels and the austenitic stainless steels in the presence of elemental sulfur at high temperatures. Severe localized corrosion is indicated by the weight loss values (mpy) in Table 3. These values are reported as "uniform penetration measurements" although the weight loss was caused by corrosion in the localized regions at crevices. Consequently, crevice penetration rates are much higher than reported in Table 3. No weight loss was observed on alloys 8700 or C-276 in the elevated temperature tests containing elemental sulfur.

The reader is reminded that in the presence of H_2S the results are from deaerated solutions. If the solutions were aerated, the environments would become much more aggressive. Even solutions at pH 8.5 with air, but no H_2S or elemental sulfur, were almost as aggressive as the pH = 6 solutions with sulfur. This information reinforces the knowledge that air should be precluded from any fluid that is injected into severe sour gas wells. It is

® TEFLON is a registered trademark of E.I. duPont.

believed that elemental sulfur and oxygen play a similar role in participating in a reduction reaction, thus accelerating crevice corrosion.

In some of the austenitic stainless steels, stress corrosion cracking occurred at punch marks or other stressed areas. Also, the expected more noble potential of the alloys, resulting from the presence of elemental sulfur or oxygen, would tend to accelerate stress corrosion cracking as is shown in Table 3.

HYDROGEN EMBRITTLEMENT

While much information has been developed on hydrogen embrittlement of the martensitic and precipitation hardenable alloys, this section will focus on nickel-base and cobalt-base alloys which have been studied to a lesser extent. Much of the earlier work (late 1970s and early 1980s) on environmental embrittlement of nickel-base alloys for the oil and gas industry was directed at hydrogen embrittlement. Table 4 displays a partial list of alloys that had been evaluated in this investigation of hydrogen embrittlement resistance. The test environment was the "NACE solution" described in NACE specification TM-01-77. Specimens were also aged at various temperatures. Over 2,000 specimens were tested. Either C-shaped or C-ring samples were employed, typically above the yield strengths of the alloys. Exposure times exceeded 1,000 hours. No cracking of the cobalt- or nickel-base alloys was observed in the absence of galvanic coupling with steel. Of the alloys listed in Table 4, only the cobalt-base alloys, such as alloys No. 25, 188, or MP35N® alloy, the 400 series stainless steels and alloy 718 exhibited cracking when coupled to carbon steel. The cobalt-base alloys exhibited cracking only at hardness levels exceeding about HRC 40. A contributing factor in producing sensitivity of the cobalt-base alloys to cracking is that they achieve a much higher strength level by cold working than do nickel-base alloys.

An example of the type of data used to construct Table 4 is shown in Table 5. For MP35N alloy, notice that hardness of the alloy does not necessarily reflect the susceptibility to embrittlement, as can be seen by comparing the different conditions at HRC 42-44 in Table 5. Also notice that the remedy for eliminating the susceptibility to hydrogen embrittlement of the cobalt-base alloys, such as MP35N alloy, 188, and 25, is aging near 752° to 807°C (1,400° to 1,500°F).

Aging at bottom hole temperatures of 175° to 257°C (350° to 500°F) increases the susceptibly of nickel-base and cobalt-base alloys to embrittlement. Examples to demonstrate this effect are shown in Table 6. Typically unaged (as cold worked) alloys are not embrittled even in extremely high strength conditions.

As the environmental temperature is increased above ambient, the susceptibility of the alloys to embrittlement by hydrogen greatly decreases. Table 7 shows that no embrittlement occurs in HASTELLOY® alloy C-276, even at yield strengths of 190 Ksi, when the temperature of the "NACE solution" is raised to 43°C (110°F). This data is especially significant since the NACE solution is truly an accelerated environment to test for hydrogen embrittlement.

The severity of an environment toward hydrogen embrittlement in nickel-base alloys is determined by the corrosivity of that environment toward steel, the conductivity of that environment and the presence of hydrogen poisons. The corrosivity toward steel is important since the hydrogen evolution in a steel coupled nickel-base alloy is related to the corrosion of the steel. In cases where steel does not corrode, embrittlement of nickel- or cobalt-base alloys, even in the most embrittlement sensitive condition, does not occur. On the basis of laboratory tests, materials selection has been made to minimize the incidence of hydrogen embrittlement especially of cold worked tubing. In liners or downhole applications, higher strength alloy C-276 components, with minimum yield strengths to 160 Ksi, have been used. Because of the higher operating temperature downhole, there is much less concern about hydrogen embrittlement. Other alloys such as alloy G-3 or alloy 825 do not have maximum strength restrictions imposed by hydrogen embrittlement resistance since these alloys are not particularly susceptible to cracking in these environments. Rather, the ductility of these alloys is reduced if their strength level is increased to too high a level.

The present practice, when using downhole tubulars in the oil and gas industry, is to control the yield strength of alloy C-276 in the range 110 to 150 Ksi, in cases where the tubing can reach ambient temperature. This restriction is thought to be overly conservative and will probably be relaxed as more experience is gained.

PRODUCTION FLUIDS

Historically, laboratory testing with simulated production fluids has been in unbuffered environments usually containing sodium chloride and various partial pressures of carbon dioxide and hydrogen sulfide. Earlier evaluations were performed with the addition of acetic acid to accelerate the rate of stress corrosion cracking.

® MP35N is a registered trademark of SPS Technologies, Inc.
® HASTELLOY is a registered trademark of Cabot Corporation.

More recently, attempts have been made to more nearly simulate production fluid environments without the use of acetic acid. The importance of acidity in accelerating stress corrosion cracking has established the results of earlier tests to be especially aggressive in relationship to existing oil and gas wells.

While considerable information exists on the sulfide stress cracking of martensitic stainless steels in severe H_2S containing environments, an attempt was made to determine the high temperature limits above which 420 stainless steel tubulars no longer exhibit sulfide stress cracking. Table 8 presents this information on sulfide stress cracking of 13% chromium martensitic stainless tubular steel in a low partial pressure H_2S containing environment at various temperatures. The limiting conditions imposed on 420 stainless steel are susceptibility to corrosion and sulfide stress corrosion cracking. Therefore, the elevated temperature environments are more severe from a corrosion standpoint but low temperature environments are more severe toward sulfide stress cracking. Stress corrosion cracking did occur in laboratory tests with a partial pressure of .03 psi H_2S at 90°C (195°F). However, the mode of cracking was blunt as seen in Figure 1. Possibly much corrosion occurred after cracking. As the temperature decreased or the strength level increased, the cracking became sharper and more typical of classical sulfide stress corrosion cracking in martensitic steels. Thus in this environment, no cracking occurred above about 92°C (200°F).

Stress corrosion cracking of duplex stainless steels is controlled by the same environmental parameters as in nickel-base alloys. However, the response to some of these parameters, for example temperature, may not be the same as for nickel-base alloys. Table 9 shows the effect of only two parameters, namely temperature and hydrogen sulfide content. In duplex stainless steels, certainly strength levels, stress, time, and all of the other parameters must be considered to fully establish the regime for successful use. Table 9, however, does demonstrate that low alkalinity solution, in the presence of hydrogen sulfide, cause stress corrosion cracking of the duplex stainless steels. Because of the incidence of cracking of duplex stainless steels at relatively low partial pressures of H_2S as shown in Table 9 and numerous other references, duplex stainless steels should be used only in low hydrogen sulfide containing environments. Only when conditions such as low stress levels or high alkalinity in the solutions are met should duplex stainless steels be considered for higher hydrogen sulfide containing environments.

The highly alloyed austenitic stainless steels and nickel-base alloys exhibit considerable improvements in stress corrosion cracking resistance over the duplex stainless steels. Table 10 presents stress corrosion cracking data of austenitic alloys in four different environments. These environments can establish the relative stress corrosion cracking resistance of these alloys. As is established in the oil and gas industry, the stress corrosion cracking resistance in production fluids has the relative rating, with alloy C-276 showing the highest resistant to stress corrosion cracking, and alloys G-3, 825, 535, and alloy 28 with correspondingly reduced resistance. Nevertheless, in deaerated environments containing high partial pressures of hydrogen sulfide, the stress corrosion cracking resistance of alloy 28 is excellent. With lowered pH and incidence of oxidants, higher alloys than alloy 28 are required for tubing applications. These environments utilized in the laboratory demonstrate the importance of the parameters outlined in Table 2. While the laboratory data is comprehensive in determining the stress corrosion cracking resistance of a number of alloys, there is a lack of published field data where all of the important parameters, which determine stress corrosion cracking resistance, are known. Therefore, the limitations placed presently on alloy selection are not on the quality of laboratory data, but rather are on the quality of information that is presently known from field operations utilizing corrosion-resistance alloys. Table 11 shows the relative importance of two environmental components, elemental sulfur and alkalinity. These tests were conducted for a one-year period using 25% NaCl solutions that were deaerated and purged with appropriate gases. As the pressure of the gases is increased and as the temperature is raised, these pH values are expected to change somewhat. In low alkalinity environments, alloy C-276 is the only alloy that has shown resistance to stress corrosion cracking in the presence of elemental sulfur at temperatures above 180°C (350°F). Notice from Table 11 that almost all of the austenitic stainless steels showed no evidence of stress corrosion cracking in similar environments but absence of elemental sulfur to 257°C (500°F). The condition with elemental sulfur represents wells containing or producing gases with very high hydrogen sulfide partial pressures.

Notice the importance of alkalinity of the environments; the high alkalinity environments (pH of 7.5) do not readily cause stress corrosion cracking, even in duplex stainless steel, at high partial pressures of hydrogen sulfide at 230°C (450°F).

Time is an important factor; failures may not occur in the first month of exposure but may occur in the second and third months, or even after one year of exposure. For this reason, many other investigators have tried to accelerate the effect of time by increasing temperature or adding acidity above levels ordinarily expected in the particular sour gas wells.

Sulfur solvents, such as ethylamine or monoethanol amines, are often injected into extremely severe wells to control sulfur plugging of production tubing. Sulfur solvents will affect the severity of the environment in two ways. First, sulfur solvents will tend to increase the pH of the environment therefore greatly decreasing the severity towards stress corrosion cracking. Second, the sulfur solvents will dissolve the elemental sulfur, thus the redox reaction, which is involved in promoting stress corrosion cracking, may be greatly inhibited. Stress corrosion cracking tests performed in environments, such as those in Table 11 but containing additions of monoethylamine, have indeed confirmed that no stress corrosion cracking has occurred during two months exposure on those alloys listed in Table 11.

In summary, performance in production fluids is determined by the alloy-environment combination. The recent trends in laboratory testing have clearly distinguished the performance of alloys, especially in environments which closely simulate field environments.

PERFORMANCE IN ACIDIZING ENVIRONMENTS

Performance in acidizing environments may be an important consideration in material selection. Results, to date, show that only the hydrochloric acid and hydrofluoric environments can produce potential problems.

Table 12 shows the corrosion rate in simulated acidizing environments containing inhibited hydrochloric acid and sodium chloride in the presence of hydrogen sulfide. Problems can be encountered in carbon and low alloy steels as well as in nickel-base alloys if the acidizing is not carefully controlled. Above 120°C (250°F), the corrosion rate of most of the corrosion-resistant alloys become quite high, the notable exception being alloy C-276 which shows very low corrosion rates in the hydrochloric acid stimulation environments, even to 175°C (350°F). Alloying elements have large effects on corrosion resistance of materials in acidizing environments . With hydrochloric acid additions, chromium in alloys is generally detrimental and molybdenum is beneficial for corrosion resistance. Consequently, alloy C-276 shows excellent performance to corrosion resistance in acidizing environments. Corrosion problems, as identified by laboratory testing, are generally not encountered in acidizing environments containing other than hydrochloric acid. However, Table 13 shows that stress corrosion cracking in the lower alloyed austenitic stainless steels and nickel-base alloys can occur in hydrofluoric acid.

The presence of hydrogen sulfide in concentrated HCl can gave detrimental effects, even at room temperature. Tables 14 and 15 show that in the absence of hydrochloric acid inhibitors, many of the corrosion-resistant alloys are susceptible to stress corrosion cracking at room temperature and at 70°C (160°F). The addition of specific inhibitors greatly reduce the susceptibility to stress corrosion cracking. Additional investigations on inhibitor effects may prove quite valuable. Only alloy C-276 did not show cracking in the presence or absence of inhibitors . In the presence of HCl inhibitors, alloys 825, G-3, and C-276 did not crack at the two temperatures tested.

Embrittlement in room temperature HCl in the presence of H_2S is not thought to be the classical type of hydrogen embrittlement since alloy C-276, which was highly cold worked, was not susceptible, while alloy 535 and SANICRO® 28 were highly susceptible. Ordinarily, high strength alloy C-276 is more susceptible to cracking by hydrogen charging than are the other mentioned alloys. Contrary to the intergranular cracking ordinarily seen after classical hydrogen embrittlement of nickel-base alloys, the cracking at room temperature in this environment is fine, typical transgranular stress corrosion cracking, as noticed in the austenitic stainless steels in the presence of HCl and H_2S. However, as the temperature is increased, the cracking becomes increasingly blunted and becomes less of a potential for failure as shown in Figure 2. The additional corrosion that occurs during cracking greatly reduces the rate of crack propagation. Nevertheless, this mode of cracking at low temperatures in the presence of hydrogen sulfide requires additional investigation.

CLEAR PACKER FLUIDS

Clear packer fluids are utilized in deep sour gas wells because of their density. The pH of different combinations of packer fluids has not been thoroughly investigated. However, deaerated packer fluids, can by themselves, in the absence of hydrogen sulfide, present a potential for stress corrosion cracking. Table 16 presents the results of unihibited, deaerated packer fluids on the stress corrosion cracking behavior of nickel-base alloys at elevated temperatures.

The presence of hydrogen sulfide is known to accelerate the stress corrosion cracking of these alloys. For example, $MgCl_2$ solutions containing H_2S have produced stress corrosion cracking in alloys that ordinarily exhibit excellent resistance in comparable environments without H_2S. However, even in the absence of hydrogen

® SANICRO is a registered trademark of Sandvikens Jernverks AK.

sulfide, some packer fluids may be excessively aggressive to the lower alloyed nickel-base alloys at very high temperatures. Even alloy C-276 is susceptible to stress corrosion cracking in zinc bromide solutions at 202°C (400°F). This investigation has not considered the effect of inhibitors which are typically added to clear packer fluids. However, the presence of stress corrosion cracking of alloy C-276 in zinc bromide solutions requires additional testing in the presence of corrosion inhibitors before these packer fluids are used for extended periods. Notice that calcium bromide is not aggressive to many of the alloys. The stress corrosion cracking of nickel-base alloys in packer fluids, considering the effects of various combinations of chemicals, the selection of inhibitors, and influence of H_2S has taken one of the most neglected areas in laboratory investigations for sour gas wells. Much more work on the stress corrosion cracking behavior in packer fluids is warranted.

SUMMARY

While many of the fundamental aspects of stress corrosion cracking have been recognized for many years, stress corrosion cracking is still a problem to be addressed in the oil and gas industry. Two important reasons are cost and extreme severity of newly discovered wells. Alloys that exhibit the best performance (such as HASTELLOY alloy C-276) cost more to manufacture than nickel-base alloys with lesser performance. Consequently, the engineer tries to select the alloy with lowest cost and possibly lowest acceptable performance for that application. Also, because of the severity and diversity of newly discovered oil and gas environments, alloy-environment combinations have been discovered which, prior to their discovery, were not thought to cause materials embrittlement. Only recently have these embrittling alloy-environment combinations been discovered.

This paper has summarized the results of laboratory tests for addition in material selections of corrosion-resistant alloys in deep sour gas wells. While not exhaustive, the following guidelines may be utilized in material selection for each of the following categories. The specific considerations must be made.

1. For the martensitic stainless steels, the corrosion resistance in the production environment must be considered. The sulfide stress corrosion cracking resistance, at even low concentrations of H_2S, must be examined. Where hydrochloric acid acidizing is utilized, corrosion resistance and environmental embrittlement must be considered.
2. When using duplex stainless steels, localized corrosion resistance should be considered. Stress corrosion cracking resistance of duplex stainless steels, especially in high H_2S environments, is of great importance. And, finally, stress corrosion cracking in hydrochloric acid environments is of importance.
3. In the selection of the austenitic alloys, such as alloy 628 or 535, the presence of elemental sulfur and the presence of excessive acidity in production environments need to be considered. In addition, stress corrosion cracking in hydrofluoric acid stimulation fluids could pose limitations on this alloy. Finally, the use of packer fluids, such as zinc bromide, limit the use of these alloys, especially at elevated temperatures.
4. The use of alloys 825, G-3, and alloy 8700 is limited by the presence of elemental sulfur, especially in unbuffered environments at high temperatures. In addition, a potential for cracking in high temperature zinc bromide solutions occur. Therefore, in excessively high hydrogen sulfide partial pressures, the use of these alloys should be very carefully considered and alloys C-276 or C-22 should be the alloys selected for the most corrosive high hydrogen sulfide applications.
5. Alloy C-276 is the nickel-base alloy most resistant to stress corrosion cracking with the possible exception of alloy C-22. Alloy C-276 is susceptible to stress corrosion cracking in zinc bromide solutions and careful consideration must be made before using this type of packer fluid at high temperatures. Alloy C-276 has the potential for sulfide stress corrosion cracking at low temperatures. In severe low temperature applications, maximum strength levels are generally imposed appropriate to the severity of the environment.

REFERENCES

1. J. Kolts, *Journal of Materials for Energy Systems* 5, 2(1983), p. 71.
2. A.I. Asphahani, *Corrosion* 37 (1981), p. 327.
3. A.I. Asphahani, Proceedings of the Seventh International Congress on Metallic Corrosion, held Oct. 1978, paper no. 192 (Houston, TX: NACE, 1978).
4. S.B. Maldonado-Zalgal, P.J. Boden, *British Corrosion* 17, 3(1982).
5. T.D. Whitehead, "Factors Influencing Pitting and Cracking Resistance of all Type 420 Stainless Steel in CO_2 Environments" (Master's Thesis, Ohio University, 1984).

Table 1

ALLOYS USED FOR DOWNHOLE TUBING

NAME	ALLOY	STRUCTURE	CONDITION
13 Chromium Steel	13 Cr STAINLESS STEEL	MARTENSITE	HEAT TREATED
UNS S31803	22 Cr DUPLEX STAINLESS STEEL	DUPLEX AUSTENITE/FERRITE	COLD WORKED
FERRALIUM® alloy 255	25 Cr DUPLEX STAINLESS STEEL	DUPLEX AUSTENITE/FERRITE	ANNEALED
SANICRO® 28	28% Cr STAINLESS	AUSTENITE	COLD WORKED
HASTELLOY® alloy 535	Ni BASE	AUSTENITE	COLD WORKED
ALLOY 825	Ni BASE	AUSTENITE	COLD WORKED
HASTELLOY alloy G-3	Ni BASE	AUSTENITE	COLD WORKED
HASTELLOY alloy C-276	Ni BASE	AUSTENITE	COLD WORKED

TABLE 2

FACTORS AFFECTING CREVICE CORROSION

AND STRESS CORROSION CRACKING

Crevice Corrosion	Stress Corrosion Cracking
TIME	TIME
TEMPERATURE	TEMPERATURE
CHLORIDE CONTENT	CHLORIDE CONTENT
pH	pH
POTENTIAL	POTENTIAL
ALLOY CONTENT	ALLOY CONTENT
P_{CO_2}	P_{CO2}
P_{H_2S}	P_{H2S}
OXIDANTS	OXIDANTS
	GALVANIC EFFECTS
CREVICE GEOMETRY	STRESS
	STRENGTH LEVEL

TABLE 3

CERAMIC CREVICE BLOCKS - CREVICE CORROSION TESTS

400°F, 25% NaCl
115 psi Initial Pressure at Room Temperature
2 Months Exposure

Alloy	99% CO_2 1% H_2S pH = 4.5		99% CO_2 1% H_2S pH = 6		99% CO_2 1% H_2S + 1g/l S^0 pH = 4.5		99% CO_2 1% H_2S + 1g/l S^0 pH = 6		Air pH = 8.5		CO_2 pH = 4.5	
		mpy		mpy		mpy		mpy		mpy		mpy
410 SS	PC	1.2	PC	1.3	PC	21	PC	34	PC	2.5	PC	1.0
304	PC	1	PC	1	PC SCC	6.5	PC	1.2	PC SCC	2.6		*
316	P	*	P	*	PC SCC	3.8	PC	1.5	PC SCC	1.2		*
317LM	P	*	P	*	PC SCC	3.0	C	1.1	PC	1.1		*
904L	P	*	P	*	PC SCC	2.3	PC	1.1	P	*	P	*
26-1	PC	•	PC	*	PC	4.6	PC	8.0	PC	*	PC	*
254 SMO	P	*	P	*	PC	1.5	C	1.1		*	P	*
2205		*	P	*	P	*		*	C	*	P	*
255		•	P	*	PC	*	P	*	PC	*	P	*
825	P	*	P	*	P	*	P	*	C	*		*
G-3			P	•	PC	*		*	PC	*		*
G-30		*		*	P	*		*	P	*	P	*
8700		*		•		*		*	P	*		*
C-276		*		*		*		*		*		*

P = Pitted
C = Crevice Attack
SCC = Stress Corrosion Cracking at Punch Marks
* = Less than 1 mpy

TABLE 4

HYDROGEN EMBRITTLEMENT TESTS

Transverse C-Shape Specimens
(Carbon Steel Couple)

NACE SOLUTION
ROOM TEMPERATURE

One Thousand Hour Exposures

ALLOYS NOT SUSCEPTIBLE TO CRACKING AT 60% COLD WORK

Alloy 535
Alloy 825
Alloy G
Alloy G-3
MULTIMET® Alloy
Alloy S
Alloy 625
Alloy 8700
Alloy C-276
Alloy C-276
Alloy C-22

ALLOYS SUSCEPTIBLE TO CRACKING AT 60% COLD WORK

Alloy No. 25
Alloy No. 188
MP35N Alloy
Alloy No. 718
410 Stainless Steel (Heat Treated)

TABLE 5

Hydrogen Embrittlement

MP35N MULTIPHASE ALLOY
TRANSVERSE C-SHAPE SPECIMENS WITH CARBON STEEL HOLDERS

NACE SOLUTION AT ROOM TEMPERATURE

Condition	Hardness (HRC)	Time to Failure (Hours)
10% CR*	23; 24; 24	>1000; >1000; >1000
20% CR	32; 32; 33	>1000; >1000; >1000
30% CR	36; 37; 37	>1000; >1000; >1000
40% CR	40; 40; 40	384; 552; >1000
50% CR	42; 43; 43	168; 192; 552
60% CR	42; 43; 43	106; 168; 624
10% CR + 200 hrs. @ 400°F	23; 23; 24	>1000; >1000; >1000
20% CR + 200 hrs. @ 400°F	33; 33; 34	>1000; >1000; >1000
30% CR + 200 hrs. @ 400°F	37; 38; 38	>1000; >1000; >1000
40% CR + 200 hrs. @ 400°F	41; 43; 43	168; >1000; >1000
50% CR + 200 hrs. @ 400°F	43; 43; 45	960; >1000; >1000
60% CR + 200 hrs. @ 400°F	45; 46; 46	120; 240; >1000
10% CR + 4 hrs. @ 1000°F + 1 hr. @ 1500°F	20; 21; 21	>1000; >1000; >1000
20% CR + 4 hrs. @ 1000°F + 1 hr. @ 1500°F	29; 29; 30	>1000; >1000; >1000
30% CR + 4 hrs. @ 1000°F + 1 hr. @ 1500°F	34; 34; 34	>1000; >1000; >1000
40% CR + 4 hrs. @ 1000°F + 1 hr. @ 1500°F	40; 40; 41	>1000; >1000; >1000
50% CR + 4 hrs. @ 1000°F + 1 hr. @ 1500°F	42; 43; 43	>1000; >1000; >1000
60% CR + 4 hrs. @ 1000°F + 1 hr. @ 1500°F	43; 43; 44	>1000; >1000; >1000

* CR = % Reduction by Cold Rolling.

TABLE 6

Alloy No. 625

TRANSVERSE C-SHAPE SPECIMENS WITH CARBON STEEL HOLDERS

NACE SOLUTION AT ROOM TEMPERATURE

Condition	Hardness (HRC)	Time to Failure (Hours)
10% CR*	32; 32; 33	>1000; >1000; >1000
20% CR	37; 37; 37	>1000; >1000; >1000
30% CR	32; 40; 40	>1000; >1000; >1000
40% CR	42; 42; 43	>1000; >1000; >1000
50% CR	43; 44; 44	>1000; >1000; >1000
60% CR	44; 44; 44	>1000; >1000; >1000
10% CR + 200 hrs. @ 400°F	32; 32; 32	>1000; >1000; >1000
20% CR + 200 hrs. @ 400°F	33; 38; 38	>1000; >1000; >1000
30% CR + 200 hrs. @ 400°F	40; 40; 40	>1000; >1000; >1000
40% CR + 200 hrs. @ 400°F	44; 45; 45	>1000; >1000; >1000
50% CR + 200 hrs. @ 400°F	45; 46; 46	336; >1000; >1000
60% CR + 200 hrs. @ 400°F	46; 46; 47	120; 168; 336;

CR = Percent Reduction by Cold Rolling.

TABLE 7

Hydrogen Embrittlement of Alloy C-276

Effect of Environmental Temperature

C-Ring Specimens, Steel Bolts, 0.9 - 0.95 σ T and
C-Shape Specimens, Steel Holders

NACE Solution - Test Duration >1000 Hours

	Yield (Ksi)	Environmental Temperature 75°F	110°F	130°F	150°F	200°F	250°F
As-Cold Worked	191	NC**					
Aged 500°F, 250 Hours	156	NC			NC	NC	
Aged 500°F, 250 Hours	183	C*			NC	NC	NC
Aged 500°F, 250 Hours	191	C	NC***	NC***	NC	NC	

*C = Cracking

** NC = No Cracking

*** Tests performed with C-shaped samples

TABLE 8

SULFIDE STRESS CRACKING OF ALLOYS

C-RING SPECIMENS

STRESSED TO 90-95% σ_y 5000ppm Cl, 90 psi CO_2 + .03 psi H_2S

TEMPERATURE, °F	TIME TO FAILURE	
	420 STAINLESS L-80 Grade	FERRALIUM® alloy 255 Mill Annealed
195	48 Hrs.	NC
250	NC	NC
350	NC	NC
400	NC	NC

NC - No Cracking

TABLE 9

STRESS CORROSION CRACKING IN ANNEALED FERRALIUM ALLOY 255

THE EFFECT OF H_2S IN CO_2, H_2S, Cl ENVIRONMENTS

1000 HOURS EXPOSURE

C-Ring Samples Stressed to 90-95% σ_y

Temperature, (°F)	%H_2S, Pressure = 90 psia		
	0.04	1	10
78		NC	C
195	NC	NC	C
250	NC	NC	C
300		NC	C
350	NC	NC	C
400	NC	NC	C
450		NC	C

C - Cracking
NC - No Cracking

TABLE 10

STRESS CORROSION CRACKING OF VARIOUS ALLOYS

C-SHAPED SAMPLES, LIKE ALLOY HOLDERS

1000 HOUR TESTS

	DEAERATED 25% NaCl 190 psia H_2S 400°F	DEAERATED 25% NaCl 90 psia 90% CO_2 10% H_2S 500°F	BOILING $MgCl_2$ 309°F	DEAERATED 25% NaCl 0.5% CH_3 COOH 90 psia 90% CO_2 10% H_2S 400°F
Alloy 28	NC	NC	C	C
Alloy 535	NC	NC	C	C
Alloy 825	NC	NC	C	C
Alloy G-3	NC	NC	NC	C
Alloy C-276	NC	NC	NC	NC

C- Cracking
NC - No Cracking

TABLE 11

EFFECT OF ELEMENTAL SULFUR AND pH ON STRESS CORROSION CRACKING

C-SHAPED SAMPLES, LIKE ALLOY HOLDERS

DEAERATED 25% NaCl + 1 g/l Sulfur (No Acid Added)

ANNEALED ALLOYS

Time to Failure, Months, 12 Month Exposure

	350°F 100 psi H_2S pH = 4.5	450°F 100 psi H_2S pH = 4.5	450°F pH = 7.5 (90%CO_2, 10%H_2S) 100 psi
UNS S31803	1, 1, 1	1, 1, 1	NC, NC, NC
Duplex Alloy 255	1, 1, 1	1, 1, 1	NC, NC, NC
Alloy 904L	2, 2, 2	1, 1, 1	NC, NC, 12
Alloy 28	1, 2, 2	1, 1, 1	NC, NC, NC
Alloy 925, 30% CW	1, 1, 1	1, 1, 1	4, 4, 5
Alloy 925, Aged	1, 1, 1	1, 1, 1	3, 4, 4,
Alloy 535	1, 2, 2,	1, 1, 1	NC, NC, NC
Alloy 718 (Heat Treated HRC 45)	1, 1, 1	1, 1, 1	2, 2, 2
Alloy 825	2, 2, 2	1, 1, 2	NC, NC, NC
Alloy G-3	7, 8, 8,	1, 2, 3	NC, NC, NC
Alloy 8700	2, 2, 2	1, 1, 1	NC, NC, NC
Alloy C-276	NC, NC, NC	NC, NC, NC	NC, NC, NC

NC - No Cracking

TABLE 12

CORROSION RATES IN SIMULATED ACIDIZING ENVIRONMENTS

15% HCl + 5% NaCl + INHIBITOR + H_2S (75 psig)

24 HOUR TESTS, 0.040" THICK SPECIMENS, MILS PER DAY

	200°F	250°F	300°F	350°F
Alloy 28	0.2	3.3	DISSOLVED	DISSOLVED
Alloy 535	0.06	8.2	DISSOLVED	DISSOLVED
Alloy 825	0.15	6.2	DISSOLVED	DISSOLVED
Alloy G-3	0.55	4.1	DISSOLVED	DISSOLVED
Alloy C-276	0.02	0.5	2.5	3.1

TABLE 13

STRESS CORROSION CRACKING

C-SHAPED SAMPLES, LIKE ALLOY HOLDERS

INHIBITED ACIDIZING ENVIRONMENTS, 24 HOUR TESTS

ALLOY	15% HCl 5% NaCl 75% psi CO_2 350°F	20% $MgCl_2$ 5% NaCl 75% psi H_2S 350°F	3% HF 5% NaCl 75% psi CO_2 350°	12% Formic Acid 5% NaCl BOILING
Alloy 28	NC	NC	C	NC
Alloy 535	NC	NC	C	NC
Alloy 825	NC	NC	NC	NC
Alloy G-3	NC	NC	NC	NC
Alloy C-276	NC	NC	NC	NC

C - Cracking
NC - No Cracking

TABLE 14

STRESS CORROSION CRACKING

C-SHAPED SAMPLES. LIKE ALLOY HOLDERS

10% HCl + 1 ATMOSPHERE H_2S. 70°F

COLD WORKED SAMPLES. 168 HOUR TESTS

	HRC	NO INHIBITOR	2% INHIBITOR (AK 12)
UNS S31803	36	DISSOLVED	CRACKED
Alloy 255	37	DISSOLVED	CRACKED
Alloy 28	32	CRACKED	NO CRACKS
Alloy 535	32	CRACKED	NO CRACKS
Alloy 825	30	CRACKED	NO CRACKS
Alloy G-3	37	CRACKED	NO CRACKS
Alloy C-276	44	NO CRACKS	NO CRACKS

TABLE 15

STRESS CORROSION CRACKING

C-SHAPED SAMPLES, LIKE ALLOY HOLDERS

10% HCl + 1 ATMOSPHERE H_2S, 160°F

COLD WORKED SAMPLES, 168 HOUR TESTS

	NO INHIBITOR	2% INHIBITOR (AK 12)
UNS S31803	DISSOLVED	DISSOLVED
Alloy 255	DISSOLVED	NO CRACKS
Alloy 28	CRACKED	CRACKS
Alloy 535	CRACKED	CRACKS
Alloy 825	CRACKED	NO CRACKS
Alloy G-3	CRACKED	NO CRACKS
Alloy C-276	NO CRACKS	NO CRACKS

TABLE 16

STRESS CORROSION CRACKING IN SIMULATED CLEAR PACKER FLUIDS

C-SHAPE SAMPLES LIKE ALLOY HOLDERS

DEAERATED, N_2 BACKFILL, 400°F

ANNEALED ALLOYS, TIME TO FAILURE, MONTHS

ONE YEAR EXPOSURE, NO INHIBITORS

ALLOY	47% $ZnBr_2$	43% $CaBr_2$
Alloy 255	1, 1, 2	4, 4, 4
Alloy 535	1, 2, 2	4, 10, NC
Alloy 825	1, 1, 2	NC, NC, NC
Alloy G-3	1, 2, 2	NC, NC, NC
Alloy C-276	1, 1, 2	NC, NC, NC
Alloy C-22	NC, NC, NC	NC, NC, NC

NC - No Cracking

® FERRALIUM is a registered trademark of Bonar Langley Alloys Ltd.

® HASTELLOY is a registered trademark of Cabot Corporation.

® MP35N is a registered trademark of SPS Technologies, Inc.

® MULTIMET is a registered trademark of Cabot Corporation.

® SANICRO is a registered trademark of Sandvikens Jernverks AK.

® TEFLON is a registered trademark of E.I. duPont

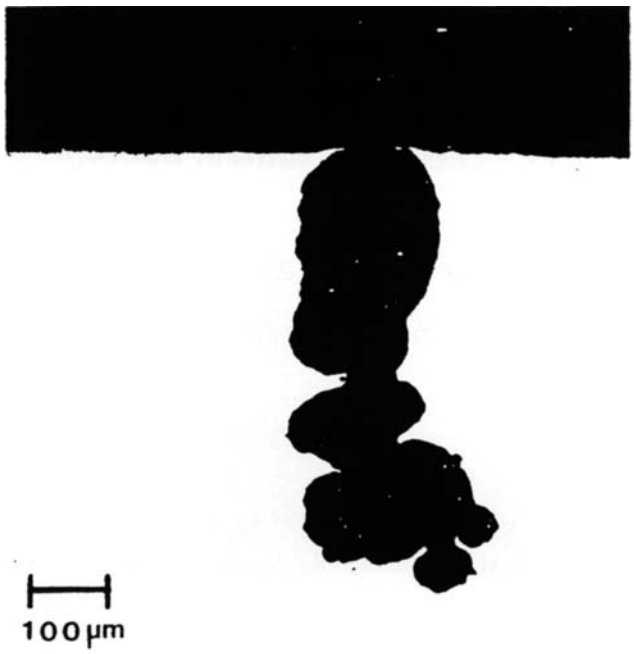


Figure 1. Fracture mode of T420 stainless steel tubing at 195°F

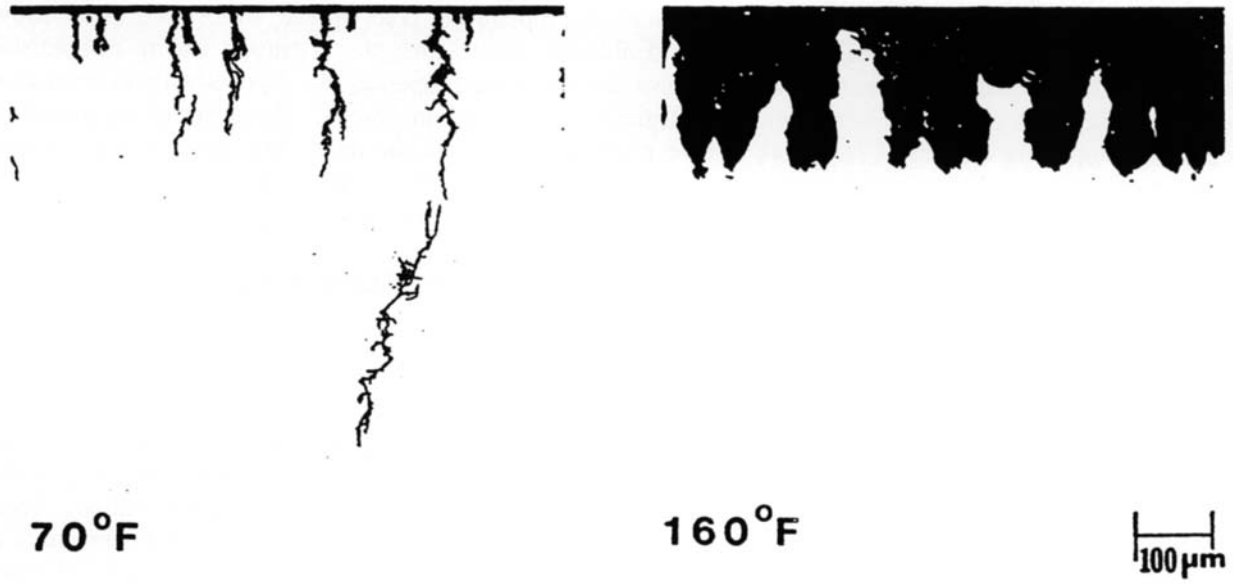


Figure 2. Cross section of stress corrosion cracks found in alloy 825 in 10% HCl at indicated temperatures.

Copyrighted Materials
Copyright © 1996 NACE International Retrieved from www.knovel.com

Paper No.
58

CORROSION 92
The NACE Annual Conference and Corrosion Show

TEMPERATURE AND TEXTURE EFFECTS ON PROPERTIES OF CRA'S

S. E. Mahmoud and C. W. Petersen
Exxon Production Research Company
Post Office Box 2189
Houston, Texas 77252-2189

M. J. Luton
Exxon Research and Engineering
Clinton Township
Route 22 East
Annandale, New Jersey 08801-9999

ABSTRACT

The results of this study show that the mechanical properties of cold-worked, corrosion-resistant alloys (CRA's) are temperature dependent. The yield and ultimate tensile strengths in tension and in compression decrease as the temperature increases. The data also show that the properties are dependent upon orientation within the tube wall; i.e., CRA materials exhibit a degree of mechanical anisotropy. The extent of the anisotropy is dependent upon the amount of cold work and the processing history of the tube. The susceptibility to stress-corrosion cracking was also found to depend upon the grain orientation developed from cold working. The significance of these results for the design of downhole tubulars for deep, sour-gas wells is discussed.

Keywords: SCC, anisotropy, corrosion-resistant alloys, cold worked, Bauschinger effect, yield criteria, texture.

INTRODUCTION

The oil and gas industry has been designing equipment and facilities made out of carbon steel for decades. In recent years, however, with the discovery of deep, sour-gas wells, often with bottom-hole temperatures in excess of 400°F (205°C), the use of corrosion- resistant alloys (CRA's) has increased. These CRA's use alloy additions, such as chromium, nickel, and molybdenum, to improve the material's resistance to corrosion and environmental cracking. Armed with no information other than that CRA's have improved corrosion/ cracking resistance, designers have continued to design equipment and facilities with the same techniques used for alloy steels. There are some distinct differences, however, between alloy steels and CRA's.

Low alloy steels are usually supplied in a heat-treatable form, which results in relatively uniform properties throughout and which results in mechanical property variations of only 5 -10% up to about 400°F

(204°C). For that reason, designers routinely use room-temperature mechanical properties with a safety factor to account for temperature effects and an assumption of isotropy when using low alloy steels.

CRA's, however, usually obtain their strength by a mechanical, cold-working process that induces strains into the material. As a result, the mechanical properties of products made this way are not uniform in all directions, thus introducing the element of anisotropy into the design. Similarly, because the strength comes from cold working, elevating the temperature of the product piece tends to relax the material. This relaxation results in reduced mechanical properties at elevated (300°-400°F or 149°-204°C) temperatures and introduces another parameter into the design equation for materials exposed to these higher temperatures. Another observation [1] has been that the manufacturing process can also have an effect on the stress-corrosion cracking (SCC) resistance of these alloys.

Therefore, to be able to properly design with CRA's, information on (a) anisotropy, (b) yield criteria, (c) temperature dependence of yield strength, and (d) SCC resistance as a function of manufacturing processes is needed. A research program was initiated to provide such information. The program included:

- Evaluating the effects of temperature on mechanical properties of selected CRA's in the temperature range 73° to 500°F (23°-260°C);
- Measuring yield strengths of the same alloys in the axial, transverse (hoop), and radial directions;
- Generating yield surfaces and therefore yield criteria for CRA's; and
- Conducting a study of the effects of manufacturing processes on the SCC resistance of selected alloys.

This paper deals with the effects of temperature and manufacturing processes on mechanical properties as well as the influence of manufacturing processes on the SCC resistance of selected CRA's. The yield criteria for anisotropic materials will be discussed in a separate publication.

RESULTS

Evaluation of Mechanical Properties

The experimental approach was, first, to perform small-scale laboratory tests (see Appendix) under uniaxial loading conditions, both tension and compression. Samples were cut from the tube wall so that the loading axis was parallel to the axial, transverse (hoop), and radial axes of the tube (Figure 1). Second, combined loading experiments were performed on full-size segments of the tube. This allowed comparison of the performance in full-size tests with the performance obtained from the uniaxial test data. Precise values of the elastic constants of materials tested were determined along with their temperature dependence [2]. The nominal compositions of some selected alloys are given in Table 1. Plain carbon steel samples were included in the test program to provide a baseline performance for essentially unalloyed material. Information on tube dimensions, cold-working method, grade, etc., is given in Table 2.

Effect of Temperature on Mechanical Properties

The test results shown in Figures 2-6, for all the materials tested, show that the yield stress and ultimate tensile strengths decrease as the temperature increases. Furthermore, the results show that all the CRA materials have a degree of anisotropy in their strength properties. The results also show that these materials behave differently than plain carbon steels (Figure 6), which are generally isotropic. The anisotropy of the CRA's is revealed, as shown in Figures 2-5, by unequal magnitude of yield stresses measured in the direction of the three major axes of the tubes.

The data for strength versus temperature, for the alloys investigated, are fitted by a relationship of the form:

$$\sigma = A \exp(B/T) \quad (1)$$

where

σ = the stress, yield or ultimate tensile, at a given absolute temperature
A = pre-exponential factor
B = materials constant
T = temperature on Kelvin Scale (°C + 273) or on the Rankin Scale (°F + 460)

The temperature dependence of the strength is embodied in the parameter B, which was found to take a constant value for each of the alloys, independent of the mode of testing (tension or compression), sample orientation (axial, transverse, or radial) and type of strength measurement (yield or ultimate tensile strength). The pre-exponential factor, A, on the other hand, is dependent on the mode of testing, orientation, and the type of strength measurement. Accordingly, we can represent the relationships between yield stress and temperature by

$$\sigma_{i,\,j,\,T} = A_{i,\,j} \exp(B/T) \quad (2)$$

where the index i represents the orientation (i.e., i = z (axial), θ (transverse) or r (radial)), while the index j represents the mode of testing (i.e., j = + (tension) or - (compression)). Since B for each material is a constant and independent of the mode of testing and the orientation of the sample, the temperature dependence is completely described by the exponential term in Equation 2.

The values obtained for parameter B are:

UNS Designation	Parameter B
N10276, pilgered	206.50
N10276, drawn	180.00
N06975, Grade 110, drawn	140.40
N06975, Grade 125, drawn	151.50

Effect of Manufacturing Processes on Mechanical Properties

As mentioned above, the yield strengths measured in the three principal directions (axial, hoop and radial) in both tension and compression were unequal. This observation indicates that the CRA materials generally exhibit anisotropic strength properties. It was also found that the degree of anisotropy depends on the processing route, that is, the sequence of cold work and annealing as well as the deformation methodology. Cold working of these alloys is achieved by two standard methods. The first is cold drawing, whereby a tube is grasped by the end and pulled through a die, causing the desired size reduction, straining, and consequential strengthening. The second is pilgering, whereby a set of rolls with a tapering groove oscillate, pounding the OD of the pipe down onto a tapered mandrel. The residual stress state induced in each piece is very different, yet the gross mechanical properties are equivalent.

Examination of Figures 2 and 3 indicates that the yield stress in axial tension is similar for the two 110-ksi materials. Furthermore, the yield stresses in the hoop direction are also similar, giving yield stress ratios of 0.95 and 0.97 for the pilgered and cold-drawn materials, respectively. Based on these data, which are commonly reported as a basis for grade specification, one could conclude that these materials are mildly anisotropic and would exhibit closely similar behavior under combined loading. This is not the case, however, because the two materials exhibit markedly different degrees of Bauschinger effect. As a result, the yielding of the two materials under compressive states of stress, particularly under biaxial compression, is not well predicted by axial and hoop

tension tests. This observation is particularly important for the design of downhole tubulars, where tubes can be subjected to combined compressive loads.

The anisotropy in the strength properties can be attributed to the preferred orientation of the grains that make up the polycrystalline tube. This preferred orientation is also known as "texture." The difference between the mechanical behavior of the pilgered and cold-drawn tubes can, in turn, be attributed to the different texture intensities that are induced by alternative processing methodologies. This aspect of the research is the subject of a separate publication.

Evaluation of SCC Behavior

As previously stated, different manufacturing processes produce different stress states in a material. Because the stress state might have an affect on cracking, a research project was developed to investigate the effect of processing on cracking.

Effect of Manufacturing Processes on SCC Behavior

In a study on N08825 [1], it was shown that the detailed thermomechanical history of a material can have a profound effect on the SCC resistance of the final product. In this study, the texture of tube samples was determined after each deformation and annealing cycle so that the process route responsible for the development of each of the texture components could be identified. It was found that tubes processed a certain way established a grain orientation that produced very high SCC resistance, while an alternate processing route produced similar mechanical properties but produced a grain orientation that was totally different and resulted in reduced SCC resistance. This effect is illustrated in Figure 7 where the SCC resistance, as measured by the area reduction ratio in the slow-strain-rate test, is seen to increase by a factor of 3-4 as the volume fraction of a specific grain orientation (e.g., (110)[001]) is increased from about 11% to 25%. This dependence of SCC resistance on texture has not yet been confirmed in the case of N10276 and N06975 materials, although alternative tube processing sequences do produce textures that contain similar volume fractions of the texture components. Research is currently under way to determine whether significant changes in SCC resistance can be achieved in these more highly alloyed materials by control of tube processing and the resultant textures.

The scientific aspects of each observation is discussed in detail in the following paragraphs.

DISCUSSION

The results of tension and compression tests show that the mechanical properties of CRA's are temperature dependent and that these properties are anisotropic. The present work also identified differences in mechanical properties and SCC resistance that can be attributed to different manufacturers and processing techniques. In this section, the following items are discussed:

- Origin of the temperature dependence;
- Anisotropy;
- Texture versus SCC resistance; and
- Design considerations for CRA's.

Origin of the Temperature Dependence

When the yield strength of pure metals and alloys are examined over the entire solid-state range, i.e., from absolute zero to the melting temperature, three distinct ranges of behavior [11] can be distinguished (Figure 8). At low temperatures, up to 0.2-0.25 T_H[1], Regime I, the yield stress is markedly temperature dependent. A similar strong dependence of the yield stress on temperature occurs at temperatures in excess of about 0.4 T_H, Regime III. At intermediate temperatures, between 0.25 and 0.4 T_H, Regime II, in Figure 8, the temperature dependence is small. Here, the temperature dependence of strength is the same as that of the elastic moduli. The marked temperature dependences in Regimes I and III arise because the motion of dislocations through the material is dependent on thermally activated processes. By contrast, in Regime II, the dislocation glide is essentially athermal. Based on these observations for pure metals, it is expected that Regime I extends up to between 180°F (82°C) and 340°F (171°C) in the present materials.

The temperature dependence of the elastic constants of the CRA materials was determined in a companion program [2]. Their temperature dependence, however, is much less than the yield strength. As an example, the strength of Alloy UNS N10276 drops approximately 17 percent between room temperature and 500°F (260°C), while the modulus changes only 5 percent. Figure 9 compares the dependence of the yield strength, modulus, and yield strength/modulus ratio on temperature, for Alloy UNS N10276. At temperatures above 400°F (204°C), the curve for σ_y versus T tends to become parallel to that of E versus T so that the curve for σ_y/E versus T tends to become temperature independent. This observation is consistent with the idea that the observed temperature dependence of the CRA materials is due to the thermally activated processes responsible for Regime I in Figure 8.

There are a number of theories describing solid-solution strengthening that can be divided into two categories. The first group is based on models for dislocation locking when the dislocation is at rest [4, 5]. The second group is concerned with the frictional resistance to dislocation glide caused by the presence of the solute [6-10]. Review of such theories and the experimental evidence suggest that the largest contribution to the flow stress arises from the resistance to movement of mobile dislocations, rather than from direct solute pinning. It is therefore postulated that the observed temperature dependence of these heavily cold-worked CRA's is due to the unpinning of mobile dislocations.

Anisotropy of the Strength Properties

The experimental results obtained in this study indicate that all the CRA materials have a degree of anisotropy in their strength properties. In this way, these materials behave differently from low alloy steels, which are generally isotropic. The anisotropy of the CRA's is revealed by the unequal magnitude of the yield stresses measured in the direction of the three major axes of the tubes. This characteristic of the CRA materials can be attributed to the fact that they are supplied in the cold-worked condition in order to develop sufficient yield strength to satisfy the specifications. Cold working combined with other tubular processing history has the effect of inducing a plastic anisotropy.

Two types of anisotropy [11] can be produced by mechanical processing; namely, crystallographic anisotropy and mechanical fibering. Crystallographic anisotropy results from the preferred orientation of the grains that make up the polycrystalline material. The most affected material properties are the yield strength, ultimate tensile strength and, to a lesser degree, the strain-hardening response. Mechanical fibering, on the other hand, is due to the preferred alignment of structural discontinuities such as inclusions, voids, segregation, and second phases in the direction of deformation. Mechanical fibering tends to have a limited effect on the yield and tensile strength; instead, it strongly influences the fracture behavior of the materials. There was no evidence generated in the present research that suggests that mechanical fibering is present in the CRA materials. Instead, the observed anisotropy can be entirely attributed to the texture or preferred orientation induced by tube processing.

---

[1] T_H is the so-called homologous temperature. It is defined as the ratio of the absolute temperature T to the absolute melting temperature.

It is notable that the anisotropy of the strength properties observed in the CRA materials has two aspects. First, the strength measured in tension along the three major axes of the tubes are unequal. This response is expected in polycrystals where there is a strong texture of preferred orientation of the grains, as is the case for the present materials. The presence of the preferred grain orientation is accompanied by a preferred orientation of the slip planes, which, in turn, leads to unequal strength for different directions in the material. The second aspect is the fact that the yield strength measured in tension along any of the major axes differs in magnitude from that measured in compression. This latter phenomenon is known as the Bauschinger effect [12] and is attributed to internal stresses due to differential crystal orientations, which inhibit slip plane glide more effectively in one direction than another. Both of these aspects are generally found in heavily worked polycrystals, but they arise from different causes and the Bauschinger effect can often be removed by mild annealing even though the preferred orientation of the grains remains.

Texture Versus SCC Resistance

The experimental results obtained earlier on N08825 [1] show that significant improvement in the stress-corrosion cracking (SCC) resistance can be obtained by increasing the (110)[001] component of the texture of this CRA alloy. Furthermore, it is shown in the present research that both N10276 and N06975 materials develop similar textures during tube processing. Both materials exhibit textures that can be considered as being made up of three ideal grain orientations; namely, (110)[1^{-}11], (110)[001] and (112)[111^{-}]. The volume fraction of grains with these orientations are present in the range of 35-45%, 15-25% and 35-45%, respectively. In the study of N08825, it was shown that the SCC resistance, as indicated by the area-reduction ratio measured in the slow-strain-rate test, increases as the volume fraction of the (110)[001] component increases from 11-25%. It is not clear why this correlation occurs. Nevertheless, it is possible to speculate that increasing the proportion of grains with the (110)[001] orientation can lead to a reduction in the total amount of surface shear when the material is loaded into the plastic range, as is the case in the slow-strain-rate test. The reduction in the size of the shear step height on the surface of the material would reduce passive film rupture and thereby decrease the access of the corrosive environment to the alloy. In this way, corrosion-driven crack initiation and growth would be similarly decreased. An alternative view is that state of stress developed within grains belonging to the various ideal orientations will be different. Since the proportion of grains which are subject to a hydrostatic tension component under any arbitrary loading will change with the intensity of the texture, it is expected the propensity of the material to take up embrittling species from the environment will similarly depend on the detailed nature of the texture. This position has the advantage that the texture dependence of SCC behavior would be observed in tests where the material is loaded elastically, that is, where subjected to stresses that are less than the yield stress. A complete analysis of this phenomena is currently under way in order to identify mechanisms responsible for the correlation between SCC behavior and preferred grain orientation.

Texture of CRA Materials

All the CRA materials examined in this research showed similar types of texture, but the intensity of specific components of the texture can be shown to be highly dependent on the processing history of the materials. The (111) - pole figures obtained on the two N10276 tube samples are shown in Figures 10a and 10b, for the pilgered and cold-drawn tubes, respectively. Examination of these and the (200) - pole figures revealed that the texture can be considered to consist of three ideal components. These were identified by comparison of the experimental figures with the idealized orientations presented in reference (13). This type of representation considers the samples to consist of three groups of grains of the type (110)[1^{-}11], (110)[001] and (122)[111^{-}]. Here (hkl) indicates the plane perpendicular to the tube radius and [uvw] indicates the crystallographic direction parallel to the tube axis. In each case, the volume fraction of grains with these ideal orientations can be estimated by summation of the diffraction intensity about the positions where the grain types occur in Euler space. Typically, the (110)[1^{-}11] and (112)[111^{-}] each represent between 35 and 45% of the grains in the material, whereas the (110)[001] component ranges from about 15 to 25%.

Design Considerations for CRA's

Compared with carbon steel, three unique characteristics for CRA's must be dealt with when sizing CRA's for completion of deep, sour-gas wells (DSGW). These characteristics are (a) anisotropy, (b) temperature dependence of strength, and (c) failure rating. All these characteristics produce adverse effects, which are not adequately covered by standard tubing design practices; the safety factors calculated by accounting for these effects are smaller than if they are ignored. Detailed analysis of the failure rating and yield criteria for CRA's will not be discussed here, and how to handle such characteristics will be published in separate publications. The present data, however, shows that de-rating of strength because of temperature should be considered in the design of CRA's for deep, sour-gas wells. The loss of strength varies from one class of CRA's to another. Equations such as shown in equation (2) were developed for each class of alloys. These equations were further simplified and embodied in manuals for design of tubing and casing. Furthermore, the yield criteria based on anisotropic behavior were developed and incorporated in design manuals.

It has been shown that the SCC resistance of N08825 can be significantly increased by enhancing the population of (110)[001] oriented grains within the material. The highest proportion of such grains was obtained when the cold reduction of the tube was achieved by the pilgering process. It is also notable that similar enhancement of the (110)[001] component is observed in N10276 and N06975 when pilgering is used as the method of cold reduction. It is of interest to note that the N10276 and N06975 tubes prepared using pilgering for the cold-working steps also exhibited the minimum anisotropy in strength properties. Although this result is largely attributable to a reduction in the Bauschinger effect, the components of texture present could be in part responsible for the difference in mechanical anisotropy. These observations together suggest that, although the mechanism by which the preferred grain orientation of cold-worked tubulars influence the SCC behavior has yet to be identified, significant improvements in field performance can be obtained by close specification of the thermomechanical processing of CRA tubular products.

CONCLUSIONS

- The mechanical properties of cold-worked CRA's are temperature dependent in the range of interest. Over the temperature range 73° to 500°F (23° to 260°C), the strength of the alloys decreases as the temperature increases. It is established that the temperature dependence of the strength parameters for each of the alloys tested is independent of the type of strength measurement or the orientation of the test sample. A general relationship describing the temperature dependence of the yield stress and tensile strength was developed.

- The CRA materials, unlike low alloy steels, exhibit anisotropic yield behavior; i.e., the yield stress is dependent on the orientation of the test sample within the tube wall. Data supporting this observation were obtained in the axial, transverse, and radial direction of the tube and presented in this paper.

- The material properties of cold-worked CRA materials are dependent on the manufacturing processes (cold drawing versus pilgering). Differences in properties are outlined in the paper. These differences were shown to affect the shape of the yield surfaces and also the residual stress pattern.

- It has been demonstrated that the SCC resistance, as measured by the reduction ratio in the slow-strain-rate test, is increased when the (110)[001] component of texture is enhanced in N08825 CRA's. This texture component is found to be maximized when cold working is achieved by pilgering. Since all the CRA's examined in the current research also exhibited the same enhancement of the (110)[001] component when prepared by pilgering, it is reasonable to conclude that similar improvements in SCC resistance accrue in tube prepared by this method.

ACKNOWLEDGMENTS

The authors would like to acknowledge the scientific and technical contributions of M. P. Anderson, M. Watkins, and S. Matras. Also we would like to express our appreciation to the management of Exxon Production Research Company and Corporate Research for approval to publish the results of this investigation.

REFERENCES

1. H. E. Chaung and M. Watkins (unpublished data).

2. S. E. Mahmoud, Elastic Constants of Selected Corrosion-Resistant Alloys, (unpublished data).

3. Standard Testing of Steel Products, A370, Annual Book of ASTM Standards, Volume 01.03, ASTM, Philadelphia, 1988.

4. A. H. Cottrell and B. A. Bilby, Proc. Phys. Soc., A62, 490, 1951.

5. H. Suzuki, Dislocations and the Mechanical Properties of Crystals, J. C. Fisher, ed., John Wiley, New York, 1957, p. 361.

6. N. F. Mott and F. R. N. Nabbarro, Report on Conference on the Strength of Solids, Physical Society, London, 1948, p. 1.

7. A. H. Cottrell, Dislocations and Plastic Flow in Metals, Oxford University Press, London, 1953.

8. R. L. Fleischer, Acta Metall., 11, 203, 1963.

9. N. G. Ainslie, R. W. Gerard and W. R. Hibbard, Trans. AIME, 215, 42, 1959.

10. M. J. Luton and J. J. Jonas, Canadian Metallurgical Quarterly, 11, pp. 79-90, 1972.

11. G. E. Dieter, Mechanical Metallurgy, McGraw-Hill, New York, 1961.

12. J. Bauschinger, Zivlingur, 27, pp. 289-347, 1881.

13. G. J. Davis, D. J. Goodwill and J. S. Kallend, J. Appl. Cryst. 4 (1971), pp. 67-70.

APPENDIX

EXPERIMENTAL PROCEDURES

Tensile Tests. The uniaxial mechanical tests were performed in an MTS 810 test apparatus equipped with a PDP 11-based data acquisition and control system. All tests were run under the control of a program designed to impose a constant true strain rate to the specimen while it undergoes uniform elongation of the gauge section.

A high-temperature extensometer was used for measuring specimen extension. The device clips onto the specimen gauge section and transmits the extension through a push-rod assembly to the LVDT. The use of this apparatus (Figure 11) provides for accurate measurement of specimen strain, even at elevated temperatures, where the specimen is enclosed in a high-temperature furnace and the strain measuring devices must be at room temperature. For all tests, the specimen strain is measured to a precision of 5×10^{-5}, and the load is measured to 0.1 percent. The load-elongation data acquired during each test is converted to true stress-true strain data pairs and plotted directly. The yield stress, ultimate tensile strength (UTS) and elongation to failure are obtained automatically. A 0.2 percent offset method was used to obtain the yield stress [3], while the UTS is obtained from the maximum force developed during the test.

Compression Tests. Compression samples consisting of right cylinders measuring 0.17 inch in diameter and 0.22 inch in height (4.32 mm x 5.6 mm) were machined from the tube wall so that the axis of the cylinder was parallel to the tube axis, tube radius, circumference and at 45 degrees to the tube axis in the circumferential plane. The compression apparatus consists of opposing anvils, measuring 2.156 inches in diameter and 0.562 inch in thickness (54.8 mm x 14.3 mm), fabricated from H13 tool steel and hardened to RC58. The anvils are supported on support columns, measuring 2.156 inches (54.8 mm) in diameter and 10 (254 mm) and 18 inches (457.2 mm) in length for the upper and lower support, respectively. This design was adopted to provide sufficient column stability during loading to 10,000 lb (4535 kg) to avoid buckling and the attendant shearing of the test specimens. The apparatus is equipped with extensometer push rods connected to collars clamped between the anvils and their respective support columns. The push-rod extensometer allows the specimen height to be monitored continuously during the compression test when the anvil and column assembly is surrounded by the heating furnace.

All tests were conducted in the MTS 810 test system described above. The tests were all run under computer control at a constant true-strain rate of 3×10^{-3} s^{-1}, which is equivalent to a crosshead approach rate of 0.04 in/min (1.016 mm/min), consistent with the rates embodied in the ASTM 370 Standard. The compression tests were all run to a true strain of 0.2. The yield stress was obtained from the true stress-true strain curve using the 0.2 percent offset method.

Texture Determination. The crystallographic textures of the samples were obtained with the aid of a Geigerflex DMAX-II-A diffractometer equipped with a semiautomatic pole figure goniometer. Samples were prepared for analysis by cutting 2-cm square samples from the tube walls with the sides parallel to the axial and hoop directions. The samples were then ground and polished, on a plane perpendicular to the radial direction, to a thickness of 80 μm.

Full pole figures were obtained for each sample by normalizing and combining data obtained in both the reflection and transmission modes. In this way, full (111) - and (200) - pole figures were obtained for each of the tubes examined in this research.

Slow-Strain-Rate Tests (SSRT). Slow-strain-rate tensile specimens were 4-inch-long (101.6 mm), round bars with a 1-inch gauge section and a 0.15-inch (3.8 mm) gauge diameter. The gauge was machined to a finished surface roughness of 30 microinches. Prior to testing, the gauge of each specimen was prepared to a 600-grit finish using silicon carbide paper. The final finish was applied in the longitudinal direction to eliminate any machining marks perpendicular to the tensile axis. The tensile specimens were pulled to failure in uniaxial tension at a constant extension rate of 4×10^{-6} inches per second (1.02×10^{-4} mm/sec) using a Constant Extension Rate machine.

Tests were conducted at two temperatures, 300° and 350°F (149° and 177°C), in air and in a sour, brine solution. The solution consisted of 25 percent NaCl and 0.5 percent acetic acid in deionized water. The solution was deaerated with nitrogen for one hour, then charged at room temperature with 100 psig (6.9 bars) of H_2S gas. All tests were begun within two hours after the solutions were prepared.

During the tests, specimens were electrically isolated from the autoclave using heat-shrink Teflon™ tubing. The adapters used for the tests were made from the same materials as the tensile specimen to minimize galvanic effects.

After the tests were completed, specimens were rinsed with distilled water. The gage sections and fracture surfaces were examined at magnifications up to 30X for evidence of SCC. Some specimens were prepared metallographically to examine the gauge sections for secondary cracks.

TABLE 1

NOMINAL COMPOSITION OF ALLOYS

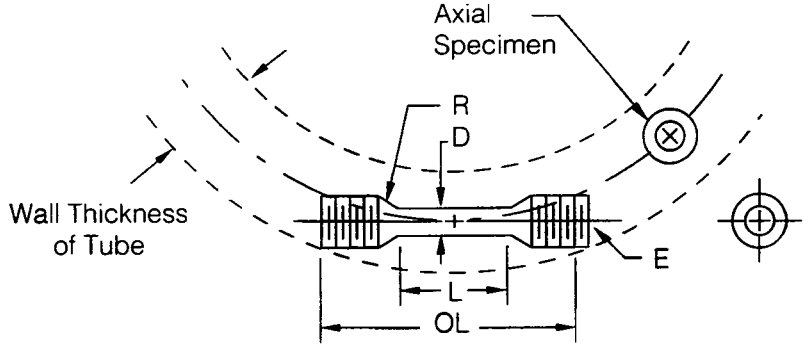
UNS Designation	Ni	Cr	Fe	Mo	W
N10276	60	16	5	16	4
N06975	50	25	17	6	--
N08825	45	22	28	3.5	--
P-105 steel	--	0.20	Bal.	0.10	--

TABLE 2

DIMENSIONS AND GRADES OF CRA TUBULARS

UNS Designation	OD (in)	OD (mm)	Wall Thickness (in)	Wall Thickness (mm)	Grade (ksi)	Grade (MPa)	Cold Work*
N10276	(5.5)	(139.7)	(0.476)	(12.1)	(110)	(758)	D
N10276	(3.5)	(88.9)	(0.254)	(6.45)	(125)	(862)	P
N06975	(4.0)	(101.6)	(0.265)	(6.73)	(125)	(862)	D
N08825	(3.5)	(88.9)	(0.625)	(15.88)	(110)	(758)	P
N08825	(3.5)	(88.9)	(0.289)	(7.34)	(110)	(758)	P
P-105 Steel	(3.5)	(88.9)	(0.254)	(6.45)	(105)	(724)	Q&T

*D - Cold drawn. P - Pilgered. Q&T - Quenched and Tempered.



Transverse Specimen

		0.25 in. Specimen	0.188 in. Specimen	0.160 in. Specimen	Tolerance (0.001)
Gage Diameter	(D)	0.252	0.188	0.160	+0 / -2
Gage Length	(T)	2.500	2.000	1.875	+2 / -0
Radius	(R)	0.187	0.156	0.156	-
Thread	(E)	0.5 in./13	0.375 in/16	0.375 in./16	-

Figure 1. Standard tension test specimens.

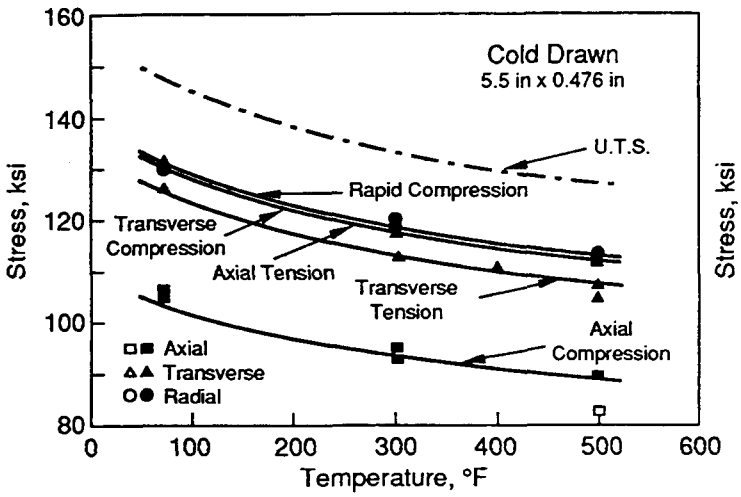


Figure 2. A combined plot of yield stress versus temperature for the three principal directions in the tube wall for cold-drawn Material N10276.

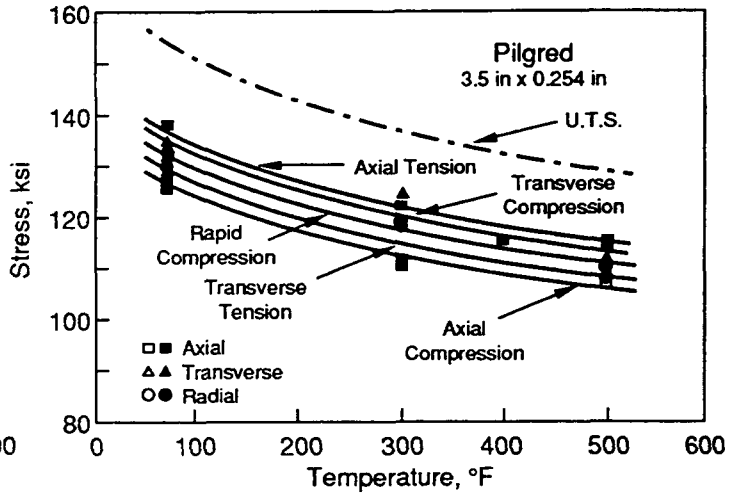


Figure 3. A combined plot of yield stress versus temperature for the three principal directions in the tube wall for pilgered Material N10276.

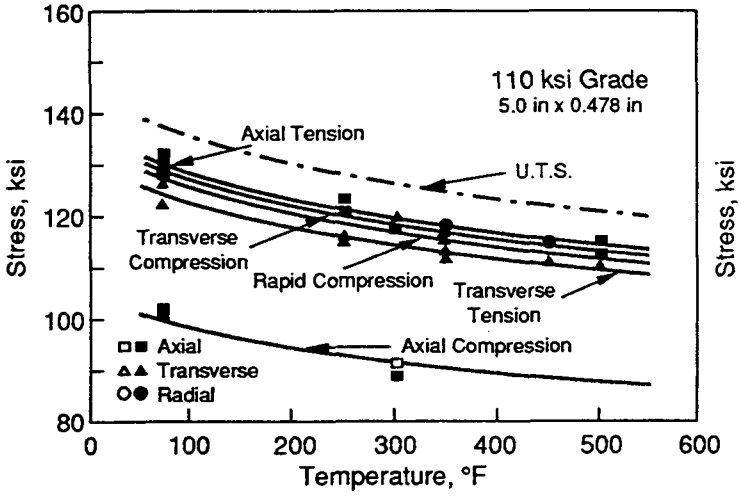


Figure 4. A combined plot of yield stress versus temperature for the three principal directions in the tube wall for cold-drawn Alloy UNS N06975, Grade 110.

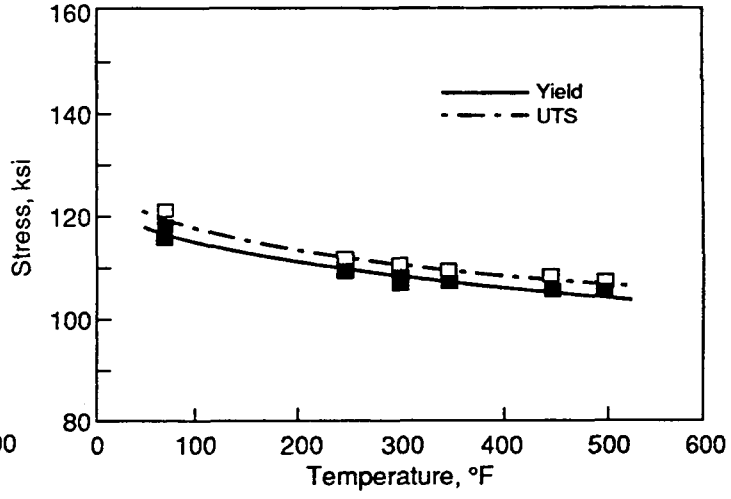


Figure 5. A plot of yield and ultimate tensile strengths versus temperature for pilgered UNS N08825. Only samples cut parallel to the tube axis were tested.

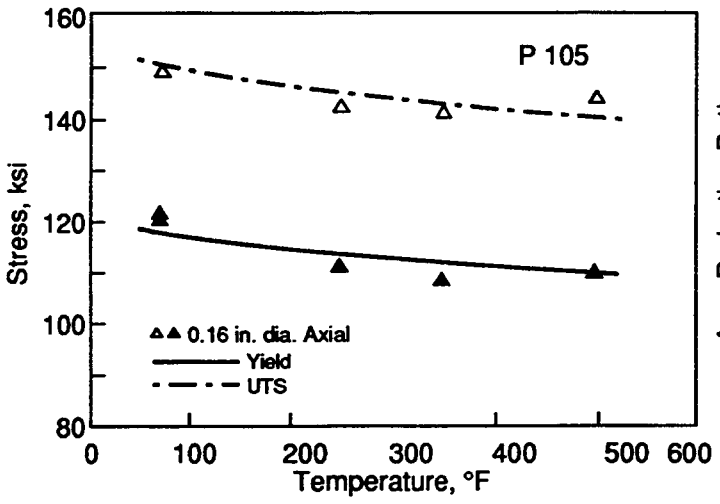


Figure 6. A plot of yield and ultimate tensile strengths versus temperature for the plain carbon steel P105. Only samples cut parallel to the tube axis were tested.

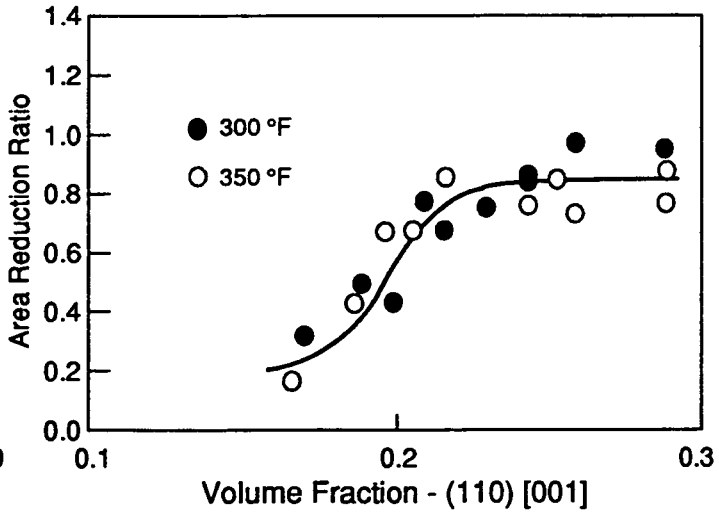


Figure 7. Influence of texture on the SCC resistance of Alloy UNS N08825.

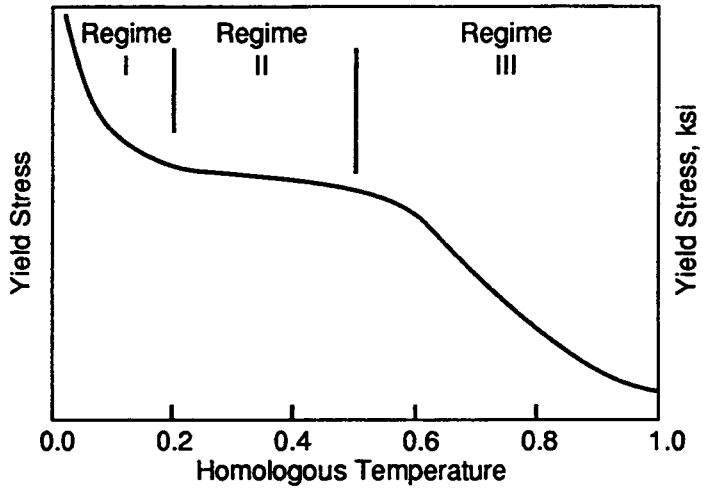


Figure 8. A schematic representation of the temperature dependence of the yield stress for metals and alloys over the entire solid-state range.

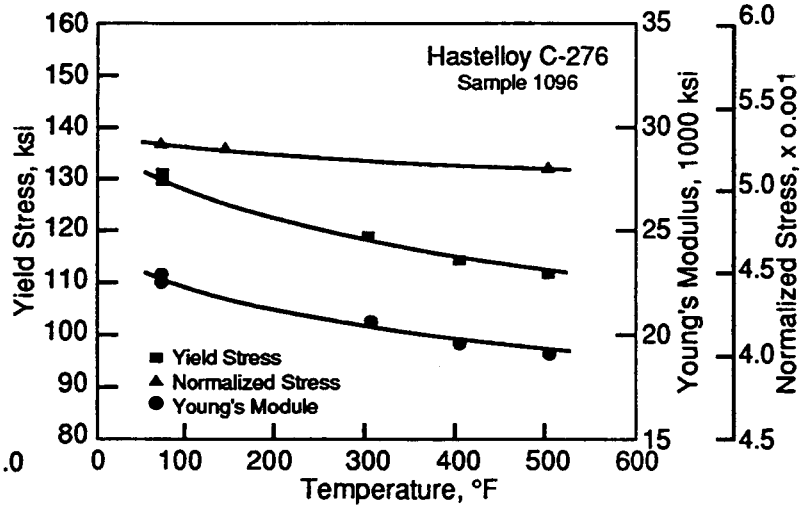


Figure 9. Comparison yield stress, σ_Y, and σ_Y/E versus temperature for Alloy UNS N10276.

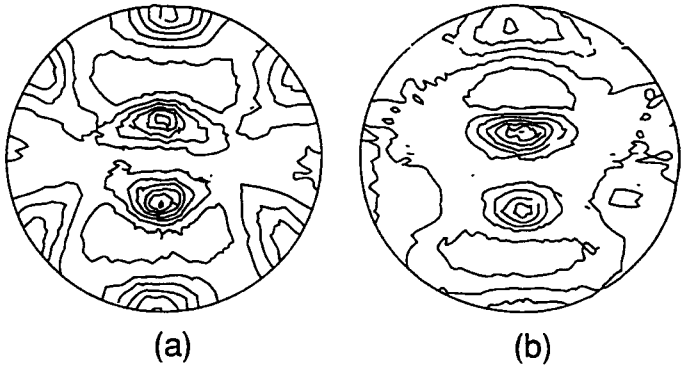


Figure 10. (111) Pole figures for N10276 materials made by (a) cold pilgering and (b) cold drawing.

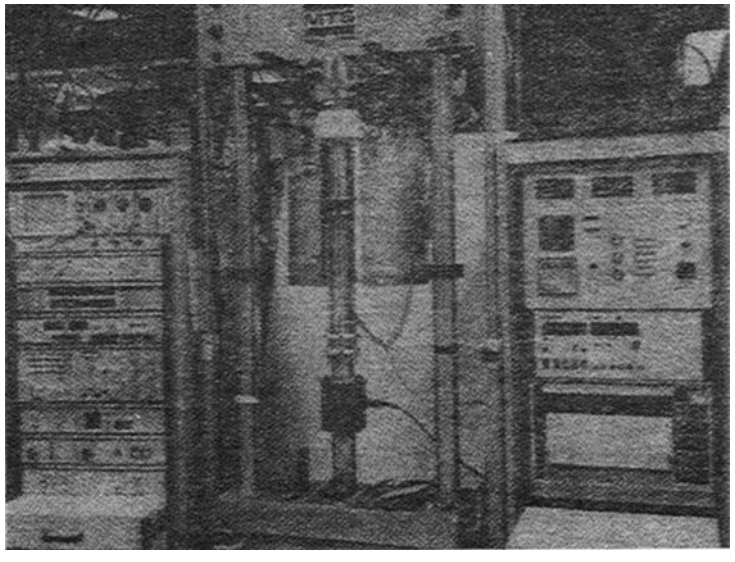


Figure 11. Test apparatus used to perform the uniaxial mechanical tests.

Copyrighted Materials
Copyright © 1996 NACE International Retrieved from www.knovel.com

Paper No.
70

NACE International

CORROSION 94
The Annual Conference and Corrosion Show
Sponsored by NACE International

THE USE OF SLOW STRAIN RATE TESTING TO DETERMINE THE EFFECT OF ELEMENTAL SULFUR ON STRESS CORROSION CRACKING OF NICKEL-BASE ALLOYS

C. J. Martin
Battelle
505 King Ave
Columbus, Ohio 43201-2693

H. S. Ahluwalia[1]
Haynes International
1020 West Park Ave
Kokomo, Indiana 46901

F. Blanchard
Vallourec Research Center
B.P. No. 17
Aulnoye, France 59620

J. Skogsberg
Chevron Petroleum
Technology Company
2202 Oil Center Court
Houston, Texas 77073

ABSTRACT

To understand the role of elemental sulfur in the stress corrosion cracking (SCC) of corrosion resistant alloys, researchers have tried various test techniques and methodologies with limited success. We feel we have developed a reliable test method for charging sulfur into Slow Strain Rate Test (SSRT) autoclaves.

An effective SSRT method using a special cup-sulfur cell, has been described to evaluate the susceptibility to SCC in sulfur containing environments. The results obtained are reproducible and reliable. Using this test method, the effect of chloride concentration on the threshold temperature for SCC in sulfur containing sour brine has been initially evaluated. UNS N06950 was determined to have a higher temperature threshold compared with UNS N06255 and UNS N06985.

Key Words: SSR testing, test method, oil and gas, stress corrosion cracking, sulfur, corrosion resistant alloys.

---

(1) Now with Ciba-Geigy Corporation, Toms River, New Jersey.

INTRODUCTION

The influence of elemental sulfur on the SCC susceptibility of nickel-base alloys is of concern to the oil and gas industry both in the production of some deep sour gas wells, where sulfur is the unwanted product, and in super-sour gas production, where sulfur is the end product desired. The exact role of elemental sulfur is unclear; however, it appears that the accelerating effect of sulfur is dependent on whether it is in solution or undissolved as a separate solid or liquid phase. When sulfur is in solution, in the form of hydrogen polysulfides, the cathodic reaction is diffusion controlled, similar to the oxygen corrosion mechanism. Under these conditions, susceptibility to SCC is only moderate. If, however, elemental sulfur particles are in direct contact with the sulfide covered metal surface, then susceptibility to SCC is dramatically increased[1].

To understand the role of sulfur, researchers have tried various test techniques and methodologies with limited success.[2,3,4] Currently, no standard test method exists for charging sulfur into SSRT autoclaves or in static test autoclaves. The way sulfur is charged into a SSRT autoclave system greatly affects the susceptibility to stress corrosion cracking. Previously, the methods used have included dry charging, charging by using a sleeve around the specimen, and by charging sulfur in a capsule in the autoclave, away from the specimen, at low test pressures ranging from 500 to 2500 psig (3.4 to 17.2 MPag). The results obtained from these tests have not always been reliable. This inconsistency is of concern, since some oil and gas company specifications include testing in sour gas environments in the presence of free sulfur.

This paper describes an effective methodology for testing nickel-base alloys using the SSR technique in the presence of free sulfur. The test methodology described has been used successfully in initially evaluating and screening various nickel-base corrosion resistant alloys. The influence of chloride content and temperature on SCC in sulfur containing sour gas environments is discussed.

EXPERIMENTAL PROCEDURE

Materials

The materials used in this investigation were Hastelloy G50[(1)] UNS N06950, Hastelloy G3[(1)] UNS N06985, and SM2550M UNS N06255.

Table 1 summarizes the chemical composition of alloys evaluated. These alloys are solid solution strengthened nickel-base alloys that are cold worked to achieve the required high yield strengths for downhole use. The yield strength of these materials, at ambient temperature in the longitudinal direction, were in the range of 130 ksi (896 MPa) to 140 ksi (965 MPa).

Environments

The simulated downhole sour environments used in this investigation are outlined in Table 2. The hydrogen sulfide (H_2S) was of 99.5% commercial purity grade. The other chemicals used were reagent grade.

---

(1) Hastelloy G50 and G3 are registered trademarks of Haynes International.

SSR Testing

Details of the test technique have been described by a number of authors. Essentially, the testing procedure outlined in a draft NACE standard test method, proposed by Task Group T-1F-9[5], was followed. Specimens machined from tubulars had a nominal gage length of 1 in. (2.54 cm) and a gage diameter of 0.15 in. (0.38 cm). The surface roughness of the specimens was less than 10 microinches (0.25 micrometers).

Special Cup-Sulfur Cell Set Up. SSRT were conducted by three independent laboratories: B, H, and V. For the experiments with sulfur, a special cup-sulfur cell, made from Teflon[(1)], nominally 2 inches (5.08 cm) long and 0.75 inch (1.905 cm) inside diameter was used. The cup formed a cell around the test specimen, as shown in Figure 1. Two methods were used to load the sulfur into the special cup-sulfer cell. The first method consisted of loading a pre-weighed charge (10 grams) of dry sulfur into the cup, prior to loading the test sample into the autoclave. It had previously been determined that only half the gage section of the specimen would be in contact with the molten sulfur. The other method was to pour molten sulfur into the cell so that exactly half the test section would be in contact with the specimen. This method ensures no contamination of the other half of the gage section.

By charging the sulfur as described above, essentially three environmental conditions are created. At the interface of the sulfur and brine, a sulfur-saturated sour brine environment exists. Above this region mainly a sour brine environment exists. Below the interface, sulfur is in direct contact with the specimen gage section and no sour brine is present.

Loading Procedure. Laboratory B's test procedure for loading the vessel was that after the sample had been loaded into the SSR machine and the autoclave had been evacuated, a measured amount of deaerated test solution was drawn into it. The vessel was then re-evacuated and the test temperature equilibrated. H_2S liquid was added, at temperature, until a steady state condition with a partial pressure of 150 psig (1.03 MPag) H_2S, plus steam pressure, was obtained. The same procedure was then used for the addition of the CO_2.

The test procedure followed by Laboratory H involved drawing an appropriate amount of brine solution into the autoclave. The vessel was then deaerated using a cyclic vacuum and nitrogen purge procedure. Several cycles of evacuation (5 min) followed by nitrogen purge (5 min) at 30 psi (207 kPa) were carried out. H_2S was then introduced at the required pressure and the cell was purged for 2 hours before final pressurization. CO_2 was then added over the H_2S partial pressure. Subsequently, the autoclave was heated to the operating temperature.

Laboratory V's loading procedure consisted of loading the sample into the SSR machine after filling cold free sulfur into the special sulfur-cup. The appropriate NaCl solution was degassed in a separate vessel with pure nitrogen for 1 hour, then with H_2S for 1 hour. The solution was then pushed into the test autoclave with an overpressure of gas mixture, at room temperature. The autoclave was then heated to operating temperature.

In all laboratories, the SSRT's were run at a nominal strain rate of 4×10^{-6} in/in/sec.

At the conclusion of each test, the failed sample was removed and the location of the fracture relative to the sulfur level noted, prior to washing the sample with deionized water and drying.

Data Analysis. For this study, SSR tests were conducted in a benign environment for each of the candidate alloy microstructure as well as a series of SSR tests in the sour environment at varying temperatures. At the conclusion of each test, the samples were measured and calculations were made of the

(1) Teflon is a registered trademark of E. I. DuPont.

various physical parameters that characterize a material's ductility; i.e., reduction in area and elongation, as well as time-to-failure. These data then were compared with the benign test data. A few of the failed samples were cross-sectioned and examined metallographically for the presence of secondary cracks, while the remaining half of the specimen was examined in the scanning electron microscope (SEM), where the morphology of the fracture surface was determined.

TEST RESULTS

UNS N06950

The SSRT data obtained by the three laboratories are presented in Table 3. The data using a pass/fail criteria based on the absence or presence of secondary cracks are plotted in Figure 2. The data clearly show good inter-laboratory agreement. As the chloride concentration increased, the threshold temperature for SCC decreased. Chloride concentration is clearly the predominant factor in determining the threshold temperature for the susceptibility to SCC in the presence of sulfur. Figure 3 shows a photograph of the gage section of a specimen tested at 425 F (218 C) and 100,000 ppm chloride. The photograph shows the presence of secondary cracks in the interface region between the sulfur and the sour brine. The conditions here are most aggressive.

Several tests also were conducted in this study in which sulfur was wrapped around the specimen using an inert tape. The data for these tests are shown in Table 4. All of the tests showed no cracking. The result is not surprising since no aqueous phase was in contact with the specimen. The current test methodology is clearly more consistent.

Quality assurance test data from in excess of 150 SSRT's, manufactured from UNS N06950 on production tubing orders, conducted by Chevron at 425 F (218 C) and chloride concentration of 162,000 ppm, with similar H_2S and CO_2 contents, but containing no sulfur have shown no failures[6]. This clearly indicates that the presence of sulfur is detrimental to the resistance of the alloy to stress corrosion cracking.

UNS N06985

The SSRT data for all of UNS N06985 material are presented in Table 5 and Figure 4. Figure 5a is a photograph of the failed sample tested at 400 F (204 C) and 50,000 ppm chloride, and Figure 5b is a photograph of the cross-sectional view through the fracture area. Similar to UNS N06950, as the chloride concentration increases the threshold temperature for SSC decreases. Again, chloride concentration is clearly the predominant factor in determining the threshold temperature for the susceptibility to SCC in the presence of sulfur. The threshold temperature for UNS N06985 is lower than that of UNS N06950.

UNS N06255

The SSRT data for UNS N06255 are presented in Table 6. These data show that several of the tested specimens have low ratio values in all three ductility parameters. When any of these samples are viewed in cross-section, evidence is found of secondary cracking being present, indicating that the failure was due to SCC. The sample tested at 400 F (204 C) and 50,000 ppm chloride, Figures 6a and 6b, typifies this. The location of the fracture is usually at the sour brine and sulfur interface, where the conditions are most aggressive. The data using a pass/fail criteria based on the materials susceptibility to SCC are plotted in Figure 7. When the ratios for this material showed indications of susceptibility, the failed sample generally had a thick crusty film deposited on the portion of the gauge length that was outside of the molten sulfur, thus making low power visual observation impossible. This then shows the importance of metallographic examinations to determining SCC. General pitting corrosion was also noted on these samples. With this alloy the effect of sulfur is equally as important as the chloride concentration.

The effect of chloride on the threshold temperature for susceptibility for the three alloys is plotted in Figure 8. The plot clearly shows that UNS N06950 has the highest threshold temperature.

DISCUSSION

To understand the role of sulfur, various test methodologies have been used with limited success. Choi[2] has reported that the way sulfur is charged into an SSRT autoclave greatly affects the susceptibility to SCC. The methods investigated included dry charging, where a weighed amount of dry sulfur is added into the autoclave along with the test solution. This method is the one most frequently used in the industry. Other methods included sleeve charging, where sulfur is intentionally contacted with the specimen surface for the entire length of the gage section; capsule charging, where the sulfur is placed in a capsule and suspended in the vapor space within the test autoclave. Choi's data clearly show the inconsistence with the various charging methods. Sridhar and Corey[3] charged sulfur in their autoclave using the dry charging method. They reported a wide scatter in their data. This scatter was attributed to possible segregation of sulfur and partly due to the difficulty in detecting cracks masked by crevice corrosion. In their experiments sulfur was undissolved at the start of the test, generally floating at the top of the solution, and appeared as a ball at the bottom of the autoclave at the end of the test. Coyle[4] also used the dry charging technique and added 1 g/L of dry sulfur powder to the test vessel. He observed wide variation in test results and reported the difficulty of predicting resistance to SCC. The test data varied depending on whether or not molten sulfur contacted the gage section of the specimen. From the data produced for this program, it is obvious that more testing needs to be done to help more accurately predict the thresholds.

The test method described in this paper has shown that it provides reproducible data, and that the effect of sulfur can be evaluated reliably.

CONCLUSIONS

An effective test method, using a special-cup sulfur cell, has been described to evaluate the susceptibility to SCC in sulfur containing environments. The initial results obtained are reproducible and reliable.

Using the test method described, the effect of chloride concentration on the threshold temperature for SCC in sulfur containing sour brine has been evaluated. UNS N06950 has a higher temperature threshold limit than UNS N06255 and N06985.

ACKNOWLEDGMENTS

The authors wish to acknowledge Mr. L.A. Highfill of Battelle, Mr. D. C. LaCluyse of Haynes International, and Mr. P. Cravet of Vallourec for invaluable help in performing the experiments.

REFERENCES

1. Ahluwalia, H.S., "Problems Associated with Slow Strain Rate Quality Assurance Testing of Nickel-Base Corrosion Resistant Alloy Tubulars In Hydrogen Sulfide Environments," ASTP STP 1210, R.D. Kane Ed., American Society for Testing and Materials, Philadelphia, 1993, pp. 225-239.

2. Choi, H.J., "The Effect of Elemental Sulfur and Surface Condition on Stress Corrosion Cracking of High Nickel Alloys Under Hot Sour Environments," CORROSION/92, paper no. 59 (Houston, TX: NACE, 1988).

3. Sridhar, N. and Corey, S.M., "The effect of Elemental Sulfur on Stress Cracking of Nickel Base Alloys," CORROSION/89, paper no. 12, (Houston, TX: NACE, 1989).

4. Coyle, W.R. "Effect of Free Sulfur on Cracking Behavior of CRA's in Simulated Downhole Environments," CORROSION/93, paper no. 131, (Houston, TX: NACE, 93).

5. Draft NACE Standard, proposed by Task Group T-IF-9, "Slow Strain Rate Test Method for Screening Corrosion Resistant Alloys (CRA's) for Sour Oilfield Service," NACE.

6. Chevron Document, MCQA-06, "Specification for Corrosion Resistant Alloy Tubulars for Deep Sour Gas Wells".

TABLE 1
CHEMICAL COMPOSITION OF ALLOYS TESTED (WEIGHT PERCENT)
ONLY MAIN ALLOYING ELEMENTS LISTED

UNS No.	Ni	Fe	Cr	Mo	W	C
N06950	52.58	15.80	20.00	9.08	0.38	0.009
N06255	51.20	15.30	24.25	6.85	–	0.01
N06985	43.56	18.70	22.88	6.56	0.98	0.009

TABLE 2
SIMULATED DOWNHOLE ENVIRONMENT

1000 to 100,000 ppm Cl-
150 psig H_2S (1.03 MPag)
150 psig CO_2 (1.03 MPag)
425 F (218 C)

TABLE 3
SSRT DATA FOR UNS N06950

Testing Laboratory	Temp. F	Temp. C	Cl (ppm)	T/Ta	E/Ea	R/Ra	Secondary Cracking
B	425	218	0[a]	--	--	--	No
H	425	218	0	--	--	--	No
V	425	218	0	--	--	--	No
B	425	218	1,000	1.06	1.06	0.98	No
B	425	218	1,000	0.93	0.93	1.08	No
H	425	218	1,000	1.09	1.11	0.99	No
B	425	218	10,000	1.05	1.05	0.99	No
H	475	246	10,000	1.08	1.52	1.09	No
H	350	177	20,000	1.29	1.18	1.03	No
V	425	218	20,000	1.01	1.01	1.03	No
H	475	246	20,000	0.85	0.91	1.11	Yes
B	350	177	50,000	1.06	1.06	1.08	No
V	400	204	50,000	0.92	1.28	0.66	Yes
B	425	218	50,000	0.38	0.38	0.78	Yes
V	425	218	50,000	0.67	0.67	0.33	Yes
H	450	232	50,000	0.72	0.98	0.45	Yes
B	350	177	100,000	0.97	0.98	1.02	No
H	350	177	100,000	0.63	0.53	0.41	Yes
H	350	177	100,000	0.88	1.12	1.16	No
V	375	191	100,000	1.05	1.05	1.10	No
H	400	204	100,000	0.82	0.94	0.39	Yes
B	425	218	100,000	0.58	0.58	0.39	Yes
B	425	218	100,000	0.44	0.44	0.73	Yes
H	425	218	100,000	0.5	0.38	0.25	Yes
H	425	218	100,000	0.62	0.53	0.31	Yes
V	425	218	100,000	0.60	0.61	0.35	Yes

[a] Benign tests.

TABLE 4
SSRT DATA FOR UNS N06950 WITH ALL TESTS USING A TIGHT SLEEVE CONTAINING THE SULFUR AROUND THE TEST SAMPLE.

Testing Laboratory	Temp. F	Temp. C	Cl (ppm)	T/Ta	E/Ea	R/Ra	Secondary Cracking
V	425	218	1,000	1.04	1.04	1.01	No
V	425	218	1,000	0.97	0.97	0.93	No
V	425	218	10,000	1.06	1.06	1.12	No
V	425	218	50,000	0.99	0.99	0.99	No
V	425	218	100,000	1.03	1.03	0.94	No

TABLE 5
SSRT DATA FOR UNS N06985

Specimen	Temp. F	Temp. C	Cl (ppm)	T/Ta	E/Ea	R/Ra	Secondary Cracking
1	325	163	0[a]	–	–	–	No
2	300	149	100,000	0.97	0.97	1.04	No
3	325	163	100,000	0.55	0.55	0.79	Yes
4	325	163	50,000	0.96	0.96	0.97	No
5	350	177	50,000	0.85	0.85	1.02	No
8	400	204	50,000	0.68	0.68	0.74	Yes
6	375	191	10,000	0.93	0.93	0.98	No
7	400	204	10,000	0.83	0.84	0.98	No
9	425	218	10,000	0.59	0.64	0.98	Yes

[a] Benign test.

TABLE 6
SSRT DATA FOR UNS N06255

Specimen	Temp. F	Temp. C	Cl (ppm)	T/Ta	E/Ea	R/Ra	Secondary Cracking
A/1	475	246	0[a]	–	–	–	No
E/7	325	163	100,000	0.64	0.39	0.68	Yes
E/4	400	204	50,000	0.59	0.26	0.37	Yes
E/3	325	163	50,000	0.92	0.83	1.01	No
E/8	400	204	10,000	0.93	0.91	0.99	No
E/2	425	218	10,000	0.59	0.23	0.58	Yes
E/5	425	218	10,000	0.53	0.21	0.25	Yes
E/1	325	163	10,000	0.91	0.8	1.04	No
E/6	325	163	10,000	0.90	0.79	1.00	No

[a] Benign test.

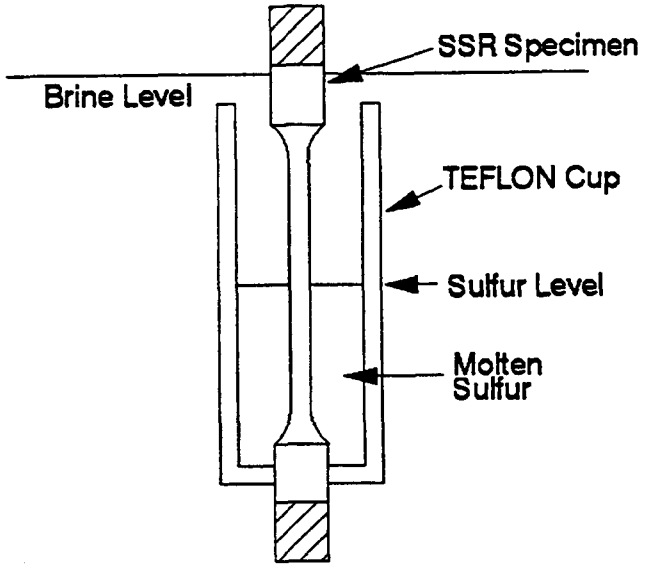


FIGURE 1 - Schematic drawing showing test sample with the special sulfur-cup cell mounted

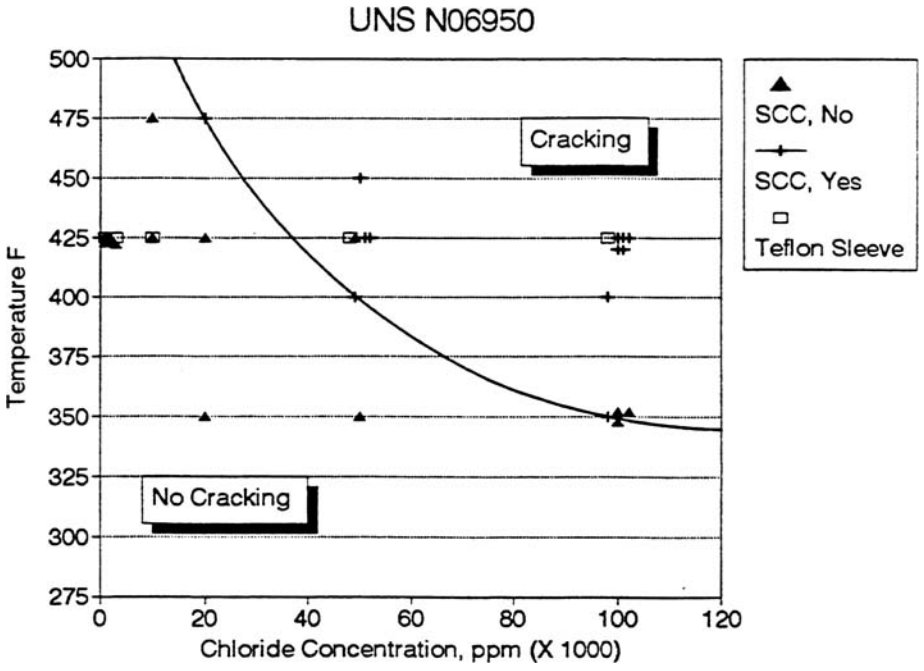


FIGURE 2 - Plot of data using pass/fail criteria for UNS N06950

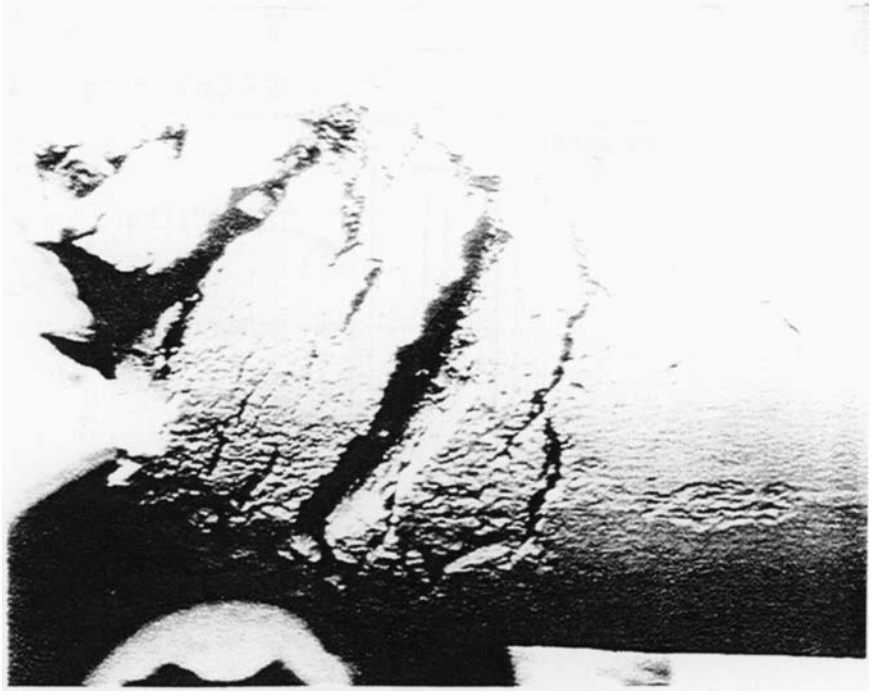


FIGURE 3 - Photomacrograph of a failed UNS N06950 sample, tested at 425 F and 100,000 ppm chloride

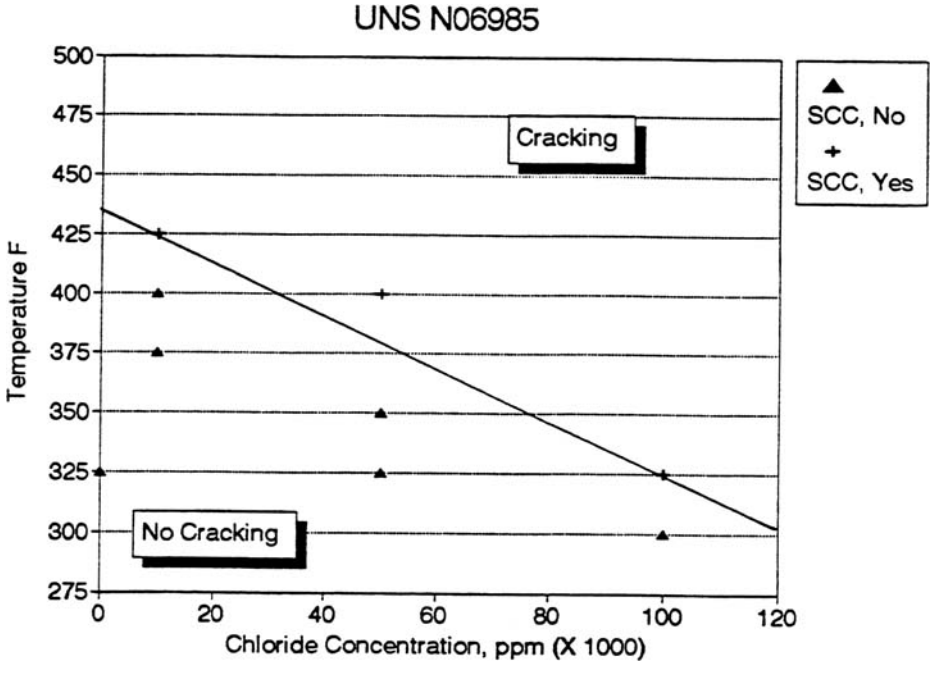


FIGURE 4 - Plot of data using pass/fail criteria for UNS N06985



FIGURE 5a - Photomacrograph of a failed UNS N06985 sample, tested at 400 F and 50,000 ppm chloride

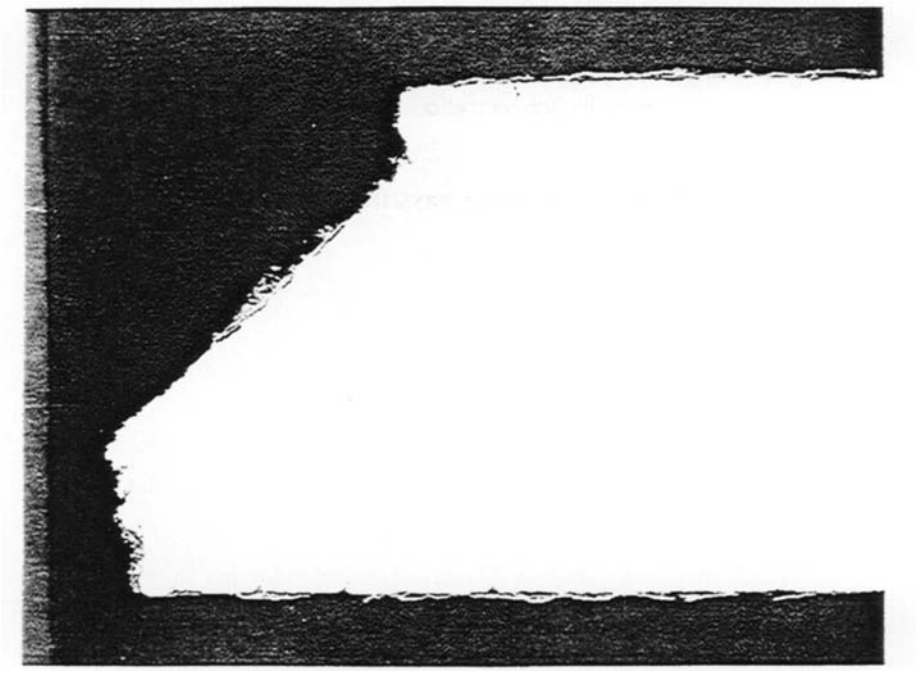


FIGURE 5b - Photograph showing cross sectional view of above samples showing the presence of secondary cracks



FIGURE 6a - Photomacrograph of a failed UNS N06255 sample, tested at 400 F and 50,000 ppm chloride

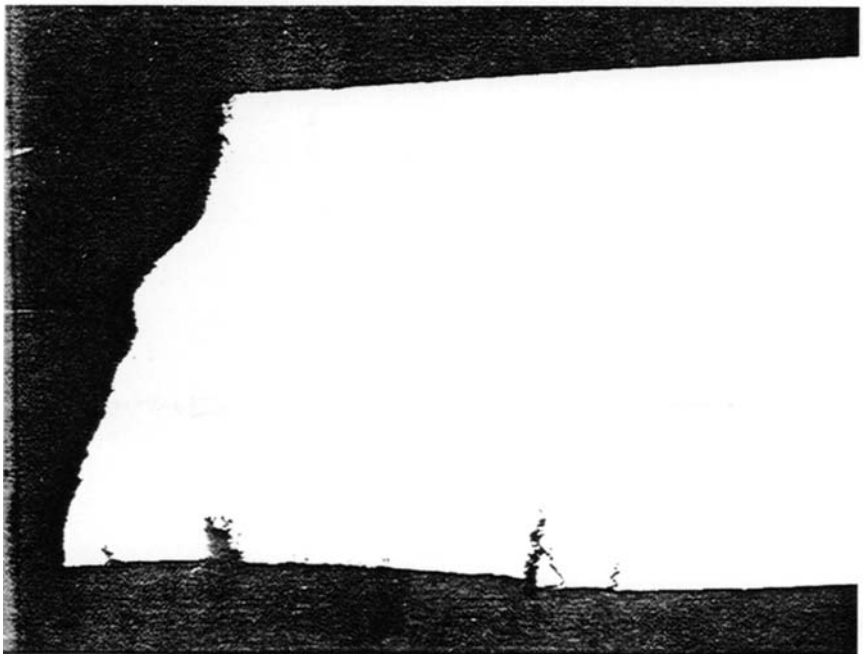


FIGURE 6b - Photograph showing cross sectional view of above samples showing the presence of secondary cracks

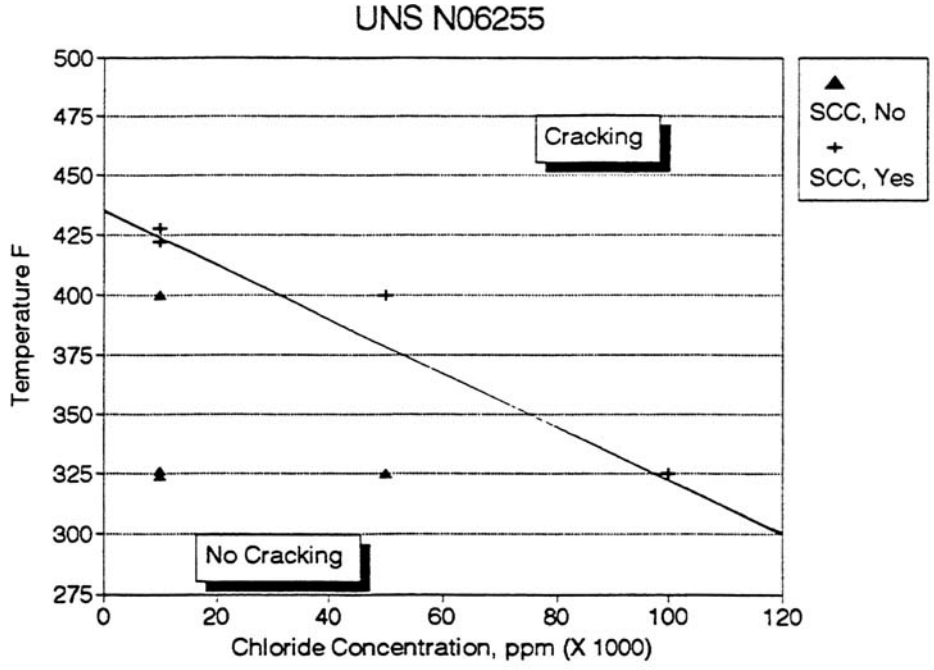


FIGURE 7 - Plot of data using pass/fail criteria for UNS N06255

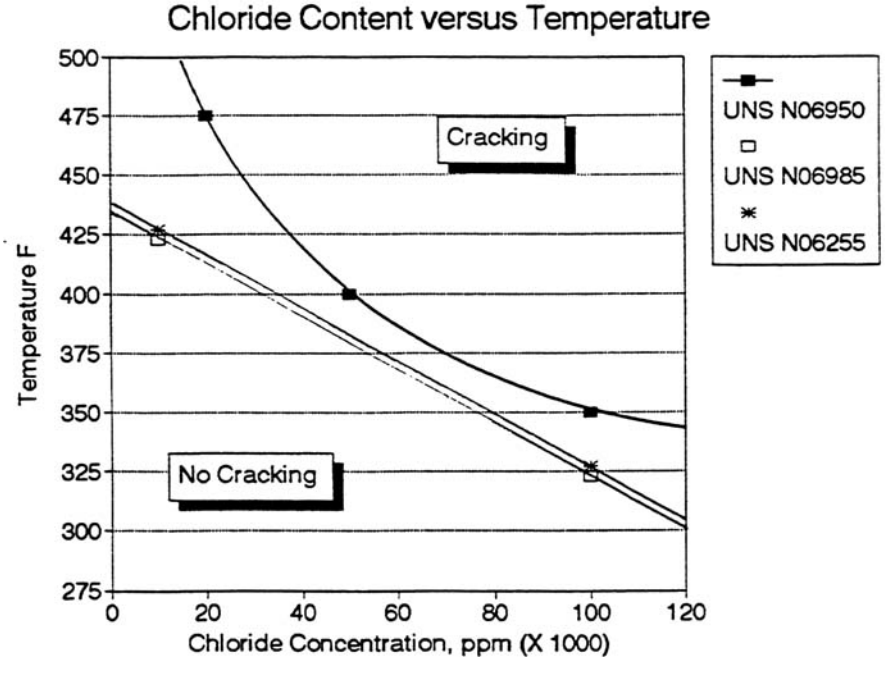


FIGURE 8 - Typical threshold data determined using new test method

Copyrighted Materials
Copyright © 1996 NACE International Retrieved from www.knovel.com

NIPPON STEEL TECHNICAL REPORT NO. 38 JULY 1988

UDC669.15-194.3-462.3

Development of High-Alloy Tubular Goods for Sour Wells

Hiroyuki Ogawa*1 Akihiro Miyasaka*1
Kohzoh Denpoh*1 Hitoshi Asahi*1
Katsutoshi Ina*1 Shunji Sakamoto*1
Kensai Shitani*1 Masao Onoyama*1

Abstract:

High-alloy oil country tubular goods (OCTG) with service performance required for sour gas environments were designed. The alloy compositions designed are 22Cr-25/30Ni-4Mo, 25Cr-35Ni-4/6Mo and 25Cr-40/50Ni-6/8Mo. OCTG made of these high-alloy steels on a trial basis exhibited satisfactory properties as expected. To ensure the optimum applicaiton of high-alloy OCTG in actual environments, it is essential to evaluate their service performance by suitable methods.

1. Introduction

The first oil crisis of 1973 drastically pushed up the world oil and natural gas prices, which had the effects of a) encouraging the drilling of the previously unlapped oil and gas resources of poor quality (contiaining hydrogen sulfide, in particular) in the United States and other countries to secure indigenous energy resources, and b) promoting enhanced oil and gas recovery (EOR) in intensified well exploitation throughout the world requiring the transport and feeding of carbon dioxide for injection into the well. For those purposes, OCTG and flow line pipes*1 of conventional low alloy steels are insufficient in service performance*2.

Stainless steels containing 13% or more chromium are alloy steels that can withstand service in environments containing CO_2 or H_2S. Before high-alloy tubular products came to be used as OCTG on a trial basis towards the end of the 1970s, the existing nickel-base alloys developed for chemical plants were employed in such severe environments.[1-3, 7] Alloys designed for use in chemical plants were not of optimum composition for service in oil and gas well environments. Research work has been carried out on the development of new high-alloy OCTG based on the alloy designing to meet the oil and gas well environments.[6,8,9]

2. Establishment of Service Performance Evaluation Method for Alloy Designing

To develop a material that suits a particular service environment, alloy designing must adopt an evaluation method that precisely simulates the environmental and service conditions involved. The sour oil and gas well environments in which high-alloy OCTG are to be used are shown in terms of temperature versus H_2S partial pressure in **Fig. 1**. The factors that comprise corrosive oil and gas well environments are H_2S, CO_2, Cl^- and temperature. Among these environmental factors, CO_2 affects only the PH value of the environment, and is included in the effect of H_2S. When Cl^- is present in a solution, it is enriched in crevices and deposits formed on materials. Stress corrosion cracking (SCC) is the typical corrosion morphology that limits the service preformance of, or, in other words, afflicts a fatal damage to, high-alloy tubular products. It often originates from such precursors as pitting corrosion and crevice corrosion. In view of this corrosion mecahnism, the service performance of the high alloy OCTGs is evaluated on the basis of their resistance to SCC, and, thus, the SCC evaluation test environment was established in a concentrated chloride ion solution in which H_2S was dissolved in equilibrium at the prescribed

*1 Central R & D Bureau

*1 Mainly refers to line pipe for the flow line and gathering line, relatively short distances of line pipe from the wellhead to the gathering station. The as-produced crude oil or gas flows through the flow line and gathering line.
*2 Mechanical properties and corrosion resistance that meet the intended service environment.

Courtesy Nippon Steel

temperature and partial pressure. Two specimens were held with a crevice and stressed as exposed to the test environment to evaluate service performance. The critical service environment was established with the initiation of SCC taken as the critical condition.

Specimens were machined from the test materials which were vacuum melted, hot rolled, solution heat treated and hardening treated. SCC test specimen geometry and SCC test conditions are shown in **Fig. 2** and **Table 1**, respectively.

Using the test jigs illustrated in **Fig. 2**, the specimens were

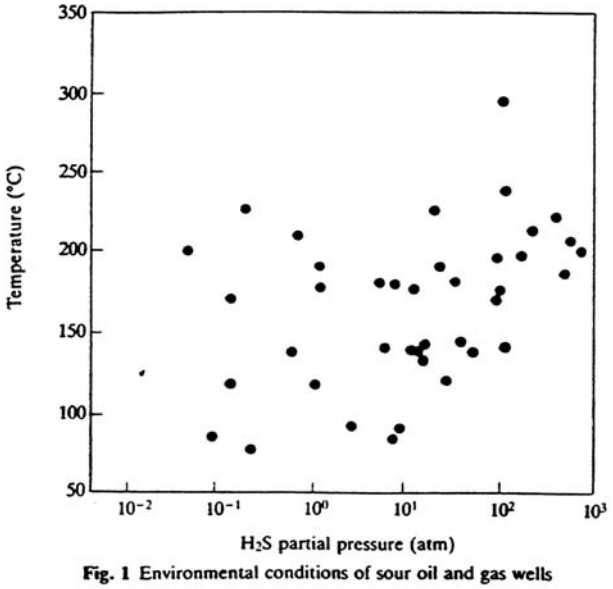
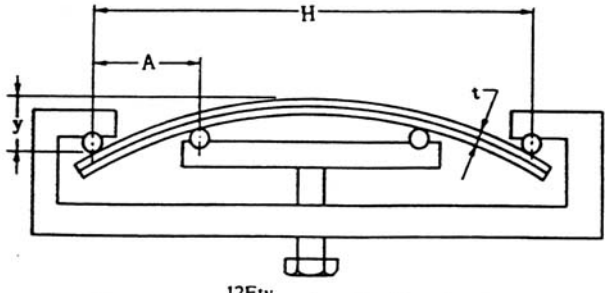
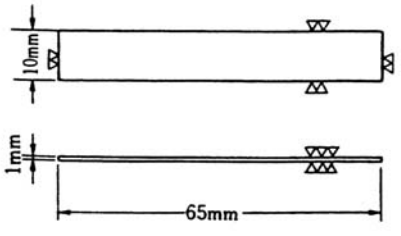


Fig. 1 Environmental conditions of sour oil and gas wells



$$\text{Test stress} = \frac{12Ety}{3H^2 - 4A^2}$$ where E = Young's modulus

(a) Test jigs and test stress calculation formula



(b) Specimen geometry

Fig. 2 Four-point double bent beam specimen test jigs and specimen geometry

loaded as specified in ASTM G 39-73. The specimens were mounted in the jigs, placed in an autoclave and tested under the specified conditions.

Table 1 SCC test conditions

Test environment	
Solution: 20% NaCl solution	
H_2S partial pressure (atm): 0.1-100	
CO_2 partial pressure (atm): 100	
Test stress (kgf/mm²): 87.5, 140*1	
Test temperature (°C): 100-300	
Test time (h): 168	

*1 Set as specified in ASTM G 39-73

3. Strengthening Method

If an alloy of the austenitic microstructure is used as an OCTG material, it is not directly subject to any existing specifications, API 5AC, for example, but is requried to assure an 0.2% offset yield strength of at least 77.3 kgf/mm² (110 ksi). A Ni-Cr-Mo alloy of the austenitic microstructure has a low 0.2% offset yield strength in the as-annealed condition.*1 Some strengthening method is thus necessary to increase the 0.2% offset yield strength. Precipitation hardening and work hardening are common methods of strengthening. The former method strengthens the material by hardening through the precipitation of γ' phase or Ni_3 (Al, Ti), for instance. It provides a relatively high yield strength compared with the latter as shown in **Fig. 3**, but increases the SCC susceptibility as shown in **Table 2. 3**, but increases the SCC susceptibility as shown in **Table 2.** The increase in yield strength achieved by the latter method depends on the alloy composition in general and the chromium and molybdenum contents in particular, as shown in **Fig. 4**, but the level of strength obtained is lower than that accomplished by precipitation hardening. As shown in **Fig. 5**, yield strength levels off when the amount of cold working has reached 20%, and increases little despite any further cold working. These results also depend on the method of hot working and the grain size of the microstructure prior to cold working. Nevertheless, the absolute SCC susceptibility of the cold worked material with respect to the test stress is low when compared with the precipitation hardening method (refer to **Tables 2** and **3**). When the service performance of OCTG is the consideration, therefore, strengthening by work hardening seems preferable to precipitation hardening.

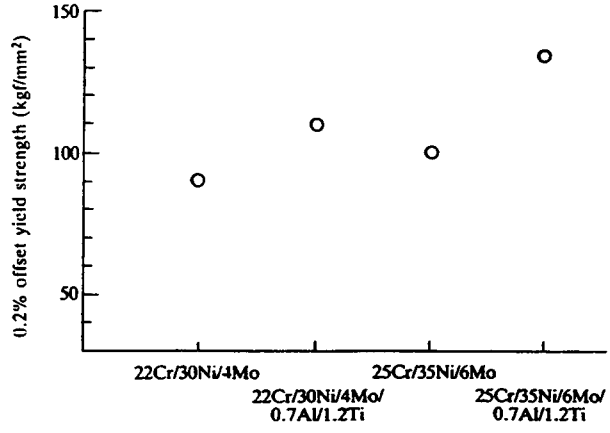


Fig. 3 Strengthenig by precipitation hardening
Test materials of base compositions were cold worked by 30% and precipitation-hardened materials had 0.75% Al and 1.25% Ti added to base composition.

*1 For example, the 0.2% offset yield strength of Inconel 625, a material of the 21Cr-62Ni-9Mo-3.5Nb composition, is approximately 40 kgf/mm².

For the reasons noted above, cold working was adopted as the method of material strengthening for the high-alloy OCTG reported here. The test specimens described below were all cold worked by 30%.

Table 2 Effect of precipitate forming elements on SCC susceptibility
Base composition: 25%Cr-35%Ni-6%Mo

Test stress (kgf/mm²)	87.5	140
Test temperature (°C)	250	
H_2S partial pressure (atm)	10	
Base composition	NF*2	NF
0.75%Al-1.25%Ti*1	F*2	F

*1 Test material had 0.75%Al and 1.25%Ti added to the base composition and was precipitation hardened.
*2 NF: Not failed
F: Failed

Table 3 Effect of cold working on SCC susceptibility

Test steel: 22%Cr-25%Ni-4%Mo
Test conditions
Test stress: 140 kgf/mm²
Test temperature: 150°C
H_2S partial pressure: 10 atm
CO_2 partial pressure: 10 atm

Amount of working (%)*	20	30	40
Test result	NF	NF	NF

*1 Expressed in reduction of area
NF: Not failed

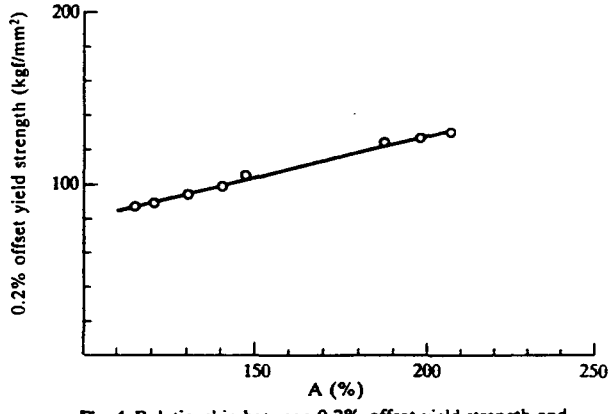


Fig. 4 Relationship between 0.2% offset yield strength and alloy content after cold working
Amount of cold working (reduction of area): 30%
A(%) = 2.5Cr(%) + Ni(%) + 9Mo(%)
Measuring temperature: 25°C

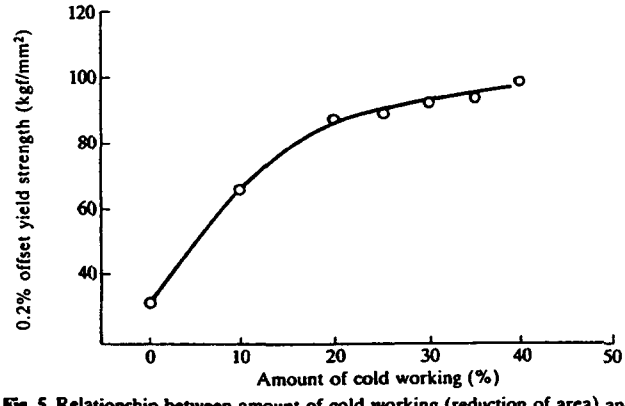


Fig. 5 Relationship between amount of cold working (reduction of area) and 0.2% offset yield strength after cold working
Test steel: 22%Cr-25%Ni-4%Mo
Measuring temperature: 25°C

4. Establishment of Alloy Contents

The temperature and H_2S partial pressure, which represent the environmental conditions under which OCTG are used in oil and gas wells as previously described, continuously change as shown in **Fig. 1**, if all the possible service environments are summarized. There is a limit to the range of environments where any given alloy can satisfactorily perform. To cover the whole range of service environments shown in **Fig. 1**, it is not a rational choice to develop an alloy of high corrosion resistance and thus run a risk of excess quality in practical applications. A reasonable response instead is to develop a series of alloy steels that can cover the whole range on a selective basis. The alloy contents were established from this standpoint.

The effects of nicekl, molybdenum and chromium on the critical environmental limits for the SCC initiation are shown in **Figs. 6.7** and **Table 4**, respectively. The nickel and molybdenum additions decrease the SCC susceptibility and thus expand the SCC-free range of service environment. There is a limit to the

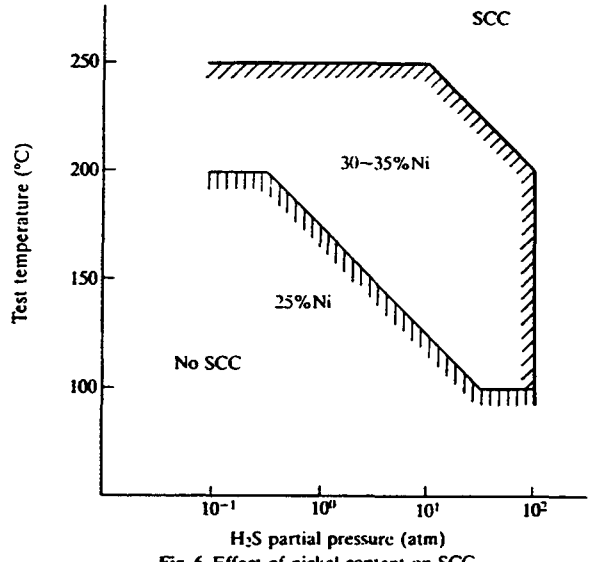


Fig. 6 Effect of nickel content on SCC
Base composition: 22%Cr-4%Mo
Stress: 87.5 kgf/mm²

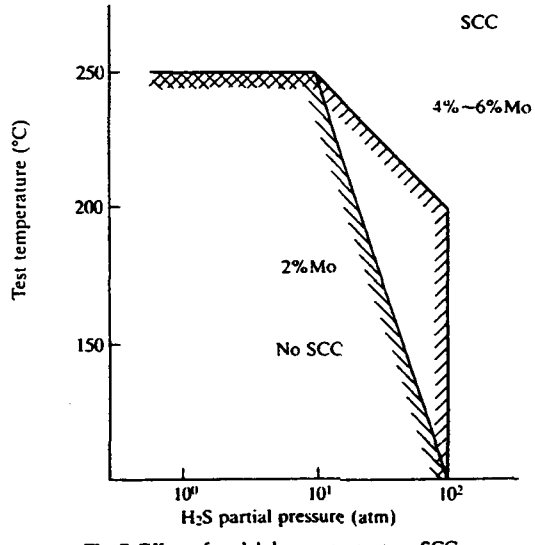


Fig. 7 Effect of molybdenum content on SCC
Base composition: 22%Cr-30%Ni
Stress: 87.5 kgf/mm²

effectiveness of alloying elements added to a given base composition. In the case of **Fig. 7**, for instance, the SCC-free range does not expand even if 4% or more molybdenum is added to the 22%Cr-30%Ni base composition. Nickel and molybdenum are very effective in reducing the SCC susceptibility, but chromium is less effective. The fact that nickel is more effective than chromium is a characteristic feature of the effectiveness of alloying elements in increasing corrosion resistance in sour environments as compared with that in neutral chloride environments like seawater.[10,11]

Table 4 Effect of chromium content on SCC

Base composition: 30%Ni-4%Mo

Test stress (kgf/mm²)	87.5				140			
Test temperature (°C)	150		200		150		200	
H_2S partial pressure (atm)	10	100	10	100	10	100	10	100
22%Cr	NF	F	NF	F	NF	F	NF	F
25%Cr	NF	F	NF	F	NF	F	NF	F
28%Cr	NF	F	NF	F	NF	F	NF	F

NF: Not failed F: Failed

Table 5 Effects of chromium, molybdenum and nickel contents on SCC

Test stress: 87.5 kgf/mm²

Test temperature (°C)	150		200	
H_2S partial pressure (atm)	1	10	1	10
22Cr-25Ni-4Mo	NF	F	NF	F
22Cr-25Ni-6Mo	NF	NF	NF	F
25Cr-25Ni-6Mo	F	F	F	F
25Cr-30Ni-6Mo	—	NF	—	NF

NF: Not failed F: Failed

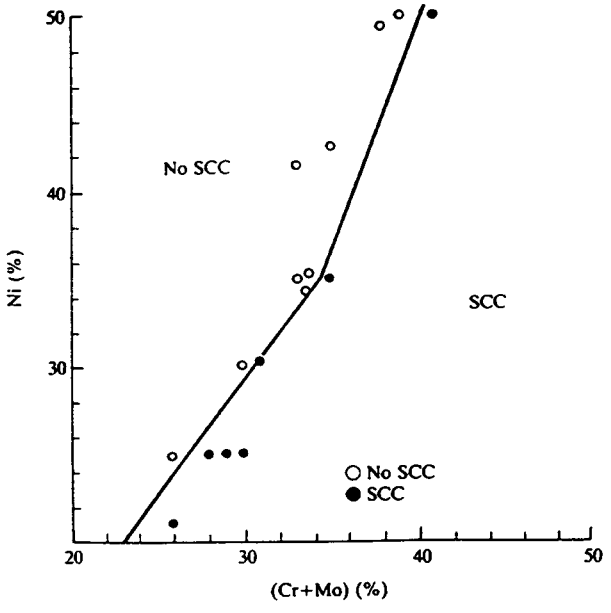


Fig. 8 Effects of nickel content and combined chromium and molybdenum content on SCC

The results of **Table 5** implies that the excess contents of chromium and molybdenum increase the SCC susceptibility, unless nickel is present in a certain amount in relation to chromium and molybdenum combined. The relationship between the combined chromium and molybdenum content and the nickel content with respect to the SCC susceptibility was investigated over a wide chemistry range. The results obtained are shown in **Fig. 8**. According to **Fig. 8**, the limit nickel content that prevents SCC is $3Ni > 4(Cr + Mo)$ for $(Cr + Mo) \leq 34\%$ and is $2Ni > 5(Cr + Mo) - 102$ for $(Cr + Mo) > 34\%$. A similar relationship was observed in $MgCl_2$ environments.[12]

The test results mentioned above led to the establishment of an OCTG alloy series which are resistant to SCC in the H_2S environment. The alloy series in shown in **Fig. 9** as superimposed on the temperature — H_2S partial pressure diagram. The alloy series shown in **Fig. 9** indicate the chemical compositions of high-alloy OCTG that can accommodate all the sour oil and gas well environments shown in **Fig. 1**.

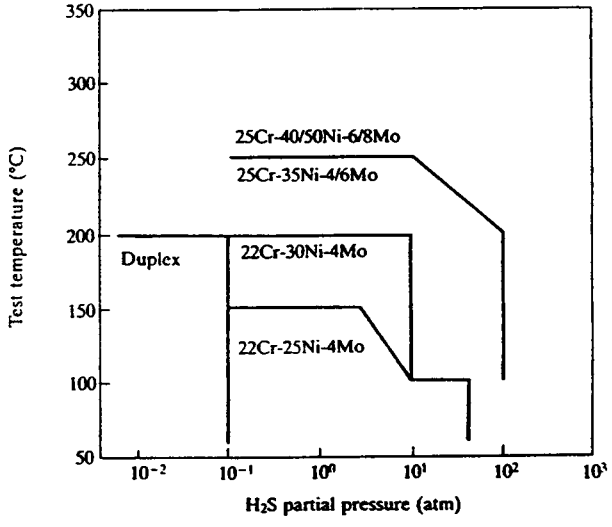


Fig. 9 Limiting environmnetal conditions for high-alloy OCTG with initiation of SCC taken as critical condition

5. Properties of Trial Tubes

The properties of trially-produced tubes in the OCTG series shown in **Fig. 9** are described below.

Fig. 10 is a schematic illustration of the production process and typical chemical compositions of hot-extruded tubes. An example of trial tube is shown in **Photo. 1**. The mechanical properties of trial tubes are given in **Table 6**. The 0.2% offset yield strength indicates the 110-ksi grade. The SCC test results of trial tubes in the H_2S environment are shown in **Fig. 11**[*1], which closely agree with the test results of the Labo-melt 22%Cr-25%Ni-4%Mo alloy shown in **Fig. 9**. **Table 7** shows the intergranular corrosion resistance and pitting corrosion resistance of the trial steel. The steel has good resistance to intergranular and pitting corrosion.

[*1] The test stress values shown in **Fig. 11** are higher than the tensile strength value in **Table 6**. This is because the test stress is set according to the formula specified in ASTM G 39-73 for calculating the elastic stress at the mid-portion of four-point loaded specimens as previously noted. The specimen actually deforms plastically and the test stress is lower than the initial stress setting.

(1) Production process
Vacuum melting in high-frequency induction furnace → Soaking → Hot extrusion → Heat treatment → Pickling → Cold drawing → Straightening → Nondestructive inspection → Product

(2) Chemical composition

	C	Si	Mn	P	S	Ni	Cr	Mo	N	O
Target composition (%)	<0.015	<0.15	<0.15	<0.02	<0.01	24/36	20/25	4/4.5	<0.02	<0.01
Typical composition (%)	0.012	0.1	0.01	0.01	0.002	25.5	22.3	4.3	0.01	0.002

Fig. 10 Schematic illustration of production process of hot-extruded trial tubes, and typical composition (22Cr-25Ni-4Mo)

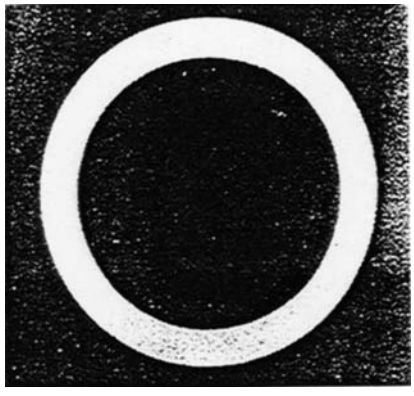


Photo. 1 Example of trial tube
22Cr-25Ni-4Mo
Hot-extruded tube

Table 6 Example of mechanical properties of trial tubes

Tensile strength (kgf/mm²)	0.2% offset yield strength (kgf/mm²)	Elongation (%)	Hardness (Hv)	Grain size number
82	76	24	260	5.5

Amount of cold drawing: 23%
Product tube size
Outside diameter: 60.3 mm
Wall thickness: 6.45 mm

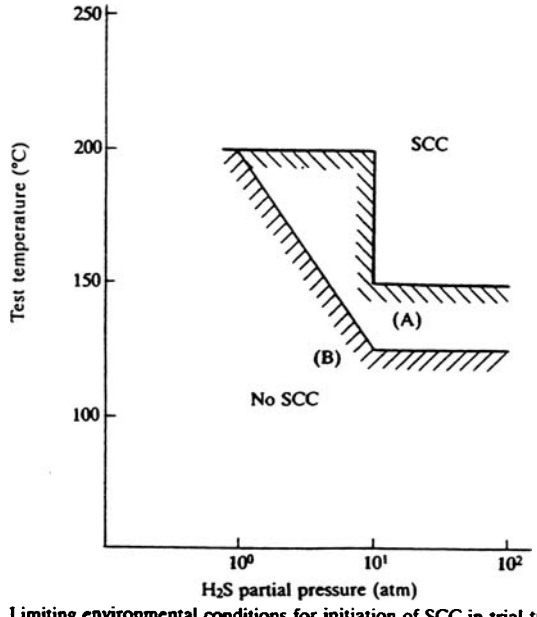


Fig. 11 Limiting environmental conditions for initiation of SCC in trial tubes
(A) Test stress: 87.5 kgf/mm²
(B) Test stress: 140 kgf/mm²

Table 7 Intergranular corrosion and pitting corrosion test results of trial steel

Intergranular corrosion test		Pitting corrosion test	
ASTM A 262 C	ASTM A 262 E	ASTM G 48 A	ASTM G 48 B
NC	0.125 g/m²/h	CPT: 40°C	CCT: 30°C

NC: No cracking
CPT: Critical pitting temperature
CCT: Critical crevice corrosion temperature

6. Methods for Evaluating Service Performance of High-Alloy OCTG

When high-alloy OCTG are planned for application in sour environments, establishing an OCTG evaluation method suited for the service environment is as important as developing an appropriate alloy series. The type of corrosion that restricts the service performance of high-alloy steels is localized corrosion.

When the service performance of high-alloy steel OCTG is evaluated, the type of corrosion may be divided into two groups. One is the type which can be uniquely evaluated by thermodynamic mechanism without time dependence (pitting corrosion, for instance) and the other belongs to the secondary corrosion morphology with time-dependent nucleation process (like SCC which initiates at pitting as precursor). It is very difficult to rationally establish service limits for the latter type of corrosion morphology.

In this paper, the initiation of SCC is taken as the critical condition to establish the service limit of high alloy steel OCTG. As the test duration is prolonged, there is a possibility that SCC may originate from pitting corrosion under such environmental conditions that SCC does not otherwise occur in a short test duration. Accordingly, the service limit line varies corresponding to the evaluation method.

The predicted transition of corrosion morphology in duplex stainless steel is shown in **Fig. 12**[13] and the corrosion test results of the tested steel are shown in **Fig. 13**.[14] The initiation of pitting corrosion and the transition between passive and active corrosion can be thermodynamically predicted. The prediction results are indicated by lines A and B in **Fig. 12**. The prediction results closely agree with the test results, as can be seen from **Fig. 13**. Line C in **Fig. 12** is a limit line for the initiation of SCC

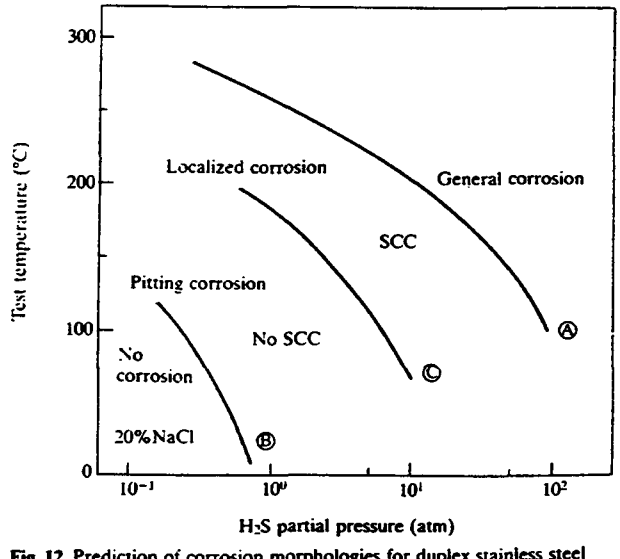


Fig. 12 Prediction of corrosion morphologies for duplex stainless steel
Test steel: DIN 1.4462

as determined by the test method shown in Fig. 2. As the test duration extends (for example, 1,000 or 3,000 h), SCC begins to originate from pitting corrosion and limit line C for the initiation of SCC approaches limit line B for the initiation of pitting corrosion. Lines A and B indicate the results of prediction, while line C indicates the results of experimentation. The former are not dependent on time and are uniquely determined, while the latter depends on the measuring conditions, the test duration, in particular.

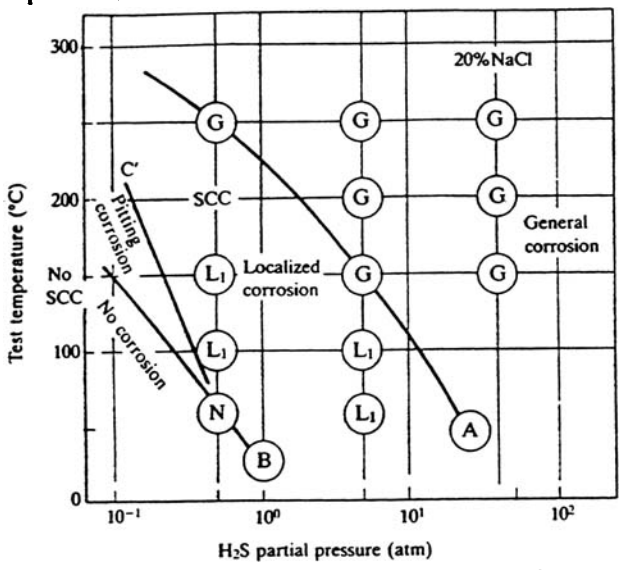


Fig. 13 Corrosion test results of duplex stainless steel
Test steel: DIN 1.4462

Limit line C' for the initiation of SCC in Fig. 13 indicates the measurement of SCC nucleation by the slow strain rate test (SSRT),[15] a test method that can evaluate SCC susceptibility without time dependence. Line C' approximately agrees with limit line B for the initiation of pitting corrosion and suggests that when a long-time evaluation test is conducted, the limit line obtained for the initiation of SCC virtually coincides with limit line B for the initiation of pitting corrosion.[16]

Pitting corrosion resistance in the H_2S environment was evaluated by measuring the pitting potential. The results are shown in Fig. 14. The pitting potential of the alloy series shown in Fig. 9 is related to the chromium, nickel and molybdenum contents of the alloys in Fig. 14. As the contents of these alloying elements increase, the pitting potential becomes nobler and the pitting corrosion resistance becomes higher. It can be seen that the higher the limiting test temperature and H_2S partial pressure above which SCC occurs in Fig. 9, the nobler the pitting potential and the higher the pitting corrosion resistance.

If the limit line for the initiation of SCC agrees with that for the initiation of pitting corrosion as discussed above, the limit line can be drawn irrespective of time dependence.*1 This, however, generally represents slightly stricter evaluation. Since what method to employ for evaluating the service performance of materials is related to the user's concept of material selection, it is not appropriate to stipulate a specific evaluation method for all the materials to be used. It is at least necessary that any established evaluation method be based on the mechanism of nucleation of the corrosion morphology that occurs in actual service environments.

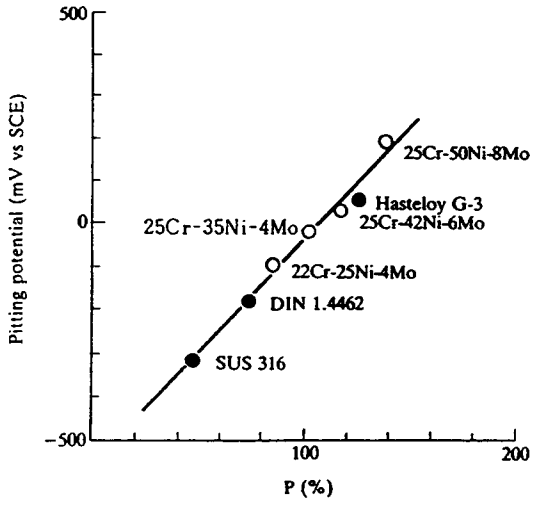


Fig. 14 Effect of alloying elements on pitting potential
P = Cr (%) + 2Ni (%) + 1.5Mo (%)
Measuring environment: 20%NaCl solution; H_2S partial pressure 1 atm; pH 4; temperature 80°C

7. Conclusions

An alloy series for OCTG that are compatible with high-temperature, high-pressure environments where H_2S is present were established with reference to SCC. Three alloy systems, 22Cr-25/30Ni-4Mo, 25Cr-35Ni-4/6Mo and 25Cr-40/50Ni-6/8Mo, were presented as alloy compositions that meet the predicted environmental conditions. Trial tubes were found to have good properties, and their test results verified the feasibility of manufacturing high-alloy OCTG of the prescribed design service performance from these materials.

It was also proposed that the service performance of high-alloy OCTG should be evaluated by methods that meet actual service conditions in order to assure rational use of OCTG.

8. Acknowledgments

The authors gratefully thank many people in the research, production and technical administration divisions of Nippon Steel for their cooperation in the present work.

*1 When stres corrosion nucleates at pitting or crevice corrosion as a precursor, there arise such time dependence question as incubation time until the initiation of crevice corrosion, and the timing of transition from pitting or crevice corrsion to SCC.

References

1) Irving, R.R.: Iron Age. (Nov. 12), 52 (1980)
2) Kohut, G.B., Caldwell, J.R., Morris, R.A.: Alloys for the Eighties. Barr. R.Q., ed. Greenwitch, Climax Molybdenum, 1981, p. 235
3) Kane, R.D., Boyd, W.K.: Alloys for the Eighties. Barr, R.Q., ed. Greenwitch, Climax Molybdenum, 1981, p. 225
4) Place, M.C.Jr.: Corrosion/87, Paper No. 282. San Francisco, 1987, NACE
5) Terasaki, F., Ikeda, A.: Journal of the Japanese Association of Petroleum Technologists. 50 (2), 43 (1980)
6) Kudo, T., Terasaki, F.: Bulletin of the Japan Institute of Metals. 26 (4), 247 (1987)
7) Rhodes, P.R.: Corrosion/86, Paper No. 322. Houston, 1986, NACE
8) Ikeda, A., Kudo, T., Okada, Y., Mukai, S., Terasaki, F.: Corrosion/84, Paper No. 206. New Orleans, 1984, NACE
9) Matsushima, I., Shimada, T., Masamura, K., Sakai, J., Tanimura, M.: Corrosion/85, Paper No. 233. Boston, 1985, NACE

Copyrighted Materials
Copyright © 1996 NACE International Retrieved from www.knovel.com

CORROSION 84

207

The International Corrosion Forum Devoted Exclusively to The Protection and Performance of Materials

April 2-6, 1984/New Orleans Hilton Hotel/Rivergate Exhibition Center/New Orleans, Louisiana

CRITICAL CONTENTS OF NICKEL AND CHROMIUM REQUIRED FOR SCC RESISTANCE OF HIGH ALLOY OCTG

Jun-ichi Sakai, Masaharu Honda,
Katsumi Masamura, Iwao Matsushima,
Yoshiichi Ishizawa

Technical Research Center
Nippon Kokan K.K

1-1, Minami-watarida-cho,
Kawasaki-ku, Kawasaki,
Kanagawa-ken, Japan T210

Takanori Ono

NKK America Inc.
Capital National Bank Plaza Building,
333 Clay st. Suite 1500
Houston, Texas 77002

ABSTRACT

Based on the laboratory SCC test results of 10 - 37% Cr, 25 - 45% Ni, 3% Mo, bal. Fe alloys, it is shown that the beneficial effect of increased Ni contents on SCC resistance is retained only when the Cr content is appropriate. Good SCC resistance is obtained when the stability of austenite is above a critical value so that the content of ferrite formers, e.g., Cr and Mo, should not exceed a certain limit which is determined by the content of austenite formers, e.g., Ni. The critical stability of austenite depends on the annealing temperature, a higher temperature requiring a higher stability of austenite. The lower limit of the Cr and Mo contents, on the other hand, is determined in view of pitting corrosion resistance.

1. INTRODUCTION

It has long been established that the resistance of austenitic chromium-nickel stainless steels to transgranular stress corrosion cracking (SCC) in aqueous chloride media is improved by increasing the nickel content. For example, Copson (1) showed that austenitic stainless steels containing more than 45% Ni were immune to SCC in a boiling $MgCl_2$ solution and probably in other chloride solutions as well (2). The environmental and metallurgical factors affecting susceptibility of Cr - Ni - Fe alloys to chloride SCC have been reviewed by Staehle and his co-authors (3)(4)(5). These authors also reviewed in detail many mechanistic postulates that had been presented to account for the occurrence of chloride SCC.

Recently, high Ni austenitic alloys have been attracting attention as the tubulars for use in oil and gas wells of high corrosivity because of their excellent resistance to corrosion and SCC. Such alloys naturally contain large amounts of Ni, Cr, and Mo. The beneficial effect of Ni on SCC resistance is widely accepted, while the effect of Cr (6)(7)(8)(9) has not been firmly established. Evans, et al,(5) concluded that the resistance to SCC depended upon the (Cr + Ni) content. Truman, et al,(6) found that additions of 15-20% Cr to Ni-Fe alloys resulted maximum susceptibility to SCC. On the other hand, Staehle, et al,(9) reported, based on their test results in $MgCl_2$ (154°C) solutions, that lowering the chromium content to 10 to 15% was very effective in preventing SCC of austenitic alloys. Sedriks(10) reached a conclusion that the effect of Cr on the SCC susceptibility of an alloy was variable.

In view of the situation, a study was undertaken to determine the effects of Cr on SCC resistance with particular attention to the amount of coexisting Ni. The annealing temperature was also taken as a factor considering its potential influence.

2. EXPERIMENTAL

Materials

Alloys for testing were melted in the laboratory by using a 150kg high frequency induction furnace. The chemical composition and the yield strength are listed in Table 1. Most of the alloys had a composition of X% Cr - Y% Ni - 3% Mo - 1.4% Cu, where X=10.8-36.8 and Y=24.9-45.7. Si and Mn were controlled to

0.3% and 0.8%, respectively. Less than 50ppm P and 20ppm S were ensured by using high purity raw materials. The C content was analyzed between 0.002 to 0.026%. The ingots were hot rolled to 10mm thick sheets which were heat treated at 950°C and 1050°C for 30 minutes and were water quenched.

Test Procedures

Resistance to chloride SCC was examined in a 45% $MgCl_2$ solution boiling at 154°C. All specimens were machined after heat treatment and thoroughly degreased prior to test. Tensile specimens (3.0 diam. x 10mm in the gauge section) were stress loaded uniaxially and immersed in the test solution contained in a glass cell equipped with a reflux condenser. Tests were conducted under an applied stress equivalent to 120% of the yield strength measured at room temperature. Tests were continued over 600 hours and then terminated in case of non-failure.

3. RESULTS

Crack Morphology

A typical crack morphology is shown in Figures 1 a-c. These photographs were taken from a specimen, i.e., 1050°C solution treated 21Cr-29Ni-Fe alloy, which failed in 28 hours. From the general appearance (Fig.1 a), microstructure (Fig.1 b), and SEM observation (Fig.1 c) of the specimen, it is readily seen that many cracks initiate in the gauge section, and propagate transgranularly. The final stage of the failure is caused by ductile fracture due to the reduction of the effective crosssection. All the specimens which showed susceptibility to SCC failed in the same manner.

Effect of Metallurgical Factors

1) Alloying Elements ----- The effects of the Cr contents and the annealing temperature on time to failure (TTF) in alloys containing 30 and 45% Ni with 3% Mo are shown in Figures 2 a and 2 b, respectively. Evidently, Cr is detrimental for SCC resistance and its degree depends both on the Ni contents and annealing temperature, and becomes greater as the Ni content decreases and the annealing temperature rises. When the Ni content is high (45%) and the annealing temperature is low (950°C), failure does not occur regardless of the Cr content.

The effects of the Ni contents and the annealing temperature on SCC susceptibility in alloys containing 22 and 27% Cr are shown in Figure 3. The Cr content and the annealing temperature being the same, an increase of the Ni content always makes the alloy more resistant to SCC. The beneficial effect of Ni is more pronounced when the Cr content and the annealing temperature are low.

2) Annealing Temperature ----- As is obvious from Figures 2 and 3, an alloy is more resistant to SCC when the alloy is annealed at 950°C rather than at 1050°C. This applies to all the alloys tested in the present study, in spite of the fact that better homogeneity of the microstructure is expected when an alloy is annealed at higher temperatures.

3) Austenite Stability ----- SCC test results are plotted on a %(Ni) vs %(Cr+1.5Mo) diagram and shown in Figures 4 a and 4 b. Open marks show survival in 600 hours, and filled ones indicate failure. The austenite stability, Δ(11), as defined as

$$\Delta = Ni - \frac{(Cr + 1.5Mo - 20)^2}{12} - 0.5Mn - 35C - Cu - 27N + 15 \quad ---(1)$$

was calculated for the alloys tested and the values are listed in Table 1. Curves showing iso-austenite stability are drawn in Figures 4 a and 4 b. It is evident that a curve corresponding to an austenite stability divides the failure and no-failure regions in the Ni vs (Cr + 1.5Mo) diagram; alloys having a Δvalue less than critical fail. The critical value depends on the annealing temperature; Δ=10 for annealing temperature of 950°C and 20 for 1050°C.

4. DISCUSSION

It is interesting that the effects of the metallurgical factors, i.e., alloy composition and heat treatment, on resistance to SCC by chloride can be expressed consistently in terms of the austenite stability. Taking the austenite stability (11)(12) as the criterion of SCC, it is expected that Cr would be beneficial up to the %(Cr + 1.5Mo) value of 20 and detrimental above this value. According to Equation (1), susceptibility to SCC would be highest at 20% Cr in Cr-Ni-Fe alloys. The present results are in good agreement with that reported by Evans, et al,(6) and Truman, et al, (7). Almost the same tendency was

obtained by Gras, et al, (13) for high purity Cr-Ni-Fe alloys. No account for the effect of Cr has been given.

The new finding in the present study that susceptibility to SCC is related to the austenite stability can be discussed in terms of tendency for an austenite alloy to be transformed to martensite by application of stresses. The critical composition of the alloys heat treated at 950°C is very close to that for stable/metastable austenite transition in the Cr-Ni-Fe ternary alloy diagram (14)(15). Martensite in metastable alloys is induced not only by deformation but also by hydrogen occlusion, the latter having been proposed as a possible cause of SCC (16). The metastable/stable austenite transition has a close relationship to the dislocation arrangement and stacking fault energy which were claimed to be associated with susceptibility to SCC.

In order to use the austenite stability as a criterion for susceptibility to SCC, there are some aspects that should be accounted for by further study. First, the reason why the annealing temperature also affects susceptibility to SCC can not be readily explained based on the austenite stability. It is not likely that the stable/metastable transition is easier in alloys annealed at higher temperatures. Second, the critical values of the austenite stability were obtained in the present study using a boiling $MgCl_2$ solution. The value could be different in other chloride environments, although very close values were determined for similar alloys tested in H_2S-CO_2-Cl^- at 230°C (17).

In spite of the fact that concentrated boiling $MgCl_2$ solutions do not correspond to any practical environments that cause SCC by chlorides, they have been used widely and found useful as SCC test media, because they are very aggressive and therefore can differentiate SCC resistance among highly resistant alloys. The primary objective of the present study is to find some basic principle with respect to alloy composition that controls SCC resistance, rather than to obtain practical values. Therefore, the use of the most aggressive media, e.g., $MgCl_2$, was desirable. Along the same lines, the applied stress was high, i.e., 120% YS.

In designing an alloy that is used in chloride bearing environments, the greatest concern is to provide resistance to both SCC and pitting corrosion. Cr and Mo that are detrimental to

SCC if contained in amounts more than critical, as demonstrated in this study, are well known as beneficial elements to resist pitting corrosion. For example, the pitting corrosion resistance of highly alloyed commercial stainless steels, evaluated in terms of weight loss in 10% $FeCl_3.6H_2O$ solution (50°C, 24hr), is shown in Figure 5 with respect to Cr and Ni equivalents (18),

$$Cr_{eq} = \%Cr + \%Mo + 1.5 \times \%Si + 0.5 \times \%Nb \quad \text{----- (2)}$$

$$Ni_{eq} = \%Ni + 30 \times \%C + 30 \times \%N + 0.5 \times \%Mn \quad \text{----- (3)}$$

Thus, a sort of trade-off in the amount of (Cr+Mo) is necessary. The present results, therefore, provide a useful basis in developing a resistant alloy for use in chloride environments.

5. CONCLUSIONS

From the data obtained in this study, the following conclusions can be drawn as to the SCC resistance of highly alloyed austenitic stainless steels in chloride media.

1) Ni always shows beneficial effect regardless of the Cr contents and the annealing temperature.

2) The effect of Cr on susceptibility to SCC depends on its content, i.e., it is beneficial up to a (Cr + 1.5Mo) value of 20% and detrimental above it.

3) SCC resistance among various Cr-Ni-Mo-Fe alloys can be classified systematically in terms of the austenite stability, Δ .

4) The critical value of Δ depends on the annealing temperature; ten when annealed at 950°C and twenty at 1050°C.

5) An alloy is more resistant to SCC when annealed at 950°C than at 1050°C.

6) Pitting resistance mainly depends on Cr equivalent (Cr+Mo,%).

6. ACKNOWLEDGMENT

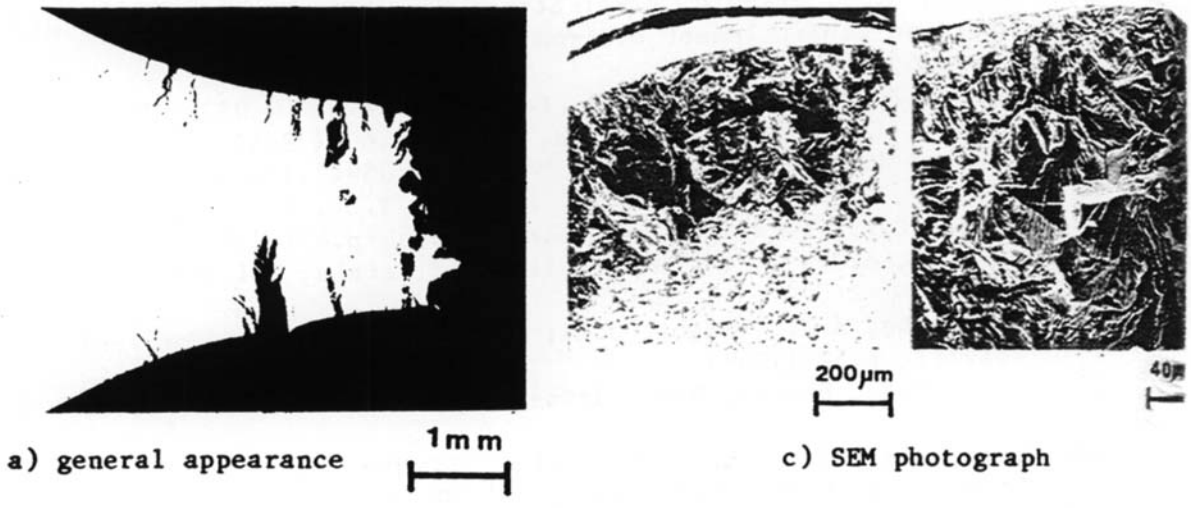
The authors wish to thank Dr. M. Tanimura and Mr. Y. Kamemura for their helpful discussions during this study.

7. REFERENCES

1) Copson, H.R.; Physical metallurgy of stress corrosion fracture. p.247, ed. T.N. Rhoden, Interscience, New York (1959).
2) Speidel, M.O.; Met. Trans.A, Vol.12A, p.779 (1981)
3) Staehle, R.W.; The Theory of Stress Corrosion Cracking in Alloys. p.223, ed. J.C. Scully, NATO, Brussels (1971).
4) Latanision, R.M., Staehle, R.W.; Proceedings of Conference Fundamental Aspects of Stress Corrosion Cracking, p.214, NACE, Houston, Texas (1969).
5) Theus, G.J., Staehle, R.W.; Stress Corrosion Cracking and Hydrogen Embrittlement of Iron Base Alloys, p.845 NACE, Houston, Texas (1977).
6) Evans, T.E., Burr, D.J.; Br. Corr. J., Vol.1, p.192 (1966).
7) Truman, J.E., Perry, R.; ibid, Vol.1, p.60 (1966).
8) Denhard Jr, E.E.; Corrosion, Vol.16, p.359t (1960).
9) Staehle, R.W., Royuela, J.J., Raredon, T.L., Serrate, E., Morin, C.R., Farrar, R.V.; ibid, Vol.26, p.451 (1970).
10) Sedriks, A.J.; J. of the Institute of Metals, Vol.101, p.225 (1973).
11) Griffiths, A.J., Wright, J.C.; Iron Steel Inst. London Publ. Vol.117, p.52 (1969)
12) Post, C.B., Eberly, W.S.; Trans. Am. Soc. Met., Vol.39 p.868 (1947).
13) Gras, J.M., Belo, M.C., Montuelle, J.; Memoires Scientifiques Rev. Metallurg., Vol.70, p.953 (1973)
14) Rhodes, C.G., Thompson, A.W.; Met. Trans. A, Vol.8A, p.1901 (1977).
15) Hirayama, T., Kogirima, M.; Nippon Kinzoku Gakkaishi, Vol.34, p.507 (1970).
16) Rhodes, P.R.; Corrosion, Vol.25, p.462 (1969).
17) Masamura, K., Hashizume, S., Matsushima, I.; unpublished data.
18) DeLong, W.T.; Welding J., Vol.35, p.521S (1956).

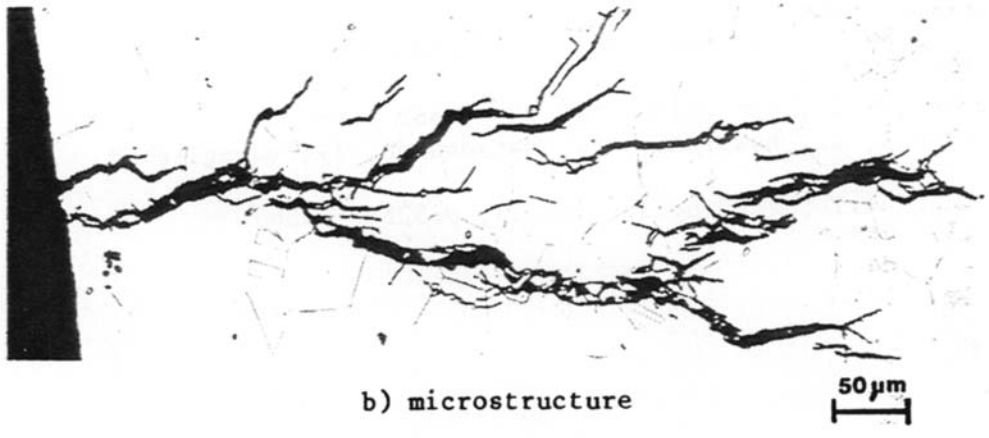
Table 1. Chemical composition, yield strength and Δ value of alloys.

	Code	Cr	Ni	Y.S. (Kg/mm^2) 950°C	Y.S. (Kg/mm^2) 1050°C	Δ value
F	1	21.75	25.50	34.7	31.3	9.22
	2	21.01	29.44	32.0	27.8	15.05
	3	21.33	34.60	35.1	31.8	19.08
	42	18.89	40.13	33.2	32.5	27.04
	45	21.55	39.57	35.1	34.7	24.09
	5	23.69	45.71	37.5	32.5	27.22
	6	25.97	25.09	36.3	35.4	3.31
	7	25.69	29.30	36.5	36.5	8.13
	8	26.28	34.46	38.6	36.8	13.14
	9	28.20	41.23	40.1	36.8	14.66
	102	28.34	43.95	39.9	35.8	17.74
A	1	10.76	24.88	29.0	24.0	9.96
	2	13.90	30.07	25.0	23.3	16.99
	3	16.67	33.60	24.4	23.9	20.44
	4	25.17	45.05	30.9	27.3	24.85
	5	29.15	35.20	38.5	36.1	7.52
	6	32.73	40.03	50.9	41.0	3.60
	7	36.83	44.33	66.2	49.8	- 5.39



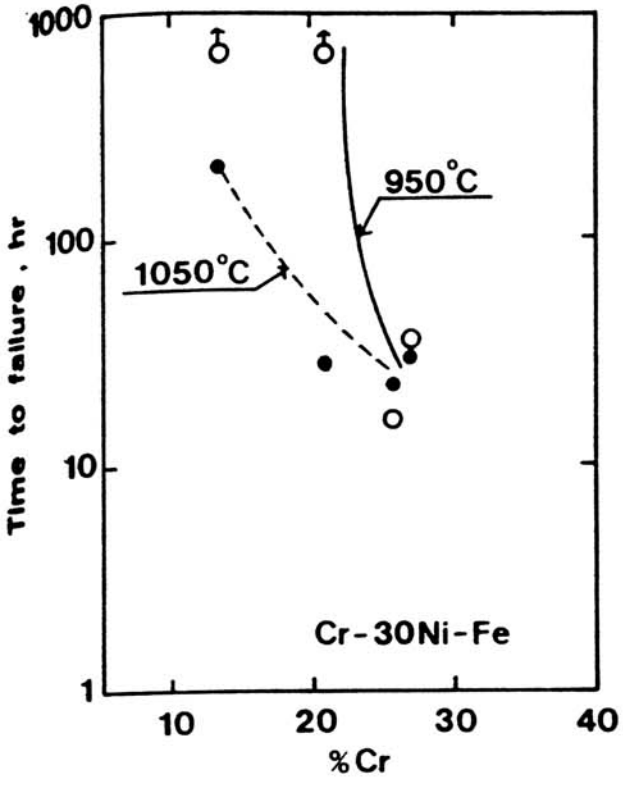
a) general appearance

c) SEM photograph



b) microstructure

Figure 1 : A typical morphology of failed specimen, 21% Cr-29% Ni-3% Mo.



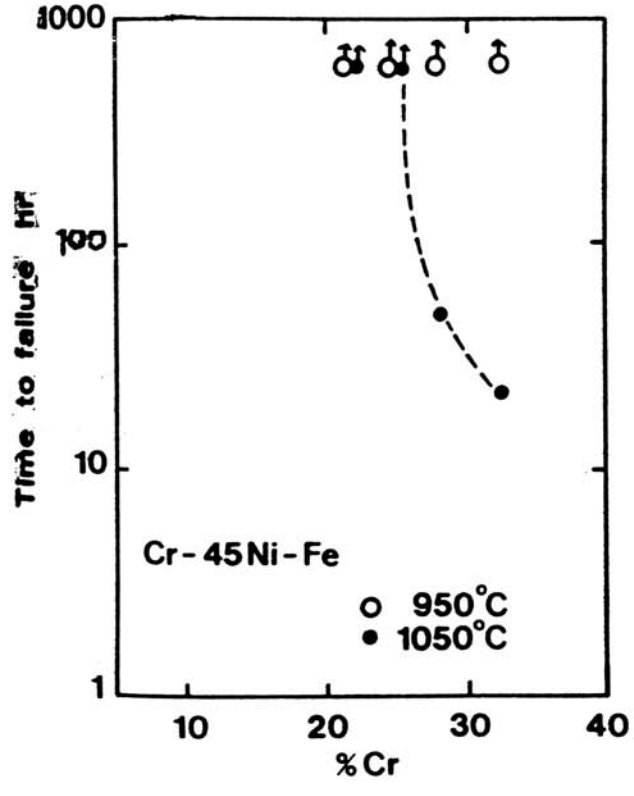


Figure 2 : Effects of the Cr contents and the annealing temperature on TTF.
a) X% Cr-30% Ni-3% Mo-Fe
b) X% Cr-45% Ni-3% Mo-Fe

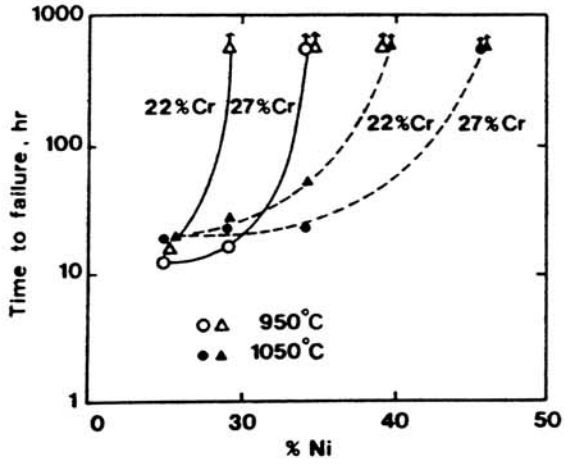


Figure 3 : Effects of the Ni contents and the annealing temperature on SCC resistance of 22% Cr- and 27% Cr-Y% Ni- 3% Mo -Fe.

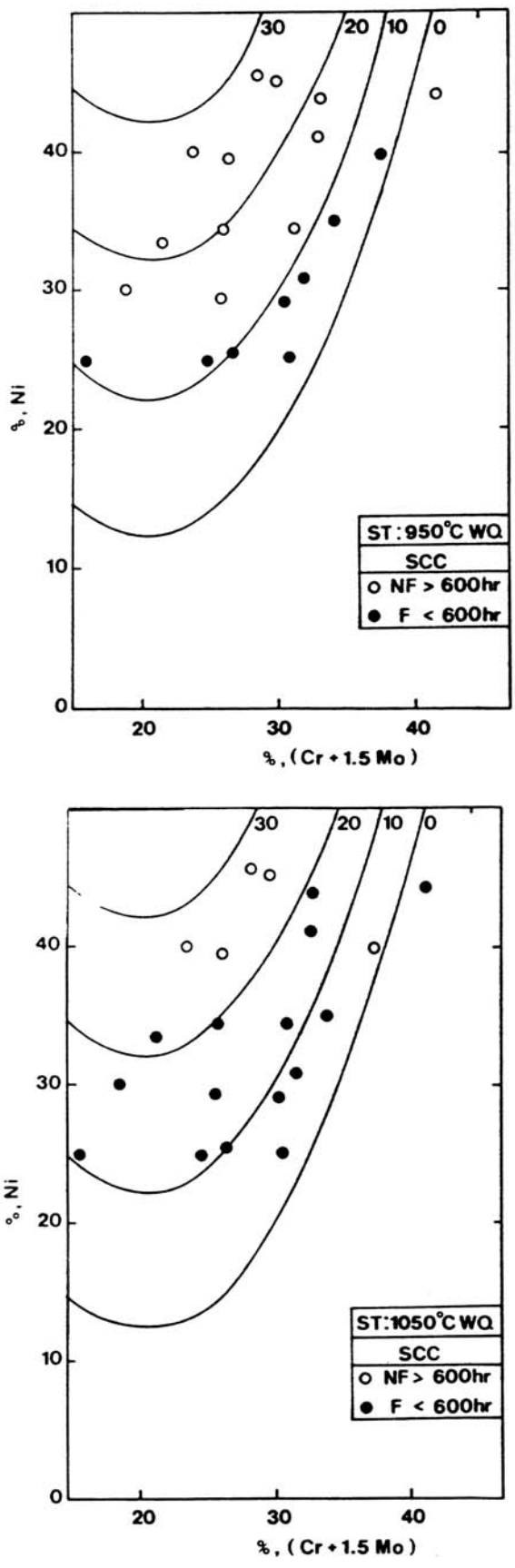


Figure 4 : Effects of the Cr and Ni contents on SCC susceptibility. The curves and the numbers are representing iso-austenite stability.
a) Annealed at 950°C
b) Annealed at 1050°C

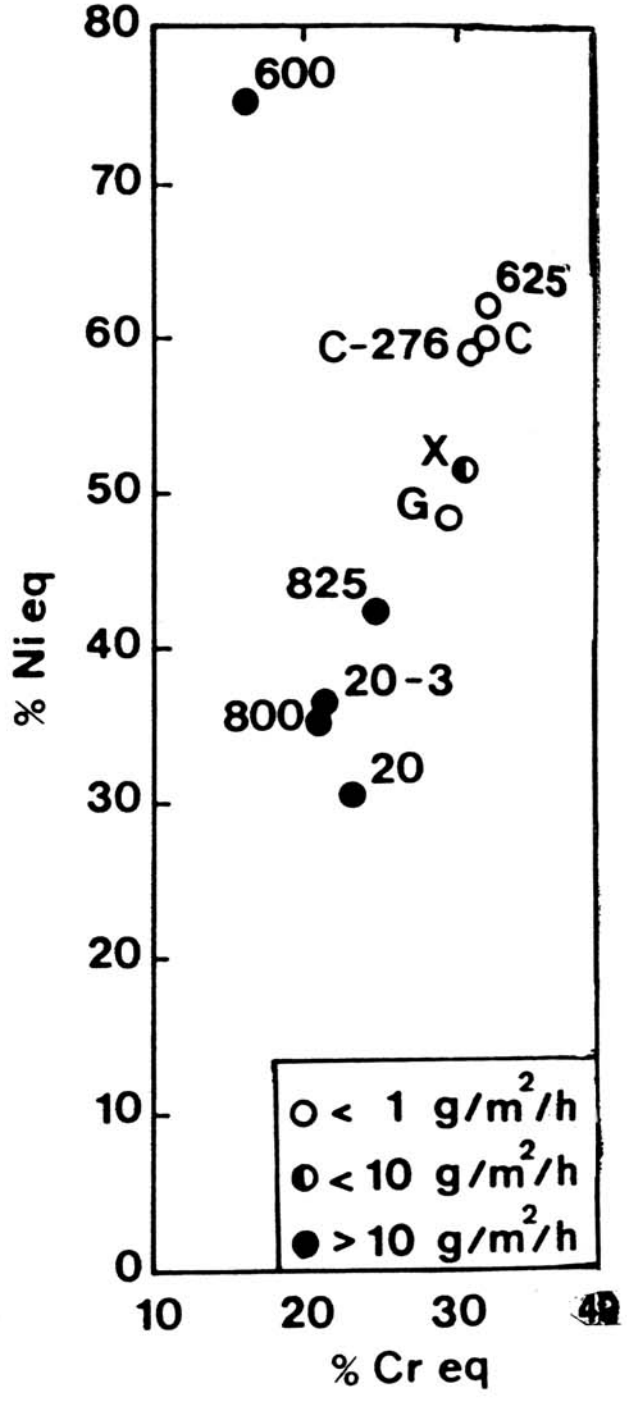


Figure 5 : Effect of Cr and Ni equivalents of commercial highly alloyed stainless steels on pitting corrosion resistance (10% $FeCl_3 \cdot 6H_2O$, 50°C, 24hr).

Copyrighted Materials
Copyright © 1996 NACE International Retrieved from www.knovel.com



OTC 6071

Laboratory and Field Evaluations of Clad Christmas Tree Equipment

by W.J. Sisak, Exxon Production Research Co., and J.R. Gordon, Exxon Co. U.S.A.

Copyright 1989, Offshore Technology Conference

This paper was presented at the 21st Annual OTC in Houston, Texas, May 1–4, 1989.

This paper was selected for presentation by the OTC Program Committee following review of information contained in an abstract submitted by the author(s). Contents of the paper, as presented, have not been reviewed by the Offshore Technology Conference and are subject to correction by the author(s). The material, as presented, does not necessarily reflect any position of the Offshore Technology Conference or its officers. Permission to copy is restricted to an abstract of not more than 300 words. Illustrations may not be copied. The abstract should contain conspicuous acknowledgment of where and by whom the paper is presented.

ABSTRACT

A methodology is presented for evaluating the corrosion resistance of clad equipment in sour environments. The paper describes the laboratory and field test programs used to evaluate the suitability for sour service of gate valves clad with Alloy UNS N06625 by weld overlay and by hot isostatic pressing (HIP). The laboratory tests that were used to evaluate the corrosion and cracking resistance of the clads are reviewed. Experience with actual field installations of both types of clad valves is presented and the test/inspection methods used to evaluate the equipment during and after the service period are discussed. Finally, laboratory and field results are compared to highlight key findings related to the clad valve bodies as well as to the trim components.

In general, successful performance in the field trials confirmed the laboratory test results. However, the field trials highlighted the importance of the performance of the mechanical components in the sour environment, an area not targeted in the original laboratory test program. The methodology employed emphasizes the synergism of laboratory and field programs in evaluating component performance.

INTRODUCTION

Service environments encountered in the production of hot, sour gas reservoirs can be extremely corrosive to conventional alloy steel equipment. A class of nickel-base materials known as corrosion-resistant alloys (CRAs) are being used increasingly as tubulars and downhole equipment in these applications because of their good corrosion resistance. CRA materials may also be required for the christmas tree in environments that are too corrosive for alloy steels or martensitic stainless steels. As a result, many operators have selected valves that are internally clad with Alloy UNS N06625 to provide the needed corrosion resistance.

The primary commercial processes for cladding are weld overlay and hot isostatic pressing, or HIP. Welding procedures for the overlay are qualified in accordance with ASME Section IX with primary controls on hardness and chemistry dilution. The HIP process uses heat (2000-2100°F) and pressure (up to 15,000 psi) to consolidate a CRA powder into a fully-dense layer bonded to a steel body.

METHODOLOGY

To gain greater assurance that specific materials and designs would perform satisfactorily under given conditions, laboratory and field test programs were used to evaluate corrosion properties and mechanical reliability for the life cycle of the clad equipment. A joint laboratory and field test approach was considered essential to compensate for deficiencies in a singular laboratory or field test program. Laboratory programs typically use small-sized specimens that are tested in a variety of environments. It generally is not possible, however, to simulate actual production conditions in these experiments, making it difficult to correlate lab data with field performance. Field tests, on the other hand, allow evaluation of the equipment of interest in actual producing conditions under real operating stresses. Field tests are limited to available producing environments and thus cannot simulate the range of conditions possible in the laboratory.

Reference and illustrations at end of paper.

© OTC Reprinted with the permission
of the Offshore Technology Conference

OBJECTIVES

The principal objectives of the laboratory and field test programs were the assessment of the corrosion and cracking susceptibility of the clad layer in sour environments as well as the disbonding tendency of the clad/steel interface for both the weld overlay and HIP clads. In addition, in the field test program, the performance of CRA ring gaskets and premium stem packing assemblies was observed.

EXPERIMENTAL

It was recognized at the outset of this program that available well completions were not sufficiently harsh to model all sour service conditions of interest. This dictated the use of more severe laboratory test conditions and provided unavoidable mismatch of field and lab environments. This hindered precise correlation of lab and field results.

Laboratory Tests

Stress-corrosion-cracking (SCC) resistance was determined using the slow-strain-rate tensile (SSRT) test. The SSRT specimens were machined from the clad layer of test blocks that were manufactured in the same manner as clad equipment. The compositions of the test blocks are listed in Table I. The specimens were pulled to failure at an initial strain rate of 4×10^{-6} per second in an autoclave. The sour environment was a solution of 25 weight percent NaCl and 0.5 weight percent acetic acid in deionized water. The solution was charged with 100 psig hydrogen sulfide gas at ambient temperature. Identical specimens were tested in air for comparison to the solution tests. Following fracture, the specimens were examined for indications of SCC such as brittle fracture mode, secondary cracks, or corrosion on the fracture surface.

Mechanical disbond tests studied factors affecting disbond at the clad/steel interface. Specimens were machined from spacer spools that were manufactured identically to clad equipment (Table II). The interface bond was tested using Charpy V-notch specimens similar to specimens used in an earlier study of clad [1]. The Charpy notch was perpendicular to the clad/steel interface so that fracture occurred in the clad and steel simultaneously (Fig. 1). Specimens were fractured at ambient temperature and examined for disbond at the interface.

Hydrogen disbond tests studied the effect of hydrogen accumulation on cracking at the interface. Spools were machined to a tubular shape that had an outer layer of steel and an inner layer of clad. The specimens were charged as the cathode in a solution of 1.0 N H_2SO_4 containing 0.5 cc per liter of As_2O_3 as a hydrogen recombination poison. The test set-up is shown in Figure 2. Specimens were charged at current densities of 1 mA/cm^2 and 10 mA/cm^2 at ambient temperature for 240 hours. After charging, the interface was inspected using a straight beam ultrasonic technique. The test pieces were also sectioned for direct metallographic examination of the bond line.

Field Tests

The test valves were 2-9/16-inch, 10M psi working pressure and were installed as wing valves on two test wells. Both valves featured special alloy trim components and were manufactured to critical service specifications. Materials used in the test valves met the requirements of NACE MR-01-75 and are listed in Table III.

The valves were installed at readily accessible land locations and experienced producing conditions as shown in Table IV. Both oil and gas producers were selected in order to evaluate a wide range of flowing wellhead temperature, saltwater production, and H_2S content. Total production for both test valves is also included in Table IV. Arbitrarily, the valve clad by weld overlay was installed on Well A for 25 months while the HIP clad valve was installed on Well B for 18 months.

Periodic onsite inspections monitored the performance of the test valves while in field service. Visual and dye-penetrant examination, dimensional checking and hydrostatic testing were conducted at approximately six-month intervals. Both valves received a thorough final inspection, witnessed in the manufacturer's plant, that included the procedures outlined in Table V.

RESULTS AND DISCUSSION

Laboratory Tests

SCC. Both the weld overlay and HIP clads performed well in this test. No indications of SCC or localized corrosion were found at 200, 250, and 300°F, indicating good resistance to cracking in this temperature range.

Mechanical disbond. No disbond was observed in weld clad specimens, whereas some disbonding occurred in the HIP clad samples (Fig. 3). Disbond cracks were in a region of dense carbides near the clad/steel interface (Fig. 4). It was found that the carbon content of the base steel influenced the extent of disbond. Disbond cracks were longer in the AISI 4130 base steel samples (~0.30% C) than in the 2-1/4 Cr-1 Mo base steel samples (~0.19% C). While the Charpy disbond test provided a qualitative assessment of bond integrity, we have not conducted sufficient testing to develop a quantitative acceptance criteria for mechanical disbond using this test.

Hydrogen disbond. No disbond was detected at the clad/steel interface in either clad tested at 1 mA/cm^2. In tests at 10 mA/cm^2, no cracks were found in the HIP specimen; however, cracks were detected by ultrasonic examination and confirmed by metallographic sectioning in the weld overlay specimen. Hydrogen disbond cracks were oriented parallel to the interface (Fig. 5), but did not cause collapse of the clad layer.

Field Test Program

The field test program successfully addressed its materials-related objectives. It also yielded additional information on performance of the trim components that was not an initial target of the program. Results are highlighted below.

- No defects in the clad surface of either test valve were indicated by dye-penetrant inspection during and after the service period.
- No disbonding of the clad layer was detected by ultrasonic examination of the clad interface after the service period.
- No corrosion could be documented by visual inspection or dimensional checking of the clad bodies and flowbores.
- CRA ring gaskets and stem packing stacks functioned properly and were virtually undamaged.

Both valves failed in-plant gas tests upon return to the manufacturers. Large gate-to-seat leakage was observed and was attributed to scoring and flaking of the hardfaced surfaces. The valves were not operated regularly throughout the test period and mechanical damage or wear of the closure parts was not anticipated. Flaking of the hardfacing material was an unexpected corrosion problem.

The problems uncovered in the field test program emphasized the need for full evaluation of all materials and manufacturing processes as well as the need for a thorough analysis of design practices. As a result of these problems, a new suite of laboratory and field tests was defined. These tests would:

1. Evaluate various substrate/hardfacing material combinations and hardfacing application processes for corrosion/pitting resistance, and
2. Evaluate specific hardfacings and valve designs for wear endurance through differential pressure openings and thermal cycling.

CONCLUSIONS

For the laboratory and field conditions cited earlier in this paper, the following conclusions about clad valves are made.

- Laboratory and field results both confirm the corrosion and cracking resistance of the clad layer.
- No disbonding at the clad interface could be detected after 18-24 months of field exposure.
- Disbonds from laboratory experiments cannot be directly correlated to field service limits at present.
- Mechanical disbond resistance at the interface was better in lower carbon 2-1/4 Cr-1 Mo steel base metal than in higher carbon AISI 4130 steel.
- Full-scale field testing is invaluable in appraising the overall mechanical performance of actual materials and designs.

REFERENCE

[1] P. J. Kovach and T. D. Williams, Low-Heat Input Welding Process for Corrosion-Resistant Cladding of Wellhead Components, SPE/IADC Drilling Conference, Paper No. SPE/IADC 13452, 1985.

Table I Chemical Analysis of Clad Layer from Clad Test Blocks

(in weight percent)

Material Description	Element										
	Ni	Cr	Mo	Nb & Ta	Ti	Al	C	P	S	Si	Fe
Weld	63.8	21.4	7.9	3.2	0.26	0.21	0.02	0.008	0.001	0.06	3.1
HIP	65.2	21.8	8.0	3.3	0.30	0.18	0.04	0.010	0.009	0.06	1.09

Table II Description of Clad Spacer Spools
Used for Disbond Tests

	Weld	HIP
Description:	2-1/16-inch ID 5000 psi working pressure	2-1/16-inch ID 5000 psi working pressure
Base Steel:	AISI 4130	AISI 4130
Clad Material:	UNS NO6625	UNS NO6625
Clad Thickness:	Nominal 1/8 inch	Nominal 1/8 inch
Description:	2-9/16-inch ID 20,000 psi working pressure	2-9/16-inch ID 20,000 psi working pressure
Base Steel:	2-1/4 Cr-1 Mo	2-1/4 Cr-1 Mo
Clad Material:	UNS NO6625	UNS NO6625
Clad Thickness:	Nominal 1/8 inch	Nominal 1/4 inch

Table III 2-9/16", 10 Mpsi Test Valve Descriptions

	Weld Clad	HIP Clad
Body	AISI 4130	2-1/4 Cr-1 Mo
Gate	UNS NO6625	UNS NO7718
Seat	UNS NO6625	Cobalt base
Stem	UNS NO7718	UNS NO7718
Hardfacing	Cobalt base	Nickel base

Table IV Test Well Description

	Well A	Well B
Type Well	Gas	Oil
H_2S Content (%)	19	4
CO_2 Content (%)	44	10
Flow Rate	10 MCFD	800 BOPD
Liquid Production	100 BCPM	8000 BWPD
FWHP - psi	1100	360
FWHT - degrees F	125	225
Gas Production	3.22 GCF	0.99 GCF
Oil Production	322 MB	321 MB
Water Prodution	21 MB	3940 MB

Table V Final Plant Inspection

	Clad Layer	Stem	Gate/ Seat	Packing/ Bonnet Seal
Gas Test			X	X
Visual Exam	X	X	X	X
Photograph	X	X	X	X
Dye Penetrant	X	X	X	
Ultrasonic	X			
Dimensions*	X			

*Dimensional checking duplicated field procedure where internal diameters were measured 90 degrees apart at one-inch and two-inch distances in from each flange face.

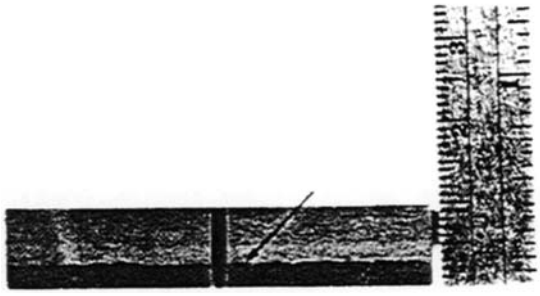


Fig. 1. Charpy V-notch specimen used for mechanical-disbond tests.

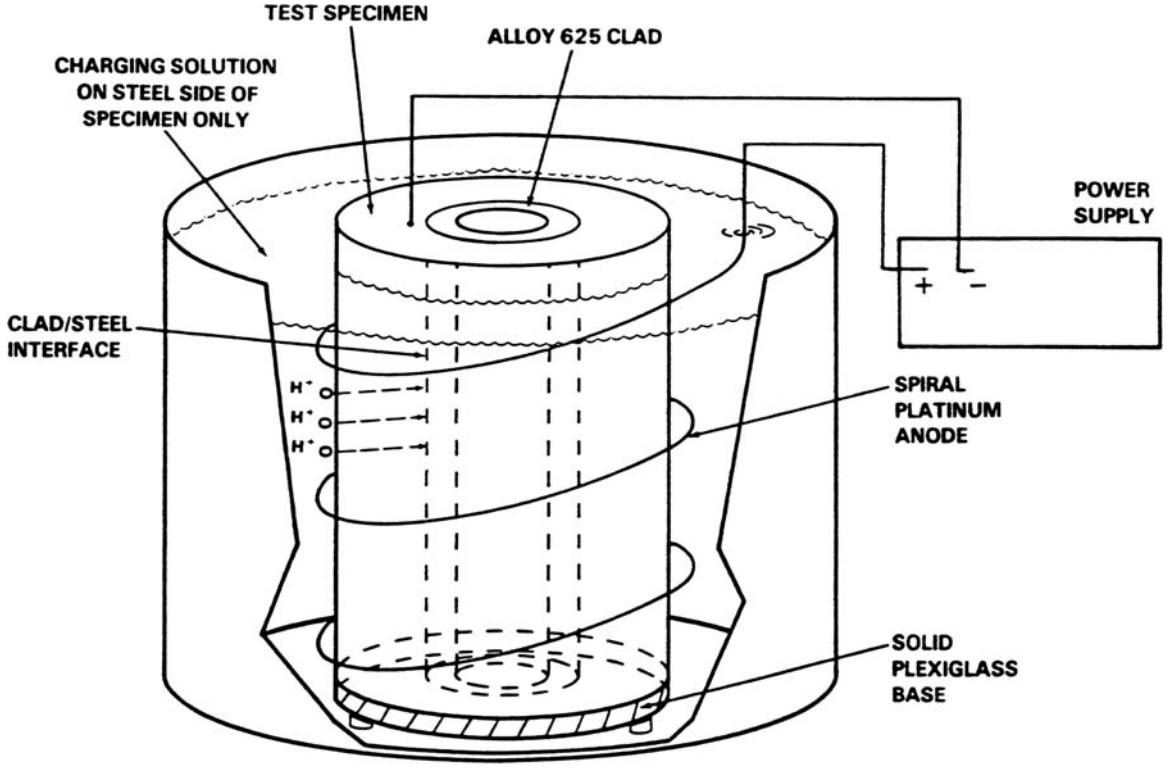


Fig. 2. Schematic of hydrogen-disbond test apparatus.

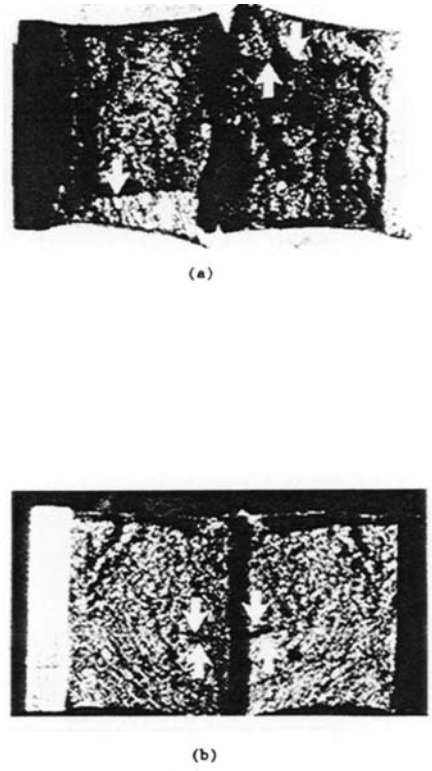


Fig. 3. Fracture surfaces of mechanical-disbond specimens. (a) Weld-clad; no cracks. (b) HIP-clad; arrows indicate cracks.

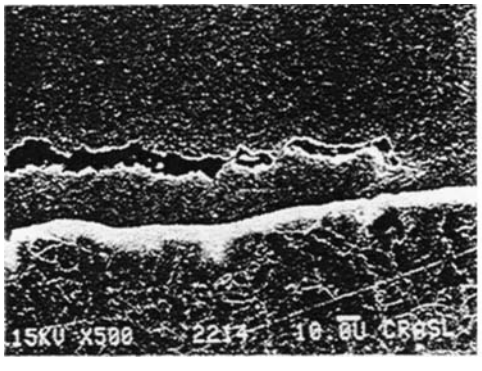


Fig. 4. Scanning-electron micrograph of HIP-clad specimen showing mechanical disbond near the clad/steel interface.

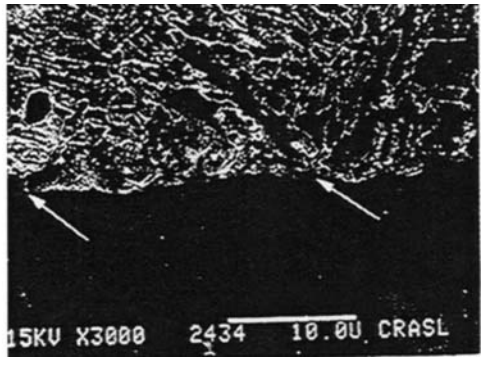


Fig. 5. Scanning-electron micrograph of hydrogen-disbond cracks near the clad/steel interface in a weld-overlay sample.

Copyrighted Materials
Copyright © 1996 NACE International Retrieved from www.knovel.com

Paper No. 12—CORROSION/89

THE EFFECT OF ELEMENTAL SULFUR ON STRESS CRACKING OF NICKEL BASE ALLOYS

N. Sridhar and S.M. Corey
Haynes International Inc.
Kokomo, Indiana 46901

ABSTRACT

The effects of elemental sulfur additions to sour gas environments on the stress corrosion cracking (SCC) resistance of Ni-base alloys are examined in this paper. Attention is focused on low accounts of sulfur, less than 1 g/l. It is found that the detrimental effects of sulfur, depending on the alloy, can be found even at concentrations of 0.02 g/l at 204°C (399°F). The effects of pH, chloride levels, sulfur solvents, strength, and temperature are also examined. The effects of alloying elements are examined through various commercial alloys. Alloys containing molybdenum about 13% or higher (UNS N06022 and N10276) showed the best resistance of the Ni-base alloys tested.

INTRODUCTION

The effects of elemental sulfur is of great interest both in the production of some of the sour oil and gas wells, where sulfur is an unwanted component, and in super-sour gas production, where sulfur is the end product desired.[1,2] The detrimental effect of elemental sulfur on the sour-gas stress corrosion cracking (SSCC) of corrosion resistant alloys (CRAs) is well documented.[1-8] However, several questions remain largely unanswered: (1) What is the lowest concentration of elemental sulfur causing a detrimental effect? (2) Is the effect of elemental sulfur purely mechanical (crevice formation and localized generation of H_2S) or electrochemical (change in redox potential), and if electrochemical, does sulfur change the redox potential or does it merely increase the cathodic reaction kinetics? (3) What effect does testing technique have on the correlation between alloying elements and SSCC? (4) What is the effect of strength level? Compounding the above uncertainties is the uncertainty about the state of sulfur at the temperatures and pressures used in laboratory tests. Some investigators have assumed that sulfur is essentially undissolved and molten while others have proposed mechanisms based on the formation of polysulfides from the reaction of elemental sulfur and H_2S.[3,4]

To attempt to answer all of the above questions is, perhaps, too ambitious. Attention in this paper will be focused on the concentration necessary to observe the detrimental effect of sulfur. Additionally, a number of alloys of varying strength levels will be examined, to study the effect of alloying elements on corrosion and SSCC. The effects of other environmental variables such as temperature, pH, and sulfur solvents will also be presented.

EXPERIMENTAL TECHNIQUES

The compositions of the alloys tested are shown in Table 1. Two types of SSCC tests were performed: (1) 2-point bend tests (or C-shaped bend tests) using cold-rolled sheet 1 mm (0.040 in.) thick, and (2) C-ring tests on cold-worked tubulars. For the 2-point bend tests, samples were cut with the stressing direction perpendicular to the rolling direction. They were then polished wet to 120-grit finish. The sample-holder was made of the same alloy as the sample. The strain in the outer fiber was measured for a number of samples and ranged from 2.4% to 4.6%. The effect of various degrees of cold rolling on hardness of the sheet samples tested is shown in Table 2. The effect of cold rolling on yield strength is shown in Figure 1. The samples were placed in individual glass boats which were then placed in HASTELLOY® alloy C-276 (UNS N10276) autoclaves. The placement of the boats was such that not all three samples of an alloy were located at the same depth in the autoclave. This was to avoid any spurious effects due to segregation of the sulfur. Tests were conducted for a maximum time period

® HASTELLOY is a registered trademark of Haynes International, Inc.

of 1,008 hours. The samples were examined for cracking, after 48, 96, 168, 240, 336, 504, 744, and 1,008 hours from the start, by visual observation at 40X. At the end of the tests, selected samples were examined metallographically and by SEM.

In addition, tests were conducted on unstressed samples 2.5 cm x 2.3 cm x 0.3 cm in dimension. The samples were in the mill-annealed condition and wet-ground to a 120-grit finish. Tests were conducted in a solution of 25% NaCl + 0.5% acetic acid + 0.1 gm/l sulfur + 100 psi H_2S for 96 hours at temperatures ranging from 121° to 204°C (249° to 399°F). The samples were cleaned in a wet, mildly abrasive slurry to remove the deposited sulfur corrosion products and examined for pitting or crevice corrosion.

C-ring samples were stressed to 70-90% of transverse, room-temperature yield strength and placed in autoclave with various alloys touching each other. The calculation of deflection for the applied stress is shown in Appendix I.

RESULTS

The rather dramatic effect of sulfur is shown in Tables 3 and 4. It can be seen that even 0.02 g/l of elemental sulfur causes a steep fall in time-to-failure of alloys N06985 and H-9M. Alloy N10276 was not affected by sulfur at these concentrations within the time period tested. The results are shown graphically in Figures 2 and 3. It must be emphasized that the 2-point bend samples are severely strained and hence are to be considered as accelerated laboratory tests.

The time-to-failure values also showed wide scatter in these tests, partly because of possible segregation of sulfur and partly due to the difficulty in detecting cracks masked by crevice corrosion. Cracking was almost always noted below crevice corrosion as illustrated in Figure 4. The type of scatter in the results is shown in Table 5, where the same heat was tested at two different times.

The addition of acetic acid had little effect on the 2-point bend tests as shown in Table 6. However, this could have been the result of the severity of the tests.

As can be seen from the previous results, there did not seem to be any significant differences between various Ni-base alloys containing less than about 16% Mo and 4% W. Alloy N10276 exhibited higher resistance than lesser alloyed materials. The effect of strength level on time to failure is shown in Table 7 and Figure 5. In these tests, the fully annealed material did not show any cracking in the time period tested, while no significant difference in cracking time was found between the 30% and 50% cold-rolled samples.

While the 2-point bend samples provide an accelerated and economical method to examine a variety of variables, the very severity of the test method prevents elucidation of the effects of certain variables such as applied stress level. C-ring tests were performed on selected alloy tubular samples. These results are shown in Tables 8 and 9. The times to failure are rather long and are significantly reduced by an increase in temperature, while applied stress has a lesser role at stresses below the gross yield point.

DISCUSSION

Effect of Elemental Sulfur

There is considerable uncertainty regarding the physical and chemical state of elemental sulfur in brine solutions containing moderate amounts of H_2S. Wilhelm hypothesized that sulfur in H_2S containing brines forms polysulfides of formulae H_2Sx+1, with x ranging from 2 to 4.[3] Similar proposals have been advanced by others.[1,3] Ikeda et al. proposed that sulfur existed as molten, free sulfur and acted as a crevice former as well as an oxidant.[4] Miyasaka was unclear about the state of sulfur (undissolved or dissolved either as sulfur or polysulfides), but did propose that elemental sulfur in either case increased the cathodic reaction kinetics.[5] Hyne has shown that the dissolution of sulfur is very low in environments containing less than about 10% H_2S at temperatures up to 135°C (275°F), the solubility equation for sulfur exhibiting an inverse relationship with temperature at least at low H_2S concentrations.[2] In all the experiments described in this paper, sulfur was undissolved at the start of the test, generally floating at the top of the solution, and appeared as a ball at the bottom of the autoclave at the end of the test.

The observed effects of elemental sulfur, however, seem to be universal:

1. Considerable increase in corrosion in almost all alloys
2. Formation of crevices and corrosion product deposits
3. Cracking under the crevices
4. Increase in cracking tendency

Since the detrimental effects of sulfur have been observed in this investigation at quite low levels (Figure 2), it is likely that the role of sulfur is more than that of a mechanical, crevice former. It is unlikely that molten sulfur at a concentration of 0.02g/l would be deposited over all the samples tested in an autoclave. Yet all the samples of alloy N06985 showed a considerable reduction in cracking time. The change in redox potential or cathodic reaction kinetics could, however, be felt at low concentrations.

Effect of Strength

Some of the results are shown in Figure 5. These are representative of all the results observed so far on various alloys. While there is a great difference in cracking susceptibility between the annealed material and the cold worked material, the differences between the 30% cold rolled and the 50% cold-rolled samples are insignificant. This is reflected even in the less severe, C-ring tests, as shown in Table 8, where the differences due to strength level are minor compared to those due to test temperature. It must be noted, however, that strength levels intermediate between that of mill-annealed and 30% cold-rolled conditions have not been examined. These strength effects are similar to the strength effects seen for low-temperature, hydrogen embrittlement observed by Vaughn and Greer.[6]

Effect of Alloying Elements

The effects of alloying elements can be seen in Tables 4, 6, and 7. While systematic variations in alloying elements have not been examined here, the data show in general that the alloy UNS N10276 shows superior resistance over alloys UNS N06985, H-9M, N06625, N08825, and N06975. Ciaraldi has shown that higher nickel content is beneficial, while chromium had a secondary role.[7] Ikeda et al. have shown that alloys containing greater than about 12% molybdenum and 15% chromium are suitable for service in sulfur-containing environments.[4] Both these conclusions are in general agreement with the current investigation although N06625, with considerably higher Ni content than alloy H-9M, did not show significantly higher cracking resistance (Table 6). It must be noted that correlations of SSCC resistance to pitting resistance in oxidizing chloride environments not containing sulfides or sulfur must be done with care. For example, Tsujikawa has shown that the pitting resistance in H_2S solution had a poor correlation to pitting resistance in ASTM C-48 solution (6% $FeCl_3$).[8]

Localized corrosion underneath deposits was noted in all cases where cracking had occurred. Hence, it would appear that the crevice corrosion resistance of an alloy can be used as a guide for judging the SCC resistance. The results of corrosion tests on unstressed samples in an elemental sulfur containing environment are shown in Table 10. It can be seen that the alloys containing up to about 7% Mo exhibit the same degree of crevice corrosion resistance, while the 9% Mo alloys exhibit a slightly superior resistance.

The alloy containing 16% Mo and 4% W showed the best resistance to crevice corrosion. In contrast, the localized corrosion resistance of the 7% Mo alloy in oxidizing chloride environments containing oxidants such as ferric and cupric chlorides would be superior to that of the 3% Mo alloy.[9,10] Hence there is no one to one correspondence between the localized corrosion resistance in the two types of environments. The trend in the SCC resistance has a greater correlation to the relative behavior in crevice corrosion in the H_2S-sulfur environment than in oxidizing chloride media such as ferric chloride.

Effect of Acidity and Sulfur Solvents

As shown in Table 6, acidity changes caused by the addition of acetic acid did not seem to have a significant effect on cracking in the 2-point bend tests. This may be related to the severity of the tests. Ikeda et al. observed that acetic acid increased the susceptibility of the alloys to cracking.[4] Ciaraldi did not find any accelerating effect of acetic acid in DCB tests.[7] Kolts showed that, in 2-point bend tests of annealed alloys N08825, N06985, and H-9N, addition of NaOH to increase the pH of a 25% NaCl + 1g/l sulfur + 100 psi(RT) H_2S solution from 4.5 to 7.5 at room temperature resulted in a considerable increase in time-to-failure.[11]

Sulfur solvents have a significant effect of the cracking susceptibility of many alloys. This is shown in Table 11. In the presence of diethylamine, even the duplex stainless steel UNS S32550 shows high resistance to cracking. The beneficial effect of diethylamine is observed even at lower pH levels.

Effect of Temperature

As expected, increase in temperature resulted in reduced time to failure (Table 8). This has been observed by a number of investigators and the data in Table 8 is in agreement with that found by Vaughn and Greer.[5,6]

CONCLUSIONS

1. Detrimental effects of elemental sulfur on sulfide stress corrosion cracking resistance was observed at concentrations down to 0.02 g/l at a temperature of 204°C (399°F).
2. The detrimental effect of elemental sulfur was a function of yield strength of the materials. The annealed alloys showed a much higher cracking resistance than the cold-rolled alloys. The differences in cracking susceptibility were small between 30% cold-rolling and 50% cold-rolling in the 2-point bend test.
3. Increase in temperature resulted in lower cracking times especially in the C-ring tests.
4. The alloy with high molybdenum and tungsten contents (UNS N10276) showed higher resistance to cracking. The tests did not examine the effects of alloying elements systematically enough to gauge the effects nickel vs. other elements.
5. Increase in pH or presence of sulfur solvents reduced cracking significantly even in lower alloys such as UNS S32550.
6. The effect of elemental sulfur is more likely to be due to a change in electrochemical conditions (redox potential or cathodic reaction kinetics) than due to a purely mechanical, crevice forming event. However, crevice corrosion was noted in almost all the cracked samples exposed to elemental sulfur. It is postulated that crevice formation could be due to the localized corrosion in the presence of elemental sulfur which then led to the deposition of corrosion products.
7. Further clarification on the mechanisms of sulfur-effects could only be attained by a better understanding of the physical chemistry of the system.

REFERENCES

1. P.R. Rhodes, CORROSION/87, paper no. 322 (Houston, TX: NACE, 1987).
2. J.B. Hyne, Proceedings of the Annual Gas Conditioning Conference, 1985.
3. S.M. Wilhelm, CORROSION/88, paper no. 77 (Houston, TX: NACE, 1988).
4. A. Ikeda, M. Igarashi, M. Ueda, Y. Okada, H. Tsuge, CORROSION/88, paper no. 65 (Houston, TX: NACE, 1988).
5. A. Miyasaka, K. Denpo, H. Ogawa, CORROSION/88, paper no. 70 (Houston, TX: NACE, 1988).
6. G. Vaughn, J.B. Greer, SPE-AIME Annual Meeting in Dallas, TX., Sept. 1980, Paper 9240.
7. S.W. Ciaraldi, CORROSION/87, paper no. 284 (Houston, TX: NACE, 1987).
8 S. Tsujikawa, CORROSION/88, paper no. 64 (Houston, TX: NACE, 1988).
9. P.E. Manning, CORROSION/82, paper no. 176 (Houston, TX: NACE, 1982).
10. A.I. Asphahani, *Materials Performance* 19, 8(1980), pp. 9-21.
11. J. Kolts, CORROSION/86, paper no. 323 (Houston, TX: NACE, 1986).

ACKNOWLEDGMENT

The authors wish to acknowledge the efforts of the Corrosion Laboratory, specifically D.C. LaCluyse, in performing the tests. They also thank R.A. Dague for typing the manuscript, and J. Kolts and A.I. Asphahani for initiating some of the test programs.

Table 1

Nominal Chemical Compositions of Various Alloys Examined

Alloy	UNS No.	C	Cb	Cr	Cu	Fe	Mo	N	Ni	W	Others
FERRALIUM® alloy 255	S32550	0.04*	-	26	1.7	Bal.	3	0.17	5.5	-	-
Alloy 825	N08825	0.05*	-	21.5	2.0	29	3	-	42	-	Ti = 1.0
Alloy 625	N06625	0.10*	3.7	21.5	-	5.0*	9	-	62	-	-
Sumitomo SM2550®	N06975	0.02	-	25	1.0	19	5	-	50	-	-
HASTELLOY® alloy G-3	N06985	0.015*	0.03*	22	2.0	20	7	-	44	-	-
HASTELLOY alloy H-9M	-	0.03*	-	22	-	18.5	9	-	45	2	-
HASTELLOY alloy C-276	N10276	0.01*	-	15.5	-	5.5	16	-	57	4	-

* Maximum

FERRALIUM is a registered trademark of Bonar Langley Alloys Ltd.
SM2550 is a registered trademark of Sumitomo.
HASTELLOY is a registered trademark of Haynes International, Inc.

Table 2. Effect of cold-rolling on hardness of sheet samples used for 2-point bend tests.

Alloy	Hardness, Rockwell		
	0% CR	30% CR	50% CR
N08825	B70	C24	C31
N06985	B75	C31	C36
N06625	B84	C41	C44
H-9M	-	C33	C38
N10276	B79	C39	C42

Table 3. Effect of Sulfur Concentration on SSCC Susceptibility

2-Point Bend Samples, 177°C (350°F)
25% NaCl + 100 psi (RT) H_2S + Sulfur
Samples Cold-Rolled 30% Except Where Indicated

Sulfur, g/l	Alloy	Time to Failure, Hrs.
0 + 0.5% Acetic	N06985 (50% CR)	NC, NC, NC*
0.1 (No Acetic)	N06985	336, 48, 338
1.0 (No Acetic)	N06985	48, 48, 48
0.1 (No Acetic)	H-9M	48, 336, 480
1.0 (No Acetic)	H-9M	96, 48, 48

* No cracking in 1008 hours.

Table 4. Effect of sulfur concentration on SSCC susceptibility of a number of alloys.

2-point bend samples, 204°C (400°F)
25% NaCl + 100 psi(RT) H_2S + sulfur
Samples cold-rolled 30% except where indicated

Environment	Alloy	Time To Failure (hours)
0 g/l S	N06985 (50% CR)	NC (1008)
	N10276 (50% CR)	NC (1008)
0.02 g/l S	N06985	48,48,48
	H-9M	168,96, 1008
	N10276	NC(1008), NC(1008), NC(1008)
1.0 g/l S	N06985	48,48,48
	H-9M	48,168,48
	N10276	168,1008,1008
0.1 g/l S+0.5% Acetic	N06985	96,48,96
	H-9M	96,96,96
	N10276	NC(1008),504,504
1.0 g/l S+0.5% Acetic	N06985	48,48,48
	H-9M	48,96,96
	N10276	168,504,504

Table 5. Scatter observed in the test results on two alloys

25% NaCl + 1g/l sulfur + 100 psi(RT) H_2S, 204°C(400°F)

2-point bend samples, 50% cold-rolled

Test Series	Alloy	Hardness	Time to Failure, Hours
1	N10276	C42	NC(1008), NC(1008),168
2	N10276	C43	1008,1008,48

Table 6. Effect of acetic acid addition on SSCC in sulfur containing solutions.

25% NaCl +100 psi(RT) H_2S + 1.0 g/l S
Temperature = 204°C (400°F)

Alloy	Hardness Rockwell	Time to Failure, Hours	
		No Acetic	0.5% Acetic
N06985	C31	48,48,48	48,48,48
H-9M	C33	48,168,48	48,96,96
N06625	C41	48,48,48	96,48,48
N10276	C39	168,1008,1008	168,504,504

Table 7. Effect of strength level on SSCC

25% NaCl + 100 psi(RT) H_2S + 1g/l S
2-point Bend samples

Alloy	% Cold Roll	Hardness Rockwell	Time to Failure, Hours		
			177°C	204°C	232°C
N08825	0	B70	1488	-	791
	30	C24		48	
	50	C31		48	
N06985	0	B77	5136	-	1031
	30	C31	48	48	
	50	C36		48	
N10276	0	B79	NC(8736)	-	NC(8736)
	30	C39		728	
	50	C43		688	

Table 8. Results of C-Ring Tests

5% NaCl + 1.0 g/l Sulfur + 0.1% Acetic + H_2S

N10276, CW + Aged 204°C/200 Hrs.

% Yield Stress	Yield ksi	Time to Failure (Hours) 177°C	204°C	232°C
70	155	NC (8600)	-	528
	183	NC (8640)	-	300
	191	NC (8640)	864	144
90	155	NC (8688)	1584	528
	183	NC (8688)	-	312
	191	NC (8688)	-	168

Table 9. C-Ring Tests on Various Commercial Alloys

25% NaCl + 100 psi(RT) H_2S + 1g/l Sulfur

177°C (350°F)

Alloy	Yield Strength MPa (Ksi)	% Yield	TTF (Hours)
N06975	862 (125)	90	2160
N06985	1172(170)	90-96	2160,2160
N10276	1117(162)	91-95	NC, NC*

* - No Cracking in 4320 hours

Table 10. Corrosion Tests on Unstressed Samples

25% NaCl + 0.5% Acetic Acid + 0.1 gm/l Sulfur + 100 psi H_2S, 96 hours
Mill Annealed Samples

Alloy	Cr	Mo	W	Results 121°C	149°C	177°C	204°C
N08825	21.5	3	-	CA, CA*	CA, CA	CA, CA	CA, CA
N06985	22	7	-	CA, CA	CA, CA	CA, CA	CA, CA
H-9M	22	9	2	NCA, NCA**	NCA, CA	CA, CA	CA, CA
N06625	22	9	-	NCA, NCA	NCA, NCA	CA, CA	CA, CA
N10276	16	16	4	NCA, NCA	NCA, NCA	NCA, NCA	NCA, NCA

CA - Crevice Attack
NCA - No Crevice Attack

Table 11. Effect of sulfur solvents on SSCC.

25% NaCl + 100 psi(RT) H_2S + 1g/l sulfur , 232°C (450°F)

Mill-annealed Alloys, 2-point bend tests

Alloy	TTF, Hours		
	No Solvent	5%Diethylamine pH =10-11.2	5%Diethylamine pH = 3.3 -5.5
S32550	720	NC*	NC
N03825	960	NC*	NC*
N06985	1440	NC*	NC*
N10276	NC**	NC*	NC*

* - No Cracking in 1440 hours

** - No Cracking in 8640 hours

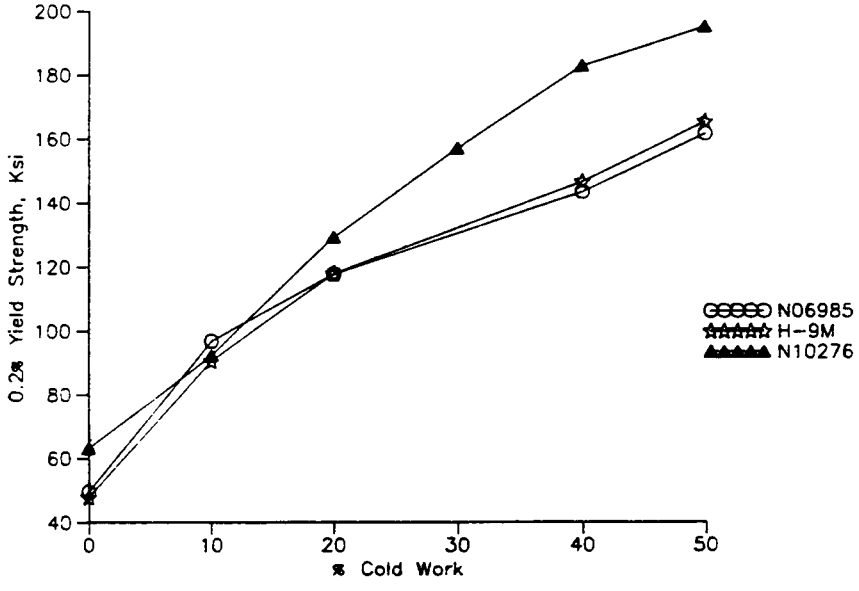


Figure 1. Effect Of Cold-Rolling On RT Yield Strength Of Sheet Samples.

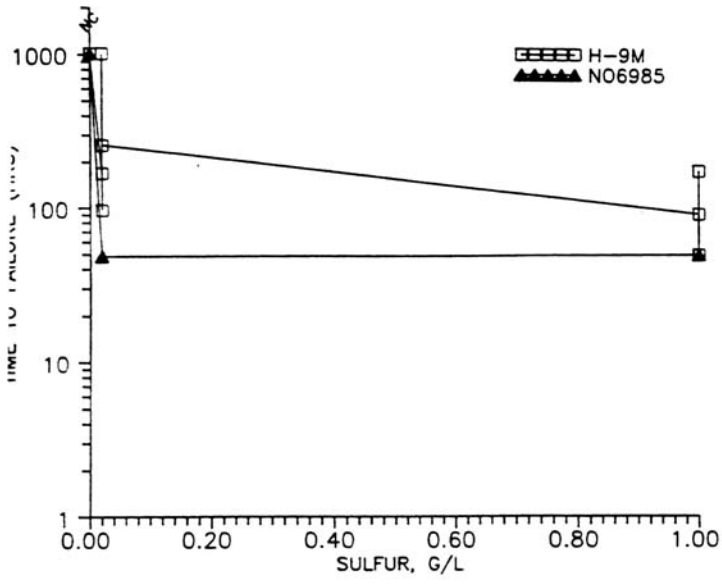


Figure 2. Effect Of Sulfur On SSCC Of 2-Point Bend Samples 25% NaCl + 100 psi H_2S , 204°C

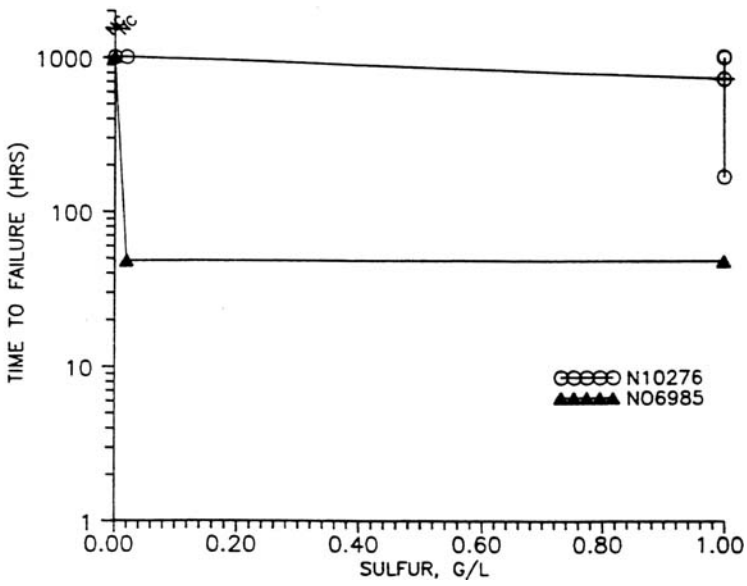


Figure 3. Effect Of Sulfur On SSCC Of 2-Point Bend Samples 25% NaCl + 100 psi H_2S , 204°C



Figure 4. Cross-section of a 2-point bend sample of alloy N10276 tested in 25% NaCl + 100 psi H_2S + 1 g/l sulfur at 204°C. 200X

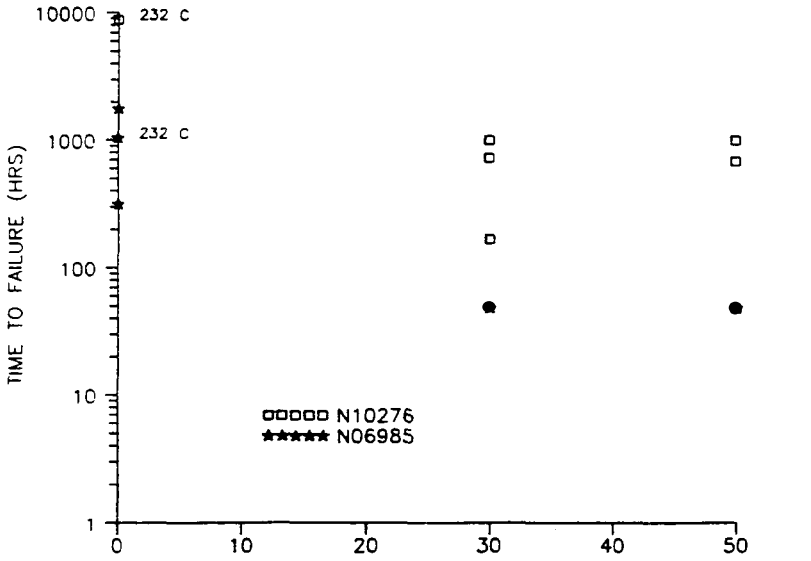


Figure 5. Effect Of Strength On SSCC Of 2-Point Bend Samples
25% NaCl + 100 psi H_2S + 1G/L S^0 204 C

APPENDIX I

Calculation used for deflection of C-ring samples

(S. O. Fernandez and G. F. Tisinai, J. Of Engineering for Industry, Trans ASME, February, 1968, p.147.)

D_o = O.D. of tube (inch)
t = Wall Thickness (inches)
Y = RT longitudinal yield strength, ksi
p = Applied stress level as % of yield
q = ratio of transverse to longitudinal yield = 0.85
E = modulus of elasticity, ksi
d = deflection, inches
A = 0.94, Correction Factor to account for the difference between calculated and measured deflection.
$e = t^2/6D$
$D = D_o - t$
$t_1 = t/2 - e$

$$\text{deflection, } d = \frac{(A) \times (q) \times (pY)}{\frac{8Ec}{\pi D^2}\left[\frac{t_1 D}{e D_o} - 1\right]}$$

Copyrighted Materials
Copyright © 1996 NACE International Retrieved from www.knovel.com

PAPER NUMBER

8

CORROSION 89

April 17-21, 1989
New Orleans Convention Center, New Orleans, Louisiana

INFLUENCE OF ELEMENTAL S ON CORROSION BEHAVIOR OF CRA IN H_2S-CO_2-Cl^- ENVIRONMENT

M.Ueda[1], H.Tsuge[2] and A.Ikeda[3]

Sumitomo Metal Industries,LTD.,
Iron & Steel Research Labs.[1]
Advanced Technology Research Labs.[2]
3-1, Nishinagasu-Hondori, Amagasaki
Osaka Head Office[3], 5-15 Kitahama, Osaka, Japan

ABSTRACT

Phase transition of elemental S in H_2S-CO_2-Cl^- environment is observed and this behavior is indicated to be the same as physical properties of elemental S itself. Electrochemical behavior in S, H_2S and S+H_2S environment at high temperature is also investigated potentiodynamically by means of a pressure equilibrium type autoclave and it is clarified that elemental S accelerate cathodic reaction by the reaction of S → H_2S, spontaneous potential(E_{sp}) in S-H_2O system become noble compared to E_{sp} in nonsulfur-containing environment. Electrochemical reactivity of elemental S is related to increase of viscosity due to production of liquid μ sulfur over 160°C and reformation of sulfur at the corrosion site due to the reverse dissolution reaction of dissolved species(SO_4^{2-}, H_2S, polysulfide). Furthermore, it is also clarified that critical pitting potential(V_c') of corrosion resistant alloy(CRA) of UNS No; N10276 alloy is less noble in order of S, H_2S and S+H_2S environment at 200°C. Mo content is important to improve V_c'. Solubilities of elemental S by self-oxidation-reduction reaction and production of polysulfide(S_x^{2-};x=2,3,4,5) are estimated by thermodynamic calculation. Calculated-solubility of elemental S is between 0.1g/l S and 1g/l S at 200°C in S-H_2O system. It is discussed in relation with electrochemical behavior of elemental S. Finally, Corrosion mechanism at S-deposited portion in S-containing environment is discussed on the basis of those experimental results.

1. Introduction

Environments encountered in the exploration and production of high temperature hostile wells usually contain substantial amounts of hydrogen sulfide(H_2S), carbon dioxide(CO_2) and concentrated brine solution. Temperature could be exceed 200°C. In addition to those wells,recently, the more severe environments which contain free sulfur have appeared[1]. On the other hand, corrosion problems due to elemental S have also occurred in transportation line and tubing in sulfur source wells with neutral aqueous solution at about room temperature[2-4]. The corrosion problems in sulfur source wells were thought to relate with S-deposition at materials. Further, effect of dissolved species(H_2S, SO_4^{2-}, polysulfide) on corrosion was investigated. McDonald et al were suggested that the corrosion process was subject to catalysis of the cathodic reaction considering an action of polysulfide on the direct contact portion between the steel and sulfur[2].

For corrosion phenomena in S-containing sour well at high temperature over 200°C, in spite of its importance, little fundamental work has been performed. Phodes et al noted that the introduction of sulfur in H_2S-containing environment might provide an oxidant to accelerate cathodic reaction, which could be either H_2S_x,HS_x^-,H^+ or S_x[5-7].

In this article, phase and electrochemical reaction of elemental S are investigated. Further, effect of elemental S on pitting corrosion of CRA's is also investigated. Finally, a role of elemental S for corrosion behavior in S-containing environment is discussed from the viewpoint of dissolution and electrochemical reactivity of elemental S.

2. Experimental

Observation of phase transition of elemental S in H_2S-CO_2-Cl^- environment was carried out by means of an autoclave with observation window shown in Fig.1. A solution with 25wt%NaCl and elemental S(volume ratio;1:1) was filled in a test tube, and the test tube was set in the autoclave and pure water is charged around the test tube, and then the autoclave is closed. Evacuation and nitrogen gas bubbling operation were carried out, and H_2S gas and CO_2 gas were purged ,and then pressure in the autoclave was raised to the experimental condition of 0.1MPa H_2S and 1.0MPa CO_2. A test schedule for observation of elemental S is indicated in Fig.2.

Electrochemical reaction of elemental S on Pt electrode was investigated in H_2O-Cl^- environment containing N_2, S, H_2S and S+H_2S. Effect of elemental S on critical pitting potential(V_C') using alloys of UNS No; N06975* alloy and UNS No; N10276** alloy of which the chemical composition is shown in Table 1. Those were cold-worked materials melted in mill. Effect of alloying element(Cr, Ni, Mo) on critical pitting potential(V_C') was investigated with alloys of the chemical composition range of 15-20wt%Cr, 10-16wt%Mo and 52-64%Ni shown in Table 2. Those were melted in the vacuum furnace in laboratory, forged, hot rolled to the plates of 12mm in thickness and then solution heat treated at 1150°C for 1hour followed by water quenching, and then 20% cold-worked.

Electrochemical measurement was curried out potentiodynamically at a sweep rate of 20mV/min with a potentiostats in pressure equilibrium type autoclave shown in Fig. 3. Standard test condition in S, H_2S, S+H_2S environment is shown in Table 3. A Ag/AgCl(3.3N KCl solution) reference electrode which reversible potential was -0.045V

---

*: UNS No N06975; SM2550(25Cr-50Ni-6Mo)
**: UNS No N10276; C276 (15Cr-58Ni-16Mo),registered name in Hynes International Co.

vs. SCE at 25°C and a Pt counter electrode were used in this study. The pressure inthe lower autoclave shown in Fig.3, which is kept at room temperature, is the same as that in the upper autoclave.

A working electrode used was a disk of 15mm in diameter and 2mm in thickness. The specimen was polished with silicon carbide No 600 paper, washed with water, and then degreased with alcohol and acetone. It was set as the working electrode in upper autoclave shown in Fig.3. After the test solution either with or without free-S was filled in both autoclaves, the apparatus was closed. In the examination in the solution with free sulfur, it was added only in the upper autoclave. Then, the test solution bubbled with the nitrogen gas for about 1hour to deaerate and pressurized to 1.0MPa N_2. After that, the temperature was raised to test condition and the elctrochemical measurement was carried out.

3. Results

3.1 Observation of elemental sulfur in H_2S-CO_2-Cl^- environment at high temperature

The autoclave with observation window shown in Fig.1 was used to observe the behavior of elemental S in H_2S-CO_2-Cl^- environment at high temperature. Sulfur in H_2S-CO_2-Cl^- environment showed solid(β sulfur)-liquid(λ sulfur) phase transition at about 120°C as same as that in the system to be constituted only by sulfur[8]. The liquid λ sulfur had a light yellow color. Further, the color of liquid λ sulfur changed a dull orange color at about 160°C. This phenomenon could be closely related to the phase transition of liquid sulfur, ie λ to μ[8]. Liquid λ sulfur consists of S_8 molecule. It is recognized that liquid μ sulfur consists of a molecule connecting lots of atoms and therefore has a high viscosity, because a loop of S_8 molecule is broken at the high temperature[8].

3.2 Electrochemical reaction in H_2O-Cl^- containing elemental sulfur at high temperature

3.2.1. Effect of temperature

Electrochemical reaction of S has been mainly investigated in S+H_2S environment. In the case of S+H_2S environment, it is difficult to define electrochemical reaction due to elemental sulfur because of an effect of electrochemical reaction of H_2S. Accordingly, electrochemical reaction of S in S-H_2O-Cl^- environment was investigated with Pt electrode. Fig.4 and Fig.5 show results at high temperature that potential of Pt electrode polarized to 0.7V cathodic side from spontaneous potential(E_{sp}) and polarized reversely to anodic side. Fig.6 and Fig.7 show cathodic and anodic polarization respectively.

Test results are summarized as follows.

a. Increase of current density on anodic and cathodic region occurs when S is added in H_2O-Cl^- system.

b. Both cathodic and anodic reactions due to S addition are remarkably accelerated by the temperature change from 150°C to 200°C. This behavior might be related to a contact rate of S-deposition on the surface of Pt electrode due to increase of viscosity of S(liquid μ sulfur).

After the measurement of the polarization curves at 200°C shown in Fig.4 , H_2S was detected over 100ppm in gas phase by a portable H_2S detector and pH in the solution after degassed H_2S was about 2.8. Therefore, it is thought that the following cathodic reaction occurs:

$$S + 2H^+ + 2e^- \rightarrow H_2S \quad \text{----------} \quad (1)$$

The following anodic reaction could be suggested including both a oxidation product of S and the product of H^+ ion:

$$S + 4H_2O \rightarrow SO_4^{2-} + 8H^+ + 6e^- \quad \text{----------} \quad (2)$$

Therefore, chemical analysis of SO_4^{2-} concentration was carried out and SO_4^{2-} of 614mg/l was detected in the solution after tested at 250°C.

Reactions of (1) and (2) requires S-deposition on the Pt electrode. The current density due to the anodic polarization after the cathodic polarization shown in Fig.4 is about 10 times larger than one due to anodic polarization without the preceding cathodic polarization shown in Fig.7.

This behavior would indicate that reaction (1) occurs in cathodic polarization and reverse reaction of (1) adds in anodic polarization. Although the reverse reaction rate of (1) would be small, it is noted that the anodic current could significantly increase. That is to say, a newly deposited sulfur from H_2S dissolved in brine could decisively affect an increase of anodic current due to the reaction (2). It suggests that a deposited sulfur reduced from H_2S plays a role of catalysis and results in a increase of contact rate of free sulfur which is been originally charged.

3.2.2 Effect of sulfur concentration

Measured results of spontaneous potential(E_{sp}), current density of anode peak(J_{max}) and pH of degassed brine(pH^*) after test are shown in Fig.8 and Fig.9. H_2S-Cl^- environments containing sulfur of 0.1, 1 and 10g/l at 150 and 200°C were examined. Polarization curves are measured with the same method as shown in Fig.4.

In the case of 150°C, E_{sp}, J_{max} and pH^* had almost the same values in the environment of 0.1, 1 and 10g/l sulfur, respectively.

In the case of 200°C, E_{sp} in the various environment indicated almost the same value. However, J_{max} and pH^* occurred remarkable change between 1g/l sulfur to 0.1g/l sulfur. Accordingly, increase of J_{max} and decrease of pH^* indicate the increase of electrochemical reactivities on the surface of Pt electrode probably due to S-deposition. These behaviors indicate that the solubility of S at 200°C would be between 0.1g/l and 1g/l.

3.3 Electrochemical reaction of H_2S-CO_2-Cl^- containing elemental sulfur at high temperature.

Polarization curves in cathodic region and anode region due to Pt electrode at 200°C in H_2O-Cl^- environment containing N_2, S, H_2S and S+H_2S are shown in Fig.10 and Fig.11. Further, the time dependence of spontaneous potential(E_{sp}) in H_2O-Cl^- environment containing S, H_2S and S+H_2S is investigated. The results are shown in Fig.12. An electrochemical anodic reaction is very high in H_2S-containing environment. An electrochemical cathodic reaction in S-containing environment is also very high. The cathodic polarization behavior in H_2S-H_2O-Cl^- environment is similar to that in the acid media, although the diffusion current density in the former is remarkably larger than the latter's one, because of an action of dissolved CO_2 or H_2S gases[9]. The following reaction is thought:

$$2H^+ + 2e^- \rightarrow H_2 \quad \text{----------} \quad (3)$$

In S-H_2S-H_2O-Cl^- environment, electrochemical reactivity is very high by a superposition of both reactions due to H_2S and S.

On the other hand, E_{sp} in S-H_2O-Cl^- environment is about 0.1V higher than E_{sp} in

H_2O-Cl^- environment containing H_2S and S+H_2S . E_{sp} in H_2O-Cl^- environment containing H_2S is almost the same as that in S+H_2S environment.

3.4 Effect of elemental sulfur and H_2S on critical pitting potential of CRA's.

Critical pitting potential(V_c') of the alloys of UNS No; N06975 alloy and UNS No; N10276 alloy in H_2O-Cl^- environment containing N_2, S, H_2S and S+H_2S were measured and effect of elemental sulfur and H_2S on V_c' were investigated. V_c' was measured in the region of high current density(over 10^2 $\mu A/cm^2$), because of a masking action due to a high current density of reaction (1) and (2).

3.4.1 Effect of elemental sulfur

Anodic polarization curves of UNS No; N06975 alloy at 150 and 200°C in S-H_2O-Cl^- environment are shown in Fig.13 and Fig.14.

V_c' in S-H_2O-Cl^- environment at 150°C is almost the same as that in H_2O-Cl^- environment. V_c' in S-H_2O-Cl^- environment at 200°C is less noble than V_c' in H_2O-Cl^- environment. This means that the effect of S on V_c' is not detected at 150°C, but detected at 200°C. This is thought that an aggressiveness in electrochemical reaction of S remarkably increases at 200°C.

3.4.2 Effect of Sulfur and H_2S

Anodic polarization curves of UNS No; N10276 alloy at 200°C in H_2O-Cl^- environment containing N_2, S, H_2S and S+H_2S are shown in Fig.15. Spontaneous potential in S-H_2O-Cl^- environment is noble in the same manner as the result of Pt electrode. V_c' is less noble in order of S, H_2S and S+H_2S.

3.5 Effect of alloying elements(Cr,Ni,Mo) on critical pitting potential(V_c') in S-containing environment.

Effect of alloying element in S-H_2O-Cl^- environment on critical pitting potential of corrosion resistant alloys(CRA's) is investigated in the environmental condition of 10g/l S, 25%NaCl and 200°C. As for CRA's, Alloys with the chemical composition range of 15-20%Cr, 10-16%Mo and 52-64%Ni are used for this study. Effect of Ni and Mo contents on critical pitting potential($V_c'_{1000}$) measured as a potential in 1000 $\mu A/cm^2$ is shown in Fig.16 and Fig.17. The addition of Mo remarkably improves pitting corrosion resistance, as it contributes to increase V_c'. But, the addition of Ni does not almost affect on V_c'.

Accordingly, it is thought that Mo content in alloy is important to improve pitting corrosion resistance of alloys containing 15-20%Cr and 52-64%Ni.

4. Discussion

There are two main theories of corrosion mechanism in S-H_2S-H_2O system, ie free sulfur deposition and formation of polysulfide[1,5-7]. Specifically, on the former, a dissolution behavior of sulfur in H_2O is very critical. Hence, a solubility of sulfur in S-H_2S-H_2O system is firstly discussed and a discussion of corrosion mechanism is followed in this article.

4.1 Solubility of elemental S in S-H_2O and S-H_2S-H_2O environment

Elemental S in S-H_2O environment where some electrochemical reaction occurs, contributes to formation of H_2S(aq) , SO_4^{2-} ion and H^+ ion through (1) and (2) reactions. The authors call this phenomenon " self-oxidation-reduction reaction".

These formed species affect a solubility of sulfur. Therefore, dissolution behavior of elemental S in S-H_2S-H_2O environment is thought in the same manner as that in S-H_2O environment. But production of polysulfide supposing by Rhodes,Wilhelm and Miyasaka et al should be also considered[5-7]. The following reaction is thought as the production reaction of polysulfide:

$$H_2S + S_{x-1} \rightarrow H_2S_x \quad \text{---------- (4)}$$
$$HS^- + S_{x-1} \rightarrow HS_x^- \quad \text{---------- (5)}$$
$$S^{2-} + S_{x-1} \rightarrow S_x^{2-} \quad \text{---------- (6)}$$

Therefore, solubility of elemental S in H_2S-containing environment is calculated by the following two methods:

1. Solubility based on the self-oxidation-reduction reaction
2. Solubility based on dissolution constants of polysulfide(S_x^{2-})

4.1.1 Solubility of elemental S by self-oxidation-reduction reaction

As self-oxidation-reduction reaction, the following reactions are considered:

$$4S + 4H_2O \rightarrow 3H_2S + HSO_4^{2-} + H^+ \quad \text{---------- (7)}$$
$$4S + 4H_2O \rightarrow 3H_2S + SO_4^{2-} + 2H^+ \quad \text{---------- (8)}$$
$$4S + 4H_2O \rightarrow 3HS^- + SO_4^{2-} + 5H^+ \quad \text{---------- (9)}$$
$$4S + 4H_2O \rightarrow 3S^{2-} + SO_4^{2-} + 8H^+ \quad \text{---------- (10)}$$

S-solubilities due to these reactions are calculated by thermodynamic data of dissolution species(H_2S, HS^-, S^{2-}, SO_4^{2-} and HSO_4^{2-})[10-11] and dissolution constant of H_2S[12].

a) Solubility of elemental S in S-H_2O system

Solubilities of elemental S at elevated temperature are shown in Fig.18. In pH 3, solubility of elemental S is 0.01-0.001g/l at R.T., about 0.1g/l at 150°C and 0.1-1g/l at 200°C. The remarkable increase of J_{max} between 0.1g/l S and 1g/l S in S-H_2O-Cl^- environment over 200°C was recognized in measuring the effect of S content on the anodic current density on Pt. This behavior could be closely to solubility value(0.1-1g/l) of S at 200°C.

b) Solubility of elemental S in S-H_2S-H_2O system

Calculation results for solubility of elemental S in S-0.1MPa H_2S-H_2O system show in Fig.19. Solubilities of elemental S under the existence of H_2S are very small in low pH region. In pH3, solubility of elemental S at 200°C is 10^{-4}-10^{-5} g/l. That is to say, co-existence of H_2S decreases a solubility of sulfur in self-oxidation-reduction reaction.

4.1.2 Solubility of elemental S by the production of polysulfide

Dissolution constant of S_x^{2-} at elevated temperature is estimated by Murry et al[11]. The following reactions are considered as dissolution reaction of polysulfide:

$$S(s,l) + S^{2-} \rightarrow S_2^{2-} \quad \text{---------- (11)}$$
$$S(s,l) + S_2^{2-} \rightarrow S_3^{2-} \quad \text{---------- (12)}$$

$S(s,l) + S_3^{2-} \rightarrow S_4^{2-}$ ---------- (13)
$S(s,l) + S_4^{2-} \rightarrow S_5^{2-}$ ---------- (14)

The solubilities at pH 7 of elemental S calculated to use the dissolution constant of S^{2-}, S_2^{2-}, S_3^{2-}, S_4^{2-} and S_5^{2-} in S-0.1MPa H_2S-H_2O environment are shown in Fig.20. Because S_x^{2-} is thought to be stable in neutral and basic solution, calculation is carried out at pH7. Solubility of elemental S due to self-oxidation-reduction reaction is also shown in Fig.20. In comparison with the self-oxidation-reduction reaction, contribution of polysulfide to dissolution of sulfur is larger in low temperature than in high temperature. In acid solution, dissolution of elemental S due to H_2S_x and HS_x^- is thought from the analogy to dissolution behavior of H_2S. The higher partial pressure of H_2S, the more remarkable the solubility of sulfur due to polysulfide.

4.2 Corrosion mechanism in S-containing environment.

Corrosion mechanism of CRA's under the 0.1MPa H_2S - 10g/l S - brine condition is discussed. Increase of spontaneous potential(E_{sp}) due to S-deposition and corrosion behavior at S-deposited portion in S-containing environment is thought to be the important factor for clarification of corrosion mechanism. Then, corrosion mechanism in S-containing environment is discussed with respect to these two points.

4.2.1 Increase of Spontaneous Potential(E_{sp}) in S-containing environment.

E_{sp} in S-H_2O-Cl^- environment is about 0.1V more noble than E_{sp} in H_2S and S+H_2S environment. Based on analyzed concentration of H_2S and SO_4^{2-}, potentials of anodic and cathodic reactions at 200°C in S, H_2S and S+H_2S environment are estimated to clarify these behavior. The results estimated are shown in Fig.21. Calculated-E_{sp} in S-H_2O environment at 200°C is about -0.3V and is almost consistent with measured-E_{sp}. In H_2S-H_2O environment, E_{sp} presumed from calculation results is the hybrid potential between hydrogen evolution reaction(reaction (3)) as cathodic reaction and an oxidation reaction as anodic reaction. But, measured-E_{sp} in H_2S-H_2O-Cl environment at 200°C is almost equal to the potential of the reaction of $H_2S \rightarrow S$(reaction (1)). This behavior might be related to oxidation reaction of H_2S(reaction (1)) due to oxygen contamination such as absorbed oxygen on metals in autoclave. In S-H_2S-H_2O environment, E_{sp} is the hybrid reaction between the potential due to elemental S and the potential due to H_2S. Potential related to elemental S becomes almost equal to measured-E_{sp} in H_2S-H_2O-Cl^- environment because of the potential of cathodic reaction(reaction (1)) decreases owing to increase of H_2S partial pressure. Accordingly, E_{sp} in S-H_2S-H_2O environment is almost the same as that in H_2S-H_2O environment. However, in S-H_2S-H_2O environment, E_{sp} would be kept noble potential to stabilize at S-deposition portion of electrode in comparison with the case in H_2S-H_2O environment.

4.2.2 Corrosion behavior at S-deposited portion

Elemental S at high temperature accelerates cathodic reaction and dissolved due to the self-oxidation-reduction reaction. Dissolved ion species such as SO_4^{2-}, H_2S, H_2Sx, HSx^- and Sx^{2-} are thought to accelerate S-deposition at metal surface shown in Fig.22 because of S could be produced by a pair reaction of corrosion reaction including anodic and cathodic reactions. The S-deposition would easily occur over 200°C due to the increase of viscosity of S(liquid μ Sulfur). Effect of elemental S on corrosion is schematically shown in Fig.23. The locally enriched H_2S concentration by reaction (1) could make poor a stability of corrosion resistant film. It is thought that corrosion due to elemental S occurs at the S-metal interface and the S-metal crevice because of acceleration of cathodic reaction, making noble potential at S-deposited portion and forming high H_2S concentration locally.

5. Conclusions

The effect of elemental S on corrosion behavior of CRA's in S-containing environment at high temperature was investigated by the direct observation of elemental S in H_2S-H_2O-Cl^- environment, electrochemical measurement and thermodynamic calculation of solubility of S and spontaneous potential(E_{sp}). The results obtained are summarized as follows:

1. Physical behavior of elemental S in H_2S-H_2O-Cl^- environment was almost the same as that of elemental sulfur itself.

2. Electrochemical reactivity of S in both cathodic and anodic region remarkably increases with the high temperature region over 200°C. This should be related to the increase of S-deposition due to the increase of viscosity of S.

3. Spontaneous potential(E_{sp}) in S-containing environment is more noble than E_{sp} in nonS-containing environment at 200°C, E_{sp} in that is about 100mV more noble than E_{sp} in H_2S-H_2O-Cl^- environment. E_{sp} in H_2S environment is almost the same as that in S+H_2S environment because of E_{sp} in H_2S environment is thought to be affected by an oxidant such as contaminated-O_2.

4. Critical pitting potential(V_C') of UNS No; N06975 alloy in S-H_2O-Cl^- environment at 150°C is almost the same as V_C' in H_2O-Cl^- environment and that at 200°C is less noble than Vc' in H_2O-Cl^- environment. V_C' of UNS No; N10276 alloy in S and H_2S containing environment at 200°C is less noble in a sequence of S, H_2S and S+H_2S.

5. Mo content in alloy is important to improve pitting corrosion resistance of alloy such as UNS No; N10276 alloy in S-H_2O-Cl^- environment at 200°C.

6. Solubility of S in S-H_2O environment at 200°C corresponds to a remarkable change of polarization curve. S content between 0.1 and 1 g/l S is criteria at 200°C. Solubility of S by self-oxidation-reduction reaction in S-H_2S-H_2O environment is smaller than that in S-H_2O environment.

7. The formed species by the self-oxidation-reduction reaction such as H_2S, SO_4^{2-}, H_2S_x, HS_x^- contribute to make nuclei of sulfur deposition.

8. Corrosion in S-containing environment occurs at S-metal interface and the S-metal crevice because of acceleration of cathodic reaction , sustaining noble potential at S-deposited portion and forming high H_2S concentration locally.

ACKNOWLEDGEMENTS

The authors are indebted to Dr.H.Ohtani ,General Manager of Tube & Pipe Research Department of Iron & Steel Research Laboratories for allowing them to publish this investigations. The discussion of co-workers in Tube & Pipe Corrosion Research Laboratory is gratefully acknowledged. Thanks they owe to Messrs. T.Miki, Y.Imai and H.Kusagi for their helps in the experimental works.

References

1. A.Ikeda, M.Igarasi, M.Ueda, Y.Okada and H.Tsuge, Corrosion/88, Paper No. (1988)
2. D.D.MacDonald, B.Roberts and J.B.Hyne, Corrosion Science, Vol.18, p411(1978)
3. W.Küster, H.Sclerkmann, G.Schmitt, W.Schwenk and D.Steinmetz, Werkstoffe und Korrosion, Vol.35, p556(1984)
4. E.Schaschl, Material Performance, p9, July(1975)
5. P.R.Rhodes, Corrosion/86, Paper No.322, NACE(1986)
6. S.M.Wilhelm, Corrosion/88, Paper No.77, NACE(1988)
7. A.Miyasaka,K.Denpo and H.Ogawa, Corrosion/88, Paper No.70, NACE(1988)
8. M.Mizunoe, Kisokagaku kiso-mukihen, tokyoshoseki, p65(1965)
9. A.Ikeda,M.ueda and S.Mukai, Corrosion/83, Paper No.45, NACE(1983)
10. R.C.Weast, Handbook of Chemistry and Physics 59th Edition,D-61, CRC Press(1979)
11. R.J.Biernat and R.G.Robins, Electrochemica Acta, Vol.17, p1261(1972)
12. H.C.Helgeson, J. Phy. Chem., Vol.71, No.10, p3127(1967)
13. R.C.Murry,Jr and D.Cubicciotti, J. Electrochem. Soc., Vol.130, No.4,p866(1983)

Table 1. Chemical composition of materials melted in mill used for this study (wt%)

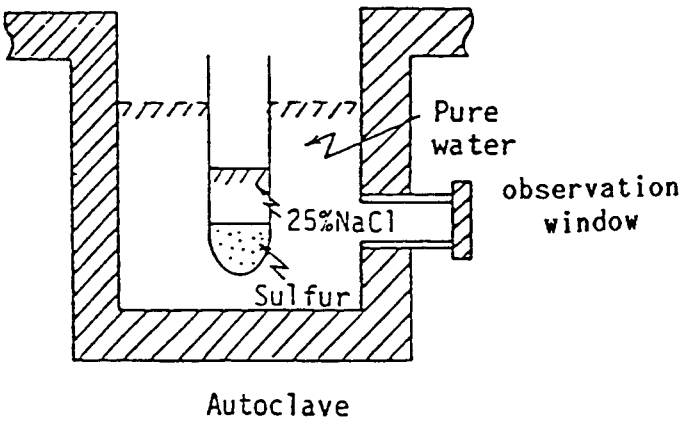
UNS No.	C	Si	Mn	P	S	Ni	Cr	Mo	W	Co	Cu
N06975	0.018	0.31	0.59	0.013	0.001	50	24	5.7	0.1	---	0.79
N10276	0.005	0.10	0.50	0.008	0.001	58	15.4	16.0	13.4	0.91	---

Table 2. Chemical composition of materials melted in lab. used for this study (wt%)

Mark	C	Si	Mn	P	S	Cu	Ni	Cr	Mo	Al	Nb	W
G1	.003	.020	.310	.001	.001	---	58.09	15.29	15.34	.130	---	3.83
G2	.005	.010	.320	.001	.001	---	63.15	15.10	15.25	.120	---	3.78
G4	.004	.010	.310	.001	.001	.97	57.35	19.88	9.80	.130	.96	---
G5	.003	.010	.310	.001	.001	.97	54.62	19.89	9.88	.120	.97	---
G6	.003	.010	.320	.001	.001	.96	51.80	19.96	9.90	.120	.97	---
G7	.003	.020	.310	.001	.001	.96	58.19	19.96	12.30	.110	.95	.7
G8	.005	.020	.320	.001	.001	.97	52.32	20.08	12.33	.120	.96	.7

Table 3. Standard test conditicen of electrochemical measurement

Environment	S	H_2S	$S+H_2S$
Temperature (℃)	200	200	200
S (g/l)	10	---	10
H_2S (MPa)	---	0.1	0.1
NaCl	5	5	5
Sweep rate (mV/min)	20	20	20



Autoclave

Test condition
Solution : 25%NaCl + S
Gas : 1atmH_2S + 10atmCO_2
Temp. : 20°C ~ 177°C

Fig. 1. Schematic illustration of autoclave apparatus with observation window

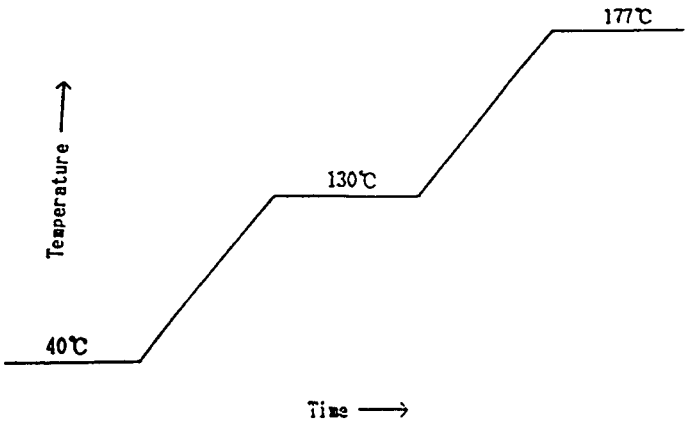


Fig. 2. Observation schedule of elemental S in H_2S-CO_2-Cl^- environment.

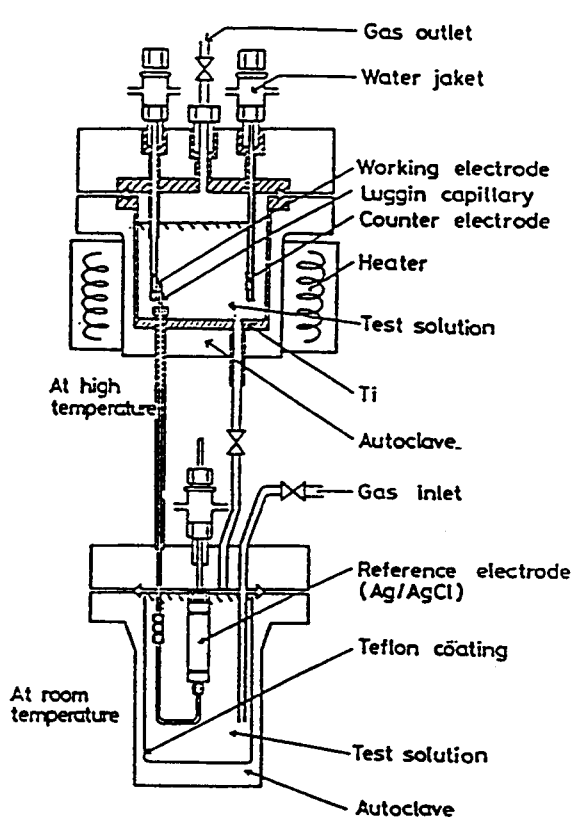


Fig. 3. Test apparatus for electrochemical measurement at high temperature

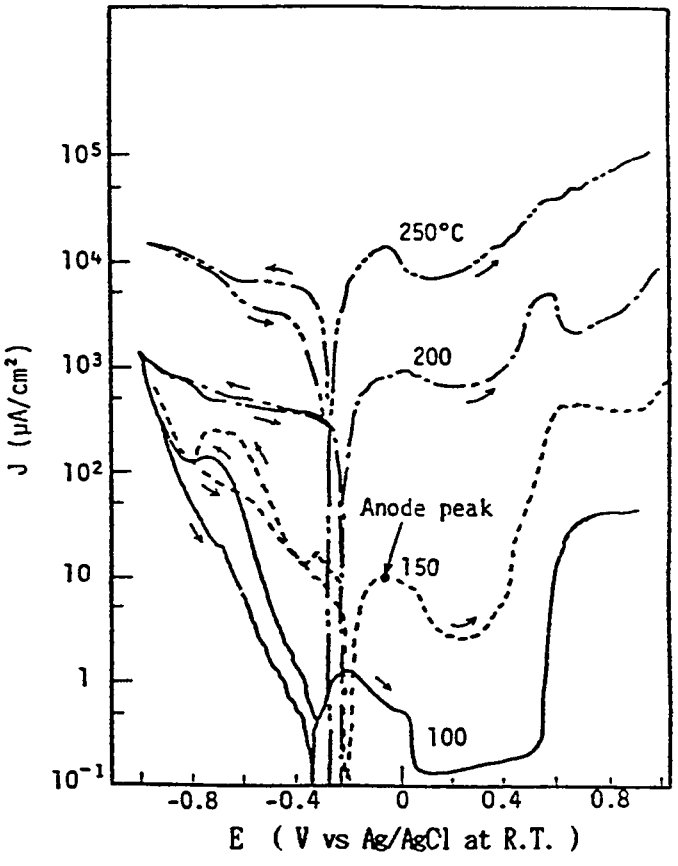


Fig. 4. Polarization behavior of sulfur at high temperature
(Pt electrode, 5%NaCl + 10g/lS
sweep rate: 20mV/min, 0.1MPa N_2)

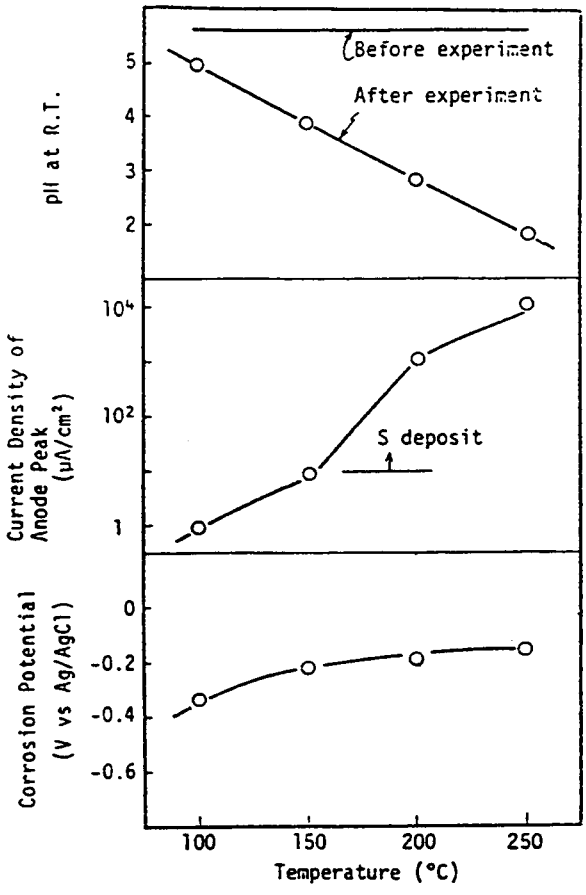


Fig. 5. Effect of temperature on corrosion potential, current density of anode peak and pH (before and after experiment) in S-H_2O-Cl^- environment.
(Pt electrode, 5%NaCl + 10g/lS
sweep rate: 20mV/min, 0.1MPa N_2)

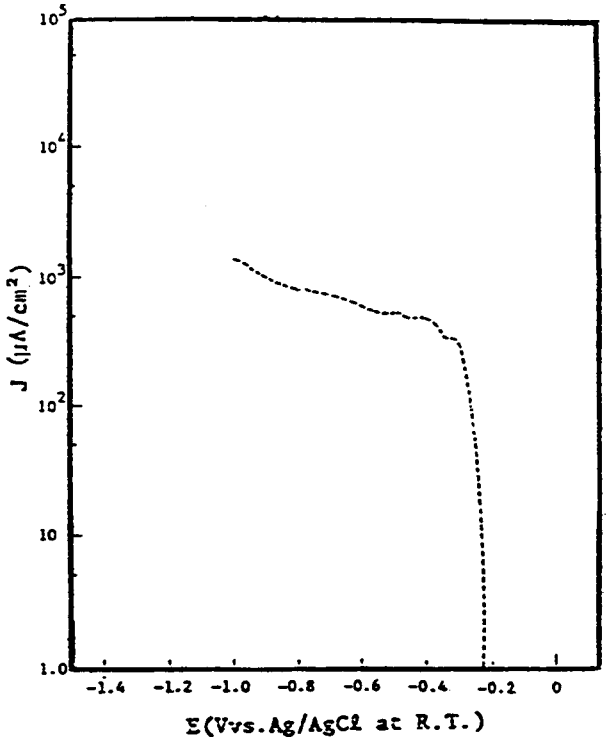


Fig. 6. Cathodic polarization curve of Pt electrode in S-H_2O environment
(200℃, 5%NaCl + 10g/lS,
sweep rate: 20mV/min)

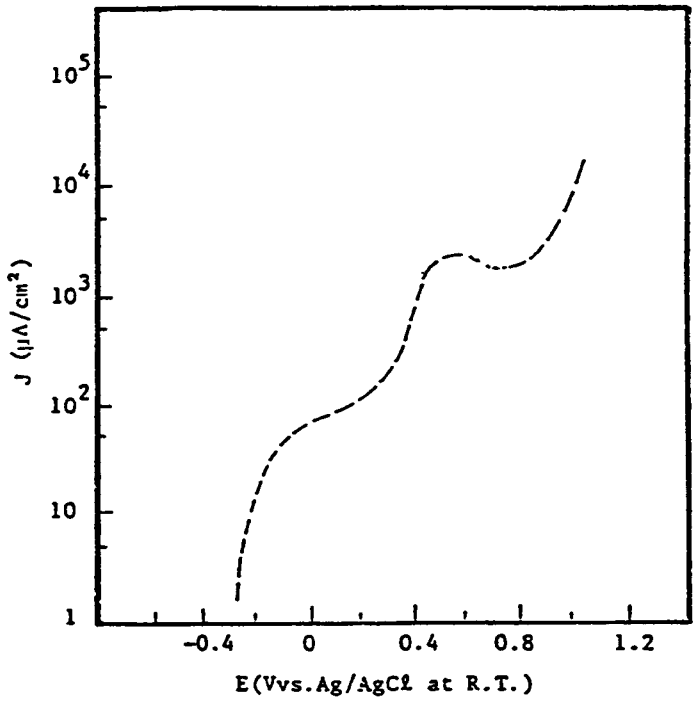


Fig. 7. Anodic polarization curve of Pt electrode in N2, S, H_2S and S+H_2S environment
(200℃, 5%NaCl + 10g/lS,
sweep rate: 20mV/min)

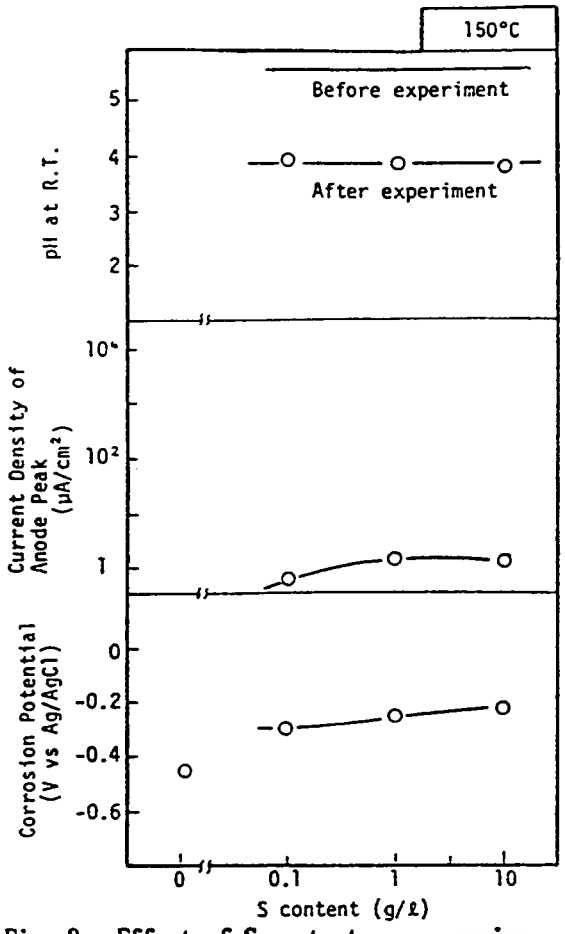


Fig. 8. Effect of S content on corrosion potential, current density of anode peak and pH (before and after experiment) in S-H_2O-Cl^- environment. (Pt electrode, 5%NaCl + x g/lS, 150℃ sweep rate; 20mV/min, 0.1MPa N_2)

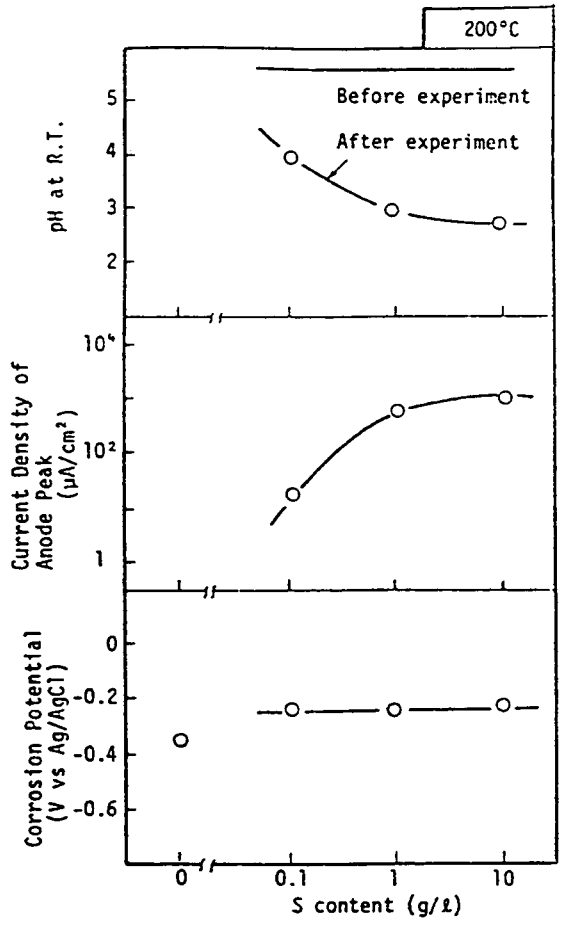


Fig. 9. Effect of S content on corrosion potential, current density of anode peak and pH (before and after experiment) in S-H_2O-Cl^- environment. (Pt electrode, 5%NaCl + x g/lS, 200℃ sweep rate; 20mV/min, 0.1MPa N_2)

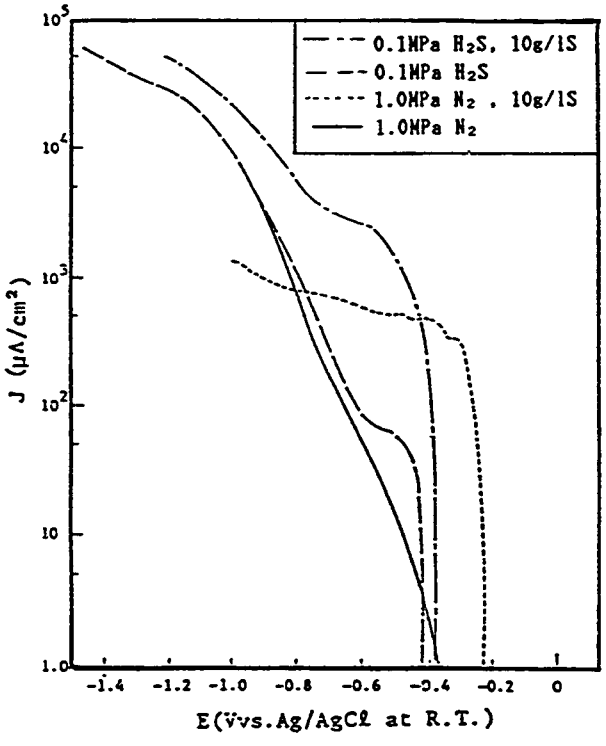


Fig. 10. Cathodic polarization curve of Pt electrode in N2, S, H_2S and S+H_2S environment (200℃, 5%NaCl, sweep rate; 20mV/min)

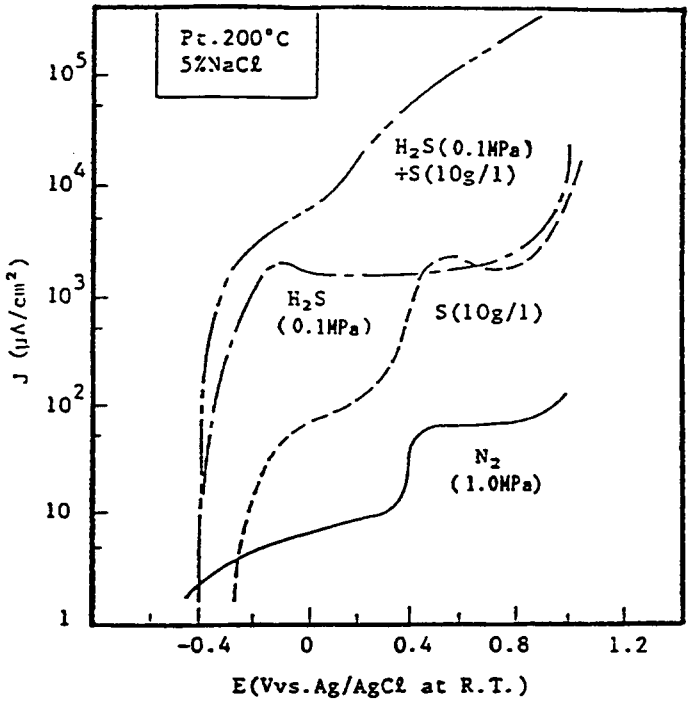


Fig. 11. Anodic polarization curve of Pt electrode in N2,S,H_2S and S+H_2S environment
(200℃, 5%NaCl, sweep rate; 20mV/min)

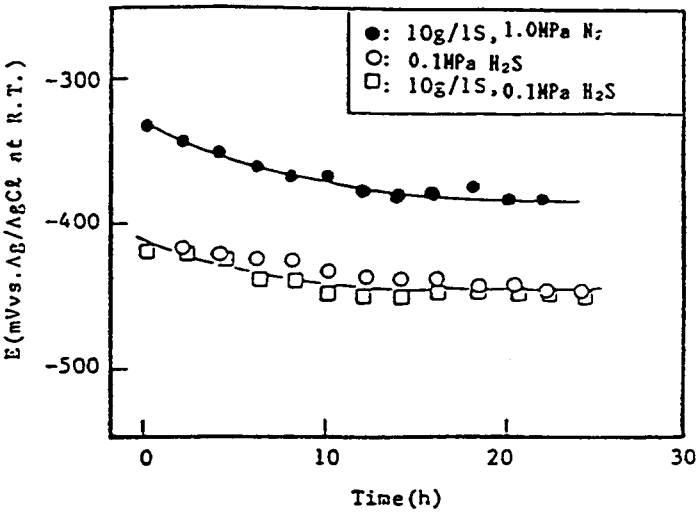


Fig. 12. Dependence of time on spontaneaous potential of Pt electrode in S-Cl^--H_2O environment
(200℃, 5%NaCl)

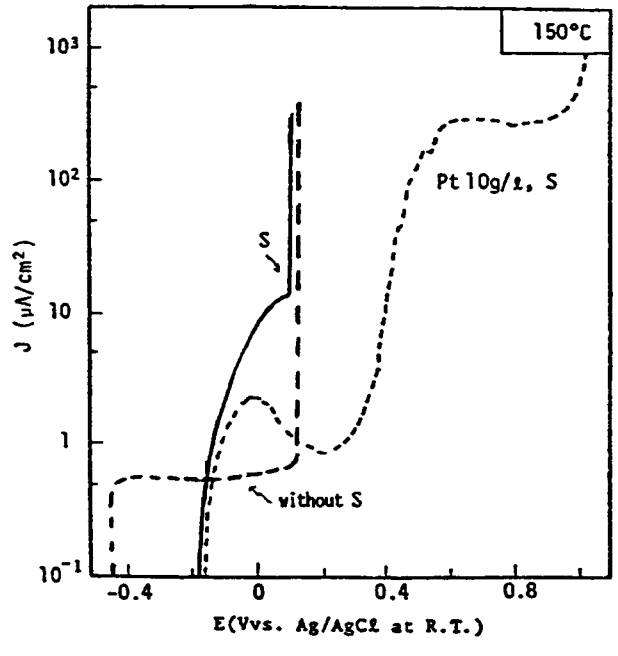


Fig. 13. Anodic polarization behavior of UNS No. N06975 alloy in S-H_2O-Cl^- environment at 150°C
(5%NaCl + 10g/1S, 150℃ sweep rate; 20mV/min, 0.1MPa N_2)

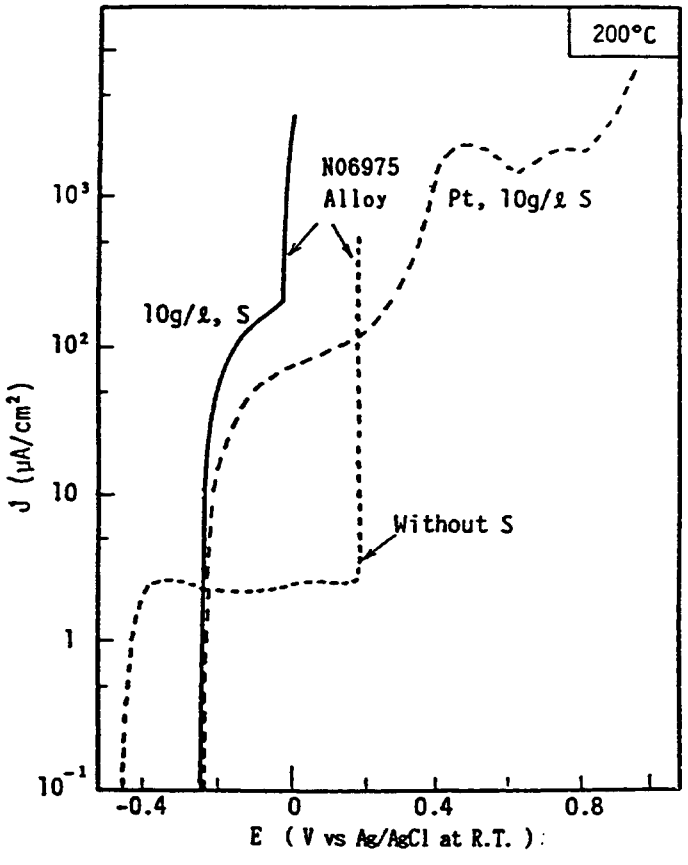


Fig. 14. Anodic polarization behavior of UNS No. N06975 alloy in S-H_2O-Cl^- environment at 200°C
(5%NaCl + 10g/1S, 200℃ sweep rate; 20mV/min, 0.1MPa N_2)

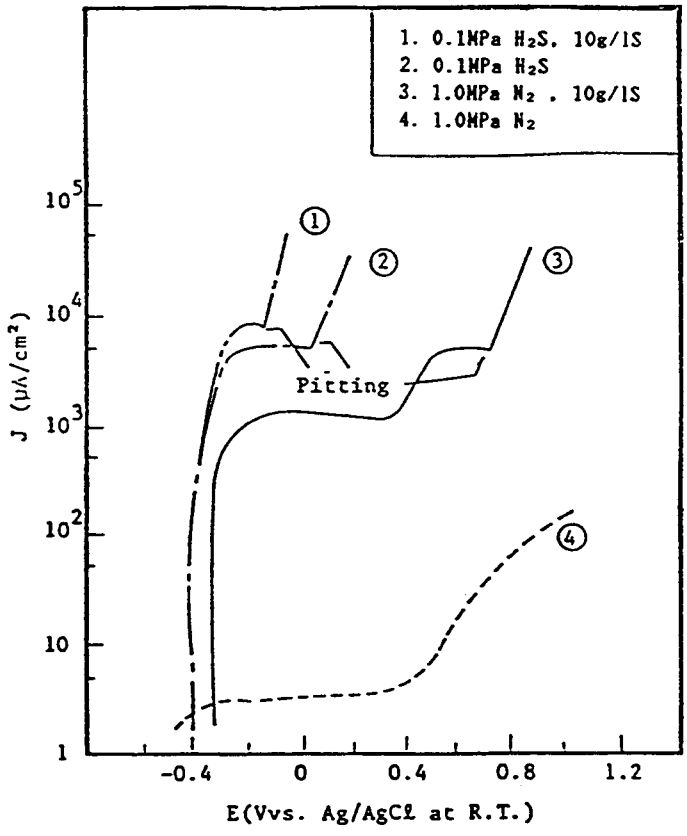


Fig. 15. Anodic polarization curve of UNS No. N10276 alloy in N2,S,H_2S and S+H_2S environment (5%NaCl, 200℃, sweep rate; 20mV/min, 0.1MPa N_2)

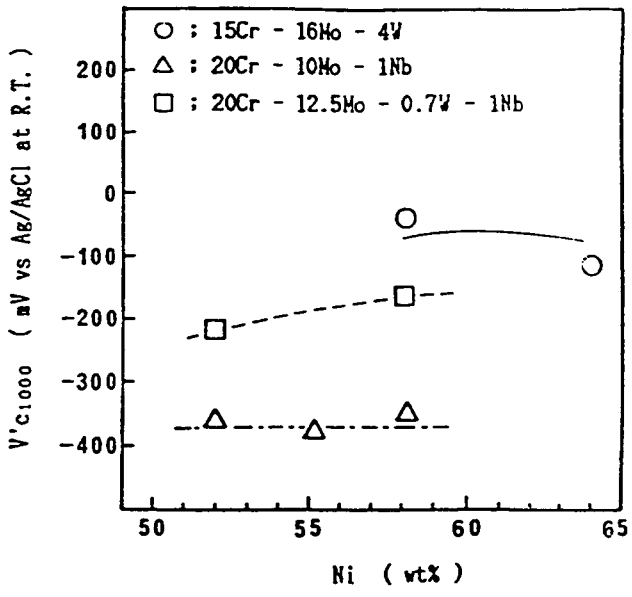


Fig. 16. Effect of Ni content in alloys on critical pitting potential in S-H_2O-Cl^- environment (200℃, 25%NaCl, 10g/lS sweep rate ; 20mV/min)

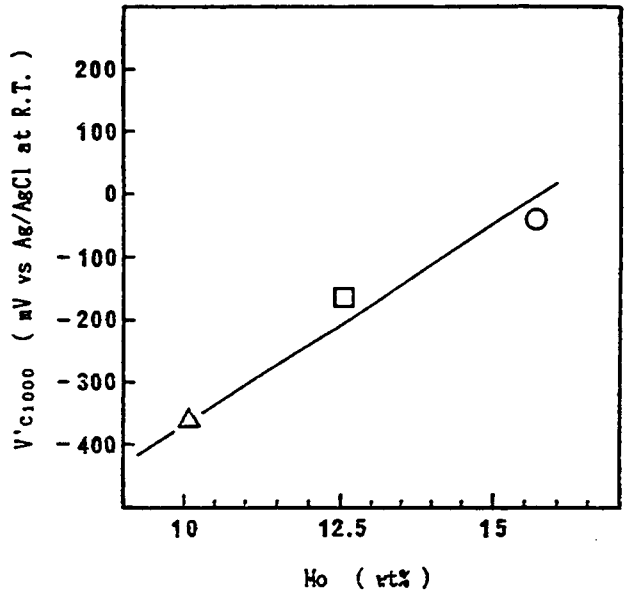


Fig. 17. Effect of Mo content in alloys on critical pitting potential in S-H_2O-Cl^- environment (200℃, 25%NaCl, 10g/lS sweep rate ; 20mV/min)

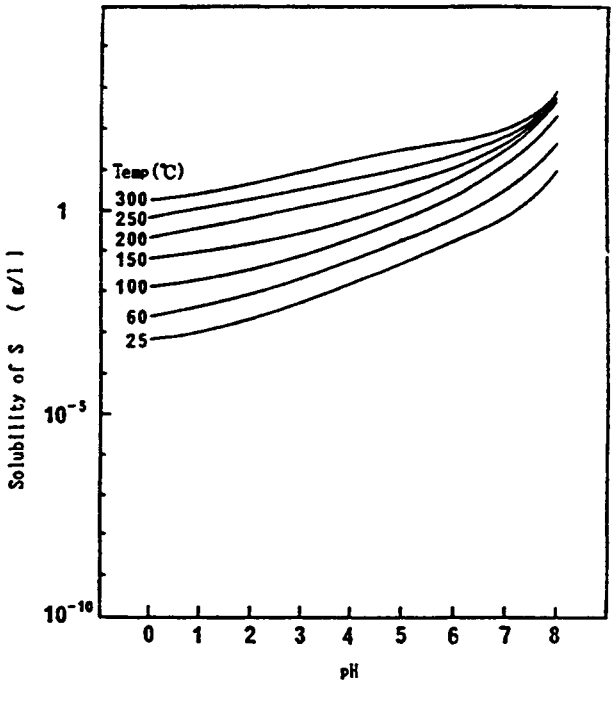


Fig. 18. Solubility of S estimated by thermodynamic calculation to assume the self-oxidation-reduction reaction(H_2O system)

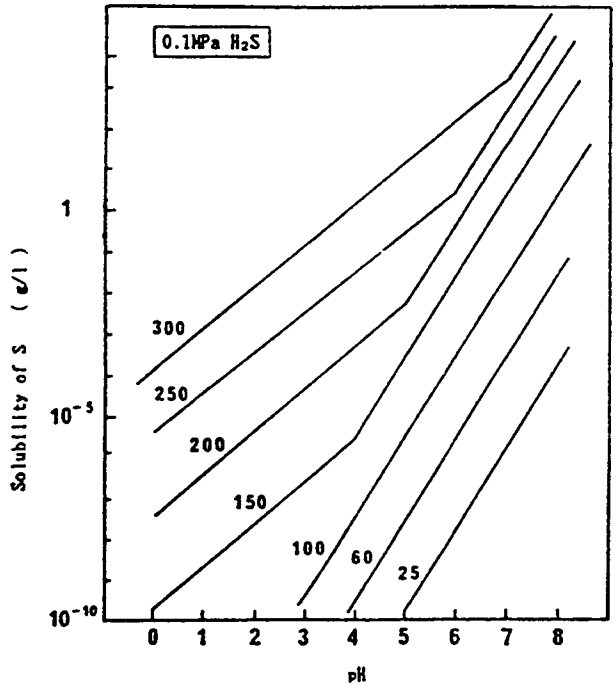


Fig. 19. Solubility of S estimated by thermodynamic calculation to assume the self-oxidation-reduction reaction(0.1MPa H_2S-H_2O system)

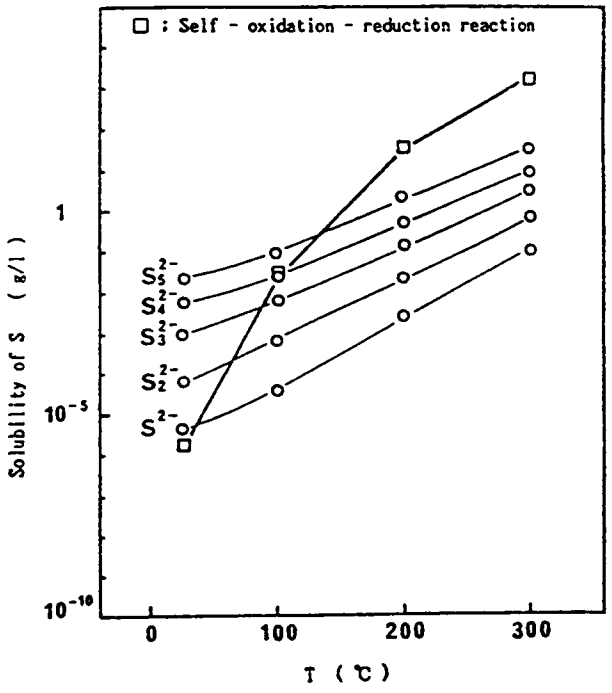
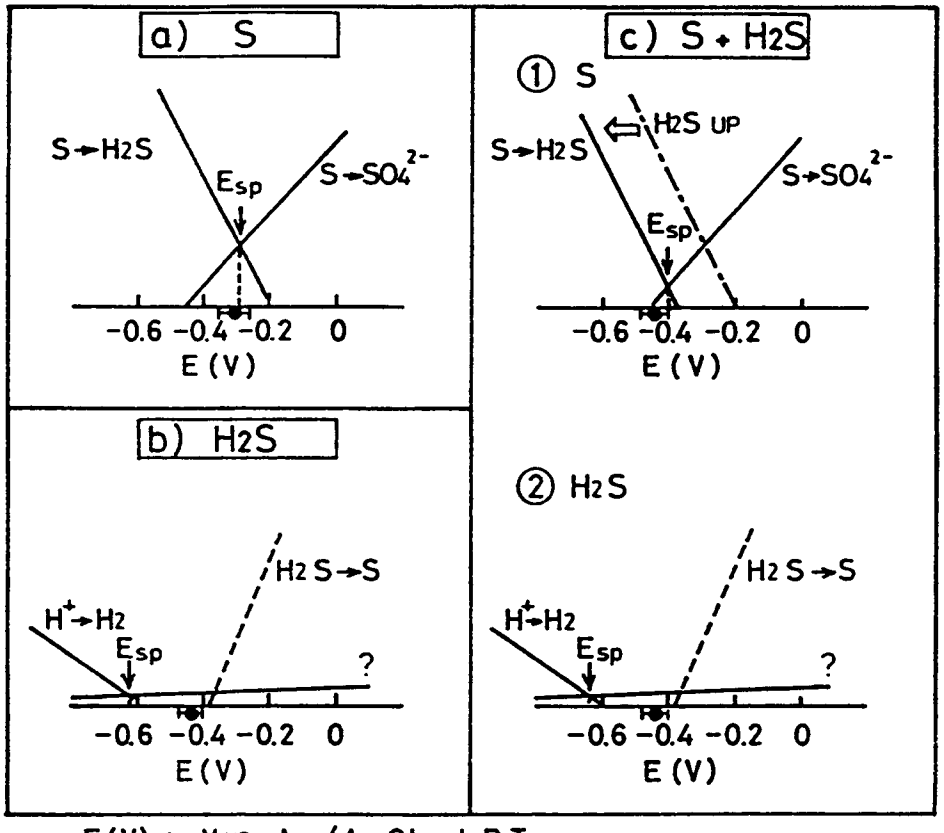


Fig. 20. Solubility of S by production of polysulfide at pH 7.
(S-0.1MPa H_2S-H_2O system)



E(V) : V vs Ag/AgCl at R.T.

Fig. 21. Schematic illustration of spontaneous potential(Esp) estimated by thermodynamic calculation in H_2O-Cl^- environment containing S,H_2S and S+H_2S
(200℃. S : H_2S ; 10^{-5}MPa, SO_4^{2-} ; 10^{-6}mol/l, pH 3 H_2S : H_2S ; 0.1MPa, pH 3
● ; measured Esp in S(10g/lS) , H_2S(0.1MPaH_2S) and S+H_2S (200℃ , 5%NaCl))

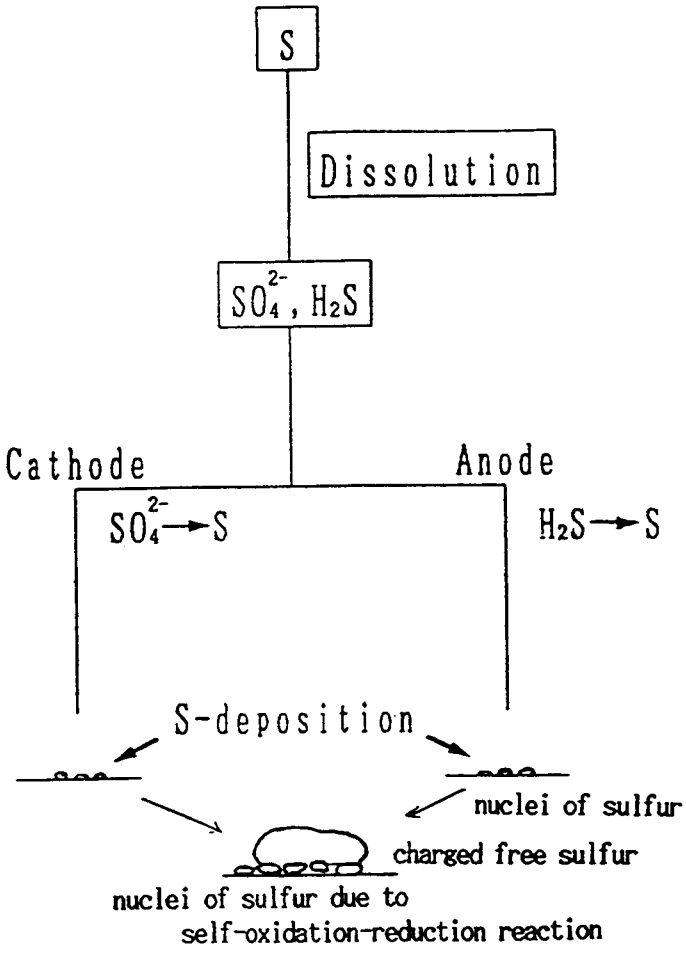


Fig. 22. A mechanism of S-deposition due to reverse dissolution reaction

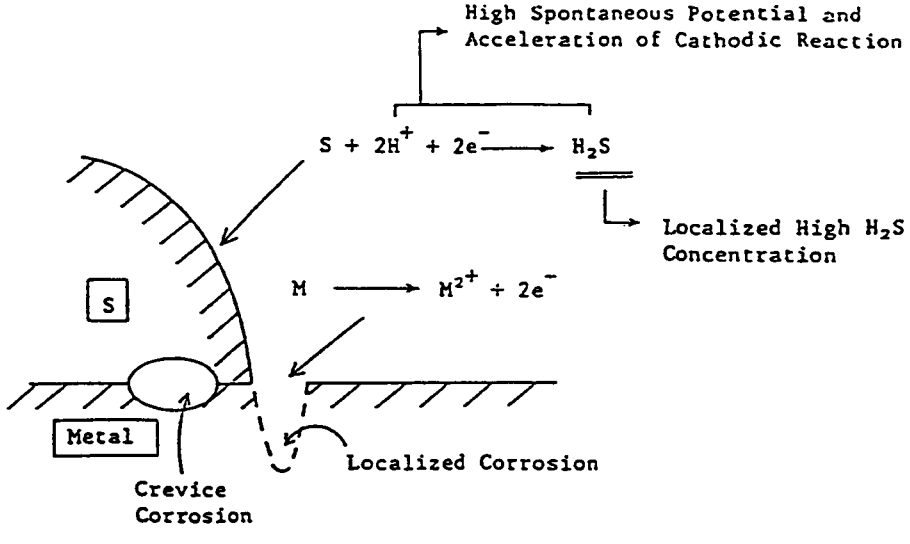


Fig. 23. A model of corrosion in environment with elemental sulfur

Copyrighted Materials
Copyright © 1996 NACE International Retrieved from www.knovel.com

Wireline Materials for Sour Service*

GLEN A. VAUGHN and HUNG-ERH CHAUNG*

Operators have experienced a significant increase in wireline failures due to stress corrosion cracking (SCC) in sour oil and gas wells. To identify materials that will perform effectively in sour environments, the SCC resistance of potential wireline materials was evaluated in both the field and the laboratory. Four categories of wireline materials were investigated: (1) austenitic stainless steels, (2) duplex (austenitic-ferritic) stainless steels, (3) nickel base alloys, and (4) nickel/cobalt base alloys. The SCC data obtained from testing these materials showed that, in general, a wireline material must contain a minimum of 30% nickel to operate for extended periods of time in 93 C, H_2S + Cl containing environments.

Introduction

WIRELINES HAVE BEEN EMPLOYED in oil and gas wells since the early days of the industry. The uses of wireline include depth determinations; temperature and pressure surveys; removing paraffin, scale, and sand accumulations from the flow path; and setting, retrieving, and manipulating such devices as chokes, circulating plugs, gage cutters, and safety valves.

The surface equipment required for wireline operations varies with operating conditions. However, it usually consists of the wireline, wireline reel and power unit, a wireline measuring device, a weight indicator, and a pulley to provide entrance into the well. In addition, since most wireline operations are conducted under pressure, a stuffing box, staff, blowout preventer, and lubricator are used. A typical installation is shown in Figure 1.

The most common wireline diameters utilized are between 1.7 and 2.3 mm (0.066 and 0.092 inch). The diameter of the wireline is important, since the equipment used to provide entrance into a wellbore under pressure becomes bulky and complicated as the diameter of the wireline increases. The ultimate tensile strength of wirelines is generally near 1600 MPa (230 ksi). Conventional wireline materials are usually available in one piece from wire-drawing mills in lengths up to 7620 meters (25,000 feet).

One of the major material problems encountered in wireline operations is stress corrosion cracking (SCC); this is especially the case in sour wells. In recent years, a significant increase in wireline failures has been experienced in sour oil and gas wells. Of particular concern is the parting of the wirelines in the well with no loading other than the weight of the tool string. Many of the wirelines had been subjected to temperatures up to 143 C (290 F) in the presence of H_2S, CO_2, and chloride-containing water. After repeated SCC failures of AISI 304, AISI 316, and 18-18-2 (18% Cr, 18% Ni, 2% Si) stainless steel wirelines in these sour wells, the use of austenitic-ferritic duplex stainless steel wirelines was tried. The number of failures decreased, but failures continued to occur, making the use of the duplex alloy wirelines marginal in sour wells. Thus, an investigation was initiated to determine the SCC resistance of several other potential wireline materials. In addition to environments conducive to SCC, these alloys may be exposed to conditions that promote hydrogen embrittlement cracking (HEC); therefore, the HEC resistance of these wireline materials was also evaluated.

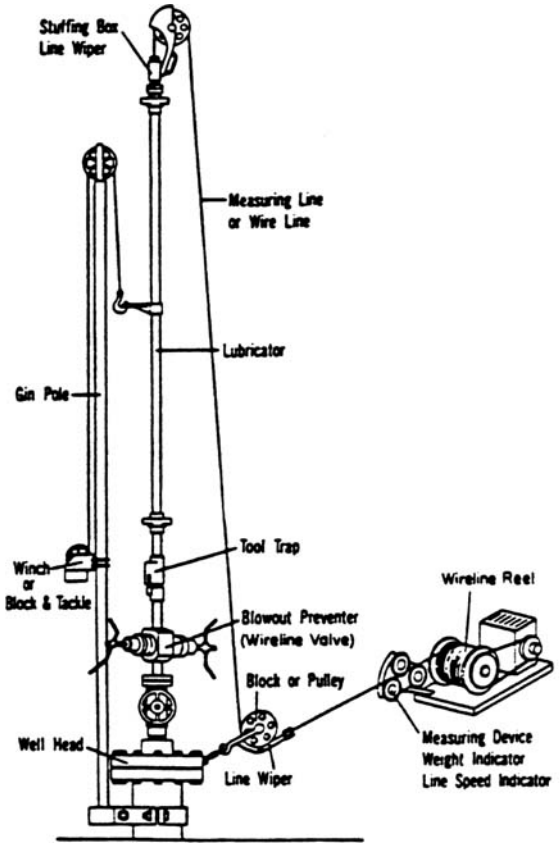


FIGURE 1 — Wireline servicing installation.

Experimental Procedure

Materials

The wireline materials[1] examined in this study included the following: (1) austenitic stainless steels AISI 316, 18-18-2, Uranus B6, Sandvik 2RK65, Sanicro 28, Carpenter 20Cb-3, Incoloy Alloy 825, and Hastelloy G; (2) duplex (austenitic-ferritic) stainless steels Uranus 50 and SAF-2205; (3) nickel alloys Pyromet 31, Alloy 718, Inconel 617, Inconel 625, and Hastelloy

*Presented during Corrosion/81 (Paper 182), April, 1981, Toronto, Ontario.

*Exxon Production Research Company, Houston, Texas.

[1]All trade names are acknowledged in Table 1.

TABLE 1 — Nominal Composition of Wireline Materials Tested

Material	Description	Weight Percent Fe	Cr	Ni	Mo	Co	Others
AISI 316	Austenitic	67	17	12	2.2	—	1.88 Mn
18-18-2	Austenitic	60	18	18	—	—	2.0 Si, 1.5 Mn
Uranus 50[1]	Duplex	67	21	7	2.5	—	1.5 Cu, 1.0 Mn
SAF-2205[2]	Duplex	66	23	6	2.9	—	1.6 Mn, 0.4 Si
Uranus B6[1]	Austenitic	49	20	25	4.5	—	1.5 Cu
Sandvik 2RK65[2]	Austenitic	47	19.5	25	4.5	—	1.5 Cu, 1.8 Mn
Sanicro 28[2]	Austenitic	34	27	31	3.5	—	1.0 Cu, 2.0 Mn, 1.0 Si
Carpenter 20Cb-3[3]	Austenitic	36	20	34	2.5	—	2.0 Mn, 3.5 Cu, 1.0 Si, 1.0 Ta + Cb
Incoloy Alloy 825[4]	Austenitic	28	22	44	3.0	—	1.7 Cu, 0.97 Ti
Hastelloy G[5]	Austenitic	22	20	43	6.3	2.1	1.9 Cu, 1.98 Ta + Cb, 1.43 Mn, 0.62 W
Alloy 718	Nickel alloy	18	18	53	3.0	—	5.2 Ta + Cb
Pyromet 31[3]	Nickel alloy	16	23	55	2.0	—	1.4 Al, 2.3 Ti
Inconel Alloy 625[4]	Nickel alloy	4	21	61	9.0	—	3.6 Ta + Cb
Inconel Alloy 617[4]	Nickel alloy	—	22	57	9.0	12.5	
Hastelloy C-276[5]	Nickel alloy	5.5	15.5	60	16	2.0	
MP35N[6]	Nickel/cobalt alloy	—	20	35	9.5	35	

[1]Trademark, Creusot-Loire Steels.
[2]Trademark, Sandvik Steel, Inc.
[3]Registered trademark, Carpenter Technology Co.
[4]Registered trademark, Huntington Alloys, Inc.
[5]Registered trademark, Cabot Corporation.
[6]Registered trademark, Standard Pressed Steel Co.

TABLE 2 — Mechanical Properties of Wireline Materials Tested

Material	Yield Strength MPa	ksi	Tensile Strength MPa	ksi
AISI 316	1410	205	1460	212
18-18-2	1460	212	1540	223
Uranus 50	1410	205	1590	230
SAF-2205	1580	229	—	—
Uranus B6	—	—	1560	226
Sandvik 2RK65	1420	206	—	—
Sanicro 28	—	—	1490	216
Carpenter 20Cb-3	1400	203	—	—
Incoloy Alloy 825	1190	173	1280	185
Hastelloy G	—	—	1680	243
Alloy 718	1480	215	1660	240
Pyromet 31	—	—	1450	210
Inconel Alloy 625	1540	223	1550	225
Inconel Alloy 617	1510	219	1770	257
Hastelloy C-276	1400	203	1590	230
MP35N	1480	215	1720	249

C-276; and (4) the cobalt base alloy MP35N. The nominal compositions of these alloys are given in Table 1.

All the wireline materials were obtained and tested in the cold worked condition. Austenitic-type alloys strain-harden rapidly, so cold working was used to increase their hardness and strength. As shown in Table 2, the ultimate tensile strengths of the alloys varied from 1280 MPa (185 ksi) to 1770 MPa (257 ksi).

Test Specimens

The wireline materials were tested in the form of modified U-bend specimens. Wirelines 15 cm (6 inches) in length were

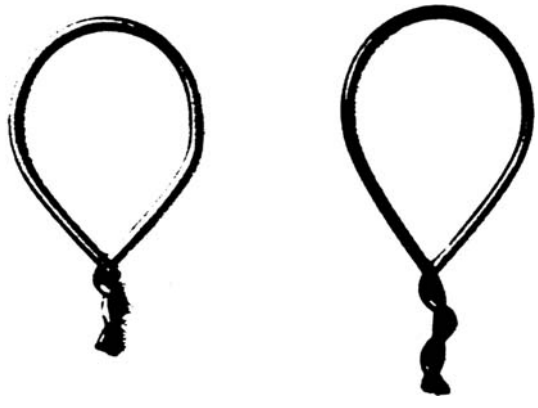


FIGURE 2 — Stressed wireline specimens, uncoupled.

formed around a mandrel 2.5 cm (1 inch) in diameter and then stressed by deflecting the ends of the specimens until they touched. Thus, the specimens were severely stressed, with the applied stress being above the yield strength of the material.

For the elevated temperature SCC tests, specimens of the type shown in Figure 2 were used. To evaluate the HEC resistance, two types of specimens were employed: a U-bend specimen galvanically coupled to steel, as shown in Figure 3, and an uncoupled U-bend specimen of the type used in the SCC tests.

Test Environments

SCC tests were conducted in our field test facility, and in simulated field environments in autoclaves in the laboratory. The field environments consisted of chloride-containing water (206,000 mg/L Cl^-) and the field gas, which contains approximately 11% H_2S and 40% CO_2. The analyses of the field water

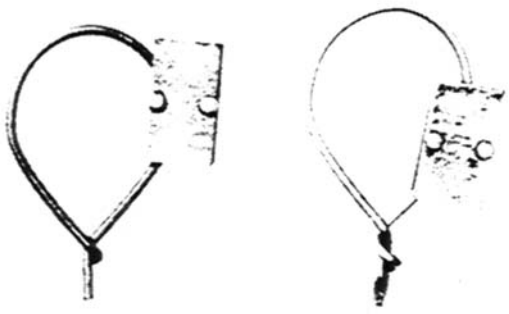


FIGURE 3 — Stressed wireline specimens, coupled to steel.

TABLE 3 — Composition of Field Water

Specific Gravity @ 24 C = 1.227
pH @ 24 C = 5.7

	Mg/L	Meq/L
Sodium	80,000	3400
Calcium	39,000	2000
Magnesium	4,200	345
Chloride	206,000	5800
Sulfate	0	0
Iron	0	0
Bicarbonate	342	5.6
Carbonate	0	0
Total	330,484	
Total Iron	0	
Barium	66	

and gas are shown in Tables 3 and 4, respectively. The field test vessels were equipped with heating bands and temperature controlling equipment so that SCC tests could be conducted at elevated temperatures. The field tests were carried out for 30 days at 93 C (200 F) and 149 C (300 F).

In the laboratory, SCC tests were performed in aqueous solutions containing 25% NaCl (180,000 mg/L Cl^-), 0.5% acetic acid, and saturated with H_2S. These tests were conducted for seven days at 93, 149, 177, and 204 C (200, 300, 350, and 400 F). To determine the role of chlorides and H_2S on SCC, tests were conducted for seven days at 93, 149, and 204 C in 25% NaCl/0.5% acetic acid solution containing no H_2S; and one test was carried out at 204 C in an H_2S saturated, 0.5% acetic acid solution without the presence of chlorides. In all tests, the pH was between 3 and 3.5

The laboratory HEC tests were performed in a room temperature NACE solution (5% NaCl, 0.5% acetic acid, saturated with H_2S).

Results

Elevated Temperature Tests in H_2S + NaCl Environments

Table 5 presents the results obtained from the 93 and 204 C field tests and the 93, 149, 177, and 204 C laboratory tests.

TABLE 4 — Composition of Field Gas

Constitutent	Concentration (mol %)
H_2S	10.9
CO_2	39.8
N_2	1.7
C_1	29.7
C_2	5.0
C_3	3.2
iC_4	0.89
nC_4	2.0
iC_5	0.67
nC_5	1.0
C_6	1.4
C_7	1.2
C_8	0.77
C_9	0.58
C_{10}	1.1
Carbonyl Sulfide	0.069

The field tests were 30 days in duration and the laboratory tests seven days. Not all the wirelines in this study were investigated in the field, since some of the materials were not available at the time of the field evaluations.

Of those investigated in the elevated temperature, sour field environment, only AISI 316 failed at both 93 and 149 C. Type 18-18-2 did not crack during the field tests, but did show evidence of pitting at both temperatures. Uranus 50 and Uranus B6 both failed at 149 C, but not at 93 C in these environments. Sandvik 2RK65, Carpenter 20Cb-3, Alloy 718, Inconel 617, Inconel 625, Hastelloy C-276, and MP35N did not fail in the 30 day, 149 C field test.

The results obtained from the laboratory SCC test were similar to those observed in the field tests. In the laboratory tests, two materials, AISI 316 and 18-18-2, failed at 93 C. Uranus 50, SAF-2205, Uranus B6, and Sandvik 2RK65 failed in the 149 C test. Pyromet 31 wireline specimens were observed to have a 50% chance of failing in the seven day, 149 C test. The following materials survived the 149 C sour laboratory environment: Sanicro 28, Carpenter 20Cb-3, Incoloy Alloy 825, Alloy 718, Hastelloy G, Inconel 625, Hastelloy C-276, Inconel 617, and MP35N. All the materials tested above 149 C failed with the exception of MP35N, which did not fail in the SCC test at 177 or 204 C.

The SCC laboratory results are plotted in Figure 4 as a function of the Ni content of the wireline. In this plot, the Co content of the MP35N and Inconel 617 wirelines was considered to be equivalent to the Ni content (*e.g.*, MP35N was considered to contain 70% Ni). The plot shows the tendency of increased Ni to increase the SCC resistance of the wireline materials. In general, a Ni content of approximately 25% is needed to prevent wireline SCC failures in 93 C, H_2S-containing, NaCl solutions. However, the Uranus 50 and SAF-2205 wirelines, which contained less than 10% Ni, did not fail at 93 C. This is attributed to their duplex austenitic-ferritic microstructure. A wireline with approximately 30% Ni was needed to endure the 149 C sour test environment. Pyromet 31 was an exception, however, with laboratory tests indicating this alloy had a 50% chance of failure when subjected to the 149 C sour environments. The dashed line in Figure 4 attempts to establish general failure/no failure zones; as previously mentioned, the duplex alloys and Pyromet 31 are exceptions.

Figure 5 shows the field data plotted as a function of Ni content. The dashed line established from the laboratory test data (Figure 4) is superimposed on the graph. As can be seen, the correlation between laboratory and field tests was excellent.

TABLE 5 — SCC Results on Wireline Materials Tested

Environment:
Field: NaCl + $MgCl_2$ + $CaCl_2$ contacted with 11% H_2S, 40% CO_2 gas
Lab: NaCl contacted with 100% H_2S gas

Material	7 Days @ 93 C Lab	30 Days @ 93 C Field	7 Days @ 149 C Lab	30 Days @ 149 C Field	7 Days @ 177 C Lab	7 Days @ 204 C Lab
AISI 316	F	F	F	F	—	F
18-18-2	F	P	F	P	—	F
Uranus 50	NF	NF	F	F	F	F
SAF-2205	NF	—	F	—	F	F
Uranus B6	NF	NF	F	F	F	F
Sandvik 2RK65	NF	NF	F	NF	F	F
Sanicro 28	NF	—	NF	—	F	F
Carpenter 20Cb-3	NF	—	NF	NF	F	F
Incoloy Alloy 825	NF	—	NF	—	F	F
Hastelloy G	NF	—	NF	—	—	F
Alloy 718	—	NF	NF	NF	—	F
Pyromet 31	NF	—	F*	—	F	F
Inconel Alloy 625	—	—	NF	NF	—	F
Inconel Alloy 617	—	—	NF	NF	F	F
Hastelloy C-276	—	NF	NF	NF	F	F
MP35N	—	—	NF	NF	NF	NF

NF = No failure.
F = Failure.
P = Pitted, but no failure.
F* = Six specimens were tested in separate vessels; three failed, and three did not fail.

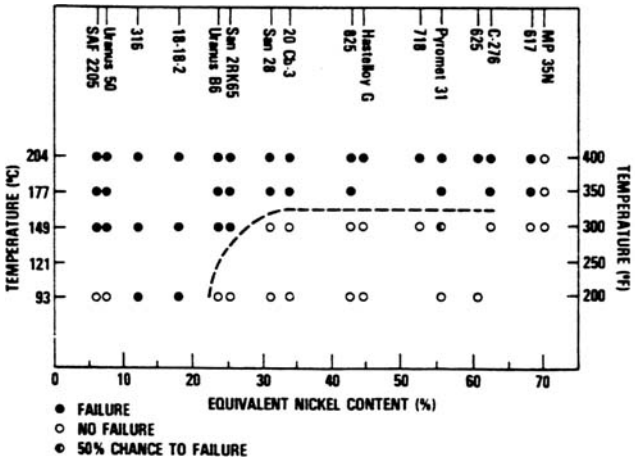


FIGURE 4 — Effect of equivalent nickel content (Ni + Co) on SCC resistance of wireline materials in laboratory environments.

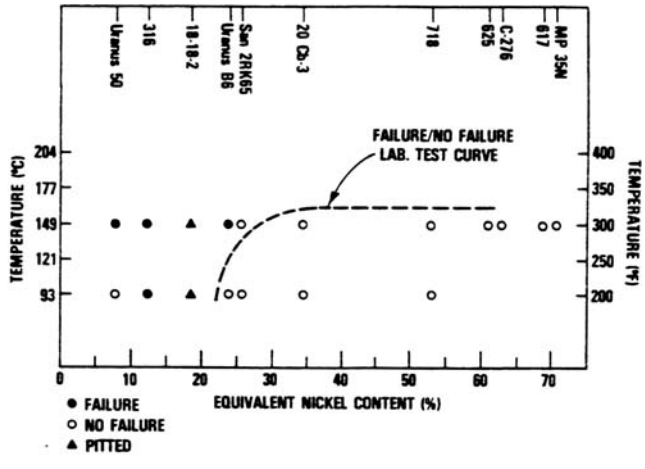


FIGURE 5 — Effect of equivalent nickel content (Ni + Co) on SCC resistance of wireline materials in field environments.

NaCl Environment Containing No H_2S

To determine the effect of H_2S on the SCC susceptibility of the materials, seven day tests were conducted at 93, 149, and 204 C in a 25% NaCl solution containing no H_2S. The pH of the solution was adjusted to between 3 and 3.5 with acetic acid. The test results are given in Table 6. No failures were observed at 93 and 149 C; only one material, 18-18-2, failed at 204 C.

Aqueous Solutions Containing H_2S and No Chlorides

An effort was made to determine the role of chlorides in the SCC of these materials. A seven day test was performed at 204 C in an H_2S saturated solution (pH 3-3.5) without chlorides. As seen in Table 7, no failures were observed in this test.

Room Temperature Tests in NACE Solution

As part of the alloy evaluation program, the materials were tested in a room temperature NACE solution. Specimens of each material were tested in the galvanically coupled-to-steel and in the uncoupled condition. As shown in Table 8, in the galvanically coupled condition, AISI 316, 18-18-2, and Uranus 50 failed in the NACE solution. The other coupled wireline materials did not fail during the test period. However, when the specimens were not coupled to steel, AISI 316, 18-18-2, and the two duplex alloys, Uranus 50 and SAF-2205, failed in much

TABLE 6 — SCC in Chloride Environment Containing No H_2S

Material	7 Days @ 93 C	7 Days @ 149 C	7 Days @ 204 C
AISI 316	NF	NF	NF
18-18-2	NF	NF	F
Uranus 50	NF	NF	NF
SAF-2205	NF	NF	NF
Uranus B6	NF	NF	NF
Sandvik 2RK65	NF	NF	NF
Sanicro 28	NF	NF	NF
Carpenter 20Cb-3	NF	NF	NF
Pyromet 31	NF	NF	NF

F = Failed.
NF = Did not fail.

TABLE 7 — SCC in Deionized H_2S Saturated with H_2S

Material	7 Days @ 204 C
AISI 316	NF
18-18-2	NF
Uranus 50	NF
SAF-2205	NF
Uranus B6	NF
Sandvik 2RK65	NF
Sanicro 28	NF
Carpenter 20Cb-3	NF
Pyromet 31	NF
Incoloy Alloy 825	NF
Inconel 617	NF
Hastelloy C-276	NF
MP35N	NF

NF = No failure.

TABLE 8 — Evaluation of Wireline Specimens in NACE Solution

Material	U-Bend Specimens Coupled to Steel (Exposure time in days)	U-Bend Specimens Uncoupled (Exposure time in days)
AISI 316	(118)	(34), (57)
18-18-2	(153)	(11), (85)
Uranus 50	(153)	(34), (57)
SAF-2205	209	(34), 113
Uranus B6	242	191
Sandvik 2RK65	191	191
Sanicro 28	242	191
Carpenter 20Cb-3	242	191
Incoloy Alloy 825	33	33
Hastelloy G	47	47
Alloy 718	61	61
Pyromet 31	242	191
Inconel Alloy 625	33	33
Inconel Alloy 617	75	75
Hastelloy C-276	—	—
MP35N	144	144

() = Specimen failed in days indicated.

shorter times than in the coupled condition, (*i.e.*, 18-18-2 failed in the coupled condition in 153 days and in the uncoupled condition in 11 days). The other materials showed no evidence of failure in either the coupled or uncoupled condition in the NACE solution.

Observation of Fractographs

The first was a complete fracture directly across the diameter of the wire, *i.e.*, transverse to the drawing direction (*e.g.*, Uranus B-6 and Sanicro 28). The second was a transverse crack that proceeded a short distance inward from the surface and then shifted to a longitudinal direction until failure occurred (*e.g.*, Uranus 50). The third was a combination of 1 and 2 (*e.g.*, AISI 316 and 18-18-2). Metallographic and SEM examinations revealed that transgranular cracking was the predominant mode in all failed specimens.

Discussion

Effect of Hydrogen Sulfide and Chlorides

The results revealed that most of the materials evaluated were susceptible to SCC in varying degrees depending upon the test conditions. Laboratory SCC tests in H_2S-containing NaCl solutions showed that only the AISI 316 and 18-18-2 wirelines failed at 93 C, but all the specimens, with the exception of MP35N, failed at 177 and 204 C. However, in H_2S solutions containing no chlorides, no materials failed at 204 C, while in 204 C, chloride-containing solutions without H_2S, only one material, 18-18-2, failed. Thus, it appears that the combination of H_2S and chloride creates a synergistic effect to promote SCC, even though chlorides may have a more pronounced effect.

Effect of Nickel on SCC

The Ni content in the materials tested varied from 6 to over 60%. The SCC test results showed that, in general, the greater the Ni content of the wireline material, the higher its resistance to failure. It has been shown previously[1,2] that adding Ni to austenitic alloys has a beneficial effect on the resistance to SCC in chloride solutions. Furthermore, adding Ni to the material could increase the hydrogen solubility, and decrease the hydrogen diffusivity in the alloy.[3] Thus, it is implied that the higher Ni-containing alloys are less likely to suffer HEC and chloride SCC.

No failures were noted in the MP35N wireline specimens in either the field or laboratory environments. This material contains only 35% Ni, but it also contains 35% Co. The effect of Co on chloride SCC has not been studied extensively. A small addition of Co to AISI 304 was found[4] to render the alloy less susceptible to chloride SCC. Since Co and Ni are similar electrochemically, adding Co should be equivalent to adding Ni.[5] Still others[6] have concluded that alloys such as MP35N, which was found to resist SCC in boiling $MgCl_2$, can have some of the Ni replaced by Co without changing the observed resistance, but replacing all of the Ni with Co leads to SCC in boiling $MgCl_2$.

Effect of Metallurgical Structure

With the exception of the duplex stainless steel alloys, the wireline materials used in this study were austenitic-type alloys. In general, austenitic alloys have good resistance to HEC.[7] However, most austenitic alloys are susceptible to chloride SCC under certain conditions.[5,8] It has been demonstrated that ferrite-containing alloys have good resistance to chloride SCC;[9,10] therefore, it might be expected that austenitic-ferritic steels, such as Uranus 50 and SAF-2205, with approximately equal proportions of austenite and ferrite, would have a higher SCC resistance than similarly alloyed austenitic materials. Although the duplex stainless steel wirelines did not fail in the 30 day field or seven day laboratory SCC tests at 93 C, they did fail at 149 C. Additionally, the uncoupled duplex alloy failed in the room temperature NACE solution.

TABLE 9 — Effect of Polarization on SCC of Wirelines

Test Specimen: U-bend.
Test Environment: NACE solution at room temperature.

Material	Open Circuit Potential (MVsce)[1]	Applied Potential (MVsce)	Time to Failure (hr)
18-18-2	−375	OP[2]	264
18-18-2	−375	−275	4
18-18-2	−375	−350	72
18-18-2	−375	−600	NF − 168[3]
AISI 316	−384	OP	816
AISI 316	−384	−275	6
AISI 316	−384	−600	NF − 168
SAF-2205	−440	OP	816
SAF-2205	−440	−275	12
Uranus 50	−435	OP	816
Uranus 50	−435	−275	6

[1]Potentials against saturated calomel electrode.
[2]OP = Open circuit potential.
[3]NF = No failure at 168 hours of test.

Thus, in these high H_2S-containing, NaCl-saturated solutions, the use of duplex stainless steel wirelines does not appear promising.

Metallographic examination revealed that all failed specimens experienced predominantly transgranular cracking with branching, which is the typical mode of fracture for nonsensitized austenitic alloys at elevated temperatures in chloride-containing solutions.[5] Materials such as Uranus 50 and AISI 316 showed some degree of intergranular cracking. The cracks in these specimens initiated in the transverse direction and then became partially intergranular in the longitudinal direction. This behavior implies either a stress dependency of the crystalline orientation due to cold work or a precipitation of a second phase along the grain boundaries in the longitudinal direction.

Mechanism of SCC in Room Temperature NACE Solutions

The uncoupled AISI 316, 18-18-2, SAF-2205, and Uranus 50 specimens failed in the room temperature NACE test; however, their times to failure were shorter than those observed when these same wireline materials were coupled to steel (Table 8). Since these materials are more noble than steel, coupling these alloys to steel polarizes them in the negative direction from their free corrosion potentials. Generally, this would favor hydrogen liberation on the wireline surface (cathode) and tend to promote HEC. However, in these four materials, the results did not indicate such a tendency, but rather indicated that the steel couple appeared to provide some degree of cathodic protection.

Constant potential tests were conducted in NACE solutions on these stressed materials to determine the effect of potential on their times to failure. The specimens were polarized at the desired potentials with a potentiostat. A calomel electrode connected through a salt bridge served as the reference. Results of these tests are shown in Table 9. A stressed 18-18-2 wireline specimen in the NACE solution failed in four hours at a potential 100 mV above the open potential and in 72 hours at 25 mV above the open potential; however, no failures were experienced at 225 mV below the open potential of this material in H_2S-containing, NaCl solutions. Tests on AISI 316, SAF-2205, and Uranus 50 specimens also showed the more noble the applied potential, the shorter the times to failure. Additionally, it was found that in the NACE solution, pitting occurred in these four materials at approximately 300 mV above their open potentials. Therefore, the pitting potentials are close to the open potentials of the materials, and these materials would have a tendency to pit in the NACE solution. These constant potential findings indicate that pitting initiation and chloride induced SCC are the failure mechanisms for 18-18-2, AISI 316, and the duplex stainless steel in the NACE solution. This agrees with other work[11] that showed duplex stainless steels failed by chloride-induced SCC rather than HEC in ambient temperature solutions containing both H_2S and chlorides.

Correlation Between Laboratory and Field Tests

The laboratory and field test results were in good agreement, as shown in Figure 5. There were indications, however, that the laboratory environment was slightly more severe than field conditions. For example, the 18-18-2 wirelines pitted in the 30 day field tests at 93 and 149 C, whereas in the laboratory environment at the same temperatures, these wireline materials failed in less than seven days. Furthermore, Sandvik 2RK65 did not fail in the 30 day field test at 149 C, but failed in less than seven days in the laboratory. With these exceptions, there was good agreement between the field and laboratory results.

There were differences between the field and laboratory test environments. The field gas used to saturate the field solution consisted of 11% H_2S and 40% CO_2; in addition, the field water had a higher chloride content (206,000 mg/L) than the laboratory solution (180,000 mg/L). The laboratory solution contained only sodium and chloride ions, whereas the field water contained sodium, calcium, magnesium, and chloride ions. In general, the susceptibility of austenitic stainless steels to chloride induced SCC increases as the chloride concentration of the test solution increases.[12] The effects of various metallic cations, such as Mg^{++}, Ca^{++}, and Na^{+}, on the SCC resistance of stainless steels have been investigated,[13] but no clear understanding was obtained of their influence. It was noted that more rapid cracking occurred in $MgCl_2$ vs $CaCl_2$ and $CaCl_2$ vs NaCl; however, it was thought this may have been caused by the difference in pH,[14] since increasing the pH will reduce the cathodic reaction rate. The pH of the field test solution was not measured after it was saturated with the field gas; the H_2S saturated laboratory solution had a pH of 3-3.5.

The following explanations are offered regarding why the lower chloride ion, metallic-cation-containing laboratory solution was more severe than the field environment:

1. The higher concentration of H_2S dissolved in the laboratory solution (contacted with 100% H_2S, while the field solution was contacted with 11% H_2S) had a greater effect on SCC than did the chloride concentration difference (11% lower in the laboratory environment).

2. The pH of the laboratory solution may have been lower.

3. A combination of 1 and 2.

Summary

1. The field and laboratory test results were in good agreement, with the laboratory test being slightly more severe.

2. In general, a wireline material must contain a minimum of 30% nickel to operate for extended periods of time in 93 C, H_2S + Cl-containing solutions. However, wirelines of the nickel base alloy Pyromet 31 were observed to have a 50% chance of failing in a 93 C sour environment.

3. Of the materials tested, only the stressed MP35N wirelines survived in the 204 C laboratory NaCl solution saturated with H_2S.

4. AISI 316, 18-18-2, Uranus 50, and SAF-2205 uncoupled wireline specimens had shorter times to failure in room temperature NACE solutions than those for the same wireline materials coupled to steel. Subsequent constant-potential tests indicated that chloride induced SCC was the failure mechanism for AISI 316, 18-18-2, and the duplex stainless steel wirelines in the NACE solution.

5. No wireline failures were observed in 204 C deionized water saturated with H_2S. Additionally, 18-18-2 was the only wireline specimen to fail in 204 C NaCl solutions containing no H_2S; however, all the wireline materials except MP35N failed in 204 C solutions containing H_2S and chlorides. Thus, it was concluded that the combination of H_2S and chlorides creates a synergistic effect to promote SCC, even though the chlorides may have a more pronounced effect.

6. Transgranular cracking was the predominant failure mode.

Acknowledgments

The authors thank A. R. Hagedorn, D. S. Foster, and S. K. Sangani for their technical assistance. They also acknowledge the other members of the research and administrative staff of Exxon Production Research Company for their support and guidance.

References

1. Copson, H. R. Physical Metallurgy of Stress Corrosion Fracture, Interscience, New York (1959).
2. Staehle, R. W. The Theory of Stress Corrosion Cracking in Alloys, edited by J. Scully, NATO, Brussels (1971).
3. Beck, W. et al., Met. Trans., Vol. 2, p. 883 (1971).
4. Uhlig, H. H., White, R. A. Trans. ASM, Vol. 52, p. 830 (1960).
5. Latanision, R. M., Staehle, R. W. Fundamental Aspects of Stress Corrosion Cracking, Ohio State Unviersity (1967).
6. Uhlig, H. H., Asphahani, A. I. Materials Performance, Vol. 18, No. 11, p. 9 (1979).
7. Uhlig, H. H. Trans. Am. Inst. Mining Met. Engrs., Vol. 158, p. 183 (1944).
8. Rhodin, T. N. Physical Metallurgy of Stress Corrosion Fracture, Interscience, New York (1959).
9. Flowers, J. W. et al., Corrosion, Vol. 19, p. 186t (1963).
10. Troiano, A. R., Hekermann, R. F. Materials Performance, Vol. 18, No. 1 (1979).
11. Herbsleb, G., Popperling, R. Corrosion Properties of Austenitic-ferritic Duplex Steel AF22 in Chloride and Sulfide Containing Environments. NACE Annual Conference 1980, Chicago, unpublished paper No. 13.
12. Warren, D. Proceedings of the Fifteenth Annual Industrial Work Conference, Purdue University (1960).
13. Berg, S., Henriksoh, S. Recent Advances in Stress Corrosion, Bulletin No. 25, Corrosion Committee, Royal Swedish Academy of Engineering Sciences, Stockholm, Vol. 63 (1961).
14. Thomas, K. C. et al., Corrosion, Vol. 20, p. 89t (1964).

Copyrighted Materials
Copyright © 1996 NACE International Retrieved from www.knovel.com

Section 6

OTHER ALLOYS

SPE
Society of Petroleum Engineers

SPE 18050

Corrosion and Stress-Corrosion Cracking of Aluminum Alloy Drillpipe in a Water-Base, Low-Solids, Non-Dispersed Drilling Mud

by S.W. Ciaraldi, D.R. Grimes, and H.F. Nichols, Amoco Corp., and S.O. Moore,* Amoco Production Co.

*SPE Member

Copyright 1988, Society of Petroleum Engineers

This paper was prepared for presentation at the 63rd Annual Technical Conference and Exhibition of the Society of Petroleum Engineers held in Houston, TX, October 2-5, 1988.

This paper was selected for presentation by an SPE Program Committee following review of information contained in an abstract submitted by the author(s). Contents of the paper, as presented, have not been reviewed by the Society of Petroleum Engineers and are subject to correction by the author(s). The material, as presented, does not necessarily reflect any position of the Society of Petroleum Engineers, its officers, or members. Papers presented at SPE meetings are subject to publication review by Editorial Committees of the Society of Petroleum Engineers. Permission to copy is restricted to an abstract of not more than 300 words. Illustrations may not be copied. The abstract should contain conspicuous acknowledgment of where and by whom the paper is presented. Write Publications Manager, SPE, P.O. Box 833836, Richardson, TX 75083-3836. Telex, 730989 SPEDAL.



ABSTRACT

Corrosion and stress-corrosion cracking (SCC) tests were performed on aluminum drill pipe alloy 2014-T6 in a water-base, low-solids, non-dispersed (LSND) drilling mud. Variables examined included chloride concentration, temperature, state of aeration, and effects of galvanic coupling to tool joint steel. Electrochemical corrosion test results suggested the aluminum alloy to have adequate corrosion resistance to at least 71°C (160°F), even when galvanically coupled to steel in aerated muds. However, SCC susceptibility of the alloy in aerated muds was clearly demonstrated by slow strain rate technique and Rising-K SCC tests. SCC did not occur in deaerated muds. It was concluded that oxygen scavenging and monitoring are essential to successful performance of aluminum alloy drill strings in chloride-containing, water-base, LSND drilling muds. These conclusions were subsequently confirmed by excellent field performance.

INTRODUCTION

A highly deviated well was recently drilled from a fixed offshore platform. A vertical section view plot of this well is shown in Figure 1. The well was kicked off at 427 m (1400 ft) and angle was built at a rate of 1.5 degrees per 30 m (100 ft) to an inclination of 58 degrees from vertical at 1615 m (5300 ft) measured depth (MD), 1416 m (4647 ft) true vertical depth (TVD). The inclination angle was held at 58 degrees to 1640 m (5380 ft) MD, 1429 m (4689 ft) TVD, where 340 mm (13 3/8 in) casing was set. Drilling continued below the 340 mm (13 3/8 in) casing shoe, holding the inclination angle between 57 and 60 degrees to 2830 m (9285 ft) MD, 2054 m (6739 ft) TVD, where 225 mm (9 5/8 in) casing was set.

References and illustrations at end of paper.

Courtesy SPE

As will be explained below, continued drilling of the well required that sections of the steel drill string be replaced with aluminum drill pipe. Thus at the 225 mm (9 5/8 in) casing point, approximately 1372 m (4500 ft) of 127 mm (5 in) aluminum drill pipe was substituted for the steel pipe previously used. The aluminum pipe was positioned immediately above the heavy weight drill pipe of the bottom hole assembly (BHA). The remainder of the drill string above the aluminum drill pipe to surface was 127 mm (5 in) steel drill pipe.

Drilling continued below the 225 mm (9 5/8 in) casing shoe with the combination aluminum/steel drill string, holding the inclination angle at about 59 degrees to 3155 m (10351 ft) MD, 2206 m (7236 ft) TVD. At this point, an additional 457 m (1500 ft) of steel drill pipe was removed from the drill string and replaced with 127 mm (5 in) aluminum drill pipe in the same manner as previously described. Drilling then continued at an inclination angle between 58 and 64 degrees to the final total depth (TD) of 4007 m (13145 ft) MD, 2635 m (8645 ft) TVD. The total departure at this final TD was 2642 m (8667 ft) from the surface location.

The aluminum pipe used in this project was Reynolds Aluminum drill pipe with internal-flush, Reed Alstan tool joints (1). Approximately 2286 m (7500 ft) of the aluminum drill pipe (250 joints) was obtained on a rental basis. Of these, 191 joints were new and 59 joints were used, but in premium condition. The seamless drill pipe was specified as alloy 2014-T6, with a minimum yield strength of 400 MPa (58 ksi). Outside diameter (OD) and internal diameter (ID) of the aluminum drill pipe was 131 mm (5.15 in) and 104 mm (4.10-in), respectively. Pipe body wall thickness was

13.3 mm (0.525 in) and the OD of the steel tool joints was 178 mm (7 in). Corrected weight of the aluminum drill pipe in air, including the tool joints, was 8.85 kg/m (13.2 lb/ft).

The reason aluminum drill pipe was required to drill the well was that experience in the area indicated formation friction factors would be high. Previously drilled wells had not exceeded 1830 m (6000 ft) in departure due to the rig rotary table torque limitation of 27,100 J (20,000 ft lbs) and excessive drag. Computer simulations of the well made prior to drilling also had indicated that high torque and drag levels would be encountered. The predicted levels were sufficiently high such that the rotary table torque limitation of the rig would be exceeded unless aluminum drill pipe was incorporated into the drill string. A combination aluminum/steel drill string was used rather than a full string of aluminum drill pipe due to the greater abrasion resistance of steel. Had a full string of aluminum been used, excessive pipe body wear may have occurred to joints positioned in the "build" portion of the well bore. Due to the well curvature, drill pipe in this region would probably have been in contact with the well bore walls or casing during drilling.

A chloride-containing, fresh-water, low-solids, non-dispersed (LSND) mud was used during drilling. As both corrosion and stress-corrosion cracking (SCC) of alloy 2014-T6 is possible in aqueous brines (2,3), a laboratory investigation of these potential problems was performed prior to drilling. Chemical composition, hardness and mechanical properties of the aluminum pipe were also determined. The following summarizes results of this study, and suggests corrosion control was vital to the subsequent excellent success of the drilling operations.

EXPERIMENTAL PROCEDURE

Electrochemical Corrosion Testing

Electrochemical testing was performed in order to rapidly determine which parameters had the greatest effect on corrosion behavior. These tests were performed in stirred, water-base drilling fluids with the chemical composition and physical properties listed in Table I. The fluid was modified to simulate different levels of chloride and aeration. Test temperature was either ambient or 71°C (160°F), the approximate maximum downhole temperature. Aeration was obtained by continuous air purging at ambient pressure. Deaeration was accomplished by continuous nitrogen purging and by periodically adding small doses of ammonium bisulfite oxygen scavenger.

Cylindrical specimens were machined from a section of drill pipe and an attached tool joint. The longitudinal axis of specimens was oriented parallel to the pipe axis. Following machining, specimens were polished through 600 grit using silicon carbide abrasive prior to testing. Specimens were then rinsed in distilled water and acetone. A brush-applied lacquer was used to mask the top and bottom faces of the cylindrical specimens to avoid end-grain effects. All electrochemical tests were performed in pyrex glassware using saturated calomel reference electrodes (SCE) and graphite counter electrodes. Potentials in this report are given in mV vs. SCE (saturated calomel electrode).

Two different electrochemical tests were performed, cyclic polarization and galvanic coupling. In the cyclic polarization test a controlled voltage (potential) is applied to the specimen and the resultant current is monitored. Controlling the potential effectively controls the driving force for corrosion. These tests were used to determine the ability of the aluminum to passivate and thereby resist corrosion in the drilling fluid.

The galvanic coupling test is slightly different from the cyclic polarization test in that two dissimilar metal specimens are placed in the cell. In this study, equal size cylinders of drill pipe aluminum and tool joint steel were used. Once again the current is monitored to determine the corrosion rate. However, the current between the specimens in this test is self-inducing due to galvanic differences. These corrosion tests were performed to semiquantitatively estimate corrosion rates due to the coupling of the aluminum to the steel. Two additional galvanic coupling tests were performed for 48 hours to determine the effect of the coupling on the potential of the aluminum pipe under equilibrium conditions. Potentials of the coupled specimens were compared to pit nucleation potentials determined in cyclic polarization tests.

Stress-Corrosion Cracking (SCC) Studies

SCC tests were performed using round tensile bars and sub-size, mini-compact tension (MCT) specimens in modified drilling fluids. The base fluid was modified to simulate different levels of chloride and oxygen contamination. Round tensile bars having 4.2 mm (0.165 in) diameters and 19 mm (0.75 in) gauge lengths were machined from blanks taken parallel to the pipe axis, Figure 2. MCT specimens were machined from blanks cut both parallel and perpendicular with respect to the pipe axis. These specimens were prepared according to ASTM E-399 (4) with a depth (W) of 25.4 mm (1.0 in) and a "straight-thru" notch. As exceptions to ASTM E-399, thickness (B) was 6.4 mm (0.25 in) and specimens were side-grooved 20 pct on both sides. A brush-applied lacquer was used to mask specimen grip regions and machine fixtures so that only the specimen gauge length (tensile bars) or the notch and side grooves (MCT specimens) were exposed to the drilling fluid during SCC testing. MCT specimens were insulated from the loading fixtures using non-metallic spacers. All SCC tests were performed in pyrex glassware. Electrochemical monitoring was obtained using saturated calomel reference electrodes.

SCC tests were performed using the slow strain rate technique (SSRT). The strain rate used for tensile bar specimens was 10^{-6} sec^{-1} (mm/mm-sec). MCT specimens were pulled at an elongation rate of 1.9×10^{-5} mm/sec (7.5×10^{-7} in/sec). The slow strain rate system used allowed the drilling fluid to be heated and specimens to be electrochemically monitored during the SCC evaluation.

Briefly, SSRT studies are performed by slowly increasing load on a specimen while simultaneously exposing it to a corrosive solution. The critical environment and dynamic strain generally allows rapid SCC assessment of metals. Degree of SCC susceptibility can be semi-quantitatively measured on tensile bars by comparing ultimate tensile strength, elongation (or time to failure), and the reduction-of-area in corrosive solutions to values obtained in an inert environment. Evidence of secondary cracking is also generally a positive indication of SCC.

SSRT testing using MCT specimens is generally referred to as a "Rising Stress-Intensity" or "Rising-K" test. ASTM Standard E-399 details calculation of the fracture mechanics stress-intensity (K) based on specimen geometry and applied load (4). As load slowly increases during SSRT testing, applied K likewise increases. In an inert environment, K increases until a critical K_c for rapid fracture is reached. Although much the same behavior occurs in a corrosive environment, sub-critical crack growth by SCC can occur prior to reaching K_c. If SCC occurs, load will increase at a decreased slope with respect to time, since the crack (or notch) length has increased. The point at which deviation from inert behavior is detected gives an approximate initiation load for SCC. From this load, an SCC threshold stress-intensity can be calculated.

Specimens were examined after testing for evidence of SCC. Some specimens were mounted for metallographic examination. Many fracture surfaces produced by SSRT testing were examined using a scanning electron microscope (SEM).

RESULTS

Results of chemical composition analyses of the aluminum alloy drill pipe are shown in Table II. Composition corresponded to alloy 2014, which is an age hardenable alloy based on the aluminum-copper system. Average mechanical properties from duplicate tests on 6.4 mm (0.25 in) diameter x 25.4 mm (1.0 in) gauge length tensile bars, obtained mid-wall parallel to the pipe axis, are shown in Table III. Properties were typical of the 2014 alloy as solution annealed, quenched and artificially aged (T6 temper).

Results of Rockwell A scale (HRA) hardness tests performed on ground ring samples obtained from the pipe body and box upset are shown in Table IV. Tests were performed through-wall in four equally spaced quadrants. Values reported represent averages of triplicate readings taken near the I.D., at mid-wall and near the O.D. As can be seen, hardness varied rather insignificantly, indicating effective quenching after solution annealing heat treatment.

Table V lists results of cyclic polarization, electrochemical corrosion tests. Current densities observed during these tests were low. Equilibrium potentials observed were well below the corresponding pit nucleation potentials. Aluminum specimens readily passivated with low critical currents during the anodic sweep of the cyclic polarization testing, indicating the ready formation of a protective surface film. Typical polarization results obtained are shown in Figure 3.

Cyclic polarization results were statistically analyzed. Of the three variables studied (oxygen concentration, temperature, and chloride concentration), temperature appeared to have contributed most significantly to the electrochemical behavior. Raising the temperature to 71°C (160°F) from ambient increased the equilibrium potential approximately 100 mV and the pit repassivation potential 125 mV. The critical current for passivation and the current in the passive region increased with increasing temperature. However, both current values remained low, indicating low corrosion rates. Aeration of the drilling fluid appeared to decrease the equilibrium potential approximately 70 mV, but did not affect other parameters. Increasing the chloride concentration from 3000 to 10,000 ppm apparently increased the equilibrium potential slightly (45 mV) and decreased the pit repassivation potential 75 mV.

Results of galvanic coupling tests are shown in Table VI. The low current densities observed in these tests would correspond to an aluminum corrosion rate of less than 0.025 mm/year (1 mil/year). Coupling shifted the potential of the aluminum in the positive direction, as expected, Table VII. However, the potential remained well below the pit nucleation potential as determined by cyclic polarization tests.

Table VIII lists results of SSRT-SCC tests performed using aluminum alloy tensile bar specimens. Note that only a very slight decrease in total elongation and no decrease in tensile strength were observed in deaerated drilling muds compared to results obtained in air. By contrast, a significant reduction in total elongation and slight decrease in tensile strength occurred in aerated muds, both at 21°C (70°F) and 71°C (160°F). Comparison of applied stress-elongation results for specimens tested in aerated and deaerated muds is shown in Figure 4.

As noted in Table VIII, specimens tested in aerated muds exhibited corrosion pits and associated secondary cracks along their gauge lengths. SEM appearance of this attack is shown in Figure 5. These characteristics were not observed for specimens tested in deaerated muds.

Overall SEM fractographic appearance of a tensile bar specimen tested in aerated mud is shown in Figure 6. Although the majority of the fracture surface exhibited ductile overload, some brittle appearing regions initiated by surface pits were evident. At high magnification, Figure 7, these brittle appearing areas exhibited an intergranular fracture mode appearance. Grain size was apparently quite fine, i.e., $5\text{-}8 \times 10^{-3}$ mm ($2\text{-}3 \times 10^{-4}$ in) in diameter.

Fine grain size was confirmed metallographically to be $5\text{-}10 \times 10^{-3}$ mm ($2\text{-}4 \times 10^{-4}$ in). These fine grains were contained within larger grains possibly originally produced during ingot solidification. This structure is termed a "fragmented" grain structure and is common to the 2014 alloy (5).

Results of Rising-K SCC tests performed using MCT specimens are shown in Table IX. Initial rapid fracture stress-intensity (K_c) in air was lower for cracking parallel to the pipe axis, as anticipated. Load-time behavior of MCT specimens in deaerated muds closely followed air curves, although K_c values showed slight reductions. No evidence of subcritical crack growth (SCC) was observed on resultant fracture surfaces. By contrast, curves for specimens tested in aerated muds significantly deviated from deaerated curves, as shown in Figure 7, possibly indicating SCC propagation prior to rapid fracture. Visual and SEM examination of resultant fracture surfaces indicated that subcritical crack growth by SCC had indeed occurred and had propagated 3.2-6.4 mm (0.12-0.25 in) prior to initial overload. Because of this sub-critical crack growth, load increase was less rapid to reach K_c, actually increasing failure time. Based on curve deviation loads, K_{SCC} values of 11.3 and 15.6 MPa$\cdot\sqrt{m}$ (10.3 and 14.2 ksi$\cdot\sqrt{in}$) were calculated for transverse and longitudinal MCT specimens, respectively. Note, however, that specimens lacked sufficient thickness to meet ASTM plane strain requirements (4), so that both lower K_{SCC} and K_c values

would be expected as the alloy's inherent materials properties (independent of geometry).

DISCUSSION

The aluminum alloy drill pipe evaluated conformed well to the properties of the 2014-T6 alloy. Further, hardness uniformity indicated good heat treatment practice.

Cyclic polarization tests suggested that corrosion of aluminum alloy drill pipe should not be a problem in LSND, water base drilling muds, up to at least 71°C (160°F), as evidenced by low corrosion currents, high pitting potentials, and ready passivation. This was true even at chloride levels of 10,000 ppm in aerated fluids. Galvanic coupling to steel, although anodically polarizing the aluminum, did not produce a sufficient effect to significantly affect corrosion resistance. Interestingly, the galvanic attack observed on some of the actual, used drill pipe joints probably resulted due to upset conditions. Although official details were unknown, it was suspected that the drill pipe was allowed to remain downhole in stagnant fluids for an extended period of time following a failure in a previously drilled well.

Susceptibility of the aluminum drill pipe to SCC in aerated drilling fluids was clearly demonstrated by tensile bar SSRT and MCT Rising-K tests. SCC initiated from corrosion pits, which were possibly strain induced, and propagated intergranularly, which is common for SCC in high-strength aluminum alloys (6). Similar reductions in elongation were observed at both 21° and 71°C (70° and 160°F), although tensile strength showed greater reduction at the higher temperature. This greater reduction was, however, probably more due to temperature-plasticity effects rather than to enhanced SCC. Aluminum alloys generally exhibit maximum SCC susceptibility at or below room temperature, which is typical of the hydrogen embrittlement mechanism believed to be responsible for SCC (7,8).

Deaeration of drilling muds by oxygen scavenging and nitrogen purging restored the aluminum alloy's SSRT and Rising-K behavior almost completely to that obtained in air. No pitting or evidence of SCC was observed for such specimens. These results indicate that oxygen scavenging is critical for avoiding SCC of aluminum drill pipe in water-base LSND muds.

As mentioned previously, MCT specimens lacked sufficient thickness for plane strain conditions (4). As confirmation, lower plane strain fracture toughness (K_{IC}) values are reported in the literature (9) compared to the K_c values obtained in this study. Therefore, K_c and K_{SCC} results obtained should be considered qualitatively. Also, although numeric values were close, K_{SCC} results obtained in this study indicated somewhat increased susceptibility to SCC transverse to the pipe axis, which is contrary to literature reports (10). However, MCT Rising-K test procedures were not fully established at the time of testing and are still in the process of being more quantitatively developed.

During actual drilling, oxygen scavenger additions were regularly made to the drilling mud and residual scavenger concentrations were monitored. Torque levels experienced were approximately 30 to 50 pct lower than expected. However, actual drag was about three times the forecast value. Steerable directional drilling assemblies were used for initial drilling, but at 2743 m (8998 ft) MD, 1971 m (6467 ft) TVD, drag had increased to the point that further drilling in the sliding mode was impossible. Therefore, from 2743 m (8998 ft) MD to 2830 m (9285 ft) MD at the 225 mm (9 5/8 in) casing point, a rotary BHA was used. After incorporating aluminum pipe into the drill string, torque and drag were reduced to acceptable levels due to the lighter weight of the aluminum, and drilling to TD proceeded without fruther problems. The final TD was reached on the 50th day from spud.

No aluminum drill pipe failures were encountered during the nearly two week use of the combination steel/aluminum drill string. No evidence of aluminum drill pipe deterioration by corrosion or cracking was observed following drilling.

CONCLUSIONS

1. Electrochemical studies suggested corrosion of aluminum alloy drill pipe in stirred LSND, water-base muds to 71°C (160°F) was not a potential problem, even in aerated fluids. Galvanic coupling to steel tool joints did not modify this conclusion.

2. The 2014-T6 aluminum alloy drill pipe was susceptible to stress-corrosion cracking (SCC) in aerated muds. SCC did not occur when muds were nitrogen purged and oxygen scavenged.

3. Effective oxygen scavenging and monitoring are essential to successful performance of aluminum alloy drill pipe in chloride-containing, water-base, LSND drilling muds.

4. A steel/aluminum drill string was used for drilling a highly deviated offshore well with corrosion control guidelines developed from this study. Excellent success was obtained and the drilling was completed ahead of schedule, with significant associated cost savings.

5. Due to the high formation friction factors in the area, it probably would have been impossible to have drilled the well without using aluminum drill pipe.

ACKNOWLEDGEMENTS

The authors would like to acknowledge A. D. Beckett for his work in analyzing the feasibility of the drilling operation and for developing the fundamental plan for using aluminum drill pipe. Thanks are also owed to D. B. Assell, M. Horvat, and S. M. Polomchak for their valuable contributions to the laboratory investiations.

REFERENCES

1. Reynolds Metals Co., "Reynolds Aluminum Drill Pipe", Engineering Data, Edition No. 8, Richmond, VA, 1982, 33 pp.

2. Amer. Soc. for Metals, Metals Handbook Desk Edition, Amer. Soc. for Metals, Metals Park, OH, November 1984, p. 6-69.

3. Canzolino, F., Private Communications to S. W. Ciaraldi, Sikorsky Aircraft Co., New Haven, CT, February 1987.

4. Amer. Soc. for Testing and Matls. (ASTM), "Standard Method of Test for Plane-Strain Fracture Toughness of Metallic Materials", E-399-74, 1974, p. 561.

5. Amer. Soc. for Metals, Metals Handbook, 8th Ed., Vol. 7, Amer. Soc. for Metals, Metals Park, OH, August 1972, p. 245.

6. Gruhl, W. and D. Brungs, Metall., Vol. 23, 1969, p. 1020.

7. Gest, R. J. and A. R. Troiano, Corrosion, Vol. 30, No. 3, March 1974, p. 274.

8. Ciaraldi, S. W., J. L. Nelson, R. A. Yeske and E. N. Pugh, Hydrogen Effects in Metals, American Institute of Mining, Metallurgical and Petroleum Engineers, Inc., New York, NY, 1981, p. 437.

9. Ibid Ref. 1, p. 6-47.

10. Ibid Ref. 1, p. 6-69.

TABLE I

Composition and Properties of Drilling Mud Used for Corrosion and SCC Tests

Composition

Constituent	Amount (kg/m^3)	(lb/bbl)
Bentonite	71	25
Caustic	0.3	0.1
Polymeric Dispersant Deflocculant	0.06	0.02
Polyanionic Cellulose (fluid loss control)	0.71	0.25
Heat-Stable Synthetic Resin (fluid loss control)	2.8	1
Emulsifier	0.11	0.04
Gilsonite	17.1	6
Barite	85.6	30
Biocide	0.14	0.05

Properties

Density	110 kg/m^3 (9.25 lb/gal)
Plastic Viscosity	0.02 Pa•s (20 Cp)
Yield Point	0.8 kg/m^2 (16 lb/100 ft sq)
Gel Strength	0.3/0.9 kg/m^2 (6/18 lb/100 ft sq)
Filtrate (30 min)	7200 mm^3
pH	9.2
Methylene Blue Capacity	5.2
Calcium	80 ppm
Chlorides	3000 to 10,000 ppm

TABLE II

Chemical Composition of 2014-T6 Aluminum Alloy Drill Pipe

	Weight Pct
Aluminum	93.10
Copper	4.05
Silicon	0.97
Manganese	0.80
Magnesium	0.64
Zinc	0.09
Chromium	0.02
Iron	0.21
Titanium	0.01
Others (each)	<0.05
Others (total)	<0.15

TABLE III

Average Mechanical Properties of 2014-T6 Aluminum Alloy Drill Pipe

Yield strength - 486.1 MPa (70.5 ksi)

Tensile strength - 519.2 MPa (75.3 ksi)

Elongation - 11.5 pct

Reduction of area - 23.8 pct

TABLE IV

Results of Rockwell A (HRA) Hardness Tests on 2014-T6 Aluminum Alloy Drill Pipe

1. Pipe Body	Average Hardness (HRA)			
	Quadrant			
Location	0°	90°	180°	270°
ID	50.0	50.3	49.6	49.0
Mid-wall	50.6	51.0	50.6	51.0
OD	51.0	50.6	50.6	50.6

2. Box Upset	Average Hardness (HRA)			
	Quadrant			
Location	0°	90°	180°	270°
ID	50.6	50.3	51.0	50.6
Mid-wall	52.0	52.0	51.6	52.0
OD	52.0	52.0	52.0	52.0

TABLE V

Cyclic Polarization Electrochemical Test Results

Test No.	Temperature (°C)	(°F)	Chloride (ppm)	State of Aeration	E_θ (mV)	E_{pp} (mV)	I_c (mA)	I_R (mA)	E_{pp} (mV)	E_{rp} (mV)
1	21	70	3000	Aerated	-1205	-1060	.0048	.0034	-570	-840
2	71	160	3000	Deaerated	-1034	- 895	.0170	.0160	-570	-700
3	21	70	10000	Deaerated	-1090	-1020	.0022	.0022	-590	-900
4	71	160	10000	Aerated	-1060	- 880	.0120	.0120	-650	-790

TABLE VI

Results of Electrochemical Galvanic Coupling Tests

Test No.	Temperature (°C)	(°F)	Chloride (ppm)	Sate of Aeration	Imax (mV)	Ifinal (mA)
1	21	70	3000	Aerated	-0.0005	-0.0008
2	71	160	3000	Deaerated	-0.0001	-0.0003
3	21	70	10000	Aerated	-0.0004	-0.0008
4	71	160	10000	Deaerated	-0.0032	-0.0005

TABLE VII

Steady State Potential (E_o) of Aluminum Alloy Coupled to Steel Tool Joint

Temperature (°C)	(°F)	Chloride (ppm)	State of Aeration	Potential (mV)
21	70	3000	Aerated	-872
21	70	10000	Aerated	-772

TABLE VIII

Results of SSRT Tests Using Aluminum Alloy Tensile Bar Specimens

Test No.	Temperature (°C)	(°F)	Chloride (ppm)	State of Aeration	Potential	Tensile Strength (MPa)	(ksi)	Total Elongation (in)	Comments
1	21	70	----Tested in		Air ---	483	70	14.8	Air standard
2	21	70	3000	Deaerated	Coupled	483	70	14.1	--
3	21	70	10000	Deaerated	Open Circuit	490	71	14.0	--
4	21	70	10000	Aerated	Open Circuit	476	69	12.6	Corrosion pits and secondary cracks
5	71	160	10000	Aerated	Open Circuit	455	66	12.6	Corrosion pits and secondary cracks

TABLE IX

Results of Ambient Temperature Rising-K SCC Tests Using Aluminum Alloy MCT Specimen

Test No.	Chloride (ppm)	Specimen Orientation	State of Aeration	SCC?	K_{SCC} [1] (MPa$\sqrt{m}$)	Rapid Fracture Load [2] (kg)	K_Q (MPa$\sqrt{m}$)
6	N/A	T[3]	Tested in Air		--	884	57.0
7	N/A	L[4]	Tested in Air		--	644	41.5
8	10000	T	Deaerated	No	--	816	52.6
9	10000	T	Aerated	Yes	11.2	--	--
10	10000	L	Deaerated	No	--	544	35.1
11	10000	L	Aerated	Yes	15.5	--	--

(1) To obtain values in ksi$\sqrt{in}$, multiply by 0.92.
(2) To obtain values in lbs., multiply by 2.2.
(3) Cracking transverse to pipe axis.
(4) Cracking parallel (longitudinal) to pipe axis.

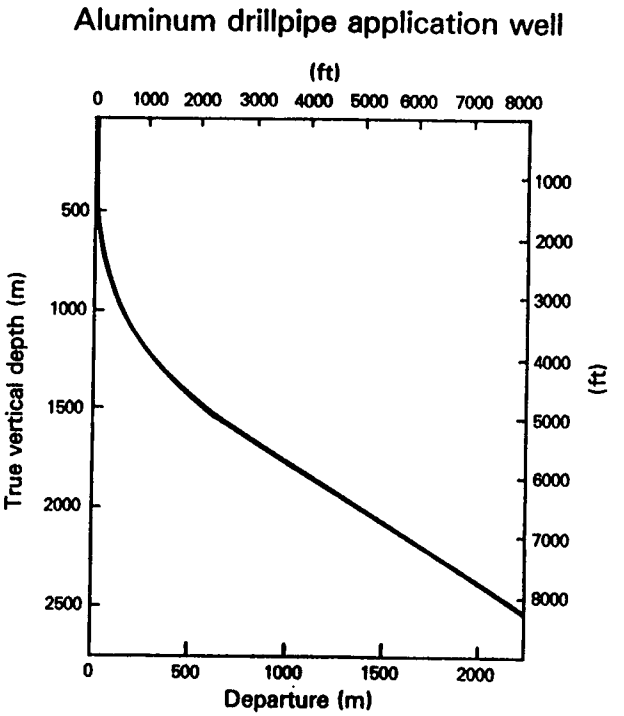


Fig. 1—Vertical section view of highly deviated offshore well drilled using aluminum drillpipe.

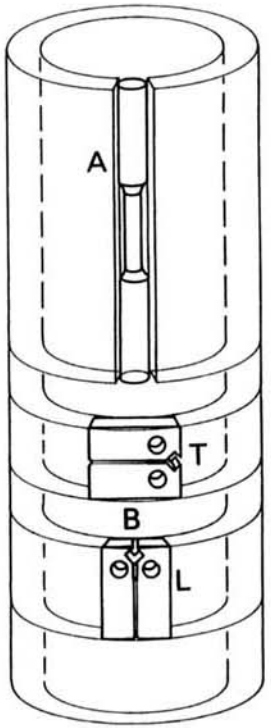


Fig. 2—Tensile bar (A) and MCT (B) specimen orientations used for stress-corrosion cracking tests (L—longitudinal and T—transverse).

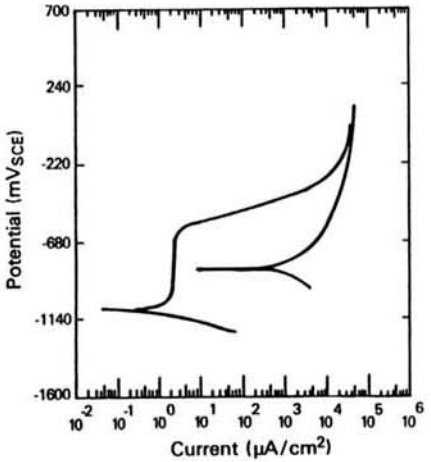


Fig. 3—Typical cyclic polarization test results, aluminum alloy in drilling fluid.

SCC of Aluminum drill pipe
Type 2014—T6 Aluminum in drilling fluid

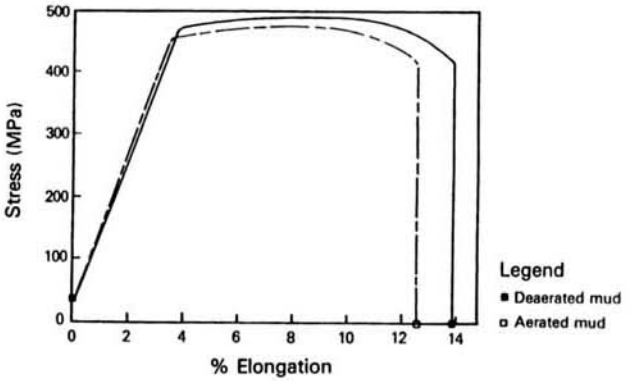


Fig. 4—Aluminum alloy tensile bar SSRT behavior in aerated and deaerated muds at ambient temperature. Note reduced elongation and tensile strength in aerated mud.

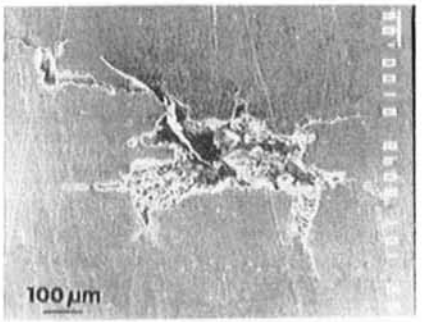


Fig. 5—SEM appearance of tensile bar specimen gauge length showing corrosion pit and secondary cracks from SSRT testing in aerated mud.

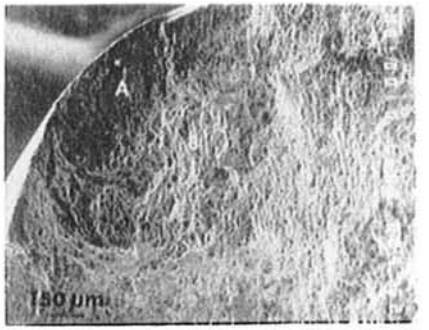


Fig. 6—SEM fractograph of tensile bar specimen SSRT tested in aerated mud. Regions of SCC (A) and ductile overload (B) are indicated.

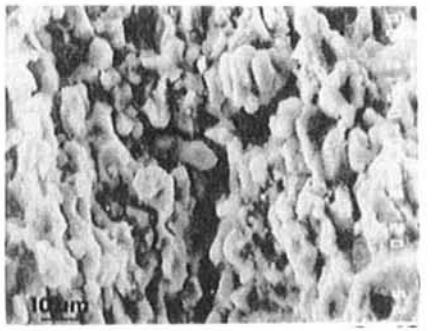


Fig. 7—Intergranular SCC from Region A, Fig. 6. Microcrystalline grains are indicative of a fragmented grain structure common to the 2014 alloy (5).

SCC of Aluminum drill pipe
Type 2014—T6 Aluminum in drilling fluid

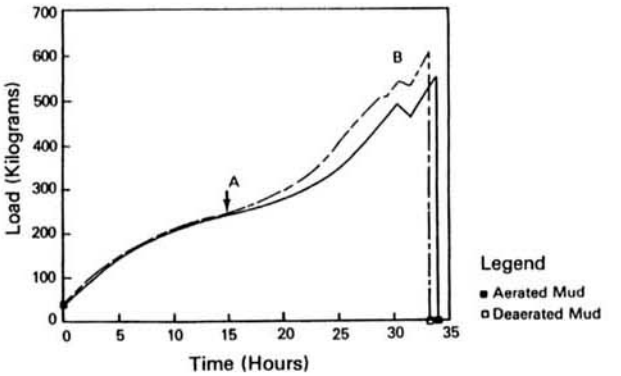


Fig. 8—Rising-K SSRT behavior in aerated and deaerated drilling muds. SCC initiated in aerated mud at curve deviation point (A). Sharp peaks (B) indicate overload.

Copyrighted Materials
Copyright © 1996 NACE International Retrieved from www.knovel.com

54

CORROSION 95

The NACE International Annual Conference and Corrosion Show

YELLOW METAL (UNS C69100) FOR SOUR SERVICE

T. Clark and W. Inglis
Tungum Hydraulics Ltd.,
The White House, Arle,
CHELTENHAM, Glos. GL51 0AD, United Kingdom

C.M. Fowler
CAPCIS Ltd.,
Bainbridge House, Granby Row,
MANCHESTER. M1 2PW, United Kingdom

ABSTRACT

UNS C69100, a 'yellow metal', copper-based alloy, is used extensively in the European Oil and Gas industry. The work reported herein was designed to assess the susceptibility of the material to sour environments, in terms of general corrosion and cracking.

A series of sour environmental tests was conducted at ambient temperature and at elevated temperature and pressure. The ambient temperature tests indicated high resistance to sulphide stress corrosion cracking (SSCC). Additionally, tests including free sulphur exhibited no evidence of cracking. The high temperature and pressure tests also showed no tendency to SSCC.

The corrosion rate tests at ambient temperature indicated corrosion rates well below those of carbon steel tested in an identical environment. Hydrogen permeation measurements confirmed the corrosion rate measurements.

This alloy should be considered for sour service use. Further work will be undertaken to confirm the high temperature properties.

Keywords: Sour service, SSCC, UNS C69100, Hydrogen Sulphide, Hydrogen Permeation.

INTRODUCTION

UNS C69100 is an aluminium-nickel-silicon-brass alloy, generally classed as a copper-based alloy under Section 4.3.1.2 of NACE MR0175 [1]. This material is used extensively in marine and industrial applications and is currently enjoying an ever-increasing penetration into the 'offshore oil platform' sector. Initially, used in the U.K.'s aircraft industry, user experience quickly confirmed its ideal suitability for naval marine and military fighting vehicle use where its excellent resistance to marine corrosion and shock/vibration were highly attractive. Commercial marine and industrial applications, including cryogenic systems were added to its uses. From the outset of the U.K.'s offshore oil industry, the inherent safety of the alloy made it the 'industry standard' tubing for dive systems and, more recently, because of an increasing recognition of the shortcomings of stainless steels, UNS C69100 is penetrating the integral instrumentation tubing market on offshore installations. The alloy has exceptional corrosion resistance in a range of environments. Its mechanical properties are given in Table 1. The chemical composition and other important properties are presented in Tables 2 and 3.

Although the material is included in NACE MR0175, no documented cases of its use in sour service have been found. It is the purpose of this paper to describe the material and present sour service test data to support its use in H_2S environments. Some corrosion rate and hydrogen permeation data are also reported. Further work is ongoing to obtain high temperature corrosion data which will further support the use of this material in sour service environments.

GENERAL MATERIAL PROPERTIES

UNS C69100 is an unusual copper-based alloy in that the heat treatment includes precipitate hardening which enables a wide range of strength levels to be made available. The alloy also has a high strength to weight ratio which can afford considerable savings when compared to alternative materials. In addition, the material is spark-proof, possesses exceptional resistance to shock and vibration-induced fatigue, has a very, very low magnetic signature and offers an excellent cryogenic performance (typically its elongation increased by 70% as the material cools from +15 to -198° Celsius). Appendix A details usage and benefits of UNS C69100.

SSCC RESISTANCE AT AMBIENT TEMPERATURE

The determination of SSCC resistance was initially demonstrated by testing in NACE TM0177 [2] solution using an internally loaded C-ring specimen. This configuration was selected such that the internal surface of the tube was the 'test surface'. As such, the influence of any areas of damage caused by the manufacturing process could be assessed. (It has been noted, for instance, that Pilger marks, can be sites for initiation of SSCC in some corrosion resistant alloys (CRAs).

Two different test conditions were used:

a. The standard NACE TM0177 solution
b. A modified NACE TM0177 solution containing elemental sulphur.

The test matrix is reproduced as Table 4.

HYDROGEN PERMEATION AND CORROSION RATE MEASUREMENT

The overall corrosion rate and hydrogen permeation properties were studied using a combined test cell. For comparison purposes, a second cell was also run using carbon steel samples machined from a typical API 5L linepipe steel.

For the purposes of this test, an environment more typical of North Sea field conditions was selected, i.e. 5% NaCl, 0.5% acetic acid, 94.5% distilled water, saturated with H_2S/CO_2 gas mixture of 3.5% H_2S and 6.5% CO_2, balance N_2. The temperature was controlled at 25°C ± 1°C and test duration was 14 days.

EXPERIMENTAL

The test cell is illustrated in Figure 1. Each cell had two 3mm plates of material clamped to 'ports' and electrochemical hydrogen permeation cells were attached. This test configuration allows duplicate samples to be tested. The cell contained the test solution. Additionally; 'finger type' corrosion coupons were inserted through the top of the cell and these were monitored for corrosion rates using linear polarisation and electrochemical noise described below, and weight loss measurements. The chemical composition of the linepipe steel is given in Table 5.

All metal samples were cleaned, polished and degreased and the finger-type electrode samples weighed prior to insertion in the test cell. The 3mm thin plate samples used for the hydrogen permeation studies were plated with palladium on the hydrogen collection (the permeation cell) side prior to connection to the test cell.

After filling the hydrogen permeation cell with electrolyte and connection to the corrosion test cells, the cells were purged with high purity nitrogen to remove air/oxygen. This was followed by the introduction of pre-saturated test solution which was continuously sparged with the gas mixture for the duration of the test.

Hydrogen permeation was measured using an electrolytic cell containing 1M NaOH which is polarised to 300 mV with respect to a reference electrode.

The internal C-rings were loaded using strain gauges to monitor the strain. 'T' gauges were applied such that compensation for the Poisson's Effect could be made.

RESULTS

Weight Loss Measurements

The weight loss measurements and calculated corrosion rates obtained from the finger-type samples are presented in Table 6.

The mean corrosion rate during the test was estimated from weight loss measurements and the results show that the corrosion rate of UNS C69100 was some **3 times lower** than that of carbon steel as indicated by weight loss data.

Corrosion Monitoring

A range of corrosion monitoring techniques were applied during the test in order to compare the corrosion behaviour of the UNS C69100 alloy and carbon steel samples. These included corrosion potential, linear polarisation, electrochemical impedance and electrochemical noise.

Electrochemical monitoring indicated that the corrosion potential of UNS C69100 stabilised quite rapidly at -550 to -580 mV vs. SCE (saturated calomel electrode) (Figure 2). The potential of the carbon steel was more erratic but was in a similar range (-570 to -600 mV) than that of the UNS C69100 alloy in this environment.

Polarisation resistance vs. time for each material is shown in Figure 3. The polarisation resistance is inversely proportional to the corrosion rate. The corrosion current (i_{corr}) can be calculated from the polarisation resistance (R_p) using the following equation:

$$i_{corr} = \frac{B}{R_p}$$

Where B = constant.

From the literature, a B constant value of 20 mV can be assumed for UNS C69100 alloy, i.e. the same as that for carbon steel.

Approximate corrosion rates have therefore been calculated from linear polarisation resistance data and the change in corrosion rate with time is given in Figure 4.

This graph shows that immediately after the introduction of H_2S (after ~48 hours) the corrosion rates of UNS C69100 alloy and carbon steel were similar at approximately 0.4 mm/yr. The corrosion rate of carbon steel remained reasonably constant for the remainder of the test.

The corrosion rate of UNS C69100 alloy fell rapidly to a mean value of **approximately 0.06 mm/yr some 60 hours** after the introduction of H_2S. This suggests that protective film formation occurred. Although weight loss data indicated a 3X difference between the average corrosion rates of UNS C69100 and carbon steel taken over the full duration of the test, the corrosion rate vs. time data show that when rates had stabilised the corrosion rate of UNS C69100 alloy **was at least six times lower** than that of carbon steel. Similar trends in corrosion rate with time were indicated by electrochemical impedance measurements.

Electrochemical noise data (Figures 5 and 6) also indicate significantly less corrosion activity on the UNS C69100 alloy compared with carbon steel with current noise values on UNS C69100 alloy some 2 orders of magnitude lower than on carbon steel. The resistance noise values did not correlate with polarisation resistance data obtained from linear polarisation and electrochemical impedance..

HYDROGEN PERMEATION RESULTS

Hydrogen permeation measurements on both UNS C69100 alloy and carbon steel were obtained.

The hydrogen permeation transients are presented in Figure 7. The carbon steel exhibited a gradual increase in hydrogen permeation until a value of 13 $\mu A/cm^2$ was reached. Hydrogen permeation on the UNS C69100 alloy was not measurable.

HIGH TEMPERATURE SULPHIDE STRESS CORROSION AND CREVICE PROPERTIES

In addition to the ambient temperature investigation, some of the high temperature properties of UNS C69100 alloy have been studied. These properties are particularly important if the material is to be considered for use in the North Sea where the operating temperatures are increasing. Currently, duplex stainless steel, which has limited H_2S tolerance, is often used in these environments. The test conditions were selected to duplicate NACE TM0177 test solution conditions at 90°C. To achieve this, an autoclave was used with 16 bar of H_2S pressure.

Six internally loaded C-rings, two each loaded at 80%, 90% and 100% of specified minimum yield strength (SMYS). In addition six crevice coupons were included in the autoclave. The test duration was 30 days.

The results of these tests are summarised in Table 7. None of the samples exhibited any form of cracking and, in addition, none of the crevice corrosion test coupons exhibited crevicing greater than 0.01 mm. General corrosion was noted on all samples and a scale build up was evident.

DISCUSSION

UNS C69100 alloy has been tested for SSCC resistance, corrosion rate determination and hydrogen permeation flux at ambient temperature. In addition, high temperature SSCC performance and crevice corrosion properties have been assessed.

The alloy has been shown to be immune to sulphide stress corrosion cracking at stress levels as high as 100% SMYS were tested. The measured corrosion rates were found to be 3 to 6 times lower than those of a standard carbon steel. The good performance of the alloy was further substantiated by almost zero hydrogen permeation flux measurements.

CONCLUSIONS

1. UNS C69100 alloy shows high resistance to SSCC at both ambient and high temperatures.

2. The corrosion rate of UNS C69100 alloy has been shown to be considerably lower than that of linepipe carbon steel at ambient temperature.

3. The crevice corrosion susceptibility of UNS C69100 alloy was determined to be very low.

4. The material was shown to be resistant to sour conditions and should be considered for use in such environments in all but the highest strength applications.

FURTHER WORK

The high temperature corrosion rates are to be determined in typical field environments.

REFERENCES

1. NACE Standard MR0175, National Association of Corrosion Engineers, Houston, U.S.A.

2. NACE Standard TM0177, National Association of Corrosion Engineers, Houston, U.S.A.

3. Naval Engineering Standard 749, Requirements for Aluminium-Nickel-Silicon-Brass, Part 3, Issue 2, Tubes, Ministry of Defence, Foxhill, Bath.

4. Specification TCL 100 for Tungum Alloy Tubing, Tungum Hydraulics Ltd., Arle, Cheltenham, U.K.

5. Specification DTD 5019, Aircraft Material Specification, Aluminium-Nickel-Silicon-Brass Tubes (suitable for pipelines and high pressure hydraulic systems especially where flaring is required), Ministry of Aviation, HMSO, 1964.

TABLE 1
MECHANICAL PROPERTIES OF ALLOY UNS C69100

SPECIFIC GRAVITY WEIGHT		 Kg/mm^3 lb. per cu. in.	8.60 8.52×10^{-6} 0.308
ULTIMATE TENSILE STRENGTH:	Mean value Min. value for NES.749 PT.3 [3] Min. value for TCL 100 [4] Min . value for DTD 5019 [5]	N/mm^2 Tons per sq. in. N/mm^2 Tons per sq. in. N/mm^2 Tons per sq. in. N/mm^2 Tons per sq. in.	480 31.07 450 29.13 430 27.84 4.17 27.00
0.2% PROOF STRENGTH	Mean value Min. value for NES.749 PT. 3 [3] Min. value for DTD 5019 [5]	N/mm^2 Tons per sq. in. N/mm^2 Tons per sq. in. N/mm^2 Tons per sq. in.	240 15.54 230 14.89 216 14.00
ELONGATION	Mean value Min. value for NES.740 PT. 3 and DTD 5019 [5]	% on 5.65 $\sqrt{A}$ % on 5.65 $\sqrt{A}$	45 40
HARDNESS	Range for TCL 100 [4] Range for NES.749 PT. 3 [3]	HV5 HV5	120-140 125-140
MODULUS OF ELASTICITY	In tension or compression In torsion or shear	N/mm^2 lb. per sq. in. N/mm^2 lb. per sq. in.	116.5×10^3 16.9×10^6 43.8×10^3 6.35×10^6
POISSONS RATIO			0.33
ULTIMATE SHEAR STRENGTH		N/mm^2 Tons per sq. in.	253 16.4
YIELD POINT IN SHEAR		N/mm^2 Tons per sq. in.	143 9.3
IZOD IMPACT VALUE		J	41.7

TABLE 2
ELECTRICAL PROPERTIES OF ALLOY UNS C69100

ELECTRICAL CONDUCTIVITY AT 20°C	Referred to copper	15% ± 5%
SPECIFIC RESISTANCE AT 20°C	Microhms per mm	1.13
ELECTROCHEMICAL EQUIVALENT	Kg per coulomb	32.4
SOLUTION POTENTIAL	mV calomel scale	230
MAGNETIC PERMEABILITY	μ	1.0015
THERMAL PROPERTIES OF ALLOY UNS C69100		
MELTING TEMPERATURE	°C	1008
STRESS RELIEVING TEMPERATURE	°C (for 15/20 minutes)	300
SOLUTION TREATMENT TEMPERATURE	°C (for 60 minutes)	800
THERMAL CONDUCTIVITY	W/m°C	77 at 100°C 103 at 300°C
TEMPERATURE COEFFICIENT	per °C	0.000748

TABLE 3
CHEMICAL COMPOSITION

ELEMENT	%
Copper	81.00 - 86.00
Aluminium	0.70 - 1.20
Nickel	0.80 - 1.40
Silicon	0.80 - 1.30
Iron	0.25 max.
Lead	0.05 max.
Tin	0.10 max.
Manganese	0.10 max.
Total Other Impurities	0.50 max.
Zinc*	Balance

The material is non-dezincifiable in both fresh and seawater, even when the zinc content is at its maximum possible level of 16.7%.

TABLE 4
SUMMARY OF INTERNALLY LOADED, C-RING, SSCC TESTS ON ALLOY UNS C69100 IN NACE TM0177 SOLUTION AT AMBIENT TEMPERATURE

SAMPLE NO.	STRESS LEVEL (% SMYS)	TEST SOLUTION	RESULTS
1	80	NACE TM0177	NO FAILURE
2	80	NACE TM0177	NO FAILURE
3	90	NACE TM0177	NO FAILURE
4	90	NACE TM0177	NO FAILURE
5	90	NACE TM0177 PLUS FREE SULPHUR	NO FAILURE
6	90	NACE TM0177 PLUS FREE SULPHUR	NO FAILURE

TABLE 5
CHEMICAL COMPOSITION OF CARBON STEEL LINEPIPE MATERIAL API 5L GRADE X65

ELEMENT	%
Carbon	0.045
Silicon	0.28
Manganese	1.38
Phosphorus	0.011
Sulphur	<0.003
Chromium	0.04
Molybdenum	0.01
Nickel	0.03
Aluminium	0.039
Copper	0.02
Vanadium	0.06
Calcium	<0.001
Niobium	0.041
Titanium	<0.005

TABLE 6
WEIGHT LOSS AND CORROSION RATES OBTAINED FROM FINGER SAMPLES

Sample	Material	Initial Weight (gms)	Final Weight (gms)	Weight Loss (gms)	Corrosion Rate (mm/yr)
1	UNS C69100	4.2529	4.2311	0.0218	0.12
2	UNS C69100	4.2135	4.1992	0.0143	0.07
3	C Steel	3.6120	3.5557	0.0563	0.31
4	C Steel	3.7430	3.6872	0.0558	0.31

TABLE 7
RESULTS OF SSCC TESTS

SAMPLE NO.	STRESS LEVEL % SMYS	SSCC RESULTS
H1	80	No failure
H2	90	No failure
H3	90	No failure
H4	90	No failure
H5	100	No failure
H6	100	No failure

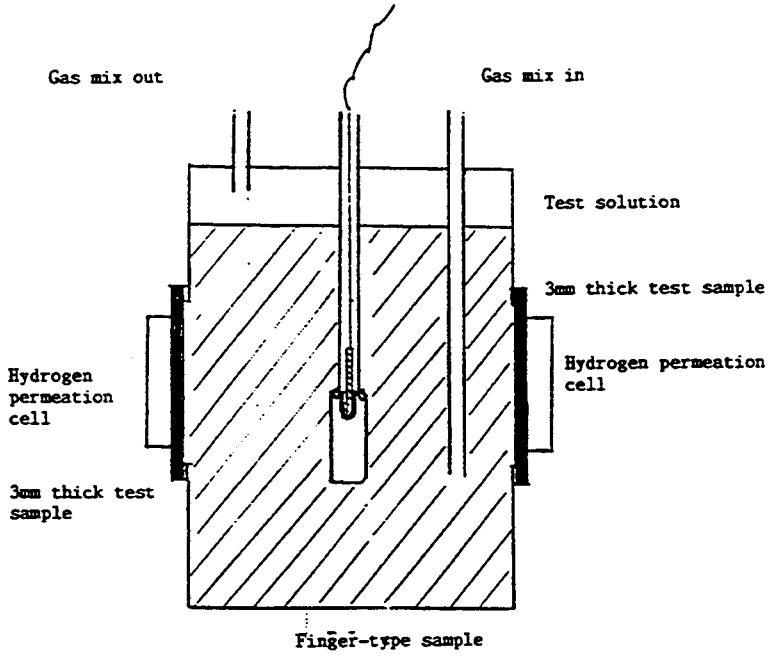


FIGURE 1. Hydrogen permeation and corrosion rate measurement cell.

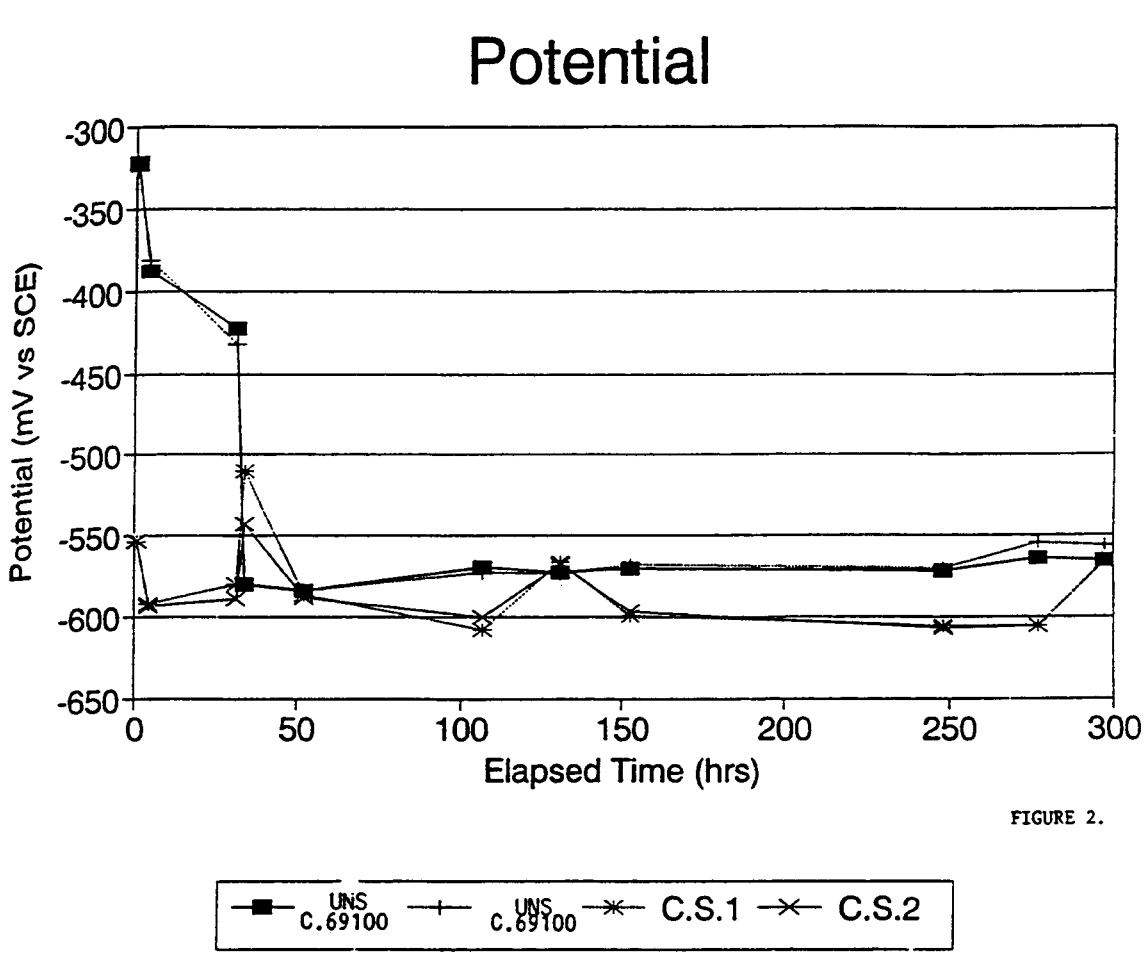


FIGURE 2.

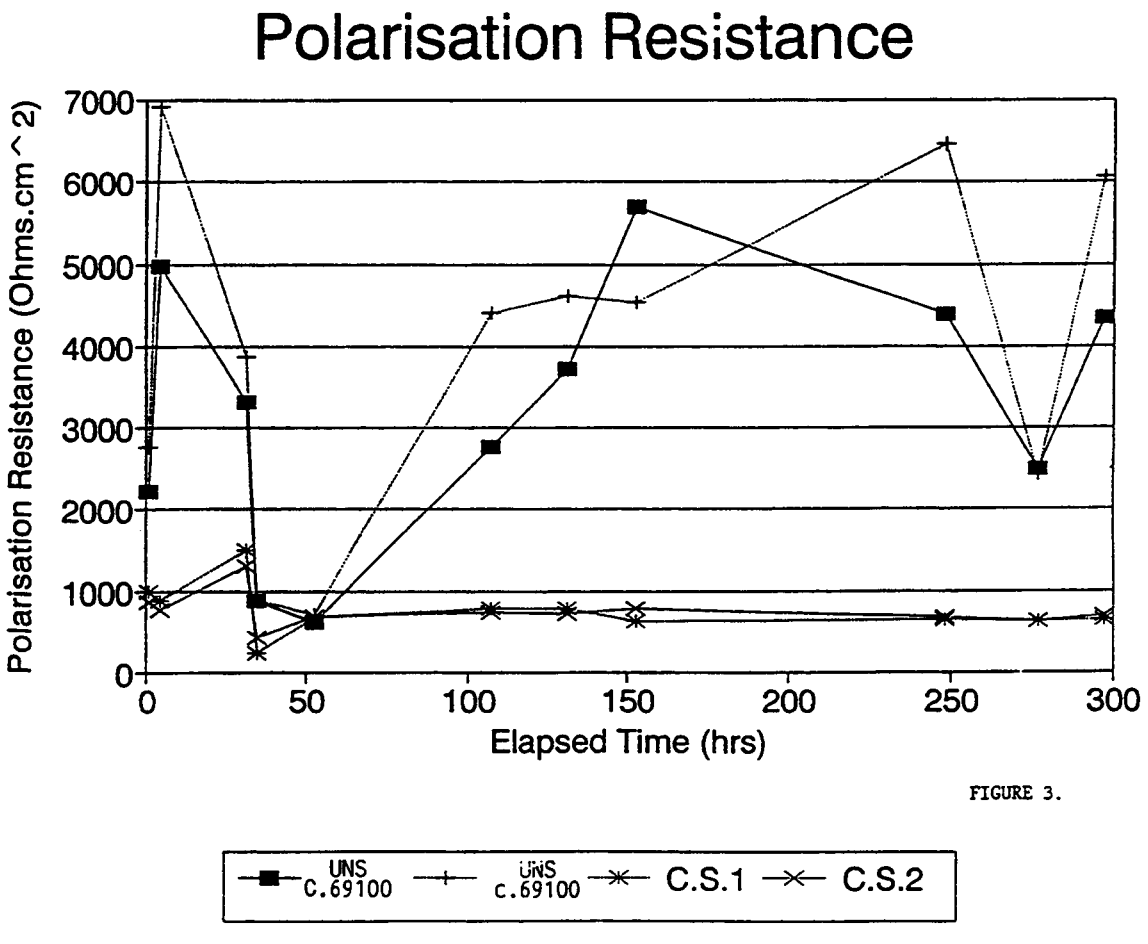


FIGURE 3.

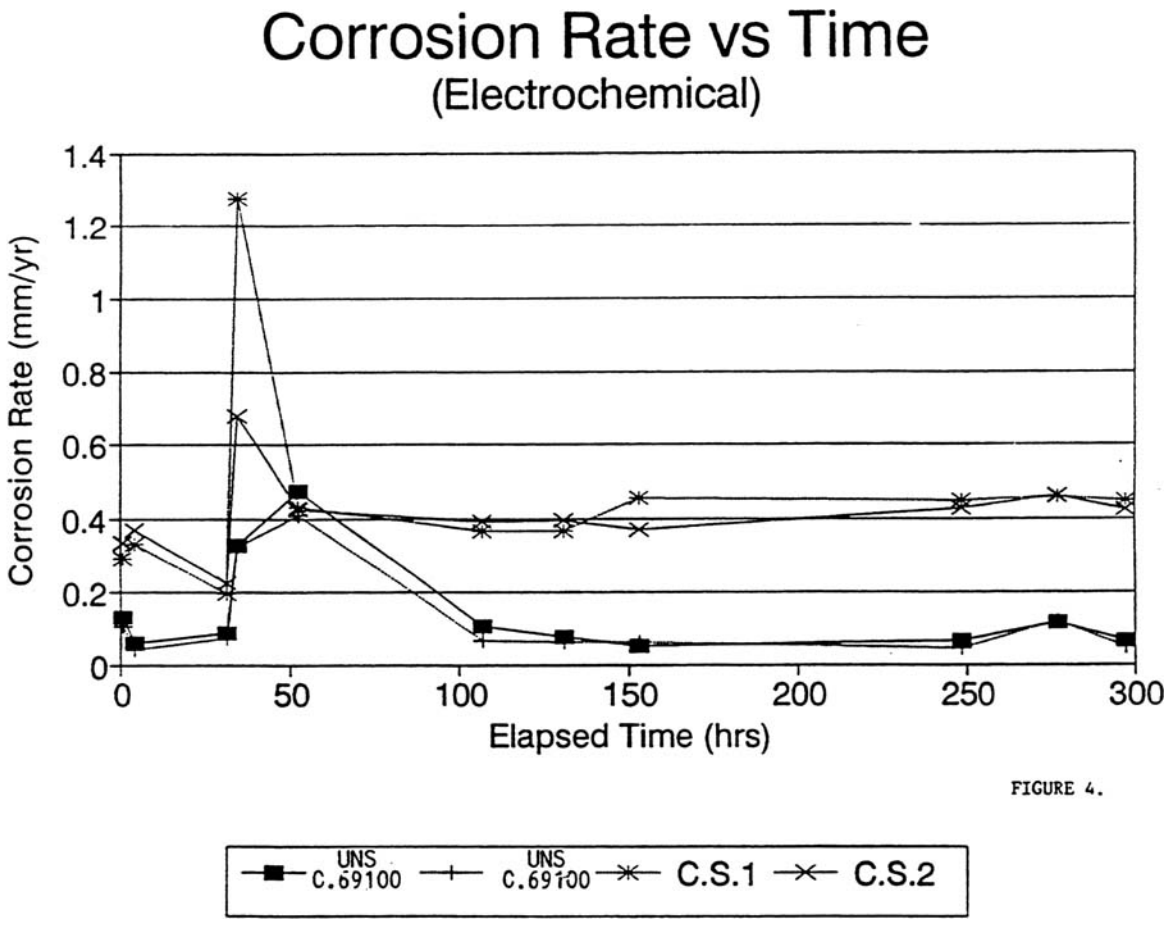

Corrosion Rate vs Time
(Electrochemical)
Corrosion Rate (mm/yr)
1.4
1.2
1
0.8
0.6
0.4
0.2
0
0
50
100
150
200
250
300
Elapsed Time (hrs)
UNS C.69100
UNS C.69100
C.S.1
C.S.2

FIGURE 4.

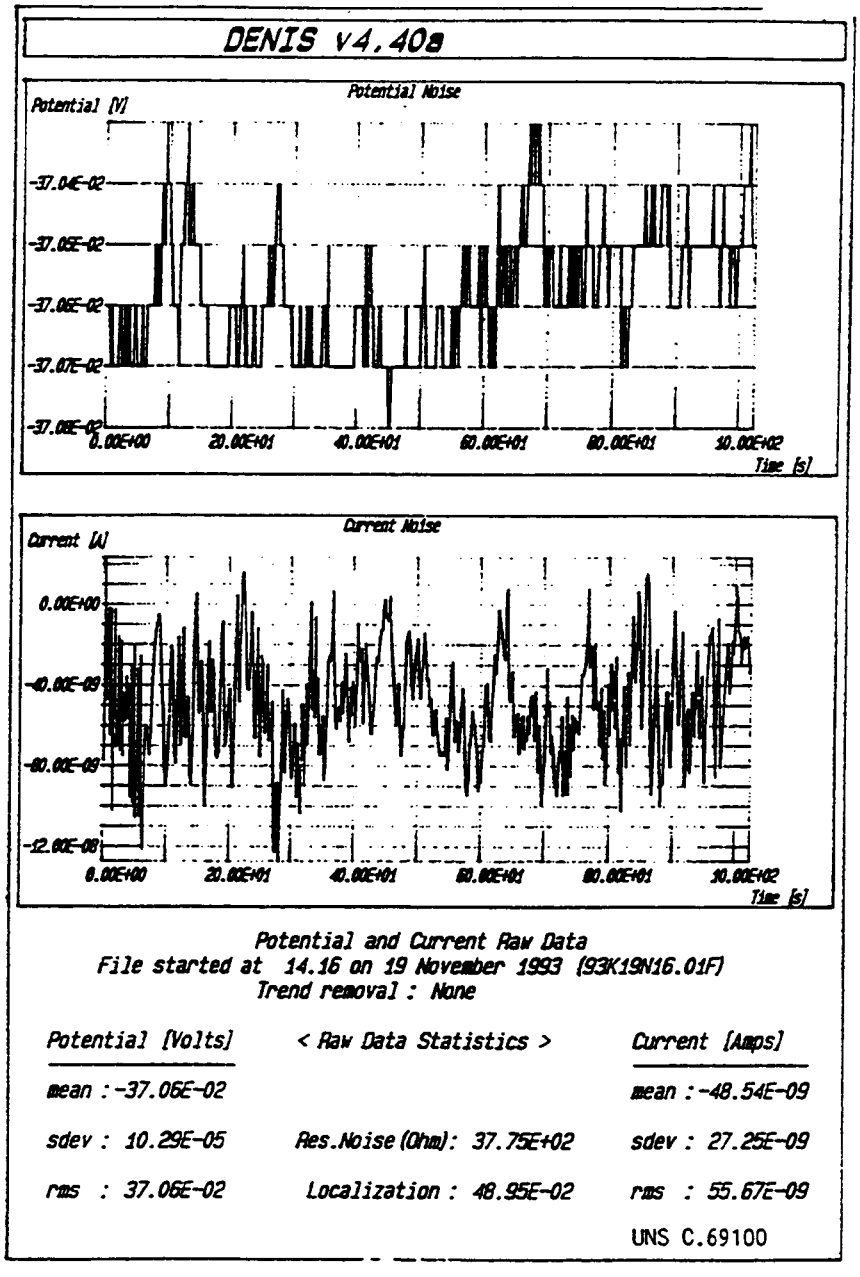


FIGURE 5. Potential and current noise data for UNS C69100

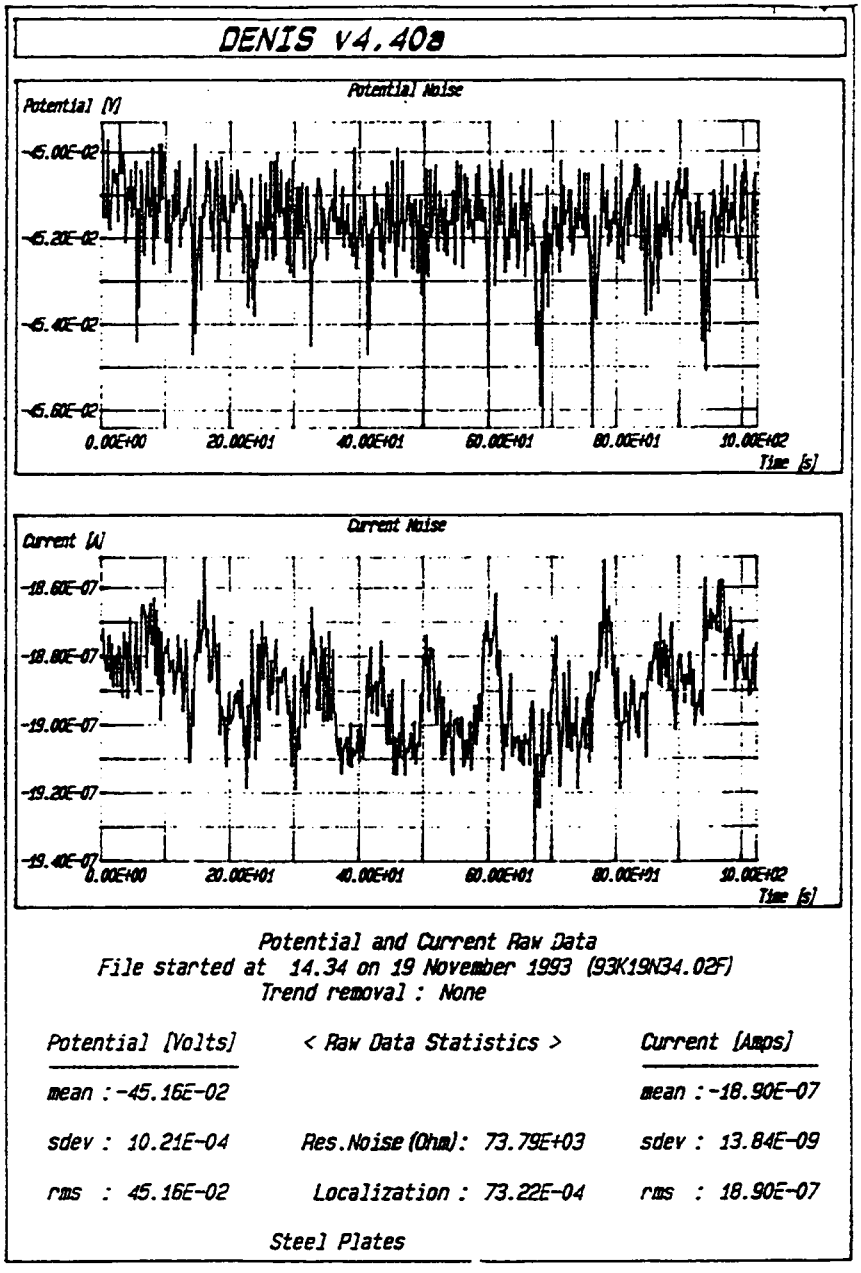
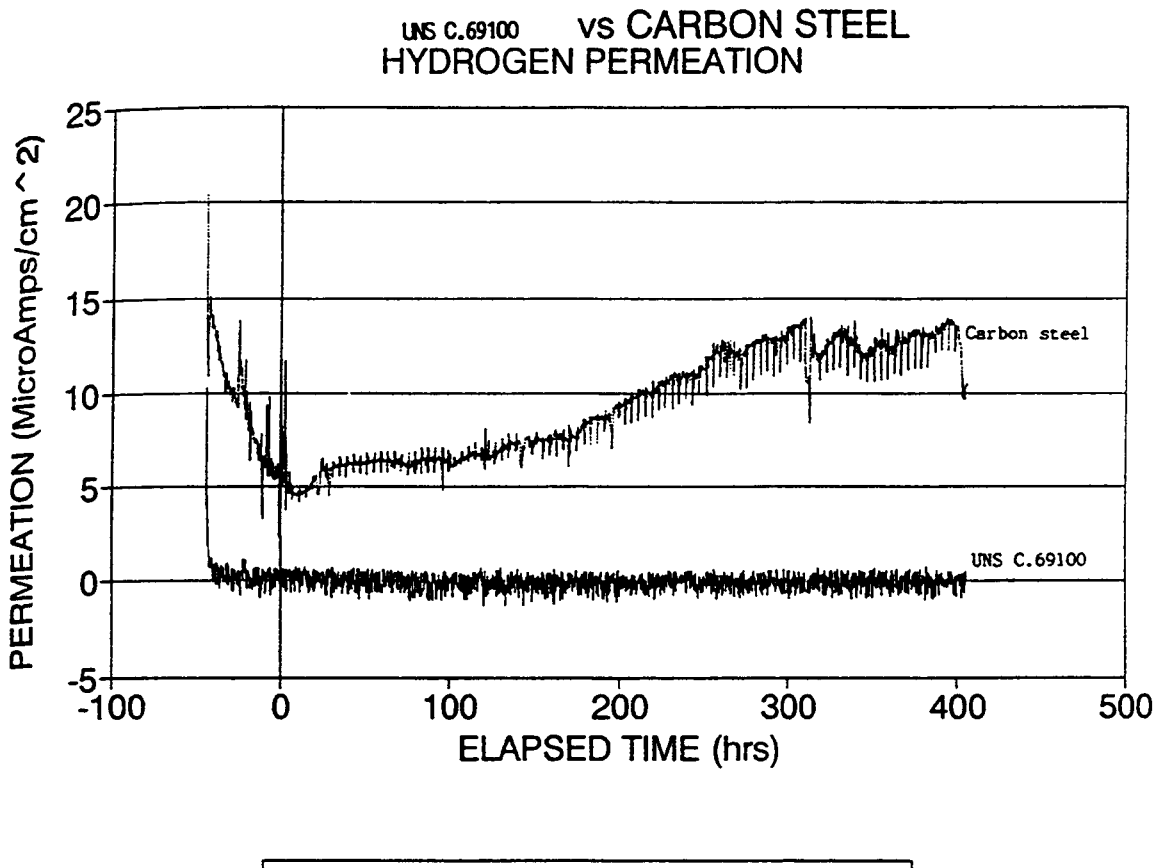


FIGURE 6. Potential and current noise data for steel samples.



UNS C.69100 — Carbon Steel

FIGURE 7.

APPENDIX A

UNS C69100 - TABLES OF USAGE AND BENEFITS

APPLICATION	TECHNICAL BENEFIT									
	1	2	3	4	5	6	7	8	9	10
OFFSHORE PLATFORMS										
Integral instrumentation/control lines	X	X	X	X	X	-	-	X	-	X
Life support systems	X	X	-	X	X	X	-	-	X	X
Miscellaneous auxiliaries (e.g. cranes)	X	X	X	-	X	-	-	X	-	X
OFFSHORE DIVING SYSTEMS										
Life support gases	X	X	-	X	X	X	-	-	X	X
Divers' heating circuits	X	-	-	X	-	-	-	X	-	X
Hydraulic retrieval systems	X	X	X	-	X	-	-	X	-	X
NAVAL MARINE APPLICATIONS										
Hydraulic auxiliaries	X	X	X	-	X	-	X	X	-	X
Pneumatic auxiliaries	X	X	-	X	X	X	X	X	X	X
COMMERCIAL MARINE APPLICATIONS										
Hydraulic auxiliaries	X	X	X	-	X	-	-	X	-	X
Pneumatic auxiliaries	X	X	-	X	X	X	-	X	X	X
FIGHTING VEHICLES										
(Battle tanks, large howitzers, GAPCs)	X	X	X	-	X	-	-	X	-	X
AIRCRAFT APPLICATIONS										
Power control systems	-	X	X	-	X	-	-	X	-	X
Braking systems	-	X	X	-	X	-	-	X	-	X
Test (fatigue) rigs	-	X	X	-	X	-	-	X	-	X
HP GAS STORAGE SYSTEMS										
(O_2, H_2, N_2, CO_2, He)	-	X	X	X	X	X	-	X	X	X
GENERAL 'INDUSTRIAL' PROJECTS										
HP water washdown systems	X	X	-	-	X	-	-	X	-	X
Rail transportation systems	-	X	X	-	X	-	-	X	-	X
CIVIL ENGINEERING PROJECTS										
Bridge and linkspans	X	X	X	-	X	-	-	X	-	X
Dock gates/river barrages	X	X	X	-	X	-	-	X	-	X

Key to Benefits

1. Excellent resistance to marine corrosion.
2. High strength-to-weight ratio.
3. Resistance to shock and fatigue.
4. Non-sparking.
5. Lasting clean-bore properties.
6. Thermal characteristics in safety conveying high pressure oxygen.
7. Very low magnetic signature.
8. Excellent ductility - ease of installation.
9. Cryogenic strength.
10. Extended maintenance free life.

Copyrighted Materials
Copyright © 1996 NACE International Retrieved from www.knovel.com

SPE
Society of Petroleum Engineers of AIME

SPE 13025

Performance of a Beryllium Copper Nonmagnetic Drill Collar Alloy

by F. Dunlevey, *Brush Wellman Inc.*

SPE Member

Copyright 1984 Society of Petroleum Engineers of AIME

This paper was presented at the 59th Annual Technical Conference and Exhibition held in Houston, Texas, September 16-19, 1984. The material is subject to correction by the author. Permission to copy is restricted to an abstract of not more than 300 words. Write SPE, 6200 North Central Expressway, Drawer 64706, Dallas, Texas 75206 USA. Telex 730989 SPEDAL.

ABSTRACT

Laboratory characterization and field testing show the advantages of beryllium copper Alloy 25 for use in non-magnetic drill collars, stabilizers, and subs. Beryllium copper is resistant to stress corrosion cracking failures at elevated temperature and pressure in the presence of hydrogen sulfide and dissolved chloride solutions. The alloy is more resistant than stainless steel to galling failure in threaded joints.

INTRODUCTION

Non-magnetic drill collars (NMDC) see the same service conditions as alloy steel drill collars, however, the special requirements placed on their magnetic properties often limit the selection of alloys for this application. Austenitic stainless steels are frequently specified for NMDC service. Their use requires careful attention to lubrication practice to prevent tool joint damage which may lead to galling and loss of the drill collar's magnetic quality. Additionally, improper material selection can lead to catastrophic stress corrosion cracking failures[1] in the presence of high chloride drilling fluids. For severe service, nickel-base alloys are sometimes substituted for stainless steels, but their availability is not always certain.

Beryllium copper alloys have been successfully used in many downhole applications requiring difficult combinations of strength, corrosion resistance, fabricability and non-magnetic properties. Recent laboratory and full size field testing of beryllium copper drill collars have demonstrated that the alloy performs well in severe service conditions.

References and illustrations at end of paper

Copper-base alloys are not generally used in applications requiring high mechanical properties; dilute alloys of beryllium in copper are the exceptions. For certain applications, beryllium copper alloys can be produced with tensile strength exceeding 200 ksi (1380 MPa).

BERYLLIUM COPPER ALLOY 25

The beryllium copper alloy system encompasses several commercial alloys. The strongest of these is Alloy 25 (UNS Alloy No. C17200). Alloy 25 contains nominal 2% beryllium by weight. Because of the wide difference in atomic weights between beryllium and copper, Alloy 25 contains approximately 13% beryllium on a volume basis. It is much more heavily alloyed than its composition suggests, which explains its relatively high mechanical properties.

The physical properties of Alloy 25 (Table 1) are typical of copper alloys, particularly its high conductivity and low magnetic permeability. Physical properties are largely unaffected by processing and service conditions, and are difficult to change under any circumstances. Conversely, the mechanical properties of the alloy can be modified over wide ranges. The tailoring of mechanical properties to particular application requirements accounts for the wide use of Alloy 25.

Alloy 25 - Mechanical Properties

Dilute beryllium copper alloys are strengthened by precipitation hardening. A series of specific thermal treatments, rather than mechanical deformation, provide the consistently high strength of these alloys. The strength of Alloy 25 for mechanical applications can be precisely controlled to $\pm$ 5 ksi within the 0.2% offset yield strength range of 90 to 150 ksi (620-1034 MPa) or a tensile strength range of 125 to 170 ksi (862-1172 MPa).

© 1984 Courtesy SPE

For a particular application, the combined requirements of strength and ductility will dictate the strength specification. Alloy 25 NMDC are supplied to a strength specification, and require no further treatments before or after machining.

For the NMDC application, Alloy 25 is manufactured within the strength range of 100 to 120 ksi (690-827 MPa) yield strength. Figure 1 shows the relationship of Alloy 25's yield and tensile strengths with ductility (percent elongation) in the tensile test. In the yield strength range of 100 to 120 ksi (690-827 MPa), the tensile strength varies from 135 to 148 ksi (930-1020 MPa). Ductility normally falls within the range of 13 to 18% elongation. These properties meet the API strength requirements[2] for drill collars and subs.

Figure 2 shows schematically the stress-strain curve from a tensile test. In addition to the 0.2% offset yield point at 110 ksi (758 MPa) the curve shows the relationship of other design criteria such as the 0.01% offset yield at 75 ksi (517 MPa) and the proportional limit (0% offset) at 61 ksi (420 MPa). Alloy 25's strain hardening coefficient of 0.35 and high uniform elongation result in a large spread between the yield and tensile strengths. Even after the start of local yielding, Alloy 25 is capable of absorbing additional strain before reaching the ultimate tensile strength.

The impact strength of Alloy 25 varies in the same manner as ductility. Figure 3 depicts the relationship between tensile properties and Charpy impact strength. Alloy 25, prepared to the NMDC specification, will have Charpy V-Notch impact energy between 13 and 22 ft lb (18-29 J).

Resistance to fatigue failure is an important consideration for rotating drill string components. Figure 4 shows the fatigue strength of Alloy 25 in a fully reversed, smooth, rotating beam test. The curve has the characteristic S-N shape and exhibits an endurance limit of about 45 ksi (310 MPa) at 200 million rotational cycles.

Alloy 25's tensile properties are relatively insensitive to temperature below 300°F (150°C). Tests conducted between -50°F and 500°F (-45 to 260°C) are summarized in Figure 5 which shows no strength loss at low temperatures, and at 500°F the alloy retains about 95% of its room temperature strength. Above 500°F, the mechanical properties begin to significantly decrease.

The tensile data reported here were generated using smooth, unnotched test samples. Materials used in shock loaded mechanical applications are frequently tested using notched tensile specimens to determine if the presence of sharp defects will affect the material's strength. The presence of notches should be avoided, but, typically they occur in the form of threads, sharp radii, machining marks, scratches, gouges, etc. If these stress intensifiers decrease the material's strength, the material is termed "notch sensitive." The tensile strength of a notched sample of Alloy 25 is about 1.35 times GREATER than a smooth sample. Notched tensile samples contain a ground circumferential notch (0.006 in. (0.15 mm) root radius) to simulate a sharp crack in the materials. This crack did not easily propagate in the tensile test as evidenced by the higher strength of the notched test pieces. Figure 6 summarizes the notched tensile data and shows that Alloy 25 for NMDC application is not notch sensitive.

Plane-strain fracture toughness tests were performed on 1.5 in. (38.1 mm) thick samples. The methods for testing and determination of K_{IC} as outlined in ASTM 399 were followed. Testing was conducted at 70°F (20°C) and yielded K_{IC} values of 75-80 ksi $\sqrt{in}$ (82-88 MPa $\sqrt{m}$)for Alloy 25 samples which had yield strength in the NMDC range of 100 to 120 ksi (690-827 MPa).

Alloy 25 - Corrosion Resistance

Table 2 briefly summarizes the corrosion properties of beryllium copper. Its corrosion performance is typical of many copper alloys. Beryllium copper is suitable for use in any atmospheric environment; it resists chemical attack in dilute inorganic acids and organic compounds. Service in strongly basic solutions is not recommended.

Unlike some other high strength materials, Alloy 25 resists stress corrosion cracking (SCC) in the presence of dissolved chloride solutions and it resists sulfide stress cracking (SSC) in the presence of hydrogen sulfide. SCC and SSC failures are usually catastrophic, occurring with little deformation or warning. Susceptible materials fail in a brittle fashion from a combination of tensile stress, less than the material's yield strength, and the presence of a corrosive medium which is usually considered chemically innocuous to the material. In some susceptible steels, SCC failures can be initiated in solutions containing as little as a few parts per million dissolved chloride. The tensile stress may occur from an operating load or from residual stresses induced in processing the material. The NACE TM 01-77 test procedure[3] measures materials SSC susceptibility by exposing the stressed specimens to 5% sodium chloride solution which is hydrogen sulfide saturated (0.3-0.4%) and acidified with acetic acid. The NACE testing is done at ambient temperature and atmospheric pressure. Alloy 25, stressed at 90% of its tensile yield strength, survived the 30 day NACE test without failure[4].

Additional SCC testing was performed by Brush Wellman under conditions more severe than the NACE test and more typical of some downhole environments. Tests were performed in an autoclave at 1000 psi (6.9 MPa), at temperatures up to 300°F (150°C), with gases of up to 10% hydrogen sulfide and 20% carbon dioxide, and an aqueous phase with the equivalent of up to 11% dissolved sodium chloride. Reference 4 details the test conditions and procedures. The results, summarized in Table 3, show that Alloy 25 is not susceptible to cracking under conditions which led to failure in three non-magnetic stainless steel drill collar alloys.

In separate evaluations, Alloy 25 was exposed to a boiling 45% magnesium chloride solution at 311°F (155°C), following ASTM G36 procedures. Test samples (diametrically loaded C-rings) were stressed to 100% of their yield strength. The tests were concluded when the Alloy 25 samples reached 1000 hrs without failure. The tests demonstrate Alloy 25's SCC resistance particularly at high stresses and in the presence of aggressive cations and very high chloride concentrations. Stainless steel (AISI 304 and 316) samples, tested in the same manner, failed in less than 24 hrs.

Alloy 25 - Magnetic Properties

Beryllium copper alloys are not ferromagnetic. They are weakly paramagnetic, having a magnetic permeability slightly greater than unity. Alloy 25's magnetic permeability is less than 1.003 c.g.s. units. In addition to low magnetic permeability, the magnetic properties of Alloy 25 do not deteriorate in service. Figure 7 compares the magnetic permeability of Alloy 25 with two nickel-stabilized, non-magnetic stainless steel alloys[5], and shows the effect of deformation on magnetic properties. The change in permeability of the stainless alloys is the result of strain induced transformations which can be locally generated by machining, thread wear, abrasion, or tong scarring. Such localized deformation can cause magnetic hot spots. Alloy 25's properties do not change as a result of machining or service deformation.

Alloy 25 - Resistance to Galling

Alloy 25 is frequently specified in severe service (high load/low speed) bearing and bushing applications because of its resistance to failure from seizing and galling. The properties of Alloy 25 which contribute to its anti-galling characteristics are its low coefficient of friction which is not heavily temperature sensitive, and high thermal conductivity which allows rapid dissipation of frictional heat from the rubbing surfaces.

Since there are no generally accepted procedures to measure galling resistance, Brush Wellman conducted tests using full size API threaded joints. The joints were made and broken at progressively higher torques until a galling failure was visually detected at the joint. When galling occurred, it was usually seen on the sealing face and not on the threads. There was no correlation between the galling failures and the make-up/break-out torque ratios to indicate the onset of the galling failure. Various combinations of Alloy 25, stainless steel and alloy steel (shown in Table 4) were used in the galling tests which were conducted both unlubricated and with normal lubrication practice.

The test results show that a stainless/stainless couple fails at less than the API recommended minimum torque - unlubricated; and at a 30% overload in a lubricated test. The Alloy 25/Alloy 25 couple did not fail by galling when the torque was 200% of the API recommended value. A mixed couple of Alloy 25/stainless resisted galling failure when lubricated. The Alloy 25/stainless couple showed indications of galling only when the test was conducted unlubricated at double the API recommended torque.

Alloy 25 - Machinability

The economics of using a NMDC alloy depend upon its performance and maintenance costs, as well as the purchase price. Among the items contributing to the cost of a NMDC alloy is machinability which affects the fabrication cost as well as post-purchase maintenance costs through re-threading when required over the life of the drill collar. Figure 8 compares the machinability of Alloy 25 with several other alloys which have oilfield applications. Although not a standard measurement, the machinability rating was based on the metal removal rate in two different machining operations, turning and drilling. The machining parameters were selected to optimize surface quality and tool life. The machinability of Alloy 25 is about double that of stainless and alloy steels and about ten times higher than Monel K-500[6,7].

Alloy 25 is weldable but, as with any strengthened alloy, welding will affect the mechanical properties in the vicinity of the weldment.

Alloy 25 can be safely machined using conventional methods and tools. Machining is usually performed wet. Welding and grinding operations on beryllium copper and any other metal are performed in ventilated areas to eliminate worker exposure to airborne particulate material.

ALLOY 25 - PERFORMANCE IN NMDC APPLICATIONS

The laboratory testing conducted on Alloy 25 suggests its suitability as an acceptable NMDC alloy. No laboratory testing, however, exactly simulates the conditions seen in service. Beryllium copper Alloy 25 has a successful history of downhole service in applications including logging tool housings, directional instrument housings, sucker rod pump barrels, and drill bit bushings. The success in these applications, as well as the laboratory tests, led to service evaluations. Field tests have been in progress since 1982 on Alloy 25 drill collars and subs. Brush Wellman has encouraged the use of Alloy 25 in service conditions where other alloys have demonstrated limitations. Table 5 briefly summarizes the service history of full size (30 ft) beryllium copper Alloy 25 drill collars. In addition, many more subs are in use as thread savers and in MWD applications. In all cases, the drill collars and subs have not received special treatment with regard to use conditions, thread lubricants, or handling.

The drill collar with the longest service history has been in use since March, 1983. Most of its life has been spent in the Williston Basin area in drilling fluids with about 180,000 ppm chloride ion content. It has performed without problem. It has remained in service longer than the average for stainless steel alloys in that geographical area, and its maintenance costs from thread reworking are considerably less than those of stainless.

CONCLUSIONS

Beryllium copper Alloy 25 is suitable for non-magnetic drill collar use. It can be produced to meet the API mechanical properties specification. The particular advantages that Alloy 25 offers are:

a) resistance to stress corrosion cracking in the presence of chloride solutions,
b) resistance to sulfide stress cracking in the presence of hydrogen sulfide,
c) protection of tool joints from galling under lubrication-poor and over-torque conditions,
d) low magnetic permeability and resistance to formation of magnetic hot spots,
e) ease of machining.

Field tests of beryllium copper drill collars and subs have been successful in a variety of service conditions including high chloride muds and some oil-based drilling fluids.

REFERENCES

1. Kane, R.D.: "High Alloy Tubulars Hold Promise for Sour Service Tolerance," Pet. Engr. Int'l. (Jan 1983) 98-112.

2. API Specification 7 for Rotary Drilling Equipment, Section 6, American Petroleum Institute, Dallas, 1981.

3. NACE Standard TM 01-77, National Association of Corrosion Engineers, Houston, 1977.

4. Booker, J., Cribb, W.R., Turn, J.C. Jr. and Kane, R.D.: "Corrosion Behavior of Beryllium Copper and Other Nonmagnetic Alloys in Simulated Drilling Environments," Paper 220, presented at NACE Corrosion 84, New Orleans, April, 1984.

5. ASM Source Book on Industrial Alloy and Engineering Data, American Society for Metals, Cleveland, 1978.

6. Machining Beryllium Copper, Brush Wellman Inc., Cleveland, 1976.

7. Machining Data Handbook, Machinability Data Center, Cincinnati, 1972.

Gammaloy is a registered trademark of Armco Inc.
18-18 Plus is a registered trademark of Carpenter Technology Corp.
NMS-100 is a registered trademark of Earle M. Jorgensen Co.
Monel is a registered trademark of International Nickel Co., Inc.

Table 1

BERYLLIUM COPPER ALLOY 25

PHYSICAL PROPERTIES

DENSITY	0.302 lb/in^3	8.36 g/cm^3
MELTING RANGE	1600-1800°F	870-980°C
ELASTIC MODULUS	18.5 x 10^6 psi	128 GPa
TORSIONAL MODULUS	7.3 x 10^6 psi	50 GPa
POISSON'S RATIO	0.30	0.30
THERMAL CONDUCTIVITY	60 Btu/ft hr°F	1.0 J/cm sec°C
ELECTRICAL CONDUCTIVITY	22% IACS	0.13 megmho cm
ELECTRICAL RESISTIVITY	46 ohms circ mil/ft	7.7 microhm cm
THERMAL EXPANSION COEFFICIENT	9.7 x 10^{-6}/°F (70-400°F)	17.4 x 10^{-6}/°C (20-200°C)
SPECIFIC HEAT	0.10 Btu/lb °F	0.43 J/g °C
MAGNETIC PERMEABILITY		<1.003 C.G.S. units

Table 2

BERYLLIUM COPPER ALLOY 25

CORROSION PROPERTIES

	ACCEPTABLE	NOT RECOMMENDED
ATMOSPHERE	INDUSTRIAL MARINE RURAL	
GAS (DRY)	CHLORINE OXYGEN/OZONE CARBON DIOXIDE SULFUR DIOXIDE AMMONIA FUEL GASES	ACETYLENE
ORGANIC COMPOUNDS	MOST ORGANIC ACIDS ALCOHOLS KETONES CHLORINATED SOLVENTS FUELS LUBRICATING/ HYDRAULIC OILS	PYRIDINE
INROGANIC CHEMICALS	NON-OXIDIZING ACIDS ACETIC ACID HYDROCHLORIC ACID DILUTE SULFURIC ACID PHOSPHORIC ACID AQUEOUS SOLUTIONS CARBONATES CHLORIDES SULFATES	AMMONIUM HYDROXIDE SODIUM HYDROXIDE HYDROGEN PEROXIDE OXIDIZING ACIDS/SALTS CHROMIC ACID NITRIC ACID FERRIC CHLORIDE MERCURY
CORROSION CAN BE AFFECTED BY TEMPERATURE, CONCENTRATIONS, VELOCITY, AND THE PRESENCE OF OTHER CHEMICALS.		

Table 3

BERYLLIUM COPPER ALLOY 25

CORROSION CRACKING RESISTANCE

	AUTOCLAVE TEST (1000 psi					
					TEST RESULTS 90% YIELD STRENGTH	
ALLOY	TEMPERATURE °F	H_2S %			SHELL BENT BEAM	C-RING
ALLOY 25	150	1	0	3	NF	NF
	150	10	20	3	NF	NF
	250	10	20	3	NF	NF
	300	0	20	11	NF	NF
	300	1	20	3	NF	NF
	300	10	20	3	NF	NF
AUSTENITIC STAINLESS ALLOY						
GAMMALOY	250	10	20	3	F	-
18-18 PLUS	250	10	20	3	F	-
NMS-100	250	10	20	3	F	-
NF - NO FAILURE IN 720 HRS.			F - FAILED IN LESS THAN 720 HRS.			

Table 4

BERYLLIUM COPPER ALLOY 25

GALLING RESISTANCE

COUPLE (PIN/BOX)	ONSET OF GALLING FAILURE (% OF API MINIMUM TORQUE)	
	LUBRICATED	NONLUBRICATED
STAINLESS/STAINLESS[1]	130%	<100%
ALLOY 25/STAINLESS[2]	N.F. (180%)*	---
ALLOY 25/STAINLESS[1]	N.F. (200%)	200%
ALLOY 25/AISI 4140[2]	N.F. (205%)	---
ALLOY 25/ALLOY 25[1]	N.F. (200%)	N.F. (200%)

[1] API 3-1/2 IF
[2] API 6-5/8 REG

*NO FAILURE (TEST LIMIT)

TABLE 5

BERYLLIUM COPPER ALLOY 25

DRILL COLLAR PERFORMANCE

LOCATION	APPROXIMATE SERVICE LIFE (rotating hours)	IN SERVICE SINCE
U.S. WILLISTON BASIN	5000	MARCH 1983
CANADA WILLISTON BASIN	2500	FEBRUARY 1984
CANADA	1500	MARCH 1984
CANADA ATLANTIC COAST		APRIL 1984
NORTH SEA		JUNE 1984
NORTH SEA		JUNE 1984
NORTH SEA		AUGUST 1984
NORTH SEA		AUGUST 1984

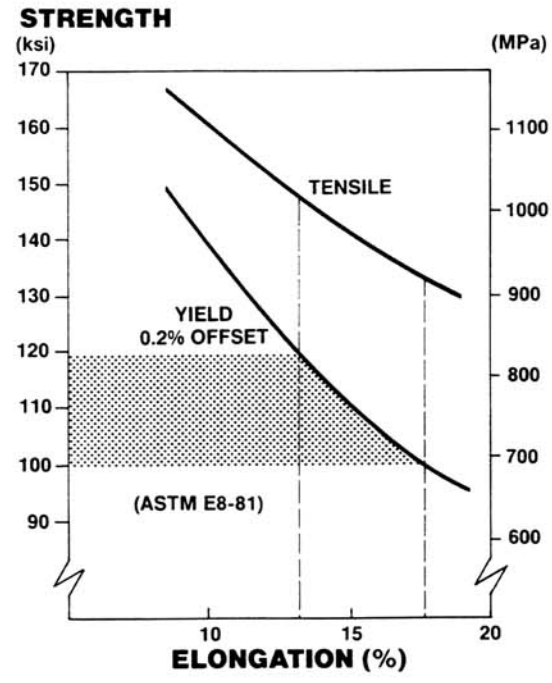


Fig. 1—Beryllium Copper Alloy 25 strength — elongation relationship.

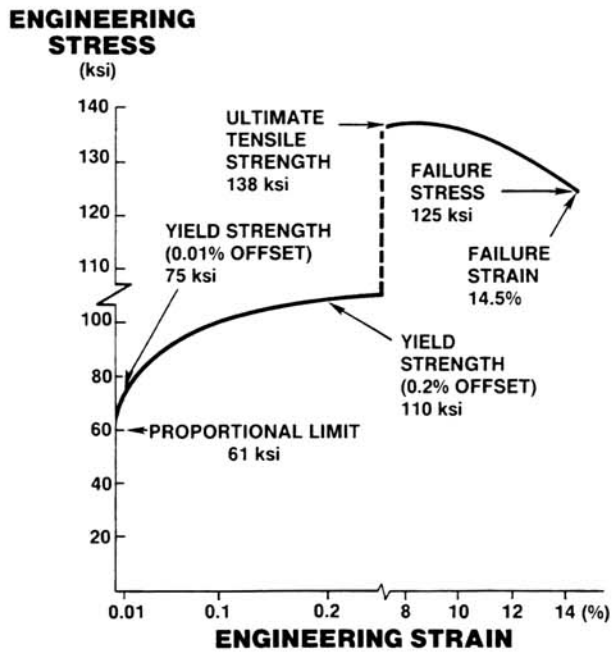


Fig. 2—Beryllium Copper Alloy 25 room temperature tensile test.

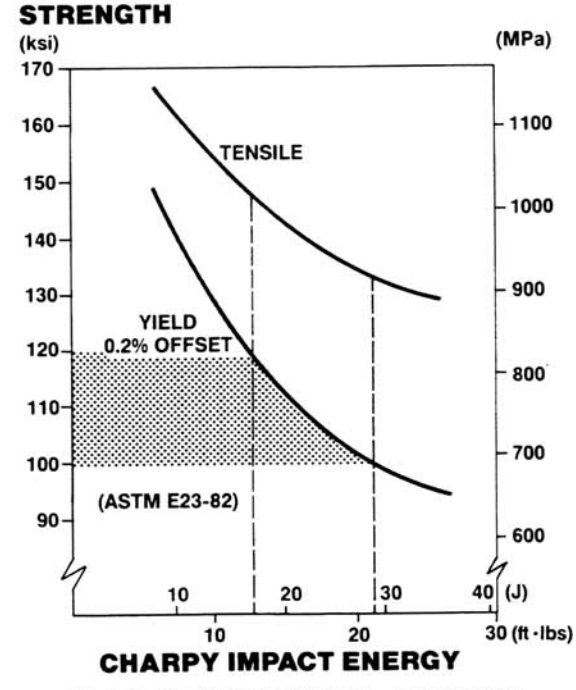


Fig. 3—Beryllium Copper Alloy 25 strength — impact relationship.

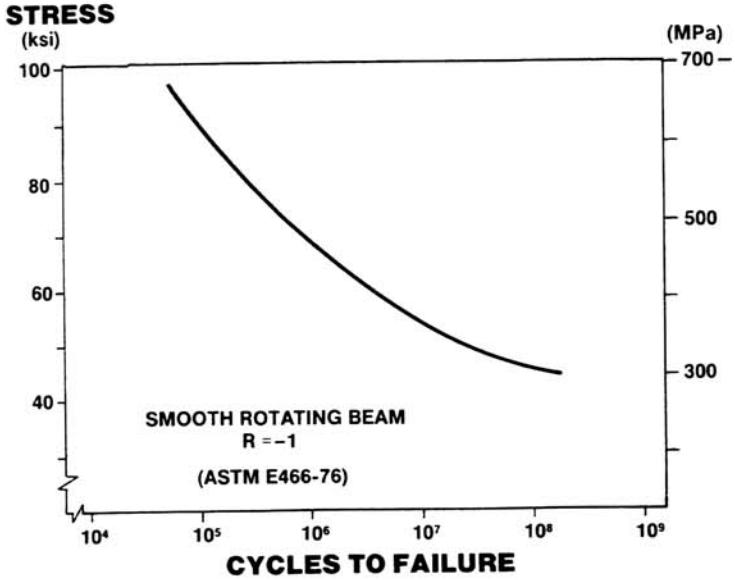


Fig. 4—Beryllium Copper Alloy 25 fatigue test performance.

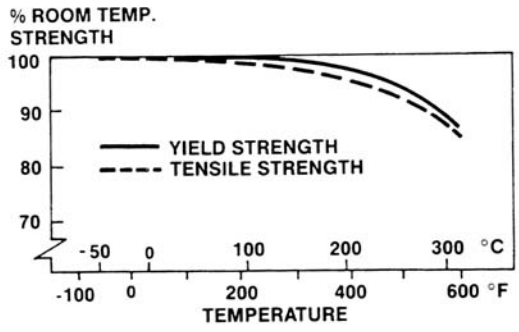


Fig. 5—Beryllium Copper Alloy 25 elevated temperature properties.

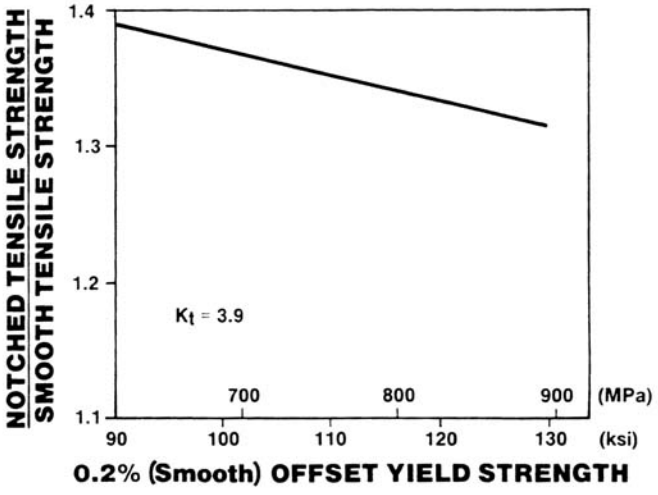


Fig. 6—Beryllium Copper Alloy 25 notched tensile test data.

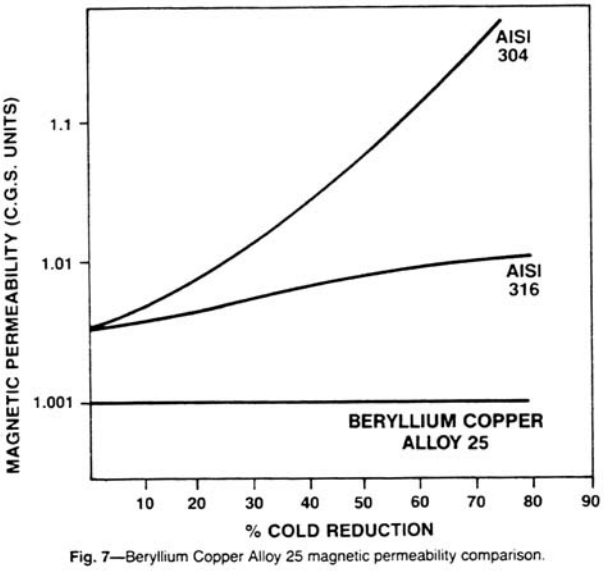


Fig. 7—Beryllium Copper Alloy 25 magnetic permeability comparison.

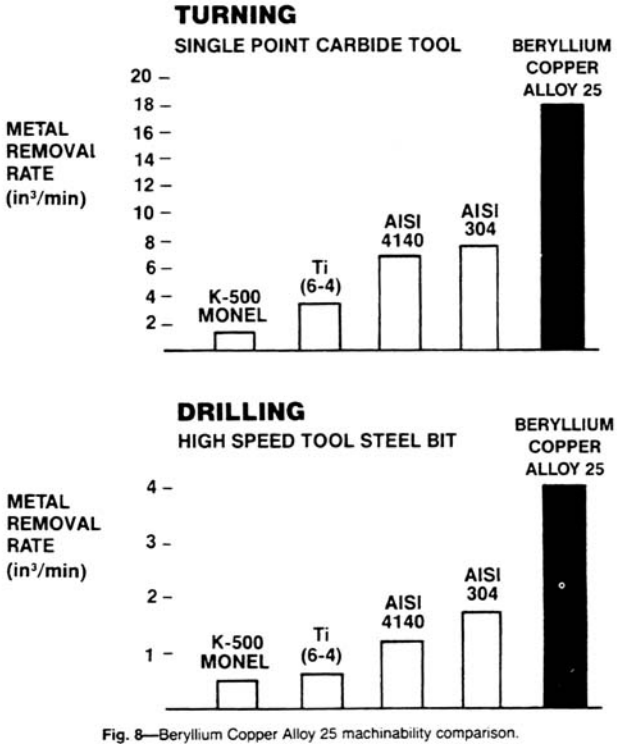


Fig. 8—Beryllium Copper Alloy 25 machinability comparison.

Copyrighted Materials
Copyright © 1996 NACE International Retrieved from www.knovel.com

Technical Paper

Boshoku Gijutsu, **29**, 113–121 (1980)

Corrosion and Hydrogen Embrittlement Behavior of Titanium in Aqueous Sulfidic Solutions

Z. A. Foroulis*

**Exxon Research and Engineering Co.*

Aqueous sulfidic solutions which contain H_2S, or mixtures of H_2S and NH_3 are corrosive to carbon steel and other commonly used alloys particularly if the sulfidic solutions also contain chloride and cyanide ions. Titanium has been considered as a candidate construction material for services in petroleum refining and related processes, which involve handling aggressive aqueous sulfidic solutions. The corrosion and electrochemical behavior of titanium in aqueous sulfidic solutions was therefore investigated to provide answers regarding the corrosion and embrittlement behavior of titanium in these solutions. This paper summarizes the results of this study of the corrosion and electrochemical behavior, including galvanic effects, of titanium in aqueous acidic and alkaline sulfidic solutions. Variables investigated include the effect of solution pH, temperature and solution composition on the corrosion and electrochemical behavior of titanium. The effect of chloride and cyanide ions in aqueous sulfidic solutions on the corrosion behavior of titanium was also studied. Surfaces of titanium electrodes exposed to sulfidic solutions were also examined by reflection electron diffraction and the results of these tests are compared with thermodynamic predictions (Pourbaix diagrams).

An important factor which may also limit the utilization of titanium as a heat exchanger material is its ability under certain conditions to absorb hydrogen due to either superficial corrosion or galvanic coupling to more active materials. The absorbed hydrogen may lead to titanium hydride formation and embrittlement of titanium. This paper also discusses the results of an investigation of the effect of solution pH and composition, temperature, and impurity elements such as chlorides, cyanides, phosphates, etc. in solutions on the mechanism and rate of hydrogen absorption and formation of titanium hydride. In addition the effect of hydrogen and mechanical loading rate (strain-rate) on the ductility and embrittlement of titanium is also discussed.

Introduction

Titanium has been finding increasing acceptance as a construction material in the chemical and petroleum industries because of attractive mechanical properties and generally good corrosion resistance. As a result, there has been a growing literature on the corrosion behavior of titanium in acidic solutions of HCl, H_2SO_4 and in nearly neutral chloride solutions[1~7], but not in sulfidic solutions. Aqueous sulfidic solutions which contain H_2S or mixtures of H_2S and NH_3 are corrosive to carbon steel and other commonly used alloys, particularly if the sulfidic solutions contain also chloride and cyanide ions.[8]

The corrosion and electrochemical behavior of titanium in aqueous sulfidic solutions, including galvanic effect and cathodic hydrogen absorption was therefore investigated to provide answers regarding the corrosion and embrittlement behavior of titanium in aggressive sulfidic solutions. This paper discusses the corrosion, electrochemical and hydrogen embrittlement behavior of titanium in aqueous sulfidic solutions. In addition, the effect of hydrogen on the ductility of titanium will also be considered.

The topics which are discussed in this paper, after the above brief introduction include: (a) corrosion and electrochemical behavior of titanium in sulfidic solutions, (b) galvanic behavior of titanium in sulfidic solutions, (c) factors influencing hydrogen absorption and embrittlement of titanium.

Corrosion Behavior of Titanium in Sulfidic Solutions

The aqueous sulfidic solutions used in this study included acidic sulfidic solutions prepared by saturating distilled water at different temperatures with H_2S, and alkaline sulfide solutions (pH 9~10) prepared with ammonium sulfide in the concentration range 2 to 20% $(NH_4)_2S$ with and without

* P. O. Box 101, Florham Park, NJ 07932 USA

Courtesy Boshoku Gijutsu

the addition of smaller concentrations of chloride and cyanide ions in the form of their sodium salts. The chemistry of aqueous sulfidic solutions is fairly complex and the stability of different species as described previously[9),10)] depends on both solution pH and the redox potential of the solution. In the potential region corresponding to the natural corrosion potential of titanium in aqueous sulfidic solutions the predominant stable species are H_2S in acidic solutions, SH^- in neutral and mildly alkaline solutions and $S^=$ in fairly alkaline solutions, as shown schematically in Fig. 1.

Fig. 2 shows the thermodynamic equilibrium potential−pH diagram for the system Ti-H_2O[9)]. This diagram shows that at very active potentials Ti is the stable species and corrosion is not expected to occur. In the active potential region at high cathodic polarizing potentials cathodic hydrogen evolution occurs and titanium hydride (TiH_2) becomes a thermodynamically stable phase (not shown in the diagram).

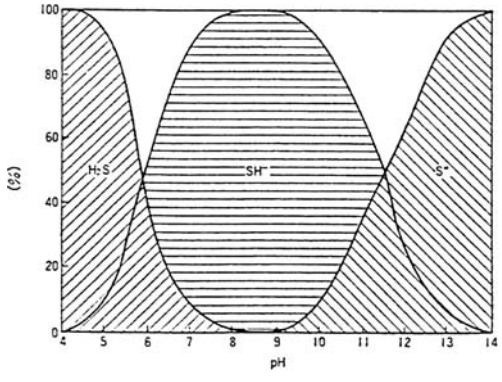


Fig. 1. Percentage Variation of Concentration of H_2S, SH^- and $S^=$ with Solution pH (25°C, Oxygen Free).

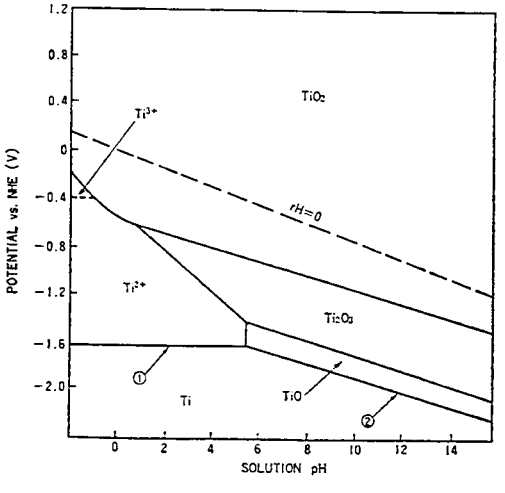


Fig. 2. Potential −pH Equilibrium Diagram for the Ti-H_2O System, 25°C.

In strong acidic solutions at more noble potentials Ti^{2+} and Ti^{3+} as soluble corrosion products become the thermodynamically stable species. In mildly acidic and neutral to alkaline pH solutions, a series of titanium oxides with increasing titanium valence, i.e., TiO, Ti_2O_3 and TiO_2, become thermodynamically stable with increasing potential. It is noted that although these oxides are thermodynamically stable in their respective potential −pH regions, formation of these oxides in many instances depends on kinetic factors and these oxides may not be formed. For example, the steady-state corrosion potentials of Ti in the sulfidic solutions investigated in this study, were found to be within the region of stability of TiO_2. However, examination of the surface of titanium specimens, which were exposed in aqueous sulfidic solutions, with reflection electron diffraction failed to reveal the presence of a titanium oxide film. This suggests that either the film was amorphous or too thin to be detected.

Previous studies by other investigators also indicate that TiO_2 forms only under extreme conditions of oxidation, i.e., air at elevated temperature, or anodic treatment at high anodic potentials. Soviet investigators[11)] who studied the nature of films of titanium polarized in H_2SO_4, also reported the absence of a well defined cystalline oxide film in the above potential regions; they were able to detect TiO_2 in the form of anatase only on specimens polarized at potentials greater than +0.1 V (NHE).

The corrosion behavior of titanium in sulfidic solutions was investigated by weight loss measurements of titanium coupons exposed in different sulfidic solutions and temperatures for up to 332 hrs. and by corrosion potential and polarization measurements. Typical corrosion data of titanium in acidic and alkaline sulfidic solutions, shown in Table 1, indicated that titanium remains passive and is subject to negligible corrosion. Passivation of titanium in these solutions is also confirmed by the data on the time variation of the natural corrosion potential of pre-activated titanium in aqueous sulfidic solutions shown in Fig. 3. The specimens were activated with HF prior to immersion in test solution.

The data in Fig. 3 show that the corrosion potential of titanium immediately upon immersion in test solutions was about −0.8 V (SCE) and pro-

Table 1. Corrosion Behavior of Titanium in Aqueous Sulfidic Solutions.

Test Solution	Temp.°C	Corrosion Rate+	
		mpy	mm/y
H_2O Sat'd with H_2S (Atm, Pres.)	72	0.3	<0.01
2% $(NH_4)_2S$	80	0.1	<0.01
10% $(NH_4)_2S$	80	0.1	<0.01
20% $(NH_4)S$	80	0.1	<0.01
2% $(NH_4)_2S$ +100ppm NaCN	80	0.0	0.00
2% $(NH_4)_2S$ + 2% NaCN	80	0.1	<0.01
20% $(NH_4)_2S$ +50ppm NaCN	80	0.0	0.00
20% $(NH_4)_2S$ + 1% NaCN	80	0.0	0.00

+Corrosion rates were calculated from weight loss differences (before and after test). Test coupons were honed after test to remove surface oxide film formed during test. Test coupons after test and before honing had generally small weight gain.

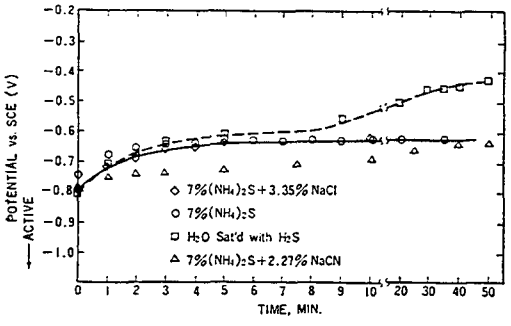


Fig. 3. Time Dependence of the Corrosion Potential of Titanium in Sulfidic Solutions. Titanium was Activated with HF prior to Immersion in Test Solution.

gressively increased reaching a steady-state value after several minutes. In H_2O sat'd with H_2S, the steady-state corrosion potential of about −0.45 V (SCE) was not achieved until about 35 minutes. In 7% $(NH_4)_2S$ solution as well as in alkaline sulfidic solutions containing NaCl, the corrosion potential was stabilized at about −0.65 V (SCE) after about 5 minutes of immersion. In a solution which contained 7% $(NH_4)_2S$ and 2.27% NaCN a steady-state corrosion potential of about −0.65 V (SCE) was also attained, but only after exposure time of about 40~50 minutes.

The progressive increase in the corrosion potential of active titanium with immersion time is interpreted as due to formation of a passive film. Although the exact nature of the passive film on titanium in these solutions has not been established it is reasonable to assume that it is a thin oxide film (50~100Å). The passive film is also assumed to be free of pores or cracks since at the steady-state corrosion potential any exposure of base metal through defects of this type is unlikely. It should be noted that the steady-state corrosion potential of titanium in these solutions is almost 0.5 V above the equilibrium potential for the reaction $Ti+2\,H_2O=TiO_2+4\,H^+ +4\,e$ and that titanium is extremely reactive metal. The argument against the existence of pores in passive films on iron has been given by Vetter[12] and similar arguments apply to titanium.

The considerable hysteresis observed in the potential time dependence of titanium in solutions containing cyanide ions (Fig. 3) is attributed to adsorption of cyanide ions in competition with water molecules on the titanium surface which tend to interfere with the passivation reaction. Chloride ions apparently exhibit no similar effect.

Typical anodic and cathodic potentiostatic quasi-steady-state polarization behavior of passive titanium in sulfidic solutions is shown in Fig. 4. The polarization curves in Figs. 4 and 5 were obtained after the titanium electrode had attained a steady-state corrosion potential. The polarization curves were determined beginning from −0.1 V (SCE) toward higher potentials at 25 to 50 mv internals by measuring the steady-state current at the end of a 3 minute arrest at each potential.

The cathodic polarization in both acidic and alkaline sulfidic solutions on "passive" titanium (Fig. 4) exhibits a Tafel type behavior with a slope

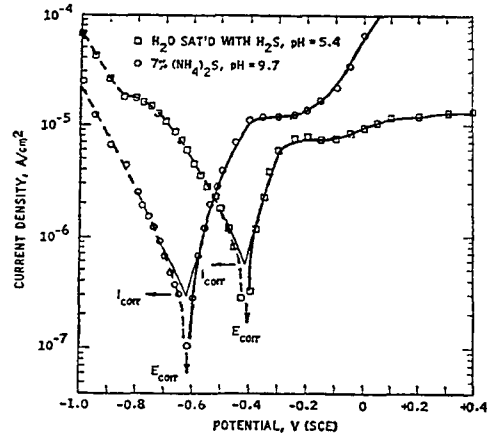


Fig. 4. Typical Anodic and Cathodic Potentiostatic Polarization Behavior of Passive Titanium in Sulfidic Solutions at 60°C.

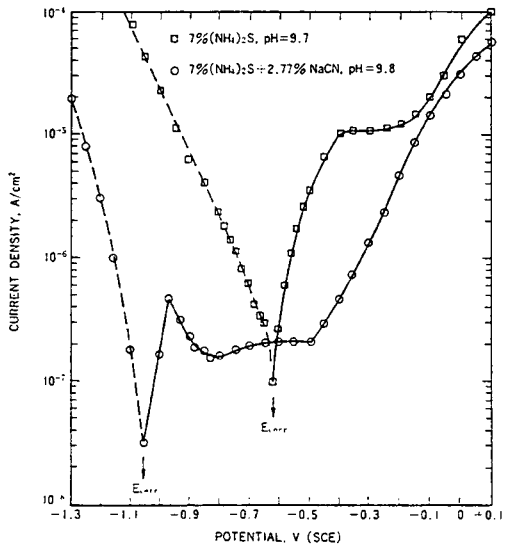


Fig. 5. Anodic and Cathodic Potentiostatic Polarization of Passive Titanium in 7% $(NH_4)_2S$ Solution at 60°C with and without cyanide ions.

of about 150 mv/decade of current. In the acidic solution (3.34% NaCl sat'd with H_2S) the cathodic reaction corresponds to the overall reaction: $2\,H_2S+2\,e=H_2+2\,HS^-$ and it is limited by hydrogen overvoltage at low polarizing potentials and by H_2S diffusion at more negative potentials.[13] In alkaline sulfidic solutions, the cathodic reaction corresponds to decomposition of H_2O. The experimentally determined cathodic Tafel slopes are consistent with a model proposed by Meyer[14] for passive zirconium, which assumes that the overall kinetics of the cathodic reaction is controlled by both charge transfer through the passive oxide film and through the Helmholtz layer at the oxide–solution interface. Additions of chloride ions in sulfidic solutions were found to have no significant effect on cathodic polarization of passive titanium. Cyanide ions, however, were found to promote the cathodic activation of passive titanium[13] as shown in Fig. 5.

The anodic polarization behavior of passive titanium in sulfidic solutions is more complex due to redox processes involving various sulfur species.[15] In acidic solutions, redox interferences are less significant. The anodic polarization curve in this solution (Fig. 4) shows an initial Tafel like behavior which is attributed to activation controlled growth of the passive oxide film, prior to development of the oxide as a diffusion barrier. At potentials higher than −0.3 V (SCE) the oxide film apparently becomes of sufficient thicknesses to act as an ionic diffusion barrier and the current becomes essentially constant as the voltage increases giving a plateau on the *i–E* plot. This is likely due to the fact that the decrease in current due to oxide film thickening is counter-balanced by the increase in current resulting from the voltage rise. The anodic polarization behavior of passive titanium in alkaline solutions shows similar Tafel like behavior near the corrosion potential, but exhibits interference from oxidation reactions involving SH^-. These effects are discussed in more detail elsewhere.[15]

Galvanic Behavior of Titanium in Sulfidic Solutions

A knowledge of the polarity of titanium with respect to other commonly used construction materials when it is galvanically connected to them in contact with aqueous sulfidic solutions is necessary in order to be able to predict whether or not titanium is anodic or to predict conditions which may lead to hydrogen uptake and embrittlement (when it is the cathodic member of a galvanic couple).

To study the galvanic behavior of titanium in aqueous sulfidic solutions the following experimental methods were used: (a) open circuit potential measurements of uncoupled titanium and other commonly used materials, (b) corrosion rates of uncoupled titanium and titanium galvanically coupled to several alloys, and (c) measurements of galvanic currents flowing between titanium and several commonly used alloys in contact with aqueous sulfidic solutions.

The open circuit potential measurements of uncoupled titanium and several other commonly used metals and alloys in sulfidic solutions are

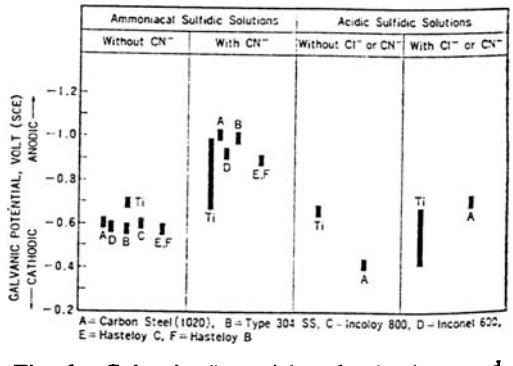


Fig. 6. Galvanic Potentials of Titanium and Several Commonly Used Alloys in Sulfidic Solutions.

Table 2. Galvanic Corrosion Effects Between Titanium and Several Other Materials in Sulfidic Solutions Containing Cyanides, 175°F (79°C), 168 hrs Test. (A/C~1)*

Galvanic Couple	Metal or Alloy	Composition of test solution					
		10% $(NH_4)_2S$+10% NaCN			2% $(NH_4)_2S$+10% NaCN		
		Corrosion Rate		Galvanic Corrosion++ Acceleration	Corrosion Rate		Galvanic Corrosion++ Acceleration
		mpy	mm/y		mpy	mm/y	
Ti−Inconel 600	Ti	0.1	0.01		0.0	0.0	
Ti−Inconel 600	Inconel 600	15.8	0.4	1.25	45.8	1.16	1.31
Uncoupled	Ti	0.0	0.0		0.1	0.01	
Uncoupled	Inconel 600	12.6	0.3		34.8	0.9	
Ti−Incoloy 800	Ti	0.1	0.01		0.0	0.0	
Ti−Incoloy 800	Incoloy 800	23.7	0.6	1.22	32.7	0.8	1.75
Uncoupled	Incoloy 800	19.4	0.5		18.6	0.5	
Ti−Type 304SS	Ti	0.1	0.01		0.0	0.0	
Ti−Type 304SS	Type 304SS	25.5	0.6	1.18	0.0	0.0	0.0
Uncoupled	Type 304SS	21.6	0.5		5.8	0.15	
Ti−Carbon Steel	Ti	0.1	0.01		0.0	0.0	
Ti−Carbon Steel	Carbon Steel	38.4	1	1.56	8.8	0.2	1.35
Uncoupled	Carbon Steel	24.6	0.6		6.5	0.16	

* A/C=anode-cathode area ratio.
++ Galvanic corrosion acceleration=Corrosion rate in galvanic couple/corrosion rate of uncoupled material.

summarized in Fig. 6. The data in Fig. 6 show that titanium is slightly anodic by about 100 to 250 mV to other commonly used metals and alloys in aqueous sulfidic solutions which are free of cyanide ions. On the other hand, in sulfidic solutions which also contain cyanides and chlorides titanium is cathodic by about 200 to 300 mV as compared with other commonly used materials. The observed reversal is galvanic polarity of titanium in sulfidic solutions containing cyanide and chloride ions is attributed to breakdown of protective sulfides or other "passive" films[15], present on carbon steel and commonly used alloys, by the cyanide or chloride ions which results in active corrosion and the more active corrosion potential for these alloys.

The galvanic potential measurement were supplemented with corrosion data obtained in sulfidic solutions by exposing uncoupled titanium test coupons as well as test coupons coupled to several commonly used construction materials. In cyanide-free sulfidic solutions, titanium is anodic to several materials such as carbon steel, Type 304 SS, Inconel 600 or Incoloy 800, and these materials were not subject to any corrosion acceleration due to galvanic coupling. Titanium although anodic in these tests did not corrode, or suffer any other adverse effects. This immunity to corrosion of titanium when anodic in a galvanic couple is attributed to self-passivation of titanium in these solutions, which is further enhanced by the anodic growth of the oxide film.

In sulfidic solutions containing cyanides or chlorides, in which titanium is cathodic the data shown in Table 2 indicate that carbon steel, Type 304 SS, Inconel 600 and Incoloy 800 when galvanically coulped to titanium, corrode at a higher rate than when exposed in the same solution uncoupled.

It should be noted theat the data shown in Table 2 are weight loss data when the anode to cathode area ratio A/C~1:1. To determine the effect of different anode to cathode area ratios on corrosion acceleration due to galvanic coupling to titanium, the galvanic currents flowing between carbon steel and titanium for different A/C values were determined in a sulfidic solution containing cyanides. The data shown in Fig. 7 indicate that the galvanic current and, therefore, the corrosion rate acceleration of carbon steel when galvanically coupled to titanium, in cyanide containing sulfidic solutions, is maximum at A/C~1:1 and decrease by about a facrot of 5 as the A/C becomes 4/1 and higher.

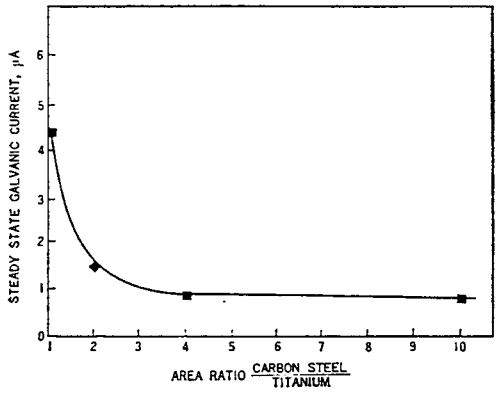


Fig. 7. Variation of the Galvanic Current Between Titanium and Carbon Steel for Different CS/Ti Area Ratios in 10% $(NH_4)_2S$+10% NaCN Solution at 79.4°C.

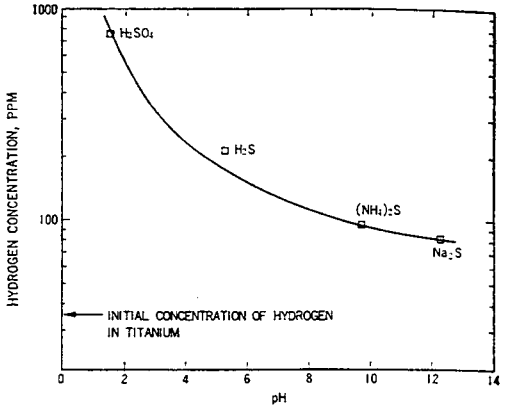


Fig. 8. Effect of Solution pH on the Rate of Hydrogen Absorption in Titanium. Identical Titanium Electrodes Cathodically Polarized at 10 ma/cm² for 24 hrs at 82°C.

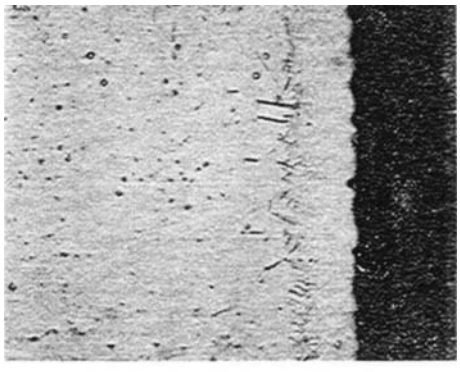
Factors Influencing Hydrogen Absorption and Embrittlement of Titanium

Hydrogen is one of the most dangerous impurities in titanium and titanium-base alloys and therefore absorption of hydrogen in titanium is a phenomenon of considerable technological importance.

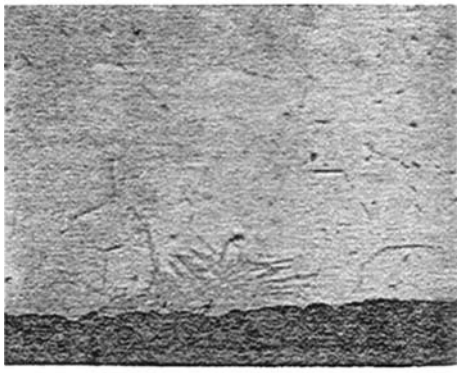
The TiH system forms an interesting contrast to the well known Fe–H system. In the Fe–H system, the affinity between metal and hydrogen is only slight, they form no chemical compounds and the hydrogen gas dissolves in the metal in comparatively small concentrations. In the Ti–H system on the other hand, the mutual affinity is great, a chemical compound is formed, and hydrogen dissolves in the metal in relatively large quantities. The maximum concentration of hydrogen which can be absorbed by titanium corresponds approximately to the composition of TiH_2.

One of the ways in which hydrogen can be absorbed in titanium is either by atomic hydrogen generated on the metal surface during natural corrosion or during cathodic polarization, i.e., when titanium is galvanically connected to a more active metal. A study of hydorgen absorption under conditions of cathodic polarization is therefore of significance from a practical standpoint, since absorption of hydrogen in titanium may lead to formation of titanium hydride (TiH_2) and embrittlement of titanium.

For the hydrogen absorption studies the electrode and cell design was similar to that described previously.[16] The titanium electrodes were cathodically polarized at 10 ma/cm² at different times and the amount of hydrogen absorbed in the ti-



a. H_2O sat'd with H_2S (pH=4.3)



b. 10% Na_2S (pH=12.3)

Fig. 9. Effect of Solution pH on the Morphology of Titanium Hydride Formed on Titanium Cathodically Polarized at 10 ma/cm² for 24 hrs at 82°C. a. H_2O sat'd with H_2S (pH 4.3), b. 10% Na_2S (pH 12.3).

tanium electrodes was determined using a high vacuum extraction method at 1400°C. Fig. 8 shows the effect of solution pH on the amount of hydrogen absorbed when identical electrodes were polarized at 10 ma/cm^2 for 24 hrs. in solutions of different pH at 82°C. The data shows quite a pronounced effect of solution pH on the rate of hydrogen absorption, with considerably higher rate in acidic than nearly neutral to alkaline solutions.

It is also of interest that not only the amount of hydrogen is affected by pH, but also the morphology of the titanium hydride phase formed on the metal surface as a result of hydrogen absorption. As shown in Fig. 9, in acidic solutions the titanium hydride forms a continuous layer on the metal surface.* On the other hand, in mildly alkaline sulfidic solutions only isolated patches of titanium hydride were detectable on the metal surface with most of the surface area being free of titanium hydride. This is attributed to different kinetic mechanisms which control the rate of hydrogen absorption in acidic and mildly alkaline solutions.

As shown in Fig. 10 in acidic solutions hydrogen absorption appears to follow a parabolic time dependence which apparently implies that the overall kinetics of hydrogen absorption is controlled by solid state diffusion of hydrogen in titanium and growth of the titanium hydride layer. In mildly alkaline sulfidic solutions on the other hand, the overall kinetics of hydrogen absorption shows a

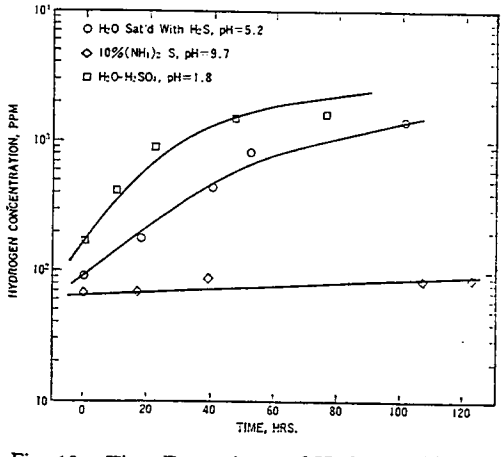


Fig. 10. Time Dependence of Hydrogen Absorption Rate in Titanium Cathodically Polarized at 10 ma/cm^2 at 77°C.

* After prolong exposure, diffusion of hydrogen and formation of titanium hydride thin plates far deep into the metal structure were also detectable.

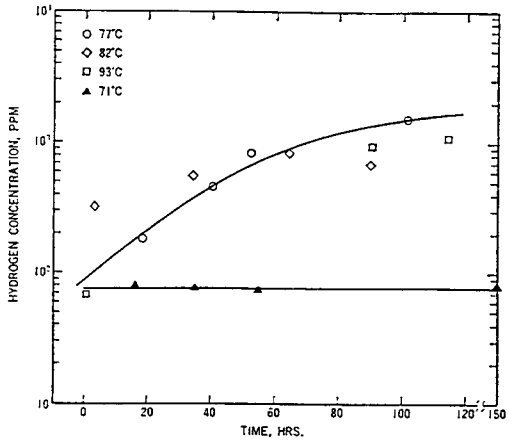


Fig. 11. Effect of Temperature on the Rate of Hydrogen Absorption in Titanium Cathodically Polarized at 10 ma/cm^2 for 24 hrs in Distilled Water Sat'd with H_2S (1 Atm) at Different Temperatures.

linear time dependence, and the overall rate is controlled by the interface hydrogen generating reaction.[17] The spotty formation of titanium hydride on titanium in mildly alkaline solutions is probably due to competitive adsorption of hydroxyl ions or water molecules which tend to promote passivation of titanium and thus interfere with hydrogen absorption.

Temperature is another important parameter affecting hydrogen absorption in titanium. Experiments with a variety of sulfidic as well as acidic sulfate solutions, indicate that the rate of hydrogen absorption in titanium is significant at temperatures higher than 72°C, but negligible at lower temperatures. The role of temperature on the rate of hydrogen absorption is illustrated with data in Fig. 11 which show hydrogen absorption of titanium cathodically polarized at 10 ma/cm^2 in distilled water sat'd with H_2S (1 Atm) at different temperatures[17].

Several experiments were also carried out to determine the effect of promoter elements on the rate of hydrogen absorption in titanium cathodically polarized at 10 ma/cm^2 in an acid sulface solution of pH≈1. The data[18] shown in Fig. 12 demonstrate the pronounced effect of sulfur and phosphorus containing impurities in increasing the rate of hydrogen absorption as indicated with thickness measurements of the titanium hydride ilayer. The influence of arsenic and antimony con taining impurities was not as pronounced.

There is little doubt that the promoter elements exert their influence on increasing hydrogen ab-

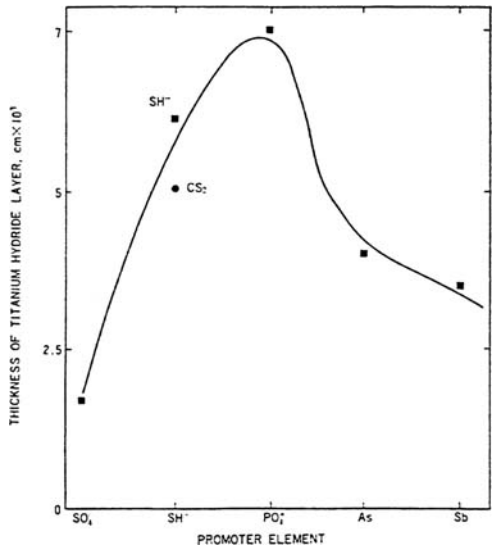


Fig. 12. Effect of Various Promoter Species (3×10^{-3} g-equ./lit) on the Rate of Hydrogen Absorption in Titanium Cathodically Polarized at 10 ma/cm² for 24 hrs in 0.1 N H_2SO_4 (pH = 1.2) at 93°C.

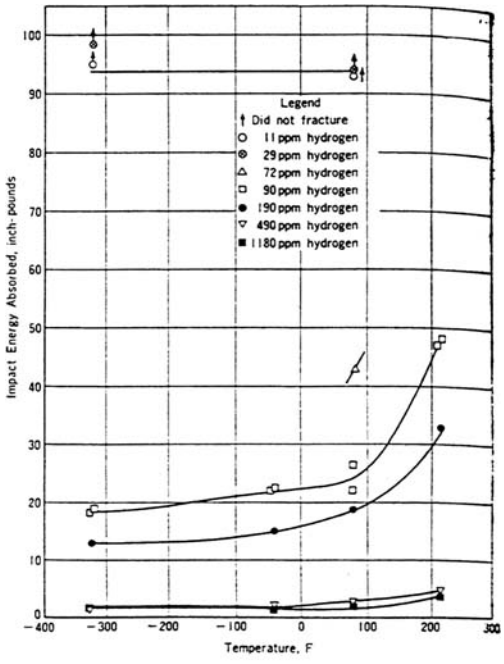


Fig. 13. Effect of Hydrogen and Temperature on the Notch-Bend Impact Strength of High-Purity Titanium (From Reference 19).

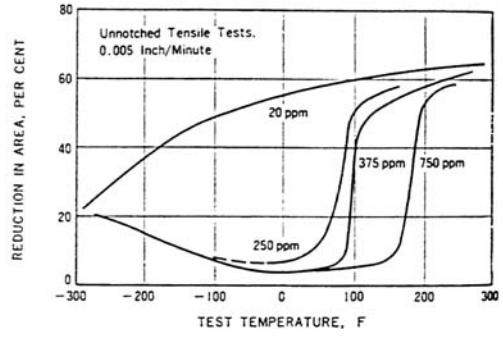


Fig. 14. Effect of Hydrogen and Temperature on the Low-Strain-Rate Embrittlement of α/β-Titanium Alloys (From Reference 20).

sorption by adsorbing on the titanium metal surface. However, the mechanism of their action in promoting absorption of hydrogen is not known. It is possible that the promoter increases the Ti–H bond on the metal surface and thus increases the coverage of adsorbed atomic hydrogen which thereby increases the permeation rate. Other explanations such as formation of hydride of the promoter element during cathodic polarization as an essential element of hydrogen entry is also possible[18]. Similar experiments with sulfidic solutions showed thar cyanide ions tend to promote hydrogen uptake, whereas chloride ions have essentially no effect[10].

The presence of even comparatively small concentration (a few tens of ppm or more) of hydrogen in titanium and titanium alloys can lead to brittle failure. This effect, referred to as hydrogen embrittlement can be devided into two quite dissimilar types. Because the most striking difference between these two types of embrittlement is the strain rate at which they appear, the two types of hydrogen embrittlement are generally referred to as **impact embrittlement** and **low-strain-rate** embrittlement.

Impact embrittlement becomes more severe with increasing hydrogen content, decreasing temperature, increasing strain-rate (or loading rate) and when notches are introduced into the sample. In contrast to impact embrittlement, low-strain-rate embrittlement becomes more severe as the strain rate decreases. In addition, ductility is lost over a finite intermediate temperature range, so that an alloy susceptible to slow-strain-rate embtittlement will often be ductile if tested at either a higher or lower temperature range.

With commercially pure titanium (almost entirely alpha-titanium) contaminated with hydrogen, impact embrittlement is the most common form of failure, but low-strain-rate embrittlement also is known to occur. The role of hydrogen and tem-

perature on the impact embrittlement of titanium is shown schematically in Fig. 13 which is reproduced from the paper by Lenning et al.[19]. With α/β–titanium alloys, low–strain–rate embrittlement is most often observed. The effect of small additions of hydrogen and temperature on low–strain–rate embrittlement of α/β–titanium alloys was demonstrated by Williams[20] and illustrated in Fig. 14.

Embrittlement of titanium and its alloys is attributed to formation of titanium hydride crystallites in the from of thin plates. Titanium hydride may be formed either by thermal precipitation due to rapidly decreasing solubility of hydrogen in Ti with decreasing temperature, or may precipitate from supersaturated solution when the alloy is stressed. If the excess of hydrogen before testing is present in the form of titanium hydride, impact embrittlement is observed. When, on the other hand, the excess of hydrogen before testing is present in supersaturated solution, low–strain–rate embrittlement is observed.

Concluding Remarks

- Titanium in both acidic and alkaline sulfidic solutions exhibits stable passivity and negligible corrosion.
- Titanium when galvanically coupled to carbon steel and commonly used alloys in sulfidic solutions may be cathodic or anodic depending on the aggressiveness of the corrosive solution.
- Cathodic polarization in sulfidic solutions promotes hydrogen uptake and embrittlement of titanium. The rate of hydrogen uptake is strongly influenced by solution pH, the presence of promoter impurities, and is significant only at temperature of 72°C and higher.
- Even comparatively small hydrogen contents (a few tens of ppm or more) are sufficient to cause embrittlement of titanium. With commercially pure titanium contaminated with hydrogen, impact embrittlement is the most common form of failure. With α/β–titanium alloys low–strain–rate embrittlement is most often observed.

(Received September 1, 1979)

References

1) M. Stern and H. Wissenberg: *J. Electroch. Soc.*, **106**, 755 (1959).
2) M. Levy: *Corrosion*, **23**, 236 (1967).
3) J. M. Peters and J. R. Myers: *J. Electroch. Soc.*, **23**, 326 (1967).
4) J. C. Griess: *Corrosion*, **24**, 96 (1968).
5) R. R. Sayano and K. Nobe: *Corrosion*, **22**, 81 (1966).
6) N. T. Thomas and K. Nobe: *J. Electroch. Soc.*, **116**, 1748 (1969).
7) N. D. Tomashov and G. P. Chernova and R. M. Atltovskii: *Russ J. Phys. Chem.*, **35**, 523 (1961).
8) Z. A. Foroulis: Proc. 4th Latin-American Congress on Electrochemistry and Corrosion, Caracas, Venezuela, 1979.
9) M. Pourbaix: "Thermodynamics of Dilute Aqueous Solutions", Arnold London (1949).
10) Z. A. Foroulis: *Werkstoffe u. Korrosion*, in press.
11) E. E. Rider, V. I. Orcharenko, V. Y. Dudarev and V. M. Novakovskii: *Protection of Metals*, **11**, 170 (1975).
12) K. J. Vetter: *Z. Electrochem.*, **55**, 274 (1951).
13) Z. A. Forouli: *J. Electroch. Soc.*, to be submitted.
14) R. E. Meyer: *J. Electroch. Soc.*, **107**, 847 (1960).
15) Z. A. Foroulis: *Corrosion*, to be submitted.
16) Z. A. Foroulis: *J. Electroch. Soc.*, **113**, 532 (1966).
17) Z. A. Foroulis: *Met. Trans.*, to be submitted.
18) Z. A. Foroulis: *J. Electroch. Soc.*, to be submitted.
19) G. A. Lenning: C. M. Craighead and R. I. Jaffe, *Trans, AIME*, **200**, 367 (1954).
20) D. N. Williams: *J. Inst. Metals*, **91**, 147 (1962–63).

Copyrighted Materials
Copyright © 1996 NACE International Retrieved from www.knovel.com

Paper No.
63

CORROSION 92
The NACE Annual Conference and Corrosion Show

ENGINEERING INCENTIVES FOR UTILIZING Ti-3Al-8V-6Cr-4Zr-4Mo ALLOY TUBULARS IN HIGHLY AGGRESSIVE DEEP SOUR GAS WELLS

D. R. Klink
RMI Titanium Company
11200 Westheimer
Houston, TX 77042

R. W. Schutz
RMI Titanium Company
1000 Warren Ave.
Niles, OH 44446

ABSTRACT

The cold pilgered Pd-enhanced Ti-38644 titanium tubular represents an optimized production tubular product for worst-case deep sour gas well service. Tubular processing and heat treatment improvements have resulted in enhanced ductility, age uniformity, and thermal stability compared to first generation hot extruded Ti-38644 tubulars. Alloy compositional enhancement with a minor Pd level, in conjunction with these microstructural improvements, have elevated both stress corrosion and crevice corrosion temperature thresholds to at least 246° C in worst-case sour gas well fluids. Excellent resistance in common chloride and bromide completion fluid brines is also observed up to at least 232° C in laboratory tests.

Specific guidelines for acidizing treatments and methanol injection in gas wells must be observed to assure compatibility with Ti-38644 tubulars. Suggested guidelines developed from laboratory testing of tubulars are presented.

Finally, a Pd-enhanced Ti-38644 titanium tubing string can offer substantial potential cost savings over a C-276 alloy string in very deep, high pressure, sour gas wells. This is derived from this titanium alloy's unique combination of physical properties and higher design allowables at temperature, permitting downsizing of tubing and reduction or elimination of seal-bore assemblies.

INTRODUCTION

The Ti-38644 alloy (Ti-3Al-8V-6Cr-4Zr-4Mo, or Beta-C™ titanium), developed by RMI Titanium Company more than 20 years ago, has been commercially utilized in numerous critical aerospace component applications, including springs and fasteners. These applications have been driven by the Ti-38644 alloy's ability, as a solute-rich beta titanium alloy, to be aged to very high strengths, provide deep hardenability in thick sections, and exhibit an elevated strength-to-density ratio. By virtue of its significant molybdenum content, however, this alloy has also been shown to be endowed with superior resistance to reducing acid and localized chloride corrosion[1] compared to most other commercial titanium alloys. This attractive combination of high strength, low density, and hot chloride corrosion resistance was first exploited commercially when the Ti-38644 alloy was selected for production tubular casings in several Salton Sea hypersaline geothermal wells in the mid-1980's.[2] These rather large hot-extruded casings, still in service today, represent a technical and economic success in material selection for handling corrosive, high temperature produced brine fluids.

As highly sour and sulfur-laden produced brine fluids in deep gas wells exceed approximately 175-190°C, traditional CRA alloy tubulars, such as duplex stainless steel and Ni-Cr-Mo alloy tubing, can exhibit susceptibility to localized chloride attack and/or stress corrosion cracking. The rather high density and cost of these alloy tubulars are additional negative aspects with respect to deep gas well design. Based on its favorable strength to density trait and superior hot brine resistance, supported by the parallel geothermal well service experience, Ti-38644 titanium became a natural candidate for high temperature, deep sour gas well production tubulars.

This paper provides an overview of relevant metallurgy, and mechanical, physical, and corrosion properties of the Ti-38644 alloy which are applicable to deep sour gas tubular service. Alloy adjustments and optimization which were necessary to achieve a reliable, corrosion-resistant, and cost-competitive production tubular product are discussed. Implications of Ti-38644 alloy tubulars on gas well design and economics are also considered.

Ti-38644 ALLOY METALLURGY

Ti-38644 (UNS #R58640), defined by the chemical composition range outlined in Table 1, is a solute-rich metastable-beta titanium alloy. The chromium, vanadium, and molybdenum alloying elements serve to stabilize the beta (bcc structure) phase, such that 100% beta phase is retained upon rapid or air-cooling from temperatures above the beta transus (~760°C). The aluminum addition, by stabilizing alpha phase (hcp structure), enhances final aging response. The alloy is basically strengthened via two mechanisms: solid solution hardening derived from all alloying elements, and by aging which involves precipitation of fine alpha phase within the beta phase matrix. Due to its high beta stabilizing alloy content, the alloy has exceptional deep section age hardenability and is ageable to strengths in excess of 1380 MPa (200 ksi).

Due to the bcc crystal structure symmetry and multiple active slip planes available in the beta phase, this alloy exhibits excellent hot workability at temperatures above 815°C and, unlike alpha-beta alloys, excellent cold workability in the annealed (or solution-treated) condition. In the manufacture of Ti-38644 oil field tubulars, ingot is forged at temperatures above 980°C to produce billet. After trepanning, this billet stock is extruded at temperatures above 980°C to produce the basic tubular form. After solution treatment, this tubular can either be aged to achieve aim properties; or surface-conditioned, cold-pilgered, and subsequently solution-treated and aged (STA) to produce thin walled tubular products.

The precipitate size, degree, and uniformity of aging and, thus, strength of tubulars can be consistently controlled within a wide range of values. This is achieved by standardizing prior processing, and controlling final

solution-treat temperature and age time and temperature. For gas well service above 177°C, it is vital that Ti-38644 alloy tubulars be thoroughly aged to a stable metallurgical condition, thereby assuring thermal stability of strength and ductility properties with time. Finally, it is also paramount that final tubular surface conditioning, (i.e., machining and/or sandblast and pickle) completely eliminate oxide scale, alpha case, and oxygen-rich ID/OD surface layers incurred from hot processing and final heat treatment. These hard, brittle surface layers may promote pipe crack initiation and SCC, and will preclude acceptance under pipe flattening test criteria.

Ti-38644 GAS WELL TUBULAR OPTIMIZATION

The traditional production method for alpha-beta and beta titanium alloy tubulars was direct hot extrusion to size. For the Ti-38644 alloy, this meant extruding well above the beta transus temperature where significant grain growth occurs. Depending on the extrusion rate and reduction ratio, nonuniform recrystallization can result in a mixture of coarse equiaxed and very elongated (L-direction) beta grains exhibiting some variable aging response. Due to these microstructural traits, pictured in Figure 1, tubular ductility may be marginal for gas well tubular service. Elongation values of 10-15% (with RA ~20-30%) are typical for the 896-1034 MPa (130-150 ksi) yield strength window. Although minimum ductility limits for production tubulars are generally not specified, it is generally agreed that a minimum elongation of 15% is desirable. Improved ductility enhances tubular damage tolerance during handling, particularly in regard to running and extracting the string from a well.

Tubular ductility was increased to a typical elongation value of 18-21% by incorporating an intermediate cold-pilger (tube reduction) step prior to final heat treatment. Once significantly cold-worked, the subsequent solution treatment fully recrystallizes the beta grains, reducing average grain size from ASTM No. 2.5 (in extruded product) to ASTM No. 5, as shown in Figure 2. The beta grains are refined and equiaxed, thereby enhancing ductility.

Once the cold-pilgered Ti-38644 tubular is solution-treated, it is directly aged to meet the nominal 965 MPa (140 ksi) yield strength aim. However, due to the fully annealed condition achieved by solution treatment and the rich stable beta phase of this alloy, aging may be highly nonuniform, sluggish, and intergranular. This results in inadequate tubular strength from practical age cycles, and a thermally unstable microstructure at downhole temperatures.

This undesirable age condition was remedied by incorporating a proprietary solution treat and age (STA) heat treatment. This final tubular heat-treat sequence, developed by RMI Titanium Company and dubbed the PASTA treatment,[3] enhances aging kinetics and uniformity with minimum grain boundary alpha formation, while retaining excellent tubular ductility. Figure 2 reveals the uniformly aged, thermally stable microstructure achievable by this treatment.

Another major limitation of standard Ti-38644 tubulars identified from extensive downhole simulation corrosion testing at the RMI R&D Laboratory is possible susceptibility to crevice corrosion and stress corrosion cracking (SCC). Standard extruded/STA or cold-pilgered/STA Ti-38644 tubulars can exhibit chloride-induced crevice corrosion within severe crevices (i.e., Teflon to metal) exposed to deaerated NaCl brine containing sulfide or sulfur species at temperatures above 177°C. Although C-ring tests indicate cracking resistance to 232°C, these tubulars may exhibit susceptibility to SCC under slow strain rate testing (SSRT) in these sour brines above 177-191°C.[4] Similar crevice and stress corrosion limitations were indicated in high temperature chloride and bromide well completion fluid brines as well.

These corrosion performance limitations were alleviated by enhancing the standard Ti-38644 alloy composition with palladium in the 0.04-0.10 wt% range. This Pd-enhanced Ti-38644 alloy resists crevice attack

in production and completion fluids to temperatures as high as 246°C, while raising SCC thresholds of cold-pilgered pipe to temperatures of 246-260°C.[4]

Finally, production of thin-walled titanium alloy tubulars via hot extrusion may be physically limited or very costly, depending on available extrusion press size and capacity, extrusion temperature, and required reduction ratios. Furthermore, extruded titanium alloy hollows often exhibit significant wall thickness variability, eccentricity, and poor, irregular surfaces. This means excessive OD/ID surface machining and yield losses, increasing pipe cost.

These production cost issues were alleviated by producing Ti-38644 tubulars through cold-pilgering of extruded hollows to near-final size and length. This near-net process produces thin-walled pipe in API Range II lengths with exceptional ID/OD surface profile and overall dimensional tolerances. This translates into minimal surface conditioning, improved yields, and significant reductions in tubular cost.

This evolution in Ti-38644 tubular product development, outlined in Figure 3, was essential for Ti-38644 titanium to evolve into a prime candidate for deep sour gas well production tubular service.

Ti-38644 TUBULAR PROPERTY CHARACTERIZATION

Relevant mechanical, physical, and corrosion properties of Ti-38644 tubulars for gas well production are described in the following sections. Most of these properties were determined from the three lots of mill-produced tubulars described in Table 2. These three lots represent the extruded and cold-pilgered forms of standard Ti-38644 pipe, and the optimized cold-pilgered, Pd-enhanced Ti-38644 pipe for comparative purposes.

Mechanical Properties

Typical tensile properties for Ti-38644 production tubulars are outlined in Table 3. Gas well pipe generally requires yield strength limits of 896-1034 MPa (130-150 ksi) at room temperature with typical values of 724-793 MPa (105-115 ksi) at downhole temperatures to minimize tubular wall and weight. Cold pilgered tubulars are readily aged to L direction yield strengths in the 931-1000 MPa (135-145 ksi) range, which will drop ~172-207 MPa (~25-30 ksi) to values of 758-793 MPa (~110-115 ksi) at 200-260°C. Higher minimum strength values at temperature are easily adjusted upward through a minor reduction in final age temperature.

Table 3 data also reveals that the cold-pilgered Ti-38644 pipe offers a significant margin of comfort in ductility over the extruded product. However, neither product exhibits notch sensitivity over this temperature range. The relatively low modulus of beta titanium alloy tubulars offers improved elastic bending and flexibility downhole compared to conventional downhole alloys, and is more than adequate from a collapse standpoint. Note that compressive strength, and not modulus, is the limiting factor in pipe collapse at OD thickness ratios below ~13.

Fracture toughness (K_c) values for both beta tubular forms were measured to be in the 44-62 MPa $\sqrt{m}$ (40-56 ksi $\sqrt{in.}$) range in the C-R direction. Note that this represents the most conservative (worst-case, lowest K_c value) direction in the tubular, based on texture considerations. Because of their bcc structure, all beta titanium alloys characteristically exhibit relatively low Charpy impact toughness values compared to conventional downhole alloys with fcc structures. Values measured for Ti-38644 were relatively unchanged at 11-16 Joules over the -20° to 20°C temperature range. No ductile to brittle transition is observed, and gradually increasing Charpy values can be expected with increasing temperature. Note that Ti-38644 tubular impact toughness is totally

independent of strength, ductility, hardness, or fracture toughness properties. Based on this and known downhole service dynamics, this seemingly low high-strain-rate toughness in these tubulars is not perceived to be a real or practical limitation of these alloys in downhole tubular applications.

Finally, the creep resistance of both Ti-38644 tubulars was evaluated at maximum loads and temperatures anticipated downhole to assure that high pressure connection seal integrity will be maintained with time. Applied stress levels of 586-758 MPa at 204-232°C produced primary creep strain values below 0.1%, and steady state creep rates of 3-30 x 10^{-7}%/hour. These creep values translate into net tubular strains that are less than 0.3% after 10 years, which are well within acceptable limits.

Physical Properties

The two physical properties that especially distinguish beta titanium tubulars from ferrous and nickel base alloy tubulars are low density and low thermal expansion coefficient. With a density of 4.8 gm/cm^3 and an expansion coefficient of 9.4 x 10^{-6}/°C, Ti-38644 tubulars are 46% and 27% lower than corresponding C-276 tubular values, respectively. Their beneficial impact on deep sour gas well design is discussed in the final "well design/economics" section.

A strong linear correlation between hardness and yield strength exists in Ti-38644 tubulars. Rockwell C hardness values in the 31-36 range can be expected within the 896-1034 MPa (130-150 ksi) yield strength window. These are well below the maximum HRC value of 42 allowed for this alloy under the NACE MR-01-75 specification.

Corrosion Performance

A suitable deep sour gas well tubular must not only resist worst-case produced fluid environments (including liquid mercury), but must also exhibit compatibility with various completion fluids, acidizing treatments, and injected methanol at downhole temperatures. The following sections review the results of extensive laboratory testing conducted on Ti-38644 tubulars under diverse, simulated, worst-case well conditions.

Produced Well Fluids. Autoclave testing was conducted on Ti-38644 tubulars in a worst-case deep sour gas well fluid brine environment, described by the following parameters:

- fully deaerated 20% NaCl brine[4]
- 6.9 MPa (1000 psi) H_2S
- 3.4 MPa (500 psi) CO_2
- 1 gpl elemental sulfur
- with and without 0.5 wt% acetic acid
- 163-274°C

C-ring, SSR, and crevice corrosion testing revealed that standard Ti-38644 tubulars are susceptible to both crevice and stress corrosion under these worst-case conditions at temperatures above ~177°C. Although 3-6 month C-ring exposures (loaded to 90-105% YS) demonstrated SCC resistance up to 232°C, the more discriminating SSR tests (at 4 x 10^{-6} sec^{-1} strain rate) produced more conservative SCC temperature thresholds by 42-56°C. This SCC test program and data are detailed in another paper.[4] The crevice attack was observed in Teflon® gasket to metal crevices and, to a lesser degree, in metal to metal crevices; and was considered to be the result of crevice acidification by retained and adsorbed oxygen reacting with sulfur/sulfide species.

The Pd-enhanced cold-pilgered Ti-38644 tubular, in contrast, demonstrated full resistance to localized corrosion up to temperatures of 246°C, even in Teflon to metal crevices. SSR testing similarly revealed that SCC threshold temperatures were elevated to 246-288°C,[4] even with 0.5% acetic acid and excessive sulfur additions to the brine. This significantly expanded window of resistance to produced sour brine fluids achievable with the Pd-enhanced tubular is indicated in Figure 4.

No significant uniform corrosion or hydrogen absorption (ΔH) of any Ti-38644 tubulars was detected in any high temperature sour brine exposures. No significant hydrogen absorption can be expected as long as the alloy is not coupled to an active, nonresistant metal (i.e. steel) in the hot sour brine fluid.

A limited number of gas wells have been known to produce minor quantities of liquid mercury, which creates concern for possible liquid metal embrittlement of tubulars in these few cases. This risk was evaluated by immersing several extruded and cold-pilgered Ti-38644 tubular C-rings, loaded to 90% YS, under liquid mercury for 30 days at 25° and 232°C. To assess the role of the oxide surface film on metal embrittlement, the C-rings were exposed in unabraded and severely abraded (in situ) conditions. The tests revealed that no cracking or dissolution occurred in liquid mercury when the stressed pipe was left unabraded. Once the protective, nonwetting oxide film was severely damaged under the liquid mercury, cracking was possible at 232°C. Since oxide film damage is not anticipated under produced liquid mercury pockets contacting pipe ID surfaces, Ti-38644 tubulars, protected by their surface oxide films, can be expected to resist amalgamation and associated embrittlement in produced fluids containing mercury.

Completion Fluids. Titanium alloy tubulars are known to be fully resistant to the more benign completion fluids, such as fresh water and oil-based muds. However, consideration must be given to localized corrosion and SCC resistance of Ti-38644 tubulars exposed to the more dense, highly concentrated sodium or calcium chloride or bromide brine fluids (at downhole temperatures), often considered for high pressure deep gas well completion. These fully deaerated brines, described in Table 4, also represent excellent electrolytes for galvanic interaction between the steel casing ID surface and the tubular OD surface. These potential galvanic effects between the noble Ti-38644 tubular and the active steel casing must be assessed in regards to possible hydrogen absorption by the titanium alloy cathode and aggravated attack on the anodic member (steel).

These corrosion issues were evaluated via 30 day autoclave tests conducted on cold-pilgered Ti-38644 tubulars in fully deaerated completion fluid brines at 232°C. SCC performance was evaluated on C-ring tubular samples stressed to 95% yield strength (at 232°C). Both metal to metal and Teflon gasket to metal crevices were exposed. A 1:1 cathode to anode surface area ratio was reflected in the carbon steel to Ti-38644 bolted galvanic assembly tested.

The test results, summarized in Table 4, reveal that both standard and Pd-enhanced Ti-38644 tubulars resisted localized corrosion, stress cracking, and significant hydrogen uptake (even when coupled to steel) in the sodium-based brines. In the more aggressive, hydrolyzable calcium brines, standard Ti-38644 exhibited susceptibility to crevice corrosion and SCC. In contrast, the Pd-enhanced tubulars exhibited total resistance to all completion fluid brines tested.

Well Acidizing Treatments. Gas well flow may require periodic stimulation by injecting and circulating acidizing solutions downhole during well workover cycles. Common acidizing fluids include 12% HCl-3% HF, 15% HCl, 10% formic acid, and 10% acetic acid solutions. The more aggressive HCl-based solutions are generally injected into the well for a total exposure of approximately six hours, after which the weak, spent acid slowly flows or is pumped back out of the well. The temperature achieved by these solutions within the tubular depends on maximum downhole temperature, and can be varied by controlling the fluid circulation rate through the well.

The weaker, slower acting organic acids are generally injected for three day periods, to break up carbonate-based formations and debris.

Like most CRA tubulars, Ti-38644 titanium may experience severe corrosion degradation when exposed to strong concentrated reducing acids at downhole temperatures. As shown in the laboratory acidizing test results outlined in Table 5, the 15% HCl and, especially, the 12% HCl-3% HF solutions produce excessive corrosion rates and hydrogen absorption in Ti-38644 tubulars. These cannot be adequately inhibited at downhole temperatures, and should be strictly avoided with titanium alloy strings. Although HF-containing acids represent a serious corrosion hazard for titanium alloys, adequate inhibition of less concentrated ($\leq$10%) HCl solutions appears to be a practical strategy. Although traditional amine-type acid inhibitors are ineffective with titanium alloys, highly oxidizing species in sufficient concentrations can mitigate uniform corrosion while alleviating hydrogen absorption. Some potent candidate oxidizing inhibitors such as ferric, nitrate, and molybdate ion additions were further evaluated in 6 hour laboratory autoclave test exposures. As indicated in Table 5, a 4.0-4.5% sodium molybdate addition can effectively mitigate corrosion in $\leq$10% HCl, while avoiding stress cracking to temperatures below ~180°C. Above this temperature, SCC becomes the limiting factor, as detected in tubular C-rings stressed to 90% of yield stress at test temperature. Although this provides a reasonable avenue for utilizing 5-10% HCl acidizing fluids at temperatures up to ~180°C with Pd-enhanced or standard Ti-38644 tubulars, further studies with this and other inhibitor systems are warranted for optimizing inhibitor cost and concentration. Furthermore, compatibility of these specific inhibitors with conventional amine-type inhibitors and other downhole alloys has yet to be established.

The safest and most highly recommended well acidizing treatment that is fully compatible with Ti-38644 titanium tubulars involves injection of organic acids. As revealed in Table 5, Ti-38644 tubulars exhibit exceptional resistance to either 10% acetic or formic acids up to at least 232°C without any inhibitor addition. The presence of significant background levels of chloride in these organic acid solutions will not compromise alloy resistance.

Injected Methanol. Methanol may be periodically injected downhole to stimulate flow by dissolving hydrate pluggages. Although conventional downhole materials generally resist methanol quite well, titanium alloys are known to be highly susceptible to SCC in near-anhydrous methanol[5,6]. Although chlorides may accelerate cracking, sufficient concentrations of water have been shown to effectively suppress this stress cracking phenomenon. Since commercial grades of methanol injected are near-anhydrous (i.e. $\geq$ 97% methanol), minimum safe levels of water in methanol required for full SCC inhibition need to be identified for highly stressed Ti-38644 tubulars at downhole temperatures.

A laboratory tubular C-ring test program was conducted in NaCl-saturated methanol solutions containing 0-3 wt.% water additions at 25°, 63° (boiling), and 232°C. Tubular C-rings of standard and Pd-enhanced Ti-38644 titanium were loaded to 90% yield strength (at test temperature) prior to exposure for 300 hours. The minimum safe levels of water necessary for full cracking inhibition, derived from Figure 5 results, lie in the 1.5 - 3.0% water content range depending on tubular type. It is interesting to note that increasing temperature actually decreases the minimum water required, indicating a reduced stress cracking tendency.

Based on these results, a conservative safe minimum water content of $\geq$ 3 wt.% is recommended for methanol injected into Ti-38644 tubulars. This "safe" methanol may be obtained commercially, or formulated by adding either fresh water or seawater to anhydrous methanol prior to injection.

IMPLICATIONS ON GAS WELL DESIGN/ECONOMICS

Having established the corrosion resistance of Pd-enhanced Ti-38644 tubulars in the most severe downhole environments, the alloy's unique combination of mechanical and physical properties facilitate design changes which dramatically diminish the overall cost of drilling and completing deep sour gas wells. Critical tubular properties directly impacting tubular string design include yield strength, density, elastic modulus, and coefficient of thermal expansion. With the significantly reduced density, modulus, and thermal expansion of Ti-38644 titanium compared to Ni-Cr-Mo alloys, combined with accepted tubular design allowables (Table 6), tubing string cost is reduced and certain ancillary equipment can be eliminated.

These improved well design concepts are readily illustrated when comparing Ti-38644 titanium and C-276 alloy string completion options for a very deep, high pressure sour gas well. In this example, a 7,620 m (25,000 ft.) deep well with a bottom hole pressure of 138 MPa (20,000 psi), downhole and flowing wellhead temperatures of 224°C and 191°C, respectively, and freshwater packer fluid completion was assumed. Utilizing tubular design allowables in Table 6, resultant well string design and estimated costs are outlined in Figure 6. Note that almost 1.4 million U.S. dollars may be saved in the case through the selection of Pd-enhanced Ti-38644 tubulars over the heavier, "telescoping" C-276 tubing string.

In addition to reduced string cost, additional cost is saved by downsizing or even eliminating the seal-bore assembly. The thermally induced movement of a Ti-38644 string is calculated to be 4.3 m, compared to a projected movement of 5.5 m for the C-276 string. This means that the seal-bore assembly required to accomodate tubing expansion and contraction for the titanium alloy string may be shortened by 1.2 m. In fact, the thermal stress imparted into the Ti-38644 string (~19,680 lbs.) can be readily superimposed onto the tension load (~117,750 lbs.), and still maintain a tension design factor of 2.2. Therefore, if desired, the seal bore assembly can be totally eliminated from the string design. This eliminates a very costly component while replacing a moveable seal with a fixed one, thereby reducing the probability of leakage.

As a final note, gas well drilling costs may be significantly reduced by the utilization of Pd-enhanced Ti-38644 subsurface safety valves in offshore gas well tubing strings. This is derived from the higher yield strengths (at temperatures) achievable by aging hot forged or extruded Ti-38644 titanium safety valve bodies, compared to cold worked Ni-Cr-Mo alloy analogies. Higher strength translates into decreased valve OD and increased ID valve dimensions, thereby increasing valve throughput and favorably impacting well casing size.

CONCLUSIONS

The cold pilgered, Pd-enhanced Ti-38644 titanium tubular represents evolution of an optimized production tubular for worst-case deep sour gas well service. This cold pilgered tubular exhibits a refined, recrystallized beta microstructure which significantly elevates ductility over hot worked tubulars. A relatively uniform age is achieved by a simple modification in final heat treatment, resulting in good thermal stability at downhole temperatures. These features, in conjunction with enhancement of alloy composition with 0.04 - 0.10% Pd, elevates both SCC and chloride crevice corrosion temperature thresholds to at least 246°C in worst-case deep sour gas well fluids in laboratory tests. Excellent resistance is similarly noted in common chloride and bromide completion fluid brines up to at least 232°C.

Specific guidelines for acidizing treatments and methanol injection in gas wells will need to be observed to assure compatibility with Ti-38644 tubulars. Laboratory tests suggest that $\geq$ 3 wt.% water additions to injected methanol will very safely preclude stress cracking, and indicate that compatible acidizing fluids may consist of either organic acids, or of lower concentration ($\leq$10%) HCl solutions containing special oxidizing inhibitors at

temperatures below 180°C.

Finally, a Pd-enhanced Ti-38644 tubing string can offer substantial potential cost savings over a C-276 alloy string in very deep high pressure sour gas wells. This is derived from the alloy's reduced density, modulus, and thermal expansion coefficient, combined with higher design allowables with titanium alloy tubulars. These features permit reductions in pipe OD and wall sizes over the entire string compared to C-276 tubing, and possible downsizing or elimination of devices needed to compensate for thermally-induced tubing movement.

REFERENCES

1. D. E. Thomas, et. al., "Ti-38644: An Emerging Titanium Alloy for the Industrial Marketplace," Industrial Applications of Titanium and Zirconium: 4th Volume, ASTM STP 917, 1986, pp. 144-163.

2. W. W. Love, et. al., "The Use of Ti-38644 Titanium for Downhole Production Casing in Geothermal Wells," Sixth World Conference on Titanium Proceedings, Cannes, June 6-9, 1988, Société Française de Métallurgie, Les Ulis Cedex, France, pp. 443-448.

3. R. W. Schutz and S. R. Seagle, "Method for Improving Aging Response and Uniformity in Beta Titanium Alloys," U.S. Patent applied for, RMI Titanium Company, Niles, OH.

4. R. W. Schutz, M. Xiao and T. A. Bednarowicz, "Stress Corrosion Behavior of the Ti-3Al-8V-6Cr-4Zr-4Mo Titanium Under Deep Sour Gas Well Conditions," Paper No. 92051, presented at NACE Corrosion '92, Nashville, TN, April 27 - May 1, 1992.

5. W. F. Czyrklis, M. Levy, Corrosion, 1976, Vol. 32, pg. 99.

6. Metals Handbook - Ninth Edition: Vol. 13 - Corrosion, American Society of Materials, 1987, page 687.

ACKNOWLEDGEMENTS

The authors wish to recognize significant contributions by Ming Xiao of RMI Titanium Company in assisting in the development of the laboratory corrosion test data presented in this paper. Finally, the enormous commitment and support provided by RMI Titanium Company in pursuing development of this optimized Ti-38644 gas well tubular product is recognized and appreciated.

Table 1. Chemical Composition Range for the Ti-38644 Titanium Alloy

CHEMICAL COMPOSITION	% BY WEIGHT
Aluminum	3.0 to 4.0
Vanadium	7.5 to 8.5
Chromium	5.5 to 6.5
Molybdenum	3.5 to 4.5
Zirconium	3.5 to 4.5
Iron	0.30 maximum
Nitrogen	0.03 maximum
Carbon	0.05 maximum
Oxygen	0.12 maximum
Hydrogen	0.020 maximum
Others: 0.40 total (0.10 maximum each element)	

Table 2. Compositions of the Three Mill-Produced Ti-38644 Tubular Products Evaluated

		EXTRUDED/ STA STD. Ti-38644 PIPE	COLD PILGERED/STA STD. Ti-38644 PIPE	COLD PILGERED/ PASTA Pd-ENHANCED Ti-38644 PIPE
RMI Heat No.		881457	881457	882836
Composition	%Al	3.3	3.3	3.1
	%V	7.8	7.8	7.9
	%Cr	6.2	6.2	6.0
	%Zr	3.8	3.8	4.0
	%Mo	4.0	4.0	4.2
	%0	0.08-0.11	0.08-0.11	0.08
	%Pd	--	--	0.06
Size	OD mm (in.)	89 (3.50)	73 (2.875)	73 (2.875)
	Wall mm (in.)	11 (0.430)	5.5 (0.217)	7 (0.276)

Table 3. Typical Tensile Properties of Ti-38644 Titanium Production Tubulars (L-direction)

PROPERTY	TEMP. (°C)	EXTRUDED PIPE	COLD-PILGERED PIPE*
Yield Strength MPa (ksi)	25 204	965 (140) 841 (122)	965 (140) 765 (111)
Tensile Strength MPa (ksi)	25	1048 (152)	1020 (148)
Notched/Unnotched Tensile Ratio (K_t=4.5)	25 260	1.2 1.3	1.5 1.5
% Elongation	25 232	14 14	20 21
% Reduction of Area	25 232	26 28	46 48
Elastic Modulus 10^3 MPa (10^6 psi)	25 204	100 (14.5) 95 (13.8)	97 (14.0) 93 (13.5)

*Equivalent tensile properties for standard and Pd-enhanced alloy versions in STA and PASTA heat treated conditions.

Table 4. Corrosion Performance of Ti-38644 Production Tubulars in Deaerated Completion Fluids at 232°C

CORROSION MODE	26% NaCl (10 lb/gal)	46% NaBr (12.5 lb/gal)	44% $CaCl_2$ (12 lb/gal)	60% $CaBr_2$ (16-18 lb/gal)
Pitting	R (R)*	R (R)*	R (R)*	R
Crevice	R (R)	R (R)	R (N)	R
SCC	R (R)	R (R)	R (N)	R
ΔH**	R (R)	R (R)	-	-

R = Resistant
N = Not Resistant

* Standard Ti-38644 cold-pilgered pipe result within parenthesis; Pd-enhanced Ti-38644 cold-pilgered pipe result without parenthesis

** 1:1 galvanic couple with carbon steel

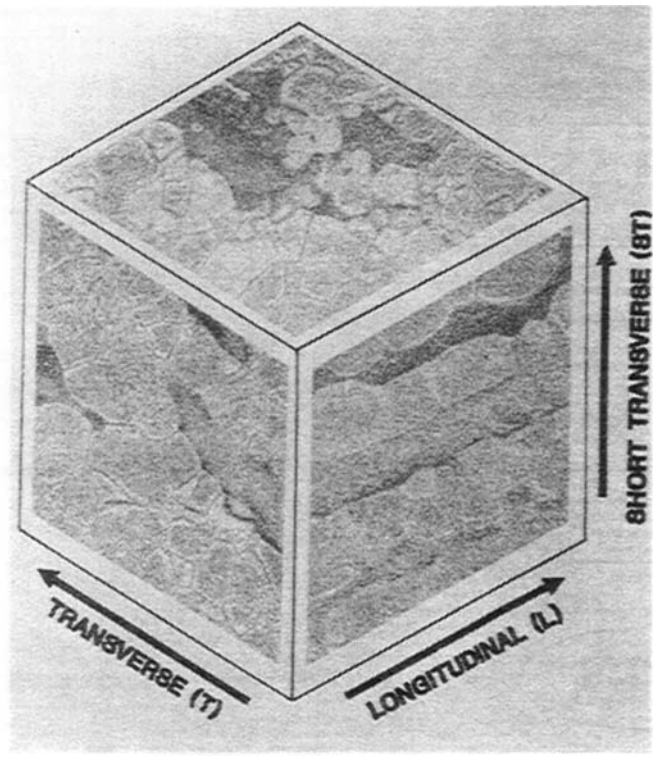
Table 5. Corrosion Performance of Pd-Enhanced Ti-38644 Tubulars in Candidate Well Acidizing Fluids

ACIDIZING FLUID	FLUID TEMP. (°C)	INHIBITOR ADDITION (WT.%)	UNIFORM CORROSION RATE μm/6Hrs. (mils/6Hrs.)	SCC?	ΔH (ppm)	COMMENTS
12% HCl - 3% HF	>25	None	>520 (>20)	--	>500	Excessive corrosion and ΔH
15% HCl	>120	None	>350 (>14)	--	>500	Excessive corrosion and ΔH
10% HCl	100	None	10 (0.4)	No	Nil	Compatible
7.5% HCl	100	None	1.6 (0.06)	No	Nil	Compatible
7.5% HCl	177	4.0% Na_2MoO_4	<0.5 (<0.02)	No	Nil	Compatible
10% HCl	177	4.0% Na_2MoO_4	1.0 (0.04)	No	Nil	Compatible
10% HCl	204	4.0% Na_2MoO_4	2.1 (0.08)	Yes	Nil	SCC limited
15% HCl	177	4% Na_2MoO_4	20.9 (0.8)	Yes	Nil	SCC limited
10% Formic Acid*	232	None	0	No	Nil	Highly compatible
10% Acetic Acid*	232	None	0	No	Nil	Highly compatible
10% Acetic Acid + 10% NaCl*	232	None	0	No	Nil	Highly compatible

* - 72 hour exposures, all other acids were 6 hours exposures.

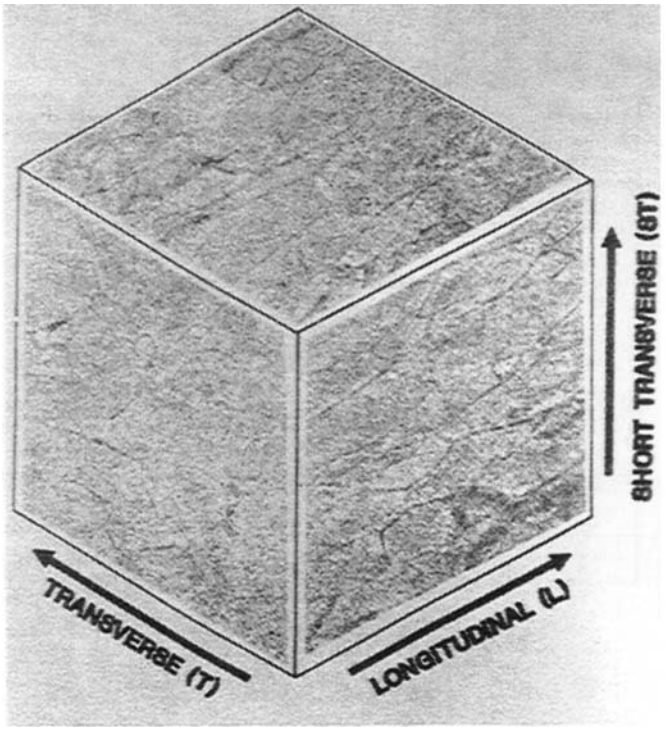
Table 6. Ti-38644 and C-276 Alloy Pipe Parameters Assumed in the Deep Gas Well String Design/Cost Analysis

PARAMETER	Pd-ENHANCED Ti-38644	COLD-WORKED C-276	COLD-WORKED C-276	COLD-WORKED C-276
Pipe OD, mm (in.)	73 (2.875)	73 (2.875)	89 (3.50)	73 (2.875)
Pipe Wall, mm (in.)	7 (0.276)	7 (0.276)	9.5 (0.375)	7.8 (0.308)
Weight, ft. (lbs.)	4.7	8.7	14.2	9.5
Pipe Body Yield (10^3 lbs.)	259	239	390	263
Min. Yield Strength MPa (ksi)	896 (130)	862 (125)	862 (125)	862 (125)
Min. Tensile Strength MPa (ksi)	965 (140)	931 (135)	931 (135)	931 (135)
Min. Yield Strength @ 204°C MPa (ksi)	793 (115)	731 (106)	731 (106)	731 (106)
Burst Strength MPa (ksi)	137 (19.9)	126 (18.3)	141 (20.4)	141 (20.4)
Collapse Strength MPa (ksi)	93 (13.5)	86 (12.5)	99 (14.3)	99 (14.3)

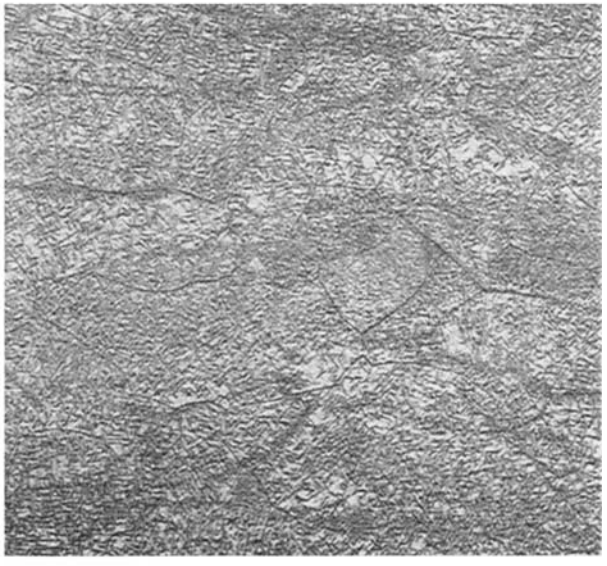


(60X)

Figure 1. Typical microstructure of a hot extruded/STA Ti-38644 tubular. Note the coarse, irregular, and elongated beta grain structure.



a. (60X)



b. (200X) Note the refined, equiaxed beta grains.

Figure 2. Typical microstructure of cold pilgered/PASTA heat treated Ti-38644 tubulars.

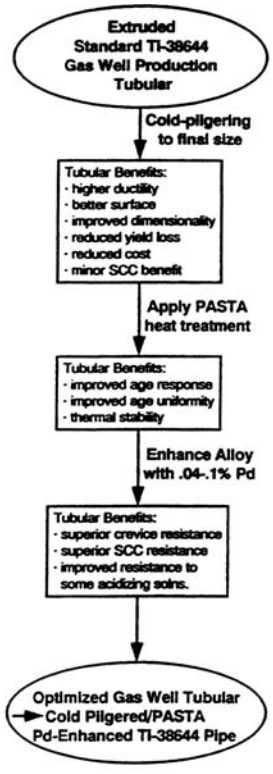


Figure 3. Evolution of the Ti-38644 titanium tubular product for deep sour gas well production tubular service.

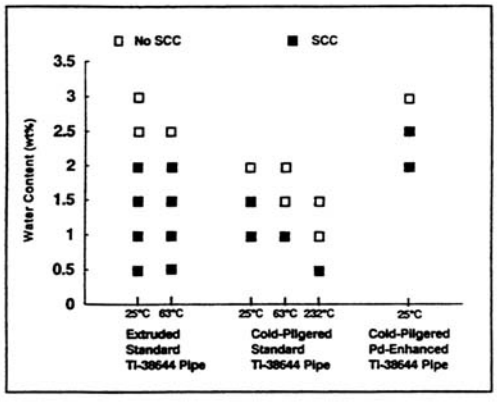


Figure 5. C-ring test data revealing the minimum water content necessary to inhibit Ti-38644 tubular stress cracking in NaCl-saturated methanol solutions.

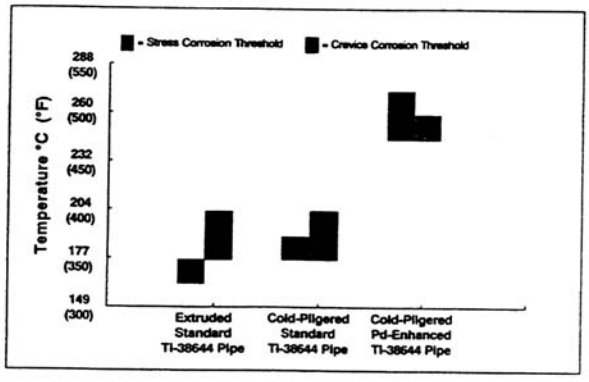
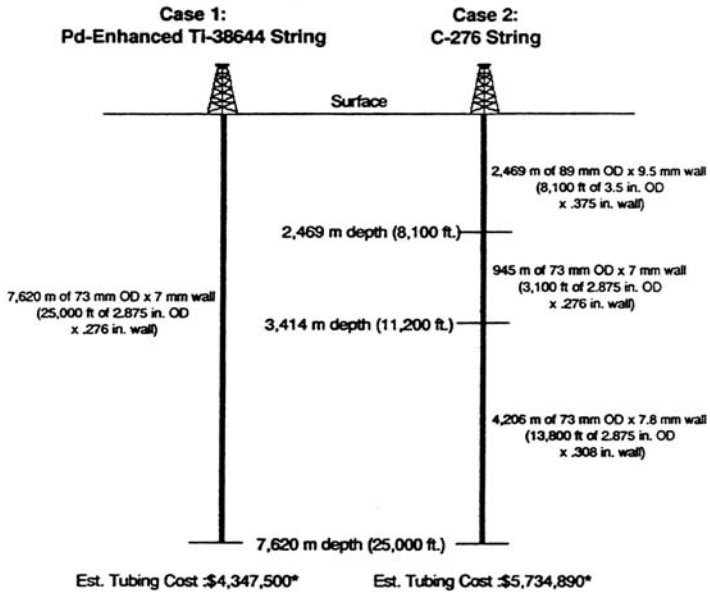


Figure 4. Stress corrosion and chloride crevice corrosion temperature thresholds for various Ti-38644 tubular products in a worst-case deep sour gas well environment.



Estimated savings due to tubing cost:	$1,387,390
Estimated savings due to shorter seal bore:	$20,000
Total estimated savings:	$1,407,390

*Costs based on actual quotes made in August 1991.

Figure 6. A comparison of economics and string designs for Ti-38644 titanium vs. C-276 alloy production tubulars utilized in a very deep sour gas well.

Copyrighted Materials
Copyright © 1996 NACE International Retrieved from www.knovel.com

Paper No.
51

CORROSION 92
The NACE Annual Conference and Corrosion Show

STRESS CORROSION BEHAVIOR OF Ti-3Al-8V-6Cr-4Zr-4Mo ALLOY UNDER DEEP SOUR GAS WELL CONDITIONS

R. W. Schutz and M. Xiao
RMI Titanium Company
1000 Warren Avenue
Niles, OH 44446

T. A. Bednarowicz
Cameron Forge Company
P.O. Box 1212
Houston, TX 77251

ABSTRACT

Standard and Pd-enhanced Ti-3Al-8V-6Cr-4Zr-4Mo (Ti-38644 or Beta-C™ titanium) alloy plate, billet, and tubular materials were evaluated with respect to their SCC resistance in a simulated worst-case deep sour gas well environment up to 274°C (525°F). Long term C-ring tests of standard Ti-38644 tubulars revealed no SCC susceptibility below 232°C (450°F) within test matrix parameters. Slow strain rate (SSR) testing of standard Ti-38644 tubulars, however, produced much more conservative SCC thresholds of 163-177°C (325-350°F) for extruded/STA pipe and 177-191°C (350-375°F) for the more ductile cold pilgered/STA pipe. Stress cracking above these threshold temperatures was primarily transgranular cleavage and probably anodically controlled.

SSR testing of all Pd-enhanced Ti-38644 products revealed SCC threshold improvements over standard Ti-38644 in the range of 42-83°C (75-150°F) in this worst-case environment. SCC resistance was synergistically elevated when both cold processing and Pd enhancement were incorporated into the Ti-38644 alloy product, achieving SCC thresholds in excess of 246°C (475°F). This SSR data base suggests that Pd-enhanced Ti-38644 can provide more than adequate SCC resistance for the worst-case deep sour gas well environments currently anticipated.

BACKGROUND

By virtue of its combination of high strength, low density, and excellent resistance to hot chloride brines, the Ti-38644 titanium alloy (Ti-3Al-8V-6Cr-4Zr-4Mo and UNS #R58640) offers potential design, cost, and performance advantages over costly, heavy Ni-Cr-Mo alloys in deep gas well tubular applications. As a beta

titanium alloy, the Ti-38644 alloy also offers definite production and cost advantages when producing thin walled production tubulars and casings via cold pilgering, a process which is not practical with alpha-beta titanium alloys. These deeper gas wells, however, generally entail higher downhole temperatures and pressures, sour conditions (high H_2S pressures) with or without elemental sulfur, and concentrated brines together which are highly corrosive to conventional downhole alloys. Numerous gas wells currently being developed in the Mobile Bay (Gulf of Mexico), Madden (Western Wyoming), and Arun (Indonesia) fields reflect these conditions, involving minimum partial pressures in excess of 0.7 MPa each of H_2S and CO_2, elemental sulfur, and near saturated NaCl brine at temperatures of 190-230°C.

The Ti-38644 alloy has logged a successful service record as production liners and tubulars handling hypersaline geothermal brines containing traces of H_2S at temperatures as high as 260°C. Furthermore, the alloy's resistance to stress corrosion cracking (SCC) has also been demonstrated in highly loaded, smooth, notched, and precracked samples exposed to ambient sweet and sour salt solutions[1-4], including NACE Standard TM-01-77 test conditions. However, no significant information addressing the SCC behavior of this alloy in highly sour, concentrated brines at temperatures above 177°C, with and without elemental sulfur, is available. The alloys's SCC resistance is of critical concern in these highly stressed tubular applications. It is generally agreed among gas producers that long term (≥3 month) tubular C-ring tests, supplemented by slow strain rate testing (SSRT), under worst-case gas well conditions can provide a satisfactory data base for assessment of alloy SCC performance.

This study was intended to generate this needed C-ring and SSRT SCC data base for Ti-38644 titanium in the most aggressive production fluid environment conceivable in deep sour gas wells. Both standard and Pd-enhanced Ti-38644 alloy samples were evaluated at strength levels and in metallurgical conditions relevant to gas well tubular and component service.

EXPERIMENTAL

Test Environment - The C-ring and SSR tests on Ti-38644 samples were all conducted in laboratory autoclaves containing a simulated worst-case sour gas well production environment which consisted of:

- fully deaerated 20 wt.% NaCl
- 6.9 MPa (1000 psi) H_2S
- 3.4 MPa (500 psi) CO_2
- 1 gpl S°
- with or without 0.5 wt.% acetic acid
- 177-274°C (350-525°F)

The partial pressures of H_2S and CO_2 indicated are those at test temperature. The addition of 0.5% acetic acid was made in a few tests to further reduce brine pH and create ultra-aggressive test conditions.

Successful simulation of downhole production fluids in laboratory tests requires the achievement of total deoxygenation within the autoclave. This includes de-adsorption of oxygen from autoclave internals and specimen surfaces and crevices, in conjunction with complete brine and gas phase deaeration. Inadequate removal of oxygen may aggravate localized attack on CRA test samples as a result of oxygen reacting with sulfide and sulfur species at temperature to locally form highly acidic chloride and sulfate conditions. This resultant localized attack can seriously compromise or even invalidate alloy SCC test evaluation.

An autoclave loading procedure was utilized that reproducibly precluded significant oxygen contamination, and best simulated the fully deaerated fluid environment downhole. This procedure incorporates multiple autoclave evacuation and argon backfilling cycles prior to charging the fully deaerated (argon sparged) brine into the autoclave. Once filled with brine, the autoclave is sequentially charged with liquid H_2S and liquid CO_2 at room temperature. Appropriate partial pressures for each gas to be "cold charged" are derived from pressure calibration curves empirically established in prior autoclave trials. Final autoclave heat-up to test temperature raises the partial pressures to desired values. This eliminates the need for a high pressure "hot charging" procedure for the H_2S and CO_2 gases, which introduces an increased probability of leakage and air intrusion into the autoclave.

C-Ring Testing - C-ring testing was conducted on two tubular products of standard Ti-38644 titanium which were mill produced at RMI Titanium Company (Niles, OH). One tubular was 89 mm (3.5 in.) OD x 11 mm (0.430 in.) wall in size produced by direct extrusion, followed by solution treating and aging (extruded/STA). This process results in a tubular exhibiting reasonable strength, but less than optimum microstructure, ductility, and flattenability. The other tubular, 73 mm (2.875 in.) OD x 5.5 mm (0.217 in.) wall, was produced by cold pilgering the as-extruded form of the first tubular, followed by solution treating and aging (cold pilger/STA). This final cold reduction, recrystallization, and age processing produced more refined, equiaxed beta grains, exhibiting enhanced ductility and flattenability at the same strength level. Tubular composition and properties are outlined in Table 1.

C-ring samples tested were 25.4 mm in width, and were prepared and loaded by deflection measurement in accordance with ASTM G-38 specifications. Specimen surfaces were either as-machined to a 25-30 RMS finish, or left as mill produced (i.e. sandblasted and pickled). C-rings were stressed using Ti-38644 titanium bolts, washers and nuts to avoid galvanic interferences. These samples were loaded to either 90, 95, or 105% of tubular L-direction yield strength at test temperature. C-ring stressing calculations were based on tubular yield strength and elastic modulus values measured at temperature.

Testing was conducted in Ti-38644 titanium autoclaves of sizes outlined in Table 2, two autoclaves offered continuous magnetic stirring capability to provide constant suspension of elemental sulfur within the brine, thereby maximizing specimen contact. C-ring samples were mounted to a central titanium sheet fixture attached to the autoclave lid, as pictured in Figure 1, via ceramic washers to assure galvanic isolation. Testing was conducted at 218°C (425°F), 232°C (450°F), 246°C (475°F), and 260°C (500°F), for 3 and 6 month duration as indicated in Table 2. The number of C-ring samples exposed per test temperature/time condition ranged between three and six for each tubular product. Post-exposure C-ring evaluation consisted of visual examination for cracking at 1-40X, and high magnification SEM examination of failed sample fracture surfaces.

Slow Strain Rate Testing (SSRT) - SSRT was performed on the two standard Ti-38644 tubular products (Table 1), in addition to two laboratory heats and one production heat of Pd-enhanced Ti-38644. The Pd-enhanced alloy product forms tested include 73 mm OD x 7 mm wall and 73 mm OD x 11 mm wall pipes, 6.4 and 25 mm plates, and 105 mm and 152 mm diameter billets, as described in Table 3. Note that the Pd-enhanced alloy tubular has been cold pilgered (~50%), and heat treated with a proprietary solution treat and age (dubbed the PASTA heat treatment)[5], and is representative of mill product designated for gas well use. The plate products were prepared in the laboratory to simulate hot forged/STA bar and cold pilgered/PASTA tubular products at various strength levels. L-direction samples were tested from all products.

SSRT was performed in Ti-38644 titanium autoclaves at a strain rate of 4×10^{-6} sec^{-1} utilizing a 4.8 mm diameter x 25.4 mm length gage SSRT sample. Ceramic washers assured electrical isolation of the sample from the load train and autoclave. This strain rate was chosen based on its empirically demonstrated ability to

stimulate SCC in standard Ti-38644 in sour brines above 190°C, and the lack of strain rate dependence indicated in this study (see Figure 11). Samples were all tested in the worst-case gas well environment described over the temperature range of 177-274°C. Sample % RA (Reduction of Area) and TTF (Time to Failure) values derived from the environment were compared (by ratio) to those measured in an inert helium gas atmosphere at each test temperature. Post exposure evaluation of SSRT samples included visual examination of fracture surfaces at 1-40X for secondary cracking, and SEM examination at 50-2000X for fracture mode determination.

RESULTS/DISCUSSION

Standard Ti-38644 Titanium

C-Ring Testing - Table 4 indicates the incidence of SCC observed in extruded/STA and cold pilgered/STA standard Ti-38644 tubulars after 3 and 6 months exposure in the worst-case gas well environment. SCC susceptibility, graphically depicted in Figure 2, was found in both tubulars at temperatures above 232°C. The frequency of C-ring failure, however, was generally 20-40%, suggesting somewhat borderline behavior. Although no SCC was noted at or below 232°C, cracking susceptibility was observed after 3 months at 232°C with the extruded/STA tubular when 0.5% acetic acid was added to the brine.

Tubular SCC susceptibility appeared to be relatively insensitive to several variables incorporated into the test matrix. No apparent effect of stress level (within 90-105% YS), surface condition (as-produced vs. machined), and brine flow (stirred vs. stagnant) was observed. The lack of dependence on brine slurry stirring suggests that sample surface contact with elemental sulfur may not be critical for SCC initiation, and/or that sulfur adequately contacted sample surfaces in stagnant brine tests.

When SCC did occur, SEM fracture examination clearly revealed initiation via transgranular cleavage in both Ti-38644 tubulars. Stress crack propagation was primarily transgranular, with finite branching via transgranular and intergranular modes. No general corrosion of C-ring samples was detected via gage or weight loss measurements, and less than 15 ppm hydrogen pickup was measured after 6 months exposure. No forms of localized surface attack were noted either, attesting to the thoroughness of oxygen removal during autoclave loading. Ti-38644 tubulars and stressing bolts and nuts proved to be resistant to crevice corrosion within metal-to-metal contact zones, except for several samples at 246°C. These minor isolated cases are attributed to entrapped residual oxygen (air) within bolt/nut crevices, which reacts with sulfur species to locally acidify crevices. Prior autoclave tests employing inadequate deaeration procedures have consistently experienced severe crevice corrosion under surface sulfur deposits and within metal-to-metal contact sites of standard Ti-38644 C-rings (and other CRA's including Ni-Cr-Mo alloys) after several days exposure at or above 204°C. This highly localized attack on stressed surfaces has resulted in premature C-ring cracking and an invalid SCC evaluation. Similar problems can be anticipated with DCB specimens involving residual oxygen retained within precracks.

SSR Testing - SSR test results for the standard Ti-38644 extruded/STA tubular are plotted as a function of temperature in Figures 3 and 4. SSRT results for the standard Ti-38644 cold pilgered/STA tubular are similarly presented in Figures 5 and 6. In almost all cases, tubular RA and TTF ratio values correspond with and parallel each other quite well, gradually decreasing as temperature increases.

If the common acceptance criteria of RA ratio ≥ 0.8 is applied, an apparent SCC threshold of 163-177°C is derived for the extruded/STA tubular. Similar analysis reveals a threshold of 177-191°C for the cold pilgered/STA tubular. A somewhat improved SCC threshold of ~204°C is obtained for the cold pilgered/STA tubular if a ≥ 0.8 TTF is invoked. These SCC thresholds are relatively unaffected by the addition of 0.5% acetic acid.

Examination of tubular SSRT specimen fracture surfaces, however, reveals that finite transgranular cleavage and, hence, incipient SCC still occurs at RA ratio values as high as 0.8. This was also evidenced by blackened sites on fracture surfaces, which represent sites of Ti-38644 alloy corrosion (product) produced by hot acid chloride (HCl) solution exposure. These SCC indications disappear above RA ratios of 0.9, and do not alter the estimated temperature thresholds for standard Ti-38644 tubular SCC.

Typical fractographs of standard Ti-38644 tubular samples exhibiting SCC susceptibility are presented in Figures 7 and 8. Note that SCC initiation and propagation occur predominantly by transgranular cleavage, with finite secondary cracking occurring via transgranular and intergranular modes. This correlates with the stress corrosion fracture characteristics noted in failed tubular C-rings. The significantly higher inherent ductility of the cold pilgered/STA tubular over the extruded/STA product is obvious in sample overload areas. This enhanced ductility may also explain the increased depth (fracture area) of SCC-affected cracking observed with the cold pilgered/STA tubular. Higher ductility increased resistance to crack growth and accommodated a larger critical crack size prior to tensile overload, resulting in somewhat improved RA and TTF values.

Pd-Enhanced Ti-38644 Titanium

SSR Testing - SSR test results for the Pd-enhanced Ti-38644 products evaluated are presented in Table 5 for hot forged products, and in Table 6 for cold processed products. The hot forged/STA plate and billet products revealed SCC thresholds in range of 204-246°C, based on a pass criteria of $\geq$ 0.85 RA ratio and the absence of fractographic evidence of cleavage. These thresholds were somewhat variable, and found to be sensitive to product microstructure, processing history, and location within the product. The billet product SSRT results, for example, indicated more consistent and somewhat improved values in the mid-radius location compared to outer radius sites, but were less dependent on strength level.

The cold processed Pd-enhanced Ti-38644 products, on the other hand, exhibited less variable SCC thresholds which consistently fell within the 246-274°C temperature window. This was found to the case for both solution treated (ST) and solution treated and age (STA or PASTA) conditions spanning the yield strength range of 793-1145 MPa. It should be noted from Table 6 that the further addition of either elemental sulfur (to 20 gpl) or 0.5 wt.% acetic acid did not significantly influence or degrade alloy SCC performance.

The SSRT results for two mill produced cold pilgered/PASTA Pd-enhanced Ti-38644 pipe products are plotted in Figure 9 as a function of temperature. Note again that RA and TTF ratio values tend to correlate quite well, and reveal an apparent SCC threshold at ~260°C. At RA ratios $\geq$0.85, SEM fractographic examination of these and other cold processed Pd-enhanced Ti-38644 samples revealed classic ductile void coalescence with no evidence of cleavage, as shown in Figure 10. Transgranular cleavage, like that pictured in Figure 8, became evident at RA ratios below ~0.85 and when blackened spots appeared on fractured surfaces. Although some transgranular and intergranual secondary cracking is also prominent with SCC occurrence, some minor crack branching can be found in pulled, inert environment samples as well.

A strain rate sensitivity study was performed to assure that the reference strain rate of 4×10^{-6} sec^{-1} represents a conservative, discriminating strain rate for Pd-enhanced Ti-38644 SSRT evaluation. Cold worked/PASTA plate (Ht. No. 882836) was tested in the worst case gas well test environment at 246°C at five strain rates spanning the range 2×10^{-6} to 35×10^{-6} sec^{-1}. The SSRT ratio data, plotted in Figure 11, reveals that

no significant reduction in SCC threshold temperature occurred over this strain rate range. Thus, the reference strain rate employed in this study (i.e. 4 x 10^{-6} sec^{-1}) may be considered a reasonable, conservative choice for Pd-enhanced Ti-38644 materials.

Standard vs. Pd-Enhanced Ti-38644 SCC Performance

The SCC temperature threshold windows indicated for the products evaluated in this SSR study are graphically compared in Figure 12. An assessment of relative SCC performance between standard and Pd-enhanced Ti-38644 alloys can be obtained by comparing SCC (SSR) thresholds at similar alloy strength levels and metallurgical conditions. For the hot worked/STA products (i.e. extruded pipe and forged billet/plate), the Pd enhancement raises the average SCC threshold approximately 42-56°C (75-100°F). The cold processed/STA or PASTA products, however, experienced an average SCC threshold increase of 69-83°C (125-150°F) through Pd enhancement.

The effect of metallurgical condition (i.e. extruded/STA vs. cold pilger/STA) alone in standard Ti-38644 only accounts for ~14C (~25°F) improvement in SCC threshold. For Pd-enhanced Ti-38644, the threshold increase derived from cold processing and PASTA heat treatment is on the order of 42°C (75°F). This 28°C (50°F) threshold differential (improvement) implies a significant beneficial synergistic effect achieved when Pd enhancement and cold processing (and final heat treatment) are both incorporated into the Ti-38644 alloy.

A comparison of SCC thresholds derived from C-ring vs. SSR testing of standard Ti-38644 tubulars suggests that SSRT derived SCC thresholds may be conservative by approximately 56°C (100°F) (i.e. 232°C vs. 177°C). If this is true, then SCC thresholds for cold pilgered/STA Pd-enhanced Ti-38644 pipe C-rings can be expected to be well in excess of 260°C under these worst-case sour gas well test conditions. Actual C-ring test data on Pd-enhanced Ti-38644 tubulars are currently in test to confirm this assumption.

The practical implications of the alloy SCC performance results generated in this study suggest that standard Ti-38644 may be reasonably resistant in the 170-232°C temperature range under worst-case sour gas well conditions. However, based on highly discriminating SSRT data, a very conservative guideline would be to limit standard Ti-38644 use to a maximum of ~177-191°C in highly stressed, critical downhole components. The Pd-enhanced alloy, in contrast, can be very safely considered for critical sour gas well applications to temperatures of ~204-218°C in hot worked products, and at least to 246°C for cold processed and heat treated products.

SCC/Pd Enhancement Mechanism

Although the mechanism of SCC in Ti-38644 titanium in high temperature sour brine is not fully understood, SCC must be either a cathodic (hydrogen embrittlement) or an anodic (chloride-assisted) controlled phenomenon. Considering the high solubility and diffusivity of hydrogen in beta titanium at these service temperatures and the lack of profuse generation of atomic hydrogen at the metal surface, a cathodic mechanism is considered unlikely. An anodic explanation appears more plausible, and has been diagnosed in a moly-rich alpha-beta titanium alloy under similar conditions.[6] In fact, the case for anodic control is enhanced by observations that standard Ti-38644 SCC (SSR) thresholds are relatively unaffected by the presence of sulfur and sulfide species in high temperature deaerated NaCl brine.[7,8]

The predominantly transgranular mode of SCC suggests that the beta phase itself may be susceptible, and would explain the beneficial effect of cold processing. Cold work followed by heat treatment results in refined, recrystallized beta grains, providing improved ductility and a reduced mean free path of susceptible phase. This improves SCC resistance by reducing the ability to achieve critical stress crack size. The observation that solution

treated Ti-38644 (all beta phase) has very similar SCC thresholds to the alloy in the aged condition in high temperature sour brines also suggests that the beta phase and not alpha phase, is susceptible.

The positive influence of Pd-enhancement on Ti-38644 alloy SCC resistance is expected based on palladium's known ennobling effect. By reducing hydrogen overvoltage and depolarizing cathode processes, palladium serves to shift titanium alloy potential in the positive direction, thereby promoting formation of protective oxide films. Thus, passivity of Ti-38644 titanium is extended into hotter, more reducing acid conditions, and manifests itself as improved resistance to hot HCl solutions and chloride crevice corrosion[9]. Palladium's positive effect on SCC resistance can be rationalized whether the cracking mechanism is cathodically (hydrogen) or anodically (chloride) controlled. Rate of oxide film repassivation is enhanced, thereby limiting hydrogen absorption or anodic attack when localized film breakdown occurs, such as during slow straining. Resistance to crack initiation on stressed metal surfaces where local sites of reducing acid chlorides may develop (i.e. within crevices, under deposits) is also realized.

CONCLUSIONS

Standard and Pd-enhanced Ti-38644 alloy plate, billet, and pipe materials were evaluated with respect to their SCC resistance in a simulated worst-case deep sour gas well environment up to 274°C (525°F). SCC susceptibility in standard Ti-38644 tubulars was not indicated below 232°C (450°F) in long term (3 - 6 month) C-ring tests, regardless of metallurgical condition, surface condition, brine stirring, and stress level tested. Brine acidification with 0.5% acetic acid did impart a minor negative effect on SCC threshold temperature. Slow strain rate (SSR) testing of standard Ti-38644 tubulars, on the other hand, produced more conservative SCC thresholds of 163-177°C (325-350°F) for extruded/STA pipe and 177-191°C (350-375°F) for cold pilgered/STA tubulars. Transgranular cleavage predominated in stress crack initiation and propagation above these threshold temperatures.

SSR testing of Pd-enhanced Ti-38644 products processed to a wide range of strength levels revealed SCC threshold improvements over standard Ti-38644 in the approximate range of 42-83°C (75-150°F) in this worst-case gas well environment. SCC resistance was synergistically elevated when both cold processing and Pd enhancement were incorporated into the Ti-38644 alloy product form, achieving SCC thresholds in excess of 246°C (475°F). Alloy SCC resistance was not significantly influenced by elemental sulfur and 0.5% acetic acid brine additions, nor by increasing or decreasing strain rate. The lower ductility, coarser grained hot forged/STA products exhibited somewhat lower and more variable SCC threshold temperatures compared to the cold processed/PASTA heat treated products. Based on this SSRT data base, Pd-enhanced Ti-38644, especially with intermediate cold processing (i.e. production tubulars) appears to exhibit more than adequate SCC resistance for the worst-case deep sour gas well production environments currently anticipated.

REFERENCES

1. W. F. Czyrklis, M. Levy, Corrosion, 1976, Vol. 32, pg. 99.

2. W. L. Silence, K. A. Groeneveld, "High Strength Alloy Wirelines for Deep Oil and Gas Well Service," Paper #11, NACE Corrosion '89, April 17-21, 1989, New Orleans, LA.

3. D. E. Thomas and S. R. Seagle, "Stress Corrosion Cracking Behavior of Ti-38-6-44 In Sour Gas Environments," Titanium Science and Technology, Proceedings of the 5th International Conference on Titanium, Munich, Germany, Sept. 10-14, 1984, Deutsche Gesellschaft für Metallkunde E.V., pp. 2533-2540.

4. W. W. Love, et. al., "The Use of Ti-38644 Titanium for Downhole Production Casing in Geothermal Wells," Sixth World Conference on Titanium Proceedings, Cannes, June 6-9, 1988, Société Française de Métallurgie, Les Ulis Cedex, France, pp. 443-448.

5. R. W. Schutz and S. R. Seagle, "Method For Improving Aging Response and Uniformity in Beta Titanium Alloys," U.S. Patent applied for, RMI Titanium Company, Niles, OH.

6. M. Ueda, et. al., "Corrosion Behavior of Titanium Alloys In a Sulfur-Containing H_2S-CO_2-Cl Environment," Paper #271, NACE Corrosion '90, Las Vegas, NV, April 23-27, 1990.

7. Unpublished data, R. W. Schutz and M. Xiao, RMI Titanium Company R&TD Laboratory, Niles, OH 1991.

8. W. J. Sisak and D. E. Knox, "Stress Corrosion Cracking of Ti-3Al-8V-6Cr-4Mo-4Zr in a Sour Brine," presentation made at an AIME-TMS Annual Meeting Symposium, New Orleans, LA, Feb. 17-18, 1991.

9. D. R. Klink and R. W. Schutz, "Engineering Incentives for Utilizing Ti-3Al-8V-6Cr-4Zr-4Mo Titanium Tubulars in Highly Aggressive Deep Sour Gas Wells," Paper No. 92063, presented at NACE Corrosion '92, Nashville, TN, Apr. 27 - May 1, 1992.

Table 1. Properties and Composition of the Two Standard Ti-38644 Tubular Products Tested

		EXTRUDED/STA STD. Ti-38644 PIPE	COLD PILGERED/STA STD. Ti-38644 PIPE
• RMI HEAT NO.		881457	881457
• Composition	%Al	3.3	3.3
	% V	7.8	7.8
	%Cr	6.2	6.2
	%Zr	3.8	3.8
	%Mo	4.0	4.0
	%O	0.08-0.11	0.08 - 0.11
• Tensile Properties	YS MPa (ksi)	993 (144)	952 (138)
	UTS MPa (ksi)	1069 (155)	1000 (145)
	%El	14	27
	%RA	27	45

Table 2. C-Ring Test Matrix for Standard Ti-38644 Tubulars

TEST TEMP. °C (°F)	EXPOSURE (MONTHS)	AUTOCLAVE VOLUME (LITERS)	CONTINUOUS STIRRING?	0.5% ACETIC ACID ADDED?
218 (425)	3	5.1	No	No
218 (425)	6	5.6	No	No
232 (450)	3	5.6	No	No
232 (450)	3	5.1	No	Yes
232 (450)	6	14.8	Yes	No
246 (475)	3	5.1	No	No
260 (500)	3	5.1	No	No
260 (500)	6	12.4	Yes	No

Table 3. Composition of Pd-Enhanced Ti-38644 Product Forms Tested

	RMI HEAT NUMBER		
COMPOSITION	X-20040	X-20041	882836
%Al	2.7	2.8	3.1
%V	7.8	8.0	7.9
%Cr	6.0	5.8	6.0
%Zr	4.0	3.8	4.0
%Mo	4.1	4.2	4.2
%Pd	0.045	0.075	0.062
%0	0.08		0.08
Product Forms Tested	• 6.4 mm plate • 25 mm plate	• 6.4 mm plate	• 6.4 mm plate • 73 mm OD x 7 mm AW pipe* • 73 mm OD x 11 mm wall pipe* • 152 mm billet • 105 mm billet

* - Pipe Tensile Properties: YS = 945 MPa (137 ksi)
UTS = 993 MPa (144 ksi)
El = 21%
RA = 47%

Table 4. Results of Ti-38644 C-ring Testing In a Worst-Case Sour Gas Well Environment

(20% NaCl, 6.9 MPa H_2S, 3.4 MPa CO_2, 1 gpl S°)

Temp.	Time	Extruded/STA Std. Ti-38644 Tubular		Cold Pilg./STA Std. Ti-38644 Tubular	
°C (°F)	Months	As Prod.	Machined	As Prod.	Machined
218 (425)	3	0/1	0/2	0/1	0/2
	6	0/1	0/2	0/1	0/2
232 (450)	3	0/1	0/2	0/1	0/2
	6**	0/1	0/3	0/1	0/5*
246 (475)	3	--	--	0/1	1/3
260 (500)	3	1/1	1/2	0/1	0/2
	6**	0/1	1/4*	0/1	1/5*
232 (450) w/Acetic acid	3	--	1/3	--	0/3

Note:

1. X / Y = Number of cracked C-rings/Number of C-rings tested
2. C-rings loaded to 95% test temp. L-YS, except where indicated
3. * One of the C-rings was loaded to 105% yield strength
4. No cracking occurred in 105% YS loaded C-rings
5. ** Continuously stirred solution tests, other tests involved stagnant solutions

Table 5. SSRT Results for Various Hot Forged and Heat Treated Pd-Enhanced Ti-38644 Products Tested in A Worst-Case Sour Gas Well Environment

(L Direction Samples)

PRODUCT FORM (Heat #)	CONDITION	RT YS MPA (ksi)	TEST TEMP (°C)	PROP. LIMIT AT TEMP. MPa (ksi)	ENVIRON-MENTAL % RA	RA RATIO	TTF RATIO	SCC?
25 mm plate (X20040)	Forged and ST	786 (114)	218	634 (92)	66.4	1.00	1.00	No
25 mm plate (X20040)	Forged, ST, and Duplex Aged	979 (142) " "	232 246	848 (123) " "	32.9 9.8	0.96 0.29	0.98 0.39	No Yes
152 mm billet (882836)	Forged and STA (mid-radius location)	1110 (161) " " " "	204 218 232	945 (137) " " " "	19.8 14.3 15.4	1.00 0.93 1.00	1.00 0.85 0.75	No No No
	Forged and STA (outer radius location)	1110 (161) " " " "	204 218 218	945 (137) " " " "	16.2 17.3 10.5	1.00 1.00 0.71	1.00 1.00 0.71	No Yes Yes
	Forged and STA (mid-radius location)	1013 (147) " "	218 232	846 (123) " "	24.7 20.5	0.95 0.79	0.99 0.91	No Yes
	Forged and STA (outer radius location)	1013 (147)	218	846 (123)	18.3	0.81	0.63	Yes
105 mm billet (882836)	Forged, ST and Duplex Aged	1000 (145) " "	204 218	821 (119) " "	19.5 13.8	1.00 0.71	0.91 0.44	No Yes

Table 6. SSRT Results Cold-Process and Heat Treated Pd-Enhanced Ti-38644 Products Tested In A Worst-Case Sour Gas Well Environment

(L Direction Samples)

PRODUCT FORM (Heat #)	CONDITION	RT YS MPA (ksi)	TEST TEMP (°C)	PROP. LIMIT AT TEMP. MPa (ksi)	ENVIRON-MENTAL % RA	RA RATIO	TTF RATIO	SCC?
6.4 mm plate (X20040)	Cold Worked and STA	793 (115) " " 896 (130) " "	218 232 246 260	670 (100) " " 703 (102) " "	57.1 57.1 54.4 54.6	1.00 1.00 1.00 1.00	0.91 0.98 1.00 1.00	No No No No
6.4 mm plate (X20041)	Cold Worked and PASTA	931 (135) " " " "	232 246 260	724 (105) 703 (102) " "	44.2 43.9 43.8	0.98 0.97 0.97	0.98 0.95 0.98	No No No
6.4 mm plate (882836)	Cold Worked and PASTA	1000 (145) " "	218 232	800 (116) " "	32.9 30.6	0.92 0.85	0.99 0.99	No No
6.4 mm plate (882836)	Cold Worked and PASTA	979 (141) " " " "	232 246 260	786 (114) " " " "	36.3 35.3 17.7	1.00 1.00 0.50	0.95 1.00 0.62	No No Yes
6.4 mm plate (X20040)	Cold Worked and Direct Aged	1145 (166) " " " "	218 218 232	958 (139) " " " "	20.5 21.6* 19.6	1.00 1.00* 1.00	0.99 1.00* 0.95	No No No
73 mm OD x 7 mm wall pipe (882836)	Cold Pilgered and PASTA	945 (137) " " " " " " " "	232 246 246 260 274	772 (112) " " " " " " " "	36.5 40.6 42.4 43.9 18.6	0.94 1.00 1.00** 1.00 0.48	0.94 1.00 1.00** 1.00 0.72	No No No No Yes
73 mm OD x 11 mm wall pipe (882836)	Cold Pilgered and PASTA	945 (137) " " " " " "	246 246 260 260	772 (112) " " " " " "	39.4 35.0** 39.8 30.4	0.99 0.90** 1.00 0.83	0.97 1.00** 1.00 0.91	No No No Yes

* - 20 gpl sulfur added

** - 0.5% acetic acid added

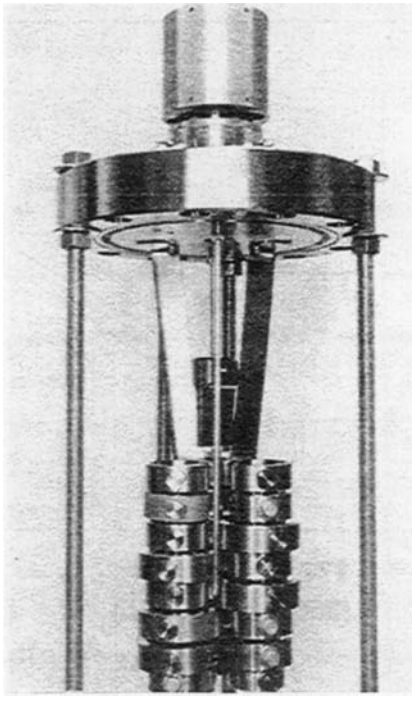


Figure 1. Ti-38644 pipe C-ring samples affixed to a titanium fixture which was fastened to an autoclave lid, and which suspended electrically-isolated samples within the autoclave.

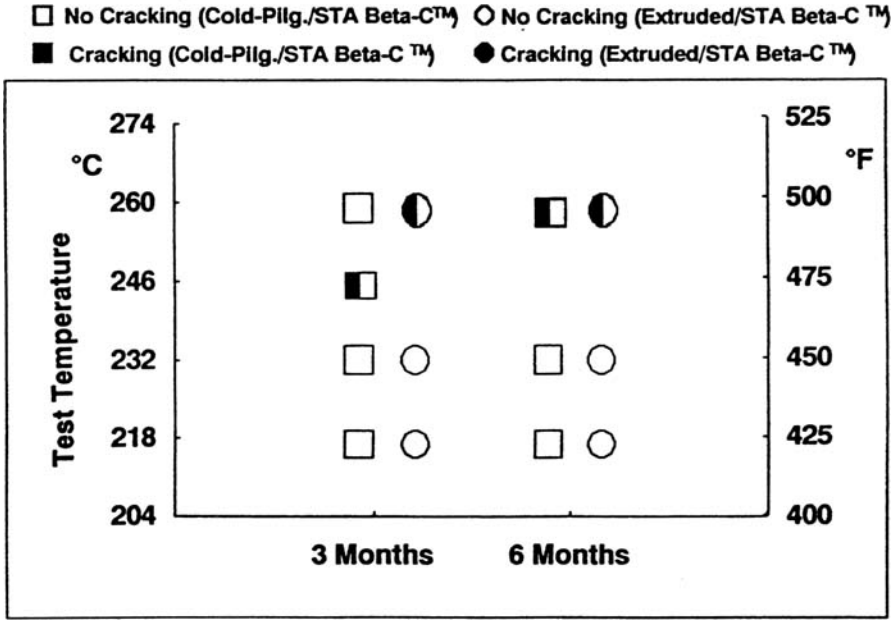


Figure 2. Standard Ti-38644 tubular C-ring test results in a worst-case deep sour gas well environment.

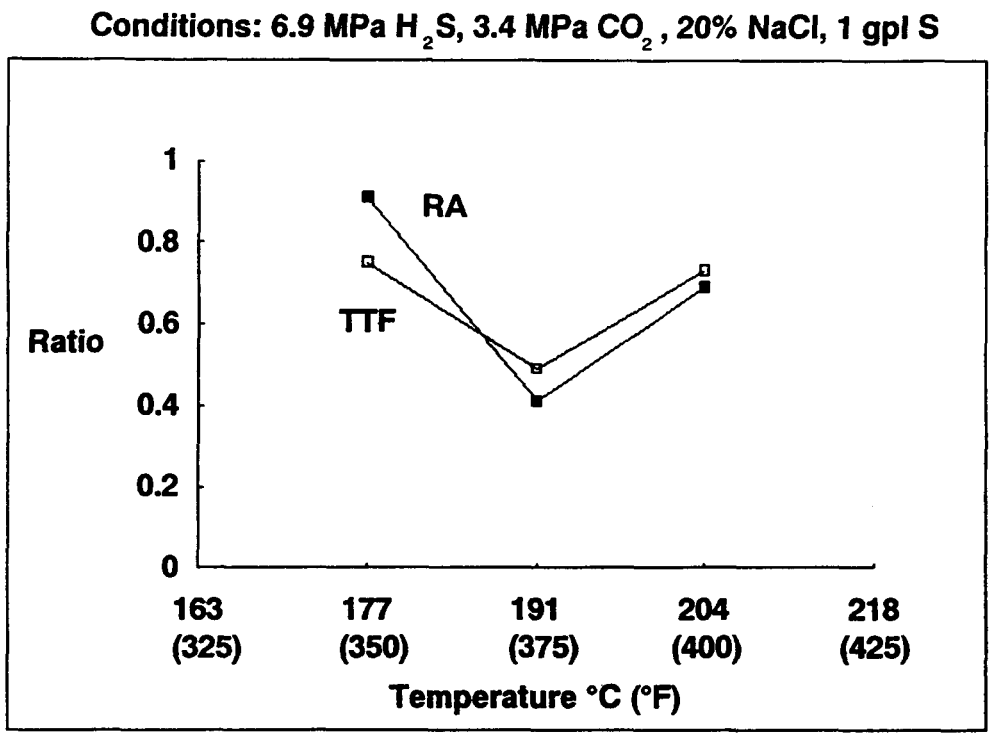


Figure 3. SSRT ratios for extruded/STA standard Ti-38644 pipe in a worst-case deep sour gas well environment.

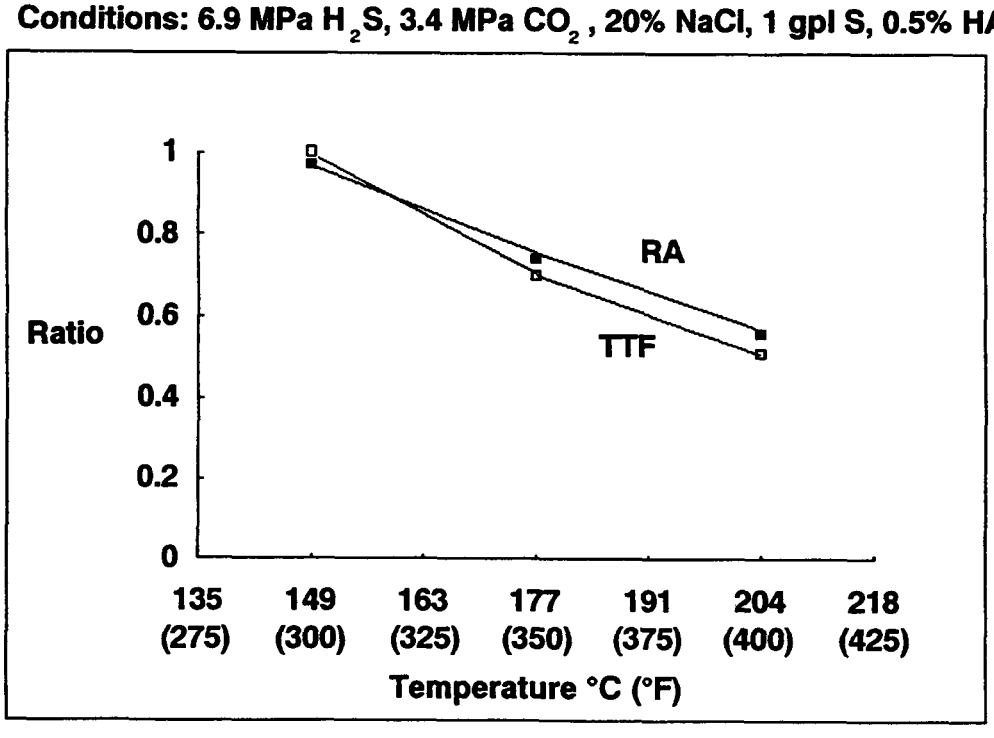


Figure 4. SSRT ratios for extruded/STA standard Ti-38644 pipe in a worst-case deep sour gas well environment with 0.5% acetic acid added.

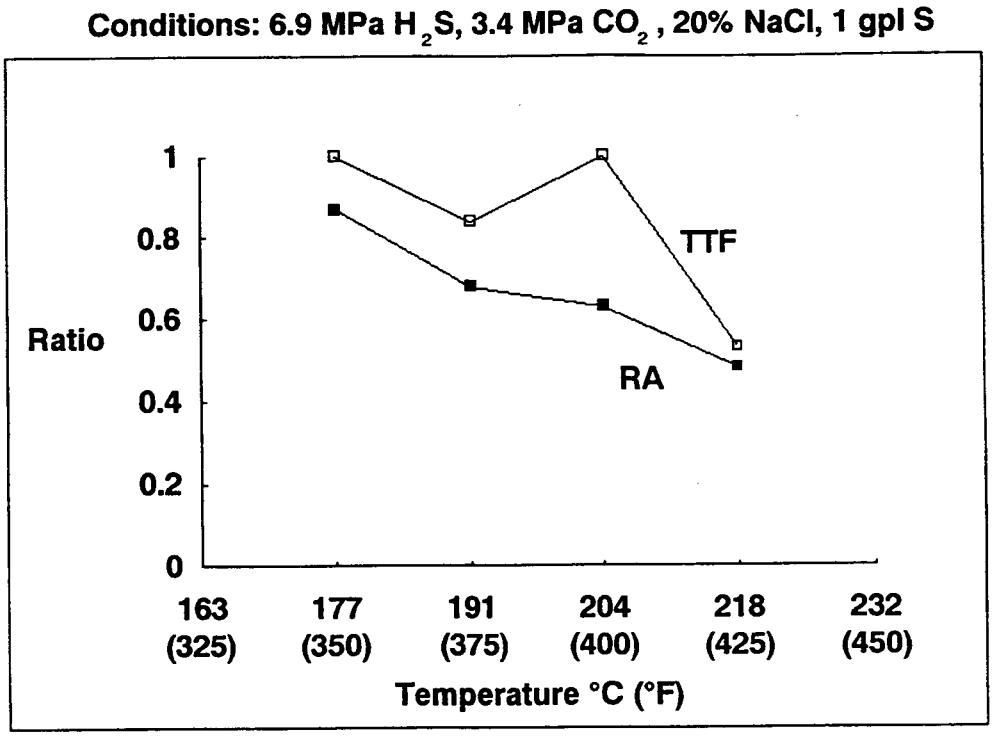


Figure 5. SSRT ratios for cold pilgered/STA standard Ti-38644 pipe in a worst-case deep sour gas well environment.

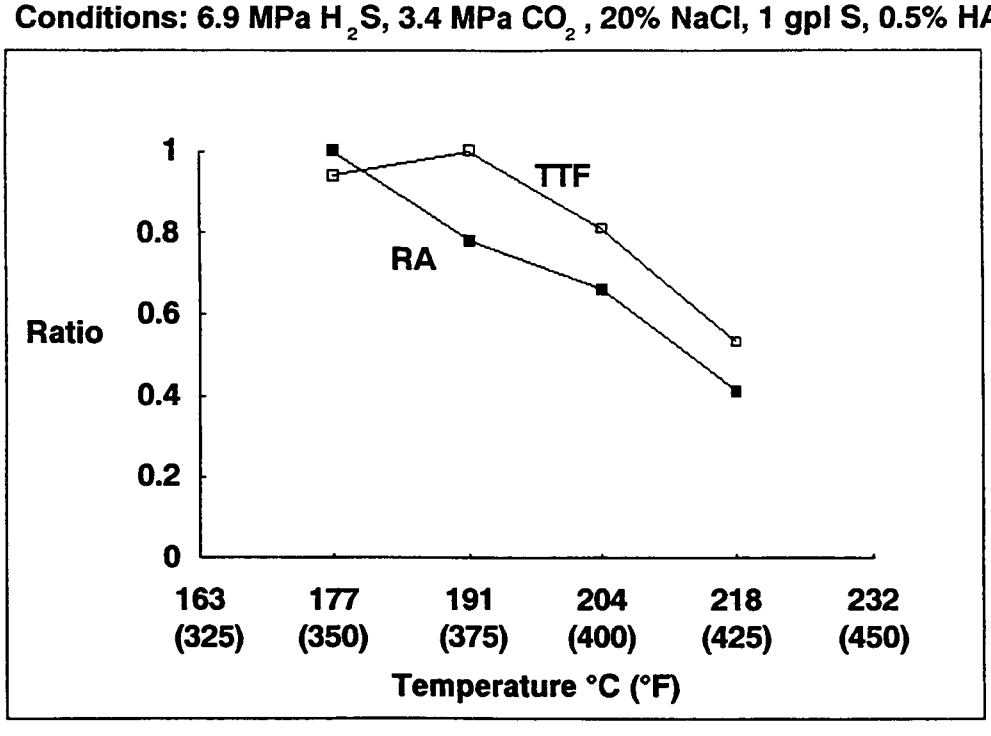
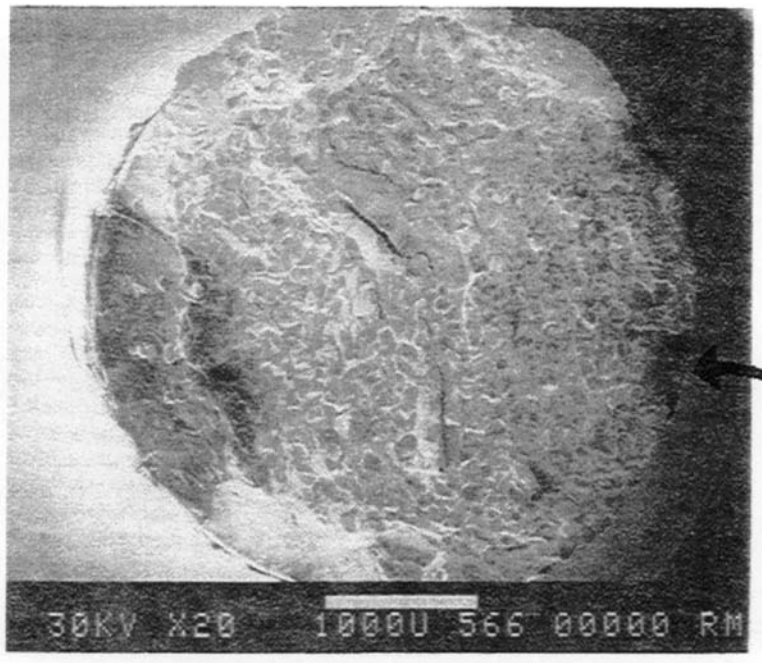
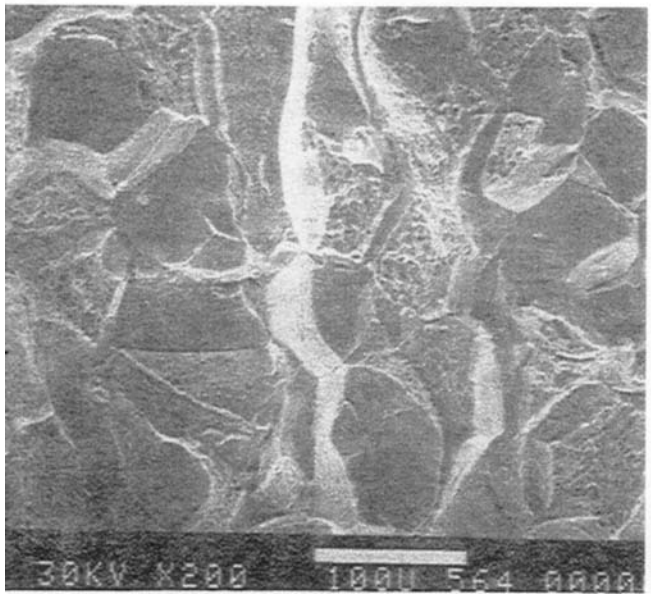


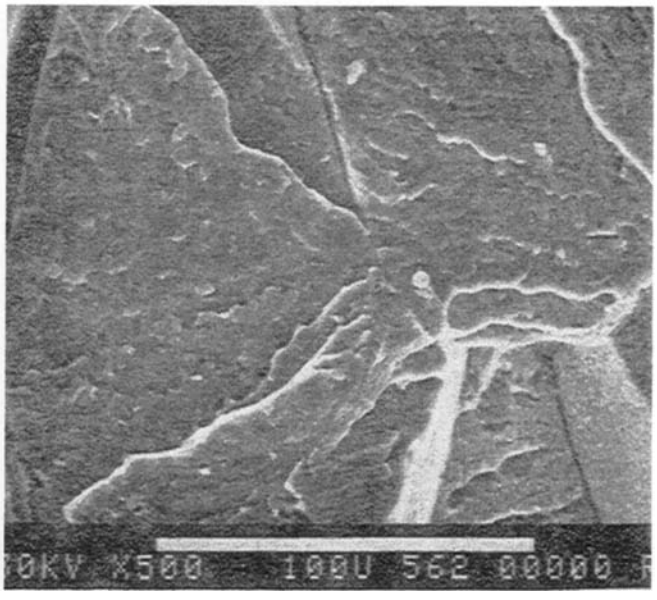
Figure 6. SSRT ratios for cold pilgered/STA standard Ti-38644 pipe in a worst-case deep sour gas well environment with 0.5% acetic acid added.



(20X)

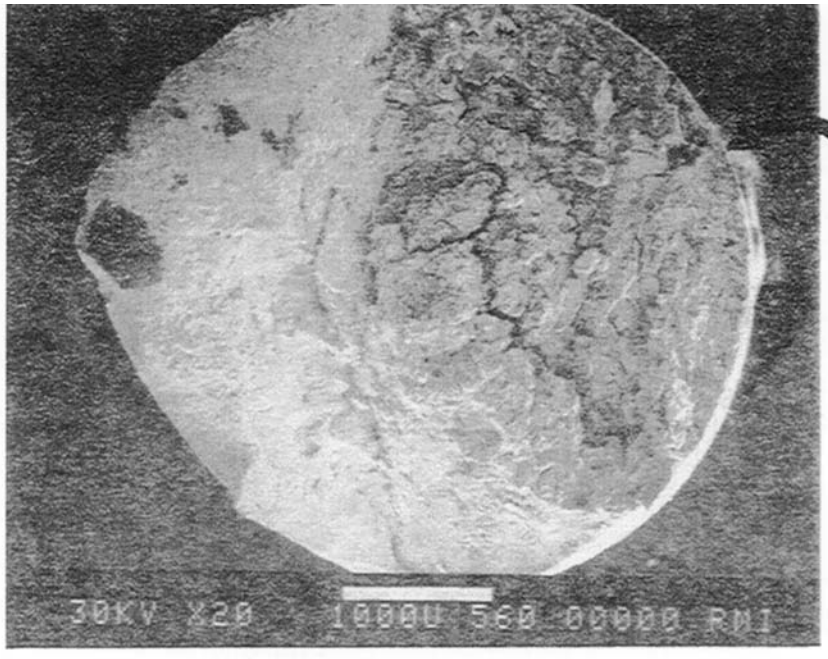


Variable ductility in overload zone near core (200X)



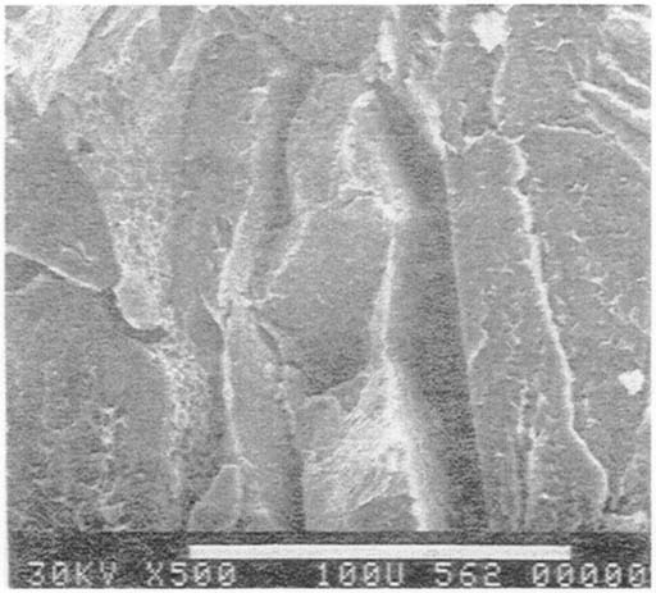
Transgranular SCC cleavage at edge initiation site (500X)

Figure 7. SEM fractographs of an extruded/STA standard Ti-38644 tubular SSRT specimen in a worst-case deep sour gas well environment at 204°C.

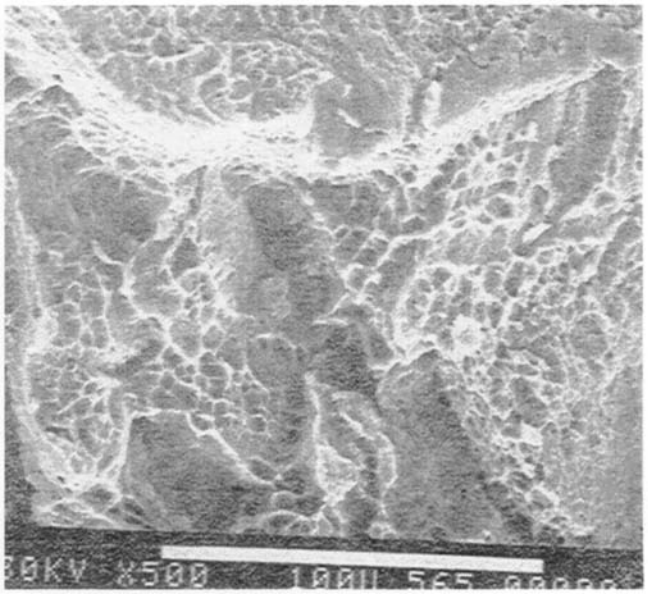


SCC Crack Initiation Site

(20X)



Fully ductile near SSRT sample core (500X)



Transgranular SCC cleavage at edge initiation site (500X)

Figure 8. SEM fractographs of cold pilgered/STA standard Ti-38644 tubular SSRT specimen pulled at 204° C in worst-case deep sour gas well environment.

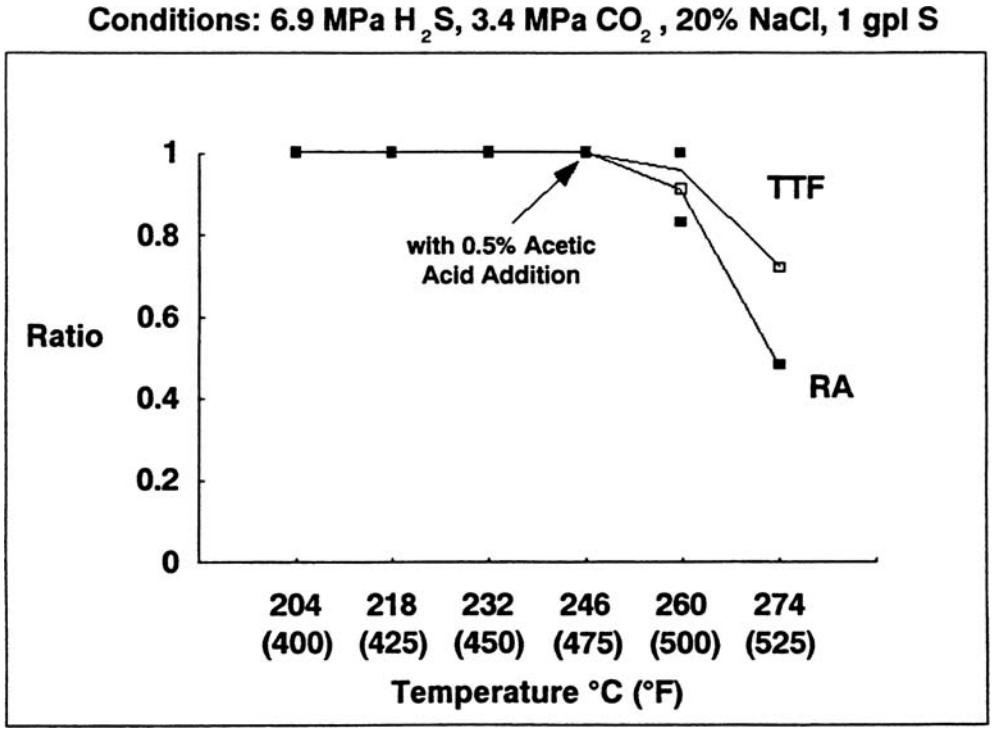
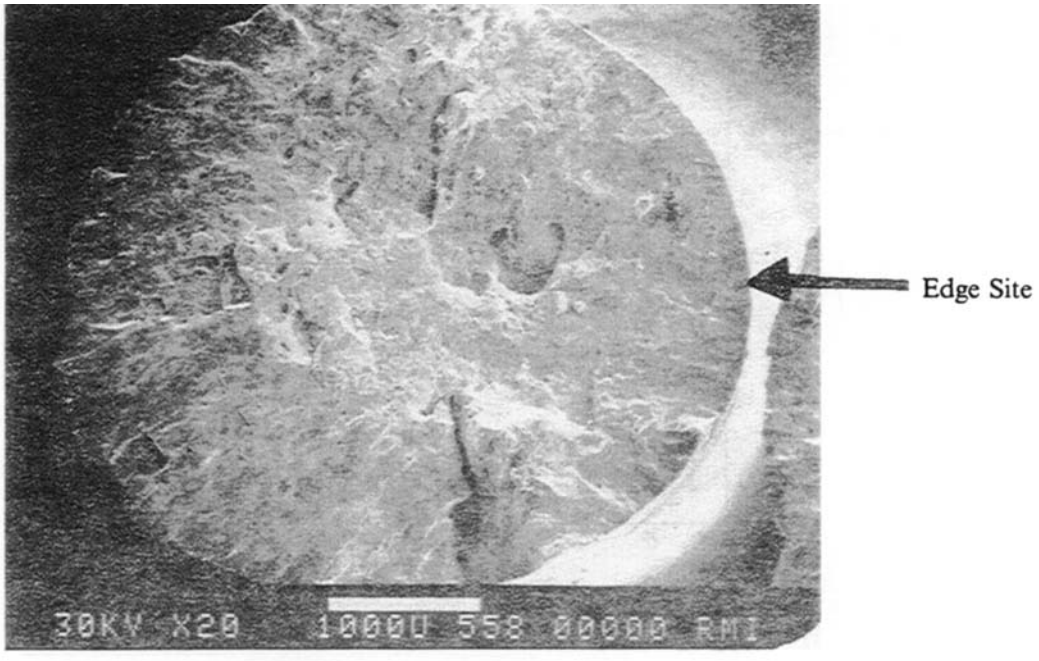
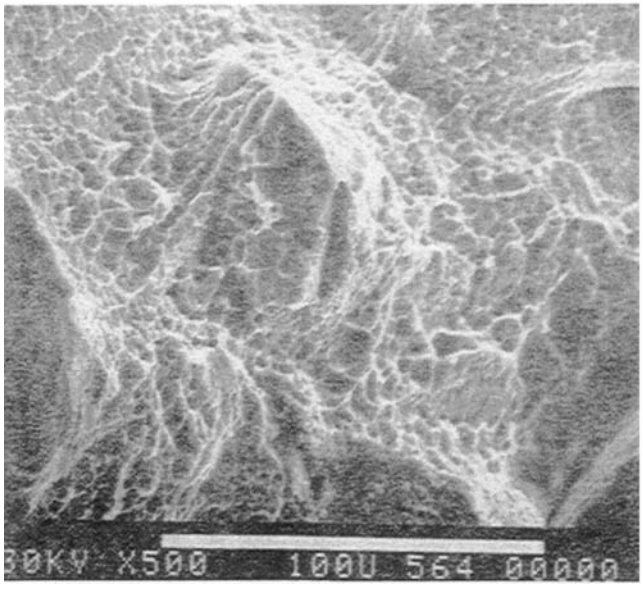


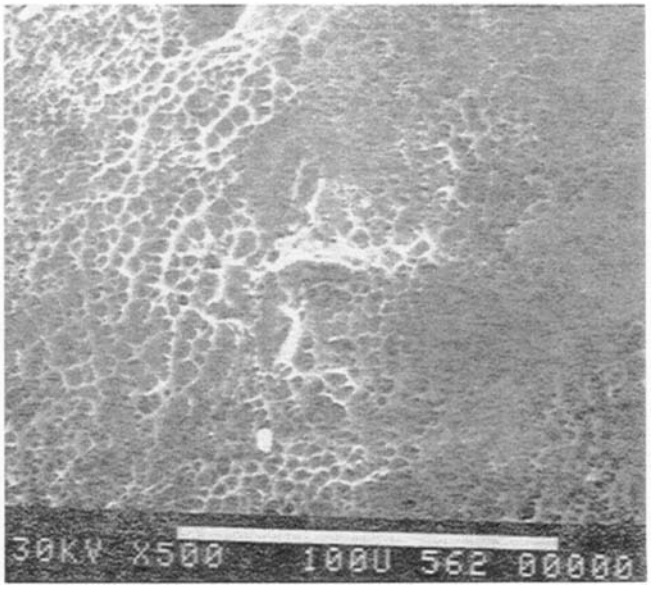
Figure 9. SSRT ratios for cold pilgered/PASTA Pd-enhanced Ti-38644 pipe in a worst-case sour gas well environment.



(20X)



Fully ductile near SSRT sample core (500X)



Fully ductile near edge (500X)

Figure 10. SEM fractographs of cold pilgered PASTA Pd-enhanced Ti-38644 SSRT specimen pulled at 232°C in worst-case deep sour gas well environment. No SCC indicated.

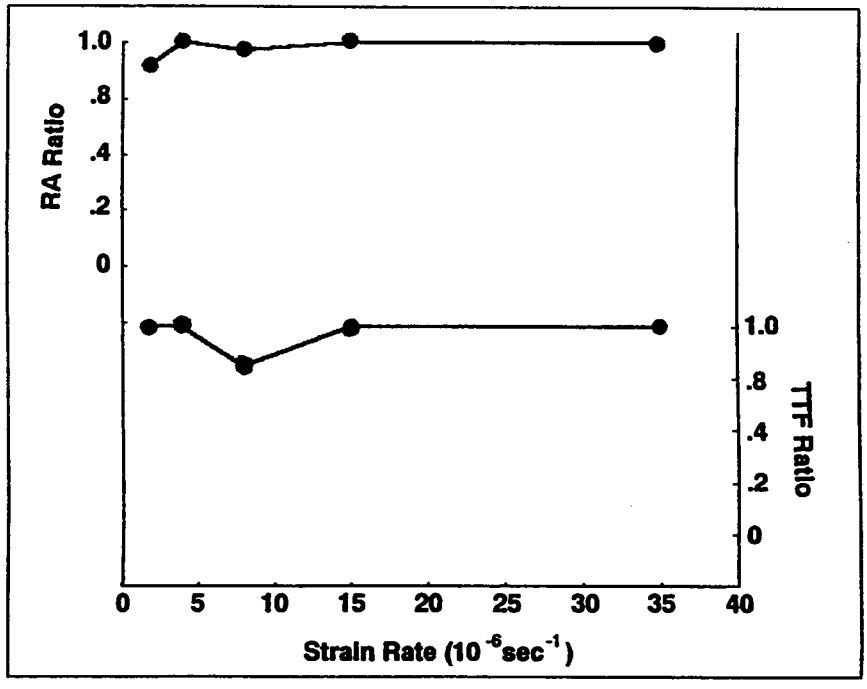


Figure 11. Effect of strain rate on the SSR behavior of cold worked PASTA Pd-enhanced Ti-38644 in a worst-case sour gas well environment at 246°C.

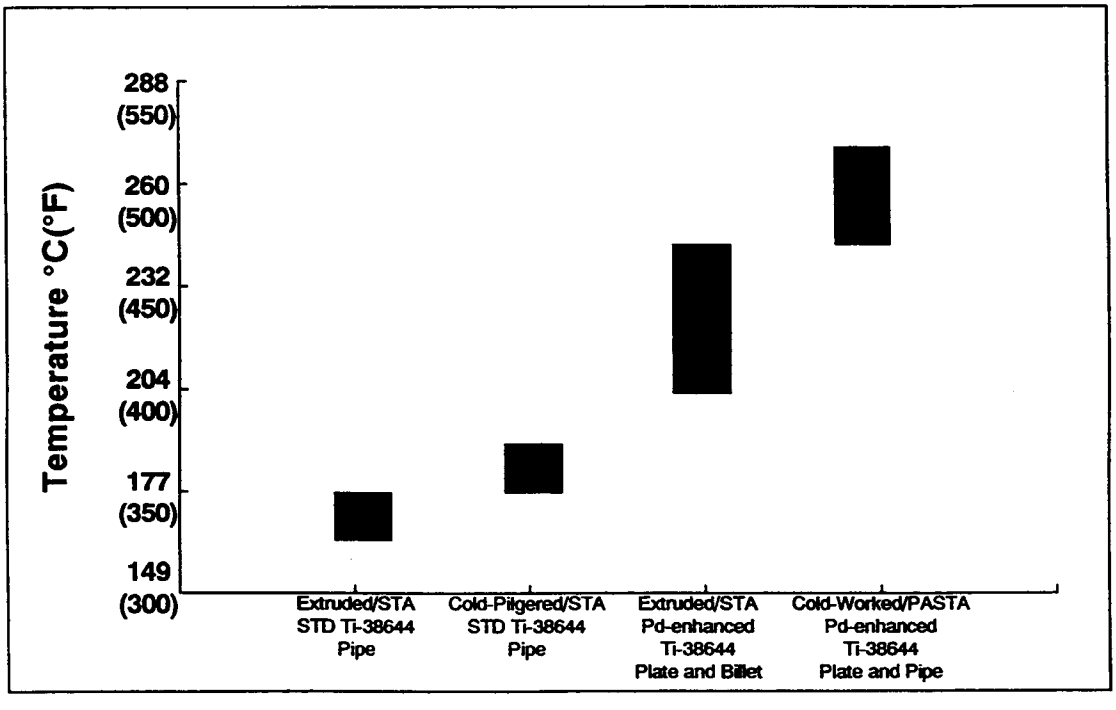


Figure 12. Conservative SCC temperature thresholds for standard and Pd-enhanced Ti-38644 products in a worst-case sour gas well environment based on SSR testing.

Copyrighted Materials
Copyright © 1996 NACE International Retrieved from www.knovel.com

STRESS CORROSION CRACKING BEHAVIOR OF Ti-38-6-44 IN SOUR GAS ENVIRONMENTS

D. E. Thomas and S. R. Seagle, Research & Technical Development, Niles, Ohio, USA

Introduction

Environmental cracking of materials exposed to corrosive, hydrogen sulfide-containing environments has plagued the oil and gas industry for many years (1). As a result, this industry has turned to the high performance metal producers for answers. Materials must possess high strength at elevated temperatures, good corrosion resistance and, above all, resistance to environmental cracking. Of the many metals options, high strength beta titanium alloys appear to have several advantages. Unfortunately very little information has been reported concerning cracking behavior of these alloys (2-6). Previous investigators that have examined the beta alloys have limited their attention to ambient temperature, NaCl environments and found that several beta alloys, notably Ti-3Al-8V-6Cr-4Mo-4Zr, have excellent resistance to stress corrosion cracking. However, little, if anything, is known about the effect of hydrogen pickup and possible embrittlement during exposure to hydrogen sulfide. This may be particularly important because of the known effect of hydrogen sulfide on hydrogen absorption response.

This paper presents initial results on the environmental cracking behavior of one beta alloy, Ti-3Al-8V-6Cr-4Mo-4Zr (also known as Beta-C). Because the alloy is a metastable beta alloy acquiring its high strength by aging, attention has been devoted to examining the effect of heat treatment. Environmental variables such as stress level and hydrogen charging are also examined.

Experimental

Three mill heats of Ti-3Al-8V-6Cr-4Mo-4Zr were selected for this investigation. Alloy compositions of final production are given in Table 1. Heat treatments and resultant mechanical properties are presented in Table 2. Note that each of the mill heats was processed into different mill products (e.g., bar, billet, etc.) so that microstructural effects, before heat treatment, could be evaluated.

	A	B	C
C	0.02	0.04	0.02
N	0.012	0.006	0.014
O	0.083	0.082	0.088
H	0.0099	0.0046	0.012
Fe	0.06	0.10	0.04
Al	3.4	3.5	3.2
V	8.2	8.0	7.6
Cr	6.2	5.8	5.9
Mo	4.0	3.9	3.8
Zr	4.0	4.0	3.6
Product:	Hot Rolled 0.710Ø Bar	3"Ø Pipe	Cold Drawn 0.310Ø Bar

Table 1: Alloy Chemistry - Ti-3Al-8V-6Cr-4Mo-4Zr (Weight Percent)

Courtesy DGM (Deutsche Gesellschaft für Materialkunde)

Heat	Test Sample Code	Heat Treatment	Mechanical Properties			
			Ultimate MPa(Ksi)	Yield 0.2% Offset MPa(Ksi)	Percent Elongation	Percent Reduction In Area
A	A-1	780C-1Hr-AC*	925(134)	897(130)	18	47
	A-2	780C-1Hr-AC+ 482C-8Hrs-AC	1490(216)	1415(205)	10	21
B	B-1	870C-1Hr-AC	849(123)	800(116)	19	48
	B-2	780C-1Hr-AC+ 482C-8Hrs-AC	1408(204)	1297(188)	8	11
	B-3	780C-1Hr-AC+ 593C-8Hrs-AC	1056(153)	952(138)	14	25
C	C-1	454C-24Hrs-AC	1711(248)	1622(235)	7	16
	C-2	As Drawn	1166(169)	1076(156)	8	34

*AC - Air Cool

Table 2: Heat Treatments and Mechanical Properties

Environmental cracking susceptibility was evaluated using several techniques. Sustained load smooth and notched tensile samples were tested using the apparatus illustrated in Figure 1. This apparatus uses a compressed ring to maintain a constant deflection which, when used properly, maintains an essentially constant load. If required, a cathodic current was applied using the coated titanium anode as shown. All of the tests were performed in a solution containing 5 wt. % NaCl and 0.5 wt. CH_3COOH. After loading each sample the solution was purged with nitrogen for 1 hour and hydrogen sulfide for 1 hour. Thereafter a steady flow of hydrogen sulfide was maintained to ensure the solution remained saturated. Throughout the test the solution was maintained at 25C $\pm$ 2C.

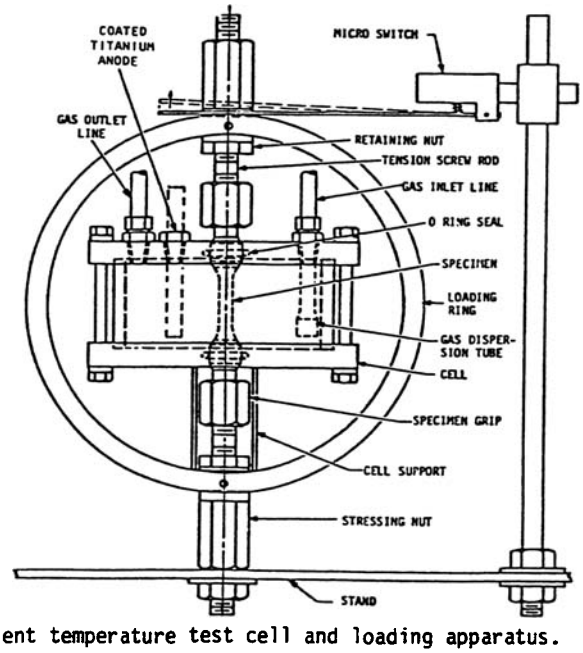


Fig. 1: Ambient temperature test cell and loading apparatus.

Results

Smooth tensile results are shown in Table 3. In each case the test was terminated after 30 days (720 hours). No evidence of cracking was observed irrespective to heat treatment, mill chemistry or product form. Duplicate tests with a cathodic current density of 0.5mA/cm^2 produced similar results. This is not surprising since several investigators have indicated that it is nearly impossible to initiate cracking of titanium alloys exposed to aqueous, chloride solutions using smooth test samples (7-9).

Test Sample Code	Stress Level MPa (Ksi)	Percent of Yield Strength	Results	
			No Charging	Charged at 0.5mA/cm^2
A-1	462 (67)	50	NC*	NC*
A-1	876 (127)	95	NC	NC
A-2	711 (103)	50	NC	NC
A-2	1063 (154)	75	NC	NC
A-2	1350 (195)	95	NC	NC
B-1	759 (110)	95	NC	NC
B-2	649 (94)	50	NC	NC
B-2	1235 (179)	95	NC	NC
B-3	476 (69)	50	NC	NC
B-3	904 (131)	95	NC	NC
C-1$^\Delta$	1539 (223)	95	NC	--
C-2$^\Delta$	538 (78)	50	NC	--
C-2$^\Delta$	1022 (148)	95	NC	--

Tensile sample - 2.5cm gage length, 0.65cm gage diameter

*NC - no cracking observed in 30 days (720 hours)

$^\Delta$Substandard tensile sample - 0.32cm gage diameter

Table 3: Smooth Tensile, Constant Deflection Stress Cracking Test Results (5% NaCl, 0.5% CH_3COOH, Saturated H_2S, 25C).

Because of the initiation difficulty, notched, fatigue precracked tensile samples were tested. The stress concentration factor, K_t, was approximately 3.0. Samples were loaded to stress levels calculated on the basis of the notched region cross sectional area neglecting any stress concentrating effects. Cracking results are presented in Table 4. In the absence of an applied current no cracking was observed. This included both solution treated (ST) and solution treated and aged (STA) microstructural conditions.

Test Sample Code	Stress Level* MPa(Ksi)	Percent of Yield Strength	Results	
			No Charging	Charged at 0.5mA/cm^2
A1	876 (127)	95	NC**	NC**
A2	1350 (195)	95	NC	C-175 Hrs.

Tensile specimen - 2.5cm gage length, 0.64cm gage diameter, 0.51cm diameter in notch, K_t = 3.0.

*Stress level determined using notched region cross-sectional area.
**NC - no cracking, 30 days (720 Hrs.)
C - total separation by cracking

Table 4: Notched Tensile, Constant Deflection Stress Cracking Test Results (5% NaCl, 0.5% CH_3COOH, Saturated H_2S, 25C).

Testing with an applied cathodic current density of 0.5 mA/cm^2 produced quite different results. The ST condition consisting of essentially all β phase did not crack during the 30 day exposure. The STA condition consisting of equiaxed beta with a fine dispersion of precipitated alpha particles cracked after 175 hours. Total separation of the sample occurred in the notched area. Examination of the fracture surface indicated a small, flat cleavage-like fracture near the outside diameter of the notch and a ductile overload region toward the notch center. Fracture appeared to initiate from a single area on the notch perimeter.

Small diameter smooth tensile samples were tested to see whether the stress concentration produced by the notch or simply the reduced cross-sectional area was responsible for the observed cracking. In order to magnify the effect of second phase particles a heavily cold worked bar aged to produce high volume fraction of alpha phase was employed. In addition, charging current density was varied to examine the effect of charging rate. Results for these subsize samples are presented in Table 5.

Test Sample Code	Impressed Current Density mA/cm^2	Results
C-1	0	NF* - 500 Hrs.
C-1	.15	F - 494 Hrs.
C-1	1.5	F - 115 Hrs.
C-1	15	F - 180 Hrs.
C-1	150	F - 29.4 Hrs.

Tensile - 2.5cm gage length, 0.318cm gage diameter
Stress Level - 1539 MPa (223 Ksi), 95% tensile yield strength

*NF - no failure
F - complete failure (i.e., total separation)

Table 5: Subsize Tensile, Constant Deflection Stress Cracking Test Results (5% NaCl, 0.5% CH_3COOH, Saturated H_2S, 25C).

Once again, samples tested without an impressed current did not crack in 500 hours. Impressed current tests did, however, produce cracking. As the current density was increased the time to failure dropped initially. Unexpectedly, further increasing current density raised time to failure approximately 50% and then lowered it again. Clearly, hydrogen-related embrittlement was not related to hydrogen generation rate in a simple straightforward way.

Discussion

At least two previous investigators have indicated the immunity of Ti-3Al-8V-6Cr-4Mo-Zr to stress corrosion cracking in aqueous brines (10, 11). These investigations included both the ST and STA conditions. However, neither of these investigations considered the effect of hydrogen charging on sustained load cracking behavior. While hydrogen charging may not be particularly important for seawater applications it can be extremely important in longtime service where galvanic interactions with active metals (e.g., steel, aluminum, etc.) are unavoidable. The question is, what level of hydrogen does it take to adversely affect the mechanical

properties of a material and what is the likelihood that this level will ever be attained? To answer this first question one must consider the type of sample configuration, metallurgical condition, stress state, environment and hydrogen charging rate.

Without an impressed cathodic current, corrosion of the test sample provides all of the driving force for discharge and subsequent absorption of hydrogen. If the sample does not corrode there is no driving force. This is the suggested mechanism for hydrogen embrittlement of carbon steels in hydrogen sulfide environments (known as sulfide stress cracking). However, titanium alloys do not corrode in hydrogen sulfide so there is no driving force for generation of surface hydrogen and therefore no hydrogen absorption. This was demonstrated by data in Tables 3, 4 and 5 where no cracking was observed in tests run without impressed cathodic current. These results were independent of all other factors which indicates the importance of hydrogen on Ti-3Al-8V-6Cr-4Mo-4Zr environmental cracking. Recent work has shown the corrosion resistance of Ti-3Al-8V-6Cr-4Mo-4Zr is very good (12) in elevated temperature environments containing hydrogen sulfide. As a result there is essentially no hydrogen generation and hence, very good cracking resistance (12).

Hydrogen, however, can be generated on a titanium surface by a galvanic couple. Because titanium alloys are quite noble metals (i.e., no corrosion) they are very good at accelerating corrosion when galvanically coupled to active (i.e. rapid corrosion) metals. Since titanium is the cathode, hydrogen reduction occurs. The production rate of hydrogen on this titanium surface is dependent primarily on the corrosion rate of the active metal. Simulating this situation with an impressed cathodic current provided several interesting results.

Testing notched precracked tensile samples revealed that the STA condition was susceptible to cracking while the ST condition was not. This is consistent with previous stress-corrosion cracking studies on other beta titanium alloys that showed the ST condition was immune to cracking while the STA condition was not (13,14). Unfortunately, because of the parameter used to compare cracking behavior, namely percent of yield strength, it is not clear whether stress level or microstructure was the controlling factor. Possibly the STA condition would not have cracked had it been stressed to the same level as the ST sample. If hydriding plays a role in Ti-3Al-8V-6Cr-4Mo-4Zr cracking behavior then, based upon the work of others, the STA condition with its higher fraction of alpha would be more susceptible than the ST condition.

If hydrogen causes the failures, then changing the rate at which hydrogen evolves on the sample's surface (the surface hydrogen flux) should have an effect on time to failure. This was shown in Table 5 where the STA condition was found to be sensitive to surface hydrogen flux. However, the effect was not consistent for a simple diffusion model. Instead of observing a continuous decline in failure time as surface flux increased, there was an initial decrease through a minimum followed by an increase through a maximum and then a further decrease. Assuming hydrogen diffusion rate within the metal was constant throughout the exposure, two transport steps may be responsible for this behavior: 1) the adsorption rate (i.e., the rate at which the hydrogen atom attaches to the titanium surface)

and/or 2) the absorption rate from the surface into the metal. Both of these steps are influenced by metal surface characteristics.

At least two investigators have indicated that the oxide film on titanium affects hydrogen transport (15,16). These investigators also indicated that transport through titanium's passive oxide was a slow, possibly rate-limiting process. However, a surface layer rich in hydrogen, possibly a hydride, could also have a significant affect on hydrogen transport. Investigations of commercially pure titanium under cathodic polarization have shown that development of a surface hydride dramatically reduces hydrogen absorption rates (17).

The photos given in Figure 2 show typical fracture surfaces for samples fractured under impressed cathodic current. All of the samples exhibited this fracture mode irrespective of the degree of impressed current. Note that the fracture appeared to propagate stepwise in waves similar to a fatigue fracture. Fracture waves appeared to initiate from discrete sites at several areas visible around the perimeter of the sample.

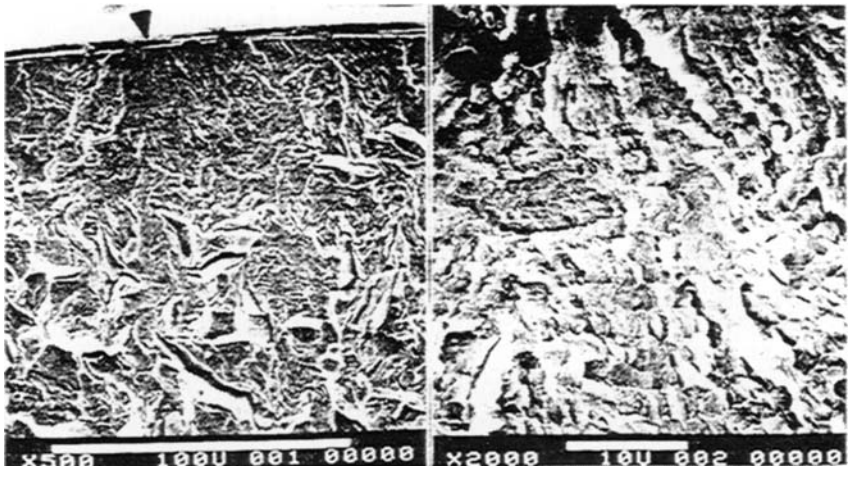


Fig. 2: Fracture surface photograph. Beta-C sample tested at 95% of yield strength (i.e., 1540 MPa) with an applied current density of 1.5mA/cm^2. Failure occurred after 115 hrs. Note wavelike striations.

Based upon these fracture surface features the following model seems possible. Defects in the surface layer may promote rapid local hydrogen absorption. Within this area local stress concentrations may promote the buildup of hydrogen to some critical concentration. Once this critical concentration is reached cracking can initiate. The cracks can then

propagate until they grow beyond the region of critical hydrogen concentration. Crack growth would then cease and the buildup process would start again along the freshly generated surface. This process would continue until the crack had moved far enough into the sample cross-section to cause ductile overload and failure of the sample.

Microstructure would most likely affect both surface and bulk diffusion rates. If hydride-induced embrittlement is responsible for mechnical property degradation then lowering the volume fraction of alpha phase would tend to reduce the likelihood that hydrides form. Thus, solution treatments without aging or higher aging temperatures (i.e., > 454C) would be preferred. Unfortunately, the data presented here only hints at this possibility. Further work must be performed to clarify to what extent microstructure affects environmental cracking susceptibility.

Conclusions

The high strength beta titanium alloy, Ti-3Al-8V-6Cr-4Mo-4Zr, has been shown to have excellent environmental cracking resistance in aqueous, hydrogen sulfide environments under open circuit conditions. This was true irrespective of thermomechanical condition, stress level, and yield strength.

Under an impressed cathodic current at 95% of the yield strength, the alloy was susceptible to environmental cracking in the solution treated and aged condition. The solution treated condition was not susceptible to cracking. As the impressed current was increased, time to failure went through a minimum and a maximum indicating a complex hydrogen diffusion model dependent on several unknown factors.

Acknowledgement

The authors thank RMI Company for its generous support of this work.

References

(1) P. W. Rice, R. A. Beverly, C. E. Ivey, B. R. Keevey: Materials Performance, Vol. 12(10), p. 35, 1973.
(2) S. Ohtani, T. Nishimura, Y. Mosiguch: Presentation at 50th Anniversary of Foundation of Climax Molybdenum Research Institute, 1980.
(3) Z. A. Foroulis: Werkstoffe und Korrosion, 30, p. 477, 1979.
(4) Anon: Iron Age, Nov. 22, 1976.
(5) M. Watkins, J. B. Greer: Journal of Petroleum Technology, June, 1976, p. 698.
(6) Z. A. Foroulis: Materials Performance, Vol. 19(9), p. 29, 1980.
(7) B. F. Brown, T. J. Lennox, Jr., R. L. Newbegin, M. H. Peterson, J. A. Smith, L. J. Waldron: Marine Corrosion Studies, NRL Memorandum Report 1574, Second Interim Report of Progress, U.S. Navy Research Laboratory, Nov. 1964.
(8) R. E. Curtis, R. R. Boyer, J. C. Williams: Trans. ASM, Vol. 62, 1969, p. 457.
(9) D. N. Fager and W. F. Spurr: Trans. ASM, Vol. 61, 1968, p. 283.
(10) R. J. Stokes: Thermomechanical Properties and Stress Corrosion Cracking of RMI Ti-3Al-8V-6Cr-4Mo-4Zr, Master Thesis, Univ. of Kentucky, 1976.
(11) W. F. Czyrklis, M. Levy: Corrosion, 1976, Vol. 32, p. 99.
(12) D. E. Thomas: To be published.
(13) B. S. Hickman, J. C. Williams, H. L. Marcus: AIME Spring Meeting, Las Vegas, NV, 1970.
(14) J. Feeney, M. J. Blackburn: Met. Trans. 1, p. 3309, 1970.
(15) G. R. Gaskey, Jr.: Hydrogen in Metals, I. M. Bernstein and A. W. Thompson eds., p. 465, American Society for Metals, 1974.
(16) K. K. Shah, D. L. Johnson: Hydrogen in Metals, I. M. Bernstein and A. W. Thompson eds., p. 475, American Society for Metals, 1974.
(17) D. E. Thomas: Unpublished work.

Copyrighted Materials
Copyright © 1996 NACE International Retrieved from www.knovel.com

PAPER NUMBER
303

Corrosion 87
March 9-13, 1987
Moscone Center / San Francisco, California

THE CHLORIDE STRESS CORROSION CRACKING BEHAVIOR OF BERYLLIUM COPPER AND OTHER NONMAGNETIC DRILL COLLAR ALLOYS

John C. Turn, Jr.
Brush Wellman Inc.
17876 St. Clair Ave.
Cleveland, OH 44110

ABSTRACT

Nonmagnetic drill collars and other structural components are used to provide a region in the bottom hole assembly near the bit in which sensitive magnetic measurements can be made. Beryllium copper, C17200, is paramagnetic with low magnetic permeability which makes it aptly suited for nonmagnetic components. Not only are the magnetic properties of the alloys for these components important, but the integrity of the alloys under dynamic loading in a range of hostile drilling fluids is critical as well. Chlorides in certain drilling muds can cause unpredictable stress corrosion cracking (SCC) of susceptible alloys. In a standard test for chloride SCC, ASTM G 36-73, beryllium copper, C17200, showed no failure after 1000 hr of exposure to boiling 45 weight percent magnesium chloride solution. The applied stresses were 100 percent of the 0.2 percent offset yield strength for the alloy. Failures for austenitic stainless steels generally occurred in less than 200 hr in this environment at applied stresses of 25 percent of the yield strength. Although benefits can be obtained by controlling the environment and introducing residual compressive stresses to austenitic stainless steel components, these remedies cannot permanently eliminate the underlying susceptibility of these alloys to chloride SCC. Beryllium copper is immune to chloride SCC.

INTRODUCTION

Nonmagnetic drill collars help drillers intersect hydrocarbon reservoirs in the earth's crust. Reservoirs of interest are being found at greater depths which increases the operating temperatures of drilling muds. The composition of drilling fluids changes as the requirements for drilling change, and water-based, chloride-containing muds may be necessary at some point during a campaign. These two factors, increasing temperatures and presence of chlorides, must be considered in selecting materials for nonmagnetic drill collars.

In the past these special collars have been fabricated from austenitic stainless steels which are also susceptible to stress corrosion cracking (SCC) in chloride environments. Evidence of SCC failures of these alloys during drilling have begun to appear[1]. Higher mud temperatures at any chloride level increase the chances of a SCC failure[2,3]. Especially offshore, drilling rig costs are high and downtime must be avoided. Materials which are resistant to SCC and, hence, more reliable are required for such demanding situations.

Since SCC resistance in chloride environments is an important criterion for selecting alloys for nonmagnetic drill collars and similar components, the performance of alloys in a standard test enables a direct comparison of the materials on an equal basis. It also provides perspective of the performance of nonmagnetic drill collar alloys to alloys which have been often evaluated and have well-known SCC behavior. These two benefits from conducting a standard SCC test provide confidence in the reliability of an alloy for nonmagnetic drill collars.

This paper reports results and conclusions from a standard SCC test in boiling magnesium chloride for twelve alloys, nine of which serve as materials of construction for nonmagnetic drill collars.

EXPERIMENTAL PROCEDURES

Materials

The alloys that were evaluated are listed in Table 1 with the respective commercial product forms and nominal compositions. Table 2 lists the mechanical properties of these alloys. Brush Alloy 25, UNS number C17200, was evaluated for two substantially different strengths. The bar for a drill collar application had a yield strength of 103 ksi (710 MPa), and the peak aged extruded tube had a yield strength of 160 ksi (1103 MPa).

C-ring Specimens

C-ring specimens for stress corrosion cracking tests were machined from each of the alloys. The dimensions were nominally 1 inch outside diameter by 0.093 inch thick wall by 0.75 inch wide and conform to ASTM Specification G 38-73[4]. The diameter to thickness ratio was 10.8 and assured linear elastic loading during deflection. Load was applied to the C-rings for C17200, N05500, N09925, S30403 and S31600 transverse to the axis of product, while the other C-rings were loaded in the longitudinal direction. For either orientation any cracks propagated in the radial direction of the product.

Figure 1 is a graph of the outer fiber stress as a function of the deflection for C17200 C-rings. This graph was constructed by attaching strain gauges to the outer surface of two C-rings opposite the ring gap and measuring the circumferential and transverse strains with increasing deflections of the C-ring. From these assumed elastic strains, the applied stresses were calculated and are represented in this graph as individual points. The line was calculated from the following formula[4]:

$$d = \frac{\sigma \pi (D - h)^2}{4 E h z}$$

where d is the deflection of the C-ring, D is its outside diameter, h is its wall thickness, z is a correction factor for its geometry, E is elastic modulus of the alloy, σ is the applied stress and π is 3.14159. For each alloy this C-ring geometry provided good agreement between applied stresses from strain measurements and those calculated from the above formula up to about the 0.2 percent offset yield strength.

To stress the C-rings for exposure, a bolt was tightened against an insulating spacer to compress the C-ring. Having experimentally developed the relationship between deflection and outer fiber stress, the deflection was selected to obtain the desired applied stress on the outer fiber of the C-ring. Generally, the alloys were tested at 100, 50 and 25 percent of the respective 0.2 percent offset yield strength.

SCC Test Procedure

Preparation of the magnesium chloride solution and the test procedure are described in ASTM Specification G 36-73[5]. The glassware apparatus that was used to conduct this test is shown in Figure 2 and consists of three parts with a thermometer similar to one described by Streicher and Sweet[6]. The boiling solution is in a flask which is capped by a water-cooled condenser and water vapor trap.

The solution of magnesium chloride and demineralized water was heated to boiling. By adjusting the amount of water in the solution the boiling point of the solution was established at 155 C +/-1 C (311 F +/-1.8 F). From the equation of Casale[7], the concentration of the solution should be 45 weight percent magnesium chloride. Two identically stressed C-rings of the same alloy were placed in the solution, and the condenser and vapor trap were connected to the flask. This glassware apparatus maintained the boiling point of this solution within +/-1 C (+/-1.8 F) for the 1000-hour duration of this test.

The C-rings were examined periodically during the exposure for cracks. At the first evidence of cracking, C-ring exposure was stopped, and the time to failure was recorded.

At the end of the exposure, each C-ring was thoroughly rinsed, dried and photographed. The loading bolt was removed, and the C-ring cut in half to metallographically evaluate the crack path.

RESULTS

Table 3 lists the results from the SCC tests in boiling magnesium chloride at 155 C. These data were collected as a function of the applied stress. C17200, N05500 and N07031 were evaluated only at 100 percent of their respective yield strengths because no failures occurred at that applied stress during 1000 hr of exposure. The other alloys cracked at this level of applied stress. Only one of the nonmagnetic stainless steels, S28200, survived 1000-hour exposure in this environment at 25 percent of the yield strength. N09925 with 42 weight percent nickel cracked at 25 percent of its yield strength. Figure 3 shows the individual C-ring data for C17200 and five of the other alloys. These data are a subset of Table 3.

Figures 4 and 5 show microstructures of six of the alloys that developed cracks during exposure to the boiling magnesium chloride solution. Figures 4a and 4b show, respectively, cracks that propagated in S30403 and S31600. The crack path in both of these cases was transgranular. For the other alloys in Figures 4 and 5 and the remaining alloys not shown, the crack paths were also transgranular. This behavior was observed for all levels of the applied stress.

DISCUSSION

The ASTM G 36-73 test is a standard materials practice for evaluating the SCC resistance of alloys in an environment that will definitely cause rapid failures of susceptible alloys. It is a procedure to evaluate materials. It is not an applications test. That is, it will not establish whether a particular alloy will perform adequately in a particular drilling mud at certain levels of temperature and chloride content in the field. ASTM G 36-73 can only rank alloys and variables like composition, heat treatment, surface finish, microstructure and stress with respect to chloride SCC resistance.

Two recent studies[1,8] underscore the caution which should be used in interpreting applications test data. Although early work[2,3] in chloride SCC showed that increases in temperature for any chloride content reduce the time to failure, the recent investigators neglected to provide test temperature and sodium chloride concentration for the most aggressive environment that they used. This oversight makes comparison to other data difficult.

The data from this investigation show that C17200 exhibits comparable performance to N05500 and N07031. No evidence of cracking was found for these alloys after 1000 hr of exposure to boiling 45 percent magnesium chloride. Also the applied stress could be as high as the 0.2 percent offset yield strength without causing cracking or fracture in these alloys. N05500 is often cited as resistant to chloride SCC[2,9,10]. These current data show that C17200 offers the same resistance to chloride SCC as offered by highly resistant, high nickel alloys.

Intermediate between the highly resistant copper and nickel base alloys and highly susceptible stainless steels is N09925 with about 42 weight percent nickel. This alloy appears to have chloride cracking resistance similar to other nickel-rich alloys with about the same nickel content[2,9,10].

Susceptible alloys fail rapidly in this test. S30400 is well-known to have low resistance to chloride SCC[2,3,10]. The current data show S30403 is susceptible, and the other austenitic stainless steels exhibit about the same high susceptibility to chloride SCC. Whether the austenite is stabilized by nickel, such as for S30403, S31600 or S20910, by manganese, as S28200 or NMS-100®, or by a combination of the two elements, as Gammaloy® or SCF-19®, the cracking performance is similar. The evaluations by Couper[2] support this contention, since he showed that stainless steels with 6 to 15 percent manganese and 0.5 to 5 percent nickel fail rapidly as do S30400 and S31600.

As shown in Figures 4 and 5, these susceptible alloys failed with the cracks propagating transgranularly. Smith *et al.*[1] also reported that the austenitic, nonmagnetic, drill collar alloys that they investigated cracked rapidly in boiling 42 percent magnesium chloride by transgranular crack propagation.

Some of the factors that influence SCC performance can be controlled to some extent at the drilling rig. These factors include the applied stress, mud temperature, chloride salt, chloride concentration, oxygen content, pH and time of exposure. Susceptible alloys can be treated to introduce compressive stresses on the exposed surface thus significantly changing the local stress condition. The degree to which these factors or remedies can be consistently and permanently controlled dictates the type of materials, susceptible or resistant, that can used with confidence to provide reliable service. Of course, alloys that are immune to chloride SCC can provide consistent performance and permit attention to be focused in other areas.

CONCLUSIONS

The results of these experiments support the following conclusions:

1. Beryllium copper, C17200, is immune to stress corrosion cracking in this chloride environment and ranks with high nickel base alloys in chloride cracking resistance.

2. Beryllium copper should be considered as a "materials solution" to the problem of chloride stress corrosion cracking for nonmagnetic drill collars and drill stem components.

3. Austenitic stainless steels, whether the austenite is stabilized by additions of nickel or manganese, are extremely susceptible to chloride stress corrosion cracking.

REFERENCES

1. P. G. Smith, J. E. Truman, H. T. Gisborne and G. Oakes, J. Materials for Energy Systems, Vol. 6, No. 4, p.300 (1985).

2. A. S. Couper, Materials Protection, Vol. 8, No. 10, p. 17 (1969).

3. K. C. Thomas, H. M. Ferrari and R. J. Allio, Corrosion, Vol. 20, No. 3, p. 89t (1964).

4. ASTM Standard Recommended Practice, G 38-73, "Making and Using C-ring Stress-Corrosion Test Specimens".

5. ASTM Standard Practice, G 36-73, "Performing Stress-Corrosion Cracking Tests in a Boiling Magnesium Chloride Solution".

6. M. A. Streicher and A. J. Sweet, Corrosion, Vol. 25, No. 1, p. 1 (1969).

7. I. B. Casale, Corrosion, Vol. 23, No. 10, p. 314 (1967).

8. T. Nakazawa, T. Suzuki, T. Sakamoto, Y. Yazaki and Y. Tsukano, Offshore Technology Conference, Paper No. OTC 5151, Houston, TX, 1986.

9. W. K. Boyd and W. E. Berry, "Stress Corrosion Cracking Behavior of Nickel and Nickel Alloys" in Stress Corrosion Cracking of Metals -- A State of the Art, STP 518, ASTM, 1916 Race St., Philadelphia, PA, 1972.

10. M. Watkins and J. B. Greer, "Corrosion Testing of Highly Alloyed Materials for Deep Sour Gas Well Environments", CORROSION/76, Paper No. 139, NACE, Houston, TX, 1976.

Table 1 - Nominal Composition and Product Form of Alloys

Alloy Designation	Common Name	Product Form	Principle Alloying Elements (wt.%)
Beryllium Copper			
C17200	Brush Alloy 25	Drill Collar & Tube	1.8Be 0.25Co
Nickel Alloys			
N05500	Monel K500[1]	Bar	30Cu 2Al 0.5Ti
N09925	Incoloy 925[1]	Bar	28Fe 22Cr 3Mo 2Cu 2Ti 0.25Al
N07031	Pyromet 31[2]	Bar	22Cr 15Fe 2Mo 2Ti 1Al
Stainless Steels			
S30403	AISI 304L	Tube	18Cr 8Ni
S31600	AISI 316	Tube	18Cr 10Ni 2Mo
S28200	18-18 Plus[2]	Drill Collar	18Cr 18Mn 1Cu 1Mo 0.5N
NMS-100[3]	NMS-100	Drill Collar	18Mn 13Cr 2Ni
Gammaloy[4]	Gammaloy	Drill Collar	15Cr 10Mn 10Ni
SCF-19[2]	SCF-19	Drill Collar	20Cr 18Ni 5Mn 5Mo 0.3N
S17400	17-4 PH[4]	Bar	15Cr 3Cu 3Ni 1Ti 0.4Al
S20910	Nitronic 50[4]	Bar	23Cr 13Ni 2Mo 0.3N

[1]Monel and Incoloy are registered trademarks of Huntington Alloys, Inc.
[2]Pyromet, 18-18 Plus and SCF-19 are registered trademarks of Carpenter Technology Corp.
[3]NMS-100 is a registered trademark of Earle M. Jorgensen Co.
[4]Gammaloy, 17-4 PH and Nitronic are registered trademarks of ARMCO Inc.

Table 2 - Mechanical Properties of Alloys

Alloy	0.2% Offset Yield Strength (ksi)	0.2% Offset Yield Strength (MPa)	Ultimate Tensile Strength (ksi)	Ultimate Tensile Strength (MPa)	Elongation (%)	Reduction-in-Area (%)
C17200						
Drill Collar	103	710	134	924	20	38
Tube	160	1103	177	1220	7	15
N05500	112	772	163	1124	29	48
Incoloy® 925	106	731	164	1131	28	42
N07031	106	731	160	1103	33	47
S30403	40	276	93	641	72	68
S31600	40	276	90	621	69	71
S28200	134	924	158	1089	39	66
NMS-100®	114	786	135	931	38	68
Gammaloy®	97	669	125	862	38	60
SCF-19®	120	827	145	1000	28	62
S17400	127	876	142	979	23	72
S20910	103	710	134	924	34	63

Table 3 - Stress Corrosion Cracking Results

Alloy	Applied Stress (ksi)	Applied Stress (MPa)	Time to Failure (hr)
C17200			
Drill Collar	110	758	N.F.[1]
Tube	150	1034	N.F.
N05500	110	758	N.F.
Incoloy® 925	110	758	24
	55	379	67
	28	193	940
N07031	100	690	N.F.
S30403	150	1034	24
	100	690	18
	50	345	24
	20	138	135
S31600	150	1034	8
	100	690	23
	50	345	23
	20	138	130
S28200	120	827	5
	70	483	83
	35	241	N.F.
NMS-100®	100	690	22
	60	414	28
	30	207	91
Gammaloy®	90	620	20
	50	345	27
	25	172	66
SCF-19®	115	793	66
	60	414	17
	30	207	24
S17400	130	896	3
	65	448	5
	32	220	5
S20910	110	758	4
	55	379	5
	28	193	5

[1]N.F. means that no failure occurred during 1000 hr of exposure.

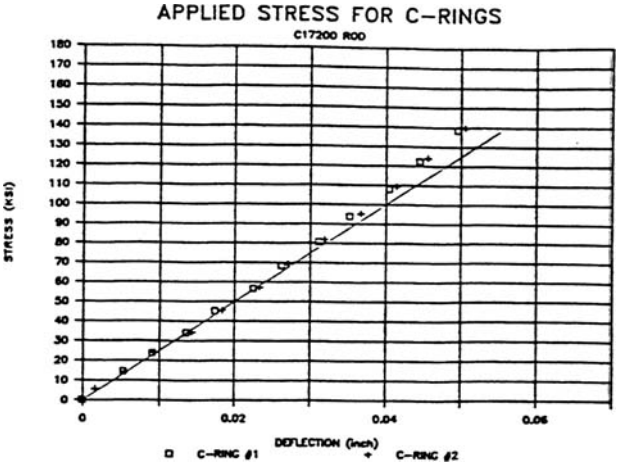


Figure 1 - This graph shows the relation between C-ring deflection and the resulting applied stress for C-rings from C17200 rod.

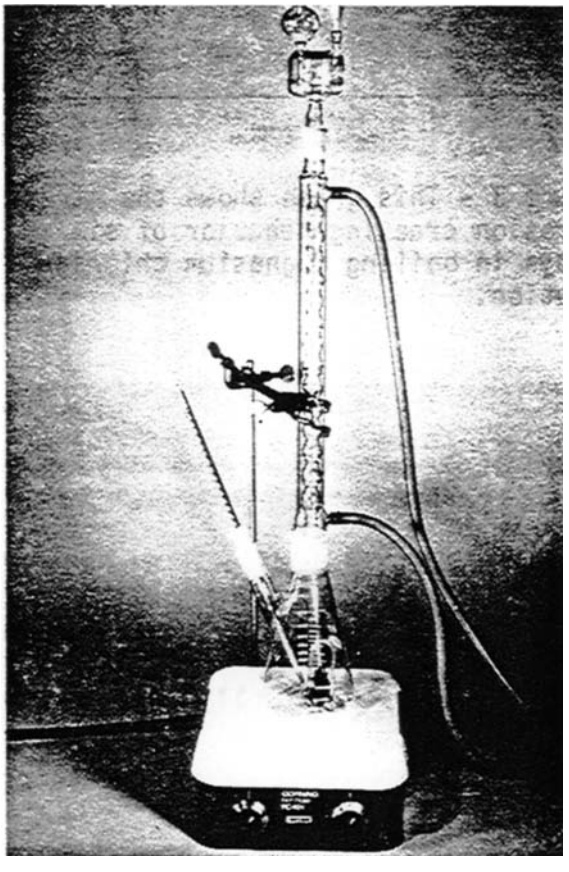


Figure 2 - This photograph shows the apparatus for the boiling magnesium chloride tests. Note that a glass stand was used to support a C-ring in the boiling solution.

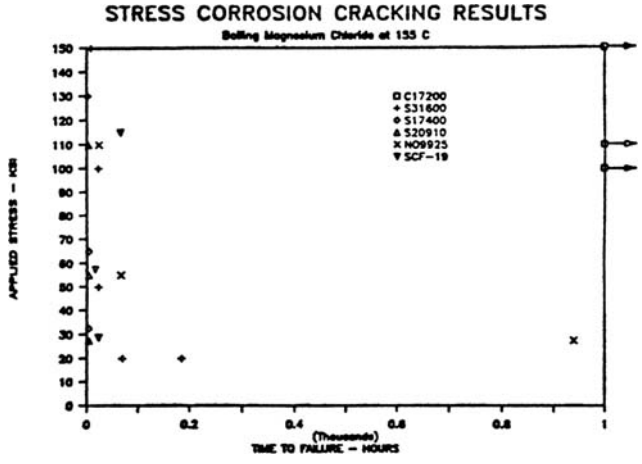


Figure 3 - This graph shows the stress corrosion cracking behavior of six alloys in boiling magnesium chloride solution.

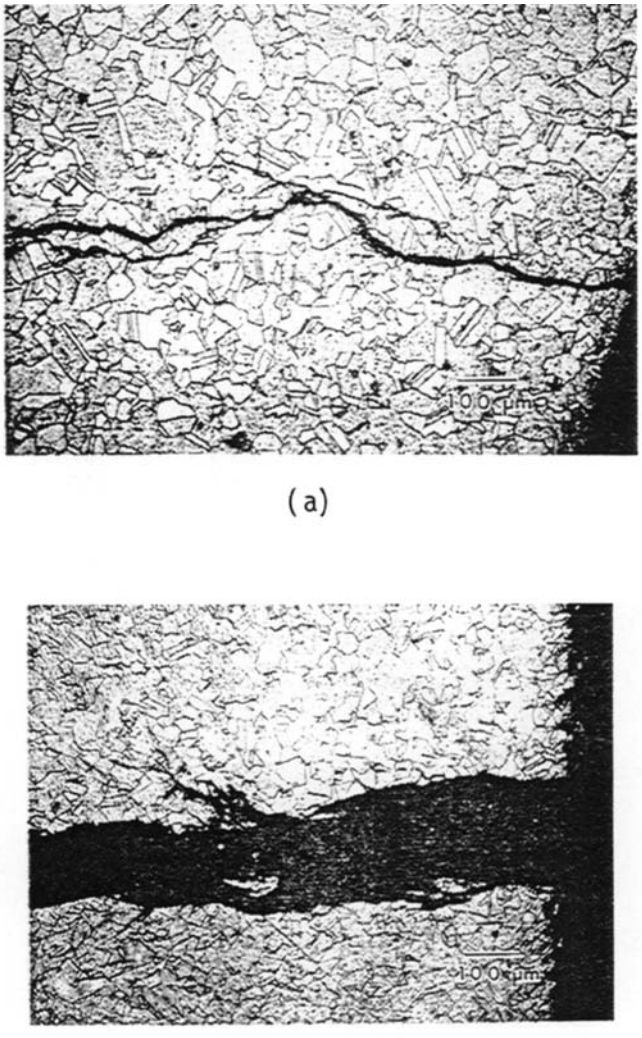
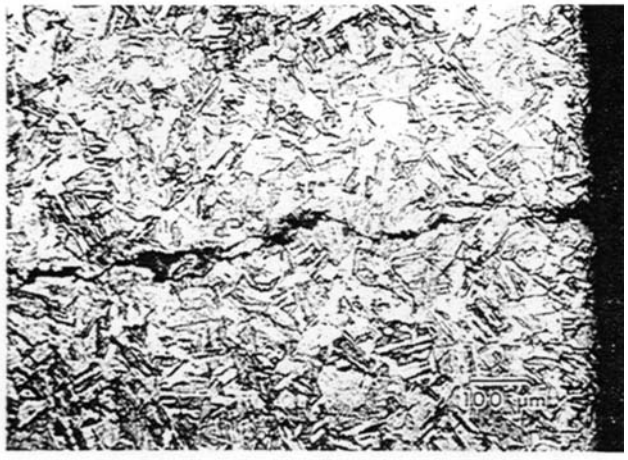


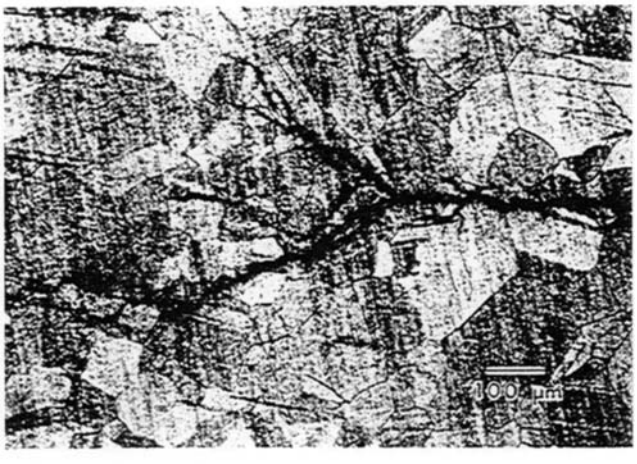
Figure 4 - These micrographs show the transgranular cracks that develop after exposure to boiling magnesium chloride (a) S30403, (b) S31600, (c) SCF-19®.



(a)



(b)



(c)

Figure 5 - These micrographs show the transgranular cracks that develop after exposure to boiling magnesium chloride (a) S17400, (b) S20910, (c) N09925.

Copyrighted Materials
Copyright © 1996 NACE International Retrieved from www.knovel.com

PAPER NUMBER

69

Corrosion 88

March 21-25, 1988
Cervantes Convention Center / St. Louis, Missouri

THE EFFECT OF OXYGEN AND TEMPERATURE ON CHLORIDE STRESS CORROSION CRACKING OF BERYLLIUM COPPER AND OTHER NONMAGNETIC ALLOYS IN A SIMULATED CHLORIDE DRILLING ENVIRONMENT

John C. Turn, Jr.
Brush Wellman Inc.
17876 St. Clair Avenue
Cleveland, OH 44110

ABSTRACT

The chloride SCC behaviors of beryllium copper C17200 and other nonmagnetic stainless alloys were evaluated in an applications test. The environment was a mixed chloride drilling fluid that contained 6% potassium chloride and 25% magnesium chloride at a near neutral pH. The dissolved oxygen content of the fluid was changed by varying the composition of the saturating nitrogen gas from 50 to 20,000 ppm of oxygen. Temperature of the fluid was also varied from 175 F (79 C) to 300 F (149 C). The time to failure by SCC decreased as the oxygen content and temperature of the drilling fluid increased. C17200 showed no evidence of cracking in these tests after 1000 hr. The average corrosion rate for C17200 is 2 mpy (0.05 mm/yr) under laboratory conditions of 5,000 ppm oxygen and 300 F (149 C) for exposures of 1000 hr. Beryllium copper resists chloride SCC and corrosion in these simulated drilling environments.

INTRODUCTION

Nonmagnetic drill collars and other nonmagnetic components are used during the drilling of oil and gas wells to make sensitive measurements of the earth's magnetic field. Such measurements, when made accurately, describe the trajectory of the bit toward the desired reservoir. Water-based chloride-containing drilling muds are routinely used during drilling. As the depth to reach hydrocarbon deposits increases so does the temperature. The combination of elevated temperatures and high concentrations of chloride ions are well-known to cause chloride stress corrosion cracking (SCC) of austenitic stainless

steels. These alloys have been used extensively for nonmagnetic components. Besides the susceptibility to chloride SCC, these alloys tend to gall at the threaded connections and the magnetic properties can be degraded by cold work.

Previous work showed that beryllium copper C17200 resists chloride SCC[1] in a standard test, ASTM G 36-73[2]. Although this test shows susceptibility of an alloy to SCC, it is an aggressive test. For applications like nonmagnetic components that are used in drilling, an applications test is needed to more closely simulate the environmental conditions in a water-based, chloride drilling fluid. The variables that must be controlled for a test to simulate conditions during drilling are: pH, chloride ion content, dissolved oxygen content, temperature and tensile stress. In these laboratory experiments the pH of a mixed drilling fuild was adjusted to near neutral. The chloride ion content was fixed. Only the oxygen content, temperature and applied stress were systematically varied.

This paper reports the results of laboratory SCC and corrosion tests that simulate the conditions of oxygen content and temperature that can exist during drilling in a water based chloride mud. Beryllium copper C17200 and other stainless nonmagnetic alloys were evaluated in these applications tests at two levels of applied stress.

EXPERIMENTAL PROCEDURES

Materials

The alloys that were examined are listed in Table 1 with the nominal compositions and product forms. These alloys were obtained from commerical sources. Table 2 lists the longitudinal mechanical properties of the alloys in Table 1. No additional mechanical or thermal treatments were given to these products before evaluation. Brush Alloy 25, C17200, was evaluated from two product forms with different strengths. The drill collar had a 0.2 percent offset yield strength of 103 ksi (710 MPa), while the extruded tube had a yield strength of 160 ksi (1103 MPa).

C-rings for stress corrosion cracking tests were machined from the product forms. The dimensions were the same as those previously employed[1], a nominal 1 inch outside diameter by 0.093 inch thickness by 0.75 inch wide. This size conforms to ASTM G38[3]. The C-rings were oriented such that any crack would propagate in the radial direction of the product form.

Tensile stress was applied to the outer surface of the C-ring by tightening a loading bolt. The relationship between the deflection of the C-ring and the applied stress was described earlier[1,3]. The level of the applied stress was 50 and 100 percent of the measured yield strength of the product. Two C-rings at both levels of applied stress were concurrently exposed to the laboratory environment.

Weight loss coupons of C17200 were concurrently exposed with C-ring specimens. These coupons were 0.75 x 1.5 x 0.125 inch.

Applications Test for SCC

The composition of the aqueous solution that was the environment for SCC tests is listed in Table 3. This composition simulates a drilling fluid with

high chloride ion content. On a weight basis the fluid contains 6% potassium chloride and 25% magnesium chloride. The pH of the solution is adjusted with calcium hydroxide to near neutral as shown in Table 3.

A 5 liter N10276 autoclave was filled with 1.8 liter of the mixed chloride drilling fluid. The C-rings or C-rings and corrosion coupons were suspended on a glass fixture in the drilling fluid. The lid was bolted closed, and the saturating gas bubbled through the sealed vessel for 30 min. This gas was either purified nitrogen (99.999 percent pure) or nitrogen and oxygen gas mixtures which contained 50, 500, 5000 or 20,000 ppm of oxygen. After purging, the autoclave was pressurized with the saturating gas and heated to the desired temperature. Regardless of the test temperature the total pressure was 1000 psi. Temperatures during the exposures were 175 F (79 C), 250 F (121 C) or 300 F (149 C). C-rings of the nickel and iron alloys were tested together, and C17200 was tested separately.

C-rings were examined weekly after the first week of exposure. During the first week the C-rings were examined after 3 days. Examination consisted of looking at the C-ring with the unaided eye. If no cracks were observed during 1000 hr of exposure, the C-ring was sectioned and examined metallographically for cracks. If either unmagnified or magnified examination of the specimen revealed a crack, the specimen was classified as a one that failed. The exposure time of the specimen in the mixed chloride fluid was termed the time to failure. Two C-rings were exposed at each stress level, and the average of the individual times to failure is reported here.

Corrosion coupons of C17200 were measured and weighed before exposure to the drilling fluid, and these values were recorded. The two coupons were removed after 3, 7, 21 and 42 days of exposure. Each coupon was cleaned in a solution of 50% concentrated hydrocloric acid, 10% concentrated sulphuric acid and 40% deionized water for 3 min at room temperature. Each coupon was rinsed, dried and reweighed. The weight loss per unit area and average corrosion rate were calculated. The average corrosion rate in this case is the weight loss per unit area divided by the specific exposure time. This value was converted to a penetration rate in thousandths of an inch per year (mpy).

RESULTS

Table 4 lists the average time to failure data for C-rings stressed to 50 and 100% of yield strength. The environment for these tests was the mixed chloride drilling fluid that was saturated and pressurized with nitrogen with different oxygen contents. The temperature inside the autoclave during each individual test was 300 F, and the total pressure was 1000 psi. The data for C-rings stressed to 50% of the yield strength are plotted in Figure 1, while the data for C-rings tested at 100% of the yield strength are graphed in Figure 2.

Cracking was observed in the deaerated drilling fluid (about 1 ppm oxygen) for S17400, NMS-100® and Gammaloy® for both stress levels, Figures 1 and 2. C-rings of S20910, SCF-19® and N09925 were more resistant and showed no failures in deaerated fluid after more than 1000 hr exposure. By purging the solution with nitrogen gas that contained 50 ppm of oxygen, cracking occurred for S20910 and N09925 at the 100% stress level in 1000 hr as shown in Table 4. SCF-19® did not crack in this environment at this level of stress for a similar period of exposure. For the fluid saturated with 500 ppm of oxygen, cracks were found in C-rings of S20910, SCF-19® and N09925. The time to failure for S20910 that was stressed to 100% of the yield strength was about half the value for 500 ppm

oxygen in the gas, as it was with 50 ppm oxygen in the gas. Increasing the oxygen content of the gas phase to 5000 ppm substantially decreased the times to failure for S20910, SCF-19® and N09925. Increasing the oxygen content even further to 20,000 ppm reduced the times to failure even further. This effect of the oxygen on the time to produce cracks is displayed in Figures 1 and 2. Beyond 50 ppm of oxygen, the times to failure decrease dramatically with increasing oxygen content in the saturating gas phase for these stainless alloys.

Table 4 and Figure 2 also contain results of cracking tests for beryllium copper C17200 in both product forms. The mixed chloride drilling fluid for this test was saturated with gas with 5000 ppm of oxygen, and the temperature was 300 F. Both the drill collar and extruded tube showed no evidence of cracking after more than 1000 hr in this environment.

Table 5 contains the average time to failure for four alloys in the mixed chloride drilling fluid. The temperatures during the exposures were 175 F (79 C), 250 F (121 C) and 300 F (149 C). The drilling fluid was saturated and pressurized with nitrogen that contained 5000 ppm of oxygen. Data for both applied stress levels appear in Table 5.

N09925 showed no failures at 175 and 250 F, but failure occurred in less than 443 hrs at 300 F for both 50 and 100% stress levels. SCF-19® showed failures at both stress levels and each temperature. The time to failures were 1000, 600 and 400 hr at 175, 250 and 300 F, respectively. S20910 exhibited failures at each temperature with times to failure that ranged from 500 hr at 175 F to 40 hr at 300 F. The times to failure were similar for these alloys at the 50 and 100% stress levels.

Beryllium copper was evaluated at 300 F and showed no cracking at this temperature for an oxygen content in the gas of 5000 ppm. The data from Table 5 are presented in Figures 3 and 4. In both of these figures the stainless alloys exhibit cracking behaviors that show poorer resistance to cracking at elevated temperatures. At the highest temperature, 300 F, C17200 showed no evidence of cracking in either drill collar or high strength tube.

Figure 5 shows the weight loss corrosion of C17200 in mixed chloride drilling fluid at 300 F with 5000 ppm of oxygen in the saturating gas. Both product forms showed similar weight loss behavior. Corrosion was general with no localized attack. Regressed lines were fitted to this weight loss data. The equations for the particular product forms are given in Figure 5. Generally, the corrosion rate slows over the duration of the exposure. The regression equations predict that the instantaneous rate at 1000 hr is less than 1 mpy (0.03 mm/yr) for both product forms.

The average corrosion rates were calculated from the weight loss data. Figure 6 shows the trend for the average corrosion rate with exposure time. The highest average rate is about 4 mpy (0.1 mm/yr). With longer exposures corrosion slows to an average rate of 2 mpy (0.05 mm/yr). Although the product forms are shown as distinct sets of data, the weight loss values and average corrosion rates are not significantly different. These low corrosion rates indicate that beryllium copper is resistant to corrosion in a mixed chloride drilling fluid at 300 F with as much as 5000 ppm of oxygen in the saturating gas.

DISCUSSION

A major benefit of a standard materials test is that it is a consistent and reliable method to evaluate the specific performance of a material under well defined and closely controlled conditions. The ASTM G 36-73 is such a standard test[2]. The variables are controlled that influence the chloride SCC of susceptible alloys. The pH is 3.5 to 4.0. The solution contains 45% magnesium chloride. Boiling deaerates the solution. The temperature is fixed by carefully controlling the water content of the solution, and the applied stress on a specimen can be calculated from elastic equations or measurements of strain. One problem with such a test is that these conditions are too aggressive to predict whether a certain alloy may be acceptable under less aggressive conditions. What is required is an applications test. In this type of evaluation the variables of the standard test are carefully controlled to reduce the aggressiveness of the test to match the conditions in service. Problems can result if this transformation is not executed correctly.

SCC of nonmagnetic stainless steels as drill collars in chloride drilling muds is becoming more well publicized[4,5]. Applications tests could provide information to successfully select materials for this demanding application, but the variables of pH, chloride ion content, dissolved oxygen content and temperature must be properly controlled. Either a combination of these variables must be found that permits a margin of safety to avoid failures by SCC or alloys that are resistant can be identified to aid proper materials selection. Thus, an applications test can establish whether a particular alloy will be likely to perform well in a particular application. The current results showed that by manipulating the environmental variables, susceptible alloys can exhibit good or poor performance.

Chloride drilling muds contain large quantities of chlorides. The pH of the mud is usually controlled to be neutral or slightly basic. The oxygen content should be kept low, but during operation, equipment may allow some oxygen to dissolve in the mud. Mud temperature is a function of the depth being drilled and can be above 250 F. In the current series of results and those previously published[1], the SCC behavior of beryllium copper C17200 in chloride environments was documented. This alloy resists SCC under aggressive conditions (ASTM G 36-73) and under those that simulate a wide range of mud conditions. No cracking was observed under any of these laboratory conditions. Furthermore, in a chloride drilling fluid beryllium copper exhibited a low corrosion rate which tended to decrease with exposure time. This type of corrosion performance is superior to that of stainless steels.

The good corrosion performance of beryllium copper combined with excellent resistance to galling and low, stable magnetic permeability make this alloy a good candidate for nonmagnetic drill collars and other nonmagnetic components.

CONCLUSIONS

1. Beryllium copper resists SCC and general corrosion under environmental conditions and stress levels that simulate drilling muds.

2. An applications test for evaluating materials for SCC in drilling environments should account for the solution pH, chloride ion concentration, oxygen content and temperature as well as the applied tensile stress.

3. The chloride SCC behavior of nonmagnetic alloys other than C17200 depends on the oxygen content and temperature of the drilling fluid.

4. For similar oxygen contents and temperatures, a low pH, high chloride solution (ASTM G 36-73) was substantially more aggressive in initiating SCC than a high pH, mixed chloride drilling fluid.

REFERENCES

1. J. C. Turn, Jr., "The Chloride Stress Corrosion Cracking Behavior of Beryllium Copper and Other Nonmagnetic Drill Collar Alloys," CORROSION/87, Paper No. 303, National Association of Corrosion Engineers, Houston, TX, 1987.

2. ASTM Standard Practice, G 36-73, "Performing Stress-Corrosion Cracking Tests in a Boiling Magnesium Chloride Solution".

3. ASTM Standard Recommended Practice, G 38-73, "Making and Using C-ring Stress-Corrosion Test Specimens".

4. P. G. Smith, J. E. Truman, H. T. Gisborne and G. Oakes, J. Materials for Energy Systems, Vol. 6, No. 4, p. 300 (1985).

5. J. N. Cordea, H. V. Sheth and J. C. Jasper, Materials Performance, Vol. 26, No. 9, p. 50 (1987).

Table 1 - Nominal Composition and Product Forms of Alloys

Alloy Designation	Common Name	Product Form	Principal Alloying Elements (wt.%)
Beryllium Copper			
C17200	Brush Alloy 25	Drill Collar & Tube	1.88Be 0.25Co
Nickel Alloy			
N09925	Incoloy 925[1]	Bar	28Fe 22Cr 3Mo 2Cu 2Ti 0.25Al
Stainless Steels			
S28200	18-18 Plus[2]	Drill Collar	18Cr 18Mn 1Cu 1Mo 0.5N
NMS-100[3]	NMS-100	Drill Collar	18Mn 13Cr 2Ni
Gammaloy[4]	Gammaloy	Drill Collar	15Cr 10Mn 10Ni
SCF-19[2]	SCF-19	Drill Collar	20Cr 18Ni 5Mn 5Mo 0.3N
S17400	17-4 PH[4]	Bar	15Cr 3Cu 3Ni 1Ti 0.4Al
S20910	Nitronic 50[4]	Bar	23Cr 13Ni 2Mo 0.3N

1. Incoloy is a registered trademark of Huntington Alloys, Inc.
2. 18-18 Plus and SCF-19 are registered trademarks of Carpenter Technology Corp.
3. NMS-100 is a registered trademark of Earle M. Jorgensen Co.
4. Gammaloy, 17-4 PH and Nitronic are registered trademarks of ARMCO Inc.

Table 2 - Mechanical Properties of Alloys

Alloy	0.2% Offset Yield Strength (ksi)	0.2% Offset Yield Strength (MPa)	Ultimate Tensile Strength (ksi)	Ultimate Tensile Strength (MPa)	Elongation (%)	Reduction-in-Area (%)
C17200						
Drill Collar	103	710	134	924	20	38
Tube	160	1103	177	1220	7	15
N09925	106	731	164	1131	28	42
S28200	134	924	158	1089	39	66
NMS-100®	114	786	135	931	38	68
Gammaloy®	97	669	125	862	38	60
SCF-19®	120	827	145	1000	28	62
S17400	127	876	142	979	23	72
S20910	103	710	134	924	34	63

Table 3 - Composition of a Mixed Chloride Drilling Fluid

1 liter of deionized water

145 gm of KCl

1274 gm of $MgCl_2 \cdot 6H_2O$

6 gm of $Ca(OH)_2$

6.7 to 7.1 pH

Table 4 - Time to Failure versus Oxygen Content

Oxygen Content (ppm)	Time to Failure (hr)*			
	N09925	SCF-19®	S20910	C17200
0	NF/NF	NF/NF	NF/NF	
50	NF/1000	NF/NF	1000/1000	
500	1000/1000	1000/1000	844/580	
5000	443/443	400/400	40/40	/NF
20000	336/336	120/16	16/16	

* NF = no failure after more than a 1000 hr exposure.

The first time to failure value is the average for the two C-rings stressed at 50% of the yield strength, while the second value is the average of the two stressed to 100%.

Table 5 - Time to Failure versus Temperature

Temperature (F)	Time to Failure (hr)*			
	N09925	SCF-19®	S20910	C17200
175	NF/NF	1000/1000	500/500	
250	NF/NF	590/670	96/64	
300	443/443	400/400	40/40	/NF

* NF = no failure after more than a 1000 hr exposure.
The first time to failure value is the average for the two C-rings stressed at 50% of the yield strength, while the second value is the average of the two stressed to 100%.

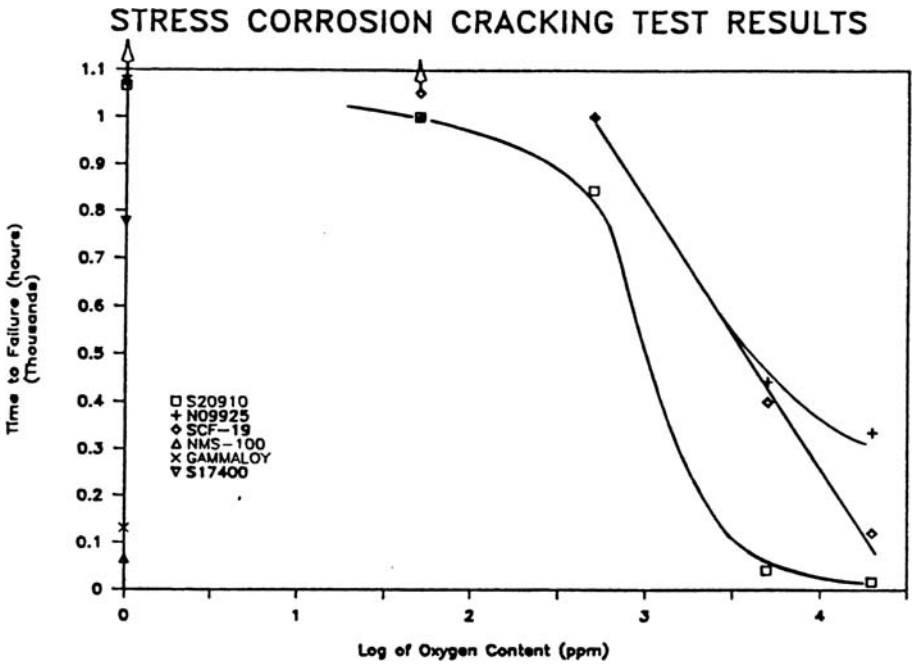


Figure 1 - The time to failure for C-rings stressed to 50% of the yield strength is plotted versus the oxygen content in the saturating gas for a temperature of the drilling fluid of 300 F. Arrows indicate no failure after 1000 hr.

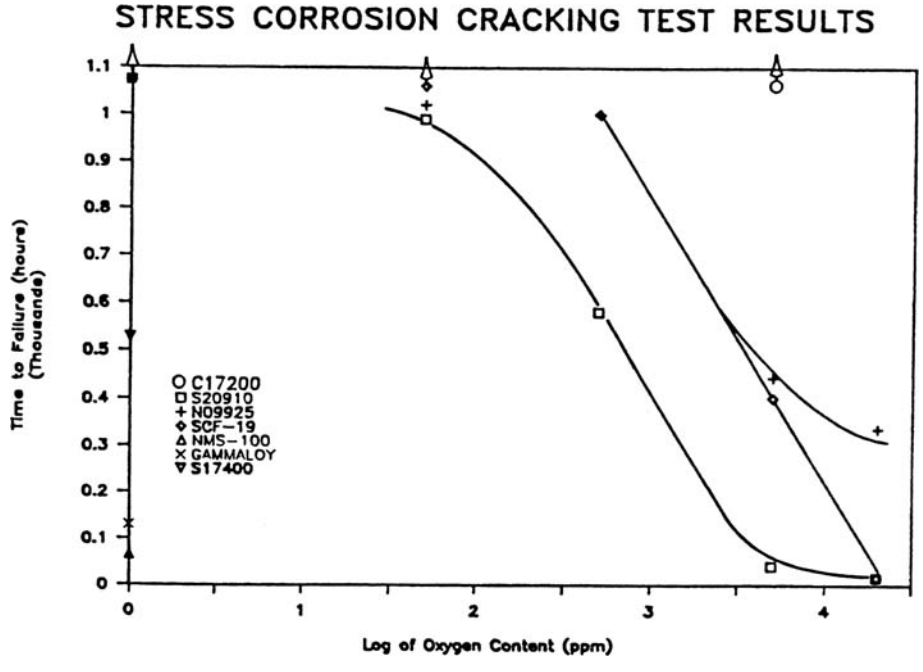


Figure 2 - The time to failure for C-rings stressed to 100% of the yield strength is plotted versus the oxygen content of the gas for a temperature of 300 F. Arrows indicate no failure after 1000 hr.

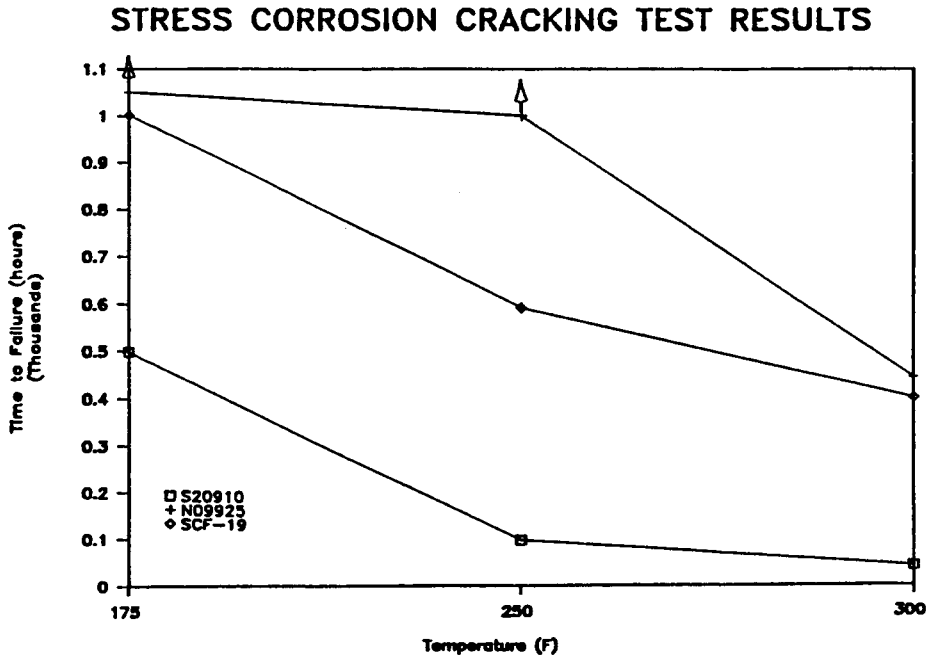


Figure 3 - At an oxygen content of 5000 ppm in the gas, the time to failure for C-rings stressed to 50% of the yield strength is plotted versus the temperature of the drilling fluid. Arrows indicate no failure after 1000 hr.

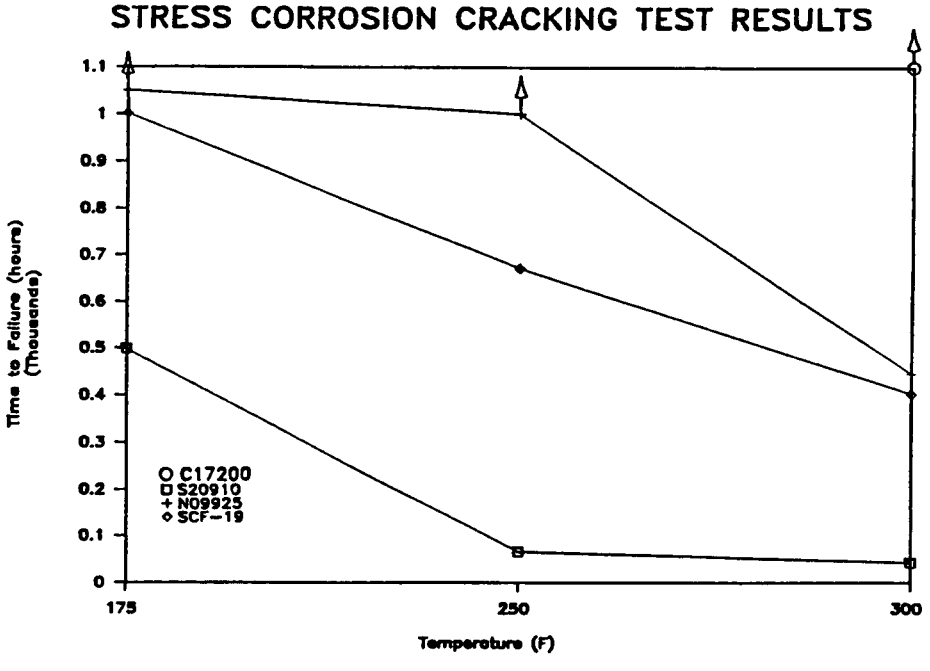


Figure 4 - At an oxygen content of 5000 ppm in the gas, the time to failure for C-rings stressed to 100% of the yield strength is plotted versus the temperature of the drilling fluid. Arrows indicate no failure after 1000 hr.

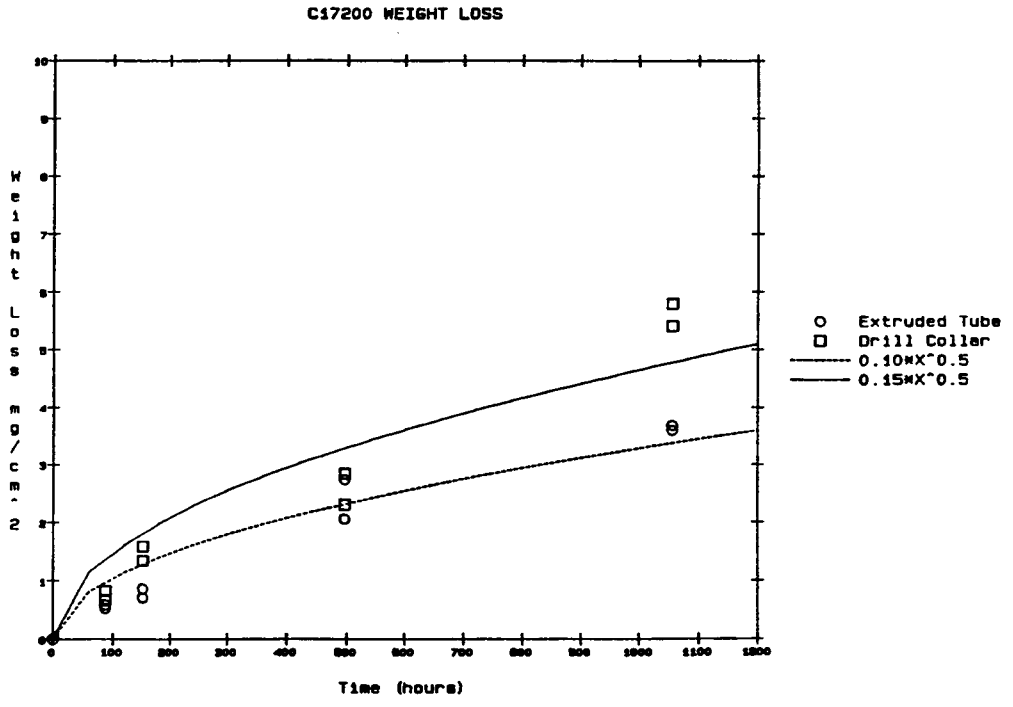


Figure 5 - The weight loss corrosion is plotted for exposure time for C17200 in drilling fluid at an oxygen level of 5000 ppm and a temperature of 300 F.

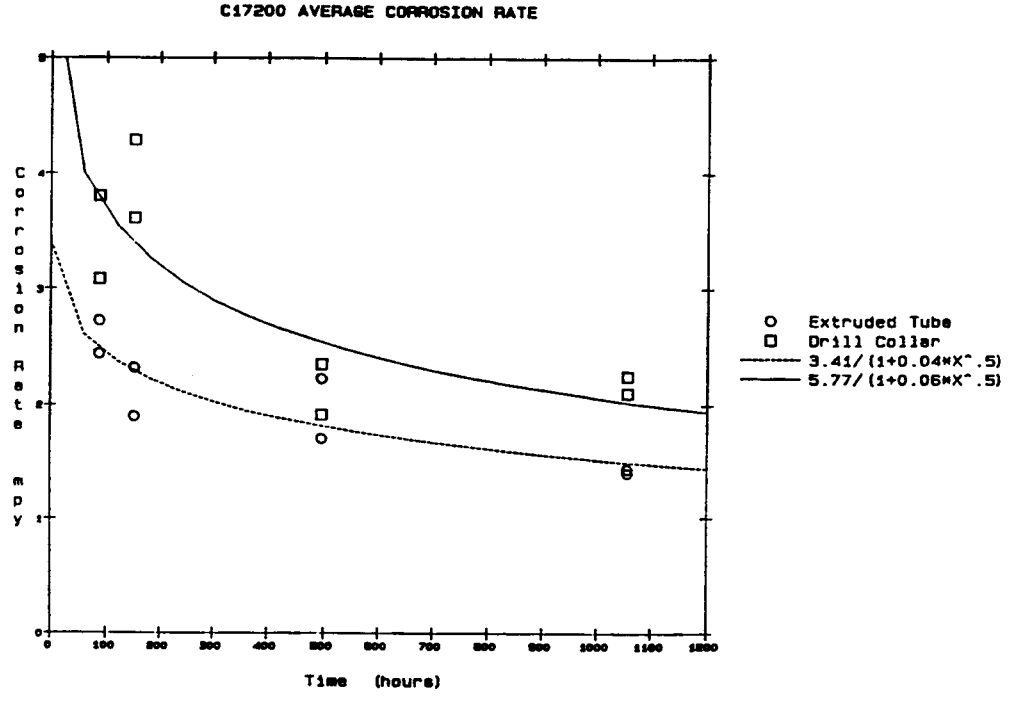


Figure 6 - The average weight loss corrosion rate is plotted from the data from Figure 5.

Copyrighted Materials
Copyright © 1996 NACE International Retrieved from www.knovel.com

The Performance of Zirconium Alloys in Sulfide Solutions*

TE-LIN YAU*

Abstract

Zirconium Grades R 60702, R 60704, and R 60705 were investigated for deep sour gas well applications. Test methods include autoclave, constant strain, sustained load, and constant strain rate techniques. Test results indicate that these alloys have excellent resistance to general corrosion and to stress corrosion cracking in sulfide environments. No cracking was detected in all grades of zirconium in 5% NaCl + 0.5% CH_3COOH + saturated H_2S at room and boiling temperatures. Hydrogen sulfide seems to play a neutral role in the corrosion reactions of zirconium because of zirconium's low affinity for sulfur.

Introduction

Hydrogen sulfide in aqueous environments is known as a powerful promoter for sulfide stress cracking (SSC). Hudgins, *et al.*, observed cracking of HRC 21 hardness steel in a 5% NaCl solution with only 1 ppm H_2S at a stress corresponding to 130% of the yield strength.[1] Treseder and Swanson defined a 0.001 atmosphere H_2S partial pressure (3 ppm) as the criteria for a sour environment since they could produce cracking of API P-110 and 9Ni steels in a 0.5% CH_3COOH + 3 ppm H_2S solution.[2]

Thermodynamic analyses indicate that the electromotive force of the corrosion elements is much higher for metal-hydrogen sulfide-water ternary systems than for metal-water binary systems.[3-6] Hydrogen sulfide can react with many metals to form metal sulfides as main corrosion products in sulfide containing solutions:

$$H_2S + Me \xrightarrow{H_2O} MeS + 2H. \quad (1)$$

Hydrogen released during corrosion is generally thought to be responsible for SSC failures. The atomic hydrogen is considerably more deleterious than hydrogen gas. According to Kerns and Staehle's studies, cracking velocities of double cantilever beam specimens (AISI 4335 V steel) in hydrogen sulfide are at least three orders of magnitude greater than in hydrogen gas at the same pressure and stress intensity.[7]

The main areas that may be affected by H_2S are sewage disposal equipment, geothermal energy systems, equipment handling sour crudes and natural gases, and deep sour oil and gas well drilling. Among these fields, deep sour gas well drilling appears to be the most challenging problem for corrosion and materials researchers.[8-10] Down-hole environments can have pressures exceeding 138 MPa (20,000 psi) and temperatures exceeding 204 C (400 F), and contain 35-45% H_2S, 10% CO_2, and 45-55% CH_4 plus organic acids and brine solutions.[8-10] Materials selected for the deep drilling must be high strength and have high resistance to chloride stress corrosion cracking (SCC) in addition to hydrogen sulfide attack. It is well-known that high strength steels are susceptible to SSC and that this susceptibility increases with increased strength of the steel.[1,2,11-15] SSC is the most important factor that limits the use of the high strength steels in handling H_2S containing solutions. Also, deep sour gas well environments can induce severe attack in the forms of general corrosion, pitting, and crevice corrosion.

In the last few years, the high alloy materials (highly alloyed stainless steels and nickel-base alloys) have been evaluated and used for the deep drilling.[8,10,16-26] These corrosion resistant materials may also experience stress cracking failure in deep sour gas well environments. It seems that, at this time, no commercial alloy with sufficient yield strength has been found to be resistant to SSC and/or chloride SCC for use in deep sour gas wells.[27]

It is the purpose of this paper to evaluate the corrosion and stress cracking resistance of zirconium alloys in sulfide containing chloride solutions.

Corrosion Properties of Zirconium Alloys

The corrosion properties of zirconium and its alloys in a carbon dioxide atmosphere have been studied extensively because they are candidate materials for CO_2-cooled reactors.[28-38] This subject has been reviewed by Parfenov, *et al.*,[39] Cox,[40] and Tyzack and Cowen.[41] The weight gain data shows that zirconium should not be heated in CO_2 above 650 C for extended periods if excessive corrosion is to be avoided.[29] The Zircaloy type alloys (Zr-1.5Sn alloys) should not be used for CO_2 at temperatures higher than 400 C.[30] The Zr-Nb type alloys may show considerable weight gains during oxidation in CO_2, but oxide films are compact and well-adherent. The Zr-1.5Nb alloy does not exhibit breakaway during oxidation in CO_2 at 500 C after 3000 hours.[30] Cladding alloys of zirconium, copper, and molybdenum are resistant to oxidation under irradiation in carbon dioxide and steam at temperatures up to 600 C.[38]

Zirconium is regarded as a high performance material in corrosive applications. It resists attack in a broad range of corrosive chemicals, which includes most mineral acids, salt solutions, organic acids, alkalis, molten salts, and molten metals.[42-44]

Zirconium can naturally passivate in reducing acids, *e.g.*, up to 37% HCl or 70% H_2SO_4, even at elevated temperatures

*Presented during Corrosion/82 (Paper 129), March, 1982, Houston, Texas.

*Metallurgical Research & Development, Teledyne Wah Chang Albany, Albany, Oregon.

TABLE 1 — Properties of Annealed Zirconium Alloys

	Zr 702		Zr 704		Zr 705	
Composition, Wt%						
Zr + Hf, min.	99.2		97.5		5.5	
Hafnium, max.	4.5		4.5		4.5	
Fe + Cr	0.2 max.		0.2-0.4		0.2 max.	
Hydrogen, max.	0.005		0.005		0.005	
Nitrogen, max.	0.025		0.025		0.025	
Carbon, max.	0.05		0.05		0.05	
Oxygen	0.16		0.18		0.18	
Niobium	—		—		2.0-3.0	
Tin	—		1.0-2.0		—	
	20 C (70 F)	**315 C (600 F)**	**20 C (70 F)**	**315 C (600 F)**	**20 C (70 F)**	**315 C (600 F)**
Mechanical Properties						
Tensile Strength MPa (10^3 psi)	450 (65)	125 (18)	485 (70)	140 (20)	585 (85)	330 (48)
Yield Strength MPa (10^3 psi)	310 (45)	85 (12)	380 (55)	105 (15)	450 (65)	205 (30)
Elongation, %	25	35	20	32	20	30
Reduction in area, %	50	65	42	60	45	65

and pressures. Dissolved oxygen or anodic protection systems are not needed for the passivation processes. Also, zirconium exhibits excellent resistance to many salt solutions, except ferric and cupric chloride solutions.[45] This resistant property is not affected by chloride ion concentration and pH (if pH > -1). Furthermore, zirconium's resistance to acidic chloride solutions makes it very resistant to crevice corrosion.

Zirconium is more vulnerable in highly oxidizing and oxygen deficient solutions. It corrodes in concentrated sulfuric acid and aqua regia. The presence of oxidizing agents, *e.g.*, Fe^{+3} or Cu^{+2}, in halide solutions may cause pitting. Environments that can induce SCC include $FeCl_3$ or $CuCl_2$ solutions,[46,47] concentrated HNO_3,[48,49] and CH_3OH + HCl.[50]

Experimental

Three zirconium alloys were used in the present investigation; namely, Grades R 60702 (Zr 702), R 60704 (Zr 704), and R 60705 (Zr 705). The nominal compositions and mechanical properties of these materials are given in Table 1. Zr 702 is generally chosen for chemical process industrial applications because of its excellent corrosion resistant properties. However, it may not have adequate strength for high temperature applications if high strength is required. The corrosion resistant properties of Zr 704 are similar to those of Zr 702. Zr 705 has and can retain higher strength than Zr 702 and 704 at high temperatures.

Four types of specimens were prepared from mill annealed sheets or plates as shown in Figure 1. Immersion tests were performed on Type A specimens, 50.8 mm × 25.4 mm × about 1.5 mm. U-bend tests were performed on Type B specimens, 114.3 mm × 19.1 mm × about 1.5 mm. Stressing was achieved by a two-stage operation to a radius of 15.9 mm according to ASTM G-30 specification. Teflon insulators were used to prevent the contact between the U-bend and the bolt. Sustained load tests were performed on tensile specimens whose gauge length was 25.4 mm and 6.5 mm in diameter (Type C). Constant strain rate tests were performed on tensile specimens whose gauge length was 12.7 mm and 2.5 mm in diameter (Type D). Both longitudinal and transverse cut speci-

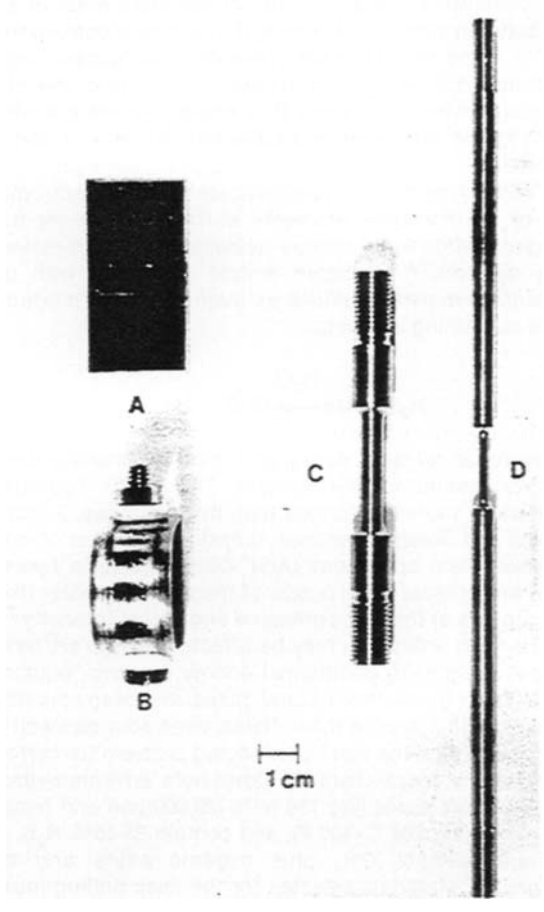


FIGURE 1 — Specimens used in corrosion tests: (A) corrosion coupon; (B) U-bend specimen; (C) tensile specimen for sustained load tests; and (D) tensile specimen for constant strain rate tests.

TABLE 2 — Successive 24 Hour Exposure Tests in 125 ml HCl + 192.3 g $Na_2S \cdot 9H_2O$ + 1.19 CH_3COOH + 81 ml H_2O at 200 C

Alloy[1]	Corrosion Rate[2] (mm/y) 1st Day	2nd Day	3rd Day	4th Day	Average
Zr 702	+0.02	+0.04	+0.0	+0.01	+0.02
Zr 702W	+0.10	+0.11	+0.02	+0.02	+0.06
Zr 704	+0.01	−0.01	+0.06	+0.0	+0.02
Zr 704W	+0.01	−0.0	+0.12	−0.09	+0.01
Zr 705	+0.02	+0.0	+0.03	+0.04	+0.02
Zr 705W	+0.01	+0.0	+0.03	+0.01	+0.01

[1]W = Weld.
[2]+ = Weight Gain; − = Weight Loss.

TABLE 3 — Results of U-Bend Tests in 5% NaCl + 0.5% CH_3COOH + Saturated H_2S for 60 Days

Alloy	Condition	Room Temperature	Boiling Temperature
Zr 702	LCNW	No Cracking	No Cracking
Zr 702	TCNW	No Cracking	No Cracking
Zr 702	LCWW	No Cracking	No Cracking
Zr 702	TCWW	No Cracking	No Cracking
Zr 704	LCNW	No Cracking	No Cracking
Zr 704	TCNW	No Cracking	No Cracking
Zr 704	LCWW	No Cracking	No Cracking
Zr 704	TCWW	No Cracking	No Cracking
Zr 705	LCNW	No Cracking	No Cracking
Zr 705	TCNW	No Cracking	No Cracking
Zr 705	LCWW	No Cracking	No Cracking
Zr 705	TCWW	No Cracking	No Cracking

LCNW = Longitudinal Cut Non-Welded.
TCNW = Transverse Cut Non-Welded.
LCWW = Longitudinal Cut With Weld.
TCWW = Transverse Cut With Weld.

mens were used for SSC tests. Welded specimens were made by butt welding sheets using a gas tungsten arc welder. After machining, specimens were ultrasonically cleaned in Cole-Primer's MICRO solution and distilled water. Test solutions were prepared from reagent grade chemicals, standard grade gases, and distilled water.

Immersion corrosion tests were conducted in Berghof 750 ml autoclaves. The pressure vessel is manufactured of Type 316 stainless steel. The interior of the top lid, the removable liner, lid inlets, and fittings are all made of Teflon. For each test, H_2S was generated by adding 125 ml HCl into 192.3 g $Na_2S \cdot 9H_2O$ + 1.19 ml CH_3COOH + 81 ml H_2O. This solution was used because it has a high sulfide content. The pH was about 3, and the pressure reached about 5 MPa at 200 C. The testing schedule consisted of four one-day intervals, with the test solution changed after each interval. After each interval, sample coupons were washed, dried, and weighed.

TABLE 4 — Results of Sustained Load Tests in 5% NaCl + 0.5% CH_3COOH + Saturated H_2S for 60 Days

Alloy[1]	Applied Stress MPa (10^3 psi)	Room Temperature
Zr 702L	310 (45)	No Cracking
Zr 702T	310 (45)	No Cracking
Zr 704L	380 (55)	No Cracking
Zr 704T	380 (55)	No Cracking
Zr 705L	450 (65)	No Cracking
Zr 705T	450 (65)	No Cracking

[1]L = Longitudinal cut specimens.
T = Transverse cut specimens.

U-bends and tensile specimens were tested in an aqueous NACE solution (5% NaCl + 0.5% CH_3COOH saturated with H_2S). H_2S was bubbled through the test cells continuously for constant strain and sustained load tests. The pH value of the solution was checked frequently and did not exceed 4.5 during the testing. U-bends were tested in a two-liter resin flask (4 per flask) equipped with a reflex condenser at room or boiling temperature. The sustained load tests were conducted by using CORTEST proof rings. Each specimen was stressed to the average room temperature yield strength, which was 310, 380, and 450 MPa for Zr 702, 704, and 705, respectively. The requirements of the proposed NACE Standard TM-01-77 were followed for this work. The constant strain rate tests were conducted by using WT Specialty P-2000 constant extension rate tensile machine.[51] For testing in an aqueous solution with a one-liter Teflon cell, the specimen was covered with shrinkable Teflon tubing, leaving only the gauge section exposed. The open circuit potential of the specimen was continuously monitored during straining using a Luggin probe, a saturated clomel electrode, a Wenking Model LB75M potentiostat, and a recorder.

Results

Corrosion Rate Measurements

Corrosion rate measurements were attempted in 125 ml HCl + 192.3 g $Na_2S \cdot 9H_2O$ + 1.19 ml CH_3COOH + 81 ml H_2O solutions at 200 C using autoclaves. Test results are given in Table 2. Table 2 indicates that Type A specimens of all three zirconium alloys exhibited negligible weight changes. No localized attack was detected. All specimens were covered by a tarnished film. These results are consistant with Shannon's findings, which indicate that H_2S in geothermal brines at 250 C has no observable effect on zirconium.[52]

Stress Cracking Tests

Three types of stress cracking tests were conducted. Results of U-bend tests are given in Table 3. Nonwelded and welded Type B specimens showed no cracking after 60 days of exposure in the NACE solution at room or boiling temperature (Table 3). Also, no corrosive attack was observed. Overstressing the tested U-bends indicated that they were still ductile.

Results of standard NACE SSC tests are given in Table 4. Again, Type C specimens of all alloys did not fail after 60 days of exposure in the NACE solution at room temperature. All specimens retained their metallic luster after testing.

Zr alloys are high performance materials. Therefore, conventional SCC test methods may be too mild to reveal their SSC and/or SCC susceptibility. The slow strain rate technique was used to assure the genuineness of their cracking resist-

TABLE 5 — Maximum Stress and Strain Data from Constant Strain Rate Tests Zr 702 Longitudinal Cut Specimen in Air and in the NACE Solution at Room Temperature

	Longitudinal Cut Specimen				Transverse Cut Specimen			
	AIR		NACE SOLUTION		AIR		NACE SOLUTION	
Strain Rate (Sec^{-1})	Max. Stress MPa (10^3 psi)	Max. Strain %	Max. Stress MPa (10^3 psi)	Max. Strain %	Max. Stress MPa (10^3 psi)	Max. Strain %	Max. Stress MPa (10^3 psi)	Max. Strain %
2.5×10^{-4}	499.5 (72.5)	24.0	509.9 (74.0)	26.9	503.7 (73.1)	23.8	492.0 (71.4)	22.7
2.5×10^{-5}	475.4 (69.0)	23.4	477.5 (69.3)	26.6	476.8 (69.2)	23.8	476.1 (69.1)	24.9
2.5×10^{-6}	449.9 (65.3)	29.3	441.7 (64.1)	28.4	454.1 (65.9)	25.9	442.3 (64.2)	29.1
7.5×10^{-7}	429.9 (62.4)	25.0	430.6 (62.5)	27.6	425.8 (61.8)	24.4	424.4 (61.6)	26.0

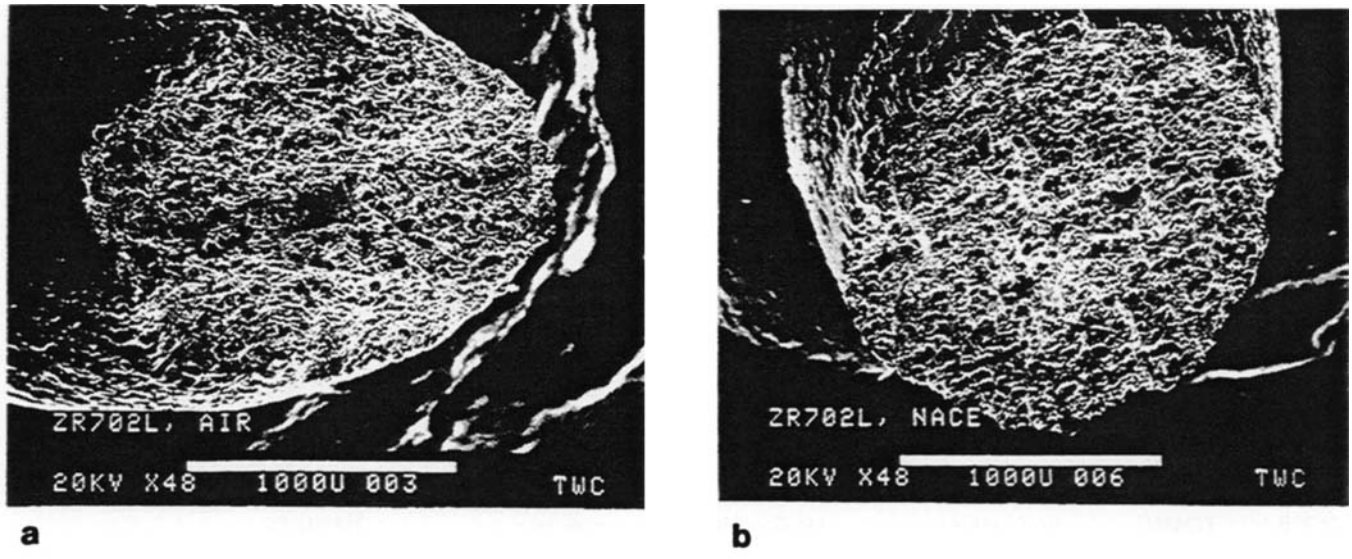


FIGURE 2 — Comparison of the fractured specimens of Zr 702 longitudinal cut specimens at a strain rate = 2.5×10^{-6}/second; (a) in air; and (b) in the NACE solution.

ance in the NACE solution at room temperature. The tensile strength and maximum strain of Zr 702 in air or in the NACE solution at strain rates, 2.5×10^{-4}, 2.5×10^{-5}, 2.5×10^{-6}, and 7.5×10^{-7}/second are tabulated in Table 5. It can be seen that the tensile strength and maximum strain of Zr 702 in the NACE solution are only slightly different from those in air. The differences are less than 10%, which is considered minor. The fractured specimens of Zr 702 longitudinal cut specimens in air and in NACE solution at a strain rate = 2.5×10^{-6}/second are shown in Figure 2. No significant difference is noticeable, with both specimens showing similar ductile fracture. The engineering stress versus strain curves obtained with Zr 702 longitudinal cut specimens in air, in the NACE solution, and in the solution containing 5% NaCl + 0.5 CH_3COOH at a strain rate = 2.5×10^{-6}/second are shown in Figure 3. The change in the open circuit potential of the specimen during straining is also shown in the figure. It is apparent from these results that Zr 702 is very resistant to SSC and SCC in this sulfide containing brine solution.

Discussion

Because zirconium is a reactive metal, it can readily passivate in an environment containing a sufficient amount of oxygen, and dissolved oxygen is not necessary for the passivation of zirconium. Any break in the integrity of the surface film will be healed spontaneously. For example, an addition of about 3% water to methanol-hydrochloric acid solutions can prevent the SCC of zirconium U-bends.[50] It should be noted that zirconium can react with several ingredients in deep sour gas well environments to form protective zirconium oxides. These ingredients include water, steam, carbon dioxide, and organic acids. Also, zirconium oxide may form via hydrolysis of ZrO^{2+}.[53,54]

Secondly, zirconium has very little affinity for sulfur. The sulfur atoms are significantly larger than the oxygen atoms, and, unlike the latter, they cannot fit into the interstitial site of a zirconium crystal lattice. Furthermore, the zirconium crystal lattice is a highly stable one, and an energetic reagent is required for the breakdown and the rebonding of its constituent

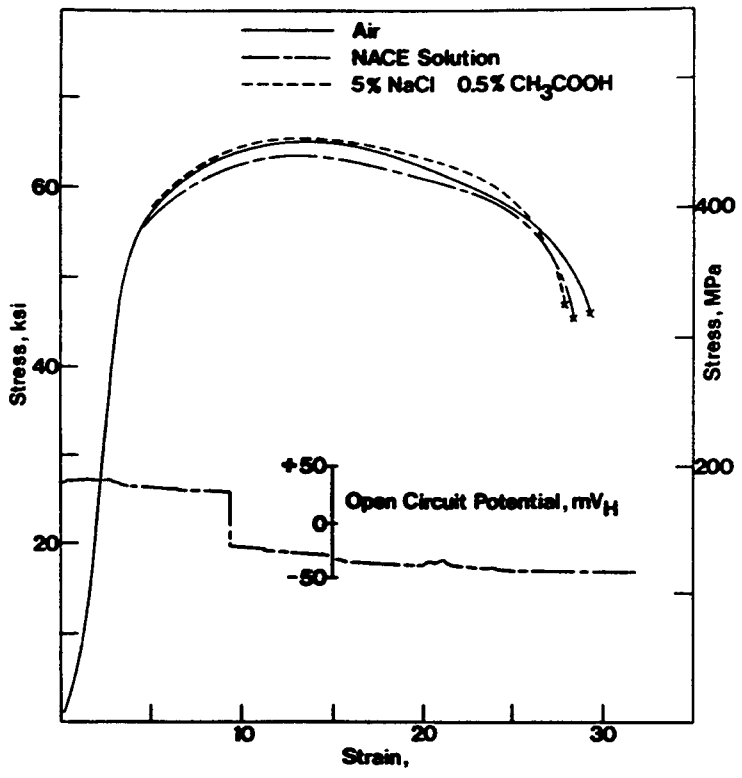


FIGURE 3 — Stress and open circuit potential vs strain curves of Zr 702 longitudinal cut specimens in air, the NACE solution and the solution containing 5% NCl + 0.5% CH_3COOH at a strain rate = 2.5 × 10^{-6}/second.

atoms in new combinations. The free energy of formation of the known interactions of zirconium with sulfur is insufficient to bring about complete destruction of zirconium's hcp structure. The combinations are described by the term semimetallic rather than metallic.[55] Zirconium-sulfur compounds have been found to form only at temperatures greater than 500 C; namely, ZrS_3, ZrS_2, ZrS_{1+x} (x = 0.0-0.5), ZrS, ZrS_{1-x} (x = 0.2-0.5), Zr_2S, $Zr_{21}S_8$, and Zr_9S_2.[56-61] A more important fact is that there is no instance of zirconium-sulfur bonds forming in aqueous systems.[62-63] It seems that hydrogen sulfide will play a neutral role in the corrosion reactions of zirconium in sulfide containing solutions.

The open circuit potential of Zr 702 at the beginning of the test was approximately 40 mV_H (Figure 3). This potential remained steady during straining through the elastic region. However, there were sudden drops during straining through the plastic region. These drops may be related to the generation of film-free surfaces and/or the interactions between dislocations and oxygen clusters with zirconium.[64] The open circuit potential was approximately −50 mV_H at the end of the test. The potential range of this straining electrode is at least 120 mV_H above the H/H^+ equilibrium potential in a pH 3 solution. Therefore, the presence of hydrogen in the specimen surface is not very likely. In other tests, the open circuit potential of Zr 702 during straining behaved similarly. The exception was that the open circuit potential dropped drastically to a very active potential (~ −1 V_H) and recovered to the original value at the end of the test when straining at 2.5 × 10^{-4}, 2.5 × 10^{-5}, and 7.5 × 10^{-7}/second.

It is expected that zirconium alloys will have excellent corrosion properties in sulfide environments. The limitation for using these alloys in deep drilling would be the strength: they may not have adequate strength at high temperatures. However, they can be used in cladding materials. Techniques are available for cladding high-strength alloys with an alloy chosen for corrosion resistance. At this time, cladding materials could be applicable to material problems in the deep drilling.

Conclusions and Recommendations

The results of this study justify the following observations:

1. Zirconium alloys have excellent corrosion resistance in a sulfide containing chloride solution at 200 C.
2. Hydrogen sulfide does not seem to be a corrodent or a cracking promoter to zirconium alloys.
3. Zirconium alloys have high SSC and SCC resistance in the simulated sour gas well brine.

This work is not completed. The following recommendations are made for future work in this area:

1. To evaluate corrosion and the SCC and SSC resistance of zirconium alloys in concentrated chloride solutions containing hydrogen sulfide, *e.g.*, 25% NaCl + 0.5% CH_3COOH + 0.1% S + Saturated H_2S at elevated temperatures.
2. To study the hydrogen embrittlement resistance of zirconium alloys when coupled with steels in sour brine solutions.
3. To test zirconium alloys in deep sour gas wells.

Acknowledgments

The author is grateful to M. Cross, J. A. Andrews, and R. Henson for performing the experiments; to A. F. Condliff and F. L. Shubert for supporting this study; and to Teledyne Wah Chang Albany for permission to publish these results.

References

1. Hudgins, C. M., HcGlasson, R. L., Mehdizadeh, P., and Rosborough, W. M., Corrosion, Vol. 22, p. 238 (1966).
2. Treseder, R. S. and Swanson, T. M., Corrosion, Vol. 24, p. 31 (1968).

3. Horvath, J., Electrochemical Studies on the Corrosion of Steel by the Microbiological Oxidation of Reduced Inorganic Sulfur Compounds, First International Congress on Metallic Corrosion, Butterworths, London (1961).
4. Bouet, J. and Brenet, J. P., Corrosion Science, Vol. 3, p. 51 (1963).
5. Horvath, J. and Novak, M., Corrosion Science, Vol. 4, p. 159 (1964).
6. Macdonald, D. D. and Syrett, B. C., Corrosion, Vol. 35, p. 471 (1979).
7. Kerns, G. E. and Staehle, R. W., Scripta Met., Vol. 6, p. 631 (1972).
8. Tuttle, R. N., Materials Performance, Vol. 13, No. 2, p. 42 (1974).
9. Tuttle, R. N. and Hamby, T. W., Materials Performance, Vol. 16, No. 10, p. 9 (1977).
10. Kane, R. D. and Boyd, W. K., Metal Progress, Vol. 119, No. 2, p. 54 (1981).
11. Fraser, J. P. and Treseder, R. S., Corrosion, Vol. 8, p. 342 (1952).
12. Vollmer, L. W., Corrosion, Vol. 8, p. 326 (1952).
13. Bates, J. F., Materials Protection, January, p. 33 (1969).
14. Treseder, R. S., Stress Corrosion Cracking and Hydrogen Embrittlement of Iron Base Alloys, NACE, Houston, Texas, p. 147 (1977).
15. Kane, R. D., J. Petroleum Technology, Vol. 29, p. 1483 (1977).
16. Watkins, M. and Greer, I. B., Corrosion Testing of Highly Alloyed Materials for Deep Sour Gas Well Environments, 1975 SPE Conference (Paper 5622) September-October, Dallas, Texas (1975).
17. Stroup, J. R., Bauman, A. H., and Simkovich, A., Multiphase MP35N—An Alloy for Deep Sour Well Service, CORROSION/76 (Paper 136) March, Houston, Texas (1976).
18. Bernhardsson, S. O. and Oredsson, Tynell, M., Properties of a Duplex Stainless Steel for Use in Corrosive Oil and Gas Wells, CORROSION/80 (Paper 14) March, Chicago, Illinois (1980).
19. Asphahani, A. I., Highly Alloyed Stainless Materials for CO_2/H_2S Environments, CORROSION/80 (Paper 12) March, Chicago, Illinois (1980).
20. Asphahani, A. I., High Performance Alloys for Deep Sour Gas Wells, CORROSION/78 (Paper 42) March, Houston, Texas (1978).
21. Kochera, J. W., Dunlop, A. K., and Tralmer, J. P., Experience With Stress Corrosion Cracking of Nickel-Base Alloys in Sour Hydrocarbon Production, CORROSION/76 (Paper 50) March, Houston, Texas (1976).
22. Rice, P. W., Materials Performance, Vol. 17, No. 9, p. 16 (1978).
23. Kane, R. D., Watkins, M., Jacobs, D. F., and Hancock, G. L., Corrosion, Vol. 33, p. 309 (1977).
24. Berkowitz, B. J. and Kane, R. D., Corrosion, Vol. 36, p. 24 (1980).
25. Kane, R. D. and Berkowitz, B. J., Corrosion, Vol. 36, p. 29 (1980).
26. Whelan, E. P., Sulfide Stress Cracking Resistance of Super-Alloy for Sour Gas Well Applications, RP-57-77-03, Climax Molybdenum Company of Michigan, January (1979).
27. Flannery, J. W., Nickel Topics, Vol. 32, No. 4, p. 3 (1979).
28. Guldner, W. G. and Wooten, L. A., Trans. Electrochem. Soc., Vol. 93, p. 223 (1948).
29. Hayes, E. T., Roberson, A. H., and Robertson, R. H., J. Electrochem. Soc., Vol. 97, p. 316 (1950).
30. O'Driscoll, W. G., Tyzack, C., and Raine, T., 2nd U.N. International Conf. Peaceful Uses of Atomic Energy (Paper 1450) (1958).
31. Gregg, S. J., Hussey, R. J., and Jepon, W. B., Corrosion, Vol. 17, p. 575t (1961).
32. Asher, R. C., Davies, D., Hall, A., Kirstein, T. B. A., Marriott, J. W., and White, P. J., Electrochem. Technol., Vol. 4, p. 231 (1966).
33. Asher, R. C., Davies, D., Kirstein, T. B. A., McCullen, P. A. J., and White, J. F., Corrosion Science, Vol. 10, p. 695 (1970).
34. Asher, R. C., Davies, D., and Kirstein, T. B. A., J. Nucl. Mater., Vol. 49, p. 189 (1973/74).
35. Hurst, P. and Tyzack, C., Proc. Intern. Conf. on Effects of Environment on Material Properties in Nuclear Systems, Brit. Nucl. Energy Soc., London, p. 37 (1971).
36. Berezina, N. N. and Vorontsov, E. S., Zh. Fiz. Khim., Vol. 54, No. 4, p. 1045 (1980).
37. Bradhurst, D. H. and Heuer, P. M., J. Nucl. Materials, Vol. 96, p. 196 (1981).
38. Ringot, C. and Orsier, G., Proc. Intern. Conf. on Nuclear Fuel Performance, Brit. Nucl. Energy Soc. (Paper 93), London (1973).
39. Parafenov, B. G., Gerasimov, U. V., and Venediktova, G. I., USAEC Report AEC-tr-6978 (Israel Program for Scientific Translations), p. 134 (1969).
40. Cox, B., Advan. Corrosion Sci. Technol., Vol. 5, p. 216 (1976).
41. Tyzack, C. and Cowen, H. C., At Energy Rev., Vol. 14, p. 2 (1976).
42. Zircadyne Corrosion Data, Teledyne Wah Chang Albany.
43. Knittel, D. R. and Webster, R. T., Industrial Applications of Titanium and Zirconium, Kleefisch, F. W., ed., ASTM STP-728, p. 191 (1981).
44. Yau, T. L., Corrosion Properties of Zirconium, Presented at Pacific Northwest Metals and Minerals Conference, April 26-29, Portland, Oregon (1981).
45. Zirconium Outlook, Vol. 2, No. 3, Teledyne Wah Chang Albany (1981).
46. Dunham, J. T. and Kato, H., SCC Susceptibility of Zirconium in Ferric Chloride Solution, Bureau of Mines Report of Investigations 5784 (1961).
47. Thomas, K. C. and Allio, R. J., Nuclear Applications, Vol. 1, p. 252 (1965).
48. Beavers, J. A., Griess, J. C., and Boyd, W. K., Corrosion, Vol. 37, p. 292 (1981).
49. Yau, T. L., SCC of Zirconium and Its Alloys in Nitric Acid, CORROSION/81 (Paper 102), April, Toronto, Canada (1981).
50. Mori, K., Takamura, A., and Shimose, T., Corrosion, Vol. 22, p. 29 (1966).
51. Nutter, W. T., Agrawal, A. K., and Staehle, R. W., Stress Corrosion Cracking—The Slow Strain Rate Technique, Ugrausky, G. M. and Payer, J. H., eds., ASTM STP-665, p. 375 (1979).
52. Shannon, D. W., Corrosion of Iron-Base Alloys Versus Alternate Materials in Geothermal Brines, Interim Report—Period Ending October, 1977, PNL-2456 UC-66d, Battelle Pacific Northwest Laboratories.
53. Mesmer, R. E., and Baes, C. F., Jr., Inorg. Chem., Vol. 10, p. 2290 (1971).
54. MacDonald, D. D., Butler, P., and Owen, D., J. Phys. Chem., Vol. 77, p. 2474 (1973).
55. Blumenthal, W. B., The Chemical Behavior of Zirconium, D. Van Nostrand Co., Princeton, N.J., p. 84 (1958).
56. Bloom, H., Ph.D. Thesis, Univ. of London (1947).
57. Hahn, H., Ness, P., Z. Anorg. Allg. Chem., Vol. 292, p. 82 (1957).
58. Larson, A. H., Schlechten, A. W., Trans. Met. Soc. AIME, Vol. 230, p. 862 (1964).
59. Tijera, S. and Elliott, J. F., Met. Trans., Vol. 2, p. 903 (1971).
60. Brattas, H. and Kjekshus, A., Acta Chem. Scand., Vol. 26, p. 3441 (1972).
61. Conrad, B. R. and Franzen, H. F., High Temp. Sci., Vol. 3, p. 49 (1971).
62. Blumenthal, W. B., Zirconium Compounds, National Lead Co., TAM Division, September 3, p. 65 (1969).
63. Latimer, W. M., The Oxidation States of the Elements and Their Potentials in Aqueous Solutions, Prentice-Hall, Englewood Cliffs, N. J., p. 272 (1952).
64. Westlake, D. G., Acta Met.. Vol. 12, p. 1373 (1964).

Copyrighted Materials
Copyright © 1996 NACE International Retrieved from www.knovel.com

Section 7

ACIDIZING CORROSION-RESISTANT ALLOYS

Paper No.
73

CORROSION 95
The NACE International Annual Conference and Corrosion Show

DUPLEX STAINLESS STEEL CORROSION BEHAVIOUR DURING ACIDIFICATION: LABORATORY VERSUS FIELD TEST RESULTS

T. Cheldi, I. Obracaj
AGIP S.p.A. CORM: Corrosion & Materials Technologies Dpt.
via Emilia 1,
20097 San Donato Milanese (MI), Italy

A. Cigada, M. Cabrini
Politecnico di Milano - Dipartimento di Chimica Fisica Applicata
Piazza Leonardo da Vinci 32,
20133 Milano, Italy

B. Vicentini, G. Rondelli
C.N.R. - I.T.M.
via Bassini 15
20133 Milano, Italy

ABSTRACT

Laboratory tests and field acidizing operations have been conducted on a 25% Cr-140 ksi duplex stainless steel utilizing a 90% HCl 15% + 10% CH_3COOH acid mixture inhibited with a commercial package. Laboratory tests proved that the duplex stainless steel can be effectively protected in the adopted experimental conditions at 150°C. Examination of parts of tubings extracted from a real completion showed appreciable corrosion attack only in the sections of the string placed at higher depth (operating temperatures ~130°C): in these cases the estimated rates of corrosion attack can be about one order of magnitude higher than that foreseeable on the basis of laboratory tests. However even in these cases the severity of attack is maintained within acceptable limits.

Keywords: duplex, stimulation, acid mixture, inhibitors, oil wells.

INTRODUCTION

In the exploitation of deep sour oil wells duplex stainless steels represent a reasonable compromise, among corrosion resistance to aggressive environments, mechanical properties and cost.

One or more times during the life of a well, acidizing jobs are carried out in order to improve the well output. During this operation strong acid mixtures are injected through the string together with inhibitor commercial packages since, owing to active conditions, also stainless steels are heavily corroded in these aggressive conditions due to the high temperatures present at high depth.

Through laboratory tests it has been shown that duplex stainless steels are more difficult to protect than high alloy austenitic stainless steels[1,2]. This is due to the fact that in active conditions a galvanic coupling is operating between the austenitic and ferritic phases, that constitute (roughly 50% in volume) the structure of duplex stainless steels. The ferritic phase is the less noble phase and is preferentially dissolved by acid mixtures[3].

Starting from inhibitor packages originally set up for carbon steels, new packages have been developed in order to overcome the problem; in particular attention has been given to new Sb-based intensifiers[4,5]. These new packages have been found to be effective in 15%HCl solutions up to 160°C[6]. According to other authors, using proper experimental packages it would be possible to protect duplex in 28% HCl up to 135°C[1]. With other acid mixtures such as 10.2% HCl + 9.9% CH_3COOH and 12% HCl + 3% HF maximum allowable temperature limits of 180°C and up to 130°C respectively have been determined[7].

All the above reported data were obtained by laboratory tests conducted in autoclaves under static conditions. These kind of tests are useful in establishing the performances of inhibitor packages, the order of severity of different acid mixtures and the ranking of several steels belonging to the same class; however it should be considered that, at least at the authors' knowledge, there is a lack of data obtained in real field operative conditions.

For these reasons it was deemed interesting to report, besides laboratory data, also some findings obtained by field experiences of acidizing jobs conducted on a 25% Cr duplex stainless steel utilizing the same inhibitor package and the same acid mixture (90% HCl 15% + 10% CH_3COOH).

EXPERIMENTAL

Material

All tests have been conducted on a 25% Cr - 140 ksi duplex stainless steel (0.023%C, 0.82%Mn, 0.47%Si, 25.1%Cr, 6.82%Ni, 3.16%Mo, 0.002% S max., 0.023%P, 0.35%Cu, 0.196%N, 0.2%W.

Inhibitor and Acid Mixture

Both laboratory tests and field experience were conducted utilizing an acid mixture made of 90% (by volume) HCl 15% and 10% of CH_3COOH.

As inhibitor a proprietary package made of inhibitor and intensifier was employed. The inhibitor is a mixture of acetilenic alcohols, dispersants, quaternized heterocyclic amines and inorganic salts, while the intensifier is a liquid containing primarily an antimony salt. The concentration of both the inhibitor and the intensifier was 2% by volume. In fields operative conditions also a surfactant to inhibit emulsion (0.5% by volume) was added.

Corrosion Tests

Lab 1 The specimens have been obtained from cold worked tubulars by means of cutting, turning and milling operations. All machined surfaces have been afterward polished using wet emery papers up to 320 mesh, leaving unchanged the original finish of the remaining surfaces. Lastly the specimens have been degreased in trichloroethylene and acetone and then rinsed in distilled water.

Oxygen was not removed from the solutions and no pressure control was accomplished during the tests. Experiments have been performed in tantalum lined autoclaves at total initial pressure 50 MPa, by pressurizing with high purity nitrogen. The ratio volume of aggressive solution/total surface of exposed specimens was higher than 7.5 ml/cm^2. Test pieces have been arranged on a suitable rack (made of glass or PTFE) to avoid contact between them and autoclave walls. In all experiments the temperature was held within ±1.5°C of the selected value (150°C); the duration time, at the selected temperature, was 5 hours.

Lab 2 The experimental conditions adopted by Lab 2 were similar to those of Lab 1 but in this case only one specimen was allocated in a 85 ml PTFE beaker which was than placed in an autoclave made of alloy C-276. The autoclave was filled with kerosene which acted as heat transfer and hydraulic fluid. The ratio volume of aggressive solution/total surface of exposed metal was about 5 ml/cm^2.

Well No.1 Field Tests For these experiments cylindrical specimens (110 mm length, 6 mm diameter) obtained from commercially available tubulars goods were utilized. The coupons, after degreasing and weighting, were fitted in a suitable specimen holder made of the same steel (Figure 1) that was placed inside the production string at the bottom of the field (depth = 5777 m). At the end of acidizing job, conduced with 15.3 m^3 of acid mixture, the specimen holder was recovered by means of a wireline operation. The coupons were accurately cleaned in trichloroethylene to remove a thick the black oily film, dried and weighted. The acid contact time was 34 minutes; the mean acid velocity in the string was 3 m/s while, due to the configuration of the specimen holder, the velocity on the specimens was about 22 m/s. The temperature range evaluated by simulation software was 77-117°C[8].

Mechanical tests were performed on the specimens to verify the effect of acidizing treatment on the yield strength of the steel.

Well No.2 Field Tests In this case the corrosion behaviour was evaluated by examining sections of tubular goods utilized for the production string of an oil field subjected to acidizing operations. Figure 2 reports a schematic drawing of the string and shows the zones from which the test pieces were extracted.

The acidizing was performed at the level 5640-5670 m with 39 m^3 of acid mixture. For the section 1 and 2 the acid contact times was 76 minutes and the mean acid velocities were 2 and 3.2 m/s respectively. For section 6 and 7 the acid contact time was 62 minutes and the mean acid velocity was 3.9 m/s. The temperatures at the different levels calculated using the simulation software are shown in Figure 3[8].

It should be remarked that, besides the first batch above mentioned, the string was subjected to a further acid treatment (60 m^3 acid mixture, ~80 minutes contact time, 3.2-5 m/s mean acid velocity).

However this batch was conducted at a temperature ≤ 80°C that implies low corrosion losses[9]. For this reason this second batch was considered practically insignificant as regards the effects on the extent of corrosion attack.

After the acid stimulations and extraction of the string, sections coming from zones 1, 2, 6 and 7 have been examined. They were firstly cleaned with trichloroethylene to remove the black oily film in order to allow the observation of the surface appearance. These tube parts were also utilized to obtain samples for metallographic examination of the corrosion attack. For this purpose the test pieces were subjected to nickel deposition (minimum thickness 0.2 mm) before mounting in epoxy resin to avoid blunting of the edges during polishing.

RESULTS AND DISCUSSION

The results of laboratory tests are reported in Table 1. It can be observed that, under the adopted experimental conditions, the utilized inhibitor package is suitable for protecting the duplex steel.

The corrosion losses are lower than the maximum limit generally accepted for single acidizing operation. Figure 4 shows, as an example, the preferential attack of the ferritic phase detected on a coupon tested in Lab 2.

The weight losses determined on specimens extracted from Well No.1 field experiment (Table 1) even thought higher then those of laboratory tests are lower than the maximum allowed limit generally accepted for each acidizing operation: 0.05 lb/ft^2 (244 g/m^2). An example of the morphology of attack of the ferritic phase is shown in Figure 5.

Mechanical tests did not show any influence of acidizing operation on the yield strength of the steel.

Concerning the Well No.2 field experiences it was observed that tubing sections coming from the higher levels of the completion (zones 1 and 2) do not display any visually detectable attack: the surface appearance is practically identical to that of brand new tubulars. Also the microscopic examination of these sections (Figures 6 and 7) confirm the almost absence of corrosion attack. This behaviour can be ascribable to the low temperature acting at these levels (Figure 3).

On the sections extracted from higher depth (zones 6 and 7) the presence of some uniformly distributed corrosion attack can be observed (Figure 8). Nevertheless, it can be deduced that also these sections of the string have been proved to be sufficient corrosion resistant and the extent of the attack is still acceptable. Metallographic examination display attack of the ferritic phase and the maximum wall thickness reduction is about 50 μm (Figure 9). However, since the corrosion attack is disuniformly distributed (Figure 10) an average corrosion penetration of 25 μm seems to be a reasonable estimation of the extent of the attack.

From this value a corrosion loss of about 0.04 lb/ft^2 (195.5 g/m^2), lower than the maximum accepted limit, can be calculated, so confirming the judgements made on the basis of visual observation. However by comparing the corrosion rates normalized for one hour of treatment (Table 1) it can be observed that, for the Well No.2 tested sections coming from the zones of higher corrosion attack (zones 6 and 7) and coupons exposed in Well No.1, the corrosion losses are higher

(up to about one order of magnitude) than those obtained from laboratory tests conducted in similar conditions. This can be related to the fact that laboratory tests are conducted in static conditions while in field experiences dynamic flow conditions are realized[10].

Lastly, from the examination of test specimens coming from tubulars of Well No.2 it can be observed that the sections of the string that presented high attack are those located at the lower levels where the requirements of high mechanical properties are less important, hence the completion structure is preserved.

CONCLUSIONS

Laboratory tests and field acidizing operations have been conducted on a 25% Cr - 140 ksi duplex stainless steel utilizing a 90% HCl 15% + 10% CH_3COOH acid mixture inhibited with a commercial inhibitor package. The following conclusions can be drawn:

1. Autoclave laboratory tests indicated that the duplex stainless steel can be effectively protected at 150°C also for long exposure time (5 hours).

2. Field experiences indicated for the sections located at high depth (about 5600-5770 m, temperatures up to ~130°C) observable attack of the ferritic phase with estimated corrosion losses that can be even one order of magnitude higher than those obtained in comparable laboratory test conditions

3. Also in the cases reported in point 2, the corrosion attack evaluated both on the basis of visual observation of the corrosion attack of section test pieces and on metallographic examination is still maintained within acceptable levels. Since these sections are located at high depth, where less important are the mechanical strength requirements, the structure of the of completion is preserved.

REFERENCES

1. R.Jasinski, W.W.Frenier, S.Grannan, "Inhibiting HCl Corrosion of High Chrome Tubulars Steels", Corrosion/88, paper No. 188, (Houston, TX: NACE, 1988).

2. B.Vicentini, at al., "High Alloy Steels for Oil Wells: Behaviour in Acidizing Conditions", 11th International Corrosion Congress, Vol. 4, p.455, (Milano, Italy: AIM, 1990).

3. Y.Yau, M.A.Streicher, "Galvanic Corrosion of Duplex-Fe-Cr-10%Ni: Alloys in Reducing Acids", Corrosion/85, paper No. 228, (Houston, TX: NACE, 1985).

4. M.L.Walker, J.M.Cassidy, K.R.Lancaster, T.H.McCoy, "Acid Inhibition of CRA's: a Review", Corrosion /94, paper No. 19 (Houston, TX: NACE, 1994).

5. A.Cizek, Material Performance 33, 1(1994): p. 56.

6. M.L.Walker, T.H.McCoy, "Effect and Inhibition of Stimulation Acids on Corrosion Resistant Alloys", Corrosion/86, paper No. 154, (Houston, TX: NACE, 1986).

7. B.Vicentini, G.Rondelli, A.Cigada, T.Cheldi, "Resistance to Acidizing Treatments of Duplex Stainless Steels for Oil Wells", presented at the NACE Conference on Life Prediction of Corrodible Structures, Kauai, Hawaii USA, November 5-8, 1991.

8. Technical Report AGIP-CORM No.T08-94, 1994.

9. M.L.Walker, T.H.McCoy, "Inhibition of High Alloy Tubulars II: Effect of Fluoride Ion and Acid Strength", Corrosion/88, paper No. 189, (Houston, TX: NACE, 1988).

10. C.F.Smith, F.E.Dollarhide, N.B.Byth, "Acid corrosion inhibitors - are we getting what we need?", J. Petroleum Technology, May 1978, p. 737

Table 1
Laboratory and field test results

	Temperature [°C]	Time [h]	Weight loss / area (2) [lb/ft^2]	[lb/ft^2/1h]	Wall thickness reduction [µm]	[µm/1 h]
Lab 1 (1)	150	5	0.022 ±0.003	0.004	13.7 ±1,6	2.75
Lab 2	150	5	0.013 ±0.001	0.003	8.0 ±0.6	1.6
Well No.1	77 - 117	~0.5	0.011 ±0.001	0.022	6.3 ±0.5	12.7
Well No.2	80 - 130	~1	~0.042(3)	0.042	~25	~25

(1) The concentration of HCl utilized for the preparation of the acid mixture was 12% instead of 15%
(2) Weight loss test conduced on at least 6 samples
(3) The weight loss was evaluated from the estimated average thickness reduction

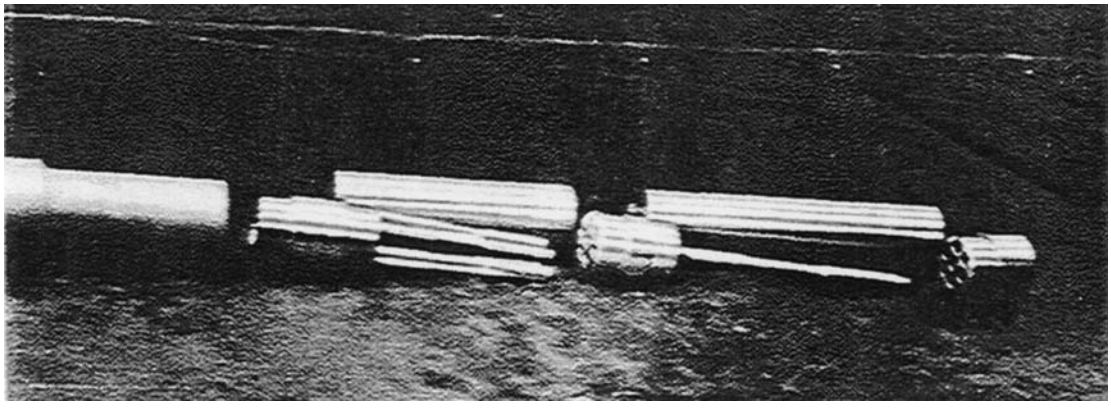


Figure 1 Specimen holder and samples utilized in Well No.1 field tests.

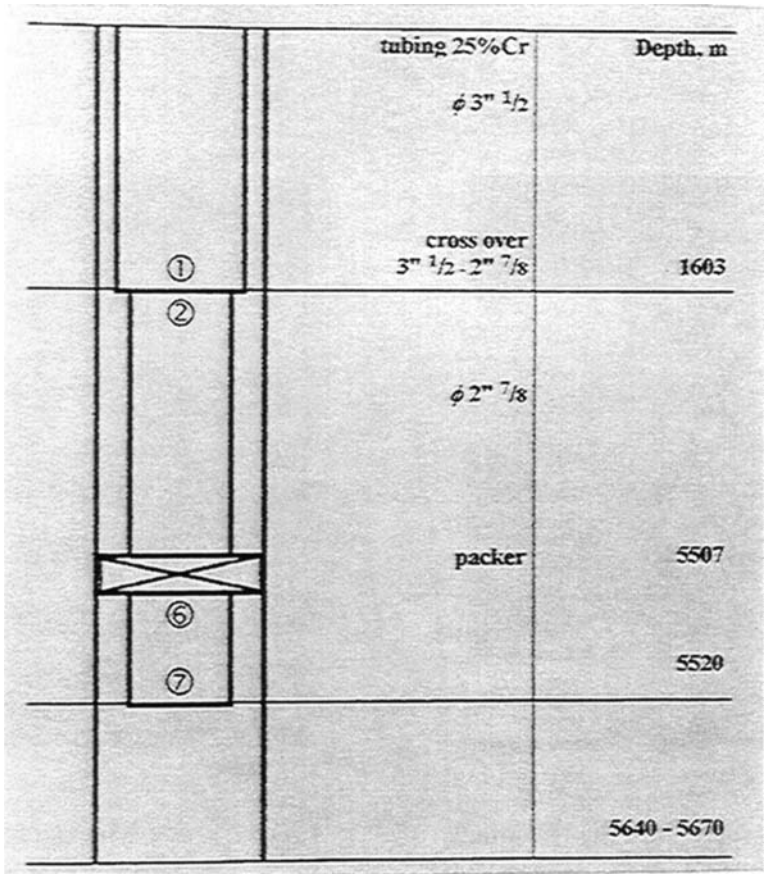


Figure 2 Schematic drawing of the string of Well No.2.

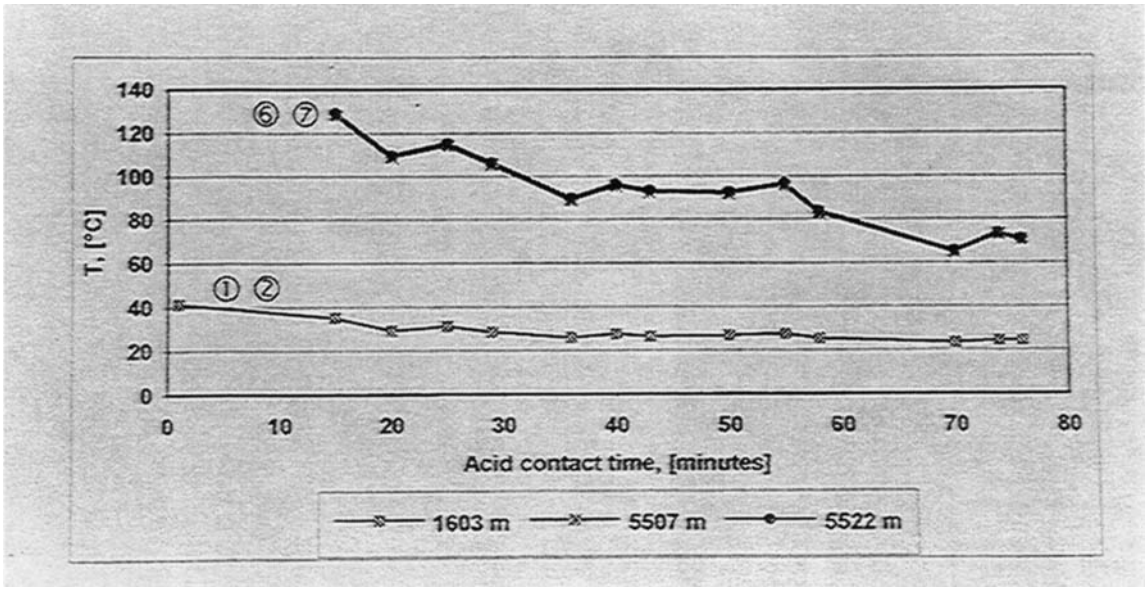


Figure 3 Acid temperature Vs time in Well No.2 for the first batch of acidification[8].

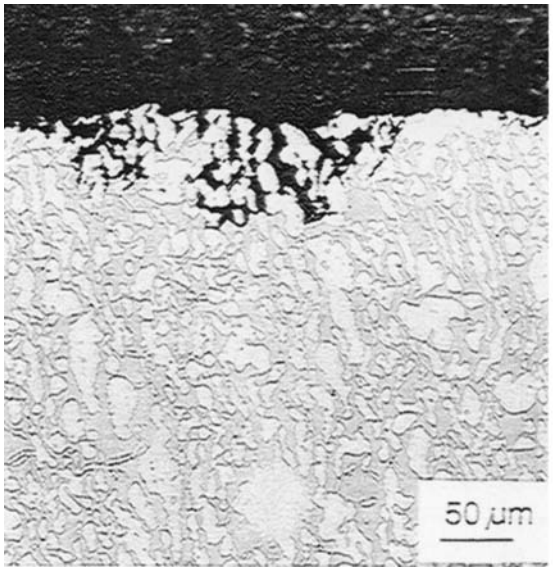


Figure 4 Micrograph showing the attack in a coupon tested in Lab 2 (Electrolytic etching in 40%NaOH).

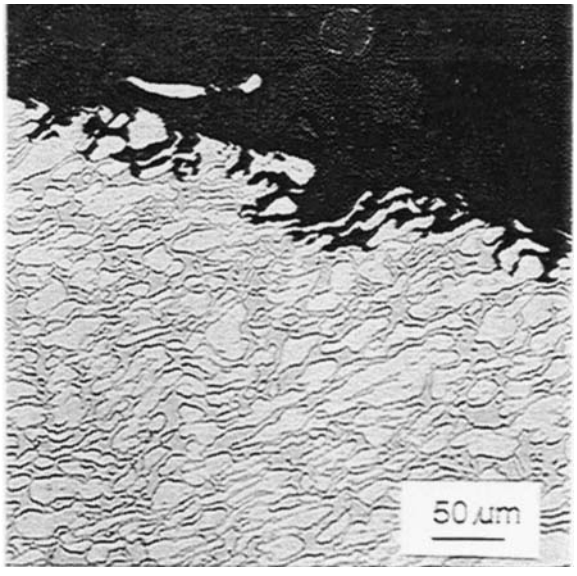


Figure 5 Micrograph showing the attack in a samples exposed in Well No.1 (Electrolytic etching in 40% NaOH).



Figure 6 Micrograph showing the attack in a tubing section coming from zone 1 of Well No.2 (Electrolytic etching in 40%NaOH).

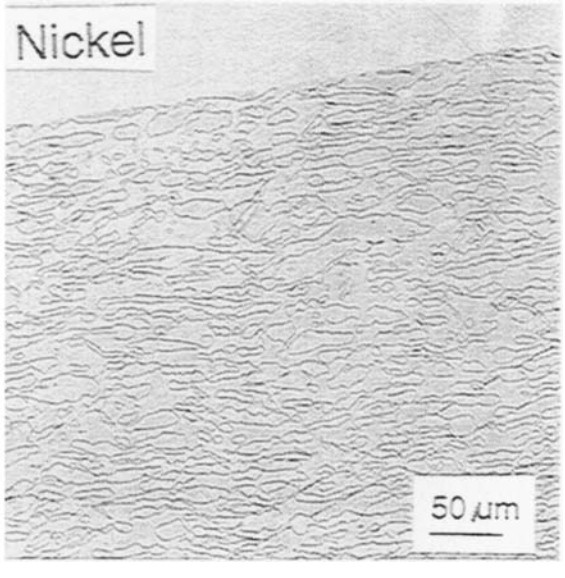


Figure 7 Micrograph showing the attack in a tubing section coming from zone 6 of Well No.2 (Electrolytic etching in 40%NaOH).

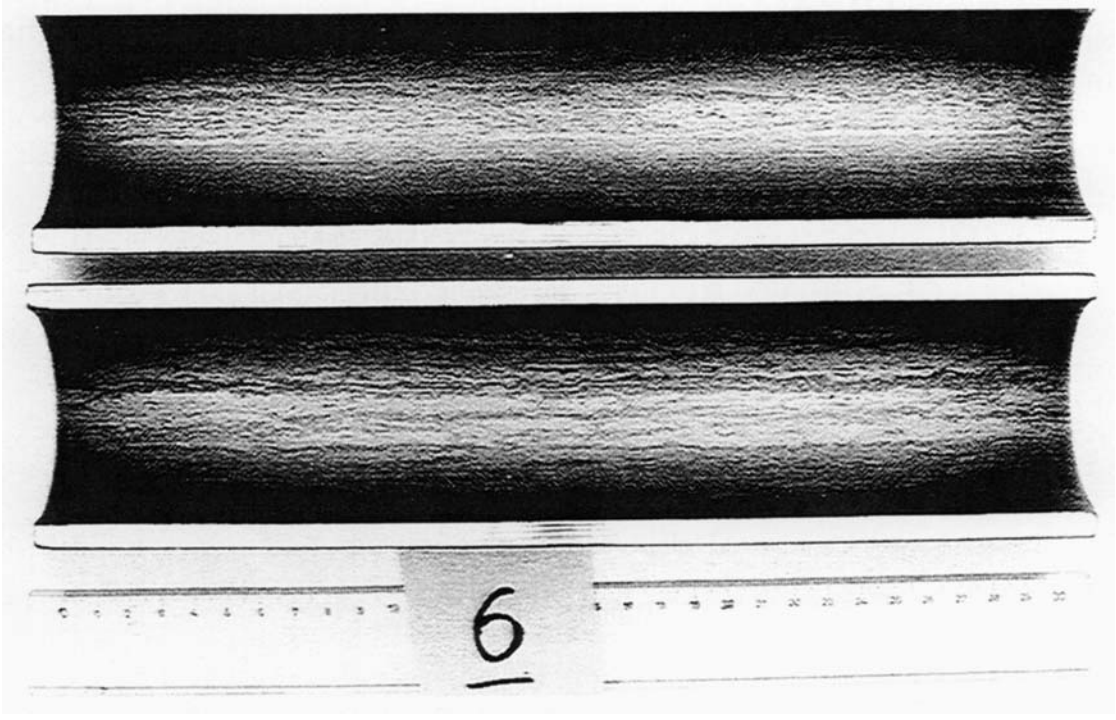


Figure 8 Surface appearance of tubing parts coming from zone 6 of Well No.2.

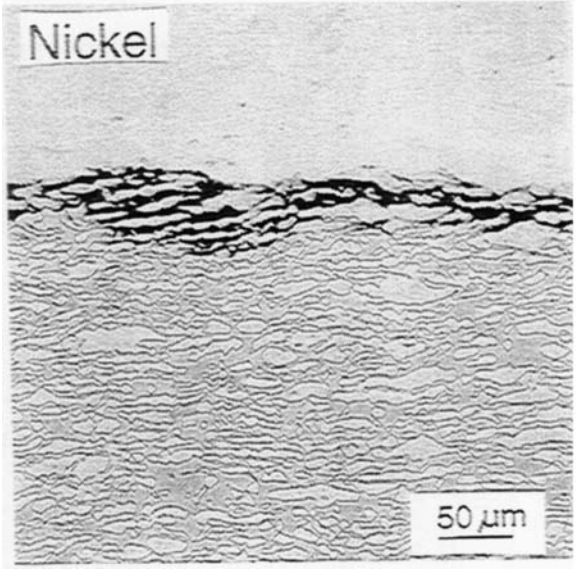


Figure 9 Micrograph showing the attack in a tubing section coming from zone 6 of Well No.2 (Electrolytic etching in 40% NaOH).

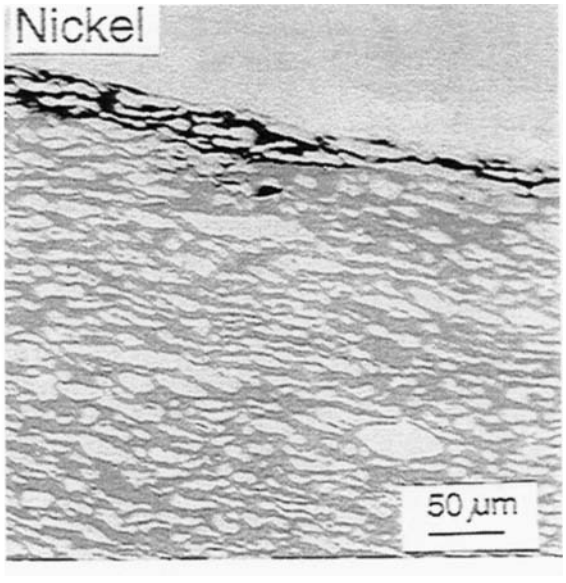


Figure 10 Micrograph showing the attack in a tubing section coming from zone 6 of Well No.2 (Electrolytic etching in 40% NaOH).

Copyrighted Materials
Copyright © 1996 NACE International Retrieved from www.knovel.com

Paper No.
81

NACE International

CORROSION 94
The Annual Conference and Corrosion Show
Sponsored by NACE International

HYDROGEN ASSISTED CRACKING AND INHIBITION OF SPRING ALLOYS IN ACIDIZING SOLUTIONS

William R. Coyle, P.E.
Greg B. Chitwood, P.E.
Patrick W. Rice, P.E.
Halliburton Energy Services
P.O. Box 819052
Dallas, TX 75381

Michael L. Walker, Ph.D.
Halliburton Energy Services
P.O. Box 1431
Duncan, OK 73536

ABSTRACT

Several experiments were conducted to investigate and compare the hydrogen assisted cracking resistance of high strength, corrosion resistant spring alloys to acidizing fluids. Two cobalt-based alloys, UNS R30035 and UNS R30003, and one nickel-based alloy, UNS N07750, were evaluated. The tests involved exposing stressed spring segments of all alloys and C-rings of R30035 to uninhibited 28% HCl, 28% HCl with two different inhibitors, and the NACE TM0177 solution.[1] Failures of N07750 spring segments in the uninhibited acid parallel field performance of this alloy. There were no failures of the R30035 or R30003 spring segments in the environments tested. Springs made from N07750 are more susceptible to hydrogen embrittlement than either R30035 or R30003. The C-ring tests of R30035 revealed the benefit of corrosion inhibition as a means of elevating the threshold cracking stress and increasing the time to failure in corrosive media. A strong beneficial effect of elevated-temperature thermal processing was observed for UNS R30035. High performance acidizing inhibitors are required in order to provide effective protection to high alloy spring materials.

Keywords: acid, corrosion inhibition, hydrogen embrittlement, spring failures, UNS R30035, UNS R30003, UNS N07750

INTRODUCTION

Nickel and cobalt-base alloys X-750 (UNS N07750), MP35N[1] (UNS R30035), and Elgiloy[2] (UNS R30003) springs are commonly used in downhole completion equipment destined for severe corrosion service. There have been intermittent failures of these springs, some being attributed to hydrogen embrittlement.[2] The difficulty of reproducing these failures in the laboratory has been attributed to dynamic loads experienced by springs failing in service compared to laboratory tests involving only statically-loaded springs. Previous studies of cold-worked tubes made from these alloys have revealed their susceptibility to hydrogen embrittlement.[3] National Association of Corrosion Engineers publication 1F192 cautions that precipitation-hardenable, nickel-base alloys such as N07750 are susceptible to hydrogen embrittlement.[4] Occasional failures of compression springs fabricated from R30035 and R30003 cobalt-base alloys are also mentioned.

Inhibitors are used to reduce the corrosive effects of hydrochloric acid on downhole metal goods. Factors to be considered in the selection of the inhibitor package include cost, performance, and availability. The beneficial effect of acid inhibitors used for protection of steel production tubing is well known; however, the capability of these same inhibitors to protect high alloy spring materials has not been established. In view of these citations in the technical literature and the frequent exposure of CRA springs to acidizing fluids and other environments known to promote hydrogen embrittlement, the need for more performance data and laboratory experimentation was indicated.

EXPERIMENTAL PROCEDURE

Materials and Sample Preparation

Three corrosion resistant alloys (CRA's) that are commonly used for springs in downhole completion equipment were investigated: cobalt-base alloys R30035 and R30003, and nickel-base alloy N07750. The chemical composition of each alloy is presented in Table 1.

For the spring testing, a spring was manufactured from each of the three materials using 0.500 inch (12.7 mm) diameter, spring-temper wire. The nominal diameter of these springs was 3.950 inches (100 mm). After coiling, the springs were age-hardened using standard industry heat treatments: the R30035 and N07750 springs were age hardened at 1200°F (650°C)/4 hrs; the R30003 spring was age hardened at 980°F (530°C)/5 hrs. The resultant mechanical properties for each alloy and heat treatment are given in Table 2.

Each spring was dye-penetrant inspected before testing to ensure that no cracks were present. The springs were then sectioned into 1 and 2-coil segments for testing (see Figure 1). The spring segments were compressed between steel plates using N10276 hardware. The 2-coil spring samples were stressed to solid height (coils touching), which is the design criterion of typical springs used in downhole completion equipment. The 1-coil spring samples were intentionally overstressed by compressing the coil beyond solid height until the ends were aligned. The stress level induced by the deflection was calculated by formulas contained in MIL STD 29A.[5] For a compression spring, Wahl predicts torsional loading of the wire and maximum stress on the spring ID.[6] Figure 2 shows stressed spring samples prior to testing.

---

[1]MP35N is a registered trademark of Standard Pressed Steel Company.

[2]Elgiloy is a registered trademark of the Elgiloy Company.

For the C-ring tests, highly cold drawn tubing was not available in the R30003 and N07750 alloys; therefore, C-rings were fabricated only from R30035 tubing. Rotorolled cold-drawn and aged tubing measuring 1.72" OD x 1.387" ID (44 mm X 35 mm) was obtained. The tubing was received in the 1050°F (565°C) aged condition and split into two lengths. One section was used in the as-received condition (i.e., standard heat treatment applied to this product at the mill: 1050°F (565°C)/4hrs), and the other section of the tubing was heat treated at 1200°F (650°C)/4hrs to simulate the heat treatment typically applied to springs used in sour service. The mechanical properties of the tubing after age-hardening are shown in Table 2.

In preparation for machining the C-rings, the OD and ID surfaces were cleaned up by light grinding and honing. The C-rings were then machined, placed in carbon steel fixtures, and compressed to the desired stress level. Duplicate C-rings were stressed to 46%, 80%, and 100% of yield strength. The level of 46% was chosen to correlate with the spring tests. Typical industry practice for design of helical compression springs involves using a maximum design stress of 45% of minimum ultimate tensile strength; for the R30035 material, this stress level corresponds to 46% of actual yield strength. Deflection calculations were performed in accordance with NACE TM0177; 2000 microstrain was added to the deflection calculations for the specimens stressed to 100% of yield to simulate 0.2% permanent set. Experience has shown that the deflections calculated by the TM0177 method are nearly identical to those determined using strain gauge techniques.[7]

Acidizing Tests

The full matrix of alloys, heat treatments, sample configurations, and stress levels were tested in acid. One test with 28% uninhibited HCl acid and two tests each with a different inhibitor in 28% HCl were conducted.

The acid solutions were prepared using field grade 22 Baumè hydrochloric acid that was diluted with tap water to a strength of 28 vol %. Bulk solutions were titrated in triplicate and were within 0.1% of the stated concentration. In the tests with inhibitors, inhibitor concentrations of 0.3% were obtained by addition of the appropriate inhibitor volume and removal of the corresponding volume of the acid mixture. Hydrogen embrittlement is typically a low-temperature phenomenon; therefore, in order to simulate a "worst case" acidizing scenario, all tests were conducted at room temperature.

The inhibitors used in this study are commercial proprietary compositions.[8] Inhibitor A is an economical, low-temperature inhibitor designed for applications in shallower wells, generally 175°F (79°C) and below. This inhibitor contains acetylenic alcohols and derivatives of coal tar amines in addition to solvents and dispersants. Inhibitor B is a high-temperature acid inhibitor designed to protect a wide range of alloys at temperatures up to 325°F (163°C). When used with 'intensifier' compounds, it can be applied at much higher temperatures. Inhibitor B contains acetylenic alcohols, dispersants, quaternized coal tar amines, and inorganic salts.

Spring and C-ring test samples were placed in separate 5 liter covered plastic containers. Three liters of acid were used in the tests of the springs, and 2 liters of acid were used in the tests of the C-rings. The samples were initially inspected every two hours for the first eight hours and then left overnight. They were inspected again in the morning and every 4 hours afterwards for the second day. For the remainder of the 7-day test period, the samples were inspected daily. If a sample was found cracked during inspection, it was removed, rinsed, and stored. If the sample showed no visible crack, it was replaced in the same acid solution. After testing, the samples were cleaned and sectioned to provide specimens for fractographic and interstitial hydrogen analyses.

TM0177 Tests

These tests were conducted using a group of the R30035 C-rings with both age-hardening heat treatments. The test environment consisted of 5% NaCl + 0.5% CH_3COOH, saturated with H_2S at room temperature. These tests were carried out in 1-gallon plastic tubs with tight-fitting lids. The plastic tubs had been "conditioned" by prior exposure to the NACE TM0177 sour test environment. As is required by NACE TM0177, the fluid was deaerated prior to introduction of the H_2S, and an outlet trap was utilized to prevent the ingress of oxygen during the test. The pH was measured before and after the test and found to be within the limits prescribed by TM0177. The test was scheduled for inspection of the C-rings on a daily interval through the first week and then weekly thereafter for the duration of the 30-day test.

RESULTS AND DISCUSSION

Only two spring segments cracked in the acid solutions, as shown in Table 3. The 1-coil N07750 spring segment cracked 2-3 hours after immersion in the uninhibited 28% HCl acid solution; the 2-coil segment cracked after 3 days. Figure 3 shows the cracked 2-coil segment after testing in uninhibited 28% HCl; the appearance of the crack in the 1-coil segment was nearly identical. The other N07750 spring segments and all other spring segments of R30035 and R30003 remained intact in both inhibited and uninhibited acids at the conclusion of the 7-day test. After the testing was complete, the springs were removed from the fixtures and reinspected using dye-penetrant. There were no cracks found on either the R30035 or R30003 springs, and only one large crack was noted on each of the 1- and 2-coil N07750 spring segments. Visual examination of the N07750 spring indicated a brittle fracture with crack propagation along a plane approximately 45° to the wire axis (plane of maximum tensile stress). The crack initiated at the ID of the spring where the stress is at a maximum. The fracture surface was prepared for examination using the scanning electron microscope (SEM). As shown in Figure 4, the fracture surface contains features of both cleavage and intergranular fracture. This fracture morphology is very similar to past spring failures attributed to hydrogen embrittlement.[2]

While no spring segments of R30035 failed, there were several instances where C-rings of this alloy failed. The results of testing R30035 C-rings in uninhibited 28% HCl, inhibited 28% HCl, and the NACE TM0177 test solution are presented in Table 4 and graphically in Figures 6 and 7. The alloy showed a strong propensity to fail at all stress levels in the uninhibited 28% HCl and TM0177 test solutions, with failure occurring within one day. There was a pronounced effect of aging temperature and inhibitor type and upon failure. As shown in Figures 6 and 7, R30035 C-rings age-hardened at 1200°F (650°C) exhibited increased time to failure and/or higher threshold cracking stress in all environments tested when compared to C-rings age-hardened at 1050°F (565°C). Inhibitor A provided a 46% threshold cracking stress on C-rings aged at a temperature of 1200°F; Inhibitor B provided increased protection as it provided an 80% threshold cracking stress. C-rings aged at 1050°F (565°C) cracked at all stress levels in 28% HCl + Inhibitor A; however, when protected by inhibitor B, a 46% threshold cracking stress was observed.

The relative insensitivity of R30035 spring segments to cracking with respect to C-rings made from this same alloy suggests a hydrogen-embrittlement mechanism. Wahl assumes that springs may be considered straight bars under torsion for purposes of determining stresses.[6] Latanision, et al, proposed that loading mode influences susceptibility to environmentally-induced cracking, and in particular, that certain alloys prone to hydrogen embrittlement are more susceptible to cracking when loaded in tension, (mode I), than when loaded in torsion, (mode III).[9] These researchers suggested that the decreased susceptibility to hydrogen embrittlement under torsional loading results from elimination of the hydrostatic tensile stresses needed to drive hydrogen into the region ahead of a

crack tip. Wahl has shown that the torsional stresses in the inner fibers or at inside diameters of compression springs exceed those at springs' outside diameters or outer fibers.[6] The inside diameter is the typical location where fracture initiates in helical compression springs. These fractures are invariably oriented 45° to the spring wire's axis along a plane of maximum tensile stress present in bars loaded in torsion.[10] Static, infinitesimal elements contained within torsionally-loaded bars are maintained in equilibrium by forces other than triaxial tensile forces associated with cracks growing under mode I loading. These significant differences in stress fields present in tensile specimens, beams or C-rings, versus those existing in components substantially loaded in torsion undoubtedly influence the respective capabilities of these geometries to localize hydrogen in the metallic lattice.

Kane has shown that the yield stress measured transverse to the primary grain direction in cold-worked R30035 tubes is less than the yield stress measured parallel to the primary grain.[3] This anisotropy complicates comparisons of properties of compression springs made from cold-worked rods to those of C-rings made from cold-worked tubes. Kane also reports that R30035 transverse C-rings aged at 1100°F (593°C) failed when coupled to steel in the NACE solution. No similarly heat-treated, R30035 tensile specimens stressed parallel to the primary grain direction failed in the NACE solution when coupled to steel. The results of the current study plus Kane's findings illustrate the difficulty of directly comparing results of embrittlement tests using spring segments to those using C-rings because of anisotropy and differing stress fields induced by test-specimen geometry. Kane's finding that R30035 C-rings cracked only when cathodically polarized by being coupled to steel further indicates a hydrogen-embrittlement mechanism for stressed CRA materials contacted by corroding steel components.

Oriani states that large stresses can concentrate interstitial hydrogen by orders of magnitude above the stress-free solubility.[11] Hydrogen atoms migrate to and concentrate in regions of high strain in a stressed metal's cross section, dwelling for some time prior to weakening and separating the bonds between metallic atoms. If the C-rings and spring samples have failed by hydrogen embrittlement, it follows that elevated hydrogen contents should be discovered at the fracture site(s). This is exactly what was found when samples of cracked C-rings were submitted to two independent analytical laboratories for determination of interstitial hydrogen content. Bulk hydrogen contents 2 to 25 times higher than those found in the control samples were discovered. The results of the hydrogen analyses are presented in Table 5.

One method to control hydrogen uptake is through the use of corrosion inhibitors. Corrosion of a metal in strong mineral acids such as hydrochloric acid is an electrochemical process. Hydrogen ions are reduced to hydrogen atoms, which then combine to form hydrogen gas. Simultaneously, iron atoms are converted to ferrous ions by releasing two electrons. For simplicity, the two reactions are separated: the cathodic reaction and the anodic reaction. Hydrogen ion reduction is the cathodic reaction, and iron oxidation is the anodic reaction.

Corrosion is an electrochemical process, and as such, several conditions must exist in order for corrosion to occur. The anodic and cathodic areas must be created or exist at the same time. Further, these areas must be electrically in contact, and the electronic charge transfer process must take place across the interface such that electrical neutrality of the solution and substrate is maintained. When all of the above conditions exist, inhibition can occur when one or more of the processes is affected. In most cases, one of the steps that occurs in sequence is slower than the others and determines the rate of the overall process. For inhibitors in solution and in contact with a solid corroding surface, interference with the mass transport or charge transfer at the surface is the most likely rate determining step.[12]

Commercial inhibitors take advantage of the complexity of the process and requirements of electrical neutrality and simultaneity by interfering with the corrosion process. Effective inhibitor

molecules or blends interfere with the rate determining step or create a new one. The inhibitors used are complex mixtures of several active components. Each component is capable of slowing either the cathodic reaction or the anodic reaction or preventing one or several species from migrating to or from a surface. Commercial inhibitors utilize quaternized heterocyclic amines, acetylenic alcohols, or unsaturated carbonyl compounds along with solvents and dispersants.[13]

The mechanism by which these inhibitors function is not fully known. However, film forming components may affect the ability of the hydrogen ion to effectively transport to the corroding surface. Likewise the film may also retard the diffusion of ferrous ion away from the surface of the metal. Some components are thought to provide inhibition by interfering with the electron transfer process. These inhibitors may retard electron transfer to the hydrogen ion to create atomic hydrogen or prevent combination of the hydrogen atoms to molecular hydrogen. Acetylenic alcohols have been proposed to work by this mechanism.[14]

There is some doubt as to the effectiveness of acid corrosion inhibitors on hydrogen-induced cracking (HIC) directly. Since it is thought that some inhibitors may stabilize atomic hydrogen or inhibit recombination as the corrosion inhibiting mechanism, the flux of hydrogen atoms into the metal matrix may increase. If this were the case, it would be expected that no noticeable effect or a high degree of failures would occur when compared to uninhibited acid.

It has also been stated that the effect of the acid inhibitors on HIC occurs externally since it is doubtful the inhibitor could penetrate the metal matrix. There is no action exerted by the inhibitor preventing the atomic hydrogen from entering the metal or preventing the atomic hydrogen from interacting with the metal atoms. The external effect is due to the reduced amounts of hydrogen atoms that are formed. The lower concentration of hydrogen atoms would lead to the assumption of a significantly reduced hydrogen atom flux into the metal matrix.

Several major oil companies have had occasional failures of N07750 springs, thus it was not surprising that the spring samples failed in the uninhibited 28% HCl acidizing test. R30035 springs age hardened for 4 hours @ 1200°F have been used in severe downhole conditions since January 1982 with good success although NACE Publication 1F1-92 reports occasional failures of this alloy and R30003. Many users consider R30035 and R30003 equivalent in resistance to corrosion and cracking in downhole environments. The results of this acidizing test support this theory.

CONCLUSIONS

1) R30035 age-hardened at 1200°F (650°C) is less susceptible to hydrogen embrittlement than when aged at lower temperatures.

2) Both inhibitors are effective in reducing cracking of CRA's in hydrochloric acid solutions, however there are differences in performance between the two inhibitors tested. In the environments tested, Inhibitor B reduced cracking of R30035 C-rings more effectively than Inhibitor A. Adequate protection of CRA spring materials requires higher performance inhibitors.

3) Even in inhibited acid solutions, exposure time is important (i.e., spring failures may be related to "soak" time and choice of inhibitor)

4) Common, corrosion resistant spring alloys are, as noted in NACE 1F1-92, susceptible to hydrogen embrittlement. N07750 is more susceptible than either R30035 or R30003.

5) Stress orientation and product form affect susceptibility to hydrogen embrittlement. Transverse-stressed C-ring specimens are more susceptible than springs.

REFERENCES

1. National Association of Corrosion Engineers, Standard TM0177, "Laboratory Testing of Metals for Resistance to Sulfide Stress Cracking in H_2S Environments."

2. G.B. Chitwood, "Environmental Cracking History of High Alloy Downhole Springs," CORROSION/87, Paper no. 298, (Houston, TX: NACE 1987).

3. R.D. Kane, M. Watkins, D.F. Jacobs, G.L. Hancock, Corrosion 33, 9(1977): p. 309.

4. NACE Publication 1F192 "Use of Corrosion Resistant Alloys for Resistance to Environmental Cracking in Oilfield Environments" (Houston, TX: NACE, 1992), p. 16.

5. MIL-STD-29A, "Military Standard, Springs, Mechanical; Drawing Requirements For," (Washington, D.C.: United States Government Printing Office, 1962).

6. A.M. Wahl, Mechanical Springs, (Cleveland, OH: Penton Publishing Company, 1944), p. 26, 34.

7. W. R. Coyle, "Effect of Free Sulfur on Cracking Behavior of CRA's in Simulated Downhole Environments," CORROSION/93, Paper no. 131, p. 2 (Houston, TX: NACE, 1993).

8. M.L. Walker, T.H. McCoy, "Effect and Inhibition of Stimulation Acids on Corrosion Resistant Alloys," CORROSION/86, Paper no. 154, (Houston, TX: NACE, 1986).

9. R.M. Latanision, O.H. Gastine, C.R. Compeau, "Stress Corrosion Cracking and Hydrogen Embrittlement: Differences and Similarities," Environment Sensitive Fracture of Engineering Materials, (TMS-AIME, 1979), p. 48

10. Metals Handbook Vol. 9, 8th Edition "Fractography and Atlas of Fractographs," (Metals Park, OH: American Society for Metals, 1974), p. 36.

11. R.A. Oriani, "Hydrogen—The Versatile Embrittler," Corrosion 43, 7(1987): p. 390.

12. R.H. Hausler, Corrosion Chemistry (Washington, D.C.: American Chemical Society, 1979), p. 266-286.

13. M.L. Walker, T.H. McCoy, "Effect and Inhibition of Stimulation Acids on Corrosion resistant Alloys," CORROSION/86, Paper no. 154, (Houston, TX: NACE, 1986).

14. S.W. Daen, H.J. Deitzer, C.A. Cooper, "Strong Acid Inhibition with Acetylenic Alcohols," CORROSION/79, Paper no. 69, (Houston, TX: NACE, 1979).

TABLE 1
CHEMICAL COMPOSITION OF ALLOYS TESTED (WT. %)

Element	UNS R30035		UNS R30003 Spring	UNS N07750 Spring
	C-rings	Spring		
C	.006	.004	.060	.03
Mn	< .01	.01	1.97	.05
Si	.02	.05	.51	.07
P	.002	.004	.009	.008
S	.001	.003	.002	.001
Cr	20.55	20.30	20.02	15.82
Ni	34.97	35.63	15.32	71.01
Mo	9.53	9.35	7.23	---
Co	Bal.	Bal.	40.17	.03
Fe	.14	.88	Bal.	8.25
Al	---	---	---	.85
Ti	.84	.89	---	2.75
Cb + Ta	---	---	---	.86

TABLE 2
MECHANICAL PROPERTIES OF ALLOYS TESTED

Material & Aging Heat Treatment		Yield Strength ksi (MPa)	Tensile Strength ksi (MPa)	% Elong.	% Reduction in Area	Hardness (HRC)
R30035	4 hours @ 1200°F (650°C) (Spring)	259.0 (1786)	263.8 (1819)	9.0	47.5	46
	4 hours @ 1050°F (565°C) (C-rings)	258.0 (1779)	263.0 (1813)	5.5	---	46.5
	4 hours @ 1200°F (650°C) (C-rings)	251.0 (1731)	259.0 (1786)	6.0	---	46
R30003, 5 hours @ 980°F (530°C) (Spring)		202.0 (1393)	256.0 (1765)	8.0	32.0	45
N07750, 4 hours @ 1200°F (650°C) (Spring)		171.0 (1179)	197.0 (1358)	13.0	31.0	43

TABLE 3
TEST MATRIX AND RESULTS OF SPRING SAMPLES

Material (UNS No.)	Condition (Heat Treatment)	Sample Type	Stress Level (% of UTS)	Environment		
				28% HCl without Inhibitor	28% HCl + Inhib. A	28% HCl + Inhib. B
R30035	4 hours @ 1200°F (650°C)	1-coil	75	NF	NF	NF
		2-coil	37	NF	NF	NF
R30003	5 hours @ 980°F (530°C)	1-coil	83	NF	NF	NF
		2-coil	46	NF	NF	NF
N07750	4 hours @ 1200°F (650°C)	1-coil	100	F	NF	NF
		2-coil	49	F	NF	NF

TABLE 4
TEST MATRIX AND RESULTS OF C-RING SAMPLES

Material (UNS No.)	Condition (Heat Treatment)	Stress Level (% of Yield)	Environment			
			28% HCl (uninhibited)	28% HCl + Inhib. A	28% HCl + Inhib. B	NACE TM0177
R30035	4 hours @ 1200°F (650°C)	46	F / F	NF / NF	NF / NF	F / F
		80	F / F	F / F	NF / NF	F / F
		100	NF / F	F / NF	F / NF	F / F
	4 hours @ 1050°F (565°C)	46	F / F	F / NF	NF / NF	F / F
		80	F / NF	F / F	F / NF	F / F
		100	F / F	F / F	F / F	F / F

TABLE 5
INTERSTITIAL HYDROGEN ANALYSES OF CRACKED C-RINGS

Description	Lab #1 (ppm)	Lab #2 (ppm)
Control Sample - 1050°F (565°C) Age	0.16, 0.15	0.1, 0.2
Control Sample - 1200°F (650°C) Age	0.18, 0.18	0.1, 0.1
1050°F (565°C) Age / 28% HCl + Inhib. A	3.30, 3.83	---
1050°F (565°C) Age / 28% HCl + Inhib. B	0.30, 0.34	---
1050°F (565°C) Age / Uninhibited 28% HCl	0.46, 0.47	---
1050°F (565°C) Age / TM0177	1.70, 1.11	0.7, 0.5, 1.3
1200°F (650°C) Age / Uninhibited 28% HCl	0.30, 0.34	0.2, 0.1, 0.2

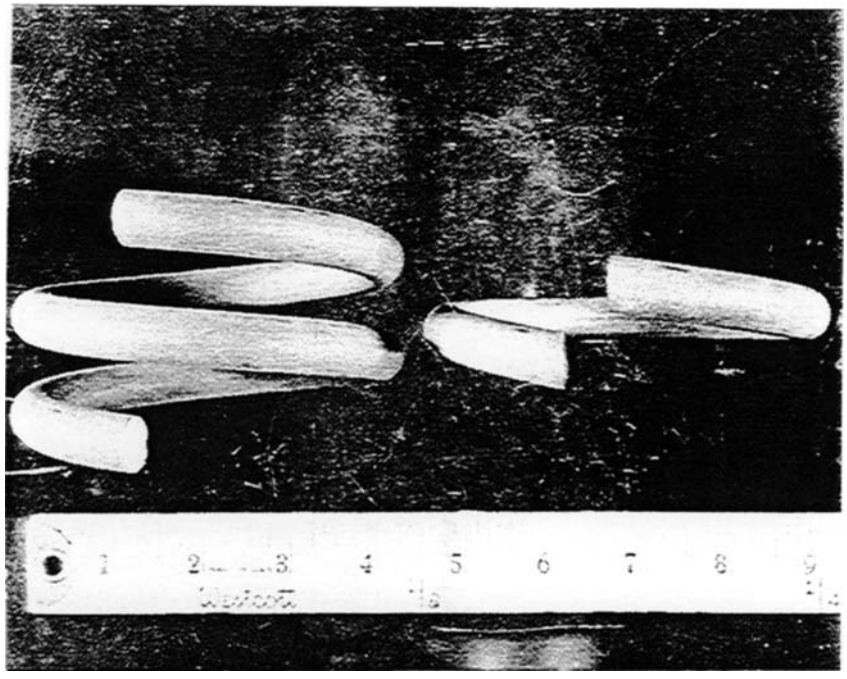


FIGURE 1. Typical 1-coil and 2-coil spring segments prior to stressing and testing.

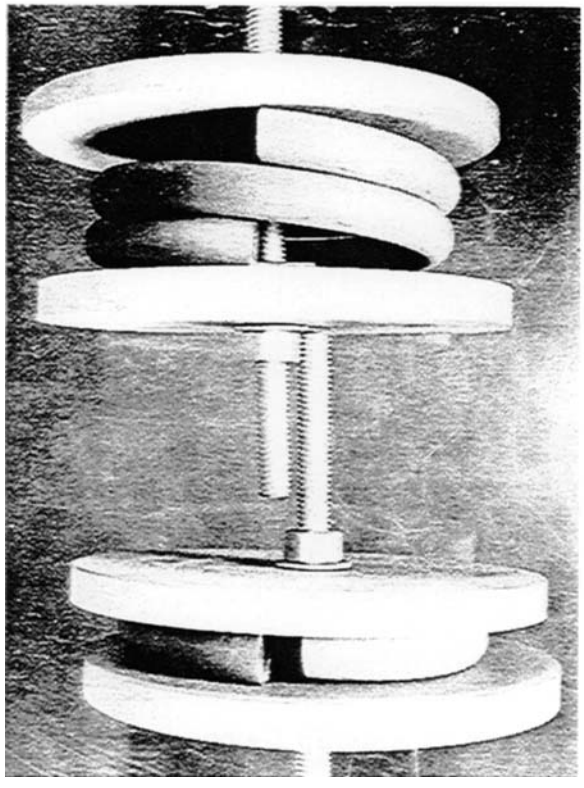


FIGURE 2. Typical test fixtures after compressing the spring samples.

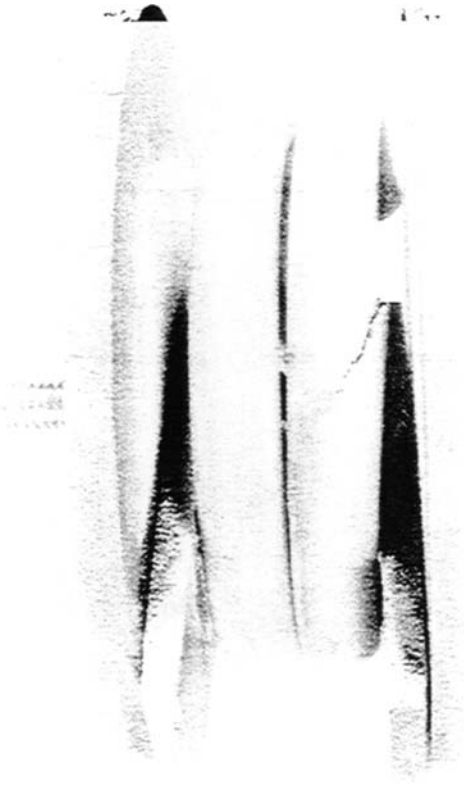


FIGURE 3. Crack in N07750 2-coil spring sample discovered after 3 days in 28% HCl.

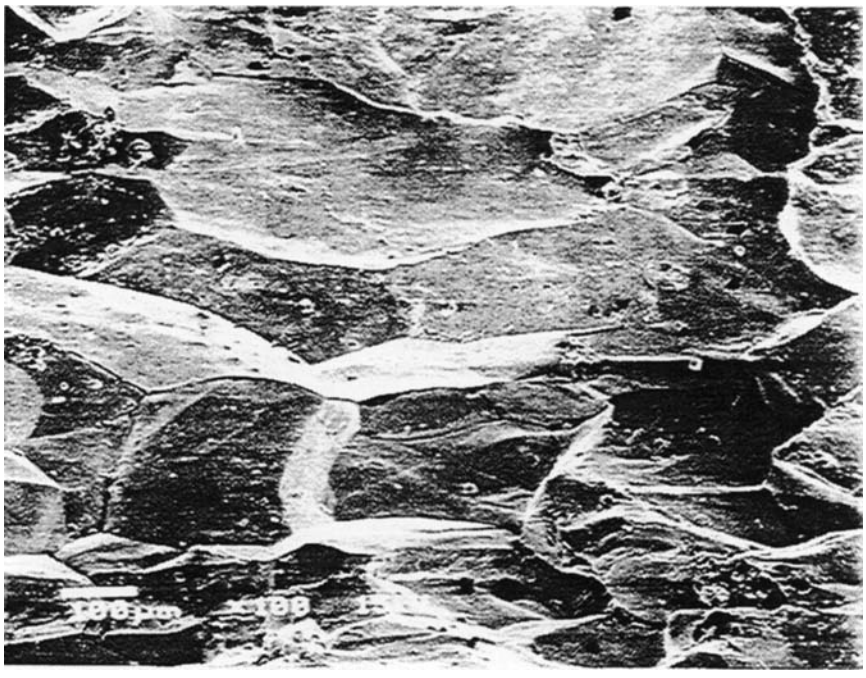


FIGURE 4. Scanning electron fractograph of N07750 spring fracture surface; the appearance is very similar to other spring failures attributed to hydrogen embrittlement.

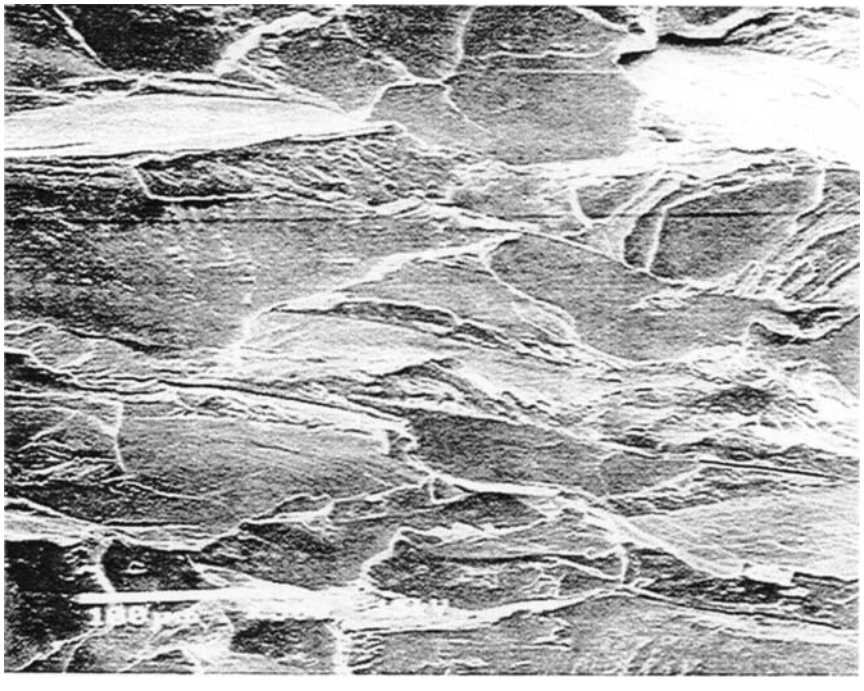


FIGURE 5. Scanning electron fractograph of R30035 C-ring fracture surface; note the similarity to Figure 4.

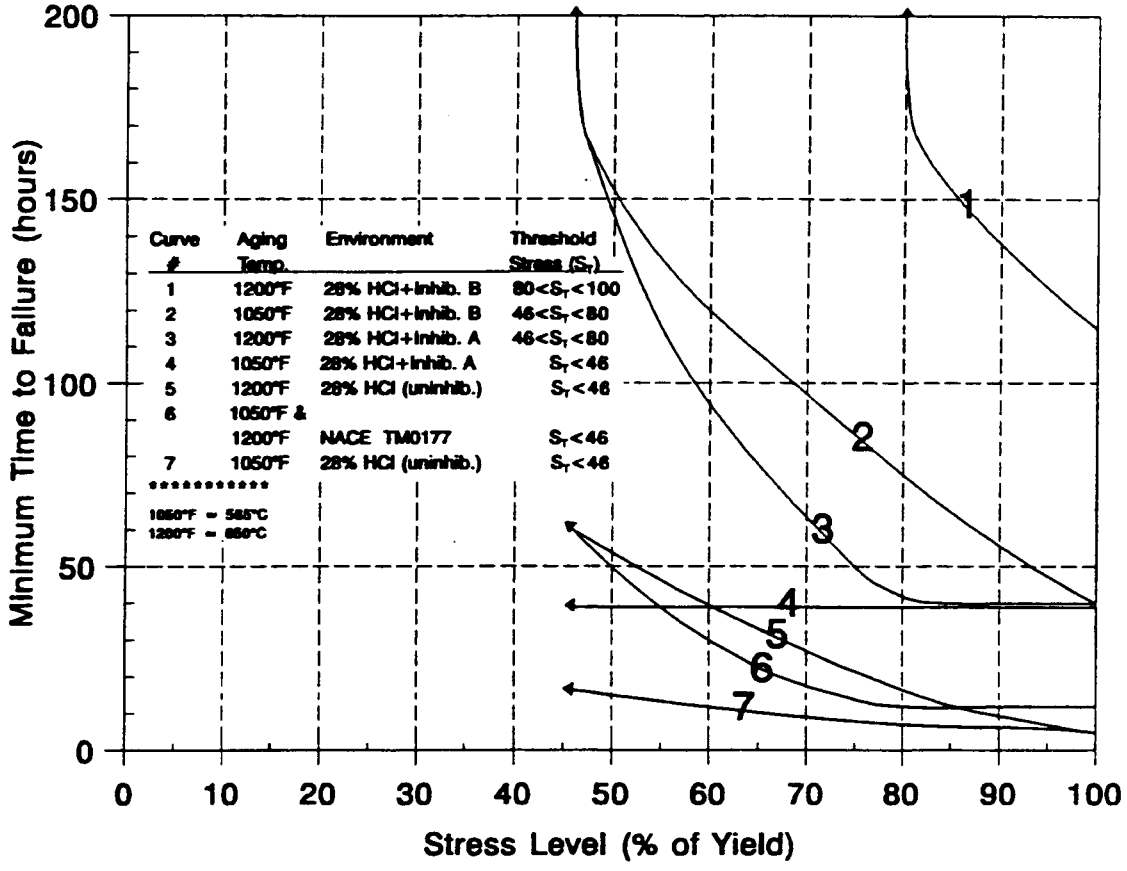


FIGURE 6. R30035 C-ring Tests; Minimum Time to Failure versus Stress Level

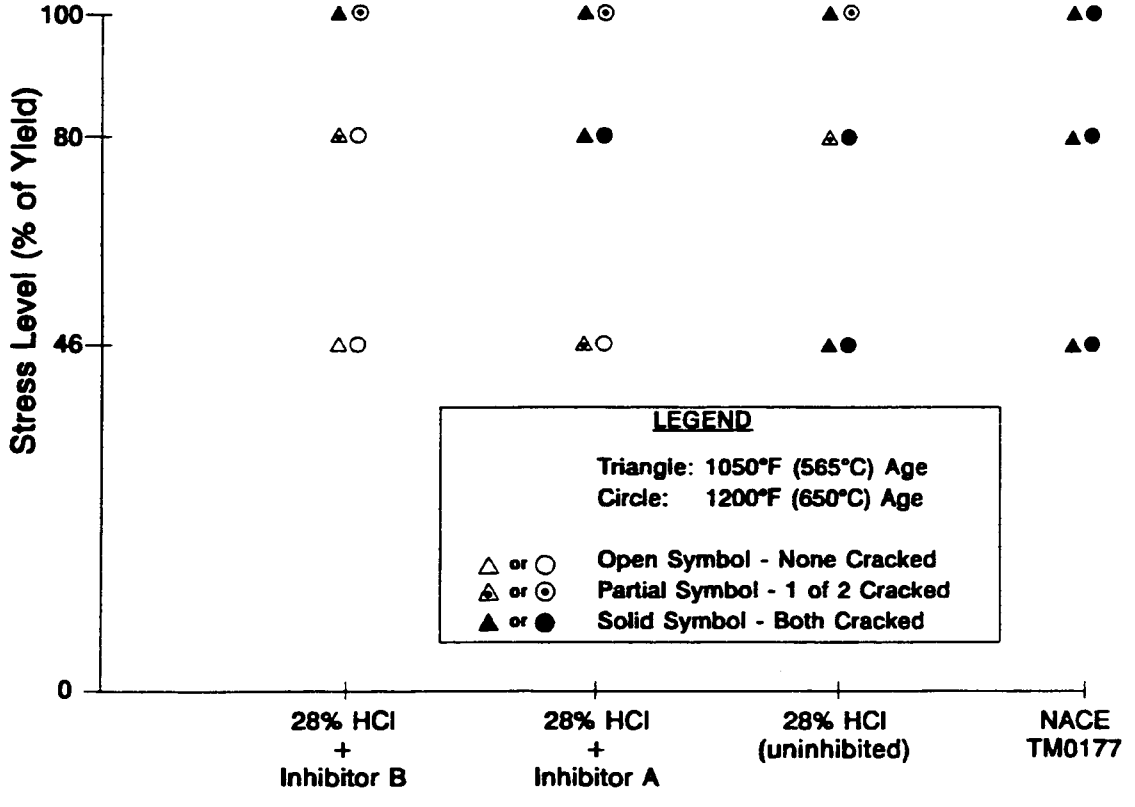


FIGURE 7. R30035 C-ring Tests; 28% HCl Acidizing Solutions and NACE TM0177

Copyrighted Materials
Copyright © 1996 NACE International Retrieved from www.knovel.com

How High-Alloy Tubulars React In Acidizing Environments

by Dr. J. D. Garber and Mohammad Kantour,
Department of Chemical Engineering,
University of Southwestern Louisiana, Lafayette, La.

Deep oil and gas reservoirs often contain extremely aggressive environments of high temperature and pressure.[1] Corrosive species such as carbon dioxide and hydrogen sulfide, in conjunction with production water and water condensate, make these environments very hostile to carbon steel tubulars.

Laboratory investigations[1-6] indicate that the use of highly alloyed steels such as martensitic and duplex stainless steels, high nickel-base alloys, and nickel-cobalt base alloys could be economically attractive in the most severe well conditions. As a result of these intensive studies, efforts are being deployed to speed up the use of such alloys on a large industrial scale.

One area that has received little attention in the literature is the effect that strong reducing conditions could have on these highly alloyed steels. For example, they can be exposed to hydrochloric acid during scale-removing operations or when acidizing the reservoir. The acidizing of carbonate formations along the Gulf Coast normally is done by injecting a 15% by weight solution of HCl, although lower concentrations are used.

This article summarizes a study[7] in which an examination has been made of the effect of various concentrations of hydrochloric acid at temperatures up to 180 F on the following tubulars: N-80 carbon steel (reference material), 410 stainless steel, ferralium 255 (duplex steel), Incoloy 80 (high nickel alloy), and Inconel 625 (nickel-base alloy). The pitting susceptibility of these alloys was also a point of focus.

Table 1. Chemical compositions of the materials tested

Material	Description (structure)	Weight, % Fe	Cr	Ni	Mo	Mn	Others	
N-80	Low carbon steel (quenched and tempered)	98.39	0.22	—	—	1.31	Si:0.07 C :0.36	
410 Stainless steel	Martensitic (quenched and double tempered)	85.29	12.75	0.43	0.07	0.61	C :0.074 P :0.024 Si:0.68	Cu:1.90 S :0.005 V :0.04
Ferralium 255	Duplex steel (50% cold rolled)	63.18	25.44	5.20	3.08	0.96	C :0.02 Si:0.44 S :0.002	Cu :0.54 P :0.018 N :0.20
Incoloy 800	High nickel alloy (annealed)	46.55	20.11	31.08	—	0.84	C :0.07 S :0.003 Ti:0.36	Cu:0.54 Si:0.25 Al:0.20
Inconel 625	Nickel-base alloy (annealed)	4.75	21.87	60.68	8.46	0.15	C :0.02 P :0.007 Si:0.24 Al:0.11	Cb + Ta:3.48 S :0.001 Ti:0.23

Courtesy Hart Publications, Inc.

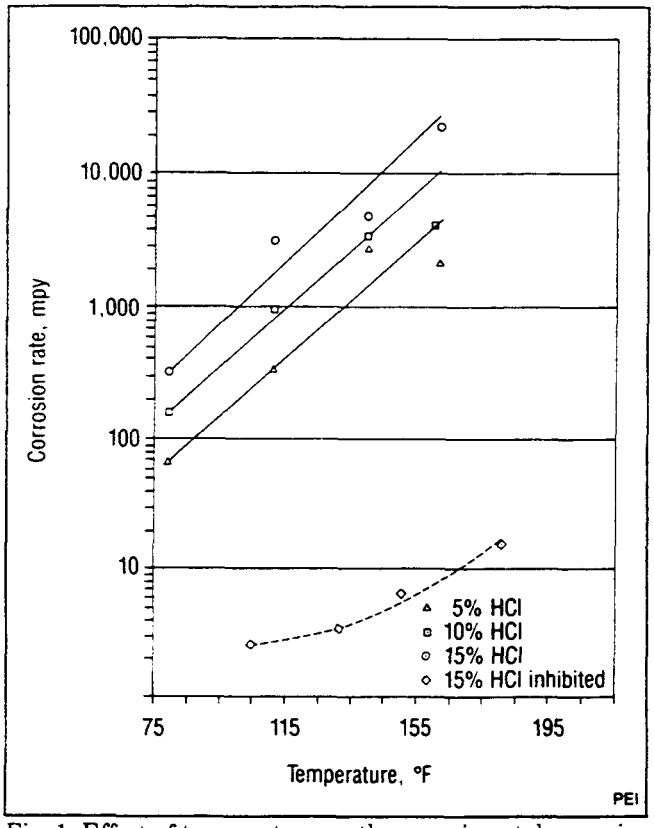


Fig. 1. Effect of temperature on the experimental corrosion rates of N-80 carbon steel in HCl solutions.

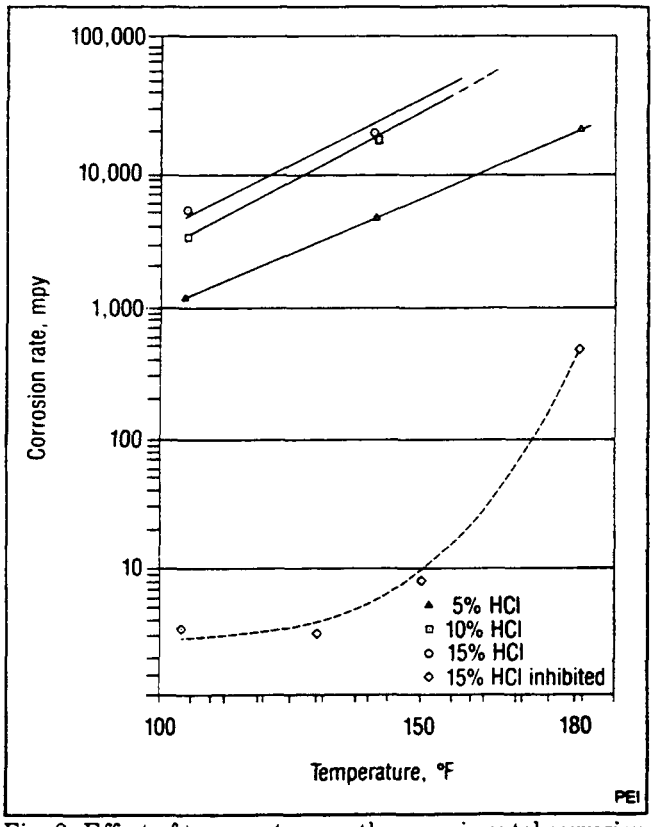


Fig. 2. Effect of temperature on the experimental corrosion rates of 410 stainless steel in HCl solutions.

In addition, potentiodynamic polarization curves at various temperatures and acid concentrations were produced for ferralium 255 and Inconel 625. Such curves provide a basis for alloy comparison and even allow calculation of corrosion rates.[8]

The composition and structure of the materials evaluated are presented in Table 1. All five metals are quite different in their chemical makeup. Hence, a substantial amount of information should be obtained about how various alloying elements affect the corrosion resistance of a metal in hydrochloric acid.

Experimental Procedure

The weight loss measurements determined were based on 12-hr exposure time of rectangular samples, with approximate surface areas of 5 sq in. in unagitated HCl solutions. The coupons were prepared for testing according to NACE Standard TM-01-69. All coupons were ground to a 120 grit finish before being hung in 750 ml of the test solution by a teflon thread. The acid solutions were purged with nitrogen to remove oxygen from the system and maintained at 1 atm pressure.

Each test was run in duplicate and the temperature was maintained at ±3 F of the set point. Tests involving the use of a high-temperature, commercial, alcohol-base acid inhibitor were run with 1% inhibitor by volume. The exposed coupons were examined under an optical microscope so that pit depth and density could be determined and to describe the type of attack of each of the materials under investigation.

The potentiodyne used in these experiments was the Model M-4100 from Petrolite Instruments. Both the auxiliary and the test electrodes were cylindrical, and identical in size and nature. The reference electrode used was a saturated calomel cell. The test electrode was prepared for polarization by standard recommended procedure, ASTM G-3, before a scan rate of 3 v/hr was applied.

Test Results

The weight loss measurements, based on 12-hr duration tests, were conducted on various metals at concentrations of 5%, 10%, and 15% HCl by weight with the inhibitor being added only to the 15% HCl solution. The normal temperature range studied was from 104 to 180 F.

Semilog plots of the results of these tests are presented in Figs. 1 through 5. In every case the corrosion rate increased with temperature. A comparison reveals that 410 stainless steel experienced the highest corrosion rates and ferralium 255 is only as good as carbon steel. The high nickel alloys showed a significant reduction in corrosion.

Although most of the corrosion rates increased with acid concentration, Figs. 4 and 5 reveal that this was not always the case. Incoloy 800 and Inconel 625 both experienced a reduction in attack with increasing acid concentration from 10% to 15%. Examination of the microstructure of these materials revealed that at 10% HCl the corrosion attack appears to be primarily intergranular in nature, which allowed some grains to simply fall out of the crystal lattice, giving large corrosion rates. At higher concentrations, the attack appeared to be more uniform and less dislodgement of grains occurred.

Materials such as N-80 carbon steel, 410 stainless

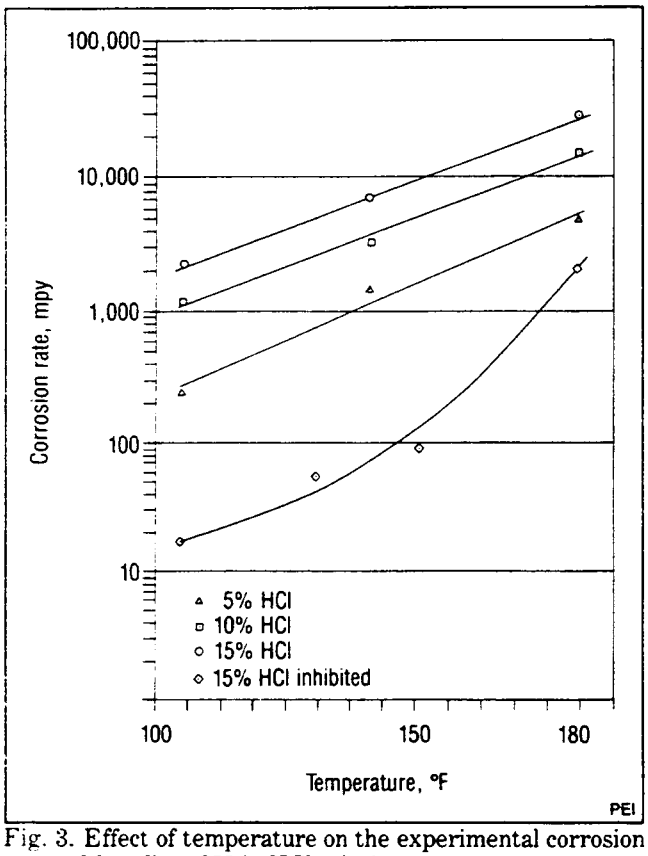


Fig. 3. Effect of temperature on the experimental corrosion rates of ferralium 255 in HCl solutions.

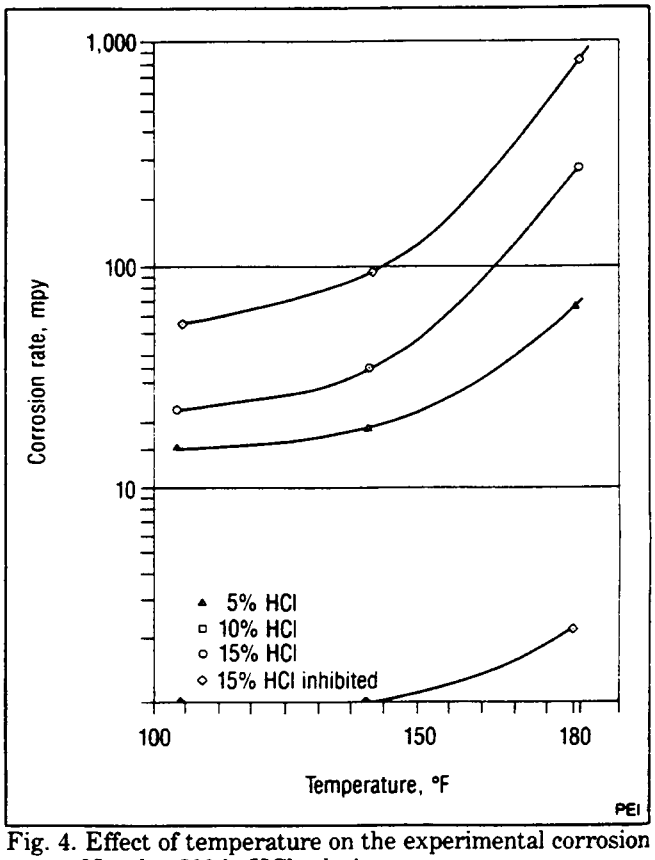


Fig. 4. Effect of temperature on the experimental corrosion rates of Incoloy 800 in HCl solutions.

steel, and ferralium 255 sustained very severe weight loss. Their respective corrosion rates were 27,000 mpy, 45,000 mpy, and 14,000 mpy in 15% HCl at 160 F.

In addition, N-80 and 410 were susceptible to pitting attack in uninhibited solutions, mainly at low acid concentrations and temperatures. In such a reducing environment, the addition of chromium did not improve the resistance to weight loss or to pitting. In fact, it even appeared to cause them to increase. The addition of nickel and molybdenum greatly improved the resistance to weight loss. A nickel content of over 30% seems to be required to provide an acceptable resistance to weight loss in such reducing environments.

Table 2 summarizes the types of attack which occurred on each of the metals in uninhibited HCl solutions. The 410 and N-80 materials showed shallow intergranular corrosion to some degree.

In every case the addition of inhibitor reduced the corrosion rate by a substantial amount. It seems that the alcohol-base inhibitor began losing its effectiveness as the temperature was increased above 150 F, however, mainly for carbon steel and chromium alloys. At 180 F, it appears to have worked better for carbon steel than 410 stainless steel, and was very ineffective in protecting ferralium 255.

Microscopic examinations showed that N-80 was susceptible to pitting in inhibited solutions, and the inhibitor actually increased the amount of pitting which occurred on 410 stainless steel. The high nickel alloys were effectively protected by the inhibitor.

Although several potentiodynamic polarization curves were obtained for duplex stainless steel and Inconel 625, the ones presented here were obtained in 5% HCl by weight at 104 F. The test electrode was polarized from −1.0 v to +1.0 v versus the saturated calomel electrode. The applied current density was simultaneously recorded on semilog paper.

Fig. 6 shows the polarization curve of Inconel 625. This nickel-base alloy shows an active-passive transition which indicates that the rate of dissolution of the metal would be about 3 mpy in such an environment if the alloy were operating in the passive region.

The reverse scan, used by investigators to predict the susceptibility to localized attack,[9] also proves that this alloy is self-repassivating in this environment and is not susceptible to localized corrosion when operating in the passive region. The reducing nature of the acid solution, however, dropped the natural corrosion potential of the alloy to −0.22 v versus the saturated calomel electrode which is located in the active region and gives a corrosion rate of 19.9 mpy.

The potentiodynamic polarization curve of the duplex stainless steel in 5% HCl at 104 F is presented in Fig. 7. Again, the metal shows active-passive transition. The current density in the passive region is relatively high and increasing, indicating a less stable passive film. When operating in its passive zone, the alloy will be susceptible to pitting above +0.16 v versus the saturated calomel electrode because of the hysteresis exhibited on the reverse scan.

The natural corrosion potential of the duplex steel in the test environment, −0.32 v versus SCE, is located in the active region. The values of the corrosion current density of these alloys suggest that the duplex stainless steel is much less resistant to weight loss than Inconel 625. The calculated corrosion rate of ferralium 255

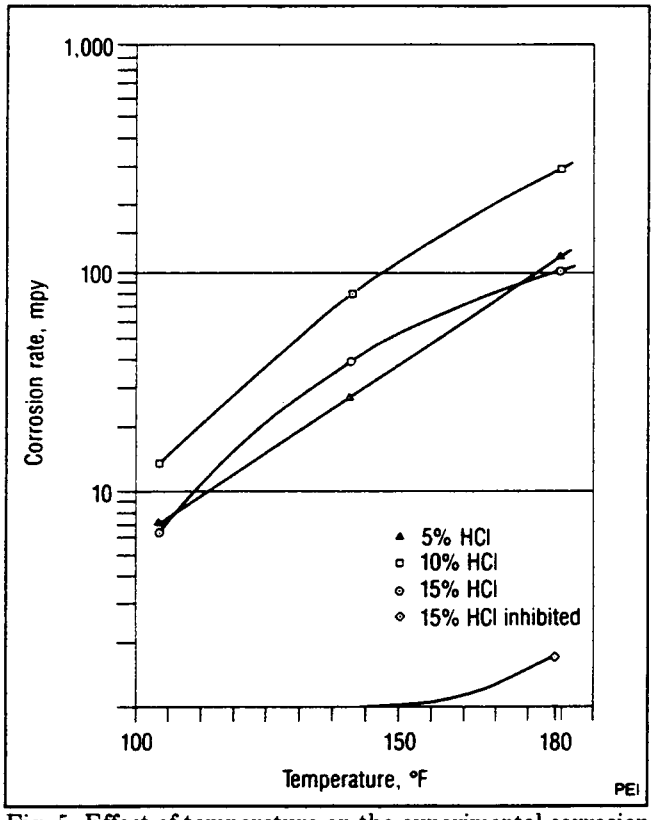


Fig. 5. Effect of temperature on the experimental corrosion rates of Inconel 625 in HCl solutions.

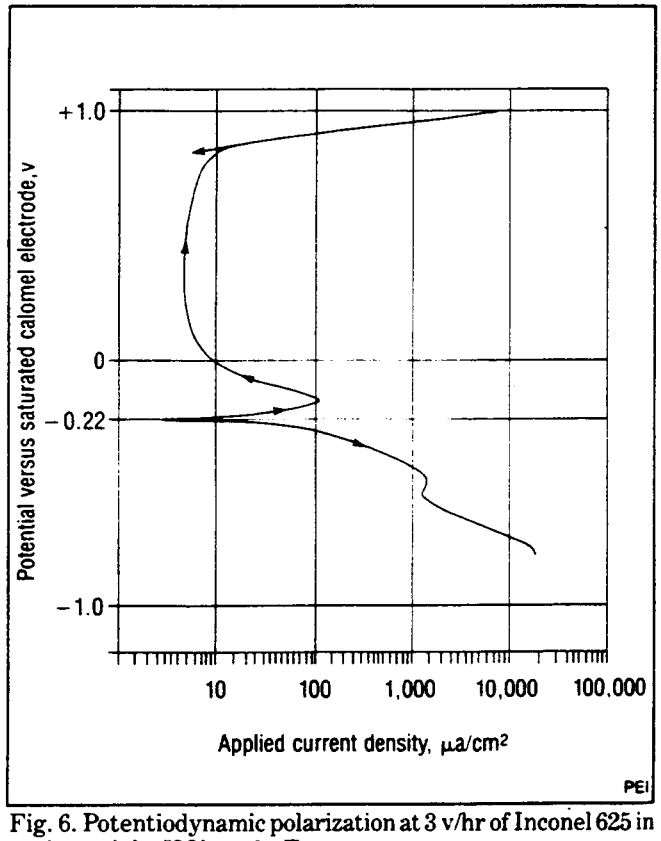


Fig. 6. Potentiodynamic polarization at 3 v/hr of Inconel 625 in 5% by weight HCl at 104 F.

TABLE 2. Summary of the type of attack which occurred during the total immersion tests

Alloy	Average pit depth, mils/12 hr	Pit density, No./sq in.	General corrosion	Intergranular corrosion	Remarks
N-80 steel	2.4	6-32	Very severe	No	More general corrosion and less pitting occurred as the temperature and acid concentration were increased. The addition of inhibitor did not improve the resistance toward pitting.
410 steel	3.0	100	Very severe	No	
Ferralium 255	NA*	NA*	NA*	NA*	Selective attack was detected on cleaned coupons. The surface became like pulp and could be removed with a rubber stopper. The inhibitor was particularly ineffective in protecting this alloy.
Incoloy 800	No	0	Acceptable	Deep	The intergranular attack was most severe in 10% HCl. Excellent effectiveness of the inhibitor in reducing weight loss and eliminating localized corrosion.
Inconel 625	No	0	Acceptable	Shallow	

*Selective attack produced a delaminated surface

duplex steel from Fig. 7 was 3,439 mpy.

Table 3 shows the corrosion current densities obtained from the various polarization curves, and the calculated corrosion rates compared to those obtained from the weight loss measurements. There is not good agreement between the two methods. The potentiodyne does appear to be able to give a good relative comparison of which metals are best in a given solution. It also tells whether a metal undergoes active-passive type of behavior. To use this method for predicting absolute corrosion rates in strong acid solutions, however, could lead to some problems.

Evaluating Test Results

Based on these reported results, a number of conclusions can be reached concerning the effect that alloying elements have on a metal's resistance to HCl, the effect that alloying elelments have on the effectiveness of the acid inhibitor, and how potentiodynamic scans can help in evaluating metals.

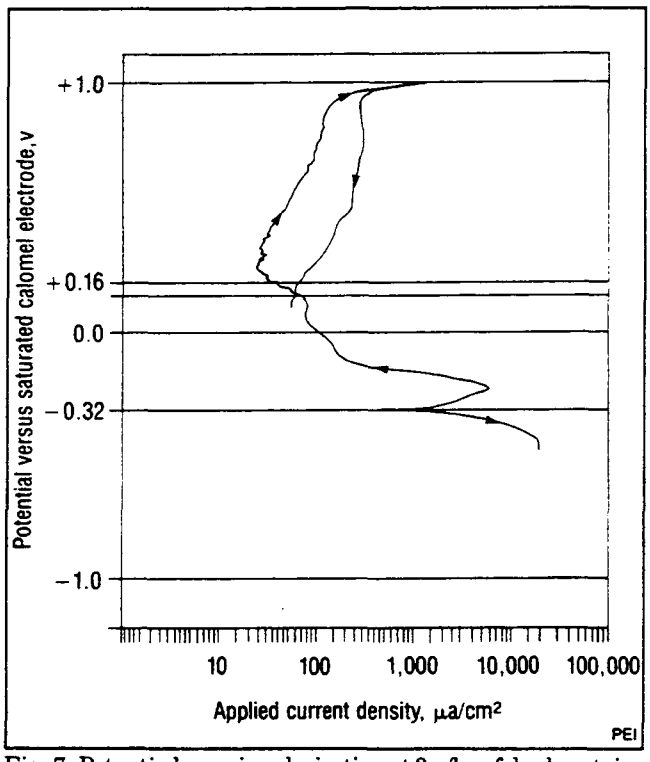


Fig. 7. Potentiodynamic polarization at 3 v/hr of duplex stainless steel in 5% by weight HCl at 104 F.

TABLE 3. Comparison of weight loss and potentiodynamic corrosion rates

Alloy	Conditions	Corrosion current density, μa/cm²	Potentiodynamic corrosion rate, mpy	Weight loss corrosion rate, mpy
	5% HCl, 104 F	33.5	19.9	6.9
	5% HCl, 180 F	33	19.6	113.2
Inconel	10% HCl, 104 F	5.5	3.3	13.2
625	10% HCl, 180 F	400	238	283.8
	15% HCl, 104 F	12	7.14	6.4
Duplex	5% HCl, 104 F	6,000	3,439	239
steel	5% HCl, 140 F	12,500	7,164	1,420.5

Comparison of these five different materials makes it possible to make some general statements about the effect that various alloying elements have on the metals' resistance to HCl.

- The addition of chromium to carbon steel, as in 410 SS, actually reduces the corrosion resistance and increases the pitting rate.
- Ferralium 255, a duplex stainless, contains high chromium in addition to small concentrations of molybdenum and nickel. Exposure of the duplex structure, 50% austenitic and 50% ferritic, did not cause pitting to occur, but produced a delaminated surface. It is most likely that the ferritic grains were selectively attacked.
- The addition of nickel reduces the general corrosion rate, but the attack becomes intergranular, especially in 10% HCl. Increasing the nickel from 31% in Incoloy 800 to 61% in Inconel 625 reduced this attack. These alloys should be used in 15% HCl when acidizing.
- Acid inhibitors have been developed for use on carbon steels and the results obtained in this study suggest how effectively they might work on high-alloy tubulars. All tests were conducted in 15% HCl solutions at a concentration of 1% by volume. On all metals examined, the inhibitor effectiveness reduced as the temperature increased. On 410 stainless steel, the inhibitor actually increased the pitting rate when compared to an uninhibited rate of 100 pits/sq in. The inhibitor was especially ineffective on duplex stainless steel. It is not clear if the increased chromium content or the duplex structure is responsible for the poor protection. The increased nickel contents of Incoloy 800 and Inconel 625 appear to have improved the inhibitor effectiveness. It can be concluded that new acid inhibitors will have to be developed for high chromium stainless steels.
- The potentiodynamic tests conducted on duplex stainless steel and Inconel 625 reveal some interesting information about this method of alloy evaluation. The corrosion rates predicted by the potentiodynamic method do not compare well to weight loss measurements. The results do give a good relative comparison of which metal will work best in a given solution, however. The potentiodynamic curves for ferralium 255 and Inconel 625 reveal that both metals exhibit active-passive behavior in HCl, although the natural corrosion potential of both metals occurs in the active regions. The potential scan of duplex stainless steel shows a relatively unstable passive region and the reverse scale intersects the passive region at a low potential. Hence, attempts to anodically protect this metal probably would not be successful.

The same scan for Inconel 625 shows a much smaller nose on the anodic branch and a more stable passive region. The reverse scan shows that the metal will not pit if it is held in this passive region. Hence, anodic protection would work effectively on this metal. In addition to corrosion rates, these curves reveal a great deal of information about a metal in a given solution.

References

1. Watkins, M. and Greer, J. B.: "Corrosion Testing of Highly Alloyed Materials for Deep Sour Gas Well Environments," paper SPE 5622, presented in Dallas, Tex.
2. Kudo, T., *et al.*: "Corrosion Behavior of Highly Alloyed Materials in H_2S-CO_2-Cl^- Environments," paper presented at Corrosion 82, NACE (March 1982) Houston, Tex.
3. Asphahani, A. I., *et al.*: "Highly Alloyed Austenitic Materials for Corrosion Services," *Metal Progress* (September 1983) 25.
4. Vaughan, G. A. and Chaung, H. E.: "Wireline Material for Sour Service," *Materials Performance* (January 1982) 44-50.
5. Asphahani, A. I.: "Highly Alloyed Stainless Materials for CO_2/H_2S Environments," paper No. 12, presented at Corrosion 1980, NACE, Chicago, Ill.
6. Oredsson, J. and Bernhardsson, S.: "The Performance of Highly Alloyed Austenitic and Duplex Stainless Steels in Sour Gas and Oil Environments," paper No. 126, presented at Corrosion 1980, NACE, Houston, Tex.
7. Kantour, M.: "High Performance Alloys for Stimulated Deep Well Tubulars," thesis, University of Southwestern Louisiana, Spring 1984.
8. Morris, P. E. and Scarberry, R. C.: "Predicting Corrosion Rates with a Potentiostat," *Corrosion, 28*, No. 12 (1972) 444.
9. Pourbaix, M.: "Significance of Protection Potential in Pitting and Intergranular Corrosion," *Corrosion, 26*, No. 16 (1970) 431.

Copyrighted Materials
Copyright © 1996 NACE International Retrieved from www.knovel.com

Paper No. 481—CORROSION/89

COMPATIBILITY OF STAINLESS AND NICKEL BASE ALLOYS IN ACIDIZING ENVIRONMENTS

Dr. Russell D. Kane and Dr. S. Mark Wilhelm
Cortest Laboratories, Inc.
11115 Mills Road, Suite 102
Cypress, Texas 77429

ABSTRACT

This paper presents results from a recent multiclient study conducted by Cortest Laboratories. It involved the evaluation of selected corrosion resistant alloys (CRA) in the following oil field acidizing media: (1) 15 percent HCl, (2) 28 percent HCl, (3) 12 percent formic acid, and (4) 13 percent HCl/2 percent HF. The tests were conducted both with and without H_2S and at 92° and 202°C (200° and 400°F) using a three phase testing sequence involving consecutive exposures to (1) concentrated acid mixtures with inhibitors, (2) reacted inhibited acids and (3) dilute, reacted acids without inhibitors. With exception of formic acid, the acidizing media were generally found to be very aggressive to CRA materials with weight loss corrosion the predominant mode of attack in concentrated acids with inhibitor and SCC in reacted and/or dilute acidizing fluids. The extent and nature of corrosive attack was widely variable depending on the specific alloy composition, inhibitor formulation, and acidizing conditions examined.

INTRODUCTION

In recent years, the use of stainless and nickel base alloys (also referred to as Corrosion Resistant Alloys — CRA's) in corrosive oil field production environments has become increasingly prevalent. Extensive laboratory testing and limited field experience has identified specific CRA materials that can be utilized under conditions of H_2S, CO_2, and brine. However, it has become apparent that the limiting situation for some of these materials may not be the production environment but the environments present during and after acidizing procedures. Therefore, there is much concern regarding (1) the inherent corrosion resistance of CRA materials in acidizing media, (2) synergistic effects of acids and acid gases — H_2S and CO_2, and (3) the effectiveness of acid inhibitors on CRA materials.

BACKGROUND

Several investigations have been conducted on the corrosion behavior of CRA materials in acidizing fluids.[1-5] Most of these studies, however, have been limited to only a few materials in concentrated acids and inhibitors. Furthermore, nearly all have been limited to studies of corrosion behavior only and not dealing with stress corrosion cracking (SCC). These studies indicate that severe corrosion of CRA's can occur in concentrated acids and that conventional acid inhibitors used for steels are of only limited effectiveness on preventing corrosion of materials such as 13 Cr and duplex stainless steels.[1,2] One of the few references on corrosion of duplex stainless steels that involved SCC testing indicated that SCC did not occur during exposure to inhibited acids.[3]

In general, the understanding of the behavior of CRA materials in acidizing environments appears unclear due to the complex nature of these fluids and wide range of potential alloys to be considered. The present study was initiated to determine the behavior of CRA materials in a range of environmental conditions that may exist during and after an acidizing operation. Whereas it would be an impossible task to try to evaluate all acid types and formulations in this program, several generic types were employed. Furthermore, conditions were simulated in this study which relate to those found downhole during the actual acidizing operations, along with those that may persist in the well for an indefinite period thereafter resulting from reacted and/or diluted acid with varying degrees of inhibitor effectiveness.

EXPERIMENTAL PROCEDURE

Materials

Tests were conducted on ten different stainless and nickel base alloys. They consisted of seven materials strengthened by coldworking:

Duplex stainless steel - 22 Cr
Duplex stainless steel - 25 Cr
Austenitic stainless steel - 28 Cr
Nickel base alloy (Alloy 825) - 42 Ni
Nickel base alloy (Alloy G) - 50 Ni
Nickel base alloy (Alloy C-276)
Nickel base alloy (Allcorr)

and three materials were strengthened by heat treatment:

Martensitic stainless steel (AISI 420) - 13 Cr
Nickel base alloy (Incoloy alloy 925)
Nickel base alloy (Alloy 718)

The nominal chemical compositions and yield strengths of the materials in this program are given in Table 1.

Specimens

Weight loss corrosion coupons were used with the nominal dimensions of 1.0-inch x 0.5-inch x 0.063-inch. A 0.25-inch hole was machined in the middle of the coupon. The coupons were electrically isolated using TFE shoulder washers.

Stress corrosion cracking (SCC) tests were conducted on the materials with the use of C-ring specimens stressed to 100 percent of the 0.2 percent offset yield strength

Environments

Four acid formulations were used in this study: (1) 15 percent HCl, (2) 28 percent HCl, (3) 12 percent formic acid, and (4) 13 percent HCl/2 percent HF mixture. Tests were conducted with the various acids with either a CO_2 (PCO_2 = 200 psig) or H_2S (PH_2S = 100 psig) cover gas added at 23°C (75°F). Tests were then run at 93°C (200°F) and 204°C (400°F). All tests were conducted in Alloy C-276 lined autoclaves with internal TFE vessels which were used to hold the acid mixtures and specimens.

The acidizing tests were conducted in a three stage sequence. Stage 1 consisted of the concentrated acid formulation with inhibitor. Specimens were exposed to this environment for a period of six hours simulating the conditions during an actual acidizing operation.

Stage 2 consisted of a six day exposure to inhibited reacted acid. The HCl and formic acid mixtures were reacted with $CaCO_3$ pellets. The HCl - HF mixture was reacted with the combination of silica flour and bentonite. The Stage 2 environment was meant to simulate downhole conditions existing immediately following the acidizing operation during the circulating out of the spent (reacted) acidizing fluids.

Stage 3 related to prolonged exposure to spent diluted acid when the inhibitor has been depleted. This may occur during production after the acidizing operation. The Stage 3 sequence consisted of exposure to reacted, diluted acid without inhibitor for a period of seven days.

More complete information regarding these reaction and dilution steps is given in Appendix I.

Inhibitors

All inhibitors used in the present study were obtained from a commercial supplier. They were based on aromatic heterocyclic nitrogen compounds and formulated for use in oil field acidizing environments. Two different inhibitors were used in separate tests with each type of acid. Inhibitors 1 and 2 were used in the HCl and HF-HCl mixtures whereas Inhibitors 3 and 4 were used in the formic acid. The concentrations of inhibitor used in the various tests are given in Appendix I.

RESULTS

The results of the corrosion and SCC tests conducted in the various inhibited acids are given in Figures 1 through 7. These figures show the severity of corrosion and the occurrence of SCC as a result of exposure to the various stages of the acidizing sequence. Corrosion rate data is presented by showing the regimes of corrosion behavior which have a general corrosion rate either less than 2,000 mpy (5.5 mpd) or greater than this value. This rate was chosen because it is typical of the corrosion rate commonly experienced and considered acceptable on steel tubulars in normal acidizing operations. The SCC data as presented has failure/no-failure data for C-ring specimens exposed for the acidizing stages indicated.

15 Percent Hydrochloric Acid

As can be seen in Figures 1 and 2, the results of the corrosion tests are highly dependent on specific alloy composition and environmental conditions (i.e., H_2S, CO_2, temperature and inhibitor). Test conditions involving H_2S and higher temperature are typically more severe from a corrosion standpoint. The predominant mode of attack was general corrosion. However, some materials did show signs of pitting in the H_2S containing acid at 92°C (200°F) (13 Cr, 28 Cr, 42 Ni, and 925) and in the CO_2 containing acid at 202°C (400°F) (52 Ni and Allcorr). Of particular interest is the evidence of selective phase attack in the duplex stainless steels which usually leads to very high corrosion rates. Similarly there are other environment/materials combinations that lead to very high corrosion rates.

Generally, in the 15 percent acidizing media, all coldworked nickel base alloys (≥ 42 percent nickel) had acceptable general corrosion rates in the Stage 1 exposure. This condition is typical of conditions experienced during the actual acidizing treatment (i.e., short duration, concentrated acid with inhibitor). Inhibitor 2 appears to have somewhat different performance than Inhibitor 1 in 15 percent HCl. Inhibitor 2 resulted in a generally less severe corrosion conditions than did Inhibitor 1.

No materials showed evidence of SCC in the relatively short (6 hours) Stage 1 acidizing exposure. SCC was limited to exposures to the reacted or reacted and diluted acid media found in Stages 2 and 3. Cracking was particularly severe in the 202°C (400°F) Stage 2 and 3 environments with either H_2S or CO_2. SCC was found in all materials which were not removed due to excessive corrosion. Whereas weight loss corrosion was generally less severe in the environment with Inhibitor 2, SCC was worse as seen by reduced failure times in the environment containing Inhibitor 2.

28 Percent Hydrochloric Acid

The results from the two tests conducted with inhibited 28 percent HCl are presented in Figures 3 and 4. Similar to the tests in 15 percent HCl, the results are both alloy and environment specific. However, comparing the results of 15 percent and 28 percent HCl with Inhibitor 1 (Figures 1 and 3), it can be seen that the 28 percent HCl acidizing environment is less corrosive at 92°C (200°F). This was particularly noticeable with respect to the lack of attack on the duplex stainless steels in the 92°C (200°F)/CO_2 tests. At 202°C (400°F), both tests with CO_2 and H_2S were of comparable severity from the standpoint of weight loss corrosion.

As in the case of the 15 percent HCl, the use of Inhibitor 2 was found to result in lower corrosion rates of most materials. This observation was particularly true for the Stage 1 exposure to the concentrated acid.

The occurrence of SCC in the 28 percent HCl acidizing sequence, was comparable to that found for the 15 percent HCl test. Only 28 Cr was observed to exhibit SCC in the Stage 1 exposure. All other materials were free of SCC in this portion of the acidizing sequence. At 202°C (400°F) with either CO_2 or H_2S, the subsequent stages of the acidizing test involving unreacted and reacted and diluted acid were extremely severe from the standpoint of SCC with cracking exhibited by all materials that were not removed from the tests due to excessive weight loss corrosion.

12 Percent Formic Acid

The results from the two tests conducted with inhibited 12 percent formic acid are both represented in Figure 5. The results of the tests with Inhibitor 3 and Inhibitor 4 were very similar. Both showed, very low corrosion rates on the CRA materials. The exception to this was the selective attack and resultant high corrosion rates on the 22 Cr duplex stainless steel. This attack was limited to tests conducted at 202°C (400°F) both with CO_2 and with H_2S.

No SCC was observed in materials exposed to the Stage 1 acidizing environment. The only occurrences of SCC were in 22 Cr and 25 Cr duplex stainless steel exposed to the reacted and diluted acid in the tests containing H_2S gas. This behavior was seen in specimens tested at both 92°C (200°F) and 202°C (400°F).

13 Percent Hydrochloric Acid/2 Percent Hydrofluoric Mixture

The results of the tests conducted in inhibited 13 percent HCl/2 percent HF are given in Figures 6 and 7. Like tests conducted in inhibited HCl which were discussed previously, the corrosion rates of the various CRA materials varies greatly depending on the specific conditions present. For example, with Inhibitor 1, significant selective attack was observed on the duplex stainless steels at 92°C (200°F) with H_2S or CO_2. With Inhibitor 2, however, high corrosion rates and selective attack were limited to duplex stainless steels tested in the Stage 1 inhibited acid mixture when CO_2 was present. Tests conducted under these conditions with H_2S did not show these results. Tests conducted with Inhibitor 2 at 92°C (200°F), showed much more severe corrosion in Stages 2 and 3 than did tests conducted with Inhibitor 1.

At 202°C (400°F), environments containing Inhibitor 1 appeared to be more corrosive than those with Inhibitor 2. However, the most noticeable differences between Inhibitors 1 and 2 were seen in the susceptibility to SCC in Stage 1 tests. In the HCl/HF mixture containing Inhibitor 1, no cracking was found to occur during this stage of the acidizing sequence under any conditions [i.e., 92°C (200°F)/202°C (400°F); CO_2/H_2S]. However, in tests containing Inhibitor 2, extensive cracking of nearly all materials was noted during the Stage 1 exposure.

DISCUSSION

Currently, there are no guidelines for determining the compatibility of acidizing environments with CRA materials. For the purposes of this study the following guidelines were used:

1. Weight Loss Corrosion Rate <2,000 mpy (5.5 mpd) during the Stage 1 exposure
2. No tendency for localized corrosion or selective phase attack, and
3. No SCC.

Applying these tentative guidelines to the results of the tests, it can be seen that the environment which simulates the actual acidizing situation (Stage 1 — exposure to concentrated acid and inhibitor) should be a concern primarily from the standpoint of weight loss corrosion. SCC was found to occur only to a very limited degree with the most severe conditions in this stage of the acidizing sequence. Attack was primarily in the form of weight loss corrosion in most CRA materials.

Localized attack was only manifested in isolated cases where specific alloys and environments showed incompatibility. The best example of this is the selective phase attack found in the duplex stainless steels. It is the result of preferential attack of the ferrite in this material and most likely due to galvanic differences between the ferritic and austenitic phases in the strong acid solution. However, this mode of attack was found to occur only in cases of specific acids and inhibitors sometimes in either 22 Cr or 25 Cr materials and sometimes in both.

The Stage 2 and 3 acidizing sequences related to conditions that may exist in oil field operations resulting from spent (reacted) and/or diluted acidizing fluids being in contact with CRA materials for prolonged periods following the actual acidizing procedure. The results of the present study indicate that SCC is the greatest corrosion related concern in spent acidizing fluids. Under these conditions, the acid strength may be reduced from reaction with formation rock or by dilution with formation water. However, it is also most likely that inhibitors will be less effective than they are in the original acidizing mixture. Such conditions would be ideal for SCC particularly at higher temperatures.

Due to the specific nature of the compatibility of CRA materials and acidizing chemicals it appears important to review the actual contents of various acidizing fluids. They may contain specific chemicals which could have a profound effect on corrosion and SCC performance. Acidizing fluid packages can contain a variety of inhibitors, inhibitor enhancers, surfactants, co-solvents, and iron control agents that may have effects that cannot be predicted beforehand.[4] This review may or may not be directly useful since the effects of many of these chemicals on CRA corrosion and SCC is not well established. It is therefore recommended that for critical applications, the specific acidizing fluids and alloys which are being considered for use be evaluated for corrosion and SCC under conditions similar to those anticipated in the field.

CONCLUSIONS

Based on the results of the program presented herein, the following conclusions were made:

1. Oil field acidizing formulations can be aggressive to CRA materials used for tubulars, valve components and trim. Severe weight loss corrosion, localized corrosion, and SCC may occur.
2. The behavior of CRA materials in inhibited acids is very specific to alloy composition, acidizing fluid composition, and environmental conditions.
3. The most prevalent mode of attack on CRA materials in the concentrated acid and inhibitor is general corrosion. Specific cases of localized corrosion, selective phase attack, and SCC can also occur. The duplex stainless steels are particularly prone to selective attack of the ferrite phase in the material in acidizing fluids.
4. The most prevalent mode of corrosive attack on CRA materials in the spent acidizing fluids is SCC particularly at higher temperatures.

ACKNOWLEDGMENTS

The author would like to extend his appreciation to the multiclient sponsor group consisting of 15 members from oil companies, equipment manufacturers, materials and inhibitor suppliers who supported this program. In addition, thanks are in order to the engineering, technical, and administrative staff of Cortest Laboratories for their collaboration and technical assistance. Special acknowledgment is also given to Ms. Delia Cuellar for her technical contribution to this study in both developing and conducting the acidizing test procedures described herein.

REFERENCES

1. R. Jasinski, W. Frenier, S. Grannan, "Inhibiting HCl Corrosion of High Chrome Tubular Steels," CORROSION/88, paper no. 188 (Houston, TX: NACE, 1988).
2. M. Walker, T.H. McCoy, "Effect and Inhibition of Stimulation Acids on Corrosion Resistant Alloys," CORROSION/86, paper no. 154 (Houston, TX: NACE, 1986).
3. B. Vincentine, et. al., "Corrosion Behavior of High Alloy Tubular Materials in Inhibited Acidizing Conditions," CORROSION/87, paper no. 43 (Houston, TX: NACE, 1987).
4. P.A. Burke, et. al., "Corrosion of Chromium Steels in Inhibited Acids," CORROSION/87, paper no. 41 (Houston. TX: NACE, 1987).
5. M. Walker, T.H. McCoy, "Inhibition of High Alloy Tubulars II: Effect of Fluoride Ion and Acid Strength," CORROSION/88, paper no. 189 (Houston, TX: NACE, 1988).

TABLE 1

Materials Included in Acidizing Tests

Stainless Steels			Nominal Yield Strength (ksi)
Martensitic	(13 Cr)	13 Cr - Fe	85
Duplex	(22 Cr)	22 Cr - 5.5 Ni - 3 Mo - Fe	125
	(25 Cr)	25 Cr - 7 Ni - 1.5 Mo - Fe	134
Austenitic	(S-28)	28 Cr - 32 Ni - 3 Mo - Fe	135
Nickel Alloys			
Cold Worked	(42 Ni)	42 Ni - 22 Cr - 3 Mo	123
	(52 Ni)	52 Ni - 22 Cr - 6 Mo	142
	(C-276)	Bal Ni - 16 Cr - 15 Mo	154
	(Allcorr)	Bal Ni - 30 Cr - 10 Mo	152
Precipitation Hardened	(Inconel 718)	55 Ni - 22 Cr - 2 Mo - Ti - Al - Cb - Fe	130
	(Incoloy 925)	42 Ni - 22 Cr - 3 Mo - Ti - Al - Fe	106

FIGURE 1

Results of Corrosion Tests with 15% HCl + Inhibitor 1

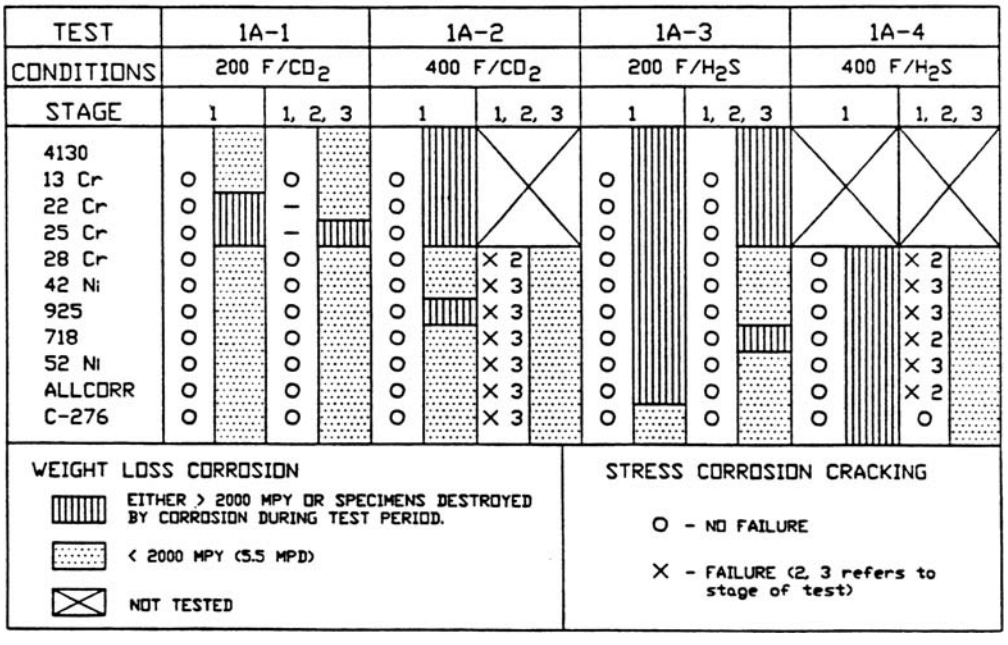


FIGURE 2

Results of Corrosion Tests with 15% HCl + Inhibitor 2

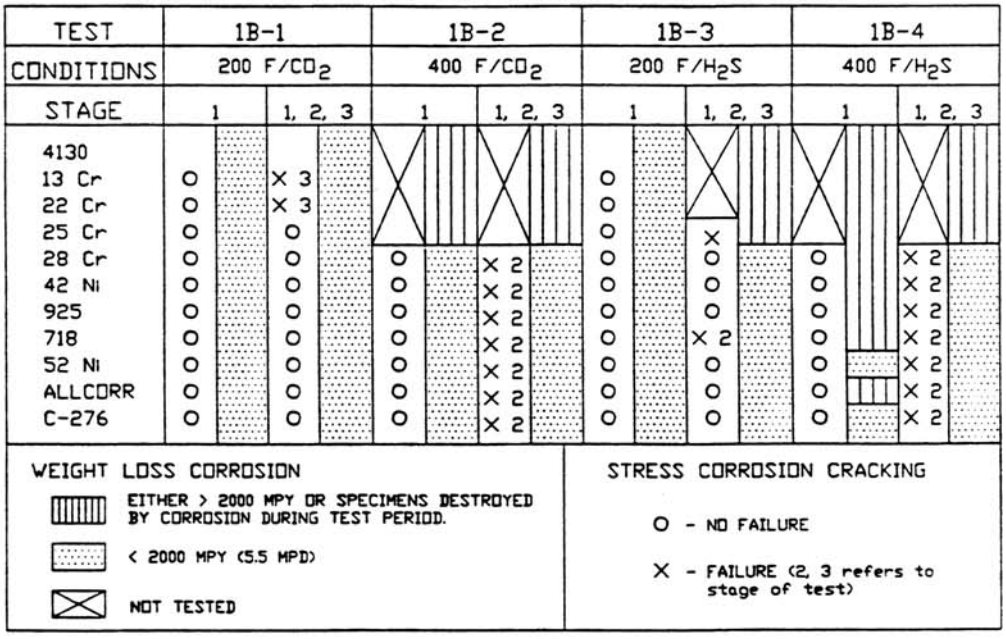


FIGURE 3

Results of Corrosion Tests with 28% HCl + Inhibitor 1

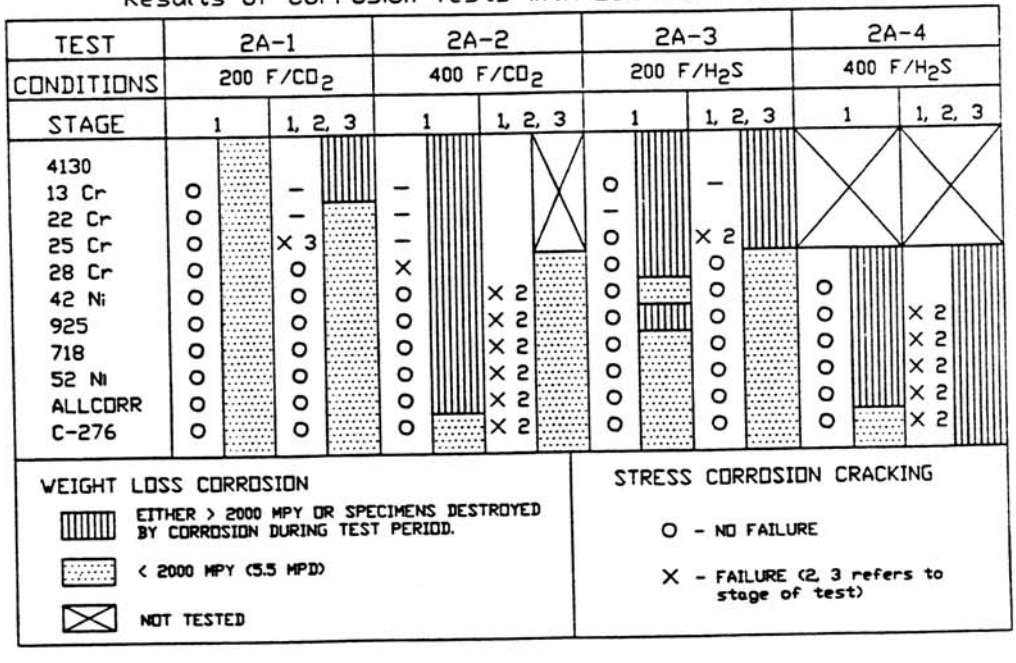


FIGURE 4

Results of Corrosion Tests with 28% HCl + Inhibitor 2

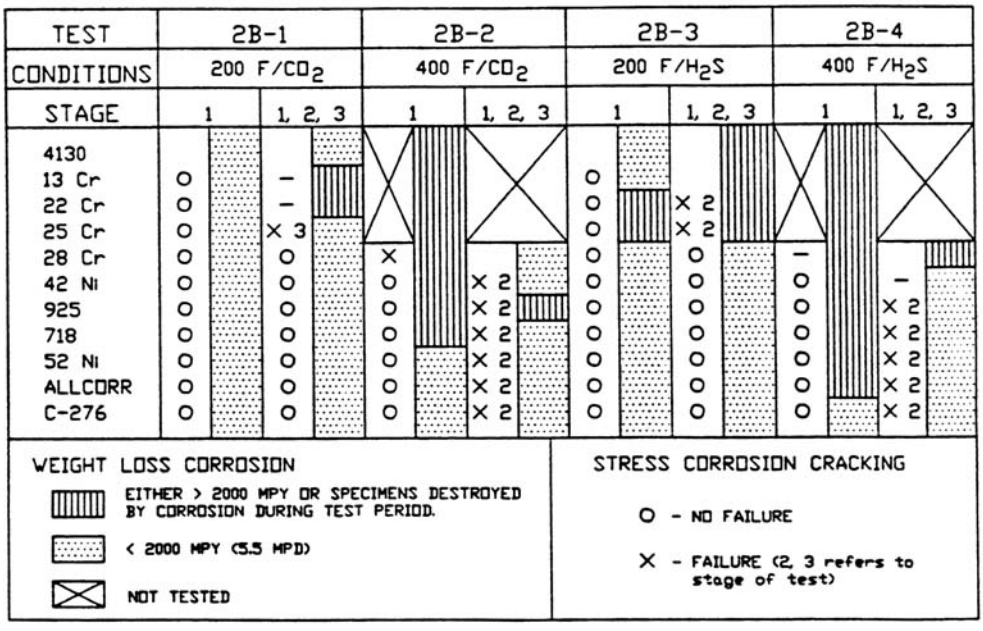


FIGURE 5

Results of Corrosion Tests with 12% Formic Acid + Inhibitor 3 or 4

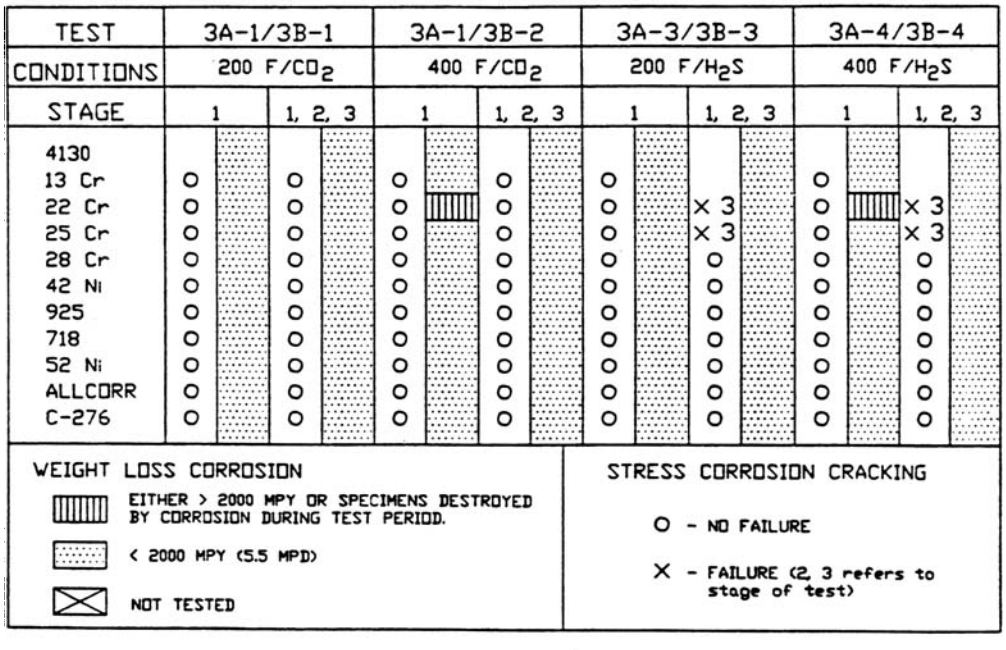


FIGURE 6

Results of Corrosion Tests with 13% HCl + 2% HF + Inhibitor 1

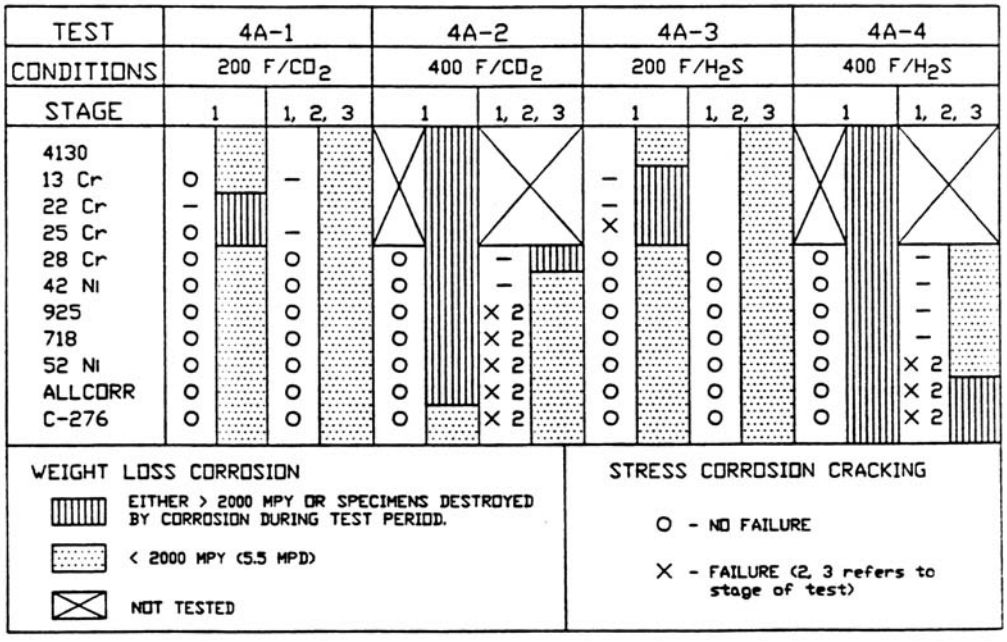
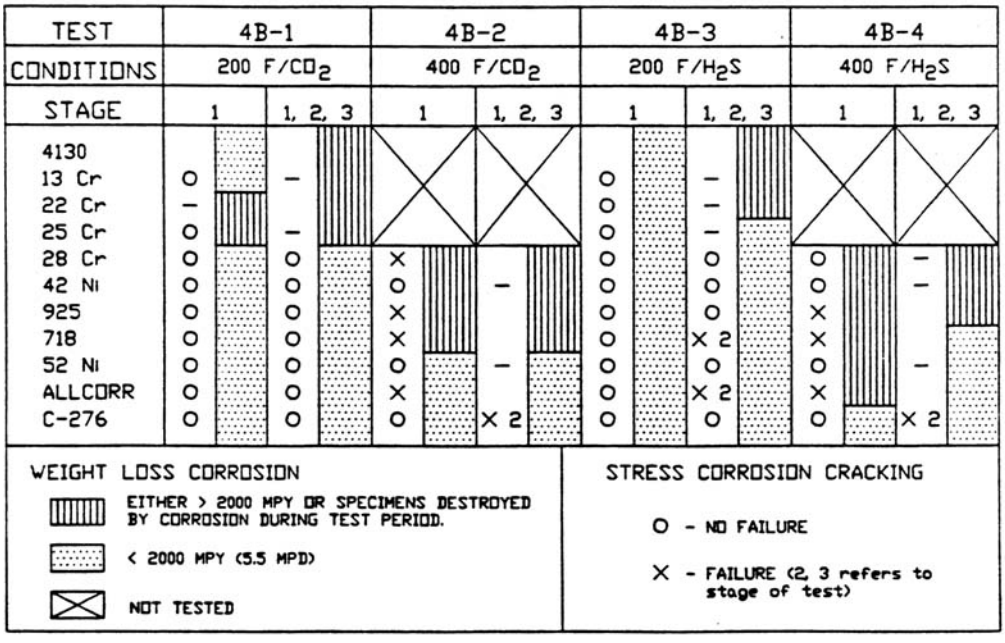


FIGURE 7

Results of Corrosion Tests with 13% HCl + 2% HF + Inhibitor 2



APPENDIX I

TABLE I-1

Exposure Sequence for 15 Percent HCl Tests

Environment 1 - Concentrated Acid + Inhibitor*

Acid - 15% HCl
Inhibitor - 0.6 to 3.0%
Duration - 6 hours

Environment 2 - Spent Acid + Inhibitor

Acid - 15% HCl
Inhibitor - 0.6 to 3.0%
Reactant - 16.5 g/100 ml $CaCO_3$
Duration - 6 days

Environment 3 - Dilute/Spent Acid + No Inhibitor

Acid - 1.5% HCl
Inhibitor - None
Reactant - 1.65 g/100 ml $CaCO_3$
Duration - 7 days

*Inhibitor 1 and 2; 0.6% at 200 F, 3.0% at 400 F

TABLE I-2

Exposure Sequence for 28% HCl Tests

Environment 1 - Concentrated Acid + Inhibitor*

Acid - 28% HCl
Inhibitor - 1.2 to 6.0%
Duration - 6 hours

Environment 2 - Spent Acid + Inhibitor

Acid - 28% HCl
Inhibitor - 1.2 to 6.0%
Reactant - 33.0 g/100 ml $CaCO_3$
Duration - 6 days

Environment 3 - Dilute/Spent Acid + No Inhibitor

Acid - 2.8% HCl
Inhibitor - None
Reactant - 3.3 g/100 ml $CaCO_3$
Duration - 7 days

*Inhibitor 1 and 2; 1.2% at 200 F, 6.0% at 400 F

TABLE I-3

Exposure Sequence for Formic Acid

Environment 1 - Concentrated Acid + Inhibitor*

Acid - 12% Formic
Inhibitor - 0.6 to 3.0%
Duration - 6 hours

Environment 2 - Spent Acid + Inhibitor

Acid - 12% Formic
Inhibitor - 0.6 to 3.0%
Reactant - 33.5 g/l $CaCO_3$
Duration - 6 days

Environment 3 - Dilute/Spent Acid + No Inhibitor

Acid - 1.2% Formic in 5% NaCl brine
Inhibitor - None
Reactant - 3.3 g/l $CaCO_3$
Duration - 7 days

*Inhibitor 3 and 4; 0.6% at 200 F, 3.0% at 400 F

TABLE I-4

Exposure Sequence for HCl/HF Tests

Environment 1 - Concentrated Acid + Inhibitor*

Acid - 13% HCl + 2% HF
Inhibitor - 0.6 to 3.0%
Duration - 6 hours

Environment 2 - Spent Acid + Inhibitor

Acid - 13% HCl + 2% HF
Inhibitor - 0.6 to 3.0%
Reactant - 30 g/l Silica Flour + 30 g/l Bentonite
Duration - 6 days

Environment 3 - Dilute/Spent Acid + No Inhibitor

Acid - 1.3% HCl + 0.2% HF
Inhibitor - None
Reactant - 30 g/l Silica Flour + 30 g/l Bentonite
Duration - 7 days

*Inhibitor 1 and 2; 0.6% at 200 F; 3.0% at 400 F

Copyrighted Materials
Copyright © 1996 NACE International Retrieved from www.knovel.com

Paper no. 217 - CORROSION/84

CORROSION AND STRESS CORROSION CRACKING OF HIGH-PERFORMANCE ALLOYS IN SIMULATED ACIDIZING ENVIRONMENTS TO 175°C (350°F)

J. Kolts, S.M. Corey
Cabot Corporation
1020 West Park Avenue
Kokomo, Indiana 46901

ABSTRACT

Laboratory corrosion and stress corrosion cracking tests were performed on commercially produced 1020 carbon steel; HASTELLOY® alloys 535, G-3, C-276, and B-2; CABOT® alloy No. 825; and alloys 28 and 904L in simulated acidizing environments containing NaCl, HCl, HCOOH, HF, and/or $MgCl_2$. A commercial inhibitor provided excellent corrosion inhibition of the high-performance alloys at the boiling point and good inhibition in 15% HCl at 175°C (350°F). The use of high- performance alloys offers additional protection to corrosion over carbon steels in the acidizing environments. Non-HCl-containing acidizing environments were not nearly as corrosive as the HCl-containing environments. Stress corrosion cracking was observed in H_2S-containing environments in HASTELLOY alloy B-2 and in HF-containing environments in the low nickel- and molybdenum-containing austenitic alloys such as alloy 904L, alloy 28, and alloy 535. Otherwise, no stress corrosion cracking was observed in the other alloys in the 24-hour tests.

INTRODUCTION

As oil and gas wells are being produced from deeper depths, the downhole temperatures are increasing. The higher temperatures in combination with the presence of acid gases have made the use of corrosion-resistant alloys economically attractive. These wells may be stimulated by the injection of various combinations of acid. Since corrosion rates in acid are known to increase with increasing temperature, acid treatment of hot wells is much more severe from a corrosion standpoint than acid treatment of lower temperature wells encountered in more typical production. One of the major problems in acid treatment of deep wells over 120°C (250°F) or 147°C (300°F) is corrosion.

The available HCl inhibitors lose their effectiveness on steels, and the less aggressive organic acids are used where possible when such conditions are encountered.[1] Often, cool down techniques or inhibitor intensifier additives can be effectively used to reduce corrosion of steel during acidizing extremely hot wells.[2,3] Possibly, acid-in-oil emulsions may be effective.[4]

Inhibitors have been developed for steels and their effectiveness on corrosion-resistant alloys is not known. Also, acids are known to accelerate stress corrosion cracking in the austenitic corrosion-resistant alloys. While the acids during well stimulation may be in contact with the corrosion-resistant alloys for only a short time, the stress corrosion cracking resistance of the alloys in the presence of acids needs to be considered. This investigation has utilized laboratory autoclave tests to measure corrosion and stress corrosion cracking behavior of a number of selected austenitic high-performance alloys in simulated downhole acidizing environments. Both the influence of HCl acidizing inhibitors and acid gases have been evaluated.

MATERIALS AND EXPERIMENTAL PROCEDURE

The alloys used in this investigation were commercially produced, high performance, corrosion-resistant alloys intended for deep sour gas applications. Normalized 1020 steel was included so that a relative comparison between steel and high-performance alloys could be made.

Corrosion rates were determined either in glass flasks for boiling solutions or in TEFLON®-lined

HASTELLOY and CABOT are registered trademarks of Cabot Corp.
TEFLON is a registered trademark of E.I. duPont de Nemours Co.

HASTELLOY alloy C-276 autoclaves. All specimens were isolated from galvanic contact with other samples by hanging them in glass boats in the autoclaves. Two-point beam samples as described previously were utilized to assess the susceptibility to stress corrosion cracking.[5]

Reagent grade chemicals were used in preparing the electrolytes. Proprietary HCl inhibitors were utilized to study the effects of inhibition. Four commercially available acidizing inhibitors from different suppliers were screened and the best inhibitor was chosen for the evaluations of alloys and environments. The selected inhibitor was Tretolite inhibitor AK12. The inhibitors were added to concentrated HCl, which was diluted as required. Autoclave solutions were deaerated with consecutive evacuations and purging with nitrogen. Acid gases were purged through the environments prior to pressurizing the system to 75 psig at room temperature. After pressurizing, the autoclaves were heated to the exposure temperature. After a 24-hour exposure, samples were brushed and ringed in distilled water prior to weighing. HCl concentrations to 15% with or without HF are common to any acidizing fluids, so this concentration was selected to simulate an HCl-acidizing fluid.[6-9] Higher concentrations of HCl have been used as acidizing solutions, but were not investigated in this work.[10,11]

RESULTS AND DISCUSSION

Corrosion Behavior

Corrosion engineers typically report metal loss rates in mils per year (or mm/y), while inhibitors are often evaluated as percent inhibitor efficiency. Table 1 presents the corrosion rates and percent inhibition of steel in a number of different environments for inhibited and uninhibited acids. In boiling environments, the inhibitor provides excellent inhibition to steel with inhibitor efficiencies often being above 99%. Both formic acid and especially H_2S have an effect on the inhibitor efficiency. The corrosion rate of steel in HCl without inhibitors does not seem to be greatly affected by the presence of H_2S, however, the corrosion rate increases by roughly a factor of 7 in inhibited boiling solutions by the addition of H_2S. In the last case, the inhibitor efficiency is still 98%.

The literature reports corrosion rates exceeding 0.01 lbs/ft^2 hr (2,000 mpy) for carbon steels in inhibited HCl up to about 2% inhibitor at 120°C (250°F). These are considered acceptable during acidizing because of the short period of time that acid is expected to contact the tubing during such treatments.[3]

In contrast to the excellent inhibition provided to steel, the HCl acid inhibitor tested is not particularly effective for the duplex stainless steel. Corrosion rates in excess of 8,000 mpy may be encountered in inhibited boiling HCl-containing environments. Care should be exercised in selecting and controlling acidizing environments when utilizing duplex stainless steels.

The high-performance alloys exhibit excellent corrosion resistance in boiling acidizing environments, often without inhibitor additions. The corrosion rate of HASTELLOY alloy G-3 in the boiling uninhibited HCl-containing environments listed in Table 2 is approximately 500 mpy. The addition of even 0.1 volume percent inhibitor reduces this rate to a negligible value in the boiling solutions. Thus the high-performance alloys offer an advantage over steel in providing an extra margin of safety during acidizing.

Since the high-performance alloys are intended for high-temperature service, the boiling solutions do not represent sufficiently severe conditions, and autoclave tests were required to assess their corrosion resistance in acidizing environments. Because of the high corrosion rates of the duplex stainless steel in boiling HCl-containing environments, the duplex stainless steel was deleted from tests at the higher temperature autoclave environments.

Steel corrosion inhibitors are effective in inhibiting nickel-base alloys in HCl at elevated temperatures. Table 3 presents the corrosion behavior of a number of alloys in the inhibited and uninhibited HCl solutions. In the uninhibited acid, the alloy 535, 825, and G-3 samples were essentially dissolved so that the corrosion rate values reported in the table represent minimum values. Additions of even 0.1 volume percent inhibitor decreases the corrosion rate to values that are considered acceptable for steel. Additions of even higher concentrations of inhibitor (2%) further decrease the corrosion rates. All of the nickel-base alloys do not exhibit identical performances in HCl, as would be expected. Increasing the molybdenum content of the alloy results in increasing resistance to corrosion by HCl-acidizing environments both in the inhibited as well as uninhibited environments.[12] The conditions were much too severe for carbon steel since all steel samples dissolved in both inhibited or uninhibited 175°C (350°F) HCl-containing environments. Thus the advantages of using high performance alloys over carbon steels are retained to the higher temperatures.

The presence of H_2S in acidizing fluids containing HCl adversely affects the corrosion performance of al-

loys. Table 4 presents the corrosion rates of alloys in HCl-containing environments with the autoclaves filled at 75 psig with N_2, CO_2, 90% CO_2 + 10% H_2S, or H_2S. While the dissolution rates with N_2 or CO_2 are quite similar, those solutions containing H_2S may be an order of magnitude more aggressive. Sulfide ions are known to be good cathodic poisons in acid environments. Perhaps the inhibitors are even better cathodic poisons and the competitive adsorption of sulfide ions results in a net decrease in inhibitor efficiency in the presence of H_2S. No experiments were conducted to test the hypothesis.

The other acid or salt additions appeared to be secondary in influence on corrosivity in comparison to HCl. The presence of formic acid may slightly accelerate corrosion in HCl acid solutions, but the corrosion behavior was controlled by the presence of HCl rather than the formic acid. Corrosion in HCl solutions and in simulated spent acidizing liquors was small in comparison to HCl as can be seen in Table 5. In the HF solution, no systematic inhibition of corrosion was noted, nor was it needed since the rates were quite low.

Stress Corrosion Cracking Behavior

Stress corrosion cracking behavior in 24 hours on plastically deformed samples was measured both in boiling solutions and at 175°C (350°F). No stress corrosion cracking was observed in any of the alloys or solutions at the boiling points as shown in Table 6.

AT 175°C (350°F) (Table 7), stress corrosion cracking occurred in two of the alloy systems. In the HASTELLOY alloy B-2, stress corrosion cracking was observed only in the presence of H_2S and occurred in both HCl, HCl + formic, and HF solutions. In the absence of H_2S, no cracking occurred in any of the environments. The latter behavior is consistent with previous work which shows that HASTELLOY alloy B-2 is the most resistant alloy of this group to stress corrosion cracking in chloride-containing environments in the absence of H_2S.[13]

Of the chromium-, molybdenum-, nickel-, and iron-containing alloys, the low nickel- and molybdenum-containing alloys such as 904L, 28, and 535 exhibited stress corrosion cracking in the HF environment at 175°C (350°F). This does not mean that these alloys would necessarily exhibit stress corrosion cracking in actual downhole service during acidizing. The test specimens used in this study are especially severe since the samples are stressed beyond their yield point. Consequently these laboratory tests represent extreme conditions. All of the other alloys tested exhibited better stress corrosion cracking resistance. Other than the previously mentioned incidences, no stress corrosion cracking was noted. Consequently, the higher alloyed alloys such as 825, G-3, or C-276 offer advantages over the 36% nickel-containing alloys in improved stress corrosion cracking resistance during acid treatments.

Additional tests on alloys 535, 825, G-3, and C-276 were performed in uninhibited HCl, $MgCl_2$, and $MgCl_2$ + $MgCO_3$ environments pressurized with N_2 under conditions similar to those listed in Table 7. No stress corrosion cracking was noticed in these uninhibited chloride-containing environments in the 24-hour tests.

CONCLUSIONS

1. The high-performance alloys offer advantages over carbon steels by providing improved corrosion resistance in acidizing environments at especially high temperatures.
2. Corrosion inhibitors which provide insufficient inhibition to carbon steels at very high temperatures such as 175°C (350°F) still provide adequate inhibition to high-performance alloys.
3. 825 adversely affects acid inhibitor performance both on steels and nickel-base alloys.
4. HASTELLOY alloy B-2 exhibited the best corrosion resistance in inhibited HCl with HASTELLOY alloy C-276, HASTELLOY alloy G-3, alloy 825, HASTELLOY alloy 535, and steel exhibiting decreasing corrosion resistance in that order.
5. Stress corrosion cracking was not observed in most of the environments in short-time tests. Alloys 904L, 28, and 535 did exhibit stress corrosion cracking in HF-containing environments.
6. HASTELLOY alloy B-2 possesses excellent resistance to corrosion and stress corrosion cracking in HCl solutions except in the presence of H_2S where it exhibits stress corrosion cracking.
7. The inhibitor tested was more effective on steel than on duplex stainless steels.

REFERENCES

1. W. B. Bleakley, *Petroleum Engineer International* 4(1982), p. 32.

2. C.F. Smith, C.W. Crowe, D.R. Wieland, SPE Paper # 3008 (New York, NY: AIME, 1920).
3. R.A. Woodroof, Jr., R.J. Baker, R.A. Jenkins, Jr., SPE Paper No. 5645 (New York, NY: AIME, 1975).
4. D.D. Knight, US Patent 3,353,603 (1967).
5. A.I. Asphahani, *Corrosion* 37 (1981), p. 329.
6. G.F. Ford, *J. of Petroleum Technology* 7(1981), p. 1,203.
7. A.W. Coulter, T.S. Claiborne, *Materials Protection* 6(1968), p. 23.
8. Anonymous, *Producers Monthly* 12(1956), p. 12.
9. G.R. Coulter, S.B. Purvis, *J. Petroleum Technology*, 6(1982), p. 1,211.
10. J.A. Knox, *Petrolium Review* 5(1972), p. 153.
11. A.R. Hendrickson, R.B. Rosene, E.N. Alderman, *World Oil* 7(1972), p. 63.
12. J. Kolts, J.B.C. Wu, A.I. Asphahani, *Metals Progress* 9(1983).
13. J. Kolts, CORROSION/82, paper no. 241 (Houston, TX: NACE, 1982).

Copyrighted Materials
Copyright © 1996 NACE International Retrieved from www.knovel.com

Paper No.
92

CORROSION 95
The NACE International Annual Conference and Corrosion Show

CORROSION INHIBITION OF 13Cr, SUPER 13Cr, AND 15Cr STAINLESS STEELS IN HCl-HF ACIDIZING FLUIDS

Robert D. Mack
Koninklijke/Shell Laboratorium, Amsterdam
Shell Research b. v.
Badhuisweg 3
1031 CM Amsterdam
The Netherlands

ABSTRACT

Acidizing is frequently used as a method to stimulate the production of oil at the onset of production or in subsequent well workovers. For some formations, "mud acids" (e.g., HCl-HF solutions) are required. As these acid packages are quite corrosive to steels and corrosion resistant alloys (CRA's), corrosion inhibitors must be added to minimize the attack on the downhole components throughout the period of the well stimulation. This paper presents and discusses the results of a laboratory study of the corrosion inhibition of 13Cr, Super 13Cr, and 15Cr martensitic stainless steel exposed to half strength mud acid solutions (7½ wt.% HCl + 1½ wt.% HF) over the temperature range of 210°-250°F (99°-121°C). Several inhibitor packages were studied as additions to fresh and simulated spent acid packages. The Super 13Cr and 15Cr stainless steels were more difficult to protect against localized attack than the straight 13Cr, but it was demonstrated that these steels can be successfully protected from excessive general corrosion and pitting during their exposure during formation stimulation.

Keywords: Acidizing, martensitic stainless steel, 13Cr, Super 13Cr, 15Cr, production tubing, mud acid, HCl, HF, inhibition, well, oil, corrosion resistant alloy, CRA, active, passive, passivity, corrosion, localized corrosion, pitting, spent acid.

INTRODUCTION

A 13Cr and its newer variations, e.g., the so-called "Super" 13Cr and 15Cr martensitic stainless steels, were candidates for the production tubing for several hydrocarbon reservoirs for which it appeared necessary to use 7½ wt.% HCl + 1½ wt.% HF as the acidizing fluid to stimulate the formations. The maximum anticipated bottomhole temperature was 225°F (107°C). As such acid packages are quite corrosive to steels and corrosion resistant alloys (CRA's), corrosion inhibitors must be added to minimize the attack on the downhole components throughout the period of the well stimulation. This paper presents and discusses the results of a laboratory study of the corrosion inhibition of 13Cr, Super 13Cr, and 15Cr martensitic stainless steel exposed to half strength mud acid solutions (7½ wt.% HCl + 1½ wt.% HF) over the temperature range of 210°-250°F (99°-121°C).

EXPERIMENTAL DETAILS

Materials

Several heats of the martensitic stainless steels 13Cr (AISI 420; API L-80 grade), two versions of the Super 13Cr (13Cr-5Ni-2Mo, and 13Cr-4Ni-1Mo), and a 15Cr (15Cr-1.5Ni-0.5Mo) were obtained from four different vendors in production tubing form. Flat corrosion coupons were machined from these heat treated products. The compositions, mechanical properties, and heat treatment are listed in Table 1.

Corrosion inhibitor packages from several vendors were obtained for evaluation. Each of these packages was designed for use in acidizing. These inhibitor chemical packages are described in Table 2.

In one experiment, a simulated "spent" acid, i.e., after exposure to the formation and produced back through the tubing, was used as the exposure medium. The acid package was "spent" in the laboratory by exposure to a mixture of finely divided minerals that was intended to simulate the formation in question. The mixture was composed of the following minerals and in the following proportions, by weight percent.

Wt.%	Mineral	Chemical Formula	
60%	Quartz	SiO_2	
10%	Albite	$NaAlSi_3O_8$	plagioclase feldspar
9%	Illite	$(K_2O)_2)(Mg,Fe)_3[(Al,Fe)_2O_3]_{0.8}(SiO_2)_{24}(H_2O)_{12}$]	a mica
9%	Montmorillonite	$(½Ca,Na)_{0.7}(Al,Mg,Fe)_4[(Si,Al)_8O_20](OH)_4 \cdot nH_2O$	
6%	Chert	SiO_2	
3%	Pyrite	FeS_2	
2%	Biotite	$K(Mg,Fe)_3AlSi_3O_{10}(OH)_2$	a mica
1%	Calcite	$CaCO_3$	

Experimental Procedures

All of the tests were performed on corrosion of the stainless steel coupons by exposing them to fresh solutions of 7½ wt.% HCl + 1½% wt. HF, which simulated the acidizing fluid of interest, i.e., a half strength mud acid. The 1½ wt.% HF was accomplished by the addition of an appropriate amount of NH_4HF_2 (ammonium bifluoride).

The exposures were conducted inside Alloy C-276 autoclaves. In all cases the specimens were isolated from the C-276 autoclave by hanging them from a quartz "tree"; this prevented deleterious galvanic effects from the autoclave. (Attack of the quartz in these HF systems was minimal.) The solution was not permitted to contact the autoclave, as the tree was placed inside a glass (borosilicate) liner in the autoclave. The liner was very important for these tests, because it was discovered in earlier tests that one of the inhibitors preferentially adheres to and protects austenitic alloys such as Alloys C-276 and 718, and the austenite phase in duplex stainless steels (preferentially adsorbs to face centered cubic structures). Without such isolation, the inhibitor could have been "consumed" by the autoclave, thereby lowering its concentration in the fluid and concomitantly lowering its effectiveness in the protection of the stainless steel corrosion specimens.

Some solutions were covered with kerosene (to simulate the presence of a hydrocarbon phase); others were not. The purpose of this was to study the effect of the presence of a hydrocarbon liquid.. A cover gas of N_2 was added to slow the loss of fluid to the vapor; the total pressure was a variable (from 15 to 2300 psi). In all cases the air from the vapor space in the autoclave was removed at room temperature prior to the test, though the fluid was not further deaerated.

For the simulated spent acid tests, the mixture of eight "formation" minerals (i.e., the silica, illite, montmorillonite, pyrite, etc.) was added to the glass liner of a 1-liter autoclave after which was added the acidizing package (acids + inhibitor package). The autoclave was closed, evacuated, then back-filled with nitrogen to 15 psia. The autoclave was heated to 225°F (107°C) for 40 hours. The "spent" acid was removed from the autoclave and then immediately used for exposure to the CRA's in another autoclave.

Test times varied from 3.0 to 17.5 hours. Base line (without inhibitor present) tests were conducted at room temperature, 210°F (99°C), and 225°F (107°C). Corrosion inhibitor additions were studied at temperatures from 210° to 250°F (99° to 121°C).

At the conclusion of each test, each specimen was examined for signs of localized corrosion, then re-weighed to determine the general weight loss corrosion rate. In some cases, the specimens were "lightly" bead blasted (glass beads) to remove the residue of the corrosion inhibitor; this gave a more accurate corrosion rate.

The experimental conditions for each test are summarized in Table 3.

RESULTS

The results are summarized in Table 3. Corrosion rates less than 1000 mpy are highlighted by bold borders in the table. The corrosion rate of each specimen exposed during each test is listed, therefore more than one value may be found within a single entry box in the table.

Pitting occurred on several of the specimens. In general the pits were small (less than 5 mils (0.1 mm) in diameter with the same depth.

With or without inhibitor package additions, the corrosion rates results were generally consistent within a given steel/corrosive system.

No effect of the addition of kerosene was observed.

DISCUSSION OF RESULTS

Inhibitor packages B and F were not effective corrosion inhibitors for 13Cr and the Super 13Cr exposed to 7½% HCl + 1½% HF acidizing fluids in the inhibitor concentrations and temperatures studied; general corrosion rates were reduced by only a factor of 2 to 4. Inhibitor B was designed for formic acid systems (not recommended by the supplier for the system studied) and was totally ineffective for the low pH halide system studied; this illustrates the importance of properly designed inhibitor packages. The specimens exposed in the Inhibitor B tests experienced very high general corrosion rates as well as large areas of "localized" attack (too large to be called pits).

The addition of kerosene in some of the tests did not seem to affect the results of the test significantly. No effect of N_2 pressure was observed, though not enough tests were conducted to reveal a small effect.

If one adopts an acceptance criteria of 1000 mpy for a 24 hour exposure during an acidizing treatment, then there are several inhibitor packages that were effective for the materials studied. At temperatures up to 225°F (107°C), Inhibitor packages A, C+D (see Table 3), and E+G, can be added in sufficient concentrations to protect 13Cr, the two versions of Super 13Cr, and the 15Cr studied without localized attack. These are highlighted in Table 3.

The Super 13Cr and 15Cr stainless steels were more difficult to inhibit than the 13Cr stainlesses in the HCl/HF system studied. The reason for this is most likely that these alloys are passive over a wider range of pH than the standard 13Cr (AISI 420).

The spent fluid test results showed a large number of very small pits. This is likely a result of a transition in the 13Cr and the Super 13Cr from general corrosion in the fresh solution (in which it would be not passive, though protected by adsorption by the inhibitor) to that of marginal passivity in the spent (higher pH) acid.

The corrosion inhibition of steels and stainless steels in acid solutions has been widely studied and many of these studies are specific to acidizing environments such as the HCl/HF system studied here [1-24]. Aliphatic alcohols, diols, and triols, and acetylenic alcohols, such as propargyl alcohol, have been reported in the literature as effective components in corrosion inhibitors for steels and stainless steels in acid media [1-4]. As noted in Table 2, such components are found in many of the inhibitor packages. In addition, inorganic salts, such as iodides and other halides [6, 14, 15] are also prominent additions in these packages. The inhibitors found to be effective in this study had one or more of these components in the package studied.

SUMMARY AND CONCLUSIONS

The results show that the corrosion of the five versions of a 13Cr (AISI 420), the two versions of the new alloys Super 13Cr, and the one of 15Cr martensitic stainless steels can be inhibited to levels less than 1000 mpy at temperatures as high as 225°F in fresh 7½ wt.% HCl + 1½ wt.% HF acidizing fluid with inclusion of an appropriate inhibitor package.

Spent acid returns of the HCl/HF system studied can be more aggressive from the viewpoint of localized corrosion for these martensitic stainless steels than fresh acids, but the degree of attack may be considered to be acceptable. An appropriate increase of a suitable inhibitor package may prevent this; more work is required to confirm this.

The new stainless steels Super 13Cr (13Cr-5Ni-2Mo and 13Cr-4Ni-1Mo) and 15Cr (15Cr-1.5Ni-0.5Mo) are more difficult to inhibit than the standard 13Cr (AISI 420) stainless steels. It is proposed that the reason for this is that these newer alloys are passive over a wider range of pH in the HCl/HF system studied and are therefore more likely to experience localized attack in this system at the temperatures studied.

ACKNOWLEDGEMENTS

The author gratefully acknowledges Lonnie Wheaton (Westhollow Technology Center, Shell Development Company, Houston, Texas) who performed all of the experiments reported in this paper, the support of Shell Offshore, Inc., which funded the research, Shell Oil Company and Shell Research b. v. for permission to publish this work, and Peter Rhodes, Scott Lester, Lee Morgenthaler, and Harold Bross for helpful discussions during this study.

REFERENCES

[1] A. Cisek, "A Review of Corrosion Inhibitors Used In Acidizing", Paper No. 92, CORROSION/93, National Association of Corrosion Engineers, Houston, Tx., 1993.
[2] R. J. Tedeschi, "Acetylenic Corrosion Inhibitors", Corrosion, Vol. 31, No. 4, April, 1975, pp. 130-34.
[3] D. D. N. Singh and A. K. Dey, "Synergystic Effects of Inorganic and Organic Cations on Inhibitive Performance of Propargyl Alcohol on Steel Dissolution in Boiling Hydrochloric Acid Solution", Corrosion, Vol. 49, No. 7, July, 1993, pp. 594-600.
[4] K. N. Edwards, L. J. Nowacki, and E. R. Mueller, "Acetylenic Alcohol-Inhibited Pickling Bath As a Pretreatment Prior to Lining Steel Pipe", Corrosion, Vol. 15, No. 5, May, 1959, pp. 275t-78t.
[5] C. C. Seastrom, "Passivity of Chromium and Stainless Steel in Hydrofluoric Acid", Corrosion, Vol. 20, No. 6, June, 1964, pp. 179t-83t.
[6] K. F. Hager and M. Rosenthal, "Halides as Acid Pickling Inhibitors", Corrosion, Vol. 6, No. 10, October, 1950, pp. 344-46.
[7] S. Hettiararachchi, Y. W. Chan, R. B. Wilson Jr., and V. S. Agarwala, "Macrocyclic Corrosion Inhibitors for Steel in Acid Chloride Environments", Corrosion, Vol. 45, No. 1, 1989, pp. 30-34.
[8] F. B. Growcock, "Corrosion Kinetics of J55 Steel in Hydrochloric Acid Inhibited with Benzoyl Allyl Alcohol", Corrosion, Vol. 45, No. 5, May, 1989, pp. 393-401.

[9] F. B. Growcock and V. R. Lopp, "Film Formation on Steel in Cinnamaldehyde-Inhibited Hydrochloric Acid", Corrosion, Vol. 44, No. 4, April, 1988, pp. 248-54.
[10] W. W. Frenier, F. B. Growcock, and V. R. Lopp, "a-Alkenylphenones -- A New Class of Acid Corrosion Inhibitors", Corrosion, Vol. 44, No. 9, September, 1988, pp. 590-98.
[11] O. L. Riggs Jr., and R. L. Every, "Study of Organic Inhibitors for Hydrochloric Acid Attack on Iron", Corrosion, Vol. 18, No. 7, July, 1962, pp. 262t-69t.
[12] J. Vosta, J. Eliasek, and P. Knizek, "A Quantum-chemical Study of the Corrosion Inhibition of Iron by Means of Aniline Derivatives in Hydrochloric Acid", Corrosion, Vol. 32, No. 5, May, 1976, pp.183-87.
[13] W. E. Billings and D. Morris, "Effect of Acid Volume and Inhibitor Quantity on Corrosion of Steel Oil Field Tubing in Hydrochloric Acid", Corrosion, Vol. 17, No. 5, 1961, pp. 86-92 (208t-14t).
[14] Y. L. Huang, C. N. Cao, M. Lu, and H. C. Lin, "Inhibition of I^- and I_2 on Stress Corrosion Cracking of Stainless Steel in Acidic Chloride Solutions", Corrosion, Vol. 49, No. 8, August, 1993, pp. 644-49.
[15] K. S. Rajagopalan and G. Venkatachari, "Mechanism of Corrosion of Iron by Hydrochloric Acid and Its Inhibition by Iodide and Quinoline", Corrosion, Vol. 36, No. 6, June, 1980, pp. 320-21.
[16] S. T. Arab and E. A. Noor, "Inhibition of Acid Corrosion of Steel by Some S-Alkylisothiouronium Iodides", Corrosion, Vol. 49, No. 2, February, 1993, pp. 122-29.
[17] E. Stupnisek-Lisac, M. Metikos-Hukovic, D. Lencic, J. Vorkapic-Furac, and K. Berkovic, "Structural Investigation of N-Arylpyrroles as Iron Corrosion Inhibitors in Hydrochloric Acid" Corrosion, Vol. 48, No. 11, November, 1992, pp. 924-30.
[18] R. A. George and N. Hackerman, "Acid Corrosion Inhibition by High Molecular Weight Nitrogen-Containing Compounds", Corrosion, Vol. 11, No. 6, June, 1955, pp. 249t-54t.
[19] C. C. Nathan, "Studies on the Inhibition by Amines of the Corrosion of Iron by Solutions of High Acidity", Corrosion, Vol. 9, No. 6, June, 1953, pp. 199-202.
[20] J. Kolts and S. M. Corey, "Corrosion and Stress Corrosion Cracking of High-Performance Alloys in Simulated Acidizing Environments to 350°F", Paper No. 217, **CORROSION/84**, National Association of Corrosion Engineers, Houston, Tx., 1984.
[21] J. Kolts, "Effect of Selected Organic Corrosion Inhibitors on Performance of Corrosion Resistant Alloys", Paper No. 121, **CORROSION/93**, National Association of Corrosion Engineers, Houston, Tx., 1993.
[22] W. R. Coyle, G. B. Chitwood, P. W. Rice, and M. L. Walker, "Hydrogen Assisted Cracking in Inhibition of Spring Alloys in Acidizing Solutions", Paper No. 81, **CORROSION/94**, NACE International, Houston, Tx., 1994.
[23] K. R. Lancaster, J. M. Cassidy, and M. L. Walker, "Effect of HCl on the Repassivation of Some Chromium-Containing Alloys", Paper No. 94, CORROSION/93, National Association of Corrosion Engineers, Houston, Tx., 1993.
[24] A. I. Williamson and M. G. Hay, "Selection of CRA Tubing and HCl Corrosion Inhibitors for Burnt Timber/Limestone Wells', Paper No. 11, CORROSION/91, National Association of Corrosion Engineers, Houston, Tx., 1991.

Table 1: Compositions and Mechanical Properties of Materials Studied

Stainless Steel Designation **	Material Number (**)	As-Received Condition (***)	σ Yield (ksi)	σ Tensile (ksi)	El./g.l. (%./in.)	Hardness (HRC)	Composition, Elements by wt.%, (balance Fe)										
							C	*Cr*	*Ni*	*Mo*							
(I) AISI 420:																	
	7213	Aus&T	101.6	123.9	35.4	22.2-25.9	0.20	12.90	0.08	---	0.45	0.45	0.017	0.001			
	7214	Aus&T	90.0	112.4	43.3	20.0-23.1	"	"	"	"							
	7216	N&T	90.3	114.9	39.0	18.8-21.5	"	"	"	"	"	"	"	"		"	
	7212	Q&T	Mechanical properties and composition are not available; composition and heat treated to API grade L-80.														
	7340	Q&T	"				"				"			"		"	
(II) Super 13Cr's:																	
	7688	Q&T	102.0	125.0	36.0/2.0	25.5-25.9	0.02	11.95	5.50	2.08	0.45	0.18	0.019	0.001	0.022		0.005
	7785	Q&T	97.0	121.0			0.02	12.94	4.13	1.00	0.44	0.44	0.008	0.002			
(II) 15Cr:																	
	7868	Q&T	86.0	114.0			0.11	14.59	1.52	0.50	0.69	0.26	0.010	0.003			

* All materials were received in the form of production tubing.

** This designation is an internal materials identification number.

*** Aus&T = Ausformed, air cooled, and tempered.

Q&T = Quenched and tempered.

N&T = Normalized and tempered.

Table 2: Description of Inhibitor Packages Studied.

Inhibitor "Package"	*Function*	*Description Provided by Supplier*
A	Inhibitor	A proprietary blend of acetylenic alcohols, dispersants, quaternized heterocyclic amines, and inorganic salts.
B	Inhibitor	A reaction product of aromatic aliphatic ketone with short chained aldehydes and sulfur compounds blended in an alcohol based system.
C	Inhibitor	An organic mixture containing an aliphatic aldehyde, ethoxylated alcohol, amine salts, formic acid, and isopropyl alcohol.
D	Inhibitor Aid	Potassium iodide
E	Inhibitor	A proprietary blend of alcohols and a quaternary ammonium salt
F	Inhibitor	A proprietary blend of alcohols & complex substituted keto-amine(s)
G	Inhibitor Intensifier	A proprietary blend of an alcohol and inorganic halides

Table 3: Summary of Experimental Conditions and Results for 13Cr, Super 13Cr's, and 15Cr Martensitic Stainless Steels Exposed to 7½ wt.% HCl + 1½ wt.% HF Acidizing Solutions With and Without Corrosion Inhibitor Additions

Summary of the Experimental Conditions					General Corrosion Rates by Stainless Steel (mils/year)							
Inhibitor Additions					(I) AISI 420 (13Cr) *					(II) Super 13Cr *		(III) 15Cr *
Chemical Designation *(See Table 2)*	Amount Added (vol.%)	Nitrogen Cover Gas Pressure (psi)	Test Duration (hours)	Temp. (°F)	(7213)	(7214)	(7216)	(7212)	(7340)	(7688)	(7785)	(7868)
None	-	15	19.0	70					265			
None	-		4.0	225						28,000	22,000	16,000
None	-	650	16.5	210			14,500	13,800	12,300	12,400		
None	-	300	16.5	210	10,150							
A (spent acid)	1.5	25	4.0	225-270					315; 530; pits	500; 500; pits		
A	1.0	2000	4.0	230	890					3,100; pits		
A	1.5	2000	4.0	225	500					2,100		
A	2.0	1850	4.5	250				1,100		1,630		
A	3.0	2350	4.0	215	170					140		
A + kerosene	3.0	2000	4.5	215				130		110		
A	2.5	2000	4.3	225				130	125	800; 1300	180; 370	100; 300
A	3.0	2000	4.4	225						220; 430	110; 120	74; 103
B	3.0	15	16.0	212	4,300	4,200	3,950			14,700		
B + kerosene	3.0	270	17.5	210			1,650			14,900		
B	4.0	2200	4.5	215				3,800		19,700		
B + kerosene	4.0	2200	4.5	220	5,300					14,700		
2.0 vol% C + 1.2 wt.% D		1200	3.0	225	290		310			2,080		
3.0 vol% C + 1.1 wt.% D		2000	4.5	225			160	360	340	1340; 1900	830; 1000	670; 725; 895
E	2.0	1200	16.5	225		512; pits	700; pits			9,910; pits		
1.0% E + 1.0% G		1200	17.5	225	57				74	173		
1.0% E + 1.0% G		2000	4.0	225				33	57	125; 153	68; 101	118; 139
F	2.0	1200	16.5	225			1,830	3,780		9,410		

* *See Table 1.*

Copyrighted Materials
Copyright © 1996 NACE International Retrieved from www.knovel.com

Paper No.
88

CORROSION 94
The Annual Conference and Corrosion Show
Sponsored by NACE International

EFFECT OF ACIDIZING SOLUTIONS ON K_{IEAC} OF 13 Cr AND 22 Cr STAINLESS STEELS

T.H. McCoy, S.T. Mackey and M.L. Walker
Halliburton Energy Services
P.O. Box 1431
Duncan, OK 73536

ABSTRACT

Fracture mechanics environment-assisted cracking tests, using pre-cracked TM0177-90 double cantilever beam (DCB) specimens, were performed on 13 Cr (UNS S42000) martensitic stainless steel and 22 Cr (UNS S31803) duplex stainless steel in stimulation acidizing solutions to simulate downhole conditions. The acidizing solutions used were 15% HCl and 12% HCl-3% HF with proprietary inhibitors. The 13 Cr material was quenched and double tempered to meet the mechanical property requirements of API Spec 5CT Grade L-80. The 22 Cr material was grade 130 (130 ksi minimum yield strength) cold reduced tubing. This paper shows that the low strength 13 Cr material is not very susceptible to crack propagation in acidizing solutions. The high strength 22 Cr material, however, did show susceptibility to crack propagation in the same acidizing solutions while no cracking occurred in NACE TM0177-90 sour brine solution.

Keywords: fracture mechanics, fracture toughness, environment-assisted cracking, double cantilever beam, acidizing, hydrochloric acid, hydrofluoric acid, inhibitor

INTRODUCTION

Corrosion resistant alloys (CRA's) such as 13 Cr and 22 Cr stainless steel play an important role in producing hydrocarbon reservoirs that contain corrosive fluids. These stainless steel alloys are inherently suited to prevent corrosion damage from sweet gas (CO_2) environments. The martensitic 13 Cr has also proven to be suitable for minimal sour reservoirs. The 22 Cr duplex stainless steels are more corrosion resistant to H_2S environments due to their austenite and ferrite duplex microstructure. The presence of salts, such as chlorides, dissolved in the aqueous phase can intensify corrosive attack and 22 Cr has more overall resistance than 13 Cr due to its higher alloy content. At times, however, there may be a need to perform a chemical stimulation treatment on wells containing these materials by using acid solutions such as hydrochloric acid perhaps with or without a hydrofluoric acid addition. Of course, the acids are always inhibited to minimize corrosion on downhole tubing, casing, and other tools that the fluid may contact.

Most studies of acid corrosion only involve determination of weight loss values. Very little work has been done to quantify the cracking resistance of the 13 Cr and 22 Cr stainless steels when stressed and exposed to acidizing solutions. Many downhole materials are subjected to corrosive environments which may lead to weight loss corrosion as well as pitting corrosion. Pitting can serve as initiation sites for cracking. If cracks are present, crack propagation could occur under certain stress conditions when aided by the environment.

Heady[1] described a test procedure using double cantilever beams (DCB's) for quantifying the sulfide stress cracking resistance of metals using crack-arrest fracture mechanics concepts. To date, most of the work has been in H_2S test environments. The authors studied crack propagation of relatively high strength 4140 (UNS G41400) low alloy steel (34 HRC) and concluded that under some circumstances, crack propagation could occur in acidizing solutions even though weight loss corrosion was minimal[2]. High strength martensitic stainless steels can also fail by hydrogen embrittlement in acidic environments where acid is the source of hydrogen. It was not known how the low strength 13 Cr or the high strength 22 Cr duplex stainless steels would perform. Hence, it was decided that the crack propagation tendency of these materials should be investigated.

Environment-assisted cracking (EAC) is brittle fracture of a normally ductile material in which the corrosive effect of the environment is a contributing factor. K_{IEAC} can be obtained using crack-arrest fracture mechanics concepts. This value can be used to quantitatively compare the effects of various acidizing solutions on the

material in question. The DCB described by NACE Standard TM0177-90 was used to determine the effects of various acid-inhibitor solutions on the cracking resistance of 13 Cr (L-80) and high strength 22 Cr duplex stainless steel. The resulting value, K_{IEAC}, was then calculated per NACE TM0177-90.

EXPERIMENTAL PROCEDURE

Test Material

Commercial materials were obtained for testing. The 13 Cr was obtained in bar form, 7 in. (17.8 cm) diameter, that was quenched and double tempered to meet the mechanical property requirements of API Spec 5CT, grade L-80. The 22 Cr material used was coupling stock, 2.875 in. OD x 0.562 in. wall (7.30 cm OD x 1.43 cm wall) that was cold reduced to meet Grade 130 requirements. Chemical composition and mechanical properties of each alloy are shown in TABLES 1 and 2 respectively. Metallographic examination verified that the microstructure of the 13 Cr material consisted of tempered martensite, FIGURE 1, and the 22 Cr material consisted of ferrite and austenite, FIGURE 2.

Test Specimens

Specimens were machined per FIGURE 3 to yield an RL[1] orientation for the 13 Cr and CL[1] orientation for the 22 Cr material. All of the DCB's from the 13 Cr material were taken near the OD. All of the specimens were side grooved before fatigue precracking except DCB No's 2-1 through 2-4 and 3-1 through 3-4, which were precracked before machining the side grooves.

The fatigue precrack on all specimens was generated by cyclically loading to about 400 lb (1779 N) at the drilled holes with the dynamic tensile testing machine operating in displacement control. The loading frequency was 20 Hz. The precrack was allowed to grow until it reached a nominal length of 0.10 in. (2.5 mm) from the root of the EDM notch. Precracking was typically accomplished in 2 to 4 hours. The fatigue precrack procedure yielded some disparity in crack lengths, ranging from about 0.03 in. (0.8 mm) for DCB No. 2-18 to 0.20 in. (5 mm) for DCB no. 2-7. Most specimens, however, had a precrack length of about 0.10 in. (2.5 mm).

---

[1] Per ASTM E616-89.

Test Solutions

Commercially available field grade hydrochloric acid, 20°Be, was diluted with tap water to the desired concentration. The acid solutions were titrated in triplicate and were adjusted to within 0.1% of the concentrations stated. The 12% HCl-3% HF acid solutions were prepared by the addition of 4.8 grams of ammonium bifluoride to 100 mL of the titrated 15% HCl.

The corrosion inhibitors were commercially available materials used in oil field practices to reduce corrosion in HCl containing fluids. The low alloy inhibitor H-J is a proprietary blend of acetylenic alcohols, dispersants, quaternized heterocyclic amines and inorganic salts. The high alloy inhibitor WW-5 is an antimony containing compound that is fully described in the referenced patent.[3]

Corrosion Testing Procedure

All tests were conducted at either 100°F (38°C) for 336 hours or 300°F (149°C) for 6 hours. At the test temperature of 100°F (38°C), the specimens were immersed in 240 mL of inhibited acid in glass or plastic jars. The solutions were then allowed to stabilize at the test temperature by placing them in a water bath. For tests at 300°F (149°C), the specimens and the test fluids were placed in an autoclave manufactured from a Ni-Mo Alloy, UNS N10665. All test specimens were isolated from galvanic contact with the autoclave body by placing them in polytetrafluoroethylene (PTFE) cells. The autoclaves were filled with kerosene which acted as the heat transfer medium and served as a hydraulic fluid. Autoclave tests were performed at 600 psi (4.14 MPa). No precautions were taken to exclude oxygen, as oxygen cannot be excluded during an actual acidizing job.

After completion of the test, the specimens were removed from the acid, rinsed in water and rapidly air dried. The specimens were then analyzed for crack propagation.

K_{IEAC} Testing Procedure

Arm displacements of 0.035 in. (0.89 mm) and 0.050 in. (1.27 mm) were used for all tests. Using load values from load versus displacement curves and the NACE TM0177-90 equation shown below, initial K_I loading was calculated to be 40 ksi$\sqrt{in}$ (44 MPa$\sqrt{m}$) for arm displacements of 0.035 in. (0.89 mm). Initial loading for arm displacements of 0.050 in. (1.27 mm) was calculated to be 57 ksi$\sqrt{in}$ (63 MPa$\sqrt{m}$).

$$K_{IEAC} = \frac{Pa(2\sqrt{3} + 2.38\,\frac{h}{a})\,(\frac{B}{B_n})^{.577}}{Bh^{1.5}}$$

where:
P = Equilibrium (final) wedge load
a = Crack length
h = Height of each arm
B = Specimen thickness
B_n = Web thickness

FIGURE 4 demonstrates how the loading wedge was inserted prior to placement in the solutions. The DCB's were placed in the test solutions as soon as possible after wedge loading. After exposure to the solution, the lift-off load of the specimens was determined. The lift-off load is the load at the abrupt change in slope of the load versus displacement curve.

The DCBs were then chilled in liquid nitrogen and pulled apart so that crack length measurements could be made. The crack length was determined by measuring from the wedge loaded end of the specimen to the crack front. The crack front was measured at the side grooves, in the middle and half way between the side grooves and the middle. The side groove measurements were averaged and treated as one value and averaged with the other three measurements. Once the distance from the end to the crack front was established, 0.250 in. (6.35 mm) was subtracted to determine the distance from the crack front to the loading plane.

The precracking, lift-off load and the final separation of the DCBs were all accomplished on a computer/microprocessor controlled dynamic tensile testing machine with a 60 KIP (267 KN) capacity load frame.

RESULTS AND DISCUSSION

13 Cr Material

TABLE 3 presents the test data for the 13 Cr material. Test solutions are listed in TABLE 4. Only one 13 Cr specimen showed any crack propagation. This specimen (DCB No. 3-2) was in the 12% HCl-3% HF acid solution with 0.1% H-J inhibitor at 100°F (38°C) for 336 hours and K_{IEAC} was calculated to be 58 ksi$\sqrt{in}$. (64 MPa$\sqrt{m}$). The fracture surface of this specimen was examined using the scanning electron microscope (SEM) and the cracking was primarily intergranular as shown in FIGURE 5. Two 13 Cr DCB specimens were also tested in the NACE TM0177-90 sour brine solution and both specimens showed side cracking after conclusion

of the 30 day test, making the test result (K_{IEAC} value) invalid. The fracture surface morphology of the sample in the acid solution was very similar to the sample in sour brine (compare FIGURE 5 to FIGURE 6) indicating that the failures were due to hydrogen induced cracking. The 13 Cr DCB's in the NACE TM0177-90 solution were wedge loaded to an arm displacement of 0.035 in. (0.89 mm).

Overall, these results suggest that 13 Cr in the L-80 condition is not very susceptible to crack propagation in acidizing solutions. It is not known why one sample cracked but there are probably two primary factors. The first factor is that the DCB which cracked was in an acid solution which contained only 0.1% inhibitor and there may have been incomplete adsorption of the inhibitor at the crack tip. However, overall corrosion rate was low at about 2 mpy (0.05 mm/y). DCB's in acid solutions with higher concentrations of inhibitor did not exhibit crack propagation. The second factor may have been the presence of the fluoride ion since the sample that cracked was in the 12% HCl-3% HF acid solution. The fluoride ion tends to increase corrosive activity in general. None of the DCB specimens in 15% HCl showed any crack propagation.

For acid stimulation treatments, an arbitrary value of 0.05 lbs/ft^2 has been commonly accepted by the industry as the maximum acceptable corrosion weight loss for a particular exposure period. For the 6 hour and 336 hour test times used herein, this yields maximum acceptable corrosion rates of 1775 mpy (45 mm/y) and 32 mpy (0.8 mm/y), respectively. In can be seen then that weight loss corrosion data were acceptable in all acidizing solutions except for the tests conducted at 300°F (149°C) for 6 hours in acid solutions with 2.0% H-J inhibitor. Severe pitting corrosion, primarily at the stressed area, occurred in the 15% HCl acid solution and severe general corrosion occurred in the 12% HCl-3% HF acid solution. When 2% of inhibitor WW-5 was added, corrosion rates dropped to acceptable levels. FIGURE 7 compares DCB No. 3-16 which was tested in 15% HCl + 2% H-J inhibitor to DCB No. 3-17 that was tested in 15% HCl + 2% H-J + 2% WW-5 inhibitor. This demonstrates the effectiveness of the high alloy inhibitor, WW-5. No pitting corrosion was noted in the tests conducted at 100°F (38°C) even in the stressed areas.

22 Cr Material

As shown in TABLE 5, several of the 22 Cr DCB's exposed to the acidizing solutions showed crack propagation. All of the samples tested in the 12% HCl-3% HF acid solution at 100°F (38°C) exhibited crack propagation. Propagation occurred even though the concentration of the H-J inhibitor was increased from 0.1% to 1%. Crack extension during acid exposure was similar for samples in acid with 0.1%, 0.5% or 1.0%

inhibitor even though the apparent corrosive attack was much greater on the DCB specimens exposed to the acid solution with 0.1% inhibitor (see FIGURES 8 and 9). The average K_{IEAC} value increased (as the inhibitor concentration was increased) from 18 ksi$\sqrt{in}$ (20 MPa$\sqrt{m}$) to 36 ksi$\sqrt{in}$ (40 MPa$\sqrt{m}$); however, this increase in K_{IEAC} is not considered significant since the material is expected to have a plane strain fracture toughness, K_{IC}, value in excess of 200 ksi$\sqrt{in}$ (220 MPa$\sqrt{m}$).[4] (Note: K_{IC} is a basic material property that describes the resistance of a material to brittle fracture. A material with a K_{IC} of 200 ksi$\sqrt{in}$ would be considered a very crack resistant material.)

Only one DCB specimen was tested in the 15% HCl acid solution with 1.0% H-J inhibitor at 100°F (38°C). Crack propagation occurred and K_{IEAC} was 35 ksi$\sqrt{in}$ (38 MPa$\sqrt{m}$). This value is similar to K_{IEAC} values determined from tests in the 12% HCl-3% HF acid with 1.0% H-J inhibitor, showing that cracking is not dependent on the presence of HF.

At the higher test temperature of 300°F (149°C), mixed results occurred with respect to crack propagation. One of the two DCB's in the 12% HCl-3% HF acid solution showed crack propagation and K_{IEAC} was calculated to be 110 ksi$\sqrt{in}$ (121 MPa$\sqrt{m}$). This result occurred in the solution containing 2% H-J + 2% WW-5 inhibitor. No crack propagation occurred in the two DCB's exposed to this same acid solution with only 2% H-J inhibitor although corrosion rates were significantly higher. Similar results occurred in the 15% HCl solution although the crack propagation which occurred in DCB No. 2-17 was less than 0.100 in. (2.5 mm) and the K_{IEAC} value was therefore considered invalid as per NACE TM0177-90.

Two 22 Cr DCB specimens were also tested in the NACE TM0177-90 sour brine solution after wedge loading to 0.035 in. (0.89 mm) arm displacement. Neither of the samples exhibited any crack propagation after the 30 day test period.

Microstructural examination of a section along the crack path of DCB No. 2-11 suggested that crack propagation was occurring by anodic dissolution. FIGURE 10 attempts to show corrosion products proceeding like "fingers" along the ferrite-austenite interface. Preferential ferrite attack in the HCl and HCl-HF acid solutions has been well documented[5]. Accelerated corrosion activity would not be unexpected at the phase interfacial area as these are high energy sites due to structural mismatching (i.e., body centered cubic ferrite to face centered cubic austenite). In addition, it has been shown that the attack is driven by galvanic action between the anodic ferrite and the cathodic austenite in stimulation acids.[6]

The 22 Cr duplex stainless steel showed much higher corrosion rates

in the acidizing solutions as compared to the 13 Cr material, as can be seen by comparison of the data in TABLES 4 and 5. At the 100°F (38°C) test temperature, corrosion rates were above the acceptable limits in all cases except DCB No. 2-19 which was in 15% HCl with 1.0% H-J inhibitor. In the 12% HCl - 3% HF acid solution, corrosion rates dropped from around 400 mpy (10 mm/y) to 60 mpy (2 mm/y) as the inhibitor concentration increased from 0.1% to 1%. Unfortunately, this lowering of corrosion losses did not significantly inhibit crack propagation tendencies.

At the 300°F (149°C) test temperature, severe corrosion losses occurred in the acid solution containing 2% H-J inhibitor. However, corrosion losses decreased dramatically to acceptable levels when 2% WW-5 inhibitor was added to the solution (compare DCB's in FIGURES 11 and 12) although crack propagation occurred. All of the 22 Cr specimens visually displayed varying degrees of a "woody" structure after testing in the acid solutions, reflecting the preferential ferrite attack.

CONCLUSIONS

1. 13 Cr martensitic stainless steel heat treated to L-80 mechanical properties is not particularly susceptible to crack propagation in 15% HCl or 12% HCl-3% HF inhibited acid solutions.

2. 22 Cr, cold worked to meet grade 130 requirements, showed significant susceptibility to crack propagation in 12% HCl-3% HF and 15% HCl even when corrosion losses were minimized. Crack propagation occurred by anodic dissolution at the ferrite and austenite phase interface.

REFERENCES

[1] R.B. Heady: "Evaluation of Sulfide Corrosion Cracking Resistance in Low Alloy Steels," Corrosion 33, 7 (1977): pp. 98-107.

[2] T.H. McCoy, M.L. Walker, S.T. Mackey: "Effects of Acidizing Solutions on K_{1EAC} of 4140 Low Alloy Steel," CORROSION/93, paper no. 123, (Houston, TX: NACE, 1993).

[3] U.S. Patent No. 4,522,658.

[4] Private correspondence with H. Eriksson, Sandvik Steel Inc., Feb, 1993.

[5] M.L. Walker, T.H. McCoy: "Effect and Inhibition of Stimulation Acids on Corrosion Resistant Alloys," CORROSION/86, paper no. 217, (Houston, TX: NACE, 1986).

[6] Y. Yau, M.A. Steicher: "Galvanic Corrosion of Duplex-Fe-Cr-10% Ni Alloys in Reducing Acids," CORROSION/85, paper no. 228, (Houston, TX: NACE, 1985).

TABLE 1
CHEMICAL COMPOSITION

Element	13 Cr	22 Cr
Carbon	0.20%	0.009%
Manganese	0.54%	1.57%
Silicon	0.44%	0.37%
Sulfur	0.004%	0.001%
Phosphorus	0.017%	0.022%
Chromium	13.02%	22.00%
Molybdenum	0.03%	2.98%
Nickel	0.19%	5.50%
Copper	0.07%	--
Nitrogen	--	0.15%

TABLE 2
MECHANICAL PROPERTIES[1]

Property	13 Cr	22 Cr
Hardness (HRC)	18	31
Yield Strength, ksi (Mpa) (0.2% offset)	88.2 (608)	152.4 (1051)
Ultimate Tensile Strength, ksi (Mpa)	115.1 (794)	160.4 (1106)
Elongation (in 4D), %	20.0	13
Reduction of Area, %	62.0	--

[1] As per mill certification documentation.

TABLE 3
K_{IEAC} OF 13 Cr MATERIAL

DCB No.	Arm Displacement in	(mm)	K_{IEAC} ksi√in	(MPa√m)	Acid System[1]	Pitting (I,M,S)[3]	Corrosion Rate[2] mpy	(mm/y)
3-19	0.050	(1.270)	NCP[4]		a (0.1)	I	1	(0.03)
3-20	0.050	(1.270)	NCP[4]		a (0.1)	I	1	(0.03)
3-21	0.050	(1.270)	NCP[4]		a (0.5)	I	1	(0.03)
3-22	0.050	(1.270)	NCP[4]		a (0.5)	I	1	(0.03)
3-23	0.050	(1.270)	NCP[4]		a (1.0)	I	0.5	(0.01)
3-24	0.050	(1.270)	NCP[4]		a (1.0)	I	0.5	(0.01)
3-15	0.050	(1.270)	NCP[4]		a (2.0)	S/M[5]	8600	(220)
3-16	0.050	(1.270)	NCP[4]		a (2.0)	S/M[5]	11000	(280)
3-17	0.050	(1.270)	NCP[4]		a (2+2)	M/I[6]	220	(6)
3-18	0.050	(1.270)	NCP[4]		a (2+2)	M/I[6]	250	(6)
3-1	0.050	(1.270)	NCP[4]		b (0.1)	I	2	(0.05)
3-2	0.050	(1.270)	58	(64)	b (0.1)	I	2	(0.05)
3-3	0.035	(0.889)	NCP[4]		b (0.1)	I	11	(0.3)
3-4	0.035	(0.889)	NCP[4]		b (0.1)	I	10	(0.3)
3-13	0.035	(0.889)	NCP[4]		b (0.5)	I	7	(0.2)
3-14	0.035	(0.889)	NCP[4]		b (0.5)	I	7	(0.2)
3-11	0.035	(0.889)	NCP[4]		b (1.0)	I	7	(0.2)
3-12	0.035	(0.889)	NCP[4]		b (1.0)	I	6	(0.2)
3-9	0.035	(0.889)	NCP[4]		b (2.0)	I	12000	(300)
3-10	0.035	(0.889)	NCP[4]		b (2.0)	I	9100	(230)
3-7	0.035	(0.889)	NCP[4]		b (2+2)	M	1500	(38)
3-8	0.035	(0.889)	NCP[4]		b (2+2)	I	620	(16)

[1] See TABLE 4
[2] Values for comparison only as DCB's not fully immersed during testing
[3] I - insignificant, M - moderate, S - severe
[4] NCP - no crack propagation
[5] Pitting severe in stressed areas, moderate otherwise
[6] Pitting moderate in stressed areas, insignificant otherwise

TABLE 4
SUMMARY OF ACID SYSTEMS

Acid System	HCl %	HF %	H-J %	WW-5 %	Test Time hours	Test Temp °F (°C)
a (0.1)	15.0	0.0	0.1	0.0	336	100 (38)
a (0.5)	15.0	0.0	0.5	0.0	336	100 (38)
a (1.0)	15.0	0.0	1.0	0.0	336	100 (38)
a (2.0)	15.0	0.0	2.0	0.0	6	300 (149)
a (2+2)	15.0	0.0	2.0	2.0	6	300 (149)
b (0.1)	12.0	3.0	0.1	0.0	336	100 (38)
b (0.5)	12.0	3.0	0.5	0.0	336	100 (38)
b (1.0)	12.0	3.0	1.0	0.0	336	100 (38)
b (2.0)	12.0	3.0	2.0	0.0	6	300 (149)
b (2+2)	12.0	3.0	2.0	2.0	6	300 (149)

TABLE 5
K_{IEAC} OF 22 Cr MATERIAL

DCB No.	Arm Displacement in	(mm)	K_{IEAC} ksi√in	(MPa√m)	Acid System[1]	Pitting (I,M,S)[3]	Corrosion Rate[2] mpy	(mm/y)
2-15	0.035	(0.889)	NCP[4]		a (2.0)	I	11900	(300)
2-16	0.035	(0.889)	NCP[4]		a (2.0)	I	11100	(280)
2-17	0.035	(0.889)	INVALID[5]		a (2+2)	M	280	(7)
2-18	0.035	(0.889)	NCP[4]		a (2+2)	M	380	(10)
2-19	0.050	(1.270)	35	(38)	a (1.0)	I	11	(0.3)
2-1	0.050	(1.270)	18	(20)	b (0.1)	I	370	(9)
2-2	0.050	(1.270)	22	(24)	b (0.1)	I	380	(10)
			avg 20	(22)				
2-3	0.035	(0.889)	15	(16)	b (0.1)	I	460	(12)
2-4	0.035	(0.889)	21	(23)	b (0.1)	I	450	(11)
			avg 18	(20)				
2-13	0.050	(1.270)	37	(41)	b (0.5)	I	110	(3)
2-14	0.050	(1.270)	30	(33)	b (0.5)	I	130	(3)
			avg 34	(37)				
2-11	0.050	(1.270)	39	(43)	b (1.0)	I	57	(1)
2-12	0.050	(1.270)	33	(36)	b (1.0)	I	60	(2)
			avg 36	(40)				
2-9	0.050	(1.270)	NCP[4]		b (2.0)	I	17500	(440)
2-10	0.050	(1.270)	NCP[4]		b (2.0)	I	15800	(400)
2-7	0.050	(1.270)	NCP[4]		b (2+2)	I	1700	(43)
2-8	0.050	(1.270)	110	(121)	b (2+2)	I	1500	(38)

[1] See TABLE 4
[2] Values for comparison only as DCB's not fully immersed during testing
[3] I - insignificant, M - moderate, S - severe
[4] NCP - no crack propagation
[5] Crack extension < 0.100 in. (2.5 mm) required by TM0177-90 for validity



FIGURE 1 - Showing tempered martensitic microstructure of 13 Cr material. Original magnification 100x. Nital etch.



FIGURE 2 - Showing ferrite - austenite microstructure of 22 Cr material. Original magnification 100x. Vilella's etch.

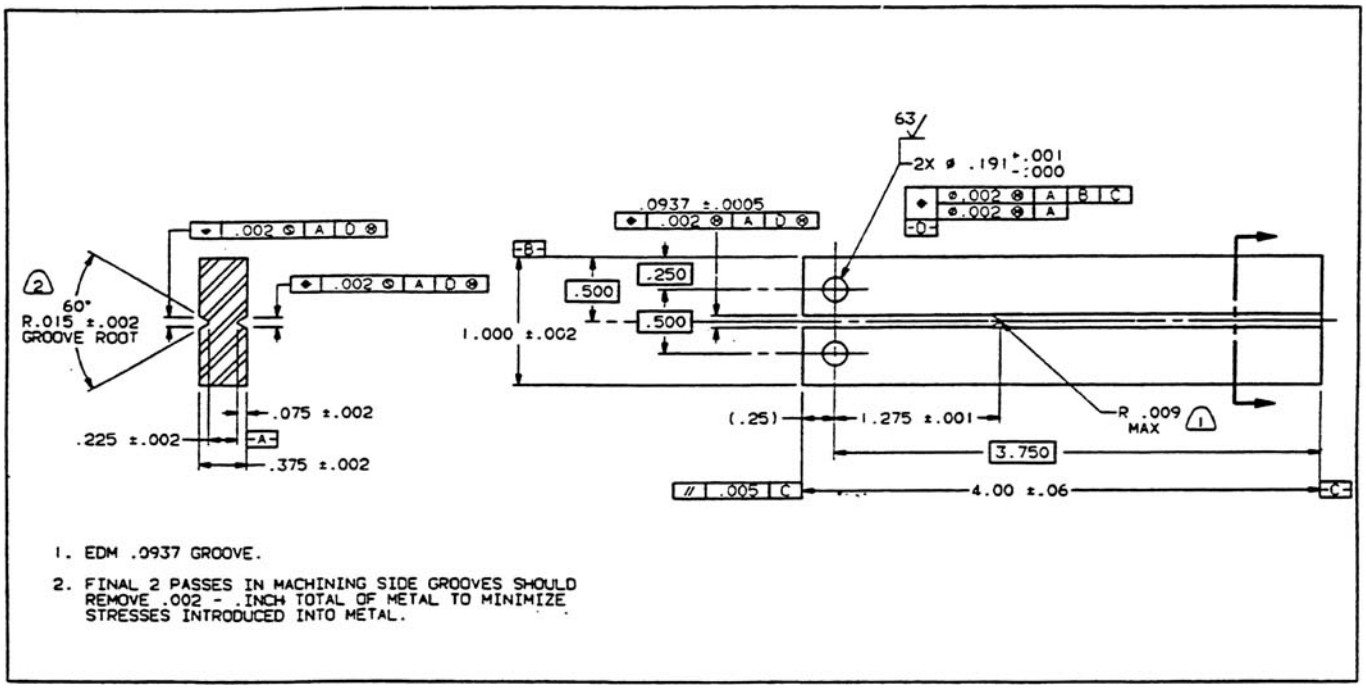


FIGURE 3 - Design of DCB specimen.

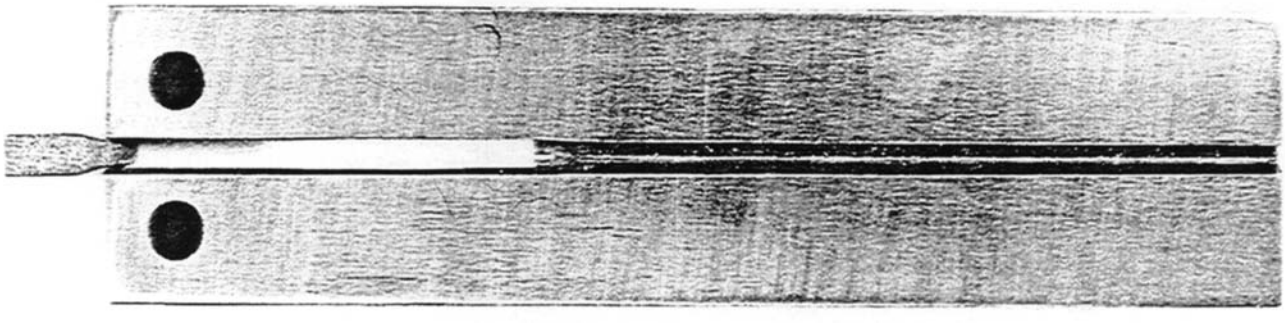


FIGURE 4 - DCB specimen ready for wedge loading.

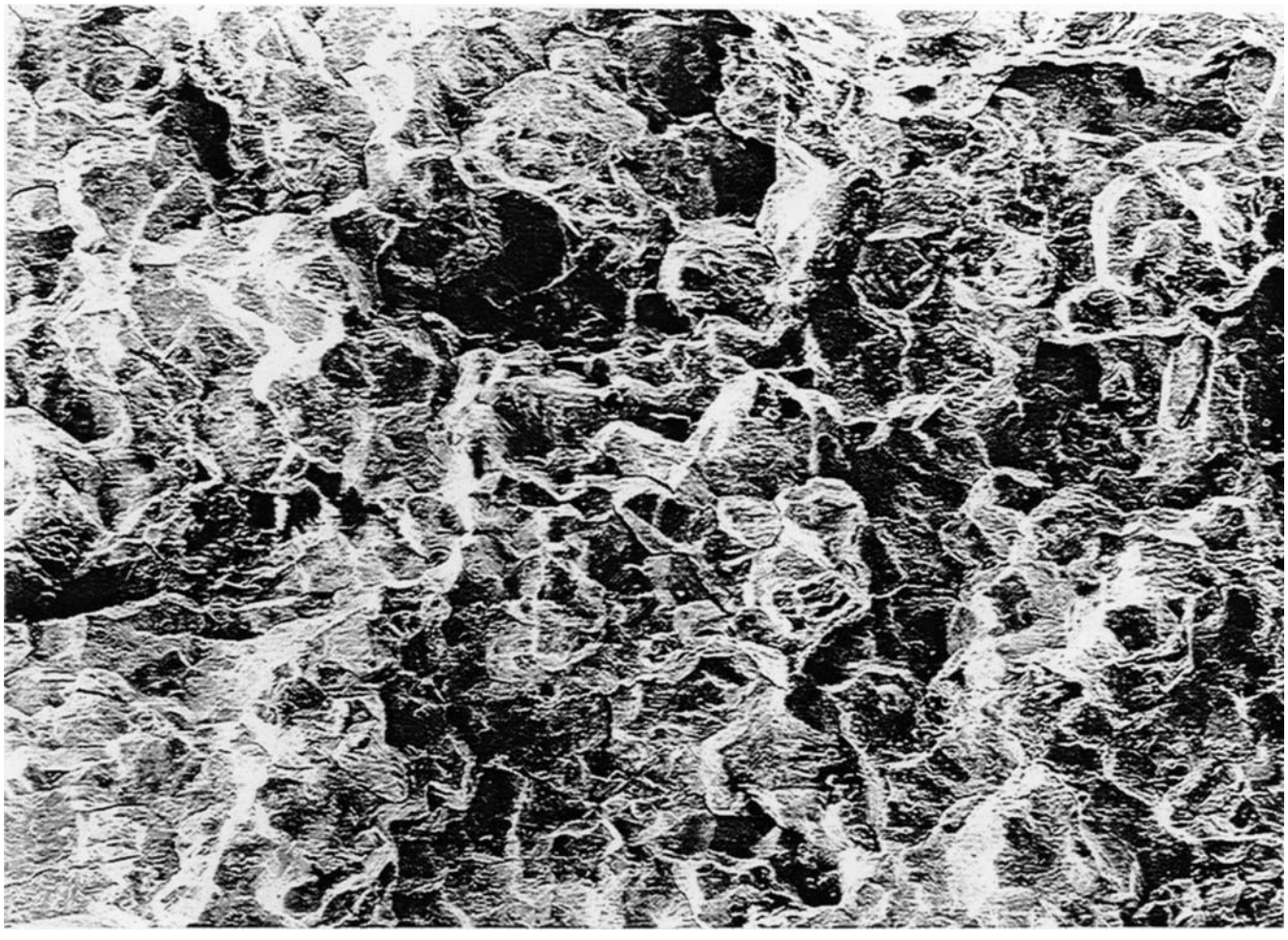


FIGURE 5 - SEM fractograph showing intergranular fracture of DCB No. 3-2 after exposure to 12% HCl-3% HF with 0.1% inhibitor. Original magnification 100x.

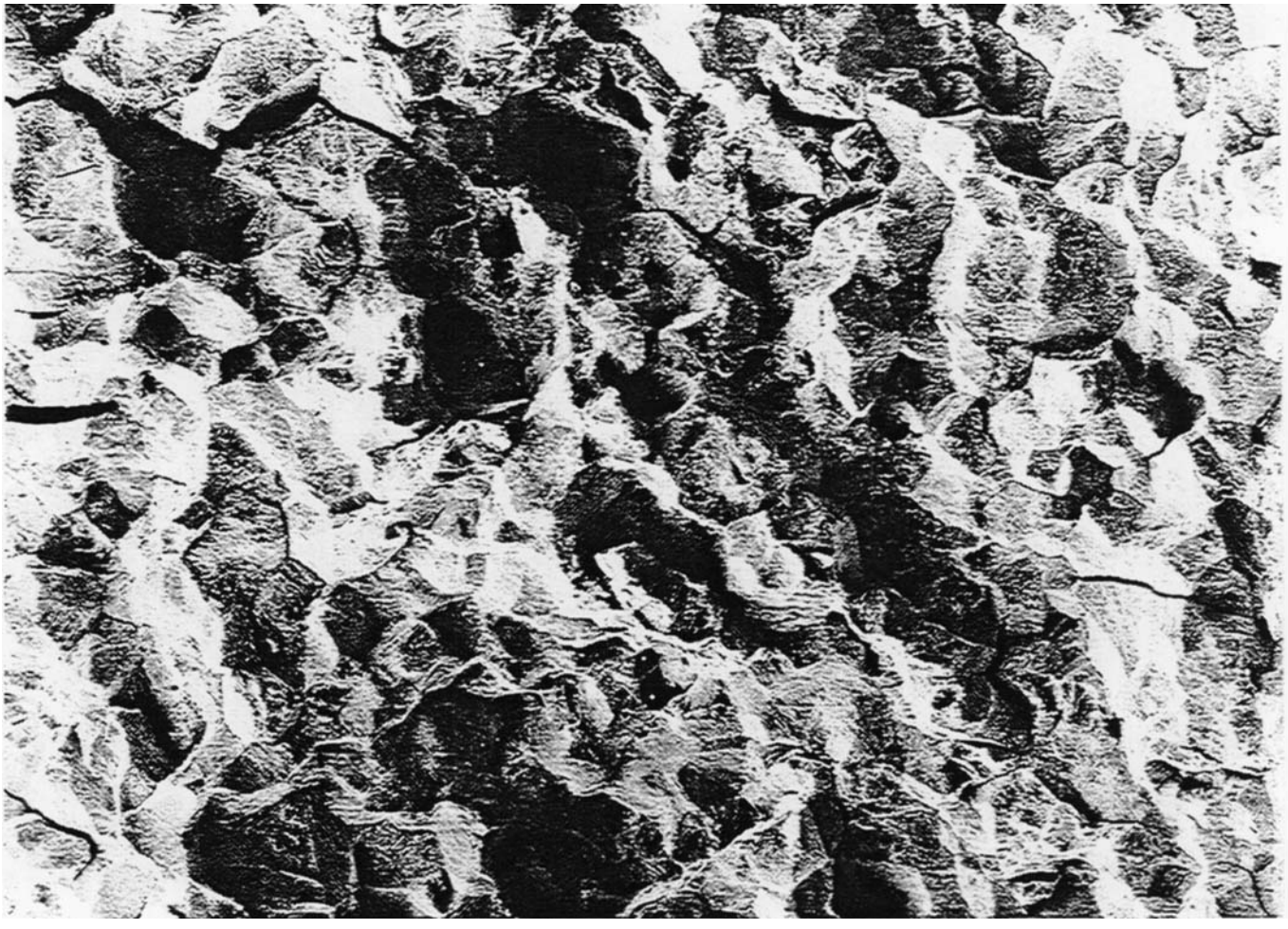


FIGURE 6 - SEM fractograph showing intergranular fracture of 13 Cr DCB specimen after exposure to NACE TM0177-90 sour brine solution. Original magnification 100x.

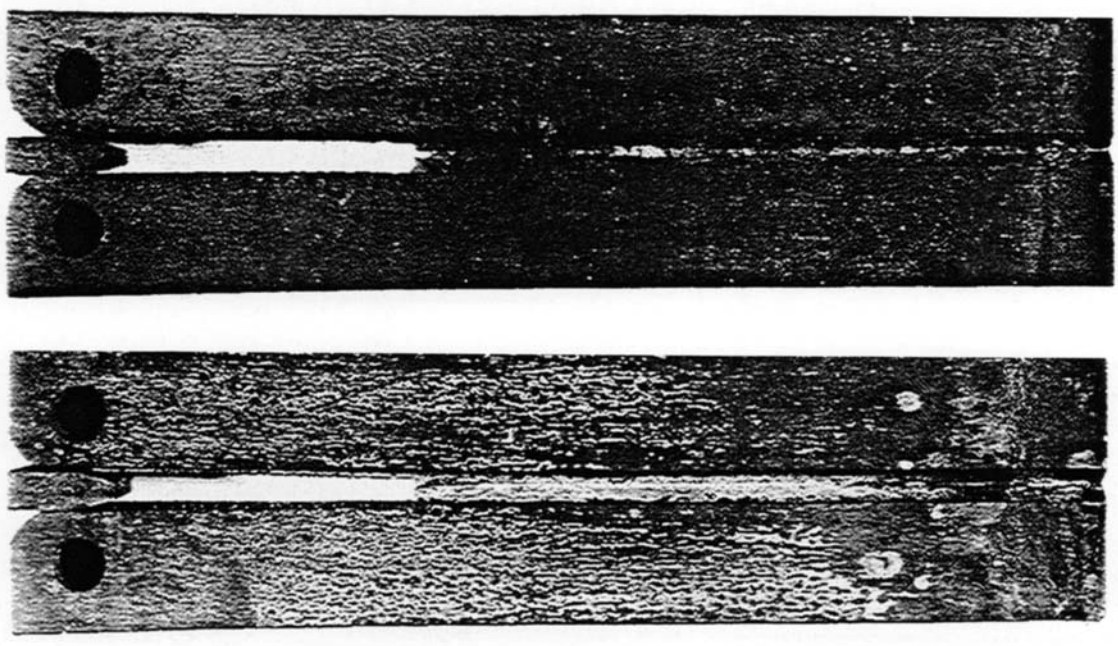


FIGURE 7 - Showing 13 Cr DCB No.'s 3-16 (top) and 3-17 after exposure to inhibited 15% HCl at 300°F (149°C).

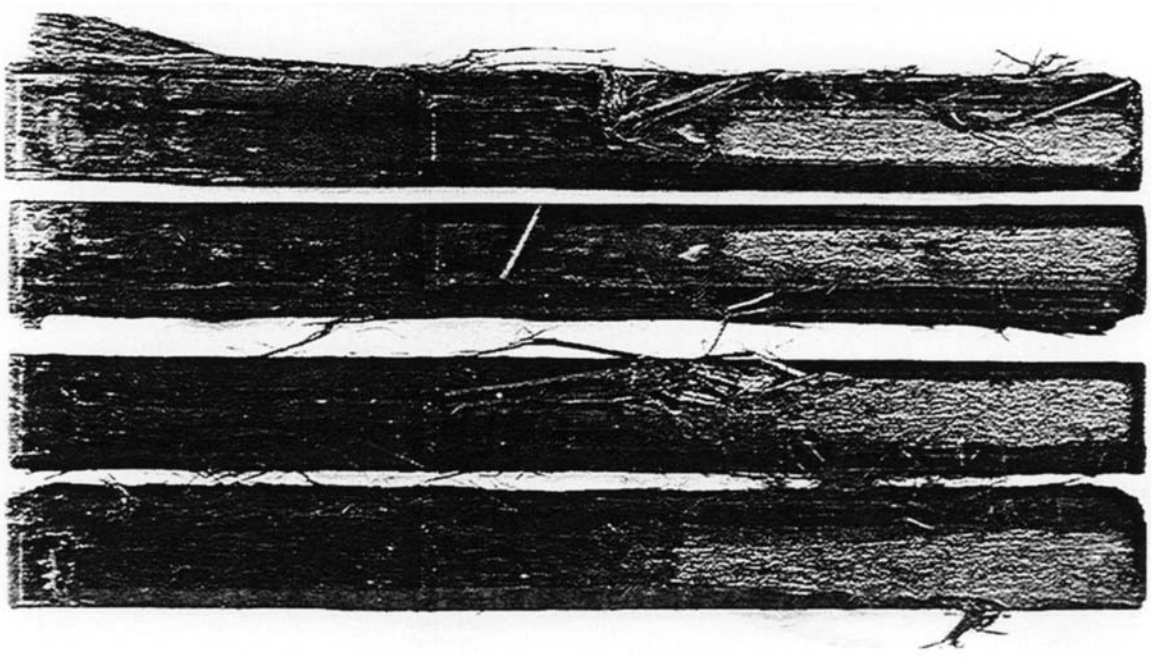


FIGURE 8 - Showing 22 Cr DCB No,'s 2-1 (top) and 2-2 after exposure to 12% HCl-3% HF with 0.1% inhibitor.

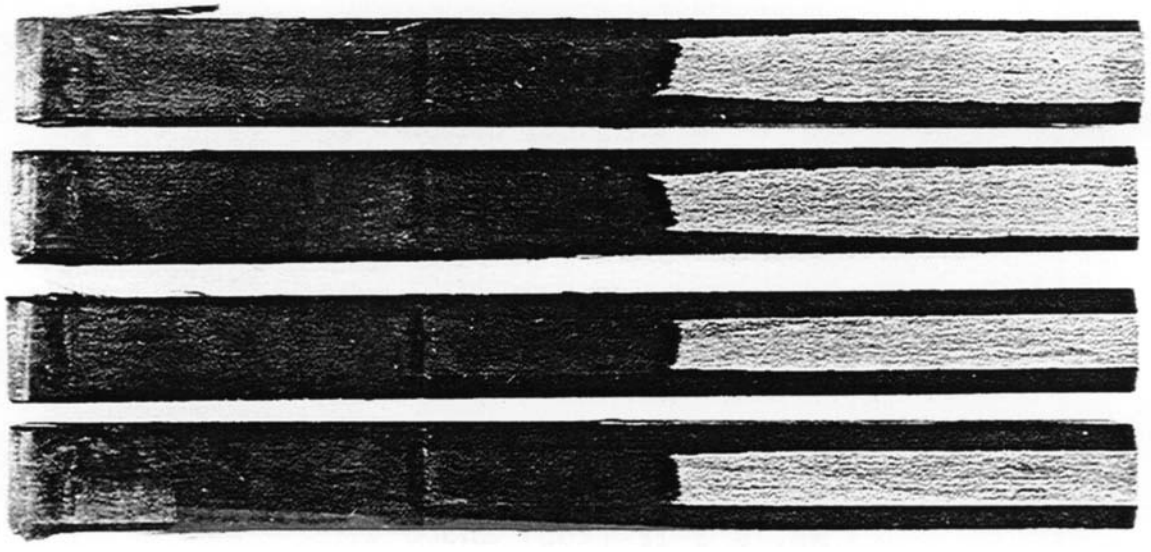


FIGURE 9 - Showing 22 Cr DCB No.'s 2-13 (top) and 2-14 after exposure to 12% HCL-3% HF with 0.5% inhibitor.

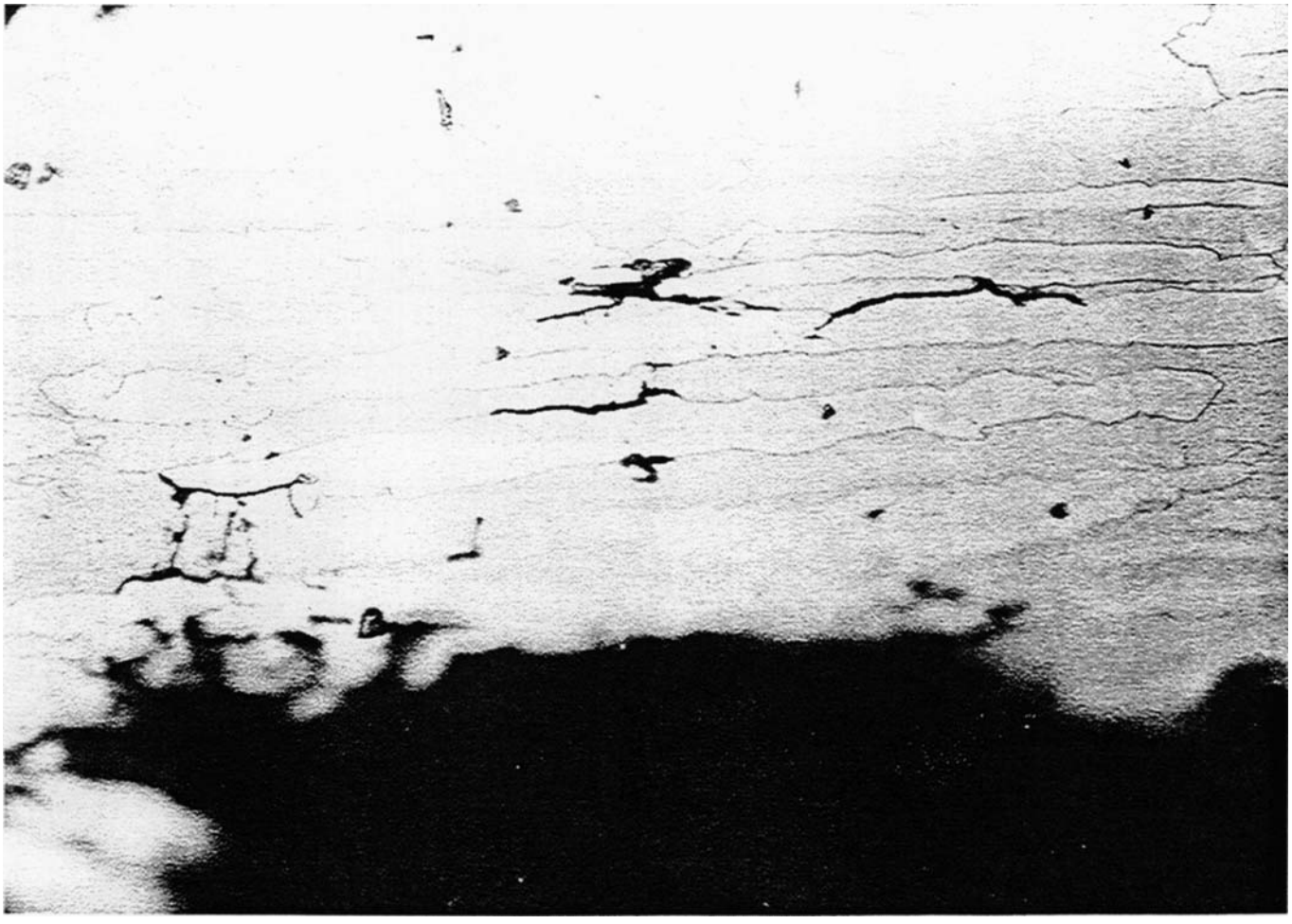


FIGURE 10 - Showing crack propagation of 22 Cr DCB No. 2-11 by corrosive attack of ferrite - austenite interface. Original magnification 500x. Vilella's etch.

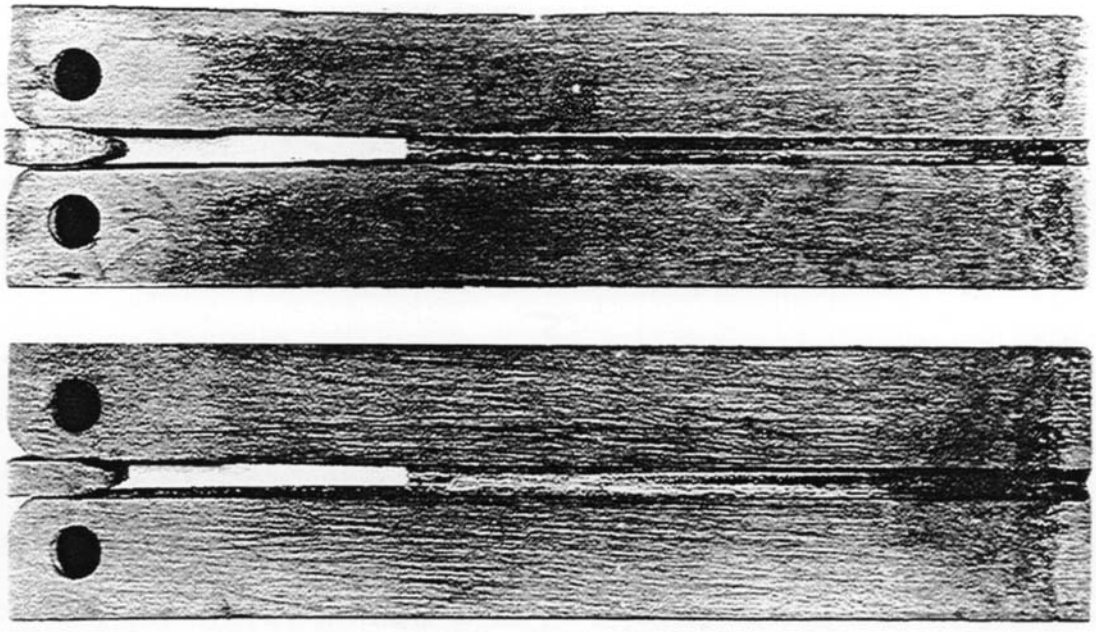


FIGURE 11 - Showing 22 Cr DCB No.'s 2-16 (top) and 2-17 after exposure to inhibited 15% HCl at 300°F (149°C).

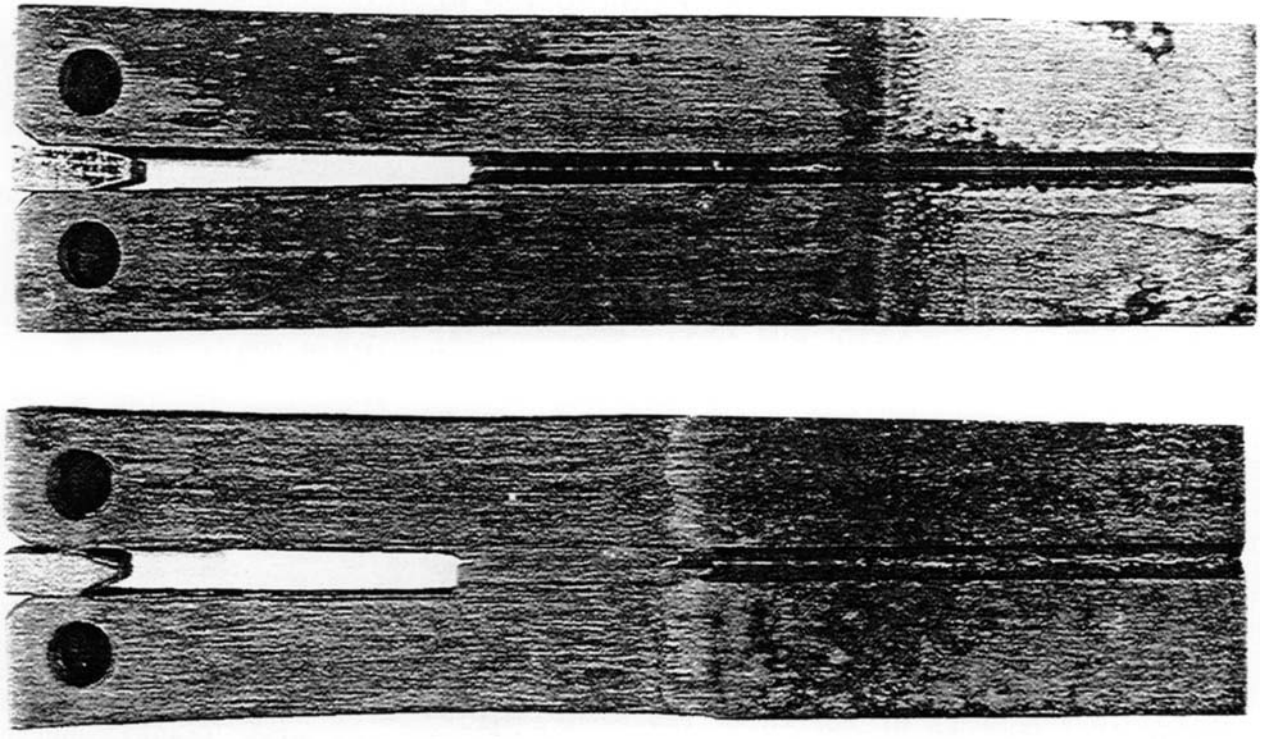


FIGURE 12 - Showing 22 Cr DCB No.'s 2-8 (top) and 2-9 after exposure to inhibited 12% HCl-3% HF at 300°F (149°C).

Copyrighted Materials
Copyright © 1996 NACE International Retrieved from www.knovel.com

PAPER NUMBER

68

CORROSION 90

April 23-27, 1990 · Bally's Hotel, Las Vegas, Nevada

CORROSION BEHAVIORS OF CORROSION RESISTANT ALLOYS IN ACID STIMULATION ENVIRONMENTS

Akihiro Miyasaka and Hiroyuki Ogawa

Nippon Steel Corporation
Pipe and Tube Research Laboratory
5-10-1 Fuchinobe, Sagamihara, Kanagawa, JAPAN 229

ABSTRACT

A series of laboratory experiments was conducted on the corrosion behaviors in acidizing environments of corrosion resistant alloys (CRAs) such as a 13% chromium martensitic stainless steel, duplex stainless steels and high nickel austenitic alloys. Corrosion tests were performed with and without a corrosion inhibitor in a stimulating acid of 15% HCl aqueous solution. Corrosion behaviors in spent acid with low pH were also examined. The effect of alloying elements on corrosion behaviors and their roles in the corrosion process were investigated by means of electrochemical measurements.

On the basis of test results, the corrosion risk of CRA OCTG during acid stimulation is discussed in relation to the necessity for the addition of corrosion inhibitors.

Key words: corrosion resistant alloys, hydrochloric acid, corrosion prevention, stainless steel, corrosion inhibitor, polarization

INTRODUCTION

Well stimulation is one of the major petroleum production technologies. Among the various stimulation techniques is acid stimulation. With an increase in the application of corrosion resistant alloys (CRAs), the corrosion behaviors of CRAs during acid stimulation and the succeeding flow back of spent acid have been attracting much attention from industry[1-3]. In the case of acid stimulation through low alloy steel tubings, chemical inhibition is inevitable because low alloy steel

does not show any corrosion resistance in any circumstances of operation. For CRAs with high corrosion resistance, there exists some possibility of abolishing chemical inhibition depending on the corrosion resistance of CRAs and the aggressiveness of the given environments. It is therefore important to clarify the risk of weight loss fatal to the integrity of tubings and the necessity for the chemical inhibition for respective CRAs.

This study reports the corrosion behaviors of representative CRAs in extremely low pH aqueous solutions of hydrochloric acid. The necessity for chemical inhibition and caution in assuring the integrity of tubings is also discussed.

EXPERIMENTAL

Test materials

Six alloys were subjected to investigation. Their chemical compositions are listed in Table 1. Alloys A (type 420 martensitic steel), B (22%Cr type duplex stainless steel) and C (25%Cr type duplex stainless steel) were the seamless pipes manufactured by the rolling process. They were quenched and tempered (alloy A) or solution heat treated (alloy B) after rolling in the steel mills and tested in as-received conditions. Alloys D (high nickel austenitic alloy) and F (nickel base CRA) are tubings made by the hot extrusion process. They were cold drawn after solution heat treatment to enhance the yield and tensile strength. Alloy E was melted, hot rolled, solution heat treated and finally cold rolled entirely in the laboratory.

Test coupons of 3 mm thick, 15 mm wide and 20 mm long were machined from these materials. They were degreased and polished with No.320 emery paper for immersion and with No.800 for polarization measurements.

Test environments and conditions

Immersion tests. Test environments and conditions are listed in Table 2. The corrosion rate was calculated on the basis of weight loss during immersion and the specimen surface area. In the case of immersion in a 15%HCl aqueous solution, the effect of a corrosion inhibitor (Halliburton HAI-75[1]) was examined. An inhibitor intensifier was not added.

Immersion in aqueous HCl solutions of pH 0.2 and 1.0 was intended to simulate the corrosion during flow back of spent acid. The corrosion inhibitor was not added because its effect cannot be expected during the flow back.

DC polarization measurements. DC polarization curves were measured in a 15%HCl solution and in pH 1.0 solution. The test temperature was 60°C. The potential scan was made from -700 mV vs. S.C.E. to +400 mV vs. S.C.E. at a scan rate of 50 mV/min. Test solutions were deaerated with high purity argon gas. Deaeration was continued during polarization measurement.

Specimens were coated with silicon resin after polishing leaving an area of 1 cm^2 for measurement. They were degreased again just before measurement. Pickling before polarization measurement to remove the air-formed film was not conducted, because most of the alloys were activated in the test solutions themselves.

(1) Trade name

RESULTS AND DISCUSSION

Corrosion in 15%HCl aqueous solution

Immersion test results in 15%HCl aqueous solution with and without the addition of the corrosion inhibitor are given in Table 3. Alloy A exhibited a significant weight loss without the addition of the corrosion inhibitor. The corrosion rates of alloys B and C without inhibition were also considerably high, whereas those of alloys D and E were fairly low. Selective dissolution of the ferrite phase was observed for duplex stainless steels (alloys B and C) both with and without the corrosion inhibitor. Figure 1 shows a typical example of preferential dissolution of ferrite phase. The corrosion rate of alloy C was slightly greater than that of alloy B. It is well known that chromium promotes the active dissolution of iron-base alloys. The corrosion rate increases with increasing chromium content. This accounts for the above-mentioned corrosion behavior in considering that the ferrite phase contains more chromium and less nickel than the austenite phase does. No localized or selective corrosion was observed for alloys A, D and E.

Generally the corrosion rate decreased as the microstructure changed from tempered martensite to ferrite+austenite duplex and finally to austenite. In other words the corrosion rate decreased with increasing nickel content. In boiling 15% hydrochloric acid all the tested alloys are in a active state. It is well known that nickel is beneficial in reducing the active dissolution rate of stainless steels.

The addition of the corrosion inhibitor gave the similar tendency to the above-mentioned results without the inhibitor. The corrosion rates were two to three times lower than those without the inhibitor. The %protections were 98.8 to 99.9%. This clearly shows the effect of chemical inhibition. It should be noted that with the addition of the corrosion inhibitor used in the study alloy A exhibited a lower corrosion rate than alloys B and C. This suggests the necessity for proper selection of a corrosion inhibitor as a function of the alloy chemical compositions of CRAs.

DC polarization curves of alloys B to F in a 15%HCl solution are shown in Fig. 2. None of the alloys tested exhibited passivity in the solution. This agrees with the immersion test results. The corrosion potentials of austenitic alloys (alloys D, E and F) was 80 to 95 mV more noble than those of duplex stainless steels. This tendency is also in good agreement with the immersion test results. This is because nickel is beneficial in reducing the active dissolution rate of alloys. The effect of nickel on the cathodic reaction is not so prominent. It seems that an increase in nickel content slightly depolarize the cathodic reaction. The higher the nickel content, the less weight loss in 15% HCl solution, because the reduction of anodic dissolution by nickel exceed the small increase in cathodic reaction.

Corrosion in spent acid

Corrosion test results in low pH aqueous solutions are tabulated in Table 4. The relationship between the alloy structures (or Ni content) and the corrosion rates was similar to that in 15%HCl acid. The corrosion rates were much lower in pH 0.2 and pH 1.0 solutions than in a 15%HCl solution. Alloys D and E exhibited the passivity at pH 1.0 but not at pH 0.2. This shows that depassivation pH (pH_d) of the two alloys is less than 1.0 but higher than 0.2. The corrosion rates of

duplex stainless steels (alloys B and C) at pH 1.0 showed considerable scatter, presumably because the pH_d of these alloys are approximately 1.0. The ferrite phase was selectively attacked in pH 0.2 solution as in the 15%HCl solution. Alloy A was still active at pH 1.0. Alloy A cannot be self passivated unless at a higher pH, because the pH_d value of this alloy in a 3%NaCl aqueous solution is 3.2[4].

DC polarization curves of alloys B to F in a pH 1.0 solution are given in Fig. 3. All the alloys tested are passivated in the solution. This result agrees well with the immersion test results. Austenitic alloys had a more noble corrosion potential than duplex stainless steels.

Corrosion risk during acid stimulation

The duration of acid injection through tubings is usually very short. Even for an actively dissolving CRA tubing in stimulation acid, corrosion prevention is not necessary as far as the weight loss during this limited time is sufficiently small compared with the wall thickness. The corrosion rates obtained in the immersion tests were converted to the reduction in wall thickness in 6 hours. The results are given in Table 3. The expected thickness loss for alloys D and E is sufficiently lower than the usual wall thickness of 5 to 8 mm for tubings. Chemical inhibition is not required for these alloys and presumably also for alloy F. Alloys A, B and C will lose the major part of the wall thickness unless chemically inhibited during acid injection. The corrosion inhibitor used in the study can successfully reduce the thickness loss so that the integrity of tubings can be retained.

Corrosion risk in flow back of spent acid

The corrosion rates of alloys in low pH solutions were also converted to the calculated thickness loss in 6 hours of flow back. The thickness loss of austenitic alloys D, E and F is negligibly small even at pH 0.2. The risk of degradation of these alloys by spent acid is not expected. The thickness loss of alloys B and C at pH 0.2 and that of alloy A at pH 1.0 cannot be ignored. Some countermeasures either from petroleum production or corrosion prevention technology should be applied when stimulating formations with strong acid.

CONCLUSIONS

The corrosion behaviors of various corrosion resistant alloys in 15%HCl solution and the resultant spent acid were studied.

(1) The risk of corrosion damage in high nickel austenitic alloys due to acid stimulation is small. Their weight loss during stimulation is expected to be much less than the wall thickness. They remain passive in the spent acid condition. Chemical inhibition is not required.

(2) The addition of corrosion inhibitor to stimulation acid is necessary for acid injection through 13%Cr and duplex stainless steel tubings. Care must be taken in the case of corrosion of 13%Cr steel in spent acid.

ACKNOWLEDGMENTS

The authors wish to express their thanks to Nippon Steel Corporation for allowing publication of this material. The assistance and discussion of co-workers in Nippon Steel's research laboratories are gratefully acknowledged.

REFERENCES

1. W. W. Frenier S. E. Grannan and R. J. Jasinski, *CORROSION/88*, Paper No.188, National Association of corrosion engineers, Houston, Texas, 1988.
2. R. D. Kane and S. M. Wilhelm, *CORROSION/89*, Paper No.481, National Association of corrosion engineers, Houston, Texas, 1989.
3. K. Masamura and T. Nishimura, *Boshoku Gijutsu*, Vol.37, p.546, 1988.
4. Un-published data.

Table 1 Chemical compositions of test alloys (%)

Alloy	Grade	C	Si	Mn	Ni	Cr	Mo	Others
A	NT-13CR*1 (type 420)	0.190	0.38	0.44	0.16	13.2	—	
B	NT-22CR*1 (UNS S31803)	0.019	0.53	1.73	5.70	22.3	3.14	N 0.184
C	NT-25CR*1	0.040	0.52	0.57	6.99	24.6	2.72	N 0.169
D	NT-2225*1	0.015	0.05	0.10	25.5	22.4	4.30	
E		0.013	0.22	0.18	31.2	26.5	3.61	Cu 1.15
F	NT-2242*1 (UNS N08825)	0.010	0.07	0.35	42.3	22.3	2.96	Cu 1.7, Ti 0.70

*1 Proprietary grades of NIPPON STEEL

Table 2 Test conditions for immersion tests

Item	Conditions
Test solution	(a) 15% HCl aq. soln. (b) 15% HCl aq. soln. with corrosion inhibitor (c) HCl aq. soln. of pH 0.2 (d) HCl aq. soln. of pH 1.0
Test temperature	Boiling (ca. 110°C)
Corrosion inhibitor	Added only for solution (b)
Test duration	10 min for solution (a) 6 hours for solutions (b), (c) and (d)

Table 3 Test results in 15%HCl solution

Alloy	Corrosion rate*2 (mm/y)		% protection*3	Calculated thickness loss in 6 hours*2 (mm)	
	(A) without corrosion inhibitor	(B) with corrosion inhibitor		without corrosion inhibitor	with corrosion inhibitor
A	16900	2.5	99.9	11.6	0.0017
B	4620	54.1	98.8	3.16	0.037
C	5890	31.1	99.5	4.03	0.021
D	99.3	0.31	99.7	0.068	0.00021
E	109.6	0.22	99.8	0.075	0.00015

*2 average of two specimens, *3 100 x (A-B)/A

Table 4 Test results in spent acids

Alloy	Corrosion rate (mm/y)		Calculated thickness loss in 6 hours*4 (mm)	
	pH 0.2	pH 1.0	pH 0.2	pH 1.0
A	---	4577, 4843	---	3.2
B	6907, 6943	40.2, 0.064	4.75	0.016
C	13130, 12950	0, 0.064	8.93	0.000022
D	147, 151	0, 0	0.102	0
E	55.1, 47.5	0, 0	0.035	0
F	27.9, 26.2	7.31, 8.08	0.019	0.0053

*4 average of two specimens

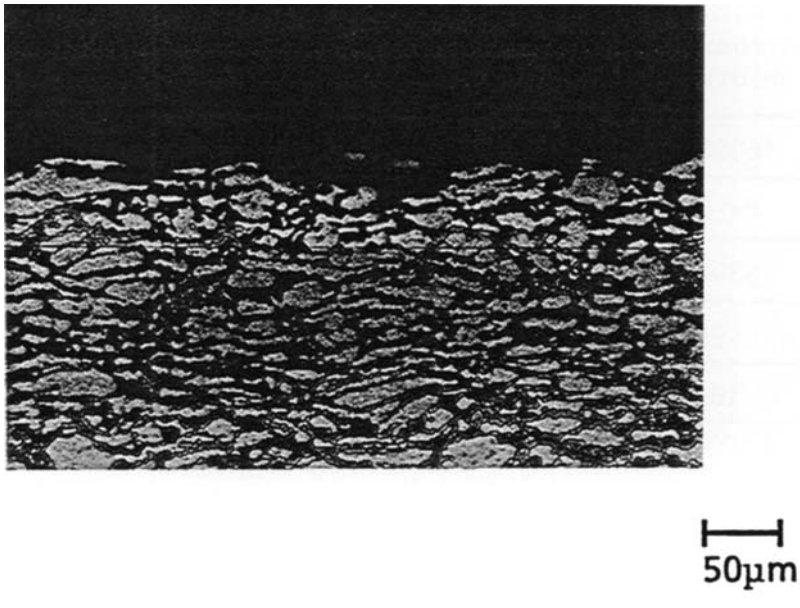


Figure 1 Selective dissolution of ferrite in boiling 15%HCl solution with corrosion inhibitor (Alloy B)

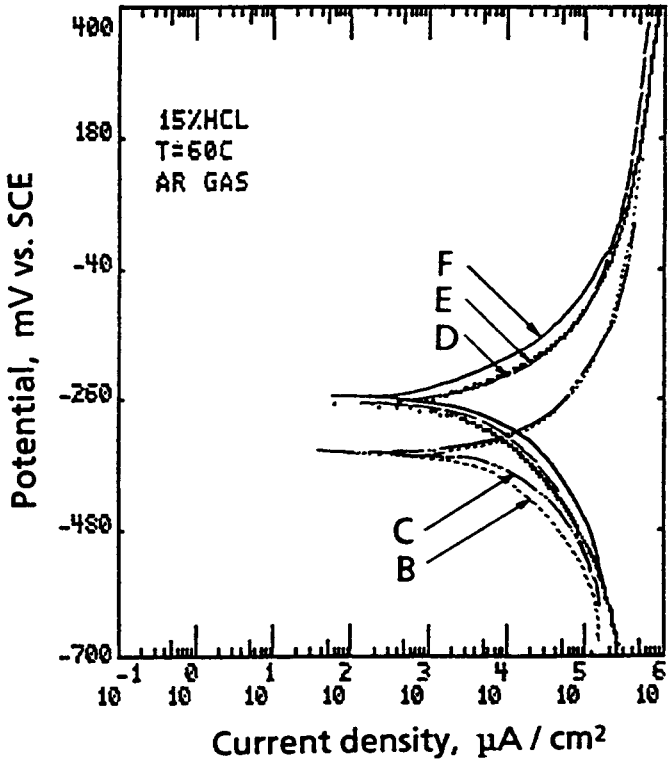


Figure 2 Polarization curves in 15%HCl solution

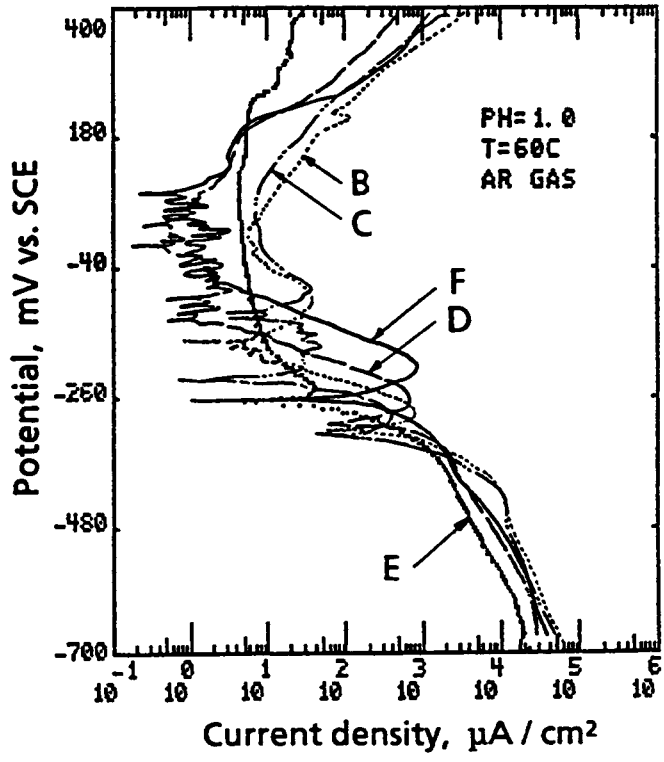


Figure 3 Polarization curves in pH 1.0 solution

Copyrighted Materials
Copyright © 1996 NACE International Retrieved from www.knovel.com

Paper No.
96

CORROSION 93
The NACE Annual Conference and Corrosion Show

A FIELD EXPERIENCE OF CORROSION INHIBITION DURING THE ACID FRACTURING OF A DEEP OIL WELL COMPLETED WITH 22 % Cr DUPLEX STEEL

Alberto Valdes, Alfredo Viloria and Sara Marcano
INTEVEP, S.A. - R & D Center affiliated to Petróleos de Venezuela, S.A.
Department of Materials Technology
P.O. Box 76343, Caracas 1070A, Venezuela

Carlos Boggio
LAGOVEN, S.A. - Department of Petroleum Engineering
Tia Juana, Estado Zulia, Venezuela

ABSTRACT

This paper reports the metal losses caused by an acid fracturing process carried out on a crude oil well completed with 22 Cr duplex steel. The composition of the acidizing fluid was formulated in order to protect the production tubing against corrosion, during the stimulation of a limestone reservoir.The fluid was formed by a strong acid, a weak acid, a surfactant and a commercial high temperature corrosion inhibitor.

The loss of metal in the production tubing was calculated from the iron, nickel and chrome concentrations in the produced fluid, once the well was open for operation. The total acid number was also measured in the same fluid samples used for the metal counts. In order to carry-out the calculations of corrosion rate, two different assumptions regarding the composition of the returning fluid were made. In both assumptions the acid was taken as the only aggressive fluid, the difference being in the aggressivity of the returning spent acid, and in the mixing inside the formation of the various fluids used during the stimulation job. The metal counts yielded a loss of production tubing, due to corrosion, in the range 0,035 - 0,040 lb/sq. ft. during the operation. For both assumptions the evolution of the total acid number showed a reasonable agreement with the variation of the metal concentrations with time.

Keywords: Corrosion, inhibitor, acidizing, oil well, duplex steel

INTRODUCTION

Traditionally wells have been completed with carbon steels but, due to the increasing amounts of hydrogen sulfide and carbon dioxide in the produced fluids, special steels are used more and more as an alternative for corrosion control. However, these materials are extremely sensitive to the fluids used in the operations of acid stimulation in which mineral and organic acids are used in high concentrations [1]. For this reason acidizing jobs must include corrosion inhibitors as a way to minimize the attack of the acid on the production tubing.

Most stimulation treatments use hydrochloric acid due to its high dissolution power of the minerals deposits present in the formation, this acid can be combined with hydrofluoric acid for the stimulation of silicate-rich formations, or with acetic acid for the stimulation of limestone formations. Acetic acid is a weak organic acid, it causes low corrosivity and is easily inhibited at high temperatures.

The main disadvantage of the mixtures for acid stimulation is their aggressivity on completion tubing, the damage caused is specially difficult to control at temperatures higher than 250 °F. Corrosion inhibitors specially adapted to the completion material have been designed in order to decrease this attack, these inhibitors are injected along with the acid mixture. Unfortunately, the efficiency of the inhibitors is very low and the metal losses are still very high.

The maximum corrosion allowance during acidizing jobs continues to be a matter of discussion. Each company follows in-house criteria which are used discretionally. Nevertheless, there seems to exist a certain consensus according to which it is reasonable to accept a metal loss of 0,05 pounds of metal per foot of surface exposed to the stimulating fluids, at temperatures above 200 °F.

FIELD JOB PERFORMED ON THE WELL

The well on which the acidizing job was done is located in the south of Lake Maracaibo in Venezuela. This well produces about 3000 barrels per day of API 42 grade oil, from two different formations, mostly limestone. The well was completed with 16461 foot of 22 % Cr (22 Cr - 5 Ni) steel pipe (3.5 inches of external diameter and 0.375 inches of wall thickness).

The decline of production over a period of several months (Fig.1) showed that it was necessary to perform an acid fracturing job stimulation. Since asphaltene deposits were detected, a preliminary cleaning stage was carried out by pumping 250 barrels of gasoil. The well was subsequently closed for a 24-hour period to allow removal of the deposits.

After this period the acid fracturing was started, Table 1 shows the different stages of the job. First a cooling stage was used to decrease the temperature of the bottom of the well from an initial value of 303 °F to about 200 °F. Next a batch of fracturing fluid, followed by a batch of acid, were injected into the well. Three stages of fracturing fluid plus acid were needed in order to stimulate each one of the producing intervals of the well, rubber balls were used as diverting material in stages 4 and 6 to drive the fluids to the wanted interval.

A few hours after finishing the job the well was opened for production and sampling of the fluids was started. These samples were used to do the measurements described below.

RESULTS

Production Results

As shown in Fig. 2, the treatment increased the production of the well from about 3500 BPD* to about 6500 BPD. From an oil production point of view the acid treatment was successful, however, the extent of the attack of the acid on the production tubing is not indicated by these results. Instead, the rate of the corrosion process on the metal needs to be determined.

Metal concentrations

Table 2 show the concentration profiles obtained for the iron, nickel and chrome. The higher metal counts were obtained in the first three hours of operation, with a distinctive maximum obtained after one hour. The corrosion rate is expressed in lb/sq.ft. of metal loss, as is customary for this type of work; 1 lb/sq.ft. per hour is equivalent to 243.3 mpy (6.2 mm/y).

Total Acid Number

The acidity of the sampled fluids was determined by means of the Total Acid Number (TAN)*. Fig 3 shows that the sample obtained after one hour of production was the more acidic. After, the acidity decreased with time until it reached very low values, practically constant, corresponding to the acidity of the crude normally produced by the well. The decrease in the acidity of the produced fluid is an indication of a progressive dilution of the injected fluids into those present in the formation.

DISCUSSION

In order to calculate the corrosion rate of the steel it is necessary to determine the total time of contact between the steel and the stimulation fluid, the volume of this fluid and the total area of metal exposed to the acid. Thus, it is necessary to do several considerations before deciding which value of these variables must be used to calculate the corrosion rates. For example, the acid is more aggressive when it enters the well, is spent by reaction over the metal walls, and in the formation, and returns to the surface with a much lower concentration, this means that the acidity is greatly reduced and therefore less aggressive. The time of contact between the metal and the injected fluids will be equal to the time required for pumping the acid stages, plus the time used for the return of those fluids when the well is opened. A number of fluids are injected into the well during the acidizing operation, doubtlessly the acid mixture is the most aggressive.

Two cases were considered in order to have better information about the actual corrosion rates in the well the difference being the extent of the mixing in the formation of the different fluid phases injected to the well. In our experience, the acid concentration of the returning fluids during acidizing jobs is more than one order of magnitude lower than that of the injected acid, when the well is immediately open for operation, and even lower when some residence time is allowed before opening the well. According to

---

* barrels per day
* mg of KOH needed to neutralize one gram of sample

this, for both cases the assumption was made that the attack on the pipe occurs only during the stages when there are acid fluids in contact with the metal. In other words, any other fluid is considered non-corrosive compared with the acid. Furthermore, it was assumed that the acid is aggressive only when it is injected to the well, but not when it returns to the surface. These cases are discussed next.

Case 1.

For this case it is assumed that the fluids pumped into the well mix completely in the formation before returning to the surface. The samples obtained were therefore a uniform mixture of: cooling and fracturing fluids, acid, gelifiers and gasoil. A total of 77960 gallons of fluids were pumped into the well, of which 20160 correspond to the acid stages. since the attack on the metal occurs only when the acid is in contact with the metal, the corrosion products appearing during these stages will be diluted in the total volume of fluids, i.e. 3.87 times. The time used for the calculation of the corrosion loss is equal to the time consumed for injection of the three acid stages (57,63 minutes). Figures 4 and 5 show the profile of the metal losses calculated for each of the samples according to this assumption.

Case 2.

For this case the assumption was made that the fluid phases do not mix completely in the formation; instead, pseudo-interfaces would be formed between successive fluid phases in such a manner that the corrosion products formed during the passage of each of the acid stages will remain dissolved in the particular stage without mixing with the neighboring phases.

Once the well was open for operation, the fluid phases would return to the surface in inverse order to the injection. Since the production flow is known, and the volume of each stage is also known, a simple calculation will indicate which is the fluid phase present at each sampling time. Then the samples will yield the metal concentrations in the particular phase passing by the sampling point at the sampling time.

Fig. 6 shows which fluid would be sequence of returning fluids, according to the production flow of 6500 BPD. As can be seen, the sample corresponding to one hour was taken while acid stage 3 was passing by the sampling point. Acid stage 3 has a pumping time of 25 minutes, the calculated loss of iron for this stage is 0.0035 lb/sq.ft. Similarly, the sample corresponding to two and a half hours was taken during acid stage 2 which had a pumping time of 17 minutes. The calculated loss of iron for this stage is 0.002 lb/sq/ ft. Table 2 shows the times used to carry out the calculations for the corrosion losses and Fig. 7 and 8 show the corresponding metal concentrations.

The results for both cases are similar, the largest metal losses were obtained for the samples collected between one and one and a half hours after opening the well for production. For larger times the losses due to corrosion did not vary with time, and were similar for both cases. This seems to indicate that the real situation may be more likely intermediate between a total mixture of fluids and the establishment of pseudo-interfaces through which the concentration profiles of iron, chrome and nickel would be established.

According to Figure 6, the half hour sample was taken in the gasoil phase, which has a very low concentration of the three metals. Between this phase and the next (acid) there will not be a significant concentration gradient for any of the metals since the gasoil is an organic phase with a low affinity for compounds of mineral nature. The acid and fracturing stages consist of aqueous phases, therefore it is easy to establish a concentration profile with significant amounts of metals on both sides of the interface. The samples taken after one a half, two and three hours will be influenced by the concentrations established by diffusion of the metal ions from the acid phases located on both sides of the interphase.

Since the concentration profiles of the metallic species present in the acid would be established by diffusion, the time frame during which the mass transfer occurs, and the local temperature during the same time, are of great importance. It is well known that temperature variations affect the kinetics of chemical and electrochemical process, a well has a temperature gradient between the bottom and the surface which has not been considered in the present case, therefore the calculated losses of metal correspond to an average on the total length of the pipe. The method used does not give any indication about the presence of localized corrosion.

The samples taken after two hours gave similar results, these samples were taken on the first injected fluids, these are the fluids that were in the well for longer time at the bottom temperature. As a result, the mass transport had more opportunity to occur and therefore to even the metal concentrations across the interphases.

The attack of the returning acid on the pipe was not taken into consideration because the largest aggressivity of the acid is available during the injection stages when the acid has not been used, once the acid reacts, initially with the pipe and later with the formation,the possibility of reacting with the pipe during the returning stage is diminished.

The (calculated) dissolved metal composition for both cases was different from that of the pipe. This in itself is not surprising, it has been shown [2,3] that during the dissolution of Fe-Cr alloys the Cr concentration of the dissolution products is the same as in the alloy only when the steady state is reached, a Cr deficiency has been observed while non-stationary conditions prevail. Also, the time required to reach the steady state increases with the Cr content of the alloy (e.g. from 30 minutes for 1 at. % Cr to 50 minutes for 14 at. % Cr [2]). Due to the contact time between the acid stages and the tube wall, and the continuous fluid flow which is constantly disturbing the concentration profiles near the surface, an steady state for Cr dissolution was probably never reached.

The alloy in the present case contains Ni, in the author's knowledge there is no information in the literature on the dissolution behavior of Fe-Cr-Ni steels under bottom hole conditions, in particular on preferential dissolution, passive film growth, changes in surface composition and pitting. Further work is being carried-out to better understand these particular points.

The gas associated to the crude produced by the well contains around 10 ppm of H_2S, but none was detected while the job was being carried-out, or during the first few hours of operation. It is assumed that H_2S was not present when the well was open for production because the fluids injected to the well pushed back into the formation the bottomhole fluids. Thus, there was no contribution from H_2S attack on the pipe and the metal dissolution was only due to the acid injected during the acidizing stages.

The content of iron measured after 19 hours of production was 13 ppm, and the content of Cr and Ni was below 0.01 ppm. It is likely that by this time all of the injected fluids had left the well, therefore these concentrations reflect reasonably well those in the oil produced by the well under normal conditions. Thus, the metal concentrations measured in the returning fluids during the first few hours of operation had a negligible contribution from the metals dissolved in the oil.

CONCLUSIONS

The largest corrosion losses calculated from the metal counts were in the range 0,0035 - 0,0040 lb/sq.ft. These losses reflect the general (uniform) corrosion of the pipe during the stimulation process; although the localized loss may be much larger.

The calculated metal concentrations were similar when either a complete mixing of the injected fluids or pseudo-interphases between these fluids were considered. This indicates that most likely the situation is intermediate between these two extremes.

The temperature gradient between the bottom of the well and the surface was not considered, therefore the calculated losses of metal correspond to an average on the total length of the pipe.

REFERENCES

[1] B. Vicentini, G. Rondelli, G. Onofrio, L. Lazzari and A. Cigada, "Corrosion Behavior of High Alloy Tubular Materials in Inhibited Acidizing Conditions", paper # 43, CORROSION/87, Houston, 1987.

[2] B. Heine and R. Kirchheim. "Dissoluton rates of Iron and Chromium and Fe-Cr-Alloys in the Passive State", Corr. Sci., 31, 533-538, (1990)

[3] G. Hultquist, M. Seo, T. Leitner, C. Leygraf and N. Sato. "Dissolution behavior of Iron, Chromium, Molibdenum and Copper for pure metals and for Ferritic Stainless Steel", Corr. Sci., 27, 937-946, (1987).

TABLE 1

STAGES OF THE JOB*

Stage	Fluid	Volume (gal)	Injection time
1	cooling stage	20000	39' 45"
2	fracturing stage	10500	25' 56"
3	acid stage	6720	15' 33"
4	fracturing stage	10500	24' 24"
5	acid stage	6720	15' 33"
6	fracturing stage	10500	25' 24"
7	acid stage	6720	25' 00"
8	gasoil	6300	27' 28"
	Total volume	77960	

* each acid stage was composed of: a mixture of hydrochloric and acetic acid, 2 % of inhibitor (mixture of phenylvinylketones and a quaternary ammonium salt), and appropriate organic solvents and surfactants.

TABLE 2

IRON, CHROME AND NICKEL CONCENTRATIONS MEASURED IN THE WELL AFTER OPENING FOR NORMAL OPERATION

Time (hrs)	Iron (mg/lt)	Chromium (mg/l)	Nickel (mg/l)
0	well opened for normal operation		
0.5	1.95	0.11	0.21
1	1125	39.3	27.8
1.5	844	1.08	5.98
2	601	1.24	2.72
2.5	625	1.53	2.63
3	580	0.64	3.35
19	13	< 0.01	< 0.01

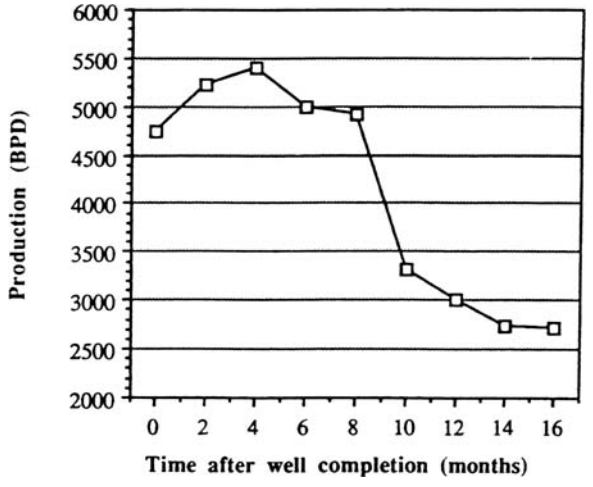


FIGURE 1. Production history of the well before the acidizing job.

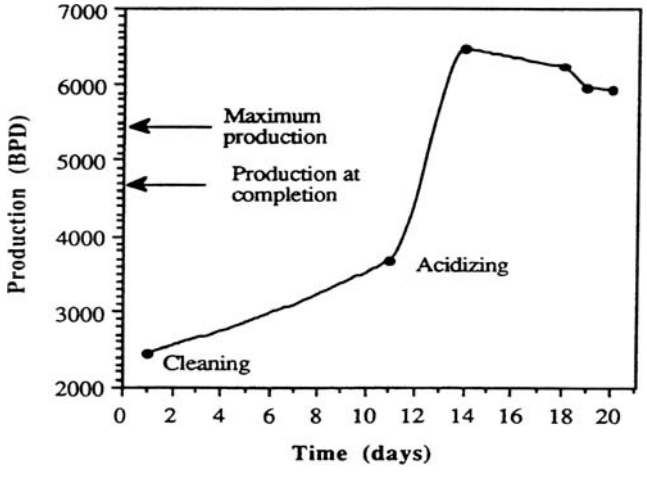


FIGURE 2. Effect of the acidizing on production.

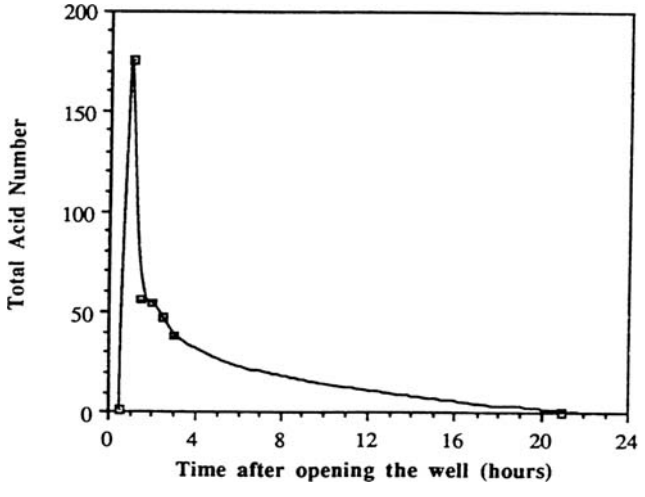


FIGURE 3. Total acid number during the first hours of production after acidizing.

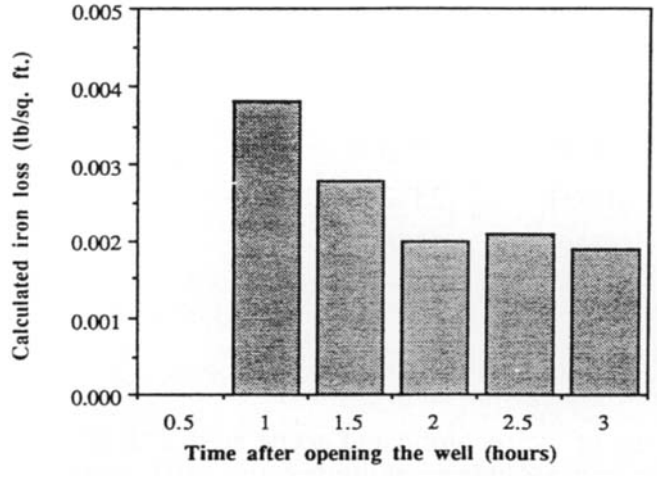


FIGURE 4. Iron losses calculated from each sample, for case 1.

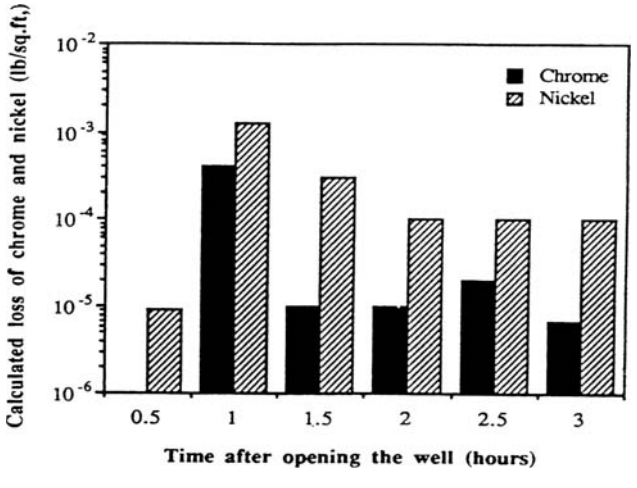


FIGURE 5. Chrome and nickel losses calculated from each sample, for case 1.

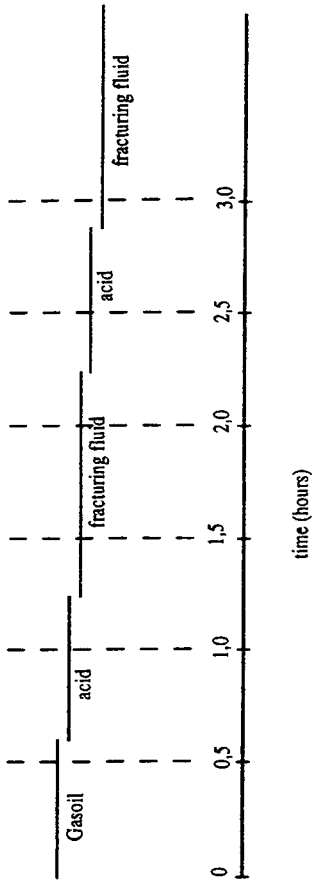


FIGURE 6. Returning fluids passing by the sampling point at different times, according to case 2.

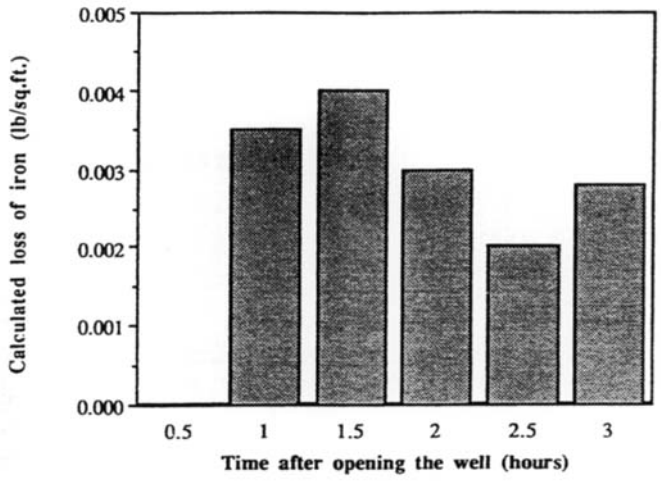


FIGURE 7. Iron losses calculated from each sample, for case 2.

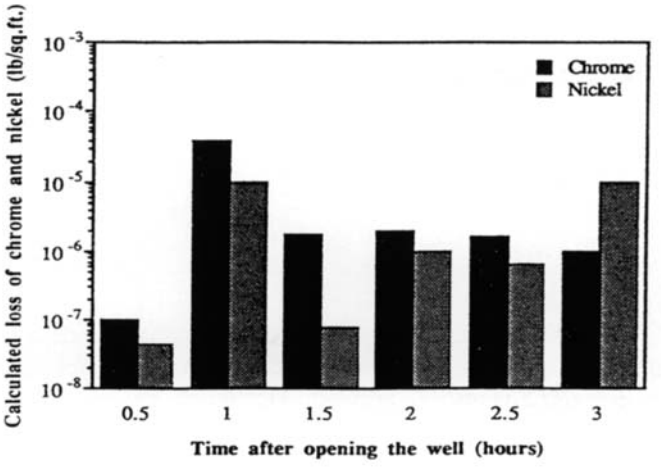


FIGURE 8. Chrome and nickel losses calculated from each sample, for case 2.

Copyrighted Materials
Copyright © 1996 NACE International Retrieved from www.knovel.com

Paper No.
19

CORROSION 94
The Annual Conference and Corrosion Show
Sponsored by NACE International

ACID INHIBITION OF CRA'S: A REVIEW

Michael L. Walker, Juanita M. Cassidy, Ken R. Lancaster, and Terry H. McCoy
Halliburton Energy Services
P.O. Box 1431
Duncan, OK 73534

ABSTRACT

This paper will review the brief history in the literature of the inhibition of corrosion resistant alloys (CRA's) in acidic stimulation fluids. This review primarily discusses the problems associated with inhibiting 13% Cr and 22% Cr duplex steels in hydrochloric (HCl) and hydrochloric-hydrofluoric (HCl-HF) acid systems using low alloy inhibitors and the successes achieved using high alloy inhibitors. Other areas briefly discussed are the repassivation of 13% Cr and 22% Cr, effect on nickel-based alloys and use of organic acids.

Keywords: corrosion resistant alloys, inhibitors, low alloy steel, hydrochloric acid, corrosion, stainless steel, nickel-based alloys.

INTRODUCTION

In the production of oil and gas, other fluids are sometimes co-produced which are corrosive to the tubulars. Typically, the use of corrosion inhibitors to mitigate the effects of these produced fluids is the method most commonly applied. However, the concept of producing these fluids through materials which are inert to the production environment is also very attractive. This concept would mean no costs over the initial capital cost of the tubulars and a trouble free production schedule, at least from a corrosion view point.

REVIEW

CRA's

A corrosion resistant alloy (CRA) is defined as an alloy whose weight loss corrosion rate in produced fluids is at least an order of magnitude less than carbon steel, thus providing an alternative method to using inhibition for corrosion control.[1] This could include relatively low cost steels with 9% chromium to expensive nickel-based alloys. CRA's can also be classified further by reference to their microstructure, such as martensitic (13% Cr), ferritic-austenitic (22% Cr duplex) and austenitic (nickel-based alloys). Emphasis of this paper is on 13% Cr and 22% Cr alloys. Nickel-based alloys will only be briefly mentioned here and may be the subject of a later presentation.

History

Corrosion from a sweet oil well was first noted in 1945 in Southeastern Louisiana.[2] Serious concern was expressed when strings of tubing required replacement after 2 to 4 years of service. Subsequently, in the late 1940's, the NACE Technical Practices Committee 1-C undertook the problem as its major project for study.[2] Carbon dioxide was listed as a primary factor. Various possible solutions were explored including coated tubulars, metal plating, inhibitors, as well as alloy steel. Also in 1950, it was reported that 9% Cr and 9% Ni materials showed significantly lower corrosion rates than ordinary steels in corrosive environments containing high CO_2 partial pressures.[3] In 1952, Chevron successfully used low hardness 9% Cr-1% Mo tubulars in the minimally sour Puckett-Ellenberger field in Texas.[4] In 1964, corrosion problems in the Brown Bassett Ellenburger gas field (Terrell County, Texas) were reported.[5] Both 9% Cr-1% Mo and 410 stainless steel were resistant to the production fluids with 9% Cr-1% Mo being the most economical. Despite this activity, the concept of using 'inert materials' to reduce the corrosive effects of the produced fluids and to increase the life of the downhole tubulars did not gain much momentum due to higher initial capital costs, long delivery times and use of 'cheaper' alternatives.

In the late 1970's and early 1980's, higher oil prices along with increased production from formations with corrosive environments and higher formation temperatures brought about another review of the use of CRA's. Successful use of 13% Cr tubulars beginning in the late 1970's in the Tuscaloosa Trend and other areas in the world confirmed that the use of CRA's was a viable alternative.[4] Duplex stainless steels were also being investigated for use as oilfield tubulars based on their success in the chemical industry.[6] The duplex stainless steels offered higher mechanical properties and better corrosion resistance to produced fluids than 13% Cr. The first production of 22% Cr duplex stainless steel made for oilfield tubulars occurred in the late 1970's. What was not realized at the time, however, was the corrosive effect of acidic stimulation fluids on the 13% Cr and 22% Cr materials.

ACID EFFECTS

In 1979, an Austrian well had the lower 2,000 feet of a string of tubing destroyed by 15% HCl. The well contained a hybrid string of low alloy L-80 with 22% Cr duplex steel for the bottom 2,000 feet. It was the duplex material that suffered the greatest degree of damage.[7] The failure of the inhibited acid treatment to prevent corrosion on the 22% Cr duplex portion of the string dramatically illustrated that the concept of general corrosion resistance attained by using CRA's for production corrosion was incorrect when applying the principle to other environments. Specifically, it was thought, the corrosion resistance showed by the alloy in production environments would also be found in stimulation fluids containing HCl. The Austrian example showed that this assumption was not correct.

Inhibited Hydrochloric Acid

Garber, et al, and Kolts, et al, appeared to be the first investigators to report the effect of inhibited hydrochloric acid on some CRA's.[8,9] Garber concluded that the inhibitors designed for low alloy steel were not very effective on the CRA's tested. He noted the difficulty with preferential attack of the ferritic phase in the duplex structure. This is illustrated in Figure 1. Although, differing in the details of some of the effects of the inhibitor on 13% Cr and 22% Cr duplex, Walker and McCoy along with independent studies by Burke

and by Vicentini and later by Jasinski and by Kane confirmed the same general trends: low alloy corrosion inhibitors (LA) did not perform as well on the chromium containing alloys in inhibited hydrochloric acid solutions as they did on the low alloy steels (Figure 2).[10-14]

The concept of low alloy corrosion inhibitors and high alloy corrosion inhibitors (HA) along with guidelines for the use of some commonly available low alloy corrosion inhibitors on 13% Cr and 22% Cr duplex at reasonable acid contact times were established in the above referenced works. Further, it was shown that inhibition could be achieved if temperatures and low alloy inhibitor type were considered. Basically, low alloy inhibitors would protect 13% Cr and 22% Cr duplex if inhibitor concentrations were increased (Figures 3 and 4). Unfortunately, the maximum temperature at which the low alloy inhibitors and intensifiers were able to protect 13% Cr and 22% Cr duplex was lower than for N-80 low alloy steel: about 250°F and about 225°F respectively. Comparable protection on N-80 with these inhibitors was obtained at 400°F.[10] However, higher temperature limits were reported by Jasinski at shorter contact times for 13% Cr.[13]

Effect of HF

In wells drilled into sandstone formations, HF acid is used as the stimulation fluid. Inhibitor performance on low alloy steels in 12%-3% HCl-HF is approximately equivalent to that obtained in 15% HCl. However, chromium containing alloys, namely 13% Cr and 22% Cr duplex, show a dependence on the presence of fluoride. Corrosion protection afforded by the low alloy inhibitor in HCl decreased in acid systems containing HF (12-3 HCl-HF) when tested under the same conditions (Figures 5 and 6).[10-14] This effect was found to be more pronounced on the duplex alloys, where preferential attack on the ferritic phase was made drastic.[9]

Inhibition of CRA's

Although the data provided by Garber and independently by Burke, demonstrated the effect of acid and the effect of low alloy inhibitors no reasonable methods for inhibition were shown.[8, 11] Walker and McCoy showed the first use of a high alloy inhibitor system for chromium containing alloyed steels.[10, 16] This inhibitor system successfully inhibited 15% HCl and 12-3 HCl-HF at high temperatures. The system consisted of using a high performing organic low alloy inhibitor containing acetylenic alcohols mixed with an antimony compound added separately to the acid.[17] Depending on the concentration of the organic inhibitor and the concentration of the antimony compound, inhibition of 13% Cr and 22% Cr duplex up to 350°F and higher was achieved. Further, the dependence on the presence of fluoride in the system was largely removed. The use of this high alloy inhibitor system did provide inhibition on low alloy steel as well as high alloy chromium tubulars (Figures 7 and 8).

In subsequent work, Jasinski and Frenier developed a high alloy inhibitor system based on antimony used in conjunction with unsaturated carbonyl compounds blended with amines and surfactants as the active organic component.[18] Analogously, bismuth has also been reported to function in addition to antimony in this inhibitor system. Williams, et al, mixed either antimony or bismuth in a composition containing amines and dimethyformamide in an aprotic system.[18] Unsaturated oxygen-containing compounds are not believed to be the active functional material in this inhibitor system.

In these works, a principle not expressly discussed, but considered, was the effect of the high alloy inhibitor on low alloy tubulars such as N-80. Just as low alloy inhibitors were not effectively performing on the CRA's, inhibitors for the CRA's may not perform on low alloy steel. The concept of a hybrid or dual function inhibitor, one that would work on both metal types, was based on the addition of copper to the low alloy inhibitor composition. This dual system worked reasonably well on duplex steel, but suffered in two areas: fluoride dependence on corrosion losses was not completely removed, and second, the performance of the antimony containing systems was superior. Work in this area was not fully investigated.

Cizek made a modification to this concept by substituting mercury for all or part of the copper content of the dual purpose inhibitor.[20] Although, the system was an improvement over the inhibitors containing copper alone, it still had difficulties in the presence of fluoride and was out performed in some cases by antimony or bismuth containing systems.

Ferritic Attack

Acid stimulation fluids based on HCl attack duplex steel at all temperatures. The mode of attack was preferential dissolution of the ferritic phase. Further, acid systems containing HF, such as 12%-3% HCl-HF, are found to be more corrosive on the chromium containing alloys than 15% HCl. The low alloy inhibitors allow preferential attack on the ferritic phase (Figures 1, 9, and 10). The exact reason why the fluoride ion enhances corrosive attack is unknown but may be that it is much smaller in diameter than the chloride ion and thus may be able to penetrate the passive oxide layer or remove the chromium atom from metal matrix more easily via the complex ion formation with the chromium. In another opinion, Yau and Streicher have shown that corrosive attack by stimulation acids (such as HCl) is driven by galvanic action between the anodic ferrite and the cathodic austenite. The corrosion rate of ferrite increases with increasing chromium and with decreasing nickel content.[21] The galvanic action may explain the ferrite dissolution preference, but did not consider the effect of fluoride. Metallographic studies of duplex alloys exposed to these acid systems by McCoy, et al, indicated that corrosion was first occurring at the ferrite-austenite boundary.[22] Corrosion at the phase interface would not be unexpected as these are high energy sites resulting from microstructure mismatching (i.e., body centered cubic ferrite to face centered cubic austenite). Since the continuous phase is ferritic, the degree of damage to the structural integrity of the metal is more pronounced than indicated by the weight loss data.

Much of the preferential ferrite dissolution is prevented by the use of the high alloy antimony inhibitor system as compared to the low alloy inhibitors. Metallographic examinations show that some preferential attack still occurs, but is greatly reduced (Figure 11).

Repassivation

The chromium-containing iron alloys, 13% Cr and duplex steel, have layers of chromium rich oxides on the surface. These oxide layers are the primary agents responsible for protecting the base metal from the corrosive action of CO_2, H_2S, etc. in the production environments. Treatment of these alloys with acid (HCl or HCl-HF) removes the protective oxide layers. Lancaster, et al, and Cassidy, et al, have shown that the alloys are placed in an active state immediately after contact with the acid fluid containing low alloy inhibitors.[23,24] Although acidizing renders both alloy types active, 22% Cr duplex steel showed restoration of the passive layer in a high chloride (5% NaCl), low pH (2% acetic acid) simulated production environment. The 13% Cr alloy has also been shown to reform the passive oxide layer in brine after acidizing, although this reformation appears to be critically dependent on pH, temperature and chloride content of the brine.[23-26]

Cassidy, et al, postulated a method for protection of 13% Cr and 22% Cr steels by introduction of a repassivating fluid following acidizing.[24] The efficacy of utilizing a common industrial cleaning passivating solution, the Navy solution (0.5% $NaNO_2$, 0.25% NaH_2PO_4, 0.25% Na_2HPO_4), following an HCl acid stimulation treatment on 13% Cr and 22% Cr has been examined.

Valdez, et al,[27] and Lancaster, et al,[23] showed in independent work in field evaluations and laboratory studies, respectively, a disturbing effect in the repassivation of 13% Cr and 22% Cr duplex. They report that although the steel alloys apparently repassivated following acidizing, a greater loss of iron with respect to chromium was observed in the repassivation of 22% Cr duplex and a greater loss of chromium with respect to iron was observed on the 13% Cr alloy (Figures 12 and 13). The results are obtained from preliminary studies and further efforts are continuing in each group.

Nickel-Based Alloys

Nickel-based alloys generally show the greatest degree of resistance to the production environments. In this case, the general rule of resistance in production environments is also found in stimulation fluids based on HCl and HCl-HF, that is, nickel is more resistant to HCl than iron. However, at elevated temperatures, 350°F and above, nickel-based alloys are found to undergo a significant amount of corrosion. Again, this is in the presence of low alloy inhibitors in the acid. Walker demonstrated that the high alloy inhibitor system based on antimony and its corresponding activating agent would perform on these widely varying alloy compositions. Further, cobalt alloys, MP35N and Monel (nickel-copper), alloys are inhibited by these same type systems (Figure 14).[27-28]

Organic Acids

Organic acids are sometimes used in well stimulations. Two acid types are used: 10% acetic and 10% formic acid. These acids are used where formation deconsolidation can occur in the presence of strong mineral acid, or where corrosion losses of the downhole metal goods are a concern. The concerns are most notable in wells at elevated temperature.

Chromium-containing CRA's show a high degree of resistance to these acids when tested with low alloy corrosion inhibitors. As expected, the higher the alloy content, the more resistant the alloy was to the acid. Lower corrosion losses were obtained on 22% Cr duplex than on 13% Cr under the same conditions. Further, formic acid, due to its greater acidity, was shown to be more corrosive than acetic acid, Figure 15.

The addition of HF to the acid system increased the corrosivity of the base fluid significantly,[29] Figure 16. However, corrosion losses were still within acceptable corrosion levels.

CONCLUSION

In conclusion, corrosion resistant alloys such as 13% Cr and 22% Cr duplex were effective in preventing excessive corrosion due to produced fluids. However, the inhibited HCl solutions were found to be surprisingly corrosive. In addition, the presence of fluoride was an unexpected component to corrosive action of stimulation fluids. Commercial inhibitors designed for protection of low alloy steel were not effective in providing adequate protection to the chromium alloys mentioned, however, systems based on activators for antimony or bismuth were effective in providing protection for a wide variety of alloys: 9% Cr-1% Mo to MP35N.

REFERENCES

1. NACE Technical Committee T-1F-21G: "Use of Corrosion Resistant Alloys in Oil Field Environments," Report 1F-192 (1993 Revision).

2. H.L. Bilhartz, "High Pressure Sweet Oil Well Corrosion," Vol. 7, No. 8 (1951).

3. NACE Publication 50-3, July 1950: "The Field Testing of 32 Alloys in the Flow Streams of Seven Condensate Wells".

4. J.D. Combes, J.G. Kerr, L.J. Klein, "13% Cr Tubulars Solve Corrosion Problems in the Tuscaloosa Trend," Petroleum Engineering International, March, 1983, p. 50-70.

5. R.F. Weeter, "A Case History - High Pressure Sour Gas Well Corrosion Central-Brown Bassett Field," Proceedings of the 11th Annual Southwestern Short Course: NACE, April, 1964, p. 55-60.

6. Private Correspondence: W. Walter, Mannesmannrohren-Werke AG.

7. Private Communications: Halliburton Energy Services, 1980.

8. J.D. Garber, M. Kontow, "How High-Alloy Tubulars React in Acidizing Environments," Petroleum Engineering International, July, 1984, p. 60.

9. J. Kolts, S.M. Corey, "Corrosion and Stress Corrosion of High Performance Alloys in Simulated Acidizing Environments," Corrosion/84, paper no. 217, (Houston, TX: NACE, 1984).

10. M.L. Walker, T.H. McCoy, "Effect and Inhibition of Stimulation Acids on Corrosion Resistant Alloys," Corrosion/86, paper no. 154, (Houston, TX: NACE, 1986).

11. P.A. Burke, J.L. Dawson, G. Bailey, R.C. Woollam, "Corrosion of Chromium Steels in Inhibited Acid," Corrosion/87, paper no. 41, (Houston, TX: NACE, 1987).

12. B. Vicentini, G. Rondelli, G. Onofrio, "Corrosion Behavior of High Alloy Tubular Materials in Inhibited Acidizing Conditions," Corrosion/87, paper no. 43, (Houston, TX: NACE, 1987).

13. R. Jasinski, W.W. Frenier, S. Grannan, "Inhibiting HCl Corrosion of High Chrome Tubular Steels," Corrosion/88, paper no. 188, (Houston, TX: NACE, 1988).

14. R.D. Kane, M.S. Wilhelm, "Compatibility of Stainless and Nickel-Based Alloys in Acidizing Environments," Corrosion/89, paper no. 481, (Houston, TX: NACE, 1989).

15. G. Trabanelli, G. Frignani, C. Brunorro, Monticelli, F. Zucchi, "Corrosion and Inhibition of Low Alloyed Chromium Steels in Hydrofluoric Acid Solutions," Corrosion/85, paper no. 376, (Houston, TX, 1985).

16. M.L. Walker, "Corrosion Inhibitors for 13% Cr Steel," Proceeding of the Southwest Petroleum Short Course, 1985, p. 529.

17. M.L. Walker, U.S. Patent No. 4,498,997 (1985).

18. R.J. Jasinski, European Patent Application 0,471,400A1 (1992).

19. D.A. Williams, P.K. Holifield, J.R. Looney, L.A. McDougall, U.S. Patent No. 4,997,040 (1991).

20. A. Cizek, U.S. Patent No. 4,997,040 (1991).

21. Y. Yau, M.A. Streicher, "Galvanic Corrosion of Duplex -Fe -Cr -10% N: Alloys in Reducing Acids," Corrosion/85, paper no. 228, (Houston, TX: NACE, 1985).

22. T.H. McCoy, M.L. Walker, S.T. Mackey, "Effect of Acidizing Solutions on K_{ISCC} of 13% Cr and 22% Cr Stainless Steels," Corrosion/94, paper no. 88, (Houston, TX: NACE, 1994).

23. K.R. Lancaster, J. Cassidy, M.L. Walker, "Effect of HCl on the Repassivation of Some Chromium-Containing Alloys," Corrosion/93, paper no. 94, (Houston, TX: NACE, 1993).

24. J.M. Cassidy, K.R. Lancaster, M.L. Walker, "Repassivation of Some Chromium-Containing Alloys," Corrosion/93, paper no. 95, (Houston, TX: NACE, 1993).

25. J.M. Cassidy, M.L. Walker, K.R. Lancaster, "Repassivation of 13% Cr After Acidizing: Electrochemical Investigation of Oxidizing Solutions" Corrosion/94, paper no. 87, (Houston, TX: NACE, 1994).

26. S. Huizinza, W. Liek, "The Performance of 13% Cr Steel in Acid Stimulations," Corrosion/93, paper no. 80, (Houston, TX: NACE, 1993).

27. A. Valdez, A. Vilario, S. Marcano, C. Boggio, "A Field Experience of Corrosion Inhibition During Acid Fracturing of a Deep Oil Well Completed with 22% Cr," Corrosion/93, paper no. 96, (Houston, TX: NACE, 1993).

28. M.L. Walker, "Tubulars in Harsh Environments Need Special Protection," Drilling, p. 30, 1988.

29. M.L. Walker, T.H. McCoy, "Inhibition of High Alloy Tubulars II: Effect of Fluoride Ion and Acid Strength," Corrosion/88, paper no. 189, (Houston, TX: NACE, 1989).

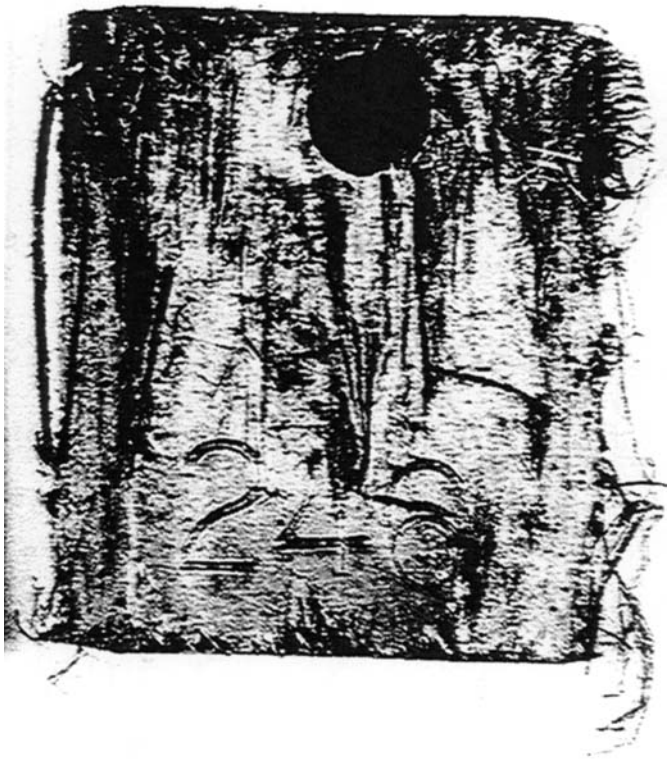


Figure 1. Picture of 22% Cr duplex steel showing preferential ferrite attack. Exfoliation of the austenite phase occurs as the ferritic phase is dissolved by the acid containing low alloy inhibitors.

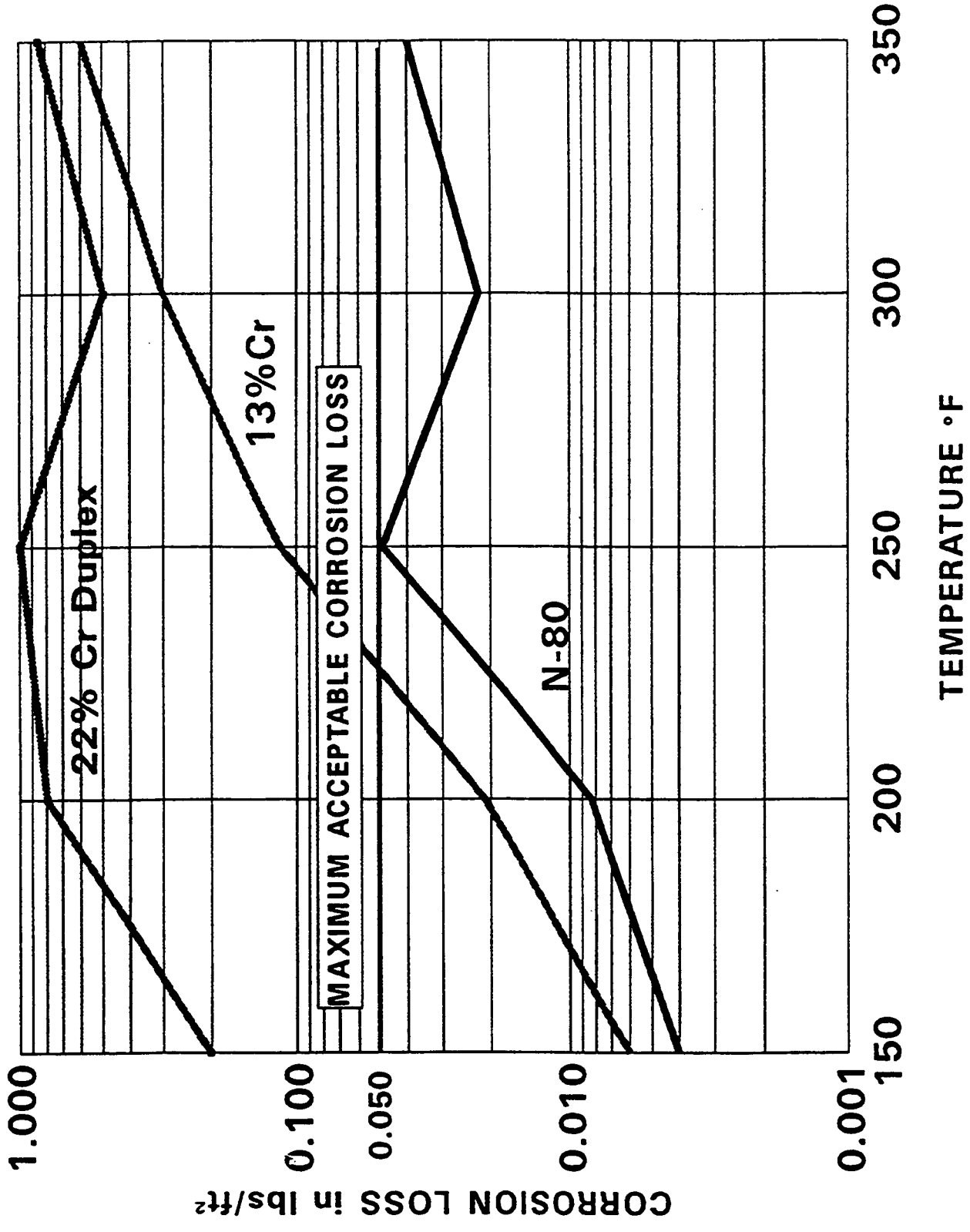


Figure 2. Corrosion losses obtained in 15% HCl. Concentration of the LA inhibitor used in obtaining data shown are those values recommended for N-80 at the corresponding temperature.

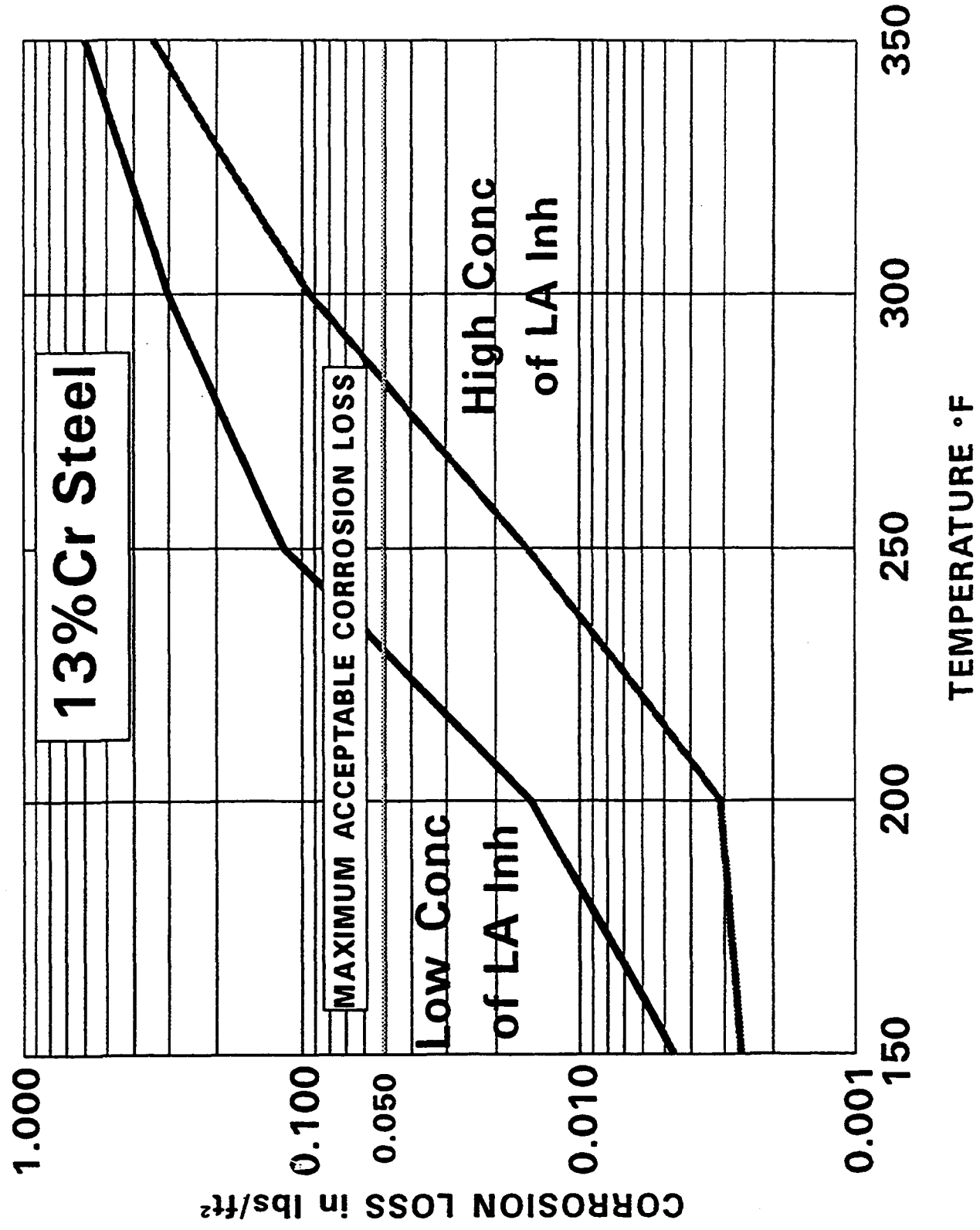


Figure 3. Performance of low alloy inhibitors on 13% Cr steel in 15% HCl at concentrations 2X-5X above that recommended for N-80.

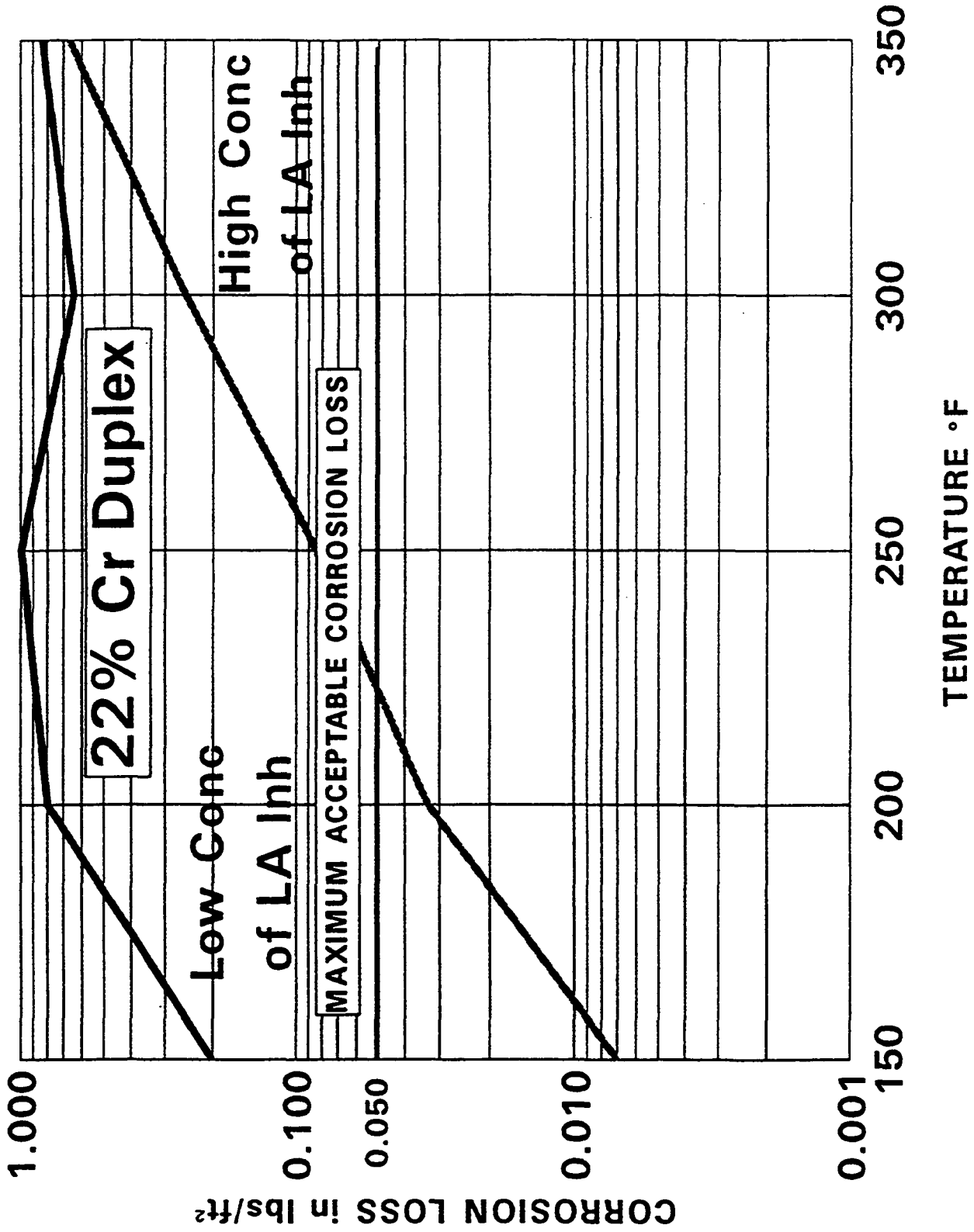


Figure 4. Performance of low alloy inhibitors on 22% Cr duplex steel in 15% HCl at concentrations 2X-10X above that recommended for N-80.

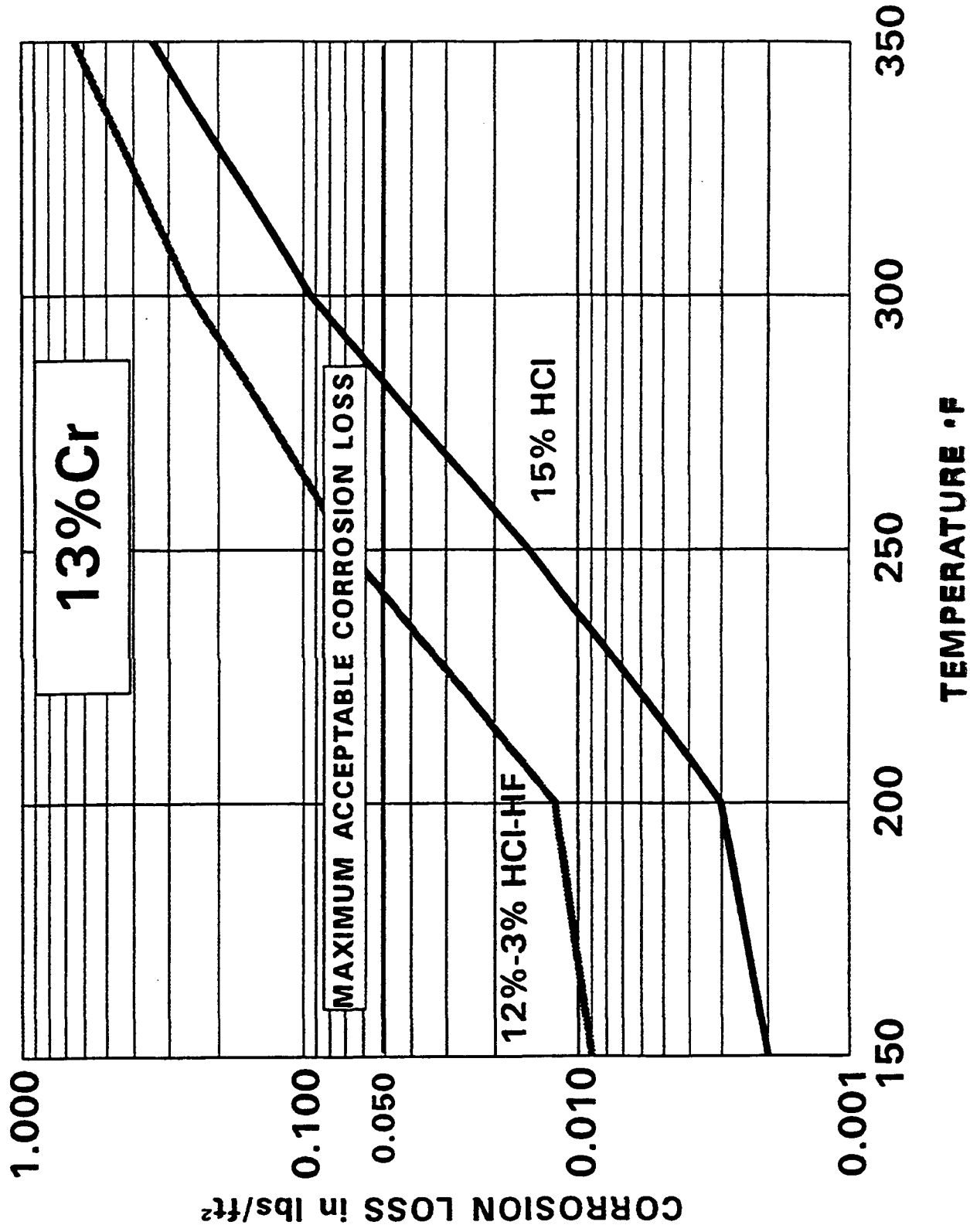


Figure 5. Effect of HF on the performance of low alloy inhibitors at high inhibitor concentration on 13% Cr.

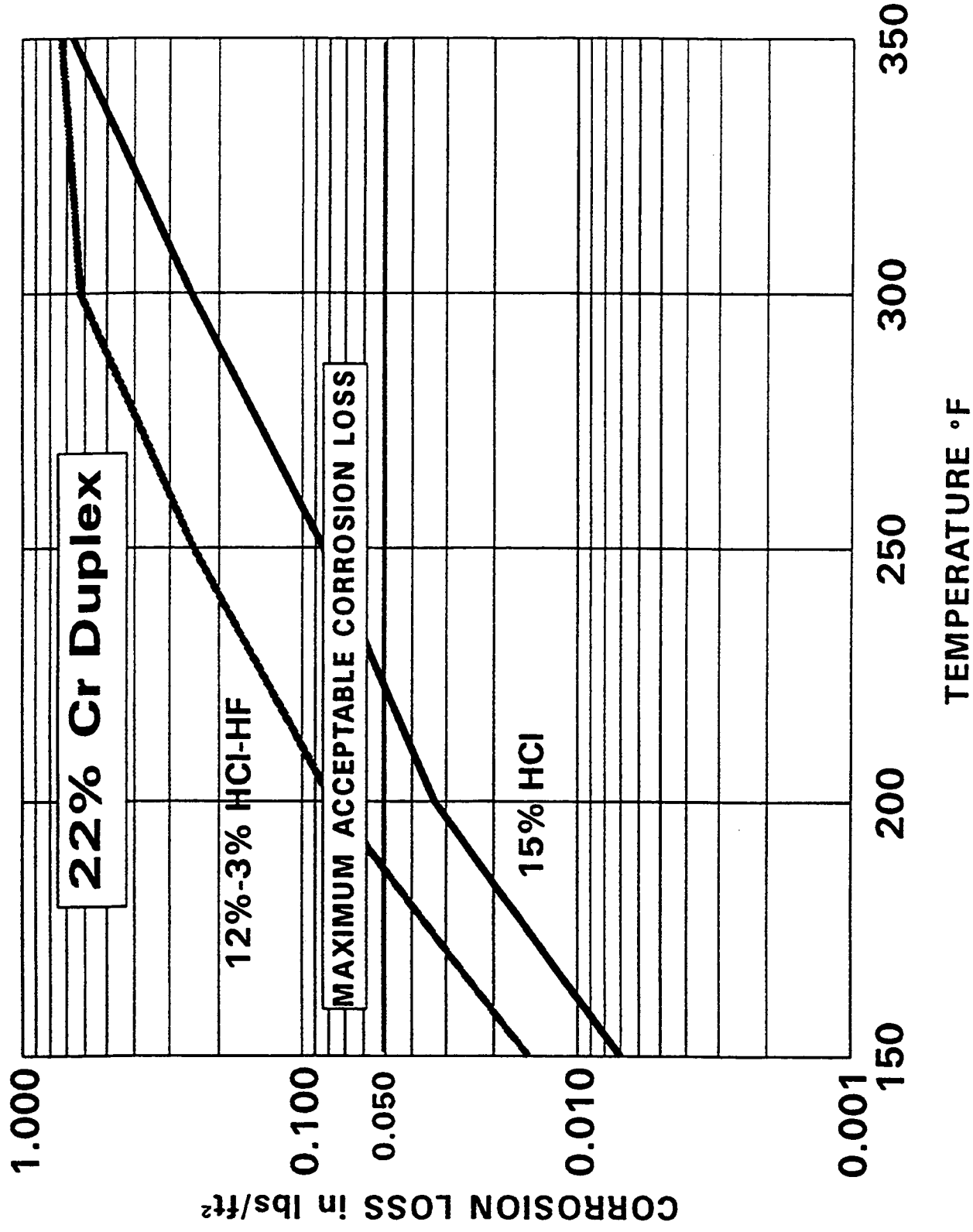


Figure 6. Effect of HF on the performance of low alloy inhibitors at high inhibitor concentrations on 22% Cr duplex steel.

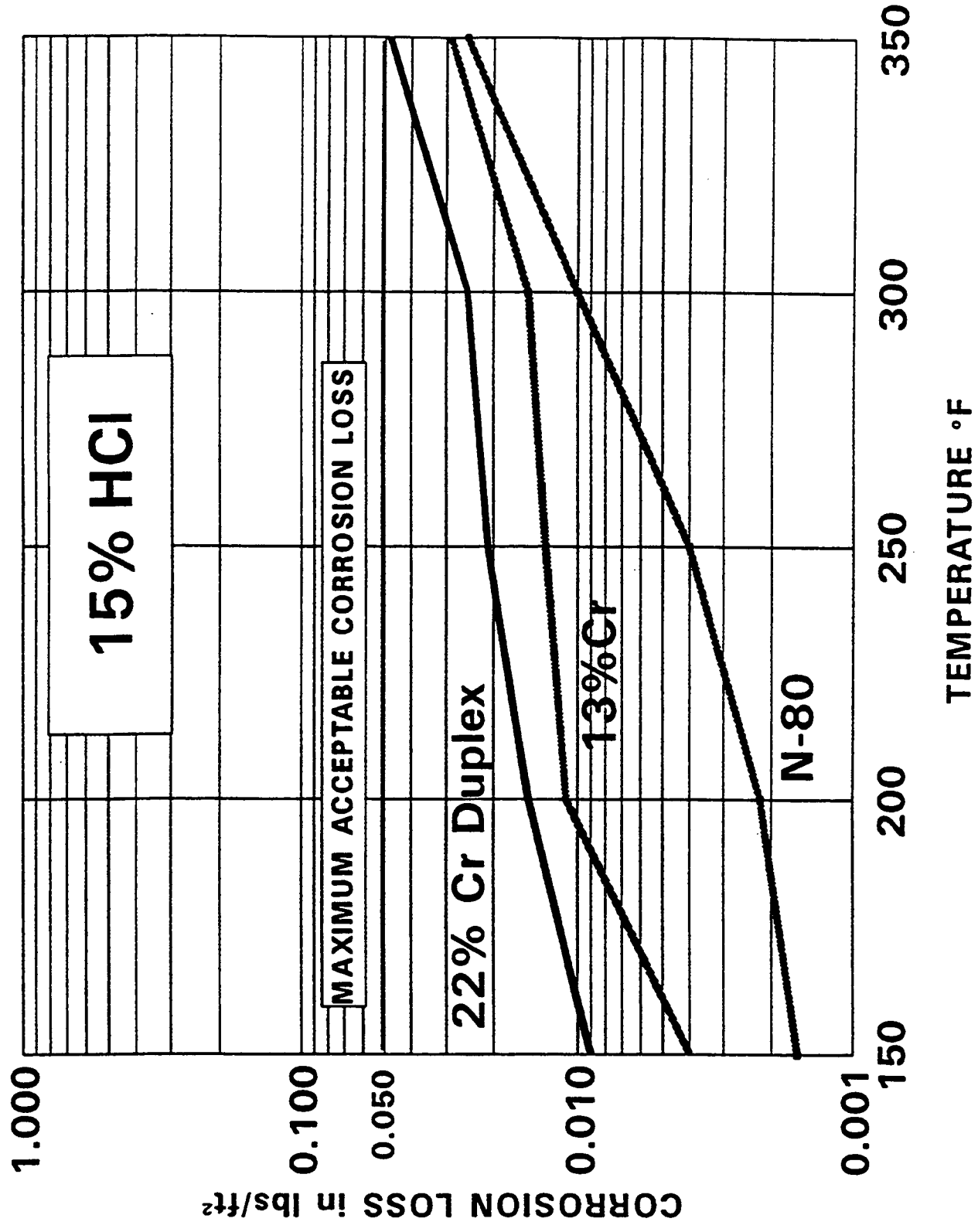


Figure 7. Corrosion losses obtained on three alloy types using the high alloy inhibitor system in 15% HCl.

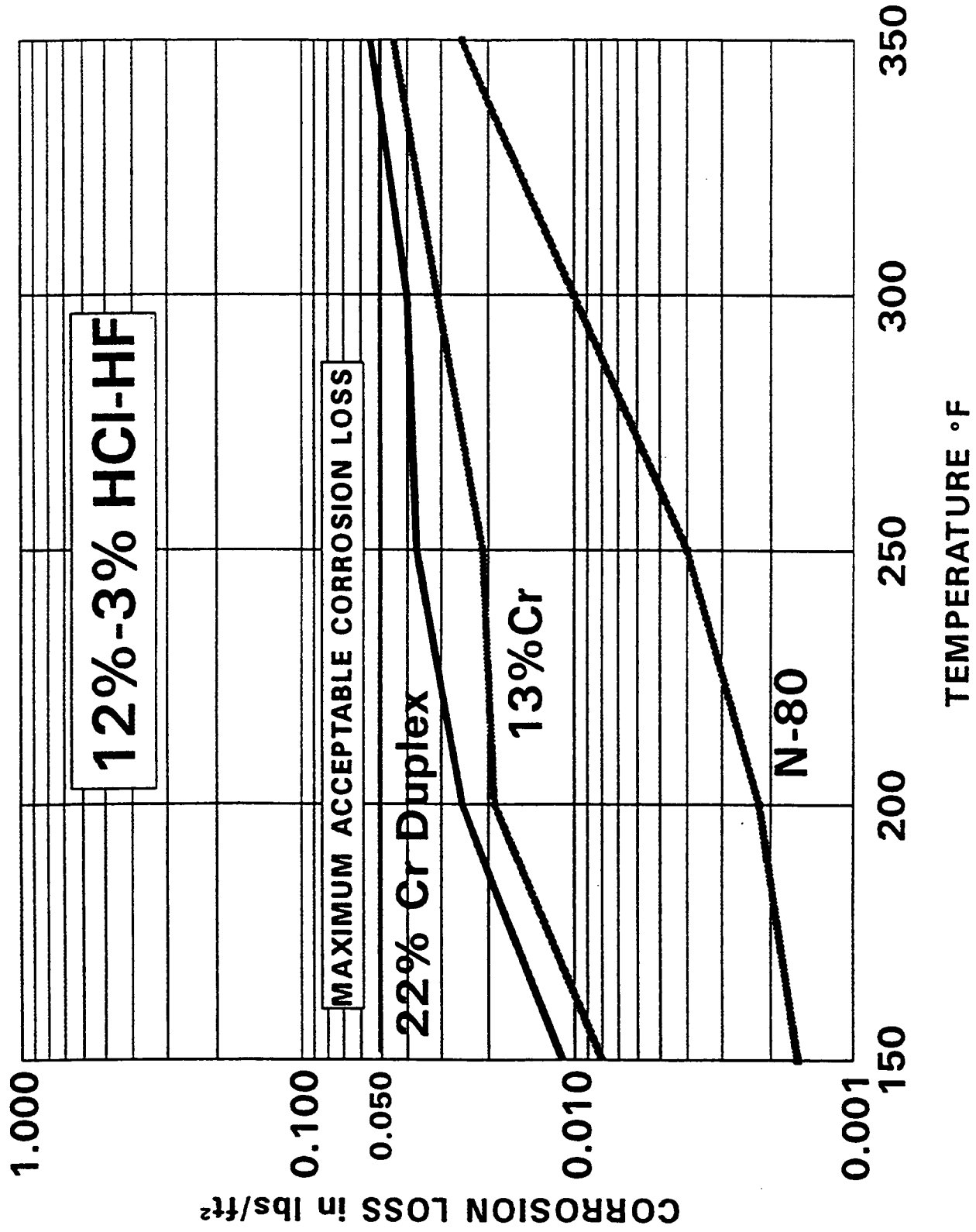


Figure 8. Corrosion losses obtained on three alloy types using the high alloy inhibitor system in 12-3 HCl-HF.

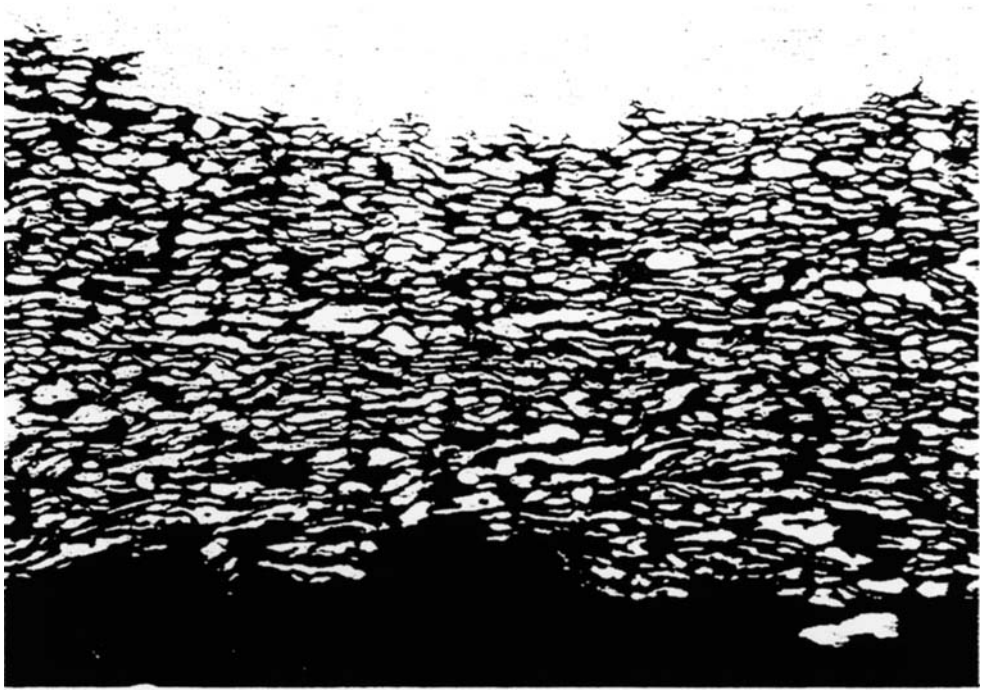


Figure 9. Photomicrograph of the surface of the coupon shown in Figure 1. Original magnification 200X. Note the complete isolation of the austenite grains at the surface. The sample was exposed to 15% HCl at 300°F using low alloy inhibitor and cuprous iodide intensifier.

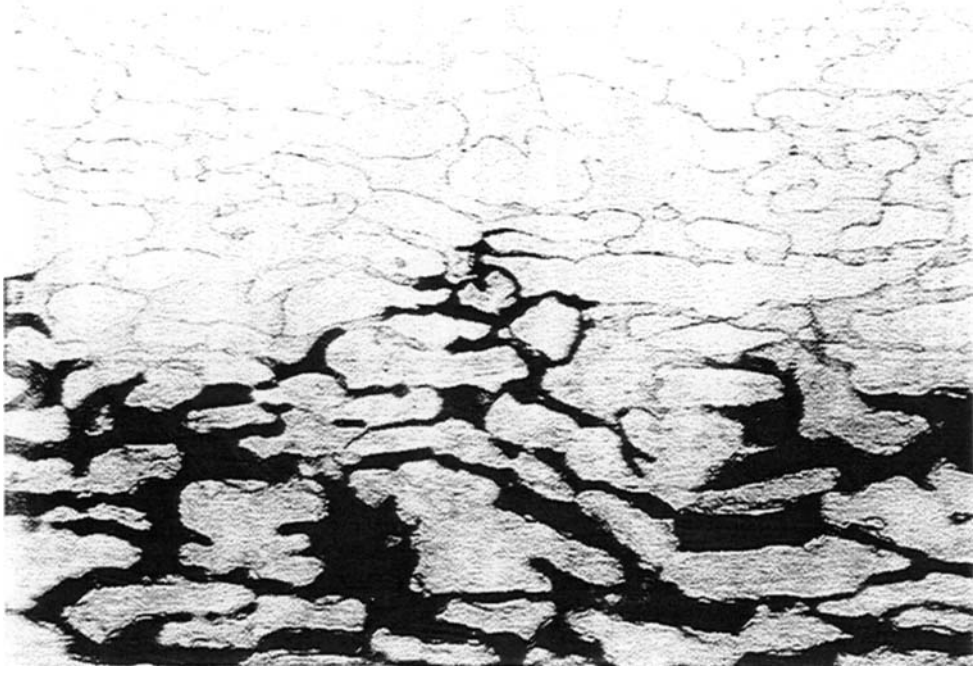


Figure 10. Photomicrograph of Figure 9 at 1000X.

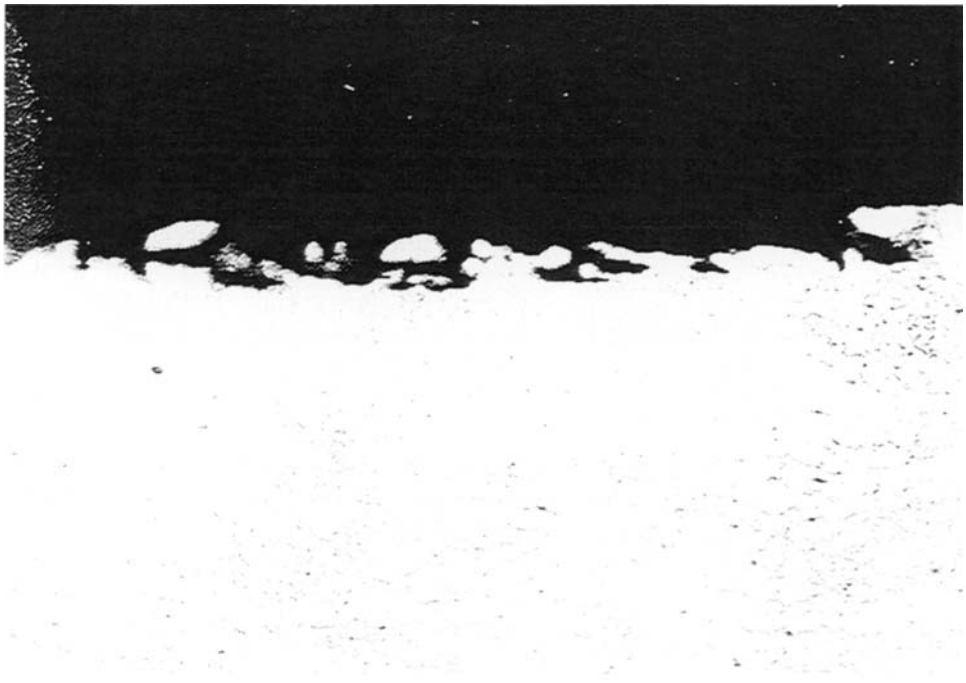


Figure 11. Photomicrograph of the surface of a 22% Cr duplex coupon exposed to 15% HCl containing the high alloy inhibitor system all other conditions were the same as quoted in the caption of Figure 9.

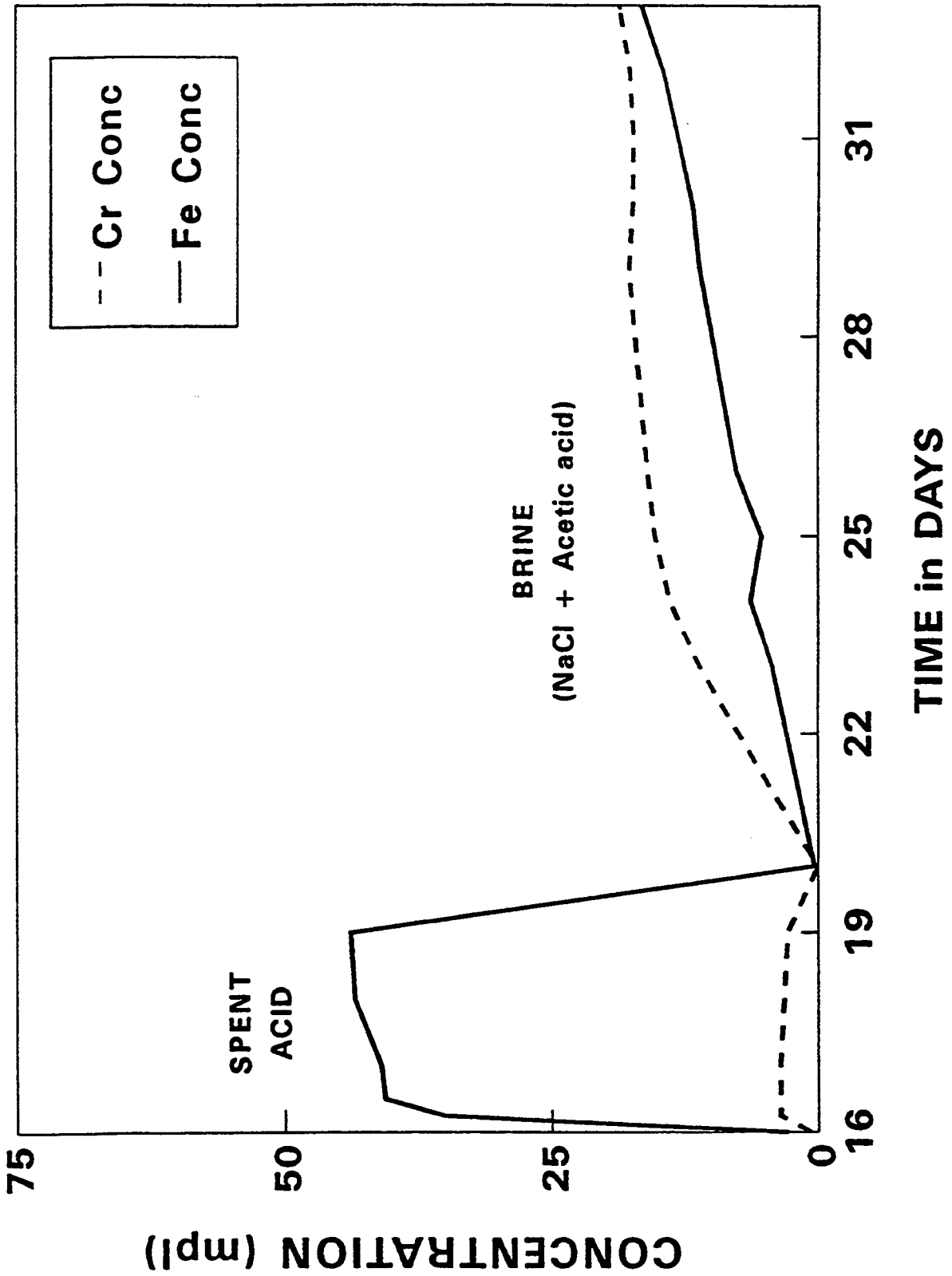


Figure 12. Solution concentrations of iron and chromium in spent acid and simulated production brine after exposure of 22% Cr duplex steel to 15% HCl containing low alloy inhibitors.

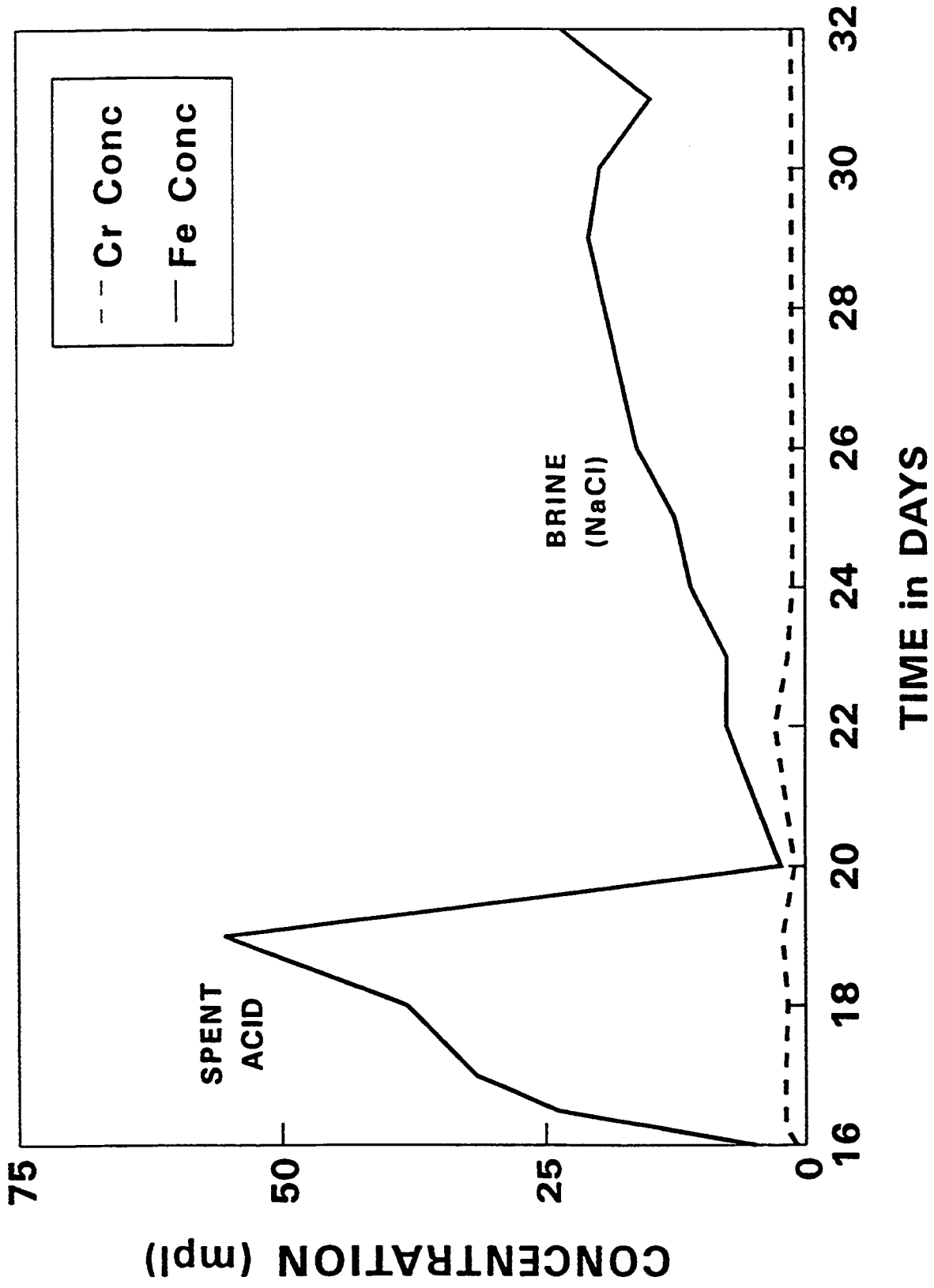


Figure 13. Solution concentrations of iron and chromium in spent acid and simulated production brine after exposure of 13% Cr steel to 15% HCl containing low alloy inhibitors.

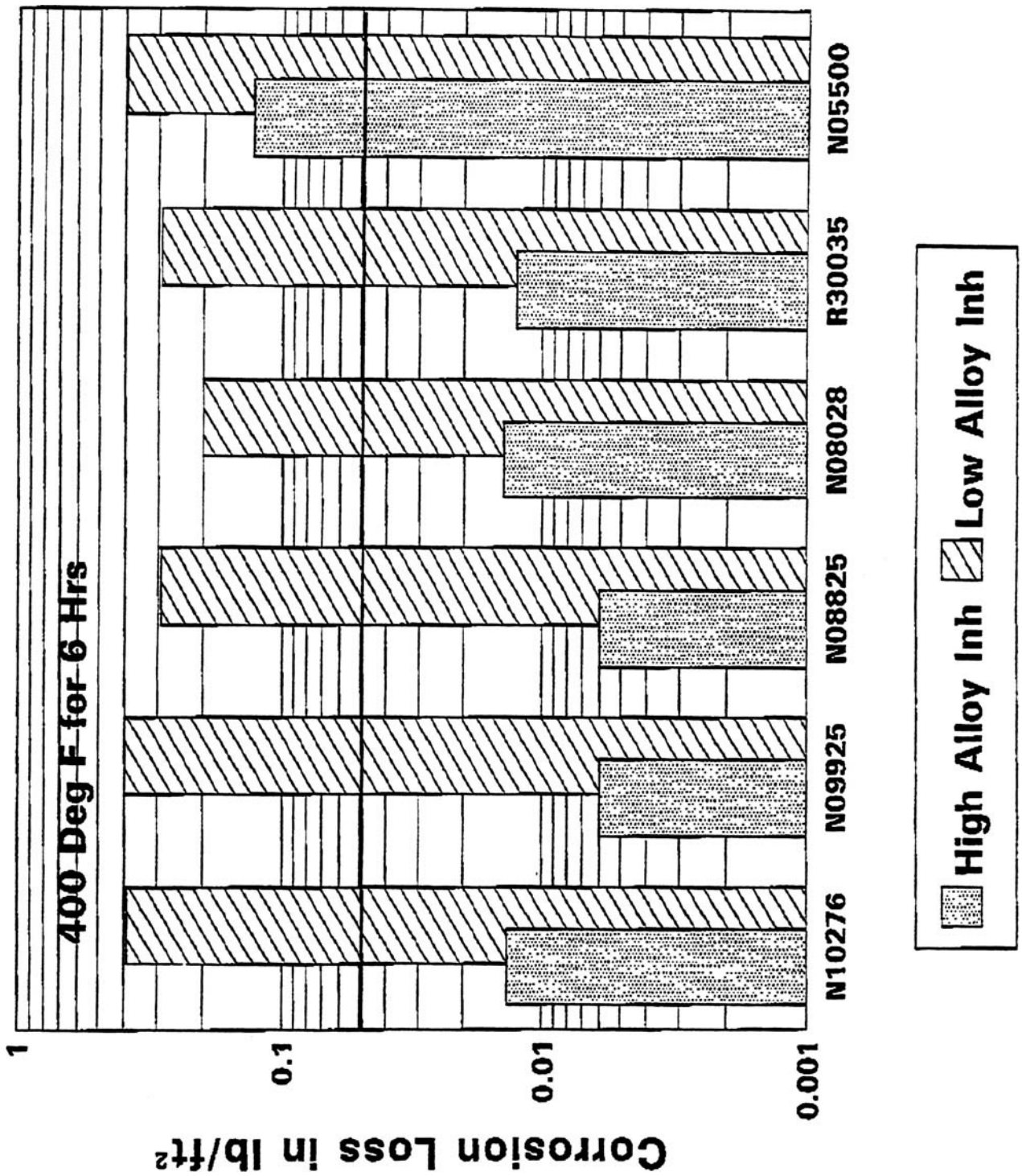


Figure 14. Comparison of the corrosion losses of some nickel-based and other alloys in 15% HCl with low alloy inhibitors and high alloy inhibitors.

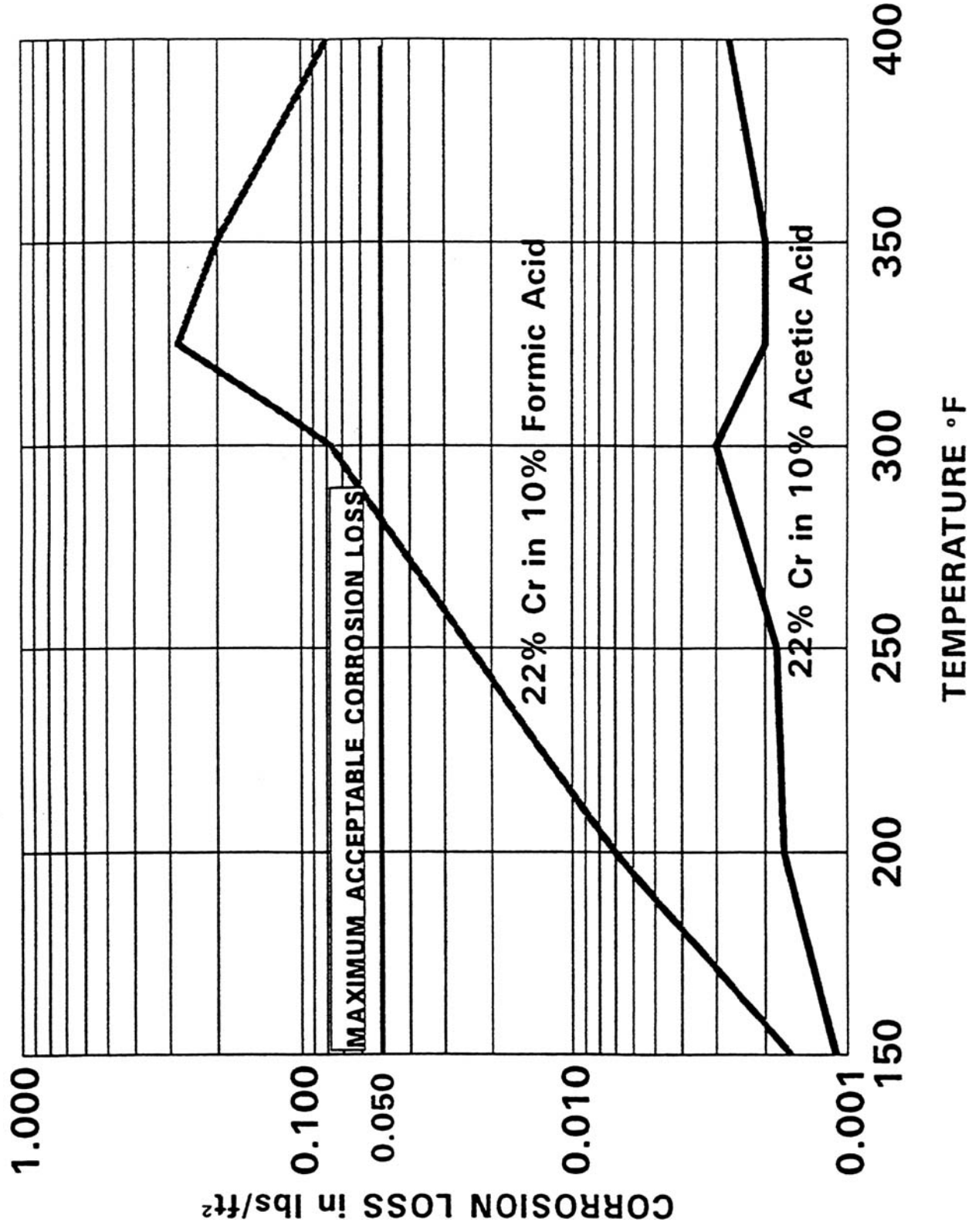


Figure 15. Comparison of corrosion losses of 22% Cr duplex in 10% acetic acid or 10% formic acid at various temperature using low alloy inhibitor for organic acids.

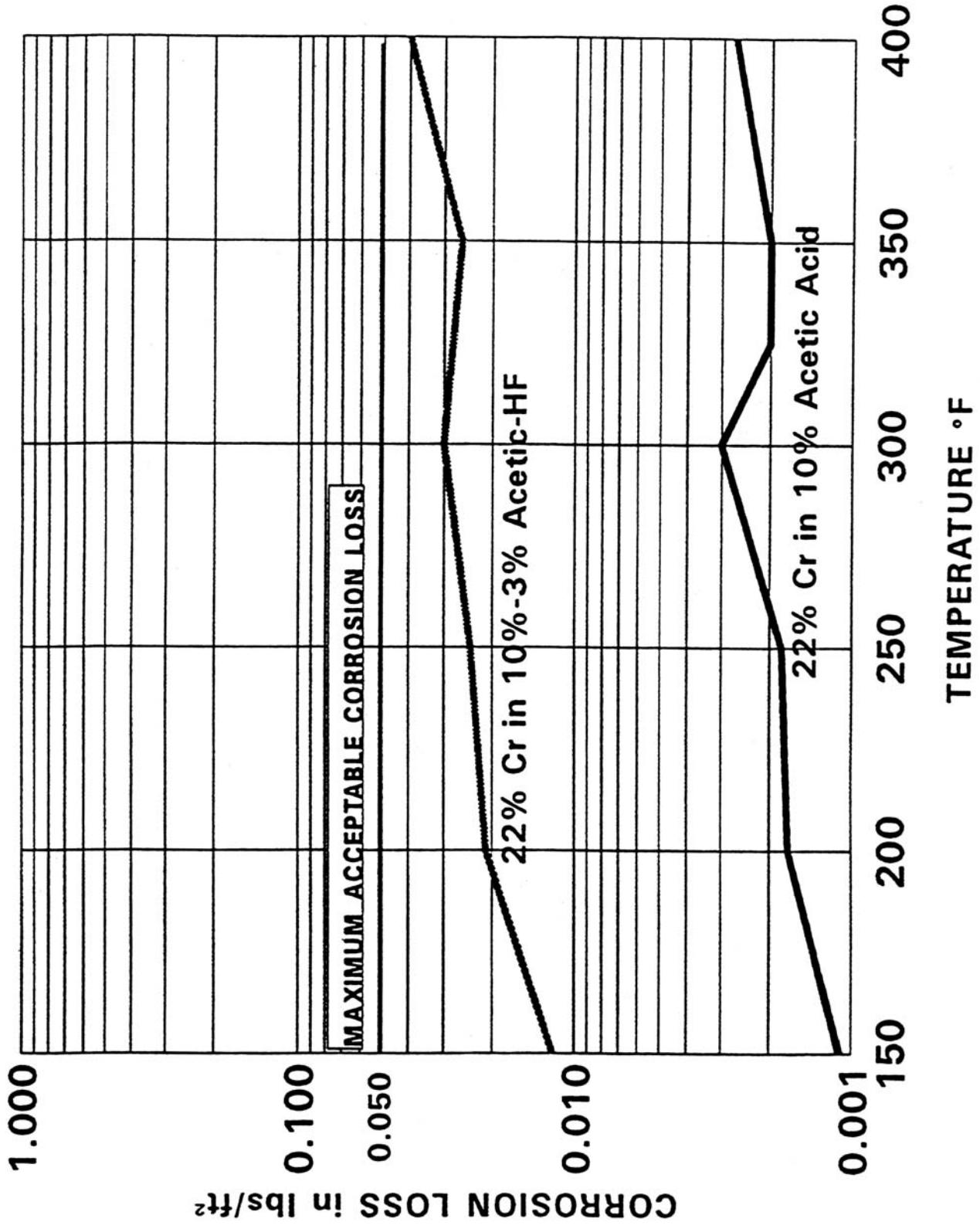


Figure 16. Effect of HF on corrosion loss of 22% Cr in 10% acetic acid containing low alloy inhibitor for organic acids.

Copyrighted Materials
Copyright © 1996 NACE International Retrieved from www.knovel.com

Bibliography

Volume I

GENERAL PAPERS INCLUDING FIELD EXPERIENCES

M. Bonis, J.-L. Crolet. "Practical Aspects of the Influence of *in situ* pH on H_2S- Induced Cracking." *Corrosion Science* 27, 10/11 (1987): pp. 1,059-1,070.

A. Cigada et al. "Sulfide stress corrosion cracking in steels for the oil industry" in *International Congress of Metallic Corrosion*, Vol. 4., p. 458-465.

J.-L. Crolet, M. Bonis. "pH Measurements under High Pressures of CO_2 and H_2S," *Materials Performance*, 23, 5 (1984): pp. 35-42.

J.-L. Crolet, M. Bonis. "Prediction of the Risks of CO_2 Corrosion in Oil and Gas Wells." Presented at the 22nd Offshore Technology Conference" 1990.

B. Craig. "Controlling Corrosion in Deep Hot Wells," *Petroleum Engineer International*, October (1987) pp. 35-38.

M.F. Galis et al. "Corrosion properties of stainless steels and nickel base alloys for O.C.T.G. purposes." Presented at the 28th Annual Conference of The Metallurgical Society of CIM, 1989.

A. Ikeda et al. "Recent Progress in Tubular Products for Oil and Gas Production," *The Sumitomo Search* 37, 11(1988): pp. 43-64.

A. Ikeda et al. "Corrosion Behavior of Low and High Alloy Tubular Products in Completion Fluids for High Temperature Deep Well." CORROSION/92, paper no. 46. NACE 1992.

R. Johnsen. "Corrosion Problems in the Oil Industry," 11th Scandinavian Corrosion Conference, April 1989, p. 12.

R.D. Kane. "Roles of H_2S in Behaviour of Engineering Alloys," *International Metals Reviews*, 1985, Vol. 30, No. 6, pp. 291-301.

J.A. King, P.S.C. Badelek. "Materials Performance of Valve Materials in Wet H_2S and CO_2 Contaminated Hydrocarbons." *Materials Performance* 1(1993).

K. Masamura et al. "Pitting corrosion resistance of high-alloy OCTG in CO_2 environment as affected by chlorides and sulfides." CORROSION/84, paper no. 292. NACE.

I. Matsushima. "Effects of Alloy Composition on Corrosion and SCC Resistance of High Alloy OCTG in Sour Well Environments." CORROSION/85, paper no. 233. NACE.

A. Miyasaka et. al. "Estimation and Measurements of pH in High Temperature and High Pressure Sour Environments," Nippon Steel Corp., ISIJ International, Vol. 29, no. 1, 1989.

A. Miyasaka et al. "Corrosion Performance and Application Limits of Materials in Oil Fields" in 12th International Corrosion Congress. 1993. NACE

H. Ogawa et al. "Criteria for passivity breakdown of high alloy materials in relation to crevice corrosion nucleation." *Corrosion Science*, Vol. 31 (1990): pp. 459-464.

M. Place Jr. "The development and application of corrosion resistant alloys in natural gas production." CORROSION/87, paper no. 282, NACE.

P.R. Rhodes, "Stress Cracking Risks in Corrosive Oil and Gas Wells." CORROSION/86, paper no. 322. NACE.

C.M. Schillmoller. "High Performance Alloys: How They are Used Offshore," *World Oil*, July (1988):

pp. 46-51.
C.M. Schillmoller. "Selection of Corrosion Resistant Alloy Tubulars for Offshore Applications," presented at the 1989 Offshore Technology Conference.
L.M. Smith et al. "Materials Selection for Gas Processing Plant." *Stainless Steel Europe*, Vol. 7, No. 1, 1995.
G.L. Swales, "Applications of Centrifugally-Cast Alloy Piping and Pipe Fittings in Onshore Oil and Gas Production," NiDI Technical Series No. 10 034. Paper prepared for presentation at the 28th Annual Conference of Metallurgists of the Canadian Institute of Mining and Metallurgy Meeting of Sea and Science, Halifax, Nova Scotia, 1989.
G.L. Swales, B. Todd. "Nickel-Containing Alloy Piping for Offshore Oil and Gas Production," Paper presented at 28th Annual Conference of Metallurgists of the Canadian Institute of Mining and Metallurgy Meeting of Sea and Science, 1989.
B. Todd. "Corrosion and Materials Selection in Seawater Systems." C76/79, Conference on Cooling with Sea Water, 1979, Process Engineering Group and the Steam Plant Group of The Institution of Mechanical Engineers.
R.S. Treseder, R.N. Tuttle. "Historical Review of the Sulfide Stress Cracking Problem in Oil and Gas Production." The 6th Asian-Pacific Corrosion Control Conference, 1989, Singapore, NACE.
S. Tsujikawa et al. "An Alternative Method for Evaluating the Sour Gas Resistance of Low Alloy Steel and CRA's." paper no. 45, CORROSION/92, NACE.
R.N. Tuttle. "Corrosion in Oil and Gas Production." *J. of Petroleum Technology*, July 1987.
R.N. Tuttle. "What Is a Sour Environment?" *Petroleum Engineers*, March 1990.
R.N. Tuttle. "Deep Drilling - A Materials Engineering Challenge," *Materials Performance*, February 1974, pp. 42-46.
R.N. Tuttle. "New Trends in Application of Steel and Corrosion Resistant Alloys in Oil and Gas Production." Lecture 3, Proceedings of the Third International Conference on Steel Rolling, Technology of Pipe and Tube and Their Application, 1985. The Iron and Steel Institute of Japan.
S.M. Wilhelm, R.D. Kane. Status Report: Corrosion Resistant Alloys, *Petroleum Engineer International*, March 1987, p. 36.
S.M. Wilhelm, R.D. Kane. "Selection of Materials for Sour Service in Petroleum Production," *Journal of Petroleum Technology*, October 1986, pp. 1,051-1,061

SECTION 1 MARTENSITIC STAINLESS STEELS

A.K. Agrawal et al. "Corrosion and Stress-Corrosion Cracking Behavior of a Martensitic 12Cr-3.5Ni-Fe Alloy in Simulated Sour Gas Environments," CORROSION/86, NACE.
B. Baroux et al. "Investigations on the Corrosion Resistance of 13% Cr Stainless Steels Used in Acid Wells." CORROSION/83, paper no. 57, NACE.
M. Barteri et al. "Corrosion Resistance of Martensitic Stainless Steels in Moderately Sour Oilfield Environments." CORROSION/95, paper no. 76, NACE.
D.S. Burns. "A Method of Evaluation of New Materials and Processes for Use in H_2S Service," CORROSION/75, NACE.
J.L. Crolet. "Acid Corrosion in Wells (CO_2, H_2S): Metallurgical Aspects," *Journal of Petroleum Technology*, August 1983, pp. 1,553-1,558.
C.S. Carter et al. "Stress Corrosion Properties of High Strength Precipitation Hardening Stainless Steels," *Corrosion*, Vol. 27, No. 5, 1971, pp. 190-197.
J.R. Corwith, "The Downhole Corrosion Control Program at Ekofisk," *Noroil* February 1984.
S.D. Cramer et al. "Corrosion and Scaling of Nickel Alloys in Salton Sea Geothermal Environments," CORROSION/83.
M.S. de Santa Maria, A. Turnbull. "Effect of H_2S Concentration and pH on the Cracking Resistance of AISI 410 Stainless Steel in 5% Brine." National Physical Laboratory (UK), PB88-166087/XAB, 1987, p. 41.
C.T. Fujii. "Electrochemical Aspects of Stress-Corrosion Cracking - Recent SCC Studies on High-Strength

Steels," Report of NRL Progress, June 1974, pp. 21-28.28.
F.S. Gareau et al. "Effect of stress and environment on failures of 17-4 pH stainless steel valve stems." CORROSION/93, paper 146, NACE.
R.R. Gaugh. "Sulfide Stress Cracking of Precipitation-Hardening Stainless Steels," CORROSION/77, NACE.
S. Hashizume et al. "Corrosion Data on Laboratory Performance of Type 420 for OCTG." CORROSION/95, paper no. 77. NACE.
P. Hewitt, B.S. Hockenhull. "The Effect of Microstructures on the Stress Corrosion Cracking Susceptibility of a 13% Cr Martensitic Stainless Steel," *Corrosion Science,* 1976, Vol. 16, pp. 47-51.
Y. Ishizawa et al. "The Sulfide Stress Corrosion Cracking Resistance of 13% CR Steels for OCTG." 3rd Asian-Pacific Corrosion Control Conference, 1983.
P.S. Jackman, H. Everson. "Development of New Martensitic Stainless Steels for OCTG: The Challenges for the Steelmaker and the Tubemaker." CORROSION/95, paper no. 89.
R.D. Kane, J.B. Greer. "Stress Cracking of High-Strength Steels in Laboratory and Oilfield Environments," *Journal of Petroleum Technology*, November 1977, pp. 1,483-1,488.
R.D. Kane et al. "The Improvement of Sulfide Stress Cracking Resistance of 12% Chromium Stainless Steels Through Heat Treatment," CORROSION/76, NACE.
T. Kawate et al. "Manufacturing and Characteristics of 13 Cr Stainless Steel Tubing," *Kawasaki Steel Technical Report* No. 14, March 1986, pp. 83-92.
T. Kushida et al. "SCC Susceptibility and its Evaluation Method of 13 CR Martensitic Steel." CORROSION/93, paper no. 124. NACE.
K.H. Lange, R.K. Popperling. "Control of CO_2 Corrosion by Special Production Tubulars in Offshore Operation," Offshore Technology Conference, 1980. OTC 3890.
B. Lefebvre et al. "Behaviour of Carbon Steel and Chronium Steels in CO_2 Environments," CORROSION/84, NACE.
U. Lotz, "CO_2 Corrosion of C-Steel and 13% Cr Steel in a Particle Laden Fluid." CORROSION/87, paper no. 440. NACE.
W.C. Mack et al. "H_2S Testing of Specialty Steels for Oil Country Tubular Applications," CORROSION/81, NACE.
D.R. McIntyre. "Pitting of AISI 410 Stainless Steel in CO_2-Saturated Synthetic Seawater and Condensate," ASTM STP 970, American Society for Testing and Materials, 1988, pp. 246- 254.
Miyasaka et al. "Influence of Metallurgical Factors on Corrosion Behaviors of Modified 13% Martensitic Stainless Steels," CORROSION/90, paper no. 67, NACE.
Y. Miyata et al. "Toughness and Sulfide Stress Cracking Resistance of 13 Cr Stainless Steel OCTG Manufactured by Ausforming," CORROSION/95, paper no. 84. NACE.
Y. Miyata et al. "Corrosion of New 13Cr Martensitic Stainless Steel OCTG in Severe CO_2 Environment." CORROSION/95, paper no. 83, NACE.
E.H. Phelps. "Stress Corrosion of Ferritic-Martensitic Stainless Steels," *Metals Engineering Quarterly*, May 1973, pp. 44-49.
G.M. Pressouyre et al. "New Steels for Use in H_2S Environments," CORROSION/81, NACE.
E.T. Sherman et al. "Processing Low Carbon CA6NM to Meet NACE Hardness Requirments," *Steel Foundry Facts* No. 353, January 1983.
T. Shiraishi, K. Toyama. "NK Cr13 Steel Pipe for CO_2 Corrosion," *Nippon Kokan Technical Report*, Overseas No. 37, 1983, pp. 59-63.
K. Tamaki, "A New 13Cr OCTG for High Temperature and High Chloride CO_2 Environments," CORROSION/89, paper no. 469, NACE.
C.J. Thomas et al. "Environmentally Assisted Crack Growth in Martensitic Stainless Steels." *Materials Science and Engineering,* Vol. 78, 1986.

SECTION 2 AUSTENITIC STAINLESS STEELS

H.E. Hanninen. "Influence of Metallurgical Variables on Environment Sensitive Cracking of Austenitic Alloys." *International Metals Reviews*, No. 3, 1979.

S. Takemura et al. "Stress Corrosion Cracking of Stainless Steels in Hydrogen Sulfide Solutions." Stress Corrosion - New Approaches. ASTM STP 610, ASTM 1976.

Xinn et al. "Effect of Cold Work Strengthening on Sulfide on Stress Cracking Performance of Austenitic Stainless Steels." *1984 International Congress on Metallic Corrosion.*

FERRITIC STAINLESS STEELS

A.P. Bond, H.J. Dundas. "Effects of Composition on the Stress Corrosion Cracking of Ferritic Stainless Steels," *Corrosion*, Vol. 24, No. 10, pp. 344-352, October 1968.

J.P. Carter, S.D. Cramer. "Field Stress Corrosion Tests in Brine Environments of the Salton Sea Known Geothermal Recource Area," CORROSION/80, paper no. 203, NACE.

K. Fässler, H. Spähn, "On the corrosion behavior of a ferritic 18 Cr-2 Mo-steel-Part I," *Anti-Corrosion*, August 1982, pp. 4-16.

K. Fässler, H. Spähn, "On the Corrosion Behavior of a Ferritic 18 Cr-2 Mo Steel," *Alloys for the Eighties*, AMAX, 1980, pp. 281-301.

H.S. Kwon et al. "Influence of Thermal and Mechanical History on the SCC of Ferritic Stainless Steels," American Society for Metals, 1982, pp. 313-318.

N.L. Makarova et al. "Influence of Thermal Aging on the Tendency of Iron-Chromium Alloys to Corrosion Cracking," *Protection of Metals*, Vol. 16, No. 1, Jan-Feb. 1980, pp. 26-29.

T.W. Mohr et al. "Stress Corrosion Cracking of Ferritic Stainless Steels in Chloride Solutions," *Corrosion* Vol. 37, No. 4, April 1981, pp. 199-208.

H. Tomari et al. "Influence of Chemical Compositions on the Intergranular Stress Corrosion Cracking Susceptibilities of Ferritic Stainless Steels in High Temperature Aqueous Environments," CORROSION/81, paper no. 121, NACE.

R.F. Hehemann, "Stress Corrosion Cracking of Stainless Steels." *Met. Trans. A*, Volume 16A, November 1985, p. 1,909.

F.B. Pickering, "Physical metallurgy of stainless steel developments," *International Metals Reviews*, December 1976, pp. 227-267.

H. Tomari et al. "Intergranular Stress Corrosion Cracking of 13% Cr and 18% Cr Ferritic Stainless Steels in High Temperature High Purity Water," *Corrosion* vol. 38, No. 5, May 1982, pp. 283-294.

J.E. Truman. "Stress-Corrosion Cracking of Martensitic and Ferritic Stainless Steels," *International Metals Reviews*, 1981, No. 6, pp. 301-349.

SECTION 3 DUPLEX STAINLESS STEELS

J.P. Audouard et al. "Duplex austenitic ferritic stainless steels in oil and gas production," *Oil & Enterprise,* No. 18, January 1985, pp. 18-21.

M. Barteri et al. "Microstructural Study and Corrosion Performance of Duplex and Superaustenitic Steels in Sour Well Environment," CORROSION/86, paper no. 157, NACE.

B. Bazzoni et al. "Field and laboratory experiences of sulfide stress corrosion of a duplex stainless steel," *Werkstoffe und Korrosion* 36, 151-156(1985).

F. Braouezec et al. "Duplex Stainless Steel for Seamless Flow Line," presented at Middle East Corrosion, NACE, Bahrein, 1988.

S. Bernhardsson et al. "Controlling Environmentally Assisted Cracking by Using Duplex Stainless Steels," CORROSION/86, paper no. 331, NACE.

S. Bernhardsson et al. "Properties of Two Highly Corrosion Resistant Duplex Stainless Steels," CORROSION/81, paper no. 124, NACE.

S.O. Bernhardsson. "The Use of Special Stainless Steel Alloys to Solve SCC Problems in the Chemical Industry," pp. 585-593.

S.O. Bernhardsson, J. Oredsson. "The Stress Corrosion Cracking Resistance of Duplex and High-Alloy Austenitic Stainless Steels," UK National Corrosion Conference, 1982, pp. 63-64.

W.B. Bleakley. "Marathon Solves Brae Field's Problems," *Petroleum Engineer International*, March 15, 1983.

R.K. Churchill. "Mechanical Properties and Corrosion Resistance of Several Cast Duplex Stainless Steels," CORROSION/87, paper no. 305, NACE.

A. Desestret. "Sulfide Stress Corrosion Cracking Resistance of Several Austenitic & Duplex Stainless Steels in Chloride Solutions Containing Hydrogen Sulfide, Influence of Structure, Hardening Heat Treatment, Cold-Work and of the Temperature of the Solutions," CORROSION/83, paper 165, NACE.

M. Estavoyer, "Corrosion Problems at LACQ Sour Gas Field," *Journal of the Institute of Petroleum*, Vol. 46, No. 439, July 1960, pp. 223-233.

R. Francis et al. "The Effect of Cathodic Protection on Duplex Stainless Steels in Sea Water." CORROSION/95, paper 290, NACE.

B. Heritier et al. "Influence of the Austenite/Ferrite Ratio on the Mechanical Properties and the Corrosion Resistance of Duplex Stainless Steels." CORROSION/86, paper 158, NACE.

G. Herbsleb, R.K. Erling. "Corrosion Properties of Austenitic-Ferritic Duplex Steel AF 22 in Chloride and Sulfide Containing Environments," CORROSION/80, paper 13, NACE.

J. Kolts, A.I. Asphahani. "Effect of Temperature on the Chloride-Sulfide Stress Cracking of Stainless Tubulars," CORROSION/81, paper 99, NACE.

J. Kolts, "Properties of Ferralium Alloy 255 Duplex Stainless Steel for Sour Gas Well Applications." *J. of Materials for Energy Systems*, vol. 5, no. 2, September 1983, p. 71.

T. Kudo et al. "Stress Corrosion Cracking Resistance of 22% Cr Duplex Stainless Steel in Simulated Sour Environments," *Corrosion*, Vol. 45, No. 10, pp. 831-838.

A.C. Madsen et al., "Weldability of Duplex Stainless Steel Pipelines," CORROSION/87, paper 295, NACE.

A. Miyasaka et al. "Critical Conditions for High Alloys in Sour Gas Environments" presented at 10th International Congress on Metallic Corrosion.

H. Miyuki et al. "Localized Corrosion of Duplex Stainless Steels in CO_2-H_2S-Cl^- Environments at Elevated Temperatures," CORROSION/84, paper 293, NACE.

K. Ogawa et al. "An Estimating Method for the Critical Limit of Corrosion Resistance of the High Alloy OCTG and Line Pipe in the Sour Environments," CORROSION/87, paper no. 294, NACE.

J. Pleva, B. Johansson. "Evaluation of Welds on a Ferritic-Austenitic Stainless Steel," CORROSION/84 paper 218, NACE.

J.C. Prouheze et al. "Production of Tubing in Duplex Steel VS22 Influence of Cold Working on Mechanical Properties Behavior in Corrosive Sour Gas and Oil Environment" *J. Materials for Energy Systems*, Vol. 5, No. 1, June 1983.

J. Sakai et al. "Corrosion Resistance of Duplex Stainless Steel and its Weldment in Pipeline Service," CORROSION/87, paper 292, NACE.

J. Sakai et al. "Effects of Metallurgical Factors on Service Performance of Duplex Stainless Steel for Deep Sour Gas Wells," *J. Materials for Energy Systems*, Vol. 5, No. 2, September 1983, pp. 105-111.

N. Sridhar et al. "Corrosion and Mechanical Properties of Duplex Stainless Steel Weldments." American Society for Metals, No. 8410- 031, pp. 341-350.

H. Tsuge. "Corrosion Behavior of Duplex Stainless Steels for Oil and Gas Field Use," *The Sumitomo Search*, No. 36, May 1988, pp. 65-72.

M. Ueda et al."Performance of High Corrosion Resistant Duplex Stainless Steel in Chloride and Sour Environments." CORROSION/93, paper 125, NACE.

K. van Gelder et al. "The Stress Corrosion Cracking of Duplex Stainless Steel in $H_2S/CO_2/Cl^-$ Environments," Shell Research, Hydrogen Sulfide Induced Environment Sensitive Fracture of Steels (Proc. Conf.) Amsterdam, 1986, *Corros. Sci.*, 1987, 27, (10-11), 1,271-1,279.

Duplex Stainless Steels, R.A. Lula, ed. Metals Park, Ohio: American Society for Metals, 1983.

Volume II

SECTION 4 PRECIPITATION HARDENED NICKEL ALLOYS

T.A. Bednarowicz, S.L. Radabaugh. "Sour Service Performance of Alloy 625," CORROSION/88, paper no. 58, NACE.

M.J. Cieslak et al. "The Welding Metallurgy of Custom Age 625 PLUS Alloy," *Welding Research Supplement,* December 1989, pp. 473-s-482-s.

L.R. Curwick. "Development of Incoloy Alloy 925, an Age-Hardenable Corrosion Resistant Alloy for Sour Gas Service," Technical Paper 1219-CP, March 15, 1983, pp. 1-8. ASM Advisory Technical Awareness Council.

D.L. Dull, L. Raymond. "Surface Cracking of Inconel 718 During Cathodic Charging," *Metallurgical Transactions*, Volume 4, June 1973, pp. 1,635-1,637.

R.B. Frank, T.A. DeBold."Heat Treatment of an Age-Hardenable, Corrosion-Resistant Alloy UNS NO7716. CORROSION/90, paper 59, NACE.

H.P. Hack. "Mechanical, Corrosion, and Fatigue Properties of 15-5 pH, Inconel 718, and Rene' 41 Weldments," National Technical Information Service, May 1975, pp. 1-35.

J.A. Harris et al. "The Development of a Corrosion-Resistant Alloy for Sour Gas Service," CORROSION/84, paper 216, NACE.

J.A. Harris et al. "Effects of Hydrogen on the Engineering Properties of MONEL Nickel-Copper Alloy K-500," *Corrosion*, Vol. 28, No. 2, February 1972, pp. 57-62.

K. Hosoya et al. "Microstructural Role in Environmentally Assisted Cracking of Ni-Base Alloys," *Corrosion*, Vol. 44, No. 11, November 1988, pp. 838-851.

R.P. Jewett et al. "Hydrogen-Environment Embrittlement of Metals," NASA.

J.W. Kochera et al. "Experience with Stress Corrosion Cracking of Nickel-Base Alloys in Sour Hydrocarbon Production," CORROSION/76, March 22-26, 1976, pp. 1-7.

J. Prybylowski, R. Ballinger. "The Influence of Microstructure on Environmentally Assisted Cracking of Alloy 718," CORROSION/86, NACE.

N.S. Stoloff et al. "Hydrogen Embrittlement of an Aligned Y/Y[1]-ä Eutectic Alloy," *Scripta Metallurgica*, Vol. 10, 1976, pp. 889-893.

R.S. Treseder, R. Wieland. "Down-Hole Corrosion in a Salton Sea Geothermal Well," Society of Petroleum Engineers of AIME, paper no. 6,613, 1977.

R.H. Tuttle, J.W. Kochera. "Control of hydrogen embrittlement in deep gas wells," Conference on Effects of Hydrogen on Behavior of Materials, 1975, pp. 531-541.

R.J. Walter et al. "Influence of Gaseous Hydrogen on Metals Interim Report," Rocketdyne, No. N71-32489.

R.J. Walter, W.T. Chandler. "Influence of Gaseous Hydrogen on Metals," October 1973, pp. v-vii.

R.J. Walter, W.T. Chandler. "Influence of Hydrogen Environments on Crack Growth in Inconel 718," Engineering Societies Library, 1977, pp. 513-522.

R.J. Walter, W.T. Chandler. "Influence of Gaseous Hydrogen on Inconel 718," Proc. of the Intl. Conference on the Effects of Hydrogen on Materials Properties & Selection & Structural Design, 1973.

SECTION 5 SOLID SOLUTION NICKEL/COBALT BASE ALLOYS

H.S. Ahluwalia. "The role of strain rate testing in evaluating nickel base corrosion resistant alloy tubulars in hydrogen sulfide environments." CORROSION/93, paper 136, NACE.

A.I. Asphahani. "Evaluation of Highly Alloyed Stainless Materials for CO_2/H_2S Environments," *Corrosion*, Vol. 37, No. 6, June 1981, pp. 327-335.

P.D. Bunch et al. "Corrosion/Galling Resistant Hardfacing Materials for Offshore Production Valves," Offshore Technology Conference, 1989.

H.C. Choi. "The effect of elemental sulfur and surface condition on stress corrosion cracking of high alloys under hot sour environments." CORROSION/92, paper 59, NACE.

A. Ikeda et al. "Corrosion Behaviors of High Alloy Oil Country Tubular Goods for Deep Sour Gas Well." CORROSION/84, paper 206, NACE.

A. Ikeda et al. "On the Evaluation Methods of Ni-Base Corrosion Resistant Alloy for Sour-Gas Exploration and Production," *Corrosion*, October 1989, pp. 838-847.

R.D. Kane, J.B. Greer. "Embrittlement of High-Strength, High-Alloy Tubular Materials in Sour Environments," SPE, October 9-12, 1977.

R.D. Kane et al. "Stress Corrosion Cracking of Nickel and Cobalt-Base Alloys in Chloride-Containing Environments," CORROSION/79, NACE.

L.J. Klingler, G.A. Kurisky. "MP35N Alloy-The Ultimate Wire Material," *Wire Journal*, July 1980.

J. Kolts et al. "Environmental Embrittlement of Nickel and Nickel Base Alloys - An analogy to Steels and Austenitic Stainless Steels." *J. of Materials for Energy Systems*, Vol. 8, no. 3, 12(1986): p. 306-318.

J. Kolts. "Environmental Embrittlement of Nickel-Base Alloys." *Metals Handbook*, Volume 13, Corrosion, ASM, 1987, p. 647.

P. Marcus, H. Talah. "Sulfur Induced Breakdown of Passive Films and Pitting of Nickel and Nickel Alloys." *Corrosion Science*, V. 29, No.4, 1989.

D.R. McIntyre et al. "Slow Strain Rate Testing for Materials Evaluation in High Pressure H_2S Environments." CORROSION/86, paper 149, NACE.

D.A. Mezzanotte et al. "Hydrogen Transport in a Ni-Base Superalloy," *Scripta Metallurgica*, Vol. 14, No. 2, 1980.

A. Miyasaka et al. "Criteria for the Prediction of Application Limits of CRA's in Sour Gas Environments." Paper presented at the Annual Conference of JSCE, June 20-22, 1986.

A. Miyasaka et al. "Environmental Aspects of SCC of High Alloys in Sour Environments." *Corrosion*, Vol. 45, No. 9, pp. 771-780 (1989) September.

J.M. Moyer, R.J. Gerlock. "A New Corrosion Resistant Nickel-Base Alloy for Gas and Oil Industry Use." CORROSION/83, NACE.

K. Mudge. C.J. Levesque. "Materials choice can cut downhole corrosion," Sept. 27, 1982, *Oil & Gas Journal*, pp. 245-248.

J. Murayama et al. "Role of Alloying Elements on Corrosion Resistant Ni Based Alloy for Sour Gas Environment." paper A84-45, The Metallurgical Society of AIME.

P.B. Needham Jr. et al. "Corrosion Studies in High-Temperature, Hypersaline Geothermal Brines," CORROSION/79, NACE.

H. Ogawa et al. "Development of High-Alloy Tubular Goods for Sour Wells." *Nippon Steel Technical Report* No. 38, July 1988.

E.L. Raymond. "Mechanisms of Sensitization and Stabilization of Incoloy Nickel-Iron-Chromium Alloy 825," *Corrosion*, vol. 24, no. 6, June 1968, pp. 180-188.

F.J. Rizzo. "New Critical Service CRA Alloys," Offshore Technology Conference, 1989.

C.M. Schillmoller. "Selection of Corrosion-Resistant Alloy Tubulars for Offshore Applications," Presented at 21st Annual Offshore Technology Conference, 1989.

C.M. Schillmoller. "High Performance Alloys: How They are used Offshore," World Oil Exploration Drilling Production, Offshore '88, July 1988.

A.J. Sedriks. "Stress-Corrosion Cracking of Stainless Steels and Nickel Alloys," *Journal of the Institute of Metals*, Vol. 101, 1973, pp. 225-232.

W.J. Sisak et al. "Corrosion and Cracking of Alloy C-276 in High Temperature Brine Solutions." paper 60, CORROSION/92, NACE.

N. Sridhar et al. "Effect of Low Temperature Aging on Hydrogen-Induced Crack Growth in a Ni-Base Superalloy," *Scripta Metallurgica*, Vol. 14, No. 11, 1980, pp. 1,257-1,260.

N. Sridhar et al. "Hydrogen-Induced Crack Growth in a Ni-Base Superalloy," *Scripta Metallurgica*, Vol. 14, No. 2, 1980, pp. 225-228.

J.P. Stroup et al. "Multiphase MP35N - An Alloy for Deep Sour Well Service," *Materials Performance*, June 1976.

S. Tsujikawa et al. "A New Method of Predicting Pitting Corrosion Resistance of CRA's in Sour Environments." paper 64, CORROSION/88, NACE.
M. Tsuji et al. "High Nickel Alloy Clad Pipe by UOE Process for H_2S-CO_2-CL^- Environment," OMAE 88.
M. Ueda et al. "Influence of Element on Corrosion Resistance of Ni Base Alloy in Sulfur Containing Sour Environment." CORROSION/94, paper 69, NACE.
G.A. Vaughn, J.B Greer. "High-Strength Nickel-Alloy Tubulars for Deep, Sour Gas Well Application," SPE, September 21-24, 1980.
Watkins et al. "Laboratory Testing of the SCC Resistance of Stainless Alloys." CORROSION/87, paper 283, NACE.
E.P. Whelan. "Sulfide Stress Cracking Resistance of Superalloys for Sour Gas Well Applications," in *Hydrogen Effects in Metals*, Metallurgical Society of AIME, 1980
S.M. Wilhelm. "Effect of Elemental Sulfur on Stress Corrosion Cracking of Nickel Base Alloys in Deep Sour Gas Well Production," CORROSION/88, paper no. 77, NACE.

SECTION 6 OTHER ALLOYS

K.C. Bendall, C.D.S. Tuck. " Development, Properties, Performance Testing of a Very High Strength Cupronickel with Resistance to Hydrogen Embrittlement." paper 46, CORROSION/95, NACE.
J. Booker et al. "Corrosion behavior of beryllium copper and other nonmagnetic alloys in simulated drilling environments." CORROSION/84, paper 220, NACE.
R.K. Conrad et al. "Corrosion of Selected Metals and a High-Temperature Thermoplastic in Hypersaline Geothermal Brine," RI No. 8792, U. S. Department of the Interior, Bureau of Mines Report of Investigations, 1983.
W.F. Czyrklis, M. Levy. "Stress Corrosion Cracking Susceptibility of β Titanium Alloy 38-6-44*," *Corrosion*, Vol. 32, No. 3, March 1976, pp. 99-102.
W.W. Love et al. "The Use of Beta-C™ Titanium for Downhole Production Casing in Geothermal Wells, "Sixth World Conference on Titanium", 1988, France, sponsored by Societe Francaise de Metallurgie et de Materiaux.
R.W. Schutz. "Performance and Application of Titanium Alloys in Geothermal Brine Service," *Materials Performance*, NACE, January 1985, pp. 9-17.
R.W. Schutz, J.S. Grauman. "Fundamental Corrosion Characterization of High-Strength Titanium Alloys," *Industrial Applications of Titanium and Zirconium*, pp. 130-142.
W.L. Silence, K.A. Groeneveld. "High Strength Alloy Wirelines for Deep Oil and Gas Well Service," CORROSION/89, paper no. 11, NACE.
D.E. Thomas et al. "Beta-C: An Emerging Titanium Alloy for the Industrial Marketplace," *Industrial Applications of Titanium and Zirconium*, ASTM STP 917, p. 144-163.
J.C. Turn, J.O. Ratka. "The Mehanical Behavior of Hydrogen Charged Beryllium Copper." paper 171, CORROSION/86, NACE.
W. Tsai et al. "Hydriding and Cracking Behavior of Titanium under Cathodic Polarization Conditions." *J. Materials Engineering*, Vol. 10, No. 2, 1988, p. 93.
A.H. Tuthill. "Guidelines for the Use of Copper Alloys in Seawater," *Materials Performance*, Vol. 26, No. 9, September 1987, pp. 12-22.
A.H. Tuthill. "The Right Metal for Heat Exchanger Tubes," *Chemical Engineering*, January 1990.
M. Ueda et al. "Corrosion behavior of titanium alloys in a sulfur-containing H_2 CO_2-CI^- environment." paper 271, CORROSION/90, NACE.
T. Yau. "Zirconium versus corrosive species in geothermal fluids." CORROSION/84, paper 140, NACE.
T. Yau. "Corrosion behavior of zirconium in H_2S-containing environments." 5th Asian-Pacific Corrosion Control Conference in conjunction with 27th Australasian Association Conference, Melbourne, Australia, 1987.

SECTION 7 ACIDIZING CORROSION-RESISTANT ALLOYS

P.A. Burke et al. "Corrosion of Chromium Steels in Inhibited Acids." CORROSION/87, paper 41, NACE.

J.M. Cassidy et al. "Repassivation of 13Cr after acidizing, Electrochemical investigation of oxidizing solutions." paper 87, CORROSION/94, NACE.

S. Huizinga, W.E. Liek. "The performance of 13Cr steel in acid stimulations." paper 80, CORROSION/93, NACE.

R. Jasinski et al. "Inhibiting HCl Corrosion of High Chrome Tubular Steels." paper 188, CORROSION/88, NACE.

J. Kolts et al. "Stress Corrosion Cracking of Nickel Base Alloys in Room Temperature HCl Containing H_2S, *Environment Induced Cracking of Metals*, ASM, 1988.

N. Nilsen. "Corrosion Behavior and Cathodic Protection of Stainless Steels for Offshore Hot Risers." CORROSION/ 85, paper 320, NACE.

A. Valdes, M.E. Afonso. "A comparison of 13%-22% Cr alloys under acidizing condtitions." paper 88, CORROSION/95, NACE.

B. Vicentini et al. "Corrosion Behavior of High Alloys Tubular Materials in Inhibited Acidizing Solutions." CORROSION/87, paper 43, NACE.

M.L. Walker, T.H. McCoy. " Effect and Inhibition of Stimulation Acids on Corrosion Resistant Alloys." paper 154, CORROSION/86, NACE.

M.L. Walker. "Inhibition of High Alloy Tubulars II: Effect of Fluoride Ion and Acid Strength." paper 189, CORROSION/88, NACE.